OIL SPILL ENVIRONMENTAL FORENSICS CASE STUDIES

Edited by
Scott A. Stout
Zhendi Wang

B
H

OIL SPILL ENVIRONMENTAL FORENSICS CASE STUDIES

OIL SPILL ENVIRONMENTAL FORENSICS CASE STUDIES

Edited by

SCOTT A. STOUT, Ph.D.
NewFields Environmental Forensics Practice, LLC, Rockland, MA, United States

ZHENDI WANG, Ph.D.
Environment and Climate Change Canada, Ottawa, ON, Canada

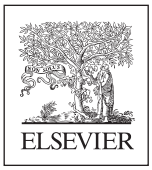

Butterworth-Heinemann
An imprint of Elsevier

Butterworth-Heinemann is an imprint of Elsevier
The Boulevard, Langford Lane, Kidlington, Oxford OX5 1GB, United Kingdom
50 Hampshire Street, 5th Floor, Cambridge, MA 02139, United States

Notices
Knowledge and best practice in this field are constantly changing. As new research and experience broaden our understanding, changes in research methods, professional practices, or medical treatment may become necessary.

Practitioners and researchers must always rely on their own experience and knowledge in evaluating and using any information, methods, compounds, or experiments described herein. In using such information or methods they should be mindful of their own safety and the safety of others, including parties for whom they have a professional responsibility.

To the fullest extent of the law, neither the Publisher nor the authors, contributors, or editors, assume any liability for any injury and/or damage to persons or property as a matter of products liability, negligence or otherwise, or from any use or operation of any methods, products, instructions, or ideas contained in the material herein.

British Library Cataloguing-in-Publication Data
A catalogue record for this book is available from the British Library

Library of Congress Cataloging-in-Publication Data
A catalog record for this book is available from the Library of Congress

ISBN: 978-0-12-804434-6

Publisher: Matthew Deans
Acquisition Editor: Ken McCombs
Editorial Project Manager: Peter Jardim
Production Project Manager: Sruthi Satheesh
Cover Designer: Matthew Limbert

Typeset by MPS Limited, Chennai, India

List of Contributors

Puspa L. Adhikari Louisiana State University, Baton Rouge, LA, United States

Matthew Adkins CSX Transportation, Inc., Lithia Springs, GA, United States

Joan Albaigés Spanish National Research Council (CSIC), Barcelona, Spain

Hernando P. Bacosa The University of Texas Marine Science Institute, Port Aransas, TX, United States

Gregory Baker NOAA, Menlo Park, CA, United States

Fred Baldassare ECHELON Applied Geochemistry Consulting, Murrysville, PA, Unites States

Josep M. Bayona Spanish National Research Council (CSIC), Barcelona, Spain

C.J. Beegle-Krause Sintef OCEAN AS, Trondheim, Norway

Mark J. Benotti NewFields Environmental Forensics, LLC, Rockland, MA, United States

Detlef A. Birkholz Analytical Consultant, Inc., Edmonton, AB, Canada

Cornelia Blaga Netherlands Forensic Institute (NFI), The Hague, The Netherlands

Chui-Wei Bong University of Malaya, Kuala Lumpur, Malaysia

Samantha H. Bosman Florida State University, Tallahassee, FL, United States

Carl E. Brown Environment and Climate Change Canada, Ottawa, ON, Canada

Pamela Brunswick Environment and Climate Change Canada, North Vancouver, BC, Canada

Jeffrey P. Chanton Florida State University, Tallahassee, FL, United States

Elizabeth Chapman ECHELON Applied Geochemistry Consulting, Murrysville, PA, Unites States

Mei-Hua Chen CPC Corporation, Miaoli, Taiwan

Fanny Chever Centre de Documentation de Recherche d'Expérimentations, Brest, France

Jan H. Christensen University of Copenhagen, Frederiksberg, Zealand, Denmark

Julie Corley FTI Consulting, San Francisco, CA, United States

Deborah Crowley RPS-ASA, South Kingstown, RI, United States

Laura de la Torre Spanish Maritime Safety Agency (SASEMAR), Madrid, Spain

Olívia M.C. de Oliveira Universidade Federal da Bahia (UFBA), Salvador, Bahia, Brazil

Antônio F. de Souza Queiroz Universidade Federal da Bahia (UFBA), Salvador, Bahia, Brazil

Majbrit Dela Cruz University of Copenhagen, Frederiksberg, Zealand, Denmark

Carmen Domínguez Spanish National Research Council (CSIC), Barcelona, Spain

Gregory S. Douglas NewFields Environmental Forensics Practice, LLC, Rockland, MA, United States

William B. Driskell Consultant, Seattle, WA, United States

Stephen Emsbo-Mattingly NewFields Environmental Forensics Practice, LLC, Rockland, MA, United States

Noemi Esquinas University of Oviedo, Mieres, Spain

Meredith M. Evans The University of Texas Marine Science Institute, Port Aransas, TX, United States

Nicolas Fitz Federal Maritime and Hydrographic Agency, Hamburg, Germany

James S. Franks The University of Southern Mississippi, Ocean Springs, MS, United States

Deborah P. French-McCay RPS-ASA, South Kingstown, RI, United States

José Luis R. Gallego University of Oviedo, Mieres, Spain

Fabiana D.C. Gallotta Petrobras Research Center, Rio de Janeiro, Brazil

A.J. Gravel FTI Consulting, Rockville, MD, United States

Julien Guyomarch Centre de Documentation de Recherche d'Expérimentations, Brest, France

Jeffery Hardenstine NewFields Environmental Forensics Practice, LLC, Rockland, MA, United States

Joshua A. Harrill Center for Toxicology and Environmental Health, North Little Rock, AR, United States

Shijie He Ludong University, Yantai, China

Edward (Ted) Healey NewFields Environmental Forensics Practice, LLC, Rockland, MA, United States

Ching-Jen Ho Environmental Protection Administration Executive Yuan, Taipei, Taiwan

Bruce Hollebone Environment and Climate Change Canada, Ottawa, ON, Canada

Matthew Horn RPS-ASA, South Kingstown, RI, United States

Wei-Nung Hung Industrial Technology Research Institute, Hsinchu, Taiwan

Katherine Jayko RPS-ASA, South Kingstown, RI, United States

Ronan Jezequel Centre de Documentation de Recherche d'Expérimentations, Brest, France

Paul G.M. Kienhuis Rijkswaterstaat CIV, Lelystad, The Netherlands

Marcus Kim Agilent Technologies Inc., Mississauga, ON, Canada

John A. Kind Center for Toxicology and Environmental Health, North Little Rock, AR, United States

Kerylynn Krahforst NewFields Environmental Forensics Practice, LLC, Rockland, MA, United States

Mette Kristensen University of Copenhagen, Frederiksberg, Zealand, Denmark

Michael A. Kruge Montclair State University, Montclair, NJ, Unites States

Christopher L. Kuhlman Center for Toxicology and Environmental Health, North Little Rock, AR, United States

Patrick Lambert Environment and Climate Change Canada, Ottawa, ON, Canada

Mike Landriault Environment and Climate Change Canada, Ottawa, ON, Canada

Azucena Lara-Gonzalo University of Oviedo, Mieres, Spain

Stephen R. Larter University of Calgary, Calgary, AB, Canada

Sandra Layland FTI Consulting, Santa Barbara, CA, United States

Lisa Lefkovitz Battelle Memorial Institute, Norwell, MA, United States

Yuanwei Li Yantai Institute of Coastal Zone Research, Chinese Academy of Sciences, Yantai, China

Zhengkai Li RPS-ASA, South Kingstown, RI, United States

Danúsia F. Lima Universidade Federal da Bahia (UFBA), Salvador, Bahia, Brazil

Eric Litman NewFields Environmental Forensics Practice, LLC, Rockland, MA, United States

Bo Liu NewFields Environmental Forensics Practice, LLC, Rockland, MA, United States

Xiaoxing Liu Dalian Maritime University, Dalian, China

Zhanfei Liu The University of Texas Marine Science Institute, Port Aransas, TX, United States

Daniel Mendelsohn RPS-ASA, South Kingstown, RI, United States

Maria de F.G. Meniconi Research and Development Center (CENPES), Petroleo Brasileiro S.A (PETROBRAS), Rio de Janeiro, Brazil

Buffy M. Meyer Louisiana State University, Baton Rouge, LA, United States

Martin Scott Miles Louisiana State University, Baton Rouge, LA, United States

Glenn C. Millner Center for Toxicology and Environmental Health, North Little Rock, AR, United States

Marc A. Mills United States Environmental Protection Agency, Cincinnati, OH, United States

Ícaro T.A. Moreira Universidade Federal da Bahia (UFBA), Salvador, Bahia, Brazil Universidade Salvador—UNIFACS, Salvador, Bahia, Brazil

Paul A. Nony Center for Toxicology and Environmental Health, North Little Rock, AR, United States

Thomas B.P. Oldenburg University of Calgary, Calgary, AB, Canada

Gregory M. Olson Louisiana State University, Baton Rouge, LA, United States

Edward B. Overton Louisiana State University, Baton Rouge, LA, United States

Joseph Papineau EnviroScience, Inc., Stow, OH, United States

Grace Park Environment and Climate Change Canada, North Vancouver, BC, Canada

James R. Payne Payne Environmental Consultants, Inc., Encinitas, CA, United States

Leo Peschier Netherlands Forensic Institute (NFI), The Hague, The Netherlands

R. Paul Philp University of Oklahoma, Norman, OK, United States

Kristoffer G. Poulsen University of Copenhagen, Frederiksberg, Zealand, Denmark

Jagoš R. Radović University of Calgary, Calgary, AB, Canada

Claudia Y. Reyes Universidade Federal da Bahia (UFBA), Salvador, Bahia, Brazil

Kelsey L. Rogers Florida State University, Tallahassee, FL, United States

David Runciman Cherith, Orkney, United Kingdom

Dayue Shang Environment and Climate Change Canada, North Vancouver, BC, Canada

Carine S. Silva Universidade Federal da Bahia (UFBA), Salvador, Bahia, Brazil

Malcolm L. Spaulding University of Rhode Island, Narragansett, RI, United States

Scott A. Stout NewFields Environmental Forensics Practice, LLC, Rockland, MA, United States

Gordon Todd Heriot-Watt University, Edinburgh, United Kingdom

Imma Tolosa International Atomic Energy Agency (IAEA), Monaco-Ville, Monaco

Giorgio Tomasi University of Copenhagen, Frederiksberg, Zealand, Denmark

Vahab Vaezzadeh University of Malaya, Kuala Lumpur, Malaysia

Graham van Aggelen Environment and Climate Change Canada, North Vancouver, BC, Canada

Angela de L.R. Wagener Pontifical Catholic University of Rio de Janeiro (PUC-Rio), Rio de Janeiro, Brazil

Chuanyuan Wang Yantai Institute of Coastal Zone Research, Chinese Academy of Sciences, Yantai, China

Qing Wang The University of Texas Marine Science Institute, Port Aransas, TX, United States East China Normal University, Shanghai, China

Zhendi Wang Environment and Climate Change Canada, Ottawa, ON, Canada

Shawn M. Wnek Center for Toxicology and Environmental Health, North Little Rock, AR, United States

Wendy Wong NewFields Environmental Forensics Practice, LLC, Rockland, MA, United States

Suh-Huey Wu CPC Corporation, Miaoli, Taiwan

Chun Yang Environment and Climate Change Canada, Ottawa, ON, Canada

Zeyu Yang Environment and Climate Change Canada, Ottawa, ON, Canada

Mohamad P. Zakaria University of Malaya, Kuala Lumpur, Malaysia

Gong Zhang Environment and Climate Change Canada, Ottawa, ON, Canada

Haijiang Zhang Yantai Oil Spill Response Technical Center of Yantai MSA, Yantai, China

Preface

Advances in the environmental forensics aspects of oil spill research are continually being achieved. Our first textbook on this subject (*Oil Spill Environmental Forensics*, Academic Press, 2007) brought together researchers from 11 countries to convey what, at the time, represented a state-of-the-science compilation of the proven and emerging technologies relevant to the forensic questions surrounding oil spills' impacts on the environment. This original compilation included reviews of the methods focused on chemical fingerprinting and source identification, as well as a limited number of case studies dating back to the *Exxon Valdez* studies in the 1990s, which some recognize as the commencement of oil spill environmental forensics. The authors strove to provide thorough inventories of the relevant literature previously dispersed in chemistry, geology, oceanography, and environmental books, journals, and unpublished reports into a single volume.

Following the *Deepwater Horizon* disaster and oil spill in 2010 a new surge in oil spill research occurred that rapidly expanded the breadth of technologies and data analysis methods utilized in oil spill environmental forensics. The available literature expanded commensurate with these efforts and our second edition textbook (*Standard Handbook—Oil Spill Environmental Forensics*, Academic Press, 2016) attempted to capture the new state-of-the-science following this surge in oil spill research. That effort was intentionally focused on the most relevant topics or categories, such as sampling and study design, expanded or new diagnostic chemicals, analytical instrumentation, data analysis and interpretation, different types of petroleum, weathering effects, fate and transport, and fingerprinting different matrices (water, tissues, sediments). All along, it was our intention to follow the 2016 textbook with this one, in which we strove to assemble and present "real world" oil spill case studies.

In this book we have assembled 34 chapters that serve to present various aspects of environmental forensics in relation to "real-world" oil spill case studies from around the globe. The magnitude of the collective efforts of the chapters' lead authors and the dozens of co-authors, representing academic, government, and private researcher groups from 14 countries, is commendable. The professionalism shown by these diverse groups in respecting our deadlines and following our guidance has made our editorial task enjoyable, and we hope, has brought a more global perspective to this volume.

For the book we have broadened the definition of "oil spill" to include releases that include natural gas/methane, automotive gasoline and other petroleum fuels, lubricants, vegetable oils, paraffin waxes, bitumen, manufactured gas plant residues, urban runoff, and, of course, crude oil, the latter ranging from light Bakken shale oil to heavy Canadian oil sands oil. New challenges surrounding forensic investigations of stray gas in the shallow subsurface, volatiles in air, dissolved chemicals in water (including passive samplers), and biological tissues associated with oil spills are included in various case studies, as are the effects and long-term oil weathering, long-term monitoring in urbanized and nonurbanized environments, fate and transport, forensic historical research, new analytical and chemical data processing and interpretation methods.

In closing, it is acknowledged that all scientists at any point in their career share one common goal—to continue to learn. And although we all learn from our own experiences, the ability to learn from others' experiences cannot be understated. Therefore, we hope that this volume focused on case studies will not only be of interest and educational to experienced oil spill researchers, but also to lecturers and students alike. It is left to the reader to use the information contained herein to achieve a greater understanding, and perhaps modify and improve their thinking with respect to the various aspects of oil spill environmental forensics.

Scott A. Stout
NewFields Environmental Forensics Practice, LLC, Rockland, MA, United States
Zhendi Wang
Environment and Climate Change Canada, Ottawa, ON, Canada
September 2017

CHAPTER

1

Critical Review of an Interlaboratory Forensic Dataset: Effects on Data Interpretation in Oil Spill Studies

Eric Litman, Stephen Emsbo-Mattingly and Wendy Wong

NewFields Environmental Forensics Practice, LLC, Rockland, MA, United States

BIOGRAPHIES

Eric Litman is an environmental scientist with 15 years of laboratory and consulting experience specializing in applied chemistry and technical project management. Since 2010, he has been a consulting scientist at NewFields Environmental Forensics Practice, LLC in Rockland, Massachusetts working in support of governmental and industrial clients. During this time he has managed a variety of regulatory and industrial site investigations focused on the chemical characterization of environmental contaminants and conducted extensive research during the NRDA investigation following the *Deepwater Horizon* oil spill. His research interests include the optimization of analytical techniques and the development of emerging environmental technologies.

Wendy Wong is a consulting scientist at NewFields Environmental Forensics Practice, LLC in Rockland, Massachusetts. Ms. Wong has 19 years of experience in the field of environmental chemistry and specializes in detailed chemical analysis, chemical fingerprinting, and applications of environmental forensic principles for advanced site investigation projects. Over the years, Ms. Wong has worked on numerous site assessment and investigative projects, including roles as analyst, consulting chemist and technical project leader. She has managed laboratory operations during multiple large-scale oil spill investigations including the *Exxon Valdez*, Saudi/Gulf War, *Cosco Busan*, and *Deepwater Horizon* oil spills. As an experienced forensics chemist and a strong operations professional, she has optimized laboratory operations through staff training, process improvement, scaling of analytical capabilities, enhancement of real-time quality control measures, and augment client and laboratory communication to meet the demands of these high-profile, technical forensics programs.

Stephen Emsbo-Mattingly is a senior scientist at the NewFields Environmental Forensics Practice in Rockland, MA. He has 28 years of environmental chemistry and forensic investigation expertise. He specializes in the source identification of petroleum, tar, PAHs, PCBs, dioxins, and chlorinated solvent products in the environment. His chemical fingerprinting involve extensive research concerning the process chemistry associated with petroleum and tar refineries, coal operations, pavement producers, chemical manufacturers, metal fabricators, degreasing operations, dry cleaning, avionics, electrical utilities, wood treaters, pipelines, hydraulic fracturing, oil & natural gas development, railroading, automobile manufacturing and recycling, circuit board manufacturing, and wastewater treatment plants. He has authored or coauthored over 100 papers, book chapters, guidance documents, and presentations. His research extends to natural ambient sources of contaminants, such as petroleum seeps, coal fires, sewage and storm-water runoff. He is a member of the American Chemical Society, Society of Environmental Toxicology and Chemistry, Air and Waste Management Association, American Wood Protection Association, and Society for Industrial Archeology. His project portfolio reflects a wide range of public and private sector sponsors in support of site investigations, risk assessments, liability management, as well as civil and criminal litigation.

Oil Spill Environmental Forensics Case Studies.
DOI: http://dx.doi.org/10.1016/B978-0-12-804434-6.00001-X

1.1 INTRODUCTION

In this chapter, we consider the intra- and interlaboratory variability for traditional and nontraditional analytes generated during one of the largest environmental forensic investigation conducted to date, the NOAA *Deepwater Horizon* (DWH) oil spill natural resource damage assessment (NRDA). Large-scale and long-term environmental investigations can require the use of multiple laboratories to meet the traditional data quality objectives (DQOs) associated with regulatory programs, such as USEPA Superfund or NOAA NRDA. However, traditional quality assurance programs require accommodations and adjustments for nontraditional analytes [e.g., alkylated polycyclic aromatic hydrocarbons (PAHs) and geochemical biomarkers] and nontraditional DQOs (e.g., forensic source identification and environmental weathering). Specifically, the variability that unavoidably exists within interlaboratory data presents a challenge to forensic data users as they attempt to differentiate in-situ trends and minimize laboratory bias and variability.

The chemistry data collected during an oil spill investigation generally measures five classes of hydrocarbon compounds. These include volatile hydrocarbons, saturated hydrocarbons, total petroleum hydrocarbons (TPH_{C9-C44}) PAHs and geochemical biomarkers. This evaluation focuses on the particular measurement of PAHs, alkylated PAHs and geochemical biomarkers in interlaboratory data and considers the effects of interlaboratory variability on the reliability of these compounds in forensic data interpretation. PAH and geochemical biomarker analyses typically include both traditional EPA priority pollutant PAHs and nontraditional chemicals, including sulfur-containing heterocyclic PAHs, alkylated PAHs and terpane, sterane, and triaromatic steroid geochemical biomarkers. These nontraditional chemicals are specifically related to the identification and characterization of petroleum and petroleum-derived products.

Priority pollutant PAH data is generated using well-established environmental methods that are designed for the commercial laboratory industry. These methods attempt to limit variability that is introduced through method bias and experimental error by using mature standard operating procedures and measuring analytes that have been studied by commercial environmental laboratories since the implementation of the priority pollutant list in 1976. Environmental chemists throughout the world have cultivated years of experience measuring and evaluating the mass spectra of these compounds using gas chromatography (GC) and mass spectrometry. Priority pollutant PAHs are an important subset of data collected during an oil spill investigation and are critically important to regulatory decision making regarding ecological and human-risk assessments.

Unfortunately, priority pollutant PAH concentrations alone do not provide the chemical specificity needed to characterize the more complex mixtures of hydrocarbons found in crude petroleum. For instance, the 16 parent PAHs included on the EPA priority pollutant list are only a small subset of the parent PAHs, alkylated PAH and geochemical biomarker target compounds used in forensic oil spill investigations (NOAA DWH AQAP, 2014). By comparison, the alkylated PAH analytes represent more than 19,000 individual PAH isomers (Emsbo-Mattingly and Litman, 2016). These nontraditional petroleum-related compounds tend to demonstrate higher levels of laboratory variability due to the methodological nuances required to measure the alkylated PAHs as homolog groups. Laboratories need to modify and optimize standard operating procedures and methods to account for these complex mixtures of compounds. These method modifications are best completed by chemists experienced with the measurement of nontraditional hydrocarbon analytes, modern instruments, relevant literature, and specialized analytical standards or certified reference materials.

Program managers frequently implement quality control (QC) procedures to monitor and correct laboratory performance problems with analytical quality assurance plans (AQAPs) that may include periodic analyses of National Institute of Standards and Technology (NIST) standard reference materials (SRMs), surrogate corrected analyte concentrations, third party data validation and round robin interlaboratory calibration studies. Environmental professionals emphasize the importance of monitoring and controlling the variability for priority pollutant PAHs; however, most of these QC strategies are designed for standard EPA methodologies and standard EPA target analytes. These techniques do not provide QC measures that monitor the variability of nontraditional target analytes like alkylated PAHs and geochemical biomarkers. This is largely due to the fact that these classes of nontraditional compounds have historically been analyzed by a small number of specialized forensic laboratories. These nontraditional compounds present technical challenges that are different than standard priority pollutant analysis. Alkylated PAHs are present as homologous series that contain many isomers per carbon group.

Traditional QC techniques used to monitor precision and accuracy like blank spikes, matrix spikes and reference materials are dependent on the availability of analytical standards or certified reference materials. The geochemical biomarker compounds studied in oil spill investigations are discrete chemicals with limited commercial availability. Analytical standards for many of these compounds are expensive or difficult to purchase commercially. These factors create an analytical environment where data variability is very difficult and expensive to control. These traditional QC measures are not easily employed by laboratories for alkylated PAHs and geochemical biomarkers.

This review considers the implications of using intra- and interlaboratory data diagnostically for forensic interpretation.

1.2 LABORATORY STUDIES CONSIDERED

The NOAA DWH NRDA evaluated the environmental fate of crude oil released from the failed Macondo well following the explosion of the DWH drill rig and measured the resulting exposure of the resources in the northern Gulf of Mexico (GOM) to the oil (and chemical dispersants). The sampling and analytical plan was focused on establishing a pathway from the Macondo well to impacted natural resources and the confirmation that the observed exposure was a forensic match to the spilled Macondo oil. This required the collection and forensic analysis of tens of thousands of unique field samples that included crude oil, stranded oil, oil adsorbent devices, sea water, animal tissue, vegetation, marine sediment, and marsh soil matrices. These samples were collected from the deep benthos, water column, shoreline, marshland and various other ecological communities that comprise the GOM ecosystem. In addition to the large-scale analysis of field samples thousands of QCs samples were also analyzed to support the quality and reliability of the investigation data. In addition to standard laboratory QC samples investigators also required the analysis of NIST Standard Reference Materials (SRM) and forensic reference materials like Alaska North Slope crude oil and Macondo (MC252) crude oil (NOAA, 2014). This created a unique data environment where reference oil data from contributing laboratories could be evaluated for precision and accuracy. NOAA program managers enlisted scientists from NIST to formalize this interlaboratory comparison into a series of supporting studies that could be relied upon to evaluate the integrity and reliability of the investigation data.

1.2.1 Interlaboratory Calibration Studies Considered

During the NOAA DWH NRDA three round robin studies were conducted on behalf of NOAA investigators by NIST between 2010 and 2011. These studies were designed to evaluate the interlaboratory precision and accuracy of results reported by participating laboratories for priority pollutant parent PAHs, heterocyclic parent PAHs, alkylated PAHs and selected terpane and sterane geochemical biomarker compounds. The studies focused on the analysis of three matrices; (1) QA10OIL01 crude Macondo reference oil (NISTIR 7793, 2011), (2) hydrocarbon impacted marine sediment collected from a waterway in New York/New Jersey (NISTIR 7792, 2011), and (3) mussel tissue homogenate prepared by NOAA Status and Trends (NS&T) laboratories as QC90TC (NISTIR 7819, 2011). The NISTIR 7793 QA10OIL01 crude oil study had 26 participating laboratories, the NISTIR 7792 QA10SED01 marine sediment study had 33 participating laboratories and the NISTIR7819 QA10TIS01 mussel tissue study had 34 participating laboratories. In this chapter, the mussel tissue reference samples were only evaluated for PAHs and alkylated PAHs and not for geochemical biomarkers due to the limited amount of biomarker data generated during the NIST QA10TIS01 interlaboratory study (NIST, 2011c).

NIST instructed the laboratories that participated in the round robin studies to analyze an "unknown" reference material for each matrix (oil: QA10OIL01, sediment: QA10SED01, tissue: QA10TIS01) in triplicate and to report the data to three significant figures. NIST used a mean of the three reported replicate values to assign a target analyte mean for each laboratory. The reported mean results were assigned performance scores (z-score for accuracy and p-score for precision) according to IUPAC *Guidelines for Assessment of Precision and Accuracy in Inter-Comparison Exercises* (IUPAC, 1993). Each participating laboratory also analyzed a certified NIST SRM of a similar matrix type to the unknown reference material as an experimental control for each study. The SRMs included SRM1582 petroleum crude oil, SRM1941b marine sediment, and SRM1974b mussel tissue. After evaluating the data using the IUPAC guidelines for assessing precision and accuracy and assigning performance scores NIST removed outliers from the data set and generated target analyte consensus values for each unknown reference material (Schantz and Kucklick, 2011a,b,c).

The laboratories participating in these studies used a variety of matrix specific sample preparation techniques, extract cleanup procedures and internal analytical standards, GC capillary column phases, and GC/MS data acquisition parameters. The analytical results were generated by the participating laboratories using variations of EPA Method 8270D semivolatile analysis by GC−mass spectrometry (GC/MS) operating in select ion monitoring (SIM) mode. Laboratory-specific method details can be found in the published NIST interlaboratory studies (Schantz and Kucklick, 2011a,b,c).

1.2.2 Intralaboratory Studies Considered

Alpha Analytical Inc. (Alpha) in Mansfield, Massachusetts served as the primary laboratory during the NOAA DWH NRDA oil spill investigation, a monumental effort managed by our group on behalf of NOAA and the other designated Trustees. The traditional batch QC analyzed by environmental laboratories using EPA Method 8270D (EPA, 2014) included a method blank, laboratory control sample (LCS), LCS duplicate, laboratory duplicate, matrix spike (MS) and matrix spike duplicate. In addition, Alpha analyzed matrix specific NIST SRMs and reference oil samples with every laboratory QC batch that was analyzed during the NRDA program. These supplemental QC samples provided a critical framework for improving precision and accuracy for the traditional and nontraditional analytes throughout the project. Between 2010 and 2014, Alpha analyzed thousands of QC samples that provided critical benchmarks for future large-scale and long-term monitoring projects.

Alpha's intralaboratory standard reference material data contains hundreds of replicate analysis of the NIST intercalibration reference oil QA10OIL01 (NIST SRM 2779), NIST 1941b marine sediment and NIST SRM 1974b mussel tissue (NOAA Diver, 2017). These standard reference materials are commonly used in NRDA type investigations to monitor the accuracy of priority pollutant chemicals. In addition to priority pollutant PAHs, Alpha's NOAA DWH NRDA data provide important information about the precision of intralaboratory measurement for alkylated PAHs and geochemical biomarkers. This expanded collection of QC data provided data users with reference data capable of setting QC criteria for nontraditional target analytes for future investigations. These data were also used to test the stability of diagnostic ratios (DRs) and establish frameworks for distinguishing laboratory variability from true in-situ chemical differences.

These data were generated at Alpha using customized forensic methods that have been optimized through the modification of standard EPA methodology. Alpha performed DWH NRDA forensic chemistry analysis in accordance with the "DWH NRDA Analytical Quality Assurance Plan" (NOAA, 2014). The Q10OIL01 reference oil was prepared in the laboratory using a modification of EPA method 3580 *Waste Dilution* which involves the dissolution of hydrocarbon products or residues in dichloromethane (DCM). The marine sediment reference samples were extracted by shaker table in DCM. NOAA Status and Trends program favors the shaker table method, because particle agitation assists the solvent extraction (NOAA, 1998). The sediment sample extracts where then "cleaned-up" by elution through a gravity column filled with silica gel to remove polar organic compounds and then treated with copper to remove elemental sulfur. The mussel tissue reference samples were extracted by stainless steel tissue probe in DCM. The high lipid content of the tissue extracts required several cleanup steps. First, the extracts were eluted through a gravity column filled with alumina and silica gel powder. Second, the extracts were processed by HPLC using gel permeation chromatography to remove excess lipids.

Oil, sediment and tissue extracts were spiked with internal standard and analyzed for a suite of PAH, alkylated PAH and geochemical biomarker compounds using a modification of EPA method 8270D. The concentration of approximately 80 PAHs, alkylated PAH homologues, individual PAH isomers, and sulfur-containing heterocyclic PAHs and approximately 50 hopane and sterane geochemical biomarker compounds (Table 1.1) was determined on a gas chromatograph equipped with a mass spectrometer detector (GC/MS). The GC was equipped with a 60-m Phenomonex (Zebron) ZB-5 capillary column with a 0.25-mm diameter and 0.25 μm 5% phenyl phase thickness. The MS was operated in select ion monitoring (SIM) mode.

Over the course of the 5-year DWH analytical program Alpha operated 22 different GC/MS systems consisting of Agilent 6890 or 7890 GCs and 5973 or 5975c mass spectrometers. Approximately 10 instrument operators and data analysts operated these instruments. During the analytical program Alpha generated data for 865 analytical replicates of the QA10OIL01 Macondo reference oil. This provided the unique opportunity to monitor the accuracy and precision of target analytes, hydrocarbon features and PAH summations in crude oil in an intralaboratory environment over the course of several years, utilizing multiple instruments, instrument models and instrument operators. These data established a robust baseline for precision and accuracy for a single laboratory during a large oil spill investigation that included multiple instruments and analysts working under a common laboratory SOP and AQAP.

TABLE 1.1 Inventory of Target Analytes Considered in the Evaluation of Intra- and Interlaboratory Data

No.	Abbrev	Analytes	Class	EPA PAH16	$TPAH_{49}$	No.	Abbrev	Analytes	Class	EPA PAH16	$TPAH_{49}$
1	BT0	Benzothiophene	Parent			38	NBT2	C2-Naphthobenzothiophenes	Alkylated		x
2	BT1	C1-Benzo(*b*)thiophenes	Alkylated			39	NBT3	C3-Naphthobenzothiophenes	Alkylated		x
3	BT2	C2-Benzo(*b*)thiophenes	Alkylated			40	NBT4	C4-Naphthobenzothiophenes	Alkylated		x
4	BT3	C3-Benzo(*b*)thiophenes	Alkylated			41	BA0	Benz[*a*]anthracene	Parent	x	x
5	BT4	C4-Benzo(*b*)thiophenes	Alkylated			42	C0	Chrysene/Triphenylene	Parent	x	x
6	N0	Naphthalene	Parent	x	x	43	BC1	C1-Chrysenes	Alkylated		x
7	N1	C1-Naphthalenes	Alkylated		x	44	BC2	C2-Chrysenes	Alkylated		x
8	N2	C2-Naphthalenes	Alkylated		x	45	BC3	C3-Chrysenes	Alkylated		x
9	N3	C3-Naphthalenes	Alkylated		x	46	BC4	C4-Chrysenes	Alkylated		x
10	N4	C4-Naphthalenes	Alkylated		x	47	BBF	Benzo[*b*]fluoranthene	Parent	x	x
11	B	Biphenyl	Parent		x	48	BEP	Benzo[*e*]pyrene	Parent		x
12	DF	Dibenzofuran	Parent		x	49	BJKF	Benzo[*j*]fluoranthene/Benzo[*k*]fluoranthene	Parent	x	x
13	AY	Acenaphthylene	Parent	x	x	50	BAF	Benzo[*a*]fluoranthene	Parent		x
14	AE	Acenaphthene	Parent	x	x	51	BAP	Benzo[*a*]pyrene	Parent	x	x
15	F0	Fluorene	Parent	x	x	52	IND	Indeno[1,2,3-*cd*]pyrene	Parent	x	x
16	F1	C1-Fluorenes	Alkylated		x	53	DA	Dibenz[*ah*]anthracene/Dibenz[*ac*]anthracene	Parent	x	x
17	F2	C2-Fluorenes	Alkylated		x	54	GHI	Benzo[g,h,i]perylene	Parent	x	x

(*Continued*)

TABLE 1.1 (*Continued*)

No.	Abbrev	Analytes	Class	EPA PAH16	$TPAH_{49}$	No.	Abbrev	Analytes	Class	EPA PAH16	$TPAH_{49}$
18	F3	C3-Fluorenes	Alkylated		x	55	Ts	18α-22,29,30-Trisnorneohopane-Ts	Hopane		
19	A0	Anthracene	Parent	x	x	56	Tm	17α(*H*)-22,29,30-Trisnorhopane-Tm	Hopane		
20	P0	Phenanthrene	Parent	x	x	57	T15	30-Norhopane	Hopane		
21	PA1	C1-Phenanthrenes/Anthracenes	Alkylated		x	58	T19	17α(*H*), 21b(*H*)-Hopane	Hopane		
22	PA2	C2-Phenanthrenes/Anthracenes	Alkylated		x	59	T16	18α(*H*)-30-Norneohopane-C29Ts	Hopane		
23	PA3	C3-Phenanthrenes/Anthracenes	Alkylated		x	60	X	17α(*H*)-Diahopane	Hopane		
24	PA4	C4-Phenanthrenes/Anthracenes	Alkylated		x	61	T21	30-Homohopane-22S	Hopane		
25	DBT0	Dibenzothiophene	Parent		x	62	T22	30-Homohopane-22R	Hopane		
26	DBT1	C1-Dibenzothiophenes	Alkylated		x	63	S4	13β(*H*),17α(*H*)-20S-Diacholestane	Sterane		
27	DBT2	C2-Dibenzothiophenes	Alkylated		x	64	S12	14α(*H*),17α(*H*)-20S-Cholestane/	Sterane		
28	DBT3	C3-Dibenzothiophenes	Alkylated		x	65		13β(*H*),17α(*H*)-20S-Ethyldiacholestane			
29	DBT4	C4-Dibenzothiophenes	Alkylated		x	66	S17	14α(*H*),17α(*H*)-20R-Cholestane/	Sterane		
30	FL0	Fluoranthene	Parent	x	x	67		13β(*H*),17α(*H*)-20R-Ethyldiacholestane			
31	PY0	Pyrene	Parent	x	x	68	S25	14α(*H*),17α(*H*)-20S-Ethylcholestane	Sterane		
32	FP1	C1-Fluoranthenes/Pyrenes	Alkylated		x	69	S28	14α(*H*),17α(*H*)-20R-Ethylcholestane	Sterane		
33	FP2	C2-Fluoranthenes/Pyrenes	Alkylated		x	70	S14	14β(*H*),17β(*H*)-20R-Cholestane	Sterane		
34	FP3	C3-Fluoranthenes/Pyrenes	Alkylated		x	71	S15	14β(*H*),17β(*H*)-20S-Cholestane	Sterane		
35	FP4	C4-Fluoranthenes/Pyrenes	Alkylated		x	72	S26	14β(*H*),17β(*H*)-20R-Ethylcholestane	Sterane		
36	NBT0	Naphthobenzothiophenes	Parent		x	73	S27	14β(*H*),17β(*H*)-20S-Ethylcholestane	Sterane		
37	NBT1	C1-Naphthobenzothiophenes	Alkylated		x						

The participating round robin laboratories reported analyte concentrations in standardized units for each matrix under laboratory-specific SOPs, but using a common AQAP. The crude reference oil samples were reported on an oil weight basis (mg/kg_{oil}). The marine sediment and mussel tissue samples were reported on a dry weight basis ($\mu g/kg_{dry}$). These standard units provided more comparable data for the investigation and for this evaluation of intra- and interlaboratory variability.

1.2.3 Interlaboratory and Intralaboratory Data Considered

Most environmental programs subject environmental data to multiple levels of QC review. These QC processes are generally carried out by laboratory chemists and QC officers. Most large data collection programs contract a third party validator to verify and validate the data for completeness, precision and accuracy. These review processes are generally informed by the EPA's *Guidance on Environmental Data Verification and Data Validation* (EPA, 2002), the *EPA National Functional Guidelines for Superfund Organic Methods Data Review* (EPA, 2017) or by additional data quality requirements issued by state agencies or regulators.

Oil spill investigators offer additional recommendations on how to manage and treat interlaboratory data. The NIST Hydrocarbon Inter-calibration Experiment (HIE) NISTIR 8123 (2015) affirmed the use of certified reference materials, including weathered reference materials in routine laboratory analysis. It also recommended that laboratories gain familiarity with supplemental method information reported in relevant peer review publications and that intercalibration studies be implemented including the addition of new matrices as they become relevant to investigators. NISTIR 8123 also encouraged laboratories to continue to expand their target analyte lists to include additional nontraditional analytes. Data managers were also encouraged to gain greater awareness regarding the quantitation techniques laboratories use to quantify alkylated PAHs and geochemical biomarkers (Reddy et al., 2015). The NISTIR 8123 HIE report did suggest that it was recognized that biomarker analysis in particular only needs to be internally consistent but that laboratories should work toward biomarker data being "externally consistent" as well (NISTIR 8123, 2015).

These data validation processes help monitor the precision, bias, sensitivity, completeness, and comparability of EPA priority pollutant chemicals. These QC measures confirm that the laboratory measurement fall within acceptable control limits. If the laboratory QC results exceed the data quality criteria established in the SOPs or AQAP then the associated data is qualified by validators as estimated. Qualified data are flagged to alert the data user of potential data quality problems that should be considered when using the results. Rejected data fall far outside the acceptable control limits and may be censored from the database. During the NOAA DWH NRDA $<1\%$ of chemistry results were rejected by third party validators (NOAA DIVER, 2017).

NIST-instructed participating laboratories to analyze the QA10OIL01 reference oil "using their laboratories and/or programs analytical protocols." The data reported by each participating laboratory was done so in accordance with each laboratory's own QA/QC or data quality protocols and according to the DWH AQAP. In the QA10OIL01 reference oil study all 26 laboratories reported parent PAH results, 23 out of the 26 laboratories reported alkylated PAH results and 14 out of the 26 laboratories reported at least one biomarker result. This is worth noting that 12 of the participating laboratories did not report geochemical biomarker results. This observation indicates that more environmental laboratories determined the concentrations of alkylated PAHs than geochemical biomarkers. Forensic investigators may need to be involved in the laboratory selection to assure that the PAH and geochemical biomarker results are generated using consistent laboratory SOPs to minimize variability. Geochemical biomarker data is critical to the efforts of oil spill investigators to characterize the source oil and then to perform source identification on oil residues found in the environment.

NIST utilized the IUPAC guidelines (IUPAC, 1993) for the Assessment of Precision and Accuracy in Intercomparison studies. These guidelines focus on controlled interlaboratory proficiency testing studies and are designed to identify outliers based on the relative comparison of any given result to the consensus values of the data set as a whole for a common, homogenous reference material. For the purposes of this review, in an attempt to simulate the challenges of the interlaboratory data environment that investigators are frequently tasked to work with, no reported data points are censored. This type of data evaluation is not used, nor is it applicable for use in evaluating interlaboratory data that is generated for use in a true oil spill or site investigation. The IUPAC guidelines would not be applied to interlaboratory data generated from native field samples for a large-scale oil spill investigation. In the case of a true oil spill investigation the data would go through data quality review processes at the laboratory and the program level. With true native field data there are no expected values among target analytes that can be evaluated for precision and accuracy. Only the laboratory QC data can be used for this. Outliers can be observed within field-derived interlaboratory data but without consensus values there is no technical basis to censor results if there are no associated QC issues. All of the reported data was generated in agreement with

each participating laboratories or programs QC parameters so no data is being censored or removed from the data set due to a deviation from the NIST-generated consensus values. The NIST interlaboratory studies will be treated as true investigation data and not as a controlled interlaboratory study.

The participating laboratories used different instrument acquisition parameters and column phases. These differences affected the elution order and the resolution of coeluting PAH isomers. Select laboratories were able to chromatographically separate benzo[*b*]fluoranthene from benzo[*j*]fluoranthene and benzo[*k*]fluoranthene, whereas other laboratories reported these compounds as unresolved or partially coeluting results. Similarly, some laboratories reported dibenz[*a*,*h*]anthracene and dibenz[*a*,*c*]anthracene separately and others reported the sum of both compounds as a coelution. Separating PAH isomers that have similar molecular weight and structure is a common laboratory challenge.

Many of the participating laboratories in these studies used GC capillary columns with a 5% phenyl column phase. This low polarity column phase is useful in achieving the separation of a wide range of compounds but it does not effectively separate heavy molecular weight PAH isomers (Phenomonex, 2017). Due to the limited number of laboratories reporting these PAHs in a consistent fashion, benzo[*b*]fluoranthene, benzo[*j*]fluoranthene, benzo[*k*]fluoranthene, dibenz[*a*,*h*]anthracene and dibenz[*a*,*c*]anthracene are not included in this evaluation of interlaboratory or intralaboratory data. Another lesson learned from the DWH project is that AQAP's associated with large or long-term projects should assure that participating laboratories report parent PAHs as individual analytes when possible as opposed to coeluting analytes to maximize interlaboratory comparability.

Parent PAHs are present in the QA10OIL01 reference oil at varying concentrations. For the purpose of this review a subset of analytes were excluded due to their low relative abundance in the QA10OIL01reference oil. At lower relative concentrations analytical variability increases due to the limitations of the instrumentation. Including these compounds will confound general method variability with variability introduced by the sensitivity threshold of the instrumentation. This type of variability is largely a function of the lower relative level of target analyte concentration and not necessarily a function of a given laboratories ability to accurately and precisely report target compounds. Including these compounds would artificially increase the mean variability of each data set. The DWH AQAP target reporting limit for oil is 2.0 mg/kg_{oil}. In agreement with the DWH AQAP, analytes detected at less than 2× the reporting limit (4.0 mg/kg_{oil}) were considered to be estimated values and were omitted from the statistical consideration of this study. In forensic interpretation diagnostic chemicals are chosen based on their abundance in the source material, their analytical resolution and their resistance to environmental weathering. Chemicals that are present at lower relative levels would likely not be used forensically. The compounds considered in this study are listed in Table 1.1. The low-level compounds detected at $<4.0\ mg/kg_{oil}$ on average that are not being considered statistically are anthracene, fluoranthene, benzo(*a*)fluoranthene, benzo(*a*)pyrene, perylene, indeno(1,2,3-*cd*)pyrene and benzo(*g*,*h*,*i*)perylene.

1.3 INTERPRETIVE METHODS

During the DWH investigation forensic investigators determined the extent and the magnitude of Macondo oil in the northern GOM. DRs composed of saturated hydrocarbons, PAHs, and geochemical biomarkers helped confirm the presence of Macondo oil in resources of the GOM and differentiate it from ambient hydrocarbons composed of terrestrial runoff, coastal detritus, natural oil seeps, unrelated oil spills, and others (Stout, 2016; Stout et al., 2016; Stout and Payne, 2016; Payne and Driskell, 2017; Douglas et al., 2017; Stout et al., 2017).

The DRs reflected distinct chemical features of Macondo oil capable of distinguishing petroleum sources and monitoring the degree of environmental weathering associated with evaporation, dissolution, photo-degradation, in-situ burning, and biodegradation. Previous publications provide the basis for most of the recalcitrant DRs used by petroleum geologists (Peters and Moldowan, 1993) and oil spill investigators (Wang et al., 1999; Stout and Wang, 2008; CEN, 2012; Nordtest, 2002).

For the purpose of this review 9 DRs are used to analyze and interpret the data (Table 1.2). DRs 1 and 2 are the ratios of the sulfur content of the QA10OIL01 reference oil as calculated by the ratio of the C2-dibenzothiophenes to the C2-phenanthrene/anthracenes (DBT2/PA2) and the C3-dibenzothiophenes to the C3-phenanthrene/anthracenes (DBT3/PA3). DRs 3 to 7 are based on the ratios of the abundances of diagnostic triterpanes relative to hopanes and DRs 8 and 9 consider the comparative abundances of select steranes. These DRs are based on target compounds that are relatively abundant in the QA10OIL01 reference oil, exhibit good chromatographic resolution, and exhibit slow, but well-characterized changes when environmentally weathered

TABLE 1.2 Inventory of Common Diagnostic Ratios Considered in This Study to Evaluate Intra- and Interlaboratory Data

No.	Ratio abbreviations
1	DBT2/(DBT2 + PA2)
2	DBT3/(DBT3 + PA3)
3	T15/(T15 + Hopane)
4	Ts/(Ts + Tm)
5	T21/(T21 + T22)
6	Tm/(Tm + T21)
7	Tm/(Tm + T22)
8	S25/S25 + S28
9	S26 + S27/(S26 + S27) + (S25 + S28)

(CEN, 2012). These DRs are commonly used in forensic chemistry and represent reliable metrics for directly comparing petroleum residues in the source oil to petroleum residues in field samples. However, DRs are sensitive to the precision and the accuracy of the laboratory data. The reproducibility of these DRs reflects the reliability of the results being reported by the participating laboratories. The DRs used in this study are the comparison of the stated chemical results and the ratios are calculated using the $(a/(a + b))$ configuration. This approach normalizes ratios between 0 and 1 and it avoids generating ratios that contain insignificant figures when the two results being evaluated are of substantially different values (SINTEF, 2002).

Forensic investigators also use PAH summations to evaluate the magnitude of oil exposure to the environment. Two common groups of PAH summations used by investigators are total 16 EPA priority pollutant PAHs (EPAPAH16) and total parent + alkylated PAHs ($TPAH_{49}$). $TPAH_{49}$ includes the 52 analytes listed between naphthalene and benzo(*ghi*)perylene, excluding retene, benzo(*b*)fluorene and perylene on Table 1.1. Retene (RET) and perylene (PER) are excluded because they are diagenetic PAHs (naturally occurring). Benzo(*b*)fluorene is excluded because its concentration is accounted for within the C1-fluoranthene/pyrene total.

1.4 RESULTS—QA10OIL01 CRUDE OIL

The NIST QA10OIL01 crude reference oil data serves as the primary means for evaluating and comparing interlaboratory and intralaboratory variability in this study. The QA10OIL01 crude oil is useful for this type of assessment for a variety of reasons. First, it is composed of fresh Macondo oil. Second, the laboratory preparation process for neat crude oil is simply a function of dissolution into solvent. Most of the participating laboratories reported performing a simple dilution of the crude oil using DCM or another organic solvent. This eliminates variability that can be introduced through preparation procedures that require additional laboratory manipulations. The QA10OIL01 data provides a means of comparison that largely represents the influences of the analytical process on data variability and not issues associated with field collection, sample handling, matrix homogeneity, or other matrix-related phenomena that may contribute to variability. Capturing the variability that is introduced through target analyte identification and quantitation allows for a more focused evaluation of how different laboratory's analytical methods affect the precision and accuracy of reported data. By contrast, NIST interlaboratory marine sediment and mussel tissue data are also considered in this review to evaluate how the preparation techniques required for these matrices may introduce additional types of laboratory variability through the presence of native matrix interferences, the need to employ additional laboratory cleanup steps and the challenges that environmental weathering of target analytes can have on data interpretation.

In this study laboratory variability is evaluated for target analytes, DRs and PAH summations by calculating the percent relative standard deviation (%RSD) for each parameter in both the interlaboratory and intralaboratory data. Percent RSD is calculated by dividing the standard deviation (STD) for a given target analyte, DR or PAH summation by the mean value for that same parameter and then multiplying the result by 100 to generate a

TABLE 1.3 Comparison of Parent PAH Concentration Metrics in the QA10OIL01 Macondo Reference Oil Used in the Evaluation of Intra- and Interlaboratory Data. **All concentrations in mg/Kg oil weight**

Parent PAHs			Intralaboratory data				Interlaboratory data			
			QA10OIL01				QA10OIL01			
No.	Abbrev	Analytes	Count	Mean	STD	%RSD	Count	Mean	STD	%RSD
1	BT0	Benzothiophene	865	6.60	0.85	12.8	8	13.6	7.30	53.7
2	N0	Naphthalene	865	781	92.1	11.8	26	837	126	15.0
3	B	Biphenyl	865	171	16.5	9.7	25	194	34.0	17.6
4	DF	Dibenzofuran	865	26.4	2.33	8.8	13	26.7	5.9	22.0
5	AY	Acenaphthylene	865	7.50	0.91	12.1	15	11.68	7.23	61.9
6	AE	Acenaphthene	865	21.4	5.55	26.0	19	20.1	17.3	86.4
7	F0	Fluorene	865	132	10	7.8	26	145	37	25.8
8	A0	Anthracene	865	1.09	NC	NC	16	9.66	5.8	60.1
9	P0	Phenanthrene	865	275	23	8.3	26	272	61.4	22.6
10	DBT0	Dibenzothiophene	865	48.4	4.44	9.2	24	51.5	13.3	25.8
11	FL0	Fluoranthene	865	3.46	NC	NC	18	5.07	1.98	39.0
12	PY0	Pyrene	865	16.2	2.06	12.7	23	15.5	3.47	22.4
13	NBT0	Naphthobenzothiophenes	865	19.2	2.33	12.1	9	14.5	9.39	64.6
14	BA0	Benz[*a*]anthracene	865	6.29	0.72	11.5	19	8.40	3.47	41.3
15	C0	Chrysene/Triphenylene	865	50.6	4.03	8.0	25	46.3	10.9	23.5
19	BEP	Benzo[*e*]pyrene	865	11.4	0.93	8.2	21	11.41	2.12	18.6
20	RSD	Average Parent PAH %RSD	–	–	–	11.4	–	–	–	37.5

percent ((STD/Mean)*100 = %RSD) (SINTEF, 2002). This basic statistical test measures the precision of the reported results and the reproducibility of each DR. The %RSD provides a framework to assess the reliability of each parameter within the interlaboratory and intralaboratory data.

1.4.1 Parent PAH Results

Among the classes of analytes studied through the analysis of the QA10OIL01 crude reference oil parent PAH data demonstrated lower relative levels of variability when compared to nontraditional compounds. The interlaboratory data set ($n = 26$) reported %RSD values for individual analytes that ranged from 15% to 86.4% with a mean %RSD of 37.5% for parent PAHs. The intralaboratory data ($n = 865$) reported %RSD values for parent PAHs that ranged from 7.8% to 26% with a mean %RSD of 11.4% (Table 1.3).

1.4.2 Alkylated PAHs Results

The QA10OIL01 crude reference oil data demonstrated higher relative levels of interlaboratory variability for alkylated PAHs, whereas the intralaboratory data demonstrated only a slight increase in variability as compared to intralaboratory parent PAH precision. The alkylated PAH compounds studied (Table 1.4) reported interlaboratory results that ranged from 12.1% to 265% with a mean %RSD of 55.6%. The %RSD values for the intralaboratory alkylated PAH results ($n = 865$) ranged from 8.4% to 20.2% with a mean %RSD of 13.0%.

TABLE 1.4 Comparison of Alkylated PAH Concentration Metrics in the QA10OIL01 Macondo Reference Oil Used in the Evaluation of Intra- and Interlaboratory Data. **All concentrations in mg/Kg oil weight**

Alkylated PAHs			Intralaboratory data				Interlaboratory data			
			QA10OIL01				QA10OIL01			
No.	Abbrev	Analytes	Count	Mean	STD	%RSD	Count	Mean	STD	%RSD
1	BT1	C1-Benzo(*b*)thiophenes	865	27.0	3.59	13.3	8	61.6	63.0	102
2	BT2	C2-Benzo(*b*)thiophenes	865	24.9	3.02	12.1	8	607	1611	265
3	BT3	C3-Benzo(*b*)thiophenes	865	40.4	5.54	13.7	8	122	156	127
4	BT4	C4-Benzo(*b*)thiophenes	865	29.9	4.91	16.4	8	28.8	3.49	12.1
5	N1	C1-Naphthalenes	865	1655	160	9.7	21	2115	544	25.7
6	N2	C2-Naphthalenes	865	1913	193	10.1	23	2409	830	34.5
7	N3	C3-Naphthalenes	865	1239	143	11.5	23	1861	1508	81.1
9	N4	C4-Naphthalenes	865	581	81.1	14.0	23	712	308	43.3
10	F1	C1-Fluorenes	865	276	23.1	8.4	23	332	146	43.9
12	F2	C2-Fluorenes	865	357	36.4	10.2	22	360	101	28.1
13	F3	C3-Fluorenes	865	264	34.3	13.0	23	274	91.6	33.5
14	PA1	C1-Phenanthrenes/Anthracenes	865	597	56.3	9.4	23	731	204	27.9
15	PA2	C2-Phenanthrenes/Anthracenes	865	589	66.5	11.3	23	1063	1892	178
16	PA3	C3-Phenanthrenes/Anthracenes	865	328	46.4	14.2	22	441	176	39.9
17	PA4	C4-Phenanthrenes/Anthracenes	865	138	22.3	16.2	22	216	151	69.7
18	DBT1	C1-Dibenzothiophenes	865	144	13.9	9.6	23	120	43.0	35.8
19	DBT2	C2-Dibenzothiophenes	865	181	19.8	11.0	23	152	54.9	36.0
20	DBT3	C3-Dibenzothiophenes	865	133	16.9	12.7	20	116	26.5	22.8
21	DBT4	C4-Dibenzothiophenes	865	66.6	10.7	16.1	18	57.4	20.2	35.2
22	FP1	C1-Fluoranthenes/Pyrenes	865	76.5	8.83	11.5	22	90.6	63.9	70.5
23	FP2	C2-Fluoranthenes/Pyrenes	865	125	15.9	12.8	19	131	32.7	25.0
24	FP3	C3-Fluoranthenes/Pyrenes	865	146	21.7	14.9	21	138	61.8	44.8
25	FP4	C4-Fluoranthenes/Pyrenes	865	115	20.1	17.5	13	88.3	39.4	44.7
27	NBT1	C1-Naphthobenzothiophenes	865	56.0	7.24	12.9	9	50.0	22.3	44.5
28	NBT2	C2-Naphthobenzothiophenes	865	75.2	11.1	14.8	8	68.4	22.6	33.1
29	NBT3	C3-Naphthobenzothiophenes	865	54.4	9.22	16.9	8	47.0	14.0	29.7
30	NBT4	C4-Naphthobenzothiophenes	865	39.2	7.90	20.2	7	28.9	10.3	35.6
31	BC1	C1-Chrysenes	865	113	9.98	8.8	22	117	35.6	30.3
32	BC2	C2-Chrysenes	865	139	14.8	10.6	21	136	60.6	44.6
33	BC3	C3-Chrysenes	865	138	18.4	13.3	19	87.1	30.3	34.8
34	BC4	C4-Chrysenes	865	80.3	13.7	17.1	15	57.5	25.6	44.6
35	RSD	Average Alkylated PAH %RSD	–	–	–	13.0	–	–	–	55.6

TABLE 1.5 Comparison of Geochemical Biomarker Concentration Metrics in the QA10OIL01 Macondo Reference Oil Used in the Evaluation of Intra- and Interlaboratory Data. All concentrations in mg/Kg oil weight

Geochemical biomarkers			Intralaboratory data QA10OIL01				Interlaboratory data QA10OIL01			
No.	**Abbrev**	**Analytes**	**Count**	**Mean**	**STD**	**%RSD**	**Count**	**Mean**	**STD**	**%RSD**
1	Ts	18a-22,29,30-Trisnorneohopane-TS	865	12.2	1.47	12.1	8	6.97	1.35	19.4
2	Tm	17a(*H*)-22,29,30-Trisnorhopane-TM	865	9.94	1.20	12.1	12	9.95	7.10	71.3
3	T15	30-Norhopane	865	27.2	2.90	10.7	11	20.02	15.8	79.1
5	T16	18a(*H*)-30-Norneohopane-C29Ts	865	10.7	1.21	11.4	8	7.8	4.23	54.4
6	X	17a(*H*)-Diahopane	865	7.71	1.1	14.5	7	4.2	1.33	31.7
4	T19	17a(*H*), 21b(*H*)-Hopane	865	62.5	6.01	9.6	14	43.8	9.21	21.0
7	T21	30-Homohopane-22S	865	25.9	2.7	10.5	11	15.7	2.84	18.1
8	T22	30-Homohopane-22R	865	21.5	2.4	11.0	11	12.8	3.42	26.7
9	S4	13b(*H*),17a(*H*)-20S-Diacholestane	865	49.0	4.5	9.3	8	46.8	14.5	31.1
10	S12	14a(*H*),17a(*H*)-20S-Cholestane/ 13b(*H*),17a(*H*)-20S-Ethyldiacholestane	865	57.0	5.1	9.0	8	46.5	25.2	54.1
11	S17	14a(*H*),17a(*H*)-20R-Cholestane/ 13b(*H*),17a(*H*)-20R-Ethyldiacholestane	865	63.5	5.8	9.1	13	44.4	23.9	53.8
12	S25	14a(*H*),17a(*H*)-20S-Ethylcholestane	865	33.3	4.2	12.5	8	26.1	11.2	42.8
13	S28	14a(*H*),17a(*H*)-20R-Ethylcholestane	865	23.2	2.6	11.4	11	22.7	9.80	43.1
14	S14	14b(*H*),17b(*H*)-20R-Cholestane	865	29.4	2.6	8.8	11	25.5	8.08	31.7
15	S15	14b(*H*),17b(*H*)-20S-Cholestane	865	29.2	2.6	9.0	9	24.9	9.75	39.2
16	S26	14b(*H*),17b(*H*)-20R-Ethylcholestane	865	38.4	4.2	11.0	12	26.0	9.66	37.2
17	S27	14b(*H*),17b(*H*)-20S-Ethylcholestane	865	24.9	3.7	14.9	9	25.4	8.35	32.9
18	RSD	Average biomarker %RSD	–	–	–	11.0	–	–	–	40.5

1.4.3 Geochemical Biomarkers Results

The QA10OIL01 crude reference oil data demonstrated slightly lower variability for geochemical biomarker results than for interlaboratory parent PAHs. One reason for this is that only 14 of the 26 participating laboratories reported at least one biomarker result. This decreased the sample size of interlaboratory contributors and decreased the introduction of additional sources of variability. The geochemical biomarkers studied (Table 1.5) reported interlaboratory data ($n = 7-14$) results that ranged from 19.4% to 79.1% with a mean %RSD of 40.5%. The %RSD for the intralaboratory geochemical biomarker results ($n = 865$) ranged from 8.8% to 14.9% with a mean %RSD of 11.0%.

1.5 DISCUSSION

1.5.1 Parent PAHs

The parent PAH compounds demonstrate lower relative levels of variability when compared to alkylated PAHs for both the interlaboratory and the intralaboratory studies. Laboratories generally have technical and historical experience with parent PAH analysis. In addition, commercial vendors have offered a variety of analytical standards containing these compounds at affordable prices for decades. The lower levels of overall variability among parent PAHs are a direct function of these factors. Parent PAHs represent a class of target analyte that demonstrate accuracy and precision in an interlaboratory study. However, there is a notable difference in the relative level of variability between the interlaboratory results and the intralaboratory results. On average, parent

PAHs in the interlaboratory study demonstrate a %RSD value of 37.5%, whereas parent PAHs in the intralaboratory study demonstrate a mean %RSD value of 11.4%. This comparison demonstrates that the variability present in the interlaboratory data is >3× the variability found in the intralaboratory data.

In general, the concentrations of PAHs in crude oil tend to decrease with increasing molecular weights or boiling point (Stout, 2002). This trend holds true in the QA10OIL01 reference oil. For example, PAHs with 4-, 5-, and 6-rings such as fluoranthene, benzo(*a*)fluoranthene, benzo(*a*)pyrene, perylene, indeno(1,2,3-*cd*)pyrene and benzo(*g*,*h*,*i*)perylene, are all present at concentrations below 2× the DWH AQAP target reporting limit of 4.0 mg/kg_{oil}. These compounds demonstrate higher levels of variability and are not included in this statistical evaluation.

The most abundant parent PAHs in the QA10OIL01 reference oil contain two- and three-rings. Naphthalene, fluorene, phenanthrene, and dibenzothiophene are detected in the interlaboratory data at concentrations ranging between 51.5 mg/kg and 837 mg/kg. These four PAHs together have a means %RSD of 22.3%. Variability decreases with an increase of target analyte abundance among the parent PAHs in the interlaboratory data. This is still 2× the %RSD found in the mean %RSD for all parent PAHs in the intralaboratory data set. This represents an important baseline for comparison between interlaboratory and intralaboratory data. Intralaboratory data demonstrates lower relative levels of variability even when evaluating compounds that are most likely to be reproducible, such as parent PAHs.

1.5.2 Alkylated PAHs and Geochemical Biomarkers

Alkylated PAH compounds in the QA10OIL01 reference oil demonstrate higher relative levels of variability when compared to parent PAHs and geochemical biomarker data in both the interlaboratory and the intralaboratory studies. However, the interlaboratory data demonstrates substantially higher relative levels of variability when compared to the intralaboratory data (Tables 1.4 and 1.5). The interlaboratory alkylated PAH data in the QA10OIL01 reference oil on average reports a %RSD value for alkylated PAHs of 55.6%, whereas the intralaboratory alkylated PAH data on average reports a %RSD value of 13.0%. In the QA10OIL01 reference oil the interlaboratory geochemical biomarker data on average reports a %RSD value of 40.5%, whereas the intralaboratory geochemical biomarker data on average reports a %RSD value of 11.0%. This comparison demonstrates that the variability present in the interlaboratory data for alkylated PAHs and for geochemical biomarkers are >3× the variability found in the intralaboratory data. It is worth noting that this is approximately the same difference in variability that was observed between the interlaboratory and intralaboratory parent PAH data.

Alkylated PAH and geochemical biomarker analyses are not new technologies, having originated in the petroleum geochemistry field in the 1950s and adopted in the environmental forensics field in the 1980s with ongoing improvements. Investigators used these methods for decades to generate more comprehensive chemical profiles of hydrocarbon materials like crude oil (Douglas et al., 1996). Historically, alkylated PAH and geochemical biomarker measurements were performed by academic and specialty laboratories that customized and optimized analytical techniques for nontraditional forensic target analytes. Large-scale oil spill investigations can rapidly expand the demand for overall commercial laboratory services. This increase in demand provides an opportunity for less experienced laboratories to enter the laboratory service market for alkylated PAH and biomarker analysis. Increased demand for specialty analytical services builds capacity in the commercial laboratory industry. However, the interlaboratory study results demonstrate there is an increase in variability as more laboratories with varying levels of expertise contribute alkylated PAH and geochemical biomarker data into an interlaboratory data set.

1.6 DISCUSSION—SOURCES OF ANALYTICAL VARIABILITY

The sources of laboratory variability found in interlaboratory data are associated with the development and operation of modified analytical methods. The variability arises from the changes to the analytical method, the learning curve associated with chemists and instrument operators, and the use of new analytical standards for nontraditional compounds. The quantitation techniques used by different laboratories in their analytical environments also introduce variability based on what internal standards or relative response factors are used for quantitation. The native sample material is also a source of potential variability depending on the complexity of the matrix and the preparation techniques that may be used to isolate the target analytes. Time is also a source of variability in the laboratory environment. Data that is acquired over the course of time, whether it is days,

months or years in the case of the NOAA DWH NRDA investigation. Equipment conditions change and hardware degrades and fails, standard manufacturers change lots, laboratory staff rotates. All of these different parameters are potential sources of variability (ASTM E177-04, 2004).

1.6.1 Availability of Analytical Standards

The analyses of alkylated PAHs and geochemical biomarkers present unique analytical challenges, because these nonstandard analytes differ in several respects from the measurement of priority pollutant PAHs. Alkylated PAHs are analyzed and reported as groups of PAH isomers that elute in homologous series. Although the availability of individual alkylated PAH isomers is growing slowly, it still only accounts for less than 1% of the total isomers represented in Table 1.1. The available commercial standards for most of these isomers are substantially more expensive than the priority pollutant PAH compounds and the isomer price increases with increased levels of alkylation. Due to the high number and cost of alkylated PAH isomers, it is not practical for laboratories to routinely measure more than a handful of PAH isomers individually.

Geochemical biomarker standards have also become more readily available for selected classes, like triterpanes and steranes, but they are also prohibitively expensive to use on a routine basis. Many laboratories will only purchase a subset of biomarker compounds to be used as representative calibration standards. Without discrete standards instrument operators must use reference materials, mass spectral analysis and literature to identify the proper alkylated PAH homologue ranges and geochemical biomarker compounds. Running these methods requires analytical experience, modern instrumentation, reference materials with known or consensus concentrations, and familiarity with the applicable literature. Without a firm grasp of these resources it is likely that laboratories will introduce both method bias and experimental error through the inconsistent processing of raw data.

1.6.2 Instrument Acquisition Parameters

Forensic laboratories developed GC/MS data acquisition parameters that are designed to increase the chromatographic resolution, and instrument response for higher mass compounds. The increase in chromatographic resolution through longer acquisition methods, customized pressure programs and longer capillary columns more clearly isolates the isomer components of each alkyl group. This makes the alkyl ranges more distinctive and readily identifiable. Without method modifications that enhance chromatographic resolution and sensitivity, alkylated PAH ranges may not be sufficiently distinguished from other chemical residues present in the sample or from native matrix interferences.

Geochemical biomarker analysis also requires chromatographic resolution that can separate series of biomarker compounds. Sets of hopane and sterane epimers elute in doublets due to their similar molecular weight and structures (Wang et al., 2006). Epimers are isomers with different configurations of atoms around an asymmetric carbon. These epimers can easily coelute if the acquisition method is not configured properly. This loss of resolution is also a loss of chemical specificity and the ability to more fully and accurately characterize source oils. If the needed instrumental resolution is not achieved then identifying alkylated PAHs and geochemical biomarker compounds cannot be done accurately or reproducibly.

1.6.3 Raw Data Analysis

The lack of adequate commercial standards requires that alkylated PAHs and geochemical biomarkers be identified using literature, reference materials, and spectral analysis. This strategy benefits greatly from the analysis of at least one reference crude oil sample and a familiarity with the patterns of each alkylated PAH homolog and geochemical biomarker class. Crude petroleum derived from different geologic formations contain similar PAH isomers with different relative abundances that range from subtle to completely distinct. In this way, a reference sample, such as North Slope Crude or Macondo oil, can help the laboratory measure nontraditional analytes consistently over time without the need to measure every isomer individually.

Analyst experience and reference sample libraries help interpret changes in the alkylated PAH homolog and geochemical biomarker patterns. These changes are typically caused by environmental weathering or mixing with thermogenic byproducts (e.g., tar and soot), anthropogenic discharges (e.g., sewage and runoff), and mixing with natural organic matter (e.g., detrital vegetation). Forensic investigators benefit greatly when the laboratory

measures the traditional and nontraditional analytes with maximum accuracy and minimal variability. Patterns of PAH homologs and geochemical biomarkers need to be measured accurately and precisely so that laboratory artifacts are not mistaken as environmental weathering or mixing.

1.6.4 Quantification Techniques

Laboratories integrate alkylated PAHs as ranges of target analytes. The alkyl ranges are quantified using the relative quantitation factor of a surrogate compound in the instrument calibration standard. Surrogate calibration compounds are generally the response factor of the alkyl groups parent PAH or the quantitation factor from a single isomer within the homologue group. In both cases a relative quantitation factor is used to quantify the range of alkyl PAHs. In general quantitation factors decrease with increased levels of alkylation so using a parent PAH, which would have a higher quantitation factor, to quantify alkylated PAH ranges will introduce a low bias into the data. This low bias increases with increased levels of alkylation, so the low bias in C1-alkylated PAH ranges is not as pronounced as the low bias in C4-alkylated PAH ranges. Laboratories that use the quantitation factor from a native isomer may generate more accurate quantitation results for C1- or C2 alkyl groups but discrete standards become less available for C3- and C4-alkylated PAHs. This could lead to an environment where some alkyl groups are being quantified using the quantitation factor derived from a native isomer, whereas other alkyl groups are being quantified using a parent PAH quantitation factor. This makes the data internally incoherent and difficult for use in diagnostic work. In practice, the use of surrogate parent PAHs and a single biomarker isomer to quantify alkylated PAH homologs and biomarker analytes exchanges some accuracy for greatly improved precision, analytical efficiency, and forensic power.

Laboratories participating in the interlaboratory study also applied different strategies to quantifying geochemical biomarkers. In addition to reporting geochemical biomarker results a sub set of participating laboratories also reported the representative surrogate compound that was used in quantitation. During the QA10OIL01 crude oil interlaboratory study five laboratories reported quantitating hopane using the relative quantitation factor of 17β(*H*), 21β(*H*)-hopane (nontarget analyte), whereas three laboratories reported using the quantitation factor of 17α(*H*), 21β(*H*)-hopane (target analyte). These two hopane isomers, due to their unique structures, respond differently in the GC/MS analytical environment and as a result have different quantitation factors. If we compare the average hopane concentrations of laboratories using 17β(*H*), 21β(*H*)-hopane (38.9 mg/kg) for quantitation to the average hopane concentrations of laboratories using 17α(*H*), 21β(*H*)-hopane for quantitation (47.3 mg/kg) we see the corresponding results are approximately 19% difference. This type of systematic methodological difference introduces variability into interlaboratory data sets that challenge the ability of data users to differentiate a true increase in measured field impact from bias introduced by method variation.

1.7 DISCUSSION—IMPLICATIONS ON USE OF DATA IN FORENSIC APPLICATIONS

1.7.1 PAH and Alkylated PAH Summations

PAH summations are commonly used in oil spill investigations to assess the level of oil exposure to the environment. There are a variety of possible PAH summations that investigators may consider in evaluating the degree of oiling. In this review, two common PAH summations are considered; EPAPAH16 which is comprised of the sum of the 16 priority pollutant parent PAHs and $TPAH_{49}$, which is comprised of 22 parent PAHs ($PARPAH_{22}$) and 27 alkylated PAHs ($ALKPAH_{27}$; Table 1.1). During oil spill investigations it is important for investigators to accurately characterize source oils. Selected components of the PAH pattern are critically important for identifying fugitive oil, monitoring its degradation and mixing, and estimating environmental exposure. Crude petroleum is enriched in alkylated PAHs and generally contains lower relative abundances of parent PAHs. This is true of the QA10OIL01 reference oil, according to the interlaboratory PAH and alkylated PAH concentration data the QA10OIL01 reference oil on average is comprised of 87% alkylated PAHs and 13% parent PAHs. The reliability of using a PAH summation that includes alkylated PAHs is a function of the reliability of the alkylated PAH data. The interlaboratory alkylated PAH data for the QA10OIL01 oil demonstrated high relative levels of variability (55.6% avg. RSD), whereas the intralaboratory data demonstrate lower relative levels (13.0% avg. RSD).

The relationship between the aggregate concentrations of EPAPAH16 and $TPAH_{49}$ demonstrates some of the challenges faced by scientists using interlaboratory ($n = 26$) and the intralaboratory ($n = 865$) data for the analysis

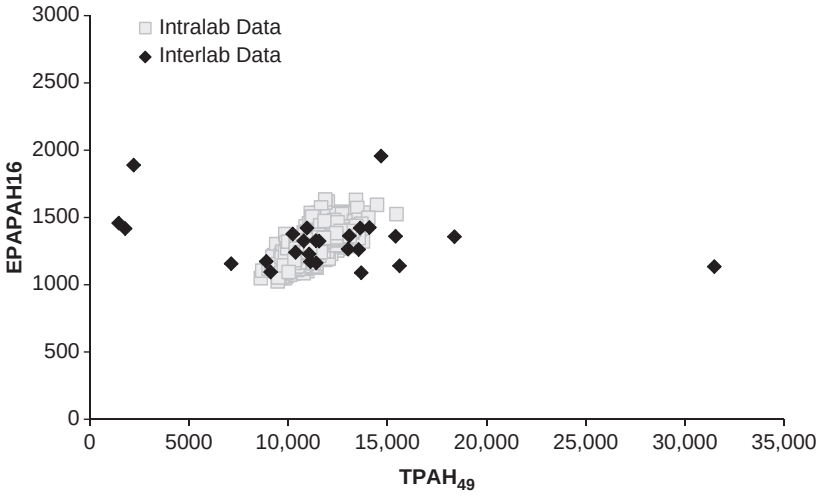

FIGURE 1.1 Cross-plot showing the measured concentrations (mg/kg_{oil}) of EPAHPAH16 vs $TPAH_{49}$ in the QA10OIL01 reference crude oil. Interlaboratory data: QA10OIL01 reference crude oil ($n = 26$). Intralaboratory data: QA10OIL01 reference crude oil ($n = 865$).

TABLE 1.6 Comparison of the Diagnostic Ratio Precision Used in the Evaluation of Intralaboratory- and Interlaboratory Data Generated from Crude Oil, Marine Sediment and Mussel Tissue Reference Samples

Diagnostic ratios and PAH summations		Intra-laboratory data						Inter-laboratory data					
		Crude oil		Marine sediment		Mussel tissue		Crude oil		Marine sediment		Mussel tissue	
No.	Analytes	*n*	Avg. % RSD	*n*	Avg. % RSD	*n*	Avg. % RSD	*n*	Avg. % RSD	*n*	Avg. % RSD	*n*	Avg. % RSD
1	DBT2/(DBT2 + PA2)	865	3.1	40	3.4	40	6.1	23	35.6	25	26.3	22	72.5
2	DBT3/(DBT3 + PA3)	865	4.1	40	3.7	40	5.2	20	26.6	24	19.7	19	68.2
3	T15/(T15 + Hopane)	865	3.4	40	1.9	0	NA	14	77.0	19	64.7	0	NA
4	Ts/(Ts + Tm)	865	5.1	40	3.2	0	NA	12	76.0	0	NA	0	NA
5	T21/(T21 + T22)	865	2.6	40	2.7	0	NA	11	10.1	14	29.0	0	NA
6	Tm/(Tm + T21)	865	6.6	40	3.4	0	NA	11	39.0	13	18.8	0	NA
7	Tm/(Tm + T22)	865	6.5	40	3.8	0	NA	11	36.1	14	16.0	0	NA
8	S25/S25 + S28	865	3.9	40	5.3	0	NA	11	68.0	0	NA	0	NA
9	S26 + S27/(S26 + S27) + (S25 + S28)	865	4.0	40	3.2	0	NA	12	43.3	0	NA	0	NA
10	EPATPAH16	865	8.4	40	7.5	40	8.1	26	15.1	33	27.3	35	100
11	$TPAH_{49}$	865	8.7	40	8.3	40	9.9	26	48.9	33	43.6	35	150

of an identical Macondo source oil (Fig. 1.1, QA10OIL01). As discussed previously, the EPAPAH16 results exhibit a reasonable degree of variability among the interlaboratory data (15.1% avg. RSD) and the intralaboratory data (8.4% avg. RSD; Table 1.6). However, the $TPAH_{49}$ results demonstrate substantially higher levels of variability in the interlaboratory data (48.9% avg. RSD), whereas the intralaboratory data demonstrates low relative levels of variability in $TPAH_{49}$ results (8.7% avg. RSD). These intralaboratory $TPAH_{49}$ results compare well with the intralaboratory EPAPAH16 results (Table 1.6). The variability evident in the replicate analyses of the same QA10OIL01 reference oil by participating laboratories present in the interlaboratory data significantly complicates the determination of total $TPAH_{49}$ concentration in oil samples. The high interlaboratory variability associated with alkylated PAH measurement raises concern about the accuracy of these measurements for source identification and exposure assessments in the environment.

The identification of fugitive oil in marine sediments is a critical objective for forensic investigators and other environmental professionals. The detection of fugitive oil in marine sediment samples is in many ways more difficult than the analysis of pure oil samples for two primary reasons. First, the oil must be efficiently extracted

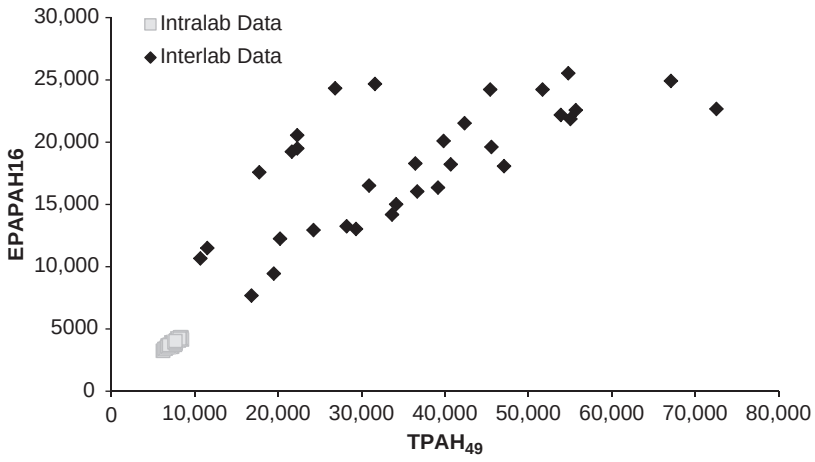

FIGURE 1.2 Cross-plot showing the measured concentrations ($\mu g/kg_{dry}$) of EPAHPAH16 vs $TPAH_{49}$ in the marine sediment reference materials. Interlaboratory data: QA10SED01 reference material ($n = 33$). Intralaboratory data: NIST SRM 1941b ($n = 40$).

from the sediment. Second, compounds that might otherwise interfere with the measurements of traditional and nontraditional analytes must be removed before analysis. Although designed to improve accuracy, additional laboratory preparation procedures can introduce additional method variability.

The PAH and alkylated PAH data generated during the NIST QA10SED01 marine sediment interlaboratory study allow data users to evaluate how interlaboratory and intralaboratory variability affects the reliability of parent PAH and alkylated PAH results generated from the analysis of marine sediment samples (Fig. 1.2). These interlaboratory results were generated from the analysis of a common, homogenous marine sediment reference material. The variability of interlaboratory ($n = 33$) results for EPAPAH16 (27.3% Avg. RSD) and TPAH49 (43.6%) demonstrate high variability for QA10SED01 results as compared to the results for the intralaboratory ($n = 40$) data which reported lower relative levels of variability in the EPAPAH16 (7.5% Avg. RSD) and TPAH49 (8.3% Avg. RSD) results for the NIST 1941b SRM (marine sediment collected at the mouth of Baltimore Harbor, MD). These data show that interlaboratory alkylated PAH summations can range substantially in concentration. The QA10SED01 marine sediment interlaboratory data reported a minimum $TPAH_{49}$ concentration of 10,600 μg/kg, a maximum concentration of 72,200 μg/kg and a mean concentration of 35,600 μg/kg. This high degree of variability poses a challenge to environmental professionals involved in oil spill impact assessments.

The accurate and precise detection of oil residues in animal and plant tissue is an important capability for laboratories involved in oil spill investigations. These data allow investigators to assess the nature and extent of oil exposure to regional biota. The laboratory preparation techniques used to analyze marine animal tissue are more complex than oil and sediment matrices. The more extensive extraction, concentration, and cleanup procedures introduce additional sources of potential laboratory variability.

The NIST mussel tissue interlaboratory study QA10TIS01 provides an opportunity to assess the implications of interlaboratory and intralaboratory alkylated PAH variability on the reliability of PAH summations generated from the analysis of mussel tissue. These interlaboratory results were generated from the analysis of a common, homogenous mussel tissue reference material.

The relationship between the EPAPAH16 and $TPAH_{49}$ concentrations illustrate the interlaboratory ($n = 35$) and the intralaboratory ($n = 40$) variability associated with the QA10TIS01 and NIST 1974b SRM mussel tissue reference samples (Fig. 1.3). The interlaboratory results for EPAPAH16 (100% Avg. RSD) and $TPAH_{49}$ (150%) demonstrate high variability for the QA10TIS01 results compared to the intralaboratory data for EPAPAH16 (8.1% Avg. RSD) and $TPAH_{49}$ (9.9% Avg. RSD). These data also show that interlaboratory alkylated PAH summations can range substantially in concentration. The interlaboratory QA10TIS01 mussel tissue concentrations for $TPAH_{49}$ range from 235 μg/kg to 33,500 μg/kg with a mean of 3,730 μg/kg. This extreme degree of variability should be considered when designing tissue sampling plans for the assessment of oil impacts to plants and marine organisms.

The interlaboratory $TPAH_{49}$ results in sediment and tissue matrices demonstrate a high bias. This can be attributed to false positive results driven by matrix-related interferences, differences in quantitation techniques and varying approaches to accurately recognizing alkylated PAH patterns.

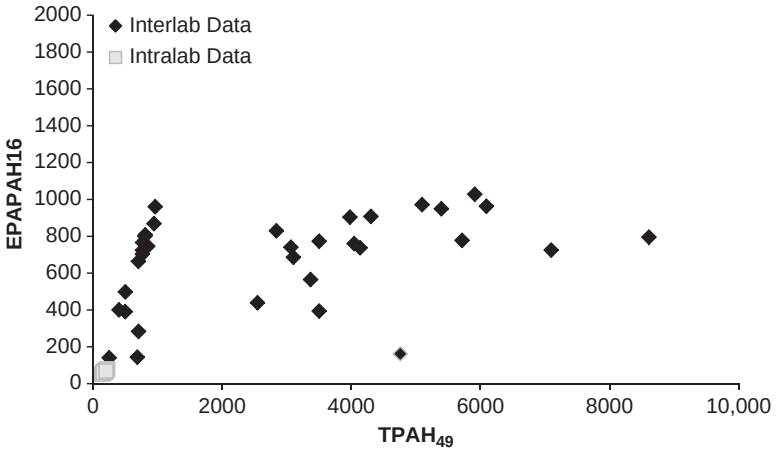

FIGURE 1.3 Cross-plot showing the measured concentrations (μg/kg$_{wet}$) of EPAHPAH16 vs TPAH$_{49}$ in the mussel tissue reference materials. Interlaboratory data: QA10TIS01 reference material ($n = 35$). Intralaboratory data: NIST SRM 1974b ($n = 40$). TPAH$_{49}$ result 33,500 μg/kg is not plotted with the interlaboratory data because it obscured the distribution of the other data points.

1.7.2 Alkylated PAH and Geochemical Biomarker Diagnostic Ratios

Alkylated PAH and geochemical biomarker DRs are metrics used by oil spill investigators to chemically characterize source oils for comparison to oils spilled in the environment. Forensic chemists employ a wide range of possible alkylated PAH and geochemical biomarker DRs that investigators may consider in performing source oil identification. In this review two common alkylated PAH DRs are considered; DBT2/ PA2 and the DBT3/PA3. In addition, seven geochemical biomarker DRs are considered; T15/hopane, Ts/Tm, T21/T22, Tm/T21, Tm/T22, S25/S28, S26 + S27/S25 + S28 (Table 1.2). These alkylated PAHs and geochemical biomarker compounds are all relatively abundant in the QA10OIL01 Macondo reference oil and illustrate the reliability of intralaboratory alkylated PAH and geochemical biomarker DRs for source identification purposes.

Forensic investigators use published protocols to evaluate DR data for quality and statistical stability. *The Center for European Norms: Oil spill identification protocol* (CEN, 2012) provides guidance on the laboratory precision needed for forensic investigators to confidently observe differences in the chemical composition of the oils being evaluated. The CEN protocol recommends a 5% RSD threshold for the laboratory precision of all DRs being used in the interpretation. CEN (2012) recommends that laboratories perform a method validation by analyzing a standard reference oil 8 times and then calculating the normative DRs. This method validation needs to yield diagnostic precision of 5% RSD or less for each ratio for the CEN protocol to be appropriate and effective. If the laboratory variability is greater than 5% RSD it becomes difficult for investigators to recognize true statistical variation in oil chemistry from laboratory variability.

The %RSD values for the DRs in this study exhibit predicable trends (Table 1.6). The intralaboratory variability satisfied the CEN criteria, but the interlaboratory %RSD results far exceed the CEN 5% RSD threshold. This observation signifies that interlaboratory variability alone obscures the forensic resolution needed to differentiate hydrocarbon sources. If the QA10OIL01 reference oil results submitted by the participating laboratories were analyzed using the CEN protocol, in spite of mean %RSD values being >5%, and the NISTIR 7793 consensus values were used to generate mean diagnostic source ratio values, none of the individually submitted QA10OIL01 reference oil results would be recognized as a "match" to the "source" oil for the DRs considered. In short, interlaboratory data should not be used for forensic purposes unless the participating laboratories collectively satisfy the CEN criteria for laboratory precision.

The intralaboratory data demonstrate relatively high levels of precision for the reported DRs. There are intralaboratory ratios that do slightly exceed the recommended 5% RSD threshold. The intralaboratory data represent a relatively large data set that was generated over the course of five years, using many instruments, generations of instrument technology and instrument operators. Nonetheless, the intralaboratory data represents the type of precision that can be achieved using advanced forensic methods and intentional forensic review protocols for a large dataset generated under conditions of nonrepeatability. When the intralaboratory data is analyzed using the CEN protocol for the DRs considered in this study using the mean intralaboratory DRs as the comparative source, all 865 replicates are recognized as matches to the source oil. The intralaboratory data represents a robust method validation for a large-scale, long-term project that incorporates instrument variability, multiple operators and typical laboratory turnover rates for batches of solvents, reagents and laboratory equipment.

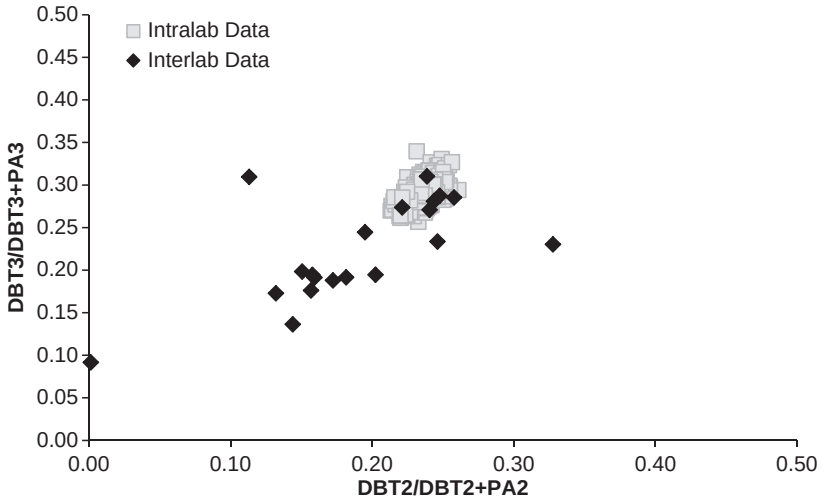

FIGURE 1.4 Cross-plot showing the measured concentrations ($\mu g/kg_{oil}$) of DBT2/(DBT2 + PA2) vs DBT3/(DBT3 + PA3) in the QA10OIL01 reference crude oil. Interlaboratory data: QA10OIL01 reference crude oil ($n = 23$). Intralaboratory data: QA10OIL01 reference crude oil ($n = 865$).

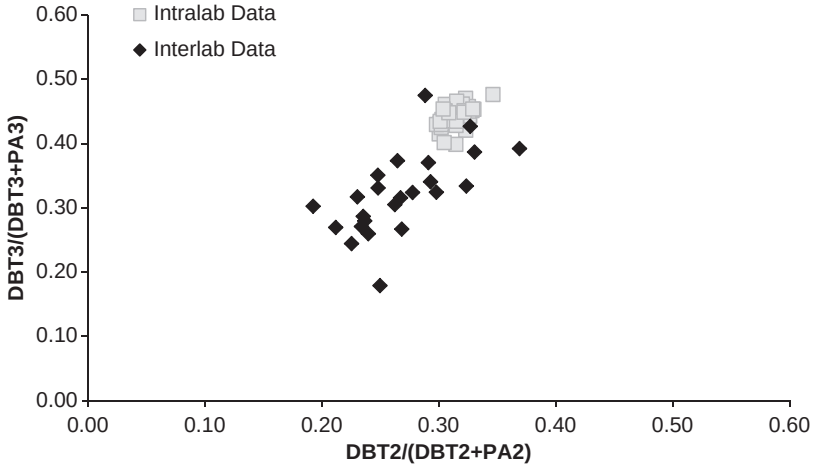

FIGURE 1.5 Cross-plot showing the measured concentrations ($\mu g/kg_{dry}$) of DBT2/(DBT2 + PA2) vs DBT3/(DBT3 + PA3) in the marine sediment reference materials. Interlaboratory data: QA10SED01 reference material ($n = 25$). Intralaboratory data: NIST SRM 1941b ($n = 40$).

The variability among interlaboratory and intralaboratory DRs is represented well by a cross-plot of the DBT2/(DBT2 + PA2) ratio vs DBT3/(DBT3 + PA3) ratio (Fig. 1.4). These widely used PAH source ratios and include some of the most easily quantified alkylated PAH analytes; consequently, they approximate a best case scenario for evaluating laboratory performance in forensically significant terms. The interlaboratory ($n = 26$) and the intralaboratory ($n = 865$) data for the QA10OIL01 Macondo reference oil demonstrate the challenge that forensic investigators may encounter when trying to use alkylated PAH results obtained from different laboratories for DR-based source identification. The variability present in the interlaboratory data generated by analyzing the same Macondo source oil creates the appearance that the analyzed oils arise from several different sources with distinct alkylated PAH characteristics. The intralaboratory data more accurately and precisely reflects a consistent source signature.

The NIST 1941b marine sediment exhibited similar results for the DBT2/(DBT2 + PA2) and DBT3/(DBT3 + PA3) ratios (Fig. 1.5). The CEN protocol is intended for use in oil to oil comparisons, but if it were adopted for oil-to-sediment comparisons, the interlaboratory results from the QA10SED01 reference material are elevated in excess of 3× the recommended 5% RSD threshold for the DRs considered in this study. This observation indicates that interlaboratory data is strongly biased in favor of determining that oil DR signatures will not match sediment samples simply because of interlaboratory variability. By contrast, the intralaboratory variability for DRs generated by an experienced forensic laboratory satisfied the <5% RSD CEN criteria (Table 1.6) even in a marine sediment matrix. In short, interlaboratory PAH data are not compatible with the CEN method for oil-to-sediment source identification purposes.

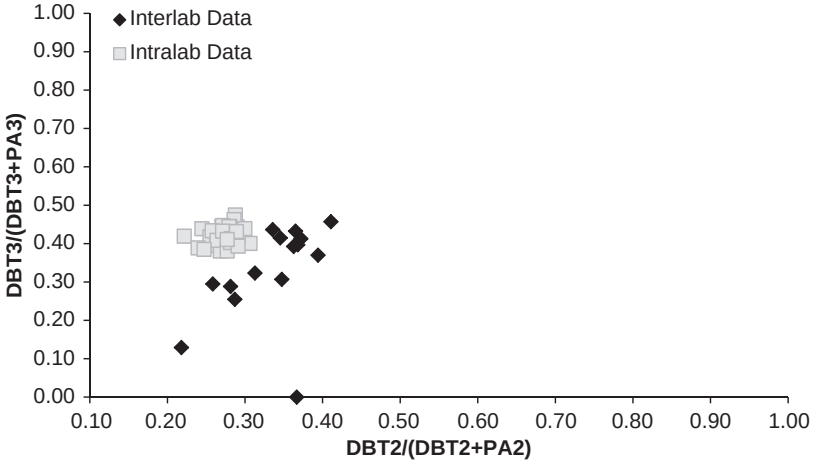

FIGURE 1.6 Cross-plot showing the measured concentrations ($\mu g/kg_{wet}$) of DBT2/(DBT2 + PA2) vs DBT3/(DBT3 + PA3) in the mussel tissue reference materials. Interlaboratory data: QA10TIS01 reference material ($n = 22$). Intralaboratory data: NIST SRM 1974b ($n = 40$).

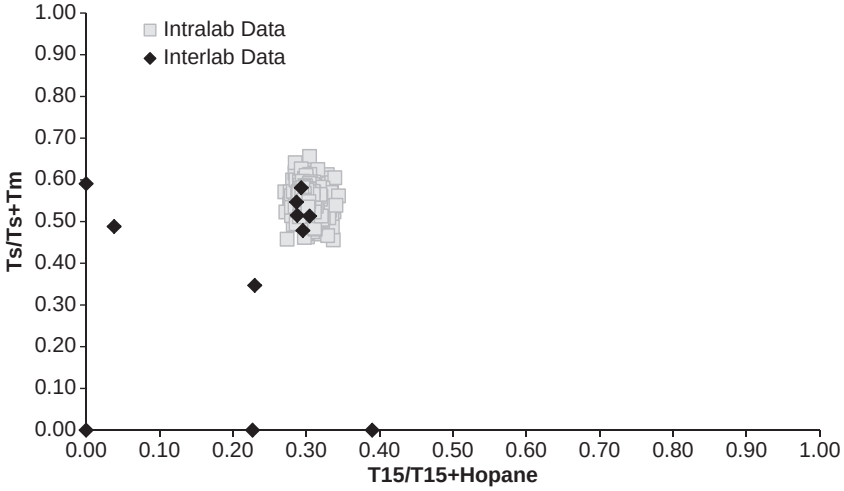

FIGURE 1.7 Cross-plot showing the measured concentrations ($\mu g/kg_{oil}$) of T15/(T15 + Hopane) vs(Ts/Ts + Tm) in the QA10OIL01 reference crude oil. Interlaboratory data: QA10OIL01 reference crude oil ($n = 12$). Intralaboratory data: QA10OIL01reference crude oil ($n = 865$).

The NIST 1974b mussel tissue SRM also exhibited similar results for the DBT2/(DBT2 + PA2) and DBT3/(DBT3 + PA3) ratios (Fig. 1.6). The mean interlaboratory DRs generated from the analysis of the QA10TIS01 reference material demonstrate high relative levels of variability well in excess of the recommended 5% RSD threshold. Like the sediment results, the tissue samples also appear to contain a variety of potential sources when the petroleum was, in fact, identical. By contrast, the mean DRs generated from the intralaboratory data are just above the recommended 5% RSD threshold. The intralaboratory samples demonstrate a discrete population of data that represent samples that contain chemical characteristics that arise from a common source (Table 1.6).

The use of geochemical biomarker DRs within the CEN framework works well for the intralaboratory data, but poorly for the interlaboratory results. This trend is illustrated well with the geochemical biomarker DRs T15/Hopane vs Ts/Tm and S25/ S28 vs (S26 + S27)/(S25 + S28) generated from the interlaboratory and intralaboratory analysis of the QA10OIL01 Macondo reference oil (Figs. 1.7 and 1.8). The mean %RSD values for the interlaboratory DRs are elevated and demonstrate similar variability that was observed in the interlaboratory alkyl PAH DRs. In other words, the geochemical biomarkers erroneously indicated that the samples contained different petroleum even when the samples contained identical material. By contrast, the intralaboratory QA10OIL01 data reports low variability and demonstrates a discrete sample population attributable to a common source.

A cross-plot of T15/Hopane vs the Tm/T21 generated from the interlaboratory (QA10SED01) and intralaboratory (SRM 1941b) analysis of the marine sediment reference materials demonstrates high variability in these biomarker DRs (Fig. 1.9) for the interlaboratory data set. The high variability among interlaboratory biomarker data confounds the ability to match source oil to marine sediment samples using interlaboratory data. By contrast, the intralaboratory data demonstrate low variability for the biomarker DRs indicating a discrete population of samples and that demonstrate common source characteristics (Fig. 1.9).

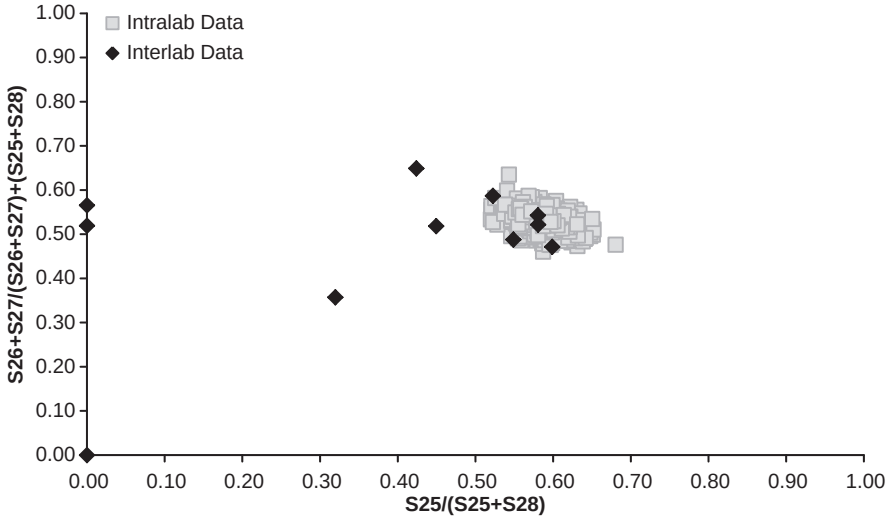

FIGURE 1.8 Cross-plot showing the measured concentrations ($\mu g/kg_{oil}$) of S25/S28 vs (S26 + S27)/(S25 + S28). in the QA10OIL01 reference crude oil. Interlaboratory data: QA10OIL01 reference crude oil ($n = 12$). Intralaboratory data: QA10OIL01reference crude oil ($n = 865$).

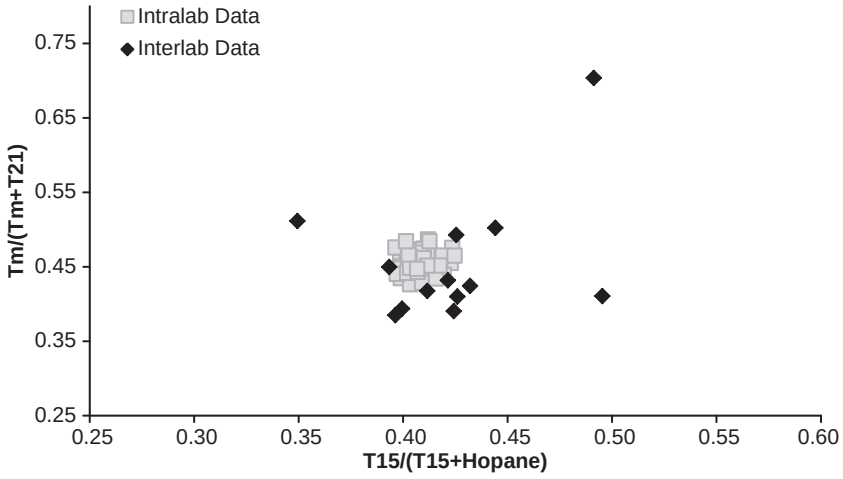

FIGURE 1.9 Cross-plot showing the measured concentrations ($\mu g/kg_{dry}$) of T15/(T15 + Hopane) vs (Tm/Tm + T21) in the marine sediment reference materials. Interlaboratory data: QA10SED01 reference material ($n = 13$). Intralaboratory data: NIST SRM 1941b ($n = 40$).

1.8 CONCLUSIONS AND RECOMMENDATIONS

This review evaluates the effects of intra- and interlaboratory variability on the ability of investigators to use traditional and nontraditional analyte concentrations in support of large-scale and long-term environmental investigations. Routine analyses of Macondo oil and NIST SRMs by one laboratory and comprehensive QC testing of oil, sediment, and tissue by multiple laboratories provide a comprehensive database for the evaluation of intra- and interlaboratory performance, respectively. The study data also provides a robust framework for comparing the accuracy and precision of traditional (i.e., 16 priority pollutant PAHs) and nontraditional analytes (i.e., alkylated PAHs and geochemical biomarkers). These data support the use of interlaboratory data for projects requiring the rapid analysis of large numbers of samples for regulatory compliance monitoring of priority pollutant analytes. However, single experienced forensic laboratories generate superior quality data for traditional and nontraditional analytes measured for source identification and other forensic purposes. These observations merit consideration for large-scale and long-term monitoring programs, like those used during oil spill investigations.

This evaluation demonstrates several important points for environmental scientists. First, interlaboratory variability is greater than intralaboratory variability, as expected. This observation is true for traditional parent PAHs and nontraditional heterocyclic parent PAHs, alkylated PAHs and geochemical biomarkers. Second, the interlaboratory variability of petroleum-related EPA priority pollutant PAHs is lower than the interlaboratory variability of alkylated PAHs and geochemical biomarkers. Interlaboratory data is not sufficiently precise for use in forensic investigations that require detailed comparisons of source oil and field samples consisting of oil residues,

sediment, or tissue. Third, the sources of laboratory variability are not well controlled in an interlaboratory analytical environment. Fourth, large-scale long-term projects benefit from extra QC strategies implemented to monitor and control interlaboratory variability. These QC strategies may include analytical QC plans, more routine laboratory QC audits, third party data validation, routine analysis of reference materials and periodic interlaboratory studies. It is important to note that the intralaboratory data discussed herein was generated under an advanced QA program that featured real-time or nearly real-time data review of most QC parameters and chromatographic integrations, which enabled the laboratory to correct analytical problems and efficiently generate high quality data. Fifth, even with an enhanced QA program, the data in this study indicate that the measurement of nontraditional compounds, like alkylated PAHs and geochemical biomarkers, fail to limit the high degree of variability found in interlaboratory data. This variability precludes the use of interlaboratory dataset in drawing conclusions requiring comparisons between alkylated PAH and biomarker concentrations or DRs produced by different laboratories.

The precision needed to meet the demands of oil spill identification protocols are very difficult to achieve using interlaboratory and clearly not achieved among multiple laboratories during the DWH investigation. The single, internal laboratory consistency for alkylated PAH and geochemical biomarker data is critical to reliable data forensic interpretations and conclusions. Diagnostic forensic data that is accurate and precise was only generated in an intralaboratory environment. Although the interlaboratory results appear to satisfy laboratory specific SOPs, QA plans, and conventional data validation protocols for regulatory compliance, traditional analytes and nontraditional analytes, such as alkylated PAHs and geochemical biomarkers, compiled from multiple laboratories demonstrate a degree of variability that render them unreliable for use in source determination and related forensic applications. For these reasons and others, NIST offers guidance that calls for increasing the precision and accuracy of "routine" laboratory analysis (Murray et al., 2015).

Our evaluation of the NOAA DWH NRDA dataset described herein finds that the most reliable and immediately available method for generating sufficiently accurate and precise alkylated PAH and geochemical biomarker data is the use of a single forensic laboratory operated with real-time QC review. Although this option may limit the overall capacity of the analytical program, laboratories can be scaled up by experienced forensic laboratory managers with the addition of instrumentation and trained staff to meet increased sample throughput demands. This was the strategy implemented by investigators during the NOAA DWH NRDA and the result was a robust and reliable forensic data set that was useful in the determination of injury and exposure to the GOM. Increased capacity realized through the use of many multiple laboratories, at the expense of forensic experience, is not an effective strategy to produce large amounts of reliable data. Quickly creating a large interlaboratory analytical program may quickly determine reasonably accurate concentrations for priority pollutant PAHs in many samples, but this approach is poorly suited for the determination of alkylated PAH and geochemical biomarker in any volume of samples collected to assess the origin and the extent of oil spill impacts.

References

ASTM, 2004. Standard Practice for Use of the Terms Precision and Bias in ASTM Test Methods. E 177–14. Am. Soc. Testing & Materials, Conshohocken, PA.

CEN. Oil spill identification—Waterborne Petroleum and Petroleum Products—Part 2: Analytical Methodology and Interpretation of Results Based Upon GC–FID and GC–MS Low Resolution Analysis. Center for European Norms Technical Report 15522-2 Oct. 3, 2012.

Douglas, G.S., Bence, A.E., Prince, R.C., McMillen, S.J., Butler, E.L., 1996. Environmental stability of selected petroleum hydrocarbon source and weathering ratios. Environ. Sci. Technol. 30, 2332–2339.

Douglas, G.S., Liu, B., Hardenstine, J., Wong, W., Litman, E., 2017. Chemical evidence for exposure of red crabs to Macondo oil after the Deepwater Horizon oil spill. In: Stout, S.A., Wang, Z. (Eds.), Case Studies in Oil Spill Forensics. Elsevier Publishing Co., Boston, MA.

Emsbo-Mattingly, S.D., Litman, E., 2016. Polycyclic aromatic hydrocarbon homolog and isomer fingerprinting. In: Stout, S.A., Wang, Z. (Eds.), Standard Handbook of Oil Spill Environmental Forensics: Fingerprinting and Source Identification, second ed. Elsevier Publishing Co., Boston, MA. ISBN 978012803821.

EPA, 2002. Guidance on Environmental Data Verification and Data Validation: EPA QA/G-8.

EPA, 2014. EPA Method 8270D: Semivolatile Organic Compounds by Gas Chromatography/Mass Spectrometry.

EPA, 2017. National Functional Guidelines for Organic Superfund Methods Data Review.

IUPAC, 1993. The International Harmonized Protocol for the Proficiency Testing of (Chemical) Analytical Laboratories. Pure Appl. Chem. 65 (9), 2123–2144.

Murray, J., Sander, L., Wise, S., Reddy, C.,2015. Gulf of Mexico Research Initiative 2014/2015 Hydrocarbon Intercalibration Experiment: Description and Results for SRM 2779 Gulf of Mexico Crude Oil and Candidate SRM 2777 Weathered Gulf of Mexico Crude Oil. NISTIR 8123, Gaithersburg, MD.

NIST Certificate of Analysis for Standard Reference Material (SRM) 1582 Petroleum Crude Oil, 1984. National Institute of Standards and Technology (NIST), Gaithersburg, MD, 1984.
NIST Certificate of Analysis for Standard Reference Material (SRM) 1974b Organics in Mussel Tissue (*Mytilus edulis*), 2003. National Institute of Standards and Technology (NIST), Gaithersburg, MD.
NIST Certificate of Analysis for Standard Reference Material (SRM) 1941b Organics in Marine Sediment, 2004. National Institute of Standards and Technology (NIST), Gaithersburg, MD.
NIST Certificate of Analysis for Standard Reference Material (SRM) 2779 Gulf of Mexico Crude Oil, 2012. National Institute of Standards and Technology (NIST), Gaithersburg, MD.
NOAA, 1998. National Status and Trends: Sampling and Analytical Methods of the NS&T Program 1993–1996.
NOAA, 2014. Analytical Quality Assurance Plan, Mississippi Canyon 252 (Deepwater Horizon) Natural Resource Damage Assessment, Version 4.0. May 30, 2014.
NOAA, 2017. Diver Explorer DWH NRDA: Lab Results and Field Measurements. <http://ww.diver.orr.noaa.gov>.
Payne, J.R., Driskell, W.B., 2017. Forensic identification and distribution of Deepwater Horizon oil in the Gulf of Mexico subsurface waters. In: Stout, S.A., Wang, Z. (Eds.), Case Studies in Oil Spill Forensics. Elsevier Publishing Co., Boston, MA.
Peters, K.E., Moldowan, J.M., 1993. The Biomarker Guide: Interpreting Molecular Fossils in Petroleum and Ancient Sediments. Prentice Hall, Englewood Cliffs, NJ.
Phenomenex, 2017. Zebron ZB-5 Product Technical Specifications.
Reddy, Christopher M., Murray, J., Sander, L., Wise, S., 2015. Summary of Results from the 2014/2015 Hydrocarbon Inter-calibration Experiment (HIE). Gulf of Mexico Research Initiative, Gaithersburg, MD.
Schantz, M.M., Kucklick, J.R., 2011a. Interlaboratory Analytical Comparisons Study to Support Deepwater Horizon Natural Resource Damage Assessment: Description and Results for Crude Oil QA10OIL01. NISTIR 7793, Gaithersburg, MD.
Schantz, M.M., Kucklick, J.R., 2011b. Interlaboratory Analytical Comparisons Study to Support Deepwater Horizon Natural Resource Damage Assessment: Description and Results for Marine Sediment QA10SED01. NISTIR 7792, Gaithersburg, MD.
Schantz, M.M., Kucklick, J.R., 2011c. Interlaboratory Analytical Comparisons Study to Support Deepwater Horizon Natural Resource Damage Assessment: Description and Results for Mussel Tissue QA10TIS01. NISTIR 7819, Gaithersburg, MD.
SINTEF, 2002. Nordtest Methodology for Oil Spill Identification. SINTEF Applied Chemistry Trondheim, Norway, May 8, 2002.
Stout, S.A., 2016. Oil spill fingerprinting method for oily matrices used in the Deepwater Horizon NRDA. Environ. Forensics 17 (3), 218–243.
Stout, S.A., Payne, J.R., 2016. Macondo oil in deep-sea sediments: Part 1—sub-sea weathering of oil deposited on the seafloor. Mar. Pollut. Bull. 111, 365–380.
Stout, S.A., Wang, Z., 2008. Diagnostic compounds for fingerprinting petroleum in the environment. Environ. Forensics R. E. H. Hester, R.M. London. Special Publication No. 26, 54–104.
Stout, S.A., Uhler, A.D., McCarthy, K.J., Emsbo-Mattingly, S., 2002. Chemical fingerprinting of hydrocarbons. In: Murphy, B.L., Morrison, R.D. (Eds.), Introduction to Environmental Forensics. Academic Press, Boston, MA, pp. 137–260.
Stout, S.A., Payne, J.R., Emsbo-Mattingly, S.D., Baker, G., 2016. Weathering of field-collected floating and stranded Macondo oils during and shortly after the Deepwater Horizon oil spill. Mar. Pollut. Bull. 105, 7–22.
Stout, S.A., Litman, E., Baker, G., Franks, J., 2017. Novel biological exposures following the Deepwater Horizon oil spill revealed by chemical fingerprinting. In: Stout, S.A., Wang, Z. (Eds.), Case Studies in Oil Spill Forensics. Elsevier Publishing Co., Boston, MA.
Wang, Z., Fingas, M., Page, D.S., 1999. Oil spill identification. J. Chromatogr. A 843, 369–411.
Wang, Z., Stout, S.A., Fingas, M., 2006. Forensic fingerprinting of biomarkers for oil spill characterization and source identification (Review). Environ. Forensics 7 (2), 105–146.

Further Reading

ASTM, 2002. Standard Practice for Dealing with Outlying Observations. *E 178-02*. Am. Soc. Testing & Materials, Conshohocken, PA.
Douglas, G.S., Stout, S.A., Uhler, A.D., McCarthy, K.J., Emsbo-Mattingly, S.D., 2016. Advantages of quantitative chemical fingerprinting in oil spill identification and allocation of mixed hydrocarbon contaminants. In: Stout, S.A., Wang, Z.(Eds.), Standard Handbook of Oil Spill Environmental Forensics: Fingerprinting and Source Identification. Elsevier Publishing Co., Boston, MA, pp. 789–847.
International Organization for Standardization (ISO) and International Electrochemical Commission (IEC) 17043: 2010 Conformity Assessment-General Requirements for Proficiency Testing, 2010.
Schantz, M.M., Parris, R.M., Wise, S.A., 2008. NIST Intercomparison Exercise Program for Organic Contaminants in the Marine Environment: Description and Results of 2007 Organic Intercomparison Exercises. NISTIR 7501, Gaithersburg, MD.
Stout, S.A., Uhler, A.D., McCarthy, K.J., 2001. A strategy and methodology for defensibly correlating spilled oil to source candidates. Environ. Forensics 2 (1), 87–98.

CHAPTER

2

Fifty Years of Petroleum Geochemistry: A Valuable Asset in Oil Spill Environmental Forensics

R. Paul Philp

University of Oklahoma, Norman, OK, United States

BIOGRAPHY

R. Paul Philp received his Ph.D. in organic chemistry from the University of Sydney (Australia) in 1972 and D.Sc. degree from the same University in 1998. He then spent one and a half years as a postdoctoral fellow with Professor G. Eglinton at the University of Bristol (England) undertaking research in various aspects of organic geochemistry and the application of analytical techniques such as gas chromatography–mass spectrometry to this area of research. Following this, he spent 4 years at the University of California, Berkeley, as a research associate, directing the organic geochemistry research group of Professor Melvin Calvin. He returned to Sydney in 1977 to join the CSIRO, Fuel Geoscience Unit where he was a principal research scientist studying various aspects of petroleum geochemistry. In June 1984, he joined the faculty at the University of Oklahoma. Recently a large amount of his research has been concerned with environmental studies and particularly investigating the use of stable carbon isotopes as a means of monitoring and tracking pollutants in the environment. He is now an Emeritus Professor at the University of Oklahoma having retired in December 2015 but continues to be actively involved in various aspects of geochemical research.

2.1 INTRODUCTION

Environmental forensic investigations can generally be summarized with a few basic questions. What is the product that has been released, when did the release occur, and can the spilled product be related back to the source or point of release? Such investigations can be many and varied but this chapter will focus primarily on issues related to oils spills. However, rather than provide numerous examples of specific oils spills this chapter will focus on diagnostic aspects related to crude oil compositions that are evident from decades of oil exploration and production petroleum geochemistry research, which have been demonstrated to be invaluable in resolving issues related to identifying the source of any spill. It is important to emphasize that not every spill resembles the *Exxon Valdez* or *Deepwater Horizon* incident where the major sources of oil were clearly evident, although it was still necessary to demonstrate that the spilled product was related to those sources and not, for example, naturally seeped oils, for litigation purposes. Some cases may be related to rogue spills in the ocean with no tanker within miles or a plume of hydrocarbons under multiple pipelines and in such cases, forensic investigations become even more important.

Hydrocarbon spills, or releases, into the environment can take many forms with a significant number of variables involved but can generally be divided into a number of basic categories. First, they can be divided on

Oil Spill Environmental Forensics Case Studies.
DOI: http://dx.doi.org/10.1016/B978-0-12-804434-6.00002-1

the basis of the type of product released: crude oils, condensates, heavy oils, light oils, refined products, or natural gas. Second, they can be divided on the basis of the environment into which the spill or release occurred: marine, estuarine, lacustrine, onshore, offshore, above ground, below ground, cold climates, warm climates, wet environments, dry environments. Third, releases may occur from tankers, trains, pipelines, underground storage tanks, above ground storage tanks and probably many other unknown sources. These are some of the many variables that need to be taken into consideration when undertaking forensic investigations designed to determine the point of release of a particular product and relate the released product to the original product that was released. Many of the factors mentioned above, along with many others, will control what happens to the product after it is released and these will be discussed in the following sections.

The initial purpose of this chapter is to provide an overview of factors that control the original composition of a crude oil and why crude oils from different sources will differ both in terms of their bulk properties and their molecular composition. Another important issue related to this is the impact of weathering on the oils after they are released. Weathering, either through evaporation, water washing or biodegradation, has the ability to alter crude oil compositions such that the characteristics of the spilled product may ultimately be quite different from that of the original product at the time of release. Finally, there is the problem with onshore releases of crude oils where it becomes necessary to distinguish the fingerprints from the spilled oil versus those of the naturally occurring organic matter in the environment (e.g., vegetation). Much of what is known regarding crude oil's composition, weathering, and naturally occurring organic matter applied in environmental forensics comes from petroleum geochemistry research documented in literature spanning the last 50 years. Thus, another purpose of this chapter is to reintroduce those aspects of oil spill environmental forensics that have derived from conventional petroleum exploration and production geochemistry.

2.2 THE ORIGIN OF CRUDE OILS

Forensic investigations of crude oil spills require extensive fingerprinting of the oils that may have been responsible for the release and also samples of the spilled product. The most commonly used analytical tools for fingerprinting purposes will be gas chromatography (GC), GC−mass spectrometry (GC−MS) and related ancillary techniques and stable isotopes. Stable isotopes can either be determined as bulk values—the isotopic composition of the whole oil—or the isotopic composition of individual compounds as determined by GC-isotope ratio MS (GCIRMS). Much of the information in the following sections is derived from the vast source of information that can be found in the petroleum geochemistry literature. Since the dawn of molecular geochemistry in the late 1960s, early 1970s, petroleum geochemists have been using the molecular composition of crude oils to obtain information on the origin and history of crude oils (Burlingame and Simoneit, 1969; Eglinton and Murphy, 1969; Henderson et al., 1968; Hunt et al., 2002; Mackenzie, 1984; Peters and Moldowan, 1992; Peters and Fowler, 2002; Peters et al., 2005; Philp, 1985, 2014; Philp and Lewis, 1987). In my opinion it is extremely important that the environmental investigators be aware of this body of knowledge since application of geochemical concepts to an exploration problem, such as relating an oil to potential source rocks, is no different than trying to relate a spilled product back to its source. In both cases, it is an exercise in fingerprinting but the key is an understanding of the content of the fingerprints and what constitutes diagnostic similarities or differences in these fingerprints.

Crude oils are derived from mixtures of organic matter deposited in a wide variety of depositional environments and may vary in age from a few tens of millions of years to several hundred millions of years. Over geologic time, as a result of the evolution of various plant types, algae and phytoplankton, bacteria and other source materials, the compositions of source materials of crude oils have changed on both a bulk and molecular level. The key processes involved in crude oil formation start with photosynthesis and the primary photosynthesizers, such as plants and phytoplankton, incorporating CO_2 from the atmosphere into their cell walls. As will be shown below the isotopic composition of the atmosphere has also changed over time as a result of continuing photosynthetic activity, and therefore, the isotopic composition of crude oils has changed over time providing another variable that can ultimately be useful to distinguish crude oils from different sources.

As the primary photosynthesizers ultimately die and are deposited into a variety of depositional environments, a variety of complex processes can occur depending on the nature of the organic matter and nature of the depositional environment. Very oxic environments will degrade organic matter relatively quickly and only leave the more recalcitrant organic residues that are generally not very oil prone but will generate gas rather than oil. More highly reducing, or anoxic environments, will generally preserve the organic matter far more effectively

and ultimately lead to the formation of organic rich sediments which, as they are buried, will start to generate or release hydrocarbons as a result of increasing temperatures the rocks experience with increasing depth of burial. The ultimate result of this synthesis of organic matter followed by deposition, preservation, burial and heating is the production of a crude oil and/or natural gas. It should be noted that oil and gas generation is a very complex process and there are a number of different situations that may occur. A popular topic today is that of unconventional resources (Slatt et al., 2009; 2012a,b; Slatt and Rodriguez, 2012). In the case of shale gas, the gas is actually being formed from oil that was trapped in the shale from which it was generated and as a result of being trapped is ultimately converted to gas. Shale oil is similar but the trapped oil has not been heated enough to generate gas and it remains as oil. As a result of the low permeability of the rocks preventing expulsion of the oil or gas to a reservoir, the concept of hydraulic fracturing was developed to release the trapped products by fracturing the rocks using primarily water and sand. However, regardless of whether the oil was derived from conventional or unconventional sources, once the oil is produced it has to be transported and, regardless of whether it came from a conventional or unconventional source, will face the same problems if it is released into the environment.

As mentioned above the primary source of organic matter responsible for the formation of crude oils is derived from the primary photosynthesizers such as plants, phytoplankton, and photosynthetic bacteria. Atmospheric CO_2 is incorporated into the living organisms and through the process of photosynthesis incorporated into cell wall components. Atmospheric CO_2 is composed of $^{12}CO_2$ and $^{13}CO_2$ with an approximate relative abundance of 99 to 1. During the process of photosynthesis, the lighter isotope is incorporated at a faster rate than the heavier isotope, leading to the process of isotopic fractionation. The extent of this fractionation will vary depending on the nature of the plant or organism incorporating the CO_2. Variations in isotopic compositions are determined by completely combusting the organic material and then measuring the relative proportions of the $^{12}CO_2$ and $^{13}CO_2$ and ultimately converting this into a $\delta^{13}C$ value which is expressed:

$$\delta^{13}C = \frac{(R_{sample} - R_{standard})}{R_{standard}} \times 1000$$

In the above expression, $R = {}^{13}C/{}^{12}C$ for sample and standard, respectively, as measured from the intensity of masses 45 and 44 in the isotope ratio mass spectrometer. The values are measured relative to international standards, which in the case of C is a marine carbonate known as Pee Dee Belemnite or PDB (Fuex, 1977; Stahl, 1978). For the benefit of those not familiar with this expression it should be noted that as the isotope values become more negative that means they contain less of the heavier isotope and the product, or compound, becomes isotopically lighter. As mentioned above over geologic time the isotopic composition of atmospheric CO_2 and resulting oils have changed. In the Precambrian times oils had isotopic values around -35 per mill but today the youngest crude oils are isotopically much heavier with values around -20 per mill (Andrusevich et al., 1998). The reason for that change was primarily due to increasing diversity of the primary photosynthesizers utilizing more and more of the lighter CO_2 with the net result being that the residual CO_2 in the atmosphere became isotopically heavier, and ultimately the compounds produced by photosynthesis will also become isotopically heavier. The net result being that the isotopic values for crude oils over time have varied considerably meaning that this is another tool that can be used for correlation or discrimination of sources. There is not an infinite range of isotopic compositions for crude oils so there will be many cases when crude oils from different sources do indeed have very similar values. In any case, isotopes should not be used as the sole tool to differentiate samples but should be used in conjunction with the additional fingerprinting tools to be described below.

2.3 CRUDE OIL COMPOSITION

The composition of a crude oil can be characterized in various ways. First, there is the bulk composition, including properties such as the API gravity, optical activity, bulk isotope values, S content; composition in terms of relative proportions of saturate, aromatic, polar, and asphaltene fractions (Hunt, 1979, 1996; Tissot and Welte, 1984). All of these bulk parameters have been used in the past to correlate or discriminate oils from the same or different sources. However, they are bulk parameters and, therefore, not very specific and oils from totally different sources may coincidently have the same bulk parameters. However, since the early 1970s, with the development of the GC and GC–MS systems, the fingerprinting has become far more specific and predictable. In other words, differences in the fingerprints of crude oils can now be interpreted in terms of different source materials being deposited in different depositional environments and subjected to differing levels of maturity (Philp, 2014).

2.4 ANALYTICAL TECHNIQUES

Before looking at some of these differences and why they occur, a brief summary of the analytical techniques is appropriate. GC is basically a separation tool not an identification technique. However, with experience certain components can be recognized on the chromatograms and tentatively identified. For example, the chromatogram shown below in Fig. 2.1 is derived from a crude oil and certain components have been identified. The reason being that the homologous series of major components is easily recognized as being comprised of *n*-alkanes and if the C_{19} and C_{20} isoprenoids, pristane and phytane, can be identified it is easy to label the major *n*-alkanes in the chromatogram since these compounds always elute adjacent to *n*-C_{17} and *n*-C_{18}. At the same time, it is important to point that even though it may not always be possible to tentatively identify peaks in the chromatogram it is still possible to differentiate between say gasoline and jet fuel or diesel based using the gas chromatograms. The problems arise of course when you have multiple crude oil samples or gasoline samples and they all look very similar chromatographically and then it is generally impossible to differentiate them by GC alone.

The next, and more powerful, level of analysis is based on the GC–MS approach. There are many different types of mass spectrometers and this is not the forum to describe all of these instruments. Basically, a mass spectrometer can operate in two ways, either it can collect complete mass spectra of every compound or it can be used in the form of an ancillary technique known as multiple ion detection (MID). For forensic investigations, the most commonly used approach is the latter since you are looking for specific compounds and want to use the most specific, sensitive, and selective technique to detect these compounds.

For those investigators not as familiar with the MID technique as they are with GC, a brief explanation will follow here. In the ion source of a mass spectrometer, compounds are ionized and fragment in a very characteristic manner which depends on the actual structure of the compound under investigation. In the case of crude oils, a number of compound classes are typically monitored and the majority of these compounds can be classified as biomarkers, a term discussed in more detail below. Two common classes of biomarkers are steranes and terpanes and typical structures for these compounds are shown below along with an indication as to how these molecules fragment and the most stable fragment ion that is formed during ionization. As seen toward the right of Fig. 2.2, for steranes, the major fragment has a mass of *m*/*z* 217 and for terpanes it is *m*/*z* 191. So, when the mass spectrometer is operated in the MID mode instead of collecting all the ions that are formed in the ion source of the mass spectrometer, if only steranes and terpanes are being analyzed, only the ions at *m*/*z* 217 and 191 are monitored, making the system more selective, specific, and sensitive. One word of caution though needs to be introduced and that is the chromatograms that are produced from these MID methods are basically showing all compounds in the sample that have *m*/*z* 217 as one of their fragment ions. It is commonly assumed that all of these compounds are going to be steranes and for the most part that is correct. However, there are exceptions to this common observation and one should be aware of this possibility. In a normal crude oil, these compounds of interest are generally present in relatively low concentrations, meaning they are not normally observable on a gas

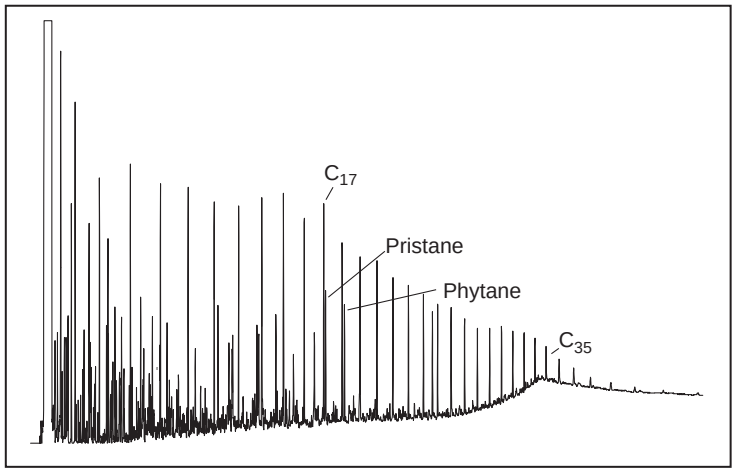

FIGURE 2.1 A gas chromatogram for a typical crude showing a well-defined distribution of *n*-alkanes and the major isoprenoids, pristane, and phytane.

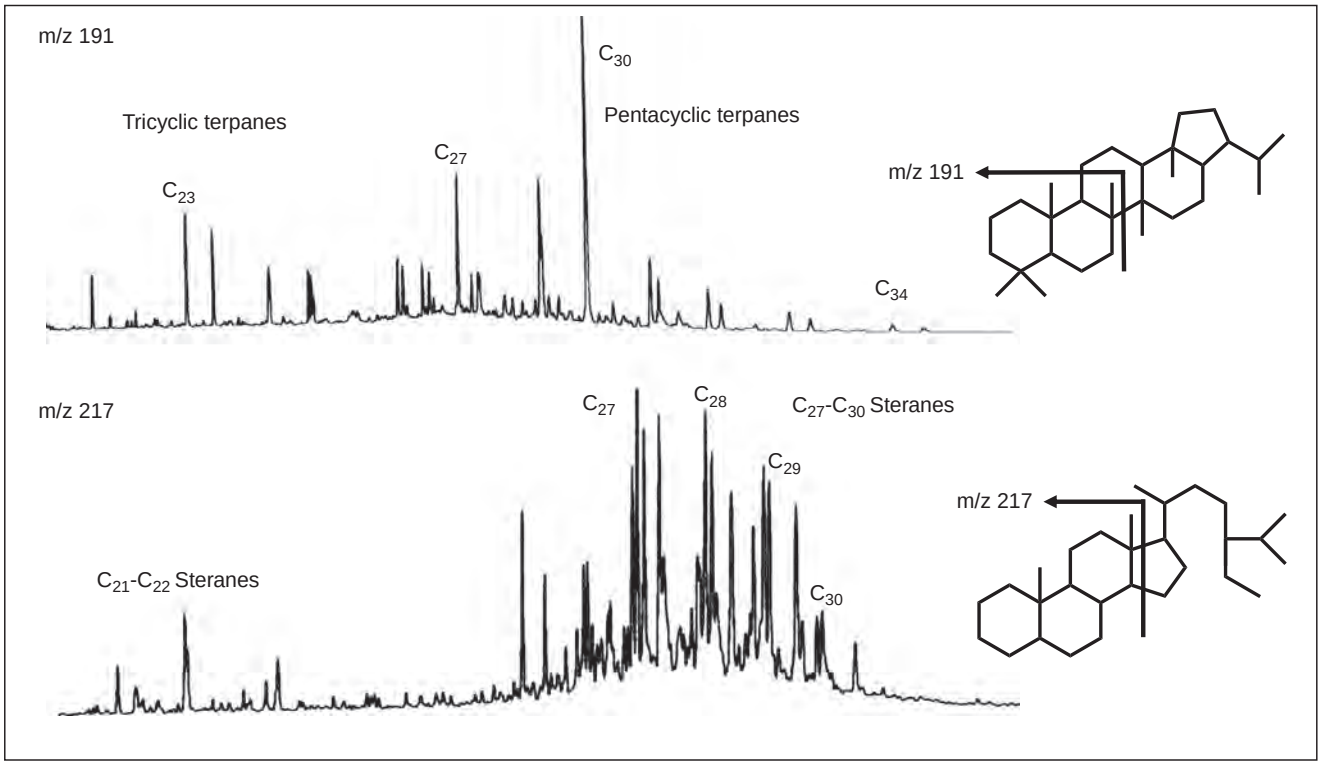

FIGURE 2.2 GC–MS chromatograms showing typical terpane and sterane distribution in a crude oil as determined through MID using the ions at *m/z* 191 and 217, respectively. Major peaks are identified in these chromatograms but the identity of all components is well documented in the literature. Structures to the right show fragmentation that give rise to the characteristic *m/z* 191 and 217 fragments.

chromatogram since they are hidden in the baseline of the chromatogram. Use of the MID approach permits detection of these compounds to produce fingerprints of the type shown in Fig. 2.2.

As mentioned, the MID approach has been the standard technique for many years in many different areas of geochemistry and has been a very important tool. However, there is another sophisticated approach that can be used for solving more difficult problems and that is the approach known as tandem mass spectrometry or MS–MS. This is a more complex technique but provides an additional degree of separation. As mentioned above the *m/z* 217 chromatogram is assumed only to show steranes. However, as it is known that the major series of steranes are the compounds at C_{27}, C_{28}, C_{29}, and C_{30} the molecular masses of these compounds are known to have parent ions of *m/z* 372, 386, 400, and 414, respectively. In the MS–MS approach, the molecule is ionized in the ion source of the mass spectrometer. But then only the parent ions are allowed to pass through the first quadrupole into a collision cell where that parent fragment ion is allowed to collide with an inert gas such as argon where it will fragment with the major fragment ion being that at *m/z* 217. The *m/z* 217 ion is allowed to pass through the third, quadrupole and it is ultimately detected by the electron multiplier. However, the data system is able to relate the ion at mass 217 with the parent from which it was derived. Therefore, at the end of the analyses it is possible to deconvolute the complex sterane mixture shown in Fig. 2.2 into the individual members of the series as shown below (Fig. 2.3). This is not a technique that needs to be used on every sample but it is useful to know the method is available if needed to identify individual compounds or resolve complex mixtures.

The final technique to briefly introduce is that of GCIRMS (Freeman et al., 1990; Mansuy et al., 1997; Philp and Kuder, 2008; Philp, 2009; Smallwood et al., 2002). It was mentioned above that for many years stable isotopes were measured as the so called bulk numbers, where one value was obtained for each crude oil, corresponding to the weighted average of the isotopic composition of all the individual compounds in the oil. These numbers have been used extensively but have limited use due to the fact many oils worldwide will coincidently have the same isotope values. Bulk isotopes can be made a little more useful by separating the samples into saturate and aromatic components and determining the isotopic composition of the individual fractions and plotting them against each other as shown below (Fig. 2.4; Stahl, 1978). The oils in this figure have different in geologic ages but show a trend toward isotopically heavier values as they become geologically younger and provides an initial

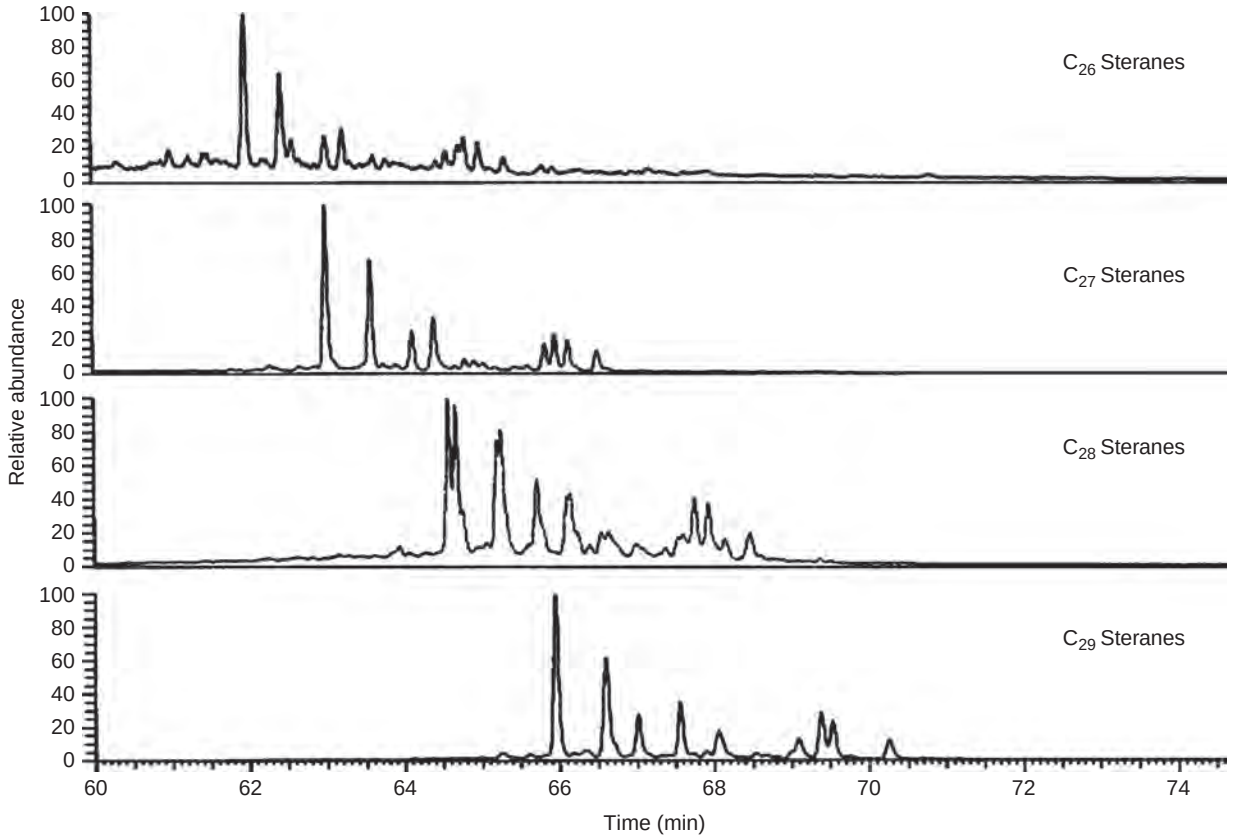

FIGURE 2.3 MSMS permits an additional element of separation to be introduced based on parent/daughter relationships of components in the mixture. In this example the transitions for the parent ions of the C_{27}, C_{28}, C_{29}, and C_{30} steranes (m/z 372, 386, 400, and 414, respectively) and the m/z 217 daughter ion are used to resolve the mixture.

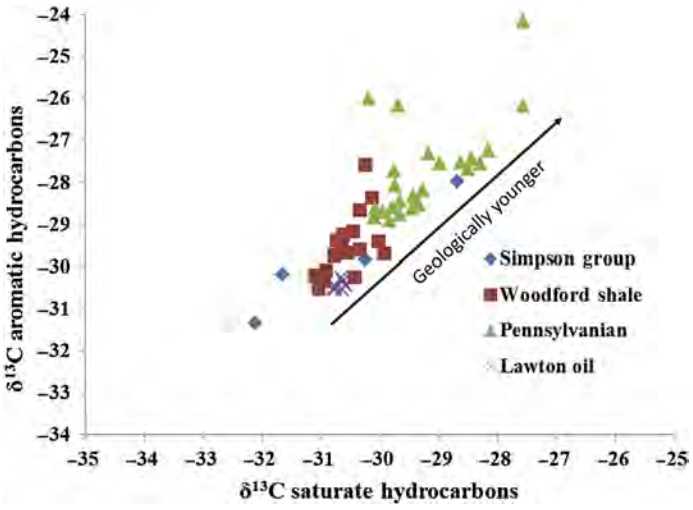

FIGURE 2.4 Examples showing several oils that have been separated into saturate and aromatic fractions and then the carbon isotope values of the individual fractions have been determined. The oils shown on this diagram are of different geological ages and as the oils become younger they are also becoming isotopically heavier.

guideline for differentiating oils derived from different sources in this particular region. More recently, the GCIRMS combination has become available such that the isotopic composition of individual compounds in a mixture can now be obtained. Again some words of caution prior to looking at some examples of the results. First, if you cannot see a compound on the chromatogram (i.e., it is hidden in the baseline) you will not be able to get an isotope value for it unless it is physically isolated from the oil or fraction being analyzed. Second, high resolution chromatography is of the utmost importance and ideally baseline resolution is desirable. The GCIRMS

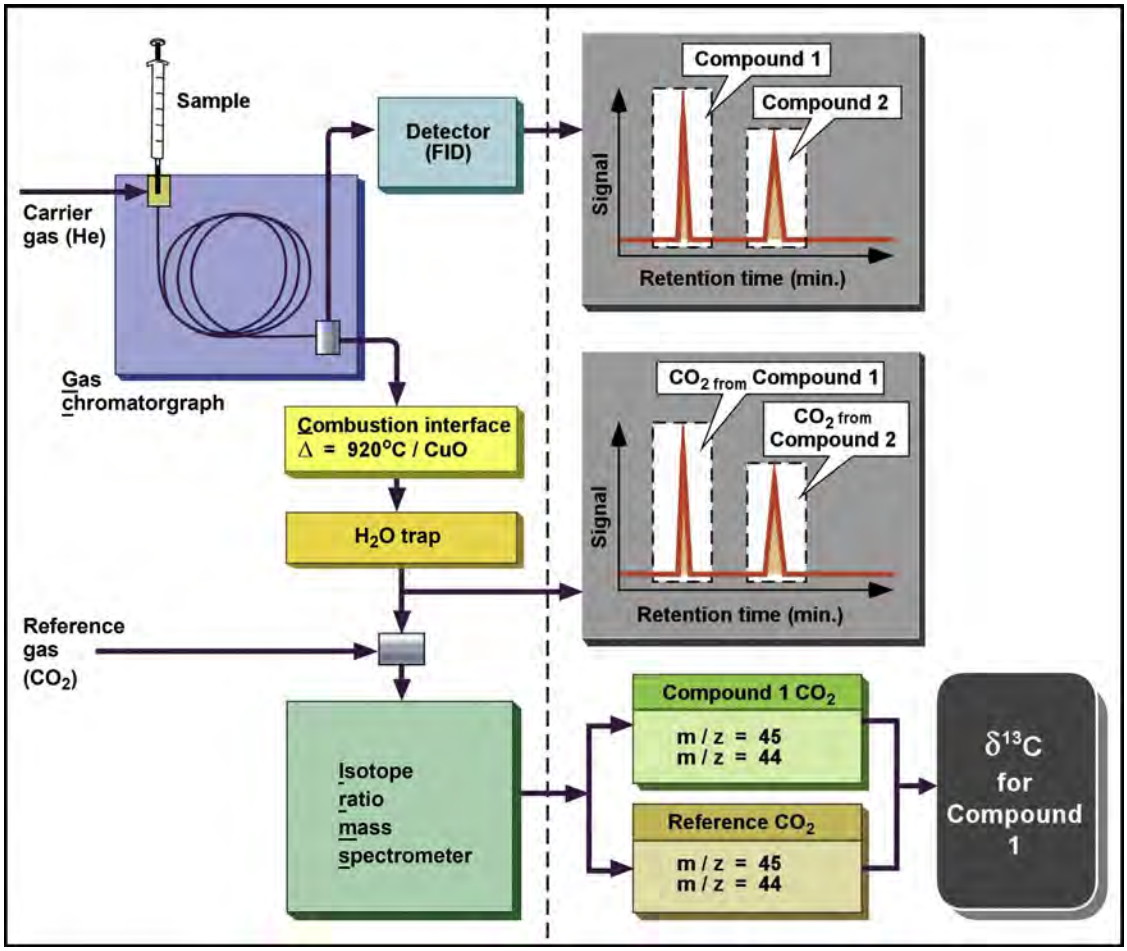

FIGURE 2.5 The GCIRMS system combines the GC with an isotope ratio mass spectrometer. After GC separation the separated components are combusted to CO_2 and the resulting CO_2 is transferred to the mass spectrometer and the relative proportions of $^{13}CO_2$ and $^{12}CO_2$ are determined and converted into a $\delta^{13}C$ value for each component.

system is basically a conventional GC but as the compounds elute from the GC they pass through a combustion reactor where they are converted to CO_2 and water. The water is removed and the $^{12}CO_2$ and $^{13}CO_2$ from the combustion process enters the mass spectrometer where the intensities are determined and ultimately converted into a $\delta^{13}C$ value. A schematic of the system is shown below (Fig. 2.5) and an example showing the results from the analyses of the isotopic composition of *n*-alkanes in 5 oils is shown in the accompanying figure (Fig. 2.6). It can be seen from this figure that the isotopic data are separated into three groups suggesting the oils are possibly derived from 3 different sources. However, this is not necessarily definitive but should be used as preliminary data or guidelines that can be used in conjunction with the biomarker data to confirm these differences (Kvenvolden et al., 1995; Mackenzie et al., 1982; Waples, 1985; Waples and Machihara, 1991).

2.5 THE BIOMARKER CONCEPT

The tools available for fingerprinting crude oils have been described above and now the question is how to utilize the information that is obtained from these techniques since there are two levels for interpretation and utilization of the data. First, the chromatograms can be simply used as fingerprints with little or no idea where the compounds in the fingerprint came from, how they change with source and weathering, or for that matter the identity of the compounds. Interpretation at this level can be very dangerous and probably not successful if the data are to be used in litigation. At a higher level of interpretation the ability to recognize specific compounds and utilize information about their geological origin takes the interpretation to a much higher level. In the following sections the occurrence of specific compounds and families of compounds present in crude oils

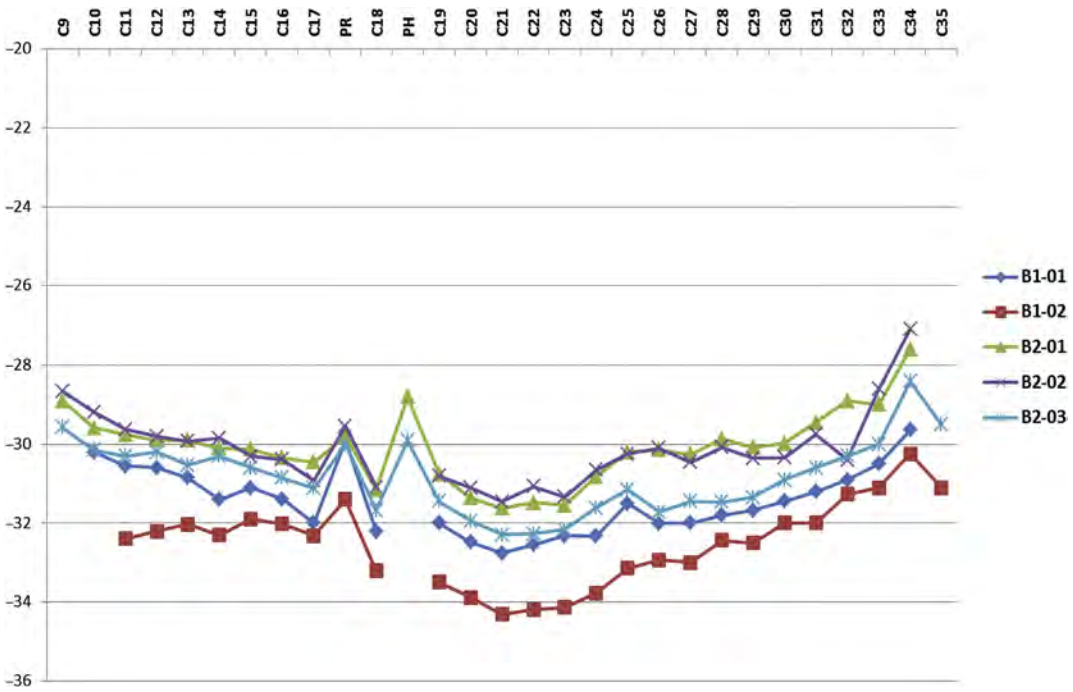

FIGURE 2.6 The stable carbon isotopic composition of individual *n*-alkanes from five different samples plotted against carbon number showing differences in the oils resulting from differences in the source materials on these samples.

will be given along with how these compounds can be used to differentiate crude oils coming from different sources.

As indicated above a great of information developed in the petroleum exploration and production industry is directly applicable to environmental forensic studies. There is little difference between trying to correlate a crude oil with its suspected source rock than trying to correlate a spilled oil with a sample from its suspected point of release. In many ways it is even easier since even if spilled oil is altered by weathering processes, the degree of alteration may be fairly insignificant compared to the level of alteration of a crude oil that may have been subject to biodegradation over a period of many millions of years. The real breakthrough in the crude oil fingerprinting came with the development of GC and GC–MS. Initially, these systems were not available commercially and a review of the literature will reveal many papers related to the development of the systems in laboratories that were working on origin of life studies or lunar related projects, such as the University of California at Berkeley and University of Bristol in England (Eglinton et al., 1964; Kimble et al., 1974; Hites and Bieman, 1970; Maxwell et al., 1971; Seifert and Moldowan, 1978, 1979). These early studies required the ability to detect trace amounts of complex mixtures in rock extracts. It should also be noted at that time data systems were in their infancy and many of the early commercial GC–MS systems were sold without data systems, making analyses and data processing a very time consuming and tedious task. This early work gave birth to the concept that was originally christened chemical fossils by Calvin and Eglinton, a term that went through several iterations through terms such as biological markers and biomarkers appeared at different times but today the term "biomarker" is the most commonly used term to describe specific compounds in crude oils. A classic definition of this term would be that biomarkers are hydrocarbons that occur in oils and source rocks whose hydrocarbon skeletons can be related to the structure of their functionalized precursor molecules present in source materials deposited into the geological record millions of years ago. A simple example of this concept is shown below where a sterol, a common constituent of many living systems, is ultimately converted to a sterane but note the similarity in the basic carbon skeleton of the sterol and sterane (Fig. 2.7).

The ability to relate molecules present in crude oils and source rocks today with those precursor molecules deposited millions of years ago, provides a wealth of information for the explorationist in reconstructing the origin and history of the oil. The fingerprints that can be obtained from multiple biomarkers present in crude oils and source rocks can also be used for oil/oil or oil/source rock correlations. This is where the cross over with environmental forensics enters since precisely the same approach can be applied to the correlation of a spilled oil with its suspected source. Some knowledge of the origin and source of specific compounds can be extremely

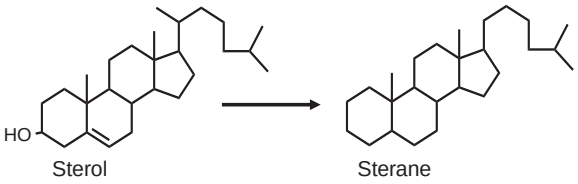

FIGURE 2.7 A classic example illustrating the biomarker concept based on the sterol/sterane relationship.

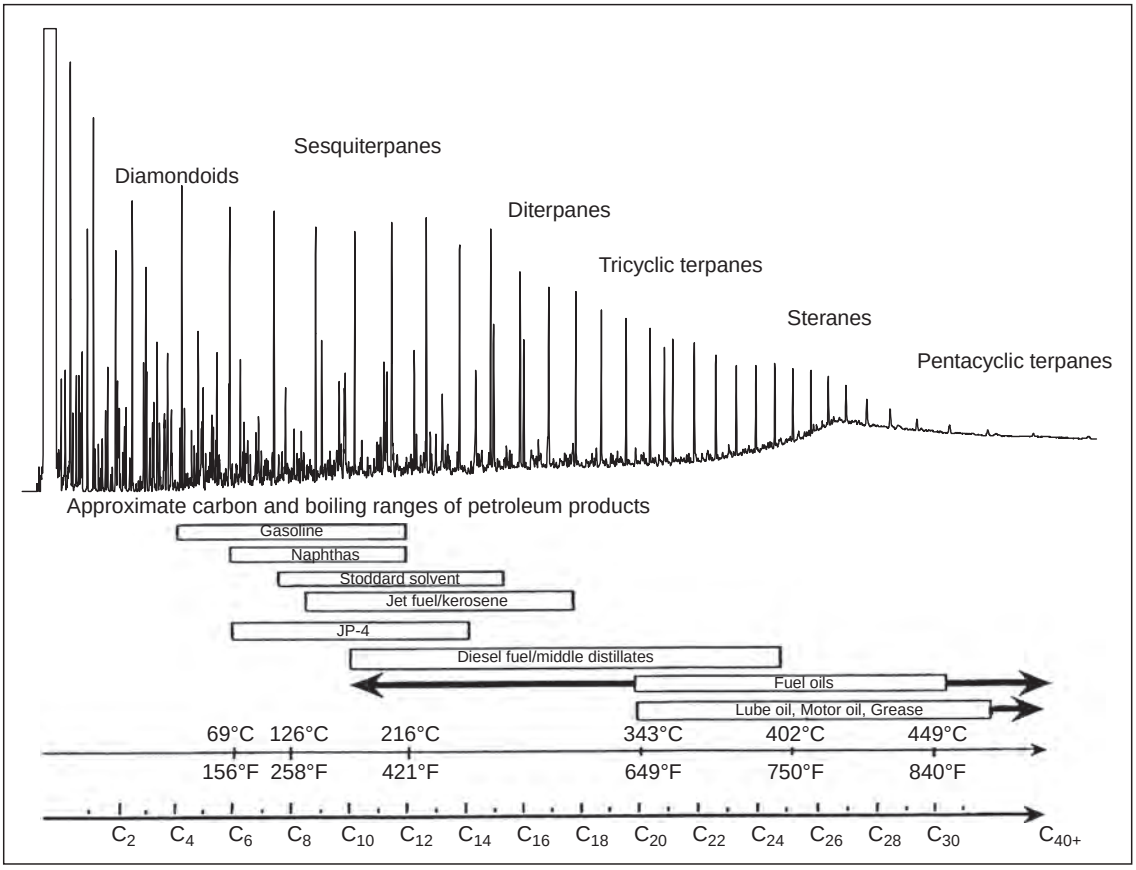

FIGURE 2.8 Carbon number ranges for crude oil and refined products along with the carbon number ranges for most common biomarkers. From this example it can be seen that not all biomarkers will be present in all refined products.

useful in determining the origin of "rogue" or mystery spills, particularly oils spills at sea, where no obvious source can be observed. In the exploration context a detailed knowledge of the origin of the biomarkers and how their distributions change over time is critical in obtaining information on source, maturity, biodegradation, depositional environment and geological age of the oil. In the following section, a brief review of biomarkers will be provided. Clearly this will not be totally comprehensive or inclusive since that would justify a chapter or book by itself and indeed one book that is an invaluable reference is *The Biomarker Guide, 2nd Ed.* by Peters et al. (2005). It is impossible to review all the biomarkers that have been discovered and utilized but the idea of this short review is to provide information on the most useful compounds and how they can be successfully applied to forensic problems. However, another word of caution is necessary here before going into a more detailed discussion. This chapter is primarily about crude oils but it would be remiss not to mention refined products and the fact that crude oils can have properties ranging from very light oils or condensates to very heavy oils that are severely biodegraded. The most useful and widely used biomarkers occur in the range C_{15}–C_{35} range. There are biomarkers that are more volatile but most of these compounds are going to volatilize or evaporate relatively quickly when a spill or release occurs. The carbon number ranges for a crude oil and common refined products are shown in Fig. 2.8, and it can be clearly seen from that figure that not all biomarkers will work for all

products. Gasolines for example are devoid of any biomarkers and correlation of gasolines will depend on ratios that have been developed using various aromatic compounds or utilization of the C and H isotopes of the individual compounds in the gasolines (Smallwood et al., 2002). Condensates are also dominated by lower carbon hydrocarbons ranging up to around C_{15} or C_{20}, will not contain the steranes or terpanes or at least only the lowest carbon number member of the series. Another aspect of biomarker distributions, which will not be discussed in detail in this paper since we are primarily dealing with crude oils and not refined products, is the fact that biomarker distributions in refined products may vary slightly as a result of variations in refinery processes. For example diesel products will contain the tricyclic terpanes but depending upon the upper temperature cut off for the distillation process there may be differences in the carbon number distribution of the tricyclic compounds since their separation is based upon boiling points, hence enabling the products from different refineries to be differentiated.

A typical nondegraded crude oil is dominated by *n*-alkanes and by conventional chromatography these compounds are shown to range from C_1 to approximately C_{40}. However, it should be noted that in reality most crude oils contain varying amounts of *n*-alkanes that extend far beyond C_{40} as far as C_{120} or maybe even higher. In order to detect those compounds it is necessary to utilize high temperature GC. Condensates are at the other extreme and are light oils with a limited range of *n*-alkanes and biomarkers but condensates do contain compounds known as diamondoids that can be useful for correlation purposes and will be discussed below. *n*-Alkanes in the oils can be derived from a variety of source materials including plants, algae and bacteria with very characteristic signatures, in particular a pronounced odd/even predominance (Bray and Evans, 1964). However, as the organic maturity increases with burial those signatures are gradually lost due to the thermal cracking of the *n*-alkanes leading to the relatively smooth distribution of these alkanes with no noticeable odd/over even predominance. The number at which the alkanes maximize will also shift toward lower carbon numbers with increasing maturity. The two most important features of the *n*-alkane distribution from an environmental perspective is the fact that the smooth distribution of the *n*-alkanes is quite different to the *n*-alkane distribution for a contemporary depositional environment. In the latter the alkanes will show a very marked odd/even predominance due to the presence of plant material (Fig. 2.9) or if it is a marine environment with no plant material it will show a very narrow *n*-alkane distribution dominated by hydrocarbons around C_{17}. These features by themselves provide valuable information in terms of determining areas that have been impacted by the release of crude oil into the environment. Areas close to the point of release will be dominated by alkanes with no odd/even predominance but as one moves further from the point of release the signature of the natural vegetation will become more evident until the pronounced odd/even predominance becomes dominant.

The impact of weathering and biodegradation will be discussed in more detail below but suffice it to say at the present time that the first group of compounds to be removed by biodegradation are the *n*-alkanes with the lighter components being removed first followed by the higher carbon numbered compounds, ultimately leading to a chromatogram dominated by an unresolved complex mixture (UCM) devoid of any *n*-alkanes.

The second family of compounds that need to be described is the isoprenoids, with the most common isoprenoids being the C_{19} pristane and C_{20} phytane (Brooks et al., 1969; Powell and McKirdy, 1973; Didyk et al., 1978). These compounds are commonly thought to be derived from chlorophyll, the compound present in the leaves

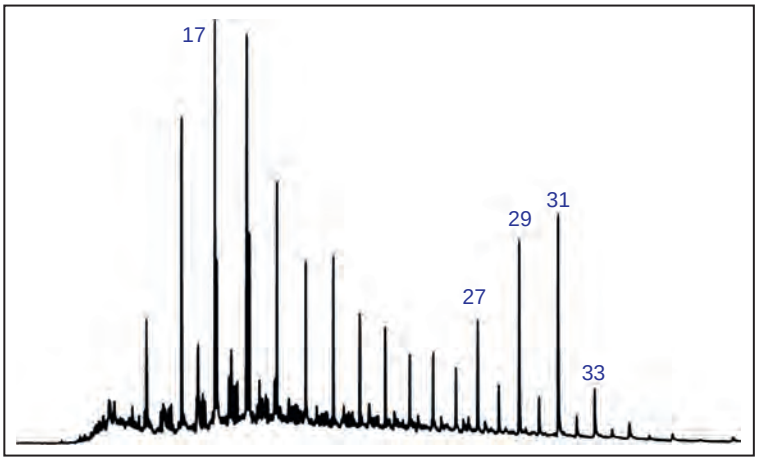

FIGURE 2.9 This chromatogram shows the result of a sediment sample that has been contaminated with a light oil. The odd/even distribution of hydrocarbons in the higher carbon number range C_{27}–C_{35} is indicative of plant material. The lighter hydrocarbons have been lost by evaporation.

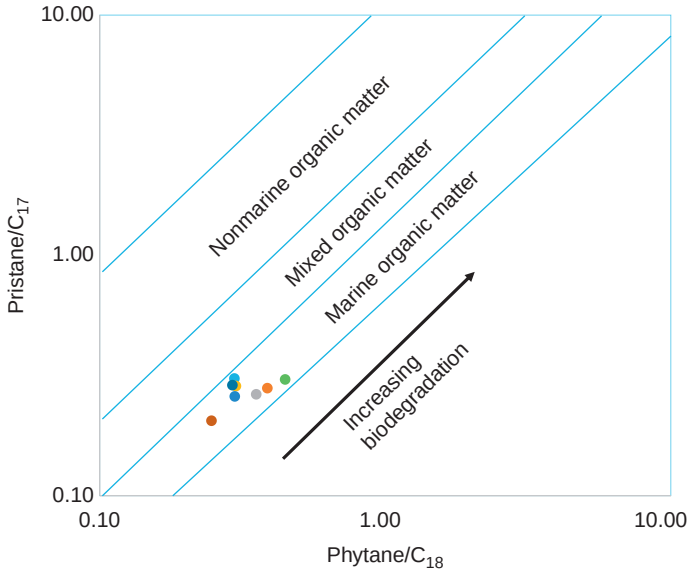

FIGURE 2.10 A cross plot of Pr/C_{17} and Ph/C_{18} that can be used in environmental studies to group oils that are possibly related to each other. Increasing biodegradation will decrease the relative concentration of the *n*-alkanes shifting degraded samples toward higher values for each ratio. *Modified from Shanmugam, G., 1985, Significance of coniferous rain forests and related organic matter in generating commercial quantities of oil, Gippsland Basin, Australia. Am. Assoc. Pet. Geol. Bull.; 69, 1241–1254.*

of plants responsible for driving photosynthesis. Pristane and phytane are easy to identify on the gas chromatogram, eluting adjacent to *n*-C_{17} and *n*-C18. The Pr/Ph ratio was one of the first biomarker parameters proposed in the literature as an indicator of the oxicity of a depositional environment. There has been much debate over the years about the use of the Pr/Ph ratio for this purpose since there are a number of factors that can impact the values, such as possible alternative sources of both pristane and phytane. However, from an environmental perspective the ratio itself is a very useful correlation parameter if you have a large series of samples that you are trying to relate to each other. The Pr/Ph ratio is not significantly affected by biodegradation and these compounds are more resistant to biodegradation than the *n*-alkanes. Two other ratios that also evolved from petroleum exploration studies are the Pr/C_{17} and Ph/C_{18}. A widely used diagram in the exploration field is that of the Pr/C_{17} and Ph/C_{18} illustrated below (Shanmugam, 1985; Fig. 2.10). This diagram is often over interpreted in terms of the amount of information that can be extracted from it in an exploration context. As can be seen there are different areas that have been labeled in terms of source of the oil, increasing maturity and increasing biodegradation. From a forensic point of view the diagram can still be very useful since it will be used in a more limited manner. First, if data from a group of samples from an oil spill are plotted on the diagram it will provide preliminary information on whether or not they are related based on similarities in these ratios. The most significant changes you will expect to see between a group of environmental samples will of course be related to biodegradation or weathering. Biodegradation will lead to the removal of the normal alkanes preferentially over the isoprenoids. Hence, the ratios as plotted will show an increasing trend with increased biodegradation. So on this plot if all samples collected as well as possible original source samples are related they will plot closely on this diagram. However, if they have experienced increasing levels of biodegradation they will show the trend noted on Fig. 2.10. In terms of correlations or establishing relationships between spilled product and potential source, this is preliminary data since a correlation between two samples simply based on the Pr/C_{17} and Ph/C_{18} ratios can be very ambiguous with many oils worldwide having similar values for this ratio. So the results provide a guideline leading into the more detailed evaluation of the more source specific biomarkers determined by GC–MS and described in detail below.

The biomarker parameters described to date will provide some very general information on possible relationships between the spilled product samples and samples possibly responsible for the release. However, these parameters are not very specific and it is necessary to go to the next level of biomarkers that are generally not clearly evident from the GC data and require GC–MS and MID to detect them and resolve them from the baseline components. As indicated at the outset this is not a comprehensive biomarker review but is presented with the intention to highlight some very important compounds and fingerprints that are potentially very useful for correlation purposes both from an exploration point of view as well as an environmental forensic viewpoint.

There are four major families of biomarkers that are present in the saturate fraction of a crude oil that are extremely useful in both petroleum exploration and production and environmental forensic investigations. As indicated previously from a forensic point of view it is not necessary to know the exact identity of every

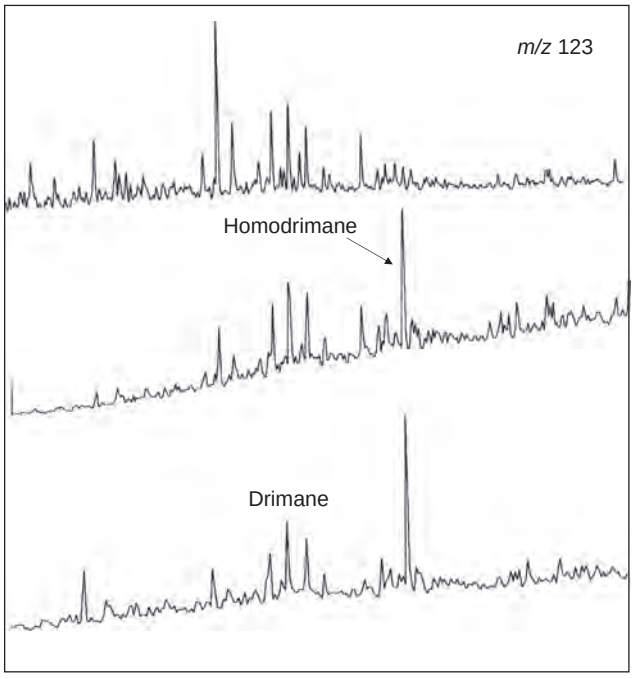

FIGURE 2.11 Sesquiterpanes occur in the early eluting region of the chromatogram. On this diagram sesquiterpanes from several unrelated oils are shown to illustrate potential differences between the sesquiterpanes in these oils from different sources.

component as it is an exploration case. It is more important when correlating to ensure you are comparing the same peaks in different samples. The four groups of compounds are the sesquiterpanes, steranes, terpanes and diamondoids and below a brief summary for each of these compounds is provided.

2.5.1 Sesquiterpanes

The family of sesquiterpanes is generally comprised of C_{14}–C_{16} bicyclic sesquiterpanes which are generally present in virtually all crude oils in varying proportions (Alexander et al., 1983). Care needs to be taken such they are not lost during sample preparation since a little too much enthusiasm in evaporating the solvent during sample preparation can greatly affect the distribution of these compounds. The identity of most of these compounds can be found in the Biomarker Guide (Peters et al., 2005) or papers in the exploration literature going back to the late 1970s. However, basically it is sufficient to know the identity of the compounds known as drimane and homodrimane in order to use these simply for correlation purposes as shown in Fig. 2.11. There are variations in the distributions of these compounds between oils coming from different sources and this provides one of the First, set of fingerprints for differentiating oils from different sources. The impact of weathering on these compounds has not been widely studied since the major weathering impact with these samples is evaporation rather than biodegradation which will remove the compounds faster than the biodegradation. However, if fresh samples of a spill can be collected and carefully preserved then this is one fingerprint that can be used in the correlation toolbox for forensic studies.

2.5.2 Terpanes

The second important family of biomarkers is referred to as the terpanes (Aquino Neto et al., 1981; Peters et al., 2005). This is a family of compounds widely used in exploration studies and despite the fact that the pentacyclic compounds are derived from precursors ubiquitous in bacteria and the tricyclic compounds are thought to probably be sourced from *Tasmanites*, a tremendous amount of useful exploration information can be derived from these fingerprints. A classic terpane fingerprint is shown below (Fig. 2.12) and the areas where the tricyclic and pentacyclic compounds elute clearly labeled. The identity of all the other compounds in this chromatogram are known but not necessarily needed for the forensic type correlation.

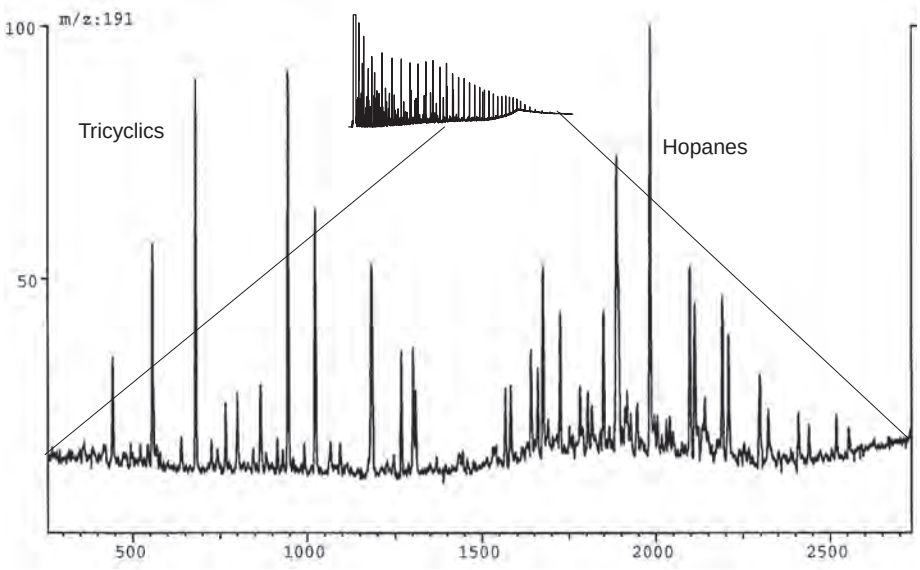

FIGURE 2.12 A classic distribution of terpanes in a crude oil. The major components are tricyclic and pentacyclic terpanes as indicated. Variations in these distributions can occur as a result of various factors such as source, depositional environment, maturity, and biodegradation.

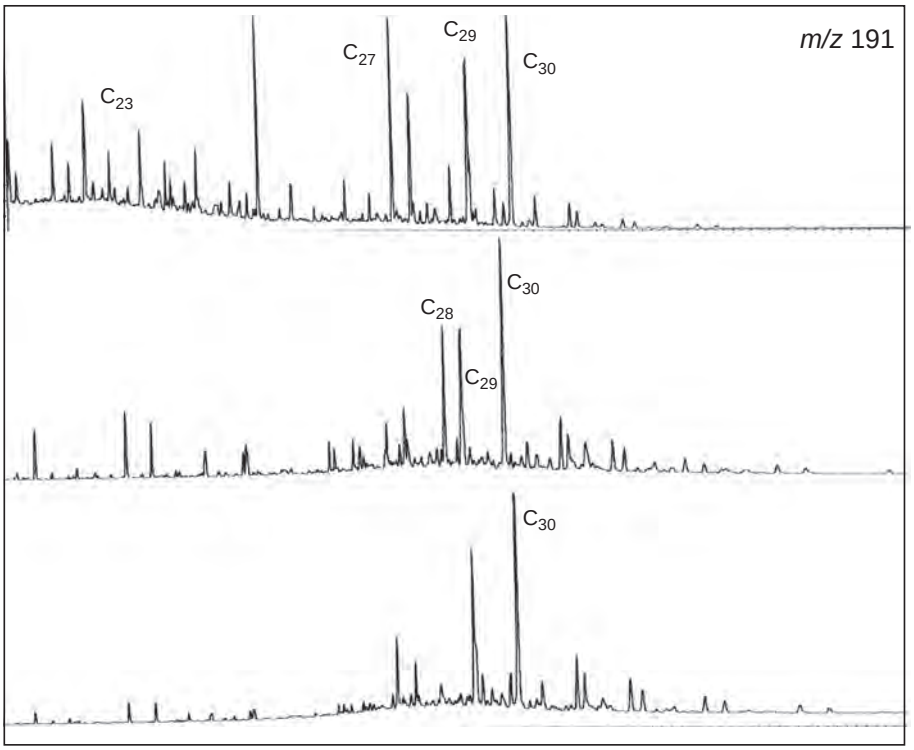

FIGURE 2.13 A comparison between the terpane chromatograms for three oils from different sources to illustrate differences in these fingerprints. Only the major compounds are identified on these chromatograms but the identity of all the components is known.

In Fig. 2.13, a number of different terpane chromatograms are illustrated simply to show differences that may be expected for oils coming from different sources (in this context source means the original source rock not the point of release although at the same time it is possible that different points of release in the sample area may have different terpane fingerprints if the oils were derived from different source materials. Close examination of

these fingerprints reveal both relatively subtle differences and some significant differences. In general, the major differences should be used initially to differentiate samples coming from different sources or samples that are not related and then once samples that have significantly different fingerprints are excluded further differentiation can be undertaken using these more subtle differences. It should also be noted that over geological time periods the terpanes can be impacted by biodegradation but over the relatively short time involved with oil spills or releases virtually no degradation will occur and indeed in the Exxon Valdez spill the C_{30} hopane was actually used as an internal standard to measure changes resulting from biodegradation (Prince et al., 1994).

An illustration of the power of individual biomarkers to differentiate samples can be shown with the use of 18αH-oleanane. This compound is uniquely sourced from angiosperms or flowering plants. The presence of oleanane in one oil and not another is a very strong piece of evidence to suggest that the two oils are not related. However, as with all of these compounds, one should not depend upon one parameter alone. This piece of information is one line of evidence and can be used to build the case that the two samples are not related. Another individual terpane that can be used in this manner is a compound called gammacerane (ten Haven et al., 1989). This is generally associated with oils coming from a saline or hypersaline depositional environment, but present in one sample and absence in another would be strong evidence the two samples are not related.

2.5.3 Steranes

There are multiple families of steranes in most crude oils and these typically range in carbon number from C_{20} to C_{30} with additional minor series of steranes present extending to C_{35}. The sterane families that are commonly used for correlation purposes in exploration studies and can also be used in forensic studies include regular steranes, rearranged steranes, monoaromatic steroid hydrocarbons, triaromatic steroid hydrocarbons, methylsteranes, and minor series of alkylsteranes (Mackenzie et al., 1982). There are multiple components within each family as can be seen in Fig. 2.14 that shows examples of sterane and diasteranes from two crude oils. These sterane fingerprints clearly show the complexity of these mixtures although with increasing aromaticity, the number of isomers and epimers tend to decrease due to removal of hydrogens with the aromatization process (Fig. 2.15).

As with all the other biomarkers discussed above the structures of the majority of these compounds are known but the identities are not necessarily needed in environmental investigations. In an exploration context these compounds would be used to provide information on source, maturity, depositional environments, of the source for the oil as well as any biodegradation, age of the oil and then for oil/oil and oil/source rock correlations. However, in addition to using the fingerprints of these families in environmental investigations there are some ratios that may be useful in forensic studies that can easily be derived from these fingerprints. The most useful being the relative proportions of the $C_{27}/C_{28}/C_{29}$ steranes plotted on a ternary diagram (Fig. 2.16). The relative proportions of the steranes can be determined using either the distribution of the regular steranes or the monoaromatic steroid hydrocarbon fingerprint that is less complex making it easier to calculate the relative proportions of these individual steranes. However, the goal here is to establish the relationship between groups of samples. Those that are related will group very close to each other whilst those from a different source will show signs of separation.

It is worth noting here that if a more detailed separation of the steranes is required, then these families can be analyzed by the GC−MS−MS approach, as discussed above, which will introduce an additional element of separation based on mass spectral characteristics rather than chromatography. In most environmental cases, this level of investigation may not be necessary but suffice it to mention that it may provide additional pieces of information when evaluating points of release or looking for an unknown source of release. For example, components which may be present in relatively low concentrations can be very important is establishing relationships between samples. Such compounds may be the C_{30} *n*-propylsteranes or the C_{26} steranes (Moldowan et al., 1990; Holba et al., 1998). The former which are uniquely related to marine sourced oils are clearly evident from the regular GC−MS analyses. The C_{26} steranes can only be detected through the use of GC−MS−MS as illustrated below (Fig. 2.17). The important point to indicate here is that minor components such as these, which are relatively unique, may provide important correlation parameters may differentiate between two samples that were previously thought to be related.

2.5.4 Diamondoids

Diamondoids are another family of compounds used in exploration studies for many years prior to their First, use in forensic studies (Moldowan et al., 2015; Liu et al., 2016). Diamondoids exist as a series of structural isomers and homologies, ranging from admantanes, diamantanes, triamantanes, and continuing into significantly

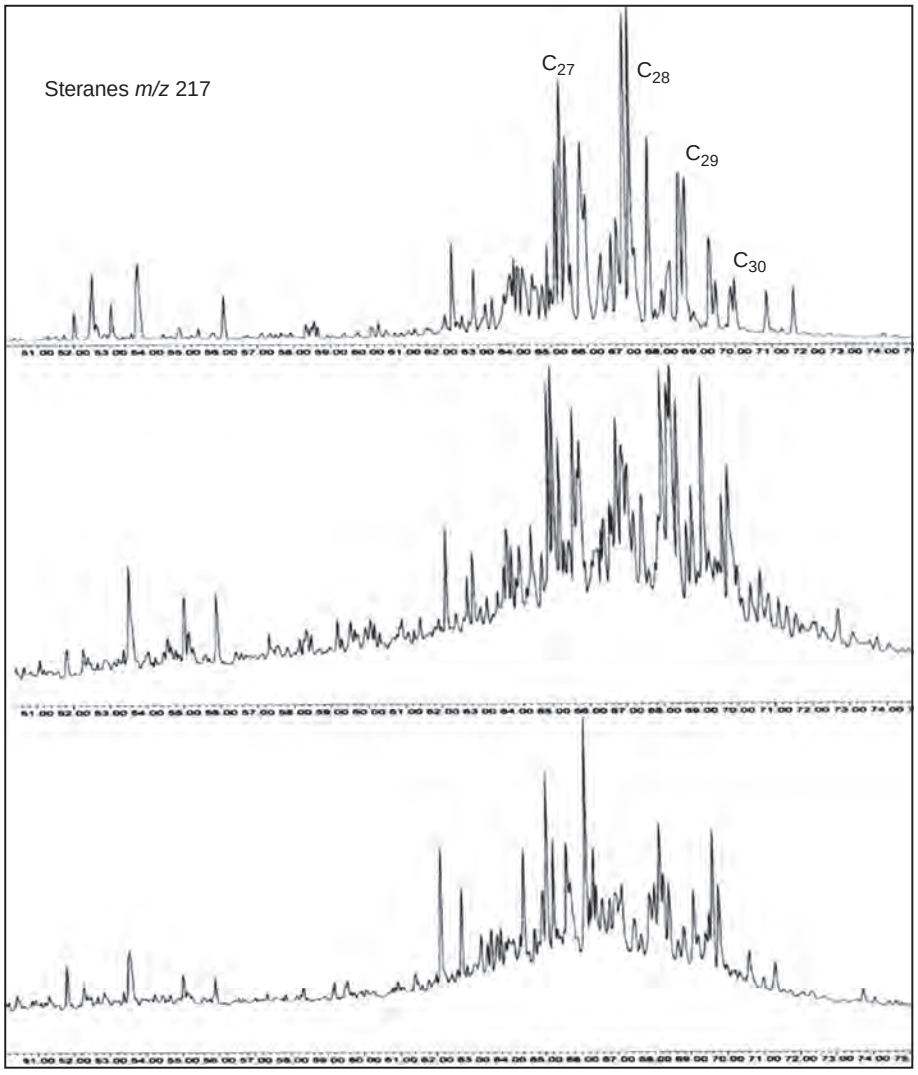

FIGURE 2.14 Sterane chromatograms (m/z 217) from three crude oils. Differences between these fingerprints may sometimes be quite small but can still indicate whether or not the oils are related. At each of the carbon numbers indicated there are mixtures of regular steranes, rearranged (dia-) steranes, stereoisomers and optical isomers.

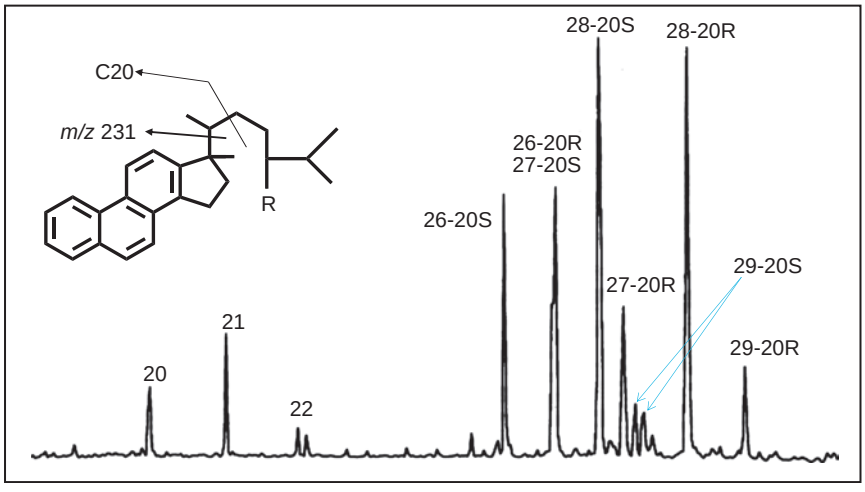

FIGURE 2.15 A chromatogram (m/z 231) showing the distribution of the triaromatic steroid hydrocarbons from a crude oil. As mentioned with increasing maturity the number of isomers significantly decreases making it easier to identify remaining components.

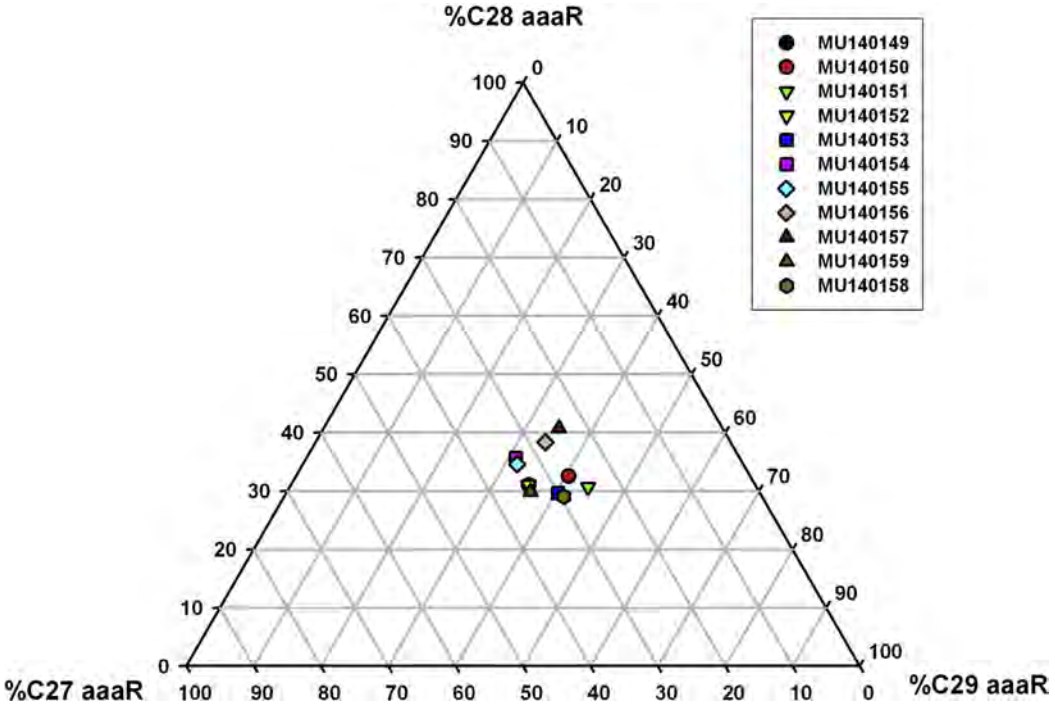

FIGURE 2.16 The relative proportions of the $C_{27}/C_{28}/C_{29}$ steranes can be plotted on a ternary diagram to evaluate relationships between a number of samples and determine whether or not they are derived from the same source.

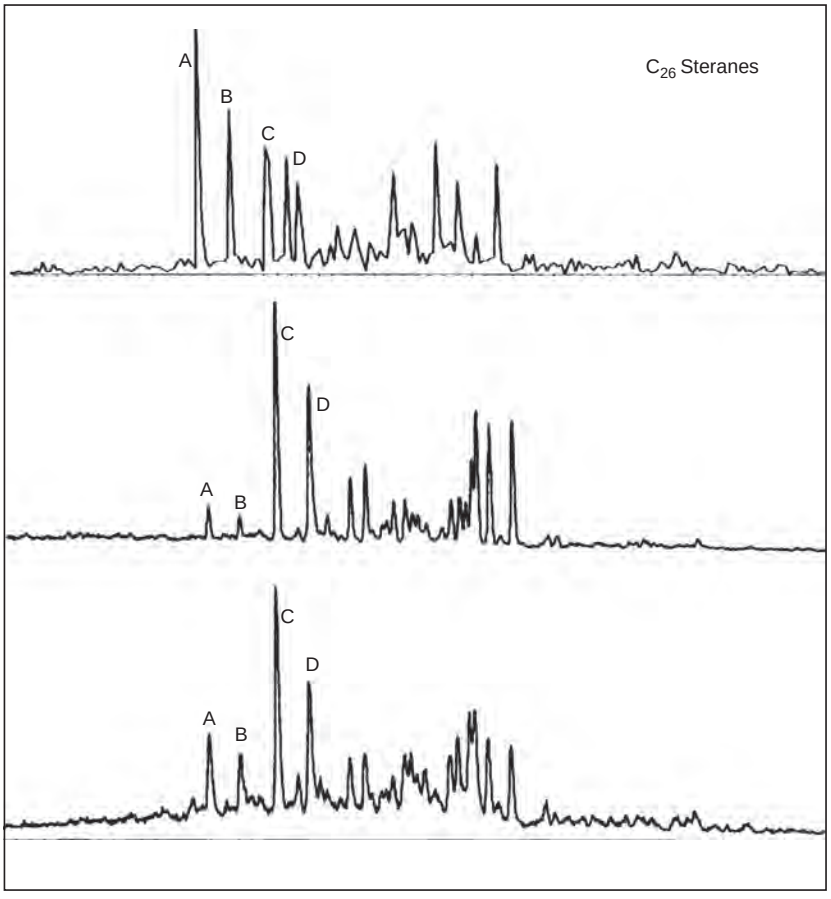

FIGURE 2.17 Minor components such as the C_{26} steranes can also provide valuable clues to differentiate oils from different sources or geologic ages. The two examples below were determined by MSMS and only show the C_{26} steranes. In particular note the difference between the ratio of first two components (A and B) relative to the second pair of peaks (C and D). These ratios change with the geologic age of the oil and can in many cases be used as another parameter to determine whether oils are related to each other or not.

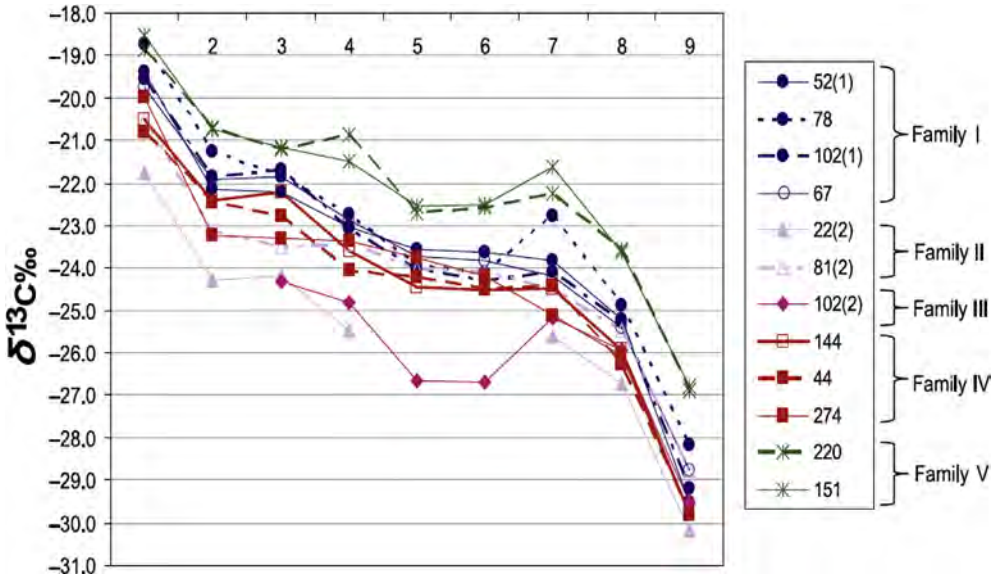

FIGURE 2.18 An example showing where stable isotopes of individual diamondoids have been used to differentiate oils from different sources. *Reprinted by permission of the AAPG. Taken from Liu, Z., Moldowan, J.M., Nemchenko-Rovenskaya, A., Peters, K.E., 2016. Oil families and mixed oil of the North–Central West Siberian basin, Russia. AAPG Bull. 100(3), 319–343.*

higher carbon numbers. These compounds can be readily detected by GC–MS and MID. The lower members of the adamantanes series are volatile and can easily be lost during sample preparation. If it is necessary to obtain the isotopic composition of individual diamondoids it is possible to isolate the diamondoids using published methods REF. There are several papers in the literature describing examples where diamondoids and their isotopic values determined and used for correlations purposes (Fig. 2.18; Wei et al., 2007; Moldowan et al., 2015). Unfortunately, the majority of those papers do not provide any specific details on the isolation of the diamondoids.

These compounds are extremely resistant to biodegradation that makes them very useful for correlating degraded and nondegraded samples, providing another powerful group of fingerprints that can be used in environmental studies. Most applications are restricted to using the adamantanes and diamantanes since these are the more abundant diamondoid components. These compounds are also extremely stable and tend to increase in concentrations with increasing maturity of the source rocks responsible for their generation. Condensates have particularly high concentrations of diamondoids but may be the only family of compounds available for correlation purposes due to the loss of the more traditional biomarkers at these higher levels of maturity.

2.5.5 C7 Compounds

The term C7 compounds can often be found in the petroleum geochemistry literature referring to those compounds with 7 carbon atoms, including heptane, toluene, branched hydrocarbons and cyclic hydrocarbons. The reason these compounds are of interest from an exploration point of view is twofold. First, they are the highest carbon number where all the isomers can be resolved chromatographically; Second, from an exploration prospective they are invaluable maturity indicators as well as having a role in correlation studies. From a forensic point of view they are not quite as useful for correlation purposes as a result of volatilization and samples sitting around in the environment will lose these compounds relatively rapidly (Fig. 2.19). However, subsurface samples, releases from broken pipelines or underground storage tanks may still contain these compounds which can then be used for correlations (Halpern, 1995).

2.5.6 Aromatic Hydrocarbons

Aromatic hydrocarbons in crude oils and condensates are present as very complex mixtures of a wide variety of compounds (Radke and Welte, 1981; Strachan et al., 1988; van Aarssen et al., 1999). Many of these compounds

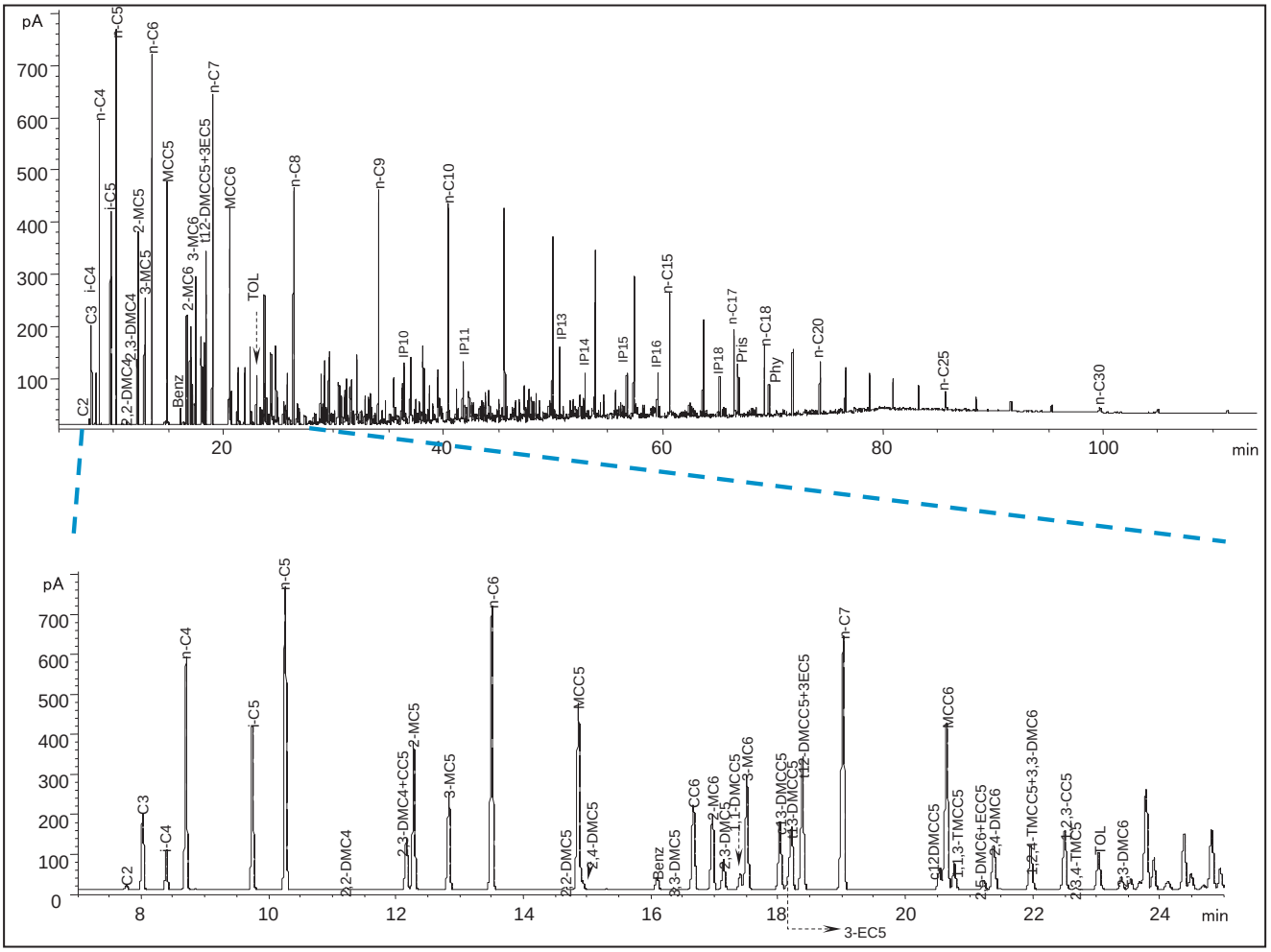

FIGURE 2.19 A chromatogram illustrating the early part of a whole oil to show the C7 compounds. Whilst these compounds will evaporate relatively rapidly on the surface, subsurface releases from a pipeline for example will retain the compounds and then various ratios, such as those described by Halpern (1995) can be used for correlation purposes.

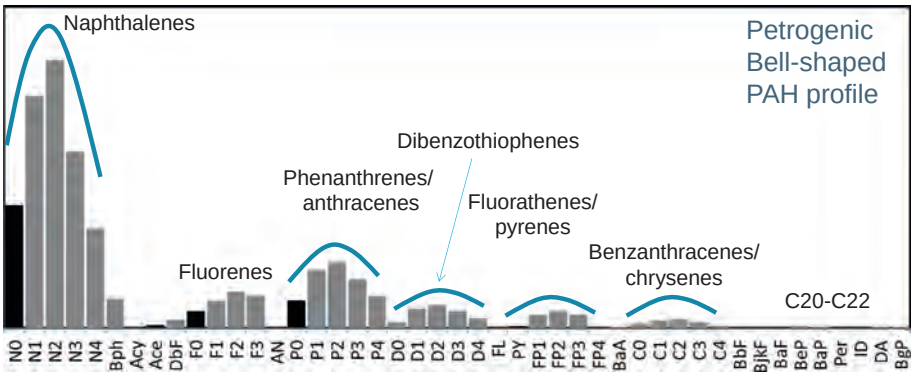

FIGURE 2.20 A histogram showing the distribution of alkylated aromatics in a crude oil. In the histograms the individual isomers are all grouped together.

have been used extensively in the past in forensics studies but in general previous work has been restricted to histograms showing the relative abundance the more abundant series of compounds and their alkylated homologies. Clearly, this approach has been successful and yields a great deal of useful information for establishing relationships or differences between samples from a spill site (Fig. 2.20).

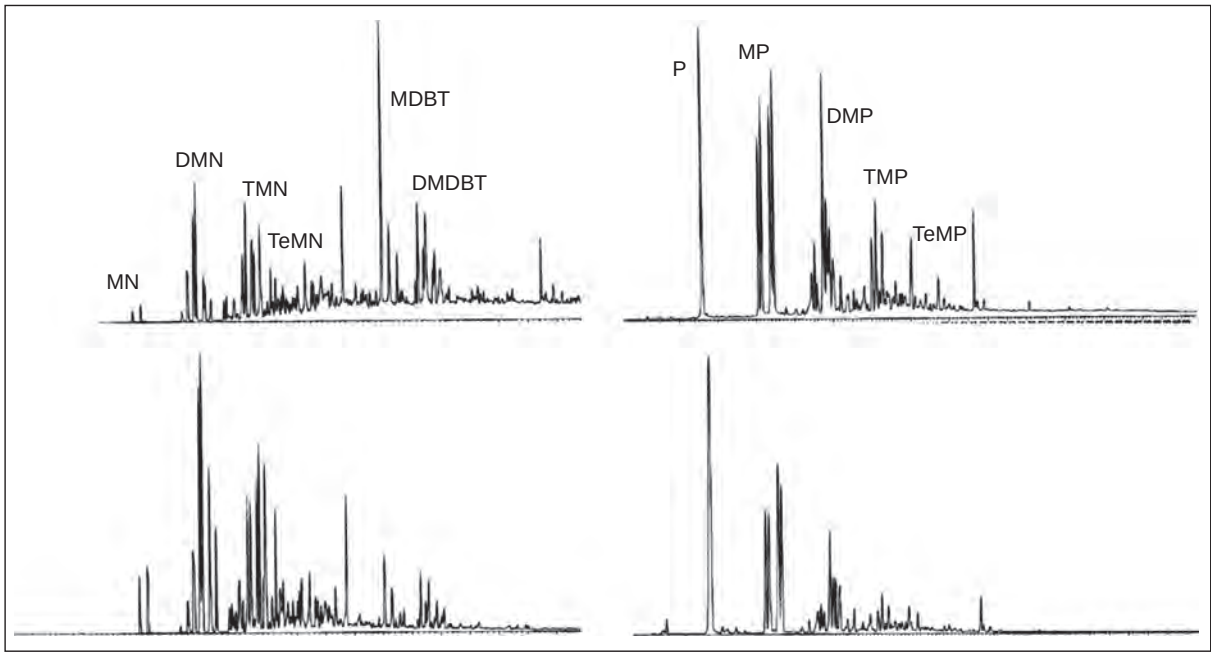

FIGURE 2.21 Chromatograms showing the distributions of alkylnaphthalenes and alkylphenanthrenes in a crude oil, illustrating the distribution of all the isomers at each carbon number (*DMN*, dimethylnaphthalenes; *TMN*, trimethylnaphthalenes; *TeMN*, tetramethylnaphthalenes; *MDBT*, methyldibenzothiophenes; *DMDBT*, dimethyl-dibenzothiophenenes; *P*, phenanthrene; *MP*, methylphenanthrenes; *DMP*, dimethyl-phenanthrenes; *TMP*, trimethylphenanthrenes; *TeMP*, tetramethylphenanthrenes).

However, in addition to utilizing the histograms, a far more comprehensive manner of utilizing the aromatic data is to compare the complete distributions of the aromatic compounds and initially separate the major classes of compounds such as the naphthalenes, phenanthrenes, and dibenzothiophenes (Fig. 2.21). Following that initial separation, the various alkylated members of these series can be separated based on the multiple ion chromatograms. These chromatograms provide the raw data needed to construct the histograms but more importantly the distribution of the individual isomers at each carbon number vary between oils derived from different source materials. In some cases these differences may be very subtle but they are significant and reproducible. Many of these differences are indirectly related to differences in source material and such differences, albeit small may be sufficient to differentiate between oils that were initially thought to be related on the basis of the more commonly used biomarker parameters. For example, 1,2,7-trimethylnaphthalene has been proposed to be a degradation product of oleanane, a higher plant derivative. If it is present in certain samples but not others that will indicate that these oils are not related. Aromatic compounds are susceptible to biodegradation over geologic time but over the shorter time periods of contemporary spills the extent of any alteration to these higher carbon aromatics will be negligible. Lower carbon aromatics such as benzene and toluene will be much more prone to weathering and will be removed relatively rapidly but from a forensics point of view these compounds are not of great value.

2.6 COMPOUND-SPECIFIC ISOTOPE ANALYSES

The preceding sections have discussed individual and families of biomarkers that can be very important for correlation purposes of distinguishing oils or condensates derived from the same or different release points respectively. The use of these compounds is a very powerful tool with applications in both forensic studies and exploration studies. In general it is very important to use multiple parameters or fingerprints and not a single compound. Not all the individual fingerprints within a group of oils from a single release point will have identical fingerprints. Small variations can be expected from weathering affects and maybe in the oil bring released.

In addition to using the biomarker fingerprints, the stable isotopes of the individual compounds provide an additional supporting evidence to establish relationships between samples as shown in Fig. 2.6 (Philp et al., 2002).

In the case of oils, the biomarkers will be the primary correlation tool with the isotopes providing a supporting role. However, in the case of a condensate release stable isotopes will be a primary tool for undertaking correlations. As mentioned above the classic biomarkers are absent from the lower boiling products and alternative correlation tools have to be used. Similarly refined products such as gasoline are also devoid to biomarkers and isotopes have been shown to be useful for correlating or discriminating between samples. At the other extreme, heavy lubricating oils do not have any resolved compounds that can be characterized isotopically. However, the bulk isotope numbers for products with no resolved peaks may be of limited use but provide a bulk parameter than provides supporting correlation information.

Whilst the lighter hydrocarbons will show small isotopic shift as a result of biodegradation as the carbon number of the sample increases any isotopic shits resulting from biodegradation are no longer detectable and hence the isotopic fingerprints become useful for correlation purposes. Furthermore it is possible now to determine both C and H isotopes of individual compounds if necessary.

2.7 WEATHERING–EVAPORATION, WATER WASHING, BIODEGRADATION

Weathering has been mentioned in many places in the preceding discussion. This is a very important issue since a combination of these three effects can have a significant impact on the characteristics of any released into the environment. Evaporation and water washing will for the most part impact the more volatile hydrocarbons and have an impact immediately following the release of the oil. The extent of the impact via evaporation will of course depend upon temperature and other environmental factors such as wind speed but under fairly normal temperature and wind conditions it could be expected that hydrocarbons up to around C_{12}–C_{15} will be lost via evaporation. Water washing will also be impacted by factors such as water salinity and temperature but it is generally the low carbon numbered compounds, primarily aromatics such as benzene and toluene. Low carbon numbered compounds are more water soluble than the higher carbon numbered compounds but overall the solubility is low and other factors such as evaporation and biodegradation will have a far greater impact than water washing.

Biodegradation of crude oils in reservoirs has been widely studied and there are many reports in the literature describing the rate at which different compound classes are removed under both aerobic and anaerobic conditions. A number of tables summarizing these effects have been published with the better known of those being the Peters and Moldowan (1992) scale which was originally published many years ago but is still cited extensively. One of the more interesting observations of crude oil biodegradation is that the relative rate of different compound classes is very similar for all crude oils even down to the rate of removal of selected isomers within a particular family of compounds. However, the big difference between crude oil biodegradation in a reservoir and degradation of a recent release is that the extent to which compound classes are removed in a recent spill is far more limited than what happens in a reservoir over millions of years.

The most commonly observed effect from biodegradation is removal of the *n*-alkanes. Generally, the *n*-alkanes are removed starting with the lower carbon numbered compounds and then moving toward the higher carbon numbers. In a simulated degradation experiment in which crude oil was biodegraded shows there are obvious effects on the *n*-alkanes (Fig. 2.22). This experiment was performed in the laboratory where the crude oil was treated with sewage sludge that provided the bacteria necessary to degraded the oil. The concentrated source of bacteria may have impacted the rate of degradation somewhat more rapidly than natural degradation in the environment but the relative rate of removal on the hydrocarbons would be similar. After 1 month there has been significant removal of the alkanes around C_{18}. It should be noted that these are relative concentrations that are being observed in these chromatograms and the longer chain compounds that now appear to be present in much greater concentrations are basically present in the same absolute concentrations as they were in the original oil. After 4 months all of the *n*-alkanes have been removed and a significant "hump" has appeared, which again was present in the original sample but not clearly evident since it was suppressed by the normalization on the most intense *n*-alkane. The "humps" or UCMs are very complex mixtures of many thousands of compounds that cannot be resolved chromatographically. Most of the major biomarkers described above are hidden in that UCM and their distributions can be determined by GC–MS and MID. Despite the significant changes in the overall character of the crude oil after 4 months of biodegradation the sterane and terpane biomarkers have remained unchanged (Fig. 2.23), which demonstrates their utility in correlating fresh and weathered crude oils at this level of alteration.

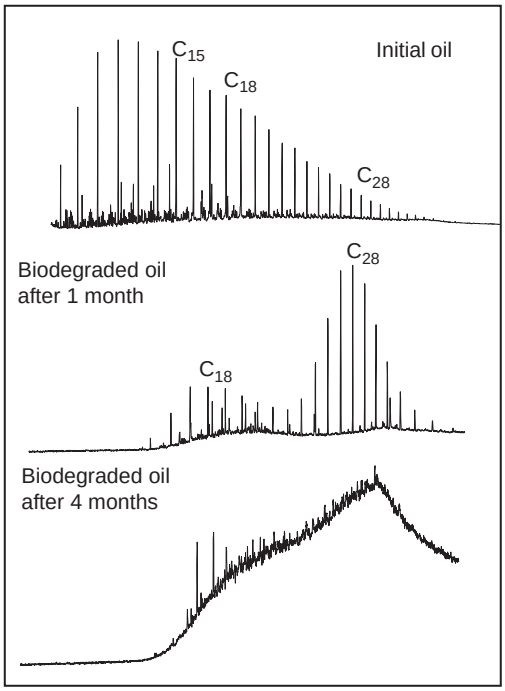

FIGURE 2.22 The impact of biodegradation on a crude oil illustrating the relatively rapid removal of the *n*-alkanes.

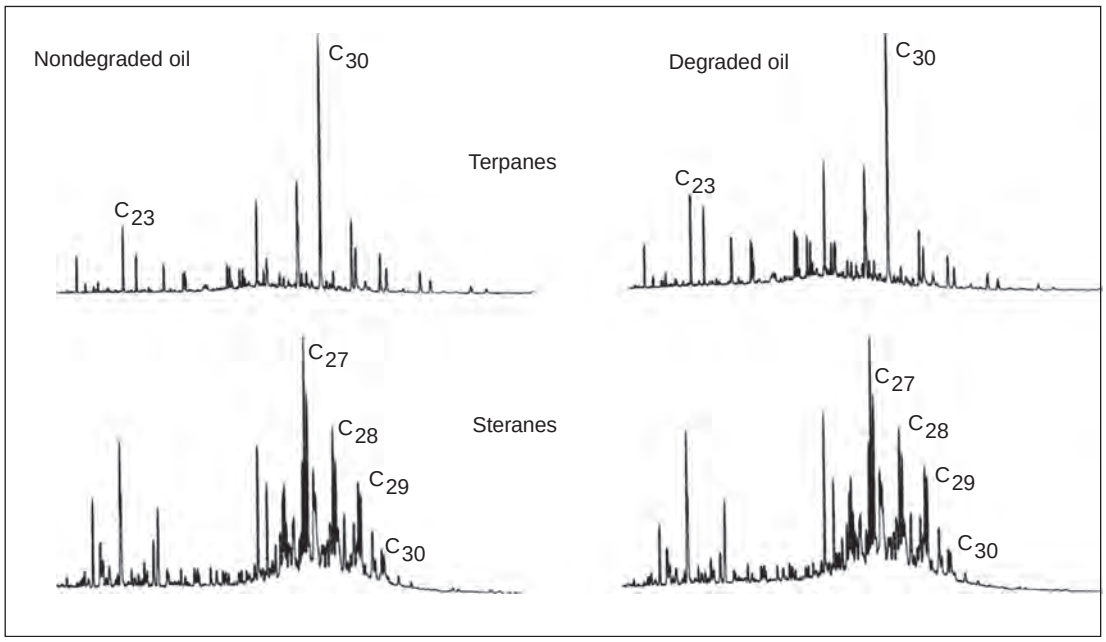

FIGURE 2.23 Sterane and terpane chromatograms for the initial oil and oil degraded for 4 months shown in Fig. 2.22 illustrating the fact that although the second oil is extensively degraded, the steranes and terpanes are unaltered at this level of alteration and can still be used for correlation purposes.

Another point of interest, often overlooked, is related to the higher molecular weight hydrocarbons present in virtually all crude oils but are not seen by conventional GC. Fig. 2.24 shows the result of analyzing an oil by high temperature GC and illustrates *n*-alkanes extending to almost C_{100}, whereas conventional GC would have only revealed *n*-alkanes extending to C_{40}. Biodegradation of a crude oil and monitoring the high molecular weight hydrocarbons showed that hydrocarbons above C_{45} were very resistant to biodegradation (Fig. 2.24). The oil in

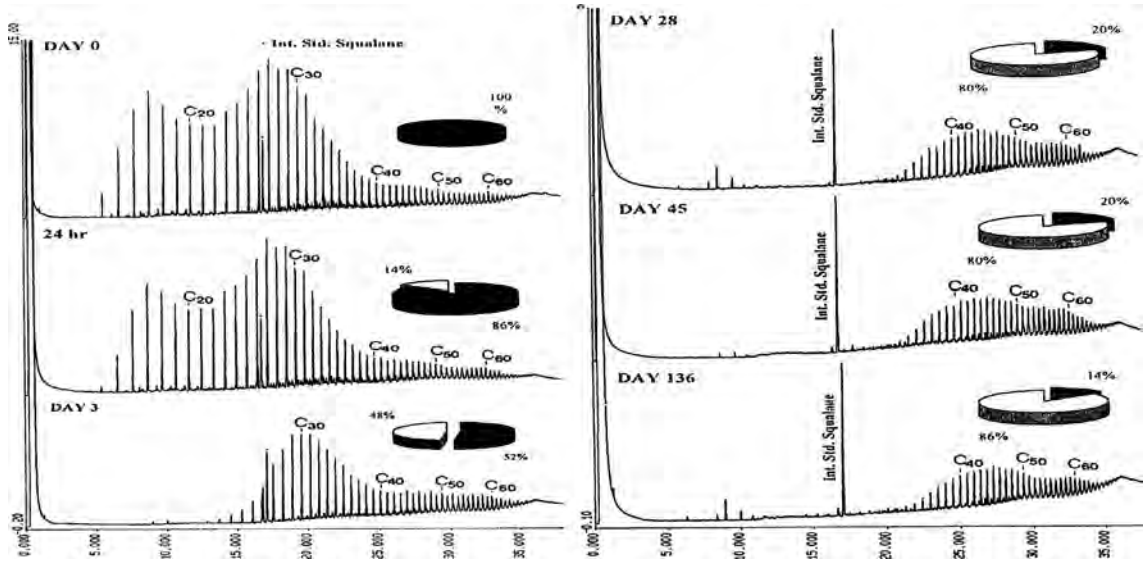

FIGURE 2.24 A laboratory degradation study of a waxy crude oil shows that despite removal of lower carbon numbered alkanes in a relatively short period of time, the longer chain compounds ($>C_{40}$) appear to be recalcitrant and relatively resistant to biodegradation. In this figure the black portion of each pie chart represents the fraction of nondegraded oil which at day 0 is 100% and after day 136 has decreased to 14%. *After Heath, D.J., C.A. Lewis, S.J. Rowland. The use of high temperature gas chromatography to study biodegradation of high molecular weight hydrocarbons. Org. Geochem.: 1997; 26, 769–785.*

this laboratory experiment was a waxy Indonesian crude that was degraded in the laboratory over a 136 day period by *Pseudomonas fluorescens* (Heath et al., 1997). This observation may have relevance to environmental studies but is generally overlooked. However, the point that it is relevant is that with increasing biodegradation, the relative concentration of these high molecular weight hydrocarbons will effectively increase and leave a waxy residue that will be more intractable and more difficult to remediate and clean up.

The section above has discussed changes in the *n*-alkanes, which is where the major changes will be observed. However, with extensive and longer term biodegradation, changes to the isoprenoids may also be observed. Pristane and phytane are the two most abundant isoprenoids observed in crude oils and they are relatively resistant to biodegradation since these are branched hydrocarbons which degrade more slowly. Over the short term, steranes and terpanes are not going to be impacted by biodegradation and can still be used for correlation purposes of released and probably degraded product with the original nondegraded source material.

Aromatic compounds are general thought to be relatively resistant to biodegradation. The aromatic compounds in crude oils, particularly the naphthalenes and phenanthrenes, are complex mixtures of alkylated homologues as shown above (Fig. 2.21). Several interesting papers were published following the *Exxon Valdez* incident many years ago by Douglas et al. (1996). Following extensive quantitative analyses of the aromatic compounds it was observed the over several years selected aromatic compounds did degrade under the conditions present in the Prince William Sound area where the spill occurred. Based on the rate of removal of selected aromatic compounds phenanthrenes, chrysenes, and dibenzothiophenes, two parameters were determined that could be used as source correlation parameter based on C3 dibenzothiophenes and C3 phenanthrenes. A second parameter was a weathering parameter based on C3 dibenzothiophenes and C3 chrysenes, where the chrysenes were observed to degrade faster than the dibenzothiophenes. The resulting plot of these ratios permitted oils that were not degraded to be correlated with those oils that had been released and undergone extensive degradation.

2.8 SUMMARY

Decades of research by petroleum geochemists involved in the exploration and production of crude oil have provided a foundation upon which oil spill environmental forensics is based. An understanding of the geologic basis for oil's composition, the effects of weathering and the occurrence of naturally occurring organic matter in the environment gained from the petroleum geochemistry literature is available for use in assessing oil spill environmental forensics questions. As mentioned at the outset of this chapter, the intent was not to provide a set of

oil spill examples but rather provide some detailed background information from decades of petroleum geochemistry research illustrating why crude oils have differing compositions and how these differences provide valuable information in any forensic investigation. The key to a successful case is to acquire as many fingerprints as possible and look for similarities and differences. Some of these differences may be significant, such as presence or absence of certain compounds. Other differences may be more subtle like a simple ratio. Some of the diagnostic features may be bulk parameters. However, the more parameters or fingerprints that can be determined the more confident you can be in determining whether samples are related or not. Much of the discussion in this chapter has been related to crude oils and the heavier refined products that will still contain some of the biomarkers. Volatile products such as gasoline which are devoid of biomarkers are better suited to characterization using stable isotopes of the individual compounds.

Finally it is important to emphasize that there is a wealth of information in the petroleum geochemistry literature that is as applicable to environmental forensic cases as it is to exploration and production problems. There are far too many papers in the environmental literature that have basically "rediscovered the wheel," whereas lot of time and effort could be saved by carefully reviewing the appropriate historic literature.

References

van Aarssen, B.G.K., Bastow, T.P., Alexander, R., Kagi, R.I., 1999. Distributions of methylated naphthalenes in crude oils: indicators of maturity, biodegradation and mixing. Org. Geochem. 30, 1213–1227.

Alexander, R., Kagi, R., Noble, R.A., Volkman, J.K., 1983. Identification of some bicyclic alkanes in petroleum. In: Schenck, P.A., De Leeuw, J.W., Lijmbach, G.W.M. (Eds.), Advances in Organic Geochemistry. Pergamon Press, Oxford.

Andrusevich, V.E., Engel, M.H., Zumberge, J.E., Brothers, L.A., 1998. Secular, episodic changes in stable carbon isotope composition of crude oils. Chem. Geol. 152, 59–72.

Aquino Neto, F.R., Trendel, J.M., Restle, A., Connan, J., Albrecht, P.A., 1981. Occurrence and formation of tricyclic and tetracyclic terpanes in sediments and petroleums. 1983. In: Bjorøy, M., et al. (Eds.), Advances in Organic Geochemistry, pp. 659–667.

Bray, E.E., Evans, E.D., 1964. Distribution of *n*-paraffins as a clue to recognition of source beds. Geochim. Cosmochim. Acta 22, 2–15.

Brooks, J.D., Gould, K., Smith, J.W., 1969. Isoprenoid hydrocarbons in coal and petroleum. Nature 222, 257–259.

Burlingame, A.L., Simoneit, B.R., 1969. High resolution mass spectrometry of Green River kerogen oxidations. Nature 222, 741–747.

Didyk, B.M., Simoneit, B.R.T., Brassell, S.C., Eglinton, G., 1978. Organic geochemical indicators of palaeoenvironmental conditions of sedimentation. Nature 272, 216–222.

Douglas, G.S., Bence, A.E., Prince, R.C., McMillen, S.J., Butler, E.L., 1996. Environmental stability of selected petroleum hydrocarbon source and weathering ratios. Environ. Sci. Technol. 30 (7), 2332–2339.

Eglinton, G., Murphy, M. T.J. (Eds.), 1969. Organic Geochemistry: Methods and Results. Springer Verlag, New York.

Eglinton, G., Scott, P.M., Belsky, T., Burlingame, A.L., Calvin, M., 1964. Hydrocarbons of biological origin from a one billion year old sediment. Science 145, 263–264.

Freeman, K.H., Hayes, J.M., Trendel, J.M., Albrecht, P., 1990. Evidence from carbon isotope measurements for diverse origins of sedimentary hydrocarbons. Nature 343, 254–256.

Fuex, A., 1977. The use of stable isotopes in hydrocarbon exploration. J. Geochem. Explor. 7, 155–188, 1990.

Halpern, H.I., 1995. Development and applications of light-hydrocarbon based star diagrams. Am. Assoc. Petrol. Geol. Bull. 79, 801–815.

ten Haven, H.L., Rohmer, M., Rullkötter, J., Bisseret, P., 1989. Tetrahymanol, the most likely precursor of gammacerane, occurs ubiquitously in marine sediments. Geochim. Cosmochim. Acta 53, 3073–3079.

Heath, D.J., Lewis, C.A., Rowland, S.J., 1997. The use of high temperature gas chromatography to study the biodegradation of high molecular weight hydrocarbons. Org. Geochem. 26, 769–785.

Henderson, W., Wollrab, V., Eglinton, G., 1968. Identification of steranes and triterpanes from a geological source by capillary gas liquid chromatography and mass spectrometry. In: Schenck, P.A., Havenaar, I. (Eds.), Advances in Organic Geochemistry. Pergamon Press, London, pp. 181–207, 1969.

Hites, R.A., Bieman, K., 1970. Computer evaluation of continuously scanned mass spectra of gas chromatographic effluents. Anal. Chem. 42, 855–860.

Holba, A.G., Tegelaar, E.W., Huizinga, B.J., 1998. 24-Norcholestanes as age sensitive molecular fossils. Geology 26 (9), 783–786.

Hunt, J.M., 1979. Petroleum Geochemistry and Geology. Freeman, San Francisco.

Hunt, J.M., 1996. Petroleum Geochemistry and Geology, second ed. Freeman, New York.

Hunt, J.M., Philp, R.P., Kvenvolden, K., 2002. Early developments in petroleum geochemistry. Org. Geochem. 33 (9), 1025–1052.

Kimble, B.J., Maxwell, J.R., Philp, R.P., 1974. Tri- and tetraterpenoids in mussel oil shale. Geochim. Cosmochim. Acta 38, 1165–1181.

Kvenvolden, K.A., Hostettler, F.D., Carlson, P.R., Rapp, J.B., Threlkeld, C.N., Warden, A., 1995. Ubiquitous tar balls with a California-source signature on shorelines of Prince William Sound, Alaska. Environ. Sci. Technol. 29 (10), 2684–2694.

Liu, Z., Moldowan, J.M., Nemchenko-Rovenskaya, A., Peters, K.E., 2016. Oil families and mixed oil of the North–Central West Siberian basin, Russia. AAPG Bull. 100 (3), 319–343.

Mackenzie, A.S., 1984, Application of biological markers in petroleum geochemistry. In: Brooks, J., Welte, D.H. (Eds.), Advances in Petroleum Geochemistry, vol. 1, pp. 115–214.

Mackenzie, A.S., Brassell, S.C., Eglinton, G., Maxwell, J.R., 1982. Chemical fossils: the geological fate of steroids. Science 217, 491–504.

Mansuy, L., Philp, R.P., Allen, J., 1997. Source identification of oil spills based on the isotopic composition of individual components in weathered oil samples. Environ. Sci. Technol. 31 (12), 3417–3425.

Maxwell, J.R., Pillinger, C.T., Eglinton, G., 1971. Organic geochemistry. Q. Rev. Chem. Soc. 25, 628.
Moldowan, J.M., Fago, F.J., Lee, C.Y., Jacobson, S.R., Watt, D.S., Slougui, N.-E., et al., 1990. Sedimentary 24-*n*-propylcholestanes, molecular fossils diagnostic of marine algae. Science 247, 309–312.
Moldowan, J.M., Dahl, J., Zinniker, D., Barbanti, S.M., 2015. Underutilized advanced geochemical technologies for oil and gas exploration and production-1. The diamondoids. J. Petrol. Sci. Eng. 126, 87–96.
Peters, K.E., Fowler, M.G., 2002. Applications of petroleum geochemistry to exploration and reservoir management. Org. Geochem. 332 (1), 5–36.
Peters, K.E., Moldowan, J.M., 1992. The Biomarker Guide: Interpreting Molecular Fossils in Petroleum and Ancient Sediments. Prentice Hall, Englewood Cliffs, NJ.
Peters, K.E., Walters, C.C., Moldowan, J.M., 2005. The Biomarker Guide: Biomarkers and Isotopes in the Environment and Human History, vol. 2. Cambridge University Press, Cambridge, 1155 p.
Philp, R.P., 1985. Fossil Fuel Biomarkers. Applications and Spectra. Elsevier, Amsterdam.
Philp, R.P., 2009. The utilization of stable isotopes in environmental and forensic geochemistry studies. In: Halley, G.T., Fridian, Y.T. (Eds.), Environmental Impact Assessments. Nova Science Publishers, New York, pp. 31–334, Chapter 10.
Philp, R.P., 2014. Formation and geochemistry of oil and gas. In: second ed. Holland, H.D., Turekian, K.K. (Eds.), Treatise on Geochemistry, vol. 9. Elsevier, Oxford, pp. 233–265.
Philp, R.P., Kuder, T., 2008. Biomarkers and stable isotopes in environmental forensic studies. In: Mudge, S.M. (Ed.), Methods in Environmental Forensics. CRC Press, Boca Raton, Florida, pp. 315–334, Ch. 4. pp. 113-171.
Philp, R.P., Lewis, C.A., 1987. Organic geochemistry of biomarkers. Annu. Rev. Earth Planet. Sci. 15, 363–395.
Philp, R.P., Allen, J., Kuder, T., 2002. The use of the isotopic composition of individual compounds for correlating spilled oils and refined products in the environment with suspected sources. Environ. Forensics 3 (3–4), 341–348.
Powell, T., McKirdy, D., 1973. Relationship between ratio of pristane to phytane, crude oil composition and geological environment in Australia. Nat. Phys. Sci. 243, 37–39.
Prince, R.C., Elmendorf, D.L., Lute, J.R., Hsu, C.S., Haith, C.E., Senius, J.D., et al., 1994. 17α(H), 21β(H)-Hopane as a conserved internal marker for estimating the biodegradation of crude oil. Environ. Sci. Technol. 28, 142–145.
Radke, M., Welte, D., 1981. The methylphenanthrene index (MPI): a maturity parameter based on aromatic hydrocarbons. Adv. Org. Geochem. 1983, 504–512.
Seifert, W.K., Moldowan, J.M., 1978. Applications of steranes, terpanes and monoaromatics to the maturation, migration and source of crude oils. Geochim. Cosmochim. Acta 42, 77–95.
Seifert, W.K., Moldowan, M.J., 1979. The effect of biodegradation on steranes and terpanes in crude oils. Geochim. Cosmochim. Acta 43, 111–126.
Shanmugam, G., 1985. Significance of coniferous rain forests and related organic matter in generating commercial quantities of oil, Gippsland Basin, Australia. Am. Assoc. Pet. Geol. Bull. 69, 1241–1254.
Slatt, R.M., Rodriguez, N., 2012. Comparative sequence stratigraphy and organic geochemistry of gas shales: commonality or coincidence? J. Nat. Gas Sci. Eng. 8, 68–84.
Slatt, R.M., Singh, P., Philp, R.P., Marfurt, K.J., Abousleiman, Y., O'Brien, N.R., et al., 2009. Workflow for stratigraphic characterization of unconventional gas shales. Gulf Coast Assoc. Geol. Trans. 59, 699–710.
Slatt, R.M., O'Brien, N.R., Miceli Romero, A., Rodriguez, H., 2012a. Eagle ford condensed section and its oil and gas storage and flow potential (abs.): AAPG Search and Discovery Article 90142. http://www.searchanddiscovery.com/documents/2012/80245slatt/ndx_slatt.pdf.
Slatt, R.M., Buckner, T.N., Abousleiman, Y., Sierra, R., Philp, R.P., Miceli Romero, A., et al., 2012b. Outcrop-behind outcrop (quarry), multiscale characterization of the Woodford Gas Shale, Oklahoma. In: Breyer, J. (Ed.), Shale Reservoirs—Giant Resources for the 21st Century, 97. AAPG Memoir, Tulsa, pp. 382–402.
Smallwood, B.J., Philp, R.P., Allen, J., 2002. Stable carbon isotopic composition of gasolines determined by isotope ratio monitoring gas chromatography mass spectrometry. Org. Geochem. 33 (2), 149–159.
Stahl, W.J., 1978. Source rock-crude oil correlation by isotopic type-curves. Geochim. Cosmochim. Acta 42, 1573–1577.
Strachan, M.G., Alexander, R., Kagi, R.I., 1988. Trimethylnaphthalenes in crude oils and sediments: effects of source and maturity. Geochim. Cosmochim. Acta 52, 1255–1264.
Tissot, B.P., Welte, D.H., 1984. Petroleum Formation and Occurrence. Springer-Verlag Berlin Heidelberg, Germany, 699 p.
Waples, D.W., 1985. Geochemistry in Petroleum Exploration. D. Reidel Publishing Company, Boston, USA, 217 p.
Waples, D.W., Machihara, T., 1991. Biomarkers for geologists—a practical guide to the application of steranes and triterpanes in petroleum geology. AAPG Methods Explor. 9, 85.
Wei, Z., Moldowan, J.M., Peters, K.E., Wang, Y., Xiang, W., 2007. The abundance and distribution of diamondoids in biodegraded oils from the San Joaquin Valley: implications for biodegradation of diamondoids in petroleum reservoirs. Org. Geochem. 38, 1910–1926.

CHAPTER

3

Fingerprinting Analysis and Source Differentiation of Petroleum-Contaminated Environmental Samples

Chun Yang, Zhendi Wang, Carl E. Brown, Mike Landriault, Zeyu Yang, Bruce Hollebone, Patrick Lambert and Gong Zhang

Environment and Climate Change Canada, Ottawa, ON, Canada

BIOGRAPHIES

Dr. Chun Yang is Head of the Chemical Research Laboratory, Emergencies Science and Technology Section of Environment and Climate Change Canada, Ottawa, Canada. He has a Ph.D. in analytical chemistry and environmental process from Nanyang Technological University of Singapore, a master degree in organic-analytical chemistry from the Research Centre for Eco-Environmental Sciences of Chinese Academy of Sciences, and a bachelor degree in organic chemistry from Beijing Normal University of China. His specialties include environmental sciences, analytical chemistry, and natural products. His current researches mainly focuses on environmental forensics of oils and other potential spill candidates, environmental behaviors of organic pollutants and application of high resolution mass spectrometry in target and nontarget analysis of emerging environmental contaminants. Dr. Yang has authored over 120 academic publications including about 60 peer-reviewed journal papers and invited book chapters. E-mail: chun.yang@canada.ca.

Dr. Zhendi Wang was a Senior Research Scientist and Head of Oil Spill Research Lab at Environment and Climate Change Canada, and currently is an Emeritus Scientist. He received degrees in analytical chemistry and environmental chemistry from Peking University and Concordia University. He has devoted the last 30 years on the forensic oil and toxic chemical spill research. His specialties and research interests include development of oil spill fingerprinting and tracing technologies; properties, fate and behavior of oil and other hazardous organics in the environment; contaminated sediments assessment; oil burn emission and products study; oil biodegradation; and application of modern analytical techniques to oil and chemical spill studies. Dr. Wang has authored or coauthored about 400 publications including peer-reviewed journal papers, invited journal reviews, books and book chapters, departmental reports, conference proceedings, and other publications. He has also received numerous national and international academic honors. He was one of the *Editors-in-Chief* of *Environmental Forensics* (June 2006 to Dec 2010). E-mail: wangzhendi47@hotmail.com.

Dr. Carl E. Brown is the Manager of the Emergencies Science and Technology Section in the Water Science and Technology Directorate of Environment and Climate Change Canada. Dr. Brown has a doctorate degree in physical chemistry from McMaster University and a Bachelor of Technology degree in laboratory science from Ryerson Polytechnical University. Prior to joining Environment and Climate Change Canada, Dr. Brown was a research scientist on a Natural Sciences and Engineering Research Council (NSERC) Industrial Fellowship with Intera Information Technologies (now Intermap). Dr. Brown has postdoctoral experience as a research associate with the Organic Reaction Dynamics and the Laser Chemistry Groups at the Steacie Institute for Molecular

Oil Spill Environmental Forensics Case Studies.
DOI: http://dx.doi.org/10.1016/B978-0-12-804434-6.00003-3

Sciences, at the National Research Council of Canada, and held a Canadian Government Laboratory Visiting Fellowship in Chemistry, with the Laser Chemistry Group, Division of Chemistry, National Research Council of Canada in Ottawa. His specialties include airborne oil spill sensor development and the application of laser technologies to environmental problems. He has authored over 290 scientific papers and publications. E-mail: carl.brown@canada.ca.

Dr. Zeyu Yang is a scientist in the Emergencies Science and Technology Section, Environment and Climate Change Canada, Ottawa, Canada. She received her Ph.D. in environmental science from Guangzhou Institute of Geosciences, Chinese Academy of Sciences, a master degree in environmental engineering from Huazhong University of Science and Technology of China, and a bachelor degree in chemistry from Hunan University of China. Her specialties and research interests include fate and behavior of oil and other hazardous organics in environment, development of oil (including biodiesel) spill fingerprinting and tracing technology, development of biomimic methods based on passive sampling techniques for the simulation of bioaccessibility and bioavailability of organic contaminants. She has authored over 50 academic publications, over 30 of them published in the internationally recognized and respected peer-reviewed journals. E-mail: zeyu.yang@canada.ca.

Dr. Bruce P. Hollebone Bruce Hollebone is a chemist over 20 years of experience in the field of chemical and oil spill research and development. He has a Ph.D. in chemistry from the University of British Colombia. His research interests include the fate and behavior of oil and petroleum products in the environment, including simulation of spill behaviors in the laboratory; the development of new methods for physical and chemical analyses relevant to spills studies; environmental forensics for oil spill suspect-source identification; and environmental emergencies response. He currently works at the Oil Research Laboratory of Environment and Climate Change Canada. E-mail: bruce.hollebone@canada.ca.

Patrick Lambert is a chemist 25 years of experience in the environmental field of chemical and oil spill research and development in both the private and public sectors. His specialties include environmental emergencies, enforcement, counter-terrorism and contaminated site remediation. R&D efforts have focused on health and safety programs, impact of oil and chemicals in the environment, the development and evaluation of methods and equipment for sampling and on-site analysis and laboratory analysis of hazardous materials and studies on the fate and behavior of spilled oil on shorelines. He is Head of Field Work and Response, Emergencies Science and Technology Section, Environment and Climate Change Canada. Throughout his career, he has been involved in hundreds of environmental emergencies, lead laboratory and field R&D projects and Research Support Activities (RSA) and has extensive experience with response to environmental emergencies, counter-terrorism and contaminated site incidents both nationally and internationally. E-mail: patrick.lambert@canada.ca.

Dr. Gong Zhang is a scientist in the Emergency Science and Technology Section, Environment and Climate Change Canada, Ottawa, Canada. He received his Ph.D. in nutrition and food hygiene from the National Institute for Nutrition and Food Safety, Chinese Center for Disease Control and Prevention, Beijing, China. His current specialties and research interests include application of high resolution mass spectrometry in the analysis of naphthenic acids and other environmental contaminants. E-mail: gong.zhang@canada.ca.

Michael Landriault is a senior research technician in the Emergencies Science and Technology Section (ESTS), Environment and Climate Change Canada, Ottawa, Canada. Mr. Landriault received his Chemical Engineering Technology Diploma from Algonquin Collage, Ottawa, Canada. He has worked for over 25 years in oil spill forensic identification and emergency chemical spill analysis. He is a veteran of instrumental analysis using techniques such as gas chromatography and high performance liquid chromatography-mass spectroscopy. E-mail: mike.landriault@canada.ca.

3.1 INTRODUCTION

Petroleum hydrocarbons (PHCs) are ubiquitous constituents in the environment. In addition to PHC, there are other potential sources of hydrocarbons to the environment, i.e., naturally occurring biogenic organic compounds (BOC), formed in-situ through biological process; and pyrogenic compounds, generated from natural forest fires and combustion of fossil fuel, organic material or waste, and potentially air transported over long distances (Wang et al., 2009, 2012, 2014). It is important to characterize and differentiate between PHC, BOC, and pyrogenic hydrocarbons in oil-contaminated environmental samples. Naturally occurring BOC in environmental samples can be mistakenly identified and quantified as regulated toxic PHCs, thus leading to unnecessary and costly cleanup or remediation measures (Wang et al., 2009, 2012, 2014).

Oil fingerprinting analysis is essential to monitor the contamination, to evaluate the damage, and to overlook the environmental recovery. Accurate analysis and unambiguous results are critical in order to identify the source of the hydrocarbons and to allocate the legal liability. The fingerprinting of oil spills can be a considerable challenge to analytical chemists due to the complexity of petroleum oil and the low concentrations of many constituents of interest. In addition, once released into the environment, oil is immediately subjected to a series of weathering processes that alter its compositional distribution, and environmental samples are often a mixture of more than one oil and background matrices, and subsequently becomes difficult to recognize its original spill source.

The types of environmental samples are diverse and unlimited. Many previous approaches have focused on the identification and differentiation of petrogenic, pyrogenic, and biogenic inputs (Volkman et al., 1992; Boehm et al., 1997; Benlahcen et al., 1997; Page et al., 1999; Yunker et al., 1999, 2002, 2011; Micić, et al., 2011; Wang et al., 2009, 2012, 2014; Aboul-Kassim and Williamson, 2013; Kelly-Hooper et al., 2013), but accurate apportionment (even estimation) of the contamination source still remains to be a great challenge. This chapter presents results on specific environmental samples that we have investigated, which demonstrate the application of chemical fingerprinting in their identification. The environmental samples selected to demonstrate this include; (1) sediment collected from a century old recreational pond, (2) sediment from the Athabasca River, Alberta, (3) melted snow water collected in an oil sands bitumen industry area, (4) bilge from a suspected vessel which illegally released waste into a river, and (5) used lubricating oil from diesel-powered truck motor crankcases.

3.2 FINGERPRINTING ANALYSIS OF TARGET ANALYTES

Previous literatures have well described the methodologies of oil analysis in detail (Wang et al., 2006; Stout et al., 2001, 2002; Yang et al., 2015, 2017; Kienhuis et al., 2016). These established analytical methods, generally based on gas chromatography (GC), have been demonstrated to be efficient and suitable for identification and quantitative characterization of PHCs in both crude oils and refined products. However, the analysis of oils in environmental samples can be more difficult and complex due to environmental weathering processes and mixing with background substances, which alter oil characteristics and complicate identification.

Sample preparation of representative oil or environmental samples is crucial to a successful forensic approach. The analysis of oil-contaminated environmental samples first involves the recovery of extractable organic materials from their matrices such as water and soil. Briefly, hexane and dichloromethane (DCM) are often used to extract the oil for analysis, but DCM needs to be replaced by hexane if a silica gel column is used for subsequent extract cleanup and fractionation. It is necessary to determine the total solvent extractable materials (TSEMs) for environmental samples, in order to calculate the proper aliquot of the extract to load on the chromatographic column.

It is not a rare practice to directly inject diluted oil solutions or extracts into an instrument, particularly for fast screening oil types. However, due to the complex nature of petroleum and the environmental sample matrices, proper sample cleanup and further fractionation is essential prior to instrumental analysis in order to achieve accurate quantification of individual components and unbiased identification of the spill source, while protecting the instrument from contamination. Various procedures for cleanup and fractionation of petroleum into aliphatic, aromatic, and other hydrocarbon groups were reported in many previous studies (Wang et al., 2006; Yang et al., 2015, 2017).

A forensic chemical fingerprinting methodology using GC−mass spectrometry (GC−MS) and GC−flame ionization detection (GC−FID) was widely applied to characterize and to differentiate pyrogenic and biogenic from petrogenic hydrocarbons in environmental matrices. Numerous target PHCs were quantitatively determined and applied for differentiation and indication of the presence or absence of PHC, pyrogenic and/or BOC compounds in environmental samples. The analysis of specific PHCs is of particular importance in oil forensic studies as they can provide valuable information toward improving characterization and identification of petroleum samples. Target compounds frequently used in oil fingerprinting analysis include a large number of saturated and aromatic PHCs, such as total petroleum hydrocarbons (TPHs) and unresolved complex materials (UCMs), normal alkanes and isoprenoids, unsubstituted PAHs and their alkylated series, aromatic steroids, biomarker terpanes, and steranes (Wang et al., 2006; Stout et al., 2001, 2002; Yang et al., 2015, 2017; Kienhuis et al., 2016). Identification of target analytes is generally based on specific spectral fragments and positive match of the peak retention times with authentic standards or reference materials. Certain biogenic compounds producing the same

TABLE 3.1 Characterization Results of Target Hydrocarbon Groups in Representative Environmental Samples

Sample	Recreational pond sediment (μg/g, dry weight)	Athabasca River sediment (μg/g, dry weight)	Snowmelt water (μg/kg water)	Vessel bilge (μg/g TSEM)	Used lubricating oil (μg/g)
TPHs	338	251	4,764	783,000	745,000
TSH/TPHs (%)	–	41.4	38.3	81.5	94.8
TAH/TPHs (%)	–	58.6	61.7	18.5	5.2
Resolved peaks/TPHs (%)	44.9	14.7	16.8	29.6	4.7
UCM/TPHs (%)	55.1	85.3	83.2	70.4	95.3
Total *n*-alkanes	27.5	5.83	54.6	86,800	12,100
Total target PAHs	0.18	1.41	273	14,613	934
Unsubstituted PAHs	0.13	0.17	47.0	252	94.9
Alkylated PAHs	0.06	1.24	226	14,361	859
Biomarkers	0.00	1.56	10.9	506	599
Diagnostic ratios					
P/An	5.07	–	2.26	16.7	7.31
C_1-P/C_0-P	0.00	0.91	2.69	2.41	2.69
2-MAn/C_1-P	–	0.01	0.20	0.04	0.04
Fl/Py	1.46	0.18	0.22	0.11	0.36
BaA/C	0.57	0.16	0.73	0.64	0.54
Carbon preference index (CPI)	9.41	1.97	1.35	1.02	0.97
Pyrogenic index (PI)	1.18	0.09	0.21	0.02	0.09
Perylene index (%)	90.5	70.4	3.0	0.0	6.1

TPHs, total petroleum hydrocarbons; *TSH*, total saturated hydrocarbons; *TAH*, total aromatic hydrocarbons. Normal alkanes include *n*-C_9 to *n*-C_{44}, pristane and phytane. Unsubstituted PAHs include biphenyl (Bph), acenaphthylene (Acl), acenaphthene (Ace), anthracene (An), fluoranthene (Fl), pyrene (Py), benz[*a*]anthracene (BaA), benzo[*b*]fluoranthene (BbF), benzo[*k*]fluoranthene (BkF), benzo[*e*]pyrene (BeP), benzo[*a*]pyrene (BaP), perylene (Pe), indeno[1,2,3-*cd*]pyrene (IP), dibenz[*a*,*h*]anthracene (DA), and dibenzo[*ghi*]perylene (BgP). Alkylated PAH homologues include C_0- to C_4-naphthalenes, C_0- to C_4-phenanthrenes, C_0- to C_3-dibenzothiophenes, C_0- to C_3-fluorenes, and C_0- to C_3-chrysenes. Petroleum biomarkers include C_{21} to C_{24} tricyclic terpanes, C_{27} 18α(*H*),21β(*H*)-22,29,30-trisnorneohopane (Ts), C_{27} 17α(*H*),21β(*H*)-22,29,30-trisnorhopane (Tm), C_{29} 17α(*H*),21β(*H*)-30-norhopane (H29), C_{30} 17α(*H*),21β(*H*)-hopane (H30), C_{31} to C_{35} homohopanes, and C_{27} to C_{29} αββ steranes. The PI values of the pond and river sediments were calculated using target unsubstituted PAHs excluding biogenic perylene.

mass fragments could be misidentified as target PHCs in environmental samples. As the petrogenic compounds generally do not occur alone in petroleum oil, their unique chromatographic features and distribution patterns could be used to avoid mismatch with interferences.

Table 3.1 presents target hydrocarbon group characterization of the environmental samples including quantitative results of TPHs, *n*-alkanes, target unsubstituted PAHs and alkylated PAHs, as well as selected critical diagnostic ratios to differentiate the hydrocarbon sources. For environmental samples such as water and sediment, the final resulting target analytes can be expressed in terms of total solvent extractable materials or TPHs, instead of units per whole sample. This kind of expression can truly reflect the type of oils and contamination level present in the environmental samples, and facilitate a convenient and meaningful comparison of analytical results among samples and with a database.

3.3 ASSESSMENT OF HYDROCARBON GROUPS IN ENVIRONMENTAL SAMPLES

Generally, preliminary identification of oil type and degree of weathering can be readily achieved from their GC–FID traces, especially when the oil contamination is at a high-level relative to the background levels in a

petroleum impacted environment. Rather than determining individual components, GC–FID analysis aims to identify the types of contamination and the type of oil content, and to investigate if the oil is weathered through the overall of PHC profiles. GC–FID analysis measures the concentrations of hydrocarbon groups including normal alkanes, TPHs, total saturated hydrocarbons, total aromatic hydrocarbons, total resolved components, and UCM content.

The chromatographic features of typical crude oils and petroleum products have been well discussed in our previous publications (Wang et al., 2006; Yang et al., 2015, 2017). For example, Fig. 3.1 displays GC–FID chromatograms of PHCs in some crude oils and refined petroleum products. Each oil has its own distinct fingerprint in chemical composition depending on the geological conditions of oil formation and migration. For most conventional crude oils, their GC-chromatograms generally demonstrate significant *n*-alkanes (in *n*-C_8 to *n*-C_{44} range) over a broad UCM hump with different profiles and shapes. Refined petroleum products vary significantly from type to type and oil to oil in the carbon range and hydrocarbon distribution profiles. The distinguishable characteristics for various types of products are attributed to parent crude oil feedstocks, refining processes, and the materials added in the products for specific purposes (Yang et al., 2015, 2017). Lubricating oils (or simply lube oils) are distinguishable from other refined products by their unique characteristic, such as a UCM hump eluted at high-boiling-point hydrocarbons range, and as an example in Fig. 3.1E, these oils generally contain very low resolved chromatographic content concentration of normal alkanes and aromatic hydrocarbons (Lu and Kaplan, 2008; Yang et al., 2016).

Once oil enters into the environment it is immediately subjected to a series of natural weathering processes. The effect of evaporation is particularly significant during the initial stages of an oil spill on land or water.

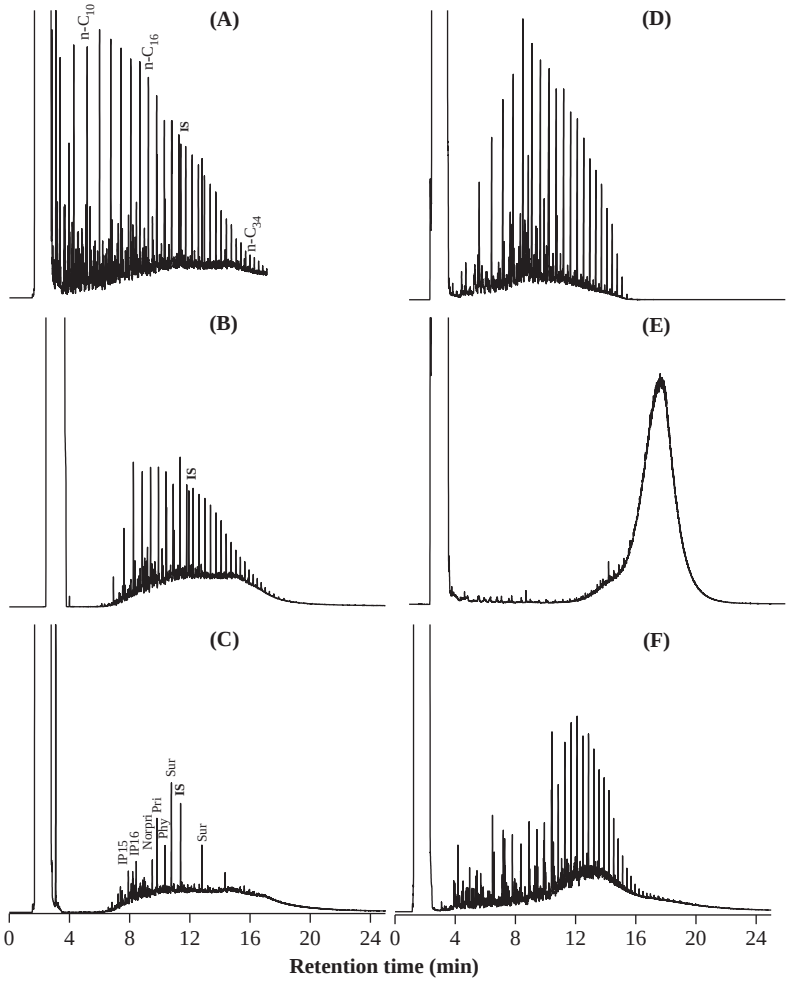

FIGURE 3.1 GC–FID chromatograms of PHCs in selected oil samples: (A) ANS crude (fresh), (B) Prudhoe Bay crude (20% evaporation), (C) ANS (biodegraded), (D) diesel, (E) lube 20W-50, and (F) bunker C.

Fig. 3.1B displays the chromatographic change of PHC in Prudhoe Bay crude oil (Alaska, USA) at 20% w/w evaporative weathering. In theory, evaporating oil loses lighter compounds with low boiling points first, whereas the distributions of certain hydrocarbons, particularly high molecular biomarkers and PAHs, remain consistent through the evaporation process. In addition, evaporation does not significantly remove UCM and probably results in an increased UCM proportion in evaporated oils (Wang et al., 2006; Yang et al., 2015, 2017). It has been well established that biodegradation over long term can considerably affect the hydrocarbon distributions in petroleum released into the environment. The effects of microbial degradation on oil composition are significantly different from those of physical weathering processes. Different classes of PHCs have varying susceptibilities to biodegradation. Overall, this process preferentially affects straight-chain *n*-alkanes over branched alkanes, alkanes over other hydrocarbon groups, GC-resolved compounds over the UCMs, and small aromatics over large aromatic compounds. It is apparent in Fig. 3.1C that *n*-alkanes were completely removed, whereas certain isoprenoids remain fairly consistent in moderately biodegraded Alaska North Slope crude oil.

The *n*-alkanes are derived from a variety of sources. Normal alkane distributions are often used to distinguish biogenic sources from petrogenic contamination sources in environmental samples. In general, most crude oils exhibit an *n*-alkane distribution profile of decreasing abundances with increasing carbon number. A wide range of alkanes commonly found in soil and sediments, with a marked predominance of odd-numbered hydrocarbons in the span of *n*-C_{23} to *n*-C_{35}, originate from higher vascular plants (concentrations of *n*-C_{27}, *n*-C_{29}, and *n*-C_{31} hydrocarbons are particularly high). Algae produce *n*-alkanes with shorter lengths between C_{11} and C_{25} (Meyers and Ishiwatari, 1993). Therefore, environmental samples with significant biogenic contributions exhibit a unique *n*-alkanes distribution pattern with odd carbon-numbered alkanes being much more abundant than even carbon-numbered alkanes in the range of *n*-C_{21} to *n*-C_{35}. Using this distinguishable phenomena, carbon preference index (CPI) is widely used to identify hydrocarbon sources in an environmental sample by environmental chemists and to estimate thermal maturity of crude oil by geochemists. CPI is a ratio of the total of *n*-alkanes with odd carbon numbers divided by the total of *n*-alkanes with even carbon numbers in the GC−FID detectable carbon range (approximately C_8 to C_{44}). CPI values of most high maturity petroleum are ~1.0. The CPI values can be used as indicator for distinguishing input of petrogenic or biogenic (CPI >2) hydrocarbons in contaminated samples.

Fig. 3.2A presents the hydrocarbons determined in the sediment from a century old recreational pond (Ontario, Canada). The C_{16}−C_{34} fraction totally accounts for 65.4% of the total GC−FID detectable components in this sediment (338 μg/g by dry weight). The predominance of odd carbon numbers in the *n*-C_{21}−*n*-C_{35} range results in an exceedingly high CPI value of 9.4. The ratio of GC-resolved area to the total GC area was measured to be 44.9%. These substance were further identified by GC−MS analysis as biogenic organics including normal alkanes, fatty acids (or alkanoic acids), fatty alcohols, and steroids (Wang et al., 2009). The naturally occurring organics present in BOC-rich environmental samples are generally nonhazardous or less hazardous than petrogenic and pyrogenic compounds, and they pose relatively low impact to the environment.

Organic matter in river sediment is derived from both natural (aquatic and terrestrial) and anthropogenic sources. As an example, Fig. 3.2B presents a GC−FID chromatogram and the *n*-alkane distribution in sediment collected from the Athabasca River, Alberta (upstream, wet fine sands). The concentration of TPH was determined to be 251 μg/g (dry weight), equivalent to about 60~70% of that in typical oil sands bitumen (Yang et al., 2011; Wang et al., 2014). Unresolved peaks dominate 85.3% of the GC−FID chromatogram but this proportion is lower than ~98% of oil sands bitumen reported by Yang et al. (2011). These evidences indicate oil sands bitumen as the main contributor but also imply other sources to PHC determined in this river sediment. Predominance of odd carbon numbers with maxima at the long-chain *n*-C_{27} or *n*-C_{29} alkanes was also observed, indicating a contribution of biogenic input from organic matter from terrigenous higher plants. In contrast, the heavily degraded Athabasca oil sands bitumen only contains little or no *n*-alkanes (Yang et al., 2011).

PHC in the water of melted snow collected from the oil sands region (Alberta, Canada) was determined to be 4,764 μg/kg. About 17% of them present as resolved peaks in GC−FID chromatogram, obviously higher than ~15% for the studied Athabasca River sediment and ~2.5% for typical oil sands bitumen (Yang et al., 2011). In addition, the *n*-alkane profile in Fig. 3.2C suggests multiple sources of contamination in this sample. Only trace amount of *n*-alkanes were determined at 54.6 μg/kg of water (or 1.1% in terms of TPH) in this sediment sample, and their distribution patterns show a predominance of odd carbon numbers, such as *n*-C_{25} and *n*-C_{27}. Correspondingly, the CPI value was calculated to be 1.35. These results imply a biogenic input from organic matter from terrigenous higher plants into the snow water.

As seen in Fig. 3.2D, the resolved *n*-alkanes in the vessel bilge fall mostly within the diesel carbon range of *n*-C_9 to *n*-C_{24} with maxima at *n*-C_{13} or *n*-C_{16}, and almost no resolved peaks were detected in the lube oil carbon range. Two UCM humps are clearly visible with the first hump being in the diesel-range and the second small

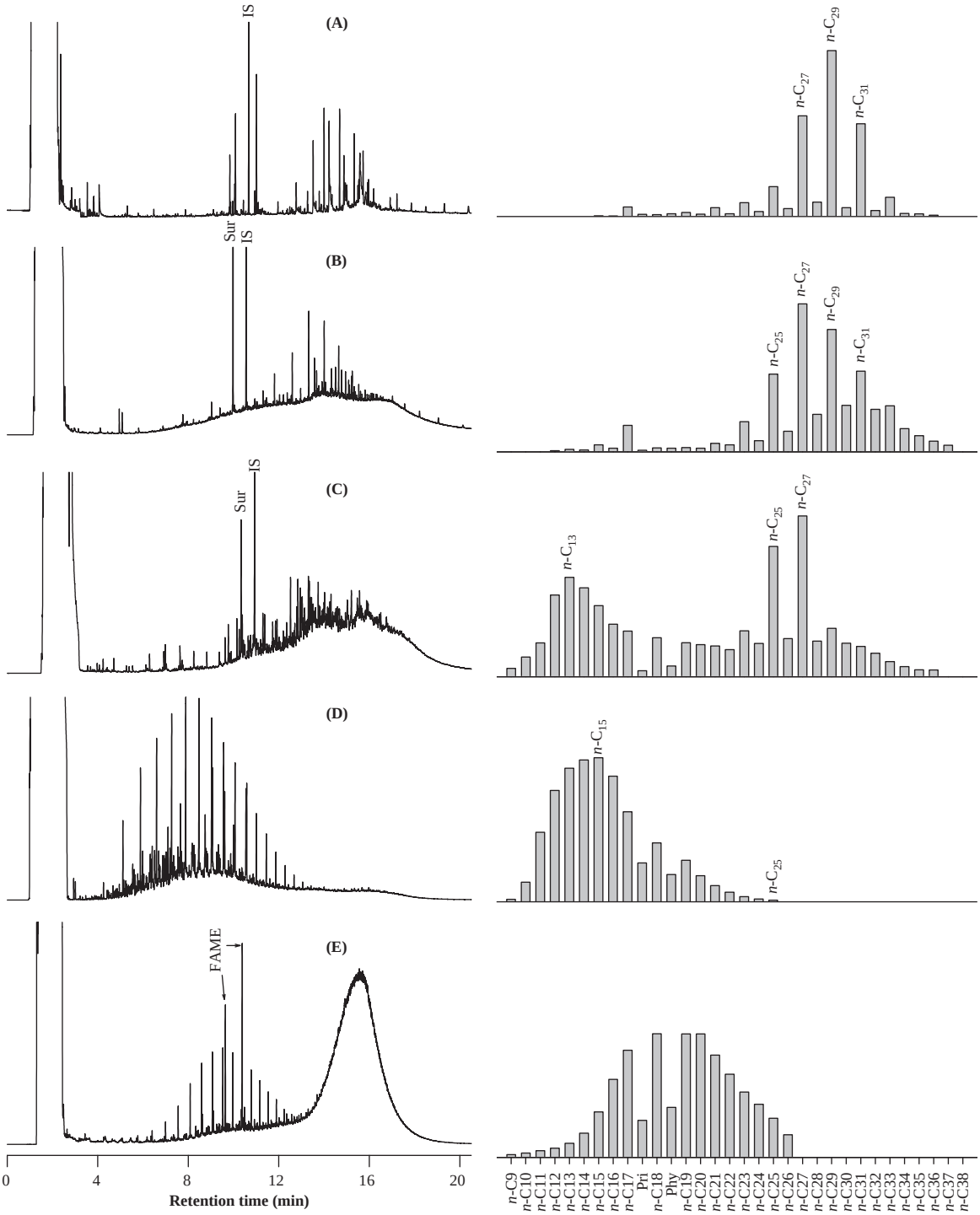

FIGURE 3.2 GC–FID chromatograms of hydrocarbons and distribution of normal alkanes in environmental samples: (A) recreational pond sediment, (B) Athabasca River sediment, (C) snowmelt water, (D) bilge water, and (E) used lubricating oil.

hump being in the lube oil-range ($\sim C_{24}$ up to $\sim C_{50}$). The GC–FID profiles, carbon ranges of GC-TPH, *n*-alkane distribution, and the characteristic shapes of the UCM humps all suggest that the vessel bilge clearly consist of primarily a diesel range fuel ($\sim$90%) and a slight amount of a lube oil ($\sim$10%) eluted at the high-boiling-point hydrocarbons range.

Used oil can be illegally dumped into waterways or dumped on land or in landfills to avoid payment of disposal fees. In some regions, used lube oils or other materials have occasionally been deliberately added into lube

oil to extend the volume sold. Used or waste lube oils have special chemical composition characteristics which are different from those of the unused lube oils. The used lube oil in Fig. 3.2E was collected from a diesel-engine vehicle. A large typical UCM hump from *n*-C_{20} to *n*-C_{50} of lube oil represents roughly 90% of detected hydrocarbons. A small amount of *n*-alkanes between *n*-C_{12} to *n*-C_{26} and 4.7% resolved peaks of TPH were also noted in the GC−FID chromatogram, which are certainly attributable to unburned diesel fuel, and combustion residue from the engine. Two pronounced peaks eluted after *n*-C_{19} and coeluted with *n*-C_{21} were identified as fatty acid methyl esters, further suggesting the fuel contamination from a biodiesel blend (Yang et al., 2016).

From the examples presented above, we can understand that chromatographic profile and normal alkane distribution by GC−FID analysis provides diagnostic information for the identification and differentiation of biogenic and petrogenic contamination sources. However, this technique is unable to unambiguously verify the contamination sources or to allocate their contribution, particularly when biogenic input is dominant and the characteristics of petrogenic hydrocarbons become indistinct. The analysis of specific PHCs using GC−MS are necessary and of particular importance in forensic studies as they can provide valuable information toward improving characterization and identification of environmental samples.

3.4 ASSESSMENT OF POLYCYCLIC AROMATIC HYDROCARBONS IN ENVIRONMENTAL SAMPLES

Petrogenic PAHs generally occur in significant amounts in crude oils and refined products. Their relative concentrations also vary significantly among different oils, making them source-specific. Petrogenic PAHs are characterized by high C_0−C_4 alkylated homologues, in particular by five commonly analyzed naphthalene, phenanthrene, dibenzothiophene, fluorene, and chrysene series; in addition, naphthalene series is often the most abundant, followed by phenanthrene series. Each alkylated PAH homologous group distributes in an overall bell-shaped curve. Unsubstituted PAHs, particularly high molecular weight (MW) 4−6 ring PAHs, are very minor components in most crude oils (Wang et al., 1999; Stout et al., 2002; Yang et al., 2015, 2017). Pyrogenic PAHs, particularly higher MW PAHs ranging from benzo[*a*]anthracene to coronene, are prevalent contaminants from heavy anthropogenic and industrial activities such as incomplete combustion of fuel, industrial petrochemical practices, residential wood burning, vehicular emissions, power plant emissions, and so on (Boehm et al., 1997; Stout et al., 2001, Wang et al., 2007). Biogenic PAHs are produced by organisms or formed during early stage of diagenesis in sediments. Unlike petrogenic and pyrogenic PAHs, biogenic PAHs are generally found individually or in very simple mixtures.

An abundance of literature has discussed the use of PAHs to identify and to differentiate contamination sources in environmental samples, particularly in oil-contaminated soils and sediments (Venkatesan, 1988; Boehm et al., 1997; Yunker et al., 1999, 2002, 2011; Pereira et al., 1999; Lima et al., 2003, 2005; Jautzy et al., 2013; Wang et al., 2009, 2012, 2014). Many PAHs can be employed for identification and differentiation contamination sources according to the specific situation of each case. For example, Fig. 3.3 illustrates the selected ion chromatograms of phenanthrene and anthracene (*m*/*z* 178), C_1-phenanthrenes/anthracenes (*m*/*z* 192), triaromatic steranes (*m*/*z* 231) and 5-ring PAHs (*m*/*z* 252) in the environmental samples. Methylanthracenes (MAns) are generally absent or in low concentrations relative to methylphenanthrenes in most conventional crude oils. 2-MAn elutes between two pairs of methylphenanthrene isomers and is in variable concentration in different types of oils. Relatively high presence of 2-MAn in oil sample generally indicates cracking. Tricyclic aromatic steroids are a series of naphthenoaromatic hydrocarbons (*m*/*z* 231). Although aromatic steroids can occur in relatively low concentrations in oils, their specific fingerprints and high weathering resistance make them desirable biomarkers for forensic investigation. In addition, pentacyclic PAHs determined from environmental samples could originate from petrogenic, biogenic or pyrogenic contribution. A cluster of isomers at *m*/*z* 252 (i.e., benzo[*b*]fluoranthene, benzo[*k*]fluoranthene, benzo[*e*]pyrene, benzo[*a*]pyrene, and perylene) provides valuable information to disclose the contamination sources.

Numerous quantitative diagnostic ratios were applied to differentiate petrogenic PAHs from other hydrocarbon sources. The ratios derived from less thermodynamically stable versus stable PAH isomers, such as fluoranthene to pyrene (Fl/Py), phenanthrene to anthracene (P/An), and methylphenanthrenes to phenanthrene (C_1-P/C_0-P), are often used to investigate petrogenic contamination against pyrogenic input in environmental samples (Yunker et al., 1999, 2002; Benlahcen et al., 1997, Lima et al., 2005). Petrogenic sources are characterized by high ratios of P/An (>15) and C_1-P/C_0-P (>2) in association with lower ratios of fluoranthene/pyrene

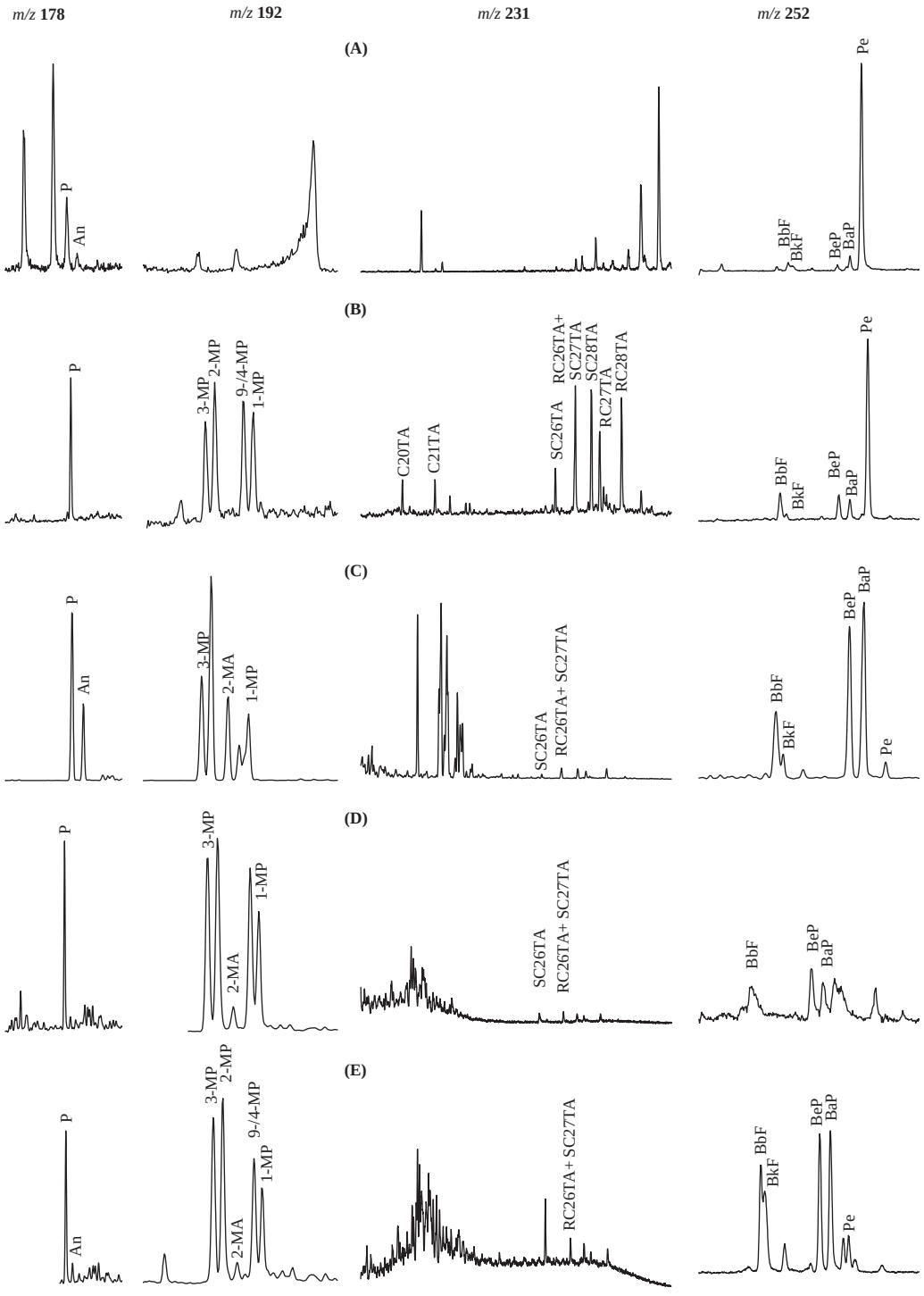

FIGURE 3.3 GC–MS chromatograms of phenanthrene and anthracene (*m*/*z* 178), methylphenanthrenes (*m*/*z* 192), triaromatic steranes (*m*/*z* 231) and *m*/*z* 252 PAH isomers in environmental samples: (A) recreational pond sediment, (B) Athabasca River sediment, (C) snowmelt water, (D) bilge water, and (E) used lubricating oil.

(Fl/Py <1) and benzo(*a*)anthracene/chrysene (BaA/C < 0.4) (Benlahcen et al., 1997). Diagnostic ratios with contrary values could point to a pyrogenic source. The ratio of 2-MAn relative to the total of methylphenanthrenes ranges from 0 to 0.03 for most crude oils, diesels and lube oils studied, whereas this ratio is generally greater than 0.03 for heavier refined petroleum products, such as Bunker C (Yang et al., 2017). Yunker et al. (1999, 2002,

2011) reported that the ratio of IP/(IP + BgP) <0.20 likely implies petroleum; between 0.20 and 0.50 liquid fossil fuel (vehicle and crude oil) combustion; and over 0.50 implies grass, wood, and coal combustion.

Pyrogenic index (PI) is an indispensable diagnostic parameter of identification and differentiation of pyrogenic and petrogenic PAHs. PI is defined as the ratios of the total of 15 unsubstituted 2–6 ring PAHs to the total of five alkylated PAH homologues (Wang et al., 1999). Lighter refined products and many crude oils have PI ratios <0.01, whereas heavy oils and heavy fuels have higher ratios in the range of 0.02 to 0.05 (Wang et al., 1999). The ratio dramatically increases as the proportion of pyrogenic PAHs increases. This index has demonstrated its vantage for identification of pyrogenic PAHs and for differentiation of pyrogenic and petrogenic PAHs in many spill case studies.

PAHs synthesized by organisms can be easily differentiated from those occurring in petroleum. Perylene is often the most abundant 5-ring PAHs detected in environmental samples with biogenic input. Perylene is a common substance in sediments which is produced biologically under anaerobic conditions (Venkatesan, 1988). Perylene index, defined as the concentration of perylene divided by the total of five 5-ring PAHs (m/z 252), is a very useful tool to distinguish biogenic from pyrogenic hydrocarbons. Perylene indices greater than 10% often indicate diagenetic (biogenic) inputs, whereas those $<10\%$ indicate a pyrogenic or petrogenic origin.

Fig. 3.3 shows the selected ion chromatograms of some target PAHs, and Fig. 3.4 depicts the distribution of target PAHs determined from five environmental samples.

Anthropogenic input is one of the major sources causing significant accumulation of sedimentary PAHs in river and marine beds. Most PAHs do not dissolve easily in water and their hydrophobicity generally increases with increasing molecular mass. Consequently, these compounds tend to deposit and accumulate in sediments, soils, and biota, resulting in long-term hazards to the environment. As seen in Fig. 3.4A, only traces of unsubstituted PAHs plus C_1-naphthalenes were detected, but no other petroleum-characteristic alkylated PAH homologues were detected in the recreation pond sediment. PAHs were determined to be 0.18 μg/g of dry weight (Table 3.1). These trace amount of PAHs are probably attributed to anthropogenic input such as runoff and atmospheric deposition. Perylene in this sample is at an unusually high concentration compared with other 5-ring PAH compounds, accordingly resulting in a high perylene index of 90.5% which is far higher than the pyrogenic input criteria of 10%. Therefore, the contribution of natural biogenic source to the hydrocarbons in the sediment is evident.

PAHs in the Athabasca River sediment in Fig. 3.4B are obviously dominated by alkylated PAHs. Except the naphthalene series, the alkylated PAH families show an overall decreasing distribution pattern of $C_0 < C_1 < C_2 < C_3$, which is consistent of the typical PAHs distribution of the oil sands bitumen (Yang et al., 2011; Wang et al., 2014). Meanwhile, alkylated naphthalenes are highly abundant and in a bell-shape distribution profile. This may indicate some anthropogenic contribution of oil hydrocarbons from lighter petroleum products, in addition to oil sands bitumen contribution to the sample (Wang et al., 2014). As seen from Figs. 3.3 and 3.4, among target unsubstituted PAHs, perylene is the most abundant component, accounting for about 34.6% of the sum of unsubstituted PAHs and over 70% of total 5-ring PAHs, clearly indicating contribution of biogenic input to this sediment. Excluding the outstanding contribution of biogenic perylene, the PI was calculated to be 0.09, still slightly higher than the PI value of 0.06 for general oils and refined products. It may indicate certain contribution of PAHs from pyrogenic sources (such as emission particulates) to the sediment sample.

Five target alkylated PAH homologous series in the snowmelt water were all detected with a total concentration of 226 μg/kg, accounting for about 4.7% of GC-detectable TPHs. This concentration is significantly higher than $\sim$0.8% for oil sands bitumen but at a comparable abundance of PAHs in medium to heavy fuels (Yang et al., 2015, 2017). Meanwhile, this sample also contains 47.0 μg/kg of unsubstituted PAHs with the dominance of the high molecular mass 4–6 ring PAHs over the low molecular mass 2–3 ring PAHs (Fig. 3.4C). These unsubstituted PAHs totally make up about 1.0% of GC-detectable TPHs, which is unusually higher than in common crude oils and refined petroleum products. As seen in Fig. 3.3C, anthracene, benzo[*e*]pyrene and benzo[*e*]pyrene all increased significantly. The diagnostic ratios in Table 3.1 such as P/An (2.26), C_1-P/C_0-P (2.69), 2-MAn/C_1-P (0.20), BaA/C (0.73) and PI (0.21) all imply significant contributions of PAHs from pyrogenic sources to the snow sample. These pyrogenic PAHs could be either formed locally or were from far away through long distance atmospheric transport. A perylene index of 3.0% represents only a minor biogenic contribution to the detected PHCs in the sample.

The total PAHs were determined to be 14,613 μg/g TSEM with a predominance of alkylated PAHs and no detection of the high MW alkylated chrysenes among 5 target alkylated PAH homologous series in the bilge (Table 3.1 and Fig. 3.4D). Unsubstituted PAHs are dominated by low MW two and three ring PAHs. This is typical features in the chemical composition of light diesel fuels. It has been well known that in general, PAH

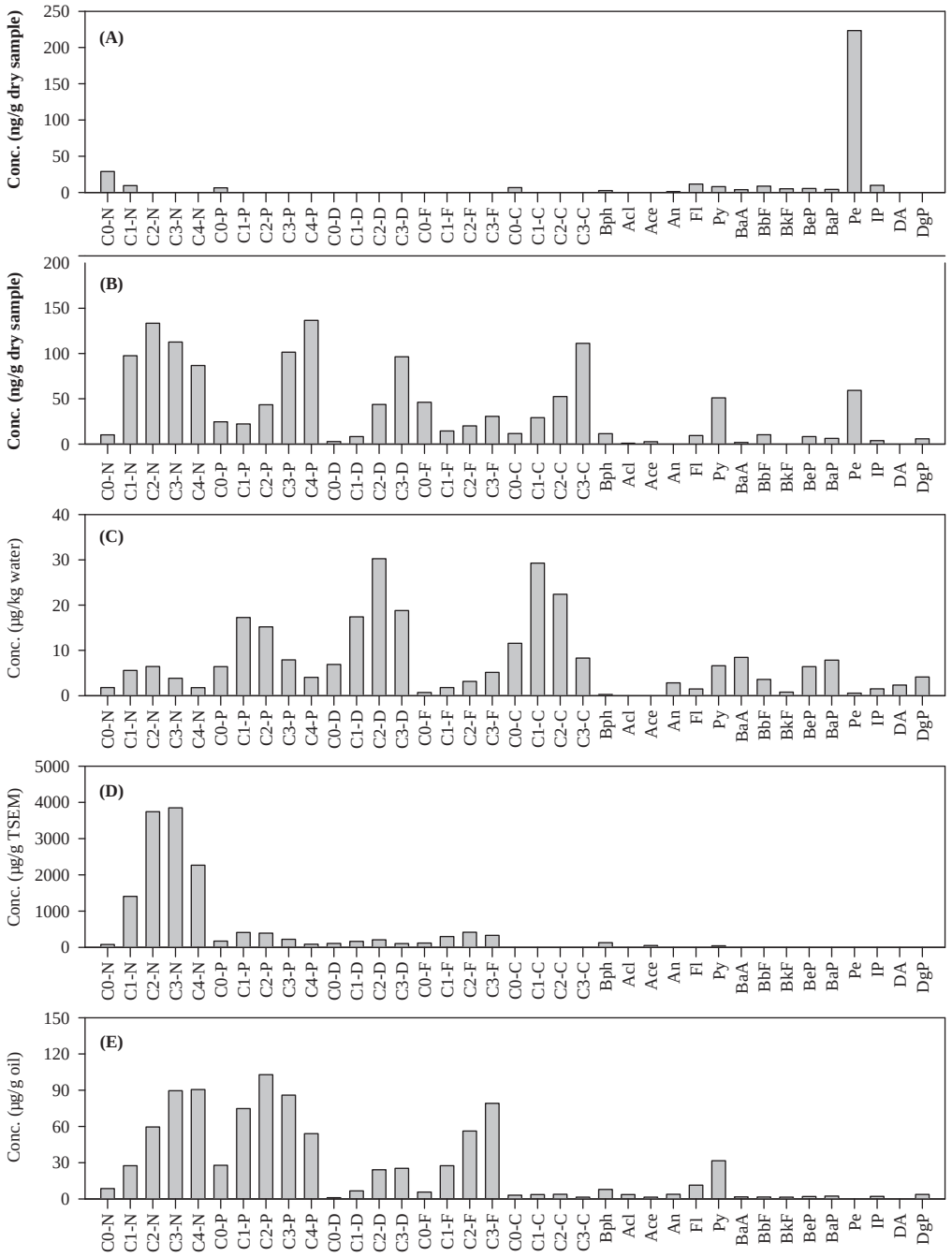

FIGURE 3.4 Distribution of PAHs in environmental samples: (A) recreational pond sediment, (B) Athabasca River sediment, (C) snowmelt water, (D) bilge water, and (E) used lubricating oil.

concentrations are high in diesels, whereas lube oils only contain trace amount of alkylated PAHs (Yang et al., 2015, 2016, 2017). Therefore, it can be expected that the portion of lube oil in a mixture of diesel and lube oil would only have minimum effects on the PAH distribution pattern and profile. In addition, biogenic and pyrogenic contribution to the bilge sample was not observed from PAH fingerprinting analysis.

Most of the aromatic hydrocarbons including PAHs in the base oil are purposely removed during the refining process in the production of lube oils. Therefore, commercial high quality lube oils in principle contain very little of these aromatic compounds. Although most lube oils alone only contain very low concentrations of PAHs, the used lube oil could become hazardous as they are usually contaminated by low MW PAHs and pyrogenic high MW PAHs from unburned fuel oil and combustion residue (Kaplan et al., 2001; Yang et al., 2016). The used lube

oil retained some characteristics of the diesel oil but presents some characteristics of additional pyrogenic PAHs. It was noted that relative to other smaller PAHs, 4- to 6-ring PAHs were very prominent in the used lube oil (Fig. 3.4E), resulting in a PI of 0.09. These high MW PAHs are largely formed from combustion, although their absolute amount is only a very small fraction of the total determined PAHs. This indicates that the used lube oil was a mixture of lube oil, unburned diesel, and combustion exhaust of oils (Yang et al., 2016).

3.5 ASSESSMENT OF PETROLEUM BIOMARKERS IN ENVIRONMENTAL SAMPLES

Petroleum biomarkers in crude oils retain all or part of the molecular structures from their original biological molecules produced by organisms. Different oils often have highly distinguishable chemical fingerprints of their biomarkers, varying in both concentration and distribution patterns. Their relevant diagnostic ratios are robust for oil-to-oil correlation and oil source tracking. Because of their inherent specificity and resistance to biodegradation, petroleum biomarkers have also proven particularly useful in the discrimination of petrogenic sources from biogenic and pyrogenic sources of environmental contamination. These petroleum biomarkers are unlikely generated through pyrogenic processes and are generally absent from modern sediments lacking petroleum contamination although these modern sediments contain a variety of compounds of biogenic origin that could ultimately form petroleum. Likewise, those biomarkers determined in the environmental samples should be exclusively attributed to a petrogenic source and serve as strong evidence of petrogenic contamination (Wei et al., 2006; Yang et al., 2012).

Biomarker analysis provides backbone information to investigate the source and history of petroleum-derived environmental contaminants. Commonly used biomarkers include tri- to pentacyclic terpanes (e.g., hopanes), regular and rearranged steranes and mono- and triaromatic steranes (Stout et al., 2002; Wang et al., 1999; Yang et al., 2015, 2017; Kienhuis et al., 2016). Light petroleum biomarkers including bicyclic sesquiterpanes with drimane skeletons and diamondoids with cage molecules are also applicable to forensic oil source identification, particularly for those cases where tri- to pentacyclic biomarker terpanes and steranes are absent (Stout and Douglas, 2004; Stout et al., 2005; Yang et al., 2006, 2009, 2012). Fig. 3.5 illustrates the biomarker terpanes and steranes determined at their characteristic fragment ions of *m/z* 191, *m/z* 217 and *m/z* 218, respectively, and Fig. 3.6 presents selected GC−MS chromatograms of bicyclic sesquiterpanes (*m/z* 123), C_3-admantanes (*m/z* 163) and C_2-diamantanes (*m/z* 201) in studied environmental samples. Clearly, the fingerprints and quantitation data of biomarker terpanes and steranes further confirm the conclusion obtained from the fingerprinting results of TPH, *n*-alkanes, and target PAHs.

As seen in Figs. 3.5A and 3.6A, the biomarker terpanes and steranes and bicyclic sesquiterpanes and diamondoids were all undetectable in the sediment from the recreational pond. Nondetection of these petroleum biomarkers would be a clear indication of the absence of PHCs in this sediment. This is in agreement with the PAH characterization results. On the other hand, this confirmed the compounds detected by GC−FID analysis are mostly from biogenic source.

A wide range of terpanes, from C_{19} to C_{35}, are present in the Athabasca River sediment sample (Fig. 3.5B). Among these biomarkers, C_{21} to C_{25} tricyclic terpanes are in considerable concentrations, and C_{29} 17α(*H*),21β(*H*)-30-norhopane (H29) and C_{30} 17α(*H*),21β(*H*)-hopane (H30) are the most abundant terpanes. In addition, the presence of C_{28} 28,30-bisnorhopane and gammacerane (a unique biomarker which is not often seen in many other crude oils) is evident in this sample. It can be clearly seen from the chromatograms at *m/z* 191 that these samples display a clear distribution pattern of $C_{29} < C_{30}$, and C_{31} to C_{35} homohopanes display a regular decreasing profile in the abundance of C_{31} to C_{34} and a specific feature of C_{34} (S) $< C_{35}$ (S) and C_{34} (R) $< C_{35}$ (R). The concentrations of target steranes were found to be much lower than target terpanes. C_{21} ββ- and C_{22} ββ-steranes at *m/z* 218 are relatively more abundant than C_{27} αββ, C_{28} αββ, and C_{29} αββ steranes in the sample. Biomarker characteristics and relevant molecular ratios closely resemble those of typical oil sands bitumen, implying that most hydrocarbons detected in the river sediment were associated with oil sands bitumen (Yang et al., 2011; Wang et al., 2014). Target biomarkers were determined to be 1.56 μg/g by dry weight, accounting for a small portion (~0.6%) of TPH and slightly higher biomarkers in oil sands bitumen (~0.5% of TPH) (Yang et al., 2011). From another point of view, this further confirms petrogenic hydrocarbons to be the major organic contaminants in the sediment. Alberta oil sands bitumen is well known as a naturally degraded heavy crude oil. According to the oil sands studied in Yang et al. (2011), oil sands averagely contains 31.9 μg/g of H29 and 37.9 μg/g of H30, which are highly resistant to biodegradation and can be considered to be highly stable in the environment. H29 and H30 in

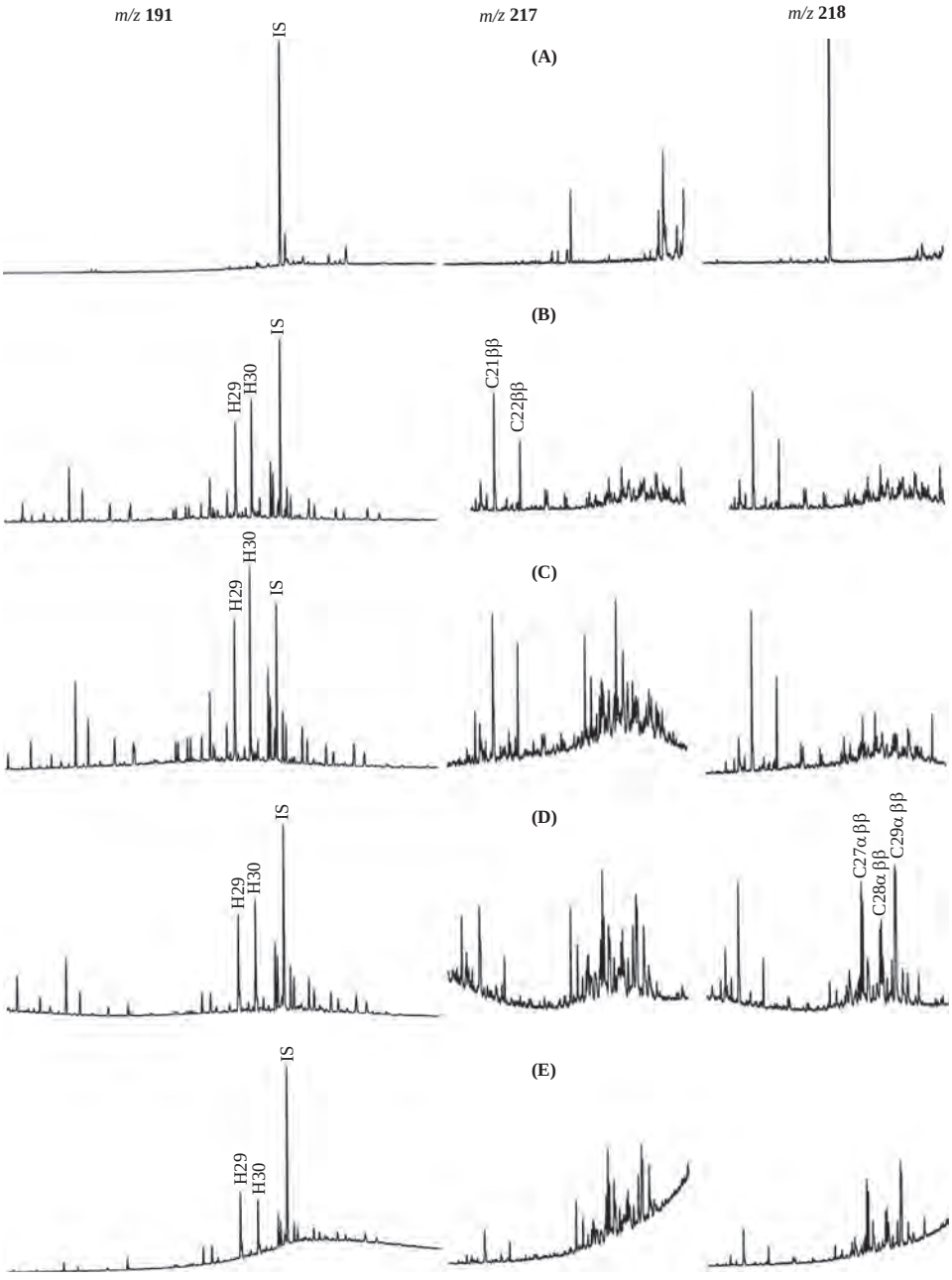

FIGURE 3.5 GC–MS chromatograms of biomarker terpanes (*m*/*z* 191) and steranes (*m*/*z* 217 and *m*/*z* 218) in environmental samples: (A) recreational pond sediment, (B) Athabasca River sediment, (C) snowmelt water, (D) bilge water, and (E) used lubricating oil.

this sediment were determined to be 0.22 μg/g and 0.24 μg/g (by dry weight), respectively. Assuming these biomarkers in the sediment are all attributed to bitumen, it can be estimated that the river sediment consists of about 0.1% (by dry weight) of oil sands bitumen, and the oil sands bitumen contributes almost all of the TPH determined in this sample.

Previous *n*-alkane and PAH analysis suggested that PHCs in the snowmelt water were from multiple contributors including biogenic source, pyrogenic source and various petroleum oils. A wide range of terpanes, from tricyclic C_{19} to pentacyclic C_{35}, is clearly present in the snowmelt water sample. In general, the target biomarker distribution characteristics are consistent with the typical features of oils sands bitumen. Interestingly, the diagnostic ratios of target biomarkers were found also to be almost identical with the Alberta oil sands bitumen sample #1 reported in Yang et al. (2011). The total target biomarkers were determined to be 10.9 μg/kg of water,

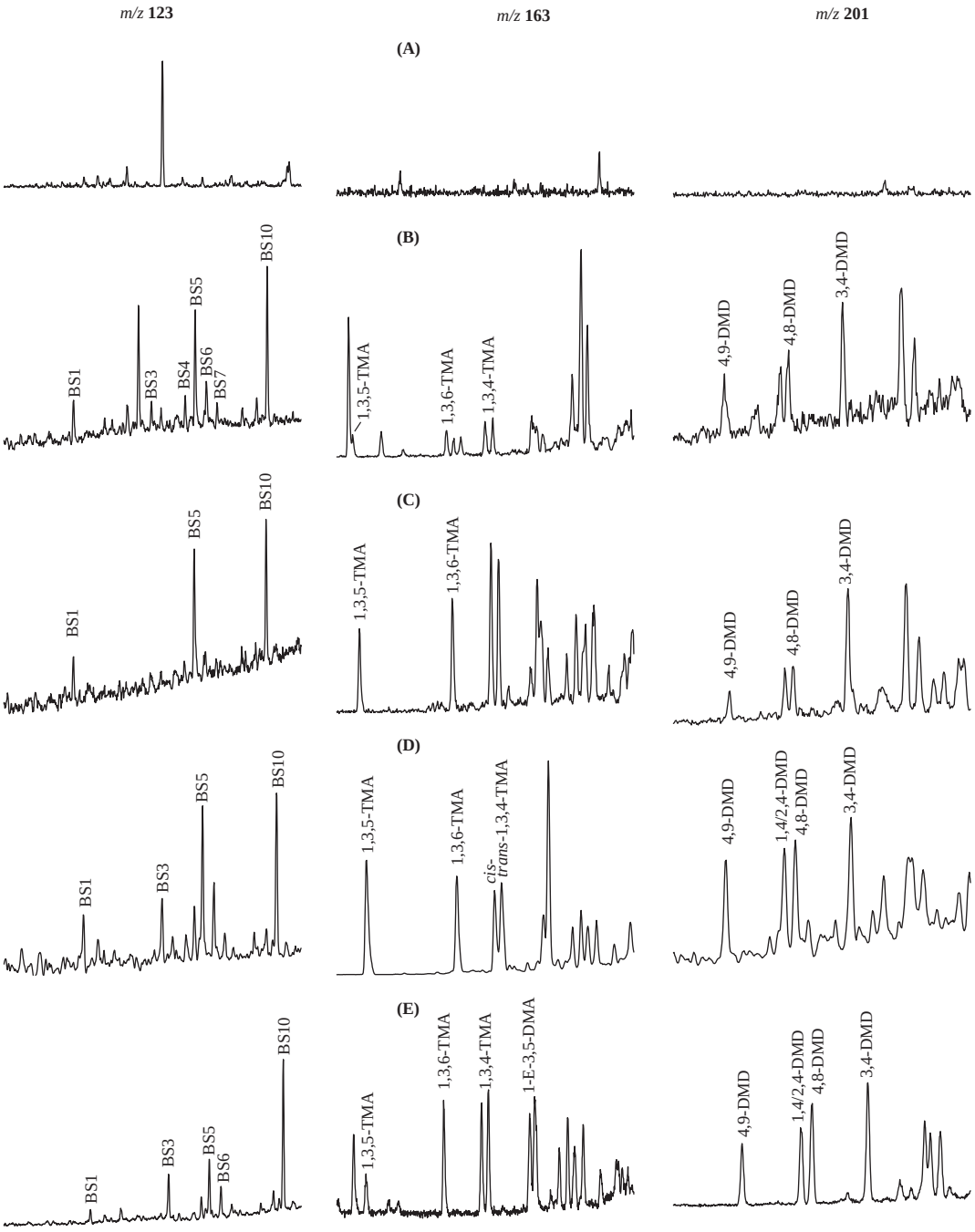

FIGURE 3.6 GC–MS chromatograms of bicyclic sesquiterpanes (*m/z* 123), C_3-admantanes (*m/z* 163) and C_2-diamantanes (*m/z* 201) in environmental samples: (A) recreational pond sediment, (B) Athabasca River sediment, (C) snowmelt water, (D) bilge water, and (E) used lubricating oil.

accounting for 0.2% relative to detected TPH. This concentration is apparently lower compared with 0.5% for those of the studied Athabasca River sediment and typical oil sands bitumen (Yang et al., 2011; Wang et al., 2014). This could be explained by the dilution effect by other types of petroleum and other sources of hydrocarbons in the snowmelt water. If H29 and H30 determined in the water are attributed to the portion of oil sands, based on the above methodology used for the Athabasca river sediment, it is estimated that oil sand bitumen in this sample contributed to roughly 45% of 4764 μg/kg of TPH and only about 5% of 273 μg/kg of PAHs. Further study of the particulates filtered from snowmelt waters indicated that PAHs, biomarkers and other hydrocarbons found in whole water sample were nearly all derived from particulates, with almost no hydrocarbons detected in

the filtered water phase, likely attributable to low water solubilities of oil sands hydrocarbons in general (Wang et al., 2014).

The concentrations of biomarkers in lube oils refined from petroleum base oils are significantly influenced by the crude oil feedstocks used in production and the distillation cut point of the petroleum products. Lubricating oils are generally rich in high MW terpanes and steranes but contain relatively low lighter tricyclic terpanes (Yang et al., 2016). This is because most low MW biomarker compounds have been removed from their stocks during the refining processes. Similarly, diesels generally contain much less biomarker terpanes and steranes because most high MW biomarker compounds have been removed from their stocks during the refining processes. Commercial lube oil usually has a distinct fingerprint of petroleum biomarkers; therefore, forensic analysis of biomarkers in environmental samples containing lube oils, such as herein the bilge water and the used lube oil, could play a critical role in oil identification.

The total biomarkers in the bilge sample were determined to be 506 μg/g TSEM. The dominance of C_{29} and C_{30} hopanes and C_{31} to C_{35} homohopanes over smaller terpanes is pronounced (Fig. 3.5D). Therefore, in combination of the TPH and PAH characterization results, it can be concluded that biomarkers in the sample were largely originated from the lube oil portion. This bilge also consists of some low-molecular-weight biomarker terpanes such as C_{19} to C_{24} and abundant bicyclic sesquiterpanes and diamondoid hydrocarbons because of a small diesel oil portion in the sample.

As noticed from Fig. 3.5E, the dominance of pentacyclic C_{29} and C_{30} hopanes over smaller terpanes is pronounced in the used lube oil sample, and tricyclic C_{19} and C_{24} terpanes are significantly less abundant. The total biomarkers were detected to be 599 μg/g in the used lube oil. In Fig. 3.6E, the presence of bicyclic sesquiterpanes and diamondoid hydrocarbons in the used oil is a clear evidence of diesel contamination as these compounds originate exclusively from the petroleum and are unlikely to be generated during fuel combustion. In addition, the biomarker concentration can be applied to accurately assess the proportion of lube oil and diesel if the original source oils are available.

3.6 CONCLUSIONS

Chromatographic profile and normal alkane distribution by GC–FID analysis provide primary diagnostic information for the identification and differentiation of petrogenic and biogenic sources. PAH distribution and associated diagnostic ratios such as PI and perylene index are useful tools in distinguishing petrogenic hydrocarbons from both pyrogenic and biogenic hydrocarbons. As petroleum-characteristic alkylated PAH homologues and biomarkers are absent in biogenic and pyrogenic source hydrocarbons, their co-occurrence can be used as unambiguous indicators of petrogenic contamination, whereas the absence of these petroleum-characteristic component and presence of abundant biogenic compounds (such as dominant odd-numbered *n*-alkanes, sterols, fatty acids, and alcohols) can be used as unambiguous indicators for predominance of natural organic compounds in samples. Normal alkanes and PAHs can be used to further to establish the proportion from each source.

Based on the chemical fingerprints of the studied environmental samples, it can be concluded that: (1) the hydrocarbons in the recreational pond sediment mainly originate to biogenic matters. This sample is basically free of petroleum contamination and only contains trace amount of PAHs from anthropogenic inputs; (2) the hydrocarbons detected in the Athabasca River sediment are largely attributed to oil sands bitumen, whereas contribution from other lighter petroleum is also apparent. Contributions of both pyrogenic and biogenic sources are also evident in terms of relatively high pyrogenic and perylene indices, respectively; (3) various petroleum oils are the principal contributors of the hydrocarbons determined in the snowmelt water. Meanwhile, many evidences also strongly indicate significant pyrogenic input; (4) the bilge sample clearly consists of primarily a diesel range fuel and a slight amount of a lubricating oil (~10%); and (5) *n*-C_9 to *n*-C_{24} alkanes, PAHs and biomarkers were detected in the used lube oil at considerable concentrations. This used oil is comprised of approximately ~90% of lube oil mixed with unburned diesel fuel and combustion exhaust of oils.

References

Aboul-Kassim, T.A.T., Williamson, K.J., 2003. Forensic analysis and genetic source partitioning model for Portland Harbor contaminated sediments. J. Environ. Info. 1, 58–75.

Benlahcen, K.T., Chaoui, A., Budzinski, H., Bellocq, J., Garrigues, P., 1997. Distribution and sources of polycyclic aromatic hydrocarbons in some Mediterranean coastal sediments. Mar. Pollut. Bull. 34, 298–305.

Boehm, P.D., Douglas, G.S., Burns, W.A., Mankiewicz, P.J., Page, D.S., Bence, A.E., 1997. Application of petroleum hydrocarbon chemical fingerprinting and allocation techniques after the *Exxon Valdez* oil spill. Mar. Pollut. Bull. 34, 599–613.

Jautzy, J.J., Ahad, M.E., Gobeil, C., Savard, M.M., 2013. Century-long source apportionment of PAHs in Athabasca Oil Sands Region Lakes using diagnostic ratios and compound-specific carbon isotope signatures. Environ. Sci. Technol. 47, 6155–6163.

Kaplan, I.R., Lu, S.T., Alimi, H.M., MacMerphey, J., 2001. Fingerprinting of high boiling hydrocarbon fuels, asphalts and lubricants. Environ Forensics 2, 231–248.

Kelly-Hooper, F., Farwell, A., Pike, G., Kenedy, J., Wang, Z.D., Grunsky, E.C., et al., 2013. Is it clean or contaminated soil? Using petrogenic versus biogenic GC–FID chromatogram patterns to mathematically resolve false petroleum hydrocarbon detections in clean organic soils: a crude oil-spiked peat microcosm experiment. Environ. Tox. Chem. 32, 2197–2206.

Kienhuis, P.G.M., Hansen, A.B., Faksness, L., Stout, S.A., Dahlmann, G., 2016. CEN methodology for oil spill identification. In: Stout, S.A., Wang, Z.D. (Eds.), Standard Handbook Oil Spill Environmental Forensics, second ed., Academic Press, Cambridge, MA, pp. 685–728.

Lima, A.L., Eglinton, T.I., Reddy, C.M., 2003. High-resolution record of pyrogenic polycyclic aromatic hydrocarbon deposition during the 20th century. Environ. Sci. Technol. 37, 53–61.

Lima, A.L., Farrington, J.W., Reddy, C.M., 2005. Combustion-derived polycyclic aromatic hydrocarbons in the environment—a review. Environ. Forensics 6, 109–131.

Lu, S.T., Kaplan, I.R., 2008. Characterization of motor lubricating oils and their oil-water partition. Environ. Forensics 9, 295–309.

Meyers, P.A., Ishiwatari, R., 1993. Lacustrine organic geochemistry—an overview of indicators of organic-matter sources and diagenesis in lake-sediments. Org. Geochem. 20, 867–900.

Mićić, V., Kruge, M.A., Köster, J., Hofmann, T., 2011. Natural, anthropogenic and fossil organic matter in river sediments and suspended particulate matter: a multi-molecular marker approach. Sci. Total. Environ. 409, 905–919.

Page, D.S., Douglas, G.S., Bence, A.E., Burns, W.A., Mankiewiczet, P.J., 1999. Pyrogenic PAHs in sediments record past human activity: a case study in Prince William Sound, Alaska. Mar. Pollut. Bull. 38, 247–260.

Pereira, W.E., Hostettler, F.D., Luoma, S.N., Van Geen, A., Fuller, C.C., Anima, R.J., 1999. Sedimentary record of anthropogenic and biogenic polycyclic aromatic hydrocarbons in San Francisco Bay, California. Mar. Chem. 64, 99–113.

Stout, S.A., Douglas, G.S., 2004. Diamondoid hydrocarbons application in the chemical fingerprinting of natural gas condensate and gasoline. Environ. Forensics 5, 225–235.

Stout, S.A., Uhler, A.D., McCarthy, K.J., 2001. A strategy and methodology for defensibly correlating spilled oil to source candidates. Environ. Forensics 2, 87–98.

Stout, S.A., Uhler, A.D., McCarthy, K.J., 2005. Middle distillate fuel fingerprinting using drimane-based bicyclic sesquiterpanes. Environ. Forensics 6, 241–251.

Stout, S.A., Uhler, A.D., McCarthy, K.J., Emsbo-Mattingly, S., 2002. Chemical fingerprinting of hydrocarbons. In: Murphy, B.L., Morrison, R.D. (Eds.), Introduction to Environmental Forensics. Academic Press, London, pp. 137–260.

Venkatesan, M.I., 1988. The occurrence and possible sources of perylene in marine sediments—a review. Mar. Chem. 25, 1–27.

Volkman, J.K., Holdsworth, D.G., Neill, G.P., Bavor Jr., H.J., 1992. Identification of natural, anthropogenic and petroleum hydrocarbons in aquatic sediments. Sci. Total Environ. 112, 203–219.

Wang, Z.D., Fingas, M., Shu, Y.Y., Sigouin, L., Landriault, M., Lambert, P., 1999. Quantitative characterization of PAHs in burn residue and soot samples and differentiation of pyrogenic PAHs from petrogenic PAHs—the 1994 Mobile Burn Study. Environ. Sci. Technol. 33, 3100–3109.

Wang, Z.D., Fingas, M., Yang, C., Christensen, H.J., 2006. Crude oils and refined products fingerprinting: principles. In: Morrison, R.D., Murphy, B.L. (Eds.), Environmental Forensics: Contaminant Specific Guide, first ed. Elsevier Academic Press, New York, pp. 339–407.

Wang, Z.D., Li, K., Lambert, P., Yang, C., 2007. Identification, characterization and quantitation of pyrogenic polycylic aromatic hydrocarbons and other organic compounds in tire fire products. J. Chromatogr. A. 1139, 14–26.

Wang, Z.D., Yang, C., Kelly-Hooper, F., Hollebone, B., Peng, X., Brown, C.E., et al., 2009. Forensic differentiation of biogenic organic compounds from petroleum hydrocarbons in biogenic and petrogenic compounds cross-contaminated soils and sediments. J. Chromatogr. A. 1216, 1174–1191.

Wang, Z.D., Yang, C., Yang, Z.Y., Hollebone, B., Brown, C.E., Landriault, M., 2012. Fingerprinting of petroleum hydrocarbons (PHC) and other biogenic organic compounds (BOC) in oil-contaminated and paired background soil samples. J. Environ. Mon. 14, 2367–2381.

Wang, Z.D., Yang, C., Parrott, J.L., Frank, R.A., Yang, Z., Brown, C.E., et al., 2014. Forensic source differentiation of petrogenic, pyrogenic, and biogenic hydrocarbons in Canadian oil sands environmental samples. J. Hazard. Mater. 271, 166–177.

Wei, Z.B., Moldowan, J.M., Paytan, A., 2006. Diamondoids and molecular biomarkers generated from modern sediments in the absence and presence of minerals during hydrous pyrolysis. Org. Geochem. 37, 891–911.

Yang, C., Wang, Z.D., Hollebone, B., Peng, X., Fingas, M., Landriault, M., 2006. GC/MS quantitation analysis of diamondoid compounds in crude oils and petroleum products. Environ. Forensics 7, 377–390.

Yang, C., Wang, Z.D., Hollebone, B., Brown, C.E., Landriault, M., 2009. Characteristics of bicyclic sesquiterpanes in crude oils and petroleum products. J. Chromatogr. A. 1216, 4475–4484.

Yang, C., Wang, Z.D., Yang, Z.Y., Hollebone, B., Brown, C.E., Landriault, M., et al., 2011. Chemical fingerprints of Alberta oil sands bitumen and related petroleum products. Environ. Forensics 12, 173–188.

Yang, C., Wang, Z.D., Hollebone, B., Brown, C.E., Landriault, M., Fieldhouse, B., 2012. Application of light petroleum biomarkers for forensic characterization and source identification of spilled light refined oils. Environ. Forensics 13, 298–311.

Yang, C., Wang, Z.D., Hollebone, B., Brown, C.E., Yang, Z.Y., Landriault, M., 2015. Chromatographic fingerprinting analysis of crude oil and petroleum products. In: Fingas, M. (Ed.), Handbook of Oil Spill Science and Technology. John Wiley & Sons, Inc., Hoboken, NJ, pp. 95–163.

Yang, C., Yang, Z.Y., Zhang, G., Hollebone, B., Landriault, M., Wang, Z.D., et al., 2016. Characterization and differentiation of chemical fingerprints of virgin and used lubricating oils for identification of contamination or adulteration sources. Fuel 163, 271–281.

Yang, C., Brown, C.E., Hollebone, B., Yang, Z., Lambert, P., Fieldhouse, B., et al., 2017. Chemical fingerprints of crude oil and petroleum products. In: Fingas, M. (Ed.), Oil Spill Science and Technology, second ed. Gulf Professional Publishing, Huston, TX, pp. 209–304.

Yunker, M.B., Macdonald, R.W., Goyette, D., Paton, D.W., Fowler, B.R., Sullivan, D., et al., 1999. Natural and anthropogenic inputs of hydrocarbons to the Strait of Georgia. Sci. Total Environ. 225, 181–209.

Yunker, M.B., Macdonald, R.W., Vingarzan, R., Mitchell, H.R., Goyette, D., Sylvestre, S., 2002. PAHs in the Fraser River basin: a critical appraisal of PAH ratios as indicators of PAH source and composition. Org. Geochem. 33, 489–515.

Yunker, M.B., Macdonald, R.W., Snowdon, L.R., Fowler, B.R., 2011. Alkane and PAH biomarkers as tracers of terrigenous organic carbon in Arctic Ocean sediments. Org. Geochem. 42, 1109–1146.

CHAPTER

4

The Application of Isotope Geochemistry in Stray Gas Investigations: Case Studies

Fred Baldassare and Elizabeth Chapman

ECHELON Applied Geochemistry Consulting, Murrysville, PA, Unites States

BIOGRAPHIES

Fred Baldassare has more than 25 years of experience as a geologist and more than 20 years of experience investigating more than 300 reported incidents of stray gas migration. He is an experienced investigator and researcher who has helped pioneer the application and advancement of isotope geochemistry to identify and distinguish the origin of different microbial and thermogenic gases in the Appalachian Basin. Fred was the lead author for Pennsylvania's Oil & Gas regulations (25 PA. CODE CH. 78, §78,89) for stray gas incident response, the Marcellus Shale Coalition's technical guidance for stray gas investigations, and coauthor of the first comprehensive manual for investigating and characterizing incidents of stray gas migration: *Technical Measures For The Investigation And Mitigation Of Fugitive Methane Hazards In Areas of Coal Mining*. Fred has authored and coauthored professional papers for peer-reviewed journals on the application of isotope geochemistry since 1997. He has taught and lectured internationally, and at his alma maters, The Pennsylvania State University and The University of Pittsburgh.

Elizabeth Chapman received her Ph.D. from the University of Pittsburgh in 2011 under the advisement of Dr. Rosemary Capo. Liz's work focuses on combining strontium (Sr) isotopic data with major and trace element geochemistry to characterize groundwater, surface water, and produced water from various fossil fuel sources. This characterization allows for contaminant tracking through the environment as well as identifying and quantifying water–rock interactions. Recent publications include: *Geochemical and strontium isotope characterization of produced waters from Marcellus Shale natural gas extraction* (Environmental Science & Technology, 2012) and *Strontium isotope quantification of siderite, brine, and acid mine drainage contributions to abandoned gas well discharges in the Appalachian Plateau* (Applied Geochemistry, 2013).

4.1 INTRODUCTION

Petroleum occurs in gaseous, liquid, and solid forms. In its gaseous form, i.e., natural gas, it consists of methane and small straight and branched hydrocarbons, generally containing one to five carbons as well as various nonhydrocarbons (e.g., CO, N_2, H_2S, etc.). Natural gas occurring in groundwater and/or soils in the near-surface environment and of an unknown origin, is referred to as "stray gas", which is an emerging environmental hazard.

Oil Spill Environmental Forensics Case Studies.
DOI: http://dx.doi.org/10.1016/B978-0-12-804434-6.00004-5

In this chapter, we discuss environmental forensic aspects of stray gas. Determining the source(s) of natural gas and methane in the environment has often been a subject of environmental forensics (Coleman et al., 1977; Harrison, 1983; Coleman et al., 1995; Baldassare and Laughrey, 1997; Hackley et al., 1999; Révész et al., 2010). Incidents of stray gas migration have resulted in catastrophic consequences (Figs. 4.1 and 4.2).

In recent years, the application of high-volume hydraulic fracturing (HVHF) and horizontal well design has revolutionized the natural gas industry and increased natural gas production throughout North America. This process has also created more awareness regarding the migration of "stray gas" to shallow aquifer systems. However, as noted above, incidents of stray gas migration are relatively rare and not only recent phenomena.

"Stray gas" can be defined as gaseous matter of undetermined origin found in an area that presents a threat to public health and safety or has impacted the shallow subsurface or aquifer system. Methane is the principal migrated gas for the vast majority of stray alkane hydrocarbon gases. Unlike most environmental investigations, stray gas incidents often require immediate and rapid response. "Gas forensics" is an interpretive process using the molecular and isotopic gas compositions as empirical geochemical evidence to define gas origin and constrain the gas source. Properly interpreted, these geochemical markers provide evidence to focus on potential stray gas sources and to advance the investigation to evaluate the mechanism of migration and identify the specific source (s) of the subject stray gas investigation.

Methane in the shallow subsurface either as a dissolved gas in groundwater or in the gas phase is not unusual in aquifer systems above coal-bearing or petroliferous basins. The origin may be a natural condition, the result of legacy conditions, or due to recent activity. In general, the manifestation of stray gas incidents can be categorized as:

1. Nonthreatening,
2. Initially as nonthreatening and escalating to potentially threatening
3. Threatening or catastrophic

FIGURE 4.1 1995: Photograph showing the remains of a residence after an explosion caused by the migration of stray combustible gas from the subsurface. The investigation revealed the gas origin was a natural condition in the aquifer.

FIGURE 4.2 1999: Photograph showing the remains of a residence after an explosion caused by the migration of stray combustible gas. The investigation revealed the migration of stray gas was due to underground coal mining.

Methane is classified as a simple asphyxiant and explosion hazard; it is not toxic and there is no ingestion hazard. It has a specific gravity of 0.555, is explosive between 5% and 15% in ambient air, and is soluble in water between ~24 and 28 mg/L at 1 atmosphere of pressure; however, its solubility in water is proportional to pressure (Henry's law). Every foot of hydrostatic head exerts 0.43 psi, or 2.31 ft of water is under 1 psi. As such, groundwater at depth can contain much higher concentrations of dissolved methane than is possible at atmospheric conditions. It is for this reason that homeowners utilizing local groundwater sometimes report effervescence from their water, as dissolved gas under pressure at depth exsolves upon reaching surface pressures.

The diffusivity in air (Da) of methane is 0.23 cm^2/s; this value is about twice as high as that of benzene, toluene, ethylbenzene and xylene (BTEX) compounds. The rate of diffusion for a compound is proportional to its diffusivity in air. Thus, the diffusion rate of methane is about twice as fast as diffusion of most volatile organic compounds (VOCs) commonly associated with petroleum. The viscosity of methane is about 1.1E-04 g/cm-s, which is less than the viscosity of air (but within a factor of 2x), and therefore, the pressure-driven flow of methane is somewhat faster than that of air.

If methane is introduced (or any organic carbon, including that in the soil zone above an aquifer that can recharge the aquifer) into the groundwater system, it can create reducing conditions which may cause sulfate, nitrate, and dissolved oxygen concentrations to decrease and dissolved iron, dissolved manganese, dissolved inorganic carbon (DIC), alkalinity, and pH to increase. As the oxygen level in water drops (becoming anoxic), the groundwater becomes more reducing. These geochemical changes are often recognized by the homeowner as the water turns black or yellow in color and has a "rotten eggs" odor. Because of the chemical changes, the introduction of methane can alter the water redox (reduction-oxidation) state to be anoxic. Additionally, introducing methane into groundwater can cause variations in the concentrations of common cations (sodium, calcium,

potassium, magnesium). Also, of note is that the redox state of the groundwater can vary seasonally due to any number of factors.

Contaminant solute transport in accordance with Darcy's law is the dominant transport mechanism for conventional groundwater investigations. However, unlike water, gas is compressible and gas migration in an aquifer system can migrate under pressure from a source as a dissolved gas, or in the gas phase, or as both simultaneously. Migration pathways may occur over long distances in short timeframes and therefore the distance from a potential source to a receptor cannot be the sole basis to rule out (or in) the gas source a priori. Stray gas migration typically exhibits strong vertical gradients, lateral migration along bedding planes, preferred migration along faults/fracture networks and pathway/flow rates subject to pressure gradient.

Stray gas forensics and gas origin-to-source correlation should be an iterative process to include different data types and multiple lines of evidence (Baldassare and Laughrey, 1997; Baldassare et al., 2014; Dusseault and Jackson, 2014; Sherwood et al., 2016; Zhang and Soeder, 2016). The investigation process can be described, generally as follows:

- Define and characterize the stray gas at the receptor (manner of manifestation, time series gas concentrations, gas and groundwater geochemistry)
- Evaluate stray gas geochemistry for possible secondary effects such as mixing and oxidation
- Identify the potential source(s) of the stray gas
- Define the molecular and isotopic characteristics that distinguish the potential gas sources
- Identify the best match between the stray gas and potential source(s) to focus the investigation
- Define, to the extent possible, the gas migration pathway(s)
- Monitoring—frequency and timeframe specific to the investigation
- Evaluate mechanism of migration

4.2 GAS GEOCHEMISTRY

The application of molecular and isotopic compositions to constrain the origin of natural gases in the subsurface is well established. Various researchers have determined by examination of stable carbon and hydrogen isotopes of methane that there are common carbon and hydrogen isotopic compositions for thermogenic gas associated with coal and natural gas, drift gas, and other near-surface microbial gases (Craig, 1953; Coleman et al., 1977; Deines, 1980; Schoell, 1980; Rice and Claypool, 1981; Schoell, 1983; Whiticar et al., 1986; Wiese and Kvenvolden, 1993; Coleman et al., 1995; Baldassare and Laughrey, 1997; Kaplan et al., 1997; Rowe and Muehlenbachs, 1999; Osborn and McIntosh, 2010; Révész et al., 2010; Baldassare et al., 2014; Dusseault and Jackson, 2014).

Two distinct processes on Earth produce hydrocarbon gases: microbial and thermogenic degradation of organic matter. Microbial gas is formed at shallow depths and low temperatures by anaerobic bacterial decomposition of sedimentary organic matter. In contrast, thermogenic gas is formed at higher temperature regimes and at deeper depths by thermal cracking of sedimentary organic matter into hydrocarbon liquids and gas ("primary" thermogenic gas) and thermal cracking of oil at high temperatures into gas ("secondary" thermogenic gas) and pyrobitumen.

Microbial gas is very dry (i.e., consisting almost entirely of methane). In contrast, thermogenic gas can be dry or can contain significant concentrations of "wet gas" components (ethane, propane, butanes) and condensate (C5+ hydrocarbons). Although thermogenic gas is typically the dominant type of natural gas in coal and petroleum reservoirs, those reservoirs often contain a component of microbial gas.

Geochemical analysis of a gas includes both molecular composition (relative abundance of C1 to C6+ hydrocarbons and nonhydrocarbon gases such as He, H_2, CO_2, and N_2 in the gas sample) and isotopic composition. The isotopic composition of a gas may include the stable carbon and hydrogen isotope ratios of the C1 to C5 hydrocarbon gas species, stable isotope composition of nonhydrocarbon gases, and radioactive carbon (carbon-14) of methane.

Normal carbon is composed of approximately 98.9% carbon-12 (^{12}C) and about 1.1% carbon-13 (^{13}C). The difference in the mass of the carbon isotopes results in a difference in the rates at which the isotopic species undergo certain physical and chemical processes. Isotopic fractionation, or the partial separation of carbon isotopic species, can occur in certain natural processes. The $^{13}C/^{12}C$ of carbon is expressed as a $\delta^{13}C$ value in units of per mil (parts per

thousand, ‰). A $\delta^{13}C$ value of −40‰ indicates that the material is 40 parts per thousand (or 4%) lighter than the standard. That is, the material is enriched in ^{12}C by 40‰ relative to the standard.

Stable isotope compositions are expressed as:

$\delta^{13}C_{CH4}$ (per mil, or ‰) = [($^{13}C/^{12}C$) gas sample − ($^{13}C/^{12}C$)standard]/($^{13}C/^{12}C$)standard] × 1000

A positive value indicates that the sample is more enriched in the heavy isotope (^{13}C) than the international measurement standard, whereas a negative value indicates that the sample is depleted in the heavy isotope (^{13}C) relative to the international measurement standard. Stable carbon isotope ratios are reported relative to the Vienna Peedee belemnite (VPDB) standard and hydrogen isotope ratios are relative to the Vienna standard mean ocean water (VSMOW) standard (Gat and Gonfiantini, 1981).

There are two principal pathways by which microbial CH_4 is produced (Schoell, 1980):

1. Acetic acid fermentation: $CH_3COOH \rightarrow CH_4 + CO_2$
2. CO_2 reduction: $CO_2 + 4H_2 \rightarrow CH_4 + 2H_2O$

For microbial methane found in near-surface environments due to acetate fermentation (marsh gas and landfill gas), $\delta^{13}C_{CH4}$ (or $\delta^{13}C_1$) ranges from about −40‰ to −62‰ and δD_{CH4} (or δDC_1) ranges from about −270‰ to −350‰. Microbial methane in due to CO_2 reduction (drift gas) generally has $\delta^{13}C_1$ values ranging from about −62‰ to −90‰ and δDC_1 values ranging from about −180‰ to −240‰.

The $\delta^{13}C_1$ and δDC_1 range historically associated with and reported for thermogenic gas has changed in recent years as the result of the proliferation of HVHF and horizontal well technology in shale gas production in more thermally mature areas of petroliferous basins throughout North America. Taking these newer shale gas data into consideration, the $\delta^{13}C_1$ of thermogenic gas more accurately ranges from about −23‰ to −50‰ or −60‰ and δDC_1 ranges from about −110‰ to −250‰. Contrary to normal kinetic isotope effects (KIE), we also see reversal of the normal trend of carbon isotopic composition, where $\delta^{13}C_1 > \delta^{13}C_2 > \delta^{13}C_3$ (Baldassare et al., 2014; Burruss and Laughrey, 2010; Curiale and Curtis, 2016). Values of $\delta^{13}C_1$ near −60‰ associated with δDC_1 values in the −160‰ to −260‰ range generally are attributed to diagenesis or mixing of thermogenic and microbial methane. Fig. 4.3 provides a revised Schoell diagram expanding the thermogenic region based on shale gas production from more thermally mature basins.

Fig. 4.4 includes methane isotope data for a thermally mature and dry gas area of the Appalachian Basin. The data indicate isotope reversals universally in the Marcellus. Fig. 4.5 reveals a thermal maturity trend and

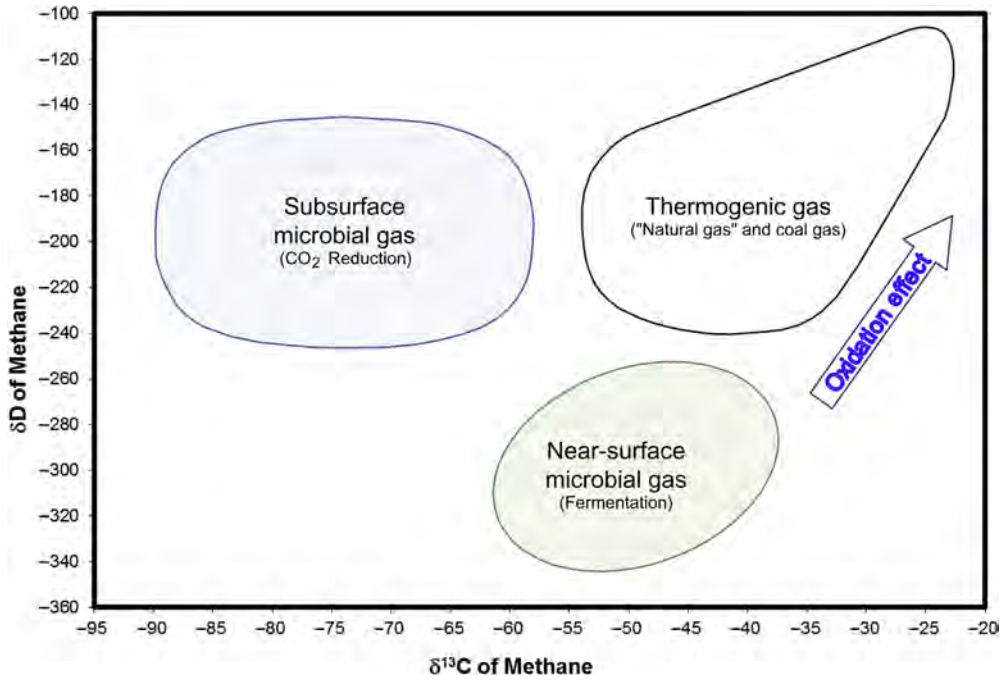

FIGURE 4.3 Modified Schoell plot in which the thermogenic gas region is expanded to include more thermally mature shale gas production common in recent years. *Source: Modified from Schoell, M., 1983. Genetic characterization of natural gases. Am. Assoc. Pet. Geol. Bull. 67 (12), 2225–2238.*

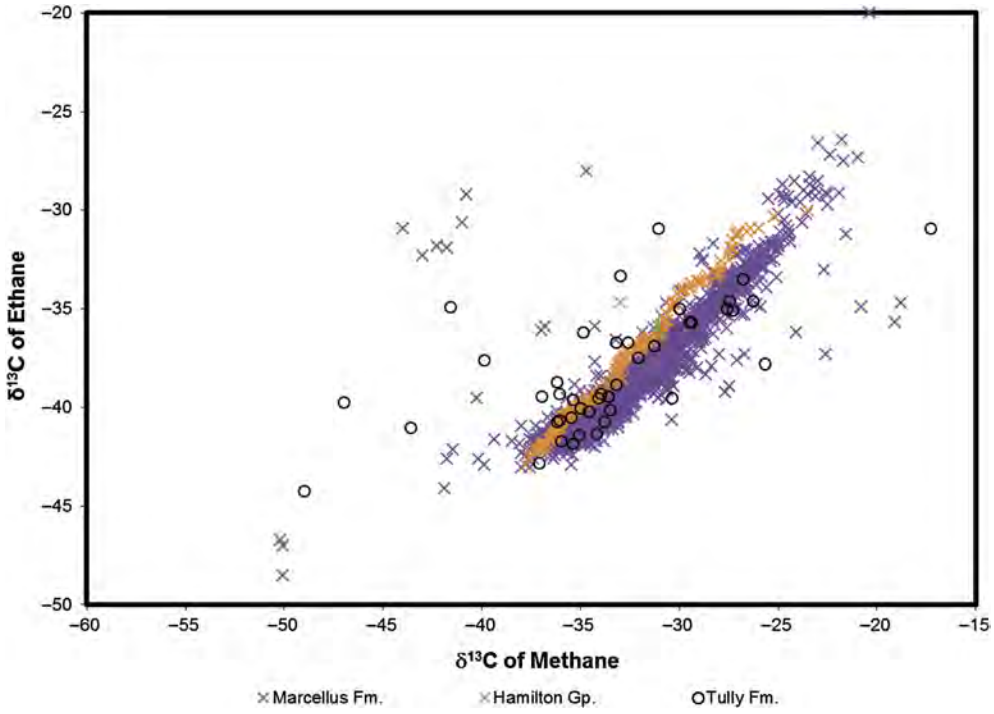

FIGURE 4.4 $\delta^{13}C_1$ versus $\delta^{13}C_2$ Mudgas isotope concentrations for gas shows >1524 m (5000 ft.) in the northeastern part of the Appalachian Basin. Interval is generally representative of Tully Limestone, Hamilton Group, and Marcellus Formation (Fm.) strata. *Reprinted by permission of the AAPG. Taken from Baldassare, F.J., McCaffrey, M.A., Harper, J.A., 2014. A geochemical context for stray gas investigations in the northern Appalachian Basin: Implications of analyses of natural gases from Neogene-through Devonian-age strata. AAPG bull. 98(2), 341–372.*

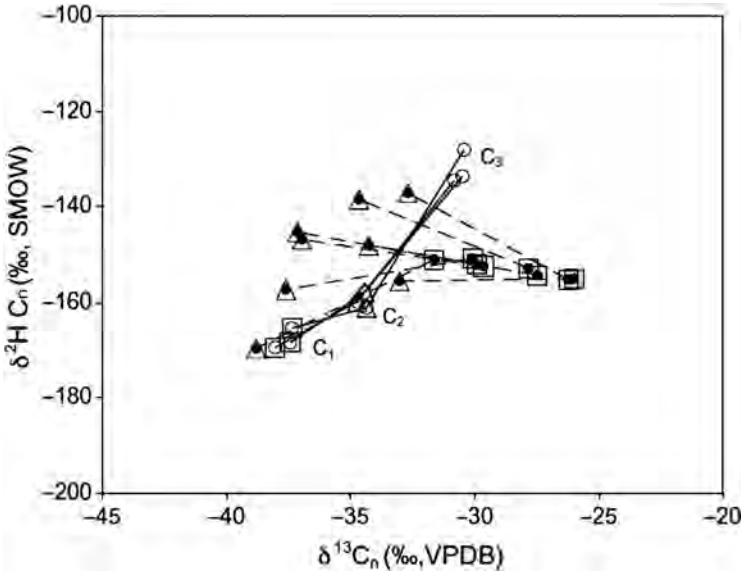

FIGURE 4.5 Compound specific $\delta^{13}C$ versus $\delta^{2}H$ for C1 to C3 in Ordovician OAG gases in three samples from the York field, Ohio and NAG from several fields in New York. The OAG are shown as open symbols connected with solid lines. The data indicate normal KIE. The NAG are shown as solid symbols connected with dashed lines and the isotopic compositions are reversed. The normal and reversed trends are further highlighted by outlining the values for C1 in squares and C2 in triangles (Burruss and Laughrey, 2010).

comparison of isotope compositions for oil-associated (OAG) and nonassociated gases (NAG) for areas of the Appalachian basin. Fig. 4.6 provides a comparison of gases from unconventional source-rock reservoirs exhibiting normal KIE versus those showing a reversed trend.

The molecular and isotopic composition of stray gas may be modified by secondary effects that can alter their molecular and isotopic compositions. Common secondary effects may include oxidation or mixing. Bacterial oxidation of methane can affect its carbon isotopic composition (as indicated in Fig. 4.3). The light isotope (^{12}C) is oxidized more rapidly than the heavy isotope (^{13}C) and therefore the residual CH_4 becomes more enriched in ^{13}C

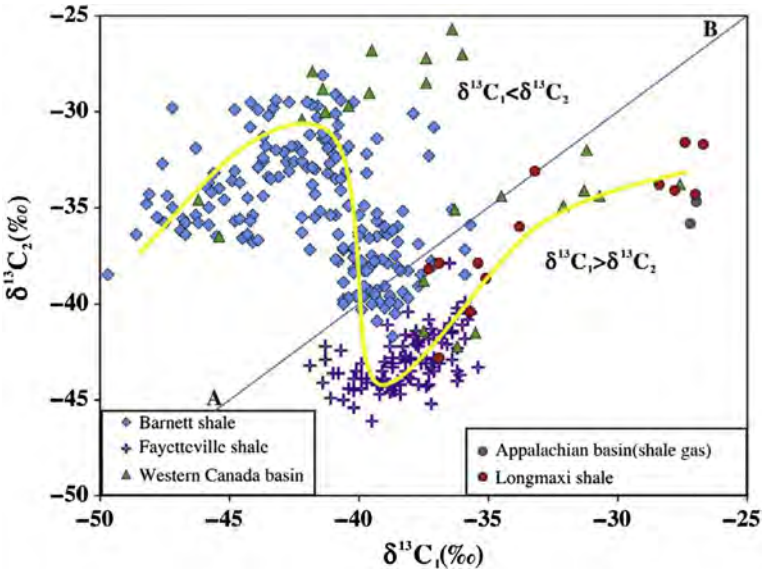

FIGURE 4.6 Trend of $\delta^{13}C_1$ versus $\delta^{13}C_2$ variation for a set of gases from unconventional source-rock reservoirs. The A–B line segment separates the gases with normal KIE trend (above) from those showing a reversed trend (below; Curiale and Curtis, 2016).

(Coleman et al., 1981; Whiticar and Faber, 1985). Additionally, the C2+ hydrocarbons oxidize preferentially over methane. Similarly, mixing of different gases in the subsurface can alter the molecular and isotopic composition of a stray gas from its original source gas.

In the remainder of this chapter, we present two stray gas case studies that serve to demonstrate the forensic approach and geochemical principles described above.

4.3 CASE STUDY #1—INTRODUCTION

In 2014, multiple property owners notify local emergency management officials of a natural gas odor and areas of stressed vegetation on their properties. The homeowners report that the onset of the stressed vegetation occurred earlier than they reported as it was initially thought the area of stressed vegetation was due to a combination of drought conditions, poor-quality grass seed, or occasional flooding of the small tributary that borders the properties.

State and local environmental officials respond and conduct monitoring with a combustible gas indicator calibrated to methane. Combustible gas is not detected in any of the nearby homes; however, monitoring of the soil gas indicates >10% range combustible gas. The area of impact is delineated to be approximately 100 ft in length and 3–5 ft wide.

Potential stray gas sources in the area were subsequently identified, including several operating and plugged and abandoned gas wells within 1000 ft of the area of impact and an active coal mine approximately 400 ft below the surface that had been mined by room and pillar methods. One of the plugged and abandoned gas wells was identified as the nearest potential source to the area of stressed vegetation (within 50 ft). Records reveal this particular well was drilled in 1921 to a depth of 2800 ft and was plugged and abandoned in 1966. The method of plugging was approved by the regulatory agency. Because the plugged well was located within the boundaries of the coal mine, which was also operating at the time, a two-inch vent was installed, in accordance with the regulations, as an added measure of safety should the well plug fail.

Soil gas monitoring points were installed throughout the area of stressed vegetation for delineation and long-term monitoring. Soil gas samples were collected on numerous occasions for molecular and isotopic analyses from the area of stressed vegetation and also from soils adjacent to the proximal plugged gas well. Gas was also collected from the vent on the nearby plugged gas well.

The objective of the collection and analysis of these soil gases was to determine the origin of the gas, in particular whether or not gas leaking from the nearby plugged gas well and/or the coal-mining operation was the source of the stray gas.

4.4 CASE STUDY #1—RESULTS AND DISCUSSION

4.4.1 Gas Geochemistry

The molecular and isotopic results for 16 gas samples were evaluated for the investigation:

- Four gas samples were collected and analyzed specifically during this investigation in 2014 and 2015. These included two soil gas locations and gas collected on two occasions from the vent on the nearby plugged gas well.
- Earlier data for samples collected nearby in 2009 were also evaluated. These included gas geochemistry data for two nearby water well gas samples, a gas sample from the coal mine degas borehole, and two production gas samples from nearby natural gas-producing wells. These earlier data were obtained from a 2010 report by the regulatory agency in the vicinity of their investigation of a site located approximately 1500 ft south of the subject investigation.
- In addition, previously published gas isotope results for production gas samples collected from seven nearby (active) gas wells in 2012 and 2013, which produced from the same formations as the nearby plugged gas well, were averaged and evaluated.

All analytical results are summarized in Table 4.1 and plotted on interpretive gas geochemistry plots in Figs. 4.7 and 4.8.

The gas geochemistry reveals that two distinct gas types are present in the areas of investigation. These are early thermogenic and mature thermogenic gases, which are further described below.

4.4.2 Early Thermogenic Gas

Early thermogenic gas was found in both soil gas samples, in both samples from the two-inch vent on the nearby plugged gas well and also in the mine degas borehole and two water well samples collected for the nearby prior investigation (Table 4.1; Figs. 4.7 and 4.8). Early thermogenic gas is known to be naturally occurring within the shallow system in this part of the basin. Specifically, early thermogenic gas is found in coalbeds and carbonaceous rocks in the Permian and Upper Pennsylvanian formations, generally within the upper 1000 ft locally. Nonetheless, anthropogenic activity can mobilize preexisting gas and create a potential public health and safety hazard.

The mine degas borehole was drilled to a total depth of 620 ft and constructed with 200 ft of slotted casing. It was terminated at ~40 ft above the active coal mine and was designed specifically to degas the mine. The early thermogenic gas found in the mine degas borehole is interpreted as having been formed during diagenesis and/or late-stage microbial activity within the coal(s) by anaerobic microorganisms, and possibly mixed with the thermogenic gases that formed earlier within the area's coals. Groundwater flow creates a favorable environment for late-stage microbial activity and the associated generation of late-stage gases.

The presence of early thermogenic gas in the water well samples collected for the nearby and prior (2009) investigation was confirmation that early thermogenic gas was indeed present throughout the shallow (upper 1000 ft) aquifers of the area.

The presence of early thermogenic gas in both samples collected from the plugged well's vent, rather than mature thermogenic gas as was produced from depth when this well was active, provided proof that the well plug for the deeper producing formations was still effective. If the plug were not effective, we would have expected to see a mature thermogenic gas component from the original producing formation comprising the vent gas. While both samples collected from this plugged well's vent are early thermogenic, there was a notable change in the $\delta^{13}C_1$ of 6.96‰ between the 2014 (−50.46‰) and 2015 (−57.42‰) sampling events (Table 4.1). Review of the well logs for the plugged well indicated the well's vent was open to multiple shallow gas shows within the shallow system. We attribute the isotopic (and other) differences in gas composition in the plugged well's vent gas between 2014 and 2015 to variable mixing of the different early thermogenic gases within the shallow system and some oxidation.

4.4.3 Mature Thermogenic Gas

Several produced gas samples from operating wells in the area provided baseline molecular and isotopic compositions of local production gas. As part of the prior (2009) investigation, gas samples were collected for

TABLE 4.1 Summary of Gas Geochemistry for Samples From Case Study #1

Sample date	Sample name	CO_2 %	N_2/O_2	N_2/Ar	C1 %	C2 %	C1/CO_2	C1/C2	C1/C2 +	C1/(C2 + C3)	C2 + C3 + iC4 + nC4 %	$\delta^{13}C_1$ ‰	δDC_1 ‰	$\delta^{13}C_2$ ‰	Gas type
12-08-2014	Soil gas	0.33	3.739	81.76	14.47	0.040	43.8	366.3	352.9	362.7	0.040	−54.46	−223.3		ET
20-07-2015	Soil gas	0.58	3.861	82.83	29.00	0.090	50.0	322.6	309.2	316.2	0.093	−56.04	−222.2		ET
12-08-2014	Plugged well (vent)	1.30	4.109	81.95	24.16	0.044	18.6	544.1	520.7	540.5	0.045	−50.46	−220.8		ET
20-07-2015	Plugged well (vent)	2.71	27.04	78.74	75.44	0.269	27.8	280.4	269.3	273.0	0.279	−57.42	−219.8	−32.46	ET
11-05-2009	Water well (prior investigation)	2.06	7.149	77.70	83.17	0.264	40.4	315.0	235.4	252.7	0.350	−58.10	−229.1		ET
11-05-2009	Water well (prior investigation)	1.01	4.020	88.70	10.66	0.028	10.6	386.2	302.8	302.8	0.035	−59.05	−229.5		ET
16-07-2009	Mine degas borehole	1.06			58.29	1.02	55.0	57.1	41.0	45.3	1.382	−53.85	−209.0		ET
28-07-2009	Operating area gas well	0.094			85.35	5.63	908.0	15.2	9.7	11.5	8.307	−42.93	−180.5		MT
28-07-2009	Operating area gas well	0.064			85.97	4.78	1343	18.0	11.5	13.7	7.008	−42.68	−179.4		MT
3/2012−2/2013	U.Devonian/L. Mississipian[a]											−43.43	−191.65		MT

[a]*Published Data; average for seven area Upper Devonian/Lower Mississipian producing gas wells.*
ET: early thermogenic.
MT: mature thermogenic.

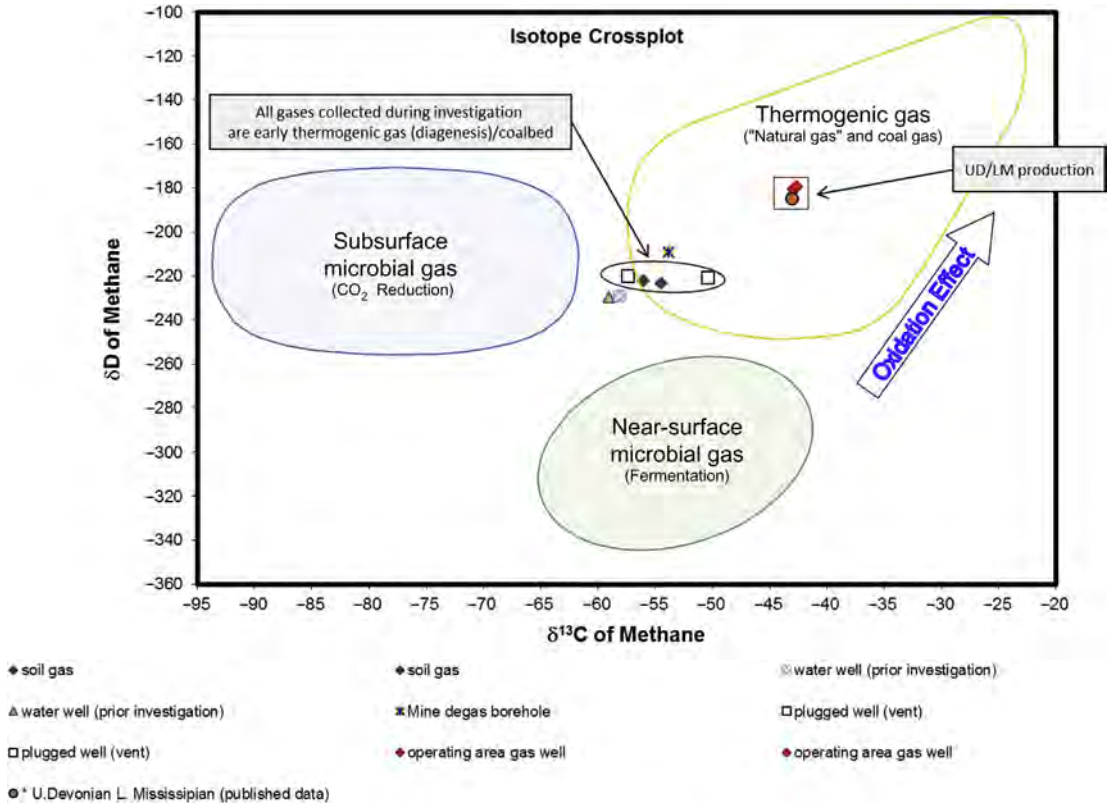

FIGURE 4.7 Isotope crossplot for methane in gas samples from case study #1. (Genetic fields indicated are modified from Schoell, 1983.) Data contained in Table 4.1.

both molecular and isotopic analyses from an Upper Devonian gas well located approximately 1500 ft south of the study area in this case study. Results from these production wells indicated mature thermogenic gas was present, as is typical of Upper Devonian production. These produced gases exhibited clearly different in molecular and isotopic compositions from the stray gas found in the study area's soils and in the vent for the nearby plugged gas well (Table 4.1; Figs. 4.7 and 4.8).

In addition, previously published isotopic data for seven production gas samples in the area (collected in 2012–2013) were obtained and averaged (Table 4.1). These data were reported in a previous study by the National Energy Technology Laboratory (NETL) that included data from nearby gas wells producing from deeper Upper Devonian and Lower Mississippian formations. These data also indicate that the deeper gases were more thermally mature and clearly different in origin than the stray gas found in the study area's soils and the vent at the plugged well. As such, it was concluded that migration of mature thermogenic gas from deeper Upper Devonian and/or Lower Mississippian formations could not be the source of subject stray gas investigation.

4.4.4 Mechanism of Migration

After evaluation of well records and diagnostic measurements at the wellhead, there was no physical evidence that inadequate plugging or failure of the plugs at the plugged well proximal to the stressed vegetation was the source of the methane detected in the soils. The geochemistry for the gas samples also corroborates the integrity of the well plugging. If the plugs were leaking, we would have expected to see mature thermogenic gas in the soils, such as was typical of the gases from wells producing within the Upper Devonian/Lower Mississippian formations in the area. The fact that the soil gas, as well as gas sampled from the plugged well's vent, were all comprised of early thermogenic gas indicated that the source of gas is not from the deeper Upper Devonian/Lower Mississippian formations.

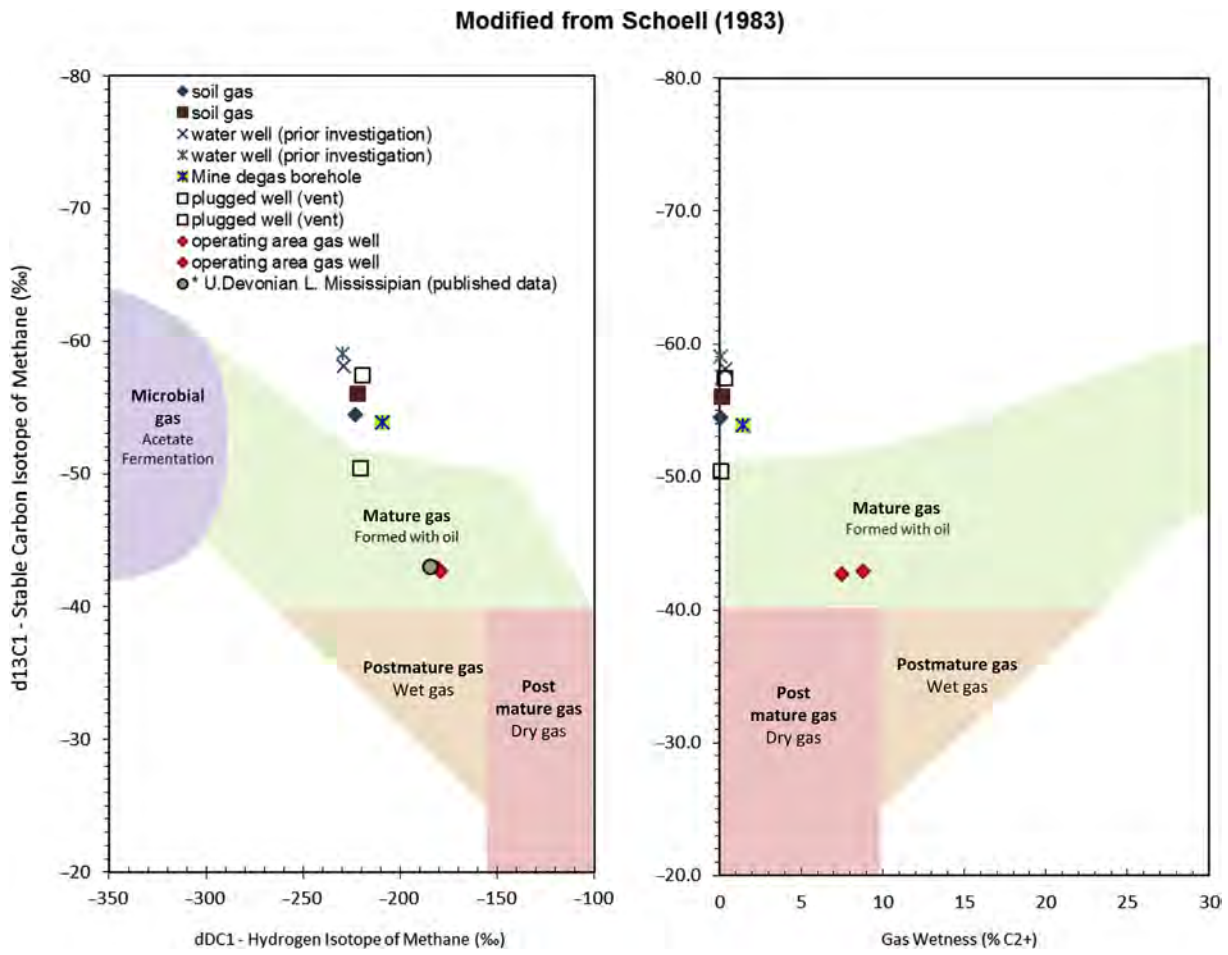

FIGURE 4.8 Isotopic and gas wetness plots for gas samples from case study #1. (Genetic field indicated are modified from Schoell, 1983.) Data contained in Table 4.1.

In addition, there is no physical evidence that the nearby plugged well could be the source of the stray gas. Recall, the proximal gas well was plugged and abandoned in 1966. At that time a "Certificate of Plugging Well through Workable Coal Seams" was submitted to the regulatory agency. Typical gas well abandonment procedures involve removal of casings and installation of cement plugs at specific intervals, and in this case, installation of a vent below the area's workable coal seam. Casing removal is typically achieved by determining the free point in the casing string by applying a pull on the casing string and measuring the stretch in the casing. That is the point at which a charge is set to loosen a pipe collar, and then the free casing is then recovered.

Dead pull to free and remove casing would not be conducted except on very shallow casing strings. The issues with that process are that tremendous pulling capacity would be required and there would be no control over where the casing parts. Casing parting at an unwanted depth would create both delays and costly recovery operations to retrieve the casing, in addition to jeopardizing the integrity of the abandonment.

Once the casing was removed, plugging and filling the subject well consisted of the placement of cement and wood plugs through specific intervals, based on the well drilling record and depths of gas shows. Wood plugs were driven down on top of fill to provide a stable bottom for cement placement.

Our review of the available well record indicated a coal bed existed at 407–412 ft, "little gas" was present at 922 ft, and "gas" was present at 1246, 1883, 2188, and 2720 ft. Water was encountered at 1320 ft. Well plugging included:

- A 20-feet cement plug set from 2784 to 2764 ft, above the deepest two gas-producing zones.
- A 20-feet cement plug set from 1977 to 1957 ft, which provides a seal above the gas encountered at 1983 ft.
- Cement plugs (20-feet) set from 1312 to 1292 ft and from 1240 to 1220 ft, which isolated the gas encountered at 1246 ft.
- A final cement seal from 504 to 484 ft, at which point 32 ft of gravel and a vapor point assembly was installed.

Plugging was completed with 100 ft of cement (452 to 352 ft), aquagel (352 to 15 ft), and concrete (15 ft to surface).

Thus, based upon the clear disparity in molecular and isotopic composition between the early thermogenic stray soil gas and the region's mature thermogenic gas (Table 4.1; Figs. 4.7 and 4.8) and the thoroughness and integrity evident in the plugging of the nearby gas well, we were able to exclude the plugged well as a source of the area's stray gas.

4.4.5 Underground Coal Mining

The coal seam that was deep mined directly below and in the adjacent areas of the stray gas remained a viable source. Our research of available records indicated that room and pillar mining had progressed from south to north in 2005, stopping approximately 500 ft south of the subject/nearby plugged gas well (described above). Room and pillar mining then resumed in 2007 and progressed northward; the immediate vicinity of the subject plugged well was mined between March and June 2007. The mine's plans showed that coal was eventually removed to within 50 ft of the plugged well, most likely during retreat from the mine to maintain roof integrity.

The timing for the onset of the stray gas in the area's shallow soils as explained by the property owners, and as documented in a set of time series aerial photographs, was determined to be consistent with the timing of the progression of underground coal mining in the area of the deep mine. Historical photographs spanning 2006 through 2013 were compiled for the area of investigation. The stressed/dead grass area was clearly visible in the photos from 2008, 2010, and 2013. However, the earlier photo from 2006 did not show indications of impacted vegetation.

Additionally, the manifestation of the stray gas (dead vegetation) was in a linear, north–south trend, which occurred to the west of the plugged well. If early thermogenic gas leaked from shallower Permian and Upper Pennsylvanian strata within the plugged well were the source of the stray gas, we would have expected to see evidence of migration and impact in a more radial pattern around the plugged well. However, the linear pattern observed (west of the plugged well) was considered to be more consistent both spatially and temporally with leakage of gas associated with the progression of underground, room, and pillar mining.

Underground coal mining, as such that occurred in the time prior to the manifestation of stray gas in this case study, is characteristically accompanied by rock fracturing, dilation of joints, and separation along bedding planes. Rock movements typically occur vertically above the mine workings and at an angle projected away from the mined-out area. Mining-induced fracturing within this angle can result in hydrologic impacts, including dewatering of the overlying strata beyond the margins of the mine workings.

Underground mine openings can intercept and convey surface water and groundwater. When excavated below the water table, mine voids serve as low-pressure sinks inducing groundwater to move to the openings from the surrounding saturated rock. The result is the dewatering of nearby rock units via drainage of fractures and water-bearing strata in contact with the mine workings.

These changes to the rock mass can change the water transmitting capabilities of the rock by creating new fractures and enlarging existing fractures. This may result in the mobilization and migration of preexisting methane gas to migrate vertically.

4.5 CASE STUDY #1—CONCLUSION

The gas geochemistry and lack of mechanism of migration indicate the plugged abandoned gas well proximal to the area of stressed vegetation was not the source of the stray gas found during this investigation. Conversely, the gas geochemistry indicates the stray gas in the shallow subsurface in this investigation clearly comprised early thermogenic gas associated with the shallow overburden, specifically, coalbeds and carbonaceous rocks in the Permian and Upper Pennsylvanian systems, generally within the upper 1000 ft in this area of the basin—and not thermally mature gas from deeper (Upper Devonian and Lower Mississippian) natural gas-producing formations. The timing of the expansion of the underground coal mine preceded the occurrence of stressed vegetation and shallow subsurface gas in the study area. Specifically, underground mining provides a mechanism of migration for naturally occurring coal-associated methane to mobilize and migrate to areas of lower pressure, such as the shallow soils impacted in this investigation.

4.6 CASE STUDY #2—INTRODUCTION

In 2011, a homeowner notified the state regulatory agency of a change in the water quality of their water well. The report included the recent onset of effervescing water. Sample results confirmed a methane concentration of 42 mg/L, a concentration which exceeds methane's solubility at 1 atm. Gas well drilling and operations were ongoing within a radius of 2000 ft at the time of the homeowner's report. Prior to the drilling and operations, the concentration of methane in the homeowner's water had been nondetect at a 0.0001 mg/L detection limit.

Subsequent sampling took place over a period of almost five years and included gas and water samples from three water wells in the area (Water Wells 1, 2, and 3) as well as gas samples collected from the production and casing annuli of six horizontal gas wells in the area (Gas Wells 1–6). The objective of the investigation was to determine if one or more of the recently drilled gas wells was the source of methane in the homeowner's effervescing water.

Gas samples were analyzed for molecular composition and stable carbon and hydrogen isotopes. In addition, the water samples were analyzed for major and trace cations and anions. The results of this sampling are summarized in Tables 4.2 and 4.3.

4.7 CASE STUDY #2—RESULTS AND DISCUSSION

4.7.1 Gas Geochemistry

The molecular and isotopic compositions for all samples collected and analyzed from Water Wells 1 to 3 revealed no evidence that the isotope compositions had been affected by bacterial oxidation or other secondary effects. Analytical results for DIC also corroborated the absence of oxidation or other secondary impact. The results also revealed the gas in Water Wells 1 and 2 was early thermogenic in origin, consistent with what occurs in the shallow stratigraphy for this area of the basin. The early thermogenic gas type was consistent for all sampling events for both Water Wells 1 and 2. The gas collected from a single sample from Water Well 3 was thermally less mature.

All gas samples collected and analyzed from the production and casing annuli of six nearby gas wells revealed the gas was also thermogenic; however, these gases were all more thermally mature than what occurs in Water Wells 1 to 3 (Figs. 4.9 and 4.10). The gas from production and intermediate casing intervals is postmature thermogenic gas characterized by partial isotope reversals ($\delta^{13}C_1 > \delta^{13}C_2$; Table 4.2). Both dissolved phase and gas phase results from Water Wells 1, 2, and 3 reveal a markedly different hydrocarbon ratio [C1/(C2 + C3)] and stable carbon and hydrogen isotope composition than the gas from all of the gas well samples (Figs. 4.9 and 4.10).

Postmature gas was found in the surface casings of Gas Wells 1 and 3. However, postmature gas is not typical for shallow formations exposed to this casing annulus. Thus, the occurrence of postmature gas in the surface casing may be an indication of gas migration from deeper formations into the shallow section of the gas wells. A mechanism for gas migration from one of the area's gas well is possible if, for example, pressure at the surface casing exceeds the allowable gradient and results in migration away from the wellbore. However, all geochemical data provided for this investigation reveal the gas in the head space and dissolved in the groundwater of Water Wells 1–3 was not sourced from the tubing or casings of nearby gas wells (Figs. 4.9 and 4.10).

Despite the evident geochemical differences in gas composition, and because of the possible surface casing migration mechanism, a comprehensive evaluation of well integrity was performed. This included review of casing, cement, and wellhead design; wellhead seal testing; multiple annular build-up tests; ongoing extended build up testing; balloon vent rate testing; and fluid caliper communication tests. Well integrity evaluation revealed good cement returns fully isolating production gas. Testing further demonstrated cement isolation at the intermediate casing shoe. However, some of the testing indicated the possibility for very small pressure build up in the surface casing. Though this level of testing is considered comprehensive by the regulatory agency, there was some equivocation in the results and ongoing pressure build-up testing is recommended.

4.7.2 Water Geochemistry

Evaluation of the water quality data for Water Well 1 indicated the water type present was bicarbonate alkali, sodium bicarbonate type. This water type was consistent throughout all five sampling events (Fig. 4.11A).

TABLE 4.2 Summary of Gas Geochemistry for Samples From Case Study #2

Sample date	Sample name	He %	CO_2 %	N_2/O_2	N_2/Ar	C_1 %	C_2 %	C1/He	C1/CO_2	C1/C2	C1/C2+	C1/(C2 + C3)	C2 + C3 + iC4 + nC4 %	$\delta^{13}C_1$ ‰	δDC_1 ‰	$\delta^{13}C_2$ ‰	Gas type
16-07-2010	Gas Well 1 tubing	0.0205	0.012			97.35	2.07	4749	8113	47.0	45.7	45.8	2.1279	−36.58	−164.7	−42.31	PM
16-07-2010	Gas Well 2 tubing	0.017	0.011	10.2		96.98	2.36	5705	8816	41.1	40.0	40.1	2.4224	−36.90	−163.8	−42.82	PM
04-11-2010	Gas Well 2 prod casing (csng)	0.0171		38.6		97.08	2.43	5677		40.0	38.9	39.0	2.4934	−37.02	−163.3	−42.94	PM
11-12-2009	Gas Well 3	0.0195	0.014			97.43	2.2	4996	6959	44.3	43.0	43.0	2.2682	−36.66	−163.3		PM
16-07-2010	Gas Well 3 surf csng	0.0208		15.8		97.86	1.59	4705		61.5	59.2	59.4	1.6540	−35.94	−165.1	−41.76	PM
16-07-2010	Gas Well 3 tubing	0.0189	0.012			97.35	2.23	5151	8113	43.7	42.5	42.5	2.2919	−36.71	−162.7	−42.47	PM
10-03-2011	Gas Well 3 surf csng	0.0214	0.005	4.7	94.1	97.32	1.53	4548	19464	63.6	61.2	61.4	1.5896	−35.88	−168.9	−41.66	PM
11-12-2009	Gas Well 4	0.0212	0.014			97.68	1.93	4608	6977	50.6	49.3	49.4	1.9812	−36.46	−162.0		PM*
10-03-2011	Gas Well 4 surf csng	0.0199	0.006	3.8	90.1	86.81	1.41	4362	14468	61.6	59.1	59.4	1.4684	−35.88	−171.3	−41.67	PM
16-07-2010	Gas Well 4 tubing	0.0194	0.016	40.0		97.33	2.24	5017	6083	43.5	42.3	42.3	2.3036	−36.74	−162.1	−42.47	PM
16-07-2010	Gas Well 5 tubing	0.0167	0.010	7.4		96.83	2.36	5798	9683	41.0	40.1	40.1	2.4151	−37.17	−163.7	−42.92	PM
04-11-2010	Gas Well 5 prod csng	0.0158	0.010			97.14	2.43	6148	9714	40.0	39.1	39.1	2.4851	−37.29	−163.1	−43.00	PM
04-11-2010	Gas Well 5 surf csng	0.0208		17.4		97.32	2.07	4679		47.0	45.1	45.2	2.1594	−36.11	−164.2	−42.46	PM
16-07-2010	Gas Well 6 tubing	0.0165	0.015	6.7		96.65	2.52	5858	6443	38.4	37.4	37.4	2.5847	−36.92	−162.1	−42.89	PM
04-11-2010	Gas Well 6 prod csng	0.0188	0.066	48.3		97.17	2.23	5169	1472	43.6	42.4	42.5	2.2917	−37.04	−165.6	−42.56	PM
04-11-2010	Gas Well 6 tubing	0.0155	0.018			97.01	2.59	6259	5389	37.5	36.5	36.6	2.6549	−37.03	−168.5	−42.99	PM
10-03-2011	Water Well 1	0.0089	0.094	40.6	46.8	95.63	0.0182	10745	1017	5254	5254	5254	0.0182	−40.20	−203.6		ET
25-10-2011	Water Well 1	0.0069	0.130	1.6	38.9	86.07	0.0178	12474	662	4835	4782	4835	0.0179	−39.54	−200.6		ET
11-11-2011	Water Well 1	0.0081	0.170	3.1	52.6	85.70	0.0174	10580	504	4925	4925	4925	0.0174	−39.69	−200.9		ET
25-04-2012	Water Well 1	0.0157	0.190	2.6	49.6	86.52	0.0179	5511	455	4834	4834	4834	0.0179	−39.68	−201.6		ET
13-05-2013	Water Well 1	0.0081	0.150	1.4	38.6	72.01	0.0162	8890	480	4445	4391	4445	0.0162	−38.85	−204.3		ET
25-06-2010	Water Well 2	0.0015	0.049	3.7	82.4	5.21	0.0010	3473	106	5210	3065	5210	0.0010	−40.34	−205.1		ET
25-06-2010	Water Well 2		0.270	3.2	47.6	83.79	0.0243		310	3448	3365	3448	0.0243	−38.59	−206.5		ET
10-03-2011	Water Well 2	0.0136	0.190	6.4	64.8	91.73	0.0226	6745	483	4059	4059	4059	0.0226	−39.35	−202.6		ET
10-03-2011	Water Well 2		0.056	3.7	84.0	1.35			24					−40.78	−201.2		ET
25-04-2012	Water Well 2	0.0202	0.310	1.8	45.7	88.25	0.0279	4369	285	3163	3163	3163	0.0279	−38.28	−205.2	−31.1	ET
12-06-2014	Water Well 2	0.0100	0.270	1.8	41.0	93.93	0.0339	9393	348	2771	2771	2771	0.0339	−37.80	−206.4	−30.1	ET
11-11-2011	Water Well 3		0.780	4.6	47.2	70.25	0.0078		90	9006	7983	9006	0.0082	−47.41	−200.4		ET*

Gas Types: ET: early thermogenic; ET*: early thermogenic, thermally less mature; PM: Postmature; PM*: Likely PM gas, however, lack of C2 isotope data constrains interpretation.

TABLE 4.3 Cation–Anion Balance for Water Samples From Case Study #2

Name	Calcium mg/l	Magnesium mg/l	Sodium mg/l	Potassium mg/l	Alkalinity mg/l	Chloride mg/l	Sulfate mg/l	Nitrate mg/l	Barium mg/l	Iron mg/l	Manganese mg/l	Strontium mg/l	TDS mg/l	pH S.U.	Methane mg/l	Deviation %
Water Well 1 6/12/08[a]						21				0.117			332	8.42		
Water Well 1 4/27/09[a]						18				0.0956			363	8.49	< 0.00001	
Water Well 1 3/10/11	12.5	1.98	122	1.93	221	45	2.5		0.94	0.0542	0.008		346	8.30	53.4	3.52
Water Well 1 10/25/11	12.8	2.15	118	1.75	231	56	2.5	0.25	0.84	0.0715	0.007	1.75	348	7.90	55.3	-1.68
Water Well 1 11/11/11	12.7	2.23	118	1.87	220	44	2.5		0.92	0.0707	0.008	1.76	340	8.30	51.8	3.08
Water Well 1 4/25/12	12.3	2.03	126	1.89	228	56.8	0.5	0.05	0.84	0.025	0.006	1.7	304	8.40	58.8	1.52
Water Well 1 5/13/13	12.7	2.16	118	1.8	259	53.1	0.5	0.05	0.76	0.0415	0.007	1.76	346	8.20	46.6	-5.06
Water Well 2 6/12/08[a]						10							295	8.00		
Water Well 2 4/27/09[a]						43				0.243			343	7.92	< 0.00001	
Water Well 2 6/25/10	29.8	7.30	65.4	2.02	277	23.1	1.29		1.76	0.275	0.0260		305	7.80	12.3	-10.64[b]
Water Well 2 2/15/11	24.5	5.16	90.4	2.08	233	29.3	2.5		1.45	0.237	0.0194		289	8.00	45.5	1.12
Water Well 2 3/10/11	27.5	6.24	82.2	2.22	237	25.4	2.5		1.7	**0.325**	0.0238		288	8.20	41.5	0.44
Water Well 2 3/29/12	30.5	7.21	80.4	2.39	240	18.8			1.78	**0.356**	0.0263	3.26		8.10	77.2	4.13
Water Well 2 4/25/12	28.6	6.34	76	2.13	216	34.2	0.5	0.05	1.59	0.103	0.017	2.89	289	8.00	63.0	1.01
Water Well 2 6/27/12	23.8	5.36	84.5	2.05	230	24.5			1.43	0.188	0.0191	2.64		8.30	69.6	1.45
Water Well 2 9/20/12	17.8	3.94	73.1	1.74	222	26.6			1.19	0.296	0.0152	2.08	284	8.50	84.3	-6.97
Water Well 2 12/26/12	24.6	6.10	72.0	2.02	234	20.6			1.51	0.230	0.0187	2.72	294	8.40	19.4	-2.47
Water Well 2 3/20/13	22.4	5.24	80.0	2.28	227	21.6			1.42	0.218	0.0168	2.49	271	7.80	60.8	0.24
Water Well 2 6/20/13	24.8	5.69	83.3	2.21	234	21.6			1.53	0.222	0.0197	2.74	295	7.50	64.6	1.78
Water Well 2 9/26/13	23.5	5.13	78.5	2.01	211	23.7			1.41	0.261	0.0173	2.64	287	8.43	38.4	2.63
Water Well 2 12/23/13	22.6	5.20	75.4	1.97	221	23.9			1.37	**0.373**	0.0177	2.56	302	8.43	36.3	-1.14
Water Well 2 3/25/14	23	5.51	81.5	2.17	254	29.5			1.44	**0.406**	0.017	2.61	291	**8.57**	61.2	-5.47
Water Well 2 6/12/14	24.3	5.8	74.9	2.14	228	24		0.05	1.47	**0.338**	0.018	2.67	302	**8.53**	1.6	-1.34
Water Well 2 9/17/14	23.9	5.9	77.4	2.12	233	23.8			1.53	**0.356**	0.020	2.79	288	8.43	14.3	-1.25
Water Well 2 12/31/14	31.2	8.08	73	2.29	243	18.9			1.79	**0.354**	0.022	3.24	291	7.76	10.4	1.62
Water Well 2 12/31/14	31.4	7.39	77.6	2.41	233	18.9	0.5		1.85	**0.645**	0.026	3.62	296	8.22	7.92	4.96
Water Well 2 3/30/15	26.7	6.47	77.7	2.21	242	22.1		0.25	1.58	0.1	0.021	2.89	276	8.20	69	-0.66
Water Well 2 6/4/15	25.3	6.12	75.7	2.18	235	23.7	0.5		1.51	0.27	0.020	2.77	293	8.20	78	-1.58

(*Continued*)

TABLE 4.3 (*Continued*)

Name	Calcium mg/l	Magnesium mg/l	Sodium mg/l	Potassium mg/l	Alkalinity mg/l	Chloride mg/l	Sulfate mg/l	Nitrate mg/l	Barium mg/l	Iron mg/l	Manganese mg/l	Strontium mg/l	TDS mg/l	pH S.U.	Methane mg/l	Deviation %
Water Well 2 6/4/15	26.7	6.43	75.1	2.12	233	24.8			1.61	0.256	0.023	2.89	288	8.30	76	-0.72
Water Well 2 9/14/15	23.8	5.55	84.4	2.12	233	28.8			1.43	0.276	0.019	2.55	316	8.20	62	-0.11
Water Well 2 9/14/15	22.2	5.08	78.4	1.96	228	26.2	0.5		1.39	0.271	0.018	2.5	307	8.10	63	-2.26
Water Well 2 3/29/16	29.2	6.77	79.2	2.21	236	20.9			1.65	**0.331**	0.023	2.98	265	8.20	60	2.86
Water Well 2 9/8/16	25.2	5.98	77.4	2.21	234	21.4			1.52	0.1	0.019	2.76	306	8.10	61	-0.19
Water Well 3 5/12/11	59.8	10.5	162	1.63	198	248	10.1		**3.30**	**1.95**	**0.419**		**626**	7.30	7.63	-0.43
Water Well 3 11/11/11	65.8	12.2	165	1.68	186	**269**	2.5		**3.61**	**1.92**	**0.450**	5.39	**684**	7.70	24.2	1.77

[a]*Insufficient data to determine cation-anion balance*
[b]*Error exceeds generally accepted threshold of ± 10%*
Dissolved metals results used instead of total where available.
Value used is 1/2 of detection limit.
Exceeds primary or secondary maximum contaminant level (MCL), or falls outside of reasonable pH goal range.

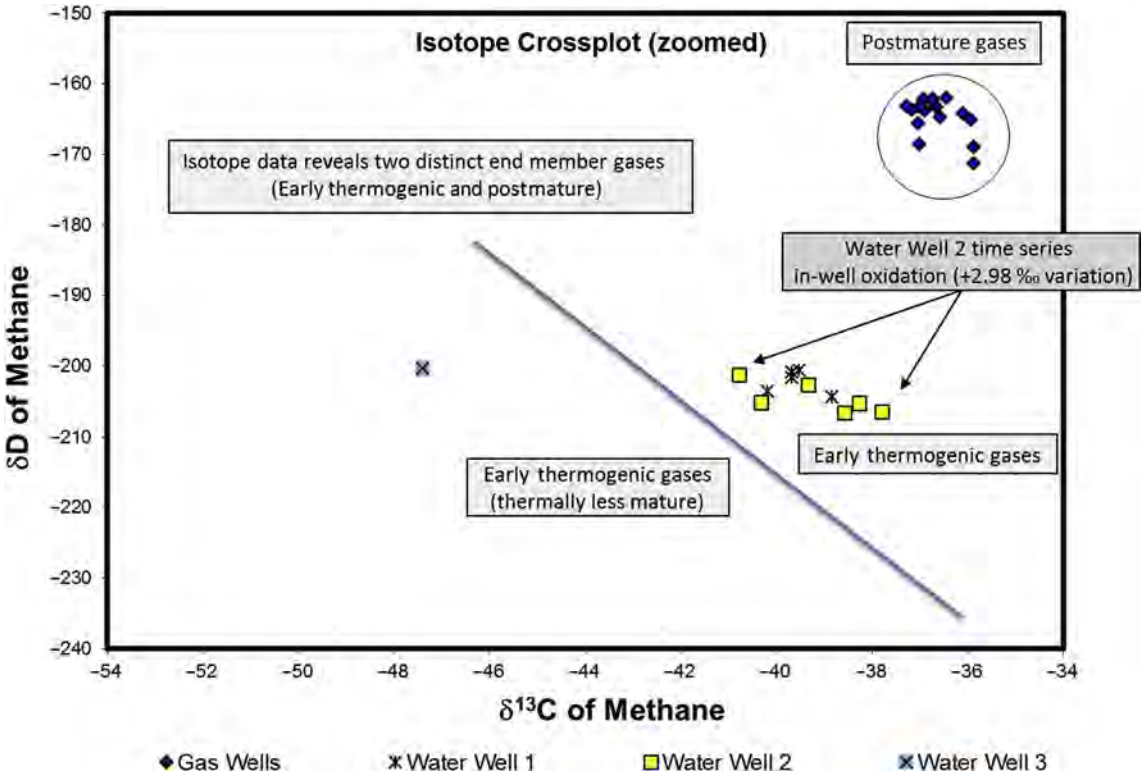

FIGURE 4.9 Isotope crossplot for methane in gas samples from case study #2. Data contained in Table 4.2.

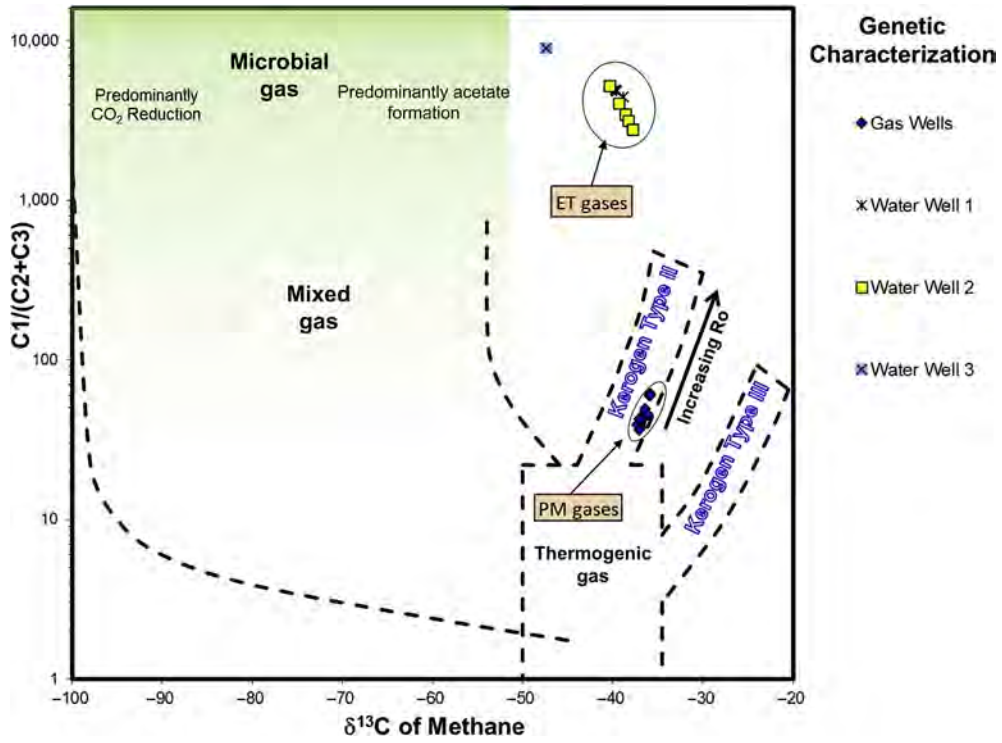

FIGURE 4.10 Methane carbon isotope versus gas wetness plot for gas samples from case study #2. Data contained in Table 4.2.

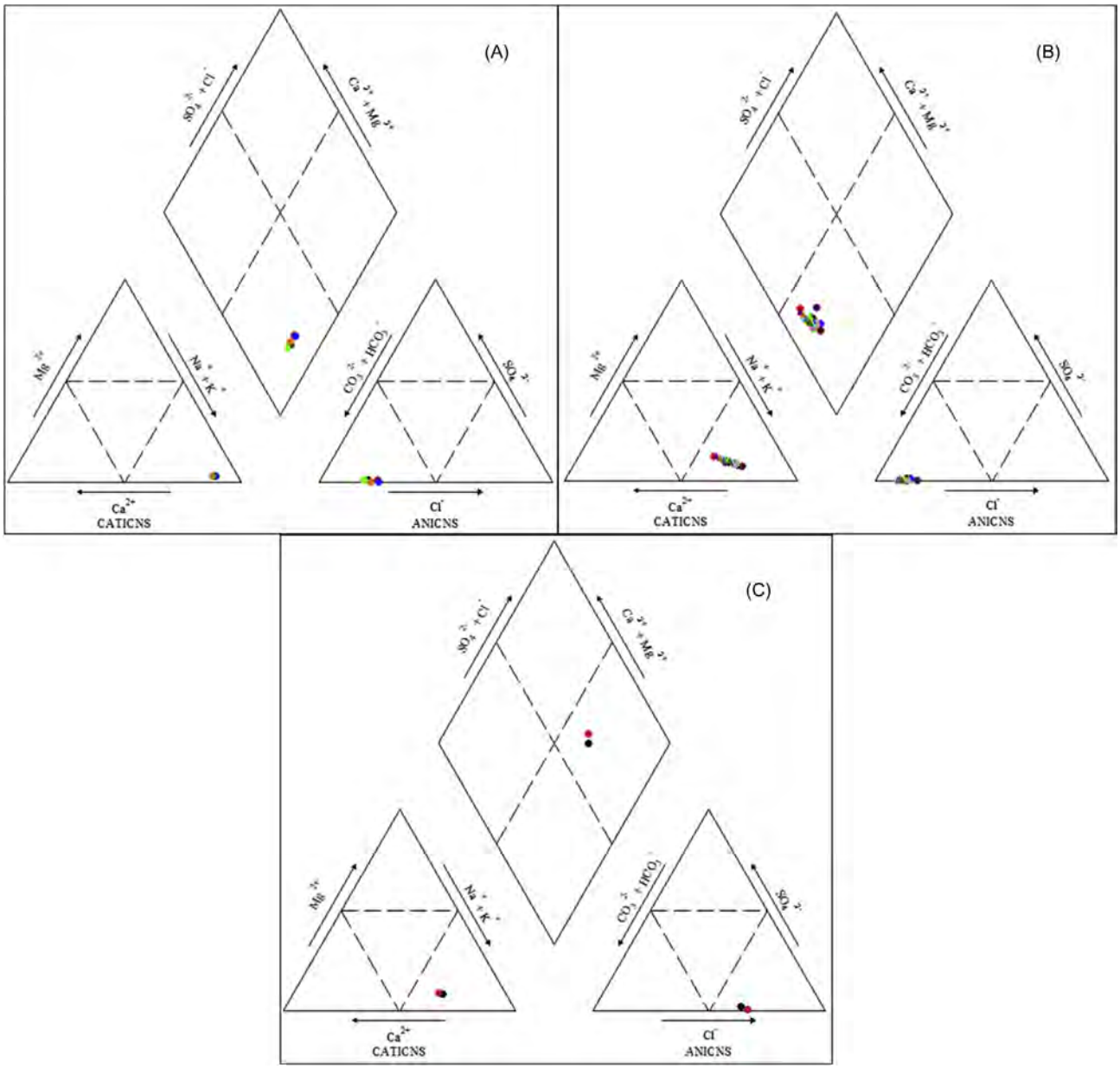

FIGURE 4.11 Trilinear plots for Water Wells 1 (A), 2 (B), and 3 (C) from case study #2.

Although there are no drinking water standards for sodium, the concentration of sodium was elevated (118–126 mg/L) for all sampling events. Evaluation of the redox process in Water Well 1 (for samples with sufficient parameters) reveals a suboxic category for all sampling events. Therefore, the occurrence of methane in the water supply well had not affected water quality nor altered the redox state.

Evaluation of the water quality data for Water Well 2 indicated the water type was bicarbonate alkali, sodium bicarbonate type (Fig. 4.11B). This water type was the same as found in Water Well 1, except for samples collected on May 1, 2010 and on April 29, 2012 (no dominant cation–anion pair), and was consistent for all sampling events. As was the case with Water Well 1, sodium was elevated in Water Well 2 (65.4–90.4 mg/L) for all sampling events. Only one Water Well 2 sample contained sufficient parameters for evaluation of redox process. This evaluation reveals a mixed anoxic–oxic category (Table 4.3).

Unlike Water Wells 1 and 2, the water from Water Well 3 was noncarbonate alkali, sodium chloride water type (Fig. 4.11C). It had higher total dissolved solids, including calcium, sodium, and chloride, and also had

barium concentrations, which exceeded its primary maximum contaminant level of 2 mg/L (EPA, 2009). In the area of investigation, this water chemistry was consistent with a shallow, restricted flow aquifer.

4.8 DISCUSSION

At the onset of this investigation, the state regulatory agency was involved in an investigation of at least one additional alleged stray gas incident in the area of investigation. The origin, influence, and status of this incident are unknown to us. Details of this incident, and any other ongoing or recent stray gas incidents in the area, should be evaluated to determine if those source(s) could be impacting Water Wells 1−3.

Records on file with the state geological survey revealed that formations in the shallow subsurface that also serve as the aquifer in this area contain methane as a natural condition. Isotope geochemistry for gas wells drilled in the area also revealed the occurrence of both microbial and early thermogenic gases throughout the shallow formations.

Our results showed that the water quality for Water Wells 1 and 2 had not been affected by the introduction of methane. Typically, when methane is introduced to a system, the change in redox toward more reducing conditions causes predictable changes in major and trace element concentrations. These changes include decreased sulfate, nitrate, and dissolved oxygen; and increased iron, manganese, pH, alkalinity, and barium (Baldi et al., 1996, Carbonell, et al., 1999).These changes were not observed in either water well over the time series (Table 4.3).

Historical information from the study area reveals that low volatile bituminous rank coal exists just southeast of the area of investigation. Records indicate coal mining in this area occurred from 1856−1867 with production totaling over 420,000 tons mined. Coalbed elevations and mining details are not available; however, historical maps indicate two coal beds separated by approximately 50 feet of rock. The area coal mines were abandoned in 1880. It is unknown if any coalbeds occur below the surface of the properties on which Water Wells 1 to 3 are located; however, the presence of coal in the area is significant because the availability of carbonaceous precursor materials and the paleo-environment are favorable to form coal and methane. Even thin, unminable coalbeds or associated shale can yield the concentrations of methane observed in the water supply wells. Furthermore, as noted above, early thermogenic gas and microbial gas can be generated in coal beds.

4.9 CASE STUDY #2—CONCLUSION

The type of early thermogenic gas apparent in Water Wells 1 to 3 was consistent throughout all sampling events. The geochemical evidence reveals the origin and source of the stray gas is not from the tubing or casings of nearby gas wells, which were consistently comprised of postmature gas. The gas in Water Wells 1 to 3 was of a different thermogenic origin than any of the gas wells sampled. Additionally, water quality for Wells 1 and 2 was not affected by the presence of the gas.

The manifestation (effervescing water) at the onset of the gas in Water Wells 1 and 2 occurred suddenly. This sudden onset appears to be related to an undefined shallow sourced disturbance of the aquifer system − and not to recent gas well drilling or operations in the area. The nearest operating gas well was comprehensively evaluated for well integrity. Those results confirmed well integrity; however, results revealed the possibility for pressure build-up at the surface casing and ongoing pressure build-up testing was recommended. Area gas wells should also be evaluated individually to determine if a pressure gradient at the surface casing has created a condition to mobilize preexisting gas in the aquifer to areas of lower pressure, such as nearby water wells.

4.10 CONCLUSION

Stray gas investigations require investigation at the site-specific level in order to identify gas origin and a specific stray gas source(s). Gas and groundwater geochemistry data provide evidence of gas origin and focus to identify potential sources. Ongoing monitoring and additional sampling for laboratory analyses are necessary to identify and secondary effects, define dosing, and to further delineate the plume. Potential sources require establishing and then determining a mechanism of migration. Potential stray gas sources should be evaluated

individually and not simultaneously. For anthropogenic stray gas incidents, monitoring subsequent to any remediation is required to ensure an effective remedy.

References

Baldassare, F.J., Laughrey, C.D., 1997. Identifying the sources of stray methane by using geochemical and isotopic fingerprinting. Environ. Geosci. 4 (2), 85–94.

Baldassare, F.J., McCaffrey, M.A., Harper, J.A., 2014. A geochemical context for stray gas investigations in the northern Appalachian Basin: implications of analyses of natural gases from Neogene-through Devonian-age strata. AAPG Bull. 98 (2), 341–372.

Baldi, F., Pepi, M., Burrini, D., Kniewald, G., Scali, D., Lanciotti, E., 1996. Dissolution of barium from barite in sewage sludges and cultures of desulfovibrio desulfuricans. Appl. Environ. Microbiol. 62 (7), 2398–2404.

Burruss, R.C., Laughrey, C.D., 2010. Carbon and hydrogen isotopic reversals in deep basin gas: evidence for limits to the stability of hydrocarbons. Org. Geochem. 41 (12), 1285–1296.

Carbonell, A.A., Pulido, R., DeLaune, R.D., Patrick, W.H., 1999. Soluble barium in barite and phosphogypsum amended Mississippi River alluvial sediment. J. Environ. Qual. 28 (1), 316–321.

Coleman, D.D., Meents, W.F., Liu, C.-L., Keogh, R.A., 1977. Isotopic identification of leakage gas from underground storage reservoirs-a progress report.". SPE Midwest Gas Storage and Production Symposium. Society of Petroleum Engineers.

Coleman, D.D., Risatti, J.B., Schoell, M., 1981. Fractionation of carbon and hydrogen isotopes by methane-oxidizing bacteria. Geochim. Cosmochim. Acta 45 (7), 1033–1037.

Coleman, D.D., Liu, C.L., Hackley, K.C., Pelphrey, S.R., 1995. Isotopic identification of landfill methane. Environ. Geosci. 2 (2), 95–103.

Craig, H., 1953. The geochemistry of the stable carbon isotopes. Geochim. Cosmochim. Acta 3 (2–3), 53–92.

Curiale, J.A., Curtis, J.B., 2016. Organic geochemical applications to the exploration for source-rock reservoirs–a review. J. Unconv. Oil Gas Resour. 13, 1–31.

Deines, P., 1980. The carbon isotopic composition of diamonds: relationship to diamond shape, color, occurrence and vapor composition. Geochim. Cosmochim. Acta 44 (7), 943–961.

Dusseault, M., Jackson, R., 2014. Seepage pathway assessment for natural gas to shallow groundwater during well stimulation, in production, and after abandonment. Environ. Geosci. 21 (3), 107–126.

Environmental Protection Agency (EPA), 2009. National Primary Drinking Water Regulations. <https://www.epa.gov/sites/production/files/2016-06/documents/npwdr_complete_table.pdf> (accessed 22.03.17.).

Gat, J.R., Gonfiantini, R., 1981. Stable isotope hydrology. Deuterium and oxygen-18 in the water cycle.

Hackley, K.C., Liu, C.L., Trainor, D., 1999. Isotopic identification of the source of methane in subsurface sediments of an area surrounded by waste disposal facilities. Appl. Geochem. 14 (1), 119–131.

Harrison, S.S., 1983. Evaluating system for ground-water contamination hazards due to gas-well drilling on the glaciated appalachian plateau. Ground Water 21 (6), 689–700.

Kaplan, I.R., Galperin, Y., Lu, S.T., Lee, R.P., 1997. Forensic environmental geochemistry: differentiation of fuel-types, their sources and release time. Org. Geochem. 27 (5), 289–317.

Osborn, S.G., McIntosh, J.C., 2010. Chemical and isotopic tracers of the contribution of microbial gas in Devonian organic-rich shales and reservoir sandstones, northern Appalachian Basin. Appl. Geochem. 25 (3), 456–471.

Révész, K.M., Breen, K.J., Baldassare, A.J., Burruss, R.C., 2010. Carbon and hydrogen isotopic evidence for the origin of combustible gases in water-supply wells in north-central Pennsylvania. Appl. Geochem. 25 (12), 1845–1859.

Rice, D.D., Claypool, G.E., 1981. Generation, accumulation, and resource potential of biogenic gas. Am. Assoc. Pet. Geol. Bull. 65 (1), 5–25.

Rowe, D., Muehlenbachs, K., 1999. Isotopic fingerprints of shallow gases in the Western Canadian sedimentary basin: tools for remediation of leaking heavy oil wells. Org. Geochem. 30 (8), 861–871.

Schoell, M., 1980. The hydrogen and carbon isotopic composition of methane from natural gases of various origins. Geochim. Cosmochim. Acta 44 (5), 649–661.

Schoell, M., 1983. Genetic characterization of natural gases. Am. Assoc. Pet. Geol. Bull. 67 (12), 2225–2238.

Sherwood, O.A., Rogers, J.D., Lackey, G., Burke, T.L., Osborn, S.G., Ryan, J.N., 2016. Groundwater methane in relation to oil and gas development and shallow coal seams in the Denver-Julesburg Basin of Colorado. Proc. Natl. Acad. Sci. U.S.A. 113 (30), 8391–8396.

Whiticar, M.J., Faber, E., 1985. Methane oxidation in sediment and water column environments-isotope evidence. Adv. Org. Geochem. 10, 759–768.

Whiticar, M.J., Faber, E., Schoell, M., 1986. Biogenic methane formation in marine and freshwater environments: CO_2 reduction vs. acetate fermentation—isotope evidence. Geochim. Cosmochim. Acta 50 (5), 693–709.

Wiese, K., Kvenvolden, K.A., 1993. Introduction to Microbial and Thermal Methane. US Geological Survey Professional Paper 1570, pp. 13–20.

Zhang, L., Soeder, D.J., 2016. Modeling of methane migration in shallow aquifers from shale gas well drilling. Ground Water 54 (3), 345–353.

Further Reading

Heverly, C.F., 1924. History and Geography of Bradford County, Pennsylvania, 1615–1924, 594p. Reproduction of Unigraphic Inc., Evansville, Indiana, 1976 with subject index by C.W. Northrup, 1936 and name index by E.R. Gleck 1976.

CHAPTER

5

Forensic Aspects of Airborne Constituents Following Releases of Crude Oil Into the Environment

Shawn M. Wnek, Christopher L. Kuhlman, Joshua A. Harrill, Paul A. Nony, Glenn C. Millner and John A. Kind

Center for Toxicology and Environmental Health, North Little Rock, AR, United States

BIOGRAPHIES

John A. Kind, PhD is a toxicologist and industrial hygienist with 17 years of experience addressing worker and public health issues. Since receiving his PhD in toxicology from The University of Georgia in 2000, Dr. Kind has been employed as a toxicology and industrial hygiene consultant, and has been employed at The Center for Toxicology and Environmental Health (CTEH) since 2007. As a Principal Toxicologist at CTEH, Dr. Kind leads air-monitoring and environmental sampling teams and has supported multiple petroleum responses ranging from crude oil train derailments to gasoline and crude oil pipeline releases to large-scale marine oil spills. During the Deepwater Horizon incident, Dr. Kind served in unified command in both the safety and environmental sections. Dr. Kind has presented on oil spill worker safety and health at multiple national scientific meetings. He is a member of the Society of Toxicology, the American Conference of Governmental Industrial Hygienists, and the American Industrial Hygiene Association (AIHA).

Glenn C. Millner, PhD is a founding partner and Principal Toxicologist at CTEH, L.L.C., an environmental consulting firm that is part of the University of Arkansas for Medical Sciences Incubator Program. He is an assistant professor in the Department of Environmental and Occupational Health, College of Public Health, University of Arkansas for Medical Sciences (UAMS) and College of Medicine, Division of Interdisciplinary Toxicology, UAMS. Dr. Millner has more than 30 years' experience responding to hazardous materials releases and more than 21 years' experience as a primary responder to the transportation industry, oil and gas industry, and the chemical industry. Some of the more noteworthy recent emergency response projects he and CTEH were responsible for include the BP Gulf Oil Spill, President Barrack Obama's Inauguration, 2010 Winter Olympics in Vancouver for Health Canada, 2010 NBA All-Star Game, and 2010 and 2015 live releases of Toxic Inhalation Hazard chemicals (TIHs) at Dugway Proving Grounds.

Joshua A. Harrill, PhD is a toxicologist with over 9 years of professional experience in a variety of sectors including academia, government and industry. Dr. Harrill received his PhD in toxicology from the University of North Carolina at Chapel Hill and completed a postdoctoral traineeship at the US Environmental Protection Agency (US EPA) National Health and Environmental Effects Research Laboratory (NHEERL), Integrated Systems Toxicology Division. Dr. Harrill has also served as principal investigator at a nonprofit research organization, the Hamner Institutes for Health Sciences—Institute for Chemical Safety Sciences, a toxicology consultant at CTEH, LLC and a toxicologist at the US EPA National Center for Computational Toxicology (NCCT). Dr. Harrill's research has focused on modernizing chemical hazard identification, characterization and risk

Oil Spill Environmental Forensics Case Studies.
DOI: http://dx.doi.org/10.1016/B978-0-12-804434-6.00005-7

assessment practices using high-/medium-throughput cell-based assay systems. Dr. Harrill also has experience conducting human health risk assessment using US EPA and state-level guidance as well as devising and managing rapid-phase environmental sampling, analysis and data interpretation programs during events involving the release of potentially hazardous chemicals, including crude oil and petrochemicals.

Paul A. Nony, PhD is a Senior Toxicologist and Certified Industrial Hygienist at CTEH, L.L.C. Dr. Nony has 20 years of training and professional experience in the fields of chemical emergency response, worker health and safety, environmental toxicology, and cancer research. He received his PhD in Interdisciplinary Toxicology from the University of Arkansas for Medical Sciences (UAMS) and spent 2 years in a postdoctoral fellowship at the National Institute of Environmental Health Sciences (NIEHS) in Research Triangle Park, NC. Dr. Nony is consulted for his expertise in worker chemical exposure incidents and is asked to convey toxicological information to workers, supervisors, and health care providers to improve the communication of health risks to workers and employers and the quality of toxicological information used by treating physicians. He also is called by government agencies as well as chemical manufacturing and transportation clients to provide emergency preparedness and expert toxicological and human health risk support for emergency situations where releases of hazardous materials pose a threat to workers, residents, and the environment. Dr. Nony is a member of the Society of Toxicology and the AIHA.

Shawn M. Wnek, PhD is a board-certified toxicologist (DABT) with consulting experience in the fields of occupational toxicology, environmental toxicology, industrial hygiene, and human health risk assessment. Dr. Wnek has training and professional experience in the fields of pharmacology and toxicology, cell biology, and cancer research. Dr. Wnek's background includes a BS in Biology from Baldwin-Wallace University in Berea, Ohio (2005) with education and training focusing on microbiology, immunology, biochemistry, gross anatomy, physiology, and genetics. Upon graduation from Baldwin Wallace, Dr. Wnek worked as a biologist within a contract research organization having roles in product safety assessment and testing. He attended the University of Arizona to complete a PhD in the field of Pharmacology and Toxicology where his graduate research focused on metals toxicology and mechanistic studies on cancer development. Upon completion of his PhD (2011), Dr. Wnek accepted a position as Toxicologist at CTEH in Little Rock, AR where he participates in a variety of project work involving the evaluation of chemicals in industrial and environmental settings. Dr. Wnek specializes in environmental and occupational toxicology, risk assessment, toxicity evaluations, and emergency response toxicology. Dr. Wnek provides support to industrial and regulatory agencies during chemical emergencies where hazardous materials pose a threat to first responders, remediation workers, the general public, and the environment.

Christopher L. Kuhlman, PhD is a Toxicologist at the CTEH, L.L.C with 4 years of consulting experience in the fields of human health risk assessment, industrial hygiene, and environmental toxicology. Dr. Kuhlman's background includes a BS in Biochemistry from the University of California, Los Angeles (UCLA). Upon graduation from UCLA, he worked at Bachem Americas, Inc. in Torrance, California, as a research and development chemist. In a good laboratory practice (GLP) environment, he was involved in the synthesis, purification, and analytical characterization of active pharmaceutical ingredients. He later attended the University of Arizona to complete a PhD in Pharmacology and Toxicology with research focused on chemical toxicology and proteomics. Dr. Kuhlman has extensive experience in the chemical composition and human health risks of petroleum products. His graduate research at the University of Arizona investigated renal- and hematopoietic-tissue proteins targeted by the reactive metabolites of benzene. While at CTEH, Dr. Kuhlman has responded to numerous petroleum spills in the United States and Canada where he conducted human health and ecological risk assessments, community and worker health evaluations, and regulatory compliance consultations. Dr. Kuhlman also participates in the preparation of emergency response guides for the AIHA and the American Petroleum Institute (API). He is a member of AIHA and the Society of Toxicology.

5.1 INTRODUCTION

Crude oil and refined petroleum products are complex mixtures of hydrocarbons that present unique challenges with regards to air monitoring and potential inhalation exposures following an environmental release. In the event of an environmental crude oil release, protecting the health of response workers and the general public is of the utmost importance. As such, an understanding of the chemical composition of crude oil, the types of crude oil, and the factors that contribute to the release of airborne constituents following a crude oil release are critical to conducting the air monitoring and sampling necessary to evaluate site conditions to protect

remediation workers and the general public from potential hazards. First responders, public officials, and remediation workers often use air monitoring data to evaluate the presence of potential airborne chemicals to determine the delineation of safety zones and to assist stakeholders in making informed decisions related to worker and public health and safety.

The airborne constituents associated with an environmental release of crude oil are dependent on many factors including the type of crude oil released, the nature of the release, the weathering process (i.e., the changes in chemical and physical composition of crude oil over time caused by exposure to sunlight, weather conditions, and microorganisms), the local meteorological conditions, and the presence or absence of fire. Air monitoring and sampling conducted during crude oil spills provide valuable information regarding the potential for responder and community exposures. Information regarding the concentrations of volatile organics emitted from crude oil releases has been used to focus air monitoring and analytical air sampling efforts on those constituents with the greatest potential to impact human health.

In this chapter, we review the forensic aspects of airborne crude oil volatiles following the release of crude oil in the environment. This chapter also provides an overview of the types of crude oil and a discussion of the constituents of concern associated with airborne exposures to crude oil volatiles, including common target analytes and tentatively identified compounds (TICs). Furthermore, as releases of crude oil may be accompanied by fire, adjustments to air monitoring strategies under such circumstances will be evaluated. In order to evaluate potential inhalation hazards following a crude oil release, airborne concentrations of chemicals need to be measured and compared to relevant health-based exposure limits. As there are no occupational or community exposure limits for crude oil hydrocarbon mixtures, specific crude oil constituents of concern will be discussed relative to their respective occupational and community exposure standards and guidelines along with a detailed description of available air monitoring and sampling techniques for the evaluation of airborne crude oil constituents. In addition, an analysis of Bakken crude oil compared to non-Bakken crude oil will presented, and an overview of specific environmental crude oil releases will be provided to demonstrate the air sampling conducted under various release scenarios.

5.2 CRUDE OIL HETEROGENEITY AND WEATHERING

Crude oil is categorized as a single substance, petroleum (CAS# 8002-05-9); however, this classification can be misleading as petroleum encompasses a complex combination of hydrocarbons consisting predominantly of aliphatic, alicyclic, and aromatic hydrocarbons as well as trace amounts of nonhydrocarbon elements including nitrogen, oxygen, and sulfur (API, 2011).

Although commonalities exist in the identity of chemicals found in different types of crude oil, marked heterogeneity in the percent mass of constituent chemicals across crude oil types is not uncommon. Some of the chemical constituents of crude oils, such as benzene, toluene, ethylbenzene, and xylene (i.e., BTEX compounds) are classified as volatile organic compounds (VOCs) which can enter the air surrounding spilled crude oil following a spill. The concentrations of BTEX compounds vary widely among different crude oils. For example, evaluations of different crude oils performed by Environment Canada and the United States Environmental Protection Agency (USEPA) demonstrated the concentrations of BTEX compounds varied as much as 200% from one crude oil type to another (Wang et al., 2003). In particular, benzene levels in West Texas Intermediate Crude Oil were more than 400% higher than benzene levels found in Arabian Light crude oil (Wang et al., 2003). In addition, similar heterogeneities were observed following the evaluation of other USEPA priority hazardous air pollutants (HAPs), a list of 187 compounds regulated under the Clean Air Act of 1990. The volatile component of crude oils includes some chemicals which are considered HAPs and other chemicals which are not considered HAPs, but for which occupational and community health standards and/or guidelines for air quality exist. In the event of a crude oil release, it is critical to identify the chemical composition of crude oil that may have been released as this will help to determine which chemicals should be considered chemicals of concern with respect to the protection of worker and community health.

There are multiple schemes for the classification of crude oil. Crude oils are often classified according to their density, hydrocarbon composition and molecular structure, and presence of dissolved gases. Common classifications of crude oil include light/heavy crude oils, paraffinic/naphthenic crude oils, and sweet/sour crude oils (e.g., API, 2011; McMillen et al., 2001). An additional method for classifying petroleum oils is based on their chemical and physical characteristics within the environment following a release (Table 5.1).

TABLE 5.1 Oil Groups and General Behaviors After Environmental Release (Michel and Rutherford, 2013)

Oil group	Physical and chemical characteristics
Group 1: Gasoline; jet fuel	• Specific gravity is <0.80; American Petroleum Institute (API) gravity >45 • Very volatile and highly flammable • Evaporate and dissolve rapidly (in a matter of hours) • Narrow cut fraction with no residues • Low viscosity; spreads rapidly into thin sheens • Will penetrate substrates but are not sticky • High acute toxicity to animals and plants
Group 2: Diesel-like products and light crude oils	• Specific gravity range of 0.80–0.85; API gravity range of 35–45 • Moderately volatile and soluble • Crude oils can leave residue after evaporation is complete • Low to moderate viscosity; spreads rapidly into thin slicks • Are more bioavailable than lighter oils (in part because they persist longer), so are more likely to affect animals in water and sediments
Group 3: Medium crude oils and intermediate products	• Specific gravity range of 0.85–0.95; API gravity range of 17.5–35 • Moderately volatile • For crude oils, up to one-third will evaporate in the first 24 h • Moderate to high viscosity; will spread into thick slicks • Are more bioavailable than lighter oils (because they persist longer), so are more likely to affect animals in water and sediments
Group 4: Heavy crude oils and residual products	• Specific gravity range of 0.95–1.00; API gravity range of 10–17.5 • Very little product loss by evaporation or dissolution • Very viscous to semi-solid; might require heating during transport • Can form stable emulsions and become even more viscous • Tend to break into tar balls quickly • Low acute toxicity to water-column biota • Penetration into substrates will be limited at first, but can increase over time • Can cause long-term effects via smothering or coating, or as residues in the water column and sediments
Group 5: Sinking oils	• Specific gravity >1.00; API gravity <10. • Very little product loss by evaporation or dissolution • Very viscous to semi-solid; might require heating during transport or blended with a diluent which can evaporate if spilled into the environment • Low acute toxicity to water-column biota • Penetration into substrates will be limited at first, but can increase over time • Can cause long-term effects via smothering or coating, and as residues in sediments

The type of crude oil can reveal limited information regarding the types of volatile and HAPs potentially present. This is particularly true in the case of sulfur-containing sour crudes. As a general rule, crude oils with less than 1% sulfur are categorized as "sweet" and crude oils with over 1% sulfur are categorized as "sour" (API, 2011). Some "sour" oils contain hydrogen sulfide (H_2S), a toxic, flammable gas that has an easily recognizable rotten-egg odor discernable at low concentrations (less than 1 part per million, ppm) (Roth, 1993). Hydrogen sulfide can act as an irritant and an asphyxiant in humans, leading to eye and respiratory tract irritation at concentrations ranging from 20 to 50 ppm (Beauchamp et al., 1984). Although the low odor threshold associated with H_2S provides adequate warning for the presence and potential for exposure, as concentration of H_2S reach 100 to 200 ppm loss of smell (olfactory paralysis) can rapidly occur (Beauchamp et al., 1984; Guidotti, 2010). Olfactory paralysis at higher concentrations results in a loss of perception of the presence of H_2S and the warning properties of odor disappear (Guidotti, 1996). H_2S is a recognized hazard in the oil and gas industry, where it may be emitted or released during exploration, development, extraction, treatment and storage, transportation (i.e., pipeline and rail), and refining (USEPA, 1993), but it can also be of significant concern in oil spills involving sour crude.

Despite the differing physical and chemical characteristics of crude oil, some generalizations can be made regarding its behavior in the environment. Freshly spilled crude oil, in which the composition of the oil residue resembles that of the unspilled source oil, will often release initially high concentrations of airborne volatile organics that gradually decline as the oil weathers and the lighter fractions volatilize. The volatile components of crude oil will rapidly evaporate when oil is spilled in well-ventilated, warm environments, resulting in the loss of the more volatile constituents of crude oil over hours to a few days. Previous studies have evaluated the

presence of VOC air concentrations in ambient air samples collected in the breathing zone above or in the direct vicinity of unweathered crude oil (Harrill et al., 2014). A time course analysis from various crude oil releases demonstrates that VOCs released from crude oil typically dissipate over a period of a few days. However, this may not always be the case, particularly in scenarios where fresh oil continues to be released throughout and beyond the initial phase of the response, and/or during remediation when unweathered reservoirs such as subsurface deposits are accessed during remediation (Harrill et al., 2014).

As the chemical and physical parameters of the crude oil change due to weathering, the potential airborne hazards will change as well. Due to changes associated with weathering in the environment, petroleum hydrocarbon mixtures may become toxicologically different from the original petroleum mixture. In order for a direct inhalation pathway to exist (i.e., volatilization of constituents from water or soil), constituents must have a sufficient vapor pressure to volatilize from soil or surface water and become airborne at concentrations resulting in a meaningful dose. Initially, the lighter components of crude oils (e.g., hexane, benzene, ethylbenzene, toluene, and xylenes), which fall in the range of gasoline-range organics (GRO) may rapidly volatilize and will not be present in a weathered mixture. These compounds typically represent the greatest inhalation and dermal hazard to workers and the general public following a crude oil release. As the product weathers, these more volatile compounds rapidly dissipate through the weathering process, leaving behind compounds with little or no volatility (Osuji et al., 2006; Thayer et al., 2001; Stout et al., 2006). The physical and chemical properties of the weathered crude oil will reflect hydrocarbons of the diesel-range organics (DRO) and oil-range organics (ORO). For example, total petroleum hydrocarbon (TPH)-DRO (C_{10}−C_{20}) has a low vapor pressure of 0.0063 atm, and TPH-ORO (C_{20}−C_{28}) has a vapor pressure of 0.0000011 atm (TPHCWG, 1997). Aromatic hydrocarbons in these ranges have even lower vapor pressures (ATSDR, 1999). Thus, due to loss of the more volatile components, from a toxicological standpoint the weathered crude oil becomes less of an inhalation hazard and dermal contact becomes the primary hazard.

5.3 AIRBORNE CHEMICALS OF CONCERN FOLLOWING CRUDE OIL SPILLS

5.3.1 Spills Unaccompanied by Fire

Of particular concern during an emergency response to a spill of crude oil is monitoring for the potential presence of the lighter aliphatic hydrocarbons and aromatic compounds, such as benzene and toluene, which can volatilize and create a potential for airborne exposures and can pose a flammability hazard. Some “sour” oils contain H_2S as previously discussed. Occupational exposures to these compounds and other volatile components of crude oil are regulated by Occupational Safety and Health Administration (OSHA), and the USEPA promulgates community exposure guidelines for many of these volatile components as well.

There can be marked heterogeneity in the percent mass of crude oil volatiles across crude oil types (USEPA, 1999). Identifying the specific chemicals releasing into the air is possible via sampling and rapid analysis of air captured above or in the direct vicinity of freshly released crude oil during the initial phase of a response. Air sampling can provide critical information in the initial phases of a response. However, as laboratory turnaround time for analysis of VOC air samples generally takes 24 hours or more, and it is often not practical to wait for the delivery of analytical data before implementing protective measures for workers and the general public, knowledge of likely airborne constituents is critical to initiating and implementing an appropriate air-monitoring strategy.

Retrospective analysis of analytical air sampling data from previous spills can provide useful guidance on potential target analytes to be monitored during the initial phase of an oil spill response. A detailed discussion of the use of air sampling data from historic crude oil events to prioritize chemicals of concern is presented below. The list of potential analytes may be refined as analytical results become available. Table 5.2 lists the general volatile chemicals of concern associated with spilled crude oil based upon prior air sampling data. Air monitoring of these volatile hydrocarbon constituents and comparison to occupational and community exposure limits can aid in determining where an exclusion zone and/or evacuation zone boundary should be established.

It is important to note that the acute and chronic health effects listed in Table 5.2 would not automatically be expected to occur upon exposure to crude oil volatiles. The potential to experience health effects is determined by the intensity, duration, frequency, and route of exposure as well as interindividual sensitivity. Different acute and chronic health effects will occur at different dose thresholds. In a properly controlled spill-response work environment, exposure to crude oil volatiles should not occur at levels and durations that would be associated with adverse health effects.

TABLE 5.2 Potential Health Effects of Selected Volatile Chemicals of Concern Associated with Crude Oil Spills

		Benzene	Cyclohexane	Ethylbenzene	*n*-Hexane	Toluene	Xylenes	Naphthalene	Butane	Hydrogen sulfide
Acute health effects	Eye, nose, and/or upper respiratory tract irritation	•	•	•	•	•	•	•		•
	Central nervous system effects (dizziness, headaches, narcosis)	•	•	•	•	•	•	•	•	•
	Dyspnea, shortness of breath	•						•		
	Nausea	•	•	•	•	•	•	•	•	•
	Dermatitis		•	•	•	•	•			•
	Numbness, muscle weakness				•					
	Respiratory sensitization							•		
	Dilated pupils and lacrimation									•
	Eye injury		•			•	•			
Chronic health effects	Known human carcinogen (IARC-1)	•								
	Possible carcinogen (IARC-2B)		•	•				•		
	Dermatitis, defatting, or drying/cracking of skin	•	•		•	•	•			
	Peripheral nervous system effects				•					
	CNS effects	•				•	•		•	•
	Weight loss									•
	Liver injury					•	•			
	Kidney injury					•	•			
	Cataracts							•		
	Anemia (aplastic/hemolytic)	•						•		

Source: NIOSH (2007).

5.3.2 Crude Oil Spills Accompanied by Fires

A release of crude oil into the environment is often accompanied with a chance of explosion, fire, and the production of smoke. Fires can be either accidental or intentional, the latter being a common response to waterborne oil spills, referred to as *in situ* burning. Although petroleum hydrocarbons are consumed during combustion, the resulting byproducts have the potential for significant human health and environmental impacts, and thus warrant discussion. The ability of crude oil to burn is related to the content of volatile hydrocarbons within the source product. The volatile hydrocarbon vapors of freshly spilled crude oil can act as a fuel source which readily facilitates product ignition. Conversely, heavy, viscous crude oils, such as bitumen, typically contain few volatile compounds; as a result, these types of crude oil do not burn as readily.

Crude oil fires can produce large amounts of heavy black smoke. Smoke produced by burning crude oil is a combination of black carbon particulate matter (PM) (soot), liquid droplets, and combustion gases. The flame

temperature, availability of oxygen, and fuel type will influence the burn efficiency and the quantity and composition of smoke generated during a fire. In a well-ventilated, oxygen-rich environment, complete combustion of petroleum products would generate only water vapor, carbon dioxide, and heat (Wakefield, 2010). In comparison, an oxygen-starved crude oil fire can cause incomplete combustion leading to the subsequent conversion of the crude oil into black smoke (Ferek et al., 1997). Thus, the presence of fire following a crude oil release will require modifications to the overall air monitoring strategy focusing on PM and other combustion by-products that would not be of concern in the absence of fire.

5.3.2.1 General Composition of Petroleum Oil Smoke

Water vapor, carbon dioxide (92%), carbon monoxide (3%), and PM (5%) are the primary compounds emitted during the burning of crude oil. In addition, noncombusted constituents including VOCs, aldehydes and ketones, oxides of nitrogen and sulfur, and carbon monoxide are emitted during the burning of hydrocarbons present in crude oil (Booher and Janke, 1997; Ross et al., 1996). VOCs released during a crude oil fire represent 0.3% of the total emissions and are predominantly mono-aromatic hydrocarbons such as benzene and alkylbenzenes. The release of VOCs during the burning of crude oil is significantly less than the volume that can be released from standing pools of freshly spilled crude oil, as these VOCs are consumed if the source product is on fire (Ross et al., 1996; Fingas, 2011). A breakdown of the emissions from hydrocarbon fires is presented in Fig. 5.1.

The visible black PM that is released from a petroleum fire consists of 80% to 90% elemental carbon with trace amounts of organic compounds (Booher and Janke, 1997). It should be noted that the quantity of PM produced during an oil fire can range from 1% to 15% and is influenced by the type of source oil (Fingas, 2011; Ferek et al., 1997). Fingas (2011) reported about 5% to 8% of the volume of burning diesel fuel is emitted as PM, whereas particulate emissions from a crude oil fire may only amount to 1% to 2% of the volume. The concentration of PM produced during oil fires is comparable to the levels produced during forest wildfires. For instance, an oil fire burning 200 barrels of oil per hour will emit smoke particulates at a rate of 4050 kg/hour, which is comparable to the smoke emission rate from a 9-acre controlled agricultural burn (Ross et al., 1996).

5.3.2.2 Hazardous Constituents of Petroleum Smoke

Of the constituents released during the burning of petroleum oil, exposure to PM represents the greatest potential health hazard to response and remediation workers and the general public. Depending upon particle size, PM can be transported considerable distances from the fire source. VOCs, polycyclic aromatic hydrocarbons

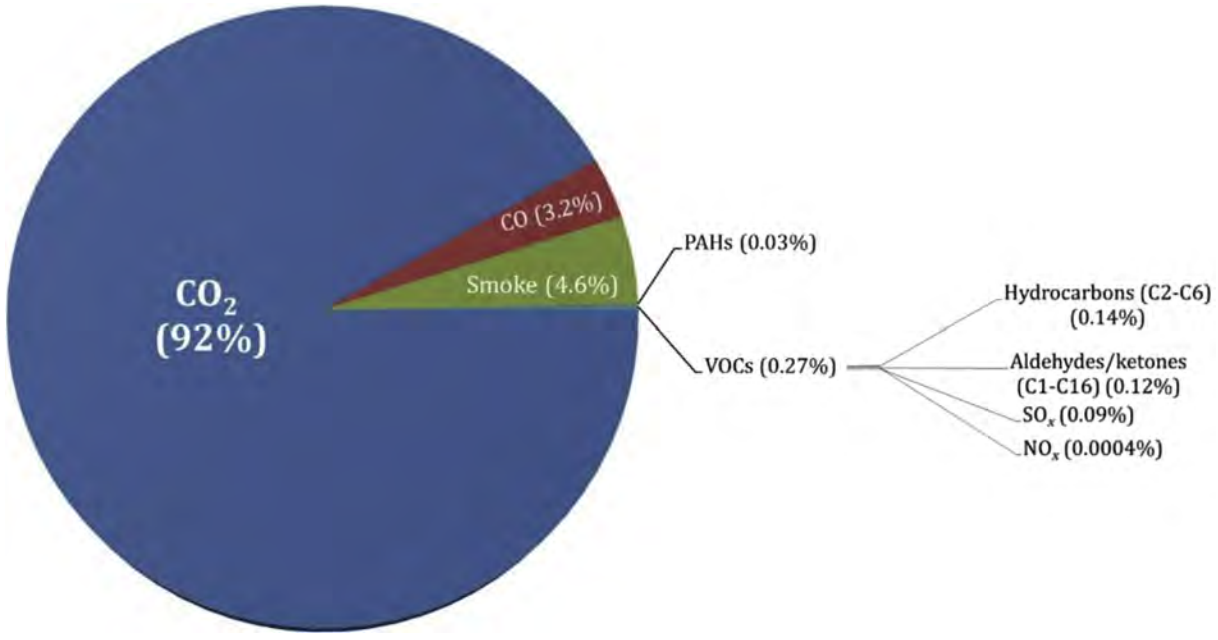

FIGURE 5.1 Composition of emissions from petroleum hydrocarbon fires (excluding water). *Adapted from Booher, L.E. and Janke, B. (1997) Air emissions from petroleum hydrocarbon fires during controlled burning*, Am. Ind. Hyg. Assoc. J., *58(5), pp. 359–365.*

(PAHs), and combustion by-products are additional decomposition products of burning petroleum oil that need to be considered when evaluating chemicals of concern following a fire.

5.3.2.2.1 Carbon PM

PM from a petroleum oil fire is composed of small elemental carbon particles that, due to the generally intense heat produced, will initially loft high into the air in a plume of black smoke (Middlebrook et al., 2012). Wind conditions will dictate the movement of these smoke particulates, diluting and spreading smoke downwind from the source. The high levels of PM emitted from a petroleum fire will often cause the air to appear hazy, decreasing the range of visibility.

The particles comprising petroleum smoke are not uniform in size. Some components of PM are large enough to be seen as smoke, whereas smaller particles can be visible as smoke depending upon the density of the smoke plume emitted from the fire source. The dilution of PM in the atmosphere increases with distance from the fire location. Larger particles can remain in the air for a few minutes to hours before settling to the ground near the source; whereas smaller particles (aerodynamic diameter of 10 μm and smaller, PM_{10}) can remain in the air from several days to weeks and can be dispersed by winds over wide areas or long distances from the original source (Middlebrook et al., 2012). These particles are generally removed from the atmosphere by wet precipitation or through contact with other surfaces. Only the smallest particles (aerodynamic diameter of 2.5 μm and smaller, $PM_{2.5}$) tend to remain in the air for longer periods. The airborne smoke particles generated in a petroleum fire are on average less than 1 μm in diameter, which is small enough to penetrate into the gas exchange regions of the lung (Buist and Nedwed, 2011; Ross et al., 1996). Generally, finer particles are considered to pose a greater toxicological concern due to their deeper penetration into the lung.

5.3.2.2.2 Polycyclic Aromatic Hydrocarbons

In smoke collected above large test burns of crude oil during the Newfoundland Offshore Burn Experiment (NOBE), PAH concentrations were found to be lower in fire smoke PM than in the starting oil (USEPA, 2016). The NOBE results and the findings from many other oil-burning experiments indicated that PAHs are consumed by petroleum fires to a large degree (Fingas et al., 1995; Fingas et al., 2001). During the NOBE test burns, naphthalene and acenaphthylene were the predominant PAH compounds detected downwind of smoke plumes from burning #2 fuel oil and crude oil. Naphthalene reached concentrations of 2.5 $\mu g/m^3$ and 1.5 $\mu g/m^3$ at a sampling site 100 ft away from the fuel oil and crude oil smoke plumes, respectively (Booher and Janke, 1997). Acenaphthylene was detected at 0.12 $\mu g/m^3$ and 0.11 $\mu g/m^3$ at the same locations. At distances beyond 100 ft, concentrations of these PAHs were at or below instrument detection limits.

During the *Deepwater Horizon* oil spill, the USEPA developed health-based screening levels for PAHs, using information regarding exposure levels that might pose an increased risk of cancer and noncancer health effects (USEPA, 2016). These screening-level concentrations assume continuous exposure (24 hours a day, 7 days a week) for a year. For naphthalene, the USEPA screening level for a 1-year average exposure is 30 $\mu g/m^3$. The 2.5 $\mu g/m^3$ of naphthalene detected 100 ft away from burning fuel oil during the NOBE test burn is well below the USEPA screening-level value. Thus, an acute-duration exposure to naphthalene or other PAHs at the concentrations detected adjacent to burning crude oil fires is unlikely to be a health concern for workers or the general public.

5.3.2.2.3 Volatile Organic Compounds

Although VOC emissions are a larger concern for nonburning pools of crude oil, the potential still exists for the emission of VOCs during petroleum fires (Buist et al., 1999; Fingas et al., 2001). VOCs, including benzene and alkylbenzenes, are readily detectable within the smoke plume above burning crude oil (Bowes, 1996; Booher and Janke, 1997; Buist, 2005). Booher and Janke (1997) reported that concentrations of VOCs dropped significantly with distance downwind from 500-gal test burns of either #2 fuel oil or light crude oil. Of the individual VOCs evaluated, benzene was the only compound detected outside of the smoke plume. Benzene concentrations 50 ft away from the #2 fuel oil and crude oil smoke plumes were 34 ppb (110 $\mu g/m^3$) and 81 ppb (260 $\mu g/m^3$), respectively. Samples collected a mile downwind of the burning crude oil and fuel oil contained no detectable levels of benzene.

5.3.2.2.4 Combustion Gases

Some gaseous combustion byproducts of petroleum hydrocarbon fires have asphyxiant properties with the potential to displace oxygen in breathing air or interfere with oxygen transport in the human body. Carbon dioxide and nitrogen oxide gases released from a petroleum fire can behave as simple asphyxiants. Simple asphyxiants act to displace oxygen and create suffocating atmospheres when accumulated in poorly ventilated areas or

TABLE 5.3 Estimated Airborne Emissions From the Burning of Crude Oil

Component of concern		Concentration at the burn site	Concentration 1 km downwind of burn site
Smoke particulates	$PM_{2.5}$	2.4 mg/m^3 [a] (from diesel)	NA
	PM_{10}	850 $\mu g/m^3$ [b]	86 $\mu g/m^3$ [c]
PAHs	–	0.0–13.1 $\mu g/m^3$ [a]	NA
Gases and vapors	SO_2	2 ppm[d,e]	<0.0012 ppm[e]
	NO_2	0.0001–0.0006 average ppm[f]	0.0001 ppm[f]
	CO	0.14–0.15 average ppb[f]	0.14 ppb[f]
	Total VOCs	0.0026–0.0083 average ppm[f]	0.0013–0.0016 ppb[f]

[a] *Fingas and Punt (2000).*
[b] *Buist et al. (1999).*
[c] *Fingas et al. (1994).*
[d] *Booher and Janke (1997).*
[e] *Note that the level of SO_2 is dependent on the amount of sulfur in the oil. SO_2 levels are typically very low. Colorimetric detector tubes can be used to perform real time air monitoring (Buist et al., 1999).*
[f] *Middlebrook et al. (2012).*
Notes: NA, data not available. Units of ppm are most appropriate for gases and vapors, and $\mu g/m^3$ is more appropriate for particulates and fumes.

enclosed spaces. In contrast to simple asphyxiants, carbon monoxide inhalation has the potential to reduce the oxygen-carrying capacity of the blood. Carbon monoxide is a chemical asphyxiant with 200–250 times greater affinity for blood hemoglobin than oxygen (Wakefield, 2010). For the general public, exposures to the simple and chemical asphyxiant gases emitted from a petroleum fire will be limited as petroleum fires will likely occur in open environments, and the levels of these gases rapidly decrease with increased distance from the source fire and as the petroleum smoke plume dissipates (Wakefield et al., 2010).

Emissions of sulfur dioxide from burning crude oil will depend on the amount of sulfur present in the oil. Sulfur dioxide is a highly water-soluble irritant gas that is readily absorbed by the mucous membranes of the nose and respiratory tract, resulting in irritation primarily within the upper airways (ACGIH, 2014a). Sulfur dioxide has been reported to reach concentrations of 2 ppm at the site of a crude oil fire (Buist et al., 1999). At this concentration, a healthy individual may experience symptoms of irritation and bronchoconstriction; however, for the general public, exposures to sulfur dioxide will be limited as the levels of sulfur dioxide rapidly decrease with increased distance from the source fire (Buist et al., 1999).

Carbon dioxide has been reported to reach concentrations of 500 ppm at a distance of 1 m from an open burn of crude oil or diesel fuel (Fingas et al., 1996). It is notable that acute exposure to 500 ppm of carbon dioxide does not pose a danger to the health of responders in the vicinity of a petroleum fire, as this concentration is below the OSHA Permissible exposure limit (PEL) of 5000 ppm for carbon dioxide. At a distance of 4 m from the smoke plume, the levels of carbon dioxide returned to ambient concentrations (300 ppm) (Ferek et al., 1997; Fingas et al., 1996). In experiments monitoring the levels of combustion gases present downwind of burning crude oil, carbon monoxide emissions from an oil fire were observed to be more than 25 times lower than carbon dioxide emissions, and nitrogen oxides were present at a concentration 1000 times lower than carbon dioxide (Ferek et al., 1997). Thus, carbon monoxide and nitrogen oxide levels adjacent to a petroleum fire are likely to be below the detection limits of air-monitoring equipment, and at these concentrations are of little concern to response workers or the general public during a petroleum-related fire (Booher and Janke, 1997).

In summary of the discussion above, Table 5.3 summarizes estimates of airborne emission of smoke particulates, PAHs, and combustion gases and vapors from burning crude oil 1 km downwind.

5.4 HEALTH PROTECTIVE VALUES

In order to evaluate potential inhalation hazards for responders and the general public, airborne concentrations of volatile chemicals and gases can be compared to their respective occupational or community exposure standards or guidelines selected for use as action levels during a crude oil response. The OSHA and The American Conference of Governmental Industrial Hygienists (ACGIH) have established workplace exposure

standards and guidelines, respectively. Many regulatory agencies, default to using the ACGIH Threshold Limit Values (TLVs) as an occupational exposure limit (OEL) for response activities. TLVs are typically based on the most current science and are more health-protective than OSHA Permissible Exposure Limits (PELs). There are no occupational exposure standards or guidelines specifically for crude oil hydrocarbon vapor mixtures. However, analyses may be conducted for the individual constituents of crude oil as described above, and concentrations can be compared to the respective occupational exposure standards and guidelines. In addition, readings of total VOCs may be compared to occupational values for hydrocarbon vapor mixtures which have a similar composition as what would be expected to be released from crude oil (i.e., gasoline-range vapors). It is important to note that OELs, such as ACGIH TLVs and OSHA PELs, can be applied to responder exposures; however, different exposure guidelines are used for evaluating airborne exposures to the general public.

5.4.1 Occupational Exposure Levels

OSHA and the ACGIH have established workplace exposure standards and guidelines, respectively, to protect the health and safety of workers from overexposure to many of the individual constituents of crude oil. In addition, the National Institute for Occupational Safety and Health (NIOSH) has derived Recommended Exposure Limits (RELs) for the same purpose. These values are expressed as 8-hour (OSHA PELs and ACGIH TLVs) or 10-hour (NIOSH RELs) Time-Weighted Averages (TWA) and are intended to address daily worker exposures occurring over a working lifetime. Others may be expressed as Short-Term Exposure Limits (STEL; 15-minute average exposures) or Ceilings (maximum values allowed during a work period). The STEL and Ceiling values are applicable to exposures of shorter duration that can occur during chemical release emergencies. The 8-hour TWA values may also be relevant to emergency settings if intended to protect against short-term health effects such as irritation, central nervous system depression, etc. Together, the worker exposure guidelines and standards provide useful information for the development of action levels and in the interpretation of the results of air monitoring and sampling performed during crude oil releases. Table 5.4 summarizes the OSHA worker exposure standards and the NIOSH and ACGIH guidelines for target analytes associated with crude oil.

5.4.2 Community Exposure Guidelines

5.4.2.1 Protective Action Criteria

The US Department of Energy Subcommittee on Consequence Assessment and Protective Actions (SCAPA) has established Protective Action Criteria (PACs) for over 3300 chemicals for planning and response to uncontrolled releases of hazardous chemicals. These criteria, combined with estimates of exposure, provide the information necessary to evaluate chemical release events for the purpose of taking appropriate protective actions. During an emergency response, these criteria may be used to evaluate the severity of the event and to inform decision makers regarding what protective actions should be taken.

PAC values are based on the following exposure limit values:

- Acute Exposure Guideline Level (AEGL) values published by USEPA;
- Emergency Response Planning Guideline (ERPG) values produced by the American Industrial Hygiene Association; and
- Temporary Emergency Exposure Limit (TEEL) values developed by SCAPA.

For any particular chemical, the following hierarchy is used to establish its PAC:

- Use AEGLs (including final or interim values) if they are available;
- If AEGLs are not available, use ERPGs; and
- If neither AEGLs nor ERPGs are available, use TEELs.

AEGLs, ERPGs, and TEELs have three common benchmark values for each chemical. Each successive benchmark is associated with an increased severity of potential health effect(s). The three benchmarks present estimated threshold levels for:

1. Mild, transient health effects.
   a. AEGL-1: The airborne concentration of a substance above which it is predicted that the general population, including susceptible individuals, could experience notable discomfort, irritation, or certain asymptomatic nonsensory effects. However, the effects are not disabling and are transient and reversible upon cessation of exposure (Subcommittee on Acute Exposure Guideline Levels; National Research Council, 2001).

TABLE 5.4 Occupational Exposure Standards and Guidelines

		OSHA		ACGIH		NIOSH	
Analyte		**PEL-TWA[a]**	**PEL-STEL[b]**	**TLV-TWA[c]**	**TLV-STEL[d]**	**REL-TWA[e]**	**REL-STEL[f]**
Volatiles	Benzene	1 ppm	5 ppm	0.5 ppm	2.5 ppm	0.1 ppm	1 ppm
	Cyclohexane	300 ppm	NE	100 ppm	NE	300 ppm	NE
	Ethylbenzene	100 ppm	NE	20 ppm	NE	100 ppm	125 ppm
	Hexane	500 ppm	NE	50 ppm	NE	50 ppm	NE
	H_2S	NE	20 ppm (C); 50 ppm[g]	1 ppm	5 ppm	NE	10 ppm (C)
	Naphthalene	10 ppm	NE	10 ppm	NE	10 ppm	15 ppm
	Toluene	200 ppm	300 ppm (C); 500 ppm[g]	20 ppm	NE	100 ppm	150 ppm
	Xylene	100 ppm	NE	100 ppm	150 ppm	100 ppm	150 ppm
Combustion products	$PM_{2.5}/PM_{10}$	NE	NE	NE	NE	NE	NE
	PAHs[h]	200 $\mu g/m^3$	NE	200 $\mu g/m^3$	NE	100 $\mu g/m^3$	NE
	CO_2	5000 ppm	NE	5000 ppm	30,000 ppm	5000 ppm	30,000 ppm
	SO_2	5 ppm	NE	NE	0.25 ppm	2 ppm	5 ppm
	NO_2	NE	5 ppm (C)	0.2 ppm	NE	NE	1 ppm
	CO	50 ppm	NE	25 ppm	NE	35 ppm	200 ppm (C)

[a]*OSHA PEL-TWA = Permissible Exposure Limit − Time Weighted Average = The employee's average airborne exposure in any 8-h work shift of a 40-h work week which shall not be exceeded. It is intended to be the highest level of exposure an employee may be exposed to without incurring the risk of adverse health effects (OSHA 29 CFR: 1910.1000).*
[b]*OSHA PEL-STEL = Permissible Exposure Limit − Short-Term Exposure Limit (PEL-STEL). A 15-min TWA exposure that should not be exceeded at any time during a workday. (OSHA 29 CFR: 1910.1000).*
[c]*ACGIH TLV-TWA = Threshold Limit Value − Time Weighted Average (TLV-TWA). The TWA concentration for a conventional 8-h workday and a 40-h workweek, to which it is believed that nearly all workers may be repeatedly exposed, day after day, without adverse effect (ACGIH, 2014b).*
[d]*ACGIH TLV-STEL = Threshold Limit Value − Short-Term Exposure Limit (TLV-STEL). A 15-min TWA exposure that should not be exceeded at any time during a workday, even if the 8-h TWA is within the TLV-TWA. The TLV-STEL is the concentration to which it is believed that workers can be exposed continuously for a short period of time without suffering from (1) irritation, (2) chronic or irreversible tissue damage, (3) dose-rate dependent toxic effects, or (4) narcosis of sufficient degree to increase the likelihood of accidental injury, impaired self-rescue, or materially reduced work efficiency. Exposures above the TLV-TWA up to the TLV-STEL should be less than 15 minutes, should occur not more than 4 times per day, and there should be at least 60 minutes between successive exposures in this range. (ACGIH, 2014b).*
[e]*NIOSH REL-TWA = Recommended Exposure Limit − Time Weighted Average (REL-TWA). The TWA concentration for up to a 10-h workday during a 40-h workweek.*
[f]*NIOSH REL-STEL = Recommended Exposure Limit − Short-Term Exposure Limit (REL-STEL). A 15-min TWA exposure that should not be exceeded at any time during a workday.*
[g]*10-min peak; once per 8-h shift.*
[h]*Although OSHA, ACGIH, and NIOSH have not established an occupational exposure limits for PAHs, there are exposure limits for volatiles from coal tar pitch that cover the PAHs anthracene, benzo(a)pyrene, phenanthrene, acridine, chrysene, and pyrene.*
(ACGIH, 2014a), *NE*, Not Established; (C), Ceiling.

b. ERPG-1: The maximum concentration in air below which it is believed nearly all individuals could be exposed for up to 1 hour without experiencing other than mild transient adverse health effects or perceiving a clearly defined objectionable odor (AIHA, 2015).
c. TEEL-1: is the airborne concentration [expressed as ppm (parts per million) or mg/m^3 (milligrams per cubic meter)] of a substance above which it is predicted that the general population, including susceptible individuals, when exposed for more than 1 hour, could experience notable discomfort, irritation, or certain asymptomatic, nonsensory effects. However, these effects are not disabling and are transient and reversible upon cessation of exposure (U.S. Department of Energy, 2016).

2. Irreversible or other serious health effects that could impair the ability to take protective action.
a. AEGL-2: The airborne concentration of a substance above which it is predicted that the general population, including susceptible individuals, could experience irreversible or other serious, long-lasting adverse health effects or an impaired ability to escape (Subcommittee on Acute Exposure Guideline Levels; National Research Council, 2001).
b. ERPG-2: The maximum concentration in air below which it is believed nearly all individuals could be exposed for up to 1 hour without experiencing or developing irreversible or other serious health effects or symptoms that could impair an individual's ability to take protective action (AIHA, 2015).

TABLE 5.5 Community Exposure Guidelines for Selected Crude Oil Constituents

Analyte	PAC-1	PAC-2	PAC-3
Benzene	52_A ppm	800_A ppm	4000_A ppm*
Hexane	300 ppm	3300_A ppm*	8600_A ppm**
Hydrogen sulfide	0.51_A ppm	27_A ppm	50_A ppm
Toluene	200_A ppm	1200_A ppm*	4500_A ppm*
Xylene	130_A ppm	920_A ppm*	2500_A ppm*

* USDOE (2016); PAC values marked with a subscript "A" correspond to 60-min AEGL values; PAC values marked by * are >10% lower explosive limit (LEL) but <50% LEL; PAC values marked by ** are >50% LEL.

   c. TEEL-2: is the airborne concentration (expressed as ppm or mg/m^3) of a substance above which it is predicted that the general population, including susceptible individuals, when exposed for more than 1 hour, could experience irreversible or other serious, long-lasting, adverse health effects or an impaired ability to escape (U.S. Department of Energy, 2016).

3. Life-threatening health effects
   a. AEGL-3: The airborne concentration of a substance above which it is predicted that the general population, including susceptible individuals, could experience life-threatening health effects or death (Subcommittee on Acute Exposure Guideline Levels; National Research Council, 2001).
   b. ERPG-3: The maximum concentration in air below which it is believed nearly all individuals could be exposed for up to 1 hour without experiencing or developing life-threatening health effects (AIHA, 2015).
   c. TEEL-3: is the airborne concentration (expressed as ppm or mg/m^3) of a substance above which it is predicted that the general population, including susceptible individuals, when exposed for more than 1 hour, could experience life-threatening adverse health effects or death (U.S. Department of Energy, 2016).

Table 5.5 provides community exposure guidelines for target analytes of crude oil.

There are currently no occupational or community exposure guidelines for exposure to fire smoke PM. However, as wildfire smoke PM is substantially similar to that formed during the combustion of crude oil, wildfire smoke exposure guidelines represent an acceptable surrogate for establishing action levels for community and worker protection during petroleum fires. In "*Wildfire Smoke: A Guide for Public Health Officials*" (Lipsett et al., 2013), particles from wildfire smoke range from 0.4 to 0.7 μm in diameter and fall completely within the fine PM fraction of $PM_{2.5}$ (Lipsett et al., 2013). This is similar to smoke PM generated during a petroleum fire, with PM generally less than 1 μm in diameter (Buist et al., 1999; Ross et al., 1996). Based on knowledge of the similar size fractions of PM produced during the burning of petroleum products and wildfire smoke it is acceptable to use existing recommended action levels developed for wildfire smoke (Table 5.6). Table 5.6 can be used as guidance for public health officials with regards to measures that can be taken to protect public health at different air quality index (AQI) categories. These AQI categories correspond to PM levels ($PM_{2.5}$ and PM_{10}) at different averaging times. The AQI value for PM is derived from estimated or measured 24-hour average concentrations; PM levels for shorter averaging times (e.g., 1- to 3-hour and 8-hour averages) are not "official" AQI values, but have been mathematically derived from the $PM_{2.5}$ AQI breakpoints for 24-hour concentrations, and are based on epidemiological studies associating long- and short-term $PM_{2.5}$ exposures with respiratory and cardiovascular morbidity and mortality (USEPA, 2012; Lipsett et al., 2013).

5.4.2.2 ATSDR Minimal Risk Levels

The Agency for Toxic Substances and Disease Registry (ATSDR) prepares toxicological profiles for numerous hazardous substances in accordance with guidelines developed by ATSDR and the USEPA. These toxicological profiles include an examination, summary, and interpretation of available toxicological information and epidemiologic evaluations of a hazardous substance. During the development of toxicological profiles, Minimal Risk Levels (MRLs) are derived when reliable and sufficient data exist to identify the target organ(s) or the most sensitive health effect(s) for a specific duration for a given route of exposure. "An MRL is an estimate of the daily human exposure to a hazardous substance that is likely to be without appreciable risk of adverse noncancer health effects over a specified duration of exposure." These substance-specific estimates are intended only to serve as screening levels and are used by ATSDR health assessors to identify contaminants and potential health effects that may be of concern at hazardous waste sites. They may also be viewed as a mechanism to identify those hazardous waste sites that are not expected to cause adverse health effects (ATSDR, 2016).

TABLE 5.6 Levels of Concern Associated With Airborne Particulate Levels

Levels of health concern (AQI values)	$PM_{2.5-10}$ levels ($\mu g/m^3$)[a] 1–3-h average[b]	8-h average[b]	24-h average[c]	Visibility–arid conditions (miles)	Recommended actions for general public
Good (0 to 50)	0–38	0–22	0–12	≥11	• If smoke event forecasted, implement communication plan
Moderate (51 to 100)	39–88	23–50	13–35	6–10	• Issue public service announcements advising public about health effects/symptoms and corrective actions • Distribute information about exposure avoidance
Unhealthy for sensitive groups (101 to 150)	89–138	51–79	36–55	3–5	• If smoke event projected to be prolonged, evaluate and notify possible sites for clean air shelters and prepare evacuation plans
Unhealthy (151 to 200)	139–351	80–200	56–150	1.5–2.75	• Consider "Smoke Day" for schools, possibly based on school environment and travel conditions • Consider canceling public events
Very unhealthy (201 to 300)	352–526	201–300	151–250	1–1.25	• Consider closing some or all schools • Cancel outdoor events (e.g., concerts and competitive sports)
Hazardous (>300)	>526	>300	>251–500	<1	• Close schools • Cancel outdoor events (e.g., concerts and competitive sports) • Consider closing workplaces not essential to public health • If PM level projected to continue to remain high for a prolonged time consider evacuation of sensitive populations

[a]*Most fire smoke particles are less than 1 μm, so the values obtained by measuring either PM_{10} or $PM_{2.5}$ are virtually interchangeable as reported in Lipsett et al. (2013).*
[b]*These 1- to 3-h and 8-h $PM_{2.5}$ levels are estimated using the 24-h breakpoints of the $PM_{2.5}$ Air Quality Index included in the February 7, 2007 paper (http://www.epa.gov/airnow/aqi_issue_paper_020707.pdf) by dividing the 24-h concentrations by the following ratios: 8-h ratio is 0.7, 1-h ratio is 0.4.*
[c]*Revised 24-h average breakpoints from the Revised Air Quality Standards for Particle Pollution and Updates to the Air Quality Index, US Environmental Protection Agency, December 14, 2012.*

TABLE 5.7 ATSDR[a] Minimal Risk Levels for Selected Volatile Crude Oil Constituents

Analyte	Acute MRL	Intermediate MRL	Chronic MRL
Benzene	0.009 ppm	0.006 ppm	0.003 ppm
Cyclohexane	NE	NE	NE
Ethylbenzene	5 ppm	2 ppm	0.06 ppm
Hexane	NE	NE	0.6 ppm
Hydrogen sulfide	0.07 ppm	0.02 ppm	NE
Naphthalene	NE	NE	0.0007 ppm
Toluene	2 ppm	NE	1 ppm
Xylene	2 ppm	0.6 ppm	0.05 ppm

[a]ATSDR (2016), NE, No inhalation MRL has been established.

MRLs are derived using the no-observed-adverse-effect level/uncertainty factor approach. They are established below concentrations that might cause adverse health effects in the people most sensitive to such chemical-induced effects. MRLs are derived for acute (1–14 days), intermediate (15–364 days), and chronic (365 days and longer) durations and for the oral and inhalation routes of exposure. Exposure to a level above the MRL does not mean that adverse health effects will occur (ATSDR, 2016).

Table 5.7 provides the published MRLs for volatile crude oil constituents.

5.5 IDENTIFICATION OF CRITICAL VOLATILE ORGANICS DURING CRUDE OIL RELEASES

The USEPA has established standardized analytical methods for profiling VOC content in ambient air using gas chromatography/mass spectrometry (GC/MS) technology. These methods are appropriate for use in

TABLE 5.8 Description of Three Crude Oil Release Events[a]

	Events 1A and 1B	Event 2	Event 3
Event type	Pipeline Release	Pipeline Release	Railcar release
Type of oil released	Heavy crude oil	Crude petroleum oil	Light sweet crude oil
Flash point	<21°C	<23°C	<40°C
Shipping name	Petroleum crude oil (sour)	Petroleum crude oil (sweet)	Petroleum crude oil
Hazard class and division	3	3	3
Packing group	II	NA	II
Sulfur content	>1%	<1%	<1%
Boiling point/range	>35°C	>38°C	>35°C
Average temperature	53.6°F	53.8°F	48°F
Average humidity	90	88	66
Average atmospheric pressure at sea level	30.2 mmHg	30.1 mmHg	30.2 mmHg

[a]*Events 1A and 1B are samples taken during the initial phase of the same event in two geographically distinct locations. To maintain anonymity, the identity of the responsible parties and locations of the releases have been withheld (Harrill et al., 2014).*

profiling VOCs released from crude oil. In order to identify the chemicals of concern following a release of crude oil, the analysis of airborne VOC levels in the context of community and worker health protective standards and guidelines provides a means to prioritize chemicals during crude oil releases. Previous analysis has been conducted using the PAC value database to analyze VOCs detected in the breathing zone air above or in the direct vicinity of freshly released crude oil to prioritize target analytes for worker and community air monitoring (Harrill et al., 2014). Similar to the criteria used to establish PAC values for use in the community, critical health protective values (CHPV) were established for crude oil release response workers based on chemical specific OELs derived from the lower of the OSHA PEL-TWA, NIOSH REL-TWA, or ACGIH TLV-TWA values. The CHPV was then used to prioritize target analytes in a work zone surrounding a crude oil release (Harrill et al., 2014).

Harrill et al. (2014) evaluated VOC air concentrations derived from samples of ambient air taken in the breathing zones above or in the direct vicinity of various pipeline and rail transportation crude oil releases. Analytical air samples were collected over a 24-hour period in stainless steel canisters prepared for analysis of VOCs as target analytes and Tentatively Identified Compounds (TICs) using USEPA Method TO-15. Target compounds are those for which standard curves have been measured by the analytical laboratory for use in quantifying a chemical concentration. TICs are chemicals which can be identified and whose quantity can be estimated using an analytical method, but for which a standard curve has not been established. A description of the crude oil release scenarios is provided in Table 5.8.

A summary of the VOC concentrations of target compounds and TICs detected in crude oil air samples is presented in Table 5.9. Detections of VOCs included aromatic hydrocarbons (BTEX compounds), cyclic hydrocarbons with varying degrees of ethyl and methyl substitutions, aliphatic straight chain hydrocarbons, and aliphatic branched chain hydrocarbons. The frequency of detection across samples varied for different VOCs. Benzene, toluene, hexane, heptane, octane, cyclohexane, methylcyclohexane, trans-1,2-dimethylcyclopentane, 2-methylpentane, 2-methylhexane and 2-methylheptane were reported in all samples collected. The mean concentrations of the majority of VOCs were below 1 ppm. The highest reported concentrations included isobutane, hexane, pentane, and 2-methylbutane at concentrations of 1.10, 1.15, 2.30 and 3.40 ppm, respectively (Harrill et al., 2014).

Table 5.10 lists PAC-1 and PAC-2 values as well as the worker CHPVs for VOCs detected in crude oil releases. Ratios were calculated by dividing the mean VOC concentration detected in crude oil air samples by either the PAC-1, PAC-2, or CHPV values. PAC-1, PAC-2, or CHPV ratios higher than 1.0 demonstrate concentrations of chemicals in the air in the vicinity of released crude oil exceeded these exposure values. As demonstrated in Table 5.10, none of the VOCs detected in crude oil air samples exceeded the PAC-1 or PAC-2 health protective criteria. Benzene was detected at levels approximately 1.5 times greater than the CHPV value of 0.1 ppm.

VOCs were ranked according to the respective PAC-1, PAC-2, or worker CHPV ratios in order to prioritize which VOCs may represent potential target analytes for community and worker exposure during an oil release response as presented in Table 5.11.

These data indicate the prioritization of potential target analytes will vary depending upon the receptor (i.e., worker or general public) under consideration for implementing a health protective air-monitoring plan

TABLE 5.9 Air Concentrations (ppm) of VOCs and TICs Detected in Air Sampled in Proximity to Released Crude Oil

			Concentration (ppm)				
			Event				
Analyte	CAS	Classification[a]	1A	1B	2	3	Mean conc. (ppm)
AROMATIC HYDROCARBONS							
Benzene	71-43-2	Target	0.04	0.11	0.29	0.18	0.16
Toluene	108-88-3	Target	0.05	0.11	0.58	0.12	0.21
Ethylbenzene	100-41-4	Target	–	–	0.10	–	0.10
Xylenes[b]	Multiple	Target	–	–	0.54	–	0.54
Trimethylbenzene[c]	Multiple	Target	–	–	0.18	–	0.18
4-Ethyltoluene	622-96-8	Target	–	–	0.03	–	0.03
CYCLIC HYDROCARBONS							
Methylcyclobutane	598-61-8	TIC	0.15	0.47	–	–	0.31
Cyclohexane	110-82-7	Target	0.09	0.27	0.73	0.35	0.36
Methylcyclohexane	108-87-2	TIC	0.15	0.40	0.98	0.16	0.42
Ethylcyclohexane	1678-91-7	TIC	–	–	0.13	–	0.13
1,3-Dimethylcyclohexane	591-21-9	TIC	–	–	0.14	–	0.14
cis-1,3-Dimethylcyclohexane	638-04-0	TIC	0.03	0.06	–	0.06	0.05
1,1,3-Trimethylcyclohexane	3073-66-3	TIC	–	–	0.08	–	0.08
Methylcyclopentane	96-37-7	TIC	0.24	0.73	0.07	–	0.35
Ethylcyclopentane	1640-89-7	TIC	–	–	0.20	–	0.20
1,1-Dimethylcyclopentane	1638-26-2	TIC	–	–	0.10	–	0.10
cis-1,2-Dimethylcyclopentane	1192-18-3	TIC	0.03	0.08	–	0.06	0.06
trans-1,2-Dimethylcyclopentane	822-50-4	TIC	0.04	0.10	0.27	0.09	0.12
1,3-Dimethylcyclopentane	2453-00-1	TIC	0.03	0.08	–	0.06	0.05
cis-1,3-Dimethylcyclopentane	1759-58-6	TIC	–	–	0.18	–	0.18
1,2,3-Trimethylcyclopentane	15890-40-1	TIC	–	–	–	0.03	0.03
1,2,4-Trimethylcyclopentane	4850-28-6	TIC	–	–	–	0.03	0.03
ALIPHATIC STRAIGHT CHAIN HYDROCARBONS							
Propane	74-98-6	TIC	0.04	0.12	–	–	0.08
Butane	106-97-8	TIC	0.72	2.10	–	0.08	0.97
Pentane	109-66-0	TIC	1.10	3.50	–	–	2.30
Hexane	110-54-3	Target	0.30	1.10	1.30	1.90	1.15
Heptane	142-82-5	Target	0.10	0.24	0.84	0.49	0.42
Octane	111-65-9	TIC	0.04	0.10	0.28	0.06	0.12
Nonane	111-84-2	TIC	–	–	0.17	0.03	0.10
Decane	124-18-5	TIC	–	–	0.12	–	0.12
ALIPHATIC BRANCHED CHAIN HYDROCARBONS							
2-Methylbutane	78-78-4	TIC	–	3.40	–	–	3.40
2,2-Dimethylbutane	75-83-2	TIC	0.04	0.12	–	–	0.08
Isobutane	75-28-5	TIC	–	1.10	–	–	1.10
2-Methylpentane	107-83-5	TIC	0.46	1.40	0.08	0.13	0.52
3-Methylpentane	96-14-0	TIC	0.25	0.74	–	0.08	0.36

(*Continued*)

TABLE 5.9 (*Continued*)

			Concentration (ppm)				
			Event				
Analyte	CAS	Classification[a]	1A	1B	2	3	Mean conc. (ppm)
2,3-Dimethylpentane	565-59-3	TIC	–	–	0.16	0.03	0.09
2-Methylhexane	591-76-4	TIC	0.07	0.16	0.44	0.07	0.18
3-Methylhexane	589-34-4	TIC	0.07	0.17	0.48	–	0.24
2-Methylheptane	592-27-8	TIC	0.04	0.09	0.22	0.07	0.10
3-Methylheptane	589-81-1	TIC	–	–	0.12	–	0.12
2,6-Dimethyl-2-octene	2216-33-3	TIC	–	–	0.10	–	0.10
2,3-Dimethylnonane	4057-42-5	TIC	–	–	0.07	–	0.07

[a]*Target = target compounds for USEPA TO-15 GC/MS. TIC = Tentatively identified compound for US EPA TO-15 GC/MS.*
[b]*There are three isomers of xylene including* m-, p-, *and* o-*xylene (CAS #: 103-38-3, 106-42-3 and 108-38-3, respectively). In the PAC database, CAS# 1330-20-7 refers to total xylene isomers. Here all xylene isomers detected were summed within each event and averaged to obtain the mean concentration.*
[c]*There are three isomers of trimethylbenzene including 1,2,3-trimethylbenzene, 1,2,4-trimethylbenzene and 1,3,5-trimethylbenzene (CAS #: 526-73-8, 95-63-6, 108-67-8, respectively). In the PAC database, each isomer is individually indexed. In this analysis, all trimethylbenzene isomers detected were summed within each event and averaged to obtain the mean concentration (Harrill et al., 2014).*

TABLE 5.10 PAC and CHPV Values for Selected VOCs Detected in Air Samples Collected in the Vicinity of Released Crude Oil

	PAC-1 value		PAC-2 value		Worker CHPV[a]				
Analyte	ppm	Source	ppm	Source	ppm	Source	PAC-1 ratio	PAC-2 ratio	CHPV ratio
Benzene[b]	52	AEGL	800	AEGL	0.1	NIOSH	0.0030	0.0002	1.5500
Toluene[b]	200	AEGL	1200	AEGL	20	ACGIH	0.0011	0.0002	0.0107
Ethylbenzene[b]	33	AEGL	1100	AEGL	100	OSHA/NIOSH/ACGIH	0.0030	0.0001	0.0010
Xylenes[b]	130	AEGL	920	AEGL	100	OSHA/NIOSH/ACGIH	0.0042	0.0006	0.0054
Trimethylbenzenes[b]	140	AEGL	360	AEGL	25	NIOSH/ACGIH	0.0013	0.0005	0.0070
4-Ethyltoluene[b]	12	TEEL	130	TEEL	–	–	0.0028	0.0003	–
Cyclohexane[b]	100	TEEL	100	TEEL	100	ACGIH	0.0036	0.0036	0.0036
Methylcyclohexane[c]	400	TEEL	400	TEEL	400	NIOSH/ACGIH	0.0011	0.0011	0.0011
Methylcyclopentane[c]	0.77	TEEL	8.5	TEEL	–	–	0.4489	0.0407	–
Propane[c]	5500	AEGL	17,000	AEGL	1000	OSHA/NIOSH/ACGIH	>0.0001	>0.0001	0.0001
Butane[c]	5500	AEGL	17,000	AEGL	800	NIOSH	0.0002	0.0001	0.0012
Pentane[c]	120	TEEL	610	TEEL	120	NIOSH	0.0192	0.0038	0.0192
Hexane[b]	300	TEEL	3300	AEGL	50	NIOSH/ACGIH	0.0038	0.0003	0.0230
Heptane[b]	440	TEEL	440	TEEL	85	NIOSH	0.0009	0.0009	0.0049
Octane[c]	300	TEEL	385	TEEL	75	NIOSH	0.0004	0.0003	0.0016
Nonane[c]	200	TEEL	200	TEEL	200	NIOSH/ACGIH	0.0005	0.0005	0.0005
Decane[c]	1.9	TEEL	20	TEEL	–	–	0.0632	0.0060	–
2-Methylbutane[c]	600	TEEL	610	TEEL	–	–	0.0057	0.0056	–
2,2-Dimethylbutane[c]	510	TEEL	510	TEEL	–	–	0.0002	0.0002	–
Isobutane[c]	800	TEEL	800	TEEL	800	NIOSH	0.0014	0.0014	0.0014
2-Methylpentane[c]	510	TEEL	510	TEEL	–	–	0.0010	0.0010	–
3-Methylpentane[c]	510	TEEL	510	TEEL	–	–	0.0007	0.0007	–
2-Methylheptane[c]	300	TEEL	385	TEEL	–	–	0.0003	0.0003	–

[a]*The worker critical health protective value (CHPV) is the minimum value amongst OSHA, NIOSH, and ACGIH TWA values. Where multiple sources are listed, values are the same from each source (Harrill et al., 2014).*
[b]*Target, USEPA TO-15 method.*
[c]*TIC, USEPA TO-15 method.*

TABLE 5.11 Comparative Ranking of Selected VOCs Using Worker or Community Health Criteria

Analyte	Worker CHPV ratio rank	PAC-1 ratio rank	PAC-2 ratio rank
Benzene	1	9	18
Hexane	2	6	14
Pentane	3	3	4
Toluene	4	13	19
Trimethylbenzenes	5	12	13
Xylenes	6	5	11
Heptane	7	16	9
Cyclohexane	8	7	5
Octane	9	19	15
Isobutane	10	11	6
Butane	11	21	22
Methylcyclohexane	12	14	7
Ethylbenzene	13	8	21
Nonane	14	18	12
Propane	15	23	23
4-Ethyltoluene	–	10	17
2,2-Dimethylbutane	–	22	20
2-Methylbutane	–	4	3
Methylcyclopentane	–	1	1
Decane	–	2	2
2-Methylheptane	–	20	16
2-Methylpentane	–	15	8
3-Methylpentane	–	17	10

As presented in Harrill et al. (2014).

and what standards or guidelines are considered. In addition, these data provide insight on potential chemicals that should be considered for air-monitoring analysis following a crude oil release scenario.

5.6 AIR MONITORING STRATEGIES

Continuous or frequent air monitoring should be employed following a crude oil release to measure concentrations of different constituents in the air during the response. Common examples of real-time instruments which can be used to monitor hydrocarbon vapors and gases include multigas meters equipped with photoionization detectors (PIDs) and chemical-specific colorimetric detection tubes. PID equipped multigas meters are not chemical-specific; however, these instruments provide a readout for total VOCs which is appropriate for general monitoring of the complex mixtures of hydrocarbon vapors which are emitted from crude oil. Colorimetric detector tubes are chemical-specific and can be used to detect individual hydrocarbon constituents of crude oil which may be present as vapors. There are also some chemical-specific real-time instruments, such as benzene and hydrogen sulfide monitors. In addition to real-time air monitoring, analytical air sampling should be performed as a method to supplement real-time air-monitoring efforts during a crude oil release. Analytical air sampling may include ambient air and personal exposure sampling. As previously discussed, it is important to determine the potential chemicals of concern which will require air monitoring during a crude oil release as well as establishment of health-protective occupational and community exposure levels as a comparison for air monitoring

results. In order to conduct air monitoring during a crude oil release, it is necessary to select the appropriate air monitoring equipment and methodologies as well as have an understanding of the strengths and limitations of the air monitoring equipment which may be available during an oil-spill response.

5.6.1 Real-Time Air Monitoring

Real-time air monitoring refers to the use of direct-reading instruments that report nearly instantaneous measurements of an airborne substance in real-time. These data can be used to quickly evaluate air quality and identify conditions that may have an impact on community and/or worker health and safety. Real-time air monitoring can be performed at locations accessible by workers or community members using handheld instruments or stationary, remote-telemetering instruments. Real-time air monitoring may be performed using multigas meters with PIDs, flammability and chemical-specific sensors. The PIDs can be used to detect volatile components of the spilled oil and chemical specific sensors (or colorimetric detector tubes as a secondary instrument) may be used for chemical specific analysis in the event that elevated VOCs are detected using a PID.

Air monitoring should be conducted at selected locations that address remediation worker and potential off-site receptors, accounting for possible changes in wind direction. In addition, air monitoring should be conducted as needed in response to potential concerns or complaints raised on- or off-site during a crude oil response. The locations selected and the level of real-time-monitoring efforts should be determined based on the type, size, and location of the operation. At a minimum, real-time air-monitoring readings should be taken at several locations around the operations and at different distances from the operations in order to characterize the site and its perimeter. In addition, real-time air monitoring should be conducted at continuous intervals downwind until there are sufficient data to indicate a crude-oil-related constituent is not a concern for potential inhalation hazards.

Table 5.12 presents examples of available instrumentation for real-time air monitoring of crude oil constituents. Real-time instruments should be calibrated in accordance with the manufacturer's recommendations.

5.6.2 Analytical Air Sampling

Analytical air sampling refers to the collection of discrete air samples over a specified time period. Collected samples are submitted to an analytical laboratory for chemical analysis. Laboratory analysis of analytical air samples generally provides chemical-specific results at lower detection limits than real-time instrumentation. Depending upon the sampling duration, the results of analytical air samples may be directly compared to available screening criteria or standards, such as the ATSDR acute MRLs, ACGIH TLVs, and OSHA PELs. Many of the analytical methods used for analysis of crude oil constituents in analytical air samples are approved by federal agencies and organizations such as the USEPA, OSHA, and NIOSH. Table 5.13 presents analytical air sampling methodology for crude oil constituents.

The turnaround time for laboratory analysis of analytical air samples is generally 24 hours or more. To effectively monitor a community potentially impacted by an emergency release of crude oil, responders should

TABLE 5.12 Real-Time Air-Monitoring Equipment

	Instrument/Sensor	Constituent
Particulate monitor	Size-selective impactor	PM_{10}
		$PM_{2.5}$
Multigas meter	Photoionization detector (PID)	VOCs
	Photoionization detector with chemical separator tube	Benzene
	Flammable atmosphere sensor	LEL
	Electrochemical-specific sensors	SO_x, NO_x, CO, CO_2, H_2S
Gas sampling pumps	Colorimetric detector tubes + piston pump	SO_x, NO_x, CO, CO_2, H_2S, benzene, hexane, naphthalene, toluene, xylene

TABLE 5.13 Analytical Air Sampling Methods for Crude Oil-Associated Constituents

Constituent(s)	Sampling method(s)	Sampling media
Volatile organic compounds	USEPA Method TO-15	Evacuated canisters (e.g., Minican and SUMMA Canister)
Polycyclic aromatic hydrocarbons	USEPA Method TO-13	Sorbent cartridges (e.g., polymeric adsorbent)
Benzene, toluene, ethylbenzene, xylene, hexane (BTEX + hexane)	NIOSH Methods 1500/1501	Solid sorbent tubes; passive dosimeter badges (e.g., organic vapor monitors)
Hydrogen sulfide	OSHA Method 1008	Sampling tubes with silver nitrate coated silica gel.
Formaldehyde	OSHA Method 52	Sampling tubes with polymeric adsorbent coating
Sulfur dioxide	OSHA Method ID-200	Impregnated activated beaded carbon tubes
Nitrogen dioxide	OSHA Method ID-182	Triethanolamine impregnated molecular sieves

consider an air monitoring and sampling strategy that includes real-time air monitoring to rapidly identify areas of potential concern, in addition to the collection of analytical air samples for comparison to screening criteria.

5.7 CASE STUDY—AIR MONITORING DURING THE *DEEPWATER HORIZON* OIL SPILL

A key role for various environmental consultants during the Deepwater Horizon oil spill included addressing potential worker and community health concerns related to crude oil vapors. The following sections describe the approach used to identify chemicals of concern in air samples taken above fresh crude oil emerging at the surface of the Gulf of Mexico directly above the release site in addition to heavily weathered floating crude oils distant from the source where manual oil recovery operations (i.e., skimming) were conducted.

5.7.1 Sampling and Analysis of *Deepwater Horizon* Crude Oil From the Sea Surface

The crude oil released by the *Deepwater Horizon* oil spill was a "light, sweet" crude oil, which is often referred to as MC252 or Macondo oil. Due to the presence of volatile organics in the source oil, the released product was affected by dissolution of more water soluble organics as the oil traveled to the ocean surface. Surfaced oil also experienced significant weathering over time and distance through the effects of wind, sun, and wave action as the floating oils traveled with the ocean currents. Three samples of significantly weathered MC252 oil, collected from the sea surface at various distances from the source and several days after surfacing, were submitted for whole oil (C3−C44) analysis at a forensic laboratory. These weathered crude oil samples were also analyzed for PAHs using a modified EPA Method 8270. The lowest molecular weight hydrocarbon detected in the whole oil analysis was the alkane *n*-C14 (labeled on Fig. 5.2). Naphthalene, a semivolatile PAH compound, which elutes earlier than *n*-C14 and was present above detection limits at only 0.1 mg/kg oil. The more volatile VOCs, including BTEX, were not detected. Analysis of VOCs in six other less weathered MC252 oils also found no detections of benzene, whereas variable levels of toluene, ethylbenzene, and xylene were detected (Stout et al., 2016).

Results of whole oil analysis from the forensic laboratory demonstrated that the significantly weathered oil was comprised of hydrocarbons greater than C14, indicating that the volatile fraction of the oil was lost to weathering prior to sampling. The chromatogram presented in Fig. 5.2 illustrates the distribution and relative abundance of hydrocarbons in a significantly weathered MC252 oil, including an absence of hydrocarbons below C14.

Results of PAH analysis indicate that naphthalene, the lightest and most volatile PAH tested was detected slightly above the 0.1-mg/kg detection limit. The chromatogram presented in Fig. 5.2 illustrates the distribution and relative abundance of PAHs and alkylated PAHs in the highly weathered MC252 crude oil samples studied. It is notable that the most abundant PAH species present were the phenanthrenes/anthracenes, and there were very small concentrations of the higher molecular weight (carcinogenic) PAHs, if any (Fig. 5.3). An extensive analysis of weathering in 62 floating MC252 oils showed a range of naphthalene concentrations from 0.2 to 346 mg/kg in floating oils of various weathering conditions (Stout et al., 2016). Fig. 5.3

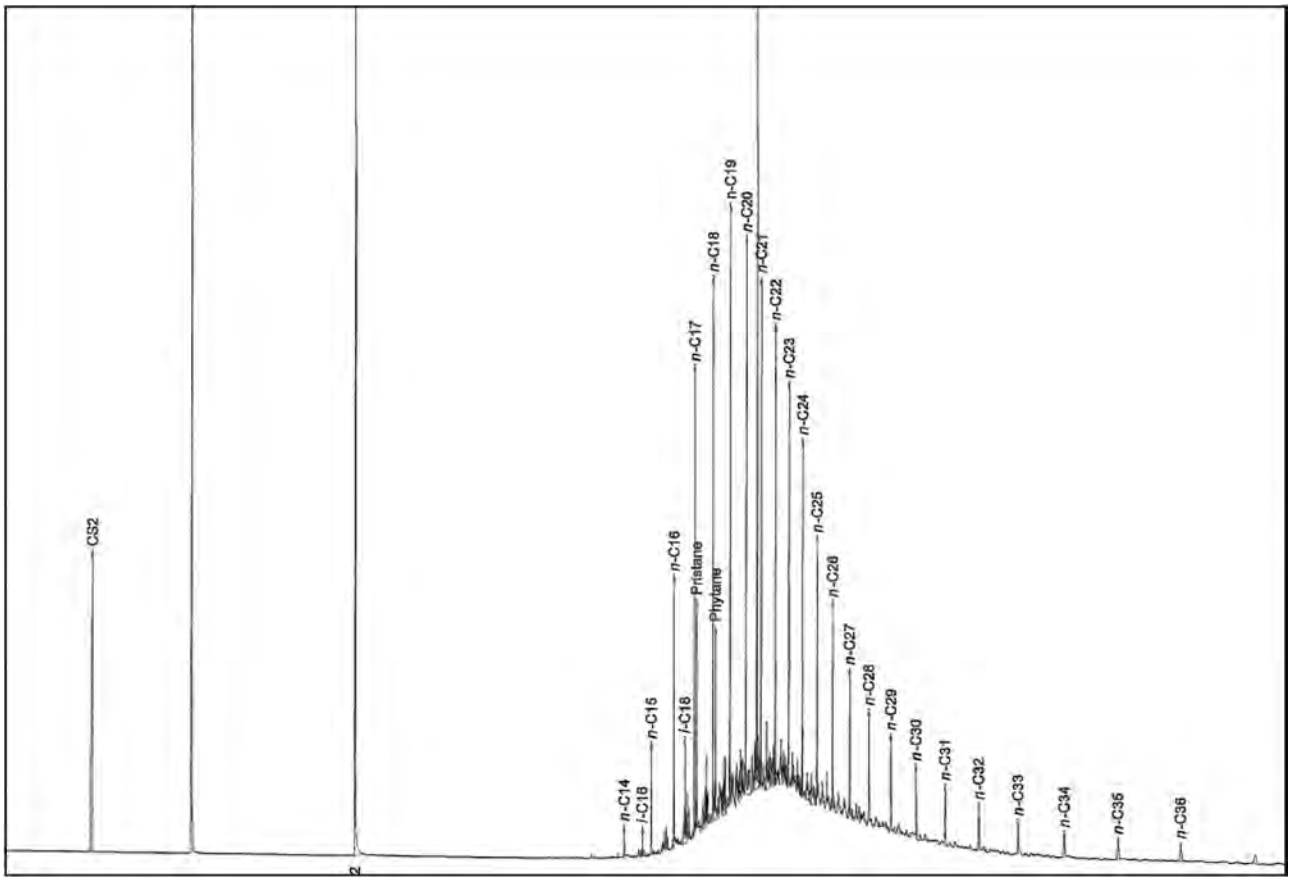

FIGURE 5.2 GC/FID chromatogram for a weathered MC252 crude oil.

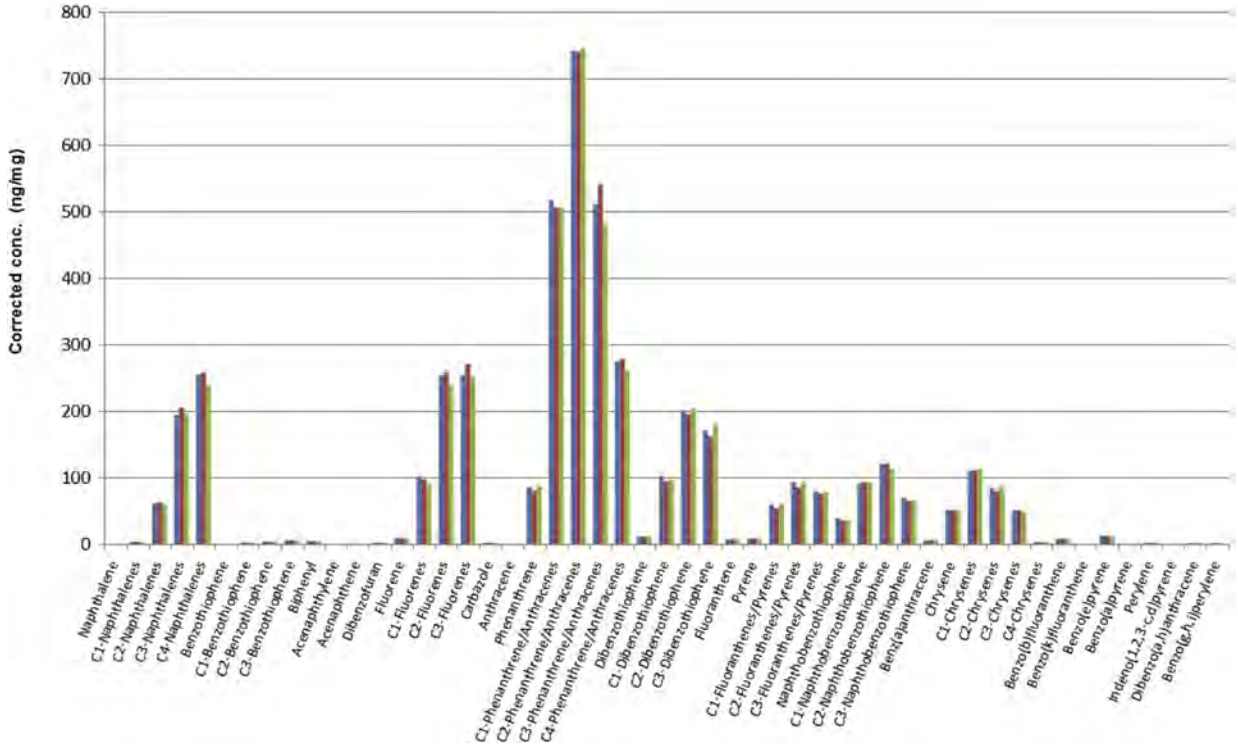

FIGURE 5.3 Distribution and relative abundance of PAHs in three weathered MC252 crude oils collected from the sea surface.

5.7.2 Chemistry of Vapors From the *Deepwater Horizon* Oil Spill

In order to identify the chemical composition and concentration of crude oil vapors present in air from MC252 crude oil reaching the sea surface, environmental consultants collected a series of whole air samples using evacuated canisters from directly above freshly surfaced MC252 crude oil upon reaching the surface of the Gulf of Mexico at the release point. The data obtained from these studies were then used to help guide decisions regarding the potential chemicals of concern in crude oil vapor to the public and to workers engaged in cleanup activities.

Two 6-L evacuated canisters were used to collect whole air samples approximately 3 ft above the surface of freshly surfaced MC252 crude oil from the construction vessel Skandi Neptune. Samples were sent to an analytical laboratory for analysis using USEPA Method TO-15 with analysis of TICs. An additional four evacuated canister whole air samples were collected from the relief well drilling rig Q4000 adjacent to the leaking well and from the multipurpose offshore vessel BOA SUB C that was positioned directly above the surfacing oil. These air samples were collected approximately 3 ft above the surface of crude oil slicks and also on the decks of the Q4000 and BOA SUB C and sent to the same analytical laboratory for analysis. The results of all six evacuated canister air samples are provided in Table 5.14. Samples 1 and 2 were collected approximately 3 ft about the surface of freshly surfaced MC252 oil from the Skandi Neptune. Sample 3 was collected approximately 3 ft above the surface of the crude oil slick by the Q4000. Sample 4 was collected from the deck of the Q4000 and is representative of worker locations. Sample 5 was collected immediately above the surface of crude oil by the BOA SUB C positioned above the leaking well. Sample 6 was collected from the deck of the BOA SUB C and is representative of worker locations, areas where combustion engines were operating, and locations other petroleum sources were present.

Inspection of Table 5.14 shows very low concentrations of benzene and naphthalene were detected, if any, and the levels of toluene, ethylbenzene, and xylene, traditionally some of the chemicals of greatest concern in fresh crude oil releases, were very low. The most likely cause of the low concentrations of BTEX compounds and naphthalene was their significant dissolution into the water column during the MC252 oil's ascent to the sea surface from the spill site near the sea floor, more than 5000 ft below the surface of the Gulf of Mexico (Stout et al., 2016) Thus, the product that reached the water surface was already "weathered" crude oil, in a sense, with the least water soluble, heavier organics predominating. As indicated by extensive real-time air monitoring during weathered crude oil recovery operations, the surfaced oil continued to weather over time due to sunlight, wind, and wave action until very low to nondetectable concentrations of VOCs were observed in the worker breathing space or in communities whose shores were impacted by crude oil. In essence, due to weathering processes, the primary risk of exposures being attributed to crude oil vapors gave way to that of dermal exposures in workers during recovery of oil and equipment decontamination.

The other chemicals detected in the analyses of air samples over freshly surfaced crude oil consisted mainly of methylated alkanes and aromatics (Table 5.14). These results were then used to inform the development of a list of indicator compounds for the *Deepwater Horizon* oil and subsequent worker and community health approaches. Finally, as expected with a light sweet crude oil, hydrogen sulfide was not detected in the air over freshly surfaced oil or weathered oil at sea.

5.8 CASE STUDY—COMPARISON OF HYDROCARBON VAPOR PROFILES AND INHALATION HAZARD POTENTIAL IN BAKKEN VS NON-BAKKEN LIGHT SWEET CRUDE OILS

Since the beginning of this century, a large increase in oil production from the Bakken formation in the northern United States (i.e., Montana, North Dakota) and southern Canada (i.e., Saskatchewan and Manitoba) has occurred, due largely to the widespread application of horizontal drilling and hydraulic fracturing technologies (Nordeng, 2010). Coincident with this increased production was an increase in the volume of crude oil being shipped via railroad and a series of train derailments which involved full or partial loss of lading from crude oil tank cars and large fires. The events prompted speculation that the properties of Bakken light sweet crude oil (API Gravity 40°–43°) (Auers et al., 2014) may differ from light crude oils produced in other geographical regions, particularly in terms of light end hydrocarbon content and flammability. It follows, that if the volatile components of Bakken crude oil produced using hydraulic fracturing technologies differ significantly from that

TABLE 5.14 Compounds Detected in Air Samples Collected Above Freshly Surfaced MC252 Crude Oil and on a Rig or Vessels Near Spilled Oil During the *Deepwater Horizon* Oil Spill Response

	Analytical air sample results					
Chemical	**Sample 1 (ppb)**	**Sample 2 (ppb)**	**Sample 3 (ppb)**	**Sample 4 (ppb)**	**Sample 5 (ppb)**	**Sample 6 (ppb)**
Benzene	4.8J	ND	ND	ND	ND	6.4
Cyclohexane	107	204	36.4	5.9	14.9	372
Dichlorodifluoromethane	ND	ND	ND	1.6	1.4	ND
Ethanol	41.1	6.8	ND	ND	ND	ND
Ethyl acetate	162	ND	ND	ND	3.3	ND
Ethylbenzene	6.1J	8.9	10.8	ND	1.6	69.1
4-Ethyltoluene	4.1J	7.8	17.8	ND	ND	131
n-Heptane	143	302	52.0	10	19.7	237
Toluene	25.4	22.6	14.3	ND	4.6	99
1,2,4-Trimethylbenzene	13.1	29.7	92.4	4.7	3.0	145
1,3,5-Trimethylbenzene	4.7J	11.4	31.2	1.9	ND	63.6
m&p-Xylene	29.1	50.4	70.8	3.7	8.0	237
o-Xylene	9.1	15.4	27.3	1.5	2.6	109
n-Hexane	ND	300	50.9	10.2	22.6	222
2-Propanol	4.6J	ND	ND	ND	ND	ND
Naphthalene	3.5J	11.9	19.2	ND	ND	ND
Propylene	17.6	23.1	ND	ND	ND	ND
Tetrachloroethene	ND	ND	ND	2.0	ND	ND
THC as Gas	3730	5370	5550	847	645	15200
TENTATIVELY IDENTIFIED COMPOUNDS						
Carbon dioxide	314	66.0	ND	ND	ND	ND
Isobutane	63.6	ND	ND	ND	ND	ND
Butane, 2-methyl-	43.4	68.4	ND	ND	13.8	ND
Pentane, 2-methyl	40.4	76.4	ND	5.51	13.1	ND
Pentane, 3-methyl-	ND	ND	ND	ND	6.26	13.2
1H-Tetrazole, 5-methyl-	41.8	ND	ND	ND	8.42	ND
Pentane, 3-ethyl-3-methyl-	34.8	ND	ND	ND	ND	ND
Hexane, 3-methyl-	134	ND	ND	ND	6.42	ND
Cyclohexane, methyl-	108	218	78.0	1.08	25.9	38.0
Hexane, 2,5-dimethyl	32.5	ND	ND	ND	ND	ND
Cyclohexane, 1,3-dimethyl-	51.8	113	ND	ND	12.0	1330
Octane	83.6	174	98.7	13.7	21.5	1620
Cyclohexane, 1,2-dimethyl-	19.0	ND	ND	ND	6.80	ND
Cyclohexane, ethyl-	28.0	61.6	ND	ND	6.13	1400
Heptane, 2,3-dimethyl	21.8	53.6	ND	ND	ND	ND
Octane, 4-methyl-	32.0	ND	95.7	ND	11.2	ND

(*Continued*)

TABLE 5.14 (*Continued*)

	Analytical air sample results					
Chemical	**Sample 1 (ppb)**	**Sample 2 (ppb)**	**Sample 3 (ppb)**	**Sample 4 (ppb)**	**Sample 5 (ppb)**	**Sample 6 (ppb)**
Nonane	66.4	ND	186	22.1	21.4	ND
Cyclohexane, propyl-	33.5	78.5	134	12.4	9.96	1110
Decane	47.4	118	191	22.5	11.2	704
Cyclohexane, butyl-	20.8	ND	ND	ND	ND	ND
Butane	ND	47.5	ND	ND	ND	ND
Pentane	ND	88.8	ND	ND	ND	ND
Cyclopentane, methyl-	ND	56.5	ND	ND	ND	16.2
Hexane, 2-methyl-	ND	62.5	ND	ND	5.86	ND
Pentane, 2,3,4-trimethyl-	ND	141	ND	ND	ND	ND
Cyclohexane, 1-ethyl-2-meth	ND	59.9	ND	ND	ND	806
Cyclohexane, 1-ethyl-2-meth	ND	54.8	ND	ND	ND	ND
Undecane	ND	97.5	220	18.2	6.01	ND
Dodecane	ND	65.6	ND	ND	ND	ND
Benzene, 1-ethyl-2-methyl-	ND	ND	69.8	ND	ND	731
Cyclohexane, 1-methyl-2-pro	ND	ND	91.6	5.95	ND	ND
Benzene, 1-ethyl-3-methyl-	ND	ND	60.9	ND	ND	ND
Cyclohexane, butyl-	ND	ND	81.2	7.25	ND	ND
Benzene, 1-methyl-3-propyl	ND	ND	73.0	ND	ND	ND
Benzene, 1-methyl-4-(1-meth	ND	ND	67.1	ND	ND	ND
Benzene, propyl-	ND	ND	ND	ND	ND	950
Naphthalene, decahydro-2-me	ND	ND	67.1	ND	ND	ND
Naphthalene, decahydro-2-me	ND	ND	98.5	ND	ND	ND
Cyclohexane, pentyl-	ND	ND	85.3	5.38	ND	ND
Naphthalene, decahydro-	ND	ND	ND	6.12	ND	ND
Cyclopentane, 1,2,3-trimeth	ND	ND	ND	1.08	ND	7.87
Cyclopentane, 1,2,4-trimeth	ND	ND	ND	ND	ND	8.16
Heptane, 2-methyl-	ND	ND	ND	5.53	9.48	ND
Cyclohexane, 1,4-dimethyl	ND	ND	ND	6.52	ND	528
Nonane, 2-methyl	ND	ND	ND	5.90	ND	ND
Benzene, 1-methyl-2-propyl-	ND	ND	ND	5.38	ND	ND
Cyclopentane, 1,2-dimethyl	ND	ND	ND	ND	5.35	ND
Cyclopentane, 1,3-dimethyl-	ND	ND	ND	ND	ND	13.7
Hexanedioic acid, .alpha. −k	ND	ND	ND	ND	4.63	ND
Hexane, 3-ethyl-	ND	ND	ND	ND	ND	390
2,2-Dimethyl-1-oxa02-silacy	ND	ND	ND	ND	ND	987
Undecane, 2,5-dimethyl-	ND	ND	ND	ND	ND	371

ppb, parts per billion; *ND*, not detected.

of light sweet crude oils produced outside the Bakken formation, then the human health hazards associated with inhalation of Bakken crude oil vapors may also differ.

To test this hypothesis, a headspace sampling and analysis method was used to characterize hydrocarbon vapor profiles from Bakken and non-Bakken crude oils. Fresh crude oil samples were collected in 16 oz. glass jars from various facilities producing oil from the Bakken shale ($n = 3$) or other areas within the Williston Basin of North Dakota, but not within the Bakken formation ($n = 3$). The sample jars were filled to approximately 3/4 capacity and sealed immediately after sample collection. Each sample jar was allowed to equilibrate to ambient temperature for 10 minutes. The jar was then opened and an instantaneous (i.e., "grab") whole air sample was collected inches above the captured oil using a 6-L SUMMA canister. The canisters were then shipped to a certified industrial hygiene laboratory for analysis of VOCs using US EPA GC/MS TO-15 Method. The concentrations of target analytes and TICs were compared across samples.

The pie charts in Fig. 5.4 summarize the volatile hydrocarbon mixtures (VHMs) detected in each of the Bakken and non-Bakken whole air samples. The VHM constituents are coded by hydrocarbon type (i.e., aromatic, straight or branched-chain paraffinic or naphthenic) and carbon content. Bar graphs to the right of each set of pie charts present the average VHM composition for each type of crude. Individual constituents detected in the vapor sample are listed in the chart on the right of Fig. 5.4. Qualitatively, there was no marked, systematic difference in the vapor profiles corresponding to Bakken and non-Bakken oil samples. Vapors from both types of oils contained a small percentage of benzene and other C7–C8 aromatic hydrocarbons with a near complete absence of C9–C15 aromatics (save 1,2,4-trimethylbenzene detected in a single Bakken sample). The VHM from each oil type primarily consisted of straight and branched-chain aliphatic hydrocarbons in the C5–C6 range.

To compare the hazardous potential of VHMs from Bakken and non-Bakken crude oil, OELs were calculated for each using the ACGIH Reciprocal Calculation Method for Refined Hydrocarbon Vapor Mixtures (ACGIH, 2014a). Although this method is primarily intended to evaluate the inhalation hazard of refined petroleum products where the composition of light hydrocarbons in the liquid phase has been characterized, this method is also applicable for evaluating inhalation hazards from unrefined hydrocarbon sources where vapor phase constituents have been measured (ACGIH, 2014a). The method calculates an OEL by quantifying the relative percentage of aromatic, paraffinic (i.e., alkanes) and naphthenic (i.e., cycloalkanes) in a VHM using group guidance values (GGVs) which are representative toxicity values assigned to each hydrocarbon class. The equation shown in Fig. 5.5 is then used to calculate a GGV for the mixture ($GGV_{mixture}$), which serves as a single OEL. To calculate the $GGV_{mixture}$, ACGIH recommends GGV values from two different literature sources: McKee et al. (2005) and UKHSE (2000) as listed in Table 5.15. Of note, the Reciprocal Calculation Method is applicable if the individual components of a VHM have similar toxicological effects on the same target organ or system and assumes that the principal effects from exposure to the VHM are acute nervous system depression and eye/respiratory tract irritation. Benzene, a known human carcinogen with an ACGIH TLV of 0.5 ppm, is not included in the Reciprocal Calculation Method and should always be monitored in parallel with total hydrocarbons during instances where exposure to crude oil vapors is a possibility. The Reciprocal Calculation Method also indicates that chemicals which could potentially be present in the VHM and have either individual TLVs below the calculated $GGV_{mixture}$ or critical effects outside of CNS depression or acute respiratory irritation be monitored in parallel with total hydrocarbons. Such hydrocarbons are listed in the last two columns of Table 5.15. The concentrations & percentages of these individual hydrocarbons did not differ significantly between Bakken and non-Bakken VHM profiles.

In Table 5.16, $GGV_{mixture}$ values for each Bakken and non-Bakken crude oil VHM sample were calculated using the GGV values from either McKee et al. (2005) and UKHSE (2000). The average $GGV_{mixture}$ for each oil type was also calculated and rounded up to the nearest 100th based on the lower average in order to define a range of $GGV_{mixture}$ values. Using the GGV values from McKee et al. (2005), the average $GGV_{mixture}$ value for Bakken and non-Bakken crude oil was 1416 mg/m^3 and 1362 mg/m^3, respectively. When rounded, both types of crude oil had a $GGV_{mixture}$ of 1400 mg/m^3. Likewise, using the GGV values from UKHSE, the average $GGV_{mixture}$ value for Bakken and non-Bakken crude oil was 1526 mg/m^3 and 1543 mg/m^3. When rounded up , both types of crude oil had a $GGV_{mixture}$ of 1600 mg/m^3. A graph illustrating the range and average of $GGV_{mixture}$ values calculated for these two oil types is presented in Fig. 5.6. Overall, data from this small sample set indicate that there is no difference in the potential inhalation hazard for VHMs from Bakken and non-Bakken crude oil. Additional studies of VHMs from light sweet crude oil samples from other geographical regions are needed to support or refute these observations.

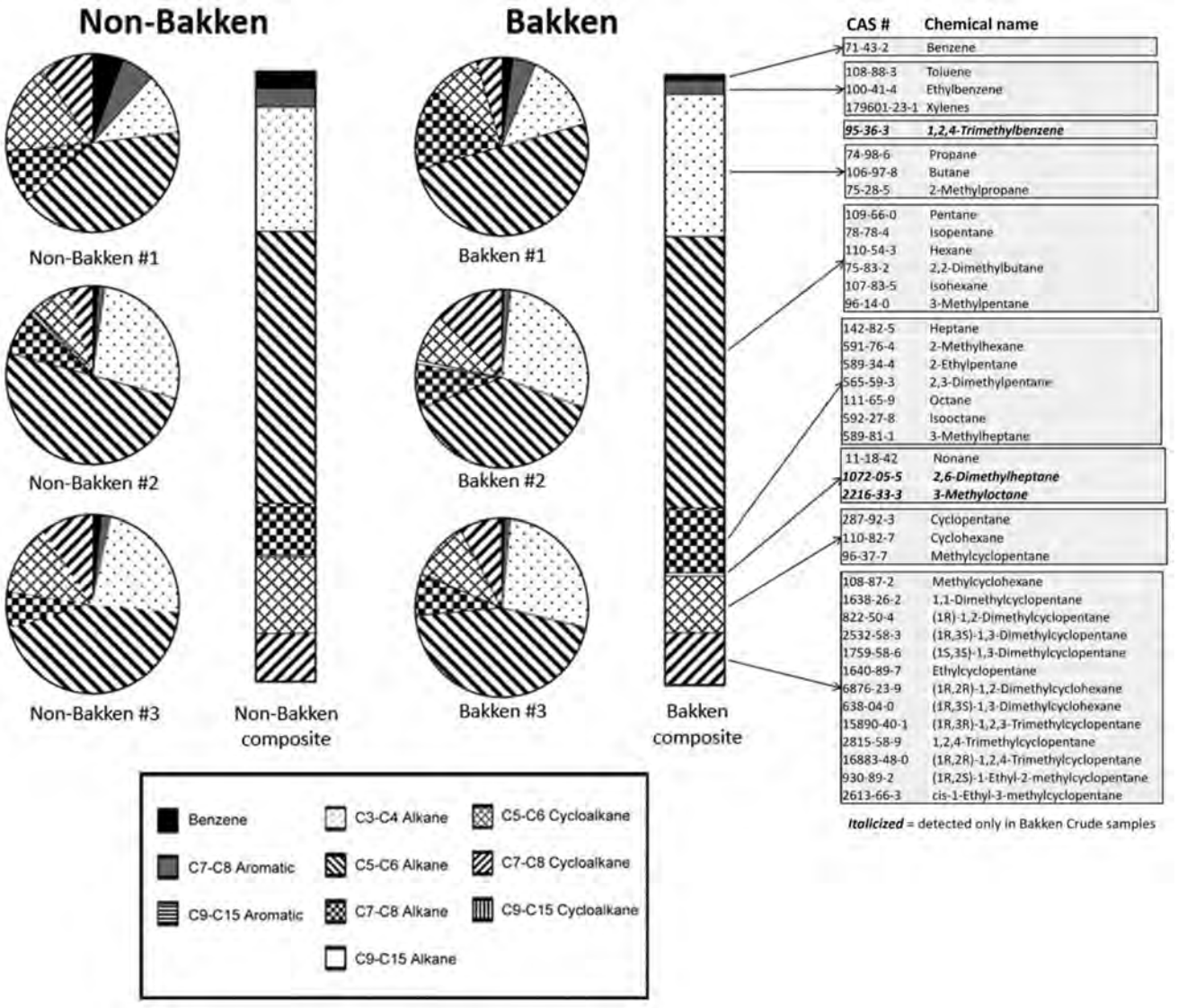

FIGURE 5.4 Volatile hydrocarbon mixture composition in air samples collected above Bakken and non-Bakken light sweet crude oils.

$$GGV_{mixture} = \frac{1}{\frac{F_a}{GGV_a} + \ldots + \frac{F_n}{GGV_n}}$$

$GGV_{mixture}$ = calculated 8-h TWA-OEL for mixture
GGV_a = Guidance value (or TLV®) for group or component, *a*
F_a = The vapor mass fraction of group or component *a* in the hydrocarbon mixture
GGV_n = Guidance values (or TLV®) for group or component, *n*
F_n = The vapor mass fraction of group or component *n* in the hydrocarbon mixture

FIGURE 5.5 Equation for $GGV_{mixture}$ calculations.

TABLE 5.15 Group Guidance Values (GGV) Used to Calculate $GGV_{mixture}$

Hydrocarbon group	McKee et al. (2005) (mg/m^3)	UKHSE (2000) (mg/m^3)	Volatiles with unique TLVs (mg/m^3)	Volatiles with differing or additional critical effects from acute CNS depression or eye/airway irritation (TLVs, mg/m^3)
C7–C8 aromatics	200	500	Xylene, all isomers (434) Ethylbenzene (87)	Toluene (75), visual impairment, reproductive
C9–C15 aromatics	100	500	–	Naphthalene (52), hematological effects Methylnaphthalene (3), lung damage Indene (24), liver damage
C3–C4 alkanes[a]	2000	2000	–	–
C5–C6 alkanes	1500	1800	Pentane, all isomers (2950) Hexane isomers (1760)	*n*-Hexane (175), peripheral neuropathy
C7–C8 alkanes	1500	1200	Heptane, all isomers (1640) Octane, all isomers (1401)	–
C9–C15 alkanes	1200	1200	*n*-Nonane (1050)	–
C5–C6 cycloalkanes	1500	1800	Cyclopentane (1720) Cyclohexane (350)	–
C7–C8 cycloalkanes	1500	800	Methyl cyclohexane (1610)	–
C9–C15 cycloalkanes	1200	800	–	–

[a]*The GGV for C3–C4 alkanes is derived from the STEL values for* n*-butane.*

TABLE 5.16 Bakken and Non-Bakken $GGV_{mixture}$ Values Are Similar

Sample	$GGV_{mixture}$ McKee et al. (2005) (mg/m^3)	$GGV_{mixture}$ UKHSE (2000) (mg/m^3)
Non-Bakken #1	1143	1428
Non-Bakken #2	1509	1651
Non-Bakken #3	1434	1550
Non-Bakken, average	**1362 (*1400*)**	**1543 (*1600*)**
Bakken #1	1224	1482
Bakken #2	1491	1500
Bakken #3	1534	1598
Bakken, average	**1416 (*1400*)**	**1526 (*1600*)**

Lastly, Fig. 5.7 presents the range of determined $GGV_{mixture}$ values for VHMs from Bakken and non-Bakken light sweet crude oil and compares them to the individual hydrocarbon components of crude oil for which individual ACGIH TLV values have been established. This comparison may help guide the development of air-monitoring protocols during events which involve potential exposures to crude oil VHMs. For example, action levels for central nervous system depression and upper respiratory irritation from the VHM mixture would be greater than action levels for individual petroleum hydrocarbons which have lower TLVs based on non-nervous system or airway irritancy effects. It may be advisable to individually monitor these constituents, particularly benzene, individually in the interest of protecting worker health.

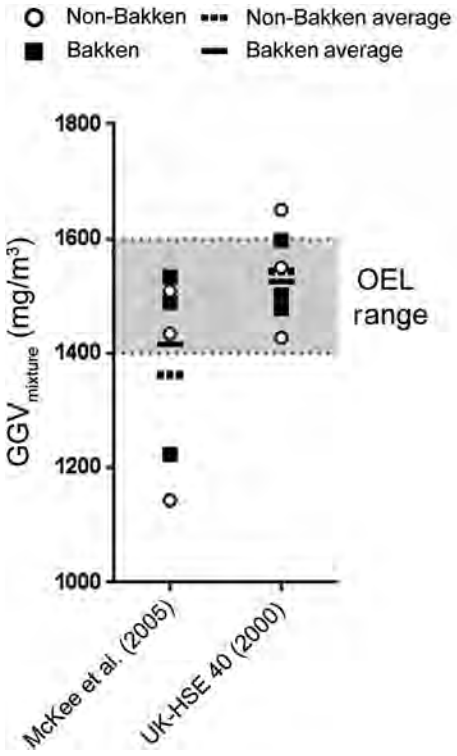

FIGURE 5.6 Comparison of Bakken and non-Bakken $GGV_{mixture}$ values.

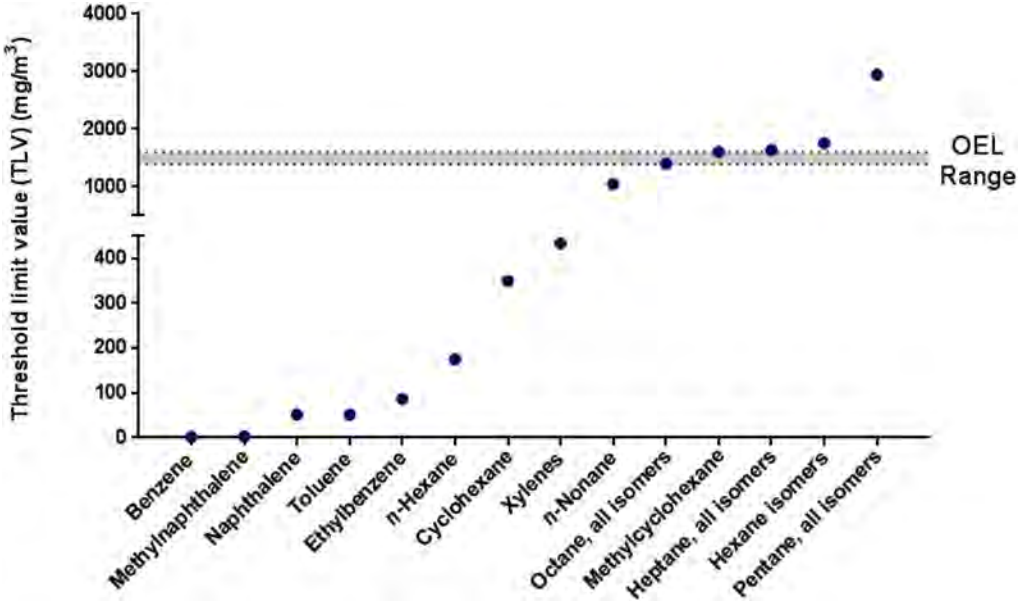

FIGURE 5.7 Comparison of crude oil OEL range to individual constituent TLVs.

5.9 CONCLUSION

Environmental releases of crude oil present unique challenges with regards to the assessment of potential airborne exposures. The unforeseen release of crude oil can result in various emergency situations for responders and key stakeholders including industry personnel, emergency responders, public officials, regulatory agencies,

and the general public. Knowledge of the chemical and physical characteristics, toxicological information, exposure standards and guidelines, potential chemicals of concern, and air monitoring and sampling strategies is critical when evaluating hazards and communicating precautions to site personnel and the general public. As presented above, many factors contribute to the different chemicals that may be present in air following a crude oil release. These include, but are not limited to, the type of crude oil released, the nature of the release, crude oil weathering, meteorological conditions during the release, and the presence or absence of fire. Historical air monitoring data have provided information necessary to determine and prioritize chemicals of potential concern following a crude oil release. The rapid collection, analysis, and interpretation of crude oil composition and volatilization data early in an oil spill can aid decision makers in the development of plans to protect worker and community health that are tailored to the type of oil that is spilled. As additional data from future crude oil releases or additional toxicity data for crude oil components become available, it will be important to continue to refine and expand upon the analysis presented here.

References

ACGIH®, 2014a. 2014 TLVs and BEIs: Based on the Documentation of the Threshold Limit Values for Chemical Substances and Physical Agents and Biological Exposure Indices. ACGIH®, Cincinnati, OH.

ACGIH® (Ed.), 2014b. Guide to Occupational Exposure Values 2014. American Conference of Governmental Industrial Hygienists, Cincinnati, Ohio.

AIHA (Ed.), 2015. Emergency Response Planning Guidelines. American Industrial Hygiene Association, Fairfax, VA.

API, 2011. High Production Volume Chemical Challenge Program. Lubricating Oil Basestocks Category Assessment Document. American Petroleum Institute Petroleum HPV Testing Group, Washington, DC.

ATSDR, 1999. Toxicological Profile for Total Petroleum Hydrocarbons (TPH). Agency for Toxic Substances and Disease Registry, Atlanta, Georgia.

ATSDR, Sciences, D.o.T.a.H.H, 2016. Minimal Risks Levels (MRLs) [March 2016]. Agency for Toxic Substances and Disease Registry, Atlanta, Georgia.

Auers, J.R., Couture, R.M. and Sutton, D.L. 2014. The North Dakota Petroleum Council Study on Bakken Crude Properties. Bakken Crude Characterization Task Force, Dallas.

Beauchamp, R.O., Bus, J.S., Popp, J.A., Boreiko, C.J., Andjelkovich, D.A., 1984. A critical review of the literature on hydrogen sulfide toxicity. Crit. Rev. Toxicol. 13 (1), 25–97.

Booher, L.E., Janke, B., 1997. Air emissions from petroleum hydrocarbon fires during controlled burning. Am. Ind. Hyg. Assoc. J. 58 (5), 359–365.

Bowes III, S.M., 1996. Volatile hydrocarbon exposure during in situ burning of crude oil at sea. Am. Ind. Hyg. Assoc. J. 57 (1), 62–67.

Buist, I., 2005. In Situ Burning for Oil Spills in Ice-Covered Waters. SL Ross Environmental Research, Ottawa, ON, Canada.

Buist, I., Nedwed, T., 2011. Using Herders for Rapid In Situ Burning Of Oil Spills on Open Water. Int. Oil Spill Conf. Proc. 2011 (1), pp. Paper 231.

Buist, I., McCourt, J., Potter, S., Ross, S., Trudel, K., 1999. In situ burning. Pure Appl. Chem. 71 (1), 43–66.

Ferek, R.J., Allen, A.A., Kucklick, J.H., 1997. Air Quality Considerations Involving In-Situ Burning. Marine Preservation Association, Scottsdale, AZ.

Fingas, M.F., 2011. Soot production from in-situ oil fires. Int. Oil Spill Conf. Proc. 2011, pp. abs8.

Fingas, M.F., Halley, G., Ackerman, F., Nelson, R., Bissonnette, M., Laroche, N., et al., 1995. The Newfoundland Offshore Burn Experiment—NOBE. Int. Oil Spill Conf. Proc. 1995 (1), 123–132.

Fingas, M.F., Li, K., Ackerman, F., Campagna, P.R., Turpin, R.D., Getty, S.J., et al., 1996. Emissions from mesoscale in situ oil fires: the Mobile 1991 experiments. Spill Sci. Technol. Bull. 3 (3), 123–137.

Fingas, M.F., Lambert, P., Li, K., Wang, Z., Ackerman, F., Whiticar, S., et al., 2001. Studies of Emissions From Oil Fires. Int. Oil Spill Conf. Proc. 2001 (1), 539–544.

Guidotti, T.L., 1996. Hydrogen sulphide. Occup. Med. (London) 46 (5), 367–371.

Guidotti, T.L., 2010. Hydrogen sulfide: advances in understanding human toxicity. Int. J. Toxicol. 29 (6), 569–581.

Harrill, J.A., Wnek, S.M., Pandey, R.B., Cawthon, D., Nony, P., Goad, P.T., 2014. Strategies for assessing human health impacts of crude oil releases. Int. Oil Spill Conf. Proc. 2014 (1), 1668–1685.

Lipsett, M., Materna, B.L., Stone, S., Therriault, S., Blasidell, R., Cook, J., et al., 2013. Wildfire Smoke: A Guide for Public Health Officials. California Office of Environmental Health Hazard Assessment, Sacramento, CA, <http://oehha.ca.gov/air/risk_assess/wildfirev8.pdf>. Available at: L:\043501-044000\043574.pdf.

McKee, R.H., Medeiros, A.M., Daughtrey, W.C., 2005. A proposed methodology for setting occupational exposure limits for hydrocarbon solvents. J. Occup. Environ. Hyg. 2 (10), 524–542.

Middlebrook, A.M., Murphy, D.M., Ahmadov, R., Atlas, E.L., Bahreini, R., Blake, D.R., et al., 2012. Air quality implications of the Deepwater Horizon oil spill. Proc. Natl. Acad. Sci. U.S.A. 109 (50), 20280–20285 + supporting information.

Nordeng, S., 2010. A Brief History of Oil Production from the Bakken Formation in the Williston Basin. North Dakota Department of Mineral Resources.

Osuji, L.C., Udoetok, I.A., Ogali, R.E., 2006. Attenuation of petroleum hydrocarbons by weathering: a case study. Chem. Biodivers. 3 (4), 422–433.

Ross, J.L., Ferek, R.J., Hobbs, P.V., 1996. Particle and gas emissions from an in situ burn of crude oil on the ocean. J. Air Waste Manage. Assoc. 46 (3), 251–259.

Roth, S.H., 1993. Hydrogen sulfide. In: Corn, M. (Ed.), Handbook of Hazardous Materials. Academic Press, San Diego, pp. 367–376.

Stout, S.A., Millner, G.C., Hamlin, D., Liu, B., 2006. The role of chemical fingerprinting in assessing the impact of a crude oil spill following Hurricane Katrina. Environ. Claims J. 18 (2), 169–184.

Stout, S.A., Payne, J.R., Emsbo-Mattingly, S.D., Baker, G., 2016. Weathering of field-collected floating and stranded Macondo oils during and shortly after the Deepwater Horizon oil spill. Mar. Pollut. Bull. 105 (1), 7–22.

Subcommittee on Acute Exposure Guideline Levels; National Research Council, 2001. Standing Operating Procedures for Developing Acute Exposure Guideline Levels for Hazardous Chemicals [Online]. National Research Council, Washington, DC. Available at: https://www.epa.gov/sites/production/files/2015-09/documents/sop_final_standing_operating_procedures_2001.pdf.

Thayer, E.C., George-Ares, A., Plutnick, R.T., Kaufman, R.A., 2001. Chemical Human Health Hazards Associated with Oil Spill Response. American Petroleum Institute, Washington, DC, API Publication Number 4689.

TPHCWG, 1997. Selection Of Representative TPH Fractions Based on Fate and Transport Considerations. Total Petroleum Hydrocarbon Criteria Working Group. Available at: <http://www.aehs.com/>.

UK Health and Safety Executive (UKHSE) 2000. EH40/2000. Occupational Exposure Limits.

U.S. Department of Energy, 2016. Protective Action Criteria (PAC): Chemicals with AEGLs, ERPGs, & TEELs [Online]. Available at: https://sp.eota.energy.gov/pac/teel/teeldef.html (Accessed: March 13, 2017).

USEPA, 1993. Report to Congress on Hydrogen Sulfide Air Emissions Associated with the Extraction of Oil and Natural Gas. U.S. Environmental Protection Agency, Research Triangle Park, NC (EPA/453/R-93/045).

USEPA, 2016. Polycyclic Aromatic Hydrocarbons on the Gulf Coastline. U.S. Environmental Protection Agency, Washington, DC, <https://archive.epa.gov/bpspill/web/html/pahs.html>.

USEPA, Development, O.o.R.a, 1999. Compendium Method TO-15. Determination of Volatile Organic Compounds (VOCs) in Air Collected in Specially Prepared Canisters and Analyzed by Gas Chromatography/Mass Spectrometry (GC/MS). U.S. Environmental Protection Agency, Cincinnati, Ohio (EPA/625/R-96/010b).

Wakefield, J., 2010. A Toxicological Review of the Products of Combustion. Health Protection Agency, Chilton, Didcot, Oxfordshire. Available at: http://www.hpa.org.uk/.

Wang, Z., Hollebone, B.P., Fingas, M., Fieldhouse, B., Sigouin, L., Landriault, M., et al., 2003. Characteristics of Spilled Oils, Fuels, and Petroleum Products: Composition and Properties of Selected Oils. National Exposure Research Laboratory, U.S. Environmental Protection Agency, Research Triangle Park, NC (EPA/600/R-03/072).

CHAPTER

6

Combined Gas and Liquid Chromatography Tandem Mass Spectrometry Applications for Forensic Lubricant and Vegetable Oil Spill Identification

Dayue Shang[1], *Grace Park*[1], *Pamela Brunswick*[1], *Graham van Aggelen*[1], *Chun Yang*[2] *and Marcus Kim*[3]

[1]Environment and Climate Change Canada, North Vancouver, BC, Canada [2]Environment and Climate Change Canada, Ottawa, ON, Canada [3]Agilent Technologies Inc., Mississauga, ON, Canada

BIOGRAPHIES

Dr. Dayue Shang is a Senior Chemist at the Pacific Environmental Sciences Centre of the Pacific and Yukon Laboratories for Environmental Testing, Environment and Climate Change Canada. He is specialized in environmental oil spill forensics and has over 20 years of extensive experience in characterization, quantitative work, and method development using LC/MS/MS and GC/MS instruments. He has a Doctorate and Master of Science degrees in Chemical Engineering from Laval University, Quebec, Canada and a Bachelor of Science degree in Chemical Engineering from the Shanghai Institute of Chemical Technology. He has published over 40 peer-reviewed manuscripts and more than 60 presentations in national and international conferences.

Grace Park is chemical analyst assistant at the Pacific Environmental Sciences Centre of the Pacific and Yukon Laboratories for Environmental Testing, Environment and Climate Change Canada. She has studied Environmental Sciences at the University of British Columbia and has coauthored a paper on the longevity and fate of ocean oil spill dispersants.

Dr. Pamela Brunswick is currently a chemist specializing in mass spectrometry for the Organic Chemistry division of Environment and Climate Change Canada, North Vancouver, BC, Canada. Pamela graduated University in the United Kingdom with a Ph.D. degree in Biochemistry. Her laboratory experience includes research at the University of Helsinki (Finland), University of Witwatersrand (South Africa), and University of British Columbia (Canada). During 20 years of employment in commercial analytical laboratories, Pamela gained extensive training in GMP and GLP under OECD and ISOIEC 17025 quality systems and was Study Director for multiple research projects, including studies for multinational companies. Pamela has authored scientific papers, presented research data at international conferences, and has lectured a biochemical techniques course at University level. Her current focus is on the application of high resolution mass spectrometry methods to support environmental law enforcement, including the identification of contamination by oil spills, fracking additives, surfactants, pesticides, and unknowns. Although thriving on analytical problem solving, Pamela continues to appreciate the alternative technical challenges of playing squash league without performance enhancing options!

Graham van Aggelen is Manager of the Pacific Environmental Sciences Centre, Environment and Climate Change Canada. He has been instrumental in the development of aquatic toxicological testing methods relevant

Oil Spill Environmental Forensics Case Studies.
DOI: http://dx.doi.org/10.1016/B978-0-12-804434-6.00006-9

to Canada's aquatic ecosystems. He established national protocols to ensure standardized approaches to testing of individual compounds and complex mixtures of industrial effluents for both private and public laboratories and is actively engaged in integrating toxicogenomics into testing methodology for which he has received numerous citations of merit from the Government of Canada. His laboratory has extensive experience and expertise in aquatic toxicology and analytical chemistry. He has published over 30 peer-reviewed manuscripts.

Dr. Chun Yang is Head of the Chemical Research Laboratory, Emergencies Science and Technology Section of Environment and Climate Change Canada, Ottawa, Canada. He has a Ph.D. in analytical chemistry and environmental process from Nanyang Technological University of Singapore, a master degree in organic-analytical chemistry from the Research Centre for Eco-Environmental Sciences of Chinese Academy of Sciences, and a bachelor degree in organic chemistry from Beijing Normal University of China. His specialties include environmental sciences, analytical chemistry, and natural products. His current researches mainly focuses on environmental forensics of oils and other potential spill candidates, environmental behaviors of organic pollutants and application of high resolution mass spectrometry in target and nontarget analysis of emerging environmental contaminants. Dr. Yang has authored over 120 academic publications including about 60 peer-reviewed journal papers and invited book chapters. E-mail: chun.yang@canada.ca.

Dr. Marcus Kim is the mass spectrometry specialist for Agilent Technologies in Canada where he brings a decade of experience helping a wide range of clients across a broad diversity of applications and needs with technical expertise and industry market knowledge. Marcus received his Bachelor's degree from York University and a Ph.D. from McMaster University with a focus on analytical chemistry and polymer characterization. Marcus is a coauthor of many scientific papers, frequent guest lecturer and holds a patent for a technology related to functionalizing macroporous materials for high throughput separations. Marcus spends all his spare time devoted to exploring the wonders of our universe with the tools of science with his young son, Atom.

6.1 INTRODUCTION

Although the vast majority of oil spill cases are related to the transportation of petroleum crude oil, due to increased production and wide use in modern society, cases of lube oil environmental releases have increased in urban centers (Fingas, 2015; Stout and Wang, 2016). Lube oils, including hydraulic oil, pump oil, transmission oil, and engine oil, play an important role in daily life, and their storage, transportation, and disposal are common in a modern economy. Although large volumes of motor oil (approximately 800 million gallons) are recycled annually for reuse (U.S. EPA, 2001), significant amounts of used motor oil continue to be discharged into the environment. It is estimated that 30% of motor oil may not be disposed of properly (Dominquez-Rosado and Pichtel, 2003). Small-scale spills and contamination by lube oil has become a serious concern for environmental protection. The inappropriate or illegal disposal of used motor oil could have a significant impact on ecosystems and public health. For example, polycyclic aromatic hydrocarbons (PAH) compounds, a component of motor and lubricant oils, represent a direct hazard to the environment and human health (Hewstone, 1994).

The analytical characterization of lube oils is hindered by their complex chemical structure. Lube oil is largely composed of saturated hydrocarbons and various additives, such surfactants, antioxidants, antifoaming agents, etc. During forensic oil spill analysis, gas chromatography with flame ionization detection (GC/FID) and gas chromatography with mass spectrometry detection (GC/MS) are commonly applied. PAHs and other biomarkers have commonly been used in the characterization of lube oil (Wang and Stout, 2007) , although the peaks of unresolved complex materials (UCMs) often dominate GC traces, making the oil fingerprint study complex (Wang and Stout, 2007). The PAH and biomarker comparison approach is particularly useful in distinguishing the type of lube oil, as well as oil products formulated using different base oil stock. However, often many motor oil products with various brand names are sourced from the same manufacturer and made with the same base oil stock in the formulation. Their only difference is generally in the quantity and variety of additives within the product. In this case, two dimensional GC/MS and gas chromatography quadrupole time-of-flight mass spectrometry (GC/QToF) can be powerful tools in detecting and distinguishing differences in the additives. Unfortunately the availability of these high end instruments is still rare in routine environment chemistry laboratories and traditional GC/FID and GC/MS approaches often cannot distinguish between different lube oil products when the same base oil is used in the formulation.

Similar to the situation of lube oils, worldwide vegetable or plant-based oil production and transportation are increasing steadily. Vegetable oil spilled into the environment is not uncommon and its environmental damage

can be significant (Fingas, 2015). Vegetable oils mainly consist of triacylglycerols, generally with 20−32 carbon atoms in the alkyl chain. The GC/MS profile of the vegetable oils present few peaks and are often difficult to interpret for forensic oil spill cases. To the analyst's advantage, however, vegetable oils are complemented by the addition of coloring agents and antioxidants, such as butylated hydroxytoluene (BHT), butylated hydroxyanisole (BHA), vitamin C, etc., many of which are water soluble and more suited to liquid chromatography tandem mass spectrometry (LC/MS) analysis.

In published literature there is a paucity of methods relating to the environmental forensic characterization of lube and vegetable oil. Caravaggio et al. (2007) determined *n*-alkane profiles of engine lubricating oil by molecular sieve extraction followed by GC/MS analysis. The sieve method yielded better chromatography, unambiguous identification of *n*-alkanes, and allowed examination of differences between light and heavy-duty vehicle lubricating oils. According to the author, the extraction of *n*-alkanes into sieves proved very challenging and no effort was made to identify lube oil products from the same type of base oil. Dominquez-Rosado and Pichtel (2003) reported some preliminary results from the characterization of a small number of engine lubricating oils using GC/MS, nuclear mass resonance (NMR), and Fourier transform infrared spectroscopy (FTIR). A number of degradation products of aliphatic and aromatic compounds in the oil were reported by these authors. UCM was noticed in the fresh oil samples but no forensic characterization was performed. For vegetable oil, most of the methods developed are for quality control and adulteration prevention purposes (Lerma-Garcia et al., 2009; Blumhorst, 2011; Mata-Espinosa et al., 2011; Elzey et al., 2016). Few systematic environmental forensic study of vegetable oil spill has been found in open literature (Fingas, 2015).

In today's industry, lube oil additives are (as corrected) necessary components added to ensure performance of the product. In fact, lube oils can contain about 10% to 20% of additives such as detergents, antifoam agents, dispersants, emulsifiers, antioxidants, friction modifiers, color stabilizers, and corrosion inhibitors (Ghosh et al., 2017). Different lube oil products generally have various additive components of differing concentrations that can provide useful fingerprint information for forensic oil identification. For compatibility purposes, the additives need to be extracted into a solvent applicable to both GC and LC techniques. It is noted that some of the extracted compounds can only be analyzed by the GC, such as low polarity and high volatility compounds, whereas others by LC, such as high polarity and low volatility compounds. The wide range of additive polarities and characteristics of additives mean that the extraction step is critical to the success of the forensic oil identification. This chapter describes a method for rapid comparative characterization of additives in engine lubricating oil and vegetable oil. This procedure is based on a fast solvent liquid−liquid sample extraction combined with use of GC/FID, GC/MS, and LC/MS techniques. A number of real world cases will be presented to demonstrate the usefulness as well as limitations of this method. Another potential application of the current method is for laboratories only equipped with LC/MS or even LC/UV to be able to explore the possibility of oil source identification.

6.2 EXPERIMENTAL

6.2.1 Reagents and Materials

Ultrapure water used in the sample preparation and instrument analysis was purified using a Milli-*Q* water purification system (Millipore, Billerica, MA, USA). Hexane (pesticide grade), acetonitrile (LC−MS and HPLC grade), dichloromethane (spectrophotometry grade), and formic acid (Analar grade) were obtained from EM Science (Gibbstown, NJ, USA). GHP Acrodisc syringe filter (0.2 μM) was purchased from Pall Life Sciences (Mississauga, Canada). Syringes with BD Luer-Lock tip, BD Medical, 3 mL, were obtained from VWR (Mississauga, Canada).

6.2.2 Sample Preparation

Sample extraction is summarized in the flowchart shown in Fig. 6.1. Briefly, each batch of samples consisted of up to six oil samples (both source and environmental), method blanks and a QC sample. A positive displacement pipette was used for adding 1 mL of lube or vegetable oil to the 15 mL centrifuge tube. Method blank samples were prepared using 1 mL of hexane instead of lube or vegetable oil and a QC sample was prepared using 1 mL of well-characterized vegetable or lube oil. A volume of 3 mL of acetonitrile was added to each centrifuge tube; following this, 0.1 mL of formic acid was added to facilitate the extraction of aromatic amine additives in the lube oil case (note: this is recommended for lube oil but optional for vegetable oil). A volume of 8 mL of hexane was added to the centrifuge tube that was then vortexed prior to centrifugation at ~4500 g for 3 minutes. The top layer of

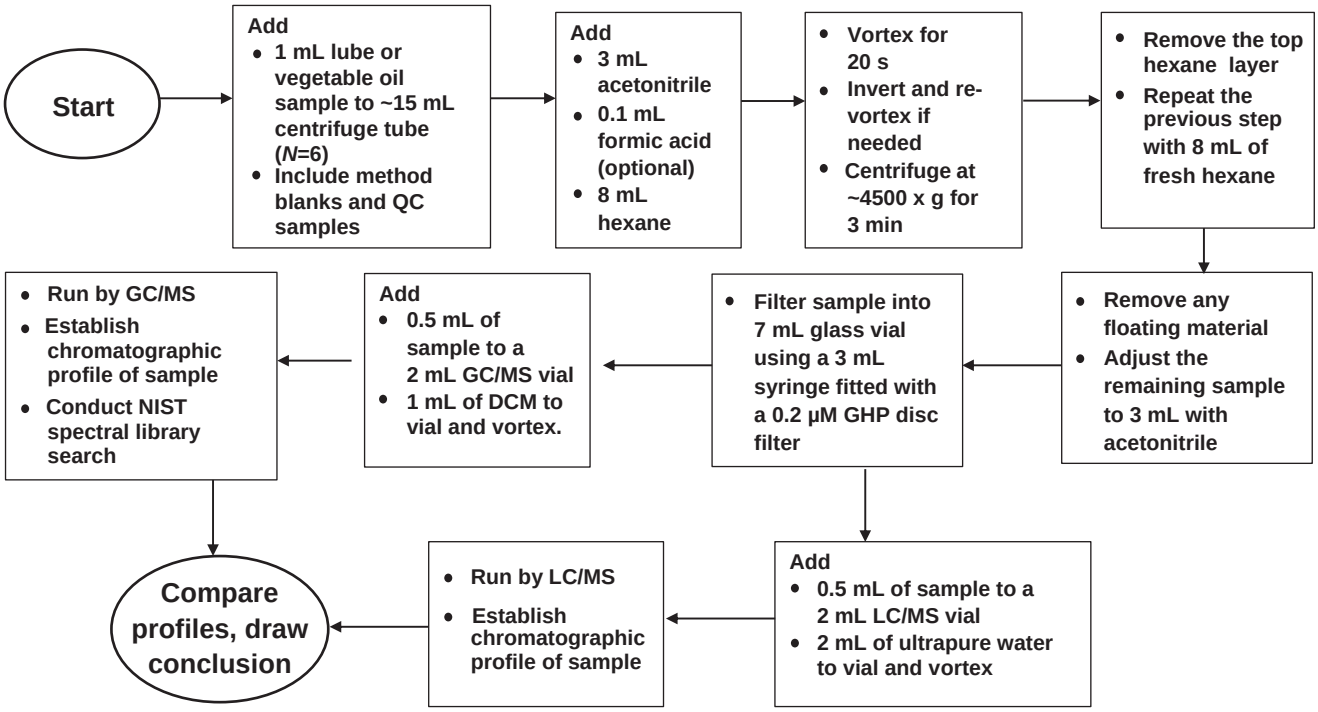

FIGURE 6.1 Sample extraction method flowchart.

hexane with lube or vegetable oil was then removed and discarded. This process was repeated with 8 mL of fresh hexane. Particular attention was paid to removing any floating aggregated materials before adjusting the remaining sample volume to 3 mL with acetonitrile. The sample was filtered into a 7 mL glass vial using a 3 mL syringe fitted with a GHP 0.2 μM disk filter. Aliquots of 0.5 mL sample were transferred into separate GC and LC vials. To the GC vials, 1 mL of dichloromethane was added, and to the LC vials 1 mL of ultrahigh purity water was added. The final sample extracts were vortexed before being analyzed by GC/MS, GC/FID, and LC/MS.

6.2.3 Sample Analysis

6.2.3.1 GC/FID

The GC/FID analysis, while not essential, can still be an integral part of this forensic characterization. In most cases, the GC/MS results reveal much richer forensic information than that of GC/FID. Nonetheless, the GC/FID analysis remains useful because of its low cost and wide availability in many laboratories.

An initial screening analysis of lube or vegetable oil was performed by aliquot of 0.2 mL of the original oil sample, direct dilution with 5 mL of hexane, vortex and analysis using an Agilent 6890 N GC equipped with a flame ionization detector and the Agilent 7683 injector. The injection volume was 2 μL in split mode with split ratio of 25:1. The separation was performed with a Restek Rtx-5 capillary GC column (30 m, 0.32 mm ID, 0.25 μm film thickness). Injector temperature was set at 250°C and detector temperature set at 325°C. Helium carrier gas flow rate was regulated at 1.4 mL/minutes. The temperature ramp program started with an initial temperature at 55°C held for 2 minutes, then increased at a rate of 8°C/minutes to reach 325°C, and then held for 24.25 minutes. The total method run time was 60 minutes. System control and data acquisition were achieved using the Agilent MassHunter chromatography software.

6.2.3.2 GC/MS

For GC/MS analysis, the chromatographic separation and MS scan were carried out on an Agilent 7890A gas chromatograph (Mississauga, ON, Canada) equipped with a 5975 mass-selective detector (MSD) and a 7683B autosampler. A Restex Rtx-5ms fused silica column (30 m, 0.25 mm ID, 0.25 μm film thickness) with Integra-guard guard column was used. Helium carrier gas flow rate was 0.86 mL/minutes. The injector temperature was set at 280°C and source temperature set at 350°C. The GC oven temperature program started at 42°C held for

2 minutes, then heated at a rate of 5.5°C/minutes to 325°C and held for 16 minutes, with a 5 minutes post run time. The total run time was 58 minutes. The sample injection volume was 2 μL and injected in pulsed splitless mode. The MS was operated in the ion scan monitoring mode and the NIST database spectral library (Build 1, 2002) was used for the compound identity search. System control and data acquisition were achieved with the Agilent MassHunter software. Observed ions of interest were extracted from the total ion scan chromatography.

6.2.3.3 LC/MS/MS

LC/MS/MS analysis was performed using an Agilent Infinity 1290 HPLC system with Infinity 1260 autosampler and an Agilent 6490 iFunnel Series Liquid Chromatograph Tandem Mass Spectrometer controlled by MassHunter 6400 series software. High sensitivity and good separation of analytes from a 10-μL injection sample injection volume was achieved on an Agilent Poroshell 120 SB-C18 column (2.7 μM, 2.1 × 100 mm). Ultrapure water was used as mobile phase A and acetonitrile as mobile phase B, both containing 0.1% formic acid (by volume) as a mobile phase modifier. Method development reviewed a variety of chromatographic elution conditions and the final selected conditions employed an initial composition of 95% A and 5% B mobile phase. Analyte elution employed a linear gradient to 95% B over 12 minutes, with a final hold at that concentration for another 13 minutes before adjusting back to 5% B and final reequilibration to initial conditions over 5 minutes. A flow rate of 0.4 mL/minutes was used throughout the entire gradient program of 30 minutes. MS tuning conditions employed source parameters as follows; nebulizer 30 psi, gas temperature 260°C, gas flow 15 L/minutes, sheath gas temperature 375°C, sheath gas flow 12 L/minutes, and capillary voltage 3000 V.

For initial scanning runs, the mass range was set from 150 to 800 m/z in ESI positive or negative mode. During the method development for LC/MS/MS, it was observed to be necessary to limit the mass range from 260 to 500 m/z for lube oil in order to avoid an elevated baseline and presence of numerous small peaks that made interpretation difficult. The injection volume was also limited to 10 μL because higher volumes would compromise the peak shape. Initially, both positive and negative modes were used in the screening process.

6.3 RESULTS AND DISCUSSIONS

6.3.1 Selection of Extraction Solvent

For both lube oils and vegetable oils, direct analysis for forensic characterization with GC/FID or GC/MS is difficult due to the overwhelming presence of unresolved hydrocarbon peaks as shown in Fig. 6.2, or featureless as in Fig. 6.3. The direct injection of oil based samples into reversed-phase LC is not recommended due to compatibility issues. Normal phase LC may help but conversion from commonly used reverse phase to normal phase LC is time consuming and often troublesome due to incompatibility of mobile phases. In consequence, an efficient sample extraction and clean-up procedure is proposed to extract additives and less hydrophobic compounds from lube and vegetable oils. Ideally, the extraction method should be compatible to both GC and LC analysis, while at the same time remove as much base oil as possible from the sample. During method development liquid−liquid extractions and solid phase extraction (SPE) experiments were performed which included acidified or alkalinized water, methanol, and binary solvents of acetonitrile/water and isopropanol/water, and a variety of SPE cartridges. A high extraction efficiency and a very clean baseline was achieved by using a two-step back-extraction procedure, i.e. first extraction with water acidified with 1% formic acid then readjusted to pH 11 with ammonium hydroxide, followed with hexane extraction. However, this process was not pursued because it was very laborious and sometimes sample specific.

During method development, acetonitrile was found to be the most satisfactory multipurpose extraction solvent. With the additional optional aid of formic acid to improve the extraction of amine additives in lube oil, acetonitrile demonstrated a number of advantages over that of other solvents. First, acetonitrile extracted a large amount of the additives, while separating distinctly from the hexane. The hexane was able to remove most of the hydrocarbons or hydrophobic triacylglycerols from the base matrices of the lube or vegetable oil. Secondly, compared to methanol, acetonitrile is aprotic and associates less strongly with water, an advantage to GC capillary column analysis. Third, acetonitrile is miscible with dichloromethane, a GC/FID and GC/MS friendly solvent. During our work with GC/FID and GC/MS analysis, the ideal ratio was found to be acetonitrile 1:2 dichloromethane. Over the course of the original method development, 120 injections were carried out using this binary injection solvent with no apparent deterioration of the GC column performance. Fourth, acetonitrile is also ideal for LC/MS/MS analysis. During our application, the acetonitrile extract was diluted with ultrahigh purity water

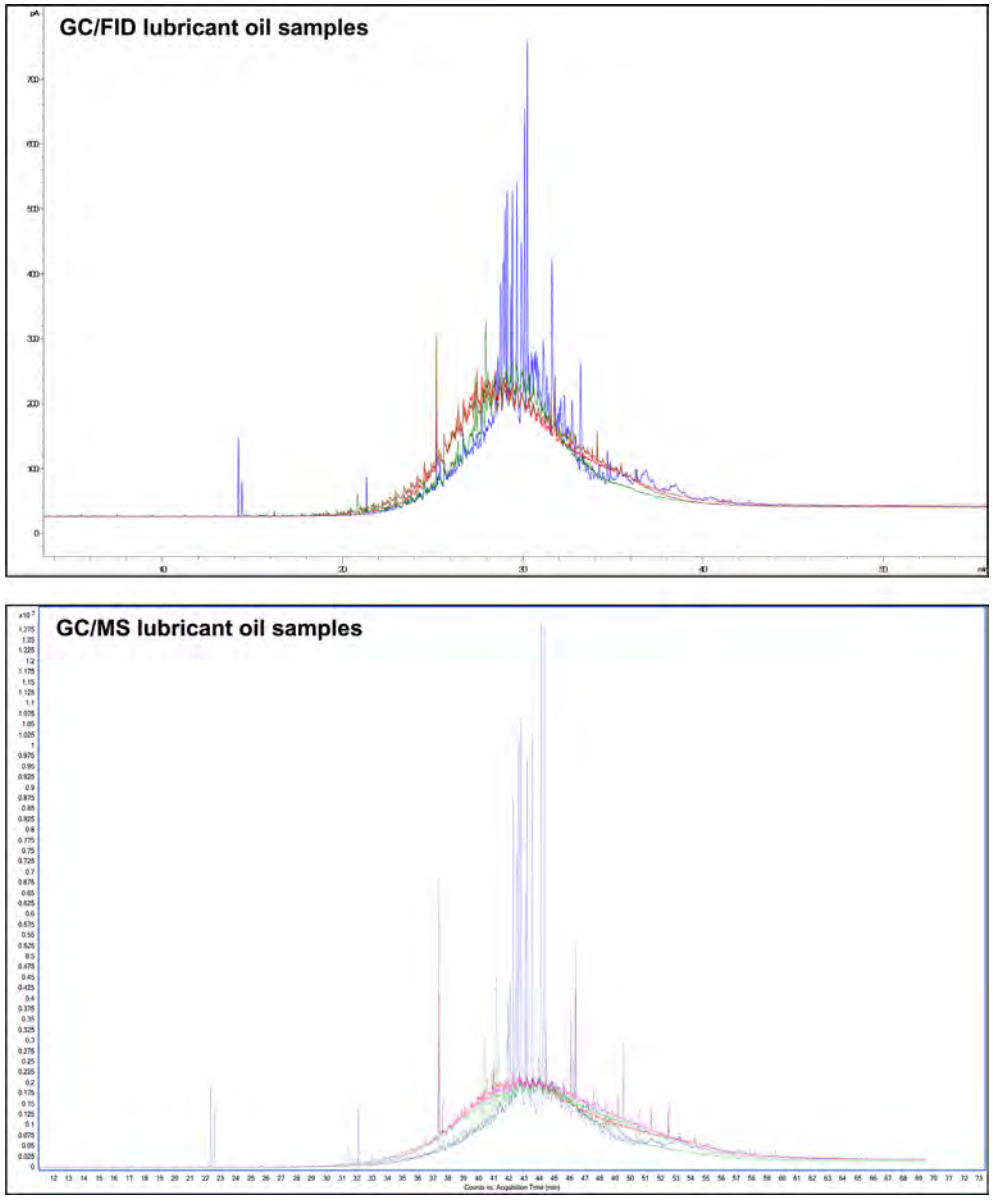

FIGURE 6.2 Above—GC/FID chromatogram of five overlaid lubricant oil samples (1 spill sample and 4 different source samples) prepared with the "dilute and shoot method". Below—GC/MS chromatogram of five overlaid lubricant oil samples (1 spill sample and 4 different source samples) prepared with the "dilute and shoot method." See Case No. 1 for additional details.

at a ratio of 1:2 for analysis. If the sample appeared "foggy" after dilution, low volumes of acetonitrile were added back to clarify the sample. At an injection volume of 10 μL, the sample produced rich chromatographic peaks in LC/MS/MS runs, suitable for further forensic study (refer to later data). Using only small amounts of solvents and no time consuming SPE procedure, this simple and rapid sample preparation method can process a batch of 6 environmental samples, a method blank, and a QC sample in less than 2 hours by one analyst. The prepared samples were free from particulates and were stable for storage up to 6 months (data not shown).

6.3.2 Case No. 1—Application to Lube Oil Spill Identification

Surface oil was observed in an urban area creek in a light industry area. Fish mortality was reported and public concern was high. A number of abandoned lube oil containers were found near the site and suspended to be related to the spill. One environmental Spill and four Source oil samples were collected for analysis.

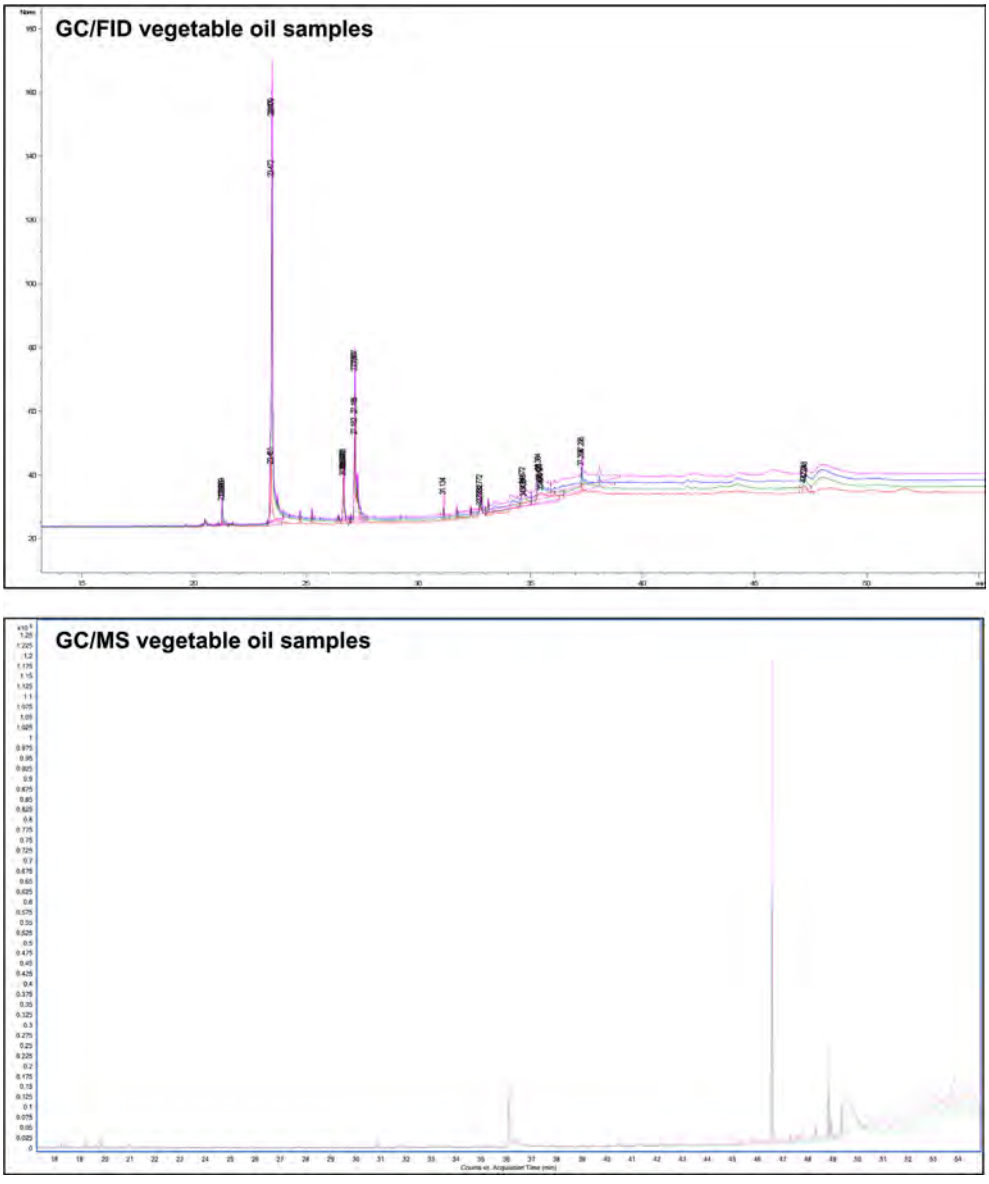

FIGURE 6.3 Above—GC/FID chromatogram of four overlaid vegetable oil samples (1 "Unknown" sample and three vegetable oil source samples) prepared with the "dilute and shoot method". Below—GC/MS chromatogram of four overlaid vegetable oil samples (1 "Unknown" sample and three vegetable oil source samples) prepared with the "dilute and shoot method" run using the TIC scan method. See Case No. 2 for additional details.

6.3.2.1 GC/FID Characterization—Lube Oil Spill

As previously shown in the examples of Fig. 6.2, the original oil samples directly diluted with hexane exhibited a typical profile of lube oil but with the exception that Source 4 had a narrow carbon range which may indicate synthetic oil (result not shown). Example GC/FID chromatographic profiles of the acetonitrile prepared extracts of the four lube oil Source samples and a method blank are shown in Fig. 6.4. The acetonitrile extract produced a minimal UCM between 23 and 26 minutes for Source 4 and a number of distinctive peaks for the other Source samples. The retention time of each of the peaks, the intensity of the peaks, and the ratio of the neighboring peaks all contributed to the characterization of the Spill sample. Evidently, the profile of the Spill sample is distinctly different from Source 2, 3, and 4 samples (refer to the circled areas in Fig. 6.4), but similar to Source sample 1. In summary, whereas initial GC/FID by sample dilution in hexane could only be applied for identification of the type of lube oils present (Fig. 6.2), it was not useful for the purpose of spill oil source

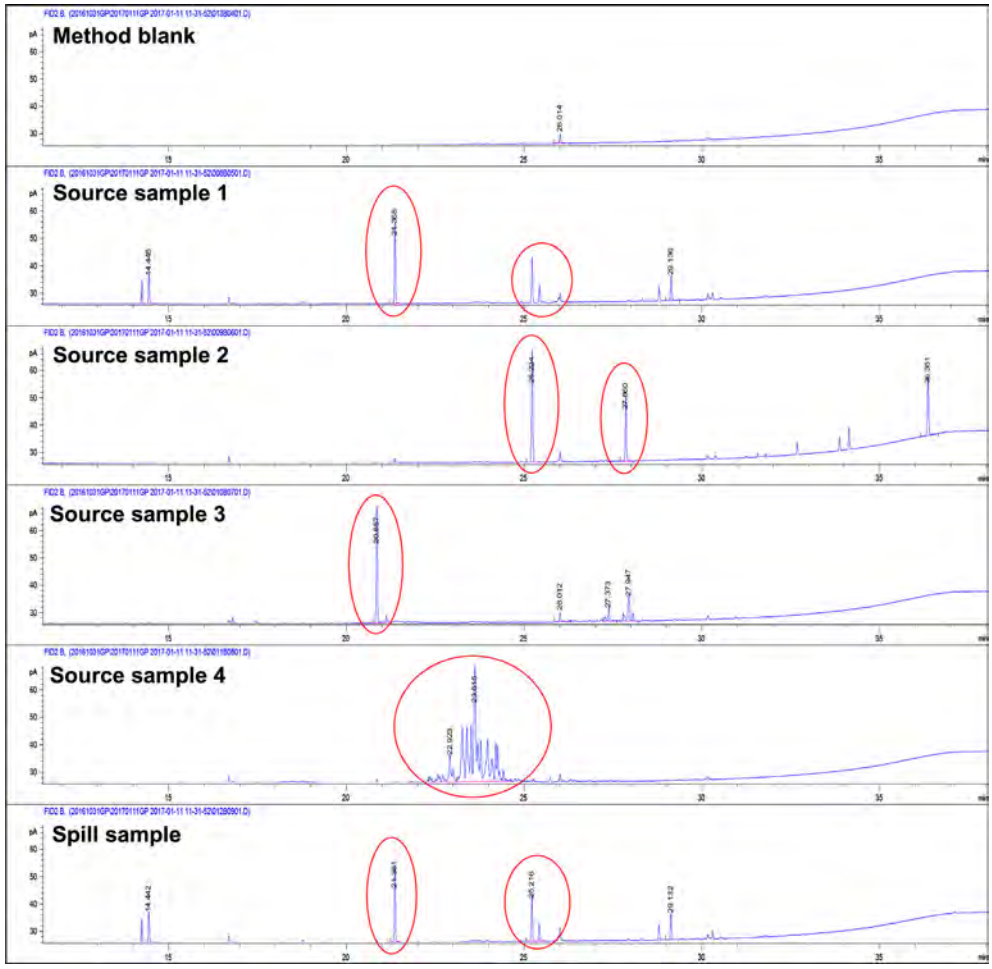

FIGURE 6.4 GC/FID chromatogram of lubricant oil samples, which includes method blank, four source samples, and a spill sample, prepared with the acetonitrile sample extraction method.

identification. In contrast, results from the acetonitrile extraction method demonstrated that GC/FID can still be used for the distinction between very similar lubricating oils.

6.3.2.2 GC/MS Characterization—Lube Oil Spill

The GC/MS chromatographic profiles of the same five lube oil sample acetonitrile extracts described in the previous section are shown in Fig. 6.5. Similar to the GC/FID results, the total ion chromatogram (TIC) scan of these extracts showed a minimal UCM in the case of Source 4 sample and a number of sharp peaks for the other samples. Many of the distinctive peaks found in Source 2, 3, and 4 samples were missing from the Spill sample (refer to the circled areas in Fig. 6.5), narrowing down the identity of the Spill to the matching Source sample 1.

In addition, a combined single ion mode (SIM) analysis of the acetonitrile extracts was included to monitor for the traditional set of PAH and biomarker peaks (Fig. 6.6). The resulting chromatography showed sharp peaks that enable distinction between the lube oils analyzed (Fig. 6.6). Results for both GC/MS TIC and SIM procedures applied to the acetonitrile extracts confirmed that the spill oil was related to Source sample 1. From the results obtained, it was tentatively concluded that the lube oil samples had the same formulation (GC/FID) but with different additives (GC/MS). This result was further supported by LC/MS/MS characterization detailed in the next section.

An added advantage of the acetonitrile extraction method allows a NIST spectral library search to characterize peaks of interest. The very clean baseline and sharp peaks from the acetonitrile extract aids significantly in this process. A number of the peaks observed in lube oils were identified as aromatic amine compounds, sulfurized phenols, fatty acids, fatty amides, and fatty alcohols.

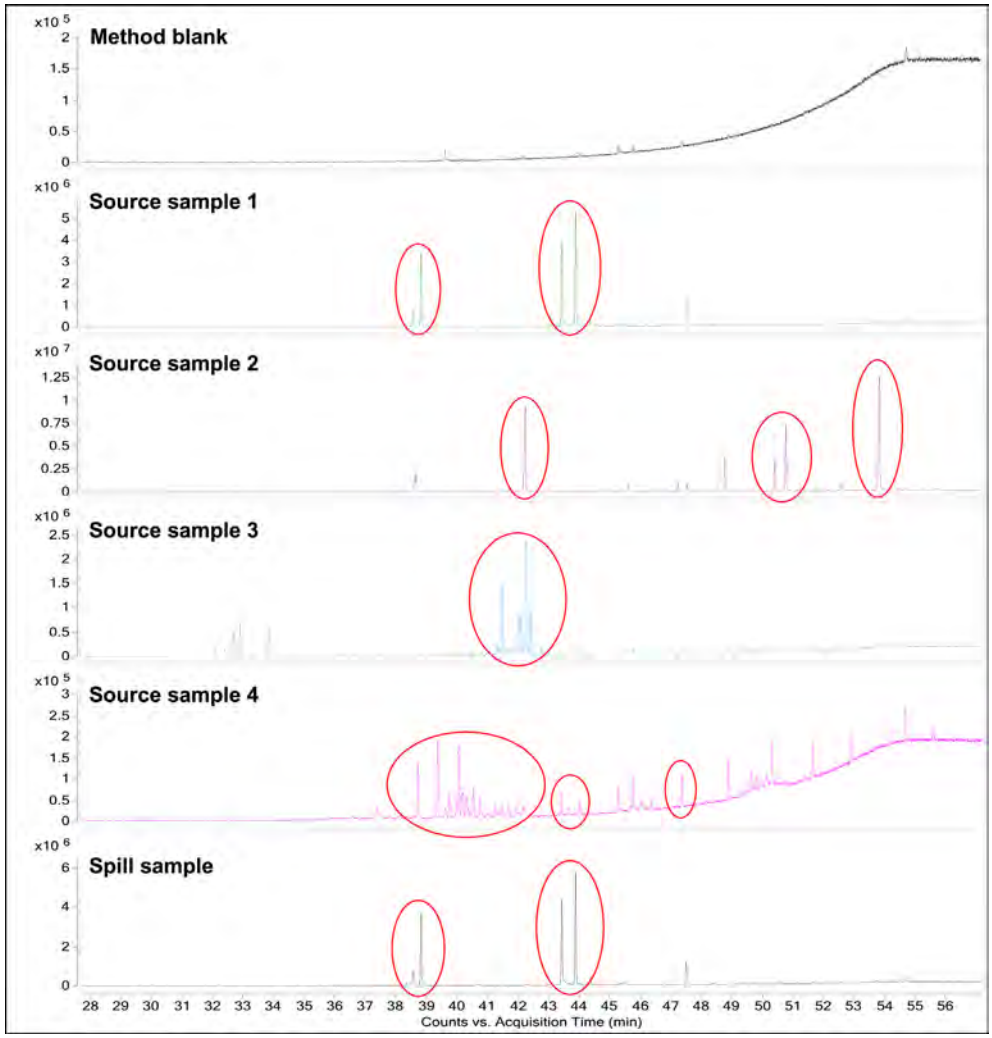

FIGURE 6.5 GC/MS TIC chromatogram of lubricant oil samples, which includes method blank, four source samples, and a spill sample, prepared with the acetonitrile sample extraction method.

The current acetonitrile extraction method has been successfully applied to a number of other lube oil products including: synthetic engine oils, snowmobile oil, transmission gear oil, and hydraulic oil (data not shown). Although routine "dilute and shoot" GC/FID or GC/MS analysis can produce distinctive profiles for oil type determination and fingerprinting, this additional extraction procedure can improve on the approach by yielding unique peaks that make the sample comparative characterization easier. Although not the intended objective in the development of this method, it could readily be applied to the study of the fate/release of fuel additives. Additives in fuel that are priority substances include biphenyl *i*-butyl phenyl phosphate and alkylphenols. The release of such compounds into the environment following fuel combustion and their potential fate is currently unknown.

6.3.2.3 LC/MS/MS Characterization—Lube Oil Spill

In many cases, the previous GC/FID and GC/MS analysis are sufficient for the characterization of the lube oil samples. However, particularly for those laboratories without access to GC/FID or GC/MS, this current extraction method also offers an alternative LC/MS/MS approach for the forensic determination of lube oil. In the present example, there were striking similarities between Spill and Source 1 sample LC/MS/MS total ion scan (TIC) chromatographic profiles which eliminated the three other Source samples as possible matches (Fig. 6.7). With Source 1 sample, there was a pair of two distinctive peaks at retention times 6.8 and 8.2 minutes that distinguished this from Source 2, 3, and 4 samples (Fig. 6.7). There were a number of other subtle differences in the

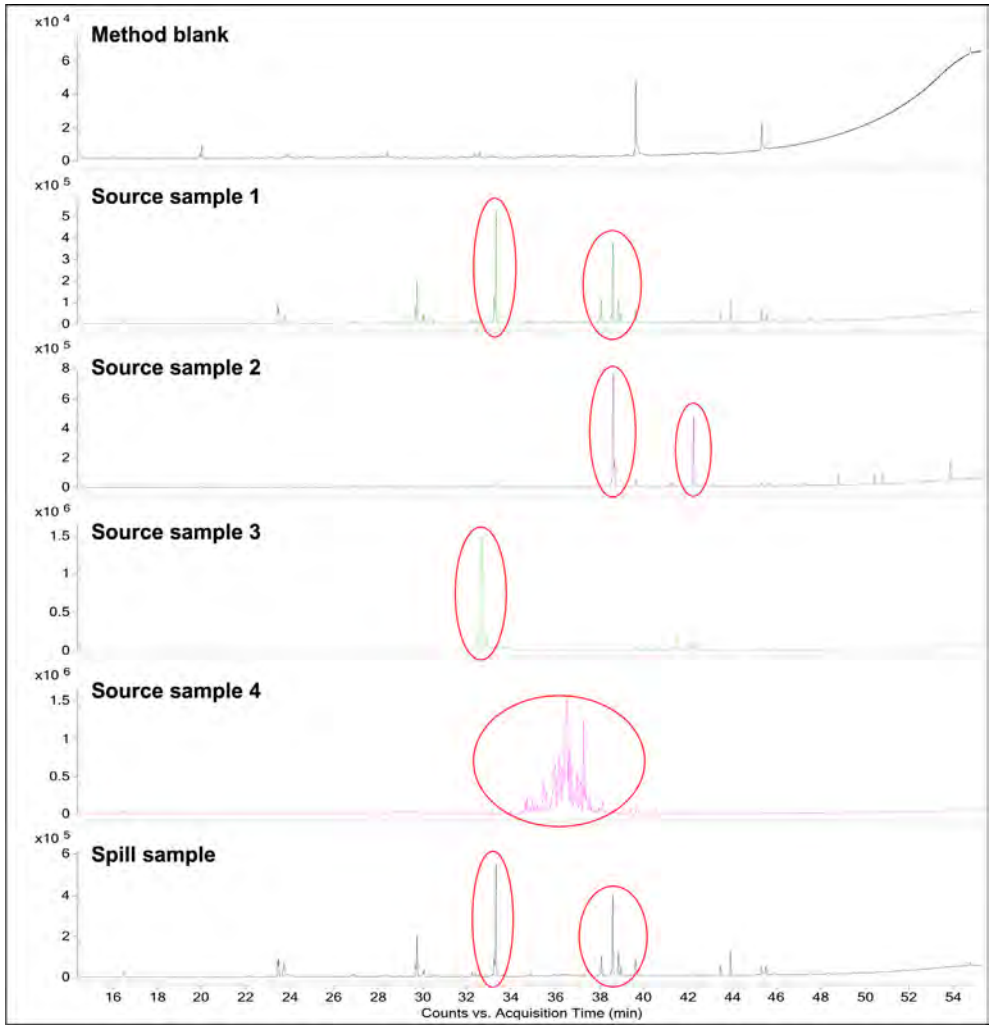

FIGURE 6.6 GC/MS PAH SIM chromatography of lubricant oil samples, including method blank, four source samples, and a spill sample, prepared with the acetonitrile sample extraction method. SIM chromatography combines PAH biomarker ions at 73, 74, 82, 83, 85, 92, 106, 121, 123, 128, 132, 134, 136, 137, 138, 142, 148, 152, 153, 154, 156, 162, 166, 166, 168, 170, 176, 178, 180, 184, 188, 189,189, 190, 191, 192, 194, 198, 202, 205, 206, 208, 212, 215, 216, 217, 218, 219, 220, 226, 228, 230, 231, 234, 240, 242, 244, 245, 252, 253, 256, 264, 270, 276, 278, 284 m/z over defined chromatographic sections.

chromatography that helped to set Source 1 sample apart (refer to the circled areas in Fig. 6.7). For example, the peak at 4.5 minutes for Source 1 sample is much larger than that of Source 2, 3, and 4 samples. In summary, the "fingerprint" of Source 1 sample is distinctly different from Source 2, 3, and 4 samples and results indicated that Source 1 sample was a "match" to the Spill sample.

Although the current comparison procedures allow for the matching of Spill versus Source samples, identification of observed additive compounds is more complex. Employing the current extraction method with the discussed techniques can offer environmental forensic chemists the ability to identify complex lube oils adulterated with deleterious chemicals. When available, application of high resolution mass spectrometry such as LC/QToF can aid in identification of additives used in lube oils.

6.3.3 Case No. 2—Application to Plant Base Oil Cases, Vegetable Oil Coloring Agent

A significant amount of rusty colored oil was found in an urban area creek and some dead fish were noticed. Public concern on the environment impact was intense. The area is a light industry zone with a number of wood products manufacturers and food process plants. LC-50 toxicity tests indicated that the spilled oil was deleterious

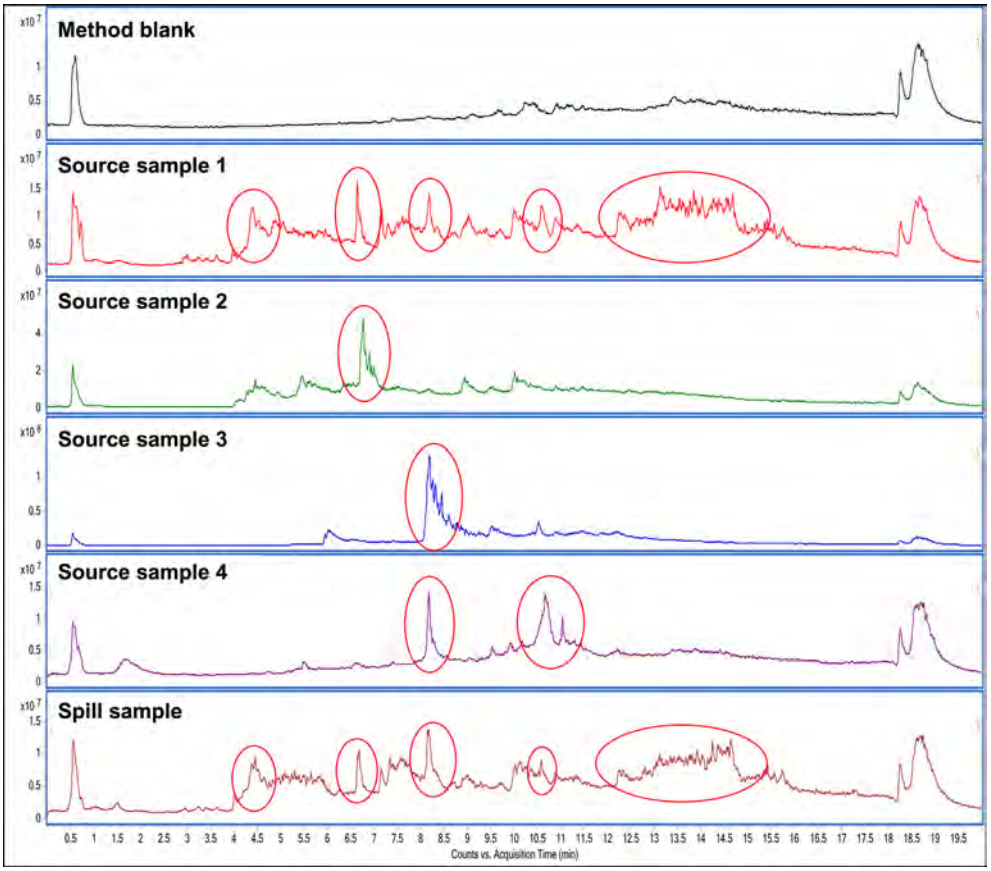

FIGURE 6.7 LC/MS/MS chromatogram of lubricant oil samples prepared with the acetonitrile sample extraction method.

to fish. One environmental "Unknown" sample and three Source samples were collected for chemical assessment. The sample submitter requested to have the results as soon as possible.

A quick FTIR test indicated that all the oil samples were vegetable oil. GC/MS and GC/FID runs produced inconclusive results regarding a match between any of the Source samples to the environmental "Unknown" sample. Based on the color of the spilled sample, a food coloring agent such as astaxanthin was suspected. However, with the "dilute and shoot" method, GC/FID and GC/MS scan runs were unable to detect those compounds, as shown in Fig. 6.3.

The Source and environmental "Unknown" samples were extracted following the established acetonitrile extraction method. The extracts were then subjected to both a GC/MS scan (Fig. 6.8) and an LC/MS/MS MRM method (Fig. 6.9) created to confirm the presence or absence of astaxanthin. GC/MS scan run could not identify this compound due to its high mass and low volatility. Meanwhile, LC/MS/MS results indicated that this same coloring agent was present in both environmental "Unknown" sample and one of the Source samples collected near a large food processing plant. No such coloring agent was found in the two other Source samples (Fig. 6.9).

6.3.4 Case No. 3—Application to Plant Base Oil Cases, Application to Neem Oil Determination

An oil spill was reported in a creek that was connected to a moat surrounded a rural property. This particular property was suspected of ongoing marijuana grow-op activities. The samples were submitted by law enforcement officers for evidence of possible chemical dumping and illegal activities. Communicating with law enforcement officers, a piece of critical information was obtained that local grow-ops often use neem oil for pest control.

Application of both GC/FID and GC/MS routine analysis for identification was unable to confirm the identity of the spilled oil (data not shown). The submitted samples were therefore further processed by the current

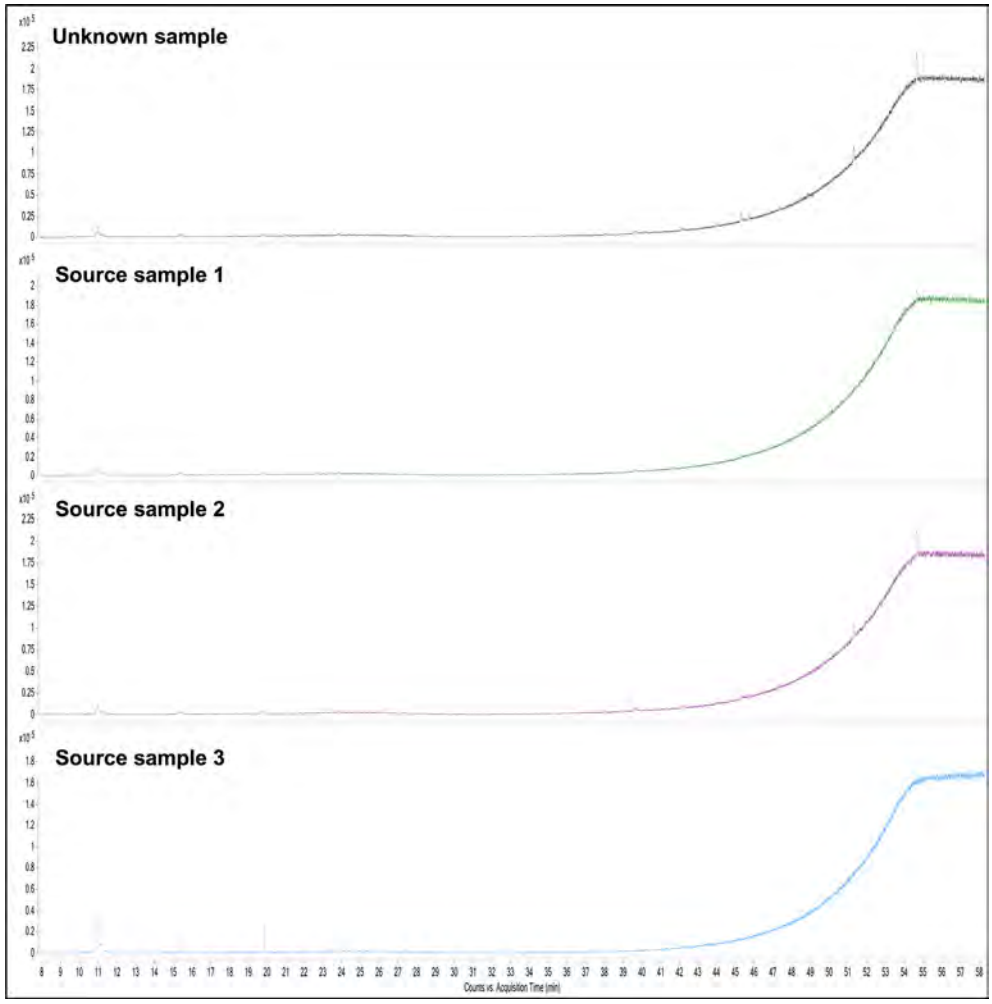

FIGURE 6.8 GC/MS TIC scan method chromatogram of vegetable oil spill samples prepared with the acetonitrile sample extraction method.

acetonitrile extraction procedure. Since it is well recognized that the active ingredient of neem oil is a complex limonoid compound, also known as azadirachtin, this compound was specifically targeted by a MRM LC/MS/MS analysis, using literature based data for instrument set up. Results showed no azadirachtin in the method and field blanks, but produced a distinct an azadirachtin peak in the oil sample collected from the creek (Fig. 6.10). Although at the time no chemical reference standard of azadirachtin was available and later confirmation was confirmed, we were able to affirm its tentative presence. This conclusion was based on the compound having a particularly high molecular weight (743.2 m/z) and the presence of a definitive ion fragmentation pattern by LC/MS/MS that was unlikely to be derived from other compounds. This piece of critical information provided law enforcement officers with enough evidence to pursue further investigation for illegal activities.

6.4 CONCLUSIONS

The novel inclusion of oil "additive" analysis, employing combined parallel GC/FID, GC/MS, and LC/MS instrumentation, was successfully applied to a case of engine lubricating oil spill and vegetable oils for forensic identification. The current method was based on the use of a simple liquid–liquid sample extraction procedure

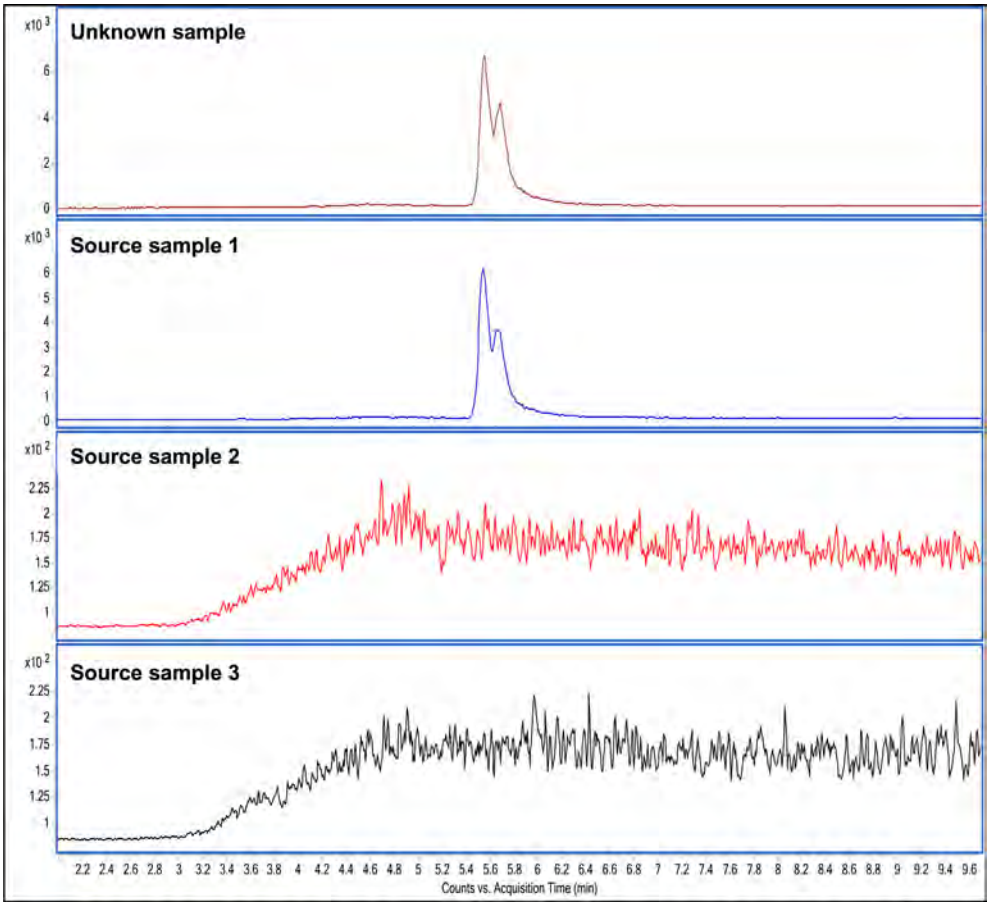

FIGURE 6.9 LC/MS/MS MRM chromatogram of coloring agent, *Astaxanthin*, identified in the spill sample compared to three source samples. Conditions for the instrument are detailed in the text with the exception of gas temperature at 16 mL/min, nebulizer pressure of 20 psi, sheath gas flow 11 mL/min, and capillary voltage 3500 V. The MRM ion transition for Astaxanthin was 597.3938 $m/z \rightarrow 147.1$ m/z in positive mode ionization with collision energy of 22 V.

to concentrate the additives in acetonitrile (optionally acidified), while removing background hydrophobic oil components from the sample by hexane washes. Simple filtration and dilution with appropriate solvents allowed for the application of the three instrument applications. The procedure was designed to tackle a wide range of additive-rich petroleum products including engine oil, transmission gear oil, brake oil, and hydraulic oil and plant-based oils.

The current method allows GC/FID, GC/FID, and LC/MS to be used either as separate tools or as a combined approach for oil fingerprinting analysis. The combined use of GC/MS with its NIST spectrum library search and LC/MS for nonvolatile compounds significantly enhances the confidence of source identification. As demonstrated in two environmental oil spill cases, LC/MS with its ability to detect many larger, more hydrophilic organic compounds unsuitable for GC/MS, can play an important role in determining additives or active ingredients in plant-based oils. In addition, the potential of the method to analyze the fate of oil additives and by-products post fuel combustion, and their fate in the environment, could be explored in the future studies.

Acknowledgments

The authors gratefully acknowledge the support and input of their colleagues, notably Liane Chow, Oxana Blajkevitch, Honoria Kwok, Jeffrey Yan, Lauretta Liem, and Norman Berke of the Pacific Environmental Science Centre of Environment and Climate Change Canada, North Vancouver, BC.

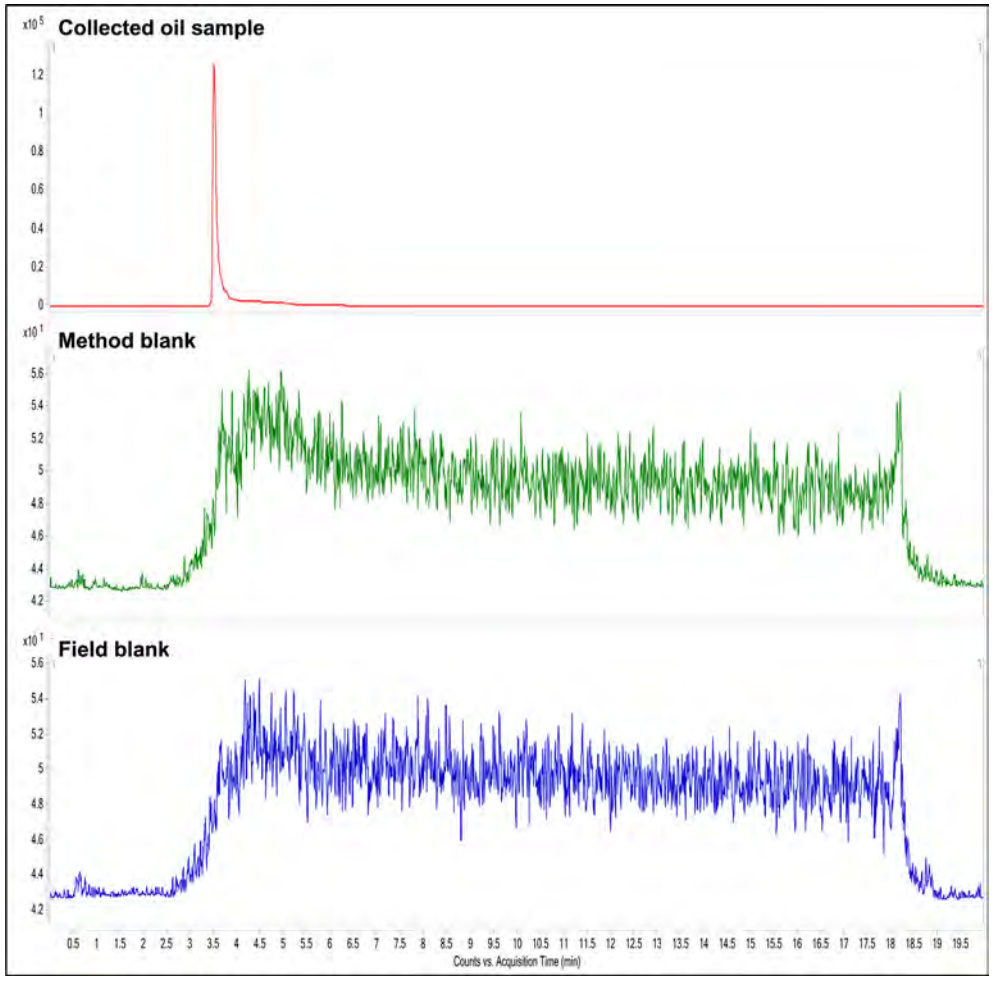

FIGURE 6.10 LC/MS/MS MRM chromatogram of *Azadirachtin* from a collected oil sample compared to method blank and field blank. Conditions for the instrument are detailed in the text with the exception of gas temperature at 16 mL/min, nebulizer pressure of 20 psi, sheath gas flow 11 mL/min, and capillary voltage 3500 V. The MRM ion transition for Azadirachtin was 743.25216 $m/z \rightarrow 725.2$ m/z in positive mode ionization with collision energy of 32 V.

References

Blumhorst, M.R., 2011. Direct determination of glycidyl esters of fatty acids in vegetable oils by LC–MS. J. Am. Oil Chem. Soc. 88, 1275–1283.

Caravaggio, G.A., Charland, J.-P., Macdonald, P., Graham, L., 2007. *n*-Alkane profiles of engine lubricating oil and particulate matter by molecular sieve extraction. Environ. Sci. Technol. 41, 3697–3701.

Dominguez-Rosado, E., Pichtel, J., 2003. Chemical characterization of fresh, used and weathered motor oil via GC/MS, NMR and FTIR techniques. Proc. Indiana Acad. Sci. 112, 109–116.

Elzey, B., Pollard, D., Fakayode, S.O., 2016. Determination of adulterated neem and flaxseed oil compositions by FTIR spectroscopy and multivariate regression analysis. Food Control. 68, 303–309.

Fingas, M., 2015. Vegetable Oil Spills: Oil Properties and Behavior. John Wiley & Sons, Edmonton, AB, 79 p.

Ghosh, P., Dey, K., Upadhyay, M., Das, T., 2017. Multifunctional biodegradable lube oil additives: synthesis, characterization, and performance evaluation. Petrol. Sci. Technol. 35, 66–71.

Hewstone, R.K., 1994. Health, safety and environmental aspects of used crankcase lubricating oils. Sci. Total Environ. 156, 255–268.

Lerma-Garcia, M.J., Ramis-Ramos, G., Herroro-Martinez, J.M., Gimeno-Adelantado, J.V., Simo-Alfonso, E.F., 2009. Characterization of the alcoholic fraction of vegetable oils by derivatization with diphenic anhydride followed by high-performance liquid chromatography with spectrophotometric and mass spectrometric detection. J. Chromatogr. A 1216, 230–236.

Mata-Espinosa, P., Bosque-Sendra, J.M., Bro, R., Cuadros-Rodriguez, L., 2011. Olive oil quantification of edible vegetable oil blends using triacylglycerols chromatographic fingerprints and chemometric tools. Talanta 85, 177–182.

Stout, S.A., Wang, Z., 2016. Chemical fingerprinting methods and factors affecting petroleum fingerprints in the environment. Standard Handbook Oil Spill Environmental Forensics – Fingerprinting and Source Identification. Elsevier, London, UK, pp. 61–129.

U.S. Environmental Protection Agency (EPA), Office of Solid Waste and Emergency Response, 2001. Introduction to Used Motor Oil, 530-K-0200251. Washington, DC.

Wang, Z., Stout, S., 2007. Oil Spill Environmental Forensics. Academic Press, New York, NY, 554 p.

CHAPTER

7

Environmental Forensics Study of Crude Oil and Petroleum Product Spills in Coastal and Oilfield Settings: Combined Insights From Conventional GC–MS, Thermodesorption–GC–MS, and Pyrolysis–GC–MS

Michael A. Kruge[1], *José Luis R. Gallego*[2], *Azucena Lara-Gonzalo*[2] *and Noemi Esquinas*[2]

[1]Montclair State University, Montclair, NJ, Unites States [2]University of Oviedo, Mieres, Spain

BIOGRAPHIES

Dr. Michael A. Kruge is Professor of Earth and Environmental Studies at Montclair State University (MSU) in New Jersey (Unites States). He was formerly Associate Dean of the College of Science and Mathematics at MSU, Professor and Chair in the Department of Geology at Southern Illinois University Carbondale, and a Geochemist for Standard Oil (Ohio)/British Petroleum. He holds a PhD in Geology (1985) from the University of California, Berkeley. His research interests include environmental geochemistry and forensics of organic contaminants in sediments; marine, estuarine, and lacustrine biogeochemistry; geochemistry of peat; fossil organic matter as indicator of environmental change; applications of analytical pyrolysis–GC–MS; biological marker compounds and polycyclic aromatic hydrocarbons in petroleum, petroleum source rocks, oil shales, coal, and sediments; nature of organic sulfur in fossil fuels. He is the author of numerous peer-reviewed scientific publications.

Dr. José Luis R. Gallego is currently Associate Professor at the University of Oviedo (Spain). He holds a PhD (2004) in Mining, Environmental and Civil Engineering. Dr. Gallego has performed basic and applied research, heading projects in the areas of environmental engineering, organic and inorganic geochemistry, and environmental forensics, in cooperation with private industry as well as with European and Spanish public entities. He has coauthored 45 articles in ISI-indexed journals, mainly focused on site remediation and organic geochemistry.

Dr. Azucena Lara-Gonzalo holds a PhD (2015) in Analytical Chemistry. She is currently in charge of the Environmental Assay Unit of the Scientific and Technical Services (SCTs) of the University of Oviedo (Spain). Her main specialization is mass spectrometry applied to organic contaminants, including GC, GCxGC, and more recently Pyrolysis–GC–MS techniques.

Noemi Esquinas (MSc in geological engineering) has recently joined the University of Huelva (Spain) as a research assistant. She is doing a PhD in environmental engineering and her thesis is focused in the analytics of heavy oil fractions.

Oil Spill Environmental Forensics Case Studies.
DOI: http://dx.doi.org/10.1016/B978-0-12-804434-6.00007-0

7.1 INTRODUCTION

Techniques and applications for the chemical fingerprinting of spilled crude oil and petroleum products have developed increasing sophistication over recent decades (Stout and Wang, 2007). Besides conventional gas chromatography–mass spectrometry (GC–MS), advanced methods including compound specific stable isotope ratio mass spectrometry, two-dimensional GC, and Fourier transform ion cyclotron resonance mass spectrometry have proven their effectiveness (Gaines et al., 2007; Jeffrey, 2007; Chen et al., 2016). In studies of contaminated sites, when rapid analytical results with minimum sample preparation are desired, analytical pyrolysis–gas chromatography–mass spectrometry (Py–GC–MS) has been employed (De Leeuw et al., 1986; Richnow et al., 1995; Kruge and Permanyer, 2004; Kruge et al., 2010; Kruge, 2015). Contaminants that escape detection by conventional analytical methods may be discovered (Lara-Gonzalo et al., 2015). At temperatures and durations commonly used for analytical pyrolysis (e.g., 610°C for 20 seconds) volatile and semivolatile constituents may also be thermally desorbed and mixed with true pyrolysis products. To isolate the two types of materials, a separate thermodesorption step can be performed first, heating the sample at a lower temperature (e.g., 350°C). The thermodesorption method (TD–GC–MS) employs the same instrumentation as Py–GC–MS. Thus, after the GC–MS analysis of the thermally desorbed volatiles and semivolatiles has finished, the remaining sample residue can be heated at the higher pyrolysis temperature and a second GC–MS analysis effected. The thermodesorption–sequential pyrolysis approach for the study of environmental contamination was pioneered decades ago (Whelan et al., 1980) and has been used fruitfully since (Faure and Landais, 2001; Kruge, 2015). Thermodesorption alone, without subsequent residue pyrolysis, has been recommended by regulators as an alternative analytical method (USEPA, 1996).

For this study, a diverse collection of five samples affected by spills at locations around the world has been assembled. These include the (1) Aboño fuel oil spill (oiled rocks on the Asturian coast, Spain), (2) *Prestige* heavy fuel spill (oiled rocks on the Galician coast, Spain), (3) *Deepwater Horizon* tarball (Alabama coast, Unites States), (4) Kuwait crude oil spill (oilfield soil, deliberate spill during the first Gulf war), and (5) an Angolan light crude oil spill (oilfield soil). In addition to conventional GC–MS analyses, TD–GC–MS and Py–GC–MS were employed. The data are interpreted in the context of the samples' diverse origins, emplacement, and weathering using a standard environmental forensics approach. In addition, insights from the thermodesorption and pyrolysis methods are presented, including an evaluation of their effectiveness as forensic screening tools.

7.2 MATERIALS AND METHODS

7.2.1 Samples

A representative set of five samples obtained in four very different regions was selected in order to obtain a mixture of well-known spills and unknown cases, different product characteristics, and different levels of weathering. Three of them were taken in shorelines affected by marine oil spills and the other two were taken inland in areas where oil spill incidents had occurred.

The Kuwait sample is an oiled sandy soil partially preserved for years from weathering effects in very dry/anoxic conditions. It was taken in 2014 in one of the areas (Burgan field) affected by the huge spills that took place in the first Gulf War (Brown et al., 1998). A detailed description of oil geochemistry of Burgan field can be found in Kaufman et al. (2000). The sample is from a "dry oil lake" in which the polluted sand [taken at 40 cm depth, having 20,000 ppm total petroleum hydrocarbons (TPH)] was encrusted with a surficial layer of weathered heavy oil that preserved the product permeating the sand below from rapid degradation. The soil is sealed by a tar mat (Balba et al., 1998), forming a layer about 1 cm thick that was peeled off to reveal the underlying polluted sand that was sampled. The soil sampled revealed an alkaline pH, high salinity, sandy texture (less than 10% of silt and clay), and very low concentrations of nitrogen, phosphorus, and natural organic matter. Information on the composition of this particular fresh oil was not available, but reported mean values for three topped fresh Burgan field oils are 37.7% saturated hydrocarbons, 46.0% aromatics, 8.1% polar compounds, and 8.3% asphaltenes with 2.93% sulfur in the whole oil (Abdullah and Connan, 2002).

The sample from Angola was taken in 2012 in a sandy soil affected by oil spills (TPH: 11,000 ppm) as a result of oil exploration and production activity at a confidential location. The soil sampled shown a neutral pH, low conductivity, sandy texture (less than 10% of silt and clay), and low concentrations of nitrogen, phosphorus, and natural organic matter. Compositional data on the fresh crude oil were not obtainable.

At the end of June 2012, the Cantabrian shoreline of Asturias (Spain) was affected by a heavy fuel oil spill (around 20 tons) from an industrial facility close to the coast. The Aboño sample was taken in a study site with a relatively homogenous 500 m stretch of pristine rocky shore affected by the fuel immediately after the spill. In order to obtain representative data, composite samples comprised 10 increments of 4 cm^2 of fuel geometrically distributed at sampling stations, corresponding to rocks from the upper intertidal zone (Gallego et al., 2013). The Aboño spill was originated by a heavy fuel oil (δ15°C = 0.991 kg/L; sulfur = 2.25%) composed when fresh of 24.3% saturates, 44.2% aromatics, 11.5% polars, and 20.0% asphaltenes.

Like the Aboño, the *Prestige* sample is a rock scraping. It was obtained in 2010, more than seven years after the *Prestige* fuel oil spill (Alzaga et al., 2004), at the beach site called Moreira, located on the Atlantic coast of Galicia (northwestern Spain), 80 km from La Coruña. Significant weathering and specifically (bio)degradation was expected given that this area was subjected to bioremediation with oleophilic fertilizers between 2003 and 2005 (Gallego et al., 2006). The spilled cargo of the *Prestige* tanker was a heavy residual fuel oil (δ15°C = 0.993 kg/L; sulfur = 2.6%; nitrogen = 0.69%) that was composed of 26.8% saturates, 39.1% aromatics, 17.3% polars, and 16.8% asphaltenes (Díez et al., 2005; Gallego et al., 2007).

The Macondo sample is a tarball recovered along the Alabama shoreline approximately six weeks following the explosion of the *Deepwater Horizon* oil rig on April 20, 2010. That tragic event led to a release of more than 70,000 tons of petroleum hydrocarbons from the Macondo well (Atlas and Hazen, 2011). The Macondo oil has been intensively studied in recent years, and therefore its composition (chemical fingerprint, biomarkers, weathering evolution etc.) is well known (Aeppli et al., 2012; Aeppli et al., 2014; White et al., 2016). The fresh Macondo oil was a light crude oil (δ15°C = 0.820 kg/L; sulfur = 0.4%; nitrogen = 0.38%) with 74% saturates, 16% aromatics, and 10% resins and asphaltenes (Reddy et al., 2012).

7.2.2 Experimental Methods

Fig. 7.1 presents an overview of the experimental procedures, the details of which are given below.

7.2.2.1 Extraction and LC Fractionation

The sandy samples (Kuwait and Angola) were extracted with dichloromethane:methanol (3:1, v/v) in a Soxtherm system (Gerhardt). The extract was concentrated by rotary evaporation. The shoreline samples (rock

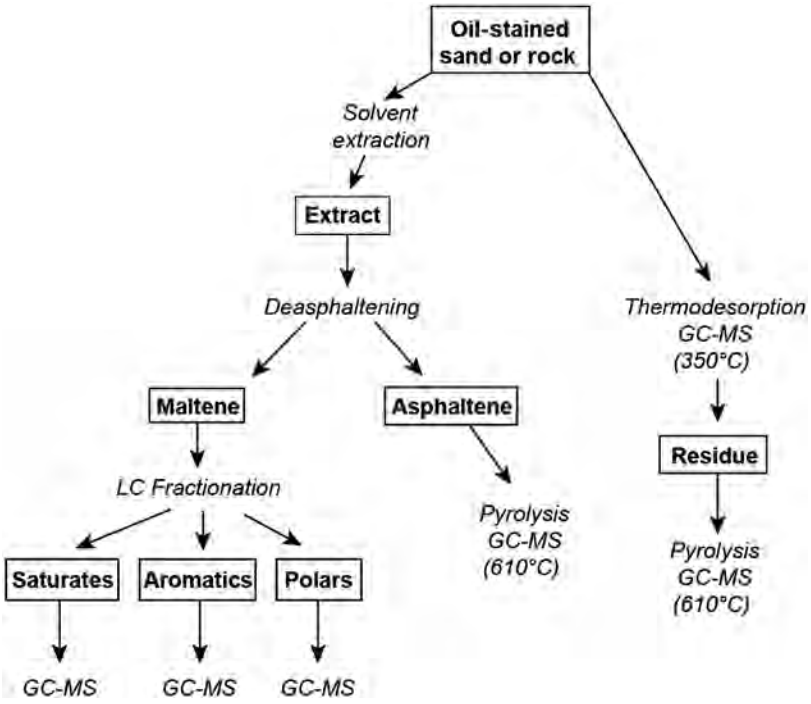

FIGURE 7.1 Analytical scheme used in this study.

scrapings from *Prestige* and Aboño spills, and sand from deepwater horizon (DWH) spill) were extracted as follows: 1-g representative subsamples were extracted with dichloromethane in an ultrasonic bath for 15 min; the extracts were then carefully filtered (Whatman 42 filter) to eliminate impurities such as sand, clay particles, algae.

Aliquots of the extracts (both soil and shoreline samples) were fractionated and gravimetrically quantified by liquid chromatography (LC) into saturated and aromatic hydrocarbon, polar compound, and asphaltene fractions. In brief, LC was carried out in two steps: in the first one, maltenes and asphaltenes were separated by filtering through 0.45 μm filters using hexane and dichloromethane, respectively; then, in the second step, maltenes were fractionated into saturated, aromatic, and polar fractions by LC in columns filled with silica gel and alumina. The saturated fraction was eluted with hexane, the aromatics with a mix of dichloromethane:hexane (4:1, v/v), and finally, the polar fraction with dichloromethane:methanol (1:1, v/v).

7.2.2.2 Conventional GC–MS

The analyses of the saturate, aromatic, and polar fractions were carried out by GC–MS. The injection of the extracts was performed on a GCMS-QP2010 Plus from Shimadzu. A capillary column DB-5MS (5% phenyl 95% dimethylpolysiloxane; 60 m × 0.25 mm i.d. × 0.25 μm film) from Agilent Technologies was used with helium as carried gas at 1 mL min^{-1}. The initial oven temperature was 40°C (held for 5 min) and ramped at 5°C min^{-1} up to 300°C and held for 20 min. The mass spectrometer was operated in electron ionization mode (EI) at 70 eV. It was calibrated daily by autotuning with perfluorotributylamine (PFTBA) and the chromatograms were acquired in full scan mode (mass range acquisition was performed from 45 to 500 *m*/*z*). For quality control, solvent blanks were periodically injected.

7.2.2.3 Thermodesorption–GC–MS and Pyrolysis–GC–MS

Aboño, Angola, Kuwait oil-stained rock and sands. Oil scraped from the stained rock (Aboño, <0.1 mg) and oil-stained sand (Angola, Kuwait, ca. 5–6 mg) were analyzed by TD–GC–MS using a CDS 5150 Pyroprobe coupled to a Thermo Finnigan Focus DSQ GC/MS equipped with an Agilent DB-1MS column (30 m × 0.25 mm i.d. × 0.25 μm film thickness). The GC oven temperature was programmed from 50°C to 300°C (at 5°C min^{-1}), with an initial hold of 5 minutes at 50°C and a final hold of 15 minutes at 300°C. The MS was operated in full scan mode (50–500 Da, 1.08 scans sec^{-1}). After the thermodesorption run ended, the sample (which had remained untouched in the Pyroprobe) was heated at 610°C for 20 sec, pyrolyzing the postthermodesorption residue ("sequential pyrolysis"). Pyrolysis products were analyzed by GC–MS (Py–GC–MS) using the conditions employed for the thermodesorption products.

Prestige oil-stained rock. Rock scraping of the *Prestige* spilled oil (0.22 mg) was analyzed with a PY-2020iD double-shot pyrolyzer (Frontier Lab) coupled to a Shimadzu GCMS-QP2010 equipped with a DB-5MS column (30 m × 0.25 mm i.d. × 0.25 μm film). The GC oven temperature was programmed from 50°C to 300°C (at 5°C min^{-1}), with an initial hold of 5 minutes at 50°C and a final hold of 30 minutes at 300°C. Thermodesorption was affected for 20 seconds at 350°C. Upon completion of the GC run, the residue was pyrolyzed for 20 seconds at 610°C and a second GC run completed. The MS was operated in full scan mode from 50 to 500 Da.

Asphaltenes. Py–GC–MS (610°C, 20 sec) was performed directly on the asphaltene fractions (<0.1 mg), without the thermodesorption step. Py–GC–MS instrumentation and conditions were the same as those used for the Aboño, Angola, and Kuwait oil-stained rock and sands.

Macondo tarball. Unlike the others, this sample (<0.1 mg) was analyzed in a "single shot" run at 610°C for a rapid, combined thermodesorption–pyrolysis experiment. For this experiment, a chemical data systems (CDS) 2000 Pyroprobe was coupled to a Thermo Finnigan Focus DSQ GC/MS equipped with a J&W scientific DB-1MS column (15 m × 0.25 mm i.d. × 0.25 μm film thickness). The GC oven temperature was programmed from 50°C to 300°C (at 5°C min^{-1}), with an initial hold of 5 minutes at 50°C and a final hold of 5 minutes at 300°C. Pyrolysis was performed for 20 seconds at 610°C. The MS was operated in full scan mode (50–500 Da, 1.08 scans sec^{-1}).

7.3 RESULTS AND DISCUSSION

7.3.1 Overview of General Characteristics

The five samples discussed in this chapter represent a variety of spill types (crude oils and petroleum products) from marine and terrestrial settings. They are genetically unrelated and represent wide compositional variety. The Kuwait sample was a normal, sulfur-rich crude oil spilled in the oil field at the end of the first Gulf War,

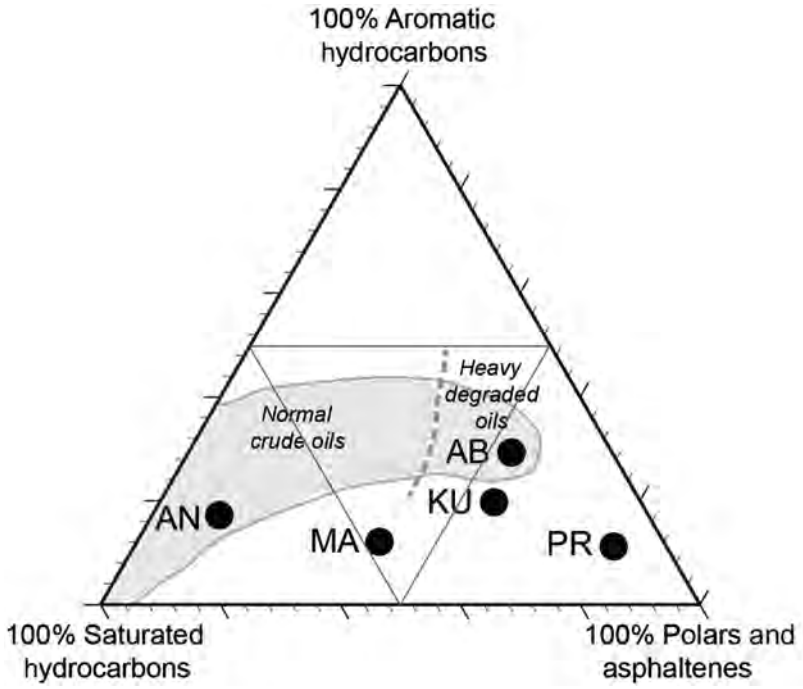

FIGURE 7.2 Ternary diagram showing the bulk composition of the five degraded oil samples as reported in Table 7.1. *AB*, Aboño; *AN*, Angola; *KU*, Kuwait; *MA*, Macondo; *PR*, Prestige. The "normal" and "heavy degraded" zonations follow Tissot and Welte (1984).

TABLE 7.1 Bulk Composition of the Degraded Oils as Received

Sample	Saturates (%)	Aromatics (%)	Polars (%)	Asphaltenes (%)	Sulfur (%)
Aboño	16.8	29.3	26.2	27.7	3.2
Angola	71.6	17.2	7.9	3.3	0.9
Kuwait	24.5	19.7	35.6	20.2	6.3
Macondo	47.4	12.1	22.1	18.4	0.9
Prestige	8.8	11.2	12.5	67.5	3.2

and degraded during years of residence at the surface. The Aboño sample was a fuel oil product spilled at sea, subsequently contaminating shore areas. The *Prestige* sample had a similar history but originated as a heavier fuel oil fraction. The Angola sample is a light crude oil, spilled in the oil field. The Macondo sample was spilled at sea and subsequently collected after it made landfall. In their present state, the Kuwait and Aboño samples are considered to be heavy degraded oils, following the classification of Tissot and Welte (1984), with the Aboño sample richer in aromatic hydrocarbons (Fig. 7.2; Table 7.1). The *Prestige* sample exhibits a more extreme level of degradation, composed primarily of polar compounds and especially, asphaltenes. In contrast, the Angola sample contains mostly saturated hydrocarbons. Saturated hydrocarbons comprise nearly half of the Macondo sample which is also notably poor in aromatics. In their present degraded state, the Angola and Macondo samples are low in sulfur, while the other three are sulfur rich, in particular the Kuwait, having 6.3 % sulfur (Table 7.1).

For an overview of their principal molecular characteristics, total ion chromatograms (TIC) of the saturated and aromatic hydrocarbon fractions derived from the solvent extract are presented along with traces from thermodesorption of the whole sample at 350°C, the subsequent pyrolysis of the same sample aliquot at 610°C, and the pyrolysis of the asphaltene fraction, also at 610°C. Chromatographic conditions and instrumentation varied depending on sample type, as discussed in detail above. Details of specific compounds (including normal alkanes, biological marker compounds, and aromatic hydrocarbons) are presented subsequently in Section 3.2.

7.3.1.1 *Kuwait Oil Spill*

The total ion current trace of the Kuwait oil's saturated hydrocarbon fraction displays prominent normal alkanes from C_{16} to at least C_{30}, phytane, pristane, and C_{29}–C_{35} hopanes (Fig. 7.3A). Their peaks crown a broad unresolved complex mixture (UCM) hump in the n–C_{15}–C_{40} retention time range. The aromatic fraction exhibits a UCM hump spanning the same retention times (Fig. 7.3B). Clearly evident aromatic compounds include a series of C_1 to C_4-alkylated dibenzothiophenes, consistent with this oil's high sulfur content (Table 7.1). Also noteworthy are aromatic biomarkers, including 8,14-secohopanoids and benzohopanes (Table 7.2).

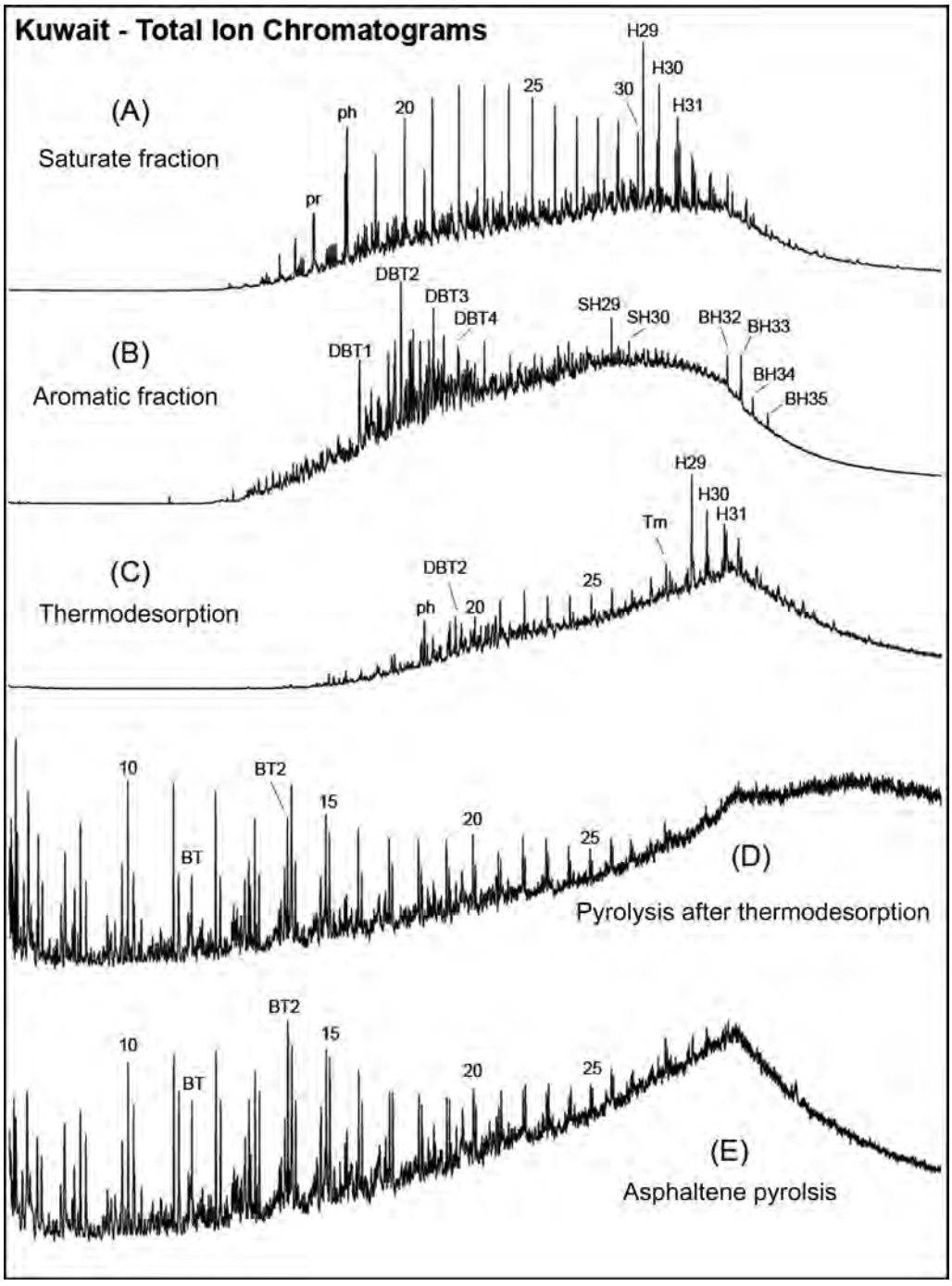

FIGURE 7.3 Total ion current chromatograms for the Kuwait oil. (A) Saturated hydrocarbon fraction, (B) aromatic fraction, (C) thermodesorption products, (D) products of sequential pyrolysis of the postthermodesorption residue, and (E) asphaltene pyrolysis products. See Table 7.2 for peak identification.

TABLE 7.2 Symbols Used for Peak Identification in Figs. 7.3 through 7.12, 7.14, and 7.15

SATURATED HYDROCARBONS	
numerals	normal alkanes (*n*-alk-1-ene/*n*-alkane doublets for pyrolyzates)
pr	pristane
ph	phytane
Hx	hopanes ("x" indicates the carbon number, C_{29}–C_{35})
Ts	18α(H)-22,29,30-trisnorhopane
Tm	17α(H)-22,29,30-trisnorhopane
TRx	tricyclic terpanes ("x" indicates the carbon number)
Sx	regular steranes ("x" indicates the carbon number)
Dx	diasteranes ("x" indicates the carbon number)
#	*n*-alkylcyclohexanes
AROMATIC COMPOUNDS	
For alkyl-substituted aromatic compounds, "x" indicates the degree of substitution.	
	1: methyl, 2: dimethyl or ethyl, etc.
Bx	alkylbenzene isomers
ST	styrene
*	*o*-alkyltoluenes
N	naphthalene
Nx	alkylnaphthalene isomers
PHN	phenenanthrene
PHNx	alkylphenanthrene isomers
ANT	anthracene
PYRx	alkylpyrene isomers
CHR	chrysene
CHRx	alkylchrysene isomers
BAN	benzo[*a*]anthracene
BANx	alkylbenzo[*a*]anthracene isomers
BT	benzothiophene
BTx	alkylbenzothiophene isomers
DBT	dibenzothiophene
DBTx	alkyldibenzothiophene isomers
BNT	benzonaphthothiophene
SHx	8,14-secohopanoids ("x" indicates the carbon number)
BHx	benzohopanes ("x" indicates the carbon number)
TASx	triaromatic steroids ("x" indicates the carbon number)
OTHER COMPOUNDS	
Ax	*n*-alkanoic acids ("x" indicates the carbon number)
IBx	isobutylene oligomers ("x" indicates the carbon number)

The composition of thermodesorption products is expected to resemble that of the full solvent extract prior to fractionation. This is generally the case with the Kuwait sample, for which the thermodesorption TIC shows a pronounced UCM hump in the $n-C_{15}-C_{40}$ range, with hopanes, minor *n*-alkanes, phytane, and alkyldibenzothiophenes clearly in evidence (Fig. 7.3C). These compounds were all detected in either the saturated or aromatic fractions, but occur in different proportions in the thermally desorbed components. The thermodesorption results provide a convenient means for assessing the extent of biodegradation, providing in effect a "whole oil" chromatogram that also shows some of the volatiles lost when using the solvent extraction method. From examination of Fig. 7.3C, it is evident that the oil is heavily biodegraded, i.e., having a value of 3–4 on the 10-point biodegradation scale of Peters et al. (2005), since relatively minor amounts of *n*-alkanes are still present. The residue remaining after thermodesorption was pyrolyzed, yielding a mixture of lower molecular weight compounds contrasting strongly with the thermally desorbed mixture (Figs. 7.3C and 7.3D). Most notably, the trace displays a series of C_7-C_{27} *n*-alk-1-ene/*n*-alkane doublets characteristic of the pyrolysis products of aliphatic-rich material (e.g., Kruge, 2015). Benzothiophenes are also present, indicative of the sulfurous nature of the sample. While isoprenoids and hopanes are important thermodesorption products, they are not detectable in the pyrolyzate. The pyrolyzate of the extract's asphaltene fraction (Fig. 7.3E) closely resembles that of the residue (Fig. 7.3D), with prominent *n*-alk-1-ene/*n*-alkane pairs and benzothiophenes. This suggests that much of the material remaining after thermodesorption is asphaltene.

7.3.1.2 *Aboño Fuel Oil Spill*

The saturated hydrocarbon fraction of the degraded Aboño fuel oil notably contains long-chain *n*-alkanes ($C_{23}-C_{33}$), hopanes, and isoprenoids. Its TIC trace displays a prominent UCM hump in the *n*-C_{14} to C_{40} retention time range (Fig. 7.4A). Its aromatic fraction is characterized by a UCM hump over the same retention times, with a complex distribution of polycyclic aromatic hydrocarbons (PAHs), particularly alkylphenanthrenes and alkylchrysenes (Fig. 7.4B). As with the Kuwait sample, the thermodesorption products combine features detected in the saturated and aromatic fractions, in this case, prominent UCM hump, alkylated PAHs, and lesser amounts of long-chain *n*-alkanes (Fig. 7.4C). The relatively abundant PAHs evident in the aromatic fraction and thermally desorbed material are consistent with the sample's elevated aromatic content (Table 7.1). This heavily biodegraded sample fits the description corresponding to levels 3–4 on the Peters et al. (2005) biodegradation scale. The pyrolyzates of both the postthermodesorption residue and the asphaltenes show a predominance of aliphatic hydrocarbons (short to mid-chain *n*-alkanes and alkenes) with secondary amounts of aromatic compounds such as methylnaphthalene and benzothiophene (Figs. 7.4D and 7.4E).

7.3.1.3 *Prestige Fuel Oil Spill*

The saturated hydrocarbons isolated from the degraded *Prestige* heavy fuel oil contain long-chain *n*-alkanes ranging from C_{24} to C_{42} and beyond, along with hopanes. The UCM hump also reflects the predominance of heavier hydrocarbons, covering the *n*-C_{19} to *n*-C_{42} retention time range, with its maximum coeluting with *n*-C_{36} (Fig. 7.5A). The TIC trace of the aromatics exhibits a prominent UCM hump with a plateau in the *n*-C_{29} to C_{36} retention time range (Fig. 7.5B). PAHs (phenanthrenes, pyrenes, chrysenes) and aromatic biomarkers including 8,14-secohopanoids, benzohopanes, and triaromatic steroids are also in evidence. Upon thermodesorption, the sample yielded long-chain *n*-alkanes and hopanes consistent with those seen in the saturated fraction (Figs. 7.5A and 7.5C) as well as a prominent UCM hump having a maximum coincident with *n*-C_{30}. The C_{16} and C_{18} fatty acids are likely from residue of an oleophilic fertilizer sprayed at the spill site to favor biodegradation (Gallego et al., 2006), as the material to be thermodesorbed was scraped directly from a tar-stained rock sample with no preparative steps. This sample exhibits severe biodegradation or 4–6 on the Peters et al. (2005) scale, although for reasons of bioavailability it has long-chain *n*-alkanes still evident as major components. The residue after thermodesorption is predominantly aliphatic (Fig. 7.5D) as is the asphaltene pyrolyzate (Fig. 7.5E), although the latter has relatively more aromatic hydrocarbons, particularly alkylbenzenes and alkylnaphthalenes, and a pronounced UCM hump.

7.3.1.4 *Angola Oil Spill*

The light Angola petroleum is distinguished from the other samples in this study by its very high saturated hydrocarbon content (71.6 %; Table 7.1). Its TIC chromatograms reflect its distinctiveness. The saturated fraction exhibits a series of *n*-alkanes from C_{13} to C_{27}, with a maximum at C_{20} along with lesser amounts of isoprenoids and hopanes (Fig. 7.6A). Its UCM hump attains its maximum coincident with *n*-C_{28} and extends to the *n*-C_{37} retention time. The aromatic TIC trace is dominated by a similar UCM hump (Fig. 7.6B). With PAHs relatively less abundant, this fraction is instead notable for a series of $C_{16}-C_{29}$ *o*-alkyltoluenes and other long-chain

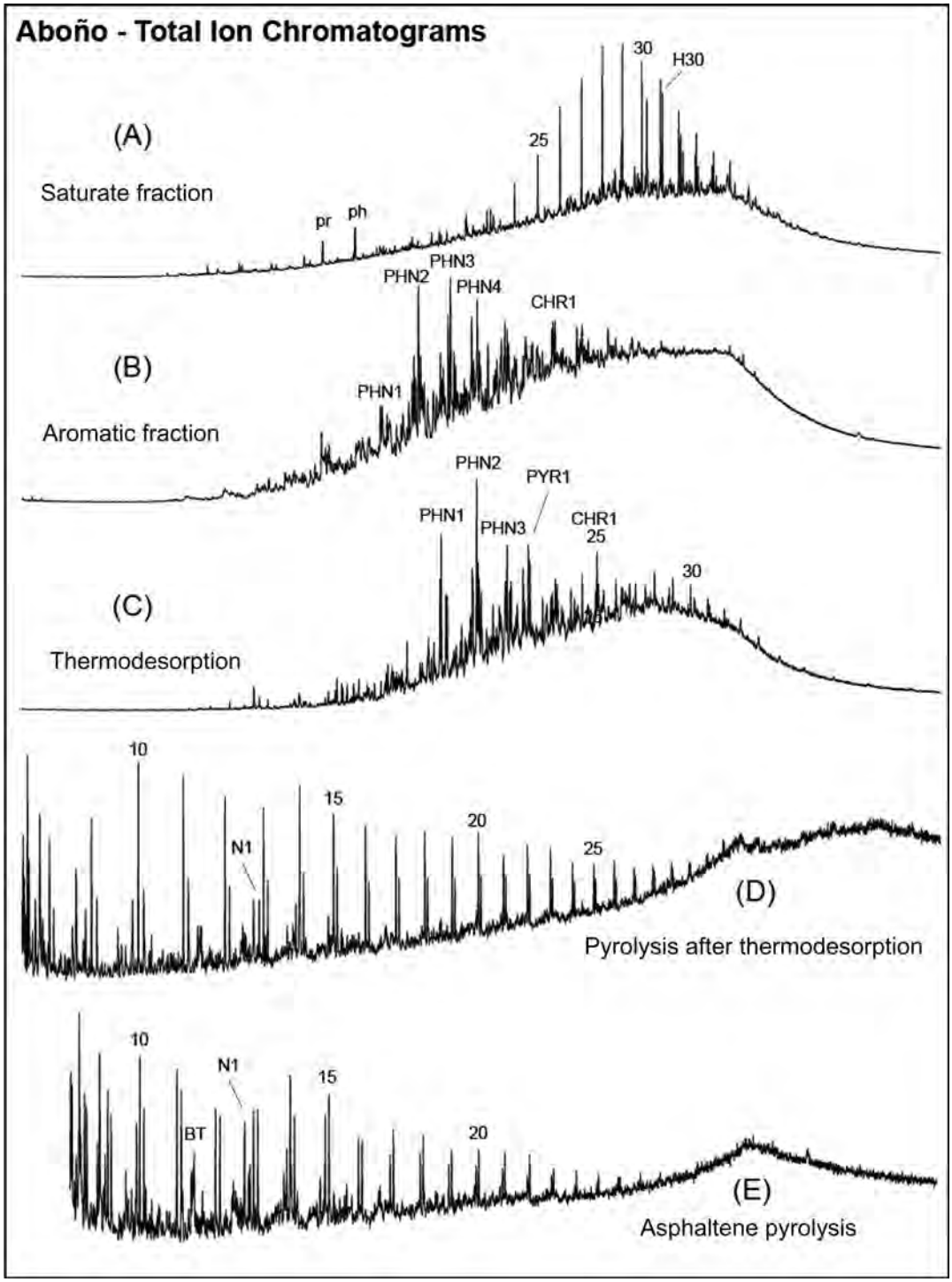

FIGURE 7.4 Total ion current chromatograms for the Aboño fuel oil. (A) Saturated hydrocarbon fraction, (B) aromatic fraction, (C) thermodesorption products, (D) products of sequential pyrolysis of the postthermodesorption residue, and (E) asphaltene pyrolysis products. See Table 7.2 for peak identification.

alkylbenzenes, indicating that even its aromatic hydrocarbons have an "aliphatic" character. The thermally desorbed components closely resemble those of the dominant saturated fraction, having a similar distribution of normal alkanes, isoprenoids, and hopanes (Fig. 7.6C). There is also a relatively narrow UCM hump maximizing near n-C_{30}. With n-alkanes still present, this sample can be considered to be lightly to moderately biodegraded, i.e., at level 1–2 on the Peters et al. (2005) scale. Very little residue remained after thermodesorption. The most

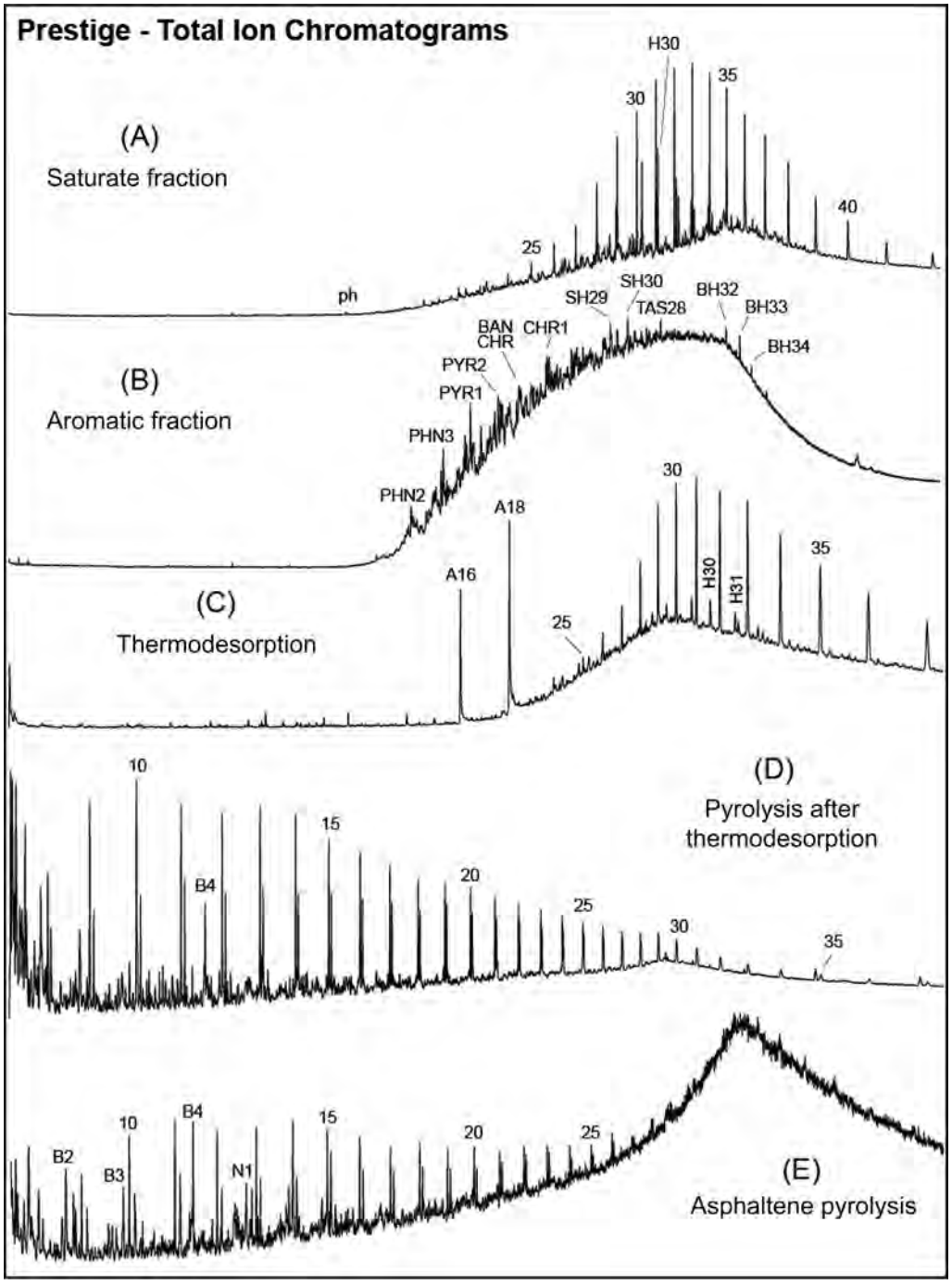

FIGURE 7.5 Total ion current chromatograms for the Prestige fuel oil. (A) Saturated hydrocarbon fraction, (B) aromatic fraction, (C) thermodesorption products, (D) products of sequential pyrolysis of the postthermodesorption residue, and (E) asphaltene pyrolysis products. See Table 7.2 for peak identification.

prominent peaks evident on its TIC chromatogram are interpreted to correspond to isobutylene oligomers ($(C_4H_8)_n$) from the pyrolysis of polyisobutylene. This polymer is employed in oil spill cleanup (Vollhardt and Schore, 2002) and its detection here is forensic evidence suggesting that it may have been used for remediation at the Angolan site. These compounds were not detected in any of the extract fractions and therefore must only be present as pyrolysis products. They were not found in the asphaltene pyrolyzate either (Fig. 7.6E). The only prominent peak on its TIC trace is due to styrene, suggesting polystyrene contamination at the collection site or during handling. In any case, asphaltenes constitute only a very minor portion of this oil (3.3%; Table 7.1).

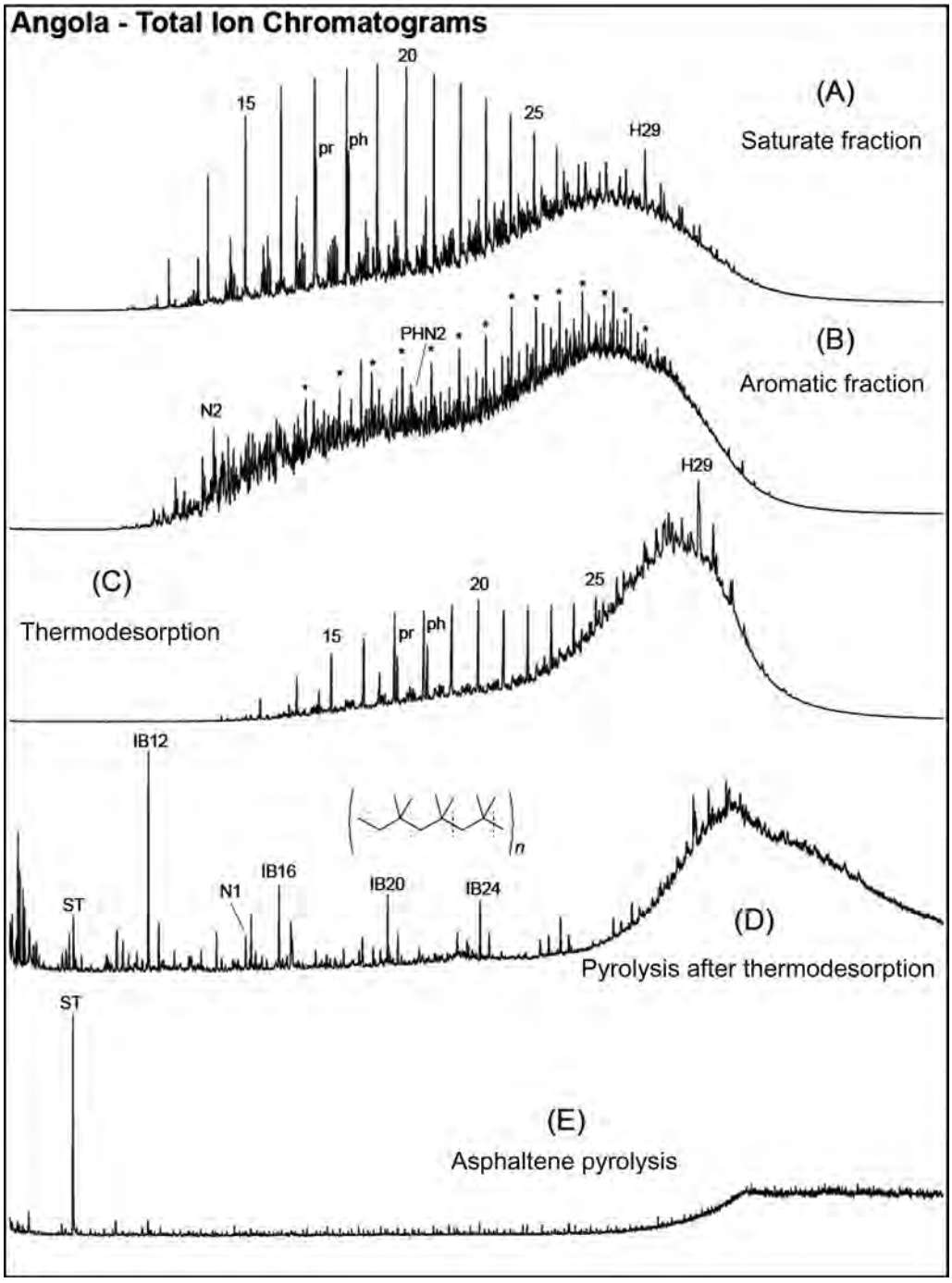

FIGURE 7.6 Total ion current chromatograms for the Angola oil. (A) Saturated hydrocarbon fraction, (B) aromatic fraction, (C) thermodesorption products, (D) products of sequential pyrolysis of the postthermodesorption residue, and (E) asphaltene pyrolysis products. See Table 7.2 for peak identification.

7.3.1.5 Macondo Oil Spill

The Macondo tarball sample was collected about six weeks after the start of the spill event, shortly after the material reached the Alabama shore. It is relatively fresh, with abundant *n*-alkanes (C_{16}–C_{42}, maximum at C_{20}) in its saturated fraction, along with subordinate isoprenoids and *n*-alkylcyclohexanes (Fig. 7.7A). The UCM hump is more apparent in the aromatic fraction, along with phenanthrenes and benzo[*a*]anthracenes (Fig. 7.7B). As with the Angola sample, there are also long-chain alkylbenzenes present, most notably, the *o*-alkyltoluene series from

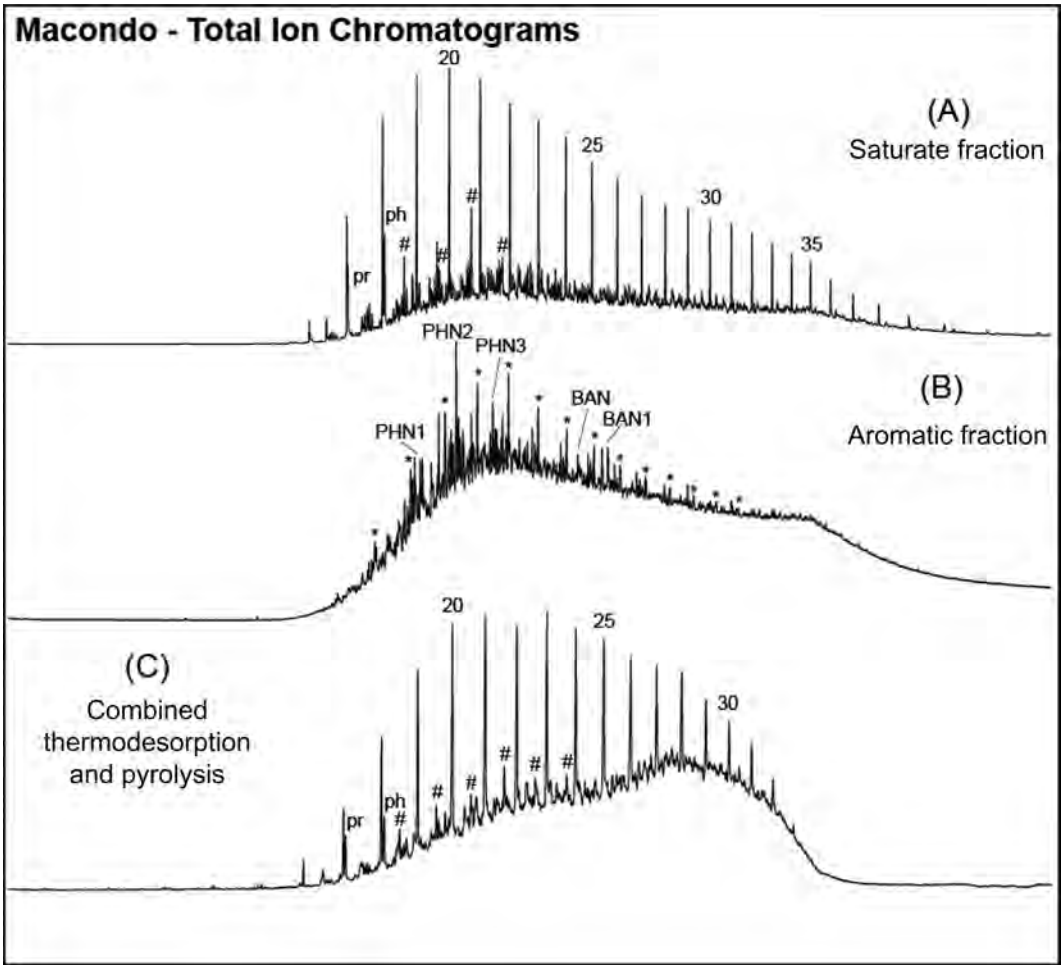

FIGURE 7.7 Total ion current chromatograms for the Macondo oil. (A) Saturated hydrocarbon fraction, (B) aromatic fraction, (C) combined thermodesorption and pyrolysis products produced in a single shot run at 610°C. See Table 7.2 for peak identification.

C_{17} to C_{30}. For this sample, a "single shot" combined thermodesorption and pyrolysis experiment was employed, heating the sample only once at 610°C and using a short (15 m) GC column to reduce analysis time and favor the elution of the heavier compounds. The results are essentially similar to those in the saturate fraction (Figs. 7.7A and 7.7C), with a predominance of C_{16}–C_{33} *n*-alkanes, pristane, phytane, and C_{18}–C_{23} *n*-alkylcyclohexanes. This is to be expected since saturated hydrocarbons comprise nearly half of the sample (Table 7.1). Notably absent from Fig. 7.7C are the normal alkane/alkene doublets characteristic of the pyrolysis of aliphatic-rich material and seen in the pyrolyzates of the other samples (Figs. 7.3D, 7.4D, and 7.5D). It is evident therefore that nearly all of the sample was thermally desorbed and thereby avoided pyrolysis. It will be treated as the equivalent of a thermodesorption product in the discussions below. In contrast with the other samples in this study, the Macondo tarball is only moderately biodegraded, having approximately a value of 2 on the 10-point scale of Peters et al. (2005).

7.3.2 Principal Compound Groups

7.3.2.1 Aliphatic Hydrocarbons

For a clearer picture of the normal and isoprenoid alkane distributions in the sample set, *m*/*z* 71 mass chromatograms are plotted in Fig. 7.8. From the top to the bottom of the diagram, the samples are arranged in order of decreasing saturated hydrocarbon content (Table 7.1). Coincidently, there is a corresponding shift from predominantly shorter to longer chains proceeding from the Angola sample (Figs. 7.8A and 7.8B) to the *Prestige* (Figs. 7.8I and 7.8J). The traces from the saturate fractions are arrayed on the left side of Fig. 7.8 with their thermodesorption counterparts on the right. While similarities were noted when comparing the TIC chromatograms of the

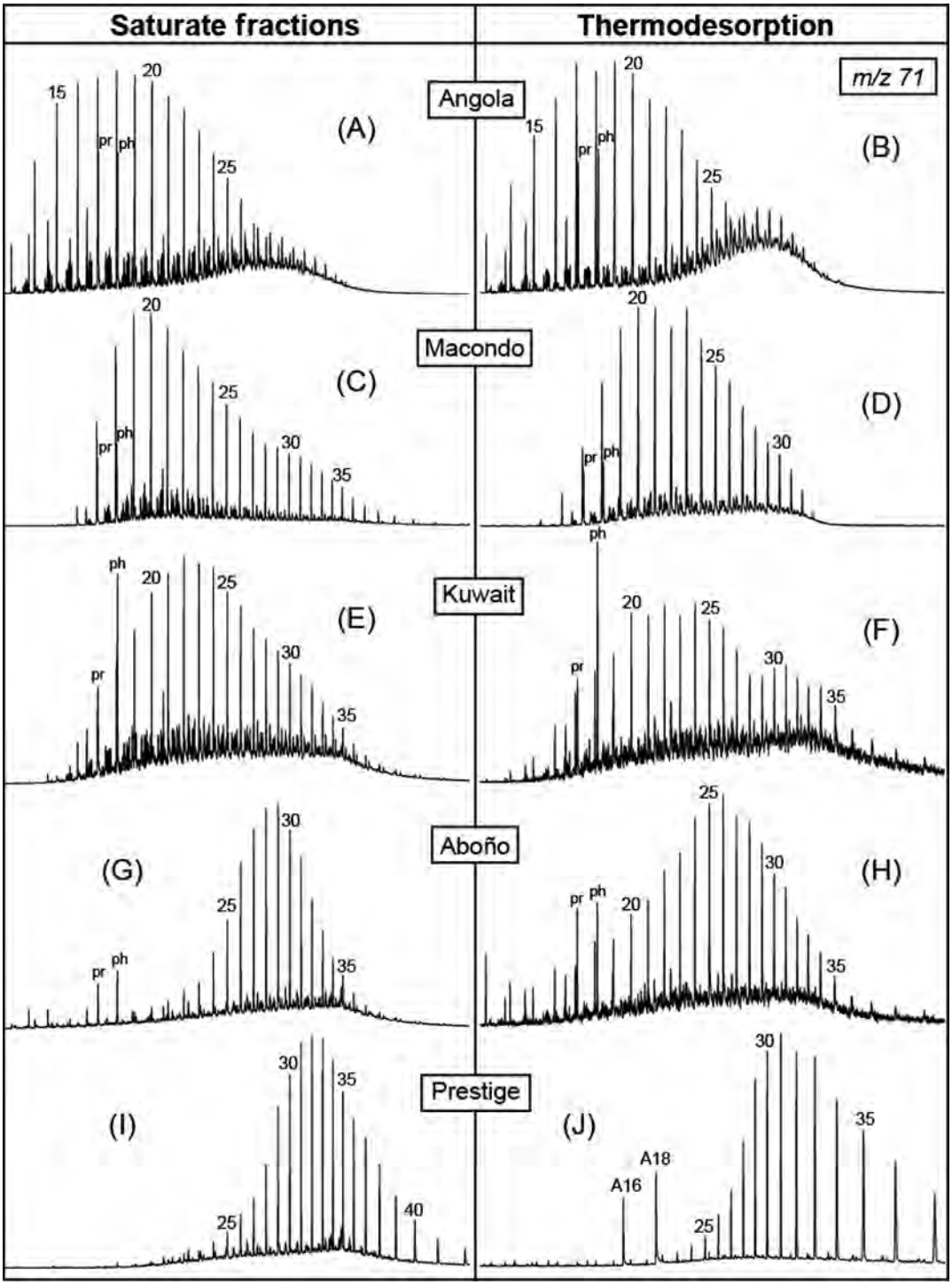

FIGURE 7.8 Mass chromatograms (*m*/*z* 71) showing the distribution of normal and isoprenoid alkanes in the saturate fractions (A, C, E, G, I) and corresponding thermodesorption products (B, D, F, H, J) of the five oils. See Table 7.2 for peak identifications.

Angola saturates and thermodesorption products (Section 3.1.4; Figs. 7.6A and 7.6C), the *m*/*z* 71 traces show a much stronger correspondence in the distribution of alkanes (Figs. 7.8A and 7.8B), all the more so when taking into account the differences in chromatographic conditions employed (Section 7.2.2). On both chromatograms, one observes a predominance of C_{14} to C_{25} *n*-alkanes, with a maximum around C_{18} or C_{19}, and a pristane/phytane ratio close to unity. For the Macondo sample, the longer chain *n*-alkanes ($> C_{33}$) are more effectively

TABLE 7.3 Diagnostic molecular ratios for the saturated (SAT) and aromatic (ARO) fractions and the thermodesorption products (TD), computed using the indicated ions for the five oil samples

m/z	192	198	71	191
Diagnostic ratio	**2-mPHN/1-mPHN**	**4-mDBT/1-mDBT**	**Pr/Ph**	**H29/H30**
Aboño TD	1.83	2.50	0.92	0.88
Aboño ARO/SAT	1.35	2.88	0.84	0.75
Angola TD	1.28	3.09	0.93	1.47
Angola ARO/SAT	1.21	3.29	0.87	1.24
Kuwait TD	0.83	1.73	0.48	1.20
Kuwait ARO/SAT	0.75	1.83	0.43	1.26
Macondo TD**	1.51	3.02	0.84	0.38
Macondo ARO/SAT	1.23	2.95	0.90	0.43
Prestige TD	1.5	(*)	(*)	0.86
Prestige ARO/SAT	(*)	(*)	0.28	0.79

mPHN: methylphenanthrene, mDBT: methyldibenzothiophene, Pr: pristane, Ph: phytane, H29: 17α(H),21β(H)-30-norhopane, H30: 17α(H),21β(H)-hopane.
* compound concentrations too low; ** combined thermodesorption/pyrolysis "single-shot" data employed.

detected by the injection technique (Fig. 7.8C) than by thermodesorption (Fig. 7.8D). Otherwise, the alkane distributions correspond closely, beginning with *n*-C_{16} and maximizing at C_{20}. The Kuwait chromatograms display the same range of *n*-alkanes (C_{16}–C_{36}, maximum at C_{22}), but there are variations in the distributions (Figs. 7.8E and 7.8F). Both techniques revealed a low pristane/phytane ratio, although phytane appears relatively more abundant overall in the thermodesorption products. The mid-length alkanes appear more abundant in the thermally desorbed components of the Aboño oil than in its saturate fraction, with a maximum at *n*-C_{26} rather than C_{29} (Figs 7.8G and 7.8H). With both methods, however, the *n*-alkane range is shown to extend to about C_{36} and phytane is marginally more abundant than pristane. With the heavy *Prestige* fuel oil, both techniques revealed a preponderance of long-chain *n*-alkanes, with the maximum at C_{30} or C_{31} and very little eluting prior to C_{24} (Figs. 7.8I and 7.8J). The thermodesorption results indicate the presence of *n*-alkanes up to C_{42} (not shown in Fig. 7.8J). Fatty acids noted on the thermodesorption TIC trace (Fig. 7.5C) are also evident here. Pristane/phytane ratios in the thermodesorption products are close to those in the saturate fraction (Table 7.3).

7.3.2.2 *Hopanes and Steranes*

The *m/z* 191 mass chromatograms displaying hopane distributions are arrayed in Fig. 7.9 using the same sequence employed in Fig. 7.8, with the sample most enriched in saturated hydrocarbons on top of the diagram and the thermodesorption results placed to the right of the corresponding saturate fraction data. The Angola hopanes show a predominance of the C_{29} 17α(H),21β(H)-30-norhopane over the C_{30} 17α(H),21β(H)-hopane (peaks H29 and H30 in Figs. 7.9A and 7.9B, respectively; Table 7.3) and a gradual decrease in relative abundance out to C_{35}. The C_{27} 18α(H)-22,29,30-trisnorhopane is nearly as abundant as the 17α(H)-22,29,30-trisnorhopane (Ts and Tm, respectively) and the C_{28} and C_{29} tricyclic terpanes are detectable as very minor components. The saturate fraction and thermodesorption *m/z* 191 traces for this sample correspond closely. The hopane distribution in the Macondo oil's saturate fraction shows a strong predominance of the C_{30} hopane, slightly more Ts than Tm, and a gradual decline in abundance from C_{31} to C_{35} (Fig. 7.9C, Table 7.3). In Fig. 7.9D, C_{30} hopane predominance is clear, but the other details are poorly registered. As indicated in Section 7.2.2.3, the data shown in Fig. 7.9D were produced by a single heating at 610°C and indicate that some quality was sacrificed for the advantages provided by a rapid screening procedure.

The Kuwait oil hopanes show a maximum at C_{29}, a low Ts/Tm ratio, and an elevated C_{35}/C_{34} ratio (Fig. 7.9E), all characteristics of petroleums derived from carbonate source rocks (Connan et al., 1986; Peters et al., 2005). The hopane distribution in the thermally desorbed material is quite similar, but also showing benzohopanes previously noted in the aromatic fraction (Fig. 7.3B). Since thermodesorption was performed on the whole oil sample, saturated and aromatic compounds may both be detected. Aromatic hopanes are also characteristic of carbonate-sourced oils (Connan et al., 1986). The Aboño and *Prestige* fuel oils have similar hopane distributions, with a

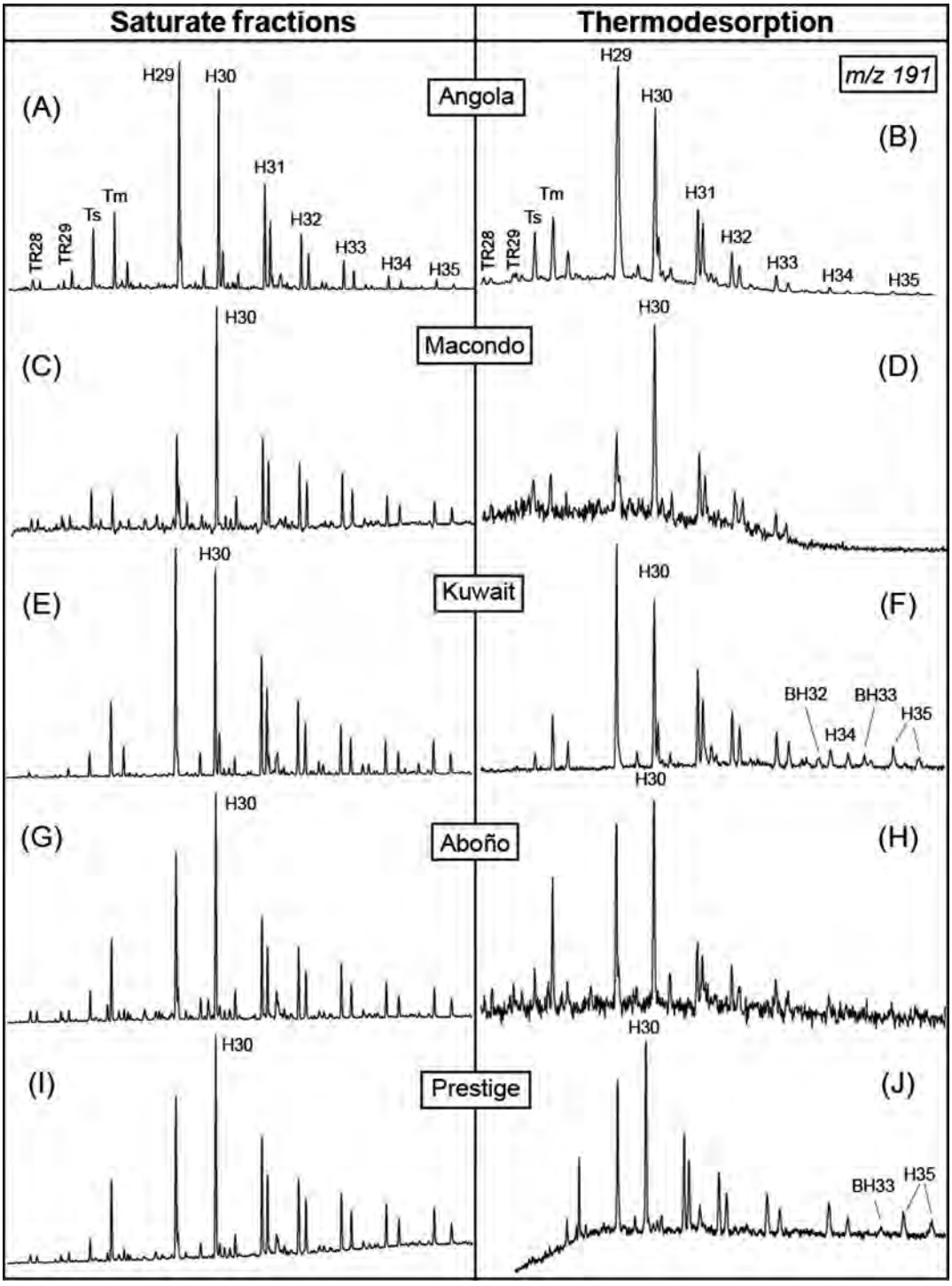

FIGURE 7.9 Mass chromatograms (*m/z* 191) showing the distribution of hopanes in the saturate fractions (A, C, E, G, I) and corresponding thermodesorption products (B, D, F, H, J) of the five oils. See Table 7.2 for peak identifications.

maximum at C_{30}, relatively abundant C_{29}, Tm, and C_{31}, and a gradual reduction in abundance from C_{31} to C_{35} (Figs. 7.9G and 7.9I; Table 7.3). In the Aboño thermodesorption products, the C_{27}, C_{29}, and C_{30} proportions resemble those in the saturated fraction (Figs. 7.9G and 7.9H) but the C_{31}–C_{35} hopanes are poorly resolved, likely due to insufficient concentrations. In contrast, the *Prestige* thermodesorption results compare favorably with those from the saturated fraction (Figs. 7.9I and 7.9J). The aromatic C_{33} benzohopane, also detected in the aromatic fraction (Fig 7.5B), is seen here as a relatively minor component.

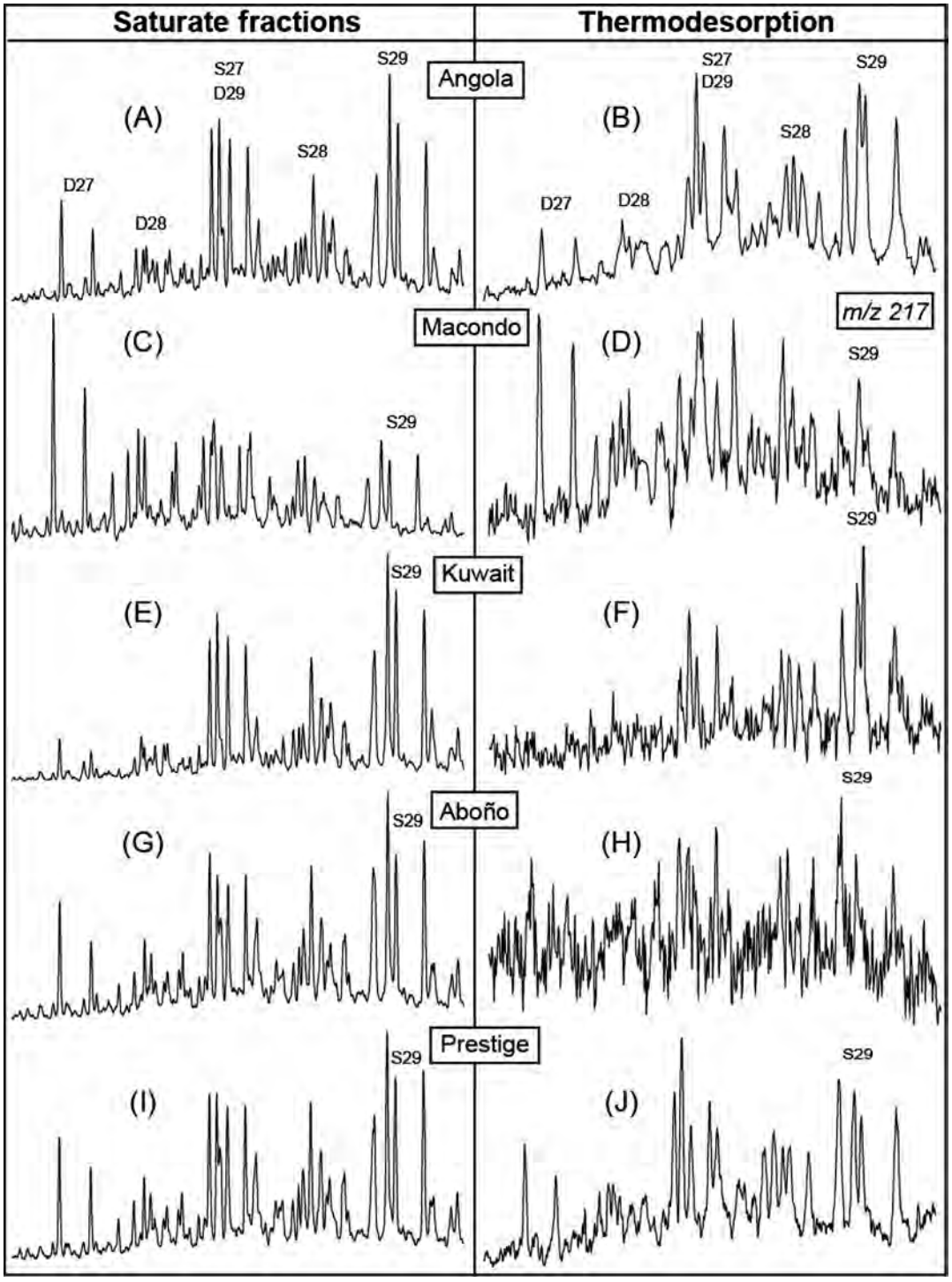

FIGURE 7.10 Mass chromatograms (*m/z* 71) showing the distribution of steranes in the saturate fractions (A, C, E, G, I) and corresponding thermodesorption products (B, D, F, H, J) of the five oils. See Table 7.2 for peak identifications.

The sterane results in Fig. 7.10 are arranged in the same manner as Figs. 7.8 and 7.9. In the Angola saturated fraction, the regular steranes are relatively more abundant than the rearranged, with $C_{29} > C_{27} > C_{28}$ (Fig. 7.10A). Chromatographic conditions were optimized for biomarker work and near-baseline resolution was achieved for individual compounds. Although chromatographic resolution is evidently inferior in the case of the thermodesorption data, the same general picture nonetheless emerges (Fig. 7.10B) in half the analysis time. The Macondo

oil is distinguished by a predominance of C_{27} diasteranes (Fig. 7.10C). Although the single temperature, rapid screening experiment poorly resolved the steranes, the importance of the C_{27} diasteranes is clearly evident (Fig. 7.10D). The Kuwait oil has a regular sterane carbon number distribution showing $C_{29} > C_{27} > C_{28}$ with relatively minor diasteranes (Fig. 7.10E), consistent with derivation from carbonate source rock (Connan et al., 1986; Peters et al., 2005). The thermodesorption results provide the same general information, but with poorer chromatographic resolution and signal to noise ratio (Fig. 7.10F). The Aboño and *Prestige* fuel oils have similar sterane distributions with a modest preference for C_{29} over C_{27} and relatively moderate amounts of C_{28} (Figs. 7.10G and 7.10I). Rearranged steranes are nearly as abundant as the regular. The steranes in the Aboño thermodesorption products are poorly discernable with a low signal to noise ratio (Fig. 7.10H). This would likely have been improved with a larger sample size. Upon thermodesorption, the *Prestige* oil yielded a sterane distribution comparable to that seen in the saturated fraction (Figs. 7.10I and 7.10J).

7.3.2.3 Polycyclic Aromatic Compounds

7.3.2.3.1 Phenanthrenes and Dibenzothiophenes in Aromatic Fractions and Thermodesorption Products

As an example, the distribution of phenanthrene and C_1 to C_4-alkylphenanthrenes in the Kuwait oil are displayed on composite mass chromatograms employing the respective molecular ions (Fig. 7.11). In spite of differences in the chromatographic conditions employed (different instruments, GC columns, and GC temperature programs), the results from the aromatic fraction and the thermodesorption of the whole oil exhibit striking similarities. Small variations in the relative retention times of several isomers produced some variation in coelution or separation, as revealed by close comparison of the C_2 and C_3-alkylphenenanthrene fingerprints on both traces

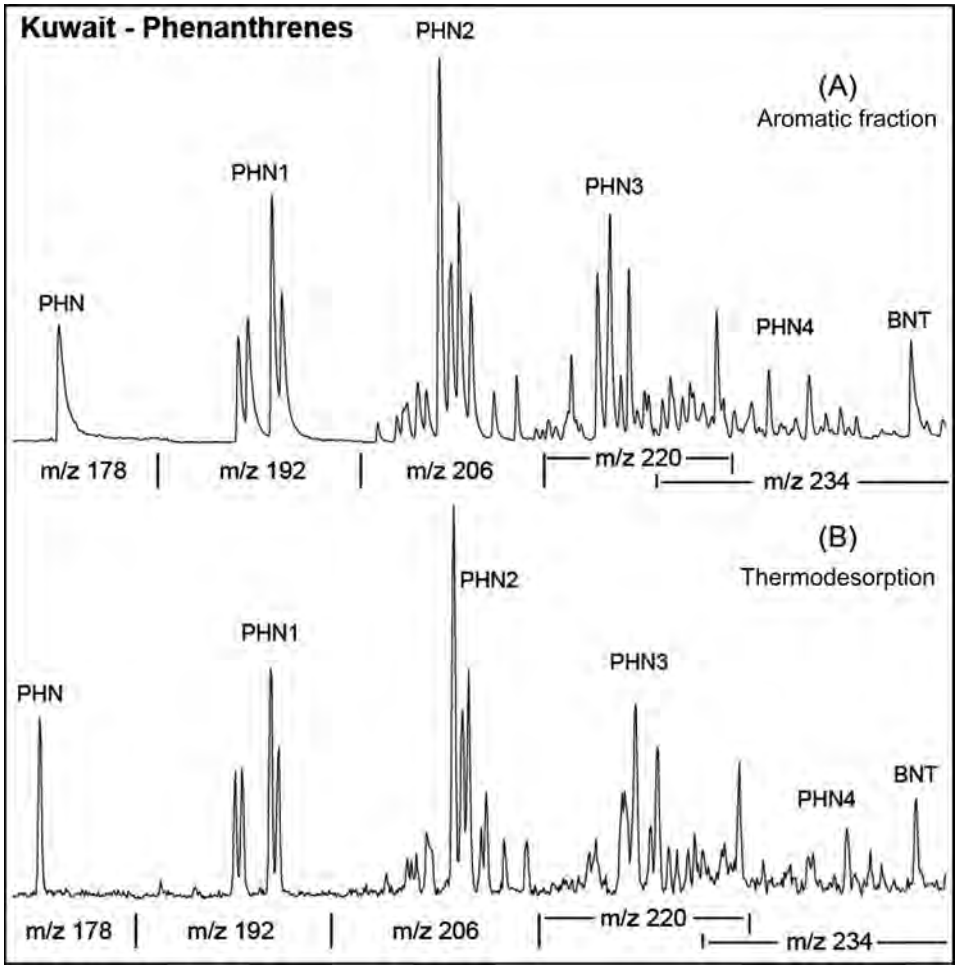

FIGURE 7.11 Composite mass chromatograms of the molecular ions of phenanthrene and the C_1 to C_4-alkylphenanthrenes in the (A) saturate fraction and (B) thermodesorption products of the Kuwait oil. See Table 7.2 for peak identification.

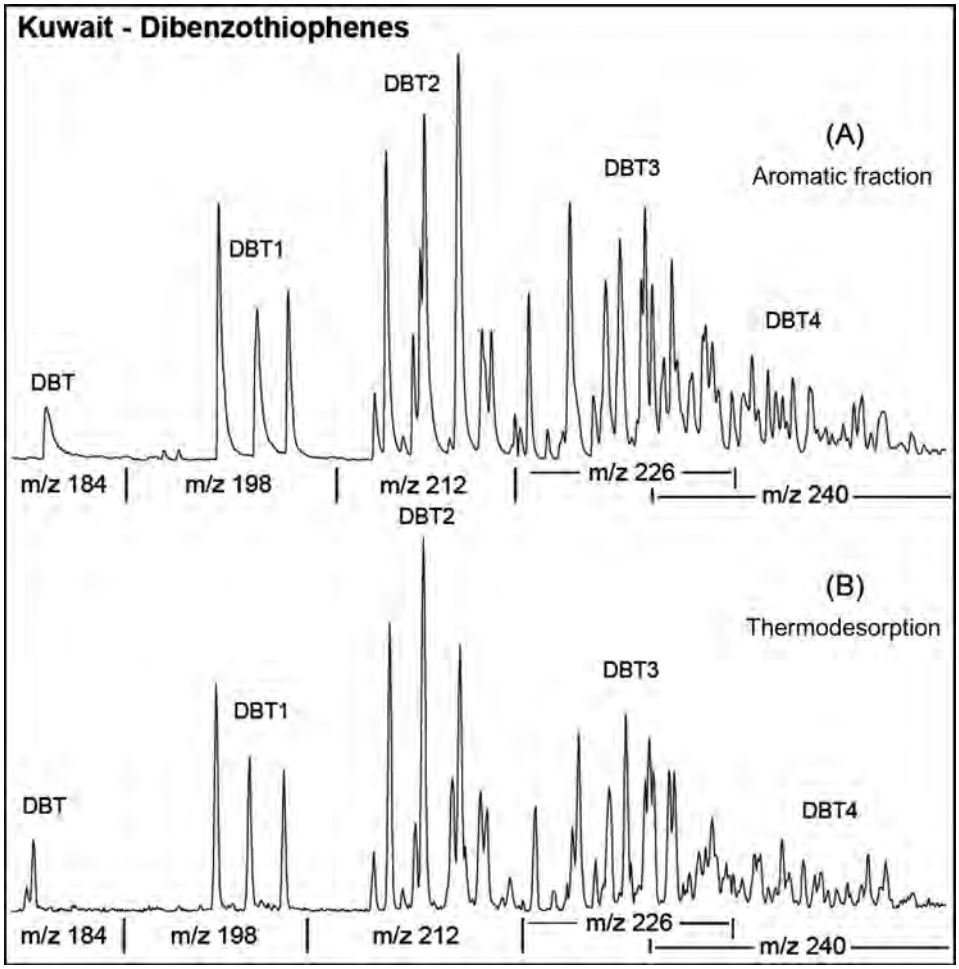

FIGURE 7.12 Composite mass chromatograms of the molecular ions of dibenzothiophene and the C_1 to C_4-alkyldibenzothiophenes in the (A) saturate fraction and (B) thermodesorption products of the Kuwait oil. See Table 7.2 for peak identification.

(Figs. 7.11A and 7.11B). The more complex C_4-alkylphenanthrene isomer clusters display the greatest differences. In both cases, the C_2-alkylphenanthrenes are relatively the most abundant.

In analogous fashion, dibenzothiophene and C_1 to C_4-alkyldibenzothiophene fingerprints are shown in Fig. 7.12. The results for the aromatic fraction and thermodesorption closely correspond in overall architecture as well as in detail. As in the phenanthrene example, there are more variations in peak distributions as the degree of alkylation increases. These likely arise due to minor changes in the relative retention times of isomers in response to the differences in the chromatographic conditions. Methylphenanthrene and methyldibenzothiophene ratios show similar trends when calculated for the aromatic fraction and the thermally desorbed products, but exhibit greater variation than that observed with the computed saturated compound ratios (Table 7.3). Comparisons of polycyclic aromatic compound (PAC) ratios based on thermodesorption results with those from solvent extract data should be exercised with caution.

Environmental forensics studies concerned with PACs often sum the quantitative results for each isomer cluster (Bence et al., 2007; Stout and Wang, 2007; Wang et al., 2007). For example, the concentrations of all C_2-alkylphenanthrenes are reported as a single composite number, rather than separately presenting the values for the individual constituent isomers. In the case of the phenanthrenes and dibenzothiophenes detected in the Kuwait oil, this can be presented as a simple bar graph, based on the normalized, relative quantitation results employing the relevant molecular ions (Fig. 7.13A). The relatively greater importance of the thiophenic components is clearly evident, consistent with the sample's high sulfur content (Table 7.1). Among the dibenzothiophenes as well as the phenanthrenes, the C_2 and C_3-alkyl compounds are the most important. Overall the distribution of these compound groups in the aromatic fraction closely resembles that in the thermodesorption products (Fig. 7.13A). The same holds true for the full set of five samples (Fig. 7.13B) which strongly correlate ($r^2 = 0.89$).

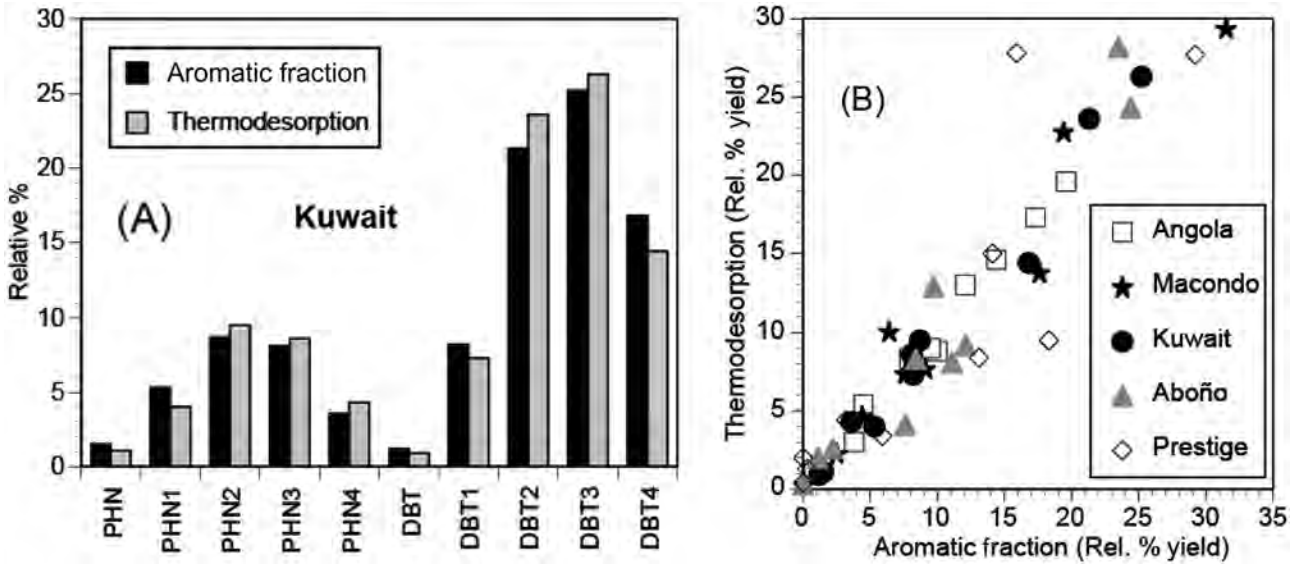

FIGURE 7.13 (A) Summary bar graphs for the PAC data from Figs. 7.11 and 7.12 for the aromatic fraction and thermally desorbed products of the Kuwait oil. See Table 7.2 for compound codes. (B) Comparison of the relative PAC yields for the aromatic fractions and thermodesorption products of the five oils. Values for isomer groups have been summed, as in Fig. 7.13A.

7.3.2.3.2 PACs in Pyrolyzates

The molecular weight of the pyrolysis products tends to be lower than that of the thermally desorbed and extracted material, as evident when comparing Figs. 7.3D and 7.3E with Figs. 7.3A, 7.3B, and 7.3C for example. This general observation applies to the occurrence of PACs. These degraded oils have lost their lighter PACs (if they had them originally), but they are produced anew during pyrolysis at 610°C from the thermodesorption residues and asphaltenes. As an example of this phenomenon, composite mass chromatograms employing molecular ions depict the distributions of naphthalenes and phenanthrenes in the Kuwait oil's pyrolysis products (Fig. 7.14). Among the C_1 to C_3-alkylnaphthalenes, the methylnaphthalenes are relatively the most abundant in both the postthermodesorption residue and the asphaltene pyrolyzates (Figs. 7.14A and 7.14B). In overall architecture as well as in the contributions of the individual isomers, the results strongly resemble one another. The samples were analyzed under identical conditions in these experiments, eliminating the instrumental variability discussed in Section 3.2.3.1.

The phenanthrene group fingerprints are also similar in both pyrolyzates, although there is more variation in the proportions of particular isomers (Figs. 7.14C and 7.14D). The differences between the pyrolysis and thermodesorption products (Fig. 7.11B) are more pronounced. One key difference is the presence of anthracene and its alkylated derivatives in pyrolyzates. The C_3 and C_4-alkylphenanthrenes are not well-resolved in the pyrolysis data produced by these samples and are therefore not presented here.

There is a strong resemblance between the alkylbenzothiophene fingerprints of the residue and asphaltene pyrolysis products (Figs. 7.15A and 7.15B). The three-ring sulfur compounds in both pyrolyzates are also very similar, overall and in the distribution of individual isomers (Figs. 7.15C and 7.15D).

These observations are summarized graphically using the normalized, relative quantitation results based on the respective molecular ions, summed by PAC compound group (Fig. 7.16A), showing a strong resemblance between the Kuwait residue and asphaltene pyrolyzates. This is also evident for the other samples for which pyrolysis data are available (Fig. 7.16B), which exhibit a robust overall correlation ($r^2 = 0.85$). It can be concluded that the residue pyrolyzed sequentially after thermodesorption is largely comprised of asphaltenes, a conclusion supported by inspection of the pyrolysis TIC traces in Figs. 7.3, 7.4, and 7.5. While Angola pyrolyzates (Figs. 7.6D and 7.6E) appear dominated by contaminants, the PACs are nonetheless revealed on the mass chromatograms of their respective molecular ions, although its asphaltene pyrolysis results are weak and must be interpreted with caution.

It is evident that thiophenic compounds are particularly important in the sulfur-rich Kuwait oil sample (Figs. 7.3B, 7.13A, and 7.16A). This observation is generalized using the Benzothiophene Naphthalene Ratio, defined for pyrolyzates as:

$$C_1 \text{ to } C_3\text{-alkylbenzothiophenes}/(C_1 \text{ to } C_3\text{-alkylnaphthalenes} + C_1 \text{ to } C_3\text{-alkylbenzothiophenes})$$

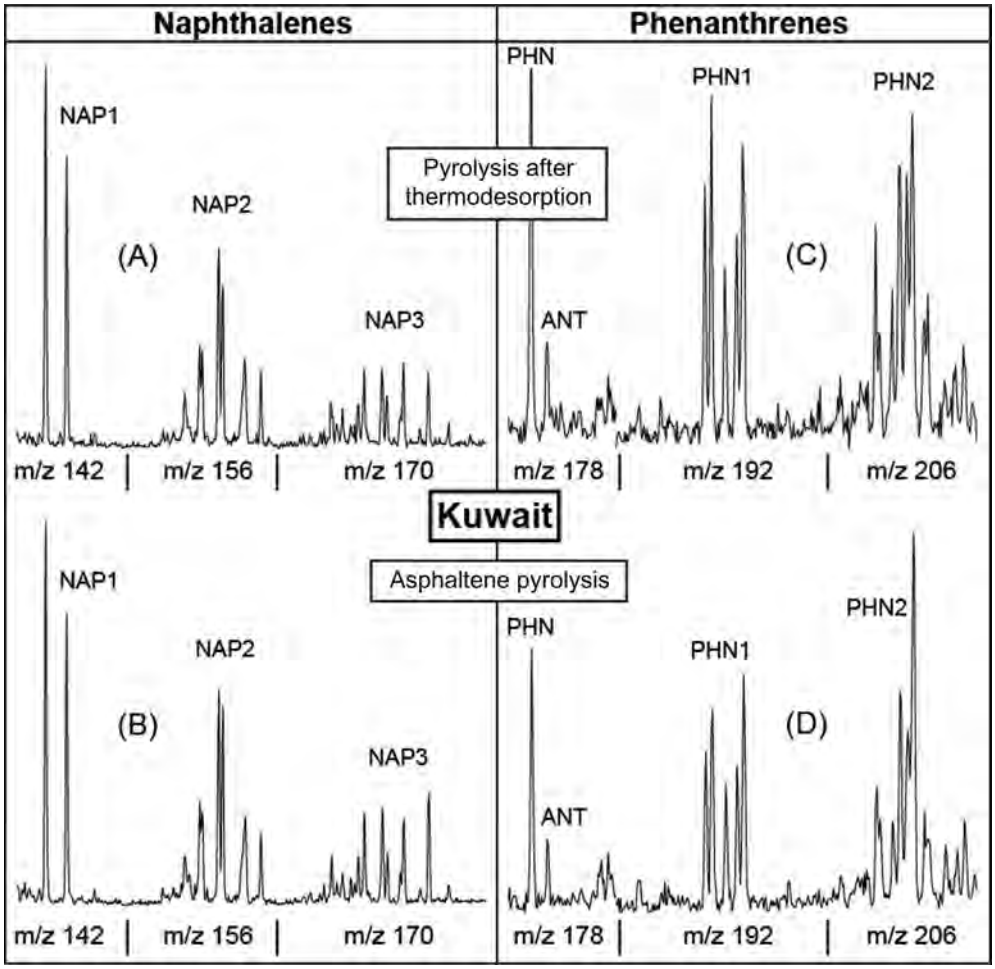

FIGURE 7.14 Composite mass chromatograms of the molecular ions of C_1 to C_3-alkylnaphthalenes, phenanthrene, and the C_1 to C_2-alkylphenanthrenes in the pyrolysis products of the (A) postthermodesorption residue and (B) asphaltenes of the Kuwait oil. See Table 7.2 for peak identification.

This ratio increases linearly as a function of sulfur content. Notably, the asphaltene pyrolyzates consistently exhibit slightly higher values than those from the corresponding residues (Fig. 7.17).

7.3.2.4 Alkanones

The polar fractions of the five samples were analyzed by GC–MS without prior derivatization (derivatization being beyond the scope of the project). The nonderivatized Aboño, Kuwait, and *Prestige* samples revealed little beyond phthalates likely introduced during sample handling and UCM. However, the Angola and Macondo samples contained series of long-chain alkanone isomer groups, C_{14} to C_{27} for the Angola oil, and C_{17} to C_{33} for the Macondo, crowning broad UCM humps (Fig. 7.18). Each cluster contains a similar group of peaks, for which the C_{20} provides a representative example (Fig. 7.19), distinguishable here due to the high-resolution gas chromatographic conditions employed. Isomer assignments can be made on the basis of the mass spectra and elution patterns, by reference to the work of Leif and Simoneit (1995) that employed authentic standards. The carbonyl oxygen can attach to the straight hydrocarbon chain at any position. Thus in the case of C_{20}, there is eicosan-2-one, eicosane-3-one, etc., up to at least eicosan-7-one (Fig. 7.19). The 7-one peak is large and likely includes as coeluants the remaining possible isomers up to the 10-one, which is the limit for the C_{20} alkanone.

The eicosanone isomers in the Macondo oil are readily discernable on the total ion current trace (Fig. 7.19A). Eicosan-3-one and 7-one are emphasized on the *m*/*z* 57 trace, while the 2-one and 5-one appear stronger on the *m*/*z* 58 (Figs. 7.19B and 7.19C). The 4-one and 6-one are best observed on the *m*/*z* 71 mass chromatogram and *m*/*z* 72 highlights eicosan-3-one (Figs. 7.19D and 7.19E). The same pattern is observed in the Angola oil's polar fraction, but with the addition of the C_{22} n-alkane coeluting with the eicosan-3-one (Figs. 7.19F–J). This oil is so

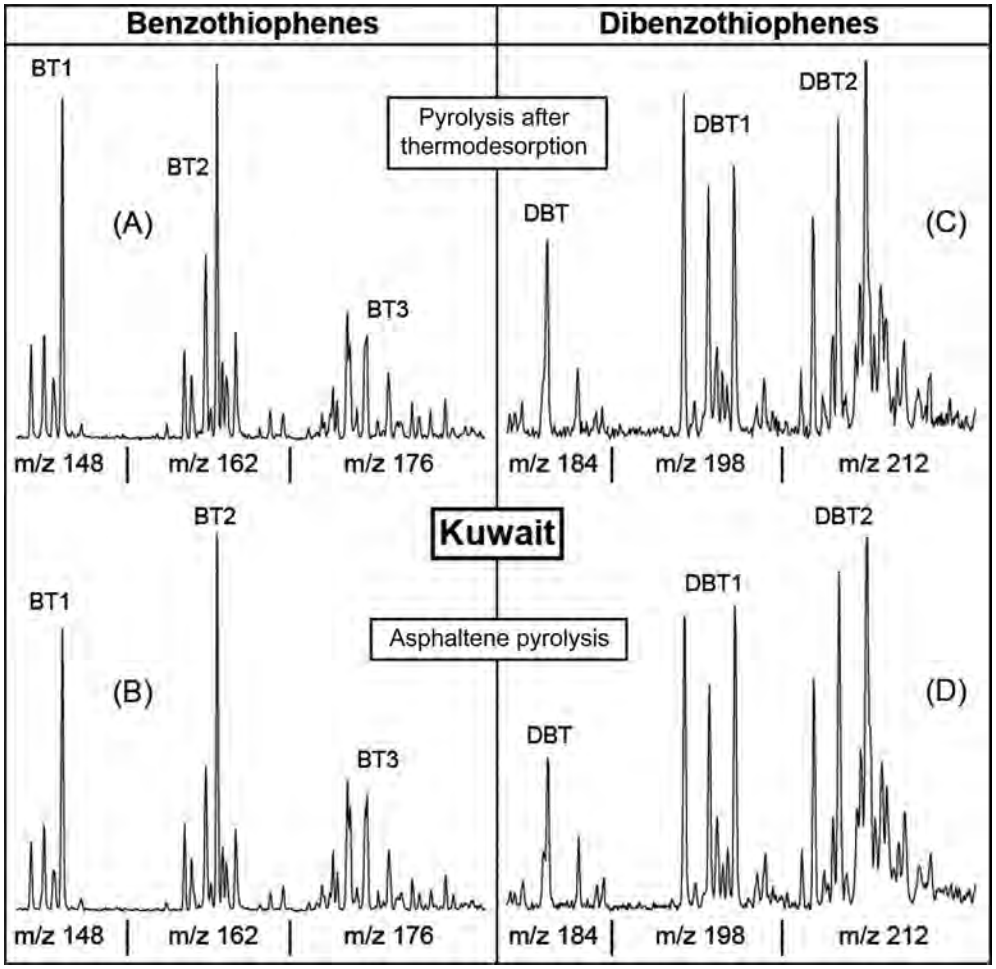

FIGURE 7.15 Composite mass chromatograms of the molecular ions of C_1 to C_3-benzothiophenes, dibenzothiophene, and the C_1 to C_2-alkyldibenzothiophenes in the pyrolysis products of the (A) postthermodesorption residue and (B) asphaltenes of the Kuwait oil. See Table 7.2 for peak identification.

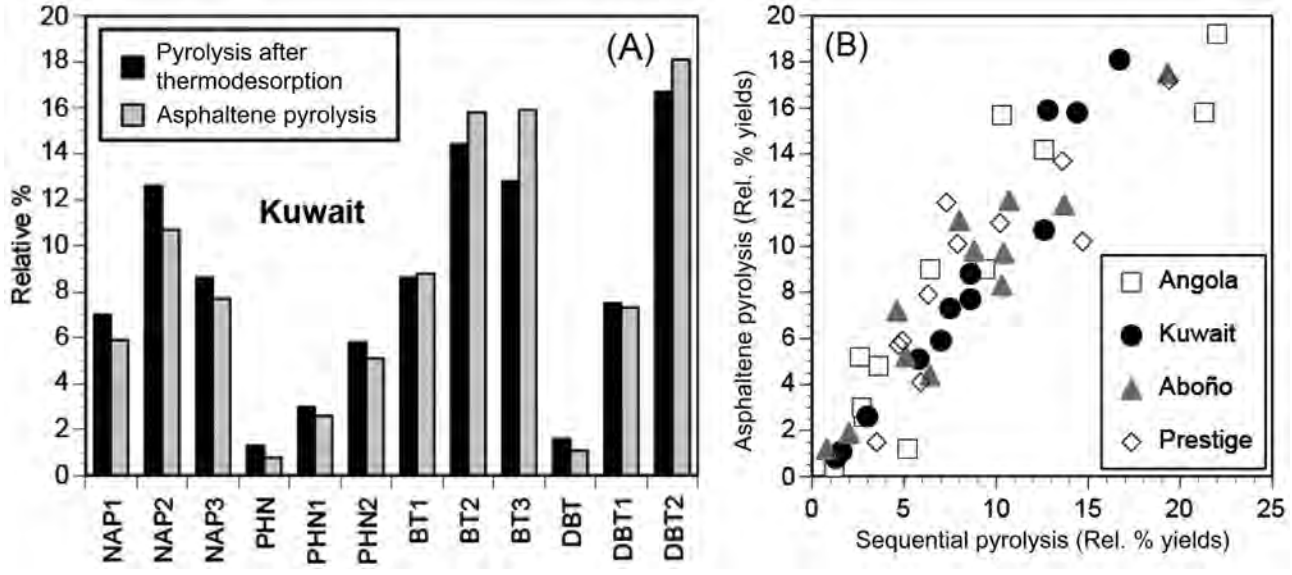

FIGURE 7.16 (A) Summary bar graphs for the PAC data from Figs. 7.14 and 7.15 for the pyrolysis products of the postthermodesorption residue and asphaltenes of the Kuwait oil. See Table 7.2 for compound codes. (B) Comparison of the relative PAC yields for the pyrolysis products of the postthermodesorption residue and asphaltenes of the four oils for which data are available. Values for isomer groups have been summed, as in Fig. 7.16A.

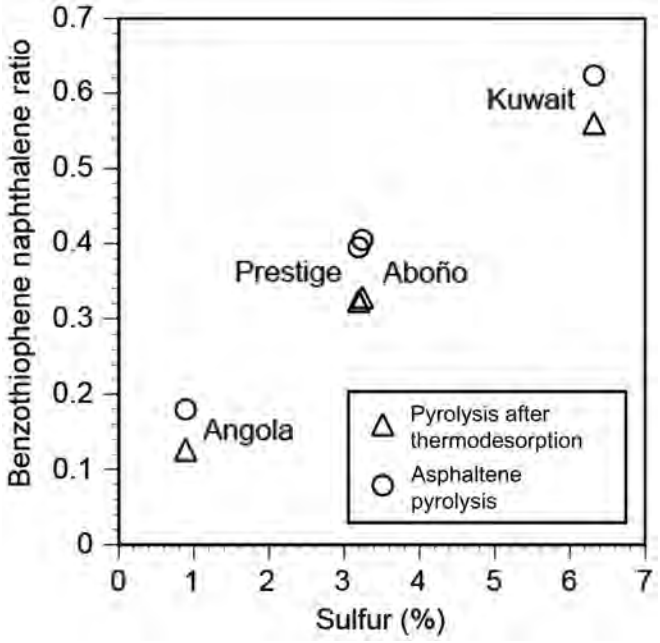

FIGURE 7.17 Cross-plot of total oil sulfur vs. the Benzothiophene Naphthalene Ratio values computed for the pyrolysis products of the post-thermodesorption residue and asphaltenes of the four oils for which data are available. The ratio is computed as [C_1 to C_3-alkylbenzothiophenes/(C_1 to C_3-alkylnaphthalenes + C_1 to C_3-alkylbenzothiophenes)] employing the respective molecular ions (*m*/*z* 142, 148, 156, 162, 170, 178).

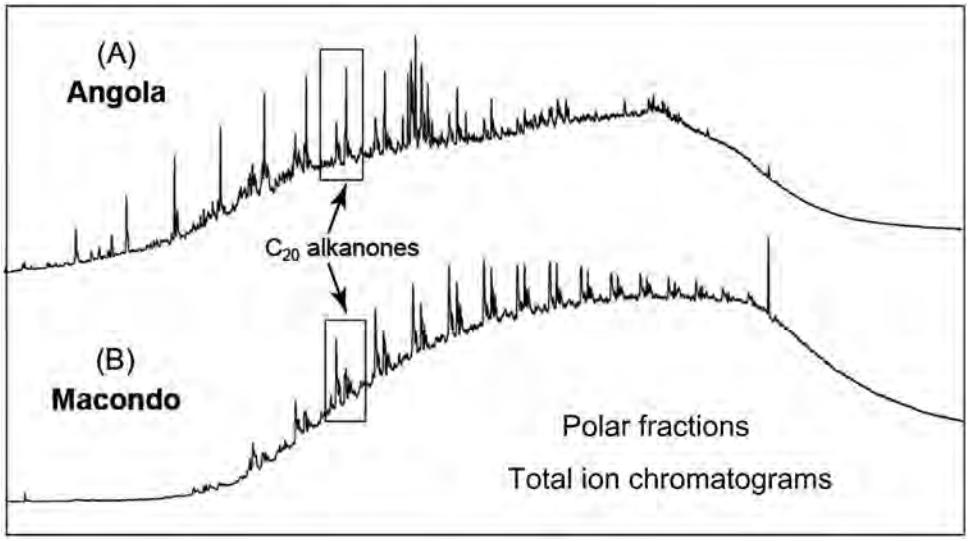

FIGURE 7.18 Total ion current traces of the polar fractions of the (A) Angola oil and (B) Macondo oil samples. The elution region of the C_{20} alkanones is highlighted.

enriched in saturated hydrocarbons (71.6%; Table 7.1), that the liquid chromatographic system was evidently overwhelmed and some normal alkanes eluted with the polar fraction. Alkanones were not detected in the thermodesorption and pyrolysis products.

Oxygen-containing compounds occur in significant variety and abundance in weathered Macondo oil, evidently as products of postspill alteration (Aeppli et al., 2012; Ruddy et al., 2014; Chen et al., 2016; White et al., 2016), with alkan-2-ones among them (Ruddy et al., 2014). In the present study, additional alkanone isomers are identified in Macondo oil as well as in the Angola sample. However, the alkanones were not detected in the Kuwait, Aboño, and *Prestige* oils. While all five oils are weathered, a key distinction is that the Angola and Macondo samples are particularly enriched in saturated hydrocarbons but the others are not (Table 7.1). It would appear that aliphatic-rich oils are the most prone to formation of ketones upon weathering.

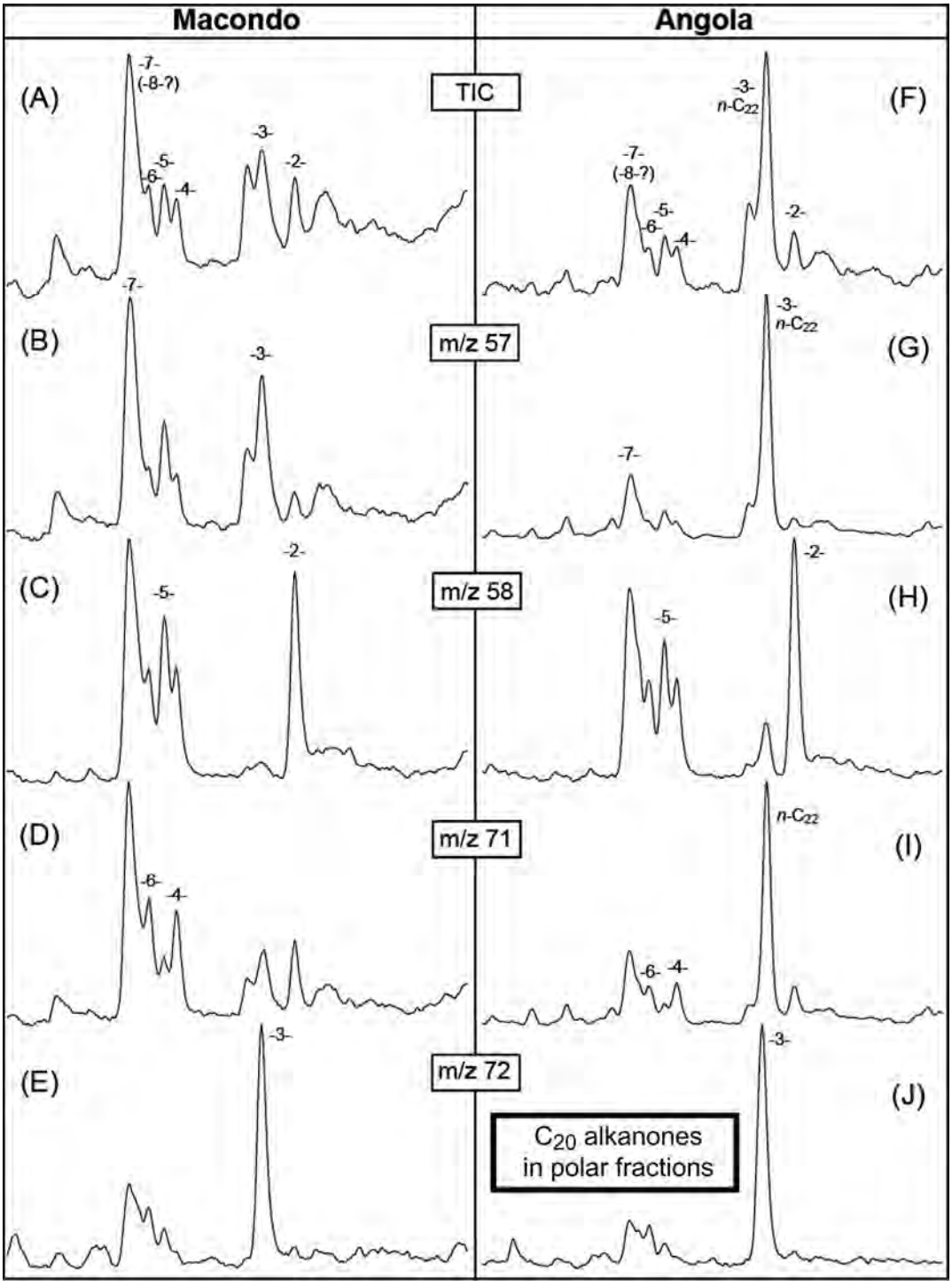

FIGURE 7.19 Details of the C_{20} alkanones detected in the Macondo (A–E) and Angola (F–J) oil samples, employing the total ion current and the *m/z* 57, 58, 71, and 72 traces. Peaks are labeled according to the position of the carbonyl function (-2-: eicosan-2-one, -3-: eicosan-3-one, etc.); *n*-C_{22} is *n*-docosane.

The Macondo and Angola oils are also the ones containing long-chain alkylbenzenes in their aromatic fractions (Figs. 7.6B and 7.7B), compounds that have been previously noted in aliphatic-rich source rock and petroleum (Ellis et al., 1996; Zhang et al., 2014). In contrast to the ketones, these compounds are likely primary components rather than weathering products. Together with the normal alkanes and ketones, the alkylbenzenes reflect the aliphatic nature of the oils.

7.4 CONCLUSION

A multifaceted environmental forensics approach revealed key molecular features of a diverse, genetically unrelated suite of weathered spilled oils. In addition to the commonly employed GC−MS analysis of saturated and aromatic fractions, the polar fractions were investigated. These experiments led to the recognition of a complex series of linear alkanones in those oil samples particularly enriched in aliphatics. TD−GC−MS of the whole oils was used to further test its efficacy as a tool for the rapid fingerprinting of environmental contamination. The method was shown to accurately detect most of the essential features recognized in the conventional analysis of the saturated and aromatic fractions, although in some instances with less sensitivity and poorer resolution. Characteristics so recognized included the distributions of normal and isoprenoid alkanes, saturate, and aromatic biomarkers, and PACs such as alkylphenanthrenes and alkyldibenzothiophenes.

Sequential pyrolysis of the postthermodesorption residue and asphaltene pyrolysis yielded similar results, indicating that the residue is likely to consist primarily of asphaltenes. A ratio of pyrolytic benzothiophenes to naphthalenes correlates with the sulfur content of the oils. Thermodesorption and pyrolysis also recognized substances likely to be associated with spill cleanup efforts that were not detected by conventional analysis.

References

Abdullah, F.H., Connan, J., 2002. Geochemical study of some Cretaceous rocks from Kuwait: comparison with oils from Cretaceous and Jurassic reservoirs. Org. Geochem. 33, 125−148.

Aeppli, C., Carmichael, C.A., Nelson, R.K., Lemkau, K.L., Graham, W.M., Redmond, M.C., et al., 2012. Oil weathering after the Deepwater Horizon disaster led to the formation of oxygenated residues. Environ. Sci. Technol. 46, 8799−8807.

Aeppli, C., Nelson, R.K., Radović, J.R., Carmichael, C.A., Valentine, D.L., Reddy, C.M., 2014. Recalcitrance and degradation of petroleum biomarkers upon abiotic and biotic natural weathering of Deepwater Horizon oil. Environ. Sci. Technol. 48, 6726−6734.

Alzaga, R., Montuori, P., Ortiz, L., Bayona, J.M., Albaigés, J., 2004. Fast solid-phase extraction−gas chromatography−mass spectrometry procedure for oil fingerprinting: Application to the *Prestige* oil spill. J. Chromatogr. A. 1025, 133−138.

Atlas, R.M., Hazen, T.C., 2011. Oil biodegradation and bioremediation: A tale of the two worst spills in U.S. history. Environ. Sci. Technol. 45, 6709−6715.

Balba, M.T., Al-Daher, R., Al-Awadhi, N., Chino, H., Tsuji, H., 1998. Bioremediation of oil-contaminated desert soil: The Kuwaiti experience. Environ. Int. 24, 163−173.

Bence, A.E., Page, D.S., Boehm, P.D., 2007. Advances in forensic techniques for petroleum hydrocarbons: The Exxon Valdez experience. In: Wang, Z., Stout, S.A. (Eds.), Oil Spill Environmental Forensics. Academic Press, Burlington (MA), pp. 449−487.

Brown, L.D., Cologgi, D.L., Gee, K.F., Ulrich, A.C., 1998. Bioremediation of oil spills on land. In: Fingas, M. (Ed.), Oil Spill Science and Technology. Gulf Professional Publishing, Boston, pp. 699−729.

Chen, H., Hou, A., Corilo, Y.E., Lin, Q., Lu, J., Mendelssohn, I.A., et al., 2016. 4 Years after the Deepwater Horizon spill: Molecular transformation of Macondo well oil in Louisiana salt marsh sediments revealed by FT-ICR mass spectrometry. Environ. Sci. Technol. 50, 9061−9069.

Connan, J., Bouroullec, J., Dessort, D., Albrecht, P., 1986. The microbial input in carbonate-anhydrite facies of a sabkha palaeoenvironment from Guatemala: A molecular approach. Org. Geochem. 10, 29−50.

De Leeuw, J.W., De Leer, E.W.B., Damste, J.S.S., Schuyl, P.J.W., 1986. Screening of anthropogenic compounds in polluted sediments and soils by flash evaporation/pyrolysis gas chromatography-mass spectrometry. Anal. Chem. 58, 1852−1857.

Díez, S., Sabaté, J., Viñas, M., Bayona, J.M., Solanas, A.M., Albaigés, J., 2005. The *Prestige* oil spill. I. Biodegradation of a heavy fuel oil under simulated conditions. Environ. Toxicol. Chem. 24, 2203−2217.

Ellis, L., Langworthy, T.A., Winans, R., 1996. Occurrence of phenylalkanes in some Australian crude oils and sediments. Org. Geochem. 24, 57−69.

Faure, P., Landais, P., 2001. Rapid contamination screening of river sediments by flash pyrolysis-gas chromatography−mass spectrometry (PyGC−MS) and thermodesorption GC−MS (TdGC−MS). J. Anal. Appl. Pyrolysis. 57, 187−202.

Gaines, R.B., Frysinger, G.S., Reddy, C.M., Nelson, R.K., 2007. Oil spill source identification by comprehensive two-dimensional gas chromatography (GCXGC). In: Wang, Z., Stout, S.A. (Eds.), Oil Spill Environmental Forensics. Academic Press, Burlington (MA), pp. 169−206.

Gallego, J.R., González-Rojas, E., Peláez, A.I., Sánchez, J., García-Martínez, M.J., Ortiz, J.E., et al., 2006. Natural attenuation and bioremediation of *Prestige* fuel oil along the Atlantic coast of Galicia (Spain). Org. Geochem. 37, 1869−1884.

Gallego, J.R., Fernández, J.R., Díez-Sanz, F., Ordoñez, S., Sastre, H., González-Rojas, E., et al., 2007. Bioremediation for shoreline cleanup: In situ vs. on-site treatments. Environ. Eng. Sci. 24, 493−504.

Gallego, J.R., A. Lara-Gonzalo, E. Rodríguez-Valdés, G. Márquez, M. Escobar, 2013. Natural attenuation of heavy fuel oil components along oiled shores. 26th International Meeting on Organic Geochemistry; Tenerife (Spain).

Jeffrey, A.W.A., 2007. Application of stable isotope ratios in spilled oil identification. In: Wang, Z., Stout, S.A. (Eds.), Oil Spill Environmental Forensics. Academic Press, Burlington, MA, pp. 207−227.

Kaufman, R.L., Kabir, C.S., Abdul-Rahman, B., Quttainah, R., Dashti, H., Pederson, J.M., et al., 2000. Characterizing the Greater Burgan field with geochemical and other field data. SPE Reserv. Eval. Eng. 3, 118−126.

Kruge, M.A., 2015. Analytical pyrolysis principles and applications to environmental science. In: Barbooti, M. (Ed.), Environmental Applications of Instrumental Chemical Analysis. CRC Press, Boca Raton, FL, pp. 533−569.

Kruge, M.A., Permanyer, A., 2004. Application of pyrolysis-GC/MS for rapid assessment of organic contamination in sediments from Barcelona harbor. Org. Geochem. 35, 1395−1408.

Kruge, M.A., Permanyer, A., Serra, J., Yu, D., 2010. Geochemical investigation of an offshore sewage sludge deposit, Barcelona, Catalonia, Spain. J. Anal. Appl. Pyrolysis. 89, 204–217.
Lara-Gonzalo, A., Kruge, M.A., Lores, I., Gutiérrez, B., Gallego, J.R., 2015. Pyrolysis GC–MS for the rapid environmental forensic screening of contaminated brownfield soil. Org. Geochem. 87, 9–20.
Leif, R.N., Simoneit, B.R.T., 1995. Ketones in hydrothermal petroleums and sediment extracts from Guaymas Basin, Gulf of California. Org. Geochem. 23, 889–904.
Peters, K.E., Walters, C.C., Moldowan, J.M., 2005. The Biomarker Guide, Biomarkers and Isotopes in Petroleum Exploration and Earth History, Vol. 2. Cambridge University Press, Cambridge, 1155 p.
Reddy, C.M., Arey, J.S., Seewald, J.S., Sylva, S.P., Lemkau, K.L., Nelson, R.K., et al., 2012. Composition and fate of gas and oil released to the water column during the Deepwater Horizon oil spill. Proc. Natl. Acad. Sci. U.S.A. 109, 20229–20234.
Richnow, H.H., Seifert, R., Kästner, M., Mahro, B., Horsfield, B., Tiedgen, U., et al., 1995. Rapid screening of PAH-residues in bioremediated soils. Chemosphere. 31, 3991–3999.
Ruddy, B.M., Huettel, M., Kostka, J.E., Lobodin, V.V., Bythell, B.J., McKenna, A.M., et al., 2014. Targeted petroleomics: Analytical investigation of Macondo well oil oxidation products from Pensacola Beach. Energy Fuels. 28, 4043–4050.
Stout, S.A., Wang, Z., 2007. Chemical fingerprinting of spilled or discharged petroleum — methods and factors affecting petroleum fingerprints in the environment. In: Wang, Z., Stout, S.A. (Eds.), Oil Spill Environmental Forensics. Academic Press, Burlington, MA, pp. 1–53.
Tissot, B.P., Welte, D.H., 1984. Petroleum Formation and Occurrence. Springer, Berlin, 702 p.
USEPA, 1996. Semivolatile organic compounds (PAHs and PCBs) in soils/sludges and solid wastes using thermal extraction/gas chromatography/mass spectrometry (TE/GC/MS). EPA Method 8275A.; U.S. Environmental Protection Agency; Washington, DC, 1–23 p.
Vollhardt, K.P.C., Schore, N.E., 2002. Organic Chemistry: Structure and Function. W. H. Freeman, New York, 1203 p.
Wang, Z., Yang, C., Fingas, M., Hollebone, B., Hyuk Yim, U., Ryoung Oh, J., 2007. Petroleum biomarker fingerprinting for oil spill characterization and source identification. In: Wang, Z., Stout, S.A. (Eds.), Oil Spill Environmental Forensics. Academic Press, Burlington, MA, pp. 73–146.
Whelan, J.K., Hunt, J.M., Huc, A.Y., 1980. Applications of thermal distillation—pyrolysis to petroleum source rock studies and marine pollution. J. Anal. Appl. Pyrolysis. 2, 79–96.
White, H.K., Wang, C.H., Williams, P.L., Findley, D.M., Thurston, A.M., Simister, R.L., et al., 2016. Long-term weathering and continued oxidation of oil residues from the Deepwater Horizon spill. Mar. Pollut. Bull. 113, 380–386.
Zhang, S., Huang, H., Su, J., Liu, M., Zhang, H., 2014. Geochemistry of alkylbenzenes in the Paleozoic oils from the Tarim Basin, NW China. Org. Geochem. 77, 126–139.

CHAPTER

8

Paraffin Wax Spill Identification by GC–FID and GC–MS

Paul G.M. Kienhuis[1], *Nicolas Fitz*[2], *Imma Tolosa*[3], *Cornelia Blaga*[4] *and Leo Peschier*[4]

[1]Rijkswaterstaat CIV, Lelystad, The Netherlands [2]Federal Maritime and Hydrographic Agency, Hamburg, Germany [3]International Atomic Energy Agency (IAEA), Monaco-Ville, Monaco [4]Netherlands Forensic Institute (NFI), The Hague, The Netherlands

BIOGRAPHIES

Paul G.M. Kienhuis (B.Sc.) works at the lab of the Ministry of Environment and Infrastructure and has 40 years' experience in analytical chemistry. Since 1999, he is responsible for the identification of waterborne petroleum and petroleum products from the inland waters of the Netherlands and the Dutch part of the North Sea. He has to handle about 25 cases a year ranging from small diesel overruns to large spills of HFO in harbors. Oil spill identification is used to confirm responsibility in illegal discharges, but also to reclaim cleaning costs for contaminated quays and ships in harbors. In 2004, together with Dr. G. Dahlmann (BSH, Hamburg) he started with an annual international ring test for oil spill identification to share and improve knowledge about analytical techniques and limitations in comparing oil samples.

In 2005 on request of Bonnagreement (an agreement by North Sea coastal states to protect the environment), Gerhard Dahlmann and Paul Kienhuis started an oil spill identification expert group (OSINET) of which the ring test has become part of 40 labs from all over the world participated in the ring test of 2016. OSINET has worked on a now general accepted method for oil spill identification (CEN/Tr 15522), that has been published by the European Committee for Standardization (CEN) in 2006 and an updated version in 2012. Email: paul.kienhuis@rws.nl

Cornelia Iulia Blaga was born in 1981. She obtained her Doctoral degree at Utrecht University (The Netherlands) in 2010. She has been a Postdoctoral researcher at The Netherlands Forensic Institute. Her main research field in organic biogeochemistry is in the development of new analytical methods to determine biomarkers used to reconstruct climate change and development and validation of methods for doping and forensic analyses.

Leo Peschier is forensic chemist working at the Netherlands Forensic Institute as a forensic expert. He has 20 years of experience in forensic casework, in several areas of forensic chemistry such as analytical toxicology, environmental chemistry, fire debris analysis and forensic comparisons of different materials, such as fuels, cosmetics and other substances. He worked in several research projects developing new methods for the forensic field, amongst which a project for comparison of gasoline samples from fire scenes.

Ms. Imma Tolosa holds a PhD in analytical chemistry from the University of Barcelona, where she was supervised by Professor Joan Albaiges and Josep M. Bayona. She has been working as a senior scientist for over 20 years at the International Atomic Energy Agency (IAEA) in Monaco, where she has developed and applied analytical methods for trace organic contaminants and stable isotopes in marine pollution studies. As a result, she has authored and coauthored more than 60 research papers published in peer reviewed journals. She also

Oil Spill Environmental Forensics Case Studies.
DOI: http://dx.doi.org/10.1016/B978-0-12-804434-6.00008-2

acts as a training officer at the IAEA for the determination of organic contaminants (including persistent organic pollutants, petroleum hydrocarbons, organophosphorous pesticides) and of stable isotopes, and leads the production and certification of organic reference materials. Dr. Tolosa has been involved in compound specific carbon isotope analyses to assess the sources of oil slicks from the Prestige shipwreck and is a member of Bonn-OSINET (oil spill identification network of experts within the Bonn Agreement) since 2013.

Nicolas Fitz is a chemical engineer at the Federal Maritime and Hydrographic Agency (BSH) in Hamburg (Germany), where he works in the working group of oil forensics and visible pollutions. He is mainly involved in the analytical and technical aspects of forensics of oil spill identification. His former employments included work for the Federal Institute for Geosciences and Natural Resources (BGR), where he focused on chemical mineral oil characterization in special matrices.

For the Schleswig-Holstein Agency for Coastal Defence, National Park and Marine Conservation (LKN.SH) he worked on a research project investigating the occurrence, nature and distribution of mineral oil and paraffin wax like pollutants in the German Bight and the North Sea. Within this research project, a first CEN-method orientated effort for a paraffin wax spill identification and characterization was conducted in a joined study with the RWS (Rijkswaterstaat-Laboratory), NFI (Netherlands Forensic Institute), IAEA (International Atomic Energy Agency).

8.1 INTRODUCTION

Paraffin waxes are highly refined products of slack wax, a mixture of oil and wax produced as a by-product of the lubricating oil refinery process. After hydrotreatment (dearomatization) of slack wax, several crystallization steps proceed to remove any remaining oil, odor and color, and the addition of polyethylene, for example, to improve softness, yield final paraffin wax products that vary in color (white to yellow), oil content (0.5%–3.5%), and physical properties (liquid, solid soft to solid/brittle at room temperature). Chemically speaking, paraffin waxes are overwhelming composed of *n*-alkanes, branched alkanes and alkyl-substituted cyclic alkanes (naphthenes). Paraffin waxes are used for a range of applications including food (e.g., covering cheese for surface protection, chewing gum), cosmetics, skiing waxes and candles (Stepanski, 2014).

Paraffin waxes are typically solids at ambient temperatures with melting points ranging from 35 to 50°C. Thus, heated tankers are used for bulk transport at sea. After unloading, the remnants have a higher melting point due to selective crystallization of long chain alkanes and need to be cleaned from the tanks and pipelines with steam, hot water and manually with, for example, a wooden hammer (Sanjay et al., 1995; Vadakayil, 2011). Because paraffin wax is indicated by Marpol as a nontoxic product (Annex II category Y) it is allowed to be discharged outside the 12 nm zone in small quantities while sailing. However, several times a year large amounts of wax can be found along European beaches for many kilometers. The particle sizes of paraffin wax that appear on shorelines can vary from very small (<1 cm) to very large (>25 cm). Minor amounts of small wax particles are left on the beaches for practical reasons, but larger spills have to be removed.

In recent years, numerous major incidents involving paraffin wax were observed along the North Sea coast from Denmark to The Netherlands (Roose et al., 2011; UEG, 2014). In March 2014, for example, more than 50 t of paraffin wax washed ashore on the island of Sylt (Germany). In 2012 and 2016, The Netherlands spent €350 and €450k, respectively, for shoreline clean-up in response to two large paraffin wax spills.

Between May 2013 and June 2016, The Federal Maritime and Hydrographic Agency (BSH) conducted a research project called "*Untersuchung über verölte Seevögel und Strandverölungen*" (or, *Investigations Concerning Oiled Birds and Oil Contamination on Beaches*) that focused on monitoring of drift lines along the German North Sea coast (including most of the Frisian islands) for mineral oil and for oil-derived products (e.g., paraffin wax, lubrication oil, HFO; Fitz et al., 2017). Apart from plastics, all kinds of oil-like "persistent floaters" also were monitored with the aid of NGSs and local institutions. The project's results revealed that 62% of the samples encountered during the monitoring period consisted of paraffin wax (UEG, 2014).

Determining the specific source of paraffin wax on shorelines is important but a distinct problem for conventional chemical fingerprinting of oil spills. In this chapter, we describe our efforts to develop and provide a standard methodology conforming with the European guideline for oil spill identification, CEN/Tr 15522-2:2012 (CEN, 2012), but that is appropriate for paraffin spill identification. Our efforts included a round robin analysis of paraffin samples among our four laboratories, from which the lessons learned were subsequently applied to a real world paraffin spill case study in The Netherlands. We conclude with an evaluation of the method that was developed and applied.

8.1.1 Round Robin 2015

In 2015, our laboratories (BSH, RWS, NFI, and IAEA) conducted a round robin study of 10 paraffin samples with the objective of assessing the usefulness of the European guideline for Oil Spill Identification CEN/Tr 15522-2:2012 (CEN, 2012) in distinguishing among different paraffin samples (Fitz et al., 2017). In addition, some participants also used methods of analysis and data evaluation (described below) beyond CEN (2012). Thus, the scope of the round robin was broadened and the evaluation provided an overview of the possibilities for paraffin comparison, which are described in this section.

The design of the study was to prepare three sets of three samples (plus a reference sample; described below), where each set consisted of paraffin samples with comparable compositions but derived from different origins. The intent was to test if the analytical methods were capable of discriminating between paraffin waxes with generally comparable compositions. In order to improve the likelihood that some of the paraffin samples included in the round robin had different sources, two of the samples (provided by LASEM Toulon, FR) were from distinct spills found in 2010 and 2013 on the Mediterranean part of the French coast were used as base stocks for the sample sets prepared. After Gas chromatography-flame ionization detection (GC-FID) analysis at BSH each alkane pattern has been compared with the patterns of 1509 paraffin samples available from the BSH research project (mentioned above). Two approaches were used to find the best matching samples between the LASEM and large number of BSH samples:

1. correlation of ratios calculated by normalizing each n-alkane to the n-alkane with the highest signal, e.g., the ratios of *n*-C20/*n*-C26, *n*-C21/*n*-C26, *n*-C22/*n*-C26, etc. would be calculated for a sample with *n*-C26 as the highest concentration *n*-alkane;
2. correlation of ratios calculated from adjacent alkanes, i.e., *n*-C20/*n*-C21, *n*-C21/*n*-C22, *n*-C22/*n*-C23 etc.

Approaches (1) and (2) resulted in identifying different although very comparable paraffin samples to include in the study. From these preliminary results three different sets of paraffin samples were prepared: *Set 1* consisted of samples which came from different countries, but were found within a relatively short period of time; *Set 2* consisted of samples which were also retrieved from very distant origins, but exhibited a dissimilar *n*-alkane profile (FID) from the Set 1 samples and also were found over a long period of time (2010–14); *Set 3* had the function of a control group and consisted of samples that were found within a small area and within a short period of time (07/08-2013) suggesting that they were samples from the exact same paraffin-wax product. *Set 4* was a duplicate (from the same stock solution) of the very first sample from Set 1 (from France). The Set 4 sample was added to the sample sets as a means to estimate the variance of the methods among the four laboratories' analyses of the same sample, and to study the influence on the column performance after injection of the samples of Set 2 with long chain *n*-alkanes (Fig. 8.3 and Table 8.1). Each participating laboratory analyzed all of the samples in one sequence and in duplicate, sorted on RR-number from 1 to 10.

GC–FID analyses were used to characterize the 10 round robin samples. To distinguish between samples the paraffin *n*-alkanes shape can be treated as a distribution of chain lengths from which a weighted mean and standard deviation could be calculated. This method had the elegance of characterizing a sample with only two parameters, making it possible to compare a collection of samples in one 2D plot.

To improve specificity while comparing spill and source samples additional methods are required. CEN (2012) utilizes Gas chromatography-mass spectrometry (GC-MS) for analysis of PAHs and petroleum biomarkers,

TABLE 8.1 Sample Sets Used for the Round Robin

Set	Origin, date	Origin, date	*r*
1	RR-1: LASEM, FR, 05-2013	RR-2: Amrum, DE, 05-2013	0.9977 (1)
		RR-3: Ockholm, DE, 12-2013	0.9980 (2)
2	RR-4: LASEM, FR, 2010	RR-5: Trischen, DE, 05-2013	0.9949 (1)
		RR-6: Hooge, DE, 08-2014	0.9609 (2)
3	RR-7: Buesum, DE, 08-2013	RR-8: Buesum, DE, 07-2013	0.9991 (1)
		RR-9: HaHaKoog, DE, 07-2013	0.9910 (2)
4	RR-10: Same extract as RR-1		

The correlation (*r*) of e.g., RR-2 with RR-1 is based on ratios from alkanes normalized to the highest alkane (1). The correlation (*r*) of e.g., RR-3 with RR-1 is based on ratios from adjacent alkanes (2).

but due to the dearomatization and deoiling steps in paraffin wax production all aromatic compounds including aromatic steranes are absent, whereas the biomarker concentrations are relatively low.

Therefore, as a supplement to the standard methods within CEN (2012), compound specific isotope analysis (CSIA) using gas chromatography coupled to isotope ratio mass spectrometry (GC–IRMS) was included in the round robin to study the carbon and hydrogen stable isotope ratio variation among the samples involved (Chesson et al., 2014). The common approach of GC–IRMS in forensic science is based on the exploitation of stable isotopes in order to infer the source of a trace. The method resulted in ^{13}C and ^{2}H isotope ratios of individual *n*-alkanes, which vary depending on the crude oil feedstock used to produce the paraffin (Carter and Barwick, 2011). As it is common that refineries use crude oil batches from many different sources, it can be expected that GC–IRMS can give valuable additional information to the GC–FID and GC–MS results (Jeffry et al. 2016). The $\delta^{13}C$ values of paraffin waxes derived from mineral oil are reported to vary in the same range as their petroleum sources (−35‰ to −20‰). However, in CSIA, the differences between sources must be greater than the measurement error of the GC–IRMS (±0.5‰), and thus, to ensure a reliable interpretation, the difference in the $\delta^{13}C$ values of *n*-alkanes must be at least 1‰.

Multiple lessons were learned from the round robin (Fitz et al., 2017), including:

- Isoprenoid ratios can often not be used because pristane and phytane are very low or absent in most of the paraffin samples. Therefore ratios between the *n*-alkanes have to be defined and utilized.
- It is advised to integrate *n*-alkanes based on area, because of their high variance in concentration and due to the influence that samples containing long chain *n*-alkanes have on the column performance.
- The CEN (2012) method uses many compounds for comparison that are absent or low in paraffin wax (e.g., PAHs and biomarkers) so it is important to scan the samples for useful additional compounds.
- The "weighted mean and standard deviation" method provides an overview comparison among the collection of samples, which can be used to select potentially matching samples for further analyses using more elaborate methods.
- Different GC–FID instruments equipped with different columns and applied with different settings produce different GC–FID profiles. This is even valid to some extend for sequences analyzed with the same settings on the same instrument over a longer period of time. To be able to combine the GC–FID patterns of many samples into a "weighted mean and standard deviation" database normalization of the *n*-alkanes to the *n*-alkanes standard analyzed at the beginning and end of each sequence is useful.
- CSIA on individual *n*-alkanes in paraffins showed the ability of GC–IRMS to discriminate some paraffin samples with similar hydrocarbon pattern based on the $\delta^{13}C$ of the *n*-alkanes. Therefore, combined techniques of chemical and isotopic fingerprinting might allow fine-tuning of each paraffin fingerprint. Nevertheless, GC–IRMS is an expensive, complex and labor-intensive technique compared to the most cost-effective GC–FID or –MS analytical technologies. In particular, the CSIA technique requires extensive sample purification and high chromatographic resolution of the individual compounds to get accurate and reliable isotope data. For this reason, GC–IRMS is not considered as a routine analysis technique but it may be applied in difficult cases where multiple decision tools are needed.

8.1.2 Case Study—Paraffin Wax on a Dutch Beach

In November 2015, paraffin was found on a Dutch beach. Based on shipping information (AIS, type of ship and oil spill trajectory models) one ship was suspected to be the source of the paraffin. On board a sealed can was confiscated and represented the cargo the ship was transporting at the suspected time of the spillage. The RWS-laboratory was asked to compare the contents of the can with paraffin samples collected from the impacted beach in order to determine if the paraffin on the beach and vessel were matched. For this case study, the lessons learned from the round robin (summarized above) were used.

8.2 EXPERIMENTAL AND DATA ANALYSIS METHODS

8.2.1 Samples

Two small (about 10 cm in diameter) and a large piece (about 20 × 50 cm) of paraffin were received from the spill discovered on the Dutch beach in November 2015. The reference source sample to which these were to be compared consisted of the content of a 1-L can filled with paraffin collected from the suspected source vessel.

A small aliquot of the inside of one of the small paraffin samples was weighted and dissolved in dichloromethane: sample **beach-small**. From the large piece, two aliquots were collected: one from the outside layer (sample **beach-outside**) and one from the inner layer (sample **beach-inside**). Sample **can-1** represents an aliquot collected from just under the lid of the 1-L can with paraffin. Sample **can-2** was taken from the same can at a depth of approx. 2 cm under the lid.

In order to compare and estimate the uniqueness of the case study samples, paraffin wax samples from other spills were included within the case study. These included; (1) two paraffin samples from the May 2016 Noordwijk spill (samples **Noordwijk-1** and **Noordwijk-4**), (2) one paraffin sample from the June 2016 Rottermerplaat spill (beach sample **Rottermerplaat**), (3) two paraffin samples from the July 2016 spill (beach samples **Moddergat** and **Eemshaven**), and (4) 10 paraffin samples from the 2015 round robin study described above (**RR-1** to **RR-10**).

The character of the round robin samples are described in the next paragraph.

Two paraffin samples were received from LASEM, Toulon (France). The samples were combined with seven selected paraffin samples from the BSH project (as described in Section 1.2) resulting in the four sets listed in Table 8.1.

The round robin participants received the samples dissolved in 9:1 hexane/DCM (v/v) at a concentration of approx. 1.5 mg/mL.

8.2.2 Sample Preparation

In general, a clean-up step for paraffin samples is not necessary unless a sample contains a lot of sand or debris. Even then it is often possible to wipe any contaminants away and to find a clean piece of paraffin within the sample. In this study, none of the samples were subjected to clean-up steps prior to the analysis. However, if this would have been considered necessary the samples would have been eluted over a Na_2SO_4/Florisil column using DCM as solvent following the procedure described in CEN (2012) and Albaigés et al. (2015). An injection concentration of about 1 mg/mL was used so as to not overload the 0.25 mm ID column with the *n*-alkanes at the highest concentrations.

8.2.3 Standards

One microliter of an alkane standard mixture (AccuStandard DRH-008S-R2; Hydrocarbon Window Defining Standard 35 compounds: C8-C40 500 μg/mL in chloroform diluted with DCM to a concentration of 5 mg/mL each) was injected at the start and end of each GC–FID sequence. Compounds, *n*-C13, *n*-C20, and *n*-C40 were integrated and used as absolute value (*n*-C20), as ratios within a chromatogram (*n*-C13/*n*-C20 and *n*-C40/*n*-C20) and as ratios between the first and last standard (*n*-C13 first/*n*-C13 last and *n*-C40 first/*n*-C40 last) for the GC–FID control chart to keep track of the system performance.

One microliter of a Brent standard (crude oil from the Brent field in the North Sea obtained in 1994 from Steve Grigson, University of Edinburgh) and diluted to a concentration of 30 mg/mL in DCM was injected at the start and end of each GC–MS sequence. The heights of the highest peak of the dimethylnaphthalenes, 3-methylphenantrene (3-MP) and 17α(*H*), 21β(*H*)-hopane (30ab) are used for the MS control chart in the same way as mentioned for the GC–FID control chart.

8.2.4 Instrumentation and Analytical Methods

An Agilent 7890A gas chromatograph equipped with a FID detector and mass spectrometer 5975C inert MSD (EI mode) with Triple-Axis Detector was used to analyze the samples. For the GC–FID analysis 1 μL was injected through an Agilent split-splitless injector, which was kept at a temperature of 325°C, on a 15 m DB-1 (J&W) column (ID 250 μm and phase 25 μm) to a FID detector working at 375 °C with an oven program of 35°C–(1.5 minutes)–35°C–(10°C/minute)–325°C–(10 minutes)–325°C. For the GC–MS analysis, 1 μL was injected on an Agilent split-splitless injector, which was kept at a temperature of 325°C, on a 30 m DB-5 (J&W) column (ID 250 μm and phase 25 μm) to a MS with a transfer line at 300°C and with an oven program of 42°C–(1 minute)–42°C–(5.52°C/minute)–330°C–(13 minutes)–330°C. After each sequence the retention times were checked and when needed adjusted by optimizing the initial time (in general after 3 to 4 sequences) and slope (seldom) in order to have stable retention times of 30.0 minutes for 3-MP and 47.8 minutes for hopane (30ab; as per CEN, 2012 Annex B). The SIM method applied is listed in Table 8.2

TABLE 8.2 Start and Dwell Times and m/z Values Used for the Analysis of Paraffin Samples

Group	1		2			3			
Start	5 min		26 min			35.8 min			
Dwell	50 ms		40 ms			30 ms			
	83	148	83	148	197	83	191	218	337
	85	184	85	184	212	85	197	253	351
	92		92	191	226	92	205	309	365
	106		106	192	240	106	217	323	379

8.2.5 Calculations

As per CEN (2012), the GC–FID and GC–MS percentage weathering (PW) plots were used to evaluate the analytical results as a means to estimate the influence of weathering and to visualize the analytical data. A data point (% $C_{N\text{spill}}$) in a PW plot represents the concentration of a compound in the spill sample ($C_{N\text{spill}}$) relative to the concentration of the same compound in the source sample ($C_{N\text{source}}$). To compensate for the total amount of a sample injected, the result is normalized to a compound or compound range present in both samples (C_{norm}) (Eq. 8.1)

$$\%C_{N\ \text{spill}} = \frac{C_{N\text{spill}}/C_{\text{norm spill}}}{C_{N\text{source}}/C_{\text{norm source}}} \times 100\% \tag{8.1}$$

For the assessment of the paraffin samples, data points of the GC–PW plots were normalized to the mean of the areas of the compounds *n*-C24 to *n*-C28 and data points of the MS–PW plots were normalized to the height of *n*-C30.

The diagnostic ratios (DR) between peaks A and B were calculated from the height or area of these peaks based on Eqs. (8.2 or 8.3) depending on the preference of the user:

$$\text{DR} = A/B \tag{8.2}$$

$$\text{DR} = 100 \times A/B \ \ (\text{in } \%) \tag{8.3}$$

CEN (2012) defines a relative standard deviation (RSD) limited to 5% for all DRs for samples analyzed in one sequence. The difference between two ratios should only in one of twenty comparisons exceed the repeatability limit. The repeatability limit, $r_{95\%}$, is calculated using the following equation:

$$r_{95\%} = 2.8 \times \text{RSD} \tag{8.4}$$

Appling the predefined RSD of 5% leads to a repeatability limit of 14%.

In this chapter ratio comparisons are presented in graphs, in which the line in the middle represents the repeatability limit of 14% (Fig. 8.1). For this example, it is obvious that all of the *n*-alkane ratios used for the comparison of the duplicate analysis of sample can-1 are far below the 14% limit, showing that the RSD of the GC–FID method for the sample involved is far below the upper limit of 5%.

Ratios are selected based on presence and properties of compounds in the samples. CEN (2012) advises to build ratios between two compounds with about the same relative retention time and in case of a GC–MS analysis with about the same m/z value. As a result ratios are more robust against variations in performance of the analytical column and MS source.

A ratio is most valuable and diagnostic if its value varies widely between samples from different sources. To calculate the diagnostic value of a ratio the diagnostic power (DP) has been introduced by (Christensen et al., 2004) and used by Yang et al. (2008) and Malmborg and Nordgaard (2016). DP is defined by the following equation:

$$\text{DP} = \frac{\text{RSD}_V}{\text{RSD}_A} \tag{8.5}$$

wherein the RSD of the ratio in samples of different origin (RSD_V) is divided by the random error arising from the analytical method (RSD_A).

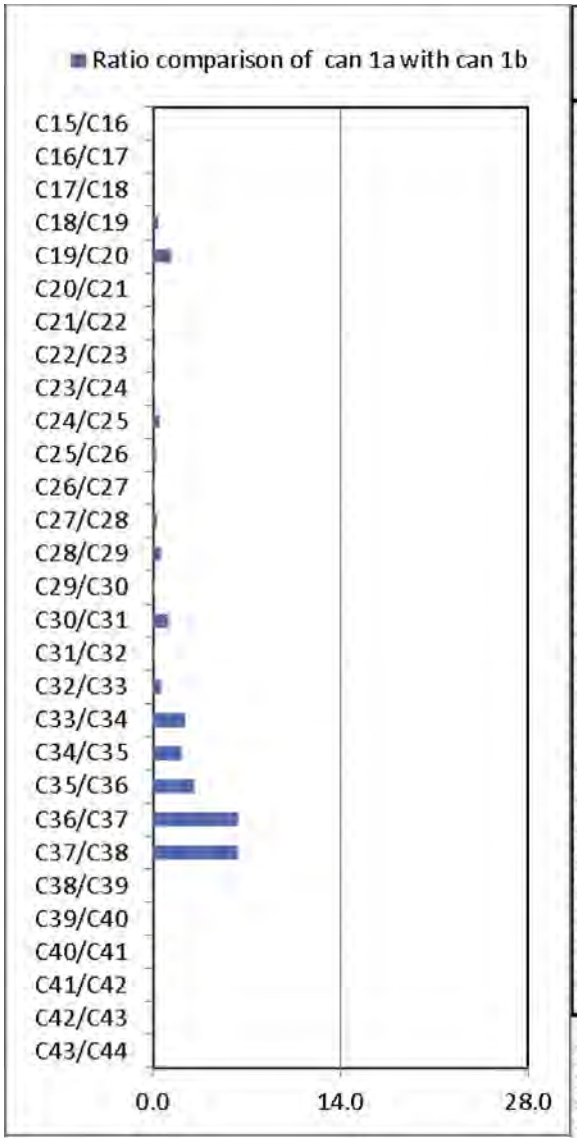

Ratios	1 is selected	Square of relative difference
C15/C16		
C16/C17		
C17/C18		
C18/C19	1	0
C19/C20	1	2
C20/C21	1	0
C21/C22	1	0
C22/C23	1	0
C23/C24	1	0
C24/C25	1	0
C25/C26	1	0
C26/C27	1	0
C27/C28	1	0
C28/C29	1	0
C29/C30	1	0
C30/C31	1	1
C31/C32	1	0
C32/C33	1	0
C33/C34	1	6
C34/C35	1	5
C35/C36	1	10
C36/C37	1	41
C37/C38	1	41
C38/C39		
C39/C40		
C40/C41		
C41/C42		
C42/C43		
C43/C44		
# of ratio comparisons used		20
Σ square of the rel. differences		107
st dev of the paired ratios		1.63

FIGURE 8.1 GC–FID ratio comparison based on a critical difference of 14% (left) and calculation of the standard deviation of paired ratios for the duplicate measurements of sample can-1 paraffin sample (right). The column "is selected" is used to select ratios of compounds present at a sufficient level in the samples involved.

The standard deviation of a ratio can be calculated by analyzing a sample at least seven times and to use the resulting ratios for calculation. The standard deviation of paired ratios makes use of the possibility to calculate a standard deviation based on the differences between ratios of two sample analyses. Combining the differences of a range of ratios results in an overall standard deviation of the applied analytical method (Ettre, 1993). If m ratios are analyzed with the results x_{i1} and x_{i2} (pertaining to the ith paired measurement), the standard deviation can be calculated by the following equation:

$$s = \sqrt{\frac{\sum (x_{i1} - x_{i2})^2}{2m}} \tag{8.6}$$

In this chapter, the differences between ratios of two samples were used to calculate the standard deviation of paired ratios for those two samples. An example of the calculation of the standard deviation of paired ratios for the GC–FID duplicate measurement of sample can-1 is shown in Fig. 8.1. All GC–FID ratios used for the

comparison of the duplicate analysis of sample can-1 are far below the 14% limit, whereas the standard deviation of the paired ratios calculation results in a value of 1.63%.

Standard formulae were used to calculate the weighted mean and standard deviation for a discrete distribution of n compounds, as follows:

$$A_n = \text{area of peak } C_n \tag{8.7}$$

$$\text{weighted mean} = \overline{n} = \frac{\sum_n nA_n}{\sum_n A_n} \tag{8.8}$$

$$\text{standard deviation} = \sqrt{\frac{\sum_n (n-\overline{n})^2 A_n}{\sum_n A_n}} \tag{8.9}$$

where n is taken from 15 to 40.

8.2.6 Spreadsheet Files

An Excel spreadsheet file was prepared to plot the weighted mean versus the standard deviation values for the large number of GC–FID paraffin wax analyses (Fig. 8.2). To compensate for performance variations between sequences the combined results of the two n-alkane standards analyzed around each sequence are used. The n-alkane standard contains the n-alkanes n-C8–n-C40 at a concentration of 5 mg/L each. Theoretically the area of each n-alkane peak should be the same but in practice this varies within a chromatogram and between sequences due to mass discrimination. To compensate for these variations the area of each n-alkane in a sample is corrected using the following equation:

$$C_{N\text{sample}} \text{ corrected} = \frac{C_{N\text{sample}}}{C_{N\text{standard}}} \times \sum C_{N\text{standard}}/26 \tag{8.10}$$

where C_N are the n-alkanes from n-C15 to n-C40.

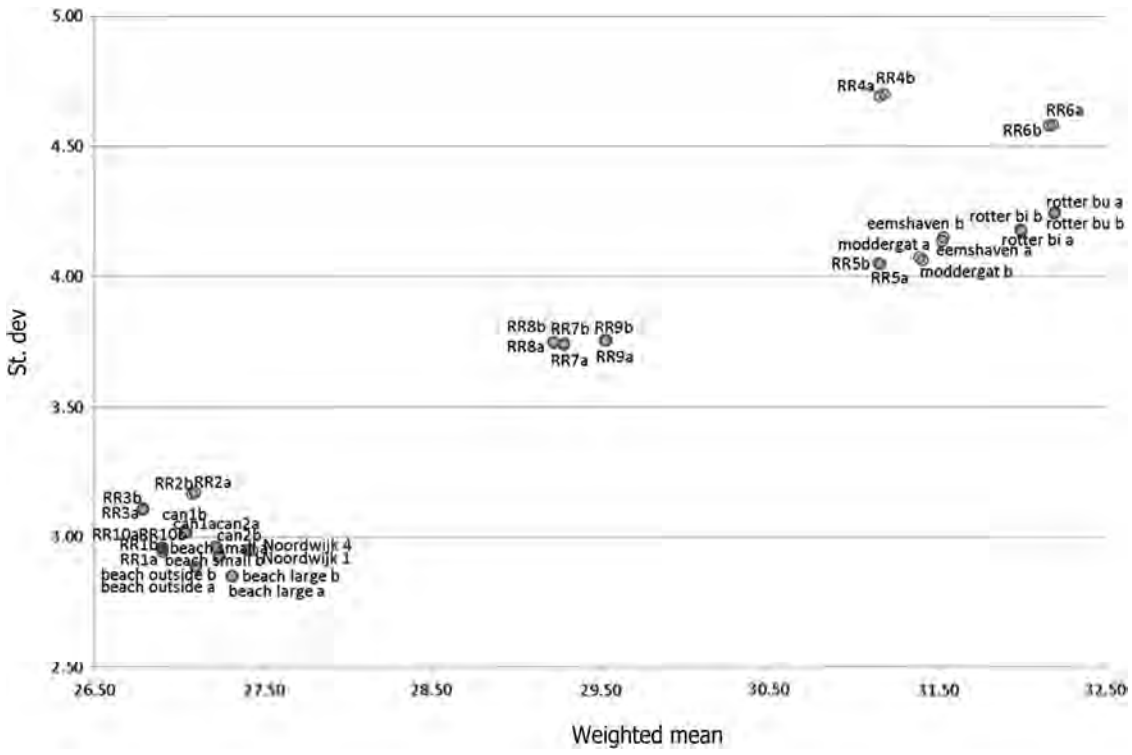

FIGURE 8.2 Weighted mean versus standard deviation of the GC–FID paraffin profiles.

Excel spreadsheet files also were prepared to evaluate the GC–FID and GC–MS data in such a way that the raw data of a paraffin case can be entered in a so-called "datasheet." "Evaluation sheets" are available and can be used to compare samples, selected from the samples available in the "datasheet." After selecting a pair of samples to be compared, the statistical evaluations by means of ratio comparison, PW plots and paired ratio calculation are generated and presented as tables and plots. (The authors are willing to provide these spreadsheet files upon request.)

8.3 GC–FID RESULTS EVALUATION

8.3.1 Weighted Mean Versus Standard Deviation

Except the samples Noordwijk-1 and Noordwijk-4, all samples mentioned in Section 8.2.1 were analyzed in duplicate and entered in the paraffin database spreadsheet file, which was used to calculate the weighted mean and the standard deviation of each chromatogram. The resulting values are crossplotted in Fig. 8.2.

Fig. 8.2 shows the relation existing between the weighted mean and the standard deviation with a higher standard deviation, when the weighted mean is higher. This is in agreement with the peak shapes observed in the sample chromatograms. The results show that the samples cluster in three groups with weighted mean values of around C27, C29.5, and C32 (Fig. 8.2), which can be seen in selected samples' GC–FID chromatograms (Fig. 8.3). As noted above, most samples were analyzed in duplicate, but these are only visible for some of the samples (Fig. 8.2), indicating that the precision of the analytical method is very high in relation with the sample range.

The group of paraffin samples with a weighted mean of about C27 includes the case study samples collected from the Dutch beach and the source samples collected from the can of paraffin from the suspected vessel (Fig. 8.4).

The distances between the duplicate analyses of the same extracts can be used as a reference for the differences between the samples. Samples RR-1 and RR-10 represent the same sample extract and show comparable results. Samples Noordwijk-1 and Noordwijk-4 represent two different samples from the same spill, but are probably very similar because the difference between the results are in line with the duplicate analyses.

The case study samples—can-1 (outside), can-2 (inside), and beach (small, large inside, and large outside)—each show a relative much higher difference. Only the samples can-2 and beach-small plot within a reasonable distance from each other (Fig. 8.4). The samples Noordwijk-1, Noordwijk-4, RR-1, and RR-10 are in the variance range of the samples can-1 and can-2, so it is useful to compare these samples also with the case samples.

8.3.2 GC–FID Sample Comparison

To access the GC–FID analytical results, CEN (2012) makes use of the GC–PW plot and isoprenoid ratios. However, the paraffin samples involved in both the round robin and case study do not show useful relative concentrations of isoprenoids. Therefore, it was necessary to add extra ratios based on the *n*-alkanes pattern. Ratios of *n*-alkanes relative to the highest *n*-alkane can be used, but this is very similar to what is used for the GC–PW plot. One of the CEN (2012) criteria for ratios is to define ratios between compounds within a limited retention time range so ratios between adjacent peaks are the obvious choice.

To test the analytical results first the duplicate analyses must be evaluated. The GC–PW and ratio plots of the duplicates of can-1 and can-2 are shown in Fig. 8.5.

For duplicate analyses, the theoretical value of each data point in a PW plot should be 100%. CEN (2012) accepts a range of 85%–118% as variance caused by the analytical method. For sample can-1 the highest integrated alkane (C38) is above 118%, which is related to the low concentration of the compound. The difference in higher alkane pattern is also visible in the ratio comparison graph of samples can-1a and can-1b. For sample can-2 the similarity between duplicates is better and all data points are between 85% and 118%. On the right side of Fig. 8.1, the calculation of the standard deviation of paired ratios is shown for the duplicates of sample can-1 with 1.63 as result. The standard deviation values for all samples of the case study are shown in Table 8.3.

The upper section of Table 8.3 shows that all duplicates compare better than the comparison of the duplicate samples of can-1 and similar or even better than can-2, which is acceptable. The lower section of Table 8.3 shows all the possible comparisons of the combined duplicate values of the samples of the paraffin wax case study. For the comparison of sample can-1 with can-2, one relative ratio difference above 14% is found, whereas the paired ratio standard deviation is much higher than found for the duplicate comparisons. The alkane pattern,

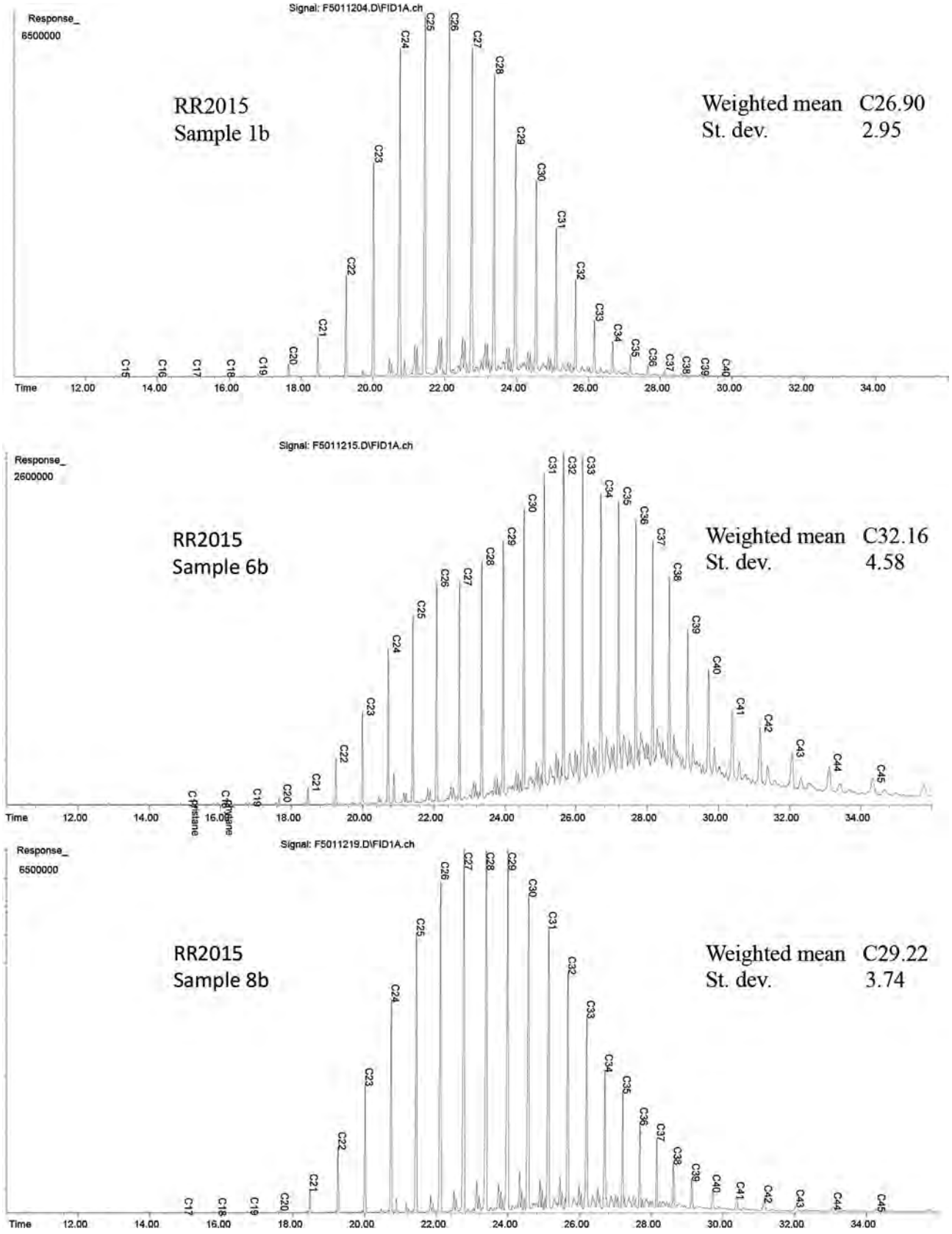

FIGURE 8.3 Chromatograms of samples representing three different types of paraffin samples used in the round robin.

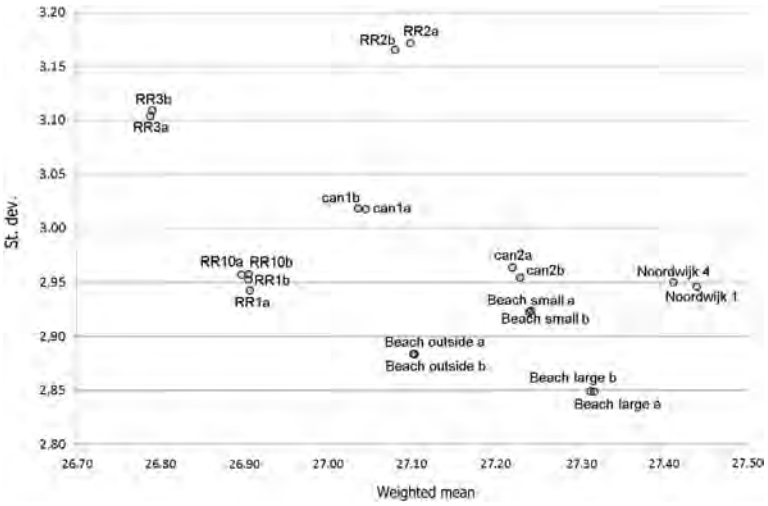

FIGURE 8.4 Group of paraffin samples with a weighted mean around C27. Duplicate analyses of the same extracts are indicated by a and b.

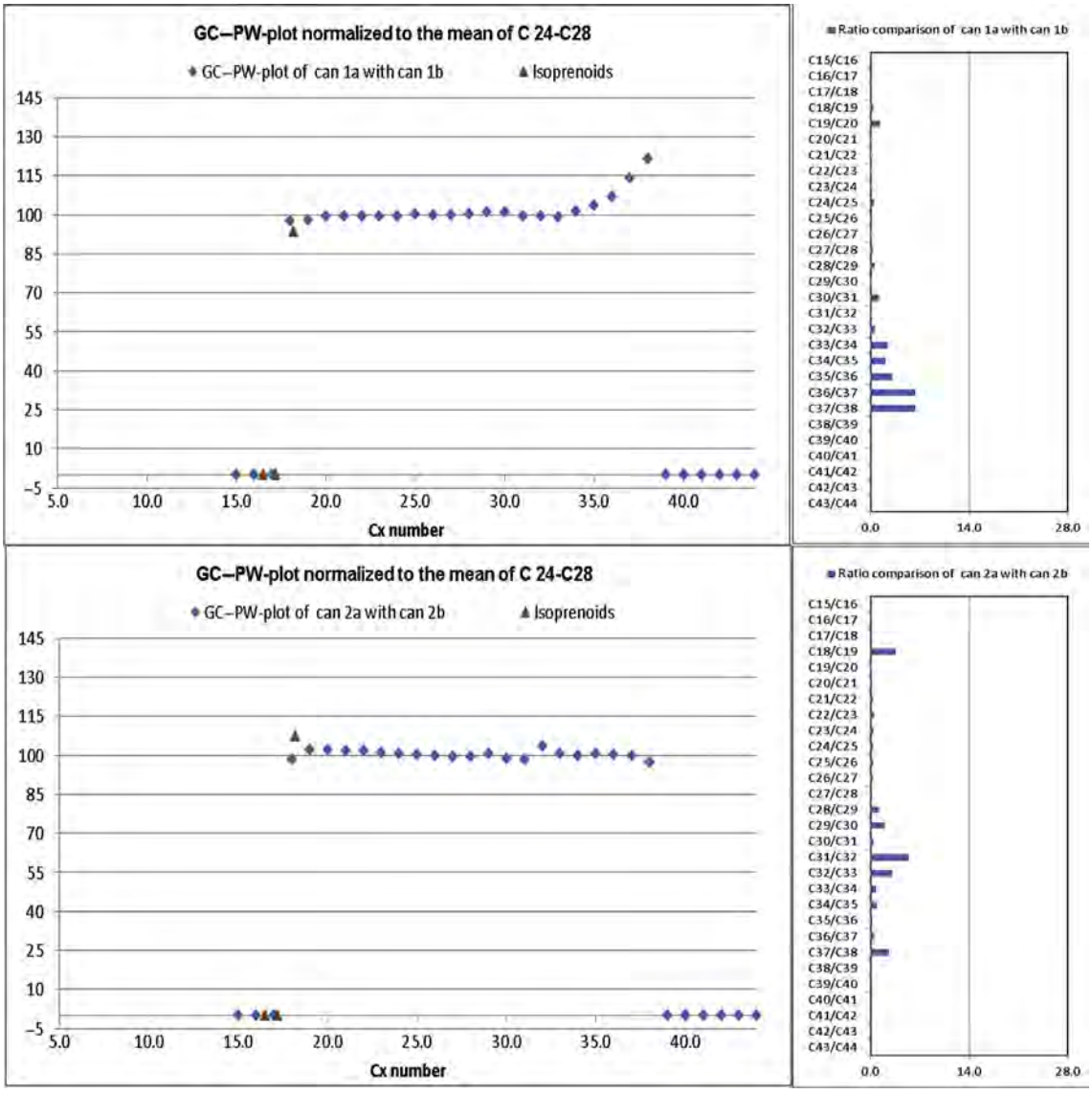

FIGURE 8.5 GC–PW plots and ratio graphs for the duplicates of paraffin samples from can-1 and can-2.

TABLE 8.3 Duplicate and Sample Comparison based on Ratio Differences >14% and the Standard Deviation of the Paired Ratios

Duplicate comparison			
Sample a	**Sample b**	**Ratios >14%**	**St. dev. paired**
Can-1	Can-1	0	1.63
Can-2	Can-2	0	1.30
Beach large inside	Beach large inside	0	1.32
Beach large outside	Beach large outside	0	1.15
Beach small	Beach small	0	1.06
Comparison of samples with combined duplicate analyses			
Sample	**Sample**	**Ratios >14%**	**St. dev. paired**
Can-1	Can-2	1	4.45
Can-1	Beach large inside	6	8.00
Can-1	Beach small	1	4.52
Can-1	Beach large outside	5	7.77
Can-2	Beach large inside	0	4.53
Can-2	Beach small	0	2.48
Can-2	Beach large outside	0	4.47
Beach large inside	Beach small	2	5.15
Beach large inside	Beach large outside	0	2.04
Beach small	Beach large outside	2	4.84

GC–PW-plot ratio comparison plot and standard deviation of the paired ratio calculation of the combined duplicates of samples can-1 with can-2 is shown in Fig. 8.6.

Fig. 8.6 shows that sample can-2 (inside of the can) contained higher concentrations of *n*-alkanes in the range of *n*-C26 to about *n*-C33 than the sample can-1 (top of the can). The reason for this difference is very likely related to wax redistribution as is also observed among spill samples (e.g., see Fig. G6 of CEN, 2012) and wax crystallization during crude oil and wax transports (Sanjay et al., 1995). Wax redistribution is caused by the fact that the compounds in the paraffin wax mixture have different melting points and that the higher *n*-alkanes with a higher melting point are dissolved in the lighter compounds when fluid. When the can was filled with a warm fluid, as is typical of wax when being transported, becomes cooled wax redistribution can take place.

An option for analysis could have been to heat the can until the content became fluid again, before taking a sample. But by taking multiple samples from the inside and top of the can gives a better chance that one of the samples matches with one or more of the paraffin beach samples, which may also have experienced wax redistribution during or after discharge.

Table 8.3 shows that the best match can be found between samples can-2 and beach-small followed by beach-inside with beach-outside. The analytical results of the comparisons are shown in Fig. 8.7.

For the GC–PW plot of sample can-2 with sample beach-small phytane and C38 are slightly outside the range of 85% to 118%, which can be explained by a higher variance due to very low compound concentrations. For the GC–PW plot of beach-inside with beach-outside the same effect can be seen as for samples can-1 and can-2. Thus, differences can be found within the same piece of paraffin collected from the Dutch beach, although the differences are smaller than the ones observed for the two can samples. For both comparisons the standard deviation of paired ratios is at a level of 2%, whereas all relative ratios differences are below to far below the 14% level (Fig. 8.7).

Fig. 8.8 shows the comparison of sample beach-small with samples RR-1 and Noordwijk-1 based on results presented in Fig. 8.4. Both comparisons show large differences between the samples despite the fact that the samples are quite close in the weighted mean versus standard deviation plot (Fig. 8.4).

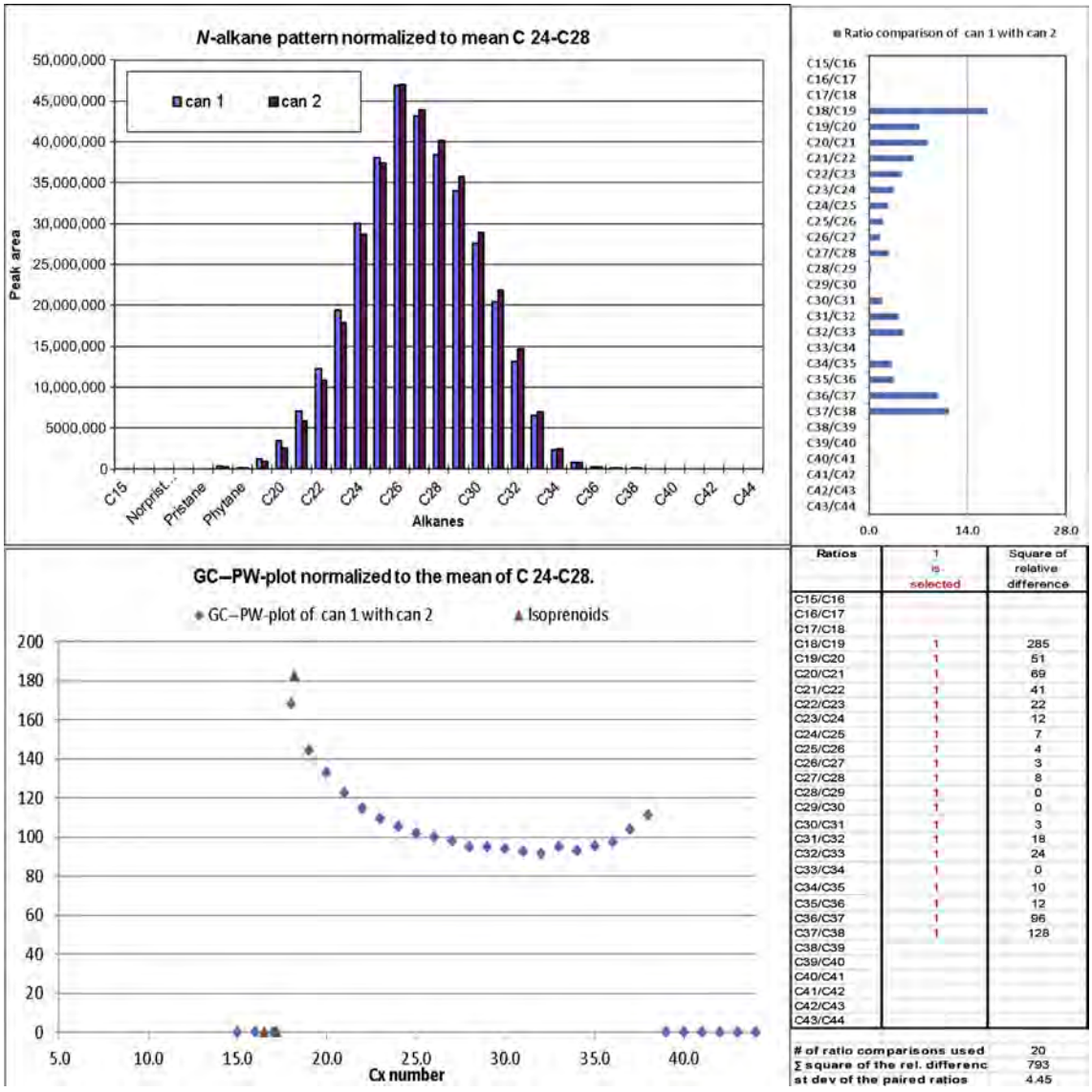

FIGURE 8.6 Samples can-1 and can-2 compared by means of pattern, GC–PW and ratio plots and calculation of the standard deviation of the paired ratios.

8.3.3 Conclusions GC–FID

Based upon the GC–FID results described above the following conclusions could be drawn:

- The sample comparisons between the inside and outside of a piece of paraffin collected from the Dutch beach, or paraffin collected from different depths in a can, show that the composition of the *n*-alkanes can vary, which is probably caused by wax redistribution as the paraffin wax cooled from a fluid to a solid.
- The duplicate samples show only small differences indicating, that the analytical system works within the variance accepted by CEN (2012).
- The differences between samples beach-small and can-2 are larger than were found for the duplicates, but smaller than for the comparison between samples can-1 and can-2 and the beach samples between each other, respectively.
- The sample beach-small is different from the samples RR-1 and Noordwijk-1 although the weighted mean versus standard deviation graph (Fig. 8.4) shows that the samples were in a close distance to the can and beach samples.

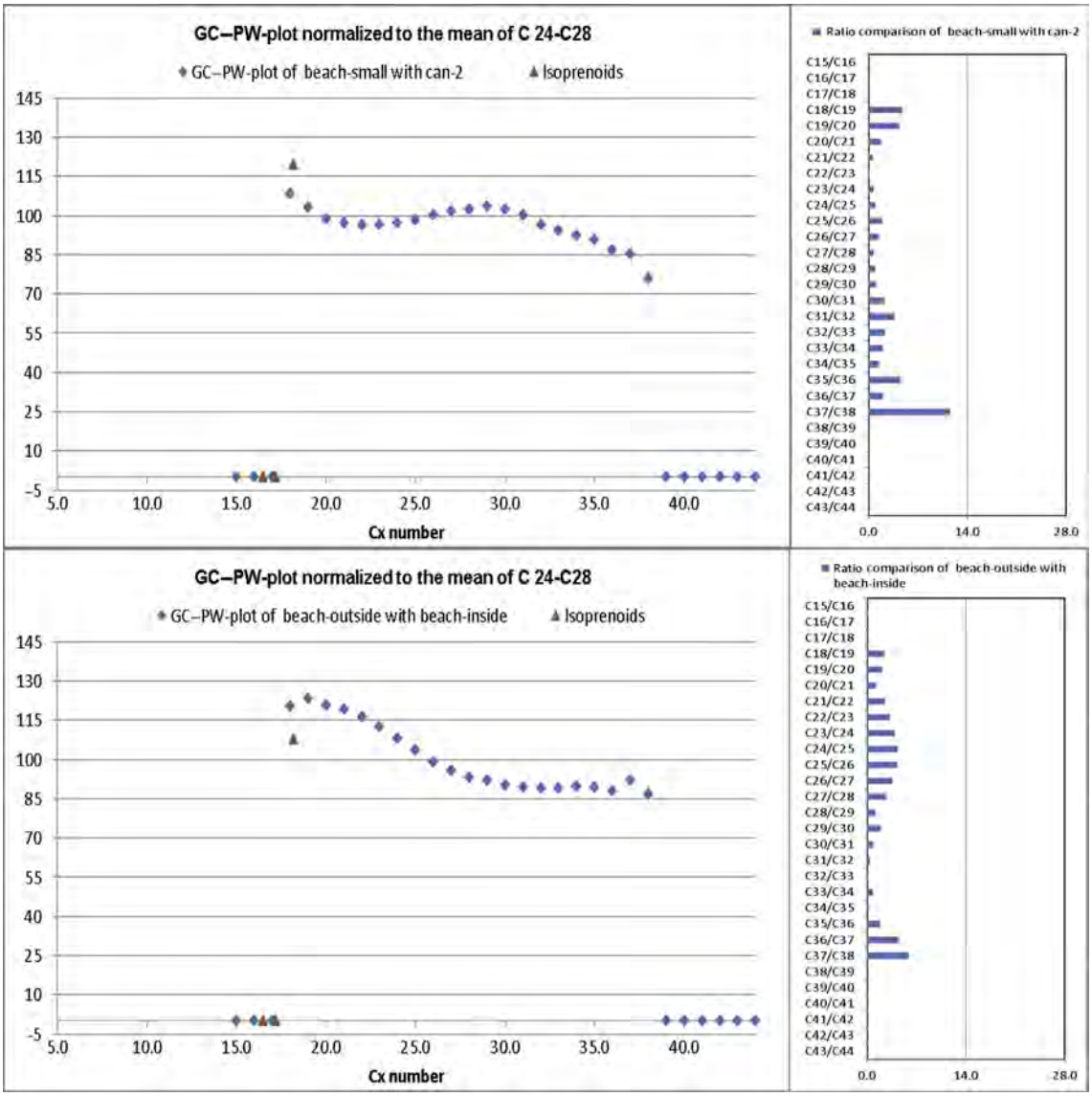

FIGURE 8.7 Comparison of combined duplicate integration results of the samples beach-small with can-2 and samples beach-outside with beach-inside by means of the GC–PW plot and ratio comparison plot.

- Based on the CEN (2012) criteria (viz., GC–PW plot 85%–118% and ratio differences <14%) samples beach-small and can-2 were considered to "match."

8.4 GC–MS RESULTS EVALUATION

The paraffin round robin made clear that the acquisition method used for oil spill identification conforming with CEN (2012) was not very suitable to compare paraffin wax samples, because PAHs and aromatic steranes are absent due to the dearomatization step and the steranes and hopanes are low in concentration due to the deoiling step in the manufacturing process. This makes a study of alternative compounds within the paraffin wax recognized using GC–MS worth investigating.

8.4.1 GC–MS Compound and Ratio Selection

Several of the paraffin wax samples were analyzed by GC–MS operated in the full scan mode and the results were studied by means of deconvolution (AMDIS) and library search. In addition to *n*-alkanes, a range of

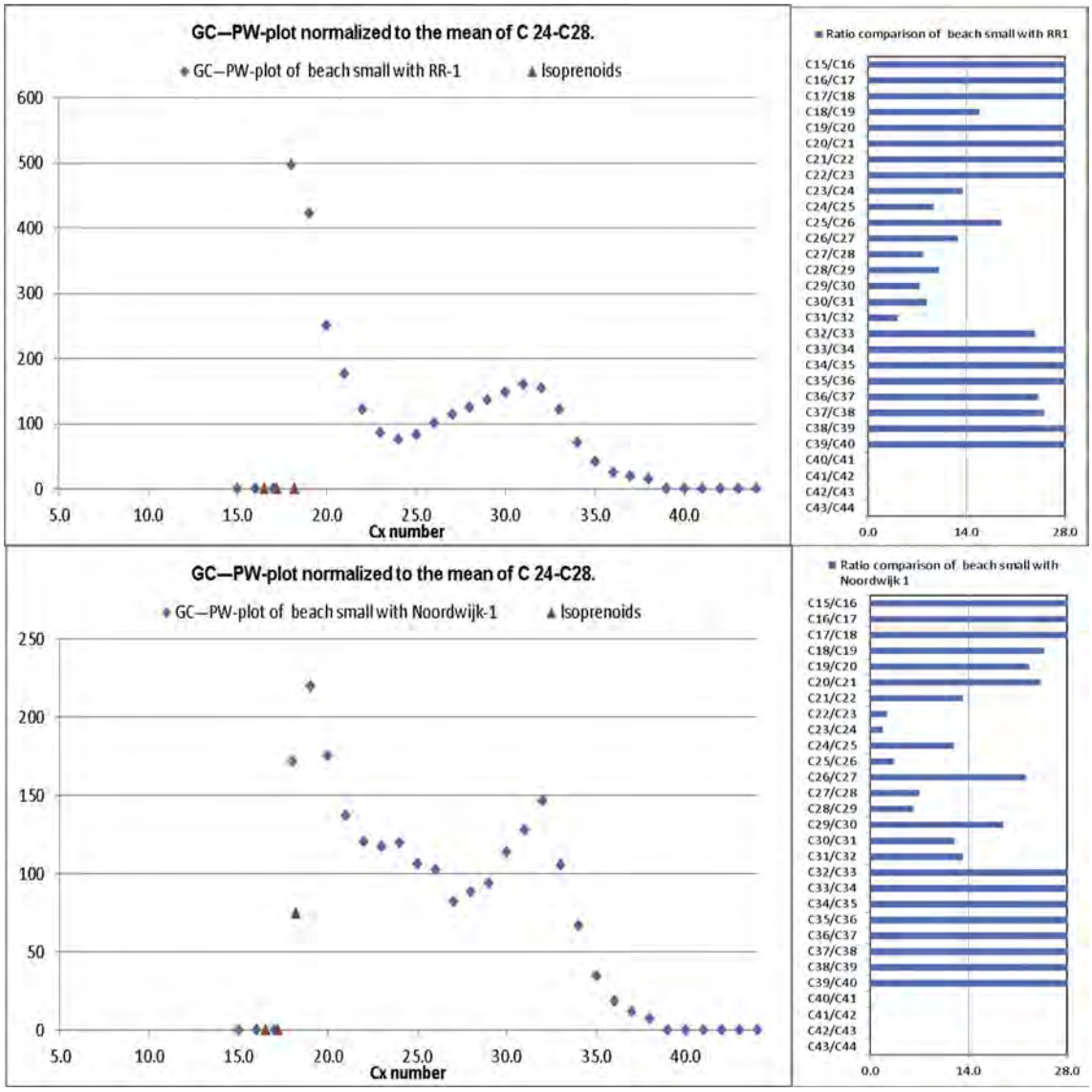

FIGURE 8.8 Comparison of samples beach-small with RR-1 and samples beach-small with Noordwijk-1 by means of the GC–PW plot and ratio comparison plot.

branched alkanes were present in all samples. Those branched alkanes clearly separated from the *n*-alkanes were used as additional compounds for comparison (Figs. 8.9 and 8.10).

The left panel of Fig. 8.9 shows ion-chromatograms applied in CEN (2012) with *m*/*z* 85 representing the alkanes and *m*/*z* 83 the alkenes. However, the highest peaks of the *m*/*z* 83 pattern coelute with the *n*-alkanes indicating that those peaks actually are generated by an ion fragment of the *n*-alkanes. See also sample Noordwijk-1 in Fig. 8.10. Additional *m*/*z* 83 peaks that are believed to truly be alkenes (and do not derive from *n*-alkane fragments) can be seen in sample RR-1 of Fig. 8.10. In fact, several of the paraffin samples studied show these additional *m*/*z* 83 peaks in the lower *n*-alkane range eluting just before the *n*-alkanes (Fig. 8.10). Polyethylene is sometimes added to improve the softness of the final product (Stepanski, 2014). As almost all poly-olefins of practical or commercial importance are poly-alpha-olefins, which generate a dominant *m*/*z* 83 ion fragment, it is most likely that the extra *m*/*z* 83 peaks are related to the addition of polyethylene. The concentrations of these, however are such that also these small peaks can only be a part of the visual (qualitative) comparison.

The ion-chromatograms of *m*/*z* 92 and 106 in Fig. 8.9 were used to check the patterns of the long-chain alkylbenzenes and alkyltoluenes (Albaigés et al., 2013). The patterns are similar to what is seen in crude oil for these monoaromatic compounds, but unexpected because of the absence of PAHs due to dearomatization of the paraffin wax. Compared with the Brent standard in SIM mode the retention times are identical, but it was not possible

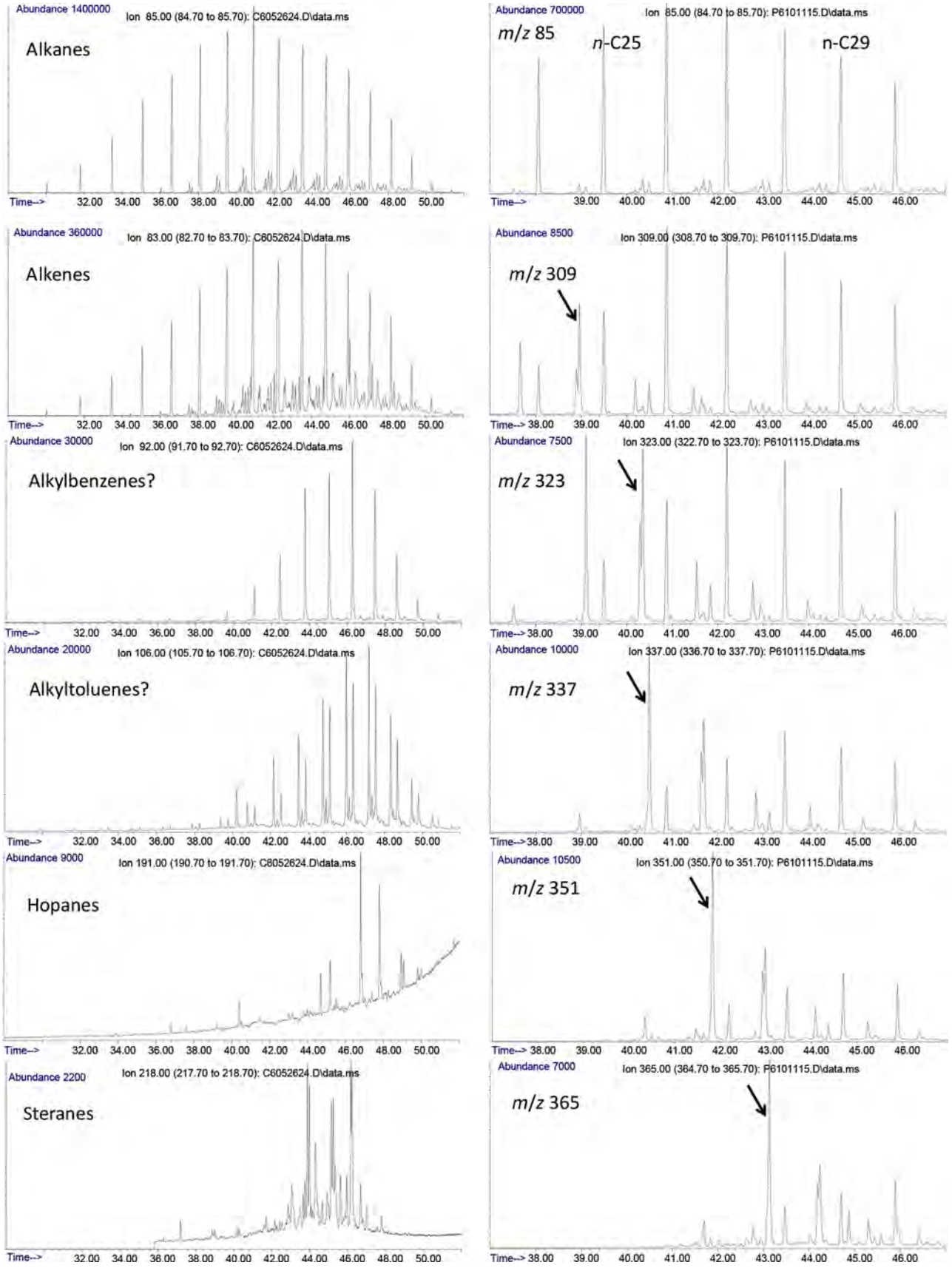

FIGURE 8.9 Ion-chromatograms of compounds and compound groups selected for the comparison of paraffin wax samples.

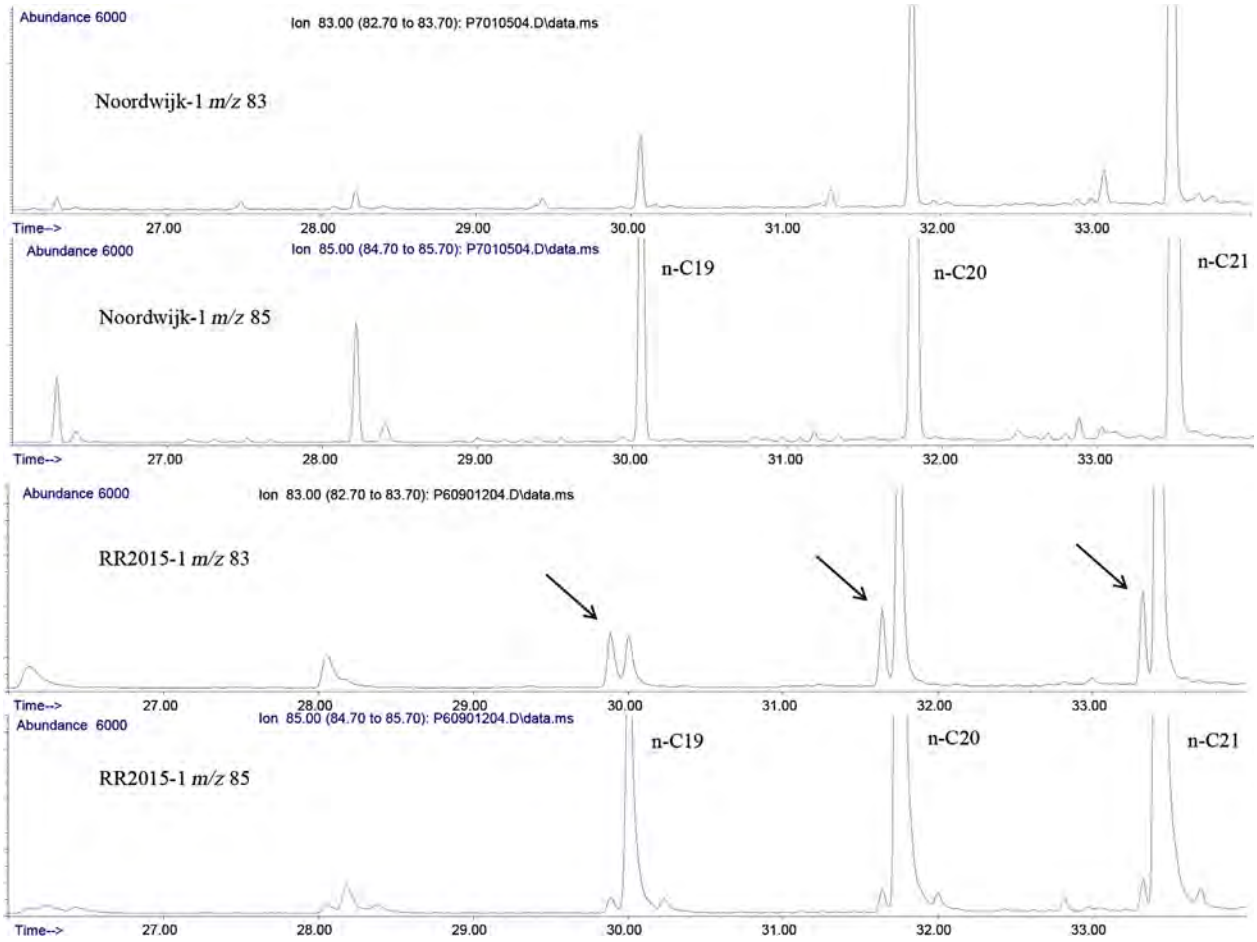

FIGURE 8.10 Ion chromatograms of samples Noordwijk-1 and RR-1. *n*-alkanes (*m*/*z* 85) and *m*/*z* 83 peaks coelute in sample Noordwijk-1, whereas sample RR-1 contains additional *m*/*z* 83 peaks.

to confirm their identity by means of a library search of the full scan spectra, because of their low intensity. Therefore the identifications as alkylbenzenes and alkyltoluenes are indicated as tentative. The ion-chromatograms of *m*/*z* 191 and 218 show the hopanes and steranes, respectively. Their concentrations are relatively low, but due to their specificity some of the compounds with the highest concentration can still be used for the MS–PW plot and ratio comparison. In CEN (2012) the hopane ratios are normalized to hopane (30ab), but because of the distillation range of most of the paraffin samples norhopane (29ab) can be used instead for paraffin fingerprinting.

The right panel of Fig. 8.9 shows a part of the *n*-alkanes together with a range of branched alkanes of which the indicated peaks are used for the MS–PW plot and ratio comparison. The resulting compounds and ratios used for a numerical evaluation of the paraffin wax samples studied are shown in Table 8.4. The SIM method used to acquire the samples was shown in Table 8.2.

Peak areas for the GC–FID analyses have been integrated to compensate peak broadening of high concentrated compounds. However, for the GC–MS it was decided to use peak heights because smaller and more difficult peaks have to be quantified. Some of the *n*-alkanes have been integrated on more than one *m*/*z* value to be able to define ratios between peaks of about the same retention time and analyzed by about the same *m*/*z* value (CEN, 2012, section 6.5.3).

8.4.2 GC–MS Sample Comparison

The first step in the evaluation of the GC–MS data is to check the quality of the analysis and the integration of the chromatograms by comparing the duplicate analyses. Table 8.5 gives a summary of the ratio comparison results. The upper part of Table 8.5 shows that all duplicates compare better than the comparison of the duplicate

TABLE 8.4 Compounds and Ratios Used for the Numerical Comparison of Paraffin Wax Samples

Compound	Ret.time	Compound	Ret.time	Compound	Ret.time
C17	26.29	C26 *m/z* 337	40.95	Compound 1 *m/z* 92	46.32
Pristane	26.41	Branched C27 *m/z* 351	41.9	29ab *m/z* 191	46.81
C18	28.22	C27	42.28	C31	47.11
Phytane	28.40	C27 *m/z* 351	42.28	C31 *m/z* 197	47.11
C19	30.06	Branched C28 *m/z* 365	43.2	Compound 1 *m/z* 106	47.22
C20	31.81	C28	43.56	30ab *m/z* 191	47.8
C21	33.49	C28 *m/z* 365	43.56	C32	48.23
C22	35.11	27bb(R + S) *m/z* 218	43.9	C33	49.31
C23	36.65	Branched C29 *m/z* 379	44.44	Compound 2 *m/z* 106	49.49
C24	38.14	Ts *m/z* 191	44.7	C34	50.35
Branched C25 *m/z* 309	39.03	C29	44.78	C35	51.38
C25	39.58	C29 *m/z* 379	44.78	C36	52.37
C25 *m/z* 309	39.58	Tm *m/z* 191	45.19	C37	53.33
Branched C26 *m/z* 323	40.42	28bb(R + S) *m/z* 218	45.27	C38	54.32
Branched C26 *m/z* 337	40.56	C30	45.97	C39	55.43
C26	40.95	C30 *m/z* 197	45.97	C40	56.68
C26 *m/z* 323	40.95	29bb(R + S) *m/z* 218	46.26	C41	58.12
RATIOS					
Biomarkers	***n*-alk.**	**Biomarker/*n*-alkanes**	***n*-alk.**	**Branches alkanes/*n*-alk.**	***n*-alk.**
Hopane ratios:	C17/pris	29bb/C30 *m/z* 197	C25/C26	Branched C25/C25 *m/z* 309	C34/C35
Ts/29ab	C18/phy	29ab/C30 *m/z* 197	C26/C27	Branched C26/C26 *m/z* 323	C35/C36
Tm/29ab	C18/C19	30ab/C31 *m/z* 197	C27/C28	Branched C26/C26 *m/z* 337	C36/C37
30ab/29ab	C19/C20		C28/C29	Branched C27/C27 *m/z* 351	C37/C38
Sterane ratios:	C20/C21	**Other compounds/*n*-alk.**	C29/C30	Branched C28/C28 *m/z* 365	C38/C39
27bb/29bb	C21/C22	Comp 1 *m/z* 92/C30	C30/C31	Branched C29/C29 *m/z* 379	C39/C40
28bb/29bb	C22/C23	Comp 2 *m/z* 106/C31	C31/C32		C40/C41
Sterane/hopane ratio:	C23/C24		C32/C33		
29bb/29ab	C24/C25		C33/C34		

n-Alkanes are integrated based on *m/z* 85 unless indicated otherwise; "branched C25 *m/z* 309" indicates a branched alkane eluting just before C25 and integrated based on *m/z* 309, etc. Compound abbreviations of the hopanes and steranes are applied according CEN (2012) and Kienhuis et al. (2016).

analyses of sample can-1 (standard deviation of the paired ratios is lower than 3.9), whereas the duplicate sample comparison of can-2 shows the lowest value. This is also visible in the MS–PW plots of the duplicates of samples can-1 and can-2 (Fig. 8.11). Sample can-1 shows that the highest integrated *n*-alkane has a value above 118%, but the higher variance can be related to its low concentration (Fig. 8.11). The ratio comparison plot shows that relative differences are all below 14%. The data points of the MS–PW plot of sample can-2 are all between 85% and 118%, whereas the ratio comparison plot shows relative differences much lower than 14% for all ratios. It can be concluded, that no significant differences have been found for all duplicates of the compounds used for the numerical comparison.

The lower part of Table 8.5 shows the numerical results of the comparison of the combined duplicates of the samples of the paraffin wax case study. The comparison of samples beach-small with can-2 is at the same level as that of the duplicates, whereas the rest of the combinations show many ratios with relative differences exceeding

TABLE 8.5 Relative Ratio Differences >14% and the Standard Deviation of the Paired Ratios for the Duplicate Analyses and Combined Duplicate Sample Results for all Sample Combinations of the Paraffin Wax Case Based Upon GC–MS Ratios (Table 8.4)

Duplicate comparison			
Sample a	**Sample b**	**Ratios >14%**	**St. dev. paired**
Can-1	Can-1	0	3.9
Can-2	Can-2	0	2.6
Beach-inside	Beach-inside	0	2.7
Beach-small	Beach-small	0	3.3
Beach-outside	Beach-outside	0	3.2
Comparison of samples with combined duplicate analyses			
Source sample	**Spill sample**	**Ratios >14%**	**St. dev. paired**
Can-1	Can-2	8	16.7
Can-1	Beach-inside	13	32.9
Can-1	Beach-small	11	17.4
Can-1	Beach-outside	12	26.2
Can-2	Beach-inside	9	20
Can-2	Beach-small	0	3.7
Can-2	Beach-outside	8	11.8
Beach-inside	Beach-small	10	19.9
Beach-inside	Beach-outside	5	10.5
Beach-small	Beach-outside	8	11.7

14% and high standard deviations for the paired ratios calculations. MS–PW plots and ratio graphs for the comparisons of samples can-1 with can-2 and of samples beach-small with can-2 are shown in Fig. 8.12. The MS–PW plot of the *n*-alkanes (Fig. 8.12 top) shows the same trend line as found for the GC–PW plot of the GC–FID analysis (Fig. 8.6), which as described above, is very likely caused by wax redistribution differences between the two can samples. The MS–PW plot shows that the biomarkers deviate significantly from the 100% line and are clearly separated from the other compound groups. They are grouped and at the level of the lighter *n*-alkanes (C18–C20).

The ratio comparison plot (Fig. 8.12, top right and Fig. 8.13, enlarged) shows that the *n*-alkane ratios from *n*-C21/*n*-C22 to *n*-C34/*n*-C35 and all hopane and sterane biomarker ratios are far below the relative difference of 14% indicating a relation between the two can samples. But the lower molecular weight *n*-alkanes from *n*-C18 to C21, most of the branched alkanes ratios, the alkylbenzene/alkyltoluene ratios, and biomarker/*n*-C30 ratios are significantly different. As is typical for the relationship between branched alkanes and *n*-alkanes is that their physical properties are very different. For example, *n*-C17 ($C_{17}H_{36}$) has a melting point of 21°C and a boiling point of 302°C, whereas pristane ($C_{19}H_{40}$) as branched alkane has a melting point of −100°C and a boiling point of 296°C. This difference indicates that the compounds with a lower melting point behave in different way than the long-chain *n*-alkanes.

The MS–PW plot of sample can-2 with sample beach-small (Fig. 8.12) shows that two data points, representing the two highest *n*-alkanes integrated, are outside the range of 85% to 118%. Their concentrations are low, and therefore the lower values for these highest boiling *n*-alkanes are not seen as significant differences. The ratio comparison plot shows low relative differences.

Before concluding that a match exists between a paraffin spill and a source sample their ion-chromatograms should be compared visually in order to assure that differences have not been missed in the selection of the ratios. A macro has been developed to produce pdf files of the samples showing all ion-chromatograms analyzed, allowing for convenient comparisons. In the case study described herein, comparisons of the ion chromatograms for the samples can-2 and beach-small showed no significant visual differences. Therefore, it can be concluded

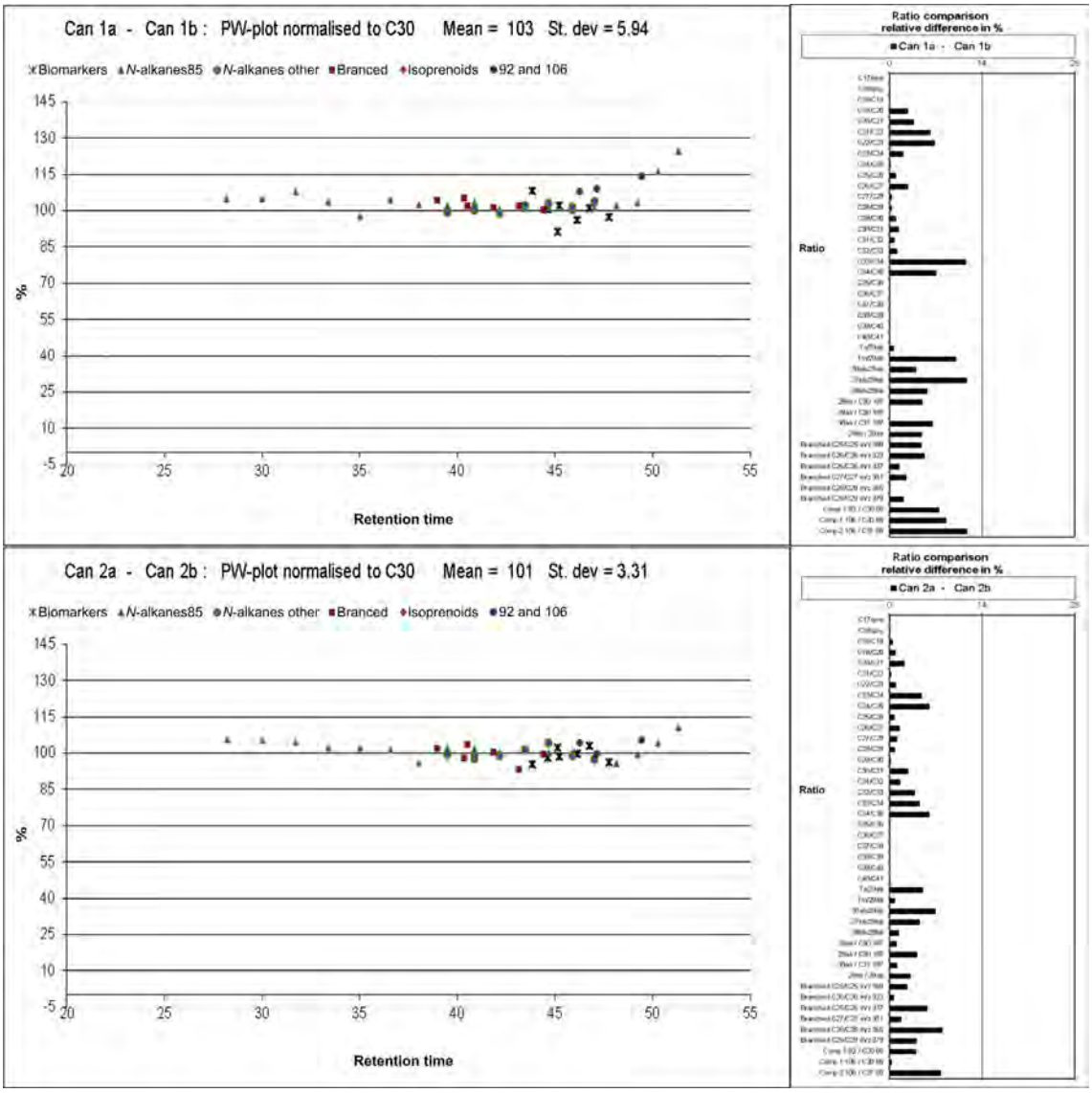

FIGURE 8.11 MS–PW plot and ratio graph of the comparison of the duplicates of samples can-1 and can-2.

that no significant differences between samples beach-small and can-2 have been found for the MS–PW plot, ratio comparison and the visual comparison of all ions-chromatograms analyzed.

The weighted mean versus standard deviation plot (Fig. 8.4) had indicated that the FID patterns of the samples Noordwijk-1 and RR-1 were close to the sample beach-small; hence, it might be useful to compare these samples using the GC–MS data (Fig. 8.14). The MS–PW plot comparing Noordwijk-1 with beach-small shows large differences exist, which cannot be explained by weathering or wax redistribution. The composition of the biomarkers is different as well, as are the concentrations of the branched alkanes. Strange, however is the fact that the "*n*-alkanes other" follows a different line than the *n*-alkanes. The "*n*-alkanes other" represents *n*-alkanes that were integrated at higher *m*/*z* values (Table 8.4). The difference observed in the MS–PW plot is probably related to the fact that the samples have been analyzed in different sequences, between which time the MS source had been cleaned, increasing the relative sensitivity of the MS for higher *m*/*z* ions. The ratio comparison plot reveals that relative differences for the ratios Ts/29ab (*m*/*z* 191) and 28bb/29bb (*m*/*z* 218) are much larger and larger than 14% indicating significant differences (Fig. 8.14). The conclusion is confirmed by a visual check of the chromatograms.

It should be noted that the comparison of samples analyzed in different sequences is not a problem as long as it is used to exclude samples for comparison, and as long as the differences are clear and cannot be caused by

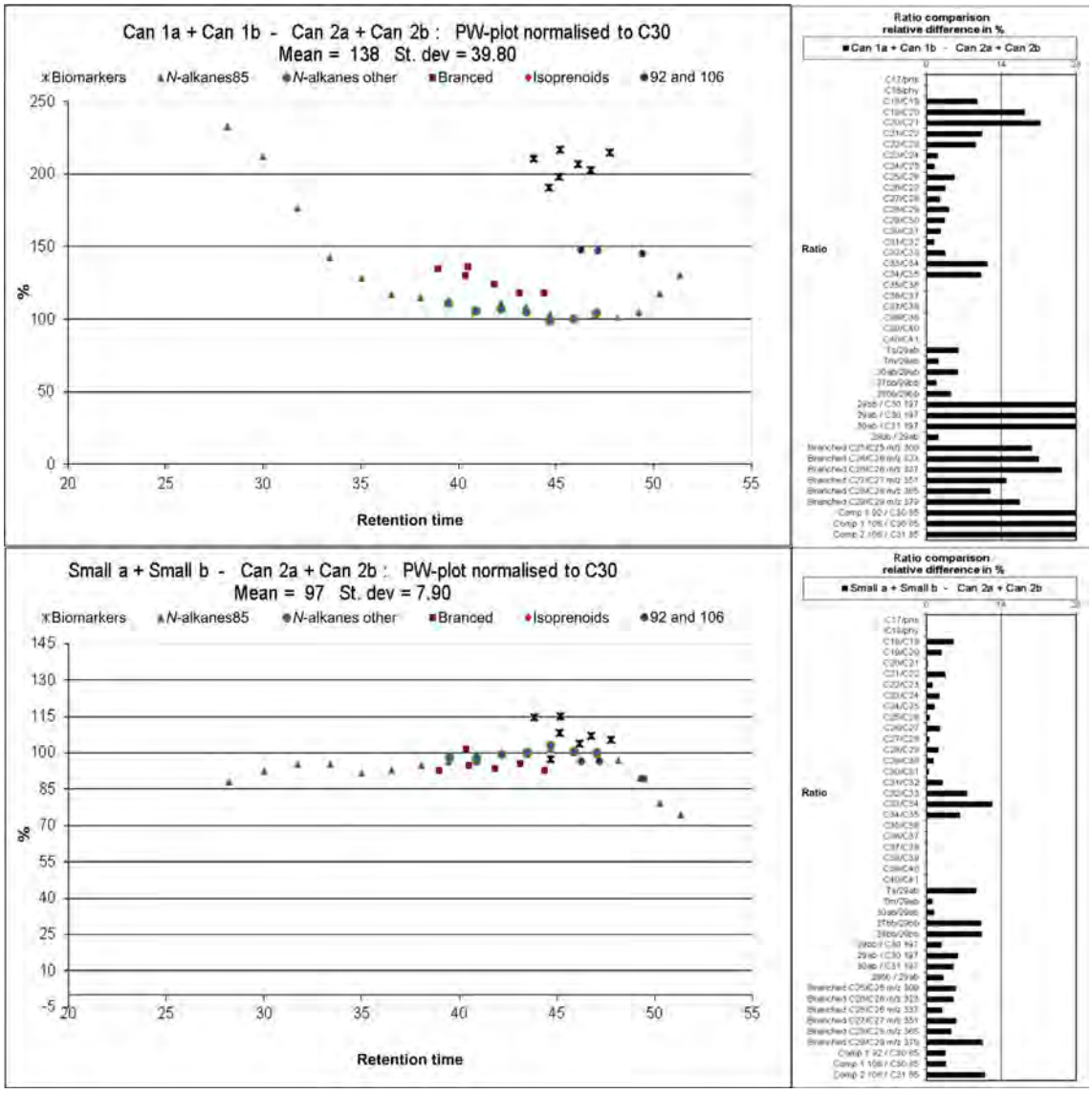

FIGURE 8.12 MS–PW plots and ratio graphs of the comparison of the combined duplicates of samples can-1 with can-2 and of samples beach-small with can-2.

instrument variations. To match two samples it is strongly advised to analyze them in the same sequence or at least on a system with the same performance.

From Fig. 8.15, it is clear that the Noordwijk-1 and beach small paraffin samples have a very similar *n*-alkanes profile, as expected from Fig. 8.4, but for the other compounds very different patterns are observed. The ion-chromatogram of *m*/*z* 92 for Noordwijk-1 seems to be caused by an analytical problem related to a SIM section, but the SIM section starts before 36 minutes so that cause was refuted. Because sample Noordwijk-4 shows the same pattern (not shown) it is expected that the Noordwijk-1 sample's pattern is the result of mixing from different sources or products before or during paraffin production. Also the steranes (*m*/*z* 218) and branched alkanes/*n*-alkanes (*m*/*z* 337) show clear differences (Fig. 8.15). Thus, it can be concluded that samples Noordwijk-1 and beach-small show significant differences.

The RR-1 and beach-small paraffin samples were analyzed within a time difference of one month, but using the same column and source performance. The MS–PW plot (Fig. 8.14, bottom) shows that the "*n*-alkanes-other" line follows the *n*-alkanes line. Most of the *n*-alkane ratios, the branched alkanes and the steranes ratio 28bb/29bb show relative differences clearly above 14%. The pattern of the *n*-alkanes with a hump in the middle is different from what is expected for wax redistribution between samples, e.g., as was evident between samples

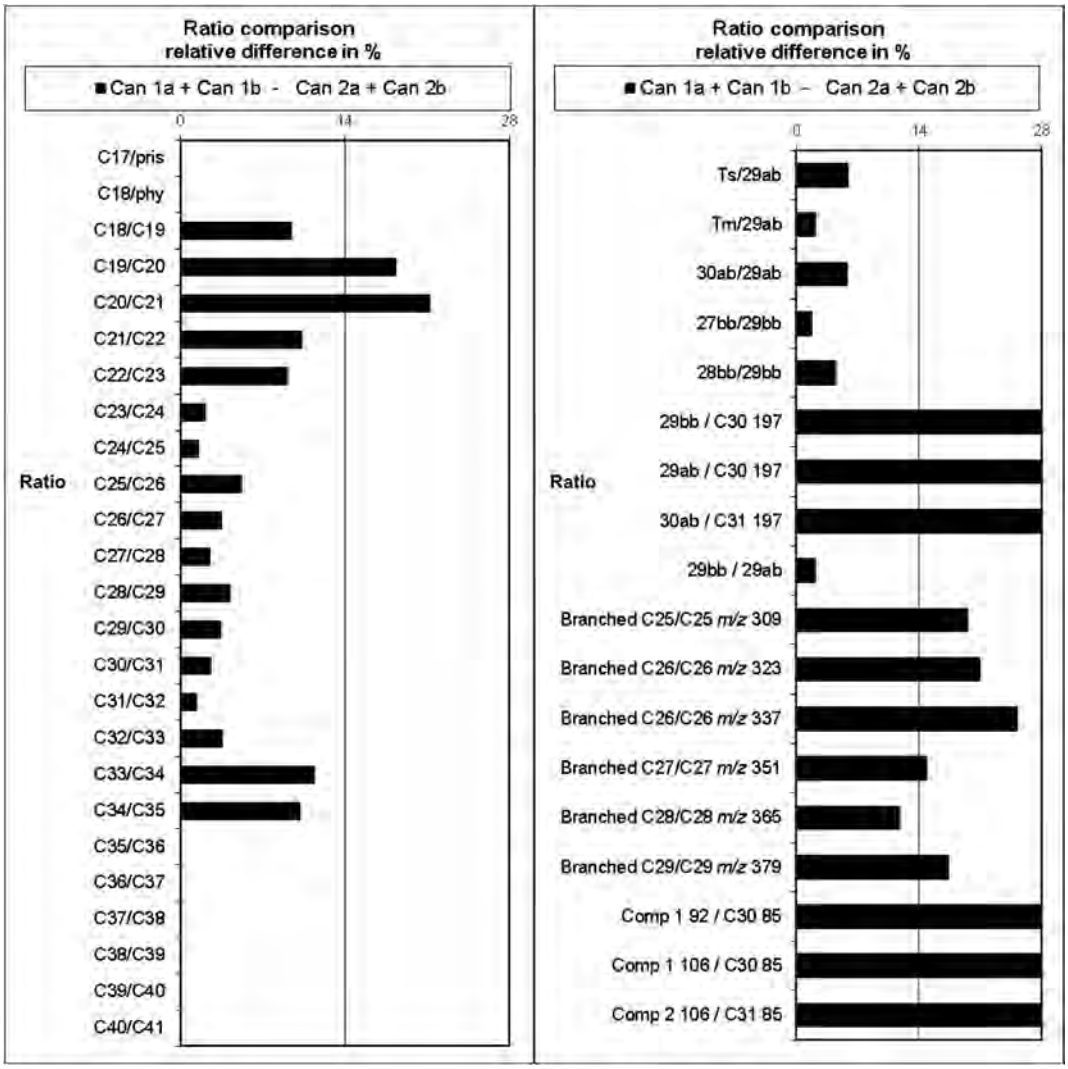

FIGURE 8.13 Ratio graph of the comparison of the combined duplicates of samples can-1 with can-2.

can-1 and can-2. A visual inspection of the ion chromatograms reveals many additional differences in which the steranes and branched alkanes are most informative. It can be concluded that samples RR-1 and beach-small show significant differences.

Fig. 8.16 shows the comparison of the RR-1 and RR-10 round robin samples that were obtained from the same extract. These two samples should be equal, but instead show that the biomarker concentrations normalized to *n*-C30 are at a level of around 145% in RR-1 relative to RR-10). All analyzed biomarkers show the same difference, whereas the differences between the ratios of the biomarkers are at a very low level (Fig. 8.17) indicating good analytical precision, despite their relative low concentration.

All samples of the round robin were analyzed in one sequence from RR-1 to RR-10. Injecting paraffin samples with a high concentration of long-chain *n*-alkanes above *n*-C45 (e.g., sample 6 of Fig. 8.3) has an impact on system performance, resulting in lower peak heights for low concentration compounds in the later analyzed samples.

The comparison of samples RR-1 and RR-2 (Fig. 8.16) also shows biomarkers above the *n*-alkanes lines. Here the effect of the column performance is less likely, because these are the first samples analyzed in the sequence and both samples do not show *n*-alkanes above *n*-C40 (Fig. 8.3 sample 1). Therefore, it is more likely that these two samples have a relative difference in biomarker concentrations. The biomarker ratios in the ratio graph on the right side of Fig. 8.17 show low relative differences except for the ratio 29bb/29ab, which has a 14% relative difference. The ratios between the branched alkanes and alkanes show relative differences above 14% and also

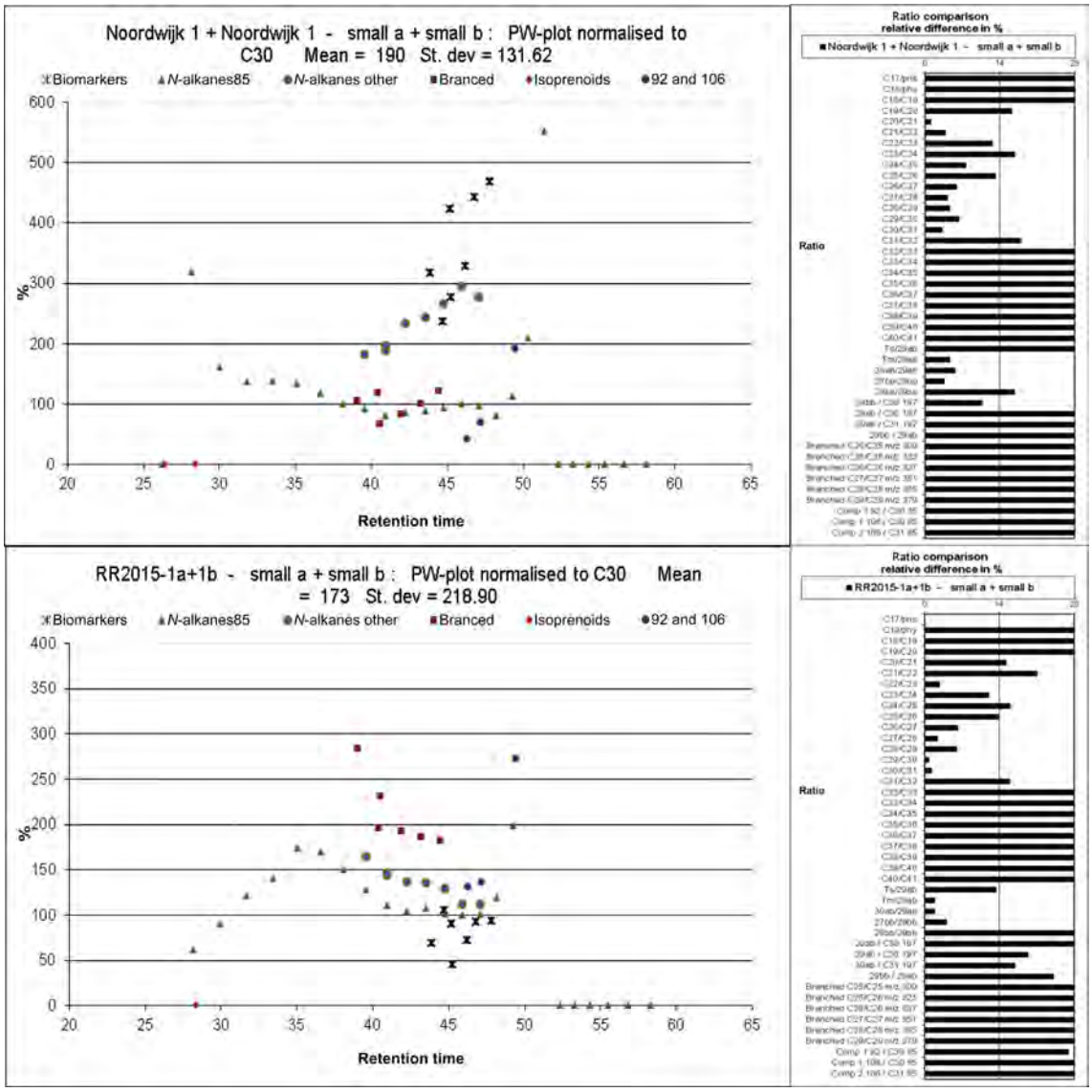

FIGURE 8.14 MS–PW plot and ratio graph of the comparison of the combined duplicates of Noordwijk-1 with beach-small and of RR-1 with beach-small.

the *m*/*z* 92 and 106 compounds show differences in concentration. A visual inspection of the ion-chromatograms indicates a clear difference in the concentrations of the *m*/*z* 92 and *m*/*z* 106 ions relative to the *n*-alkanes. Therefore, it can be concluded that samples RR-1 and RR-2 show significant differences.

8.5 CASE STUDY CONCLUSIONS

The comparison between the paraffin wax samples collected from the Dutch beach and the paraffin wax samples collected from a can on the suspected source vessel indicates a close relation exists between the samples beach-small and can-2. Inspection of the available data provide no basis to conclude these samples are a non-match. However, multiple bases exist to conclude a match between these samples, viz.,

- GC–FID chromatograms do not show significant differences.
- GC–MS ion-chromatograms do not show significant differences.

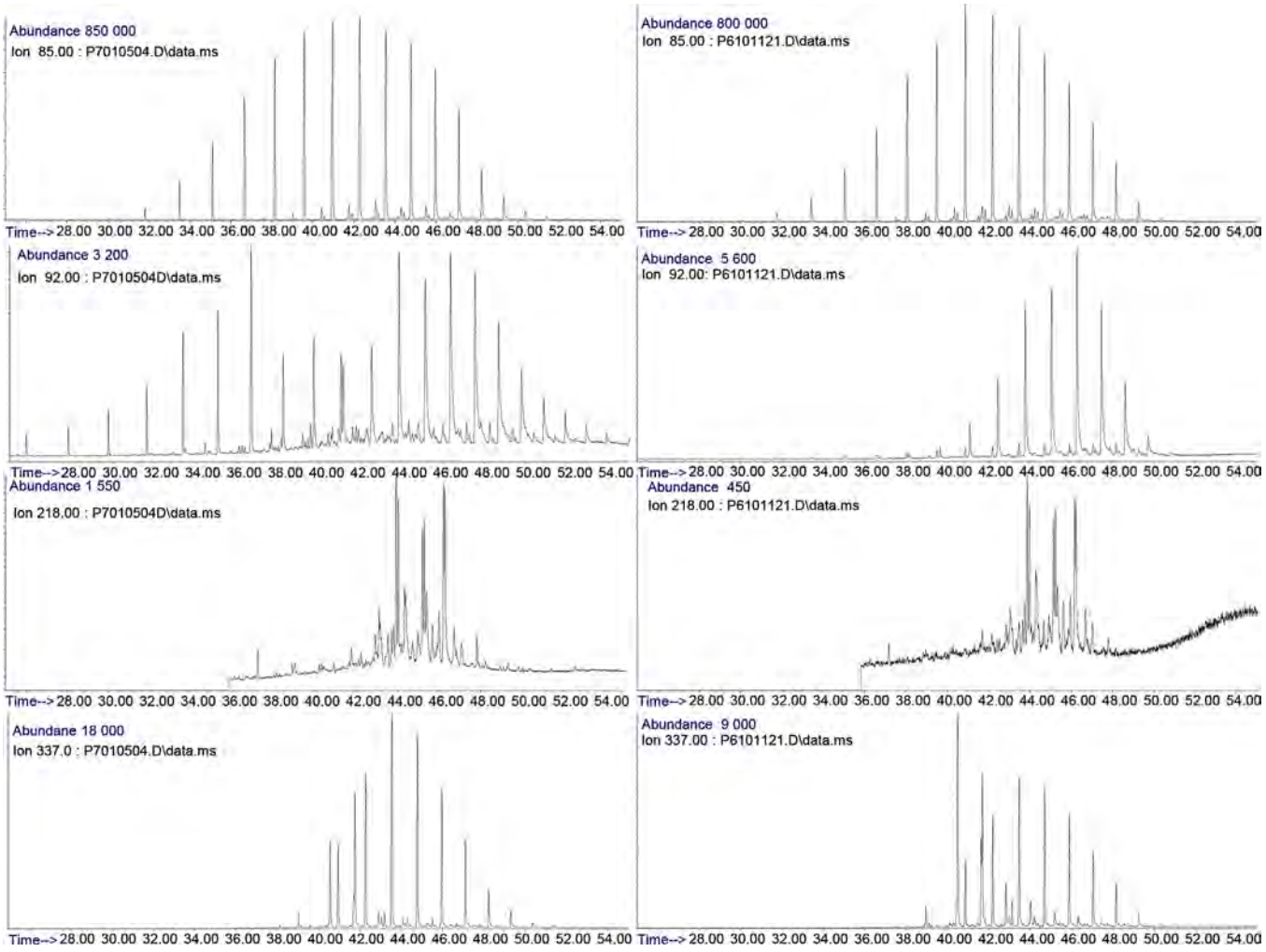

FIGURE 8.15 Visual check of the ion chromatograms *m/z* 85, 92, 218, and 337 between samples Noordwijk-1(left) and beach small (right).

– Numerical evaluation of the chromatograms by means of the GC–PW plot, MS-PW plot and comparison of the selected ratios does not indicate significant differences exist.

Therefore, it can be concluded that the paraffin samples beach-small and can-2 match.

8.6 METHOD EVALUATION

8.6.1 Weighted Mean Versus Standard Deviation Plot

The weighted mean versus standard deviation plot is not described in CEN (2012) but has been incorporated into the methodology used in comparison of paraffin waxes. In the plot, a sample can be represented as a single point, which has the advantage that it is possible to give an overview of a large collection of samples in one plot (Figs. 8.2 and 8.4). If a structuring in the sample set is present, for example, with groups of samples which are alike plotting near to one another, this will become apparent in this type of plot. As such, this plot can quickly reveal candidates for matching samples, which will plot as nearby points. However, it must be remembered that nearby points only share the same mean and standard deviation of the *n*-alkane distribution. This is only part of the evidence to conclude a match, as has been demonstrated in the comparison of samples can-2 with Noordwijk-1 and RR-1. The reason for this is that the *shape* of the *n*-alkane distribution might be different. The discriminating power of the method could be increased if the shape of the distribution would also be accounted for. This would mean that higher moments of the distribution have to be calculated, such as the skewness and

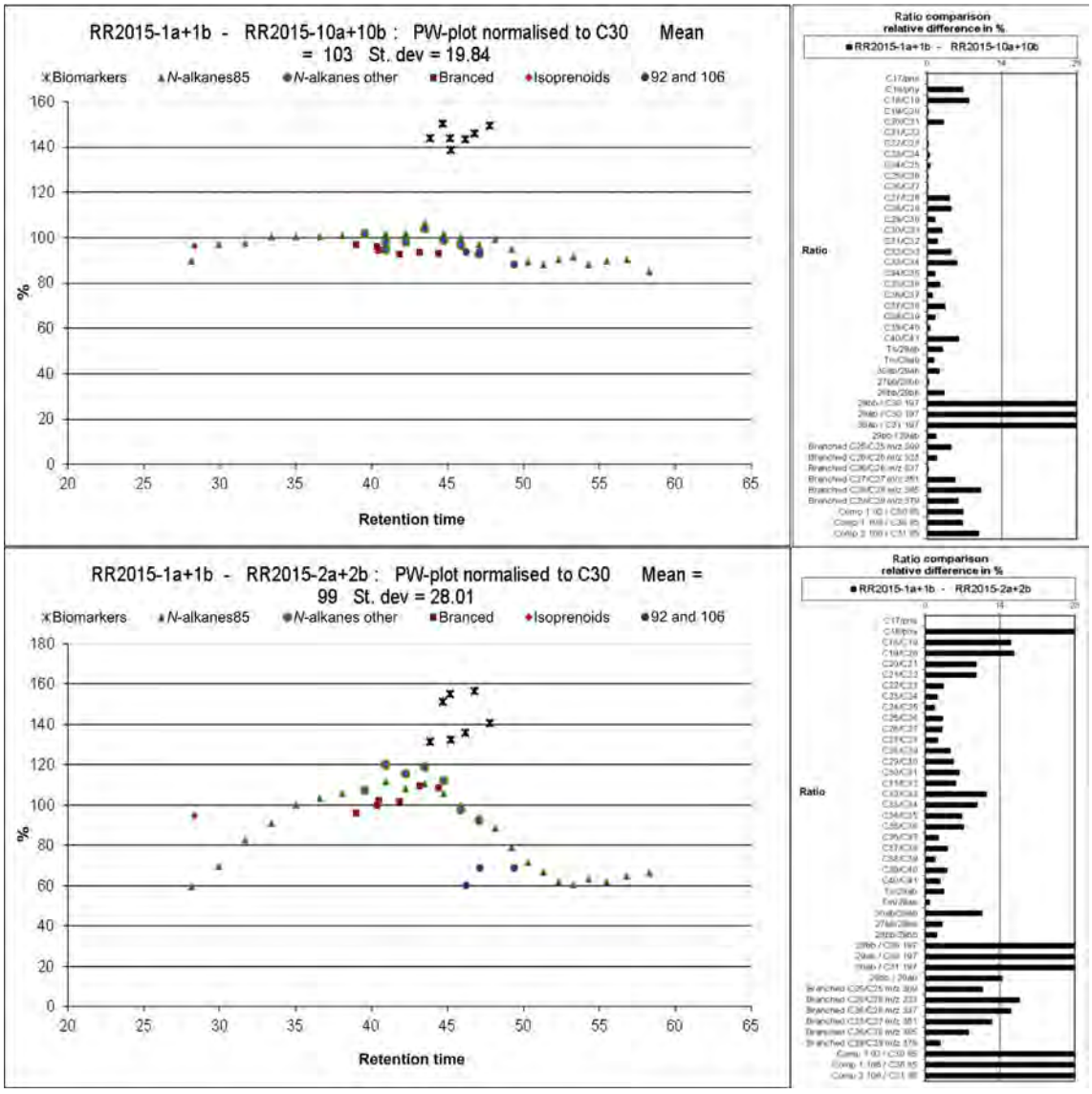

FIGURE 8.16 MS–PW plot and ratio graph of the comparison of the combined duplicates of RR-1 with RR-10 and of RR-1 with RR-2.

kurtosis (3rd and 4th central moment). Although this is certainly possible, the elegance of characterizing the sample with only two parameters is then lost. Instead of trying to resolve differences in the shape of the *n*-alkane distributions between samples with higher moments, it seems more sensible to restrict this method to two dimensions, employ it as a means to exclude obvious nonmatching samples, and to further investigate candidates for matching samples with the more elaborate ratio limits and PW plot methods, as modified from CEN (2012) appropriately for paraffin wax.

8.6.2 Diagnostic Power

The ratios used to access the paraffin spill case study described above have been selected based on the presence of specific compounds found in the samples studied. These ratios may not be appropriate for all paraffin studies. The DP calculation, shown and discussed in Section 2.5, is a useful tool to determine whether a candidate ratio shows minimal (nondiagnostic) or significant (diagnostic) variation among the samples under study. The calculation has been applied on the combined duplicate GC–MS ratios for the suite of paraffin samples studied herein. The results are shown in Table 8.6. Mean, minimum, maximum and RSD_V values of the applied ratios are shown. For the RSD contribution of the analytical method (RSD_A) the limit of 5% defined by CEN (2012) could

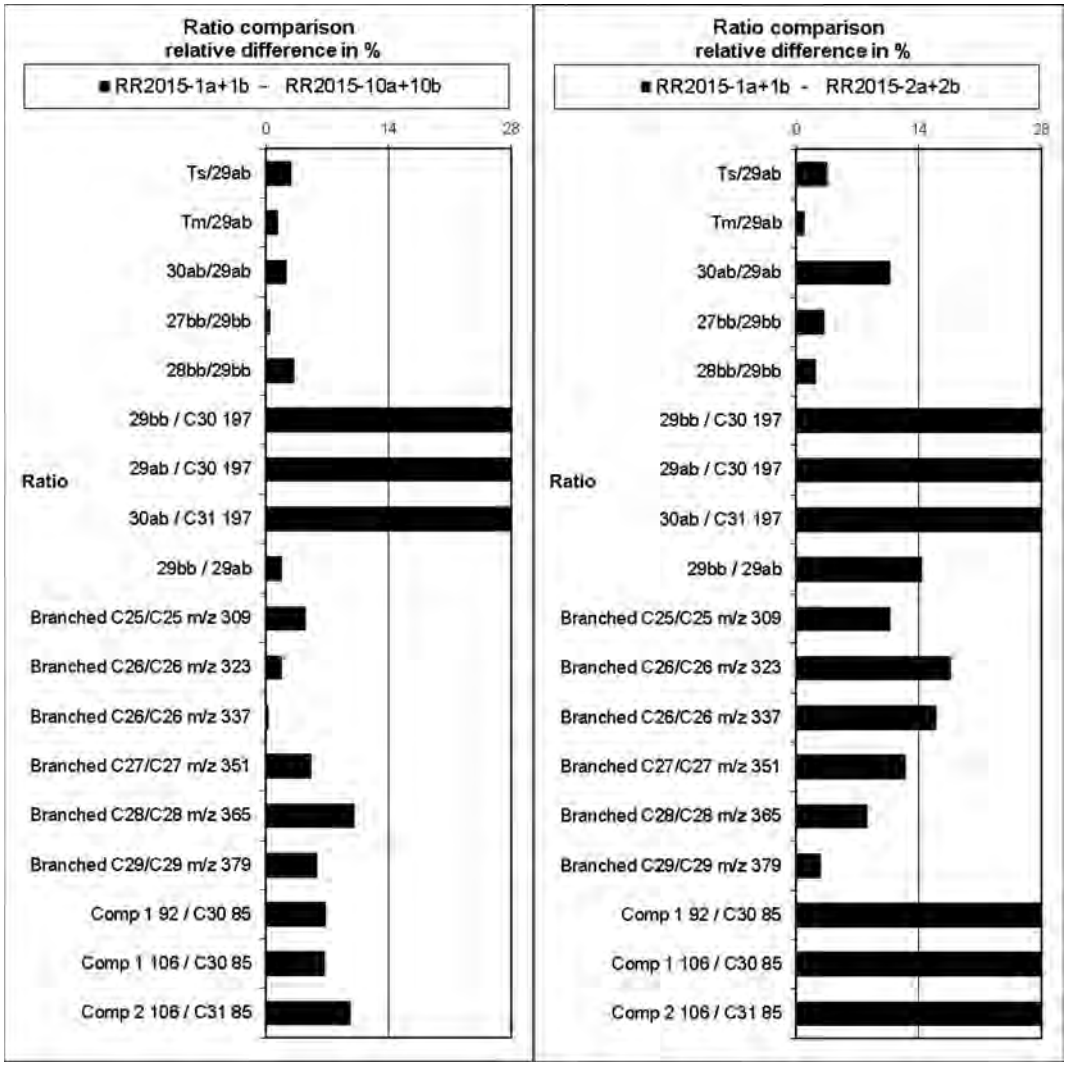

FIGURE 8.17 Part of the ratio comparison graphs for the comparison of the combined duplicates of RR-1 with RR-10 (left) and of RR-1 with RR-2 (right).

have been taken, but the standard deviation of paired ratio calculations of Table 8.5 shows that for the samples studied a value of 4% is more realistic.

Yang et al. (2008) used a set of 14 fresh crude oils to study the DP of 83 potentially DRs. The resulting DP values varied from 0.2 to 43.2 with 32 values above 10. Table 8.6 shows 42 ratios evaluated herein within a DP ranging from 2 to 33, with 19 ratios have DP above 10. Although partly related the paraffin sample set is large enough to show that many of the ratios applied vary between the samples. Low DP results are found for the ratios between adjacent *n*-alkanes. Only a few related to the shape variation of the *n*-alkanes show DP values above 10. The biomarker ratios between the hopanes and steranes show higher DP values ranging from 5 to 15. The highest DP values have been found for the three ratios between the biomarkers and the *n*-alkanes by using the peak heights of *n*-C30 and *n*-C31 integrated on *m*/*z* 197. These three ratios are all related to the concentration of the remaining oil in the paraffin samples.

The DP values of the six ratios used for the branched alkanes related to the *n*-alkanes vary from 11 to 18 (Table 8.6). The individual sample results are shown in Fig. 8.18. In limiting the number of ratios applied in a method, it is useful to determine whether ratios are related (Malmborg and Nordgaard, 2016). Fig. 8.18 shows a strong relation between the ratios "branched C25/C25 *m*/*z* 309" and "branched C26/C26 *m*/*z* 323." All the other ratios of the branched alkanes show individual properties.

TABLE 8.6 Mean, Minimum, and Maximum Values of the Ratios Applied, Combined with the Standard Deviation, Relative Standard Deviation and Diagnostic Power

Ratios applied	Ratio mean	Ratio min.	Ratio max.	St. dev	RSD_V in %	DP
C18/phytane	375.66	141	770	232	62	15
C18/C19	22.81	10	49	12	53	13
C19/C20	18.33	6	39	7	40	10
C20/C21	27.76	16	40	6	23	6
C21/C22	41.70	33	52	7	16	4
C22/C23	56.01	48	69	6	11	3
C23/C24	66.67	58	79	7	10	2
C24/C25	80.91	67	95	9	11	3
C25/C26	86.45	72	99	9	10	3
C26/C27	96.50	76	112	13	13	3
C27/C28	102.81	90	113	8	8	2
C28/C29	104.65	87	119	11	11	3
C29/C30	112.19	94	126	10	9	2
C30/C31	119.02	94	143	18	15	4
C31/C32	142.19	100	206	32	23	6
C32/C33	177.60	107	316	73	41	10
C33/C34	234.63	110	501	135	58	14
C34/C35	250.96	115	570	168	67	17
C35/C36	182.76	117	248	42	23	6
C36/C37	164.43	122	242	46	28	7
C37/C38	187.62	132	245	36	19	5
C38/C39	180.25	135	246	39	21	5
C39/C40	179.19	134	226	27	15	4
C40/C41	169.61	134	222	28	17	4
Ts/29ab	22.36	0	41	13	59	15
Tm/29ab	29.47	0	39	9	31	8
30ab/29ab	83.96	0	145	27	32	8
27bb/29bb	84.17	50	109	23	27	7
28bb/29bb	66.37	49	89	14	22	5
29bb/C30 *m/z* 197	3.58	0	19	5	127	32
29ab/C30 *m/z* 197	23.38	4	81	23	99	25
30ab/C31 *m/z* 197	23.32	1	123	31	131	33
29bb/29ab	17.53	0	26	7	42	11
Branched C25/C25 *m/z* 309	75.55	26	163	44	59	15
Branched C26/C26 *m/z* 323	101.33	43	199	46	46	11
Branched C26/C26 *m/z* 337	229.58	42	563	165	72	18
Branched C27/C27 *m/z* 351	307.20	65	669	197	64	16

(*Continued*)

TABLE 8.6 (*Continued*)

Ratios applied	Ratio mean	Ratio min.	Ratio max.	St. dev	RSD_V in %	DP
Branched C28/C28 *m/z* 365	309.36	104	614	168	54	14
Branched C29/C29 *m/z* 379	333.75	163	585	148	44	11
Comp 1 *m/z* 92/C30 *m/z* 85	0.91	0	2	1	60	15
Comp 1 *m/z* 106/C30 *m/z* 85	0.76	0	1	0	37	9
Comp 2 *m/z* 106/C31 *m/z* 85	0.93	0	2	1	74	18

The values are based on the combined duplicate values of the paraffin samples mentioned in Section 2.1.

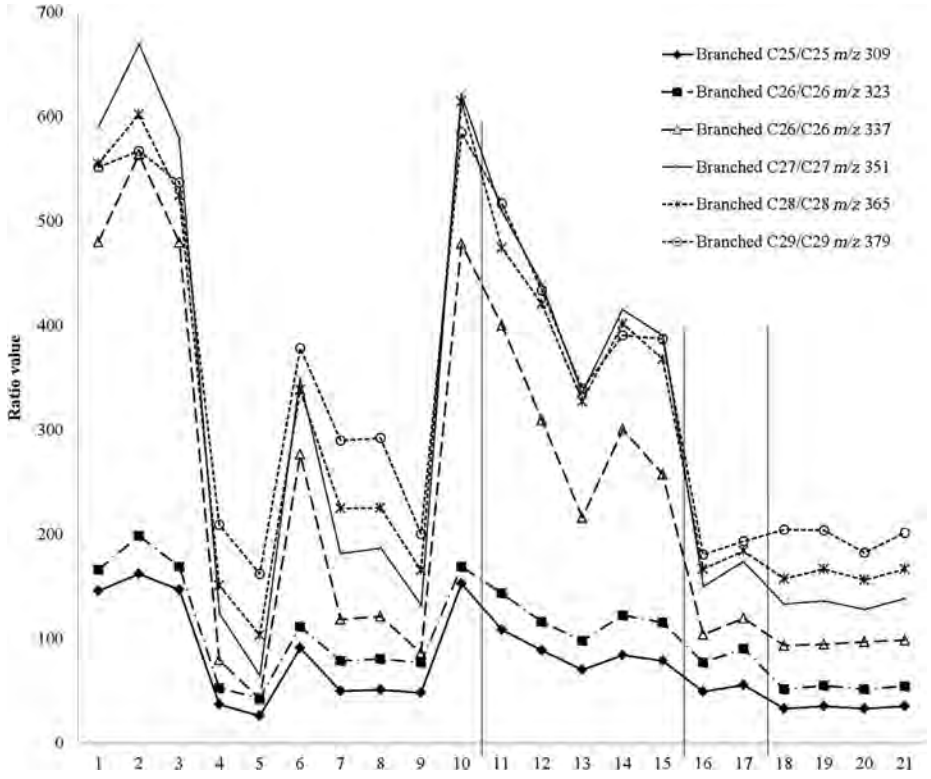

FIGURE 8.18 Branched alkanes/*n*-alkanes ratio values of the combined duplicate analyses of the RR (1–10), can—beach (11–15), Noordwijk-1 and 4 (16–17) and Eemshaven (18), Moddergat (19), and Rottermerplaat (20–21) samples.

The three ratios based on the *m/z* 92 and 106 compounds show a variation of 9 to 18. In the comparison of the samples described in Section 8.4, they often show a more or less unique pattern and are therefore a useful addition to the method. To limit the number of ratios in reporting, some ratios can be excluded, such as the ratio "branched C25/C25 *m/z* 309" (which is related to C26/C26 *m/z* 233; Fig. 8.18). Similarly, several of the adjacent *n*-alkane ratios could be eliminated based on their low DP values. Overall, it can be concluded that many of the proposed ratios (Table 8.6) used can be considered diagnostic among paraffin wax samples from different origins.

8.6.3 Weathering

CEN (2012) defines weathering as "*changes in oil composition which take place after the spillage, including evaporation, dissolution, emulsification, oxidation and biological decomposition*". The protocol describes the effects of different types of weathering on spill samples, which does not preclude the ability to conclude a match by explaining the differences caused by weathering.

Paraffin spill samples are very robust against these weathering effects because the outer layer of a piece of paraffin protects the inside. Wax-redistribution is mentioned in CEN (2012), but the effect on the composition of paraffin wax samples in particular is not described. As indicated by the apparent effects of wax redistribution in some of the samples studied herein, however, it is useful to study these effects further.

8.6.4 CEN (2012) Conformity

The paraffin spill evaluation method developed and applied herein is based on CEN (2012) in that it follows the protocol and makes use of the criteria for the numerical assessment of the PW plots and ratio comparisons. The main difference is the application of other ratios appropriate for paraffin. CEN (2012) provides a list of normative ratios that have to be used unless the compounds involved are below a signal-to-noise ratio of 3–5. Besides the normative ratios it is advised to make use of additional ratios based on the presence of compounds specific for the samples involved.

Due to the specific properties of paraffin samples most of the normative ratios defined in CEN (2012) could not be used in evaluating paraffin spill samples, and only a limited number of other compounds were available for comparison.

A weakness in the comparison of paraffin spill samples is the phenomenon of wax-redistribution, which was evident in aliquots taken from the same paraffin sample. For the comparison of samples beach-small and can-2 in the case study, however, wax redistribution was not needed to explain the difference caused by weathering.

The application of the selected ratios diagnostic within a paraffin wax sample set derived from several paraffin spills teaches us that the composition of different paraffin samples varies considerably and that the combination of the selected ratios and the applied CEN (2012) criteria is capable of achieving robust final decisions in the comparisons of paraffin wax spill and source samples.

Acknowledgments

The IAEA-lab participation in the paraffin round robin with GC–FID and GC–IRMS analyses and in preparing this publication has been partially funded by the US through the Peaceful Uses Initiatives (PUI) program under the project, "*Implementation of a Comprehensive Sampling and Analytical Methodology to Determine and Trace Oil Pollution in Marine Waters*". The IAEA is grateful for the support provided to its Environment Laboratories by the Government of the Principality of Monaco.

References

Albaigés, J., Jimenez, N., Arcos, A., Dominguez, C., Bayona, J.M., 2013. The use of long-chain alkylbenzenes and alkyltoluenes for fingerprinting marine oil wastes. Chemosphere 91 (3), 336–343.

Albaigés, J., Kienhuis, P.G.M., Dahlmann, G., 2015. Oil spill identification. In: Fingas, M. (Ed.), Handbook of Oil Spill Science and Technology. Chapter 6, Wiley, pp. 165–203. http://dx.doi.org.10.1002/9781118989982.ch6.

Carter, J.F., Barwick, V.J. (Eds.), 2011. Good practice guide for isotope ratio mass spectrometry. In: FIRMS. ISBN 978-0-948926-31-0.

CEN/TR 15522-2:2012, 2012. Oil Spill Identification—Waterborne Petroleum and Petroleum Products—Part 2: Analytical Methodology and Interpretation of Results. European Committee for Standardization, 138 p.

Chesson, L.A., Tipple, B.J., Howa, J.D., Bowen, G.J., Barnette, J.E., Cerling, T.E., Ehleringer, J.R., 2014. Stable isotopes in forensics applications. In: second ed. Holland, H.D., Turekian, K.K. (Eds.), Treatise on Geochemistry, vol. 14. Elsevier, Oxford, pp. 285–317.

Christensen, J.H., Hansen, A.B., Tomasi, G., Mortensen, J., Andersen, O., 2004. Integrated methodology for forensic oil spill identification. Environ. Sci. Technol. 38, 2912–2918.

Ettre, L.S., 1993. Nomenclature for chromatography; IUPAC recommendations 1993; Section 4.3. Pure Appl. Chem. 65 (4), 819–872.

Fitz, N., Kienhuis, P., Tolosa, I., Blaga, C., de Bruyn, R., Kraus, U., 2017. Usability of GC–FID, GC–MS and GC–IRMS for Paraffin Wax Spill Identification. Berichte des BSH 56. ISBN 978-3-86987-782-2. http://www.bsh.de/de/Produkte/Buecher/Berichte_/index.jsp.

Jeffry, A., McLoughin, P., Pirkle, R., 2016. Application of isotopic compositions in fugitive petroleum product identification and correlation. In: Stout, S.A., Wang, Z. (Eds.), Standard Handbook Oil Spill Environmental Forensics. Fingerprinting and Source Identification, second ed. Chapter 10, Academic Press/Elsevier, San Diego, CA, pp. 481–508.

Kienhuis, P., Hansen, A.B., Faksness, L.-G., Dahlmann, G., 2016. CEN methodology for oil spill identification. In: Stout, S.A., Wang, Z. (Eds.), Standard Handbook Oil Spill Environmental Forensics. Fingerprinting and Source Identification, second ed. Chapter 14, Academic Press/Elsevier, San Diego, CA, pp. 685–728.

Malmborg, J., Nordgaard, A., 2016. Forensic characterization of mid-range petroleum distillates using light biomarkers. Environ. Forens. 17 (3), 244–252.

Roose, P., Albaigés, J., Bebianno, M.J., Camphuysen, C., Cronin, M., de Leeuw, J., et al., 2011. In: Calewaert, J.B., McDonough, N. (Eds.), Chemical Pollution in Europe's Seas: Programmes, Practices and Priorities for Research, Marine Board Position Paper 16. Marine Board-ESF, Ostend, Belgium.

Sanjay, M., Simanta, B., Kulwant, S., 1995. Paraffin problems in crude oil production and transportation: a review. Soc. Petrol. Eng. Available from: http://dx.doi.org/10.2118/28181-PA.

Stepanski, M., 2014. Wax deoiling technology for the future. Sulzer Tech. Rev. 1, 12–15.

UEG, 2014. Independent Environmental Group of Experts "Consequences of Pollution Incidents" (UEG). Pollution of the North and Baltic Seas with Paraffin, Opinion dated 22 July 2014. http://www.bfr.bund.de/cm/349/pollution-of-the-north-and-baltic-seas-with-paraffin.pdf.

Vadakayil, A., 2011. http://ajitvadakayil.blogspot.nl/2011/09/paraffin-wax-on-chemical-tankers-capt.html.

Yang, C., Wang, Z., Hollebone, B., Brown, C.E., Landriault, M., 2008. Application of statistical analysis in the selection of diagnostic ratios for forensic identification of an oil spill source. In: International Oil Spill Conference Proceedings, pp. 297–310.

CHAPTER

9

Challenges and Mysteries in Oil Spill Fate and Transport Modeling

C.J. Beegle-Krause
Sintef OCEAN AS, Trondheim, Norway

BIOGRAPHY

CJ Beegle-Krause is an oceanographer interested in finding better answers for Decision Support questions. She has provided operational support for over 200 oil spills in the US and internationally, including the Deepwater Horizon (DWH) oil spill, the T/V Prestige oil spill, and supported the US military in the Persian (Arabian) Gulf. During her last 5 years at NOAA, she was one of two lead trajectory modelers for the US government. She was called back to NOAA to assist with operational modeling for the DWH oil spill, as she had been the lead trajectory modeler during the BP Thunderhorse riser break and begun developments to improve response modeling for these types of events. She also provided daily forecasts of the DWH subsurface oil layer during the oil spill response. She is interested in Lagrangian Drift Problems, such as oil spills, marine debris and larval fish. At present, she is leading a team developing new under ice turbulence and trajectory models, and improving simulation of dispersed oil droplets in the SINTEF oil spill contingency and response (OSCAR) oil spill model. She is also a lead in the EU Seabasins Checkpoints Arctic project to evaluate data sets used in oil spill response around the Arctic. She recently published work on areas of the world ocean where oil biodegradation from a well blowout could potentially lead to subsurface hypoxic conditions even without subsurface dispersant injection, and in applications of chaos theory to oil spill problems. Two years ago, she had a short fellowship with the University of Osaka, Japan, for research into NaTech events: Natural events that lead to Technological Disasters, such as oil spills caused by tsunamis.

9.1 INTRODUCTION TO OIL SPILL MODELING

Modeling is a tool for looking forward and backward in time as well as spatially in three dimensions. Most commonly in oil spills, modeling is used:

- in oil spill response to allow responders to "get ahead" of the spill by providing time to mobilize and position response equipment and personnel, and to plan daily activities and
- after a spill to reconstruct the spill scenario in order to understand the evolution of the spill for Natural Resource Damage Assessment, particularly to reconcile conflicting information, data or viewpoints.

Oil spills are caused by events, which may have their own stories: an unknown sunken vessel leaking after many years, the explosion of a well blowout, bad weather leading to an accident or unknown damage that later causes an accident. An oil spill can also be a clue leading to understanding of a more scenario, such as a search-and-rescue (SAR) or search-and-recovery operation.

Oil Spill Environmental Forensics Case Studies.
DOI: http://dx.doi.org/10.1016/B978-0-12-804434-6.00009-4

This chapter examines cases studies in which oil spill modeling was or *could have been applied* to assist in understanding the situation. The *Deepwater Horizon* (DWH) oil spill, T/V *Exxon Valdez* oil spill (EVOS) and Nella Dan oil spills capture modeling challenging in the surface and subsurface, and sets the stage for discussion of a modern interpretation of on old mystery spill in the Caribbean Sea. The subsurface/sunken oil spills examined are the integrated tank barge (ITB) DBL-152, Kalamazoo River Spill, T/V *Athos I*, USS *Jacob Luckenbach*, USS *Mississinewa*. This chapter does not go into extensive details of specific oil spills models or algorithms, as there are extensive reviews on oil spill modeling, e.g., Spaulding (2017), Beegle-Krause (2015), Fingas (2015), and Reed et al. (1999b). Prognostic (e.g., forward) spill modeling software is both freely and commercially available for oil spill modeling, e.g., Beegle-Krause (2001), Reed et al. (1999a), Rye et al. (2008), and Socolofsky et al. (2015).

Oil and other drifting objects that are at the water surface move with both the wind and currents, though the effect of the wind changes depending how high the object/substance reaches into the atmosphere. Trajectory calculations combine the wind and current vectors together. The wind is adjusted with a multiplier applied to the standard (10 m) wind value, called a "windage" or "leeway" factor. For oil and chemical spills, this factor is related to the density of the substance, see Youssef and Spaulding (1994) and Anderson et al. (1998). For oil spills, the drift factor for oil is a value is between 0% and 6% of the wind vector added to the water current vector. Due to oil weathering, the windage factor will decrease over time. As persistent oils weather, eventually the windage will be near zero as the oil weathers to floating tarball fields. Simple surface drift models can be modified to simulate other chemicals or objects in order to predict their trajectory. There are also factors for particular types of objects, e.g., vessels, barrels, etc. which could be leaking oil as they drift. These windage are often in the same windage range as oils but can be much higher, for example: shipping containers (1.4% semisubmerged), oil drums (0.8%) and old WW II mines (2%). Standard methods outline how to estimate these values, for examples, see Breivik et al. (2011, 2013). Whale carcass drift is an example of how many applications require such drift modeling. Included at the end of the chapter are references related to notable nonoil spill drift problems of public interest for further reading.

Surface and subsurface oil spreads out to lower thicknesses/concentrations in the ocean by eddy diffusion (the time scale for physical spreading of liquid oil on the water surface is only minutes). Oil spills can also begin subsurface from a pipeline or well blowout. Through oil weathering processes, the oil will change over time, as components evaporate, dissolve are biodegrade. Dense oils or highly weathered and biodegraded oils can sink to the bottom. Oil droplets can also combine with suspended sediments or biological material in the water column to form oil-mineral aggregates (OMA) or Marine Oil Snow Sedimentation and Flocculent Accumulation (MOSSFA), which both sink in the water column. Mechanisms, such as waves, bring surface oil into the water column. Sediments that contain OMA or MOSSFA can be identified by their petrogenic molecular and isotopic signatures (radiocarbon) and put into context with other radiotracers (e.g., ^{210}Pb (lead), ^{238}Uranium, and daughter products).

What unifies/simplifies all these cases is that in the farfield, away from the source release dynamics, the larger environment controls the trajectory. Thus, we can reduce the complexity of studying many aspects of oil spill transport because the movement is primarily horizontal. We understand this simplifies the overall problem at the surface, but in the deeper ocean, we can apply these principles as first approximations (except in cases of sinking oil). Above the main ocean thermocline ($\sim$1000 m), there is wind induced vertical mixing, so chemical signals do not remain in intact very long—usually erased during winter wind induced mixing when surface waters are colder (denser). Within the main thermocline and deep ocean, chemical signals can last for years due to low mixing, which will be discussed in more detail later. Also, in the deep ocean, chemical transport is along constant density surfaces (isopycnals) which are approximately horizontal. The density surfaces tilt in order to balance the transport with the earth's rotation, which is called "geostrophic balance," so transforming deep chemical signatures from vertical coordinates to density coordinates can simplify understanding the dynamics.

9.2 FORENSICS IN OIL SPILLS

The most common forensic issues in oil spill modeling are "*Where did this spill come from?*" and "*Who spilled this oil*?" When a mystery spill is located, forward trajectory analysis can inform the response, but a secondary task is to identify the source location and Responsible Party. Ideally, the Responsible Party will be identified and provide both information on the oil and reparations for any damage by the oil spill. Chemical fingerprinting can assist with identifying and matching specific oils between a spill and vessel, but is less helpful for discharges from fuel tanks that are refilled from a variety of sources as the vessel moves about. Identifying the Responsible Party often involves determining aspects of the scenario, particularly the spill staring location.

Initial observations of the oil location and chemistry will provide a sense of timing in terms of the release into the environment. Highly weathered tarballs are much older than fresh oil at the surface. Lighter oils, such as gasoline or jet fuels, will evaporate and disperse into the water column over a relatively short time. Observations of the oil ideally narrow down the options of the type of oil spilled and chemical analysis can provide further insight.

Oil thickness can be a clue to source location, changes in spill rate, and/or complexities in the water flow. A stable, continuous subsurface release in a tidal area lasting more than one tidal cycle can have a complex pattern of thicker and thinner oil, so multiple observations are often needs to determine the source location. Overall, spreading of the oil increases over time, so this information should be evaluated with knowledge of the local circulation and potential spill sources. Convergence zones, either from freshwater overlying salt water or from convergences in the wind or current field, can complicate the scenario by thickening oil in particular areas. Docks and other harbor areas add complexities to the water circulation that creates complex circulation and difficulty in obtaining accurate oil observations.

Next, obtain recent weather information, particularly the wind history. Wind observations are increasingly easy to download from online meteorological stations, but these data must be quality controlled. Significant topography, such as headlands or large man-made structures, can cause changes in the winds, as well as large, manmade structures. In ports and harbors, docks and other structures can modify the winds near the water surface, which can make the oil movement much more complicated.

To begin further analysis to determine where a spill came from, start with the details of the oil location: position, extent, observable properties at initial siting and through the response. A chart of the area will provide bathymetric information, which in coastal and shallow waters informs the general sense of the coastal flow. Flow in rivers, estuaries, coast and the open ocean all follow known but separate physics. River flow will move along streamlines, but the overall flow can change greatly due to significant rain or other events. Rivers discharging into the ocean can mix into the ocean within an estuary, creating a two layer system. Rivers discharging into the ocean, when moving very quickly, can overlay coastal water as a defined layer of freshwater. This sharp interface between freshwater overlaying salt water can be a barrier to transport, and thus a collection area, of the oil moving in toward the coast.

Coastal areas require knowledge of tidal predictions, and these currents are stronger in deeper areas (shallow water wave theory). In areas along the continental shelf, the water will behave as stiff columns of fluid akin to the well-known concept of Taylor Columns. The Taylor Proudman Theorem states that for a slow, steady 2-dimensonal flow in a rotating system (e.g., coastal flows on the continental shelf), the fluid will behave as a stiff column. For bays, estuaries and the continental shelf, this assumption works well: in the absence of wind, the spill will move along bathymetry. The assumption breaks down with large changes in latitude (planetary rotation), such as was the case with the T/V *Prestige* oil spill in 2002. In the deep ocean, the upper water is primarily wind driven, so a first proxy could be a 2D wind field if ocean surface currents are unavailable. Ocean circulation models need to assimilate satellite altimetry in order to reproduce more detailed eddy dynamics.

Sea breeze can complicate understanding an oil spill, as these light, small-scale winds can lead to oil approaching a beach or beaching. The effect is not simulated within most atmospheric models, so research into archive weather forecasts are needed in order to determine information such as potential for sea breezes and timing. Winds, even as light as sea breezes, can lead to oil beaching. Winds can also "pin" oil in place, so that when the tide goes out, the oil strands on the beach. The slight upward slope of the freshwater is thought to provide the barrier, but the circulation at this sharp boundary likely plays a role as well.

Not enough can be said regarding checking data and model resolution (temporal, horizontal and vertical) and the associated metadata (where these data are from, quality control, model version and settings, underlying grid) of the information used to recreate the spill. Each of these aspects can change trajectory modeling results. Data at too coarse a resolution, mismatch between the real shoreline and the model edges, lack of relevant physics—these can all lead to erroneous analyses.

With the combined information available: source, oil type, amount (or rate) spilled, bathymetry, winds, and currents, one can begin to reconstruct the spill. Ideally, the exact scenario can be recreated. Commonly one or more of these pieces of information will be missing, so auxiliary or information at hand must constrain the scenario. This may lead to a one or more "possible scenarios" that can be created for the event. For further reading, the NOAA report on the oil spill from the Barge *Morris J. Berman* (HAZMAT Report 95-10) includes a section on the selection of the different types of physics for modeling the oil spill trajectories.

9.3 OIL FINGERPRINTING

"*Know your oil*" is a key mantra in oil spill response. In forensics the same is true, and oil fingerprinting is the method to identify the oil in great detail. Determining the product and source are keys to recreating the release

correctly—thus getting the trajectory correct, which can identify an overall search area for further evidence of the oil. The goal of fingerprinting is to determine all significant components of the oil and their relative quantities in order to both identify the source of the oil and to understand the fate and possible effects of the oil on the ecosystem. Wang and Stout (2010) and Stout and Wang (2016) are both detailed summaries of oil spill identification/fingerprinting. Bayona et al. (2015) discuss details in oil fingerprinting analytics in three tiers based on analytics methods and the inherent weathering of an oil spill over time:

1. Gas chromatography (GC)−flame ionization detector profiling to determining the *n*-alkanes, the isoprenoids, pristane (Pr), and phytane (Ph). This identifies the type of oil/product, but the signal degrades as the oil biodegrades.
2. Gas chromatography−mass spectrometry (GC−MS) profiles for *n*-alkanes, acyclic isoprenoids, bicyclic sesquiterpanes, triterpanes, steranes (and counterparts), aromatics, alkylated naphthalenes, phenanthrenes, pyrenes, chrysenes, heterocyclic sulfurs, and carbazoles.
3. Diagnostic ratios for the measured compounds use to compare source and spill oils to one another and against standards.

From this process, the oil can be broadly identified, and the carefully matched with oil samples. Corilo et al. (2013) have identified a fingerprinting technique using principle component analysis of electrospray ionization Fourier transform−ion cyclotron resonance−mass spectrometry (FT−ICR−MS) for identifying components of multiple spills (e.g., multiple tank ruptures, as during a natural disaster or significant marine accident) or for highly weathered products. Biodegradation studies are becoming more detailed, with identification of specific microbial groups that biodegrade specific components and calculations of biodegradation rates for individual components, e.g., Brakstad et al. (2014, 2015a,b). The consumption of dissolved oxygen (DO) from oil biodegradation as a persistent marker of oil in the deep ocean will be discussed later in the chapter.

An important note in oil spills is that illegal dumping of another oil into an existing oil spill is not uncommon. Oil can appear in odd places that do not match with the scenario, drawing a red flag requiring sampling, or oil can be released within the bounds of the spill, which is why multiple oil samples are taken. False observations of oil are also possible, requiring investigation related to the siting.

9.4 EXAMPLE OIL TRANSPORT

Surface oil moves with the water currents, winds and eddy diffusion (randomness in the flow). These each add different effects to an oil spill. Fig. 9.1 shows a series of pictures using the NOAA GNOME model with different aspects of the physics of the spill simulated, but no weathering (e.g., evaporation or dissolution). Oil weathering is commonly not used during a first level of trajectory analysis for spill locations. The series shows how the oil spill trajectory changes as tides, wind, and eddy diffusion are added into the simulation. The spill starts at 29° 37.97 N, 94° 52.64 W on March 9, 2017 at 11:00 and continues for 5 days. At first (A), the spill moves only with the tidal currents. Next (B), a light wind from the Northeast at 1-knot (51.44 cm/s) wind is added to the currents, making the tidal currents less visible as the spill now directed toward the higher currents in the main channel. Note how the tidal signal becomes stretched and less obvious, as the transport turns. Next (C), a low eddy diffusion of 100 cm^2/s or (D, with a higher eddy diffusion of) 10^5 cm/s is included with the winds and tides. Note how the tidal signal becomes more difficult to distinguish with the larger eddy diffusion, and could be confused with release rate changes. The tidal signal has disappeared (D), and the oil moves far enough to enter into the swifter channel currents to travel much farther toward the ocean, with the wind direction leading to some oil beaching.

Next, you can do further exploration with GNOME by using the model's "Diagnostic Mode" and turning the different physics on/off with the checkbox to combine any of the dynamics together: diffusion, winds and currents in different combinations. By turning on the visualization of the grid used by the currents, any areas where the grid for the currents overlap or have a gap in between could lead the oil to beach inappropriately. In the model, the horizontal mixing physics can cause oil to beach as the oil approaches the land; thus, the value for this parameter needs to be selected carefully with consideration of errors and knowledge of the area. Both winds and diffusion can cause oil to beach in the model. You may wish to change the winds to different directions and/or speeds to build intuition for spill trajectories in an area.

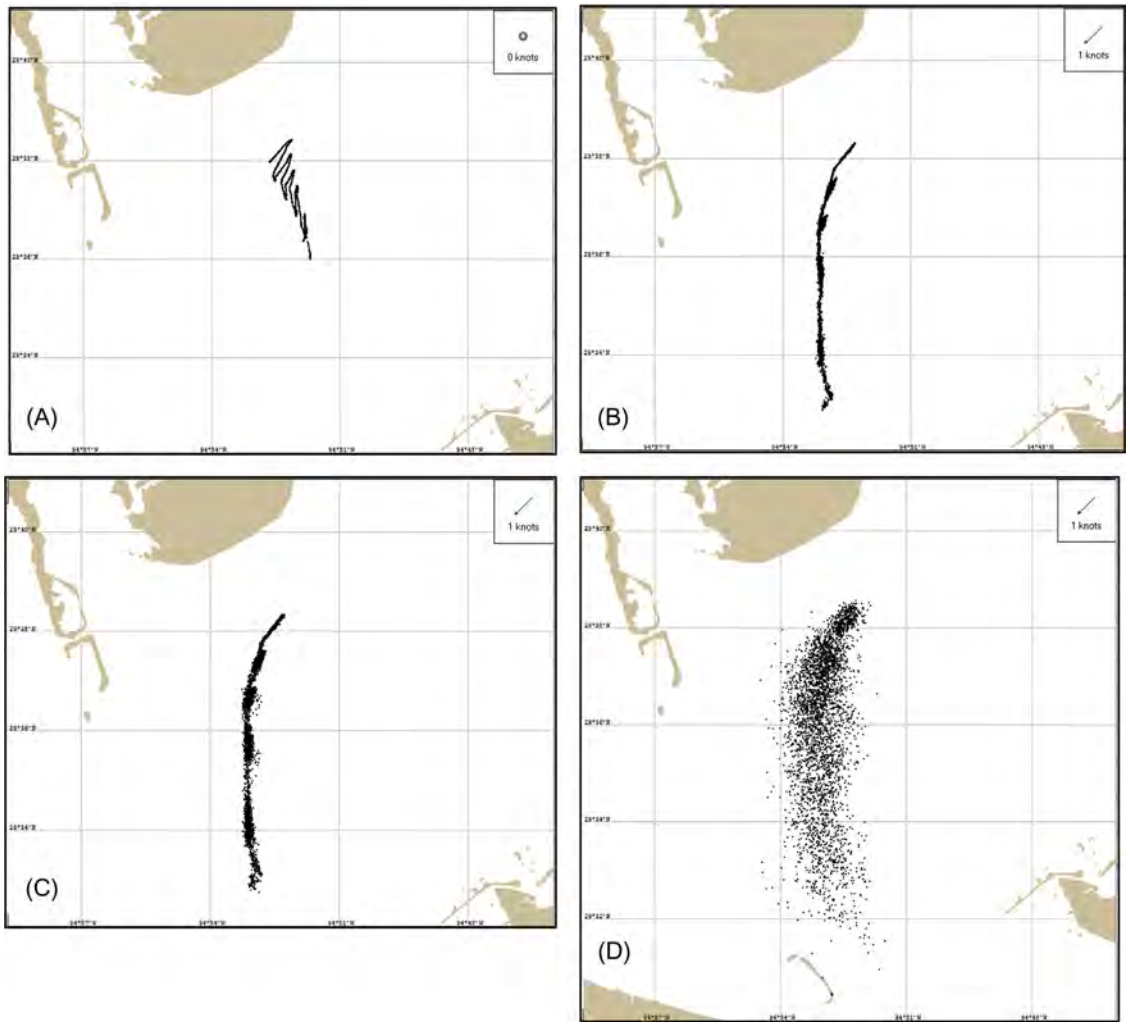

FIGURE 9.1 An example oil spill in Galveston Bay in order to show to the different dynamics control and oil spill using the GNOME model and the Galveston Bay Location File. Note that weathering, e.g., dissolution, evaporation, etc., have been turned off. (A) The spill is subject only to currents (particularly tides) and low river runoff. (B) The spill is subject to a 1-knot (~50 cm/s) wind from the northeast, which pushes the oil into the main channel where the channel is deeper, so that currents are stronger. (C) The spill is subject to tides, winds and a low eddy diffusion of 100 cm^2/s. Note how the tidal signal becomes more difficult to distinguish, and could be confused with release rate changes. (D) The eddy diffusion in increased to 100 cm^2/s, while all other conditions are the same as in part (C). The tidal signal has disappeared, and the oil moves far enough into the swifter channel currents to travel much farther toward the ocean, leading so some oil beaching.

9.5 CASE STUDIES FOR SUBSURFACE WELL BLOWOUTS

The unusual discussion during the DWH oil spill was the subsurface layer of oil droplets, which was also noted during the IXTOC I oil spill, NOAA (1980). What is important for forensics is that (1) the 3D problem can often be simplified to 2D and (2) within and below the ocean's main thermocline (~1000 m), circulation and changes are much slower than in the surface wind-mixed layer. We usually think of our experience at the ocean surface meaning that ocean currents flowing along a constant depth, but deep ocean flow is along density surfaces (isopycnals). A good example of this from the DWH oil spil is Figure 4 in Socolofsky et al. (2011) and the detailed Joint Analysis Report (2012) on the DWH subsurface oil droplet layer. The evolution of a spill is also much slower in the deep ocean, so inert materials or tracers of an oil spill (e.g., reduction in DO) can be followed for a long time. For example the chemical tracer *sulfur hexaflouride*, SF_6, was released in the main thermocline offshore of the Canary Islands, as described in 1992 (Ledwell et al., 1993) and followed for 30 months, as reported in Ledwell et al. (1998).

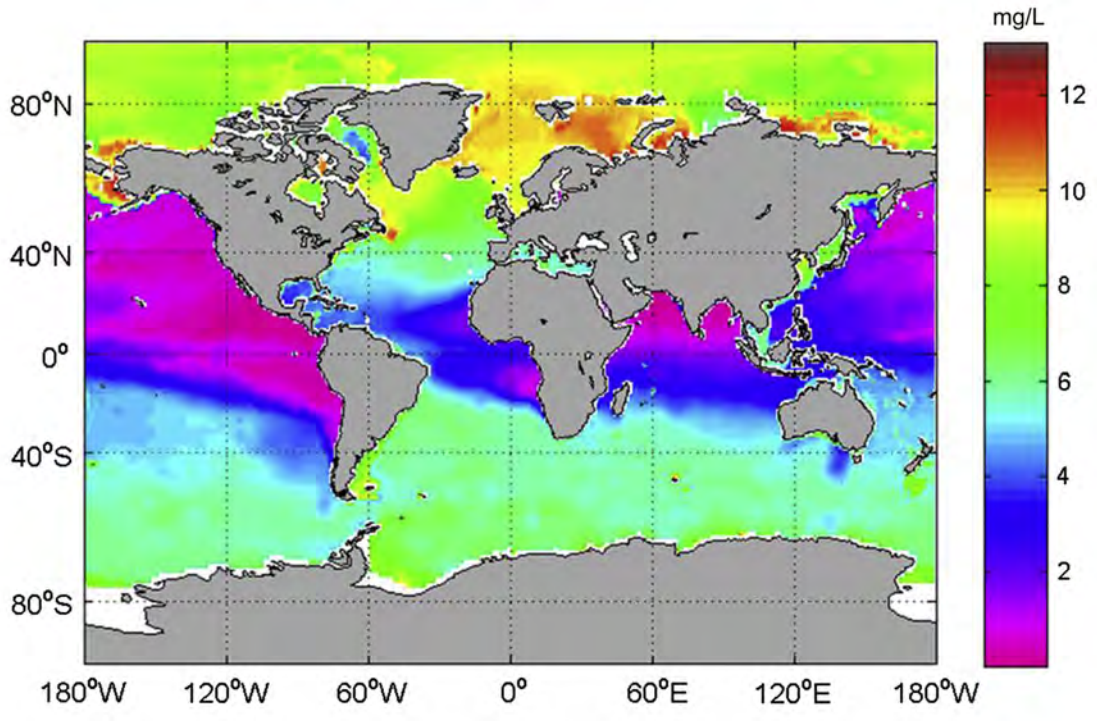

FIGURE 9.2 World-wide Dissolve Oxygen Minima. The 2005 World Ocean Atlas was analyzed for the minimum vertical DO concentration in the water column. This map shows large areas in the world ocean's eastern basins with minima at or below hypoxic levels. Note that the minimum is not at the same depth everywhere in the world ocean.

Many questions arose during the DWH oil spill regarding the subsurface layer of tiny oil droplets and the long-term implications. Based on these earlier SF_6 experiments, after the DWH oil spill, a 25-km streak of CF_3SF_5 (which is more environment friendly than SF6) was released 70 km southwest (SW) of the DWH well location, at approximately 1100 m (the depth of the subsurface layer of oil droplets). The release was approximately 150 m above the bottom along the continental slope and sampled at 5 days, 12 days, 4 months, and 12 months after release. The deepwater circulation in the Gulf of Mexico is roughly counter-clockwise (Dehaan and Sturges 2005; Sturges 2005). This Ledwell et al. (2016) field and modeling study shows that any remnant hydrocarbon in the DWH subsurface layer could begin to exit the Gulf of Mexico within about 1 year.

Biodegradation would be more likely to remove the DWH oil from that subsurface layer in less than 1 year, as biodegraded oil droplets become more dense over time. Large-scale MOSSFA is a likely removal mechanism for oil droplets in the water column during larger spills, such as the DWH, 1979 IXTOC 1, and 1969 Santa Barbara oil spills. The significance of MOSSFA is not a clear issue for small spills, as discussed in Vonk et al. (2015), though this is an emerging area of concern.

Biodegradation of the subsurface layer of oil droplets during the DWH utilized ~25% of the available DO in the subsurface layer of oil droplets (Joint Analysis Group, 2012). Beegle-Krause et al. (2016) discusses new modeling capabilities to estimate the DO consumed by oil biodegradation of subsurface oil droplets. The two example case studies from Brazil and Angola show how different the DO concentrations are in the deep world ocean and the potential for a realistic well blowout to lead to subsurface hypoxic conditions without SubSurface Dispersant Injection (SSDI), so with SSDI more DO would be utilized, thus driving DO levels lower and/or transiting over a wider area. As seen in Fig. 9.2, extensive areas of the world ocean have significant DO depletion at some level in the water column.

9.6 CASE STUDY: WAS THERE A MEGA-SEEP OR A WELL BLOWOUT OFFSHORE OF VENEZUELA IN THE 1970s?

Well blowouts, such at the IXTOC I and DWH oil spill, have a known source, with oil on the ocean surface, in the water column and on the seafloor. However, Harvey et al. (1979) and Requejo and Boehm (1985) describe

sampling in 1978 that found a 1400-km layer of oil rich water at approximately 200 m depth (see Fig. 9.3 for the vicnity of the area where the oil layer was found). Harvey et al. (1979) found 3–12 mg/L oil using hexane extracts of water samples. GC was used to analyze the hydrocarbons, fatty acid methyl esters and silylated sterol fractions while at sea. These analyses identified the samples as 60%–70% biodegraded hydrocarbon. The volume of biodegraded oil was estimated at greater than 1 megaton of oil (10^8 kg). The conclusion at the time was that the oil was from a large seep on the Venezuelan shelf at a similar depth, though chemical analysis could not determine with the weathering occurred prior or during drift in the ocean.

From this map in Harvey et al. (1979), one sees a sampling plan that samples roughly along the coast in along a WestNorthwest (WNW) to EastSoutheast (ESE) and another transect roughly Southwest (SW) to Northeast (NE). Looking only at the sampling plan, one might agree with Harvey et al. that the source must be from Venezuela. Without looking at the currents in the region, you might envision an oil source advecting and diffusing outward from Venezuela reaching into the central Atlantic. However, eastern continental margins have strong Western Boundary Currents, e.g., the Brail Current, the Gulf Stream and the Kuroshio Current. The Caribbean Current flows *along the coast* of Venezuela toward the Yucatan Straits, just as the North and South Atlantic Equatorial currents flow northward along the western continental margin. The seasonal winds are steady *from* the northeast or southeast, so the winds do not have a component to move the oil *to* the northeast of the Venezuelan coast. So where could this oil found offshore have come from?

The history of offshore oil drilling indicates that jackup rigs were being used in 45 m to almost 100 m of water depth in the late 1970s and 1980s. Oil development in Venezuela at the time was in the Gulf of Paria and the Orinoco Delta (Perez et al., 2010). In Brazil, Petrobas first found offshore oil in Serigipe Basin around 1970 and the Campos Basin in 1975 (Offshore Center Denmark, 2009).

Today, discovery of such an unusual layer of oil droplets would be investigated with the consideration in mind of a large unreported well blowout. Modern research might be leveraged to reconstruct the biodegraded oil

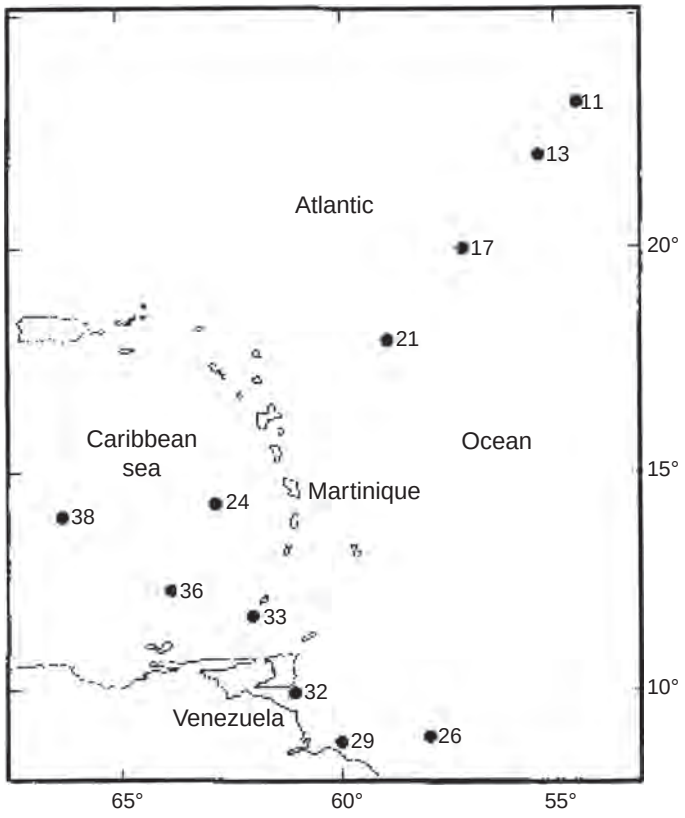

FIGURE 9.3 Sampling stations from the NOAA R/V *Researcher* cruise R-78-1. Oil was found at stations 11 (12.6 mg, 200 m), 13 (5.8 mg, 200 m), 17 (9.6 mg, 270 m), 21 (3.2 mg, 145 m), and 24 (2.8 mg, 150 m and 5.7 mg, 200 m). *From G.R. Harvey, A.G. Requejo, P.A. Mc Gillivary and J.M. Tokar (1979) "Observation of a Subsurface Oil-Rich Layer in the Open Ocean" Volume 205, pp. 999–1000. Reprinted with the permission of the AAAS.*

droplets from biodegradation rates, knowledge of crude oil chemistry and composition variation. Oil spill trajectory modeling (oil from various "start site" locations in Venezuela) could be analyzed for potential oil release locations with the NOAA Trajectory Analysis Planner, Barker (2011, 2000) or Lagrangian Coherent Structure methodology, e.g., Allshouse et al. (2016) and Beegle-Krause et al. (2011b), could be used to constrain the starting position of the release.

The mystery oil was analyzed by Requejo and Boehm (1985), which showed very heavy oil constituents. Modern chemical analysis might point to more detailed source information for the oil in terms of fingerprinting. New biodegradation methodologies are leading to biodegradation rates for individual oil and gas components, e.g., Brakstad et al. (2014, 2015a, 2015b). Potentially, weathered mystery oil droplets or tarballs could be chemically reconstructed to begin identifying a range of possible sources. An oil sample that shows more lighter constituents would be easier to recreate. The layer at 200 m is too shallow to use DO as an indicator of the amount of biodegradation (potentially setting a time for range for the release e.g., Beegle-Krause et al., 2016). Over winter, the seasonal thermocline disappears, so wind mixing homogenizes the water column down to the main thermocline, so this may be a clue to when the release could have happened along with an estimate of the speed of the local currents.

9.7 CASE STUDIES IN SUNKEN OILS

Oil can sink to the bottom due for various reasons: (1) the oil is denser than the local water, (2) the oil weathers to become denser than the local water, or (3) the oil combines with minerals (e.g., sand, mineral particles in the water column) to become denser than the local water. Notable spills of heavy oil with good reference material are the tank barge (T/B) *Morris J. Berman* oil spill in 1992, the ITB DBL-152 oil spill in 2005, and the T/V *Athos I* oil spill in 2004. The towline between the Tug Emily S and the T/B Morris J. Berman broke during the night, leading the barge to drift and ground on a reef, rupturing seven of the nine holding tanks, U.S Dept of the Interior (2017). Anecdotal evidence exists that the heavy oil from the Berman spill repeatedly moved between the surface and subsurface: (1) reached the beached in the evening with the onshore winds, (2) was mixed with beach sand and sank, then, (3) in the heat and calm of the day, the oil warmed enough to separate from the sand and rise to the surface. The sea breeze generated waves during the day were thought to provide the energy for the sediment to separate from the oil as the oil warmed (decreasing viscosity) through the day (Michel and Galt, 1995). Otherwise, rumors that oil can travel along the bottom to resurface later need to be carefully considered, as oil in the ocean does not change to become lighter density—floating oils need to attach to something denser than water in order to sink, (Beegle-Krause et al., 2006). A recent review of detection and recovery of sunken oil by Michel et al. (2016) is a good general reference for understanding these spills.

In the ITB DBL-152 was holed by uncharted debris from Hurricane Rita on November 11, 2005. Three million gallons of slurry oil was spilled and sank to the bottom with few sheens at the surface. A Vessel-Submerged Oil Recovery System, snare sentinels (generally weighted sorbants), and a Remotely Operated Vehicle camera system were used to locate and track the oil. The submerged oil followed the curving bathymetry of the continental shelf in the area of the spill (the author, personal experience) due to the fluid behaving as Taylor Columns, which are "stiff" fluid columns, which was not intuitive to nonoceanographers. Sampling was limited, but the oil would settle into the trough between sand small undulations of approximately 10−20 cm diameter lenths of oil, and move when the currents increased. Though there was concern that the oil could reach the beaches of Texas, oil does not travel "uphill" to shallower water, nor roll up onto beaches, Beegle-Krause et al. (2006).

The T/V *Athos* spill of heavy Brazilian Crude in 2004 was caused by an uncharted obstruction in the Delaware River. The heavy crude oil leads to both surface and sunken oil. The spill occurred on November 26, 2004 and by December 1, 2004 sheens were near the Salem nuclear power plant. Tarballs observed on water intake screens lead the power plant management to choose to do a controlled shutdown. The big question was determining a safe time to restart the nuclear power plant. Both monitoring and modeling were used to determine the safe time for restarting the plant. Modeling the subsurface oil was based on estimated bottom transport speeds later calibrated with observations of varying concentrations of submerged oil (the author, personal experience). The field of highest tarball concentrations was thought to be increasing in size (along-river length) due to the difference in speeds of various sizes of sunken oil transiting along the river bottom. Observations of oil combined with observations and predictions of river flow were key to assisting Decision Makers to determine when conditions were safe to restart the nuclear power plant after 11 days. The period of shutdown cost $33.1 M in claims.

Submerged spills are challenging due to lack of observations. Potentially, AUVs could be fitted with sensors that could detect oil on the seafloor. Hansen et al. (2009) reported on heavy oil sensing equipment tests, recommending requirements included: ease of deployment, off-the-shelf/easily integrated with existing systems, and combining the oil recovery, as submerged oil moves under water and is not easy to detect again. Autonomous systems, yet to be developed, that could continuously monitor or search for oil overnight might be able to solve some of these issues.

An important note on "submerged oil" is that oil does not sink unless either (1) the original density is greater than seawater or (2) the oil is mixed with sediment. As floating oil types weather, the density increases, but usually only after extensive weathering and/or biodegration could the oil sink to the bottom in salt water. Scattered tarball fields floating just below the water surface can be very difficult to see from the air (e.g., NOAA OR&R Open Water Identification Job Air for Aerial Observation, 2016). These tarballs fields can drift hundreds of kilometers while being difficult to detect. In the 1989 EVOS, the tarballs resulting from a storm were brought together in large tidal convergence zones to reform slicks, giving the illusion that "the oil sank to the bottom and then rose up again" as discussed in Galt et al. (1991). Such reports need to be evaluated relative to the observer qualifications and viewing conditions (e.g., sun angle). Trained oil spill observers flying in helicopters very low over the water with the door off *may be able to see* such tarball fields.

An emerging issue is bitumen products that have been modified with a diluent to create a pump-able material: Diluted Bitumen (DilBit). The Kalamazoo River Spill in 2010 is the most notable spill occurrence in the United States (Dollhopf and Durno, 2011). The National Academy of Sciences, Engineering, and Medicine (2016) reviewed DilBit pipeline spills with recommendations for specific modeling tools to be developed. The diluent can be a variety of very light oils, usually soluble light oils that are highly toxic, and may cause an inhalation hazard to responders. The bitumen product then collects along the bottom of the riverbed and travels downstream. Theoretically, the bitumen density, which is intermediate between fresh and open ocean water, could settle on an intermediate density layer. An early statistical modeling study for the Gitxaala First Nation in Canada for potential effects of fuel spills from DilBit tankers included research needs for the DilBit product itself and was presented to the National Energy Board of Canada (Beegle-Krause et al., 2011a).

The Sunken Oil Simulation model (SOSim) is an open source Bayesian predictive model both for inferring the total observed mass of sunken oil, and for predicting where the oil will go, Englehardt et al. (2010) and Echavarria and Englehardt (2015). SOSim has been applied to the ITB DBL-152 slurry oil release. The model uses observed data to infer the spatial distribution of oil mass. The model uses noninformative Bayesian priors for the prediction inferential. This could be used to information and adjust sampling plans in near-realtime. Englehardt (1995) has also developed methods for prediction of the size of large, infrequent incidents, such as oil spills.

9.8 MYSTERY SPILLS AND MYSTERIOUS OILED WILDLIFE

What happens when oil is located on the water, but no one claims to have caused the spill or has contacted the US National Response Center? When simple analysis and modeling does not provide any hint of the source, the case becomes a Mystery Spill. Note that at this point, the oil spill modeler should confirm with those that discovered the oil that the observation is really oil rather than an oil mimic such as natural sheens, cloud shadows, schooling fish or jellyfish clusters (see NOAA Oil Identification Job Aid, 2016 for more information). Mystery spills are a challenge, and can be caused by aging infrastructure, aging sunken vessels, illegal dumping, unnoticed/unreported accidents or pipeline breaks.

WW II vessels of both US and other flags are a known source of oil worldwide, but are often difficult to uniquely identify as the source of an oil spill. Spills from aging wrecks commonly lead to tarball events, where weathered oil is newly observed on a beach. As the oil is highly weathered, oil fingerprinting may only be able to identify a general/potential source of the oil.

Examples of spills from known sunken wrecks are the USS *Mississinewa* in Ulithi Atoll, Micronesia, *see* Gilbert et al. (2003), and the SS *Jacob Luckenbach*; both vessels have undergone subsurface oil removal. The SS *Jacob Luckenbach* is a most interesting case, and is discussed in McGrath et al. (2003). After repeated investigation of local wrecks by divers, the source was identified. Only during the clean-up operations was modeling used (NOAA), but new techniques could have been applied to aid in the search for the source of the oil. Chaos theory has been applied to analyzing trajectory information and could be used to improve our understanding of the evolution on an oil spill and the controlling transport mechanisms, as discussed Beegle-Krause et al. (2011a). Allshouse et al. (2016)

shows how oil spill drift is controlled by these invisible structures in the ocean surface that block transport or identify areas where very subtle changes in the location of a spill can have widely varying trajectories. This work will be of particular interest to forensics.

9.9 SEAWEED AND OIL SPILLS—AN EMERGING TOPIC

Direct seaweed impacts from an oil spill contacting seaweed are not unusual, as reviewed in Moller et al. (1989). Delayed seaweed ecosystem impacts from oil spills are an emerging issue. For example, Felder et al. (2014) discuss the loss of decapods during the DWH oil spill leading to loss of seaweeds. An oil spill could have cascading effects; as the natural organisms are lost due to a spill, seaweed grazers have an opportunity to colonize and graze down the seaweed. Smith and Simpson (1995) discuss the ecosystem changes from the Nella Dan spill at Macquarie Island in the Southern Ocean. If the invasive species taking advantage of the spill is stable in the new habitat, the seaweed may not be able to return. This is an open topic that requires more research.

9.10 WHAT DO YOU DO WITH A DEAD WHALE?

As mentioned earlier, one might expect that trajectory models for drifting oil are only used for oil spills, but there are many other applications. An unusual but important use can be in disposal of large, dead marine mammals, particularly from ship strikes. These carcasses must be removed, as they can be linked to increases in toxins in the food chain leading to mortality in marine birds and other wildlife, as discussed by Stede (1997). Disposal of carcasses in landfills can be done, as reported in Sorensen (2017) but because whale falls (a whale carcass that has sunken down to the seafloor) are important in the food chain, disposal at sea is a better option than on land, Roman et al. (2014); Smith et al. (2015). Altering shipping/vessel traffic can reduce the number of ship strikes. Irvine et al. (2014) discussed tagging data for blue whales (*Balaenoptera musculus*) from 1983 to 2008. Vessel traffic alterations can be successful because data, such as Irvine et al. (2014), shows the high fidelity of blue whales (and likely other whale species) to specific locations.

Whale strikes by large vessels are a concern for marine mammal conservationists. News articles show that cruise ships at times arrive in port with dead whales on their bows. Planning for disposal can be difficult, e.g., due to accumulated gases from the decomposing whale, the dead whale could sit rather high in the water, so the wind drift portion of a predictive drift model can be very high. Whale carcasses after necropsy activities or newly dead do not have large amounts of internally trapped gases, so do not sit so high in the water. For whales to be disposed of offshore, estimating the potential for the winds to bring the whale carcass back to shore or into vessel traffic lanes is key.

9.11 SUMMARY

Forensic work with oil spills varies greatly, from identification of a particular oil and locating positions backwards in time to discovering the source location. Oils vary in composition and density, so oils can be at the surface, along the bottom or in the water column between. The release scenario and dynamics also play a roll, e.g., a leaking vessel in transit, a sunken vessel, a pipeline break or a well blowout. Learning spill modeling in general is a good start to learning forensic modeling, as these teach one how to deconstruct a spill scenario. The transport mechanisms for oil spills are applicable to other drift questions, such as chemical spills, whale strikes, chemical releases, shipping container releases or items released from various containers such as chemicals, Nike shoes or rubber ducks.

9.12 FURTHER READING

The methodologies for oil spill forecasting and forensics have uses with other types of spills. Of note are unusual spills that attract public attention:

- 1990 Nike Shoe Spill—80,000 Nike shoes were lost in the North Pacific in May 1990, with shoes washing up in the Pacific NE from 6 months to a year, analyzed by Ebbesmeyer and Ingraham (1992).

- 1992 Rubber Duck bath toy spill—The story led to the 2011 novel *Moby Duck: The True Story of 28,800 Bath Toys Lost at Sea and of the Beachcombers, Oceanographers, Environmentalists, and Fools, Including the Author, Who Went in Search of Them* by Donovan Hohn. Note that beaver, turtle and frog toys were also lost.
- 2011 Fukushima Nuclear Disaster—The spread of radioactive chemicals was a concern, see Buesseler et al. (2011). This spill will be a new, unintentional chemical tracer release that could be used to date how old a specific water mass is, if found to that contain this radioactive Cesium in the years to come.
- 2011 Tohoku Tsunami Debris Field—The spread of debris across the North Pacific, see (Lebreton and Borrero 2013) and NOAA GNOME model (https://marinedebris.noaa.gov/sites/default/files/JTMD_Visualization_October.pdf).
- 2001 Ehimi Maru victim recovery and oil removal—A tragic accident when a Japanese fishing vessel was accidentally struck by a US submarine practicing emergency procedures, leading to complex and challenging victim and recovery and oil removal operations (Navy, 2006).

Acknowledgments

The author would like to thank her mentors at the NOAA Office of Response and Restoration. Mr. Glen Y. "Bushy" Watabayashi always shared his knowledge and great breadth of experience. Discussions and opportunities with Dr. Bill Lehr and Dr Jerry Galt were great sources of experience and perspective.

References

Allshouse, M.R., Ivey, G.N., Xu, J., Beegle-Krause, C.J., Lowe, R.J., Jones, N.L., et al., 2016. The impact of wind on the Lagrangian structure of ocean surface transport. Environ. Fluid Dyn. 17, 473–483.

Anderson, E., Adalo, A., Spaulding, M.L., 1998. Modeling Leeway Drift. United States Coast Guard, Washington, DC, p. 57.

Barker, C.H., 2000. The NOAA Trajectory Analysis Planner: TAP II.

Barker, C.H., 2011. A statistical outlook for the deepwater horizon oil spill. In: Monitoring and Modeling the Deepwater Horizon Oil Spill: A Record-Breaking Enterprise. American Geophysical Union.

Bayona, J.M., Domínguez, C., Albaigés, J., 2015. Analytical developments for oil spill fingerprinting. Trends Environ. Anal. Chem. 5, 26–34.

Beegle-Krause, C.J., 2001. General NOAA Oil Modeling Environment (GNOME): a new spill trajectory model. In: 2001 International Oil Spill Conference, pp. 865–871.

Beegle-Krause, C.J., 2015. Oceanographic and meteorological effects on spilled oil. In: Fingas, M.F. (Ed.), Handbook of Oil Spill Science and Technology. Wiley & Sons, Inc., Hoboken, NJ.

Beegle-Krause, C.J., Barker, C.H., Watabayashi, G.Y., 2006. Long-term transport of oil from the T/B DBL-152: lessons learned for oil heavier than seawater. In: Arctic and Marine Ocean Pollution (AMOP) Conference. Environment Canada.

Beegle-Krause, C.J., Emmet, B., Hammond, M., Short, J., Spies, R., 2011a. In: Beckman, L. (Ed.), Expert Opinion on Petroleum Tanker Accidents and Malfunctions in Browning Entrance and Principe Channel: Potential Marine Effects on Gitxaala Traditional Lands and Waters of a Spill During Tanker Transportation of Bitumen from the Northern Gateway Pipeline Project (NGP). JKF Law Corporation, Vancouver, British Columbia, Canada.

Beegle-Krause, C.J., Peacock, T., Allshouse, M.R., 2011b. Exploiting Lagrangian coherent structures (LCS) for the calculations of oil spill and search and rescue drift patters in the ocean. In: Arctic and Marine Oil Spill Conference (AMOP). Environment Canada, Banff, AB.

Beegle-Krause, C.J., Daae, R.L., Skancke, J., Brakstad, O.G., Stefanakos, C., 2016. Deepwater wells and the subsurface dissolved oxygen minimum: a tale of two sides of the Atlantic Ocean. In: Arctic and Marine Oil Pollution Conference. Environment Canada, Halifax, NS, Canada.

Brakstad, O.G., Daling, P., Faksness, L.-G., Almas, I.K., Vang, S.-H., Syslak, L., et al., 2014. Depletion and biodegradation of hydrocarbons in dispersions and emulsions of the Macondo 252 oil generated in an oil-on-seawater mesocosm flume basin. Mar. Pollut. Bull. 84, 125–134.

Brakstad, O.G., Nordtug, T., Throne-Holst, M., 2015a. Biodegradation of dispersed Macondo oil in seawater at low temperature and different oil droplet sizes. Mar. Pollut. Bull. 93, 144–152.

Brakstad, O.G., Throne-Holst, M., Netzer, R., Stoeckel, D.M., Atlas, R.M., 2015b. Microbial communities related to biodegradation of dispersed Macondo oil at low seawater temperature with Norwegian coastal seawater. Microb. Biotechnol. 8, 989–998.

Breivik, Ø., Allen, A.A., Maisondieu, C., Roth, J.C., 2011. Wind-induced drift of objects at sea: the leeway field method. Appl. Ocean Res. 33, 100–109.

Breivik, Ø., Allen, A.A., Maisondieu, C., Olagnon, M., 2013. Advances in search and rescue at sea. Ocean Dyn. 63, 83–88.

Buesseler, K., Aoyama, M., Fukasawa, M., 2011. Impacts of the Fukushima nuclear power plants on marine radioactivity. Environ. Sci. Technol. 45, 9931–9935.

Corilo, Y.E., Podgorski, D.C., McKenna, A.M., Lemkau, K.L., Reddy, C.M., Marshall, A.G., et al., 2013. Oil spill source identification by principle component analysis of electrospray ionization Fourier transform ion cyclotron resonance mass spectroscopy. Anal. Chem. 85, 9064–9069.

DeHaan, C.J., Sturges, W., 2005. Deep cyclonic circulation in the Gulf of Mexico. J. Phys. Oceanogr. 35, 1801–1812.

Denmark, Offshore Center, 2009. Overview of the Brazil Oil and Gas Industry. Offshore Center Denmark, p. 53.

Dollhopf, R., Durno, M., 2011. Kalamazoo river/Enbridge pipeline spill 2010. In: International Oil Spill Conference, 2011-422. International Oil Spill Conference.

Ebbesmeyer, C.C., Ingraham, W.J., 1992. Shoe spill in the North Pacific. In: EOS: Earth & Space Science News. Washington, DC.

Echavarria, G., Englehardt, J., 2015. A predictive Bayesian data-derived Gaussian model of sunken oil mass (SOSim). Environ. Modell. Softw. 69, 1–13.
Englehardt, J., 1995. Predicting incident size from limited information. J. Environ. Eng. 121, 455–464.
Englehardt, J., Echavarria, G., Avellaneda, P., 2010. Development of a Predictive Bayesian Data-Derived Multimodal Gaussian Model of Sunken Oil Mass Location and Transport.
Felder, D.L., Thoma, B.P., Schmidt, W.E., Sauvage, T., Self-Krayesky, S.L., Chistoserdov, A., et al., 2014. Seaweeds and decapod crustaceans on Gulf Deep Banks after Macondo oil spill. Bioscience. 69, 808–819.
Fingas, M.F., 2015. Introduction to spill modeling. In: Fingas, M.F. (Ed.), Handbook of Oil Spill Science and Technology. Wiley & Sons, Inc, Hoboken, NJ.
Galt, J.A., Lehr, W.J., Payton, D.L., 1991. Fate and transport of the Exxon Valdez oil spill. Part 4. Environ. Sci. Technol. 25, 202–209.
Gilbert, T., Nawadra, S., Tafileichig, A., Yinug, L., 2003. Response to an oil spill from a sunken WWII oil tanker in Yap state, Micronesia. In: International Oil Spill Conference Proceedings, 2003, pp. 175–182.
Hansen, K.A., Fitzpatrick, M., Herring, P.R., VanHaverbeke, M., 2009. Heavy Oil Detection (Prototypes). U.S. Coast Guard R&D Center, Washington, DC, p. 74.
Harvey, G.R., Requejo, A.G., McGilliavary, P.A., Tokar, J.M., 1979. Observation of a subsurface oil-rich layer in the open ocean. Science 205, 999–1000.
Interior, U.S. Department of the, 2017. Barge Morris J. Berman Fuel Oil Spill. U.S. Department of the Interior (accessed 18.03.17).
Irvine, L.M., Mate, B.R., Winsor, M.H., Palacios, C.M., Bograd, S.J., Coasta, D.P., et al., 2014. Spatial and temporal occurrence of blue whales off the U.S. West Coast, with implications for management. PLoS One 9 (7), e102959.
Joint Analysis Group, Deepwater Horizon Oil Spill, 2012. Review of subsurface dispersed oil and oxygen levels associated with the deepwater horizon MC 252 spill of national significance. In: NOAA Technical Report NOS OR&R, 113. not published: NOAA.
Lebreton, L.C.M., Borrero, J.C., 2013. Modeling the transport and accumulation floating debris generated by the 11 March 2011 Tohoku tsunami. Mar. Pollut. Bull. 66, 53–58.
Ledwell, J.R., Watson, A.J., Law, C.S., 1993. Evidence for slow mixing across the pycnocline from an open-ocean tracer-release experiment. Nature 364, 701–703.
Ledwell, J.R., Watson, A.J., Law, C.S., 1998. Mixing of a tracer in the pycnocline. J. Geophys. Res. Oceans 103, 21499–21529.
Ledwell, J.R., He, R.R., Xue, Z., DiMarco, S.F., Spencer, L.J., Chapman, P., 2016. Dispersion of a tracer in the deep Gulf of Mexico. J. Geophys. Res. Oceans 1212, 1110–1132.
McGrath, G.G., Parker-Hall, H.A., Tarpley, J.A., Nack, A., 2003. The investigation to identify the SS Jacob Luckenbach—using technology to locate a hidden source of oil that caused years of impacts and the future implications of sunken shipwrecks. In: International Oil Spill Conference Proceedings, 2003, pp. 1219–1224.
Michel, J., Galt, J.A., 1995. Conditions under which floating slicks can sink in marine settings. International Oil Spill Conference. IOSC, Long Beach, CA, USA, pp. 573–576.
Michel, J., Ploen, M., Elliot, J., Key, W., 2016. Sunken oil detection and recovery. API Technical Report, 116. American Petroleum Institute, Washington, DC.
Moller, T.H., Dicks, B., Goodman, C.N., 1989. Fisheries and mariculture affected by oil spills. International Oil Spill Conference. American Petroleum Institute, pp. 389–394.
National Academy of Sciences, Engineering, and Medicine, 2016. Spills of Diluted Bitumen from Pipelines. That National Academies Press, Washington, DC.
Navy, U.S., 2006. U.S. Navy Salvage Report F/V Ehime Maru. U.S. Navy Salvage, p. 416.
NOAA, 1980. Proceedings of the symposium on preliminary results from the September 1979 Researcher/Pierce IXTOC-I Cruise. In: Preliminary Results From the September 1979 Researcher/Pierce IXTOC-I Cruise, 604. NOAA, Key Biscayne, FL.
Perez, P., Fernandez, E., Beiras, R., 2010. Fuel toxicity on *Isochrysis galbana* and a coastal phytoplankton assemblage: growth rate vs. variable fluorescence. Ecotoxicol. Environ. Saf. 73, 254–261.
Reed, M., Ekrol, N., Rye, H., Turner, L., 1999a. Oil spill contingency and response (OSCAR) analysis in support of environmental impact assessment offshore Namibia. Spill Sci. Technol. Bull. 5, 29–98.
Reed, M., Johansen, Ø., Brandvik, P.J., Daling, P., Lewis, A., Fiocco, R., et al., 1999b. Oil spill modeling towards the close of the 20th century: overview of the state of the art. Spill Sci. Technol. Bull. 5, 3–16.
Requejo, A.G., Boehm, P.D., 1985. Characterization of hydrocarbons in the subsurface oil-rich layer in the Sargasso sea. Mar. Environ. Res. 17, 45–64.
Roman, J., Estes, J.A., Morissette, L., Smith, C., Costa, D., McCarthy, J., et al., 2014. Whales as marine ecosystem engineers. Front. Ecol. Environ. 12, 377–385.
Rye, H., Reed, M., Frost, T.K., Smit, M.G.D., Durgut, I., Johansen, Ø., et al., 2008. Development of a numerical model for calculating exposure to toxic and nontoxic stressors in the water column and sediment from drilling discharges. Integr. Environ. Assess. Manage. 4, 194–203.
Smith, C.R., Glover, A.G., Treude, T., Higgs, N.D., Amon, D.J., 2015. Whale-fall ecosystems: recent insights into ecology, paleoecology, and evolution. Annu. Rev. Mar. Sci. 7, 571–596.
Smith, S.D.A., Simpson, R.D., 1995. Effects of the 'Nella Dan' oil spill on the fauna of *Durvillaea antarctica* holdfasts. Mar. Ecol. Prog. Ser. 121, 73–89.
Socolofsky, S.A., Adams, E.E., Sherwood, C.R., 2011. Formation dynamics of subsurface hydrocarbon intrusions following the Deepwater Horizon blowout. Geophys. Res. Lett. 38 (9), L09602.
Socolofsky, S.A., Adams, E.E., Boufadel, M.C., Aman, Z.M., Johansen, Ø., Konkel, W.U., et al., 2015. Case study: inter-comparison of oil spill prediction models for accidental blowout scenarios with and without subsea chemical dispersant injection. Mar. Pollut. Bull. 96, 110–126.
Sorensen, P., 2017. Disposal of a beached whale: an account. Int. J. Environ. Stud. 74, 177–181.
Spaulding, M.L., 2017. State of the art review and future directions in oil spill modeling. Mar. Pollut. Bull. 115, 7–19.
Stede, M., 1997. Problems of disposal of dead marine mammals. Dtsch. Tierarztl. Wochenschr. 104, 245–247.

Stout, S., Wang, Z., 2016. Standard Handbook Oil Spill Environmental Forensics: Fingerprinting and Source Identification. Academic Press, Burlington, MA.

Sturges, W., 2005. Deep-water exchange between the Atlantic, Caribbean, and Gulf of Mexico. In: Circulation in the Gulf of Mexico: Observations and Models.

U.S. Department of Commerce, National Oceanic and Atmospheric Administration, National Ocean Service, Office of Response and Restoration. 2016. Open Water Oil Identification Job Aid for Aerial Observation, Version 3. 54. Washington, DC.

Vonk, S.M., Hollander, D.J., Murk, A.J., 2015. Was the extreme and wide-spread marine oil-snow sedimentation and flocculent accumulation (MOSSFA) event during the Deepwater Horizon blow-out unique?. Mar. Pollut. Bull. 100, 5–12.

Wang, Z., Stout, S., 2010. Oil spill environmental forensics: fingerprinting and source identification. Academic Press, Burlington, MA.

Youssef, J., Spaulding, M.L., 1994. Drift current under the combined action of wind and waves in shallow water. Arctic and Marine Oilspill Program Technical Seminar. Ministry of Supply and Services, Canada.

CHAPTER

10

Unraveling the Complexities of Upland Spilled Fuels: Selected Case Studies

Kerylynn Krahforst and Edward (Ted) Healey

NewFields Environmental Forensics Practice, LLC, Rockland, MA, United States

BIOGRAPHIES

Kerylynn Krahforst holds a BA in chemistry from the University of Rhode Island and is a staff scientist at NewFields Environmental Forensics Practice, LLC in Rockland, Massachusetts. She has over 25 years of experience specializing in analytical and forensic chemistry. Her main focus is characterizing the source and extent of environmental contamination (i.e., petroleum products, manufactured gas plant residues and tar-derived wastes). She has managed a variety of environmental investigations involving both marine and terrestrial environments and has direct experience in the area of petroleum characterization and identification.

Edward (Ted) Healey is a scientist and project manager with NewFields Environmental Forensics Practice, LLC in Rockland, Massachusetts. Mr. Healey has a B.S. in Environmental Management from University of Rhode Island. Mr. Healey has over 20 years' experience in the field of environmental chemistry. Mr. Healey has coauthored and contributed to numerous publications/presentations in scientific journals and books. Much of the focus of his work is the molecular-level characterization of petroleum and petroleum products and investigations of the chemical alteration of petroleum/tar due to physical and biological weathering. He is fully trained in standard US Environmental Protection Agency (EPA) and ASTM chemical analytical methodologies. Mr. Healey has managed the planning and technical work of hundreds of projects involving the study of fate and transport of organic contaminants in aquatic and terrestrial environments.

10.1 INTRODUCTION

Petroleum and refined petroleum products represent the single largest source of chemical contamination of marine, terrestrial, and groundwater environments. To address this problem, many federal and state regulatory agencies have imposed requirements for the reporting and investigation of petroleum and hazardous releases into the environment. These regulations include the Clean Water Act, 1972, the Resource Conservation and Recovery Act, 1976, the Toxic Substance Control Act, 1976, Comprehensive Environmental Response and Compensation, and Liability Act, 1980, and the Natural Resource Damage Assessment, 1986.

One of the primary regulatory requirements for responsible parties following a petroleum release is an assessment of the nature and extent of contamination at the impacted site. During a site assessment, responsible parties typically employ standard chemical analysis such as US EPA's SW-846 methods (e.g., EPA Methods 8260D, 8015D, 8270C, etc.) in support of site investigation (EPA, 2015). While such data is adequate for basic site characterization, it is inherently limited in terms of chemical specificity. Standard methods of chemical analysis such as the SW-846 methods provide virtually no meaningful data about detailed composition of petroleum. Such detailed chemical composition data—essential to an investigator who wishes to develop a sophisticated chemical fingerprint of spilled petroleum and impacted media, and differentiate and allocate between impacts from a spill

Oil Spill Environmental Forensics Case Studies.
DOI: http://dx.doi.org/10.1016/B978-0-12-804434-6.00010-0

event versus preexisting impacts from historic or nonsite-related impacts—can only be derived using forensic methods of chemical analysis.

The chemical compounds reported using standard methods of chemical analysis are only a small subset of a much larger group of hydrocarbon compounds that actually comprise petroleum. For example, standard EPA Method 8260 *Volatile Organic Compounds by Gas Chromatography/Mass Spectrometry (GC/MS)*—used routinely in contaminated site investigations to measure volatile range chemicals—measures only 6 common gasoline-derived hydrocarbons. In contrast, the forensic adaptation of EPA Method 8260 measures nearly 100 important volatile paraffins, isoparaffins, aromatics, naphthenes, olefins, and gasoline additive compounds that are essential for fingerprinting of automotive gasoline and light distillate petroleum products. Analysis of media impacted by higher boiling petroleum that rely only upon the 16 US EPA Priority Pollutant PAHs that are reported by standard EPA Method 8270 *Semi-volatile Organic Compounds by Gas Chromatography/Mass Spectrometry (GC/MS)* provide data that is information limited, as these few compounds lack the specificity to distinguish among different polycyclic aromatic hydrocarbon (PAH) sources in the environment (Stout et al., 2015). On the other hand, the forensic adaptation of EPA Method 8270 reports over 50 parent and C_1−C_4 alkylated homologues of PAH, and over 50 petroleum biomarker compounds that, collectively, provide a detailed chemical depiction of the petroleum found in impacted media.

Chemical fingerprinting is defined as "the generation and comparison of diagnostic chemical features among oil samples (i.e., both spill and source oils) and potentially impacted samples (e.g., shorelines, sediments, or biological tissues), can play an important role in assessing this liability and monitoring ecological effects" (Stout et al., 2016). The ability to conduct a chemical fingerprinting investigation depends on the use of analytical methods especially designed for the detailed analysis of petroleum. Such methods measure classes of petroleum hydrocarbons related to spilled fuels in the environment and include volatile organic hydrocarbons, *n*-alkanes, acyclic isoprenoids, PAHs, alkylated PAHs and sulfur containing PAHs, and sterane and triterpane petroleum biomarkers (Douglas and Uhler, 1993; Sauer and Boehm, 1995; Wang and Page, 1999, Wang et al., 2000; Wang and Fingas, 2003, Stout, 2003; Stout et al., 2006; Douglas et al., 2007, 2016). A summary of these methods is provided below. The benefits of the forensic-quality data developed using these methods of chemical analysis for investigations at petroleum impacted, upland sites are illustrated in the four diverse case studies presented in this chapter.

10.2 CHEMICAL FINGERPRINTING METHODOLOGIES

The chemical fingerprinting methods relied upon by contemporary forensic chemists collectively provide both general (e.g., boiling ranges) and detailed (e.g., diagnostic compounds) information on the composition of petroleum. Most forensic methods of chemical analysis are straightforward adaptations of standard methods that have been optimized for measurements of hydrocarbons in petroleum impacted media. The most common methods used in the forensic analysis of petroleum—referenced in the case studies that follow—include:

Whole Oil Fingerprinting: A "whole oil" GC technique that uses tandem high resolution GC−flame ionization detection (FID) and high resolution GC−MS following adaptations of Modified EPA Method 8015 and Modified EPA Method 8270, respectively. This analysis is conducted on nonaqueous phase liquid samples (NAPLs). These analyses provide detailed information about the occurrence and distribution of hydrocarbons over the C_4 to C_{44+} carbon range. The resulting GC profile depicts the type or types of petroleum products that compose NAPL.

Total Petroleum Hydrocarbons (TPH) and Selected Alkane Quantification and Fingerprinting: A modified EPA method 8015B high resolution GC/FID method that determines concentrations of TPH (C_8−C_{44}), as well as of selected normal and branched-chain alkanes, such as *n*-C_{17}, *n*-C_{18}, pristane, and phytane. The slightly higher carbon range for this analysis (compared to the whole oil fingerprinting) owes to the fact it is appropriate for analysis of the solvent extracts of soil, sediment, water or other matrices, which must be concentrated prior to instrument analysis. This analysis provides a synoptic depiction of the hydrocarbon makeup of samples, provides data to characterize the type(s) of petroleum that compose a sample, and provides certain diagnostic information about the product formulation and relative weathering state. The target analytes are listed in Table 10.1.

PAH and Petroleum Biomarker Quantification and Fingerprinting: A modified EPA Method 8270C high resolution GC/MS (GC/MS-SIM) method that determines the concentrations of semivolatile compounds or compound groups, including decalins, parent and alkylated PAH, sulfur-containing aromatics, and petroleum biomarker compounds (triaromatic steroids, steranes, and triterpanes). These compounds can provide specific information regarding the origin/source of PAHs and type(s) of hydrocarbons found in NAPLs or impacted samples. The occurrence, distribution, and relative ratios of key PAH and biomarker compounds can be used to distinguish among crude oil sources of middle boiling (i.e., kerosene, diesel fuel, etc.) and higher boiling petroleum products [i.e., lubricating oil, heavy fuel oil (HFO), etc]. Tables 10.2 and 10.3 list the PAH and biomarker target analytes, respectively.

TABLE 10.1 *n*-Alkane and Branched Chain Alkane Target Compounds

Abbr.	Compound
C9	*n*-Nonane (C9)
C10	*n*-Decane (C10)
C11	*n*-Undecane (C11)
C12	*n*-Dodecane (C12)
C13	*n*-Tridecane (C13)
1380	2,6,10 Trimethyldodecane (1380)
C14	*n*-Tetradecane (C14)
1470	2,6,10 Trimethyltridecane (1470)
C15	*n*-Pentadecane (C15)
C16	*n*-Hexadecane (C16)
NP	Norpristane (1650)
C17	*n*-Heptadecane (C17)
Pr	Pristane
C18	*n*-Octadecane (C18)
Ph	Phytane
C19	*n*-Nonadecane (C19)
C20	*n*-Eicosane (C20)
C21	*n*-Heneicosane (C21)
C22	*n*-Docosane (C22)
C23	*n*-Tricosane (C23)
C24	*n*-Tetracosane (C24)
C25	*n*-Pentacosane (C25)
C26	*n*-Hexacosane (C26)
C27	*n*-Heptacosane (C27)
C28	*n*-Octacosane (C28)
C29	*n*-Nonacosane (C29)
C30	*n*-Triacontane (C30)
C31	*n*-Hentriacontane (C31)
C32	*n*-Dotriacontane (C32)
C33	*n*-Tritriacontane (C33)
C34	*n*-Tetratriacontane (C34)
C35	*n*-Pentatriacontane (C35)
C36	*n*-Hexatriacontane (C36)
C37	*n*-Heptatriacontane (C37)
C38	*n*-Octatriacontane (C38)
C39	*n*-Nonatriacontane (C39)
C40	*n*-Tetracontane (C40)
TPH	Total petroleum hydrocarbons (C9–C44)

TABLE 10.2 PAH and Alkyl-PAH Target Compounds

Abbr.	Compound	Abbr.	Compound
D0	*cis*/*trans*-Decalin	FL0	Fluoranthene
D1	C1-Decalins	PY0	Pyrene
D2	C2-Decalins	FP1	C1-Fluoranthenes/Pyrenes
D3	C3-Decalins	FP2	C2-Fluoranthenes/Pyrenes
D4	C4-Decalins	FP3	C3-Fluoranthenes/Pyrenes
BT0	Benzothiophene	FP4	C4-Fluoranthenes/Pyrenes
BT1	C1-Benzo(*b*)thiophenes	NBT0	Naphthobenzothiophenes
BT2	C2-Benzo(*b*)thiophenes	NBT1	C1-Naphthobenzothiophenes
BT3	C3-Benzo(*b*)thiophenes	NBT2	C2-Naphthobenzothiophenes
BT4	C4-Benzo(*b*)thiophenes	NBT3	C3-Naphthobenzothiophenes
N0	Naphthalene	NBT4	C4-Naphthobenzothiophenes
N1	C1-Naphthalenes	BA0	Benz[*a*]anthracene
N2	C2-Naphthalenes	C0	Chrysene/Triphenylene
N3	C3-Naphthalenes	BC1	C1-Chrysenes
N4	C4-Naphthalenes	BC2	C2-Chrysenes
B	Biphenyl	BC3	C3-Chrysenes
DF	Dibenzofuran	BC4	C4-Chrysenes
AY	Acenaphthylene	BBF	Benzo[*b*]fluoranthene
AE	Acenaphthene	BJKF	Benzo[*k*]fluoranthene
F0	Fluorene	BAF	Benzo[*a*]fluoranthene
F1	C1-Fluorenes	BEP	Benzo[*e*]pyrene
F2	C2-Fluorenes	BAP	Benzo[*a*]pyrene
F3	C3-Fluorenes	PER	Perylene
A0	Anthracene	IND	Indeno[1,2,3-cd]pyrene
P0	Phenanthrene	DA	Dibenz[*a*,*h*]anthracene
PA1	C1-Phenanthrenes/Anthracenes	GHI	Benzo[*g*,*h*,*i*]perylene
PA2	C2-Phenanthrenes/Anthracenes		
PA3	C3-Phenanthrenes/Anthracenes		
PA4	C4-Phenanthrenes/Anthracenes		
RET	Retene		
DBT0	Dibenzothiophene		
DBT1	C1-Dibenzothiophenes		
DBT2	C2-Dibenzothiophenes		
DBT3	C3-Dibenzothiophenes		
DBT4	C4-Dibenzothiophenes		
BF	Benzo(*b*)fluorene		

PIANO Quantification and Fingerprinting: A modified EPA Method 8260B purge-and-trap GC/MS method that measures 88 (C_5–C_{12}) volatile hydrocarbons from five major hydrocarbon classes: paraffins (p), isoparaffins (I), aromatics (A), naphthenes (N), and olefins (O). In addition, various oxygenated compounds commonly found in oxygenated and reformulated gasolines are targeted, including *tert*-butyl alcohol (TBA), methyl-*tert*-butyl ether

TABLE 10.3 Triterpane and Sterane Biomarker Target Compounds

Abbr.	Compound	Abbr.	Compound
T5	C24 Tricyclic terpane	S5	13β(*H*),17α(*H*)-20R-Diacholestane
T6	C25 Tricyclic terpane	S8	13β(*H*),17α(*H*)-20S-Methyldiacholestane
T6a	C24 Tetracyclic terpane	S12	14α(*H*),17α(*H*)-20S-Cholestane
T6b	C26 Tricyclic terpane-22S	S17	14α(*H*),17α(*H*)-20R-Cholestane
T6c	C26 Tricyclic terpane-22R	S18	13β(*H*),17α(*H*)-20R-Ethyldiacholestane
T7	C28 Tricyclic terpane-22S	S19	13α(*H*),17β(*H*)-20S-Ethyldiacholestane
T8	C28 Tricyclic terpane-22R	S20	14α(*H*),17α(*H*)-20S-Methylcholestane
T9	C29 Tricyclic terpane-22S	S24	14α(*H*),17α(*H*)-20R-Methylcholestane
T10	C29 Tricyclic terpane-22R	S25	14α(*H*),17α(*H*)-20S-Ethylcholestane
T11	18α-22,29,30-Trisnorneohopane-Ts	S28	14α(*H*),17α(*H*)-20R-Ethylcholestane
T11a	C30 Tricyclic terpane-22S	S14	14β(*H*),17β(*H*)-20R-Cholestane
T11b	C30 Tricyclic terpane-22R	S15	14β(*H*),17β(*H*)-20S-Cholestane
T12	17α(*H*)-22,29,30-Trisnorhopane-Tm	S22	14β(*H*),17β(*H*)-20R-Methylcholestane
T14a	17α/β,21β/α 28,30-Bisnorhopanes	S23	14β(*H*),17β(*H*)-20S-Methylcholestane
T14b	17α(*H*),21β(*H*)-25-Norhopane	S26	14β(*H*),17β(*H*)-20R-Ethylcholestane
T15	30-Norhopane	S27	14β(*H*),17β(*H*)-20S-Ethylcholestane
T16	18α(*H*)-30-Norneohopane-C29Ts	RC26/SC27TA	C26,20R- + C27,20S-Triaromatic steroids
X	17α(*H*)-Diahopane	SC28TA	C28,20S-Triaromatic steroid
T17	30-Normoretane	RC27TA	C27,20R-Triaromatic steroid
T18	18α(*H*)&18β(*H*)-Oleananes	RC28TA	C28,20R-Triaromatic steroid
T19	Hopane		
T20	Moretane		
T21	30-Homohopane-22S		
T22	30-Homohopane-22S		
T26	30,31-Bishomohopane-22S		
T27	30,31-Bishomohopane-22R		
T30	30,31-Trishomohopane-22S		
T31	30,31-Trishomohopane-22R		
T32	Tetrakishomohopane-22S		
T33	Tetrakishomohopane-22R		
T34	Pentakishomohopane-22S		
T35	Pentakishomohopane-22R		

(MTBE), di-isopropyl ether (DIPE), ethyl-*tert*-butyl ether (ETBE), and *tert*-amyl-methyl ether (TAME). Lead scavengers historically used in leaded gasoline (1,2-dichloroethane and 1,2-dibromoethane) and various volatile sulfur species are also analyzed. This analysis provides data that can be used to ascertain the makeup and weathering state of gasoline, solvents or other light distillates that may be present in a NAPL or impacted sample. This analysis also produces a chromatographic "fingerprint" useful for the qualitative identification of gasoline or other solvents or low boing distillates that compose samples. The target analytes are listed in Table 10.4.

Organic Lead Quantification and Speciation. A modified EPA Method 8270C GC/MS technique that measures the concentrations of five organic lead compounds—tetraethyl lead (TEL), trimethylethyl lead (TMEL),

TABLE 10.4 Volatile Hydrocarbon Target Compounds (PIANO)

Abbr.	Compound	Abbr.	Compound
IP	Isopentane	C8	Octane
1P	1-Pentene	12DBE	1,2-Dibromoethane
2M1B	2-Methyl-1-butene	EB	Ethylbenzene
C5	Pentane	2ETHIO	2-Ethylthiophene
T2P	2-Pentene (*trans*)	MPX	*p*/*m*-Xylene
C2P	2-Pentene (*cis*)	1N	1-Nonene
TBA	Tertiary butanol	C9	Nonane
CYP	Cyclopentane	STY	Styrene
23DMB	2,3-Dimethylbutane	OX	*o*-Xylene
2MP	2-Methylpentane	IPB	Isopropylbenzene
MTBE	Methyl-*tert*-butyl ether	PROPB	*n*-Propylbenzene
3MP	3-Methylpentane	1M3EB	1-Methyl-3-ethylbenzene
1HEX	1-Hexene	1M4EB	1-Methyl-4-ethylbenzene
C6	Hexane	135TMB	1,3,5-Trimethylbenzene
DIPE	Di-isopropyl ether	1D	1-Decene
ETBE	Ethyl-*tert*-butyl ether	1M2EB	1-Methyl-2-ethylbenzene
22DMP	2,2-Dimethylpentane	C10	Decane
MCYP	Methylcyclopentane	124TMB	1,2,4-Trimethylbenzene
24DMP	2,4-Dimethylpentane	SECBUT	sec-Butylbenzene
12DCA	1,2-Dichloroethane	1M3IPB	1-Methyl-3-isopropylbenzene
CH	Cyclohexane	1M4IPB	1-Methyl-4-isopropylbenzene
2MH	2-Methylhexane	1M2IPB	1-Methyl-2-isopropylbenzene
B	Benzene	IN	Indane
23DMP	2,3-Dimethylpentane	1M3PB	1-Methyl-3-propylbenzene
THIO	Thiophene	1M4PB	1-Methyl-4-propylbenzene
3MH	3-Methylhexane	BUTB	*n*-Butylbenzene
TAME	*Tert*-Amyl-methyl ether	12DM4EB	1,2-Dimethyl-4-ethylbenzene
1H	1-Heptene/1,2-DMCP (*trans*)	12DEB	1,2-Diethylbenzene
ISO	Isooctane	1M2PB	1-Methyl-2-propylbenzene
C7	Heptane	14DM2EB	1,4-Dimethyl-2-ethylbenzene
MCYH	Methylcyclohexane	C11	Undecane
25DMH	2,5-Dimethylhexane	13DM4EB	1,3-Dimethyl-4-ethylbenzene
24DMH	2,4-Dimethylhexane	13DM5EB	1,3-Dimethyl-5-ethylbenzene
223TMP	2,2,3-Trimethylpentane	13DM2EB	1,3-Dimethyl-2-ethylbenzene
234TMP	2,3,4-Trimethylpentane	12DM3EB	1,2-Dimethyl-3-ethylbenzene
233TMP	2,3,3-Trimethylpentane	1245TMP	1,2,4,5-Tetramethylbenzene
23DMH	2,3-Dimethylhexane	PENTB	Pentylbenzene
3EH	3-Ethylhexane	C12	Dodecane

(*Continued*)

TABLE 10.4 (*Continued*)

Abbr.	Compound	Abbr.	Compound
2MHEP	2-Methylheptane	N0	Naphthalene
3MHEP	3-Methylheptane	BT0	Benzothiophene
T	Toluene	MMT	MMT
2MTHIO	2-Methylthiophene	C13	Tridecane
3MTHIO	3-Methylthiophene	2MN	2-Methylnaphthalene
1O	1-Octene	1MN	1-Methylnaphthalene

dimethyldiethyl lead (DEDML), triethylmethyl lead (TEML), and tetramethyl lead (TML)—historically used in the formulation of leaded gasoline additive packages. The type(s) and concentrations of organic lead compounds found in (or absent from) gasoline-bearing or -derived NAPL can provide insight into the production period of gasoline that contains organic lead.

Sulfur: various ASTM or other international standards can be used to measure the total sulfur content of NAPL. With federally mandated reduction of sulfur in fuels, the sulfur analysis can be useful in gaining insight into the possible vintage of the fugitive NAPL.

10.3 SELECTED CASE STUDIES

10.3.1 Case Study 1: Allocation and Spatial Extent of the Spilled Gasoline Attributed to Two Retail Gasoline Stations

Retail gasoline stations are ubiquitous and one of the most frequent subjects of environmental forensic investigations. There are more than 150,000 active retail gasoline stations in the United States alone (NACS, 2015). Gasoline contamination arising from leaking underground storage tanks (USTs) has historically, and continues to occur frequently at retail stations. Leaking USTs were particularly problematic at older (pre-1980s) sites where the use of corrosion-susceptible steel-built UST was common (EPA, 2017). Many retail gasoline stations have a history of multiple owners, often leading to the need to determine the party(s) responsible for response and cleanup costs when contamination is discovered. Finally, retail gasoline stations are often found sited in close proximity to one another, e.g., multiple retail stations at busy intersections. When contamination is discovered at a multiretail site setting, environmental forensic investigations are often called upon to unravel the source or sources of the contamination.

This case study describes an environmental forensic investigation focused on identifying the source or sources of gasoline-derived NAPLs found in the vicinity of two neighboring retail gasoline stations in Australia (Fig. 10.1). One site was a decommissioned service station (Station A), the other nearby site is an active service station (Station B). NAPL was discovered on both properties, and in the street that separated the two stations. Historical site operation information suggested that both stations had experienced releases of product at various times during their operations. The forensic issue at hand was to (1) determine the nature of the fugitive NAPL on each site and in the street, (2) differentiate the petroleum products arising from both sites, and (3) if necessary, estimate contribution of petroleum from the two stations to NAPLs found in the subsurface of the street and residential properties proximal to the two sites.

NAPL samples were collected from the ten locations shown in Fig. 10.1. Two grades of dispensed gasoline were also collected from the active service Station B. These dispensed gasoline samples are referred to as ULP Bowser 3 (regular unleaded gasoline) and PULP Bowser 9 (unleaded premium gasoline). The NAPL samples and dispensed gasoline were analyzed using a series of forensic methods referenced above that included, Whole Oil Fingerprinting, PIANO Quantification and Fingerprinting, and Organic Lead Quantification and Speciation. Table 10.5 presents a summary of selected chemical parameters measured for the NAPLs and two dispensed gasolines. The basis for the various blending and refining parameters presented in Table 10.5 are taken from Stout et al. (2006).

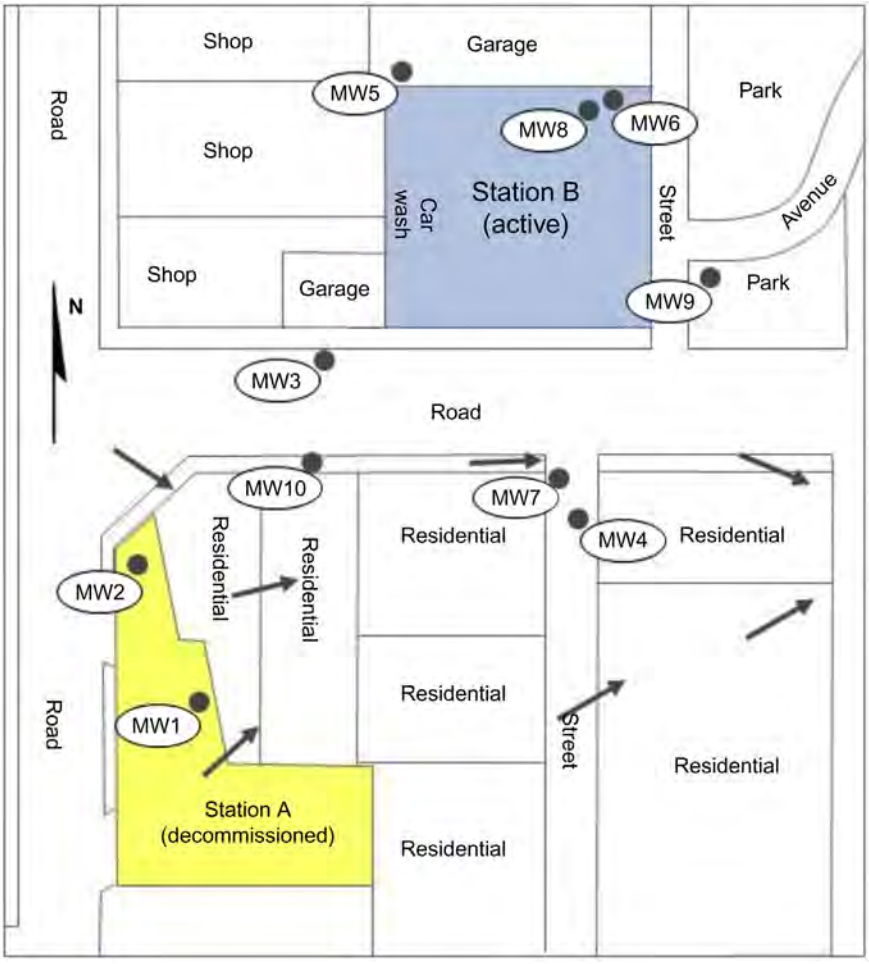

FIGURE 10.1 Map showing the study area and the locations of the monitoring wells sampled for NAPL in Case Study 1. Light shaded area represents a decommissioned service station (Station A) and the dark shaded area represents the active service station (Station B). Arrows indicate groundwater flow direction.

10.3.1.1 Chemical Fingerprinting Analysis

Whole oil GC and PIANO analysis revealed that all of the NAPL samples are composed of C_5 to C_{12} hydrocarbons in proportions that are consistent with automotive gasoline, i.e., prominent relative amounts of compounds that include isopentane, certain *n*-alkanes, monoaromatic compounds that include benzene, toluene, ethylbenzene, and xylenes (BTEX), numerous C3- and C4-alkylated benzenes, and trimethylpentane (TMP) isomers, particularly iso-octane. Representative chromatograms are illustrated in Fig. 10.2. There was no chromatographic evidence for higher boiling petroleum fuels or lubricants among the samples.

MTBE and other oxygenate additives were not detected in any of the NAPL samples. The lead scavenger historically used in leaded gasoline, 1,2-dibromoethane was detected at trace levels in the NAPL samples from monitoring wells MW4, MW6, MW8, and MW9, e.g., at the northwest margin of the entire study area (Fig. 10.1).

10.3.1.2 Organic Lead

All of the NAPL samples contained detectable and significant concentrations of organic lead. The concentration of organic lead measured in the samples ranged from 0.1 glpg (MW9) to 1.3 glpg (MW2), with tetraethyl lead being the major alkyl lead component in all samples (Table 10.5). Leaded gasoline has been banned for on-road use in Australia since January 1, 2002 (Fuel Standard (Petrol) Determination, 2001). The detection of organic lead in all of the NAPLs indicates that the samples are comprised of, or contain a significant fraction, of leaded gasoline that had been released prior to that date.

TABLE 10.5 Summary of the Gasoline Parameters Measured in the NAPLs and Dispensed Gasoline in Case Study 1

Sample ID	MW1	MW2	MW3	MW4	MW5	ULP-bowser 3	PULP-bowser 9	MW6	MW7	MW8	MW9	MW10
BULK PROPERTIES												
%Paraffins	15.9	16.5	20.1	13.1	16	13.1	9.7	15	22.1	14.3	15.8	10.6
%Isoparaffins	19.5	28.8	42.4	27.1	35	32	42.2	30	44.5	27.3	29.8	23.7
%Aromatics	61.3	48.9	31.6	54.9	44	40.7	35.7	50	27.9	54.3	49	61.4
%Naphthenes	2.7	4.9	4.7	4.4	3.9	9.2	6.3	4	4.8	3.3	4.8	4
%Olefins	0.5	0.8	1.2	0.6	1.2	5.1	6.1	1	0.7	0.8	0.7	0.2
%Oxygenates	0	0	0	0	0	0	0	0	0	0	0	0
LEAD CHARACTERISTICS												
glpg as TML	ND	ND	ND	ND	ND	NA	NA	ND	ND	ND	ND	ND
glpg as TMEL	ND	ND	ND	ND	ND	NA	NA	ND	ND	ND	ND	ND
glpg as DEDML	ND	ND	ND	ND	ND	NA	NA	ND	ND	ND	ND	ND
glpg as MTEL	0.005	0.001	0.001	0.001	0.001	NA	NA	0.001	ND	0.001	ND	ND
glpg as TEL	1.20	1.26	1.02	0.84	0.05	NA	NA	0.91	0.70	0.88	0.14	0.75
Lead (glpg)	1.20	1.26	1.02	0.84	0.50	NA	NA	0.91	0.70	0.88	0.14	0.75
REFINING CHARACTERISTICS OF GASOLINE												
ALKYLATE CHARACTER												
Alkylate type-%Iso ratio	39.6	48	45.1	49.3	53.3	52.9	64	58	51.6	52.1	54.1	50.2
Alkylate amount—$\sum$TMP/(nC7 + MCH)	0.74	0.51	0.67	0.62	0.79	1.3	9.9	0.64	0.6	0.62	0.53	0.62
WEATHERING CHARACTERISTICS OF GASOLINE												
Evaporation—nC7/(nC5 + nC7)	91	64	32	58	29	10	13	34	34	32	37	89
Water-washing—CH/(CH + B)	95	62	90	39	31	85	82	29	99	26	48	85

10.3.1.3 Weathering State of the Fugitive Gasoline

The three principal weathering processes that can affect the composition of spilled petroleum in the subsurface are evaporation, water-washing, and biodegradation. Of those three, the two most prevalent weathering pathways relevant to fugitive gasoline in the subsurface are typically evaporation and water-washing. A number of weathering indices that have been published are used to monitor the weathering state of fugitive gasoline (Stout et al., 2016). These weathering parameters provide a basis to measure changes in gasoline-derived NAPL composition brought about by both natural processes, and, in the case of sites under corrective action, by the influences of certain remedial actions such as pump-and-treat or vapor extraction.

Isopentane is the most volatile chemical measured in gasoline, and thus is a useful compound for evaluating potential evaporative weathering of gasoline-containing NAPL. The isopentane concentration measured in the study samples ranged from 1320 mg/kg (MW1) to 76,700 mg/kg (MW3). All of the values among the NAPLs are lower than the two dispensed gasoline samples (102,000 and 99,100 mg/kg)—a result of evaporative weathering of the most volatile components in the NAPLs. The NAPLs that exhibit the least evaporation (freshest) are from MW3, located proximal to the Station B property.

The most water soluble hydrocarbon compounds in gasoline are the mono-aromatic BTEX compounds, with benzene being the most soluble of the group. These chemicals can become depleted in gasoline NAPL via dissolution into groundwater. Compared to freshly dispensed gasoline, the NAPL samples in this study exhibited a range in water-washing character (Table 10.5). However, it was evident that the least water washed samples were found on located on or near Station B (MW5, MW8, and MW6).

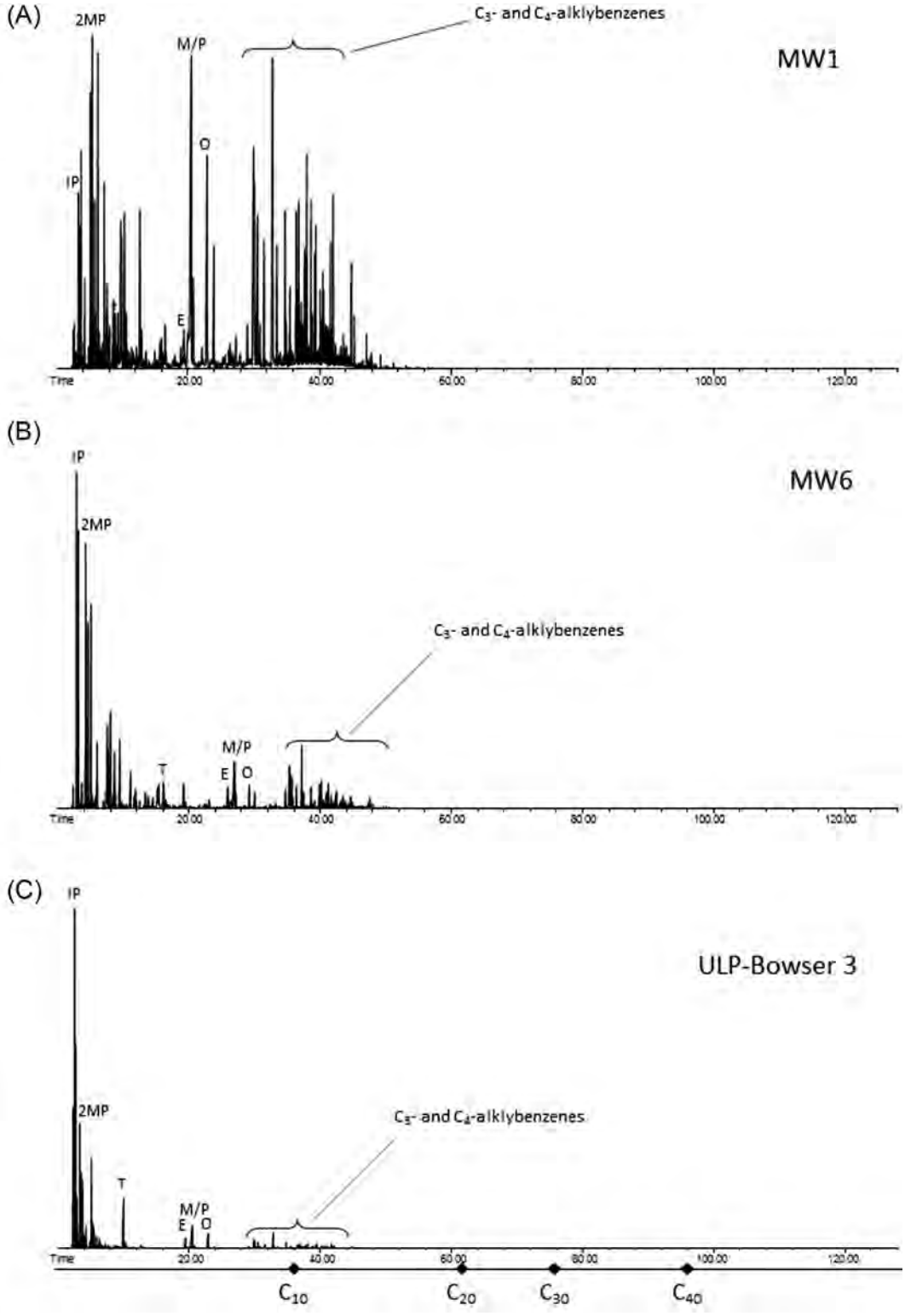

FIGURE 10.2 Representative whole oil gas chromatograms of the samples investigated: (A) Highly weathered gasoline NAPL MW1 collected from Station A; (B) slightly weathered gasoline NAPL MW6 collected from Station B; and (C) freshly dispensed unleaded premium gasoline reference sample gasoline taken from ULP Bowser 3. Compound abbreviations are listed in Table 10.4.

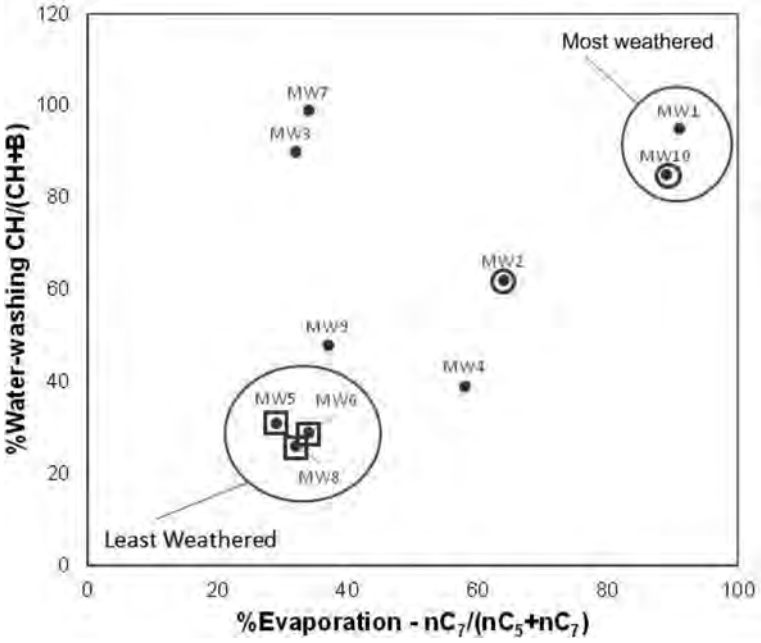

FIGURE 10.3 Graphical summary of the relative degree of weathering that has affected the NAPLs from Case Study 1 in terms of evaporation and water-washing. Circle symbols represent NAPLs collected from Station A and square symbols represent NAPLs collected from Station B.

Fig. 10.3 is a crossplot of two weathering metrics sensitive to evaporation [$nC_7/(nC_5 + nC_7)$, x-axis] and water-washing ($CH/CH + B$, y-axis), respectively. Used together, these two metrics provide an integrated view of the weathering state of the NAPLs. Overall, the NAPLs that have undergone the least collective relative weathering occur on or proximal to Station B (MW5, MW6, MW8, and MW9). All things being equal, this suggests that these NAPLs were released more recently than the more highly weathered samples found on or near Station A.

10.3.1.4 *Alkylate Character of the NAPLs*

Insight into similarity and/or difference's in the chemical composition of the NAPLs was explored by examining the characteristics of the alkylate blending components that comprised the gasolines. Alkylate is a blending stock added to many modern gasolines to achieve fuel octane requirements. Alkylate contains various isoparaffins, particularly the high octane TMPs. Alkylate is produced in refineries by acid-catalysis processes. There are two common refining processed used in alkylation—either sulfuric acid (H_2SO_4) or hydrofluoric acid (HF) mediated. During the alkylation process, isoalkanes are formed, in particular iso-octane (2,2,4-TMP) and its three-related isomers (2,2,3-TMP, 2,3,4-TMP, and 2,3,3-TMP). The iso-octane isomers are formed in different proportions, depending on which acid catalyst is used in their production. For example, the HF process produces higher relative amounts of 2,2,4-TMP compared to alkylate produced with H_2SO_4.

The percentage of isooctane (%Iso) is a convenient means for distinguishing between HF and H_2SO_4 produced alkylates. The %Iso in a TMP-rich alkylate is computed as:

$$\%\text{Iso} = \frac{(2,2,4-\text{TMP})}{(2,2,4-\text{TMP}) + (2,2,3-\text{TMP}) + (2,3,4-\text{TMP}) + (2,3,3-\text{TMP})} \times 100$$

Published values of %Iso for alkylate from H_2SO_4 production units range from 0.39 to 0.45, whereas the %Iso for alkylate from HF production units is higher, and ranges from 0.54 to 0.73 (Beall et al., 2002). Owing to TMPs' resistance to weathering (except when affected by evaporation), using these published %Iso ranges, it is possible to identify the type of alkylate found in gasoline (i.e., HF or H_2SO_4). As such, the %Iso is a forensic probe that can be used to compare, and potentially distinguish among alkylate-containing gasoline NAPLs (Stout and Wang, 2008).

The relative amount of alkylate in gasoline varies, depending on the octane level for which the gasoline is blended. The relative amount of alkylated in gasoline can be estimated using the ratio $\sum$TMP/(n-C_7 + MCH). As the amount of alkylate in gasoline increases, the amount of total TMP isomers ($\sum$TMP) increases relative to the sum of two common gasoline hydrocarbons n-C_7 and MCH.

Fig. 10.4 shows a cross plot of the %Iso versus the $\sum$TMP/(n-C_7 + MCH) for the study NAPLs. It is interesting to note that most of the NAPLs are blended with similar amounts of alkylate [$\sum$TMP/(n-C_7 + MCH) $\sim$ 0.7]—the

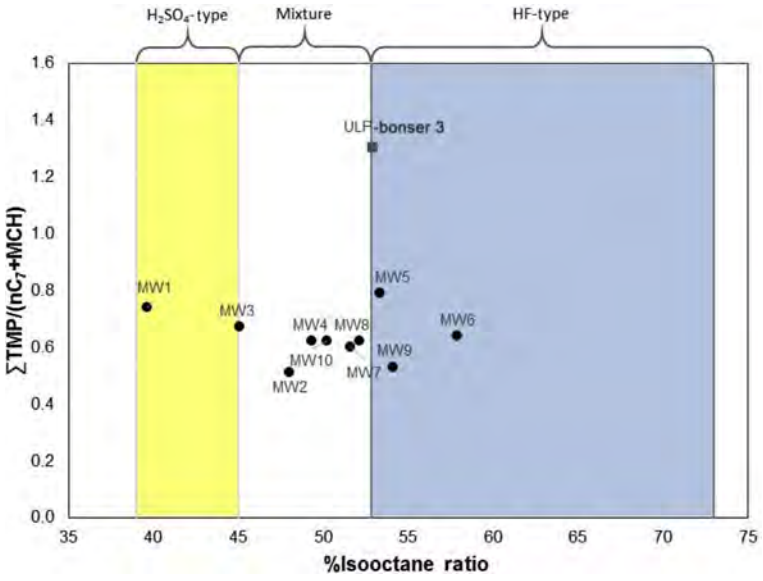

FIGURE 10.4 Cross plot of the %Iso (reflecting the alkylate type) versus $\sum$TMP/(n-C_7 + MCH) (reflecting the alkylate amount) in the NAPLs from Case Study 1. The light and dark shading span the range in end-members considered representative of H_2SO_4-type and HF-type alkylation, respectively.

exception being the dispensed unleaded premium gasoline reference sample "ULP-Bowser 3". However, Fig. 10.4 clearly illustrates that there are NAPLs containing both H_2SO_4 and HF alkylate gasoline "end members", as well as multiple intermediate NAPLs that are composed of mixtures of H_2SO_4 and HF type alkylate-bearing gasolines. Specifically, it is evident in Fig. 10.4 that NAPLs from wells MW1 (Station A) and MW3 were blended from a H_2SO_4-type alkylate blending stock, NAPLs from wells MW5, MW6, MW8, and MW9 (located on Station B) were blended from an HF-type alkylate blending stock, and NAPLs from wells MW2, MW4, MW7, MW8, and MW10 mixtures of these two types of alkylate gasoline.

10.3.1.5 Comingled Mixtures of Gasoline in the Study Area

Consideration of the weathering and compositional features of the NAPLs (Figs. 10.3 and 10.4) reveals some trends that point to the likely origins of the NAPLs. On one hand, the H_2SO_4-type alkylate gasoline NAPL collected from MW1 (Station A) was severely weathered, and contained the highest concentration of lead (Table 10.5). On the other hand, the HF-type alkylate gasoline collected from MW5 (Station B) was mildly weathered and contained low concentrations of lead (Table 10.5)—suggestive of a product containing lower lead or composed of unleaded gasoline from releases more recent than observed on Station A.

The relationship among the NAPLs between the alkylate character (%Iso) and the organic lead concentration is further revealing. Fig. 10.5 is a crossplot between %Iso and organic lead concentration for the samples. This graph indicated that the H_2SO_4-type alkylate NAPLs have among the highest lead contents, whereas the HF-type alkylate NAPLs have among the lowest lead contents of the population of NAPL samples. NAPLs with %Iso values between the H_2SO_4- and HF-type gasolines having intermediate lead contents.

In summary, consideration of the compositional and weathering features of the NAPLs supports a hypothesis for two "end members"—a relatively older, higher lead, H_2SO_4-type gasoline originating from Station A, and a less weathered, lower lead-bearing HF-type gasoline originating on Station B. The remainder of NAPLs are arguably comingled analogs of the two end members originating from the two stations.

10.3.1.6 Allocation of the End Member Sources

Most of the NAPLs in the study area are mixtures of the two "end member" gasoline NAPLs—the H_2SO_4-like alkylate gasoline from Station A, and the HF-type alkylate gasoline from Station B. A simple mixing model was developed in order to estimate contributions of the two "end member" gasolines for those otherwise mixed source NAPLs. The mixing model developed was based on the alkylated character of the "end member" NAPLs. Two candidate end-member NAPLs were chosen to represent the H_2SO_4-like alkylate gasolines from Station A—MW1 and MW3. Similarly, two end-members selected to represent HF-type alkylate gasoline NAPLs from Station B—MW5 and MW6.

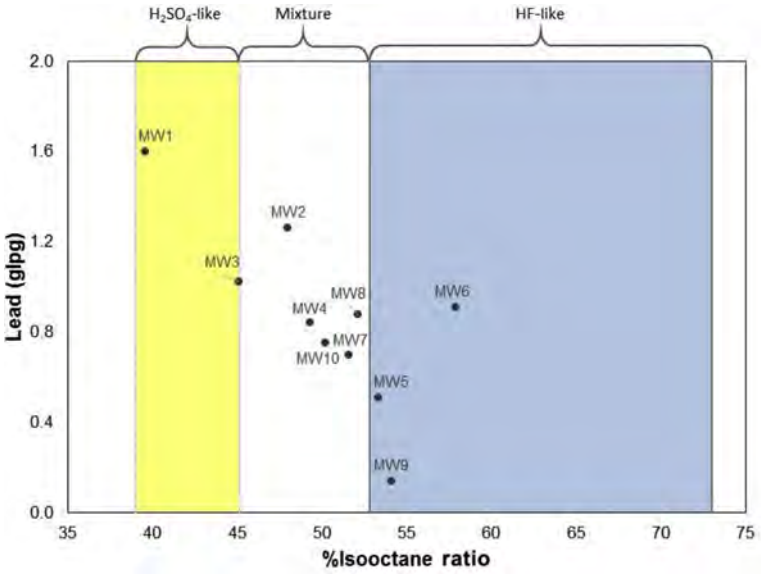

FIGURE 10.5 Cross plot of the %Iso (reflecting alkylate type) and the organic lead content in the NAPLs from Case Study 1. The light and dark shading span the range in end-members considered representative of H_2SO_4-type and HF-type alkylation, respectively.

TABLE 10.6 Predicted %HF-Like Gasoline Mixtures

Mixing end members	MW1	MW3	MW2	MW4	MW5	MW6	MW7	MW8	MW9	MW10
H_2SO_4-type MW5/HF-type MW1	0	54	84	97	100	100	100	100	100	100
H_2SO_4-type MW6/HF-type MW1	0	28	44	51	73	98	64	67	78	56
H_2SO_4-type MW5/HF-type MW3	0	2	71	100	100	100	100	100	100	100
H_2SO_4-type MW6/HF-type MW3	0	4	26	36	68	100	55	59	74	43
Min %HF-type	0	2	26	36	68	98	55	59	74	43
Max %HF-type	0	54	84	100	100	100	100	100	100	100
Average %HF-type	0	22	56	71	85	100	80	82	88	75
Average %H_2SO_4-type	100	78	44	29	15	0	20	18	12	25

Using these end members, four mixing scenarios were considered:

1. HF-type MW5 mixed with H_2SO_4-type MW1
2. HF-type MW6 mixed with H_2SO_4-type MW1
3. HF-type MW5 mixed with H_2SO_4-type MW3
4. HF-type MW6 mixed with H_2SO_4-type MW3

For each scenario, the percent HF-type gasoline mixed was determined by linearly combining varying proportions of the mixing end members:

$$y = mx + b$$

where:

y = %HF-type gasoline
m = the slope derived from the linear regression
x = calculated TMP ratio
b = y intercept

The tabulated percent of HF-type and H_2SO_4-type gasolines calculated for each NAPL sample for each of the four mixing scenario is presented in Table 10.6. The range (min and max) and average of the calculated mixtures are compiled at the bottom of the table. Fig. 10.6 depicts, geographically, the average proportions of the percent HF-type and H_2SO_4-type gasoline found in the NAPL at the study area.

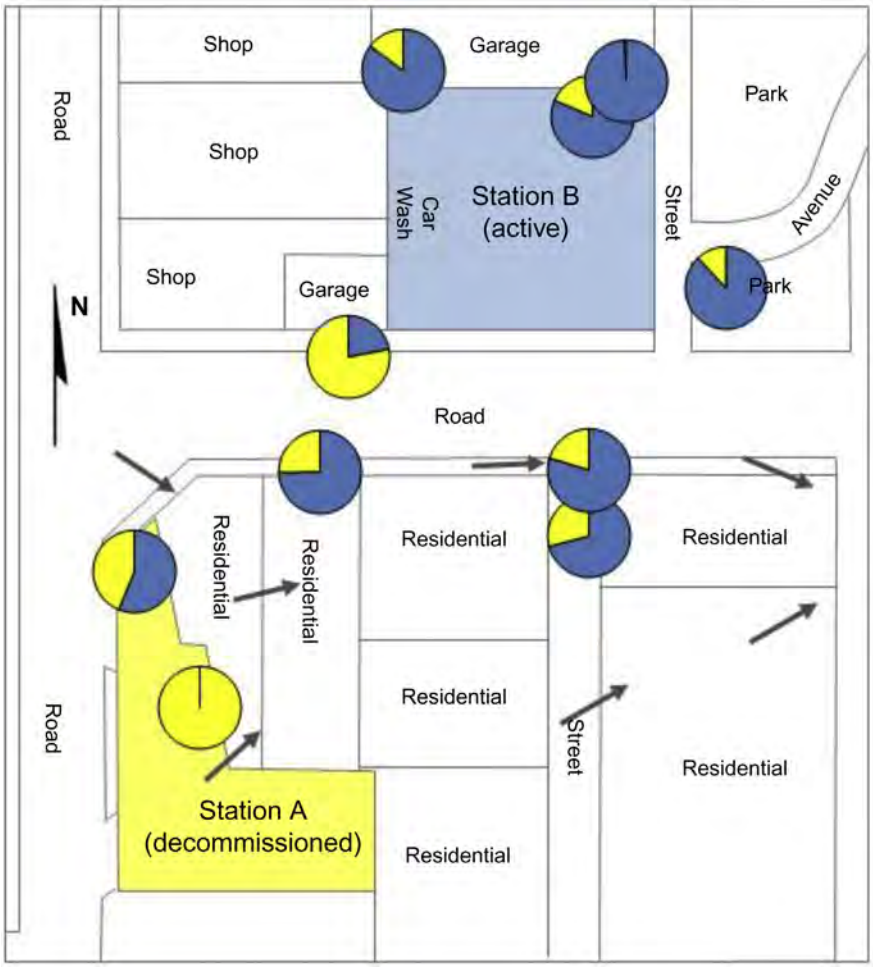

FIGURE 10.6 Graphical representation of the percent H_2SO_4-type gasoline (light shade) versus HF-type gasoline (dark shade) for the NAPLs from Case Study 1. Arrows indicated groundwater direction.

There is undoubtedly some uncertainty inherent in the mixing model presented above, due to the variability in the alkylate composition of the proposed gasoline end-members. Nonetheless the results provide a credible estimate for establishing the composition and source contribution of HF-type and H_2SO_4-type gasoline to fugitive NAPLs in the study area.

In summary, it is apparent that the NAPL from MW1 (Station A) is comprised exclusively of H_2SO_4-type gasoline, while the NAPLs from MW5 and MW6 (Station B) are comprised exclusively of HF-type gasoline. These locations likely represent each site's principal gasoline release areas. High percentages of HF-type gasoline were calculated in NAPLs from MW8 (also on the Station B site), MW7 (just south of the Station B site), and MW9 (just east of the Station B site). There is basis to suggest that there may be some influence of the HF-type gasoline at MW2, which is located on the Site (Station A). The presence of HF-type gasoline component at these diverse locations around the Station B site argues that the migration of NAPL in the area was not necessarily toward the North. Rather the diverse migration directions of Station B-like gasoline could be the result of the ground water mounding sometimes observed in the area.

10.3.2 Case Study 2: Identifying Fugitive Petroleum at an Automobile Repair Shop

There are approximately 175,000 active automotive repair shops in the United States (Sunkin, 2000). These facilities offer a variety of services including gasoline and diesel fueling, crankcase and transmission oil changes,

hydraulic brake repair, antifreeze replacement, lubrication, repainting, and degreasing. Some of the common types of waste generated at automobile maintenance facilities arising from these services include:

- Petroleum solvents (e.g., paint thinners, Stoddard solvent, etc.)
- Chlorinated solvents
- Antifreeze
- Brake fluids, hydraulic
- Batteries
- Motor oils
- Fuels (gasoline, diesel, kerosene)
- Lubricating grease

In many communities, auto repair shops and garages represent the largest generators of hazardous waste among small businesses (Kansas State University, 2000). Liquid petroleum wastes, inclusive of fuels, lubricants and solvents are among the most volumetrically important waste streams at automobile repair facilities. For example, it has been estimated that each year over 180 million gallons of used engine oil alone are improperly disposed of improperly in the United States (Alameda CCWP, 1992). The mismanagement of waste petroleum liquids can result in significant damage to the environment and costly cleanup. Environmental forensic investigators are often called upon to identify the nature of fugitive oil found at automobile repair shops, and to ascertain if spilled oil at one location matches (compositionally and sometimes "genetically") oily waste found elsewhere on or nearby a site under investigation.

At most automobile repair shops, forensic investigations are usually relegated to simple identification and delineation of the type(s) of waste oils found at a site. Since most petroleum contamination at repair facilities are the result of spills and releases of a chronic nature, it stands to reason that the resultant fugitive petroleum is inherently heterogeneous in chemical composition. As such, it would be expected that molecular chemical fingerprinting/matching (often associated with large acute oil spill investigations) would not be of value in most investigations of fugitive oil at automobile repair facilities since the likelihood of rigorous compositional "matches" among chronically spilled oils and suspected sources would be unexpected.

Nonetheless, there are instances where traditional molecular chemical fingerprinting is of value in the investigation of spilled petroleum at automobile repair facilities. For instance, large instantaneous releases of waste oil such as from a ruptured waste holding tank, or illegal disposal of waste oil into a sewer drain, can require the forensic investigator to answer the question "does fugitive oil found [on site, at the end of a pipe, etc.] "match" the oil released during the spill event?". In such cases, molecular chemical fingerprinting can be brought to bear to answer such questions in a quantitative fashion.

In this case study, we introduce gas chromatograms and molecular chemical data for a number of common petroleum liquids that can be encountered during investigation of automobile repair facilities. We then provide an example of the use of molecular chemical fingerprinting to ascertain if fugitive oil found in contaminated soil and groundwater are "matches" for waste oils suspected of being the source of the contamination.

10.3.2.1 Examples of Common Petroleum Products at Automobile Repair Facilities

There are a variety of common petroleum fuels and products that, in our experience, can be encountered during site investigation work at auto repair shops. Such petroleum materials include a variety of fuels, lubricants, and solvents. Among the most common are:

- Automotive gasoline
- Paint thinner
- Kerosene
- Diesel fuel
- Motor oil
- Greases
- Hydraulic oil
- Heavy fuel oils

Each of these candidate petroleum products are formulated differently to meet intended end uses. As such, each of the products have different boiling ranges and molecular compositions (Table 10.7). The varying bulk and molecular chemical differences lead in turn to unique product-specific gas chromatograms that the forensic investigator can rely upon for product identification.

TABLE 10.7 Boiling Points and Carbon Ranges for Common Petroleum Products

Petroleum product	Boiling point (°C)	Carbon range
Organic solvents	25–130	C_7–C_{12}
Gasoline	25–215	C_4–C_{12}
Kerosene	200–290	C_9–C_{17}
Fuel oil #2, diesel fuel	150–400	C_{10}–C_{25}
Heavy fuel oils	150–575	C_9–C_{45}
Lubricating oils	270–525	C_{15}–C_{40}

The high resolution TPH-type gas chromatograms or "fingerprints" for fresh analogs of the candidate petroleum products are shown in Fig. 10.7. It is apparent that each product has a unique chromatographic profile. Note how the dominant portions of each chromatogram align well with the boiling ranges listed in Table 10.7. Although weathering—the combined effects of evaporation, dissolution and biodegradation—can affect certain aspects of the molecular chemistry and thus the resulting gas chromatogram of petroleum products, the basic compositional (and thus chromatographic) features of most petroleum products remain intact, allowing the investigator to identify both fresh and weathered analogs of such petroleum in the environment (Stout et al., 2003).

The molecular chemistry of each of the candidate products are distinctive. For example, gasoline is compositionally dominated by a unique mixture of low boiling ($<C_{12}$) paraffinic, isoparaffinic, aromatic, naphthenic and olefin compounds (Stout et al., 2006); diesel fuel, kerosene, and paint thinner are composed of varying amounts of C_{10}–C_{20} *n*-alkanes, and 2- and 3-ring PAH compounds (Douglas et al., 2007). Heavier boiling mineral oil-derived materials like motor oil, transmission oil and greases contain few if any *n*-alkanes and (because of the result of dearomatization during refining) only sporadic, low concentrations of PAH compounds; these mineral oil-derived products are primarily composed of complex mixtures of chromatographically unresolved nonpolar hydrocarbons (Uhler et al., 2016). HFOs contain the broadest range of 2-, 3-, and 4-ring PAH and in fresh form, often a broad range of *n*-alkanes spanning the C_{10}–C_{40} range (Uhler et al., 2016).

10.3.2.2 Use of Gas Chromatography and Molecular Fingerprinting to Reconcile Fugitive Oil with a Suspected Source

Instantaneous, large releases of waste oils or fuels can occur at automobile repair facilities. Waste oil tanks usually hold a multifarious mixture of petroleum products. However, at any one point in time, such a mixture of petroleum has its own unique chemical composition. Of course, catastrophic releases of fuels, solvents, or wastes (from above- or below-ground tanks or illegal discharges to drains) can lead to a fugitive product that is compositionally simple (i.e., unicomponent), with its own distinct chemical fingerprint. In other words, instantaneous releases of fuels, solvents or even a mixture of waste oils have distinctive molecular compositions amenable to quantitative chemical fingerprinting assessment.

Consider two cases described herein, wherein forensic investigations were carried out following release or discharge of significant quantities of petroleum fuel and solvent, respectively.

- Case #1. A repair facility where HFO tank bottoms had been discharged to the ground surface. The goal of the investigation was to determine if the spilled HFO had impacted a nearby surface water body.
- Case #2: A facility where illegal disposal of an organic cleanup solvent was alleged to have occurred on the paved surface of the site. The objective of the investigation was to ascertain if the spilled solvent had impacted nearby offsite soil.

Case # 1: A sample of soil ("B-2") that had been heavily impacted with HFO tank bottoms was collected from the land surface at an auto repair facility where HFO tank bottoms had been dumped. A downgradient, nearby drainage swale with weakly flowing water was observed to have been impacted by a sheen of floating hydrocarbons. The drainage swale was located in a busy industrial corridor, so the possibility for multiple sources for the sheen had to be considered. A sample of sheen from this waterbody ("M-20") was obtained for analysis.

The gas chromatogram (Fig. 10.8A) for soil sample B-2 was consistent with a typical HFO, viz., a broad boiling mixture of hydrocarbons between about C_{10} and C_{40}, that included a prominent unresolved complex mixture (UCM) between about C_{20} and C_{40}, and C_{10}–C_{25} distillate range petroleum, blended into the product as a

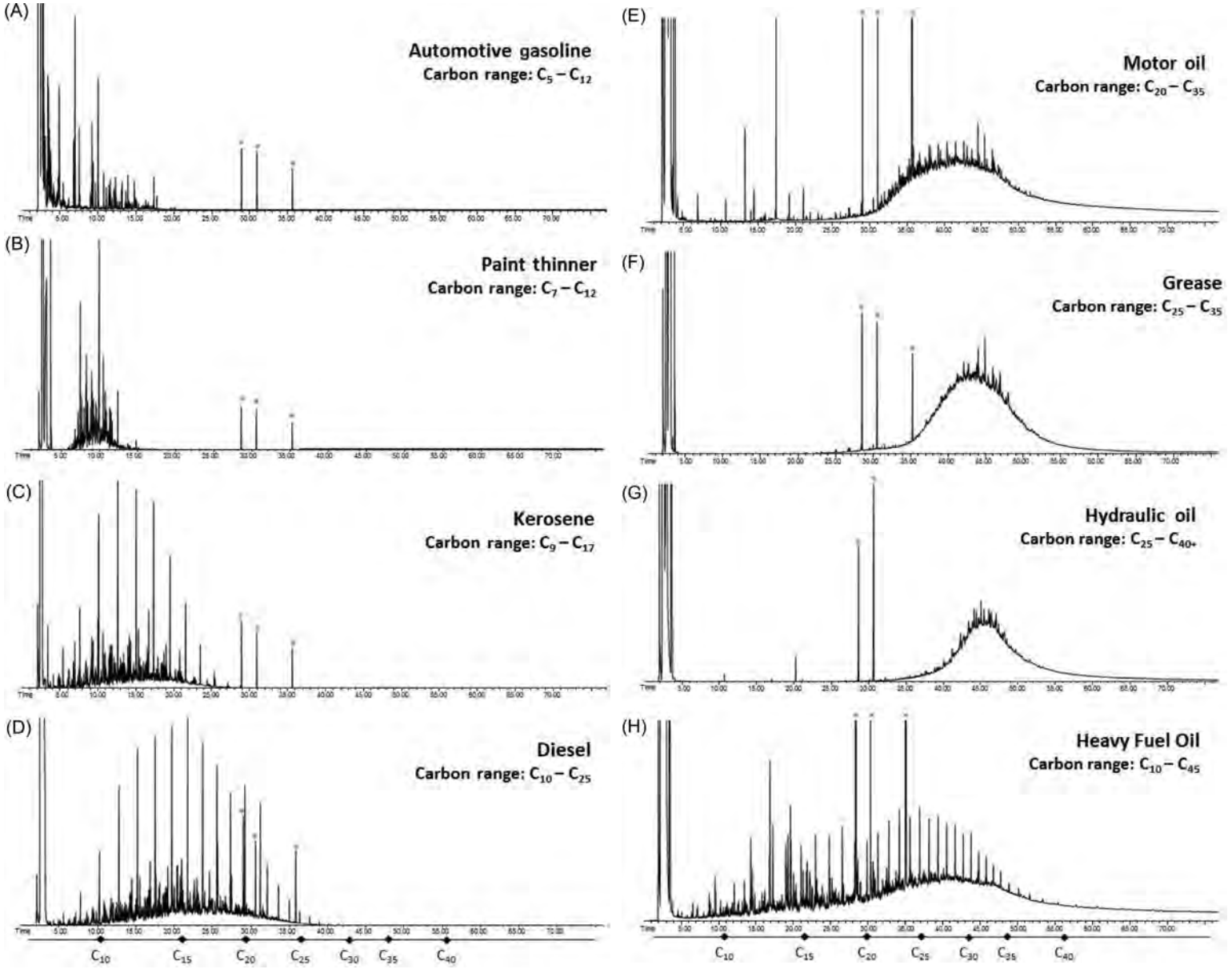

FIGURE 10.7 Gas chromatograms of petroleum products that are typically found at an automotive repair shop: (A) automotive gasoline, (B) paint thinner, (C) kerosene, (D) diesel, (E) motor oil, (F) grease, (G) hydraulic oil, and (H) heavy fuel oil (HFO). Carbon range is annotated at the bottom of the figure. "*": laboratory-added internal standard.

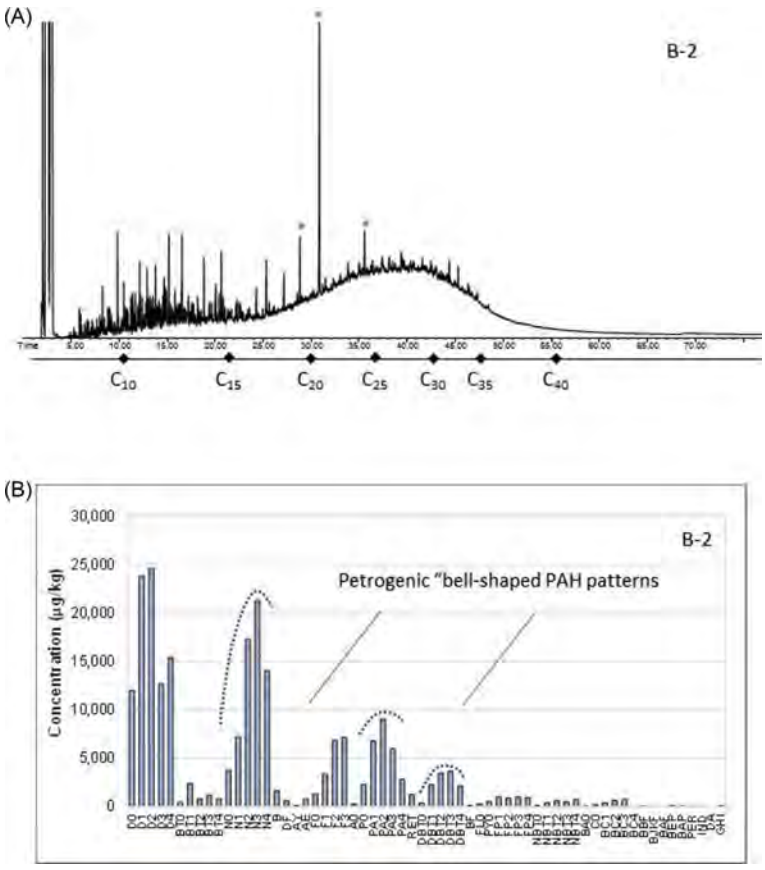

FIGURE 10.8 Compositional analysis of soil sample B-2: (A) gas chromatogram; and (B) PAH histogram.

cutter stock to improve the fuel's viscosity characteristics (Uhler et al., 2016). The PAH distribution (Fig. 10.8B) was consistent with an unweathered HFO, i.e., a broad range of 2 through 4-ring PAH. The petrogenic, "bell shaped" distribution of the PAH alkyl homologue groups is consistent with unweathered analogs of petroleum-derived PAH.

The GC/FID chromatogram for the surface water sample M-20 had features different than the suspected "source" soil sample (Fig. 10.9A). However, alone those differences did not necessarily rule out the petroleum found in soil sample B-2 as its source. The chromatogram of M-20 illustrates that the floating hydrocarbons was a high boiling petroleum material. The chromatogram is dominated by a UCM that spans the C_{15}–C_{45+} range. There is no evidence for the lower boiling C_{10}–C_{25} distillate range cutter stock noted for soil sample B-2. The shape of the UCM for the water sample is more pyramidal than the more Gaussian-shaped UCM noted for soil sample B-2. The carbon maxima for the UCMs of the two samples are different—the soil sample carbon maximum occurs near C_{25}, whereas the carbon maximum for the water sample occurs near C_{30}. While these qualitative features suggest compositional differences between the petroleum in the two samples, an argument could be made that the features of water sample M-20 are the result of weathering—particularly evaporation—of the petroleum found in soil sample B-2.

Detailed molecular chemical analysis conclusively shows that the petroleum found in the two samples are in fact, different. Consider the PAH compositional histograms for the two samples (Figs. 10.8Band 10.9B). Whereas the PAH homologues found in soil sample B-2 are consistent with petroleum that has undergone little if any biodegradation, the PAH found in water sample M-20 are highly biodegraded, i.e., diminution of parent and lower alkylated (C1–C3) homologues have occurred, leading to "inverse sloped" distributions of PAH that are emblematic of highly biodegraded petroleum. Even more informative is the stark differences in the ratio of the recalcitrant, source-specific diagnostic ratio of the sulfur-containing C3-alkylated dibenzothiophenes to C3-phenanthrenes (DBT3/PA3). This diagnostic ratio is documented to be a sensitive marker of source chemistry among petroleum fuels (Douglas et al., 1996), which can be measured with a precision better than 5% relative (Hansen et al., 2006). The DBT3/PA3 source ratio measured in soil sample B-2 (0.62) is dramatically different

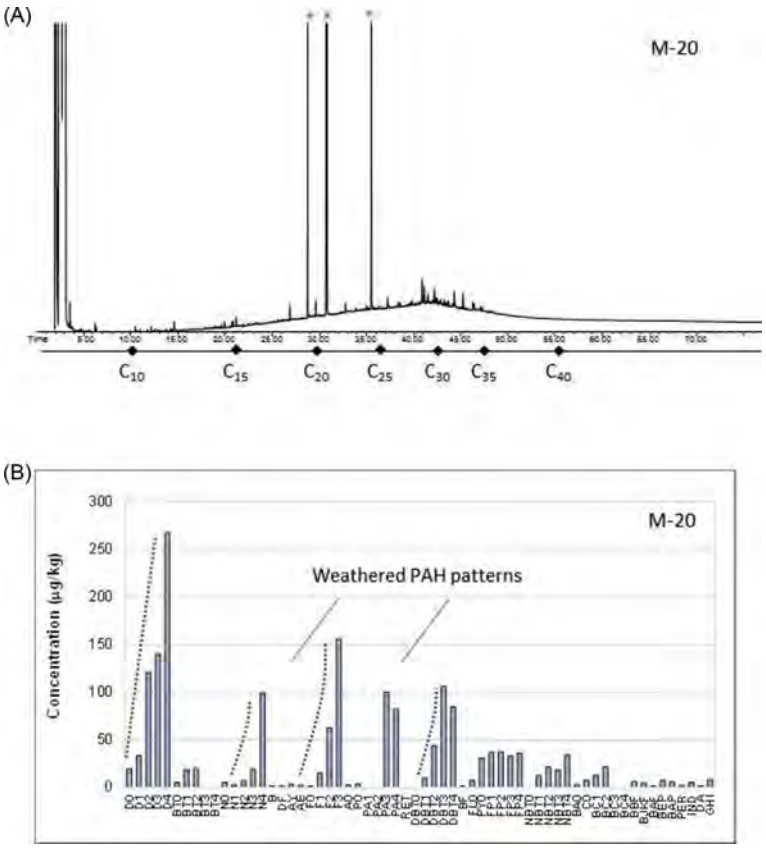

FIGURE 10.9 Compositional analysis of soil sample M-20: (A) gas chromatogram; and (B) PAH histogram.

TABLE 10.8 PAH and Biomarker Diagnostic Ratios Evaluated for Source Character for Heavy Fuels

DR	Definition
%Pr/Ph	[Pr]/[Pr] + [Ph] × 100
%NorPr/Pr	[NoPr]/[NoPr] + [Pr] × 100
%DBT3/PA3	[DBT3]/([DBT3] + [PA3]) × 100
%4MDT	[4MDT]/[4MDT] + [1MDT] × 100
%Tri (1)	([T7] + [T8] + [T9] + [T10])/([T7] + [T8] + [T9] + [T10] + [T19]) × 100
%Tri (2)	([T7] + [T8] + [T9] + [T10])/([T7] + [T8] + [T9] + [T10] + [T11] + [T12]) × 100
%27Ts	(T11]/([T11] + [T12]) × 100
%29Ts	[T16]/([T16] + [T19]) × 100
%29ab	[T15]/([T15] + [T19]) × 100
%31abS	[T21]/([T21] + [T22]) × 100

than that for water sample M-20 (1.1). This fact alone rules out the possibility that the petroleum found in the soil sample B-2 as the singular source of the petroleum found in the surface water sample M-20.

Further evidence for compositional differences between the petroleum found in soil sample B-2 and water sample M-20 is evident in significant differences among other documented petroleum diagnostic source ratios that are considered highly stable during weathering. A list of diagnostic PAH and biomarker ratios appropriate for evaluating source relationships for heavy fuels (Daling et al., 2002) was considered (Table 10.8).

Analysis of a duplicate aliquot of the soil sample B-2 was carried out to demonstrate the precision in measurements of the diagnostic ratios found in the sample's petroleum. The results of those analyses yielded a diagnostic

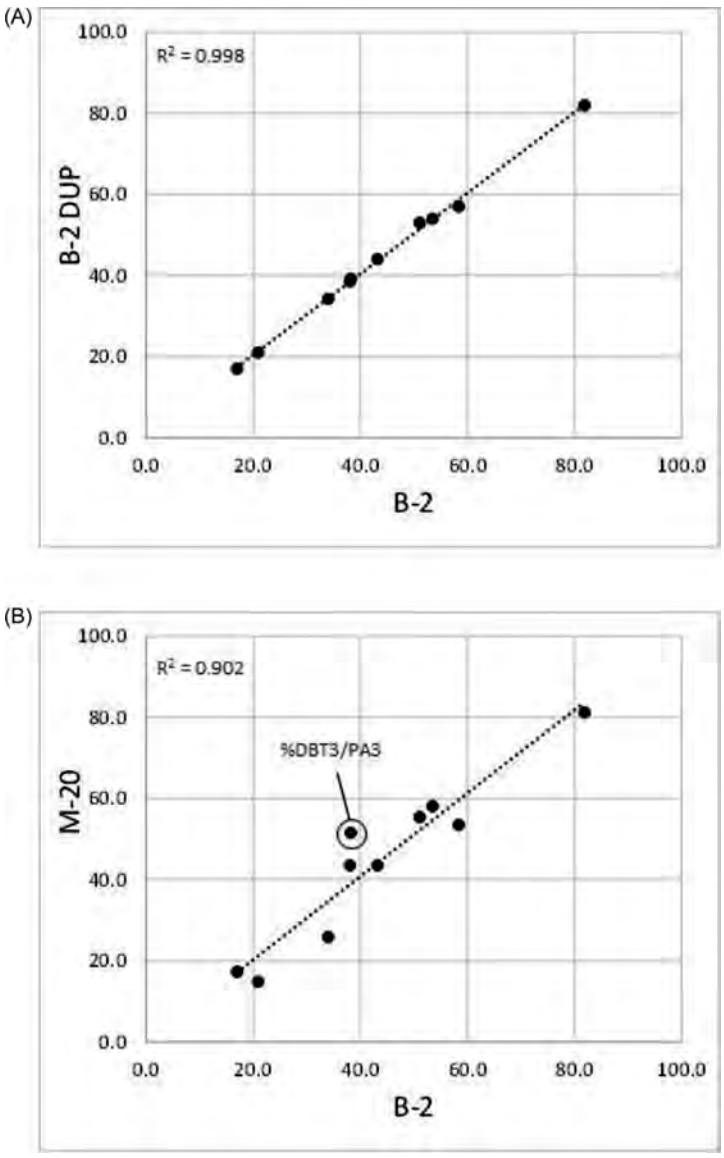

FIGURE 10.10 Crossplots of the PAH and biomarker diagnostic ratios from Table 10.8 (A) between duplicate samples B-2/B-2 DUP; and (B) between B-2 and M-20.

ratio crossplot with linear regression coefficient of 0.998—all of the measured diagnostic ratios fell squarely upon the regression line for the duplicate samples (Fig. 10.10A). By contrast, the diagnostic ratio cross plot comparing soil sample B-2 and water sample M-20 shows that many of the DRs fall well off the expected linear regression line (Fig. 10.10B), confirming that the heavy petroleum found in the off-site water sample M-20 was chemically different than the HFO found in the on-site soil sample B-2.

Consideration of GC/FID chromatogram profiles, PAH histograms, and source specific diagnostic ratio analysis leads to the conclusion that the petroleum found in offsite water sample M-20 had a source different that the HFO found in the on-site, impacted soil sample B-2.

Case #2: A significant amount of liquid waste was found accumulated on the paved surface in the back lot of an automotive repair facility. Physical evidence, i.e., staining, suggested that the liquid waste had migrated across the paved surface, and impacted the unpaved soil of a neighboring industrial property. A forensic investigation was carried out to determine if the petroleum residue found in the offsite soil (B-1) matched the NAPL that had been discharged onto the paved lot of the facility (M-41).

The TPH-type gas chromatogram of the NAPL from the paved lot (M-41) had the characteristics of a light solvent (Fig. 10.11A, **left panel**). The light boiling product was composed of hydrocarbons between approximately C_7 and C_{12}. While arguably this material falls in the so-called "gasoline range", its basic chromatographic features align with those of a light petroleum distillate solvent, i.e., a narrow but distinctive UCM of hydrocarbons,

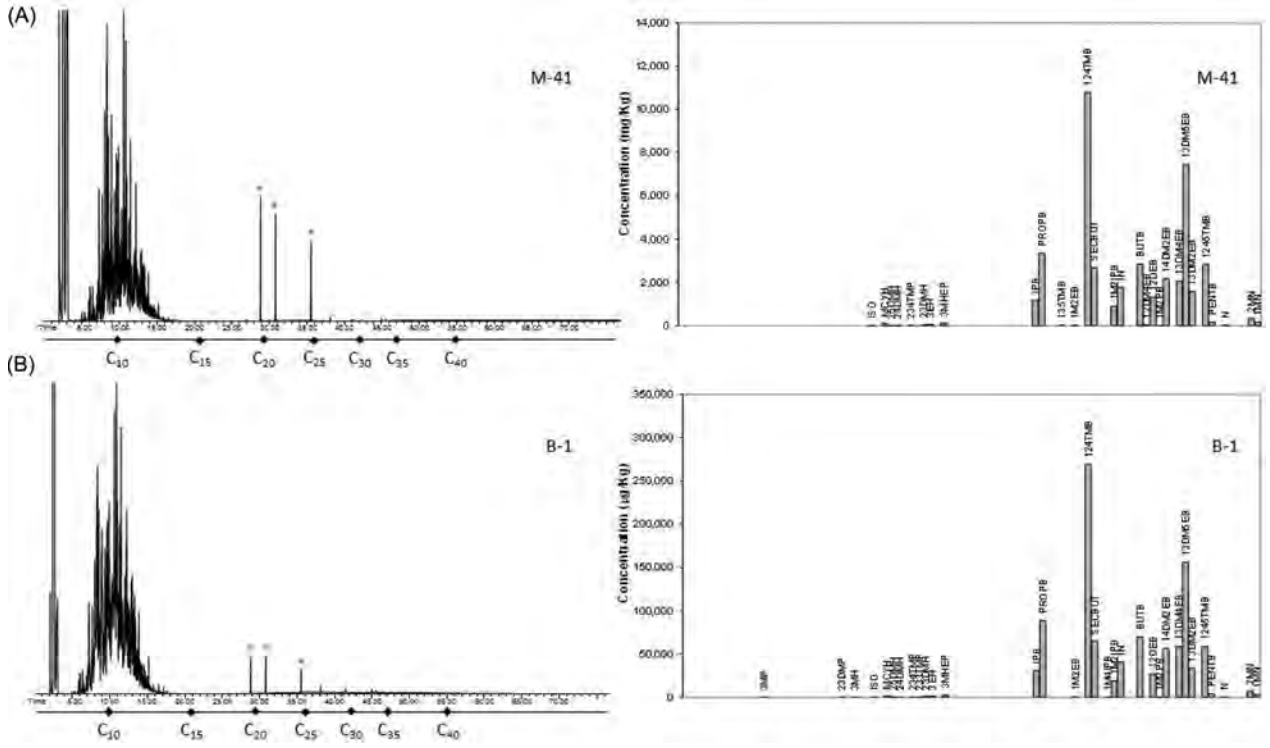

FIGURE 10.11 Compositional analysis: (A) candidate NAPL source sample MW41 and (B) impacted soil sample B1. The GC/FID chromatograms are shown on the left panel and the PIANO histograms are shown on the right panel. "*" represent internal standards added.

TABLE 10.9 PIANO Composition of M-41 and B-1

Component	Sample M-41 liquid petroleum (%)	Sample B-1 soil sample (%)
%Paraffins	0.0	0.0
%Isoparaffins	0.73	0.66
%Aromatics	99.0	99.1
%Naphthenes	0.23	0.19
%Olefins	0.0	0.0

superimposed with a number of close-eluting resolved peaks (Uhler et al., 1999). This chromatographic pattern is distinct from automotive gasoline, which is characterized by prominent monoaromatic compounds and a regular series of clearly resolved paraffins, isoparaffins, naphthenes, and/or olefins that occur in proportions reflective of manufactured automotive gasoline (Stout et al., 2016).

The C_5–C_{12} range PIANO analysis provides more detailed quantitative insight into the composition of the M-41 NAPL (Fig. 10.11A, **right panel**). Here, it is evident that NAPL sample M-41 is highly aromatic in composition—the results of PIANO analyses indicate that 99% of the 88 compounds reported in the PIANO analysis (Table 10.4) are C_1–C_5 alkyl-substituted monoaromatic compounds. Virtually no paraffins, isoparaffins, naphthenes or olefins were detected in the sample. This categorizes the M-41 NAPL as an aromatic solvent. There are a wide variety of low boiling, aromatic solvents marketed by the chemical industry. Aromatic solvents have myriad uses, including as paint stripers and engine cleaners (EPA, 1979).

Qualitatively, the gas chromatogram of the impacted offsite soil B-1 bore a striking similarity to the candidate source NAPL sample M-41 (Fig. 10.11B, **left panel**). The gas chromatogram has virtually the same narrow but distinctive UCM of hydrocarbons, superimposed with a number of close-eluting resolved peaks as seen in the NAPL source sample M-41. In addition, the C_5–C_{12} range PIANO analysis of soil B-1 has a virtually identical bulk hydrocarbon class compositions as measured for the on-site liquid petroleum sample M-41 (Table 10.9).

Qualitatively, the distribution of measured C_5–C_{12} PIANO for soil sample B-1 (Fig. 10.11B, **right panel**) was strikingly similar to the on-site liquid petroleum (Fig. 10.11A, **right panel**). In fact, a simple crossplot measured concentrations of the 88 compounds measured in the PIANO analysis for the two samples yields a highly linear compositional regression, with an r^2 of better than 0.990.

Quantitative comparison of the composition of the on-site liquid petroleum sample M-41 and off-site soil sample B-1 was also examined using diagnostic ratio analysis based upon the PIANO results. In this case, eight DRs were selected for evaluating the source chemistry of the samples. Since the petroleum products under comparison are overwhelmingly aromatic in nature, it stood to reason to use monoaromatic hydrocarbons and alkylated naphthalenes as the basis for the diagnostic ratios. The occurrence and relative amounts of alkylated benzenes and alkylated naphthalenes in petroleum products are a function of crude oil source and refining practices. Thus, their relative abundances, i.e., ratios, are diagnostic of source but the potential effects of weathering must also be considered. In this case, diagnostic ratio pairs of alkylated benzene and alkylated naphthalene compounds were selected following published guidelines (Sauer and Costa, 2003), wherein the selection of diagnostic ratios were based on pairs of alkylbenzene and alkylnaphthalene compounds with similar volatilities and aqueous solubilities, and therefore, expectedly similar environmental behavior. In this way, the values of the diagnostic ratios remain relatively stable, even in the face of environmental weathering—particularly dissolution. Eight such diagnostic ratios were computed (per compound identifications in Table 10.4) as,

2MN/1MN
PROB/124TMB
1M2EB/PROPB
124MB/IPB
SECBUT/12DEB
12DEB/13DM5EB
13DM4EB/14DM2EB
1M2E/124TMB

When the values for the these eight source-specific diagnostic ratios for the on-site liquid petroleum sample M-41 are plotted versus those values for the off-site soil B-1, a highly linear relationship is observed, with a linear regression coefficient (r^2) of 0.997 (Fig. 10.12). Based on this analysis, the on-site liquid petroleum sample M-41 and the off-site soil B-1 contain petroleum that are concluded to be compositionally indistinguishable.

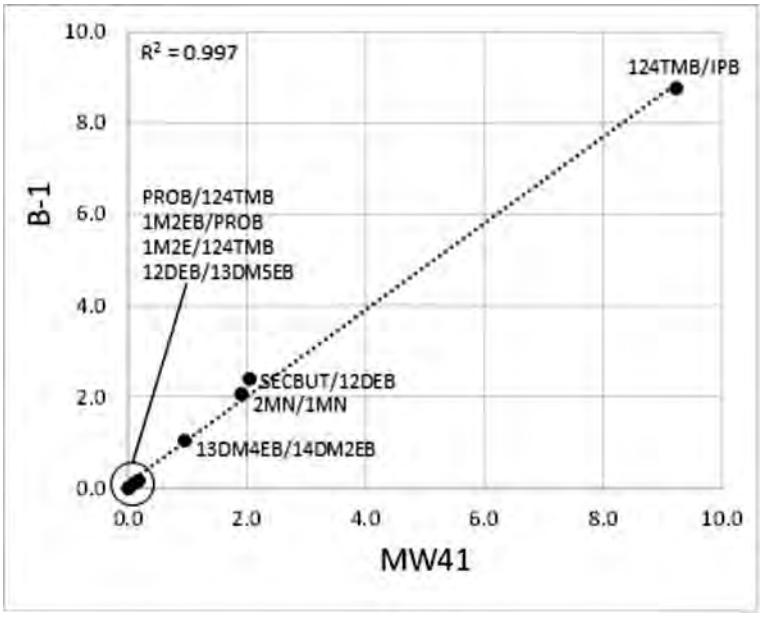

FIGURE 10.12 A crossplot of source-specific diagnostic ratios for aromatic hydrocarbon pair for the on-site liquid petroleum sample M-41 and the off-site soil B-1.

In summary, the qualitative gas chromatograms for on-site NAPL sample M-41 and off-site soil B-1 are strikingly similar and indicated both samples are composed of similar, light petroleum solvent. Quantitative PIANO analysis further demonstrated that the solvent found in both samples was highly aromatic in nature (99% of PIANO compounds), leading to the conclusion that the petroleum in both samples could be classified as aromatic solvents. The detailed molecular comparison between on-site NAPL sample M-41 and off-site soil B-1 were remarkably similar—there was an r^2 correlation of 0.990 between the relative concentrations of 88 PIANO compounds measured in the two samples. Lastly, eight source-specific and environmentally stable alkylbenzene and alkylnaphthalene diagnostic ratios were highly correlated ($r^2 = 0.997$). In summary, chemical fingerprinting indicated that the petroleum found in the off-site impacted soil B-1 was a compositional match for the light aromatic solvent found to compose the on-site NAPL sample M-41.

10.3.3 Case Study 3: Allocation Between Petrogenic and Pyrogenic Sources of PAH at a Contaminated Industrial Site

Industrial manufacturing sites—particularly older sites with long histories of varied operations—often are contaminated by multifarious products and/or waste of hydrocarbon origin. Such hydrocarbon contaminants are frequently of petroleum (petrogenic) origin, i.e., fuels, lubricants and solvents utilized in industrial operations. However, it is not uncommon to encounter hydrocarbon contamination of pyrogenic (combustion or pyrolysis) origin at older industrial sites. Notable pyrogenic wastes include former manufactured gas plant (MGP) wastes such as coal or oil tars (in this chapter, collectively referred to as pyrogenic tar), and/or pyrogenic tar-derived products such as creosote and pitch. Further, there are other common wastes—notably combustion residues like ash, cinders, and general atmospheric fallout and roadway dust that are enriched in combustion-type chemicals that can often confound the identification of the nature and sources of hydrocarbon-derived contaminants at industrial sites.

Many site investigations are driven by regulatory limits or remedial action levels established for PAHs. Both petroleum- and coal tar-derived contamination (as well as general combustion wastes, albeit at lower concentrations) contain significant levels of PAH. However, because of their genesis, the inherent nature of the PAH are distinct and differentiable.

This case study presents the results of an investigation at a former industrial site regarding the nature and sources of PAH contamination in soils from the site. The site once housed a MGP, but in more recent decades, was used for storage of petroleum in above ground tanks. Remedial investigators had identified a geographic area on the site impacted by PAH above concentrations of regulatory concern. There was a need to ascertain the nature and source of the PAH impacts—specifically to ascertain if the PAH arose from historic MGP-operations, from more contemporary handling of petroleum fuels, or some combination of both. We describe herein a study that differentiated between the likely sources of PAH at the site, as well as a methodology to unravel contribution of mixed pyrogenic and petrogenic PAH to the impacted soils.

10.3.3.1 PAH Content and Character of Petroleum and MGP Tar

PAHs are ubiquitous compounds in the environment (ATSDR, 1995). They originate from a large number of sources which can be broadly classified as either (1) diagenetic, (2) petroleum-derived (petrogenic), or (3) combustion-derived (pyrogenic) (Emsbo-Mattingly et al., 2002). *Diagenetic sources* of PAH are of natural origin and arise from geological processes that accompany the degradation of natural organic matter. *Petroleum-derived (petrogenic) sources* are both natural and anthropogenic sources of PAH. Natural sources of PAH include natural seeps and petroleum source rocks (shales). Anthropogenic sources of PAH arises directly from crude oil or refined petroleum products. *Combustion-derived (pyrogenic) sources* are generally anthropogenic in origin and include those derived from fires, combustion of petroleum products, combustion and conversion of coal, and metallurgical processing. Included in this pyrogenic category are products produced from the pyrolytic destruction of coal and/or oil.

While petroleum and MGP-derived tar wastes both contain PAH, the latter contain ten or more times higher concentration of PAH than does petroleum, making pyrogenic tars on an equivalent mass basis a much more potent source of PAH than petroleum. Table 10.10 lists examples of the concentrations of individual PAH, and the sum of the 16 EPA Priority Pollutant PAH (PAH16) compounds in some representative petroleum products (gasoline, diesel fuel, and HFO), coal tar, and creosote. Here, the disparity in PAH16 between petroleum and coal tar-derived materials is evident. Generally, petroleum contains only hundreds of parts per million of PAH16,

TABLE 10.10 Concentrations of Individual PAH, and the Sum of the 16 EPA Priority Pollutant PAH (PAH16) Compounds in Some Representative Petroleum Products (Concentrations in mg/kg)

Compound	Gasoline	Diesel fuel	Heavy fuel oil	Coal tar	Creosote
cis/*trans*-Decalin	25.4	780	40.0	30	29.8
C1-Decalins	36.8	1600	78.3	140	54.1
C2-Decalins	42.9	1700	95.8	310	66.9
C3-Decalins	10.6	1100	72.1	210	ND
C4-Decalins	ND	1500	91.1	230	ND
Benzothiophene	71.9	51	53.6	3800	1540
C1-Benzo[*b*]thiophene	155	140	297	980	344
C2-Benzo[*b*]thiophene	3.70	72	476	620	152
C3-Benzo[*b*]thiophene	2.20	130	364	400	63.2
C4-Benzo[*b*]thiophene	1.03	72	204	160	25.4
Naphthalene	3220	1000	1170	160,000	54,500
C1-Naphthalenes	2820	3000	2020	20,000	9240
C2-Naphthalenes	419	4400	2550	8400	3290
C3-Naphthalenes	134	3900	1780	3500	1080
C4-Naphthalenes	39.7	2300	872	1000	265
Biphenyl	ND	540	109	9400	1600
Dibenzofuran	ND	62	32.7	1000	6090
Acenaphthylene	ND	12	11.0	14,000	5940
Acenaphthene	ND	110	110	1300	1080
Fluorene	ND	230	114	6100	8360
C1-Fluorenes	ND	640	272	2400	1130
C2-Fluorenes	ND	1300	448	1300	418
C3-Fluorenes	ND	1200	462	780	199
Anthracene	ND	ND	77.0	8600	7580
Phenanthrene	ND	420	506	58,000	22,500
C1-Phenanthrenes/anthracenes	ND	1200	1210	12,000	4980
C2-Phenanthrenes/anthracenes	ND	1200	1660	3800	1440
C3-Phenanthrenes/anthracenes	ND	620	1320	1200	414
C4-Phenanthrenes/anthracenes	ND	200	678	280	113
Retene	ND	ND	ND	ND	ND
Dibenzothiophene	ND	13	134	4700	1240
C1-Dibenzothiophenes	ND	100	397	1600	449
C2-Dibenzothiophenes	ND	240	570	1000	242
C3-Dibenzothiophenes	ND	240	538	480	122
C4-Dibenzothiophenes	ND	120	302	170	63.6
Benzo[*b*]fluorene	ND	ND	50.8	780	1810
Fluoranthene	ND	13	43.2	30,000	13,100

(*Continued*)

TABLE 10.10 (*Continued*)

Compound	Gasoline	Diesel fuel	Heavy fuel oil	Coal tar	Creosote
Pyrene	ND	120	261	40,000	9380
C1-Fluoranthenes/pyrenes	ND	120	679	8800	5890
C2-Fluoranthenes/pyrenes	ND	67	815	1900	1410
C3-Fluoranthenes/pyrenes	ND	28	729	520	457
C4-Fluoranthenes/pyrenes	ND	12	483	140	241
Naphthobenzothiophenes	ND	ND	66.0	1900	789
C1-Naphthobenzothiophenes	ND	ND	217	490	369
C2-Naphthobenzothiophenes	ND	1.5	301	150	168
C3-Naphthobenzothiophenes	ND	ND	245	220	89.5
C4-Naphthobenzothiophenes	ND	ND	162	48	ND
Benz[*a*]anthracene	ND	0.96	89.7	7800	5500
Chrysene/triphenylene	ND	3	141	8800	4820
C1-Chrysenes	ND	6.1	484	2000	1920
C2-Chrysenes	ND	4.8	717	490	730
C3-Chrysenes	ND	ND	738	220	548
C4-Chrysenes	ND	ND	402	ND	252
Benzo[*b*]fluoranthene	ND	0.43	17.0	5700	2830
Benzo[*k*]fluoranthene	ND	ND	6.53	5600	3500
Benzo[*a*]fluoranthene	ND	ND	ND	1300	1020
Benzo[*e*]pyrene	ND	0.58	44.7	6400	2290
Benzo[*a*]pyrene	ND	0.73	48.1	10,000	4540
Perylene	ND	ND	20.8	2400	1020
Indeno[1,2,3-c,d]pyrene	ND	0.34	4.49	7400	2140
Dibenz[*a*,*h*]anthracene	ND	0.26	8.12	880	700
Benzo[*g*,*h*,*i*]perylene	ND	0.77	20.0	8200	1800
Total PAH52	6633	23,426	24,136	473,148	199,649
PAH16	3220	1911	2627	372,380	148,270
%API	51	89	87	15	18

whereas coal tar materials contain tens of thousands of parts per million PAH16. Further, tar products are enriched in high molecular weight 4-, 5- and 6-ring PAH, a subset of which are those regarded as probable human carcinogens and primary drivers in risk-based assessments of PAH [i.e., benz(*a*)anthracene, benzo(*a*)pyrene, benzo(*b*)fluoranthene, benzo(*k*)fluoranthene, chrysene, dibenz(*a*,*h*)anthracene, and indeno(1,2,3-*c*,*d*)pyrene (EPA, 1993)].

10.3.3.2 PAH Character and the Alkyl-PAH Index (%API)

The origins of PAH are generally classified as either petroleum-derived (petrogenic) or combustion-derived (pyrogenic) (Douglas et al., 2007). Petroleum-derived PAH are dominated by lower molecular weight 2- through 3-ring PAH and their C_1 to C_4 alkyl homologues occur in "bell shaped" distributions. Pyrogenic PAH are dominated by 4- through 6-ring PAH, with lesser amounts of alkyl homologues. Pyrogenic PAH occur in patterns dominated by the parent PAH, with systematically decreasing amounts of higher alkyl homologues, resulting in

TABLE 10.11 %API Values for Various Source Hydrocarbon Material

Hydrocarbon material	%API
Fresh coal tar	15
Weathered coal tar	18
Fresh crude oil	91
Weathered crude oil	94
Fresh heavy fuel oil	91
Weathered heavy fuel oil	97
Fresh diesel fuel	89
Weathered diesel fuel	98

a "sloped" distribution. These distinctive PAH homologue distributions are key chemical features used to distinguish the nature of PAH that compose the environmental samples.

Datasets that contain alkylated PAH data allow the investigator to more accurately identify contributions from both pyrogenic and petrogenic PAH. A convenient means to express the character of PAH (i.e., petroleum-derived PAH, pyrogenic-derived PAH) in soils is the alkyl PAH index (API). This index is the ratio of the sum of the alkyl PAH homologues to the sum of parent plus alkylated PAH homologues in a sample from naphthalene to benzo(*g*,*h*,*i*)perylene (Douglas et al., 2016). The %API can be calculated from environmental data and compared to literature reference materials in order to ascertain the PAH source characteristics and approximate percentages of petroleum- and pyrogenic-derived PAH found in soil samples. The index is defined as:

$$\%\text{API} = \left(\sum C_1\text{-}, C_2\text{-}, C_3\text{-}, \text{and } C_4\text{-alkly homologues of 2-, 3-, and 4-ring PAH}\right) / \left(\sum \text{Parent and alkylated PAH}\right) \times 100$$

This ratio compares the relative amount of the sum of the alky-substituted PAH (abundant in petroleum) to the sum of total PAH in samples. Review of data for various types of petroleum (i.e., crude oils, HFOs, and middle distillates) and pyrogenic material (i.e., coal tar, creosote) offer a framework to classify %API as source materials, or mixtures thereof. Previously published data (Douglas et al., 2016) have %API values for various source hydrocarbon materials is presented in Table 10.11. Similar %API values for these different products are evident in the sample data provided in Table 10.10.

For this case study, we identified PAH with an overwhelming petroleum origin to exhibit %API greater than 80%, and PAH with an overwhelming pyrogenic tar origin to exhibit %API less than 30%. Mixtures of petrogenic and pyrogenic products have %API values in between these two benchmarks. The %API is the basis for which the allocation of the proportion of petroleum- and pyrogenic-derived PAH in the Site soils was made. In summary, knowledge of the fundamental PAH chemistry for petroleum and MGP tar-derived PAH provides risk assessment and site assessment professionals a means to identify the likely source, and ascribe responsibility for, the PAH that drive risk-based corrective actions at contaminated sites.

10.3.3.3 Example Case—Allocating Sources of PAH in Soils at an Industrial Site

Twenty soil samples were collected from various depths in an area of an industrial site where screening studies had identified hydrocarbon (measured as TPH) and PAH impacts of regulatory concern. The soil samples were analyzed using forensic methods referenced above that included, *Total Petroleum Hydrocarbons (TPH) and Selected Alkane Quantification and Fingerprinting* (Table 10.1), and *PAH and Petroleum Biomarker Quantification and Fingerprinting* (Table 10.2).

The GC/FID hydrocarbon measurements, i.e., GC "fingerprints", and the alkylated PAH data provide two complimentary lines of data that proved useful in identifying and characterizing the bulk hydrocarbon source signatures and the underlying PAH composition of hydrocarbons measured in the environmental samples. The GC/FID fingerprints provide qualitative evidence for the petroleum and/or pyrogenic tar product(s) that make up the dominant material that comprise the TPH of the sample. As described above, the alkylated PAH data, including the %API, provide information about the proportions of petroleum and pyrogenic tar that contribute to the PAH burden of the sample.

TABLE 10.12 Summary of the Tar and Petroleum Composition of the Site Soil Samples

Boring ID	Depth (ft)	Dominant hydrocarbon fingerprint	TPH (mg/kg)	Total PAH (mg/kg)	PAH16 (mg/kg)	% Tar (TPH)	% Petroleum (TPH)	% API	% Tar (PAH)	% Petroleum (PAH)
SB1	(5–7)	Weathered HFO	4432	45	8	3	97	78	30	70
SB2	(11–13)	Pyrogenic tar	5085	1339	889	100	0	29	96	4
SB3	(0–1)	Weathered middle distillate/pyrogenic tar	3403	516	338	48	52	29	96	4
SB3	(5–7)	Weathered middle distillate/pyrogenic tar	2161	225	133	33	67	35	94	6
SB3	(9–11)	Pyrogenic tar	4537	1559	1129	100	0	20	93	7
SB3	(13–15)	Pyrogenic tar	9457	3363	2427	100	0	20	98	2
SB3	(17–19)	Pyrogenic tar	6281	1934	1337	100	0	24	90	10
SB4	(0–1)	Weathered HFO	19,700	269	23	6	94	91	0	100
SB4	(5–7)	Weathered middle distillate/pyrogenic tar	6804	597	383	28	72	26	87	13
SB4	(9–11)	Weathered middle distillate/pyrogenic tar	3960	328	193	26	74	33	95	5
SB4	(13–15)	Pyrogenic tar	5572	1874	1250	100	0	28	97	3
SB5	(0–1)	Weathered middle distillate/pyrogenic tar	17,286	585	147	11	89	72	36	64
SB5	(5–7)	Weathered middle distillate/pyrogenic tar	2099	72	14	11	89	78	28	72
SB6	(0–1)	Weathered middle distillate/pyrogenic tar	4368	145	70	10	90	45	69	31
SB6	(5–7)	Weathered middle distillate/pyrogenic tar	11,960	835	375	22	78	51	62	38
SB6	(9–11)	Pyrogenic tar	60,596	15,805	9695	100	0	33	81	19
SB7	(0–1)	Weathered middle distillate/pyrogenic tar	95,719	4425	1536	15	85	61	64	36
SB8	(13–15)	Pyrogenic tar	3105	1210	868	100	0	21	92	8
SB9	(0–1)	Weathered HFO	1761	15	6	3	97	55	57	43
SB9	(3–7)	Weathered middle distillate/pyrogenic tar	6261	609	282	31	69	49	64	36
SB9	(9–11)	Weathered middle distillate/pyrogenic tar	6151	949	657	49	51	23	94	6
SB9	(14–15)	Pyrogenic tar	2060	475	348	73	27	19	96	4

A summary of the results of relevant chemical parameters measured in the soil samples from this case study are listed in Table 10.12. The table includes characterization of the overall hydrocarbon composition of the sample, percentage of the pyrogenic tar and petroleum hydrocarbons that compose the measured TPH, the %API, and the percentage of the pyrogenic- and petrogenic-derived PAH. These results are further described in the following sections.

10.3.3.4 GC/FID Fingerprinting Results

The GC/FID chromatograms indicated that the study samples were composed of hydrocarbons that could be segregated into three categories, i.e., where the dominant hydrocarbon composition of the TPH was (1) weathered HFO, (2) pyrogenic tar, or (3) a mixture of weathered middle distillate and pyrogenic tar. Fig. 10.13 shows a representative gas chromatogram for each category type.

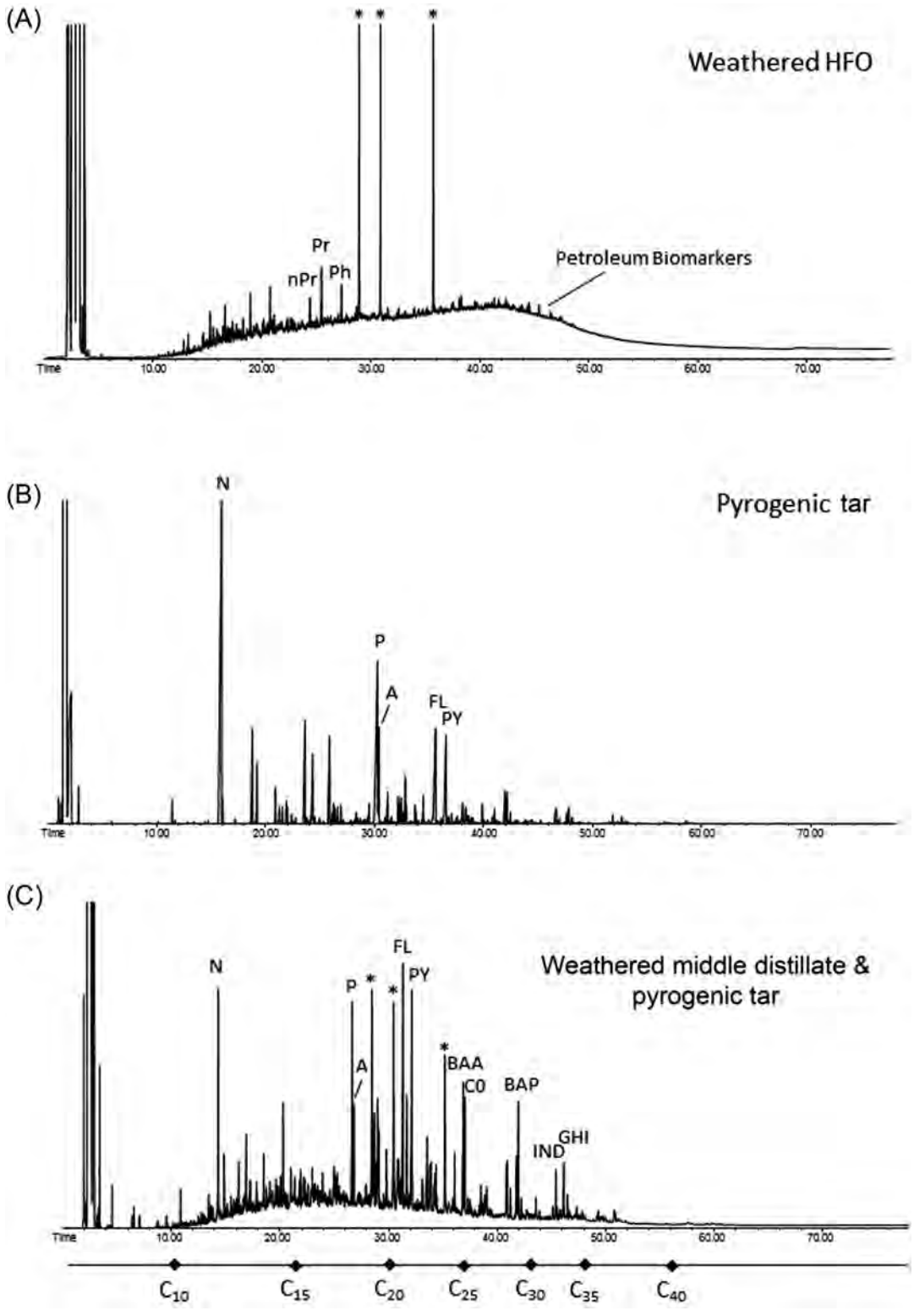

FIGURE 10.13 Gas chromatograms for samples that represent the dominant hydrocarbon product-types that compose the Site samples. (A) weathered heavy fuel oil (HFO); (B) pyrogenic tar; and (C) weathered middle distillate and pyrogenic tar mixture. "*": laboratory-added internal standard. Chromatograms are annotated with abbreviations found in Tables 10.1 and 10.2.

The majority of the bulk hydrocarbons in the samples in this case study, measured as TPH, are mixtures of petroleum and pyrogenic tar. The approximate proportions of the petroleum and pyrogenic tar that make up the TPH was extrapolated from the GC/FID data. The distribution between the hydrocarbon types (tar and petroleum) was determined by the following equation:

$$\%\text{Tar} = \frac{\text{TPAH}}{\text{TPH}} * \text{PF}$$

where

% Tar is the percentage of pyrogenic tar comprising the measured TPH;
TPAH (mg/kg) is the sum of the parent and alkylated 2- to 6-ring PAH (Table 10.2);
TPH (mg/kg) is the total petroleum hydrocarbon (TPH) concentration (C_9–C_{44}); and
PF is the Tar:TPH proportionality factor (PF). For this case study, the PF was determined by averaging the ratio of TPH:TPAH for samples identified in this study as pure pyrogenic tar.

The percentage of petroleum is the difference between the TPH and the fraction of tar. Implicit in the estimate of %Tar is the understanding that pyrogenic tars contain significantly higher proportional amounts of PAH than petroleum products, and that any PAH recognized in a GC/FID chromatogram are due solely to the presence of tar. Tar products yield TPH measurements that are typically about 30% less than the actual mass of tar. Thus the PF is used to correct tar-derived TPH values for this mass bias. Table 10.12 lists the percentage of pyrogenic tar and petroleum that compose the total petroleum hydrocarbons residues in the soil samples. The results show that fourteen percent of the Site soil samples were composed of HFO, 36% were composed of pyrogenic tar, and 50% were composed of a mixture of weathered middle distillate and pyrogenic tar.

10.3.3.5 PAH Results

While the GC/FID chromatograms provided a qualitative means to identify the bulk makeup of the total hydrocarbon residues in the Site soil samples, the "fingerprints" themselves do not directly provide insight in the makeup of the underlying PAH. Since pyrogenic tar contains disproportional larger relative amounts of pyrogenic PAH compared to the equivalent mass of petroleum, some samples that exhibit hydrocarbon fingerprints that appear petroleum dominant, or as mixtures of petroleum and pyrogenic tar, have PAH compositions that can be dominantly pyrogenic in nature. This concept is illustrated in Fig. 10.14. Fig. 10.14A is a gas chromatogram of a Site soil sample SB4 (9–11). The bulk character of the TPH of the sample, as determined by the %Tar calculation listed above, is a mixture of 74% weathered diesel fuel and 26% pyrogenic tar. However, inspection of the PAH profile for SB4 (9–11) (Fig. 10.14B) reveals that the PAH are dominantly pyrogenic in nature, i.e., the PAH pattern is dominated by parent PAH, with systematically decreasing amounts of higher alkylated homologs that occur in a "sloped" pattern. The sample also contains high concentrations of 5- and 6-ring PAH emblematic of pyrogenic-derived PAH. In addition, this Site sample has an %API of 33%—PAH of virtually 100% tar origin (Table 10.12).

Synoptically, ten (45%) of the 22 samples have an %API less than 30%, indicating that the PAH in these samples align with strictly pyrogenic tars. Only one sample had a %API greater than 80%, i.e., PAH of strictly petroleum origin. About half of the site samples (11) had %API values between the petroleum and pyrogenic tar benchmarks, indicating that they were composed of mixtures of petroleum- and pyrogenic-derived PAH (Table 10.12). A simple mix model was used to estimate the proportions of petroleum- and tar-derived PAH that made up these mixed-source samples.

In this case, a mixing model based on the %API was used to estimate the proportion of petroleum- and pyrogenic-derived PAH that composed samples. Incremental mixtures of tar and petroleum were computed using data from the analysis of laboratory reference materials. For each theoretical mixture, the percentage of petroleum-derived PAH and the %API were calculated. The types of hydrocarbons recognized in the soil were used as the two surrogate end members, viz., pyrogenic tar mixed with HFO and pyrogenic tar mixed with weathered diesel fuel. Next, the percent petroleum PAH was plotted against the %API, for mixtures that ranged from 0% to 100% of each end member. The best-fit polynomial curve for was fitted for each relationship.

Fig. 10.15A shows the best-fit polynomial curve for weathered HFO and pyrogenic tar mixture. Fig. 10.15B shows the best-fit polynomial curve for weathered diesel fuel oil and pyrogenic tar mixture. The shape of the mixing curves depicted in Fig. 10.15A and B vary somewhat, which is a result of the different distribution and relative amounts of PAH in the petroleum used in the mixing models. Using these mixing curves, the percentage

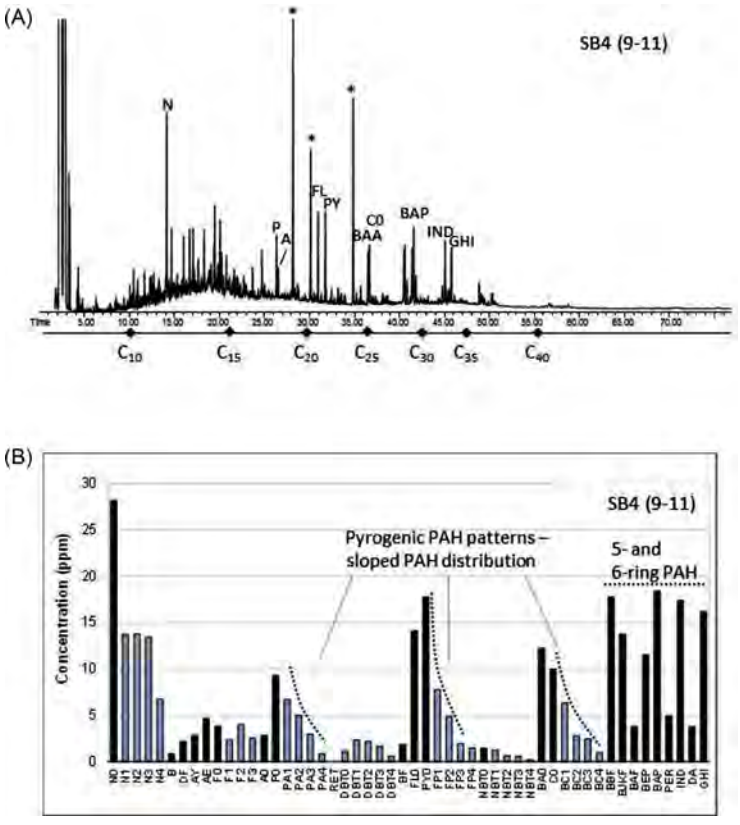

FIGURE 10.14 Compositional analysis of Site soil sample SB4 (9–11) in Case Study 3. (A) Gas Chromatogram showing the TPH makeup of the sample. PAH compounds annotated. "*" represent internal standards added. (B) PAH profile illustrating the dominate pyrogenic nature of the PAH. Black bars represent parent PAH; gray bars represent alkylated PAH.

of petroleum- and tar-derived PAH was computed for each sample, using the %API for the authentic sample as the input parameter to the best-fit mixing curve (Table 10.12).

Using this mixing model approach, it was found that in general, the majority of samples at the site contained PAH of pyrogenic tar-derived origin. Seventy-seven percent of the Site samples contained tar-derived PAH greater than 60%, and 55% contained tar-derived PAH greater than 80%. Only one sample contained petroleum-derived PAH greater than 80% (Table 10.12).

In summary conventional GC/FID fingerprinting provided a basis to identify the major sources of total hydrocarbon (TPH) contamination in soils at the contaminated site under investigation. Detailed PAH analysis revealed that the underlying PAH signatures in the site soils did not correlate directly with what the overly simplistic qualitative TPH fingerprints. Since MGP tar derived hydrocarbons contain significantly more PAH than equivalent amounts of petroleum, even small amounts of pyrogenic tar, associated with former MGP operations, in the site soils imparted a significant contribution to the PAH loads. A PAH mix model, using surrogate end members consistent with the nature of site contamination, provided a technical basis to allocate contribution of PAH in site soils to the appropriate petroleum and pyrogenic tar sources.

10.3.4 Case Study 4: Chemical Fingerprinting of Dissolved Phase Petroleum-Derived Hydrocarbons.

Many chemical fingerprinting investigations of petroleum and other hydrocarbons focus on chemical characterization of NAPL or residuals of hydrocarbons entrained in soil or sediment. The advantages of focusing on NAPL and contaminated soil is that such media contain significant concentrations of soluble, sparingly soluble, and virtually insoluble chemical compounds, thereby affording chemically diverse and information-rich chemical fingerprints. In turn, such data afford the forensic investigator the opportunity to robustly characterize and differentiate among the nature and sources of contamination at a site by drawing upon the varied similarities (or differences) observed in the compositional data among samples.

Groundwater contamination is, however, an often critical element of site investigations. As such, forensic investigators are often tasked with interpreting groundwater data in the context of understanding the likely

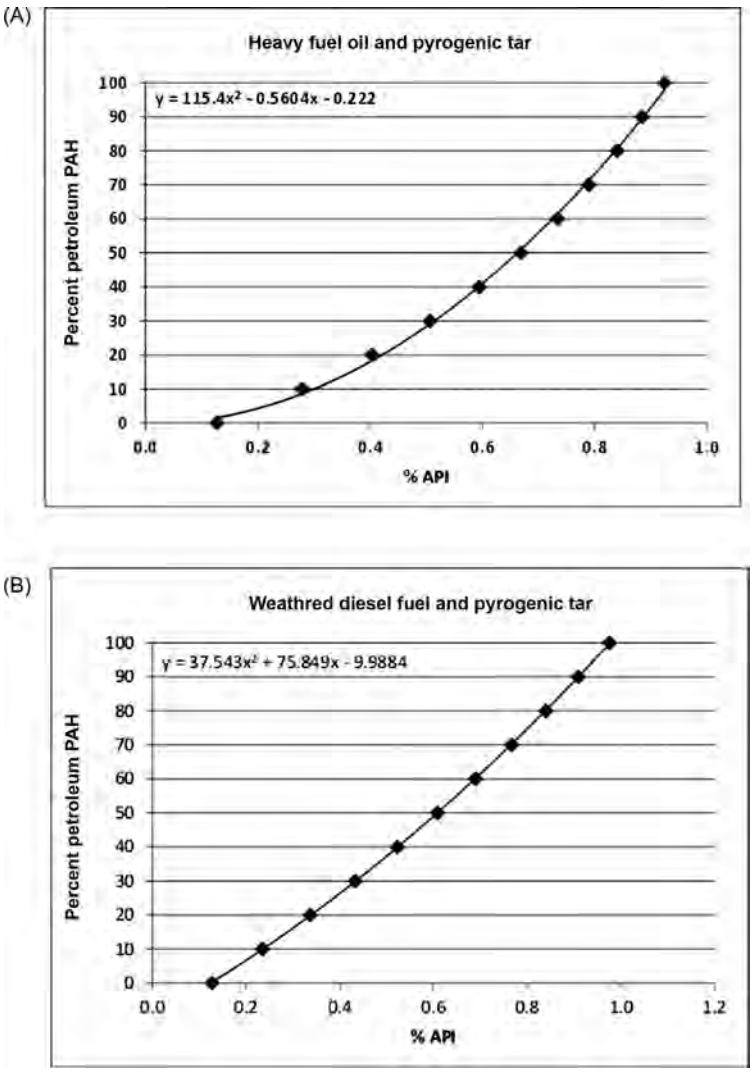

FIGURE 10.15 Plot of the percent petroleum versus APU for the two types of petroleum mixtures including (A) heavy fuel oil and pyrogenic tar, and (B) weathered middle distillate and pyrogenic tar. The best fit polynomial curve is shown in the upper left corner of each plot.

source or sources of dissolved phase contamination. There are inherent challenges in interpreting the "chemical fingerprints" of dissolved phase groundwater data. In some cases, the only data available are the limited list of regulatory hydrocarbons such as BTEX. In other cases, such as described herein, groundwater samples have been analyzed for an extended forensic-appropriate list of low molecular weight PIANO compounds (Table 10.4). However, because these compounds have highly varied water solubilities (Table 10.13), the patterns of the PIANO hydrocarbons measured in groundwater in equilibrium with a NAPL source are altered by these differential solubilities. Variable solubility among PIANO compounds can result in a loss of some chemical specificity (i.e., detectability) among dissolved phase petroleum-derived constituents due to the effects of partitioning, i.e., the interphase transfer of individual chemicals from NAPL into groundwater (Stout et al., 2010). As suggested above, the groundwater "fingerprints" of dissolved phase hydrocarbons differ from the parent product or NAPL "fingerprints" due to the preferential transfer of more soluble compounds into groundwater. The degree of partitioning of a hydrocarbon from NAPL into groundwater is a function of both the compounds' aqueous solubility and its relative mole fraction in the NAPL.

Because petroleum-derived hydrocarbon concentrations in groundwater are greatly affected by partitioning from NAPL, the direct use of the measured concentrations of water borne hydrocarbons as a "fingerprint" for the source of the chemicals can be unreliable. The use of solubility-adjusted fingerprinting techniques (Sauer and Costa, 2003) allows for intercomparison of petroleum-derived constituents among groundwater samples, and linkage of the dissolved phase chemical pattern with that of the source NAPL. Herein, we present a case study where solubility theory is used to back-calculate the predicted chemical fingerprint of the source hydrocarbon

TABLE 10.13 PIANO Concentrations Measured in GW-01, The Reference Jet Fuel and Unleaded Gasoline NAPL, and The Predicted Jet Fuel and Unleaded Gasoline NAPL WAF

Analytes	MW (g/mol)	Solubility, 20°C (mg/L)	GW-01 (μg/L)	Jet fuel NAPL (mg/kg)	Unleaded gasoline NAPL (mg/kg)	WAF jet fuel (μg/L)	WAF unleaded gas (μg/L)
Isopentane	72.15	44.59	73.2	59.7	84,300	6.09	5470
1-Pentene	70.13	114.2	ND	ND	4,760	ND	814
2-Methyl-1-butene	70.13	153.4	ND	ND	9170	ND	2106
Pentane	72.15	50.06	50.6	31.8	27,900	3.64	2033
2-Pentene (*trans*)	70.13	147.6	0.570	ND	11,400	ND	2519
2-Pentene (*cis*)	70.13	147.6	ND	ND	6,020	ND	1330
Tertiary butanol	74.12	96,600	ND	ND	ND	ND	ND
Cyclopentane	70.13	234.8	63.0	ND	4,460	ND	1,568
2,3-Dimethylbutane	86.18	13.64	20.7	33.0	8710	0.86	145
2-Methylpentane	86.18	12.52	52.7	112	30,200	2.68	461
MTBE	88.15	19,600	ND	ND	105	ND	2451
3-Methylpentane	86.18	14.82	77.1	95.5	19,500	2.71	352
1-Hexene	84.16	29.84	ND	ND	802	ND	30
Hexane	86.18	13.81	34.6	61.9	19,900	1.64	335
Diisopropyl ether (DIPE)	102.17	3740	ND	ND	ND	ND	ND
Ethyl tertiary butyl ether (ETBE)	102.2	4980	ND	ND	135	ND	691
2,2-Dimethylpentane	100.2	2.43	1.50	8.20	1940	0.033	4.94
Methylcyclopentane	84.16	52.56	328	127	15,700	13.1	1030
2,4-Dimethylpentane	100.2	2.97	2.80	49.6	5670	0.243	17.6
1,2-Dichloroethane	98.96	13,900	ND	ND	ND	ND	ND
Cyclohexane	84.16	65.97	531	122	5760	15.8	474
2-Methylhexane	100.2	3.24	13.3	103	14,600	0.550	50
Benzene	78.11	1270	7.80	ND	4390	ND	7495
2,3-Dimethylpentane	100.2	4.12	15.3	127	7840	0.862	34
Thiophene	84.14	1540	ND	ND	ND	ND	ND
3-Methylhexane	100.2	3.66	22.9	195	15,300	1.18	59
TAME	102.17	6460	ND	ND	ND	ND	ND
1-Heptene/1,2-DMCP (trans)	98.19	7.34	135	227	2500	2.80	20
Isooctane	114.22	0.61	ND	109	18,600	0.10	10
Heptane	100.23	3.48	20.3	325	10,400	1.86	38
Methylcyclohexane	98.19	13.74	358	885	5700	20.4	84
2,5-Dimethylhexane	114.23	0.76	0.642	62.4	3360	0.069	2.35
2,4-Dimethylhexane	114.23	0.87	2.35	110	3530	0.138	2.82
2,2,3-Trimethylpentane	114.23	0.9	ND	11.6	890	0.015	0.74
2,3,4-Trimethylpentane	114.23	1.13	ND	93.0	8140	0.152	8.45

(*Continued*)

TABLE 10.13 (*Continued*)

Analytes	MW (g/mol)	Solubility, 20°C (mg/L)	GW-01 (μg/L)	Jet fuel NAPL (mg/kg)	Unleaded gasoline NAPL (mg/kg)	WAF jet fuel (μg/L)	WAF unleaded gas (μg/L)
2,3,3-Trimethylpentane	114.23	1.06	ND	61.3	7820	0.094	7.62
2,3-Dimethylhexane	114.23	1.01	1.16	134	2800	0.195	2.60
3-Ethylhexane	114.23	1.08	0.742	134	915	0.209	0.91
2-Methylheptane	114.23	0.81	3.92	605	5240	0.708	3.90
3-Methylheptane	114.23	0.95	2.58	504	5340	0.692	4.66
Toluene	92.14	398	27.5	84.6	58,800	60.3	26,669
2-Methylthiophene	98.17	504.1	ND	ND	ND	ND	ND
3-Methylthiophene	98.17	529.1	ND	ND	ND	ND	ND
1-Octene	112.22	1.79	ND	ND	ND	ND	ND
Octane	114.22	0.86	3.31	1430	4430	1.78	3.50
1,2-Dibromoethane	187.86	8830	ND	ND	ND	ND	ND
Ethylbenzene	106.17	140.9	49.4	217	13,800	47.5	1923
2-Ethylthiophene	112.19	124.2	ND	ND	ND	ND	ND
p/*m*-Xylene	106.17	121.7	376	987	38,400	187	4622
1-Nonene	126.24	0.42	ND	ND	ND	ND	ND
Nonane	128.25	0.21	ND	5230	2080	1.41	0.36
Styrene	104.15	142.2	ND	ND	29.9	ND	4.29
o-Xylene	106.17	164.8	188	619	14,400	159	2347
Isopropylbenzene	120.19	49.25	6.47	149	941	10.1	40.5
n-Propylbenzene	120.19	31.05	0.501	340	3650	14.5	99.0
1-Methyl-3-ethylbenzene	120.19	47.65	158	1100	9960	72.0	415
1-Methyl-4-ethylbenzene	120.19	43.88	78.5	657	5210	39.6	200
1,3,5-Trimethylbenzene	120.2	43.46	71.8	1360	4690	81.1	178
1-Decene	140.3	0.0936	ND	ND	ND	ND	ND
1-Methyl-2-ethylbenzene	120.2	63.9	112	1030	3990	90.3	223
Decane	142.3	0.0504	0.419	12,400	1460	0.725	0.05
1,2,4-Trimethylbenzene	120.2	51.94	205	3620	14,400	258	653
sec-Butylbenzene	120.2	16.77	4.00	302	224	6.95	3.28
1-Methyl-3-isopropylbenzene	134.22	16.84	16.9	497	417	10.3	5.49
1-Methyl-4-isopropylbenzene	134.22	15.26	9.11	408	150	7.65	1.79
1-Methyl-2-isopropylbenzene	134.22	23.17	3.66	194	44.5	5.53	0.81
Indan	118.18	98.1	10.7	379	3,430	51.9	299
1-Methyl-3-propylbenzene	134.22	10.66	18.9	1020	1740	13.4	14.5

(*Continued*)

TABLE 10.13 (*Continued*)

Analytes	MW (g/mol)	Solubility, 20°C (mg/L)	GW-01 (μg/L)	Jet fuel NAPL (mg/kg)	Unleaded gasoline NAPL (mg/kg)	WAF jet fuel (μg/L)	WAF unleaded gas (μg/L)
1-Methyl-4-propylbenzene	134.22	9.85	ND	622	874	7.53	6.73
n-Butylbenzene	134.22	7.16	ND	478	650	4.21	3.64
1,2-Dimethyl-4-ethylbenzene	134.22	18.47	17.9	1380	1740	31.3	25.1
1,2-Diethylbenzene	134.22	16.03	5.81	613	140	12.1	1.76
1-Methyl-2-propylbenzene	134.22	14.21	15.5	1260	566	22.0	6.29
1,4-Dimethyl-2-ethylbenzene	134.22	18.46	17.6	1390	1100	31.5	15.9
Undecane	156.3	0.0118	ND	16,400	364	0.204	0.00
1,3-Dimethyl-4-ethylbenzene	134.22	20.21	17.2	1540	925	38.3	14.6
1,3-Dimethyl-5-ethylbenzene	134.22	16	21.2	2180	1650	42.9	20.7
1,3-Dimethyl-2-ethylbenzene	134.22	25.66	5.46	477	126	15.0	2.53
1,2-Dimethyl-3-ethylbenzene	134.22	25.83	12.5	1130	299	35.9	6.04
1,2,4,5-Tetramethylbenzene	134.22	9.01	7.76	1100	715	12.2	5.04
Pentylbenzene	148.24	1.68	0.344	240	46.7	0.449	0.06
Dodecane	170.34	0.00272	ND	12,400	102	0.033	0.00
Naphthalene	142.28	142.1	47.4	487	903	80.3	94.7
Benzothiophene	134.2	191.6	ND	ND	ND	ND	ND
MMT	218.09	24.39	ND	ND	ND	ND	ND
Tridecane	184.36	0.02746	ND	3620	ND	0.089	ND
2-Methylnaphthalene	170.33	40.62	44.5	1730	346	68.1	8.66
1-Methylnaphthalene	170.33	40.62	49.8	1280	162	50.4	4.06

from dissolved phase groundwater data, using equilibrium partitioning theory based on Raoult's law of partitioning between liquid phase hydrocarbon and groundwater (Lane and Loehr, 1992; Luthy et al., 1993; Mahjoub et al., 2000; Sauer and Costa, 2003; Burris et al., 2006). The basic Raoult's law equation that describes the partitioning of a chemical between liquid phase petroleum and the dissolved phase is:

$$C_w = X_o S$$

where C_w is the effective solubility of a compound, X_o is the mole fraction (of a chemical in fuel), and S is the solubility (mg/L).

The estimate of the mole fraction of a chemical found in a NAPL depends in part on the estimated molecular weight of the parent NAPL. Estimated molecular weights for different petroleum products are available in the literature. EPA has published such data (Wilson et al., 1990), and they are available on the U.S. EPA web site "On-line Tools for Site Assessment Calculation" (https://www3.epa.gov/ceampubl/learn2model/part-two/onsite/es.html) wherein the mole fraction for common fuels including gasoline (105 g/mol), jet fuel/kerosene (165 g/mol), and diesel fuel (230 g/mol) are reported.

An application of dissolve phase hydrocarbon fingerprinting is presented in the following case study conducted at an active bulk fuel storage facility. The subject of this case is a terminal located on an eight acre site in a rural area of New Mexico. The facility consists of six above ground storage tanks (ASTs) containing jet fuel and automotive gasoline. The terminal is interconnected with a pipeline system and contains a product blending facility as well as a truck loading and offloading rack. Residential and commercial properties border the terminal. Dissolved phase hydrocarbon impacts were found in a monitoring well located on a neighboring property just downgradient of the terminal. The terminal environmental management team needed to understand the likely source(s) of the contamination discovered in the offsite monitoring well. While various environmental site assessments and limited remediation activities were conducted on the terminal property by consultants contracted by the owners/operators of the terminal, these undertakings did not develop suitable data to adequately characterize the nature (and thus source) of the contaminants in groundwater off-site. A forensic investigation was undertaken to identify the chemical characteristics and likely source(s) of the dissolved phase hydrocarbon contamination found in the impacted offsite monitoring well.

In support of this study, a groundwater sample was collected from the offsite monitoring well where dissolved phase BTEX had previously been reported (GW-01). The groundwater was analyzed using the forensic methods describe above that included a high resolution TPH-type GC and measurement of volatile-range PIANO hydrocarbons (Table 10.4).

Inspection of the gas chromatogram for groundwater sample GW-01 (Fig. 10.16) reveals a relatively uncomplicated mixture of hydrocarbons, composed primarily of individual C_5 to C_{12} compounds; there is no evidence for an UCM that is typically associated with a "whole oil" fingerprint of middle distillate and higher boiling petroleum fuels. The absence of a UCM does not rule out distillate fuels as source of the dissolved phase hydrocarbons, because most of the constituents of the UCM are effectively insoluble. Further compositional analysis of the true dissolved phase hydrocarbons was needed to identify the source of the compounds found in the GW-01 groundwater.

Compositional analysis of the dissolved phase PIANO compounds shed light on the nature of the hydrocarbons observed in the gas chromatogram. The total concentration of the 88 dissolved-phase PIANO analytes in the GW-01 groundwater is 3423 μg/L. The compositional histogram for the PIANO compounds measured in GW-01 is presented in Fig. 10.17A. The most prominent compounds present include methylcyclohexane, xylenes and numerous C3- and C4-alkylbenzenes. Many of these compounds are common to both jet fuel and gasoline. However, the presence of substantial relative concentrations of naphthenic hydrocarbons (i.e., methylcyclopentane, cyclohexane, and methylcyclohexane) and the absence of important additives found in modern gasolines (e.g., alkylate blending stock or any oxygenated compounds, i.e., TBA, MTBE, DIPE, ETBE, and TAME) are inconsistent with a gasoline source, and more commonly reconcile with the water soluble fraction of a naphthene-rich, light distillate product such as jet fuel.

In an effort to illustrate the likely source of the water soluble hydrocarbons observed in GW-01, we calculated the water accommodated fraction (WAF) of both gasoline and jet fuel reference samples, based on the measured concentrations of PIANO compounds in the two types of fuels (Table 10.13). Fig. 10.17 presents the predicted dissolved PIANO distributions of dissolved phase hydrocarbons for the jet fuel (Fig. 10.17B) and unleaded, alkylate grade gasoline reference samples (Fig. 10.17C). For comparison, the PIANO compositional histogram for the dissolved phase chemicals measured in GW-01 is shown in Fig. 10.17A.

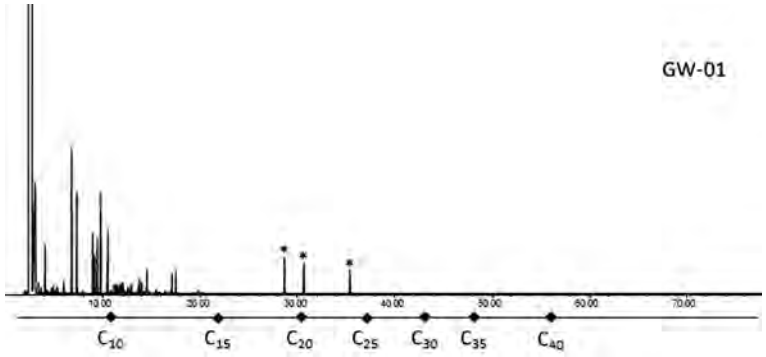

FIGURE 10.16 Gas chromatograms of groundwater sample GW-01 from Case Study 4.

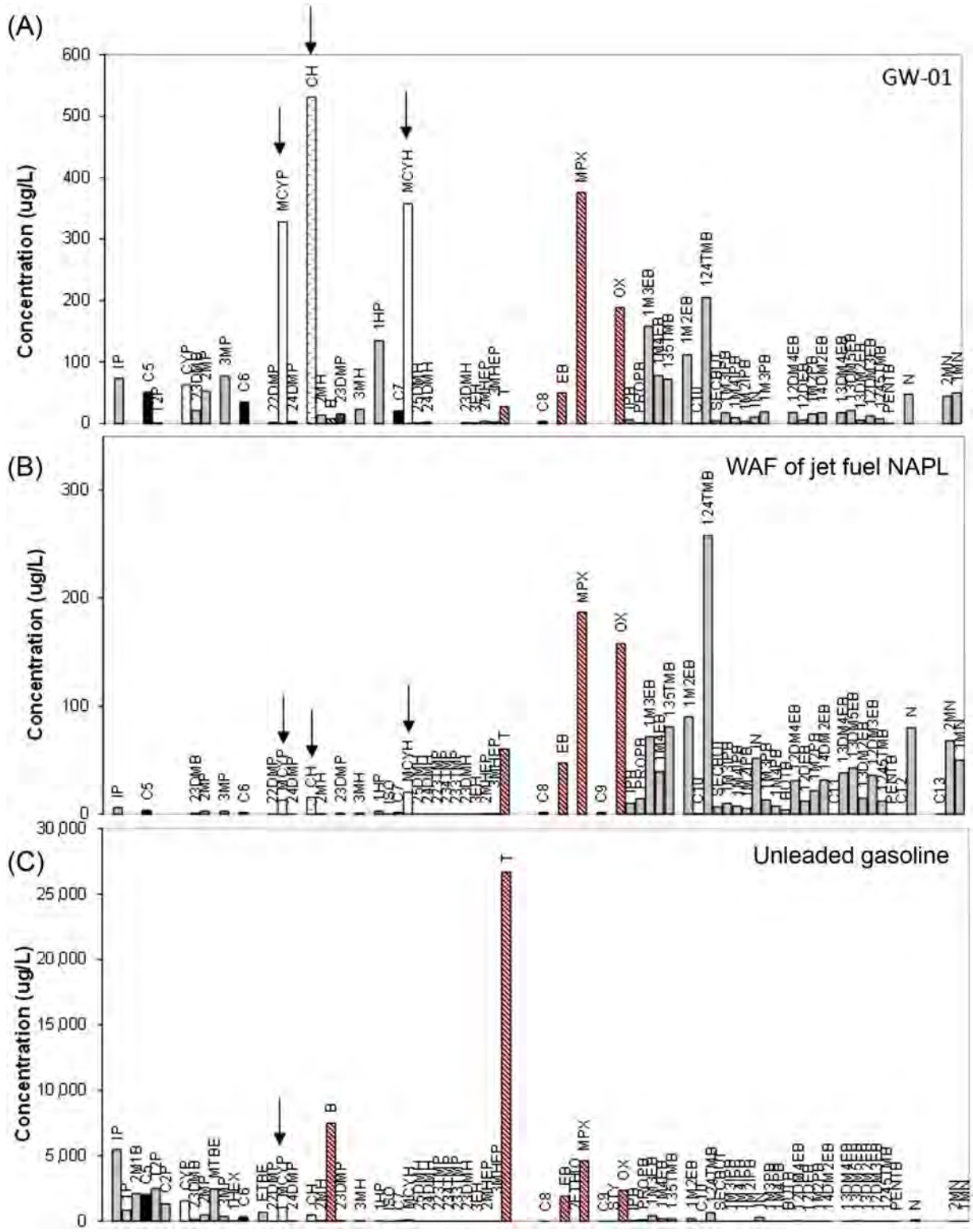

FIGURE 10.17 PIANO histograms: (A) measured concentrations in the GW-01 groundwater and WAF predicted groundwater concentrations of reference (B) jet fuel NAPL; and (C) unleaded gasoline.

It is readily apparent that the predicted WAF of the gasoline reference sample is dominated by simple BTEX chemicals, whereas the predicted WAF of the jet fuel reference sample is composed of a more complex mixture of higher boiling monoaromatics and to a lesser extent, naphthenic hydrocarbons. The PIANO histogram of the GW-01 groundwater sample has strong compositional similarity with jet fuel, albeit with significantly higher relative concentrations of naphthenic compounds, notably methyl-cyclopentane, cyclohexane, and methylcyclohexane. We attribute the elevated relative concentrations of these naphthenic compounds in the GW-01 groundwater to a jet fuel source that is more highly weathered, namely water-washed, than the fresh jet fuel used as the reference sample in this exercise.

Based on this analysis, we concluded that the dissolved phase hydrocarbons found in GW-01 best reconciled with a weathered jet fuel source. Armed with this information, the site management team was able to locate and repair a chronic subsurface leak in the bulk fuel facility's jet fuel handling system.

References

Agency for Toxic Substances and Disease Registry, 1995. Toxicological profile for polycyclic aromatic hydrocarbons. Agency for Toxic Substances and Disease Registry Division of Toxicology/Toxicology Information Branch 1600 Clifton Road NE, E-29 Atlanta, Georgia 30333.

Alameda Countywide Clean Water Program (CCWP), 1992. Keeping It All in Tune: Car Repair and Pollution Prevention. Alameda Countywide Clean Water Program, Hayward, CA.

Beall, P.W., Stout, S.A., Douglas, G.S., Uhler, A.D., 2002. On the role of process forensics in the characterization of fugitive gasoline. Environ. Claims J. 14, 487–506.

Burris, D.R., Reisinger, H.J., Lundegard, P.D., 2006. Fingerprinting approach for relating non-aqueous phase liquid, soil, and groundwater data. Environ. Forensics 7, 247–257.

Daling, P.S., Faksness, L.G., Hansen, A.B., Stout, S.A., 2002. Improved and standardized methodology for oil spill fingerprinting. Environ. Forensics 3, 263–278.

Douglas, G.D., Emsbo-Mattingly, S.D., Stout, S.A., Uhler, A.D., McCarthy, K.J., 2007. Chemical fingerprinting of hydrocarbons and polychlorinated biphenyls. In: Murphy, B., Morrison, R. (Eds.), Introduction to Environmental Forensics, second ed. Academic Press, New York, pp. 317–459.

Douglas, G.D., Stout, S.A., Uhler, A.D., McCarthy, K.J., Emsbo-Mattingly, S.D., 2016. Advantages of quantitative chemical fingerprinting in oil spill identification and allocation of mixed hydrocarbon contaminants. In: Stout, S.A., Wang, Z. (Eds.), Standard Handbook Oil Spill Environmental Forensics Fingerprinting and Source Identification, second ed. Academic Press, New York, pp. 789–847.

Douglas, G.S., Uhler, A.D., 1993. Optimizing EPA methods for petroleum contaminated site assessments. Environ. Test. Anal. 2, 46–53.

Douglas, G.S., Bence, A.E., Prince, R.C., McMillen, S.J., Butler, E.L., 1996. Environmental stability of selected petroleum hydrocarbon source and weathering ratios. Environ. Sci. Technol. 30 (7), 2332–2339.

Emsbo-Mattingly, S.D., Uhler, A.D., Stout, S.A., McCarthy, K.J., Douglas, G.D., Brown, J.S., et al., 2002. Polycyclic aromatic hydrocarbon (PAH) chemistry of MGP tar and source identification in sediment. In: Coleman, A. (Ed.), Sediments Guidance Compendium. Electric Power Research Institute, Palo Alto, CA, pp. 1–41, Technical Report 1005216.

EPA, 1979. Organic Solvent Cleaners—Background Information for Proposed Standards. Office of Air, Noise. Office of Air quality Planning and Standards, Washington, DC, EPA-450/2-78-045a.

EPA, 1993. Provisional Guidance for Quantitative Risk Assessment of Polycyclic Aromatic Hydrocarbons. Office of Research and Development, Washington, DC, EPA/600/R-93/089.

EPA, 2015. Test Methods for Evaluating Solid Waste, Physical/Chemical Methods, third ed. EPA Publication SW-846, Washington, DC, Final Updates I (1993), II (1995), IIA (1994), IIB (1995), III (1997), IIIA (1999), IIIB (2005), IV (2008), and V (2015).

EPA, 2017. Underground storage tanks. https://www.epa.gov/ust/learn-about-underground-storage-tanks-usts.

Fuel Standard (Petrol) Determination, 2001. Section 21 of the fuel quality standards act 2000. Federal Registry of Legislative Instruments F2006C00555.

Hansen, A.B., Daling, P., Faksness, L.G., Sorheim, K.R., Kienhuis, P., Duus, R., 2006. Emerging CEN methodology for oil spill identification. In: Wang, Z., Stout, S.A. (Eds.), Oil Spill Environmental Forensics. Elsevier, New York.

Kansas State University, 2000. Pollution Prevention for Auto Maintenance and Repair Shops. Kansas State University Pollution Prevention Institute, Manhattan, KS.

Lane, W.F., Loehr, R.C., 1992. Estimating the equilibrium aqueous concentrations of polynuclear aromatic hydrocarbons in complex mixtures. Environ. Sci. Technol. 26 (5), 983–990.

Luthy, R.G., Ramaswami, A., Goshal, S., Merkel, W., 1993. Interfacial films in coal tar non-aqueous phase liquid water systems. Environ. Sci. Technol. 27 (13), 2914–2918.

Mahjoub, B., Jayr, E., Bayard, R., Gourdon, R., 2000. Phase partition of organic pollutants between coal tar and water under variable experimental conditions. Wt. Res. 34 (14), 3551–3560.

NACS, 2015. 2015 Retail Fuels Report. The Association for Convenience & Fuel Retailing (NACS), Alexandria, CA.

Sauer, T.C., Boehm, P.D., 1995. Hydrocarbon chemistry analytical methods for oil spill assessment. Marine Spill Response Corporation Technical Report Series 95-032.

Sauer, T.C., Costa, H., 2003. Fingerprinting of Gasoline and Coal Tar NAPL Volatile Hydrocarbons Dissolved in Groundwater. Environ. Forensics 4, 319–329.

Stout, S.A., 2003. Applications of petroleum fingerprinting in known and suspected pipeline releases—two case studies. Appl. Geochem. 18, 915–926.

Stout, S.A., Wang, Z., 2008. Diagnostic compounds for fingerprinting petroleum in the environment. In: Hester, R.E., Harrison, R.M. (Eds.), *Environmental Forensics*, Issues in Environmental Science and Technology Publ. No. 26. Royal Society of Chemistry, Cambridge, pp. 54–104.

Stout, S.A., Douglas, G.S., Uhler, A.D., 2006. Automotive gasoline. In: Murphy, B., Morrison, R. (Eds.), Environmental Forensics: A Contaminant Specific Approach. Elsevier Publishing Co, San Francisco, CA, pp. 466–531.

Stout, S.A., Douglas, G.S., Uhler, A.D., 2010. Assessing temporal and spatial variations of gasoline-impacted groundwater using relative mole fractions and PIANO fingerprinting. Environ. Forensics 11 (4), 328–341.

Stout, S.A., Emsbo-Mattingly, S.D., Douglas, G.S., Uhler, A.D., McCarthy, K.J., 2015. Beyond 16 priority pollutant PAHs: a review of PACs used in environmental forensic chemistry. Poly. Aromat. Compd. 35 (2–4), 285–315.

Stout, S.A., Douglas, G.S., Uhler, A.D., 2016. Chemical fingerprinting of gasoline and distillate fuels. In: Stout, S.A., Wang, Z. (Eds.), Standard Handbook of Oil Spill Environmental Forensics: Fingerprinting and Source Identification, second ed. Elsevier Publishing Co, Boston, MA, pp. 509–564.

Sunkin, E., 2000. Repair market industry profile, Ed Sunkin, Underhood Service, March 2000. http://www.babcox.com/editorial/us/us30044.htm.

Uhler, A.D., Stout, S.A., McCarthy, K.J., Seavey, J.A., Uhler, R.M., 1999. Identification and differentiation of light- and middle-distillate petroleum for NRDA using chemical forensics. In: Proceedings of the International Oil Spill Conference, Seattle, WA.

Uhler, A.D., Stout, S.A., Douglas, Gregory S., Healey, E.M., Emsbo-Mattingly, Stephen D., 2016. Chemical character of marine heavy fuel oils and lubricants. In: Stout, S.A., Wang, Z. (Eds.), Standard Handbook of Oil Spill Environmental Forensics: Fingerprinting and Source Identification, second ed. Elsevier Publishing Co, Boston, MA, pp. 641–683.

Wang, Z., Fingas, M., 2003. Development of oil hydrocarbon fingerprinting and identification techniques. Mar. Pollut. Bull. 47, 423–452.

Wang, Z., Fingas, M., Page, D.S., 1999. Oil spill identification. J. Chromatogr. A 843, 369–411.

Wang, Z., Fingas, M., Sigouin, L., 2000. Characterization and source identification of an unknown spilled oil using fingerprinting techniques by GC-MS and GC-FID. LC GC N. Am. 18, 1058–1067.

Wilson, J.L., Conrad, S.H., Mason, W.R., Peplinski, W., Hagan, E., 1990. Laboratory investigation of residual liquid organics. United States Environmental Protection Agency, EPA. 600/6-90/004.

CHAPTER

11

Advantages of Multidimensional Chemical Fingerprinting in Identifying the Source of Marine Oil Spills in Bohai Bay, China

Xiaoxing Liu

Dalian Maritime University, Dalian, China

BIOGRAPHY

Dr. Xiaoxing Liu obtained a doctoral degree in Eco-systems Engineering from Tokushima University (Japan) in 2002. He now works as a Professor at the College of Environmental Science & Engineering at Dalian Maritime University in China, and is mainly engaged in the study and development of analytical technology for environmental pollutants. He has completed major projects such as, "*Distribution and sources of polycyclic aromatic hydrocarbons in Tokushima*", as a regional project supported by the Japanese Science and Technology Agency, "*Development of biochemical chip making use of local surface plasmon resonance*" supported by the Hitachi Corporation of Japan, and "*Study on characteristics, drift prediction and recovery technology of sunken and submerged oil in Bohai, China*" supported by the Maritime Safety Administration of China. In recent years, his research has mainly focused on the identification of the nature and source marine oil spills in China derived from unknown sources. The relative research achievements including: ten publication articles, a co-authored monograph, three China invention patents, one second class prize of China Institute of Navigation's Science and Technology Rewards.

11.1 INTRODUCTION

With the expanding development of China's economy the demand for petroleum is rising rapidly. Since more than 90% of oil transportation relies on maritime routes, and coupled with offshore drilling operations, the risk of oil spills is increasing in coastal waters. It is often very difficult to the confirm the identity of the responsible party for oil spills and the resulting damage claims due to the escape and concealment of the perpetrators after oil spills occurred. Over the past two decades, the claims for only 17 oil spill cases have been compensated in 44 cases oil spill accidents in which 50 t of oil were discharged in the coastal areas of China. The main reason for this was the difficulty of identifying the source of oil after long-term weathering of the spilled oil reduced the ability to accurately identify the original source oil. As most perpetrators were not held liable, it was difficult to provide the cost of cleanup following the incident. As a result the oil spills were not removed in time and many potential losses were irreversible. Therefore, a better means for the identification of oil spills after long-term weathering has great significance for the protection of the marine environment.

Bohai Bay is located between Liaoning, Hebei, Shandong and Tianjin and surrounded by land on three sides. The Bay is a semienclosed sea with an area of about 77,000 square kilometers and an average depth of 44 m and the coastline is about 3800 km. As noted above, in recent years, there has been an increasing problem surrounding marine pollution control of China. Specifically, there has been repeated incidents where unknown sources of

Oil Spill Environmental Forensics Case Studies.
DOI: http://dx.doi.org/10.1016/B978-0-12-804434-6.00011-2

FIGURE 11.1 The map of Bohai Bay.

FIGURE 11.2 The oil pollution on the beach of Qinhuangdao.

spilled oil went ashore in Bohai Bay. More than 20 cases consecutively occurred on the shore of Qinhuangdao during the 2006–2014 years. Figs. 11.1 and 11.2 show the locations and character of oils that went ashore on Qinhuangdao during March to July in 2012, mostly in April, May, and June. Because there was no known oil spill(s) occurred in the nearby sea area when the oil washed ashore, it hypothesized that an oil spill in the past that had resulted in sunken and submerged oil had been remobilized and then floated in the appropriate environment conditions until becoming stranded on the shore. These mysterious events had seriously damaged the local tourism and aquaculture.

Sunken and submerged oil settled down the coastal waters through the interaction between oil spills and the sediments in the sea. The main reasons for such behavior of oil spills were believed to be:

1. Sinking of oil spills with high density
   The density of spilled oil was greater than water resulted in settling to the seabed.
2. Oil spills suspending in the water
   The volatilization of the light components in oil spill led to its density becoming closer to that of water, and it became suspended in the water under the wave action.
3. Sinking of floating oil after becoming adhered to the suspended sand in the water
   In shallow or turbulent sea area, the floating oil adhered to suspended sand led to agglomeration and increased density of oil–sand particles causing sinking of the oil with as little as 2 wt% sand was present.
4. Resuspension, stranding, transport, and settlement of oil spills

Oil spills stranded on the shore due to adhered to sediments or sands, which were previously submerged under the seawater with the tide rise.

5. Sinking after artificial intervention

The use of in situ burning as an emergency response treatment for oil spill would form an unburned residue of higher density that would sink. In addition, the use of chemical dispersant emulsified oils into the seawater.

Previously sunken and submerged oil could subsequently float again under the action of sand falling, changes in water temperature, or greater hydraulic energy. The migration and fate of previously sunken and submerged oil are not entirely clear yet, and most of the existing oil transport models are unable to simulate the movement of oil heavier than water.

Since the source oil pollution in Bohai Bay derives mainly from the leakage of crude oil and marine fuel, understanding the chemical compositions of, and distinctions between, these petroleums was an important basis for their accurate identification. Bohai crude oils are considered heavy crude oils because their density is usually 0.93–0.98 (g/cm^3, 20°C). Bohai crude oils elemental compositions include 85.5–87.6 (wt%) carbon, 10.4–13.0 (wt%) hydrogen, 0.04–0.60 (wt%) sulfur, 0.07–0.79 (wt%) nitrogen, 15.00–46.80 (ppm) nickel, and 0.40–1.54 (ppm) vanadium. The alkane content is only 32.8–44.6 (wt%) due to biodegradation, but the content of gum is 18.9–29.8 (wt%). Normal paraffins are an important constituent in Bohai crude oil and show a continuous distribution easily measured using gas chromatography. The maximum *n*-alkane in crude oils varies with the different of geological age of crude oil but also with the degree of weathering (Wang et al., 1999). The distribution of *n*-alkanes in a typical Bohai crude oil is shown in Fig. 11.3, although it should be noted that the *n*-alkanes in a few Bohai crude oils (e.g., Penglai 19–3) vary owing to partial or complete biodegradation (Deng and Li, 2001).

The composition of refined petroleum product are different from the parent crude oil due to changes experienced during the refining process. For example, marine fuel is composed of a heavier residual oil and lighter diesel fuel (gas oil) that are blended in certain proportions. Marine fuels often contain rich polycyclic aromatic hydrocarbons and *n*-alkanes, and appear dark brown in color, i.e., the same as most Bohai crude oils. The density of marine fuel is close to that of water and as such, it can be expected to float or sink and submerge in the sea after leakage.

The physical properties and chemical composition of petroleum are as unique as the human fingerprinting. The conventional way to identify the source of oil spills is comparison between the chemical fingerprints of a spilled oil and suspected source oil(s). Because of the complexity of oil composition, there is no one analytical method that can express all information of oil products. With the development of analytical technology, a variety of test methods have been used for the characterization of oil chemistry, resulting in a variety of approaches to oil fingerprinting. For example, the US exploited GC, GC/MS to identify the source of oil spills (Frame et al., 1979; Blumer et al., 1971). Canada used fluorescence spectroscopy (FL) to resolve the feature of oil spills (Wang et al., 2006). France developed the model software for identification of oil spills by GC–IR (Staniloac et al., 2001), Japan utilized GC, GC/MS, FT/IR to distinguish oil spills, and Korea has used GC, FT/IR, and FL to identify oils from ships leakage. Oil spill fingerprinting methods in China have only recently been evolving. In recent years, the State Oceanic Administration and Ocean University of China has utilized GC/MS and FL to identify the

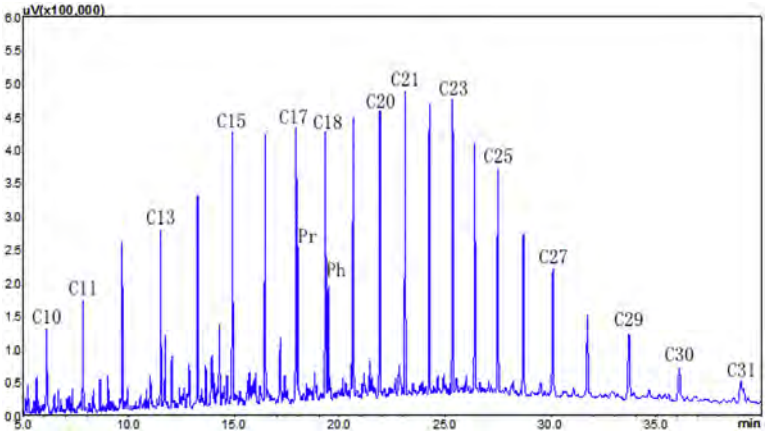

FIGURE 11.3 The gas chromatograph of *n*-alkanes of Bohai crude oil.

source of oil spills (Yang et al., 2008; Li et al., 1998; Zhu et al., 2009), Guangzhou Institute of Geochemistry has used GC/MS to trace the origin of crude oil (Peng et al., 2004), and Dalian Maritime University has used GC/IrMS to analyze the characteristic of $\delta^{13}C$ in crude oil and marine fuel (Wang et al., 2013; Liu et al., 2014). Because the indicator that expresses petroleum information is different in each analytical method, the oil characteristics can only be described using the most representative information which is extracted from the experimental data (Wang et al., 2002). At present, the indicators most commonly used for oil fingerprinting include *n*-alkanes, pristine (Pr), phytane (Ph), polycyclic aromatic hydrocarbons, steranes, and terpanes as biomarker compounds. The distribution of *n*-alkanes, Pr, and Ph can be directly showed in GC or GC/MS chromatograms. Identification of oil samples is realized by GC chromatogram and selected diagnostic ratios (n-C_{17}/Pr, n-C_{18}/Ph, Pr/Ph; Wang et al., 1997, 1998). Benzene, naphthalene and phenanthrene in petroleum are common aromatic hydrocarbons in most petroleum. Some aromatic hydrocarbons with four and five rings are related to steranes and terpanes biomarkers. The distributions of polycyclic aromatic hydrocarbons can vary in different crude oils and refined oil products, and are generally more stable than saturated hydrocarbons in most weathering processes, and as such, are often useful in oil fingerprinting. Petroleum geochemical studies have shown that terpane and sterane biomarkers vary widely among different crude oils, and that their volatility, susceptibility to biodegradation, and water solubility are very small. As such, biomarkers play an important role in identification of weathered oil since they are among the most stable hydrocarbons in crude oil (Christensen et al., 2005). However, biomarkers have no advantage at all on identification of some marine fuel due to easy damage or loss in petroleum refining process. In order to distinguish oil products which refined from different crude oil, using the stable isotope ratio method to obtain data of the total hydrocarbon isotopic composition and individual hydrocarbon isotope composition, the latter can provide more useful isotope fingerprinting (Philp et al., 2002). The stable isotope ratio method is not only useful for identification of oil containing no biomarkers, but can supplement identification of oil containing biomarkers.

Most of studies on oil fingerprinting focus on the determination of some diagnostic component characteristics especially revealed by the chromatographic fingerprinting of various hydrocarbons. However, chromatographic fingerprinting has some uncertainties owing to the complexity of petroleum components and the variable influences of weathering. For instance, the US Coast Guard's Oil Identification Laboratory pointed out that some marine fuels with low-boiling point were not correctly and effectively detected by GC, FL, FT/IR, and HPLC because of the action of a long-term weathering (Kaplan et al., 2001). Spotts et al. (2005) made use of tracking metals (nickel, iron, copper, manganese, and chromium) to distinguish 14 different kinds of light marine fuel, and the metals results were in good agreement with the results of organic analysis.

The study of human fingerprints indicated that the so-called fingerprinting recognition was not only according to fingerprinting lines, but also to several characteristics of the fingerprint, such as endpoint, fingerprinting center, bifurcation and delta (Mori et al., 2003; Fig. 11.4). By analogy, the various indicators that reflect petroleums' different chemical properties should also be combined and considered when using d chemical fingerprinting for the identification of oil spills. In view of abundant *n*-alkanes, polycyclic aromatic hydrocarbons, nickel and vanadium in crude oil and marine fuel, Liu et al. (2013) proposed a "multidimensional-chemical-oil-fingerprinting" method aimed at the identification of oil spills after a long-term weathering. This chemical fingerprinting approach represents a multidimensional concept that combines multiple components from traditional oil fingerprinting. This approach can improve singleness and limitation of existing chromatographic fingerprinting, and

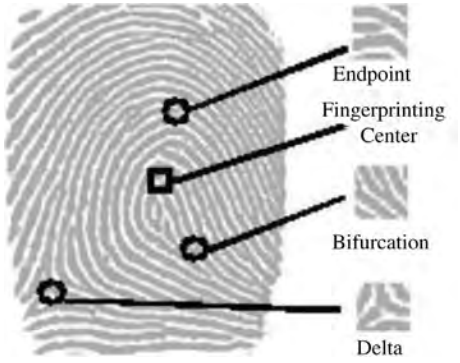

FIGURE 11.4 The feature points of human fingerprinting.

provide a reliable means for assessment and claims regarding marine oil pollution. In this chapter, we demonstrate the multidimensional approach to fingerprinting in the recognition and distinction among crude oils and marine fuels in Bohai Bay after varying degrees of long-term weathering.

11.2 METHODS AND SAMPLES

Bohai crude oil and marine fuel were weathered naturally for 240 days at ambient outdoor conditions. For the weathering the fresh oils were cast atop 2 m^3 vessels containing Bohai Sea water achieving an oil film thickness of 2 mm. The vessels were exposed to the atmosphere and natural light throughout the experiment. Oil samples were regularly collected from the surface of each vessel as described below.

In order to systematically investigate the influence of a long-term weathering on the composition of crude oil and marine fuel, the samples were analyzed in sequence at selected time intervals throughout the weathering time sequence. Weathered samples collected between 1 and 14 days are considered to have experienced short-term weathering, and samples collected after 15 days are considered to have experienced long-term weathering. The collection and analysis of samples was relatively intensive during short-term weathering in order to understand the weathering effects on light components of *n*-alkanes and polycyclic aromatic hydrocarbons. The collection and analysis frequency for oils experiencing long-term weathering was once a month. The analytical tests performed on all samples included *n*-alkanes, fluorescent, nickel, and vanadium of oil samples, as described in the following sections.

11.2.1 Determination of *n*-Alkane Distributions

Silica gel as the stationary phase was packed in a glass column, and was washed by C_6H_{14} solvent. The oil samples were loaded and washed into the column by the eluent CH_2Cl_2:C_6H_{14} at 2:1 (v/v). The eluted hydrocarbon fractions were analyzed by GC with temperature programming, and then, *n*-alkanes in oil samples were qualitatively or quantitatively analyzed through comparing with standard chromatograms using peak areas.

11.2.2 Determination of Fluorescence Spectra

The oil samples were dissolved in *n*-hexane which was purified with activated carbon, the stock solution was prepared and refrigerated, and then the stock solution was diluted to a test solution. PAHs standard samples and the test solutions were scanned by constant wavelength synchronous fluorescence spectrophotometer.

11.2.3 Determination of Nickel and Vanadium Concentrations

The concentrations of Ni and V in oil samples were detected by graphite furnace atomic absorption spectrometry. The calibration curve of Ni as $A = 0.2611C - 0.0012$, the correlation coefficient was 0.9989. The calibration curve of V as $A = 0.0777C - 0.0003$, the correlation coefficient was 0.9992. The preparation of standard solutions of nickel and vanadium and the pretreatment of oil samples referred to National Standard of the People's Republic of China GB/T 18608-2001.

11.3 RESULTS AND DISCUSSION

11.3.1 The Distribution of *n*-Alkanes in Bohai Crude Oil After Short- and Long-Term Weathering

The change trend of *n*-alkanes in Bohai crude oil after a short-term weathering for 14 days is shown in Fig. 11.5. After 8 hours, the light components of n-C_{10}–n-C_{15} decreased obviously. After the 4th day, n-C_{10} and n-C_{11} had not been detected, which indicated that a short-term weathering had a great influence on *n*-alkanes below n-C_{12}, but the distribution of n-C_{15}–n-C_{29} exhibited little change. In addition, the *n*-alkane and isoprenoid diagnostic ratios of the crude oil were essentially unchanged during short-term weathering (Fig. 11.6); Pr/Ph was 1.08 ± 0.17, C_{17}/Pr was 1.69 ± 0.09, and C_{18}/Ph was 1.73 ± 0.21.

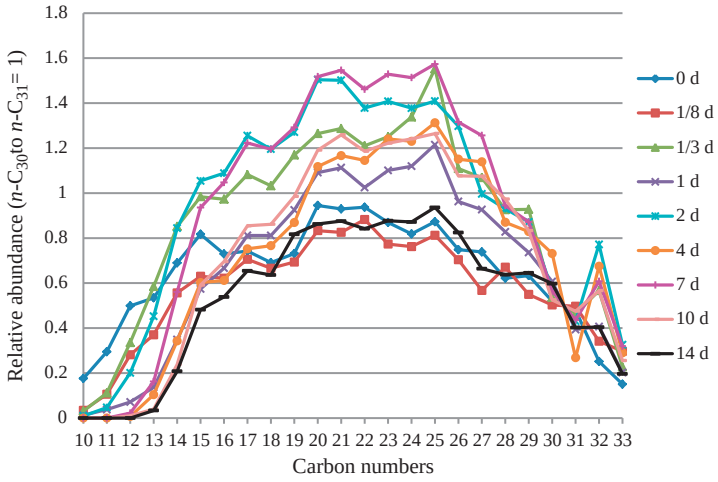

FIGURE 11.5 The distribution of *n*-alkanes in Bohai crude oil during short-term weathering.

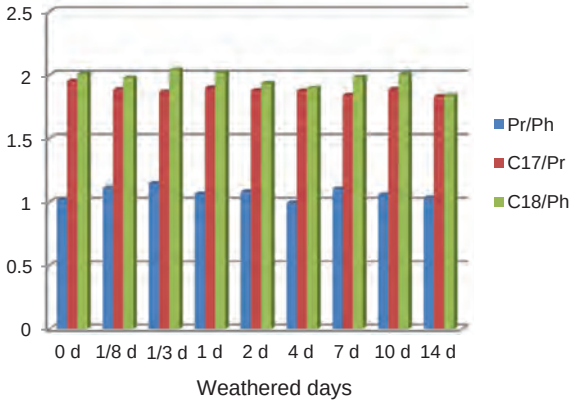

FIGURE 11.6 The diagnostic ratios of Bohai crude oil during short-term weathering.

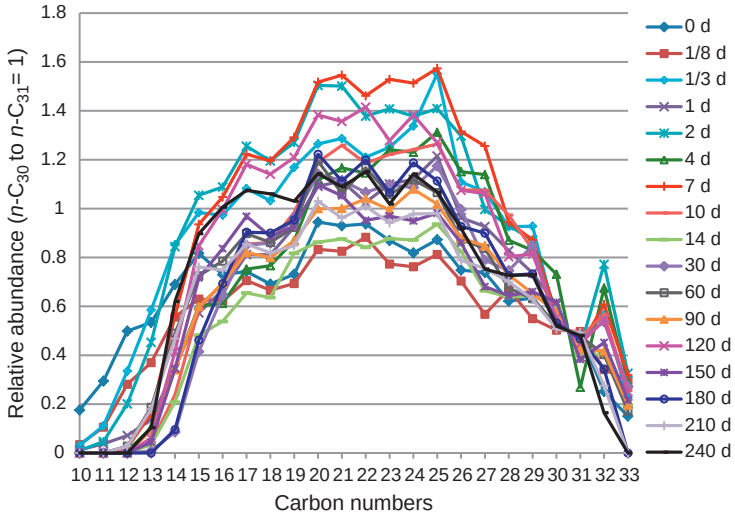

FIGURE 11.7 The distribution of *n*-alkanes in Bohai crude oil during long-term weathering.

Fig. 11.7 shows the changes of *n*-alkanes in Bohai crude oil during long-term weathering for up to 240 days. The light *n*-alkanes boiling below *n*-C_{13} were not basically detected, and *n*-C_{13}–*n*-C_{15} had significantly decreased. The dominant *n*-alkanes varied between *n*-C_{17}–*n*-C_{27} during 240 days weathering, the distribution got

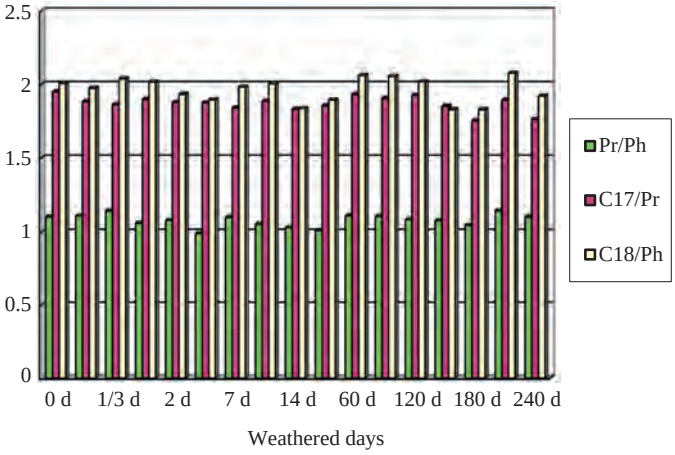

FIGURE 11.8 The diagnostic ratios of Bohai crude oil during long-term weathering.

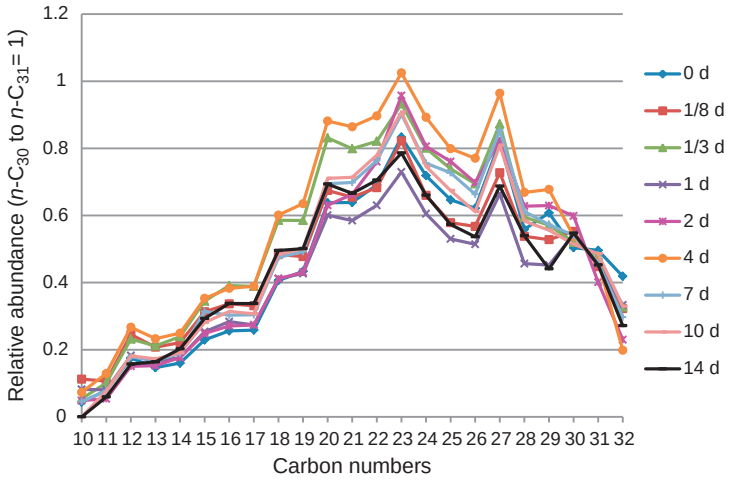

FIGURE 11.9 The distribution of *n*-alkanes in marine fuel weathered for 14 days.

narrower than *n*-C_{15}−*n*-C_{29} after 14 days weathering, which indicated that a long-term weathering had a great influence on the distribution of *n*-alkanes. The relative contents of *n*-alkanes above *n*-C_{16} became progressively higher as the loss of light components led to the relative increase of heavier *n*-alkanes. The diagnostic ratios of Bohai crude oil were basically not affected after weathering for 8 months (see Fig. 11.8), Pr/Ph was 1.10 ± 0.04, C_{17}/Pr was 1.76 ± 0.05, and C_{18}/Ph was 1.92 ± 0.08.

11.3.2 The Distribution Feature of *n*-Alkanes in Marine Fuel After Short- and Long-Term Weathering

The distribution of *n*-alkanes in marine fuel derives mainly from blending components, such as diesel fuel and residual oil, and is generally not as abundant as in crude oil (Fig. 11.9). The dominant *n*-alkanes concentrated in *n*-C_{19}−*n*-C_{28} during short-term weathering, although the distribution range became markedly narrower than in crude oil after short-term weathering (compare Figs. 11.5 and 11.9). The diagnostic ratios of Pr/Ph, C_{17}/Pr, and C_{18}/Ph of marine fuel exhibit minor but irregular changes with short-term weathering (Fig. 11.10).

The dominant *n*-alkanes in marine fuel experiencing long-term weathering occurred in the *n*-C_{20}−*n*-C_{27} range (Fig. 11.11). With increased weathering the distribution range became narrower than the *n*-C_{19}−*n*-C_{28} range exhibiting following short-term weathering. Because marine fuel was composed of the residual oil and diesel fuel which were refined from different crude oils, its diagnostic ratios are expected to exhibit a greater variability than Bohai crude oil. As shown in Fig. 11.12, Pr/Ph, C_{17}/Pr and C_{18}/Ph were also irregular changes.

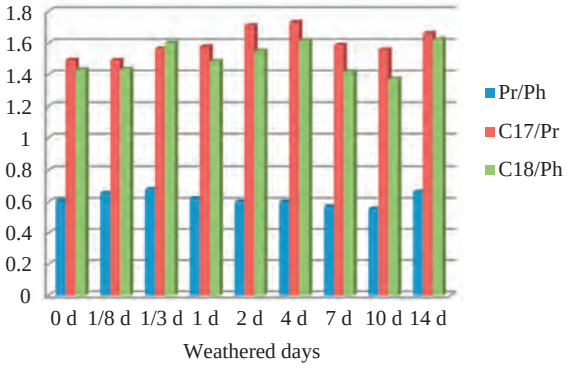

FIGURE 11.10 The diagnostic ratios of marine fuel during 14 days weathering.

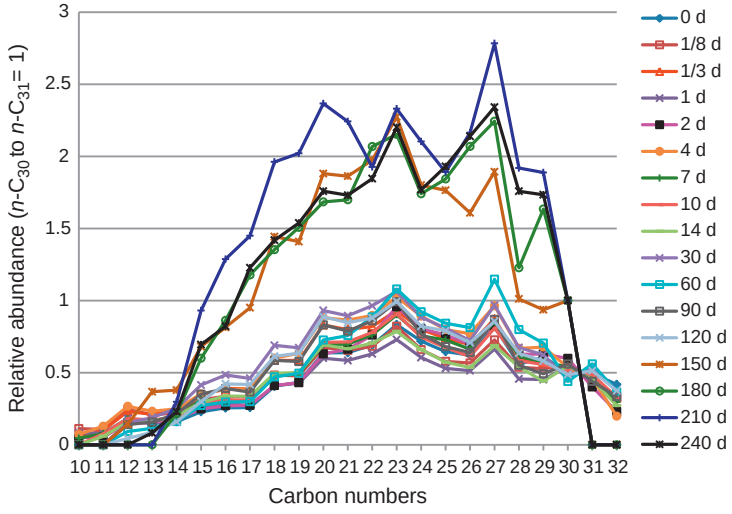

FIGURE 11.11 The distribution of *n*-alkanes in marine fuel weathered for 240 days.

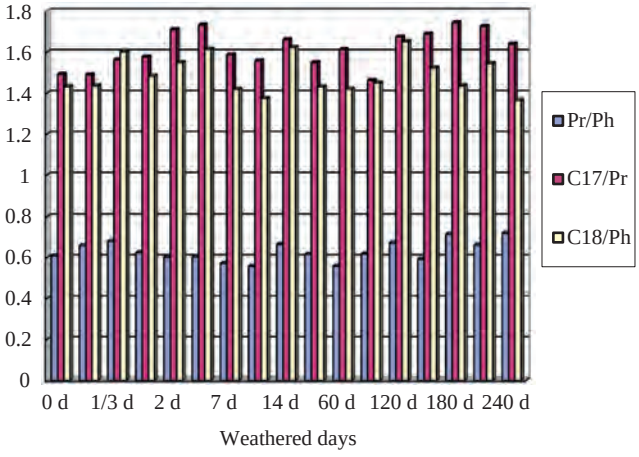

FIGURE 11.12 The diagnostic ratios of marine fuel during 240 days weathering.

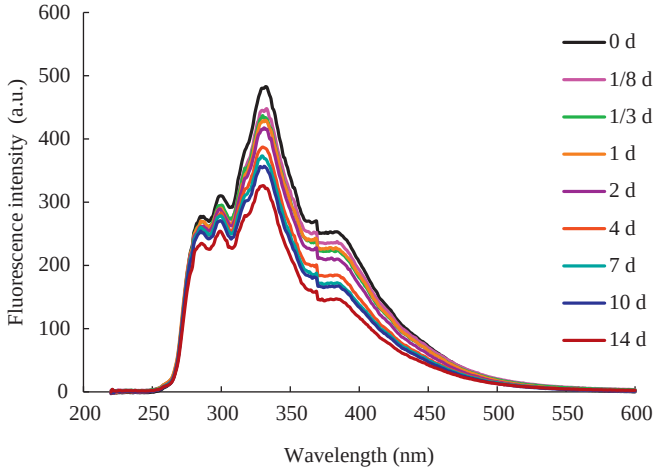

FIGURE 11.13 Fluorescence spectra of Bohai crude oil during short-term weathering.

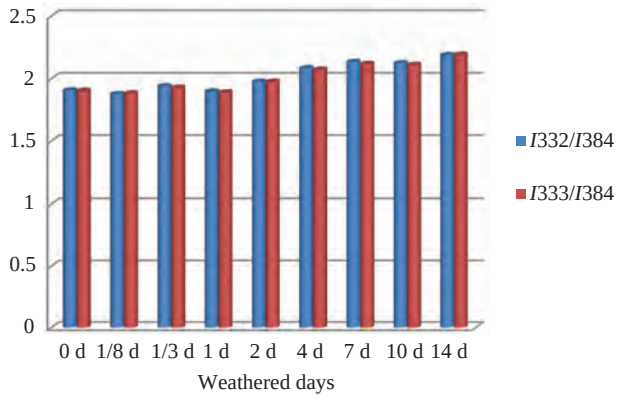

FIGURE 11.14 The ratio of I_{332nm} to I_{384nm} during short-term weathering.

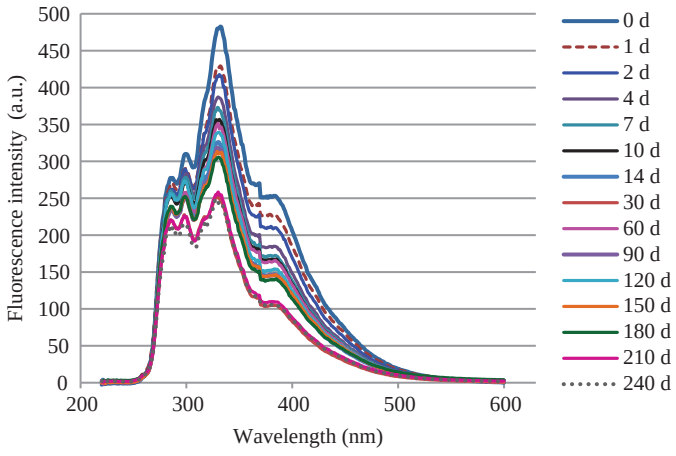

FIGURE 11.15 Fluorescence spectra of Bohai crude oil during long-term weathering.

11.3.3 The Fluorescence Characteristics of Bohai Crude Oil After Short- and Long-Term Weathering

Benzene, naphthalene and phenanthrene are abundant aromatic hydrocarbons in petroleum, and these were characterized by fluorescence at 250–300 nm, 300–365 nm, 366 nm, and 385 nm, respectively (Xia, 1992).

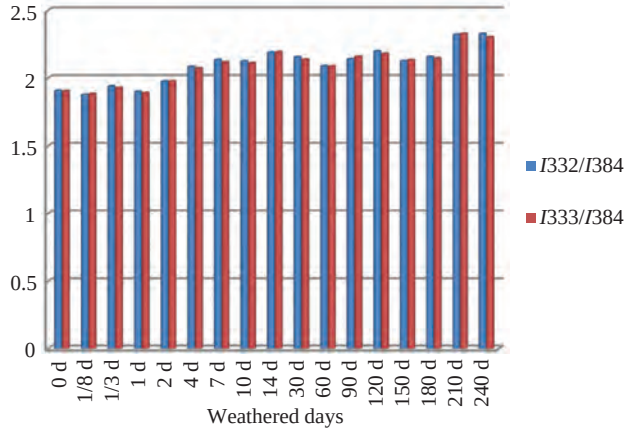

FIGURE 11.16 The I_{332nm}/I_{384nm} of Bohai crude oil during long-term weathering.

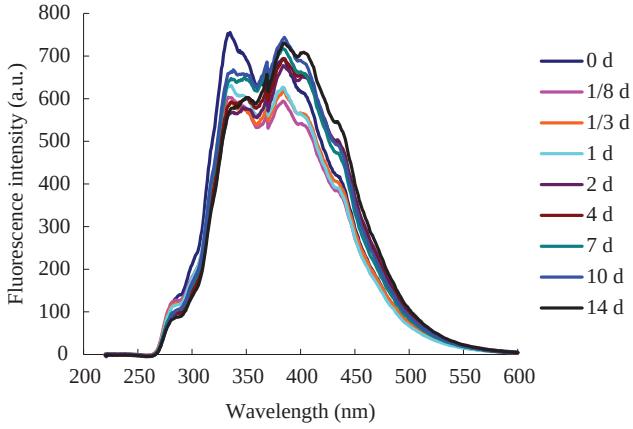

FIGURE 11.17 Fluorescence spectra of marine fuel during short-term weathering.

Synchronous fluorescence spectra of Bohai crude oil during short-term weathering as shown in Fig. 11.13, in which the strongest fluorescence peaks, is located at 332−334 nm. Fluorescence intensity decreased gradually with increasing weathering time, but the fluorescence characteristic remained basically unchanged. The ratio of I_{332nm} to I_{384nm} was between 1.8 and 2.2 (Fig. 11.14).

The fluorescence characteristics of crude oil after long-term weathering for 240 days were consistent with those exhibited following short-term weathering, the strongest fluorescence peaks remained located at 332−334 nm (Fig. 11.15). However, the attenuation of fluorescence intensity during long-term weathering was much greater than that experienced during short-term weathering, which indicated that a long-term weathering promoted the loss of polycyclic aromatic hydrocarbons. Although the fluorescence intensity decreases greatly with weathering, I_{332nm}/I_{384nm} was still stable between 1.8 and 2.4 (see Fig. 11.16). That was to say, the ratio of $I_{332-334nm}$ to I_{384nm} of crude oil had a strong weathering resistance.

11.3.4 The Fluorescence Characteristics of Marine Fuel After Short- and Long-Term Weathering

The fluorescence characteristic of marine fuel was clearly different from that of crude oil, with the former exhibiting only two strong fluorescence peaks (Fig. 11.17). The fluorescence peak located between 332 and 334 nm were similar to crude oil. The other peak located at 384 nm was a unique fluorescence characteristic of marine fuel, which was useful in distinguishing marine fuel from crude oil. During a short-term weathering, the ratio of I_{333nm} to I_{384nm} of the marine fuel was at 1.1, which was smaller than for Bohai crude oil.

The fluorescence spectra of marine fuel exhibited significant changes after 240 days weathering. The attenuation of fluorescence peaks at 384 nm was very large, and this characteristic gradually disappeared. After

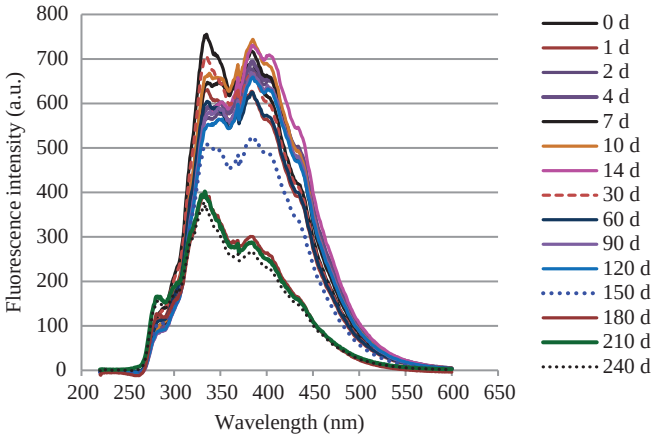

FIGURE 11.18 Fluorescence spectra of marine fuel during long-term weathering.

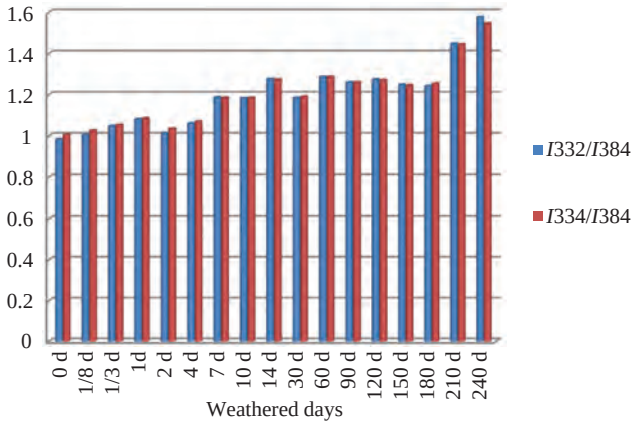

FIGURE 11.19 The I_{332nm}/I_{384nm} of marine fuel during long-term weathering.

TABLE 11.1 The Ratio of Nickel to Vanadium of Oil After a Long-Term Weathering

Days	Light Bohai crude oil	Heavy Bohai crude oil	Light marine fuel	Heavy marine fuel
0	55.16	28.24	0.27	0.30
30	53.81	28.45	0.27	0.31
60	55.13	27.59	0.26	0.29
90	51.43	29.27	0.26	0.31
120	54.59	27.96	0.27	0.30
150	56.77	26.73	0.27	0.30
180	56.96	27.98	0.27	0.30
210	53.71	28.78	0.27	0.31
240	55.51	28.27	0.26	0.31

weathering for 180 days, the original two characteristic peaks became a single peak which more closely resembled the feature of crude oil (Fig. 11.18). The ratios of $I_{332-334nm}$ to I_{384nm} were between 1.0 and 1.6 (Fig. 11.19), wherein the upper limit for marine fuel had a little overlap with lower limit of crude oil. In other words, although the fluorescence spectra of marine fuel after a long-term weathering were similar to crude oil, $I_{332-334nm}/I_{384nm}$ ratio was still able to distinguish of the marine fuel versus crude oil fluorescence characteristics.

11.3.5 The Characteristics of Ratio of Nickel to Vanadium of Bohai Crude Oil and Marine Fuel After Long-Term Weathering

The ratio of nickel to vanadium of Bohai crude oil and marine fuel did not change much after a long-term weathering (Table 11.1). The stability of this ratio indicated that Ni/V had a strong weathering resistance; however, the Ni/V of Bohai crude oil was much higher than in marine fuel.

11.3.6 Summary of Distinguishing Features—Bohai Crude Oil Versus Marine Fuel

In summary, the distribution of the dominant *n*-alkanes (C_{17}−C_{27}) in Bohai crude oil after long-term weathering was very close to that (C_{19}−C_{28}) of marine fuel after short-term weathering. Thus, there might be a misjudgment in distinguishing these petroleum if only GC fingerprinting were to be used. The fluorescence characteristic of marine fuel was similar to that of crude oil following long-term weathering; however, the $I_{332-334nm}/I_{384nm}$ ratio exhibited a good weathering resistance. An $I_{332-334nm}/I_{384nm} = 1.4-1.6$ as a threshold could be used for distinguishing both, with Bohai crude oil exhibiting higher ratios and marine fuel exhibiting lower ratios. The ratio of nickel to vanadium also had a strong resistance to weathering, although the Ni/V ratio of crude oil was much higher than in marine fuel, which provided another distinguishing feature between Bohai crude oil and marine fuel.

11.4 APPLICATION OF MULTIDIMENSIONAL CHEMICAL FINGERPRINTING TO IDENTIFICATION OF MYSTERY OIL SPILLS IN BOHAI BAY

Sixteen oil samples identified as L1 to L8, T1 to T6, and Q1 to Q2 were collected on the beaches of Laoting, Tangshan, and Qinhuangdao in March 2012, respectively. The *n*-alkanes, fluorescence and Ni/V of these samples were analyzed, and their properties were identified using the multidimensional approach to chemical fingerprinting described in Section 11.3.

11.4.1 Determination of Oil Attribution Based Upon *n*-alkanes

The distribution of *n*-alkanes in L1 to L8 samples is shown in Fig. 11.20. Except L4, the dominant *n*-alkanes in the other seven Laoting samples concentrated within the C_{18}−C_{27} range, with the light components below C_{14} not being detected. Their distributions were similar to Bohai crude oil after a long-term weathering. The dominant hydrocarbon of L4 focused on C_{18}−C_{29}, and the light component C_{10} was also detected. Thus, based upon comparison to the earlier results (Fig. 11.5), L4 was most similar to nonweathered Bohai crude oil.

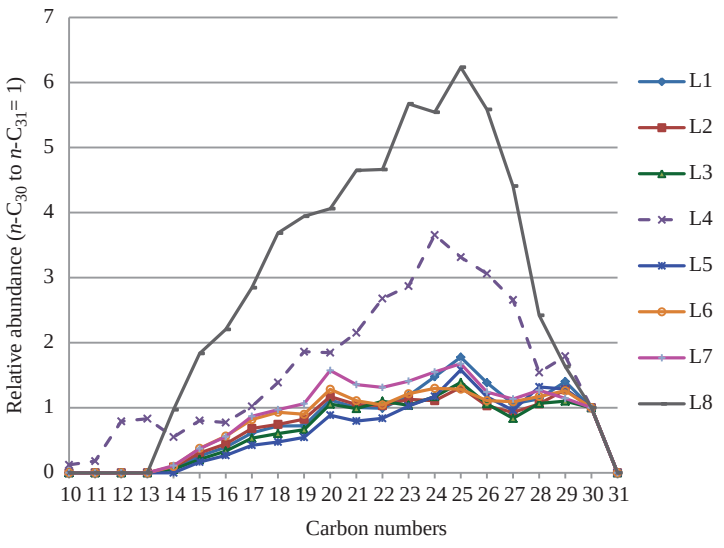

FIGURE 11.20 The distribution of *n*-alkanes in oil samples from Laoting (March 2012).

The distribution of *n*-alkanes in T1 to T6 samples is shown in Fig. 11.21. The dominant *n*-alkanes were concentrated in the $C_{20}-C_{28}$ range. The light *n*-alkanes less than C_{12} were detected except in T2, and their distribution was most similar to marine fuel after a short-term weathering (compare to Fig. 11.9).

The dominant *n*-alkanes in the Q1 and Q2 samples were focused within the *n*-C_{17}−*n*-C_{30} range (Fig. 11.22). Q2 showed a distribution consistent with crude oil that had experienced short-term weathering because of *n*-C_{10} and *n*-C_{11} were not detected. The *n*-alkanes distribution of the Q1 samples was similar to nonweathered Bohai crude oils.

11.4.2 Determination of Oil Attribution Based Upon Fluorescence

Most of fluorescence spectra of L samples exhibited the features of crude oil after a long-term weathering except for the L4 samples (Fig. 11.23), $I_{332-334nm}/I_{384nm} \approx 1.8$. The L4 sample showed a strong fluorescence consistent with a nonweathered Bohai crude oil; its $I_{332-334nm}/I_{384nm} \approx 2$. Thus, the fluorescence character of the Laoting samples was consistent with the results obtained using *n*-alkanes.

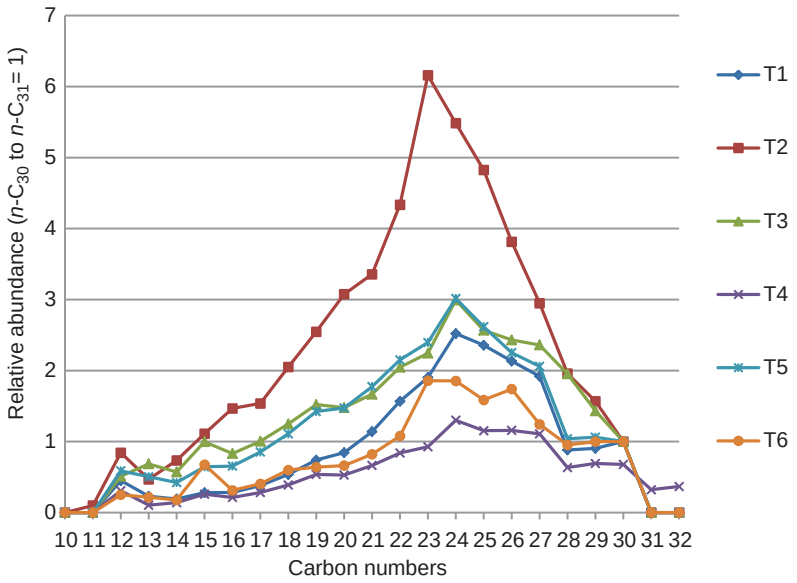

FIGURE 11.21 The distribution of *n*-alkanes in oil samples from Tangshan (March 2012).

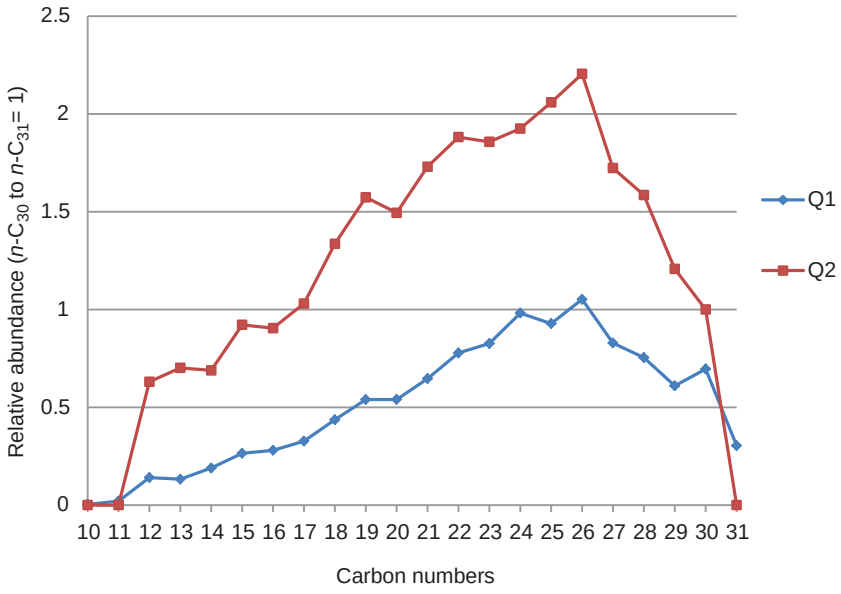

FIGURE 11.22 The distribution of *n*-alkanes in oil samples from Qinhuangdao (March 2012).

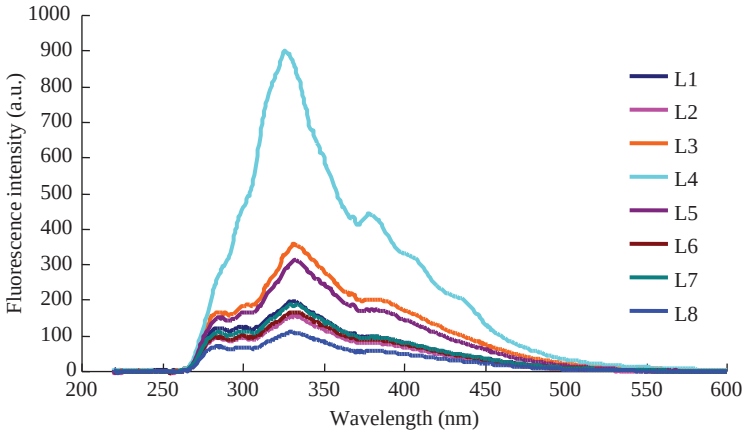

FIGURE 11.23 Fluorescence spectra of oil samples from Laoting.

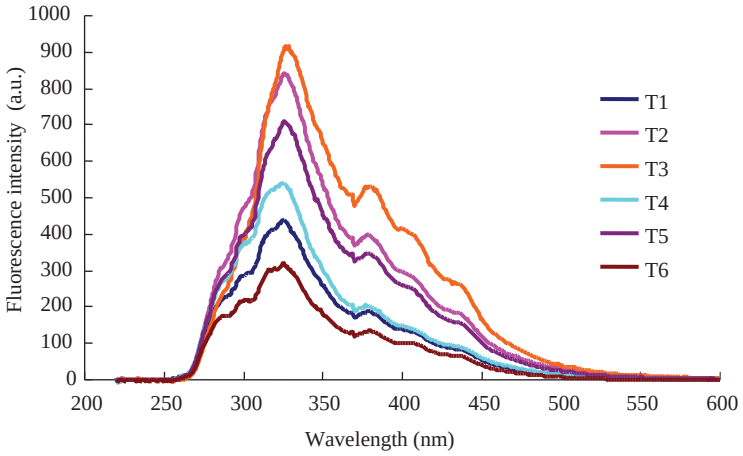

FIGURE 11.24 Fluorescence spectra of oil samples from Tangshan.

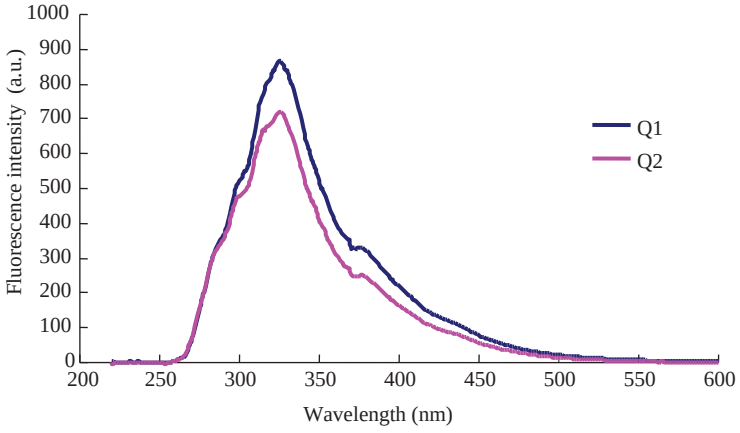

FIGURE 11.25 Fluorescence spectra of oil samples from Qinhuangdao.

Fig. 11.24 showed the fluorescence spectra of Tangshan oils. The $I_{332-334nm}/I_{384nm}$ ratios of the T1 to T6 samples were 2.1, 2.1, 1.9, 2.8, 1.8, and 2.0, respectively, and they exhibited the fluorescence characteristics of crude oils after both long- or short-term weathering ($I_{332-334nm}/I_{384nm} = 1.8-2.4$). However, these results had conflict with them identified as marine fuels in Section 11.4.1. This confirmed that there were some shortcomings in using only chromatographic fingerprinting for identification.

The $I_{332-334nm}/I_{384nm}$ ratios of the Q1 and Q2 samples were 2.5 and 2.3, respectively, with distinct characteristics of crude oil being evident. This result was consistent with the two Qinhuangdao oils' identification of crude oil based upon *n*-alkanes (Fig 11.25).

11.4.3 Determination of Oil Attribution Based Upon Ni/V

The Ni/V ratio for the T1 to T6 samples ranged from 28.0 to 29.0 and was far higher than Ni/V (0.2–0.3) of marine fuel (Table 11.1). Thus, contrary to the *n*-alkane and fluorescence spectra results described above, the high Ni/V ratios for the T1 to T6 oils inferred these oils to be heavy Bohai crude oils that had experienced long-term weathering.

The Ni/V ratios of the L1, L5, L6, and L7 samples ranged from 13.0 to 15.0, and those of the L2, L3, L4, and L8 samples ranged from 7.0 to 9.0. Referred to their *n*-alkanes distribution and fluorescence spectra, these Laoting oils were inferred to be two different types of Bohai crude oil. The Ni/V ratios of the Q1 and Q2 samples were 46.0 and 47.0, respectively, both consistent with light Bohai crude oils.

11.5 CONCLUSION

The application examples described above show that multidimensional chemical fingerprinting, which are composed of normalized *n*-alkane distributions, fluorescence spectrophotometry, and Ni/V ratios, is capable of distinguishing crude oil and marine fuel oil spills even after these oils may have experienced significant changes due to long-term weathering.

References

Blumer, M., Ehrhardt, M., 1971. Identification of oil spills by means of gas chromatographic and spectrometric data. Abstr. Papers Am. Chem. Soc.15 (MAR-A).

Christensen, J.H., Tomasl, G., Hansen, A.B., 2005. Chemical fingerprinting of petroleum biomarkers using time warping and PCA. Environ. Sci. Technol. 39, 255–260.

Frame, G.M., Flanigan, G.A., Carmody, D.C., 1979. Application of gas-chromatography using nitrogen-selective detection to oil spill identification. J. Chromatogr. 168 (2), 365–376.

Kaplan, I.R., Lu, S.T., Alimi, H.M., MacMurphey, J., 2001. Fingerprinting of high boiling hydrocarbon fuels, asphalts and lubricants. Environ. Forensics 2, 231–248.

Li, H., Lv, J.B., 1998. Identification of spilled oi1 using fluorescence Spectroscopy and Capillary GC-FID. Mar. Sci. Bull. 17 (6), 66–70.

Liu, X.X., Liu, Z.J., Zhang, S.H., Yang, Y., Zhong, M., 2013. A multidimensional chemical fingerprint for identification of crude oil and marine fuel after long-term weathering. Mar. Environ. Sci. 32 (4), 605–609.

Liu, X.X., Tang, X.H., Lian, H.Y., Gong, W.M., 2014. Identification of oil spill from marine fuel and crude oil by carbon stable isotopes ratio. J. Dalian Mar. Univ. 40 (4), 109–112.

Mori, M., Shinzaki, T., Sasaki, S., 2003. Biometric authentication technology. Fujitsu 7, 272–279.

Peng, X.Z., Liu, X., Ye, Z.X., Wu, J.X., Zhang, G., 2004. Applications of chemical and stable isotopic fingerprints for oil contamination identification: case studies of two heavy oil spills in Nanhai, Guangdong province, China. Geochimica 33 (3), 317–323.

Philp, R.P., Allen, J., Kuder, T., 2002. The use of the isotopic composition of individual compounds for correlating spilled oils and refined products in the environment with suspected sources. Environ. Forensics 3, 341–348.

Spotts, E.J.P., Reilly, T., Plourde, K., 2005. Trace metal analysis for finger printing oil spill samples. 2005 Int. Oil Spill Conf. 8, 517.

Staniloac, D., Petrescu, B., Patroeseu, C., 2001. Pattern recognition based software for oil spills identification by gas-chromatography and IR spectrophotometry. Environ. Forensics 2 (4), 363–366.

Wang, Y., Liu, X.X., Sun, Y.Q., Lian, H.Y., Tang, X.H., 2013. Identification of oil spill from imported crude oils in china using GC/IrMS. Environ. Forensics 14 (4), 306–311.

Wang, Z.D., Fingas, M., Landriault, M., Sigouin, L., Feng, Y., Mullin, J., 1997. Using systematic and comparative analytical data to identify the source of unknown oil on contaminated birds. J. Chromatogr. A 775 (1–2), 251–265.

Wang, Z.D., Fingas, M., Blenkinsopp, S., Sergy, G., Landriault, M., Sigouin, L., et al., 1998. Comparison of oil composition changes due to biodegradation and physical weathering in different oils. J. Chromatogr. A 809 (1–2), 89–107.

Wang, Z.D., Fingas, M., Page, D.S., 1999. Oil spill identification. J. Chromatogr. A 843 (1–2), 369–411.

Wang, Z.D., Fingas, M., Sigouin, L., 2002. Using multiple criteria for fingerprinting unknown oil samples having very similar chemical composition. Environ. Forensics 3, 251–262.

Wang, Z.D., Stout, S.A., Fingas, M., 2006. Forensic fingerprinting of biomarkers for oil spill characterization and source identification. Environ. Forensics 7 (2), 105–146.

Xia, J., 1992. Practical Fluorescence Analysis. Chinese People's Public Security University Press, Beijing, 335 p.

Yang, B.J., Xiu, X.Q., Li, Q.L., 2008. Application of oil spill identification by GCMS—a case study. Mar. Environ. Sci. 27 (6), 661–665.

Zhu, L.L., 2009. Characterization and identification of spilled oils using synchronous fluorescence spectroscopy and gas chromatography–mass spectrometry. Ocean University of China.

Deng, Y.H., Li, X.F., 2001. The geological characters and enlightenment of Penglai 19–3 oil field. China Pet. Explor. 6 (1), 68–71.

CHAPTER

12

Distinguishing Genetically-Similar Diesel Fuels in Taiwan Using Principal Component Analysis of Diagnostic Ratios

Suh-Huey Wu[1], *Mei-Hua Chen*[1], *Wei-Nung Hung*[2] *and Ching-Jen Ho*[3]

[1]CPC Corporation, Miaoli, Taiwan [2]Industrial Technology Research Institute, Hsinchu, Taiwan [3]Environmental Protection Administration Executive Yuan, Taipei, Taiwan

BIOGRAPHIES

Dr. Suh-Huey Wu is a senior researcher at Exploration and Development Research Institute, CPC Corporation, Taiwan. She has over 35 years of experience in the field of geochemistry focusing oil–oil/oil–source rock biomarker correlation of petroleum exploration, and also has over 15 years of experience in the oil spill environmental forensic. She carries out six relative oil spill forensic technique established plans for Taiwan EPA, since 2008. Dr. Wu obtained Ph.D. degree in chemistry at National Cheng Kung University in 2002. E-mail: 048682@cpc.com.tw.

Mei-Hua Chen obtained her M.S. degree in department of Safety, health and environmental engineering at National United University in 2011. Her primarily studied oil spill and environmental forensic. Since 2013, she has been a plan assistant on Exploration and Development Research Institute, CPC Corporation, and joined Soil and Groundwater Pollution Remediation Found Management Board, Taiwan EPA's plan. She specializes in oil spill and petroleum-contaminated soil fingerprinting, accumulating 6 years of experience.

Dr. Wei-Nung Hung is a researcher in the Green Energy and Environment Research Laboratories, Industrial Technology Research Institute (ITRI), Hsinchu, Taiwan. Dr. Hung received his Ph.D. degree in environmental engineering from National Chung Kung University, Taiwan. His current research interests involve the chemical fingerprinting and environmental forensics of oil products and other possible spill candidates.

Dr. Ching-Jen Ho obtained his Ph.D. degree in environment engineering at National Taiwan University in 2015. He primarily studied risk assessment based on soil digestion and bioavailability. In 1992, he joined the Environmental Protection Administration, he has worked on the Department of Solid Waste Resource Recycling Plant Installation, and specializes in open tender bidding, installation, and management of incinerators. 8 years later, he moved to the National Institute of Environmental Analysis, Taiwan EPA, and served as an environmental analyst. Since 2003, he has been serving as the Chief of the Technology Evaluation Section of Soil and Groundwater Remediation Fund Management Board, Taiwan EPA, accumulating 13 years of experience in environmental planning, soil and groundwater pollution investigation, remediation management. He has been responsible for establishing environmental forensics capability, pollution investigation and remediation of active manufacturing plants utilizing chlorinated organic compounds, promotion of green and sustainable remediation, pollution prevention, investigation, and remediation of gas stations, pollution prevention, investigation, and remediation of farmlands.

Oil Spill Environmental Forensics Case Studies.
DOI: http://dx.doi.org/10.1016/B978-0-12-804434-6.00012-4

12.1 INTRODUCTION

Biomarkers are complex molecular fossils derived from biochemicals, particularly lipids in once-living organisms. Biomarkers which are generally resistant to secondary processes can provide useful geochemical information on the depositional environment, thermal maturity, and the origin of oils (Peters et al., 2005). Analysis of biomarkers in petroleum can generate information of great importance to environmental forensic investigations in terms of determining the source of spilled oil, differentiating and correlating oils and weathering state of oils under a wide variety of conditions (Wang et al., 1999; Daling et al., 2002; Peters et al., 2005).

For lighter petroleum products such diesels, refining processes remove polycyclic biomarkers with high boiling point from crude oil feedstocks. Smaller, lower boiling biomarkers, such as bicyclic sesquiterpanes and adamantanes, still exist in diesel fuels. The distributions of bicyclic sesquiterpanes, adamantanes and diamantanes in different oils (crude oils and refined products) in the environment have been characterized and quantitatively evaluated (Wang et al., 2005, 2006, 2008; Yang et al., 2006, 2008, 2009; Stout and Douglas, 2004; Stout et al., 2005). Examination of Gas Chromatography–Mass Spectrometry (GC–MS) chromatograms of the characteristic fragment ions and diagnostics ratios (DRs) for bicyclic sesquiterpanes, adamantanes, alkyl PAHs (polycyclic aromatic hydrocarbons) and PAH isomers provides a useful means of differentiation and source identification for light to middle distillate refined products.

Due to the high similarity of the crude oil feedstocks supplying the two refinery companies in Taiwan, referred to as A and B herein, it is difficult to distinguish the diesel fuel products produced by companies A and B using conventional fingerprinting correlation or selected DRs match evaluation techniques. In this study, we present an approach based on the use of a large number of DRs between source-specific compounds in conjunction with principal component analysis (PCA–DRs approach) as a means to distinguish fresh and weathered diesel fuel products produced by Taiwan's refining companies A and B. The source-specific compounds used in the PCA–DRs approach included bicyclic sesquiterpanes, adamantanes, isomers of PAHs, and alkylated PAHs. The DRs employed in the approach were first evaluated in their ability to distinguish fresh biodiesel (BD) and premium diesel (PD) samples, followed by their ability to distinguish weathered diesel fuels from authentic sites where the source of contamination was uncertain.

12.2 EXPERIMENTAL

12.2.1 Materials

Unweathered (fresh) diesel oil samples were directly obtained from various gasoline stations supplied by A and B Refinery Company in Taiwan. Two types of diesel oils were collected, i.e. BD and PD, and the total number of unweathered oil samples was 267 in this study. There were a total 141 BD (2% BD blended with petroleum diesel) samples, 77 samples from A Refinery Company and 64 samples from B Refinery Company, received between June 2013 and March 2014. Due to oil policy adjustment in Taiwan, the gasoline stations stopped selling BD and started to offer PD after March 2014. Consequently, total amounts of 126 samples of PD were obtained, including 63 samples from A Refinery Company and 63 samples from B Refinery Company, between August 2014 and May 2015. Finally, 33 real-site samples including two free-phase oil samples from monitoring wells and 31 contaminated soil samples from six petroleum-impacted sites were collected and analyzed. All the diesel oils and samples obtained were stored at 4°C until analysis.

12.2.2 Sample Preparation and Analysis Method

All the diesel oil samples were dissolved in the solvent of dichloromethane and prepared to a determined concentration of 10 μg/μL for further analyses. For impacted soil samples, an adequate volume of dichloromethane (approximate 15 mL) was used to extract the oil in the soil matrix. Analyses of oils and soil extracted samples were accomplished on an Agilent 7890A model gas chromatography interfaced to an Agilent 5975C mass selective detector by an electron impact at 70 eV and detector gain at 1.5 kV. A DB-1-ms capillary column

(60 m × 0.25 mm inner diameter with 0.25 μm film thickness from Agilent Technologies Inc., USA) was used. The GC oven temperature was initially held at 40°C for 5 min, increased to 300°C at a rate of 4°C/min, and then held for 10 min. The total run time was 80 min. The carrier gas was ultrahigh-purity helium at a constant flow of 1 mL/min. Samples were injected in splitless mode and injection volume is 0.2 μL. The injection port and interface of GC was heated at 310 and 300°C, respectively.

12.2.3 Data Analysis

The diagnostic ratios (DRs) were calculated to obtain qualitative information of the unique characteristic for all of the tested diesel oils. The DRs were calculated as the ratio of the reported peak areas measured from total ion chromatograms (TIC) or extracted ion chromatograms as follows; bicyclic sesquiterpanes (*m*/*z* 123), adamantane (*m*/*z* 135, 149), alkyl PAHs and isomer PAHs (*m*/*z* 142, 156, 170, 184, 178, 192, 206, 220, 166, 180, 194; after Wang et al., 2007). To achieve the uncertainties to a minimum and yield reliable results, the peaks with low abundances and poor separation were not conducted. The DR values were accepted only when the relative standard deviations (RSD) or relative percent difference (RPD) of measured replicate samples were less than 10% or 14%, respectively.

12.3 RESULTS AND DISCUSSION

12.3.1 PCA–DRs Approach Development

Fig. 12.1 shows the typical GC–MS chromatograms of TIC and bicyclic sesquiterpanes at *m*/*z* 123 for representative BD and PD samples selected from A and B refinery companies. The TICs of all BD and PD samples from two refinery companies have similar hydrocarbon range distribution. The ratio of pristine (Pr) to phytane (Ph) ranged from 0.8 to 1.54 for all the BD and PD samples from A refinery company, while that from B refinery company ranged from 0.62 to 0.90.

For the samples from A refinery company, the fingerprints of bicyclic sesquiterpanes at *m*/*z* 123 are variable. For example, the fingerprinting of bicyclic sesquiterpanes the for PD A_PD_N033 sample has a characteristic unknown peak between BS2 and BS3 sesquiterpanes, whereas the A_BD_S011 and A_PD_S172 samples exhibit bicyclic sesquiterpanes that are nearly identical (Fig. 12.1). The bicyclic sesquiterpanes for all four BD and PD samples from B refinery company are highly consistent with one another and exhibit nearly identical fingerprintings of bicyclic sesquiterpanes (Fig. 12.1). Notably, the bicyclic sesquiterpane fingerprintings for some samples from both refiners, such as A_PD_S172, B_PD_N023 and B_PD_S172, were nearly identical. It was shown that commonly used fingerprinting correlation and DRs match evaluation techniques using bicyclic sesquiterpanes to differentiate between BD and PD samples from A and B refinery companies were rarely achieved.

Owing to the inability of sesquiterpanes to distinguish among various diesel fuels, we expanded the list of DRs among numerous other diesel range analytes, as indicated in Table 12.1. The DRs were calculated from reported peak areas from TIC, bicyclic sesquiterpanes, adamantanes, alkyl PAHs, and isomer PAHs. Based upon analytical precision and specific refining procedure, we evaluated the ability of 45 different DRs for BD and 41 DRs for PD to distinguish among the fuels and refiners using the PCA–DRs approach. Table 12.1 lists the precise and specific DRs derived from BD and PD in the PCA–DRs approach. The peak number and the abbreviation of bicyclic sesquiterpanes, adamantanes, alkyl PAHs, and isomer PAHs are based upon those found elsewhere (Wang et al., 2006, 2007; Yang et al., 2009). Listed at the bottom of Table 12.1 are several DRs involving unknown compounds, designated by the label U, that have been previously recognized as distinctive of the different refining procedures employed the two refining companies in Taiwan (Wu et al., 2013).

The resulting factor score plots of the PCA–DRs approach utilizing the 45 and 41 DRs of BD and PD, respectively, are indicated in Fig. 12.2. As can be seen, the sample populations representing the two refinery companies were divided into two groups along the first principal component (PC1), revealing that the PCA–DRs approach can distinguish the genetically-similar diesel fuels from the two refining companies. The scores of PC1 are 39.82%, 40.94%, and 34.66% with 45 DRs of 141 BD samples (Fig. 12.2A), 41 DRs of 126 PD

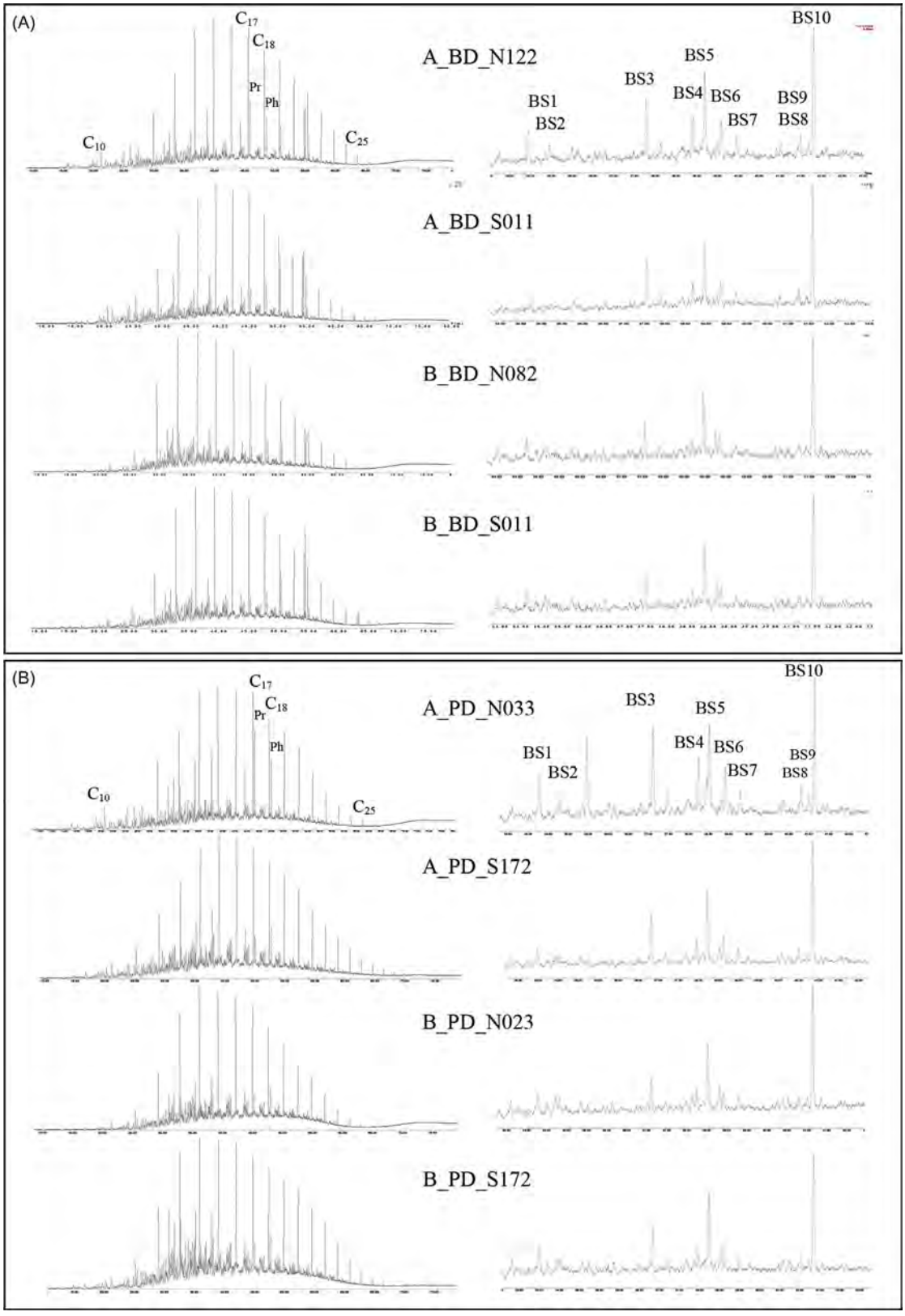

FIGURE 12.1 GC–MS chromatograms of total ion chromatograph (left) and bicyclic sesquiterpanes (*m*/*z* 123; right) for (A) biodiesel (BD); (B) premium diesel (PD) samples from A and B refinery companies in Taiwan. The "A" and "B" sample designations refer to the refinery companies, respectively.

TABLE 12.1 PCA–DRs Approach with 45 and 41 DRs of Biodiesel and Premium Diesel From A and B Refinery Companies in Taiwan

	45 DRs (biodiesel)	**41 DRs (premium diesel)**	**41 DRs (biodiesel & premium diesel)**
TIC	*n*-C_{17}/Pr	*n*-C_{17}/Pr	*n*-C_{17}/Pr
	n-C_{18}/Ph	*n*-C_{18}/Ph	*n*-C_{18}/Ph
	Pr/Ph	Pr/Ph	Pr/Ph
m/*z* 123	BS1/BS4	BS1/BS4	BS1/BS4
	BS3/BS5	BS3/BS5	BS3/BS5
	BS3/BS4	BS3/BS4	BS3/BS4
	BS4/BS5	BS4/BS5	BS4/BS5
	BS4/BS6	BS4/BS6	BS4/BS6
	BS6/BS5	BS6/BS5	BS6/BS5
	BS10/BS5	BS10/BS5	BS10/BS5
	BS3/BS10	BS3/BS10	BS3/BS10
Adamantanes	A2/A6	A2/A6	A2/A6
	A2/A17	A2/A17	A2/A17
	A6/A17	A6/A17	A6/A17
	A6/A14	A6/A14	A6/A14
	A2/A3	A2/A3	A2/A3
	A2/A10	A2/A10	A2/A10
	A3/A(7 + 8)	A3/A(7 + 8)	A3/A(7 + 8)
	A3/A10	A3/A10	A3/A10
	A(7 + 8)/A10	A(7 + 8)/A10	A(7 + 8)/A10
	A17/A10	A17/A10	A17/A10
	A10/A15	A10/A15	A10/A15
PAHs	C_1N/C_2N	C_1N/C_2N	C_1N/C_2N
	C_2N/C_3N	C_2N/C_3N	C_2N/C_3N
	C_3N/C_4N	C_3N/C_4N	C_3N/C_4N
	C_2N/C_4N	C_2N/C_4N	C_2N/C_4N
	C_0P/C_1P		
	C_1P/C_2P	C_1P/C_2P	C_1P/C_2P
	C_2P/C_3P	C_2P/C_3P	C_2P/C_3P
	C_1P/C_3P	C_1P/C_3P	C_1P/C_3P
	C_0F/C_1F		
	C_1F/C_2F	C_1F/C_2F	C_1F/C_2F
	C_1N/C_1P	C_1N/C_1P	C_1N/C_1P
	C_2N/C_2P	C_2N/C_2P	C_2N/C_2P
	C_3N/C_3P	C_3N/C_3P	C_3N/C_3P
	C_0P/C_0F		
	C_1P/C_1F	C_1P/C_1F	C_1P/C_1F
	C_2P/C_2F	C_2P/C_2F	C_2P/C_2F
	2-MN/1-MN	2-MN/1-MN	2-MN/1-MN
	(3 + 2)MP/(9 + 1)MP	(3 + 2)MP/(9 + 1)MP	(3 + 2)MP/(9 + 1)MP

(*Continued*)

TABLE 12.1 (*Continued*)

	45 DRs (biodiesel)	41 DRs (premium diesel)	41 DRs (biodiesel & premium diesel)
Refining procedure	U1/BS6	U1/BS6	U1/BS6
	U2/C_1P4		
	U3/C_2P4	U3/C_2P4	U3/C_2P4
	U4/C_1F3	U4/C_1F3	U4/C_1F3
	U6/C_2F5	U6/C_2F5	U6/C_2F5

See text for description.

samples (Fig. 12.2B), and 41 DRs for the combined total of 267 BD and PD samples (Fig. 12.2C), respectively. The scatter along the second principal component (PC2) among A group diesel is larger than that of B group, which we attribute to the fact that A refinery company has three refineries producing diesel fuel from varying feedstocks, whereas B refinery company employs a single refinery to provide its diesel fuel throughout Taiwan.

An option for selecting the most distinctive DRs used in the PCA−DRs approach was to evaluate each DR's diagnostic power (DP; Wang et al., 2007). In this study, DP is calculated from the RSD of the DR among the amounts of 45 DRs for ten oils of different refining companies divided by the RSD of the same ratios from six measurements of B refining company's oil. The DP employed can effectively select the most distinctive DRs and thereby reduce the number of DRs used in the PCA−DRs approach. DRs with DP values >5 were recognized as particularly distinctive in distinguishing between the diesel fuels from A and B refinery companies. This identified 28 DRs were useful in distinguishing among the BDs, 29 DRs were useful in distinguishing among the PD fuels, and 21 DRs were useful in distinguishing among the combined BD and PD samples. The distinctive DRs with DP values >5 identified are listed in Table 12.2. Fig. 12.3 shows the factor score plots resulting from PCA−DRs approach using only these distinctive DRs (DP >5; Table 12.2) of all the BD and PD samples studied. As expected, similar results were found when the PCA−DRs approach used only those DRs with DP >5 (as had been found when all DRs were utilized; Figs. 12.2 and 12.3). Again, the samples were readily divided into two groups representing the A and B refining companies. However, the scores of PC1 using only those DRs with DP >5 in the PCA−DRs approach were increased to 44.67%, 44.85%, and 44.43% respectively. Thus, the approach using only those DRs with DP >5 (Table 12.2) provided an excellent means to distinguish between the genetically-similar diesel fuels from each refinery company.

12.3.2 Evaluation of PCA−DRs Approach—Gasoline Interference and Weathering Effect

To evaluate the effect of gasoline interference (mixing) and weathering effect on diesel fuel on the PCA−DRs approach, liquid phase hydrocarbon (LPH) samples and soil samples were collected from the site of an oil spill that occurred on the No. 61 west coastal highway (at location of 53.5 km) in 2007, herein referred to as F site. The accident resulted in spillage of both gasoline and PD from pipelines operated by A refinery company. Two LPH samples were sampled from monitoring wells SW-10W and SW-20W in 2008, and eight soil samples were collected at a depth of 3.5 to 5.5 m from eight boring (S02, S03, and S05 to S10) installed in 2015, i.e. 8 years after the spill occurred.

Fig. 12.4 shows the GC−MS chromatograms of TIC and bicyclic sesquiterpanes at m/z 123 for LPH samples (2008) and soil samples (2015) collected from the F site. The two LPH samples from 2008 exhibit only light weathering involving dissolution of some compounds within the gasoline hydrocarbon range while the *n*-alkanes within the diesel range hydrocarbons are still abundant. The soil samples from 2015 showed that gasoline hydrocarbons had been mostly lost and that *n*-alkanes in the diesel range were depleted, especially for samples of S02, S06, S07, S08, S09, and S10 (where more than 90% of the *n*-alkanes were removed compared to the LPH samples), suggesting that the diesel fuel residues in the soils had experienced light to moderate biodegradation.

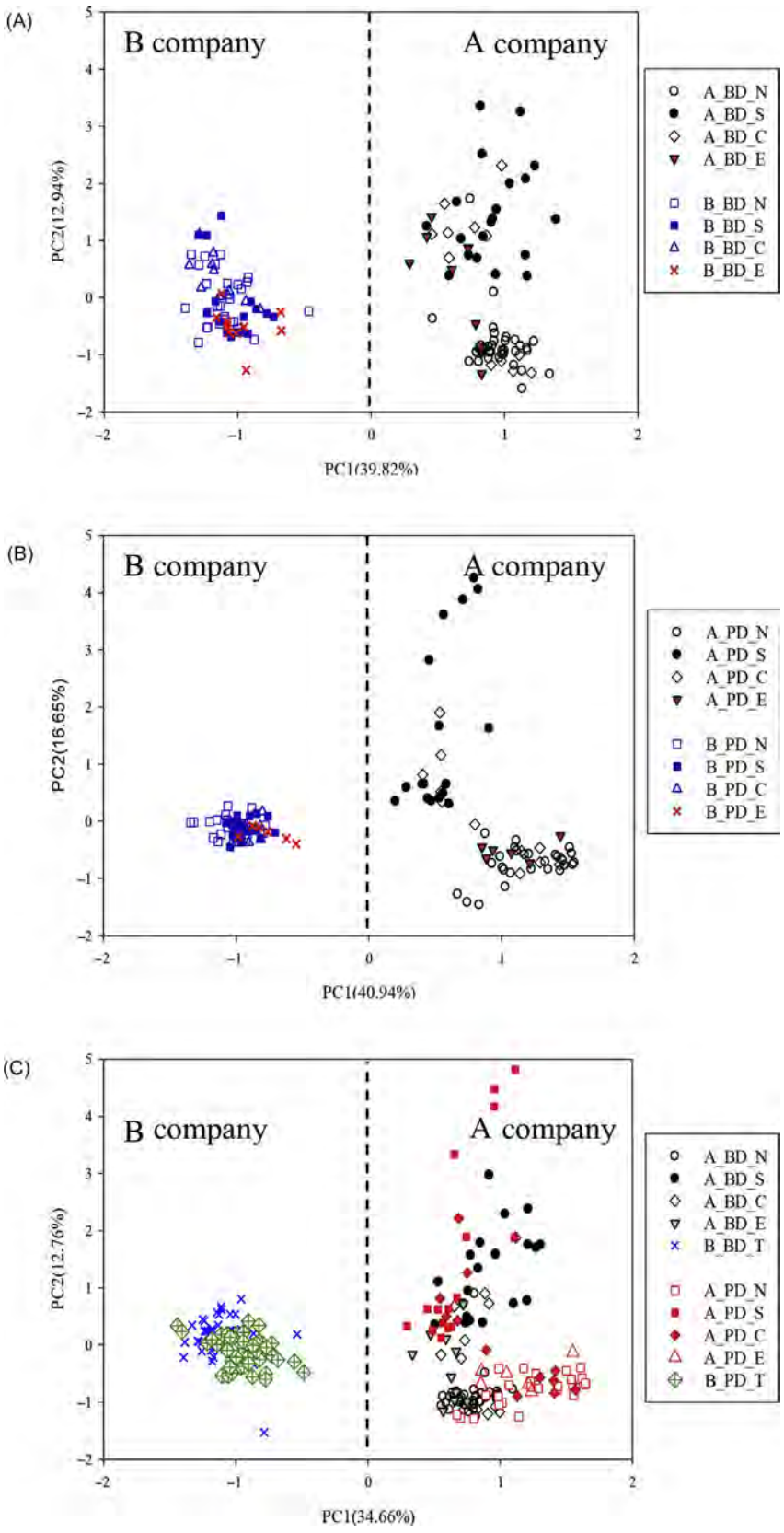

FIGURE 12.2 Resulting PCA–DRs factor score plots for (A) biodiesel samples with 45 DRs; (B) premium diesel samples with 41 DRs; (C) both biodiesel and premium diesel samples with 41 DRs from A and B refinery companies in Taiwan. See Table 12.1 for DR lists.

TABLE 12.2 The DRs with DP > 5 in the PCA–DR Approach of Biodiesels and Premium Diesels From A and B Refinery Companies in Taiwan

	28 DRs (biodiesel)	**29 DRs (premium diesel)**	**21 DRs (biodiesel & premium diesel)**
TIC	*n*-C_{17}/Pr	*n*-C_{17}/Pr	*n*-C_{17}/Pr
		n-C_{18}/Ph	
	Pr/Ph	Pr/Ph	Pr/Ph
m/*z* 123	BS1/BS4		
	BS3/BS5	BS3/BS5	BS3/BS5
		BS3/BS4	
	BS4/BS5	BS4/BS5	BS4/BS5
		BS10/BS5	
	BS3/BS10	BS3/BS10	BS3/BS10
Adamantanes	A2/A6	A2/A6	A2/A6
	A2/A17	A2/A17	A2/A17
	A6/A17	A6/A17	A6/A17
	A6/A14	A6/A14	A6/A14
	A2/A10	A2/A10	A2/A10
	A17/A10	A17/A10	A17/A10
	A10/A15	A10/A15	A10/A15
PAHs	C_1N/C_2N	C_1N/C_2N	C_1N/C_2N
		C_2N/C_3N	
	C_3N/C_4N		
	C_2N/C_4N	C_2N/C_4N	C_2N/C_4N
	C_0P/C_1P		
		C_1P/C_2P	
	C_2P/C_3P		
		C_1P/C_3P	
	C_0F/C_1F		
	C_1N/C_1P	C_1N/C_1P	C_1N/C_1P
	C_2N/C_2P	C_2N/C_2P	C_2N/C_2P
	C_3N/C_3P	C_3N/C_3P	C_3N/C_3P
	C_0P/C_0F		
		C_1P/C_1F	
		C_2P/C_2F	
Refining procedure	U1/BS6	U1/BS6	U1/BS6
	$U2/C_1P4$		
	$U3/C_2P4$	$U3/C_2P4$	$U3/C_2P4$
	$U4/C_1F3$	$U4/C_1F3$	$U4/C_1F3$
	$U6/C_2F5$	$U6/C_2F5$	$U6/C_2F5$

See text for description.

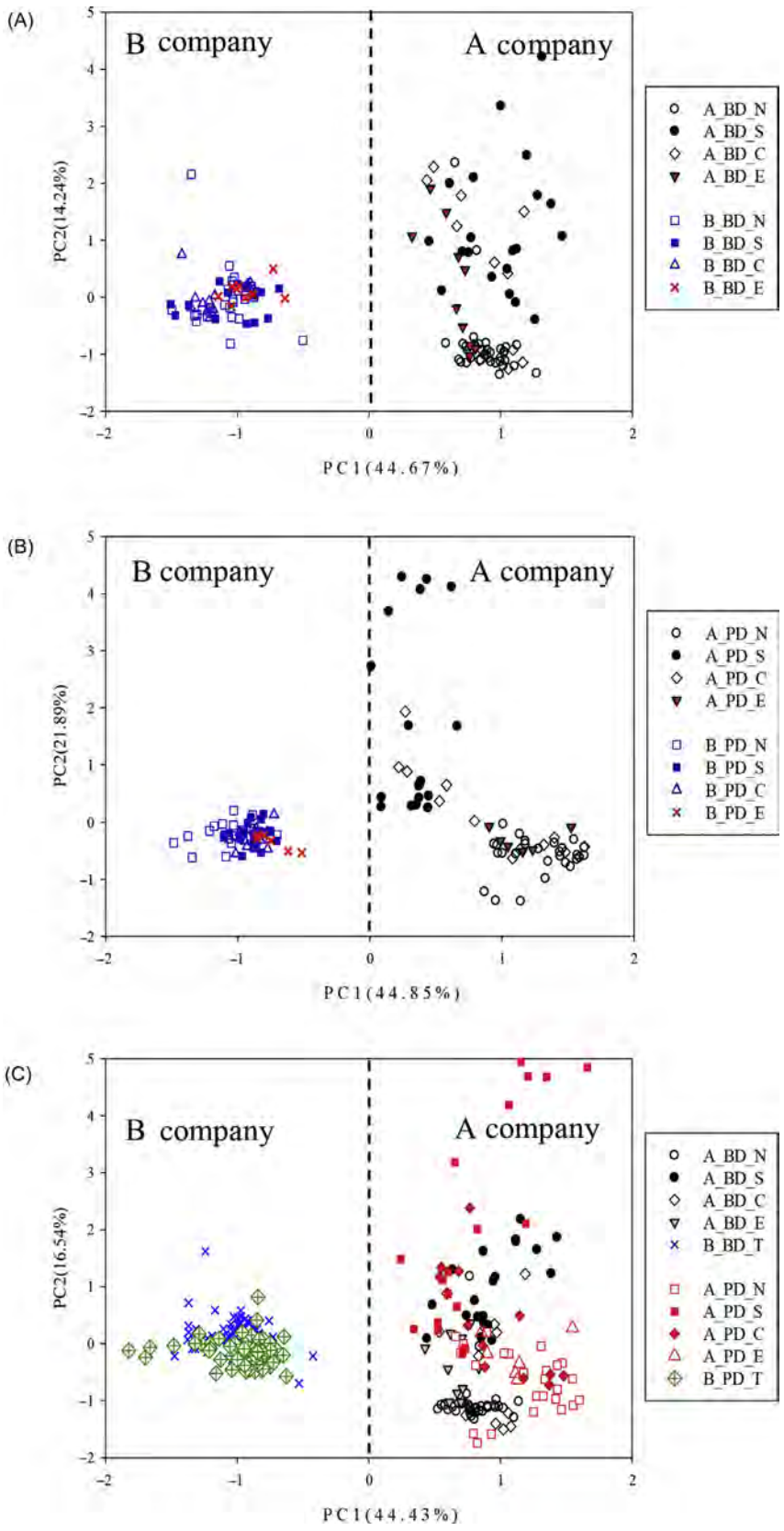

FIGURE 12.3 Resulting PCA–DRs factor score plots for (A) biodiesel samples with 28 DRs (DP > 5); (B) premium diesel samples with 29 DRs (DP > 5); (C) both biodiesel and premium diesel samples with 21 DRs (DP > 5) from A and B refinery companies in Taiwan. See Table 12.2 for DR lists.

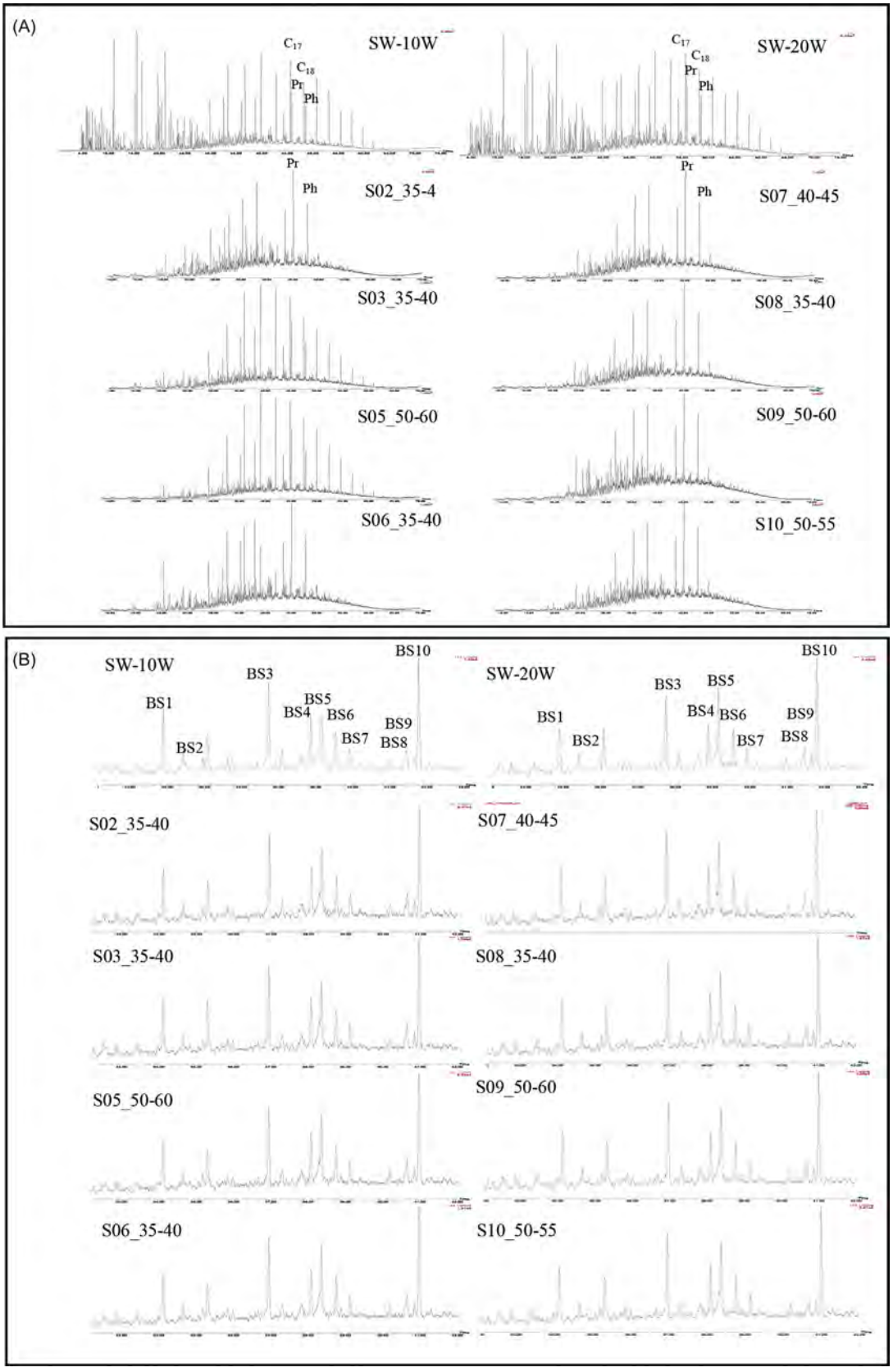

FIGURE 12.4 GC–MS chromatograms of (A) total ion chromatograph and (B) bicyclic sesquiterpanes (*m*/*z* 123) for two LPH samples collected in 2008 (SW-10W and SW-20W) and eight soil samples (S##) collected in 2015 from the F site.

TABLE 12.3 PCA–DRs Approach With 36 DRs, 31 DRs and 18 DRs With DP > 5 From Biodiesel, Premium Diesel and F Site Samples in Taiwan

	Unweathering effect		Weathering effects		
	41 DRs	**21 DRs (DP > 5)**	**36 DRs**	**31 DRs**	**18 DRs (DP > 5)**
TIC	*n*-C_{17}/Pr	*n*-C_{17}/Pr	**Biodegradation**	**Biodegradation**	**Biodegradation**
	n-C_{18}/Ph		**Biodegradation**	**Biodegradation**	
	Pr/Ph	Pr/Ph	Pr/Ph	Pr/Ph	Pr/Ph
m/*z* 123	BS1/BS4		BS1/BS4	BS1/BS4	
	BS3/BS5	BS3/BS5	BS3/BS5		BS3/BS5
	BS3/BS4		BS3/BS4	BS3/BS4	
	BS4/BS5	BS4/BS5	BS4/BS5	BS4/BS5	BS4/BS5
	BS4/BS6		BS4/BS6	BS4/BS6	
	BS6/BS5		BS6/BS5	BS6/BS5	
	BS10/BS5		BS10/BS5	BS10/BS5	
	BS3/BS10	BS3/BS10	BS3/BS10	BS3/BS10	BS3/BS10
Adamantanes	A2/A6	A2/A6	A2/A6	A2/A6	A2/A6
	A2/A17	A2/A17	A2/A17	**Dissolution**	A2/A17
	A6/A17	A6/A17	A6/A17	**Bio + dissolution**	A6/A17
	A6/A14	A6/A14	A6/A14	A6/A14	A6/A14
	A2/A3		A2/A3	A2/A3	
	A2/A10	A2/A10	A2/A10	A2/A10	A2/A10
	A3/A(7 + 8)		A3/A(7 + 8)	A3/A(7 + 8)	
	A3/A10		A3/A10	A3/A10	
	A(7 + 8)/A10		A(7 + 8)/A10	A(7 + 8)/A10	
	A17/A10	A17/A10	A17/A10	A17/A10	A17/A10
	A10/A15	A10/A15	A10/A15	A10/A15	A10/A15
PAHs	C_1N/C_2N	C_1N/C_2N	**Gasoline interference**	**Gasoline interference**	**Gasoline interference**
	C_2N/C_3N		C_2N/C_3N	**Dissolution**	
	C_3N/C_4N		C_3N/C_4N	C_3N/C_4N	
	C_2N/C_4N	C_2N/C_4N	C_2N/C_4N	**Dissolution**	C_2N/C_4N
	C_1P/C_2P		C_1P/C_2P	C_1P/C_2P	
	C_2P/C_3P		C_2P/C_3P	C_2P/C_3P	
	C_1P/C_3P		C_1P/C_3P	C_1P/C_3P	
	C_1F/C_2F		C_1F/C_2F	C_1F/C_2F	
	C_1N/C_1P	C_1N/C_1P	**Gasoline interference**	**Gasoline interference**	**Gasoline interference**
	C_2N/C_2P	C_2N/C_2P	C_2N/C_2P	C_2N/C_2P	C_2N/C_2P
	C_3N/C_3P	C_3N/C_3P	C_3N/C_3P	C_3N/C_3P	C_3N/C_3P
	C_1P/C_1F		C_1P/C_1F	C_1P/C_1F	
	C_2P/C_2F		C_2P/C_2F	C_2P/C_2F	
	2-MN/1-MN		**Gasoline interference**	**Gasoline interference**	
	(3 + 2)MP/(9 + 1)MP		(3 + 2)MP/(9 + 1)MP	(3 + 2)MP/(9 + 1)MP	

(*Continued*)

TABLE 12.3 (*Continued*)

	Unweathering effect		Weathering effects		
	41 DRs	**21 DRs (DP > 5)**	**36 DRs**	**31 DRs**	**18 DRs (DP > 5)**
Refining process	U1/BS6	U1/BS6	U1/BS6	U1/BS6	U1/BS6
	U3/C_2P4	U3/C_2P4	U3/C_2P4	U3/C_2P4	U3/C_2P4
	U4/C_1F3	U4/C_1F3	U4/C_1F3	U4/C_1F3	U4/C_1F3
	U6/C_2F5	U6/C_2F5	U6/C_2F5	U6/C_2F5	U6/C_2F5

The 41 DR values' RPDs of the two LPH samples and the 41 DR values' RSD of eight soil samples were calculated (data not shown). Larger variations among the DRs for *n*-C_{17}/Pr, *n*-C_{18}/Ph, C_1N/C_2N, C_1N/C_1P, and 2-MN/1-MN were found because of the effects of biodegradation and gasoline interference. Based on the results, the PCA−DRs approach eliminated the affected DRs and proceeded with the 36 DRs, 31 DRs and 18 DRs with DP > 5. Table 12.3 lists precise and specific DRs unaffected by the gasoline interference and weathering effect from BD, PD and F site samples. Again, this PCA−DRs approach was easily capable of distinguishing the two populations among the 126 fresh PDs—using 36 DRs (Fig. 12.5A), 31 DRs (Fig. 12.5B), and 18 DRs (Fig. 12.5C)—that had been obtained from various gasoline station supplied by the two refinery companies in Taiwan. (Only PD fuels were included in this evaluation because the F site diesel fuel spill involved PD fuel.) The PC1 scores of PCA−DRs approach with 36 DRs, 31 DRs and 18 DRs with DP > 5 are 38.86%, 38.32%, and 52.44%, respectively. In each case, the 10 LPH and soil samples from F site are most closely related to one another and to diesel fuels from the A refinery company. This result is consistent with the known history of the 2007 accidental release of PD fuel from A refining company's pipeline at F site. Thus, despite mixing of gasoline in the LPH samples and weathering in the soils samples, spilled diesel fuel could still be recognized to have come from A refining company using the PCA−DRs approach.

12.3.3 Application to Contaminated Sites

The PCA−DRs approach was further apply to five contaminated sites impacted by diesel fuel from A or B refinery company. Three contaminated sites (G, H, and I Sites) were impacted with BD or PD fuel known to have come from A refinery company, while two contaminated sites (B and C sites) were impacted by diesel fuel from B refinery company. Fig. 12.6 shows the GC−MS chromatograms (TICs) of samples collected from these five sites. As can be seen, different degrees of weathering was evident among the five contaminated sites. Light weathering was found in the sample from G Site, while severe weathering had occurred in the B and H Sites. The PCA−DRs approach of samples from these five impacted sites (B, C, G, H, and I), and from the F site (described above) was conducted using 36 DRs and 18 DRs of DP > 5 (Table 12.3) and the resulting factor score plots are displayed in Fig. 12.7. The PCA−DRs approach using 36 DRs and 18 DRs with DP > 5 was able to distinguish all of the samples of both fresh and weathered diesel fuels into two groups, A and B group, corresponding to the A and B refining companies. The PC1 scores with 36 DRs and 18 DRs with DP >5 were 31.92% and 44.48%, respectively, indicating the approach using 18 DRs (DP > 5) had increased the PC1 score by 12.56%. These results reveal that the PCA−DRs approach using 18 DRs (DP > 5) had a greater ability to distinguish among the two main groups of diesel fuels than when all 36 DRs were used. Thus, these 18 DRs (DP > 5; Table 12.3) were the most useful for distinguishing between genetically-similar diesel fuels from A and B refining companies at real spilled sites.

12.4 CONCLUSION

The PCA−DRs approach was developed and tested in this study as a means to distinguish between genetically-similar fresh diesel fuels produced by the two refinery companies in Taiwan. The approach was

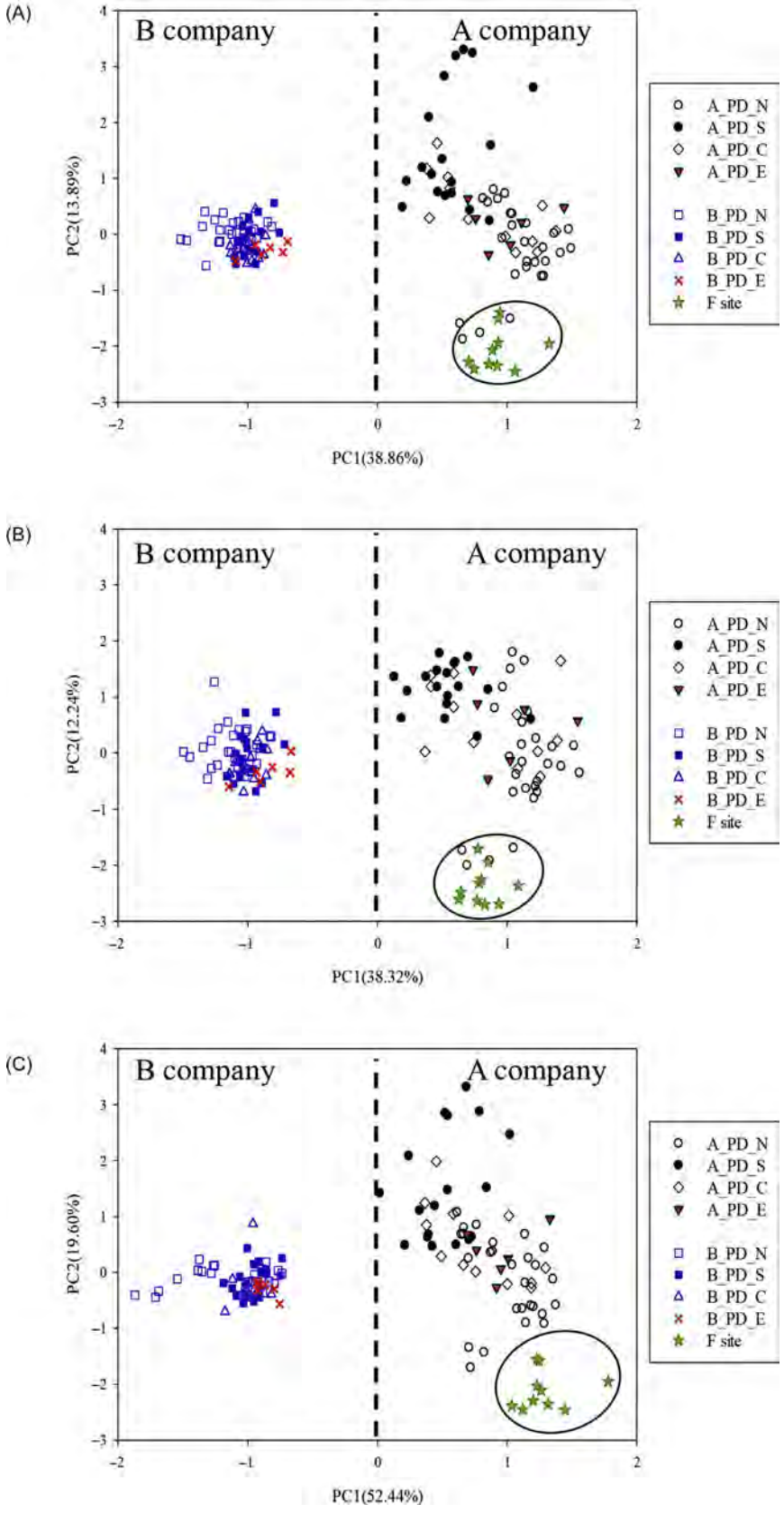

FIGURE 12.5 PCA–DRs approach of (A) fresh premium diesel and weathered F site samples with 36 DRs; (B) fresh premium diesel and weathered F site samples with 31 DRs; (C) fresh premium diesel and weathered F site samples with 18 DRs (DP > 5) in Taiwan. (N = North, S = South, C = Central, and E = East; T = Total, BD = Biodiesel, and PD = Premium diesel).

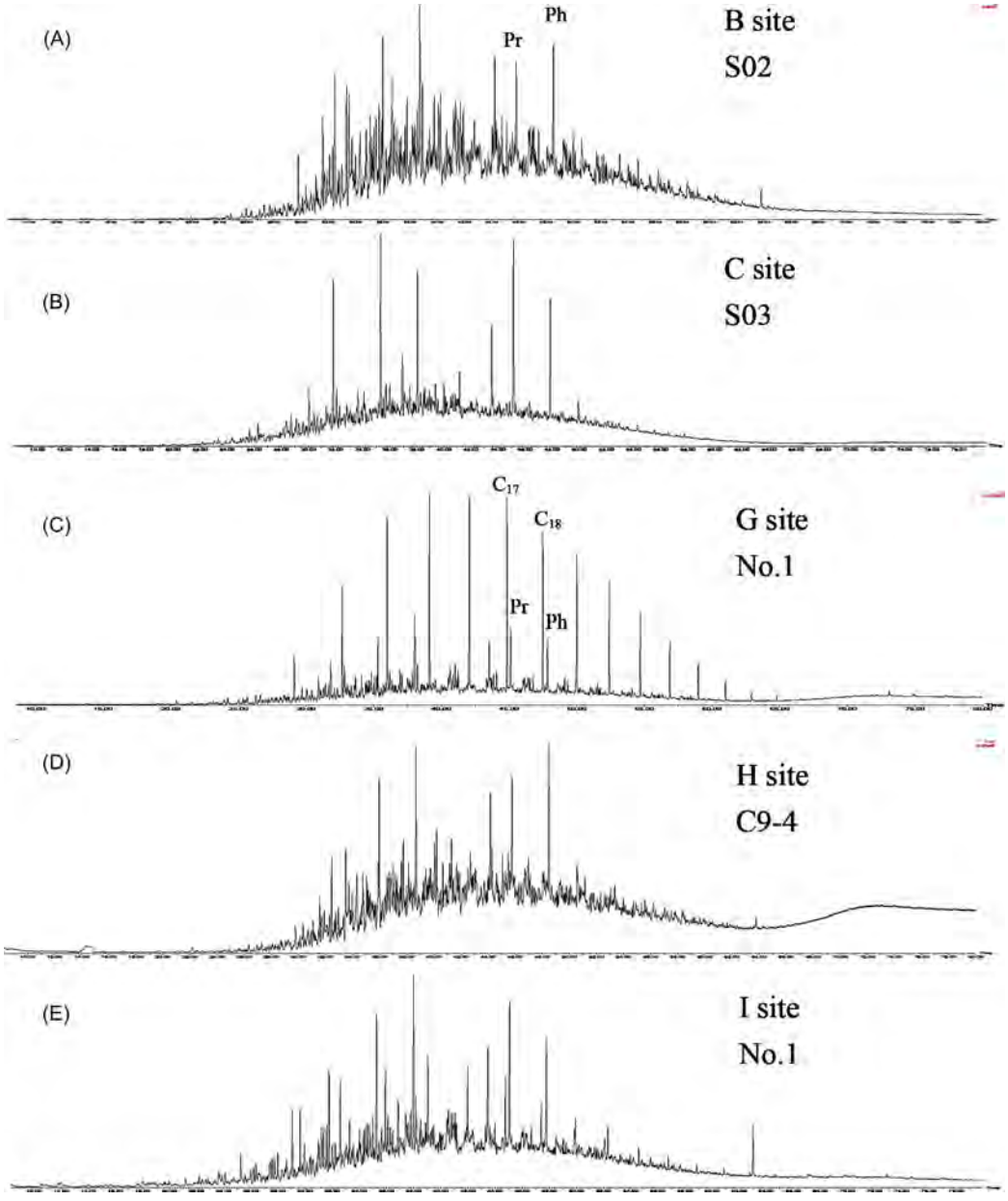

FIGURE 12.6 GC–MS chromatograms of total ion chromatograph (A) B Site; (B) C Site; (C) G Site; (D) H Site; (E) I Site in Taiwan.

successfully applied to a large population of fresh BDs and PDs and also to contaminated sites, where the fuels produced by the two refinery companies in Taiwan could be distinguished despite the effects of weathering. The PCA–DRs approach combines fingerprinting and DRs techniques, including up to 45 DRs among Pr, Ph, bicyclic sesquiterpanes, admantanes, alkyl PAHs and refining U compounds. The PCA–DRs approach applied to fresh diesel fuels, the scores of PC1 were best (44.43%) using 21 DRs with DP $>$ 5, which was better than when 41 DRs were used (34.66%). When spilled diesel fuel samples from contaminated sites are combined with fresh diesel oils, the scores of PC1 using 18 DRs with DP $>$ 5 were better (44.48%) than when 36 DRs were used (31.92%). The PC1 scores using 21 DRs (DP $>$ 5) for evaluating fresh diesel fuels and 18 DRs (DP $>$ 5) for evaluating spilled (weathered) diesel fuel samples were increased 9.77% and 12.56%, respectively, which indicates that the PCA–DRs approach using DRs with DP $>$ 5 can better distinguish fresh and weathered diesel fuels from the two refinery companies in Taiwan.

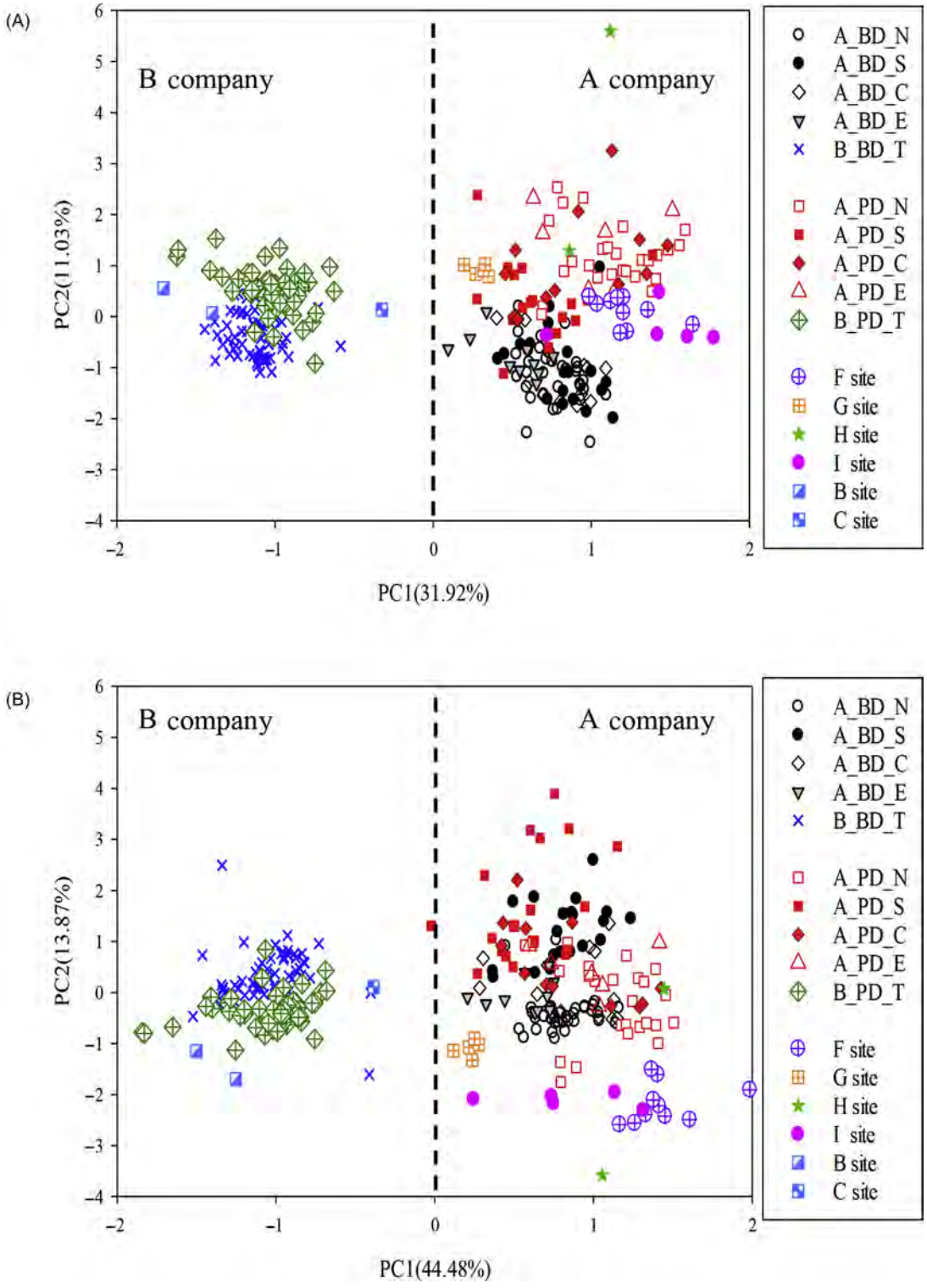

FIGURE 12.7 PCA–DRs factor score plot for fresh biodiesel and premium diesel and variably weathered diesel fuels from six impacted sites (F, G, H, I, B, and C) using (a) 36 DRs and (b) 18 DRs of DP > 5 (per Table 12.3) in Taiwan. (N = North, S = South, C = Central, and E = East; T = Total, BD = Biodiesel, and PD = Premium diesel.)

Acknowledgments

This project was funded by the Environmental Protection Administration Executive Yuan, R.O.C. (Taiwan) under the contract number EPA-102-GA13-03-A318 and EPA-103-GA13-03-A230.

References

Daling, P.S., Faksness, L.G., Hansen, A.B., Stout, S.A., 2002. Improved and standardized methodology for oil spill fingerprinting. Environ. Forensics 3, 263–278.

Peters, K.E., Walters, C.C., Moldowan, J.M., 2005. second ed. Chapter 1. The Biomarker Guide, Volume I. Cambridge University Press, New York.

Stout, S.A., Douglas, G.S., 2004. Diamondoid hydrocarbons application in the chemical fingerprinting of natural gas condensate and gasoline. Environ. Forensics 5, 225–235.

Stout, S.A., Uhler, A.D., McCarthy, K.J., 2005. Middle distillate fuel fingerprinting using drimane-based bicyclic sesquiterpanes. Environ. Forensics 6, 241–251.

Wang, Z., Fingas, M., Page, D., 1999. Oil spill identification. J. Chromatogr. A. 846, 369–411.

Wang, Z., Yang, C., Fingas, M., Hollebone, B., Peng, X., Hansen, A.B., et al., 2005. Characterization, weathering, and application of sesquiterpanes to source identification of spilled petroleum products. Environ. Sci. Technol. 39, 8700–8707.

Wang, Z., Yang, C., Hollebone, B., Fingas, M., 2006. Forensic fingerprinting of diamondoids for correlation and differentiation of spilled oil and petroleum products. Environ. Sci. Technol. 40, 5636–5646.

Wang, Z., Yang, C., Fingas, M., Hollebone, B., Yim, U.H., Oh, J.R., 2007. Petroleum biomarker fingerprinting for oil spill characterization and source identification. In: Wang, Z., Stout, S.A. (Eds.), Oil Spill Environmental Forensics: Fingerprinting and Source Identification. Academic Press, Burlington, MA, pp. 73–146.

Wang, Z., Yang, C., Hollebone, B., Brown, C., Landriault, M., 2008. Source identification of spilled diesel using diagnostic sesquiterpanes and diamondoids. In: International Oil Spill Conference, pp. 285–296.

Wu, S.H., et al., 2013. Apply environmental forensic techniques to establish commercial diesel fingerprint investigation plan. In: EPA-102-GA13-03-A318. Miaoli, Taiwan (in Chinese).

Yang, C., Wang, Z., Hollebone, B., Peng, X., Fingas, M., Landriault, M., 2006. GC/MS quantitation analysis of diamondoid compounds in crude oils and petroleum products. Environ. Forensics 7, 292–305.

Yang, C., Wang, Z., Hollebone, B., Brown, C.E., Landriault, M., 2008. Application of statistical analysis in the selection of diagnostic ratios for forensic identification of an oil spill source. In: International Oil Spill Conference, pp. 298–310.

Yang, C., Wang, Z., Hollebone, B., Brown, C.E., Landriault, M., 2009. Characteristics of bicyclic sesquiterpanes in crude oils and petroleum products. J. Chromatogr. A. 1216, 4475–4484.

Further Reading

Murphy, B.L., Morrison, R.D., 2002. Introduction to Environmental Forensics. Chapter 6. Academic Press, New York.

CHAPTER

13

Application of CEN Methodology in Evaluating Sources of Multiple Land-Based Fuel Spills in Alberta, Canada

Detlef A. Birkholz

Analytical Consultant, Inc., Edmonton, AB, Canada

BIOGRAPHY

Detlef (Deib) Birkholz, MSc, PhD, P.Chem has over forty years of practical experience in analytical chemistry, research, environmental and human toxicology, and business. Major industrial clients include: transportation, oil and gas, petrochemical, mining and pulp and paper industries. Dr. Birkholz has worked for both the Federal government (Canada) and industry. Deib, has proven a valuable resource to industry, government, and consultants, offering expertise in sampling, chemical analyses, data interpretation, toxicology, industrial problem solving, and forensic analyses. He has given numerous hours of court testimony and provided evidence in Provincial Court, Queens Bench and Federal Court. He has also provided training in evidence collection to industry and consultants and has organized several litigation seminars at key conferences with the assistance of defense lawyers, prosecutors and judges. Dr. Birkholz is currently an adjunct professor with the University of Alberta in Edmonton with teaching responsibilities at both the undergraduate and graduate level. He is a member of the oil spill identification network of experts within the Bonn Agreement (Bonn-OSINET).

13.1 INTRODUCTION

Information obtained from the Alberta Energy Regulator and reported by Global News claim that between 1975 and 2012, 28,666 oils spills occurred in the province of Alberta (Young, 2013). According to the Alberta Energy Regulator, 1.5 incidents were reported per 1000 km of pipe in 2011. Alberta has over 415,000 km of pipeline and this suggests that 775 spills occurred in 2011. Spillage from well pads, pipelines, batteries and spills resulting from train derailments and tanker accidents can and do release hydrocarbons onto farmland, forests, muskeg and into waterbodies such as creeks, rivers, ponds and lakes. A report commissioned by First Nations, raised concerns about under reporting of spills by the Alberta Energy Regulator as well as inadequate cleanup following spill events (Nikiforuk, 2017). This report claims that prior to 1975 there were thousands of spills from federally regulated pipelines which were not reported. Recent restructuring of the Alberta Energy Regulator has resulted in marked improvement in spill management and reporting, and this trend is likely to continue (Young, 2013). Although Global News obtained information from the Alberta Energy Regulator, Nikiforuk (2017) has not been subject to peer review.

The above information suggests that investigations following petroleum and chemical spills can result in surprises, i.e., detection of hydrocarbons from one or more sources, or from past spill events in the same area that may be encountered. Because the cost of cleanup can be expensive, it is in the interest of government and

Oil Spill Environmental Forensics Case Studies.
DOI: http://dx.doi.org/10.1016/B978-0-12-804434-6.00013-6

industry to determine the extent of a reported spill as well as evaluate the potential environmental damage. It is also important to determine if other mitigating factors exist, such as the discovery of previous spills, which may have been inadequately cleaned up or have been unreported.

Existing oil spill fingerprinting protocols, designed to identify sources of spilled oil, are either qualitative or quantitative in nature (Stout, 2016). Qualitative methods rely on visual comparison of chromatograms obtained following gas chromatography/flame ionization detection (GC/FID) or gas chromatography/mass spectrometry (GC/MS) analyses. The latter relies on comparisons of extracted ion profiles (EIPs) for polycyclic aromatic hydrocarbons or petroleum biomarkers. These qualitative protocols have been formalized in two standards of the American Society for Testing and Materials (ASTM, 1995, 2000).

Quantitative methods such as the technical guideline prepared by the Centre for European Norms (CEN, 2012), rely on a tiered approach that includes (1) a qualitative assessment of GC/FID and GC/MS chromatograms to assess the overall character of oil in a sample or potential source, (2) a quantitative comparison of diagnostic ratios (DRs) of polycyclic aromatic hydrocarbons (PAHs) and petroleum biomarkers in a sample and source, as well as weathering assessments, and (3) a postanalysis synthesis of the data to confirm resulting scientific conclusions.

The procedures advocated by CEN (2012), were designed to defensibly identify the source of oil spills in marine, estuarine, and other aquatic environments by comparing the chemical compositions of oil samples from spills with those of suspected sources. The method relies upon detailed chemical characterization and statistical comparisons between spill and potential source samples via a largely prescribed analytical and interpretive procedure.

The CEN (2012) method is not directly intended for oil spill impacting groundwater, vegetation, wildlife/tissues, soils or sediments, although its application in these matrices is not precluded. However, when utilizing the CEN (2012) protocol in these nonoil matrices caution must be exercised in applying this method. The reason is that unlike aquatic oil spills in which "pure" oils can be obtained for study, the samples often collected while investigating land-based spills can contribute interfering compounds following extraction of vegetation, soil, wildlife and tissue. These interfering compounds can lead to complicate comparisons between spill and source samples and lead to incorrect conclusions if left unrecognized. Furthermore, contribution of hydrocarbons from previous spills that had historically impacted the same area, if not accounted for can also lead to false conclusions. It should be pointed out that following a land-based spill, both terrestrial and aquatic environments may be impacted. The CEN (2012) method is certainly applicable to waterborne petroleum (CEN, 2012).

In this chapter, we applied the CEN (2012) method to three land-based spill events in Alberta Province, Canada involving diesel fuel, crude oil and heavy oil. Samples of potential sources, soil and wildlife were collected with the objective of defensibly determining if the potential sources identified in each case were the source of contaminated soil and wildlife in each spill area.

13.2 METHODS

Adaptations in the preparation of samples prior to analysis were included so as to minimize the effects of interfering compounds in the soil and wildlife samples studied, as described in this section.

Soil samples (6–50 g) were mixed with anhydrous sodium sulfate and subjected to Soxhlet extraction with dichloromethane overnight. The solvent was concentrated and an aliquot removed and subjected to gravimetric analysis. Based upon the gravimetric results, differing amounts of the extract were subjected to column cleanup. Cleanup was performed using a mixed phase adsorbent consisting of 2.5 g of fully activated neutral alumina (2%, w/w, water deactivated) and 5 g of silica gel. Both adsorbents were preconditioned in a tube furnace maintained at 350°C prior to use. Following addition of the extract to the mixed phase column, saturates were removed by elution with 50 mL pentane. Aromatics were removed by elution with 100 mL dichloromethane. We noted the formation of sulfur crystals in the saturated fraction of some soil samples and further cleaned these extracts using elemental mercury. The combined aromatic and saturate fraction was concentrated to 0.5–1.0 mL prior to instrumental analysis.

For some oil product samples, such as heavy oil or crude oil, an aliquot of approximately 0.5 g was split using two 50 mL test tubes. Following the addition of 1 mL of toluene the mixture was vortexed. Forty milliliters of pentane was added to each tube, vortexed and allowed to sit for 2 hours in order to accommodate the precipitation of asphaltenes. It was found that this 2 hours duration is not long enough to deasphaltene heavy oil samples; it has been previously demonstrated that at least 12 hours is required (Strausz and Lown, 2003). Accordingly, the

tubes were centrifuged and the pentane layer combined into a round bottom flask and concentrated to 4.0 mL. An aliquot was removed for gravimetric analysis and based upon that information, an appropriate aliquot (20−50 mg) was subjected to alumina−silica cleanup as described above. The lighter oil product samples studied, such as diesel fuel, were simply diluted with dichloromethane.

For wildlife samples, oil contaminated fur and/or feathers were removed and an aliquot (2−7 g) was mixed with anhydrous sodium sulfate and Soxhlet extracted with dichloromethane overnight. The resulting extract was concentrated and reconstituted with 5−10 mL of toluene. An aliquot of the toluene extract (1−2 mL) was deasphaltened and then subjected to alumina−silica cleanup as described above.

The combined saturate and aromatic fractions from all matrices were subjected to analysis using gas chromatography/selected ion-monitoring mass spectrometry (GC/MS) for target analytes (alkanes, terpanes, hopanes, sesquiterpanes, regular steranes, diasteranes, triaromatic steranes, and informative polycyclic aromatic hydrocarbons) consistent with those described by CEN (2012). The analytical and interpretive procedures of CEN (2012) were followed. Reference oil obtained from SINTEF Material and Chemistry, Trondheim, Norway, was also prepared and analyzed to aid in diagnostic peak identification.

13.3 CASE STUDY 1—ALLEGED DIESEL FUEL IMPACTS TO SURFACE SOILS

Two hydrocarbon contaminated soil samples were received from a large industrial site. The two soil samples collected were separated by a large distance—referred to herein as Site A and Site B. Despite the distance between the Sites it was believed by the operating company that the soils had been impacted by spills from a fuel truck, such as are commonly used to transport fuel to and from various locations across this large site. Tare weights from one particular fuel truck did not meet expectation and it was hypothesized that both the Site A and Site B soils may have been impacted by diesel fuel from the suspect fuel truck. Fresh diesel fuel from the suspected truck was collected for comparison to the soils. The soils and fuel originally were analyzed by a commercial laboratory who, employing a limited assessment of GC/FID data, concluded that the impacted soils from Sites A and B were related to one another and to the suspect fuel truck. We were subsequently asked to evaluate these results.

Aliquots of the soils and fuel were supplied and analyzed as described above, and the CEN (2012) method was applied. However, upon reanalysis the samples were not first analyzed by GC/FID. Although GC/FID analysis is recommended to screen samples prior to GC/MS analyses, the GC/FID analyses performed originally by the commercial laboratory provided a sufficient basis to screen the samples, so GC/FID was not repeated. Therefore, sample extracts (prepared as described above) were directly analyzed by GC/MS.

Fig. 13.1 shows an EIP obtained for soil from Site A, soil from Site B and fresh diesel fuel from the suspected fuel truck. The *m*/*z* 85 EIPs shown are characteristic of *n*-alkanes and isoprenoids (Wang et al., 2006).

From Fig. 13.1, it is apparent that the chromatograms obtained from Site A and Site B appear similar to the suspected fuel. It is also apparent that both soil samples contain diesel fuel (C_9−C_{22}) and that both sites are weathered (evaporated) relative to the suspected source. The diesel fuel present in the soil from Site B appears to be slightly more weathered than that present in the soil from Site A, as revealed by Site B's diesel containing *n*-alkanes between C_{11} and C_{22}, while Site A's diesel contained *n*-alkanes in the range C_{10}−C_{22}. The weathering of diesel fuel in the Site A and B soils, however, is not sufficient to have impacted the abundances of *n*-alkanes or isoprenoids beyond *n*-C_{15}.

Table 13.1 shows selected *n*-alkane and isoprenoid DRs obtained for the soils from Site A and Site B and for the suspected source. Also reported is the percent relative difference (%RD) between the source sample and the site soil samples. (These ratios were calculated from the peak heights shown in the *m*/*z* 85 EIP shown in Fig. 13.1.) Per CEN (2012), %RD is obtained by dividing the absolute difference by the mean obtained for a particular ratio when comparing a spill and a source sample. The result is multiplied by 100 to give a percentage. Also in accordance with CEN (2012) a %RD of less than 14% is indicative the two samples' DRs are statistically comparable, i.e., source and spill are a positive match. Samples whose DRs have a %RD exceeding 14% are considered a nonmatch (CEN, 2012).

Thus, from Table 13.1, it is apparent that the %RD for *n*-alkane and isoprenoid ratios are all below 14% when the Site A soil and the Site B soil are compared to the suspected source. Based upon this level of information, as well as the similarity of the chromatogram (Fig. 13.1), it is understandable why the commercial laboratory had originally concluded that the diesel fuel from suspected fuel truck was the source of diesel fuel contamination of

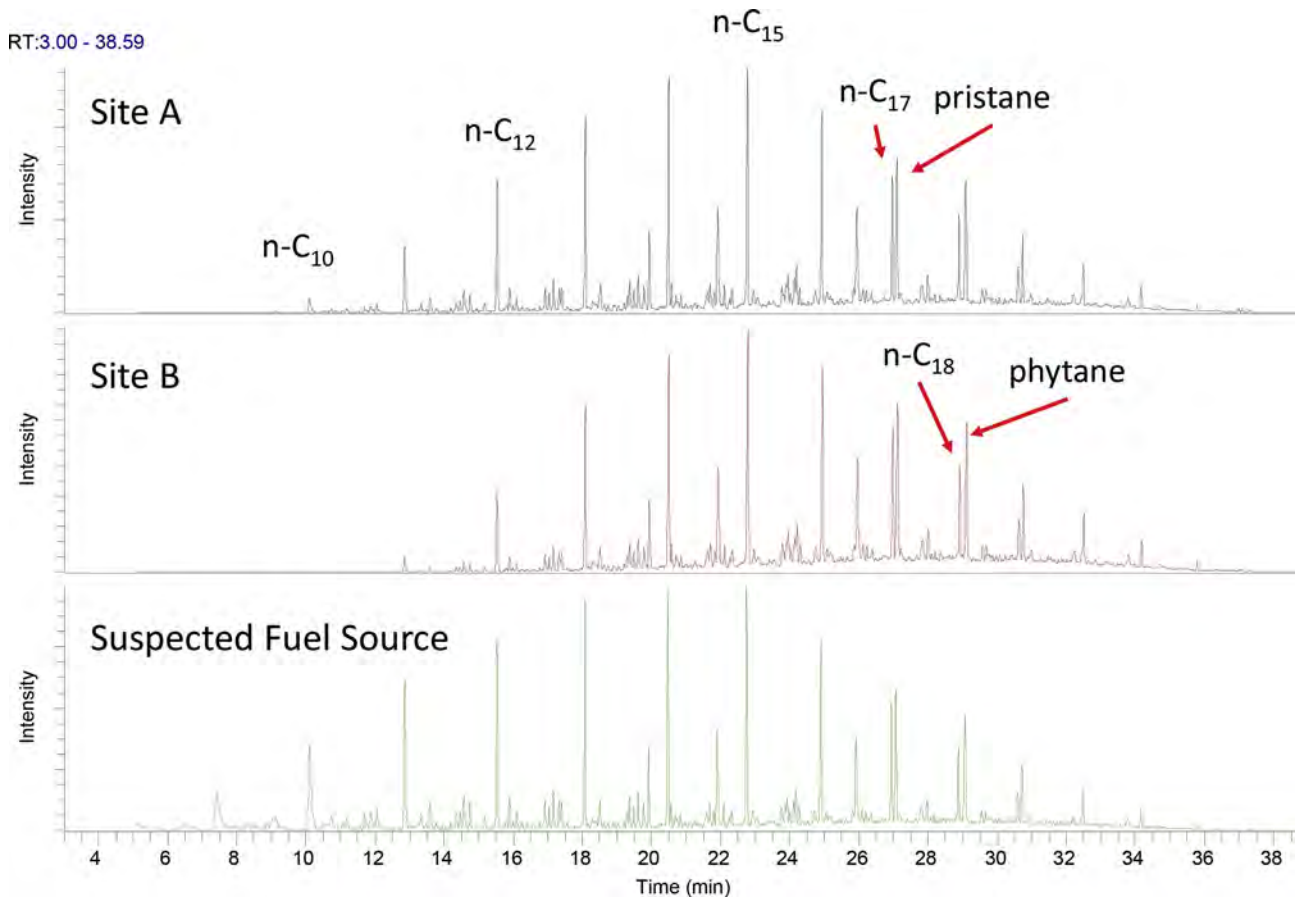

FIGURE 13.1 GC/MS EIP for *m*/*z* 85 comparing soil from Site A, soil from Site B, and fresh diesel fuel from the suspected source from Case Study 1.

TABLE 13.1 Alkane and Isoprenoid Ratios and Percent Relative Difference for Samples From Case Study 1

Sample identification	*n*-C17/pristane	*n*-C18/phytane	Pristane/phytane
Site A	0.88	0.71	1.18
Site B	0.86	0.67	1.14
Suspected source	0.91	0.69	1.23
% Relative difference	5.7	2.8%	7.6

the soils at both Site A and Site B. However, as will be evident below, more detailed chemical analysis and assessment was warranted before this conclusion can be reached.

Fig. 13.2 shows a GC/MS EIP for *m*/*z* 191, which is characteristic of terpanes including tricyclic terpanes, pentacyclic triterpanes, and hopanes for the soils from Site A and Site B and for the suspected source.

From Fig. 13.2, it is apparent that tricyclic terpanes and hopanes are present in the Site A and Site B soils but are absent in the suspected source. This observation suggests that hydrocarbons observed in Site A and Site B are not derived from the suspected source. As was the case with the terpanes, inspection of *m*/*z* 217 and *m*/*z* 218 EIPs (not shown) showed that soils from Sites A and B each contained a suite of ααα- and αββ-steranes, whereas the suspected fuel source did not.

The presence of these biomarkers in the Site A and Site B soil due to earlier spills prior to the discovery of the diesel fuel contamination at Site A and Site B is a valid concern. Mixing of petroleum derived from previous spills with the diesel fuel discovered at these Sites' soils could account for presence of petroleum biomarkers in

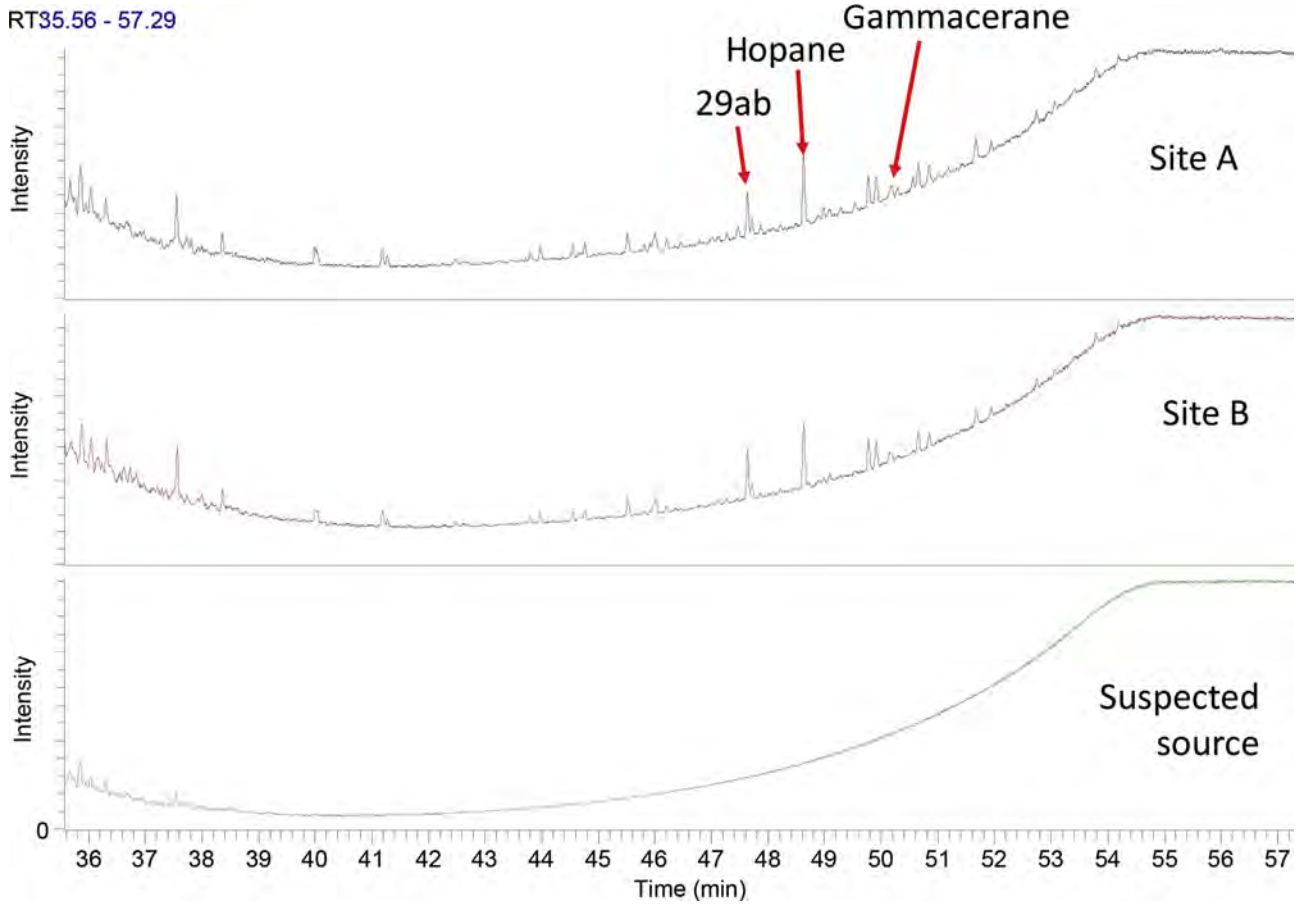

FIGURE 13.2 GC/MS EIP for *m/z* 191 comparing terpanes from the Site A soil, Site B soil, and the suspected source from Case Study 1.

the soils (Fig. 13.2) and, thereby be ignored, leading to erroneous "match" conclusions. However, the industrial site in question was a remote Northern mining site and the expectation of previous spills in the same locations was considered highly unlikely. As a result, the potential for any mixing of the suspected source diesel fuel with any preexisting petroleum (containing biomarkers) in the soils at Site A and Site B was ruled out. To bolster this conclusion, it would have been preferred to obtain and analyze soil samples from outside the Site A and Site B areas impacted by diesel fuel, as means to confirm the "clean" nature of soils. However, this was not possible within the timeframe of this investigation.

The lack of terpanes, hopanes, and steranes in the suspected source sample diesel fuel (Fig. 13.2) clearly shows that petroleum present in soils from Site A and Site B cannot have been derived from the suspected fuel truck, and that a different source (which contained trace amounts of biomarkers) must exist. Thus, in this instance when the Site's history was considered, a simple qualitative assessment of the biomarkers was capable of showing that the conclusions reached by a commercial laboratory using GC/FID chromatography, as well as simple *n*-alkane and isoprenoid based ratios (Table 13.1) were erroneous.

Our analysis of the data did not stop here however. Fig. 13.3 shows the normative and informative ratios associated with the comparison of the petroleum present in the Site A and Site B soils. Four normative ratios are shown which exceed 14% RD. The ratio of 2-methylpyrene/4-methylpyrene (2-MPy/4-MPy) could be explained by differential weathering through photooxidation (CEN, 2012; Stout et al., 2015; Radovic et al., 2014). Photooxidation could easily affect surface spills of diesel fuel to soil prior to the fuel infiltrating the soil. However, ratios such as 29ab/30ab [17α(*H*), 21β(*H*)-30-norhopane/17α(*H*),21β(*H*)-hopane], 30G/30ab [gammacerane/17α(*H*),21β(*H*)-hopane], and 27bb/29bb [5α(*H*),14β(*H*), 17β(*H*), 20R and 20S cholestane/24-ethyl-5α(*H*), 14β(*H*), 17β(*H*) 20R and 20S cholestane] are derived from stable compounds, which are generally not affected by weathering (CEN, 2012; Stout, 2016). The observation that these stable ratios exceed the 14%RD threshold of CEN (2012) (Fig. 13.3) indicates that the specific diesel fuels present in the soil samples taken from Site A and Site B are derived from differing sources.

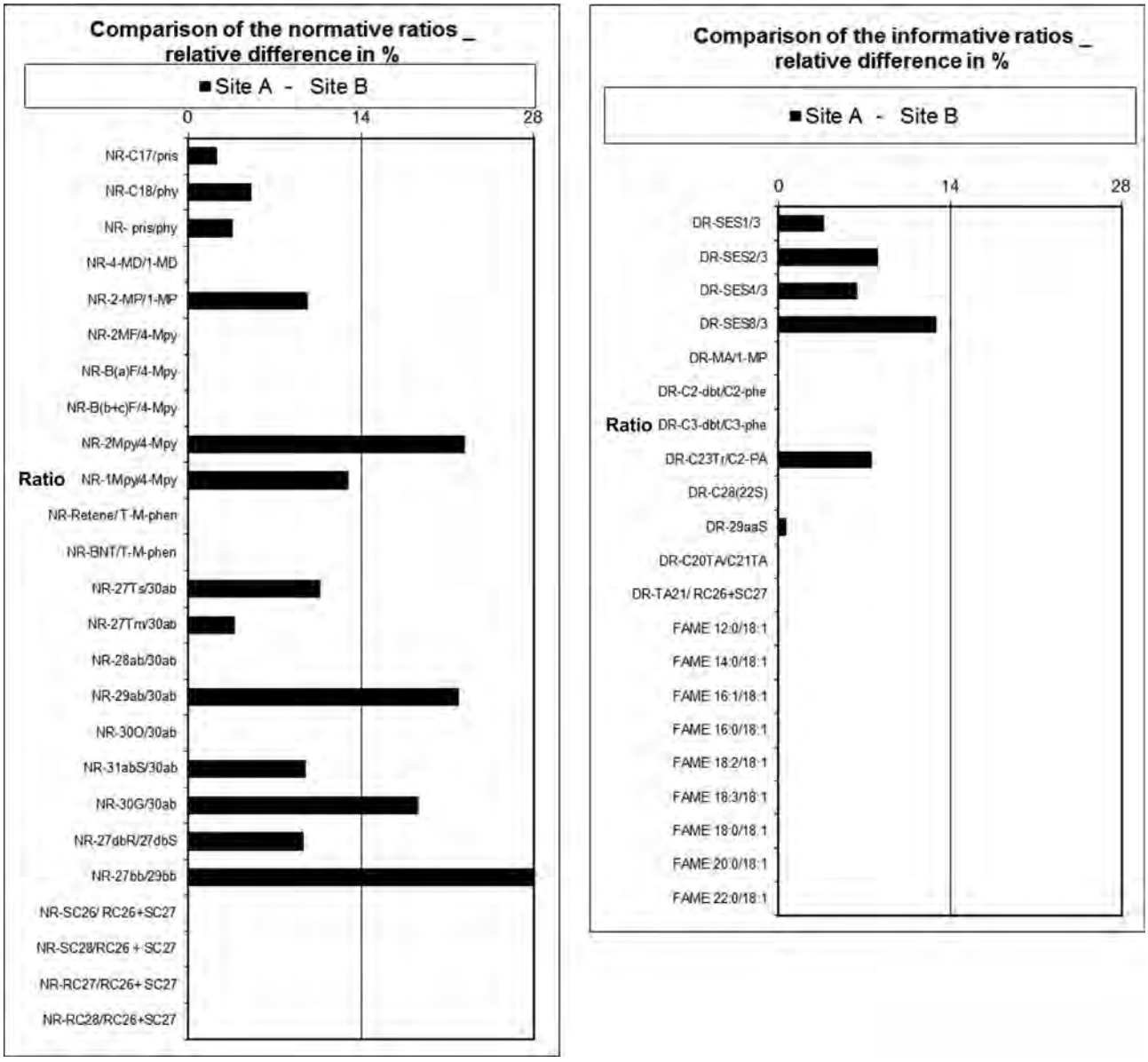

FIGURE 13.3 Comparison of normative and informative ratios for diesel fuel in soils from Site A and Site B in Case Study 1.

13.3.1 Conclusion—Case Study 1

Contaminated soil samples taken from two disparate locations on a large industrial site were compared to a source sample obtained from a fuel tanker, which based upon tare weight data, was suspected of leaking or discharging fuel at both locations. Chemical analyses using gas chromatography/mass spectrometry as well as *n*-alkane and isoprenoid based ratios supported this conclusion, which had originally been reached by a commercial laboratory. Subsequently, the soils and fuel were analyzed using more detailed analyses (i.e., PAHs and biomarkers) and these data were evaluated using CEN (2012). The results revealed that the contaminated soil samples from both Site A and Site B contained petroleum biomarkers, including tricyclic terpanes, hopanes, and steranes. None of these petroleum biomarkers were detected in the suspected source diesel fuel suggesting the soils were impacted by another source of contamination. Because the site investigated was a remote Northern mining site, no evidence was brought forward that previous spills occurred at the site, which may have contributed biomarker-containing petroleum to the soil samples. Furthermore, it was originally believed that the petroleum detected in the soil samples were derived from a single source. Calculation and statistical comparison (%RD) among numerous PAH and biomarker based normative and informative ratios revealed that the petroleum present in the soils was actually derived from differing sources—and as noted above, neither was derived from the suspected fuel truck.

13.4 CASE STUDY 2—EXTENT OF CRUDE OIL IN SOILS FOLLOWING A PIPELINE FRACTURE

A spill was investigated following a crude oil pipeline fracture. The crude oil spill occurred in a remote area and by the time investigators appeared upon the scene cleanup of the spill site was well underway. Sample of product from the repaired pipeline was collected although its relevance was uncertain because the pipeline had been purged and cleaned to facilitate repair—and as will be shown below this sample is not simply a fresh crude oil that was within the pipeline after the repair. The only authentic source sample of the spilled crude oil available was that obtained from a vacuum truck involved in the cleanup of the spill site. In order to determine the extent of spill, and its environmental impact, five surface soil samples from around the spill site were taken. Soil staining and visible impact on vegetation were drivers for selecting the locations of the soil samples. In light of introductory remarks to this chapter concerning oil spills in the province of Alberta, the objective of the study was to determine whether the crude oil from the vacuum truck was the same as the oil within the five soil samples collected around the spill site—referred to herein as Sites A through E.

An aliquot of each soil (~50 g) was Soxhlet extracted and cleaned up using a alumina–silica column as described above. The saturate fraction was further cleaned using elemental mercury in order to remove sulfur. The crude oil samples from the vacuum truck and pipeline were deasphaltened and cleaned up using a alumina–silica column as described above. Chemical analyses were performed using gas chromatography/selected ion-monitoring as described above using CEN (2012) procedures. GC/FID screening was not performed due to time and budget constraints.

Fig. 13.4 shows a GC/MS EIP for *m*/*z* 85 obtained for the oil in the vacuum truck, crude oil from the repaired pipeline, and soil samples taken from Site A, B, D, and E.

From this figure it is apparent that the product from the pipeline is unusual, and not readily compared to the site soils. This sample contained hydrocarbons in the C_{23} to C_{34} range, including some longer chain *n*-alkanes, but also repetitive clusters of peaks. The overall pattern is inconsistent with crude oil and likely represents a combination of pipeline cleaning agent, fire retardant used during pipeline repair, and some waxy residue within the pipeline. This sample is not seemingly appropriate for comparison to the site soils, but interesting and is addressed further below.

The oil collected from the vacuum truck is consistent with an evaporated crude oil and appears obviously most similar to oil extracted from soil samples from Sites B and D. The presence of crude oil in the Site B and D soils is apparent, i.e., the *n*-alkane distribution spans *n*-C_{10} to *n*-C_{40}. The *m*/*z* 85 EIPs obtained for extracts of the soils rom Site A and Site E do not appear similar to oil recovered from the vacuum truck, or the Site B and Site D soils. The Site A and Site E soils are dominated by odd-numbered *n*-alkanes that are associated with naturally occurring plant waxes found in soil and vegetation (Wang et al., 2009). This result suggests that naturally occurring (biogenic) hydrocarbons predominates in the extracts obtained from soils taken at Site A and Site E, and that crude oil, if present at all, is present at minor concentrations.

Table 13.2 shows *n*-alkane and isoprenoid ratios obtained for the vacuum truck product, pipeline product and soil extracts obtained from Sites A, B, C, D, and E.

All ratios obtained for the pipeline and soil samples were compared to the vacuum truck product, which (as discussed above) was the only source material available for study. %RD were calculated for each sample relative to the vacuum truck source sample. Those ratios appearing in bold had %RD greater that 14%, which per CEN (2012) suggests that these samples are different and a nonmatch to the vacuum source sample.

Based upon chromatographic observations (Fig. 13.4) as well as *n*-alkane and isoprenoid ratios, it is clear that the unusual pipeline sample and soil samples derived from Sites A and E, the latter of which are clearly dominated by biogenic hydrocarbons (Fig. 13.4), do not match the crude oil source sample taken from the vacuum truck and as such are removed from further consideration. These results are also suggesting that the crude oil present in soils samples from Sites B and D is consistent with the source sample, although this is further investigated below using additional GC/MS data.

Further analyses of the unusual product taken from the pipeline revealed the absence of aromatic compounds, which were mainly PAHs, following GC/MS analysis of the aromatic fraction. One is reminded that all samples were chemically fractionated into a saturate and aromatic fraction following alumina–silica cleanup as described in the methods section. A weak response for PAHs was also observed for the

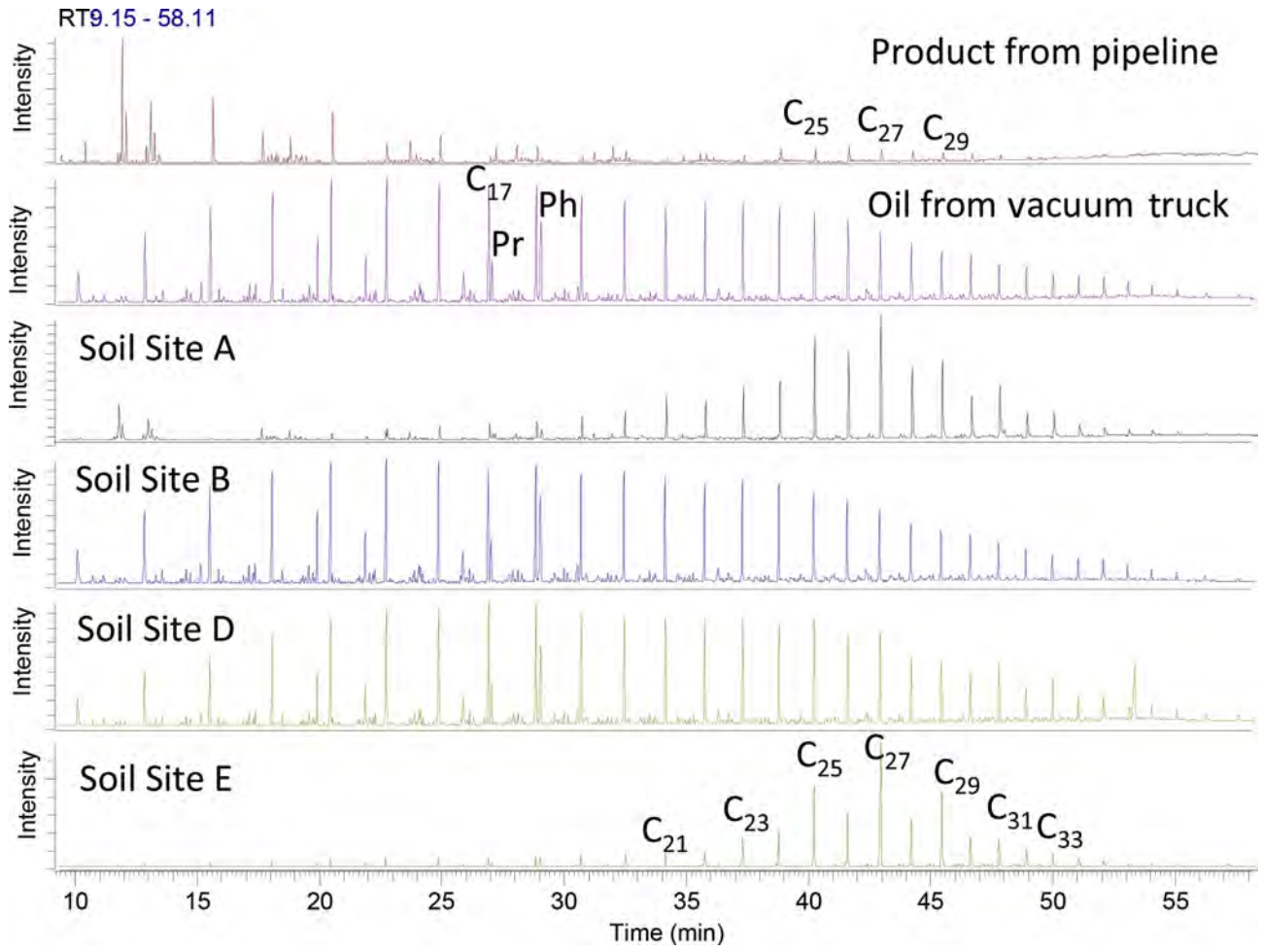

FIGURE 13.4 GC/MS EIP for *m/z* 85 comparing oil from product from pipeline, oil from vacuum truck, and soil samples A, B, D, and E in Case Study 2.

TABLE 13.2 Alkane and Isoprenoid Ratios for Samples From Case Study 2

Ratio	Source	Soil A	Soil B	Soil C	Soil D	Soil E
n-C_{17}/pristane	2.82	2.64	2.68	2.69	2.97	**2.40**
n-C_{18}/phytane	1.46	**1.79**	1.34	**3.89**	1.54	**1.24**
Pristine/phytane	0.51	**0.61**	0.49	0.53	0.53	**0.44**

The bold values represent DRs which exceed 14% RD and indicate a non-match with source material.

biogenic-rich soils taken from Site A and Site E. A strong response for PAHs was observed in the source oil taken from the vacuum truck and in soil samples taken from Site B and Site D. This is further evidence to support exclusion of the unusual product collected from the pipeline, and soils taken from Site A and Site E from further consideration. The Site A and Site E soils clearly were not impacted by crude oil released during the pipeline fracture. It also suggests that a nonpetroleum based cleaning agent may have been used to flush the pipeline prior to or during its repair.

Fig. 13.5 shows %RDs for the normative and informative ratios obtained following comparison of the vacuum truck product and the soil sample from Site B. Two ratios are observed to have a %RD greater than 14% indicating a nonmatch scenario. These ratios include: benzo(*a*)fluorene/4-methyl pyrene (BaF/4-MPy) and benzo($b + c$)fluorene/4-methyl pyrene (B($b + c$)F/4-MPy). These ratios' exceedance of 14% RD can be explained by

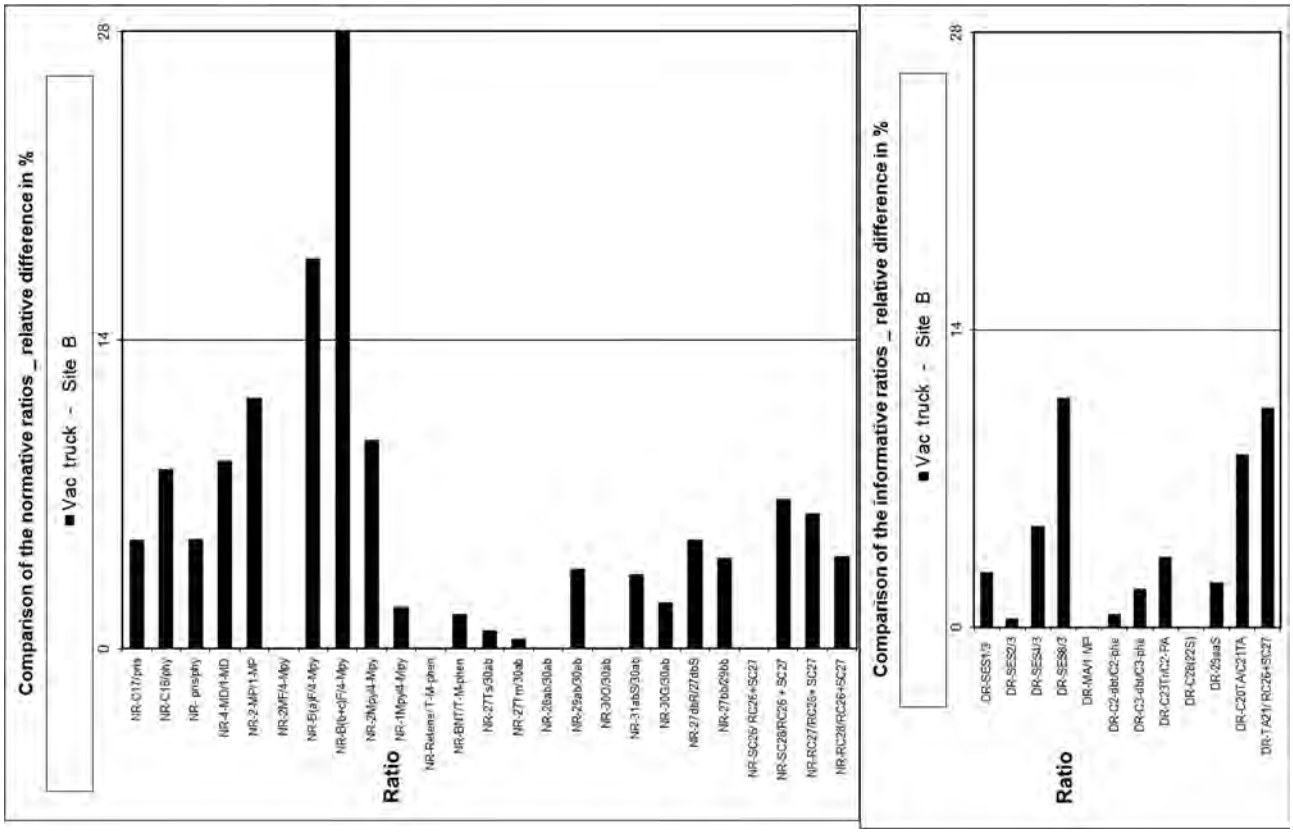

FIGURE 13.5 Normative and informative ratios following comparison of vacuum truck product and soil sample B.

weathering through photooxidation (Radovic et al., 2014; Melville et al., 2009). Peri-condensed structures such as pyrenes are very sensitive to photooxidation because they are very efficient absorbents of UV-radiation (Radovic et al., 2014) and it is reasonable that crude oil spilled from the pipeline experienced UV exposure after spillage to the site surface. As such these ratios are compromised if a sample is subject to photooxidation relative to a source oil sample. Because these two ratio exceedances can be explained by weathering (photooxidation) it was concluded that the product sample taken from the vacuum truck and soil from site B were a positive match.

Fig. 13.6 shows the normative and informative ratios following comparison of the vacuum truck oil to soil taken from Site D. Six ratios are observed to exceed 14% RD namely, including the two noted above as susceptible to photooxidation, plus BNT/T-M-Phe (benzo(*b*)naphtha(1,2-*d*)thiophene/tetra-methyl-phenanthrene), 27Ts/30ab (18α(*H*)-22,29,30-trisnorhopane/17α(*H*),21β(*H*)-hopane), RC27/RC26 + SC27 (C_{27}, 20R-triaromatic sterane/C_{26}, 20R- + C27, 20S-triaromatic steranes), and C_3-dbt/C_3-phe (C_3-dibenzothiophenes/C_3-phenanthrenes).

As was the case for the Site B soil, the failing ratios of B(*a*)F/4-MPy, B(*b* + *c*)F/4-Mpy can be explained by photooxidation (Radovic et al., 2014). Although triaromatic steroids are excellent biomarkers that generally defy most forms of weathering, they are subject to photooxidation (Radovic et al., 2014; Stout et al., 2016). The problem in this case is that, if the benzofluorene and methylpyrene-base ratios were affected by photooxidation (as believed), the C21TA/RC26 + SC27 and RC28TA/RC26 + SC27 should also have been effected by photoxidation resulting in failing ratios, which was not observed (Fig. 13.6). The most susceptible ratio to photooxidation is C21TA/RC26 + SC27 (Radovic et al., 2014), and if photoxidation affected the triaromatic steroids, then it would have expected this ratio to fail to a greater degree than RC27/RC26 + SC27 (Radovic et al., 2014). However, this was not observed; the %RD for this ratio was slightly over 5% which is excellent agreement between oil obtained from the vacuum truck and soil obtained from Site D. The ratio of RC28TA/RC26 + SC26 was less than 3%RD. Therefore, based on the varying results concerning the triaromatic steroids it was concluded that weathering cannot explain the failing RC27/RC26 + SC27 (Fig. 13.6) ratio and hence, a nonmatch between oil in the vacuum truck and oil in soil sample D was concluded. The ratio 27Ts/30 ab is a stable DR and not subject to weathering (CEN, 2012). This exceedance of the 14% RD threshold for this ratio is further evidence that a nonmatch conclusion was justified.

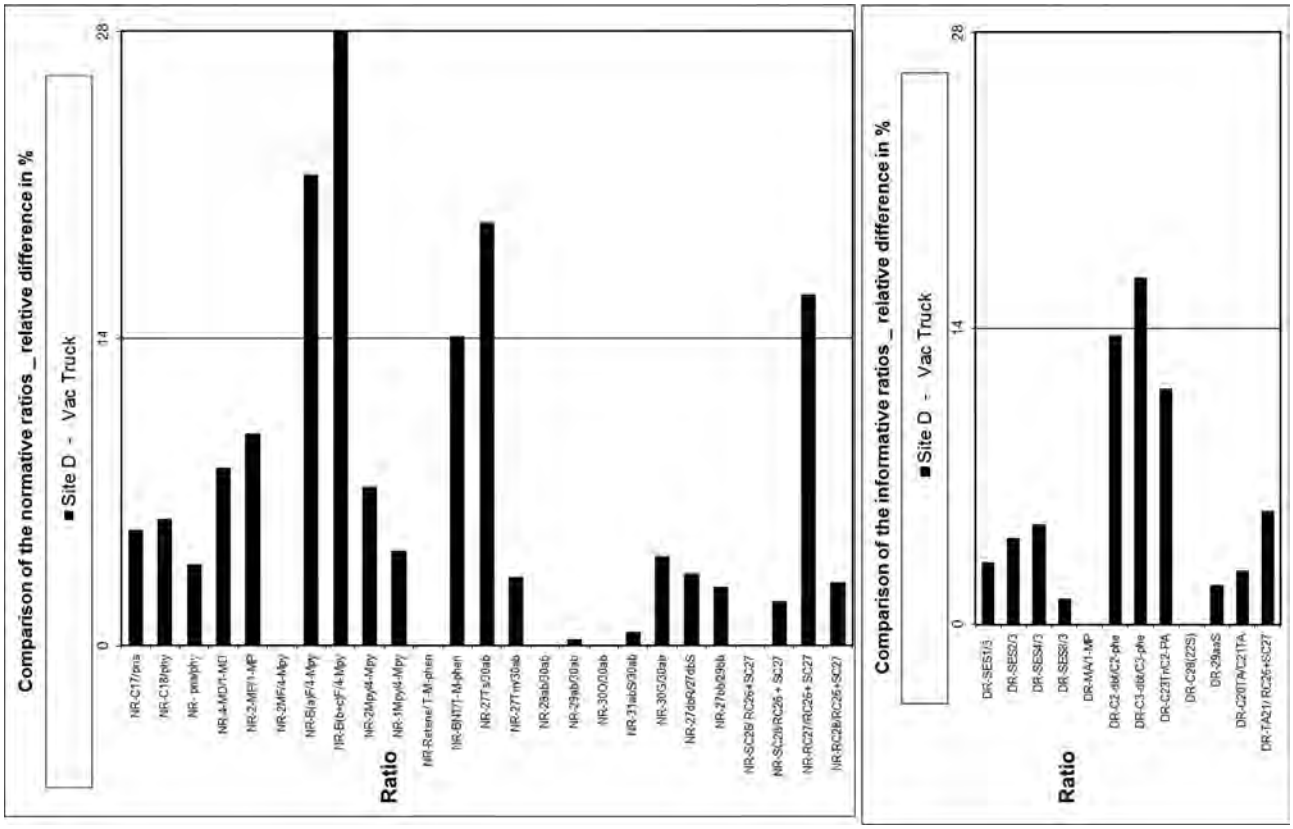

FIGURE 13.6 Normative and informative ratios following comparison of product from vacuum truck and soil from Site D.

Other DRs that exceed 14%RD include BNT/T-M-Phe and C_3-dbt/C_3-phe. Both of these ratios have a common element namely the presence of sulfur (i.e., BNT and C_3-dbt). The presence of a sulfur heteroatom can increase dissolution into water, (CEN, 2012) and as a result, flushing of the pipeline prior to repairs may have removed these compounds and affected the resulting DR. We know that flushing occurred because little or no oil was obtained from the pipeline during the investigation.

13.4.1 Conclusion—Case Study 2

Following an observed spill, samples of product were obtained from a fractured pipeline and a vacuum truck deployed during cleanup. Comparison of chromatograms obtained for the saturate fraction from the pipeline and vacuum truck product revealed they were dissimilar. Although the chromatogram obtained from the vacuum truck was crude oil, the product taken from the pipeline was not. A similar observation was observed for soil taken from Site A and E. Furthermore, comparison of total ion chromatograms (TICs) obtained for the aromatic fraction of vacuum truck oil, as well as product from the pipeline and extracts from Site A and E, revealed a lack of aromatic compounds such as PAHs removing these samples from further consideration. Comparison of oil obtained from the vacuum truck and soil taken from Site B and D revealed similar chromatograms for saturates as well as *n*-alkane and isoprenoid DRs. Chromatograms obtained for the aromatic fraction revealed similar profiles. The DRs obtained for petroleum biomarkers and PAHs revealed that %RDs exceeding 14% could be explained by weathering (photooxidation) for Site B but not for Site D. As a result we concluded that oil from the vacuum truck was a positive match with Soil B but a nonmatch with Soil D.

13.5 CASE STUDY 3—SOURCE OF OIL ON OILED WATERFOWL AND MUSKRAT

A large heavy oil spill was observed and reported in a heavy crude oil production area in Alberta. Sometime following the spill the dead and oiled carcasses of several waterfowl and a muskrat also were discovered. It is

well known that waterfowl exposed to oil can lead to death as oil can adhere to the feathers, destroying their waterproofing and insulating properties and hinder thermoregulation, buoyancy and flight. Furthermore, ingestion of toxic chemicals during preening is likely. The latter exposure mechanism also applies to muskrats that may have been exposed to oil (Beck et al., 2014). Since waterfowl and muskrats can migrate after exposure to oil but prior to death, the issue at hand was whether the oil found on the deceased waterfowl and muskrat came from the reported heavy oil spill or from some other source, such as a holding pond, sump, etc. Since heavy oil production activity is widespread in both Saskatchewan and Alberta, a forensic investigation was undertaken to determine the specific source of the oil found on the waterfowl and muskrat.

Samples of oil contaminated feathers and fur were removed from each individual and Soxhlet extracted. The resulting extract was concentrated, deasphaltened and cleaned up using an alumina−silica chromatography column as described above. Separate saturate and aromatic fractions were obtained and subjected to GC/MS analyses as described above following the procedures of CEN (2012). Two samples of the heavy oil from the known spill were also provided and were deasphaltened and cleaned up using an alumina−silica column as described above.

Fig. 13.7 shows a GC/MS TIC obtained from the saturate fraction of the muskrat and waterfowl samples B through D, as well as two heavy oil source samples from the known spill. A TIC was obtained instead of an EIP for m/z 85 because heavy oil and bitumen are usually devoid of n-alkanes.

The saturate fraction, obtained from heavy crude oil, is typically dominated by acyclic isoprenoids, phytane, pristane, mono-, di- and tricyclic terpenoid hydrocarbons, tetracyclic steranes and pentacyclic triterpenoids and

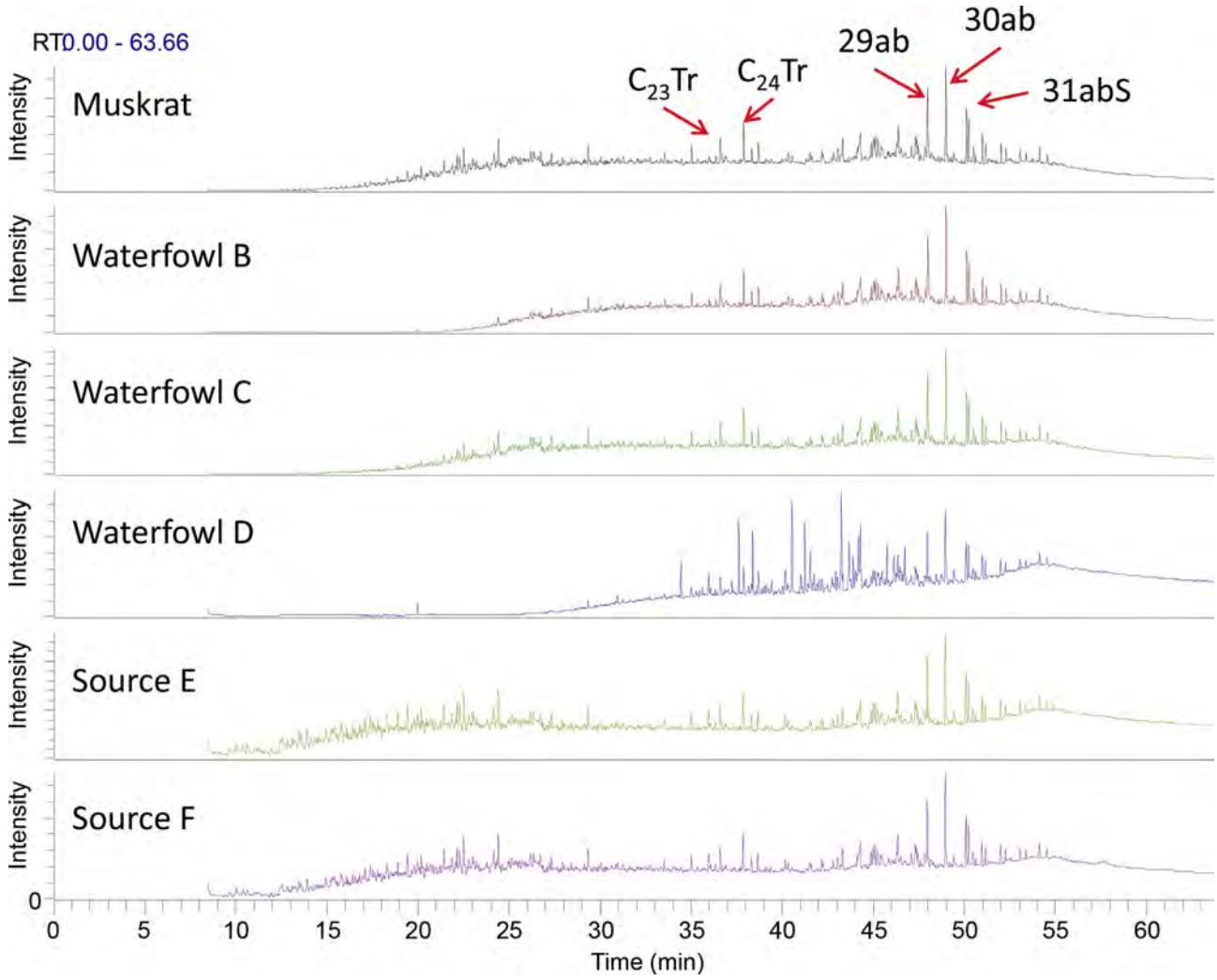

FIGURE 13.7 GC/MS TIC saturate fractions for samples from Case Study 3.

hopanes (Strausz and Lown, 2003). Fig. 13.7 shows the heavy oil source samples are dominated by presence of C_{23} and C_{24} tricyclic diterpane (C_{23}Tr and C_{24}Tr) as well as 29ab (17α(*H*), 21β(*H*)-30-norhopane), 30ab (17α(*H*), 21β(*H*)-hopane and 31abS (17α(*H*), 21β(H_, 22S-homohopane). Further inspection of Fig. 13.7 reveals that the two heavy oil source samples (Source E and Source F) appear most similar to the muskrat and two of the waterfowl samples, viz., B and C. However, waterfowl sample D appears to be different from the heavy oil source samples (Source E and Source F) owing to a prominence of additional peaks in the Waterfowl D sample (Fig. 13.7).

Fig. 13.8 shows the GC/MS TICs (of PAH ions) obtained from the aromatic fractions of the biological samples as well as the two heavy oil source samples.

The TICs in Fig. 13.8 are dominated by PAHs, such as C_3−C_4-napthalenes, C_0−C_4-phenanthrenes, and dibenzothiophenes. Although the TICs obtained were through a GC/MS-SIM run, an overlay with SINTEF reference oil, allows for the general identification of these compounds (realizing significant overlap of the many isomers is likely). From Fig. 13.8, it is apparent that the heavy oil sources (Source E and Source F) and the muskrat and waterfowl C all have very similar aromatic hydrocarbon distributions. The distributions of aromatic hydrocarbons obtained for the waterfowl B and D samples also appear similar, however, lower boiling PAHs (retention times 18−28 minutes) are reduced or absent. This could be explained through weathering, namely evaporation and water dissolution.

Comparison of the normative and informative ratios obtained for the Source E and Source F heavy oils revealed that the %RD was 1.8 ± 1.6 ($n = 36$) revealing that both these samples were derived from a common source and are a positive match. This is consistent with the understanding both these samples were obtained

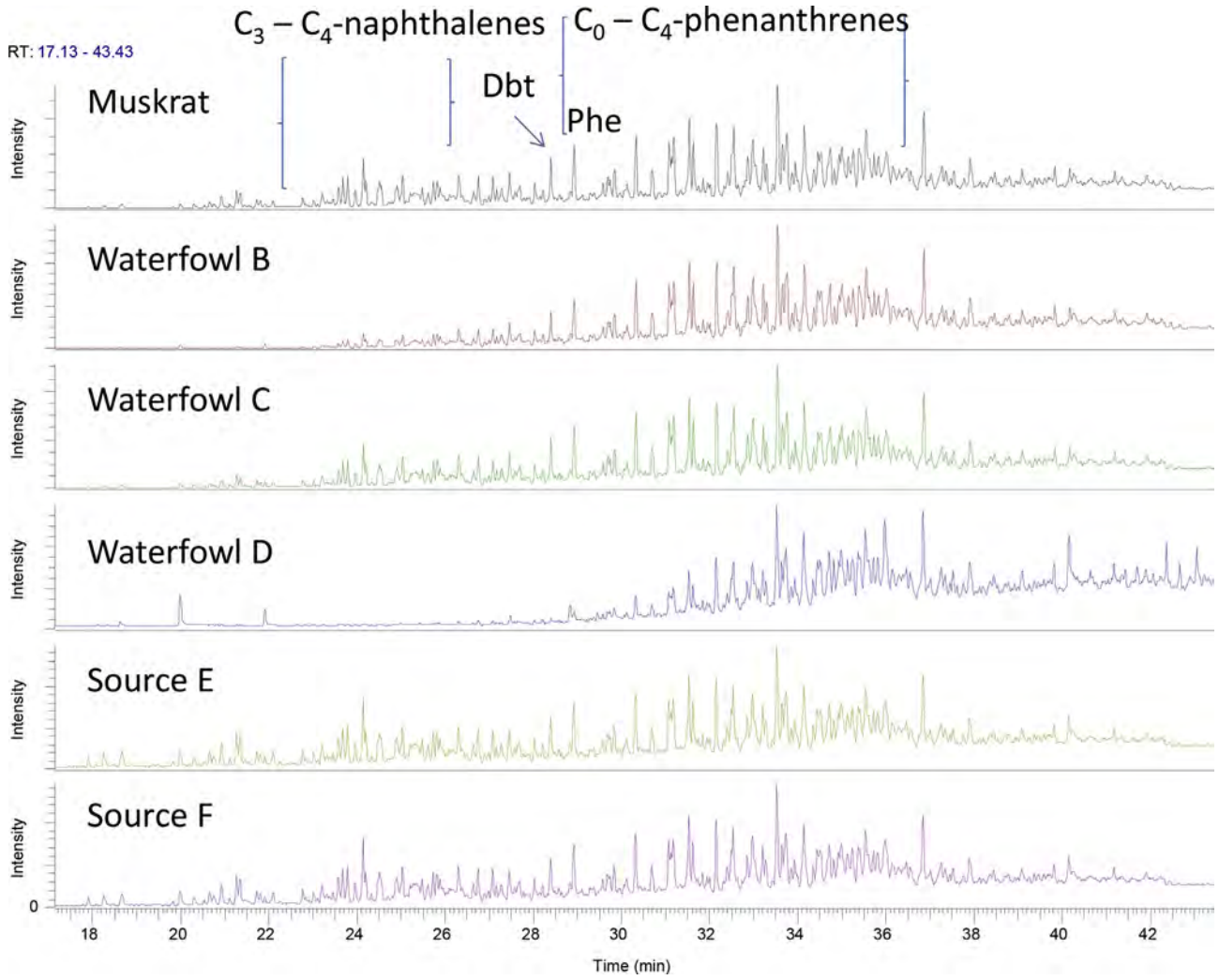

FIGURE 13.8 GC/MS TIC Aromatic Fraction for Samples from Case Study 3.

from the known spill site. Because these two source oils are matches to one another, Source F is used below to make comparisons to the muskrat and waterfowl samples.

Fig. 13.9 show the normative and informative ratios following comparison of the oil recovered from the dead muskrat and Source F. From Fig. 13.9, it is apparent that ratios associated with n-C_{17}/pristane, as well as numerous sesquiterpanes (SES 1/3, SES 4/3, and SES 8/4) have %RD exceeding 14% indicating a nonmatch according to CEN (2012). However, these failing ratios can be explained by weathering. For example, the n-C_{17}/pristane ratio in the muskrat sample has been impacted by biodegradation of n-C_{17} (Fig. 13.7) and the sesquiterpane ratios have been impacted by evaporation. These weathering impacts can be visualized on the GC/MS−PW plot which is shown in Fig. 13.10. Because the ratios exceeding 14%RD (Fig. 13.9) can be explained by weathering, i.e., biodegradation and evaporation, it was concluded that the oil recovered from the muskrat sample was a positive match with the heavy oil represented by Source F.

Fig. 13.11 shows the normative and informative ratios obtained when we compare oil recovered from the waterfowl sample B to Source oil F. Several ratio are observed to exceed the 14%RD threshold, namely, n-C_{17}/pristane, n-C_{18}/phytane, BNT/T-M-Phe, SES 1/3, SES 4/3, SES 8/3 and MA/1-MP. All of these ratios exceedance of the 14%RD threshold can be explained by weathering.

The alkane and isoprenoid ratios exceeding 14%RD can be explained by biodegradation. The sesquiterpane ratios exceed 14%RD is attributable to evaporation. The BNT/T-M-Phe ratio exceeds 14%RD because of photooxidation of T-M-Phe and similarly the methyl anthracene (MA)/ 1-methylphenanthrene (1-MP) ratio can be explained by photooxidation of MA in possible combination with evaporation of 1-MP. These weathering mechanisms are clearly illustrated in the GC/MS PW plot (Fig. 13.12) obtained when the oil recovered from the feathers of waterfowl B is compared to Source oil F.

As is characteristic of the GC/MS−PW plots utilized within CEN (2012), the different coding of the biomarkers along with description of the weathering process and the delineation of an evaporation line provides guidance to the investigator in interpreting the observed biomarker ratios. Since the alkane/isoprenoid, sesquiterpane-based biomarker ratios, and PAH-based ratios exceeding 14%RD (Fig. 13.11) can all be explained by weathering (i.e., evaporation, biodegradation and photooxidation) it was concluded that the oil recovered from waterfowl B

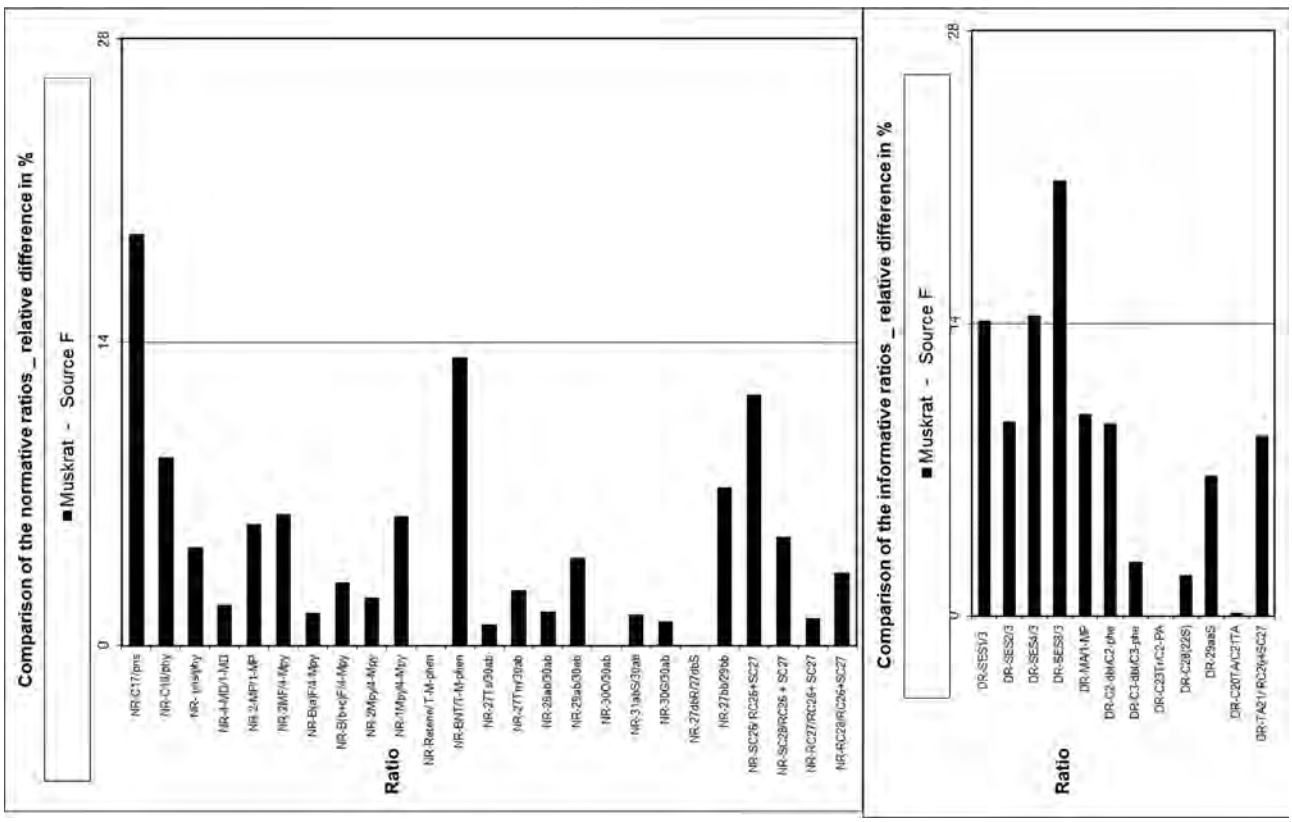

FIGURE 13.9 Normative and informative ratios comparing Source F and oil recovered from Muskrat in Case Study 3.

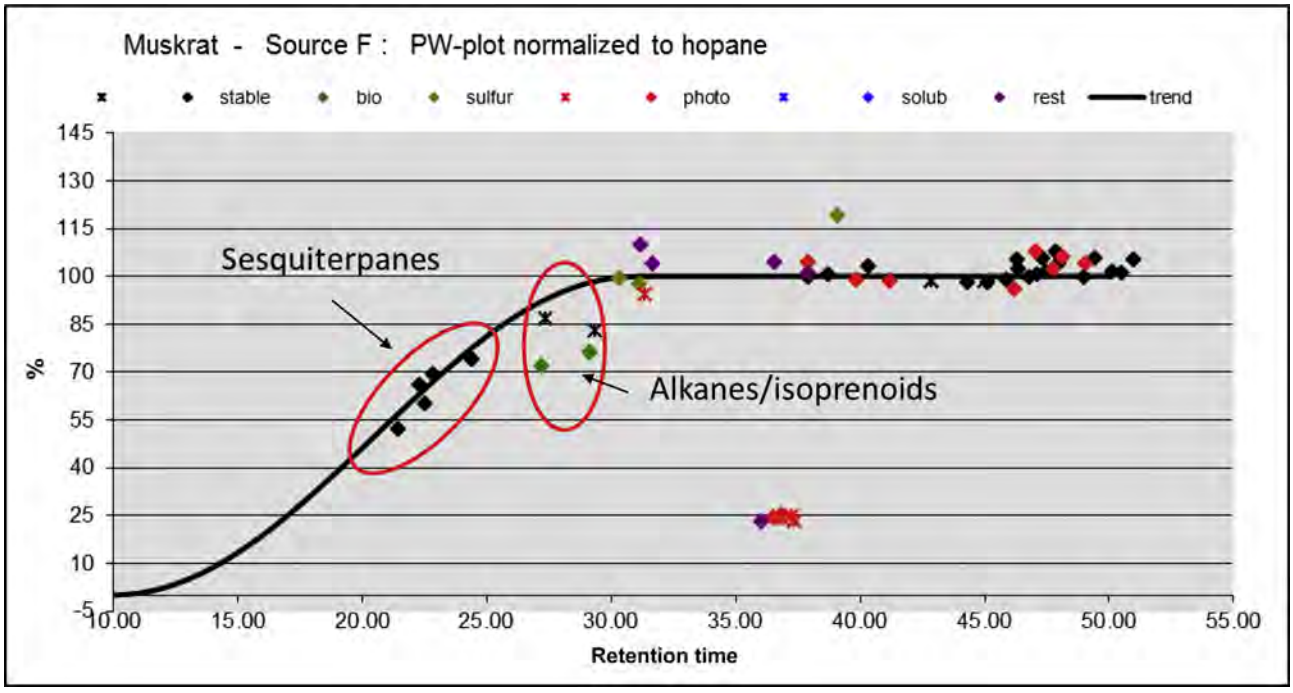

FIGURE 13.10 GC/MS PW plot comparing oil from source F and oil recovered from Muskrat from Case Study 3.

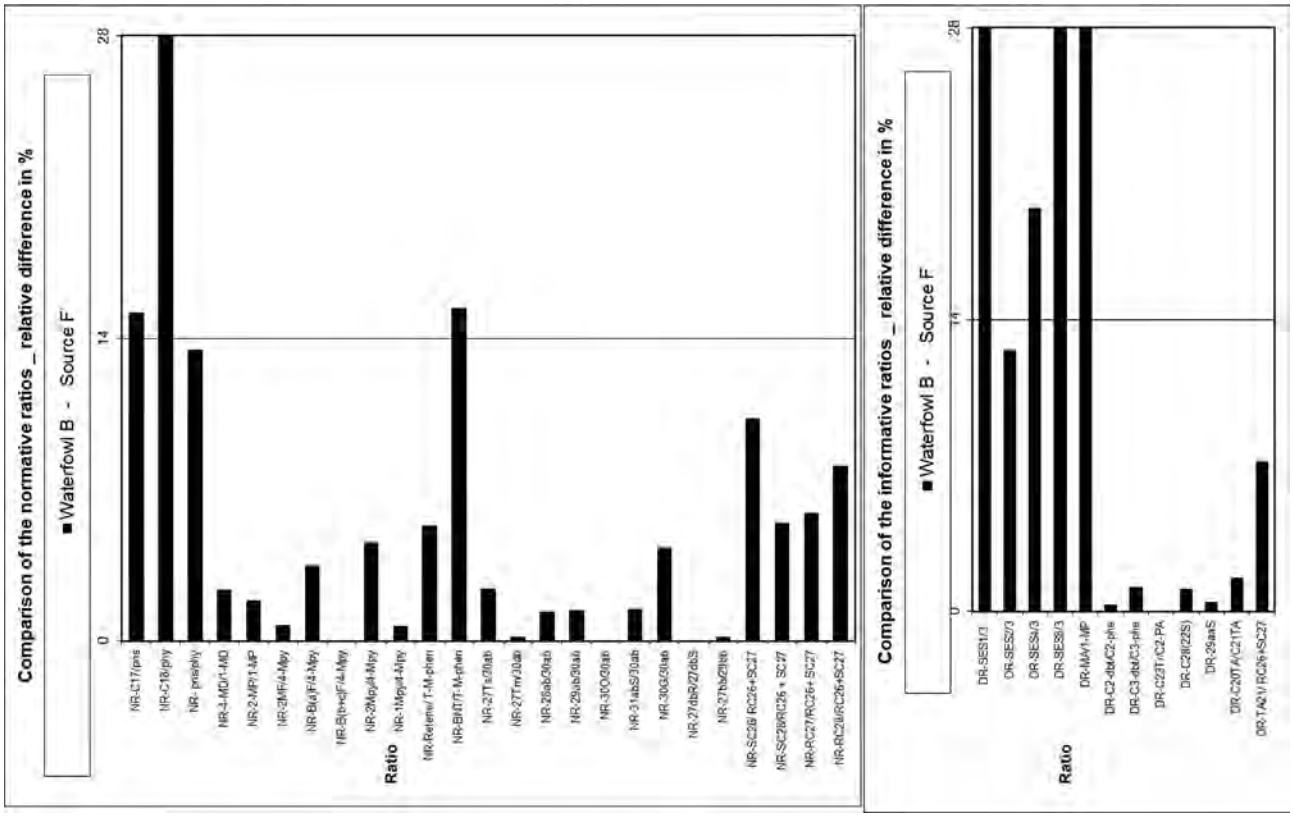

FIGURE 13.11 Normative and informative ratio obtained following comparison of oil recovered from Waterfowl B and Source F in Case Study 3.

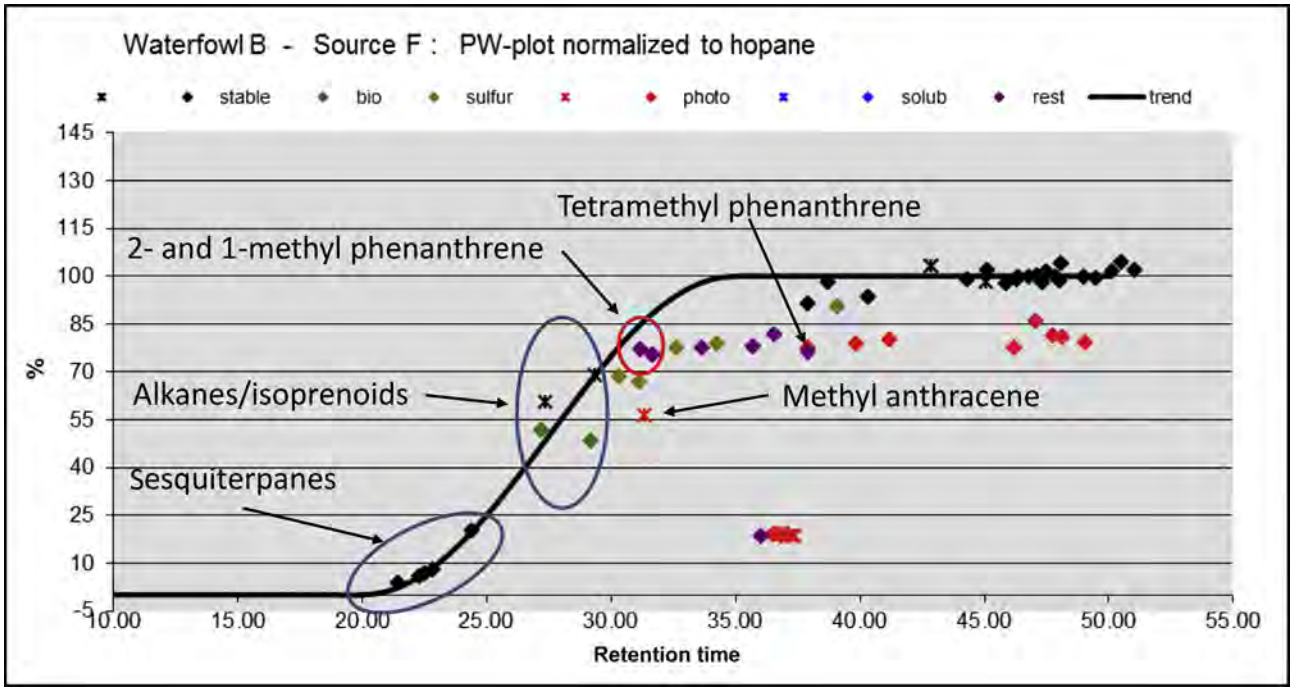

FIGURE 13.12 GC/MS PW plot comparing oil recovered from Waterfowl B and source oil F in Case Study 3.

was a positive match with the heavy oil represented by Source F. Methylpyrenes and benzofluorenes are also affected by weathering (Fig. 13.12); however, the DRs for these PAHs are not affected when we compare source F with Waterfowl B. This can be explained by similar susceptibility of the DRs' numerators and denominators to weathering, such as photooxidation, since samples of spill material and wildlife were collected well after the onset of the spill event.

Fig. 13.13 shows the normative and informative ratios obtained when we compare oil obtained from waterfowl C to Source oil F.

From Fig. 13.13, it is revealed that several ratios exceed 14%RD (n-C_{17}/pristine, n-C_{18}/phytane, SES 1/3, SES 8/3 and MA/1-MP) but, as described above, these ratios differences can be explained by weathering. Reference to the GCMS-PW plot (not shown, but comparable to that of the Waterfowl B sample shown in Fig. 13.12) revealed that biodegradation (alkanes/isoprenoids), evaporation (sesquiterpanes) and photooxidation (MA) can explain the 14%RD exceedances for these ratios. Based upon these observations, it was concluded that oil recovered from waterfowl C and source oil F were a positive match.

Finally, Fig. 13.14 shows the normative and informative ratio obtained when we compare oil obtained from waterfowl D to Source oil F. Again several normative and informative ratios exceed the 14%RD threshold when the oil obtained from waterfowl D is compared to Source F. As was the case in the other waterfowl studied, these ratios include: n-C_{17}/pristane, n-C_{18}/phytane, pristane/phytane, 4-Mdbt/1-Mdbt (4-methyl dibenzothiophene/1-methyl dibenzothiophene), 2-MPy/4-MPy (2-methyl pyrene/4-methyl pyrene), SES 4/3 and SES 8/3. Not surprisingly, inspection of the corresponding GC/MS–PW plot (Fig. 13.15) shows that these ratios (which exceed 14%RD) can also be explained through weathering. The alkanes and isoprenoid ratios are affected by biodegradation, the sesquiterpane ratios are affected by evaporation, the methyl dibenzothiophene ratios are affected by water dissolution (CEN, 2012), and the methyl pyrene ratios are affected by photooxidation (Radovic et al., 2014).

Because the ratios exceeding 14%RD are affected by various weathering processes, it was concluded that oil recovered from waterfowl D was a positive match with Source F.

13.5.1 Conclusion—Case Study 3

Source oil obtained from a large spill site (source E and F) and oil extracted from the exterior of deceased muskrat and three waterfowl (B, C, and D) were compared. Oil from these samples was deasphaltened and separated into separate saturate and aromatic fractions. Chemical analyses of the saturate fractions revealed the

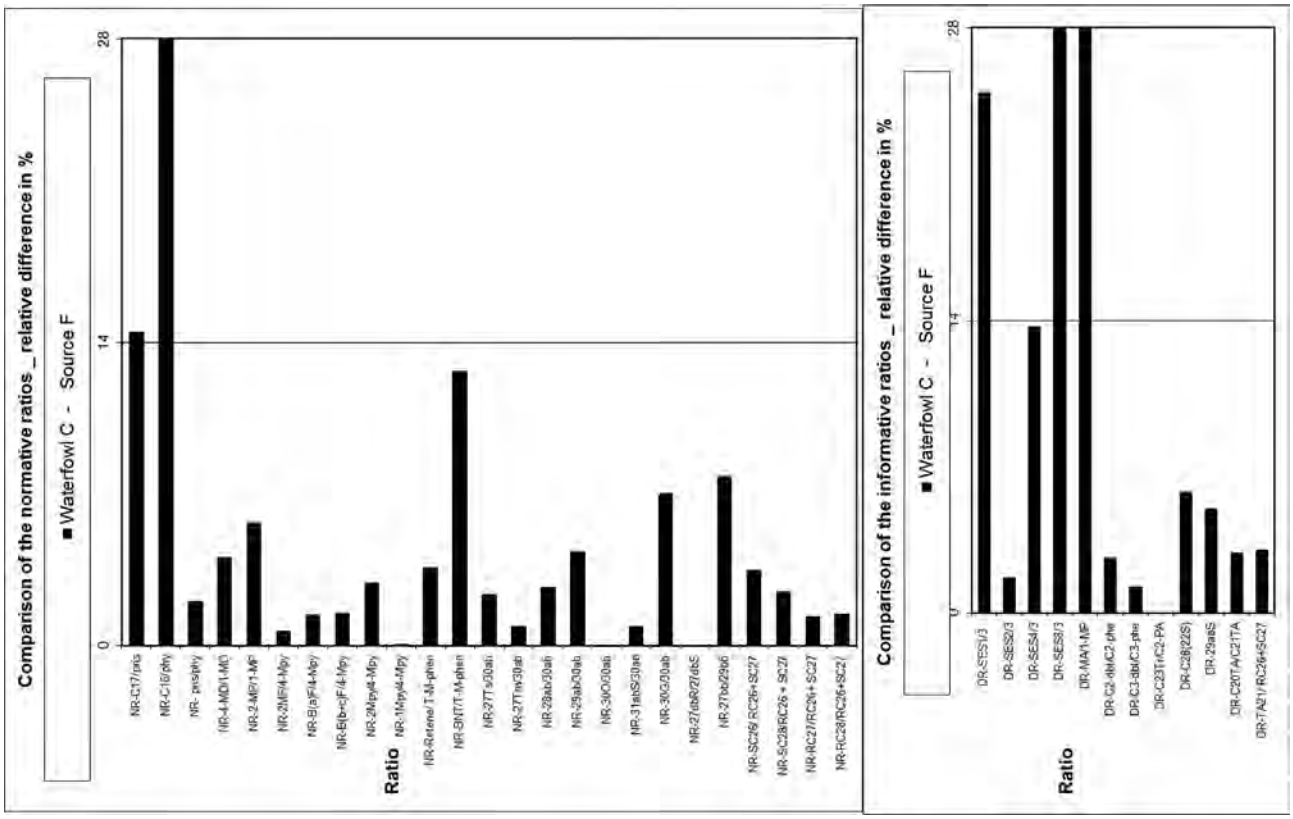

FIGURE 13.13 Normative and informative ratios obtained following comparison of oil recovered from Waterfowl C and source oil F in Case Study 3.

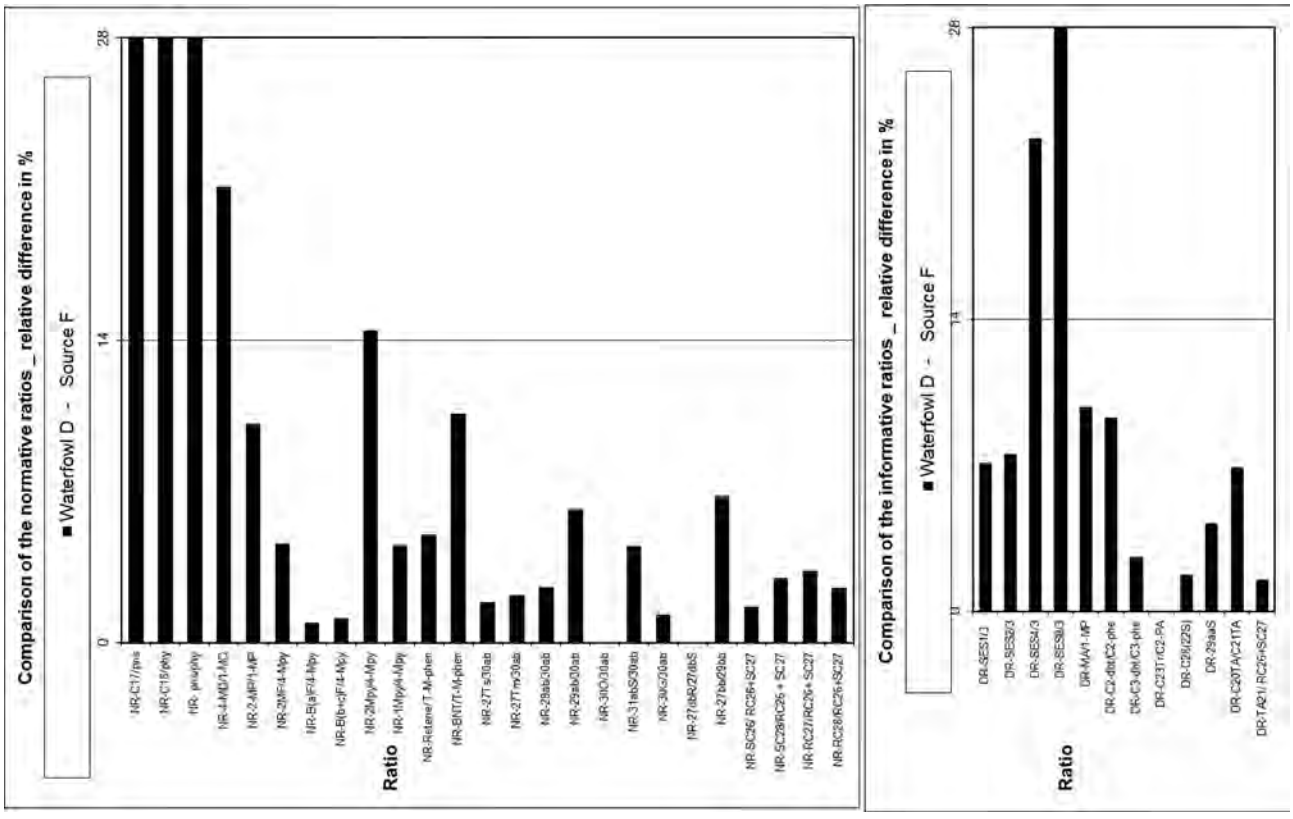

FIGURE 13.14 Normative and informative ratios obtained following comparison of oil recovered from Waterfowl D and Source F in Case Study 3.

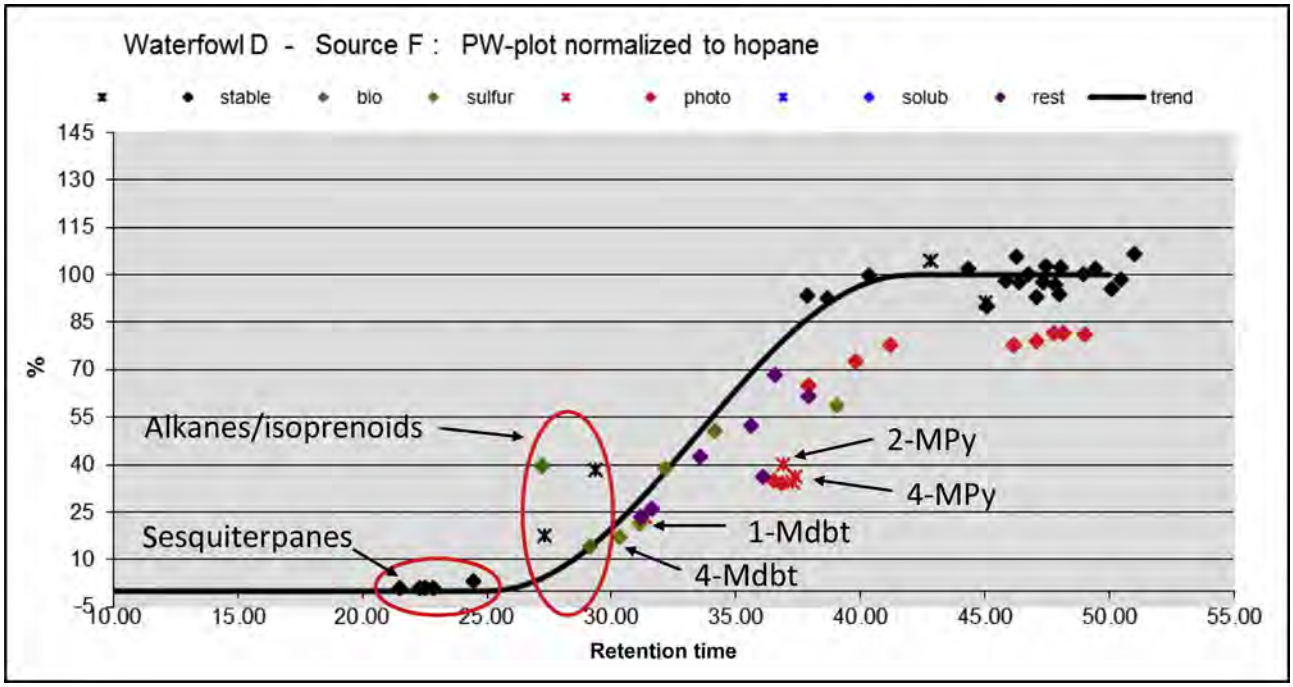

FIGURE 13.15 GC/MS PW plot comparing oil recovered from oil obtained from Waterfowl D and Source F in Case Study 3.

presence of heavy oil. Comparison of GC/MS TICs revealed that source oil (E and F) and oil recovered from muskrat, waterfowl B and C appeared similar; however the oil recovered from waterfowl D appeared dissimilar. Chromatograms obtained for the aromatic fraction revealed similarities for all samples analyzed. DRs among petroleum biomarkers and PAHs were obtained and compared. Sources E and F revealed similar ratios with a % RD of <2%, indicating excellent agreement. Comparison of DRs obtained from the muskrat and waterfowl samples (B, C and D) versus Source F revealed that several DRs > 14%RD. These included alkanes, isoprenoids, sesquiterpanes, PAHs (methyl anthracene, methyl pyrene, methylphenanthrene) as well as methyl dibenzothiophenes. Evaporation, water dissolution, biodegradation, and photooxidation can impact these ratios resulting in %RD > 14%. GC/MS–PW plots identified which compounds and DRs were affected by weathering, allowing focus on unaffected DRs. When only DRs unaffected by weathering were considered the oils recovered from the wildlife samples were determined to match the Source F oil.

13.6 CONCLUSION

Oil and gas development in Alberta along with the transportation of the products derived from these activities to refineries located in Canada and the United States are likely to result in spills. The impact of these spills can be significant affecting large tracts of land, freshwater, as well as wildlife. In consideration of the long history of such activity in Alberta, it is important to assess the impact of spills and to correctly assign liability. CEN (2012) can be used for this purpose; however, careful consideration has to be given to possible interferences from coextractives and biogenic material when applied to terrestrial environments, and wildlife. This can be addressed through proper sample preparation and cleanup. Furthermore, consideration of mixing of spilled material with unreported or uncleaned petroleum derived from previous spills has to be taken into consideration. Weathering assessments of DRs and chromatograms are particularly useful when comparing spilled material with impacted environmental samples. This is especially true for wildlife samples collected at some distance removed from the spill site. The necessity of collecting a large amount of information (chromatograms and DRs) as prescribed by CEN (2012) has been illustrated in the three case studies discussed above. Furthermore, weathering assessments are critical to determine which data are pertinent for sample and source comparisons and which are not.

References

American Society for Testing and Materials (ASTM), 1995. Standard Practice for Oil Spill Source Identification by Gas Chromatography and Positive Ion Electron Impact Low Resolution Mass Spectrometry. American Society for Testing and Materials, Conshohocken, PA, D 5739-95.

ASTM, 2000. Standard Test Methods for Comparison of Water-Borne Petroleum Oils by Gas Chromatography. American Society for Testing and Materials, Conshohocken, PA, D 3328-00.

Beck, E.M., Smits, J.E.G., Cassady, C., 2014. Health of domestic mallards (*Anas platyrhnchos domestica*) following exposure to oil sands process-affected water. Environ. Sci. Technol 48, 8847–8854.

Center for European Norms (CEN), 2012. Oil Spill Identification–Waterborne Petroleum and Petroleum Products—Part 2: Analytical Methodology and Interpretation of Results Based Upon GC–FID and GC–MS Low Resolution Analysis. Center for European Norms, Brussels, Belgium, Technical Report 15522-2, Oct 3, 2012.

Melville, F., Anersen, L.E., Jolley, D.F., 2009. The Gladstone (Australia) oil spill–impacts on intertidal areas: baseline and six months post-spill. Mar. Pollut. Bull. 58, 263–271.

Nikiforuk, A. 2017. On Oil Spills, Alberta Regulator Can't Be Believed: New Report. The Tyre News, Culture, Solutions.

Radovic, J.R., Aeppli, C., Nelson, R.K., Jimenez, A., Reddy, C.M., Bayona, J.M., et al., 2014. Assessment of photochemical processes in marine oil spill fingerprinting. Mar. Pollut. Bull. 79, 268–277.

Stout, S.A., 2016. Oil spill fingerprinting method for oily matrices used in the Deepwater Horizon NRDA. Environ. Forensics 17, 218–243.

Stout, S.A., Emsbo-Mattingly, S.D., Douglas, G.S., Uhler, A.D., McCarthy, K.J., 2015. Beyond 16 priority pollutant PAHs: a review of PACs used in environmental forensic chemistry. Poly. Arom. Compd. 35, 285–315.

Stout, S.A., Payne, J.R., Emsbo-Mattingly, S.D., Baker, G., 2016. Weathering of field-collected floating and stranded Macondo oils during and shortly after the Deepwater Horizon oil spill. Mar. Pollut. Bull. 105 (1), 7–22.

Strausz, O.P., Lown, E.M., 2003. The Chemistry of Alberta Oil Sands, Bitumens and Heavy Oils. Alberta Energy Research Institute, Calgary, Alberta, 695 p.

Wang, Z., Yang, C., Kelly-Hooper, F., Hollebone, B.P., Peng, X., Brown, C.E., et al., 2009. Forensic differentiation of biogenic organic compounds from petroleum hydrocarbons in biogenic and petrogenic compounds cross-contaminated soils and sediments. J. Chromatography A 1216, 1174–1191, 2009.

Wang, Z., Stout, S.A., Fingas, M., 2006. Forensic fingerprinting of biomarkers for oil spill characterization and source identification. Environ. Forensics 7, 105–146.

Young, L., 2013. Crude Awakening: 37 Years of Oil Spills in Alberta. Global News.

CHAPTER

14

Development and Application of Phase-Specific Methods in Oiled-Water Forensic Studies

William B. Driskell[1] *and James R. Payne*[2]

[1]Consultant, Seattle, WA, United States [2]Payne Environmental Consultants, Inc., Encinitas, CA, United States

BIOGRAPHIES

William B. Driskell, an independent consultant in Seattle, has been a marine biologist by experience and a biological oceanographer by degree (MS University of Washington) but for the last two decades has worked as an oil-spill forensic chemist in collaboration with Jim Payne. The *Exxon Valdez* spill (1989) marked his debut into assessing oil spill impacts—for that incident, as a biologist. Several events later, forensically reviewing and interpreting *Deepwater Horizon* water samples has provided the most recent professional challenge while also fulfilling the personal satisfaction of "eureka!" moments in achieving the incremental gains of understanding how natural systems function. Occasional marine fieldwork in the Alaskan coastal wilderness keeps the biology spark glowing.

James R. Payne received a B.A. with honors in chemistry from California State University at Fullerton in 1969 and his Ph.D. in chemistry from the University of Wisconsin-Madison in 1974. He has been involved in oil-spill research for over 43 years, including a postdoctoral fellowship at the Woods Hole Oceanographic Institution, work at the University of California-Bodega Marine Laboratory, Science Applications International Corporation, Sound Environmental Services, Ogden Environmental, and the last 20 years as president of Payne Environmental Consultants, Incorporated (PECI). Dr. Payne has conducted oil fate and behavior research and studies on oil-spill dispersants since the 1979 IXTOC I blowout in the Bay of Campeche, Gulf of Mexico, and he was principal investigator on 11 years of NOAA-sponsored laboratory and Kasitsna Bay, Alaska wave-tank studies on the rates of oil weathering, including: evaporation, dissolution, microbial degradation, water-in-oil emulsification, oil−droplet interactions with suspended particulate material, and sedimentation. In collaboration with other investigators, these research efforts were utilized to develop and verify computer models to predict oil weathering fate and behavior as a function of a variety of oil types and environmental conditions. As a result of his field and laboratory efforts, he has authored or coauthored three books and chapters in six others. He has published over 50 peer-reviewed articles and/or papers in various conference proceedings and prepared over 80 environmental reports for use by various governmental agencies and private clients. Dr. Payne contributed background chapters for the 1985 National Academy of Sciences publication, *Oil in the Sea—Inputs, Fates, and Effects*, and he served on four other National Academy of Sciences/National Research Council Committees dealing with petroleum spills and the use of oil-spill dispersants in the marine environment. He was Chief Scientist on spill-of-opportunity dispersant trials during the 1987 *Pac Baroness* oil spill off Point Conception, California, and the 1990 *Mega Borg* oil spill and fire off Galveston, Texas. After the 1989 *Exxon Valdez* oil spill in Prince William Sound, Alaska, he has supported several federal and state trustee agencies working on Natural Resource Damage Assessment (NRDA) programs for numerous oil spills, including the 1990 *American Trader* off Huntington Beach, California, the 1997 Platform Irene pipeline blowout off Santa Maria, California, the 1999 *New Carissa* grounding and oil spill off Coos Bay, Oregon, the 2000 *T/V Westchester* oil spill in the Mississippi

Oil Spill Environmental Forensics Case Studies.
DOI: http://dx.doi.org/10.1016/B978-0-12-804434-6.00014-8

River, the 2007 *Cosco Busan* oil spill in San Francisco Bay, and the 2010 British Petroleum (BP) Deepwater Horizon blowout and spill in the Gulf of Mexico where he served as Chief Scientist on nine separate water and sediment sampling cruises in 2010 and 2011.

14.1 INTRODUCTION

Typically, oil floats. But sinking oils, seeps, blowouts, leaking pipelines and sunken vessels, outfalls, shoreline cleaning, waves, storms, and chemical dispersant ops, all introduce oil to water and leave behind some record, either dissolved or particulate, copious or trace, of their infusions. The forensic task is to identify oil components, match them to their sources, and eventually develop/support fate and transport scenarios that can provide or confirm estimated contaminant concentrations. Note that this task list becomes more estimated (error prone) and/or speculative as the sequence proceeds—but it is possible and often doable. In this chapter, we present the evolution of our forensic insights from early studies, suggest forensic methods relative to dissolved and particulate oil phases, and ultimately show how the subsurface plume from the *Deepwater Horizon* (DWH) blowout was tracked 412 km across the Gulf of Mexico to a final point confirmed with only a trace dissolved-polycyclic aromatic hydrocarbon (PAH) pattern and supporting information.

Due to entrainment and dissolution/weathering processes, oil spilled in a water environment is present in both dissolved and particulate (oil-droplet) phases (Payne and McNabb, 1984; Payne et al., 1984). The two phases, capable of physically separating and remixing in a body of water, can easily complicate forensic evaluations. However, the extra effort expended in identifying and tracking the oft-ignored phases has high forensic value for developing interpretive scenarios of weathering and exposure processes and for providing data germane to modeling and toxicology studies for damage assessments. Samples can be parsed into phase components either physically in the field using portable filtration equipment or later, with foresight and preparation, using data evaluation methods developed to parse out unfiltered samples. For the DWH Natural Resource Damage Assessment (NRDA), field-filtered, phase-separated samples were purposefully generated to use as a weathered particulate-oil reference series that could be used to better assess the spill's impact to thousands of whole water samples collected during the NRDA.

14.2 METHODS

14.2.1 Field Collection Techniques

Offshore water-column samples are primarily collected using Niskin or GoFlo bottles mounted on instrumented multibottle, rosette frames or, for the DWH blowout event, using a submersible remotely operated vehicle (Payne and Driskell, 2015a, 2016). Combining live fluorescence, dissolved-oxygen (DO), and conductivity/temperature/depth (CTD) sensors onto the collection devices was particularly effective for adaptively tracking and sampling oil during the DWH event (as opposed to random or systematic fixed depth collections). Note that offshore water sampling techniques require meticulous methods, foresight, and awareness to avoid collecting confounded or worthless samples—topics addressed in Payne and Driskell (2016). For example, one major concern is how to collect water samples through a surface sheen or slick, while avoiding cross-contaminating the collection gear. And unfortunately, there is no feedback on the efficacy of field efforts until the data come back from the lab. For smaller scale or nearshore spills, most whole-water field collections are taken directly into sample jars by hand or with a sampling pole, removing the lid underwater to avoid surface slicks or films.

14.2.2 Phase Filtration

Certain components of oil dissolve in water and subsequently, by natural transport processes, can become separated from the particulate oil (visible droplets and/or slicks). This predictable dissolution and loss of components is part of the weathering process that dynamically modifies the chemical profile and challenges the forensic scientist. One may encounter water samples with dissolved only, particulate only, or mixtures of both phases. During the DWH event, some profiles even showed enhanced dissolved content due to the dynamics of the plume rising above the wellhead (discussed below). Initially in our projects, phase information was used to inform and aid in interpreting oil fate and transport processes, but its utility has since evolved into parsing

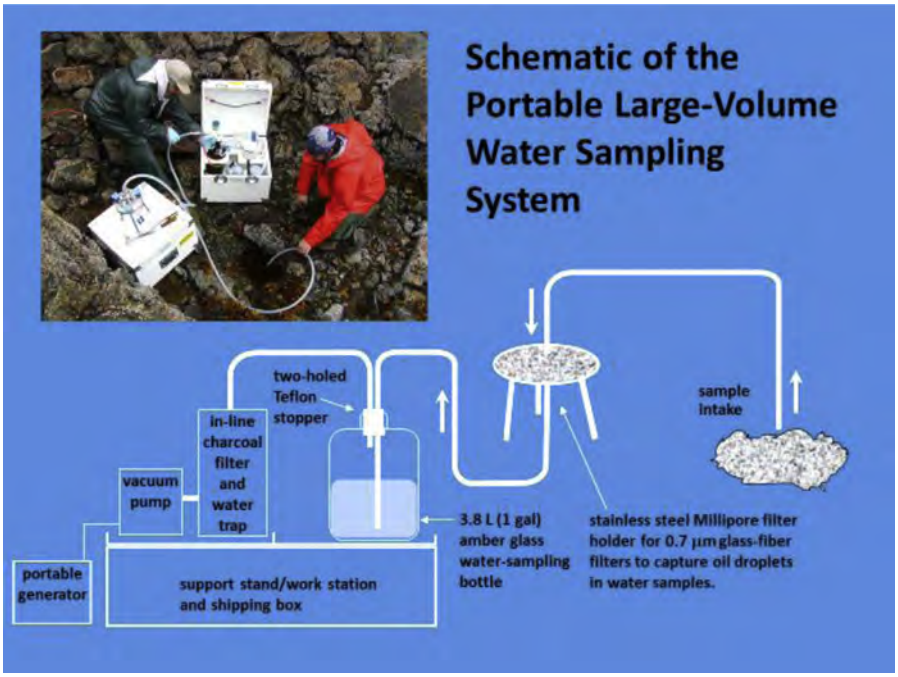

FIGURE 14.1 Schematic diagram of field water-filtration system and use during interstitial water sampling.

confounded patterns, estimating portions, and informing insights into weathering and transport. This chapter is meant to highlight its evolving utility and insights gained.

Concerted efforts were thus made during recent spill events to obtain phase-discriminated subsamples using portable field-filtration equipment (Payne et al., 1999). The process vacuums a 3.5-L water sample through an inert 0.7-μm glass fiber filter immediately after the sample is collected (Fig. 14.1). The larger volume allows the lab to achieve much higher sensitivity (lower detection limits) than that obtained from typical 1-L grabs. With detection limits from current analytical methods, 3.5 L sample volumes permit analyte detection in the 1–5 ng/L (parts per trillion, ppt) range, plus one-gallon (3.8 L) jugs are still small enough to routinely transport in iced coolers for express delivery.

Other filtering methods using liquid–liquid extractors, granular-activated carbon, resins, and polyurethane foam plugs have been developed for sampling seawater (de Lappe et al., 1978, 1980, 1983; Payne, 1997), but both resins and foam plugs can introduce background contaminants that may interfere with trace organic analyses. In addition, numerous problems associated with channeling of water around the adsorbents packed into columns or containers of varying dimensions, maintaining clean adsorbent blanks, devising ways to extract the petroleum or chlorinated hydrocarbons of interest off of the adsorbents, and preparing and maintaining ready stockpiles of cleaned adsorbent materials, all made previous in situ sampling approaches anything but a routine operation (Payne, 1997). Filtration on the lab bench is another alternative but the relative phases can change during shipment. Because of these potential limitations, the field system used herein (Fig. 14.1) filters and transfers the filtered water sample directly into commercially available, certified precleaned amber glass jugs that accompany their filters to the analytical laboratory.

14.2.3 Analytic Methods

Laboratory analyses have shown significant advancement in recent years both in instruments and method refinement. Rather than reviewing historic practices, presented here are the methods used during the recent DWH (aka MC252) incident. In the laboratory, whole and dissolved-phase (filtered) water samples are spiked with appropriate deuterated surrogate (or recovery) standards and triple-extracted with dichloromethane. Particulate-phase (filter) samples are cut up or macerated, spiked with surrogate standards, and extracted by refluxing whole with dichloromethane. Silica gel cleanup is not performed for water or particulate-phase extracts,

and internal standards are added before instrumental analysis. Analyses are typically performed in accordance with the relevant lab and/or project quality assurance plans (e.g., Analytical Quality Assurance Plan (AQAP) (2014)—NOAA) that include:

- Saturated hydrocarbon (SHC) quantification and fingerprinting. A modified EPA Method 8015B is used to determine the concentration of total extractable materials (C_9−C_{44}) and concentrations of *n*-alkanes (C_9−C_{40}) and selected (C_{15}−C_{20}) acyclic isoprenoids (e.g., pristane and phytane), and simultaneously provide a high-resolution gas chromatography−flame ionization detector (GC/FID) fingerprint of the samples.
- PAH, alkylated PAH, and petroleum biomarkers. Semivolatile compounds are analyzed using selected ion monitoring gas chromatography/mass spectrometry (SIM GC/MS) via a modified EPA Method 8270. This analysis provides the concentration of (1) approximately 80 PAH, alkylated PAH homologs, individual PAH isomers, and sulfur-containing aromatics and (2) approximately 50 tricyclic and pentacyclic triterpanes, regular and rearranged steranes, and triaromatic steroids.
- Volatiles, primarily benzene, toluene, ethylbenzene, and xylene(s) (BTEX), are analyzed by a purge-and-trap method (modified EPA method 8260) on separate, whole-water aliquots collected in the field before vacuum filtration with the PLVWSS.

Using dispersants has always been a major concern in spill response. Dioctyl-sulfosuccinate (DOSS) has been the surfactant ingredient in recently used commercial blends. It comprises 10−30% by weight of the Corexit formulations used during the DWH incident but was too large and too polar for conventional GC/MS analyses. It is, however, amenable to using a high-performance liquid chromatography/mass spectrometry method (Gray et al., 2010; Kujawinski, et al., 2011). At the primary DWH NRDA forensic laboratory, Alpha Analytical Laboratory (Mansfield, MA), just the confirmation of dispersants was considered sufficient for forensic needs and thus for waters, standard SIM GC/MS without further fractionation or cleanup was used to semiquantify Corexit-derived components in water. Dispersant indicators reported (Stout, 2015) included:

- di(propyleneglycol)-*n*-butyl ethers, designated as "GE" for glycol ethers, and dearomatized C_9−C_{14} petroleum distillates (commercially Nopar 13), the major solvents in Corexit 9500,
- 2-butoxyethanol, a major solvent in Corexit 9527 designated herein as "2BE" but also a filter contaminant in the field-filtered samples, and
- bis(2-ethylhexyl)fumerate, a GC-injection-port heat-breakdown product of DOSS, associated with both Corexit 9527 and 9500 (Stout, 2015).

SHC and volatiles were typically reported in concentrations of μg/L (parts per billion, ppb). PAH, biomarkers, and dispersant indicators were reported in ng/L (parts per trillion, ppt). From the field filtrations, particulate (filter) samples were extracted and analyzed separately from the associated (dissolved) 3.5 L water portion. Dissolved-phase sample volumes were used to calculate concentration in both the dissolved and related particulate (filter) samples on a whole sample, per-volume basis.

Notable advances in analytic technology being embraced by the oil forensics community include improved analyte resolution and sensitivity using two-stage chromatography (GC × GC, generally, nonpolar and polar columns) that renders the results in two dimensions (Reddy et al., 2011; Aeppli et al., 2012, among others). Another method, Fourier-transformed ion cyclotron resonance (FT-ICR) mass spectrometry, has proven capable in detecting compounds too polar or molecularly massive for GC/MS. Using ultrahigh resolution FT-ICR MS, McKenna et al. (2013) reported detecting more than 30,000 compounds in the MC252 source oil from BP's Gulf of Mexico spill (vs the relevant ~200 PAH, biomarkers, and SHC typically reported from GC/MS and GC/FID analyses). It has yet to be determined just which of these compounds are relevant to environmental impacts (e.g., toxicity and persistence) or how knowledge of their existence (and possible quantification) might lead to changes in resource damage assessments. Another developing topic is tracking the weathering of petroleum, a process that "increases the polarity of the molecules and requires advanced analytical techniques to provide molecular level characterization of acidic (i.e., carboxylic acids, alcohols, pyrrolic nitrogen), basic (i.e., pyridinnic nitrogen), and nonpolar components" (Aeppli et al., 2012). In this context, Q Exactive Orbitrap MS has been used with different ionization modes to discriminate among different non-GC-amenable functional groups of weathered DWH oil (Huba and Gardianali, 2016). Of specific interest is the conversion of the saturates and aromatics into assorted oxygenated hydrocarbons, either by microbial degradation or photooxidation. Again, relevance to toxicity or other impacts is currently under development.

14.3 FORENSIC ASSESSMENT METHODS

Forensic assessment methods have been steadily advancing through the decades as progress in oil analytic methods have been providing higher precision and resolution data from an expanding list of analytes of interest. In the past, forensic source identification involved comparing two chromatographic profiles visually or overlaid on a light table to qualitatively assess matching or absent spikes and patterns. Later progress in quantifying the data brought significant advantages to the oil fingerprinting process including, among others, comparing standardized data, computer processing, the use of mixing-models, statistical inference, and libraries of sources (reviewed in Douglas et al., 2016; Stout and Wang, 2016).

Assessment protocols have been developed (e.g., CEN and NORDTEST) to codify forensic judgments and create legally defensible opinions. While these approaches are useful and sufficient for many circumstances (e.g., floating oil or tarballs), the complexity of the mixtures with background contaminants (e.g., Galveston or San Francisco Bays) or scale of distribution and extent of weathering (DWH) suggests other approaches may be more insightful particularly for water samples. While we have, on occasion, relied on various indices and multivariate approaches, we find their ultimate discrimination sometimes hides the underlying causes. We prefer pattern recognition, looking for expected correlated concentrations and losses within groups of analytes, to build a scenario of weathering, distributions, and mixing. Essential to this approach are deconvoluting or at least recognizing background contaminants and source−oil phase mixtures in field samples.

14.4 CASE STUDIES—RESULTS AND IMPLICATIONS

During oil spill damage assessments, it's obvious to look for oil where it's visible as slicks, or where it stranded or was deposited in sediments or perhaps taken up in tissues of concern. The waterborne components, on the other hand, tend to be overlooked and yet they are the most likely to transport further and expose unseen populations.

Herein, the case studies begin with the 1989 *Exxon Valdez* spill, an example in which awareness of oil phases while reviewing PAH profiles led to a subtler interpretation of oiling effects on tissues; somewhat more insightful than just assigning a total PAH (TPAH) concentration. By the time of the 1999 *New Carissa* incident, field-filtration methods provided phase-separated data to reveal exposures to visibly unoiled environments. Other examples from studies in Port Valdez, Alaska, provide variations on the phase theme until the *Cosco Busan* in 2007. For this San Francisco Bay spill, a rather sophisticated mixing-model was created to parse the spilled-oil PAH profile from the urban background contamination but primarily for nonwater matrices. This same forensic mixing-model approach was later modified and refined for the DWH event and NRDA to actually parse out the oil phase profiles in the thousands of whole-water samples.

14.4.1 *Exxon Valdez* Oil Spill Tissues

Although many environmental chemistry studies followed in the wake of the 1989 *Exxon Valdez* oil spill (EVOS), only a couple have directly overlapped with our own forensic work. Brown et al. (1996) utilized mussels (*Mytilus trossulus*) in Prince William Sound (PWS) at the time of the spill to corroborate the exposure of herring eggs to oil in the water column. For this purpose, the data showed a statistically significant correlation between mussel hydrocarbon burdens and anaphase aberrations in herring eggs collected from the intertidal zone in oiled areas. These results have led some investigators to propose that uptake in mussels may be a surrogate for predicting effects in other species, but as Baumard et al. (1999a,b) emphasized, it is important to recognize the route of exposure in interpreting such assessments. Brown et al. had to use mussel tissue residues to corroborate the hydrocarbon exposure in herring eggs because the available limited herring-egg sample sizes would have resulted in higher method detection limits (MDLs) and, thus, the less sensitivity to detect analytes of interest. However, the herring egg samples eventually were analyzed and even though reported with elevated MDLs, the PAH profiles (Figs. 14.2 and 14.3) showed that the eggs' dissolved-phase PAH signature was different from the mussels' mixed particulate and dissolved phases (Payne and Driskell, 2003). The herring eggs' profile reflected a water-soluble source with naphthalenes predominant and with N0 > N1 > N2, etc., while the SHC profile showed dominant $n\mathrm{C}_{15}$ and pristane from biogenic marine sources (Short, 2005) with little evidence of particulate oil (e.g., expecting minor phytane and the alkanes $n\mathrm{C}_{18}$ through $n\mathrm{C}_{34}$ without an elevated odd carbon number ratio) (Fig. 14.3). For definitions of compound-specific abbreviations used in these and other figures in this chapter, see

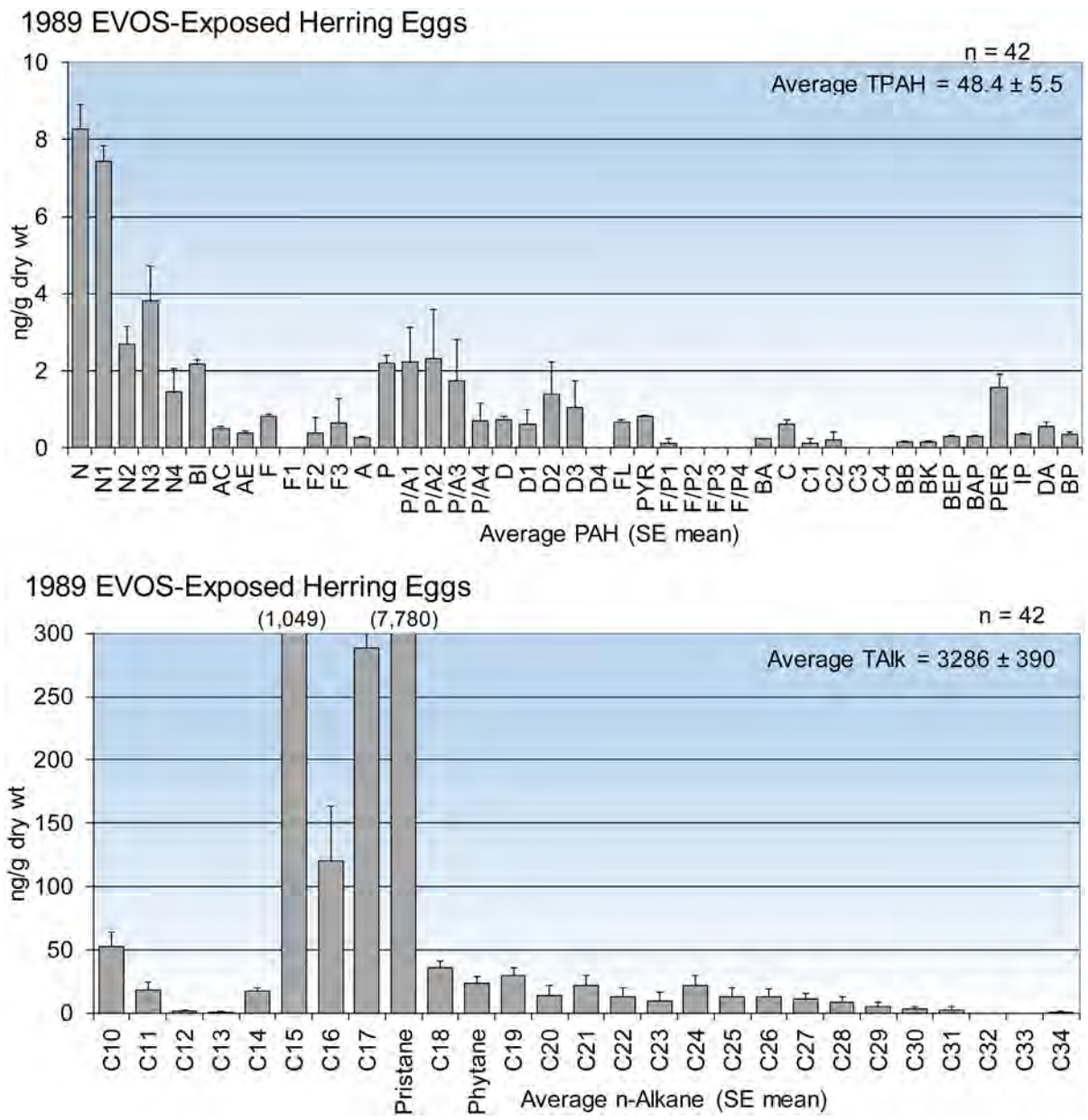

FIGURE 14.2 Average PAH and AHC histograms of herring egg extracts from samples collected from oiled areas of Cabin Bay, Naked Island (co-located with the mussel samples in Fig. 14.4) in Prince William Sound in May 1989 after the *Exxon Valdez* oil spill (EVOS) (data from EVTHD, the EVOS Trustees Database). PAH show a mostly dissolved-phase profile; SHC profile is dominated by biogenics. PAH and biomarker abbreviations are presented in Chapter 33, Novel Biological Exposures Following the Deepwater Horizon Oil Spill Revealed by Chemical Fingerprinting (Table 33.2). Adapted from Payne and Driskell (2003), reproduced with permission from the IOSC.

Chapter 33, Novel Biological Exposures Following the Deepwater Horizon Oil Spill Revealed by Chemical Fingerprinting (Table 33.2).

It appears that, in 1989, the filter-feeding mussels collected adjacent to the herring eggs were misused for TPAH correlations as the mussels showed a different weathered PAH signal. The profile was of a particulate rather than a dissolved signal, i.e., with alkylated PAH greater than the parent aromatic for each homolog group (N, F, P/A, DBT, and C) and the full suite of both even- and odd-numbered SHC from weathered oil (Fig. 14.3). The concentrations of the two phases were incidental and essentially independent and conclusively represented non-correlatable concentrations. One year later, the situation had changed when the slicks were gone, waterborne particulate oil was absent and the mussels were only showing dissolved-phase PAH from constituents leaching off the oiled shores, i.e., primarily naphthalenes and phenanthrenes with the parent PAH greater than the alkylated homologs (in

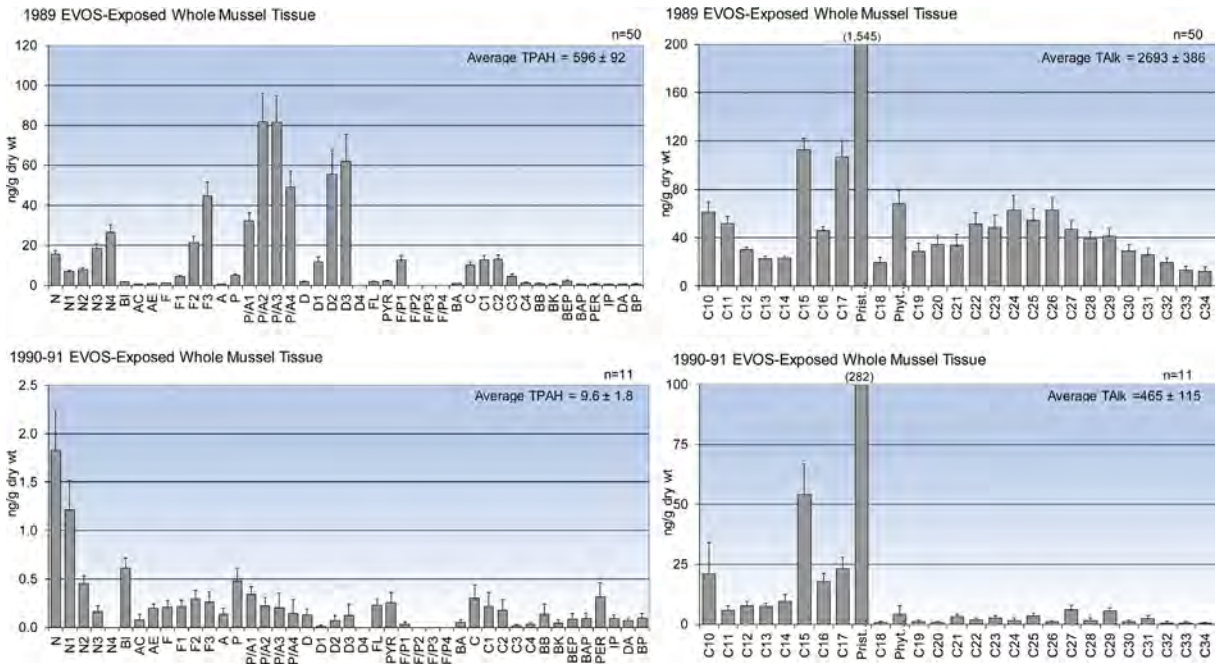

FIGURE 14.3 Average PAH and AHC histograms of whole mussel extracts from samples collected from EVOS-oiled areas of Cabin Bay, Naked Island in Prince William Sound in May 1989 after the *Exxon Valdez* oil spill (EVOS) and again in 1990 and 1991 (data from EVTHD, the EVOS Trustees Database). Profiles from 1989 were mostly particulate oil. In 1990–91, PAH profiles were mostly dissolved with biogenic SHC. Adapted from Payne and Driskell (2003), reproduced with permission from the IOSC.

descending concentrations). There was no evidence of particulate oil being available to these filter feeders (albeit a trace of pyrogenic PAH was present). The SHC patterns at that time primarily showed biogenic components with very little evidence of particulate oil. Under these circumstances, herring-egg PAH exposures may have been justifiably more correlated but the samples were not collected.

14.4.2 EVOS—Nearshore and Intertidal Seepage

Most shoreline-stranded oil from the *Exxon Valdez* visually disappeared after the first winter (1989) but was still present in subsurface intertidal sediments (mixed gravel, sand, and fines) in less-exposed embayments. Concern about these lingering deposits eventually led to a follow-up study in 2002 looking for seepage or leaching of water-soluble components from these lingering deposits. For these collections, initial samples were taken while carefully approaching the nondisturbed shoreline to collect the beach-edge water during a falling tide. After landing, interstitial water was sampled and field-filtered from zones above, amid, and below the oiled sediments (Payne et al., 2005a,b). Results confirmed the seepage of oil components into the overlaying water from EVOS oil deposited 13 years earlier (Figs. 14.4 and 14.5). Seepage-derived PAH show a more weathered state and increased dissolved portions relative to the buried intertidal oil as would be expected from a tidal-wash and interstitial-drainage scenario removing surficial oil components from the bulk mass. Similar scenarios were reported from nearshore water sampling during the 2010 DWH blowout with dissolved profiles appearing off oiled shorelines (Driskell and Payne, 2015).

14.4.3 *New Carissa* Oil Spill

During a February storm in 1999, the M/V *New Carissa*, a bulk-wood-chip cargo ship ran aground on the sandy coastline near the harbor entrance to Coos Bay, Oregon, and eventually broke into two sections, releasing four different fuels (two marine diesels and two marine fuel oils). For NRDA efforts, the field-filtration system was used for the first time on this spill (Payne et al., 1999; Payne and Driskell, 2001), thus confirming the dissolved fingerprint patterns in the environmental samples.

The bulk of the oil released during the *New Carissa* spill was a combination of two marine fuel oils. Because of their relatively high viscosities and the lack of lower molecular-weight one-ring aromatics, these oil types

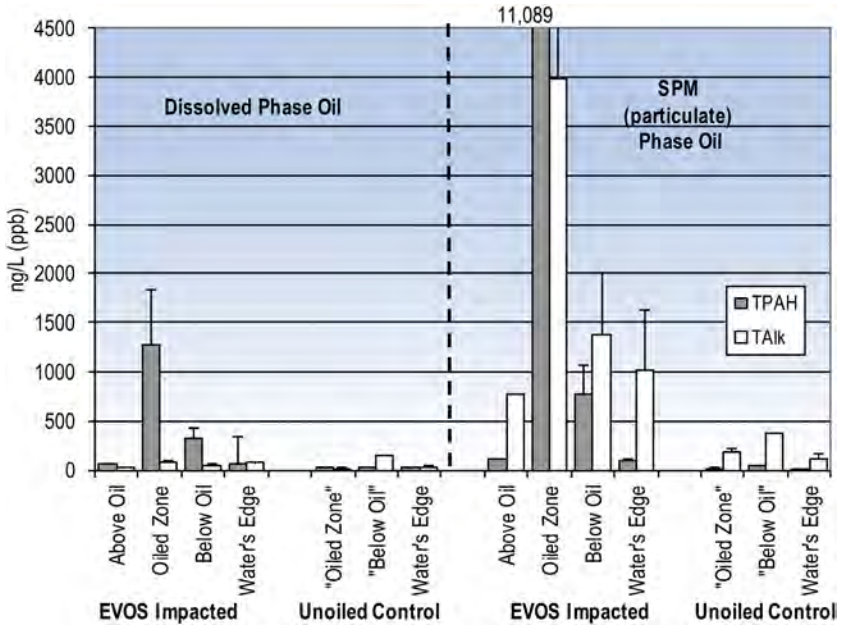

FIGURE 14.4 Average total PAH (TPAH) and total alkane (TALK) distributions of dissolved and particulate oil phases in near-shore and interstitial water from oiled and unoiled intertidal areas in Prince William Sound 13 years after EVOS. Error bars are SE of means. Adapted from Payne et al. (2005b), reproduced with permission from the IOSC.

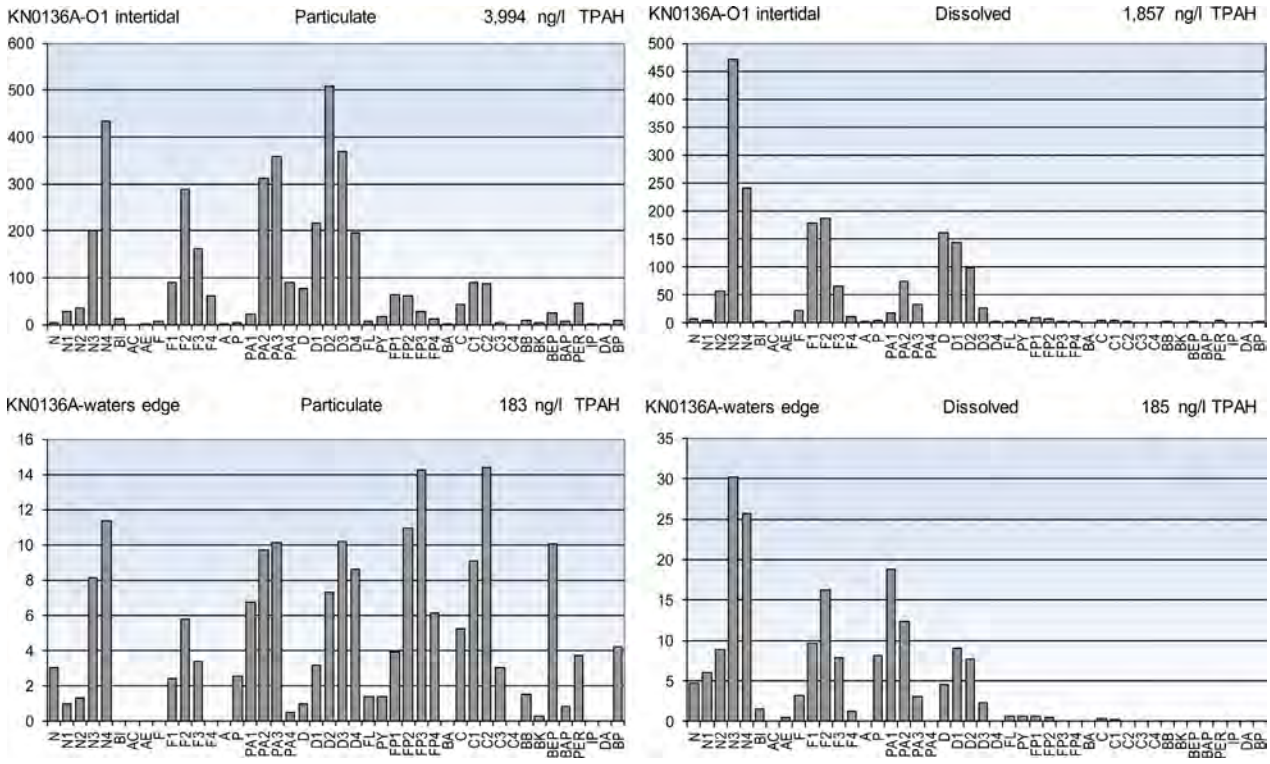

FIGURE 14.5 Particulate and dissolved PAH (ng/L) from EVOS-impacted site, Bay of Isles, showing oil profiles in oiled intertidal (upper) and in undisturbed waters immediately nearshore (lower). Extent of weathering and dissolved portion increases in water's edge samples suggesting chronic seepage from buried intertidal oil. Adapted from Payne et al. (2005a,b), reproduced with permission from the IOSC.

had generally been classified previously as not contributing persistent levels of finely dispersed oil droplets nor a significant fraction of dissolved constituents into the water column. The forensic results demonstrated, however, that low-concentration water-column and concomitant tissue-burden impacts could occur with bunker-type fuels (Fig. 14.6). Furthermore, adjacent to visibly clean beaches (likely to be reported as un-impacted by spill-response surveyors), dissolved hydrocarbons from offshore waters occurred in low concentrations in the beach's interstitial waters (0.3 to 470 μg/kg (ppb); Figs. 14.6 and 14.7). Elsewhere, on another visibly unoiled but hard-packed sand beach 3 mi north of the grounding, diatoms, locally blooming near-shore during the spill were thickly accumulated in the upper-most intertidal wrack line. PAH analyses demonstrated that as lipidic organisms often occurring at or near the ocean surface, the diatoms had accumulated significant quantities of weathered *New Carissa* oil (Fig. 14.8) and by bulk depositing (live or dead?) on the beach created a novel exposure route to intertidal fauna, scavenging birds, and unsuspecting recreational users. Similar accumulations have been noted in copepods actually ingesting oil microdroplets (Carls et al., 2006, in Alaska) and anecdotally in crab larvae during the DWH (pers. comm., Harriet Perry, 2010).

Combining pattern fingerprinting with a multivariate statistical method, *New Carissa* oil could be differentiated from background combustion-derived (and sediment-associated) PAH in clam, oyster, and crab tissue samples from inside Coos Bay. Results showed two different mechanisms of hydrocarbon uptake into affected organisms: (1) direct uptake of dissolved-phase PAH from the water column (via gills) into Dungeness crab tissues (Figs. 14.9 and 14.10), and (2) PAH and aliphatic constituents accumulating from ingesting dispersed oil droplets and oiled, suspended-particulate material (SPM) inside the bay in filter-feeding oysters (Fig. 14.11), and in mussels on the outer, ocean-exposed jetties (Fig. 14.12). Inner bay oysters showed evidence of low-level contamination of PAH (naphthalenes through dibenzothiophenes) consistent with weathered *New Carissa* oil plus significantly higher concentrations of background combustion products (fluoranthenes/pyrenes, benzo(*a*)anthracene, chrysenes, benzo(*b*)fluoranthene, and benzo(*e*)pyrene). The lower molecular-weight PAH (through the dibenzothiophenes) are almost identical to the dispersed oil/SPM samples (Fig. 14.10) filtered from the water over the oyster beds while the combustion-derived PAH appeared almost certainly associated with the background PAH from the sediments in this location (Fig. 14.13).

In contrast, the tissue samples from the filter-feeding mussels located on the exposed ocean-side of the harbor entrance ocean side of Coos Bay, North Jetty (Fig. 14.12) illustrated the uptake of particulate-phase oil directly from the water column (compared to Fig. 14.6 particulate phase) without the sediment-associated combustion products noted in the inner bay oysters (Figs. 14.11 and 14.13). The almost complete loss of naphthalenes in the mussel tissues compared to the particulate-phase oil collected near the vessel is a result of the higher surface-

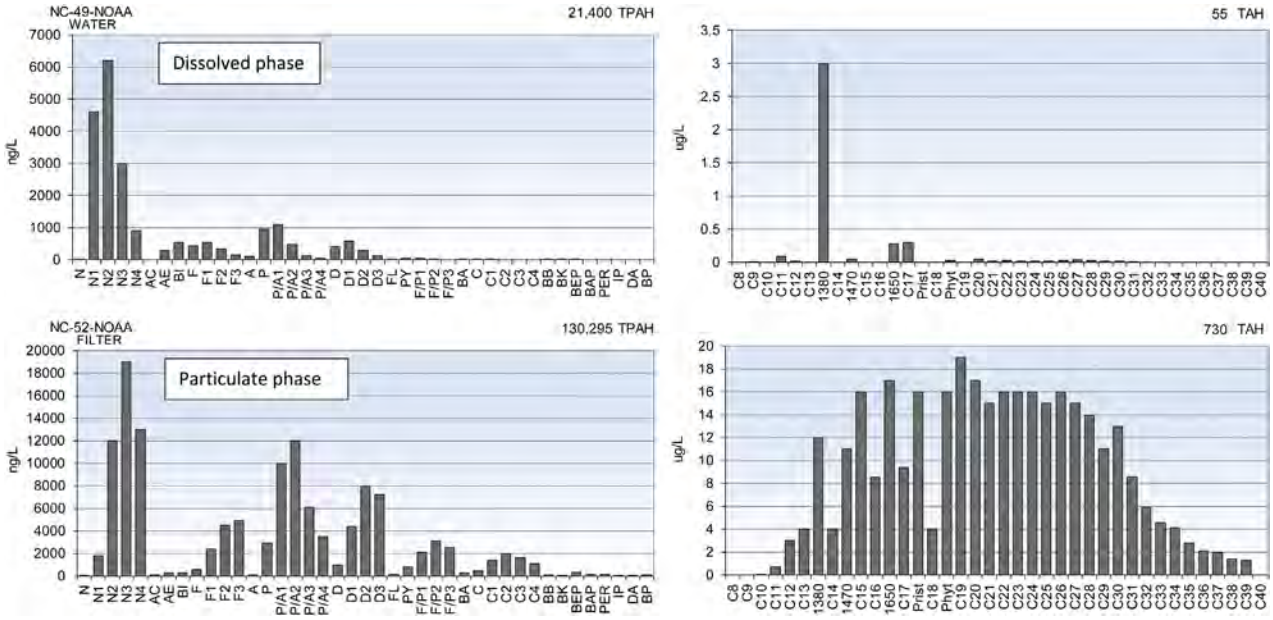

FIGURE 14.6 PAH and SHC profiles of dissolved and particulate phases water sample from surf-zone station adjacent to the bow of the *New Carissa*.

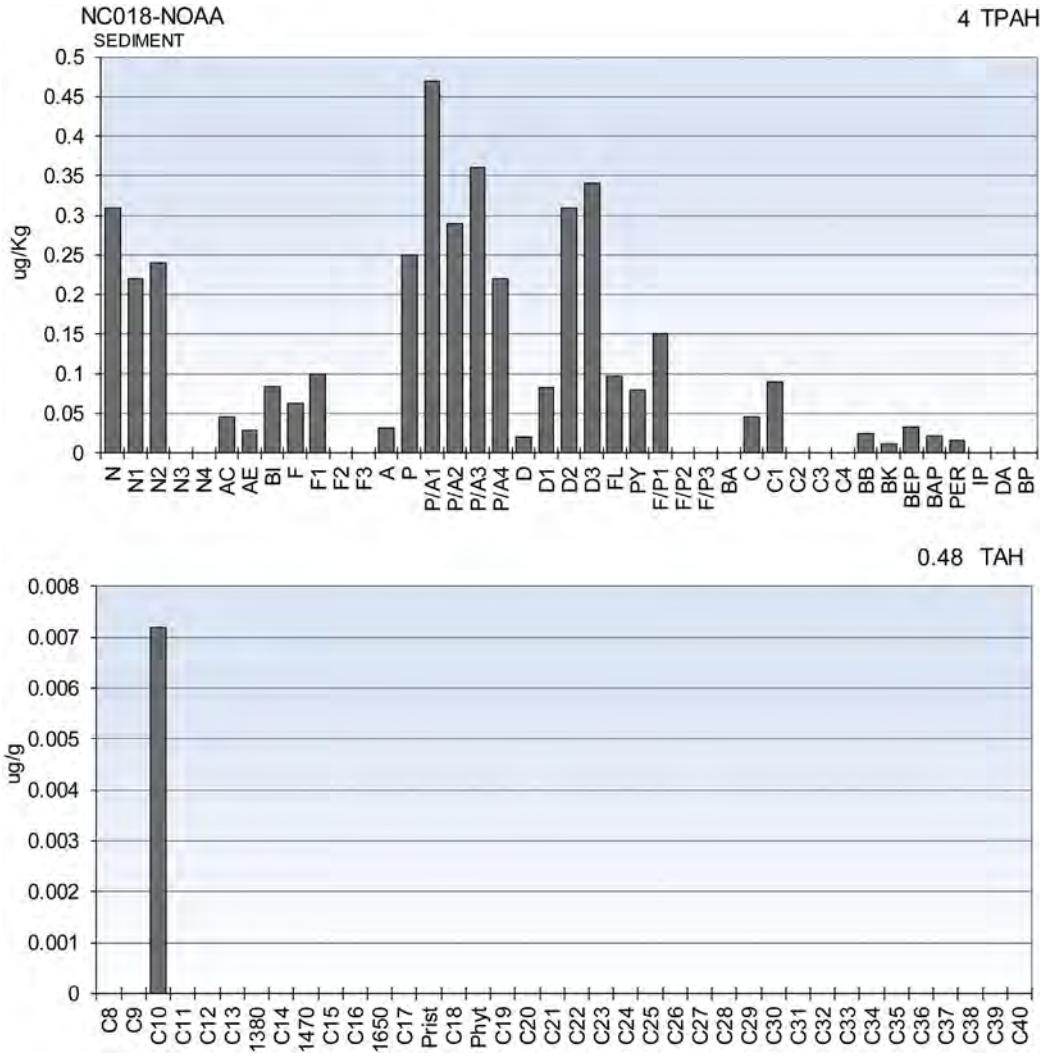

FIGURE 14.7 Source characterization data for intertidal sediment sample collected on an otherwise clean beach with no visible oil contamination 5 mi north of the *New Carissa*. Note the absence of particulate *n*-alkanes in the interstitial water vs the surf-zone sample collected adjacent to the vessel (Fig. 14.6). This sample shows only dissolved-phase PAH contamination of the interstitial water and the complete absence of any free oil or (dispersed oil droplets) as demonstrated by the lack of any aliphatic signal.

area-to-volume ratio of the very fine droplets and sheens that promotes the rapid loss of the more volatile and water-soluble naphthalene components. The remaining constituents exactly matched one of the particulate-phase source oils.

In these examples, the phase information was crucial to understanding the exposure pathways and in revealing previously unexplored mechanisms of exposure and toxicity (Payne and Driskell, 2001).

14.4.4 Port Valdez—Long-Term Monitoring

In Port Valdez, Alaska, the Trans-Alaskan pipeline delivers Alaska North Slope (ANS) crude oil for transfer to tankers at the Alyeska Marine Terminal (AMT). In the wake of the 1989 *Exxon Valdez* event on a nearby shoal, a citizen oversight group, the Prince William Sound Citizens' Advisory Council, was established by the Oil Pollution Act (1990) to oversee the terminal and tanker operations and conduct a Long-Term Environmental Monitoring Program (LTEMP) for oil contamination. Since 1993, intertidal mussel tissues and subtidal sediment samples from Port Valdez and several EVOS-impacted and reference (nonimpacted) sites within Prince William Sound (PWS) have been sampled and analyzed for hydrocarbon contamination. These data, plus occasional treated ballast-water samples, serve as a sentinel indicator and independent quality control check for terminal

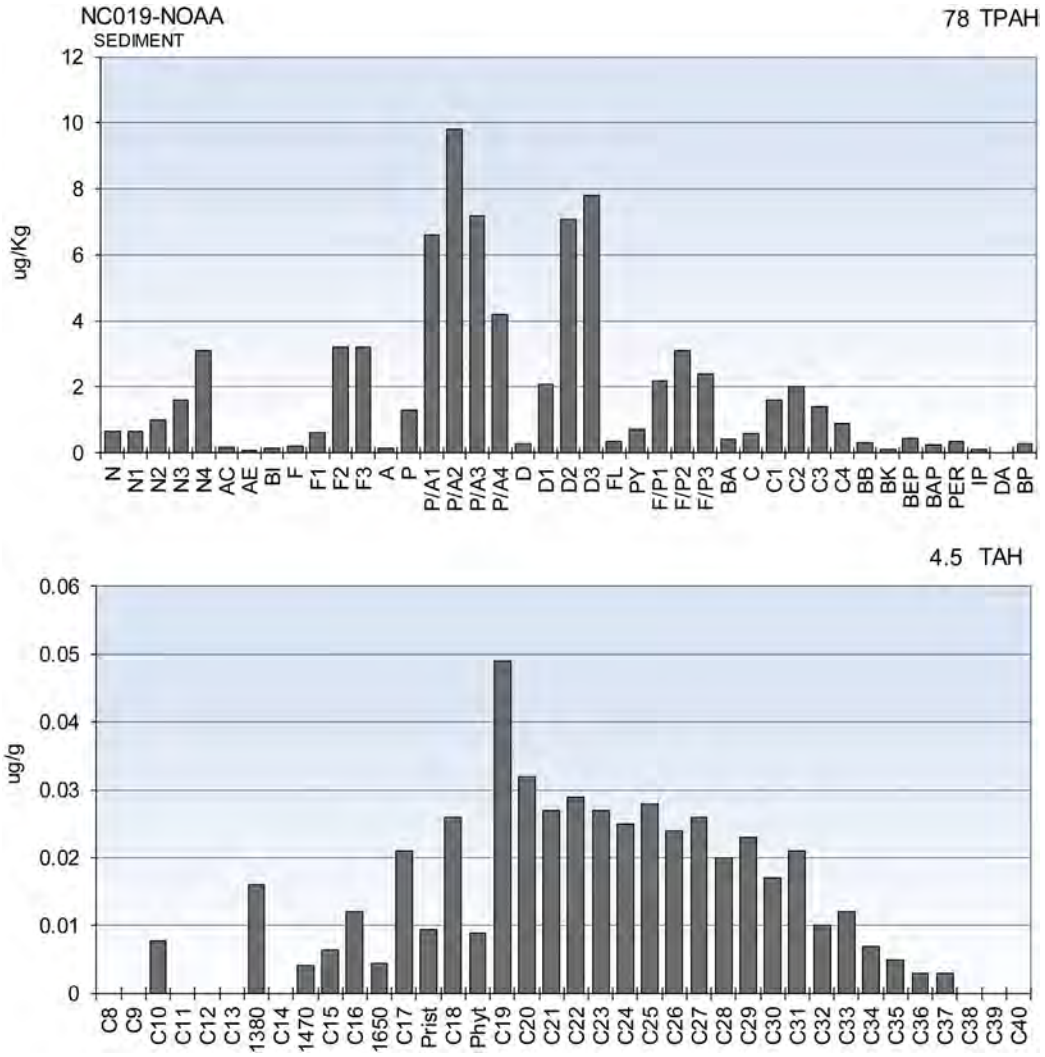

FIGURE 14.8 PAH and SHC profiles of oil-contaminated, stranded diatoms scraped from the upper strand-line on an otherwise completely unoiled hard-packed sand beach 3 mi north of the *New Carissa* release.

and tanker-operation impacts within PWS (Payne et al., 2003, 2005c, 2016). Integral to the terminal's operation is Alyeska's Ballast Water Treatment Facility (BWTF) which treats and discharges oil-contaminated ballast water offloaded from tankers returning to the terminal. Phase-discriminated effluent data were initially obtained in 2001 from filtered water samples collected in the offshore-mixing zone adjacent to the diffuser as part of a caged-mussel study (Salazar et al., 2002) and later directly from the outfall pipe in 2003/2004 (Payne et al., 2005d,e), and then again in 2016 following a treatment facility redesign project.

Two stations, AMT adjacent to the offshore BWTF diffusers and Gold Creek (GOC), a reference station 6 km across the Port, track the effects from the treated ballast discharge (Fig. 14.14). Measured parameters include polycyclic aromatic and SHC levels (PAH and SHC) in mussel tissues and sediments from the two stations within the Port, and in mussels only at two stations in the eastern PWS area, Knowles Head near a tanker-holding anchorage and the regional control site, Sheep Bay north of Cordova (Fig. 14.14). Sediment samples from the two port stations are analyzed for PAH, SHC, particle grain size, and total organic carbon content to monitor the site environments, and for the past 3 years, oil biomarkers have been added to confirm petrogenic sources. Sampling and analytical methods are modeled after the protocols developed by the National Oceanic and Atmospheric Administration (NOAA) Status and Trends Mussel Watch Program.

Data from AMT and the nearby GOC control site suggested that ANS crude oil residues from the terminal's BWTF accumulated in the intertidal mussels within the port (Payne et al., 2001), but the sediment and tissue (and the estimated water-column) PAH and SHC levels were very low. More importantly, the signatures allowed

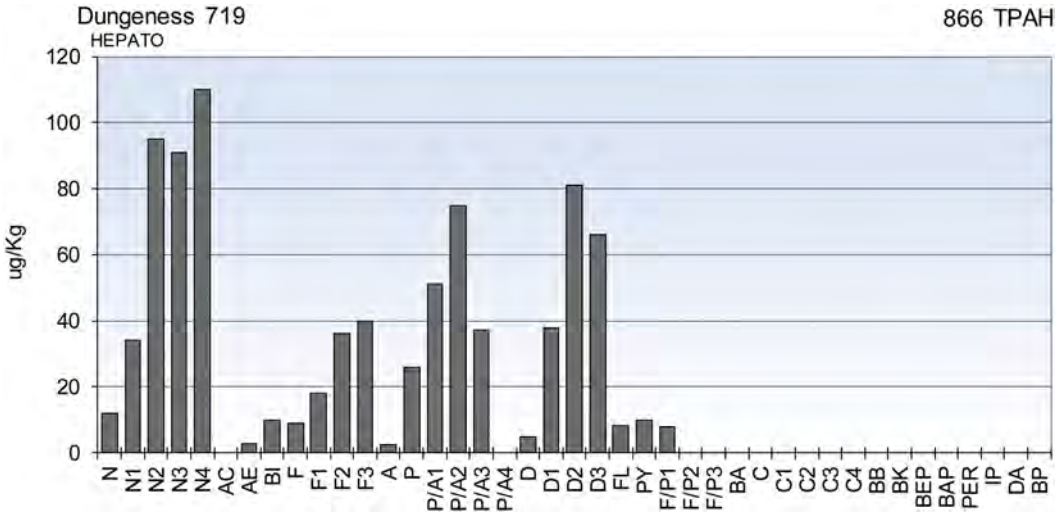

FIGURE 14.9 Tissue data for Dungeness crab collected inside Coos Bay. The PAH profile is almost identical to the dissolved-phase (filtered) water sample collected above and adjacent to the oyster beds 6 days earlier (Fig. 14.10). Similar PAH histograms were obtained from all the other crab samples collected inside the bay; however, the sediments in this region (Fig. 14.13) reflected very low concentrations of naphthalenes and predominantly higher molecular-weight combustion products.

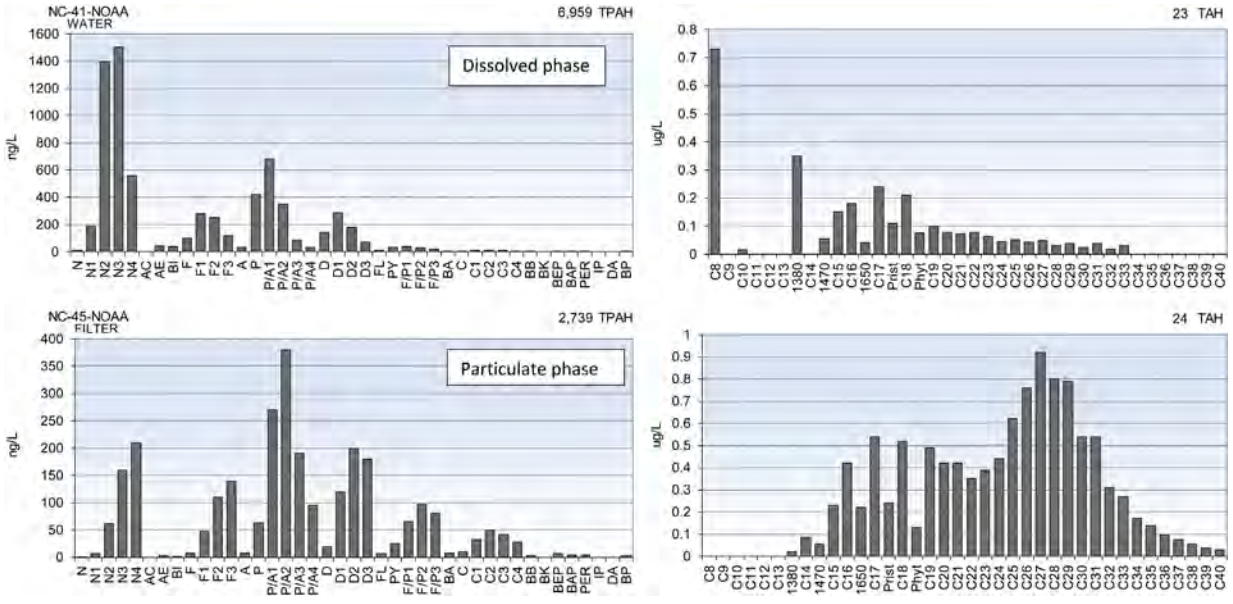

FIGURE 14.10 Phase-filtered water sample from outgoing-tide transect over the oyster beds inside Coos Bay.

discrimination of particulate (oil droplet) and dissolved-phase signals in the water column that correlated with seasonal uptake in mussels and, from other studies, with absorption in herring eggs (see Section 14.4.1). These findings gave new insight into the transport and exposure pathways in Port Valdez. The results also suggested a surface microlayer mechanism may be responsible for seasonal transport of ANS weathered oil residues from the BWTF diffuser to intertidal zones across the fjord (Payne et al., 2001, 2003, 2005c).

During strong fall and winter-wind events, the fjord's water column destratifies (Fig. 14.15), allowing both dissolved- and oil-droplet phase contaminants discharged from the BWTF's seabed diffuser to reach the upper water column where a surface microlayer of particulate-phase oil could be transported by winds and surface currents to spread throughout the fjord. When concentrations were sufficiently elevated, filter-feeding mussels, tidally immersed twice daily through the surface layer, exhibited the particulate oil profile (Fig. 14.16). During lighter

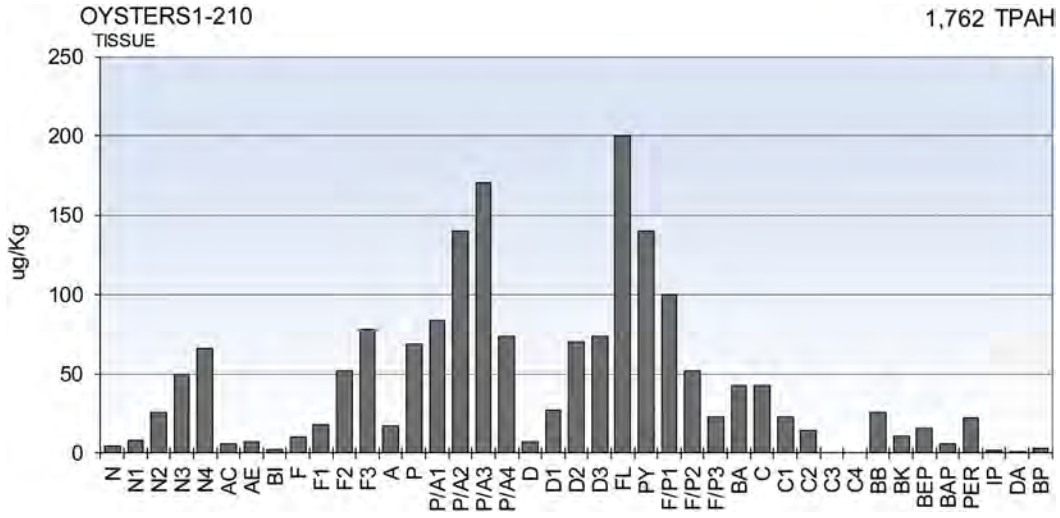

FIGURE 14.11 Tissue data for oyster sample collected at the north end of Coos Bay showing lower molecular-weight PAH (Ns, Fs, P/As, and Ds) contamination from particulate-phase *New Carissa* oil in the overlaying water (Fig. 14.10) plus sediment associated pyrogenic (FL through BAP) components from the surrounding sediments (Fig. 14.13).

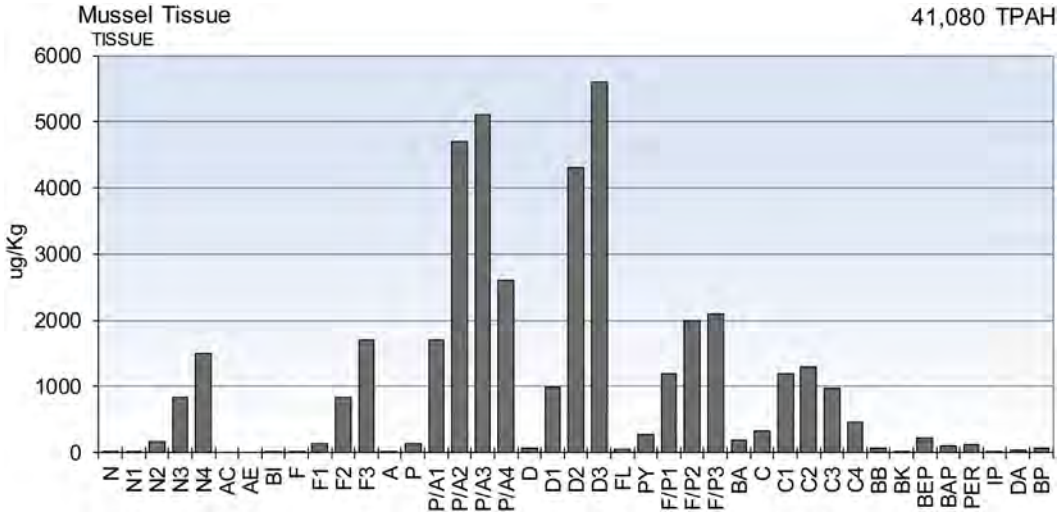

FIGURE 14.12 PAH for mussels collected from the ocean side of Coos Bay, North Jetty showing selective uptake of particulate-oil-phase PAH directly from the water column without sediment-associated, higher molecular-weight pyrogenics (Fig. 14.13).

winds and larger river inputs in the late spring, summer, and fall, the water column becomes highly stratified. During this period, primarily dissolved-phase components were observed in the mussels along the shoreline, as the oil droplets became trapped below the thermocline.

Recent years have brought change to the system as pipeline production has dropped from 2 million barrels of oil per day at its peak in 1988 to current levels of 0.5 million barrels per day in 2015. Likewise, post-EVOS tanker regulations have instituted double-hulled tankers with segregated ballast. Aboard the new segregated-ballast (double-hulled) vessels, empty cargo tanks are only used for supplemental ballast when operationally necessary (e.g., during winter storms). As a result, treated-ballast water discharges to the port have also dropped from around 15 million gallons per day (MGD) in 1990 to only 1.1 MGD in 2015. Facility operators estimate that during seasonal low-flow situations, more than half of the current discharge is treated storm water runoff (Rich Loftin, pers. comm., 2016 as cited in Payne et al., 2016). In summary, less tanker traffic, cleaner ballast, and a redesigned, more efficient, ballast-water-treatment configuration at the AMT have resulted in substantial changes in detected hydrocarbon concentrations (Fig. 14.17) and composition in the field samples in both mussels and sediments.

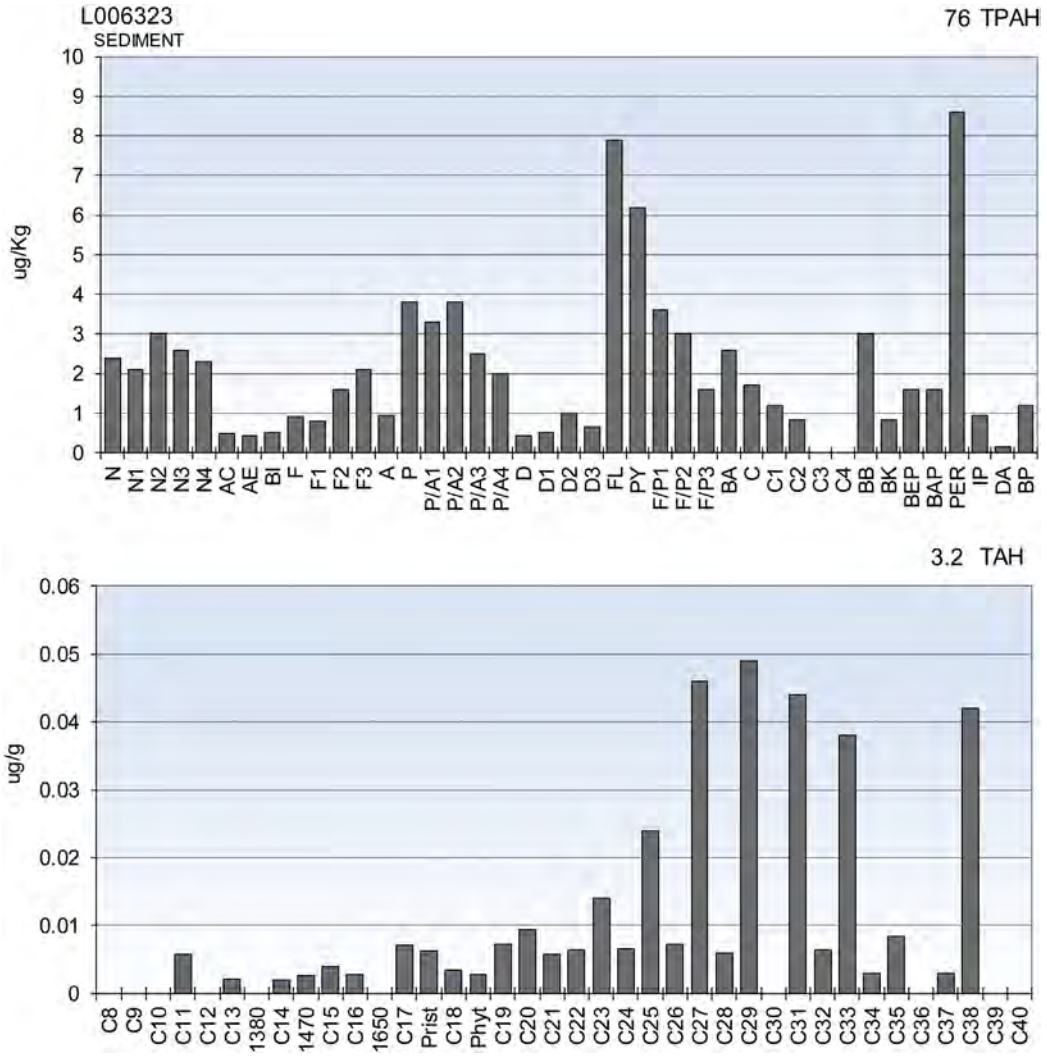

FIGURE 14.13 Background hydrocarbon profiles of sediment sample collected near the oyster beds in upper Coos Bay. The PAH profile shows primarily pyrogenic components with the parent PAH generally greater than the higher alkylated components within each homolog group, and the SHC reflect very low-level C_{17}–C_{18} petrogenic components plus more dominant odd-carbon numbered terrestrial plant wax components between C_{23} and C_{35}.

Over the last several years, mussel contamination at AMT has been generally shifting away from the terminal's earlier petrogenic profiles to background dissolved-phase or pyrogenic PAH patterns (Fig. 14.18). The sediments depositing in Port Valdez, primarily from local glacier flour SPM, associate with the oil droplets and accumulate rapidly (~1 cm/year). These new surface sediments still contain ANS oil but in decreasing amounts and portions from previous years (Fig. 14.19).

14.4.5 Gulf of Alaska Region—Long-Term Monitoring

Beyond the Port of Valdez, multiyear LTEMP samplings at eight stations comprising the geographic reach of the EVOS throughout PWS, along the Gulf of Alaska coast and down to Kodiak (Fig. 14.14) have tracked mussel tissues currently trending into the single-to-double digit PAH range (ppb). Currently lacking oil signatures, their phase profiles suggest trace dissolved phase source(s), possibly transferred from the atmosphere to water, being picked up by the mussel populations. While water samples were not collected as part of the LTEMP program, samples taken in the PWS ocean entrance in 2007 showed, not surprisingly, a similar trace dissolved-phase pattern (Fig. 14.20). Recent mussel sample profiles each comprise only a few analytes but the components show a common complexity of dissolved and pyrogenic patterns that implies effects from a region-wide process. In some

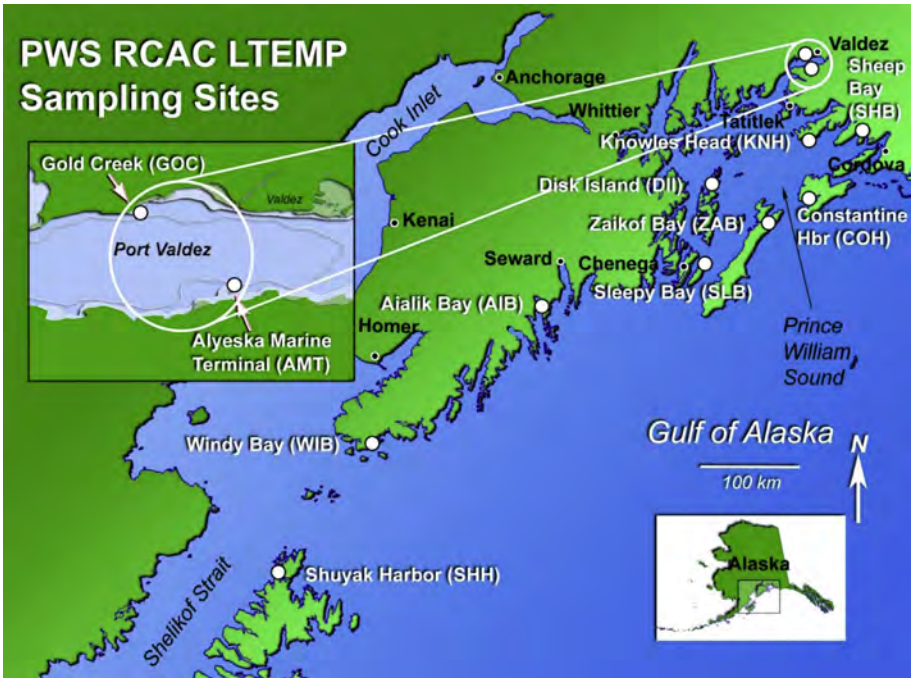

FIGURE 14.14 Map of the Alaskan LTEMP sites. Adapted from Payne et al. (2016), reproduced with permission of the PWSRCAC.

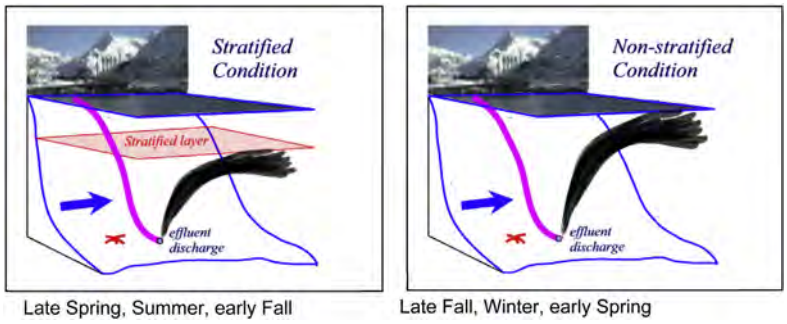

FIGURE 14.15 Seasonal stratification of the Port Valdez water column promoting surface microlayer transport of particulate-phase oil constituents to intertidal mussels during nonstratified conditions.

years, the mussels also showed higher traces of PAH combustion products, most likely from perennial Alaskan wildfires. Compared to the most recent West Coast NOAA Mussel Watch data (2004–05) and the more recent 2008–10 Alaskan Mussel Watch sites, LTEMP results continue to demonstrate that the sampled region is exceptionally clean (Payne et al., 2016).

Regional deep-sea sediments tell a different story. In the EVOS aftermath, an intriguing question arose regarding the source of PAH detected in PWS' deep basin sediments; its fingerprint appeared as petrogenic but was it deposited from EVOS or some other source (upstream oil seeps were initially suggested), and if from another source, was it bioavailable (and thus "precontributing" to EVOS impacts)? While many conflicting opinions were tendered, eventual consensus was that the material was most likely from an eroding shale formation located east (upstream) of the region, which had arrived in PWS via coastal currents. This scenario was later corroborated with sampling by MMS, EPA's EMAP program, and a series of studies coordinated or contracted by the Cook Inlet Regional Citizens Advisory Council that showed the same ambient PAH signal moving along the entire northern Gulf of Alaska (Fig. 14.21). More importantly, the persistent unweathered appearance of the readily dissolvable naphthalenes in these samples confirmed that the PAH were indeed locked into the rock matrix and were not bioavailable (and not contributing to EVOS impacts). Any dissolution losses would be confined to the particle's outer surface microlayer and would not be reflected in the bulk sediment grab samples.

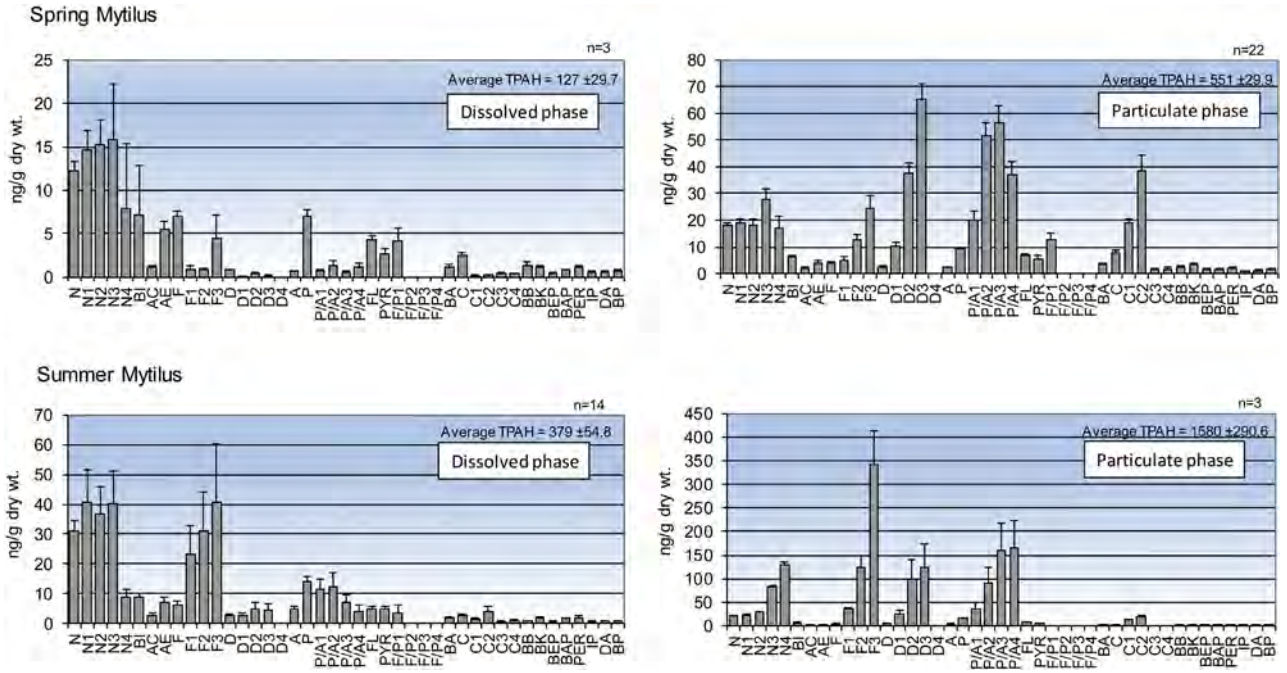

FIGURE 14.16 Mean PAH histograms from 1993 to 2000 LTEMP intertidal mussel samples from Alyeska Marine Terminal. The samples are separated vertically by season and horizontally by physical state of the hydrocarbon source. The number of samples contributing to each composite illustrates the predominant oil–droplet phase signal in the spring (22 out of 25 samples) and the predominant dissolved-phase signal in the summer (14 out of 17 samples). Adapted from Payne et al. (2001) and Payne and Driskell (2003), reproduced with permission from the IOSC.

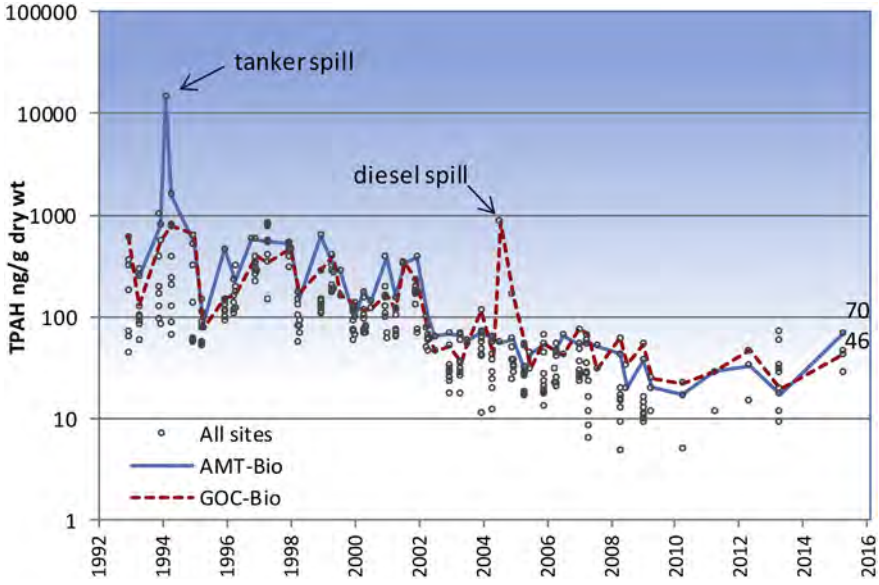

FIGURE 14.17 Time series of mean mussel log(TPAH) comparing 2015 Alyeska Terminal and Gold Creek with other regional LTEMP collections. The 1994 tanker spill occurred during a loading incident at the terminal; the 2005 diesel spill was likely a fishing vessel refueling incident. Both demonstrate monitoring successes and regional degradation rates. Adapted from Payne et al. (2016), reproduced by permission of the PWSRCAC.

14.4.6 *Cosco Busan* Oil Spill

Under thick fog in November 2007, the container ship *Cosco Busan* struck a pylon on the San Francisco-Oakland Bridge, rupturing the hull and spilling 54,000 gal of bunker fuel into San Francisco Bay. Rapidly spread

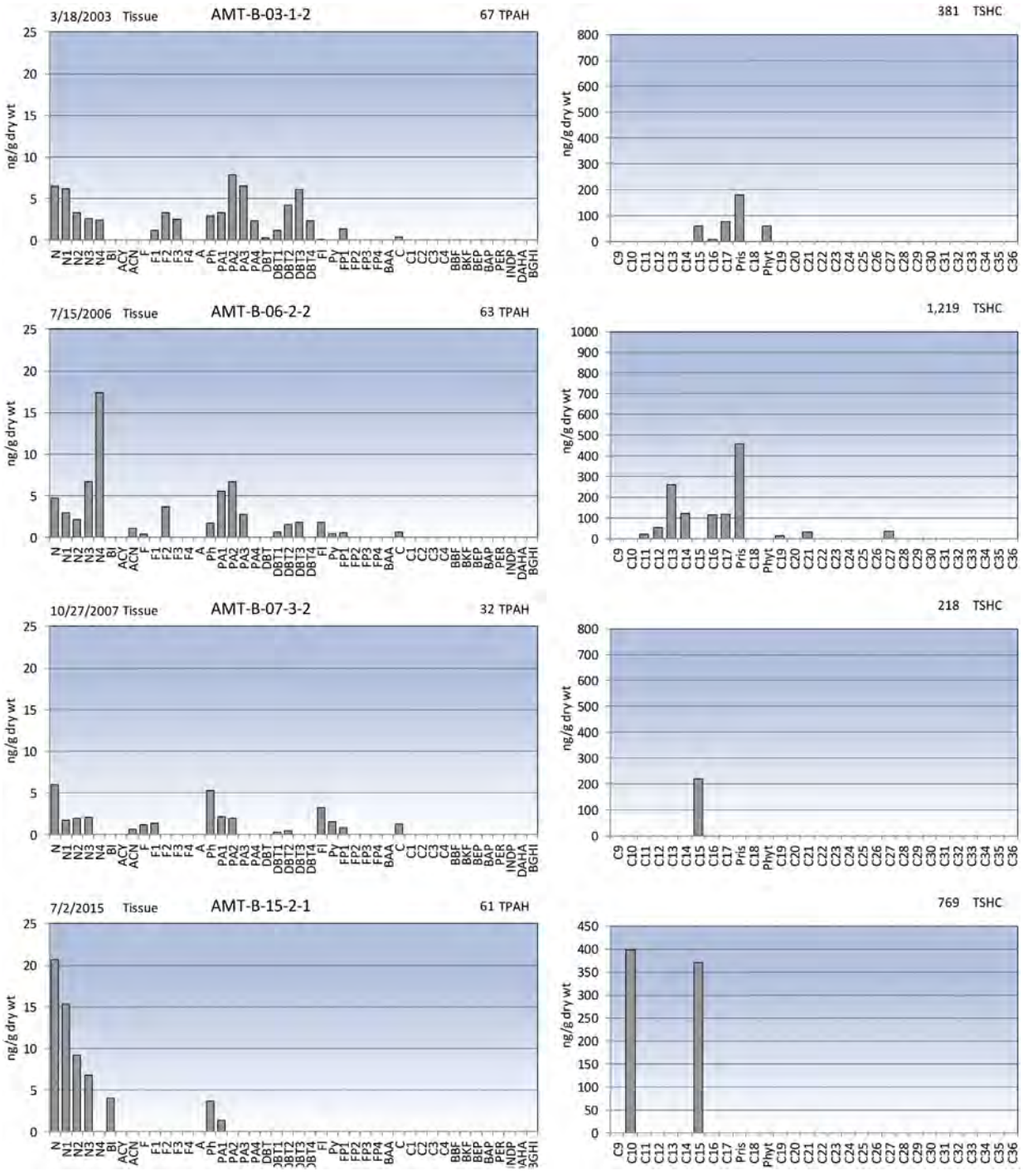

FIGURE 14.18 PAH and SHC profiles showing low-level TPAH with variable source signals (particulate/oil-, dissolved-phase, and trace-level combustion products) in AMT mussel samples from 2003 to 2015. MDL line (subnanogram) omitted for scaling perspective.

by the tides, the modest spill eventually reached a large area of the California North Coast, including the Golden Gate National Recreation Area, Ocean Beach, and the Marin Headlands, closing beaches and impacting wildlife. Water sampling for this surface release was, by management decision, minimal during the spill itself, but it was later implemented during shoreline-cleanup trials (in next section). Presented here is the forensic method used for the event's nonwater matrices that later contributed to the approach used and further developed for DWH waters.

FIGURE 14.19 Sediment PAH in Port Valdez, Alaska. Adapted from Payne et al. (2016), reproduced with permission from the PWSRCAC.

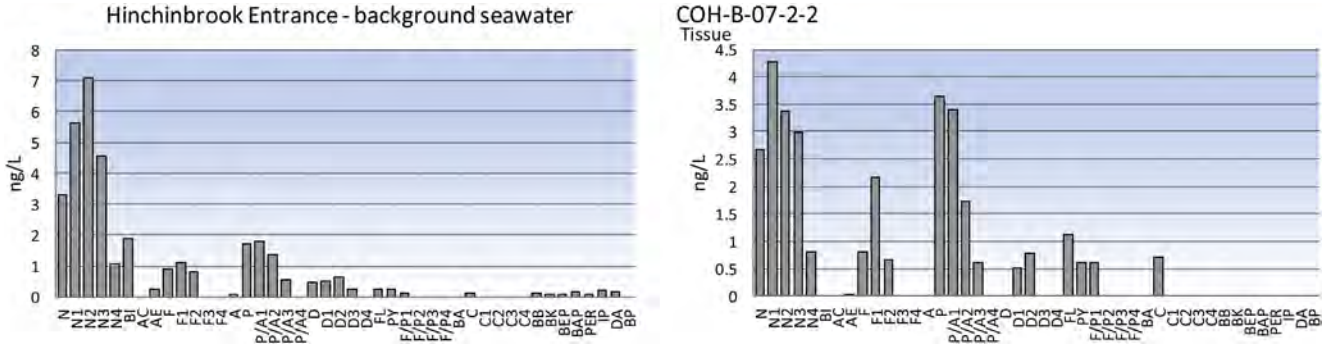

FIGURE 14.20 PAH profiles of water in Hinchinbrook Entrance, PWS, July 2007 and mussel tissue from nearby Constantine Harbor on Gulf of Alaska; both showing a trace predominantly dissolved-phase naphthalene pattern plus pyrogenics.

14.4.6.1 Forensic Assessments

For any spill, forensically evaluating samples with high concentrations of spill-source oil is a fairly straightforward task, i.e., when the source signal rises well above the background noise. But when lower concentrations are confounded by elevated background hydrocarbon levels such as found in this urban marine bay environment, parsing out the spill-oil contribution can be challenging. For this spill, our approach was to use mixing-models of both PAH and biomarker data to interactively deconvolute the source signal from background. Briefly, some novel graphical mixing-models for extracting the source from background, an empirical weathering model, a small number of prespill sediment and tissue samples, and knowledge of specific shellfish habits eventually lead to a defensible scheme of assessing samples containing low but nontrivial amounts of source oil.

For the *Cosco Busan* NRDA, the authors and Greg Douglas (NewFields Environmental Forensics, LLC) worked as a cooperative Trustee/Responsible Party (RP) forensic team in evaluating the hydrocarbon profiles of various oil, sediment, and tissues samples (Driskell et al., 2010). Although there was only one source of oil from the vessel, San Francisco Bay held multiple background sources to confound the profile-matching task. Even the biomarkers were confounded from other sources. By necessity, we developed a parsing, mixing-model approach whereby a reference sample's PAH pattern, normalized to the amount of hopane, chrysene, or napthobenzothiophene in the field sample of interest, was graphically overlaid as a line atop the sample's bar plot pattern. For this example, let's assume the sample contains fresh nearly unweathered oil. The normalized reference

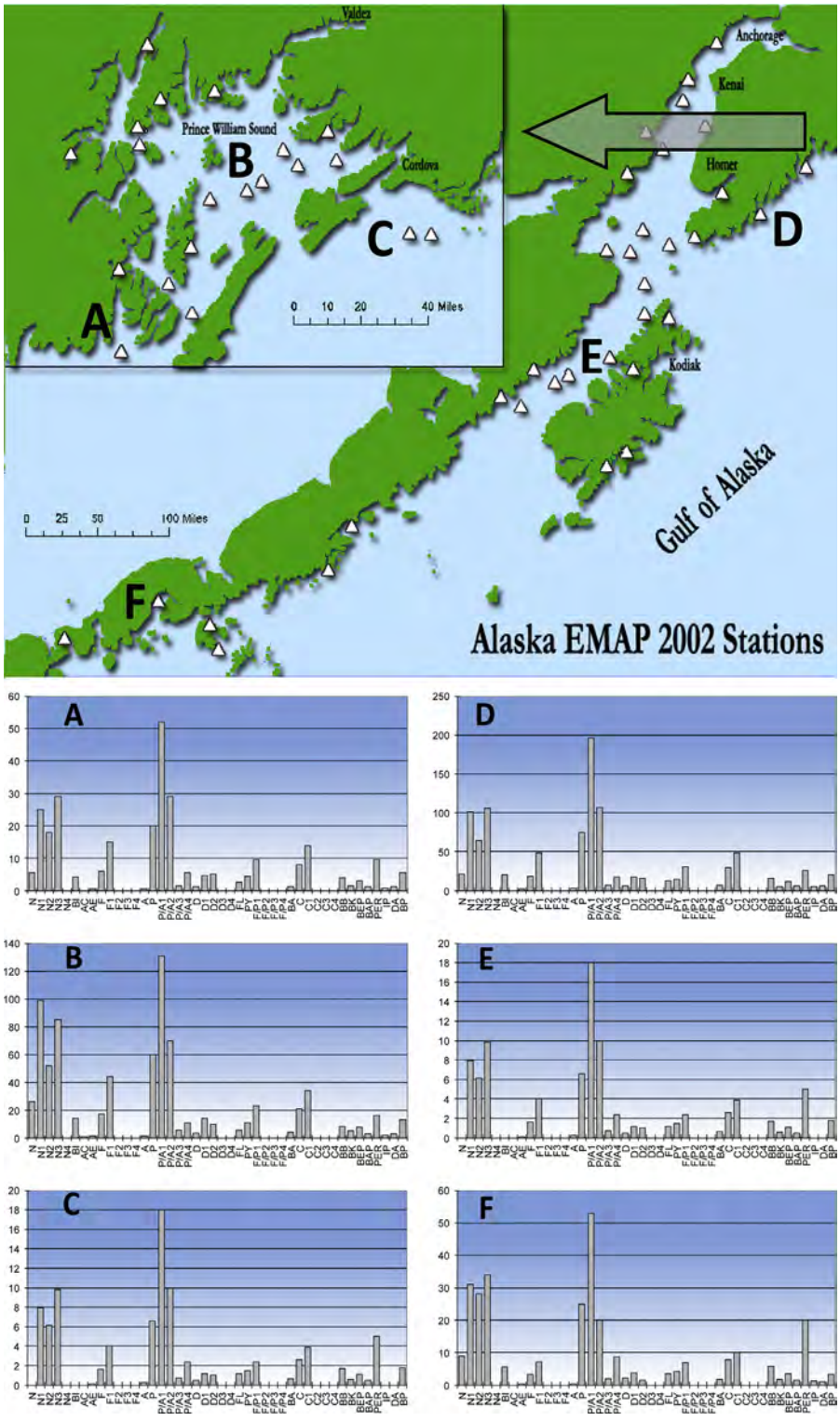

FIGURE 14.21 Benthic sediment PAH profiles from EPA EMAP surveys in PWS basin and the GOA showing the relative consistency of composition from source rock and shale erosion upstream (east) of the region.

pattern was then either manually rescaled or re-normalized to another appropriate single analyte to fit the reference pattern within the profile of the field sample, i.e., could the full reference pattern be found within the sample profile? If a logical fit was convincing, then its relative contribution could be parsed with the excess individual PAH above the scaled reference pattern representing the residual background. Because the field samples were almost always weathered, however, the weathering state of the reference oil must also be adjusted prior to comparing and parsing the sample. For adjustments, we created a weathering regression model for each PAH analyte based on an empirical series of field-weathered oil samples from the event collections (Fig. 14.22). Hence, when scaling and overlaying the reference oil, the reference sample could also be statistically weathered for the comparisons and assessments. To facilitate the process, all of the rescalings and weathering adjustments were built into an interactive Excel spreadsheet dashboard with various reference analyte scaling choices, weathering sliders, manual scalings, comparative samples, ad hoc sample and reference sample retrieval, diagnostic ratio plots, optimal solvers, mapping, and record keeping.

Knowing that the sterane/triterpane biomarkers are less susceptible to weathering, these analytes would normally provide solid confirmation of the spilled oil's presence—but biomarkers were already present in the urban background and there were no prespill biomarker data. So, a similar mixing-model was constructed (without weathering) to parse out the source biomarkers in correlation with the portions assessed in parsing out the PAH. To partially depict the process, two examples, a tarball and a tissue, are presented (Fig. 14.23). The tarball is simply a weathered sample of the *Cosco Busan* source oil, thus, the reference (dashed line) fits the pattern nicely when scaled to NBT2. Here, the bar-to-line gaps represent the weathering losses while the residuals (lower plot) are the excess trace PAH in the upper plot (above the reference line) and likely derive from some minor background contamination. In the model, the reference could be weathered down to better fit the sample but here, was not informative. The other sample, a whole mussel, initially showed a residual excess from background contamination. Proceeding, the reference oil was first fitted to NBT2 in the sample but then noting that the residual contained both NBT0 and NBT1 but not the NBT2, NBT3, or NBT4 homologs, the scalar was decreased slightly further until a logical pyrogenic pattern of NBTs was visible in the residual. For this estimated solution, the source oil PAH comprised 51% of the original profile. After confirming the potential presence of source oil, the next step would be to evaluate the other lines of evidence before proclaiming the sample a "match."

Note that the goal of this assessment was to defensibly confirm the presence of the *Cosco Busan* source oil rather than derive the precise portion contributions of PAH. One problem with this approach is seeing false positives—when the source oil profile is scaled down to miniscule proportions and/or in a highly weathered

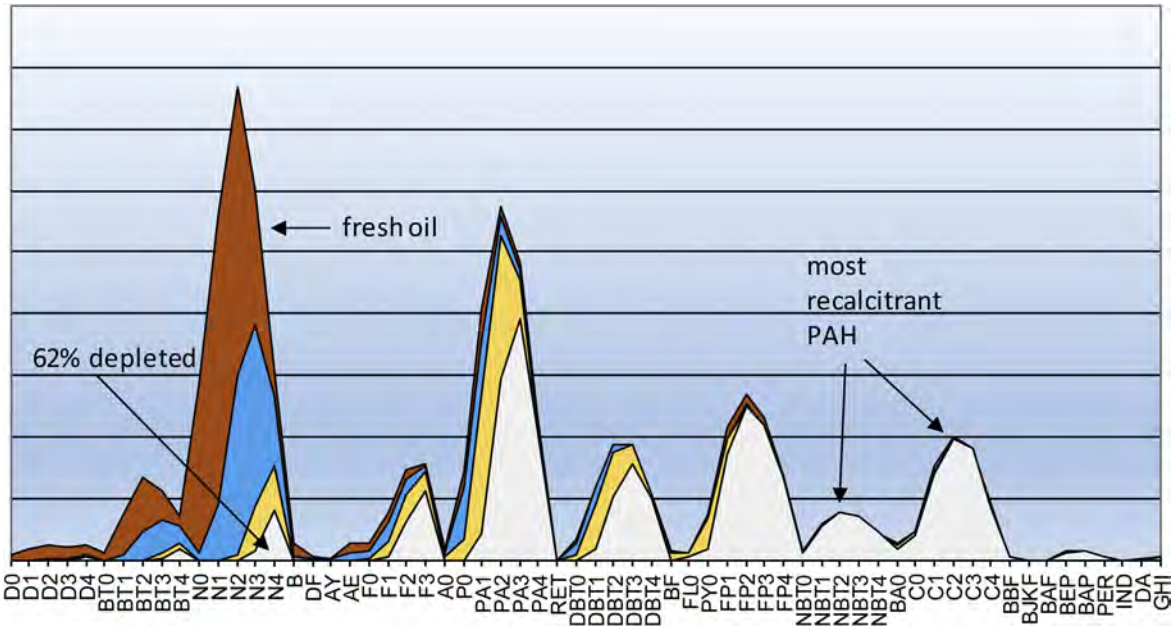

FIGURE 14.22 Weathering regression model of individual PAH using 16 weathered *Cosco Busan* oil samples, 60 PAH parameters. Overlaid shapes represent four weathered stages from fresh source oil (dark) to the most highly weathered matched sample (light).

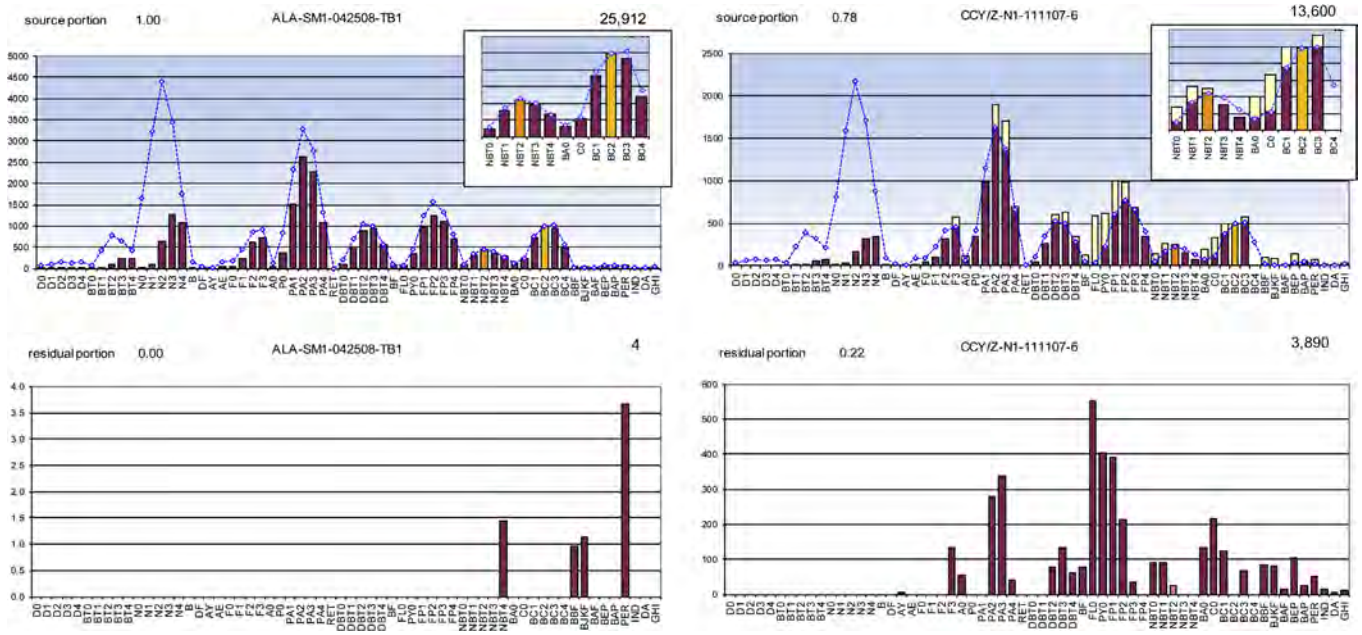

FIGURE 14.23 Example of parsing source-oil PAH profiles from *Cosco Busan* tar ball (left) and mussel sample (right) where reference oil (dotted line) is here scaled to each sample's NBT2 and overlaid on bar plot of field sample (top panels). Any analytes exceeding the reference appear as white-bar portions. The inset zooms into crucial details of fitting the oft-selected recalcitrant naphthobenzothiophenes and chrysenes. Lower panels show background residual (excess from top panel). Reference oil could be further adjusted using an interactive slider control for the weathering regression model (not shown). Other criteria determine optimal parsing.

state, the pattern could be found in almost any sample containing a broad PAH suite (even in prespill samples). Cooperatively confirming the fit by the joint Trustee/RP team, however, was not a casual task. Consensus was that a sample's pattern could be minimally justified by teasing out spill portions representing greater than 25% of the sample. Furthermore, the match/no-match decisions relied on multiple lines of evidence including PAH and biomarker fits, various diagnostic ratios for the parsed portion, prespill conditions, weathering state, species type and feeding behavior, local background patterns, and spatial patterns to build confidence and consensus in the final classification of each tissue sample.

Trustee/RP consensus tissue assessments confirmed 24 matches, 13 probable matches, 8 undecided, 21 indeterminate, and 60 nonmatching samples throughout the spill region (as defined by the spatial extent of 73 matching of 89 tarballs; Fig. 14.24).

14.4.6.2 Shoreline Cleanup-Agent Tests of Cosco Busan *Oil*

For a multitude of reasons, oil-spill responders undertake extraordinary efforts to keep oil from stranding on shorelines and to remove any that does. Shoreline washing is one of many techniques used whereby oil, in some manner or with some surfactant product, is loosened and washed back into the water to be trapped and recaptured from within encircling booms. But always during this process, a certain amount of brown water, presumably containing oil components, is seen escaping beneath the booms.

In order to select an appropriate product and optimize cleaning methods for the specific environment, some testing of product must occur. During the *Cosco Busan* event, field trials were conducted with two shoreline cleaning agents and a water-wash only control (Payne et al., 2008). The objectives of the tests were to (1) assess the efficacy of two products promoted as "lifting agents" in cleaning sections of riprap outside a marina, and somewhat uniquely; and (2) through water chemistry analyses, determine if either product resulted in entrainment (or suspension) of the "liberated oil" into the water column rather than just reforming into a recoverable slick. Both products, CytoSol (methyl soyate−vegetable oil) and Corexit 9580 (kerosene-base petroleum distillate), were on the National Contingency Plan Product Schedule and were licensed Oil Spill Cleanup Agents in the state of California.

Three adjacent zones of spill-contaminated riprap were selected and boom curtains deployed to contain oil released from the trials (Fig. 14.25). Efficacy was evaluated by before- and after-treatment observations and photo

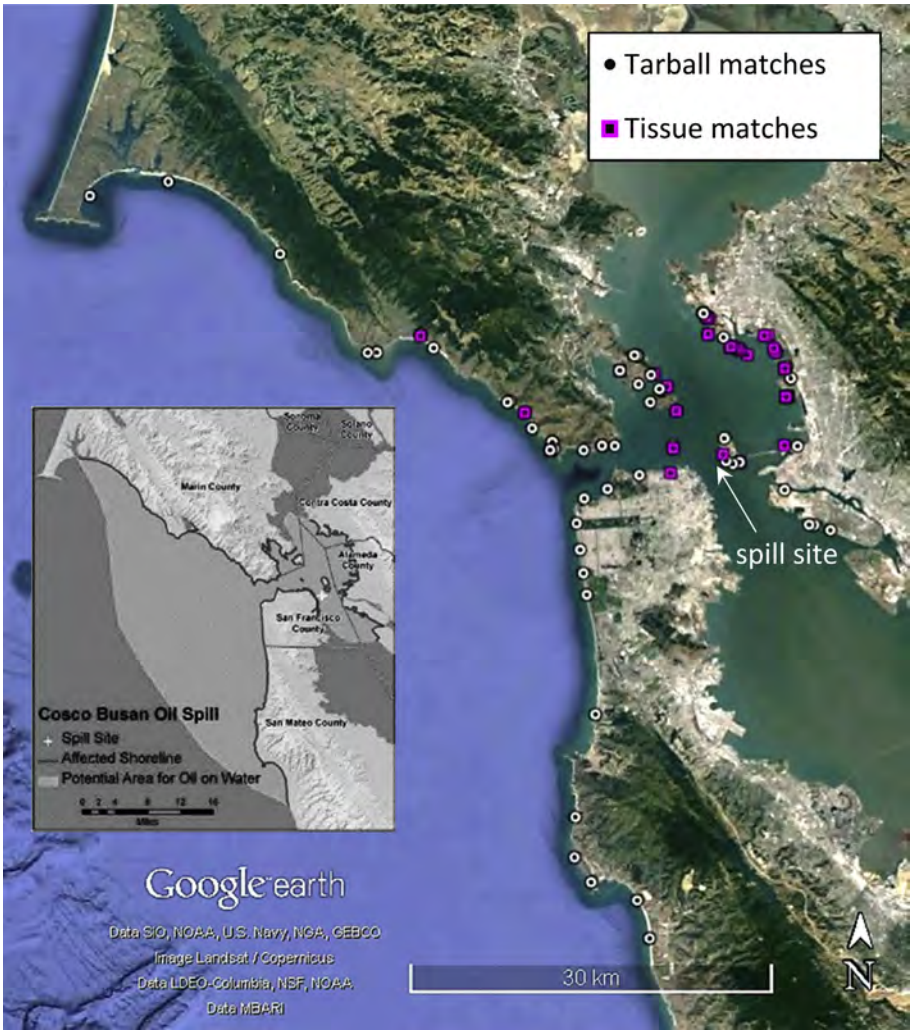

FIGURE 14.24 Results of *Cosco Busan* forensics, matching tarballs, and tissues ($n = 73, 24$). Inset from *Cosco Busan* Final NRDA depicting reach of spill.

documentation of residual oil on the treated test areas. Two different treatments were tested: (1) spraying the two products on the oiled riprap, passive soaking, deluge and pressure-washing with ambient bay water, and collecting released oily product into floating sorbents (booms and pads) and (2) spraying the products on an oiled area combined with active treatment involving light brushing, and wiping the oil immediately with a sorbent pad prior to deluge and pressure wash. A control treatment comprised washing oiled riprap with bay water only.

Pretreatment estimates of oil in the test areas averaged 20% cover. Posttesting, oil cover following passive treatment with CytoSol or Corexit 9580 was estimated at 7–10% cover; thick, sticky oil coatings remained but light oil cover was diminished. No observable change was noted in a control using only bay water with no product. The active treatment, brushing and wiping, was more effective, removing virtually all thick oil coating from the test rock and leaving only a light stain.

For the second objective, water-column contamination was quantified using in-situ fluorescence measurements Scientific Monitoring of Advanced Response Technologies (SMART) Protocols (Henry et al., 1999; Henry and Roberts, 2001; USCG et al., 2001) and by simultaneous collections of filtered water samples to assess dissolved- and particulate/oil-droplet phase concentrations of PAH and SHC (Payne et al., 1999, 2008).

Before the tests began, a background water sample was obtained offshore. During the tests, in-situ fluorescence measurements and filtered water and oil/SPM samples were collected from the water-only and CytoSol tests. For both tests, samples were obtained from 1 to 2 ft outside the lateral east and west sides of the containment boom (Figs. 14.26 and 14.27) and then from inside the boom near the apex. Unfortunately, due to the rapidly falling tide and exposed mudflat, no water-column data were obtained for the Corexit 9580 test.

FIGURE 14.25 Test site at Berkeley Marina showing the three treatment zones. *Source: Photo by L. Cotsapas.*

FIGURE 14.26 Sampling water just outside of boomed CytoSol-treatment area during pressure washing. The intake tubing for both the fluorometer and the filtration unit were clamped together at the end of the boat-hook deployed over the side of the skiff. *Source: Photo by Ken Wilson.*

The background water was very clean with few PAHs detected (Fig. 14.28). The control water-only wash showed slightly elevated PAHs both inside and outside the boom with dissolved- and particulate/oil-phase PAH levels 2–3 times higher than the background water sample but mostly below the laboratory reporting levels (sample-specific reporting limit (SSRL)) (Fig. 14.29). Outside the CytoSol containment boom, the dissolved-phase PAH increased by another factor of two (reaching levels 3–7 times above the background

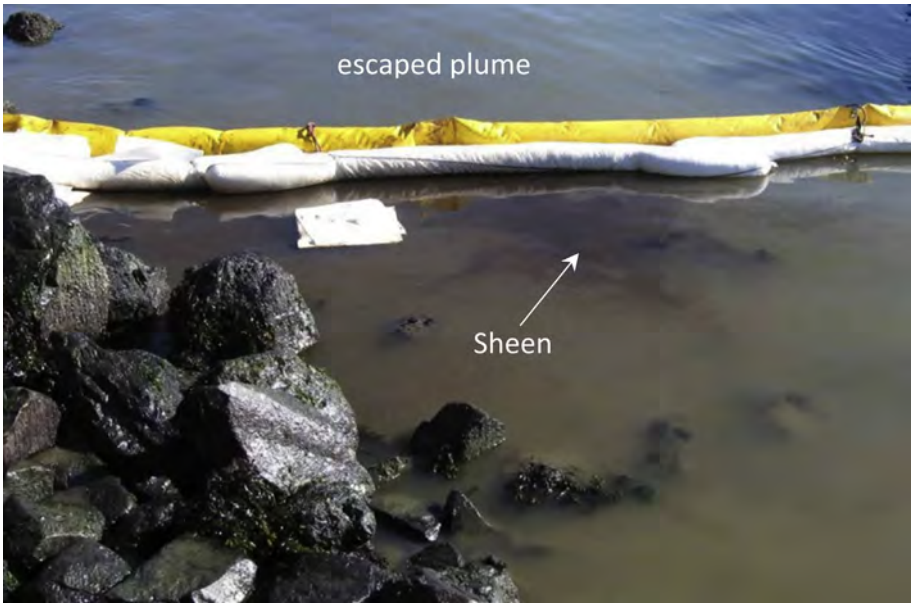

FIGURE 14.27 Free oil film and separate droplets in the CytoSol-treatment containment area during pressure wash and water deluge. Note the subsurface plume appeared both inside and outside of the boom. *Source: Photo by L. Cotsapas.*

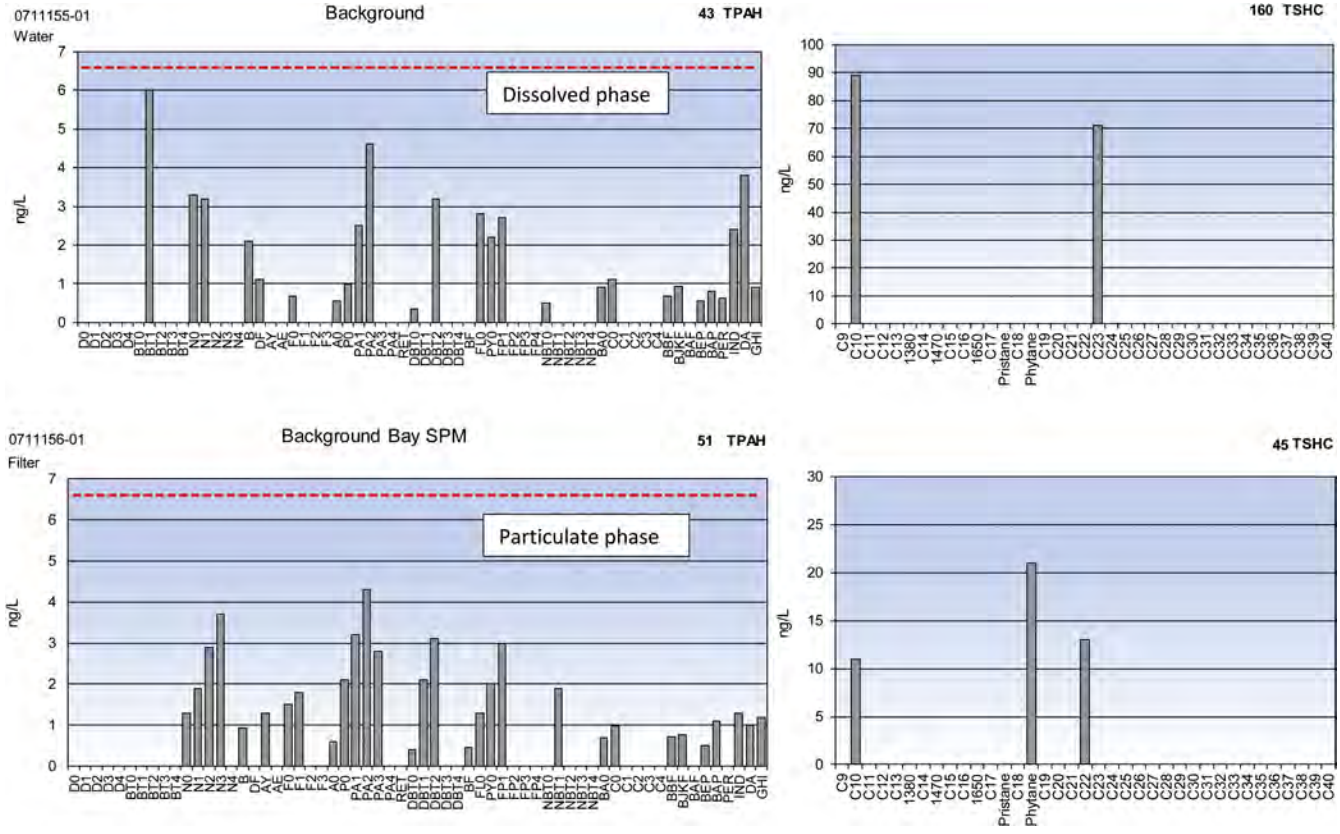

FIGURE 14.28 Background dissolved-phase and particulate/oil-phase PAH (left) and SHC (right) fractions obtained in open water 0.7 mi from the experimental site. The dashed horizontal line represents the sample-specific reporting limit (SSRL); off-scale for SHC. Components below the SSRL are considered as only trace-level concentrations.

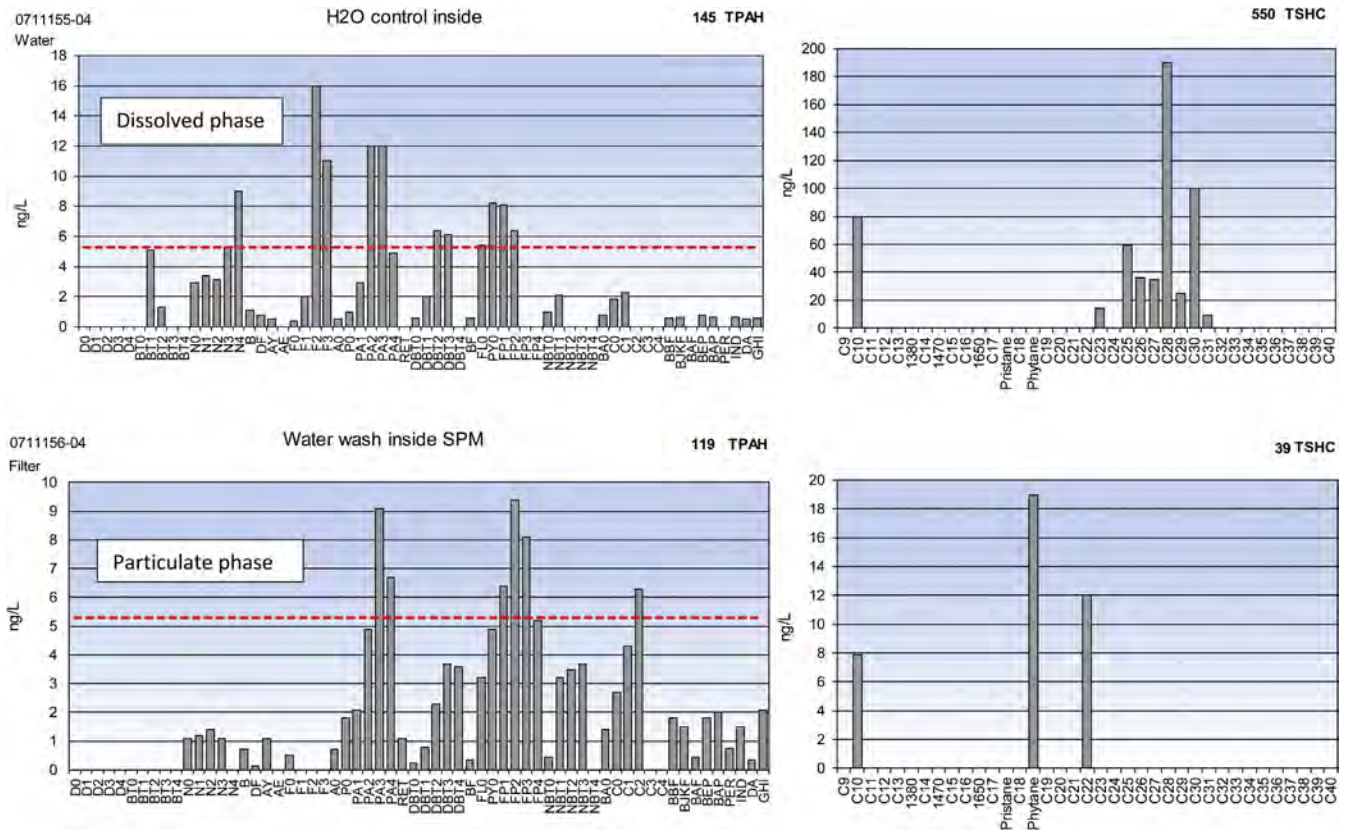

FIGURE 14.29 Dissolved-phase and particulate/oil-phase PAH and SHC fractions from inside the control, bay water-only wash, containment boom.

water levels; Fig. 14.30), while inside the boom, the dissolved-phase PAHs were almost 8 times above background levels (Fig. 14.31). The vast majority of the released CytoSol-treatment PAH was associated with oil/SPM agglomerates (Figs. 14.30 and 14.31). The particulate/oil phase TPAH level outside the eastern side of the CytoSol containment boom was 23 times higher than the pretest background levels. Carried by a slight westerly current, the particulate/oil-phase TPAH level outside the western boom edge was over 28 times higher than the east side and over 600 times higher than the particulate oil-phase levels in the open bay water.

Inside the CytoSol boom, the particulate/oil-phase TPAH level was another factor of 2 higher than outside the boom (on the higher west side), and over 1,300 times higher than the reference background. Total SHC) on the particulate/oil-phase CytoSol-treated samples followed similar trends.

These data document that sediment-bound oil was liberated from the shoreline washing operation (particularly with more effective shoreline-washing agents) and that booms placed against the shoreline were not capable of containing all the dissolved and particulate-phase oil and sedimentary material released during shoreline cleaning operations. But it was not possible to categorically state how much entrained oil/SPM (or free oil-phase droplets) might be expected to escape the booms in actual applications. It is clear that some form of boom-configuration/wash-volume/flow/dilution-factor calculations based on threshold effects values would be appropriate to better inform regulators and response personnel about what concentrations might be expected at different locations around shoreline cleaning operations and what effects might be projected onto exposed biological communities.

A similar release of dissolved- and particulate-phase oil was measured downstream of high-pressure shoreline washing operations in the lower Mississippi River main river channel following the *Westchester* spill in late November 2000 (Payne et al., unpublished data). Dissolved- and particulate-phase TPAH concentrations ranged from 17,000 to 28,000 and 43,000 to 60,000 ng/L, respectively, 20–40 m immediately down river from the spraying operations.

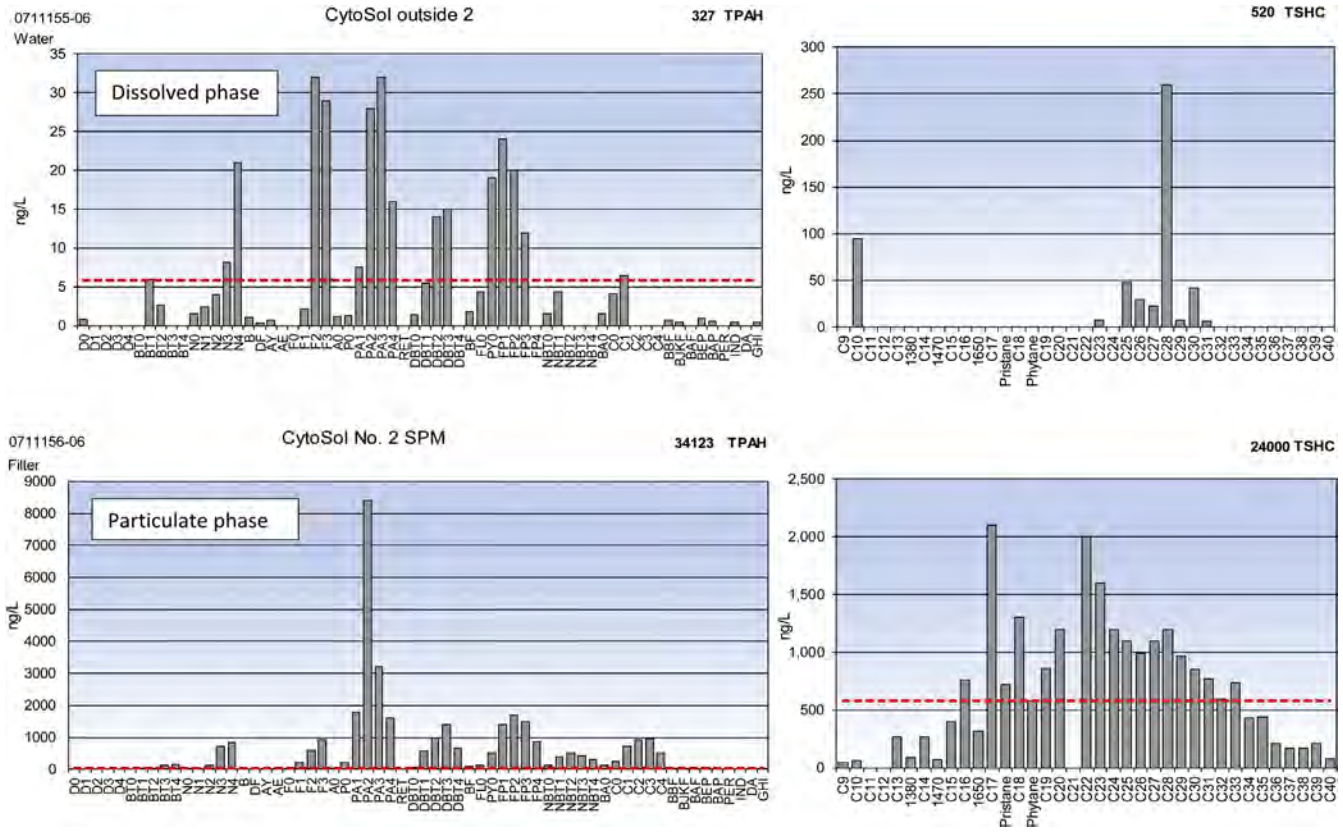

FIGURE 14.30 Dissolved-phase and particulate/oil-phase PAH and SHC fractions from outside the west side of the CytoSol-wash containment boom.

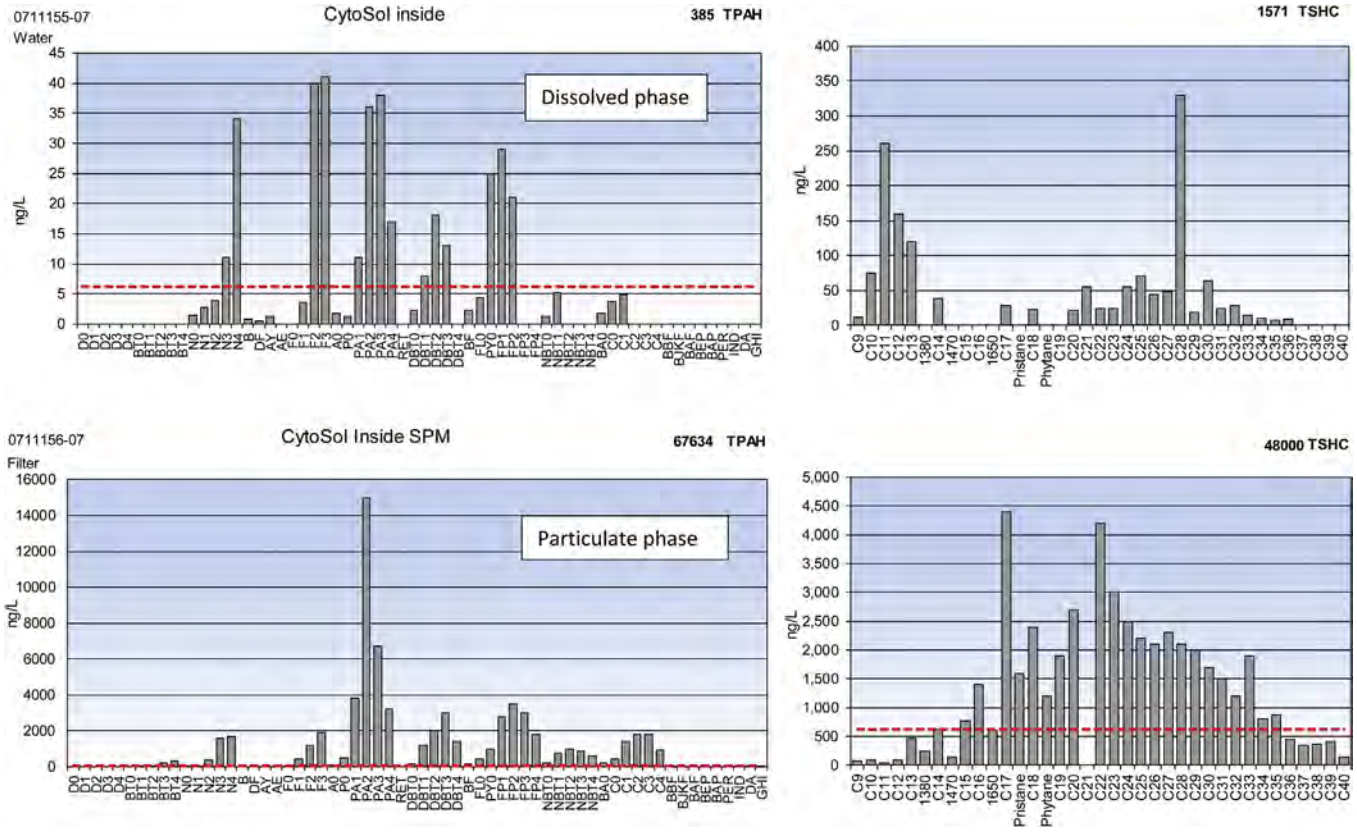

FIGURE 14.31 Dissolved-phase and particulate/oil-phase PAH and SHC fractions from inside the CytoSol-wash containment boom.

14.4.7 DWH Oil Spill

And most recently, there was the 2010 DWH blowout, a ruptured well at 1,500 m depth in north-central Gulf of Mexico that while spewing gas and oil for 87 days, had oil droplets continuously rising to the surface while shedding trails of dissolved components (Camilli et al., 2010; Reddy et al., 2011). Surface slicks were driven north toward coastal landfalls while above the wellhead, an entrapped plume of microdroplets developed at ~1,000 m (Socolofsky et al., 2011; Spaulding et al., 2015) and eventually transported dissolved- and particulate-phase oil 300–400 km to the southwest (Kujawinski et al., 2011; Payne and Driskell, 2015b,c, 2016). Further complicating the initial event, water parcels at depth containing dissolved constituents and slower rising, smaller oil droplets were swept back and forth across the basin (Valentine et al., 2012). If/When an earlier oiled water parcel recrossed the blowout and rising oil droplets at depth, the water could acquire an extra dose of dissolved components from these later ascending droplets and create an even more complex mixture.

For DWH water sample forensics, the *Cosco Busan* mixing-model approach was adopted with two major differences. First, rather than statistically weathering the source oil for sample matchings, a representative series of weathered particulate-oil profiles assembled from field samples was used for the comparative reference oil(s) (Payne and Driskell, 2015c, 2016). While losing the *Cosco Busan*-style continuously adjustable reference, using actual DWH field samples gave us a set of empirically validated profiles and diagnostic ratios. The reference-series samples were collected at depth during the release event and in the vicinity of the wellhead (2–8 km), filtered aboard the cruise vessel, and later confirmed as MC252 oil based upon biomarker fingerprinting (Fig. 14.32). This filtered-particulate reference series reflected the sequential patterns and relative rates of dissolution losses in the water column as the larger droplets rose from the wellhead to the surface or as the entrapped microdroplets advected within the deep plume.

Also, different from simply parsing the *Cosco Busan* mixtures, the circumstances of the DWH spill permitted using the mixing-model for more than sample matching. With the forensic task constrained to just the NRDA water samples, most of which were only exposed to simplified weathering factors (dissolution and biodegradation, i.e., no evaporation or photooxidation occurred at depth), it became possible to use the reference patterns and ratios to discriminate phase portions in the 1-L *unfiltered* whole-water samples (most of the collections) (briefly detailed below). Elucidating the extra details of phase state and weathering suggested patterns and trends that subsequently gave insights to confirm source matching, elucidate weathering trends, define the plume track, and reveal dispersant effects (Payne and Driskell, 2015b,c,d, 2016). Also note that this forensic task was not intended to directly establish impacts from the reported concentrations, phase partitioning, and distributions. Rather, by design, the results and interpretations were intended to inform and confirm the NRDA modeling efforts (French McCay et al., 2015a,b, 2016). Despite other publications using the samples to propose or document background and exposure averages for the event and the region (Wade et al., 2016, Boehm et al., 2016), the bias incurred from the ad hoc exploratory sampling design was not amenable to statistical inference.

As with the *Cosco Busan*, for DWH offshore waters, additional lines of forensic evidence used in confirming a profile match might include the presence of dispersant indicators, BTEX volatiles, depth, location, and date of the sample collection. For the entrained deep oil plume, unique features in CTD, DO, and fluorometry sensor data provided strong corroborating evidence. Specifically, in the field, a fluorescence spike and DO sag at approximately 1000–1300 m meant the sampler had found the plume. Thus, the typical workflow and hierarchy for evaluating each sample became:

1. PAH weathering patterns and diagnostics (e.g., dibenzothiophene/phenanthrene ratios, hopane/TPAH ratio matching);
2. biomarker patterns (if available) and diagnostic ratios;
3. dispersant indicators;
4. CTD, DO and fluorometry signals;
5. volatiles (BTEX only);
6. SHC patterns;
7. sampling date and proximity to wellhead; and
8. nearby sample trends and patterns

Our primary forensic approach, pattern recognition and parsing of the signatures, relied heavily on graphic displays to compare samples to reference sources and highlight any anomalies. Retooling the *Cosco Busan* approach to visualize and assimilate the multiple lines of evidence, a proprietary Excel dashboard utility brought together, for two samples, all relevant data in a single display of multiple graphics, maps, and diagnostic values,

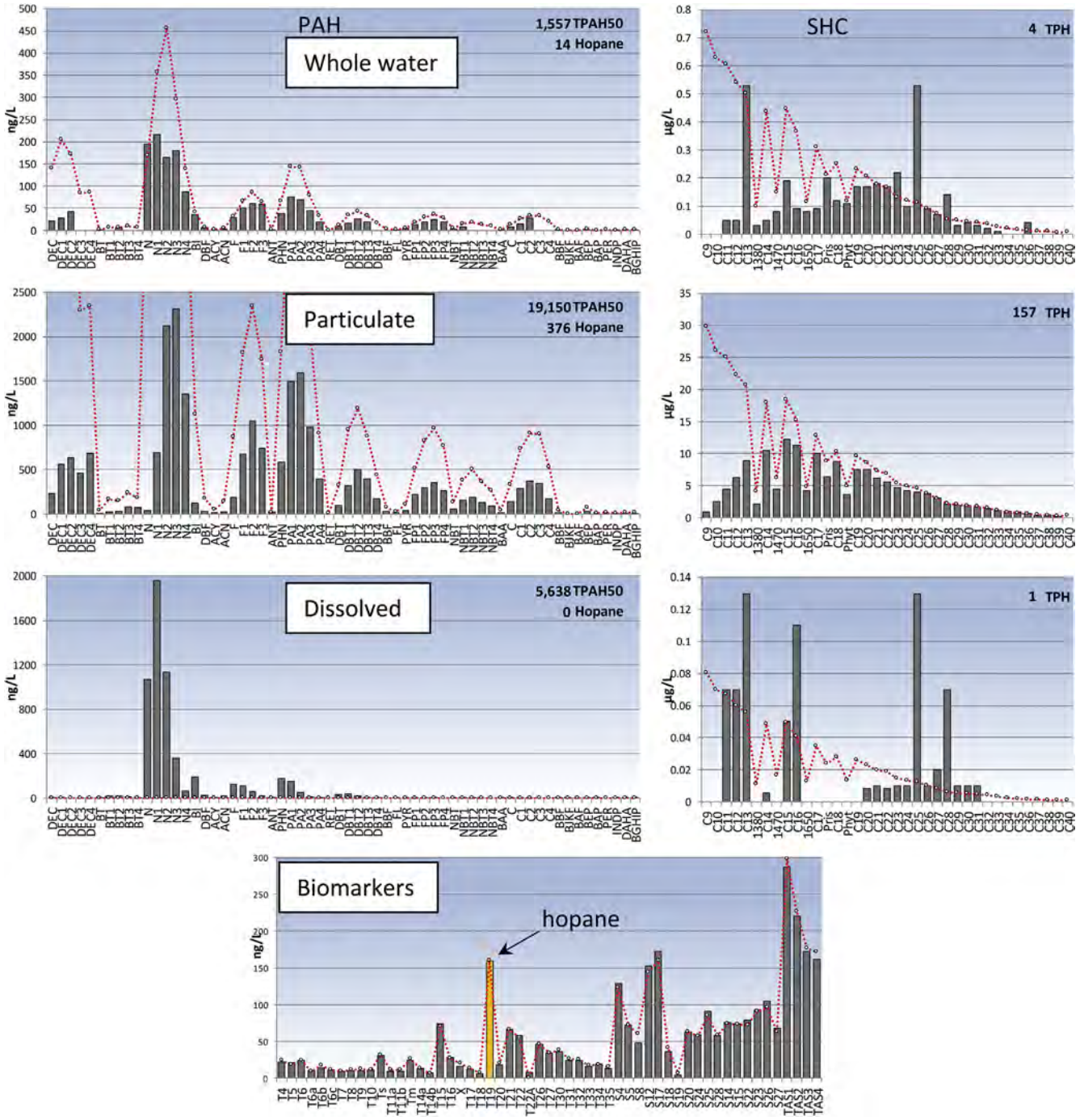

FIGURE 14.32 Example of PAH and SHC from 1 L whole water, and a 3.5-L particulate-filter fraction and dissolved (i.e., filtered) fraction from a single water grab June 16, 2010, 252 ft (77 m) depth. Biomarkers from particulate fraction in separate sample. Dotted line represents fresh MC252 oil scaled to the sample's C2-chrysene (none in dissolved fraction). Whole-water sample was subsampled from the GoFlo bottle prior to the filtered/dissolved sample aliquot. Adapted from Payne and Driskell (2016), reproduced with permission from Elsevier/Academic Press.

superimposed with a comparatively scaled reference oil sample. These data were retrieved as needed from a data table within the application, diagnostic ratios calculated, and results plotted in the interactive displays. The method and examples are presented elsewhere in Payne and Driskell (2015b,c, 2016).

After parsing oiled water samples into their dissolved and particulate phase portions, essentially four phase categories of MC252 contamination were revealed: (1) samples with either particulate only, (2) dissolved only, (3) particulate plus dissolved, or (4) particulate with extra dissolved (the latter in Fig. 14.33). From the parsed particulate portion, two additional checks could be made confirming a MC252 source match. First, the amount of expected hopane in the scaled weathered particulate reference should be similar to the hopane in the sample. Second, the traditional alkylated-dibenzothiophenes/alkylated-phenanthrenes ratios (plotted as DBT2/P2 vs DBT3/P3) should be similar to the weathered reference. These double-ratio plots were insightful as to state of weathering due to slightly different trends in losses of DBTs vs Ps. But more importantly, they also provided the first documentation of effects of dispersant on the PAH profile (e.g., accelerated dissolution discussed below). It should be noted that normally an ample list of diagnostic biomarker ratios would also be consulted but for much of the NRDA water data, the laboratory's GC/MS had scanned for biomarkers but did not quantify the data. However, if needed to confirm an equivocal sample, the biomarker extraction ion profiles (m/z 191, 217, etc.) could be reexamined and compared to MC252 oil to aid in the sample's classification.

In samples containing both dissolved- and particulate-phase mixtures, the dissolved phase was generally attributed to the companion particulate source. But what of matching a dissolved-phase-only sample where none of the usual diagnostics are germane, i.e., no biomarkers available (insoluble) and dissolved patterns from any petrogenic source are all similar in appearance? Fortunately, in most offshore ocean environments, background oil contaminants are quite low, thus, tilting the odds toward forensic resolution. And excepting the particulate-only-characteristic items 1, 2, 4, and 6 in the multiple lines of evidence listed above, there was plenty of secondary evidence to suggest a logical and defensible classification.

Because unprecedented, copious amounts of dispersant were used during the DWH event, the presence of dispersants, particularly offshore, also became a solid line of evidence. Recall that the NRDA data set only reported dispersant indicators, namely, the glycol ethers and bis(2-ethylhexyl)fumerate (the GC injection port DOSS breakdown product) and not the actual surfactant measured by other investigators (a GC/MS limitation).

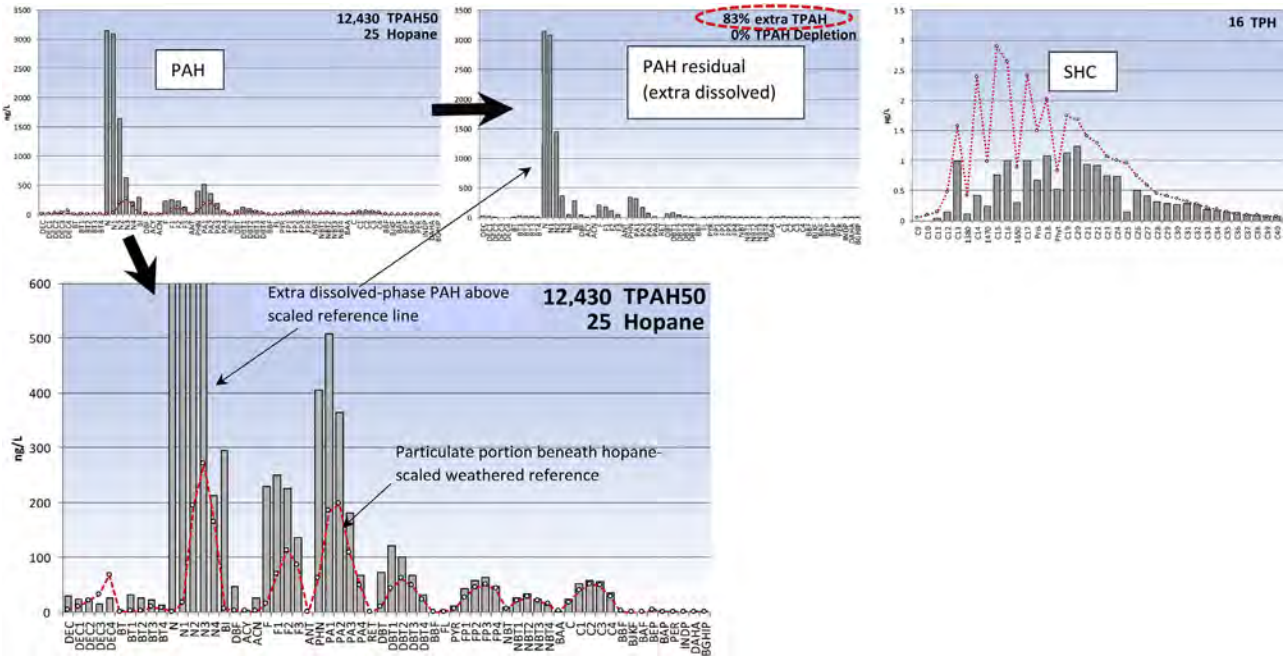

FIGURE 14.33 Example of extra dissolved on particulate PAH. Left upper plot, full PAH profile with weathered series Reference 3 overlaid; center, the 83% extra dissolved residual profile after hopane-based parsing; right, weathered SHC from the particulate portion. Presence of hopane and SHC precludes this being a purely dissolved-phase sample. Lower plot zoomed in to show weathered particulate portion beneath dotted reference line, here using weathered reference 3 scaled to hopane where expected reference hopane (defined by scaling) was 25 ng/L vs reported 25 ng/L in sample, i.e., confirmation by pattern matching and hopane mass balance.

Using dispersants at depth, directly injecting it into the escaping plume (~771 kgal), provided a novel tracer for the deep plume in its extended drift along the shelf slope. Earlier, Payne and Beegle-Krause (2011) documented the presence of dispersant indicators within the subsurface plume, but from available NRDA data at that time, it wasn't clear if the dispersants were actually present in the oil phase or if the dispersant was simply being entrained and laterally transported as a water-soluble product with the subsurface plume. It wasn't until the dispersant was actually measured in the filtered oil phase at depth (a first in field data) that showed some portion of dispersants were retained on oil droplets rather than completely diffusing back into the water column. As described in Payne and Driskell (2015d) and Driskell and Payne (in submission), these observations confirmed the functional effectiveness of dispersant injections at depth. Kujawinski et al. (2011) concluded from their own data that DOSS was selectively associated with the oil and gas phases in the deepwater plume. They also reported that 64 days after stoppage of dispersant application (following 61 days of usage), DOSS was found 300 km SW from the wellhead vs NRDA's record of 412 km in 44 days post for dispersant glycol ethers. These findings support the concept that dispersants underwent negligible, or slow, rates of biodegradation in the affected waters. Both studies emphasize the importance of these findings to responders, modelers, and toxicologists.

Another finding came from NRDA water samples containing high levels of dispersant indicators; there was a noticeable anomaly in the oil dissolution patterns, the more soluble PAH were being removed at an accelerated rate, even faster and different than natural oil degradation processes (Payne and Driskell, 2015d; Driskell and Payne, in submission). Conceptually, on an oil droplet, as the dispersant weakens the surface tension, a streaming eruption of oil occurs eventually to reform into smaller droplets (Katz, 2009; Gopalan and Katz, 2010; Murphy et al., 2015; Katz et al., 2013; Li et al., 2013; Nagamine, 2014). During this transition stage, the more soluble PAH components (lesser alkylated homologs) quickly dissolve before the surface area diminishes into the newly forming smaller droplets. We found there are several pattern characteristics and some diagnostic ratios to indicate dispersant-mediation effects but perhaps the most dramatic is the D/P double-ratio plot (Fig. 14.34). Due to an accelerated loss of C2-phenanthrene relative to the other three components in the ratios, the dispersant-mediated samples trend very sharply to the right in comparison to the more vertical trend of normally weathered samples. Enhanced dissolution of water-soluble PAH with dispersant treatment had been hypothesized (NAS, 2005) but had not observed in field data. This previously undocumented effect, again, has relevance to forensic chemists, spill modelers, and toxicologists.

With increasing time and distance from the wellhead event, relevant profiles of both the SHC and PAH eventually disappeared in the entrapped deep plume samples, albeit occasionally with some fresher dissolved signals presumably from unknown background sources. Normally, these negative observations would have defined the outer influence of the spill—no discernible impacts beyond the region of particulate PAH profiles. But because of the deep plume's nature as a coherent water mass upwardly entrapped by a deep pycnocline amidst the Gulf's nearly pristine background, further insights into the oil's transport were

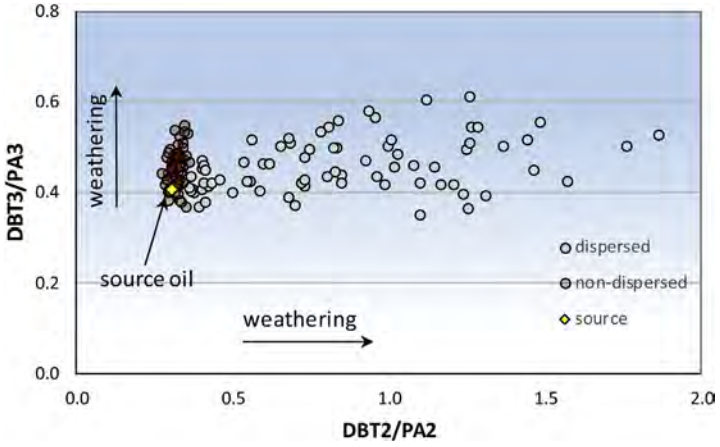

FIGURE 14.34 Comparison of dispersed vs nondispersed DWH water samples in double-ratio weathering plot of C2- and C3-alkylated dibenzothiophenes (DBT) and phenanthrene/anthracenes (PA). Lateral spread in dispersed samples is attributed primarily to accelerated loss of C2-phenanthrenes. Data are from filters and whole waters with only particulate profiles (whole oil only, no dissolved components) from the DWH NRDA data set.

revealed. While particulate oil was collected at ~1,000 m depth out to 155 km SW from the wellhead, dissolved-oil profiles in the plume attributed to MC252 were matched out to 267 km (Fig. 14.35). At the trackable distal reaches of the deep plume, 412 km SW from the wellhead, NRDA samples showed a trace of dissolved PAH that was not necessarily attributable to MC252 but with a fluorescent spike, DO sag, and dispersant indicators (GE) persisting at the appropriate plume depth (Figs. 14.36 and 14.37). These secondary

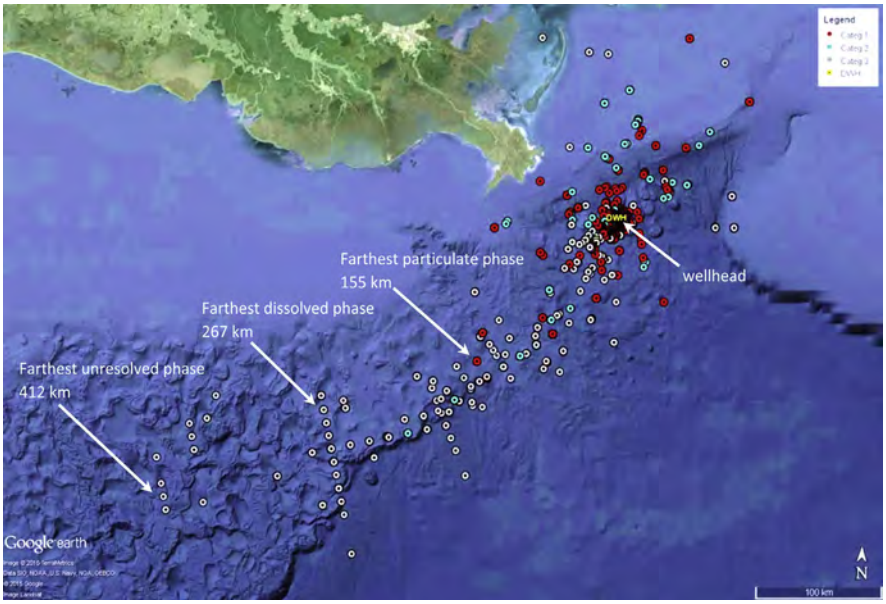

FIGURE 14.35 Distribution of offshore water samples matching MC252 source oil. Matched particulate, dissolved, and unresolved phase samples range to 155, 267, and 412 km from wellhead, respectively. Each location may have multiple depths with overlapping symbols. $n = 1766$ matches.

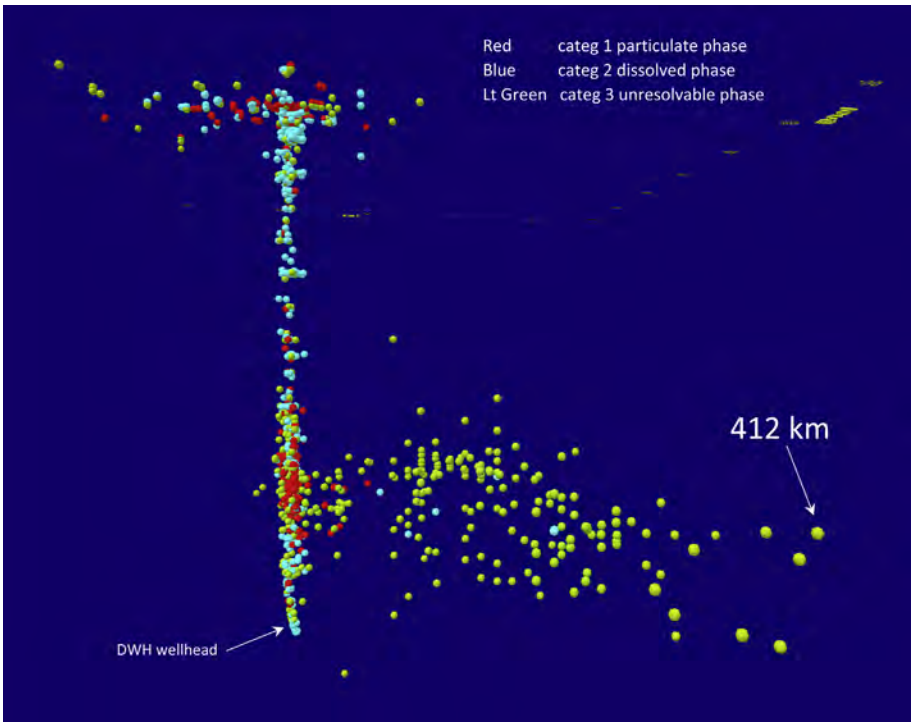

FIGURE 14.36 MC252 matched samples in 3D spatial view at 1,000 m plume depth looking east from beyond plume's SW distal end.

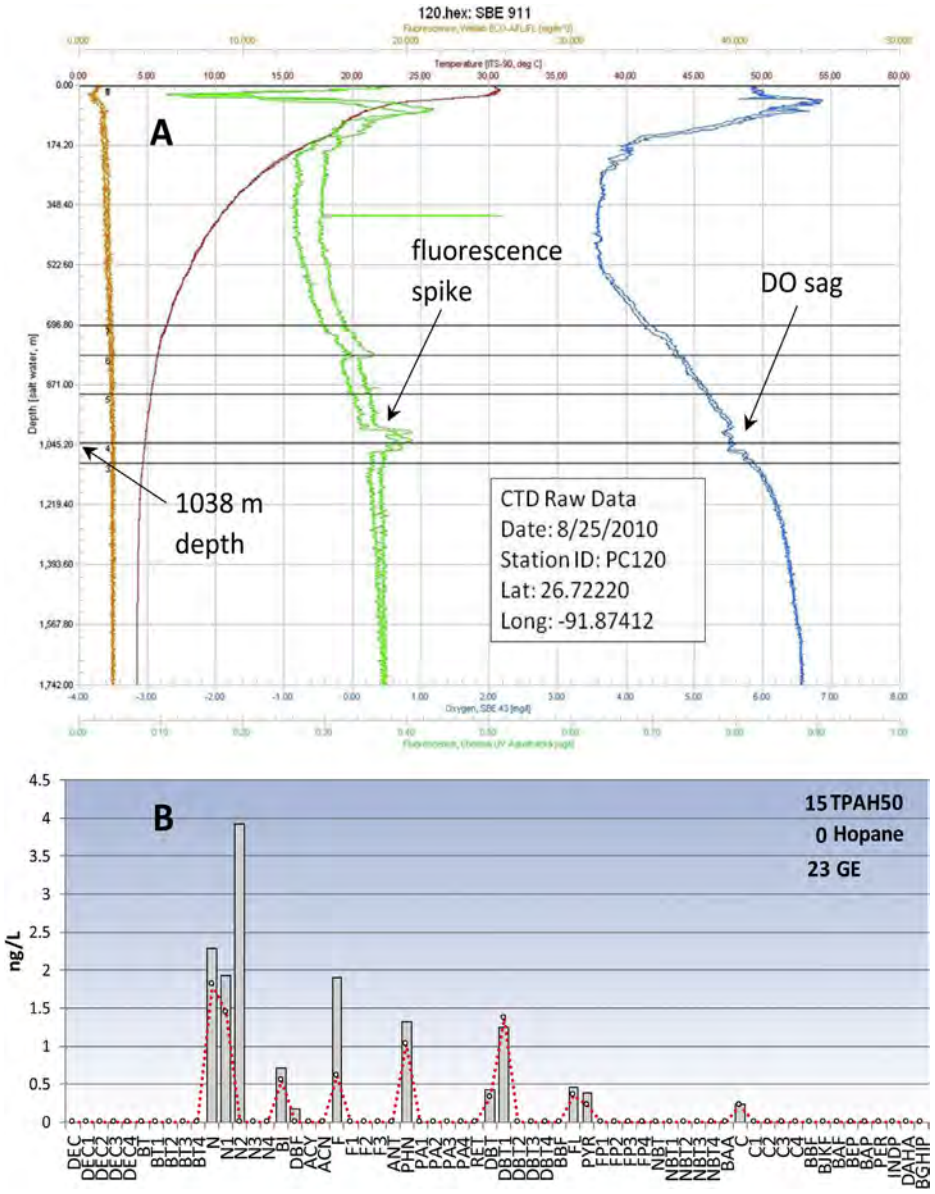

FIGURE 14.37 Instrument profile of most distant forensically matched sample (412 km SW from wellhead) showing (A) fluorescence spike and DO sag at 1,038 m while (B) TPAH was 15 ng/L as an inconsequential dissolved signal mostly negated by lab method blank (dotted line overlay). Dispersant glycol ethers (GE) were 23 ng/L. These confirming indicators suggest that the plume was still extant but, based on other studies, that the hydrocarbons had been transformed into polar heterocyclics not amenable to traditional GC/MS detection.

data suggest that even without a relevant residual PAH profile, the plume was extant (Fig. 14.36). Mentioned above, Kujawinski et al. (2011) came to a similar conclusion after finding dispersant DOSS at plume depth 300 km from the wellhead.

While deep-plume NRDA water samples have not yet been analyzed by methods capable of resolving the polar components resulting from microbial degradation, the obvious expectation is that results would show oxygenated hydrocarbons becoming more prevalent as the oil's hydrocarbons were degraded, i.e., become more polar and less resolvable by GC/MS. We interpret the fluorescent spike and DO sag still present 412 km from the wellhead with no relevant diagnostic PAH (Fig. 14.36) to suggest the presence of oxidized microbial-degraded hydrocarbons. But until samples can be analyzed using an appropriate method such as thin layer chromatography/flame ionization detection (TLC FID; Aeppli et al., 2012), Fourier Transform Ion Cyclotron Resonance Mass Spectrometry (McKenna et al., 2013), Orbitrap Q Exactive Mass Spectrometry (Huba and

Gardinali, 2016), or a similar instrument capable of detecting these compounds, the oxygenated or other transformed heteroatomic hydrocarbons in the far reaches of the plume are mostly undocumented.

14.5 CONCLUSIONS

While slicks and sheens are certainly the most visible form of oil-and-water mixtures at release events, they do not tell the entire story. Also germane to developing the event's scenario of oil fate, transport, and exposure are the entrained oil droplets and dissolved-phase components within the water. The case studies in this chapter highlight the relevance and utility of analyzing oil-contaminated water whereby the analyte profiles' details subtly reveal differential impacts based on a species' feeding mode, the pervasive presence of dissolved phase contaminants without visible oiling, seepage from shoreline oiling, stratification controlling seasonal availability of droplets, the nonavailability of PAH from a source rock matrix, contaminants escaping from shoreline containment booms, deep-ocean plume tracking, and chemical dispersant effects on dissolution behavior and droplet profiles. Some of these revelations were obvious from just the sample profiles, others required sample processing by field-filtering the sample to discriminate the two phases. And finally, mixing-model methods were presented to demonstrate how to discriminate spill-oil-impacted water from the confounded background and how to parse phase portions from an unfiltered whole water sample. The traditional alternative is to present a table of phase-lumped TPAH values and ignore the insights described herein.

Acknowledgments

Funding for the NRDA studies was provided by the National Oceanic and Atmospheric Administration (NOAA) through subcontracts with Industrial Economics, Inc. (IEc). *Cosco Busan* studies were supported by NOAA/IEc and California Department of Fish and Game—Office of Oil Spill Prevention and Response. Studies of the *Exxon Valdez* Oil Spill (EVOS) were supported directly by NOAA and the EVOS Trustees Council. Prince William Sound Regional Citizens' Advisory Council funded the Port Valdez and the Long-Term Environmental Monitoring Program studies. Data analysis of Alaska EMAP sediment samples was supported by the Cook Inlet Regional Citizens Advisory Council. The findings and conclusions expressed herein are those of the authors and do not necessarily reflect the views of the funding groups or spill trustees.

References

Aeppli, C., Carmichael, C.A., Nelson, R.K., Lemkau, K.L., Graham, W.M., Redmond, M.C., et al., 2012. Oil weathering after the *Deepwater Horizon* disaster led to the formation of oxygenated residues. Environ. Sci. Technol. 46, 8799–8807.

Analytical Quality Assurance Plan (AQAP), 2014. Mississippi Canyon 252 (*Deepwater Horizon*) Natural Resource Damage Assessment, Version 4.0; U.S. Department of Commerce/National Oceanic and Atmospheric Administration, 41 p.

Baumard, P., Budzinski, H., Garrigues, P., Dizer, H., Hansen, P.D., 1999a. Polycyclic aromatic hydrocarbon (PAH) in recent sediment and mussels (*Mytilus edulis*) from the Western Baltic Sea: occurrence, bioavailability and seasonal variations. Mar. Environ. Res. 47, 17–47.

Baumard, P., Budzinski, H., Garrigues, P., Burgeot, T., Michel, X., Bellocq, J., 1999b. Polycyclic aromatic hydrocarbon (PAH) burden of mussels (*Mytilus* sp.) in different marine environments in relation with sediment PAH contamination, and bioavailability. Mar. Environ. Res. 47, 415–439.

Boehm, P.D., Murray, K.J., Cook, L.L., 2016. Distribution and attenuation of polycyclic aromatic hydrocarbons in Gulf of Mexico seawater from the *Deepwater Horizon* oil accident. Environ. Sci. Technol. 50 (2), 584–592.

Brown, E.D., Baker, T.T., Hose, J.E., Kocan, R.M., Marty, G.D., McGurk, M.D., et al., 1996. Injury to the early life history stages of Pacific Herring in Prince William Sound after the *Exxon Valdez* oil spill. Am. Fish. Soc. Symp. 18, 448–462.

Camilli, R., Reddy, C.M., Yoerger, D.R., VanMooy, B.A.S., Jakuba, M.V., Linsey, J.C., et al., 2010. Tracking hydrocarbon plume transport and biodegradation at the *Deepwater Horizon*. Science 330, 201–204.

Carls, M.G., Short, J.W., Payne, J.R., 2006. Accumulation of polycyclic aromatic hydrocarbons by *Neocalanus* copepods in Port Valdez, Alaska. Mar. Pollut. Bull. 52, 1480–1489.

de Lappe, B.W., Risebrough, R.W., Clayton, Jr., J.R., Millikin, P.L., Okazaki, R.K., Parkin, J.S., et al., 1978. Development of methodologies for the *in situ* extraction of petroleum compounds from seawater. Southern California Baseline Study, Vol. III, Report 3.2.4. Final Report to the Bureau of Land Management. Washington, DC by the Bodega Marine Laboratory, University of California, Bodega Bay, CA and Science Applications, Inc., La Jolla, CA, 164 p.

de Lappe, B.W., Risebrough, R.W., Springer, A.M., Schmidt, T.T., Shropshire, J.C., Letterman, E.F., et al., 1980. The sampling and measurement of hydrocarbons in natural waters. In: Afghan, B.K., Mackay, D. (Eds.), Hydrocarbons and Halogenated Hydrocarbons in the Aquatic Environment. Plenum Press, New York, NY, pp. 29–69.

de Lappe, B.W., Risebrough, R.W., Walker II, W., 1983. A large-volume sampling assembly for the determination of synthetic organic and petroleum compounds in the dissolved and particulate phases of seawater. Can. J. Fish. Aquat. Sci. 40 (2), 322–336.

Douglas, G.S., Stout, S.A., Uhler, A.D., McCarthy, K.J., Emsbo-Mattingly, S.D., 2016. Advantages of quantitative chemical fingerprinting in oil spill source identification. In: Stout, S.A., Wang, Z. (Eds.), Standard Handbook. Oil Spill Environmental Forensics: Fingerprinting and Source Identification, second ed. Elsevier/Academic Press, Boston, MA, pp. 789–847.

Driskell, W.B., Payne, J.R., 2015. Forensic assessment of 2010 DWH nearshore water samples. U.S. Dept. of Interior, *Deepwater Horizon* Response & Restoration, Admin. Record, DWH-AR0039223, DWH NRDA Chemistry Technical Working Group Report, 32 p. <www.doi.gov/deepwaterhorizon/adminrecord>.

Driskell, W.B., Payne, J.R., Douglas, G.S., 2010. Forensic fingerprinting of *Cosco Busan* samples containing mixed-oil sources (Platform 164). In: Soc. Environ. Toxicol. Chem. (SETAC), 31st Annual Meeting, Portland, Oregon, November 7–11, 2010.

French McCay, D.P., Rowe, J., Balouskus, R., Morandi, A., McManus, M.C., 2015a. WC-TR.28: injury quantification for planktonic fish and invertebrates in estuarine, shelf and offshore waters. U.S. Dept. of Interior, *Deepwater Horizon* Response & Restoration, Admin. Record, DWH-AR0172019, 41 p. <www.doi.gov/deepwaterhorizon/adminrecord>.

French McCay, D.P., Jayko, K., Li, Z., Horn, M., Kim, Y., Isaji, T., et al., 2015b. WC_TR.14: modeling oil fate and exposure concentrations in the deepwater plume and rising oil resulting from the *Deepwater Horizon* oil spill. U.S. Dept. of Interior, *Deepwater Horizon* Response & Restoration, Admin. Record. RPS ASA, South Kingstown, RI. <www.doi.gov/deepwaterhorizon/adminrecord>.

French McCay, D., Horn, M., Li, Z., Crowley, D., Spaulding, M., Mendelsohn, D., et al., 2016. Simulation modeling of ocean circulation and oil spills in the Gulf of Mexico—appendix VI data collection, analysis and model validation. Prepared by RPS ASA for the US Department of the Interior, Bureau of Ocean Energy Management, Gulf of Mexico OCS Region, New Orleans, LA.

Gopalan, B., Katz, J., 2010. Turbulent shearing of crude oil mixed with dispersants generates long microthreads and microdroplets. Phys. Rev. Lett. 104, 054501, 4 pp.

Gray, J.L., Kanagy, L.K., Furlong, E.T., McCoy, J.W., Kanagy, C.J., 2011. Determination of the anionic surfactant di(ethylhexyl)sodium sulfosuccinate in water samples collected from Gulf of Mexico coastal waters before and after landfall of oil from the *Deepwater Horizon* oil spill, May to October, 2010. U.S. Geological Survey Open-File Report 2010-1318, 15 p. <www.pubs.usgs.gov/of/2010/1318>.

Henry, C.B., Roberts, P.O., 2001. Background fluorescence values and matrix effects observed using SMART protocols in the Atlantic Ocean and Gulf of Mexico. Proceedings of the 2001 Oil Spill Conference. American Petroleum Institute, Washington, DC, pp. 1203–1207.

Henry, C.B., Roberts, P.O., Overton, E.B., 1999. A primer on *in situ* fluorometry to monitor dispersed oil. Proceedings of the 1999 Oil Spill Conference. American Petroleum Institute, Washington, DC, pp. 225–228.

Huba, A.K., Gardinali, P.R., 2016. Characterization of a crude oil weathering series by ultrahigh-resolution mass spectrometry using multiple ionization modes. Sci. Total. Environ. 563–564, 600–610.

Katz, J., 2009. Measurements and modeling of size distributions, settling, and dispersions (turbulent diffusion) rates. Final Report Prepared for the Coastal Response Research Center, 31 pp.

Katz, J., Murphy, D.W., Morra, D., 2013. Large scale behavior and droplet size distributions in crude oil jets and plumes. In: 66th Annual Meeting of the Division of Fluid Dynamics. American Physical Society, Pittsburgh, PA, November 24–26, 2013.

Kujawinski, E.B., Soule, M.C.K., Valentine, D.L., Boysen, A.K., Longnecker, K., Redmond, M.C., 2011. Fate of dispersants associated with the *Deepwater Horizon* oil spill. Environ. Sci. Technol. 45 (5), 1298–1306.

Li, C., Hosler, A., Katz, J., 2013. Breakup of an oil slick mixed with dispersant by breaking wave. In: 66th Annual Meeting of the Division of Fluid Dynamics. American Physical Society, Pittsburgh, PA, November 24–26, 2013.

McKenna, A.M., Nelson, R.K., Reddy, C.M., Savory, J.J., Kaiser, N.K., Fitzsimmons, J.E., et al., 2013. Expansion of the analytical window for oil spill characterization by ultrahigh resolution mass spectrometry: beyond gas chromatography. Environ. Sci. Technol. 47 (13), 7530–7539. Available from: http://dx.doi.org/10.1021/es305284t.

Murphy, D.W., Li, C., d'Albignac, V., Morra, D., Katz, J., 2015. Splash behaviour and oily marine aerosol production by raindrops impacting oil slicks. J. Fluid. Mech. 780, 536–577.

Nagamine, S.I., May 2014. The effects of chemical dispersants on buoyant oil droplets. Master's Thesis, University of Hawaii at Manoa, 122 p.

National Research Council (NRC), 2005. Oil Spill Dispersants: Efficacy and Effects. National Academy Press, Washington, DC, 377 p.

Payne, J.R., 1997. Fabrication of a portable large-volume seawater sampling system to support NRDA oil spill efforts: a needs assessment and background paper. Prepared for Industrial Economics, Incorporated and NOAA Damage Assessment Center, Rapid Assessment Program. NOAA Contract No. 50-DSNC-7-90032, 57 p.

Payne, J.R., Beegle-Krause, C.J., 2011. Physical transport and chemical behavior of dispersed oil. In: White Paper Commissioned for the CRRC Workshop: The Future of Dispersant Use in Spill Response. September 20–22, 2011. NOAA Disaster Response Center, Mobile, AL, 26 p. <http://www.crrc.unh.edu/workshops/dispersant_future_11/Dispersant_Initiative_FINALREPORT.pdf>.

Payne, J.R., Driskell, W.B., 2001. Source characterization and identification of *New Carissa* oil in NRDA environmental samples using a combined statistical and fingerprinting approach. Proceedings of the 2001 Oil Spill Conference. American Petroleum Institute, Washington, DC, pp. 1403–1409.

Payne, J.R., Driskell, W.B., 2003. The importance of distinguishing dissolved- versus oil-droplet phases in assessing the fate, transport, and toxic effects of marine oil pollution. Proceedings of the 2003 Oil Spill Conference. American Petroleum Institute, Washington, DC, pp. 771–778.

Payne, J.R., Driskell, W.B., 2015a. Offshore adaptive sampling strategies. U.S. Dept. of Interior, *Deepwater Horizon* Response & Restoration, Admin. Record. DWH-AR0023786; DWH NRDA Chemistry Technical Working Group Report, 75 p. <www.doi.gov/deepwaterhorizon/adminrecord>.

Payne, J.R., Driskell, W.B., 2015b. 2010 DWH offshore water column samples—forensic assessments and oil exposures. U.S. Dept. of Interior, *Deepwater Horizon* Response & Restoration, Admin. Record. DWH-AR0039118; DWH NRDA Chemistry Technical Working Group Report, 37 p. <www.doi.gov/deepwaterhorizon/adminrecord>.

Payne, J.R., Driskell, W.B., 2015c. Forensic fingerprinting methods and classification of *Deepwater Horizon* oil spill offshore water samples. U.S. Dept. of Interior, *Deepwater Horizon* Response & Restoration, Admin. Record. DWH-AR0039170; DWH NRDA Chemistry Technical Working Group Report, 31 p. <www.doi.gov/deepwaterhorizon/adminrecord>.

Payne, J.R., Driskell, W.B., 2015d. Dispersant effects on waterborne oil profiles and behavior during the *Deepwater Horizon* oil spill. U.S. Dept. of Interior, *Deepwater Horizon* Response & Restoration, Admin. Record. DWH-AR0039201; DWH NRDA Chemistry Technical Working Group Report, 22 p. <www.doi.gov/deepwaterhorizon/adminrecord>.

Payne, J.R., Driskell, W.B., 2016. Water column sampling for forensics. In: Stout, S., Wang, Z. (Eds.), Standard Handbook Oil Spill Environmental Forensics—Fingerprinting and Source Identification, second ed. Elsevier/Academic Press, Boston, MA, pp. 983–1014.

Payne, J.R., McNabb Jr., G.D., 1984. Weathering of petroleum in the marine environment. Mar. Technol. Soc. J. 18 (3), 24–42.

Payne, J.R., Kirstein, B.E., McNabb, Jr., G.D., Lambach, J.L., Redding, R., Jordan, R.E., et al., February 1984. Multivariate analysis of petroleum weathering in the marine environment—subarctic. Vol. I, Technical Results; vol. II, Appendices. Final Reports of Principal Investigators, vols. 21 and 22, U.S. Department of Commerce, National Oceanic and Atmospheric Administration, Ocean Assessment Division, Juneau, Alaska; 690 p. Vol. 21 NTIS Accession Number PB85-215796; vol. 22. NTIS Accession Number PB85-215739.

Payne, J.R., Reilly, T.J., French, D.P., 1999. Fabrication of a portable large-volume water sampling system to support oil spill NRDA efforts. Proceedings of the 1999 Oil Spill Conference. American Petroleum Institute, Washington, DC, pp. 1179–1184.

Payne, J.R., Driskell, W.B., Barron, M.G., Lees, D.C., 2001. Assessing transport and exposure pathways and potential petroleum toxicity to marine resources in Port Valdez, Alaska. Final Report Prepared for Prince William Sound Regional Citizens' Advisory Council Contract No. 956.02.1. Payne Environmental Consultants, Inc., Encinitas, CA, 64 pp. plus appendices.

Payne, J.R., Driskell, W.B., Short, J.W., 2003. 2002–2003 LTEMP Monitoring Report. Final Report Prepared for Prince William Sound Regional Citizens' Advisory Council, Anchorage, AK 99051. PWSRCAC Contract No. 951.03.1, prepared by Payne Environmental Consultants, Inc., Encinitas, CA, 107 p.

Payne, J.R., Driskell, W.B., Lindeberg, M.R., Fournier, W., Larsen, M.L., Short, J.W., et al., 2005a. Dissolved- and particulate-phase hydrocarbons in interstitial water from Prince William Sound beaches containing buried oil thirteen years after the *Exxon Valdez* oil spill. Final Report Prepared for the National Oceanic and Atmospheric Administration, National Marine Fisheries Service, Auke Bay, AK. Payne Environmental Consultants, Inc., Encinitas, CA.

Payne, J.R., Driskell, W.B., Lindeberg, M.R., Fournier, W., Larsen, M.L., Short, J.W., et al., 2005b. Dissolved- and particulate-phase hydrocarbons in interstitial water from Prince William Sound beaches containing buried oil thirteen years after the *Exxon Valdez* oil spill. Proceedings of the 2005 International Oil Spill Conference. American Petroleum Institute, Washington, DC, pp. 83–88.

Payne, J.R., Driskell, W.B., Short, J.W., 2005c. 2003–2004 LTEMP Monitoring Report. Final Report Prepared for the Prince William Sound Regional Citizens' Advisory Council, Anchorage, AK 99051. PWSRCAC Contract No. 951.04.1. Payne Environmental Consultants, Inc., Encinitas, CA, 123 p.

Payne, J.R., Driskell, W.B., Braddock, J.F., Bailey, J., 2005d. Hydrocarbon biodegradation in the Ballast Water Treatment Facility, Alyeska Marine Terminal. Final Report Prepared for the Prince William Sound Regional Citizens' Advisory Council, Anchorage, AK 99051. PWSRCAC Contract Numbers 558.04.01 and 560.2004.01. Payne Environmental Consultants, Inc., Encinitas, CA, 48 p.

Payne, J.R., Driskell, W.B., Braddock, J.F., Bailey, J., Short, J.W., Ka'aihue, L., et al., 2005e. From tankers to tissues—tracking the degradation and fate of oil discharges in Port Valdez, Alaska. In: Proceedings of Arctic Marine Oil Spill Conference 2005, Calgary, AB, Canada, pp. 959–991.

Payne, J.R., Wilson, K., Cotsapas, L., Kvam, B., Addassi, Y., Hebert, C., et al., 2008. Shoreline cleaning agent tests of stranded *Cosco Busan* oil contamination at the Berkeley Marina—November 20–23, 2007. Final Report Prepared for NOAA and CA OSPR, 61 p.

Payne, J.R., Driskell, W.B., Carls, M.G., Holland, L.G., 2016. Long-term environmental monitoring program—final report: 2015 sampling results and interpretations. Final Report Prepared for the Prince William Sound Regional Citizens' Advisory Council, Anchorage, AK 99051. PWSRCAC Contract Number 951.16.01. Payne Environmental Consultants, Inc., Encinitas, CA, 47 p.

Reddy, C.M., Arey, J.S., Seewald, J.S., Sylva, S.P., Lemkau, K.L., Nelson, R.K., et al., 2011. Composition and fate of gas and oil released to the water column during the *Deepwater Horizon* oil spill. Proc. Nat. Acad. Sci. 109 (50), 20229–20234, <www.pnas.org/cgi/doi/10.1073/pnas.1101242108>.

Salazar, M., Short, J.W., Salazar, S.M., Payne, J.R., 2002. 2001 Port Valdez Integrated Monitoring Report. Prince William Sound Regional Citizens' Advisory Council. Contract No. 633.01.1, 109 p. plus appendices.

Short, J.W., 2005. Seasonal variability of pristane in mussels (*Mytilus trossulus*) in Prince William Sound, Alaska. Ph.D. Thesis, Fisheries Biology, University of Alaska.

Socolofsky, S.A., Adams, E.E., Sherwood, C.R., 2011. Formation dynamics of subsurface hydrocarbon intrusions following the *Deepwater Horizon* blowout. Geophys. Res. Lett. 38, L09602.

Spaulding, M.S., Mendelsohnm, D., Crowley, D., Li, Z., Bird, A., 2015. Technical report for *Deepwater Horizon* water column injury assessment-WC_TR 13. Application of OILMAP DEEP to the *Deepwater Horizon* Blowout. RPS ASA, 55 Village Square Drive, South Kingstown, RI 02879.

Stout, S.A., 2015. Review of dispersants used in response to the *Deepwater Horizon* oil spill. NewFields Technical Report TR02 to the Trustees in Support of the PDARP, 21 p.

Stout, S.A., Wang, Z., 2007. Chemical fingerprinting of spilled or discharged petroleum—methods and factors affecting petroleum fingerprints in the environment. In: Wang, Z., Stout, S.A. (Eds.), Oil Spill Environmental Forensics—Fingerprinting and Source Identification. Academic Press, Burlington, MA, pp. 1–53.

Stout, S.A., Wang, Z., 2016. Chemical fingerprinting methods and factors affecting petroleum fingerprints in the environment. In: Stout, S.A., Wang, Z. (Eds.), Standard Handbook. Oil Spill Environmental Forensics: Fingerprinting and Source Identification, second ed Elsevier/Academic Press, Boston, MA, pp. 61–129.

US Coast Guard (USCG), 2001. National Oceanic and Atmospheric Administration, Environmental Protection Agency, Centers for Disease Control and Prevention, and Minerals Management Service. Special Monitoring of Applied Response Technologies (SMART). US Coast Guard, Washington, DC. <http://response.restoration.noaa.gov/oilaids/SMART/SMART.html>.

Valentine, D.L., Mezic, I., Macesic, S., Crnjarc-Zic, N., Ivic, S., Hogan,, P.J., et al., 2012. Dynamic autoinoculation and the microbial ecology of a deepwater hydrocarbon irruption. Proc. Nat. Acad. Sci. 1108820109. doi:10.1073/pnas.1108820109.

Wade, T.L., Sericano, J.L., Sweet, S.T., Knap, A.H., Guinasso, N.L., 2016. Spatial and temporal distribution of water column total polycyclic aromatic hydrocarbons (PAH) and total petroleum hydrocarbons (TPH) from the *Deepwater Horizon* (Macondo) incident. Mar. Pollut. Bull. 103 (1–2), 286–293. Available from: http://dx.doi.org/10.1016/j.marpolbul.2015.12.002.

CHAPTER

15

Applications of the CEN Methodology in Multiple Oil Spills in Spanish Waters

Joan Albaigés[1], *Laura de la Torre*[2], *Josep M. Bayona*[1] *and Carmen Domínguez*[1]

[1]Spanish National Research Council (CSIC), Barcelona, Spain [2]Spanish Maritime Safety Agency (SASEMAR), Madrid, Spain

BIOGRAPHIES

Joan Albaigés is Emeritus Professor of the Spanish Research Council (CSIC). He was appointed vice-chairman of the Scientific Advisory Committee on the *Prestige* accident (2002), coordinator of the European Network on Accidental Marine Pollution (Ampera) (2004–2009) and ERA-Net "Towards integrated European marine research strategy and programs" (SEAS-ERA) (2010–2014), which grouped 20 European countries. He is also a member of the oil spill identification expert group (OSINET) and former responsible for the Spanish reference laboratory for oil spill identification. He has contributed over 250 refereed articles to scientific journals, being the Editor-in-Chief of the *International Journal of Environmental Analytical Chemistry*.

Josep M. Bayona, received a PhD in Chemistry in 1985 at the Autonomous University of Barcelona. Presently, he is Research Professor at the Institute of Environmental Assessment and Water Research (IDAEA) from the Spanish Research Council (CSIC) in Barcelona (Spain). His main research field of interest is "Environmental Organic Chemistry" focusing on the transformation processes and the pathway of organic contaminants in the environment and in engineered ecosystems. He is also a member of the oil spill identification expert group (OSINET) and the responsible for the Spanish Reference Laboratory for oil spill identification. He has authored 280 publications in peer-reviewed journals.

Carmen Domínguez obtained her BS degree in chemistry at the Barcelona University in 1998 and her PhD in 2003 in the same university. She is currently a contracted researcher on the Environmental Chemistry Department from the Institute of Environmental Assessment and Water Research of the Spanish Research Council. In 2005, she started the research in the quantification and source appraisal of polycyclic aromatic hydrocarbons in core sediments. Since 2009, she is a member of the National Reference Laboratory for oil spill identification and characterization.

Laura de la Torre is an adviser at the Spanish Maritime and Safety Agency. She is a chemical industrial engineer with experience in the field of marine pollution preparedness and response, participating in recent incidents (Prestige 2002, Spabunker IV 2003, Don Pedro 2007, Oleg Naydenov 2015). She has represented the Spanish Maritime Administration in national and European forums, workshops, and working groups (OTSOPA—Working Group on Operational, Technical and Scientific Questions concerning Counter Pollution Activities, CTG—Consultative Technical Group on Marine Pollution Preparedness and Response, Bonn OSINET—Oils Spill Identification Network) and in exchange programs. She has participated in national and international research, development, and innovation projects, platforms, and networks (MONALISA 2.0, CORELNGas Hive, PREVECMA, PROTECMA) as well as twinning projects.

Oil Spill Environmental Forensics Case Studies.
DOI: http://dx.doi.org/10.1016/B978-0-12-804434-6.00015-X

15.1 INTRODUCTION

Spain has one of the largest coastlines in Europe (ca. 8000 km). In addition to the mainland territory, two archipelagos, the Balearic and Canary Islands, enlarge the Spanish territorial waters and increase the maritime search and rescue area to nearly 1.5 million of km^2, three times the size of the national territory. This very large area is highly exposed to the impact of oil spills. Maritime traffic is the major source of accidental and operational oil discharges. Moreover, eight harbors, which hold the oil terminals of coastal refineries, are the major load and discharge centers for oil products, where accidental discharges may also occur.

An overview of the occurrence and potential impact of oils spills on the Spanish coastal waters and shores has recently been published (de la Torre and Albaigés, 2016). To face with the ecological and socioeconomic consequences of such spills, a strong oil pollution prevention, preparedness, and response system has been implemented. This system is reinforced by an efficient coordination between the monitoring activities and source identification of oil spills, a key component of which is the availability of analytical methodologies for the unambiguous characterization of the spills. Analytical results are thus used to prove pollution offenses and help to recover cleanup costs incurred during an incident.

In Spain, the implementation of the oil-spill source identification mechanism started just after the *Prestige* accident (2002), and it was based on the European Committee for Standardization guideline (CEN-TR 15522, 2012). In this study, a number of case studies involving oil spills in Spanish waters will be described to illustrate the potential of this methodology for oil spill source identification.

15.2 MAJOR SOURCES OF OIL POLLUTION

Considering the data of the last 10 years, around 370 pollution incidents are managed every year by the Spanish Maritime Safety and Rescue Agency (SASEMAR), approximately one per day. However, a certain decrease has been observed since 2010, when the aerial surveillance system was consolidated (de la Torre and Albaigés, 2016). The aerial surveillance of the Spanish waters by aircraft has detected, since 2010, at least one vessel to be discharging "red-handed" every 100 flight hours. Fig. 15.1 shows the detections identified by aerial and satellite surveillance in Spanish waters in the period 2011–2014. Pollution incidents are particularly common in places with higher maritime traffic density (e.g., the northwestern corner of the peninsula and the Strait of

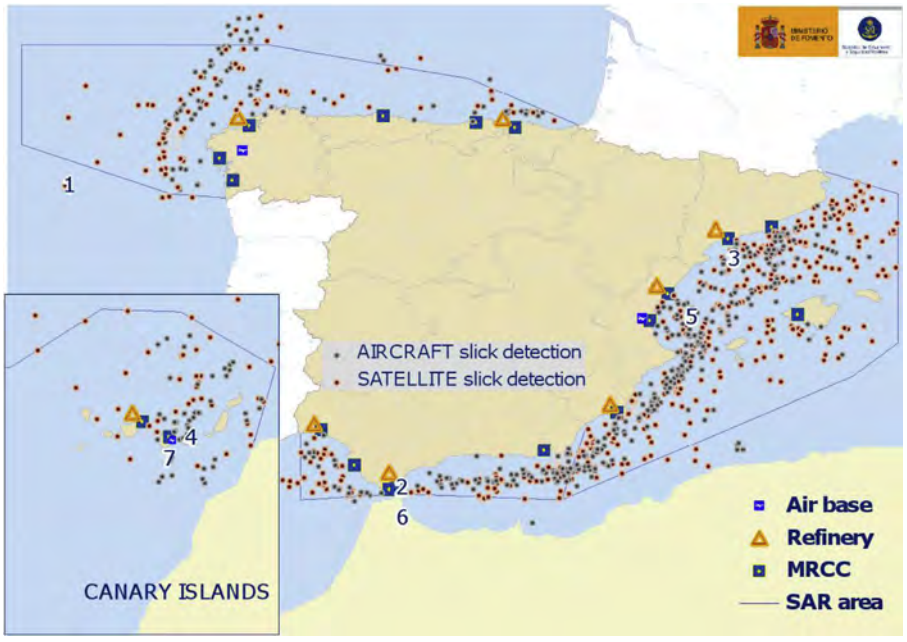

FIGURE 15.1 Aircraft and satellite slick detections in Spanish waters 2011–2014. Numbers (1–7) indicate the approximate locations of the seven case studies described herein. *MRCC*, Maritime Rescue Coordination Centre.

Gibraltar) and with greater port activity. Surprisingly, many illegal spills are detected in the Mediterranean Sea, defined by the International Convention for the Prevention of Pollution from Ships (MARPOL) as a special area of protection due to its unique oceanographic and ecological characteristics.

Although the sources of most oil spills are unknown (77.5% of the cases), confirmed spills from vessels, onshore installations, and offshore rigs represent 17.5%, 3.5%, and 0.5%, respectively. The products involved in these incidents are mainly waste oils (bilge oils, sludges, slops) derived from tanks cleaning by vessels failing to meet MARPOL requirements. A number of incidents resulting in small discharges of oil products in the inner waters of the harbors are also registered every year. The usual causes are cargo-handling operations, bunkering, oil transfers on board and cleaning operations on the deck, and the products involved are mainly heavy fuel oils.

Sometimes, accidental operational discharges are observed at sea, e.g., during the fuel transfer between tanks. More rarely, pollution may occur from time to time due to accidents, such as structural damages, collisions, or explosions, which may result with the grounding or sinking of the vessel. Of particular importance was the *Prestige* oil spill, in 2002, which extended the oil pollution over 800 km of the Atlantic coastline (Albaigés et al., 2015a).

Over the last 10 years, we have been requested to analyze samples from approximately 20 to 25 incidents per year. Among them, those involving waste oils amount, on average, 46% of the total. Additionally, on average, 25% of our investigations correspond to heavy fuel oils, 12% to gas oils, 4% to crude oils, and 13% to others (e.g., vegetable oils, biodiesel, paraffin oil, etc.).

15.3 SOURCE IDENTIFICATION OF OIL SPILLS

The methodology used in the laboratory for oil-spill identification and the prosecution of offenders is the one established in 2002 by the European Committee for Standardization (CEN-TR 15522, 2012) encompassing two guidelines:

Part I: Oil spill identification—Waterborne petroleum and petroleum products—sampling (CEN/TR 15522-1: 2006).
Part II: Oil spill identification—Waterborne petroleum and petroleum products—analytical methodology and interpretation of results (CEN/TR 15522-2: 2012).

Sampling is the first step in the process of defensibly determining the source or impact of an oil spill. Designing a comprehensive spill sampling plan is fundamental in the investigative efforts of an oil spill, and the collection of oil from both the spill and the suspected source(s) is crucial to any forensic investigation. Special attention must be paid to ensure the representativeness of the collected samples, both at sea and from the vessels tanks.

Once in the laboratory, samples are analyzed by gas chromatography–flame ionization detector (GC/FID) and gas chromatography–mass spectrometry (GC/MS), and compared using a suite of diagnostic ratios of selected compounds (molecular markers) which constitute the fingerprint of the oil (Albaigés et al., 2015b). The selection of these series of compounds lies on the combination of their source specificity and their lower susceptibility to weathering. Any differences between compound ratios, not influenced by weathering, are only relevant if the relative difference is larger than the variability of the method itself, estimated in 14%. Overlays of selected ion monitoring profiles (even some not included in the previous methodology) can also be of interest for the confirmation of the identifications.

In the sections that follow, the application of these concepts and CEN methodology is illustrated in seven case studies based upon our investigations. These seven case studies are depicted in Fig. 15.1. They offer demonstrative examples of how to identify the oil spill source and, additionally, monitor changes in oil samples due to weathering in the longer term.

15.3.1 Case Studies

Case 1. The CEN methodology was extensively used during the *Prestige* oil spill (November 13, 2002). The spill was originated by a severe structural failure of the starboard cargo tanks of the single-hulled oil tanker, under severe strong winds and extreme sea conditions (waves 8 m high). The tanker started to leak oil 30 mi off Finisterre (NW Spain) and finally, on November 19, broke in two and sank, 130 mi from the Galicia south-coast, after the spill of about 60,000 t of heavy fuel oil that affected more than 800 km of the Spanish Atlantic coast (Albaigés et al., 2006).

Following the accident, an extensive survey was carried out by SASEMAR at the northern coast of Spain to obtain a comprehensive picture of the fate of the spill in the marine environment and, indirectly, identify the possible occurrence of illegal discharges in the area after the spill. More than 200 oil samples were collected in the region (at sea, at the continental shelf, and stranded on the coast) between December 2002 and December 2003 and characterized by chemical fingerprinting (Albaigés et al., 2015a).

From the total samples analyzed during this period, 17% did not match the *Prestige* oil and most of these (52%) were found off La Coruña where the city harbor and an oil refinery support intense maritime traffic. This finding demonstrated the continued occurrence of oil discharges at sea and the need for a more strict surveillance of the areas holding heavy tanker traffic.

During that survey, the *Prestige* oil was drifting on the seawater surface for almost 1 year and thus it was highly exposed to major weathering processes (e.g., emulsification, evaporation, dissolution, photooxidation, and biodegradation). Thus, a good opportunity to monitor the resulting compositional changes for assessing the molecular indicators to be used for oil source recognition was presented (Díez et al., 2007). Over the short term, evaporation of the lower fractions (<*n*-C20 range) and dissolution of the low-molecular-weight aromatic hydrocarbons (e.g., alkylnaphthalenes) were the most evident processes, which accounted for a 5% and 2% of oil loss, respectively. A delay of about 2 months was observed before the degradation of *n*-alkanes was evidenced, and after a certain progress did not go further for the rest of the year. It is possible that the limited extension of degradation was due to the fact that the oil was in the form of compact patches, which were only available to bacteria at the surface. It should be reminded that the oil was a heavy fuel oil of high viscosity and density (11.04°API). The analysis of the collected samples did not exhibit either any noticeable photooxidation trend.

In summary, the data showed the high persistence of the spilled heavy fuel oil at sea, for 1 year after the accident, with very low incidence of the natural weathering processes, thus stressing the need for mechanical removal from the sea surface and the coastal areas.

However, 9 years later, *Prestige* oil was still recurrently arriving to some beaches. It was suggested that the morphodynamics of high-energy beaches favored a cyclic burying of the oil, down to 4 m depth, and resurfacing, with a transport from the subtidal area to the intertidal area and vice versa. During this process, a clear biodegradation signal was observed within the aliphatic and aromatic fractions. *n*-Alkanes were highly depleted (Fig. 15.2) and the C1−C2 alkylphenanthrenes and dibenzothiophenes, proposed for source recognition and weathering assessment of spilled oils, exhibited an interesting sequence of events of increasing biodegradation, as shown in Fig. 15.3 and discussed in detail elsewhere (Bernabeu et al., 2013). These features were of high

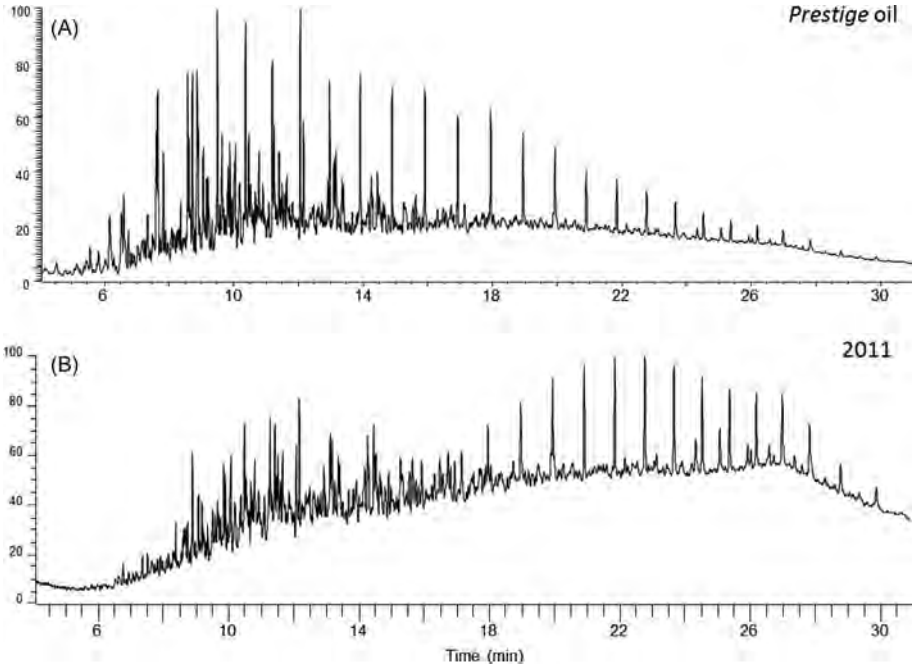

FIGURE 15.2 GC/FID profiles of (A) the *Prestige* heavy fuel oil and (B) a tar ball from the *Prestige* spill collected 9 years after the incident (2011) at a Galician beach.

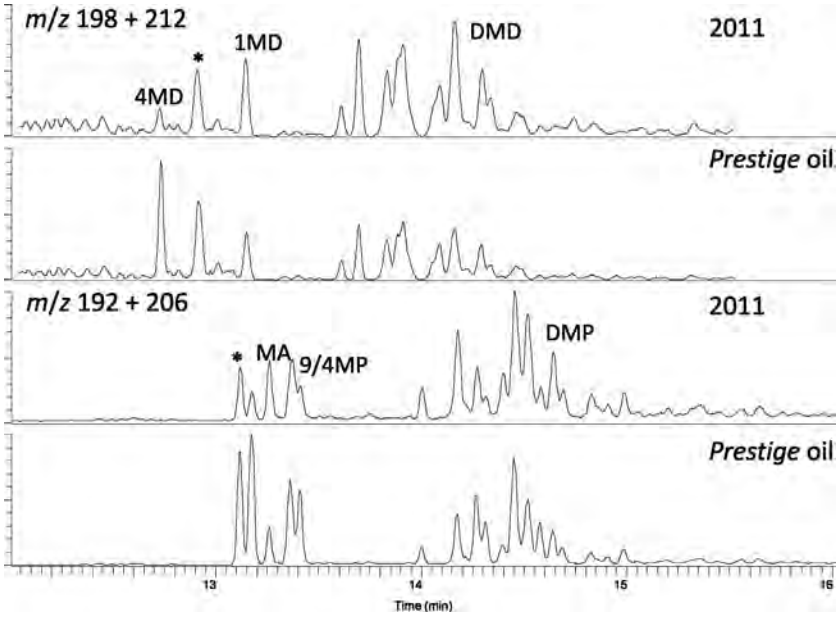

FIGURE 15.3 Ion chromatograms of methyl- and dimethyl-dibenzothiophenes (*m/z* 198 and 212) and methyl- and dimethyl-phenathrenes (*m/z* 192 and 206) of a weathered *Prestige* oil sample collected in 2011 and unweathered *Prestige* oil. *MA*, Methylanthracene; *MP*, methylphenanthrene; *MD*, methyldibenzothiophene. *2-/3-Methyl dibenzothiophene and 3-methyl phenanthrene.

significance for the assessment of future spills. However, the more recalcitrant triterpene and sterane compounds still provided the clue for source recognition.

Case 2. Another accident occurred on the evening of the October 10, 2008, when the bulk carrier of Liberian flag *Fedra* (GT 35,000 t and 225 m in length) went aground at Punta Europa in the Algeciras Bay (Cádiz, Spain), due to very rough conditions in the Strait of Gibraltar. In the following morning, the vessel broke in two and started to leak around 300 t of intermediate fuel oil (IFO 380). A few hours later, another carrier of Liberian flag (*Tawe*) stranded on the eastern part of the Bay, at Punta San García, and also started to leak oil (IFO 180), affecting 300–400 m of the coast nearby.

In the following days, the floating slick drifted toward the North-African coast, reaching the beach of Ceuta. Samples were collected from the tanks of the two vessels and from the sea, to identify the main pollution source and, eventually, to disregard other minor spills that could be present in the area. As indicated in the case of the *Prestige* spill in 2002, they are common in areas holding heavy tanker traffic like the Strait of Gibraltar.

The GC/FID profiles of the vessel fuels are shown in Fig. 15.4, which are characteristic of heavy fuel oils. Selected profiles of the marine samples are also shown in Fig. 15.4. The numbers indicate the spatial/temporal sequence, from the Algeciras Bay (1) to the coast of Ceuta (8), in the African coast (October 15).

Although the general profiles look quite similar, the determination of the diagnostic ratios defined in the CEN method enabled us to differentiate between the two vessels' fuel samples and identify vessel *Tawe* as the main source of the large spill in the area, as shown in the comparison of diagnostic ratios (Fig. 15.5). The deviation observed in the ratios in the lower boiling range (C17/pristane and C18/phytane) are clearly attributed to the effect of evaporation on the marine samples. On the other hand, the sample collected 5 days later, quite far from the source (No. 8), exhibited evidence of photooxidation on various methylpyrene and benzofluorene isomers, as already found in other spills in the area (see Case 4). It is interesting to note the rather early progression of photooxidation in these latitudes under prevailing sunny conditions.

Case 3. Since the discovery of the Amposta oil field in 1970, around 20 mi off-shore from the Ebro Delta (Spain), the area has been repeatedly explored for oil production. During the months of May and June 2009, a series of incidents took place in the area (Fig. 15.1). For example, an oil exploration platform reported the release of more than 130,000 L of oil, during the prospecting of the two new Montanazo-5D and Lubina-1 wells. The spill, covering an area of 19 km^2, was one of the most important of the decade in the coast of Tarragona and was of major concern because of its proximity to the Ebro Delta, an area of high environmental and socioeconomic value.

After the spill, May 16, 2009, samples were collected from the sea by the surveillance helicopter that confirmed the presence of a crude oil (Fig. 15.6A), associated to the Lubina-1 well according to its compositional

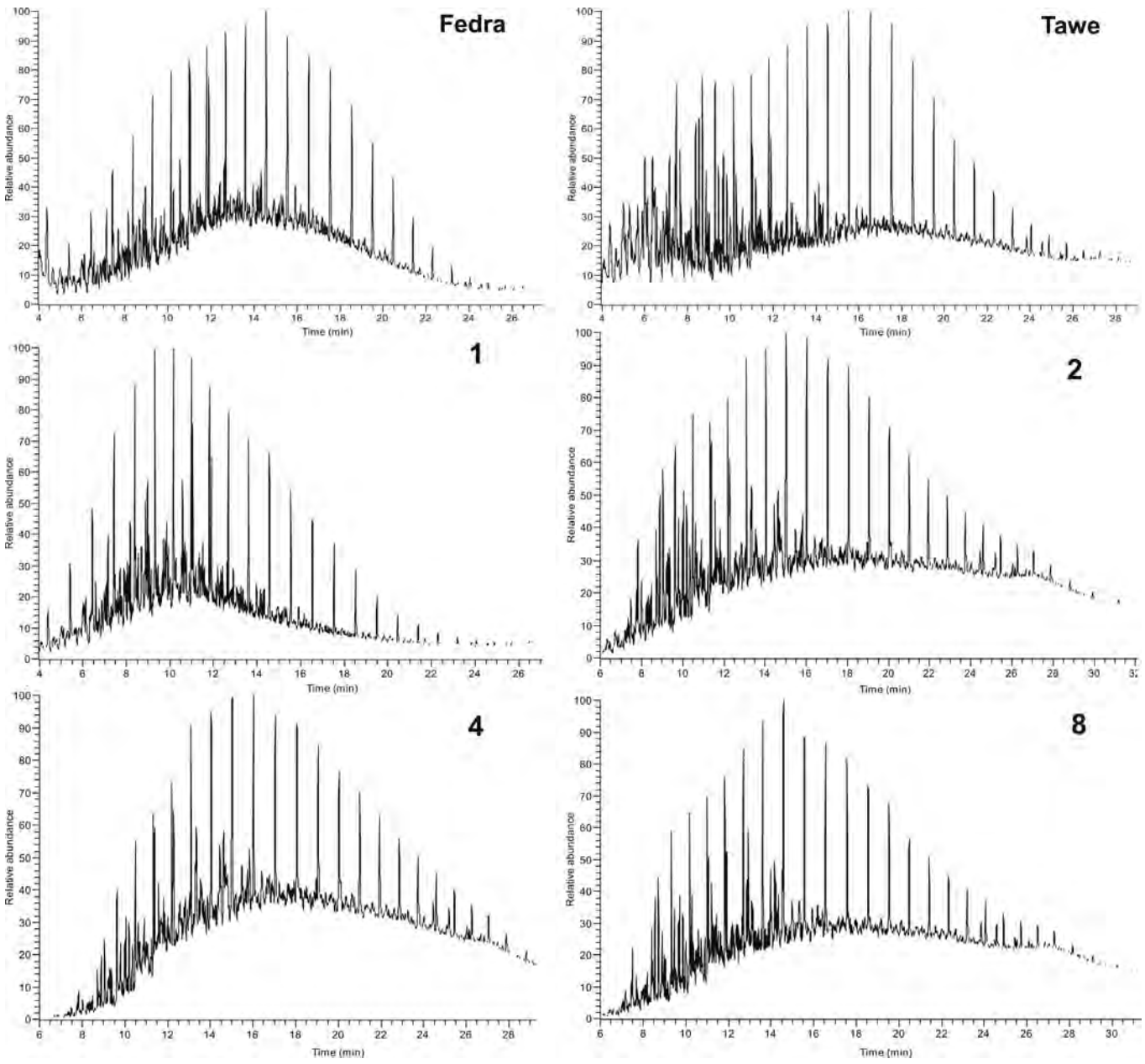

FIGURE 15.4 GC/FID profiles of the different oil samples collected in the Algeciras Bay (October 10, 2008) investigation, including fuel oils from the vessels *Fedra* and *Tawe* and four marine samples (1, 2, 4, and 8).

characteristics (diagnostic ratios). Two weeks later another oil slick appeared in the surroundings of the exploration platform, but the profile was totally different (Fig. 15.6B). The main component was a paraffin-based oil (without aromatic hydrocarbons), corresponding to a nonaqueous drilling fluid.

One month later, oil slicks and tar balls were observed in several places along the coast, and a large number of samples were collected in order to determine the source and, particularly, if they were related to the previous month's oil spill. To support the investigation, some reference samples, as potential sources, were gathered, which included crude oils from two production wells (Lubina-1 and Casablanca; Fig. 15.6A and C), oil from a pipeline connecting two oil platforms, and samples from a tanker that was in the area at that time.

The samples were processed and compared following the CEN methodology. Representative profiles of the samples collected along the coast are shown in Fig. 15.7, which based on the coincidence of the diagnostic ratios were all consisting of the same crude oil, but with different degrees of weathering. The comparison of the CEN diagnostic ratios of these samples with those of the two reference crude oils (Casablanca and Lubina-1) gave a relative difference less than 14%, with the exception of the two ratios (C2-phe/C30ab and B[a]F/4-MPy) whose values were as follows:

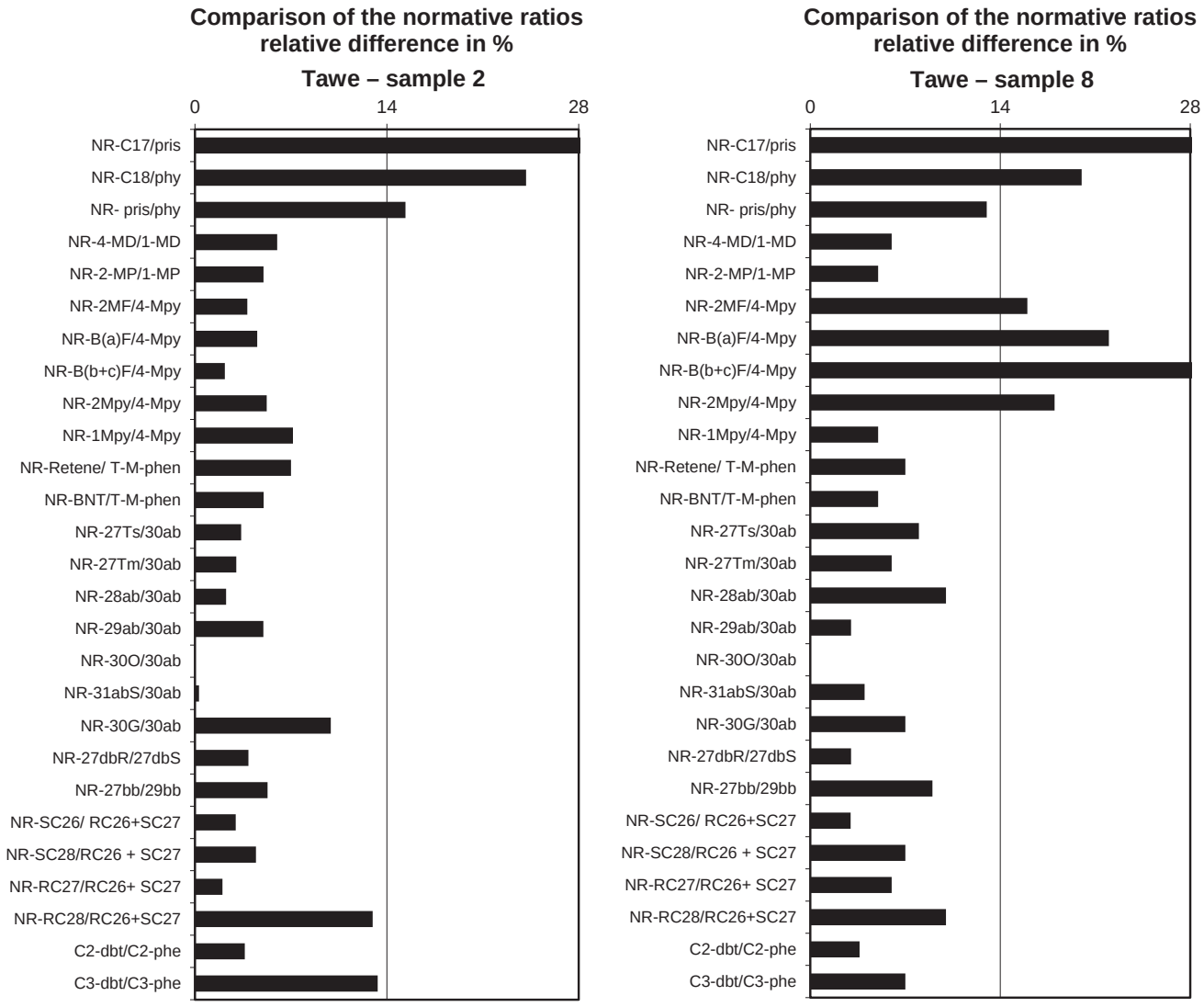

FIGURE 15.5 Comparison of diagnostic ratios of marine samples 2 and 8 with fuel oil from vessel *Tawe*.

Sample	C2-phe/C30ab)	B[a]F/4-MPy
Casablanca crude oil	60	78
Lubina-1 crude oil	31	124
Pollution samples	27–33	115–121

These ratios provided evidence that the Lubina-1 crude oil was possibly the source of the observed pollution. Certainly, the statistical comparison of the compound ratios is an important part of the evaluation of the data, however, ratios are not always conclusive. The final conclusion should be based on an overall evaluation of all available data. In this respect, it is important not only to evaluate the measured ratios but also to visually inspect all the chromatograms and identify possible characteristic features, which could be matched by overlying the profiles.

Polycyclic aromatic sulfur heterocycles (PASHs) have been identified as very useful compounds for oil fingerprinting (Hegazi and Andersson, 2016). They differ from oil to oil and several of them are stable and not affected by marine weathering. Andersson (1993) found that the PASHs are more photostable than the PAH counterparts. In fact, the presence of sulfur in the molecule (e.g., dibenzothiophenes) reduces relatively the photodegradation kinetics (Radović et al., 2014).

Fig. 15.8 shows the C2- and C3-dibenzothiophene profiles of the two reference crude oils in this case and the overlay with the pollution samples. According to this comparison, it was definitely concluded that the pollution source was the crude oil produced from the Lubina-1 platform.

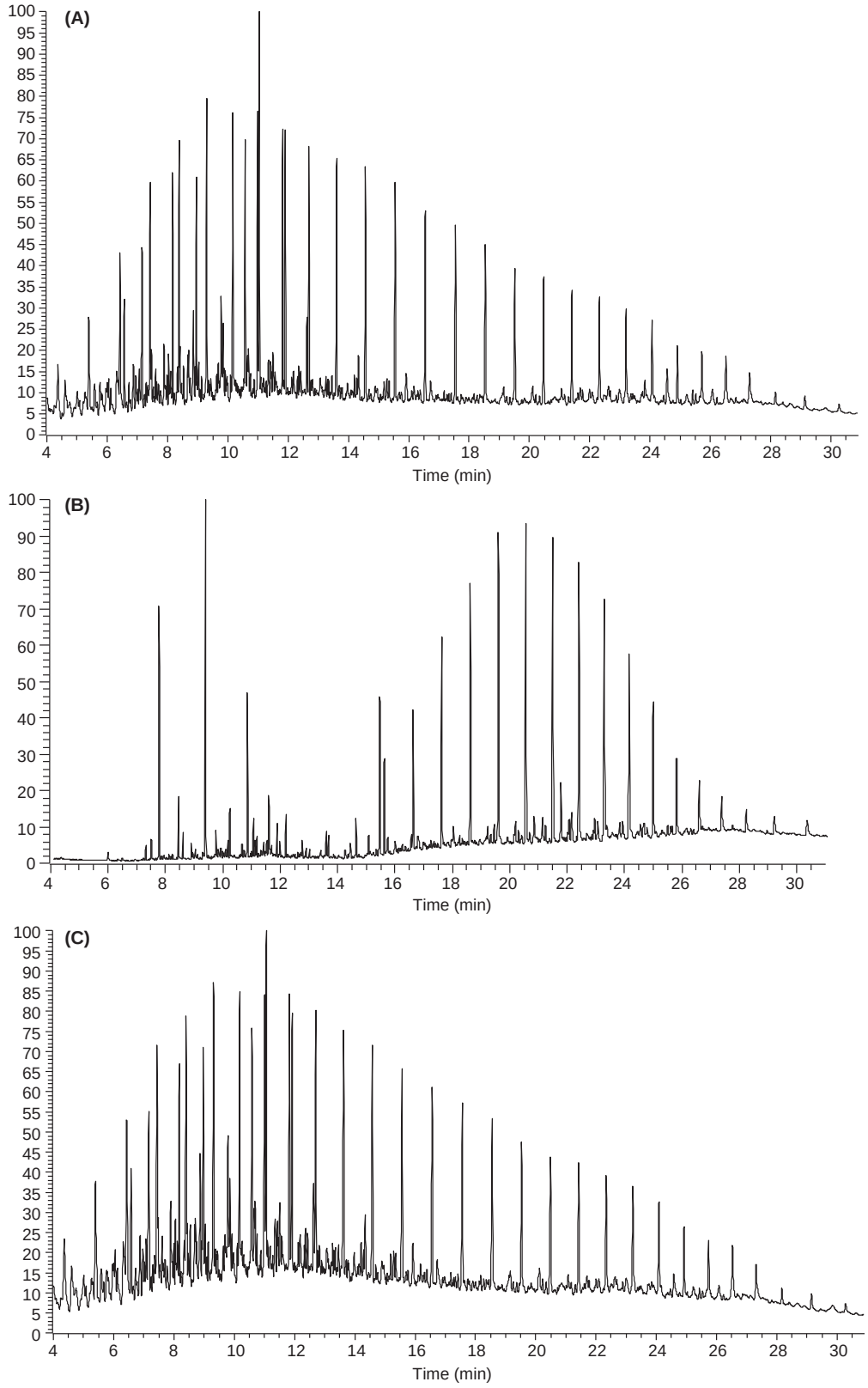

FIGURE 15.6 GC/FID profiles of (A and C) crude oils and (B) a nonaqueous drilling fluid.

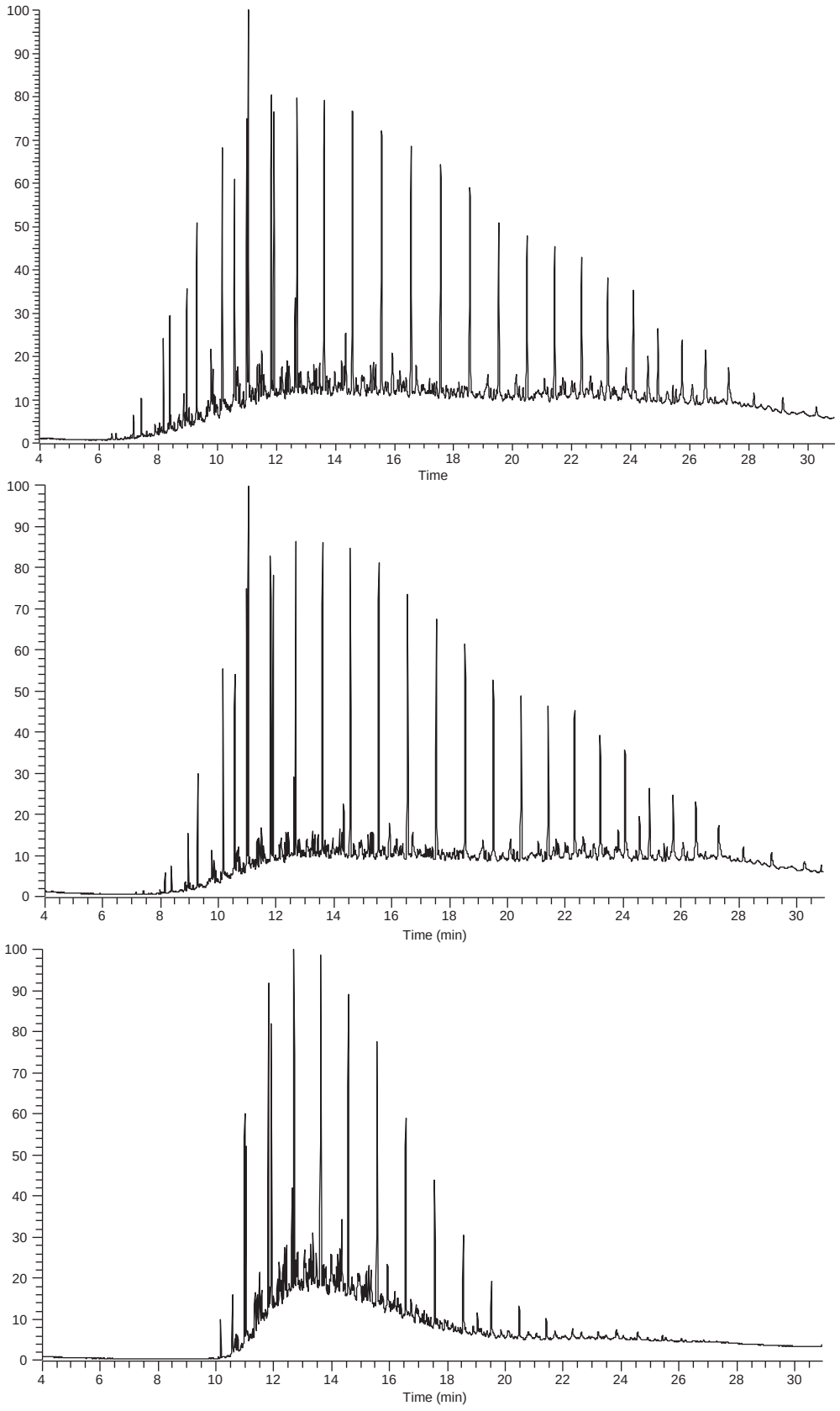

FIGURE 15.7 GC/FID profiles of variably weathered crude oil samples collected along the beaches.

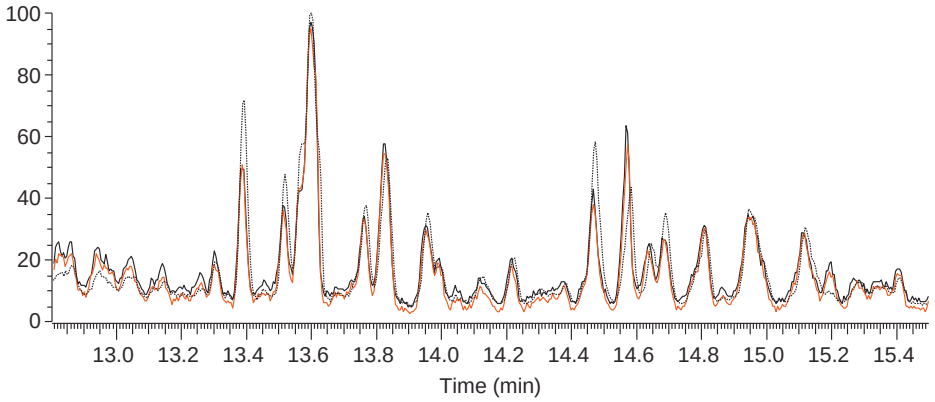

FIGURE 15.8 Overlay of the C2 and C3-dibenzothiophene profiles of the Casablanca (dotted black line) and Lubina-1 crude oils (solid black line), and pollution samples collected in the coast (*red line* (dark gray in print versions)).

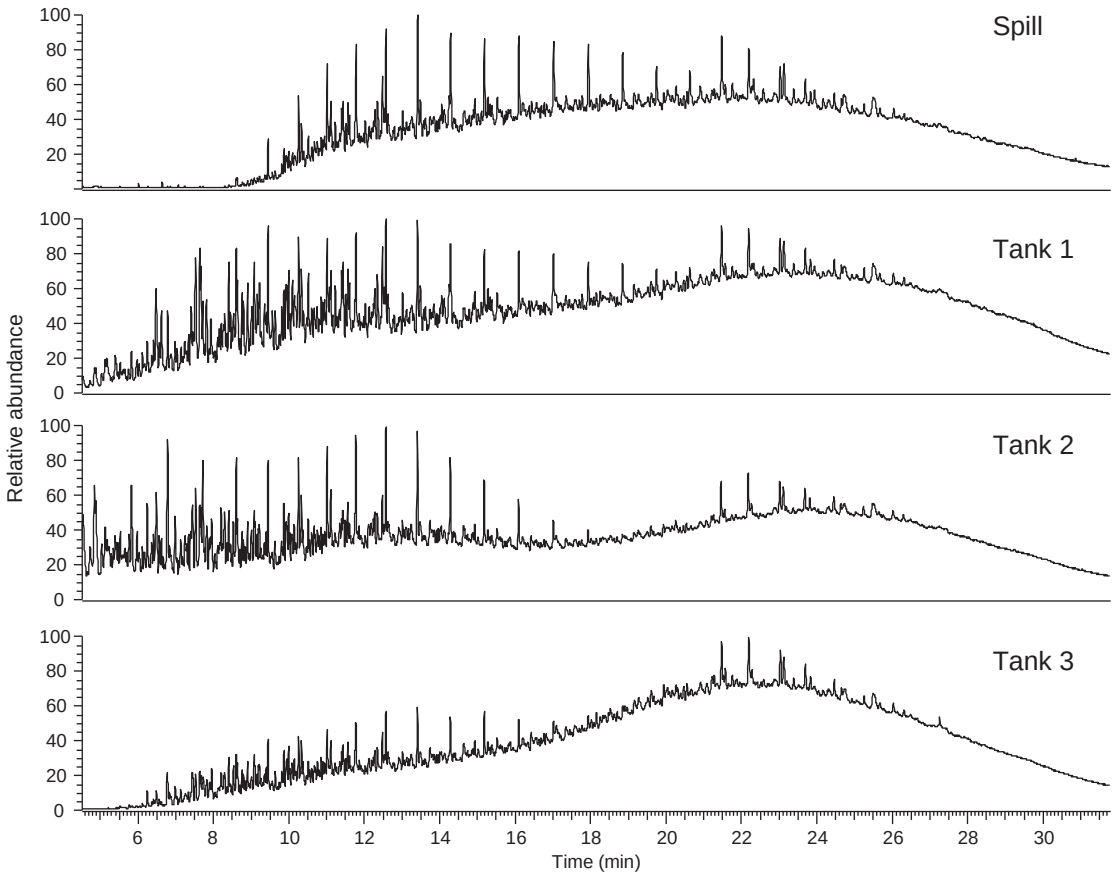

FIGURE 15.9 GC/MS TIC profiles of the spill sample and samples collected from the tanks of the suspected source vessel.

Case 4. The aerial surveillance of pollution incidents is fundamental to locate and evaluate the slicks and to guide the coastline responders. Aerial and satellite surveillance together with oil forecasting and sampling are strengths of the Spanish response system. Surveillance is carried out day and night by prepared aircrafts.

On May 14, 2012, a container carrier was detected "red-handed" during the night by the surveillance plane SASEMAR 103, at about 40 mi North of Canary Islands on his way toward Algeciras (Spain; Fig. 15.1). A slick of 34.8 km^2 was observed connected to the stern of the vessel. On the following morning, a patrol boat was sent to collect samples from the oil slick. The analysis of these samples indicated a mixture of fuel oil and lubricating oil consistent with a discharge of bilge oil (Fig. 15.9). Later, on May 29, when the suspicious vessel docked at Algeciras harbor, it was inspected by the port authorities. Although the vessel denied the discharge when

interrogated, oil samples were collected from three different tanks onboard for comparison to the slick samples. The main issue in this case was the adequate sampling of tanks. Fig. 15.9 shows the GC/MS total ion chromatograms of the collected oil residues. As it can be seen, the tank samples are composed of different mixtures of fuel oil and lubricating oil, each with a higher proportion of low boiling fractions compared with the spilled sample, which is attributed to moderate evaporation of the spilled sample.

The determination of the diagnostic ratios, according to the CEN methodology, indicated a positive matching of the spill sample with that of the vessel's sludge tank (tank 1). Relative differences of diagnostic ratios slightly above the 14% threshold defined by the CEN method could be easily explained by evaporation (e.g., pristane/phytane ratio) and photooxidation (e.g., B(a)F/4-Mpy ratio). Additional evidence of the positive matching of the tank 1 and spill oil samples was obtained by the comparison and overlaying of selected profiles. In this respect, the distributions of *n*-alkyltoluenes (m/z 106) were proposed as a complement of the m/z 85 profile for a preliminary screening of marine oil wastes (Albaigés et al., 2013). The *n*-alkyltoluene profiles shown in Fig. 15.10 clearly show the similarity between the spill and the sludge tank samples.

On the other hand, we have seen in the previous case study (Case 3) that the general distributions of certain PASHs can be useful for comparing samples. Fig. 15.11 shows the C2- and C3-dibenzothiophene (m/z 212 and 226) profiles of the samples of concern for this case study and the positive overlay of the spill and tank 1 (sludge tank) samples, thus providing further confirmation of the conclusion.

Case 5. An operational incident occurred in May 22, 2013, when the captain of a container carrier of the Maersk Line company communicated to the maritime authorities an accidental spill of fuel oil 40 mi off-shore

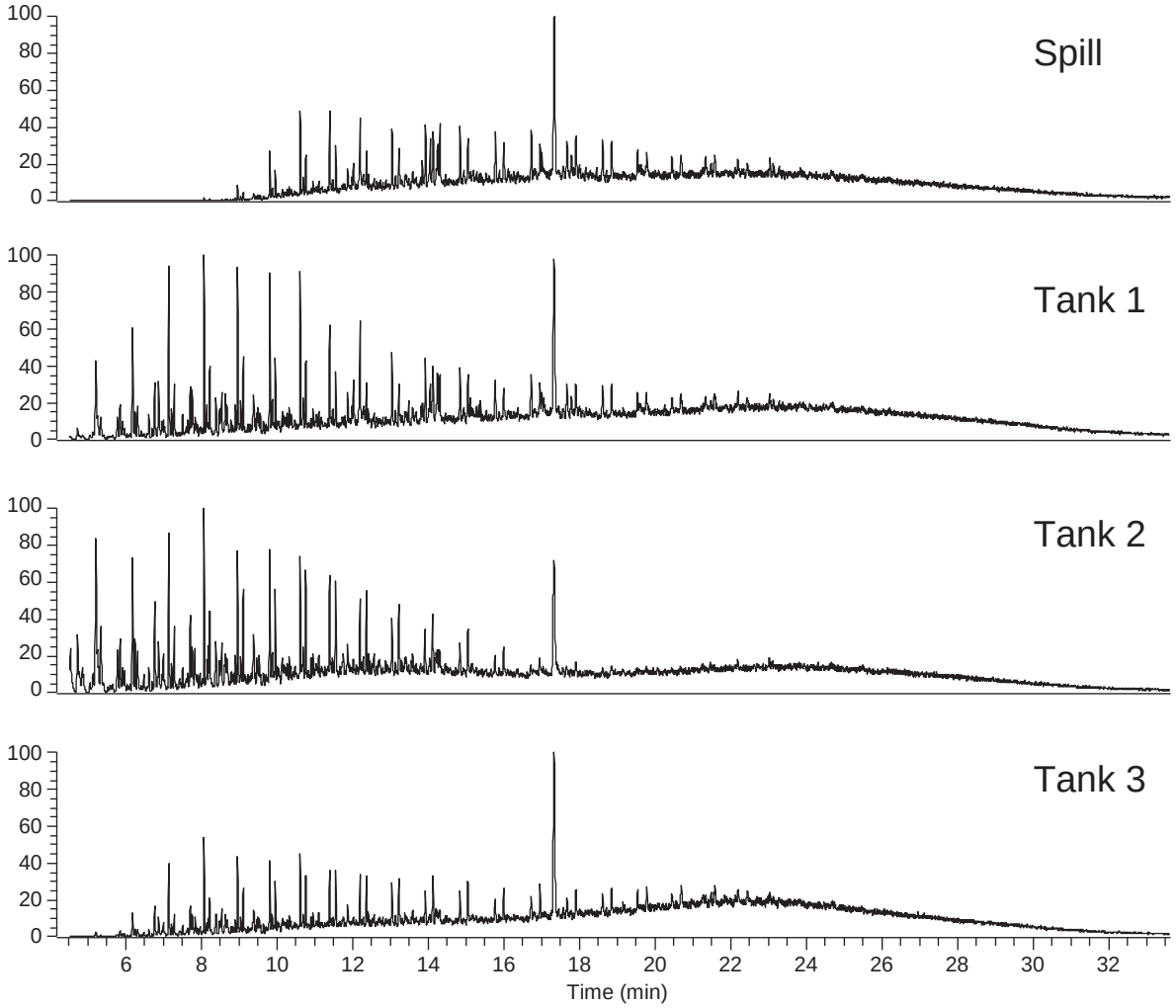

FIGURE 15.10 GC-MS profiles of *n*-alkyltoluenes (m/z 106) of the spill sample and the three tanks of the suspected source vessel.

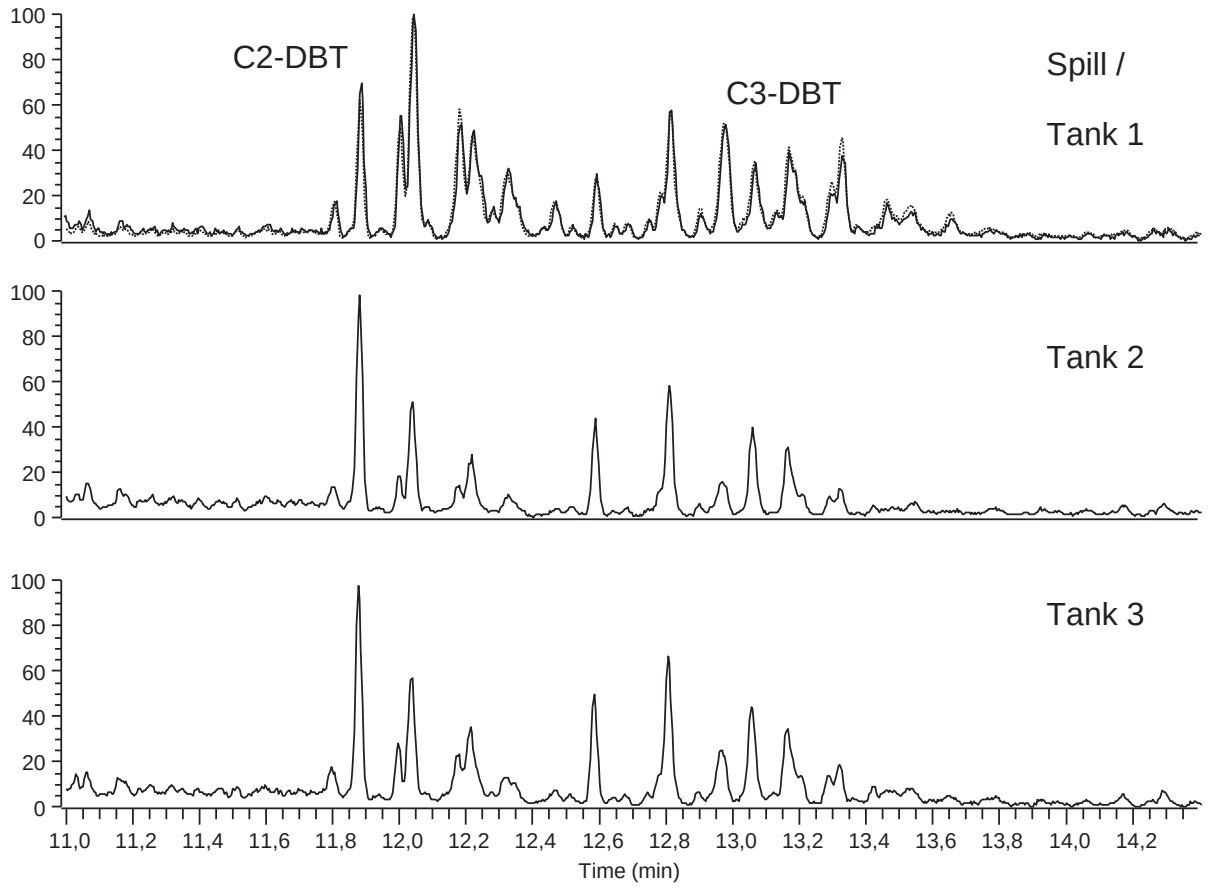

FIGURE 15.11 C2- and C3-dibenzothiophene profiles of the different tank samples. The spill sample (dotted line) overlays that of tank 1.

Valencia (Fig. 15.1). Spill samples were collected in the vicinity of the vessel and also from the suspected tank at the same day of the accident, but some days later (from May 31 to June 15) new oil slicks appeared on the sea. Almost 1 month later, from July 6 to 14, oil residues were widely spread on some Valencia and Castellón beaches. The question posed to us was to identify the source of all these samples and, particularly, if they were related to the aforementioned spill.

The comparison of the diagnostic ratios of all collected samples at sea confirmed their coincidence with the reference fuel oil sample from the container carrier's tank. Most of the ratios of the samples collected on the beaches also allowed to conclude a match to the vessel's fuel oil. However, some ratios of the spilled oils exhibited an increasing deviation from the reference fuel oil with time (Fig. 15.12). These ratios were those involving the fluorenes and benzofluorenes (2MF/4-Mpy, B(a)F/4-Mpy), and benzonaftothiophenes (BNT/T-M-phen), which are known to be affected by photooxidation (Radović et al, 2014). Photooxidation has been recognized as a rather fast process in areas where sunny conditions predominate, as was the case during this spill, which also occurred in summer when insolation was most intense.

A practical way to quantitatively illustrate these compositional changes in weathered samples is by the so-called percentage weathering plots (PW-plots) (CEN-TR 15522, 2012). The PW-plots can be obtained when the individual compounds of the original and weathered samples are normalized to the 17α(H), 21β(H)-hopane (C30-hopane), which is known to be highly refractory to weathering. Next, the calculated remaining percentage of the compounds in the weathered sample relative to the original oil is plotted against the retention time, which is a proxy for the boiling point of the corresponding compounds. If the samples are identical (e.g., a duplicate analysis), the result will be a straight line at 100%. The loss of certain compounds by weathering will be reflected by a decrease in the plot.

A summary of the effect of different environmental processes on the oil comparison is shown in Fig. 15.13, which reveals a significant depletion of compounds with low retention times (volatile) due to evaporation. At the same time, the effect of other processes, such as, i.e., dissolution, may explain the loss of C1- and C2-naphthalenes

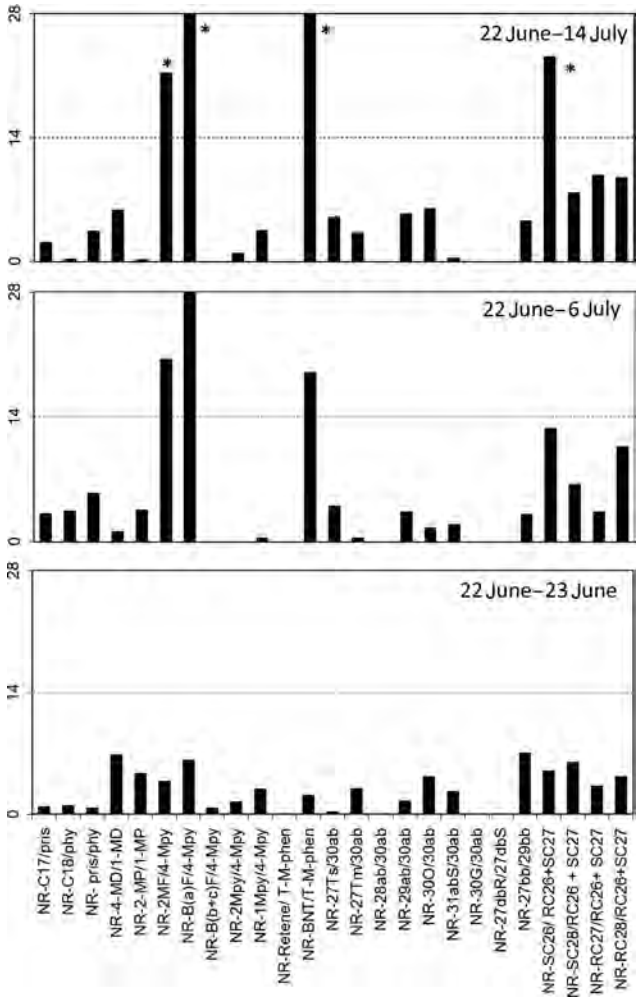

FIGURE 15.12 Comparison of diagnostic ratios of the reference fuel oil sample from the suspected vessel with those of spilled oil collected on the coast over time.*Ratios affected by photooxidation.

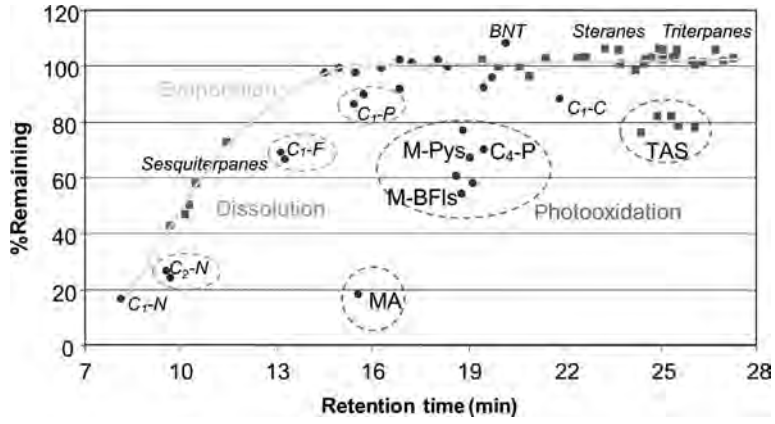

FIGURE 15.13 PW-plot showing the percent remaining of PAHs (circles) and biomarkers (squares) relative to hopane for the *Prestige* crude oil sample after simulated photooxidation in the laboratory. *Source: From Radović, J.R., Aeppli, C., Nelson, R.K., Jimenez, N., Reddy, C.M., Bayona, J.M., et al., 2014. Assessment of photochemical processes in marine oil spill fingerprinting. Mar. Pollut. Bull. 79, 268–277, reprinted with permission from Elsevier.*

TABLE 15.1 Variation of the Source Diagnostic Ratios during Extensive Oil Biodegradation and Photooxidation (*in italics*) (Albaigés et al., 2015b)

Ratio	Variation[a]
***m/z* 85**	
C17/Pr	−
C18/Ph	−
***m/z* 192**	
2-MP/1-MP	−
MA/1-MP	−
***m/z* 216**	
2-MFl/4-MPy	−
BaF/4-MPy	−
BbF/4-MPy	−
2-MPy/4-MPy	−
1-MPy/4-MPy	−
***m/z* 191**	
27Ts/27Tm	−
28ab/30ab	−
29ab/30ab	−
***m/z* 217/218**	
27dbR/27dbS	−
29aaS/29aaR	+
29bb(S + R)/29aa(S + R)	+
27bb/29bb	−
***m/z* 231**	
SC26TA/RC26TA + SC27TA	−
***m/z* 234**	
BNT/C4-P	+

[a]*Increase (+) or decrease (−) of the ratios.*

(C1-N and C2-N) and fluorenes (C1-F). Finally, the significant reduction of MA (80%), M-BFls (40%) and M-Pys (20%−40%), C4-P (30%), and TAS (20%) can be attributed to photooxidation, as it has recently been demonstrated through laboratory and field tests (Radović et al, 2014). The variation of the source diagnostic ratios during extensive oil biodegradation and photooxidation is summarized in Table 15.1. When the effects of weathering on a spilled oil are understood, any affected ratio should be eliminated or cautiously considered when comparing a weathered spill sample with an unweathered source sample.

Case 6. The port of Ceuta (Spain) is an important commercial, passenger, and sports facility that serves the traffic between the peninsula and North Africa. On December 8, 2014, a spill from an unknown source was detected in open waters (Fig. 15.1). After performing a backtracking analysis with Automatic Identification System maritime traffic data in the area, the possible pollution by any passing vessel was disregarded and the hypothesis of the leak from a pipeline somewhere in the area was considered. In a first overview of the samples collected the first day at sea, they were identified as a heavy fuel oil (see Fig. 15.14).

Between December 9 and 30 an extensive survey of the area was carried out by the Port Authority. Oil residues were collected again at sea (December 11) and along the coast nearby (stones and vegetation), as well as in

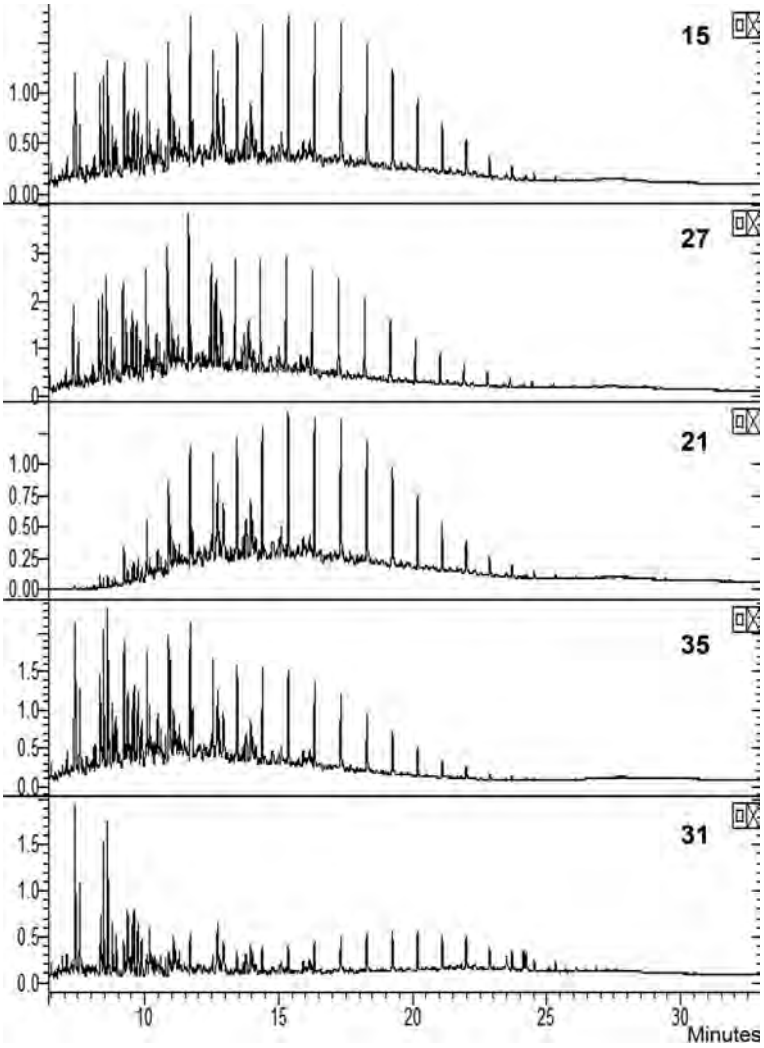

FIGURE 15.14 GC/MS TIC traces of five selected spilled oil samples from the Algeciras port investigation (references are indicated in the text below).

the port breakwater, in various fuel supply chests of two types of fuel oil (high and low in S) and in a drainer ditch. Moreover, the January 14, 2015, several soil borings, close to the fuel supply points and possibly related to the leakage, were performed. In total, 22 samples were collected that are numbered as follows, with uneven numbers (even numbers refer to the corresponding duplicates):

- marine samples (open waters) 1–17
- stones and vegetables in the coast nearby 19–23
- breakwater east 1 25
- breakwater east 2 27, 29
- fuel supply chest 1 (low S) 31
- fuel supply chest 2 (high S) 33
- fuel supply chest 3 (high S) 35
- drainer ditch 37
- soil drilled sample (east) 39
- soil drilled sample (west) 41
- soil drilled sample (south) 43

The GC/MS profiles (TIC) of some of these samples are shown in Fig. 15.14. As it can be seen, they correspond to similar heavy fuel oil residues, more or less weathered, except sample 31, which exhibits a totally different

profile. The comparison of diagnostic ratios indicated that all of the samples 1–24 (outside the port) exhibited a clear positive match to one another. The issue was, of course, to identify the pollution source. From the comparison with all other samples it was concluded that a leak of the fuel supply chest of high S fuel oil (sample 35) was the source of spilled oils.

This conclusion was reached after the comparison of the diagnostic ratios of the marine spilled oil samples with all of the suspected sources. Only sample 35 exhibited a positive matching among diagnostic ratios, as shown in Fig. 15.15. The only ratios with higher deviation from the 14% value can be explained by evaporation (C17/pristane and C18/phytane) and by photooxidation (de 2MF/4-MPy and B(b + c)F/4-MPy), as was also demonstrated in previous cases.

Although the CEN methodology can be systematically applied between each spill and suspected source sample, the comparison of diagnostic ratios from a large number of samples, like in this case, can be facilitated through the use of multivariate statistics, such as principal component analysis (PCA). The fundamentals of PCA, as a data-treatment tool in chemical fingerprinting, is that it summarizes the information in many correlated diagnostic ratios into a few so-called principal components (Christensen and Tomasi, 2006, 2016). Hence, a model with few components (e.g., 3 or 4) describes the most prominent trends in the dataset. By plotting the score of the principal components, chemical information retained in numerous diagnostic ratios for numerous samples can be simultaneously obtained.

A PCA treatment of data from this case, involving 22 determinations in duplicate and the repetition of 3 measures and 37 variables (diagnostic ratios) was carried out. Score plots (i.e., PC1-PC2) show that samples 27–28 and 31–32 are not correlated with the remaining samples (Fig. 15.16). Moreover, samples 29–30 and 37–40 clustered outside the main cluster, which includes all marine samples (1–18 and 19–24) together with sample 35–36 (high S fuel supply chest), which was (based upon CEN methodology) already suggested to be the pollution source.

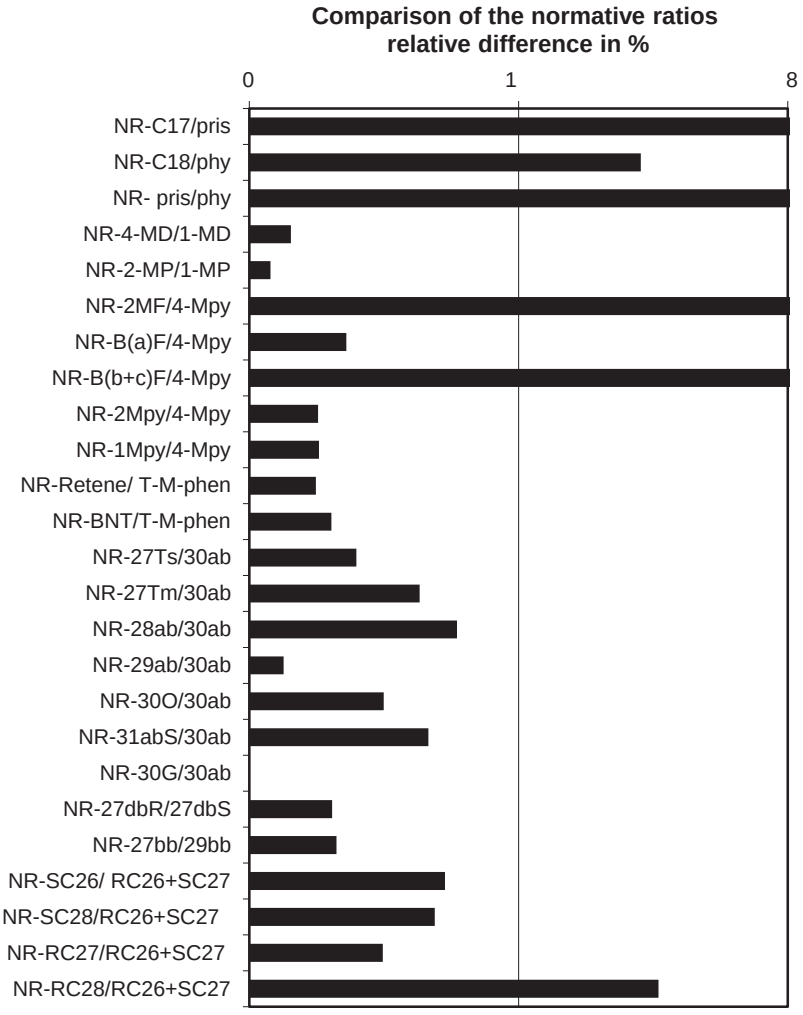

FIGURE 15.15 Comparison of diagnostic ratios between sample 15 (marine sample) and sample 35 (chest supply of low S fuel oil).

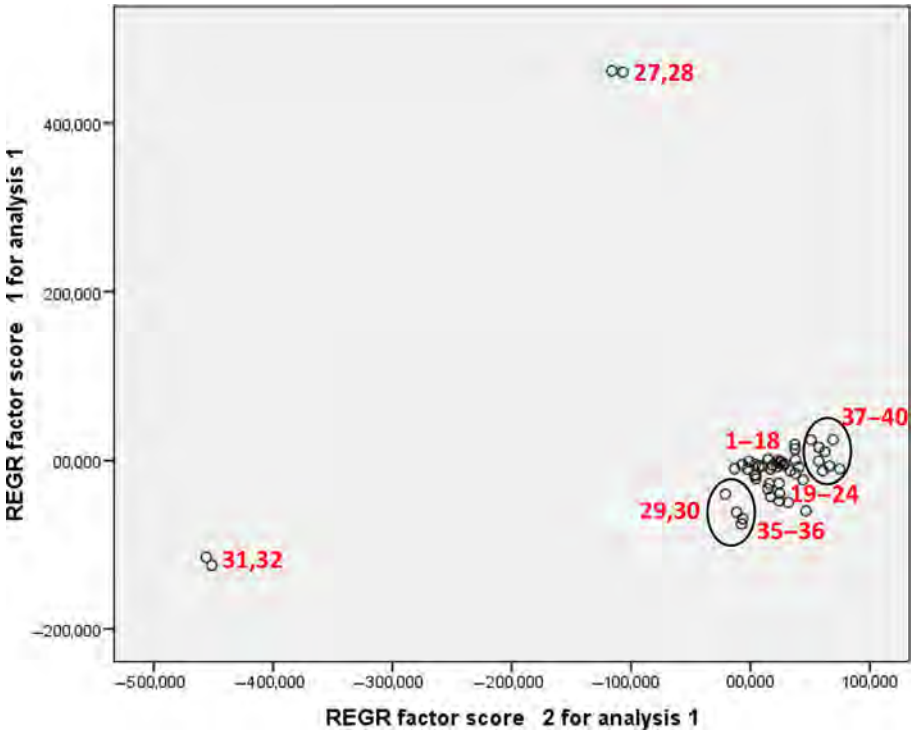

FIGURE 15.16 PCA score plot of PC1−PC2 showing clusters of samples with similar diagnostic ratios.

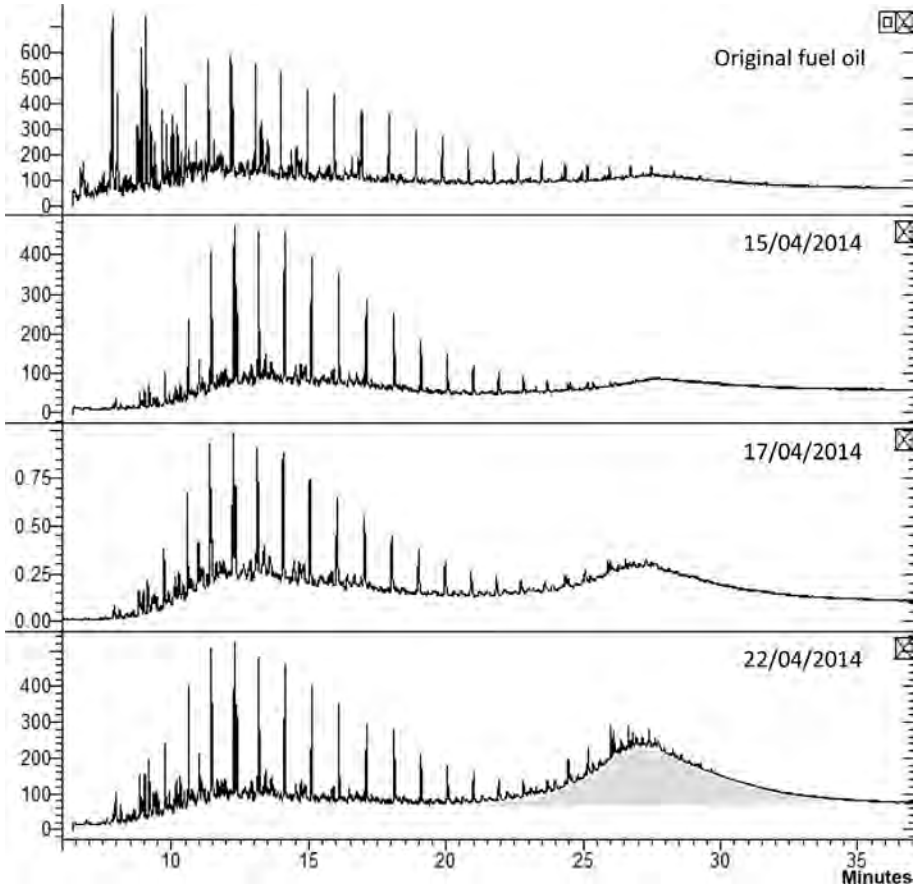

FIGURE 15.17 GC/FID profiles of the *Oleg Naydenov* fuel oil and three samples collected at sea containing varying amounts of lubricating oil (gray).

Case 7. More recently, on April 11, 2015, the Russian flag fishing vessel *Oleg Naydenov* was ready to leave the Port of Las Palmas (Gran Canaria Island; Fig. 15.1) when a fire was declared on board. Due to the risk posed by the ship's fire for the population and the environment, it was towed offshore, where it ultimately sank, on the morning of April 15, 2015, 15 mi south, at a depth of 2700 m, with 1400 t of fuel, 30 of diesel and 70 of lubricating oil. The subsequent aerial surveillance of the area quickly identified a number of oil slicks drifting to the southwest. Around 30 sets of samples were collected from April 15 to May 15, 2015, which were sent to the laboratory for identification.

As in the *Prestige* case, the main aim of the monitoring was to obtain a comprehensive picture of the spreading of the spill in the marine environment and, indirectly, to identify the possible occurrence of illegal discharges in the area after the spill. However, the problem in this case was the mixing of the different products carried by the sunken vessel during the spill. This is illustrated in the representative profiles displayed in Fig. 15.17.

The GC/FID profiles of different samples show the characteristics of a heavy fuel oil containing different proportions of lubricating oil (in gray; Fig. 15.17). The matching of the fuel oil in all samples was confirmed by the coincidence of the mid-range profiles (e.g., C1-pyrenes and C4-phenenthrenes) and the associated diagnostic ratios, whereas the contribution of different proportions of lubricating oil was evidenced by the differences in the characteristic sterane and triterpane profiles and the corresponding indices, as illustrated in Fig. 15.18.

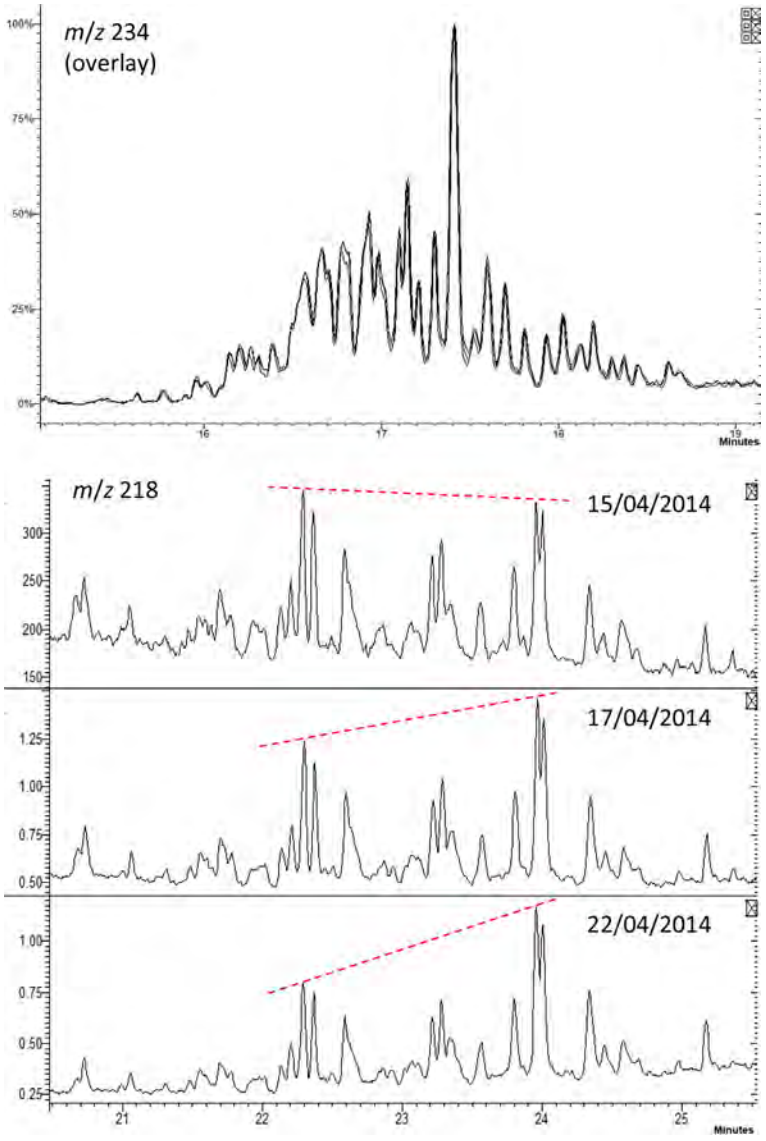

FIGURE 15.18 Ion chromatograms of C4-methyl-phenathrenes (m/z 234) and ββ-steranes (m/z 218) of *Oleg Naydenov* samples compared to three samples collected at sea.

The profiles of C4-phenanthrenes (m/z 234) exhibit a full overlay whereas the differences between the ββ-sterane distributions (m/z 218) are consistent with the increasing proportion of lube oil.

Varying features are common in spills of waste oils (e.g., bilge residues, sludge, slops) where different mixtures can be found in different tanks and samples. These differences should be considered in the assessment of chromatograms and diagnostic ratios in comparing the samples.

15.4 CONCLUSIONS

Throughout history, large oil spill incidents have allowed countries to move forward on oil spill preparedness and response. This happened to Spain in 2002 when the Maritime Authority had to deal with the *Prestige* oil spill. In response to this incident, a national oil pollution prevention and response system was set up.

Aerial and satellite surveillance together with oil forecasting and sampling are strengths of this system, as they provide reliable monitoring of the Spanish waters. These monitoring tools are essential in the enforcement processes to prove the pollution offenses in case of illegal discharges. But they are also essential to provide an effective response in oil spills incident's management.

Although a large incident hasn't occurred since 2002, Spanish authorities have dealt with medium and small oil spills, in which the whole system has been tested. The seven case studies described above demonstrate the efficiency of the CEN methodology in differentiating among qualitatively similar oils from a given oil spill and any available candidate sources. However, to be successful, a good knowledge of petroleum chemistry together with a deep understanding of the fate and weathering of the oil at sea is necessary. On the other hand, the methodology can be strengthened with the visual inspection of the different GC/MS profiles looking for particular characteristics and with the application of multivariate statistical methods.

Acknowledgments

This chapter is built on the work of the whole human team of the Spanish Maritime Safety and Rescue Agency (SASEMAR) who provided the oil samples. We acknowledge Berta Blanco for drafting Fig. 15.1.

References

Albaigés, J., Morales, B., Vilas, F., 2006. The *Prestige* oil spill: a scientific response. Mar. Pollut. Bull. 53, 205–207.

Albaigés, J., Jimenez, N., Arcos, A., Domínguez, C., Bayona, J.M., 2013. The use of long-chain alkylbenzenes and alkyltoluenes for fingerprinting marine oil wastes. Chemosphere 91, 336–343.

Albaigés, J., Bernabeu, A., Castanedo, S., Jimenez, N., Morales-Caselles, C., Puente, A., et al., 2015a. The *Prestige* oil spill. In: Fingas, M. (Ed.), Handbook of Oil Spill Science and Technology. John Wiley & Sons, Inc, Hoboken, NJ, pp. 515–546.

Albaigés, J., Kienhuis, P., Dahlmann, G., 2015b. Oil spill identification. In: Fingas, M. (Ed.), Handbook of Oil Spill Science and Technology. John Wiley & Sons, Inc, Hoboken, NJ, pp. 165–204.

Andersson, J.T., 1993. Polycyclic aromatic sulfur heterocycles. III. Photochemical stability of the potential oil pollution markers phenanthrenes and dibenzothiophenes. Chemosphere 27, 2097–2102.

Bernabeu, A.M., Fernández-Fernández, S., Bouchette, F., Rey, D., Arcos, A., Bayona, J.M., et al., 2013. Recurrent arrival of oil to Galician coast: the final step of the *Prestige* deep oil spill. J. Hazard. Mater. 250–251, 82–90.

Christensen, J.H., Tomasi, G., 2016. A multivariate approach to oil hydrocarbon fingerprinting and spill source identification. In: Stout, S.A., Wang, Z. (Eds.), Standard Handbook Oil Spill Environmental Forensics. Academic Press, London, pp. 747–788.

de la Torre, L., Albaigés, J., 2016. Oil pollution in Spanish waters. In: Carpenter, A., Kostianoy, A.G. (Eds.), Oil Pollution in the Mediterranean Sea-Part. II: National Case Studies. Springer, Heidelberg.

Díez, S., Jover, E., Bayona, J.M., Albaigés, J., 2007. *Prestige* oil spill. III. Fate of a heavy oil in the marine environment. Environ. Sci. Technol. 41, 3075–3082.

European Committee for Standardization (CEN), 2006. CEN/TR 15522–1:2006: Oil Spill Identification. In: Waterborne Petroleum and Petroleum Products. Part 1: Sampling. CEN, Brussels.

European Committee for Standardization (CEN), 2012. CEN/TR 15522-2:2012: oil spill identification. In: Waterborne Petroleum and Petroleum Products. Part 2: Analytical Methodology and Interpretation of Results Based on GC–FID and GC–MS Low Resolution Analyses. CEN, Brussels.

Hegazi, A.H., Andersson, J.T., 2016. Polycyclic aromatic sulphur heteroyccles as source diagnostics of petroleum pollutants in the marine environment. In: Stout, S.A., Wang, Z. (Eds.), Standard Handbook Oil Spill Environmental Forensics. Academic Press, London, pp. 313–342.

Radović, J.R., Aeppli, C., Nelson, R.K., Jimenez, N., Reddy, C.M., Bayona, J.M., et al., 2014. Assessment of photochemical processes in marine oil spill fingerprinting. Mar. Pollut. Bull. 79, 268–277.

Further Reading

Christensen, J.H., Tomasi, G., 2007. Practical aspects of chemometrics for oil spill fingerprinting. J. Chromatogr. 1169, 1–22.

CHAPTER

16

Fingerprinting of Petroleum Hydrocarbons in Malaysia Using Environmental Forensic Techniques: A 20-Year Field Data Review

Mohamad P. Zakaria, Chui-Wei Bong and Vahab Vaezzadeh

University of Malaya, Kuala Lumpur, Malaysia

BIOGRAPHIES

Prof. Mohamad Pauzi Zakaria is currently an associate member of the Institute of Ocean and Earth Sciences, University of Malaya, Malaysia. He obtained a Bachelor of Science from Western Michigan University, USA and Master of Science from Florida Institute of Technology and from the University of Massachusetts. Dr. Pauzi obtained his doctorate in organic geochemistry from Tokyo University of Agriculture and Technology, Japan. Pauzi's current research interest is mainly in marine pollution and environmental forensics particularly oil pollution and microplastics in the marine environment. Dr. Pauzi has published extensively in peer-reviewed journals in the subject of marine pollution.

Chui-Wei Bong is a Senior lecturer in the Microbiology, Institute of Biological Sciences and also Head of Coastal Processes Studies and Coastal Engineering Research Unit at Institute of Ocean and Earth Sciences, University of Malaya. She has a Master's degree in microbial ecology (University of Malaya, Malaysia) and a PhD in bacterial enzymology (Ehime University, Japan). Her research interests cover marine ecology, molecular ecology, marine microbiology, and coastal pollution. At present, she is actively working on the impacts of climate variability and anthropogenic activities on the occurrence of resistant and waterborne pathogen in tropical waters.

Vahab Vaezzadeh is a postdoctoral research fellow in the Institute of Ocean and Earth Sciences (IOES), University of Malaya. He began his undergraduate studies at Guilan University, Iran and graduated with a Bachelor of Science in Marine Biology. He obtained a Master of Science in Marine Sciences from Islamic Azad University, Science and Research branch of Tehran, Iran. He received his PhD in Environmental Chemistry from Universiti Putra Malaysia (UPM) under supervision of Professor Mohamad Pauzi Zakaria. He has published several research articles on petroleum and sewage pollution in high-impact journals. Currently, Dr. Vahab is continuing his research on petroleum and sewage pollution and their bioavailability in different environmental compartments of Peninsular Malaysia.

16.1 INTRODUCTION

The beginning of Industrial Revolution in the late 1870s resulted in large consumption of fossil fuels for industrial and transportation purposes. Petroleum pollution has been a prominent problem since the growth of oil production in the 19th century and the pollution from petroleum and its products seems to be increasing in the future. Petroleum contains a wide range of hydrocarbons with various molecular weights such as branched and

Oil Spill Environmental Forensics Case Studies.
DOI: http://dx.doi.org/10.1016/B978-0-12-804434-6.00016-1

saturated alkanes, alkenes, napthenes, aromatics, hydrocarbons containing heavy metals, and hopanes (Abha and Singh, 2012). Petroleum hydrocarbons (PHCs) can be introduced to the environment through various anthropogenic activities such as accidental spillage of oil, sewage sludge, and vehicular and industrial emissions. In this chapter, we include "nonpetroleum" as sources of hydrocarbons as giving rise to PHC. For example, PHCs can be released to the environment by coal, which contains identical hydrocarbons to petroleum since it is generated through similar processes as petroleum (Tripp et al., 1981). In addition, PHCs which are produced through pyrolysis of fossil fuels and wood are also present in the airborne particulate matter, especially in the urbanized and industrialized areas (Bahry et al., 2009).

Oil spills might occur accidentally due to vessel traffic or via usual tanker activities such as ballast water discharges. Spillage of oil might also originate from oil rigs, pipelines, and refineries. Such spills may result from human errors, old equipments, storms and hurricanes, and destructive weapons used during wars. PHCs can be transferred to aquatic environment by atmospheric transport and through precipitation or direct transfer from air to the surface water and also by lateral transport via runoffs which result from heavy rain storms washing out and transferring pollutants to main water bodies including rivers and subsequently coastal and marine environment (Youngblood and Blumer, 1975). Runoff from industrialized and urbanized areas as a major source of PHCs are categorized as nonpoint source pollution (Reddy et al., 2013). Some PHCs such as polycyclic aromatic hydrocarbons (PAHs) have caught great attention from scientists since they are endocrine disruptor, carcinogenic, and mutagenic chemicals. In this study, normal alkanes (*n*-alkanes), hopanes, and PAHs are used to track the sources of petroleum hydrocarbons.

Southeast Asian countries, especially Malaysia, Singapore, and Thailand have gone through massive industrialization and urbanization recently. Peninsular Malaysia maritime borders include Singapore and Indonesia in the south, while land borders with Thailand in the north. Department of Statistics Malaysia reported the Malaysia population at 31.7 million in the year 2016 (Department of Statistics Malaysia, 2016). Similar to other equatorial countries, Malaysia has tropical rainforest climate distinguished by heavy rainfall. Malaysia is characterized by an average humidity of 90%, daylight time of about 12 hours a day, and annual rainfall of around 3150 mm. Such conditions result in abundance of plant life and consequently high amounts of organic matter in the environment. Thus, organic matter which can be associated with lipophilic contaminants is washed out via equatorial precipitation and enter into aquatic environment. The main sources of petroleum pollution in Southeast Asia region were suggested to be oil platforms and heavy oil tanker traffic (Zakaria et al., 2000). Peninsular Malaysia is subject to northeast monsoon bringing atmospheric aerosols from Asian countries towards Malaysia. The mountain range located in the center of Peninsular Malaysia stops the wind currents from west to east and conversely. Peninsular Malaysia is also subject to southwest monsoon bringing hydrocarbons from biomass burning of Sumatra, Indonesia towards Malaysia (Bin Abas et al., 2004a). Burning of forests with agricultural purposes is a significant source of hydrocarbon contamination in Southeast Asia.

Peninsular Malaysia is located between two major water bodies, i.e., the Strait of Malacca in the west and the South China Sea in the east. The Strait of Malacca is similar to a funnel in shape which is narrow in the south and broadens as moving towards the north with a width range of 8 to 220 miles and an average depth of below 23 m (Kasmin, 2010). The Strait of Malacca is the shortest shipping route for transportation of oil tankers from Middle East to Asian countries, such as Japan and China. The Strait has been a strategic route for indigenous and foreign merchants for hundreds of years. On average, 60,000 vessels cross over the Strait of Malacca annually. The number of vessels reached 74,000 in the year 2010 showing heavy vessel traffic in this narrow and shallow waterway, which gives rise to vessel accidents and consequently spillage of petroleum into the marine environment (Jaswar and Maimun, 2010). Between the years 1978 and 1994, about 476 vessel accidents were reported from the Strait of Malacca, while in the five years between 2000 and 2005, 144 petroleum spill incidents were reported. It was pointed out that out of 32,000 vessels crossing over the Strait, 31% were supertankers. The ballast water from the delivered tanker is the most significant form of oil spill related to tanker transportation. An average of two tons of oil is released into the Strait of Malacca on a daily basis merely as a result of tanker ballast water. Beside environmental and ecological negative impacts to important ecosystems such as mangrove forests, spillage of petroleum can damage the tourism industry by fouling the beaches.

Oil fields in the west coast, in and offshore Sumatra Island and even east coast of Peninsular Malaysia can be the origin of oil in the Straits of Malacca (Zakaria et al., 2001). The west coast of Peninsular Malaysia is highly populated, urbanized, and industrialized having numerous rivers which receive land-based pollutants such as municipal effluents, agricultural effluents, industrial discharges, and nonpoint runoffs. There are more than 20 rivers flowing through the west coast of Peninsular Malaysia all ending in the Strait of Malacca. Emissions from large number of automobiles, especially in big cities such as the capital city of Kuala Lumpur can contribute

enormously to hydrocarbon pollution. In addition, boating activities such as fishing, sailing, and recreational activities increase the amounts of PHCs entering into aquatic environment of Peninsular Malaysia (Mirsadeghi et al., 2011). It was estimated that around 10,000 Malaysian fishing boats release up to two tons of oil into the Strait of Malacca every day. PHCs can also be transported from further areas by atmospheric transportation, global ocean circulation, and oil transportation through international marine routes. In Malaysia, the highest petroleum pollution is detected in coastal areas where majority of the human activities are performed (Mirsadeghi et al., 2011).

The South China Sea is rich in terms of oil and natural gas resources and the discovery of oil resources there during the 1950s triggered the pollution from petroleum in the east coast of Peninsular Malaysia. There are numerous offshore oil platforms in the South China Sea. Spillage of petroleum from these oil wells can be transported by water currents to the beaches or even further to the west coast due to the direction of water currents (Zakaria et al., 2001). Petroleum pollution in the east coast can also originate from oil spills as South China Sea is the route for numerous supertankers. Land-based hydrocarbon pollution in the east coast of Peninsular Malaysia commonly originates from urban locations since east coast is less industrialized. However, industrial areas are recently growing in the east coast and hydrocarbon pollution in the east coast need to be addressed as well (Sakari et al., 2008a).

16.1.1 *n*-Alkanes

n-Alkanes are saturated hydrocarbons, i.e., they consist of hydrogen and carbon with solely single bonds. *n*-Alkanes have the formula of C_nH_{2n+2} which shows the maximum bonds between carbon and hydrogen atoms. The main source of global occurrence of *n*-alkanes is petroleum; however, they also occur naturally. *n*-Alkanes can be detected in riverine, estuarine, and marine sediments as well as aquatic organisms (Arora, 2006). The proportion of *n*-alkanes in crude oil can rise up to 35%. Methane (CH_4) is the simplest alkane in the environment. *n*-Alkanes found in nature can have unlimited number of carbons. Epicuticular wax which covers the cuticle of terrestrial higher plants and protects plants from bacterial and fungal harm and water loss consists of long-chain *n*-alkanes with a predominance of odd over even carbon atoms ranging from C_{27} to C_{35}, maximizing at C_{29}. Lower molecular weight *n*-alkanes within the range of C_{15} to C_{19} with predominance of odd carbon atoms, especially C_{17} have algae and cyanobacteria origins (Eglinton and Hamilton, 1963). Higher levels of even number carbon atoms in particular among long-chained *n*-alkanes can be a sign of petrogenic inputs in the environment (Sakari et al., 2008b). Table 16.1 shows different *n*-alkane indices, their application in source type evaluation of hydrocarbons.

16.1.2 Hopanes

Hopanoids are mainly from bacterial membrane lipids and are divided into two groups, biohopanoids and geohopanoids. Biohopanoids, such as bacteriohopanetetrol (BHT), are pentacyclic triterpenoids synthesized by a diverse range of bacteria as cell membrane constituents (Ourisson et al., 1987; Rohmer et al., 1984). Biohopanoids are directly produced by bacteria as part of cell membrane, whereas geohopanoids are generated from biohopanoids through digenesis. Hopanes are among pentacyclic triterpanes, extremely found in membrane lipids of prokaryotes in marine ecosystem. Hopanoids family is also found in higher plants such as lichen, mosses, and ferns.

Being produced naturally, hopanes are found in large quantities on earth. Hopanes are not recognized as pollutants in the environment. Nevertheless, since they are persistent compounds produced through the process of diagenesis by bacteria with various compositions in different oil origins, they can be applied as geochemical biomarkers of oil pollution (Boehm et al., 1982). Hopanes were applied to fingerprint weathered oils 10 years after the release (Wang et al., 1994). Hopanes are among the last products of biohopanoids in the process of diagenesis. It is noteworthy that as gasoline and diesel are lower boiling than hopanes, they do not contain hopanes, while hopanes are present in higher boiling petroleum products, including lubricating oil and asphalt (Lough et al., 2006).

Hopanes are recognized based on the number of carbon and their side-chain and rings configuration. Three sterioisomeric forms of hopanes are as follows: 17α(H),21β(H)-, 17β(H),21β(H)-, and 17β(H),21α(H)-hopanes. Petroleum biomarkers are hopanes in the range of C_{27}−C_{35} having a naphthenic structure consisting of four six-member rings and one five-member rings and configuration of αβ. The αβ configuration is more thermodynamically persistent when compared to other configurations (ββ and βα). The ββ-isomers which are commonly found

TABLE 16.1 *n*-Alkane indices and their application in source type evaluation of hydrocarbons

n-Alkane indices	Origination	Application	References
Terrigenous/aquatic ratio (TAR)	TAR is based on abundance of C_{27}, C_{29}, and C_{31} *n*-alkanes in terrestrial plants versus abundance of C_{17}, C_{19}, and C_{21} *n*-alkanes in marine-based vegetation.	A value above 1 indicates land-based, while a value below 1 shows marine-based biogenic source *n*-alkanes.	Eglinton and Hamilton (1963)
Carbon preference indices (CPI)	CPI is derived from the predominance of odd over even carbon number *n*-alkanes in epicuticular wax of terrestrial plants.	A value from 5 to 10 is a sign of terrestrial plant origin *n*-alkanes, while a value near 1 indicates petrogenic inputs, marine organisms, and/or recycling organic materials.	Mazurek and Simoneit (1984)
Average chain length (ACL)	ACL is based on average number of carbon atoms for *n*-alkanes having vascular plant origin.	Values are constant in locations with the same source of *n*-alkanes, depending upon latitude and climatic condition, while petroleum inputs decrease the values of ACL.	Poynter and Eglinton (1987)
Low molecular weight (LMW) *n*-alkanes (C_{10}–C_{23})/high molecular weight (HMW) *n*-alkanes (C_{24}–C_{36})	LMW *n*-alkanes are abundant in fresh oil inputs, while HMW *n*-alkanes can have heavy and degraded oil as well as terrestrial plant origins.	A value below 1 can indicate higher heavy and degraded oil as well as terrestrial plant origin *n*-alkanes, whereas a value above 1 is a sign of fresh oil inputs.	Wang et al. (2006)
Unresolved complex mixture (UCM)	UCM is comprised of acyclic and branched alkanes which cannot be distinguished by the Gas chromatography (GC) and therefore, appears as a hump in GC chromatograms.	UCM is a sign of degraded oil and indicates chronic petroleum hydrocarbon pollution.	Simoneit (1982)
C_{17}/pristane (C_{17}/Pr) and C_{18}/phytane (C_{18}/Ph)	Branched alkanes (pristane and phytane) are more resistant to degradation than straight-chain C_{17} and C_{18} *n*-alkanes.	A value below 1 can be a sign of weathered oil, while a high value of C_{17}/pristane (i.e., $\gg$2) indicates phytoplankton origin of *n*-alkanes.	Readman et al. (2002) Pavlova and Papazova (2003)
Pristane/phytane (Pr/Ph)	Phytane mainly originates from petroleum, while pristane has higher biogenic contribution.	A value below 1 is a sign of petroleum inputs, while a value above 1 (commonly within the range of 3 to 5) is a sign of less contaminated areas.	Blumer et al. (1963)

in living organisms alter to more thermodynamically stable αβ and βα configuration during maturity of oil, therefore, they are depleted in petroleum (Wang et al., 2006). The αα series are more stable than ββ configuration; however, they are not produced naturally and are usually neglected (Wang et al., 2006). In order to investigate thermal maturity of different samples from similar source, T_s (18α(H)-22,29,30-trisnorneohopane) and T_m (17α(H)-22,29,30-trisnorhopane) can be applied as a sensitive tool (Wang et al., 2006). Homohopanes (C_{31} to C_{35}) can be in two homologues, i.e., 22S and 22R configurations, as they have an extra side chain on C_{22} as opposed to hopanes with 30 or less carbon atoms. In petroleum source hopanes, 22S homologues for C_{31} homohopane is slightly higher than 22R (Peters and Moldowan, 1993).

According to previous studies, the signature of two main types of crude oils, i.e., Middle East crude oil and South East Asia crude oil (MECO and SEACO) were mainly found in the west coast of Peninsular Malaysia (Zakaria et al., 2001). Both MECO and SEACO contain 17α,21β(H) C_{30} hopane (C_{30} 17α) and 17α,21β(H) C_{29} hopane (C_{29} 17α) and common 17α,21β(H), 22S and 22R homohopanes from C_{31} to C_{35}. Nonetheless, SEACO, which is the type of oil from Southeast Asia oil fields, has an abundance of hopanoids originating from higher plants. Considering the fact that SEACO originates from nonmarine (i.e., lacustrine and deltaic) shale source rocks, it has lower ratios of C_{29}/C_{30} and C_{31}–C_{35}/C_{30} than MECO oil. MECO oil originates from marine carbonate source rocks and has higher ratios of C_{29}/C_{30} and C_{31}–C_{35}/C_{30}. The decisive factor is the predominance of C_{29} 17α over C_{30} 17α in MECO and depletion of C_{31}–C_{35} homohopanes in SEACO (Zakaria et al., 2000). In other words, SEACO is less abundant in C_{29} 17α norhopane and C_{31}–C_{35}, especially C_{35} homohopanes. Thus, in order to recognize these two crude oil origins, the ratios of C_{29}/C_{30} and ΣC_{31}–C_{35}/C_{30} which are normalized by C_{30} 17α can be used. The ratio of C_{29}/C_{30} ranges between 1.41 to 2.01 and 0.85 to 1.16 in MECO and SEACO oil, respectively (Zakaria et al., 2002). The ratio of ΣC_{31}–C_{35}/C_{30} ranges between 1.80 to 2.30 and 0.41 to 0.89 in MECO and SEACO, respectively. Furthermore, the ratio of T_m/T_s ranges widely among MECO (0.35–2.31),

TABLE 16.2 Hopane-based diagnostic ratios in crude oil, fresh and used crankcase oil, street dust, and asphalt

	Hopanes ratios		
	C_{29}/C_{30} [a]	$\Sigma C_{31}-C_{35}/C_{30}$ [b]	T_m/T_s [c]
MECO			
Arabian Light	2.01	1.80	2.31
Umm Shaif	1.56	2.30	0.76
Marban	1.41	1.86	0.35
SEACO			
Labuan	0.98	0.48	2.2
Miri	0.85	0.41	1.49
Tapis	1.16	0.89	1.43
Sumatra	0.85	0.78	0.52
FRESH CRANKCASE OIL			
Petronas	1.52	3.00	0.70
BP	1.32	2.93	1.00
USED CRANKCASE OIL			
Petronas gas station	2.04	1.69	0.92
Yong motor workshop	2.66	1.2	0.62
Home auto mechanic	1.81	1.87	0.71
Motorcycle workshop	1.56	2.08	0.72
STREET DUST			
Kl-1	1.64	2.47	1.12
KL-2	1.62	2.75	1.41
KL-3	1.57	2.55	1.33
ASPHALT			
Asphalt-1	1.66	3.2	1.58
Asphalt-2	1.66	3.6	2.04

[a] *C_{29}/C_{30} = ratio of 17α, 21β (H)-30-norhopane to17α, 21β (H)-hopane.*
[b] *$\Sigma C_{31}-C_{35}/C_{30}$ = ratio of sum of 17α, 21β (H)-C_{31} homohopanes to 17α, 21β (H)-C_{35} homohopanes relative to 17α, 21β (H)-hopane.*
[c] *T_m/T_s = ratio of 17α-22,29,30-trisnorhopane over 18α-22,29,30-trisnorhopane.*

whereas the range of this ratio is narrower among SEACO (0.53 to 2.20). Such differences reveal the different geological processes in the formation of crude oils. Table 16.2 shows the values of C_{29}/C_{30}, $\Sigma C_{31}-C_{35}/C_{30}$ and T_m/T_s ratios in SEACO and MECO, fresh and used crankcase oil, street dust, and asphalt, previously reported from Peninsular Malaysia (Zakaria et al., 2002).

Another factor used to recognize SEACO from MECO is abundance of oleanane in SEACO. The origin of higher amounts of oleanane in SEACO is land plants, while MECO originates from marine source and is depleted in oleanane. However, the ratio of oleanane/C_{30} in SEACO varies in long range between 0.11 and 1.53, therefore, high ratio of oleanane/C_{30} can be an indication of SEACO oil, whereas low ratio cannot necessarily be a sign of MECO (Okui et al., 1997). Heterogeneous inputs of plants as well as thermal maturation of oil can modify this ratio.

16.1.3 Polycyclic Aromatic Hydrocarbons

PAHs have been listed by United States Environmental Protection Agency (USEPA) as priority pollutants. PAHs are ubiquitous contaminants in the environment, consisting of two or more fused aromatic rings (Blumer,

1976). Naphthalene ($C_{10}H_8$) with two fused aromatic rings has the lowest molecular weight amongst PAHs. Generally, PAHs are classified as lipophilic contaminants meaning they tend to attach to organic matter and not dissolve in water. However, LMW PAHs with two or three rings are more water soluble and are known as acute toxins to humans and organisms. HMW PAHs are less water soluble and being more carcinogenic and mutagenic, their effects are long lasting (Neff, 1979). PAHs such as chrysene, benzo(a)anthracene, benzo(a)pyrene, benzo(b)flouranthene, and benzo(ghi)perylene are among potentially carcinogenic PAHs (Guillén et al., 2000).

PAHs are released into the environment via anthropogenic and natural sources. There are two sources of anthropogenic PAHs in the environment, i.e., pyrogenic and petrogenic sources. Pyrogenic PAHs enter into aquatic environment from automobile and industrial emissions, waste incineration, and smelting. Petrogenic PAHs originate from crude and refined petroleum and petroleum products such as petrol, diesel, lubricating oil, kerosene, tar, and asphalt (Baumard et al., 1998). Petrol leaks, vehicle tire-wear particulates, used crankcase oil and asphalt road materials are among the petrogenic sources of PAHs in urban runoffs (Zakaria et al., 2002).

In addition to parent (unsubstituted) PAHs, alkylated PAHs are very applicable in source identification of PHCs. As it can be inferred from the name, alkylated PAHs such as methylphenanthrene, 7,12-dimethylchrysene, and 2,3,5-trimethylnaphthalene are PAHs that contain alkyl groups in different forms and numbers. Alkylated PAHs are abundant in crude oils, whereas parent PAHs are depleted in crude oils and exist only in small amount with predominance of LMW PAHs over HMW PAHs. For instance, crude oil or diesel fuel contain LMW PAHs concentrations at 17 to 23 times higher than HMW PAHs (Qian et al., 2001). As compared to parent PAHs, alkylated PAHs are known to be more abundant, persistent in the environment, bioaccumulative and toxic, and also less water soluble. Therefore, alkylated PAHs are a sign of petrogenic PAHs such as petroleum and its products (McGuinness and Dowling, 2009).

In order to identify source of PAHs, a number of diagnostic ratios are commonly used. These diagnostic ratios have been applied in various studies in order to infer the source of PAHs (Budzinski et al., 1997; Magi et al., 2002; Sicre et al., 1987; Soclo et al., 2000). PAHs coming from petroleum and petroleum products can be recognized from PAHs derived from petroleum or biomass combustion with the help of these ratios. These ratios are either based upon the ratio of alkylated over unsubstituted PAHs or various concentrations of parent PAHs.

The ratio of LMW/HMW PAHs is based upon a simple principle that LMW PAHs are more abundant in petrogenic PAHs, while HMW PAHs are more abundant in pyrogenic PAHs. Therefore, when the ratio of LMW/HMW PAHs is below and above 1, it is indicative of pyrogenic and petrogenic sources of PAHs in the environment, respectively. The ratio of methylphenanthrenes over phenanthrene (MP/P) is one of the ratios used commonly for source identification of PAHs. The ratio of MP/P between 0.5 to 1 shows combustion source of PAHs in the environment and the ratio between 2 to 6 demonstrates domination of fossil fuels (Budzinski et al., 1997; Garrigues et al., 1995; Prahl and Carpenter, 1983). In general, the ratio for combustion sources is lower than the ratio for petroleum (Takada et al., 1991). Despite the importance of MP/P ratio in source identification of PAHs, it can be easily affected by environmental conditions. Another ratio is sum of methylfluoranthenes and methylpyrenes to fluoranthene [(MFlu + MPyr)/Flu] (Gustafsson et al., 1996; Laflamme and Hites, 1978; Youngblood and Blumer, 1975). The ratio above 1 shows petrogenic source of PAHs, while the ratios below 1 is a sign of pyrogenic sources of PAHs. The ratio of fluoranthene to the sum of fluoranthene and pyrene [Flu/(Flu + Pyr)] is another diagnostic ratio for source identification of PAHs (Chen et al., 2012; Li et al., 2011). The ratio above 0.5, between 0.4 and 0.5, and below 0.4 indicates PAHs originating from combustion of wood, grass, and coal, petroleum combustion, and petrogenic sources, respectively. The ratio of anthracene to phenanthrene plus anthracene [Ant/(Ant + Phe)] is also used for identification of PAHs sources in the environment (Chen et al., 2012). If the ratio is more than 0.1, PAHs originate from petrogenic sources. The ratio of lower than 0.1, however, is a sign of pyrogenic sources of PAHs. The ratio of Phe/Ant > 15 is a sign of petrogenic PAHs, while lower values signify pyrogenic source PAHs. Another ratio used for source recognition of PAHs is benz(a)anthracene to the sum of benz(a)anthracene and chrysene [B(a)An/(B(a)An + Chry); (Yunker et al., 2002)]. The ratio between 0.2 and 0.35 is a sign of mixed petrogenic and pyrogenic sources of PAHs, above 0.35 shows pyrogenic source of PAHs from vehicular emission, and less than 0.2 indicates petrogenic sources of PAHs. Finally, the ratio of indeno(1,2,3-cd)pyrene to the sum of indeno(1,2,3-cd)pyrene and benzo(g,h,i)perylene [IcdP/(IcdP + BghiP)] is used to differentiate sources of PAHs. When the ratio is less than 0.2, petroleum is the most probable source of PAHs, while the ratio between 0.2−0.5 and more than 0.5 is indicative of petroleum combustion and coal, wood, and grass combustion, respectively (Yunker et al., 2002). Fig. 16.1 illustrates PAH cross plots for the ratios of mass 202 isomers Flu/(Flu + Pyr), mass 228 isomers BaA/(BaA + Chry), and mass 279 isomers IcdP/(IcdP + BghiP) versus MP/P.

Fate and behavior of PAHs are to high extents dependent upon their physical and chemical characteristics. Since PAHs are hydrophobic compounds, they have high tendency to attach to suspended matters and end up in

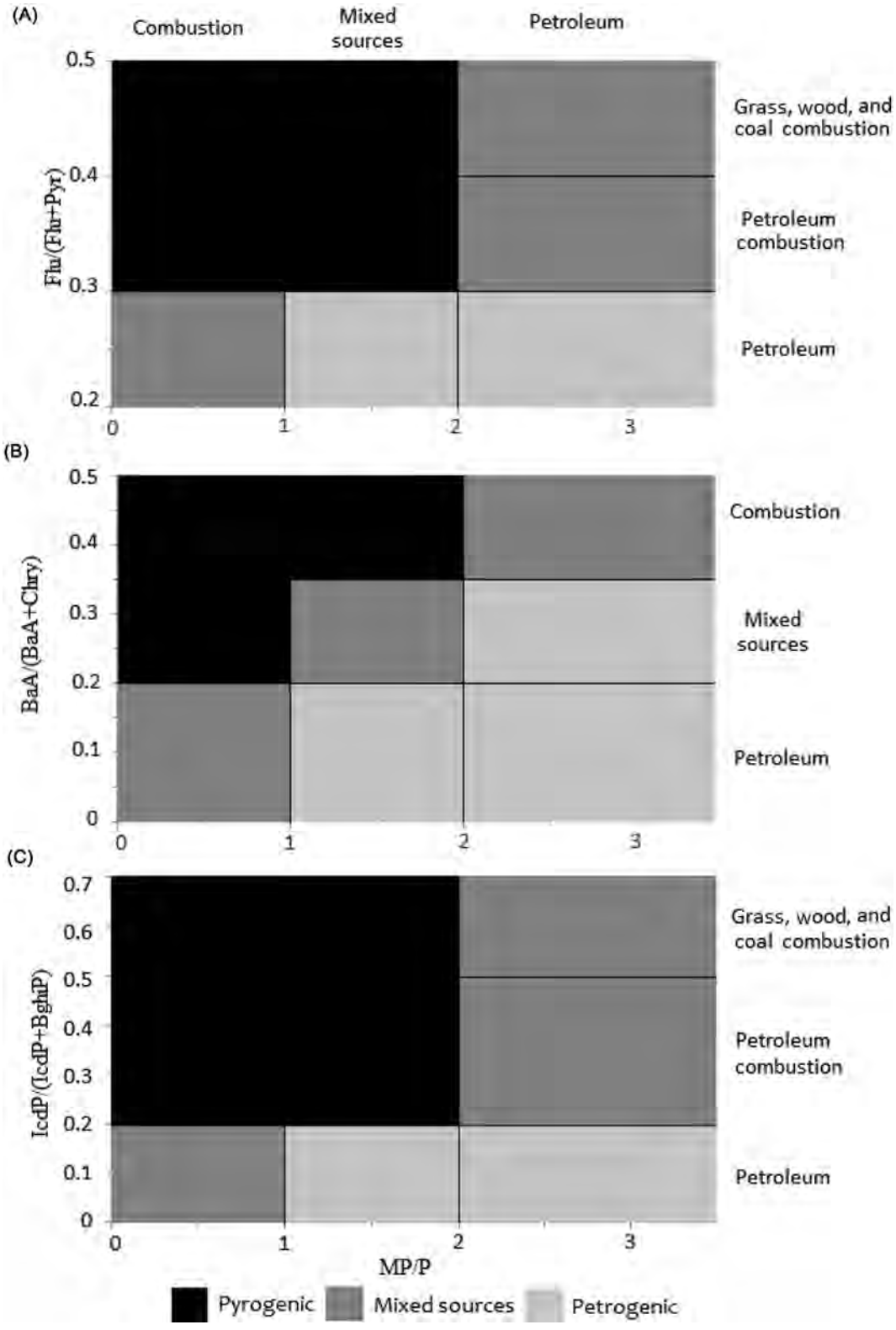

FIGURE 16.1 PAH cross plots for the ratios of (A) fluoranthene/(fluoranthene + pyrene), (B) benz(a)anthracene/(benz(a)anthracene + chrysene), (C) indeno(1,2,3-cd)pyrene/ (indeno(1,2,3-cd)pyrene + benzo[ghi]perylene) versus MP/P.

the sediment. LMW PAHs are more volatile, water soluble, and consequently more bioavailable, whereas HMW PAHs, which have high octanol–water partition coefficient (Kow), associate with particle cores and are less bioavailable and more recalcitrant to biodegradation. Higher availability of LMW PAHs results in more susceptibility of these compounds to different physicochemical loss such as evaporation, dispersion, dissolution, and photooxidation and biological loss such as digestion by benthic animals and microbial degradation. LMW PAHs are more bioavailable to filter-feeders and more probable to be absorbed by these organisms (Baumard et al., 1999).

Climatic conditions of a particular area can also have an impact on PAHs behavior and fate. Considering heavy rainfall in countries with tropical rainforest climate such as Malaysia, a great deal of sediment washout occurs. Consequently, rivers contain huge amounts of particulate matters as they enter the realm of salinity regime resulting in active sedimentation in the estuaries. Such extra sediment load causes dilution of PAHs in the sediment (Zakaria et al., 2002). This might be one of the reasons behind lower concentrations of PAHs in coastal areas of these countries as compared to other parts of the world.

16.2 MATERIALS AND METHODS

16.2.1 Sample Collection

Source materials, tar balls, aerosols, water, suspended particulate matter (SPM), sediments, and different shellfish species were collected from Peninsular Malaysia and analyzed for PHCs. Three types of MECO, including Marban, Ummu Shaif, and Arabian Light as well as four types of SEACO, including Tapis, Labuan, Miri, and Sumatra, were collected with the help of Maritime Agency of Japan. As for lubricating oils, they were randomly provided from the Malaysian market. Tar balls were collected from tidal areas of Peninsular Malaysia. Aerosols were collected from nine stations around Peninsular Malaysia. A high volume air sampler was used fitted with annealed (300°C for 8 hours) glass fiber filters (20.3 25.4 cm) situated at 2 m height for 24 hours. Water samples were collected with a Niskin bottle. SPM was immediately collected with the help of a classic vacuum system using 0.45 Millipore μm preweighed filters. Surface sediment (i.e., 0–5 cm layer, which represents modern inputs of pollution) was collected using an Ekman dredge. Core sediment was collected using a stainless steel gravity corer (i.e., 3 cm) and sliced in 3 cm intervals to record the history of pollution. A total of 20–40 individual shellfish was collected from the study area in Peninsular Malaysia. Sampling locations were selected to represent polluted areas as well as less polluted areas and remote sites of Peninsular Malaysia. The stations were selected based on their proximity to "hot spots" (i.e., locations with various anthropogenic activities). All samples were transferred on ice to the lab to avoid any microbial degradation of organic compounds during transportation and stored at −20°C until the day of analysis. The map of sampling locations is shown in Fig. 16.2.

16.2.2 Chemicals and Glassware

Chemicals and standards were purchased from Merck, Germany and Sigma Aldrich, United States. Solvents including dichloromethane (DCM), hexane, methanol (MeOH), acetone, isooctane, and diethyl ether were all high performance liquid chromatography (HPLC) grade. All kinds of glassware such as flasks, beakers, chambers, pipettes, and chromatography columns were washed with phosphate-free detergents and rinsed with tap water. Glassware was then rinsed with distilled water. Next step was to solvent-rinse glassware for three times using methanol, acetone, and *n*-hexane, respectively. After rinsing with solvents, glassware was wrapped in aluminum foil and put in an oven at 60°C for 2 hours to dry. The glassware was stored in a clean place before usage for analysis to avoid any cross contamination.

16.2.3 Standards and Standard Mixtures

External standards of *n*-alkanes consisted of even number *n*-alkanes (C_{10}–C_{40}). 17β(H), 21β(H)-hopane (C_{30}17β,21β) was applied as hopanes internal injection standard (IIS). As for hopanes standard mixtures, T_m (17α(H)-22,29,30-trisnorhopane), 17α(H), 21α(H)-30-norhopanes, 17α(H), 21β (H)-hopane, and 17β (H), 21α (H)-hopane besides proper concentrations of hopanes IIS were applied. The IIS for PAHs was p-terphenyl-d_{14}, while surrogate internal standard (SIS) for PAHs consisted of naphthalene-d_8, anthracene-d_{10}, benz[*a*]anthracene-d_{12}, and perylene-d_{14}. Standard mixtures of PAHs consist of specific concentrations of IIS and SIS for PAHs and 16

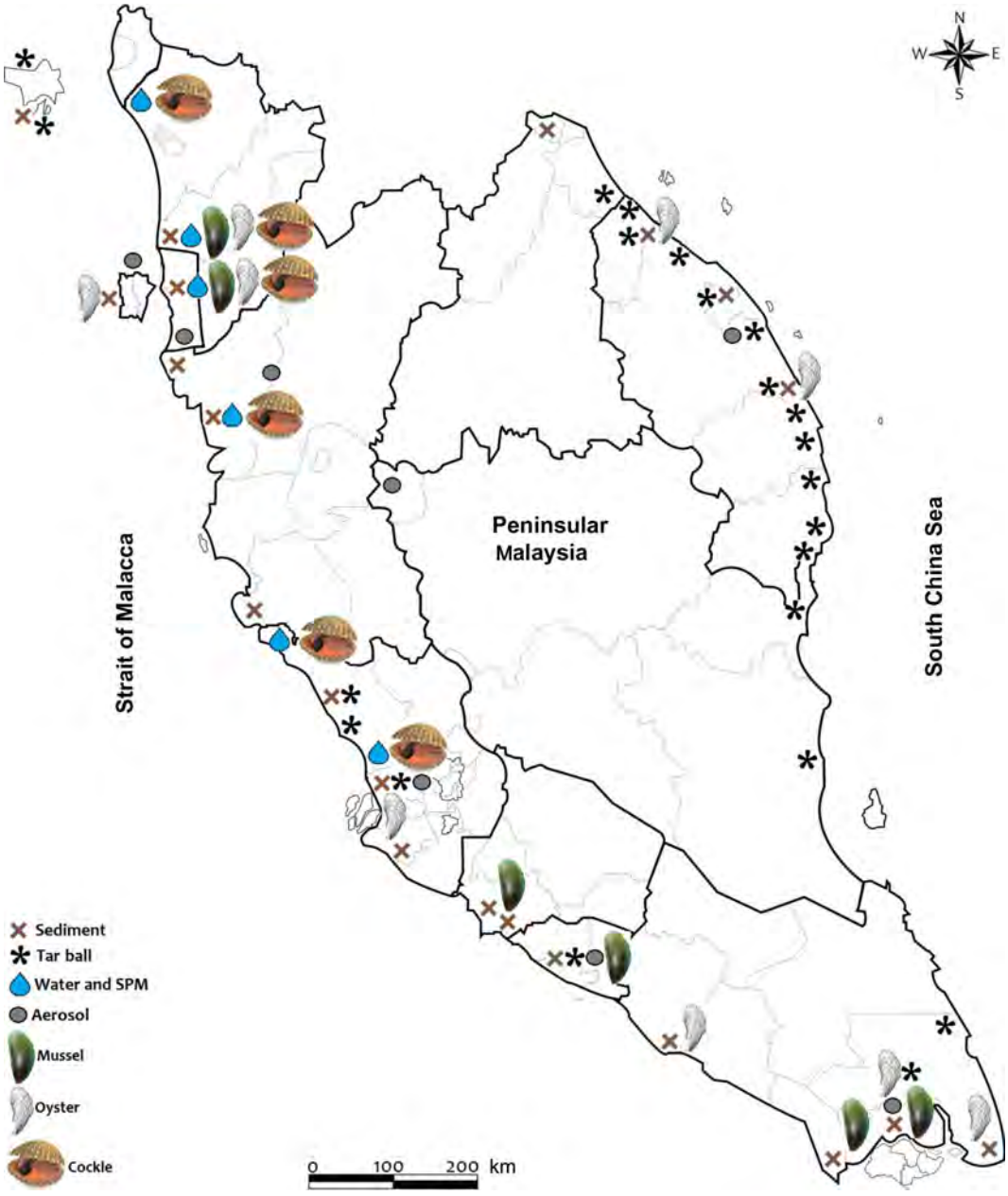

FIGURE 16.2 Map of sampling locations in Peninsular Malaysia.

USEPA priority PAHs, including naphthalene, acenaphthylene, acenaphthene, fluorine, anthracene, phenanthrene, fluoranthene, pyrene, chrysene, benz(a)anthracene, benzo(b)fluoranthene, benzo(k)fluoranthene, benzo(a) pyrene, dibenz(a,h)anthracene, benzo(g,h,i)perylene, and indeno(1,2,3-cd)pyrene.

16.2.4 Analytical Procedure

In order to remove water, samples were freeze-dried using a freeze-drier. In order to avoid possible cross-contamination while freeze-drying, samples were covered by aluminum foils with a number of pin holes on top. The process of freeze-drying might take up to 72 hours depending upon samples moisture. Freeze-dried samples were then stored frozen to perform extraction process afterwards. A soxhlet apparatus with 250 mL DCM as solvent was used for sample extraction. Up to 10 g of freeze-dried samples were weighed and added into thimble cellulous. A volume of 50 μL of 10 ppm SIS for PAHs was spiked to the samples in this stage using a

micropipette to qualify extraction and fractionation processes. Thimble cellulous was placed in glass chamber and extraction was performed for 10 hours. The extracts were collected in the bottom-round flasks and the sediment extracts were treated with copper granules. Copper granules are used to get rid of sulfur as an element which may cause pick overlaps in GC results. Sulfur is an element produced during degradation of organic matter in anoxic condition. The extracts volume was then reduced using a rotary evaporator and transferred to pear-shape flasks for further analysis.

Silica gel with pore size of 60ǫA and mesh size of 63−200 μm was applied as stationary phase for first and second-step column chromatography. Silica gel was baked at 400°C for 4 hours and at 200°C for another 4 hours. Since the purpose of first-step column chromatography is to separate polar compounds, silica gel was deactivated with 5% H_2O to trap polar compounds and separate them from nonpolar compounds. After deactivation, silica gel was packed in first-step column with 9 cm height and 0.9 cm internal diameter, gradually. Anhydrous sodium sulfate (Na_2SO_4) was added on top of packed silica gel to avoid water interference. Prior to use, Na_2SO_4 was baked at 400°C for 4 hours and cooled down to 120°C and kept in desiccator. Sample extracts were then spiked into the first-step column. Exactly 20 mL hexane/DCM (3:1, v/v) was used as an elution solvent for hydrocarbon fraction.

In order to fractionate *n*-alkanes, hopanes, and PAHs, second-step column chromatography was performed. The elution from first-step column chromatography was rotary evaporated to reduce the volume to 1−5 mL. Fully activated silica gel was packed into second-step column with 0.47 cm internal diameter and 18 cm height. After packing, samples were spiked into the column and 4 mL of *n*-hexane was used to collect *n*-alkane and hopane fraction. Another 4 mL *n*-hexane was added for linear alkylbenzenes (LABs) fraction. LABs fraction was discarded since LABs were not targeted in this research. Finally, 16 mL of hexane/DCM (3:1, v/v) was used in order to collect PAHs fractions.

The first fraction (aliphatic hydrocarbons and biomarkers) from second-step column chromatography was rotary evaporated to about 1 mL and transferred to a 1.5 mL amber vial. A gentle stream of nitrogen gas was applied to evaporate 1 mL sample to near dryness. Later, the sample was redissolved using 100 μL of isooctane and injected into GC−MS Shimadzu QP5050A model to analyze *n*-alkanes. The same elution was used for analysis of hopanes. The elution was evaporated to near dryness with gentle stream of nitrogen gas and redissolved in 50 μL of IIS for hopane [10 ppm 17β (H), 21β (H)-hopane in isooctane] prior to injection to GC−MS. After nitrogen blow down, PAHs fractions were redissolved in 200 μL of p-terphenyl-d_{14} in isooctane as PAH IIS. IIS is applied for quantification of target compounds and determination of possible error during injection. IIS is a very stable isomer and although it is not present in the samples, the pick is very near to target compounds in the samples. Helium with 99.9% purity was applied as carrier gas. A BPX-5Ms-fused silica capillary column having 30 m length, 0.25 mm internal diameter, and film thickness of 0.25 μm was applied. Temperature trend for column was 70°C for 1 minute, increased 30°C per minute to 150°C, and then 5°C per minute to 310°C and stayed in that temperature for 10 minutes. Different concentrations of external standards were injected with every batch of samples for quantification of target compounds. Identification of target compounds was made by comparing the retention time of the target compound with that of authentic standard and mass/charge ratio (m/z) of target analytes. Hopanes were detected at $m/z = 191$. Quantification was made via comparison of integrated peak area of the sample with peak area of the standard. Compounds with no corresponding peak on the standard were quantified with the help of standard peak area which bracket the target compound peak area.

16.2.5 Quality Control and Quality Assurance

The major purpose of quality control (QC) and quality assurance (QA) is to realize the possible errors during extraction procedure and justify the procedure to reduce the possibility of such errors. In the present study, various concentrations of standard mixtures from 0.5 to 10 ppm were injected with every batch of *n*-alkane, hopane, and PAH samples. In order to evaluate percentage of recovery from each sample, 50 μL of four SIS for PAHs was added to the samples before the extraction by soxhlet apparatus and PHCs analysis procedures were repeated when the recovery was not within the range 60%−120%. Concentrations of target PAHs were recovery corrected considering volatility features of PAHs, especially LMW ones. IIS was added to each sample right before injection to recognize any possible error during injection. Detection limits were estimated for individual PHC compounds as three times the baseline of measured chromatograph. Reproducibility of the analyses was tested by performing replicate analysis. The variation coefficient was below 10% for individual PHC compounds. In order to detect possible cross-contamination from various sources such as glassware or solvents during analytical procedure, a

method blank was performed with every batch of samples. Since method blank undergoes the same procedure as the rest of samples, if levels of any target compound in method blank was detected more than quality control levels or if any cross-contamination was detected that can be effective on results from GC, the whole procedures should be repeated for that batch of samples. Daily auto tuning of the gas chromatography–mass spectrometry (GC-MS) was performed in order to check the instrument condition. A column purge programme was constantly used to clean GC-MS column.

16.2.6 Determination of Total Organic Carbon

In order to dry the sediment samples, they were thawed and placed in an oven at 60°C overnight. Dried samples were ground with mortar and pestle. Then sediment samples were homogenized using a 2 mm mesh sieve. One to two g of dried samples was weighed and acidified using 1–2 mL of 1 M HCl in order to remove all inorganic carbon. Samples were dried and HCl was eliminated by placing samples at 100–105°C for 10 hours. Aliquots of the samples were weighed and analyzed to evaluate total organic carbon (TOC%). For this purpose, a LECO CR-412 Carbon Analyzer with 1350°C furnace temperature for 60 seconds was used (Raza et al., 2013).

16.2.7 Determination of Lipid Content

Since PHC are lipophilic compounds and tend to accumulate in lipid tissues of the oysters, lipid content was measured. Gravimetrical method was applied for determination of lipid content. Homogenized oyster soft tissue was weighed and dried using anhydrous sodium sulfate. Dried sample was then soxhlet extracted for 10 hours. An aliquot of the extract was separated and diethyl ether and hexane with 3:1 volume ratio was added to the aliquot and stirred. Then the sample was dried using gentle stream of nitrogen and weighed (Tanabe et al., 1987).

The following equation was applied to measure lipid content:

$$L_w = W_r \times V_f / (W_s \times V_a) \times 0.1,$$

where L_w = lipid weight (content) %; W_r = residual weight of aliquot (mg); W_s = weight of sample (g); V_f = final volume of extracted sample; V_a = volume of aliquot separated for lipid content determination.

16.3 RESULTS AND DISCUSSION

16.3.1 Use of *n*-Alkanes as Source Identifiers of PHCs in Malaysia

n-Alkanes have been investigated in various types of environmental samples in Malaysia. As it was mentioned earlier, there are various *n*-alkanes indices which are useful for source identification of hydrocarbons. The concentrations and range of different *n*-alkanes indices in various types of environmental samples of Malaysia are shown in Table 16.3. *n*-Alkanes can occur from natural sources such as terrestrial plants, algae, and other unicellular planktons. Anthropogenic *n*-alkanes, however, originate from petroleum and products of petroleum. These persistent and ubiquitous compounds are widely used for source identification of petroleum hydrocarbon in the aquatic environment.

Tar balls were collected from various beaches of Peninsular Malaysia and studied for source identification of PHCs (Zakaria et al., 2001, 2000). No UCM appeared on the gas chromatography - flame ionization detector (GC-FID) chromatograms indicating recently released oil with no weathering and biodegradation which settled down on the beach immediately after release. As shown in Table 16.3, some *n*-alkanes indices were measured in MECO and SEACO which are the two most abundant crude oils in aquatic environment of Malaysia. The range of the ratios of isoprenoids, pristane/phytane, was from 0.64 to 0.97 and 2.91 to 4.03, while the range of ratios of LMW/HMW *n*-alkanes were 3.4 to 4.6 and 1.6 to 4 in MECO and SEACO, respectively (Zakaria et al., 2000). The ratios of LMW/HMW *n*-alkanes in tar balls were between 0.21 and 0.75 which is lower than crude oil. The ratio of LMW/HMW *n*-alkanes can be easily changed via environmental conditions and other biomarkers are more reliable for source identification of petroleum hydrocarbons.

Despite depletion of LMW *n*-alkanes in tar balls, UCM as a sign of weathered oil was absent. It was concluded that the reason behind the depletion of LMW *n*-alkanes in tar balls is that petroleum pollution was coming from tanker washing and discharge of ballast water from SEACO oil tankers and not due to weathering. SEACO contains paraffin wax, which can separate from the oil during transportation and cover the tanker wall. These oil

TABLE 16.3 The concentrations (ng/g) and indices of *n*-alkanes in samples from the west and east of Peninsular Malaysia

***n*-Alkanes indices**	**SEACO**	**MECO**	**West Peninsular Malaysia**	**East Peninsular Malaysia**	**East Coast Rivers**	**Perai Strait (west)**	**Klang River (west)**	**Langet River (west)**	**Langet River (west)**	**West Peninsular Malaysia**
Sample type	Crude oil	Crude oil	Tar balls	Tar balls	SS	SS	SS	SS	SPM	SS
CPI[a]	1.07–1.34	0.90–0.96	0.99–1.09	1.05–1.08	0.02–3.35	0.00–1.22	1.09–1.21	1.9–8.96	1.43–1.97	0.35–2.11
ACL[b]	na	na	na	na	25.52–32.95	26.75–32.94	29.43–29.65	29.2–30.5	28.4–29.3	26.74–29.23
MH[c]	na	na	na	na	C_{26}&C_{32}	C_{18}&C_{20}	C_{29}	C_{29}&C_{31}	C_{24}&C_{26}	C_{29}
L/H[d]	1.62–4.52	3.35–4.60	0.00–1.72	0.80–1.31	0.04–10.73	0.01–13.32	na	na	na	0.15–1.26
Pr/Ph[e]	2.91–4.03	0.64–0.97	nd–4.14	0.69–2.19	na	nd[j]	nd	0.65–1.52	0.59–0.85	0.65–1.81
C17/Pr[f]	na	na	na	na	na	nd	0.51–0.87	0.47–0.56	0.2–0.39	0.38–2.52
C18/Ph[g]	na	na	na	na	na	nd	nd	0.38–1.13	0.99–1.11	0.29–4.80
UCM[h]	x	x	x	x	o	o	o	o	o	o
∑*n*-alkanes[i]	52,100,000–127,100,000	24,900,000–49,000,000	400,000–192,000,000	16,000,000–108,000,000	1000–7,168,000	421,000–10,770,000	9,600,000–27,200,000	1,700,000 – 8,600,000	5,900,000 – 23,000,000	27,945–254,463
References	Zakaria et al. (2000)	Zakaria et al. (2000)	Zakaria et al. (2001)	Zakaria et al. (2001)	Sakari et al. (2008a)	Sakari et al. (2008b)	Bakhtiari et al. (2010)	Bakhtiari et al. (2009)	Bakhtiari et al. (2009)	Vaezzadeh et al. (2015)

[a] *overall CPI = carbon preference index* $(C_{15}\text{-}C_{35}) = \frac{1}{2} \times [(C_{15} + C_{17} + C_{19} + C_{21} + C_{23} + C_{25} + C_{27} + C_{29} + C_{31} + C_{33}) + (C_{17} + C_{19} + C_{21} + C_{23} + C_{25} + C_{27} + C_{29} + C_{31} + C_{33} + C_{35}) \div (C_{16} + C_{18} + C_{20} + C_{22} + C_{24} + C_{26} + C_{28} + C_{30} + C_{32} + C_{34})]$.

[b] *ALC = average carbon chain value of odd carbon numbers from* C_{25} *to* $C_{33} = [(25 \times (C_{25}) + 27 \times (C_{27}) + 29 \times (C_{29}) + 31 \times (C_{31}) + 33 \times (C_{33})) \div (C_{25} + C_{27} + C_{29} + C_{31} + C_{33})]$.

[c] *MH = Maximum* n*-alkane carbon number.*

[d] *L/H = sum of LMW* n*-alkanes over sum of HMW* n*-alkanes.*

[e] *Pr/Ph = ratio of pristane over phytane.*

[f] C_{17}*/Pr = ratio of* C_{17} n*-alkane over pristine.*

[g] C_{18}*/P = ratio of* C_{18} n*-alkane over phytane.*

[h] *UCM = unresolved complex mixture, o = majority present, x = majority not present.*

[i] ∑n*-alkanes = sum of aliphatic hydrocarbons between* C_{10}–C_{36}.

[j] *nd = not detected.*

compounds consist of higher HMW *n*-alkanes and PAHs compared to the crude oil. When oil tankers are washed, these compounds are released to the aquatic environment changing the ratio of LMW/HMW *n*-alkanes and PAHs to lower values. Spillage of SEACO can also contribute to this trend. The concentrations of *n*-alkanes ranged from 24,900,000 to 49,000,000 ng/g and 52,100,000 to 127,000,000 in MECO and SEACO, respectively. The levels of *n*-alkanes in mussels from two different locations in Johor Bahru and a location in Malacca were detected at 655, 498 and 191 ng/g dw, respectively (Zakaria et al., 2000).

n-Alkanes have been widely studied in sediments of Malaysia and high concentrations were detected. Concentrations of 8170, 670, and 4670 ng/g dw were detected in the sediments of Malacca, Port Klang, and Johor Bahru in the west and south of Peninsular Malaysia (Zakaria et al., 2000). The concentrations of *n*-alkanes were between 1000 and 7,168,000 ng/g dw in sediments from the Kelantan, Besut, and Terengganu River, east coast of Peninsular Malaysia (Sakari et al., 2008a). *n*-Alkanes showed higher concentrations ranging between 421,000 and 10,770,000 ng/g dw in sediments from the Perai Strait, west coast of Peninsular Malaysia (Sakari et al., 2008b). The concentrations of *n*-alkanes were even higher in sediments from downstream of the Klang River, west coast of Peninsular Malaysia ranging from 9,600,000 to 27,200,000 ng/g dw (Bakhtiari et al., 2010). The levels of *n*-alkanes were detected between 1,700,000 and 8,600,000 ng/g dw in sediment samples and between 5,900,000 and 23,000,000 ng/g dw in SPM in the Langet River, west coast of Peninsular Malaysia (Bakhtiari et al., 2009). Core sediments collected from the Johor Strait showed *n*-alkanes concentrations between 117,000 and 4,652,000 ng/g dw (Sakari et al., 2012). The levels of *n*-alkanes in different tissues of green mussel *(Perna viridis)* from Peninsular Malaysia ranged from 554,000 to 64,012,000 ng/g dw (Shahbazi, 2009). The range of *n*-alkanes concentrations were between 27,945 and 254,463 ng/g dw in sediments from five riverine mangrove areas in the west coast of Peninsular Malaysia (Vaezzadeh et al., 2015b).

High concentrations of *n*-alkanes in the Kelantan, Besut, and Terengganu River sediments were ascribed to high shipping activities and land-based hydrocarbons transferred by urban runoffs (Sakari et al., 2008a). The concentrations of *n*-alkanes showed a drastic rise in upstream of the Besut River which was suggested to be due to urban runoffs from Jerteh Town. The ratios of LMW/HMW *n*-alkanes were below unity in the estuary of the Kelantan River which was attributed to high terrestrial plant inputs, while higher ratios in upper parts of the river were ascribed to inputs of fresh petroleum. The ratios of LMW/HMW *n*-alkanes were below unity in the Besut River indicating importance of terrestrial plant inputs as well as heavy and degraded oil in this area. As for the Terengganu River, this ratio ranged from 0.91 to 10.73 having highest values proximate to the river mouth which is a sign of fresh inputs of petroleum. The possible origins of this fresh oil input was suggested to be recreational activities including fishing and boating activities as well as spillage from numerous offshore oil platforms being transferred to the river mouth by the Monsoon currents.

Moving towards upstream, the signature of old oil was detected in sediments which could come from various discharge points throughout the river. A major source of anthropogenic hydrocarbons along the river can be urban runoffs coming from Kuala Terengganu city. The values of CPI were below unity in all three rivers except for three stations showing significance of anthropogenic sources of hydrocarbons in the study area. ACL also showed anthropogenic impacts in the study area since the range of ACL was wide in all three rivers. MH was HMW *n*-alkanes in all but two stations in the study area showing minor impacts from the sea-based sources.

The ratio of LMW/HMW *n*-alkanes showed that some of stations in the Perai Strait are influenced by fresh inputs of petroleum as the ratios were above unity in these stations (Sakari et al., 2008b). A few stations showed high impacts of vascular plant hydrocarbons. However, marine biogenic sources of hydrocarbons were rare in the study area. The ratio of C_{31}/C_{19} showed absolute predominance of terrestrial versus marine biogenic sources of hydrocarbons which can signify the importance of riverine discharge of hydrocarbons. It was suggested that either high impacts of anthropogenic hydrocarbons or higher biodegradation of marine biogenic hydrocarbons are the reason behind scarcity of these hydrocarbons in the study area. Similarly, the CPI values were indicative of high anthropogenic impacts on the Perai Strait. Wide range of ACL was another reason for the influence of anthropogenic activities on this area. MH was LMW and HMW even carbon number *n*-alkanes in all but two stations which showed the influence of different types of petroleum in the study area. The existence of UCM humps in most samples was a sign of degraded oil in the Perai Strait, while absence of pristane and phytane showed the presence of fresh oil in the environment. It was concluded based on various indices that a combination of fresh, distilled, heavy and degraded petroleum are the sources of hydrocarbons in the sediments of the Perai Strait.

Predominance of long-chain *n*-alkanes having C_{29} and C_{31} as MH was found in the sediment of the Langet River, while SPM showed an abundance of medium-chain *n*-alkanes with C_{24} and C_{26} as MH (Bakhtiari et al., 2009). Higher concentrations of *n*-alkanes in upstream of the Langet River were attributed to high anthropogenic activities in districts such as Bangi and Kajang around upstream of this river. The outcomes from CPI showed

mixed petroleum and natural origins of *n*-alkanes with higher abundance of petroleum sources in SPM. The presence of UCM in all samples was indicative of the presence of degraded oil in the Langet River.

Predominance of terrestrial biogenic sources of *n*-alkanes from tree, shrub, and grass waxes were determined in the bank of the Klang River (Bakhtiari et al., 2010). In general, HMW *n*-alkanes with either even or odd carbon atom numbers were more abundant than LMW ones. However, the CPI values signified the importance of petroleum inputs. A significant correlation was found between *n*-alkanes concentrations and TOC in the sediment from the Klang River ($r = 0.991$, $p = 0.001$).

A general increasing trend in the levels of *n*-alkanes was found in core sediments of Johor Strait from early to modern sediments with a predominance of biogenic odd carbon number *n*-alkanes from terrestrial plants in early sediments, while a predominance of anthropogenic even carbon number *n*-alkanes, especially C_{18} in modern sediments (Sakari et al., 2012). The values for CPI shows the same increase in anthropogenic inputs during modern time as the values decreased from 12.1 in sediments from 1855−1875 to 0.27 in modern sediments. According to the ratio of LMW/HMW *n*-alkanes during 1930−1990 which is between 2.87 and 8.70, high amounts of fresh oil were released to the aquatic environment of Johor Strait in this period of time.

The ratio of LMW/HMW *n*-alkanes in surface sediments of mangrove areas of the west Peninsular Malaysia showed higher levels of LMW *n*-alkanes having fresh oil origin near the mouth of the rivers, while HMW *n*-alkanes from terrestrial plant were more abundant in the upper parts of the river (Vaezzadeh et al., 2015b). Preferential biodegradation of terrestrial plant HMW *n*-alkanes by bacterioplanktons while transferring to the estuary and higher shipping activities in the estuarine area were suggested as possible reasons. CPI and ACL values showed petrogenic inputs in majority of sampling stations. Both CPI and ACL showed a decreasing trend towards the estuary which in line with the ratio of LMW/HMW *n*-alkanes showed higher petrogenic inputs near the estuaries. C_{28}, C_{29}, and C_{31} were the most frequent MH detected in the mangrove sediments. The existence of UCM hump in all the sampling locations showed the presence of degraded oil in the mangrove sediments. The ratios of C_{17}/pristane, C_{18}/phytane, and pristane/phytane were less than unity in most sampling stations which signify the presence of degraded oil. It was concluded that petrogenic *n*-alkanes originate from heavy and degraded oil and are more abundant in the estuaries, whereas biogenic *n*-alkanes originate from terrestrial plants and are more predominant in upper parts of the rivers. The Klang River and the Perai River showed the highest levels of *n*-alkanes and highest anthropogenic origin hydrocarbons based on the outcomes from *n*-alkanes indices.

Fig. 16.3 illustrates the cross plot of LMW/HMW *n*-alkanes versus CPI. As it is shown in the cross plot, the composition of *n*-alkanes is highly impacted by inputs of petroleum origin hydrocarbons in Peninsular Malaysia. Sediments from the Perai Strait and rivers of the east Peninsular Malaysia were affected by both fresh oil and heavy and degraded oil, while sediments from mangrove areas of west Peninsular Malaysia were highly influenced by heavy and degraded oil rather than fresh oil inputs. As it was mentioned earlier, tar balls collected

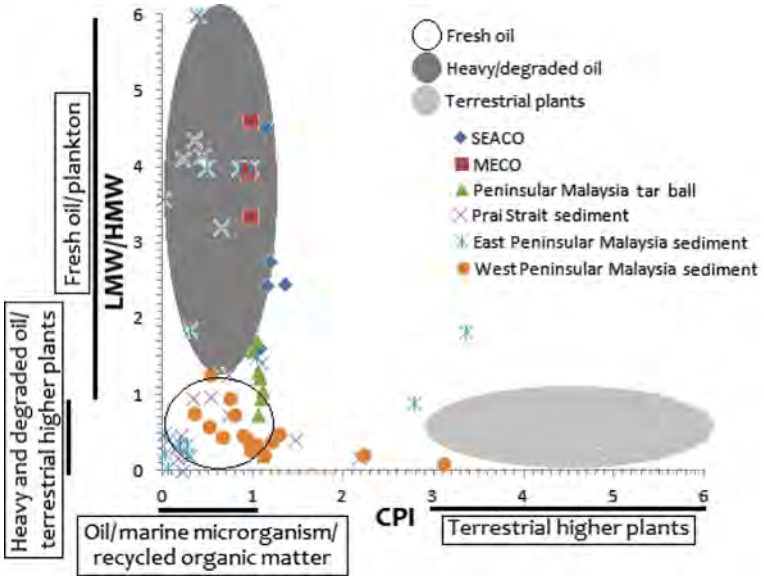

FIGURE 16.3 Cross plot of LMW/HMW *n*-alkanes versus CPI in environmental samples of Peninsular Malaysia.

from beaches of Peninsular Malaysia came from tanker washing and ballast discharge of SEACO transporting supertankers which contain high concentrations of HMW *n*-alkanes.

16.3.2 Hopanes as Source Identifiers of PHCs in Malaysia

The concentrations and indices of hopanes in different types of samples in Peninsular Malaysia are shown in Table 16.4.

Tar balls have been widely studied for hopanes in Malaysia in order to fingerprint sources of petroleum hydrocarbons. Among eight tar balls collected from west and east coast of Peninsular Malaysia, six had SEACO origin, whereas only two samples from Tanjung Rhu, Langkawi and Tanjung Karang, Selangor showed MECO origin (Zakaria et al., 2000). The ratios of C_{29}/C_{30} and $C_{31}-C_{35}/C_{30}$ were higher in these two stations than the others falling into the range of MECO. The collection of tar balls from Tanjung Karang, Selangor coincided with

TABLE 16.4 Hopane concentrations (ng/g) and hopane-based indices in different types of samples in Peninsular Malaysia

		Indices				
Location	**Type of Sample**	**∑Hopanes[a]**	**C_{29}/C_{30}[b]**	**$\Sigma C_{31}-C_{35}/C_{30}$[c]**	**T_m/T_s[d]**	**References**
Pasir Puteh, Johor Bahru	Mussel	91	1.46	1.43	0.57	Zakaria et al. (2000)
Pantai Lido, Johor Bahru	Mussel	23	1.46	1.66	0.56	Zakaria et al. (2000)
Anjung Batu, Malacca	Mussel	55	1.49	1.77	0.71	Zakaria et al. (2000)
Sungai Kajang, Selangor	Tar ball	600,000	1.97	2.21	1.55	Zakaria et al. (2001)
Pasir Puteh, Johor Bahru	Tar ball	70,000	1.53	1.41	0.37	Zakaria et al. (2001)
Tanjung Leman, Johor	Tar ball	150,000	0.7	0.91	0.73	Zakaria et al. (2001)
Merang Terengganu	Tar ball	290,000	0.81	0.8	0.52	Zakaria et al. (2001)
Tanjung Rhu, Langkawi	Tar ball	360,000	1.77	0.09	1.97	Zakaria et al. (2001)
Malacca City, Malacca	Tar ball	2,210,000	0.91	0.06	0.70	Zakaria et al. (2001)
Pinang Estuary	Surface Sediment	6515	1.59	2	0.91	Zakaria et al. (2002)
Teluk Intan	Surface Sediment	264	6.75	8.73	2.29	Zakaria et al. (2002)
Malacca River	Surface Sediment	2779	1.64	2.28	0.88	Zakaria et al. (2002)
Johor Bahru	Surface Sediment	2404	1.41	2.14	0.82	Zakaria et al. (2002)
Klang Estuary 1	Surface Sediment	3213	1.61	1.83	0.81	Zakaria et al. (2002)
Klang Estuary 2	Surface Sediment	1395	1.65	1.93	0.92	Zakaria et al. (2002)
Klang Estuary 3	Surface Sediment	98	1.67	2.04	0.89	Zakaria et al. (2002)
Pasir Putih, Kelantan	Tar ball	20,000	0.20	0.95	0.95	Chandru et al. (2008)
Dungun, Terengganu	Tar ball	28,000	0.06	0.84	1.03	Chandru et al. (2008)
Teluk Chempedak, Pahang	Tar ball	24,000	0.13	0.61	0.81	Chandru et al. (2008)
Petaling Jaya	Aerosol	10.49	1.05	2.50	0.77	Bahry et al. (2009)
Sernai	Aerosol	3.9	0.62	2.17	nd[e]	Bahry et al. (2009)
Johor Strait, Malaysia	Core Sediment	–	1.01–1.18	–	0.49–1.38	Sakari et al. (2010)
Johor Strait, Singapore border	Core Sediment	–	0.12–1.2	–	nd	Sakari et al. (2010)
Pulau Merambong	Surface Sediment	10,722	1.27	0.88	1.15	Vaezzadeh (2015)
Pulau Merambong	Oyster	7894	0.87	0.35	0.97	Vaezzadeh (2015)

[a] *∑Hopanes = sum of the concentration of* T_s, T_m, $C_{29}17\alpha$, $C_{29}17\beta$, $C_{30}17\alpha$, $C_{30}17\beta$, C_{31} *S*, C_{31} *R*, C_{32} *S*, C_{32} *R*, C_{33} *S*, C_{33} *R*, C_{34} *S*, C_{34} *R*, C_{35} *S, and* C_{35} *R.*
[b] C_{29}/C_{30} *= ratio of* 17α, 21β *(H)-30-norhopane to*17α, 21β *(H)-hopane.*
[c] ΣC_{31}-C_{35}/C_{30} *= ratio of sum of* 17α, 21β *(H)-C31 homohopane to* 17α, 21β *(H)-C35 homohopane relative to* 17α, 21β *(H)-hopane.*
[d] T_m/T_s *= ratio of* 17α*-22,29,30-trisnorhopane over* 18α*-22,29,30-trisnorhopane.*
[e] *nd = not detected.*

accidental spillage of Middle East oil in this area from a Chinese tanker coming from Kuwait. On the other hand, Tanjung Rhu, Langkawi is located on a beach that is known as the Straits of Malacca entry points for Middle East super tankers and is subject to North East Monsoon water currents. These currents could transfer MECO spilled from the tankers to the beaches (Zakaria et al., 2000). The signature of SEACO detected in other tar balls is easier to explain due to geographical locations of the sampling sites. Spillage of oil from oil platforms in the Straits of Malacca and South China Sea can be the origins of SEACO signature in other tar balls. Northeast Monsoon can transfer the spilled oil to the coastal areas of these sites. Northeast Monsoon occurs in the east coast between November and January. The major currents in South China Sea are downwards. Oleanane was depleted in the samples from Tanjung Rhu, Langkawi and Tanjung Karang, Selangor; however, oleanane was not abundant in all other tar balls (Zakaria et al., 2000). This does not contradict with the fact that these tar balls have a SEACO origin since although MECO are always depleted in oleanane, not all SEACO contain high amounts of oleanane. Therefore, the tar balls which had low amounts of oleanane can still have a SEACO origin.

In another study on tar balls in Peninsular Malaysia, similar results were detected where four out of 20 tar balls originated from MECO, while others had SEACO origin (Zakaria et al., 2001). All the four stations sampled were located in Selangor and Langkawi, similar to the previous research, and showing the dominance of MECO in tar balls of these areas. All tar balls collected from the east coast of Peninsular Malaysia showed a SEACO origin and the four tar balls with a MECO origin belong to 13 tar balls collected from the west coast. In other words, around 30% of the tar balls from the west coast showed a MECO signature, which can originate from accidental spillage or ballast water from tankers coming from the Middle East. The rest of tar balls, however, originated from SEACO indicating that the domestic oil from local oil seeps or accidental spillage was still more predominant in the west coast (Zakaria et al., 2001).

SEACO could possibly be transported to the Straits of Malacca from the spillage of oil from oil tankers transferring SEACO from east Peninsular Malaysia oil fields. Tanker ballast water and tanker washing discharges could also contribute to spillage of SEACO in the Straits of Malacca. SEACO originate from higher plants and has a waxy composition. Therefore, petroleum components might cover oil tank wall while being transported to far distances. These compounds can be released to aquatic environment, while tanks are being washed after delivery of petroleum. Moreover, oil spills as a result of drilling and other oil production activities from oil platforms of Port Dickson and Malacca in the west coast of Peninsular Malaysia besides natural oil seeps can be other sources of SEACO in the Straits of Malacca. Spilled oil in marine environment can be deposited on the sea floor or spread on the surface. The part on the sea surface can be subject to different physicochemical and biological processes. Petroleum can form sticky masses in water called chocolate mousse which is largely resistant to degradation and can be transported to far distances from the spillage point. Therefore, spillage from numerous oil platforms of the east Peninsular Malaysia can be transported intact and in the form of the chocolate mousse via the southward sea current in South China Sea. Then, the chocolate mousse can make a drastic u-turn towards the north entering the Straits of Malacca (Zakaria et al., 2001). Another possible source of SEACO in the Straits of Malacca can be Indonesian oil field activities located in east Sumatra.

Chromatograms of hopanes in the urban sediments of Malaysia showed an identical profile having a predominance of C_{30} 17R and C_{29} 17R and stair-step sequence of $C_{31}-C_{35}$ homohopanes (Zakaria et al., 2002). This identical profile can be an indication of similar origin of hopanes in the sediments of Malaysia urban areas since various oils with different source and maturation have different profiles of hopanes. The ratios of C_{29}/C_{30} and $\Sigma C_{31}-C_{35}/C_{30}$ in sediments of Malaysia were higher than SEACO range; therefore, SEACO cannot be the source of petroleum hydrocarbons. Although these ratios had similar range to those of MECO, a number of objections were raised to recognize MECO as the main source of petroleum hydrocarbons in sediments of Peninsular Malaysia (Zakaria et al. 2000, 2002). It was suggested that MECO is processed by only a very small fraction of oil refineries of west Peninsular Malaysia and therefore recognizing MECO as the main source of petroleum hydrocarbons in this area is out of question (Zakaria et al., 2002). Moreover, possible spillage of MECO from oil tankers is unlikely to affect upper parts of the rivers where many of the samples were collected. However, the fact that MECO is applied in formulation of lubricating oil in Peninsular Malaysia was reported elsewhere (Zakaria et al., 2000). Considering plants origin of SEACO, this type of crude oil is waxy in nature and is not appropriate to be used in the formulation of lubricating oil. Therefore, lubricating oil can be the source of petroleum hydrocarbons, especially in upper parts of the rivers.

The abundance of hopanes in lubricating oil was well documented before (Simoneit 1985; Rogge et al., 1993). Spillage of MECO from oil tankers in lower parts of the rivers cannot be ruled out either. In order to further clarify the issue, the ratio of C_{27} hopanes, i.e., T_m (17α (H)-22,29,30-trisnorhopane) over T_s (18α (H)-22, 29,30-trisnorhopane) was used. The ratio of T_m/T_s is a sensitive index of oil thermal maturity. This ratio ranges widely among

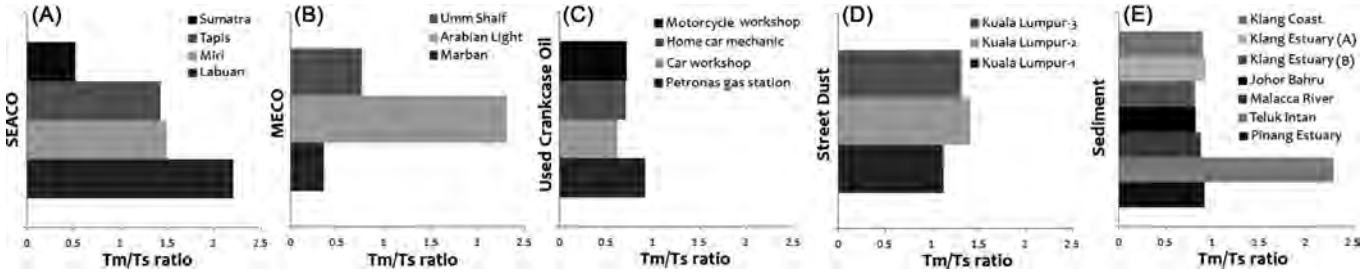

FIGURE 16.4 The range of oil thermal maturity index (T_m/T_s ratio) in source materials and sediments of Peninsular Malaysia: (A) Southeast Asian crude oil (SEACO); (B) Middle East crude oil (MECO); (C) Used crankcase oil from Kuala Lumpur; (D) Street dust from Kuala Lumpur; and (E) Sediments from west and south Peninsula. *Source: Modified from Zakaria, M.P., Takada, H., Tsutsumi, S., Ohno, K., Yamada, J., Kouno, E., et al., 2002. Distribution of polycyclic aromatic hydrocarbons (PAHs) in rivers and estuaries in Malaysia: a widespread input of petrogenic PAHs. Environ. Sci. Technol. 36, 1907–1918.*

MECO (0.35 to 2.31), while a narrow range of T_m/T_s from 0.81 to 0.92 was detected in sediments of Malaysia except for one sampling station (Zakaria et al., 2002). As a result, there must be another source of petroleum hydrocarbons except for spillage of MECO that matches the homogenous values of T_m/T_s ratios. Comparing the values of C_{29}/C_{30}, $\Sigma C_{31}-C_{35}/C_{30}$, and T_m/T_s ratios in sediments with those of SEACO and MECO, fresh and used crankcase oil, street dust, and asphalt measured in Peninsular Malaysia (Zakaria et al., 2002) showed the possibility of used crankcase oil as source of hopanes. The PAH/C_{30}-hopane ratio of used crankcase oil was the closest to the sediments having values that were an order of magnitude higher than sediments.

The ratios of LMW/HMW PAHs and MP/P in used crankcase oil were also in line with the sediments. Used crankcase oil contains petrogenic PAHs from non-combusted fuels and pyrogenic PAHs from combusted ones similar to what was observed in sediments. Moreover, the chromatogram profiles of PAHs in used crankcase oil and sediments were identical. The range of values for C_{29}/C_{30} and $\Sigma C_{31}-C_{35}/C_{30}$ and also the narrow range of T_m/T_s ratio detected in sediments match those of used crankcase oil (Zakaria et al., 2002). As it is shown in Fig. 16.4, a narrow range of T_m/T_s was detected in sediments in all but one sampling station. Despite the fact that high temperature pyrolysis process disrupt the molecular structure of hopanes (Boonyatumanond et al., 2006), used crankcase oil can perfectly reflect the composition of hopanes, since this disruption does not occur in the temperature that affects used crankcase oil (Wang et al., 2006). The importance of used crankcase oil and street dust as source of petroleum hydrocarbons in sediments and airborne particles are well documented in Peninsular Malaysia (Bahry et al., 2009; Sakari et al., 2010; Zakaria et al., 2002).

It was suggested that signature of used crankcase oil in sediments can have two origins in Peninsular Malaysia (Zakaria et al., 2002). Firstly, leakage of used crankcase oil from vehicles engines is the main source of hopanes in street dust. Street dust can subsequently be washed out by frequent rainfalls in Peninsular Malaysia and transport laterally by rivers to coastal areas. Street dust can also be transported by the atmosphere and transfer to aquatic environment either directly or via precipitation. Secondly, service shops irresponsible dumping of used crankcase oil was known to be another origin, contributing to petroleum hydrocarbons in sediments. Dumped used crankcase oil can be washed out by rainfalls and transported to the coastal areas via lateral transportation by rivers.

Signature of North Oil (NO 1) from North Sea was previously reported in one of the tar-ball samples collected from east coast of Peninsular Malaysia (Chandru et al., 2008). It was mentioned that large amounts of this type of crude oil are transported from Norway to Far East countries through the Strait of Malacca and South China Sea. However, no sign of NO 1 was recorded in other studies conducted on hopanes in different environmental media of Malaysia. The ratios of C_{29}/C_{30} and $\Sigma C_{31}-C_{35}/C_{30}$ showed SEACO origin for other tar-ball samples from the east coast of Peninsular Malaysia.

The concentrations of hopanes were detected in air samples from Peninsular Malaysia (Bahry et al., 2009). The concentrations of 17α (H), 21β (H)-hopane (C_{30} 17α) were much higher than 17α (H), 21β (H)-norhopane (C_{29} 17α). The predominance of 17α (H), 21β (H)-hopane in aerosols is a sign of combustion of fossil fuels. Noticeable concentrations of 17β (H), 21α (H)-hopane in aerosols was a signature of biomass burning origin hydrocarbons. The correlation between PAHs and hopanes in aerosols was moderate ($r = 57$). The reason behind this moderate correlation can be the fact that hopanes mainly originate from both vehicular emissions and street

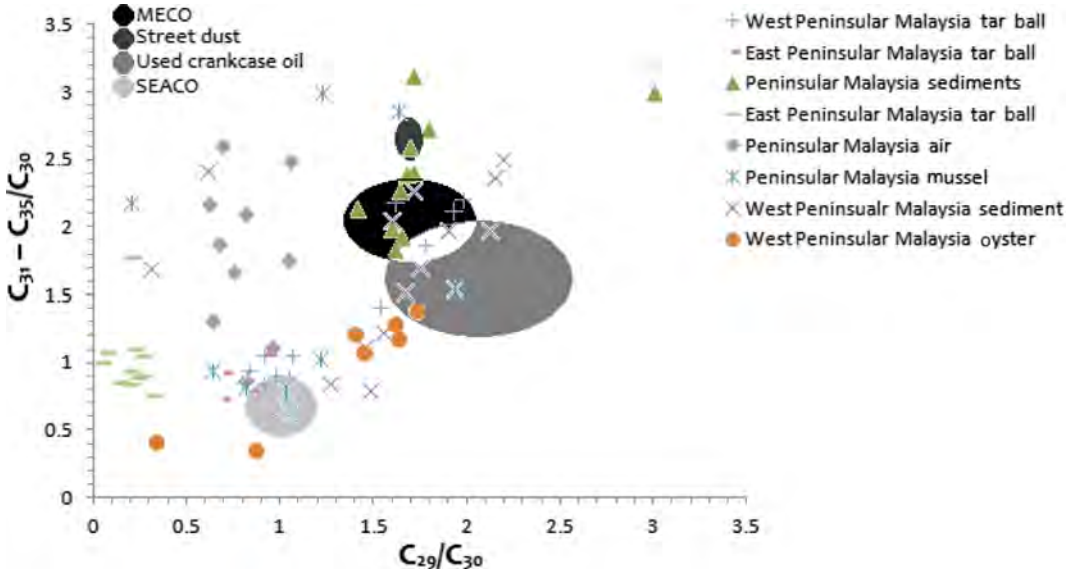

FIGURE 16.5 Cross plot of $\Sigma C_{31}-C_{35}/C_{30}$ versus C_{29}/C_{30} in environmental samples of Peninsular Malaysia.

dusts, while the major source of parent PAHs is vehicular emissions. The ratios of total PAHs/C_{30} in aerosols ranged from 1 to 10.53 overlapping with those reported by Zakaria et al. (2002) for used crankcase oil which ranged from 1.09 to 12.47. The ratio of C_{29}/C_{30} ranged from 0.62 to 1.05 in aerosols which did not fall within the range of any of the source materials detected by Zakaria et al. (2002) (Table 16.2). The ratio of $C_{31}-C_{35}/C_{30}$ fell within the range of used crankcase oil for seven aerosol samples, ranging from 1.12 to 2.17 and street dust for the other 2 having values of 2.5 and 2.6.

As it can be inferred from Fig. 16.5, the majority of tar-ball samples from east and west coast of Peninsular Malaysia fell within SEACO range of $\Sigma C_{31}-C_{35}/C_{30}$ versus C_{29}/C_{30} cross plot. However, few tar balls from the west coast fell within MECO range. Moreover, some mussel samples from Peninsular Malaysia fell within the range of SEACO. Sediment and oyster samples; however, mostly fell within the range MECO and used crankcase oil. Air samples did not fall within any of the cross plot areas for reference materials since the ratios of C_{29}/C_{30} were below those of source materials, whereas the range of $C_{31}-C_{35}/C_{30}$ were similar to those of MECO, used crankcase oil and street dust.

16.3.3 PAHs as Source Identifiers of PHCs in Malaysia

PAHs have been broadly determined in various environmental samples in Peninsular Malaysia. In a general investigation, PHCs were evaluated in water and sediments from Port Dickson, Peninsular Malaysia back in 1986–1989 (Law and Veellu, 1989). This is among the earliest literature on petroleum hydrocarbons in Malaysia. The average concentrations of PHCs were reported chrysene equivalent ranging from 0.77 to 7.87 ng/L and 1120 to 3900 ng/g dw in water and sediments, respectively. The major source of hydrocarbons was suggested to be the spillage of petroleum from oil tankers and oil platforms proximate the sampling area. Land runoff was suggested to have a minor contribution.

Aromatic hydrocarbons were detected in green mussel *(Perna viridis)* at concentrations between 16 and 14,275 ng/g wet weight in the south coast of Peninsular Malaysia. The main aromatic hydrocarbons found in mussels were 2-methylphenanthrene, benz[e]acephenanthrylene, and phenanthrene (Ramakrishnan, 1998). The main PAHs found in five water samples collected from around Peninsular Malaysia were dibenzothiophene, phenanthrene, anthracene, 2-methylanthracene, and 2-methylphenanthrene (Soon, 1999). Later, a comprehensive study was conducted on PHCs in sediments from the rivers and coastal areas of Peninsular Malaysia and the concentrations of PAHs ranged from 4 to 924 ng/g dw (Zakaria et al., 2002). Higher concentrations were determined in six sediment samples collected from different parts of the Langet Estuary, west Peninsular Malaysia where 17 out of 18 target PAHs were detected at concentrations ranging from 322 to 2480 ng/g dw (Zakaria and Mahat, 2006). A total of 14 sediment samples were collected from the Kelantan, Besut, and Terengganu Rivers in the east coast of Peninsular Malaysia and the concentrations of PAHs ranged from 58 to 1689 ng/g dw (Sakari et al., 2008a).

SPM and surface sediments were collected from six locations in the Langet River and the concentrations of PAHs ranged from 306 to 7968 and 558 to 980 ng/g dw in SPM and sediments, respectively (Bakhtiari et al., 2009). Five stations were selected in downstream of the Klang River and the concentrations of 19 PAHs ranged from 1200 to 2167 ng/g dw in sediment samples (Bakhtiari et al., 2010). The concentrations of PAHs in green mussel (*Perna viridis*) from the west and south coast of Peninsular Malaysia ranged from 17 to 2060 ng/g dw (Shahbazi et al., 2010). Sediment samples, SPM, water, and blood cockle (*Anadara granosa*) were collected from six locations in the west coast of Peninsular Malaysia (Mirsadeghi et al., 2013). The levels of PAHs ranged from 17 to 497, 221 to 1699, 24 to 153, and 26 to 265 ng/g dw in the sediment, SPM, water, and cockle samples, respectively. The concentrations of PAHs ranged from 20 to 1841 ng/g dw in sediments of 10 aquaculture areas in Peninsular Malaysia (Retnam et al., 2013). Sediment samples from mangrove forests of Rembau−Linggi estuary showed PAHs concentrations of 20 to 112 ng/g dw (Raza et al., 2013). The concentrations of PAHs ranged from 716 to 7938 ng/g dw in sediments from the Perai and Malacca River, west coast of Peninsular Malaysia (Keshavarzifard et al., 2014). The concentrations of PAHs ranged from 151 to 440 ng/g dw in sediments from the Muar River and Pulau Merambong, respectively (Vaezzadeh et al., 2015a). Thirteen sediment samples were collected from the Selangor River during dry and wet seasons and total concentrations of 25 PAHs ranged from 203 to 964 ng/g dw (Masood et al., 2016).

Two reasons were previously suggested by Zakaria et al. (2002) for low concentrations of PAHs in Malaysia compared to developed countries including lower anthropogenic activities and sediment dilution as a result of high sediment loads and SPMs that are washed out by heavy rainfall from the land and transferred to the aquatic environment. Table 16.5 shows the concentrations of PAHs in surface sediments from Malaysia and other countries. PAHs were investigated in tar balls collected from the coastal areas Peninsular Malaysia and the concentrations of PAHs ranged from 10,000 to 557,000 ng/g (Zakaria et al., 2001). PAHs were investigated in aerosol samples from nine locations all around Peninsular Malaysia and the concentrations of 18 PAHs ranged from 0.58 to 10.49 ng/m^3 in Perai and Tanah Ratah, having an average of 2.73 ng/m^3 (Bahry et al., 2009).

An abundance of HMW PAHs and depletion of LMW ones was detected in tar balls from beaches of Peninsular Malaysia (Zakaria et al., 2001). It was suggested that chemical processes such as evaporation and dissolution together with biodegradation were responsible for selective loss of LMW PAHs. Table 16.6 shows different diagnostic ratios used for source identification of PAHs in Peninsular Malaysia. Large amounts of alkylated PAHs were detected in sediments of Peninsular Malaysia indicating great petrogenic influence, whereas sediments of Tokyo like many other developed cities showed pyrogenic source PAHs (Zakaria et al., 2002). The ratio of LMW/HMW PAHs ranged from 7.7 to 50 in crude oil, while from 0.68 to 2.13 in sediments of Peninsular Malaysia. Abundance of HMW PAHs together with LMW PAHs indicated both pyrogenic and petrogenic sources of PAHs in the urban areas of Peninsular Malaysia. Thus, PAHs might not merely come from spillage of crude oil; however, selective degradation of LMW PAHs should also be taken into account. The same trend was observed for MP/P ratio with 26 out of 29 sediment samples having MP/P ratios of above unity in Peninsular Malaysia, while the MP/P ratios for most sediment samples of Tokyo were below or around unity showing predominance of pyrogenic PAHs similar to the sediments of other developed cities worldwide. A positive correlation was found between the concentrations of PAHs and MP/P in sediments of Peninsular Malaysia ($r^2 = 0.74$) indicating significance of petrogenic inputs.

In the Langet Estuary, two out of six sampling stations adjacent to downstream of the estuary showed higher concentrations (Zakaria and Mahat, 2006). High industrial and shipping activities occur proximate to these two stations suggesting the significance of ship and industrial waste discharges as the main source of PAHs. The concentrations of PAHs showed a drastic fall in the upstream of the Langet Estuary. The ratio of MP/P ranged from 0.88 to 1.27 with four stations below one, indicating predominance of pyrogenic PAHs. The ratio of LMW/HMW PAHs ranged from 0.25 to 26.96 showing significance of LMW PAHs in sediments of the Langet Estuary. Street dust and soil have higher HMW PAHs since HMW PAHs are more persistent and LMW PAHs degrade more easily. Higher concentrations of LMW PAHs in the Langet Estuary show that the pyrogenic source of PAHs should contain both LMW and HMW PAHs. PAHs in this area can originate from long or short-range atmospheric transportation or industrial discharges transferred by surface runoffs to the estuary. Street dust and crankcase oil can also contribute to PAHs concentration being washed out by run offs. Chrysene which is among the carcinogens had the highest levels among HMW PAHs.

The ratio of MP/P ranged from 0.77 to 1.83, 1.35 to 2.11, and 1.03 to 2.03, while the ratio of LMW/HMW PAHs ranged from 0.10 to 2.47, 23 to 188, and 0.03 to 3.33 in the Kelantan, Besut, and Terengganu River, respectively (Sakari et al., 2008a). The ratio of MP/P showed both petrogenic and pyrogenic inputs of PAHs in the rivers, while the ratio of LMW/HMW PAHs indicated old oil inputs in the Kelantan and Terengganu River and fresh oil inputs in the Besut River. Kuala Besut town is located in the mouth of estuary, where increased ships and boats related to fishing and recreational activities give rise to petrogenic inputs of PAHs. Moreover, urban

TABLE 16.5 Comparative PAH concentrations (ng/g) in surface sediment of Malaysia and other parts of the world

Location	*n*[a]	Range	Reference
SOUTHEAST ASIA			
Selangor River, Malaysia	25	203–964	Masood et al. (2016)
West Peninsular Malaysia	16	151–440	Vaezzadeh et al. (2015a)
West Peninsular Malaysia	16	716–7938	Keshavarzifard et al. (2014)
West Peninsular Malaysia	17	20–112	Raza et al. (2013)
Peninsular Malaysia	16	20–1841	Retnam et al. (2013)
Klang River, Malaysia	19	1304–2187	Bakhtiaria et al. (2010)
Langat River, Malaysia	18	558–980	Bakhtiaria et al. (2009)
East Peninsular Malaysia	17	59–1690	Sakari et al. (2008a)
East Peninsular Malaysia	17	260–590	Elias et al. (2007)
Langet Estuary, Malaysia	18	322–2480	Zakaria and Mahat (2006)
West Peninsular Malaysia	16	4–924	Zakaria et al. (2002)
Jakarta Bay, Indonesia	18	191–1252	Koike et al. (2012)
Iloilo River, the Philippines	12	493–3898	Taneza and Philp (2009)
Thailand	17	6–8399	Boonyatumanond et al. (2006)
EAST ASIA			
Guan River Estuary, China	21	90–218	He et al. (2014)
Yangtze Estuary, China	16	90.14–502.12	Li et al. (2012)
Kaohsiung Harbor, Taiwan	16	39–30,521	Chen et al. (2012)
Tokyo Bay, Japan	18	1232–1454	Koike et al. (2012)
Daliao Estuary, China	16	157–20,855	Liu et al. (2011)
Hong Kong SAR	16	56–3758	Ke et al. (2005)
Hong Kong	15	356–11,098	Tam et al. (2001)
MIDDLE EAST			
Imam Khomeini Port, Iran	16	2631.9–5148.9	Abdollahi et al. (2013)
AFRICA			
Lake Manzala, Egypt	39	246–9910	Barakat et al. (2013)
Black Sea coast	22	7.2–635	Readman et al. (2002)
EUROPE			
Santander Bay, Spain	16	20–344,600	Viguri et al. (2002)
Ria Formosa Lagoon, Portugal	15	1–73	Barreira et al. (2007)
SOUTH AMERICA			
Coco River, Brazil	17	3.04–2234.76	Cavalcante et al. (2009)
Ceará River, Brazil	17	3.34–1859.21	Cavalcante et al. (2009)
Angra dos Reis, Brazil	15	6–277	Azevedo et al. (2007)
CENTRAL AMERICA			
Austin in Texas, USA	16	20–82,800	DeMott et al. (2010)
San Francisco Bay, USA	17	2653–27,680	Pereira et al. (1999)
NORTH AMERICA			
Guadeloupe	20	49–1065	Ramdine et al. (2012)
Athabasca River, Canada	16	10–1130	Headley et al. (2001)

[a]*Number of PAH compounds.*

TABLE 16.6 Different diagnostic ratios of PAHs in Peninsular Malaysia

Sampling Locations	LMW/HMW[a]	MP/P[b]	FLU/(FLU + PYR)[c]	BaA/(BaA + Chry)[d]	IcdP/(IcdP + BghiP)[e]	References
Malaysian Coastal Area (Tar balls)	0.32–8.57	0.16–12.86	na	na	na	Zakaria et al. (2001)
Malaysian Aquatic Environment (Sediment)	0.68–2.13	0.39–6.65	na	na	na	Zakaria et al. (2002)
Langet Estuary (Sediment)	0.25–26.96	0.88–1.27	0.30–0.44	nd–0.60	na	Zakaria and Mahat (2006)
East Coast (Tar balls)	0.08–2.48	0.46–16.34	na	na	na	Chandru et al. (2008)
East Peninsular Rivers (Sediment)	0.03–118	0.77–2.11	na	na	na	Sakari et al. (2008a)
Langet River (Sediment)	0.17–0.39	0.7–1.9	0.3–0.4	na–0.9	na	Bakhtiari et al. (2009)
Langet River (Suspended Matter)	1.16–4.61	0.6–0.9	0.3–0.5	na–0.2	na	Bakhtiari et al. (2009)
West Peninsular Coastal Area (Mussel)	0.89–6.34	0.05–8.70	na	na	na	Shahbazi et al. (2010)
Klang River (Sediment)	16.7–202.45	1.1–1.45	0.22–0.39	na	na	Bakhtiaria et al. (2010)
West Peninsular Coastal Area (Sediment)	0.5–2.9	1–14.2	na	na	na	Mirsadeghi et al. (2013)
West Peninsular Coastal Area (Sediment)	1–3.9	0.4–13.3	na	na	na	Mirsadeghi et al. (2013)
Rembau–Linggi estuary (Sediment)	0.13–0.59	1.67–11.69	0.44–0.55	0.41–0.81	0.33–0.53	Raza et al. (2013)
Prai and Malacca Rivers (Sediment)	0.55–1.55	0.2–2.7	0.43–0.50	0.34–0.44	na–0.40	Keshavarzifard et al. (2014)
Muar River and Pulau Merambong (Sediment)	0.01–10.44	0.44–1.75	0.39–0.44	na	na	Vaezzadeh et al. (2015a)
Selangor River Dry Season (Sediment)	0.18–1.17	0.02–2.24	0.54–0.93	0.08–0.80	0.22–0.87	Masood et al. (2016)
Selangor River Rainy Season (Sediment)	0.21–1.05	0.18–2.94	0.40–1.00	0.16–0.96	na–70	Masood et al. (2016)

[a] *LMW/HMW = the ratio of sum of concentrations of PAHs from Naphthalene to Anthracene divided to the sum of concentrations of PAHs from Fluoranthene to Benzo[ghi] perylene.*
[b] *MP/P = the ratio of methylphenanthrenes/phenanthrene.*
[c] *FLU/(FLU + PYR) = the ratio of flouranthene/(flouranthene + pyrene).*
[d] *BaA/(BaA + Chry) = the ratio of benzo(a)anthracene/(benzo(a)anthracene + chrysene).*
[e] *IcdP/IcdP + BghiP = the ratio of Indeno[1,2,3-cd]pyrene/(Indeno[1,2,3-cd]pyrene + Benzo[g,h,i]perylene).*

runoffs from Jerteh Town in upstream of the river is the source of petrogenic PAHs in sediments of upstream (MP/P of 1.98), while midstream sediments showed higher pyrogenic inputs of PAHs (MP/P of 1.35–1.36). The petrogenic source of PAHs in Kuala Terengganu is consistent with *n*-alkanes and can be fresh inputs from recreational activities including fishing and boating activities as well as spillage from numerous oil platforms located in the offshore area of the river transferred to the river mouth by the Monsoon currents. The signature of old oil along the river can be from multiple discharge points releasing urban runoffs from Kuala Terengganu city into the river. The probable source of pyrogenic PAHs was suggested to be long range atmospheric transportation as the study area is less populated and industrialized.

Upstream of the Langet River showed higher concentrations of PAHs which can be due to widespread industrial areas in Kajang, Bangi, and south of Hulu Langet town along the upstream of the Langet River (Bakhtiari et al., 2009). The solely anthropogenic activities in downstream of the river are about ports and jetties with boating and shipping activities. A dominance of two, three, and four-ring PAHs was found in suspended matters, while sediments were more abundant in five-ring PAHs. Fresh inputs of oil can be the reason behind higher LMW PAHs in water, while PAHs in sediments undergo degradation either prior to or after sedimentation reducing the amounts of less persistent LMW PAHs compared to HMW ones. Furthermore, LMW PAHs are more water soluble and therefore, more dominant in water column than HMW ones. High concentrations of Naphthalene were found particularly in suspended matters ranging from 1405 to 2420 and 410 to 440 ng/g dw in

suspended matters and sediments originating from both terrigenous and combustion sources. The values of LMW/HMW PAHs showed similar trend ranging from 1.16 to 4.61 and 0.17 to 0.39 in suspended matters and sediments, respectively. Other diagnostic ratios were calculated to further explore the sources of PAHs. The range of MP/P was 0.6 to 0.9 in suspended matters and 0.7 to 1.9 in sediments indicating a mixture of petrogenic and pyrogenic sources of PAHs with predominance of pyrogenic ones. The ratios of Phe/Ant were below 10 in all samples suggesting predominance of pyrogenic PAHs. The ratios of Flu/(Flu + Pyr) were below 0.4 in most of the samples as a sign of petrogenic inputs except for two stations which had ratios between 0.4 and 0.5 showing pyrogenic inputs. The ratios of BaA/(BaA + Chr) were only applicable in four samples ranging from 0.2 to 0.9 suggesting both petrogenic and pyrogenic sources of PAHs.

Naphthalene was detected as the most predominant PAH in the sediments from downstream of the Klang River, Peninsular Malaysia which was suggested to occur naturally originating from woody materials (Bakhtiari et al., 2010). The ratio of Phe/Ant was more than 15 (i.e., 53−74), while Flu/(Flu + Pyr) was below 0.4 (i.e., 0.22−0.39) indicating predominance of petrogenic sources of PAHs in the study area. Similarly, MP/P and CombPAHs/$\sum$PAHs ratios were below 0.3 (i.e., 0.005−0.06) and above 1 (i.e., 1.1−1.45), respectively indicated petrogenic sources of PAHs. Tourism and shipping activities together with discharge of effluents from nearby port area were suggested as possible sources of petrogenic PAHs in the Klang River.

The highest PAHs concentrations in green mussel *(Perna viridis)* were detected near Penang Bridge which was ascribed to both land-based sources from populous and industrious urban areas of Penang Island and Seberang Prai as well as sea-based sources from busy port activities around the Bridge (Shahbazi et al., 2010). The residues of lubricating oil and MECO were found in the mussels with the help of hopanes indices. Second highest concentrations of PAHs were found in Kg. Pasir Puteh which is adjacent to Johor port as one of the busiest ports of Peninsular Malaysia and is an industrial area as well. A predominance of LMW PAHs was found over HMW ones in mussels which can be a sign of petrogenic sources of PAHs. Selective bioaccumulation of LMW PAHs from water through gills should also be taken into account. Other ratios were used and the ratio of Phen/Anth was below 10 in all but one sampling station indicating the importance of pyrogenic sources of PAHs. On the contrary, the ratios of Fluo/Py were below 1 showing petrogenic sources of PAHs. The ratios of MP/P were high having ratios of above 2 in three sampling locations as a sign of petrogenic sources of PAHs. As a result, a mixture of petrogenic and pyrogenic sources can be ascribed to PAHs in mussels.

The concentrations of PAH in blood cockle *(Anadara granosa)* varied enormously where the concentrations in remote areas were 10-fold lower than those of polluted areas (Mirsadeghi et al., 2013). Both petrogenic and pyrogenic PAHs inputs were detected in the cockles. A correlation was found between the concentrations of PAHs in various environmental units including sediment, SPM, water, and cockle from the same sampling location. Bioaccumulation of PAHs by the cockles was suggested to pose a risk to consumers as well as the cockle itself.

HMW PAHs, especially four and five-ring PAHs were predominant in all stations of Rembau−Linggi estuary except for station 2 which showed a predominance of three-ring PAHs (Raza et al., 2013). Benzo[b]fluoranthene was the main PAH with 10% of total PAHs in the sediment. The ratios of Ant/(Ant + Phe), Flu/(Flu + Pyr), BaA/(BaA + Chr), and IcdP/(IcdP + BghiP) all were within the range of pyrogenic source PAHs. However, the ratios of MP/P ranged from 1.67 to 11.69 indicating petrogenic inputs in the study area. It was suggested that combustion derived PAHs either originate from long range atmospheric transportation or biomass burning and automobile emissions in nearby areas. Petrogenic source PAHs, however, might originate from vessel activity as well as used crankcase oil washed out by tropical rainfalls.

A predominance of HMW PAHs was detected in sediments of aquaculture areas in Peninsular Malaysia comprising of 15%−83% of total PAHs (Retnam et al., 2013). The concentrations of PAHs classified by USEPA as potential carcinogens including chrysene, benzo(a)anthracene, benzo(b)fluoranthene, benzo(k)fluoranthene, benzo(a)pyrene, dibenzo(a,h)anthracene and indeno(1,2,3-cd)pyrene ranged from nd to 645 ng/g dw having an average of 109 ng/g dw. Benzo(a)pyrene which has the highest carcinogenic impact ranged from nd to 107 ng/g dw. The ratio of Ant/(Ant + Phe) ranged from 0.06 to 0.25 with a majority of stations above 0.1 as a source of pyrogenic PAHs. The ratio of IcdP/(IcdP + BghiP) ranged from 0.29 to 0.53 showing petroleum combustion in a majority of stations and biomass combustion in two of the stations (ratios of 0.51 and 0.53). Use of chemometric techniques together with diagnostic ratios showed automobile emissions, petroleum combustion, and biomass burning as the main sources of PAHs in the sediments. Use of absolute principle component scores-multiple linear regression revealed that automobile emissions are the source of 54% of PAHs followed by petroleum combustion and biomass burning as sources of 37% and 9% of PAHs in sediments.

A predominance of HMW PAHs was detected in sediments of the Malacca and Perai River, showing significance of pyrogenic versus petrogenic PAHs (Keshavarzifard et al., 2014). The ratios of LMW/HMW PAHs were

between 0.41 and 1.55. The ratio of Flu/(Flu + Pyr) were between 0.43 and 0.5 indicating pyrogenic inputs. The ratio of MP/P ranged from 0.2 to 2.7 having most values below 1 confirming the significance of pyrogenic PAHs in the study area. However, the ratios of MP/P were 2.5 and 2.7 in upper parts of the Malacca and Perai River indicating possible inputs of petrogenic PAHs. BaA/(BaA + Chry) were between 0.34 and 0.44 indicating pyrogenic sources of PAHs in most sampling stations. IcdP/(IcdP + BghiP) ranged from 0.24 to 0.4 which is within the range of petroleum combustion source PAHs.

Increasing of industrialization, vehicle numbers, and population growth in the state of Johor were found to be the major reasons behind the increasing trends of PAHs in the sediments of the Muar River (Vaezzadeh et al., 2015a). The Pulau Merambong, which is located in a remote area among Malaysia, Indonesia and Singapore, was studied for the first time for PAHs. Benzo[b]fluoranthene had the highest proportion among the PAHs in sediments of the study area. The ratio of LMW/HMW PAHs ranged between 0.01 and 0.38 except for one sampling station in the Pulau Merambong showing the predominance of HMW PAHs as an indication of pyrogenic PAHs. The ratio of MP/P ranged from 0.44 to 1.75 with a majority of stations below 1 showing inputs of pyrogenic PAHs. Moreover, the ratio of Flu/(Flu + Pyr) were between 0.39 and 0.44 which also dominates in the range of pyrogenic PAHs.

Higher concentrations of PAHs were detected in wet season compared to dry season in sediments of the Selangor River due to exceeding discharge of pollutants by urban runoffs and domestic sewage (Masood et al., 2016). The concentrations of 25 PAHs ranged from 203−665 ng/g dw in dry season, while the concentrations were between 215 and 965 ng/g dw in wet season. The highest concentrations were found in the estuary of the river except for one station along the river which receives high inputs from Selangor City runoffs and is surrounded by industrial activities. Furthermore, water current is quite slow in this station resulting in active sedimentation and settlement of organic pollutants such as PAHs. Higher concentrations of PAHs in the Selangor Estuary were attributed to sea-based activities such as spillage of oil and release of wastewater as well as land-based urban runoffs from areas nearby the estuary such as Kampung Telok Piai, Kampung Tanjung Keramat, and Kampung Pasir Panjang. Naphthalene merely consisted of 4% of total PAHs and LMW PAHs were generally depleted. The ratios of LMW/HMW were below unity in most sampling stations which might be due to pyrogenic sources of PAHs. At the same time, the ratios of Flu/(Flu + Pyr) were above 0.5 indicating the predominance of pyrogenic PAHs from biomass burning and coal combustion. The ratio of IcdP/(IcdP + BghiP) and BaA/(BaA + Chry) showed the contribution of petrogenic PAHs from fresh inputs of petroleum and pyrogenic PAHs from petroleum, biomass, and coal combustion with a predominance of pyrogenic sources in the study area. The ratios of MP/P were also below unity in most sampling stations confirming the significance of pyrogenic PAHs in the study area.

The levels of PAHs in aerosols from Malaysian urban areas showed an increase of 90% during haze period showing significant contribution of haze episodes in atmospheric PAHs (Bahry et al., 2009). Typically, an abundance of HMW PAHs were detected compared to LMW ones in aerosol samples originating from combustion sources such as forest fires, automobile, and industrial emissions. Benzo[e]pyrene and benzo[k]fluoranthene were the predominant PAHs in the aerosols. Benzo[e]pyrene is more resistant to photochemical degradation than other PAHs resulting in high concentrations of this PAH in aerosols. However, the reason behind predominance of benzo[k]fluoranthene can be release of this ubiquitous compound from combustion sources. Significant correlations were found between the concentrations of benzo[e]pyrene and benzo[k]fluoranthene and total PAHs ($r = 99$ and 98, respectively). The ratios of MP/P ranged from 0.41 to 2.14 with all stations below unity except for Tanah Ratah indicating significance of pyrogenic sources; however, Tanah Ratah showed petrogenic origin PAHs. As it was suggested by Zakaria et al., 2002, petrogenic PAHs from leakage of crankcase oil from automobile engines can incorporate to street dust being detected together with aerosols. It is noteworthy that Malaysia has experienced different severity of haze in years. PAHs were detected at a maximum value of 47.98 ng/m^3 during the 1997 haze episode (Bin Abas et al., 2004b).

As it is shown in Fig. 16.6, the majority of sediment samples from Peninsular Malaysia shows pyrogenic and mixed sources of PAHs based on LMW/HMW and MP/P cross plot. The ratios of LMW/HMW PAHs were mostly below 1 as a sign of pyrogenic sources in more recent studies, however, the ratios were above one as a sign of petrogenic sources in older samples reported from Peninsular Malaysia (Zakaria et al., 2002), Langet Estuary (Zakaria and Mahat, 2006), East coast rivers (Sakari et al., 2008a), and Klang River (Bakhtiari et al., 2010). The ratios of MP/P also showed pyrogenic and mixed petrogenic and pyrogenic sources for most sediments, while sediment samples analyzed by Zakaria et al. (2002) and Raza et al. (2013) had MP/P ratios of above two as a sign of petrogenic sources. Fig. 16.7 shows the cross plot between BaA/(BaA + Chry) and Flu/(Flu + Pyr). The predominance of pyrogenic sources of PAHs in sediments of Peninsular Malaysia can be clearly inferred from

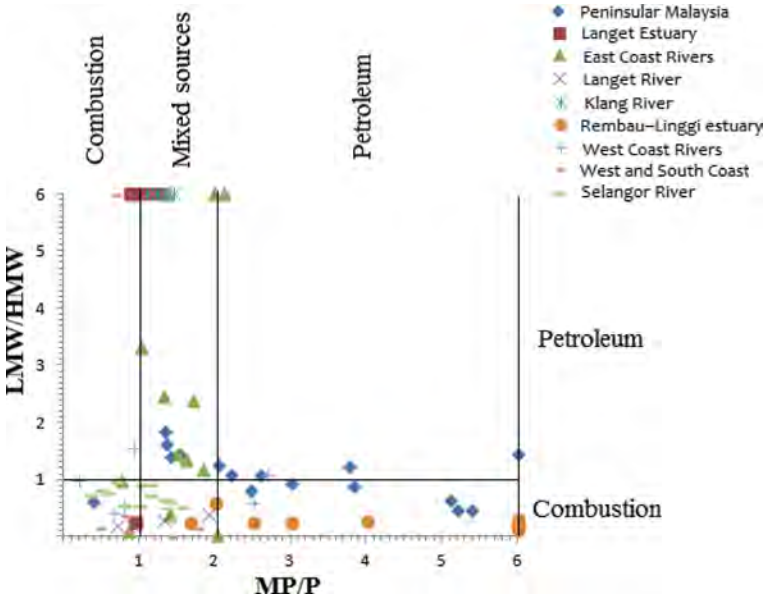

FIGURE 16.6 PAH cross plot for the ratio of LMW/HMW versus MP/P.

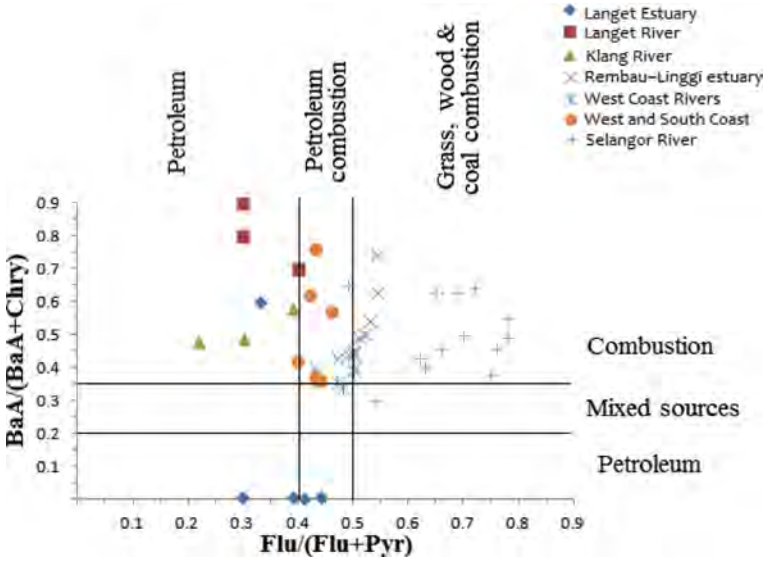

FIGURE 16.7 PAH cross plot for the ratio of BaA/(BaA + Chry) versus Flu/(Flu + Pyr).

the cross plot. Similar to LMW/HMW and MP/P cross plot, sediments from more recent studies show a predominance of pyrogenic sources, while sediments from the Langet Estuary, Langet River, and Klang River (Bakhtiari et al., 2010, 2009; Zakaria and Mahat, 2006) indicated petrogenic inputs. It was suggested that a shift has occurred from petrogenic to pyrogenic sources of PAHs in the sediments of Peninsular Malaysia (Keshavarzifard et al., 2014; Vaezzadeh et al., 2015a). This shift can be due to enforcing environmental laws against the release of petroleum resulting in a decrease in petrogenic inputs of PAHs in Malaysian environment, while pyrogenic sources of PAHs such as industrial and automobile exhaust are increasingly operational.

16.4 CONCLUSION

n-Alkanes, hopanes, and PAHs were used as molecular markers for source identification of PHCs all around Peninsular Malaysia over the past two decades. Various environmental samples including source materials, tar balls, aerosols, water, SPM, sediments, and different shellfish species were collected and analyzed for PHCs. High concentrations of *n*-alkanes showed anthropogenic inputs of PHCs. A mixture of fresh oil as well as heavy

and degraded oil was found as anthropogenic sources of *n*-alkanes in various environmental media of Peninsular Malaysia. Land-based anthropogenic PHCs were transferred to the aquatic environment via urban runoff, which is intensified by heavy tropical rainfall, whereas extreme oil tanker traffic and ballast water discharge together with tanker washing were the main sea-based sources anthropogenic PHCs. Biogenic sources of *n*-alkanes were mainly from terrestrial higher plants due to massive tropical rainforest plants in Peninsular Malaysia, while sea-based biogenic contribution of *n*-alkanes was minor. The signatures of SEACO and MECO were found in tar balls from the beaches of Peninsular Malaysia with a predominance of the former using biomarkers. In sediment and aerosol samples, however, used crankcase oil and street dust were the main sources of hopanes. A shift was found in the sources of PAHs from petrogenic to pyrogenic sources over the last decade, which seems to result from increasing enforcement of environmental laws against the release of petroleum, whereas the pyrogenic sources of PAHs has received a major increase as a result of rapid industrialization and motorization in Peninsular Malaysia.

References

Abdollahi, S., Raoufi, Z., Faghiri, I., Savari, A., Nikpour, Y., Mansouri, A., 2013. Contamination levels and spatial distributions of heavy metals and PAHs in surface sediment of Imam Khomeini Port, Persian Gulf, Iran. Mar. Pollut. Bull. 71, 336–345.

Abha, S., Singh, C.S., 2012. Hydrocarbon pollution: effects on living organisms, remediation of contaminated environments, and effects of heavy metals co-contamination on bioremediation. In: Romero-Zerón, L. (Ed.), Introduction to Enhanced Oil Recovery (EOR) Processes and Bioremediation of Oil Contaminated Sites. INTECH Open Access Publisher, Chandigrah, India, pp. 185–206.

Arora, A., 2006. Hydrocarbons (Alkanes, Alkenes and Alkynes), 2006. Discovery Publishing House, New Delhi, pp. 3–10.

Azevedo, D.A., Gonçalves, M.L., Silva, D.B., 2007. Organic geochemistry of the Angra dos Reis marine sediments: aliphatic and polycyclic aromatic hydrocarbons. Environ. Forensics 8, 245–256.

Bahry, P.S., Zakaria, M.P., Bin Abdullah, A.M., Abdullah, D.K., Sakari, M., Chandru, K., et al., 2009. Forensic characterization of polycyclic aromatic hydrocarbons and hopanes in aerosols from Peninsular Malaysia. Environ. Forensics 10, 240–252.

Bakhtiari, A.R., Zakaria, M.P., Yaziz, M.I., Lajis, M.N.H., Bi, X., 2009. Polycyclic aromatic hydrocarbons and *n*-alkanes in suspended particulate matter and sediments from the langat river, peninsular malaysia. Environ. Asia 2, 1–10.

Bakhtiari, A.R., Zakaria, M.P., Yaziz, M.I., Lajis, H., Nordin, M., Bi, X., et al., 2010. Distribution of PAHs and *n*-alkanes in Klang River surface Sediments, Malaysia. Pertanika J. Sci. Technol. 18, 167–179.

Barakat, A.O., Mostafa, A., El-Sayed, N.B., Wade, T.L., Sweet, S.T., 2013. Polycyclic aromatic hydrocarbons (PAHs) in surface sediments of Lake Manzala, Egypt. Soil Sediment Contam. 22, 315–331.

Barreira, L.A., Mudge, S.M., Bebianno, M.J., 2007. Concentration and sources of polycyclic aromatic hydrocarbons in sediments from the Ria Formosa Lagoon. Environ. Forensics 8, 231–243.

Baumard, P., Budzinski, H., Garrigues, P., 1998. Polycyclic aromatic hydrocarbons in sediments and mussels of the western Mediterranean Sea. Environ. Toxicol. Chem. 17, 765–776.

Baumard, P., Budzinski, H., Garrigues, P., Dizer, H., Hansen, P.D., 1999. Polycyclic aromatic hydrocarbons in recent sediments and mussels (Mytilus edulis) from the Western Baltic Sea: occurrence, bioavailability and seasonal variations. Mar. Environ. Res. 47, 17–47.

Bin Abas, M.R., Oros, D.R., Simoneit, B.R., 2004a. Biomass burning as the main source of organic aerosol particulate matter in Malaysia during haze episodes. Chemosphere 55, 1089–1095.

Bin Abas, M.R., Rahman, N.A., Omar, N.Y.M.J., Maah, M.J., Samah, A.A., Oros, D.R., et al., 2004b. Organic composition of aerosol particulate matter during a haze episode in Kuala Lumpur, Malaysia. Atmos. Environ. 38, 4223–4241.

Blumer, M., Mullin, M.M., Thomas, D.W., 1963. Pristane in zooplankton. Science 140, 974.

Blumer, M., 1976. Polycyclic aromatic compounds in nature. Sci. Am. 234, 35–45.

Boehm, P.D., Barak, J.E., Fiest, D.L., Elskus, A.A., 1982. A chemical investigation of the transport and fate of petroleum hydrocarbons in littoral and benthic environments: the Tsesis oil spill. Mar. Environ. Res. 6, 157–188.

Boonyatumanond, R., Wattayakorn, G., Togo, A., Takada, H., 2006. Distribution and origins of polycyclic aromatic hydrocarbons (PAHs) in riverine, estuarine, and marine sediments in Thailand. Mar. Pollut. Bull. 52, 942–956.

Budzinski, H., Jones, I., Bellocq, J., Pierard, C., Garrigues, P.H., 1997. Evaluation of sediment contamination by polycyclic aromatic hydrocarbons in the Gironde estuary. Mar. Chem. 58, 85–97.

Cavalcante, R.M., Sousa, F.W., Nascimento, R.F., Silveira, E.R., Freire, G.S.S., 2009. The impact of urbanization on tropical mangroves (Fortaleza, Brazil): evidence from PAH distribution in sediments. J. Environ. Manage. 91, 328–335.

Chandru, K., Zakaria, M.P., Anita, S., Shahbazi, A., Sakari, M., Bahry, P.S., et al., 2008. Characterization of alkanes, hopanes, and polycyclic aromatic hydrocarbons (PAHs) in tar-balls collected from the East Coast of Peninsular Malaysia. Mar. Pollut. Bull. 56, 950–962.

Chen, C.W., Chen, C.F., Dong, C., Di, T.Y.T., 2012. Composition and source apportionment of PAHs in sediments at river mouths and channel in Kaohsiung Harbor, Taiwan. J. Environ. Monit. 14, 105–115.

DeMott, R.P., Gauthier, T.D., Wiersema, J.M., Crenson, G., 2010. Polycyclic aromatic hydrocarbons (PAHs) in Austin sediments after a ban on pavement sealers. Environ. Forensics 11, 372–382.

Department of Statistics Malaysia, Official Portal. (2016). Retrieved from https://www.dosm.gov.my.

Eglinton, G., Hamilton, R.J., 1963. The distribution of alkanes. In: Swain, T. (Ed.), Chemical plant Taxonomy, 187. Academic Press, London, p. 217.

Elias, M.S., Wood, A.K., Hashim, Z., Siong, W.B., Hamzah, M.S., Rahman, S.A., et al., 2007. Polycyclic aromatic hydrocarbon (PAH) contamination in the sediments of East Coast Peninsular Malaysia. Malays. J. Anal. Sci. 11, 70–75.

Garrigues, P., Budzinski, H., Manitz, M.P., Wise, S.A., 1995. Pyrolytic and petrogenic inputs in recent sediments: a definitive signature through phenanthrene and chrysene compound distribution. Polycycl. Aromat. Compd. 7, 275–284.
Guillén, M.D., Sopelana, P., Partearroyo, M.A., 2000. Polycyclic aromatic hydrocarbons in liquid smoke flavorings obtained from different types of wood. Effect of storage in polyethylene flasks on their concentrations. J. Agric. Food Chem. 48, 5083–5087.
Gustafsson, Ö., Haghseta, F., Chan, C., MacFarlane, J., Gschwend, P.M., 1996. Quantification of the dilute sedimentary soot phase: implications for PAH speciation and bioavailability. Environ. Sci. Technol. 31, 203–209.
He, X., Pang, Y., Song, X., Chen, B., Feng, Z., Ma, Y., 2014. Distribution, sources and ecological risk assessment of PAHs in surface sediments from Guan River Estuary, China. Mar. Pollut. Bull. 80, 52–58.
Headley, J.V., Akre, C., Conly, F.M., Peru, K.M., Dickson, L.C., 2001. Preliminary characterization and source assessment of PAHs in tributary sediments of the Athabasca River, Canada. Environ. Forensics 2, 335–345.
Jaswar, M.R., Maimun, A., 2010. Effect of oil spill pollution in Malacca Strait to marine ecosystem. In: Zaharim, A., Sopian, K. (Eds.), Latest Trends in Renewable Energy and Environmental Informatics. Wseas LLC, pp. 373–377.
Kasmin, S., 2010. Enforcing ship-based marine pollution for cleaner sea in the Strait of Malacca. Environ. Asia 3, 61–65.
Ke, L., Yu, K.S.H., Wong, Y.S., Tam, N.F.Y., 2005. Spatial and vertical distribution of polycyclic aromatic hydrocarbons in mangrove sediments. Sci. Total Environ. 340, 177–187.
Keshavarzifard, M., Zakaria, M.P., Shau Hwai, T., Mustafa, S., Vaezzadeh, V., Magam, S.M., et al., 2014. Baseline distributions and sources of polycyclic aromatic hydrocarbons (PAHs) in the surface sediments from the Prai and Malacca Rivers, Peninsular Malaysia. Mar. Pollut. Bull. 88, 366–372.
Koike, T., Koike, H., Kurumisawa, R., Ito, M., Sakurai, S., Togo, A., et al., 2012. Distribution, source identification, and historical trends of organic micropollutants in coastal sediment in Jakarta Bay, Indonesia. J. Hazard. Mater. 217, 208–216.
Laflamme, R.E., Hites, R.A., 1978. The global distribution of polycyclic aromatic hydrocarbons in recent sediments. Geochim. Cosmochim. Acta 42, 289–303.
Law, A.T., Veellu, R., 1989. Petroleum hydrocarbon along the coastal areas of Port Dickson. Pertanika 12, 349–355.
Li, A., Tanabe, S., Jiang, G., Giesy, J.P., Lam, P.S.K., 2011. Persistent Organic Pollutants in Asia: Sources, Distributions, Transport and Fate. Elsevier Science, Amesterdm, p. 624.
Li, B., Feng, C., Li, X., Chen, Y., Niu, J., Shen, Z., 2012. Spatial distribution and source apportionment of PAHs in surficial sediments of the Yangtze Estuary, China. Mar. Pollut. Bull. 64, 636–643.
Liu, L., Zhang, J.H., Hu, Y.Y., Huo, C., Wang, J., 2011. Ecological risk assessment on polycyclic aromatic hydrocarbons in surface sediments of Dalian Bay. Mar. Environ. Sci. 30, 477–480.
Lough, G.C., Schauer, J.J., Lawson, D.R., 2006. Day-of-week trends in carbonaceous aerosol composition in the urban atmosphere. Atmos. Environ. 40, 4137–4149.
Magi, E., Bianco, R., Ianni, C., Di Carro, M., 2002. Distribution of polycyclic aromatic hydrocarbons in the sediments of the Adriatic Sea. Environ. Pollut. 119, 91–98.
Mazurek, M.A., Simoneit, B.R.T., 1984. Characterization of biogenic and petroleum-derived organic matter in aerosols over remote, rural and urban areas. Identif. Anal. Org. Pollut. Air 22, 353–362.
Masood, N., Zakaria, M.P., Halimoon, N., Aris, A.Z., Magam, S.M., Kannan, N., et al., 2016. Anthropogenic waste indicators (AWIs), particularly PAHs and LABs, in Malaysian sediments: application of aquatic environment for identifying anthropogenic pollution. Mar. Pollut. Bull. 102, 160–175.
McGuinness, M., Dowling, D., 2009. Plant-associated bacterial degradation of toxic organic compounds in soil. Int. J. Environ. Res. Public Health 6, 2226–2247.
Mirsadeghi, S.A., Zakaria, M.P., Yap, C.K., Shahbazi, A., 2011. Risk assessment for the daily intake of polycyclic aromatic hydrocarbons from the ingestion of cockle *(Anadara granosa)* and exposure to contaminated water and sediments along the west coast of Peninsular Malaysia. J. Environ. Sci. 23, 336–345.
Mirsadeghi, S.A., Zakaria, M.P., Yap, C.K., Gobas, F., 2013. Evaluation of the potential bioaccumulation ability of the blood cockle *(Anadara granosa)* for assessment of environmental matrices of mudflats. Sci. Total Environ. 454, 584–597.
Neff, J.M., 1979. Polycyclic Aromatic Hydrocarbons in the Aquatic Environment: Sources, Fates and Biological Effects. Applied Science, London, pp. 44–49.
Okui, A., Koshikawa, K., Yokoyama, Y. and Yokoi, K. Origin of oil with high oleanane index in southeast of Asia. In: XVIII International Meeting on Organic Geochemistry (Maastrich, The Netherlands); 1997; 807–808.
Ourisson, G., Rohmer, M., Poralla, K., 1987. Prokaryotic hopanoids and other polyterpenoid sterol surrogates. Annu. Rev. Microbiol. 41, 301–333.
Pavlova, A., Papazova, D., 2003. Oil-spill identification by gas chromatography-mass spectrometry. J. Chromatogr. Sci. 41, 271–273.
Pereira, W.E., Hostettler, F.D., Luoma, S.N., van Geen, A., Fuller, C.C., Anima, R.J., 1999. Sedimentary record of anthropogenic and biogenic polycyclic aromatic hydrocarbons in San Francisco Bay, California. Mar. Chem. 64, 99–113.
Peters, K.E., Moldowan, J.M., 1993. The Biomarker Guide: Interpreting Molecular Fossils in Petroleum and Ancient Sediments. Prentice Hall, Englewood Cliffs, NJ, p. 310.
Prahl, F.G., Carpenter, R., 1983. Polycyclic aromatic hydrocarbon (PAH)-phase associations in Washington coastal sediment. Geochim. Cosmochim. Acta 47, 1013–1023.
Poynter, J., Eglinton, G., 1987. Molecular composition of three sediments from hole 717C: The Bengal FAN1. In: Cochran, J.R., Stow, D.A.V. (Eds.), Proceedings of the Ocean Drilling Program, Scientific Results, College Station, TX (Ocean Drilling Program): Elsevier; 1987; 155–161.
Qian, Y., Wade, T.L., Sericano, J.L., 2001. Sources and bioavailability of polynuclear aromatic hydrocarbons in Galveston Bay, Texas. Estuaries 24, 817–827.
Ramakrishnan, S.N., 1998. Quantitative and qualitative analysis of hydrocarbon in green-lipped mussel (*Perna viridis*) from selected locations of south Johore coastline. Unpublished project report.

Ramdine, G., Fichet, D., Louis, M., Lemoine, S., 2012. Polycyclic aromatic hydrocarbons (PAHs) in surface sediment and oysters *(Crassostrea rhizophorae)* from mangrove of Guadeloupe: levels, bioavailability, and effects. Ecotoxicol. Environ. Saf. 79, 80–89.

Raza, M., Zakaria, M.P., Hashim, N.R., Yim, U.H., Kannan, N., Ha, S.Y., 2013. Composition and source identification of polycyclic aromatic hydrocarbons in mangrove sediments of Peninsular Malaysia: indication of anthropogenic input. Environ. Earth Sci. 70, 2425–2436.

Readman, J.W., Fillmann, G., Tolosa, I., Bartocci, J., Villeneuve, J.-P., Catinni, C., et al., 2002. Petroleum and PAH contamination of the Black Sea. Mar. Pollut. Bull. 44, 48–62.

Reddy, K.R., Xie, T., Dastgheibi, S., 2013. PAHs removal from urban storm water runoff by different filter materials. J. Hazard. Toxic Radioact. Waste 18, 04014008.

Retnam, A., Zakaria, M.P., Juahir, H., Aris, A.Z., Zali, M.A., Kasim, M.F., 2013. Chemometric techniques in distribution, characterisation and source apportionment of polycyclic aromatic hydrocarbons (PAHS) in aquaculture sediments in Malaysia. Mar. Pollut. Bull. 69, 55–66.

Rogge, W.F., Hildemann, L.M., Mazurek, M.A., Cass, G.R., Simoneit, B.R.T., 1993. Sources of fine organic aerosol. 2. Noncatalyst and catalyst-equipped automobiles and heavy-duty diesel trucks. Environ. Sci. Technol. 27, 636–651.

Rohmer, M., Bouvier-Nave, P., Ourisson, G., 1984. Distribution of hopanoid triterpenes in prokaryotes. J. Gen. Microbiol. 130, 1137–1150.

Sakari, M., Zakaria, M.P., Junos, M.B.M., Annuar, N.A., Yun, H.Y., Heng, Y.S., et al., 2008a. Spatial distribution of petroleum hydrocarbon in sediments of major rivers from east coast of peninsular Malaysia. Coast. Mar. Sci. 31, 9–18.

Sakari, M., Zakaria, M.P., Lajis, N.H., Mohamed, C.A.R., Bahry, P.S., Anita, S., 2008b. Characterization, distribution, sources and origins of aliphatic hydrocarbons from surface sediment of Prai Strait, Penang, Malaysia: a widespread anthropogenic input. Environ. Asia 2, 1–14.

Sakari, M., Zakaria, M.P., Mohamed, C.A.R., Lajis, N.H., Chandru, K., Bahry, P.S., et al., 2010. Urban vs. marine based oil pollution in the strait of Johor, Malaysia: a century record. Soil Sediment Contam. 19, 644–666.

Sakari, M., Zakaria, M.P., Lajis, N.H., Mohamed, C.R., Abdullah, M.H., 2012. Reconstruction of aliphatic hydrocarbons history and sources from sedimentary record of the Johor Strait, Malaysia. Coast. Mar. Sci. 35, 142–152.

Shahbazi, A., 2009. Green-lipped mussels (*perna viridis*) as biomarkers of petroleum hydrocarbon contamination in selected coastal waters of Peninsular Malaysia. Unpublished doctoral thesis.

Shahbazi, A., Zakaria, M.P., Yap, C.K., Surif, S., Bakhtiari, A.R., Chandru, K., et al., 2010. Spatial distribution and sources of polycyclic aromatic hydrocarbons (PAHs) in green mussels *(Perna viridis)* from coastal areas of Peninsular Malaysia: implications for source identification of perylene. Int. J. Environ. Anal. Chem. 90, 14–30.

Sicre, M.A., Marty, J.C., Saliot, A., Aparicio, X., Grimalt, J., Albaiges, J., 1987. Aliphatic and aromatic hydrocarbons in different sized aerosols over the Mediterranean Sea: occurrence and origin. Atmos. Environ. 21, 2247–2259.

Simoneit, B.R.T., 1982. Some applications of computerized GC–MS to the determination of biogenic and anthropogenic organic matter in the environment. Int. J. Environ. Anal. Chem. 12, 177–193.

Simoneit, B.R.T., 1985. Application of molecular marker analysis to vehicular exhaust for source reconciliations. Int. J. Environ. Anal. Chem. 22, 203–232.

Soclo, H.H., Garrigues, P.H., Ewald, M., 2000. Origin of polycyclic aromatic hydrocarbons (PAHs) in coastal marine sediments: case studies in Cotonou (Benin) and Aquitaine (France) areas. Mar. Pollut. Bull. 40, 387–396.

Soon, C.S., 1999. Polycyclic aromatic hydrocarbons (PAHs) in selected Peninsular Malaysia coastal water. Unpublished project report.

Takada, H., Onda, T., Harada, M., Ogura, N., 1991. Distribution and sources of polycyclic aromatic hydrocarbons (PAHs) in street dust from the Tokyo Metropolitan area. Sci. Total Environ. 107, 45–69.

Tam, N.F.Y., Ke, L., Wang, X.H., Wong, Y.S., 2001. Contamination of polycyclic aromatic hydrocarbons in surface sediments of mangrove swamps. Environ. Pollut. 114, 255–263.

Tanabe, S., Tatsukawa, R., Phillips, D.J., 1987. Mussels as bioindicators of PCB pollution: a case study on uptake and release of PCB isomers and congeners in green-lipped mussels *(Perna viridis)* in Hong Kong waters. Environ. Pollut. 47, 41–62.

Taneza, P., Philp, R.P., 2009. A preliminary study of the sources of organic pollutants in the Iloilo River, Philippines. Environ. Forensics 10, 68–81.

Tripp, B.W., Farrington, J.W., Teal, J.M., 1981. Unburned coal as a source of hydrocarbons in surface sediments. Mar. Pollut. Bull. 12, 122–126.

Vaezzadeh, V., 2015. Bioavailability of petroleum hydrocarbons to mangrove oyster (*Crassostrea belcheri* g.b. sowerby) from sediment in mangrove ecosystems of west coast of Peninsular Malaysia. Unpublished doctoral thesis.

Vaezzadeh, V., Zakaria, M.P., Shau Hwai, A., Ibrahim, Z., Mustafa, S., Keshavarzifard, M., et al., 2015a. Source type evaluation of polycyclic aromatic hydrocarbons (PAHs) in surface sediments from the Muar River and Pulau Merambong, Peninsular Malaysia. Environ. Forensics 16, 135–142.

Vaezzadeh, V., Zakaria, M.P., Shau-Hwai, A.T., Ibrahim, Z.Z., Mustafa, S., Abootalebi-Jahromi, F., et al., 2015b. Forensic investigation of aliphatic hydrocarbons in the sediments from selected mangrove ecosystems in the west coast of Peninsular Malaysia. Mar. Pollut. Bull. 100, 311–320.

Viguri, J., Verde, J., Irabien, A., 2002. Environmental assessment of polycyclic aromatic hydrocarbons (PAHs) in surface sediments of the Santander Bay, Northern Spain. Chemosphere 48, 157–165.

Wang, Z., Fingas, M., Sergy, G., 1994. Study of 22-year-old Arrow oil samples using biomarker compounds by GC/MS. Environ. Sci. Technol. 28, 1733–1746.

Wang, Z., Stout, S.A., Fingas, M., 2006. Forensic fingerprinting of biomarkers for oil spill characterization and source identification. Environ. Forensics 7, 105–146.

Youngblood, W.W., Blumer, M., 1975. Polycyclic aromatic hydrocarbons in the environment: homologous series in soils and recent marine sediments. Geochim. Cosmochim. Acta 39, 1303–1314.

Yunker, M.B., Macdonald, R.W., Vingarzan, R., Mitchell, R.H., Goyette, D., Sylvestre, S., 2002. PAHs in the Fraser River basin: a critical appraisal of PAH ratios as indicators of PAH source and composition. Org. Geochem. 33, 489–515.

Zakaria, M.P., Mahat, A.A., 2006. Distribution of polycyclic aromatic hydrocarbon (PAHs) in sediments in the Langat Estuary. Coast. Mar. Sci. 30, 387–395.

Zakaria, M.P., Horinouchi, A.I., Tsutsumi, S., Takada, H., Tanabe, S., Ismail, A., 2000. Oil pollution in the Straits of Malacca, Malaysia: application of molecular markers for source identification. Environ. Sci. Technol. 34, 1189–1196.
Zakaria, M.P., Okuda, T., Takada, H., 2001. Polycyclic aromatic hydrocarbon (PAHs) and hopanes in stranded tar-balls on the coasts of Peninsular Malaysia: applications of biomarkers for identifying sources of oil pollution. Mar. Pollut. Bull. 42, 1357–1366.
Zakaria, M.P., Takada, H., Tsutsumi, S., Ohno, K., Yamada, J., Kouno, E., et al., 2002. Distribution of polycyclic aromatic hydrocarbons (PAHs) in rivers and estuaries in Malaysia: a widespread input of petrogenic PAHs. Environ. Sci. Technol. 36, 1907–1918.

Further Reading

Masood, N., Zakaria, M.P., Ali, M.M., Magam, S.M., Alkhadher, S., Keshavarzifard, M., et al., 2014. Distribution of petroleum hydrocarbons in surface sediments from selected locations in Kuala Selangor River, Malaysia. In: Aris, A.Z., Tengku Ismail, T.H., Harun, R., Abdullah, A.M., Ishak, M.Y. (Eds.), From Sources to Solution. Springer, Singapore, pp. 351–356.
Taneza, P., Philp, R.P., 1987. A preliminary study of the sources of organic pollutants in the Iloilo River, Philippines. Environ. Forensics 10, 68–81.

CHAPTER

17

Long-Term Monitoring Study of Beached Oils Around the Shetland Isles, United Kingdom

Gordon Todd[1] *and David Runciman*[2]

[1]Heriot-Watt University, Edinburgh, United Kingdom [2]Cherith, Orkney, United Kingdom

BIOGRAPHIES

Gordon Todd is a degree-qualified chemist with a master's degree in analytical chemistry. Gordon worked for a number of years in manufacturing quality assurance before moving into environmental chemistry in 2001. He specialized in hydrocarbon analysis by gas chromatography, and this led into the forensic testing of oil spill samples. In 2005, Gordon became the expert advisor to the UK Maritime and Coastguard Agency (MCA) representing the agency within a pan-European group of experts (OSINet) on the development of oil spill identification techniques. Whilst participating in OSINet, Gordon has contributed toward the development of CEN/TR 15522-2:2012, and in 2012, he organized the group's annual proficiency testing scheme and hosted the annual workshop in Edinburgh the following year. Gordon continues to be involved in oil spill identification and has recently become involved in applying the techniques to oil seeps in support of oil exploration studies.

David Runciman is a Royal Society of Chemistry chartered chemist (MRSC CChem) with over 30 years environmental chemistry experience. He has 20 years of laboratory experience specializing in the analysis of hydrocarbons in the marine environment including the forensic analysis of oil spill samples. David has contributed to the development of national/international standardized analytical methodologies for oil spill identification (UK Environment Agency *Guide to practices, procedures and methodologies following oil spill contamination incidents (2004)* and CEN/TR 15522-2:2012). He has also worked as an expert advisor to the UK Coastguard Agency (MCA) and the International Tanker Operators Association (ITOPF). He currently works as an independent environmental scientist.

17.1 INTRODUCTION

The Shetland Isles, including Fair Isle, are composed of over 100 islands stretching approximately 100 mi from north to south and straddle the boundary where the Atlantic Ocean meets the North Sea. The islands capital Lerwick lies 125 mi northeast of the most northerly point on the British mainland, John o'Groats and only around 210 mi west of the Norwegian coastline. With the 60 degrees north line of latitude crossing the islands, they are on a similar latitude to Anchorage, Alaska and only 400 mi south of the Arctic Circle. Shetland's climate is however very different from that of Anchorage enjoying much milder conditions due to the North Atlantic Drift, or Gulf Stream, which brings warm water and air from the Gulf of Mexico to the northwest coastlines of Europe. It is this mild climate, its corresponding rich sea life, and the ca. 1700 mi of predominately rocky coastline that attracts hundreds of thousands of seabirds to the islands with some colonies vitally important in terms of global populations. These conditions also account for some of the densest populations of otters found in Europe with approximately 12% of those within the UK total living around the islands. The islands waters are also home to, or visited by, many cetaceans and seals.

Oil Spill Environmental Forensics Case Studies.
DOI: http://dx.doi.org/10.1016/B978-0-12-804434-6.00017-3

Fishing and crofting are traditional activities for the islands inhabitants with rich whitefish, herring, and shellfish grounds all around the islands. Aquaculture, and in particular salmon farming, has become an established industry with significant value to the local economy. In the late 1960s, oil was discovered in the North Sea with the Brent field approximately 100 mi east northeast of Shetland becoming one of the largest oil reserves ever discovered on the UK Continental Shelf. Following the discovery of oil at Brent and several other reservoirs (e.g., Cormorant, Dunlin, Eider, etc.) in the east of Shetland Basin (ESB), Shetland's location became of strategic importance to the developing oil and gas industry. In order to cope with the production levels from these new oilfields (ca. 130,000 m^3/day through the Brent oil pipeline in 1985), an onshore terminal was required with Sullom Voe on Shetland the site chosen. It was initially envisaged that several terminals would be built by the various operators to serve their own fields but planning consent limited it to the single terminal at Sullom Voe operated by BP on behalf of a consortium of companies. In addition, Brent pipeline system were pipelines coming from the Ninian field and latterly from the Clair field, located to the west of Shetland in the Northeast Atlantic. A shuttle tanker also brings oil to Sullom Voe from the Schiehallion field to the west of Shetland.

Construction began on the Sullom Voe Terminal in 1975 and continued until 1981. With the first oil arriving at Sullom Voe in 1978, there were obvious concerns about the possibility of a major oil spill occurring and the damage it may cause to the local environment. Unfortunately, those fears were proven valid just over 1 month after the first oil arrived at the Terminal when the tanker *Esso Bernicia* struck a mooring jetty and lost 1100 t of heavy fuel oil from a damaged bunker. Prior to and following this spill, various monitoring programs were undertaken by Sullom Voe Environmental Advisory Group (SOTEAG), including studies on bird populations and the rocky shores and seabed of Sullom Voe and the surrounding area.

In this study, we summarize the findings of a long-term monitoring program investigating the origins of beached oil collected from the Shetland shoreline between 1996 and 2015. The work is currently funded by Sullom Voe Association Limited on behalf of the operators of the Sullom Voe Terminal and managed by the SOTEAG who provide independent scientific advice to the Sullom Voe Terminal.

17.1.1 The Beached Oil-Monitoring Program

As interest grew in developing oil and gas reserves in the UK Atlantic Margin, the Atlantic Frontier Environmental Network (AFEN), composed of UK Government scientists and oil company specialists, was formed to increase the knowledge of the natural environment around Shetland and the wider the Atlantic Margin and thus supplement the environmental studies managed by SOTEAG. When the tanker *MV Braer* ran aground in January 1993 during extreme weather conditions and broke up losing its entire cargo (87,000 t) of crude and fuel oil (ESGOSS, 1994) interest in monitoring beached oil increased as attempts were made to link cases to the spill. It served as a timely reminder of the potential damage resulting from oil spills at a time when exploration and production activities in the challenging seas west of Shetland became the target of several operators. As a result, in 1996, AFEN took over management of an ad-hoc beached oil-monitoring program previously funded by Shetland Island Council with the primary objective to analyze all beached oil samples collected from the Shetland coastline to establish the oil type present and if possible, identify the source of the oil.

AFEN financing of the program ceased in 2003 and, with no other agency or industry body prepared to take up the work, SOTEAG stepped in to fund the continuation of the monitoring program. Fugro Great Britain Marine Limited (and predecessor companies; Fugro EMU, Fugro ERT, ERT Scotland, and Environment and Resource Technology) have been responsible for the provision of laboratory analyses, interpretation and reporting over the entire monitoring period thus ensuring a consistent approach throughout the program. In addition to producing summary reports for each case and periodic monitoring reports assessing the whole dataset, in 2015, Fugro EMU produced a database of all beached oil cases including details such as rationalized sample locations, sample type, oil type, and potential origin. The database has a number of search queries and forms to export the data in a tabulated format so that interested parties can extract and compare all of the results.

Sample collection around Shetland was, and largely still is carried out by volunteers following observations of spilled oil, reports of oil residues on beaches or the discovery of oiled seabirds. At the time of preparing the monitoring report, from which this chapter is based, a total of 233 samples had been collected around Shetland and Fair Isle with 229 subsequently analyzed. Samples collected are individually numbered with a designated prefix "SIC" (in reference to Shetlands Islands Council who initially collected beached oil samples on an ad-hoc basis prior to the establishment of a structured monitoring program) followed by a sequential number.

The chronological distribution of the total number of beached oil samples collected annually is shown in Fig. 17.1.

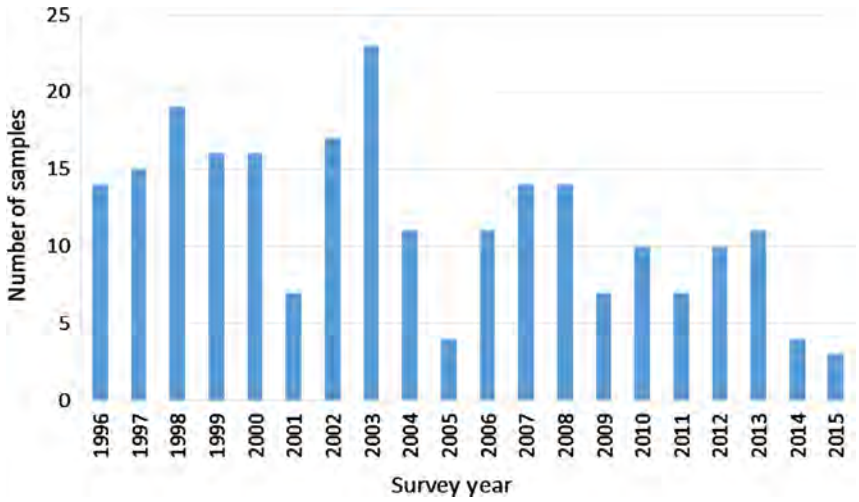

FIGURE 17.1 Chronological distribution of beached oil sample collection throughout the survey period, 1996 to February 2015.

17.1.2 Sample Locations

Over the duration of the monitoring program 204 samples have been collected from the shores around the mainland (including Burra). A total of 55 samples were collected from north of Mavis Grind (Northmavine, the northwest part of the mainland), 31 from the southeast mainland, 30 from the southwest mainland, 28 from the south mainland, 27 from the western mainland, 16 from west Burra, 11 from the eastern mainland, and 3 each from the central and northern mainland. Other than Northmavine, the geographical regions have been assigned by approximate regional splits of the mainland and are generalized locations rather than established boundaries.

Of the remaining 29 samples not collected on the mainland/Burra, 23 were collected from Yell; 3 from Fetlar; and 1 each from Bressay, Fair Isle, and Unst. Approximate sampling locations and number of samples collected are shown in Fig. 17.2, while a summarized breakdown of the sample numbers by regional location is shown in Fig. 17.3.

The locations where the beached oil samples have been collected will be influenced by the operational areas covered by the volunteer observers. The largest numbers of samples have been found on the Mainland coastline, likely related to the fact that majority of the observers effort will have been focused on this area. Between 1996 and 2015, a higher proportion of samples have been collected from the west facing coastlines. However, potential biases related to the sampling effort make the accurate determination of any long-term patterns in the deposition of beached oil difficult.

17.1.3 Sample Types

Oiled birds have accounted for the vast majority of sample types collected, numbering 202 of 233 samples, followed by tar balls (21), then general beached oil residues (10).

Guillemots were the most common bird species to be found oiled (76), followed closely by Fulmars (65). Razorbills were the next most common (16), then Gannets (14), Kittiwakes (11), Great Black-backed Gulls (6), Puffins (3), Common Gulls and Herring Gulls (2). A number of species were found only once and these single observations were Black Guillemot, Eider, Glaucous Gull, Great Northern Diver, Lesser Black-backed Gull, Red Throated Diver, and Shag.

Since 2003, there has been a shift in the ratio of oiled guillemots to fulmars recorded. The results of the annual ornithological surveys conducted as part of the SOTEAG program suggest that there may have been an overall decrease in the numbers of guillemots in the Shetland area over this period and also that this species may be spending less time in Shetland waters in winter and early spring when most oil spill incidents typically occur (Martin Heubeck, personal communication, February 2017).

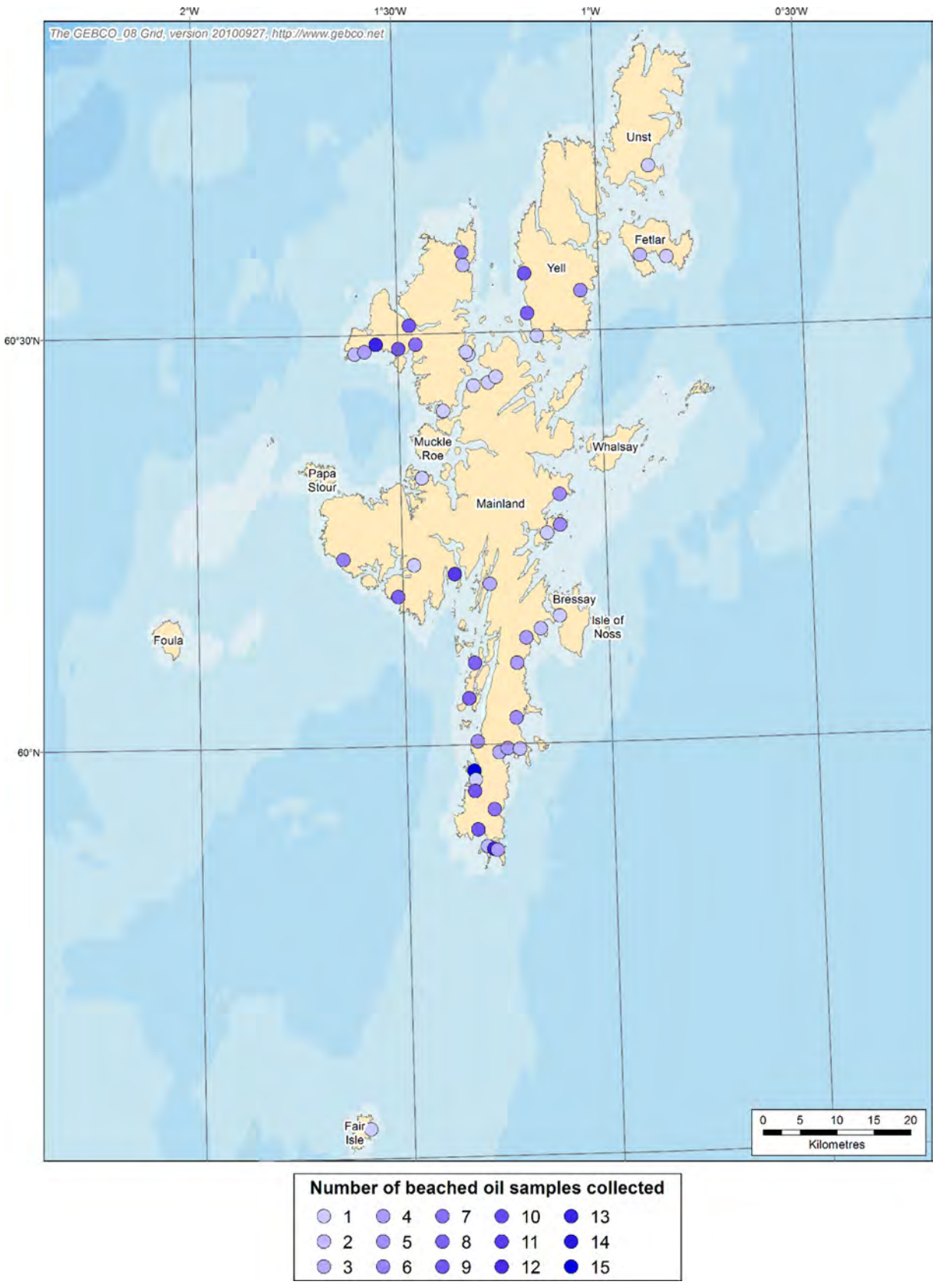

FIGURE 17.2 Map showing approximate sampling locations and number of beach oil samples collected at each site on Shetland Isles and Fair Isle throughout the survey period, 1996 to February 2015.

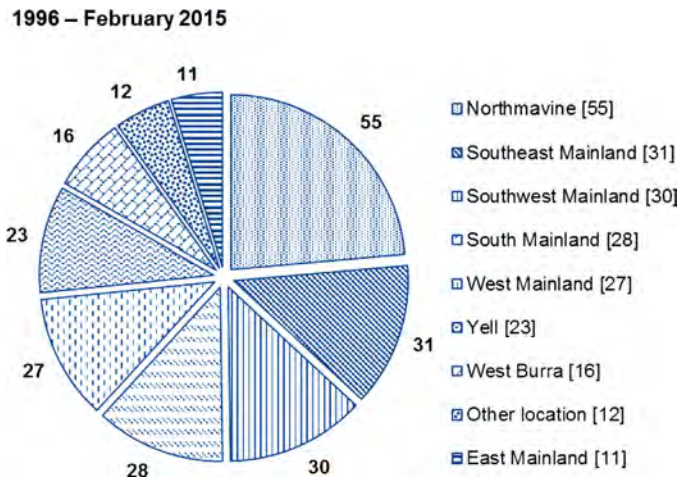

FIGURE 17.3 Geographic distribution of beached oil sampling locations throughout the survey period, 1996 to February 2015.

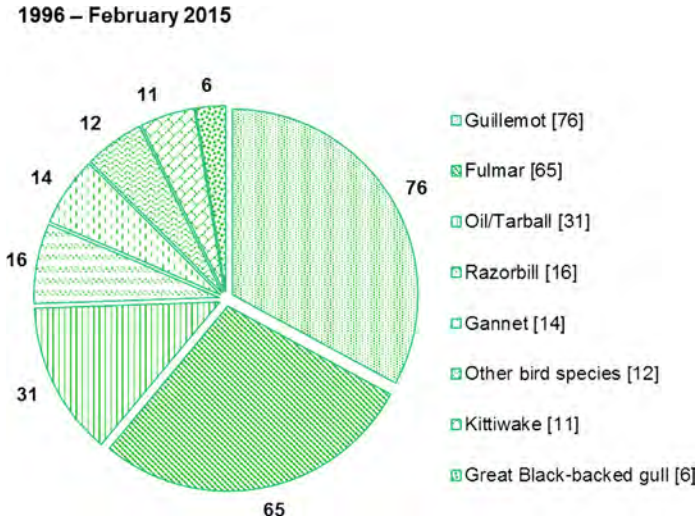

FIGURE 17.4 Sample types (oiled birds by species and oil/tarballs) supplied throughout the survey period, 1996 to February 2015.

The summarized distributions of the sample types and bird species found since monitoring began are shown in Figs. 17.4 and 17.5.

17.2 METHODOLOGY

17.2.1 Analytical Methodology

Throughout the monitoring program the samples received have been prepared for instrumental analysis using the same technique, viz., extraction with n-pentane followed by centrifugation to separate any nonsoluble material or residual water transferred from the sample matrix.

Analysis was generally consistent throughout the monitoring program, initially carried out using gas chromatography with a flame ionization detector (GC–FID) to obtain a chromatographic profile of the hydrocarbon material present in the sample. This was followed by a detailed analysis undertaken using gas chromatography with mass spectrometry (GC–MS) to study the biomarker compounds and selected polycyclic aromatic hydrocarbons.

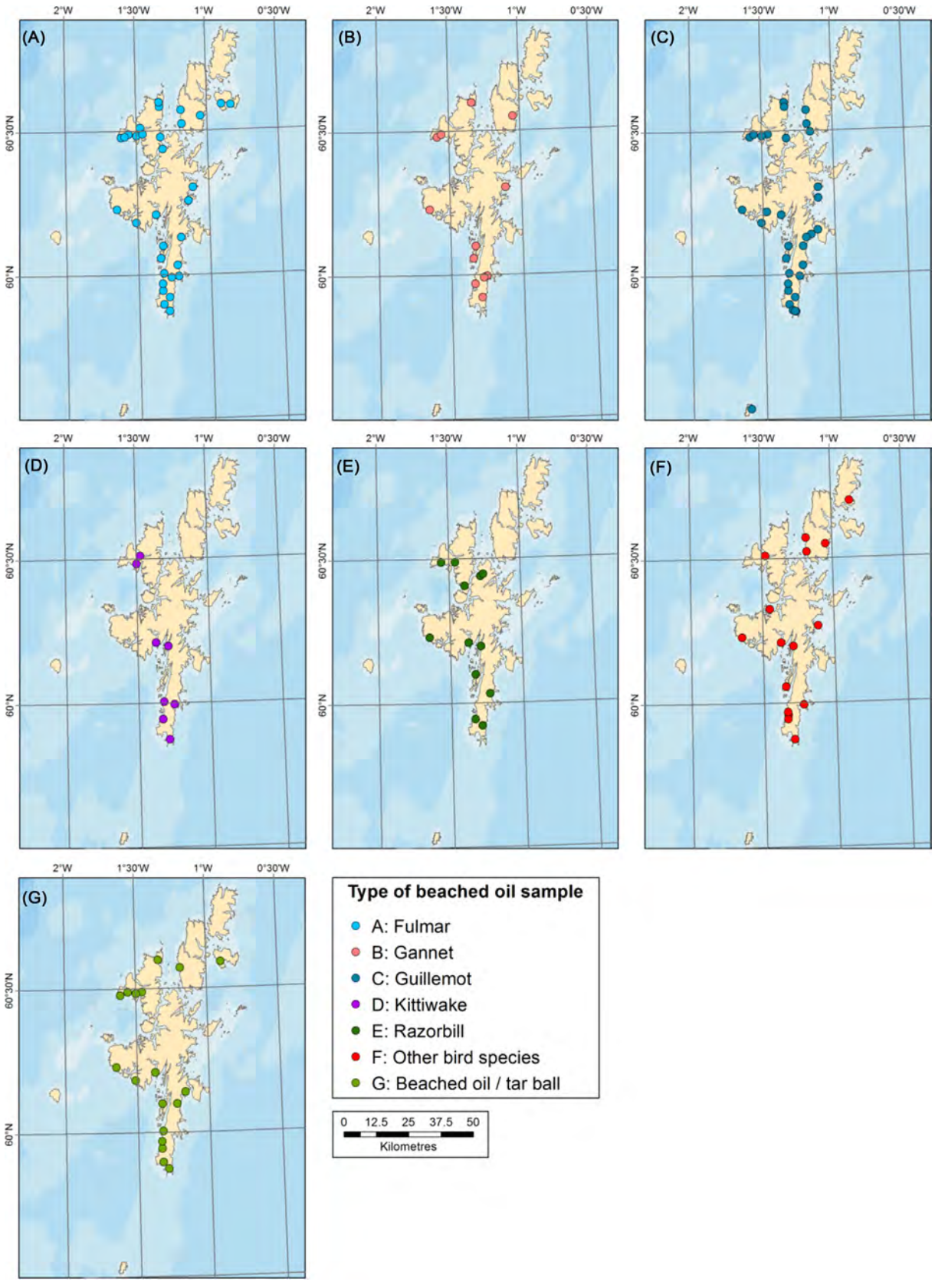

FIGURE 17.5 Main sample types (oiled birds by species and oil/tarballs) supplied by location throughout the survey period, 1996 to February 2015.

Interpretation of the analytical data has also been largely consistent throughout the duration of the program. However, the methodology has evolved over time and the approach taken to processing the data has advanced in order to continually improve the quality of the interpretation and increase the robustness of any conclusions drawn from the results.

17.2.2 Interpretation Methodology

The earliest oil identification undertaken as part of this study was based upon the Nordtest method NT CHEM 001 (Nordtest, 1991), but without the detailed *n*-alkane/isoprenoid ratio or weathering check as listed in the method.

Following on from the Nordtest method was the implementation of methodology trialed in two major research projects, first, the Joint Programme of Research on Source Identification, Behaviour and Modelling of North Sea Crudes at Sea (SIBAM) with the analytical program SLICKMATCH forming part of the project (Walker et al, 1992) and second, the European Union funded EUROCRUDE project, which aimed to create a joint European Crude Oil Identification System (Grigson and Baron, 1995). This second project was a collaborative effort from a number of institutions across six countries including the United Kingdom and coupled the latest analytical techniques with computer aided pattern recognition models to create a database of crude oil fingerprints.

The EUROCRUDE methodology introduced the concept of comparing the ratios of selected biomarker peaks and this approach to oil spill identification was continued for this study until 2002, the point at which the original Nordtest method was revised (Faksness et al., 2002). As with the original Nordtest method, not all aspects of the revised methodology were adopted for this study; however, it would become the basis for oil spill identification going forward.

For this study, not only the revised Nordtest approach to interpretation of data was abbreviated in response to the likelihood of finding the original polluter, but also a reflection of the samples typically supplied, i.e., oiled birds that had been dead for many weeks before being discovered, no source oil to match against, no other evidence (or budget to expand into this area) to help with full-scale spill investigation.

Following the sinking of the tanker *Prestige* and the vehicle carrier *Tricolor* in 2002, problems were identified by a number of laboratories in determining differences in the oil profiles and assigning beached oil samples to either wreck. This led to the creation of a working group to develop and advance the methodology and to produce a new standard to work from this would become CEN/TR 15522-2:2006 (CEN, 2006). The new CEN method initially tried to satisfy all contributing parties but was impractical to implement for many routine cases so continuing improvements were discussed prior to a revision being issued of CEN/TR 15522-2:2012 (CEN, 2012).

Where the adoption of the CEN (2012) method altered, the approach taken in this study was with the concept of critical differences, i.e., those beyond the limits of analytical uncertainties. This was the point where statistical testing of biomarker ratios became a regular part of the interpretation process and would lead to adoption of the COSIWeb program in all routine testing.

COSIWeb is a web-based interface for the computerized oil spill identification (COSI) system which was developed over many years by Dr. Gerhard Dahlmann (retired) of Bundesamt fuer Seeschifffahrt und Hydrographie (BSH) in Hamburg, Germany, as a tool for the forensic investigation of oil spills (Dahlmann and Kienhuis, 2016). The COSI system can compare oil samples against previously uploaded oils using biomarker ratios and principle components analysis (PCA) and was developed in order to speed up the identification process by reducing the level of manual integration of chromatograms whilst creating a searchable database of oil profiles.

The first sample uploaded to COSIWeb in relation to this monitoring program was SIC-211 in early 2012, and since then, all beached oil samples from Shetland have been processed through COSIWeb in addition to the more traditional comparisons. At the time of preparing the monitoring report (March 2015), upon which this chapter is based, COSIWeb contained reference data for nearly 2800 samples covering a wide range of crude and refined oils.

17.3 RESULTS

17.3.1 Introduction

As the monitoring program was initiated to identify whether beached oils were the result of spills from the Sullom Voe Terminal operations, offshore platforms, or the pipelines and tankers moving the oil around the island, the first objective of the study has always been to establish whether the oil residue found was crude oil or

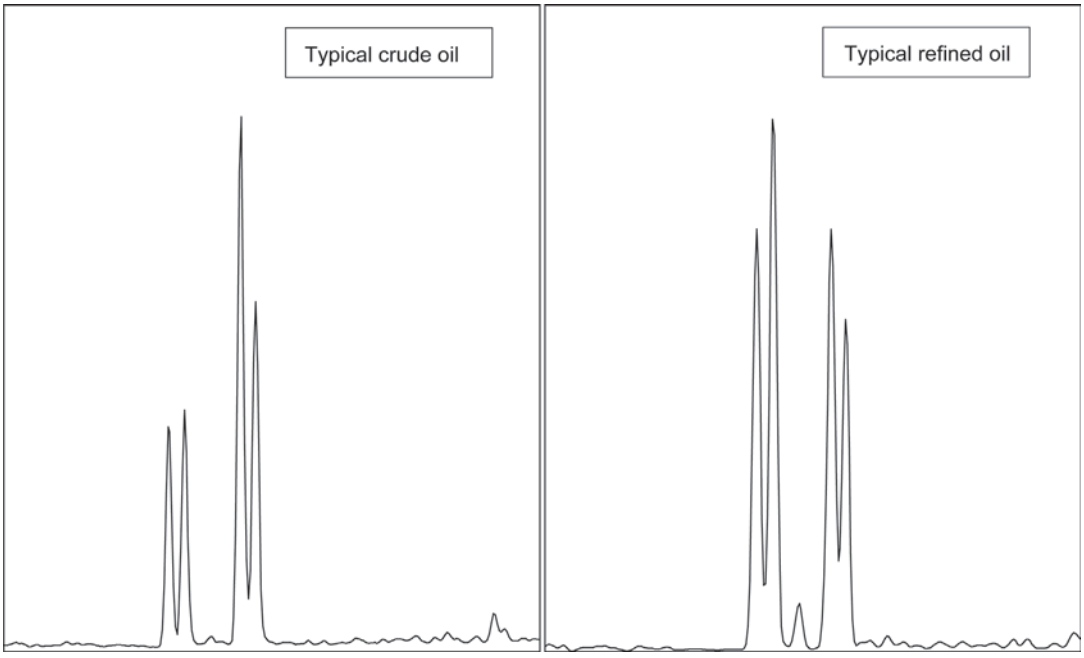

FIGURE 17.6 Typical crude and refined (fuel) oil methyl phenanthrene isomer distributions (m/z 192).

refined oil. Determining whether a spill residue is a crude oil or refined oil is critical as this can provide sufficient information to satisfy the relevant stakeholders that the oil production processes are not responsible (as spills of refined oil are highly unlikely to be related to these).

Due to the remote nature of the islands, surveillance of shipping for oil spills is substantially lower than it might be in an area like the English Channel. As such, if the beached oil is the result of an illegal bilge discharge or similar, it is highly unlikely that a suspected source will ever be identified, particularly given the time lag between the spill occurring, finding the beached oil, and then getting the samples to the laboratory for analysis.

With the program stakeholders concerned primarily with the identity of any crude oils that come ashore, and the fact that spills of refined oils are unlikely to be assigned to a suspected polluter, the determination that a beached oil sample is composed of refined oil essentially ends the investigation. When an oil residue is identified as crude oil there are clearly many more questions to answer, primarily where the oil originated from. Around Shetland, accidental crude oil spills could result from incidents such as terminal process upsets, broken oil-handling equipment, pipeline leaks, or tanker-loading failures; however, illegal discharges may also occur as tankers wash out tanks and pipelines and dump to sea. Further afield operational problems at offshore platforms could also result in beached oil coming ashore around Shetland.

The ratio of the methyl phenanthrene isomers are evaluated in order to quickly screen for oil type (Uhler et al., 2007), with refining (thermal cracking) resulting in a distinct difference to the ratio (Fig. 17.6). It is not a hard-and-fast rule as some crude oils (from high pressure high temperature reservoirs) may appear cracked while some refined oils are not cracked and simply distilled (e.g., gas oil and diesel fuels). There is also the potential risk that weathering can alter the ratios through evaporation.

17.3.2 Oil Types Found

Since 1996, crude oils accounted for a total of 56 samples (ca. 24%), while refined oils accounted for 171 samples (ca. 75%); nonoil-based residues (no distinct chromatographic profile or biomarkers found) accounted for only two samples (ca. 1%), see Fig. 17.7.

Generalized North Sea oils accounted for most of the crudes found followed closely by those most likely to have originated from the ESB. The latter crude oil residues all have key characteristics similar to oils analyzed from the region but had no direct match in the laboratory's library of oils or COSIWeb. These samples are likely to be linked to either local tanker operations or releases from offshore installations. The next most common crude oil found was Brent crude, probably related to the Sullom Voe Terminal operations, along with the oils identified

as coming from the Terminal (crude oils with characteristics very similar to a blend of Brent and Ninian but not a match to either one alone; see Fig. 17.8 for an example chromatogram of triterpanes for Brent export crude).

Around 30% of the crude oils were identified originating from Russia/Urals or other world regions. These residues almost certainly originate from oil tankers. However, it is not possible to determine the numbers of samples originating from the vessels traveling to and from the Sullom Voe Terminal compared with other tankers in transit around the north of the United Kingdom.

A summary of the geographical origin for the crude oil spill residues collected around Shetland is given in Fig. 17.9.

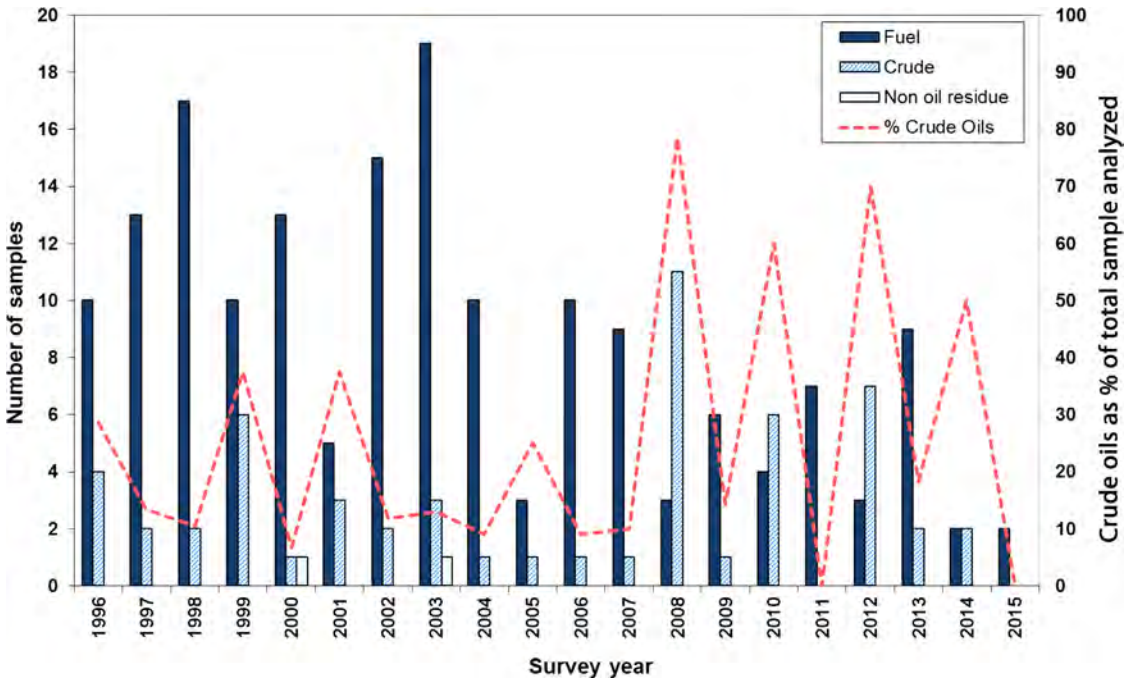

FIGURE 17.7 Oil types found among all beached oil samples throughout survey period, 1996 to February 2015.

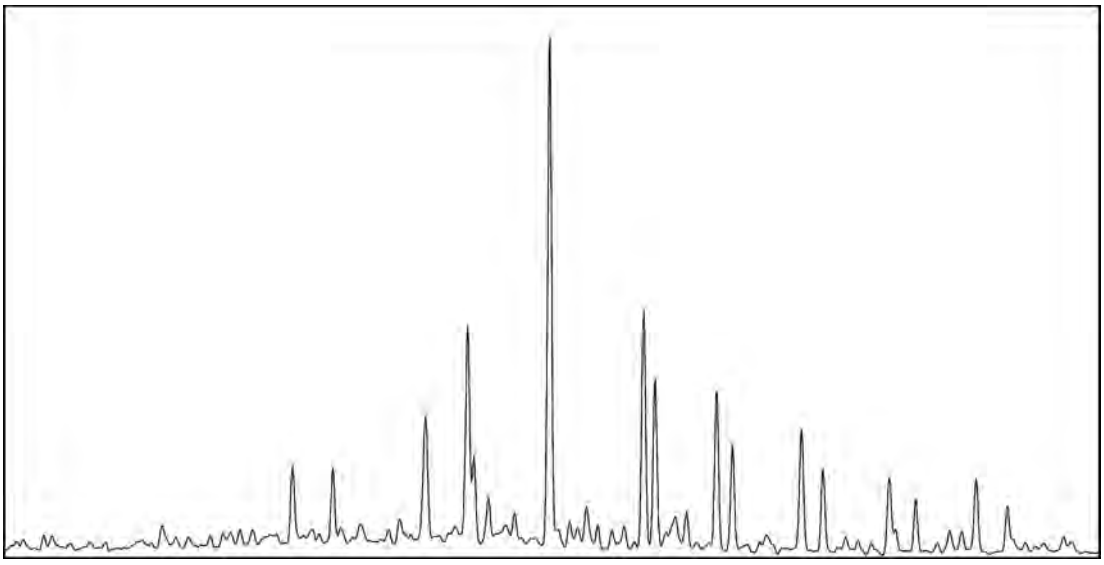

FIGURE 17.8 Triterpane profile (m/z 191) of Brent blend.

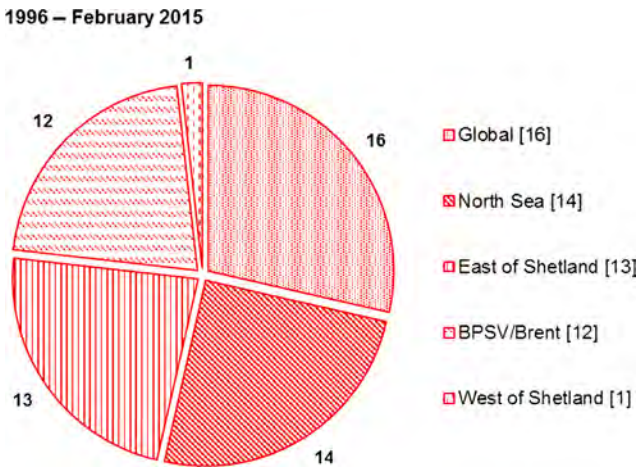

FIGURE 17.9 Crude oil samples by geographical origin throughout the survey period, 1996 to February 2015.

TABLE 17.1 List of Biomarker Compounds Selected for Multivariate Analysis of All Beached Oil Samples from January 2002 to February 2015

Peak	Compound
27Ts	18α(*H*)-22,29,30-Trisnorhopane
27Tm	17α(*H*)-22,29,30-Trisnorhopane
28ab	17α(*H*),18α(*H*),21β(*H*)-28,30-Bisnorhopane
29ab	17α(*H*),21β(*H*)-30-Norhopane
30ab	17α(*H*),21β(*H*)-Hopane
27dbS	13β,17α-Diacholestane (20S)
27dbR	13β,17α-Diacholestane (20R)
27bbRS	14β,17β-Cholestane (20R + 20S)
28bbRS	24-Methyl-14β,17β-cholestane (20R + 20S)
29bbRS	24-Ethyl-14β,17β-cholestane (20R + 20S)

17.3.3 Comparison/Visualization of the Dataset by Statistical Means

In order to summarize the structure of the data and highlight any clustering or trends, it was decided to submit the results of the diagnostic ratios to further statistical testing. Multivariate analysis techniques were applied to the all the accessible biomarker data (data files prior to January 2002 were unavailable to reprocess) to help identify any similarities in the oil residues collected. For multivariate treatment, the peak heights of 10 triterpane and sterane compounds, selected as being among the most useful diagnostic compounds for the range of oils typically found in the area, were measured and the data normalized (see Table 17.1 and Fig. 17.10).

17.3.3.1 Cluster Analysis

Cluster analysis groups samples together according to their similarity, and the results of cluster analysis are typically presented as a dendrogram. As cluster analysis is a classification technique, the dendrogram can be regarded as analogous to an evolutionary tree. If the data are amenable to cluster analysis, groups of samples that are highly self-similar will be evidently different to other groups.

Hierarchical cluster analysis was used to group samples according to the similarity in their biomarker distributions (with multiple injections of Brent crude oil used as a reference material to benchmark analytical variability). A study of the resulting dendrogram highlighted a number of samples with levels of similarity comparable to that recorded for the reference crude replicates and these are listed in Table 17.2. Although other samples than

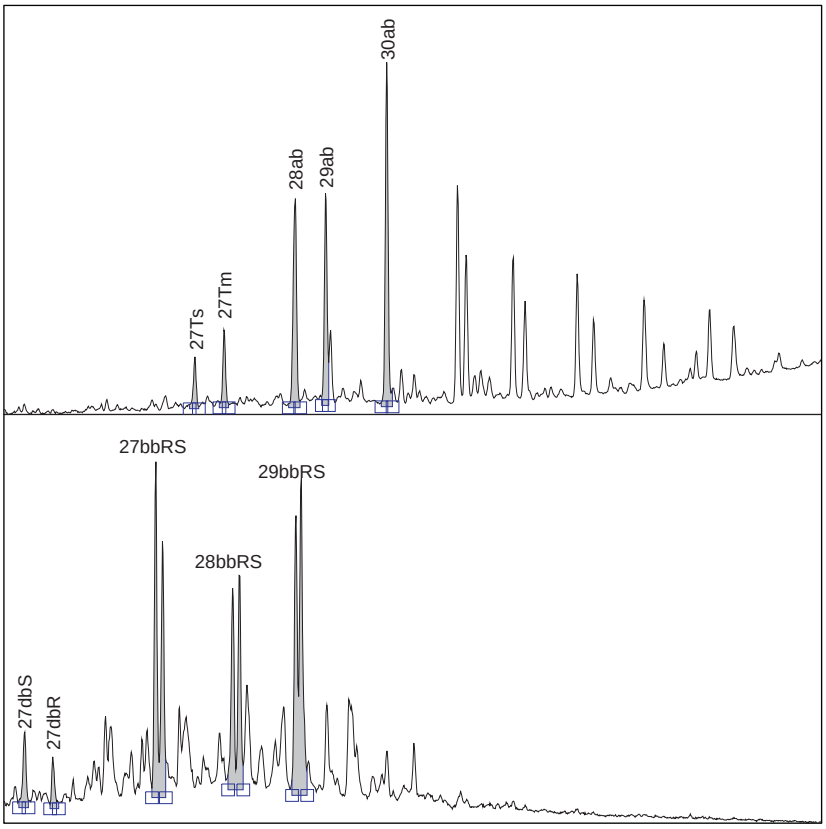

FIGURE 17.10 Triterpane (m/z 191; top) and sterane (m/z 218; bottom) profiles of central North Sea crude oil (with biomarkers from Table 17.1 highlighted).

TABLE 17.2 Selected Oil Samples with Similar Biomarker Distributions from January 2002 to February 2015

Collection dates		No. of samples	Timespan (days)	Sample identification	Oil type	Locations
First	Last					
March 26, 2002	April 24, 2002	2	29	SIC-98	Refined	Ronas Voe, Northmavine
				SIC-102		Quendale, S. Mainland
March 26, 2002	March 27, 2002	2	2	SIC-100	Refined	Urafirth, Northmavine
				SIC-101		Banna Minn, W. Burra
December 31, 2002	January 26, 2003	2	27	SIC-108	Refined	Eswick, E. Mainland
				SIC-110		Sand Voe, Northmavine
February 23, 2003	February 26, 2003	2	4	SIC-117	Refined	Gulberwick, SE Mainland
				SIC-119		Eswick, E. Mainland
November 27, 2003	November 30, 2003	2	4	SIC-128	Crude	Culswick, W. Mainland
				SIC-129		Footabrough, W. Mainland
March 30, 2004	March 30, 2004	2	1	SIC-137	Refined	West Sandwick, Yell
				SIC-140		Sand Voe, Northmavine
March 30, 2004	March 30, 2004	2	1	SIC-138	Refined	Ness of Sound, Yell
				SIC-139		Ness of Sound, Yell

(*Continued*)

TABLE 17.2 (*Continued*)

Collection dates		No. of samples	Timespan (days)	Sample identification	Oil type	Locations
First	Last					
June 27, 2008	July 01, 2008	2	5	SIC-182	Crude	Footabrough, W. Mainland
				SIC-183		Burra Voe, Northmavine
April 06, 2009	April 27, 2009	2	22	SIC-190	Refined	Tangwick, Northmavine
				SIC-191		Braewick, Northmavine
February 06, 2011	February 06, 2011	3	1	SIC-206	Refined	St. Ninian's Ayre, SW Mainland
				SIC-207		St. Ninian's Ayre, SW Mainland
				SIC-208		Culswick, W. Mainland
May 26, 2012	June 28, 2012	2	33	SIC-215	Crude	Ronas Voe, Northmavine
				SIC-217		Stenness, Northmavine
February 24, 2013	March 28, 2013	2	32	SIC-222	Refined	North Haven, Fair Isle
				SIC-225		West Voe of Sumburgh, S. Mainland
March 25, 2013	May 21, 2013	3	58	SIC-223	Refined	Boddam Voe, SE Mainland
				SIC-228		Braewick, Northmavine
				SIC-230		Burra Voe, Northmavine
May 06, 2013	July 23, 2013	3	79	SIC-227	Refined	Sandwick, Northmavine
				SIC-229		Tangwick, Northmavine
				SIC-231		Urafirth, Northmavine

those listed in Table 17.2 showed similar clustering they were not included due to the excessive date range between samples (in some cases >10 years), or the fact that, despite sharing comparable biomarker distributions, the samples were identified as different oil types (crude and refined).

As might be expected, the majority of samples within the hierarchical clusters closest to the oils produced at the Sullom Voe Terminal were identified as crude oils, and in particular, Brent and east of Shetland crudes.

17.3.3.2 Principle Components Analysis

PCA is the simplest of the true eigenvector-based multivariate analyses. Often its operation can be thought of as revealing the internal structure of the data in a way which best explains the variance in the data. The PCA plot (Fig. 17.11) shows all the samples analyzed as data points, including replicates of Brent crude analyzed to establish a control group. The figure shows a tight cluster of samples within the larger oval outline which holds the Brent crude replicates, Ninian crude oil replicates, and a number of beached oil samples. Also within the oval outline are a number of crude oils identified as originating from the ESB. To the far right of the plot is a looser clustering of samples (rectangular outline) which contains a number of samples identified with a Middle Eastern biomarker distribution. For example, those furthest to the right have the most distinctive biomarker profile with the 17α(*H*),21β(*H*)-30-norhopane (29ab) peak exceeding the height of the 17α(*H*),21β(*H*)-hopane (30ab) peak.

17.4 DISCUSSION

The monitoring of beached oils around the Shetland Isles over a 20-year period is probably one of the longest running studies of its kind anywhere in the world. The program has been managed by several different bodies since its inception, all with the remit to protect the islands' unique and sensitive environment from oil pollution.

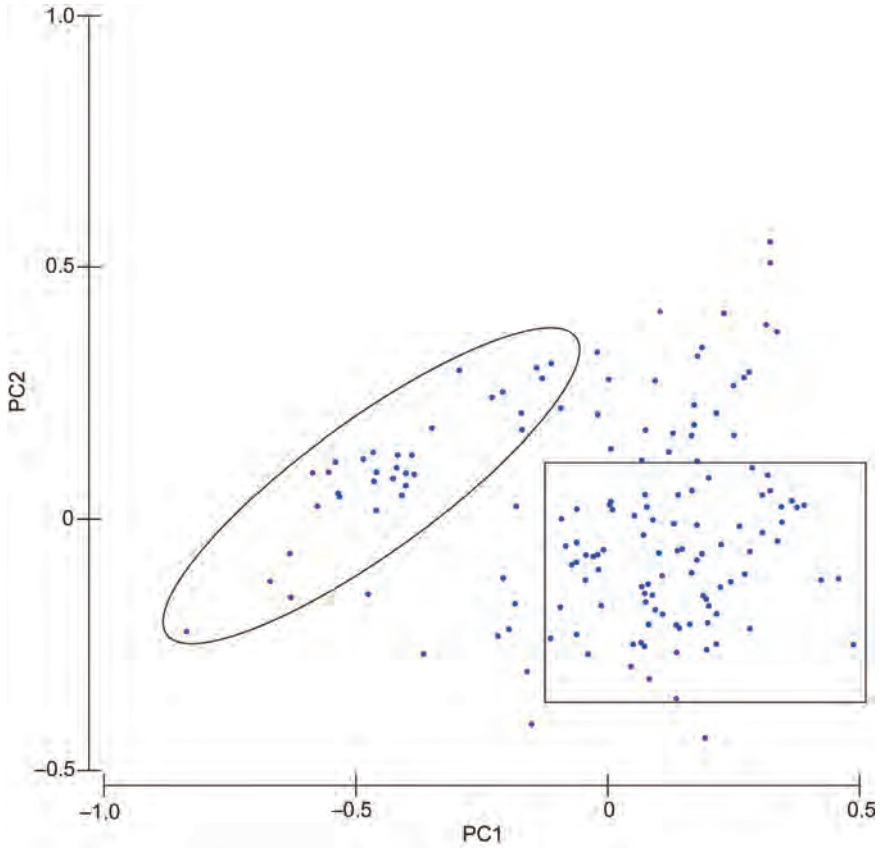

FIGURE 17.11 PCA factor score plot of all beached oil samples analyzed from January 2002 to February 2015. Variables included abundances of biomarker compounds listed in Table 17.1 in each sample. See text for description.

The program is currently funded and managed by SOTEAG and forms a part of their integrated program of environmental monitoring of the Sullom Voe Terminal.

Although the approach taken by the laboratory to identify the character and source beached oil samples has developed over the course of the program, the instrumental data acquisition has remained relatively unchanged. It is the consistency in the data acquisition that allowed samples not previously quantified to be reprocessed and included in the statistical evaluation described above.

Refined (fuel) oil was the most common residue found around the coastlines of Shetland (171 refined oil samples compared with 56 crude oil residues) since the monitoring program began. In the early years of the program, refined oils significantly dominated the samples collected; however, over the last 8 years of the monitoring period, there has been an increasing trend toward crude oil residues being found (Fig. 17.7). The GC–FID chromatographic profile for the vast majority of the refined oil residues found indicted a mixture of oils present, often fuel and lubricating oils or a mixture of fuel oil grades. These oil mixtures are normally associated with a vessel's bilge water rather than storage bunkers. Hence the greatest source of beached oil residues around the islands probably originate from illegal bilge water discharges from passing vessels.

The number of beached oil samples found appears to have been in general decline since 2003 (Fig. 17.7) suggesting that improved monitoring and surveillance of marine traffic may be encouraging more responsible attitudes toward the release of oil pollution. In addition to the declining number of beached oil residues found was the observation that crude oil residues exceeded refined oil residues in 2008, 2010, and 2012 and equaled the number collected in 2014. Taken together, the gradually decreasing number of samples and increased ratio of crude oil residues found may indicate that truly accidental discharges are now more likely to be responsible for beached oils than deliberate illegal discharges.

Whilst the aim of the monitoring program is to identify the source of an oil pollution incident whenever possible, the difficulty with relating particular oil spill incidents to the beached oil samples comes from the nature of samples themselves. As the majority of the samples collected are from dead seabirds (Fig. 17.4), there is no way

to establish where or when they became oiled, particularly those that spend the majority of their time at sea. In some cases, a bird with light oiling may have picked up the oil then flown many miles from the original location of the spill. Likewise, it is possible that a bird may have died at sea then floated through an oil spill before washing up onshore many miles away. Indeed, there is also the possibility that no spill ever occurred and that the bird in question landed on a vessel and became contaminated from oily pipes, railings, etc. on the deck of the boat.

From the 56 beached oil residues identified as crude oil, the biomarker distribution suggests that at least 18 may be directly related to oil production at the Sullom Voe Terminal (i.e., consistent with the crude oils being processed and exported from the terminal). There are a number of potential sources for the other crude oil residues recorded—they may originate from ship-to-ship transfers and other tankering operations at Sullom Voe, but may also be related to any one of the large numbers of oil tankers in transit around the north of the United Kingdom.

17.5 CONCLUSIONS

This long-term (20-year) monitoring program has provided a valuable insight into the sources of the oil being washed up on the shores of the Shetland Isles and Fair Isle. Prior to the commencement of the program in 1996, there was a perception that these residues were related to oil and gas industry activities, either at the Sullom Voe Terminal or from nearby offshore oil and gas fields (Heubeck, 1987). The results of the study have highlighted that the majority of the 229 beached oils recorded between January 1996 and February 2015 were likely to have originated from spills of marine fuel oil rather than crude oil. The program indicated a general decline in the number of oil residues being recorded in Shetland since 2003, an observation that has been replicated at other sites around the North Sea (Camphuysen and Heubeck, 2015), suggesting that improved regulation, monitoring, and surveillance of marine traffic may be encouraging more responsible attitudes toward the release of oil pollution.

References

Camphuysen, C.J., Heubeck, M., 2015. Beached bird surveys in the North Sea as an instrument to measure levels of chronic oil pollution: oil pollution in the North Sea. In: Carpenter, A. (Ed.), Handbook of Environmental Chemistry, vol. 41. Springer, Switzerland, pp. 193–208.

CEN/TR 15522-2:2006, 2006. Oil spill identification. Waterborne Petroleum and Petroleum Products. Analytical Methodology and Interpretation of Results Based on GC–FID and GC–MS Low Resolution Analyses.

CEN/TR 15522-2:2012, 2012. Oil spill identification. Waterborne Petroleum and Petroleum Products. Analytical Methodology and Interpretation of Results Based on GC–FID and GC–MS Low Resolution Analyses.

Dahlmann, G., Kienhuis, P.G.M., 2016. Development and application of online computerized oil spill identification—COSIWeb. In: Stout, S.A., Wang, Z. (Eds.), Standard Handbook Oil Spill Environmental Forensics, Fingerprinting and Source Identification, second ed Acadamic Press, Amsterdam, pp. 729–745.

ESGOSS, 1994. The Environmental Impact of the Wreck of the Braer. Scottish Office Library, Edinburgh, UK.

Faksness, L.G., Weiss, H., Daling, P.S., 2002. Revision of the Nordtest methodology for oil spill identification—technical report. SINTEF Report STF66 A01028.

Grigson, S., Baron, G.R., 1995. European crude oil identification system. In: Deutsche Hydrographische Zeitschrift; Proceedings of Akteukke Probleme der Meeresumwelt, Hamburg.

Heubeck, M., 1987. The Shetland beached bird survey, 1979–1986. Bird Study 34 (2), 97–106.

Nordtest, 1991. Oil Spill Identification, Method NT CHEM 001, second ed. Nordic Innovation Center, Espoo, Finland.

Uhler, A.D., Stout, S.A., Douglas, G.S., 2007. Chemical heterogeneity in modern residual fuel oils. In: Wang,, Z., Stout,, S.A. (Eds.), Oil Spill Environmental Forensics. Elsevier, London, pp. 327–348.

Walker, M.I., Albone, D.J., McDonagh, M., Wilkinson, A.O., Baron, G.R., Grigson, S.J.W., 1992. Final Report on the Joint Programme of Research on Source Identification, Behaviour and Modelling of North Sea Crudes at Sea, Warren Spring Laboratory, Stevenage, Report CR 3698.

CHAPTER

18

The *Erika* Oil Spill: 10 Years Monitoring Program and Effects of the Weathering Processes

Fanny Chever, Ronan Jezequel and Julien Guyomarch

Centre de Documentation de Recherche d'Expérimentations, Brest, France

BIOGRAPHIES

Dr. Fanny Chever joined Cedre (Centre of Documentation, Research and Experimentation on Accidental Water Pollution) in June 2015 after a PhD in Oceanography, applied to the speciation of iron in open ocean and its interaction with phytoplankton. At Cedre, she works as a chemist for the Analysis and Resources Department, within which she is in charge of studies on the weathering and dispersibility of oils. She is also involved as lecturer in training courses and she is a member of Cedre's Emergency Response Team since 2016, as an appointed Duty Engineer.

Dr. Ronan Jézéquel joined Cedre (Centre of Documentation, Research and Experimentation on Accidental Water Pollution) in 2000 as a PhD student. During his thesis, he studied the persistence of the *Erika* oil (1999) on the French Atlantic coastline. He works for the Research Department, within which he is in charge of studies on the medium and long-term behavior of oils. The different experiments (laboratory based and in situ) which he has overseen have enabled him to acquire a certain expertise in the chemistry of oil and in analysis techniques demonstrating natural oil weathering processes.

Julien Guyomarch joined Cedre (Centre of Documentation, Research and Experimentation on Accidental Water Pollution) in 1997 and is in charge of studies on the short to medium-term behavior of crude or refined oils. The different experiments (laboratory based, pilot scale, and in situ) which he has overseen have enabled him to acquire a certain expertise in the chemistry of hydrocarbons and more specifically in analytical techniques characterizing oils and demonstrating oil weathering processes. This knowledge also includes the assessment of response techniques (chemical dispersion, mechanical recovery, bioremediation, etc.) according to the oil nature and its weathering stage. He is also in charge of the development of analytical techniques, mainly by gas chromatography coupled to mass spectrometry, and associated with microextraction techniques. He is also member of the Oil Spill Identification Network (OSINET) working group, and was involved in the field of oil identification in the marine environment at the occasion of several major (*Erika*, *Prestige*, et al.) or minor oil spills.

18.1 INTRODUCTION

On 11 December 1999, the Maltese tanker *Erika*, laden with 31,000 tons of heavy fuel oil (HFO; fuel n°6), en route from Dunkirk (France) to Livorno (Italy) in very rough sea conditions (wind, force 8 to 9, with 6 m swell), was faced with structural problems off the Bay of Biscay. After sending an alert message, then proceeding to transfer cargo from tank to tank, the captain informed the French authorities that the situation was under control and that

Oil Spill Environmental Forensics Case Studies.
DOI: http://dx.doi.org/10.1016/B978-0-12-804434-6.00018-5

he was heading to the port of Donges at reduced speed. At 6:05 a.m. the following day, he sent a Mayday: The ship was breaking in two. A rescue operation was immediately launched and the crew was winched to safety by French Navy helicopters, backed up by Royal Navy reinforcements, in extremely difficult conditions. The *Erika* split in two at 8:15 a.m. (local time) in international waters, about thirty miles south of Penmarc'h (Southern Brittany; Fig. 18.2). The quantity of oil spilt at that time was estimated between 7000 and 10,000 tons.

The bow sank the following night, a small distance away from the place where the ship had broken up. The stern was taken in tow by a salvage tug on 12 December at 2:15 p.m., to avoid it drifting towards the French island of Belle-Ile, and it sank the following day at 2:50 p.m. The two parts of the wreck ended up 10 km apart from each other, in water 120 m deep.

Initial aerial survey missions carried out by the French Customs and French Navy planes reported slicks drifting at sea, one of which was 15 km long and estimated at 3000 tons. The slicks were moving eastwards at a speed of about 1.2 knots. The first stranded oil on the shoreline was noticed in Southern Finistere 11 days after the accident, on 23 December. Scattered oil stranding continued the following days, contaminating some islands on 25 December, and the mainland shoreline on 27 December. Owing to rough weather conditions (wind over 100 km/h, blowing perpendicular to the coast) with springtides, the pollution was thrown up to high level of the shoreline, reaching the top of cliffs exceeding 10 m. On 26 December, 14 days after the sinking, the bulk of the pollution reached the shoreline which was partly covered with a viscous oil layer, 5 to 30 cm thick and several meters wide. Ultimately, around 400 km of shoreline were impacted by the *Erika* spill.

At that time, no systematic analyses were performed on the samples collected on the shoreline in order to prove the origin of the contamination. However, from 2000, a follow-up study was initiated at Cedre with the objective of monitoring the fate and behavior of the oil, in terms of chemical composition and environmental impacts. Oil samples were regularly collected over a period of 10 years, some small areas of polluted sites being voluntarily not cleaned thereby allowing for this long-term sampling, leading to a significant set of data. In addition, some field studies were conducted using the *Erika* oil in order to better understand the modification of the oil composition according to its exposure to environmental conditions. Finally, laboratory and field samples were analyzed in the framework of a round-robin test organized within the OSINET group.

18.2 PHYSICAL–CHEMICAL PROPERTIES OF THE *ERIKA* OIL

The *Erika* oil is an HFO (fuel n° 6) characterized by a viscosity of 42,000 mPa.s (at 12°C) and a density of 1.002 (g/mL). Chemical fractions (saturates, aromatics, resins, and asphaltenes) were determined using an high pressure liquid chromatography (HPLC) technique (Jezequel, 2005). Table 18.1 presents the physical–chemical properties of the *Erika* oil. Aromatics can be subdivided in four groups depending on the number of rings contained in the compound: Monoaromatics (F1), diaromatics (F2), dibenzothiophenes/triaromatics (F3), and aromatics with four or more rings (F4). The contribution of those families to the total oil is 15%, 9%, 19%, and 12%, respectively for the F1, F2, F3, and F4 groups.

Fig. 18.1 exhibits the gas chromatography-mass spectrometry (GC-MS) chromatograms in scan mode of saturates and aromatics of the *Erika* oil. *n*-Alkanes and resolved polyaromatic hydrocarbons (PAHs) (parents and alkylated), commonly used to evaluate the potential of degradation, represent a small fraction of the total oil, respectively 2.2% and 10.1%, the largest part of saturates and aromatics being constituted of unresolved complex mixture (UCM).

18.3 NATURAL DEGRADATION OF THE *ERIKA* OIL (10-YEAR MONITORING PROGRAM)

Once spilled at sea, oils are subjected to natural weathering processes such as evaporation, dissolution, biodegradation, and photooxidation leading to changes in their chemical compositions. In order to identify the origin of oil patches washed ashore and the weathering processes that have affected it, evolution of abundance of the different chemical families are studied.

From March 2001 to December 2004, a monitoring study was carried out in the frame of a French program supported by the French Ministry of Environment in order to assess the natural degradation of the persistent *Erika* oil on different substrates and exposed to different environmental conditions (Jezequel, 2005). Seventeen sites representative of the Atlantic shoreline and affected by the pollution were selected. At those sites, oil

TABLE 18.1 Physical–Chemical Properties of the *Erika* Oil

Properties	***Erika***
Viscosity (mPa.s, 12°C)	42,000
Density	1.002
Pour point (°C)	3
Flash point (°C)	>100
Saturates (%)	23
Aromatics (%)	55
Resins (%)	14
Asphaltenes (%)	8

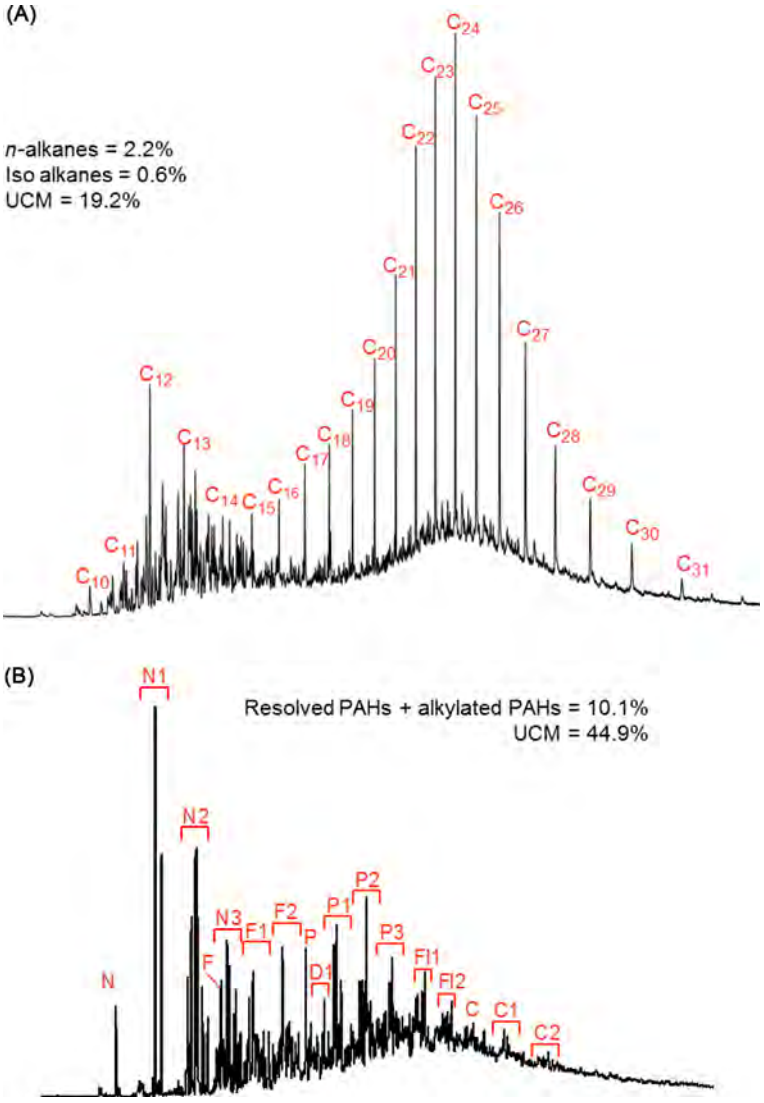

FIGURE 18.1 Chromatograms (scan mode) of the *Erika* oil, (A) saturates, (B) aromatics.

patches were voluntarily not recovered and were periodically sampled in order to monitor the fate and behavior of the oil with time. Fig. 18.2 shows the location of the selected sites. The selected sites differed by their exposition to hydrodynamic conditions (protected or exposed sites), the different types of substrates (sand, rocks, marsh), their exposition to the sun, and the littoral zones affected by the pollutant (littoral or supralittoral). The thickness of the oil layers present on the different substrates varied from <1 mm to more than 4 mm.

From this survey, a total of 189 samples were analyzed by GC-MS in Selected Ion Monitoring (SIM) mode for the quantification of *n*-alkanes (from *n*-C_{10} to *n*-C_{35} plus isoprenoids pristane and phytane), biomarkers (hopanes/steranes) and PAHs (from two to four rings, parents and alkylated up to four additional carbons).

Fig. 18.3 represents the evolution with time of heavy aromatics (from phenanthrene to C_3-chrysenes) and heavy alkanes (*n*-C_{25} to *n*-C_{35}). All values were normalized to hopane, used as a conserved internal marker within the oil to follow the disappearance of other components (Prince et al., 1994) and to the original *Erika* oil. As such, all normalized values are reported in hopane units (HU). Data collected within the same year appear with the same symbol. Most of the data were located above the 1:1 line which highlights the more important degradation of the heavy alkanes compared to the heavy PAHs. For all the field studies, data were dispersed over the whole range of data. Those results show that different environmental conditions (exposition to solar radiation, littoral zones, thickness of the oil patch, etc.) lead to different weathering processes, and so to different chemical evolutions of the oil. However, when taking into account only the mean value of each field study on a yearly basis (represented in Fig. 18.3 by bigger dots on the inserted graph at the bottom right corner), a clear trend appeared highlighting the progressive loss of heavy compounds with time.

At the end of the study in 2004, five sites were still monitored. Monitoring stopped at the other sites because of natural physical removal of the oil that led to the disappearance of the oil and/or because another major oil spill (*Prestige* in November 2002) along the Atlantic coastline had led to a new oil's arrival. Among the five sites (A, B, C, D, and E, Fig. 18.4), site A was characterized by a thick oil layer (4 cm) and was located in a sheltered environment (between rocks) not exposed to solar radiations. The other sites were characterized by a thinner oil layer (1−2 cm) and are located on rock surfaces (B, C, and E) and a maritime marsh (D). Contrary to the site A

FIGURE 18.2 Atlantic coastline impacted by the *Erika* oil (represented by the black line) and location of the monitored sites (represented by the grey circles). Figures in brackets represent the number of sites sampled in each department.

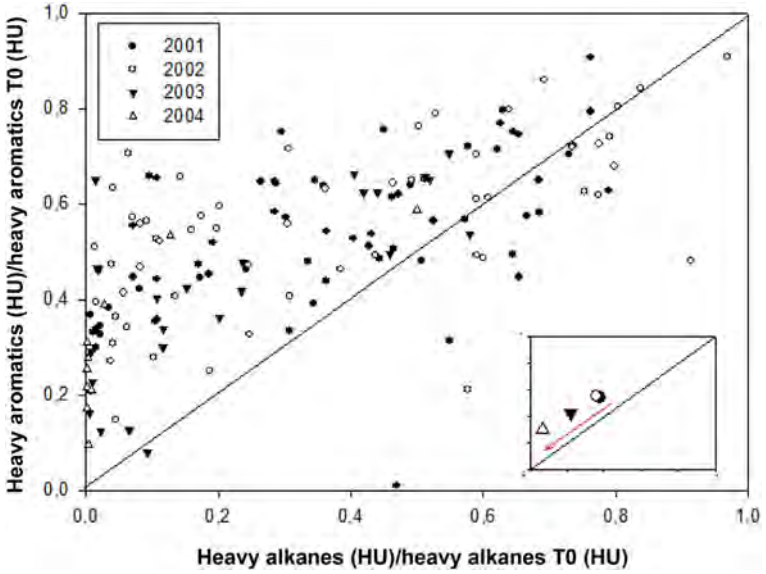

FIGURE 18.3 Heavy aromatics (HU) versus heavy alkanes (HU), normalized to the initial values. *HU*, hopane units; as data were normalized to hopane.

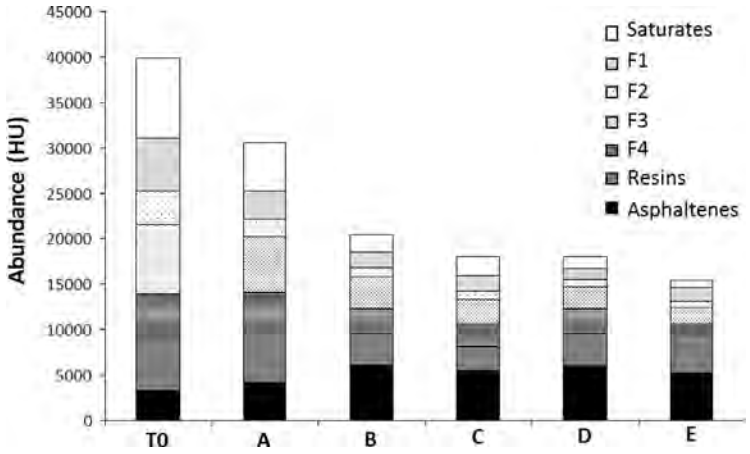

FIGURE 18.4 Relative abundances (in HU) of each chemical family for the samples collected in 2004.

where the oil was still viscous, the oil of the four other sites looked like asphalt pavement. Environmental parameters characterizing the oil collected at the five sites are detailed in Table 18.2.

Fig. 18.4 represents the repartition of the different chemical families of the five samples collected in December 2004, compared with the original *Erika* oil (T0). Samples were analyzed using scan mode in order to obtain the abundance (in HU) of the saturate + aromatic fractions (resolved peaks + UCM). The abundance of the different chemical fractions was then calculated in HU using equation 1 (X = saturates, aromatics, resins; Jezequel and Merlin, 2012). Asphaltenes content was determined by gravimetric analyses after precipitation in *n*-pentane.

$$X(\mathrm{HU}) = \%X * \frac{\mathrm{resolved(HU)} + \mathrm{UCM(HU)}}{\%\mathrm{saturates} + \%\mathrm{aromatics}}$$

Sample A clearly differed from the other samples. The main difference between the site A and the other ones was the exposition to solar radiation and so to photooxidation processes and the thickness of the oil layer. The mean degradation of the oil was 50% for samples exposed to solar radiations and 16% for the Site A. Except this last site, samples were characterized by a high abundance of polar compounds (resins and asphaltenes) that represented nearly 50% of the oil. This increase of polar compounds is due to metabolites generated during

TABLE 18.2 Environmental Parameters and Depletion Percentage of the Heavy *n*-Alkanes and Heavy PAHs of the Five Sites Monitored in 2004

	A	B	C	D	E
ENVIRONMENTAL PARAMETERS					
Solar radiation	−	+	+	+	+
Oil thickness (cm)	4	2	1	1	1
Littoral zone	Littoral	Supralittoral	Supralittoral	Littoral	Littoral
CHEMICAL EVOLUTION					
Heavy *n*-alkanes (%)	50	97	100	100	100
Heavy PAHs (%)	28	61	69	91	79

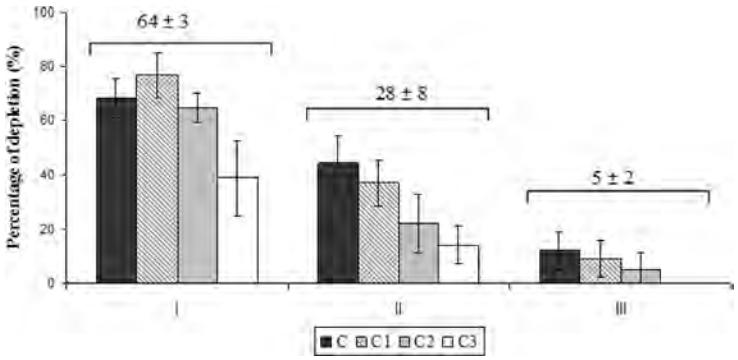

FIGURE 18.5 Degradation of chrysene (C) and some of its alkylated derivatives (C1, C2, and C3 refer to methyl, dimethyl and ethyl, and trimethyl, methyl−ethyl, and propyl-chrysenes, respectively) in oil samples from Groups I, II, and III. The number above the brackets represents the mean and standard deviation of percentage of degradation of total chrysenes (C + C1 + C2 + C3).

incomplete biodegradation of hydrocarbons (Haesler and Ballerini, 2002) and/or products of photooxidation (Garrett et al., 1998). This high amount of resins and asphaltenes explains the bituminous-like aspect of the oil collected at that time.

From the Table 18.2 it appears that for the sample characterized by a thick oil layer and that was not affected by photooxidation process (Site A), 50% of the heavy *n*-alkanes remained present in the oil. Heavy PAHs were also degraded, between 61% and 91% were lost at sites B, C, D, and E, whereas only 28% were lost for site A. Sites located in littoral zones have lost from 79% (Site E) to 91% (Site D), against 61%−69% for the sites located in supralittoral zones (Sites B and C). Hydrodynamic conditions seem to play a role in the degradation processes.

This study dedicated to the assessment of the natural degradation of the *Erika* oil in natural environment highlights the importance of the physical form (thickness especially) of the oil on the intensity of some weathering processes (especially photooxidation). However, the complexity of the natural environment does not allow for the isolation and study of only one process in controlled conditions. It was also not possible to establish a relationship statistically validated between the degradation level and the type of exposure.

Seven years after this monitoring study (from March 2001 to December 2004), a last sampling was performed in 2010 for a limited number of sites and environment conditions (Jezequel and Poncet, 2011). This study was focused on the exposure of the oil to solar radiation.

A principal component analysis (The Unscrambler v9.7, CAMO software AS) was employed as a means of easily isolating different groups of samples according to the degradation rate of *n*-alkanes and PAHs. The principal component analysis (PCA) results clearly distinguish three groups of samples/data (data not shown) that correspond to exposure conditions: Group I for the highest level of exposure, Group II for a moderate exposure, and Group III for the sheltered samples. These results show that the differences in degradation rates of *Erika* oil were mainly due to the exposure level and consequently could probably be attributed to the photooxidation process. To confirm this, losses of chrysenes (parent and alkylated forms) were calculated for the previously defined groups and are presented in Fig. 18.5. Chrysenes, as with all heavy polycyclic compounds, are known to be

sensitive to photooxidation process and not easily biodegraded (Wang et al., 1994, Garrett et al., 1998, Hadibarata et al., 2009). Fig. 18.5 demonstrates that chrysenes degradation is significantly different between each group ($63 \pm 4\%$ in Group I, $28 \pm 8\%$ in Group II, and $5 \pm 2\%$ in Group III). Nevertheless, considering each group individually, the degradation rate are inversely proportional to the degree of alkylation which is typical of the biodegradation process (C > C1 > C2 > C3; Wang et al., 1994, Wang and Fingas, 1997, Michel and Hayes, 1999) suggesting during 10 years in environment, heaviest compounds are subject to biodegradation and photooxidation.

18.4 STUDY IN CONTROLLED CONDITIONS

In order to improve the knowledge on the intensity of the natural degradation processes affecting the *Erika* oil, experiments under controlled conditions were carried out (Jezequel et al., 2003). Granite tiles coated with a thin layer of the *Erika* oil (200 μm) were fixed to the two faces of the pier of an islet located in the roadstead of Brest (Brittany, France) and were allowed to weather naturally for 216 days (Fig. 18.6).

The northern face of the pier was exposed to natural agitation and did not receive direct solar radiation. The Southern face of the pier was directly exposed to solar radiation and was less exposed to natural agitation. Those tiles were installed to a height that allowed two cycles of immersion/emersion per day and were removed at different time steps for chemical analysis.

Fig. 18.7 shows the evolution of the percentage of abundance of the three families: Saturates, aromatics, and polar (resins and asphaltenes), over the 216 days of the study.

The main observation was the chemical changes were much more important for oil on the tiles located on the South face of the pier. Fig. 18.6 shows the loss of aromatic compounds associated with the increase of the polar fraction, especially for the tiles located on the South face of the pier. This is in accordance with the results observed during the monitoring study: Exposition to solar radiation is an important, and even sometimes, a prevailing parameter explaining the degradation of the oil. Fig. 18.8 details those results. Chromatograms of the saturates/aromatics compounds in scan modes are shown (with the abundance of the resolved peaks and UCM) as well as the distribution of abundances of the different chemical families, for three time steps (T0, T1 = 33 days, and Tf = 216 days). From the chromatograms, it can be observed that the degradation rate of the UCM was more important for the samples located at the South face (67%) compared with the samples from the North face (44%) which is in accordance with the higher sensitivity of ramified compounds to photooxidation. Additionally, the total degradation of the oil was more pronounced on the South face (51%) compared with the North face (39%). At the end of the experiment, the degradation rate of the resolved compounds was of the same order for the two expositions: 76% for the samples located on the north face, 72% for the samples located on the South face. The lightest *n*-alkanes and PAHs were lost during the first month of the experiment, and in a general way, *n*-alkanes were more degraded on the North face. This last observation could be due to a warming of the substrate (tiles and oil layer) on the South face, inhibiting the bacterial growth.

Comparing the percentage of the chemical families at the end of the experiment for the North and the South pier, it appeared that the oils significantly impacted by photooxidation processes were highly weathered compared to oils mainly impacted by biodegradation. For those photooxidized oils, a drastic loss of aromatics and an increase of polar fraction (which represents nearly half of the oil) were observed, which is characteristic of asphalt pavement.

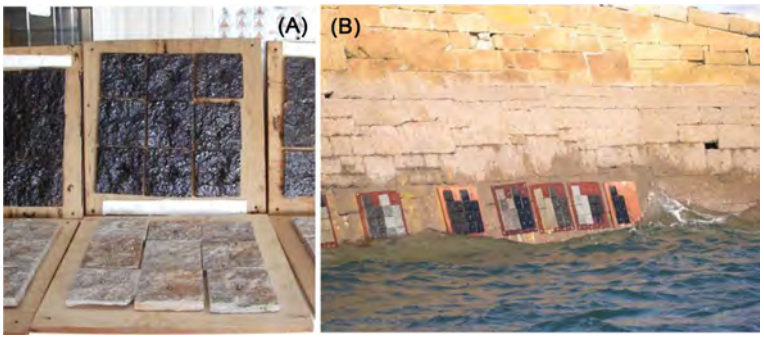

FIGURE 18.6 Pictures of (A) the tiles coated with the *Erika* oil and (B) fixed to the pier.

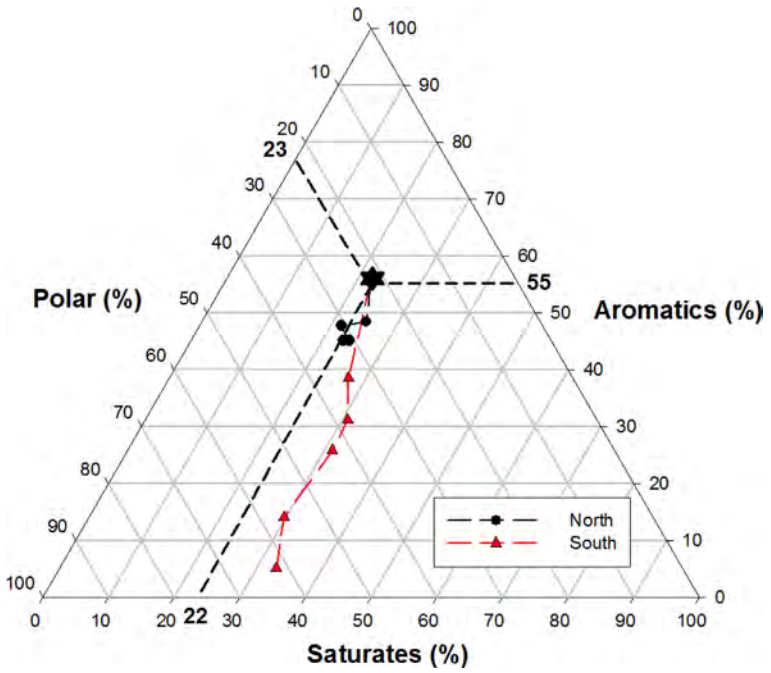

FIGURE 18.7 Ternary plot showing the evolution of the abundance (in %) of the three chemical families (saturates, aromatics, and polar) over 216 days (the original oil is represented by a star and its composition is transposed by dashed lines on the three axes).

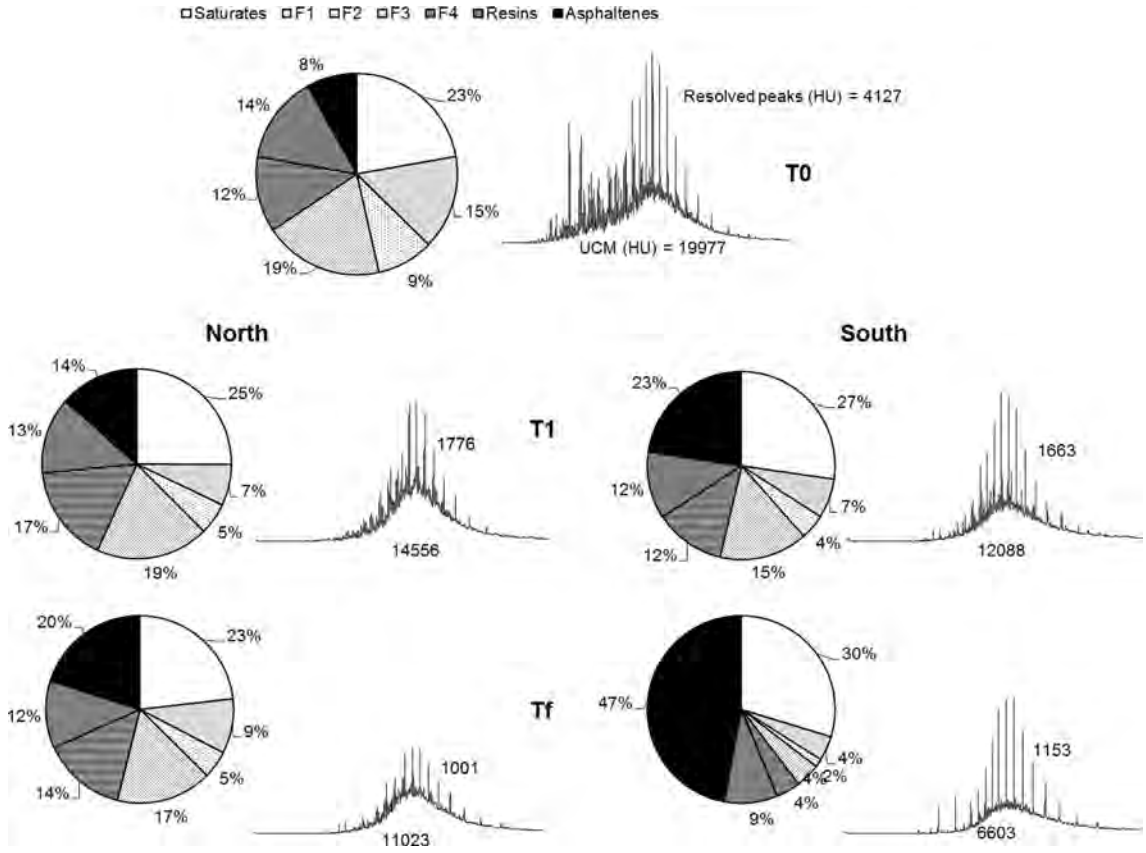

FIGURE 18.8 Percentages of chemical families and chromatograms (scan mode) of the saturates/aromatics fractions for the tiles located on the North and the South faces of the pier. T0 = 0 days, T1 = 33 days, and Tf = 216 days.

18.5 STUDY OF MOLECULAR RATIOS

During the OSINET round-robin test 2011, the original *Erika* oil was compared with several naturally and artificially weathered *Erika* oils. Artificially weathered samples were processed at CEDRE laboratory: One sample was biodegraded at the laboratory and another one was exposed outside for three months (the oil being deposited on granite tiles), prone to photooxidation processes. Naturally weathered samples were collected 11 years after the accident on the Atlantic shoreline impacted by the spill at the time of the pollution. For the OSINET round-robin testing, the discussion focused on comparisons of the fresh oil and two weathered samples: The artificially weathered oil prone to photooxidation process and a naturally weathered oil collected in the upper part of the beach, in the middle of the vegetation.

Samples were analyzed by gas chromatography / flame ionisation detection (GC/FID) and GC/MS according to conditions described in the CEN guidelines (CEN, 2012). Samples were first compared by using the GC/FID patterns to point out the most significant differences. The GC/MS analyses were then used, either to confirm the significant variations obtained from the GC/FID screening, or to enable conclusions of match or nonmatch in case of similarities of GC/FID patterns.

The GC/FID chromatograms of the three samples are presented in Fig. 18.9. Chromatogram pattern of the source sample is typical from a HFO: Abundance of light aromatics compounds eluting between 10 and 15 minutes, which correspond to aromatic-rich distillate added to a residue, which is characterized with the abundance of the UCM and the alkanes with high boiling-point range. As regards the chromatograms, the naturally weathered sample appears to be highly degraded as most of the alkanes and aromatics compounds disappeared.

Fig. 18.10 presents "percentage weathering" plots (PW-Plots) of the weathered samples based on GC/MS analyses. On these graphs, a range of PAHs and biomarkers (compound or compound group) are normalized to a nonweathered compound [here, the hopane (30ab)] and compared to the unweathered *Erika* oil. Results are sorted on retention time. A data points in the plot represent the concentration of a compound/compound group in the spill sample relative to the concentration of the same compound or compound group in the source sample (CEN, 2012).

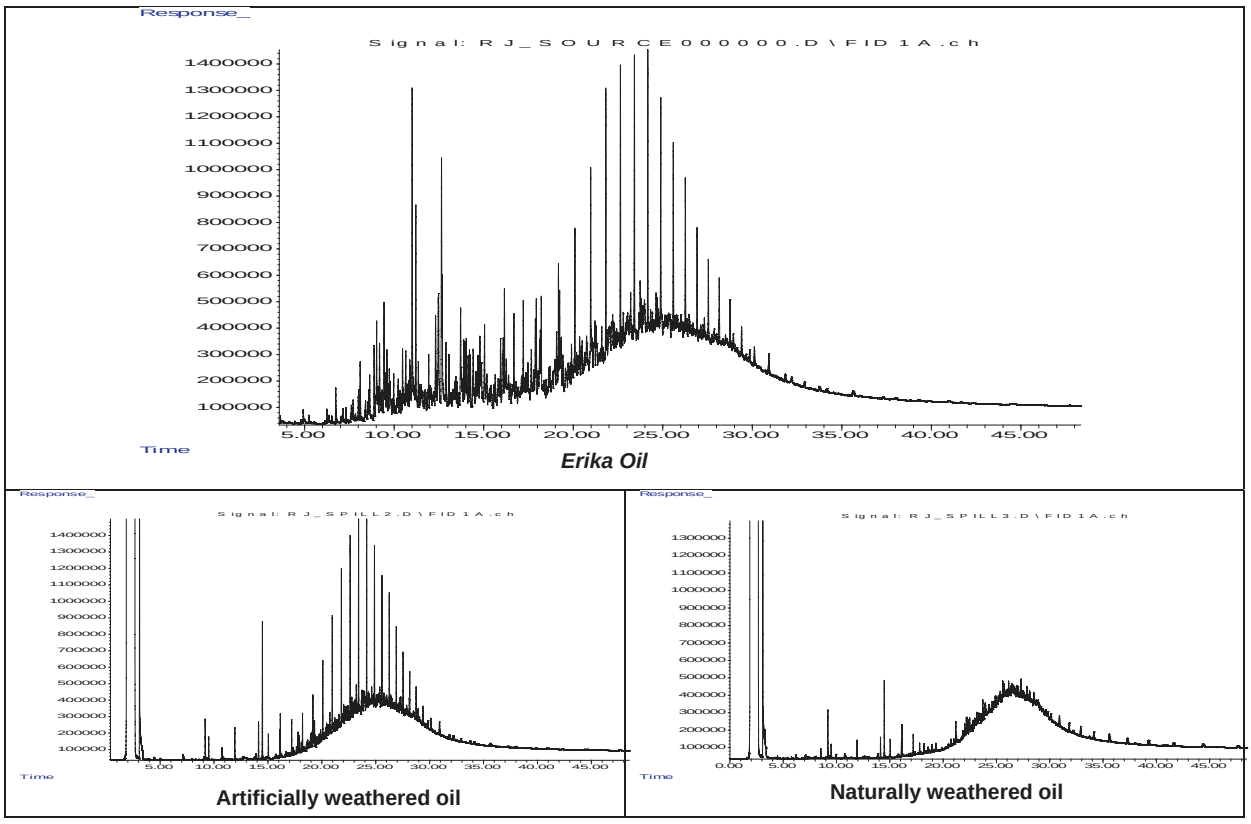

FIGURE 18.9 GC/FID chromatograms of the fresh and weathered oil samples from OSINET 2001 round-robin testing.

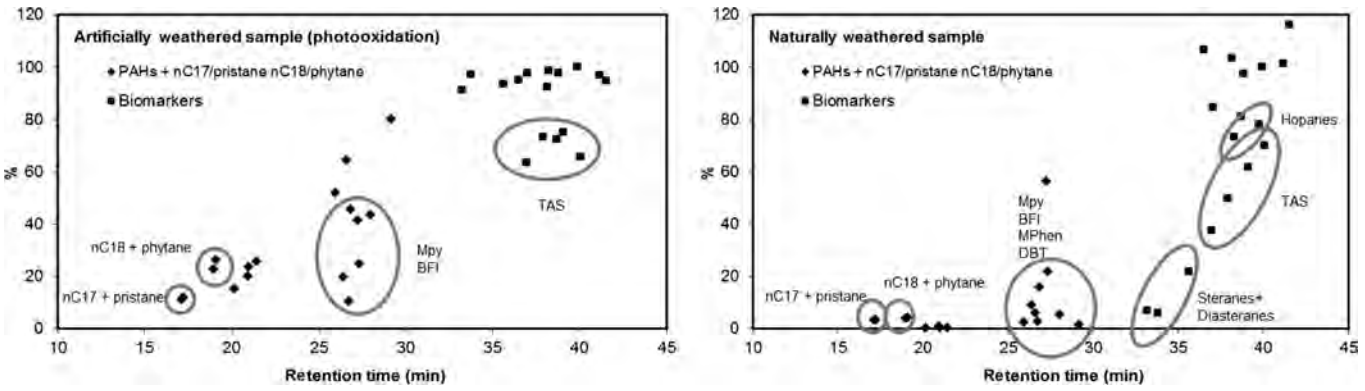

FIGURE 18.10 PW-Plots of the weathered samples compared to the source sample (*Erika* oil) and normalized to hopane (30ab). *TAS*, triaromatic steranes, *MPy*, methylpyrenes, *BFl*, Benzofluorenes, *MPhen*, methylphenanthrene, *DBT*, dibenzothiophene.

On the two PW-Plots, the lighter compounds (characterized by a lower retention time) exhibited reduced abundance compared with heaviest ones. This is a common feature reflecting evaporation processes.

The artificially weathered sample did not exhibit a reduction of n-C_{17}/n-C_{18} alkanes compared to the isoprenoids pristane and phytane, minimizing biodegradation as weathering process. A reduction of the methylpyrenes (MPy, $m/z = 216$; with the 1-methylpyrene being the most degraded) and the benzofluorenes [BFl; benzo(a) fluorene and benzo(b + c)fluorene], was also observed, demonstrating a photooxidation of the oil. Triaromatic steranes (TAS; $m/z = 231$), biomarkers extremely stable against biodegradation, were also significantly reduced ($\approx 70\%$ remaining). Photooxidation could thus also affect those aromatic biomarkers.

Considering the naturally weathered sample, identification was difficult due to the high weathering stage. GC/MS results showed a severe degradation of most of the PAHs compounds and biomarkers. As already observed for the artificially weathered sample, MPy and BFl were degraded as well as methylphenanthrenes (MPhen) and bibenzothiophenes (DBT). This result confirms the importance of the photooxidation as weathering process. n-C_{17}, n-C_{18}, and the isoprenoids pristane and phytane were absent from this sample, which highlights the biodegradation process affecting the oil. Biodegradation was also confirmed by the degradation order of C1-fluoranthenes/pyrenes. As already observed in the artificially weathered sample, TAS were strongly degraded but not all the TAS were affected in the same way (SC26TA and RC26TA + SC27TA are more impacted than RC27TA and RC28TA). Steranes and diasteranes ($m/z = 217$ and 218) that were not impacted in the sample photooxidized for three months were severely degraded in the naturally weathered sample. Steranes 27dbS and 27dbR were totally vanished from the oil (6%–7% remaining) and diasteranes 27bbR + 27bbS were highly degraded (22% remaining). Figs. 18.11 and 18.12 reflect this biomarkers degradation. Those figures present the ion chromatograms of steranes (m/z 217) and diasteranes (m/z 218) of the *Erika* oil compared with the naturally weathered oil.

By comparing the two weathered samples, it appears that TAS can be degraded after only three months of exposure to solar radiation. An extended exposure (several years) leads to an additional degradation of these compounds, but with not all the TAS being affected in the same way. Steranes and diasteranes seem to be more resistant to photooxidation as they are not affected after three months weathering but on a long term, they seem to be extremely degraded as only ~20% of the 27dbR, 27dbS, and 27bbR + 27bbS remain (Figs. 18.11 and 18.12). In both figures, degradation of the 27dbS and 27dbR diasteranes and of the 27bbR + 27bbS steranes clearly appears. Some hopanes compounds are also degraded after 10 years weathering (28ab and 30O).

Kinetic studies on oils natural degradation highlighted compound ratios (diagnostic ratios, or Dr) used to evaluate the degree of weathering of oil. Those ratios involve compounds that exhibit different behaviors depending on the dominant process of degradation. Dr are ratios between the peak height (for individual peaks) or the peak area (for compound groups) of compounds selected by their diversity in chemical composition in petroleum and petroleum products and on their known behavior in weathering process (CEN, 2012).

Any measured difference in a Dr between two samples greater than 14% relative difference is regarded as significant, meaning that these two ratios are statistically different (CEN, 2012). When looking at the relative differences of the 25 commonly studied Dr, most of them appear to be significantly higher than 14%, especially for the naturally weathered sample (Table 18.3). Several studies have already shown the degradation of biomarkers for heavily weathered oils (Munoz et al., 1997; Wang et al., 2000). Some Dr ratios are thus not robust enough to compare spill to source samples.

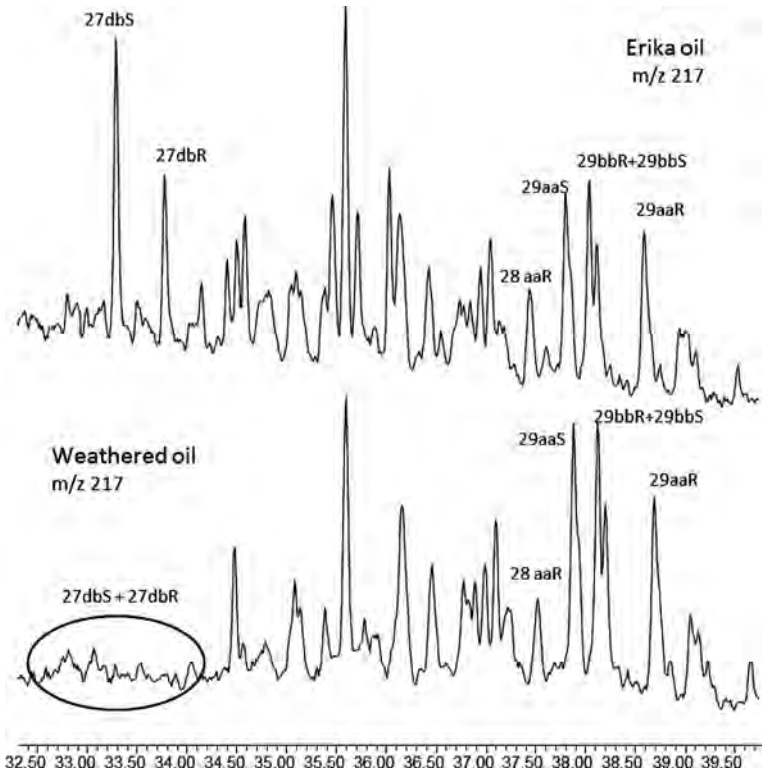

FIGURE 18.11 Ion chromatograms of steranes (*m*/*z* 217) of the *Erika* oil and the naturally weathered *Erika* oil.

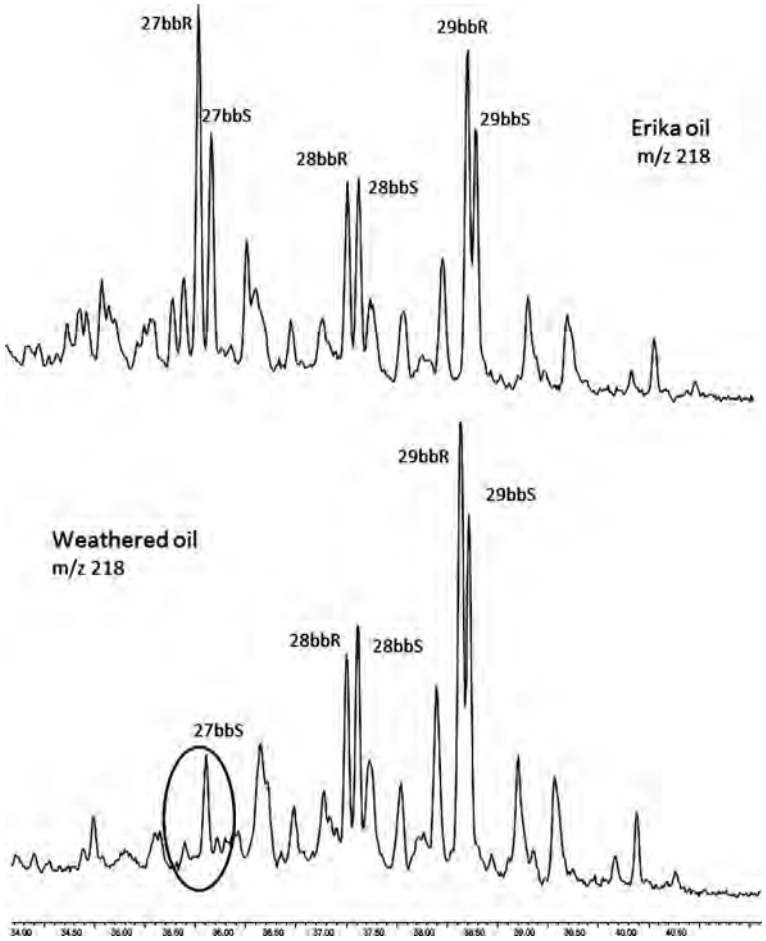

FIGURE 18.12 Ion chromatograms of steranes (*m*/*z* 218) of the *Erika* oil and the naturally weathered *Erika* oil.

TABLE 18.3 Relative Differences Between the Dr (in %) Between the Weathered Samples and the *Erika* Oil for Common Dr in the CEN (2012) Guideline

Relative difference (%)	Artificially weathered sample	Naturally weathered sample
COMMON DR		
NR-C17/pris	7	3
NR-C18/phy	14	6
NR-pris/phy	**76**	**22**
NR-4-MD/1-MD	**27**	**120**
NR-2-MP/1-MP	9	**46**
NR-2MF/4-Mpy	**22**	**184**
NR-B(a)F/4-Mpy	**71**	**145**
NR-B(b + c)F/4-Mpy	**119**	**183**
NR-2Mpy/4-Mpy	9	**112**
NR-1Mpy/4-Mpy	**50**	**89**
NR-Retene/T-M-phen	**39**	**16**
NR-BNT/T-M-phen	**59**	**117**
NR-27Ts/30ab	5	6
NR-27Tm/30ab	2	**17**
NR-28ab/30ab	1	**31**
NR-29ab/30ab	2	3
NR-30O/30ab	**26**	**25**
NR-31abS/30ab	3	1
NR-30G/30ab	5	**15**
NR-27dbR/27dbS	6	**15**
NR-27bb/29bb	1	**131**
NR-SC26/RC26 + SC27	**15**	**28**
NR-SC28/RC26 + SC27	1	**48**
NR-RC27/RC26 + SC27	2	**21**
NR-RC28/RC26 + SC27	11	**34**
ADDITIONAL RATIOS		
29aaS/29aaR	9	5
[(RC26TA + SC27TA) + SC28TA/RC28TA]	3	3

Additional ratios, taking into account stable compounds from the steranes and TAS families were analyzed in order to compare hardly weathered oils to sources. Those ratios, listed at the bottom of Table 18.3, were mainly used in geochemical investigations, as they were more stable over the long time of weathering.

18.6 CONCLUSION

The *Erika* oil was an opportunity to study the fate and behavior of an HFO experiencing natural weathering processes. Samples were collected over a period of 11 years and were analyzed in order to study the evolution of chemical families (saturates, aromatics, resins, and asphaltenes) with time and from locations with different

environmental conditions. Samples collected along the Atlantic shoreline between 2001 and 2004, demonstrate a general progressive loss of heavy alkanes and heavy aromatics with time. However, the high variability in environmental conditions characterizing the sites where the oil samples were collected during this study (e.g., variable exposure to solar radiation and tides) as well as the physical form of the oil (oil thickness) contributed to a variation in terms of alkanes and aromatics distribution.

Study in a controlled environment allowed to better understand the effect of some weathering processes such as photooxidation on the chemical composition of the *Erika* oil. Oil exposed to solar radiation (and so to photooxidation processes) is prone to a drastic decrease of aromatics compounds along with an increase of the polar compounds (resins and asphaltenes). This observation explains the bituminous consistency/aspect of the oil after a few years in the environment. Saturates seem to be preserved but when looking at the *n*-alkanes, it appears that they are more degraded under conditions where no photooxidation occurs. Bacterial growth could be inhibited when exposure to solar radiation becomes too important.

A round-robin test organized in the framework of the OSINET group allowed for the study of the evolution of compounds or group of compounds (PAHs and biomarkers) and the effects of artificial and natural weathering of *Erika* oils on the Dr commonly used to compare oils. This study highlighted the degradation of some stable biomarkers such as TAS. It also showed that the common Dr used to evaluate the potential "match" or "not match" between spills and sources via CEN (2012) are not robust enough in cases involving severely weathered oils. Additional ratios based on the specific composition of the oil, such as are used for geochemical investigations, can be used such cases.

Thanks to this 10-year, long-term monitoring study following the *Erika* oil spill, the importance of photooxidation as weathering process has been highlighted. After more than 10 years of natural weathering, it appears that even very robust compounds such as biomarkers from the steranes, disteranes, TAS, and hopanes families can be extremely degraded or even entirely removed from the oil. In the case of HFOs (such as the *Erika* oil) containing an important fraction of aromatics (and especially heavy aromatics), the photooxidation process has a strong impact on the total degradation of the oil.

Acknowledgments

The authors wish to express their sincere thanks to the OSINET (Oil Spill Identification Network) group.

References

CEN Guideline, 2012. Oil spill identification − Waterbone petroleum and petroleum products. Part 2: Analytical methodology and interpretation of results based on GC-FID and GC-MS low resolution analyses. PD CEN/TR 15522-2:2012, British Standards Publication.

Garrett, R.M., Pickering, I.J., Haith, C.E., Prince, R.C., 1998. Photooxidation of crude oils. Environ. Sci. Technol. 32, 3719−3723.

Hadibarata, T., Tachibana, S., Itoh, K., 2009. Biodegradation of chrysene, an aromatic hydrocarbon by *Polyporus* sp. S133 in liquid medium. J. Hazard. Mater. 164, 911−917.

Haesler, F., Ballerini, D. 2002. Dégradation du fuel-oil n°6 de l'Erika dans l'environnement marin. Proceedings of the 3rd R&D Forum on High-density Oil Spill Response, Brest, France. pp. 129−138.

Jezequel, R., 2005. Pollution d'un littoral par fiouls lourds : Etude de l'influence des paramètres environnementaux sur la persistance et l'évolution chimique du polluant. Thèse de doctorat de l'Université de Bretagne Occidentale.

Jezequel, R. Merlin, F.X., 2012. Influence of the nature and the weathering of oil on surfwashing efficiency: experimental study with the shoreline bench. Proceedings of the 2012 Artic and Marine Oilspill Program (AMOP) Technical Seminar, Environnement Canada, Vancouver.

Jezequel, R., Poncet, F., 2011. The Erika oil spill, 10 years after: assessment of the natural weathering of the oil and natural recovery of vegetation. Proceedings of the 2011 International Oil Spill Conference. American Petroleum Institute, Washington, DC, March 2011, 2011, pp. abs165.

Jezequel, R., Menot, L., Merlin, F.-X., Prince, R.C., 2003. Natural cleanup of heavy fuel oil on rock: an in-situ experiment. Mar. Pollut. Bull. 46, 983−990.

Michel, J., Hayes, M.O., 1999. Weathering patterns of oil residues eight years after the Exxon Valdez oil spill. Mar. Pollut. Bull. 38, 855−863.

Munoz, D., Guiliano, M., Doumenq, P., Jacquot, F., Scherrer, P., Mille, G., 1997. Long term evolution of petroleum biomarkers in mangrove soil (Guadeloupe). Mar. Pollut. Bull. 34, 868−874.

Prince, R.C., Elmendorf, D.L., Lute, J.R., Hsu, C.S., Haith, C.E., Senius, J.D., et al., 1994. 17α(H), 21β(H)-hopane as a conserved internal marker for estimating the biodegradation of crude oil. Environ. Sci. Technol. 28, 142−145.

Wang, Z., Fingas, M., 1997. Developments in the analysis of petroleum hydrocarbons in oils, petroleum products and oil-spill-related environmental samples by gas chromatography. J. Chromatogr. A. 774, 51−78.

Wang, Z., Fingas, M., Sergy, G., 1994. Study of 22-year-old Arrow spill sample using biomarker compounds by GC/MS. Environ. Sci. Technol. 28, 1733−1746.

Wang, Z., Fingas, M., Owens, E.H., Sigouin, L., 2000. Study of Long-term Spilled Metula Oil: Degradation and Persistence of Petroleum Biomarkers. Proceedings of the 23th Artic and Marine Oilspill Program (AMOP) Technical Seminar, Environment Canada, Ottawa, Ontario, pp. 99−122.

Further Reading

Guyomarch, J., Budzinski, H., Chaumery, C., Haeseler, F., Mazeas, L., Merlin, F.-X., et al., 2001. The ERIKA oil spill: laboratory studies carried out to assist responders. Proceedings of the 2001 International Oil Spill Conference. American Petroleum Institute, Washington, DC, pp. 637–647.

Jezequel, R., Simon, R, Pirot, V., 2014. Assessment of oil burning efficiency: development of a Burning Bench. In proceedings of the 2014 International Oil Spill Conference, Savanah.

CHAPTER

19

Environmental Assessment of Spills Related to Oil Exploitation in Canada's Oil Sands Region

Jagoš R. Radović, Thomas B.P. Oldenburg and Stephen R. Larter

University of Calgary, Calgary, AB, Canada

BIOGRAPHY

Jagoš R. Radović is a Postdoctoral Fellow in the PRG group, within the Department of Geoscience, at the University of Calgary, Canada. Previously, he was awarded a predoctoral fellowship of the Spanish National Research Council (CSIC) and pursued his research at the Institute of Environmental Assessment and Water Research (IDAEA) in Barcelona, leading to a doctoral degree in Environmental Analytical Chemistry from the University of Barcelona. Parts of his PhD studies were conducted in Norway (SINTEF) and in United States (Woods Hole Oceanographic Institution). To date, the main focus of his research has been the environmental fate and effects of marine oil spills in coastal, open ocean, and sedimentary settings. He worked on projects funded by the Gulf of Mexico Research Initiative (GoMRI), investigating the long-term behavior and transformations of the oil spilled after the *Deepwater Horizon* blowout. He is a member of the Bonn Agreement Oil Spill Identification Network of Experts (Bonn-OSINET). His more recent research projects are related to the investigation of signals preserved in Earth's geochemical records and how they reflect the interactions of anthropogenic activities and global biogeochemical cycles, energy transition from fossil fuels and reduction of carbon emissions, and mitigation/remediation of spills and contaminated sites.

Thomas B.P. Oldenburg received his doctoral title in Natural Science at the Research Centre Jülich and University Oldenburg, Germany. He joined the Petroleum Geochemistry group (NRG) at the University of Newcastle upon Tyne (England) in 2001 focusing on improving the understanding of in-reservoir oil biodegradation processes. In 2004, he moved together with Prof. Stephen Larter and three coworkers to Calgary to set up the PRG at the University of Calgary (UofC). He is now the Research Programs Manager at PRG and Adjunct Professor at UofC. Thomas has been the innovator and manager of the TESLA Petroleomics Centre at UofC since 2009. He is cofounder of UofC start-up companies like Gushor Inc. (now Schlumberger) and founder–CEO of Aphorist Inc. His research program focuses on transformation processes of organic matter in natural and engineered water systems, soil, sediments, and fossil fuels, which contribute to addressing critical and complex problems like supply of energy, clean water, and mitigation of climate change drivers and effects, major challenges of the 21st century.

Stephen R. Larter is Canada Research Chair and Professor of Petroleum Geology at the University of Calgary. Prior to joining the University of Calgary in 2004, he worked for the Universities of Newcastle and Oslo and in the 1980s, for Unocal in California. Dr. Larter has broad research interests ranging from understanding the phenomenon of biodegradation and predicting fluid property variations in tar sand and heavy oil reservoirs; biogenic gas generation and shale gas and coupling fluid chemistry as part of reservoir simulator history matches; through to studying the microbial life of subsurface petroleum reservoirs, and contaminated water issues. Prof. Larter is also developing transition technologies to enable society and the oil and gas industry to rapidly migrate to zero carbon emission practices. He has been active in commercialization with numerous spin-off companies including Aphorist Inc., Gushor Inc. (a Schlumberger company), and Profero Energy. He is also the former

Oil Spill Environmental Forensics Case Studies.
DOI: http://dx.doi.org/10.1016/B978-0-12-804434-6.00019-7

Scientific Director of Carbon Management Canada Inc. He has published over 190 peer-reviewed articles and has over a dozen patents. He is a member of the Norwegian Academy of Sciences, a Fellow of the Royal Society, and The Royal Society of Canada, and American Association of Petroleum Geologists (AAPG) distinguished lecturer, and has won numerous medals and awards. His degrees are from the universities of Cambridge and Newcastle.

19.1 INTRODUCTION

Oil sands are a mixture of sand, water, clay, and dense and viscous crude oil (Larter and Head, 2014). Technically, under reservoir conditions, we can differentiate "heavy" oils (gravity 10°–20° American Petroleum Institute (API), viscosity >100 centipoises, cp), which can flow; and nonflowable "bitumens" (gravity <10° API, viscosity >10,000 cp). However, since they are both part of the same physicochemical continuum, the two terms will be used interchangeably in this chapter.

One of the largest oil sand resources in the world are found in Canada, in its western province of Alberta (Fig. 19.1). Canada's Oil Sands Region (COSR) contains the third-largest proven reserves of crude oil, after Venezuela and Saudi Arabia; and it accounts for 90% of the Canadian oil production, with more than 2 million barrels per day (bbl/d) produced in 2014 and an estimated production increase to more than 5 million bbl/d by 2030 (AER, 2016; Larter and Head, 2014; NEB, 2016). These projections might change, given the recent downturn in oil production; notwithstanding, COSR will remain an important part of Canadian economy in years to come. In addition, oil producers in Alberta are still exploiting remaining conventional oil reserves, which in recent years have been contributing to the total oil output with approximately 500,000 bbl/d (AER, 2012). The main market for oil from COSR is the United States, which in 2013 imported approximately 70% of Canadian oil production

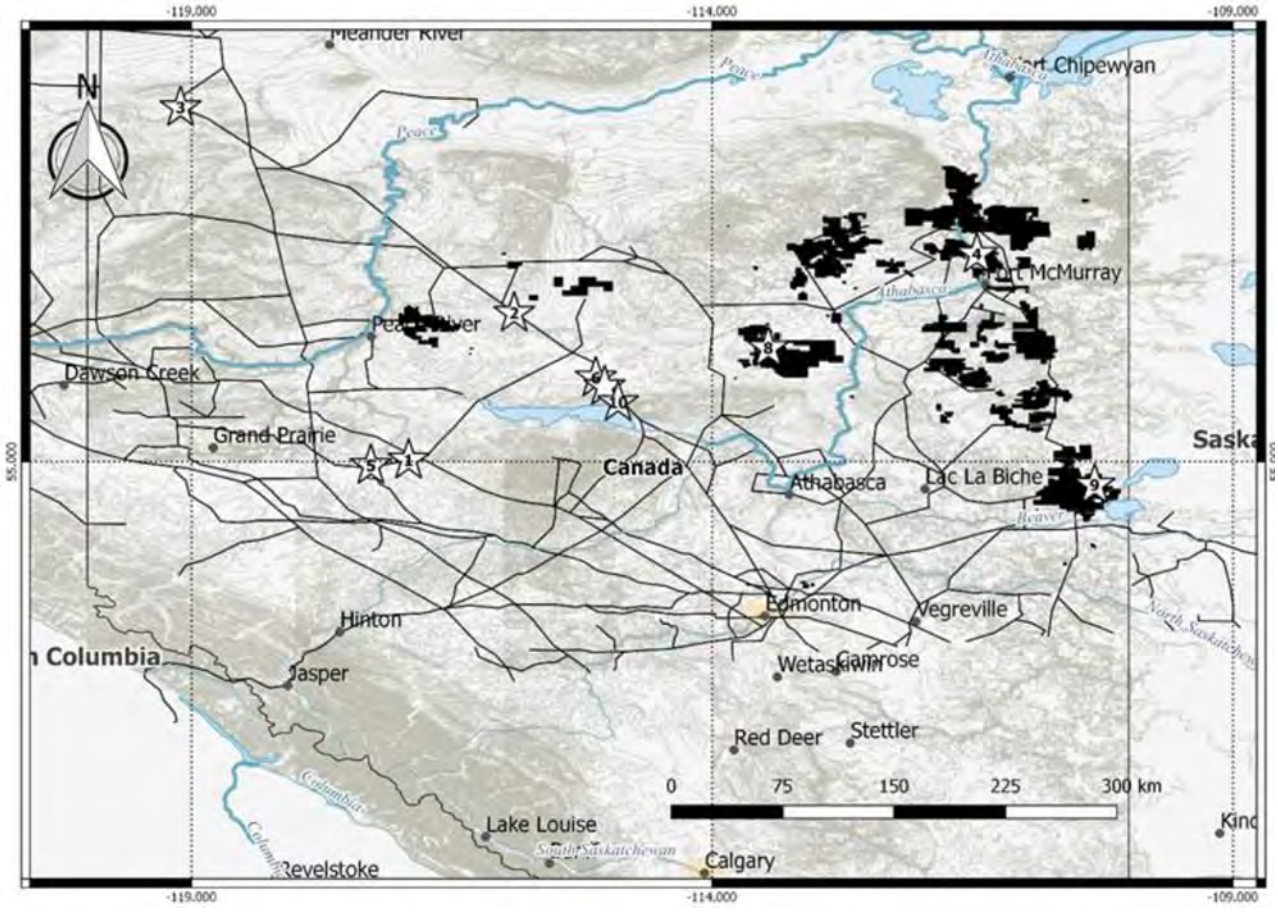

FIGURE 19.1 Polygons show all projects in the COSR, as of December 31, 2013 (Government of Alberta, 2016). Lines show pipeline network in place in 2011 (NRC, 2012). Stars mark the locations of 10 largest oil spills in Alberta from 1975 to 2012 (Young, 2013).

(NEB, 2016). Given the landlocked geographical position of Canadian oil sands resources (Fig. 19.1), extracted oil has to reach markets (refineries or marine ports) onshore.

Major (and increasing) volumes of COSR oil are transported by pipelines, while only a smaller portion, approx. 4%, is moved by rail (NEB, 2016). However, the issue of pipeline oil transport is highly contentious, due to past pipeline spill incidents and the perceived risk of future spills and related environmental impacts; which led to cancellation or delay of some major pipeline projects (Keystone XL, Northern Gateway, Energy East pipelines; Snyder, 2016). Notwithstanding, these perceptions are often not contextualized, due to the lack of comprehensive environmental assessments of the very distinct, yet variable, nonhydrocarbon-rich oil sands resources being transported.

Therefore, this chapter will aim to assess the environmental risks of spills in COSR, in relation to unique oil properties, production and transport methods, environmental characteristics of the region, and taking into account the past cases of incidental releases.

19.2 OIL SANDS PRODUCTION

Oil is extracted from the oil sands resources in two ways: Open-pit mining for shallow resources and in-situ (e.g., steam-assisted gravity drainage, SAGD, cyclic steam stimulation, CSS) for deeper resources. Oil sands recovery using open-pit mining is the smaller portion of the resources (approx. 20%; CAPP, 2016). These two oil sands process techniques are described in more detail below.

Surface (open-pit) mining includes the excavation of shallow oil sand deposits using heavy machinery followed by crushing in a facility. Hot water is added to form a slurry to separate the bitumen from the sand, clay, water, and other mineral residue in large separation vessels. After settling time the bitumen froth separates from the sediments (sand, clay, rocks) and water. The bitumen froth is further treated to reduce trapped water and clay before diluents such as naphtha or paraffin solvents are added to the bitumen to reduce the viscosity for transportation and/or further upgrading. The mixture of water with clay, sands, traces of organics, especially highly polar bitumen constituents, and process chemicals are transferred to so-called tailings ponds. Large volumes of this residual oil sands process-affected water (OSPW) are in the tailings ponds for settling and temporary containment (Fig. 19.2).

FIGURE 19.2 Satellite image of an Athabasca oil sands mine, showing the excavation area (mine) and the tailing pond holding the residues from the oil separation process (NASA, 2009).

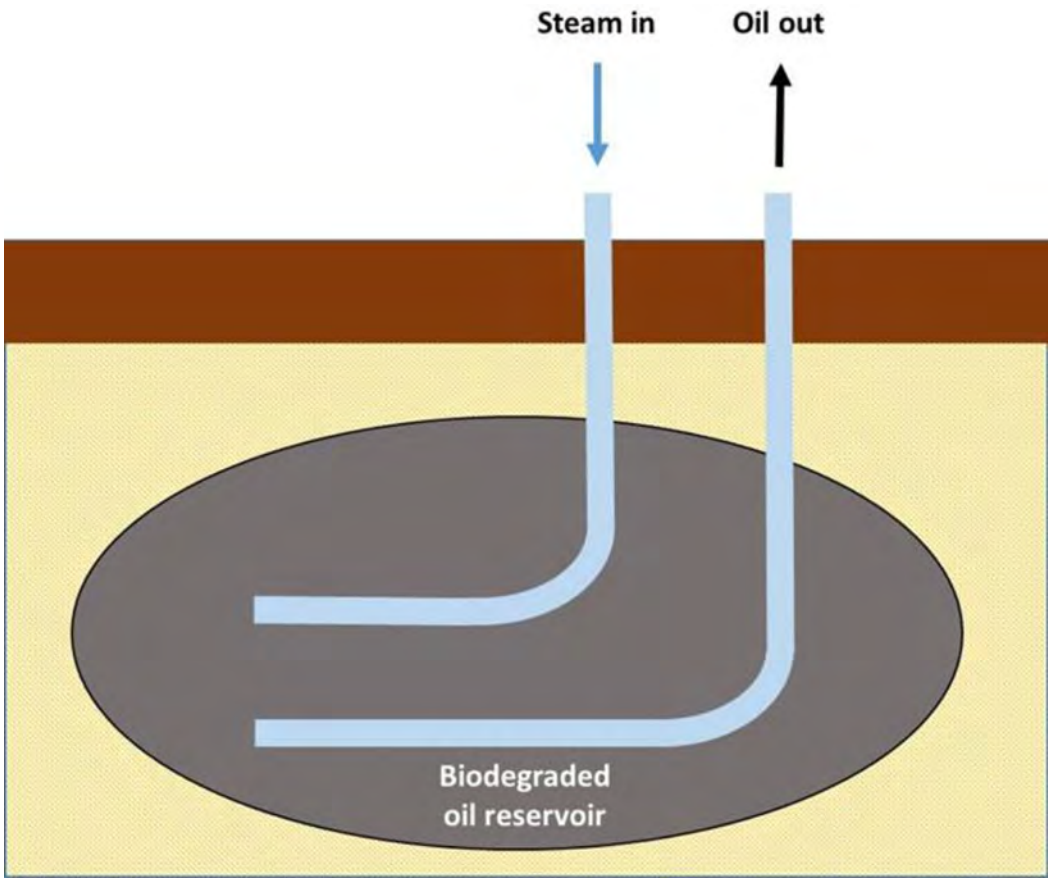

FIGURE 19.3 Schematic and conceptual representation of in-situ oil production using SAGD. Hot steam is injected to the subsurface through the upper well, where it forms a buoyant volume that rises in the reservoir, heating the oil which then, with lowered viscosity, drains to the lower recovery well, and is pumped to the surface. Much more detail is in Gates and Larter (2014) and Larter and Head (2014).

The OSPW contains a complex mixture of organic components, especially water-soluble, highly polar, carboxylic acids-containing species such as naphthenic acids (NAs), including various sulfur and nitrogen-containing analogs (Barrow et al., 2015; Headley et al., 2010; Quesnel et al., 2015). More details are described in Section 19.3.

In-situ recovery is used for extraction of more deeply (more than 130 m) buried heavy oils and bitumens, which are typically treated in situ using thermal energy (e.g., steam) to reduce oil viscosity, and then pumped to the surface (Fig. 19.3). The thermal recovery processes largely used in the oil sands are SAGD and CSS. Contrary to open-pit mining, in-situ recovery does not generate tailings ponds and therefore creates much less surface disturbance. Also, in-situ recovery typically uses less water compared to the mining process and the water used for generating steam in the bitumen production process is largely recycled in wastewater treatment plants.

The majority of extracted heavy oils and bitumens are too viscous for transportation; therefore, they have to be diluted, for example, using lighter hydrocarbon fractions such as gas condensates, naphtha, or diesel to produce the so-called "dilbit". In order to be suitable for processing in conventional refineries and as an alternative to reducing the viscosity of the bitumen to flow through the pipelines, heavy oils and bitumens are often upgraded, to break up high molecular weight compounds, add hydrogen, and remove excess sulfur. Such upgraded oil/bitumen product is known as "syncrude", or "synbit".

19.3 ORIGIN AND PHYSICOCHEMICAL PROPERTIES OF COSR OILS

Properties of COSR oil reserves were determined by the geological history of the Western-Canadian basin. Oils originated from common marine-shale source rocks in the foreland of the Rocky Mountains (Fig. 19.4A). After migration towards the East, they accumulated in shallow, cool reservoirs at the northeastern Alberta

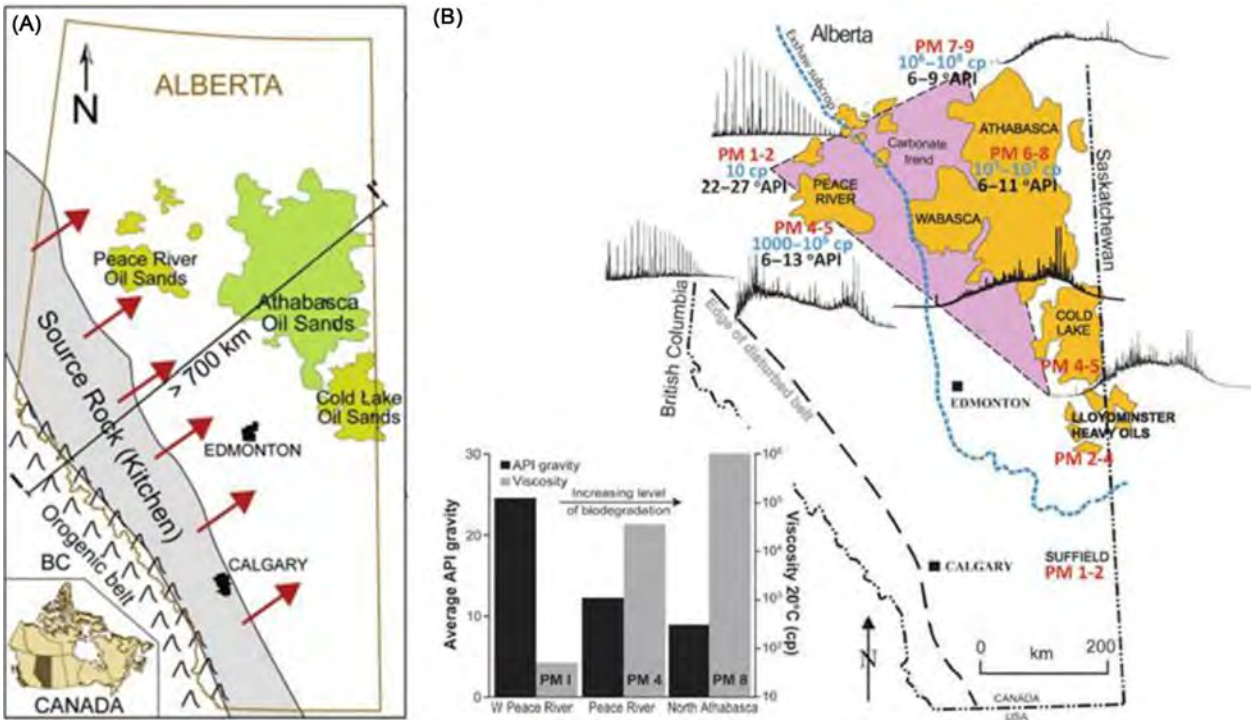

FIGURE 19.4 (A) Arrows show the direction of petroleum migration from the source rock in the foreland of the Rocky Mountains towards the Northeast. (B) Variation of physicochemical properties in heavy oil and bitumen reservoirs of COSR. Whole oil gas chromatograms show the depletion of *n*-alkanes, as the biodegradation advances towards the East. Similarly, the inset plot shows the variation of the API gravity and viscosity for the oils along the east–west cross-section, through the Athabasca and Peace River oil sands. The API gravity and viscosity (cp) ranges are shown for each of the deposits, along with the Peters and Moldowan (PM) biodegradation level of the oils [scale ranges from 0 (no biodegradation) to 10 (extreme biodegradation)]. *Adapted from Larter and Head (2014), and Fustic et al. (2012) with permission from Elsevier.*

border. Such reservoir conditions favored in-reservoir oil biodegradation, the extent of which is reflected in the unique and variable physicochemical continuum of COSR heavy oils and bitumens (Fig. 19.4B).

The degree of biodegradation and resultant increase in viscosity and decrease in API-gravity of the oils increases from west to east and south to north with the most severe biodegraded oils located in the northeastern part of Athabasca oil sands and Grosmont carbonates; for example, the API gravity spans the 38 to 6° range, while the viscosity rises up to millions of centipoises (cp), along the Peace River-Athabasca line (Larter and Head, 2014).

These trends of biodegradation are a reflection of the maximum reservoir burial depth (reservoir pasteurization >80°C) with oils in the most western part of Peace River not being biodegraded (Adams et al., 2013; Adams et al., 2006; Oldenburg et al., 2009; Wilhelms et al., 2001). The changes in the physicochemical properties of the oils are related to the changes in the molecular composition induced by biodegradation. Oil biodegradation in reservoirs follows certain paths of almost completely removing *n*-alkanes, most rapidly followed by isoprenoid alkanes, cyclic, and aromatic hydrocarbons. Over the years a few biodegradation scales were developed with the Peters and Moldowan being the most common one (Peters et al., 2005). A more detailed scale is the one based on Manco numbers (Larter et al., 2012). Whereas the saturated hydrocarbon fraction is most depleted during biodegradation, the concentration of polar oil fractions, containing nitrogen, sulfur, and oxygen (NSO) nonhydrocarbons is enriched. Polycyclic aromatic hydrocarbons (PAH) with a low number of rings are preferentially degraded, leading to an increased abundance of heavier PAH compounds. Nonhydrocarbon content ranges from 25 wt% in Peace River deposits, with significant contribution of sulfur (~10 wt%), raising up to 60 wt% of NSO compounds in the Athabasca accumulation (Larter and Head, 2014), much higher than in typical light to medium crude oils (Table 19.1). Recent comprehensive studies of hydrocarbon and nonhydrocarbon oil constituents from several biodegraded oil fields using ultrahigh resolution mass spectrometry (Fourier transform ion cyclotron resonance mass spectrometry, FTICR-MS) revealed systematic destruction of hydrocarbons, and destruction and production of high molecular weight nonhydrocarbons during progressive in-reservoir biodegradation (Oldenburg et al., 2017).

This is reflected by the SARA composition, namely an increase of the nonhydrocarbon SARA fractions of resins and asphaltenes (Table 19.1). These fractions are not GC-amenable, due to the high polarity and molecular mass, and therefore, for years, have avoided more detailed molecular characterization.

In the past decade, technical advancements in mass spectrometry, in particular, the advent of FTICR-MS, have expanded the analytical window to enable much more comprehensive characterization of polar, nonhydrocarbon oil species (McKenna et al., 2013). Due to its ultrahigh resolving power and broad mass range of detection, coupled with soft ionization techniques (e.g., atmospheric pressure photoionization, APPI and electrospray ionization, ESI), thousands of different compounds with molecular weights up to 1400 Da can be identified in a single oil sample without any previous chromatographic separation (Oldenburg et al., 2014). Such analytical improvements led to the development of "petroleomics", a field which aims to assess the properties and behavior of different oils by interpreting their complex molecular composition (Rodgers and Marshall, 2007).

FTICR-MS has also been used to characterize COSR heavy oils and bitumens (Pan et al., 2013; Shi et al., 2010). Fig. 19.5 shows the composition of a sample from Peace River deposits, obtained using FTICR-MS, in positive-ion

TABLE 19.1 Comparison of Saturates, Aromatics, Resins, and Asphaltenes (SARA) Composition of a Typical Medium Crude and Heavy Oils from COSR, Showing Much Higher Proportion of Resins and Asphaltenes, which Contain The Bulk of Nonhydrocarbon NSO Compounds (Hsu and Robinson, 2007; NAS, 2016)

	Weight percent (%)			
Oil type	**Saturates**	**Aromatics**	**Resins**	**Asphaltenes**
WTI[a]	78	15	6	1
Cold Lake	21.5	23.2	39.4	15.6
Athabasca	16.9	18.3	44.8	17.3

[a]*WTI = West Texas Intermediate.*

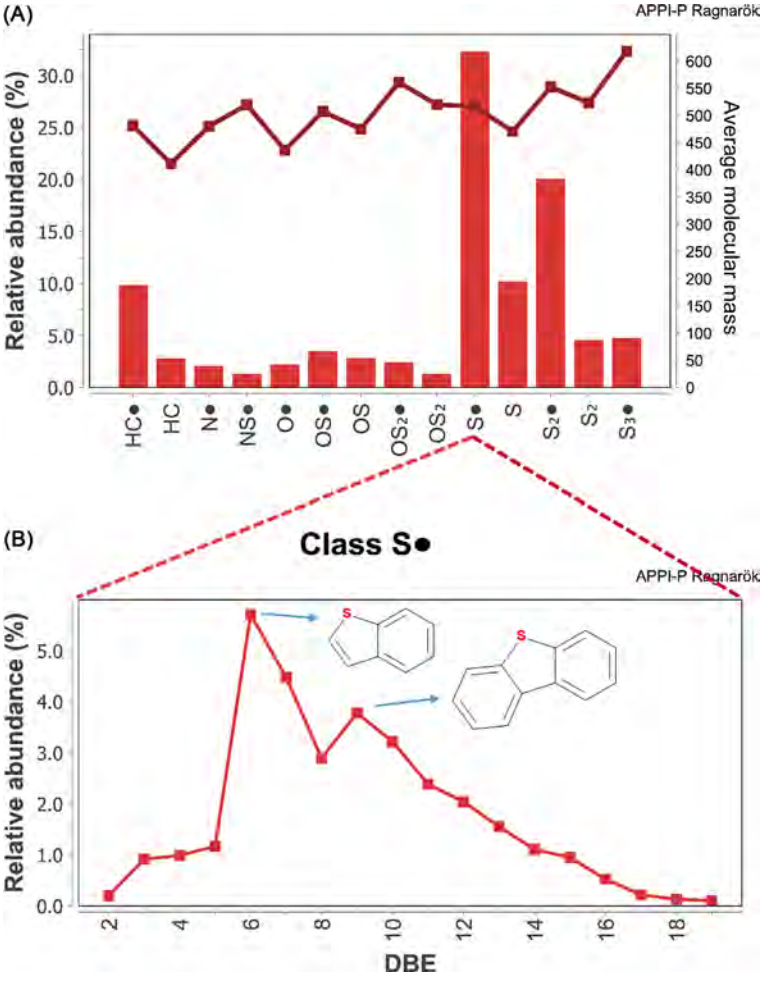

FIGURE 19.5 (A) Relative distribution of compound classes detected in an oil sample from the Peace River basin using FTICR-MS in APPI-P mode. In the APPI-P data, the dot indicates radical classes; the other classes are found as protonated species. The line shows average molecular mass for each compound class. (B) Relative distribution of species with the same DBE (rings plus double bonds) within S1 radical class in APPI-P; insert depicts example thiophenic and dibenzothiphenic structures corresponding to the most abundant DBEs within the S1 class. Data (in %) is normalized to the abundance of all assigned peaks in the sample. See Oldenburg et al. (2014) for more details on FTICR-MS ionization mechanisms, definitions, and terminology.

APPI (APPI-P) mode, which efficiently ionizes molecules containing aromatic rings and sulfur, e.g., thiophenic species. Indeed, Fig. 19.5A shows that the sulfur heteroatom compound classes (S1, S2) are dominating the oil composition, followed by hydrocarbon class species. This is not surprising, since the Peace River oils are characterized by high sulfur content due to additional sulfur-rich charge from Jurassic source rocks (Larter and Head, 2014). Plot of double-bond equivalents (DBE; the sum of rings and double bonds in the molecule; Fig. 19.5B) indicates that thiophenic (DBE 6) and dibenzothiophenic (DBE 9) analogs dominate the S1 class, including a broad range of highly substituted species with up to 60 carbon atoms (not shown). When averaged, the molecular mass of such complex mixture of sulfur-containing compounds in the S1 class is higher than 500 Da (Fig. 19.5A). For comparison, typical GC-MS based methods can detect only limited range of thiophenic species weighing up to ~250 Da (Andersson and Schade, 2004).

Positive-ion ESI (ESI-P) enables ionization and detection of basic compounds, i.e., compounds which can easily be protonated, thus accessing additional pool of compounds, in particular nitrogen-containing species, such as pyridinic molecules. For example, Fig. 19.6 shows the distribution of nitrogen-containing species in oil samples from Peace River and Athabasca basins. Compounds in the N1 class, comprised of pyridine derivatives, such as the alkylated and benzannulated homologs (Oldenburg et al., 2014), are more abundant in Athabasca oils. Athabasca samples also show higher intensity of the species in the NO class, probably including putative oxygenated analogs of the pyridinic compounds present in the N1 class. On the other hand, ESI-P analysis of Peace River samples reveals prominent distribution of sulfur-containing homologs (e.g., in the class NS and NS2; Fig. 19.6)—another evidence of sulfur-rich inputs to the Peace River deposits (Larter and Head, 2014).

Finally, negative-ion ESI (ESI-N) is optimal for the ionization of acidic species such as NAs, a class of organic compounds particularly abundant in oil sands samples (Oldenburg et al., 2014). NAs are a large group of diverse,

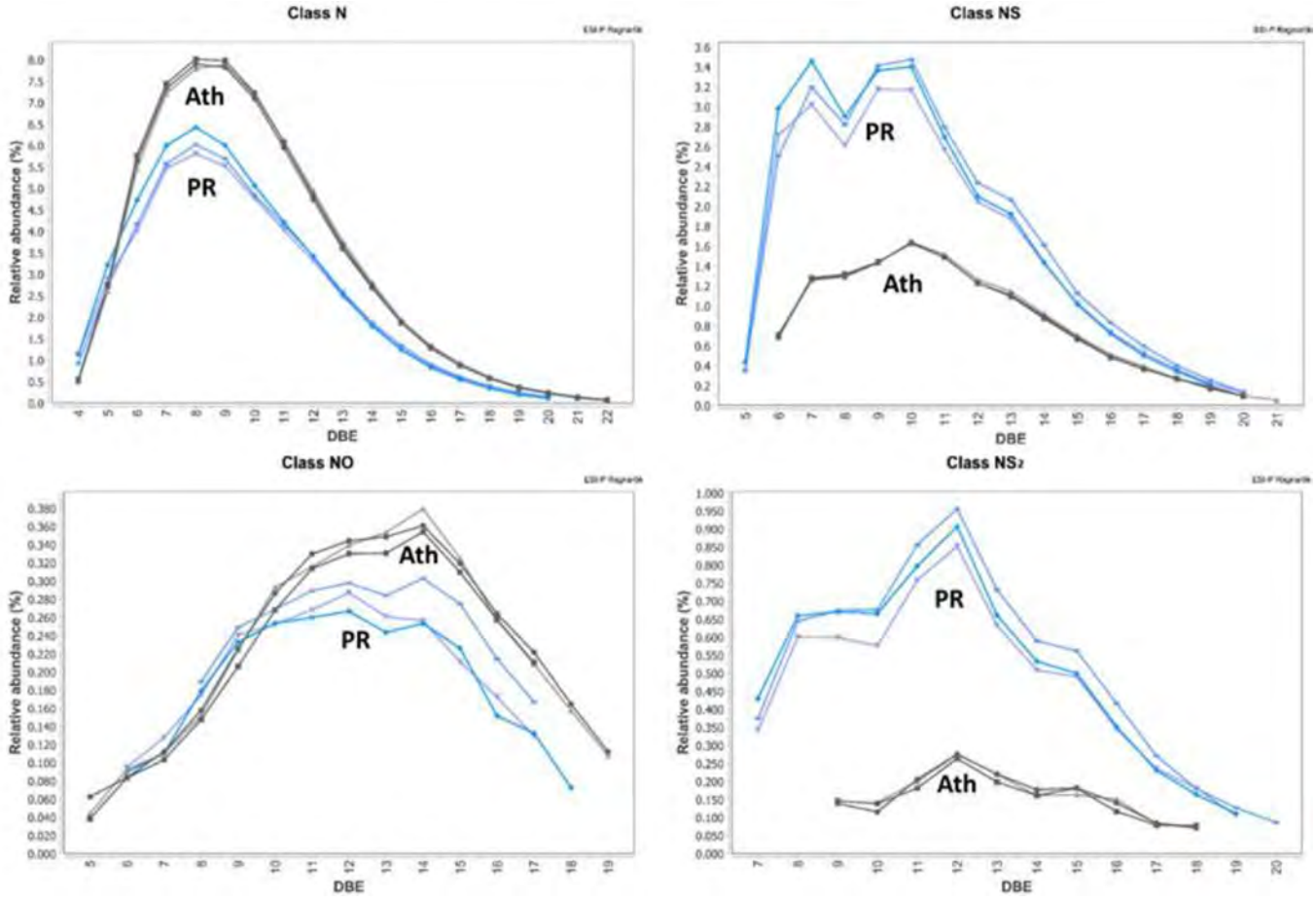

FIGURE 19.6 Distribution of nitrogen-containing species (in N, NO, NS, and NS2 heteroatom classes) in the Peace River (PR) and Athabasca (Ath) oils, grouped by their DBE, as revealed by the FTICR-MS analysis with electrospray ionization in positive-ion mode (ESI-P). Data (in %) is normalized to the abundance of all assigned peaks in the sample.

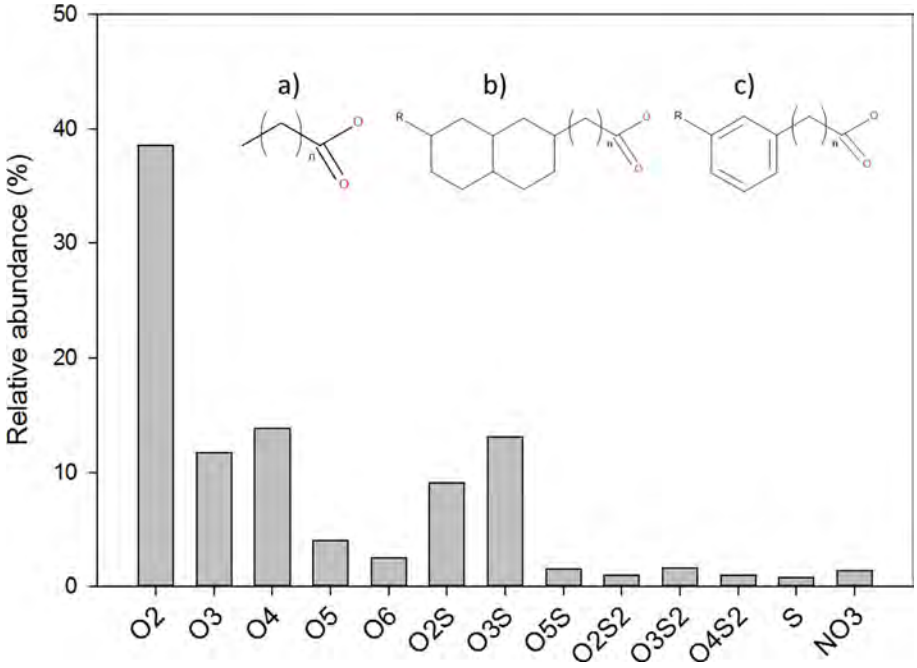

FIGURE 19.7 Relative distribution of compound classes detected in the OSPW of an active tailings pond using ESI-N FTICR-MS. Note the predominance of oxygenated compound groups, containing acidic species, such as NAs. Insert shows generalized structures of a) aliphatic, b) alicyclic and c) aromatic NAs. Data (in %) is normalized to the abundance of all assigned peaks in the sample. Figure generated from the data in Quesnel et al. (2015).

alkyl-substituted acyclic and cyclic (both saturated and aromatic) carboxylic acids, including species with multiple oxygen functional groups (e.g., dicarboxylic acids, hydroxy carboxylic acids, etc.), see insert in Fig. 19.7. These compounds are water soluble, preferentially partitioning into the water during oils sands processing, and produce the toxic OSPW, a complex concentrate of acidic, oxygen-containing compound classes, Fig. 19.7 (Quesnel et al., 2015). This illustrates different layers of compositional complexity found in nonhydrocarbon fraction of COSR oils, which can only be accessed using advanced ultrahigh resolution analytical techniques such as FTICR-MS.

In summary, extensive in-reservoir biodegradation generated oils which are often denser than water, do not readily flow at ambient temperature, and are enriched in high molecular weight aromatic hydrocarbons and nonhydrocarbons. Such chemical composition makes them more resistant to biodegradation and has important implications for the environmental behavior, fate, and effects of COSR oils in the case of a spill, which will be discussed in Sections 19.5 and 19.6.

19.4 PAST OIL SPILL CASES IN THE COSR

In order to investigate historical oil spill trends in COSR, we used a public database of releases from the oil and gas industry, based on the records from the Alberta Energy Regulator, which was compiled and made publicly available by Young (2013). Database includes the dates and locations of releases, spill source, failure type, and the volume of different types of spilled materials, such as oil, produced waters, drilling muds, etc. It does not contain data on spills from railway, road transport of oil, or from the pipelines which cross Alberta borders.

For the purpose of this chapter, we investigated a subset of 24,676 records, related to crude oil, crude bitumen, and syncrude spills in the past 37 years, from 1975 to 2012. Majority of the spills involved crude oil and bitumen. There have been large volume spills in this period which released other substances and mixtures related to oil production, e.g., wastewaters, sludges, lubricants, and many others; however, due to their diverse nature and often unknown composition, we focused only on oil spills.

In the investigated period, on average, there have been 648 spills per year and the average annual release of oil was 46,424 bbl. The number of spills does not show a clear temporal trend, nor does it correlate with the spilled volume; for example, the highest number of oil releases was recorded in 1997 (1528), more than double the average of 37 years, but the total volume spilled in the same year (55,000 bbl, approx.) was only somewhat higher than the long-term mean Fig. 19.8.

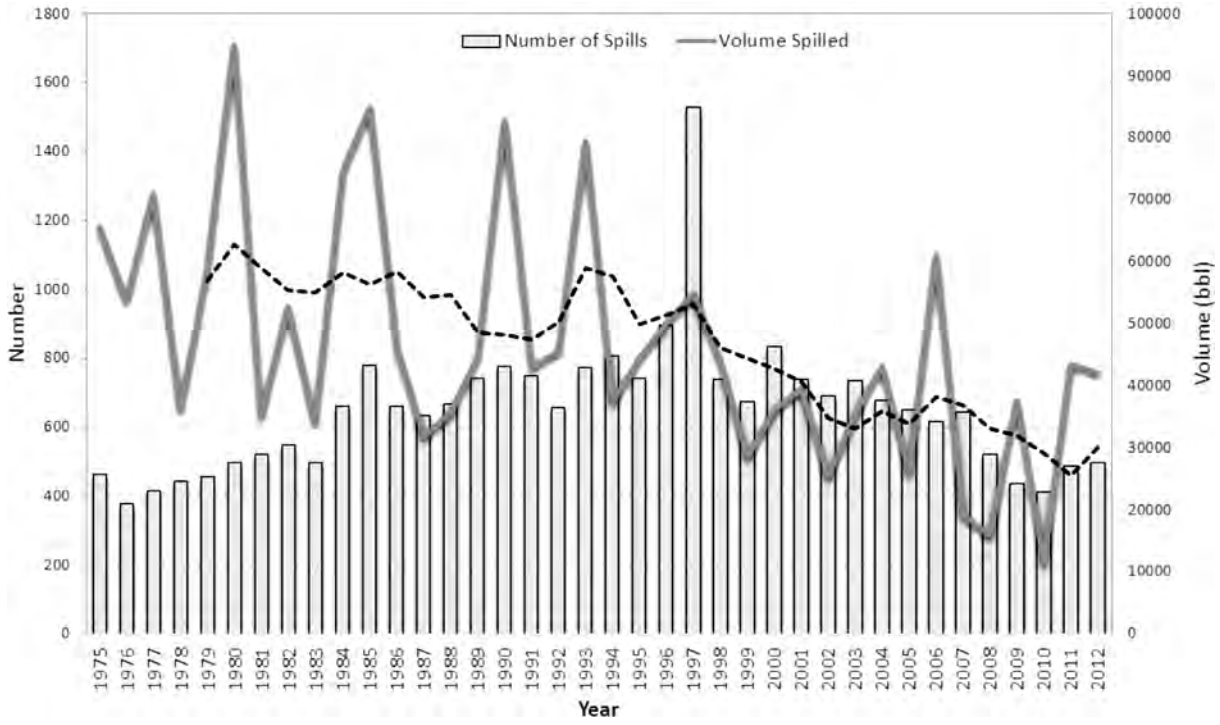

FIGURE 19.8 Number of oil spills (bars), and the released volume in barrels (full line), per year, recorded in COSR in the period from 1975 to 2012 (Young, 2013). Dashed line shows five-year moving average of spilled oil volume.

On the other hand, in this period, a variable, but decreasing trend of spilled oil volume can be observed (Fig. 19.8). During these 37 years, the oil output from COSR was raising, particularly in the past decade (CAPP, 2016). Despite higher production, the proportion of spilled oil volume relative to the total output during the investigated period was ~0.01%, on average, with a decreasing trend (Fig. 19.9). This suggests an improving spill prevention record for the oil industry in COSR during the past 37 years.

The largest oil spill in Alberta in the 1975–2012 period is the release of more than 40,000 bbl of crude oil from the Pembina pipeline, about 350 km northwest of Edmonton in 1980. According to the record, only 4500 bbl have been recovered; but, to the best of our knowledge, no additional postspill information or monitoring studies are available in the literature. The next two largest spills, both involving crude oil, occurred in 2011 and 2012; the first one was the release from the Rainbow pipeline into a stagnant muskeg area near Peace River, while the second oil spill was near Rainbow Lake due to a line failure. As seen in Table 19.2, the majority of the 10 largest spill incidents were related to pipeline infrastructure.

As commented before, we did not have a reliable and comparable database of spill incidences and released volumes related to railway and road transport of oil in COSR; however, historical cases suggest that this type of transport can be the source of notable oil releases. For example, in 2005, a train derailment led to a spill of approx. 4500 bbl of heavy fuel oil near Wabamun Lake (central Alberta), out of which an estimated 940 barrels entered the lake (deBruyn et al., 2007). This spill would classify as medium sized compared to the long-term spill record in the COSR; however, if railway oil transport would greatly increase from the current 4% of COSR oil transported (NEB, 2016), so would the risk of incidental spills, and presumably, the cumulative volume released. Some authors have analyzed Canada-wide statistical data for the number of incidental releases of hydrocarbon products (including gaseous), and suggested that the railway transport of hydrocarbons is approx. 4.5 riskier than via pipelines, based on the number of incidental releases per thousand barrels of oil equivalent (Mboe) transported (Green and Jackson, 2015).

To further contextualize the volumes spilled in the COSR, Table 19.3 contrasts them to several other sources of incidental oil releases. For example, in a comparable timeframe (1978–2007), the average annual oil spillage from the onshore petroleum industry (production wells, pipelines, refineries) in the United States was roughly three times higher than the COSR average (API, 2009). Even higher is the average volume spilled every year (between 1975 and 2012) as a consequence of tanker incidents—18 times the annual volume of releases in COSR

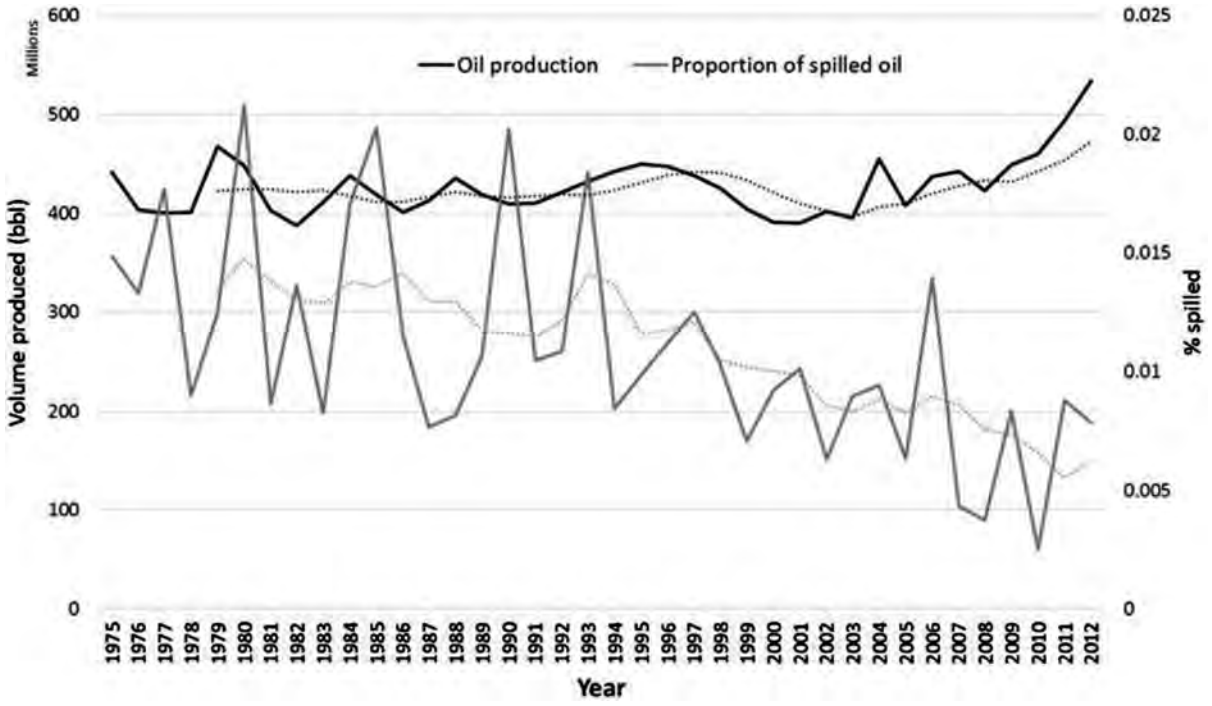

FIGURE 19.9 Annual outputs of oil from COSR from 1975 to 2012 (black line), based on the data from Canadian Association of Petroleum Producers (CAPP, 2016), and the proportion of spilled oil volume (%) relative to the total production (gray line). Dashed lines show five-year moving averages of the two variables.

TABLE 19.2 Project License, Year in Which the Release Occurred, Type and Volume of Spilled Oil for 10 Largest Oil Spills in COSR from 1975 to 2012

	License type	Year	Oil type	Volume spilled (bbl)
1.	Pipeline	1980	Crude Oil	40,885
2.	Pipeline	2011	Crude Oil	28,305
3.	Facility	2012	Crude Oil	22,015
4.	NA	2006	Crude Bitumen	18,870
5.	Pipeline	1975	Crude Oil	17,989
6.	Pipeline	1976	Crude Oil	17,989
7.	Pipeline	1993	Crude Oil	16,234
8.	Pipeline	2004	Crude Bitumen	15,863
9.	Well	2009	Crude Bitumen	15,725
10.	Pipeline	1993	Crude Oil	14,039

Locations of the spills are shown in Fig. 19.1, denoted by correspondingly numbered star symbols.

(ITOPF, 2016). Only one of the major tanker incidents, Exxon Valdez, released almost six times more oil than the annual COSR spill average (ITOPF, 2016). US offshore oil production had a better average spill record than its onshore counterparts (both in United States and Canada), Table 19.3 (API, 2009); however, when major offshore submarine spills occur, they can release unprecedented amounts of oil. For example, a blowout on the *Deepwater Horizon* platform in 2010 started an uncontrolled submarine oil release to the Gulf of Mexico which lasted 78 days and spilled a quantity of oil a hundred times greater than the average annual volume spilled in COSR (National Commission on the BP Deepwater Horizon Oil Spill and Offshore Drilling, 2011). Pursuant the marine oil spill criteria, approximately 80% of the spills which occurred in COSR over 37 years can be considered small (<50 bbl), and only 33 (0.13%) are large spills (>5,000 bbl) by the same criteria.

TABLE 19.3 Spilled Volumes from Different Incidental Spill Scenarios

	Volume (bbl)
Average annual spilled volume, US offshore (1978–2007)	6312
Pembina spill	40,885
Average annual spilled volume, COSR (1975–2012)	46,424
Average annual spilled volume, US onshore (1978–2007)	140,589
Exxon Valdez (approx.)	264,000
Average annual spilled volume, tanker incidents, globally (1975–2012)	853,383
Ixtoc-I (approx.)	3,400,000
Deepwater Horizon (approx.)	4,900,000

Based on the data from API (2009); ITOPF (2016); National Commission on the BP *Deepwater Horizon* Oil Spill and Offshore Drilling (2011); Soto et al. (2014).

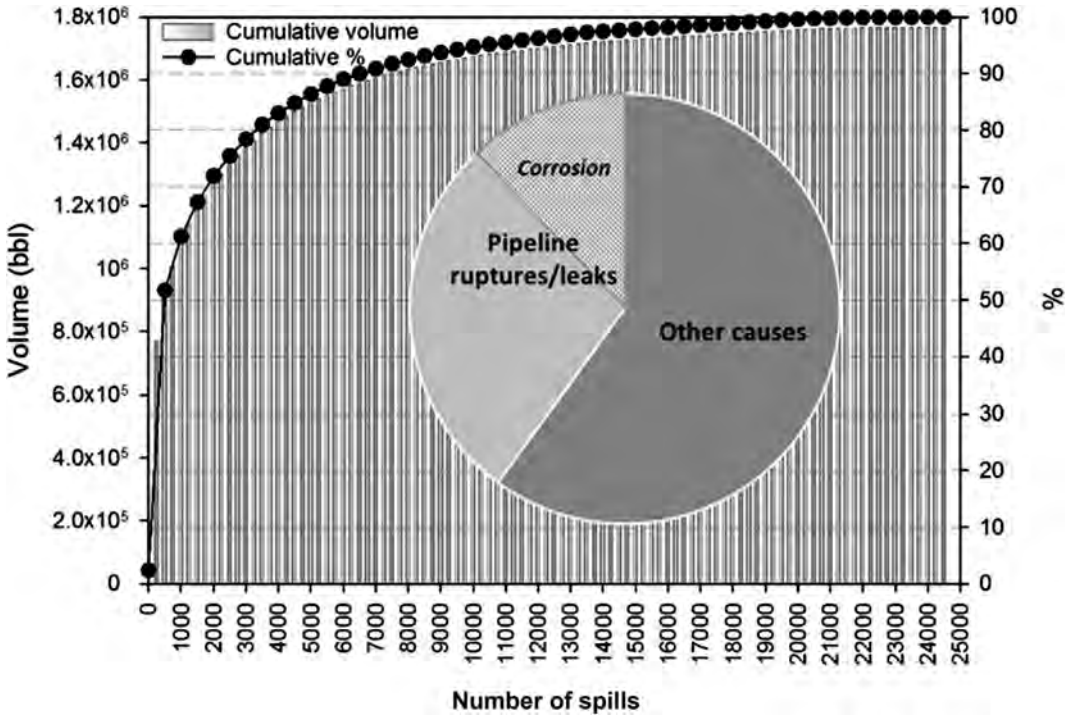

FIGURE 19.10 Pareto chart of spilled oil volume as the function of number of spills in COSR from 1975–2012, based on the data from Young (2013). Spilled volume distribution is highly skewed, 50% of cumulative spilled volume during 37 years was released by only 438 spills; out of those, 175 spills (or 40%) was due to pipeline ruptures and leaks, many of which (53 incidents) caused by corrosion, see insert pie chart.

In general, out of more than 24,000 spills in COSR during 37 years, 438 incidents (only 1.8%) released half of the total oil volume spilled (Fig. 19.10). Out of those, 175 incidents (or 40%) were due to pipeline ruptures and leaks—in the cases where spill cause could be determined, corrosion was responsible for the third (approx.) of the pipeline releases.

Pipeline corrosion is a well-known problem in the petroleum industry which for a long time focused on its monitoring, detection, and prevention (Garverick, 1994). Particularly troublesome is the internal pipeline corrosion, which occurrence and progression is hard to detect, and is exacerbated by the presence of water, often found in unprocessed oils transported in the COSR (AER, 2013). Despite mitigation efforts, internal corrosion is still responsible for a large number of incidental pipeline releases in COSR (AER, 2013); therefore, additional research and technological advancements are needed to produce reliable, early warning systems able to detect the onset and progression of internal corrosion processes prior to pipeline failure and subsequent spills. Such systems would greatly reduce the risk of unexpected, large volume pipeline spills.

19.5 ENVIRONMENTAL FATE AND BEHAVIOR OF COSR OILS

Postspill fate and behavior of oil is determined by the physicochemical properties of the spilled oil, the characteristics of the affected environment, and the conditions at the spill location (Radović et al., 2012). Due to the high viscosity and density, heavy oils and bitumens produced and transported in COSR would classify as persistent, "Group 4" oils according to marine oil spill criteria (ITOPF, 2011; Radović et al., 2012).

In the case of a spill, such oils have a tendency to adhere to surfaces, leading to pollution of plants and animals which come into contact with the oil, and making the clean-up from contaminated surfaces more complicated. On the other hand, high oil viscosity limits the spreading of the spill, both on land and in aquatic media, thus facilitating the containment efforts.

After a spill on land the risk of oil constituents migrating to groundwater resources would depend on the oil composition, the character of the soil onto which the oil is spilled, and the depth of the water table. For COSR oils, high viscosity and low content of light molecular weight hydrocarbons would limit their downward percolation through soil. Higher molecular weight compounds (e.g., larger PAH) would have the tendency to bind to the organic fraction of soil (Manzetti, 2013). Given the fact that the predominant soil types in COSR are organic-rich luvisols and chernozems (Alberta Land Resource Unit, 2005), an increased retention of such oil compounds in the soils would be expected. In turn, this means that they could be removed by reclamation measures such as excavation or using bioremediation techniques to stimulate biodegradation of retained oil compounds in soil-plant systems (Truu et al., 2015). On the other hand, diluted bitumen, or dilbit, contains light oil fractions such as diesel or naphta, added for transportation mobility, which are enriched in highly mobile compounds such as benzene, toluene, xylenes, and ethylbenzene (BTEX), lighter paraffins, and naphthenes. These dilbit components are prone to solubilization and potential migration to the subsurface, particularly in organic-lean soils. Notwithstanding, volatilization to air would still be the main environmental sink for added diluents, which has to be taken into account when protection measures for response workers are selected.

Wetland areas, which cover large portions of Alberta, are particularly sensitive to oil inputs, due to anaerobic conditions in the substrate which would slow down natural oil attenuation by biodegradation. Also, production and transportation activities in COSR are often located in the northern latitudes (Fig. 19.1), where low seasonal temperatures are an additional limiting factor for spilled oil biodegradation in soil and wetland systems.

In the case of a spill into water bodies, high density of COSR oils would increase the risk of oil sinking, due to the fact that some of the heavy oils are denser than water (API $< 10^{\circ}$); in addition, less dense oils or dilbits might also sink eventually due to evaporation of lower molecular weight compounds, and/or agglomeration with particulates, which can decrease the buoyancy to the sinking point (Winter and Haddad, 2014). For example, after the train derailment and subsequent spill to the Wabamun lake, a portion of the released heavy fuel oil was submerged due to the formation of oil-particulate agglomerates, and was resurfacing in the form of tar balls in the years after the spill (Hollebone et al., 2011). Sunken oil can affect benthic organisms in sediments and is much harder to recover and/or remediate. When sunken in deep water bodies such as oceans or deep lakes, it can be buried and persist for long time periods due to the absence of some important weathering processes, such as photooxidation or aerobic biodegradation, normally affecting oil on the surface (Daly et al., 2016; John et al., 2016; Schwing et al., 2015).

As discussed in the Section 19.3, biodegraded oils from COSR are enriched in more recalcitrant aromatic species, including families of alkyl-substituted, fused aromatic systems, such as PAH and their heteroatom analogs. These are GC-amenable, and thus very well studied compounds, which have higher octanol−water partitioning coefficients (K_{ow}) than lower molecular weight aromatic compounds (e.g., BTEX, naphthalenes). In turn, they tend to accumulate in organic-rich substrates (e.g., sediment, soil) and lipid tissues (Gachanja, 2005; Meador et al., 1995). The increased molecular size and the presence of alkyl substituents makes PAH more resistant to microbial degradation (Overton et al., 2016); on the contrary, alkyl groups promote their photooxidative degradation (Radović et al., 2014a). Heteroatom PAH analogs include simple benzothiophenes and dibenzothiophenes (contain S) or carbazoles (contain N), including alkylated species. The introduction of a heteroatom modifies their behavior in comparison with PAH; for example, introduction of nitrogen into an aromatic structure increases water solubility (Pearlman et al., 1984) and enhances the photolysis of the molecule, while the addition of sulfur reduces the photosensitivity of thiophenic species (Radović et al., 2014a).

Much less characterized are the polar, heavy molecular weight, non-hydrocarbon (NSO) oil fractions (see Section 3 above), very abundant in COSR oils and bitumens. Their exact character and environmental behavior are still the subject of contentious research. It would be expected that their large molecular weights limit the

environmental mobility and availability; however, various functional groups in a molecule can change that. Liu and Kujawinski (2015) used FTICR-MS to analyze a broad mass range of compounds solubilized from Macondo well surrogate oil. The water-soluble fraction (WSF) was prepared by mixing water and oil for seven days, after which the bulk oil was removed and the water was filtered through a 0.7 μm filter to remove residual microdroplets of dispersed oil. The FTICR-MS results demonstrated that higher heteroatom to carbon ratio (NSO:C) favors the water solubility, in particular for compounds in the 300–600 Da range (Fig. 19.11). This indicates that the introduction of heteroatoms can change water partitioning of compounds which otherwise would be very hydrophobic, if judged solely based on their carbon number (i.e., molecular weight).

This is also corroborated by various FTICR-MS analyses of OSPW (Barrow et al., 2015; Headley et al., 2010; Quesnel et al., 2015), which demonstrated the presence of oxygen-containing heteroatom compounds, including NAs, and more complex and heavier non-hydrocarbons, which preferentially partition into water during oil sands processing, Fig. 19.7. Once solubilized and concentrated in OSPW, such compounds are more environmentally mobile, with the potential to leach/seep from the tailings ponds to underground, or quickly spread to surface waters in the case of an overflow or a spill. Additional point of concern is that some of the NA compounds have been found to be recalcitrant to biodegradation (Whitby, 2010). However, no comprehensive studies have been done to date to estimate and predict the type and proportions of high molecular weight non-hydrocarbon constituents of COSR heavy oils and bitumen which may transfer to water after a spill. In addition, photooxidation and partial biodegradation of large, alkylated molecules transforms hydrocarbons and non-hydrocarbons to highly functionalized (oxygenated) high-molecular weight polar components, some of which can be solubilized in water and might be contributing to the fraction known as "dissolved organic matter", DOM (Aeppli et al., 2012; Lemkau et al., 2014; Sleighter and Hatcher, 2008).

Studies of post-spill weathering processes revealed that oxygenated transformation products in oil residues seem to persist in the environment for years after the initial oil release (White et al., 2016). Detailed molecular characterization using FTICR-MS revealed that these species are largely non-GC amenable ketone, hydroxyl, and carboxylic acid classes of molecules (Ruddy et al., 2014). Many of those species are similar to oxygen containing compounds found in non-hydrocarbon fractions of COSR oils and bitumens, and OSPW; however, it is still uncertain how similar is their environmental behavior.

In general, the main focus of future research should be a more comprehensive characterization of the polar oil fractions, present in oil sands resources, and further generated by environmental transformations of spilled oil, and/or accumulated in OSPW. Determination of the physicochemical and toxicity properties of this very complex mixture will require both model compound calibration studies and large amounts of modeling based on chemical compositions determined using advanced analytical tools such as FTICR-MS, and others (Longnecker and Kujawinski, 2016). Innovative computational models should aim to derive relationships between chemical structures and physical properties of complex NSO species, in order to reliably assess their ultimate environmental fate.

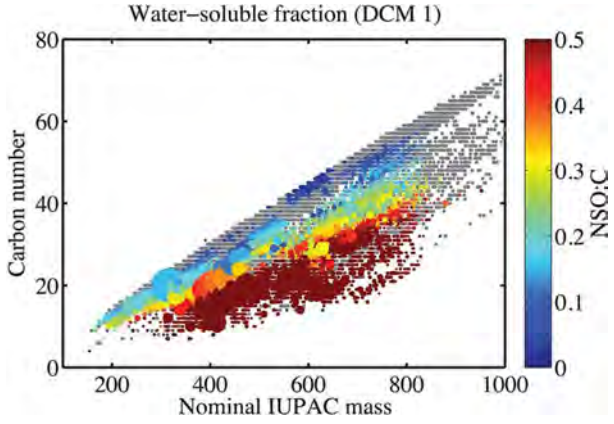

FIGURE 19.11 Carbon number versus nominal mass plot of the dichloromethane extracts of the WSF of the Macondo well oil surrogate. Each *m/z* value with an assigned elemental formula is represented by a dot on the figure. The size of each dot corresponds to relative peak height in the FTICR-MS spectra. Components in the parent oil are plotted in gray to serve as reference. Color bar indicates the ratio of total heteroatoms to carbon atoms (NSO:C). From Liu and Kujawinski (2015), under Creative Commons Attribution License (cc-by).

19.6 ENVIRONMENTAL EFFECTS OF COSR OILS

Complex chemical composition of oil translates to a very diverse range of effects spilled oil can have on organisms; ranging from acute, nonspecific (sub)lethal effects, e.g., narcosis, to more subtle and chronic changes, affecting growth, feeding, and reproduction, which can take years to fully manifest (Martínez-Gómez et al., 2010). In addition, compositional variability caused by postspill weathering transformations can modify the effects of the source oil (Rial et al., 2013).

Past decades have produced an extensive body of research focusing on the effects of the GC-amenable aromatic hydrocarbon oil fraction, in particular, PAH compounds (Hylland, 2006; Neff, 2002). It is well established that two to five-ring PAH are responsible for various toxic effects of oil, both noncarcinogenic (e.g., oxidative stress, endocrine disruption) and carcinogenic (Akcha et al., 1999; Gozgit et al., 2004). For example, in the aftermath of oil release to Wabamun Lake, deBruyn et al. (2007) observed a higher incidence of teratogenic deformities in fish larvae and linked them to exposure to PAH found in oil. More recent studies have also suggested important contributions of alkyl substituted PAH homologs in some of the overall chronic effects of oil (Radović et al., 2014b; Vrabie et al., 2012). As discussed in previous sections, in-reservoir biodegradation of COSR oil resources removed most of the *n*-alkanes, and low molecular weight aromatic compounds, enriching the content of higher ring, substituted PAH. In this context, the aromatic fraction of COSR oils has the potential to exhibit chronic PAH-related adverse effects, in the case of long-term organismal exposure, but few detailed studies have been carried out.

On the other hand, the effects of polar oil fractions and their NSO constituents came into reseach focus only recently, facilitated by the development of novel analytical tools and methods (e.g., High-performance liquid chromatography - mass spectrometry (HPLC-MS), FTICR-MS), able to resolve and characterize this complex pool of non-GC amenable compounds (Hindle et al., 2013; McKenna et al., 2013).

To date, most of the studies investigated the effects of NA, due to the concerns regarding large quantities of produced waters generated in various stages of oil exploitation, in which NAs are readily solubilized and concentrated. What has emerged from numerous studies using both model NA compounds, and real environmental samples, is that the lower molecular weight acids exhibit stronger adverse effects than high molecular weight species and that the aromatic NA analogs have higher toxicity (Fingas, 2014). As an example, Scarlett et al. (2013) showed that aromatic NA fractions of OSPW from a settling pond in the COSR had more pronounced acute toxic effects on zebrafish than the alicyclic fraction (Scarlett et al., 2013). On the other hand, a study demonstrated potential for chronic effects, such as endocrine disruption, of the offshore produced waters released to the North Sea; in this case, one to four-ring alicyclic NAs have been responsible for the bulk of the in-vitro androgenic and estrogenic effects (Thomas et al., 2009).

Many studies in recent years focused on the effects of oils which were altered in the environment, after the spillage, looking in particular at polar, oxygenated transformation products of oil weathering, which have been shown to be enriched and persist in the field, months and years after the initial oil release (Aeppli et al., 2012; White et al., 2016). The weathering processes in the aftermath of the Macondo well (*Deepwater Horizon*) oil spill yielded a mixture of ketones, hydroxyl, and carboxylic compounds—photooxidation and/or biodegradation products of the aromatic oil fraction (Ruddy et al., 2014). Model oxygenated aromatic compounds, such as diones, were previously demonstrated in laboratory tests to be more toxic than the parent molecules (Knecht et al., 2013). Experiments with artificially weathered oils, e.g., irradiated, also showed that resulting chemical alterations can increase the toxicity of the original oil (Maki et al., 2001; Rial et al., 2013).

These observations warrant further research, in order to resolve the outstanding discussions on the environmental mobility of polar degradation products of oil constituents, the mechanisms, and kinetics of their partitioning as well as their bioavailability, potential bioaccumulation, and toxicity, under real postspill conditions (Fingas, 2014; Liu and Kujawinski, 2015). The results of the toxicity tests of polar compounds should be based on and coupled to the advanced molecular characterization studies of NSO fractions in neat and weathered oils, such as the ones discussed in the previous sections.

19.7 CONCLUSION

COSR will remain an important North American oil production area in years to come, which will be mainly transported using existing, or newly constructed pipelines. This is linked to intrinsic risk of incidental oil spills

and releases; however, long-term trends suggest an improving (i.e., decreasing) trend of spilled volumes, relative to the total output of oil from COSR. A small number of spills is responsible for the bulk of released volume, and such spills are often due to pipeline corrosion. Improved corrosion monitoring and prevention could greatly reduce the volumes of released oils in COSR. On the other hand, comparatively, released volumes of oil in COSR are many times smaller than the volumes released during major offshore incidents, or from marine tanker spills.

Heavy, biodegraded oils and bitumens extracted in COSR have unique physicochemical properties, which have important considerations for their postspill behavior and effects. High oil viscosity prevents quick spreading of the spilled oil and facilitates containment, but exacerbates fouling of surfaces. On the other hand, COSR oils are often denser than water, or become so after weathering, which increases the risk of sinking, if they are spilled to aquatic media.

Chemically, COSR oils are enriched in heavier, alkyl-substituted aromatic compounds, and nonhydrocarbons, heteroatom (NSO)-containing fractions which make them, in general, more environmentally persistent. An important fraction of NSO compounds, such as NAs, is water soluble and has the tendency to preferentially partition and concentrate in the produced waters generated during oil sands treatment, which are stored in large volume tailings ponds, creating a long-term environmental liability. On the other hand, many of the high molecular weight, polar NSO species are still poorly characterized, which makes a reliable assessment of their environmental mobility and partitioning challenging.

Effects of COSR oils in the case of a spill would be driven by the heavier aromatic and NSO fraction. Aromatic compounds include higher ring number PAH, including alkylated analogs, many of which have known adverse organismal effects, in particular after prolonged exposure. On the other hand, nonhydrocarbon fractions, e.g., NAs, in particular lower molecular weight, aromatic analogs have also been extensively studied and have observable toxic effects. Similarly as in the case of their chemical composition, the effects of many heavier NSO compounds in polar oil fractions are still largely unknown. Postspill weathering, including photooxidation and biodegradation, transforms the parent oil compounds to novel complex, polar NSO analogs, which in some cases, can increase the oil toxicity and water mobility.

In conclusion, additional research and characterization of the nonhydrocarbon fractions, rich in COSR oils, using advanced analytical tools and methods is warranted and recommended (Fingas, 2014; Lee et al., 2015), in order to address fundamental gaps in the knowledge of their behavior, fate, and effects, and to create better suited response, monitoring and spill remediation measures and strategies.

Acknowledgments

This research was made possible by the Canada Foundation for Innovation (CFI), the Natural Sciences and Engineering Research Council of Canada (NSERC) and Canada Research Chairs (CRC), PRG, and the University of Calgary. We acknowledge the support of Bruker, for the FTICR-MS facility in Calgary, and Aphorist Inc. for the use of FTCIR-MS visualization software Ragnarök.

References

Adams, J., Riediger, C., Fowler, M., Larter, S., 2006. Thermal controls on biodegradation around the Peace River tar sands: Paleo-pasteurization to the west. J. Geochem. Explor. 89 (1–3), 1–4.

Adams, J., Larter, S., Bennett, B., 2013. The dynamic interplay of oil mixing, charge timing, and biodegradation in forming the Alberta oil sands: Insights from geologic modeling and biogeochemistry. Heavy-oil and Oil-sand Petroleum Systems in Alberta and Beyond: AAPG Studies in Geology 64, 23–102.

Aeppli, C., Carmichael, C.A., Nelson, R.K., Lemkau, K.L., Graham, W.M., Redmond, M.C., et al., 2012. Oil Weathering after the Deepwater Horizon disaster led to the formation of oxygenated residues. Environ. Sci. Technol. 46 (16), 8799–8807.

AER, 2012. Alberta's Energy Industry. An overview. Alberta Energy Regulator.

AER, 2013. Report 2013-B: Pipeline Performance in Alberta, 1990–2012. Alberta Enery Regulator.

AER, 2016. ST98-2016. Alberta's Energy Reserves 2015 & Supply/Demand Outlook 2016–2025. Alberta Energy Regulator.

Akcha, F., Burgeot, T., Venier, P., Narbonne, J.F., 1999. Relationship between kinetics of benzo[a]pyrene bioaccumulation and DNA binding in the Mussel Mytilus galloprovincialis. Bull. Environ. Contam. Toxicol. 62 (4), 455–462.

Alberta Land Resource Unit, 2005. Agricultural Land Resource Atlas of Alberta—Soil Groups of Alberta. http://www1.agric.gov.ab.ca/$department/deptdocs.nsf/all/agdex10307#Data.

Andersson, J.T., Schade, T., 2004. Higher alkylated dibenzothiophenes in some crude oils and hydrodesulfurized fuels. ACS Division of Fuel Chemistry, Preprints.

API, 2009. Analysis of U.S. Oil Spillage. API PUBLICATION 356. American Petroleum Institute.

Barrow, M.P., Peru, K.M., Fahlman, B., Hewitt, L.M., Frank, R.A., Headley, J.V., 2015. Beyond naphthenic acids: Environmental screening of water from natural sources and the Athabasca oil sands industry using atmospheric pressure photoionization Fourier transform ion cyclotron resonance mass spectrometry. J. Am. Soc. Mass. Spectrom. 26 (9), 150–1521.

CAPP, 2016. Statistical Handbook for Canada's Upstream Petroleum Industry. Canadian Association of Petroleum Producers.
Daly, K.L., Passow, U., Chanton, J., Hollander, D., 2016. Assessing the impacts of oil-associated marine snow formation and sedimentation during and after the Deepwater Horizon oil spill. Anthropocene 13, 18–33.
deBruyn, A., Wernick, B.G., Stefura, C., McDonald, B.G., Rudolph, B.-L., Patterson, L., et al., 2007. In situ experimental assessment of lake whitefish development following a freshwater oil spill. Environ. Sci. Technol. 41 (20), 6983–6989.
Fingas, M.F., 2014. Analyzing Oxidized and Biodegraded Hydrocarbons. 37th AMOP Technical Seminar, Canmore, NS.
Fustic, M., Bennett, B., Huang, H., Larter, S., 2012. Differential entrapment of charged oil—New insights on McMurray Formation oil trapping mechanisms. Mar. Pet. Geol. 36 (1), 50–69.
Gachanja, A.N., 2005. Polycyclic aromatic hydrocarbons/environmental applications. In: Townshend, A., Poole, C. (Eds.), Encyclopedia of analytical science, 2nd Edition. Elsevier, Oxford, pp. 234–242.
Garverick, L., 1994. Corrosion in the Petrochemical Industry. ASM International.
Gates, I.D., Larter, S.R., 2014. Energy efficiency and emissions intensity of SAGD. Fuel 115, 706–713.
Government of Alberta, 2016. Oil Sands Information Portal. http://osip.alberta.ca/map/.
Gozgit, J.M., Nestor, K.M., Fasco, M.J., Pentecost, B.T., Arcaro, K.F., 2004. Differential action of polycyclic aromatic hydrocarbons on endogenous estrogen-responsive genes and on a transfected estrogen-responsive reporter in MCF-7 cells. Toxicol. Appl. Pharmacol. 196 (1), 58–67.
Green, K.P., Jackson, T., 2015. Safety in the transportation of oil and gas: Pipelines or rail? Fraser Research Bulletin, 1–14, https://www.fraserinstitute.org/research/safety-transportation-oil-and-gas-pipelines-or-rail.
Headley, J.V., Armstrong, S.A., Peru, K.M., Mikula, R.J., Germida, J.J., Mapolelo, M.M., et al., 2010. Ultrahigh-resolution mass spectrometry of simulated runoff from treated oil sands mature fine tailings. Rapid Commun. Mass Spectrom. 24 (16), 2400–2406.
Hindle, R., Noestheden, M., Peru, K., Headley, J., 2013. Quantitative analysis of naphthenic acids in water by liquid chromatography–accurate mass time-of-flight mass spectrometry. J. Chromatogr. A. 1286, 166–174.
Hollebone, B.P., Fieldhouse, B., Sergey, G., Lambert, P., Wang, Z., Yang, C., et al., 2011. The behaviour of heavy oil in a fresh water lake. Proceedings of the 34th AMOP Technical Seminar on Environmental Contamination and Response, pp. 668–709.
Hsu, C.S., Robinson, P., 2007. Practical advances in petroleum processing. Springer, New York.
Hylland, K., 2006. Polycyclic aromatic hydrocarbon (PAH) ecotoxicology in marine ecosystems. J. Toxicol. Environ. Health Part A. 69 (1–2), 109–123.
ITOPF, 2011. Fate of marine oil spills. The International Tanker Owners Pollution Federation.
ITOPF, 2016. Oil tanker spill statistics 2015. The International Tanker Owners Pollution Federation.
John, G.F., Han, Y., Clement, T.P., 2016. Weathering patterns of polycyclic aromatic hydrocarbons contained in submerged Deepwater Horizon oil spill residues when re-exposed to sunlight. Sci. Total Environ. 573, 189–202.
Knecht, A.L., Goodale, B.C., Truong, L., Simonich, M.T., Swanson, A.J., Matzke, M.M., et al., 2013. Comparative developmental toxicity of environmentally relevant oxygenated PAHs. Toxicol. Appl. Pharmacol. 271 (2), 266–275.
Larter, S., Huang, H., Adams, J., Bennett, B., Snowdon, L.R., 2012. A practical biodegradation scale for use in reservoir geochemical studies of biodegraded oils. Org. Geochem. 45, 66–76.
Larter, S.R., Head, I.M., 2014. Oil sands and heavy oil: Origin and exploitation. Elements 10 (4), 277–283.
Lee, K., Boufadel, M., Chen, B., Foght, J., Hodson, P., Swanson, S., et al., 2015. The Royal Society of Canada Expert Panel: The behaviour and environmental impacts of crude oil released into aqueous environments. 461.
Lemkau, K.L., McKenna, A.M., Podgorski, D.C., Rodgers, R.P., Reddy, C.M., 2014. Molecular evidence of heavy-oil weathering following the M/V Cosco Busan Spill: Insights from Fourier transform ion cyclotron resonance mass spectrometry. Environ. Sci. Technol. 48 (7), 3760–3767.
Liu, Y., Kujawinski, E.B., 2015. Chemical Composition and potential environmental impacts of water-soluble polar crude oil components inferred from ESI FT-ICR MS. PLoS. ONE. 10 (9), e0136376.
Longnecker, K., Kujawinski, E.B., 2016. Using network analysis to discern compositional patterns in ultrahigh-resolution mass spectrometry data of dissolved organic matter. Rapid Commun. Mass Spectrom. 30, 2388–2394.
Maki, H., Sasaki, T., Harayama, S., 2001. Photo-oxidation of biodegraded crude oil and toxicity of the photo-oxidized products. Chemosphere 44 (5), 1145–1151.
Manzetti, S., 2013. Polycyclic aromatic hydrocarbons in the environment: Environmental fate and transformation. Polycycl Aromat Compd. 33 (4), 311–330.
Martínez-Gómez, C., Vethaak, A.D., Hylland, K., Burgeot, T., Köhler, A., Lyons, B.P., et al., 2010. A guide to toxicity assessment and monitoring effects at lower levels of biological organization following marine oil spills in European waters. ICES J. Mar. Sci. 67 (6), 1105–1118.
McKenna, A.M., Nelson, R.K., Reddy, C.M., Savory, J.J., Kaiser, N.K., Fitzsimmons, J.E., et al., 2013. Expansion of the analytical window for oil spill characterization by ultrahigh resolution mass spectrometry: Beyond gas chromatography. Environ. Sci. Technol. 47 (13), 7530–7539.
Meador, J.P., Stein, J.E., Reichert, W.L., Varanasi, U., 1995. Bioaccumulation of polycyclic aromatic hydrocarbons by marine organisms. In: Ware, G.W. (Ed.), Reviews of environmental contamination and toxicology: Continuation of residue reviews. Springer, New York, pp. 79–165.
NAS, 2016. Spills of Diluted Bitumen from Pipelines: A comparative study of environmental fate, effects, and response. National Academies of Sciences, Engineering, and Medicine, Washington, DC.
NASA, 2009. Athabasca oil sands: Image of the day. http://earthobservatory.nasa.gov/IOTD/view.php?id = 40997.
National Commission on the BP Deepwater Horizon Oil Spill and Offshore Drilling, 2011. Deep Water. The Gulf Oil Disaster and the Future of Offshore Drilling.
NEB, 2016. Crude Oil and Petroleum Products. https://www.neb-one.gc.ca/nrg/sttstc/crdlndptrlmprdct/index-eng.html.
Neff, J.M., 2002. Chapter 15—Polycyclic Aromatic Hydrocarbons in the Ocean. Bioaccumulation in marine organisms. Elsevier, Oxford, pp. 241–318.
NRC, 2012. Atlas of Canada, Northern Geodatabase (SHP).

Oldenburg, T.B.P., Larter, S.R., Adams, J.J., Clements, M., Hubert, C., Rowan, A.K., et al., 2009. Methods for recovery of microorganisms and intact microbial polar lipids from oil − water mixtures: Laboratory experiments and natural well-head fluids. Anal. Chem. 81 (10), 4130−4136.

Oldenburg, T.B.P., Brown, M., Bennett, B., Larter, S.R., 2014. The impact of thermal maturity level on the composition of crude oils, assessed using ultra-high resolution mass spectrometry. Org. Geochem. 75, 151−168.

Oldenburg, T.B.P., Brown, M., Huang, H., Bennett, B., Larter, S.R., 2017. The controls on the composition of biodegraded oils in the deep subsurface- Part 4. Degradation and production of high molecular weight aromatic and polar species during in-reservoir biodegradation. Organic Geochemistry submitted.

Overton, E.B., Wade, T.L., Radović, J.R., Meyer, B.M., Miles, M.S., Larter, S.R., 2016. Chemical composition of macondo and other crude oils and compositional alterations during oil spills. Oceanography 29 (3), 50−63.

Pan, Y., Liao, Y., Shi, Q., Hsu, C.S., 2013. Acidic and neutral polar NSO compounds in heavily biodegraded oils characterized by negative-ion ESI FT-ICR MS. Energy Fuels 27 (6), 2960−2973.

Pearlman, R.S., Yalkowsky, S.H., Banerjee, S., 1984. Water solubilities of polynuclear aromatic and heteroaromatic compounds. J. Phys. Chem. Ref. Data 13 (2), 555−562.

Peters, K.E., Walters, C.C., Moldowan, J.M., 2005. The Biomarker Guide Volume 2. Cambridge University Press, New York.

Quesnel, D.M., Oldenburg, T.B.P., Larter, S.R., Gieg, L.M., Chua, G., 2015. Biostimulation of oil sands process-affected water with phosphate yields removal of sulfur-containing organics and detoxification. Environ. Sci. Technol. 49 (21), 13012−13020.

Radović, J.R., Dominguez, C., Laffont, K., Diez, S., Readman, J.W., Albaiges, J., et al., 2012. Compositional properties characterizing commonly transported oils and controlling their fate in the marine environment. J. Environ. Monit. 14 (12), 3220−3229.

Radović, J.R., Aeppli, C., Nelson, R.K., Jimenez, N., Reddy, C.M., Bayona, J.M., et al., 2014a. Assessment of photochemical processes in marine oil spill fingerprinting. Mar. Pollut. Bull. 79 (1−2), 268−277.

Radović, J.R., Thomas, K.V., Parastar, H., Díez, S., Tauler, R., Bayona, J.M., 2014b. Chemometrics-assisted effect-directed analysis of crude and refined oil using comprehensive two-dimensional gas chromatography−time-of-flight mass spectrometry. Environ. Sci. Technol. 48 (5), 3074−3083.

Rial, D., Radović, J.R., Bayona, J.M., Macrae, K., Thomas, K.V., Beiras, R., 2013. Effects of simulated weathering on the toxicity of selected crude oils and their components to sea urchin embryos. J. Hazard. Mater. 260, 67−73.

Rodgers, R.P., Marshall, A.G., 2007. Petroleomics: Advanced characterization of petroleum-derived materials by Fourier transform ion cyclotron resonance mass spectrometry (FT-ICR MS). In: Mullins, O.C., Sheu, E.Y., Hammami, A., Marshall, A.G. (Eds.), Asphaltenes, heavy oils, and petroleomics. Springer, New York, pp. 63−93.

Ruddy, B.M., Huettel, M., Kostka, J.E., Lobodin, V.V., Bythell, B.J., McKenna, A.M., et al., 2014. Targeted Petroleomics: Analytical Investigation of Macondo Well Oil Oxidation Products from Pensacola Beach. Energy Fuels 28 (6), 4043−4050.

Scarlett, A.G., Reinardy, H.C., Henry, T.B., West, C.E., Frank, R.A., Hewitt, L.M., et al., 2013. Acute toxicity of aromatic and non-aromatic fractions of naphthenic acids extracted from oil sands process-affected water to larval zebrafish. Chemosphere 93 (2), 415−420.

Schwing, P.T., Romero, I.C., Brooks, G.R., Hastings, D.W., Larson, R.A., Hollander, D.J., 2015. A Decline in Benthic Foraminifera following the Deepwater Horizon Event in the Northeastern Gulf of Mexico. PLoS. ONE 10 (3), e0120565.

Shi, Q., Pan, N., Liu, P., Chung, K.H., Zhao, S., Zhang, Y., et al., 2010. Characterization of sulfur compounds in oilsands bitumen by methylation followed by positive-ion electrospray ionization and Fourier transform ion cyclotron resonance mass spectrometry. Energy Fuels 24 (5), 3014−3019.

Sleighter, R.L., Hatcher, P.G., 2008. Molecular characterization of dissolved organic matter (DOM) along a river to ocean transect of the lower Chesapeake Bay by ultrahigh resolution electrospray ionization Fourier transform ion cyclotron resonance mass spectrometry. Mar. Chem. 110 (3−4), 140−152.

Snyder, J., 2016. Oilsands producers face looming bottleneck, even with Trans Mountain pipeline expansion. Financial Post.

Soto, L.A., Botello, A.V., Licea-Durán, S., Lizárraga-Partida, M.L., Yáñez-Arancibia, A., 2014. The environmental legacy of the Ixtoc-I oil spill in Campeche Sound, southwestern Gulf of Mexico. Frontiers in Marine Science 1 (57).

Thomas, K.V., Langford, K., Petersen, K., Smith, A.J., Tollefsen, K.E., 2009. Effect-directed identification of naphthenic acids as important in vitro xeno-estrogens and anti-androgens in north sea offshore produced water discharges. Environ. Sci. Technol. 43 (21), 8066−8071.

Truu, J., Truu, M., Espenberg, M., Nõlvak, H., Juhanson, J., 2015. Phytoremediation and plant-assisted bioremediation in soil and treatment wetlands: A review. Open Biotechnol. J. 9 (1), 85−92.

Vrabie, C.M., Sinnige, T.L., Murk, A.J., Jonker, M.T.O., 2012. Effect-directed assessment of the bioaccumulation potential and chemical nature of Ah receptor agonists in crude and refined oils. Environ. Sci. Technol. 46 (3), 1572−1580.

Whitby, C., 2010. Microbial naphthenic acid degradation. Adv. Appl. Microbiol. 70, 93−125.

White, H.K., Wang, C.H., Williams, P.L., Findley, D.M., Thurston, A.M., Simister, R.L., et al., 2016. Long-term weathering and continued oxidation of oil residues from the Deepwater Horizon spill. Mar. Pollut. Bull.in press.

Wilhelms, A., Larter, S.R., Head, I., Farrimond, P., di-Primio, R., Zwach, C., 2001. Biodegradation of oil in uplifted basins prevented by deep-burial sterilization. Nature 411 (6841), 1034−1037.

Winter, J., Haddad, R., 2014. Ecological impacts of dilbit spills: Considerations for natural resource damage assessment. Proceedings of the 37th AMOP Technical Seminar on Environmental Contamination and Response, pp. 374−400.

Young, L., 2013. Open Data: Alberta oil spills 1975−2013. http://globalnews.ca/news/622513/open-data-alberta-oil-spills-1975-2013/.

CHAPTER

20

Chemical Fingerprinting Assessment of the Impact to River Sediments Following the Bakken Crude Oil Train Derailment and Fire, Mount Carbon, West Virginia

Scott A. Stout[1], *Joseph Papineau*[2] *and Matthew Adkins*[3]

[1]NewFields Environmental Forensics Practice, LLC, Rockland, MA, United States [2]EnviroScience, Inc., Stow, OH, United States [3]CSX Transportation, Inc., Lithia Springs, GA, United States

BIOGRAPHIES

Dr. Scott A. Stout is an organic geochemist with 28 years of petroleum and coal industry experience. Since receiving his Ph.D. from The Pennsylvania State University in 1988, he has served on the faculty at Southern Illinois University and as a researcher at Unocal Corp. and Battelle Memorial Institute. Since 2004 he has been a Sr. Consultant at NewFields Environmental Forensics, LLC in Massachusetts, serving clients in both government and industry. Dr. Stout has extensive experience in the chemical compositions of natural/shale gas-, crude oil-, coal-, gasoline-, diesel-, and other fuel-derived sources of contamination in terrestrial and aquatic environments. He has authored or coauthored over 150 papers published in scientific journals and scientific textbooks and has provided expert testimony in state, federal, and foreign courts. Along with Dr. Zhendi Wang, he has coedited two editions of the *Oil Spill Environmental Forensics*, also published by Elsevier. He is member of the Society of Environmental Forensics, Oil Spill Identification Network (OSINET; Bonn Agreement), and European Association of Organic Geochemists.

Joseph Papineau is an environmental scientist/biologist with 16 years of experience as a consultant, working principally within the industrial and transportation sectors. Mr. Papineau holds a B.S. from Mount Union College (now the University of Mount Union) and an M.S. from the University of Akron. He currently serves as EnviroScience, Inc.'s senior scientist and practice area manager for emergency response and environmental assessment at the company's Stow, Ohio headquarters. Mr. Papineau specializes in surface water and sediment contaminants and has directed a diverse array of projects, focusing primarily on contaminated media, emergency response, and management of large-scale multidisciplinary collaborations.

Matthew L. Adkins is a Certified Hazardous Materials Manager (CHMM) and is currently employed with CSX Transportation as Manager Environmental Remediation. He received a Bachelor of Science degree from Marshall University in 1994 and a Master of Science in Environmental, Safety, and Health Management from The University of Findlay in 2010. Mr. Adkins has worked in the environmental field for over 20 years and has experience developing training programs, responding to environmental emergencies, and managing large environmental remediation projects. In 2004 and 2013, he was awarded the CSX Chairman's Award of Excellence for his efforts managing multimillion dollar projects within highly public settings. The Association of American Railroads awarded Mr. Adkins its Environmental Excellence Award in 2013.

Oil Spill Environmental Forensics Case Studies.
DOI: http://dx.doi.org/10.1016/B978-0-12-804434-6.00020-3

20.1 INTRODUCTION

The Bakken Shale, located within the Williston Basin of North Dakota and Montana, is one of several major shale resources in the United States that have become economical with the advent of horizontal drilling and hydraulic fracking within the last decade. The Bakken Shale yields mostly liquid "tight" oil, as also do the Permian and Eagle Ford Shale deposits in Texas, whereas the Marcellus/Utica Shale throughout West Virginia, Eastern Ohio, and Pennsylvania yield mostly shale gas. Oil production from the Bakken Shale reached a peak in 2014 (1.2 million barrels per day), but has since declined due to the decline in world oil prices. Transport of the Bakken crude oil to refineries and terminals along the coasts also has been a limiting factor. While the tight oil produced from the Permian Basin and Eagle Ford Shales in Texas are economically transported to Gulf Coast refineries through new and extant pipelines within the State of Texas, pipelines capacity for transporting Bakken Shale oil from North Dakota and Montana to coastal refineries is generally lacking—and the construction of new mid-continent pipelines has been controversial. As a result, Bakken Shale oil has been overwhelmingly transported to refineries and terminals along the West Coast, East Coast, and Gulf Coast by rail (Fig. 20.1).

Rail transport of Bakken crude oil has not been without controversy. Over the past several years train derailments have occurred during which one or more tank cars have ruptured and leaked Bakken crude oil. Owing to the high API gravity (40−43), high Reid vapor pressure (11.5 psi at 38°C), and low flashpoint (<10°C) of Bakken crude oil, even compared to other light oils (Lord et al., 2015), derailments involving Bakken crude oil can result in significant oil fires. In one well-known tragic derailment in July 2013, 47 persons in Lac-Mégantic (Quebec) lost their lives. In addition, because railroad tracks often parallel rivers and other waterbodies, the crude oil spills and accompanying oil fires associated with derailments can also impact ecosystems along and within nearby rivers and waterbodies.

On February 16, 2015, a CSX Transportation train derailed during poor weather (−9°C with 20 cm of recent snow) along a stretch of State Route 61 and the Kanawha River near the town of Mount Carbon, Fayette County, West Virginia. The train included 107 tank cars containing 3.1 million gallons of Bakken crude oil from Manitou, North Dakota to an oil terminal in Yorktown, Virginia (NTSB, 2015). The second through the 28th railcars derailed and through a combination of punctures, valve damage, and thermal tears, the latter caused by a series of violent fireball eruptions, cars 7 to 25 released approximately 362,000 gal of crude oil, although mass balance analysis indicated most oil (~94%) was consumed in the derailment's accompanying oil fires that burned for 30 hours after the accident (Fig. 20.2A; CSX, unpublished). It's estimated that the balance of unburned oil (~22,000 gal) spilled onto

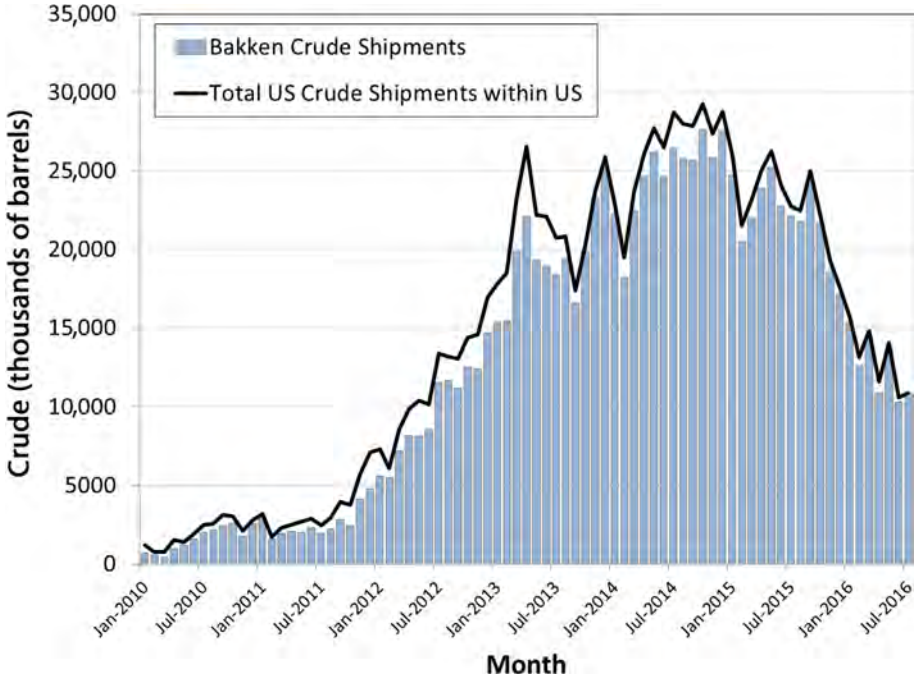

FIGURE 20.1 Trends in the total volume of crude oil shipped monthly by rail within the United States showing that Bakken crude oil comprises the vast majority of the total. *Data compiled from Energy Information Agency.*

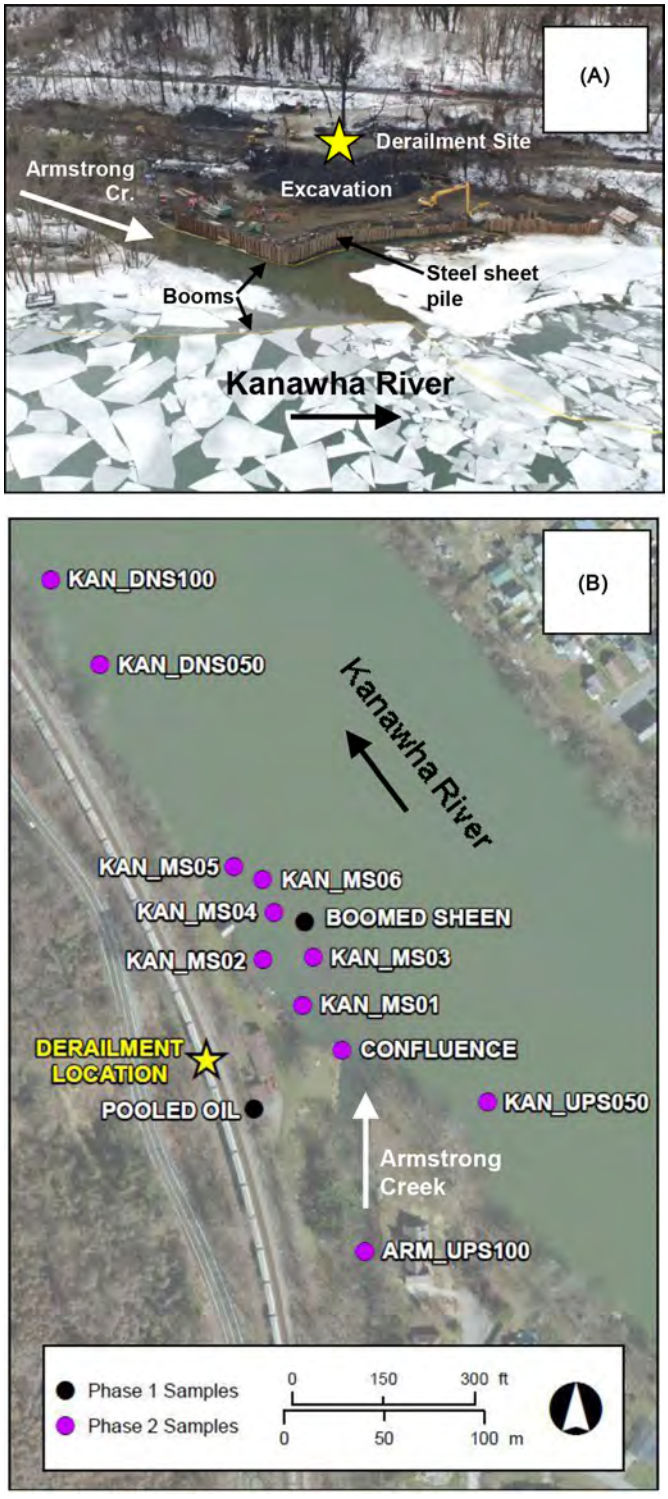

FIGURE 20.2 (A) Aerial photo of the derailment scene, February 25, 2015 and (B) map showing sample locations. Photo in (A) courtesy of CRA Rapid Rovers. Note the presence of large soil excavation at the derailment site and steel sheet pile wall and booms installed, which minimized oil transport to the River. See Table 20.1 for sample descriptions shown in (B).

soils and flowed downslope toward the nearby Kanawha River and Armstrong Creek (Fig. 20.2A). A steel sheet pile wall and floating oil booms installed along the River and Creek shorelines within days of the incident, along with the icy conditions on the River, prohibited unburned oil from impacting the River. Nonetheless, it was necessary to assess any impact of the derailment's oil spill and fires on the sediments in the River.

In this study, we present the results of a chemical fingerprinting assessment surrounding the Mount Carbon derailment oil spill and fires. The objective of the assessment was to determine the hydrocarbon impact, if any, of the spilled Bakken crude oil and fires on sediments from the Kanawha River.

20.2 SAMPLES AND ANALYTICAL METHODS

The study was conducted in two phases (described below). An inventory of the samples from both phases is provided in Table 20.1. The locations of these samples are depicted in the map shown in Fig. 20.2B. During Phase 1, fresh cargo oil and two naturally weathered cargo oils were characterized. The latter included (1) pooled oil collected at the base of the trackside slope immediately below the derailment and (2) a floating sheen collected within the boomed area on the River (Fig. 20.2B). In addition, a reference sheen observed ~650 m upstream of the derailment in the Kanawha River was also collected and studied (Fig. 20.2B). During Phase 2, surface (0–1 cm) sediment samples were collected from the Kanawha River (10) and Armstrong Creek (1). Seven of these 11 sediments were collected near and immediately downstream of the spill site with the remainder collected from two upstream and two downstream locations (Fig. 20.2B).

The samples were prepared and analyzed using methods appropriate for the study's objectives, and which have been described in detail elsewhere (Douglas et al., 2015). Prior to analysis, the samples were prepared as described in the next paragraph.

Briefly, oils were diluted in dichloromethane (DCM) and spiked with recovery and surrogate internal standards prior to analysis. The sheen and sediments samples were spiked with recovery surrogates and serially extracted (3×) using fresh DCM on a shaker table. Sheen sample extracts were combined, dried with anhydrous Na_2SO_4, concentrated to 1 mL, and spiked with surrogate internal standards prior to analysis. Sediment sample extracts were combined, filtered through glass wool, dried with anhydrous Na_2SO_4, concentrated to 1 mL, treated

TABLE 20.1 Inventory and Description of Samples Included in Phases 1 and 2 of This Study

Client ID	Matrix	Description
PHASE 1		
CBTX-742201	NAPL	Fresh cargo oil
Pooled oil	NAPL	Pooled oil on embankment
Sheen boom	Sheen	Sheen within boom on river
Sheen reference	Sheen	Upstream reference sheen
PHASE 2		
KAN-DNS100	Sediment	Downstream river
KAN-DNS050	Sediment	Downstream river
KAN-MS06	Sediment	Midstream/spill area
KAN-MS05	Sediment	Midstream/spill area
KAN-MS04	Sediment	Midstream/spill area
KAN-MS03	Sediment	Midstream/spill area
KAN-MS02	Sediment	Midstream/spill area
KAN-MS01	Sediment	Midstream/spill area
CONFLUENCE	Sediment	Creek/river confluence
KAN-UPS050	Sediment	Upstream river
ARM-UPS100	Sediment	Upstream Armstrong Creek

Phase 1 samples all collected on Feb. 27, 2015. Phase 2 samples all collected on Sept. 29, 2015.

with activated copper to remove sulfur, silica gel-cleaned using EPA Method 3630C, reconcentrated to 1 mL and spiked with surrogate internal standards prior to instrument analysis.

All samples were analyzed using the following:

1. A modified EPA Method 8015D to determine the total extractable hydrocarbon (TEH) concentration (C_9–C_{44}) and concentrations of individual *n*-alkanes (C_9–C_{40}) and selected (C_{15}–C_{20}) acyclic isoprenoids (e.g., pristane and phytane), while simultaneously providing a detailed fingerprint via high resolution gas chromatography–flame ionization detection (GC/FID).
2. A modified EPA Method 8270C employing GC/mass spectrometry (selected ion monitoring mode; GC/MS-SIM) to determine the concentrations of 66 semivolatile compounds or compound groups, included decalins, Priority Pollutant polycyclic aromatic hydrocarbons (PAHs), alkylated PAHs, and sulfur-containing aromatics. The total PAH (TPAH) concentrations reported represent the sum of the concentrations of 51 analytes (excluding retene) ranging from naphthalene through benzo(*ghi*)perylene. The total Priority Pollutant PAH (PPAH) represents the sum of 16 Priority Pollutant PAHs. (Table 20.3, presented later in the chapter, provides of list of PAH analytes, including those identified as PPAH.)
3. A modified EPA Method 8270D using GC/MS-SIM was used to determine the concentration of 53 tri-, tetra- and penta-cyclic triterpanes, regular and rearranged steranes, and triaromatic steroids (TAS). The concentration of a conservative internal marker, viz., 17α(*H*),21β(*H*)-hopane (hopane), was used to calculate percent mass depletions/enrichment of other hydrocarbons (Prince et al., 1994). This was accomplished using the following equation:

$$\%\ \text{Depletion of } A = [((A_0/H_0) - (A_s/H_s))/(A_0/H_0)] \times 100 \tag{20.1}$$

where A_s and H_s are the concentrations of analyte A and hopane in the sample, respectively, and A_0 and H_0 are the concentrations of analyte A and hopane in the fresh cargo oil.

Finally, the fresh cargo oil and pooled oil were also analyzed using the following:

4. A modified EPA Method 8260B to measure 88 volatiles ranging from C_5 to C_{13} from five major hydrocarbon classes, paraffins, isoparaffins, aromatics, naphthenes, and olefins (PIANO).

For each of the analyses above, a method blank (B), lab control sample (LCS), LCS duplicate (LCSD), sample duplicate (D), and reference oil were prepared and analyzed for quality control.

20.3 RESULTS AND DISCUSSION

Tabulated data discussed below are compiled in Table 20.2. The following sections present the results of Phases 1 and 2 separately.

20.3.1 Phase 1

GC/FID analysis showed the fresh cargo oil contained hydrocarbons ranging from C_5 up to $\sim C_{40}$ (Fig. 20.2A). [Compounds $<C_5$ were assuredly present in the cargo oil but these highly volatile compounds were not analyzed as part of this fingerprinting study, which focused on liquid oil.] Compounds spanning this range were dominated by *n*-alkanes that decreased in abundance with increasing carbon number, which is typical of fresh crude oils. The prominence of gasoline range compounds ($<C_{12}$) indicates the fresh cargo oil was a very "light" crude oil, a known feature of the Bakken crude oils (Wybenga, 2014). The specific concentrations specific volatiles present in the fresh cargo oil were revealed by the PIANO analysis (Table 20.2).

Not surprisingly the pooled oil below the derailment and sheen collected from within the boomed area on the Kanawha River (Fig. 20.2B) were comprised of weathered cargo oil (Fig. 20.3B and C). These oils exhibited a loss of volatiles due to the combined effects of natural evaporation and distillation enhanced by the fire. The latter was revealed by a depletion of *n*-alkanes (relative to hopane; per Eq. (20.1)) extending up to approximately *n*-C_{30}; i.e., far beyond losses reasonably attributable to natural evaporation (especially given the low ambient temperatures and solar radiation that existed in the area during the spill; Fig. 20.4). However, such losses are consistent with spilled crude oils that are intentionally burned as a remedial action, in the process known as *in situ* burning (Garrett et al., 2000; Stout and Payne, 2016). Of practical importance is the fact that the combined effect of natural

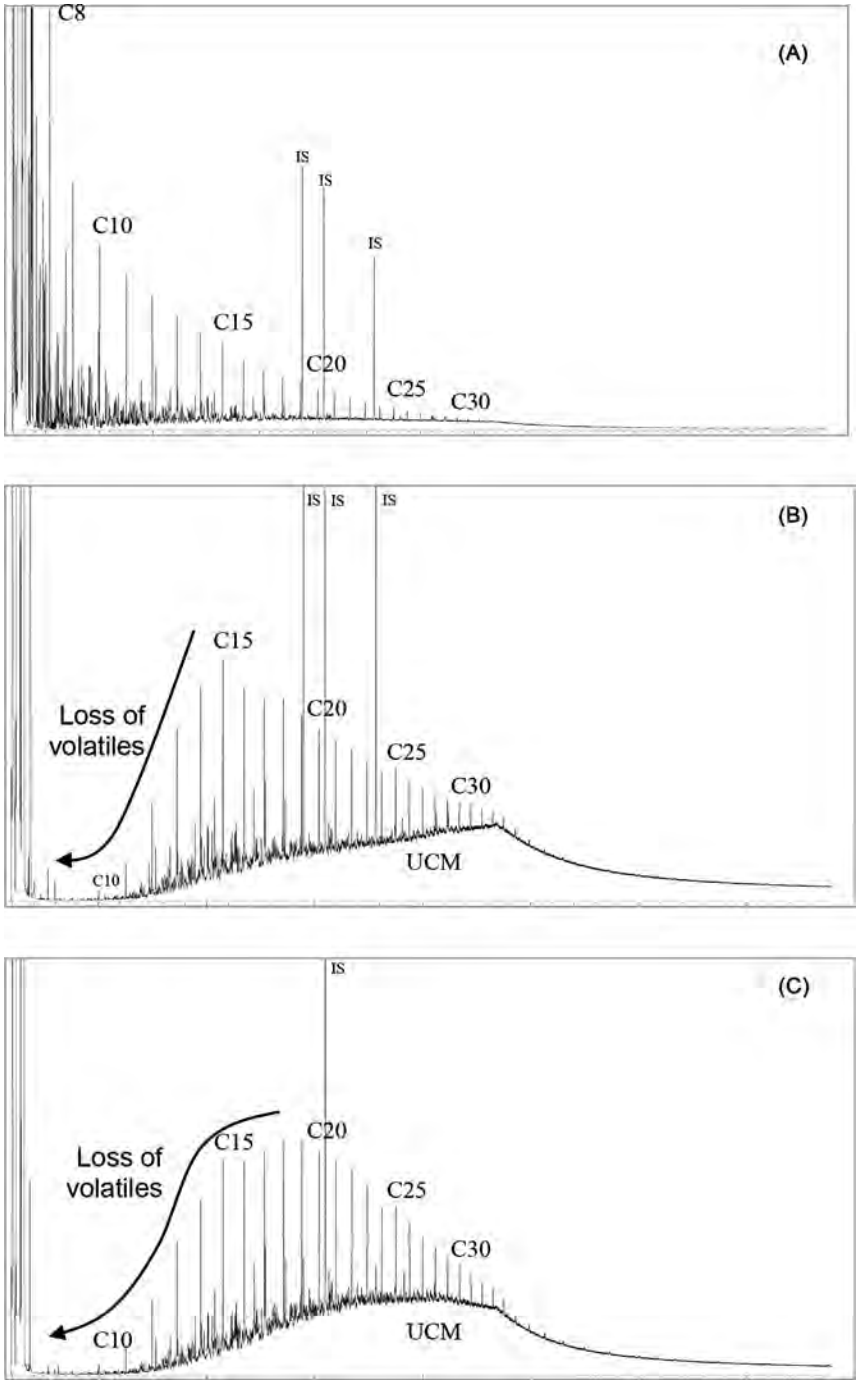

FIGURE 20.3 Gas chromatograms of (A) fresh cargo oil, (B) weathered oil pooled near the tracks, and (C) weathered oil from a sheen in boomed area of the Kanawha River. #, *n*-alkane carbon number; *UCM*, unresolved complex mixture; *IS*, internal standard.

evaporation and the derailment's accompanying fire caused the loss of virtually all volatile hydrocarbons in the weathered oils below C_{10} (Fig. 20.3B and C), including the BTEX compounds in the pooled oil (Table 20.2).

The fresh cargo oil contained 8665 mg/kg of TPAH and 360 mg/kg of PPAH. The pooled oil and oil sheen within the boom area contained 6667 and 11,043 mg/kg of TPAH and 405 to 530 mg/kg of PPAH, respectively, i.e., both lower and higher concentrations than in the fresh cargo oil (Table 20.2). This is not surprising as evaporation initially increases the concentration of PAH but as the more volatile PAHs are subsequently evaporated (or consumed via fire), the PAH concentration is reduced relative to the fresh oil. The PAH were dominated by

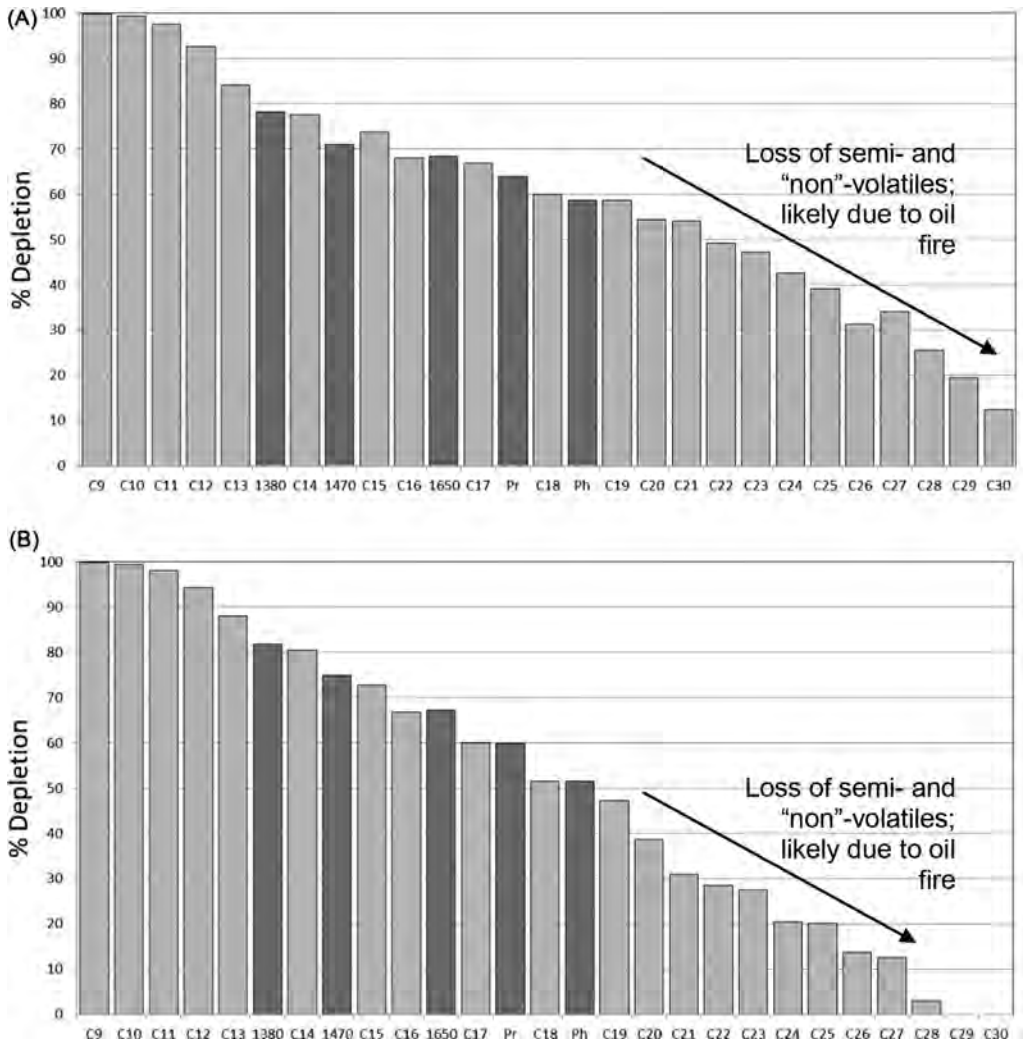

FIGURE 20.4 Histograms showing the percent mass depletion (loss) of *n*-alkanes and isoprenoids per Eq. (20.1) in the (A) weathered oil pooled near the tracks and (B) weathered oil from a sheen in boomed area of the Kanawha River relative to the fresh cargo oil. *Light gray*—*n*-alkanes; *dark gray*—isoprenoids. Loss of typically non-volatiles argues losses due to the spill's associated oil fire, which led to greater losses in the pooled oil (A) than oil sheen (B).

2- and 3-ring low molecular weight PAHs (LPAHs), which comprised 90% of the TPAH (Table 20.2), and in turn, were dominated by alkyl-naphthalenes and alkyl-phenanthrenes (Fig. 20.5A). These alkyl homologue groups exhibit a characteristic "bell-shaped" pattern that is typical of petroleum-derived (petrogenic) PAHs (Boehm, 2006). In contrast, combustion-derived (pyrogenic) PAHs have alkyl homologue groups that exhibit "skewed" patterns with much higher percentages of nonalkylated (parent) PPAH comprising the TPAH.

The evaporative loss of the volatile decalins (D0−D4) and alkyl-naphthalenes (N0−N4) was evident in both weathered oil (Fig. 20.5B and C) and resulted in a lower %LPAH in the weathered oils (77%−78%) than in the fresh cargo oil (90%; Table 20.2). The unweathered alkyl homologue groups in the weathered oils (e.g., P0−PA4) still exhibit the characteristic "bell-shaped" pattern typical of petroleum-derived (petrogenic) PAHs (Fig. 20.6).

Notably, a minor amount of "extra" PPAH were present in both weathered oils (Fig. 20.5B and C), e.g., "extra" fluoranthene (FL0) and pyrene (PY0) are present compared the fresh cargo oil. The presence of "extra" PPAH can be more easily seen when the % depletions for the PAHs are calculated (Fig. 20.6). Most homologues show a typical weathering loss that decreases with increasing degree of alkylation. However, numerous other Priority Pollutant PAHs were enriched (i.e., show negative % depletions) in the weathered oils, which (along with evaporation of naphthalenes) increased the percentage of PPAH in the weathered oils (Table 20.2).

The enrichment of numerous Priority Pollutant (nonalkylated) PAHs in the weathered oils (Fig. 20.6) clearly indicates these pyrogenic PPAH were produced during the spill's fire. While this enrichment may seem

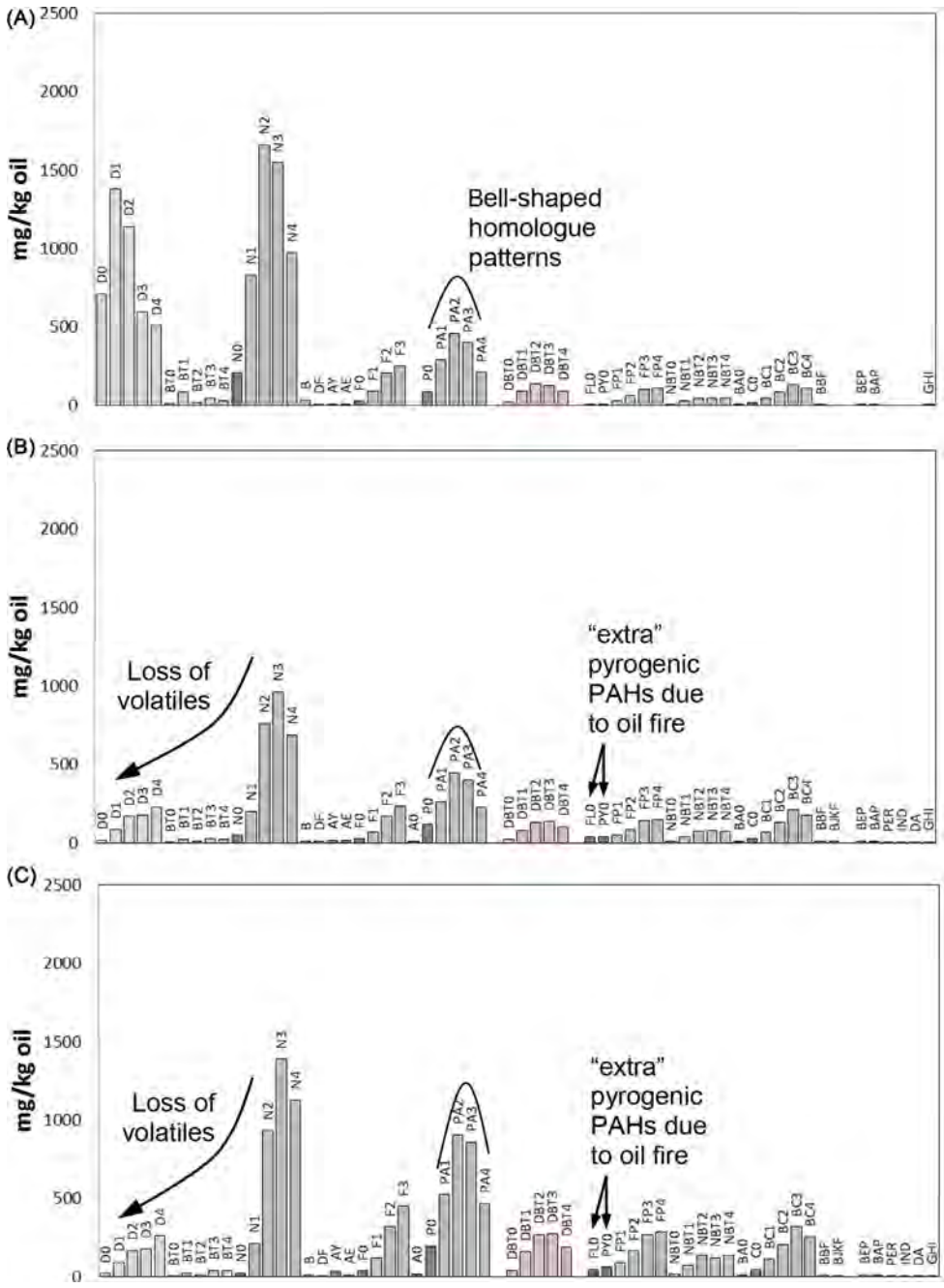

FIGURE 20.5 Histograms of PAH and sulfur-containing aromatics in (A) fresh cargo oil, (B) weathered oil pooled near the tracks, and (C) weathered oil from a sheen in boomed area of the Kanawha River. *Dark gray*—Priority Pollutant PAH; *pink (BT#, DBT#, and NBT#)*: sulfur-containing aromatics. See Table 20.3 (below) for analyte abbreviations.

"problematic" in terms of any potential ecological impact to the environment, it is important to look at the *total* mass balance (and not just individual PPAHs). Specifically, when the total depletion of all PPAHs is calculated (Eq. (20.1)), it was shown that the two weathered oils studied had actually lost 44 and 49 wt% of the PPAH originally present in the fresh cargo oil (Table 20.2). This results from the fact that naphthalene, the most abundant PPAH in the fresh oils (Fig. 20.3A) was significantly depleted in the weathered oil (~90%; Fig. 20.6). The "extra" PPAH produced during the oil fire were still only present in relatively low concentrations among the total PAH (Fig. 20.5B and C). Thus, while the oil fire may seem like it produced "extra" PPAHs, the fire actually reduced the total Priority Pollutant PAHs by nearly half (44 and 49 wt%; Table 20.2) from what was originally present.

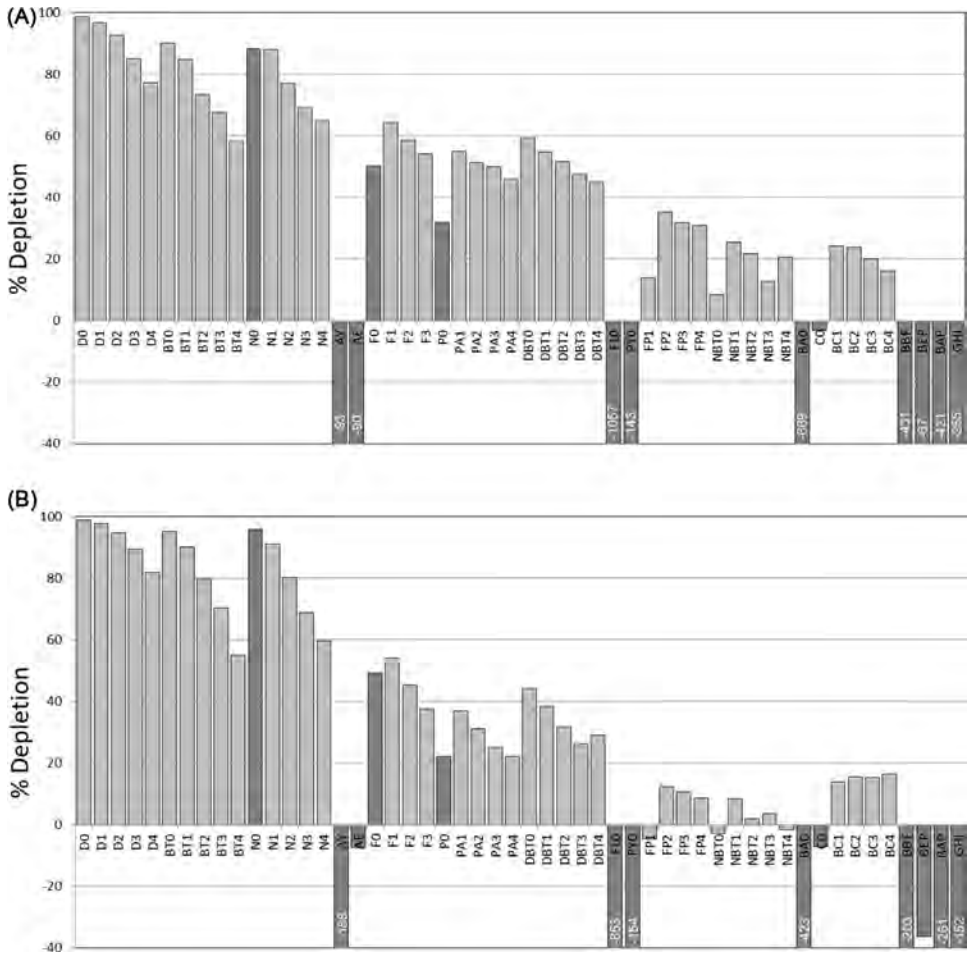

FIGURE 20.6 Histograms showing the percent depletion relative to hopane of PAH and sulfur-containing aromatics in (A) weathered oil pooled near the tracks and (B) weathered oil from a sheen in boomed area of the Kanawha River. *Dark gray*—Priority Pollutant PAH. %Depletions calculated per Eq. (20.1). Negative % depletion = % enrichment; off-scale values given in "white text". All analytes showing enrichment are Priority Pollutant PAHs. See Table 20.3 for analyte abbreviations and text for further description.

Similarly, total PAHs (TPAH) were reduced between 41 and 59 wt% (Table 20.2). This degree of reduction in PPAH and TPAH has also been observed in spilled oils that were intentionally burned (Garret et al., 2000; Stout and Payne, 2016).

A diagnostic feature revealed by the PAH results was the relative abundance of sulfur-containing aromatics (S-PAH) in the fresh and weathered source oil (*pink bars* in Fig. 20.5). These compounds' abundance was expressed by ratios between alkyl-dibenzothiophenes and alkyl-phenanthrenes (DBT2/PA2 and DBT3/PA3).

The fresh and weathered cargo oils had DBT2/PA2 and DBT3/PA3 ratios of ~0.30 and 0.32, respectively (Table 20.2).

Petroleum biomarkers are high boiling compounds that are resistant to weathering and highly specific to individual crude oils, and therefore are widely used in oil spill fingerprinting (Wang et al., 2006). As they are high boiling (~C_{30}), they are present in relatively low concentrations in the light Bakken cargo oil; e.g., hopane is present in a concentration of only ~13 mg/kg (T19 in Fig. 20.7A; Table 20.2). The concentration of hopane increased in the weathered oils (Table 20.2) allowing calculation of total mass loss of the pooled oil and oil sheen in the boom area (41–45 and 59 wt%, respectively; Table 20.2).

More importantly than the increased concentrations, the biomarker fingerprint of the fresh cargo oil (Fig. 20.7A) was unchanged in the weathered oils (Fig. 20.7B and C). Numerous biomarker diagnostic ratios remained stable during weathering allowing the two weathered oils to still be recognized and "matched" to the cargo oil (Table 20.2). These ratios will be used in Phase 2 for comparison to sediments from the River.

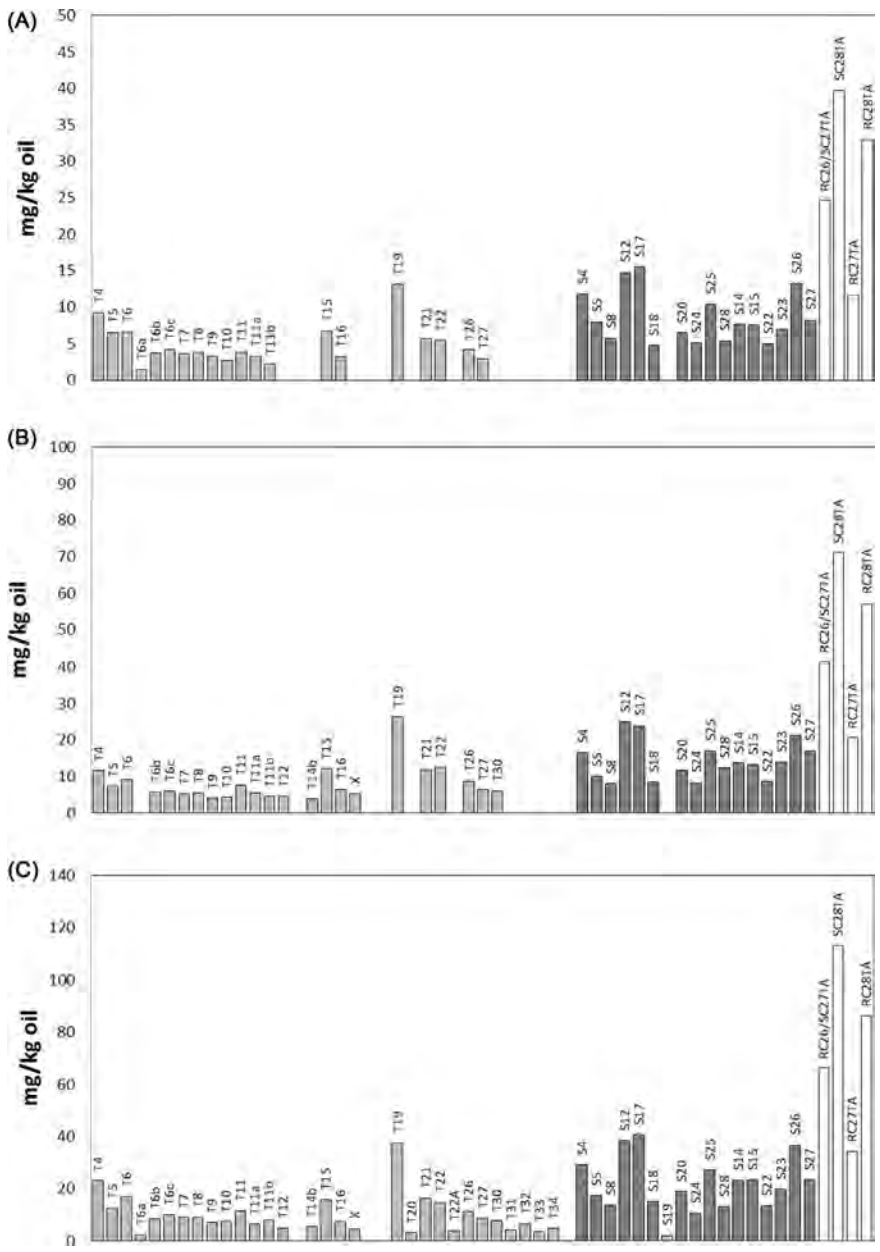

FIGURE 20.7 Histograms showing concentrations of biomarkers in (A) fresh cargo oil, (B) weathered oil pooled near the tracks, and (C) weathered oil from a sheen in boomed area of the Kanawha River. There is a good "match" between the samples indicating that weathering has not affected the biomarkers' utility for fingerprinting. *Light gray*—triterpanes; *dark gray*—steranes; *white*—TAS. *Note*: T19 = 17α(*H*),21β(*H*)-hopane (hopane).

Finally, the oil sheen collected upstream of the derailment in the Kanawha River (Fig. 20.2) exhibited a distinct chemical character revealed in its disparate GC/FID chromatograms, PAH histogram, and biomarker histogram (not shown). Every feature of this oil sheen was distinct from the fresh or weathered cargo oils discussed above (Figs. 20.2–20.5; Table 20.2). The upstream oil sheen exhibited features consistent with a severely weathered middle distillate petroleum (e.g., diesel fuel or fuel oil #2)—not Bakken or any other crude oil. Therefore, it was clear that the upstream oil sheen studied herein was unrelated to the crude oil spilled during the derailment. The existence of oil sheen, ~650 m upstream of the derailment (Fig. 20.2), was important as it indicates the Kanawha River is subject to input of petroleum from (at least one) other source(s).

TABLE 20.2 Tabulated Data for the Samples Studied in Phase 1 (left) and Phase 2 (right)

						DOWNSTREAM			MIDSTREAM							UPSTREAM	
	Fresh Cargo Oil	Pooled Oil	Pooled Oil (dup)	Boomed Sheen	Upstream Reference Sheen	KAN-DNS100	KAN-DNS100 (dup)	KAN-DNS050	KAN-MS06	KAN-MS05	KAN-MS04	KAN-MS03	KAN-MS02	KAN-MS01	CONFLUENCE	KAN-UPS050	ARM-UPS100
		NAPL	NAPL	Sheen	Sheen	Sediment	Sediment	Sediment	Sediment	Sediment	Sediment	Sediment	Sediment	Sediment	Sediment	Sediment	Sediment
TOC, TEH and Alkanes																	
TEH (C9-C44) (mg/kg)	576000	497000	528000	749000	982000	98	101	76	159	433	119	41	258	212	98	135	48
nC17/Pristane	1.7	1.5	1.6	1.6	0.1	0.8	0.7	0.9	0.8	1.2	0.9	1.1	0.8	0.6	0.9	0.9	1.0
nC18/Phytane	1.7	1.6	1.6	1.7	0.0	3.6	3.1	3.4	2.2	2.6	3.0	4.9	2.0	1.8	0.8	3.1	nc
Pristane/Phytane	1.4	1.2	1.3	1.2	1.4	3.9	4.0	3.7	3.4	3.5	4.0	2.9	3.4	3.6	0.8	3.8	nc
Carbon Preference Index	1.1	1.0	1.0	1.1	1.4	2.1	3.4	2.5	2.5	4.4	3.3	1.0	3.3	1.6	1.1	1.4	1.4
Volatiles (mg/kg)																	
Total Volatiles	190276	2267	na	na	na	na	na	na	na	na	na	na	na	na	na	na	na
Total Monoaromatics	19281	245	na	na	na	na	na	na	na	na	na	na	na	na	na	na	na
Total BTEX	8584	12	na	na	na	na	na	na	na	na	na	na	na	na	na	na	na
Benzene	917	nd	na	na	na	na	na	na	na	na	na	na	na	na	na	na	na
Toluene	2640	2	na	na	na	na	na	na	na	na	na	na	na	na	na	na	na
Ethylbenzene	757	nd	na	na	na	na	na	na	na	na	na	na	na	na	na	na	na
Total Xylenes	4270	11	na	na	na	na	na	na	na	na	na	na	na	na	na	na	na
PAH and S-PAH																	
TPAH (Σ51) (mg/kg)	8665	6667	6899	11043	3405	6.1	6.1	4.4	9.1	16.5	4.6	2.3	9.6	19.5	17.0	9.6	3.5
PPAH (Σ16) (mg/kg)	360	405	418	530	75	1.7	1.5	1.1	2.6	4.8	1.2	0.5	2.6	5.8	8.4	2.0	0.7
%TEH as TPAH	1.5	1.3	1.3	1.5	0.3	6.3	6.0	5.7	5.7	3.8	3.9	5.7	3.7	9.2	17.3	7.1	7.5
%TPAH as PP PAH	4.2	6.1	6.1	4.8	2.2	28.0	24.5	25.1	28.4	29.0	24.9	21.4	27.3	29.6	49.6	21.1	19.1
%TEH as PP PAH	0.1	0.1	0.1	0.1	0.0	1.8	1.5	1.4	1.6	1.1	1.0	1.2	1.0	2.7	8.6	1.5	1.4
%LPAH of TPAH	90	77	77	78	99	57	56	61	56	54	59	70	56	60	41	64	66
%HPAH of TPAH	10	23	23	22	1	43	44	39	44	46	41	30	44	40	59	36	34
%Petrogenic	97	91	91	92	96	63	65	66	62	61	66	73	63	62	38	69	74
%Pyrogenic	3	9	9	8	4	37	35	34	38	39	34	27	37	38	62	31	26
MPI 1	0.7	0.6	0.6	0.6	1.0	0.5	0.5	0.5	0.5	0.5	0.5	0.5	0.5	0.5	0.4	0.6	0.5
MPR	0.9	0.9	0.9	0.9	1.1	1.2	1.2	1.3	1.3	1.3	1.3	1.3	1.3	1.4	1.8	1.3	1.3
AN/P0	0.0	0.10	0.10	0.10	0.00	0.05	0.07	0.06	0.11	0.10	0.08	0.04	0.09	0.09	0.25	0.02	0.04
FL/PY	0.21	0.98	1.00	0.77	1.19	1.38	0.93	1.10	1.15	1.17	1.10	1.09	1.15	1.28	1.35	0.90	0.98
BaA/C0	0.06	0.46	0.46	0.30	0.26	0.43	0.55	0.57	0.72	0.67	0.59	0.47	0.67	0.72	1.07	0.38	0.44
DBT2/PA2	0.30	0.30	0.29	0.30	0.53	0.10	0.09	0.10	0.11	0.11	0.11	0.12	0.12	0.10	0.11	0.09	0.10
DBT3/PA3	0.32	0.34	0.33	0.32	0.67	0.13	0.11	0.13	0.14	0.14	0.14	0.17	0.16	0.11	0.15	0.11	0.14
Biomarkers																	
Hopane (T19; ug/kg)	13100	26300	28600	37600	44100	41	27	25	40	91	27	10	52	72	20	34	13
Total Triterpanes (ug/kg)	96280	180750	195890	292700	343500	272	239	192	310	1134	308	64	548	399	106	185	75
Total Steranes (ug/kg)	136400	228870	237960	366340	216880	60	43	40	66	178	51	22	113	98	33	49	29
Total TAS (ug/kg)	109100	190200	200400	299600	48010	24	18	22	34	108	25	10	71	34	13	12	13
Ts/Tm (T11/T12)	nc	1.7	1.8	2.4	0.9	0.3	0.4	0.3	0.4	0.4	0.5	0.5	0.5	0.3	0.4	0.3	0.5
H29/H29-Ts (T15/T16)	2.1	1.9	2.1	2.1	3.1	6.6	4.6	6.4	6.0	5.0	4.5	4.2	5.5	9.0	7.2	9.1	4.7
H29/Hop (T15/T19)	0.5	0.46	0.44	0.42	0.77	0.7	0.8	0.8	0.7	0.9	0.8	0.7	0.8	0.7	0.7	0.6	0.7
Tricyclics/Hop (ΣT7-10)/T19	1.0	0.73	0.75	0.86	0.00	0.0	0.1	0.1	0.1	0.2	0.1	0.2	0.2	0.1	0.1	0.0	0.1
Total Steranes/Hop	10	8702	8320	9743	4918	1.5	1.6	1.6	1.6	2.0	1.9	2.2	2.2	1.4	1.7	1.5	2.2
Total TAS/Hop	8	7232	7007	7968	1089	0.6	0.7	0.9	0.8	1.2	0.9	1.0	1.4	0.5	0.7	0.3	1.0
Percent Depletions in Weathered Oil (relative to hopane; Eq. 1)																	
TEH	0	100	100	100	na	nc	nc	nc	nc	nc	nc	nc	nc	nc	nc	nc	nc
TPAH (51)	nc	62	64	56	na	nc	nc	nc	nc	nc	nc	nc	nc	nc	nc	nc	nc
PP PAH (16)	nc	44	47	49	na	nc	nc	nc	nc	nc	nc	nc	nc	nc	nc	nc	nc
LPAH	nc	67	69	61	na	nc	nc	nc	nc	nc	nc	nc	nc	nc	nc	nc	nc
HPAH	nc	16	19	5	na	nc	nc	nc	nc	nc	nc	nc	nc	nc	nc	nc	nc

na - not analyzed
nc - not calculable
(dup) - laboratory duplicate

Percent depletions of weathered oil in sediments not calculated because no oil was present in sediments.

20.3.2 Phase 2

The sediments studied in Phase 2 each contained TEHs that ranged in concentration from 41 to 434 mg/kg (Table 20.2). The character of the TEH was revealed by the GC/FID chromatograms, which are shown in Fig. 20.8. Inspection of the sediments' chromatograms reveals them to be distinct from those of the fresh and weathered cargo oils (Fig. 20.3)—indicating the spilled oil did not appear to have obviously impacted the sediments (Fig. 20.8). For example, each of the sediments contain some lower boiling hydrocarbons ($<C_{10}$) that were absent (evaporated) from the spilled oil. Although higher boiling *n*-alkanes were present in the oil and sediments, those present in sediments exhibited distinctive profiles compared to the weathered oils, viz., the sediments were dominated by odd-carbon numbered *n*-alkanes above *n*-C_{25} (reflected in the elevated carbon preference indices in the sediments (CPI; Table 20.2). In addition, none of the sediments exhibited a prominent unresolved complex mixture (UCM) typical of weathered oil, and most contained a narrow UCM in the $C_{32}-C_{35}$ region topped by multiple peaks typical of naturally occurring terpenoids (Fig. 20.8). Pristane/phytane ratios in the sediments were much higher than in the spilled oil (Table 20.2).

Collectively, the chromatographic features of the hydrocarbons in sediments of the Kanawha River (and Armstrong Creek) are consistent with mixtures of particulate coal and naturally occurring organic matter (e.g., vegetation debris). There is no evidence for the presence of fresh or weathered crude oil contributing to the sediments' TEH. Notably, both sediments collected upstream of the derailment site contained hydrocarbons derived from particulate coal (not spilled oil), indicating this material is pervasive within the Kanawha River's sediments. The presence of particulate coal (Stout and Mattingly, 2008; Achten and Hofmann, 2009) and naturally occurring organic matter (NOM; Wang et al., 2009; Stout and Uhler, 2006; Stout et al., 2007) in sediments has been widely recognized, but fortunately can be readily distinguished from spilled petroleum (in this case, crude oil). Variability among the coal-dominated TEH fingerprints (Fig. 20.8) likely reflects varying degrees of weathering of the coal, although variable coal rank can also contribute.

Further confirmation regarding the absence of spilled Bakken crude oil in the sediments was obtained from the biomarkers results for the sediments. Fig. 20.9 shows the distributions of triterpane, sterane, and TAS biomarkers in the sediments. There was an obvious disparity in the character of these highly diagnostic compounds in the sediments (Fig. 20.9) and cargo oils (Fig. 20.7) that, like the TEH fingerprints described above, indicated the hydrocarbons in the sediments were not spilled Bakken crude oil. The disparity in biomarkers was quantified by inspection of selected diagnostic ratios among these compounds (Table 20.2). Clearly, the biomarkers in the sediments proximal and downstream of the spill site appeared consistent with those found in the upstream sediment samples recognized to contain particulate coal (Fig. 20.9). Several sediments also contained excessive relative amounts of selected biomarkers (T14b, T20, T26, T32, and T33) relative to the particulate coal (see stippled bars in Fig. 20.9). These particular excesses were attributed to coeluting terpenoids associated with modern NOM (e.g., 17β(*H*),21β(*H*)-hopanoids and other naturally occurring plant/bacteria-derived compounds; e.g., Wang et al., 2009). Thus, as was the case for the TEH, the biomarkers in the Kanawha River sediments were consistent with those derived from mixtures of particulate coal and NOM—not spilled Bakken crude oil).

The Kanawha River and Armstrong Creek sediments all contained PAHs. The concentrations TPAH and PPAH in sediments ranged from 2.3 to 19.5 mg/kg and 0.50 to 8.4 mg/kg, respectively (dry wt.; Table 20.2). Excluding the confluence sediment sample (described below), the %TPAH that occurs as PPAH in each of the sediments ranged from 19.1 to 29.6, which was markedly higher than was represented by the fresh or weathered crude oils (4.2% to 6.1%; Table 20.2). However, the higher percentages were consistent with particulate coal in all of the sediments except the confluence sample (see below). Thus, the varying concentrations of PAH in the sediments largely reflect varying concentrations of particulate coal in the River's sediments.

Fig. 20.10 shows the PAH distributions for the sediments studied. As can be seen there was an obvious disparity between the distribution of PAHs in the sediments (Fig. 20.10) versus the fresh and weathered cargo oils (Fig. 20.5). One set of metrics that quickly revealed this disparity was the DBT2/PA2 and DBT3/PA3 ratios (discussed previous in the Phase 1 results) between the Bakken crude oil ($\sim$0.30 and 0.32, respectively) and the River's sediments (0.09−0.12 and 0.11−0.17, respectively; Table 20.2), which indicated the River's coal contained markedly lower relative amounts of sulfur-containing aromatics than the spilled crude oil. Collectively, the disparity in PAH patterns and characteristics provided no basis to recognize that PAHs from the spilled oil contributed to the PAHs in the River (or Creek) sediments. Instead, most sediments (i.e., except the confluence sample) exhibited PAH distributions consistent with those found in the particulate coal-bearing sediments collected upstream of the derailment/spill site (Fig. 20.10).

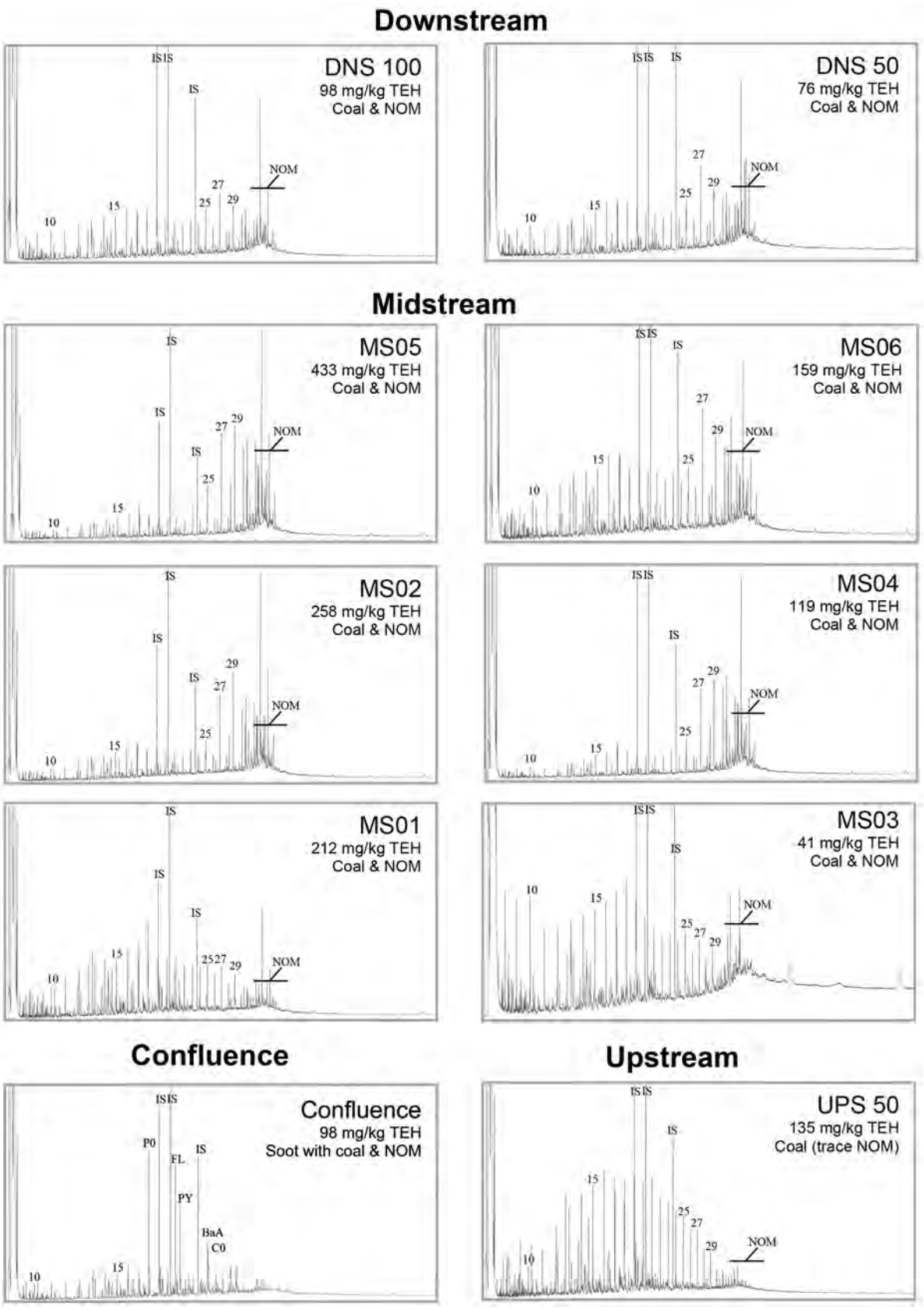

FIGURE 20.8 Gas chromatograms of selected Phase 2 sediment samples. Sediment samples are roughly arranged per location (see Fig. 20.1B). TEH concentration in sediment samples are indicated (Table 20.2) as well as description of TEH origin(s). *NOM*, natural organic matter. #, *n*-alkane carbon number; *UCM*, unresolved complex mixture; *P0*, phenanthrene; *FL*, fluoranthene; *PY*, pyrene; *BaA*, benz(*a*)anthracene; *C0*, chrysene; *IS*, internal standard.

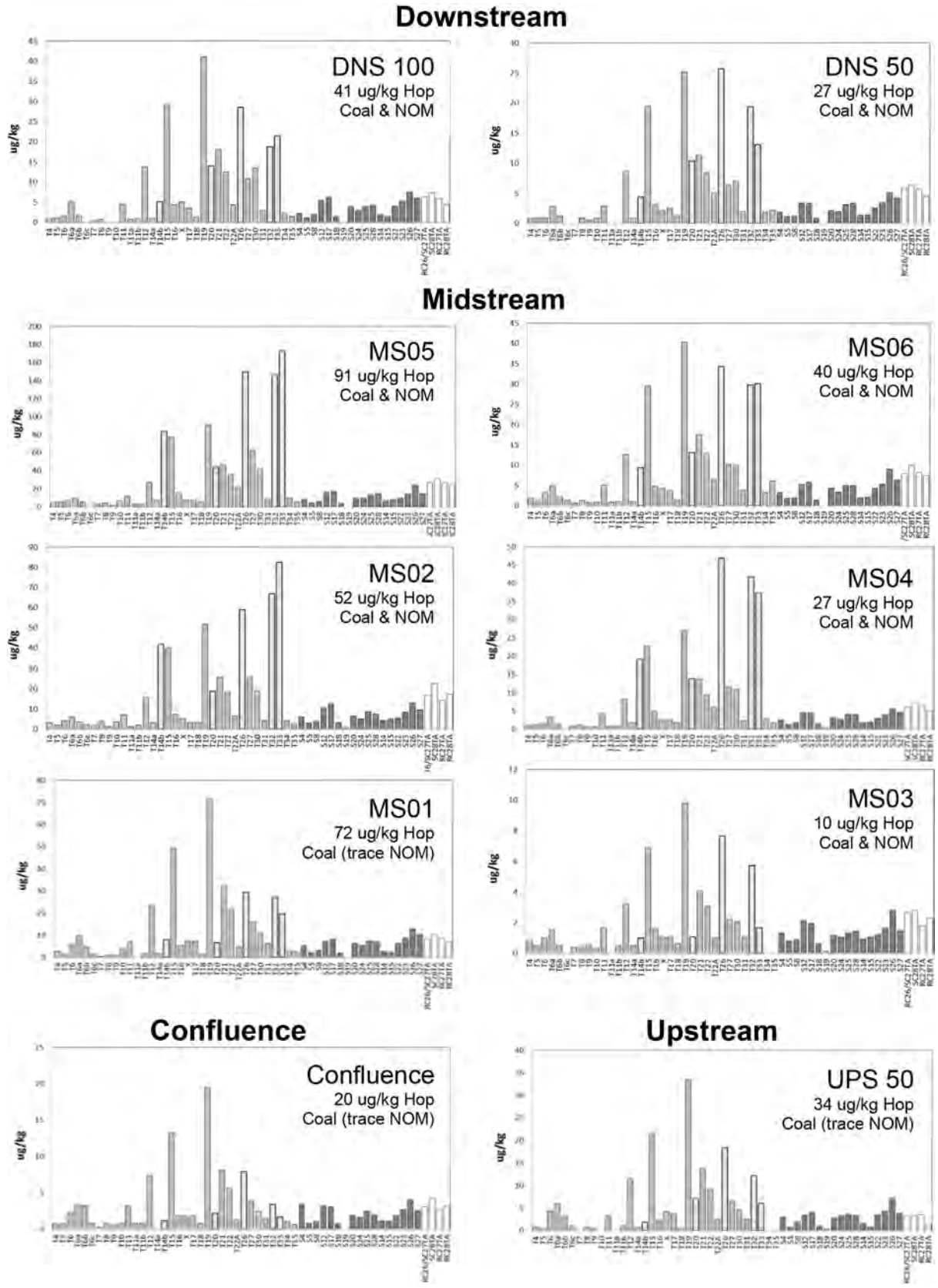

FIGURE 20.9 Biomarker histograms of selected Phase 2 sediment samples. Sediment samples are roughly arranged per location (see Fig. 20.2B). Hopane (Hop) concentration in sediment samples are indicated (Table 20.2) as well as description of biomarker origin(s). *NOM*, natural organic matter. *Light gray*—triterpanes; *dark gray*—steranes; *white*—triaromatic steroids; stippled triterpanes (T14b, 20, 26, 32, & 33) are coeluting with naturally occurring terpenoids in NOM.

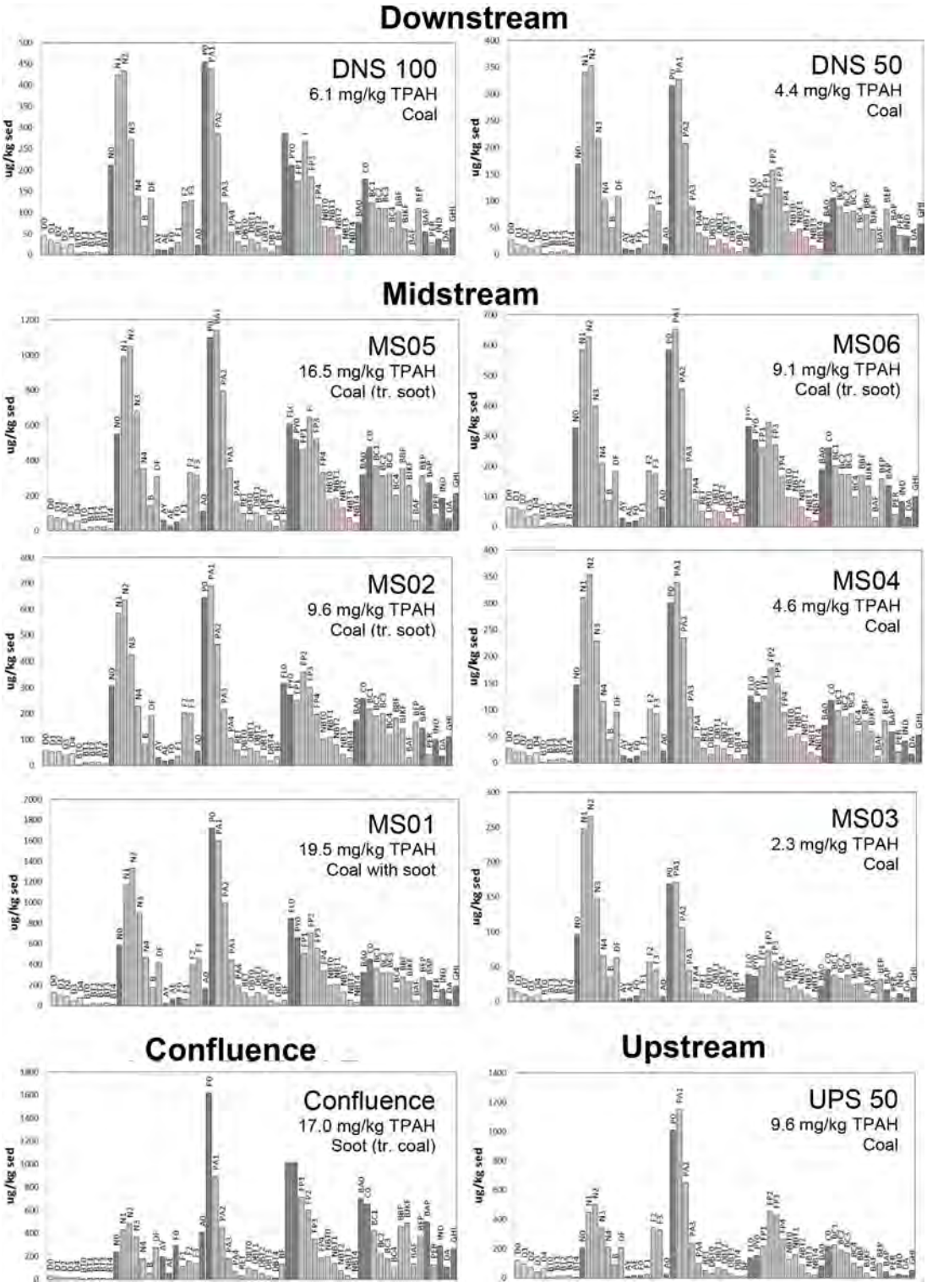

FIGURE 20.10 PAH histograms of selected Phase 2 sediment samples. Sediment samples are roughly arranged per location (see Fig. 20.2B). TPAH concentration in sediment samples are indicated (per Table 20.2) as well as description of PAH origin(s). *Dark gray*—Priority Pollutant PAH; *pink* (BT#, DBT#, NBT#): sulfur-containing aromatics. See Table 20.3 for compound abbreviations.

The confluence sediment sample was unique among the sediments studied (Fig. 20.10). This sediment contained PAHs that, unlike the other sediments, were much more strongly dominated by pyrogenic PAHs. This difference can be seen in the confluence sediment sample's higher %TPAH at PPAH (49.6), % high molecular weight PAHs (59), and % pyrogenic PAHs (62) compared to the other sediments (Table 20.2). In addition, numerous PAH isomer ratios were distinct in this sample (MPR1 through BaA/C0; Table 20.2) indicating that the manner by which the PAHs were formed (i.e., heating conditions during PAH formation) was different (e.g., Yunker et al., 2002). Collectively, these differences indicated that the dominant source of PAHs in the confluence sediment sample were distinct pyrogenic PAHs, such as occur in partially combusted organic matter, i.e., soot particles (Stout et al., 2004).

Soot particles are derived from the combustion of a variety of organic sources. For example, forest fires and combustion engines will each generate pyrogenic PAH-rich soot particles. However, given the circumstances of this investigation, viz., a proximal oil fire in which "extra" PAHs were generated and found to be enriched in the partially combusted oil found pooled below the derailment site (see above; Fig. 20.5B and C), and considering the proximity of the confluence sample in particular to the derailment site (Fig. 20.2B), it is most reasonable to attribute the unique character and elevated concentration of the confluence sediment's PAHs to the deposition of crude oil combustion-derived soot particles generated by the oil fire. Thus, while there is no evidence that the liquid oil itself impacted the Kanawha River sediments there does appear to have been an impact of PAHs generated by the derailment's accompanying oil fire to the sediments. This impact is most obvious at the confluence site (Fig. 20.10) where sheet flow off of the embankment is envisioned to have accumulated soot particles from the fire that burned for 30 hours following the derailment.

The potential contribution of such particles to the other sediments in the River was also investigated. This was achieved by calculating the %depletion of each PAH in the River's sediment samples versus the River's particulate coal—as represented by the upstream River sediment (UPS50). Any "extra" pyrogenic PAHs (relative to the "background" coal in these sediments) in the midstream and downstream sediments might be assumed to represent PAHs derived from soot particles from the oil fire that were deposited in these sediments. The % depletion was calculated using Eq. (20.1), wherein A_0 and H_0 are the concentrations of each PAH analyte, A, and hopane in the UPS50 sediment.

The results of these calculations are provided in Table 20.3 and graphically displayed in Fig. 20.11 for selected sediments (excluding UPS50, wherein all PAHs are, by definition, derived from "background" coal). The *y*-axes on the histograms plotted are shown in reverse order so that any *negative* % depletions (i.e., % enrichments) point upwards. As can be seen the confluence sediment sample exhibits hundreds to thousands percent enrichments of most Priority Pollutant (pyrogenic) PAHs—which was why it was "easy" to recognize the impact of the soot particles on this sediment (Fig. 20.10). The impact of soot particles on the other sediment is less obvious; however,

TABLE 20.3 Calculated Percent Depletion of Individual PAHs in Sediments Relative to UPS050 Sediment Per Eq. (20.1)

PAH analyte	Abbrev	DNS100	DNS050	MS06	MS05	MS04	MS03	MS02	MS01	CONFLUENCE	UPS100
Naphthalene	N0	15	−10	−32	1	11	−61	2	−33	−101	−74
C1-Naphthalenes	N1	23	−1	−8	18	14	−89	15	−22	−65	−129
C2-Naphthalenes	N2	29	6	−4	22	12	−82	17	−24	−66	−109
C3-Naphthalenes	N3	35	16	3	27	17	−48	19	−22	−85	−58
C4-Naphthalenes	N4	47	35	17	38	32	−7	29	−4	−49	−4
Biphenyl	B	40	26	20	44	40	−34	41	9	−2	−42
Dibenzofuran	DF	47	31	27	45	43	−4	41	6	−128	−17
Acenaphthylene	AY	−19	−75	−198	−172	−107	−64	−149	−31	−4064	−38
Acenaphthene	AE	34	23	17	27	27	−18	29	−91	−538	6
Fluorene	F0	5	−6	−11	−28	−11	−97	−2	−148	−3456	−105
C1-Fluorenes	F1	4	−2	0	5	−12	−140	6	−14	−672	−149
C2-Fluorenes	F2	70	64	55	64	63	43	61	46	20	50
C3-Fluorenes	F3	68	67	56	64	65	53	60	35	28	56

(*Continued*)

TABLE 20.3 (*Continued*)

PAH analyte	Abbrev	DNS100	DNS050	MS06	MS05	MS04	MS03	MS02	MS01	CONFLUENCE	UPS100
Anthracene	A0	27	−2	−120	−64	−15	−2	−47	−211	−2751	−5
Phenanthrene	P0	63	58	52	60	63	43	58	20	−176	38
C1-Phenanthrenes/Anthracenes	PA1	69	62	53	63	63	49	61	35	−34	45
C2-Phenanthrenes/Anthracenes	PA2	64	57	42	55	55	44	54	28	−20	39
C3-Phenanthrenes/Anthracenes	PA3	58	51	33	45	46	36	42	13	−29	29
C4-Phenanthrenes/Anthracenes	PA4	57	47	28	41	42	35	33	11	−18	26
Dibenzothiophene	DBT0	44	35	27	33	34	−5	29	−31	−442	−13
C1-Dibenzothiophenes	DBT1	56	48	35	47	43	19	40	15	−94	17
C2-Dibenzothiophenes	DBT2	59	50	27	44	41	23	38	18	−57	28
C3-Dibenzothiophenes	DBT3	52	42	16	31	31	5	18	14	−71	12
C4-Dibenzothiophenes	DBT4	53	46	11	30	27	9	2	15	−48	21
Fluoranthene	FL0	−73	0	−99	−62	−12	3	−48	−187	−1773	26
Pyrene	PY0	−13	17	−56	−25	8	20	−16	−102	−1150	31
C1-Fluoranthenes/Pyrenes	FP1	34	30	0	21	28	20	24	−10	−470	4
C2-Fluoranthenes/Pyrenes	FP2	52	54	37	48	51	45	48	28	−127	32
C3-Fluoranthenes/Pyrenes	FP3	65	62	48	55	57	54	55	40	−39	40
C4-Fluoranthenes/Pyrenes	FP4	64	60	48	53	55	55	51	40	−23	35
Naphthobenzothiophenes	NBT0	58	56	36	48	52	48	48	26	−166	40
C1-Naphthobenzothiophenes	NBT1	66	60	50	57	57	53	55	40	−51	29
C2-Naphthobenzothiophenes	NBT2	60	53	41	47	47	41	44	33	−39	10
C3-Naphthobenzothiophenes	NBT3	48	35	23	23	27	13	18	25	−57	−33
C4-Naphthobenzothiophenes	NBT4	42	28	10	8	18	6	−3	15	−10	−53
Benz[a]anthracene	BA0	23	2	−93	−45	−7	8	−40	−85	−1387	3
Chrysene/Triphenylene	C0	32	35	−1	18	32	27	21	2	−427	17
C1-C hrysenes	BC1	56	47	26	40	46	43	38	26	−220	2
C2-C hrysenes	BC2	53	44	24	39	42	40	34	21	−109	−17
C3-C hrysenes	BC3	47	36	16	30	32	24	24	15	−79	−39
C4-C hrysenes	BC4	49	36	18	26	27	16	22	21	−65	−36
Benzo[*b*]fluoranthene	BBF	−7	−30	−85	−70	−29	−17	−55	−72	−934	−29
Benzo[*j*/*k*]fluoranthene	BJKF	−44	−78	−221	−172	−110	−46	−162	−205	−2302	−28
Benzo[*a*]fluoranthene	BAF	−46	−141	−341	−275	−175	−81	−245	−237	−3933	−60
Benzo[*e*]pyrene	BEP	10	−15	−33	−17	0	−11	−11	−27	−546	−59
Benzo[*a*]pyrene	BAP	−12	−74	−181	−149	−80	−44	−134	−183	−2029	−53
Pyrene	PER	−107	−328	−214	−191	−136	−47	−149	−162	−1858	11
Indeno[1,2,3-cd]pyrene	IND	−32	−97	−198	−190	−116	−66	−174	−219	−2032	−41
Dibenz[ah/ac]anthracene	DA	18	−21	−67	−54	−26	−13	−45	−72	−1056	−38
Benzo[*g*,*h*,*i*]perylene	GHI	−7	−56	−66	−58	−33	−37	−48	−76	−839	−57

(See text for description). Negative depletions indicate enrichments of PAHs not attributable to particulate coal, the overwhelming source of PAHs in the River's sediments. Data are plotted in Fig. 20.11.

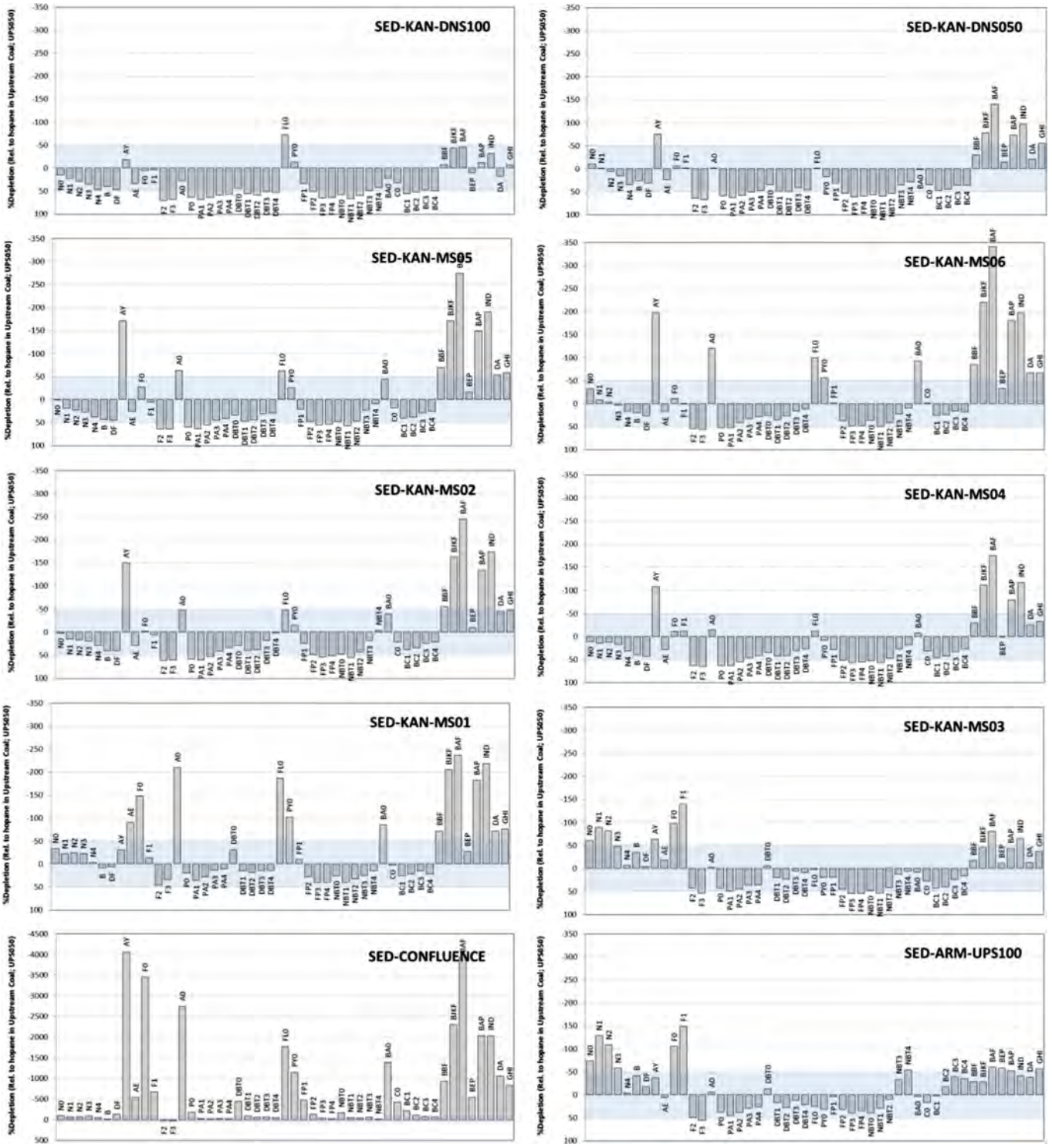

FIGURE 20.11 Histograms showing percent depletions and enrichments of PAH (relative to hopane; Eq. (20.1)) for the sediments relative to "background" coal represented by the UPS50 upstream sediment. Negative % depletions = enrichments. Shaded area depicts general error. PAHs showing significant % enrichments plot upward and extend above *shading*. Enrichments of Priority Pollutant PAHs are evident in the Confluence, MS01, MS02, MS05, and MS06 samples, whereas no enrichments are evident in the MS03, MS04, DNS50, DNS100, or UPS100. *Data from Table 20.3*.

close inspection revealed that there were enrichments of numerous pyrogenic PAHs in the MS01, MS02, MS05, and MS06 sediments. Each of these sediments contains a 100 to about 300% enrichment in acenaphthylene, fluorene, anthracene, fluoranthene, pyrene, benz(*a*)anthracene, and/or multiple 5- and 6-ring PAHs (Fig. 20.11). The location of these sediments suggests soot particles apparently entered the River and were spread downstream toward MS01, MS02, MS05, and MS06 (Fig. 20.2B).

Marginally significant and more sporadic enrichments of a few pyrogenic PAHs were also evident in the MS04 and DNS050 sediments, but these enrichments are equivocal as to whether they actually represent any "extra" PAH deposition or simply limitations of the estimates (e.g., assumed representativeness of the UPS50 upstream sample). This limitation is demonstrated by the marginal enrichment of alkylated naphthalenes in the UPS100 sediment from Armstrong Creek (Fig. 20.11), which was solely due to the higher proportion of these petrogenic PAHs in the particular (possibly less weathered) coal present in this sample (Figs. 20.10 and 20.11). No enrichment of PAHs was evident in the MS03 or DNS100 sediments (Fig. 20.11).

Because the enrichments calculated and depicted in Fig. 20.10 are percentages, they do not reflect the absolute concentrations of any "extra" PAHs due to the deposition of soot particles from the derailment's oil fire. As such, an additional calculation was performed in order to estimate the absolute concentrations of PAHs added to the sediments due to the deposition of soot. This calculation was achieved by first assuming all of the hopane present in any given sediment was derived from coal particles as represented by the upstream sediment containing particulate coal (UPS050). This was a reasonable assumption given that no crude oil was present in any of the sediments (see above; Fig. 20.8) and NOM does not contain nor contribute hopane to sediments; i.e., "background" coal was the overwhelming/only source of PAHs in the sediments (Fig. 20.10). The concentration of each PAH in a given sediments was then normalized to hopane and subtracted from the concentration of that PAH in the UPS050 (upstream) sediment containing "background" coal. Any positive resulting values reflect "extra" PAHs in the sediment that was not attributable to "background" coal.

The results of these calculations are provided in Table 20.4 and graphically displayed in Fig. 20.12. Inspection reveals that, not surprisingly, the confluence sediment sample contains the highest concentrations of "extra" PAHs—not attributable to coal. It was estimated that approximately 7.2 mg/kg of PPAH and 11.4 mg/kg of TPAH were added to this sample due to deposition of soot particles. The particles impart a strong pyrogenic character to the PAHs in this sample, as evidenced by the strongly skewed alkylated homologue patterns (Fig. 20.12).

TABLE 20.4 Calculated Concentrations (μg/kg dry wt) of "extra" PAHs in Sediments Relative to UPS050 Sediment

	DNS100	DNS050	MS06	MS05	MS04	MS03	MS02	MS01	CONFLUENCE	UPS100
N0	0	15	80	0	0	37	0	147	120	58
N1	0	4	44	0	0	117	0	212	170	223
N2	0	0	24	0	0	120	0	261	192	210
N3	0	0	0	0	0	48	0	164	169	76
N4	0	0	0	0	0	4	0	16	59	3
B	0	0	0	0	0	9	0	0	1	15
DF	0	0	0	0	0	2	0	0	154	14
AY	2	5	19	37	7	1	18	5	190	1
AE	0	0	0	0	0	1	0	27	43	0
F0	0	1	2	10	1	4	0	44	283	6
F1	0	0	0	0	2	10	0	8	97	14
F2	0	0	0	0	0	0	0	0	0	0
F3	0	0	0	0	0	0	0	0	0	0
A0	0	0	36	43	3	0	18	111	393	1
P0	0	0	0	0	0	0	0	0	1034	0
PA1	0	0	0	0	0	0	0	0	225	0

(*Continued*)

TABLE 20.4 (*Continued*)

	DNS100	DNS050	MS06	MS05	MS04	MS03	MS02	MS01	CONFLUENCE	UPS100
PA2	0	0	0	0	0	0	0	0	76	0
PA3	0	0	0	0	0	0	0	0	41	0
PA4	0	0	0	0	0	0	0	0	11	0
DBT0	0	0	0	0	0	0	0	20	79	2
DBT1	0	0	0	0	0	0	0	0	38	0
DBT2	0	0	0	0	0	0	0	0	18	0
DBT3	0	0	0	0	0	0	0	0	11	0
DBT4	0	0	0	0	0	0	0	0	3	0
FL0	123	1	165	233	14	0	102	550	1420	0
PY0	25	0	103	105	0	0	37	333	1021	0
FP1	0	0	0	0	0	0	0	45	590	0
FP2	0	0	0	0	0	0	0	0	335	0
FP3	0	0	0	0	0	0	0	0	98	0
FP4	0	0	0	0	0	0	0	0	36	0
NBT0	0	0	0	0	0	0	0	0	122	0
NBT1	0	0	0	0	0	0	0	0	47	0
NBT2	0	0	0	0	0	0	0	0	21	0
NBT3	0	0	0	0	0	0	0	0	11	4
NBT4	0	0	0	0	0	0	1	0	1	4
BA0	0	0	91	98	5	0	50	147	652	0
C0	0	0	3	0	0	0	0	0	531	0
BC1	0	0	0	0	0	0	0	0	290	0
BC2	0	0	0	0	0	0	0	0	119	13
BC3	0	0	0	0	0	0	0	0	79	26
BC4	0	0	0	0	0	0	0	0	38	14
BBF	7	17	78	145	18	4	65	117	414	9
BJKF	19	20	93	162	31	5	87	153	468	4
BAF	3	6	24	43	8	1	22	29	133	1
BEP	0	11	39	45	0	3	16	57	314	22
BAP	6	22	88	162	26	5	83	157	475	8
PER	14	27	28	57	12	2	25	38	119	0
IND	9	17	55	119	22	4	62	108	274	4
DA	0	2	13	23	3	1	11	24	97	2
GHI	4	21	39	77	13	5	36	80	239	11
PPAH	187	104	785	1070	125	63	505	1886	7239	94
TPAH	212	170	1023	1360	165	384	634	2853	11350	742

"Extra" PAHs are not attributable to particulate coal, the overwhelming source of PAHs in the River's sediments, but more likely to soot particles attributed to the derailment oil fire. Only the five shaded samples clearly contain "extra" PAH exceeding two times that of UPS100 upstream sediment, and thereby are considered significant and indicative of the addition of soot particles to the Confluence, MS01, MS02, MS05, and MS06 sediments. (See text for description). Data are plotted in Fig. 20.12.

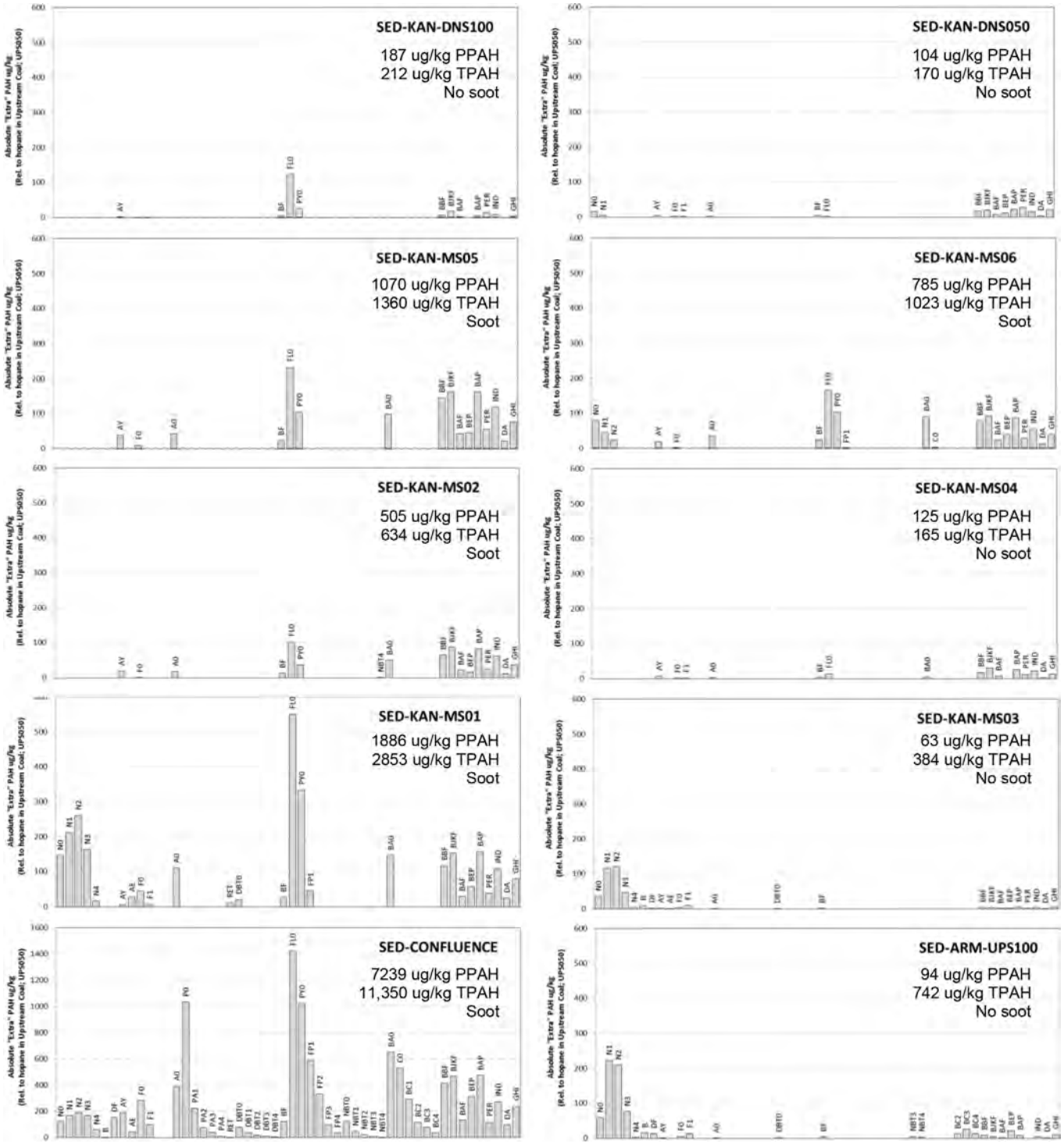

FIGURE 20.12 Histograms showing the estimated concentrations of "extra" (noncoal derived) PAH present in sediments potentially attributed to soot from the oil fire and/or variation in the nature of the coal particles. Extra PPAHs and TPAH from soot are only evident in the Confluence, MS01, MS02, MS05, and MS06 samples. Other samples reflect variation in nature of "background" coal in the region, as represented by the presence of "extra" PAH in the upstream UPS100 sample. *Data from Table 20.4*.

Not surprisingly given its immediately downstream location (Fig. 20.2B), the MS01 sediment contained the next highest concentrations of "extra" PAHs due to the presence of soot particles, viz., approximately 1.9 and 2.9 mg/kg of PPAH and TPAH, respectively (Table 20.4). These were dominated by fluoranthene and pyrene (Fig. 20.12). Further downstream, the MS02, MS05, and MS06 sediments contained even lower concentrations of "extra" PAHs ranging from 0.5 to 1.1 mg/kg PPAH and 0.6 to 1.3 mg/kg of TPAH (Table 20.4). Sediments collected further downstream at DNS100 and DNS050 contained very low concentrations of "extra" PPAH (187 and 104 μg/kg; Table 20.4), which were generally comparable to those observed in the sediment upstream in Armstrong Creek (94 μg/kg; Table 20.4). Thus, these low concentrations cannot be reasonably attributed to the deposition of soot particles at DNS100 or DNS050, but are more likely due to variations in the nature of the "background" coal in the River.

In summary, the overall spatial pattern in the concentrations of "extra" PAHs in sediments attributed to soot particles (Confluence $\ggg$ MS01 $>$ MS02 ~ MS05 ~ MS06 $>$ DNS100 ~ DNS050) indicate that PAH-bearing soot particles generated during the derailment's oil fire were mostly deposited near the confluence of Armstrong Creek and the Kanawha River and were spread downstream to have only a minor impact at MS01, MS02, MS05, and MS06.

20.4 CONCLUSIONS

Phase 1 of the chemical fingerprinting assessment of the fresh Bakken cargo oil and two weathered equivalents spilled during the February 16, 2015 train derailment in Mount Carbon, West Virginia provided for the following conclusions:

1. The fresh cargo oil was a light, highly volatile crude oil typical of Bakken crude oil that was prone to evaporation and combustion.
2. The fresh cargo oil contained 917 mg/kg of benzene, 8584 mg/kg of total BTEX, 8665 mg/kg of total PAH (TPAH) and 360 mg/kg of Priority Pollutant PAH (PPAH).
3. Numerous diagnostic features of the fresh cargo oil were measured (Table 20.2; Figs. 20.3–20.7), which were used in assessing the potential presence of Bakken oil residues in sediments of Armstrong Creek and Kanawha River during Phase 2 of the study.

   Chemical analysis of two weathered oils collected adjacent to and 11 days after the derailment (i.e., oil pooled near the track and an oil sheen within the boomed area of the Kanawha River; Fig. 20.2B) showed the weathered oils:
4. contained virtually no volatile compounds ($<C_{10}$), including the BTEX compounds, which were lost to evaporation.
5. had lost between about half to two-thirds (50% to 65%) of their total mass overwhelming due to evaporation, which was enhanced by the accompanying oil fire.
6. contained 6667 and 11,043 mg/kg of TPAH and 405 and 530 mg/kg of PPAH, the concentration of which varied depending upon the extent of evaporation.
7. contained minor amounts of "extra" combustion-derived (pyrogenic) PPAH that formed during the spill's accompanying oil fire. Although some specific PPAH were "extra", the total masses of TPAH and PPAH in the weathered oils were significantly reduced compared to the fresh cargo oil (56% to 64% and 44% to 49%, respectively). Thus, the accidental burning of the spilled oil reduced the total mass of PAH present in the unburned weathered oils by about half.
8. contained petroleum biomarkers that were consistent with the fresh cargo oil, despite the effects of evaporation and combustion, which were used in assessing the potential presence of Bakken oil residues in sediments of Armstrong Creek and Kanawha River during Phase 2 of the study.

   Chemical analysis of an oil sheen collected ~650 m upstream of, and 11 days after, the derailment on the Kanawha River showed the upstream (reference) sheen (Fig. 20.2B) was:
9. comprised of severely weathered middle distillate (diesel fuel or fuel oil #2) that was unrelated to the derailment's spilled oil. The existence of this distinct sheen indicates petroleum discharges to the Kanawha River were not unique to the derailment.

Phase 2 of the chemical fingerprinting assessment showed sediments throughout the study area:

10. contained TEHs (41 to 434 mg/kg) that are exclusively derived from variable mixtures of particulate (eroded) coal and naturally occurring organic matter (NOM; e.g., plant debris), which were ubiquitous in the River and Creek sediments.
11. did not contain liquid crude oil derived from the spilled cargo oil. The absence of fresh or weathered crude oil in the sediments was revealed by numerous diagnostic features of the sediments that were inconsistent with the fresh or weathered crude oil (Phase 1) and consistent with upstream coal-bearing sediment. Thus, any liquid oil that may have entered the Creek/River during the derailment did not accumulate in the sediments studied.
12. also did not contain middle distillate petroleum potentially attributable to the upstream (sheen) source recognized in Phase 1 (see #9 above).
13. contained TPAH concentrations that ranged from 2.3 to 19.5 mg/kg and PPAH concentrations that ranged from 0.50 to 8.4 mg/kg. The varying concentrations of TPAH largely reflect varying concentrations of particulate coal in the sediments. However, the highest concentrations of combustion-derived (pyrogenic) PPAH were found in sediment collected nearest the derailment, i.e., at the confluence of Armstrong Creek and the Kanawha River (confluence location; Fig. 20.2B).

Sediment collected proximal to the derailment/fire at the confluence of the Armstrong Creek and Kanawha River:

14. clearly contained elevated concentrations of "extra" combustion-derived (pyrogenic) PPAH that, in the absence of any other known source(s) and the observed presence of "extra" PPAH in the weathered oils (#7 above), were reasonably attributable to the deposition of PPAH-rich soot particles that were generated from the derailment's accompanying oil fire (that accumulated at the bottom of the embankment near the confluence).

Close inspection and calculations of the PAH distributions and concentration data from other River sediments—after accounting for the contribution of PAHs from "background" coal (as represented by the upstream River sediment; UPS050)—revealed:

15. only minor "extra" combustion-derived (pyrogenic) PPAH were present at the Ms01 location (Fig. 20.2B), indicating the impact of soot particles generated from the oil fire extended, but decreased downstream of the confluence.
16. traces of "extra" combustion-derived PPAH appeared also present in sediments from MS02, MS05, and MS06 (Fig. 20.2B).
17. no "extra" PAH appear to be present in sediments from MS03, MS04, DNS50, or DNS100 (Fig. 20.2B).

Estimates of the absolute concentrations of "extra" (noncoal derived) combustion-derived PAHs attributed to soot from the derailment's 30-hour long oil fires, which consumed ~94% (vol) of the spilled oil, showed:

18. the confluence sediment received approximately 7.2 mg/kg of PPAH and 11.4 mg/kg of TPAH from the soot that was deposited, probably via sheet flow off of the embankment.
19. the MS01 sediment location received approximately 1.9 and 2.9 mg/kg of PPAH and TPAH, respectively.
20. the MS02, MS05, and MS06 locations received between approximately 0.5 to 1.1 mg/kg PPAH and 0.6 to 1.3 mg/kg of TPAH.
21. downstream sediments at DNS050 and DNS100 received no "extra" PAHs from soot.

In summary, the only chemical impact of the derailment, oil spill, and oil fires on Kanawha River sediments recognized from this study was the addition of oil fire-derived, PAH-bearing soot particles to surface sediments within a limited "footprint" evident within the River (confluence, MS01, MS02, MS05, and MS06).

References

Achten, C., Hofmann, T., 2009. Native polycyclic aromatic hydrocarbons (PAH) in coals—a hardly recognized source of environmental contamination. Sci. Total. Environ. 407, 2461–2473.

Boehm, P.D., 2006. In: Murphy, B., Morrison, R. (Eds.), Environmental Forensics: A Contaminant Specific Approach. Elsevier Publishing Co., San Francisco, CA (Chapter 15).

CSX, unpublished. Mass balance analysis, Mount Carbon, West Virginia, Feb. 16, 2015 derailment. In: Internal Report. CSX Transportation, Inc.

Douglas, G.S., Emsbo-Mattingly, S.D., Stout, S.A., Uhler, A.D., McCarthy, K.J., 2015. Chemical fingerprinting methods. In: Murphy, B.L., Morrison, R.D. (Eds.), Introduction to Environmental Forensics, third ed. Acad. Press, Boston, pp. 201–309.

Garrett, R.M., Guénette, C.D., Haith, C.E., Prince, R.C., 2000. Pyrogenic polycyclic aromatic hydrocarbons in oil burn residues. Environ. Sci. Technol. 34 (10), 1934–1937.

Lord, D.A., Luketa, A., Wocken, C., Schlasner, S., Aulich, T., Allen, R., et al., 2015. Literature survey of crude oil properties relevant to handling and fire safety in transport. In: Sandia Report SAND2015-1823. Sandia National Laboratories.

National Transportation Safety Board, 2015. Tank car performance factual report, CSX Transportation, Mount Carbon, West Virginia. In: NTSB No. DCA15FR005, Report dated July 8, 2015. Washington, D.C. <https://dms.ntsb.gov/public/57500-57999/57593/578436.pdf> (accessed 29.12.16.).

Prince, R.C., Elmendorf, D.L., Lute, J.R., Hsu, C.S., Haith, C.E., Senius, J.D., et al., 1994. 17α(*H*),21β(*H*)-hopane as a conserved internal marker for estimating the biodegradation of crude oil. Environ. Sci. Technol. 28 (1), 142–145.

Stout, S.A., Emsbo-Mattingly, S.D., 2008. Concentration and character of PAHs and other hydrocarbons in coals of varying rank—implications for environmental studies of soils and sediments containing particulate coal. Org. Geochem. 39, 801–819.

Stout, S.A., Payne, J.R., 2016. Chemical composition of floating and sunken in-situ burn residues from the *Deepwater Horizon* oil spill. Mar. Pollut. Bull. 108 (1–2), 186–202.

Stout, S.A., Uhler, A.D., 2006. Distinguishing "background" hydrocarbons from contamination using chemical fingerprinting. Environ. Claims J. 15 (2), 241–259.

Stout, S.A., Uhler, A.D., Emsbo-Mattingly, S.D., 2004. Comparative evaluation of background anthropogenic hydrocarbons in surficial sediments from nine urban waterways. Environ. Sci. Technol. 38, 2987–2994.

Stout, S.A., Liu, B., Millner, G.C., Hamlin, D., Healey, E., 2007. Use of chemical fingerprinting to establish the presence of spilled crude oil in a residential area following Hurricane Katrina, St. Bernard Parish, Louisiana. Environ. Sci. Technol. 41, 7242–7251.

Wang, Z., Stout, S.A., Fingas, M., 2006. Forensic fingerprinting of biomarkers for oil spill characterization and source identification (Review). Environ. Forens. 7 (2), 105–146.

Wang, Z., Yang, C., Kelley-Hooper, F., Hollebone, B.P., Peng, X., Brown, C.E., et al., 2009. Forensic differentiation of biogenic organic compounds from petroleum hydrocarbons and petrogenic compounds cross-contaminated soils and sediments. J. Chromat. A 1216, 1174–1191.

Wybenga, F., 2014. A survey of Bakken crude oil characteristics assembled for the U.S. Department of Transportation. In: Am. Fuel & Petrochemical Manufacturers Report to U.S. DOT, dated May 14, 2014. <https://www.nrt.org/sites/2/files/AFPM%20–%20Survey%20of%20Crude%20Oil%20Characteristics.pdf> (accessed 15.02.15.).

Yunker, M.B., Macdonald, R.W., Vingarzan, R., Mitchell, R.H., Goyette, D., Sylvestre, S., 2002. PAHs in the Fraser River basin: a critical appraisal of PAH ratios as indicators of PAH source and composition. Org. Geochem. 33, 489–515.

CHAPTER

21

The Pixel-Based Chemometric Approach for Oil Spill Identification and Hydrocarbon Source Differentiation: Two Case Studies From the Persian Gulf

Kristoffer G. Poulsen, Mette Kristensen, Giorgio Tomasi, Majbrit Dela Cruz and Jan H. Christensen

University of Copenhagen, Frederiksberg, Zealand, Denmark

BIOGRAPHIES

Kristoffer G. Poulsen (born in Hillerød, Denmark, 1988) graduated in 2016 with a master's degree in Environmental Chemistry and Health and has since been employed in the Analytical Chemistry group, Department of Plant and Environmental Sciences, University of Copenhagen, Denmark. He has since 2014 been working with hydrocarbon fingerprinting including oil spill identification, source apportionment and geochemistry.

Mette Kristensen (born in Copenhagen, Denmark, 1988) is a PhD student in analytical chemistry at the Department of Plant and Environmental Sciences, University of Copenhagen, Denmark. She holds a master degree in Environmental Chemistry and Health (2014) and has been working with environmental analytical chemistry for 4 years, especially with oil hydrocarbon fingerprinting and the CHEMSIC approach (CHEMometric analysis of sections of Selected Ion Chromatograms). Her current research focus on oil degradation in extreme marine environments and the analysis of polar components in oil by comprehensive two-dimensional gas chromatography high resolution mass spectrometry.

Giorgio Tomasi obtained his MSc in Environmental Sciences in 2000 at the University of Milan Bicocca, Italy, and was awarded a PhD in chemometrics in 2006 by The Royal Veterinary and Agricultural University of Frederiksberg, Denmark. He is assistant Professor at the University of Copenhagen in the department of Plant and Environmental Sciences, section for Environmental Chemistry and Physics. He is the author of more than 20 publications on chemometrics, and oil fingerprinting, and contributed to the realization of several Matlab-based software packages for chromatographic signal processing and chemometric data analysis.

Majbrit Dela Cruz is research coordinator in the Analytical Chemistry group at Department of Plant and Environmental Sciences, University of Copenhagen, Denmark. She has a PhD in horticulture where she used the CHEMSIC method for analysis of plant mediated removal of volatile gasoline compounds.

Jan H. Christensen (born in Hillerød, Denmark, 1973) is a Full Professor in Environmental Analytical Chemistry. He is leader of the Analytical Chemistry group, Department of Plant and Environmental Sciences, University of Copenhagen, Denmark and heads the Research Centre for Advanced Analytical Chemistry (RAACE). He has pioneered cutting-edge analytical and chemometric methods for oil hydrocarbon fingerprinting and now works on all aspects of contaminant fingerprinting, petroleomics, and metabolomics. He develops

Oil Spill Environmental Forensics Case Studies.
DOI: http://dx.doi.org/10.1016/B978-0-12-804434-6.00021-5

analytical platforms and new tools to handle and process complex data from cutting-edge analytical instrumentation and apply this chemical fingerprinting concept for analysis of complex mixtures of organic contaminants and in numerous industry project collaborations with the petrochemical, environmental, and food industry. He has authored and coauthored more than 70 peer-reviewed papers and book chapters on these topics. His current research focus is on development and application of multidimensional chromatography platforms in combination with chemometric data analysis.

21.1 INTRODUCTION

Modern chromatographic systems can separate hundreds or thousands of individual compounds, but size and complexity of the derived chromatographic data can increase exponentially depending on the separation and detection method. This is especially true for complex mixtures of compounds, and often makes visual inspection and manual integration not viable even for datasets comprised of few tens of samples. Thanks to the advancement in computation power and informatics, (semi)automated methods have been devised to extract information from such complex data, which can be used for chemical fingerprinting analyses.

Pixel-based analysis represents an alternative to methods relying on peak detection and quantification (Christensen et al., 2005; Christensen and Tomasi, 2007; Groeger et al., 2008). In this approach, signal intensities are used directly as variables in the multivariate analysis instead of providing lists of features or peaks that have to be annotated and then matched between samples; the main advantage is that peak detection and quantification, and the related problems, can be avoided. The procedure can be relatively straightforward as for data from one-dimensional chromatography with single-channel detections (e.g., Gas Chromatography—flame ionization detection (GC−FID)), in which preprocessed chromatograms are stacked to form a data matrix, which is then analyzed by, e.g., principal component analysis (PCA—Christensen and Tomasi, 2007; Nielsen et al., 2012); or may require additional steps such as binning and matricization, as is the case with chromatographic data with larger dimensionality such as Gas Chromatography-Mass Spectrometry (GC−MS) and GC × GC−FID, prior to the multivariate analysis and subsequent "refolding" of the loadings before chemical interpretation (Christensen et al., 2005; Christensen and Tomasi, 2007; Furbo et al., 2014).

Pixel-based methods are the golden standard for spectroscopic data (e.g., Infrared and UV-VIS) (Esbensen and Geladi, 2009) and have been shown to work well for analysis of very complex mixtures such as mineral oils (Christensen et al., 2005; Christensen and Tomasi, 2007) and metabolomics samples (Petersen et al., 2011). However, their use for analysis of chromatographic data is rare. The slow adoption of these methods for chromatographic data is likely due to more stringent requirements with respect to preprocessing and removal of non-chemical variation (e.g., retention time shifts, peak shape changes or variations in detector response) compared to spectroscopic data and to the much larger number of variables retained which, if no filtering is applied, can lead to overfitting (Christensen and Tomasi, 2007). Despite of these drawbacks, pixel-based fingerprinting has been successfully employed for oil spill identification and hydrocarbon source differentiation; for example, the CHEMSIC [CHEMometric analysis of sections of Selected Ion Chromatograms (SICs)] method has been used to characterize sediments in the Guanabara bay and from the Iguaçu River Watershed (Christensen and Tomasi, 2007; Gallotta and Christensen, 2012) from GC−MS chromatograms obtained in selected ion monitoring mode.

In the CHEMSIC approach, which is applicable only when chromatography is used in combination with mass spectrometry detection, a number of SICs with chemical information specific to relevant classes of compounds (e.g., various classes of polycyclic aromatic hydrocarbons—PAHs, hopanes, steranes, etc.) are preprocessed and combined to be further analyzed by PCA. The objective of the analysis and environmental conditions at the sampling sites and of the samples will be decisive factors for the choice of SICs to include. For example, hopanes and steranes are often used in classical oil spill identification methods as they can be used to distinguish between source rocks and they are resistant to weathering processes (Peters et al., 2005). PAHs can also be used for hydrocarbon source differentiation and can help differentiating hydrocarbons from other sources than the petrogenic (i.e., pyrogenic, biogenic and diagenetic), but their composition profile (or fingerprint) is affected by the degree of weathering (viz., evaporation, dissolution, photodegradation and biodegradation) which in turn will depend on the environment, time, exposure, type of oil, and form of oil sample (sediment, water, emulsions, and pure oil). In areas with high temperatures and sun exposure, biodegradation and photodegradation can have an enormous impact on the compound composition while in arctic regions, biodegradation may play a minor role. Sediment samples will invariably be weathered samples, potentially exposed to all types of weathering, whereas pure oil

samples may only have been exposed to weathering in the form of evaporation and dissolution processes. For PAHs, the degree of weathering affects the composition according to number of rings and degree of alkylation. However, isomer-ratios are much more stable and only affected by photo- and biodegradation.

The more compounds or groups of compounds are included in pixel-based fingerprinting methods, the stronger the conclusions, although only the most resistant compound groups should be used if the samples are heavily weathered. The objective of this chapter is to show how the specific objectives, type of samples, and harsh environmental conditions determine the strategy for which compound groups to include in the chemical fingerprints, the data processing and the interpretation using the CHEMSIC method. The results for oil spill identification and hydrocarbon source differentiation for two case studies in the Persian Gulf will be discussed and used as examples.

21.1.1 Introduction to Case Studies

The sampling areas for the two case studies were situated around the Persian Gulf (Fig. 21.1). Samples for case study 1 were collected in the Shadegan wetland in Khuzestan province, Iran, at three sampling sites (Fig. 21.1). This is an area with a rich flora and fauna that is of vital importance for the subsistence of surrounding villages and cities such as Abadan, Bandar Mahshahr and Shadegan (CIWP, 2015). In addition, nearly 61% of the wetland area is listed as a Wildlife Refuge (UNDP/GEF 2011). Large refinery/petrochemical industries are situated in the area and transport of petroleum products takes place on a daily basis from Abadan refineries to the port of Bandar Mahshahr. In addition, Bandar Imam Khomeini, which harbors the largest marine port of Iran, is directly connected to the Shadegan wetlands.

The objectives of case study 1 were to (1) characterize hydrocarbon pollution for the three sampling sites in order to distinguish between petrogenic, pyrogenic and diagenetic hydrocarbon sources using PAH fingerprints and (2) to confirm and further investigate petrogenic pollution by evaluating petroleum biomarkers.

The samples for case study 2 were collected in the North-Northwest of Qatar from two sites at Al Zubarah (Fig. 21.1). Al Zubarah is on the UNESCO World Heritage list and is of great importance to the Qatari history (UNESCO, 2016). Oil pollution along the North-Northwest coastline of Qatar is especially problematic due to Al Zubarah and tourism in the area (UNESCO, 2016). At the time of the study, it was unknown whether the tar

FIGURE 21.1 Sampling areas for case study 1 (Iran) and case study 2 (Qatar) (Map data: Google, Landsat/ Copernicus). Squares are sampling sites and circles are cities or historic sites. In case study 1, the first sampling site was the coastal area of the Persian Gulf near the city of Hendijan; second site was at Khore Mosa river close by Bandar Imam Khomeini near the Shadegan protected wetland; and site three was at Arvandroud River between Khorramshahr and Abadan at the border to Iraq. For case study 2, both sampling sites were close to Al Zubarah and are represented by a single symbol for sampling site.

deposits that can be found on Qatari coastlines originate from highly weathered and persistent oil tar deposits following the Gulf War oil spill in 1991 or from more recent oil spills (Hayes et al., 1993; Massoud et al., 1996; Bejarano and Michel, 2010).

The objectives of case study 2 were therefore to (1) assess whether the spilled oil at North-Northwest Qatar originates from multiple sources; (2) to identify the most probable source(s) of the oil spill; and (3) to describe whether the spill samples were crude oils or heavy fuel oils (HFOs) from bunker flushes.

21.2 MATERIALS AND METHODS

21.2.1 Sampling and Sample Preparation

In the first study, sediment samples were collected from three sampling sites in Iran marked by squares in Fig. 21.1 on consecutive days in October 2014. In total, 47 samples were collected during the 3 days from depths between 0.5 and 22.9 m using a Van Veen grab sampler. Samples were later extracted by pressurized liquid extraction using a method described by Soleimani et al. (2010). For further details, see Lübeck et al. (2016).

For the second study, 34 samples were collected during two sampling campaigns (in 2014 and 2015, respectively). Fresh and heavily weathered oil spills and sediments from surface and subsurface levels were collected by hand using a sterile spatula; the oil samples were then weighed and dissolved in dichloromethane to reach a total oil concentration of 2500 μg/mL. For further details, see Al-Kaabi et al. (2017).

Both case studies include samples from a large University of Copenhagen (UCPH) database of petroleum products (e.g., crude oils and HFOs) covering a large geographical span. These samples assure an appropriate sample variation and provide specific samples with geographical relevance useful for source identification.

21.2.2 Chemical Analysis and Quality Control

In both case studies, samples were analyzed on comparable Agilent GC−MS systems using the same method as described by Gallotta and Christensen (2012), with a total of 55 mass-to-charge ratios (m/z) acquired in SIM mode.

Similar quality assurance procedures were applied in both case studies which involved full randomization of the analytical sequences which included, beside the samples, several types of quality measurements (viz., solvent blanks, instrument test solutions, and quality control—QC samples) evenly distributed along the sequence. The quality assurance samples were used to monitor crosscontamination, changes in peak shape, consistency in chromatographic resolution and sensitivity throughout the sequence and between batches.

The QC samples were constructed from samples in such a way that they would span the total sample variation both chemical and unrelated to chemical composition (e.g., retention time shifts, baselines, etc.) so that replicates could be used for the optimization and validation of the subsequent preprocessing and chemometric data analysis. The QC samples for both the "Global" sample sets in case studies 1 and 2 were constructed based on a representative subset of the UCPH oil database. For the "Local" models, in case study 1, the QC samples were based on equal amounts of all samples from the case study.

21.2.3 Data Collection and Structure

The datasets consisted of retention time windows of 55 SICs for each sample. For each SIC, the compounds of interest were identified by their retention times and m/z according to the CEN/BT/TF and Bonn-OSINet (2011) protocol. The SICs were cut to focus only on the peaks corresponding to the compounds of diagnostic relevance, and to remove sections with no chemical information (viz., trailing and leading sections).

In the first study, a total of 47 sample extracts (including sampling replicates), eight QC samples and 12 extraction blanks were analyzed. After preliminary evaluation, seven samples had to be removed due to contamination issues. This provided a total of 48 valid chromatograms of sample extracts and QC samples ($47 + 8 - 7 = 48$ chromatograms) from which a "Local" dataset was constructed. A secondary "Global" dataset of 216 samples was constructed from 214 crude oil samples from the UCPH oil database and two samples from the "Local" data (i.e., two sample extracts and eight QC samples).

In the second study, a subset of 205 samples from the UCPH database (including 46 samples from the Middle East and 18 HFOs), 27 QC samples and 34 collected spill samples were analyzed.

21.2.4 Data Preprocessing and Principal Component Analysis

The CHEMSIC method (Christensen and Tomasi, 2007; Christensen et al., 2010; Gallotta and Christensen, 2012) describes chemical variation using PCA. PCA is a bilinear decomposition method where the data is described by Principal Components (PCs), each consisting of one scores vector, and one loading vector. Scores and loadings (and therefore the PCs) are mutually orthogonal and are sorted according to the variance they explain. As PCA describes the most relevant sources of variation regardless of their nature, it is important to reduce nonchemical variation. A tiered approach was employed which includes baseline removal, retention time alignment, data normalization, variable scaling, and the combination of the distinct SICs (Christensen and Tomasi, 2007). These steps reduce nonchemical variations and focus the PCA on the chemical information; i.e., relative concentration or composition (Christensen et al., 2005). PCA is applied to the combined, preprocessed SICs, after they are stacked into a matrix in which the single SICs from all the samples form adjacent blocks of varying width, and all the SICs relative to one sample are collected in the same row. Baseline removal and alignment are performed prior to combining the SICs, whereas normalization can be applied either before and/or after.

Baselines were removed using two methods depending on the baseline complexity of the SICs in question. Complex baselines [e.g., the SICs of hopanes (191 m/z) and steranes (217 and 218 m/z)], affected by significant coelution and baseline drift, were removed by differentiation using the Savitzky–Golay algorithm, while less complex ones (e.g., for C1 to C3-PAHs) were removed by subtracting the lower part of the convex hull chromatogram (Christensen et al., 2010). The latter method is preferred for simple constant baselines, as the former requires cumulative summing of the loading coefficients in order to make these interpretable and comparable to the original chromatograms.

The single SICs were aligned independently using a combination of iCOShift or correlation optimized warping (COW) in both case studies (Nielsen et al., 1998; Tomasi et al., 2004, 2011). In both cases, the target was a sample with intermediate shifts and contains as many peaks as possible (often a QC sample). Different targets were allowed for the different SICs. The optimal parameters for COW were obtained using the optimCOW procedure (Skov et al., 2006), which is computationally more intensive but has proven effective in reducing the changes in peak shape and width due to the compression/expansion model for correction employed by COW.

The CHEMSIC method employs three types of data normalization (Schemes 1 to 3), which make the subsequent data analysis focus on either relative concentration or chemical composition (Gallotta and Christensen, 2012). In scheme 1, individual SICs are normalized, prior to combining the SICs sample wise, to the area under the curve of the SIC of an appropriate internal standard. Thus, focus is set on relative hydrocarbon concentration while the information on relative compound composition within the data is likely to show in later PCs. Schemes 2 and 3 include SIC-wise normalization to unitary Euclidean norm performed either post or prior to combining the SICs, respectively. This removes total hydrocarbon concentrations. Scheme 2 retains relative SIC abundance, focusing on differences between SICs, while Scheme 3 provides equal weights for all SICs, focusing on relative variation within SICs. Both studies, apply several normalization types depending on focus and aim of the respective models (see Section 21.3).

Finally, the variables (i.e., the intensities at the different retention times for the distinct SICs) were scaled according to the inverse of their relative analytical (or sampling) uncertainty, calculated as the relative standard deviation (RSD) of replicate samples. This scaling, provided that the PCA loadings are back-scaled using the same weights, corresponds to fitting PCA in a weighted least squares sense (Bro and Smilde, 2003). In both studies, the RSDs were calculated based on the QC replicates and ensured that the parts of the SICs with low signal-to-noise (e.g., areas without peaks) or for which preprocessing was not capable of removing the nonchemical variation had lower influence in the PCA model.

The preprocessed dataset was divided into a training- and a validation set, with the PCA models being constructed using the mean-centered training set. The QC samples, which residual variation can be taken as representative of the analytical variance after the preprocessing (and is thus also a measure of how well the preprocessing worked), were part of the validation sets.

The number of valid PCs to be included in the final model is made more complicated in the pixel-based approach by the fact that explained variance hardly ever shows a clear change in slope and that PCs can explain residual shift, making methods like cross validation less reliable (Christensen and Tomasi, 2007). Thus, it was evaluated using a tiered approach: first, the loading coefficients were visually inspected and compared to a normalized average chromatogram of the training set; at this stage the objective is to determine the presence of tell-tale residual shift artifacts, which would determine when (i.e., at which PC) the uncorrected,

nonchemical variation is starting to affect the components, thereby preventing their interpretation. The second tier is projection of the test set onto the model and evaluation of score coefficients, with low replicate variation indicative of valid PCs.

21.3 RESULTS AND DISCUSSION

21.3.1 Case Study 1

In case study 1, three PCA models are included; with the first two models being constructed using the "Local" dataset while the "Global" dataset was used for the third model.

21.3.1.1 "Local" Models for Source Identification

In both Model 1 and 2, the dataset was split into a training set consisting of 30 samples, and a validation set of eight QC samples and ten of the Hendijan Coast sampling replicates (two from each spot).

21.3.1.1.1 Model 1

Model 1 was constructed using 12 SICs including non- and alkylated, two to six ringed PAHs with well-established source specific diagnostic ability: C2- to C4-naphthalenes (m/z 156, 170 and 184), C0- to C1-phenanthrenes and anthracenes (m/z 178 and 195), C0- and C1-dibenzothiophenes (m/z 184 and 198), C0- to C1-pyrenes and fluoranthenes (m/z 202 and 216), C0-benzo(*a*)anthracene and C0- to C1-chrysenes (m/z 228 and 242), and 5- and 6-Ring PAHs (m/z 252 and 276). This selection excluded SICs with insufficient signal intensities to support pixel-based PCA and those without well-established diagnostic abilities (de Fatima et al., 2007; Gallotta and Christensen, 2012; Lübeck et al., 2016).

Normalization was carried out according to scheme 1, thus retaining information on PAH concentration as well as information on the relative composition of PAHs represented by a given SIC, but sample A12, which visual inspection and preliminary models showed to have extremely high signals, was premultiplied by a factor 0.3 to reduce its influence on the model (Christensen and Tomasi, 2007).

The final model included four components as subsequent PCs confounded chemical information with peak shape changes and residual shift (Christensen and Tomasi, 2007; Lübeck et al., 2016). PC1 (Fig. 21.2A) has positive loading coefficients for all compounds within the 12 SICs. Positive scores indicate therefore higher than average pollution levels (where the average here is represented by the mean of all the samples). PC2 (Fig. 21.2B) describes the relative concentrations of low-molecular-weight and high-molecular-weight (HMW) PAHs, indicated by negative loadings for two to three ring PAHs (i.e., C2-, C3-, C4-naphthalenes, C1-dibenzothiophenes, and C1-phenanthrenes), while three to six ring PAHs (i.e., C0-phenantrene, C0-anthracene, C0- and C1-pyrenes, fluoranthenes, chrysenes, and benzo(*a*)anthracene, as well as five and six ring PAHs) have positive coefficients. Positive scores indicate therefore higher concentrations of HMW PAHs, which are characteristic of both weathered petrogenic PAHs and pyrogenic hydrocarbon pollution (Yunker et al., 2002; Peters et al., 2005).

For PC3 (Fig. 21.2C), the nonalkylated species of anthracene, fluoranthene, pyrene, and benzo(*a*)anthracene and benzo(*b*)-/benzo(*k*)fluoranthene, which are indicative of pyrogenic sources (Peters et al., 2005), have positive loading coefficients, whereas C1-pyrenes and C1-chrysenes, indicative of weathered petrogenic input (Peters et al., 2005), have negative ones. PC3 therefore differentiates between pollution sources and negative and positive scores suggest hydrocarbon input from pyrogenic and petrogenic sources, respectively. Finally, PC4 shows large positive loading coefficients for perylene (m/z 252—Fig. 21.2D), a known indicator of diagenetic input (Silliman et al., 2001; Tissot and Welte, 2012). Hence, positive PC4 scores indicate therefore a larger diagenetic input.

Fig. 21.2E shows a bar plot of all 30 samples, sorted by their PC1 score and categorized by sampling sites. The samples from the Hendijan Coast show very little variation. All these samples have below average concentration (according to PC1) and show no characteristic PAH source pattern of either petrogenic, pyrogenic or diagenetic input (PC2 to PC4). Samples K01, K07 to K13 (Khore Mosa) and A06, A08, and A11 (Arvandroud River) have similar PC1 scores as samples from the Hendijan Coast, indicating no significant PAH contamination.

The positive PC2 and PC3 scores for samples K02 to K05 suggest that PAH contamination may have a mixed origin due to the higher than average relative concentrations of both pyrogenic- and petrogenic indicator compounds. The positive PC1 scores of K04 and K05 indicate above average PAH concentrations. K02 and K03 have a below average PAHs concentration, with K03 having an additional input from diagenetic sources (positive PC4

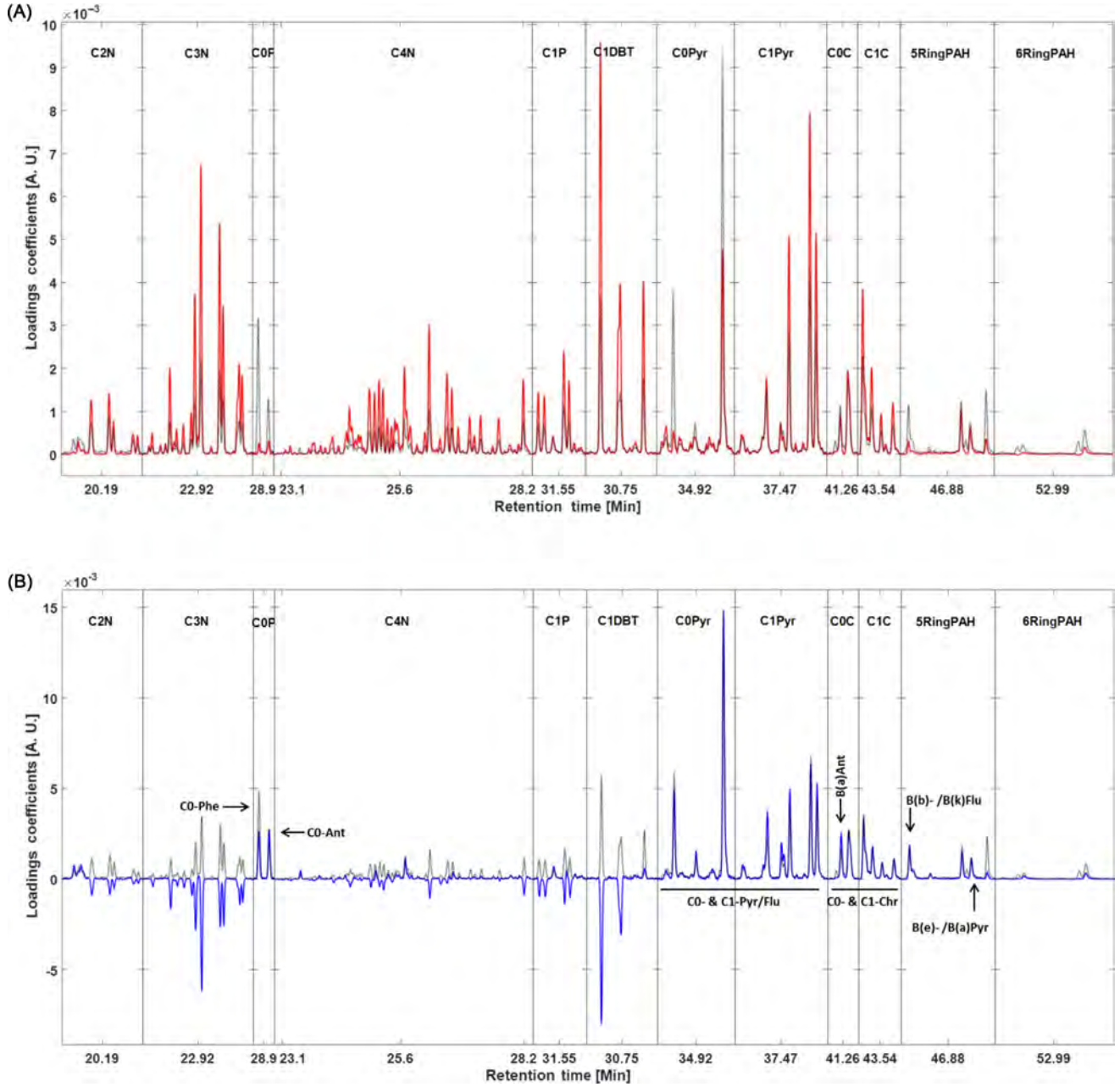

FIGURE 21.2 (A) PC1, (B) PC2, (C) PC3, and (D) PC4 loading plots for selected SICs of the Iran sediment samples: *C2N*, C2-naphthalenes; *C3N*, C3-naphthalenes; *C0P*, C0-phenanthrene and anthracene; *C4N*, C4-naphthalenes/C0-dibenzothiophene; *C1P*, C1-phenanthrenes/anthracenes; *C1DBT*, C1-dibenzothiophenes; *C0Pyr*, C0-pyrene/fluoranthene; *C1Pyr*, C1-pyrenes/fluoranthenes; *C0C*, C0-chrysene; *C1C*, C1-chrysenes; *5RingPAH*, five ring PAHs; and *6RingPAH*, six ring PAHs. The dotted chromatograms in the loading plots represent the average SIC of all samples in the training set. (E) Scores shown as a bar plot for PC1, PC2, PC3, and PC4. Symbols indicate: No significant PAH pollution (●), diagenetic input (■), fresh petrogenic input (+), weathered petrogenic input (×), and mixed anthropogenic input (Δ).

score). Sample K06 shows a significant petrogenic input with an above average PAH contamination (positive PC1) and large negative and positive PC2 and PC3 scores, respectively. This indicates that the contamination is of a weathered petrogenic nature with large relative concentrations of C1-fluoranthene, C1-pyrene, and C0-/C1-chrysenes (m/z 216, 228 and 242).

Samples A01 to A04 and A07 have negative scores for PC1 to PC3 indicating low levels of PAH contamination, while positive PC4 scores suggest diagenetic inputs (Silliman et al., 2001). The diagenetic input appears smaller for samples A04 and A07 with smaller positive scores in PC4 than A01.

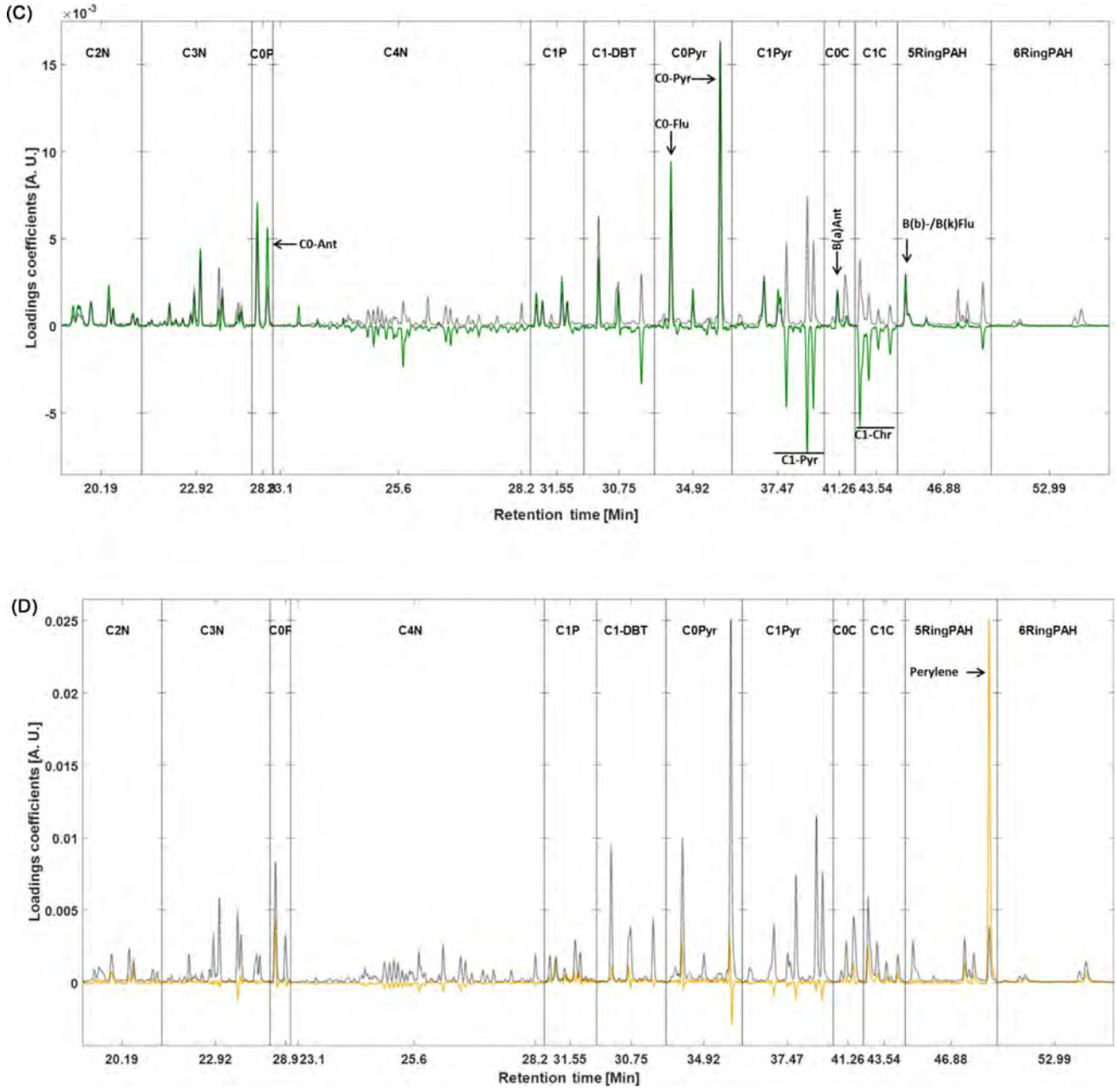

FIGURE 21.2 (Continued)

The PAH contamination in sample A05, while limited, seems to be of weathered petrogenic nature (negative PC2 and positive PC3). A small positive PC4 score also suggests, a higher than average for the sample set, diagenesis at this sampling spot. Samples A09, A10, and A12 all have positive PC1 scores and negative PC2 scores. This suggests rather fresh or nonweathered oil pollution (petrogenic input) with high relative concentrations of C3- and C4-naphthalenes and C0- and C1-dibenzothiophenes (Peters et al., 2005). A positive PC4 score for sample A09 indicates additional inputs from diagenetic sources.

21.3.1.1.2 Model 2

To confirm the results from Model 1 and the petrogenic input, a second PCA model was constructed using the hopanes (191 m/z), which are linked to oil pollution, and the same "Local" dataset (without downscaling sample A12 as it did not dictate the model) as in the previous model. The samples were normalized according to scheme

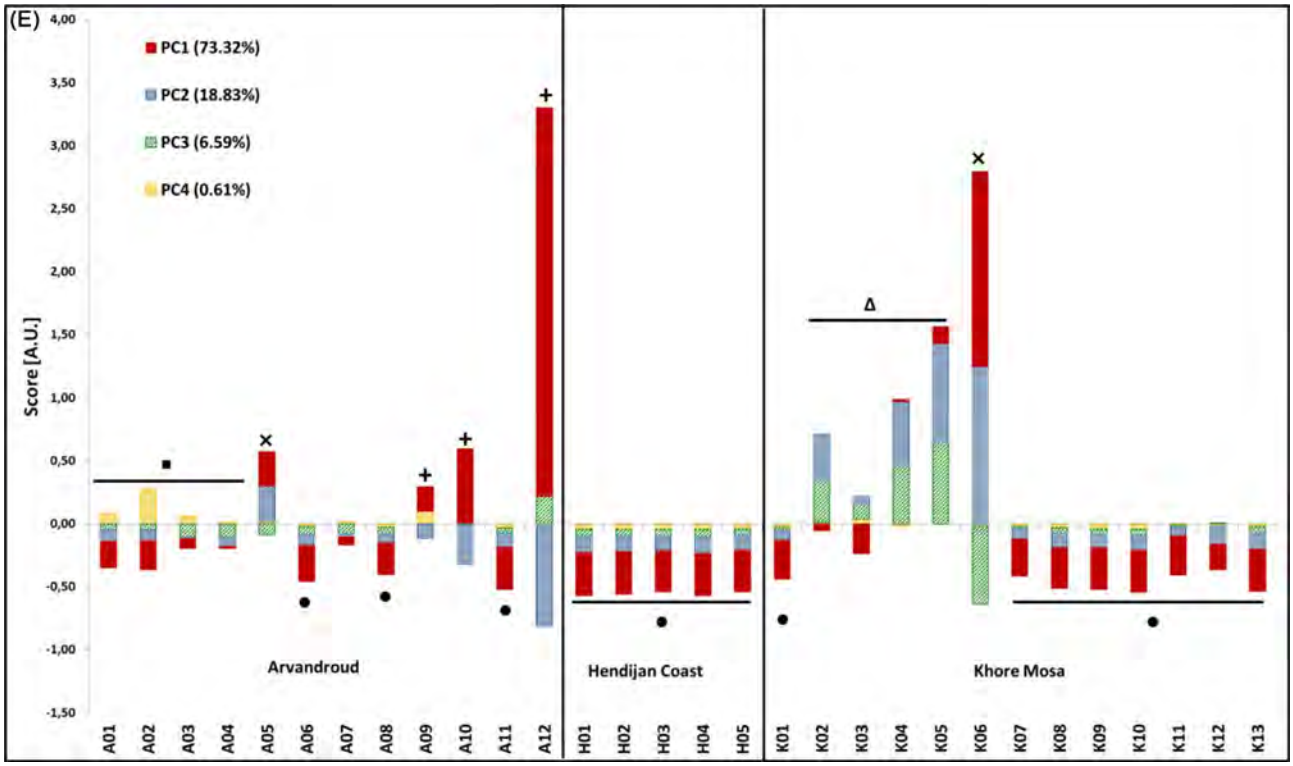

FIGURE 21.2 (Continued)

1 and without mean-centering focusing the PCA model on absolute hopane concentrations. Model 2 included only one PC describing 97.72% of the total variation. PC2 loadings described predominately noise rather than chemical information (peaks) and was therefore discarded. PC1 loading coefficients are positive for all the hopane compounds (see Fig. 21.3A) providing a hopane concentration profile with a positive PC1 score indicative of oil pollution (Fig. 21.3B). Samples characterized by insignificant overall pollution levels in Model 1 (i.e., Hendijan Coast: H01 to H05; Khore Mosa: K01, K07 to K13; Arvandroud: A06, A08, and A11), have lowest PC1 scores (i.e., lowest hopane concentrations), which supports the prior conclusions from model 1. Similarly K03, K04, and A04 have low PC1 scores, indicating limited petrogenic input. This supports the diagenetic PAH profile of A04, while suggesting a pyrogenic origin of PAH contamination detected for K03 and K04 in model 1. The remaining Khore Mosa samples (i.e., K02, K05, and K06) have higher PC1 scores in support of petrogenic input, insufficiently described by model 1. The significantly smaller score of A04 indicates lower petrogenic input compared to A07, both of which present similar low PAH concentration with no distinct source characteristics. Further source distinction is obtained for A01 to A03, as their scores also suggest petrogenic input that is not evident in model 1 which primarily indicates a diagenetic input. The higher PC1 scores of A05, A09, A10, and A12 confirm the predominately petrogenic fingerprint of their PAHs composition.

21.3.1.2 "Global" Model for Petrogenic Source Identification

21.3.1.2.1 Model 3

To further investigate the geographical source of the oil contamination a third model was constructed using the steranes (217 m/z). Steranes are common petroleum biomarkers used for petroleum identification and especially interesting when analyzing geographical origin as are the hopanes (Peters et al., 2005). The diagnostic ratio of diasteranes and regular steranes is commonly used to characterize petroleum products according to clay content of original source rock (Peters et al., 2005). The diagnostic pattern for αα- and ββ-isomers of the C_{27} to C_{30}-regular steranes is used to distinguish petroleum products according to thermal maturity, which reflects source rock conditions during crude oil generation (Peters et al., 2005). The model was constructed using a "Global" dataset which combines the 214 samples from the UCPH oil database (incl. 27 QC samples) and samples

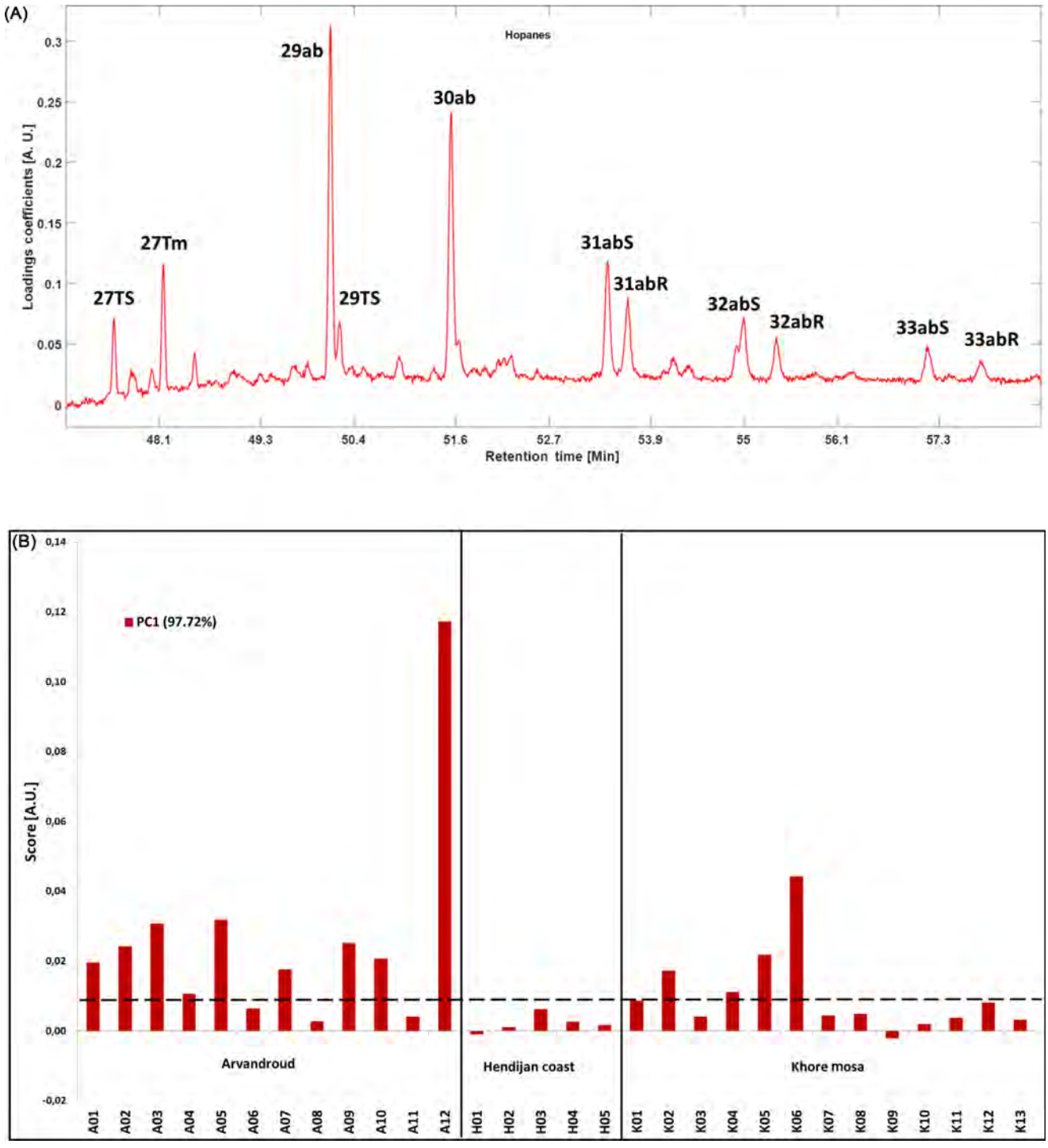

FIGURE 21.3 (A) PC1 loading plot for the hopane model (m/z 191) describing the relative concentration levels of: *27Ts*, 18α(*H*)-22,29,30-trisnorhopane; *27Tm*, 17α(*H*)-22,29,30-trisnorhopane; *29ab*, 17α(*H*),21β(*H*)-30-norhopane; *29Ts*, 18α(*H*)-30-norneohopane; *30ab*, 17α(*H*),21β(*H*)-hopane; *31abS*, 17α(*H*),21β(*H*), 22S-homohopane; *31abR*, 17α(*H*),21β(*H*), 22R-homohopane; *32abS*, 17α(*H*),21β(*H*), 22S-bishomohopane; *32abR*, 17α(*H*),21β(*H*), 22R-bishomohopane; *33abS*, 17α(*H*),21β(*H*), 22S-trishomohopane; and *3abR*, 17α(*H*),21β(*H*), 22R-trishomohopane. (B) PC1 score bar plot. The dashed line displays a score threshold for samples with insignificant pollution levels in model 1.

A12 and K06 from the "Local" dataset. These two samples were included due to their high petrogenic pollution, providing sufficient signal-to-noise levels to obtain robust results.

The "Global" dataset included a "Persian Gulf" subset of 17 oil samples from several Gulf countries relevant for the case study, including Iran and the neighboring countries of Iraq and Kuwait. Especially, the two Iraq

samples from the city of Basrah were of interest. The city is located upstream of the Arvandroud River sampling site (see Fig. 21.1) and therefore is a potential source of oil contamination. The "Global" dataset was divided into a training set ($n = 157$), based on a UCPH sample subset and a validation set ($n = 67$), including the "Persian Gulf," "Local," and QC samples. Five valid PCs were retained in the final model. PC1 and PC2 describe the predominant source variations and therefore the only PCs interpreted in the following section. PC1 loadings (see Fig. 21.4A) indicate that samples along the PC1 axis are mainly separated according to the diagnostic pattern for the diasteranes and regular steranes. Samples along the PC2 axis (see Fig. 21.4B) are separated based on the pattern for αα- and ββ-isomers of the C_{27} to C_{30}-regular steranes. Loadings for both PC1 and PC2 are therefore validated as descriptive for geographical origin of oil source (Christensen et al., 2005). PC1 and PC2 scores are shown in Fig. 21.4C. It can be seen that the 27 "Global" QC samples cluster together indicative of valid PCs. PC2 separates the Iranian oils from the Kuwait and Iraqi oils, with the A12 and K06 scoring similar to the Iranian samples. Along PC1 the separation is not as distinct, with predominately negative scores for geographical relevant oils. The Iraqi oils display some of the most negative PC1 scores, while both A12 and K06 have positive scores. This suggests similar petrogenic hydrocarbon pollution for samples A12 and K06, which does not match the petroleum biomarker fingerprint of the Iraqi oils. It also suggests that more local sources (e.g., petrochemical industry of Abadan and Bandar Mahshahr) are more likely candidates for the petrogenic pollution at the Arvandroud River and Khore Mosa sampling sites. Although the petrogenic fingerprints of the Iranian oils are the most compatible to the case study 1 samples, it does not confirms that the petrogenic pollution is from local Iranian sources as these do not score identical and no geographical information is obtained for the Iranian samples. In order to address this question more adequately, a larger number of relevant oils are needed, including samples from all of the possible local sources.

21.3.2 Case Study 2

The extreme warm weather conditions and the direct exposure of beached oil spills lead to an acceleration of the oil weathering processes, including physical removal, evaporation, and biodegradation processes. This complicates the oil spill identification process as only very recalcitrant compounds can be used to express chemical differences due to source variations. Fig. 21.5 shows the total ion chromatogram (TIC) of five Qatar spill samples together with SICs of hopanes (m/z 191), steranes (m/z 217), C1-phenanthrenes (m/z 192) and C1-pyrenes (m/z 216). Large variations in weathering degree can be observed between the Qatar spill samples. The many peaks in the TIC and in the sterane SIC together with the presence of C1-phenanthrenes and C1-pyrenes indicate that Sample 28 and X-01 are relatively unweathered. In contrast, C1-phenanthrene and C1-pyrene are absent together with most compounds in the low boiling point range of the TIC for samples 10, X-04, and 2, which can then be inferred to be highly weathered. Therefore, it is apparent that amongst the considered classes of compounds only hopanes are recalcitrant enough to be reliably used for oil spill identification if more than a few spill samples is to be included in the study.

21.3.2.1 "Global" Model for Oil Spill Identification

21.3.2.1.1 Model 1

The CHEMSIC method was used to analyze SICs of m/z 191 (hopanes). A subset of 187 samples from the UCPH oil database was used as training set for the PCA model, while 34 spill samples collected in Qatar were projected onto the model together with a set of 27 QC samples, which were used to validate the preprocessing. PC1 mainly explained the difference between samples due to heaviness of the crude oils (PC1 loading plot shown in Fig. 21.6). Sample heaviness for crude oils is confounded with evaporative weathering for hopanes. Due to these confounding effects, PC1 should in this case not be used for source identification. PC2 and PC3 from the model describe relevant variations in the dataset and loadings and score plot are shown in Fig. 21.6. PC2 is mainly controlled by high positive loadings for 29ab, whereas PC3 have high negative loadings for 30ab, 31abS, 31abR, 30G, 32abS and 32abR (Fig. 21.6).

From Fig. 21.6D, it is seen that the QC samples cluster tightly in the PCA score plot, demonstrating that the PCA model describes variations in the oil composition rather than analytical variations. Fig. 21.6D also shows that all oil spill samples from Al Zubarah cluster at high PC2 scores (representing high value of 29ab) together with oils from the Persian Gulf, especially samples from Saudi Arabia, Kuwait, and Iraq.

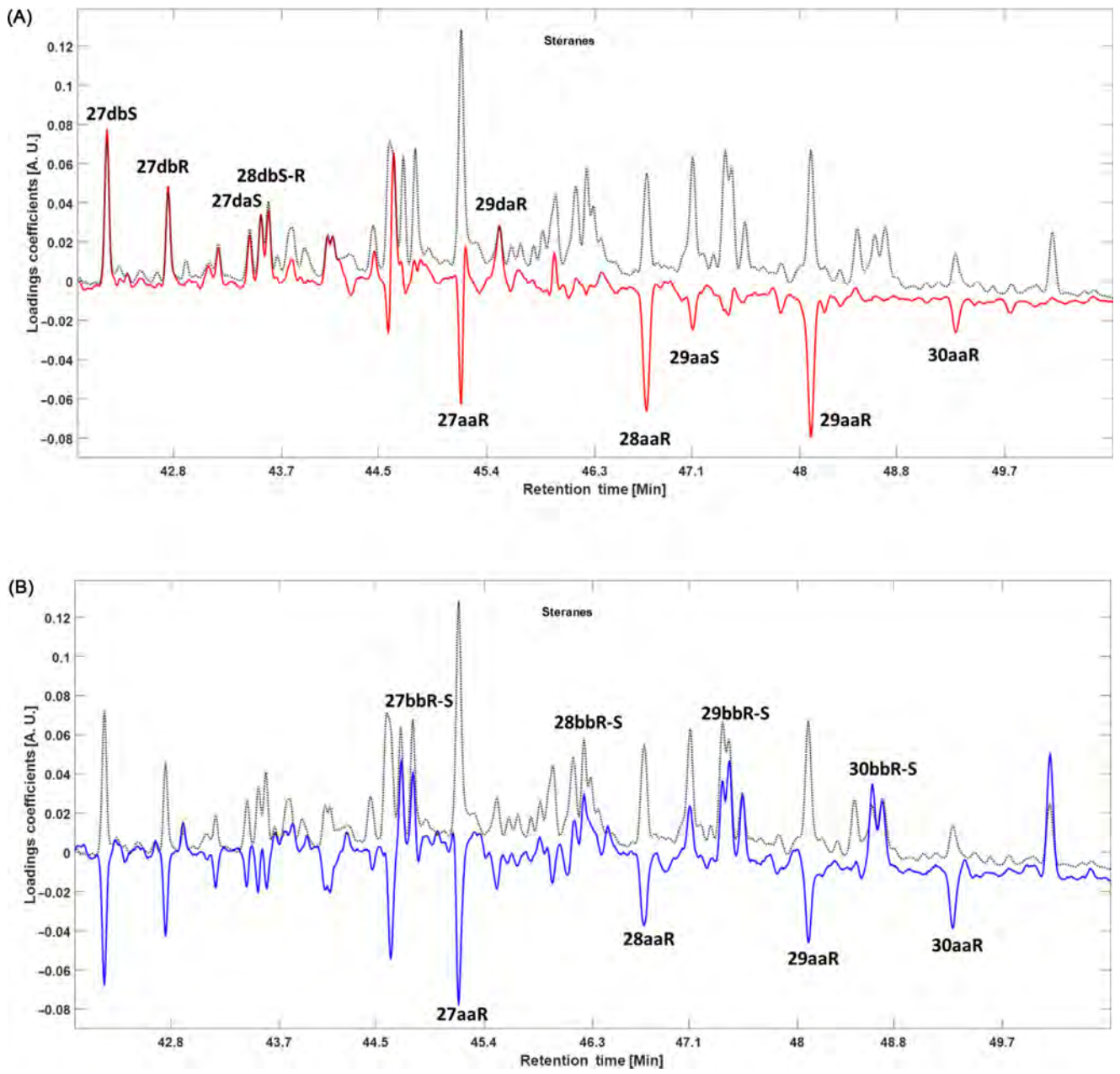

FIGURE 21.4 (A) PC1 and (B) PC2 loading plots for the sterane model (m/z 217). PC1 provides positive coefficients for diasteranes: *27dbS*, 13b(*H*), 17a(*H*), 20S-diacholestane; *27dbR*, 13b(*H*), 17a(*H*), 20R-diacholestane; *27daS*, 13a(*H*), 17b(*H*), 20S-diacholestane; *28dbS*, 24-methyl-13b(*H*), 17a(*H*), 20S-cholestane; *28dbR*, 24-methyl-13b(*H*), 17a(*H*), 20R-cholestane; *29dbR*, 24-ethyl-13b(*H*), 17a(*H*), 20R-cholestane; and *29daR*, 24-ethyl-13a(*H*), 17b(*H*), 20R-cholestane. Negative coefficients for regular steranes: *27aaR*, 5a(*H*), 14a(*H*), 17a(*H*), 20R-cholestane; *28aaR*, 24-methyl-5a(*H*), 14a(*H*), 17a(*H*), 20R-cholestane; *29aaS*, 24-ethyl-5a(*H*), 14a(*H*), 17a(*H*), 20S-cholestane; *29aaR*, 24-ethyl-5a(*H*), 14a(*H*), 17a(*H*), 20R-cholestane; and *30aaR*, 24-propyl-5a(*H*), 14a(*H*), 17a(*H*), 20R-cholestane. PC2 provides positive coefficients for ββ-isomers: *27bbR*, 5a(*H*), 14b(*H*), 17b(*H*), 20R-cholestane; *27bbS*, 5a(*H*), 14b(*H*), 17b(*H*), 20S-cholestane; *28bbR*, 24-methyl-5a(*H*), 14b(*H*), 17b(*H*), 20R-cholestane;*28bbS*, 24-methyl-5a(*H*), 14b(*H*), 17b(*H*), 20S-cholestane; *29bbR*, 24-ethyl-5a(*H*), 14b(*H*), 17b(*H*), 20R-cholestane; *29bbS*, 24-ethyl-5a(*H*), 14b(*H*), 17b(*H*), 20S-cholestane; *30bbR*, 24-propyl-5a(*H*), 14b(*H*), 17b(*H*), 20R-cholestane; and *30bbS*, 24-propyl-5a(*H*), 14b(*H*), 17b(*H*), 20S-cholestane. Negative coefficients for αα-isomers: *27aaR*, 5a(*H*), 14a(*H*), 17a(*H*), 20R-cholestane; *28aaR*, 24-methyl-5a(*H*), 14a(*H*), 17a(*H*), 20R-cholestane; *29aaR*, 24-ethyl-5a(*H*), 14a(*H*), 17a(*H*), 20R-cholestane; and *30aaR*, 24-propyl-5a(*H*), 14a(*H*), 17a(*H*), 20R-cholestane. The dotted chromatograms represent the average TIC of all samples in the training set. (C) PCA score plot of PC1 vs PC2. Model is build using the Global (circles) samples. Persian Gulf (6-point stars), Kuwait (upward triangles), Iraq (5-point stars), Iran (downward triangles), QC (crosses), A12 (rhombus), and K06 (square) are projected onto the model.

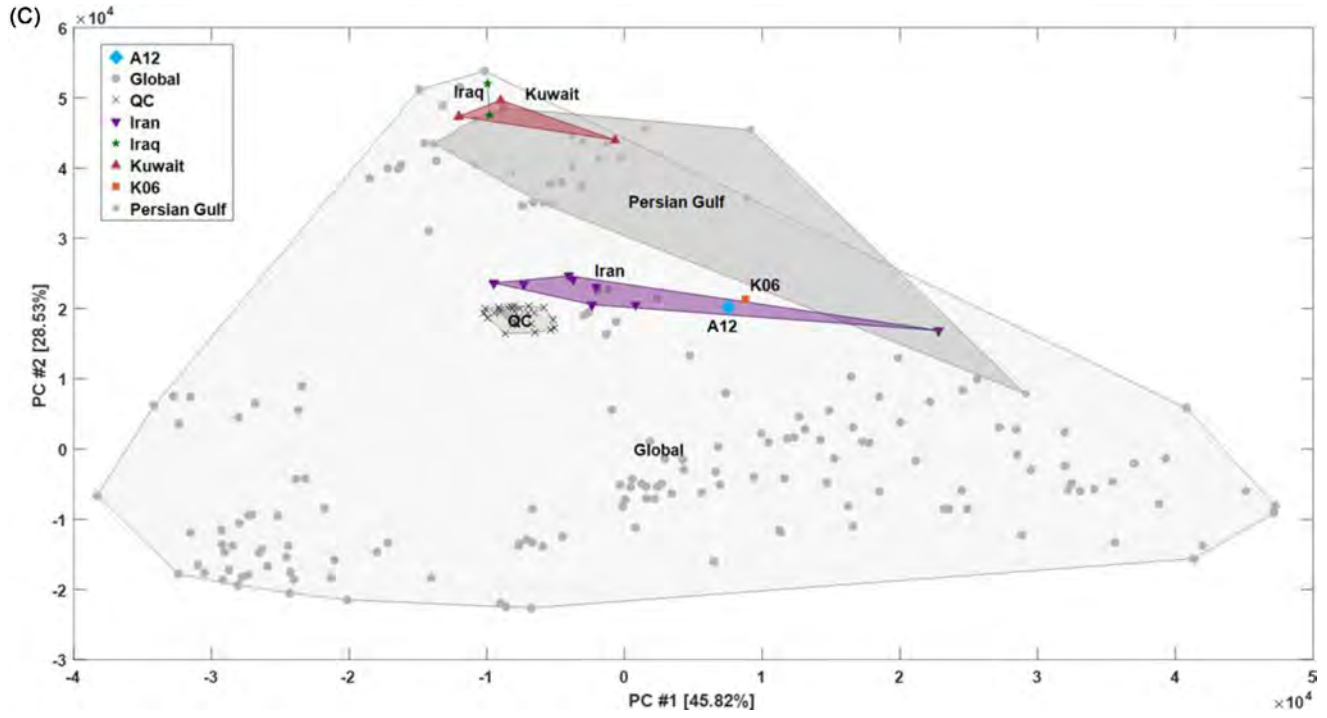

FIGURE 21.4 (Continued)

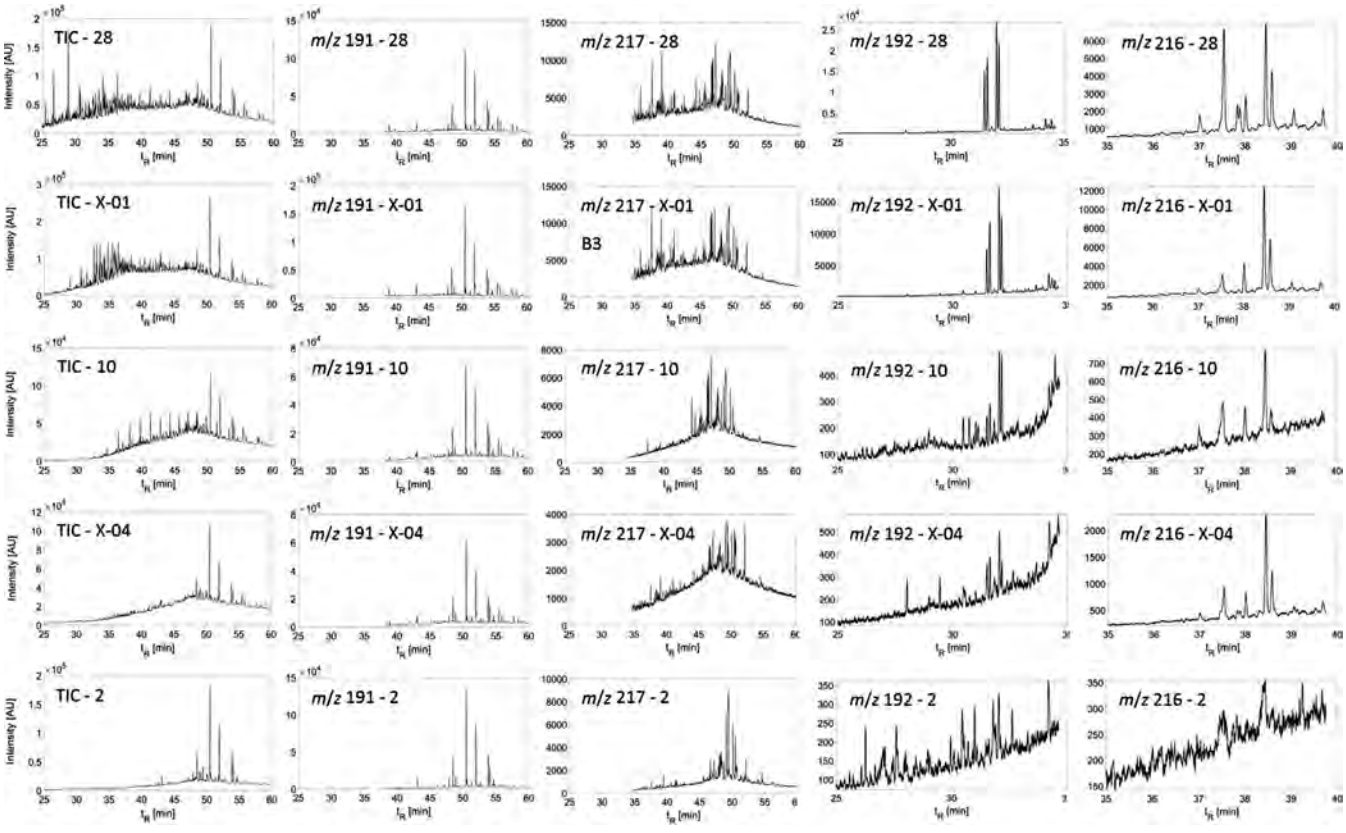

FIGURE 21.5 TIC and SICs of hopanes (m/z 191), steranes (m/z 217), C1-phenanthrene (m/z 192), and C1-pyrene (m/z 216) for five samples of various weathering degree.

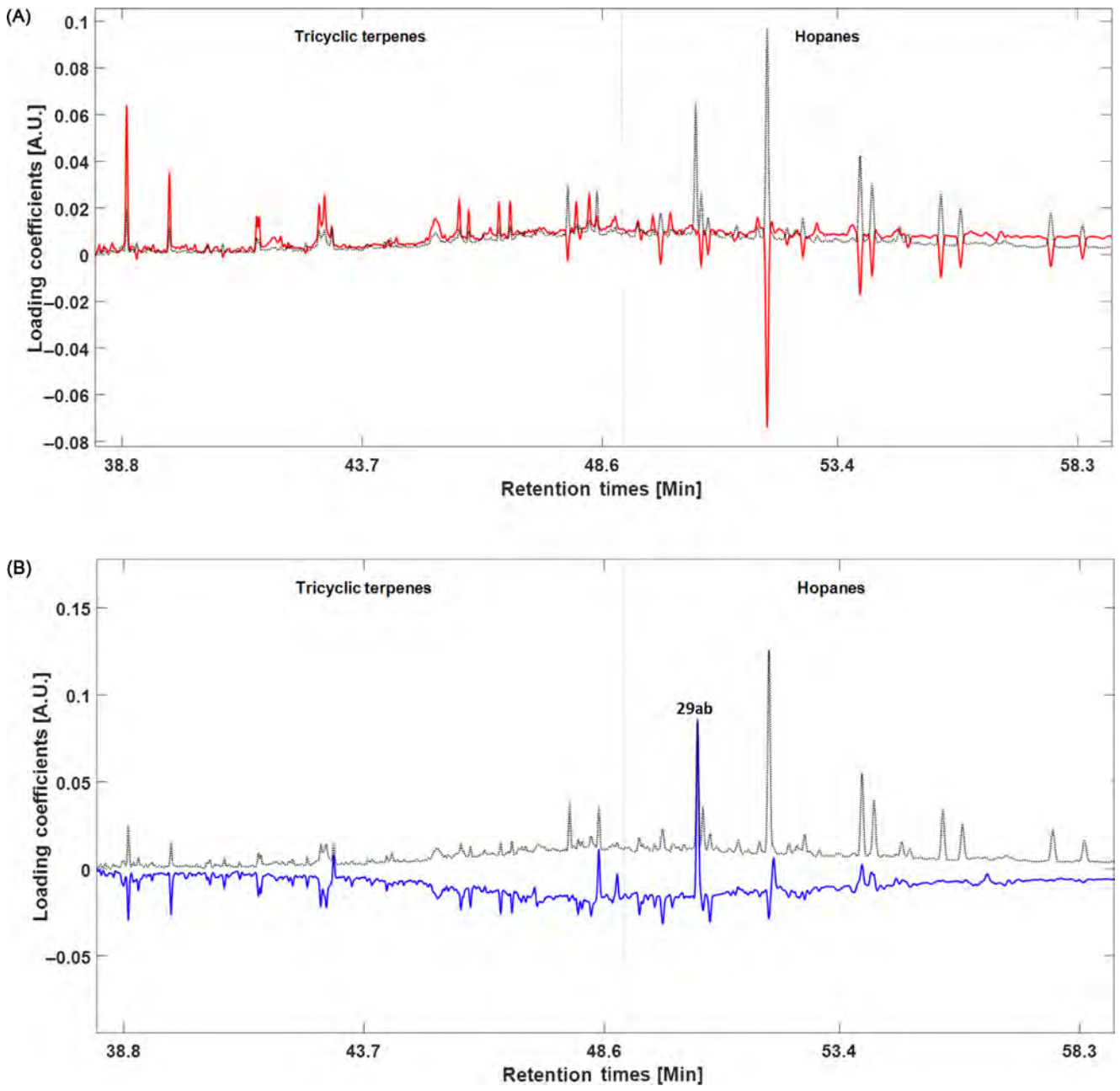

FIGURE 21.6 (A) PC1, (B) PC2, and (C) PC3 loading plots for the hopane model (m/z 191). The dotted chromatograms represent the average TIC of all samples in the training set. (D) PCA score plot of PC2 vs PC3. Qatar spill samples (stars) are projected onto the model. Inside the square are all Qatar spill samples and 11 oils from the UCPH database.

21.3.2.2 "Local" Models for Oil Spill Identification

21.3.2.2.1 Model 2

In large datasets, there is a possibility that major trends, represented by the first PCs, can mask differences between related source oils. The PCs describing these minor, but important, differences might not be a part of the "Global" PCA model. To ensure that these variations are not overlooked, a "Local" PCA model with a subset of the source oils was made. The Qatar oil spill samples cluster with 10 oil samples from the Gulf and one sample from Syria (samples inside the box in Fig. 21.6D). A "Local" model, based on these 11 samples is shown in Fig. 21.7, with the same 34 spill samples projected onto the model.

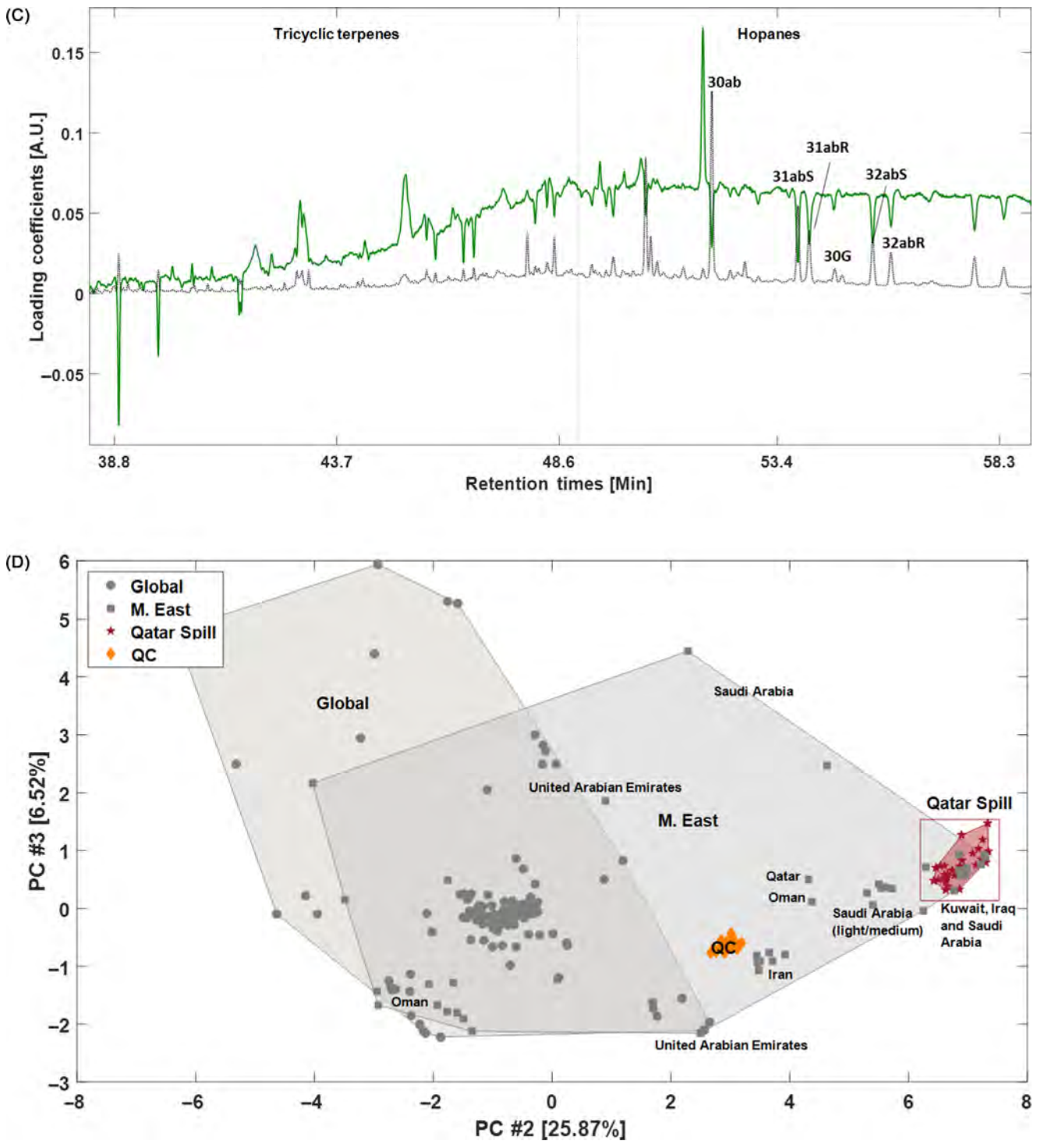

FIGURE 21.6 (Continued)

From Fig. 21.7, we can see that the spill samples most likely originate from two sources, which are similar to oils from Kuwait (dash-dotted circle in Fig. 21.7) and Saudi Arabia (dashed circle in Fig. 21.7).

21.3.2.2.2 Model 3

To gain further information for the identification, a set of the least weathered spill samples was found by analyzing selected PAHs: C0-phenanthrene to C4-phenanthrene (m/z 178, 192, 206, 220, 234), C1-benzothiophene to

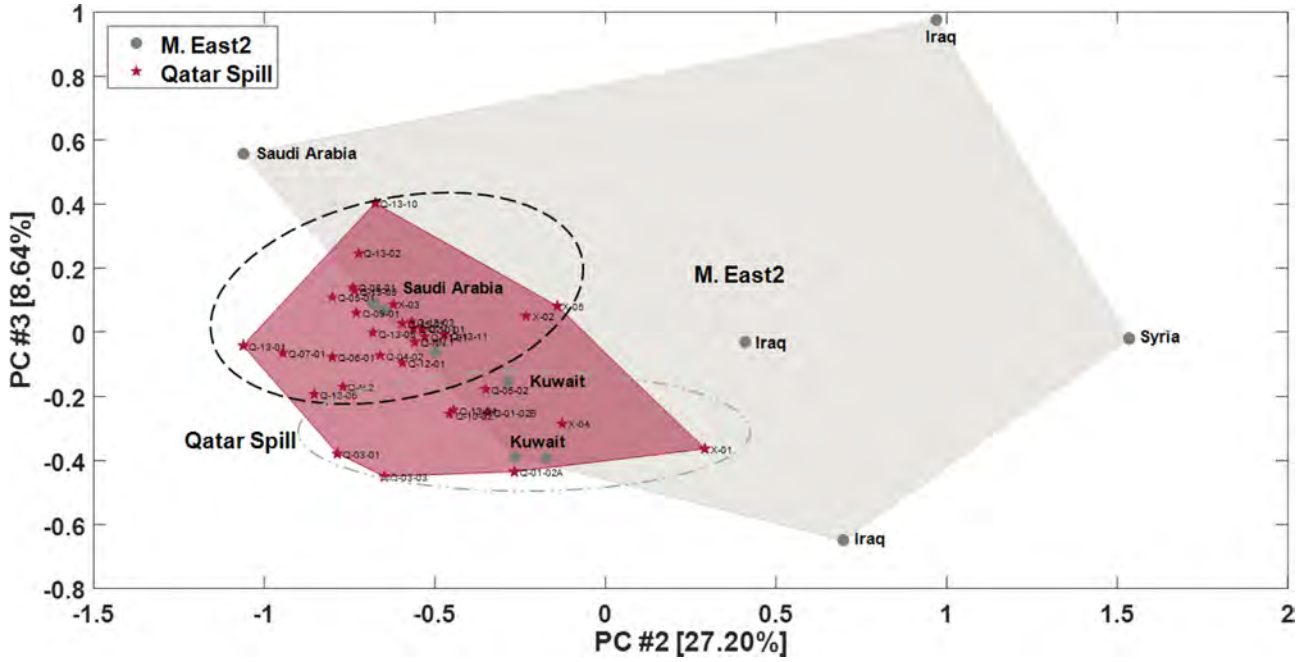

FIGURE 21.7 PCA score plot of PC2 vs PC3 of the PCA model (m/z 191 SIC) of 10 crude oil samples from the Gulf and 1 from Syria (circles) with Qatar spill samples (stars) projected onto the model (data points inside the square in Fig. 21.6D). The dash-dotted circle represents Qatar spill samples resembling Kuwait oils from the UCPH database, whereas the dashed circle represents spill samples resembling Saudi Arabia oils.

C3-benzothiophene (m/z 198, 212, and 226), C0-pyrene to C3-pyrene (m/z 202, 216, 230, 244), and C0-chrysene to C2-chrysene (m/z 228, 242, and 256). The SICs were normalized according to Scheme 2 (i.e., constant Euclidean norm after the SICs are combined). Sample Q-09-02 was excluded from the dataset as it was found to be highly weathered by visual inspection of TIC and SICs. Loadings and scores of PC1 and PC2 are shown in Fig. 21.8.

The PC1 loading plot (Fig. 21.8A) shows that negative PC1 scores characterize oil samples with high relative concentrations of three ring PAHs (phenanthrenes) and dibenzothiophene and low relative concentrations of the four ring PAHs (chrysenes and pyrenes/fluoranthenes). Negative PC1 scores are therefore characteristic for less weathered oils. Samples with positive PC2 scores have high relative concentrations of C0−C1-phenanthrenes and C1−C2-dibenzothiophenes (positive loadings in Fig. 21.8B) and low relative concentrations of four ring PAHs and highly methylated three ring PAHs (negative loadings in Fig. 21.8B). Samples with negative PC1 and positive PC2 scores are the least weathered and are selected for further analysis (109 samples shown with an asterisk in Fig. 21.8C).

For these 10 least weathered samples, it was tested whether combining hopanes with steranes or with various PAHs could improve the ability of the method to identify the sources of the Qatar spill samples. A model, based on a subset of samples from the UCPH database with 46 samples originating from the Middle East, was made and the least weathered samples were projected on it. It was tested if the model changed significantly when the spill samples were included in the model instead of being projected onto it, but this was not the case, which verifies that the spill samples contain no information not present in the source oil training set. This model (Fig. 21.9) verifies the results obtained from model 2 that the spill samples originate from multiples sources similar to oils from Saudi Arabia, Kuwait and Iraq.

21.3.2.2.3 Model 4

To test if the spill samples could be characterized as HFOs, a fourth model was calculated based on m/z 216 and 230 (C1- and C2-pyrenes/fluoranthenes) from 205 samples from the UCPH database (46 samples from the Middle East, 18 HFO's from the North Sea and 141 Global samples). The ratios of anthracenes to phenanthrenes and fluoranthenes to pyrenes can distinguish pyrogenic and petrogenic sources of PAHs (Peters et al., 2005). The ratios between phenanthrenes and anthracenes have also been used to differentiate between crude oils and HFOs

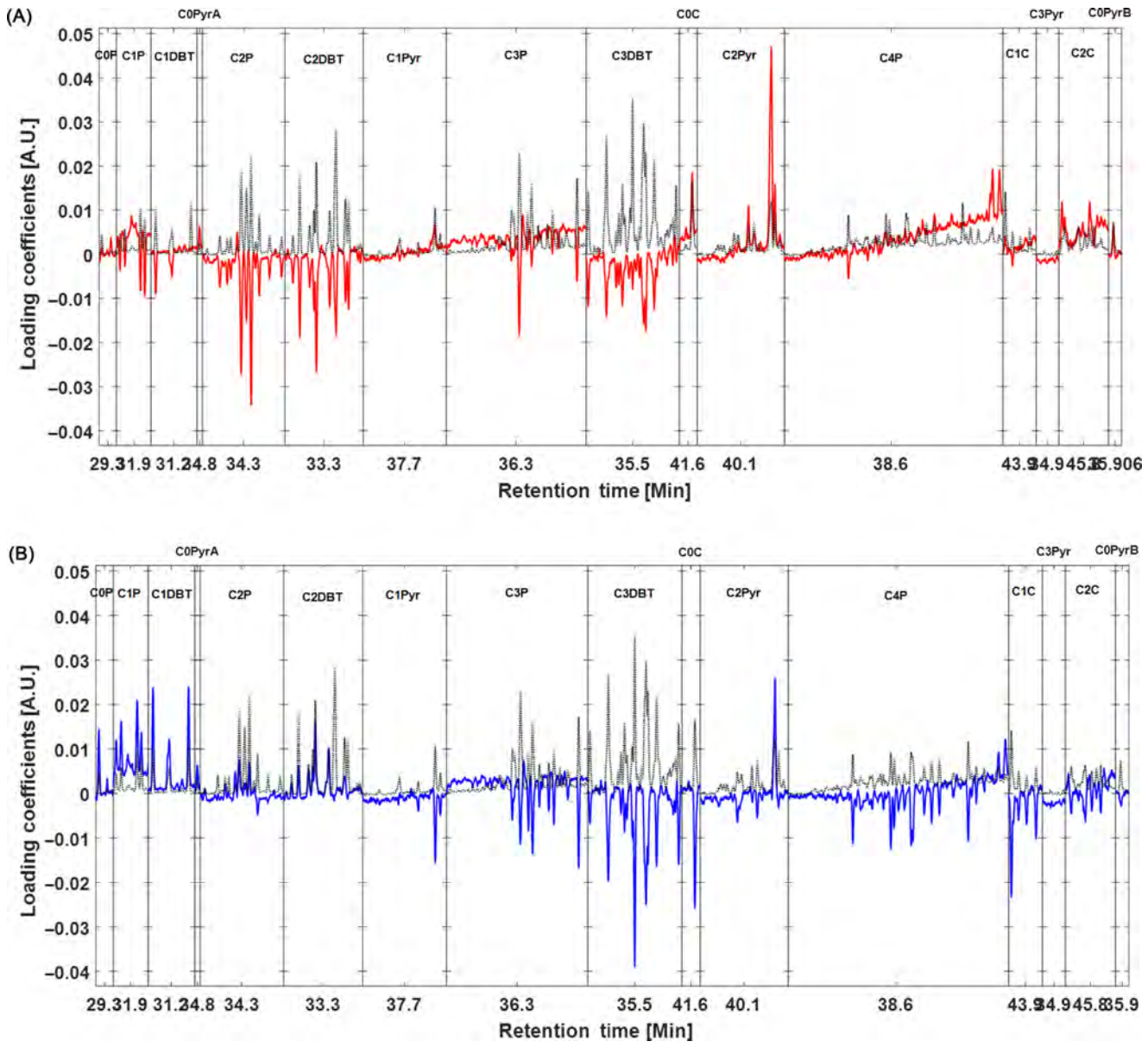

FIGURE 21.8 (A) PC1 and (B) PC2 loading plots for selected SICs in Qatar spill samples: *C0P*, C0-phenanthrene; *C1P*, C1-phenanthrenes/anthracenes; *C2P*, C2-phenanthrenes/anthracenes; *C3P*, C3-phenanthrenes/anthracenes; *C4P*, C4-phenanthrenes/anthracenes; *C1DBT*, C1-dibenzothiophenes; *C2DBT*, C2-dibenzothiophenes; *C3DBT*, C3-dibenzothiophenes; *C0Pyr*, C0-pyrene/fluoranthenes; *C1Pyr*, C1-pyrenes/fluoranthenes; *C2Pyr*, C2-pyrenes/fluoranthenes; *C3Pyr*, C3-pyrenes/fluoranthenes; *C0C*, C0-chrysene; *C1C*, C1-chrysenes; and *C2C*, C2-chrysenes. The dotted chromatograms in the loading plots represent the average TIC of all samples in the training set. (C) Score plot of PC1 (gray bars) and PC2 (black bars). The star indicates a new sample set of 10 of the least weathered samples.

due to chemical changes during the refinery process (Zhang et al., 2016) and this is hypothesized to be the case also for four ring PAHs. In this study, the parent three- and four-ring PAHs were heavily weathered but the C1-pyrenes/fluoranthenes were much less affected by weathering. The ability of C1-pyrenes/fluoranthenes to distinguish oil type where therefore tested in this study. The 10 least weathered samples identified for model 3 were projected onto the model.

Fig. 21.10 shows that the HFOs are separated from both spill samples and Middle East samples. The PC1 loadings show that PC1 distinguish between petrogenic and pyrolytic sources, as C1- and C2-fluoranthenes have negative loadings, whereas C1- and C2-pyrenes have positive loadings. Samples at positive PC1 scores are

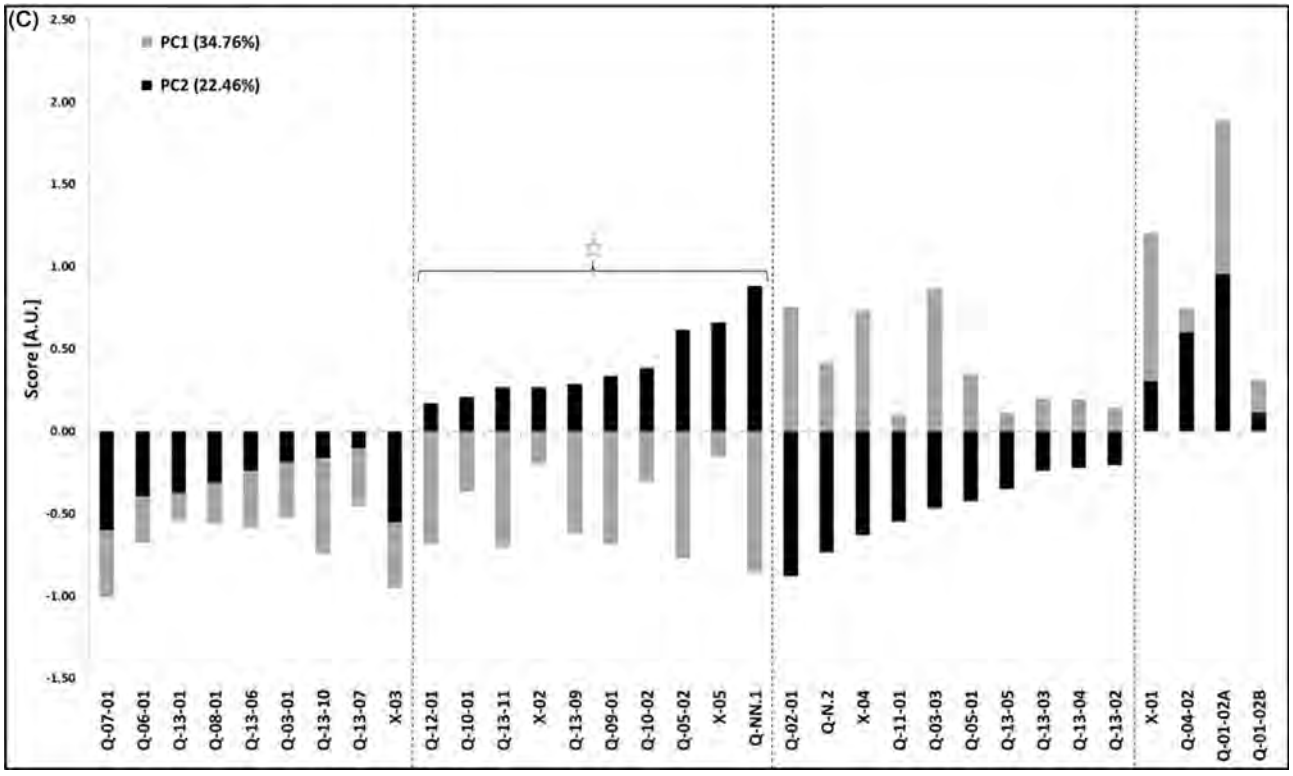

FIGURE 21.8 (Continued)

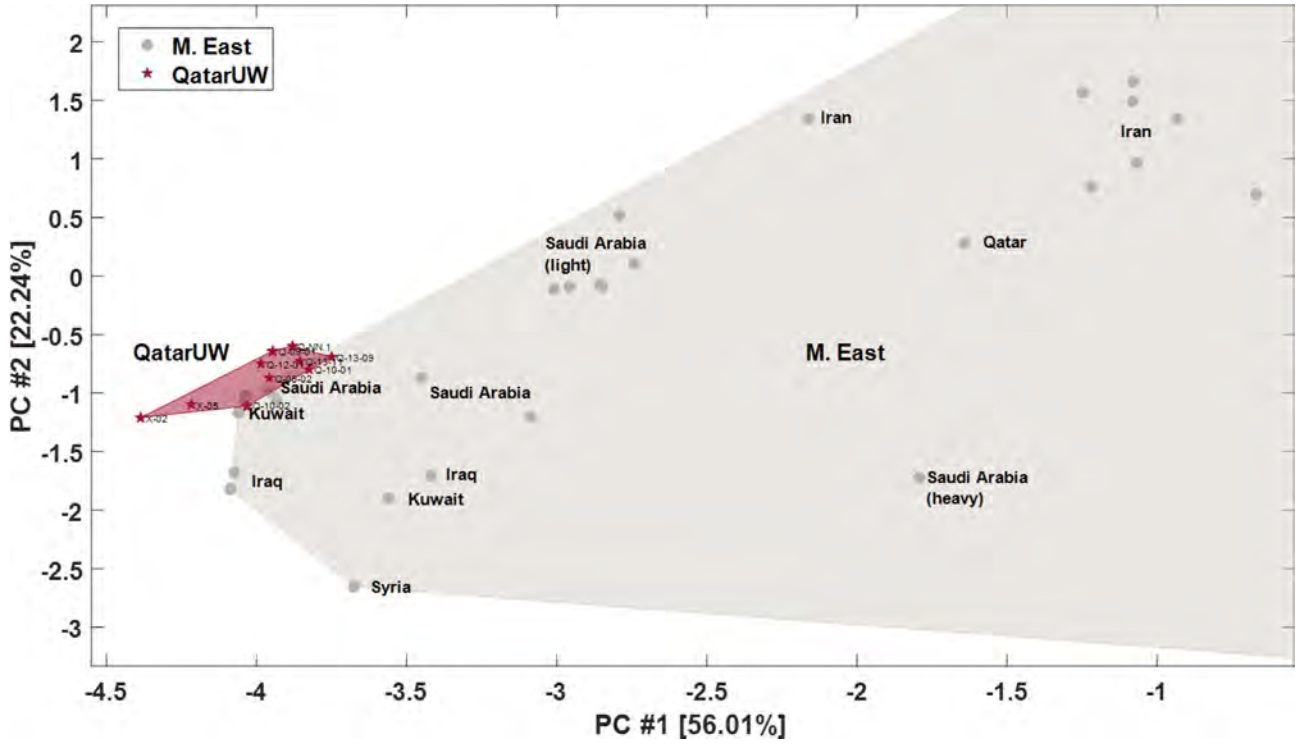

FIGURE 21.9 Zoom of the PCA score plot of PC1 vs PC2 in the hopanes (m/z 191) PCA model of 46 samples from the Middle East (circles) and 10 of the least weathered oil spill samples projected onto the model (stars).

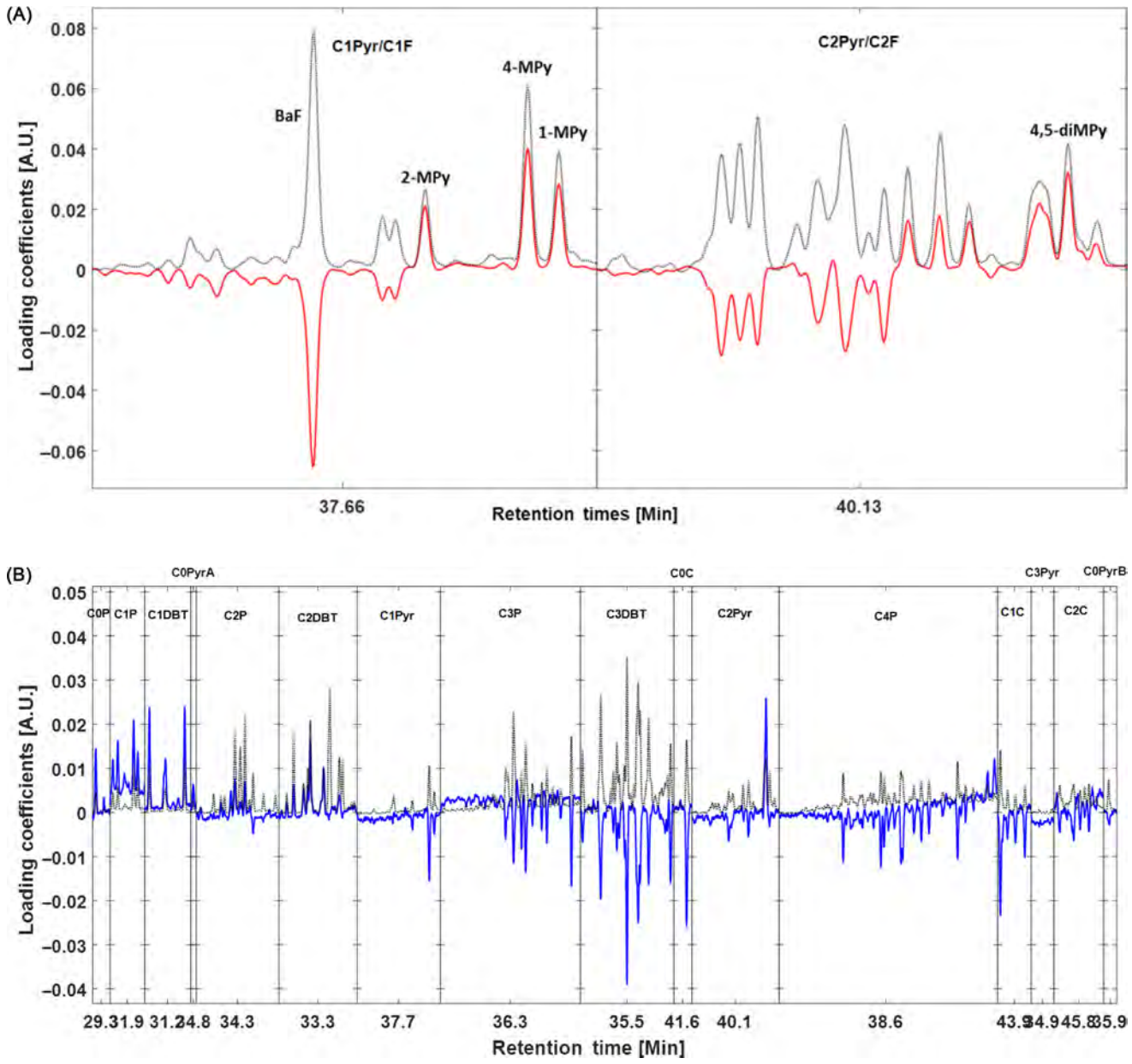

FIGURE 21.10 (A) PC1 and (B) PC2 loading plot for C1- and C2-pyrenes/fluoranthenes (C1Pyr/C1F and C2Pyr/C2F). The dotted chromatograms represent the average TIC of all samples in the training set. *BaF*, Benzo[*a*]fluorene; *2-MPy*, 2-methylpyrene; *4-MPy*, 4-methylpyrene; *1-MPy*, 1-methylpyrene; and *4,5-diMPy*, 4,5-dimethylpyrene. (C) Score plot of PC1 and PC2 for the PCA model with Global and Middle East samples (circles) and HFOs (squares) from the UCPH database. Least weathered spill samples (stars) are projected onto the model.

characterized as being from pyrolytic sources or having input from HFO fractions. PC2 further distinguish the HFOs from the spill samples. Samples at positive PC2 scores (e.g., the HFOs) has high amounts of 2-methylpyrene compared to 4-methylpyrene, whereas the spill samples have lower values of 2-methylpyrene compared to 4-methylpyrene. The C1- and C2-pyrene/fluoranthenes pattern is highly affected by photodegradation and a decrease in 1-methylpyrene relative to the other isomers can typically be explained by exposure to sunlight (CEN/BT/TF and Bonn-OSINet, 2011). The loadings show no relative decrease in 1-methylpyrene compared to the other isomers and the reason for the separation of HFOs from the cluster of spill samples was hence not photooxidation processes. The results indicate that the spill samples did not originate from HFO spills but instead from crude oil spills. To strengthen this conclusion, a larger number of HFOs from the area of interest should be included in the training set.

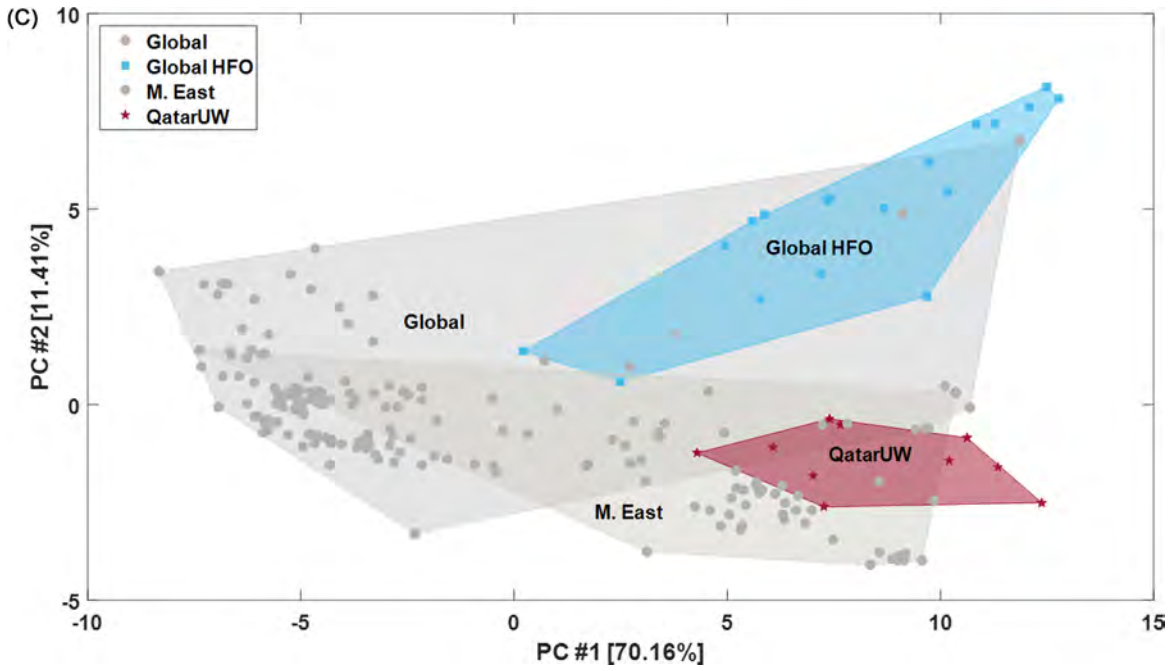

FIGURE 21.10 (Continued)

21.4 CONCLUDING REMARKS

Two case studies were presented to illustrate the use of pixel-based fingerprinting for hydrocarbon source differentiation and oil spill identification. In case study 1, it was possible to separate the sampling sites according to the level of contamination, and to discriminate the main sources of PAHs, although partly confounded with weathering. In most cases, the PAH composition allowed to characterize hydrocarbon pollution according to input of petrogenic, pyrogenic or diagenetic PAHs, as well as differentiate according to degree of weathering. Hopane biomarkers were used to further discriminate the samples with an unclear anthropogenic PAH fingerprint; and the analysis supported the prior conclusions on petrogenic samples. Sterane biomarkers were used to identify the possible source samples with clear petrogenic input. The identification of oil spill samples from Al Zubarah was the subject of case study 2. Hopane biomarkers indicated that beached oil samples originated from multiple sources which were restricted to Saudi Arabia and Kuwait using a local model on a subset of samples. The PAH composition was then analyzed to identify the least weathered spill samples so that C1- and C2-pyrenes/fluoranthenes could be used to clarify their origin as crude oils or HFOs.

CHEMSIC has been shown to be a powerful tool for oil spill identification and hydrocarbon source differentiation so long as confounding factors such as degree of weathering or the heterogeneity of the training set are taken into account. Thus, it is important to only include compounds and/or groups of compounds that are not heavily weathered and, to achieve the best possible spill identification, it is essential that all potentially relevant source samples be part of the training set for the model.

Acknowledgments

We wish to greatly acknowledge Nasser S. Al-Kaabi, Nabil Zouari, Theis I. Solling, Steffen S. Bach, and Mohammed Al-Ghouti for their work related to case study 2 and Josephine S. Lübeck, Sofie B. Knudsen, Mohsen Soleimani, and Søren Furbo for their work related to case study 1.

References

Al-Kaabi, N.S., Kristensen, M., Zouari, N., Solling, T.I., Bach, S.S., Al-Ghouti, M., et al., 2017. Source identification of beached oil at Al Zubarah, Northwestern Qatar. J. Pet. Sci. Technol. 149, 107–113.

Bejarano, A.C., Michel, J., 2010. Large-scale risk assessment of polycyclic aromatic hydrocarbons in shoreline sediments from Saudi Arabia: environmental legacy after twelve years of the Gulf war oil spill. Environ. Pollut. 158, 1561–1569.

Bro, R., Smilde, A.K., 2003. Centering and scaling in component analysis. J. Chemom. 17, 16–33.
CEN/BT/TF and Bonn-OSINet, 2011. Oil spill identification—waterborne petroleum and petroleum products—Part 2: Analytical methodology and interpretation of results based on GC–FID and GC–MS low resolution analyses. In: CEN/TR 15522-2:2011. CEN/TR European Committee for Standardization, pp. 138.
Christensen, J.H., Tomasi, G., 2007. Practical aspects of chemometrics for oil spill fingerprinting. J. Chromatogr. A 1169, 1–22.
Christensen, J.H., Tomasi, G., Hansen, A.B., 2005. Chemical fingerprinting of petroleum biomarkers using time warping and PCA. Environ. Sci. Technol. 39, 255–260.
Christensen, J.H., Mortensen, J., Hansen, A.B., Andersen, O., 2005. Chromatographic preprocessing of GC–MS data for analysis of complex chemical mixtures. J. Chromatogr. A 1062, 113–123.
Christensen, J.H., Tomasi, G., Scofield, A.D.L., Meniconi, M.D.F.G., 2010. A novel approach for characterization of polycyclic aromatic hydrocarbon (PAH) pollution patterns in sediments from Guanabara Bay, Rio de Janeiro, Brazil. Environ. Pollut. 158, 3290–3297.
CIWP, 2015. About Conservation of Iranian Wetlands Project. Conservation of Iranian Wetlands Project. Available: <http://wetlandsproject.ir/English/Default.aspx> (accessed 13.02.15).
de Fatima, M., Meniconi, G., Barbanti, S.M., 2007. 17—Case study: Evaluation of hydrocarbon sources in Guanabara Bay, Brazil. In: Stout, S., Wang, Z. (Eds.), Oil Spill Environmental Forensics. Academic Press, Burlington, pp. 505–536.
Esbensen, K.H., Geladi, P., 2009. 2.13—Principal component analysis: concept, geometrical interpretation, mathematical background, algorithms, history, practice. In: Tauler, R., Walczak, B. (Eds.), Comprehensive Chemometrics: Chemical and Biochemical Data Analysis. Elsevier, Oxford, pp. 211–226.
Furbo, S., Hansen, A.B., Skov, T., Christensen, J.H., 2014. Pixel-based analysis of comprehensive two-dimensional gas chromatograms (color plots) of petroleum: a tutorial. Anal. Chem. 86, 7160–7170.
Gallotta, F.D.C., Christensen, J.H., 2012. Source identification of petroleum hydrocarbons in soil and sediments from Iguaçu River Watershed, Paraná, Brazil using the CHEMSIC method (CHEMometric analysis of Selected Ion Chromatograms). J. Chromatogr. A 1235, 149–158.
Groeger, T., Schaeffer, M., Puetz, M., Ahrens, B., Drew, K., Eschner, M., et al., 2008. Application of two-dimensional gas chromatography combined with pixel-based chemometric processing for the chemical profiling of illicit drug samples. J. Chromatogr. A 1200, 8–16.
Hayes, M.O., Michel, J., Montello, T.M., Aurand, D.V., Almansi, A.M., Almoamen, A.H., et al., 1993. Distribution and weathering of shoreline oil one year after the Gulf War oil spill. Mar. Pollut. Bull. 27, 135–142.
Lübeck, J.S., Poulsen, K.G., Knudsen, S.B., Soleimani, M., Furbo, S., Tomasi, G., et al., 2016. Source apportionment of polycyclic aromatic hydrocarbons (PAHs) in sediments from Khuzestan province, Iran. Mar. Pollut. Bull. 110, 584–590.
Massoud, M.S., AlAbdali, F., AlGhadban, A.N., AlSarawi, M., 1996. Bottom sediments of the Arabian Gulf—II. TPH and TOC contents as indicators of oil pollution and implications for the effect and fate of the Kuwait oil slick. Environ. Pollut. 93, 271–284.
Nielsen, N.J., Ballabio, D., Tomasi, G., Todeschini, R., Christensen, J.H., 2012. Chemometric analysis of gas chromatography with flame ionisation detection chromatograms: A novel method for classification of petroleum products. J. Chromatogr. A 1238, 121–127.
Nielsen, N.P.V., Carstensen, J.M., Smedsgaard, J., 1998. Aligning of single and multiple wavelength chromatographic profiles for chemometric data analysis using correlation optimised warping. J. Chromatogr. A 805, 17–35.
Peters, K.E., Walters, C.C., Moldowan, J.M., 2005. The Biomarker Guide. Cambridge University Press, Cambridge, UK, p. 1155.
Petersen, I.L., Tomasi, G., Sorensen, H., Boll, E.S., Hansen, H.C.B., Christensen, J.H., 2011. The use of environmental metabolomics to determine glyphosate level of exposure in rapeseed (*Brassica napus* L.) seedlings. Environ. Pollut. 159, 3071–3077.
Silliman, J.E., Meyers, P.A., Eadie, B.J., Klump, J.V., 2001. A hypothesis for the origin of perylene based on its low abundance in sediments of Green Bay, Wisconsin. Chem. Geol. 177, 309–322.
Skov, T., van den Berg, F., Tomasi, G., Bro, R., 2006. Automated alignment of chromatographic data. J. Chemom. 20, 484–497.
Soleimani, M., Afyuni, M., Hajabbasi, M.A., Nourbakhsh, F., Sabzalian, M.R., Christensen, J.H., 2010. Phytoremediation of an aged petroleum contaminated soil using endophyte infected and non-infected grasses. Chemosphere 81, 1084–1090.
Tissot, B., Welte, D., 2012. Petroleum Formation and Occurrence: A New Approach to Oil and Gas Exploration. Springer-Verlag, Berlin Heidelberg New York, p. 538.
Tomasi, G., Savorani, F., Engelsen, S.B., 2011. icoshift: an effective tool for the alignment of chromatographic data. J. Chromatogr. A 1218, 7832–7840.
Tomasi, G., van den Berg, F., Andersson, C., 2004. Correlation optimized warping and dynamic time warping as preprocessing methods for chromatographic data. J. Chemom. 18, 231–241.
UNDP/GEF, 2011, Governmental-Organizations, NGO's and Local-Communities-of-Shadegan-Wetland. Shadegan Wetland Integrated Management Plan. The Ramsar Convention Secretariat. Available: <http://www.ramsar.org/sites/default/files/documents/library/shadeganmanagementplan-i.r._iran2011.pdf> (accessed 15.02.15).
UNESCO, 2016. Al Zubarah Archaeological Site. UNESCO World Heritage List. Available: <http://whc.unesco.org/en/list/1402/> (accessed: 27.11.2016).
Yunker, M.B., Macdonald, R.W., Vingarzan, R., Mitchell, R.H., Goyette, D., Sylvestre, S., 2002. PAHs in the Fraser River basin: a critical appraisal of PAH ratios as indicators of PAH source and composition. Org. Geochem. 33, 489–515.
Zhang, H.J., Wang, C.Y., Zhao, R.X., Yin, X.N., Zhou, H.Y., Tan, L.J., et al., 2016. New diagnostic ratios based on phenanthrenes and anthracenes for effective distinguishing heavy fuel oils from crude oils. Mar. Pollut. Bull. 106, 58–61.

CHAPTER

22

Use of Passive Samplers to Determine the Source of Dissolved PAHs in the Ottawa River, Toledo, Ohio

Mark J. Benotti[1], *Lisa Lefkovitz*[2] *and Marc A. Mills*[3]

[1]NewFields Environmental Forensics, LLC, Rockland, MA, United States [2]Battelle Memorial Institute, Norwell, MA, United States [3]United States Environmental Protection Agency, Cincinnati, OH, United States

BIOGRAPHIES

Mark J. Benotti, Ph.D. is a Senior Environmental Chemist with NewFields Environmental Forensics, LLC. He has more than 15 years of experience with projects related to understanding the chemical impacts of anthropogenic compounds in water systems and aquatic environments. He has managed or served as a technical advisor on projects in the United States and abroad involving the complexities of the occurrence, fate and transport of pharmaceuticals and personal care products (PPCPs), polyfluoroalkyl substances (PFASs), endocrine disrupting chemicals (EDCs), hydrocarbons, petrochemicals, polycyclic aromatic hydrocarbons (PAHs), polychlorinated biphenyls (PCBs), pesticides, and other anthropogenic contaminants in impacted aquatic, and sediment systems. His work has included study design and characterization of sites impacted by wastewater and/or combined sewer overflows (CSOs), water reuse facilities/settings, sediment remediation sites, impacted by oil spills, sites, and general investigations of waters and sediments in complex, urbanized environments. He has worked closely with risk assessors and toxicologists to incorporate aspects of environmental or human risk into interpretations of contaminant chemistry and behavior and with engineers to determine most appropriate water treatment strategies. He has published over 30 peer-reviewed manuscripts, book chapters, and reports pertaining to the forensic identification of fugitive materials, contaminant fate and transport, and water treatment. Dr. Benotti has a B.A. in Chemistry from the College of the Holy Cross and a Ph.D. in Coastal Oceanography from Stony Brook University.

Lisa F. Lefkovitz is an environmental chemist with 30 years of experience in the design and management of chemical and biological evaluations of sediments and dredged materials and the fate and transport of organic and inorganic contaminants in the environment. She is technically based in environmental chemistry with proficiency in hydrogeology, geology, regulatory affairs, and remediation, and has applied her expertise and management skills to projects where sediment quality is a prominent issue. Ms. Lefkovitz has extensive expertise in the movement, transport, and fate of contaminants in estuarine, riverine, and marine aquatic environments including the use of radio isotope analysis to study sediment deposition and contaminant history. She has participated in development and application of innovative sampling techniques such passive samplers for the measurement of hydrophobic organic compounds in the aquatic environment. Ms. Lefkovitz has applied this technology to evaluating the effectiveness of sediment remediation approaches including dredging, capping and monitored natural attenuation at numerous contaminated sediment sites including Areas of Concern in the Great Lakes and at Superfund Sites. Ms. Lefkovitz holds a B.S. in Chemistry from Case Western Reserve University and a M.S. in Water Chemistry from the University of Wisconsin.

Oil Spill Environmental Forensics Case Studies.
DOI: http://dx.doi.org/10.1016/B978-0-12-804434-6.00022-7

Marc A. Mills, Ph.D. is an Environmental Engineer at the U.S. Environmental Protection Agency (EPA)' Office of Research and Development and is a principal investigator for projects characterizing the occurrence, transport, and fate of contaminants of emerging concern (CECs) and legacy contaminants in the environment and the management of contaminated sediments. Dr. Mills leads research to identify sources of contaminants to aquatic systems and tracing their movement through the environment and the food web. He also leads the development of analytical methods for CECs (e.g., PFAS, EDCs, and PPCPs) and stable isotope chemistry for environmental samples in water, wastewater, solids, and tissues at the National Risk Management Research Laboratory for U.S. EPA. These methods are used to characterize potential sources of CECs and legacy contaminants, their management in water, wastewater treatment, and new technology development. Dr. Mills has a B.S. in Civil/Environmental Engineering from Texas A&M University and a M.S. and Ph.D. from the Texas A&M University.

22.1 INTRODUCTION

22.1.1 Use of Passive Samplers

Understanding the concentrations of contaminants of concern (COCs) in the water column, porewater, and sediments is a key component to characterize and remediate contaminated sediment sites. These sites are targeted for remediation to reduce the exposure and risk to human and ecosystem receptors. However, directly measuring the truly dissolved and bioavailable fraction of COCs is challenging, particularly for hydrophobic organic contaminants (HOCs) such as PAHs, PCBs, dioxins, organochlorine pesticides, and others. The analysis of whole water samples (as surface water or porewater) measures the dissolved contaminants and those adsorbed to suspended particulate material. For HOCs, the large majority of the contaminant mass is adsorbed to particulate materials in a whole water sample. Filtering samples simply removes particles above an operationally defined particle size and the contaminants bound to them. However, dissolved contaminants losses can occur during the filtration process, such as volatilization, partitioning to the apparatus or filters, etc. Beyond these methodological issues, the solubility of many HOCs is so low, it is necessary to extract large volumes of water to measure detectable concentrations. These large volumes are particularly problematic when collecting porewater, even in very contaminated environments. In addition, a grab water sample only characterizes the concentration at the time of sample collection, and the water concentration may be affected by transient processes, such as runoff following a heavy precipitation event. As an alternative, passive samplers can be used to calculate the time averaged dissolved concentrations of HOCs over the deployment period.

Passive sampling technologies have been around for approximately three decades, though their use in environmental investigations has increased of late and their applications are still being refined (Namiesnik et al., 2005; Vrana et al., 2005). Generally, passive samplers are composed of an organic polymer that sorbs contaminants from the dissolved phase (Parkerton et al., 2012). Thompson et al. (2016) defined a passive sampler as "a device that can be placed into sediments or surface water, in the field or laboratory, to extract chemicals from the water phase within the sediment matrix." Further, the chemical accumulated by the sampler can be used to calculate the freely dissolved HOCs. Passive samplers include semipermeable membrane devices (SPMDs), solid phase microextract (SPME) fibers, polyoxymethylene (POM), polydimethylsiloxane (PDMS), polyethylene devices (PEDs; also called polyethylene diffusion passive samplers), and others (Namiesnik et al., 2005; Vrana et al., 2005; USEPA, 2012).

Fig. 22.1 lists examples of some more common passive samplers used for characterizing water and porewater concentrations and the materials from which they are constructed. A benefit of passive samplers is that they concentrate the COCs in the samplers. This concentration and the separation of the COC from the sampling matrix typically results in much easier instrument analysis due to the higher COC concentration and lower matrix interferences. Another benefit is that contaminants partition from the dissolved phase into the passive sampler in much the same way they are accumulated from the dissolved phase into the lipids of organisms. Thus, data from passive samplers not only allow the determination of dissolved concentrations, but they can be used to determine bioavailability and as a proxy for organisms to reduce the cost of risk assessment (Vinturella et al., 2004; Friedman et al., 2009). They can be deployed in environments where organisms might not survive due to suboxic/anoxic conditions, the presence of toxic levels of contaminants, or other environmental or anthropogenic stresses.

Independent of the sampler material or physical design, conceptually, HOCs are sorbed to the passive sampler polymer over a period of days to weeks. Thus, when the passive sampler is deployed, there is a period of time,

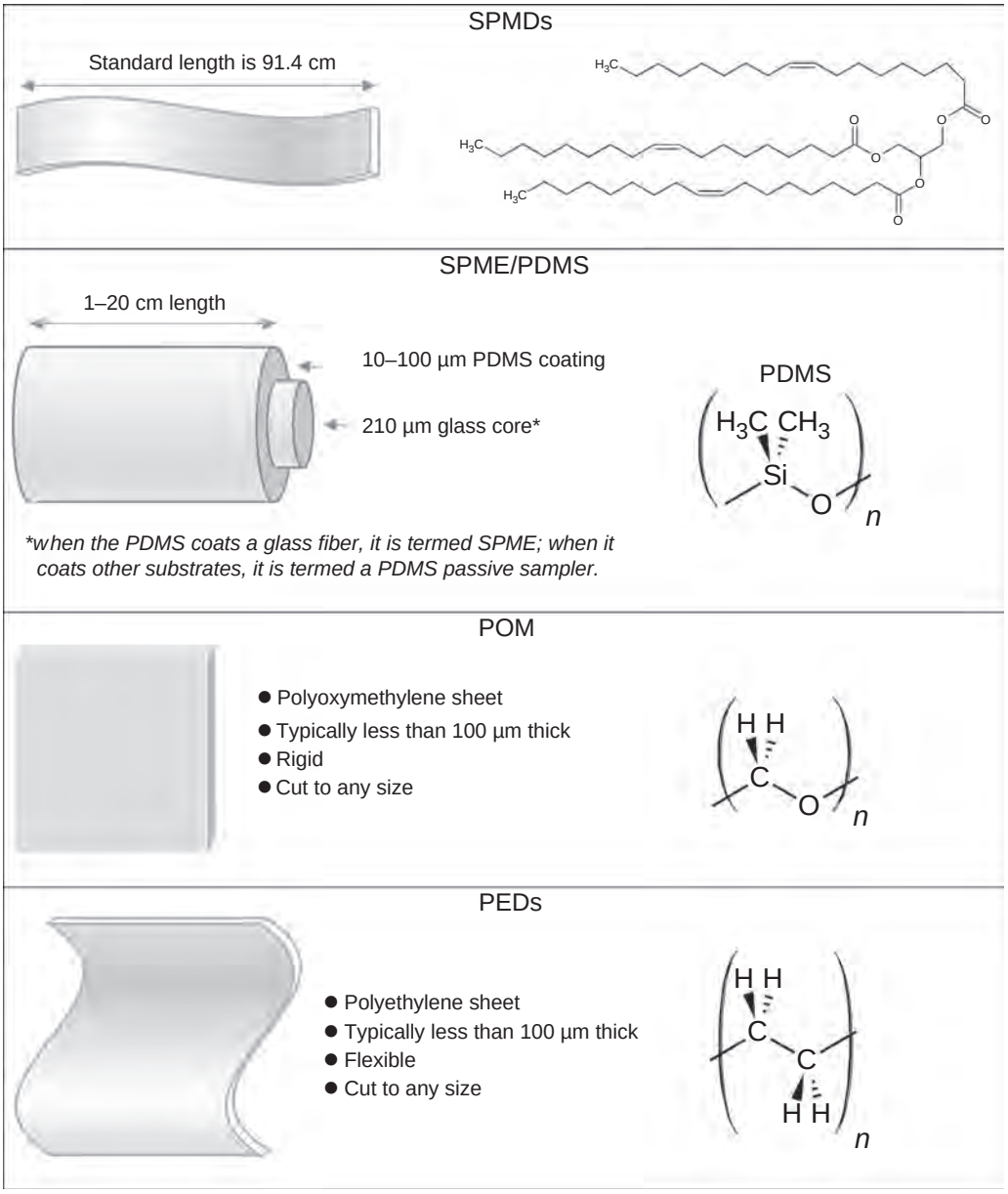

FIGURE 22.1 Inventory and selected features of common types of passive samples. SPMD: semipermeable membrane devices; SPME: solid phase microextract fibers; PDMS: polydimethylsiloxane; POM: polyoxymethylene; PED: polyethylene device.

termed the "uptake" phase, where it is out of equilibrium with the surrounding water. Once at equilibrium, the passive sampler maintains a time-integrated equilibrium concentration with the surrounding water. Typically, passive samplers take days to weeks to reach equilibrium with the water, though there are a number of factors that can affect equilibrium (Thompson et al., 2016), with some of the most important factors being the type of contaminant (particularly its hydrophobicity—less hydrophobic compounds reach equilibrium faster than more hydrophobic compounds), the type and shape/thickness of passive sampling material (e.g., thicker and higher density polymers equilibrate slower than thinner, low density polymers), and the sampled medium (e.g., overlying water typically equilibrates faster than porewater due to the limited transport of the contaminants through pore space leading to a formation of a depletion layer; ter Laak et al., 2008; Apell et al., 2016). To a lesser extend partitioning of the hydrophobic compounds to the sampler is also affected by salinity and temperature (Adams et al., 2007).

Because equilibration is not instantaneous, passive sampling results do not reflect short-term fluctuations in the contaminant concentration, and therefore provide more reliable long-term monitoring method than a one-time

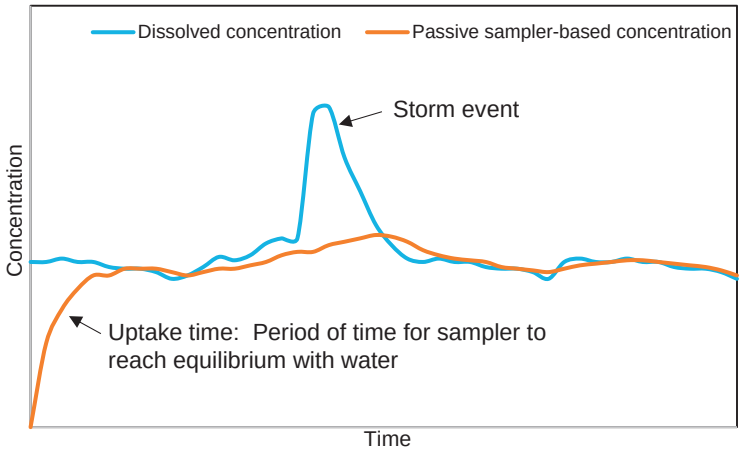

FIGURE 22.2 Conceptual dissolved water and passive sampler concentrations over time during deployment.

water sample grab measurement. Fig. 22.2 shows a conceptual relationship between the dissolved concentration of a contaminant, and the dissolved concentration calculated from passive sampler exposed over a period of time.

There are a number of considerations for using different types of passive samplers, including cost, deployment/equilibrium time, target HOCs, etc. Briefly, PEDs and POM are relatively inexpensive, they can be cut easily into any size or shape, and can be deployed in the water column or sediment in a number of configurations. However, considering the exposed surface area of the PED relates to the HOC uptake, PEDs should be deployed to avoid folding or contacting an impervious surface. POM is rigid and will not fold. However, POM can tear and break if not deployed correctly. SPME fibers can also be deployed in the water column or sediment and are available with many different polymer thicknesses, but they are brittle and need to be deployed in a specialized housing. SPMDs are fairly robust, but can only be deployed in the water column. A more complete discussion of the relative strengths and weaknesses of these different polymers and configurations for deploying them as passive samplers is available elsewhere (USEPA, 2012). The remainder of this chapter focuses on PEDs, which are often preferred due to their relative ease of use and high cost-efficiency.

22.1.2 Calculating Aqueous Concentrations From PED Data

The approach to interpreting data collected from PEDs is summarized in this section. While all passive samplers generally follow a similar approach, the water-passive sampler partition coefficients are different from polymer to polymer. All passive samplers, including PEDs, measure HOC concentration absorbed into the polymer, or lipid phase, and the calculated concentration of the HOC dissolved in water in contact with the passive sampler. Once the PED is retrieved, the polymer is extracted and prepared for analysis. The analysis technique (GC–MS, LC–MS, etc.) is dependent on the targeted HOC. Once the mass of the HOCs is calculated in the extract, it is normalized to the mass of the extracted polymer, resulting in the mass of contaminant per mass of sampler. At equilibrium, the concentration of contaminant in the PED (C_{PED}) and the dissolved concentration (C_D) are related as follows:

$$C_D = \frac{C_{PED}}{K_{PED}} \times 1000 \tag{22.1}$$

where K_{PED} is the passive sampler-dissolved phase partition coefficient (in L/kg). K_{PED} can be derived empirically (Booij et al., 2003; Adams et al., 2007) or can be estimated from the more readily available octanol–water partition coefficient (K_{OW}) using the following equation (Lohmann and Muir, 2010):

$$\log K_{PED} = -0.59 + 1.05 \log K_{OW} \tag{22.2}$$

Eq. (22.1), however, only applies when the PED is at equilibrium with the surrounding environment, and does not apply to the "uptake" phase. Recently, the use of performance reference compounds (PRCs) has been incorporated into passive sampler applications in order to correct for nonequilibrium conditions. The principle is that the passive sampler is deployed with one or more PRCs at a known concentration. The PRCs are compounds

that are not found in the environment being sampled, and they desorb from the PED with the same kinetics and at a similar rate that contaminants absorb into the PED. Therefore, when the PRC cannot be detected in the PED, absorbed contaminants are at equilibrium with concentrations in surrounding waters. Therefore, during the uptake phase (i.e., during nonequilibrium conditions), the dissolved concentration can be calculated from the passive sampler using the following equations (Adams et al., 2007):

$$C_d = \frac{C_{\mathrm{PED}}}{\left(1 - e^{-k_e t}\right) \times K_{\mathrm{PED}}} \tag{22.3}$$

and

$$k_e = \ln\left(\frac{C_{\mathrm{PRC}-t}}{C_{\mathrm{PRC}-0}}\right) \div t \tag{22.4}$$

where t is the deployment time (in days), $C_{\mathrm{PRC\text{-}0}}$ is the concentration of PRC before deployment, and $C_{\mathrm{PRC\text{-}}t}$ is the concentration of PRC after deployment. The amount of the correction decreases with increasing time, and as the PED approaches equilibrium, the value calculated from Eq. (22.2) approaches the value calculated from Eq. (22.1). In other words, as the PED approaches equilibrium, $e^{-k_e t}$ approaches 0.

In practice, not every target HOC reaches equilibrium at the same time, and nor does every PRC desorb at the same rate. Ideally, the PRCs and target HOCs are matched as closely as possible. For example, if one targeted phenanthrene with the passive sampler, an isotopically labeled phenanthrene would be an ideal PRC. However, it is impractical to isotopically match every target HOCs, and many isotopically labeled compounds are already incorporated into analytical methods as surrogate or internal standards. Therefore, it is best practice to use a number of different PRCs representative of the range of hydrophobicities or values for K_{OW} of the target HOCs. When calculating dissolved concentrations of a particular contaminant using Eqs. (22.3 and 22.4), it is also best practice to correct for nonequilibrium using the PRC that has the most similar hydrophobicity or K_{OW} to the target contaminant.

22.1.3 Site Background—Ottawa River Case Study

The Ottawa River is an urban waterway that drains into North Maumee Bay, Lake Erie in Toledo, Ohio, USA. It is 45-mi long with a drainage basin of 221 square miles; 147 of which are in Ohio. Historic industrial development along the lower portions of the river (defined as the lower 8.8 mi) includes multiple landfills, textile producers, fertilizer manufacturers, and heavy industry. As a result of the waste management practices associated with the land uses and ongoing discharge from CSO and storm sewers, sediments of the lower Ottawa River became contaminated with heavy metals, semivolatile organic compounds, and PCBs (Parametrix, 2001). In 1987, the Great Lakes Water Quality Agreement designated the Maumee River Area of Concern, which encompassed 775 square miles of the 8320-square-mile watershed, and includes the Ottawa River (Fig. 22.3; Maumee RAP, 2006). In the years that followed, substantial remediation and restoration has been completed within the Ottawa River through such programs as the Great Lakes Legacy Act (GLLA) and the Great Lakes Restoration Initiative. These actions include the identification of contaminant sources, remediation of landfills, and other upland sites along the river, characterization of the spatial extent of contamination within river sediments, completion of both ecological and human-health risk assessments, and remediation of the most contaminated areas within the lower Ottawa River.

An interdisciplinary and collaborative study started in 2009 between the U.S. EPA's Office of Research and Development (ORD), and EPA's Great Lakes National Program Office (GLNPO). The partnership has conducted a joint evaluation of the environmental dredging conducted as a GLLA project in 2009–10. Environmental dredging was selected by GLNPO as the remedy of choice to remove sediment contaminated with PCBs, PAHs, and lead from selected areas of the lower river. ORD and GLNPO are conducting an ongoing comprehensive assessment of remedy effectiveness of environmental dredging on the Ottawa River. This evaluation weight of evidence approach was used to assess the effectiveness of the selected remedy in removing contaminated sediments from the river and in restoring the river's ecosystem.

22.1.4 Potential Sources of PAH Contamination to the Ottawa River

The sediments in the Ottawa River between RM 3.2-8.8 (Reaches 2-4) historically included contamination from sources that include urban storm water runoff, commercial and residential development, municipal and industrial discharges, CSOs, sanitary sewer overflows, wastewater treatment plant bypasses, hazardous waste disposal sites,

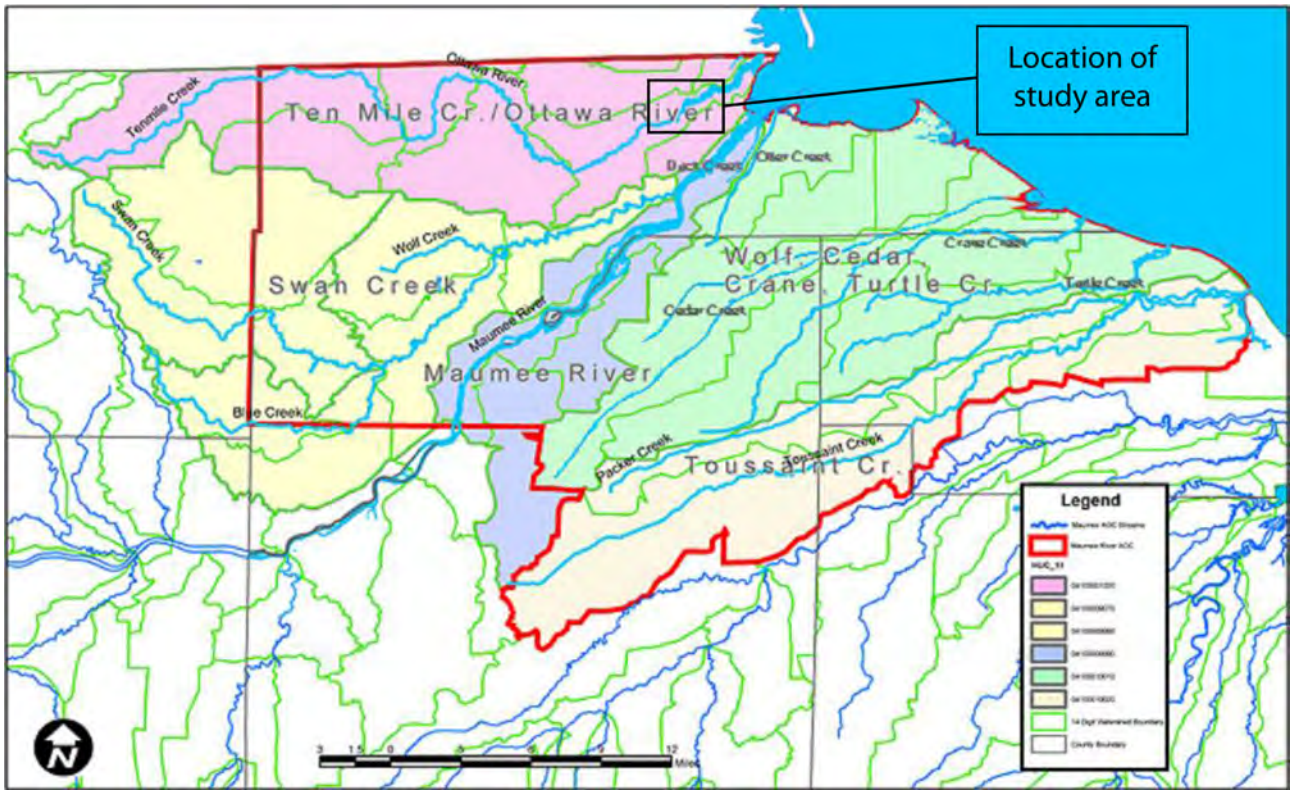

FIGURE 22.3 Maumee River Area of Concern with the Ottawa River watershed shown at the top of the figure. Location of study area within the Ottawa River watershed described herein is indicated by the black box.

and agricultural runoff. This contamination entered the waterway from direct and indirect discharge of contaminants, permitted and unregulated discharge, surface and subsurface discharge, and overflows. Current sources of contamination to this reach of the river are primarily from redistribution of currently bedded sediment, storm, sanitary, and combined server overflow discharges, and surface runoff. Major past sources are considered controlled currently (Maumee RAP, 2002). Though selected "hot spots" were dredged during the GLLA remediation project in 2009–10, elevated PAH concentration still exist in the river throughout these reaches. Historically, industrial waste such as paint waste and sludge, coal tar used in wood treating, manufacturing wastes, were discharged or disposed in dumps and landfills. Many of these legal and illegal disposal facilities continue to have uncontrolled leachate discharges directly to the river or to drainages to the river. PAHs have been detected at many of these facilities and are considered either historic or ongoing sources of contamination (Maumee RAP, 2002).

The Ottawa River continues to receive discharges from six City of Toledo CSOs, which discharge a combination of sewage and storm water runoff during heavy precipitation events. Fig. 22.4 shows a map of the study area described herein, including the location of the six active CSO outfalls.

In this study, we present our results on the use of passive samplers to determine the dissolved PAH signatures and current source(s) of the contamination using forensic methods. Our results are focused on data collected in 2013 during a post remedy assessment of the river's sediments. Dissolved PAH concentrations, calculated from PED data, are compared to PAH concentrations measured in whole water and surface sediment samples. This comparison focuses on the PAHs compositions in the media and highlights the different interpretations that arise using data from each sample matrix.

22.2 METHODS

22.2.1 Preparation of PEDs

PEDs were prepared by cutting polyethylene to size and cleaning each in solvent. One-mil (25 μM) polyethylene plastic sheets were first cut into 15 × 40 cm sections (weighing ~1 g). PED sections were cleaned by first

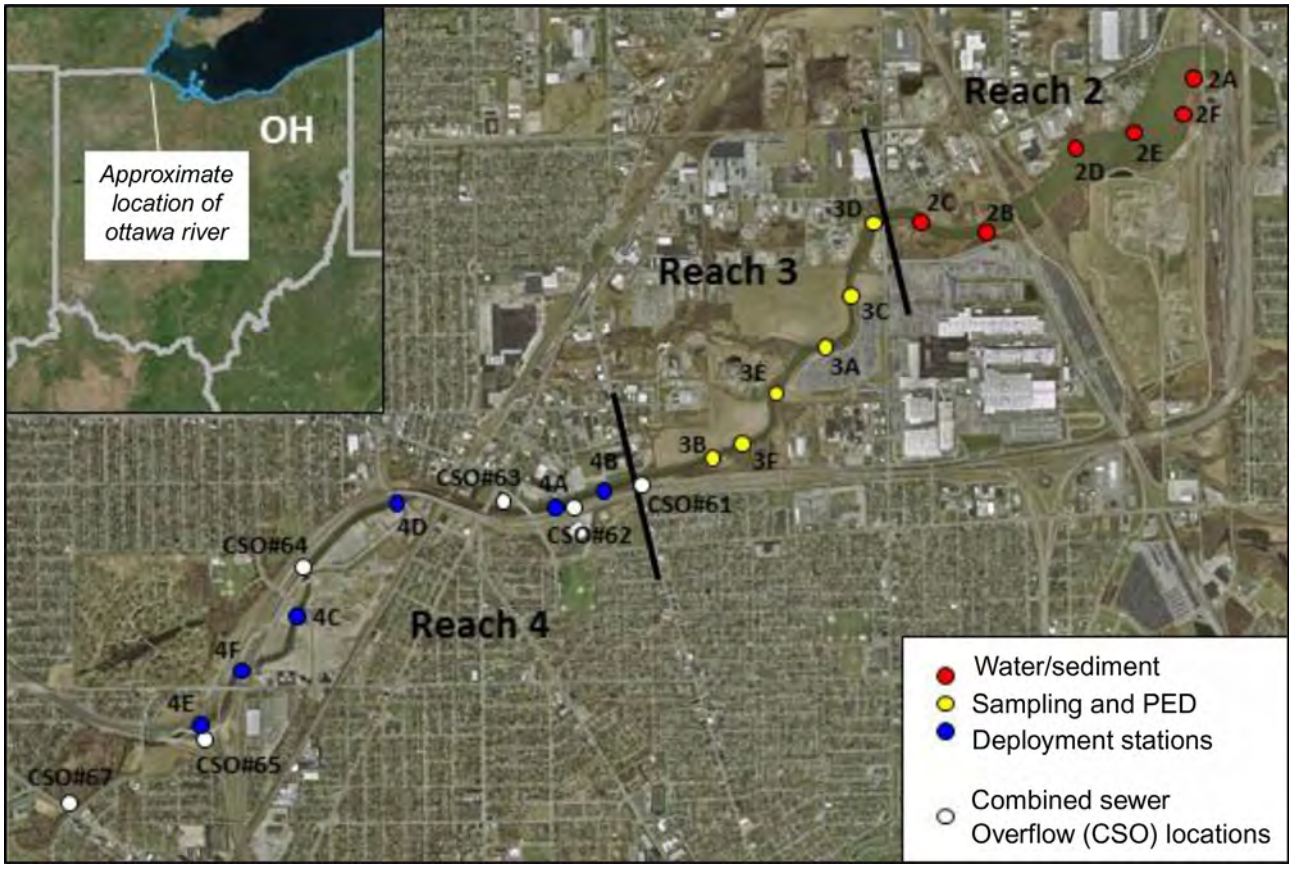

FIGURE 22.4 Map of Ottawa River study area PED deployment locations and whole water and sediment sampling locations. Sample locations (18) and CSO locations (6) in Reaches 2, 3, and 4 are indicated in different colors.

extracting for at least 12 hours in hexane, then for at least 12 hours in acetone, then for at least 12 hours in laboratory-grade water. At this point, the PEDs were removed, gently wiped dry, wrapped in cleaned aluminum foil, put into a sealed plastic bag, and stored in a freezer prior to deployment. For two reasons, PRCs were not used. First, because the deployment was planned for a relatively long period of time (i.e., greater than 40 days, see Section 22.2.2), it was assumed that the contaminants would be close to or at equilibrium. Second, since the focus of the passive samplers was to understand the forensic signature or relative distributions of PAHs, it was not necessary to use PRCs to obtain the most accurate concentration.

22.2.2 Field Activities

From July 2013 through September 2013, field activities included two primary sampling events. The first event was conducted on July 28–30, 2013 and included the deployment of PEDs and the collection of surficial sediment and water column samples. PEDs were transported to the field in their foil containers, and deployed at 18 stations in the water column (Fig. 22.4). At each station the PEDs were deployed in a triplicate set and were attached to a mooring placed on the sediment. The deployment positioned approximately 30–40 cm from the sediment bed and the PEDs were positioned perpendicular to the sediment to avoid deposition on the samplers. At two of the 18 stations, PEDs were deployed in duplicate (i.e., six PEDs attached to mooring). Composite surface sediment samples were collected from each of the 18 stations (Fig. 22.4).

Sediment was collected with a push core sampler to a depth of approximately 15 cm below the surface of the sediment-water interface. A composite sample was obtained using 16 cores collected around the perimeter of each station. Sediment samples were homogenized and subsampled in the field for multiple analyses. Composite and homogenized samples for each station were submitted to the laboratory for analysis of PCBs, PAHs, total organic carbon (TOC), moisture content, and particle size distribution.

Water column samples (1 L) were also collected at the 18 stations (Fig. 22.4). Whole water samples were collected at the approximate middepth of the water column using a Van Dorn sampler. The water samples were submitted to the laboratory for analysis of PCBs, PAHs, TOC, and total suspended solids. Fig. 22.4 shows the locations of PED deployments and whole water and surface sediment sample collection.

The PEDs were retrieved on September 9–11, 2013. PEDs were successfully retrieved from 17 of the 18 deployment stations as the sampler at Station 4F was not located during retrieval. The three PEDs from each station were placed into a sample bottle and treated as a single composite sample. PED samples were stored at 4°C and shipped to the laboratory where they were analyzed for PCBs and PAHs.

22.2.3 Analytical Methodologies

Water, sediment and PED samples were extracted and analyzed using a modified version of EPA Method 8270D (SW-846) "*Semivolatile Organic Compounds by Gas Chromatography/Mass Spectrometry (GC/MS)*." This analysis included the analysis of both parent and alkylated PAHs for a total of 36 PAHs. The extended PAH analyte list allows more detailed and comprehensive forensic analyses to be completed as compared to the more limited 16 Priority Pollutant PAH analyte list. Briefly, 1 L whole water samples (unfiltered) and 10-g sediment samples were each spiked with surrogate standards and serially extracted three times with methylene chloride. PEDs were inspected and gently wiped with a laboratory-grade tissue to remove excess water and/or biofilm. The three PEDs that composed a single sample were spiked with surrogate standards, and serially extracted with hexane. The same surrogate standards were used for all matrices and consisted of naphthalene-d_8, acenaphthalene-d_{10}, phenanthrene-d_{10} and benzo(*a*)pyrene-d_{12}. Trace water was removed by passing the extracts through anhydrous sodium sulfate and concentrated by removing solvent using Kuderna–Danish and nitrogen evaporation techniques. Sediment and PED extracts were further processed through an alumina cleanup (USEPA Method 3610B), followed by size-exclusion GPC cleanup (USEPA Method 3640A). The final extracts were concentrated by nitrogen evaporation to approximately 400 μL, spiked with internal standards (fluorene-d_{10} and chrysene-d_{10}), and the volume was adjusted to a final preinjection volume of 500 μL. Samples were analyzed by GC/MS for the 36 parent and alkylated PAHs.

22.2.4 Calculating Water Concentrations From PED Data

This section details the calculations for deriving the dissolved aqueous concentrations from the PED concentrations. The PED concentrations were initially reported in units of ng/sample, which is then divided by the mass of polyethylene contained in the composite PED sample to convert to PAH mass per mass of PED (ng/g). The calculation of the aqueous dissolved concentration of PAHs was based on Eqs. (22.1 and 22.2), using values for log K_{OW} (Durell et al., 2006) and log K_{PED} described in Table 22.1.

22.3 RESULTS

22.3.1 Concentrations of PAHs in Water and Sediment

PAHs were detected in all three media (whole water, sediment, and passive samplers) throughout the area of study (Table 22.2). Total measured concentrations of targeted PAHs in surface sediment ranged from 6030 to 72,300 μg/kg (or part-per-billion, ppb); whole water samples ranged from 0.225 to 2.39 μg/L (ppb); and PED concentrations ranged from 64,800 to 143,000 μg/kg PED. The greatest whole water, sediment, water, and PED concentrations were generally measured downriver, within Reach, and the lowest concentrations were generally measured upriver, within Reach 4, though there are locations within Reaches 3 and 4 with elevated sediment, whole water, and PED concentrations. Dissolved water concentrations calculated from the measured PED concentrations and PED deployment times are also presented in Table 22.2. Dissolved concentrations generally follow the same trend as the other data (i.e., highest concentrations downriver and lowest concentrations upriver), though the single highest value, 0.243 μg/L, was calculated from a location upriver in Reach 4, and the single lowest value, 0.063 μg/L, was calculated from a location midriver in Reach 3.

TABLE 22.1 Log K_{OW} and Log K_{PED} Values for PAHs Targeted in This Study

PAH	Abbreviation	Log K_{OW}	Log K_{PED}
Naphthalene	N0	3.37	2.95
C1-naphthalenes	N1	3.87	3.47
C2-naphthalenes	N2	4.37	4.00
C3-naphthalenes	N3	4.90	4.56
C4-naphthalenes	N4	5.30	4.98
Acenaphthylene	ACY	4.00	3.61
Acenaphthene	ACE	3.92	3.53
Fluorene	F0	4.18	3.80
C1-fluorenes	F1	4.97	4.63
C2-fluorenes	F2	5.20	4.87
C3-fluorenes	F3	5.70	5.40
Anthracene	A0	4.54	4.18
Phenanthrene	P0	4.46	4.09
C1-Phenanthrenes/anthracenes	PA1	5.14	4.81
C2-Phenanthrenes/anthracenes	PA2	5.46	5.14
C3-Phenanthrenes/anthracenes	PA3	5.92	5.63
C4-Phenanthrenes/anthracenes	PA4	6.32	6.05
Fluoranthene	FL0	5.22	4.89
Pyrene	PY0	5.18	4.85
C1-Fluoranthenes/pyrenes	FP1	5.50	5.19
C2-Fluoranthenes/pyrenes	FP2	5.80	5.50
C3-Fluoranthenes/pyrenes	FP3	6.28	6.00
Benzo(*a*)anthracene	BA0	5.91	5.62
Chrysene	C0	5.61	5.30
C1-chrysenes	BC1	6.14	5.86
C2-chrysenes	BC2	6.43	6.16
C3-chrysenes	BC3	6.94	6.70
C4-chrysenes	BC4	7.36	7.14
Benzo(*b*)fluoranthene	BBF	5.80	5.50
Benzo(*k*)fluoranthene	BKF	6.00	5.71
Benzo(*e*)pyrene	BEP	6.44	6.17
Benzo(*a*)pyrene	BAP	6.04	5.75
Perylene	PER	6.25	5.97
Indeno(1,2,3-cd)pyrene	IND	7.00	6.76
Dibenz(*a*,*h*)anthracene	AH	6.75	6.50
Benzo(*g*,*h*,*i*)perylene	GHI	6.63	6.37

TABLE 22.2 Measured Concentrations of Total Targeted PAHs in Surface Sediment, Whole Water, and PED Concentrations and Calculated Dissolved Concentrations in Water Based Upon Measured PED Concentrations

Station ID	Sediment (μg/kg)	Whole water (μg/L) (measured)	PED (μg/kg)	Calculated dissolved water (μg/L)	PED deployment time (d)
2A	26,500	2.39	131,000	0.155	44
2B	34,500	0.888	129,000	0.140	43
2C	72,300	0.911	133,000	0.163	43
2D	29,500	1.15	158,000	0.204	43
2E	26,700	0.292	143,000	0.166	44
2E DUP[a]	30,000	1.040	125,000	0.148	
2F	11,100	0.932	144,000	0.183	43
3A	7970	0.748	92,700	0.117	42
3B	12,500	0.568	64,800	0.106	44
3C	32,500	0.878	47,100	0.063	42
3D	9350	0.657	88,200	0.095	42
3D DUP[a]	14,700	0.693	92,400	0.109	
3E	37,900	0.621	70,000	0.106	43
3F	64,300	0.641	72,000	0.114	43
4A	25,700	0.562	70,600	0.095	43
4B	12,000	0.618	102,000	0.243	43
4C	6030	0.266	71,300	0.114	42
4D	23,500	0.281	67,200	0.104	43
4E	33,200	0.225	74,800	0.130	42
4F	22,700	0.249	na[b]	na[b]	na[b]

[a]*DUP = duplicate.*
[b]*PED from location 4F was not retrieved.*
na = not applicable.

22.3.2 Signature of Dissolved PAHs in Water

The forensic analyses conducted on the PAHs from the three matrices involved three primary methods. First, PAH distributions were compared between sites and relative to those of published reference materials. Second, diagnostic PAH ratios were evaluated for distinguishing among the samples site and identifying potential sources. Finally, principal component analysis was used to evaluate the degree of similarity or dissimilarity between PAH data measured or calculated for the different matrices and locations.

PAH distribution comparisons were completed for the first step of the forensic analysis of PED data. Generally speaking, the distribution of PAHs is related to the source of the material. Pyrogenic PAH signatures are characterized by higher abundances of 2- and 3-ring PAHs such as naphthalenes and phenanthrenes/anthracenes having an alkylated-PAH distribution that is dominated by the parent (i.e., C0) PAH with relative abundances decreasing with increasing degree of alkylation (i.e., C0 > C1 > C2 > C3 > C4; Boehm, 2006). This "skewed" distribution arises as a result of the formation temperatures (Neff, 1979). An urban background PAH signature is described as a variable distribution of resolved 4- to 6-ring nonalkylated (parent) PAHs, mostly dominated by fluoranthene and pyrene (Stout et al., 2004). The 2- and 3-ring PAHs in a typical urban signature are a relatively minor component. For the purposes of this case study, though their abundance is relatively minor, the distribution of 2- and 3-ring PAHs is important, as it is in part attributable to petroleum products (e.g., diesel fuel, and crank case oils) used in the urban environment impacting the Site. As such, these PAHs bear, in part, a petrogenic distribution, or a maximum around the C2- or C3-homologous. This "bell-shaped" distribution arises as a result of formation over geologic time at lower relative temperatures (Boehm, 2006). A mixture of PAHs from both petrogenic and pyrogenic sources exhibits a skewed distribution across the C0- and C1-homologues, and a

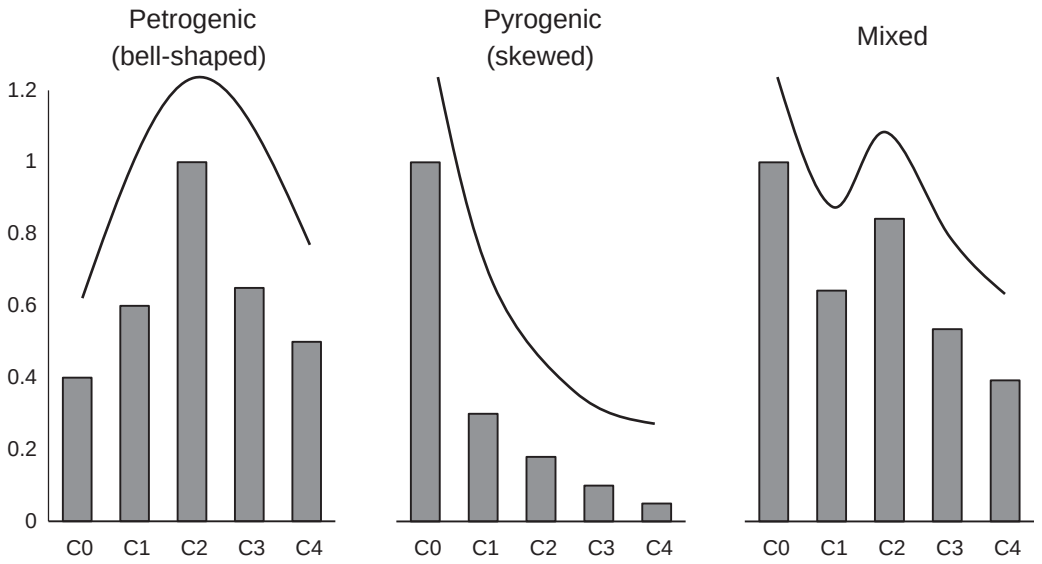

FIGURE 22.5 Representative pyrogenic, petrogenic and mixed PAH distributions within a PAH homologous series where C0 represents the parent PAH and C*n* represents the alkylated PAHs with *n* representing the number of carbons in the alkyl group.

bell-shaped distribution across the C2-, C3-, and C4-homologues. Fig. 22.5 shows representative pyrogenic, petrogenic, and mixed PAH distributions.

Fig. 22.6 shows the PAH distributions dissolved in water, as calculated from the PED results, from representative locations upriver (4B) and downriver (2A). The dissolved PAH distribution from upstream stations is consistent with a pyrogenic source, whereas that from downstream stations is consistent with an urban background source containing a mixture of petrogenic and pyrogenic features (Stout et al., 2004). Dissolved 2- and 3-ring PAHs are in greater relative abundance in the upriver sample s and their distribution is pyrogenic. However, in the downriver samples, the relative abundance of dissolved 2- and 3-ring PAHs is much lower.

For the second step in the forensic analysis, a diagnostic ratio of selected PAHs was examined. For this study, the fluoranthene to pyrene ratio (FL0/PY0), which is a useful PAH diagnostic ratio for distinguishing pyrogenic versus petrogenic PAH sources (Yunker et al., 2002; Oros and Ross 2004), also reveals a similar trend in the data as was concluded from the PAH distribution analyses described earlier. The ratio of FL0/PY0 is greater than one in the dissolved phase PAHs found in upriver stations indicative of pyrogenic source, but less than one in the dissolved phase PAHs found in downriver stations, which is indicative of a petrogenic source. Thus, dissolved PAHs are influenced by a pyrogenic source upriver and a petrogenic source downriver.

Principal component analysis (PCA) illustrates the change in dissolved PAH concentrations throughout the study area. Calculated concentrations of all 36 PAHs were normalized to the PAH in greatest relative abundance in each sample, and these data were used as the input for PCA analysis. In this way the PCA analysis was not influenced by the absolute concentrations of PAH, but only by their distributions. Fig. 22.7 shows the PCA score plot for dissolved PAH concentrations calculated from PED data at all locations throughout the study area. Notably, most of the variability in the data is explained by the first two factors: 60.1% of the variability is explained by the first factor (PCA1) and 19.7% of the variability is explained by the second factor (PCA2). The simplest interpretation of PCA score plots is to understand that PAH signatures of samples that plot proximate to one another are similar, while those that plot furthest away from one another, are dissimilar. In that regard, three of the samples from Reach 3 (4C, 4D and 4E) are similar and collectively identified as "Group 1." All samples in Reach 3 along with one sample from reach 4 (4A) and two samples from Reach 2 (2C and 2B) are similar to each other, are dissimilar from the "Group 1" samples, and are collectively identified as "Group 2." The remainder of the samples from Reach 2 are similar to each other, are dissimilar from the first two groups, and are collectively identified as "Group 3." The remaining sample (from Reach 4; location 4B, which also contained the highest calculated concentration of PAHs; Table 22.2) is dissimilar from all other samples.

When interpreting PCA results, it is most beneficial to understand *why* samples are similar or dissimilar, as these differences can shed light on valuable information. In the case of source allocation or environmental forensic efforts, such differences are often attributed to different sources of contaminants. To this end, the PAH

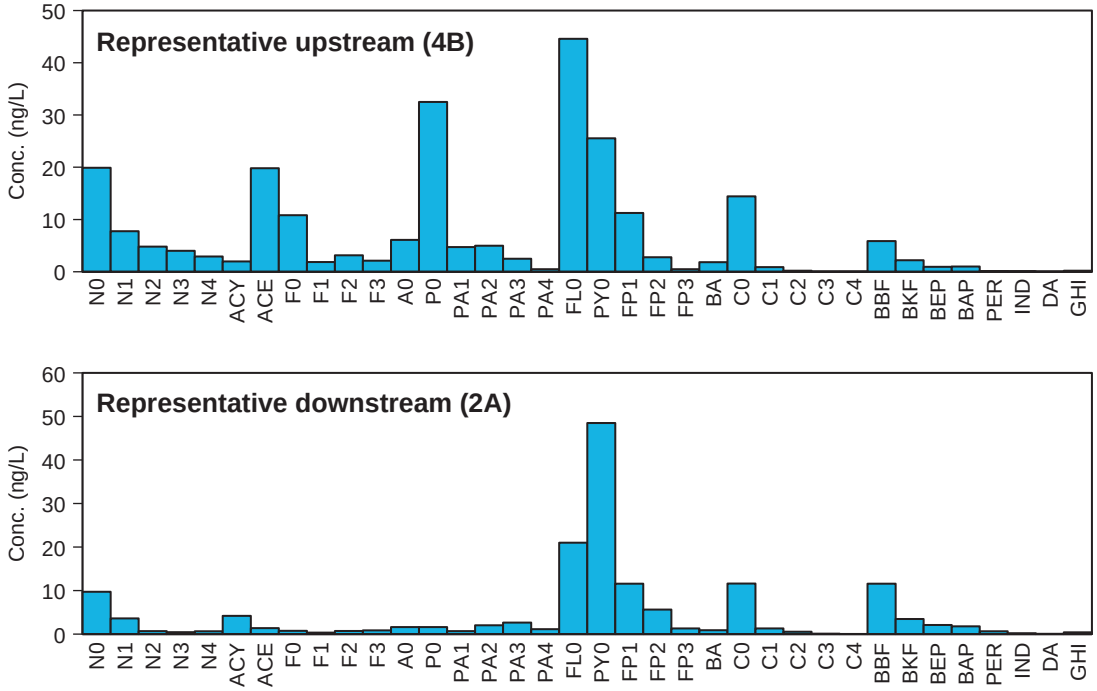

FIGURE 22.6 PAH distributions in dissolved water as calculated from PED data for representative upstream and downstream locations. See Table 22.1 for compound abbreviations.

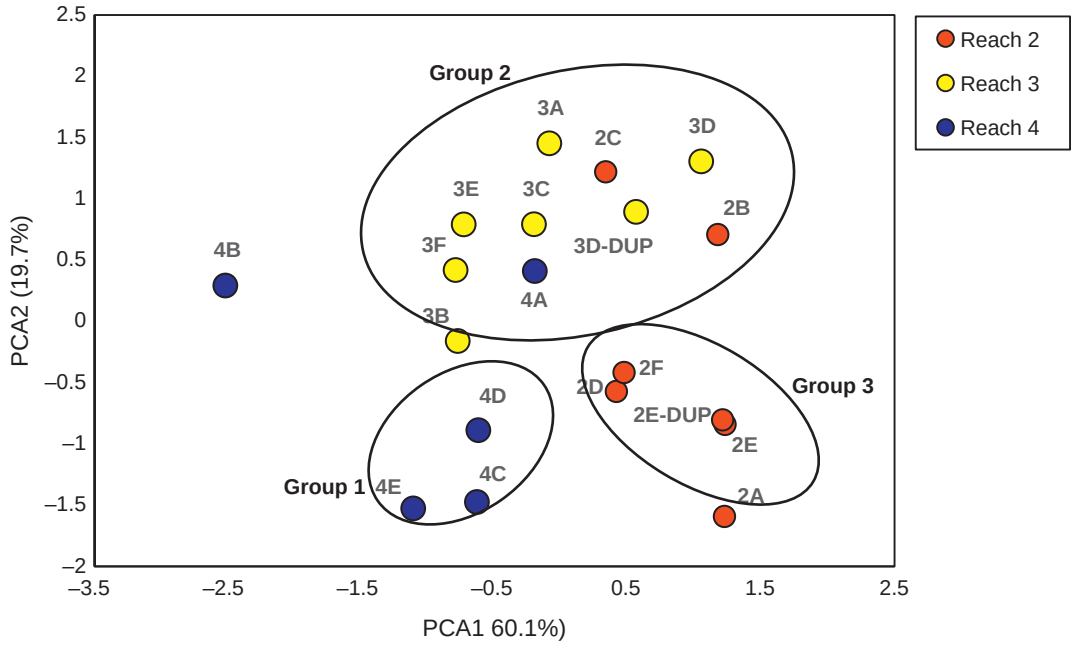

FIGURE 22.7 PCA score plot for dissolved PAH concentrations calculated from PED data at 17 stations in the Ottawa River.

distributions of individual samples were investigated to understand the differences in PAH distributions that led to the different groupings identified in Fig. 22.7. For example, the differences leading to PCA1 were examined by studying the PAH signatures of a sample that had similar PCA2 scores, but different PCA1 scores (e.g., sample 4B versus 2B). Similarly, differences leading to PCA2 were examined by studying the PAH signatures of sample that had similar PCA1 scores, but different PCA2 scores (e.g., sample 3D versus 2A). It was observed that

FL0/PY0 (which as a ratio was not used as an input variable to the PCA) varied with PCA1 scores: samples with positive PCA1 scores exhibited FL0/PY0 less than one, whereas samples with negative PCA1 scores exhibited FL0/PY0 greater than one. In addition, the overall pyrogenic/petrogenic distributions of the 2- and 3-ring PAHs varied with PCA2 scores: samples with positive PCA2 scored exhibited petrogenic 2- and 3-ring PAHs (particularly in the C1−C4 homologues), whereas samples with negative PCA2 scored exhibited pyrogenic 2- and 3-ring PAHs.

When the change in PAH distributions that is described in Figs. 22.6 and 22.7 is regarded geospatially, the nature and relative locations of different PAH sources within Reaches 2, 3 and 4 of the Ottawa River becomes clear. Specifically, the "Group 1" samples were from areas upstream of any CSO discharge. While there are active CSOs in the area, there were no recorded discharges from CSO#63, CSO#64, CSO#65, or CSO#67 during the period which PEDs were deployed (http://www.toledowaterwaysinitiative.com/tech-data/ accessed February 14, 2017). The dissolved PAH signature derived from the PEDs at these locations were also among the most pyrogenic (i.e., they exhibited pyrogenic distributions of 2- and 3-ring PAHs in relatively high abundance), and their PAH diagnostic ratios (e.g., FL0/PY0) were attributable to pyrogenic PAH sources. The "Group 2" samples were from areas immediately downstream of the two CSOs that discharged for 1199 minutes over 16 different CSO events during the period of PED deployment (CSO#61 and CSO#62; http://www.toledowaterwaysinitiative.com/tech-data/ accessed February 14, 2017). The dissolved PAH distributions derived from PEDs at these locations exhibited a mixture of pyrogenic and petrogenic characteristics. Specifically, they generally exhibited FL0/PY0 greater than one but mixed pyrogenic and petrogenic 2- and 3-ring PAH distributions. The "Group 3" samples were from areas further downstream of the CSO discharge locations. These samples exhibited a mixture of pyrogenic and petrogenic characteristics, and while the distributions of 2- and 3-ring PAHs were pyrogenic, they were in relatively low abundance compared to the "Group 2" samples immediately upriver.

Ultimately, the dissolved PAH distributions in the study area are influenced by a pyrogenic source in Reach 4, upstream of CSO discharge. Given the relative abundance and distribution of 2- and 3-ring PAHs, as well as FL0/PY0 greater than 1, the most likely source of these pyrogenic PAHs is lower boiling pyrogenic material such as creosote (Murphy and Brown, 2005), either from creosote-treated wood used in bulkheads or other structures, or from the former landfills. Immediately downriver of CSO discharge, in Reach 3, the pyrogenic/creosote signature is mixed with an urban runoff signature, as a result of CSO discharge. Further downriver, in Reach 2, the PAH signature resembles urban runoff with only minor contributions of the pyrogenic/creosote source.

22.3.3 Forensic Signature of PAHs in Whole Water Samples

The PAH distributions measured in whole water samples were different from those of dissolved PAHs calculated using measured PED concentrations. Fig. 22.8 shows the PAH distributions measured in two whole water samples from the same representative locations upriver (4B) and downriver (2A) for which calculated concentrations based on PEDs had been shown in Fig. 22.6. In general, these measured PAH distributions in whole water resemble an urban background signature, though there are minor features of the upriver sample (4B) that suggest an influence from an additional source. Specifically, the PAH distribution in the sample collected from location 4B exhibits some minor features consistent with the pyrogenic/creosote source (Fig. 22.8), but these features are not as noticeable as they were in dissolved PAH signature from this location (Fig. 22.6). Although the relative abundance of 2- and 3-ring PAHs is higher and the distribution of naphthalenes is more pyrogenic in the whole water upriver sample compared to the whole water downriver sample (Fig. 22.8), these trends are not as pronounced as they are in the dissolved phase between these same two locations (see Fig. 22.6). FL0/PY0 in both of the representative whole water samples (Fig. 22.8) is greater than one, though there is some variability. Specifically, in the upriver sample (4B) FL0/PY0 is much greater than one and similar to the ratio observed in dissolved PAH concentrations at this location, whereas in the downriver sample (2A) the ratio is closer to one. This difference in FL0/PY0 ratio reflects the transition from influence from creosote upriver to urban runoff from CSO discharge downriver.

Given that the majority of PAHs in the whole water samples are adsorbed to suspended particles, the differences between the PED-calculated dissolved PAH concentrations and measured whole water PAH concentrations speak to the forensic signatures of PAHs associated with suspended solids. In other words, the influence of the pyrogenic/creosote source upriver is most realized in the dissolved phase, as PAHs from this source are slowly released into the river's water via dissolution from impacted sediments. PAHs bound to the particle load are less influenced by this process, and look more like an urban background signature throughout the study area.

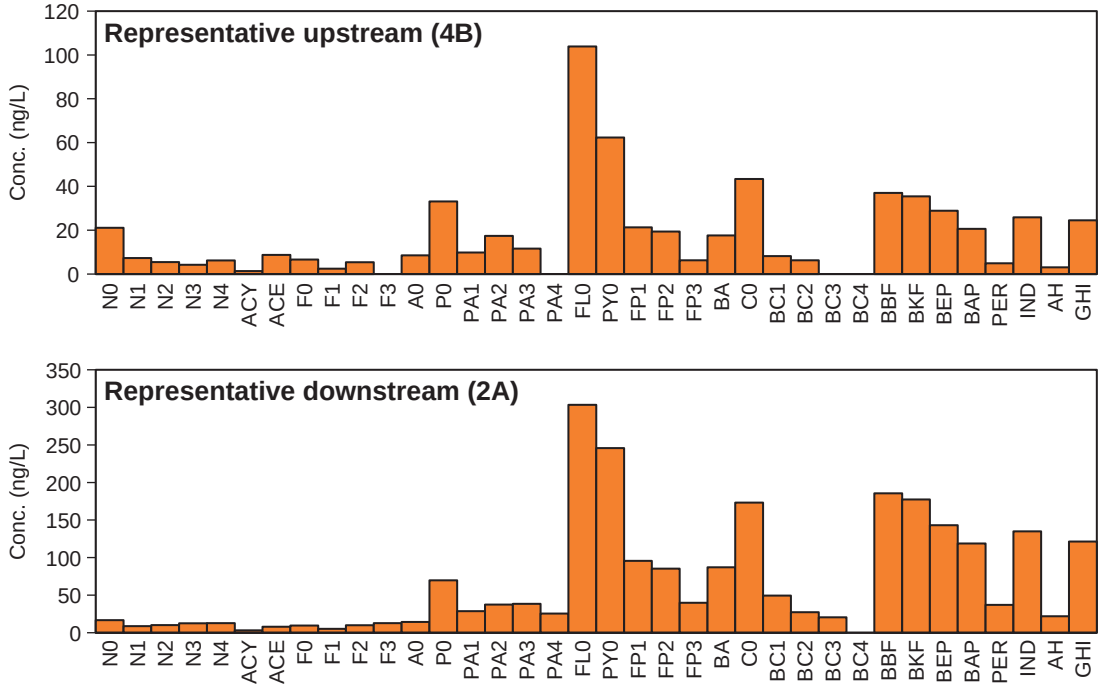

FIGURE 22.8 PAH distribution in measured in whole water samples for representative upstream and downstream locations. See Table 22.1 for compound abbreviations. These are the same locations whose PED-calculated concentrations were shown in Fig. 22.6.

22.3.4 Forensic Signature of PAHs in Surface Sediment

The PAH distribution measured in surface sediment samples is also different from that of dissolved PAHs calculated from PEDs, but similar to that of whole water samples. Fig. 22.9 shows the PAH signatures in surface sediment samples collected from the same two representative locations upriver (4B) and downriver (2A) described above. The PAH distributions both upriver and downriver are similar, and representative of all surface samples studied. Thus, the PAH distributions within surface sediment is attributed to more recent deposition of PAHs derived from urban background throughout the study area.

22.3.5 Trends in PAH Forensic Signatures

To illustrate forensic trend of PAHs in dissolved, whole water, and sediment samples throughout the study area, diagnostic PAH ratios were used to differentiate between different PAH sources. Fig. 22.10 shows the plot of anthracene to phenanthrene [A0/(A0 + P0)] versus fluoranthene to pyrene [FL0/(FL0/PY0)] in dissolved water, whole water, and sediment throughout the study area following an approach that has been used to distinguish PAH sources (Zemo, 2009). For dissolved concentrations, the diagnostic ratios change from relatively low A0/(A0 + P0) and high FL0/(FL0/PY0) in Reach 4, to intermediate FL0/(FL0/PY0) and A0/(A0 + P0) in Reach 3, to relatively high A0/(A0 + P0) and low FL0/(FL0/PY0) in Reach 2. Similar to the qualitative discussion of dissolved PAH distributions provided above, these ratios are also indicative of a source of creosote-derived PAHs upriver, transitioning to pyrogenic–petrogenic mixture or a combusted petroleum signature downriver. However, for both whole water and sediment samples, the ratios are consistent, exhibiting relatively high A0/(A0 + P0) and low FL0/(FL0/PY0) consistent with a pyrogenic source, throughout the Site.

The change in the distributions of the dissolved PAHs from upstream to downstream is attributed to the influence of CSO discharge in this region of the Ottawa River. Given FL0 and PY0 have similar hydrophobicities (log K_{OW} = 5.22 and 5.18, respectively, Table 22.1) the differences between FL0/(FL0 + PY0) (1) in dissolved PAH concentrations throughout the study area, and (2) between dissolved PAH concentrations and whole water or sediment concentrations (Fig. 22.10) is real and cannot be attributed to a solubility effect. CSO discharge contains a mixture of raw sanitary sewage and runoff from paved surfaces within the "sewershed." The forensic signature of urban runoff often contains petroleum characteristics, owing to the diesel fuel and crank case oil that is

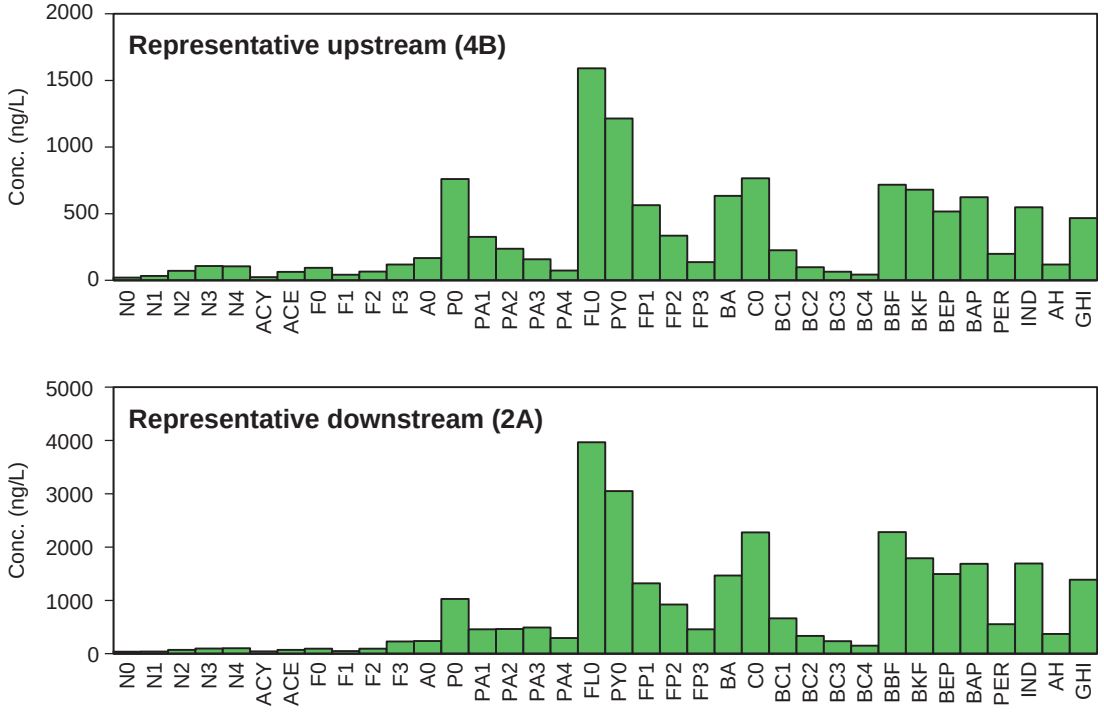

FIGURE 22.9 PAH distributions in sediment samples for representative upstream and downstream locations. See Table 22.1 for compound abbreviations. These are the same locations whose PED-calculated and whole water concentrations were shown in Figs. 22.6 and 22.8, respectively.

collected from roads and parking lots within the sewer/storm water system (Stout et al., 2004). Thus, the shift to lower FL0/(FL0 + PY0) ratios for the dissolved PAHs in Fig. 22.10 are attributed to the increasingly greater input from CSO discharge containing petroleum products, being lowest in Reach 4 and highest in Reach 2. Interestingly, the change in FL0/(FL0 + PY0) or A0/(A0 + P0) ratios are not noted for the whole water or surface sediment samples (Fig. 22.10). Therefore, dissolved PAHs change from pyrogenic/creosote to urban background/CSO-impacted within increasing distance downstream within the study area, whereas the PAHs in whole water and sediment samples resemble urban background/CSO discharge throughout the entire study area.

This discrepancy between the apparent PAH sources recognized using the dissolved PAHs and that of the whole water samples is notable. If one wanted to interpret the source of PAHs in the water column that posed an ecological or human health risk, the interpretation would vary depending on whether or not it was conducted using dissolved PAH data calculated from PED passive samplers, or measured PAH data from whole water samples. In the case of the PED passive samplers, the source of dissolved PAHs would be attributable to dissolution of creosote upriver in Reach 4, mixing with urban runoff/CSO discharge midriver in Reach 3, and transitioning to urban runoff/CSO-dominant downriver in Reach 2. However, in the case of the PAHs in whole water samples, the source of PAHs would be attributable to dissolved and particulate-derived PAHs typical of urban background/CSO discharge throughout the entire study area.

22.4 CONCLUSIONS

Passive samplers offer an alternative to the traditional analysis of water (grab) samples, and mitigate many of the challenges associated with measuring the truly dissolved concentrations of hydrophobic contaminants in water. Most commonly, they have been used to measure dissolved concentrations and estimate contaminant bioavailability. This chapter illustrates how that approach can be taken a step further to investigate the source of dissolved and bioavailable contaminants using contaminant concentrations calculated from passive samplers deployed for an extended period of time.

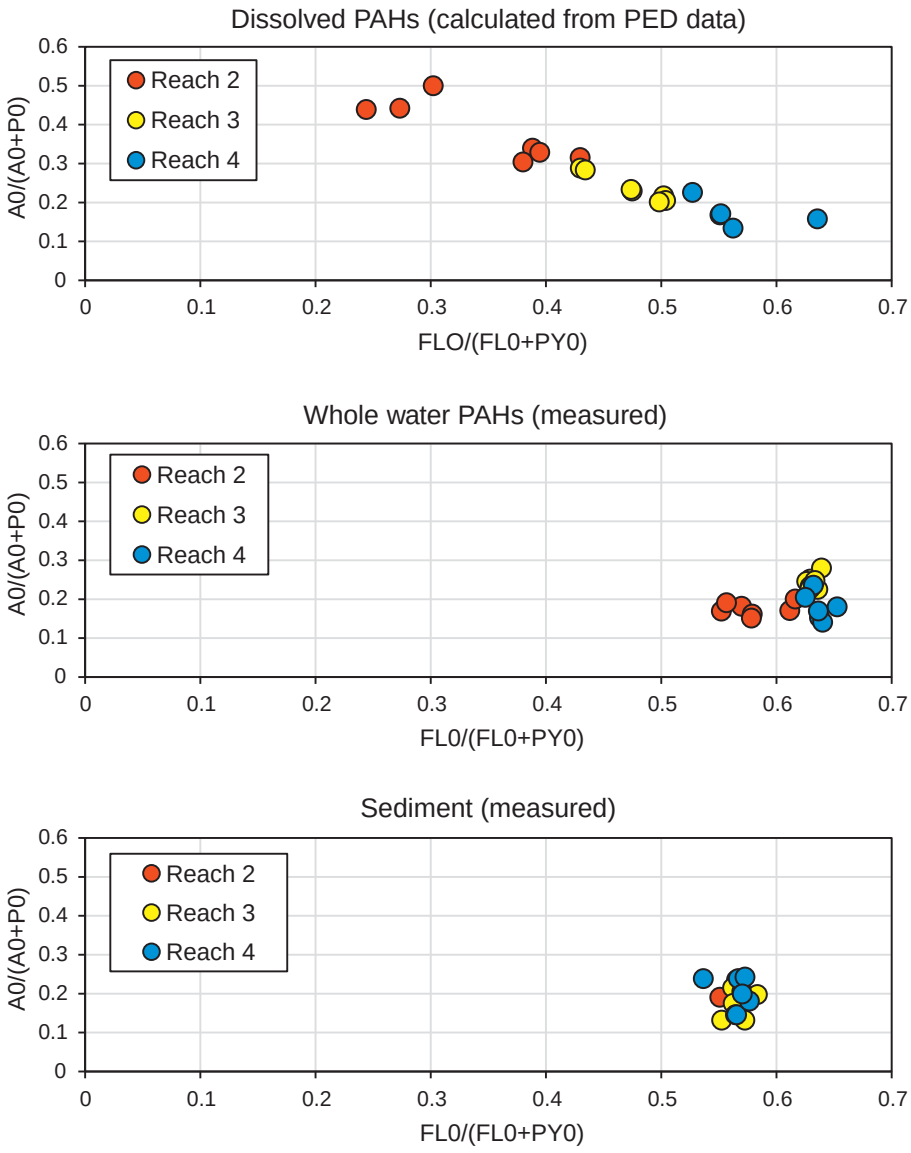

FIGURE 22.10 Diagnostic PAH ratios in PED-calculated concentration data and from measured concentrations in whole water samples and sediment samples by Reach within the Ottawa River study area.

Using a combination of PED, whole water, and surface sediment data from the Ottawa River (Ohio, USA), it has been shown that passive samples can be used to determine the forensic signatures of dissolved PAHs within the water column through a sediment remediation site, and that these signatures can vary from those evident from the whole water or surface sediment samples. Thus, the interpretation of the source(s) of PAHs in the water column can vary depending on whether or not the interpretation is based upon measured whole water samples or calculated from the passive samplers. Whole water contaminant concentrations reflect a combination of dissolved and particle-bound contamination, whereas the PED passive samplers can be used to calculate the concentrations and forensic signature of those contaminants that are truly dissolved. If the intent of the project is to study contaminant or fingerprinting associated with sediment resuspension, as for example, during dredging operations, then analysis of whole water samples may be sufficient. However, if the intent is to look at the source (s) of truly bioavailable (i.e., dissolved) contamination, or the mass or forensic signature associated with contaminants entering an aquatic system in the dissolved phase (e.g., via groundwater discharge) then passive samplers may provide more useful data. Ultimately, investigators should consider these implications when deciding whether or not to incorporate passive samplers into an environmental study.

References

Adams, R.G., Lohmann, R., Fernandez, L.A., Macfarlane, J.K., Gschwend, P.M., 2007. Polyethylene devices: passive samplers for measuring dissolved hydrophobic organic compounds in aquatic environments. Environ. Sci. Technol. 41 (4), 1317–1323.

Apell, J.N., Tcaciuc, A.P., Gschwend, P.M., 2016. Understanding the rates of nonpolar organic chemical accumulation into passive samplers deployed in the environment: guidance for passive sampler deployments. Integr. Environ. Assess. Manage. 12 (3), 486–492.

Boehm, P.D., 2006. Polycyclic aromatic hydrocarbons (PAHs). In: Morrison, R.D., Murphy, B.L. (Eds.), Environmental Forensics—Contaminant Specific Guide. Elsevier, Boston, Massachusetts, pp. 313–338.

Booij, K., Hofmans, H.E., Fischer, C.V., Van Weerlee, E.M., 2003. Temperature-dependent uptake rates of nonpolar organic compounds by semipermeable membrane devices and low-density polyethylene membranes. Environ. Sci. Technol. 37 (2), 361–366.

Durell, G., Utvik, T.R., Johnsen, S., Frost, T., Neff, J., 2006. Oil well produced water discharges to the North Sea. Part I: Comparison of deployed mussels (*Mytilus edulis*), semi-permeable membrane devices, and the DREAM model predictions to estimate the dispersion of polycyclic aromatic hydrocarbons. Mar. Environ. Res. 62 (3), 194–223.

Friedman, C.L., Burgess, R.M., Perron, M.M., Cantwell, M.G., Ho, K.T., Lohmann, R., 2009. Comparing polychaete and polyethylene uptake to assess sediment resuspension effects on PCB bioavailability. Environ. Sci. Technol. 43 (8), 2865–2870.

Lohmann, R., Muir, D., 2010. Global aquatic passive sampling (AQUA-GAPS): using passive samplers to monitor POPs in the waters of the world. Environ. Sci. Technol. 44 (3), 860–864.

Maumee, R.A.P., 2002. Activities and Accomplishments in the Maumee Area of Concern 1991–2001. Maumee RAP, Toledo, OH.

Maumee, R.A.P., 2006. Maumee Area of Concern Stage 2 Watershed Restoration Plan. Maumee RAP; Duck and Otter Creeks Partnership; Ohio Environmental Protection Agency; Toledo Metropolitan Area Council of Governments, Toledo, OH.

Murphy, B.L., Brown, J., 2005. Environmental forensics aspects of PAHs from wood treatment with creosote compounds. Environ. Forens. 6 (2), 151–159.

Namiesnik, J., Zabiegala, B., Kot-Wasik, A., Partyka, M., Wasik, A., 2005. Passive sampling and/or extraction techniques in environmental analysis: a review. Anal. Bioanal. Chem. 381 (2), 279–301.

Neff, J.M., 1979. Polycyclic Aromatic Hydrocarbons in the Aquatic Environment. Elsevier Science Ltd, Boston, Massachusetts.

Oros, D.R., Ross, J.R.M., 2004. Polycyclic aromatic hydrocarbons in San Francisco Estuary sediments. Mar. Chem. 86 (3–4), 169–184.

Parametrix, 2001. Ecological Screening-Level Risk Assessment of the Lower Ottawa River.

Parkerton, T., Maruya, K., Lydy, M., Landrum, P., Peijnenburg, W., Mayer, P., et al., 2012. Guidance on Passive Sampling Methods to Improve Management of Contaminated Sediments; Summary of a SETAC Technical Workshop. Society of Environmental Toxicology and Chemistry (SETAC), Pensacola, FL.

Stout, S.A., Uhler, A.D., Emsbo-Mattingly, S.D., 2004. Comparative evaluation of background anthropogenic hydrocarbons in surficial sediments from mine urban waterways. Environ. Sci. Technol. 38 (11), 2987–2994.

ter Laak, T.L., Busser, F.J.M., Hermens, J.L.M., 2008. Poly(dimethylsiloxane) as passive sampler material for hydrophobic chemicals: Effect of chemical properties and sampler characteristics on partitioning and equilibration times. Anal. Chem. 80 (10), 3859–3866.

Thompson, T., Menzie, C., Kane-Driscoll, S., 2016. Integrating Passive Sampling Methods into Management of Contaminated Sediment Sites: A Guide for Department of Defense Remedial Project Managers. Department of Defense Environmental Security Technology Certification Program (ESTCP).

USEPA, 2012. Guidelines for Using Passive Samplers to Monitor Organic Contaminants at Superfund Sediment Sites. United States Environmental Protection Agency Office of Superfund Remediation and Technology Innovation and Office of Research and Development.

Vinturella, A.E., Burgess, R.M., Coull, B.A., Thompson, K.M., Shine, J.P., 2004. Use of passive samplers to mimic uptake of polycyclic aromatic hydrocarbons by benthic polychaetes. Environ. Sci. Technol. 38 (4), 1154–1160.

Vrana, B., Mills, G.A., Allan, I.J., Dominiak, E., Svensson, K., Knutsson, J., et al., 2005. Passive sampling techniques for monitoring pollutants in water. TrAC, Trends Anal. Chem. 24 (10), 845–868.

Yunker, M.B., Macdonald, R.W., Vingarzan, R., Mitchell, R.H., Goyette, D., Sylvestre, S., 2002. PAHs in the Fraser River basin: a critical appraisal of PAH ratios as indicators of PAH source and composition. Org. Geochem. 33 (4), 489–515.

Zemo, D.A., 2009. Use of parent polycyclic aromatic hydrocarbon (PAH) proportions to attribute PAH sources in sediments: a case study from the Pacific Northwest. Environ. Forensics 10 (3), 229–239.

CHAPTER

23

Fingerprint and Weathering Characteristics of Petroleum Hydrocarbons in the Coastal Zone Following the "7-16" Dalian Crude Oil Spill, China

Chuanyuan Wang[1], *Shijie He*[2], *Haijiang Zhang*[3] *and Yuanwei Li*[1]

[1]Yantai Institute of Coastal Zone Research, Chinese Academy of Sciences, Yantai, China [2]Ludong University, Yantai, China [3]Yantai Oil Spill Response Technical Center of Yantai MSA, Yantai, China

BIOGRAPHIES

Dr. Chuanyuan Wang is an associate professor of the Yantai Institute of Coastal Zone Research, Chinese Academy of Sciences, where he had been working in the oil spill research field since 2007. He received his Ph.D. from Lanzhou Institute of Geology, Chinese Academy of Sciences in 2007. His research interests include: oil spill fingerprinting technology, fate and behavior of oil spill, and deposition of materials in estuaries. He has continually and extensively led and been involved in 16 scientific projects through several agencies, such as the National Natural Science Foundation of China. He has authored or coauthored over 100 papers published in scientific journals and three scientific textbooks. Between 2011 and 2016, he successively won five times the formal acceptance of your candidature for the Edition of the Eni Award.

Yuanwei Li is a master degree candidate, studying under Dr. Chuanyuan Wang, at the Yantai Institute of Coastal Zone Research, Chinese Academy of Sciences in 2016. Her major area of study is in the behavior of oil spilled in estuarine environments.

Dr. Shijie He has served on the faculty of the School of Resources and Environmental Engineering at Ludong University, China, since 2003. He received his Ph.D. from Yantai Institute of Coastal Zone Research, Chinese Academy of Sciences in 2016. His research interests include: understanding the transport of anthropogenic contaminants in marine, estuarine, and coastal systems, and chemical fingerprinting and tracing technology for mixed oil spills. He has authored or coauthored over 30 papers published in scientific journals and scientific textbooks.

Haijiang Zhang is a PhD candidate at the Ocean University of China, majoring in Marine Chemistry. Since receiving his master's degree from Changchun Institute of Applied Chemistry, Chinese Academy of Sciences in 2009, he has served on Yantai Oil Spill Response Technical Center, Maritime Safety Administration of the Peoples Republic of China, which is responsible for marine pollution prevention. He has participated in the assessment of hundreds of oil spill accidents and has extensive experience in oil spill fingerprint identification and in crude oil/fuel oil discrimination. He has authored or coauthored several papers published in scientific journals.

Oil Spill Environmental Forensics Case Studies.
DOI: http://dx.doi.org/10.1016/B978-0-12-804434-6.00023-9

23.1 INTRODUCTION

On July 16, 2010, in the northeastern port city of Dalian, a coastal city in northeast China's Liaoning Province, two crude oil pipelines exploded sending flames hundreds of feet into the air and burning for over 15 h (Fig. 23.1). About 1500 t of oil was spilled and flowed into the nearby harbor and Yellow Sea, where it spread over 165 sq. mi (Wang et al., 2013). The spilled oil had dramatic negative ecological and economic impacts on the Dalian coastal ecosystem. Evidence from other large-scale oil spills has shown that oil can persist in coastal sediments for several decades and have long-term effects on aquatic ecosystems (Peterson et al., 2003). Once oil is spilled into the environment, it is immediately subject to a variety of weathering processes, such as evaporation, dissolution, emulsification, microbial degradation, photooxidation, adsorption to suspended matter, and deposition on the sea floor, which collectively are known as weathering (Garret et al., 1998; Kennicutt, 1988; Barakat et al., 2001; Wang and Fingas, 2003; D'Auria et al., 2009; Yim et al., 2011; Stout et al., 2016). Such weathering

FIGURE 23.1 Photographs showing the scene of "7-16" Dalian crude oil spill, China. (A) terminal near the pipeline accident and (B) shoreline with crude oil residues washing ashore.

process will change the composition of the residual oil and determine its ultimate fate and impact on the marine environment (Wang and Fingas, 2003; Yim et al., 2011).

Polycyclic aromatic hydrocarbons (PAHs) are organic compounds with two or more fused aromatic rings and are one of the most important groups of toxic environmental compounds present in crude oil. Due to their carcinogenic, mutagenic, and toxic effects, some of them are on the US EPA list of priority pollutants. Therefore, many studies have examined the distribution of PAHs in coastal and oceanic sediments (e.g., Budzinski et al., 1997; Magi et al., 2002; Zeng et al., 2013). Although contamination of PAHs can result from natural and anthropogenic processes, inputs of PAHs from human activities such as oil spills, offshore oil production, and transportation and combustion are very significant and pose serious threats to coastal habitats (Lotufo and Fleeger, 1997). The 16 US EPA priority PAHs derived from oil spills may pose serious threats to coastal habitats due to their toxic effects. Detailed knowledge of PAHs weathering characteristic can provide some useful information for further understanding their environmental fate and potential ecotoxicological effect. However, prior to the "7-16" Dalian oil spill, no comprehensive surveys of PAH weathering in coastal environments of Dalian Bay were done.

The spill thereby provided an excellent opportunity to monitor the variation in the chemical composition of PAHs from the spilled residual crude oil over time and characterize the weathering processes within the impacted coastline of Dalian Bay under natural conditions. The present study aims to (1) quantitatively determine the chemical composition changes of crude oil residue and PAHs after 4 months exposure to weathering under natural coastal zone environmental condition, (2) discuss the effect of weathering process on the common diagnostic ratios commonly used for both oil spill source identification and the characterization of emission sources of PAHs, (3) determine the effects of natural weathering processes on the carbon isotopic composition of individual *n*-alkanes and evaluate the potential use of gas chromatography–combustion isotope ratio mass spectrometry (GC–C-IRMS) as a correlation tool in oil spill source identification, and (4) evaluate the environmental impacts of "7-16" Dalian crude oil spill based on toxicity guidelines for sediment.

23.2 EXPERIMENTAL

23.2.1 Sample Collection for Oil Spill in Dalian

Although large quantities of the pollution from "7-16" Dalian crude oil spill accident have been successfully removed or controlled, a significant amount of residual oil film or oil residue attached to the shoreline rocks could still be found in some heavily polluted areas even 120 days after the oil spill had occurred. The field samples were collected as oiled-coated rocks and scrapings at coastal sites from the Jinshitan area, a heavily oiled area of Dalian Bay beach. Samples were collected from this area over a period of time including 10, 60, 70, 80, 90, 100, 110 and 120 days after the oil spill occurred. In addition, a fresh crude oil sample representative of the Dalian crude oil spilled was collected from an oil storage tank located there. Oil samples were carefully taken and placed in prewashed amber bottles using a solvent-washed spatula and stored in the freezer until analysis.

In addition, the surface (0–5 cm) sediment samples from four locations (DLS-1, DLS-2, DLS-3, and DLS-4) were collected 60 days after the oil spill along the Dalian coast adjacent to the oil spill site (Fig. 23.2). Upon collection, the sediment samples were homogenized and placed into sterile polyethylene bags, sealed and frozen at −20°C in the dark until further analysis.

23.2.2 Extraction, Fractionation, and Gas Chromatography–Mass Spectrometer

In the laboratory, oil samples were Soxhlet-extracted with chloroform for a period of 72 h. Elemental sulfur was removed from the extracts using activated copper. Crude oils were deasphaltened by precipitation with *n*-hexane followed by filtration. The extract was fractionated into aliphatic and aromatic hydrocarbons by adsorption liquid chromatography using a column of alumina and silica gel, and gradient solvents as eluent: ligarine and ligarine/dichloromethane (3:9, v/v), respectively. An aliquot of 1 mL of each extract was subjected to analysis. Saturated hydrocarbon and PAHs fractions were eluted with *n*-hexane, and then analyzed by gas chromatography–mass spectrometer (GC–MS).

Sediment samples were first dried at 60°C and sieved through a 125-μm sieve to remove large particles and debris. The dried sediment samples were then ground into powder with a mortar and pestle. For total lipid extraction, about 100 g dry sediment sample was Soxhlet-extracted with chloroform for a period of 72 h. Elemental sulfur was removed from the extracts using activated copper. The extracts were fractionated by

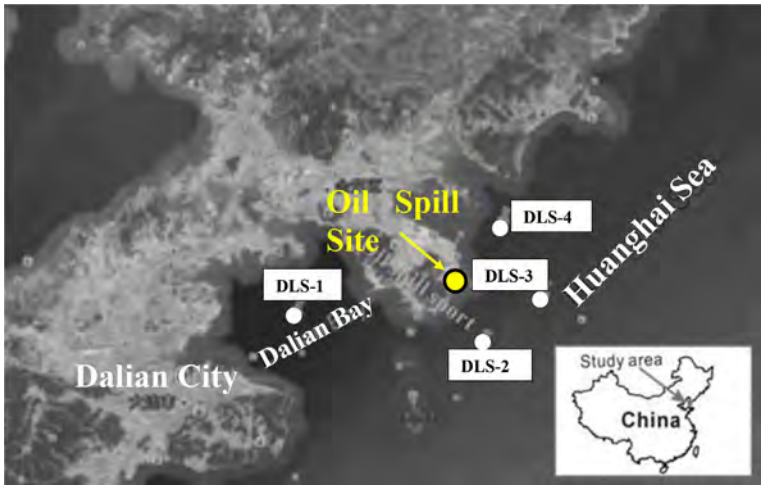

FIGURE 23.2 General location map of "7-16" Dalian oil spill showing sediment sampling sites.

column chromatography on alumina over silica gel. Saturated hydrocarbons, aromatic hydrocarbons and nonhydrocarbons were obtained by successively eluting with *n*-hexane, toluene and chloroform/methanol (98:2), respectively. The aliphatic and aromatic fractions were reconcentrated on a rotary evaporator, transferred to a vial, and then the volume was adjusted to 1 mL using a stream of filtered N_2 gas. An aliquot of 1 mL of each extract was also subjected to GC–MS analysis.

Saturated hydrocarbons and PAHs were analyzed with a 6890N GC-5973N mass spectrometer equipped with a HP-5 capillary column (50 m × 0.32 mm × 0.25 μm, Agilent Technologies, USA). The GC oven temperature was programed from 80°C to 300°C at 4°C/min, then maintained at this temperature for 30 min. Helium was used as a carrier gas. Mass spectrometer conditions were electron ionization at 70 eV with an ion source temperature at 250°C.

Individual *n*-alkanes were identified based on the retention time of the authentic standards (nC_{10-40}, Sigma), and concentrations of each *n*-alkane were calculated based on the standard calibration curve of each corresponding standard compound. The concentrations of individual PAHs were quantified based on the retention time and *m*/*z* ratio of an authentic PAHs mixed standard (Sigma), and concentrations of each PAHs were calibrated based on the standard calibration curve. For quality assurance and quality control, the method blanks (solvent) and matrix spike samples (standards spiked into soil) were analyzed. None of the target compounds was detected in method blanks. Seven surrogate standards (naphthalene-d8, acenaphthylene-d8, phenanthrene-d10, fluoranthene-d10, pyrene-d10, benzo(*a*)pyrene-d12, and benzo(*g*,*h*,*i*)perylene-d12) were added to all samples to monitor matrix effects. Recoveries of 16 PAHs ranged from 81.6% to 108%.

23.2.3 Gas Chromatography–Combustion Isotope Ratio Mass Spectrometry

GC–C-IRMS analyses were performed on a VG Isoprime instrument. The GC was equipped with a HP-5 capillary column (50 m × 0.32 mm × 0.25 μm) with helium as the carrier gas. The GC was held isothermally for 5 min at 70°C, programed to sequentially step from 70°C to 290°C at 3°C/min and then held isothermally for 40 min at 290°C. The combustion furnace was run at 880°C. Carbon isotope ratios for individual *n*-alkanes were calculated using CO_2 as a reference gas that was automatically introduced into the IRMS at the beginning and end of each analysis, and the data are reported in per mil (‰) relative to the VPDB standard. A standard mixture of *n*-alkanes (n-C_{12}–n-C_{32}) with known isotopic composition was used daily to test the performance of the instrument. Replicate analyses of this mixture showed that the standard deviation for each compound was less than 0.3‰.

23.3 RESULT AND DISCUSSION

23.3.1 Temporal Variation Characteristics of Petroleum Hydrocarbon Content

23.3.1.1 Crude Oil Adhered to the Rocks

Evaporation occurs within the first few hours after an oil spill and removes the more volatile hydrocarbons, and water-washing also occurs rapidly and removes the more water-soluble hydrocarbons, typically

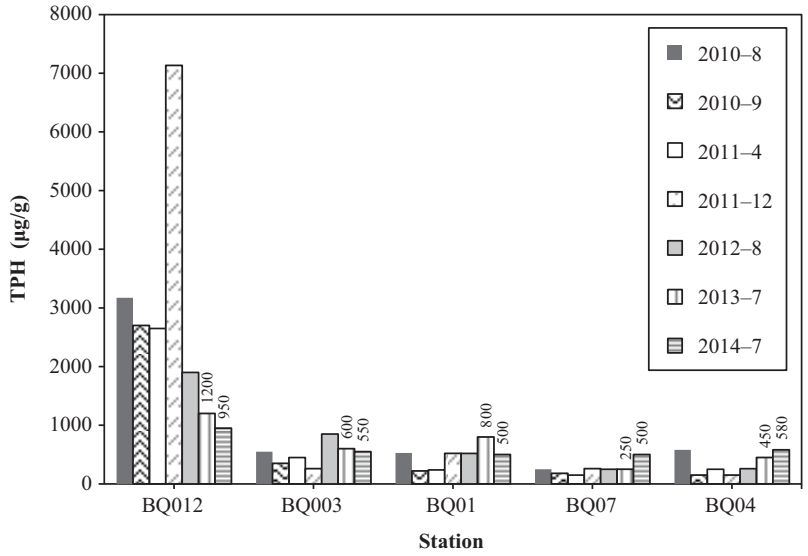

FIGURE 23.3 Annual changes of total petroleum hydrocarbons concentration in surface sediment from Dalian Bay. *Source: Revised from data from Guo, L.M., 2016. The Research of Temporal and Spatial Variations of Bacterial Community After "7.16" Oil Spill in Dalian [D]. Dalian Ocean University.*

hydrocarbons below C_{15} (Mansuy et al., 1997). At the same time, biodegradation will also start to affect the nature of the spilled oil by initially removing the *n*-alkanes before attacking the more complex branched and cyclic hydrocarbons and naphthenic compounds. These effects were evident in the crude oil residues adhered to rocks along the Dalian coastline, wherein the overall concentrations of *n*-alkanes and isoprenoids indicated some loss of 50% within 120 days after the "7-16" Dalian oil spill accident. Within 480 days, these compounds were degraded largely by up to 72.5% and, as a consequence, are of limited value in identifying the remaining oil residues.

23.3.1.2 Crude Oil Residues in Surface Sediment

The mean concentration of the total petroleum hydrocarbon (TPH) in surface sediments ranged from 2.5 to 655 μg/L in Dalian Bay during 2010−2014 (Guo, 2016). The concentrations of TPH following the "7-16" Dalian oil spill exhibited a steady decreasing trend at all station of the Bay between 2010 and 2014. The TPH concentrations had reached China's first class seawater quality standard (≤500 μg/L; *China's Marine Monitoring Standards of GB 3097-1997*) by 2012 (Guo, 2016). However, the TPH concentration in sediment from station BQ012, which was located nearest to the shore, was significantly higher than that of other stations during 2010−2012 (Fig. 23.3). The TPH concentration in surface sediments collected from the BQ012 more nearshore site were reduced from 7133 μg/g in December 2011 to 926 μg/g in July 2014, indicating these sediments' quality had recovered to the first class quality standards by 2014. Between 2013 and 2014, the TPH concentrations had increased at the BQ07 and BQ04 sites (203 and 785 μg/g), although such minor increases may be due to the heterogeneity and sedimentation of petroleum hydrocarbons. TPH concentrations in sediment from oil spill accident area was 199.25, 282.67, and 271.10 μg/g in September 2010, April 2011, and July 2011, respectively, which had reached a class of marine sediment-quality standards (Gao et al., 2013). Furthermore, the emissions and wastes from the Port of Dalian (shipbuilding, petrochemical, steel, and other industrial) activities alone have likely contributed TPH to the Gulf of Dalian, resulting in higher background concentrations of TPH in seawater and sediment in the coastal stations.

23.3.2 Distribution of Alkane and Acyclic Isoprenoids

The original Dalian crude oil contained *n*-alkanes that ranged from C_9 to C_{36} with bimodal maxima occurring at *n*-C_{15} and *n*-C_{23} (Fig. 23.4A). In the weathered crude oil collected after the spill, there was an absence of aliphatic compounds $<$*n*-C_{13} within 120 days after the spill. Over this same time, the predominant peaks were also changed from their unweathered distribution to one with maxima ranging from *n*-C_{17} and *n*-C_{23} with bimodal distribution after only 10 days to oils with a single maximum at *n*-C_{24} after 120 days (Fig. 23.4B). The residual oil samples were much more heavily biodegraded than the initial oil sample, evidenced by the large unresolved

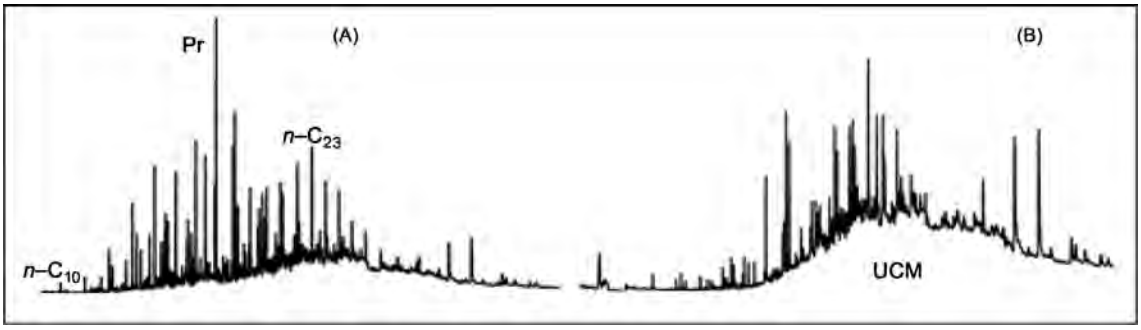

FIGURE 23.4 GC–FID chromatograms of (A) original Dalian crude oil (DL-0) and (B) weathered Dalian crude oil residual oil collected 120 days after oil spill (DL-8).

complex mixture "humps" in GC chromatograms (Fig. 23.4B). In addition, n-C_{17}/pristane and n-C_{18}/phytane ratios, which are commonly used as early indicators of biodegradation (Wang et al., 2001; Wang and Fingas, 2003; Lemkau et al., 2010), had decreased from 0.53 in the unweathered oil to 0.16 after 120 days due to biodegradation. More detailed information about the weathering of n-alkane and biomarkers for Dalian oil spill can be found in Wang et al. (2013).

23.3.3 Distribution of PAHs

23.3.3.1 Distribution of PAHs in Weathered Crude Oil Residue

The primary objective of this study was to investigate PAHs contamination in the area, identify possible PAHs sources, and evaluate their potential toxicological impacts. Given this objective, only 16 US EPA priority PAHs (16 PAHs) were measured and discussed in this work (Table 23.1). In other oil spill studies, the PAHs in floating and stranded crude oils showed dramatic reductions due to weathering (e.g., Stout et al., 2016). In our study, the concentration of total PAHs (ΣPAH_{16}) also were significantly decreased from 362.55 (ng/g oil) in the original "7-16" Dalian crude oil to 123.60 (ng/g oil) in the weathered oil after 120 days. In the original crude oil sample (DL-0), low molecular weight (LMW) PAHs (i.e., those containing 2–3 rings) were the dominant PAHs present and accounted for 70% of ΣPAH_{16}. The PAHs profiles in oil residue also changed with time. The proportion of LMW PAHs (Nap) significantly decreased from 52.32% (in DL-0) to 4.21% (in DL-8) over 120 days. The temporal changes in PAHs profile indicate that crude oil was subjected to weathering processes, wherein we suggest the LMW PAHs were dissolved in seawater and redistributed to the surrounding area.

As weathering progresses, the proportions of LMW PAHs decrease and those of heavy weight PAHs increase (Boehm et al., 1982; Yim et al., 2011). Naphthalenes are of special interest due to their toxicity, and along with other LMW PAHs, are often used to monitor recovery after an oil spill (Page et al., 2002). In the case of the *Exxon Valdez* oil spill, the proportion of naphthalenes had decreased from 40% to nearly zero in the 11 years after the accident (Page et al., 2002). Naphthalenes are more easily weathered than other PAHs. Thus, not surprisingly, naphthalene concentrations in the spilled Dalian crude oil decreased rapidly following the spill with neat oil values of 192.68 (ng/g oil) dropping to 154.14 (ng/g oil) within the first 10 days after the spill. Naphthalene concentrations continued to decrease until leveling off at approximately 12.21 (ng/g oil) 120 days postspill (Fig. 23.5A). Striking decreases in the abundance of naphthalene were very apparent (greater than 90% were lost) in comparison with the original Dalian crude oil. The proportion of naphthalenes of ΣPAH_{16} 120 days after the Dalian oil spill was still 9.88%, which indicated that the weathering process was still not complete. The depletion of other individual PAHs is shown in Fig. 23.5B. Similarly, weathering of the other 15 PAHs had already occurred demonstrating a moderate level of degradation in each. On the whole, the weathered Dalian crude oil residues were dominated by a low percent of naphthalenes but relatively enriched with 3–6 ring PAHs. These results were consistent with the preferential loss of the more volatile and soluble naphthalenes during early stages of oil weathering.

Photooxidation is considered to be another most important factor involved in the transformation of crude oil or its products released into the marine environment (Garrett et al., 1998). Photodegradation was examined using PAHs ratios, such as benz[*a*]anthracene to chrysene (BaA/Chr). These PAHs tend to weather at similar rates by most weathering processes but have been shown to photodegrade at different rates (Behymer and Hites, 1988;

TABLE 23.1 Toxicity Guidelines for PAHs in Sediments Compared to the Minimum, Maximum, and Average Concentrations Measured in Dalian Oil Residues and Surface Sediments

16 PAHs		Guideline (ng/g dw)		Residual oil (ng/g oil)			Sediment (ng/g dw)		
Abbreviation	**Compound**	**ER-L**	**ER-M**	**Min**[a]	**Avg**	**Max**[b]	**Min**	**Avg**	**Max**
Nap	Naphthalene	160	2100	12.21	72.90	192.68	10.06	26.80	77.44
Acy	Acenaphthylene	16	500	5.12	6.36	7.94	0.89	3.718	10.56
Ace	Acenaphthene	44	640	6.26	7.58	9.56	1.36	5.22	16.72
Fle	Fluorene	19	540	13.74	16.19	18.96	6.60	10.66	22.00
Phe	Phenanthrene	240	1500	11.86	14.38	16.02	24.00	55.88	149.6
Ant	Anthracene	85.3	1100	11.29	13.53	15.92	10.05	21.56	28.16
Fla	Fluoranthene	600	5100	11.68	15.85	18.74	24.22	57.00	149.6
Pyr	Pyrene	665	2600	13.29	17.12	19.20	16.36	50.40	149.6
BaA	Benz[*a*]anthracene	261	1600	4.44	6.75	8.89	12.38	42.40	123.2
Chr	Chrysene	384	2800	12.02	15.77	18.65	13.69	27.00	67.76
BbF	Benzo[*b*]fluoranthene	NA	NA	6.69	9.45	12.93	6.10	97.02	288.89
BkF	Benzo[*k*]fluoranthene	NA	NA	6.43	7.46	9.04	3.20	9.20	14.96
BaP	Benzo[*a*]pyrene	430	1600	1.84	2.29	3.01	12.36	39.60	114.4
IND	Indeno[1,2,3-*cd*]pyrene	NA	NA	1.94	3.65	6.45	13.30	38.60	105.6
DBahA	Dibenz[*a*,*h*]anthracene	63.4	260	1.53	1.87	2.37	3.30	15.14	46.64
BghiP	Benzo[*ghi*]perylene	NA	NA	3.28	4.25	5.19	11.05	35.02	98.56

[a]*Min: minimum concentration, the data from the residual oil collected 120 days after oil accident.*
[b]*Max: maximum concentration, the data from the original oil sample; NA: not available.*
ER-L, effects range-low; ER-M, effects range-median; Avg, average concentration.

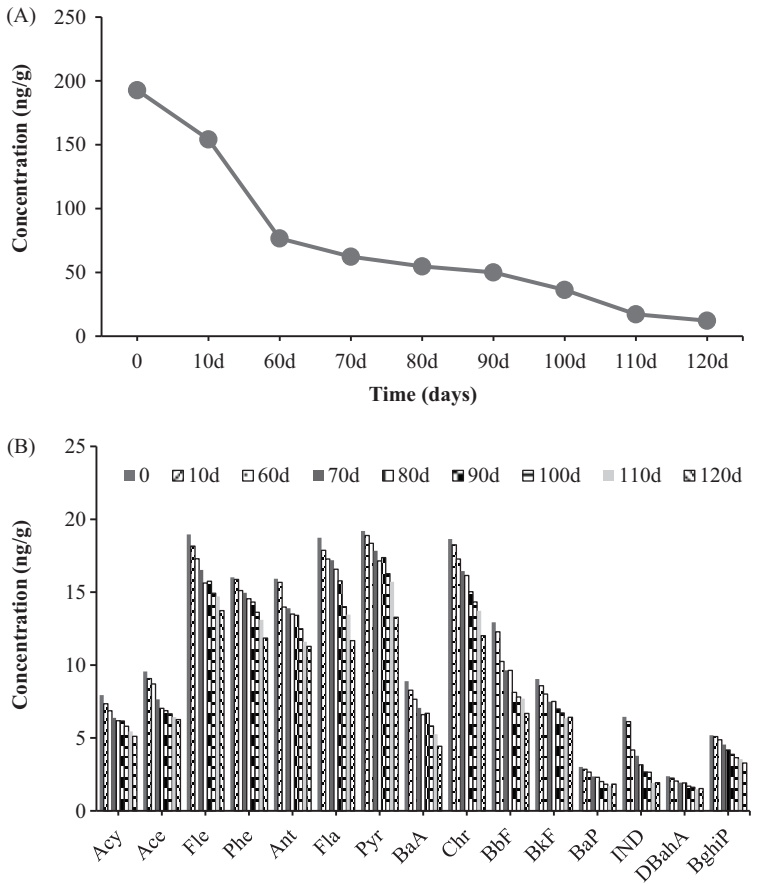

FIGURE 23.5 Trends in the concentrations of (A) naphthalene and (B) 15 other PAHs measured in Dalian crude oil residues over 120 days of weathering.

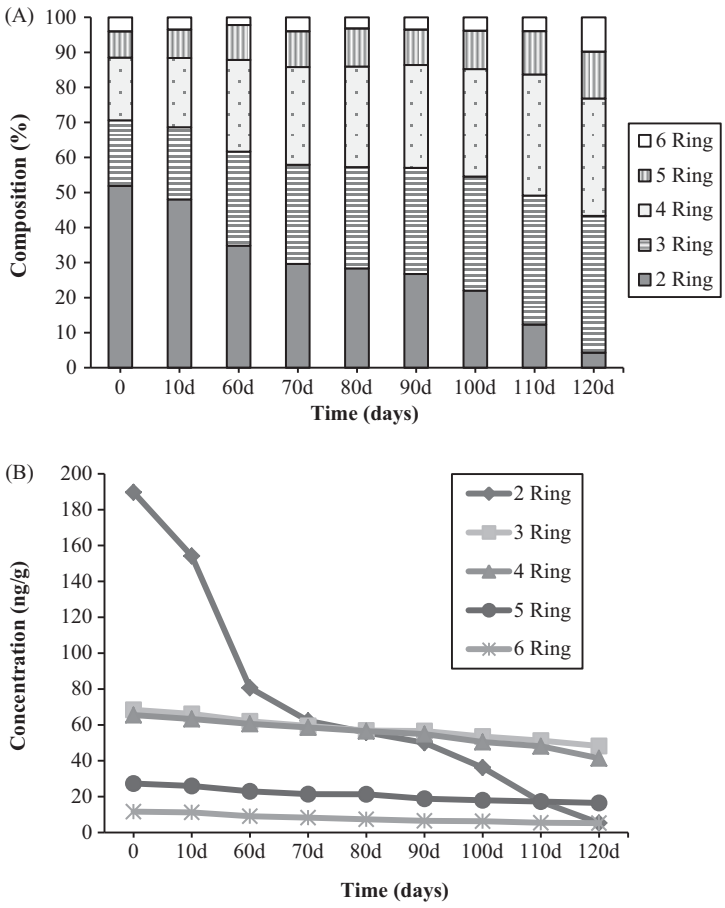

FIGURE 23.6 Trends in PAHs in Dalian crude oil over 120 days of weathering. (A) Percent of total PAHs by ring number and (B) absolute concentration by ring number.

Sauer et al., 1993; Douglas et al., 2002; Plata et al., 2008; Lemkau et al., 2010). About 1 month after the "7-16" Dalian oil spill, the BaA/Chr ratios in the oil residues began to decrease indicating the onset of photodegradation in this study. The low impact of photodegradation on samples from the other sites was similar to that observed for the *Prestige* oil samples where ratios of phenanthrene, chrysene, and their C_3-derivatives indicated no significant photodegradation 1 year after the spill (Diez et al., 2005).

The relative compositions of 16 PAHs were also evaluated (Fig. 23.6). The order of decrease among other PAHs compounds occurred in accordance with their molecular weight, i.e., the number of rings and/or size of the alkylated homologs (Ezra et al., 2000; Wang and Fingas, 2003; Lemkau et al., 2010). The relative abundance of naphthalene declined rapidly from 51.89% to 34.87% after 2 months and subsequently slowed down to 4.23% (Fig. 23.6B). On the other hand, the percent content of 3–6 ring PAHs all increased from 48.11% to 95.77% (Fig. 23.6), wherein the higher the ring number the weaker was the reduction (Fig. 23.6B). These results were in good agreement with previous work (Wang and Fingas, 2003). In this regard, it was pertinent to note that the order and the rate of weathering of 16 US EPA priority pollutant PAHs appears to decrease in accordance with the increase in the number of rings.

23.3.3.2 *Distribution of PAHs in Surface Sediment*

The concentrations of ΣPAH_{16} in sediment (DLS-1, DLS-2, DLS-3, DLS-4) ranged between 186.90 and 1304.86 ng/g dw, with a mean of 459.17 ng/g dw. The highest sediment concentrations were observed in the DLS-1 site located in the industrial areas, which was far away from oil spill site (Fig. 23.2). Thus, it is suggested that the "7-16" Dalian oil spill was not the main source of PAHs in these sediments. LMW PAHs (2–3 rings) were the dominant PAHs in crude oil sample (DL-0), account for 70% of total PAHs (Fig. 23.6A). However, a very different pattern of PAHs composition was found for sediment samples. The PAHs in sediment were mostly dominated by

high molecular weights (HMW) PAH homologs (4–6 rings), with the percentage of 58.94%–81.04%, which suggested that the elevated concentrations of PAHs in sediments were derived from pyrogenic sources.

23.3.4 Evaluation on the Diagnostic Ratios for Spilled Oil Identification

23.3.4.1 n-Alkane

Based on the evaluation method of indices suggested by Stout et al. (2001) and Li et al. (2009), relative standard deviation (%RSD) is considered as a useful indicator to evaluate the variability of diagnostic indices. The indices with %RSD <5% are probably not affected by weathering, while 5%RSD or more suggests that weathering has a remarkable effect on the index.

Weathering processes under the marine conditions in Dalian Bay caused significant changes in the chemical composition of *n*-alkanes and isoprenoids, which altered the diagnostic value of the source recognition indices based upon these compounds. For the less-weathered oils collected within 30 days of the "7-16" Dalian spill, ratios except Pr/Ph and CPI, n-C_{17}/Pr, n-C_{18}/Ph, Pr/(Pr + Ph), n-C_{17}/(Pr + n-C_{17}), n-C_{18}/(Ph + n-C_{18}), LMW/HWM, (n-C_{21} + n-C_{22})/(n-C_{28} + n-C_{29}), and n-C_{19} + n-C_{20}/n-C_{19-22} all displayed obvious changes due to weathering, indicating that these ratios are not useful for Dalian crude oil source identification. All of these ratios displayed obvious changed over weathering time (Fig. 23.7), especially for Pr/n-C_{17} and Ph/n-C_{18} which each showed a %RSD of more than 43.68, indicating that these ratios were not valid for oil source identification of the spill moderately degraded.

23.3.4.2 Polycyclic Aromatic Hydrocarbons

PAHs are relatively stable and may provide more detailed compound-specific data that can be used to identify both source and degradation extent (Yunker et al., 2002). As noted above, generally the order and rate of weathering of the PAHs appear to decrease in accordance with the increase in the number of rings and alkyl groups, i.e., molecular weight (Barakat et al., 2001; Wang and Fingas, 2003). On the other hand, unlike the preferential degradation of alkyl homologs, there appears to be no preference for degradation between different isomers of the compounds studied. In agreement with the interpretation of previous studies (Wang and Fingas, 2003), we believe that all the isomers of, e.g., the methyl-dibenzothiophenes, phenanthrenes, chrysenes are lost at more or less the same rate for lightly to moderately biodegraded oils, such as expressed in the experimental time of this study.

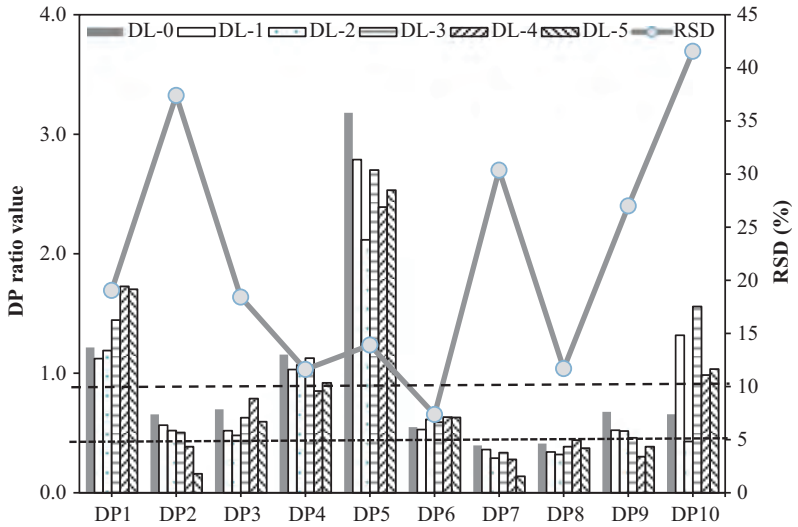

FIGURE 23.7 Trends and %RSD for ten parameters based upon *n*-alkanes and isoprenoids in Dalian oils collected at different times over 120 days. DP1: Pr/Ph; DP2: n-C_{17}/Pr; DP3: n-C_{18}/Ph; DP4: CPI; DP5: LMW/HWM; DP6: Pr/(Pr + Ph); DP7: n-C_{17}/(Pr + n-C_{17}); DP8: n-C_{18}/(Ph + n-C_{18}); DP9: n-C_{19} + n-C_{20}/n-C_{19-22}; DP10: (n-C_{21} + n-C_{22})/(n-C_{28} + n-C_{29}).
CPI: 1/2[(C_{25} + C_{27} + C_{29} + C_{31} + C_{33})/(C_{24} + C_{26} + C_{28} + C_{30} + C_{32}) + (C_{25} + C_{27} + C_{29} + C_{31} + C_{33})/(C_{26} + C_{28} + C_{30} + C_{32} + C_{34})]; LMW/HWM: n-C_9 to n-C_{21} alkanes relative to the sum of n-C_{22} to n-C_{34} alkanes. DL-0 (0 days), DL-1 (10 days), DL-2 (30 days), DL-3 (60 days), DL-4 (90 days), DL-5 (120 days).

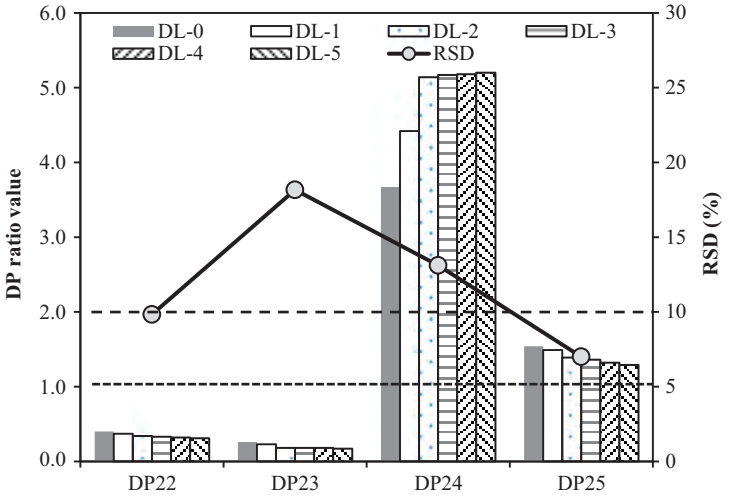

FIGURE 23.8 Trends and %RSD for four parameters based upon PAHs and dibenzothiophenes in Dalian oils collected at different times over 120 days.
DP22: C_2-dibenzothiophenes/C_2-phenanthrenes; DP23: C_3-dibenzothiophenes/C_3-phenanthrenes; DP24: ∑phenanthrenes/∑dibenzothiophenes; DP25: 4-methyldibenzothiophene/1-methyldibenzothiophene. DL-0 (0 days), DL-1 (10 days), DL-2 (30 days), DL-3 (60 days), DL-4 (90 days), DL-5 (120 days).

The weathered oil residues investigated in our study provide an opportunity to determine the stability of PAH-based diagnostic source ratios in the natural coastal zone environment. Results of this study are shown in Fig. 23.8 and indicate that the higher ratios of C_2-DBT/C_2-PHEN and C_3-DBT/C_3-PHEN, and lower ratios of ∑PHENs/∑DBTs in the weathered oil samples collected over 120 days compared to the original Dalian crude oil. This observation was also in contrast to the results of previous studies (Barakat et al., 2001), in which phenanthrenes were believed to be degraded at a faster rate relative to dibenzothiophenes in highly weathered samples in the marine environment. For example, Barakat et al. (2001) found that the ratios of C2-DBT/C2-PHEN and C3-DBT/C3-PHEN were higher in the weathered oil sample compared to the reference oil in the spill in shoreline of the Gulf of Suez, Egypt. Such variable trends might be the result of large spraying of oil spill dispersant. A large volume of oil dispersant was also sprayed in this oil accident disposal, which may have contributed to alter these diagnostic ratios.

23.3.4.3 *Terpane and Sterane Biomarkers*

Terpanes and steranes are another group of biomarker compounds that have been frequently applied in oil correlation, source identification, and maturity determination (Duan et al., 2003). The biomarker-base parameters have been playing a prominent role in almost all oil spill work for many years. Unlike the aliphatic and PAHs distributions, in our study, the terpane and sterane distributions obtained for the weathered Dalian oil residues and the original Dalian crude oil samples analyzed were similar. For example, the distribution profiles of terpanes in these oils were all dominated by hopanes composed of C_{27}–C_{35} members, with 17α,21β(*H*)-hopane being the major compound. As for steranes, the dominance of C_{27}, C_{28}, and C_{29} 20S/20R steranes was obvious, with the 20R isomers being more abundant than the 20S isomers. As mentioned above, terpanes and steranes retained their molecular distributions during the moderate weathering observed among our samples and therefore could be used in tracking the origin and sources of hydrocarbon pollution, including the Dalian crude oil, in the marine environment.

In this study, the traditional parameters among biomarkers, which are also widely used in petroleum exploration, source identifiers and weathering assessment tools, were considered. As shown in Fig. 23.9, all parameters based upon the terpane and sterane biomarkers had lower standard deviations and %RSD (<5%) demonstrating that they exhibited little change after weathering 120 days. These results were also similar to those observed in previous studies (e.g., Wang et al., 2001; Barakat et al., 2001), which showed that terpane and sterane biomarkers are more resistant to degradation than *n*-alkanes and isoprenoids.

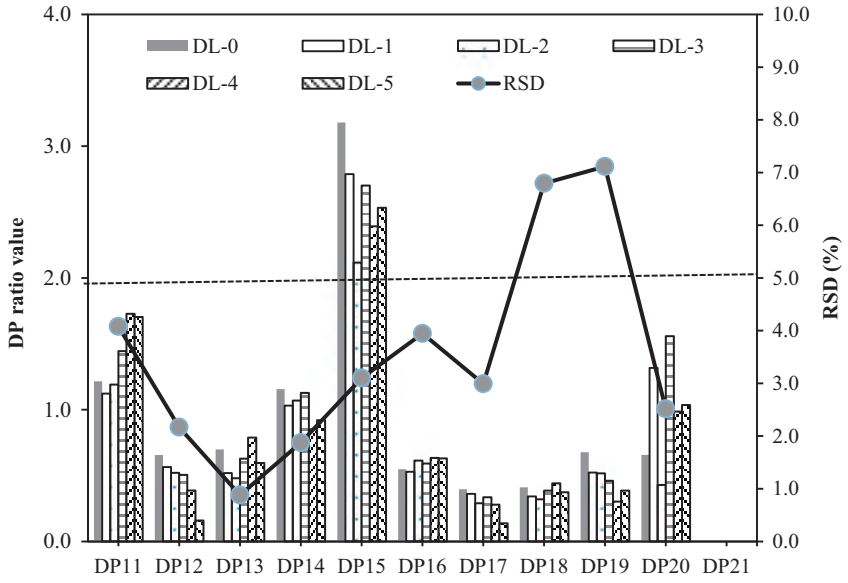

FIGURE 23.9 Trends and %RSD for 10 parameters based upon terpane and sterane biomarkers in Dalian oils collected at different times over 120 days. DP11: Ts/Tm; DP12: C_{31}22S/(22S + 22R); DP13: C_{32}22S/(22S + 22R); DP14: C_{33}22S/(22S + 22R); DP15: $C_{30}\beta\alpha/C_{30}\alpha\beta$; DP16: $C_{29}\alpha\beta/C_{30}\alpha\beta$; DP17: Gam/$C_{30}$; DP18: C_{27}/C_{29}; DP19: C_{29}20S/(20S + 20R); DP20: $C_{29}\beta\beta/(\beta\beta + \alpha\alpha)$. For terpane parameters, Ts/Tm: ratio of 18α-22,29,30-trisnorhopane relative to 17α-22,29,30-trisnorhopane; C_{31-33}22S/(22S + 22R): 22S (22S + 22R) for C_{31-33}-17α,21β(*H*)-homohopane; $C_{30}\beta\alpha/C_{30}\alpha\beta$: ratio of C_{30} Moretane to C_{30} hopane; $C_{29}\alpha\beta/C_{30}\alpha\beta$: C_{29}/C_{30} hopane ratio; 17α,21β(*H*)-30 norhopane to 17α,21β(*H*)-hopane; Gam/C_{30}: ratio of Gammacerane to 17α,21β(*H*)-hopane. For sterane parameters, $C_{27}/2C_{29}$: 20R-C_{27} to 20R-$C_{29}\alpha\alpha\alpha$ steranes ratio; C_{29}20S/(20S + 20R): 20S/(20S + 20R) C_{29} sterane ratio; $C_{29}\beta\beta/(\beta\beta + \alpha\alpha)$: $\beta\beta/(\beta\beta + \alpha\alpha)$ C_{29} sterane ratio. DL-0 (0 days), DL-1 (10 days), DL-2 (30 days), DL-3 (60 days), DL-4 (90 days), DL-5 (120 days).

23.3.4.4 *Carbon Isotopic Composition of the* n*-Alkanes*

Gas chromatography–isotope ratio mass spectrometry (GC–IRMS) is a powerful tool for identifying the source of organic matter (Freeman et al., 1990; Hayes et al., 1990) and correlating oil with possible source rocks (Bjorøy et al., 1994) in petroleum geochemistry. Compound-specific isotope analysis has been extensively applied in environmental forensic investigations related to petroleum pollution. Thus, stable carbon isotopic compositions of individual hydrocarbons in spilled oils and sediments may provide additional evidence that helps to trace oil spill sources (Mansuy et al., 1997; Mazeas and Budzinski, 2002). However, it is very important to understand the relationship between the weathering processes and the isotopic composition of individual *n*-alkanes. Previous research has indicated that short-term weathering has no significant effect on the $\delta^{13}C$ values of *n*-alkanes (Li et al., 2009). However, little work has been done about evaluation of the effect of moderate or high degrees of weathering on the carbon isotopic distribution of *n*-alkanes, as well as to determine whether stable carbon isotope ratios can be used as a weathering-resistance indicator under natural marine conditions.

For the oil sample from Dalian Bay, the $\delta^{13}C$ values for the *n*-alkanes, pristine, and phytane did not show a significant carbon isotopic fractionation with increased weathering (Fig. 23.10). The standard deviations of $\delta^{13}C$ values of individual *n*-alkanes varied from 0.07% to 0.20% for weathering over 60 days and ranged from only 0.06%–0.36% for weathering over 90 days. Even for the longer weathered samples over 120 days (DL-5), the standard deviations of $\delta^{13}C$ values of individual *n*-alkanes varied from only 0.07%–0.20%, which showed that the weathering had no significant effect on the isotopic values of individual *n*-alkanes. The carbon isotope discrimination $\Delta\delta^{13}C$ ($\Delta\delta^{13}C = \delta^{13}C(t) - \delta^{13}C(0)$) of individual *n*-alkanes were <3‰. As discussed in each of the sections above, marked differences in chemical composition were present between weathered and unweathered Dalian crude oils, which in some instance hindered the comparison of the spilled oils with the original oil. In contrast, weathering had no obvious effect on $\delta^{13}C$ values of individual *n*-alkanes, suggesting that carbon isotopic profile of *n*-alkanes could be used as a powerful tool for identifying the source of oil spills. This conclusion was in agreement with results of the three independent weathering experiments conducted by Mansuy (1997), which revealed that the ^{13}C values of *n*-alkanes are minimally affected by evaporation, water washing, or biodegradation.

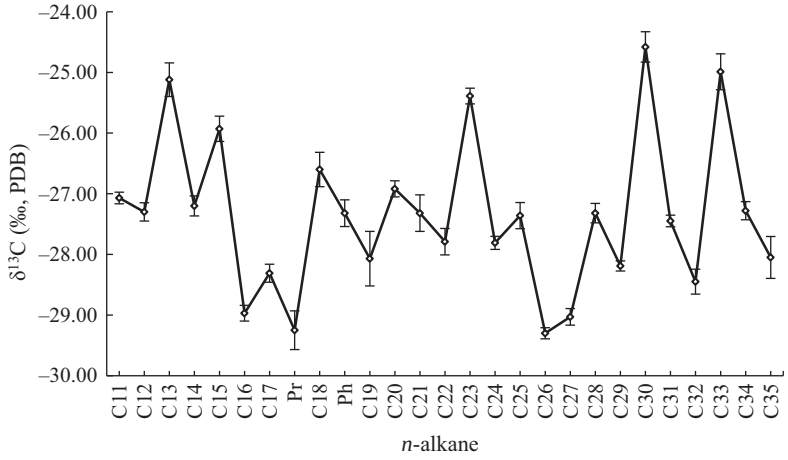

FIGURE 23.10 Distribution of $\delta^{13}C$ values of individual *n*-alkanes, pristane, and phytane in weathered Dalian crude oils and the original Dalian source oil. (Points show the average of $\delta^{13}C$ values of individual *n*-alkanes from the spilled oils studied over 120 days and the original source oil. Error bars represent standard deviations of $\delta^{13}C$ values for each individual compound.)

23.3.5 Weathering on PAH Diagnostic Ratios for the Identification of Pollution Emission Sources

PAHs in the environment originate through both from natural (organic matter diagenesis, plant synthesis, forest and prairie fires, volcanoes, etc.) and anthropogenic processes (fossil fuel burning, incomplete combustion of organic matter, petroleum, incineration, etc.). Identifying the sources of PAHs is very important to study the transport and fate of PAHs in environment. Ratios of certain PAH isomers, such as LMW (2−3-ring PAHs) to HMW (4−6-ring PAHs) (LMW/HMW), Ant/(Ant + Phe), BaA/(BaA + Chry), Fla/(Fla + Pyr), IND/(IND + BghiP), etc., can be used to identify the possible emission sources (Dickhut et al., 2000; Yunker et al., 2002; Yang et al., 2009). For example, Flu/(Flu + Pyr) values <0.4 implies petroleum, values between 0.4 and 0.5 imply petroleum combustion, and values >0.5 implies combustion of coal and biomass; Ant/(Ant + Phe) values <0.10 are seen as indicators of petroleum input or diagenetic sources, whereas values >0.1 are characteristic of combustion processes; and BaA/(Chry + BaA) values <0.20 indicate petroleum, values between 0.20 and 0.35 are seen as indicators of petroleum and combustion, and values >0.35 indicate combustion. For the sediments of this study, most of samples had values of Fla/(Fla + Pyr) >0.5, BaA/(Chry + BaA) >0.35, and Ant/(Ant + Phe) ratio >0.10, which further proved the pyrogenic origin unrelated to the Dalian oil spill (Fig. 23.11).

There was a good positive correlation ($R^2 > 0.89$, *P*-value < 0.0001) between the PAH isomers, such as Fla and Pyr, Ant and Phe, BaA and Chr, IND and BaP, IND and BghiP, for the Dalian crude oil samples collected after experiencing different weathering levels over time. This also implied that the mass 202 (Flu, Pyr), 228 (BaA, Chr), and 276 (IND, BghiP) isomers had the greatest range in stability and hence good promise as indicators of emission sources index.

Parameters generated from PAHs distributions have a tendency to change under the influence of weathering process. As noted above, the ratio of LMW/HMW dropped in crude oil residued from 2.47−0.85, 120 days after the "7-16" Dalian oil spill. In addition, except the ratios of Fla/(Fla + Pyr) and Ant/(Ant + Phe), other PAH isomer ratios displayed obvious changes over 120 days of weathering (Fig. 23.12), indicating that these other ratios (Dr-4 to Dr-7) are not valid for emission sources. Based on this, the combined effects of weathering could strongly modify the fingerprints and parameters on sources of PAHs which widely used to differentiate between pyrolytic and petrogenic sources.

23.3.6 Implication of Weathering on Ecotoxicology

The environmental impact of crude oil contamination in coastal ecosystems is potentially serious. In order to assess potential environmental impacts of PAHs from "7-16" Dalian crude oil spill on the organisms in sediment of Dalian coastal bay, the concentrations of PAHs in surface sediments were compared with sediment quality guidelines (SQGs), an important tool to assess the contamination in marine and estuarine sediments (Long et al., 1995; Long, 2006). In this study, ERL and ERM concentrations (ER-L: effects range-low; ER-M: effects range-median), were applied to evaluate the potential effects in contaminated sediments (Table 23.1). According to the Long et al.

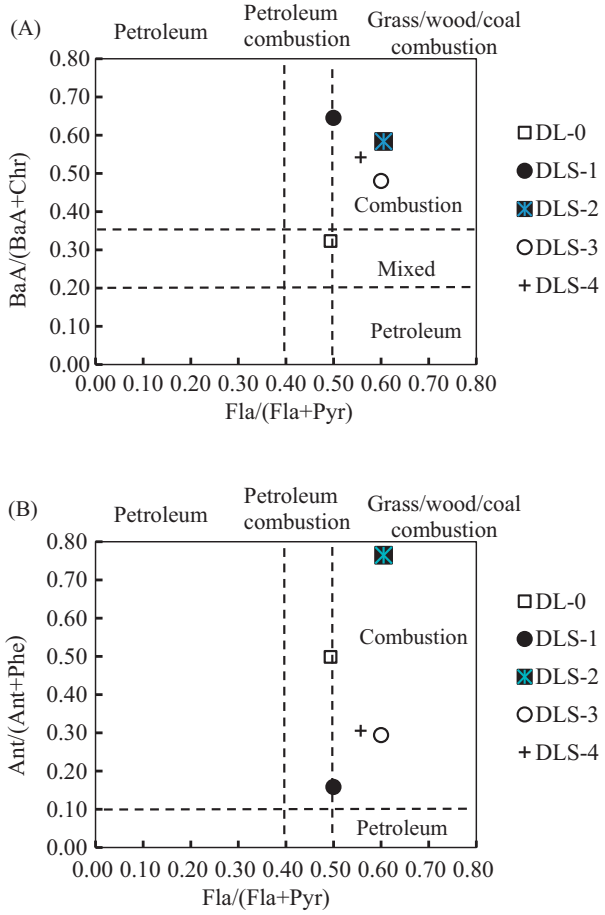

FIGURE 23.11 PAH cross plots for the ratios of (A) Fla/(Fla + Pyr) vs. BaA/(BaA + Chr) and (B) Fla/(Fla + Pyr) vs. Ant/(Ant + Phe) in surface sediments evaluated in this study.

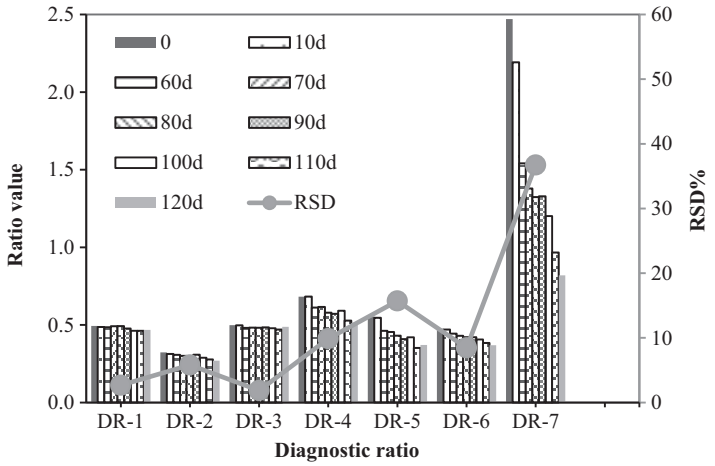

FIGURE 23.12 Diagnostic ratios of PAHs for the identification with weathering time.
Note: DR-1: Fla/(Fla + Pyr); DR-2: BaA/(Chr + BaA); DR-3: Ant/(Ant + Phe); DR-4: IND/IND + BaP; DR-5: IND/IND + BghiP; DR-6: BaA/Chr.

(1995) and Long (2006) criteria, adverse biological effects rarely occur if the observed PAH concentration is below the ER-L value (4022 ng/g dw), but if the concentration is higher than the ER-M value (44,792 ng/g dw), adverse effects are likely to occur. The results for the sediments studied herein showed that the maximum concentrations of individual PAHs compounds in sediments were much lower than the ER-M values (Table 23.1) after "7-16" Dalian oil spill accident. Thus, it may be concluded that any additional PAHs in sediments derived from the "7-16" Dalian oil spill will not cause immediately adverse biological effects in the coastline of Dalian Bay.

Weathering has significant effects on residual oil's ecotoxicology. Another important matter relevant to this study is whether potential toxicity varies according to the degree of oil weathering. As oil weathers the concentration of total PAHs required to cause, adverse effects is also lowered. According to Page et al. (2002), less-weathered samples with a high proportion of naphthalenes show higher toxicity, whereas more weathered samples with proportions of naphthalenes below 10% show lower toxicity. Our data show that only residual Dalian crude oil samples collected 120 days after the accident showed a proportion of naphthalenes below 10% (Fig. 23.6A). Thus, it can also be concluded that the potential toxicity will decrease with weathering time according to the degree of oil weathering.

23.4 CONCLUSIONS

The "7-16" Dalian crude oil spill accident in July 2010 provided an excellent opportunity to monitor the variation in the chemical composition of residual crude oil and PAHs over time along the coastline of Dalian Bay under natural conditions. The concentrations of *n*-alkanes and isoprenoids in the oil residue were reduced by 50% within 120 days after the oil spill. TPH concentration in surface sediments collected along the coastal site were reduced from 7133 μg/g in December 2011 to 926 μg/g in 2014, indicating the sediments quality recovered to the first quality standards by 2014 under natural marine conditions. In addition, the concentrations of total PAHs (ΣPAH_{16}) in residual oil decreased from 365.55 to 123.60 (ng/g oil), 120 days after the oil spill. Striking decreases in the abundance of naphthalene was very apparent in the spilled oil (greater than 90% was lost), 120 days after the accident.

Diagnostic ratios developed from *n*-alkane and selected isoprenoids, such as Pr/Ph, $n\text{-}C_{17}$/Pr, $n\text{-}C_{18}$/Ph, CPI, LMW/HWM, Pr/(Pr + Ph), $n\text{-}C_{17}$/(Pr + $n\text{-}C_{17}$), $n\text{-}C_{18}$/(Ph + $n\text{-}C_{18}$), $n\text{-}C_{19} + n\text{-}C_{20}/n\text{-}C_{19-22}$, and ($n\text{-}C_{21} + n\text{-}C_{22}$)/($n\text{-}C_{28} + n\text{-}C_{29}$), were not valid for oil source identification due to the effects of weathering. Among the sterane and terpane biomarker ratios, the Ts/Tm, C_{31}2S/(22S + 22R), C_{32}22S/(22S + 22R), C_{33}22S/(22S + 22R), $C_{30}\beta\alpha$/$C_{30}\alpha\beta$, $C_{29}\alpha\beta/C_{30}\alpha\beta$, Gam/C30, C_{27}/C_{29}, C_{29}20S/(20S + 20R), $C_{29}\beta\beta/(\beta\beta + \alpha\alpha)$ remained stable and are thereby suitable for the oil source identification and correlation. The stable carbon isotopic profile of *n*-alkanes also remained stable and thereby could also be used to identify the source of an oil spill, especially for those lower boiling oils containing prominent $C_{10}-C_{20}$ *n*-alkanes but low concentrations of sterane and terpane biomarkers. Moreover, the analysis of the weathered Dalian crude oil residues collected 120 days after the spill indicate that despite the long-term weathering, it was still possible to correlate the oil residue samples to the original source oil based on the selective use of numerous PAH-based parameters, such as Fla/(Fla + Pyr), Ant/(Ant + Phe).

Based upon the reduced concentrations of PAHs, especially naphthalene, the toxicity of the residual Dalian crude oil apparently decreased rapidly to nontoxic levels within 120 days after the oil spill accident, and thus, the "7-16" Dalian oil spill will not cause immediately adverse biological effects in the coastline of Dalian Bay. The results of this study will be useful in the risk assessment of terrestrial and other marine oil spills and in preparing management policies for future oil spills and contaminated sediments, including derivation of quality guidelines of PAHs in marine sediments.

Acknowledgments

This study was cosupported by Science and Technology Service Network Initiative, Chinese Academy of Sciences (KFJ-EW-STS-127), Project of on-site sediment microbial remediation of public area of central Bohai Sea, North China Sea Branch of State Oceanic Administration (QDZC20150420-002) and International cooperation, CAS, Chinese-foreign cooperation in key projects (133337KYSB20160002).

References

Barakat, A.O., Qian, Y., Kim, M., Kennicutt, M.C., 2001. Chemical characterization of naturally weathered oil residue in arid terrestrial environmental in Al-Alamein, Egypt. Environ. Sci. Technol. 27, 291–310.

Behymer, T.D., Hites, R.A., 1988. Photolysis of polycyclic aromatic hydrocarbons adsorbed on fly ash. Environ. Sci. Technol. 22, 1311–1319.

Bjorøy, M., Hall, K., Moe, R.P., 1994. Stable carbon isotope variations of n-alkanes in Central Graben oils. Org. Geochem. 22, 355–381.
Boehm, P.D., Fiest, D.L., Mackay, D., Paterson, S., 1982. Physical chemical weathering of petroleum hydrocarbons from the IXTOC I blowout: chemical measurements and a weathering model. Environ. Sci. Technol. 16, 498–505.
Budzinski, H., Jones, I., Bellocq, J., Pierard, C., Garrigues, P., 1997. Evaluation of sediment contamination by polycyclic aromatic hydrocarbons in The Gironde Estuary. Mar. Chem. 58, 85–97.
D'Auria, M., Emanuele, L., Racioppi, R., Velluzzi, V., 2009. Photochemical degradation of crude oil: comparison between direct irradiation, photocatalysis, and photocatalysis on zeolite. J. Hazard. Mater. 164, 32–38.
Dickhut, R.M., Canuel, E.A., Gustafson, K.E., Liu, K., Arzayus, K.M., Walker, S.E., et al., 2000. Automotive sources of carcinogenic polycyclic aromatic hydrocarbons associated with particular matter in the Chesapeake Bay region. Environ. Sci. Technol. 34, 4635–4640.
Diez, S., Sabate, J., Vinas, M., Bayona, J.M., Solanas, A.M., Albaiges, J., 2005. The Prestige oil spill. I. Biodegradation of a heavy fuel oil under simulated conditions. Environ. Toxicol. Chem. 24, 2203–2217.
Douglas, G.S., Owens, E.H., Hardenstine, J., Prince, R.C., 2002. The OSSA II pipeline oil spill: the character and weathering of the spilled oil. Spill Sci. Technol. B 7, 135–148.
Duan, Y., Zhang, H., Wu, B.X., Zheng, Z.Y., 2003. Carbon isotopic studies of individual *n*-alkanes in crude oils from Qaidam Basin. J. Mineral. Petrol. 23, 91–94.
Ezra, S., Feinstein, S., Pelly, I., Bauman, D., Miloslavsky, I., 2000. Weathering of fuel oil spill on the east Mediterranean coast, Ashdod, Israel. Org. Geochem. 31, 1733–1741.
Freeman, K.H., Hayes, J.M., Trendel, J.M., Albrecht, P., 1990. Evidence from carbon isotope measurements from diverse origins of sedimentary hydrocarbons. Nature 343, 254–256.
Gao, X.Y., Fan, J.F., Chen, J.Y., Lin, F.A., Ming, H.X., Li, J.Y., et al., 2013. Influence on marine hydrocarbon-degrading bacteria and heterotrophic bacteria abundance by Dalian "7.16" oil spill accident. Mar. Environ. Sci. 32, 688–692.
Garrett, R.M., Pickering, I.J., Haith, C.E., Prince, R.C., 1998. Photooxidation of crude oils. Environ. Sci. Technol. 32, 3719–3723.
Guo, L.M., 2016. The Research of Temporal and Spatial Variations of Bacterial Community After "7.16" Oil Spill in Dalian [D]. Dalian Ocean University.
Hayes, J.M., Freeman, K.H., Popp, B.N., Hoham, C.H., 1990. Compound-specific isotopic analyses: a novel tool for reconstruction of ancient biochemical processes. Org. Geochem. 16, 1115–1128.
Kennicutt II, M.C., 1988. The effect of biodegradation on crude oil bulk and molecular composition. Oil. Chem. Pollut. 4, 89–112.
Lemkau, K.L., Peacock, E.E., Nelson, R.K., Ventura, G.T., Kovecses, J.L., Reddy, C.M., 2010. The M/V Cosco Busan spill: source identification and short-term fate. Mar. Pollut. Bull. 60, 2123–2129.
Li, Y., Xiong, Y.Q., Yang, W.Y., Xie, Y.L., Li, S.Y., Sun, Y.G., 2009. Compound-specific stable carbon isotopic composition of petroleum hydrocarbons as a tool for tracing the source of oil spills. Mar. Pollut. Bull. 58, 114–117.
Long, E.R., 2006. Calculation and uses of mean sediment quality guideline quotients: a critical review. Environ. Sci. Technol. 40, 1726–1736.
Long, E.R., Macdonald, D.D., Smith, S.L., Calder, F.D., 1995. Incidence of adverse biological effects within ranges of chemical concentrations in marine and estuarine sediments. Environ. Manage. 19, 81–97.
Lotufo, G.R., Fleeger, J.W., 1997. Effects of sediment-associated phenanthrene on survival, development and reproduction of two species of meiobenthic copepods. Mar. Ecol. Prog. Ser. 151, 91–102.
Magi, E., Bianco, R., Ianni, C., Carro, M.D., 2002. Distribution of polycyclic aromatic hydrocarbons in the sediment of the Adriatic Sea. Environ. Pollut. 119, 91–98.
Mansuy, I., Philp, R.P., Allen, J., 1997. Source identification of oil spills based on the isotopic composition of individual components in weathered oil samples. Environ. Sci. Technol. 31, 3417–3425l7.
Mazeas, L., Budzinski, H., 2002. Stable carbon isotopic study ($^{12}C/^{13}C$) of the fate of petrogenic PAHs (methylphenanthrenes) during an in situ oil spill simulation experiment. Org. Geochem. 33, 1253–1258.
Page, D.S., Boehm, P.D., Stubblefield, W.A., Parker, K.R., Gilfillan, E.S., Neff, J.M., et al., 2002. Hydrocarbon composition and toxicity of sediments following the *Exxon Valdez* oil spill in Prince William Sound, Alaska, USA. Environ. Toxicol. Chem. 21, 1438–1450.
Peterson, C.H., Rice, S.D., Short, J.W., Esler, D., Bodkin, J.L., Ballachey, B.E., et al., 2003. Long-term ecosystem response to the Exxon Valdez oil spill. Science 302, 2082–2086.
Plata, D.L., Sharpless, C.M., Reddy, C.M., 2008. Photochemical degradation of polycyclic aromatic hydrocarbons in oil films. Environ. Sci. Technol. 42, 2432–2438.
Sauer, T.C., Brown, J.S., Boehm, P.D., Aurand, D.V., Michel, J., Hayes, M.O., 1993. Hydrocarbon source identification and weathering characterization of intertidal and subtidal sediments along the Saudi Arabian coast after the Gulf War oil spill. Mar. Pollut. Bull. 27, 117–134.
Stout, S.A., Uhler, A.D., McCarthy, K.J., 2001. A strategy and methodology for defensibly correlating spilled oil to source candidates. Environ. Forens. 2, 87–98.
Stout, S.A., Payne, J.R., Emsbo-Mattingly, S.D., Baker, G., 2016. Weathering of field-collected floating and stranded Macondo oils during and shortly after the Deepwater Horizon oil spill. Mar. Pollut. Bull. 105, 7–22.
Wang, C.Y., Chen, B., Zhang, B.Y., He, S.J., Zhao, M.M., 2013. Fingerprint and weathering characteristics of crude oils after Dalian oil spill, China. Mar. Pollut. Bull. 71, 64–68.
Wang, Z.D., Fingas, M.F., 2003. Development of oil hydrocarbon fingerprinting and techniques. Mar. Pollut. Bull. 47, 423–452.
Wang, Z.D., Fingas, M., Sigouin, L., 2001. Characterization and identification of a "mystery" oil spill from Quebec (1999). J. Chromatogr. A 909, 155–169.
Yang, Z.F., Wang, L.L., Niu, J.F., Wang, J.Y., Shen, Z.Y., 2009. Pollution assessment and source identifications of polycyclic aromatic hydrocarbons in sediments of the Yellow River Delta, a newly born wetland in China. Environ. Monit. Assess. 158, 561–571.
Yim, U.H., Ha, S.Y., An, J.G., Won, J.H., Han, J.M., Hong, S.H., et al., 2011. Fingerprint and weathering characteristics of stranded oils after the Hebei Spirit oil spill. J. Hazard. Mater. 197, 60–69.
Yunker, M.B., Macdonald, R.W., Vingarzan, R., Mitchell, R.H., Goyette, D., Sylvestre, S., 2002. PAHs in the Fraser River basin: a critical appraisal of PAH ratios as indicators of PAH source and composition. Org. Geochem. 33, 489–515.
Zeng, S.Y., Zeng, L., Dong, X., Chen, J.N., 2013. Polycyclic aromatic hydrocarbons in river sediments from the western and southern catchments of the Bohai Sea, China: toxicity assessment and source identification. Environ. Monit. Assess. 185, 4291–4303.

CHAPTER

24

Case Study in the Use of Forensic History in Matters Involving Pipeline Ruptures

A.J. Gravel[1], *Sandra Layland*[2] *and Julie Corley*[3]

[1]FTI Consulting, Rockville, MD, United States [2]FTI Consulting, Santa Barbara, CA, United States
[3]FTI Consulting, San Francisco, CA, United States

BIOGRAPHIES

A.J. Gravel is a senior managing director in FTI Consulting Inc.'s Forensic Litigation and Consulting segment. He is the copractice leader of the Environmental Solutions Practice and heads the Forensic History and Analysis group. His primary areas of expertise are in forensic history and environmental cost analysis. Mr. Gravel is based in the Washington, DC area and has over 25 years of combined experience as a consultant and expert witness. He has managed the execution of hundreds of environmental, products liability, and litigation support projects involving forensic history and environmental damages and has provided testimony as a fact witness, Rule 30(b)(6) corporate designee and expert witness.

Sandra Layland is a senior director in the FTI Consulting Forensic and Litigation Consulting, Environmental Solutions practice and is based in Santa Barbara. With over 20 years of experience as a consulting forensic historian, Ms. Layland specializes in developing historical research work plans, managing and conducting field document research; analyzing and summarizing complex information from a variety of sources; and using that information to prepare concise and cogent work products. Ms. Layland also has an extensive background in information science, corporate records management, and litigation document support.

Julie Corley is a senior director in the FTI Consulting Forensic and Litigation Consulting, Environmental Solutions practice and is based in San Francisco. With over 20 years of experience as a consulting historian, Ms. Corley specializes in forensic historical research and analysis. She specializes in developing historical research methodologies to locate and analyze disparate and complex information in order to produce a cohesive fact-based understanding of specific historical issues.

24.1 BRIEF HISTORY OF PIPELINE DEVELOPMENT

The earliest oil pipelines in the United States, laid in the 1860s, were typically constructed of 2-in cast-iron pipe threaded and screwed together in short segments. Oil was propelled through the pipeline using steam-driven, single cylinder pumps, or by gravity feed. These early pipelines, seldom more than 15 mi in length, were prone to bursting, thread stripping at the pipe joints, and frequent pump breakdowns mainly due to the percussive strain on the lines caused by each stroke of the pump which "resembled the report of a rifled gun." Development of the four-cylinder Worthington pump revolutionized the transportation of petroleum by pipeline with its constant flow and uniform pressure (The Engineering and Building Record, 1890; Scientific American, 1892; Herrick, 1949; Williamson and Daum, 1959).

Oil Spill Environmental Forensics Case Studies.
DOI: http://dx.doi.org/10.1016/B978-0-12-804434-6.00024-0

By the 1870s, a 2000-mi network of small-diameter gathering lines connected the oil-producing areas with regional refineries and storage points on the railroads and rivers where the oil could be shipped to refineries via railcars or ships and barges. Typical crude oil trunk lines were constructed of 18-ft sections of lap-welded wrought iron pipe 5 or 6 in in diameter joined with tapered, threaded joints manufactured specifically for pipeline service. The pipe was generally buried 2 or 3 ft below the ground surface. Worthington-type pumps were used as the motive power for the lines, and the pumps were powered by steam generated by coal-fired boilers. Pump stations were spaced as needed to maintain the flow of oil over the terrain crossed by the lines. At the pump stations, oil was withdrawn from the lines and passed through riveted steel receiving tanks some of which were 90 ft in diameter and 30 ft high holding about 35,000 barrels (The Engineering and Building Record, 1890; Scientific American, 1892; Herrick, 1949). Diesel-powered pumps began to replace steam power around 1913–1914 (Williamson et al., 1963).

It was not until May 1879 that the Tidewater Pipe Company, Ltd. began operation of the first long-distance crude oil pipeline covering the 100 mi between Coryville and Williamsport, Pennsylvania, to connect with the Reading Railroad. The line was constructed of 6-in wrought-iron pipe laid on the surface of the ground (except when crossing cultivated land) and relied on only two pumping stations, one at Coryville and the other near Coudersport. The expansion of the oil under the hot summer sun caused the line to shift as much as 15–20 ft from its intended position, knocking over telegraph poles and small trees, but no serious breaks occurred. In the spring of 1880, Tidewater buried the entire line (Williamson and Daum, 1959).

The success of the Tidewater pipeline set the pattern for the construction of other long-distance crude oil "trunk" lines which sprang up in the early 1880s connecting the oil regions of Pennsylvania with refining centers in Cleveland, Pittsburg, Buffalo, Philadelphia, Bayonne, and New York City (Williamson and Daum, 1959).

By 1905, the oil fields in the Oil Regions of Appalachia stretching from Wellsville, New York, through western Pennsylvania, West Virginia, eastern Ohio, Kentucky, and Tennessee were becoming depleted. The new oil fields discovered during the early 1900s in Ohio, Indiana, Illinois, southeastern Kansas, northeastern Oklahoma, and eastern Texas were quickly connected by trunk lines to the eastern refining centers as well as the new western refineries in Lima, Ohio; Whiting, Indiana; Sugar Creek, Missouri; and Neodesha, Kansas (Johnson, 1967).

The proximity of the prolific Spindle Top Field to the Gulf coast made the area around Houston, Port Arthur and Beaumont, Texas, and Baton Rouge, Louisiana into a petroleum refining center. Regional pipelines were built to carry crude oil the relatively short distances to the Gulf coast refineries (Johnson, 1967). The oil tanker ships operating from the Gulf coast ports competed for and obtained control of most of the long-distance oil transport to the refineries and markets along the eastern seaboard by the mid-1920s (Williamson et al., 1963; Johnson, 1967).

Until the 1930s, when large-diameter steel pipe was in widespread use, the carrying capacity of oil pipelines was increased by laying an additional line or lines alongside the original pipe within the same right-of-way. This practice was known as "looping." The carrying capacity of 8-in lines was about 20,000 barrels per day, while 12-in lines handled 60,000 barrels per day. Since the largest refineries operating in that era were designed to handle crude at the rate of approximately 80,000–100,000 barrels per day, the carrying capacity of the pipelines built by a refiner were carefully gauged to support the refinery with little excess capacity to offer to others (Wolbert, 1979; Willson, 1925).

By 1941, just prior to the United States' entry into World War II, there were about 127,000 mi of oil pipeline in the United States composed of about 63,000 mi of crude oil trunk lines, about 9000 mi of refined product lines, and about 55,000 mi of crude gathering lines (Frey and Ide, 1946). From February through May 1942, 50 oil tankers serving the Atlantic seaboard were sunk by German submarines. The continuing attrition of the tanker fleet by enemy action and the diversion of tankers to serve military operations abroad caused a tremendous increase in the use of pipelines to transport both crude oil and refined products to the east coast which consumed about 40% of the petroleum produced in the United States. In June 1941, before the Pearl Harbor attack, pipelines delivered about 2% of the petroleum needed by the east coast; by April 1945, pipelines carried 40% of this critical supply (Frey and Ide, 1946).

The wartime expansion of the pipeline network added more than 11,000 mi of trunk and gathering lines, repurposed over 3000 mi of existing pipelines in new locations and reversed the direction of flow of more than 3000 mi of other lines (Frey and Ide, 1946). One of the pipelines converted from products delivery and reversed in flow direction to convey crude oil to east coast refineries during the war was the Tuscarora pipeline. After the war, it was reconverted and its direction of flow was again reversed to convey gasoline from the coastal refineries to the interior (Johnson, 1967).

Noteworthy wartime pipelines owned by the federal government were the "Big Inch" crude oil line, the largest pipeline in the world at that time measuring 24 in in diameter for much of its 1254 mi length; and the "Little Big Inch," the longest refined products pipeline in the world at 1475 mi of 20-in diameter pipeline (Frey and Ide, 1946). Only during World War II did the federal government finance oil pipeline construction (Johnson, 1967).

TABLE 24.1 Crude and Product Trunk Line Mileage by Size, 1936, 1941, 1950

	Crude oil lines			Refined product lines	
Size	**June 30, 1936**	**May 1, 1941**	**January 1, 1950**	**June 30, 1936**	**January 1, 1950**
Below 4-in	1270	1050	1233	162	391
4-in	3990	3590	2768	692	1366
6-in	10,460	12,570	12,254	3781	6696
8-in	27,060	29,380	27,780	4230	9979
10-in	9450	11,710	13,500	68	1628
12-in	5510	6710	9027	68	817
Over 12-in	80	170	4811	0	4
Totals	**57,820**	**65,180**	**71,373**	**9001**	**20,881**

With the proven success of long, large-diameter crude and refined products pipelines during World War II, the rapid growth in demand for petroleum products in the post-World War II era prompted a great expansion in construction of large pipelines. The number of refined products pipelines increased about 78% from 9000 mi in 1944 to 16,000 mi in 1950. Crude oil trunk lines expanded from about 63,000 mi in 1941 to about 65,000 mi 1950. The postwar increase in the diameter of the crude oil trunk lines, and therefore their carrying capacity, far outweighed the relatively modest increase in mileage (Johnson, 1967) (Table 24.1).

The postwar shift to large-diameter pipelines (16-in or larger) was made possible by technological advances in: pipe manufacture, pipe laying, pumps and their power sources, and automation of pipeline operations (Johnson, 1967). At least 69 large-diameter crude oil pipeline projects were constructed from 1946 through 1958 covering over 17,000 mi (Johnson, 1967). An example of the activity during the postwar period, the Tuscarora line, mentioned above, had been reconverted to refined product shipment after World War II and was rebuilt in 1950 with 10- and 12-in pipe and four new and more efficient pumping stations (Johnson, 1967).

During the 1960s the trend to achieve economies of scale through increased pipeline diameter continued. The Colonial Pipeline Company constructed a product line with diameters ranging from 32 to 36 in between Houston and New York City. The Capline, a 40-in crude line from Louisiana to Patoka, Illinois, was also constructed during the 1960s (Kennedy, 1984).

The announcement of the TransAlaska Pipeline System (TAPS) in February 1969, a 48-in above-ground crude oil pipeline carrying heated oil over 800 mi from Prudhoe Bay to Valdez, Alaska ushered in a new era of pipeline technology. TAPS began operation in July 1977 after overcoming many delays, lawsuits, and political challenges at a total cost of about $9.3 billion, up from the initial estimate of $900 million (Wolbert, 1979).

TransCanada Corporation proposed the Keystone Pipeline project in February 2005 and began construction in 2008 to convey crude oil from Alberta tar sands into the United States. The first phase of the project, from Hardisty, Alberta, to Wood River and Patoka, Illinois, is about 2100 mi long and went into operation in June 2010. Phase two added a leg from Steele City, Nebraska, to Cushing, Oklahoma, about 290 mi, which went online in February 2011. Phase 3 began operations in January 2014 over an extension of the line connecting Cushing, Oklahoma, to the Nederland, Texas, area. Phase 4, also known as Keystone XL, was proposed in 2008 and consists of a second-line running from Hardisty, Alberta, to Steele City, Nebraska. The Keystone XL project has become mired in controversy over its environmental impacts, and as of this writing, it is unclear if the project will be completed (TransCanada, 2010, 2011).

24.2 REGULATION

Federal regulations were first applied to oil pipelines in 1906 with the passage of the Hepburn Amendment to the Interstate Commerce Act which authorized the Interstate Commerce Commission (ICC) to set railroad rates and also extended the Commission's authority over oil pipelines. The Hepburn Amendment placed oil pipelines in the category of common carriers (like railroads) even when a line carried only oil owned by the pipeline owner and was built in a privately owned right of way. The constitutionality of treating oil pipelines as common carriers

was challenged in the courts, but in 1914, the United States Supreme Court (*The Pipe Line Cases 234 U.S. 548, 34 Sup. Ct. 956 (1914)*) ruled that the Hepburn Amendment was constitutional (Bond, 1958; Whitesel, 1947). Ultimately, as a result of the Hepburn Amendment, oil pipelines were required to file their tariffs of rates, follow the ICC's Uniform System of Accounts, and establish their valuation under ICC rules (Bond, 1958).

In 1940, the US Department of Justice filed antitrust suits against 20 oil companies and 59 affiliated oil pipeline carriers based on alleged violations of the Elkins Act of 1903 which prohibited discriminatory rebates and concessions by railroads to shippers. When oil pipelines were brought under the Interstate Commerce Act by the Hepburn Amendment in 1906, they automatically became subject to the Elkins Act. The Justice Department alleged that the dividends paid by pipeline companies to their shipper-owners were improper rebates. On December 23, 1941 not long after Japan's attack on Pearl Harbor (December 7, 1941), the pipeline and oil company defendants agreed to a consent decree to settle this action (*U.S. v. Atlantic Refining Co., et al, C.A. 14060, U.S. District Court for the District of Columbia*). Under the decree each pipeline carrier/defendant was required to file annual reports of its earnings, dividends paid, and report on the disposition of earnings in excess of 7%, if any (Burke, 1964). The 1941 consent decree remained in effect until vacated in December 1982, but while administered by the ICC, it was not effective in controlling rates or profits (US General Accounting Office, 1979; American Bar Association, 1983).

Prior to 1960, the ICC had the authority to promulgate oil pipeline safety regulations, and investigated safety issues, but decided that oil pipelines presented no hazard to the public and found it unnecessary to issue safety regulations (Bond, 1958). In 1960, Congress inadvertently removed pipeline safety regulatory authority from the ICC. In 1965, the oil pipeline industry asked Congress to restore Federal pipeline safety authority to the ICC to overcome the inconsistencies of state-level regulations that varied from state to state. However, before the ICC could complete its rule making process, Congress transferred jurisdiction to regulate transportation of explosives and dangerous articles (including oil pipelines) to the Department of Transportation (DOT), effective April 1, 1967. DOT delegated its authority over pipelines to the Federal Railroad Administration which issued a rule on pipeline safety (adopting nearly all of the rules proposed by ICC) that became effective December 31, 1967. These regulations included accident reporting requirements (Pipeline Safety, 1969). In September 1968, the Office of Pipeline Safety (OPS) was created within DOT under the Research and Special Programs Administration (RSPA) (Pipeline Safety, 1969).

The establishment of the US Environmental Protection Agency (USEPA) in 1970 added environmental regulations to the construction and operation of pipelines.

The Department of Energy Organization Act of 1977 transferred regulation of interstate oil pipeline rates and tariffs from the ICC to the Federal Energy Regulatory Commission (FERC). FERC regulated the rates, charges, and rules for transporting oil by pipeline but was not responsible for oversight of pipeline construction, pipeline safety, or pipeline abandonment (FERC Website).

Passage of the Hazardous Liquid Pipeline Safety Act of 1979 granted DOT "substantial new regulatory and enforcement authority" over oil pipelines. Prior to 1979, while DOT inspected interstate oil pipelines, there had been no federal regulation of intrastate pipelines which was left to state and local jurisdictions. By 1984, the Materials Transportation Bureau of DOT's RSPA was responsible for gas and liquid pipeline safety (GAO, 1984).

In December 2002, Congress passed the Pipeline Safety Improvement Act which strengthened existing pipeline safety laws and enhanced the enforcement authority of the OPS while limiting its discretion. For example, the new law required the Secretary of Transportation to formally respond to pipeline recommendations by the National Transportation Safety Board (NTSB). OPS had the lowest rate, 69%, of implementation of NTSB recommendations within DOT. There had been much criticism of OPS over the years for its "weak enforcement, inaccurate records, and ineffective rules" and by 2001, over 30 years after its creation; the OPS did not have a comprehensive and detailed map of the pipelines it regulated (Parker, 2004).

In 2004, Public Law 108-426 created the Pipeline and Hazardous Materials Safety Administration ("PHMSA") within the DOT, to develop and enforce regulations for the safe and environmentally sound operation of oil pipelines. These regulations are codified in Title 49 of the Code of Federal Regulations, Parts 190-199.

24.3 NOTABLE DEVELOPMENTS IN PIPELINE TECHNOLOGY

As mentioned above, early pipelines were constructed of fairly short segments of pipe averaging 6–8-in in diameter joined by threaded, screw collars (Kiefner and Trench, 2001). By 1900, nearly all line pipe was made from steel typically from 8- to 12-in in diameter using furnace lap welding (Kiefner and Trench, 2001; Williamson et al., 1963). Eight-inch diameter pipe was the largest which could withstand the typical operating pressures until

well into the 1920s. While 10- and 12-in lines were laid, they had the unfortunate tendency "to split at the seams unless operated at less-than-desirable operating pressure" (Wolbert, 1979). By 1914, larger diameter pipes were being laid by welding the segments together using oxyacetylene welds around the circumference of the pipe (girth welding). Electric arc welding was first used in pipeline construction in 1917. Welding techniques used in pipeline construction improved over time so that by 1930, electric arc welding was the primary method of pipeline construction (Wolbert, 1979).

The first electric-resistance-welded (ERW) pipe became available in 1924. ERW pipe was formed by shaping steel plates into round cylinders which were welded closed using electric current to heat the edges to bonding temperatures while mechanically forcing the edges together. The first large-diameter (i.e., up to 24 in) seamless steel pipe was made in 1925 and by 1927, steel pipe with electric-flash-welded seams, similar to ERW, was available. These new pipes could be made in 40-ft lengths which halved the number of joints required for pipeline construction and, when properly formed, the longitudinal welded seam in the pipe was stronger than the parent metal (Kiefner and Trench, 2001).

Corrosion was a problem recognized early in the history of the operation of pipelines (Spang, 1917). In 1930, a study was undertaken by the National Bureau of Standards which confirmed that galvanic electric currents were present in pipelines and the currents were related to pipe corrosion and the electrical resistivity of the soils. Some pipelines were coated to protect against corrosion. During this period, asphalt or coal tar were among the common coatings used and in some cases pipes were then wrapped with heavy paper tape to protect the coating and exclude moisture from contact with the metal (Shepard, 1931; Wildman, 1945; Kennedy, 1984; Kiefner and Trench, 2001). By the mid-1940s, the electrochemical nature of steel pipeline corrosion was understood and cathodic protection began to be used to mitigate the problem. Cathodic protection applied an electric current and a flow of metal ions from an anode (a metal with a higher oxidation potential than iron) into a pipe to counteract the loss of metal in the flow of electrons away from the pipe into the soil. While bare pipelines could be protected in this manner, coated and wrapped pipelines required a much lower levels of electric current from the cathodic protection system (Kiefner and Trench, 2001).

Fig. 24.1 shows a typical trend line of cumulative corrosion leaks over time for a buried steel pipeline. Note the increasing rate of leaks prior to the application of cathodic protection in year 14 which sharply reduced the rate of corrosion leaks thereafter (Introduction to the Oil Pipeline Industry, 1978).

Pipeline coating technologies were expanded to include polyethylene tape, extruded polyethylene coatings, and fusion-bonded epoxies in the 1960s and 1970s. By the 1980s, combinations of polyethylene tape and fusion-bonded epoxies were used (Kiefner and Trench, 2001).

Another improvement in construction methods included the introduction of radiographic inspection of girth welds in 1948, allowing for a regular and systematic method to check on the integrity of pipelines. By 1963, radiographic inspection of a portion of all girth welds during pipeline construction became the industry standard. Some pipelines, such as the TAPS line had every girth weld radiographed. The percentage of welds so inspected increased over time until by the 1990s, nearly all pipeline welds were radiographed (Kiefner and Trench, 2001).

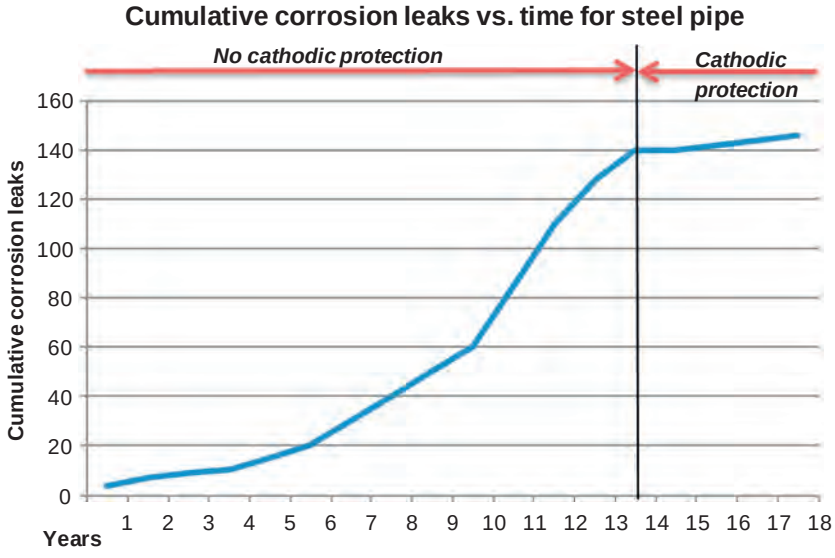

FIGURE 24.1 Cumulative corrosion leaks vs. time for steel pipe.

From the early days of pipelines, "go-devils" or internal pipeline scrappers were used to remove built up deposits of wax or other obstructions in the lines. These devices were followed by an inspector who tracked the go-devil by its sound as part of his daily inspection walking the path of the pipeline route looking for surface evidence of leaks, breaks, or tampering with the line (Scientific American, 1892). Pipeline survey and inspection technologies improved over time and were expanded significantly in 1965 with the introduction of the "smart pig" a series of instrument modules that travel through the pipeline with the oil to record pitting, corrosion, fatigue cracks, and leaks using ultrasound to measure pipe wall thickness, magnetic field anomaly detectors, and more recently GPS positioning to pinpoint problem areas (Kiefner and Trench, 2001).

24.4 AGING INFRASTRUCTURE

As illustrated in Fig. 24.2, as of 2001, three quarters of the network of crude and product pipelines was installed between 1940 and 1980. While in recent decades, improvements in pipe manufacturing, pipeline coatings, and maintenance techniques have made modern pipelines less vulnerable to failure, a high percentage of our pipelines are part of our nation's aging infrastructure upon which we rely to supply our energy needs (Kiefner and Trench, 2001).

The impact that the age of a pipeline can have on its performance is illustrated in the case of pipelines constructed prior to 1970 using steel pipe manufactured using low-frequency ERW technology. In December 1988, a 48-ft long fracture of a longitudinal seam weld in the 22-in Ozark Pipeline System in Maries County, Missouri, spilled about 20,000 barrels (over 800,000 ga) of crude oil into the Gasconade River, a tributary of the Missouri and Mississippi rivers. An investigation of the cause of the failure found that the Ozark line was constructed of ERW pipe and had been in operation since 1949 (Fields et al., 1989).

As the subsequent National Institute of Standards and Technology (NIST) investigation report stated, "[i]t is well established that ERW pipe manufactured before about 1970 contains a significant number of weld defects as a consequence of the use of a subsequently discontinued low-frequency ERW technique." It was determined that the Ozark failure "was in fact initiated at a weld defect in the ERW pipe." NIST concluded, "it is clear that ERW pipe manufactured before about 1970 is inherently susceptible to fracture and preferential corrosion. . .. Based on the failure incidence data, special standards do not appear warranted for the entire lengths of pipelines containing older ERW pipe" (*emphasis added*). Nevertheless NIST recommended "special standards be considered for locations where the risk to public safety, property and the environment is large." NIST further recommended "the replacement of the older pipe in certain critical risk locations," based in part on the fact that "the defects were known to grow with time, . . . and because present nondestructive evaluation techniques cannot detect the defects in the ERW seam welds" (Fields et al., 1989).

One question not addressed by NIST in its 1989 report was how "critical risk locations" for testing or replacing pre-1970 ERW pipe would be identified. As noted in a report prepared in November 2010, many of the nation's

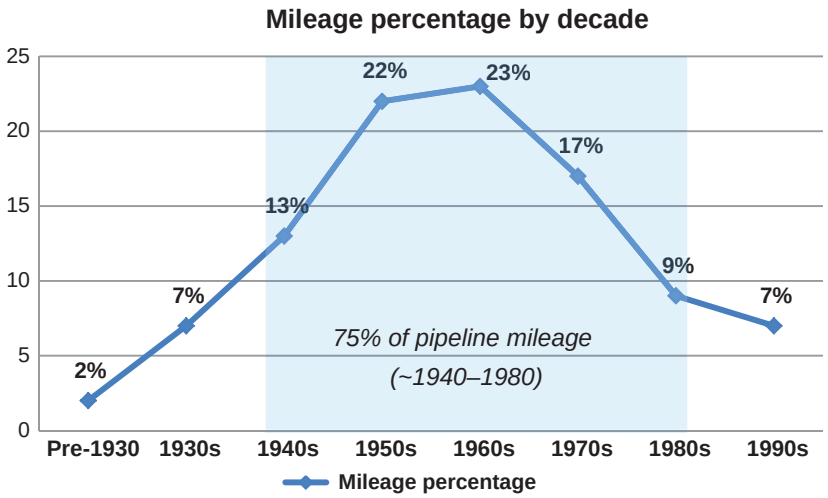

FIGURE 24.2 Pipeline mileage percentage by decade.

pipelines were originally constructed in sparsely populated areas, but subsequent population growth caused by urban and suburban development has fueled encroachment into what had been rural and even remote areas (PIPA, 2010).

The issue of encroachment of development into pipeline right-of-ways was addressed as early as 1988 by the Transportation Research Board (TRB) of the National Research Council. The TRB acknowledged the good safety record of the pipeline industry, but noted that "[d]espite this good safety record, pipeline operators reported more than 10,000 failures to liquids and gas transmission and gathering lines between 1971, the first full year of federally required reporting, and 1986." The single largest cause of pipeline failure was damage from outside forces (including both third-party excavation damage and natural causes), which in 1988 accounted for 40% of reported failures (TRB, 1988).

The following are but a few examples of the more dramatic pipeline ruptures during relatively recent times. In 1983, the NTSB investigated a pipeline accident in West Odessa, Texas involving an 8-in liquefied petroleum gas pipeline installed in 1960 in rural, undeveloped land. During the 1970s and early 1980s, the area was subdivided into residential lots. Though the pipeline operator had a permanent 50-ft easement in which the pipeline ran; the county government approved subdivision plans that placed two residential lots over the pipeline easement and allowed a mobile home to encroach on it, because the easement had not been shown on the subdivision plat map and the county had no policies about the proximity of development to hazardous materials pipelines. When drilling equipment inadvertently struck and ruptured the line in 1983, the resulting fire caused six fatalities and four serious injuries as well as considerable property damage in the residential development (TRB, 1988).

In May 1989, a train derailed in a residential neighborhood in San Bernardino, California, killing four people. The train came to rest on top of a petroleum pipeline. The line exploded in the same location, 13 days after the train derailment and after train service was restored, killing two people, injuring dozens, and destroying 10 homes (TRB, 2004).

Over a 7-day period in October 1994, up to 20 in of rain fell on the San Jacinto River floodplain near Houston, Texas, resulting in extensive flooding and causing the evacuation of over 14,000 people. Seventeen underground pipelines were exposed by the flooding, eight ruptured and 29 others were undermined at river crossings. More than 35,000 barrels (1.47 million gallons) of oil and petroleum products were released into the river. Gasoline from a ruptured 40-in pipeline ignited sending flames down the river and destroying homes, trees, and barges. Spill response costs were in excess of $7 million and estimated property losses were about $16 million (TRB, 2004). Of course, damage from outside sources was not the only source of dangerous ruptures. In 1980, a pipeline transporting naphtha (a semirefined petroleum product) through Long Beach, California ruptured as a result of corrosion and overpressure. The escaping fuel blew a hole through a paved street spraying naphtha 20 ft into the air and causing a fire that injured five and destroyed a house (TRB, 1988).

As recently as September 2016, the Colonial pipeline, a 36-in gasoline line constructed in 1963, was found to be leaking into a pond near Pelham, Shelby County, Alabama. The line delivers gasoline from Houston to the Southeast and the East Coast. A leak of about 8000 barrels of gasoline was discovered and the company initiated a response which kept the gasoline from reaching the Cahaba River (USEPA, 2016). In October, the line exploded after being struck by a trackhoe operated by a contractor repairing the line. One pipeline worker was killed, seven others injured, and the resulting fire burned for 3 days (Alabama Media Group, 2016).

24.5 CASE STUDY

When a pipeline ruptures, the pipeline owner must mobilize emergency crews to initiate cleanup. However, the damage caused by the actual spill is only a part of the problem to be addressed. Many questions arise that can best be resolved by historians experienced in both the technological history of the petroleum industry and in reconstructing a detailed land-use and other histories. As the case study below illustrates, the diversity of the inquiries related to ruptures, wide variety of sources to be examined and the ability both to integrate the information discovered and to present a concise and coherent chronicle make this an ideal assignment for forensic historians.

24.5.1 Background

In this hypothetical, an established crude oil pipeline, originally constructed in the 1950s, has ruptured. The pipeline ran through a residential development and the rupture occurred in a wooded area behind a number of homes in the development. Before the line can be shut down, 15,000 barrels (42 ga per barrel) or about 630,000 ga of crude is released into the environment. The crude pooled in the backyards of a number of homes, then flowed

between homes and down driveways and front lawns into the street. The crude then ran along the street following the normal path of the neighborhood's storm water conveyance system into storm drains that discharged to a creek and, ultimately, a river. The oil then followed the course of the river to a point where it emptied into a culvert leading to wetlands and a small lake used by community residents for fishing and other recreational activities. At least a half-dozen homes were directly impacted (i.e., crude oil was present on their properties and in their homes) and a dozen homes in the community were evacuated in what the USEPA classifies as a "major spill." Emergency response activities are immediately undertaken to address the free standing oil present in the neighborhood and stop the flow of oil into storm drains leading to the wetlands and lake. This effort is made more difficult because it begins to rain when emergency response activities are taking place.

It will potentially cost millions of dollars to clean up the neighborhood, river, wetlands, and lake. There is also a high likelihood that the pipeline company will be facing environmental cleanup and natural resources damages, toxic tort, property damage, and other potential liability exposure. In this matter, the client dispatches its cleanup crews and its research team immediately.

24.5.2 Initial Research Questions

In an effort to understand the historical context and circumstances surrounding the rupture, the pipeline company has retained a consulting firm to perform forensic historical research to obtain factual data relating to certain issues. While there are many research topics normally associated with pipeline rupture matters, the lines of inquiry are dependent on the specific circumstances, magnitude, type, and location of the rupture.

For this hypothetical, the key issues initially to be researched are represented in three lines of inquiry inventoried below and described in separate sections that follow. These were as follows:

1. The history of the pipeline, including:
   - **a.** When it was constructed?
   - **b.** Was it constructed in segments?
   - **c.** How was it constructed?
   - **d.** What type of pipe was used?
   - **e.** What types of leak prevention (e.g., wrapping, cathodic protection, etc.) techniques has it been subject to?
   - **f.** What historical leak history is publicly available?
2. The history of the subdivision development and its infrastructure, including:
   - **a.** When the subdivision was constructed?
   - **b.** When the section where the pipeline was located was constructed?
   - **c.** Who the developers were that constructed the homes?
   - **d.** Who owned the properties at the time of the rupture?
   - **e.** What does the infrastructure look like?
3. The history of the "downstream" properties:
   - **a.** Who owns the impacted areas?
   - **b.** What is the history of land and natural resources uses?
   - **c.** What types of land and natural resources were impacted?
   - **d.** Who are the Stakeholders for potential NRD claims?

24.5.3 Part 1—History of the Pipeline

In this hypothetical, there are three distinct research questions, each of which has a number of subquestions associated with them. Each requires a series of inquiries potentially researching both historical and more contemporary data. Provided below is a discussion of the types of research, collections and sources used to obtain facts which can be used to increase the pipeline company's knowledge base regarding the pipeline.

24.5.3.1 Phase 1: Obtaining Pipeline Company Data

A good starting point for reconstructing pipeline histories is to obtain as much information as possible directly from the pipeline company itself. Records relating to pipelines can reside in many different corporate departments, including:

- Real estate—pipeline easements and property ownership records;
- regulatory compliance—records focused on federal and state law compliance;

- operations—inspection, construction, as-built and maintenance records;
- legal—contract, litigation and incident records; and
- environmental, health, and safety—rupture, cleanup, and safety records.

With this in mind, conducting interviews of key staff in these departments will often identify the location of potentially relevant materials as well as other individuals that may have useful information. Casting the net as widely as possible is critical in this initial step and no lead to potentially useful information or personnel should be discounted off-hand. For example, it is important to identify company retirees and current and former consultants, legal counsel, and others who may have knowledge of the location of useful data and may be a part of the interview process. Likewise, reviewing any indices available for records housed either on-site, in company records storage facilities or at other third-party sites (i.e., consultants, former employees, legal counsel, university libraries, private archives and museums, etc.) should be a part of the process. Finally, a thorough vetting of potentially relevant electronic data sources should be completed, including data captured on data drives, CD-ROMs, microfilm, microfiche, or other storage media.

Interviews can be a critically important part of the fact-gathering process to identify the types and locations of potentially relevant materials and the identity of additional interviewees, but in some instances, they can also expose first-hand knowledge of activities relating to the research topic. When conducting interviews, great care and thorough preparation should be exercised. When possible, the preparation of recollection materials that can be used to prompt an interviewee's recollections and provide the appropriate context for the questioning should be employed. Likewise, careful consideration should be given to memorializing the interview with notes, a signed statement, or something more formal when needed. Annotated maps, drawings, and photos can also be effective ways to capture and ensure the accuracy of the information obtained.

When dealing with company documents, it should be noted that primary source company materials may no longer reside in the company's on-site files or storage facilities. For instance, given the timing of the construction of the pipeline in our hypothetical, due attention should also be focused on locating company histories and primary source materials housed in public repositories such as special collections at university libraries, private archives, and museums. The petroleum industry has a long and rich history and many collections of personal papers, company materials, and photographs have been donated to these types of institutions. These collections can be fruitful sources of information providing rich detail on construction, operations, maintenance, and historical incidents associated with the lines. In the case of company collections located in these types of repositories, a detailed review of any available finding aids can help focus the research on relevant materials. Equally important would be the review of any indices, file catalogs, box lists, or the like that can help with the identification of potentially relevant information on-site or located in storage facilities.

Once data sets containing potentially relevant information are identified and made available, a detailed examination of the materials should be undertaken. Careful procedures should be followed when reviewing historical documents and data. These procedures should be developed based on the age and condition of the data set being reviewed and should be designed to protect and preserve the materials, ensure confidentiality (when appropriate) and to record the provenance of the materials reproduced for detailed analysis. For instance, original historical documents found in company archives and/or storage facilities, or in public universities, archives or museums, may require special handling. These types of materials are typically handled with care, preferably by individuals with clean, dry hands. Surgical (or cotton) gloves may also be used to protect documents from dirt and grease, although care should be taken with thin and damaged materials as gloves (particularly cotton gloves) can reduce the user's sensitivity and cause them to damage the data under review. Even if not required by the company or public facility, researchers should follow guidelines established by archivists and historians relating to the handling of historic materials (National Archives and Records Administration; National Park Service, 1996). Of course, this type of care may not be required of all materials, but being aware of the types of materials being made available and preparing appropriately for the review will enhance the researcher's ability to obtain relevant data efficiently.

For the purpose of this hypothetical, the results of the company research revealed a limited amount of relevant information including:

1. The pipeline was constructed by a predecessor entity related to the current client.
2. The pipeline was constructed in segments between 1950 and 1953.
3. The original route of the pipeline was confirmed.

4. The company retained a number of easement documents when the pipeline was constructed.
5. The company possessed very little information relating to the construction and early operation of the pipeline because documents were destroyed in accordance with document retention policies.

However, using this information, a collection of materials related to the predecessor company was located at a public industrial library and museum. A review of the collection's finding aid revealed the presence of potentially relevant materials and photographs related to pipeline construction. These materials were analyzed, and they provided a much more detailed understanding of the construction project in general, the sequencing of the construction of specific segments, the type of pipe used to construct the line and its early operations.

Despite the results achieved in Phase 1, the company has asked that the research continue into publicly available sources to determine if additional information could be uncovered.

24.5.3.2 Phase 2: Researching Trade Literature, Technical Publications, and Other Secondary Sources

While useful information was uncovered during the review of company materials, the company was interested in understanding all it could about the pipeline. As a result, Phase 2 research was undertaken.

The objective of this task was to scour the proverbial landscape of secondary sources including but not limited to trade literature, technical publications, newspapers, and court case files. Again, casting a wide net and working toward identifying relevant materials is a critical and necessary part of this research. All of these sources will be consulted to obtain and supplement the data and information already collected.

The first step in this process is to identify journals and trade publications relevant to the research. In the case of this hypothetical, the focus would be on publications that would have reported on the construction, use, and other facts related to the subject pipeline over time. Since company data revealed that the pipeline was built between 1950 and 1953, it is necessary to both identify potentially relevant publications as well as understand how far back in time they began circulation. To do this, it is often helpful to identify trade groups and associations that serve the professionals in the oil and gas industry in general, and pipeline industry professionals in particular, that publish journals. Examples of the types of relevant trade groups and associations relevant to this inquiry might include the American Society of Mechanical Engineers (founded 1880), American Petroleum Institute (founded 1919), National Association of Corrosion Engineers (1943), Association of Oil Pipelines (founded 1947), Pipe Line Contractors Association (founded 1954), and Society of Petroleum Engineers (founded 1957). Trade groups and professional organizations typically publish journals, conference, and/or annual meeting proceedings, or special reports that could be relevant. Examples of the types of relevant journals that might be consulted include the *Oil and Gas Journal*, *Corrosion*, *Chemical Engineering*, *World Oil and The Petroleum Engineer*. It should be noted that in many instances journal names change over time so tracking the lineage of the journals of interest will be useful. A note of caution: while many journals have indices, the indices are often focused on identifying larger articles and may not include smaller articles or industry news columns of interest to the researcher. As a result, doing detailed research (i.e., a page-by-page review) to identify all potential articles published during your timeframe of interest may be necessary.

As a part of the research aimed at identifying trade groups and journals, researchers should consult other types of indices and online sources. One example of a useful index is *The Industrial Arts index*. This publication which was first made available in 1913 is a subject index to a selected list of engineering and trade periodicals. Published annually through 1958 under this title and succeeded by the *Applied Science and Technology Index*, it provides indexing of a wide range and large number of periodicals (H.W. Wilson Company, 1913). Technical studies may also provide helpful information relating to your pipeline research.

As one of the research questions posed in the hypothetical was to determine what type of pipe was used in its construction, and company information revealed the pipeline was constructed of ERW pipe, it may be useful to locate technical studies (such as those outlined above) that document the evolution of pipe technology over time and the advantages and disadvantages of using ERW versus seamless steel pipe.

Studies commissioned by trade associations, manufacturers, and/or the government may also be useful. For instance, one such source of technical studies is the National Technical Information Service, which maintains the National Technical Reports Library (NTRL), an online catalog of technical reports which can be queried to identify records of interest. This database contains a variety of technical reports and bibliographic data that can be useful in pipeline matters and is available for purchase.

Libraries, archives, museums, and other institutions have focused on digitizing materials, providing an expansive universe of digitized data available in electronic form to help researchers identify and download potentially relevant materials.

Newspaper articles may also be of interest. Many newspapers are now available through online databases. In many instances, these online repositories provide users with the ability to conduct keyword searches that comb through multiple newspapers for many years to identify articles of interest. One such database is maintained by the Library of Congress. It maintains a word searchable US Newspaper Directory which can be queried to find information contained in American newspapers published between 1690 and present (http://chroniclingamerica.loc.gov/).

Finally, in many instances, conducting court case research can also provide valuable details relating to pipeline matters. In large construction projects, such as pipelines crossing several states and local jurisdictions, disputes can arise over a multitude of issues. Often times these disputes involving construction contracts, property damage, and personal injury issues are resolved in the courts. Reviewing online databases and hard copy plaintiff/defendant indices to identify potentially relevant matters and conducting research in case files are an essential part of the research process. These types of files may reside in several locations. For example, historical Federal cases and case files reside in the National Archives and Records Administration, whereas historical state cases files may be located in State Archives and/or State Libraries and local cases may reside in county-level repositories. As with all research avenues discussed, the nature and amount of relevant materials in case files may vary, as they may contain some or all of the following types of materials: pleadings, affidavits, expert reports, and deposition and trial transcripts.

Identifying the locations of all of the materials discussed above and collecting them for detailed review and analysis is an ongoing part of the Task 2 research process. While some of the materials identified through the research performed above may be available electronically for download, a portion of the potentially relevant data set identified will undoubtedly only be available in hard copy and may be housed in a variety of repositories in multiple locations. For instance, while information on the company's construction of the pipeline may be held in a company-donated special collection at a university library, the researcher may determine that a run of company annual reports for the period of interest are housed in part at a municipal public library and in part at a private archive.

With this in mind, the ongoing collection of materials, documenting of provenance, the detailed analysis of the data, and the identification of data gaps, provide leads to additional information and affords for a continuous feedback loop that informs the research process.

With regard to the hypothetical, the research completed in Task 2 provided a substantial amount of information that was used to supplement that collected from the company-specific collection. The source and types of information uncovered included:

- Newspapers—articles reporting on the planned construction of the pipeline, litigation associated with its construction, and historical ruptures of the line.
- Trade journals—articles reporting on the construction of the pipeline, materials used to construct the line, methods used during construction, the pipeline route, the carrying capacity of the line and its pumping stations.
- Court cases—provided information on lawsuits relating to eminent domain, property damages, and construction contract claims. Each of the case files provided substantial detail on the construction of the pipeline, its route, the types (i.e., federal, state, municipal, and private) of lands and features (e.g., mountains, hills, forests, lakes, rivers, etc.) traversed, and the cost of construction.
- Technical studies—provided information on the use and leak rates for ERW pipe under certain conditions.

24.5.3.3 Interim Deliverables

In order to provide the client with the requested historical information and context related to the pipeline, a phased research plan was implemented. This plan incorporated evaluation of a variety of historical sources including both primary and secondary source materials as well as oral information gained through interviews. It also relied on the historian's ability to glean leads from available information to identify additional relevant sources. The information collected was analyzed in order to develop a chronological history of the pipeline for the client's use. The ability of the historian to construct a useful narrative will always depend on the nature, amount, and usefulness of the primary, secondary, and oral history data uncovered.

24.5.4 Part 2—History of the Subdivision

The second line of inquiry in the hypothetical involved reconstructing the history of the affected subdivision. Some of this research and sources will overlap with that identified in Part 1 and research efforts may be coordinated. However, the researcher should be aware that the goal for the work under this effort is different in that the historian is also looking for information documenting events or activities that may have impacted pipeline integrity, as well as information that will support damage claim validity and valuation. Likely categories of damages in the hypothetical include property damage, property value diminution, loss of use and enjoyment, business interruption, and crop damages. The recurring theme of casting a wide net continues to apply so as to obtain relevant information on the property and the individuals impacted by the spill.

Sources of relevant information related to this inquiry include but will not be limited to:

- County assessor records
- Recorder's office property ownership records
- Planning department records
- Public works department records
- Building department records
- Geographic Information System (GIS) data
- Court cases.

To document the historical development of the subdivision, it is useful to conduct research at the local planning department. This department typically provides information regarding the development of the subdivision, identification of builders, and, depending on the time of its construction, reports and studies such as environmental impact reports, soil surveys, infrastructure development, and the like.

Ownership and easement records are usually found at the county recorder's office and may be available online. As a part of this work, the researcher will want to obtain copies of deeds for individual target properties to track ownership over time and identify any pipeline or other easements granted over time. It may be necessary to engage the assistance of a title company for this effort.

The public works department will be able to provide information regarding activities in the area, such as road repaving, sewer replacement, or other changes to the infrastructure in the area. Building department records, particularly for the properties nearest the breach, may provide information regarding any recent activities that may have affected the area.

A key part of this research should involve developing a package of information for each impacted property. The assessor's department and local real estate professionals should have both macro- and microlevel data including sales trends, price data, inventory turnover, and owner/renter data.

Finally, for this type of inquiry, it is essential to develop spatial information to assist in the analysis of the area impacted by the pipeline breach. Typically, the county assessor will have GIS data that includes parcel boundaries, but in some instances, it may be necessary to obtain plat maps and undertake the effort to georeference them and begin to build a useable set of maps that cover the timeframe of interest. Other items to include as GIS layers may include streets, subdivision boundaries, water and sewer lines, as well as the pipeline's route and easements. Assessor's records will also provide information regarding the zoning and value of the properties involved, which will be helpful to the client in assessing property damage and other claims.

24.5.4.1 Interim Deliverables

Work conducted under this effort is used to help the client to assess the potential causes of the pipeline break, evaluate the damage to private and public property caused by the spill, and verify the value of property damage and other claims submitted. The work of the historian involves identifying and gathering the raw data and to analyze, organize, and present it to the client in a manner that is easy to understand.

24.5.5 Part 3—The History of the "Downstream" Properties

In this hypothetical, the client requested that additional research be conducted to document the history of the "downstream" properties and assess other potential issues such as natural resource damages (NRDs).

In this hypothetical, the river extends for several miles and transverses areas that are owned by various private, state, and federal entities. The wetlands and lake are part of a state-owned park and some of the land along the river is used for agricultural purposes. Coordinating cleanup activities can require negotiating various access

agreements. Moreover, the client will need to be prepared to evaluate claims for damages made by individuals, businesses, municipalities, and agencies. Ownership is again a key item for research, but it only serves as a starting point.

The first task is to define the area impacted by the pipeline spill and then to determine who owns the land, waterway, wetlands, and lake. A good starting point for this effort is the US Geological Survey (USGS) which maintains maps by state that identify ownership of all Federal- and Indian-owned lands. Federal lands are further divided by the agency ownership, such as Department of Agriculture, Forest Service, Department of Defense, and the Department of Interior. Ownership within the Department of Interior is further divided by the divisions of the Bureau of Land Management, Bureau of Reclamation, Fish and Wildlife Service, and National Parks. The USGS also has information that identifies land owned by state agencies and designated state parks, forests, and wetland areas. Moreover, much of this information can be obtained in GIS format, making it easy to incorporate into the overall project GIS system.

The next element of the research will be to determine the land uses of the larger impacted area, which in this hypothetical includes the river, wetlands, and lake. Again the USGS is a source for mapping purposes and the USGS maps provide can provide large scale detail for mapping purposes that identifies land uses such as agricultural, forest, rangeland, grazing, wetlands, and urban or industrial land uses (USEPA, 2017). However, the historian will need to dig deeper to better understand details on the subject for the client's purposes.

Much like the Part 1 research, the effort will involve looking at primary sources, literature, and other secondary sources. Some primary sources that may be of use include:

- State Fish and Game Agency
  - History of the construction of the lake or modifications to the river
  - Lake management over time
  - Water quality studies (for lake and river)
  - Fisheries division for use permits and statistical data of use of the river and lake
  - Boating statistics for the lake.
- State Environmental Agency
  - NPDES permit research for dischargers to the lake or river
  - Unpermitted dischargers to lake or river
- State Historic Commission
  - Designations of Historical Significance
- US Bureau of Land Management
- US Department of Agriculture
- Local Fish, Game, and Recreation Department.

Published literature sources may supplement the above as various items of interest may be available at state and local libraries or from various online sources discussed Part 1.

The research scope will be driven by the particulars in the matter. For instance, in this hypothetical scenario, a local agency claimed that a site where George Washington had slept had been damaged by the pipeline. Research revealed that the story was a regional myth that had never been proven, the site had not been designated a site of historical significance by State or Federal standards, and the building had been reconstructed after burning to the ground 40 years earlier. In another example, the state claimed that the lake was impacted by the pipeline spill. While there was evidence to that fact, research also revealed that the state operated a boat fueling facility on the lake, that the facility had an NPDES permit with parameters for discharges of oil and grease, that the facility had been exceeding those parameters on a regular basis, and that a local fishing group had filed suit against the state prior to the pipeline rupture for damaging the ecosystem of the lake.

In addition to assisting with individual claims that arise as a result of the pipeline rupture, the land use research will also be used to assist the client with potential NRD claims. To understand NRD issues, one must identify what has been impacted, be it fish, wildlife, biota, air, water, groundwater, drinking water supplies, or other such resources. Next, one must determine how the event (in this case the pipeline spill) changed or affected those resources and also whether there are other activities that may have contributed to the damage.

NRD claims are made by natural resources trustees. According to USEPA, federal level trustees can include the Secretaries of Agriculture, Commerce, Defense, Energy, and Interior, who can act as trustees for the natural resources subject to their respective management or control. The governor of each state may also designate state officials who may act on behalf of the public as state trustees for natural resources. Tribal chairmen (or heads of governing bodies) of Indian Tribes can also act on behalf of the Indian Tribes as tribal trustees for the natural

resources, including their supporting ecosystems, belonging to, managed by, controlled by, or appertaining to such Indian Tribe, or held in trust for the benefit of such Indian Tribe, or belonging to a member of such Indian Tribe. Finally, foreign trustees can recover NRD under certain circumstances (USEPA, 2017).

NRD claims assessments and damages calculations are a fact-intensive and complex area of research that cannot be covered in detail herein, it is important for the historian to recognize that information collected to address other areas of inquiry may also be relevant to questions related to NRD. From the historian's perspective, this research is typically focused on assisting with the documentation of baseline conditions to help the client (and other experts) understand changes in environmental conditions impacting natural resources resulting from the pipeline breach. For example, determining if nonpipeline-related petroleum impacts to resources have occurred over time might be relevant to developing NRDs calculations.

24.5.5.1 Interim Deliverable

It will be necessary to develop a mapping system to help understand the impacted area. Building on the GIS data obtained in Part 2, it will be necessary to map the affected area to better understand the potential claims. A major component of the research efforts is to help track the status of the claims and lawsuits as they are filed. Specific deliverables may likely include ongoing assistance with claim tracking, plaintiff summaries, land-use summaries for specific geographic areas, and the like.

24.6 RESULTS

The amount and nature of the information obtained from the type of effort discussed in this case study can be useful in a number of ways and in dealing with the myriad of questions posed by this type of event. Because each pipeline rupture will have its own profile, the research needed to answer questions posed by each rupture will have to be tailored to the specific circumstances of the event. The historian must be aware that research is an iterative process and that findings uncovered from answering any one question may be applicable to another. For instance, one of the property owners within the subdivision also owned a small parcel on the river and claimed that in addition to damages in the subdivision, they were entitled to substantial compensation for the loss of enjoyment for the riverfront property. Research from Part 3 revealed that the property owner had never obtained a boating, fishing, or hunting license and that the property was inaccessible except by boat. While the client may be committed to paying reasonable and verifiable claims, in this example, the riverfront claim was questionable and most likely would be denied.

The researcher must also give thought to the global resources that may assist in the effort, such as aerial photographs, which can provide information to support or refute allegations that may arise. An example is that an owner of a local quarry submitted a claim for loss of business income due to the pipeline spill. Without having to delve into business records, a straightforward review of aerial photographs revealed that the quarry had been flooded for the last 5 years and had not operated during that entire period. Additional research with the local business permit department verified the visual findings and the claim was handled in an appropriate manner.

24.7 CONCLUSION

Pipeline ruptures are potentially devastating events that require detailed and specific inquiries into causal issues. As a result, pipeline companies often must strive to gain a thorough understanding not only of the contemporary circumstances surrounding the incident but, given aging pipeline infrastructure and changes to the industry over time, the historical context as well. Forensic historians are in a unique position to provide the necessary research, analysis, and historical context for such an analysis.

References

Alabama Media Group, November 4, 2016. Alabama Explosion: Fire Is Out, Pipeline Projected to Restart Sunday.
American Bar Association, 1983. Annual Report: Section of Public Utility Law, Part IV. Oil Pipeline Regulation, pp. 147–153.
Bond, P.J., 1958. Oil pipe lines—their operation and regulation. ICC Pract. J. 25 (7), 730–742.
Burke, J.L., 1964. Oil pipelines' place in the transportation industry. ICC Pract. J. 31 (7), 780–802.

Fields, R.J., Pugh, E.N., Read, D.T., Smith, J.H., 1989. An Assessment of the Performance and Reliability of Older ERW Pipelines. US Department of Commerce and National Institute of Standards and Technology.
Frey, J.W., Ide, H.C., 1946. A History of the Petroleum Administration for War: 1941–1945. US Government Printing Office, Washington, DC.
Herrick, J.P., 1949. Empire Oil, The Story of Oil in New York State. Dodd, Mead & Company, New York.
<https://www.ferc.gov/students/regulation/oil.asp>.
<http://www.phmsa.dot.gov/about/agency>.
H.W. Wilson Company, 1913. The Industrial Arts index. White Plains: New York City.
Johnson, A.M., 1967. Petroleum Pipelines and Public Policy, 1906–1959. Harvard University Press, Cambridge, MA.
Kennedy, J.L., 1984. Oil and Gas Pipeline Fundamentals. PennWell Books, Tulsa, OK.
Kiefner, J.F., Trench, C.J., 2001. Oil Pipeline Characteristics and Risk Factors: Illustrations from the Decade of Construction. Report prepared for American Petroleum Institute's Pipeline Committee, API.
National Archives and Records Administration, National Archives Preservation Guidelines for Vendors Handling Records and Historical Materials, <https://www.archives.gov/preservation/technical/vendor-training.html>, and <https://www.archives.gov/preservation/technical/guidelines.html>.
National Park Service, September 1996. Handling Archival Documents and Manuscripts, Number 19/17, pp. 1–4.
Parker, C.M., 2004. The pipeline industry meets grief unimaginable: Congress reacts with the Pipeline Safety Improvement Act of 2002. Nat. Resour. J. 44, 243–282.
Petroleum Extension Service, University of Texas at Austin, 1978. Introduction to the Oil Pipeline Industry, second ed. American Petroleum Institute.
PIPA, November 2010. Partnering to Further Enhance Pipeline Safety in Communities Through Risk-Informed Land Use Planning, Final Report of Recommended Practices. Pipelines and Informed Planning Alliance. Last Viewed 1/30/2017 at <https://primis.phmsa.dot.gov/comm/publications/pipa/pipa-report-final-20101117.pdf>.
Pipeline Safety, 1969. Hearing Before the Subcommittee on Communications and Power of the Committee on Interstate and Foreign Commerce, House of Representatives, 91st Congress, March 5, 1969 (Serial No. 91-5).
Shepard, E.R., 1931. Pipeline currents and soil resistivity as indicators of local corrosive soil areas, Report No. 298. Bureau Standards J. Res. 6 (4), 683–708
Spang, H.W., 1917. Electrolysis—it's time remedy explained. Water Gas Rev. 27 (11), 26–28.
TransCanada, June 2010. Keystone Pipeline Starts Deliveries to US Midwest.
TransCanada, February 2011. Keystone Pipeline System.
Transportation of Crude Petroleum in the United States, July 26, 1890. The Engineering and Building Record, pp. 116–117.
Transportation of Petroleum, February 27, 1892, Scientific American, pp. 134–135.
Transportation Research Board, 1988. Pipelines and Public Safety: Damage Prevention, Land Use, and Emergency Preparedness. Special Report 219, National Research Council, Washington, DC.
Transportation Research Board, 2004. Transmission Pipelines and Land Use: A Risk-Informed Approach. Special Report 281, Washington, DC.
USEPA, September 2016. NRC 1158584, Pelham Pipeline Spill Situation Report #11.
USEPA, 2017. NRD. Last Viewed 3/10/2017 at <https://www.epa.gov/superfund/natural-resource-damages-frequently-asked-questions>.
US General Accounting Office, July 1979. Petroleum Pipeline Rates and Competition—Issues Long Neglected by Federal Regulators and in Need of Attention. Report of the US Comptroller General to Congress, EMD-79-31.
US General Accounting Office, July 1984. Need to Assess Federal Role in Regulating and Enforcing Pipeline Safety. Report by the US Comptroller General, GAO/RCED-84-102.
Whitesel, T.L., 1947. Recent Federal Regulation of the petroleum pipe line as a common carrier. Cornell Law Rev. 32 (3), 337–377.
Wildman, O., 1945. Maintenance and repair of oil pipe lines. J. Am. Weld. Soc. 24 (11), 1019–1021.
Williamson, H.F., Daum, A.R., 1959. The American Petroleum Industry: The Age of Illumination, 1859–1899. Northwestern University Press, Evanston, IL.
Williamson, H.F., Andreano, R.L., Daum, A.R., Klose, G.C., 1963. The American Petroleum Industry: The Age of Energy, 1899–1959. Northwestern University Press, Evanston, IL.
Willson, C.O., April 30, 1925. Little change in refining operations. Oil Gas J. 23 (49), 60–70.
Wolbert Jr., G.S., 1979. US Oil Pipe Lines: An Examination of How Oil Pipe Lines Operate and the Current Public Policy Issues Concerning Their Ownership. American Petroleum Institute, Washington, DC.

Further Reading

Bowie, C.P., 1932. Transportation of Gasoline by Pipe Line. US Department of Commerce, Bureau of Mines, Technical Paper 517.
DOT, 2002. Pipeline safety: gas and hazardous liquid pipeline mapping. Fed. Regis. 67 (114), 40768–40770.
<http://www.worthingtoncompressor.com/about-us>.
Johnson, A.M., 1956. The Development of American Petroleum Pipelines: A Study in Private Enterprise and Public Policy, 1862–1906. Cornell University Press, Ithaca, NY.
US Geological Survey, 2017. The National Map. Last Viewed 3/10/2017 at <https://nationalmap.gov>.
Wolbert Jr., G.S., 1951. American Pipe Lines: Their Industrial Structure, Economic Status and Legal Implications. University of Oklahoma Press, Norman, OK.

CHAPTER

25

Comparison of Quantitative and Semiquantitative Methods in Source Identification Following the OSPAR Oil Spill, in Paraná, Brazil

Fabiana D.C. Gallotta[1] *and Jan H. Christensen*[2]

[1]Petrobras Research Center, Rio de Janeiro, Brazil [2]University of Copenhagen, Frederiksberg, Denmark

BIOGRAPHIES

Fabiana D.C. Gallotta is an environmental geochemist with experience in petroleum industry since 1996. She has worked in organic analytical chemistry as technician and also as a chemist. She is also experienced in Regulatory Petroleum sector, working for the Brazilian Government as a petroleum and gas regulator for refining processes. She has received a Ph.D. in Geosciences from Fluminense Federal University in 2014, a master's degree in Optimization from Rio de Janeiro Federal University in 2004, and a chemical engineer degree from Rio de Janeiro Federal University in 2002. She is currently a research scientist of the Research and Development Center of Petrobras. Her specialties and research interests include chemical fingerprinting of petroleum and derivatives, oil spill identification, and environmental monitoring of offshore drilling activities, production wells, and oil spills in marine and terrestrial environments.

Jan H. Christensen (born in Hillerød, Denmark, 1973) is a full professor in Environmental Analytical Chemistry. He is leader of the Analytical Chemistry group, Department of Plant and Environmental Sciences, University of Copenhagen, Denmark, and heads the Research Centre for Advanced Analytical Chemistry (RAACE). He has pioneered cutting-edge analytical and chemometric methods for oil hydrocarbon fingerprinting and now works on all aspects of contaminant fingerprinting, petroleomics, and metabolomics. He develops analytical platforms and new tools to handle and process complex data from cutting-edge analytical instrumentation and apply this chemical fingerprinting concept for analysis of complex mixtures of organic contaminants and in numerous industry project collaborations with the petrochemical, environmental, and food industry. He has authored and coauthored more than 70 peer-reviewed papers and book chapters on these topics. His current research focus is on development and application of multidimensional chromatography platforms in combination with chemometric data analysis.

25.1 INTRODUCTION

The first methods for source identification of hydrocarbons were based only on visual comparison of chromatograms of samples and possible sources. Certainly, the result of these qualitative comparisons was subjective and depended on experience and critical view of the analyst. To reach more objective, reproducible, and therefore

Oil Spill Environmental Forensics Case Studies.
DOI: http://dx.doi.org/10.1016/B978-0-12-804434-6.00025-2

more reliable conclusions, strategies which involve the use of different analytical techniques and evaluation of results have been incorporated.

Currently, the most frequently used analytical techniques on source identification of hydrocarbons include: gas chromatography–flame ionization detection (GC/FID); gas chromatography coupled with mass spectrometry detector (GC/MS); and stable isotopic ratios, both for bulk oil considering total element in a sample, as for individual compounds, by separation after gas chromatography (Wang and Stout, 2007; Wang et al., 1999).

The isotopic analysis is considered an additional technique for source identification, that stands out in the evaluation of light oil or its products, where conventional biomarkers are absent. On the other hand, the isotopic analysis of individual compounds is highly complex and includes challenges related to the coelution of the target compounds (Wang and Stout, 2007). This technique will not be addressed in this chapter as it was not applied in the chemical analysis of the samples.

The chromatographic results are evaluated by the comparison of the relative abundance of compounds (CEN, 2012; Meniconi, 2007) through visual inspection of GC/FID chromatograms with the distribution of *n*-alkanes and/or histograms with the polycyclic aromatic hydrocarbons (PAHs), and selected ion chromatograms (SICs) of biomarkers and PAHs; calculation of quantitative and semiquantitative ratios of diagnostic compounds; and multivariate statistical analysis (chemometrics).

25.1.1 Diagnostic Ratios

The diagnostic ratios of hydrocarbons (DRs) have been widely used as a tool in the identification and differentiation of sources of these compounds in environmental samples. The ratios show the relative proportions between target compounds, which facilitate the interpretation of the pattern of distribution of these compounds. Depending on the objective, DRs can be calculated using concentration, peak heights for individual peaks and peak areas for compound groups in the mass chromatograms of *n*-alkanes, acyclic isoprenoids, parental PAHs, alkylated PAHs, and geochemical biomarkers.

To classify the hydrocarbons in a sample by origin (i.e., petrogenic, pyrogenic, and diagenetic), according to characteristic values available in the literature, the diagnostic reasons must be calculated using the values of concentration of the compounds (Colombo et al., 1989; Budzinski et al., 1997; Baumard et al., 1998; Wang et al., 1999; Meniconi et al., 2002, Readman et al., 2002; Yunker et al., 2002; Tolosa et al., 2004; Meniconi, 2007; Wagener et al., 2010; Puerari, 2011; Massone et al., 2013).

When comparing samples in the same case study, the DRs may be calculated directly from peaks' heights and areas in the chromatogram (Kienhuis and Dahlmann, 2004, 2007, 2009, 2014, 2015; CEN, 2012; Qing and Peiyan, 2010; Dahlmann, 2006, 2008; Lobão, 2007; Dahlmann and Kienhuis, 2005).

Among the most commonly PAHs used in the calculation of DRs are the anthracenes, pyrenes, phenantrenes, fluoranthenes, and dibenzothiophenes. For biomarkers, the main compounds include terpanes, diasteranes, regular steranes, and triaromatic steranes. Compared to *n*-paraffins and the acyclic isoprenoids, biomarkers are particularly useful because of its specificity, diversity, and resistance to weathering (Wang and Stout, 2007; Prince et al., 1994).

25.1.1.1 DRs Based on PAHs

The DRs including those of PAHs were defined based on the different distributions of these compounds in petrogenic, pyrogenic, and diagenetic sources. The most used ones are in Table 25.1, associated with their ranges of identification of sources and also the benchmark studies that have established or consolidated each of them. These DRs may involve parental PAHs, alkylated PAHs, or both.

The DRs which include only parental PAHs (Table 25.1), as phenanthrene and anthracene (Gschwend and Hites, 1981; Budzinski et al., 1997; Baumard et al., 1998; Yunker et al., 2002), fluoranthene and pyrene (Gschwend and Hites, 1981; Sicre et al., 1987; Yunker et al., 2002), benz(*a*)anthracene and chrysene (Gschwend and Hites, 1981; Sicre et al., 1987; Yunker et al., 2002), and indene(1,2,3-cd)pyrene and benzo(*ghi*)perylene (Sicre et al., 1987; Yunker et al., 2002) are based on the differences of thermodynamic stabilities of these isomers (Yunker et al., 2002). These ratios include only those compounds that have the same molecular mass and m/z monitored by GC/MS. The objective is to minimize the influence of differences in physical–chemical properties (e.g., volatility, solubility, tendency to adsorption) in the DRs values (Gschwend and Hites, 1981; Yunker et al., 2002).

While the PAHs resulting from incomplete combustion processes (pyrogenic) generally have a higher proportion of less thermodynamically stable isomers, the more thermodynamically stable PAHs originate in low-temperature processes (Yunker et al., 2002). As the process of oil generation occurs at lower temperatures compared to the combustion, the compounds with larger thermodynamic stability are preferentially formed (Yunker et al., 2002; Peters et al., 2007). Thus, the isomers are classified as representatives of petrogenic or pyrogenic

TABLE 25.1 Ranges, Classification, and Benchmark Studies for PAH Diagnostic Ratios

PAH ratio	Range	Source	References
PARENTAL PAH			
Ph/An	>15 <10	Petrogenic Pyrogenic	Gschwend and Hites (1981), Soclo (1986) *apud* Baumard et al. (1998)
An/(An + Ph)	<0.1 >0.1	Petrogenic Pyrogenic	Budzinski et al. (1997), Yunker et al. (2002)
Fl/Py	<1 >1	Petrogenic Pyrogenic	Gschwend and Hites (1981), Sicre et al. (1987)
Fl/(Fl + Py)	<0.4	Petrogenic	Yunker et al. (2002)
	>0.4 and <0.5	Liquid fossil fuel combustion	
	>0.5	Grass, wood, or coal combustion	
BaA/Ch	<0.4 >0.9	Petrogenic Pyrogenic	Gschwend and Hites (1981)
BaA/(BaA + Ch)	<0.2 >0.35	Petrogenic Pyrogenic	Sicre et al. (1987), Yunker et al. (2002)
IPy/(IPy + Bghi)	<0.2	Petrogenic	Sicre et al. (1987), Yunker et al. (2002)
	>0.2 and <0.5	Liquid fossil fuel combustion	
	>0.5	Grass, wood, or coal combustion	
Pe/(∑5 ring PAH)[a]	>10%	Diagenetic	Baumard et al. (1998)
ALKYLATED PAH			
∑C1-Ph/Ph	>2 <2	Petrogenic Pyrogenic	Prahl and Carpenter (1983), Garrigues et al. (1995)
(Ph + An)/(Ph + An + C1-Ph + An)	<0.5 >0.5	Petrogenic or pyrogenic Pyrogenic	Yunker et al. (2002)
∑(other 3–6 ring PAH)[b]/∑(5 series of alkylated PAH)[c]	<0.08 >0.50	Petrogenic Pyrogenic	Wang et al. (1998b, 1999)

[a] *∑(5 ring PAH) = Benzo*(b)*fluoranthene + benzo*(j)*fluoranthene + benzo*(k)*fluoranthene + benzo*(a)*fluoranthene + benzo*(e)*pyrene + benzo*(a)*pyrene + perylene (perylene relative abundance).*

[b] *Other 3–6 ring PAH = all PAH analyzed excluding the five series of alkylated PAH.*

[c] *Five series of alkylated PAH = naphthalenes, fluorenes, dibenzothiophenes, phenantrenes, and chrysenes.*

Abbreviations: *Ph/An*, phenanthrene/anthracene; *An/(An + Ph)*, anthracene/(anthracene + phenanthrene); *Fl/Py*, fluoranthene/pyrene; *Fl/(Fl + Py)*, fluoranthene/(fluoranthene + pyrene); *BaA/Ch*, benz(*a*)anthracene/chrysene; *BaA/(BaAn + Ch)*, benz(*a*)anthracene/(benz(*a*)anthracene + chrysene + triphenylene); *IPy/(IPy + Bghi)*, indene(1,2,3-cd)pyrene/(indene(1,2,3-cd)pyrene + benzo(*ghi*)perylene); *Pe*, perylene; *∑C1-Ph/Ph*, methyl-phenanthrenes/phenanthrene; *Ph + An/(Ph + An + C1-Ph + An)*, phenanthrene + anthracene/(phenanthrene + anthracene + methyl-phenanthrenes + methyl-anthracenes).

sources due to differences between their heats of formation (ΔHf). The larger the amplitude of ΔHf, theoretically the greater potential as an indicator of source, being fluoranthene and pyrene and indene(1,2,3-cd)pyrene and benzo(*ghi*)perylene ratios more promising than phenanthrene and anthracene and benz(*a*)anthracene and chrysene ones (Yunker et al., 2002).

The DRs which include series of alkylated PAHs (Prahl and Carpenter, 1983; Boehm and Farrington, 1984; Garrigues et al., 1995; Wang et al., 1998b, 1999; Yunker et al., 2002) (Table 25.1) are based on the predominance of the alkylated PAHs generated in oil formation, in contrast to combustion processes that favor the formation of high-molecular-weight parent PAHs. Among these, the pyrogenic index [∑(other 3–6 ring PAH)/∑(5 series of alkylated PAHs)] proposed by Wang et al. (1998b) (Table 25.1) has the additional advantage that as many compounds analyzed are included, specific problems of integration are "diluted", minimizing the interference of inaccurate concentration of a compound in the value of the DR. Values up to 0.08 for the pyrogenic index indicate the contribution of oil and refined products, while values larger than 0.5 (one order of magnitude larger) indicate pyrogenic sources. A disadvantage is that in the range of 0.08 up to 0.5 values, the source is mixed (or unspecified).

Still, the weathering can modify the DRs. The weathering reduces preferably the lower molecular weight PAH (two and three rings), increasing consequently the proportion of four to six rings PAHs (Boehm, 2005). The most important changes occur in the DRs containing alkylated PAHs, which are preferentially degraded the smaller the degree of alkylation (Page et al., 1995, Wang et al., 1999, Boehm, 2005).

Another point is that the physical weathering (e.g., evaporation) in general reduces similarly all isomers within a same group of alkylated PAHs (with the same degree of alkylation), while biodegradation processes (Wang et al., 1998a; Christensen et al., 2005b; Bernabeu et al., 2013) and photooxidation (Douglas et al., 2002; Radović et al., 2013) are influenced by the position of the alkyl group within the group of isomers. This information can be used to identify compositional changes related to each process (Wang et al., 1999).

25.1.1.2 DRs Based on Biomarkers

The DRs based on biomarkers have been widely used by geochemists in the understanding of the processes of generation, storage, and preservation of oil (Peters et al., 2007). Accordingly, many of the DRs currently used in forensic and environmental studies in oil spills come from the petroleum geochemical literature (Wang and Stout, 2007).

The most commonly used DRs involve alkanes, acyclic isoprenoids, terpanes, and steranes, in the form (biomarker1)/(biomarker2) or (biomarker1)/(biomarker1 + biomarker2) (Wang and Stout, 2007).

In contrast to PAH DRs, biomarker DRs are relatively more resistant to weathering processes. The DRs involving the terpanes practically are not affected by weathering (Wang et al., 1999).

However, in situations of extremely severe biodegradation, terpanes and steranes DRs may be altered. In the work by Wang et al. (2001) about the oil tanker *Metula*, the DRs C23 tricyclic terpane/C24 tricyclic terpane, C23 tricyclic terpane/30ab, C31abS/30ab, C32abS/30ab, C34abS/30ab, C34abR/30a, C35abS/30ab, C35abR/30a, and C27-αββ-steranes/C29-αββ-steranes have been affected over the years.

In addition, the triaromatic steranes DRs can be modified by photooxidation processes, being the C21TA/(RC26TA + SC27TA), SC26TA/(RC26TA + SC27TA), and RC27TA/(RC26TA + SC27TA) DRs the ones that present larger relative differences when compared to the original oil (Radović et al., 2013).

In 2011, OSINET (Oil Spill Identification Net of Experts) round robin (Kienhuis and Dahlmann, 2014), the triaromatic steranes were also affected by photooxidation, and additionally by dissolution and biodegradation in spill samples weathered for 10 years. Also 27dbS and 27dbR (m/z 217), 27bb (m/z 218), and 27bb(R + S) were reduced in spill samples when compared to the source.

Although it occurs rarely and only under special conditions, the changes in the biomarker DRs in environmental samples hinder the source identification and may hamper the unequivocal correlation of these samples with the spilled oil. Even an experienced analyst can have difficulties to decide, whether differences among the most stable biomarkers are caused by weathering over many years or are true differences. In these cases, one should take many samples along the years and follow the process of weathering much closer.

25.1.2 Chemometrics

Chemometrics consists of the application of statistics and mathematics to chemical methods and includes a series of techniques, e.g., principal component analysis (PCA), parallel factors analysis (PARAFAC), and partial least squares regression (PLS), which allow a more advanced treatment of data derived from complex chemical mixtures (Massart et al., 1997; Mudge, 2007; Christensen and Tomasi, 2007). The techniques of multivariate modeling can be used to explore correlations in large data sets in order to extract information from chemical composition and also to look for patterns in data associated with hidden chemical phenomena, e.g., genesis of crude oil (depositional environment, thermal maturity, migration, and intrareservoir biodegradation), refining, weathering, and oil mixture to the environment.

In addition to a more detailed and easy characterization of large data sets, the techniques of multivariate analysis that prevent the identification and quantification of the peaks in the chromatograms present potentially a positive cost benefit, considering that the processing of data is able to remove most of the variation not related to changes in chemical composition. In this line of approach, there are studies that use a method based on PCA of processed sections of chromatograms obtained by gas chromatography coupled to mass spectrometry, using selective ion monitoring, to group samples with similar characteristics (Christensen et al., 2005a, 2005b, 2010; Malmquist et al., 2007; Christensen and Tomasi, 2007).

Among the chemometric analysis methods, it was selected for this study the method proposed by Christensen and Tomasi (2007), which uses all the information contained in the SICs for the differentiation of characteristics between samples. The proposed technique (CHEMSIC) requires no effort on identification or even quantification

of the peaks in the chromatograms. It is therefore a quite attractive method when the number of samples to be evaluated is large.

Before starting the chemometric analysis itself, it is necessary to comply with a set of preprocessing procedures of the chromatographic analyses data. The goal is to reduce the variability of the data not related to chemical composition (viz., baseline drift, changes in retention times, and concentration effects). The first step is to import the relevant information (e.g., array containing signal intensity over time, name, and description of samples) for the computational environment where there will be the other steps. The data processing can be summarized in (1) baseline removal, (2) retention times alignment, (3) normalization, and (4) concatenation.

25.1.2.1 Baseline Removal

The baseline removal is performed by first order numerical differentiation, by calculating the vectors $\overline{x}_j$ (Eq. 25.1):

$$\dot{x}_j = x_{j+1} - x_j, \quad j = 1 \ldots J-1 \tag{25.1}$$

where $\dot{x}_j$ is the jth element of the derivative; x_j is the signal intensity in jth retention time; J is the length of the signal.

The result of this operation is a signal with double peaks, with a positive and a negative part, which crosses the zero in the retention time of where the original peak reaches its maximum intensity.

25.1.2.2 Retention Times Alignment

The retention times alignment of a chromatogram is accomplished by stretching or compressing sample segments along the retention time axis using linear interpolation. There are two parameters to be optimized: the length of the segments in which signals are divided and the "slack parameter," which represents how much the size of these segments is allowed to change. Sample analytical replicates can be used to determine the parameters values which maximize the variance explained by the first principal component (PC) of the matrix formed by such analytical replicates.

25.1.2.3 Normalization

The chromatographic signal intensity depends on the response factors and concentrations of the compounds. The former are affected by the instrumental variation (e.g., discrimination of masses) and chromatographic conditions (injection parameters, temperature programing, and choice of column), the latter are influenced by sampling and sample preparation (viz., extraction, fractionation, and treatment). The variation in the data concerning these factors can mask the compositional information of samples, which is the main aspect in the differentiation of hydrocarbon sources. Hence, a normalization step is required to remove this undesirable variation. The normalization to a constant Euclidean norm is a common procedure for GC/MS-SIM data (Eq. 25.2):

$$\dot{x}^N_{nj} = \frac{\dot{x}_{nj}}{a_n}, \quad a_n = \sqrt{\sum\nolimits_j \dot{x}^2_{nj}} \tag{25.2}$$

where $\dot{x}_{nj}$ is the first derivative of the nth chromatogram at the jth retention time; a_n is the Euclidean norm; N is the total number of retention times.

Other normalization methods emphasize different aspects of the data and each one has its own merits and drawbacks. The choice for a normalization method depends on the question to be answered, the properties of the data set, and the data analysis method selected (Van Den Berg et al., 2006).

25.1.2.4 Concatenation

In this step, the data of each of the m/z fragments are concatenated to form a longer signal. The goal is to keep the use of bilinear factors models. The trilinear, e.g., PARAFAC, are not recommended, since there would be many missing values and the computational time would increase unnecessarily.

25.1.2.5 Chemometrics

The preprocessed data, stacked in arrays where the rows correspond to samples and the columns correspond to the signals in each of the retention times, suggest the use of bilinear models, like PCA and PLS. In particular, in the PCA, the information is summarized in PCs that are weighted sums of the original variables (signals at a given retention time). In PCA, the variation in the data matrix, $\mathbf{X}$ $(I \times J)$ is described by the product of the scores

matrix **T** ($I \times K$), and the transpose of the loadings matrix **P** ($J \times K$) and the variation in data not described by the model is left in the residuals (**E**) (Eq. 25.3). I, J, and K are the number of samples, the number of retention times, and the number of PC, respectively.

$$\mathbf{X} = \mathbf{TP}^T + \mathbf{E} \tag{25.3}$$

The interpretation of the results is performed through the scores plots, where samples with the same compositional characteristics are grouped, and loading plots, which span the direction of the main variations in the sample set.

25.2 METHODS AND SAMPLES

25.2.1 Study Area

Araucária Municipality is located in a highly industrialized and urbanized region, in the vicinity of Curitiba City, where rivers Iguaçu and Barigüi receive intense chronic anthropogenic pollution. In the segment after Curitiba City, Iguaçu River is the second most polluted river in Brazil (IBGE, 2012). Moreover, on July 16, 2000, approximately 4000 m^3 of Cusiana crude oil were released in the area, due to a pipeline rupture at the Presidente Getúlio Vargas Refinery (REPAR), reaching the Saldanha Rivulet, the Barigüi River, and subsequently the Iguaçu River (Meniconi et al., 2002; Falkiewicz, 2003) (Fig. 25.1). Cusiana is a paraffinic crude oil with an API gravity of 41 degrees, 71% of saturates, 18% of aromatics, 10% of resins, and around 1% of asphalthenes. PAH concentration was 16 mg g^{-1}, mainly alkylated series of naphthalenes (75%), phenantrenes (17%), and fluorenes (5%).

River sediments have been collected in five campaigns in August 2000, July 2001, January 2007, July 2007, and January 2008.

For determination of hydrocarbons chromatographic raw data, soil and sediment samples were collected in July 2009 and March 2010, using augers and cores from the refinery area and from points nearby the margins of Iguaçu River (Guajuvira, General Lúcio, and Balsa Nova Municipalities). The samples were transferred into glass jars with Teflon caps, in which, they were homogenized and maintained at −20°C until preparation. Sampling location and labeling abbreviation details are shown in Fig. 25.2.

Cusiana crude oil samples, two from the refinery tanks and one from the spill at the pipeline rupture point, were included for comparison with the environmental samples. These oil samples were collected in 2000 and have been stored into glass jars with Teflon caps and kept locked up in the dark at a maximum temperature of 4°C. They are the most representative available samples of a nonweathered source of the spilled oil.

One oily water sample from an old-monitoring well close to the pipeline rupture point was withdrawn through a bailer, transferred directly into a 40-mL glass jar with Teflon cap and maintained at 4°C until preparation. This sample was expected to have higher concentrations of PAHs and biomarkers, as oil vestiges were visible. It was included in the study to test the robustness of CHEMSIC method against subsequent dilutions.

25.2.2 Analytical Techniques for Determination of Hydrocarbon Concentrations

The concentrations of PAHs from the diagnostic phase after Cusiana oil spill and from the environmental monitoring conducted since then were obtained using the method USEPA 8270 (USEPA, 2007). These analyses were performed by various laboratories, in research carried out by Petrobras (Petrobras/Cenpes/Repar, 2001) or by third parties for Petrobras (UFRGS 2003a, 2003b, 2003c, 2004; Hydrogéo Plus Inc., 2009, 2010).

25.2.3 Analytical Techniques for Determination of Hydrocarbons Raw Data

The techniques for source identification through DRs calculated from areas and heights of chromatograms and also the chemometric method required specific chemical analyses, since raw analytical data are necessary (areas, heights, and chromatograms) which were unavailable in studies conducted by third parties. The following sections describe the analytical techniques used to obtain these raw data. These analyses were carried out at Petrobras Research Center and at the University of Copenhagen by the authors of this chapter.

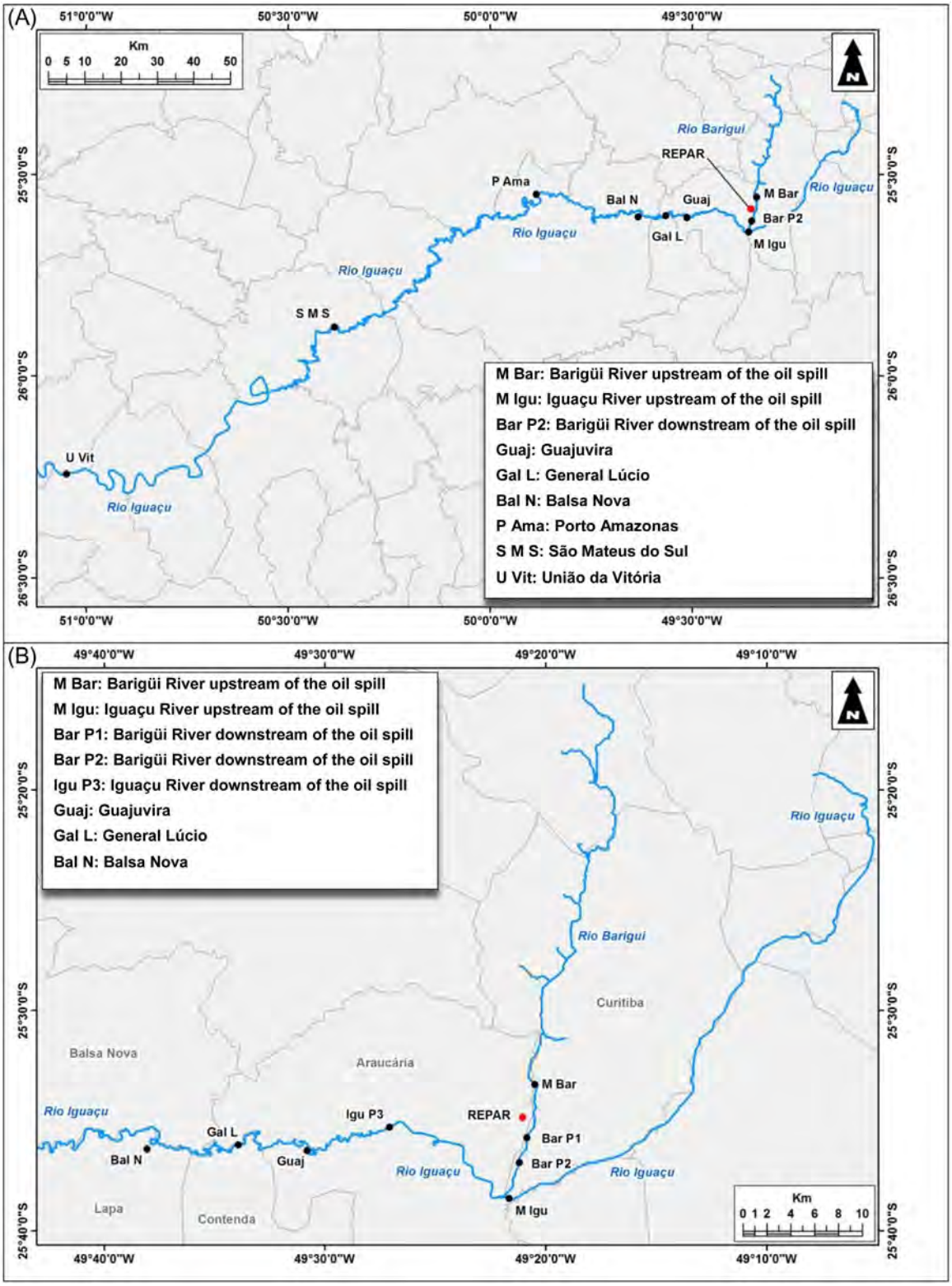

FIGURE 25.1 Map showing the study area and locations of sediment samples collected in Barigüi and Iguaçu rivers campaigns: (A) whole area and (B) amplified part of the study area. REPAR stands for Presidente Getúlio Vargas Refinery.

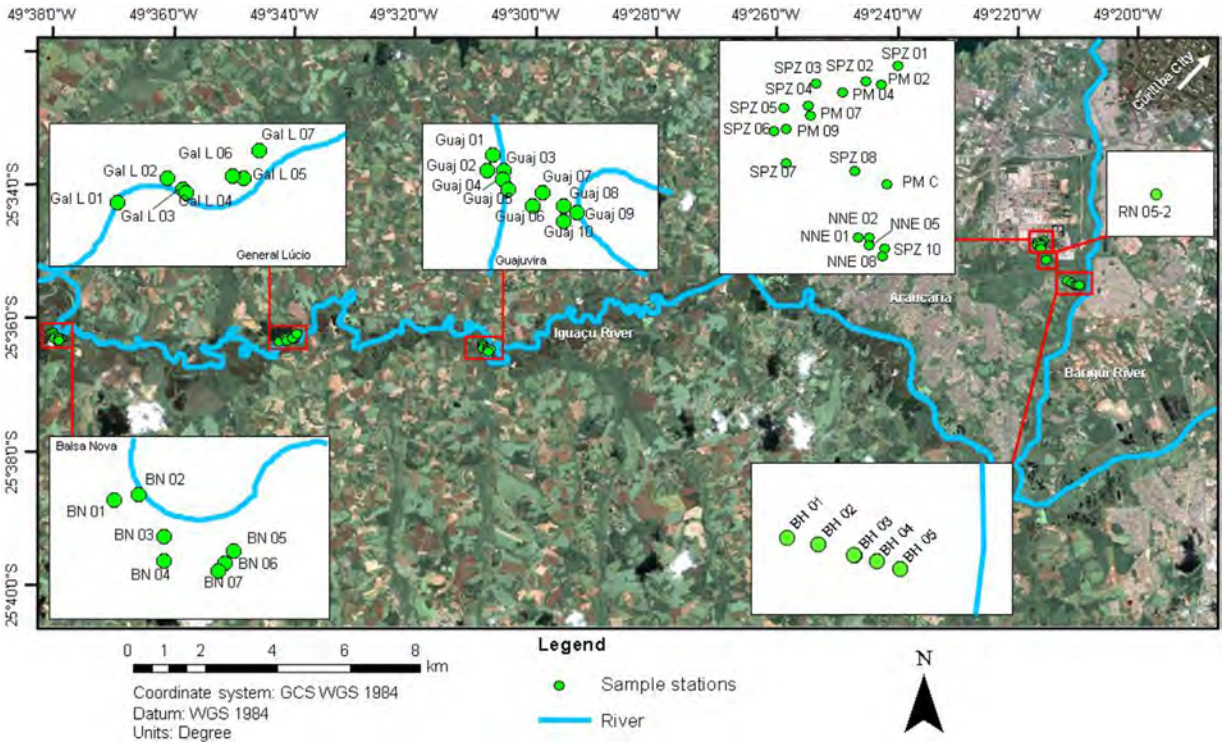

FIGURE 25.2 Map showing details of the study area and locations of sediment and soil samples collected in July 2009 and March 2010 campaigns. The sample label abbreviations stand for sample type and location; inside the refinery area: PM (composed soil collected around a monitoring well), SPZ (surface soil), NNE (surface soil collected to the north of the new road), RN (surface soil collected nearby Saldanha Rivulet water-level scale), BH (composed soil collected around a monitoring well in a swampy area); and outside the refinery area: Guaj (surface soil in Guajuvira), Gal L (surface soil in General Lúcio), and BN (surface soil in Balsa Nova). These abbreviations have been used throughout in the environmental monitoring studies, since 2000.

25.2.3.1 *Reagents and Chemicals*

Dichloromethane (Tedia, OH, USA) and *n*-hexane (Tedia, Ohio, USA) were all of residue grade. Anhydrous sodium sulfate (proanalysis, Vetec, Rio de Janeiro, RJ, Brazil) was purified by heating at 40°C for 4 h and allowed to cool in the desiccator. An aromatic surrogate standard mixture, containing naphthalene-d8, acenaphthene-d10, phenanthrene-d10, *p*-terphenyl-d14, chrysene-d12, perylene-d12 (AccuStandard, New Hawen, CT, USA), was added prior to the extraction. The instrument quality control mixture included decafluorotriphenylphosphine, 4,4′-DDT, pentachlorophenol, and benzidine (50 ng μL^{-1}, Supelco, Bellefonte, PA, USA).

25.2.3.2 *Sample Preparation*

Soil and sediment samples were mixed with anhydrous sodium sulfate and spiked with 50 μL of a 10 $\mu g\ mL^{-1}$ solution of the surrogate standard mixture. The amounts of material used for each extraction and sodium sulfate for drying were selected according to the previous knowledge about contamination levels and the water percentage, respectively (Hydrogéo Plus Inc., 2009, 2010). For samples with low total petroleum hydrocarbon (TPH) concentrations (TPH $< 3 \times 10^2$ mg kg^{-1}), 10 g of wet sample was homogenized with 30 g of sodium sulfate. For relatively more contaminated samples (TPH $3 \times 10^2 - 1 \times 10^4$ mg kg^{-1}) the amount of material was reduced to 1 g of wet sample and 5 g of sodium sulfate.

Extracts of the solid samples were obtained according to EPA Method 3545A. Samples were extracted by pressurized liquid extraction using an ASE 300 instrument (Dionex, Sunnyvale, CA, USA). The method conditions were: extraction cells size 66 mL, extraction solvent dichloromethane, oven temperature 50°C, pressure 1500 psi, preheating time 5 minutes, static time 5 minutes, flush volume of 10%, purge time 60 seconds, and three static extraction cycles. After extraction, the solvent volume was reduced to 1 mL using a TurboVap 500 (Caliper Life Science, Hopkinton, MA, USA), 30 mL of *n*-hexane was added and the extract concentrated to 1 mL.

SPE cartridges packed with 1.5 g silica and 6 g cyanopropyl (Interchim, Montluçon, France) were used for cleanup. After preconditioning of the columns with 6 mL of *n*-hexane, the extracts were applied to the top of the column, and petroleum hydrocarbons eluted with 10 mL of dichloromethane in *n*-hexane (1:9, v-v). The eluent was then concentrated to 1 mL and maintained at −20°C in amber glass vials until analysis.

The oily water sample (around 40 mL) was spiked with 50 μL of the surrogate standard mixture and liquid−liquid extracted 3 times with 5 mL of *n*-hexane. The combined extract was filtered through a funnel filled with sodium sulfate, concentrated to 1 mL and treated with the same SPE procedure as solid samples. Oil samples (1 mL of 2000 mg L^{-1} oil solution in *n*-hexane) were spiked with the surrogate standard mixture and treated by the same SPE procedure as the solid samples.

25.2.3.3 GC/MS Analysis

The samples were analyzed using an Agilent 6890N/5975 GC/MS operating in electron ionization mode. The GC was equipped with a 60 m ZB-5 (0.25 mm I.D., 0.25 μm film thickness) capillary column. Helium was used as carrier gas with a flow rate of 1.1 mL s^{-1}. Aliquots of 1 μL were injected in pulsed splitless mode with injection temperature of 315°C. The column temperature program was as follows: initial temperature 40°C held for 2 minutes, 25°C min^{-1} to 100°C, then followed by an increase of 5°C min^{-1} to 315°C (held for 13.4 min). The transfer line, ion source, and quadrupole temperatures were 315, 230, and 150°C, respectively. A total of 55 m/z's divided into 12 groups were acquired in SIM mode (cf. Table 25.2). The dwell time for each m/z was 25 milliseconds with 2.81 scans s^{-1}. The number of monitored ions (13 m/z's) was consistent between groups to avoid differences in the scanning frequency.

25.2.3.4 Quality Control

The samples were divided into six batches. In the analytical sequence, dichloromethane, an oil sample [1:1 mixture of heavy fuel oil from the Baltic Carrier and North Sea crude oil from the Brent oil field (Christensen et al., 2004)] and the instrument quality control mixture were analyzed between batches. These test solutions were used for quality control by daily monitoring for cross-contamination; changes in peak shapes, chromatographic resolution, and sensitivity; and to verify tuning, injection port inertness, and GC column performance, respectively.

Besides the regular quality control of GC/MS methods, when using CHEMSIC, additional validation samples are highly recommended, i.e., analytical replicates spread into the batches. These samples are used to ensure that the data processing is able to remove the variation unrelated to the chemical composition. Five sample extracts were included randomly in each batch: Cusiana oil sample, two samples with a weathered oil fingerprint, one sample with a high carbon preference index (CPI) value and absence of unresolved complex mixture (UCM), and one sample with both a high CPI value and UCM. The choice was based on previous GC-FID analysis (Hydrogéo Plus Inc., 2009, 2010).

Additionally, a "reference" sample extract consisting of equal amounts of eight extracts was analyzed every 10 runs. In this case study, previous GC-FID analyses were available, facilitating the selection of sample extracts representative of the whole sample set.

Furthermore, sample dilutions (1:10, 1:20, 1:40, and 1:100) of the most concentrated sample (oily water) were prepared and injected in the last batch. These dilutions were used to indicate how reproducible the CHEMSIC method is to cluster samples with the same chemical composition but with different TPH concentrations.

25.2.4 Quantitative and Semiquantitative Methods for Source Identification

Source identification in the sediment samples of Iguaçu and Barigüi rivers and in the soil of the refinery area was carried out using the three following approaches: PAH DRs calculated from compound concentrations, DRs calculated from heights and areas (signal intensity) of chromatograms, and chemometric analysis.

25.2.4.1 Diagnostic Ratios

25.2.4.1.1 Quantitative DRs Calculated from the Compounds Concentrations

For the selection of the most appropriate DRs for this case study, the DRs commonly used for source identification (Gschwend and Hites, 1981; Soclo, 1986 *apud* Baumard et al., 1998; Sicre et al., 1987; Budzinski et al., 1997; Yunker et al., 2002; Prahl and Carpenter, 1983; Garrigues et al., 1995; Wang et al., 1999; Baumard et al., 1998) were calculated for Cusiana crude oil (Table 25.3). Those that resulted in the classification of this oil as belonging

TABLE 25.2 List of Compounds, Corresponding SICs and Groups of GC/MS-SIM

Compound(s)	SIC	Group(s)	Compound(s)	SIC	Group(s)
n-Alkyl cyclohexanes	83	I–XII	C4-decalins C2-fluorenes[a]	194	I–VII
Alkanes	85	I–XII	C2-dibenzofurans[a]	196	V–VII
Alkyl toluenes	105	I–XII	C1-dibenzothiophenes[a,b]	198	VI, VII
Sesquiterpanes	123	I–VI	C0-fluoranthene[a,b] C0-pyrene[a,b]	202	VII–IX
Naphthalene[a]	128	I	C2-phenanthrenes/anthracenes[a]	206	VII–IX
Benzo(*b*)thiophene[a]	134	I	C3-fluorenes[a]	208	VI, VII
d8-naphthalene[d]	136	I	C2-dibenzothiophenes [a] d10-fluoranthene[c] d10-pyrene[c]	212	VII, VIII
C0-decalin	138	I	C1-fluoranthenes/pyrenes[a,b]	216	VIII, IX
C1-naphthalenes[a]	142	II	Steranes	217	VIII–XII
C1-benzo(*b*)thiophenes[a]	148	I, II	Steranes	218	X–XII
C1-decalinsAcenaphthylene[a]	152	I–III	C3-phenanthrenes/anthracenes[a]	220	VII–IX
Acenaphthene[a]	154	II–IV	C3-dibenzothiophenes[a]	226	VII–IX
C2-naphthalenes [a]	156	III	C0-benz(a)anthracene[a,b] C0-chrysene[a,b]	228	X
d8-acenaphthylene[c]	160	III	C2-fluoranthenes/pyrenes[a]	230	IX, X
C2-benzo(*b*)thiophenes[a]	162	II, III	Triaromatic steranes	231	X–XII
d10-acenaphthene[d]	164	III, IV	C4-phenanthrenes/anthracenes[a] retene[a] C0-benzonaphtothiophene[a]	234	VIII–X
C2-decalins C0-fluorene[a]	166	I, II, V	C4-dibenzothiophenes d12-benz(*a*)anthracene[c] d12-chrysene[d]	240	VIII–X
C0-dibenzofuran[a]	168	II–IV	C1-chrysenes[a,b]	242	X, XI
C3-naphthalenes[a]	170	IV, V	d14-*p*-terphenyl[d]	244	VIII
C3-benzo(*b*)thiophenes[a] d10-fluorene[c]	176	IV, V	C1-benzonaphtothiophenes[a]	248	X, XI
C0-phenanthrene[a,b] C0-anthracene[a,b]	178	VI	5 rings PAHs[a,b]	252	XI, XII
C3-decalins C1-fluorenes[a]	180	I–III, V	C2-chrysenes[a]	256	XI
C1-dibenzofurans[a]	182	IV–VI	d12-benzo(*k*)fluoranthene[c] d12-benzo(*a*)pyrene[c] d12-perylene[d]	264	XI, XII
C4-naphthalenes[a] C0-dibenzothiophene[a]	184	IV–VI	C3-chrysenes[a]	270	XI, XII
d10-phenanthrene[d] d10-anthracene[c]	188	VI	6 rings PAHs[a,b]	276	XII
C4-benzo(*b*)thiophenes[a]	190	IV, V	6 rings PAHs[a]	278	XII
Tricyclic terpanes hopanes	191	IX–XII	d12-indeno(1,2,3-*cd*)pyrene[c] d12-benzo(*g*,*h*,*i*)perylene[c]	288	XII
C1-phenanthrenes/anthracenes[a,b]d8-dibenzothiophene[c]	192	V–VII			

[a] *SICs included for source identification using relative fingerprints of 38 groups of PAHs.*
[b] *SICs included for the initial source identification based on a subset of SICs.*
[c] *Internal standards analyzed but not added to the samples in this particular case study.*
[d] *Internal standards used for normalization* ***Scheme I*** *in the initial source identification based on a subset of SICs.*

TABLE 25.3 DRs Commonly Used for Source Identification Calculated for Cusiana Crude Oil

PAH ratio	DRs for Cusiana crude oil	Source
PARENT PAH		
Ph/An	142	Petrogenic
An/(An + Ph)	0.01	Petrogenic
Fl/Py	1.13	Pyrogenic
Fl/(Fl + Py)	0.53	Grass, wood, or coal combustion
BaA/Ch	0.16	Petrogenic
BaA/(BaA + Ch)	0.14	Petrogenic
IPy/(IPy + Bghi)	0	Petrogenic
ALKYLATED PAH		
∑C1-Ph/Ph	4.10	Petrogenic
(Ph + An)/(Ph + An + C1-Ph + An)	0.20	Petrogenic or pyrogenic
∑(other 3–6 ring PAH)/∑(5 series of alkylated PAH)	0.02	Petrogenic

Gray scale stands for: dark gray (petrogenic), medium gray (pyrogenic), and light gray (indeterminate).

to the petrogenic range were selected as promising to identify the presence of oil in the area affected by the accident. Thus, the DRs involving fluoranthene and pyrene were excluded from the assessment (Table 25.3).

Some DRs had a limited application, as the compounds which are necessary for calculations were not evaluated in the oil and/or sediment samples (in one or more campaigns), e.g., Pe/(∑5 ring PAH).

25.2.4.1.2 Semiquantitative DRs Calculated from Heights and Areas of Chromatograms

The semiquantitative procedure for source identification through DRs calculated from heights and areas of chromatograms followed the method for waterborne oil spill identification (CEN, 2012). This method shall be applied in source identification of the hydrocarbons present in marine, estuarine environments, and other aquatic environments through comparison between spill samples and its possible sources. A match between a spill sample and a suspected source may be concluded if no significant differences (i.e., smaller than analytical variance) are observed; consequently, if differences exist and cannot be explained by weathering, mixing, or heterogeneity of the "spill sample" after the spill, a nonmatch must be concluded.

In the procedure, GC/FID (Level 1) and GC/MS (Level 2) results were evaluated through visual comparison of chromatograms (qualitative assessment) and also numerical ratios of areas or heights of target compounds (semiquantitative assessment).

The ratios were determined in two ways:

(1) *Measurements of relative abundance of target compounds normalized* by the abundance of: (1) an *n*-alkane or group of *n*-alkanes not weathered (GC/FID) or (2) the 17α(*H*),21β(*H*)-hopane (GC/MS).

The normalized results of relative abundances of the compounds were visualized through the PW plots (percentage weathering plots), which show signals (areas or heights) of chromatographic peaks of the spill sample normalized by the signal of an unweathered compound or group of compounds, with reference to the suspected source sample (Eq. 25.4). Since the samples most likely had different concentrations, this step makes them easily comparable. Thus, the percentage results (Eq. 25.5) were plotted over time. According to the analytical variability, percentage values between 85% and 118% of the compound X in the spill sample, relatively to the suspected source, are acceptable for samples having the same origin (CEN, 2012).

$$SX_{SP}^{N} = SX_{SP} \times \frac{SUW_{SO}}{SUW_{SP}} \tag{25.4}$$

where SX_{SP}^{N} is the signal (area or height of the chromatographic peak) of compound X in the spill sample, normalized by the signal of an unweathered compound, with reference to the suspected source sample; SX_{SP} is the signal of compound X in the spill sample; SUW_{SO} is the signal of unweathered compound in the suspected source sample; SUW_{SP} is the signal of unweathered compound in the spill sample.

$$\%X_{SP} = \frac{SX_{SP}^{N}}{SX_{SO}} \times 100 \tag{25.5}$$

where $\%X_{SP}$ is the percentage of compound X in the spill sample, with reference to the suspected source sample and SX_{SO} is the signal of compound X in the suspected source sample.

The comparison of the compounds normalized abundances along the whole range of retention times (C_{10}–C_{40}), through the PW plots revealed: (1) the variance of the analysis and integration of duplicates; (2) the compound concentrations differences between spill and suspected source samples; and (3) the effects of weathering on individual compounds and groups of compounds, and hence, in DRs based on these compounds. When the effects of weathering in the samples could be explained, the DRs affected were eliminated or flagged when comparing a weathered spill sample and an unweathered suspect source sample.

(2) *Diagnostic ratios* calculated from the compound heights or areas or in the chromatogram using raw data at the same m/z in a limited range of retention times. The DR between two peaks was calculated as

$$DR = \frac{A}{B} \times 100 \tag{25.6}$$

where A is the peak height or area corresponding to compound A and B is the peak height or area corresponding to compound B.

The comparison was made using relative differences between the DRs obtained for suspected source sample and spill sample (Eq. 25.7). The method establishes as a significant difference, a value above 14%. Therefore, samples having the same origin must be similar, and the differences in DRs should remain below this limit value.

$$RD_{DR}\% = 100 \times \frac{[DR_{SO} - DR_{SP}]}{DR_{SO\text{-}SP}} \tag{25.7}$$

where $RD_{DR}\%$ is the relative differences between the DRs of suspected source and spill samples; DR_{SO} is the diagnostic ratio for suspected source sample; DR_{SP} is the diagnostic ratio for spill sample; $\overline{DR}_{SO\text{-}SP}$ is the average between the DRs of suspected source and spill samples.

By visual comparison of GC/FID chromatograms (Level 1), spill samples clearly different from the source sample could be excluded of further analysis (Level 2). The differences occurred as a result of weathering were recognized by overlapping chromatograms. For samples not identified as clearly different, the peaks of *n*-alkanes and isoprenoids were integrated and the respective normalized abundances (Eqs. 25.4 and 25.5) and DRs were calculated (Eq. 25.6) and compared (Eq. 25.7).

GC/MS analysis was used for detailing the composition of the samples (Level 2). The steps were the same described for GC/FID analysis, but now a larger number of compound groups was investigated and compared between samples.

The joint evaluation of the information obtained from the DRs, PW plots, and visual comparison of chromatograms provided a detailed knowledge of the differences and similarities between the source and the spill samples. The possible conclusion were positive match, probable match, nonmatch, and inconclusive as stated in CEN Methodology (2012).

25.2.4.2 Chemometrics

25.2.4.2.1 Data

The data set consisted of retention time windows of 55 SICs per sample (cf. Table 25.2), including the deuterated standards.

A total of 127 samples were analyzed and split into a "training set" of 66 sample extracts and four "validation sets." The training set included samples collected from the study area (cf. Fig. 25.2) and samples of Cusiana oil. The four validation sets were: eight sampling duplicates ("Duplicates" in PCA plots), four dilutions of a concentrated sample ("Dilutions" in PCA plots), 19 replicate analyses of the reference sample extract ("References" in PCA plots), and 30 analytical replicates (6 injections of 5 selected sample extracts, "Replicates" in PCA plots).

25.2.4.2.2 Data Processing and Analysis

The data consisting of 55 GC/MS-SIM chromatograms for each sample were exported to the AIA file format using the commercial software ChemStation (Agilent technologies). NetCDF was used to retrieve relevant data (e.g., signal intensities, sample names, sample descriptions) in the MATLAB 7.10.0 (R2010a) programing

environment, in which the data were preprocessed and analyzed. The algorithms for import of CDF-files, correlation-optimized warping (COW) and PCA were downloaded from http://www.models.life.ku.dk.

The chromatograms comprising between 344 and 8710 data points were reduced before data processing, by visual inspection, eliminating parts with no relevant information. The parts removed included sections of the chromatogram with low signal-to-noise ratio (S/N) and sections where target compounds were not expected. The CHEMSIC procedure described by Christensen et al. (2005b, 2010) and Christensen and Tomasi (2007) was utilized in this work aiming at taking away variation that is unrelated to the chemical composition. The preprocessing consisted of baseline removal, retention time alignment, and data normalization.

The baseline was removed by calculating the first derivatives of the chromatographic data (point-by-point subtraction). The retention time alignment was performed in two steps: (1) applying rigid shifts (i.e., without compression or expansion) on the chromatograms, and (2) employing the COW algorithm (Nielsen et al., 1998; Tomasi et al., 2004). The COW algorithm aligns a sample chromatogram toward a target chromatogram by stretching or compressing sample segments along the retention time axis using linear interpolation. The optimal warping parameters (i.e., the length of the segments, in which the signals are divided, and "slack parameter," how much it is allowed to change) were determined by the use of a grid search in the parameter space followed by a discrete simplex-search on maximum values for the "warping effect" function (Skov et al., 2006).

The SICs for each m/z were always aligned separately to the SICs of a target sample. The target for the alignment was selected from the reference samples, using the one with the highest sum of correlation coefficients with the others. The reference samples were chosen in this study as they were prepared to be an average sample containing most peaks.

Although baseline removal and retention time alignment are essential steps to prepare the data, the methods involved are not important for the further interpretation of the model. However, data normalization affects the interpretation of the results and can focus the subsequent data analysis on different aspects (viz., compound concentrations, differences between groups of compounds (SICs), or differences in relative concentrations within SICs) (Gallotta and Christensen, 2012).

In this study, we therefore applied three normalization schemes that focus on these three types of variation in data.

In **Scheme I**, we normalize each SIC to an internal standard. The deuterium-labeled internal standard with most similar physicochemical properties was selected for each SIC (e.g., d10-phenanthrene for C1 and C2-phenanthrenes). Here, variations related to sample preparation and instrumental analyses are reduced, but all other chemically relevant information is retained. This normalization scheme will typically focus the analysis on variations in total hydrocarbon concentrations, followed by variations between and within groups of compounds (SICs) as the former will typically be the most pronounced variation found by PCA of semiquantitative data (Christensen and Tomasi, 2007).

In **Scheme II**, one more layer of chemical information (i.e., total hydrocarbon concentrations) is removed. This is done by combining SICs and then normalizing to constant Euclidean norm (i.e., corresponds to normalization to the sum, if data were consisting of only positive values) (Christensen et al., 2010). This normalization scheme focuses the analysis on variations between SICs followed by variations within SICs, what can provide an assessment both on the weathering (physical or biological) degree as the source of hydrocarbons present in the samples.

Finally, in **Scheme III**, data are normalized to constant Euclidean norm within each SIC and then SICs are combined. Thus, the PCA will focus solely on chemical variations within each SIC such as differences in isomer PAH patterns and biomarker fingerprints. After the removal of a large part of the variation in the data set, characteristics related to differences between compounds in the same m/z stand out, e.g., hydrocarbon sources.

The preprocessed signals for all the samples were stacked in a $I \times J$ matrix $\mathbf{X}$, where I denotes the number of samples and J the length of the signals and modeled by PCA. The PC model was calculated on the column-wise centered training set and the validation sets (viz., samples that are not present in the training set) were projected on it after centering to the mean of the training set. The model was further validated by visual inspection of the loadings and chemical interpretation of the scores and loadings.

25.3 RESULTS AND DISCUSSION

25.3.1 Assessment of Sediment from Iguaçu and Barigüi Rivers Through Quantitative DRs Calculated from the Compounds Concentrations

Comparisons between sets of PAH DRs were used for source identification of hydrocarbons in sediments of rivers and Iguaçu and Barigüi, including both parent and alkylated PAH DRs. The results for

TABLE 25.4 PAH Diagnostic Ratios Calculated from the Compounds Concentrations in Sediments of Iguaçu and Barigüi Rivers for All Campaigns

	August 2000										
	Barigüi River			Iguaçu River							
Diagnostic ratio	**M Bar**	**Bar P1**	**Bar P2**	**M Igu**	**Igu P3**	**Guaj**	**Gal L**	**Bal N**	**P Ama**	**SMS**	**U Vit**
Ph/An	30	4.5	NC	NC	4.4	NC	NC	NC	NC	NC	NC
An/(An + Ph)	0.03	0.18	0.00	0.00	0.19	0.00	0.00	0.00	NC	0.00	0.00
BaA/Ch	0.57	1.05	NC	NC	NC	0.72	0.64	0.64	NC	NC	NC
BaA/(BaA + Ch)	0.36	0.51	NC	NC	NC	0.42	0.39	0.39	NC	1.00	NC
IPy/(IPy + Bghi)	0.47	NC	NC	NC	NC	NC	0.00	NC	NC	NC	NC
∑C1-Ph/Ph	1.08	7.15	3.93	3.75	4.77	5.58	7.54	6.58	NC	2.84	2.33
(Ph + An)/(Ph + An + C1-Ph + An)	0.49	0.15	0.20	0.21	0.20	0.15	0.12	0.13	0.00	0.26	0.30
∑(other 3–6 ring PAH)/∑(5 series of alkylated PAH)	1.23	0.26	0.09	0.03	0.12	0.13	0.15	0.19	0.00	0.23	0.02
Preliminary classification	M Bar	Bar P1	Bar P2	M Igu	Igu P3	Guaj	Gal L	Bal N	P Ama	SMS	U Vit
	July 2001										
	Barigüi River			Iguaçu River							
Diagnostic ratio	M Bar	Bar P1	Bar P2	M Igu	Igu P3	Guaj	Gal L	Bal N	P Ama	SMS	U Vit
Ph/An	NC	15	NC	NC	NC	18	NC	NC	NC	NC	NC
An/(An + Ph)	0.00	0.06	0.00	0.00	0.00	0.05	0.00	0.00	0.00	0.00	0.00
BaA/Ch	1.09	1.47	NC	0.76	NC	0.74	0.63	0.73	NC	0.00	0.00
BaA/(BaA + Ch)	0.52	0.59	NC	0.43	NC	0.42	0.39	0.42	NC	0.00	0.00
IPy/(IPy + Bghi)	0.00	0.00	NC	0.00	NC	0.35	0.38	0.00	NC	NC	0.28
∑C1-Ph/Ph	1.66	2.21	2.60	3.02	2.58	4.39	3.01	1.97	0.78	3.26	0.23
(Ph + An)/(Ph + An + C1-Ph + An)	0.38	0.33	0.28	0.25	0.28	0.19	0.25	0.34	0.56	0.23	0.82
∑(other 3–6 ring PAH)/∑(5 series of alkylated PAH)	0.19	0.22	0.10	0.09	0.08	0.14	0.16	0.07	0.49	0.04	0.22
Preliminary classification	M Bar	Bar P1	Bar P2	M Igu	Igu P3	Guaj	Gal L	Bal N	P Ama	SMS	U Vit
	January 2007										
	Barigüi River			Iguaçu River							
Diagnostic ratio	M Bar	Bar P1	Bar P2	M Igu	Igu P3	Guaj	Gal L	Bal N	P Ama	SMS	U Vit
Ph/An	NC	NC	NC	NC	NC	NC	NC	NC	NC	NC	NC
An/(An + Ph)	NC	NC	NC	NC	NC	NC	NC	NC	NC	NC	NC
BaA/Ch	NC	NC	NC	NC	NC	NC	NC	NC	NC	NC	NC
BaA/(BaA + Ch)	NC	NC	NC	NC	NC	NC	NC	NC	NC	NC	NC
IPy/(IPy + Bghi)	NC	NC	NC	NC	NC	NC	NC	NC	NC	NC	NC
∑C1-Ph/Ph	NC	NC	NC	2.33	2.18	NC	NC	NC	NC	NC	NC
(Ph + An)/(Ph + An + C1-Ph + An)	NC	NC	NC	NC	NC	NC	NC	NC	NC	NC	NC
∑(other 3–6 ring PAH)/∑(5 series of alkylated PAH)	0.00	NC	NC	0.30	0.41	0.00	0.56	0.00	NC	NC	NC

(*Continued*)

2000, 2001, 2007, and 2008 campaigns are shown in Table 25.4. In cases where the compound or group of compounds presented concentration below the limit of detection, its concentration was considered equal to zero.

TABLE 25.4 (*Continued*)

	July 2007										
	Barigüi River			Iguaçu River							
Diagnostic ratio	M Bar	Bar P1	Bar P2	M Igu	Igu P3	Guaj	Gal L	Bal N	P Ama	SMS	U Vit
Ph/An	NC	NC	NC	NC	NC	NC	NC	NC	NC	NC	NC
An/(An + Ph)	NC	NC	NC	NC	NC	NC	NC	NC	NC	NC	NC
BaA/Ch	NC	NC	NC	NC	NC	NC	NC	NC	NC	NC	NC
BaA/(BaA + Ch)	NC	NC	NC	NC	NC	NC	NC	NC	NC	NC	NC
IPy/(IPy + Bghi)	NC	NC	0.18	NC	NC	NC	NC	NC	NC	NC	NC
∑C1-Ph/Ph	NC	NC	NC	NC	NC	3.42	NC	1.18	NC	NC	NC
(Ph + An)/(Ph + An + C1-Ph + An)	NC	NC	NC	NC	NC	NC	NC	NC	NC	NC	NC
∑(other 3–6 ring PAH)/∑(5 series of alkylated PAH)	NC	NC	NC	0.18	1.05	0.50	0.34	0.68	NC	NC	NC

	January 2008										
	Barigüi River			Iguaçu River							
Diagnostic ratio	M Bar	Bar P1	Bar P2	M Igu	Igu P3	Guaj	Gal L	Bal N	P Ama	SMS	U Vit
Ph/An	NC	NC	NC	NC	NC	NC	NC	NC	NC	NC	NC
An/(An + Ph)	NC	NC	NC	NC	NC	NC	NC	NC	NC	NC	NC
BaA/Ch	NC	NC	NC	NC	NC	NC	NC	NC	NC	NC	NC
BaA/(BaA + Ch)	NC	NC	NC	NC	NC	NC	NC	NC	NC	NC	NC
IPy/(IPy + Bghi)	NC	NC	NC	NC	NC	NC	NC	NC	NC	NC	NC
∑C1-Ph/Ph	NC	NC	NC	NC	NC	NC	NC	NC	NC	NC	NC
(Ph + An)/(Ph + An + C1-Ph + An)	NC	NC	NC	NC	NC	NC	NC	NC	NC	NC	NC
∑(other 3–6 ring PAH)/∑(5 series of alkylated PAH)	0.00	0.00	0.00	0.00	NC	0.28	0.00	0.00	NC	NC	NC

NC, noncalculated, as one or more compounds involved in the calculation of the DR were in concentrations below the limit of quantification. Values highlighted in gray scale stands for: dark gray (petrogenic), medium gray (pyrogenic), and light gray (indeterminate).

In 2000 and 2001 campaigns, it has been possible to calculate a fair amount of DRs, which resulted in a preliminary classification of sediment sources (Table 25.4). As expected, this preliminary classification suggested that, in most stations, the main source is petrogenic.

In the 2007 and 2008 campaigns, it was not possible to calculate most of the DRs, which impeded the source identification of the few PAHs present in sediment samples through this technique. Thus, the preliminary classification of sediments was not performed, since the results do not offer sufficiently robust conclusions. The results of more recent samples (2009–2010) were studied in the following sections, through the techniques of DRs calculated from heights and areas of chromatograms and chemometric analysis. In these last samples, no data on concentrations were available.

It is worth noting that the DRs involving the pairs pyrene and fluoranthene and benzo(*ghi*)perylene and indene(1,2,3-cd)pyrene, which theoretically has greater potential as indicator sources (i.e., petrogenic vs pyrogenic) had limited application in this study. The Fl/Py and Fl/(Fl + Py) DRs failed to classify the spilled oil (Cusiana) as having petrogenic origin, while the IPy/(IPy + Bghi) could not be calculated in several stations, because these compounds were in concentrations below the limit of quantification.

The results for Iguaçu and Barigüi river sediments of 2000 and 2001 campaigns were interpreted through PAH cross plots, two DRs in each plot, enabling a more integrated conclusion on the sources (Budizinski et al., 1997; Yunker et al., 2002).

The DRs investigated in PAH cross plots were those whose values have been calculated for most stations. Thus, the DRs selected were An/(An + Ph); ∑C1-Ph/Ph, (Ph + An)/(Ph + An + C1-Ph + An), and ∑(other 3–6 ring PAH)/∑(5 series of alkylated PAH), the latter known as pyrogenic index. Each DR including phenanthrenes/anthracenes was plotted against the pyrogenic index to prevent the results that were biased only by phenanthrenes/anthracenes (Figs. 25.3, 25.4, and 25.5).

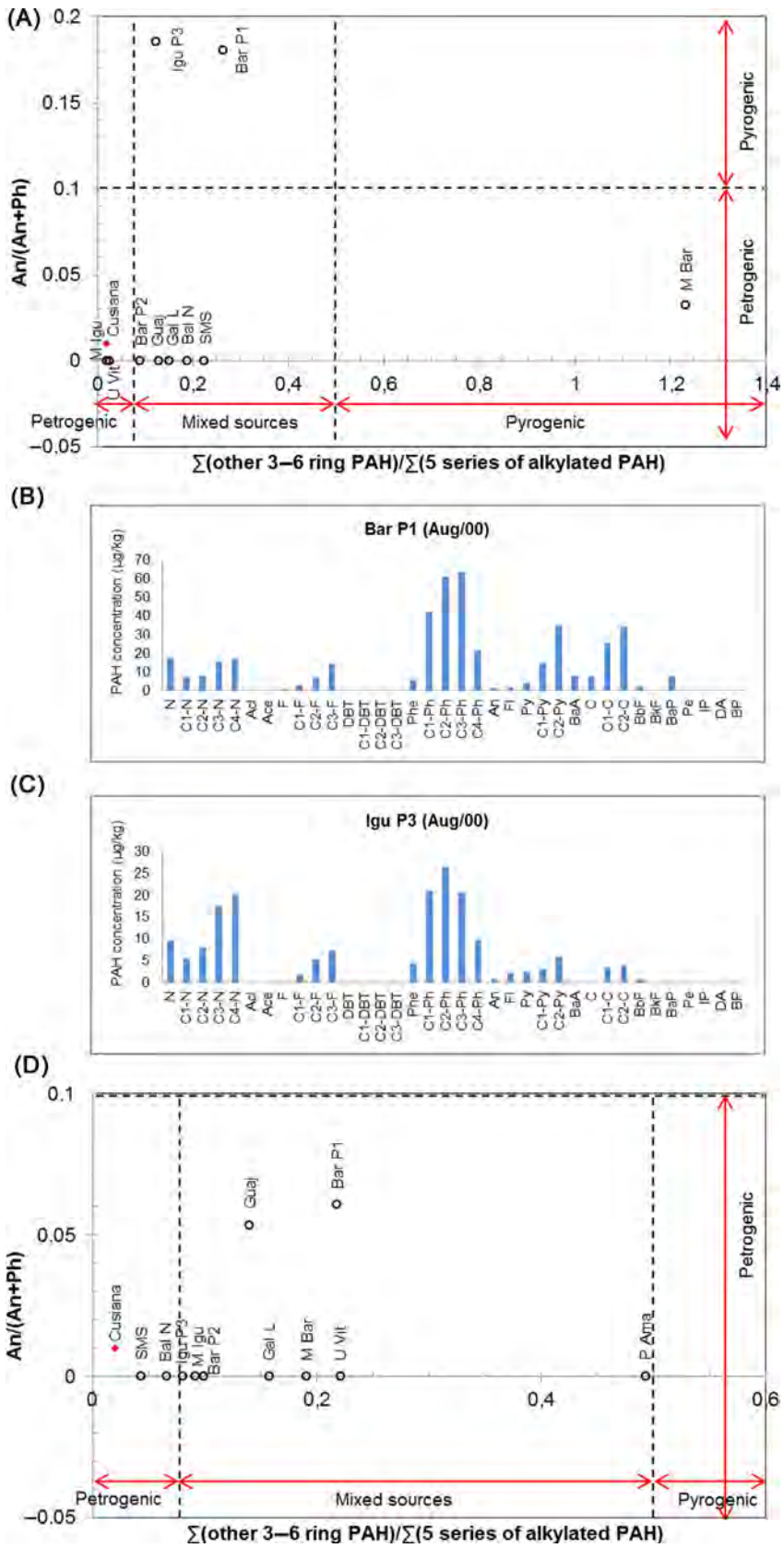

FIGURE 25.3 PAH cross plots for the DRs An/(An + Ph) versus ∑(other 3–6 ring PAH)/∑(5 series of alkylated PAHs) for Cusiana oil and Iguaçu and Barigüi river sediments in (A) 2000 and (D) 2001 campaigns. Petrogenic PAH distributions at (B) Bar P1 and (C) Igu P3 stations in 2000 campaign.

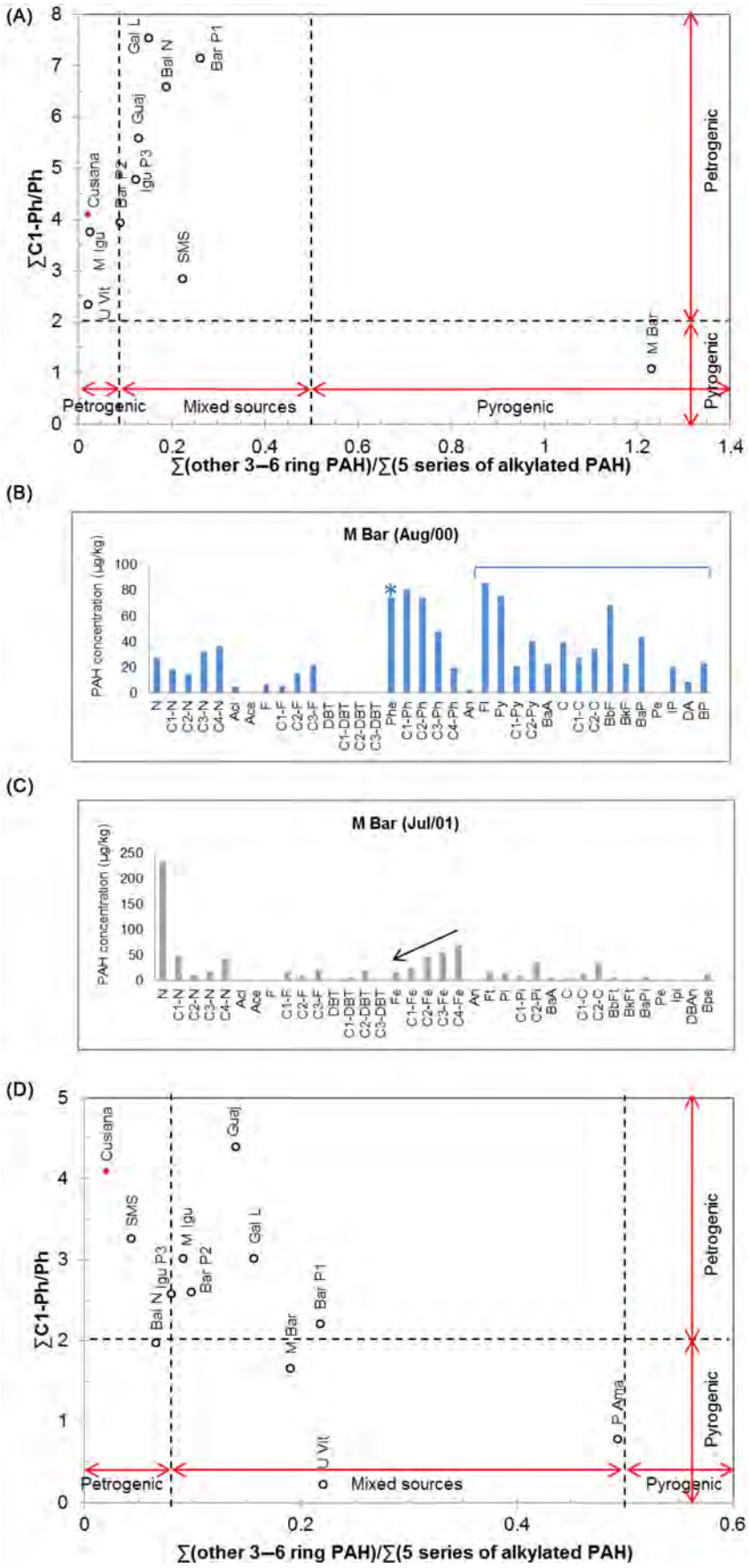

FIGURE 25.4 PAH cross plots for the DRs ∑C1-Ph/Ph versus ∑(other 3−6 ring PAH)/∑(5 series of alkylated PAHs) for Cusiana oil and Iguaçu and Barigüi river sediments in (A) 2000 and (D) 2001 campaigns; (B) presence of phenanthrene and of high molecular weight PAH at M Bar in 2000 campaign; (C) effects of weathering in phenanthrene alkylated series at M Bar in 2001 campaign.

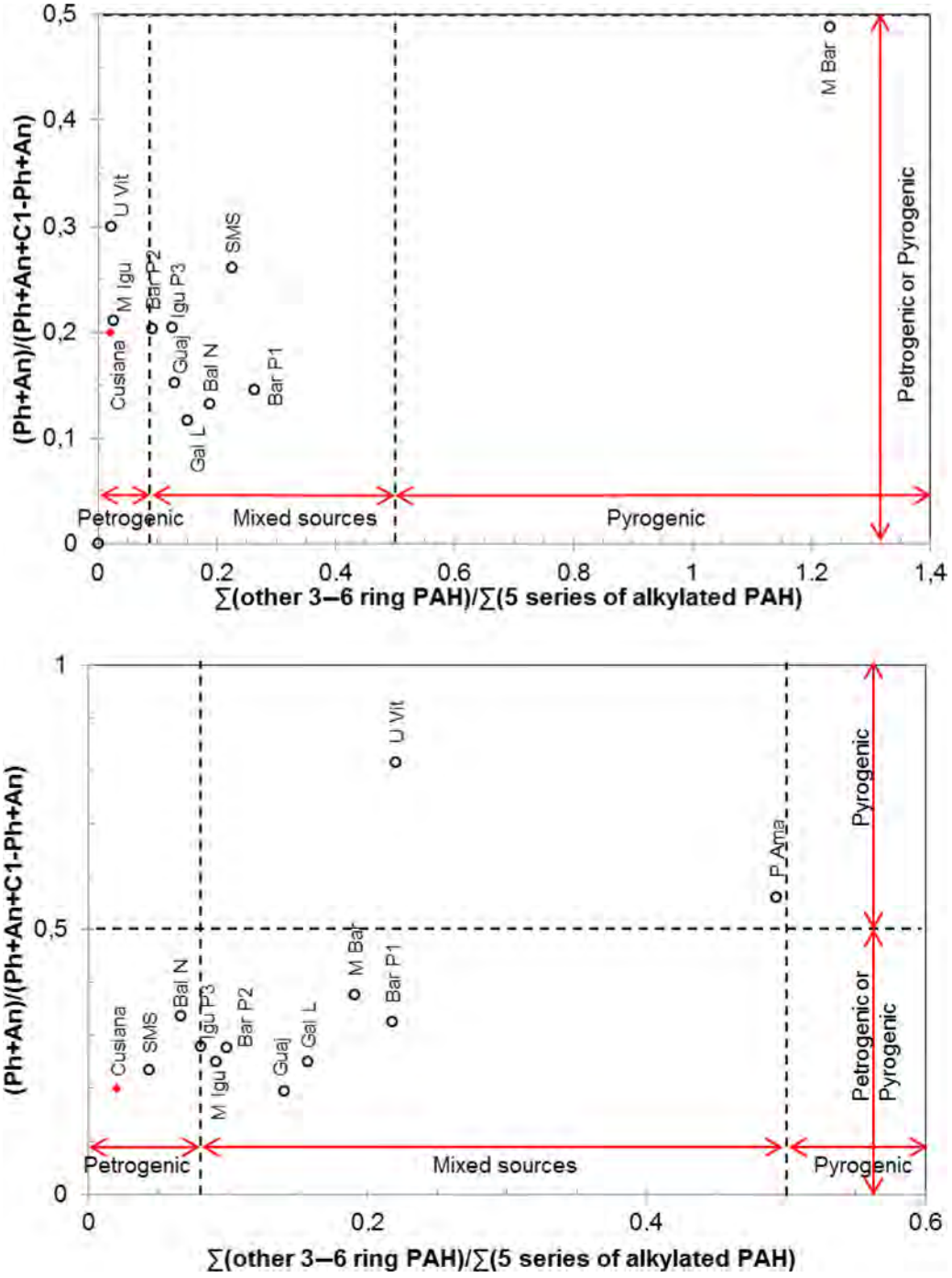

FIGURE 25.5 PAH cross plots for the DRs (Ph + An)/(Ph + An + C1-Ph + An) versus ∑(other 3–6 ring PAH)/∑(5 series of alkylated PAHs) for Cusiana oil and Iguaçu and Barigüi river sediments in (A) 2000 and (B) 2001 campaigns.

Fig. 25.3A and D shows the cross plots of An/(An + Ph) versus ∑(other 3–6 ring PAH)/∑(5 series of alkylated PAH). In the 2000 campaign (Fig. 25.3A), the An/(An + Ph) DR brought some assortment to the pyrogenic index in the range of values of 0.08–0.5, the PAHs in the sediment samples of the stations Bar P1 and P3 Igu were classified as pyrogenic source (An/(An + Ph) larger than 0.1). However, this classification does not match to the PAH petrogenic distribution pattern in these sediments (Fig. 25.3B and C). In 2001 (Fig. 25.3D), all samples were classified as petrogenic (An/(An + Ph) less than 0.1).

The second set of PAH cross plots (Fig. 25.4A and D) includes ∑C1-Ph/Ph versus ∑(other 3–6 ring PAH)/∑(5 series of alkylated PAH). In the 2000 campaign (Fig. 25.4A), all stations situated in pyrogenic index mixed sources range were classified as petrogenic by ∑C1-Ph/Ph DR (∑C1-Ph/Ph larger than 2). A single station (M Bar) was classified as having pyrogenic source for both ratios. This result can be explained by the considerable presence of phenanthrene and of high molecular weight PAHs (Fig. 25.4B). In 2001 (Fig. 25.4D), three stations classified as having mixed sources considering the pyrogenic index (M Bar, P Ama, and U Vit) were classified as pyrogenic by the ∑C1-Ph/Ph DR (∑C1-Ph/Ph less than 2). In the histogram of M Bar, the effect of weathering in phenanthrene-alkylated series explains this result of ∑C1-Ph/Ph DR (Fig. 25.4C). In P Ama and U Vit, the phenanthrene concentrations are low and therefore ∑C1-Ph/Ph DR is less robust.

The (Ph + An)/(Ph + An + C1-Ph + An) DR was studied at the last set of PAH cross plots (Fig. 25.5), plotted against ∑(other 3–6 ring PAH)/∑(5 series of alkylated PAH). In the 2000 campaign, the use of this DRs did not add information for source identification, because all the samples were in the range where the source can be both petrogenic or pyrogenic ((Ph + An)/(Ph + An + C1-Ph + An) less than 0.5). In 2001, the same two stations with low concentrations were classified as pyrogenic (P Ama and U Vit), with (Ph + An)/(Ph + An + C1-Ph + An) DR larger than 0.5.

In this particular case study, the cross diagrams added little relevant information for PAH source identification in the sediment samples of the Iguaçu and Barigüi rivers. Though more labor-intensive and dependent on the technical expertise, the observation of PAH distribution patterns (histograms) provides information on the sources and on the significance of these results, considering the concentration levels of PAHs in sediments.

There are several reasons which can explain why the DRs have been unable to point out clearly the PAH sources in this study. First, it has not been possible to use all the DRs, due to the primary failure to classify the Cusiana oil [Fl/Py and Fl/(Fl + Py)] or the absence of compounds necessary for calculation in sediments of most stations [BaA/Ch, BaA(BaA + Ch), and IPy/(IPy + Bghi)]. Among these, the Fl/(Fl + Pi) DR had been suggested by Meniconi (2007) as having a great potential to distinguish sources in tropical environments.

Considering the DRs that could be tested, some points are noteworthy. In the DRs involving anthracene [An/(An + Ph) and (Ph + An)/(Ph + An + C1-Ph + An)], the robustness of the findings may have been influenced by anthracene concentration, which was below the limit of quantification in most samples (Wagener et al., 2010). In this context, the (∑C1-Ph/Ph) and [∑(other 3–6 ring PAH)/∑(5 series of alkylated PAH)] DR would be the most appropriate, as they include compounds with concentrations above the limit of quantification in most samples.

On the other hand, the pyrogenic index includes PAH-alkylated series more susceptible to weathering (e.g., naphthalenes, fluorenes) in the denominator, which are abundant in petrogenic sources (and important in a light crude oil such as Cusiana), what can lead to inconclusive results (Wagener et al., 2010). In this study, naphthalene-alkylated series have already exhibited evidences of weathering in 2000 sediments for most stations in many of the PAH histograms (figures not shown).

Although the use of DRs for source identification of hydrocarbons is widely spread in literature, its applicability and accuracy cannot be overestimated. One of the premises of this approach is to consider that each DR has a specific range depending on the source. It turns out that the DRs are affected by processes of weathering, which can modify the values obtained in environmental samples (Massone et al., 2013; Wagener et al., 2010). Therefore, the inattentive use of DRs in environments subjected to multiple hydrocarbon sources can be of little efficiency. In these situations, the rigorous verification of the chromatograms of saturated and aromatic fractions and histograms including alkylated PAHs and the joint assessment of the largest number of possible DRs are recommended.

25.3.2 Assessment of Soil Samples Inside Refinery Area through Semiquantitative DRs Calculated from Heights and Areas of Chromatograms

After nearly a decade after the spill occurrence, the task to demonstrate that two samples have the same origin, i.e., that the compounds found in an environmental sample preserve clear relationship with the spilled oil sample is extremely complex. In addition to the influences of the various chronic anthropogenic contributions added to the environment; the spilled oil is subject to weathering processes which require explanation. Another point is that this technique for source identification is quite laborious as it requires the integration of a large number of compounds or groups of compounds, and it is impracticable its application to all samples collected along a

decade. Then, three samples of the internal area of the refinery were selected, where it is expected that the main contribution is the weathered spilled oil.

After GC/FID analysis, chromatograms of all samples collected between 2009 and 2010 have been evaluated and the most representative samples chosen, aiming at the selection of environmental samples with presence of oil in different weathering degrees. Then, the procedure for source identification through semiquantitative DRs calculated from heights and areas of chromatograms was performed (CEN, 2012).

25.3.2.1 GC/FID Analysis (Level 1)

Chromatograms of the selected samples are shown in Fig. 25.6, where an interfering peak (between 16 and 17 min), from the solid-phase extraction cartridge used in the removal of polar components, is noteworthy. The chromatogram from one of analytical blanks illustrates the presence of this compound (butylated hydroxytoluene) (Fig. 25.6E).

As expected, the chromatograms indicate a petrogenic origin for all samples (Fig. 25.6A–D), evidenced by the presence of *n*-alkanes, without preference of odd carbon-numbered alkanes to even carbon-numbered alkanes and/or presence of UCMs. The source sample (Fig. 25.6A, Cusiana crude oil) contains a wide boiling point range of *n*-alkanes, being constituted mostly by saturated compounds. The soil samples have different weathering degrees, in ascending order: PM-02 (less weathered, Fig. 25.6B), BH-03 (0.1 m) (Fig. 25.6C), and BH-04 (0.1 m) (most weathered, Fig. 25.6D). It is still possible to observe the presence of *n*-alkanes in PM-02 and BH-03 (0.1 m). In the course of weathering, the *n*-alkanes are among the first compounds to be biodegraded (Wang and Stout, 2007).

The weathering was further investigated after the integration of *n*-alkanes, pristine, and phytane peaks of the GC/FID chromatograms, plotting the results of spill and source samples in PW plots. In these charts, the *n*-alkanes, pristine, and phytane present in the spill sample were normalized by nonweathered compounds (average of *n*-C26 to *n*-C29), following Eqs. (25.4 and 25.5). Fig. 25.7 presents the PW plot of spill sample PM-02, with reference to the Cusiana oil sample, showing the evaporation process which affected the compounds up to *n*-C17 (CEN, 2012). The PW plot of spill sample BH-03 (0.1 m) confirms the significant biodegradation when compared to the Cusiana oil, evidenced by the noticeable presence of pristane and phytane in relation to less resistant *n*-C17 and *n*-C18 (Fig. 25.8). It was not possible to plot the PW plot for sample BH-04 (0.1 m), due to the absence of *n*-alkanes in this sample.

The *n*-C17/pristane, *n*-C18/phytane and pristane/phytane DRs are listed in Table 25.5. These DRs were calculated based on peak areas in GC/FID chromatograms.

There are significant differences between the *n*-C17/pristane and *n*-C18/phytane DRs of the Cusiana oil (source) and environmental "spill" samples. These differences have confirmed the occurrence of biodegradation, a process where *n*-alkanes, *n*-C17, and *n*-C18 are preferentially degraded when compared to pristane and phytane (Peters et al., 2007). The absence of *n*-C17 and *n*-C18 in BH-04 (0.1 m) corroborates that the biodegradation process was relatively more severe.

With respect to the pristane/phytane DR, no significant difference was observed between the values for the Cusiana oil and environmental "spill" samples, showing that evaporation was not the dominant weathering process for compounds with boiling point beyond *n*-C17, because pristane (more volatile) was removed in a rate similar to phytane (less volatile).

The GC/FID chromatograms, the DRs, and the PW plots led to the preliminary conclusion that Cusiana oil sample can be the source of the hydrocarbons present in environmental "spill" samples PM-02, BH-03 (0.1 m), and BH-04 (0.1 m), considering weathering processes.

25.3.2.2 GC/MS Analysis (Level 2)

The SICs of all compound groups analyzed were inspected looking for obvious differences, which were not observed. The SICs of *m*/*z* 191 did not show major differences (Fig. 25.9A–D), with the exception of the relative ratio of 17α(*H*),21β(*H*)-30-norhopane (29ab) and 17α(*H*),21β(*H*)-hopane (30ab) which are slightly different between the spill samples, but with the 30ab peak always higher than the 29ab peak. At this point, a "pure" river sediment background sample (Fig. 25.9E) was also included for comparison, in which the 29ab peak is higher than 30ab peak. These biomarkers background contribution is not insignificant and most likely affected SICs of *m*/*z* 191 fingerprints in spill samples.

Weathering assessment was performed after the integration of PAH and biomarkers peaks of GC/MS SICs, by plotting the results of the spill and source samples in PW plots. PAH and biomarkers were normalized by 17α

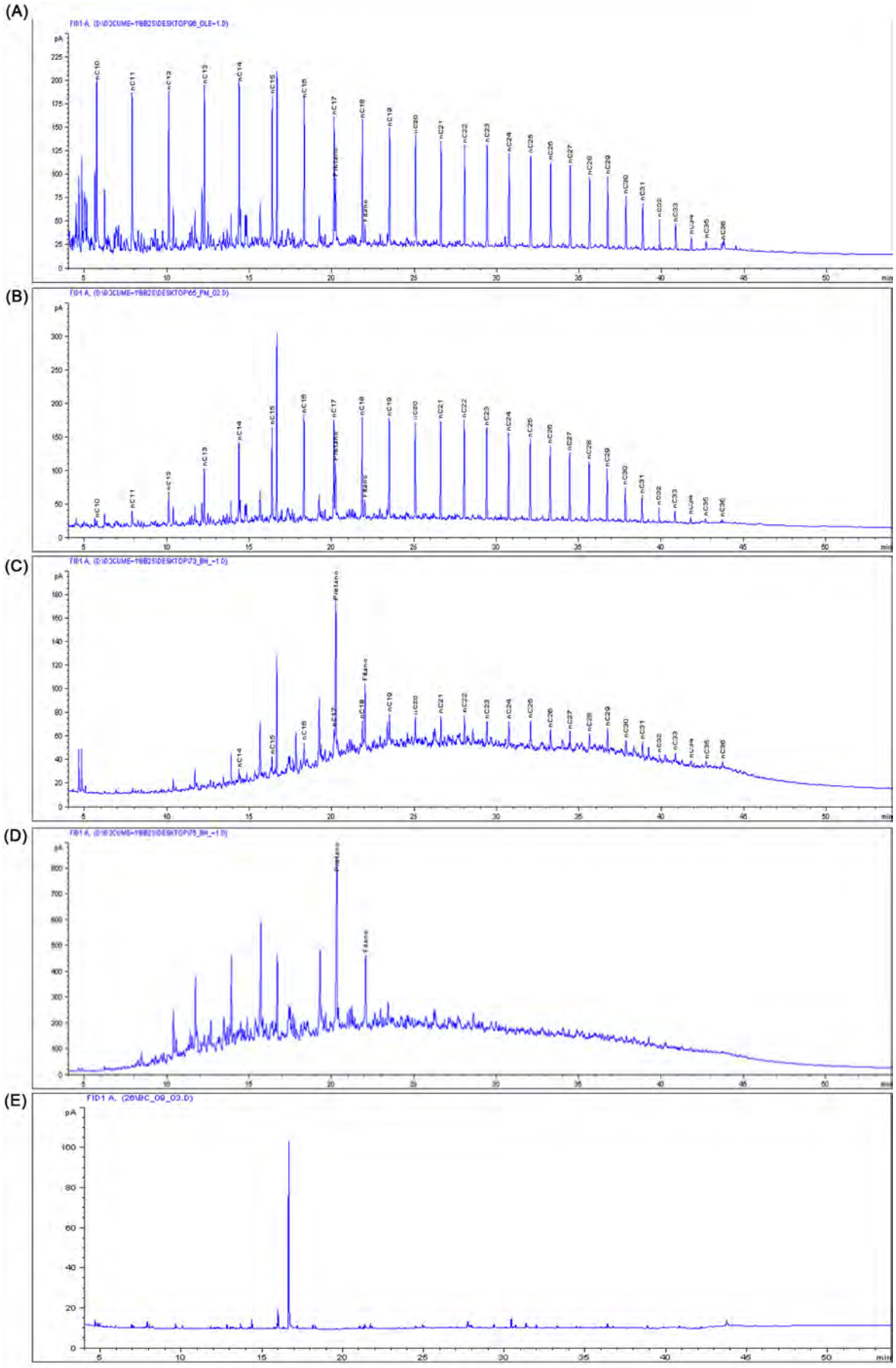

FIGURE 25.6 GC/FID chromatograms of the samples: (A) Cusiana crude oil; (B) PM-02; (C) BH-03 (0.1 m); (D) BH-04 (0.1 m); and (E) analytical blank.

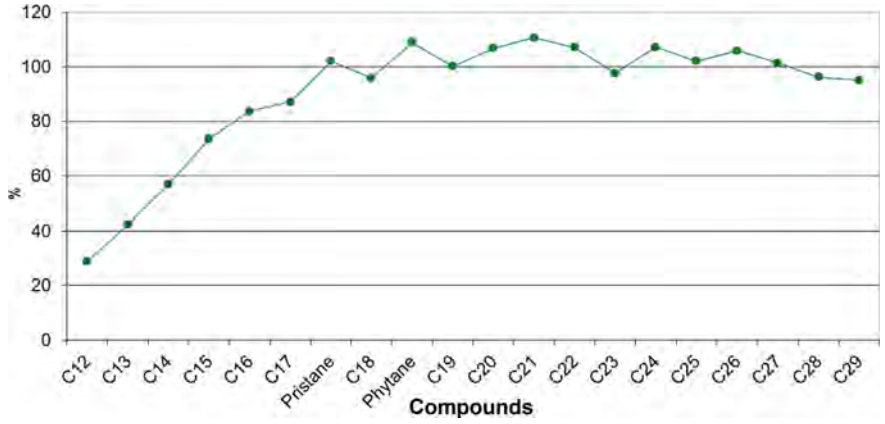

FIGURE 25.7 PW-GC/FID-plot of PM-02 sample versus Cusiana crude oil (normalized to the mean abundances of *n*-C26 to *n*-C29).

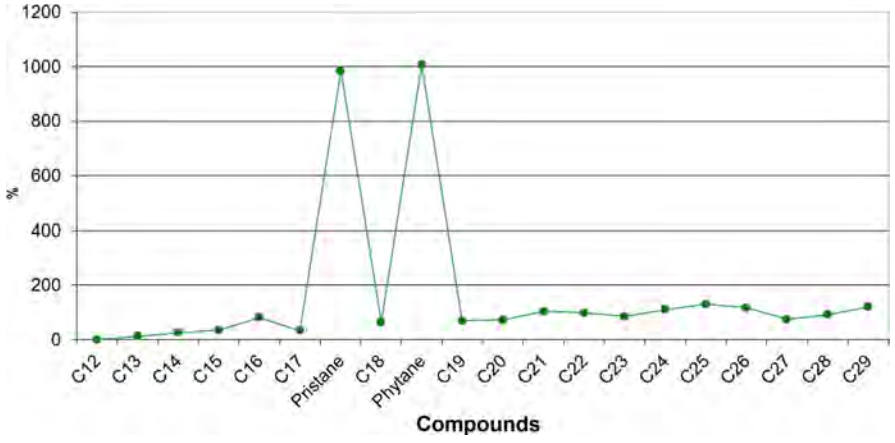

FIGURE 25.8 PW-GC-FID-plot of BH-03 (0.1 m) sample versus Cusiana crude oil (normalized to the mean abundances of *n*-C26 to *n*-C29).

TABLE 25.5 GC/FID Semiquantitative DRs

	***n*-C17/pristane**	***n*-C18/phytane**	**Pristane/phytane**
Cusiana crude oil	1,795	4,716	2,498
PM-02	1,533	4,149	2,340
Mean	1,664	4,432	2,419
Relative difference (%)	16	13	7
Cusiana crude oil	1,795	4,716	2,498
BH-03 (0.1 m)	0,060	0,294	2,442
Mean	0,927	2,505	2,470
Relative difference (%)	187	176	2
Cusiana crude oil	1,795	4,716	2,498
BH-04 (0.1 m)	0,000	0,000	2,422
Mean	0,897	2,358	2,460
Relative difference (%)	200	200	3

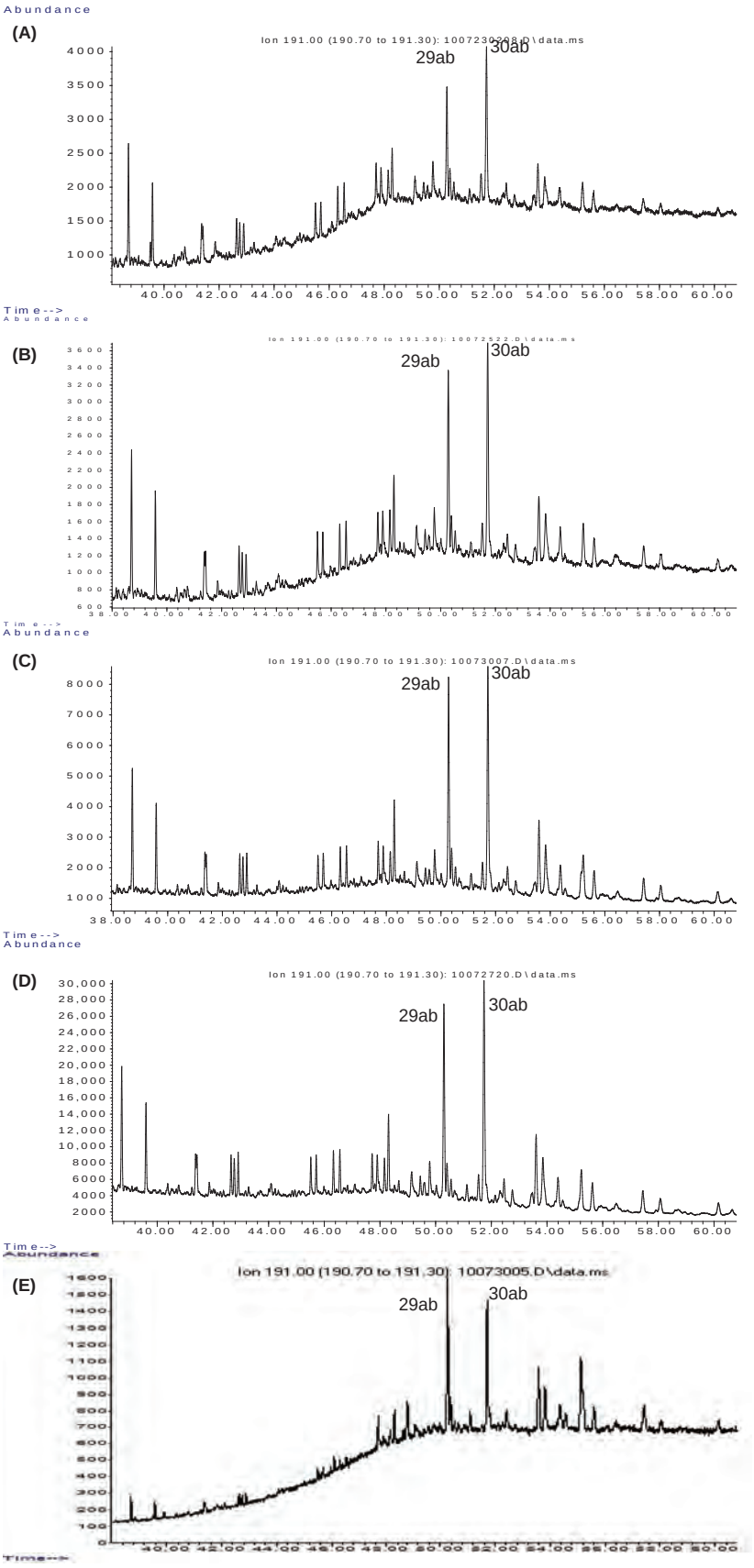

FIGURE 25.9 GC/MS mass chromatograms of m/z 191 for: (A) Cusiana oil; (B) PM-02; (C) BH-03 (0.1 m); (D) BH-04 (0.1 m); and (E) river sediment background samples.

(*H*),21β(*H*)-hopane (Figs. 25.10, 25.12, and 25.14), with Cusiana oil used as reference. Table 25.6 describes in detail the results of the PW plots, with the identification of compounds, their respective retention times, and percentages in relation to the source sample.

The DRs were calculated for all samples, based on peaks heights (or areas in the case of homologous groups) of mass chromatograms, and then compared to the DRs of the Cusiana oil. Figs. 25.11, 25.13, and 25.15 show the relative differences in bar charts. The limit of 14% is drawn by a vertical line in the middle of the graph. Some DRs were excluded from the comparison, when peaks involved in their calculations presented S/N ratio less than 3 (i.e., retene and 28ab).

25.3.2.2.1 Spill Sample PM-02 and Cusiana Oil

The PW plot of PM-02 versus Cusiana oil (normalized by 17α(*H*),21β(*H*)-hopane) (Fig. 25.10A) shows that the weathering reduced the abundance of PAH and biomarkers that elute first in the chromatographic run. This behavior is common and expected for a PW plot, as evaporation is one of the most important weathering processes, especially for the compounds with lower boiling points, which also have the lowest retention times. The compounds which elute after 44 minutes were not weathered and remain present in abundances around 100%, varying between 87% and 112%, which do not represent significant differences compared to the source, considering the variability of the method. Among the unweathered compounds are the majority of biomarkers, what gives evidence of the relationship between sample PM-02 and Cusiana oil.

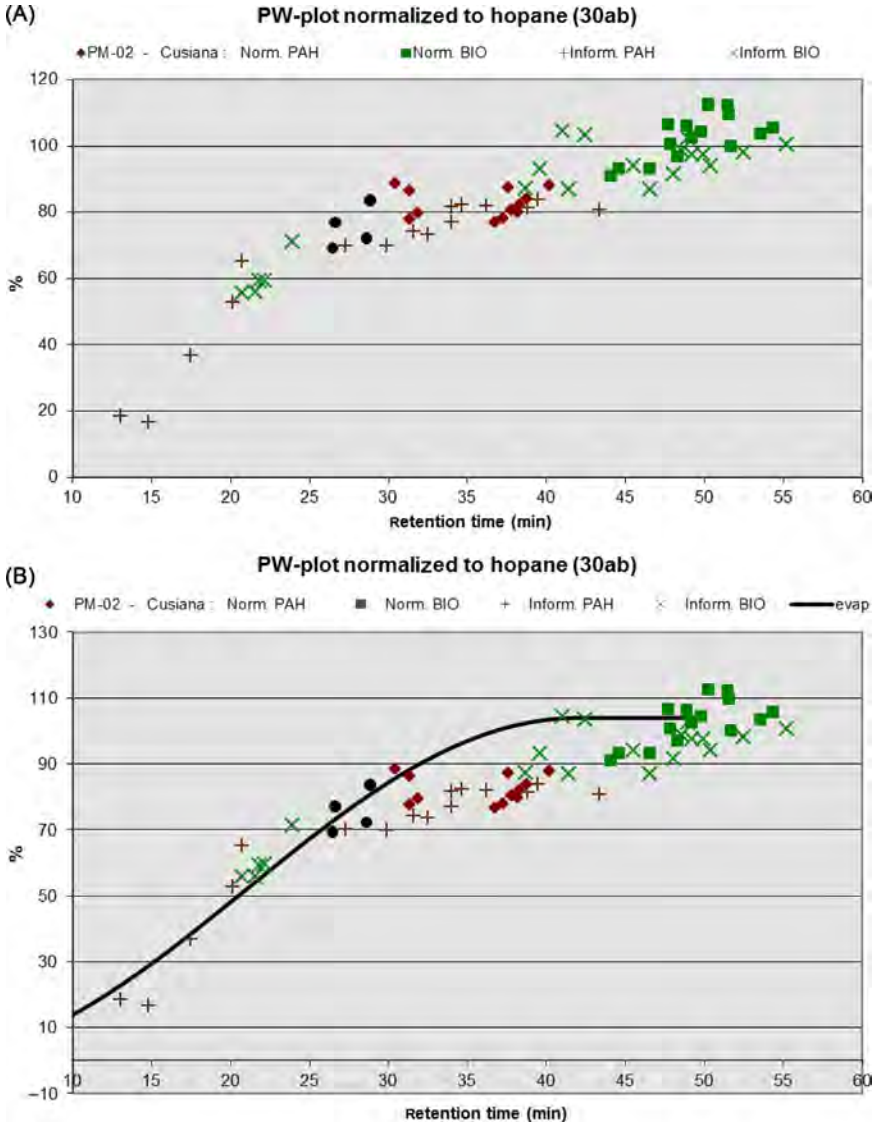

FIGURE 25.10 PW plot of PM-02 versus Cusiana oil (normalized by 17α(*H*),21β(*H*)-hopane).

TABLE 25.6 Results of the PW Plots, with the Identification of Compounds, their Respective Retention Times and Percentages in Relation to the Source Sample

Compounds	Retention time (min)	% PW PM-02	% PW BH-03 (0.1 m)	% PW BH-04 (0.1 m)
C1-decalins	13.055	19	3	16
Naphthalene	14.793	17	0	0
C1-naphthalenes	17.456	37	0	0
C2-naphthalenes	20.144	53	0	0
SES1	20.701	56	15	50
C2-benzothiophenes	20.737	65	0	0
SES2	21.591	56	17	54
SES3	21.858	59	19	55
SES4	22.172	59	19	54
SES8	23.893	71	28	62
n-C17	26.462	69	3	0
Pristane	26.598	77	35	36
C1-fluorenes	27.268	70	3	0
n-C18	28.597	72	3	0
Phytane	28.817	84	42	54
C2-fluorenes	29.867	70	9	8
4-Methyl dibenzothiophene	30.490	88	4	0
1-Methyl dibenzothiophene	31.393	86	5	0
2-Methyl phenanthrene	31.428	77	2	0
Methyl anthracene	31.606	74	9	0
1-Methyl phenanthrene	31.939	79	3	0
C2-dibenzothiophenes	32.491	73	17	15
Highest peakC2-phenanthrenes/anthracenes	34.005	81	11	11
C2-phenanthrenes/anthracenes	34.005	77	12	12
C3-dibenzothiophenes	34.652	82	38	44
C3-phenanthrenes/anthracenes	36.202	82	31	35
2-Methyl fluoranthene	36.814	77	23	29
Retene	37.313	0	0	0
Benzo(*a*)fluorene	37.343	78	15	14
Benzo(*b* + *c*)fluorene	37.640	87	17	13
2-Methyl pyrene	37.818	80	31	41
4-Methyl pyrene	38.257	80	33	42
1-Methyl pyrene	38.388	82	25	24
C23Tr	38.709	87	68	72
Tetramethyl phenanthrene	38.845	84	40	50
C4-phenanthrenes/anthracenes	38.845	81	33	47
C2-fluoranthenes/pyrenes	39.427	84	31	34
C24Tr	39.576	93	74	76

(*Continued*)

TABLE 25.6 (*Continued*)

Compounds	Retention time (min)	% PW PM-02	% PW BH-03 (0.1 m)	% PW BH-04 (0.1 m)
BNT	40.265	88	26	24
C20TA	41.001	104	65	85
C25 Tr	41.411	87	73	72
C21TA	42.468	103	65	80
C1-chrysenes	43.342	81	41	48
27dbS	44.096	91	66	72
27dbR	44.595	93	63	69
C28 (22S)	45.695	94	68	75
C29 (22S)	46.545	87	71	74
27bbR + S	46.551	93	77	94
27Ts	47.703	106	95	92
SC26TA	47.822	101	67	88
28bbR + S	48.072	92	87	91
27Tm	48.286	97	96	96
28aaR	48.547	99	75	80
RC26TA + SC27TA	48.886	106	82	98
29aaS	48.928	102	76	98
29bbR + S (m/z 218)	49.195	97	92	91
29bbR + S (m/z 217)	49.201	102	87	92
28ab	49.427	0	0	0
SC28TA	49.807	104	82	95
29aaR	49.908	97	82	88
RC27TA	50.271	112	87	108
29ab	50.277	112	124	120
29Ts	50.390	94	90	86
30O	51.519	112	92	87
RC28TA	51.543	109	86	102
30ab	51.715	100	100	100
30ba	52.441	98	105	113
31abS	53.588	104	107	111
30G	54.373	105	98	100
32abS	55.200	101	95	95

In Fig. 25.10B, an evaporation trend line was added to the PW plot. The compounds located below this line have undergone additional processes of weathering, besides evaporation. These compounds are *n*-C17 and *n*-C18, C1- and C2-fluorenes, C1–C4-phenanthrenes/anthracenes, C2- and C3-dibenzothiophenes, 2-methyl fluoranthene, benzo(*a*)fluorene, methyl pyrenes, C2-fluoranthenes/pyrenes, and C1-chrysenes. Biodegradation promoted some degradation of *n*-alkanes and may have influenced on decrease of PAH. But mainly, PAHs are subjected to photooxidation (Douglas et al., 2002; CEN, 2012; Radović et al., 2013), which explains its reduction when compared to PAHs in Cusiana oil.

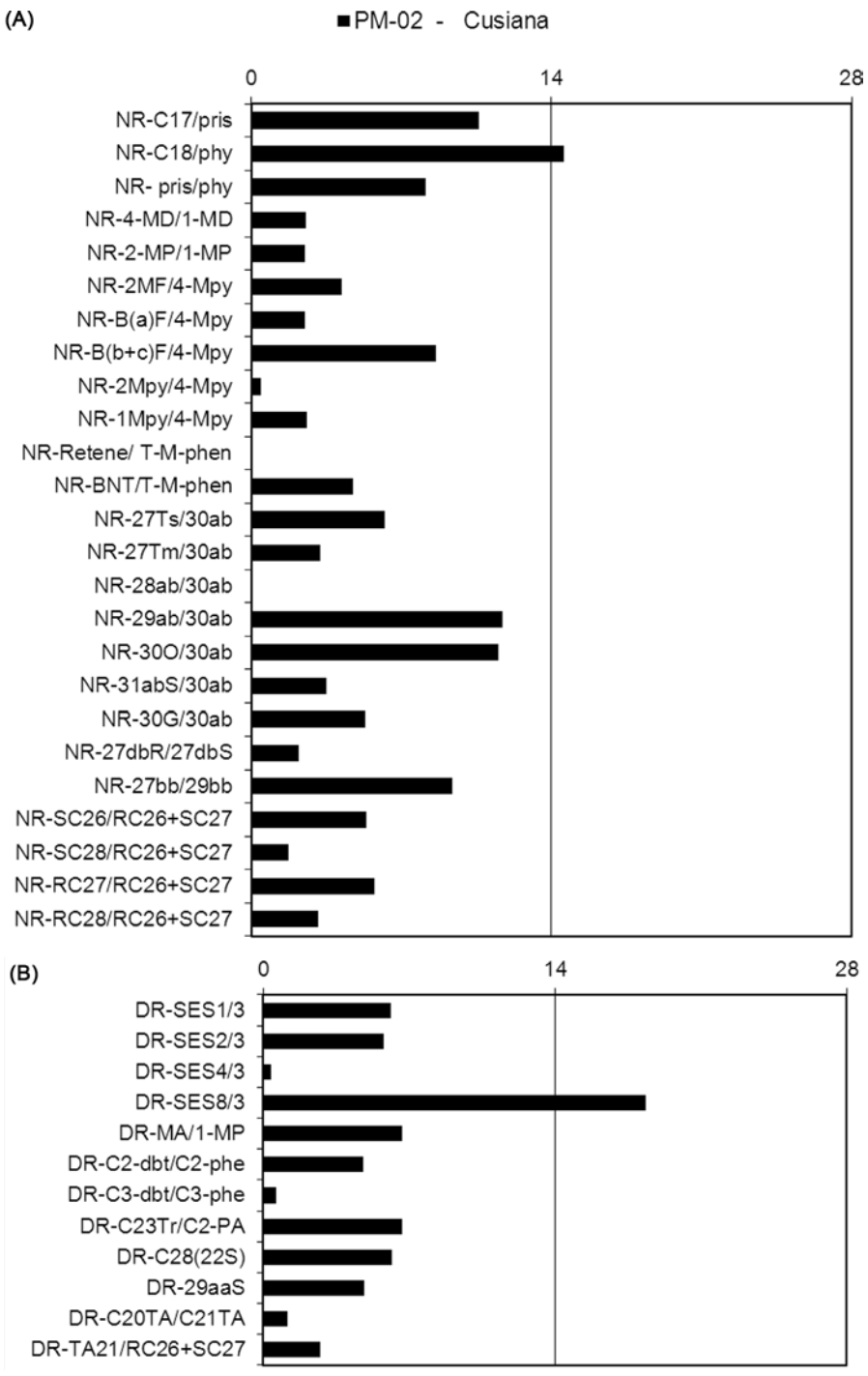

FIGURE 25.11 Relative difference between DRs of PM-02 and Cusiana oil: (A) normative DRs (NR) and (B) informative DRs (DR).

Both biodegradation and photooxidation were slight, resulting in an insignificant influence on DRs for these compounds (Fig. 25.11). Among the most important and normative DRs for this method (flagged as NR, Fig. 25.11A), only the *n*-C18/phytane exceeded the limit of 14%, which is explained by biodegradation of PM-02. For additional informative DRs (flagged as DR, Fig. 25.11B), only the ratio of the sesquiterpanes $C_{16}H_{30}$-8β(*H*)-homodrimane (SES8) and $C_{15}H_{28}$-8β(*H*)-drimane (SES3) has changed, as the evaporation process affects preferably SES3 (Table 25.6). The conclusion is that Cusiana oil is the source of sample PM-02 (positive match). Although this sample has been collected more than 9 years after the spill, the oil is still largely unaffected by weathering processes, which facilitated the comparison.

25.3.2.2.2 Spill Sample BH-03 (0.1 m) and Cusiana Oil

The PW plot of BH-03 versus Cusiana oil (normalized by 17α(*H*),21β(*H*)-hopane) (Fig. 25.12A) shows a very significant reduction of the abundance of PAH and some biomarkers. Only compounds that elute after 50 minutes were not weathered and remain present in abundances around 100%, varying between 86% and 107%, which do not represent significant differences compared to the source, considering the variability of the method. The exception is the 17α(*H*),21β(*H*)-30-norhopane (29ab), one of the most important biomarkers, which abundance is higher in BH-03 than in Cusiana oil (124%, Figs. 25.9A and C, and 25.12A).

In Fig. 25.12B, an evaporation trend line was added to the PW plot. Several compounds are located below this line, demonstrating the occurrence of multiple processes of severe weathering. The extent of biodegradation was such that the *n*-alkanes *n*-C17 and *n*-C18 have been substantially degraded; while the relatively more resilient pristane and phytane are still present (Fig. 25.12B).

Many PAH were also affected by other weathering processes, besides evaporation: C1- and C2-fluorenes, C1−C4-phenantrenes/anthracenes, C1−C3-dibenzothiophenes, 2-methylfluoranthene, benzofluorenes, methyl pyrenes, C2-fluoranthenes/pyrenes, and C1-chrysenes (Fig. 25.12B). There are several reports in the literature describing how these compounds are affected by biodegradation (Wang et al., 1998a; Wang et al., 2001;

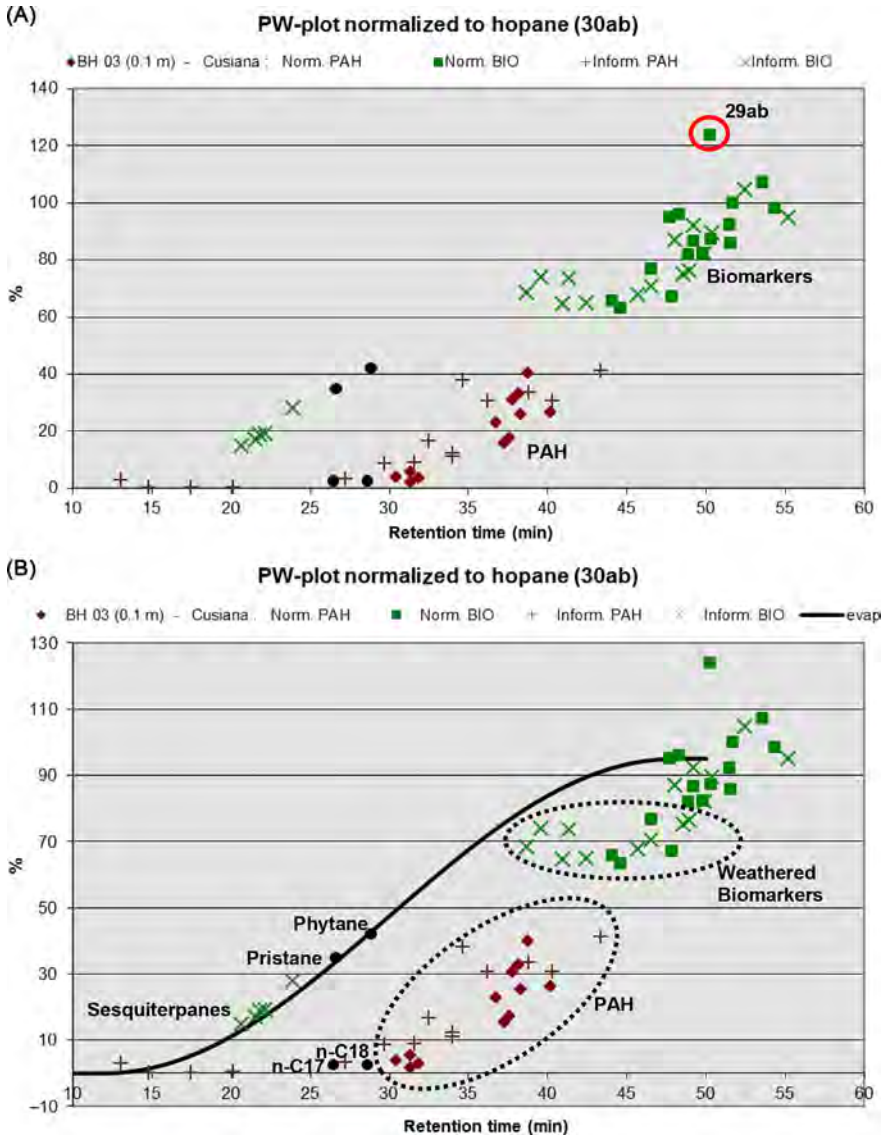

FIGURE 25.12 PW plot of BH-03 (0.1 m) versus Cusiana oil (normalized by 17α(*H*),21β(*H*)-hopane).

Christensen et al., 2005b; Wang and Stout, 2007; Bernabeu et al., 2013). Changes in the isomers distribution in C1-dibenzotiophenes and C1-phenantrenes series are known indicators of biodegradation in its initial phase, with the 2/3-methyl phenantrenes and dibenzothiophenes the most susceptible to biodegradation (Wang et al., 1998a; Bernabeu et al., 2013). As the C1-dibenzotiophenes and C1-phenantrenes were virtually removed from the sample, it has not been possible to observe these alterations. The reduction pattern in the SIC of m/z 216 with larger degradation of 1-methyl pyrene (25%) compared to 4- and 2-methylpyrene isomers (33% and 31%) and the reduction of benzofluorenes (15% and 17%) (Table 25.6) suggests that the photooxidation also contributed to the weathering (CEN, 2012).

Among biomarkers, triaromatic steranes most likely have been affected by weathering (Fig. 25.12B and Table 25.6). The reduction of C20TA, C21TA, SC26TA, RC26TA + SC27TA, SC28TA, RC27TA, and RC28TA is also an evidence that photooxidation occurred, as these compounds are known for their resistance to biodegradation (Díez et al., 2005; Peters et al., 2007; Wang and Stout, 2007). The most affected DRs were SC26/RC26 + SC27 and TA21/RC26 + SC27 (Fig. 25.13), exceeding the limit value of 14%. These results agree with those obtained by Radović et al. (2013), where these DRs were also the most affected by the effect of experimental irradiation. They suggested that the pronounced photosensitivity of triaromatic steranes is related to its aromatic backbone (structurally related to phenanthrene), and the alkyl substitution.

Other biomarkers reduced when compared to Cusiana oil (Fig. 25.12B and Table 25.6) were the terpanes C23Tr, C24Tr, C25Tr, C28 (22S), and C29 (22S), and the steranes 27dbS, 27dbR, 27bbR + S, 28aaR, and 29aaR. These compounds are known for their resistance to weathering (Peters et al., 2007) and its degradation was observed only in extreme cases (Wang et al., 2001; Bost et al., 2001; Kienhuis and Dahlmann, 2014).

Fig. 25.13 shows that in most cases, there is a significant difference between DRs in BH-03 and Cusiana oil. Among these DRs, almost all involving aromatic or *n*-alkanes, pristane, and phytane exceeded the limit of 14%, which is explained by an assemblage of weathering processes (evaporation, biodegradation, and photooxidation). However, the differences related to terpanes cannot be explained by weathering. In particular, the DR 29ab/30ab, which compounds are present in high abundance and are easily integrated, is known for its stability and robustness. In this case, only the contribution from another source of oil could cause such variation. It is possible that sample BH-03, located in the same topographic level of Barigüi River, in an area that has been frequently invaded by its waters, has gathered the influence of runoff contribution of other oil sources and also of river sediment background. This assumption is confirmed by the comparison of SICs of m/z 191 of Cusiana oil, BH-03 and a river sediment background sample (Figs. 25.9A, C, and E, respectively), where these two biomarkers proportions change depending on the sample. Hence, the river sediment background contribution increased the 29ab peak, causing the variation in the DR 29ab/30ab.

The importance of the DR 29ab/30ab is such that the difference between this DR in BH-03 and Cusiana oil would be sufficient to conclude that the samples do not have the same origin. However, considering the knowledge of the area (the oil was contained and soaked the soil), the influences of an external factor (river sediment background, Fig. 25.9E) and that the profile of SICs of terpanes is very similar in these samples (Figs. 25.9A and C), it is concluded that the Cusiana oil is probably the source of the sample BH-03.

25.3.2.2.3 Spill Sample BH-04 (0.1 m) and Cusiana Oil

The results of spill sample BH-04 are quite similar to those of sample BH-03. These samples are located close to each other in a swampy area (Fig. 25.2). The PW plot of BH-04 versus Cusiana oil (normalized by 17α(*H*),21β(*H*)-hopane) (Fig. 25.14A) shows a significant reduction in the abundance of PAHs and some biomarkers as well. Only compounds that elute after 48.8 minutes were not weathered and remain present in abundances around 100%, varying between 86% and 113%, which do not represent significant differences compared to the source, considering the variability of the method. The exception is again the 17α(*H*),21β(*H*)-30-norhopane (29ab), which has a higher abundance in BH-04 than in Cusiana oil (120%, Figs. 25.9A and D and 25.14A).

In Fig. 25.14B, an evaporation trend line was added to the PW plot. The severe biodegradation has completely removed the *n*-alkanes, *n*-C17, and *n*-C18, while pristane and phytane are still present. However, both isoprenoids were also biodegraded as they are below the evaporation trend line (Fig. 25.14B). The sesquiterpanes (Fig. 25.14B), which reduction is primarily related to evaporation (CEN, 2012), are in a larger abundance than those found in BH-03 (Table 25.6, BH-04: around 55% and BH-03; around 20%). These results show that evaporation in BH-03 was more intense than in BH-04. On the other hand, biodegradation was more severe in BH-04 than in BH-03.

PAHs were affected similarly in BH-03 and BH-04 (Figs. 25.12B and 25.14B), as PAHs more susceptible to biodegradation (e.g., C1-phenantrenes and C1-dibenzothiophenes) were completely removed and the same pattern

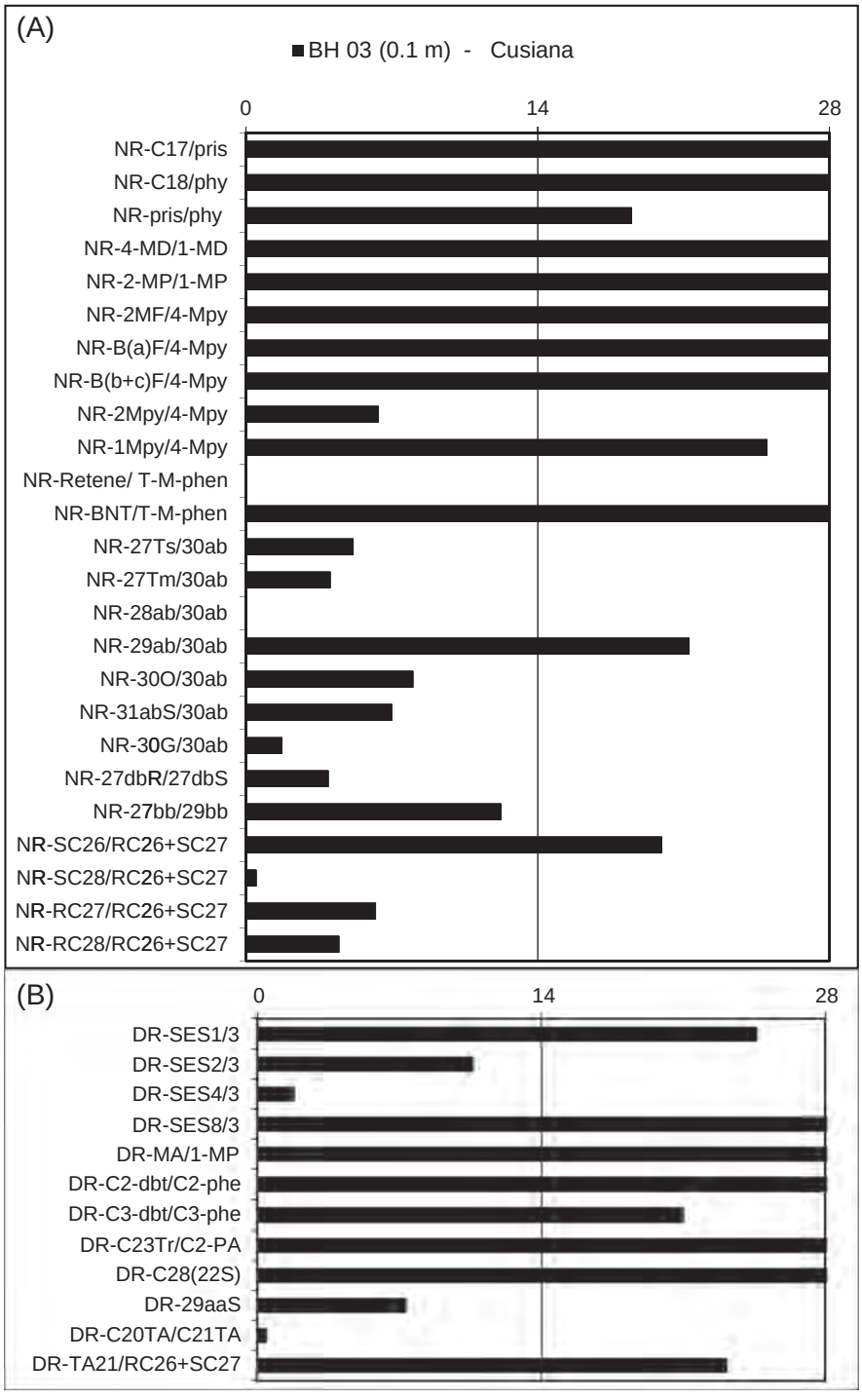

FIGURE 25.13 Relative difference between DRs of BH-03 (0.1 m) and Cusiana oil: (A) normative DRs (NR) and (B) informative DRs (DR).

of photooxidation was observed for methyl pyrenes in these samples (1-MPy more sensitive isomer) (Table 25.6). The biomarkers reduced in BH-04 when compared to Cusiana oil (Fig. 25.14B) were terpanes C23Tr, C24Tr, C25Tr, C28 (22S), and C29 (22S), and steranes 27dbS, 27dbR, and 28aaR, what has occurred in BH-03 as well.

In most cases, there was a significant difference between DRs in BH-04 and Cusiana oil (Fig. 25.15). As expected, the pattern in BH-04 is similar to that in BH-03, excluding some DRs which variation is related to evaporation (e.g., SES1/SES3 and SES8/SES3); less intense in BH-04 (Figs. 25.13 and 25.15). Again the DR 29ab/30ab in the spill sample BH-04 was significantly different from the source. These results corroborate the assumption

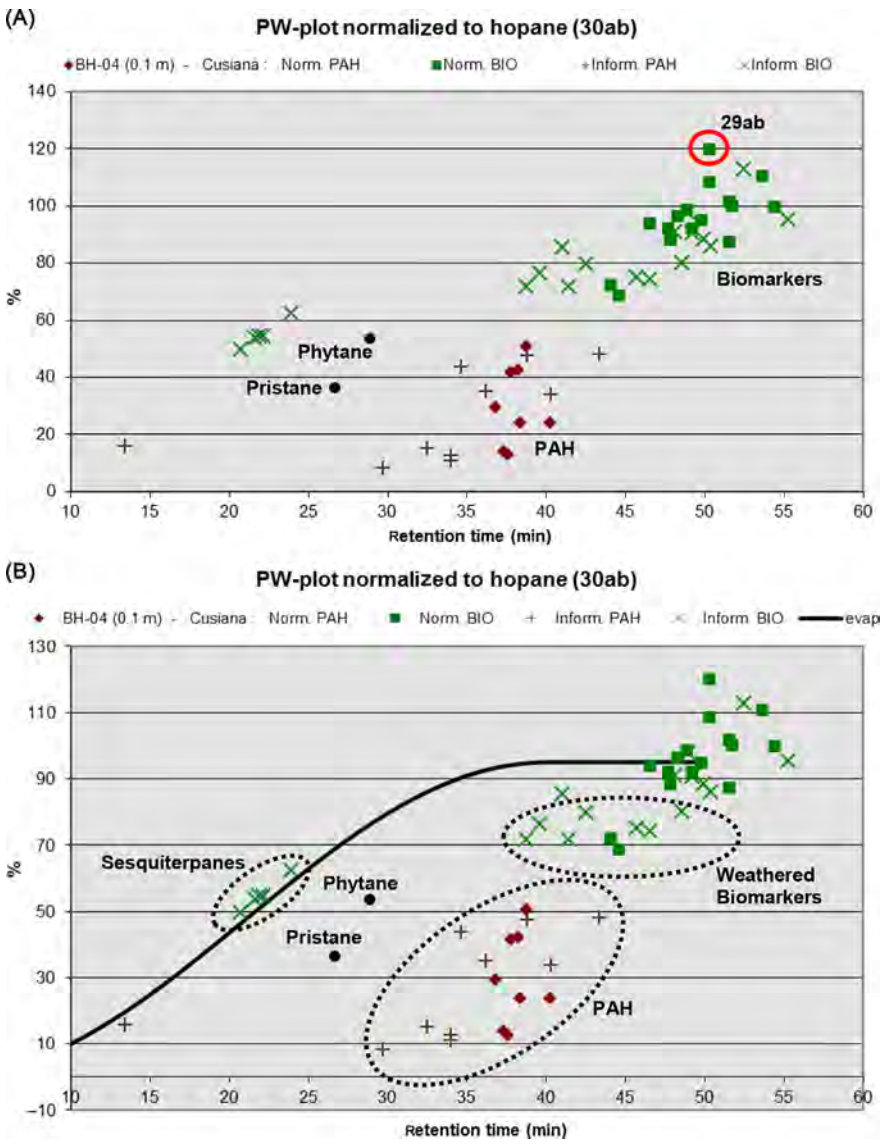

FIGURE 25.14 PW plot of BH-04 (0.1 m) versus Cusiana oil (normalized by 17α(*H*),21β(*H*)-hopane).

that the marsh where BH-03 and BH-04 were collected is influenced by river sediment background (Fig. 25.9E), which most likely have altered these biomarkers. The conclusion is that Cusiana oil is probably the source of the sample BH-04.

The method for source identification through semiquantitative DRs calculated from heights and areas of chromatograms (CEN, 2012) proved to be strict and therefore suitable for forensic investigations, where the number of samples is low and a robust and conclusive result is required. However, in every aspect analyzed, it must be confirmed that there are no differences between the spill and source samples. The similarity is proven by the absence of differences. If there are differences, they should be unequivocally explained for a match conclusion or reasonably explained for a probable match conclusion. Even within the refinery area, where it is known that the Cusiana oil represented a considerable input and soaked soil, after 9 years, it is not a trivial task to correlate hydrocarbons present in the soil with the spilled oil. Anthropogenic runoff background might alter the fingerprint of the sediment, stressing the need of recognizing the contribution of background when attempting to identify the source of hydrocarbons. Thus, this technique is not recommended for environments with multiple anthropogenic influences, as the sediments of Iguaçu and Barigüi rivers, since the degree of scientific certainty can be questionable in court trials.

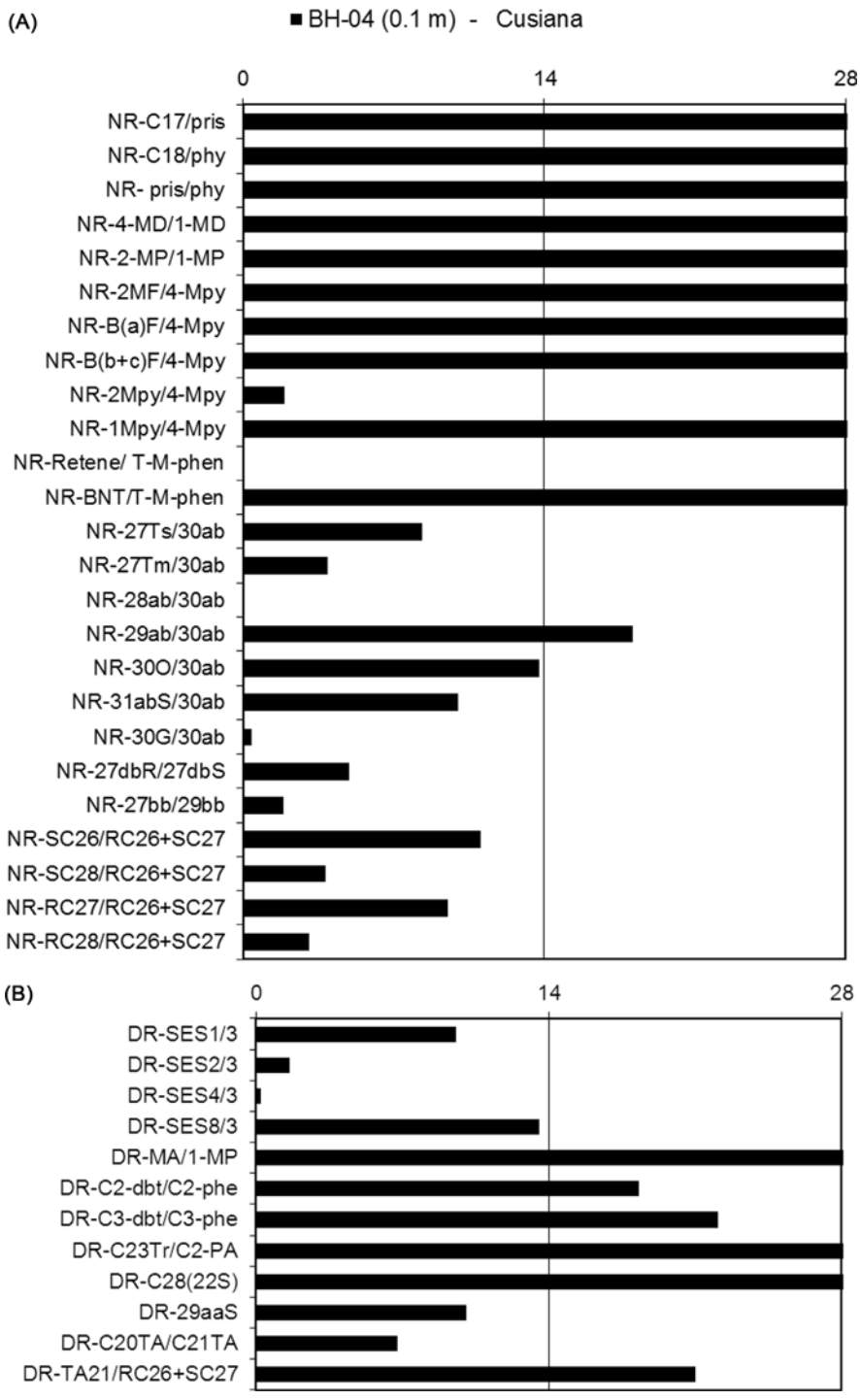

FIGURE 25.15 Relative difference between DRs of BH-04 (0.1 m) and Cusiana oil: (A) normative DRs (NR) and (B) informative DRs (DR).

25.3.3 Chemometric Assessment of Soil and Sediment Samples

25.3.3.1 Initial Source Identification Based on a Subset of SICs

For this preliminary assessment, SICs of nine groups of PAHs relevant for source identification (marked with footnote "b" in Table 25.2 and shown in Fig. 25.16A) were used (Christensen et al., 2010). Additionally, SICs of selected internal standards (marked with footnote "d" in Table 25.2) were also preprocessed and used for normalization in **Scheme I**. The baseline was removed by calculating the first derivative of the SICs. Depending on

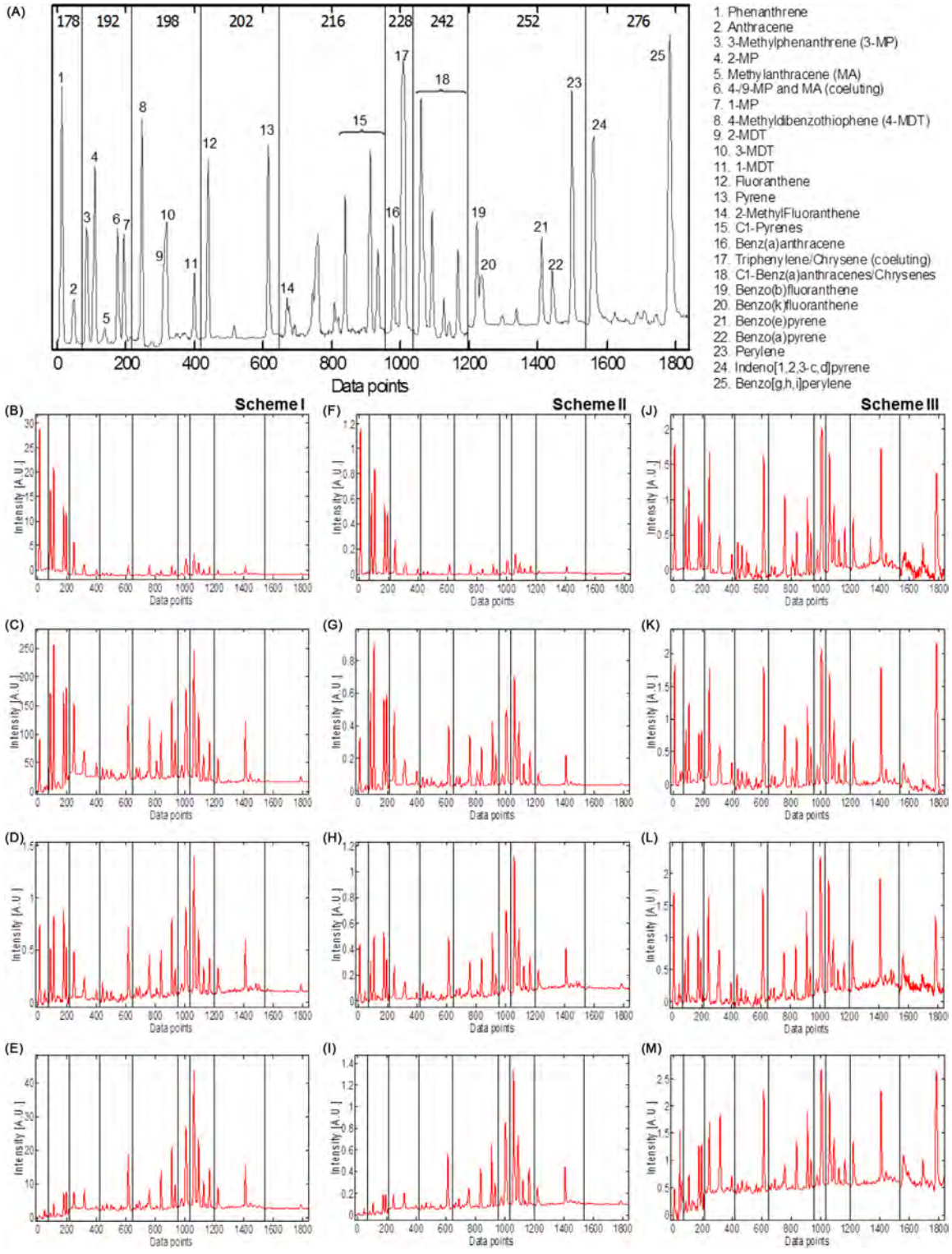

FIGURE 25.16 Data normalization: (A) peaks or peak clusters identification; **Scheme I** (normalization to internal standards): (B) Cusiana oil, (C) BH 02, (D) BH 04, (E) BH 03; **Scheme II** (concatenation and normalization to Euclidean norm): (F) Cusiana oil, (G) BH 02, (H) BH 04, (I) BH 03; **Scheme III** (normalization to Euclidean norm within SICs): (J) Cusiana oil, (K) BH 02, (L) BH 04, (M) BH 03. Note that the SICs on the top of (A) are the same showed in the other figures and were omitted to improve the readability.

the SIC, the retention time shifts in the data set were between 7 and 20 scan points. The rigid shift procedure adjusted the major part of the constant shift within each SIC. Then, COW algorithm was employed to complete the retention time alignment. For SICs with less than 200 scan points, the search for the optimal segment length was between 25 and 50 scan points (with 5 point increments) and for SICs with more than 200 scan points, the range was between 50 and 100 scan points (with 10 point increments). The slack parameter grid was 1–3 with 1 point increment for all SICs. The maximum correction allowed was 5 scan points. The optimal segment lengths were between 26 and 89 scan points and the optima for the slack parameter were between 1 and 3 points.

Fig. 25.16 shows the effect on data after the application of each one of the normalization schemes. In **Scheme I** (Fig. 25.16B–E), data exhibit intensity ranges from 1.5 up to 250, which reflect different levels of absolute PAH concentrations. The most concentrated sample is shown in Fig. 25.16C. On the other hand, the intensities are in the same range after normalization to **Scheme II** (Figs. 25.16F–I) and **Scheme III** (Figs. 25.16J–M).

In **Scheme II**, relative differences of concentrations among each group of PAHs are retained. This scheme reveals the increasing physical weathering from Fig. 25.16F–I as there is a relative decrease of low-molecular-weight (low-MW) PAHs (viz., m/z's 178, 192, and 198 SICs) when compared to high-molecular-weight (high-MW) PAHs.

Finally, in **Scheme III**, the relative difference between the concentrations of each group of PAHs is removed. Differences in the patterns of isomers within each SIC are instead brought forward. Hence, the differences between fresh oil (Fig. 25.16J) and moderated weathered samples (Fig. 25.16K) are clearly reduced by normalization **Scheme III**.

Although the differences in relative amounts of individual isomers within the alkylated families (e.g., m/z's 192 and 198) are preserved in all schemes (Figs. 25.16B–M), in **Scheme III** (Fig. 25.16J–M), these differences show up as the major variation.

25.3.3.1.1 Pollution Levels and Weathering Degree

After applying normalization **Scheme I** (normalization to internal standards), the SICs were combined (e.g., Fig. 25.16B–E). Each one of the 66 samples now consisted of 1839 data points. A bend in explained variance was observed past the third PC for the training set. Furthermore, since the loadings above PC3 contain shift patterns (Fig. 25.17) in addition to chemical variation, it was concluded that the optimal number of PCs is three (Christensen and Tomasi, 2007).

The three-component PCA model describes 98.6% of the variance. Information on relative contamination levels (relative to an average sample) included in the training set and qualitative information on PAH sources is provided by this model. The average sample is a slightly weathered crude oil, but with high levels of perylene (Fig. 25.18).

The PC1 loading is similar to the average chromatogram, except for perylene which has a small negative loading coefficient and other 4- and 6-ring PAHs which have lower positive PC1 loadings than the mean chromatogram (Fig. 25.18A). In this model, larger positive PC1 scores correspond to high concentrations of weathered crude oil, while samples with negative PC1 scores are less contaminated. Samples with PC1 scores around zero have an average contamination level relatively to the sample set (Fig. 25.19).

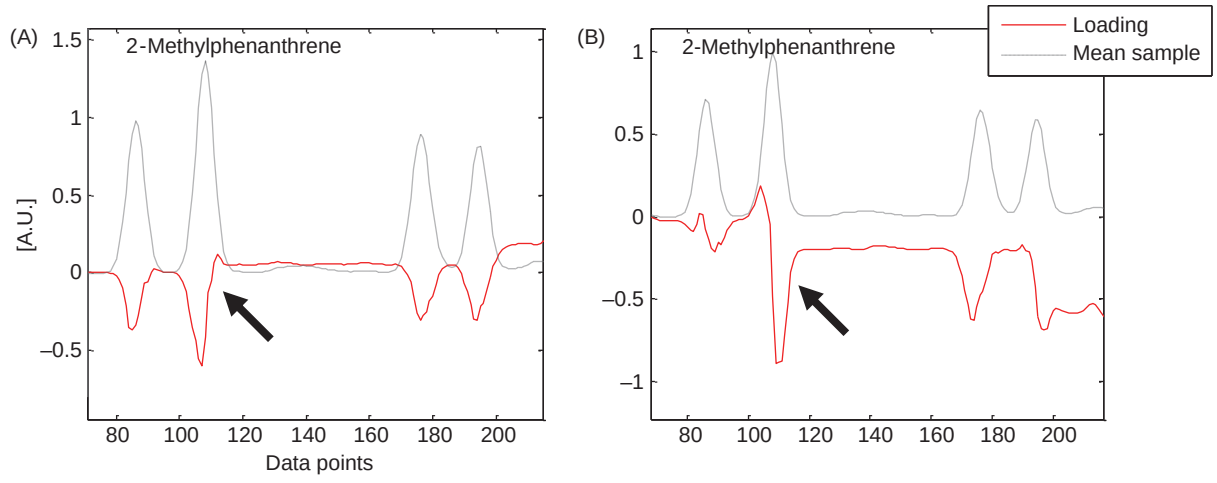

FIGURE 25.17 Example of retention time shifts at m/z 192 for (A) PC4 and (B) PC5 Loading plots for the principal component model of normalization **Scheme I** (normalization to the internal standards). Note that 2-methylphenanthrene does not coelute with other compounds.

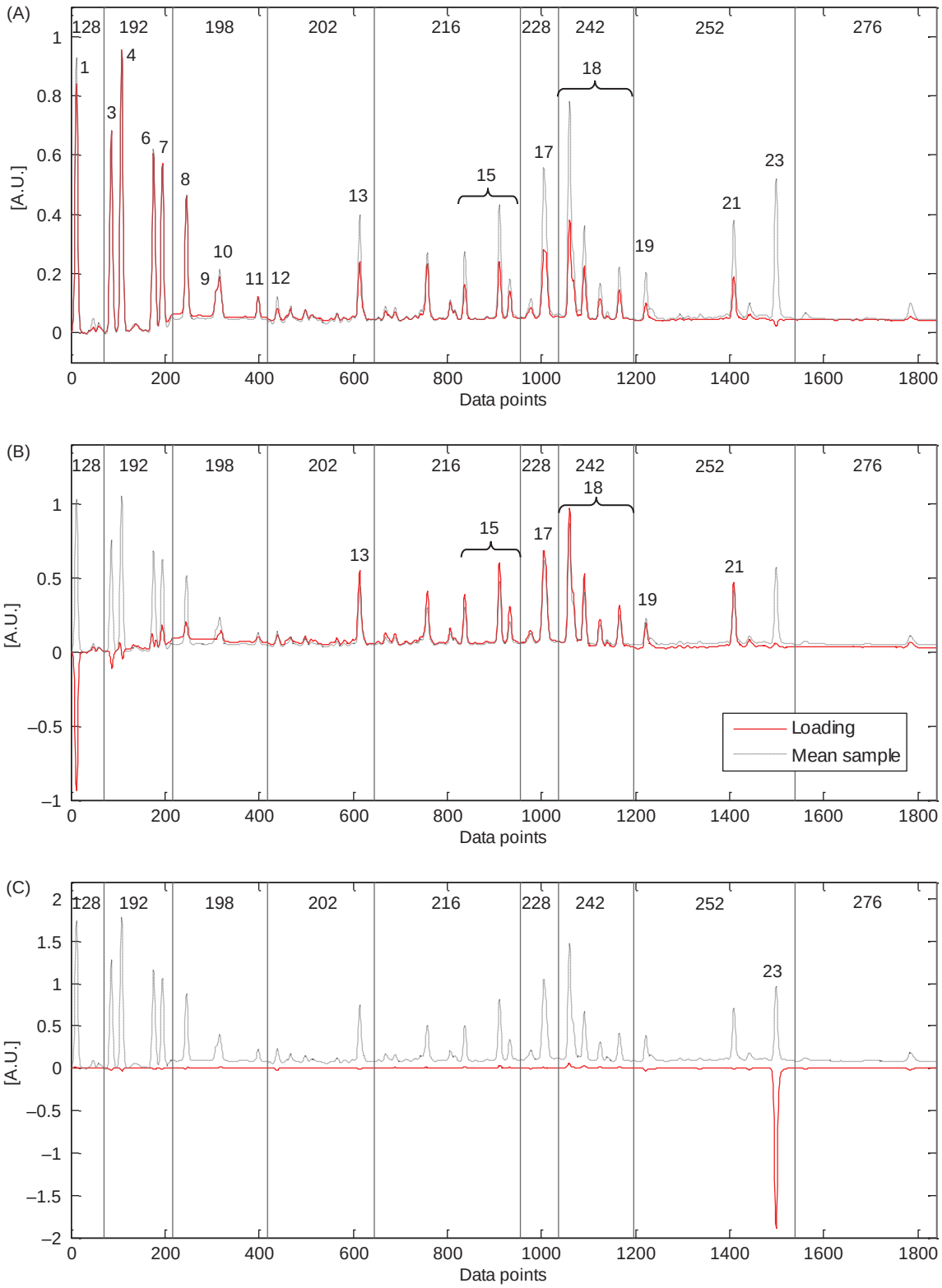

FIGURE 25.18 Subset of nine PAHs data analysis: Loading plots for the principal component model of normalization **Scheme I** (normalization to the internal standards): (A) PC1, (B) PC2, and (C) PC3. The dotted lines are the mean chromatogram of the entire training set, while the solid lines are the loadings (AU: arbitrary units). The compound numbers are specified in Fig. 25.16.

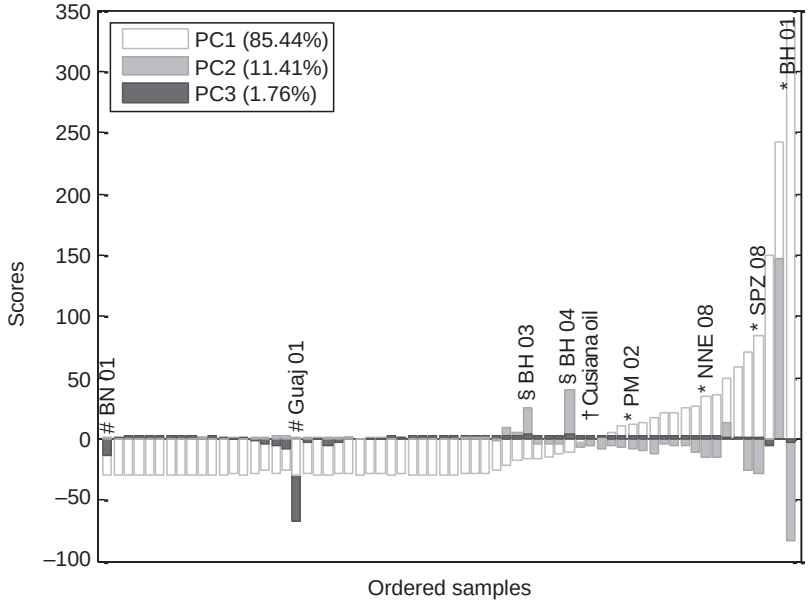

FIGURE 25.19 Subset of nine PAHs data analysis: Scores for PC1, PC2, and PC3 for the principal component model of mean-centered data of normalization **Scheme I** (normalization to the internal standards). BN, Gal L, Guaj, and Refinery denote samples from Balsa Nova, General Lúcio, Guajuvira, and from inside the Refinery area, respectively. The symbols indicate samples: *less and §more weathered than the mean sample, with significant #diagenetic input and the †Cusiana oil. Note that bars are not stacked.

Although PCA cannot provide an accurate apportionment of the different sources of PAH inputs, it can be used to determine the main sources of PAH contamination. First, as the PC2 loading coefficients are negative for (low-MW) PAHs such as phenanthrene and 3- and 2-methylphenanthrene, close to zero for anthracene, C1-anthracenes, fluoranthene, and C1-fluoranthenes, and positive for high-MW PAHs such as pyrene, C1-pyrenes, chrysene, C1-chrysenes, benzo(*e*)pyrene, and benzo(*g*,*h*,*i*)perylene (Fig. 25.18B), it can be concluded that samples with large negative PC2 scores (Fig. 25.19) contain higher concentrations of relatively fresh crude oil. Likewise, samples with large positive PC2 scores (Fig. 25.19) contain higher concentrations of a moderately weathered oil (or heavy fuel oil without cracking residues). It is also noteworthy that among the C1-phenathrenes, the 3- and 2-methyl isomers have negative PC2-loading coefficients, while the 9/4- and 1-methyl present positive coefficients. Although these coefficients are small, this pattern in the C1-phenathrenes suggests biodegradation has taken place (Christensen et al., 2005b).

The PC3 loading has a large negative coefficient for perylene, while all the other coefficients are close to zero (Fig. 25.18C). PC3 can therefore be interpreted as an indicator for in situ diagenesis. Hence, a significant diagenetic input is present in samples with large negative PC3 scores (Fig. 25.19).

Samples with positive PC1 scores and negative PC2 scores contain relatively fresh crude oil, e.g., PM 02, SPZ 08, NNE 08, BH 01 (marked with footnote "*" in Fig. 25.19) when compared to the average sample. Conversely, samples with positive PC2 scores, e.g., BH03, BH04 (marked with footnote "§" in Fig. 25.19), contain higher concentrations of weathered crude oil. As expected, Cusiana oil samples (marked with footnote "†" in Fig. 25.19) have PC1 scores close to zero and negative PC2 scores, which correspond to a typical fresh crude oil PAH pattern with average oil concentrations.

Samples with negative PC1 and PC3 scores, e.g., BN 01 and Guaj 01 (marked with footnote "#" in Fig. 25.19), are less contaminated and contain a large amount of perylene. These samples have an important diagenetic input, while PAHs of petrogenic input are limited.

Samples from outside the refinery area are less contaminated, i.e., samples from Guajuvira ("Guaj" in Fig. 25.19), General Lúcio ("Gal L" in Fig. 25.19), and Balsa Nova ("BN" in Fig. 25.19), while soil samples from inside the refinery area ("Refinery" in Fig. 25.19) are more contaminated than the mean sample.

25.3.3.1.2 Exclusion of Samples with Low Contamination Level

PCA models on the entire data set (66 sample extracts × 1839 data points) using all three normalization schemes revealed that a number of samples contain quite low levels of all PAHs. Fig. 25.20 shows the score plot of PC1 versus PC2 for the PC model on data normalized to Euclidean norm within each SIC (**Scheme III**).

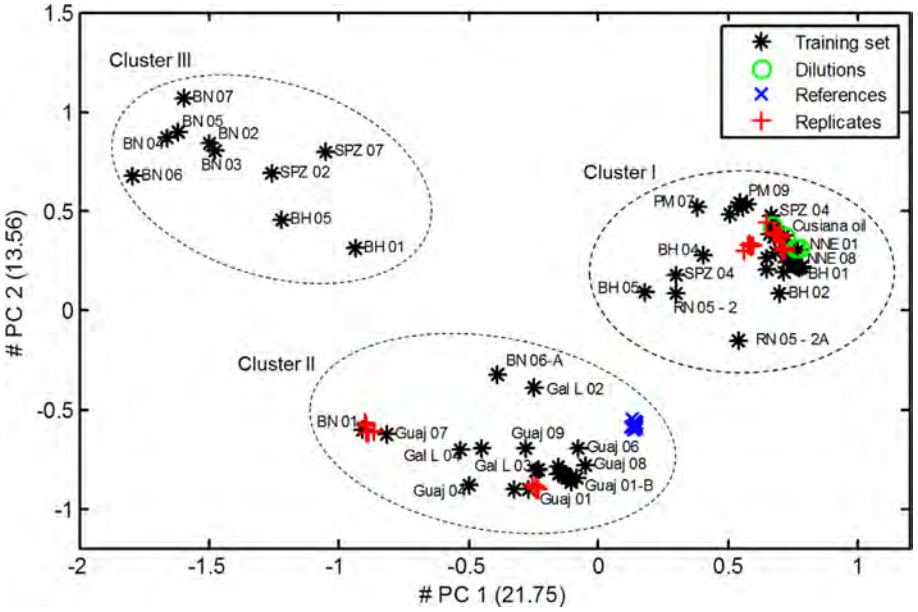

FIGURE 25.20 Subset of nine PAHs data analysis: Score plot of PC1 versus PC2 for the principal component model of normalization **Scheme III** (normalization to Euclidean norm within SICs). Some labels were omitted from the Score plot to improve the readability.

Chemical interpretation of the loading plots for this model (not shown) and of the SICs for individual samples in the three clusters (Figs. 25.21A–E) revealed that samples in Cluster I are mainly of petrogenic origin. These samples are all from inside the refinery area. Conversely, samples in Cluster II are all from outside the refinery area (Guajuvira, General Lúcio, and Balsa Nova). In these samples, a mixture of diagenetic (i.e., perylene, Fig. 25.21C: BN 01) and pyrogenic origin PAHs (i.e., fluoranthene, benz(*a*)anthracene, high-MW nonalkylated PAHs, Fig. 25.21D: Gal L 02) predominate. Finally, there were no PAHs peaks present in the SICs of samples located within Cluster III. A typical example of combined SICs for this last cluster is shown in Fig. 25.21E (BN 02). Hence, samples located in Cluster III (BN 02, BN 03, BN 04, BN 05, BN 06, BN 07, SPZ 02, SPZ 07, BH 01, and BH 05) were excluded from the subsequent chemometric analyses, as they contain no information and solely introduce noise to the models.

25.3.3.2 Source Identification Using Relative Fingerprints of 38 Groups of PAHs

A total of 38 SICs containing 2–6 ring PAHs (marked with footnote "a" in Table 25.2) were included as variables in the model. After concatenation, each one of the 56 samples consisted of 10,738 data points. The preprocessing consisted in baseline removal, as described in Section 25.1.2, and normalization **Scheme II** (concatenation and normalization to Euclidean norm). A three-component model describing 88.3% of the variance in the training set was found to be optimal. Fig. 25.22 shows the score plot for PC1 versus PC2 for this model.

PC1 distinguishes the petrogenic samples from the samples presenting mainly diagenetic and pyrogenic inputs, as the loading coefficients (Fig. 25.23A) are positive for compounds with a primarily petrogenic origin (i.e., naphthalenes, phenanthrenes, dibenzothiophenes, and fluorenes), especially large and positive for C0–C3 naphthalenes and C0–C2 phenanthrenes, and negative for the typical diagenetic (i.e., perylene) and pyrogenic (i.e., fluoranthene, benz(*a*)anthracene, indene(1,2,3-cd)pyrene) compounds (zoom in Fig. 25.23C). Perylene has the largest negative-loading coefficient (large ratio to other 5-ring PAHs), indicating a significant diagenetic background (Baumard et al., 1998) for samples outside the refinery area, which have negative PC1 score values. Moreover, the ratios of fluoranthene to pyrene, benz(*a*)anthracenes to chrysene and indene(1,2,3-cd)pyrene to benzo(*g*,*h*,*i*)perylene (Fig. 25.23C, where each pair of these peaks has approximately the same size) evidence pyrogenic input for the samples clustering in the bottom left of Fig. 25.22 as well (Yunker et al., 2002). This cluster includes all samples from outside the refinery area, i.e., samples from Guajuvira, General Lúcio, and Balsa Nova. For these samples, PC2 scores are close to zero or have small negative values, therefore, having low influence in the interpretation of results.

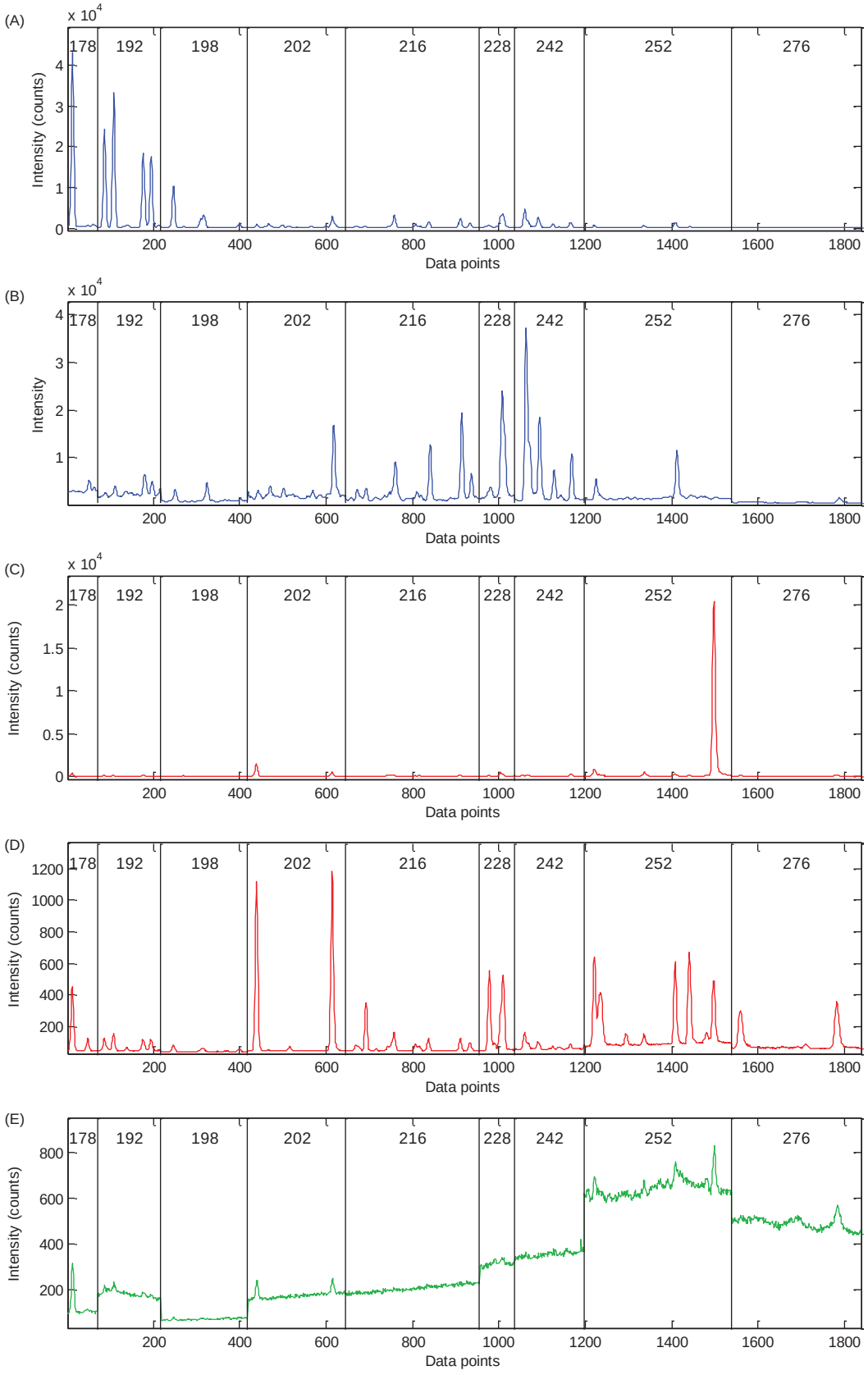

FIGURE 25.21 Untreated data of selected samples: **Cluster I**: (A) Cusiana oil, (B) BH 04; **Cluster II**: (C) BN 01, (D) Gal L 02, and **Cluster III**: (E) BN 02.

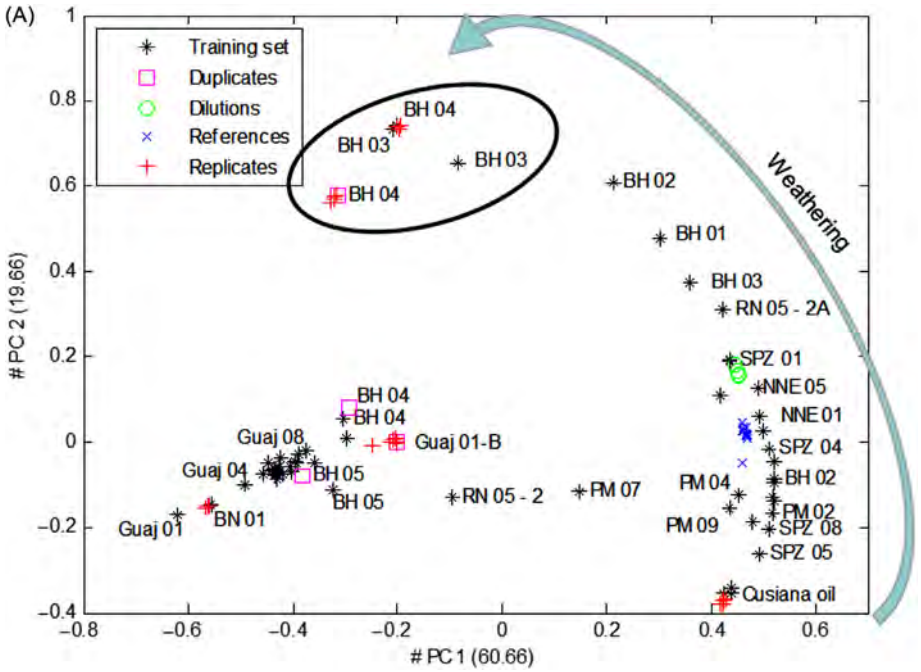

FIGURE 25.22 Thirty-eight PAHs data analysis: Score plot of PC1 versus PC2 for the principal component model of normalization **Scheme II** (concatenation and normalization to Euclidean norm). Some labels were omitted from the score plot (A) to improve the readability.

Most of the samples from inside the refinery area varies from positive PC1 and negative PC2 scores such as the Cusiana oil (Fig. 25.22, bottom right), to negative PC1 and large positive PC2, e.g., BH 04 (Fig. 25.22, top left ellipse). PC2-loading coefficients (Fig. 25.23B) are negative for C0−C2-naphthalenes and C0-phenanthrene, close to zero for C0−C1-fluorenes and positive for C3-C4-naphthalenes, C2−C3-fluorenes and C1−C4-phenanthrenes. These observed effects on the distribution among C0−C4 alkylated families indicate physical weathering but could also be caused partially by biodegradation processes as an increase in alkylation level decreases the susceptibility to microbial attack (Wang et al., 1998a).

Therefore, BH 04 and BH 03 are among the most weathered samples (Fig. 25.22, top left ellipse), while SPZ 05, SPZ 08, PM 02, PM 09, and PM 04 (Fig. 25.22, bottom right) are contaminated with relatively fresh crude oil with similar PAH composition as the Cusiana oil. The increasing weathering degree is pointed out by the arrow in Fig. 25.22. All samples following this trend were collected close to the spill accident, which provides additional evidence that these samples contain a weathered fraction of the Cusiana oil.

Besides the general physical weathering trend, changes in isomeric variations within alkylated PAHs families (e.g., the C3-naphthalene isomer more resistant to degradation in Fig. 25.23d, marked with an arrow) indicate that biodegradation has indeed occurred (Wang et al., 1998a).

Fig. 25.24 shows that perylene has the most prominent positive PC3 loading coefficient and also C2-C3-naphthalenes, C0−C1-fluorenes, and C0-C1-phenanthrenes have positive PC3 loading coefficients, while more alkylated (C2−C4) isomers and 4-ring PAHs have negative coefficients. This demonstrates that PC3 is a mixed component that mostly explains diagenetic input and intermediate weathered oils and that some samples contain significant levels of both diagenetic and petrogenic input. Therefore, a straightforward interpretation of the component is hindered by these mixed contributions and by naphthalenes series coefficients (C0-, C1-, and C4-negative in contrast to positive C2-C3-naphthalenes).

25.3.3.3 Biomarkers Data Analysis

In the last application of the chemometric approach, solely the biomarkers: terpanes; regular and diasteranes; and triaromatic steranes SICs (Table 25.2) were included as variables in the model. The preprocessing consisted of baseline removal, alignment ("training set" of 56 samples × 7654 data points per sample) and normalization to Euclidean norm within each SIC (**Scheme III**). This scheme ensures focus of the PCA on the relative composition within each of the biomarker groups. A three-component model describing 32.1% of the variance in the training

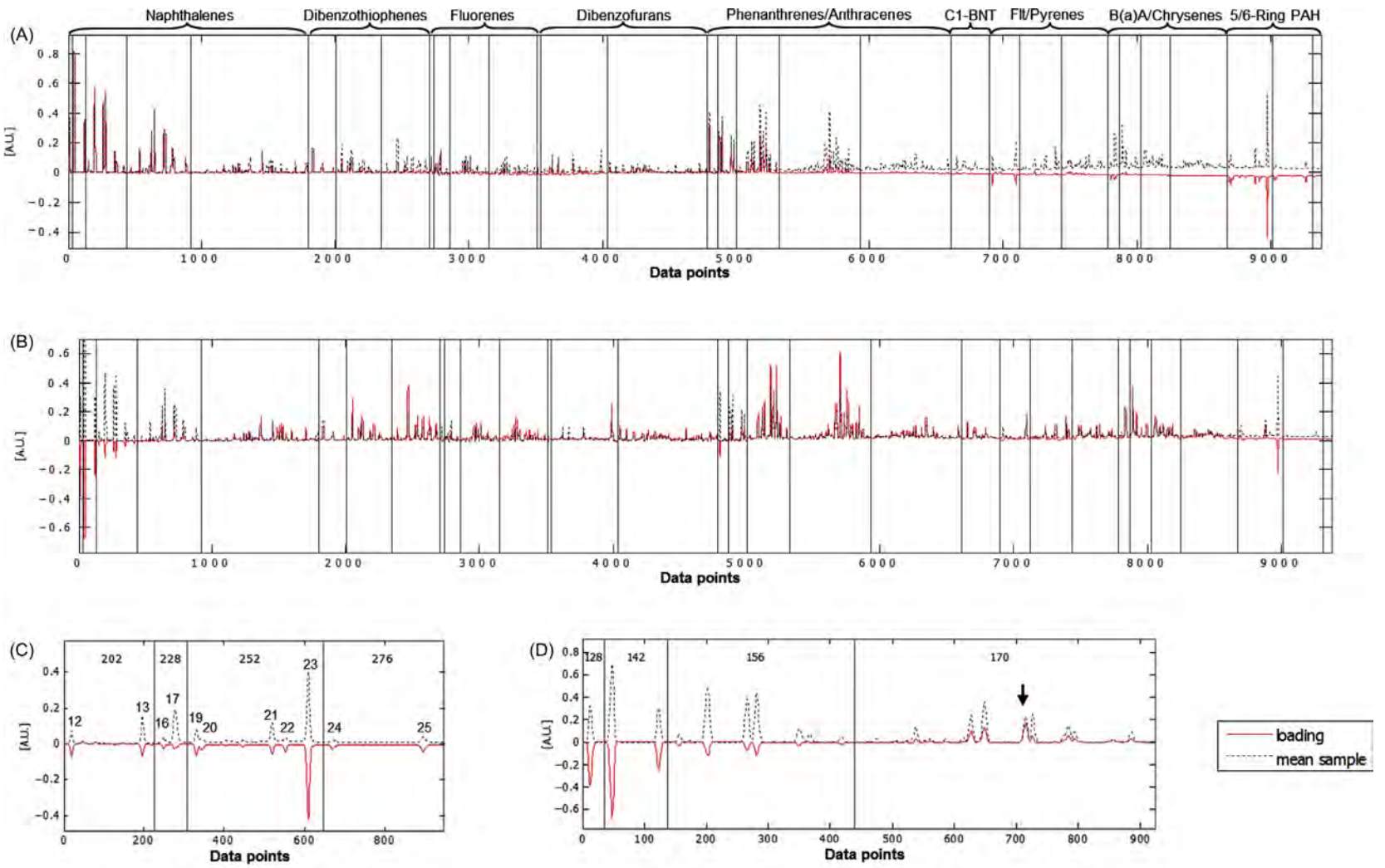

FIGURE 25.23 Thirty-eight PAHs data analysis: Loading plots for the principal component model of normalization **Scheme II** (concatenation and normalization to Euclidean norm): (A) PC1 and (B) PC2. The dotted lines are the mean chromatogram of the entire training set, while the solid lines are the loadings (AU: arbitrary units), (C) zoom of PC1 loadings for pyrogenic compounds, (D) zoom of PC2 loadings for naphthalenes (C4-naphthalenes were not included to improve the visualization). The SICs corresponding to C0−C4-benzothiophenes, acenaphthylene, and acenaphthene were omitted from the Loading plots (A) and (B) to improve the visualization. For these compounds, the loading coefficients are close to zero.

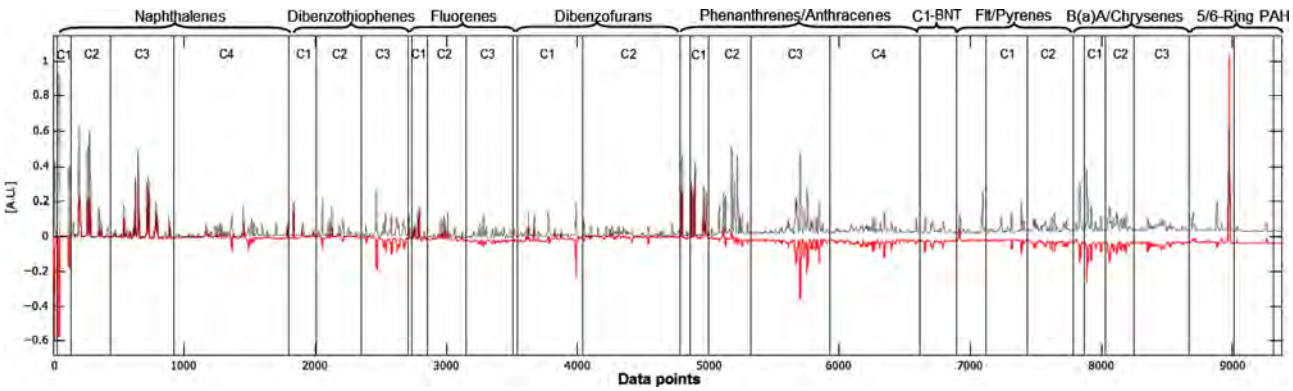

FIGURE 25.24 Thirty-eight PAHs data analysis: Loading plot of PC3 for the principal component model of normalization **Scheme II** (concatenation and normalization to Euclidean norm). The dotted lines are the mean chromatogram of the entire training set, while the solid lines are the loadings (A.U.: arbitrary units). The SICs corresponding to C0−C4-benzothiophenes, acenaphthylene, and acenaphthene were omitted to improve the visualization. For these compounds, the loading coefficients are close to zero.

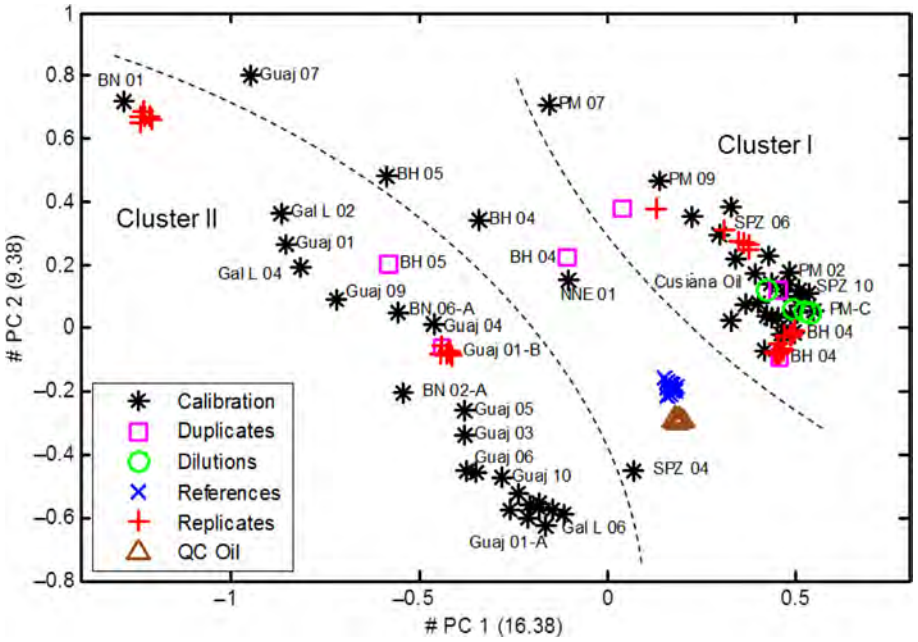

FIGURE 25.25 Biomarkers data analysis: Score plot of PC1 versus PC2 for the principal component model of normalization **Scheme III** (normalization to Euclidean norm within SICs). Some labels were omitted from the Score plot (A) to improve the readability.

set was found to be optimal as a clear bend in the explained variance of the validation set is observed and since the loadings above PC3 contain shift patterns. Fig. 25.25 shows the score plot of PC1 versus PC2 for the PC model, where two clusters can be identified.

Samples from the refinery area cluster in the upper right corner of the score plot (Fig. 25.25, Cluster I) with positive PC1 scores, and from around zero to positive PC2 scores. These samples have biomarker profiles with the highest similarity to the Cusiana oil (Fig. 25.26A). N.B. the Cusiana oil is located in the cluster of samples from the refinery area. The characteristics of these samples are among others that they have a high relative concentration of tricyclic terpanes, hopanes, particularly 17α(*H*),21β(*H*)-30-norhopane (H29) and 17α(*H*),21β(*H*)-hopane (H30), and in general a high relative concentration of steranes and triaromatic steranes (large positive PC1 loading coefficients, Fig. 25.27) and a low relative concentration of vegetation biomarkers from recent organic matter, e.g., diploptene (D) tentatively identified from literature (Venkatesan et al., 2003) (Figs. 25.26B and 25.27: BN 01). This latter peak (D) has a negative PC1 loading coefficient (Fig. 25.27).

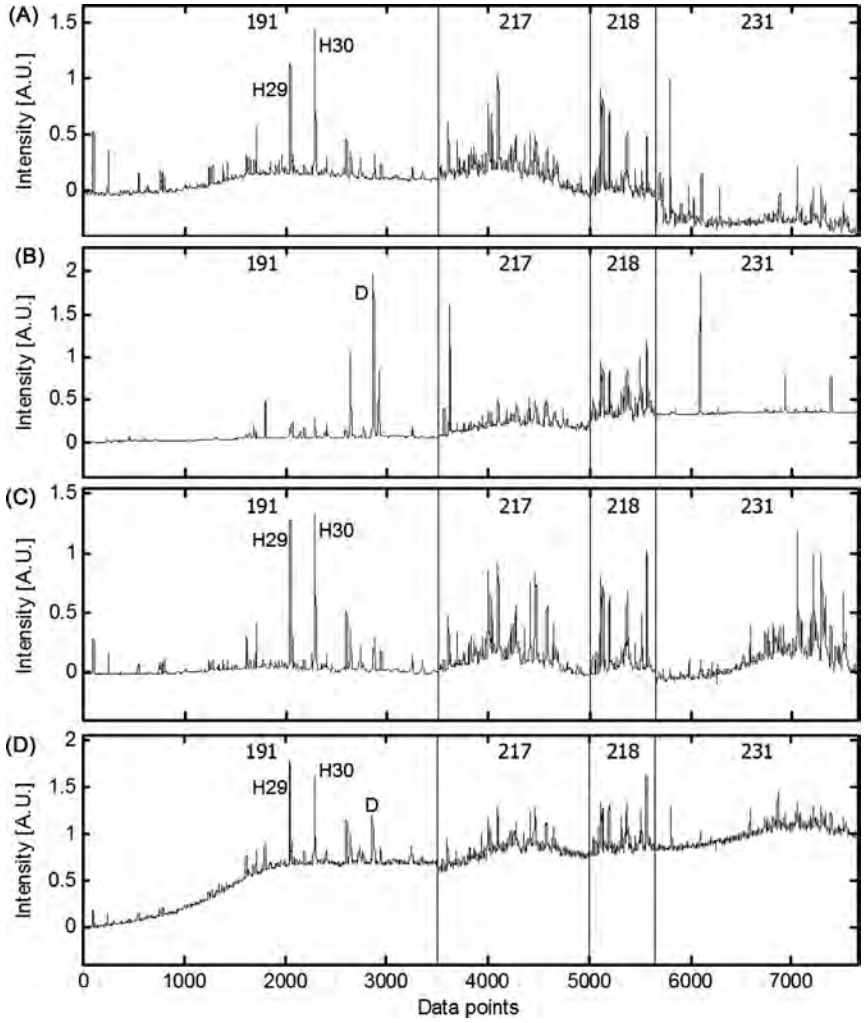

FIGURE 25.26 Biomarkers data analysis: Normalized data (**Scheme III**) of selected samples: **Cluster I**: (A) Cusiana oil; **Cluster II**: (B) BN 01, (C) Guaj 01-A, and (D) Guaj 09. The symbols stand for: diploptene (D), 17α(*H*),21β(*H*)-30-norhopane (H29) and 17α(*H*),21β(*H*)-hopane (H30).

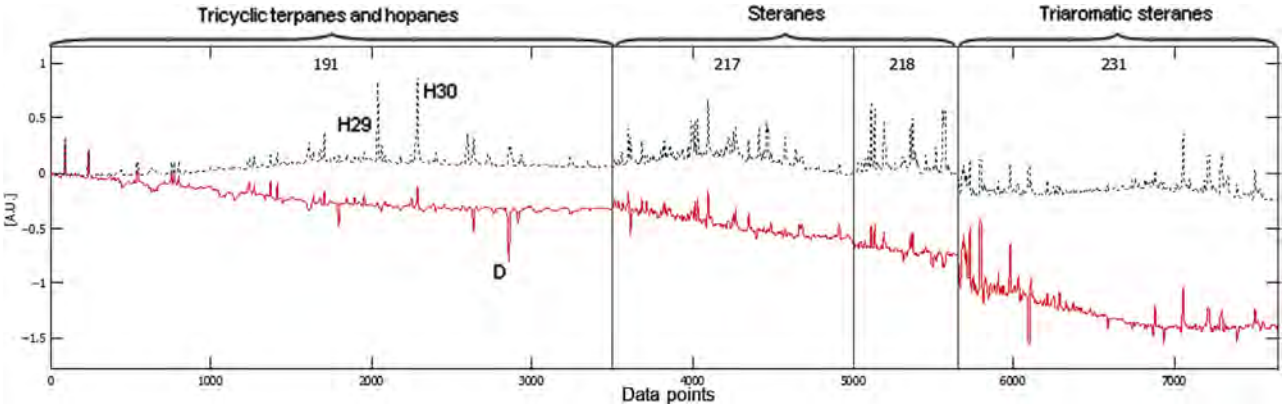

FIGURE 25.27 Biomarkers data analysis: Loading plot of PC1 for the principal component model of normalization **Scheme III** (normalization to Euclidean norm within SICs 191, 217, 218, and 231). The dotted lines are the mean chromatogram of the entire training set, while the solid lines are the loadings (A.U.: arbitrary units). The symbols stand for: diploptene (D), 17α(*H*),21β(*H*)-30-norhopane (H29) and 17α(*H*),21β(*H*)-hopane (H30).

Most of the samples in Cluster II contain petroleum biomarkers as well (Fig. 25.26C: Guaj 01-A and 25.26D: Guaj 09), however with a different composition than samples from Cluster I. Specifically, the ratio of H29 and H30 vary in samples from Cluster II. Therefore, the results showed that there are no evidences to conclude positive matches (or even a significant contribution) between the samples from outside the refinery area and the Cusiana oil.

25.4 CONCLUSIONS

DRs calculated from quantitative method through PAHs concentrations suggested that, in the majority of sediments from Iguaçu and Barigüi rivers collected in 2000 and 2001 campaigns, the main source is petrogenic. Only at the station upstream from the oil spill input in Barigüi River (M Bar), the pyrogenic source predominated in these two campaigns. The DRs that presented greater efficiency for source identification in sediments of Iguaçu and Barigüi rivers were $\sum$C1-Ph/Ph and $\sum$(other 3–6 ring PAH)/$\sum$(5 series of alkylated PAH). These DRs have the advantage of including alkylated compounds which are predominant in crude oils.

The method for source identification through semiquantitative DRs calculated from heights and areas of chromatograms (CEN, 2012) showed that after nearly a decade of occurrence of the spill, it was possible to confirm the relationship between the compounds found in soil samples of the internal area of the REPAR Refinery with the Cusiana oil spilled in the accident. However, this conclusion would not be reasonable explained without a previous knowledge on the area background, what is not a common element when dealing with waterborne spills.

The CHEMSIC method based on PCA of all signal intensity information contained in preprocessed and combined SICs showed that the most contaminated samples are inside the refinery area. These samples present a petrogenic pattern and different weathering degrees. There are indications that both physical weathering and biodegradation have occurred. The former is related to the preferential loss of whole families of less alkylated PAH isomers, while the latter is associated to changes in isomeric variations within alkylated PAH families in addition to loss of whole families. Samples from outside the refinery area are either less or not contaminated, or contain mixtures of diagenetic, pyrogenic, and petrogenic inputs where different proportions predominate. The locations farthest away from industrial activity (e.g., Balsa Nova samples) contains, as expected, the lowest levels of PAH contamination. Regarding the biomarkers results, there are no evidences to conclude positive matches between the sediment samples from outside the refinery area and the Cusiana oil.

Genuinely DRs should be able to discriminate different oils and oil products. This is often difficult to achieve when using quantitative ranges of DRs based on PAHs (Table 25.1), as known petrogenic distributions of PAHs may be affected by weathering and refining processes. There are not studies proposing new ranges when weathering has taken place. Also, for products, some of these refining processes occur at high temperatures and may form pyrogenic PAHs, e.g., 2-methyl anthracene in HFOs (Heavy Fuel Oils). Therefore, the DRs ranges in Table 25.1 should be used as a classification tool and the results should consider as many DRs as possible. Additionally, histograms with PAH distributions must be checked. These DRs are not a true-source identification method. On the other hand, they provide a quite simple way to easily assess a large number of samples.

Other quantitative methods which compare sample by sample based on PAH and biomarker DRs (not discussed in this chapter) may provide real source identification. One particular advantage of this approach is that the absolute concentration results are not biased by the period when the samples were injected, as a valid calibration curve corrects the instrumental variation over time. This is not the case of semiquantitative methods, where the relative results are more consistently comparable when samples are injected in the same instrument and sequentially. Moreover, for semiquantitative methods, one has to be certain that the results are within the linear calibration range of the instrument. The CEN (2012) Guideline provides information on advised concentrations for each type of oil/product. On the other hand, depending on the calibration target compounds and on the internal standards used by the laboratory, the quantitative results may be completely different, as many of the biomarkers do not have certified calibration standards commercially available. In this sense, the results among different laboratories are most likely incomparable.

In the past, mixing has been pointed out as a problem for semiquantitative methods, but as long as the raw data is available and the source samples are prepared in the same oil concentration (or at least at a known oil concentration which may be used to normalize raw chromatographic signals), there are simple ways to optimize the percent combination of heights (or areas) from suspect source samples, calculate mixed sources DRs, and finally compare with spill samples DRs. This has been successfully tested in OSINET-Round Robin 2014 and 2015 (no references

TABLE 25.7 Quantitative and Semiquantitative Methods in Source Identification: Advantages, Disadvantages, Applicability, and Expected Results

Method	Advantages	Disadvantages	Applicability	Expected results
Quantitative diagnostic ratios calculated from the compounds concentrations (PAHs)[a]	– Simplicity of calculation, using only basic math – Simplicity of classification, only related to ranges corresponding to each source	– Integration and quantification of PAHs are essential – Ranges have been established with oils and combustion products in temperate areas, not necessarily suitable for extrapolation to tropical conditions – For products, refining processes which occur at high temperatures may form pyrogenic PAHs – Weathering processes, which may affect the values of DRs, are not considered	– Studies with any number of samples – If there intent of establishing a relationship with a spilled oil, DRs should be tested with this oil beforehand and the result should be within the petrogenic range	– Basic sample classification depending on PAHs "theoretical" origin: petrogenic, pyrogenic, diagenetic, or mixed sources
Semiquantitative diagnostic ratios calculated from heights and areas of chromatograms (CEN, 2012)	– Quantitation of compounds is not required – Assertiveness and rigor of the results, especially for positive match conclusion	– Samples of the suspected source oils are necessary – Raw chromatographic data (peaks heights and areas) are required – Integration of chromatographic peaks of a large number of compounds – Advanced knowledge about the influence of weathering processes on DRs is indispensable to reasonable explain alteration trends – The scenario and also the background must be considered to achieve the final conclusion, what relies on analyst experience – A probable match conclusion weakens the degree of certainty	– Forensic studies with a few samples	– Establishment of unequivocal relationship between the spill sample and the suspected source oil
Semiquantitative chemometric method based on principal component analysis (PCA) of preprocessed and combined sections of selected ion chromatograms (CHEMSIC)	– Integration or quantification of the compounds is not required – Includes unknown or not traditionally analyzed compounds that may help in differentiation of samples – Allows for the separation of the contributions from coeluting compounds – Output results flexibility	– Raw chromatographic data (each point of signal intensity over time) are necessary – An erroneous chromatographic data preprocessing will ruin the results – Advanced knowledge of programing, matrix calculations, and statistics are essential – Knowledge about the composition of hydrocarbons sources and weathering effects is indispensable for loading interpretation	– Studies with any number of samples, although the more, the better	– Many possibilities depending on the type of compositional variation present in the sample set and on the preprocessing. It can provide differentiation on levels of contamination, source classification, degrees of weathering, or even strict source identification of oil or products

[a]*Based on ranges for source classification.*

available so far). The distinction of qualitatively similar oils, also previously considered a limitation of Nordtest (1991) protocol, was worked out by CEN (2012) Guideline, as PW plots took care of oils that exhibit qualitatively similar fingerprints within m/z's, but differ in absolute concentrations of different compound groups.

Semiquantitative methods are independent of calibration standards for quantification. However, the semiquantitative procedure for source identification through DRs calculated from heights and areas of chromatograms (CEN, 2012) requires the integration of a large number of compounds or compound groups, maintaining the same criteria for peak "identification" and integration, what is a quite laborious task even when a small number of samples are evaluated. This approach considers not only the conclusions themselves but as important as is the way they have been obtained. If a positive match is concluded, there are no differences between the suspected source and the spill samples and an unequivocal relationship is established, what is essential in court trials. However, a less strong output as a "probable match" will certainly raise questions on the degree of certainty of the conclusion, since it implies in causality and punitive financial consequences. In recent round robin exercises using the CEN methodology, sometimes the conclusion varied from positive, probable match or even inconclusive even though the same variations were observed by the participants. The problem lies in the analyst interpretation of the conclusion definitions. Hence, there is a need to standardize the users understanding, which again depends on experience in oil spill identification and also there is space for method improvement in the sense to establish more quantitative conclusions.

The CHEMSIC method has the distinct advantages that no prior peak integration or peak quantification is necessary and unknown or not traditionally analyzed compounds and unique chemical features are retained and can lead to the recognition of new indicator compounds for source identification. Moreover, the method allows for the separation of the contributions from coeluting compounds and most likely increase the probability for separating samples with similar hydrocarbon composition. Furthermore, different normalization approaches were tested and discussed, focusing the chemometric not only on differences in the chemical composition and concentration of samples but also on source identification and weathering behavior of petroleum compounds. A major drawback is that the mathematics behind chromatogram preprocessing is not trivial to be computationally understood and implemented. And also, although PCA is a well-known technique, not all chemists are experienced in statistics and many may find it difficult to interpret the information contained in the loading plots, which in turn explains the score plots.

Finally, understanding and explaining weathering is the most challenging task in source identification. Weathering modifies many PAH DRs and may also affect biomarker DRs depending on the severity of the process and of the time that has passed since the spill. In a recent spill, evaporation plays the main role, and it is relatively easy to understand its respective changes in oil composition. However, as time passes, other processes such as photooxidation, dissolution, and biodegradation introduce simultaneous alterations which modify differently the compound patterns, and it may be difficult to explain these changes and to reach a sound forensic positive match conclusion. Insufficient knowledge about the fate of oil in severely weathered oil samples indicate that there is a need to follow the process of weathering much closer, which means regular sampling and analysis over time. Whether qualitative, semiquantitative, or quantitative methods are used; weathering comprehension requires skills and profound experience of the analyst when analyzing the results.

Regarding the different methods for source identification shown in this chapter, Table 25.7 summarizes the authors' views on main advantages, disadvantages, and indicates the best opportunities for application and the expected results.

Acknowledgments

The study was financially supported by Petróleo Brasileiro S.A., the Torkil Holms Foundation, the Lundbeck Foundation, and the COWI Foundation. We want to thank Rafael André Lourenço and Leandro Franco Macena de Araújo for their fundamental work on sample preparation, Jette Petersen for laboratory assistance, Leandro Rodrigues de Freitas and Ivanil Ribeiro Cruz for their assistance on mapping the study area, and Maria de Fátima G. Meniconi and Irene T. Gabardo for their constructive comments on the manuscript. We would also like to acknowledge Giorgio Tomasi for development of m-files used in this study.

References

Baumard, P., Budzinski, H., Michon, Q., Garrigues, P., Burgeot, T., Bellocq, J., 1998. Origin and bioavailability of PAHs in the Mediterranean Sea from mussel and sediment records. Estuar., Coast. Shelf Sci. 47, 77–90.

Bernabeu, A.M., Fernández-Fernández, S., Bouchette, F., Rey, D., Arcos, A., Bayona, J.M., et al., 2013. Recurrent arrival of oil to Galician coast: the final step of the Prestige deep oil spill. J. Hazard. Mater. 250–251, 82–90.

Boehm, P.D., 2005. Polycyclic aromatic hydrocarbons (PAHs). In: Morrison, R.D., Murphy, B.L. (Eds.), Environmental Forensics: Contaminant Specific Guide. Academic Press, Burlington, pp. 313–337, chap. 15.

Boehm, P.D., Farrington, J.W., 1984. Aspects of the polycyclic aromatic hydrocarbons geochemistry of the recent sediments in the Georges Bank region. Environ. Sci. Technol. 18 (11), 840–845.

Bost, F.D., et al., 2001. Aerobic biodegradation of hopanes and norhopanes in Venezuelan crude oils. Org. Geochem. 32, 105–114.

Budzinski, H., Jones, I., Bellocq, J., Piérard, C., Garrigues, P., 1997. Evaluation of sediment contamination by polycyclic aromatic hydrocarbons in the Gironde estuary. Mar. Chem. 58, 85–97.

Cen, 2012. PD CEN/TR 15522-2:2012—Oil Spill Identification—Waterborne Petroleum and Petroleum Products—Part 2: Analytical Methodology and Interpretation of Results. [S.l.], BSI, p. 142.

Christensen, J.H., Tomasi, G., 2007. Review: Practical aspects of chemometrics for oil spill fingerprinting. J. Chromatogr. A 1169, 1–22.

Christensen, J.H., Tomasi, G., Hansen, A.B., 2005a. Chemical fingerprinting of petroleum biomarkers using time warping and PCA. Environ. Sci. Technol. 39, 255–260.

Christensen, J.H., Hansen, A.B., Karlson, U., Mortensen, J., Andersen, O., 2005b. Multivariate statistical methods for evaluating biodegradation of mineral oil. J. Chromatogr. A 1090, 133–145.

Christensen, J.H., Hansen, A.B., Tomasi, G., Mortensen, J., Andersen, O., 2004. Integrated methodology for forensic oil spill identification. Environ. Sci. Technol. 38 (10), 2912–2918.

Christensen, J.H., Tomasi, G., Scofield, A.L., Meniconi, M.F.G., 2010. A novel approach for characterization of polycyclic aromatic hydrocarbon (PAH) pollution patterns in sediments from Guanabara Bay, Rio de Janeiro, Brazil. Environ. Pollut. 58, 3290–3297.

Colombo, J.C., Pelletier, E., Brochu, C., Khalil, M., 1989. Determination of hydrocarbon sources using *n*-alkane and polyaromatic hydrocarbon indexes. Case study: Rio de La Plata Estuary, Argentina. Environ. Sci. Technol 23, 888–894.

Dahlmann, G., Kienhuis, P., 2005. Oil Spill Identification—Round Robin 2005. The Comparison of Four Bilge Samples. Hamburg. Available at <http://www.bonnagreement.org/osinet/oil-spill-identification> (accessed 12.07.2017).

Dahlmann, G., 2006. Report RR 2006: First round robin test within Bonn-OSINet. The comparison of 4 crude oil samples. Hamburg. Available at <http://www.bonnagreement.org/osinet/oil-spill-identification> (accessed 12.07.2017).

Dahlmann, G., 2008. Report RR 2008: The Comparison of Three Crude Oil Samples. Hamburg. Available at <http://www.bonnagreement.org/osinet/oil-spill-identification> (accessed 12.07.2017).

Díez, S., Sabaté, J., Viñas, M., Bayona, J.M., Solanas, A.M., Albaigés, J., 2005. The Prestige oil spill. I. Biodegradation of a heavy fuel oil under simulated conditions. Environ. Toxicol. Chem. 24, 2203–2217.

Douglas, G.S., Owens, E.H., Hardenstine, J., Prince, R.C., 2002. The OSSA II pipeline oil spill: the character and weathering of the spilled oil. Spill Sci. Technol. Bull. 7 (3–4), 135–148.

Falkiewicz, F.H., 2003. Oil spill in the Iguassu River—Araucaria, Parana, Brazil: cleaning and restoration of rivers and inundation areas. In: International Oil Spill Conference, 2003, Vancouver, British Columbia, Canada. American Petroleum Institute, Washington, DC, pp. 643–648. Available at <http://www.ioscproceedings.org/doi/pdf/10.7901/2169-3358-2003-1-643>.

Gallotta, F.D.C., Christensen, J.H., 2012. Source identification of petroleum hydrocarbons in soil and sediments from Iguaçu River Watershed, Paraná, Brazil using the CHEMSIC method (CHEMometric analysis of Selected Ion Chromatograms). J. Chromatogr. A 1235, 149–158.

Garrigues, P., Budzinski, H., Manitz, M.P., Wise, S.A., 1995. Pyrolytic and petrogenic inputs in recent sediments: a definitive signature through phenanthrene and chrysene compound distribution. Polycycl. Aromat. Compd. 7, 275–284.

Gschwend, P.M., Hites, R.A., 1981. Fluxes of polycyclic aromatic hydrocarbons to marine and lacustrine sediments in the north eastern United States. Geochim. Cosmochim. Acta 45, 2359–2367.

Hydrogéo Plus Inc., 2009. Avaliação dos Dados Ambientais de 2007–2008 e proposições futuras: Ponto 0 e Áreas Externas. OSPAR/REPAR. Versão Final. Araucária, PR. p. 66.

Hydrogéo Plus Inc., 2010. Avaliação dos Dados Ambientais de 2007–2010 e proposições futuras: Ponto 0. REPAR/OSPAR. Araucária, PR. p. 103.

IBGE, 2012. Água doce: Qualidade de águas interiores. In: Indicadores de Desenvolvimento Sustentável: Brasil 2012. Rio de Janeiro. cap. 10. (Série Estudos e Pesquisas. Informação Geográfica, n. 9). Available at <http://biblioteca.ibge.gov.br/visualizacao/livros/liv59908.pdf> (accessed 11.07.2017).

Kienhuis, P., Dahlmann, G., 2004. Oil Spill Identification—Round Robin 2004. The comparison of three gasoil samples. Hamburg. Available at <http://www.bonnagreement.org/osinet/oil-spill-identification> (accessed 12.07.2017).

Kienhuis, P., Dahlmann, G., 2009. Report RR 2009: The Comparison of Six Bilge Samples. Hamburg. Available at <http://www.bonnagreement.org/osinet/oil-spill-identification> (accessed 12.07.2017).

Kienhuis, P., Dahlmann, G., 2015. Round Robin 2013. The Comparison of Four Samples from an Oil Spill in a Swedish Harbor. Lelystad. Available at <http://www.bonnagreement.org/osinet/oil-spill-identification> (accessed 12.07.2017).

Kienhuis, P., Dahlmann, G., 2014. RR2011—The Comparison of 7 HFO Samples. Lelystad. Available at <http://www.bonnagreement.org/osinet/oil-spill-identification> (accessed 12.07.2017).

Kienhuis, P., Dahlmann, G., 2007. Second Intercalibration Round in the Framework of Bonn-OSINET-Round Robin 2007. The Comparison of Six HFO Samples. Hamburg. Available at <http://www.bonnagreement.org/osinet/oil-spill-identification> (accessed 12.07.2017).

Lobão, M.M., 2007. Identificação de derrames de óleo no mar: um estudo de caso. Rio de Janeiro. 158 f. Dissertação (Mestrado em Química Analítica)—Instituto de Química, Universidade Federal do Rio de Janeiro, Rio de Janeiro.

Malmquist, L.M.V., Olsen, R.R., Hansen, A.B., Andersen, O., Christensen, J.H., 2007. Assessment of oil weathering by gas chromatography–mass spectrometry, time warping and principal component analysis. J. Chromatogr. A 1164, 262–270.

Massart, D.L., Vandeginste, B.G.M., Buydens, L.M.C., De Jong, S., Lewi, P.J., Smeyers-Verbeke, J., 1997. Handbook of Chemometrics and Qualimetrics: Part A. Data Handling in Science and Technology, vol. 20A. Elsevier, Amsterdam, p. 867.

Massone, C.G., et al., 2013. Revisiting hydrocarbons source appraisal in sediments exposed to multiple inputs. Mar. Pollut. Bull. 73, 345–354.

Meniconi, M.F.G., 2007. Hidrocarbonetos policíclicos aromáticos no meio ambiente: diferenciação de fontes em sedimentos e metabólitos em bile de peixe. Natal, 2007. 231 f. Tese (Doutorado em Química)—Centro de Ciências Exatas e da Terra, Universidade Federal do Rio Grande do Norte, Natal.

Meniconi, M.F.G., Gabardo, I.T., Carneiro, M.E.R., Barbanti, S.M., Silva, G.C., Massone, C.G., 2002. Brazilian oil spills chemical characterization—case studies. Environ. Forensics 3, 303–321.

Mudge, S.M., 2007. Multivariate statistical methods in environmental forensics. Environ. Forensics 8 (1–2), 155–163.
Nielsen, N.P.V., Carstensen, J.M., Smedsgaard, J., 1998. Aligning of single and multiple wavelength chromatographic profiles for chemometric data analysis using correlation optimized warping. J. Chromatogr. A 805, 17–35.
Nordtest, 1991. Nordtest Method for Oil Spill Identification. NT Chem 001. Edition 2. Nordtest, Esbo, Finland.
Page, D.S., Boehm, P.D., Douglas, G.S., Bence, A.E., 1995. Identification of hydrocarbon sources in the benthic sediments of Prince William Sound and the Gulf of Alaska following the Exxon Valdez oil spill. In: Wells, P.G., Buttler, J.N., Hughes, J.S. (Eds), (Eds.), Exxon Valdez Oil Spill: Fate and Effects in Alaskan Waters. American Society for Testing and Materials, Philadelphia, PA, pp. 41–83.
Peters, K.E., Walters, C.C., Moldowan, J.M., 2007. The Biomarker Guide, second ed. Cambridge University Press, Cambridge, UK, p. 1196.
Petrobras, 2001. Centro de Pesquisas Leopoldo Américo Miguez de Mello (CENPES) e Refinaria Presidente Getúlio Vargas (REPAR). Caracterização química e ecotoxicológica de água e sedimentos dos rios Barigüi e Iguaçu. Rio de Janeiro, RJ.
Prahl, F.G., Carpenter, R., 1983. Polycyclic aromatic hydrocarbon (PAH)-phase associations in Washington coastal sediment. Geochim. Cosmochim. Acta 47, 1013–1023.
Prince, R.C., et al., 1994. 17α(*H*),21β(*H*)-hopane as a conserved internal marker for estimating the biodegradation of crude oil. Environ. Sci. Technol. 28, 142–145.
Puerari, L., 2011. Avaliação ambiental dos Rios Barigüi e Alto Iguaçu (Paraná): a contaminação atual e a contaminação residual relacionada ao acidente da REPAR. Porto Alegre, 2011. 110f. Dissertação (Mestrado em Geociências)—Universidade Federal do Rio Grande do Sul, Porto Alegre.
Qing, Z., Peiyan, S. Report RR 2010: The Comparison of HFO and Crude Oil Samples. Available at <http://www.bonnagreement.org/osinet/oil-spill-identification> (accessed 12.07.2017).
Radović, J.R., Aeppli, C., Nelson, R.K., Jimenez, N., Reddy, C.M., Bayona, J.M., Albaigés, J., 2013. Assessment of photochemical processes in marine oil spill fingerprinting. Mar. Pollut. Bull. 79 (1–2), 268–277. Available at <http://dx.doi.org/10.1016/j.marpolbul.2013.11.029>.
Readman, J.W., Fillmann, G., Tolosa, I., Bartocci, J., Villeneuve, J.P., Catinni, C., et al., 2002. Petroleum and PAH contamination of the Black Sea. Mar. Pollut. Bull. 44, 48–62.
Sicre, M.A., Marty, J.C., Saliot, A., 1987. Aliphatic and aromatic hydrocarbons in different sized aerosols over the Mediterranean sea: occurrence and origin. Atmos. Environ 21, 2247–2259.
Skov, T., van Den Berg, F., Tomasi, G., Bro, R., 2006. Automated alignment of chromatographic data. J. Chemom. 20, 484–497.
Soclo, H., 1986. Etude de la Distribution des Hydrocarbures Aromatiques Polycycliques dans les Sédiments Marins Récents, Identification des Sources. Bordeaux, 1986. 158 f. Ph.D. Thesis—University Bordeaux I, Bordeaux, France.
Tolosa, I., De Mora, S., Sheikholeslami, M.R., Villeneuve, J.P., Bartocci, J., Cattini, C., 2004. Aliphatic and aromatic hydrocarbons in coastal Caspian Sea sediments. Mar. Pollut. Bull. 48, 44–60.
Tomasi, G., Van Den Berg, F., Andersson, C., 2004. Correlation optimized warping and dynamic time warping as preprocessing methods for chromatographic data. J. Chemom. 18, 231–241.
UFRGS, 2003a. Instituto de Geociências. Programa de monitoramento do Ponto Zero: relatório da fase de preparação da infraestrutura. Porto Alegre, RS, p. 21.
UFRGS, 2003b. Instituto de Geociências. Programa de monitoramento diagnóstico do Ponto Zero: 2ª campanha de monitoramento. Porto Alegre, RS, p. 37.
UFRGS, 2003c. Instituto de Geociências. Programa de monitoramento diagnóstico do Ponto Zero: 3ª campanha de monitoramento. Porto Alegre, RS. p. 35.
UFRGS, 2004. Instituto de Geociências. Programa de monitoramento diagnóstico do Ponto Zero: 4ª campanha de monitoramento. Porto Alegre, RS. p. 41.
USEPA, 2007. Method 8270D: Semivolatile Organic Compounds by Gas Chromatography/Mass Spectrometry (GC/MS). Available at <http://www.epa.gov/wastes/hazard/testmethods/sw846/online/8_series.htm> (accessed 11.07.2017).
Van Den Berg, R.A., Hoefsloot, C.J.H., Westerhuis, J.A., Smilde, A.K., Van Der Werf, M.J., 2006. Centering, scaling, and transformations: improving the biological information content of metabolomics data. BMC Genom. 7, 142.
Venkatesan, M.I., Ruth, E., Rao, P.S., Nath, B.N., Rao, B.R., 2003. Hydrothermal petroleum in the sediments of the Andaman Backarc Basin, Indian Ocean. Appl. Geochem. 18, 845–861.
Yunker, M.B., Macdonald, R.W., Brewer, R., Vingarzan, R., Mitchell, R.H., Goyette, D., et al., 2002. PAHs in the Fraser River Basin: a critical appraisal of PAH ratios as indicators of PAH source and composition. Org. Geochem. 33 (4), 489–515.
Wagener, A., Hamacher, C., Farias, C., Godoy, J.M., Scofield, A., 2010. Evaluation of tools to identify hydrocarbon sources in recent and historical sediments of a tropical bay. Mar. Chem. 121, 67–79.
Wang, Z., Stout, S.A., 2007. Oil spill Environmental Forensics: Fingerprinting and Source Identification. Elsevier Academic Press, Burlington, MA, p. 554.
Wang, Z., Fingas, M., Blenkinsopp, S., Sergy, G., Landriault, M., Sigouin, L., et al., 1998a. Comparison of oil composition changes due to biodegradation and physical weathering in different oils. J. Chromatogr. A 809, 89–107.
Wang, Z., Fingas, M., Page, D.S., 1999. Review. Oil spill identification. J. Chromatogr. A 843, 369–411.
Wang, Z., Fingas, M., Owens, E.H., Sigouin, L., Brown, C.E., 2001. Long-term fate and persistence of the spilled Metula oil in a marine salt-marsh environment: degradation of petroleum biomarkers. J. Chromatogr. A 926, 275–290.
Wang. Z.D., Fingas, M., Sigouin, L., Landriault, M., Li, K., Lambert, P., et al., 1998b. Quantitative characterization of PAHs in burn residue and soot samples and differentiation of pyrogenic PAHs from petrogenic PAHs—The 1994 Mobile Burn Study. In: Proceedings of the 21st Arctic and Marine Oil Spill Program (AMOP) Technical Seminar, Environment Canada, Ottawa, pp. 673–704.

CHAPTER

26

Different Forensic Approaches for Hydrocarbons Sources Identification in an Urban Cluster Environment: Guanabara Bay

Maria de F.G. Meniconi[1], *Angela de L.R. Wagener*[2] *and Jan H. Christensen*[3]

[1]Research and Development Center (CENPES), Petroleo Brasileiro S.A (PETROBRAS), Rio de Janeiro, Brazil
[2]Pontifical Catholic University of Rio de Janeiro (PUC-Rio), Rio de Janeiro, Brazil [3]University of Copenhagen, Frederiksberg, Denmark

BIOGRAPHIES

Maria de Fatima Guadalupe Meniconi is an environmental geochemist with experience in petroleum industry for 30 years. She has carried out research on chemical fingerprinting of petroleum and derivatives, oil spill assessment and monitoring, fisheries safety evaluation, environmental off-shore production wells monitoring and source identification of hydrocarbons in the environment. She has obtained her M.Sc. (1985) in Chemical Engineering from Federal University of Rio de Janeiro (COPPE), Brazil, her MPhil. (1999) in Instrumentation and Analytical Science from University of Manchester Institute of Science and Technology (UMIST), United Kingdom, and her Ph.D. (2007) in Chemistry from Federal University of Rio Grande do Norte (UFRN), Brazil. She is currently a senior research scientist of the Research and Development Center of Petrobras, Rio de Janeiro, Brazil.

Jan H. Christensen (born in Hillerød, Denmark, 1973) is a Full Professor in Environmental Analytical Chemistry. He is leader of the Analytical Chemistry group, Department of Plant and Environmental Sciences, University of Copenhagen, Denmark and heads the Research Centre for Advanced Analytical Chemistry (RAACE). He has pioneered cutting-edge analytical and chemometric methods for oil hydrocarbon fingerprinting and now works on all aspects of contaminant fingerprinting, petroleomics, and metabolomics. He develops analytical platforms and new tools to handle and process complex data from cutting-edge analytical instrumentation and apply this chemical fingerprinting concept for analysis of complex mixtures of organic contaminants and in numerous industry project collaborations with the petrochemical, environmental, and food industry. He has authored and coauthored more than 70 peer-reviewed papers and book chapters on these topics. His current research focus is on development and application of multidimensional chromatography platforms in combination with chemometric data analysis.

Angela de Luca Rebello Wagener holds a Bachelor degree in Chemistry (UERJ, 1969) and Ph.D. in Chemistry (PUC-Rio, 1974) and was a Post-Doc at Technical University of Aachen (1978/79), received the Alexander von Humboldt Stiftung scholarship, and was a Visiting Scholar at Scripps Institution of Oceanography San Diego (USA; 1988). She was a Full Professor of Chemistry at Pontifical Catholic University of Rio de Janeiro (PUC-Rio) from 1994 to 2014 and an Emeritus Professor from 2015 to present. Dr. Wagener was also a Senior Researcher of the National Research Council (Brazil) since 1991 (1A), Scientist of the State of Rio de Janeiro (FAPERJ). Acting Head of the Marine Studies Laboratory/IAEA, Monaco (1994), Visiting Researcher at KFA/Jülich and GKSS (Germany, several occasions), and Visiting Professor at the University of Mainz, Visiting Professor at ETH/Zürich, Switzerland (2006), and Honorary Professor at the University of Plymouth (2000–02). She was member of the Scientific and Technical

Oil Spill Environmental Forensics Case Studies.
DOI: http://dx.doi.org/10.1016/B978-0-12-804434-6.00026-4

Advisory Panel of the Global Environmental Facility (1998–2002) and Director of the Chemistry Department at PUC-Rio (2011–13). She has participated of innumerous national and international scientific meetings and congresses; supervised more than 50 Dissertations and Thesis; published more than 120 scientific papers in international peer-reviewed journals and coauthored a number of book chapters. Dr. Wagener has acted as reviewer for prestigious scientific journals, acted as consultant for several companies and NGOs, and founded and coordinated the Marine Environment Laboratory at PUC-Rio dedicated to studying the presence and fate of organic and inorganic contaminants especially in the marine environment. The lab became a reference in Brazil for studies related to petroleum environmental forensic. In 2006, she received the Walter Mors Medal granted by the Brazilian Chemistry Society for contributions to the development of chemistry in Brazil and also the Zayed Prize as coauthor of the Millennium Ecosystem Assessment (UNO). She was a member of the GEOTRACES Scientific Committee, of the Honors and Recognition Committee of the AGU, and currently is member of the Brazilian Academy of Science.

26.1 INTRODUCTION

Guanabara Bay, located in Rio de Janeiro, Brazil, is a tropical estuarine system surrounded by a highly urbanized and industrialized area undergoing continuous and poorly controlled growth since 1980. Actually, it comprises the second major industrial park in the country (JICA, 1994; Pereira, 1996; Amador, 1997; FEEMA, 1998; Amador, 2013; Comite Baia de Guanabara, 2016; Inea, 2016). There are ports, oil terminals, dockyards, and marinas, supporting heavy navigation and petroleum industry activities in the bay. It is also the final destination of domestic and industrial waste from the Greater Rio de Janeiro. Guanabara Bay presents chronic pollution condition nowadays, typical of a densely populated metropolis (Carreira et al., 2004; Silva, 2004; Machado et al, 2004; Francioni et al, 2007; Fernandez et al, 2005; Baptista Neto et al., 2006; Wagener et al., 2012; Cordeiro et al., 2015). In January 2000, the bay was a scene of an oil spill of approximately 1300 m^3 of marine heavy fuel oil, reaching islands and shorelines at the northern part of the bay (Meniconi et al., 2002; Gabardo et al., 2001). In addition, the northeast shoreline mangrove of the bay was also affected by a diesel oil spill in 2005 resulting from a cargo train accident near Macacu River, also known as Caceribu River.

Among all contaminants, possibly present in Guanabara Bay sediments, hydrocarbons, notably polycyclic aromatic hydrocarbons (PAHs), are pollutants of major interest due to their ubiquitous characteristics and their potential to pose risk to organisms and human health. These compounds may be introduced into the ecosystems by different pathways, and they are mostly deposited in bottom sediments. Their input can be from natural and anthropogenic processes, including natural fires, oil seepage, diagenetic processes, sewage and industrial wastes, urban runoff, maritime transport, pipelines, oil spills, incomplete fossil fuels, and coal combustion (Tissot and Welte, 1984; Fingas, 2001; Volkman et al., 1992; Bouloubassi and Saliot, 1993; Kavouras et al., 2001; Yunker et al., 2002; Lima et al., 2005). The identification of the major sources of hydrocarbons is crucial for controlling their input into the environment and many studies have been carried out worldwide (Budzinki et al., 1997; Boehm et al., 1997; Wang et al., 1999; Soclo et al., 2000; Stout et al., 2001; Readman et al, 2002; Yunker et al., 2002; Burns et al., 2006; Meniconi and Barbanti, 2007; Gallotta and Christensen, 2012). The source identification of hydrocarbons has become of special interest in Guanabara Bay due to the rise of fossil fuel production and uses in the area.

In addition to the incidence of multiple hydrocarbons sources on the same site, it must be emphasized that these compounds, when released to the environment, are also subject to transport and transformation processes, which are major challenges to source discrimination, apportionment and identification (Budzinki et al., 1997; Wang et al., 1999; Yunker et al., 2002). These processes are of special concern in tropical estuarine systems such as Guanabara Bay, due to the complexity of the ecosystem with natural salinity gradients encompassing diverse habitats: mangroves, rivers, sandy beaches, and rocky shores (Amador, 1997). Estuaries are amongst the most threatened coastal ecosystems by anthropogenic activities (McLuski and Elliot, 2004).

In this chapter we provide a critical evaluation of results obtained from the use of three different approaches to assess Guanabara Bay hydrocarbon data. The goal is contributing to overcome the challenge of identifying sources of hydrocarbons in the Bay's sediments. The samples were collected between 2005 and 2007, from 5 to 7 years after the oil spill of January 2000, as part of the project entitled Environment Assessment of Guanabara Bay coordinated by Petrobas Research and Development Center (CENPES/Petrobras).

The efficiency for source identification of hydrocarbons in Guanabara Bay sediments shall be compared using the results from the following three different approaches, as follows: *Approach 1*: data based on gas chromatography – flame ionization detector (GC-FID) and gas chromatography - mass spectrometry (GC-MS) hydrocarbons

quantitative analyses and the application of environmental geochemistry interpretation, including diagnostic ratios and new plots such as, the five alkylated PAH series (naphthalenes, fluorenes, dibenzothiophenes, phenanthrenes and chrysenes) as function of unresolved complex mixture (UCM) and resolved peaks (RP) and the five alkylated PAH series as function of the 3–6 ring PAHs; *Approach 2*: Multivariate analysis applied to the quantitative data; and *Approach 3*: semiquantitative PAH analyses and application the CHEMSIC method.

26.2 METHODS AND SAMPLES

26.2.1 Study Area

Guanabara Bay is an estuarine system with a water surface area of 384 km^2 and a drainage basin of 4080 km^2. It encompasses 50 rivers and channels from 16 districts, housing 11 million inhabitants, and it is presently the second major industrial park in the country (JICA, 1994; Kjerfve et al., 1997; Amador, 1997; FEEMA, 1998; Meniconi and Barbanti, 2007; Amador, 2013; Comite Baia de Guanabara, 2016; Inea, 2016). Despite the fact that about 50% of the bay has shallow waters up to 5 m depths, the renew of the bay water is, in average, 11 days (Kjerfve et al., 1997). The central channel, with water depths of up to 50 m, is considered as less contaminated due to the hydrodynamics and to the greater distance from land sources. The bay is crossed by a 14-km-long bridge with a rate of 150,000 vehicles per day, contributing to hydrocarbons inputs via rain water drainage and atmospheric emissions.

The bay houses two large ports, two oil refineries, three oil terminals and several dockyards and marinas, supporting intense commercial and leisure navigation, and petroleum industry activities. Intensive inputs of largely untreated domestic sewage, constant runoff and industrial effluents contribute to the contamination (Ferreira, 1995; Consorcio Ecologus-Agar, 2005; FEEMA, 1998; Inea, 2016). Despite the severe pollution, artisanal fishery activities are intense, including 208 fixed fish traps, gillnets, hand-line and trawlers (Jablonski et al., 2006). The bay has two mangrove areas, one located at the northwest shoreline, near an urban and industrial area, and the other, the largest and more preserved one, at the northeast shoreline, inside an environmental protection area (APA in Portuguese). Fig. 26.1 shows features of the Guanabara Bay.

Data from literature provides quantitative information on the levels of pollution in the bay. Up to 465 t /day of Biochemical Oxygen Demand (BOD), predominantly from untreated domestic sewage (22 m^3/s), and about 3.1 t/day of DBO from industrial waste (0.266 m^3/s) contribute to low oxygen level of waters below the shallow photic zone (Consorcio Ecologus-Agar, 2005). About 5000 t/day of solid waste discharge is responsible for a permanent trash line along the bay coast. The chronic pollution in Guanabara Bay is typical of aquatic systems under influence of large metropolis lacking adequate infrastructure to support the continuous and intense population growth (Perin et al, 1997; Carreira et al., 2004; Silva, 2004; Machado et al, 2004; Francioni et al, 2007; Fernandez et al, 2005; Baptista Neto et al, 2006; Wagener et al., 2012; Cordeiro et al., 2015). In addition, an oil spill occurred in January 2000, with the release of approximately 1300 m^3 of marine heavy fuel oil (MF380), which spread over the water surface and reached islands and shorelines at the north part of the bay (Meniconi et al., 2002; Gabardo et al., 2001). The location of the oil spill accident is marked with a bold circle in Fig. 26.1 close to the sampling locations at Iguaçu River and Sarapuí River. The northeast shoreline mangrove was also affected by a diesel oil spill in 2005, resulted from a cargo train accident near Macacu River.

The rivers in the northwest region of the bay are the most polluted and impacted by litter disposal, domestic sewage and industrial residues. Iguacu River receives effluent from an oil refinery as well as domestic sewage. Sarapui and Sao Joao do Meriti Rivers are located in a highly urbanized and industrialized area, therefore being very contaminated. Rivers in the northeast region are less contaminated than those in the northwest area. However, Surui River receives domestic sewage and had its estuary affected by the marine heavy fuel oil spill in 2000, while the Macacu River, the least altered, was also impacted by the diesel oil spill in 2005.

26.2.2 Sampling Design

In the study Environment Assessment of Guanabara Bay (AABG in Portuguese), carried out between 2005 and 2008, the sampling design for hydrocarbons analyses in the sediments took into account not only the estuarine characteristics of the bay but also the surrounding anthropogenic activities. It encompassed 25 sampling stations, extending from the most inner part of the bay to its mouth (Fig. 26.1), and in addition, six stations located at the five most important rivers (abbreviations in parentheses) of the watershed basin: São Joao de Meriti (RioSJM), Iguaçu (RioIg1 and RioIg2), Sarapui (RioSa) Surui, (RioSu), and Macacu (RioMa). Station positioning was

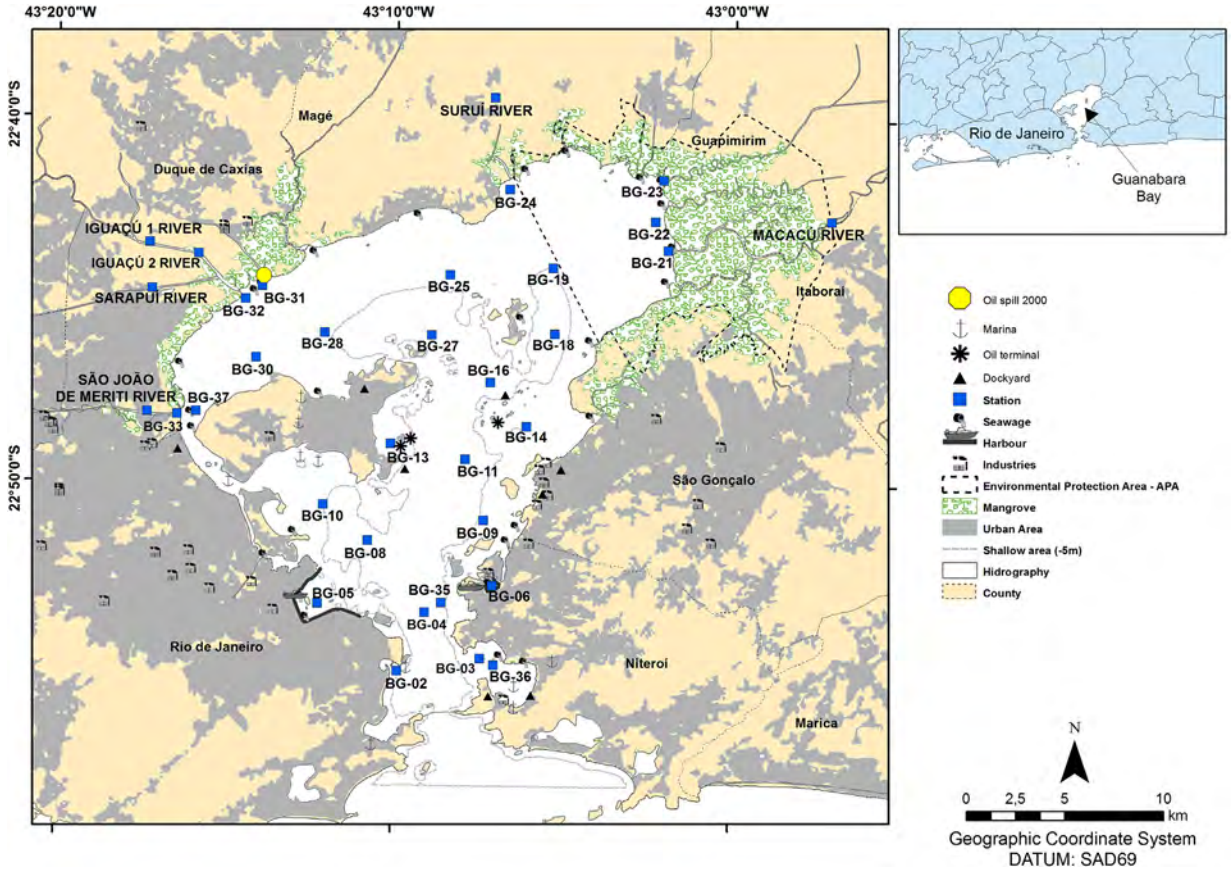

FIGURE 26.1 Map of the study area—features and sampling stations at Guanabara Bay. The prefix "BG" in the sample location names stands for Baía de Guanabara (Guanabara Bay).

determined with help of a DGPS. The prefix "BG" in the sample location names along the bay stands for Baía de Guanabara (Guanabara Bay) and the identification numbers of the stations were kept from previous studies in the bay. Abbreviations for sampling locations are used throughout the study.

Four sampling campaigns were performed along the 2 years of field work. The sediment samples were collected in July 2005 (CI), January 2006 (CII), July 2006 (CIII) and January 2007 (CIV). During the project, specifically for CIII and CIV, the sampling design was modified. Stations BG04 and BG33 were transferred to BG35 and BG37, respectively, due to logistics. Station BG36 was added to the design. Stations BG39, BG40, BG41 and BG42, situated at the north part of the bay (not shown in the map and tables), were exceptionally sampled in CIII for another study.

Surface sediments were sampled with the help of divers or using a van Veen sampler. The first 2 cm of sediments were transferred to clean aluminum boxes and kept under refrigeration until reaching the lab. Once in the lab, sediments were freeze dried, homogenized and stored until analysis (details in Wagener et al., 2012).

The forensic studies for hydrocarbons sources identification based on hydrocarbons quantitative analyses and application of environmental geochemistry interpretation and multivariate analysis of the data, utilized sediment samples from all four sampling campaigns. On the other hand, only sediments from the third campaign (CIII; July 2006) were used for the study using the CHEMIC method. Also for the CHEMIC method, only station RioIg1 (denoted as RioIG) was analyzed.

26.2.3 Methodology for Quantitative Analyses: Geochemistry Evaluation and Multivariate Analysis—Approaches 1 and 2

Detailed description of aliphatic and aromatic hydrocarbon determinations has already been described by Wagener et al. (2012). Soxhlet extraction was carried out according to EPA Method 3540C and cleanup was performed in an open glass column packed with deactivated alumina and silica gel.

Aliphatic quantitative analysis for *n*-alkanes (*n*-C12−*n*-C40), isoprenoids (phytane and pristane) and UCM were based on the U.S. EPA 8015 Method, using GC−FID and response factors obtained for individual *n*-alkane relative to *n*-dC_{24}.

Quantitative analysis of PAHs by GC−MS were based on the calibration curve of internal standards according USEPA 8270D method. Determinations included the 16 priority USEPA PAH: [naphthalene (N), acenaphthylene (ACY), acenaphthene (ACE), fluorene (F), phenanthrene (P), anthracene (AN), fluoranthene (FL), chrysene (C), pyrene (PY), benzo[*a*]pyrene (BaPY), benz[*a*]anthracene (BaA), benzo[*b*]fluoranthene (BbFL), benzo[*j*,*k*]fluoranthene (BkFL), indeno[1,2,3-cd]pyrene (IPY), dibenz[*a*,*h*]anthracene (DBA), benzo[*ghi*]perylene (BPER)] and also the compounds perylene (PER), benzo[*e*]pyrene (BePY), dibenzothiophene (D), alkylated dibenzothiophenes (C1, C2, and C3 D), alkylated naphthalenes (C1, C2, C3, and C4 N), alkylated fluorenes (C1, C2, and C3 F), alkylated phenanthrenes (C1, C2, C3, and C4 P), alkylated chrysenes (C1 and C2 C), alkylated pyrenes (C1 and C2 PY), 1,7-dimethylphenanthrene (1,7DMP) and 2,6-dimethylphenanthrene (2,6DMP).

In the text, tables, and figures, the sum of the 16 USEPA PAH was represented as 16PAH and the sum of the 37 homologs as ΣPAH or Total PAH. Also, the sum of naphthalene, phenanthrene and dibenzothiophene, including their C1-C3 alkyl homologs was represented as NPD and the 5 alkylated PAH series (naphthalenes, fluorenes, dibenzothiophenes, phenanthrenes and chrysenes) as 5 Alk. The sum of the low molecular weight PAHs was represented as LMW PAHs and the sum of the high molecular weight PAHs as HMW PAHs. Detailed description of analytical and quality assurance procedures is given in Wagener et al. (2012).

It was used surrogate standard for PAH and *n*-alkanes for recovery determination, and accuracy was successfully tested by analyzing the IAEA 383 sediment reference material. Detection limit for *n*-alkanes was of 20 μg/kg and for PAH was up to 0.1 μg/kg of sediment.

Statistical evaluation included Pearson correlation, Kruskal−Wallis test, Cluster Analysis and Factor Analysis (FA). Prior to the application of these two later tests, data were normalized by first dividing each original variable by the sum of all considered variables in the sample and then calculating the *z*-score.

26.2.4 Methodology for Semiquantitative PAH Analyses and CHEMSIC (Chemometric Analysis of Selected Ion Chromatograms)—Approach 3

26.2.4.1 GC−MS Analysis

Detailed description of the methodology of extraction, clean up, GC−MS analysis, data set and data processing has already been described by Christensen et al. (2010).

Extracts of freeze dried sediment samples were obtained according to EPA Method 3540C, using a Soxhlet apparatus. The extracts were then fractionated into an aliphatic (F1) and an aromatic (F2) fraction using an open glass column packed with activated silica gel and copper powder.

The aromatic fractions were then analyzed using a GC−MS operating in electron ionization mode. A total of 30 mass-to-charge ratios (*m*/*z*'s) divided into groups were acquired in SIM mode (see Table 26.1 for details).

Quality control was done by including control samples into all analyzed sample batches and between batches. Each batch contains 10 samples. The control samples are: one blank sample; one sample of the spilled marine fuel (MF380) from the Duque de Caxias Refinery; the solvent; a reference oil sample (1:1 mixture of heavy fuel oil from the Baltic Carrier and North Sea crude oil from the Brent oil field); a mixture of *n*-alkanes containing even number *n*-C8−*n*-C40 hydrocarbons (Florida mix). Furthermore, a sediment reference extract consisting of equal amounts of eight randomly selected extracts were analyzed every five runs. These references were used for quality control by daily monitoring for changes in peak shapes, chromatographic resolution, and sensitivity.

26.2.4.2 Data Set

The data set consisted of retention time-windows of 30 SICs per sample (Table 26.1) including the deuterated standards. Out of these, the SICs that contain PAHs that are commonly used for source identification (Yunker et al., 2002) were retained together with SICs containing new potential indicator compounds (e.g., *m*/*z* 192, 216, 242 corresponding to methylated 3−4 ring PAHs), which in this study seemed to vary significantly between samples from different locations. Nine *m*/*z*'s were retained: *m*/*z* 178 and 192 (C0−C1-phenanthrenes and anthracenes); *m*/*z* 198 (C1-dibenzothiophenes), *m*/*z* 202 and 216 (C0−C1-pyrenes and fluoranthenes), *m*/*z* 228 and 242 (C0−C1-chrysenes and benz(*a*)anthracenes), *m*/*z* 252 (5-ring PAHs), and *m*/*z* 276 (6-ring PAHs) were thus selected. The identities of compound groups and individual isomers used in the remaining sections are specified in Fig. 26.2 caption.

TABLE 26.1 List of *m/z*'s and Corresponding Groups of Aromatic Compounds. Perdeuterated Standards Are Marked in Bold

Compounds	*m/z*	Group (s)	Compounds	*m/z*	Group(s)
Naphthalene-d_8(N-d8)	***136***	***I***	C_1-dibenzothiophenes (C1D)	198	II
Naphthalene (N)	128	I	C_2-dibenzothiophenes (C2D) and ***pyrene-d_{10}(PY-d10)***	***212***	*II* + ***III*** + *IV*
C_1-naphthalenes (C1N)	142	I	C_3-dibenzothiophenes (C3D)	226	III
C_2-naphthalenes (C2N)	156	I	Pyrene (PY) and fluoranthene (FL)	202	III
C_3-naphthalenes (C3N)	170	I	C_1-pyrenes (C1PY) and C_1-fluoranthene (C1FL)	216	III
C_4-naphthalenes (C4N) and dibenzothiophene (D)	184	I	C_2-pyrenes (C2PY)	230	III
Fluorene (F)	166	I	C_3-pyrenes (C3PY) and ***p-terphenyl-d_{14}(TP-d14)***	***244***	***III***
C_1-fdluorenes (C1F)	180	I	Benzo(a)anthracene (BaA) and chrysene (C)	228	IV
C_2-fluorenes (C2F)	194	II	C_1-benzo(a)anthracenes and C_1-chrysenes (C1C)	242	IV
Phenanthrene-d_{10}(P-d10)	***188***	***II***	5-Ring PAHs	252	IV
Phenanthrene and anthrancene (P and AN)	178	II	***Benzo(a)pyrene-d_{12}(BaPY-d12)***	**264**	**IV**
C_1-phenanthrenes/C_1-anthracene (C1P and C1AN)	192	II	6-Ring PAHs	276	IV
C_2-phenanthrenes (C2P)	206	II + III	6-Ring PAHs	278	IV
C_3-phenanthrenes (C3P)	220	III	*n*-Alkanes and isoprenoids	85	I + II + III + IV
C_1-benzothiophenes (C1BT)	148	I	Triaromatic steroids	231	III + IV

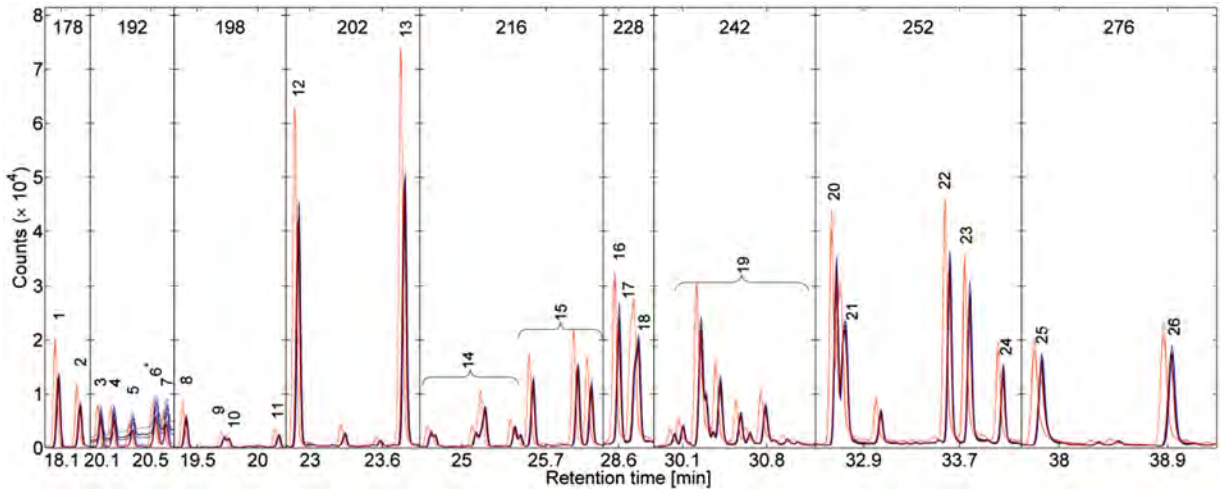

FIGURE 26.2 SICs of 18 replicate analysis of the reference sample. Nine *m/z* ratios (*m/z* 178–276) with high relevance for distinguishing between PAHs from different sources are shown. The identities of peaks or peak clusters are: 1, Phenanthrene; 2, Anthracene; 3, 3-Methylphenanthrene (3-MP); 4, 2-MP; 5, Methylanthracene (MA); 6*, 4-/9-MP and MA (coeluting); 7, 1-MP; 8, 4-Methyldibenzothiophene (4-MDT); 9, 2-MDT; 10, 3-MDT; 11, 1-MDT; 12, Fluoranthene; 13, Pyrene; 14, C1-Fluoranthenes; 15, C1-Pyrenes; 16, Benz(*a*)anthracene; 17, Triphenylene; 18, Chrysene; 19, C1-Benz(*a*)anthracenes/Chrysenes; 20, Benzo(*b*)fluoranthene; 21, Benzo(*k*)fluoranthene; 22, Benzo(*e*)pyrene; 23, Benzo(*a*)pyrene; 24, Perylene; 25, Indeno[1,2,3-*c*,*d*]pyrene; and 26, Benzo[*g*,*h*,*i*]perylene.

Sixty-six samples were analyzed and split into a "training set" of 30 sediment samples and three "validation sets": one consisting of six replicate analysis of the MF380 oil provided by Petrobras SA, one comprised of the 12 sampling duplicates ("Replicates" in PCA plots) and one comprised of 18 replicate analysis of the sediment reference sample ("Reference" in PCA plots).

26.2.4.3 Data Processing

The CHEMSIC method was employed for the processing of the chromatographic data to remove variation that is unrelated to the chemical composition (e.g., constant baselines, retention time shifts and changes in detector sensitivity), thereby retaining only variations in PAH composition that can be used to distinguish samples based on their source input. A four-step procedure has been employed here, as described by Christensen et al. (2010). It was based on a methodology previous described by Christensen et al. (2005a, 2005b) but named for the first time by Gallotta and Christensen (2012).

First, the SICs were baseline corrected, based on a procedure described by Aberg et al. (2004). Namely, the lower part of the convex hull of the chromatogram, which is by definition piece-wise linear, was subtracted from the data.

After the baseline removal, chromatograms were rigidly shifted and then further aligned using the correlation optimized warping (COW) algorithm (Nielsen et al., 1998; Christensen and Tomasi, 2007; Skov et al., 2006).

SICs of each sample were then normalized and combined. Normalization aims at removing the fluctuations in sensitivity of the detector as well as the variability of the sample preparation. Two normalization schemes were considered here: normalization to a combination of internal standards and normalization of the separate SICs to unitary Euclidean norm (Christensen et al., 2005b; Christensen and Tomasi, 2007).

The first normalization scheme reduces instrumental variation and variability introduced by the sampling and sample preparation steps (Christensen and Tomasi, 2007). Using this normalization scheme, the concentration dependency and variations between groups of PAHs (e.g., LMW PAHs vs HMW PAHs) are retained in the data set.

The second normalization scheme was based on normalization of the separate SICs to unitary Euclidean norm (Christensen et al., 2005b; Christensen and Tomasi, 2007). This normalization removes the concentration dependency and the variations between groups of PAHs and retains only chemical variations within GC–MS-SIM chromatograms (i.e., relative fingerprints).

26.2.4.4 Chemometric Data Analysis

The combined signals for all the samples were stacked in a matrix and modeled by PCA (Krzanowski, 2000).

The model was calculated on the column-wise centered training set and the validation sets were projected on it after centering to the mean of the training set. The PC model was further validated by full cross validation (Bro et al., 2008), visual inspection of loadings, and chemical interpretation.

26.2.4.5 Software

The GC–MS data was exported to the AIA file format using the commercial software ChemStation (Agilent technologies), and NetCDF was used to retrieve relevant data (e.g., signal intensities, sample names, sample descriptions) in the MATLAB programming environment, in which the data were processed and analyzed. The algorithms for import of CDF-files, COW, and PCA were downloaded from www.models.life.ku.dk.

26.3 RESULTS AND DISCUSSION

26.3.1 Approach 1—Quantitative Analyses: Geochemistry Evaluation

26.3.1.1 Aliphatic Hydrocarbons

The general feature of the aliphatics in the studied sediments is low *n*-alkanes and isoprenoids concentration and a significant UCM, usually 1 to 3 orders of magnitude higher than *n*-alkanes; the exceptions are for the samples from the NE and entrance of the bay (Table 26.2). Highest total aliphatic concentrations were found in the area of the Rio de Janeiro and Niteroi harbors (station BG05 and BG06, respectively) as well as in the northwestern region (stations BG30, BG31, BG32, RioIg1, RioIg2, RioSa, and RioSu). Stations near the entrance of bay or in areas of more effective water exchange (BG02, BG03, BG09, and BG36) and in the eastern region, inside the protected area APA (BG21, BG22, BG23, and BG24) showed the lowest concentrations.

Fig. 26.3 shows some examples of chromatograms of the aliphatic fraction obtained in the sediments of the bay from campaigns CI and CIII, where can be observed different *n*-alkane patterns: usually absence or very low concentrations of light *n*-alkanes ($<n$-C_{20}); predominance of odd to even carbon number *n*-alkanes in the high molecular range (maximum of n-C_{29}); and presence of significant UCM.

TABLE 26.2 Total Aliphatics (μg/g), Unresolved Complex Mixture—UCM (μg/g), and Diagnostic Ratios Based on Aliphatic Hydrocarbons in Guanabara Bay Sediments Sampled in Four Campaigns (CI to CIV)

Station	Total aliphatics (μg/g)				UCM (μg/g)				UCM/RP				CPI($nC_{12} - nC_{40}$)			
	CI	CII	CIII	CIV	CI	CII	CIII	CIV	CI	CII	CIII	CIV	CI	CII	CIII	CIV
BG02	342	187	22	30	303	174	21	28	7.8	13.1	16.2	9.6	1.9	1.9	1.7	1.9
BG03	7.9	40	17	0.8	5.9	32	16	–	2.9	4.1	19.1	–	4.5	1.7	1.6	1.2
BG04	158	27	–	–	140	22	–	–	7.6	4.0	–	–	2.2	2.2	–	–
BG05	21,260	1,428	1,586	3,058	21,015	1,356	1,526	2,926	85.6	19.0	25.3	22.2	2.4	1.8	2.8	1.8
BG06	866	1,565	451	907	821	1,482	430	861	18.0	17.8	20.8	19.0	1.8	2.0	1.9	1.6
BG08	600	511	354	315	566	479	334	293	16.8	15.1	16.9	13.7	2.4	2.3	2.3	3.1
BG09	69	65	86	45	64	58	80	41	11.1	7.7	14.5	10.5	2.0	2.5	2.7	3.4
BG10	900	545	689	380	848	511	657	361	16.2	15.2	20.9	19.5	3.2	3.2	2.0	2.4
BG11	493	327	411	332	461	300	381	308	14.5	11.2	12.7	13.4	3.3	2.6	2.6	4.2
BG13	260	368	348	60	240	325	327	56	12.1	7.6	15.6	12.5	2.2	2.0	3.9	2.4
BG14	573	265	389	220	536	238	360	205	14.6	8.9	12.5	14.0	3.2	3.3	3.9	3.2
BG16	425	447	553	234	398	416	523	219	14.7	13.2	17.2	14.3	3.4	3.1	3.0	2.6
BG18	374	318	235	290	335	284	217	265	8.6	8.3	11.9	10.7	3.4	3.8	5.0	3.1
BG19	177	253	239	239	150	221	217	216	5.7	6.8	9.8	9.2	2.6	3.4	5.1	3.5
BG21	52	70	82	35	37	47	66	21	2.6	2.1	4.2	1.6	4.1	5.3	4.6	4.6
BG22	56	89	66	44	33	68	40	20	1.5	3.2	1.6	0.9	4.6	5.8	4.5	4.5
BG23	16	55	19	5.7	10	37	11	1.4	1.5	2.0	1.5	0.3	2.6	5.9	5.8	2.8
BG24	166	48	88	45	124	29	61	33	3.0	1.6	2.3	2.6	4.3	5.0	5.7	5.9
BG25	463	383	513	146	428	357	478	134	12.5	13.5	13.8	11.3	3.5	3.2	3.5	3.2
BG27	1,103	540	236	263	1,032	499	217	245	14.6	12.0	11.6	13.2	3.7	3.7	2.8	2.6
BG28	733	594	174	252	676	540	161	234	11.8	10.1	12.5	13.7	2.7	2.5	4.4	3.5
BG30	767	1,281	661	440	733	1,217	627	411	17.1	19.1	18.6	13.8	3.1	3.6	5.6	3.5
BG31	886	453	652	742	820	419	607	686	12.4	12.3	13.7	12.3	4.2	5.1	6.4	4.9
BG32	1,086	1,058	989	765	1,026	979	936	719	17.1	12.3	17.6	15.6	3.1	3.2	4.9	3.0
BG33	926	737	–	–	865	685	–	–	14.4	13.2	–	–	1.7	2.6	–	–
BG35 (exBG04)	–	–	102	73	–	–	97	68	–	–	19.0	13.2	–	–	3.0	2.5
BG36	–	–	35	45	–	–	34	42	–	–	23.2	15.2	–	–	3.4	3.4
BG37 (exBG33)	–	–	1,139	706	–	–	1,063	656	–	–	14.0	13.1	–	–	1.8	2.4
RioMa	34	7.6	24	37	23	4.9	20	28	2.1	1.8	4.9	3.3	4.9	2.0	4.5	4.8
RioSu	131	52	96	46	105	36	76	38	4.0	2.2	3.8	4.5	4.1	4.2	4.4	5.1
RioIg1	1,485	27	840	14	1,355	21	774	2	10.5	3.8	11.7	0.1	2.0	1.8	2.4	6.1
RioIg2	–	–	752	631	–	–	700	586	–	–	13.5	13.3	–	–	3.1	3.0
RioSa	1,584	947	724	1,716	1,417	868	672	1,580	8.5	10.9	12.9	11.6	1.8	1.6	4.0	1.2
RioSJM	1,054	1,538	928	6,334	986	1,424	835	5,957	14.5	12.5	9.0	15.8	1.4	2.5	1.3	1.3

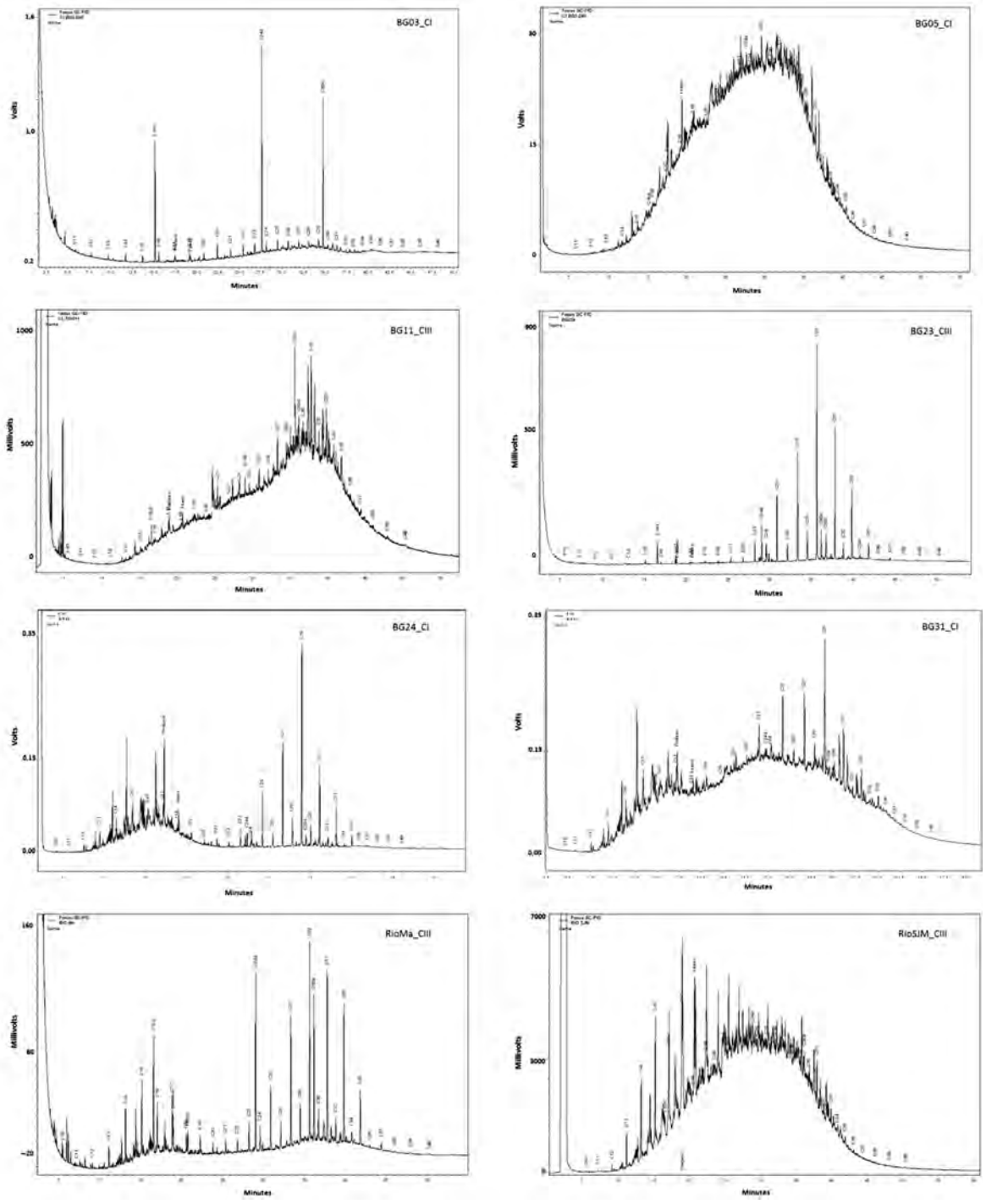

FIGURE 26.3 Gas chromatograms of the aliphatic fraction from sediments of the Guanabara Bay (BG 03, BG 05, BG 11, BG 23, BG 24, BG31, RioMa, and RioSJM)—campaigns CI and CIII.

In station BG05 (Rio de Janeiro Harbor), the most contaminated in the area, the relatively low contribution of *n*-alkanes to the RP and the high UCM/RP ratios are additional indications of highly degraded aliphatic hydrocarbons and weathered oil residues (Readman et al., 2002). In this station, *n*-alkanes comprised from 13% of the RP in CIII to 23% in CI, while the UCM/RP ratio varied between 18 (CII) to 86 (CI).

The relative proportion of odd and even carbon number *n*-alkanes expressed as Carbon Preference Index—CPI (Bray and Evans, 1961) for the bay sediments is in general $\gg 1$ (Table 26.2), indicating presence of plant residues.

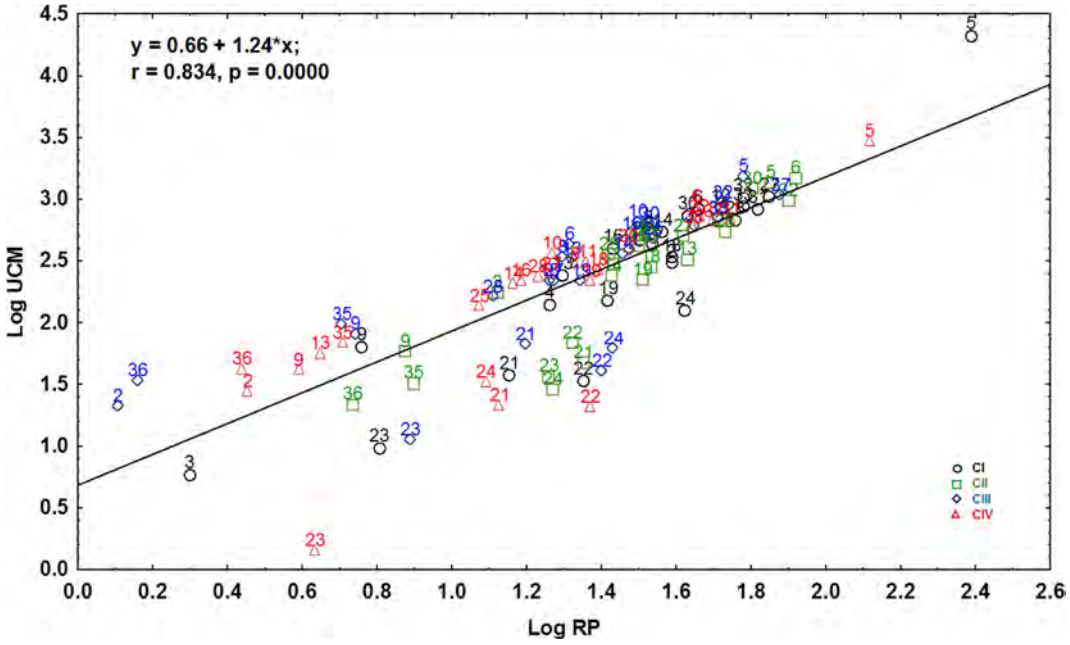

FIGURE 26.4 Log–log plot of unresolved complex mixture (UCM) versus resolved peaks (RP) from sediments of the Guanabara Bay. The prefix "BG" was removed from the sample codes for clarity within the figure.

$CPI_{n\text{-}C24-n\text{-}C40}$ varies from 1.2 in station BG03, CIV to 8.2 in station BG24 in CI. The *n*-alkane concentrations range of 7.66 μg/g (CIII) to 57.22 μg/g (CI) found in station BG05 (see Wagener et al., 2012) is similar to the reported by other authors (Lee et al., 2005) for contaminated areas. In stations BG18 and BG31 concentrations were also higher in CI, $CPI_{n\text{-}C24-n\text{-}C40}$ was $\gg 1$ and UCM/RP > 4. In general, with exception of the stations in the eastern region, all sediment samples presented UCM/RP $\gg 4$ suggesting ubiquitous contamination by degraded oil in the bay.

Fig. 26.4 shows a good correlation between UCM and RP ($r = 0.835$, $p \ll 0.01$). According to Bouloubassi and Saliot (1993), this appears if the *n*-alkanes are at low concentration and the other RP are produced by compounds of the same nature as those in the UCM. The plot, nevertheless, depicts qualitative and quantitative differences in contamination level when dealing with a large number of samples. The graph draws attention to the elevated UCM/RP in samples where both variables appear in high concentration (stations BG05, BG06, BG32, and BG31) and highlight samples with concentrations in which, however, (stations BG02 and BG36) hydrocarbons are of predominantly petrogenic origin. Most samples below the regression line are in the least contaminated areas showing UCM/RP < 4, while those with UCM/RP > 4 are close or above the regression line.

26.3.1.2 PAH

PAH concentrations obtained in the four sampling campaigns, from 2005 to 2007, are summarized in Table 26.3. Naphthalene, phenanthrene, and dibenzothiophene, including their C1–3 alkyl homologs (NPD group), were also displayed at the table to highlight the 2–3 ring compounds, the most representative range of petroleum input in the environment (OGP, 2002; Pampanin and Sydnes, 2013; Junttila et al., 2015).

Median concentrations for Total PAH were 4,906 μg/kg in CI, 2,419 μg/kg in CII, 2,306 μg/kg in CIII and 2,686 μg/kg in CIV, considering the stations of the bay and rivers. Kruskal–Wallis test indicated no significant differences among the campaigns despite the generally larger concentrations found in CI.

The highest concentrations of Total PAH were always found in station BG05, the Rio de Janeiro Harbor (68,857 to 153,316 μg/kg), and the lowest were in station BG03 (entrance of the bay), BG21, BG22 and BG23 (inside the environmental protected area). Stations in the rivers located at northwest of the bay (RioIg1, RioIg2, RioSa, and RioSJM) also showed, as expected, elevated PAH concentrations, revealing the Sao Joao de Meriti River as extremely contaminated (up to 52,025 μg/kg).

Knoppers et al. (2010) carried out a hydrocarbon fluvial load study for the five rivers analyzed herein also as part of the same project Environment Assessment of Guanabara Bay. It was carried out in situ flow measurements for the rivers and water samples were collected for PAH analyses in four surveys (July/2006; Feb/2007; April/2007; July/2007), taking into account dry and wet seasons. The methodology for load estimations is

TABLE 26.3 16PAH, Σ PAH, and NPD Concentrations (μg/kg) in Sediments Sampled in Four Campaigns (CI to CIV) in Guanabara Bay and TEL, ERL, and PEL Threshold Levels

	C I				C II				C III				C IV			
Station	16 PAH	∑PAH	NPD	NPD (%)	16 PAH	∑PAH	NPD	NPD (%)	16 PAH	∑PAH	NPD	NPD (%)	16 PAH	∑PAH	NPD	NPD (%)
BG2	34,652	52,879	26,342	50	3,889	6,680	1,415	21	176	300	38	13	1,105	2,012	335	17
BG3	146	219	24	11	86	190	47	25	8	14	4	27	23	50	12	24
BG4	3,475	5,739	756	13	72	244	106	44	–	–	–	–	–	–	–	–
BG5	68,497	1,35,114	23,028	17	43,954	1,04,261	11,469	11	78,523	1,53,316	27,551	18	37,330	68,857	9,742	15
BG6	1,636	7,574	3,408	45	6,248	21,083	8,112	38	8,471	18,851	5,026	27	7,311	14,685	3,103	21
BG8	2,532	5,036	994	20	1,812	4,140	959	23	3,119	5,464	919	17	3,374	5,677	752	13
BG9	437	858	197	23	572	724	64	9	345	571	71	12	359	676	116	17
BG10	2,941	5,530	865	16	1,264	2,586	487	19	2,693	5,311	1,016	19	5,196	8,535	1,230	14
BG11	1,252	2,813	735	26	1,294	2,954	643	22	2,304	4,124	656	16	2,699	4,390	613	14
BG13	513	988	198	20	1,014	2,226	525	24	2,143	4,425	1,285	29	450	834	143	17
BG14	1,408	2,780	569	20	1,648	3,629	771	21	2,333	4,387	873	20	1,585	3,880	983	25
BG16	2,194	4,776	910	19	15,531	18,498	1,367	7	2,822	4,895	580	12	4,604	8,366	1,179	14
BG18	1,938	9,256	6,694	72	802	1,591	416	26	1,058	2,256	482	21	1,202	2,976	674	23
BG19	4,018	11,672	7,856	67	635	1,559	359	23	817	1,708	345	20	1,075	2,396	476	20
BG21	82	355	138	39	96	404	168	42	113	228	46	20	150	471	189	40
BG22	144	425	147	35	164	410	111	27	149	422	130	31	132	399	126	31
BG23	133	274	57	21	175	590	52	9	134	280	36	13	80	162	25	15
BG24	3,380	13,772	9,868	72	182	382	87	23	147	455	114	25	130	287	61	21
BG25	938	2,107	467	22	652	2,148	634	30	1,467	2,817	495	18	1,802	4,285	1,011	24
BG27	1,222	2,779	626	23	829	2,251	661	29	2,121	4,302	722	17	1,846	3,825	809	21
BG28	1,023	2,612	755	29	1,052	2,788	599	21	370	831	178	21	763	2,070	473	23
BG30	714	1,923	565	29	610	2,195	801	37	648	1,618	422	26	640	1,854	496	27
BG31	5,153	19,379	10,603	55	424	5,439	919	17	990	7,060	1,715	24	2,651	28,511	2,905	10
BG32	661	5,729	2,272	40	711	6,592	2,916	44	685	6,761	2,676	40	959	6,536	2,504	38
BG33	8,258	28,313	17,017	60	2,162	13,550	6,640	49	–	–	–	–	–	–	–	–
BG35 (exBG04)	–	–	–	–	–	–	–	–	1,076	1,822	390	21	658	1,103	177	16
BG36	–	–	–	–	–	–	–	–	318	526	85	16	642	925	94	10
BG37 (exBG33)	–	–	–	–	–	–	–	–	4,679	17,322	4,074	24	7,870	35,296	14,755	42
RioMa	59	445	132	30	12	30	8	28	31	122	42	34	45	278	90	32
RioSu	162	1,107	466	42	52	758	347	46	134	812	395	49	38	168	53	31
RioIg1	639	8,479	4,288	51	5	164	52	32	491	5,471	2,404	44	17	86	18	20
RioIg2	–	–	–	–	–	–	–	–	326	5,429	3,055	56	357	6,096	2,875	47
RioSa	1,141	8,472	4,359	51	1,027	22,938	10,967	48	532	10,768	5,590	52	1,444	7,775	3,556	46
RioSJM	3,594	31,180	14,571	47	4,747	52,025	24,319	47	5,838	32,148	15,750	49	5,413	24,890	10,587	43

TEL Total PAH: 1,684 mg/kg; ERL Total PAH: 4,022 mg/kg; PEL total PAH: 16,770 mg/kg.

TABLE 26.4 PAH Concentrations (ng/L) and PAH Loads (kg/day) for Five Rivers of the Guanabara Bay Obtained in Four Campaigns

	Campaign 1		Campaign 2		Campaign 3		Campaign 4		Average ± S.D.	
River	PAH (ng/L)	PAH load (kg/day)	PAH (ng/L)	PAH load (kg/day)	PAH (ng/L)	PAH load (kg/day)	PAH (ng/L)	PAH load (kg/day)	PAH (ng/L)	PAH load (kg/day)
A—RioMa	55	0.02	3	0.01	83	0.16	40	0.08	45	0.07 ± 0.07
B—RioSu	20	0.01	50	0.02	87	0.01	100	0.01	64	0.01 ± 0.01
C—RioIg*	740	1.02	586	2.08	527	0.02	1,229	4.90	771	2.01 ± 2.10
D—RioSa	1,143	0.66	1,292	2.12	823	0.02	1,086	2.07	1,086	1.22 ± 1.05
E—RioSJM	2,188	3.40	1,618	4.05	1,122	1.28	503	2.04	1,358	2.70 ± 1.26

[a]RioIg corresponds to RioIg1.

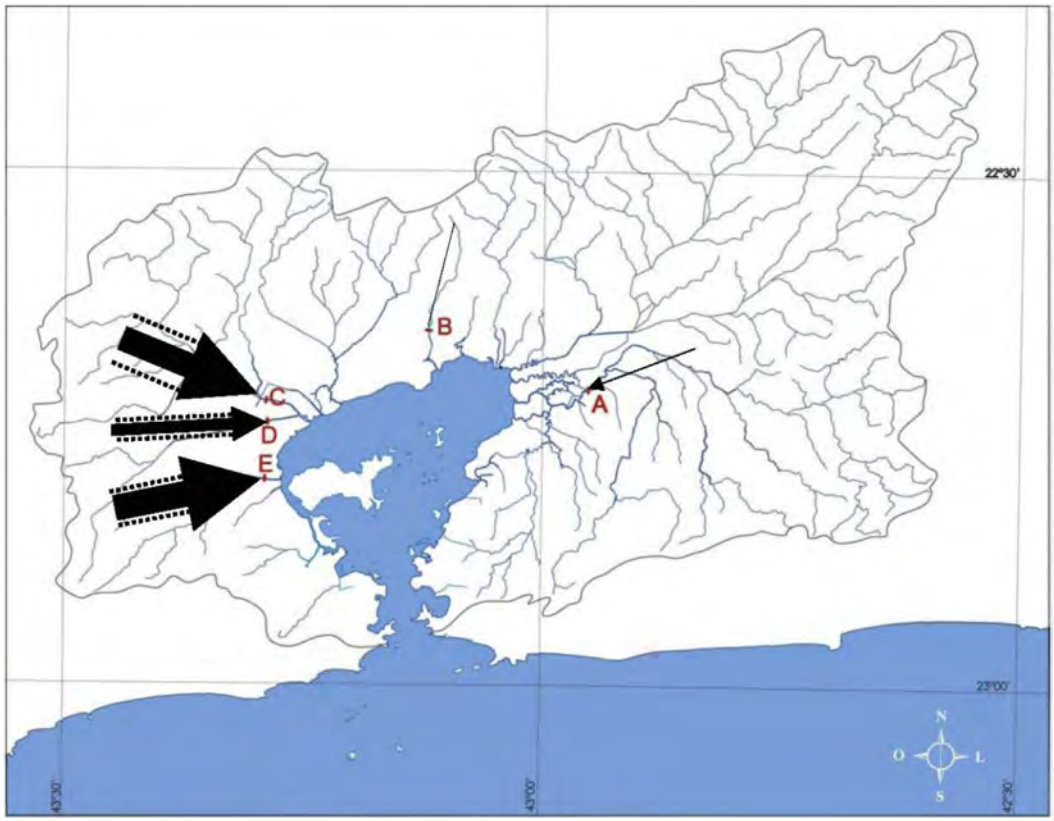

FIGURE 26.5 Display of average loads (kg/day) for five rivers of the Guanabara Bay obtained in four field campaigns.

described elsewhere (Medeiros et al., 2011) and PAH analysis was based on methods EPA 3510, EPA 3630/3610, and EPA 8270C. The PAH concentrations (sum of the 37 homologs) and PAH load results, expressed in ng/L and kg/day of PAH, respectively, are summarized in Table 26.4. The average PAH fluxes to the bay varied from 0.01 ± 0.01 kg/day (Macacu River) to 2.70 ± 1.26 kg/day (Sao Joao de Meriti River) and the highest value reached 4.90 kg/day for Iguaçu River at the campaign 4. As can be seen in Fig. 26.5, the higher loads were observed in the rivers from the northwest region of the bay, related to the intense anthropogenic activities of that highly urbanized and industrialized area.

For some stations in the bay, significant differences in concentration among samplings were observed: station BG02 (a marina area), BG06 (a shipyard area), BG31 (near a densely populated and industrialized area), BG18, BG19, and BG24. Station BG24, near the Surui mangrove contaminated by the oil spill in January 2000, presented an elevated concentration in CI, higher than previous studies, including the one carried out 14 days after the oil spill (Meniconi and Barbanti, 2007), and it was not observed in the following campaigns of this study. Such

variability observed for the stations mentioned before seem unrelated to seasonality but may rather derive from other factors, as for instance sediment heterogeneity, new inputs and remobilization due to tidal current dynamics or other removal mechanisms.

The range of ΣPAH, except for the Rio de Janeiro Harbor, was similar to the reported for the north area of Guanabara Bay by Meniconi et al. (2002) and Meniconi and Barbanti (2007). The 16PAH in Guanabara Bay are in the upper concentration range when compared to data reported by other authors (e.g., Baumard et al., 1998; Bícego et al., 2006; Oros et al., 2007) for polluted coastal systems. The Rio de Janeiro Harbor, never evaluated before, presented very high concentrations, one order of magnitude higher than the most polluted areas of the bay.

Wagener et al. (2002) analyzed total-PAH concentrations in the north area of the bay sediments sampled in February and July 2001, about 13 and 18 months, respectively, after the oil spill of January 2000. Concentrations of the same order of magnitude as those found here are reported for stations of similar geographical coordinates with exceptions of stations BG18 and BG24 for which higher concentrations were present in CI.

In relation to the specific NPD group analyses for Guanabara Bay sediments, considering the four surveys, it was observed that NPD concentrations varied in the range of 4 to 27,551 μk/kg inside the bay and 8 to 24,319 μk/kg in the rivers (Table 26.3). In average, NPD from the bay samples corresponds to 25% of total PAH concentration while 43% for the sediments from the rivers, especially for those from the northwest region of the bay, which drain the most industrialized area of Guanabara Bay watershed. These results revealed an important petrogenic hydrocarbon output from the rivers to the bay, corroborating Knoppers et al. (2010) finds mentioned before.

The environmental significance of PAH concentrations can be assessed by comparing PAH levels with the thresholds values (TEL: Threshold Effects Level; ERL: Effects Range Low; PEL: Probable Effects Level; Apparent Effect Threshold) proposed by Buchman (2008) to characterize sediments of low to high toxicity to the benthic biota. Fig. 26.6 shows the results of such comparison using, as an example, data for LMW and HMW PAH levels and BaPy and DBahA concentrations in CIV and associated thresholds values. Sediments from several locations in Guanabara Bay showed LMW PAH and HMW PAH concentrations above TEL level and some around or above PEL (BG05, BG06, BG37, BG10, BG16, Rio SJM), where adverse effects are frequently expected on the benthic biota. Similar scenario was observed for BaPY and DBA. Stations BG05, BG16, BG10 and BG31 presented elevated concentrations of these compounds, all above PEL. However, it must be highlighted that, as expected, BaPY and DBA concentrations in station BG05 (Rio de Janeiro Harbor) exceeds by a factor of 5 the Apparent Effect Level (Buchman, 2008), equal to 1,100 and 230 μg/kg, respectively.

The PAH data set was evaluated using cluster analysis. As shown in Fig. 26.7, the individual PAH are grouped in two major clusters: The first essentially includes the HMW parent PAH, which are mostly of pyrogenic origin, and few alkylated homologs of the heavier PAH chrysene and pyrene; the second cluster contains mainly the LMW parent PAH and their alkylated homologs. This cluster can be separated in two subgroups: one shows a stronger association between the LMW PAH and the alkylated PAH of lower degree of alkylation, and the other includes the homologs of higher alkylation level. The stations are also grouped in two large clusters (Fig. 26.8): in cluster 1 are stations in which pyrogenic PAH are abundant and in cluster 2 are samples enriched in LMW PAH and their alkylated homologs. The possible sources of these PAH will be further discussed ahead.

Fig. 26.9 shows PAH profile found in sediment samples of the Guanabara Bay from campaigns 1 and 3 (CI and CIII). Stations RioMa, RioSJM, and BG31 contain PAH features of degraded oil residues, including predominance of the alkylated homologs and of increasing concentration with increase in alkylation (C0 < C1 < C2 < C3 < C4) in each of the five alkylated series. Stations from Iguaçu river, BG32, Bg33, and BG37, near Rio SJM and BG31—northwest of the bay, presented similar PAH distribution (not shown). However, it must be pointed out that PAH concentration at Macacu River is very low, as expected for its location: inside the APA; besides perylene is present in considerable level. Station BG24 at first campaigns revealed a particular feature, with high PAH concentration and predominance of the lower molecular weight PAH and their alkylated homologs, distinctive of petrogenic residues. This feature has not occurred in the followings surveys, as mentioned before. Perylene, on the other hand, was predominant at BG23, due to the proximity of the mangrove forest, although PAH concentrations were low. The other stations from APA have also shown low PAH levels and important contribution of perylene, despite the presence of mixed sources of hydrocarbons. In stations BG03 (entrance of the bay), BG11 (central area of the bay), and BG05 (Rio de Janeiro Harbor) heavy pyrolytic PAHs predominate despite the difference in PAH concentrations. In general, the PAH distribution of the sediment samples from the bay corroborate the GC–FID chromatograms and in some cases, as for those samples with predominance of highly degraded oil residues (BG05, BG11), the PAH profile adds information of important contribution of another hydrocarbon source.

Based on the 16PAH/ΣPAH ratio as source indicator, stations BG31, BG32, RioIg2, and BG33 seem to be relatively more contaminated by PAH from petrogenic sources. The first three stations are near an oil refinery and in

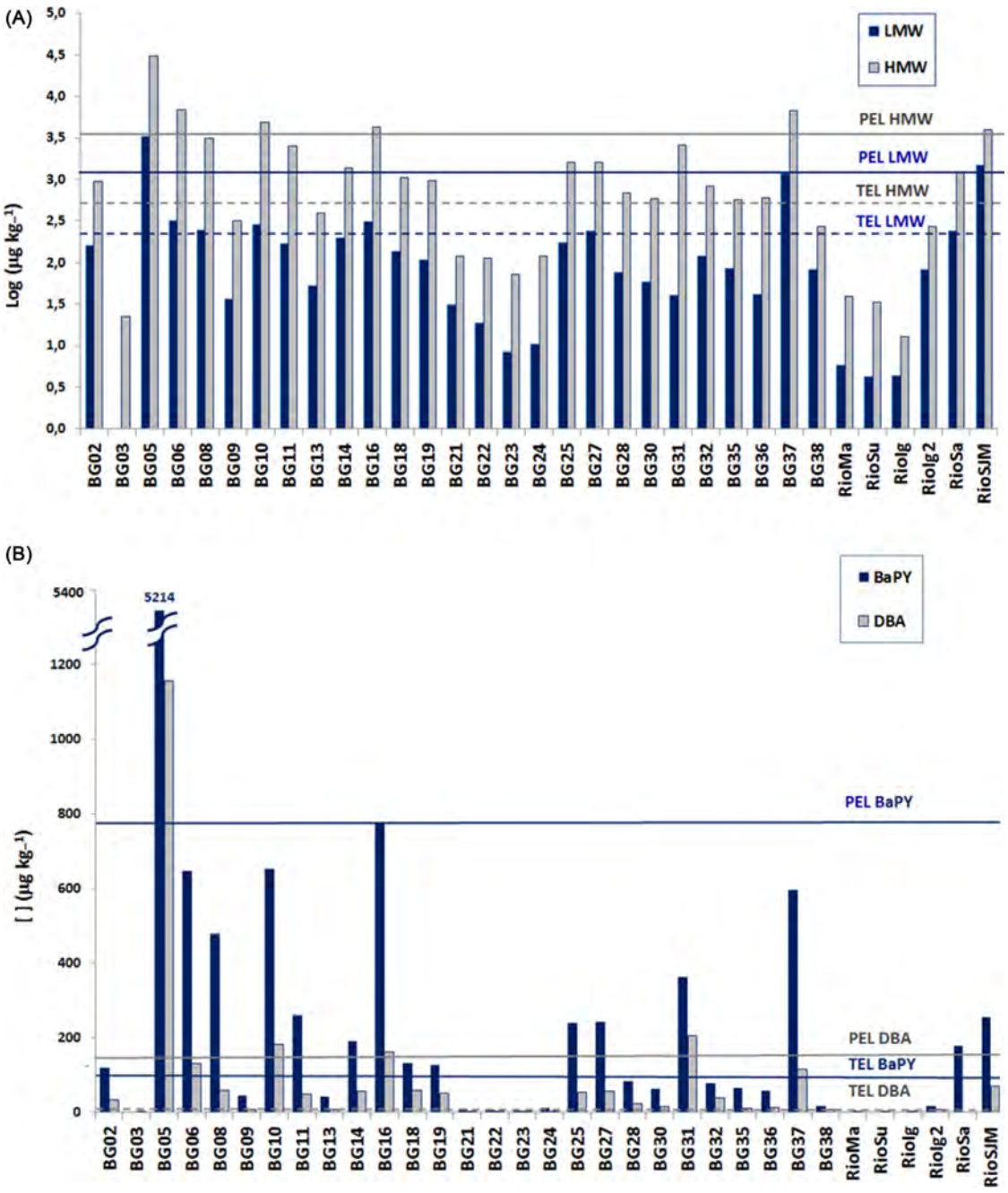

FIGURE 26.6 LMH and HMW PAH (A) and Benzo[*a*]pyrene (BaPY) and dibenz[*a,h*]anthracene (DBA) in samples from survey 4 (CIV). Thresholds TEL and PEL are also shown for the compounds. The BaPY bar for station BG05 was adjusted to fit the plot and the real value is indicated.

the area of influence of the polluted Iguaçu and Sarapui rivers, while the later receives inputs from the highly contaminated São João de Meriti River.

Cross plots of diagnostic ratios were used to distinguish PAH sources (Lima et al., 2005; Yunker and Macdonald, 2003; Yunker et al., 2002; Budzinki et al., 1997; Wang et al., 1999). The results appear in Fig. 26.10. A large group of samples show PAH deriving from mixed sources (pyrogenic and petrogenic) or from pyrogenic sources, however there are discrepancies in source assignment for some samples. According to the pyrolytic ratio (3–6 ring PAH/5 alkylated PAH series by Wang et al., 1999), PAH derive from incomplete combustion in a significant group of samples, while fluoranthene/(fluoranthene + pyrene) indicates petrogenic inputs in some of these samples. In sediments from Rio de Janeiro Harbor (station BG05) the pyrogenic ratio indicates presence of pyrogenic PAH input in

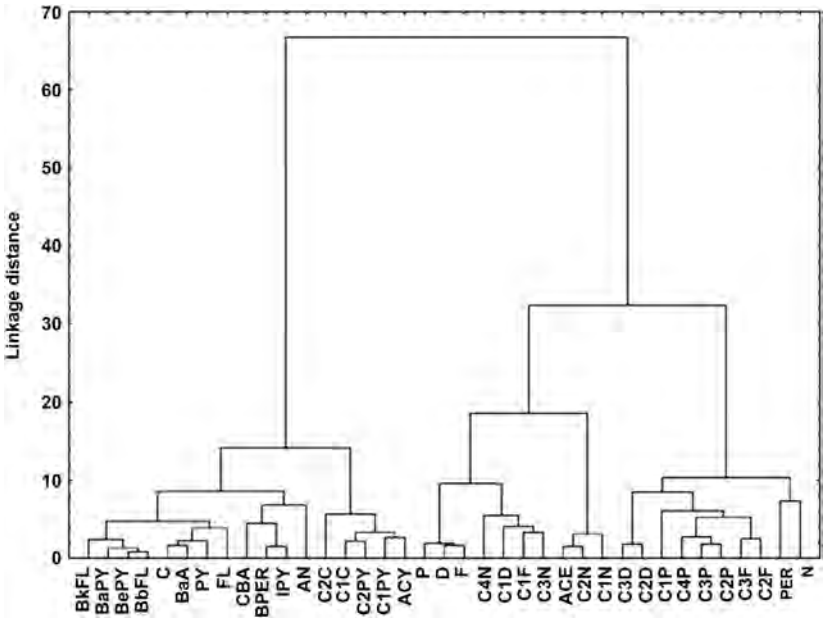

FIGURE 26.7 Cluster analysis—PAH grouping in the first survey (CI).

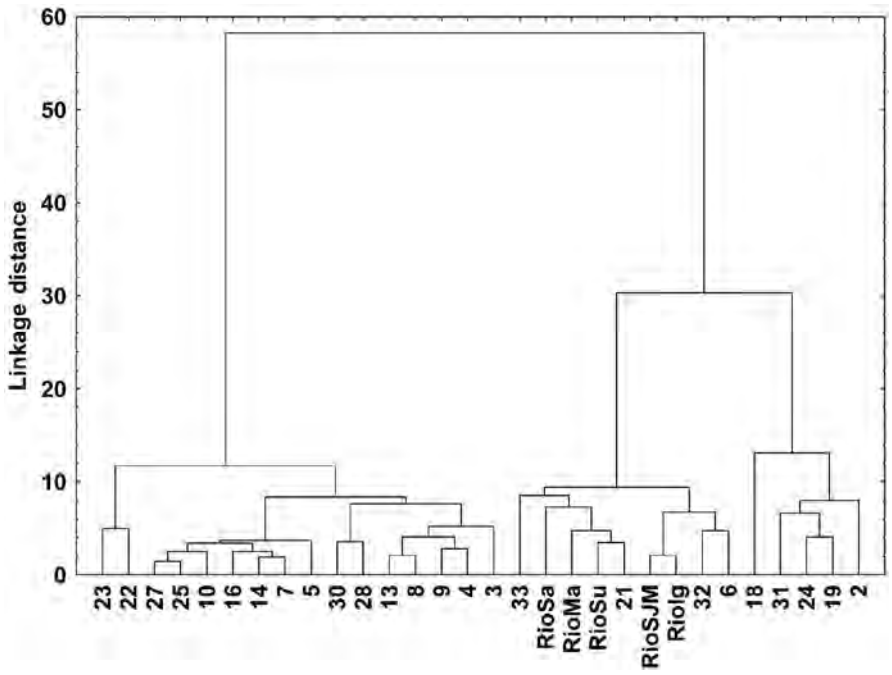

FIGURE 26.8 Cluster analysis—Sampling station grouping in the first survey (CI). The prefix "BG" was removed from the sample codes for clarity.

all sampling campaigns, although relatively high concentrations of alkylated naphthalene and other alkylated homologs of lower molecular weight PAH have been observed (Fig. 26.9 and Table 26.3).

Other diagnostic ratios were also tested which provided poorer results in terms of the ability to distinguish differences among samples. The crossplot of benzo[*b,k,j*]fluoranthene/(benzo[*b,k,j*]fluoranthene + benzo[*e*]pyrene) *versus* 1,7-dimethylphenanthrene/(1,7- + 2,6-dimethylphenanthrene) (Yunker et al., 2002) was used for combustion sources assignment and provided inadequate information for Guanabara Bay samples, considering the literature limits (see Wagener et al., 2012). The plot displayed the majority of samples as contaminated with PAH derived from biomass combustion despite the fact that biomass combustion is not a substantive practice in

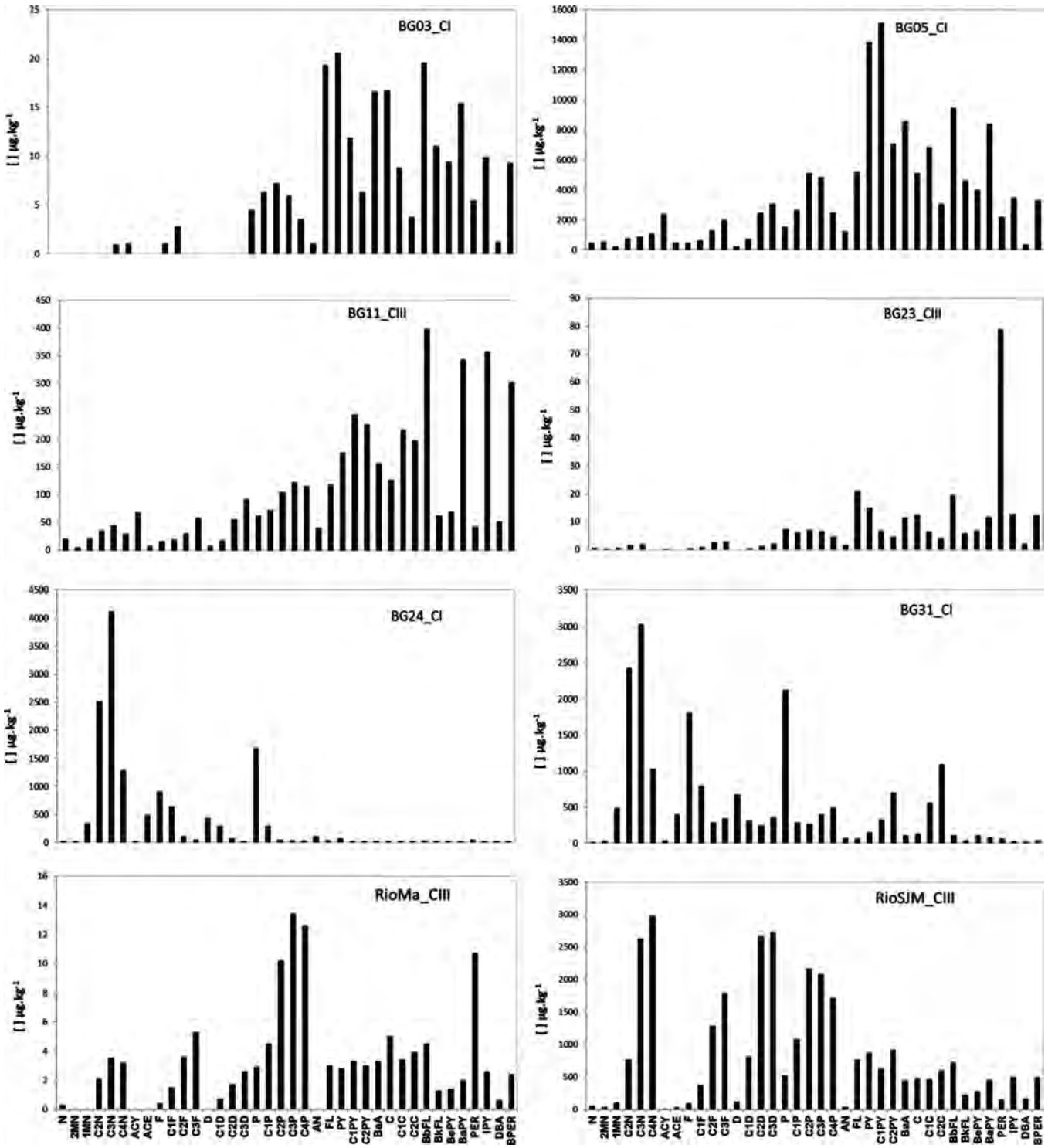

FIGURE 26.9 PAH distribution (µg/kg) for the sediment samples in Guanabara Bay (BG 03, BG 05, BG 11, BG 23, BG 24, BG31, RioMa, and RioSJM) from campaigns I and III. PAH abbreviations are specified in the text above (Section 26.2.3).

Guanabara Bay. On the contrary, the bay is the center of a highly urbanized and industrialized area, being crossed by a bridge with an intense traffic (150,000 vehicles per day) and its combustion matrix includes mainly fossil fuel combustion and vehicular emissions, similar to any other metropolis of the world (Tolosa et al., 2004; Stout et al., 2004; Yunker et al., 2002). Then these ratios call for further investigation on combustion end members which may be used as molecular markers in sediments.

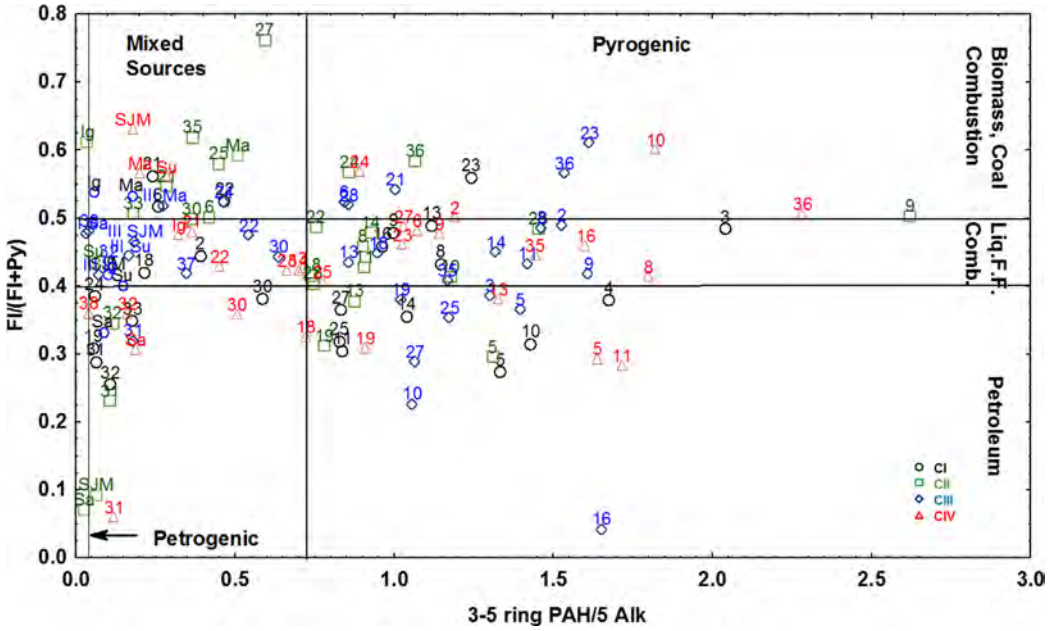

FIGURE 26.10 Cross plot of diagnostic ratios: fluoranthene/(fluoranthene + pyrene) versus sum of the 3–6 rings PAH/sum of the five alkylated PAH series. The prefixes "BG" and "Rio" were removed from the sample codes for clarity of the figure.

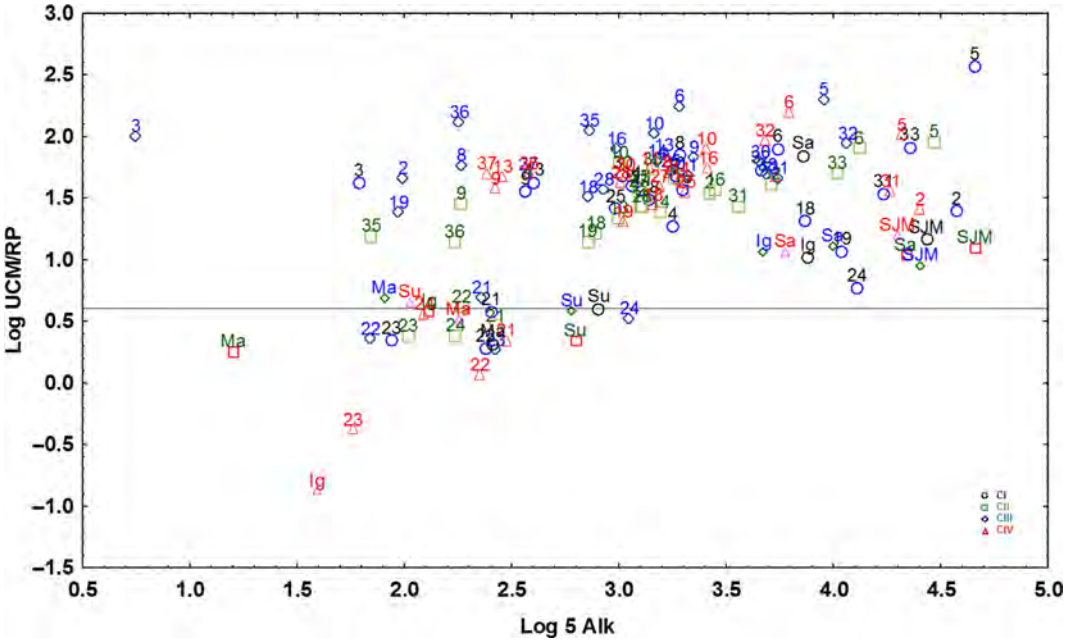

FIGURE 26.11 Log–log plot of UCM/RP and the sum of the five alkylated PAH series for Guanabara Bay sediments. The prefixes "BG" and "Rio" were removed from the sample codes for clarity of the figure.

Alternative approaches (Wagener et al., 2012) to the diagnostic ratios found in the literature will be presented below for PAH assignment in sediments of Guanabara Bay. Figs. 26.11 and 26.12 show the plots of the five alkylated PAH series as function of UCM and of the 3–6 ring PAH (those defined by Wang et al., 1999), respectively. The insert in Fig. 26.12 show the plots for the river sediments. In the first plot, the line at log UCM/RP = 0.6 specify the threshold for contamination with degraded oil (UCM/RP > 4), and there is a significant positive correlation between the UCM/RP ratio and the 5 alkylated PAH series ($r = 0.550$; $p < 0.001$). Samples from the environmental protection area (BG21, BG22, BG23, BG24), stations BG24 (CII, CIII and CIV), BG03 (CI) as well as stations from Iguaçu, Macacu and Surui Rivers (RioIg1—CIV; RioMa—CI and CII; RioSu—CII), are below this

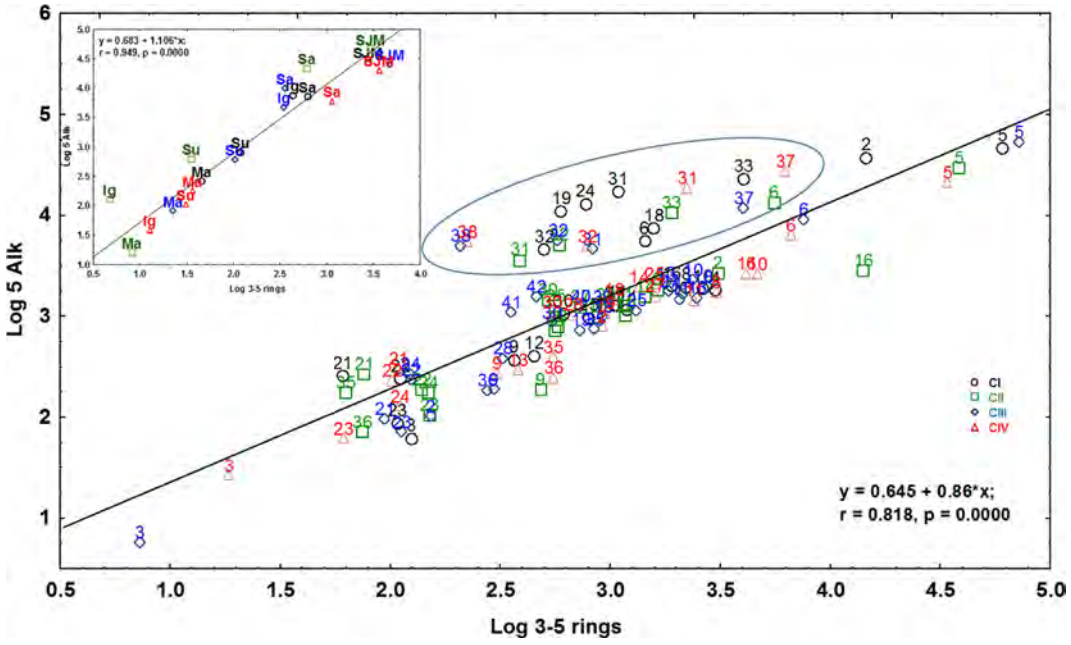

FIGURE 26.12 Log–log plot of the sum of the five alkylated PAH series and the sum of the 3–6 rings PAH for Guanabara Bay sediments. The insert in the figure shows the plot for the river sediments. The prefixes "BG" and "Rio" were removed from the sample codes for clarity of the figure. Stations BG39, BG40, BG41 and BG42 were exceptionally sampled in CIII.

threshold and in the range of low concentrations of the 5 alkylated PAH series. Through this criterion most other samples appear contaminated by degraded petrogenic residues at different levels.

The increasing trend of log UCM/RP versus log 5 alkylated PAH series can be used to distinguish the intensity of such contamination in different samples. Stations BG02, BG05, RioSJM, BG31, BG32 and BG06 (in the upper right hand side of the plot) are highly contaminated by degraded oil residues as indicate the elevated concentrations of the 5 alkylated PAH series (and the increasing concentration from C0 to Cn). Sample BG24 (CI) that display PAH typology typical of oil contamination (see Fig. 26.9) appears in the area of UCM/RP ~ 4 and high 5 alkylated PAH series content. Station BG24 faces the Surui mangrove fringe which was seriously affected by an oil spill in 2000, however, the chromatogram of the aliphatic fraction obtained by Farias et al. (2008) for the contaminated Surui mangrove sediments shows a broad UCM in the range of n-C_{15}–n-C_{33} while for sample BG24 (CI) the UCM is in the range of nC_{13}–nC_{20} and the PAH typology suggests contamination by diesel oil (Fig. 26.9). The influence of wave action and tidal currents in the dynamics of contamination in this area is evident since in later samplings hydrocarbon ascribed to oil residues decreased sharply in station BG24 as can be seen in all results including the aliphatic and aromatic compounds.

Fig. 26.12 provides direct information on the level and nature of PAH contamination which are complementary to those discussed above. There is a significant covariation of the 3–6 ring PAH and the five alkylated PAH series both for the bay and river sediments. The same trend is observed when plotting the two groups of variables calculated for oils of different origins (see Wagener et al., 2012). The slope of the curve for sediment samples is close to 1 indicating a possible common source containing PAH from pyrogenic and petrogenic origin, or a common mechanism of transfer to the sediments. In Fig. 26.12, samples in the insert above the curve are among the most contaminated with oil residues, while samples BG03 (in CIII and CIV), below the curve, are the least contaminated with PAH. Near the bay entrance and the environmental protection area [BG03, BG21, BG22, BG23, and BG24 (CII, CIII, CIV)] samples contain PAHs from both sources, despite the low concentrations. Samples from Rio de Janeiro Harbor are the most contaminated by PAH, also from pyrogenic and petrogenic origin. The insert in Fig. 26.12 shows similar plot for the rivers in which the slope of the curve slightly above 1 indicates predominance of alkylated PAH (oil derived) over pyrolytic PAH. The plot highlights sediments from SJM as the most contaminated in all four campaigns. Contamination decreases from west to east in the following sequence: Sao Joao de Meriti > Sarapui > Surui > Macacu. In Iguaçu River, station RioIg1 shows great seasonal variability with significantly higher concentrations in both winter samplings (CI and CIII) when rain fall is decreased. The complete lack of seasonality in RioSJM as well as in RioSa suggests that PAH inputs may also occur through subsurface runoff in this area.

In summary, the environmental geochemistry evaluation of the Guanabara Bay sediment related to aliphatic and aromatic hydrocarbon quantitative data, *Approach 1*, have proved to be robust and indicated a combination of ΣPAH concentrations between 14 and 153,316 μg/kg and a mixture of diagenetic, pyrogenic and petrogenic sources.

A pronounced UCM and low concentrations of *n*-alkanes, which appear mainly in the HMW range despite the high primary production in the bay, were dominant features in Guanabara Bay. This indicated sediment contamination by weathered oil and fast degradation of LMW *n*-alkanes, respectively. The exception relied on the stations located in the northeast region of the bay, inside the environmental protected area APA, with predominance of odd to even carbon number *n*-alkanes (and high relative abundance of perylene), indicating the presence of hydrocarbons derived from the mangrove forest. The same pattern of pronounced UCM was observed for the rivers from the northwest side of the bay. Highest UCM concentrations were observed in Rio de Janeiro and Niteroi harbors, followed by Sao Joao de Meriti, Sarapui and Iguacu Rivers and sites near these rivers mouths, which are close to the ruptured pipeline at the Duque de Caxias Refinery. On the other hand, sites from the entrance and environmental protected area of the bay, presented the lowest hydrocarbons concentrations, with practically no UCM.

The PAH concentrations in Guanabara Bay sediments were variable both in space and time. The random temporal variability possibly derives from the combined effect of constant inputs of different magnitudes, weathering of LMW PAHs and remobilization by tidal currents, bioturbation and other mechanism that facilitates sediment drift. Critical areas of contamination were identified, where PAH concentrations are far above the level that poses risk to the benthic organisms; special attention is given to Rio de Janeiro harbor (station BG05), extremely polluted.

Source identification of PAHs in Guanabara Bay was carried out by analyzing PAH typologies, applying traditional PAH diagnostic ratios and alternative approach of log−log plots. However, it must be highlighted that Guanabara Bay is a complex tropical environment where PAHs can be introduced by different routes and derived from several activities and processes, source identification as well as estimation of source relevance is therefore not trivial. Preferential weathering of LMW PAH may also contribute to a rapid change in the source identity.

The PAH source identification based on the alternative approaches of log−log plots provided a qualitative and quantitative evaluation of pyrogenic and petrogenic sources in Guanabara Bay sediments. The log−log plots of the five alkylated PAH series as function of UCM and RP and the five alkylated PAH series as function of the 3−6 ring PAH, have allowed the identification of the hot spots for petrogenic contamination and those where pyrogenic inputs are relatively more important. It also showed the samples with degraded petrogenic residues at different levels.

The traditional PAH diagnostic ratios have given some contradictory information for Guanabara Bay sediments at least when the present thresholds reported in the literature to differentiate sources are used, especially for combustion end members. As diagnostic ratios are widely used to distinguish PAH sources and are components of the environmental forensics literature it is highly recommendable to perform a cross evaluation with the aid of other tools, especially when chronic contamination by PAH from a diversity of sources is presumed. The predominance of biomass combustion pointed out by these ratios for a highly urbanized and industrialized area calls for further investigation on combustion end members, which may be used as molecular markers in sediments.

26.3.2 Approach 2—Quantitative Analyses: Multivariate Analysis

Another alternative methodology was tested to identify sources of PAHs in Guanabara Bay by analyzing 3 groups of compounds, related to the crude oils and derivatives. Oils used in the area (Light Arabian AL 1, Light Arabian A L 2, diesel, Marine Fuel 380), *Exxon Valdez* crude oil, Alaska North Slope Diesel, Cook Inlet oil, Katalla oil (Bence et al., 1996), Kenai-Swanson River crude, North Slope crude (Page et al., 1998), Bunker C were inspected for their PAH composition.

These oils show concentrations of PAH heavier than B(*b*)PY (i.e., BkFL, BaPY, BePY, IPY, DBA and BPER) close or below detection limit. This group of compounds are thereafter denominated "*Pyro*." The heavy Bunker C oil is an exception in the inspected group. On the other hand, these oils contain higher relative concentrations of ACE, ACY, AN, FL, PY and BaA (this group of compounds thereafter denominated "*PP*"). A third group of compounds is also identified for these 11 oils: the "*5 Alk*," with very high concentrations of the 5 alkylated PAH series—a median content of 99.5%. The median content of the PP group is of 0.44% and for Pyro group is of 0.07%.

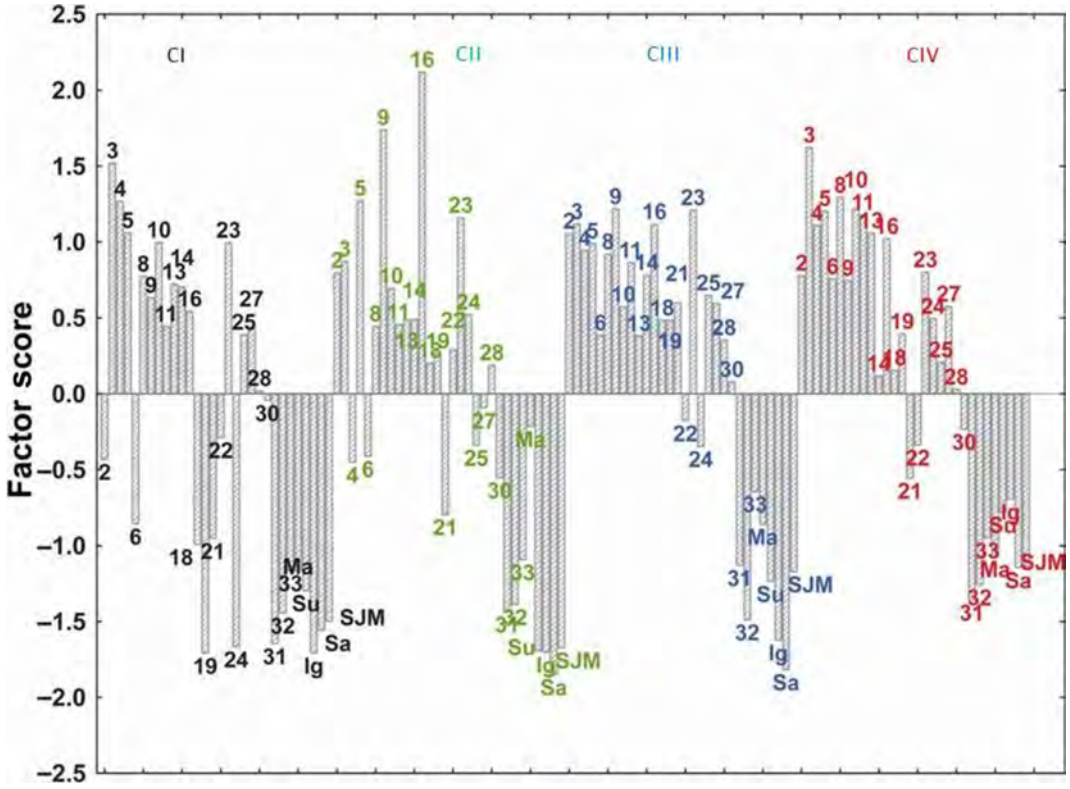

FIGURE 26.13 Factor scores obtained in the Factor Analysis of PAH in samples from Guanabara Bay. Upper bars represent samples enriched in pyrogenic PAH and lower bars stand for samples enriched in petrogenic PAH. The prefixes "BG" and "Rio" were removed from the sample codes for clarity of the figure.

The generally lower incidence of Pyro PAH in oils, although there are some exceptions, makes this set of seven compounds better indicators of pyrogenic residues than the group classified under PP. To test this hypothesis a FA of the normalized sediment concentrations of the three components was used and the result is shown in Fig. 26.13. As the original variables (3−6 ring PAH and 5 alkylated PAH series), which consist of the three components, are highly correlated, as shown in Fig. 26.12, only one factor was obtained wherein Pyro and PP are positively correlated ($r = 0.94$ and 0.91, respectively) and 5 Alk is negatively correlated ($r = 0.99$). In spite of this limitation, the FA discriminated samples with predominant petrogenic inputs (negative factor scores) and those with relative predominance of pyrogenic PAH inputs (positive factor scores). The test also indicated that in the examined sediments PP PAH are most probably deriving from pyrogenic sources. This approach allows identification of samples mainly contaminated with petrogenic PAH which appear to be in larger number than those in the group highlighted under Fig. 26.12. It also provides information on the contribution of each source in each sample. For example, sample BG03 (CI) contains the highest fraction of pyrogenic PAH even though the ΣPAH concentration is the one of the lowest observed in Guanabara Bay. Sample BG19, BG24, BG31, RioIg and RioSa (I) contain similar fractions of petrogenic PAH and the highest incidence of these compounds in the first sampling campaign. In samples such as those from station BG05, where pyrogenic PAH strongly predominate, the FA provided no information on the relevance of the petrogenic component highlighted under Figs. 26.11 and 26.12.

So, the FA of three groups of PAHs (Pyro, PP, and 5Alk), *Approach 2*, has shown to be useful but has not provided better information on the relevance of petrogenic component as observed with the new tools proposed in Approach 1: log−log plots.

26.3.3 Approach 3—Semiquantitative Analyses of PAHs and CHEMSIC (Chemometric Analysis of Selected Ion Chromatograms)

Two separate PCAs were performed on the 30 sediment sample training set. In the first analysis, each of the nine retained sections of chromatograms were normalized to the peak area of the most appropriate internal

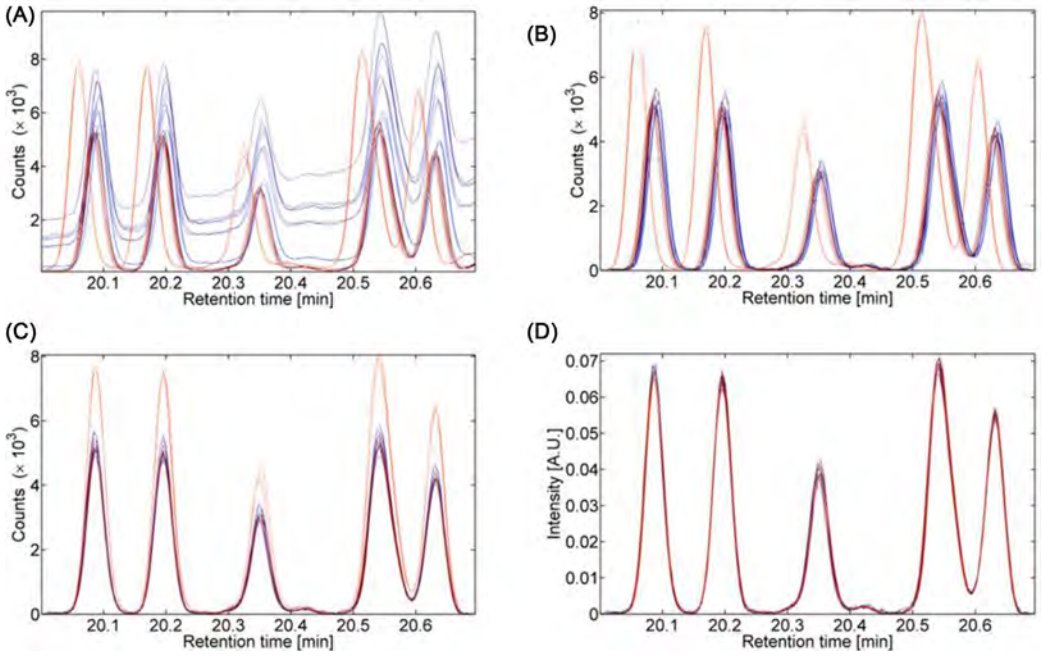

FIGURE 26.14 Data processing. Section of the *m*/*z* 192 SICs for 18 replicate analyses of reference samples: (A) raw chromatogram, (B) after offset correction, (C) after retention time alignment using COW, and (D) after normalization (A.U.: arbitrary units).

standard, while in the second analysis, each section was normalized to unitary Euclidean norm before combining the SICs. The first analysis focused on variations in PAH concentrations and the overall variations in relative patterns. The second analysis can be expected to be better at distinguishing petrogenic, pyrogenic and diagenetic input to the different locations in Guanabara Bay.

Fig. 26.2 (see Section 26.2.4) shows the SICs of the replicate analyses of the sediment reference sample. The capillary column was trimmed before the last batch, which resulted in constant retention time shifts for samples analyzed in this batch. Apart from this, limited baseline drifts, retention time shifts and changes in sensitivity of the detector were observed. However, the *m*/*z* 192 SICs (C1-phenathrenes) were affected significantly by column bleeding during the analysis of the first batches (Fig. 26.14A).

26.3.3.1 *Baseline Removal and Retention Time Alignment*

The piece-wise linear baseline correction method turned out to be adequate for all the 13 SICs (i.e., the nine relevant *m*/*z*'s plus four *m*/*z*'s relative to the internal standards) including *m*/*z* 192 (Fig. 26.14B). The maximum observed retention time shift in the data set was less than five scan points except for the samples analyzed in the last batch, in which it increased to 20 points for some samples. The rigid shift procedure took care of the main part of the constant shift within each SIC (Fig. 26.14C).

The optimal COW parameters were determined using a grid search between 25 and 150 scan points for segment length (with 25 point increments) and 1−3 for the slack parameter, followed by at most ten simplex iterations from the five best results of the grid search. The maximum correction allowed was ± 5 scan points. The 13 *m*/*z*s were aligned separately to the SICs of a reference sample with intermediate shift (the COW "target signal"—Fig. 26.14D).The optimal segment lengths were between 75 and 150 scan points and the optima for the slack parameter were between 1 and 2 points.

26.3.3.2 *Normalization Scheme 1 (Normalization to Internal Standards)*

The effects of normalization to internal standards for the *m*/*z* 192 SICs are shown in Fig. 26.14D. After the normalization, the SICs were combined and the results demonstrate high reproducibility, although minor changes in peak shape for 5−6-ring PAHs (*m*/*z* 252 and 276) could be observed.

Sample BG05, which was collected from the harbor of Rio de Janeiro, was detected as an extreme sample because of its very high PAH concentrations. The abundances for this sample were therefore scaled by a factor of

0.05 and the PCA model recalculated; this led to a more stable crossvalidated model and was accounted for in the chemical interpretation by post multiplying the scores by 20.

The three-component PCA model describes 97.0% of the variance. Loadings above PC3 describe the uncorrected retention time shift and peak shape changes, in addition to chemical variation.

The retention times that contribute the most to a PC are associated with large negative or positive coefficients in the loadings. The PC1 loading is similar to the mean chromatogram; thus larger positive PC1 scores are found for samples with higher levels of contamination. In contrast, samples with larger negative PC1 scores are the least contaminated. A PC1 score value of zero does not imply lack of contamination, but rather the closeness to the mean contamination in the collected sediment samples (Figs. 26.15A and 26.16).

The PC2 loading coefficients are large and positive for C0- and C1-phenanthrenes and for C1-dibenzothiophenes (see Fig. 26.15B), close to zero for anthracene and C1-anthracenes, and negative for 5- and 6-ring PAH. PC2 can therefore be interpreted as a source parameter for light fuel oil contamination as large ratios of C0- and C1-phenanthrenes and dibenzothiophens to C0- and C1-anthracenes and 5–6-ring PAH are indicators for LMW petrogenic input (Yunker et al., 2002). It is therefore evident that sediment samples from inside and close to the outlet of São João de Meriti River (RioSJM and BG37) marked with * in Fig. 26.16, are richer in LMW PAH as indicated by their large positive PC2 scores.

In contrast, the PC3 loading coefficients are positive for C1-pyrenes, close to zero for C1-fluoranthenes and positive for benzo(*e*)pyrene, and negative for other 5- and 6-ring PAH (Fig. 26.15C) except perylene. PC3 can therefore be interpreted as a source parameter for heavy fuel oil contamination or weathered crude oil (WCO) as high relative amounts of C1-pyrenes and benzo(*e*)pyrene are indicators for HMW petrogenic input (Yunker et al., 2002). Hence, BG31 collected closest to the ruptured pipeline at the Duque de Caxias Refinery (see Fig. 26.1) marked with † in Fig. 26.16, contains most likely a fraction of heavily WCO or some other residual fraction of petroleum as indicated by their large positive PC3 scores. The samples with positive PC2 and PC3 scores are marked with § and contain most likely a fraction of less WCO from a more recent contamination.

The PCA results indicate that there is a negative gradient in the PAH contamination level from South West to North East away from the center of Rio de Janeiro. Sediment samples from the more pristine areas inside and close to the outlet of Suruí River, and Macacu River in the North East of Guanabara Bay are the least contaminated (viz. RioMA, BG21, BG22, BG23, RioSU, and BG24), while sediments from the West (and especially the South West corner of the bay close to the harbor, BG05) are highly contaminated with PAH of mainly pyrogenic origin except for some petrogenic point sources (viz. light and heavy petroleum fractions). The contamination level in the NorthWest of Guanabara Bay inside and near the outlet of Iguaçu and Sarapuí Rivers, (viz., RioIG, RioSA, BG31 and BG32) are below the average (negative PC1 scores) and are richer in petrogenic PAH with different degrees of weathering. Conversely, sediments from inside and close to the outlet of São João de Meriti River (RioSJM and BG37) are among the most contaminated in the Bay (positive PC1 scores) and are richer in LMW PAH, which suggests light fuel oil contamination.

26.3.3.3 Normalization Scheme 2 (Euclidean Norm)

The effects of normalization to the Euclidean norm are shown in Fig. 26.17. This normalization increases the relative importance of LMW PAH (e.g., *m*/*z* 178 and 192) compared to the first analysis. A three-component model describing 83.5% of the variance in the training set was found to be optimal. The model provides detailed qualitative information on PAH sources in the bay based on patterns of PAH isomers.

The score plots in Fig. 26.18 indicate that the samples can be inscribed by a tetrahedron at whose vertices the main sources of the PAH contamination are located. Samples from inside and close to the outlet of Suruí River, and Macacu River in the North East of Guanabara Bay are found at one vertex of the tetrahedron (i.e., at positive PC1 and small negative PC2 and PC3 score values). The loadings show that these sediment samples contain large relative concentrations of perylene compared to Σ5-ring PAH, as perylene has positive PC1 and negative PC2 and PC3 loading coefficients (see Fig. 26.19). This is indicative of a dominant diagenetic source (Yunker et al., 2002).

The sediments from São João de Meriti River and BG37 are found at another vertex (i.e., at large positive PC3 and small positive PC1 and PC2 scores). These samples are characterized by high input of LMW petrogenic PAH as indicated by the large positive PC1 and PC3 loading coefficients for C0- and C1-phenanthrenes and large negative ones for C0- and C1-anthracenes (see Fig. 26.19). These observations confirm that the main source of PAH in these samples is indeed a lighter fuel oil fraction (''LFO'' in Fig. 26.18B) most likely originating from wastewater discharges and surface runoffs from the city of Rio de Janeiro.

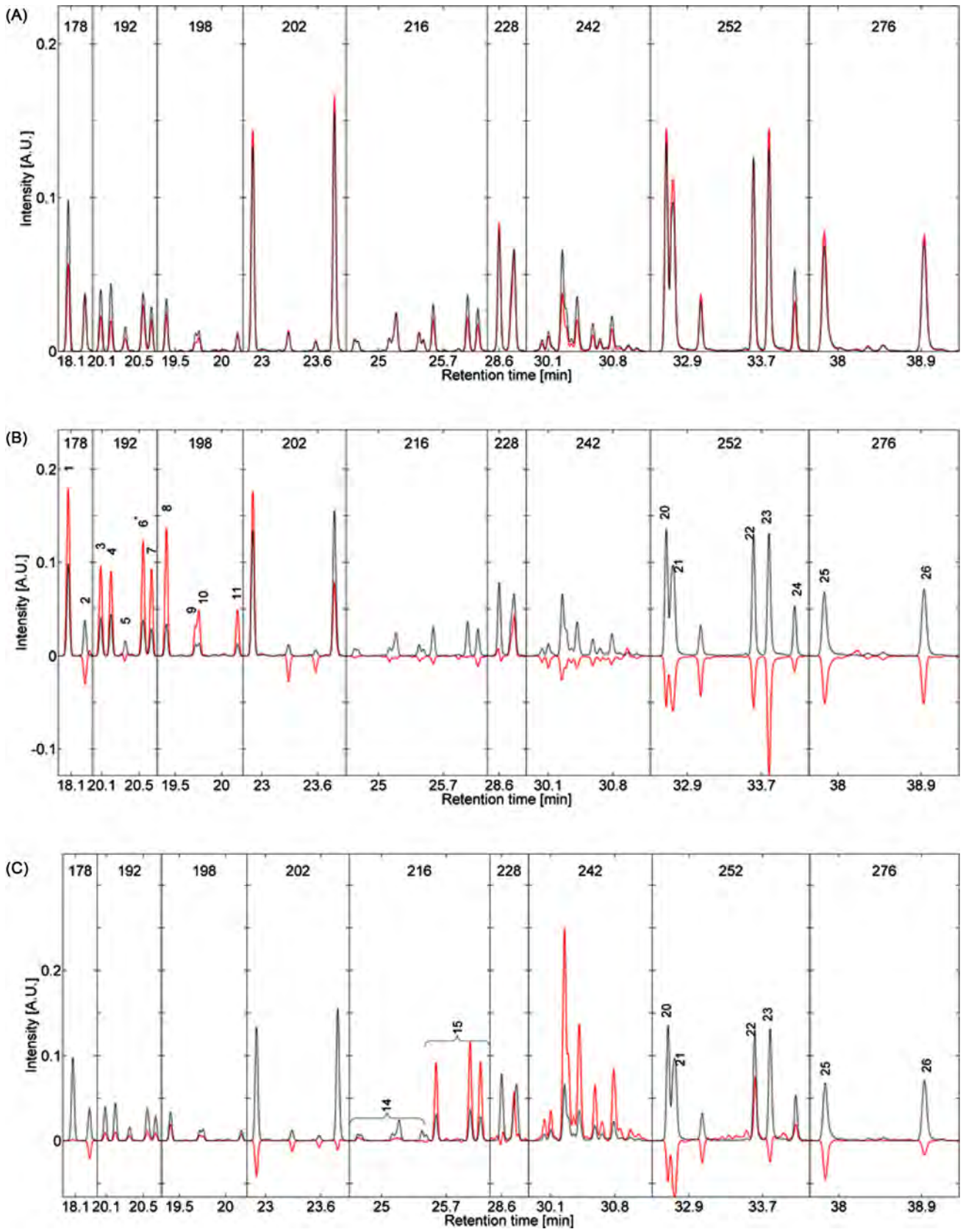

FIGURE 26.15 Loading plots: (A) PC1, (B) PC2, and (C) PC3 for the principal component model of mean-centered data normalized to the internal standards. The dotted lines are the mean chromatogram of the entire training set, while the solid lines are the loadings. The compound numbers are specified in the caption to Fig. 26.2.

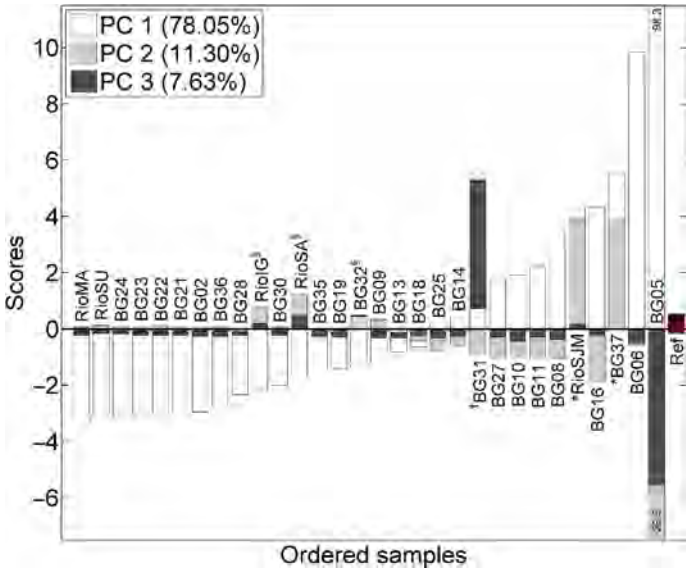

FIGURE 26.16 Scores for PC1, PC2, and PC3 for the principal component model of mean-centered data normalized to the internal standards (note that bars are not stacked). *, †, and § indicate samples heavily contaminated with LMW petrogenic PAH (e.g., light fuel oil), heavily weathered residual fraction of petroleum, and a fraction of less weathered crude oil, respectively.

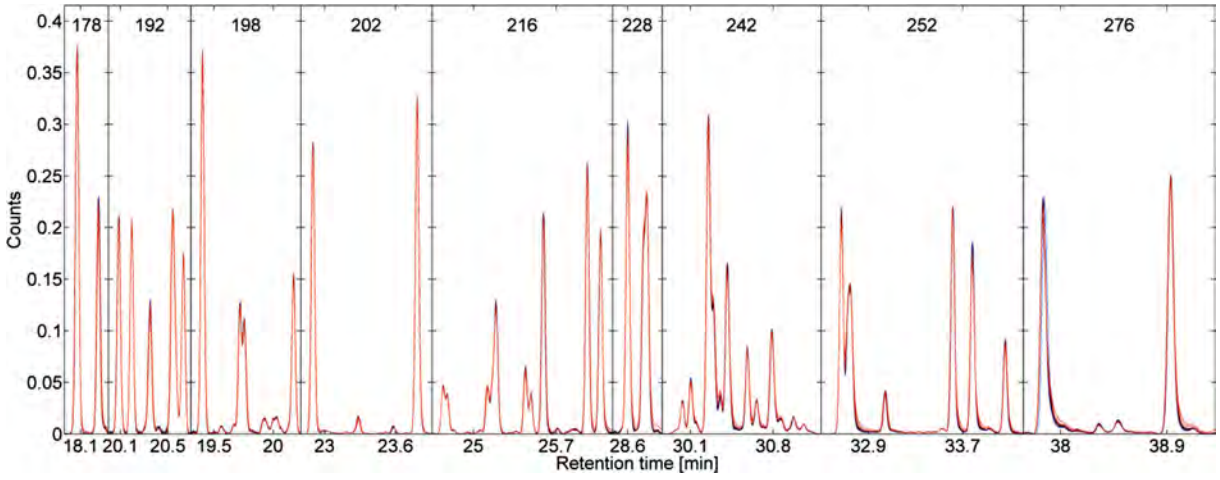

FIGURE 26.17 Combined sections of the nine SICs used in this study for 18 replicate analyses of the reference samples after normalization to the constant Euclidean norm.

The sediments from areas inside and close to the outlet of Iguaçu and Sarapuí Rivers (i.e., RioIG, RioSA, BG31, and BG32) form a cluster at large positive PC2 scores, positive PC1 scores, and both negative (BG31 and BG32) and positive (RioIG and RioSA) PC3 scores. The PC2 loading coefficients show that these samples are characterized by a heavy petroleum fraction with large ratios of C0- and C1-pyrenes to C0- and C1-fluoranthenes, benzo(*e*)pyrene to 5-ring PAH and benzo[*ghi*]perylene to indeno[1,2,3-cd]pyrene (see Fig. 26.19). The MF380 oil released into the bay from a ruptured pipeline at the Duque de Caxias Refinery in 2000 lies in the middle of this cluster which lies close to the "WCO" vertex (Fig. 26.18A). The relative concentrations of C1-pyrenes to C1-fluoranthenes and C1-chrysenes to C1-benzo(*a*)anthracenes gave additional evidence that samples close to the spill accident (e.g., BG31) contained a fraction of WCO (see Fig. 26.19) as indicated by the large positive PC2 and negative PC3 loading coefficients for C0- and C1-pyrenes and vice versa for C0- and C1-fluoranthenes (see Fig. 26.19).

The BG05 sample is located at the fourth vertex of the tetrahedron, labeled "Pyrogenic" in Fig. 26.18. In particular, the PC1 loading coefficients show that these samples contain large relative concentrations of benzo(*f*)fluoranthene, benzo(*k*)fluoranthene and benzo(*a*)pyrene compared to benzo(*e*)pyrene (indicator for petroleum input) and perylene (indicator for in situ diagenesis); large ratios of C0- and C1-benzo(*a*)anthracenes to C0- and C1-chrysenes; and of C0- and C1-anthracenes to C0- and C1-phenanthrenes (see Fig. 26.19). All these ratios demonstrate that the PAHs in the harbor of Rio de Janeiro are mainly of pyrogenic origin (Yunker et al., 2002).

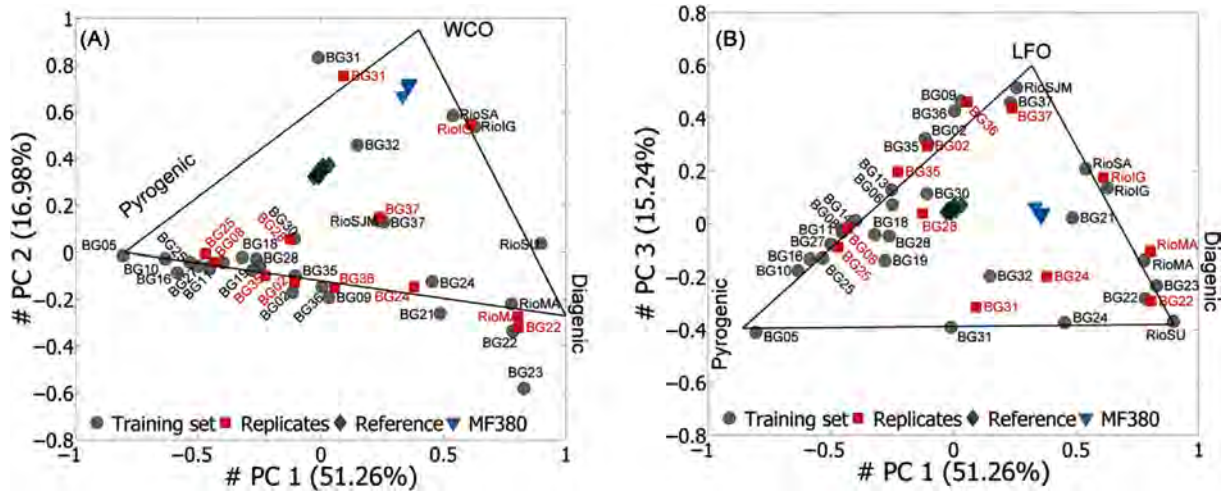

FIGURE 26.18 Score plots: (A) PC1 versus PC2 and (B) PC2 versus PC3 for the principal component model of mean-centered data normalized to the Euclidean norm. WCO and LFO are the abbreviations of "Weathered Crude Oil" and "Lighter Fuel Oils," respectively.

Samples lying inside the tetrahedron are mixtures of several sources. For example the relative contribution from the main diffuse sources in Guanabara Bay (viz., Pyrogenic, LFO, diagenetic) can be estimated from their positions in the triangle shown in Fig. 26.18B. In particular, the edge connecting the pyrogenic and LFO vertices can be used to estimate the contribution of each of these two sources to the total PAH contamination. The cluster of samples from inside and close to the outlet of Iguaçu and Sarapuí Rivers lie close to the WCO vertex as they are contaminated with WCO with high similarity to the spilled MF380 oil.

The CHEMSIC method is able to distinguish between coeluting peaks such as triphenylene and chrysene (*m*/*z* 228, see Christensen et al., 2010), 4-/9-methylphenanthrene and methylanthracene (*m*/*z* 192, Fig. 26.19C) and 2- and 3-methyldibenzothiophene (*m*/*z* 198, Fig. 26.19C) as their loading coefficients have opposite signs, which is exemplary of the high discriminative ability of the method. This was only possible because the relative concentrations of the coeluting compounds varied in the training set.

The CHEMSIC method discriminated the pollution sources in Guanabara Bay. C1-benzo(*a*)anthracenes to C1-chrysenes and C1-fluoranthenes to C1-pyrenes were found to be especially good indicators for distinguishing pyrogenic and petrogenic sources. These ratios are less affected by weathering processes than those of parent PAHs, as the additional methyl group increases the boiling point, decreases the water solubility and makes the compounds less prone to biodegradation (Wang et al.,1998). In fact, the use of alkylated PAHs in the source discrimination and identification were the main reason that heavily weathered oil with high similarity to oil from the Campos Basin could be identified as a source of PAH pollution in the bay area.

26.4 CONCLUSIONS

Guanabara Bay is a complex tropical environment, a highly urban and industrial cluster that also counts on the presence of two remaining mangrove forests. In such a system, where hydrocarbons can be introduced by different routes and be derived from several activities and processes, source identification as well as estimation of source relevance is not trivial. Preferential weathering of the LMW hydrocarbons, especially PAHs, may also contribute to rapidly change the source identity. The present work demonstrates the complexity of hydrocarbon forensics when applied to chronically contaminated sedimentary environments. Three different approaches were applied for source identification of hydrocarbons in Guanabara Bay.

Quantitative analyses and geochemistry evaluation of pyrogenic, petrogenic and diagenetic sources, as described herein as *Approach 1*, have shown an assertive approach for hydrocarbon source differentiation in Guanabara Bay. This methodology included new tools such as the five alkylated PAH series as function of UCM and RP and the five alkylated PAH series as function of the 3–6 ring PAHs, which improved the qualitative and quantitative evaluation of pyrogenic and petrogenic sources for the Guanabara Bay sediments. Approach 1 allowed identification of the hot spots for petrogenic contamination and those where pyrogenic inputs are

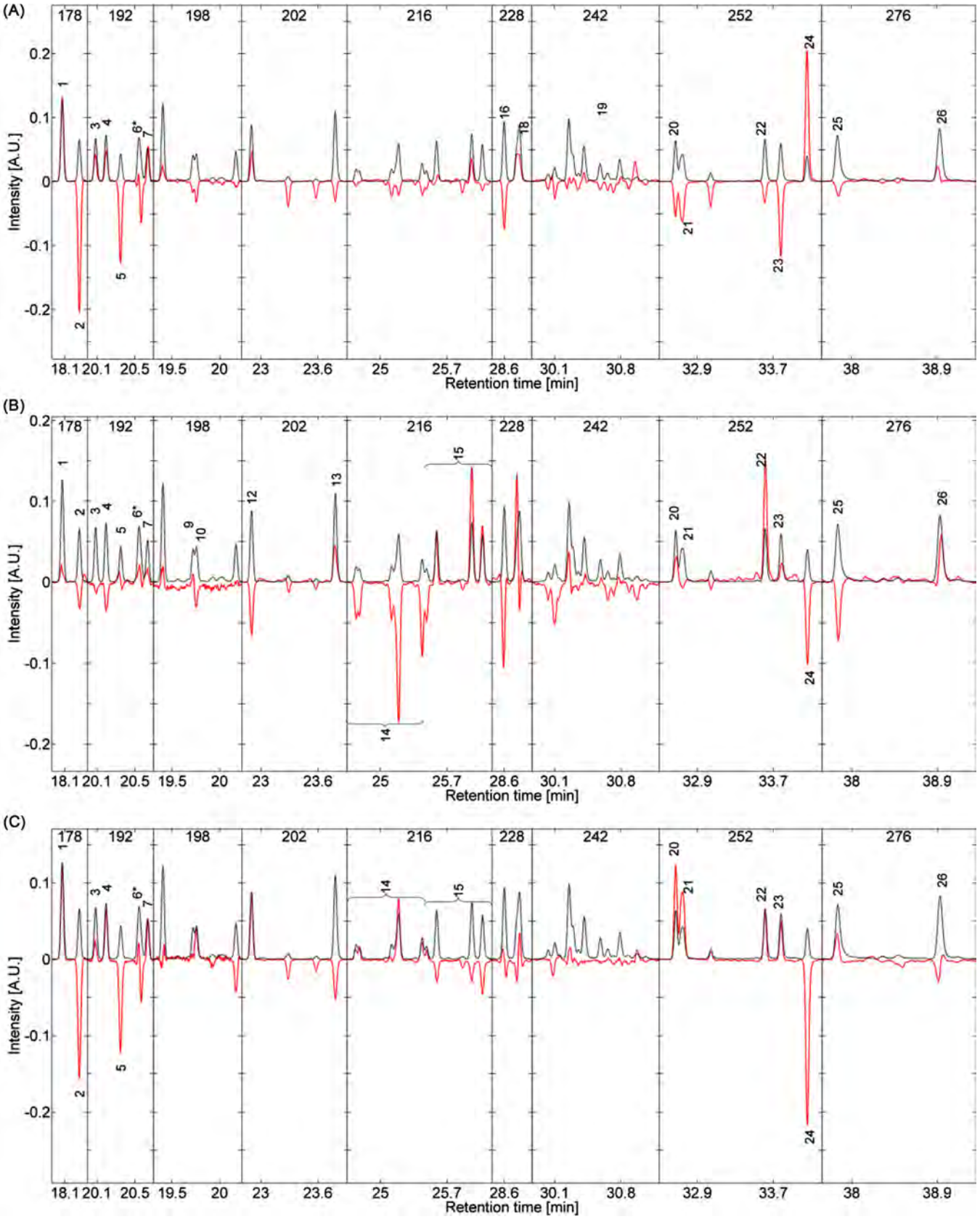

FIGURE 26.19 Loading plots: (A) PC1, (B) PC2, and (C) PC3 for the principal component model of mean-centered data normalized to the Euclidean norm. The dotted lines are the mean chromatogram of the entire training set, while the solid lines are the loadings. SICs of 18 replicate analysis of the reference sample. Nine *m*/*z* ratios (*m*/*z* 178–276) with high relevance for distinguishing between PAH from different sources are shown. The identities of peaks or peak clusters are specified in Fig. 26.2 caption.

relatively more important, and indicated a possible common source containing PAHs from pyrogenic and petrogenic origin as well. It also showed the samples with degraded petrogenic residues at different levels and a west–east contamination gradient in the bay, including the rivers, and the extreme high hydrocarbon contamination at Rio de Janeiro harbor. Yet, Approach 1 has permitted to identify diagenetic sources for some sediments of the bay, specifically for those in the environmental protection area. On the other hand, the source allocation based on PAH diagnostic ratios, using the actual thresholds reported in the literature, presented some discrepancies, especially for combustion characteristics of the Guanabara Bay sediments.

Approach 2 for source hydrocarbon assignment, which was based on the FA of GC–MS quantitative data grouped as Pyro, PP, and 5 Alk compounds, discriminated samples with predominant petrogenic characteristics from those of pyrogenic inputs, and was in agreement with the indications obtained by means of the Approach 3. However, Approach 2 does not highlight the relevance of the petrogenic component in samples where pyrogenic PAH strongly predominate.

The CHEMSIC (*Approach 3*) method based on PCA of preprocessed sections of selected ion chromatograms of PAHs chromatograms (semiquantitative data) have also shown another appropriated approach for hydrocarbon source differentiation in Guanabara Bay sediments. It must be highlighted that, despite being a semiquantitative methodology, high analytical quality is of utmost importance for the use of this technique. CHEMSIC was able to provide not only information on PAH sources in the bay but also on contamination levels of the bay sediments. Five distinct sources of 3- to 6-ring PAHs could be revealed. The harbor is the most contaminated site in the bay, its plume stretches in a South West to North East direction and the chemical profile indicates mainly pyrogenic sources mixed with a fraction of high-molecular-weight petrogenic PAHs. São João de Meriti River is the second largest source of PAHs, and introduces mainly a fraction of low-molecular-weight petrogenic PAHs from the western region of Rio de Janeiro. The sites close to the mouth of Sarapui and Iguacu Rivers and the ruptured pipeline at the Duque de Caxias Refinery (Northwest of the bay) show a distinctive pollution pattern indicating a heavy petroleum fraction.

The same overall hydrocarbon source identifications of Guanabara Bay sediments were obtained by using the three approaches. However, each of the approaches has its advantages and limitations. In the quantitative *Approach 1*, more information was included compared to the multivariate Approach 2, which allowed identification of petrogenic input in very contaminated samples with predominance of pyrogenic characteristics. Approach 1 is more time consuming and expensive due to the use of quantitative data. In contrast, *Approaches 2 and 3* use multivariate statistics to mine the data, being less dependent on the technician interpretation, and providing faster results than available via Approach 1. The CHEMSIC method (*Approach 3*) has the advantage of being a semiquantitative method and also provides information that the other methods did not, *viz*., it allows the investigation of sources with ratios involving the coeluting peaks. In general, it can be said that all three approaches corroborate each other and achieve the main findings on identifying and discriminating hydrocarbon sources in Guanabara Bay sediments.

Acknowledgments

We want to thank Petroleo Brasileiro S.A—PETROBRAS for financially supporting the project entitled Environment Assessment of Guanabara Bay, carried out between 2005 and 2008; Torkil Holms, Lundbeck Foundation and COWI Foundations for supporting the chemometric evaluations of the data. We also want to thank Jette Petersen for laboratory assistance, Gilson Cruz da Silva for their constructive comments on the manuscript and Alexandre T. Politano and Liliane Pequeno A. Heckmann for map and figures elaboration assistance.

References

Aberg, K.M., Torgrip, R.J.O., Jacobsson, S.P., 2004. Extensions to peak alignment using reduced set mapping: classification of LC/UV data from peptide mapping. J. Chemom. 18 (10), 465–473.

Amador, E.S., 1997. Baía de Guanabara e Ecossistemas Periféricos: Homem e Natureza, First edition Reproarte Gráfica e Editora Ltda, Rio de Janeiro, p. 539.

Amador, E.S., 2013. Baía de Guanabara, Ocupação Histórica e Avaliação. Ambiental, First edition Editora InterciênciaLtda, Rio de Janeiro, p. 490.

Baptista Neto, J.A., Gingele, F.X., Leipe, T., Brehme, I., 2006. Spatial distribution of heavy metals in surficial sediments from Guanabara Bay: Rio de Janeiro, Brazil. Environ. Geol. 49, 1051–1063.

Baumard, P., Budzinski, H., Garrigues, P., 1998. PAHs in Arcachon Bay, France. Origin and biomonitoring with caged organisms. Mar. Pollut. Bull. 36, 577–586.

Bence, A.E., Kvenvolden, K.A., Kennicutt, M.C., 1996. Organic geochemistry applied to environmental assessment of Prince William Sound, Alaska, after the Exxon Valdez oil spill – a review. Org. Geochem. 24, 7–42.

Bícego, M.C., Taniguchi, S., Yogui, G.T., Montone, R.C., Moreira da Silva, D.A., Lourenço, R.A., et al., 2006. Assessment of contamination by polychlorinated biphenyls and aliphatic and aromatic hydrocarbons in sediments of the Santos and São Vicente estuary system, São Paulo, Brazil. Mar. Pollut. Bull. 32, 1784–1832.

Boehm, P.D., Douglas, G.S., Burns, W.A., Mankiewicz, P.J., Page, D.S., Bence, A.E., 1997. Application of petroleum hydrocarbon chemical fingerprinting and allocation techniques after the Exxon Valdez oil spill. Mar. Pollut. Bull. 34 (8), 599–613.

Bouloubassi, I., Saliot, A., 1993. Investigation of anthropogenic and natural organic inputs in estuarine sediments using hydrocarbon markers (NAH, LAB, PAH). Oceanol. Acta 16 (2), 145–161.

Bray, E.E., Evans, E.D., 1961. Distribution of n-paraffin as a clue to recognition of source beds. Geochim. Cosmochim. Acta 22, 2–15.

Bro, R., Kjeldahl, K., Smilde, A.K., Kiers, H.A.L., 2008. Cross-validation of component models: a critical look at current methods. Anal. Bioanal. Chem. 390 (5), 1241–1251.

Buchman, F., 2008. NOAA Screening Quick Reference Table, NOAA HAZMAT Report. 08–1 Seattle, WA, Coastal Protection and Restoration Division. National Oceanic and Atmospheric Administration.

Budzinki, H., Jones, I., Bellocq, J., Piérard, C., Garrigues, P., 1997. Evaluation of sediment Contamination by Polycyclic Aromatic Hydrocarbons in the Gironde Estuary. Mar. Chem. 48, 85–97.

Burns, W.A., Mudge, S.M., Bence, A.E., Boehm, P.D., Brown, J.S., Page, D.S., et al., 2006. Source allocation by least-squares hydrocarbon fingerprinting matching. Environ. Sci. Technol. 40 (21), 6561–6567.

Carreira, R.S., Wagener, A.L.R., Readman, J.W., 2004. Sterols as markers of sewage contamination in a tropical urban estuary (Guanabara Bay, Brazil): space-time variations. Estuar. Coast. Shelf Sci. 60 (4), 587–598.

Consorcio Ecologus-Agar, 2005. Programa Diretor de Recursos Hídricos da Região Hidrográfica da Baía de Guanabara—Relatório Final Síntese, Rio de Janeiro, pp. 190.

Christensen, J.H., Hansen, A.B., Karlson, U., Mortensen, J., Andersen, O., 2005a. Multivariate statistical methods for evaluating biodegradation of mineral oil. J. Chromatogr. A 1090 (1–2), 133–145.

Christensen, J.H., Tomasi, G., Hansen, A.B., 2005b. Chemical fingerprinting of petroleum biomarkers using time warping and PCA. Environ. Sci. Technol. 39 (1), 255–260.

Christensen, J.H., Tomasi, G., 2007. Review. Practical aspects of chemometrics for oil spill fingerprinting. J. Chromatogr. A 1169, 1–22.

Christensen J.H., Tomasi, G., Scofield, A.L. and Meniconi, M.F.G. A novel approach for characterization of polycyclic aromatic hydrocarbon (PAH) pollution patterns in sediments from Guanabara Bay, Rio de Janeiro, Brazil. *Environ. Pollut*. 2010; 158, 3290–3297.

Comite Baia de Guanabara. www.comitebaiadeguanabara.org.br/sig-rhbg/ (accessed on 01.11.16).

Cordeiro, R.C., Machado, W., Santelli, R.E., Figueiredo Jr, A.G., Seoane, J.C.S., Oliveira, E.P., et al., 2015. Geochemical fractionation of metals and semimetals in surface sediments from tropical impacted estuary (Guanabara Bay, Brazil). Environ. Earth Sci 74, 1363–1378.

Farias, C.O., Hamacher, C., Wagener, A.D.L.R., Scofield, A.D.L., 2008. Origin and degradation of hydrocarbons in mangrove sediments (Rio de Janeiro, Brazil) contaminated by an oil spill. Org. Geochem. 39, 289–307.

FEEMA—Fundação Estadual de Engenharia do Meio Ambiente, 1998. Qualidade da água da Baía da Guanabara—1990 a 1997, Rio de Janeiro, pp. 100.

Fernandez, M.A., Wagener, A.L.R., Limaverde, A.M., Scofield, A.L., Pinheiro, F.M., Rodrigues, E., 2005. Imposex and surface sediment speciation: a combined approach to evaluate organotin contamination in Guanabara Bay, Rio de Janeiro, Brazil. Mar. Environ. Res. 59, 435–452.

Ferreira, H.O., 1995. Aporte de hidrocarbonetos de petróleo para a Bahia de Guanabara-RJ. M.Sc. Dissertation. Departamento de Geoquímica, UFF, Niterói, 88 pp.

Fingas, M., 2001. In: Charles, Jennifer (Ed.), The Basic of Oil Spill Cleanup, Second edition Lewis Publishers, Boca Raton.

Francioni, E., Wagener, A.L.R., Scofield, A.L., Depledge, M.H., Cavalier, B., Sette, C.B., et al., 2007. Polycyclic aromatic hydrocarbon in intertidal mussel *Perna perna*: space-time observations, source investigation and genotoxicity. Sci. Total Environ. 372 (2–3), 515–531.

Gabardo, I.T., Meniconi, M.F.G., Falcão, L.V., Vital, N.A.A., Pereira, R.C.L. and Carreira, R.S., 2001. Hydrocarbon and ecotoxicology in seawater and sediment samples of Guanabara Bay after the oil spill in January 2000. In: Proceedings of International Oil Spill Conference, Florida, EUA, 941–950.

Gallotta, F.D., Christensen, J.H., 2012. Source identification of petroleum hydrocarbons in soil and sediments from Iguaçu River Watershed, Paraná, Brazil using the CHEMSIC method (CHEMometric analysis of Selected Ion Chromatograms). J. Chromatogr A 1235, 149–158.

Inea. www.inea.rj.gov.br (Gestão das águas > Instrumentos de Gestão de Recursos Hídricos > Planos de Bacias Hidrográficas > Baía de Guanabara) (accessed on 01.11.16).

Jablonski, S., Azevedo, A.F., Moreira, L.H.A., 2006. Fisheries and conflicts in Guanabara Bay, Rio de Janeiro, Brazil. Braz. Arch. Biol. Technol.—Int. J. 49 (1), 79–91.

JICA—Japan International Cooperation Agency, 1994. The Study of Recuperation of the Guanabara Bay Ecossystem, vol. 2. Main Report; Kokusai Kogyo Co., Ltd., Tokyo.

Junttila, J., Carroll, J., Dijkstra, N., 2015. Variability of present and past PAH (polyaromatic hydrocarbons) concentrations in sediments of the SW Barents Sea. Norw. J. Geol. 95 (2), 191–210.

Kavouras, I.G., Koutrakis, P., Tsapakis, M., Lagoudaki, E., Stephanou, E.G., Von Baer, D., et al., 2001. Source apportionment of urban particulate aliphatic and polynuclear aromatic hydrocarbons (PAHs) using multivariate methods. Environ. Sci. Technol. 35 (11), 2288–2294.

Kjerfve, B., Ribeiro, C.H.A., Dias, G.T.M., Filippo, A.M., Quaresma, V.S., 1997. Oceanographic characteristics of an impacted coastal bay: Baía de Guanabara, Rio de Janeiro. Brazil. Cont. Shelf Res. 17, 1609–1643.

Knoppers, B.A., Campello, R., Loureiro, D.D., Carneiro, M.E.R. and Meniconi, M.F.G., 2010. Aporte Fluvial de Matéria Orgânica e Hidrocarbonetos de Petróleo para a Baía de Guanabara. In: Avaliação Ambiental da Baía de Guanabara. Relatório Técnico RT AMA 004/2010, PETROBRAS, Rio de Janeiro, Brazil, vol. 4, 195–228.

Krzanowski, W.J., 2000. Principles of Multivariate Analysis: A User's Perspective. Oxford University Press, Oxford, UK, p. 608.

Lima, A.L.C., Farrington, J.W., Reddy, C.M., 2005. Combustion-derived polycyclic aromatic hydrocarbons in the environment—a review. Environ. Forensics 6, 109–131.

Machado, W., Carvalho, M.F., Santelli, R.E., Maddock, J.E.L., 2004. Reactive sulfides relationship with metals in sediments from an eutrophicated estuary in southeast Brazil. Mar. Pollut. Bull. 49, 89–92.

McLuski, D.S., Elliot, D., 2004. *The Estuarine Ecosystem: Ecology, Threats, and Management*, Third edition Oxford University Press, New York.

Medeiros, P.R.P., Knoppers, B.A., Cavalcante, H.C., Souza, W.F.L., 2011. Changes in nutrient loads (N, P and Si) in the São Francisco estuary after the construction of dams. Braz. Arch. Biol. Technol. 54 (2), 387–397.

Meniconi, M.F.G., Barbanti, S.M., 2007. Case Study: evaluation of hydrocarbon sources in Guanabara Bay, Brazil. In: Wang, Z., Stout, S.A. (Eds.), Oil Spill Environmental Forensics: Fingerprinting and Source Identification. Elsevier, Amsterdam, pp. 505–536.

Meniconi, M.F.G., Gabardo, I.T., Carneiro, M.E.R., Barbanti, S.M., Silva, G.C.D., Massone, C.G., 2002. Brazilian oil spills chemical characterization—case studies. Environ. Forensics 3, 303–321.

Nielsen, N.P.V., Carstensen, J.M., Smedsgaard, J., 1998. Aligning of single and multiple wavelength chromatographic profiles for chemometric data analysis using correlation optimised warping. J. Chromatogr. A 805 (1–2), 17–35.

OGP—International Association of Oil & Gas Producers, 2002. Aromatics in Produced Water: Occurrence, Fate and Effects, and Treatment. Report No. 1.20/324, 30 pp.

Oros, D.R., Ross, J.R.M., Spies, R.B., Mumley, T., 2007. Polycyclic aromatic hydrocarbon (PAH) contamination in San Francisco Bay: a 10-year retrospective of monitoring in an urbanized estuary. Environ. Res. 105, 101–118.

Pampanin, D.M., Sydnes, M.O., 2013. Polycyclic aromatic hydrocarbons a constituent of petroleum: presence and influence in the aquatic environment. Licensee InTec83–118. Available from: http://dx.doi.org/10.5772/48176.

Page, D.S., Boehm, P.D., Douglas, G.S., Bence, A.E., Burns, W.A., Mankiewicz, P.J., 1998. Petroleum sources in the Western Gulf of Alaska/Shelikoff Strait area. Mar. Pollut. Bull. 36, 1004–1012.

Perin, G., Fabris, R., Manente, S., Rebello Wagener, A., Hamacher, C., Scotto, S., 1997. A five-year study on the heavy metal pollution of Guanabara Bay sediments (Rio de Janeiro, Brazil) and evaluation of the metal bioavailability by means of geochemical speciation. Water Res 12, 3017–3028.

Pereira, S.G., 1996. A reforma urbana de Pereira Passos e a construção da identidade carioca. Ph.D. Thesis. Escola de Comunicação, UFRJ, Rio de Janeiro, 273 pp.

Readman, J.W., Fillmann, G., Tolosa, I., Bartocci, J., Villeneuve, J.-P., Catinni, C., et al., 2002. Petroleum and PAH contamination of the Black Sea. Mar. Pollut. Bull. 44 (1), 48–62.

Silva, T.F., 2004. Monitoramento de hidrocarbonetos policíclicos aromáticos na Baía de Guanabara: sedimento, água e peixes (M.Sc. Dissertation). Departamento de Química Orgânica, UFRJ, Rio de Janeiro, pp. 102.

Skov, T., van den Berg, F., Tomasi, G., Bro, R., 2006. Automated alignment of chromatographic data. J. Chemom. 20 (11–12), 484–497.

Soclo, H.H., Garrigues, P., Ewald, M., 2000. Origin of polycyclic aromatic hydrocarbons (PAHs) in coastal marine sediments: case studies in Cotonou (Benin) and Aquitaine (France) areas. Mar. Pollut. Bull. 40 (5), 387–396.

Stout, S.A., Mager, V.S., Uhler, R.M., Ickes, J., Abbott, J., Brenne, R., 2001. Characterization of Naturally-occurring and Anthropogenic PAHs in Urban Sediments—Wycoff/Eagle Harbour Superfund Site. Environ. Forensics 2, 287–300.

Stout, S.A., Uhler, A.D., Emsbo-Mattingly, S., 2004. Comparative evaluation of background anthropogenic hydrocarbons in surficial sediments from nine urban waterways. Environ. Sci. Technol. 38, 2987–2994.

Tissot, B.P., Welte, D.H., 1984. *Petroleum formation and occurrence*. Spring-Verlag, Berlin.

Tolosa, I., de Mora, S., Sheikholeslami, M.R., Villeneuve, J.P., Bartocci, J., Cattini, C., 2004. Aliphatic and aromatic hydrocarbons in coastal Caspian Sea sediments. Mar. Pollut. Bull. 48, 44–60.

Volkman, J.K., Holdsworth, D.G., Neil, G.P., Bavor, J.R., 1992. Identification of natural anthropogenic and petroleum hydrocarbons in aquatic sediments. Sci. Total Environ. 112 (203–219), 453.

Wagener, A.de.L.R., Scofield, A.de.L., Hamacher, C., Francioni, E., Carreira, R.S., and Cardoso, J., 2002. Monitoramento Químico. In: Avaliação de Danos Causados pelo Derramamento de Óleo, em janeiro de 2000 na Baia de Guanabara. Relatório Técnico Secretaria de Meio Ambiente e Desenvolvimento Social, Rio de Janeiro, Brazil, pp. 278.

Wagener, A.L.R., Meniconi, M.F.G., Hamacher, C., Farias, C.O., Silva, G.C., Gabardo, I.T., et al., 2012. Hydrocarbons in sediments of a chronically contaminated bay: the challenge of source assignment. Mar. Pollut. Bull. 64, 284–294.

Wang, Z.D., Fingas, M., Blenkinsopp, S., Sergy, G., Landriault, M., Sigouin, L., et al., 1998. Comparison of oil composition changes due to biodegradation and physical weathering in different oils. J. Chromatogr. A 809 (1–2), 89–107.

Wang, Z., Fingas, M., Page, D.S., 1999. Oil spill identification. J. Chromatogr. A 843, 369–411.

Yunker, M.B., Macdonald, R.W., Vingarzan, R., Mitchell, R.H., Goyette, D., Sylvestre, S., 2002. PAHs in the Fraser River basin: a critical appraisal of PAH ratios as indicators of PAH source and composition. Org. Geochem. 33 (4), 489–515.

Yunker, M.B., Macdonald, R.W., 2003. Alkane and PAH depositional history, sources and fluxes in sediments from the Fraser River basin and Strait of Georgia, Canada. Org. Geochem. 34 (10), 1429–1454.

CHAPTER

27

Hydrocarbon Sources and Biotechnology Applications in Todos os Santos Bay, Brazil

Olívia M.C. de Oliveira[1], *Antônio F. de Souza Queiroz*[1], *Ícaro T.A. Moreira*[1,2], *Danúsia F. Lima*[1], *Carine S. Silva*[1] *and Claudia Y. Reyes*[1]

[1]Universidade Federal da Bahia (UFBA), Salvador, Bahia, Brazil [2]Universidade Salvador—UNIFACS, Salvador, Bahia, Brazil

BIOGRAPHIES

Dr. Olívia Maria Cordeiro de Oliveira is a Graduate in Geology from University Federal da Bahia (1992) and holds a Master's degree in Geology from University Federal da Bahia (1995) and Doctorate at Environmental Geochemistry from University Federal Fluminense (2000). She is Professor of the Federal University of Bahia (UFBA) and currently is Director of the Geoscience Institute (IGEO)/UFBA. She has experience in Geosciences, focusing on Geochemistry, acting on the following subjects: Environmental Geochemistry, Petroleum Geology and Petroleum Geochemistry and Recovery (bioremediation) of Areas Impacted by Petroleum Activities. Leader of the Research Group "Remediation of areas impacted by oil" (CNPq-UFBA).

Dr. Antônio Fernando de Souza Queiroz is a Graduate in Geology from the Federal University of Bahia (1984) and holds a Master's degree in Geosciences/Mangrove Geochemistry from the Federal University of Bahia (1989) and Doctorate in Geology/Geochemistry of the Environment/Mangrove Geochemistry from the Université Louis Pasteur de Strasbourg-France (1992). He is currently Professor of the Federal University of Bahia (UFBA) and Vice-Coordinator of the Postgraduate Program in Geochemistry: Petroleum and Environment (POSPETRO)—Master and Doctorate. Has experience in the area of Geosciences, working mainly in the following topics Environmental Geochemistry, Mangrove Geochemistry, Petrochemical Geochemistry, Analytical Geochemistry and Recovery (bioremediation) of Areas Impacted by Petroleum Activities. Leader of the Research Group "Mangroves of Bahia State" (CNPq-UFBA).

Dr. Ícaro Thiago Andrade Moreira holds a Graduate at Biological Sciences, Master in Geochemistry: Petroleum and Environment (UFBA) and Doctorate in Environmental Geology and Water Resources (Department of Oceanography/UFBA). He is currently Researcher/Collaborator of the Graduate Program in Energy (UNIFACS) and Postgraduate Program in Chemical Engineering (UFBA). He is a specialist in the interpretation of results obtained by bioremediation techniques and in the development of marine biotechnologies applied to petroleum. He has experience in ecology of communities in environments of marine influences (bays, estuaries and mangroves), with emphasis on ecological studies, assessment of risks and responses of marine organisms to environmental impacts as a function of industrial pollutants.

Dr. Danúsia Ferreira Lima is a Graduate in Biology from the Catholic University of Salvador (2002–2006) and holds a Master's degree in Geology with emphasis on environmental geology, hydrogeology and water resources by the Federal University of Bahia (UFBA) where he developed works with Bioremediation of sediment contaminated with oil (2008–2010) and Doctorate in Geology with emphasis in environmental geology, hydrogeology and water resources at the Federal University of Bahia (UFBA), where she developed studies on bioremediation of sediments contaminated with petroleum with a focus on environmental microbiology (2010–2014). Currently

Oil Spill Environmental Forensics Case Studies.
DOI: http://dx.doi.org/10.1016/B978-0-12-804434-6.00027-6

Professor Collaborator/Visitor, with capacity in the Department of Oceanography of the Institute of Geosciences of the Federal University of Bahia.

Carine Santana Silva is a Graduate in Oceanography (UFBA) and holds a Master's degree in Postgraduate Program in Geochemistry: Petroleum and Environment (POSPETRO)/UFBA. It is part of the Research Group on Remediation of Impacted Areas for Oil and Studies of Mangroves in Bahia. He has experience in the area of Oceanography, with emphasis on marine geochemistry, working mainly on the following topics: geochemistry of coastal ecosystems; Assessment/monitoring of contamination in aquatic systems; Biomarkers of oil; Remediation and recovery of areas impacted by oil activities.

Dr. Claudia Yolanda Reyes is a Graduate in Chemistry from the Industrial University of Santander—UIS, Colombia (2001) and holds a. Master's degree in Postgraduate Program in Geochemistry: Petroleum and Environment (POSPETRO)/UFBA (2010) and Doctorate in Environmental Geology and Water Resources at the Geoscience Institute, Federal University of Bahia (IGEO/UFBA). She was a Researcher in the Nucleus of Environmental Studies (NEA)/IGEO/UFBA and the Laboratory of Petroleum Studies—LEPETRO (IGEO/UFBA) and is currently Professor of the Universidad de la Amazonia in Colombia.

27.1 INTRODUCTION

Todos os Santos Bay (BTS) is the second largest navigable bay in the world and is economically very important to Brazil due to the bay's industrial activities, particularly those related to petroleum. However, several impacts of this activity have been identified and monitored by our research groups over the previous 10 years. In this chapter, we present a brief review of the main findings developed by our groups and of the biotechnology solutions that our researchers developed, patented, tested, and published.

27.2 TODOS os SANTOS BAY

BTS is a coastal inlet in the northeastern portion of the state of Bahia, Brazil, between latitudes 12°39′40″S and 13°S and longitudes 38°30′W and 38°43′30″W. The bay is regarded as the largest and most important navigable bay along Brazil's tropical coast (Leão and Dominguez, 2000). It is historically important due to its being the location of the first petroleum production in Brazil in 1939, when oil was discovered in the rail suburb of Lobato, Salvador (Bahia, 2004). The bay is surrounded by one of the largest metropolitan areas of the country, in which approximately 3.6 million people live (Bahia, 2004), and it hosts diverse ecosystems with great biodiversity in fauna and flora. The surrounding municipalities contain numerous industrial sites including the Aratu Industrial Center (Centro Industrial de Aratu), the Landulpho Alves Refinery (Refinaria Landulpho Alves), and the Paraguaçu Shipyard. This industrial activity brings a great deal of value to the economy; however, it poses significant risks to the environment (Celino et al., 2008; Hatje and Andrade, 2009). One of the coastal ecosystems considered to be most affected by oil spills in this region is the mangrove forest and its environmental compartments. These ecosystems are extensively distributed in the BTS, as Fig. 27.1 shows.

The São Paulo River flows into the northern portion of this bay, between the municipalities of São Francisco do Conde and Candeias, adjacent to the Landulpho Alves Refinery (Bahia, 2004). The estuary of the São Paulo River is protected from wave action and consequently is significantly influenced by the accumulation of organic pollutants due to the predominance of clayey sediments. According to Bahia (2004), the main problem in the São Paulo River estuary is the high concentrations of certain heavy metals and petroleum-derived hydrocarbons in the mangrove forest sediments.

The study area for the monitoring presented here corresponds to the São Paulo River basin (Fig. 27.1), which has a drainage area of 37 km^2, an average flow of 0.3 m^3/s, and a total length of 17 km. More than half of its middle reach is bordered by the mangrove ecosystem (Bahia, 2004). Flow into the São Paulo River estuary—which is located in the northern portion of the BTS, at a latitude of 12°50′S and a longitude of 38°38′W, in the state of Bahia (Cirano, Lessa, 2007)—comes from the municipality of Candeias and drains adjacent to the district of São Sebastião do Passé, on its left margin. The region has a moist climate characterized by constant high humidity; the mean annual temperature is approximately 25°C, and the mean annual precipitation varies between 1750 and 1800 mm (Bahia, 2004).

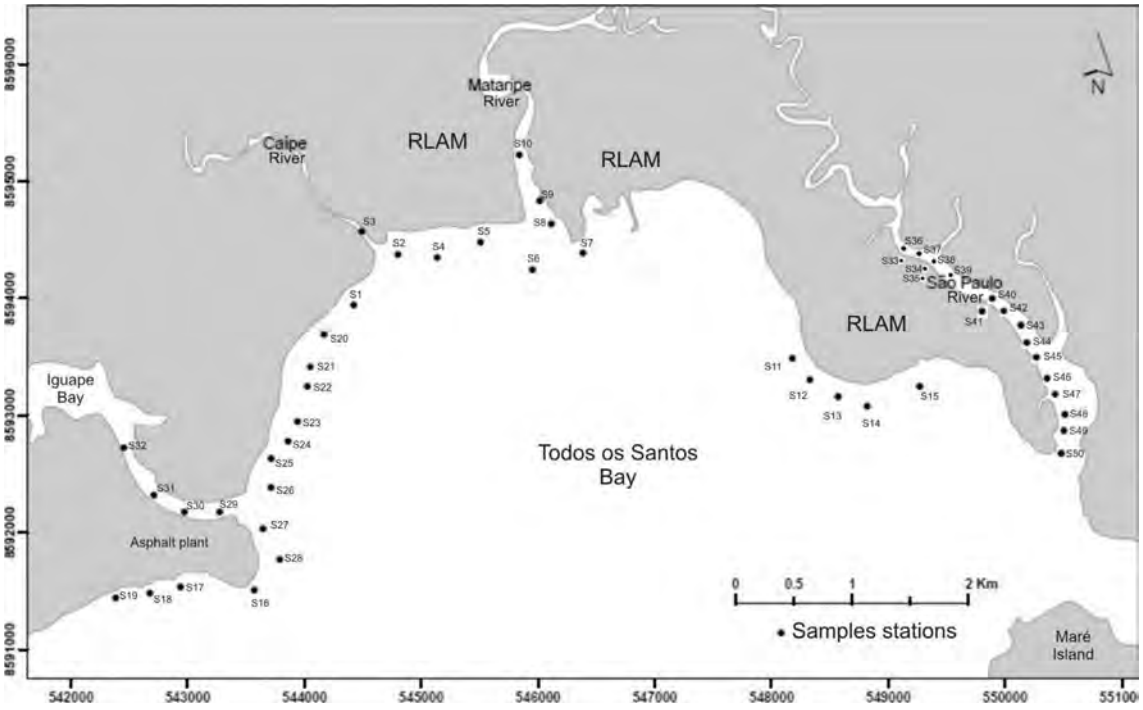

FIGURE 27.1 Map of the study area and the sediment sampling sites in Todos os Santos Bay, Brazil.

Geologically, this region is within the Recôncavo Basin, which is an intracratonic sedimentary basin of Cretaceous age with a predominance of sandy and clayey sediments. The recent sediments are predominantly of medium-high permeability, and the Cretaceous sedimentary rocks are of medium-to-high permeability (Bahia, 2004).

Several oil wells in the watershed of the São Paulo River have a historical record of blow-outs that have caused crude oil (petroleum) contamination of local ecosystems, particularly the mangrove forest. Therefore, there has been a need to develop and test methods of remediation of these areas, given that there are few studies in the literature describing similar remediation.

27.3 PETROLEUM CONTAMINATION IN TODOS OS SANTOS BAY

Organic matter in coastal sediments can show great spatial and temporal variation, is compositionally complex, and can originate from various sources (aquatic, terrestrial, atmospheric, and anthropogenic) (Volkman et al., 1992; Readman et al., 2002). Consequently, characterization of the source, transport, and fate of organic matter in coastal environments can be difficult. Geochemical-correlation parameters for comparing the relative abundance of compounds that can be directly associated with natural or anthropogenic sources are frequently used (Asia et al., 2009). Hydrocarbons, for example, differ in terms of the sizes of their carbon chains, which enables the identification of autochthonous and allochthonous sources of organic matter (Readman et al., 2002; Asia et al., 2009; Tarozo et al., 2010).

Hydrocarbons of anthropogenic origin can reach coastal environments by atmospheric deposition or by direct introduction of petroleum (Tarozo et al., 2010). Once deposited in the sediment, these organic compounds can accumulate over time (ITOPF, 2001). The hydrocarbon concentrations in the sediment may reflect the intensity of anthropogenic activities in the region and the potential for degrading the environmental quality of the ecosystems (Volkman et al., 1992). The use of these compounds in environmental diagnosis enables monitoring of ecosystems affected by spills; evaluation of environmental liability; mitigation of the environment; determination of the fate of the oil in the environment; and, in critical cases, determining needs for remediation (Douglas et al., 1992; Silva et al., 2014).

The dense local industrialization has resulted in the degradation of local ecosystems. At present, BTS is home to the largest petrochemical complex in the southern hemisphere; industries associated with chemical products, metals, foods, and fertilizers; and large ports for exporting domestic production (Hatje and Andrade, 2009).

27.3.1 Sampling and Determination of Geochemical Parameters

In 2010, in order to analyze the distribution and origin of the organic matter in BTS, samples of surface sediment (0−5 cm) were collected at 50 stations in the intertidal zone (Fig. 27.1) and stored at −20°C, in accordance with the preservation protocol for sediment samples (Method D3694-2011, ASTM, 2011). The samples were subsequently cold-dried in a lyophilizer for 72 h and passed through a 2-mm sieve and homogenized. The samples were subjected to granulometric analyses in a laser particle analyzer (CILAS 1064) (Da Silva, 2011). Total organic carbon and total nitrogen were determined using a CHNS-O elemental analyzer (Thermo Finnigan flash) following pretreatment of the samples as described by Ryba and Burgess (2002). The analysis for total petroleum hydrocarbons (TPHs) was performed by gas chromatography with a flame ionization detector (FID). A Varian CP 3800 gas chromatograph, equipped with a DB-5 capillary column (30 m long, 0.25-mm internal diameter, and 0.25-cm film thickness), and a FID were used. The chromatograph conditions were an injector temperature of 300°C, an initial oven temperature of 40°C, holding at 40°C for 2 min, ramping up at 10°C/min to 300°C, and then holding at that temperature for 12 min. Helium was used as the carrier gas at a flow rate of 1.0 mL/min and a separation ratio of 10:1. For analytical quality control and analyte quantification, the concentrations of the target compounds were within the assigned reference value at a confidence interval of 95%.

The study produced data regarding TPH levels in the surface sediments in the intertidal region of BTS. The TPH concentrations varied from 1.0 mg/g in S15 up to 40 mg/g in S35 (Table 27.1). In unpolluted environments, the TPH concentrations in estuarine sediments are typically below 10 mg/g (Volkman et al., 1992; Bouloubassi and Saliot, 1993) but can reach 30 mg/g in locations with an elevated input of organic matter (Readman et al., 2002).

The spatial distribution of petroleum hydrocarbons suggests that the proximity of the sources controls the distribution of these compounds. Only the stations located in the São Paulo River (S33 through S50) yielded TPH concentrations higher than 40 mg/g, which suggests significant contamination in that area. These values are comparable to those in sediments near this area (Bahia, 2004; Celino et al., 2008). In a previous study, Venturini et al. (2004) reported high concentrations of TPH in sediments near the petroleum refinery's area of influence. Historically, this region has suffered many blow-outs that have led to oil contamination in various environments (Bahia, 2004; Moreira et al., 2013).

The unresolved complex mixture (UCM) concentration has been used as a criterion for determining a petrogenetic source of contamination in several studies (Medeiros and Bícego, 2004; Farias et al., 2008; Tarozo et al., 2010; Guo et al., 2011; Lima et al., 2012). Low UCM concentrations may be related to bacterial transformation of sediment organic matter (Readman et al., 2002). The UCM concentrations in the surface sediment ranged from 0.11 to 17,324 mg/g (Table 27.1). Higher UCM concentrations (>100 mg/g) generally indicate contamination by oil (Readman et al., 2002). With the exception of four sampling sites (S46, S47, S48, and S50), the stations located in the São Paulo River yielded concentrations above this limit, which suggests significant contamination by oil in this area.

The concentrations of isoprenoids were also consistent with the other indices. Isoprenoid alkanes such as phytane (2,6,10,14-tetramethylhexadecane) are usually present in oil but are occasionally associated with a biogenic source (Volkman et al., 1992; Tolosa et al., 1996). This particular isoprenoid was detected in the sediment at almost all the stations (except S21 and S30)—see Table 27.1.

The relationship between the TPH concentrations in the sediment, the concentrations of pristane and phytane, and the UCM concentration, as well as possible sources, were also statistically explored using principal component analysis (PCA) (Fig. 27.2). The first PC represented 72.40% of the total variance, and the second was responsible for 18.57%; together, these PCs represented 90% of the total variance. PC1 was characterized by a high concentration of organic compounds, including petroleum hydrocarbons. The high correlation between the concentrations of TPH, UCM, pristane, and phytane indicated a common origin and similar dispersion mechanisms of these compounds.

PCA was used to establish a relationship between spatial groupings of sampling stations, the potential contaminant sources, and the geographic distribution (Fig. 27.2). It was possible to divide the region into three areal groups (I, II, and III) based on the levels of hydrocarbon contamination in the sediment in the intertidal zone. Group I is a zone of highly contaminated sediments and contains the sampling stations located in the São Paulo River. The second group consists of stations located in the Mataripe River, where the refinery's influence is less. There the hydrocarbon concentrations in the surface sediments are lower, and this area can be regarded as an area of moderate contamination by hydrocarbons. The other stations (Group III) are clustered in a zone of low contamination. The C/N ratios suggest the entry of mixed organic matter (aquatic and terrestrial) into the intertidal zone in BTS.

TABLE 27.1 Concentrations of Hydrocarbons (on a Dry Weight Basis) and Selected Ratios in Surface Sediments of Todos os Santos Bay, Brazil

Stations	TPH (μg/g)	UCM (μg/g)	Pristane (μg/g)	Phytane (μg/g)	nC17/ Pr	nC18/ Ph	Pr/ Ph	TOC (%)	OM (%)	TN (%)	C/ N	Sand (%)	Silt + Clay (%)
S1	2.25	2.17	0.002	0.003	1.12	1.47	0.64	1.58	2.72	0.09	18	97.64	2.36
S2	2.94	1.73	0.011	0.020	2.97	0.72	0.57	1.41	2.43	0.14	10	99.74	0.26
S3	13.09	7.98	0.013	0.018	2.56	0.86	0.73	1.66	2.86	0.14	12	96.36	3.64
S4	4.79	4.67	0.002	0.003	2.39	1.01	0.73	1.54	2.65	0.13	12	91.46	8.54
S5	3.15	2.47	0.011	0.016	1.14	1.00	0.68	1.00	1.72	0.08	13	97.85	2.15
S6	16.28	13.65	0.012	0.031	1.39	0.53	0.40	1.09	1.88	0.11	10	97.95	2.05
S7	22.10	15.77	0.022	0.031	1.35	0.68	0.71	0.90	1.55	0.08	11	96.95	3.05
S8	20.75	17.26	0.035	0.062	1.16	0.55	0.56	0.54	0.93	0.07	8	96.14	3.89
S9	21.95	16.25	0.041	0.087	0.51	0.49	0.47	6.94	11.97	0.16	43	95.90	4.10
S10	3.24	2.61	0.007	0.012	0.86	0.59	0.60	4.72	8.13	0.26	18	95.44	4.55
S11	3.38	3.03	0.002	0.003	0.95	1.45	0.62	3.21	5.53	0.32	10	74.14	25.62
S12	2.41	0.58	0.004	0.013	0.24	0.29	0.34	1.96	3.38	0.11	18	70.47	27.88
S13	4.74	1.85	0.051	0.111	1.48	0.91	0.46	1.91	3.30	0.11	17	75.52	23.86
S14	0.89	0.38	0.006	0.007	0.00	3.30	0.85	2.11	3.64	0.13	16	68.58	27.96
S15	0.22	0.11	0.003	0.003	1.48	1.77	1.05	3.31	5.71	0.12	27	74.80	25.20
S16	3.41	3.25	0.007	0.011	2.40	1.07	0.62	0.89	0.89	0.04	23	96.97	3.03
S17	3.58	3.02	0.027	0.043	0.00	1.78	0.63	0.48	0.48	0.05	9	99.37	0.63
S18	1.02	0.90	0.004	0.006	12.78	1.29	0.66	0.48	0.48	0.04	12	99.61	0.39
S19	2.65	1.81	0.008	0.023	4.10	2.69	0.37	2.89	2.89	0.30	10	88.15	11.85
S20	2.22	0.77	0.005	0.008	0.00	0.00	0.65	0.33	0.33	0.03	12	99.70	0.30
S21	0.32	0.18	0.000	0.000	0.00	0.00	**	0.63	0.63	0.04	14	96.10	3.90
S22	12.68	9.02	0.039	0.059	11.97	4.95	0.66	2.95	2.95	0.16	19	99.83	0.17
S23	5.88	3.57	0.024	0.034	0.00	8.40	0.72	1.14	1.14	0.11	10	99.64	0.36
S24	7.96	5.07	0.023	0.033	46.46	5.94	0.69	1.61	1.61	0.15	11	99.22	0.78
S25	13.05	2.50	0.056	0.285	28.17	9.01	0.20	4.22	4.22	0.38	11	99.57	0.43
S26	1.96	1.23	0.010	0.009	0.00	1.17	1.07	0.92	0.92	0.10	9	98.97	1.03
S27	0.46	0.29	0.004	0.005	0.00	1.18	0.84	4.04	4.04	0.38	11	99.71	0.29
S28	0.77	0.31	0.008	0.005	0.87	1.72	1.62	3.96	3.96	0.37	11	66.87	32.79
S29	12.73	4.72	0.017	0.018	1.93	2.24	0.94	3.57	3.57	0.27	13	51.24	44.44
S30	3.04	0.00	0.000	0.000	0.00	0.00	**	6.12	6.12	0.38	16	53.96	44.89
S31	0.82	0.65	0.001	0.002	1.06	1.21	0.55	4.74	4.74	0.30	16	33.82	62.37
S32	1.41	0.97	0.004	0.003	1.02	2.21	1.41	3.03	3.03	0.29	10	40.13	59.06
S33	353,234	14,130	6320	13,289	0.03	0.11	4.76	8.89	15.33	0.36	25	14.82	73.35
S34	365,421	16,079	5538	1374	0.03	0.14	4.03	9.00	15.52	0.31	29	36.60	50.89
S35	40,102	17,329	8175	1508	0.03	0.12	5.42	9.08	15.65	0.34	27	16.12	80.84
S36	33,236	14,069	4946	1250	0.01	0.11	3.96	7.65	13.20	0.36	21	23.12	65.31
S37	31,896	13,157	7707	1200	0.01	0.10	6.43	7.67	13.23	0.32	24	26.31	68.40

(*Continued*)

TABLE 27.1 (*Continued*)

Stations	TPH (μg/g)	UCM (μg/g)	Pristane (μg/g)	Phytane (μg/g)	nC17/ Pr	nC18/ Ph	Pr/ Ph	TOC (%)	OM (%)	TN (%)	C/ N	Sand (%)	Silt + Clay (%)
S38	13,914	5566	4490	524	0.01	0.12	8.58	4.94	8.52	0.31	16	15.32	82.11
S39	331	133	40	13	0.02	0.11	3.15	3.32	5.73	0.36	9	13.35	86.34
S40	3006	1203	738	114	0.02	0.10	6.53	3.21	5.53	0.30	11	36.44	59.58
S41	4909	1964	979	185	0.03	0.13	5.30	3.19	5.51	0.32	10	17.59	77.75
S42	3429	1372	314	129	0.01	0.12	2.43	2.85	4.92	0.30	10	39.93	58.09
S43	3568	1428	939	135	0.01	0.06	6.99	2.46	4.24	0.32	8	27.56	70.24
S44	499	200	140	19	0.00	0.05	7.42	2.72	4.69	0.29	9	26.70	71.74
S45	412	165	34	16	0.02	0.11	2.17	1.66	2.87	0.36	5	16.87	78.63
S46	20	8.0	2.0	1.0	0.04	0.09	2.11	3.23	5.56	0.35	9	19.55	79.54
S47	155	62	8.0	6.0	0.04	0.10	1.32	2.98	5.13	0.33	9	35.25	64.58
S48	129	52	44	5.0	0.02	0.08	8.89	2.68	4.62	0.30	9	31.76	64.09
S49	331	133	10	13	0.03	0.08	0.74	2.92	5.04	0.23	13	15.23	76.29
S50	46	19	3.0	2.0	0.02	0.07	1.82	2.72	4.69	0.21	13	24.26	73.58

***not calculated.*
TPH, Total Petroleum Hydrocarbons; *UCM*, Unresolved Complex Mixture; *Pr*, Pristane; *Ph*, Phytane; *TOC*, Total Organic Carbon; *OM*, Organic Matter; *TN*, Total Nitrogen.

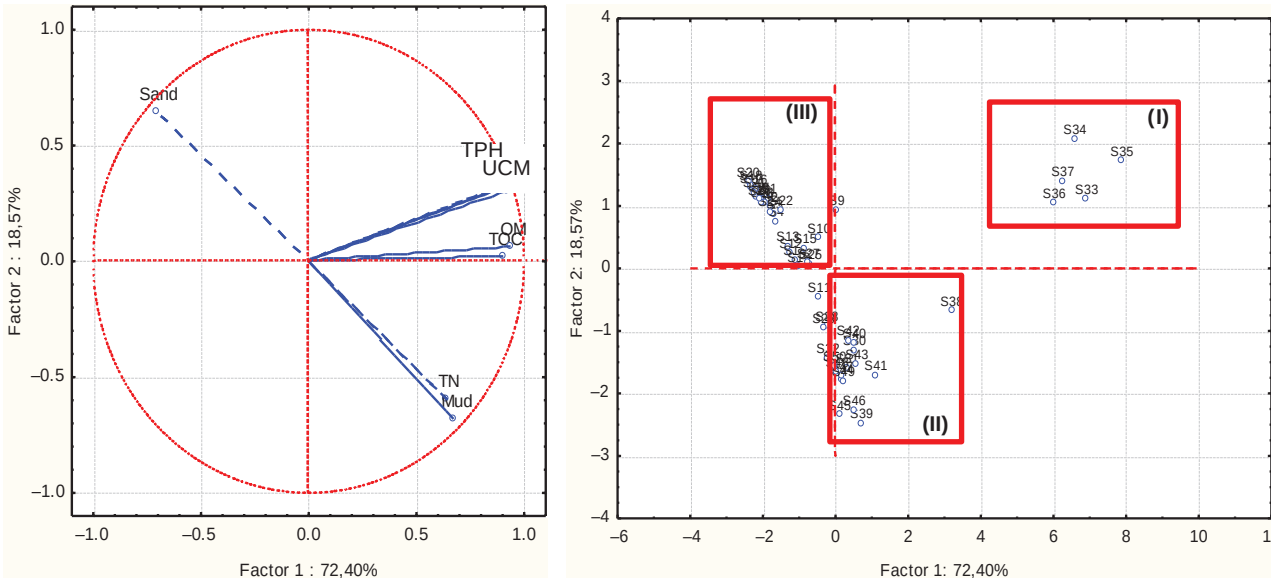

FIGURE 27.2 Principal component analysis (PCA) of geochemical parameters in surface sediments in the intertidal zone of Todos os Santos Bay, Brazil. *TPH*, Total Petroleum Hydrocarbons; *UCM*, Unresolved Complex Mixture; *TOC*, Total Organic Carbon; *OM*, Organic Matter; *TN*, Total Nitrogen.

It is evident that Group I, i.e., the stations on the São Paulo River, represents an area of significant environmental contamination. The low nC17/Pr and nC18/Ph ratios and the high UCM concentrations (Table 27.1) suggest that this contamination is not recent because they indicate that degradation of oil has occurred. This natural removal of pollutants occurs due to natural attenuation. Natural attenuation is a set of processes that promote a decrease in the concentrations of petroleum compounds over time in an environmental compartment; these processes include biodegradation, dissolution, evaporation, dispersion, emulsification, adsorption, and sorption (ITOPF, 2001). Of these, only biodegradation promotes the destruction of organic compounds. Adsorption and

sorption involve the retention of pollutants, and the other processes only cause a change of environmental compartment (Andrade et al., 2010).

The major problem of natural attenuation is the time needed for removing the compounds. The degradation rate is closely associated with the environmental conditions (e.g., hydrodynamics; level of oxygen, phosphorus, and nitrogen; salinity; and temperature), the composition of the oil, and the presence of hydrocarbon-degrading bacteria (Peters et al., 2003). Initially, this process is rapid because light and low-molecular-weight compounds are still present; however, after some time, the degradation rate decreases (Kennish, 1997).

The high concentrations still found in the São Paulo River region indicate that a management plan for contaminated areas that includes the use of remediation techniques to accelerate the natural degradation of the oil must be developed to provide better environmental quality for the region.

27.4 BIOTECHNOLOGICAL APPLICATIONS: INTRINSIC BIOREMEDIATION

Biological processes are gaining increasing importance worldwide in environmental remediation, particularly in environments contaminated with organic compounds. These methods are favored due to their lesser ecological impact, lower cost, and easier application on a large scale (Yeung et al., 1997).

Bioremediation is a process by which organic wastes are biologically degraded under controlled conditions to an innocuous state or to levels below the concentration limits established by regulatory authorities. Bioremediation is characterized by the acceleration of oil's natural degradation, in which microorganisms use the hydrocarbons as the main source of carbon in their metabolic processes (Pritchard and Costa, 1991; Prince, 1993; Atlas, 1995a and 1995b; Vidali, 2001). It is an emerging technology that involves the addition of materials (e.g., nutrients or other growth factors) in contaminated environments to accelerate natural biodegradation (EPA, 2004).

The use of bioremediation was discovered during investigations of the degradation of hydrocarbons in the natural environment. It was observed that some microorganisms are capable of using hydrocarbons as a source of carbon and energy (Zobell, 1946; Atlas, 1981). However, it was only after the analysis of biotic and abiotic factors involved in biodegradation that the technique started to be used in the cleanup of environments contaminated by oil (Lindstrom et al., 1991).

This technology is based on the premise that most of the components of petroleum are biodegradable in nature. Microorganisms use hydrocarbons as the main source of carbon in their metabolic processes under anaerobic and aerobic conditions (Atlas, 1981; 1984; Rosa, 2001; Mariano, 2006). This natural process can be accelerated by the use of biostimulation and/or bioaugmentation. In biostimulation, nutrients are added and the environmental conditions are optimized to grow the native populations of microorganisms (Feniman et al., 2009). Nutrient additives are bioremediation agents—one of the primary means for increasing the growth rate of microorganisms that degrade petroleum. This type of agent is intended to increase the biomass to a level at which the oil will be used as the primary source of food or energy. The natural environment does not contain sufficient nutrients to stimulate the metabolism and growth of the microorganisms; therefore, it is necessary to provide nutrients to maintain or increase microbial activity and natural biodegradation (Pedigo et al., 2011).

Biostimulation of populations of autochthonous microorganisms to increase the rates of biodegradation is often performed in bioremediation projects (Atlas, 1977). To use biostimulation, it must first be shown that there is a natural population of microorganisms capable of biodegrading the contaminants at a site and that the existing environmental conditions are insufficient for obtaining high rates of microbiological activity from this population (Ramaswami and Luthy, 1997).

There are limiting factors during biostimulation (e.g., nutrients and electron acceptors). Expanding these limits stimulates the metabolism and growth rate of the degraders, which accelerates the biodegradation rates under favorable environmental conditions. The addition of nutrients in contaminated environments allows for faster and more effective degradation of hydrocarbons by the native microorganisms (Vallejo et al., 2005). According to Vallejo et al. (2005), previous studies have demonstrated that biostimulation accelerates the biodegradation of contaminated soils when certain factors—such as pH, humidity, TPH concentrations (of the slower-to-degrade fractions), electron acceptors, and temperature—are controlled. Most of these studies are based on the addition of nutrients in the form of simple organic and inorganic fertilizer compounds.

Nitrogen–phosphorus–potassium (NPK) and Osmocote have been widely used as stimulators. NPK is a water-soluble fertilizer composed of ammonium sulfate $(NH_4)_2SO_4$, monoammonium phosphate $(NH_4)_3PO_4$,

potassium chloride (KCl), and cotton meal. Osmocote is another soluble fertilizer. It has the same composition as NPK but differs in that it is a slow-release type and that its inorganic nutrient granules are coated with hydrophobic materials such as paraffin or vegetable material. The goals of this study were to evaluate the degradation of saturated hydrocarbons via biostimulation in mangrove swamp sediments and to test the potential of two fertilizers (NPK and Osmocote) as accelerating agents of the biodegradation of petroleum components under experimental conditions.

In bioaugmentation, microorganisms capable of rapidly degrading specific contaminants are added (Feniman et al., 2009). In some cases, the microorganisms can be colonized in bioreactors. All commercially available agents naturally use microorganisms. Some agents may also contain nutrients to ensure the activity of the microbial cultures. Microbial agents are designed to increase the biodegradation of petroleum at any location, which is very useful in locations where the indigenous oil-degrading population is small (Pedigo et al., 2011).

Many indigenous microorganisms in water and soil are able to degrade contaminating hydrocarbons (Kumari and Amruta, 2013). These microorganisms are not restricted to a few genera: various groups of bacteria, fungi, algae, and cyanobacteria have been shown to have this capacity (Kataoka et al., 2001; Mariano, 2006). Leahy and Colwell (1990) cited the following genera of bacteria as being the most important: *Achromobacter*, *Acinetobacter*, *Alcaligenes*, *Arthobacter*, *Bacillus flavobacterium*, *Nocardia*, and *Pseudomonas*.

Riser-Roberts (1992) cited the fungi of the *Aspergillus* and *Penicillium* genera as the main species that assimilate hydrocarbons; however, this characteristic is a property of certain species and is not necessarily a particular characteristic of the genus. Notable among the genera of cyanobacteria and algae are *Oscillatoria*, *Microcoleus*, *Anabaena*, *Nostoc*, *Chlorella*, *Chlamydomonas*, and *Ulva* (Atlas, 1981).

Testing the bioaugmentation and biostimulation techniques in a benchtop experiment was one of the main steps in this study. Allied to this aspect is the internationally recognized need for the identification and isolation of microorganisms for the possible development of a consortium capable of degrading all the oil, thereby improving the bioremediation results.

27.4.1 Experimental Development

In 2007, we began using biotechnologies with the biostimulation technique. Two types of fertilizers—NPK and Osmocote—were used to stimulate the growth of microorganisms. For the experiments, 72 sediment cores were collected using a 30-cm sampler. The site for collecting the substrate samples of the mangrove forest was in a contaminated area (sampling area 1) located in the BTS, in the municipality of São Francisco do Conde, BA (Fig. 27.3).

Each core sample was then homogenized and divided into three portions. One portion, the control, was left untreated: The natural composition of the sediment was maintained. The second portion was treated by adding NPK fertilizer at a rate of 0.5 g/kg of sediment. The third portion was treated by adding Osmocote at that same rate of 0.5 g/kg of sediment. The experiment spanned 3 months.

The experiment was performed in glass tanks (aquariums) measuring 50 cm tall, 30 cm wide, and 40 cm long. Each tank contained eight glass graduated cylinders, a wooden support for the cylinders, a tap at the bottom to drain the water, and a pump for aeration (Fig. 27.4). The cylinders were covered with cotton bags, which were secured with nylon clamps at the bottom and elastic bands at the top. Seventy-two graduated cylinders were used in the setup; these were placed on wooden supports. Nine simulation units were assembled: Units 1, 2, and 3 contained the control samples; units 4, 5, and 6 contained the samples treated with NPK (Bioremediation 1); and units 7, 8, and 9 contained the samples treated with Osmocote (Bioremediation 2).

The physical–chemical parameters (salinity, dissolved oxygen [DO], pH, Eh, and temperature) were monitored throughout the experiment, and daily rising and falling tides were simulated (Fig. 27.5(A)).

In 2013, we tested the bioaugmentation technique, which involved testing the efficacy of the consortium in degrading oil from the Recôncavo and Campos Basins, with the glass tanks (aquariums) as simulation units (Fig. 27.6(A)). Uncontaminated sediment samples (sampling area 2) were collected in a mangrove area located in BTS, in the municipality of São Francisco do Conde, BA (Fig. 27.5).

Initially, filamentous fungi capable of degrading the main petroleum fractions [saturated, aromatic, and nitrogen–sulfur–oxygen (NSO) hydrocarbons] were isolated and selected. Subsequently, a consortium of fungal and encapsulated isolates formed. The sediment used in the experiment was homogenized, placed in graduated cylinders, and then sterilized for 40 min in an autoclave at 121°C. The graduated cylinders were placed on a wooden support and covered with cotton bags to minimize incident light (Fig. 27.6(B)).

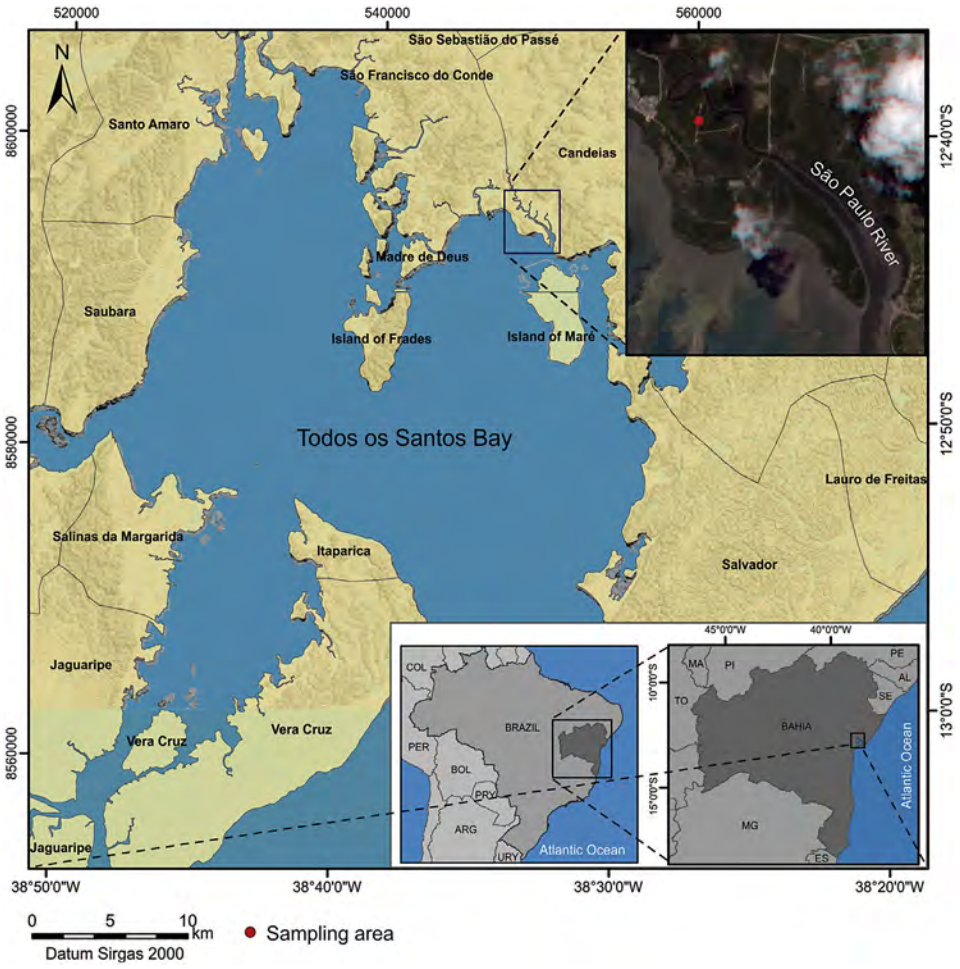

FIGURE 27.3 Location map of the study area. (A) Location of BTS and (B) satellite image of the study area showing sampling areas 1 and 2. *(A) Modified from the sheet of Todos os Santos Bay: SD-24-X-A-IV (Bahia.* Centro de Recursos Ambientais. Diagnóstico Ambiental do Grau de Contaminação da Baía de Todos os Santos por Metais Pesados e Hidrocarbonetos*; CRA; Salvador; 2004; 394 p.) and (B) Google Earth (2014).*

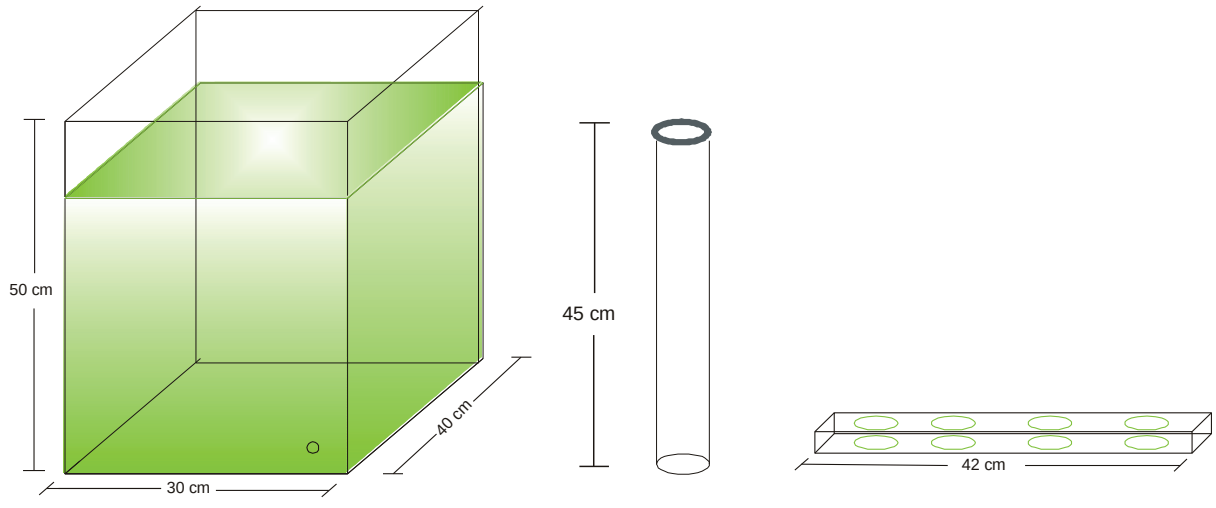

FIGURE 27.4 Schematic showing the aquarium, graduated cylinders, and wooden support for the cylinders.

FIGURE 27.5 Photographs of the biostimulation experiment: (A) simulation units, (B) monitoring of the physical–chemical parameters, (C) removal of the samples, and (D) collection of the samples.

Subsequently, the immobilized consortiums (capsules) were placed in the graduated cylinders. Ten capsules were placed in each cylinder. An oil spill was then simulated in the upper part of the cylinder (which already contained sediment and the consortium) using approximately 3% of oil from the Recôncavo Basin and 3% of oil from the Campos Basin in the respective simulation units (Fig. 27.6(C)). All the simulation units were covered and sealed with film paper to avoid contamination. All the setup procedures were performed under a laminar-flow hood. The water used in the experiment had been autoclaved at 121°C for 20 min. An oxygenation pump was placed in each aquarium. The physical–chemical parameters (salinity, DO, pH, Eh, and temperature) were measured daily.

27.4.2 Monitoring of Biological, Physical, and Chemical Parameters

In the biostimulation experiment, the samples were collected at the end of days 1, 2, 8, 15, 30, 45, 60, and 90, and the following geochemical parameters were determined: saturated hydrocarbons (following USEPA Method 8015B), ammonia and nitrate (Kjeldahl's wet method), phosphorus (method of Aspila et al., 1976), organic carbon (Walkley-Black method, 1947), and grain size (method of Folk and Ward, 1957).

In the bioaugmentation experiment, the sediment and water samples were collected at 1, 8, 15, 30, 45, 60, 75, and 90 days. The samples collected from the experiment were analyzed for physical parameters (grain size, via the method of Folk and Ward, 1957), microbiological parameters [the colony-forming units

FIGURE 27.6 Photographs of the bioaugmentation experiment: (A) graduated cylinders with sterilized sediment; and (B)–(D) collection of the samples.

(CFU) count, via the method of Da Silva, 2011 and Gerba, Pepper, 2004], geochemical and hydrocarbon parameters (via USEPA Method 8015B), total nitrogen (via Kjeldahl's wet method), phosphorus (via the method of Aspila et al., 1976), and organic carbon (via the method of Walkley-Black, 1947).

27.4.3 Bioremediation: Results and Discussion

Evaluation of the physical–chemical parameters and nutrients: The analysis for the parameters indicated that the samples were not significantly different and, therefore, that throughout the experiment, there were no large variations that adversely affected the biostimulation (Fig. 27.7; Lima et al., 2012).

The nutrients monitored during the experiment were the levels of phosphorus, ammonium, and nitrate ions in the sediment samples extracted from the graduated cylinders in the simulation units on days 1, 30, 60, and 90. Fig. 27.8 shows that the levels of phosphorus, nitrate, and ammonia in the NPK units were higher after 24 h. These higher levels can be explained by the high solubility of the NPK and by the simulated tidal action; consequently, these nutrients were released rapidly. The results also show that the dissolved nutrient levels continued to increase during the experiment. The plots in Fig. 27.8 show that the nutrients in the units treated with Osmocote were increasing at the end of the experiment, in contrast to the nutrients in the NPK unit, which were decreasing. The increase in these levels of nutrients favors the growth of the microbial population responsible for the biodegradation of oil in the environment (Lima et al., 2012).

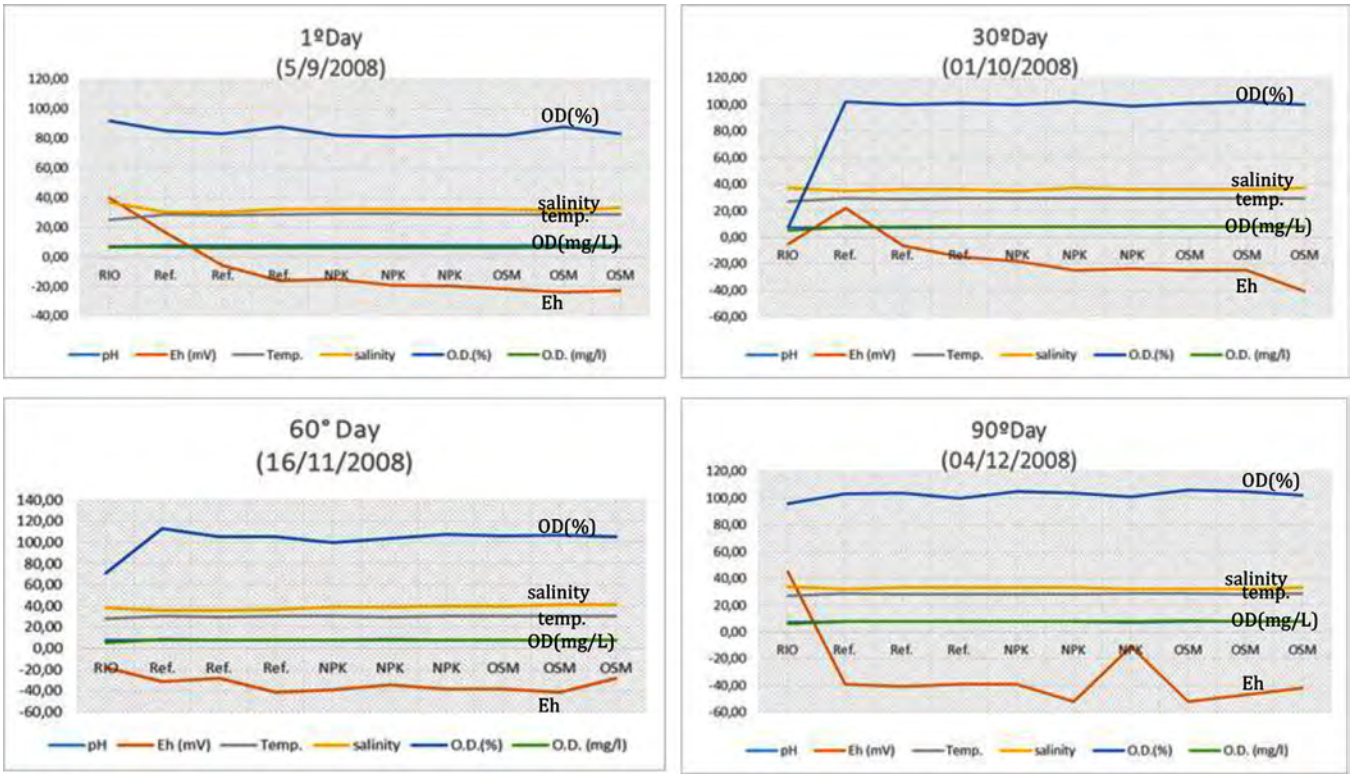

FIGURE 27.7 Variations in physical–chemical parameters during the experiment (days 1, 30, 60, and 90) in the bioremediation simulation units.

According to Vallejo et al. (2005), low phosphorus values will be present throughout such experiments because microorganisms consume phosphorus rapidly at the beginning of biodegradation. This trend was not observed in our experiment: the phosphorus values remained level throughout. This observation could be attributed to the degradation stage of the oil: No hydrocarbons of low molecular weight were detected; these hydrocarbons are the first to be degraded. The ammonia levels in the units treated with NPK were higher during the first days of the experiment and decreased appreciably from day 30 onward (Fig. 27.8). Nutrients in certain coastal environments are scarce, and the absence of bioavailable phosphorus, in particular, can lead to a reduction in the microbial population, which leads to slow degradation of oil (Leahy and Colwell, 1990; Prince, 1993). Dibble and Bartha (1976) reported that low concentrations of nitrogen and phosphorus severely limit hydrocarbon degradation and that the addition of nitrogen and phosphorus can be used to stimulate microbial degradation of hydrocarbons.

Evaluation of the liquid chromatography results: The analyses of the oil extracts collected from the simulation units on the first day of the experiment indicate a higher level of NSO compounds. Our results match the order of biodegradation proposed by some authors such as McMillen et al. (1993), in which the saturated hydrocarbons are the most susceptible to microbial degradation, whereas NSO compounds are the most persistent. The differences among the analytical results from the oil samples extracted from the simulation units indicate that the degradation of the saturated hydrocarbons was more effective in the units treated with NPK: there was greater reduction in the percentage of saturated hydrocarbons and an increase in the relative concentration of the polar (NSO) compounds (Fig. 27.9).

According to Tissot and Welte (1984), biodegradable oils contain lesser amounts of saturated hydrocarbons and, consequently, greater amounts of NSO compounds. Paraffinic oil, such as the oil found in the substrate of the mangrove forest, contains higher amounts of saturated hydrocarbons (Gaglianone and Trindade, 1988). With biodegradation, these variations probably reverse, thereby shifting the contaminant into the biodegradable class. For the most part, the analyses of the oil extracts from the control simulation units indicate that there was a decrease in the relative concentration of the saturated hydrocarbon fraction, followed by a lesser relative decrease in the aromatic fraction, which was accompanied by the relative increase in the polar fraction (NSO compounds) (Fig. 27.9).

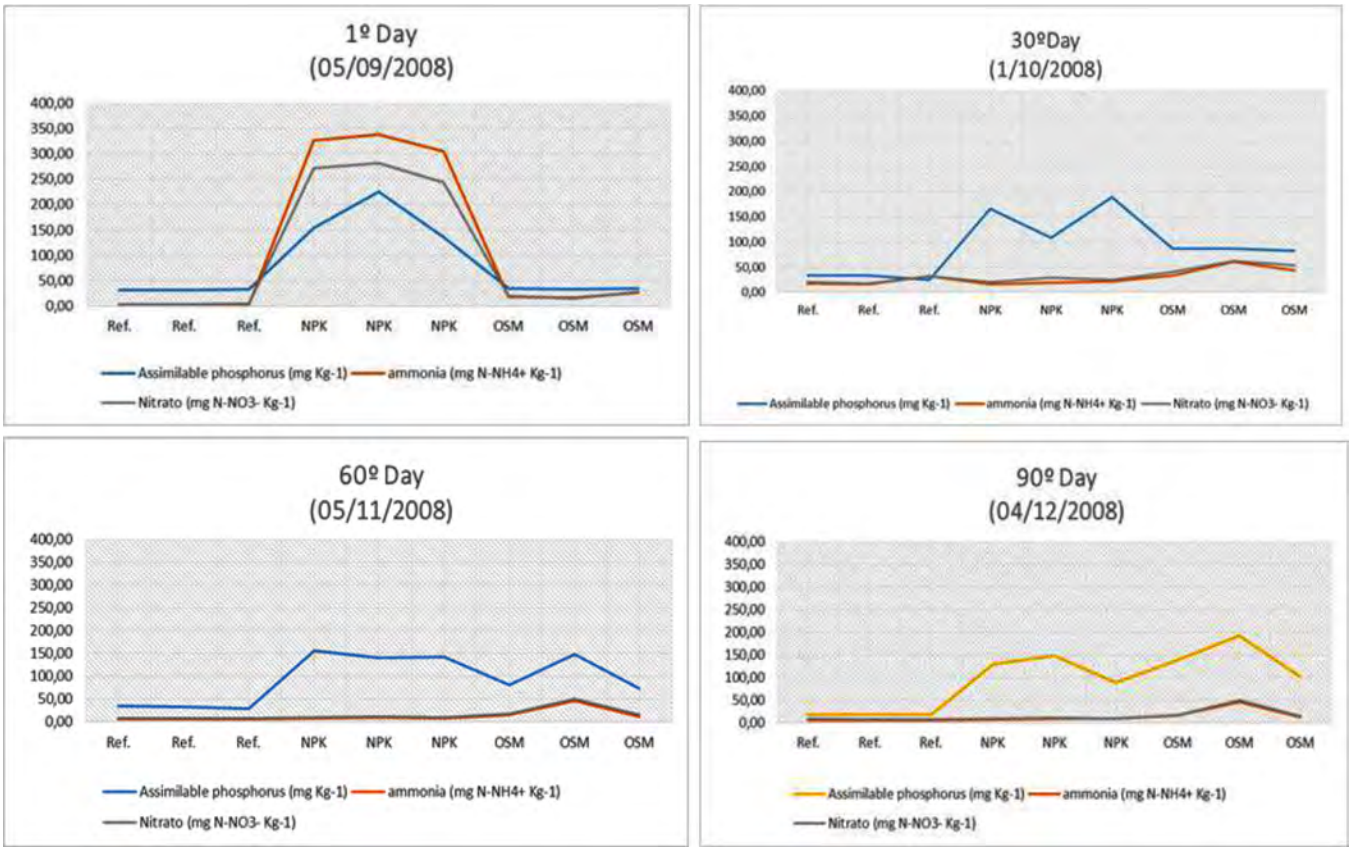

FIGURE 27.8 Concentrations of the nutrients during the experiment (days 1, 30, 60, and 90) in the bioremediation simulation units.

In the simulation units treated with NPK, liquid chromatography yielded very different values (similar to those of the control tanks): a decrease in the saturated hydrocarbons after day 90. These values may be the result of sample preparation that did not result in full homogenization; i.e., the different values reflected the heterogeneity of the samples (Fig. 27.9). This preferential reduction of saturated hydrocarbons by the microbial community is consistent with findings by several authors who performed laboratory simulations and analyses of oil spills in coastal environments (Wang and Bartha, 1990; Wolfe et al., 1994; Blenkinsopp et al., 1997). Rosa (2001) noted that the addition of nutrients in biostimulation is necessary for microorganisms to accelerate the natural biodegradation of the oil. This acceleration is directly related to the increase in microorganism populations in the contaminated environment that use hydrocarbons as an energy source. In addition, the decreases in the levels of aromatic hydrocarbons were greater in the units treated with NPK than in the control units.

The samples from the simulation unit treated with Osmocote displayed the same hydrocarbon degradation trend: an increase in NOS compounds (Fig. 27.9). Compared with the results from the other simulation units, the unit treated with Osmocote yielded a trend similar to that of the control unit and was less effective than the NPK fertilizer. This difference can be attributed to the fact that Osmocote, due to the encapsulation of its granules, releases nutrients slowly and thus requires more time to reach optimal levels for accelerating biodegradation. The NPK, in contrast, is more soluble and reaches optimum levels for accelerating the degradation more rapidly. Therefore, it is necessary to control the levels of phosphorus, ammonia, and nitrate in a shorter time interval to determine in which exact time interval the units treated with NPK and Osmocote reach the optimum levels necessary to accelerate the degradation, and whether they in fact have reached these levels. Although the use of slow-release fertilizers has been indicated by some authors (Olivieri et al., 1976; Lee et al., 1993) for providing a continuous source of nutrients to contaminated areas and has shown certain improvements in the biodegradation of oil, the major problem is the long time period required to reach the concentration of nutrients necessary for biodegradation to occur.

For the bioaugmentation experiment, data were obtained in relation to the geochemical, physical–chemical, chemical, and microbiological monitoring. Mean values were obtained from the simulation units receiving a

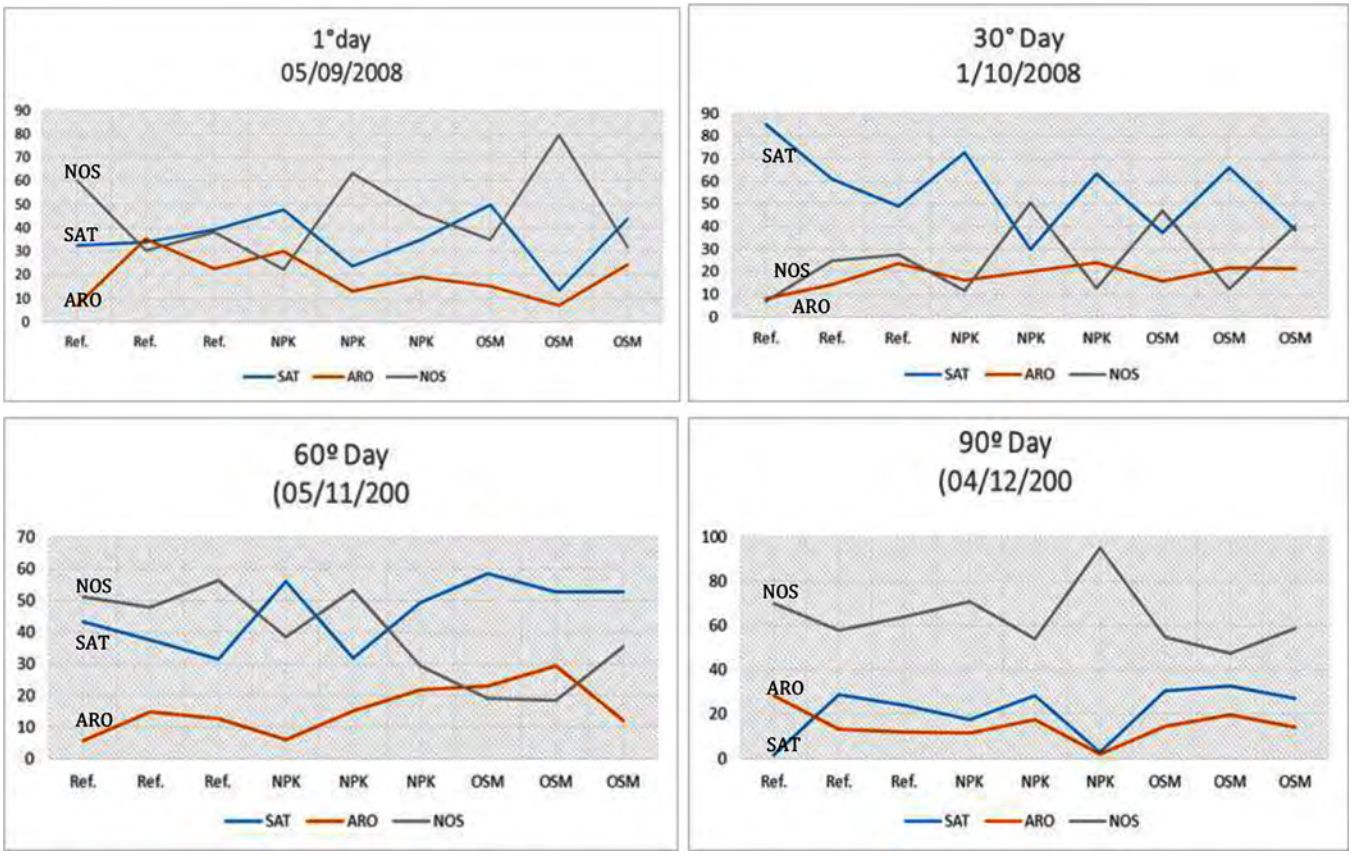

FIGURE 27.9 Percentages of saturated (SAT), aromatic (ARO), and NSO hydrocarbons in the simulation units during the bioremediation experiment (days 1, 30, 60, and 90).

given treatment. In the discussion below, the following abbreviations are used: C (control), CBR (control representing the Recôncavo basin), CBC (control representing the Campos basin), BRFI (Recôncavo basin + coconut fiber + consortium 1), BRFO (Recôncavo basin + leaf + consortium 1), BCFI (Campos basin + coconut fiber + consortium 2), and BCFO (Campos basin + leaf + consortium 2).

The data obtained from the BRFO simulation unit are plotted in Fig. 27.10. The nitrogen, phosphorus, and (to a lesser extent) CO rates decreased by day 30 of the experiment. In contrast, the fungal CFU count remained essentially constant. Again, this pattern can be attributed to the metabolic pathway of the fungal consortium: they were probably in the phase of nutrient consumption without proliferation (i.e., acclimatization). The Pr/Ph and TPH/UCM ratios increased slightly during the T30 period, indicating that biodegradation was probably minimal, which can be attributed to the adaptation of the fungi to the available carbon source in the sediment.

An increase in the CFU count was observed during the T60 period, accompanied by increases in the nitrogen and phosphorus levels. This pattern can be attributed to the acceleration of the degradation, which is consistent with an observed decrease in the Pr/Ph ratio. The CFU count decreased slightly at T90, which coincided with the reduction in nitrogen and phosphorus levels and the Pr/Ph and TPH/UCM ratios, thus indicating biodegradation (Fig. 27.11).

Based on an integration of the data from the BRFI simulation units, it was noted that by day 30, the fungal CFU count increased, followed by decreases in the amounts of nitrogen and phosphorus. The same pattern was observed in the BRFI simulation unit, thus indicating that the fungal consortium probably used the same metabolic pathway (Fig. 27.11).

The Pr/Ph and TPH/UCM ratios decreased by day 90, which suggests the occurrence of biodegradation. The Pr/nC17 and Ph/nC18 ratios increased, which is also indicative of biodegradation. At day 90, a decrease in the CFU count was observed; however, this decrease does not mean that the bioremediation was interrupted because the number of CFUs was probably sufficient to maintain the biodegradation.

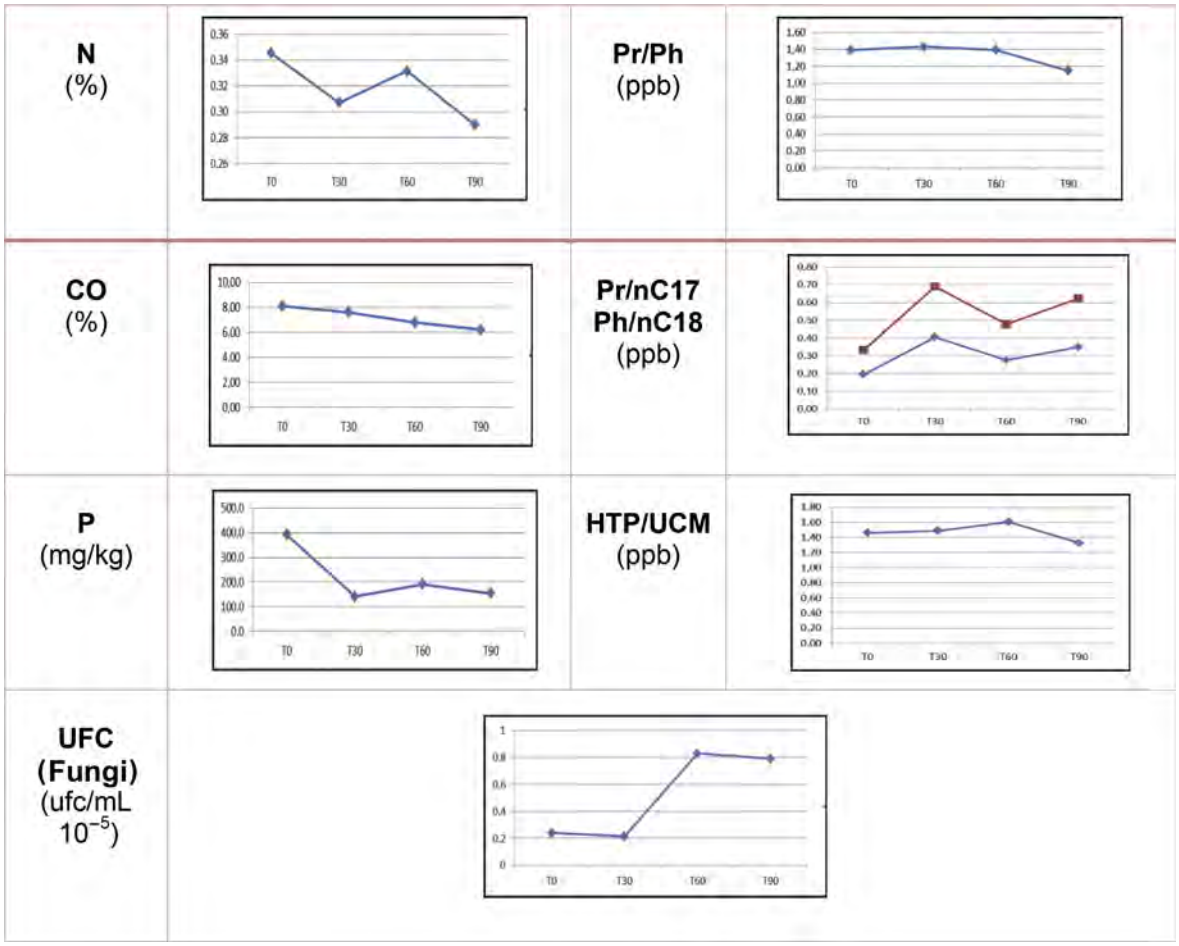

FIGURE 27.10 Variations in biogeochemical parameters for the periods T0, T30, T60, and T90 in the BRFO simulation unit.

The BCFI and BCFO simulation units behaved similarly over the 90 days of the experiment. An increase in the CFU count and decreases in the levels of nitrogen and phosphorus were observed by day 30. According to Xia et al. (2006), the microbial potential for degrading polar compounds is related to the presence of carbon, nitrogen, and phosphorus. These compounds are important for microbial metabolism, and each type of organism requires different concentrations of these compounds. Investigation of these ideal conditions is essential for development of an effective bioremediation program (Xia et al., 2006; Maciel et al., 2013).

There was also a decrease in the Pr/Ph ratio and increases in the Pr/nC17 and Ph/nC18 ratios, and these processes were still occurring at day 90 (Figs. 27.12 and 27.13).

27.5 APPLICATIONS OF NEW BIOTECHNOLOGIES: MULTIPROCESS BIOREMEDIATION AND PHYTOREMEDIATION

The presence of heavy metals and petroleum-derived hydrocarbons in mangrove sediments in BTS is one of the most important environmental problems in this ecosystem due to various factors including the biomagnification potential of these pollutants in the food chain. This biogeochemical process results in several problems such as (1) risks to human health, fauna, flora, and public safety, (2) restrictions on urban development, and (3) reductions in the quality and value of fish. The survival of a mangrove ecosystem depends on several factors that interact in complex ways. Although the predominant factor is geomorphologic change, processes that contribute to sedimentation in these areas and result in rising sea levels (e.g., damming of the rivers) and changes in the regional climate also affect the survival of mangrove ecosystems (Moreira, 2011).

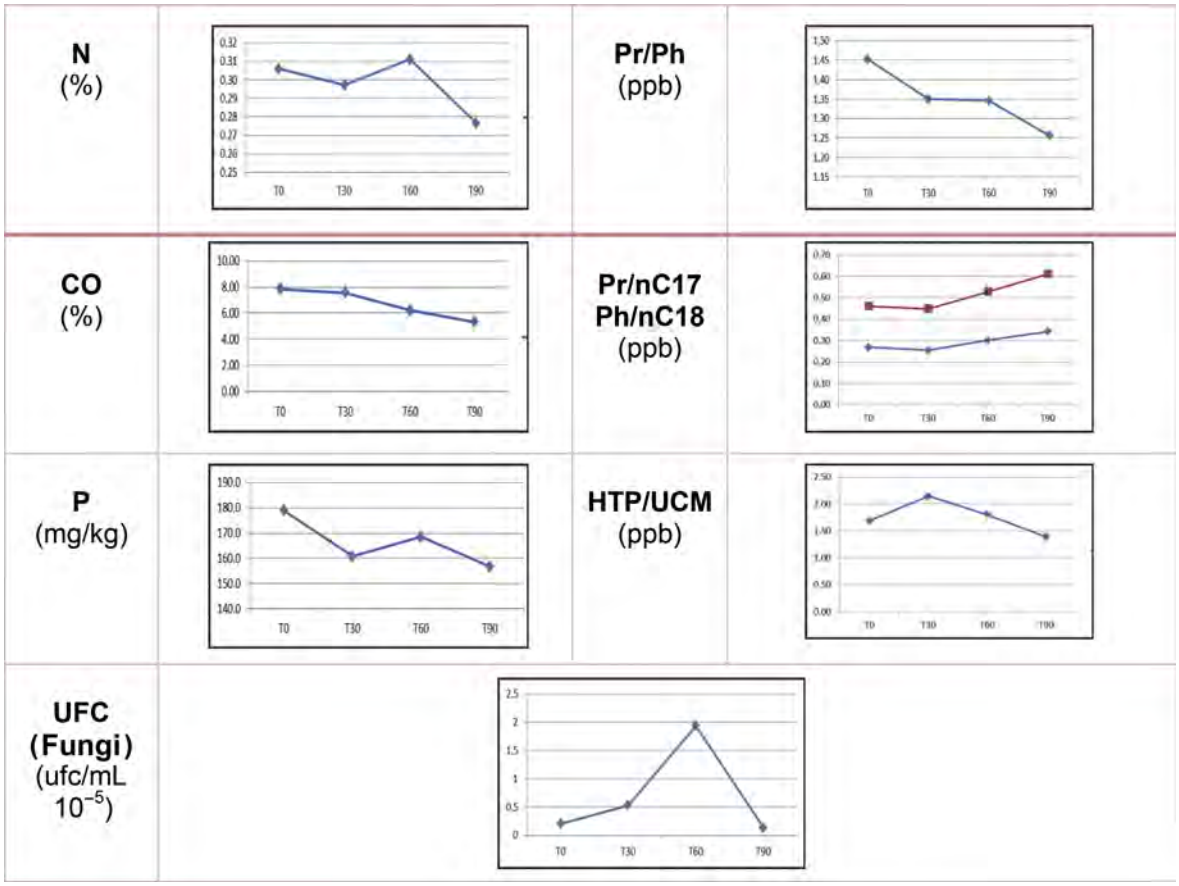

FIGURE 27.11 Variations in biogeochemical parameters for the periods T0, T30, T60, and T90 in the BRFI simulation unit.

According to Novelli (1990), the need for effective biotechnologies in the removal of petroleum-derived hydrocarbons and associated heavy metals in estuarine sediments is directly linked to the importance of the restoration, monitoring, and conservation of mangrove ecosystems. Mangrove ecosystems serve several key functions:

- provide areas for the shelter, reproduction, development, and feeding of marine, estuarine, terrestrial, and limnic species; resting areas for migratory birds; and areas for maintaining coastal biologic diversity;
- contribute to the absorption and immobilization of contaminants and to the treatment of sewage; and
- act as sources of products for coastal human communities; as places of cultural, recreational, leisure, and scientific research value; and as scenic features.

Projects aimed at restoring mangrove ecosystems impacted by petroleum-derived hydrocarbons and heavy metals have already been implemented in Brazil, but the conventional remediation technologies that are generally used are expensive. In many cases, most of these technologies have posed risks of secondary contamination when the contaminants are treated inappropriately. Thus, attention has turned to studying the effectiveness of mangrove plant species in phytoremediation, which is an innovative, inexpensive, and ecologically appropriate phytotechnology. Its application in combination with petroleum-degrading bacteria (bioremediation) in situ can be effective, particularly when the combination involves a mangrove ecosystem that provides a wealth of nutrients and other physical–chemical conditions that favor the bioremediation (Moreira et al., 2011).

Although phytoremediation is a technique that has been studied more in recent years, various specific concepts have already been employed. Carneiro et al. (2001) defined phytoremediation as simply the introduction of a plant into a contaminated soil. Ferreira et al. (2003) conceptualized it as a technique for the decontamination of soil and water using plants as a decontaminating agent. Dinardi et al. (2003) referred to it as a biotechnology tool involving the use of photosynthetic vegetation systems and their microbiota for the purpose of detoxifying degraded or polluted environments. Moreira (2011) defined it as the use of

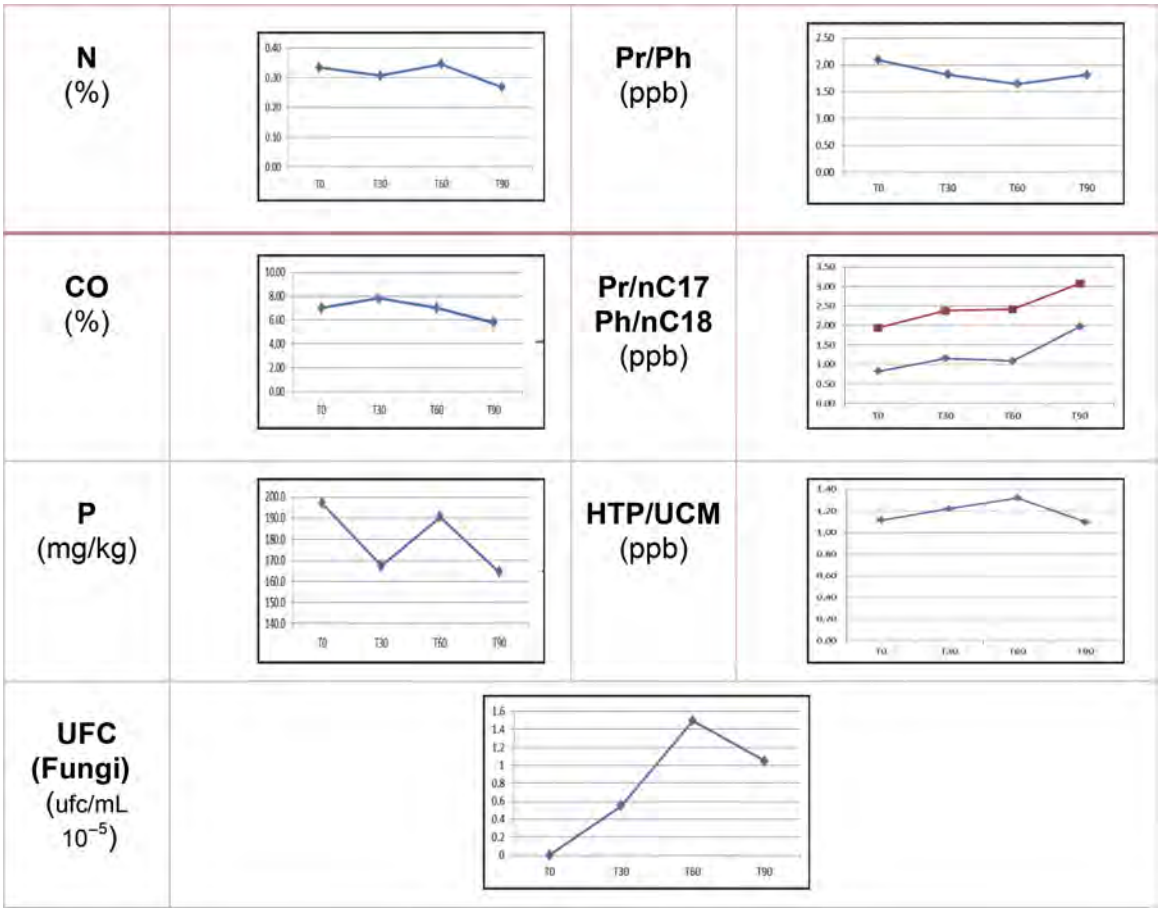

FIGURE 27.12 Variations in biogeochemical parameters for the periods T0, T30, T60, and T90 in the BCFI simulation unit.

plants—genetically modified or not—that are capable of absorbing pollutants from the soil or metabolizing the substances into their less toxic versions.

In addition to heavy metals (Pb, Cd, Zn, Cu, As, Ni, Hg, and Se), the main target substances of phytoremediation include inorganic compounds (NO_3, PO_4), radioactive elements (U, Cs, and Sr), petroleum hydrocarbons, pesticides, xenobiotics and herbicides (atrazine, bentazone, and chlorinated and nitro-aromatic compounds), explosives (TNT and DNT), chlorinated solvents (TCE and PCE), and industrial organic wastes (PCPs and PAHs). Phytoremediation offers several advantages that must be taken into account. Large areas can be restored in a variety of ways, at low cost, and the possibility exists of remediating contaminated water, soil, subsoil, and air while beautifying the environment. Unfortunately, the time needed to achieve satisfactory results can sometimes be long. According to Dinardi et al. (2003), the concentration of the contaminant and the presence of toxins must be within the tolerance limits of the plant being used so that the treatment program is not adversely affected.

Often, this technique is used incorrectly, such as when fruit plants and other important food plants are used, because there is a risk of contaminants entering the food chain. At present, there is a widespread search for nonfood-related plants that are effective but involve lower risks to human health (Moreira, 2006).

The annual expenditure on environmental cleanup worldwide is approximately 25 to 30 billion US dollars (USD). This expenditure, which is already stable in the United States (7–8 billion USD), is inclined to increase in Brazil given that investments in treatment of human, agricultural, and industrial wastes increase as society's demands increase and stricter laws are enforced. Despite certain pressures, the least-expensive technologies (e.g., phytoremediation) having the capacity to meet high demand and having greater development capacity tend to be more successful, mainly due to the increased risks of harm caused by the oil industry.

The objective of this stage of work by our research group was to develop a pilot-scale experiment spanning 3 months for evaluating the efficacy of two remediation techniques based on three models—intrinsic

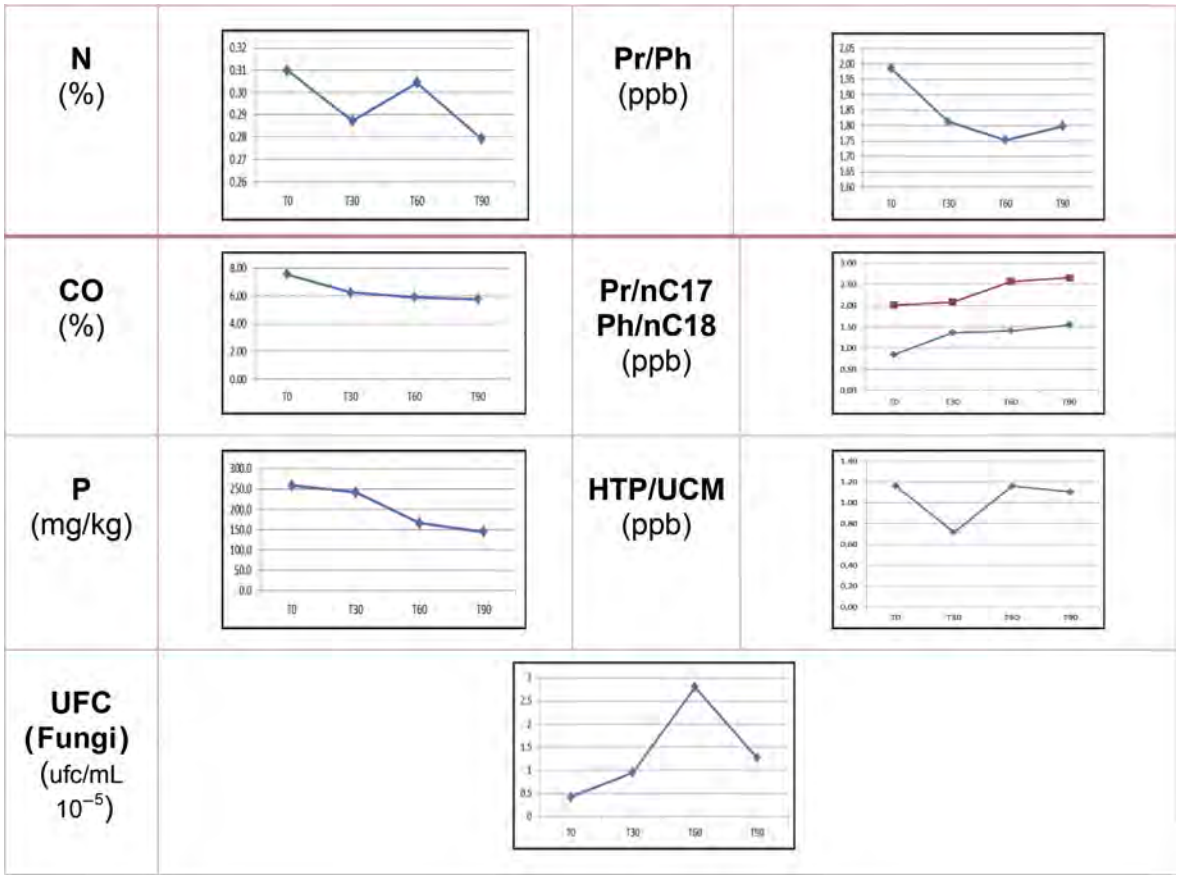

FIGURE 27.13 Variations in biogeochemical parameters for the periods T0, T30, T60, and T90 in the BCFO simulation unit.

bioremediation with autochthonous microorganisms, phytoremediation with *Avicennia Schaueriana* (black mangrove), and phytoremediation with *Rhizophora mangle* (red mangrove)—for use in mangrove swamp sediments contaminated by petroleum hydrocarbons and trace metals.

27.5.1 Experimental Development

The hypothesis of the study was as follows: "The plants and microorganisms living in mangrove swamp sediments contaminated by petroleum hydrocarbons and trace metals must have adaptive mechanisms for degradation of organic compounds in the presence of metals. What remains to be tested is whether this degradation occurs via intraspecific mechanisms or interspecific relationships (a consortium), or if, in the presence of the pollutants, these organisms can stabilize the contaminants or possibly even prevent them from developing." The hypothesis was verified by performing the following steps: (1) developing the experiment, (2) monitoring, (3) conducting chemical analyses, (4) obtaining results, (5) interpreting the results, and (6) disseminating the results by submitting articles to journals and giving presentations at scientific meetings.

To simulate the environments (in the aquarium tanks), collection sites that represent conditions nearest to the contamination in the estuary were defined. Thus, sediment samples with oil sludge were collected randomly using a stainless steel sampler in areas where exudates had been observed. In addition, in a control area defined from a preliminary evaluation, samples of sediment with no petroleum contamination were collected, based on a previous study. Subsequently, the samples containing oil residue were individually homogenized, thus defining the contaminated sediment treatment that was used in this study. The tank water was collected directly from a brackish river, the tidal regime was simulated, and the initial concentrations of the metals and total hydrocarbons were subsequently analyzed.

Three remediation models (phytotechnology I, phytotechnology II, and intrinsic bioremediation), which were monitored for 90 days, were assembled in the tanks in accordance with the following designs: (1) In the

phytotechnology I model, red mangrove seedlings (preselected in pilot research) were planted in sediments that had been collected at the site, and the following phytoremediation mechanisms were evaluated: phytodegradation, phytostimulation, and rhizodegradation. (2) In the phytotechnology II model, black mangrove seedlings (preselected in pilot research) were planted in sediments that had been collected at the site, and the following phytoremediation mechanisms were evaluated: phytodegradation, phytostimulation, and rhizodegradation. (3) In the intrinsic bioremediation model (monitored natural attenuation), degradation of petroleum-derived hydrocarbons by intrinsic petroleum-degrading bacteria was monitored. The bacterial density was characterized in the three models to evaluate the efficacy of the technique.

27.5.2 Monitoring of Biological, Physical, and Chemical Parameters

During the experiment, the plant organisms were monitored in terms of their morphophysiological growth parameters (biomonitoring). The microorganisms were monitored by determining the density of petroleum-degrading bacteria in each remediation model to establish possible relationships between the degradation capacity of the contaminants available in the sediments and the sensitivity due to the presence of metals.

The physical–chemical parameters (pH, Eh, salinity, conductivity, and DO) were also monitored in each model, specifically, in the sediments and in the water.

At the end of each established interval, designated T0, T1, T2, T3, T4, and T5 (days 0, 7, 15, 30, 45, and 60, respectively), the concentrations of total hydrocarbons (chromatographic analyses) and heavy metals (Pb, Cd, Zn, Cu, Ni, Cr, Al, and Fe) were determined in randomly selected samples in the sediments in each model using an atomic absorption spectrophotometer. In addition, the most effective phytoremediation mechanism used was evaluated in accordance with the EPA (2000). The samples were sent to the Petroleum Studies Laboratory (Laboratório de Estudos do Petróleo—LEPETRO) of the Federal University of Bahia (Universidade Federal da Bahia—UFBA) for determination of the fractions of aromatic and aliphatic hydrocarbons using USEPA Methods 8270D and 8015B. The analyses included the use of internal standards, and the analytical program was conducted under controlled laboratory conditions.

Sediment samples for microbiological analyses during the 90 days of the experiment were collected from the two models and were sent to the Laboratory of Microbiology and Clinical Analyses (Laboratório de Microbiologia e Análises Clínicas) of the Pharmacy School (UFBA) for evaluation of the bacterial density. The samples, each weighing 25 g, were transferred to Erlenmeyer flasks containing 90 mL of sterile peptone water (0.1%), and each sample was then shaken at 200 rpm for 30 min. For the colony counts, the microdrop plating technique was used (Romeiro, 2001), in which decimal dilutions were performed in nutrient agar (AGAR). The plates were incubated at 25°C ± 1°C for 24 h. After incubation, the plates selected were those containing 1 to 30 colonies. The number of colonies counted was multiplied by the inverse of the dilution, and the results were expressed as numbers of colony-forming units (CFUs).

27.6 RESULTS AND DISCUSSION

The results indicated that after 90 days, the intrinsic bioremediation, phytotechnology I (*Rhizophora mangle*), and phytotechnology II (Avicennia *schaueriana*) models achieved, respectively, 70%, 87%, and 89% removal of the petroleum hydrocarbons originally present in the estuarine sediment, as shown in Fig. 27.14. Statistically, the removal by the two phytotechnology models was significantly greater than that in the bioremediation model. These results indicate that the plant species possess greater capacity for degradation of hydrocarbons than intrinsic bioremediation in mangrove sediments.

Analysis of the hydrocarbon removal from the sediment via the phytoremediation with *R. mangle* and *A. schaueriana* and via the intrinsic bioremediation indicates that the contaminant levels in the sediment decreased from 33.2 to 4.5 mg/g, 33.2 to 4.2 mg/g, and 33.2 to 9.2 mg/g, respectively, during the 3-month period, as shown in Fig. 27.15.

The figures show that the two phytotechnology models were more effective than the intrinsic bioremediation model in the removal of petroleum hydrocarbons in the contaminated sediment. Despite this tendency having been observed in other studies (Yuan et al., 2001; Tam and Wong, 2008; Yergeau et al., 2009) that evaluated the use of remediation techniques in mangrove sediments contaminated by these contaminants, there is still a greater tendency to use other techniques in restoration of areas impacted by oil activities. One of these other techniques

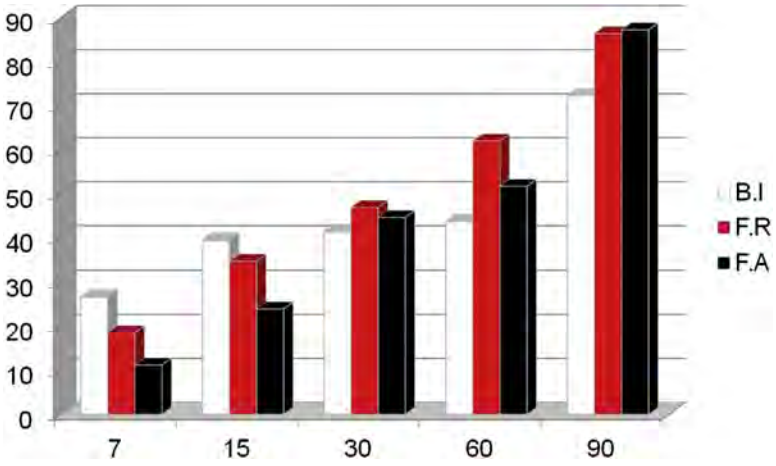

FIGURE 27.14 Efficacy of removal of petroleum hydrocarbons (%) in the three remediation models (BI = bioremediation, FR = *R. mangle*, and FA = *A. schaueriana*) during the 90 days of the experiment.

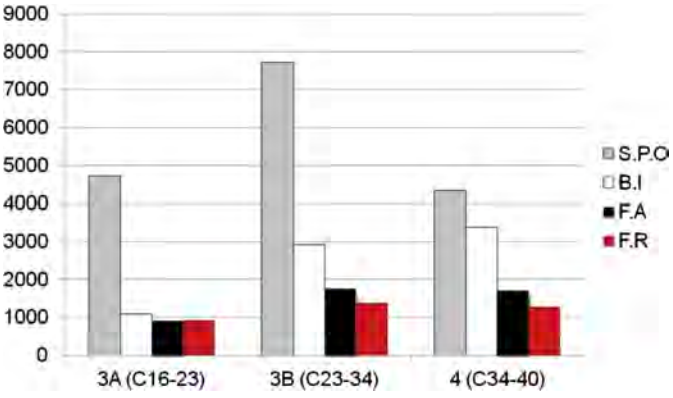

FIGURE 27.15 Removal of fractions of petroleum hydrocarbons (mg/g) in the three remediation models (SPO = initial sediment, IB = intrinsic bioremediation, PR = *R. mangle*, and PA = *A. schaueriana*) during the 90 days of the experiment.

is bioremediation with "land farming" (McCarthy et al., 2004; Huang et al., 2004, 2005), which is a field-scale bioremediation technique in which the surficial contaminated sediments are removed with the help of the wind, thereby increasing the activity of the endogenous microorganisms and, consequently, the intrinsic bioremediation. However, despite having a greater number of applications, particularly in industrial areas, these conventional techniques have severe limitations in terms of removal of hydrocarbons with higher concentrations of the heavy fraction and problems with biodegradation in sediments where the contaminant concentrations vary with depth, particularly when the techniques are applied individually.

The hydrocarbon fractions assessed were 3A (C16−23), 3B (C23−34), and 4 (C34−40), which are the most recalcitrant petroleum contaminants in the sediment. These molecules are very resistant to removal because they are hydrophobic and have a high molecular weight. The results indicated that the phytotechnology models were more effective than the intrinsic bioremediation in the removal of all the fractions in the contaminated sediment. However, both biotechnologies displayed very similar efficacy in the removal of fraction 3A (C16−C23). In the removal of fraction 3B (C23−34), the phytoremediation performed moderately better—82% with *R. mangle* and 78% with *A. schaueriana*—than the intrinsic bioremediation (63%), and these differences were greater, i.e., 70%, 61%, and 21%, respectively, in the removal of fraction 4 (C24−C40).

Fig. 27.15 shows the removal of different hydrocarbon fractions: after the 90 days of the experiment, the phytoremediation techniques were more effective than intrinsic bioremediation in the removal of the three fractions—3A (C16−23), 3B (C23−34), and 4 (C34−40). This superiority probably occurs because phytoremediation acts by removing contaminants in conjunction with the microbiota present in the rhizosphere and by stabilizing the transfer of some contaminants, and it may also destroy organic compounds in sediments (Cunningham et al., 1995, 1996). The degradation mechanisms of the plant species may, in some cases, have involved phytostabilization, which prevents absorption and functions through phytostimulation of the microorganisms present in the rhizosphere, thereby working with the rhizodegradation. It is also possible that the plants absorbed the organic compounds and there was subsequent phytodegradation.

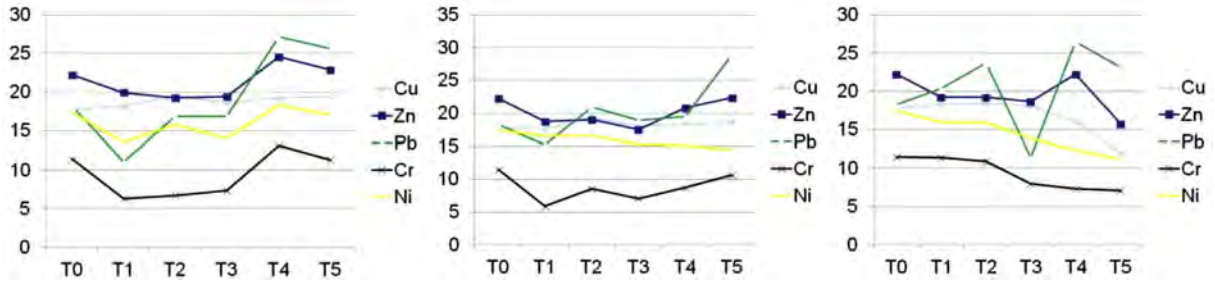

FIGURE 27.16 Metal concentrations (mg/g) in the three remediation models during the 90 days of the experiment: (A) Bioremediation, (B) *A. schaueriana*, and (C) *R. mangle*.

During the 90 days of the experiment, the total numbers of viable bacteria for remediation in the sediments were quantified in six preestablished samples. The initial mean bacteria counts were between 0.1 and 0.2×10^6 CFU/g in the uncontaminated sediment at the beginning of the experiment. After being placed in the sediment cleanup models, there was a significant increase in the number of microorganisms after day 7 in the three models, with a significant difference in comparison to the initial sediment sample—8.3×10^6 and 8.8×10^6 CFU/g, respectively. After 30 days, there was a drastic decrease in the number of microorganisms in the intrinsic bioremediation model (1.8×10^6 CFU/g). However, the microbial communities grew in the phytotechnology models: the quantified values were upward of 20.2×10^6 and 24.4×10^6 CFU/g.

Fig. 27.16 shows the concentrations of metals during the experiment. After the 90 days, the phytoremediation models with red mangrove showed a positive correlation between the degradation of the hydrocarbons and certain metals (Cu, Zn, Cr, and Ni), whereas black mangrove displayed a similar correlation with other metals (Ni and Al), thus indicating a strong tendency of phytoextraction in these models. In both of the phytoremediation models, greater growth was observed in the plants exposed to contaminated sediments than in those cultivated in the control sediments, which suggests good adaptation. No positive correlation was observed between the degradation and any of the metals in the intrinsic bioremediation model.

27.7 FINAL CONSIDERATIONS

This study yielded data regarding the TPH levels in coastal surface sediments of BTS and demonstrated that the distribution of hydrocarbons is primarily controlled by the proximity to the contaminant sources and secondarily by the physical characteristics of the sediment. Significant contamination was verified in the upstream portion of the São Paulo River near an oil refinery. Although the geochemical evaluation indicates that the petroleum hydrocarbons at the site are in an advanced stage of degradation, the high concentrations still present indicate that natural attenuation has not been effective in the removal of these compounds. Thus, it is imperative that remediation techniques be applied for the environmental restoration of the area.

Based on the biostimulation experiments, the monitoring of physical–chemical parameters (pH, temperature, salinity, and DO) indicated favorable conditions for bioremediation during the entire experiment, and these conditions were not limiting factors for the bioremediation. The evaluation of the inorganic compounds indicated that phosphorus was the only nutrient that continued to be released uniformly throughout the experiment, both in the units treated with NPK and those treated with Osmocote. This pattern of phosphorus release was attributed to the consumption of this nutrient during the first days of biodegradation of the hydrocarbons, which did not occur due to the degradation stage of the oil. The levels of ammonia and nitrate were high during the first 8 days but decreased from day 15 onward in the units treated with NPK, which can be attributed to the solubility of this fertilizer. In the units treated with Osmocote, the results showed an accelerating increase from day 15 onward, thus confirming its slow release. The ammonia levels were much higher than the nitrate levels, which suggest that ammonia was the main source of nitrogen in this experiment. The liquid chromatography results indicate a relative reduction in the saturated hydrocarbon fraction and a relative enrichment in polar (NSO) compounds in all the simulation units, with a reduction of up to 3% in the percentage of saturated hydrocarbons. When comparing all the simulation units (control, NPK, and Osmocote), the unit treated with the Osmocote tended to perform similarly to the reference units but was less effective than the units treated with NPK.

The results of the chemical and physical–chemical monitoring of the bioaugmentation were within the standards necessary for the occurrence of bioremediation. The biostimulation using the coconut fiber and immobilized mangrove leaf powder did not display a significant difference in efficacy regarding the release of nutrients. Thus, to a certain extent, suitable levels of nutrients were maintained during the 90 days of the experiment, which would not have occurred if no nutrients had been added. In addition, it was possible to observe acceleration in the biodegradation in relation to the control, in which natural attenuation was observed. The microorganisms probably use the same metabolic pathway, even if in different simulation units.

The geochemical parameters (pristane/phytane) in the bioaugmentation decreased over the 90 days, which indicates the degradation of the two types of oil. The increases in the Pr/nC17 and Ph/nC18 ratios and the decrease in the TPH/UCM ratio were also an indication of the action of microorganisms on the petroleum. The results, in general, indicate that the fungal consortiums are promising for use in bioremediation; however, more studies of the interactions between the fungi are needed.

This pilot-scale study indicates that the phytotechnology models achieved greater efficacy in the degradation of various fractions of petroleum hydrocarbons, thus confirming that this technique is promising for use in the restoration of areas contaminated by the activities of the petroleum industry. The intrinsic bioremediation had low efficacy when applied individually, despite having initially been more effective in the degradation of contaminants. The microbiological analysis revealed that the association of plants with the microorganism community in the rhizosphere increased the degradation of organic compounds in the sediment and, consequently, promoted greater growth of these plants in the contaminated sediment. The integrated analyses of the biodegradation of the petroleum compounds in the presence of heavy metals in the remediation models revealed that the plants develop phytoextraction mechanisms, which promote the removal of metals and the degradation of hydrocarbons. However, the presence of metals may have partially inhibited biodegradation by microorganisms in the intrinsic bioremediation model.

Finally, it is worth emphasizing that the application of phytoremediation in areas impacted by oil activities is of great relevance given that it is an inexpensive and ecologically and socially appropriate technique. In addition, this process contributes to the minimization of global warming via carbon sequestration by the plants, thus demonstrating its importance not only locally but also on a global level.

References

Andrade, J.D., Augusto, F., Jardim, I.C.S.F., 2010. Biorremediação de solos contaminados por petróleo e seus derivados. Eclética Quím. 35, 17–43.

Asia, L., Mazouz, S., Guiliano, M., Doumenq, P., Mille, G., 2009. Occurrence and distribution of hydrocarbons in surface sediments from Marseille Bay (France). Mar. Pollut. Bull. 58, 443–451.

Aspilla, K.I., Agemian, H., Chau, A.S.Y., 1976. A semi-automated method for the determination of inorganic, organic and total phosphate in sediments. Analyst 101, 187–197.

ASTM, 2011. D3694-2011 Standard Practices for Preparation of Sample Containers and for Preservation of Organic Constituents. American Society of Testing and Materials, West Conshohocken.

Atlas, R.M., 1977. Stimulated petroleum biodegradation. Crit. Rev. Microbiol. 5, 371–386.

Atlas, R.M., 1981. Microbial degradation of petroleum hydrocarbons: an environmental perspective. Microbiol. Rev. 45, 180–209.

Atlas, R.M., 1984. Petroleum Microbiology. Macmillan Co, New York.

Bahia, 2004. Centro de Recursos Ambientais. Diagnóstico Ambiental do Grau de Contaminação da Baía de Todos os Santos por Metais Pesados e Hidrocarbonetos. CRA, Salvador, p. 394.

Blenkinsopp, S., Sergy, G., Doe, K., Wohlgeschaffen, G., Li, K., Fingas, M., 1997. Evaluation of the toxicity of the weathered crude oil used at the Newfoundland Offshore Burn Experiment (NOBE) and the resultant burn residue. Proceedings of the Technical Seminar on Arctic and Marine Oilspill Program. Ministry of Supply and Services, Canada, pp. 677–684.

Bouloubassi, I., Saliot, A., 1993. Investigation of anthropogenic and natural organic inputs in estuarine sediments using hydrocarbon markers (NAH, LAB, PAH). Oceanol. Acta 16, 145–161.

Carneiro, M.A.C., Siqueira, J.O., Moreira, F.M.S., 2001. Estabelecimento de plantas herbáceas em solo com contaminação de metais pesados e inoculação de fungos micorrízicos arbusculares. Pesqui. Agropecu. Bras. 6, 1443–1452.

Celino, J., Veiga, I., Trigüis, J., Queiroz, A., 2008. Fonte e distribuição de hidrocarbonetos do petróleo nos sedimentos da Baía de Todos os Santos, Bahia. Braz. J. Aquat. Sci. Technol. 12, 31–38.

Cunningham, S.D., Anderson, T.A., Schwab, A.P., Hsu, F.C., 1996. Phytoremediation of soils contaminated with organic pollutants. Adv. Agron. 56, 55–71.

Cunningham, S.D., Berti, W.R., Huang, J.W., 1995. Phytoremediation of contaminated soils. Trends Biotechnol. 13, 393–397.

Da Silva, R., 2011. Técnica de Microgota Para Contagem de Células Bacterianas Viáveis em uma Suspensão. Universidade Federal de Viçosa, Viçosa, Minas Gerais, Brazil.

Dibble, J.T., Bartha, R., 1976. Effect of iron on the biodegradation of petroleum in seawater. Appl. Environ. Microbiol. 31, 544–550.

Dinardi, A.L., Formagi, V.M., Coneglian, C.M.R., Brito, N.N., Sobrinho, G.D., Tonso, S., et al., 2003. Fitorremediação: III Fórum de Estudos Contábeis. Faculdades Integradas Claretianas, Rio Claro, SP.

Douglas, G.S., McCarthy, K.J., Dahlen, D.T., Seavey, J.A., Steinhauer, W.G., Prince, R.C., et al., 1992. The use of hydrocarbon analyses for environmental assessment and remediation. J. Soil Contam. 1, 197–216.

EPA, 2000. In-situ groundwater bioremediation. Chapter 10 in how to evaluate alternative cleanup technologies for underground storage tank sites: A guide for corrective action plan reviewers. EPA, 510-R-04-002.

EPA, Environmental Protection Agency, (EUA), 2004. Design Document for Passive Bioventing. How to Evaluate Alternative Cleanup Technologies for Underground Storage Tank Sites: A Guide for Corrective Action Plan Reviewers, 2006 (EPA 510-B-94-003; EPA 510-B-95-007; and EPA 510-R-04-002). Disponível em: <http://www.epa.gov/swerust1/pubs/tum_ch3.pdf> (Acesso em: 10 de Novembro de 2008).

Farias, C.O., Hamacher, C., Wagener, A.D.L.R., Scofield, A.D.L., 2008. Origin and degradation of hydrocarbons in mangrove sediments (Rio de Janeiro, Brazil) contaminated by an oil spill. Org. Geochem. 39, 289–307.

Feniman, D.P.G., 2009 Biodegradação Ambiental: Petróleo e Pesticidas. Disponível em: <http://www.herbario.com.br/bot/toxicologia/biodegre.htm> (Acesso em: 14 nov. 2009).

Ferreira, L.R., Freitas, R.S., Berger, P.G., 2003. Manejo de plantas daninhas na cultura do algodoeiro. In: *Congresso Brasileiro da Ciência das Plantas Daninhas*, 24, 2004, São Pedro-SP. Anais, São Pedro: Sociedade Brasileira da Ciência das Plantas Daninhas.

Folk, R.L., Ward, W.C., 1957. Brazos River bar: a study in the significance of grain size parameters. J. Sediment. Res. 27, 3–26.

Gaglianone, P.C., Trindade, L.A.F., 1988. Caracterização geoquímica dos óleos da bacia do recôncavo. Geochim. Bras. 2, 15–39.

Guo, W., He, M., Yang, Z., Lin, C., Quan, X., 2011. Characteristics of petroleum hydrocarbons in surficial sediments from the Songhuajiang River (China): spatial and temporal trends. Environ. Monit. Assess. 179, 81–92.

Hatje, V., Andrade, J.B., 2009. Baía de Todos os Santos: Aspectos Oceanográficos. EDUFBA, Salvador, p. 306.

Huang, X.D., El-Alawi, Y., Penrose, D.M., Glick, B.R., Greenberg, B.M., 2004. A multi-process phytoremediation system for removal of polycyclic aromatic hydrocarbons from contaminated soils. Environ. Pollut. 130, 465–476.

Huang, X.D., El-Alawi, Y., Gurska, J., Glick, B.R., Greenberg, B.M., 2005. A multi-process phytoremediation system for decontamination of persistent total petroleum hydrocarbons (TPHs) from soils. Microchem. J. 81, 139–147.

ITOPF [International Tanker Owners Pollution Federation], 2001. Persistent vs Nonpersistent oils: What You Need to Know. Disponível em: <http://www.itopf.com> (Acesso em abril de 2011).

Kataoka, K., Harada, A., Nagasaki, Y., 2001. Block copolymer micelles for drug delivery: design, characterization and biological significance. Adv. Drug Deliv. Rev. 47, 113–131.

Kennish, M.J., 1997. Pollution Impacts on Marine Biotic Communities. CRC Press, LLC, Boca Raton, FL.

Kumari, P.S., Amruta, S.R., 2013. Analysis of biodegradation pathway of crude oil by *Pseudomonas sp*. isolated from marine water sample. Arch. Appl. Sci. Res. 5, 165–171.

Leahy, J.G., Colwell, R.R., 1990. Microbial degradation of hydrocarbons in the environment. Microbiol. Rev. 54, 305–315.

Leão, Z.M.A.N., Dominguez, J.M.L., 2000. Tropical coast of Brazil. Mar. Pollut. Bull. 41, 112–122.

Lee, K., Tremblay, G.H., Levy, E., 1993. Bioremediation: application of slow-release fertilizers on low-energy shorelines. Proceedings of the Oil Spill Conference. American Petroleum Institute, Washington, DC, pp. 449–454.

Lima, M.B., Feitosa, E.A., Emídio, E.S., Dórea, H.S., Alexandre, M.R., 2012. Distribution and sources of aliphatic hydrocarbons in surface sediments of Sergipe River estuarine system. Mar. Pollut. Bull. 64, 1721–1725.

Lindstrom, J.E., Prince, R.C., Clark, J.C., Grossman, M.J., Yeager, T.R., Braddock, J.F., et al., 1991. Microbial populations and hydrocarbon biodegradation potentials in fertilized shoreline sediments affected by the T/V Exxon Valdez oil spill. Appl. Environ. Microbiol. 57, 2514–2522.

Maciel, C.C.S., Souza, C.S., Silva, P.A., Sousa, M.D.F.V.Q., Gusmão, N.B., 2013. Cinética de degradação de querosene de aviação por Penicillium sp. através da bioestimulação. Rev. Bras. Biocienc. 11.

Mariano, A.P., 2006. Avaliação do Potencial de Biorremediação de Solos e de Águas Subterrâneas Contaminados Com Óleo Diesel. Tese (doutorado); Universidade Estadual Paulista, Instituto de Geociências e Ciências Exatas, Rio Claro, SP, 162 f.

McCarthy, K., Walker, L., Vigoren, L., Bartel, J., 2004. Remediation of spilled petroleum hydrocarbons by in situ landfarming at an arctic site. Cold Reg. Sci. Technol. 40, 31–39.

Medeiros, P.M., Bícego, M.C., 0030. Investigation of natural and anthropogenic hydrocarbon inputs in sediments using geochemical markers. II. São Sebastião, SP–Brazil. Mar. Pollut. Bull. 49, 892–8899.

Mcmillen, S.J.; Kerr, J.M.; Gray, N.R., 1993. Microcosm studies of factors that influence bioremediation of crude oils in soil. Exploration & Production Environments Conference, Texas, USA, SPE 25981, p. 389-400, 1993.

Moreira, I.T.A. et al., 2006. Coleta de solo e de folhas de Aroeirinha (*Schinus terebinthifolius*, R.) e Mamona (*Ricinus communis*, L.) para quantificação dos teores de metais pesados, para futura aplicação da técnica de Fitorremediação na área da PLUMBUM LTDA., Santo Amaro da Purificação, BA. In: *ENCOBIO-Encontro de Biólogos, VIII ENCOBIO, Resumos*, Feira de Santana, Bahia.

Moreira, I.T.A., 2011. Avaliação da Eficiência de Modelos de Remediação em Sedimentos de Manguezal Contaminados por Hidrocarbonetos Derivados do Petróleo. In: Programa de Pós-Graduação em Geoquímica: Petróleo e Meio Ambiente. Dissertação de Mestrado, p. 122.

Moreira, I.T., Oliveira, O.M., Triguis, J.A., Queiroz, A.F., Ferreira, S.L., Martins, C.M., et al., 2013. Phytoremediation in mangrove sediments impacted by persistent total petroleum hydrocarbons (TPH's) using *Avicennia schaueriana*. Mar. Pollut. Bull. 67, 130–136.

Moreira, I.T.A., Martins, C.M.S., Oliveira, M.C., Oliveira, O.M.C., Triguis, J.A., 2011. Detailed and confirmatory investigation in an area with contaminated sediment, in order for the application of phytoremediation; In: XII Workshop and Congress Geochemistry Organic American Latin Association, pp. 13–16.

NOVELLI, Y.S.,1990. Manguezal: ecossistema entre a terra e o mar – Caribbean Ecological Research, SP, 64 pp, 1990.

Olivieri, R., Bacchin, P., Robertiello, A., Oddo, N., Degen, L., Tonolo, A., 1976. Microbial degradation of oil spills enhanced by a slow-release fertilizer. Appl. Environ. Microbiol. 31, 629–634.

Pedigo, S., Marynette, H., Sammarco, P.W., 2011. Bioremediation techniques, category definitions, and modes of action in marine and freshwater environments. Originally compiled to update e and revise RRT IV Spill Response Guidance. Types of Bioremediation Section and Bioremediation Response Plan Appendix D. Science and Technology Committee.
Peters, K.E., Walters, C.C., Moldowan, J.M., 2003. The Biomarker Guide, Biomarkers and Isotopes in Petroleum Exploration and Earth History. Cambridge University Press, Cambridge.
Prince, R.C., 1993. Petroleum spill bioremediation in marine environments. Crit. Rev. Microbiol. 19, 217–242.
Pritchard, P.H., Costa, C.F., 1991. EPA's Alaska oil spill bioremediation project. Environ. Sci. Technol. 25, 372–379.
Ramaswami, A., Luthy, R.G., 1997. Mass transfer and bioavailability of PAH compounds in coal tar NAPL – Slurry Systems. 1. Model development. Environ. Sci. Technol. 31, 2260–2267.
Readman, J.W., Fillmann, G., Tolosa, I., Bartocci, J., Villeneuve, J.P., Catinni, C., et al., 2002. Petroleum and PAH contamination of the Black Sea. Mar. Pollut. Bull. 44, 48–62.
Riser-Roberts, E., 1992. Bioremediation of Petroleum Contaminated Sites. Taylor & Francis, Boca Raton.
Romeiro, D.S., 2001. Técnica de Microgota para contagem de células bacterianas viáveis em uma suspensão. Universidade Federal de Viçosa, Viçosa, Minas Gerais, Brazil, pp. 1–7.
ROSA, A.P., 2001. Processos de biorremediação na mitigação do impacto ambiental, devido a eventuais derrames de óleo na bacia de campos-experimentos laboratoriais. 145f. Tese (Mestrado em Engenharia de Reservatório e Exploração de Petróleo). Universidade Estadual do Norte Fluminense, Macaé – RJ.
Ryba, S.A., Burgess, R.M., 2002. Effects of sample preparation on the measurement of organic carbon, hydrogen, nitrogen, sulfur, and oxygen concentrations in marine sediments. Chemosphere 48, 139–147.
Silva, C.S., Moreira, I.T., de Oliveira, O.M., Queiroz, A.F., Garcia, K.S., Falcao, B.A., et al., 2014. Spatial distribution and concentration assessment of total petroleum hydrocarbons in the intertidal zone surface sediment of Todos os Santos Bay, Brazil. Environ. Monit. Assess. 186, 1271–1280.
Tam, N.F., Wong, Y.S., 2008. Effectiveness of bacterial inoculum and mangrove plants on remediation of sediment contaminated with polycyclic aromatic hydrocarbons. Mar. Pollut. Bull. 57, 716–726.
Tarozo, R., Frena, M., Madureira, L.A.S., 2010. Geochemical markers as a tool to assess sedimentary organic matter sources of the Laguna Estuarine System, south Brazil: aliphatic and polycyclic aromatic hydrocarbons. J. Braz. Chem. Soc 21, 2308–2318.
Tissot, B.P., Welte, D.H., 1984. Petroleum Formation and Occurrence. Springer-Verlag, Berlin Heidelberg, p 81.
Tolosa, I., Bayona, J.M., Albaigés, J., 1996. Aliphatic and polycyclic aromatic hydrocarbons and sulfur/oxygen derivatives in northwestern Mediterranean sediments: spatial and temporal variability, fluxes, and budgets. Environ. Sci. Technol. 30, 2495–2503.
Vallejo, V., Salgado, L., Roldan, F., 2005. Evaluación de la bioestimulación en la biodegradación de TPHs en suelos contaminados con petróleo. Bioestimulation process during the biodegradation of THH in oil contaminated soil. Rev. Colomb. Biotecnol. 7, 67–78.
Venturini, N., Tommasi, L.R., Bícego, M.C., Martins, C.C., 2004. Characterization of the benthic environment of a coastal area adjacent to an oil refinery, Todos os Santos Bay (NE-Brazil). Braz. J. Oceanogr. 52, 123–134.
Vidali, M., 2001. Bioremediation: an overview. J. Appl. Chem. 73, 1163–1172.
Volkman, J.K., Holdsworth, D.G., Neill, G.P., Bavor, H.J., 1992. Identification of natural, anthropogenic and petroleum hydrocarbons in aquatic sediments. Sci. Total Environ. 112, 203–219.
Walkley, A., Black, I.A., 1947. An examination of the Degtjareff method for determining soil organic matter and a proposed modification of the chromic acid titration method. Soil Sci. 37, 29–38.
Wang, X., Bartha, R., 1990. Effects of bioremediation on residues, activity and toxicity in soil contaminated by fuel spills. Soil Biol. Biochem. 22, 501–505.
Wolfe, D.A., Hameedi, M.J., Galt, J.A., Watabayashi, G., Short, J., O'Claire, C., et al., 1994. The fate of the oil spilled from the Exxon Valdez. Environ. Sci. Technol. 28, 560A–568A.
Xia, W., Li, J., Zheng, X., Bi, X., Shao, J., 2006. Enhanced biodegradation of diesel oil in seawater supplemented with nutrients. Eng. Life Sci. 6, 80–85.
Yergeau, E., Arbour, M., Brousseau, R., Juck, D., Lawrence, J.R., Masson, L., et al., 2009. Microarray and real-time PCR analyses of the responses of high-arctic soil bacteria to hydrocarbon pollution and bioremediation treatments. Appl. Environ. Microbiol. 75, 6258–6267.
Yeung, P., Johnson, R., Xu, J., 1997. Biodegradation of petroleum hydrocarbons in soil as affected by heating and forced aeration. J. Environ. Qual. 26, 1511–1516.
Yuan, S.Y., Chang, J.S., Yen, J.H., Chang, B.V., 2001. Biodegradation of phenanthrene in river sediment. Chemosphere 43, 273–278.
Zobell, C.E., 1946. Action of microorganisms on hydrocarbons. Bacteriol. Rev. 10, 1–49.

Further Reading

Araujo, U.C., 2000. A baía de Todos os Santos: um sistema geo-histórico resistente. Bahia Análise Dados 9, 10–23.
Ferreira, L.D., Cordeiro, O.O.M., Moreira, C.M.J., Alberto, T.J., Queiroz, A.F.S., 2012. Bioremediation in mangrove sediments impacted by oil using two types of fertilizers NPK and OSMOCOTE, Brazil. Open J. Mar. Sci. 2, 119–130.
Moreira, I.T.A., Freitas, P.F., Nascimento, R.S.A., Oliveira, O.M.C., Triguis, J.A., 2010. Selection of species plant mangrove for assessment phytoremediation of contaminated sediments by in oil and derivatives. In: Rio Oil & Gas Expo and Conference; IBP2899_10.
Rosa, A.P., Trigüis, J.A., 2006. Estudos experimentais da análise do processo de biorremediação na mitigação do impacto ambiental. Geochim. Bras. 20, 1.
Walkley, A., 1947. A critical examination of a rapid method for determining organic carbon in soils-effect of variations in digestion conditions and of inorganic soil constituents. Soil Sci. 63, 251–264.

CHAPTER

28

Assessing the Role of Environmental Conditions on the Degradation of Oil Following the *Deepwater Horizon* Oil Spill

Hernando P. Bacosa[1], *Meredith M. Evans*[1], *Qing Wang*[1,2] *and Zhanfei Liu*[1]

[1]The University of Texas Marine Science Institute, Port Aransas, TX, United States
[2]East China Normal University, Shanghai, China

BIOGRAPHIES

Hernando P. Bacosa is a postdoctoral fellow at the University of Texas at Austin Marine Science Institute (UTMSI). He has a strong interdisciplinary background, and his research interests are at the interface of environmental chemistry and microbiology particularly on understanding the interactions between microbial communities and petroleum hydrocarbons. His current work focuses on unraveling the roles of bacteria and environmental factors on the fate of oil in the Gulf of Mexico. He has published several papers on the biodegradation of petroleum hydrocarbons in both terrestrial and marine environments, oil fingerprinting, microbial communities involved in the degradation of oil, and effect of sunlight and temperature in shaping bacterial communities in oil-polluted waters. He received his B.S. Biology from Mindanao State University in the Philippines and completed his M.S. and Ph.D. in Environmental Studies from Tohoku University, Japan.

Meredith M. Evans is from Dallas, Texas and completed a Bachelor of Science in Biology at The University of Oklahoma in Norman, OK. She started her career in research science with an interest in the health of marine and aquatic systems. Following this research direction, she completed a Master of Science in Marine Science at the University of Texas at Austin Marine Science Institute in Port Aransas, TX. Here, she studied the weathering of petroleum in coastal Louisiana over the course of 3 years following the *Deepwater Horizon* oil spill. This research documented the degradation of petroleum hydrocarbons across different coastal zones, finding intense degradation along high energy beach fronts and retention of petroleum hydrocarbons, particularly polycyclic aromatic hydrocarbons, in tidal salt marshes. She also worked to adapt ramped pyrolysis–gas chromatography–mass spectrometry to efficiently analyze environmental samples of petroleum pollution. At present, Meredith is working on a Doctor of Philosophy in Marine Science at the Virginia Institute of Marine Science studying marine plastic pollution and plans to continue her career in research science.

Qing Wang was a visiting scholar at the University of Texas at Austin Marine Science Institute from March 2015 to March 2016. Meanwhile, he was also both a doctoral candidate in Physical Geography at East China Normal University and a researcher at Anhui Normal University, China. His research interests are the organic geochemistry and environmental process of polycyclic aromatic hydrocarbons in both urban system and natural environment. His work at UTMSI focused on the fate of crude oil during photooxidation under natural sunlight. He has completed his Ph.D. and his current affiliation is Department of Geography, Anhui Normal University, Wuhu, 241002, China.

Zhanfei Liu is an Associate Professor at the University of Texas at Austin Marine Science Institute. As an organic biogeochemist, his research focuses on source, degradation, transformation, and fate of natural and

Oil Spill Environmental Forensics Case Studies.
DOI: http://dx.doi.org/10.1016/B978-0-12-804434-6.00028-8

anthropogenic organic compounds. His group has been conducting oil-related research since the *Deepwater Horizon* oil spill, with funding mainly from National Science Foundation and Gulf of Mexico Research Initiative through the Dispersion Research on Oil: Physics and Plankton Studies (DROPPS) research consortium.

28.1 INTRODUCTION

On April 20, 2010, an uncontrollable blowout from the Macondo Well caused an explosion on the *Deepwater Horizon* (DWH), a mobile and deepwater semi-submersible offshore drilling rig. The Macondo Prospect is situated on Mississippi Canyon block 252 (N 28.73667, W 88.38694) located ~80 km southeast of the coast of Louisiana in the Gulf of Mexico, USA, and operated by the British Petroleum (BP). The explosion resulted to the sinking of the platform, tragic death of 11 workers and injury of 17 others. An estimated 4.9 million barrels (779 million liters, ±10%) of MC 252 crude oil (Crone and Tolstoy, 2010; The Federal Interagency Solutions Group, 2010) and 1.7×10^{11} g of natural gas (Reddy et al., 2012) flowed continuously from Macondo well over the span of about 87 days until it was capped on July 15, 2010. This unprecedented discharge of hydrocarbons to the open ocean is considered as the largest oil spill in the United States history and one of the world's largest marine oil spills in the history of petroleum industry. In addition to the volume of oil and duration, the DWH spill is also noteworthy for its distance offshore and depth. The oil and natural gas leaked from the wellhead located on the seafloor, 1500 m below the ocean surface in a high pressure (~160 atm) and low temperature (4°C) environment. Hydrocarbon compounds then partitioned between the deep ocean and the sea surface, with approximately half of the total discharge reached the ocean surface (McNutt et al., 2012; Ryerson et al., 2012).

The oil released from the Macondo well, referred to herein as Macondo oil, was a type A Louisiana light sweet crude oil which is low in sulfur and high in gasoline/kerosene fractions (Reddy et al., 2012). It has a gravity of 40°API, density of 820 g/L, and contained 74% saturated hydrocarbons, 16% aromatic hydrocarbons, and 10% polar compounds (Reddy et al., 2012). Its carbon and hydrogen composition is 86% and 13%, respectively. Oxygen, nitrogen, and sulfur comprised the polar factions spanning a wide molecular weight (MW) range. The hydrocarbon gases (C_1 to C_5) are composed primarily of methane comprising 82%, followed by ethane (8%), and propane (5%). Other gases such as *n*-pentane, isopentane, *n*-butane, and isobutane ranged from 0.5% to 2%. Aqueous methane was the most abundant hydrocarbon in the deep-sea plumes.

In an attempt to mitigate the impact of the DWH to the environment and improve safety for surface operating vehicles, an unprecedented quantity of chemical dispersants, mainly Corexit 9500 and Corexit 9527, was applied. Of the 7 million liters of Corexit used, about 40% were added at the wellhead on the ocean floor and 60% were sprayed at the surface waters. (The Federal Interagency Solutions Group, 2010; McNutt et al., 2012). The dispersants have amphiphilic properties that lower the interfacial tension between oil and water, creating smaller oil droplets. Chemical dispersants reduce oil delivery to shoreline and stimulate oil biodegradation by emulsifying surface oil slicks and increasing dissolved oil concentrations making it more bioavailable to indigenous microbial communities.

The fate of the oil at sea depends on the composition of the oil, the weathering processes, and the prevailing environmental conditions. The released oil could undergo dissolution, dispersion, emulsification, photooxidation, evaporation, sedimentation, and biodegradation, among others (Fig. 28.1) (Thibodeaux et al., 2011; McGenity et al., 2012). And as the oil accumulates, its mobility, biological uptake, and degradation are largely determined by environmental conditions. In this chapter, we focus on how these environmental variables affect the degradation of Macondo oil in the northern Gulf of Mexico (nGoM). We hope that the environmental aspects of the DWH oil spill we present in this chapter will be useful to life and physical scientists, oil spill experts, and natural resource managers on understanding the impacts and fate of oil in marine environments.

28.2 EXTENT OF OIL SPILL AND HYDROCARBON CONTAMINATION

The DWH oil spill affected the deep sea, surface, and coastal environments of the Gulf of Mexico. From a depth of 1500 m, much of the oil traveled up through the water and formed oil slicks on the surface (Fig. 28.2) (NOAA-ERMA, 2010). The maximum extent of oil slick on a single day was ~40,000 km on June 19, 2010 (DWH-NRDA, 2015; Beyer et al., 2016) and the area cumulatively covered was ~112,000 km^2 of the ocean surface during the course of the spill. Ocean currents, winds and tides carried this surface slicks to the continental shelf off

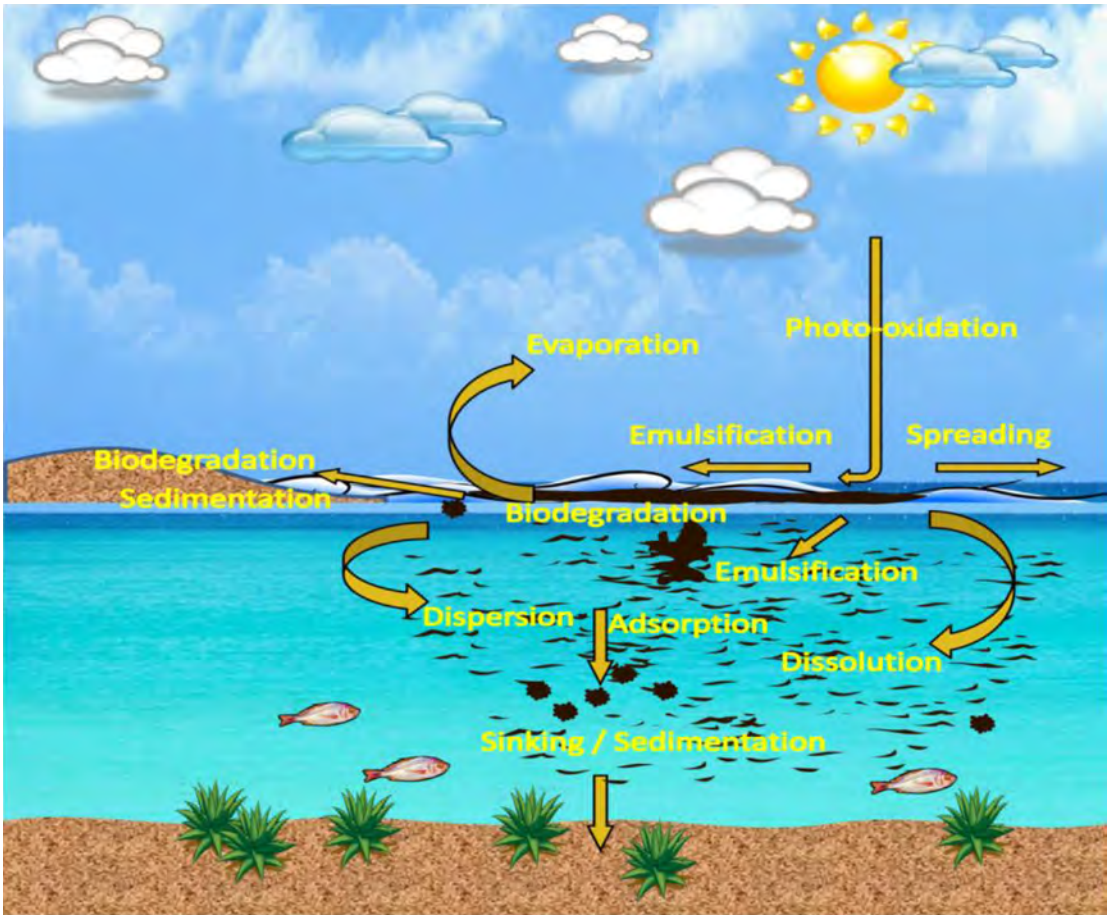

FIGURE 28.1 Fate of a marine oil spill. *Adapted from McGenity, T.J., Folwell, B.D., McKew, B.A. and G.O. Sanni. Marine crude-oil biodegradation: a central role for interspecies interactions.* Aquat. Biosyst.*; 2012; 8, 1–19.*

Texas and washed away onto the shorelines of Louisiana, Mississippi, Alabama, and Florida. The spill affected approximately 2100 km of the Gulf of Mexico coastline, fouling beaches, marshes, wetlands, and estuaries from eastern Texas to Florida Panhandle (Dietrich et al., 2012; Michel et al., 2013).

Sediment and water samples were collected from coastal waters between Galveston, Texas, and the Florida Keys, and within 50 km diameter around Macondo wellhead between May and November 2010 (Sammarco et al., 2013). Total petroleum hydrocarbon (TPH) concentrations in the sediment were highly and patchily distributed throughout the study region. In the immediate vicinity of the spill, TPH concentrations averaged 39,400 mg/kg with an overall values ranged from 0.05 to 535,000 mg/kg (Sammarco et al., 2013). TPH concentrations in seawater averaged 202 mg/L with TPH values ranging from 160 to 260 mg/L in Terrebonne, Bay Louisiana, which is close to the spill site. Varying concentrations of TPH and polycyclic aromatic hydrocarbons (PAHs) were detected both in sediment and water samples from Florida to Galveston, Texas. Wade et al. (2016) presented spatial and temporal distributions of hydrocarbon data from more than 20,000 samples collected during and after the DWH incident from 13,000 stations. These water column samples were collected from few meters to over 800 km in all directions from the wellhead and analyzed for TPH and PAHs. The TPH concentration in the samples ranged from 0 to 7,270,000 μg/L with the higher concentrations detected near the wellhead. The majority of these samples (84%) had TPH concentrations below the background concentration of 1 μg/L, about 11% had a concentration from 1 to 250 μg/L, and about 5% had a concentration >250 μg/L. Among the samples analyzed for PAHs, 78% had a concentration below the background concentration of 0.056 μg/L, while more than 21% had concentration higher than this. Highest PAH concentrations were generally found near the blowout area and from surface water samples (0 to 1 m) with large oil droplets that rise to the surface. Many samples with PAH concentrations above the background were those from the near surface water column within 25 km of the wellhead. The number of these samples exceeding the background concentration rapidly decreased

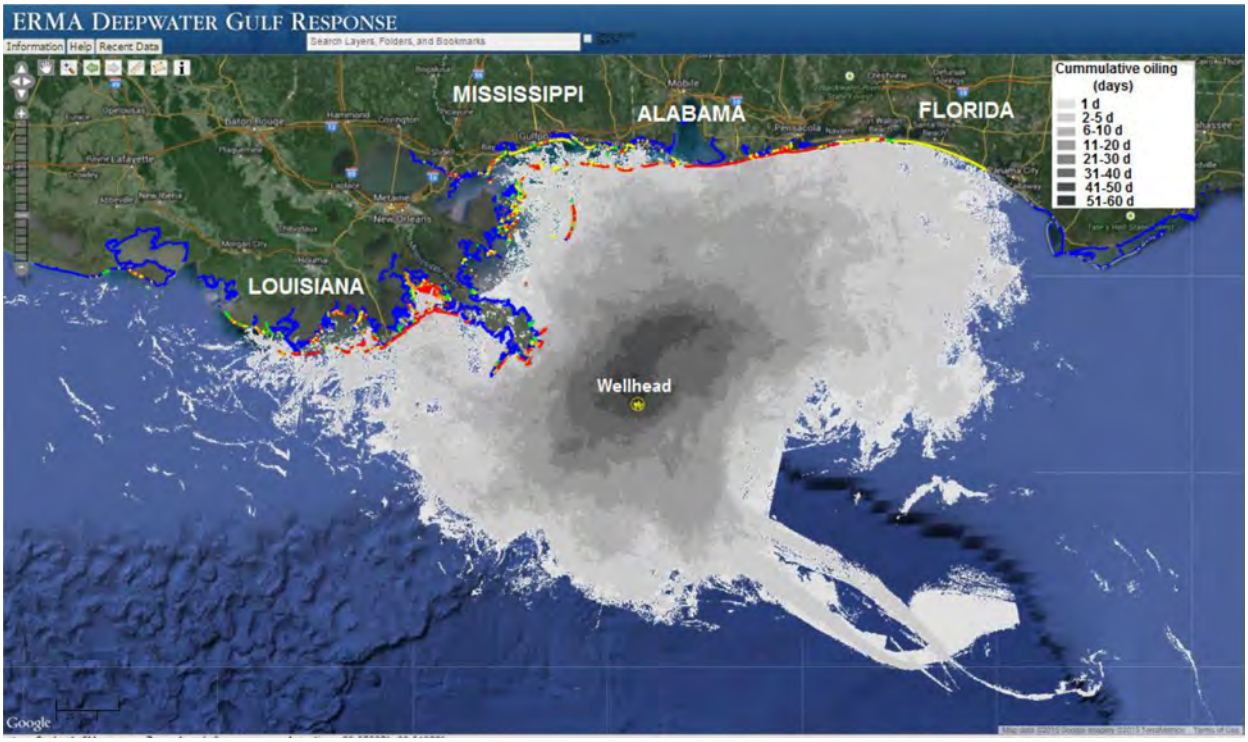

FIGURE 28.2 Map showing the location of the wellhead and the days of cumulative oiling on the ocean surface of the northern Gulf of Mexico (NOAA-Environmental Response Management Application (ERMA), 2010).

after the well was capped. This is further supported by the results of our analysis of surface water samples collected along the Louisiana shelf showing that the PAHs concentration in surface suspended particles were on the average five times higher in May 2010 than May 2011 (Liu et al., 2016).

Another notable feature of the DWH spill is the formation of deep-sea hydrocarbon plumes at the depth of 1000 to 1200 m southwest of the wellhead, in a region of at least 35 km long by 2 km wide (Hazen et al., 2010; Camilli et al., 2010). The plume is thought to have formed primarily due to application of Corexit at the wellhead combined with the environmental conditions in the deep sea resulting in the oil attaining buoyancy at this depth (Bælum et al., 2012). These plume contained high concentrations of light aromatic hydrocarbons (BTEX) and *n*-alkanes primarily C_7–C_{13} (Hazen et al., 2010) and was the focus of considerable attention especially on the potential of bacterial communities to metabolize hydrocarbons in this cold and high pressure environments. Several research groups reported the presence of the plume during the release of oil in the span of about 3 months, but these plumes were no longer detectable after the wellhead was capped (OSAT-I, 2010), presumably as a result of dispersion and microbial degradation.

28.3 BACTERIAL COMMUNITY

28.3.1 Deep-Sea Plume

Indigenous bacterial communities respond to influx and prolonged oil contamination. Following the DWH oil spill, bacterial densities significantly increased in the deep-sea oil plume and correlated with MC 252 alkane concentrations (Hazen et al., 2010). Plume water samples collected during the active phase of DWH spill in June 2010 from a location 10 km from the wellhead were dominated by bacteria closely related to order *Oceanospirillales* which comprised more than 90% of the community, while it only represented 5% of the sequences in a distal control site about 40 km away (Hazen et al., 2010). These *Oceanospirillales* form a clade of two distinct groups, one of which is largely composed of psychrophilic oil-degrading bacteria such as *Oleispira*, *Thalassolituus*, and *Oleiphilus*. Isolation and sequencing of two *Oceanospirillales* single cells revealed that both cells possessed genes coding for *n*-alkane and cycloalkane degradation, chemotaxis, motility and nutrient acquisition strategies (Fig. 28.3) (Mason et al., 2012). In another study, Redmond

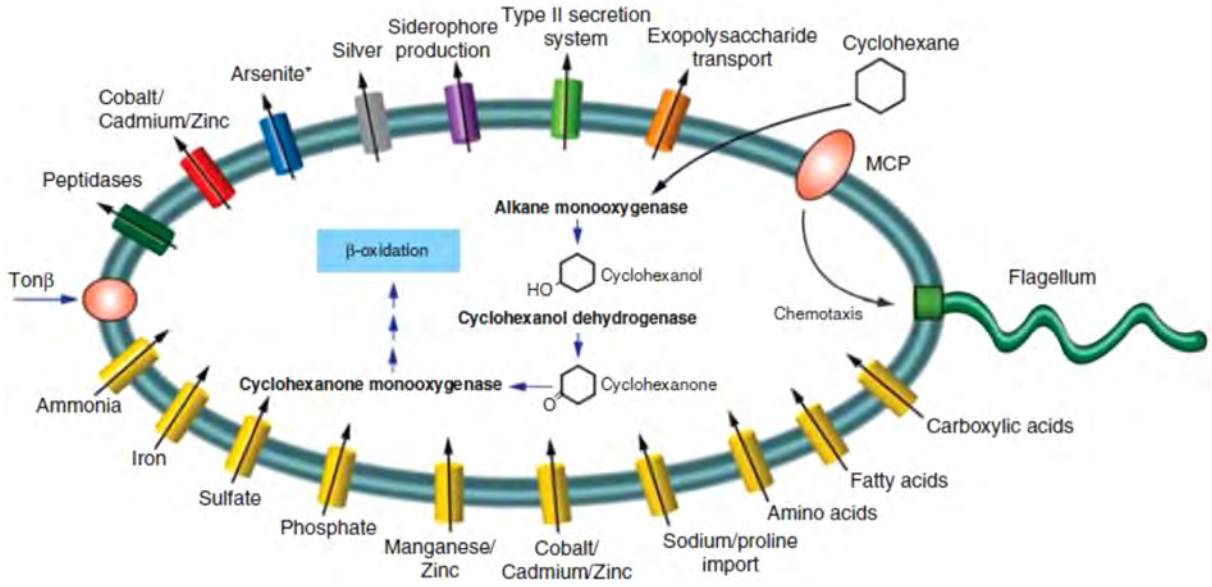

FIGURE 28.3 *Oceanospirillales* single-cell metabolic reconstruction using COG annotations of assembled sequence data and the blast comparison of unassembled single-cell reads to genes involved in hydrocarbon degradation. All genes in the single-cell metabolic reconstruction were present in the metagenomes and most were expressed in the metatranscriptome, except for those with an asterisk following the gene name. *Reprinted by permission from Macmillan Publishers Ltd: ISME J, Mason, O.U., Hazen, T.C., Borglin, S., Chain, P.S.G., Dubinsky, E.A., Fortney, J.L. et al. Metagenome, metatran-scriptome and single-cell sequencing reveal microbial response to Deepwater Horizon oil spill.* ISME J.; 2012; 6, 1715–1727.

and Valentine (2012) confirmed that *Oceanospirillales* accounted for 30% to 95% of plume samples collected in May 2010 but not detectable in June 2010 samples. Instead, *Cycloclasticus* and *Colwellia* accounted for more than 95% of the sequences. However, in September 2010 samples these bacteria were no longer detectable but methanotrophs, other methylotrophs, *Flavobacteria*, and *Rhodobacterales* were much more abundant.

DNA-stable isotope probing (SIP) incubation was conducted using the September 2010 samples amended with ^{13}C-labeled methane, ethane propane, or benzene to identify the bacteria consuming these hydrocarbons (Redmond and Valentine, 2012). Although *Oceanospirillales* was not detected in the original sample, it accounted for 3%–13% of sequences of DNA from ethane and propane but not in benzene suggesting its preference for short alkanes. *Methylococcaceae* which was initially accounted for 3% in the initial sample comprised about 84% of the heavy fraction of methane. Remarkably, *Colwellia* became dominant in heavy fraction of ethane, propane, and benzene, suggesting their ability to consume both small aromatics and short alkanes. The dominance of *Colwellia* and *Oceanospirillales* suggests that both bacteria are likely responsible for both ethane and propane oxidation in the deep-sea plume. Moreover, *Actinobacteria* and *Methylopaga* were also enriched in benzene and methane incubations, respectively. These sequences obtained in laboratory incubation were closely related to the sequences observed in the environmental samples based on phylogenetic analysis.

Initially barely undetected in water sample collected from Gulf of Mexico in June 2010, incubation using different concentrations of Macondo oil with or without Corexit resulted in the enrichment cultures dominated by *Colwelliaceae* with an abundance of 15%–30% (Bælum et al., 2012). *Oceanospirillales* and *Oleispira* also increased to 5%–10%. Oil was degraded faster in the presence of Corexit up to 60% loss compared to initial concentration. The *Colwellia* strain RC25 isolated from this enrichment has 96% similarity to *Colwellia psychrerythraea* 34H (Methé et al., 2005) and degraded 75% of the MC 252 oil after 10 days of incubation (Fig. 28.7 from Baelum). *Colwellia* abundance peaked when gaseous and simple aromatic hydrocarbons increased and supplanted *Oceanospirillales*, which dominated during the early stage of the spill. Single-cell genomics revealed that a *Colwellia* SAG isolated from the plume has genes for denitrification, chemotaxis, and motility, adaptations to cold environments and nutrient acquisitions (Mason et al., 2014a). The *Colwellia* may be also capable of degrading gaseous and aromatic hydrocarbons.

28.3.2 Deep-Sea Sediment

An estimated 3.0%–4.9% of the total hydrocarbon released during the DWH was deposited on the seafloor surrounding the wellhead in an area expanding 2.4×10^{10} m^2, based on carbon isotope analysis (Chanton et al.,

2015). High levels of PAHs (>24,000 μg/kg) were detected in sediments near the wellhead following the DWH spill, compared to distant cores (50 μg/kg) (OSAT-I, 2010). Moreover, hydrocarbon concentrations were higher during 2010–11 compared to years prior to 2010 (Liu et al., 2012; Romero et al., 2015). However, 1 to 3 years after the spill the PAH concentrations in many of these surface sediments have values similar to pre-spill concentration (Adhikari et al., 2016), suggesting degradation by active oil-degrading bacterial communities in the deep-sea sediment. Seafloor sediments harbor diverse and abundant microbial communities roughly equal to that of the seawater (Kallmeyer et al., 2012). In the northern Gulf of Mexico these bacteria are commonly influenced by hydrocarbon-rich cold-seeps and may have developed the abilities to metabolize hydrocarbons (Mills et al., 2004; Orcutt et al., 2010).

The indigenous microbial community contributed important roles in the remediation of oil spilled in the seafloor. The most heavily oil-impacted sediments collected 5 to 6 months after spill were dominated by Gammaproteobacterium and *Colwellia* species, both very similar to the sequences detected in the plume (Mason et al., 2014b). The most abundant hydrocarbon degradation pathway encoded genes involved in the degradation of aliphatic and simple aromatics. In a microcosm studies, these native microbes mineralized 48% of dodecane, 27% of toluene, and 10% phenanthrene after 90 days (Mason et al., 2014b). Moreover, sediment microbes have greater affinity for some of the compounds in the dispersant compared to that of the plume having readily degraded polyethylene glycol, a component in Corexit, with a negligible lag phase. These communities also have potential for anaerobic hydrocarbon degradation as Deltaproteobacteria and anaerobic functional genes were abundant in sediment near the wellhead (Kimes et al., 2013). In addition, genes associated with denitrification increased significantly in highly contaminated sediments.

In May 2011, 1 year after the spill, SG sediment collected 2 km from the wellhead had a total *n*-alkane concentration of 2.56 mg/g dry weight, while that of SC sediment 6 km away was 3.63×10^{-3} mg/g (Liu et al., 2012). Both of the chromatograms from the samples had resolved *n*-alkanes from C_{11} to C_{37} enriched in long-chain alkanes different from that of the MC 252 source oil (Fig. 28.4). Concentrations of total PAHs were also higher in SG (1 μg/g) than in SC sediment (0.3 μg/g), consistent with their distances from the spill site. Both sediment samples were more enriched of 3 and 4 ring PAHs. Bacterial community analysis revealed that *Pseudomonas*, a well-known hydrocarbon degrader represented 5% and 14% of the SG and SC, respectively (Liu and Liu, 2013) (Fig. 28.5). *Hyphomicrobium* and *Rhodovibrio* each accounted for 2% of the community, and *Methylococcus* and *Methylobacter* represented 3%–7% of the community suggesting low concentrations of methane in the samples. Other bacteria that were detected in these sediment samples include *Desulfobacterium* (1%), *Actinobacteria* and *Firmicutes* (4%–8%), and *Chloroflexi* (12%). The commonly observed dominant bacteria in the plume (*Oceanospirillales* and *Colwellia*) were barely detected possibly because the oil in these sediments was already depleted of natural gas components and mainly consist of heavier hydrocarbons.

28.3.3 Surface Water

Bacterial communities in oil mousses (MP, OSS, CT) were distinct from the ambient seawater without visible oil (OSS-SW, CT-SW) (Fig. 28.6; Liu and Liu, 2013). OSS and CT mousses collected in May 2010, which are depleted of *n*-alkanes C_{13} below or lighter, were represented by bacteria affiliated with *Erythrobacter, Bartonella, Rhodovulum, Stappia*, and *Thalassospira* comprising more than 50% of the total Alphaproteobacteria. Among the Gammaproteobacteria, *Marinobacter, Alcanivorax, Pseudomonas*, and *Alteromonas*, were the dominant genera. The bacteria in the oil mousses did not simply accumulate from the surrounding water but developed as they involved in the degradation of hydrocarbon compounds. Although a different type of oil, our related work on the Texas City "Y" spill showed that the bacterial communities developed in the tar balls were different from the peripheral sand (Bacosa et al., 2016). The fresher tar balls were predominated by known alkane degraders such as *Alcanivorax* and *Psychrobacter*, a predominantly PAHs-degrading *Pseudoalteromonas* dominated in the more weathered tar balls. In contrast, the peripheral sand harbor diverse microbial populations and many of those are not known to degrade hydrocarbon compounds.

The natural bacterial community shifts in the presence of oil either as the effect of the toxicity of hydrocarbons to some vulnerable bacteria or enrichment of hydrocarbon-degrading bacteria. This results to a decrease in the diversity of the community, and can be mainly dominated by known hydrocarbon degraders (Bacosa et al., 2016). The initial bacterial community as the seed for the oil-degraders explains about 20% of the variation observed using surface and deep waters in the northern Gulf of Mexico (Fig. 28.7; Liu et al., 2017). Different

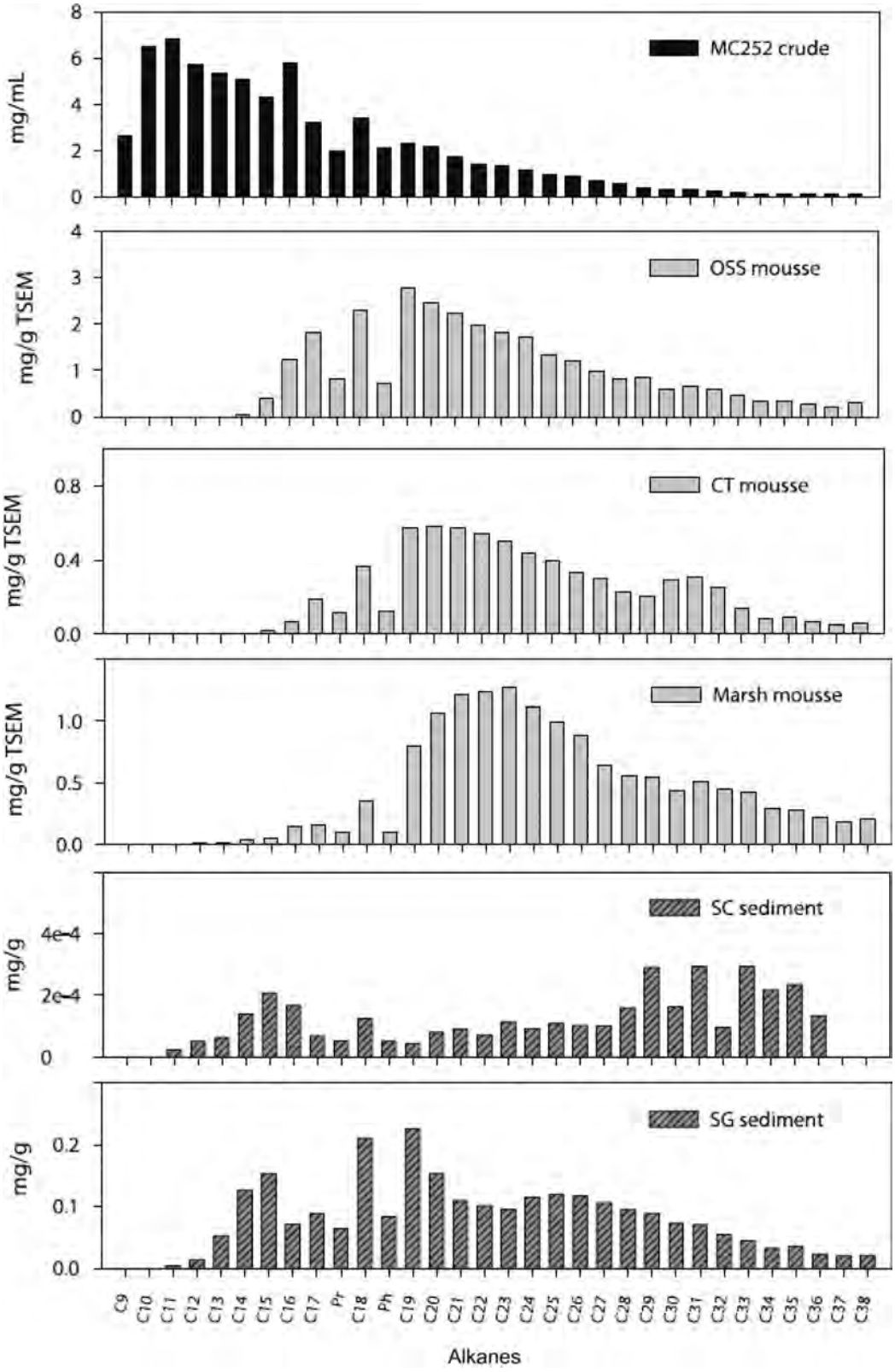

FIGURE 28.4 Concentrations of *n*-alkanes (C_9–C_{38}), pristane (Pr) and phytane (Ph) in Macondo reference oil, mousse from stations OSS, CT, and MP, and sediment oil from stations SC and SG. The alkane concentrations in oil mousse were normalized to total solvent-extractable materials (TSEM), and in sediments normalized to dried sediment weight. *Adapted from Liu, Z., Liu, J., Zhu, Q., and W. Wu. The weathering of oil after the Deepwater Horizon oil spill: insights from the chemical composition of the oil from the sea surface, salt marshes and sediments.* Environ. Res. Lett.*; 2012; 7, 035302*.

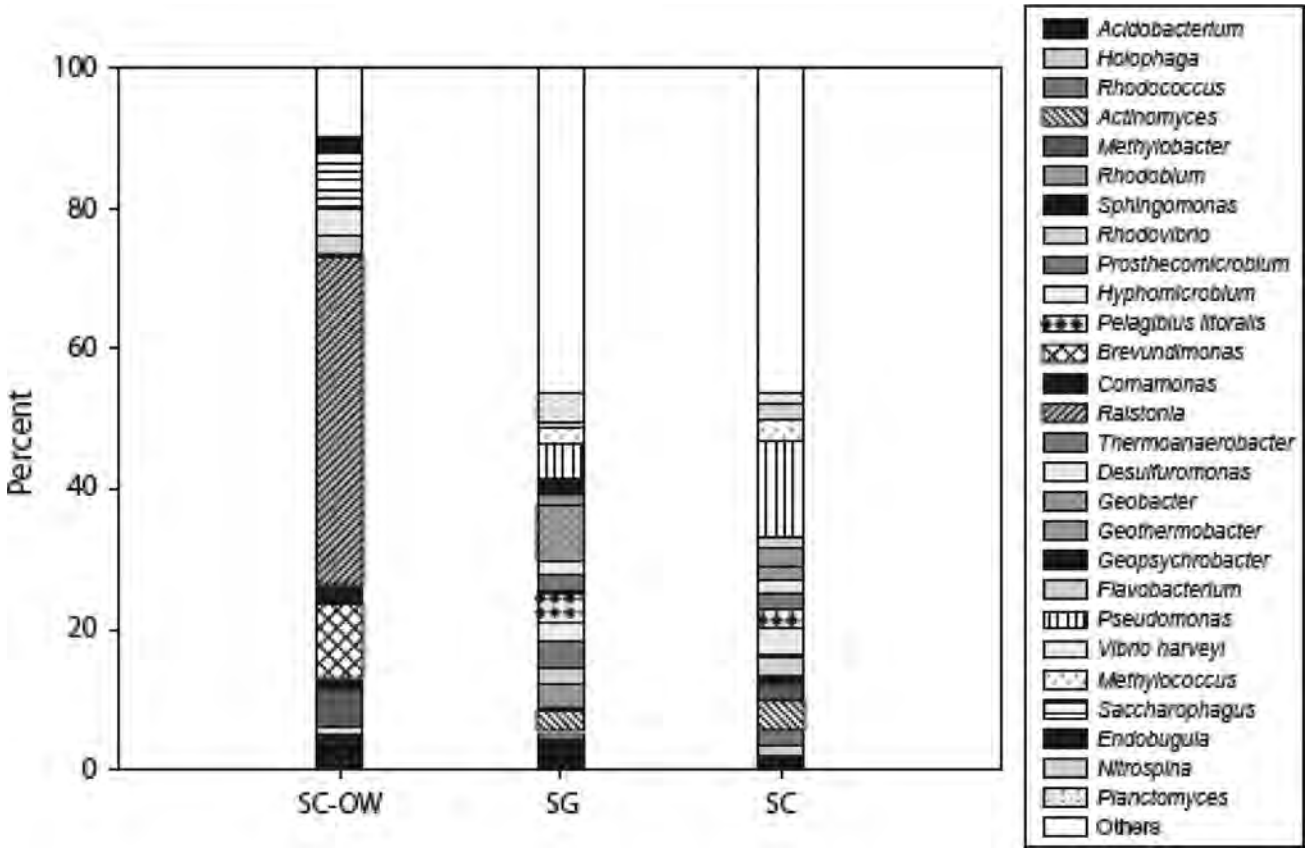

FIGURE 28.5 Compositions of bacterial communities in sediments collected at stations SG and SC, and in overlying waters of SC sediments (SC-OW). The relative abundance of each bacterial species shown in the figure was at least 2% or above in one of the three samples. The species not shown on the bar were categorized as others. Clearly, bacterial communities in the SG and SC sediments were much more diverse than those of the SC-OW. *SG*, station grab; *SC*, station core; *SC-OW*, overlying water of SC sediment. *Adapted from Liu, Z. and J. Liu. Evaluating bacterial community structures in oil collected from the sea surface and sediment in the northern Gulf of Mexico after the Deepwater Horizon oil spill.* Microbiol. Open*; 2013; 2, 492–504.*

environmental factors such as temperature, nutrients, salinity, pressure, sunlight and a combination of these might select for the oil-degrading bacteria. For example, the combination of 4°C, crude oil and deep water inoculum was a key factor for the growth of *Cycloclasticus*, while the combination of surface water inoculum and bottom water chemistry was important for the growth of *Pseudoalteromonas*.

28.4 TEMPERATURE

Temperature has significant influence on the fate of crude oil in marine environments. Both evaporation of volatile components in oil and aqueous solubility of organic compounds are strongly temperature dependent (Schwarzenbach et al., 2003). Evaporation and dilution were considered as two important ways responsible for the disappearance of spilled oil (National Research Council Committee, 2003). Both metabolic activities within microbial cells and photochemical reactions in weathering of oil are temperature dependent. Enzymatic activities in correlation with the process of oil biodegradation are abated at low temperatures (Meng et al., 2016). Temperature affects photooxidation rate of crude oil, by controlling the singlet oxygen or free-radical chain reactions (Shankar et al., 2015).

Biodegradation rates of South Louisiana crude oil, a surrogate for the Macondo crude oil, have been found related to incubation temperatures (Campo et al., 2013; Zhuang et al., 2016; Liu et al., 2017). Generally, crude oil is biodegraded faster in warmer waters such as surface waters of the northern Gulf of Mexico in summer

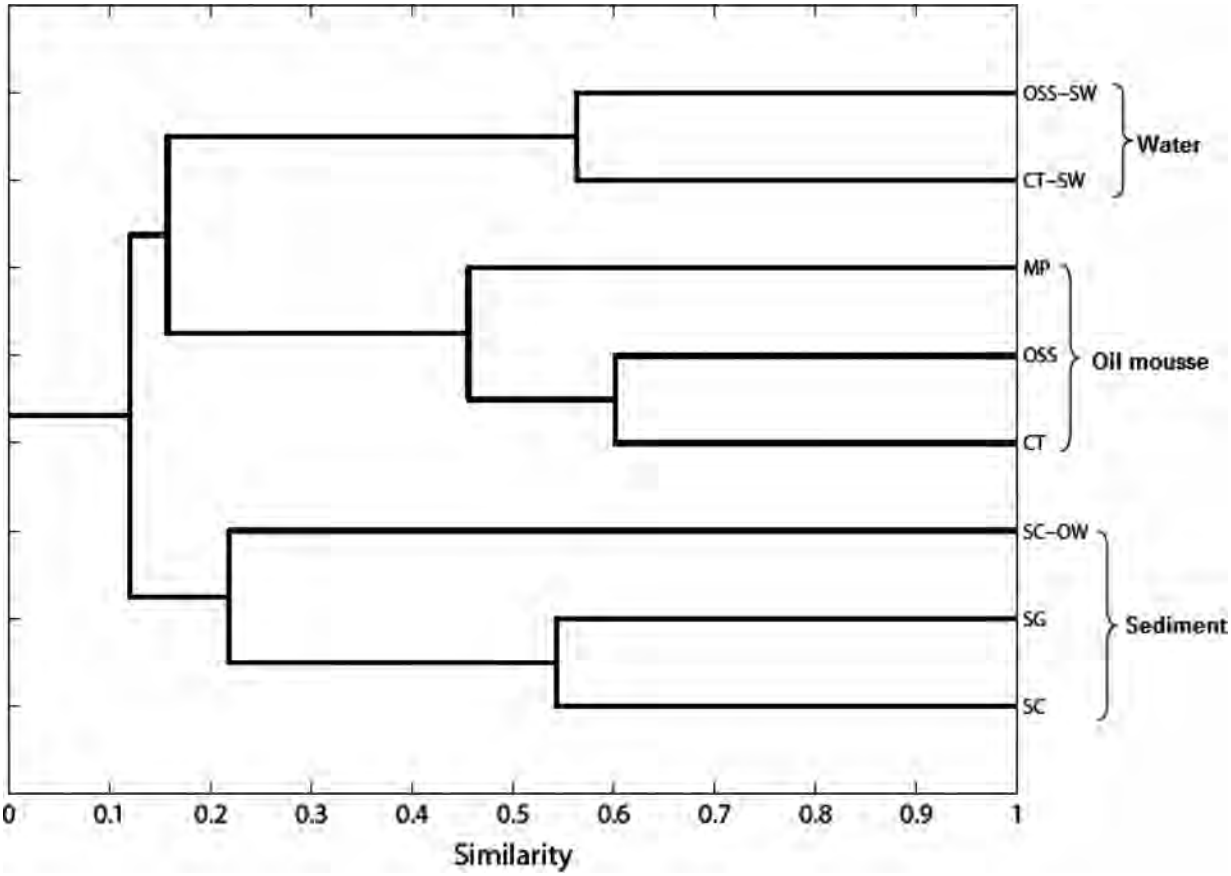

FIGURE 28.6 Bray-Curtis analysis on bacterial communities based on absence or presence of each bacterial species in oil mousses (OSS, CT, and MP), sediments (SG and SC), and overlying waters of SC sediment (SC-OW). *OSS*, oil spill site; *CT*, control; *MP*, Marsh Point; *SG*, station grab; *SC*, station core. *Adapted from Liu, Z. and J. Liu. Evaluating bacterial community structures in oil collected from the sea surface and sediment in the northern Gulf of Mexico after the Deepwater Horizon oil spill.* Microbiol. Open*; 2013; 2, 492–504.*

(28–30°C). There are two ways that temperature affects biodegradation of oil in marine environment. First, temperature changes the physical properties of oil. Temperature-dependent processes including evaporation and dissolution change the composition and bioavailability of crude oil in seawater. Low temperature might crystallize some components of oil and consequently protect them from attack of microbes (Campo et al., 2013). Second, temperature impacts microbial physiology. Temperature affects the composition of microbial communities by selecting the types of oil-degrading bacteria that can adapt to certain temperature range (Liu et al., 2017).

Temperature is one of the most important factors to consider when comparing the biodegradation of alkanes and PAHs. An example can be found in microcosm experiments with South Louisiana crude oil and dispersant Corexit 9500 incubated at 25 and 5°C, corresponding to average temperatures of seawater at surface and Macondo wellhead, respectively (Campo et al., 2013). At 25°C, the total alkane concentrations were nearly undetectable by day 11 in the absence of the dispersant and by day 4 in its presence, while PAHs did not decline until day 28 (Fig. 28.8). This was not surprising because alkanes are generally more amenable to biodegradation than PAHs (Bacosa et al., 2010, 2013, 2015a). However, at 5°C unusual higher biodegradation rates of PAHs compared to alkanes were found. The authors offered a plausible explanation that all the *n*-alkanes above tridecane crystallize at 5°C and below. Accordingly, alkanes may have been less available to the microbial communities at the lower temperature compared to the more soluble PAHs. Moreover, distinct bacterial communities develop at low temperature and may preferably degrade PAHs over alkanes (Liu et al., 2017).

Our recent work using surface water (2 m) and bottom water (1537 m) sampled near the DWH spill site and incubated with oil at 4°C and 24°C yielded results consistent with that of Campo et al. (2013) (Liu et al., 2017). Total *n*-alkanes in treatments incubated at 24°C were generally degraded faster ($k = 0.09$ to 0.22/d) than at 4°C ($k = 0.06$ to 0.12/d). However, the concentrations of PAHs decreased faster at 4°C ($k = 0.16$ to 0.34/d) than 24°C ($k = 0.10$ to 0.24/d) (*t*-test, $P < 0.05$). Moreover, different oil-degrading bacterial communities developed at 4°C and 24°C both

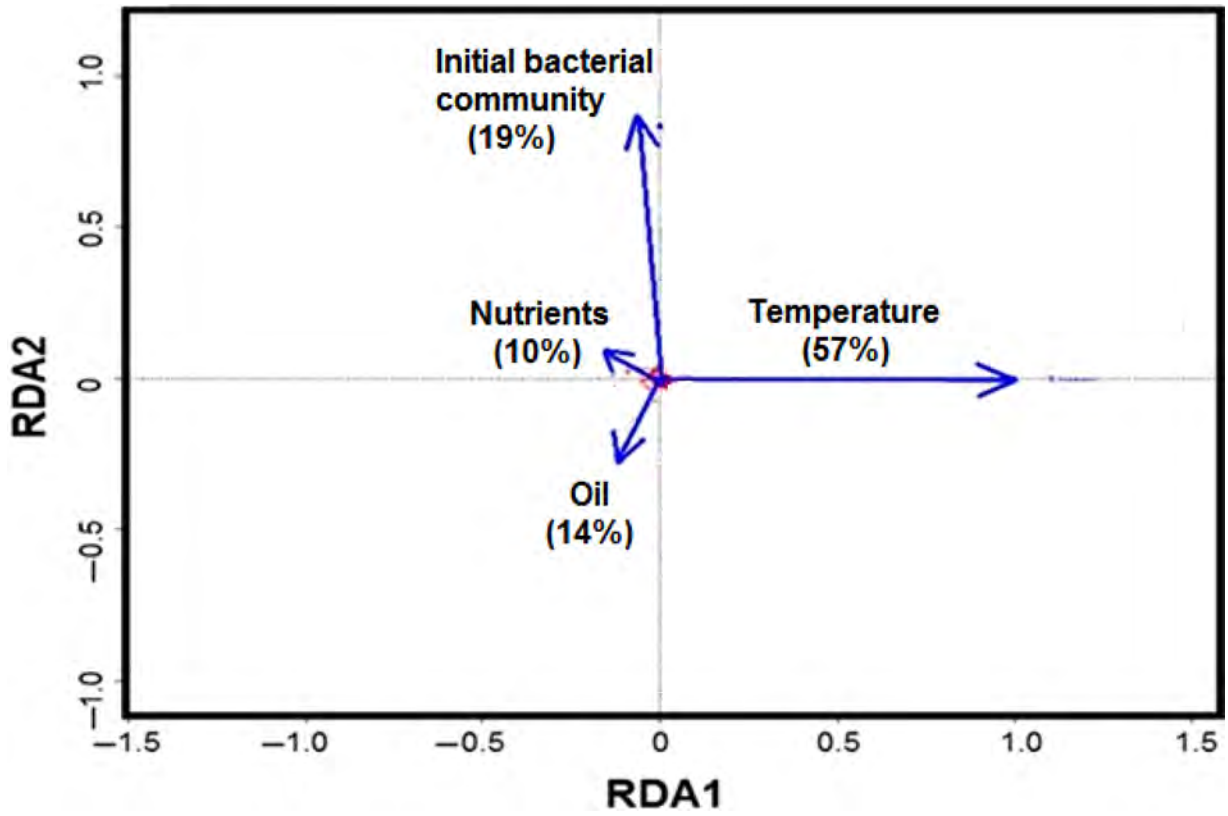

FIGURE 28.7 Biplot diagram of the redundancy analysis (RDA) on bacterial community constrained by the presence of oil, temperature, nutrients and initial community. The corresponding percentage is the result of partial RDA to determine how much of the variation in bacterial community composition is explained by the factor. *Modified from Liu, J., Bacosa, H.P. and Z. Liu. Potential environmental factors affecting oil-degrading bacterial populations in deep and surface waters of the northern Gulf of Mexico.* Front. Microbiol.*; 2017; 7, 2131.*

for surface and bottom water indicating the dominant role of temperature in selecting oil-degrading bacteria. Redundancy analysis (RDA) showed that among the environmental parameters examined, temperature has the most profound effects on bacterial community (Fig. 28.7). Further analysis using partial RDA estimated that temperature explains 57% of the variation observed in microbial community structures. Bacterial genera developed in the 4°C incubations included *Cycloclasticus*, *Pseudoalteromonas*, *Sulfitobacter*, and *Reinekea*. In contrast, the dominant bacteria in the 24°C incubations included *Oleibacter*, *Thalassobius*, *Phaeobacter*, and *Roseobacter*. Some bacteria developed well in both 4°C and 24°C such as *Alcanivorax* and *Alteromonas*. The low temperature (4°C) in the deep-sea plume also selected for psychrophilic oil-degrading bacteria. Laboratory enrichment of plume water at 4°C using crude oil produced a clone library dominated by 75%–87% of *Colwellia*, but not at room temperature (Redmond and Valentine, 2012), indicating the critical role of temperature of selecting oil-degrading bacteria.

Temperature determines whether dispersant is positive for accelerating biodegradation of oil. In their experiments, Zhuang et al. (2016) found that degradation of the aliphatic fraction in the dispersed oil occurred at a faster rate than in the South Louisiana crude oil alone treatment at cryo-culture (5°C), opposed to what they observed at 25°C. The oil-in-water emulsion created by dispersant would have attenuated the crystallization of alkanes at low temperature and thus provided more hydrocarbons to microbes. Conversely, the emulsion would have disrupted the hydrophobic interactions between long-chain alkanes and microbes at meso-culture (25°C), therefore slowed down hydrocarbon respiration.

Bacterial communities in deep water plumes of *Deepwater Horizon* spilled oil differed from those in surface oil slick samples (Redmond and Valentine, 2012). The difference could be in response to the combination of temperature and pressure. After all, the pressure is much higher at the depth below 1000 m. However, *Colwellia*, dominant in the plumes but not abundant in the surface slicks, was found abundant in oil-degrading enrichment cultures incubated at normal pressure and 4°C (like the temperature at plume depth), overwhelming its abundance at room temperature. The results suggested that the temperature may have played a significant role in determining which members of the microbial community responded to the DWH spill.

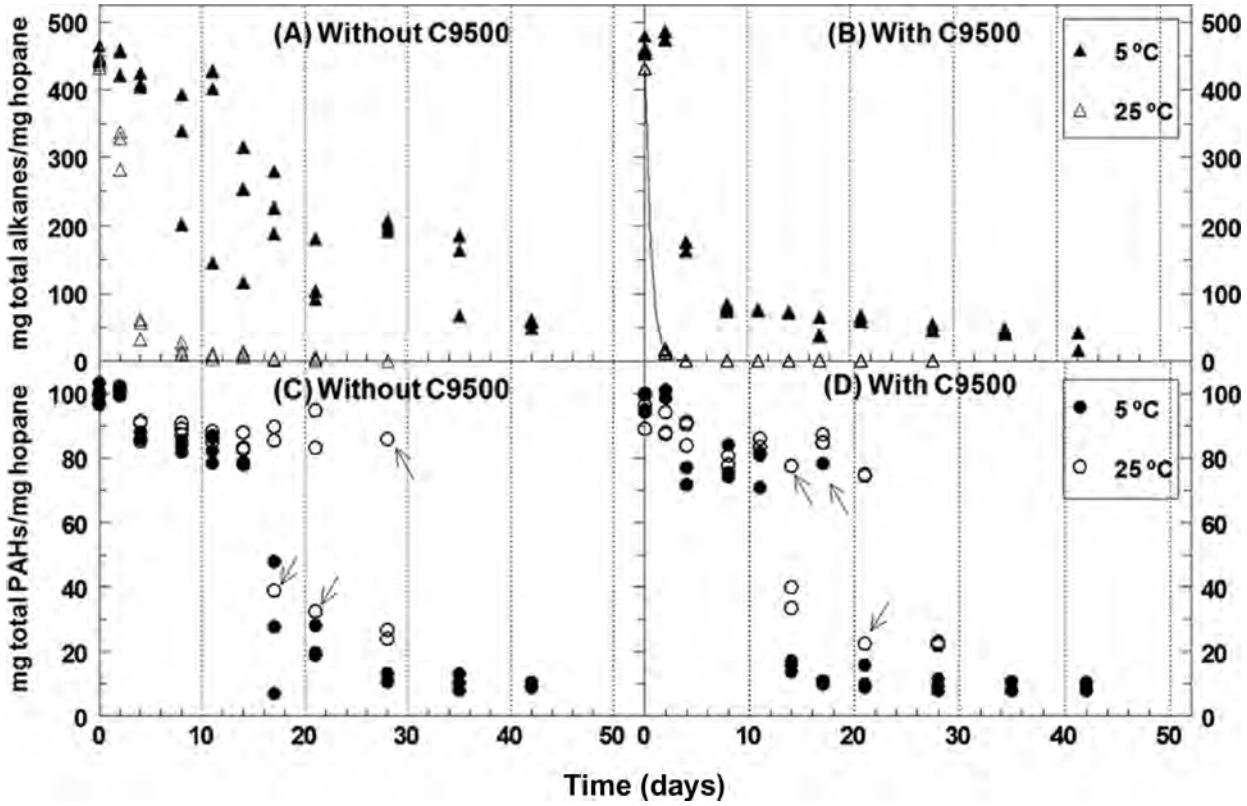

FIGURE 28.8 Biodegradation of hopane-normalized total alkanes (A, B) and PAHs (C, D) at 25 and 5°C without (A, C) and with (B, D) C9500 dispersant. The arrows in the figure panels represent statistical outliers as determined by the Grubb's outlier test.25. *Reprinted with permission from Campo, P., Venosa, A.D. and M.T. Suidan. Biodegradability of Corexit 9500 and dispersed south Louisiana crude oil at 5 and 25°C.* Environ. Sci. Technol.*; 2013; 47, 1960–1967. Copyright 2012, American Chemical Society.*

28.5 SOLAR RADIATION

Within hours after reaching the sea surface, the Macondo oil evaporated at a relatively fast rate (~258,000 kg/day) or about 14% by mass of the spilled oil (Ryerson et al., 2011). Light alkanes, BTEX, parent and alkylated naphthalene showed clear losses in oil mousses collected in May 2010 relative to the reference crude oil (Liu et al., 2012). The rest of oil was continuously exposed to the strong sunlight at northern GoM until it arrived at the coast and protected by sand/sediments. Photooxidation is one of the most important environmental processes in the weathering of spilled oil in surface seawater (Aeppli et al., 2012; Lewan et al., 2014). Many studies have observed the formation of oxygenated residues during exposure to sunlight after the DWH disaster (McKenna et al., 2013; Ray et al., 2014; Radović et al., 2014). When re-exposed to sunlight, the submerged DWH oil spill residues were significantly weathered (John et al., 2016). Besides direct photooxidation, sunlight may also affect biodegradation rate of spilled oil by, for example, selecting certain oil-degrading bacteria (Bacosa et al., 2015b).

28.5.1 Photooxidation

A given organic compound may directly undergo transformation after absorbing light energy, or be transformed by reaction with very reactive, short-lived species, or radicals, formed in the presence of light, such as hydroxyl radicals $HO^{\bullet}$ and singlet oxygen $^1O_2$ (Schwarzenbach et al., 2003; Shankar et al., 2015). In the case of DWH crude oil, a series of experiments was conducted (Ray et al., 2014; Ray and Tarr, 2014a,b; Ray and Tarr, 2015) under simulated sunlight in thin oil films over seawater to determine the intermediate products, including hydroxyl radicals, singlet oxygen, and organic triplets. Oil is a strong and important source of hydroxyl radical and singlet oxygen when exposed to sunlight (Ray and Tarr, 2014a,b). The total amount of singlet oxygen and hydroxyl radical produced in the irradiation of these thin oil films (100 mg) over Gulf of Mexico water were 2.0×10^{-5} and 3.7×10^{-7} moles, respectively.

Steady state concentrations of photo-produced singlet oxygen and hydroxyl radical were near 1×10^{-12} and 1.2×10^{-16} M in seawater under thin films of oil (Ray and Tarr, 2014a,b). Macondo oil produces higher triplet state energies than natural DOM did (Ray and Tarr, 2015), which may be explained by relatively high concentration of photosensitive PAHs in oil (Plata et al., 2008).

Different components in crude oil have different sensitivity to light. Photooxidation of saturates and aromatics were often studied because they were the most abundant in Macondo oil (Reddy et al., 2012), and partly due to the insufficient capability of GC to resolve the polar components. Aromatics were most photosensitive, followed by *n*-alkanes (King et al., 2011, 2014), although cyclic alkanes may decrease even faster than aromatic (D'Auria et al., 2009). The amounts of polar components, such as asphaltenes, which accounted for 1% of Macondo oil, increased when being exposed to light accompanied by substantial decrease of aromatics, implying the conversion of the aromatic compounds to more polar derivatives (Lewan et al., 2014; Radović et al., 2014). Using fresh Macondo oil from the gushing well and weathered oil recovered from oil splashes on jetty rocks after various days, Radović et al. (2014) determined dramatic decrease of aromatic and increase of polar fractions after a 7-day exposure to sunlight. The weight increase of photooxidized oil may partly be ascribed to the incorporation of oxygen, which was confirmed by Fourier transform infrared spectroscopy (FTIR) analyses (Dutta and Harayama, 2000), by Fourier transform ion cyclotron resonance mass spectrometry (FTICR-MS) (Ray et al., 2014), or by isotopic signals (Lewan et al., 2014).

Photooxidation rate of crude oil varied with MW and the level of alkylation. Low MW alkanes are transformed faster than high MW ones in photooxidized oil samples (King et al., 2014; Yang et al., 2015). PAHs are generally photodegraded slower than their alkylated homologues, and the removal of alkylated PAHs increased concurrently with the alkylation level in each family (Garrett et al., 1998; Radović et al., 2014).

Crude oil is typically exposed to photooxidation as a film or dissolved in surface waters known as water soluble fraction (WSF). PAHs in the WSF exhibited a high degree of photooxidation, while PAHs in oil film were less affected (Ziolli and Jardim, 2003; Griffiths et al., 2014; Shankar et al., 2015). The thickness of the oil film reduced the potential for photoreaction (Plata et al., 2008). For the Macondo oil, 90% of 350 nm radiation was attenuated in the first 9 μm of the 60 μm film and the thicker oil produced lower steady state concentrations than the thinner oil (Ray and Tarr, 2014a). Therefore, singlet oxygen formed at the very surface of the oil film is unlikely to diffuse through viscous oil to reach the aqueous layer (Ray and Tarr, 2014a).

28.5.2 Sunlight Changes Oil-Degrading Bacterial Community

Results from studies aiming to find relations between photooxidation and biodegradation showed that photooxidation increased the amount of oil components susceptible to biodegradation (Dutta and Harayama, 2000). Recently, we systematically studied the photooxidation and biodegradation of light Louisiana sweet crude oil (a surrogate for Macondo Oil) with or without Corexit dispersant using surface seawater close to the DWH spill site, and the incubation was conducted under the relevant temperature and solar radiation in the northern Gulf of Mexico (Bacosa et al., 2015a). Total *n*-alkanes in the dispersed oil degraded faster than in the non-dispersed treatments both in dark and light treatments (Fig. 28.9A). In the absence of dispersants, total *n*-alkanes decreased by 16% in the light during the first 5 days, whereas no change occurred in the dark. The light-control containing no bacteria decreased within 5 d and was static until a second burst of degradation (30%) occurred between 27 and 36 d. These findings indicate that biodegradation is the key process in controlling the disappearance of alkanes, while their photooxidation was only evident after prolonged exposure to sunlight. In contrast to alkanes, the degradation pattern of PAHs and their alkylated homologues was driven more by sunlight (Fig. 28.9B). Total PAHs in all light treatments with or without bacteria were transformed readily and nearly depleted at 20 d, while biodegradation of these group of compounds under the dark were delayed reaching only about 50% at 20 d. Overall, compared to biodegradation, photooxidation increased transformation of 4–5 ring PAHs by 70% and 3–4 ring alkylated PAHs by 36%.

In a parallel incubation, we showed how the natural solar radiation impacted the oil-degrading bacterial communities (Bacosa et al., 2015b). Sunlight significantly reduced bacterial diversity and evenness with crude oil alone, and with both crude oil and Corexit dispersant. Sunlight was also a key driver in the shifts of bacterial community structures having communities in the light-exposed treatments being more dispersed with the change in oil chemistry, while those of the dark are more clustered but distinct from those exposed to sunlight. Sunlight-favored certain bacterial genera such as *Alteromonas*, *Marinobacter*, *Labrenzia*, *Sandarakinotalea*, *Bartonella*, and *Halomonas* (Fig. 28.10). On the other hand, the dark incubation shaped a different community with the increased

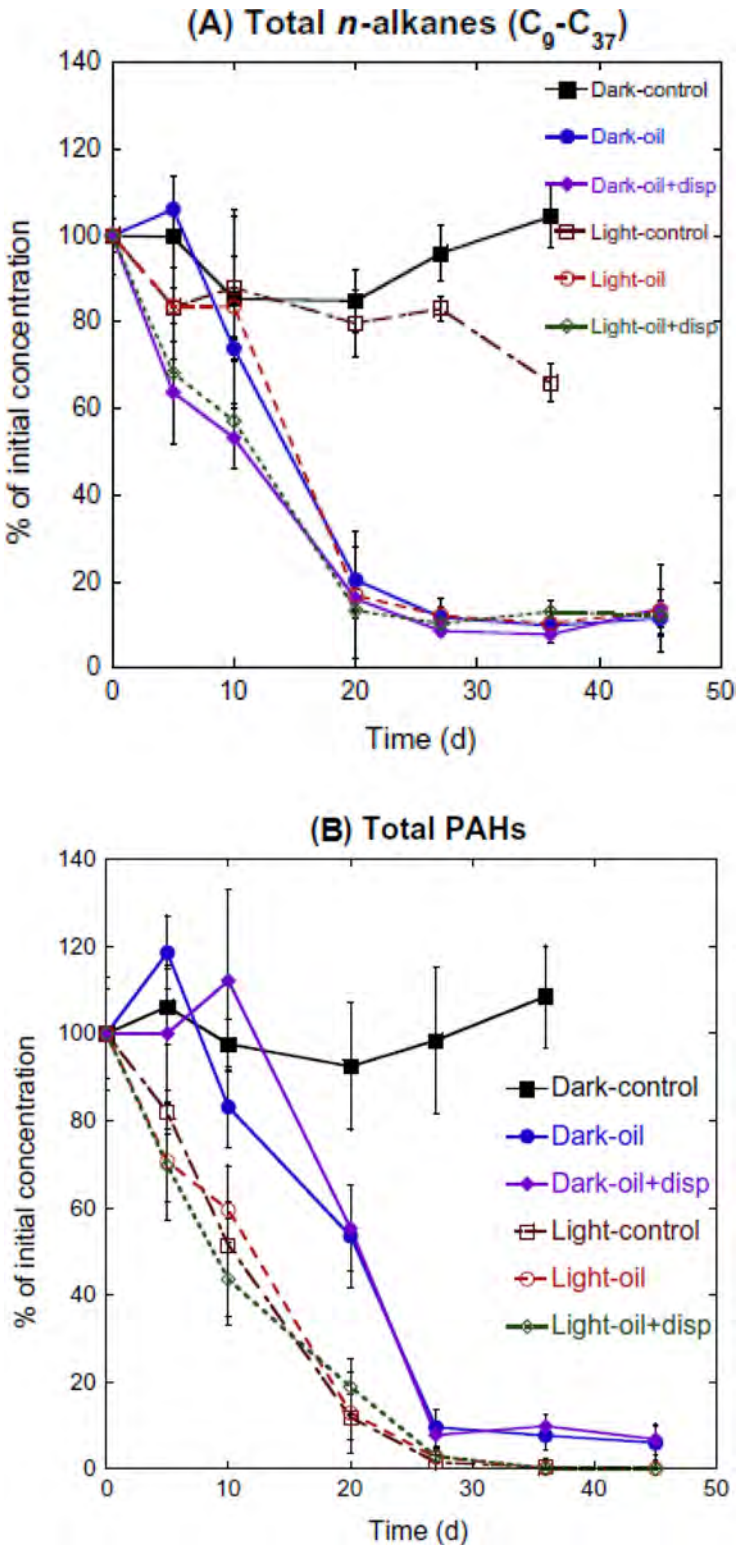

FIGURE 28.9 Degradation of total (A) *n*-alkanes and (B) PAHs under dark and light conditions. *Reprinted from Bacosa, H.P., Erdner, D.L., and Z. Liu. Differentiating the roles of photooxidation and biodegradation in the weathering of Light Louisiana Sweet crude oil in surface water from the Deepwater Horizon site.* Mar. Pollut. Bull.*; 2015a; 95, 265–272, with permission from Elsevier.*

abundances of *Thalassobius*, *Winogradskyella*, *Alcanivorax*, *Formosa*, *Pseudomonas*, *Eubacterium*, *Erythrobacter*, *Natronocella*, and *Coxiella*.

Many of these bacterial genera that developed during the incubation period were in good agreement with the field samples-OSS and CT mousses (Fig. 28.6; Liu and Liu, 2013). High abundance of *Marinobacter*, *Alteromonas*, *Erythrobacter*, *Bartonella*, *Rhodovulum*, *Thalassospira*, and *Stappia* were found in these oil mousses. *Alteromonas*

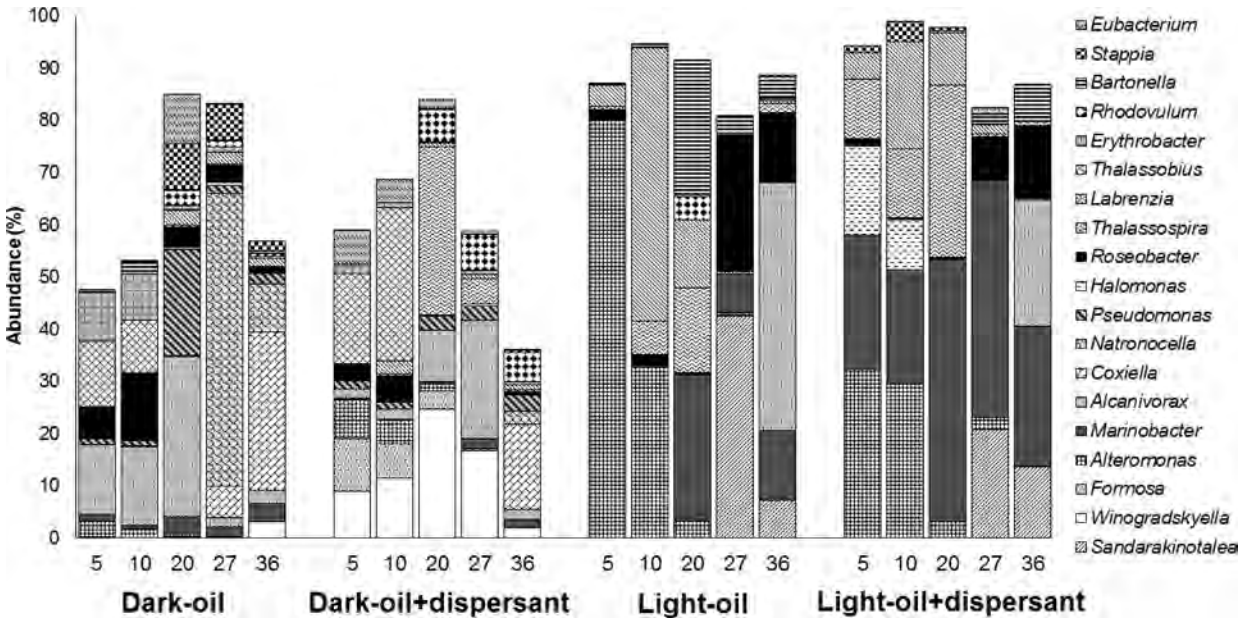

FIGURE 28.10 Abundances of bacteria at genus level in seawater amended with crude oil or both crude oil and dispersant Corexit, incubated in the dark and under the natural sunlight. The numbers indicate days of incubation. *Modified from Bacosa H.P., Liu, Z. and D.L. Erdner. Natural sunlight shapes crude oil-degrading bacterial communities in northern Gulf of Mexico surface waters.* Front. Microbiol.*; 2015b; 6, 1325.*

predominated over *Marinobacter* during the early stage of incubation which is consistent with these field samples as *Marinobacter* was more abundant in more degraded CT mousses, while *Alteromonas* was sixfold more abundant in less degraded OSS mousse. An oil mousse is a thick slick of floating oil aggregate with dark and mostly light-exposed portions, while this incubation study with a final oil concentration of 200 ppm represents an oil sheen completely exposed to sunlight. Accordingly, the bacterial communities developed in these field mousse samples were a combination of light and dark-associated bacteria, but the sunlight-favored bacteria predominated. The bacterial community developed upon exposure to oil is further shaped by various environmental parameters. The results from this incubation experiment conducted 3 years after the spill under the environmentally relevant conditions yielded results consistent to the mousses collected immediately after the spill, and substantiated our notion that high surface temperature and/or strong sunlight played an important role in the development of bacteria in oil-polluted waters in the nGoM.

28.6 NUTRIENTS

Hydrocarbon-degrading bacteria are ubiquitous in the marine environment; however, the rates that they can degrade the spilled oil depend on appropriate conditions for their growth. Since hydrocarbons only contain carbon and hydrogen, oil-degrading bacteria require utilizable adequate sources of nitrogen, phosphorous, sulfur, and iron to grow and multiply (Ron and Rosenberg, 2014). It has been widely recognized that petroleum degradation in the sea is typically limited by the availability of nutrients such as nitrogen and phosphorus. In principle, approximately 150 g of nitrogen and 30 g of phosphorus are consumed in the conversion of 1 kg of hydrocarbon to cell material. In late May 2010, nitrate concentrations inside of submerged plume waters significantly decreased (mean decrease 6 μM), but not phosphate concentrations (mean decrease 0.03 μM) (Hazen et al., 2010). However, in different samples taken from the deep plumes during May 10–14, 2010 and May 26–June 1, 2010, phosphate and nitrate anomalies had a positive correlation with the oxygen anomaly, as well as phosphate vs. nitrate anomalies (Shiller and Joung, 2012) (Fig. 28.11). These observations suggest that both nitrate and phosphate were removed together with oxygen in the subsurface plumes contrary to that of Hazen et al. (2010). These differences could be attributed to the time of sampling and stage of hydrocarbon degradation. Assuming that the nutrient depletion dominantly led to microbial growth, a substantial portion of hydrocarbons in these plumed was converted to biomass ($0.8–2 \times 10^{10}$ mol C). Notably, despite the elevated levels of PAHs in the deep plumes,

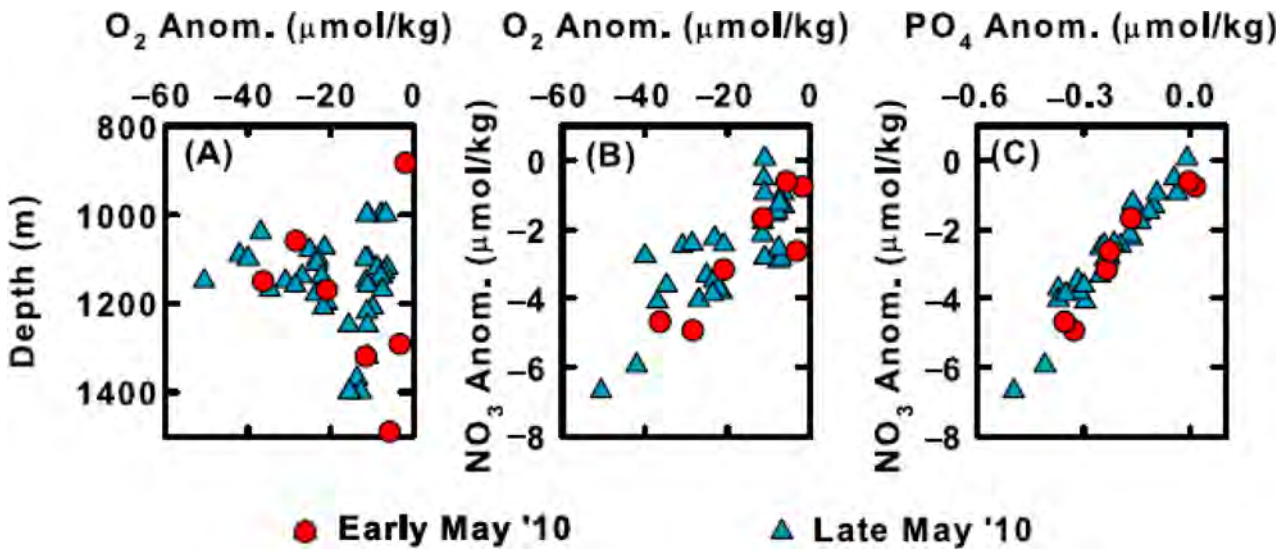

FIGURE 28.11 Dissolved nutrient and oxygen anomalies in the subsurface near the Deepwater Horizon blowout site during two cruises in May 2010. (A) Oxygen anomaly versus depth. (B) Oxygen anomaly versus nitrate anomaly. (C) Phosphate anomaly versus nitrate anomaly. *Adapted from Shiller, A.M. and D. Joung. Nutrient depletion as a proxy for microbial growth in Deepwater Horizon subsurface oil/gas plumes.* Environ. Res. Lett.*; 2012; 7, 4.*

no correlation was found between PAHs concentrations and nutrient depletions, suggesting that these heavier compounds might not have been readily biodegraded by the bacterial community, which has preference for short chain alkanes and BTEX compounds.

Comparing surface water samples from stations within 1.7−6.6 km of the Macondo well that were occupied with oil surface slick (I-1 through I-5) and more distal sites with no visible oil on surface (O-1 through O-7) (outside of slick), Edwards et al. (2011) found that the dynamic microbial community of the Gulf of Mexico supported remarkable rates of oil respiration despite a dearth of dissolve nutrients particularly phosphate. Laboratory incubations showed that the respiration rates of within the slick samples were approximately five times greater than those from outside of slick, suggesting that the microbes in these oligotrophic waters rapidly acclimated to breaking down hydrocarbon substrates (Fig. 28.12). As expected, amendments of inorganic nutrients increased the respiration and bacterial biomass in these samples. In extrapolating their observations to the entire area of the slick, Edwards et al. (2011) concluded that a large fraction of the oil had been degraded by the microbes as it arrived at the surface from the well.

Nutrients may also select for oil-degrading bacteria that develop in oil-polluted waters (Hazen et al., 2016). Our recent work demonstrated that the difference in water chemistry, which includes inorganic nutrients and trace elements, explained 10% of the variation in bacterial community structure (Liu et al., 2017). Different bacteria developed between the nutrient rich bottom water ($NO_3^- + NO_2^-$, 10.5 μM;PO_4^{3-}, 1.4 μM) and nutrient poor surface water ($NO_3^- + NO_2^-$, 0.03 μM; PO_4^{3-}, 0.29 μM). Particularly, *Alteromonas, Pseudoalteromonas, Oleibacter*, and *Winowgradskyella* developed better in the incubations using bottom water, while *Reinekea* and *Thalassobius* were favored in surface water, which suggests that high levels of nutrients may play a key role in the development of these bacteria. Moreover, using bottom water also resulted to relatively higher alkane degradation rates ($k = 0.07$ to 0.22/d) than using surface water ($k = 0.06$ to 0.09/d) (t-test, $P > 0.05$).

28.7 SHORELINE ENERGY

Evaluation of petroleum hydrocarbon weathering is mediated not only by the bacterial communities and type of perturbation, but also by the hydrography of the spill site. In particular, for spills reaching the coastal zone, researchers must factor shoreline energy (i.e., wave activity/intensity) into their evaluations. Historically, this has been studied in response to major oil spills. Following the *Exxon Valdez* spill in Alaska and *Gulf War* spill along the Saudi Arabian Coast, many researchers documented entrainment of oil in protected shorelines (Irvine et al., 1999; Michel and Hayes, 1999; Sauer et al., 1998; Peterson et al., 2003). Researchers have also summarized how

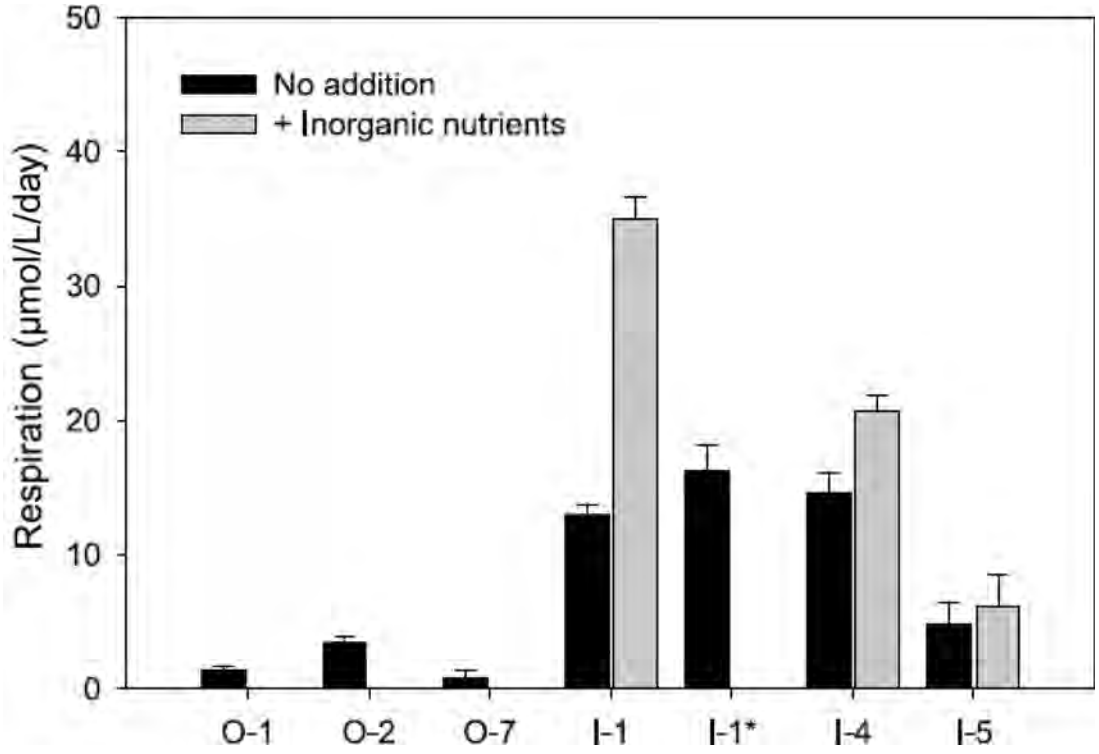

FIGURE 28.12 Community respiration rates at sampling stations within the slick and outside of the slick after incubations of approximately 36 h; except for "I-1*," which was incubated for 6 days in parallel with the hydrocarbon degradation experiment. Parallel sets of incubations at stations within the slick were amended with inorganic nutrients. Error bars indicate the magnitude of the range of respiration rates for triplicate incubations. Data from inside the slick and outside the slick are statistically distinct (Mann–Whitney, $P < 0.05$). *Adapted from Edwards, B.R., Reddy, C.M., Camilli, R., Carmichael, C.A., Longnecker, K., and Van Mooy, B.A.S. Rapid microbial respiration of oil from the Deepwater Horizon spill in offshore surface waters of the Gulf of Mexico.* Environ. Res. Lett.*; 2011; 6: 035301.*

variable combinations of low shoreline energy and protected coastal geography have led to multi-decadal persistence of petroleum following various oil spills (Owens et al., 2008), such as the *Amoco Cadiz* spill (Hayes et al., 1979), the *Gulf War* spill (Sauer et al., 1998), the *Exxon Valdez* spill (Michel and Hayes, 1999). In addition, an exposure index for predicting oil spill damage on shorelines as a function of shoreline geography and wave energy has been pioneered (Hayes, 1996).

In contrast, response to the DWH oil spill has minimally focused on shoreline energy in favor of research using advanced chemical and biological techniques. Notably, Pendergraft and Rosenheim (2014) utilized an advanced analytical technique to interpret the effects of coastal shoreline energy on hydrocarbon weathering. Pendergraft and Rosenheim (2014) sampled the Mississippi deltaic plain, barrier islands, and interlobe basins to survey a small but representative portion of coastal areas for nearly two and one-half years following the event. Using ramped pyrolysis ^{14}C analysis, they proved persistence of petrocarbon in these environments throughout the time period of their study, which in combination with specific monitoring and sampling approaches, and confirmed that subject areas had been contaminated by the *Deepwater Horizon* oil spill. Using this analysis, they also demonstrated that the thermochemical stability of hydrocarbons changed. In highly oiled samples collected soon after the spill, including surface oil sheens and surface sediment, the hydrocarbon signature consisted of relatively thermochemically reactive organic material. As weathering processes (i.e., evaporation, dissolution, biodegradation, etc.) target more volatile, low MW compounds, this suggests minimal weathering had occurred in these initial samples. In older samples (i.e., deep sediment entrainments, tars) results shifted to a more recalcitrant hydrocarbon signature, indicating volatile hydrocarbons had been weathered away. Most importantly, these patterns were found across locations, not just over time, whereby weathering was most advanced on a high energy beach, followed by a protected beach and least advanced in a sheltered bay. This was the first study of the *Deepwater Horizon* oil spill to confirm that weathering was affected by the hydrography of the coastal spill site.

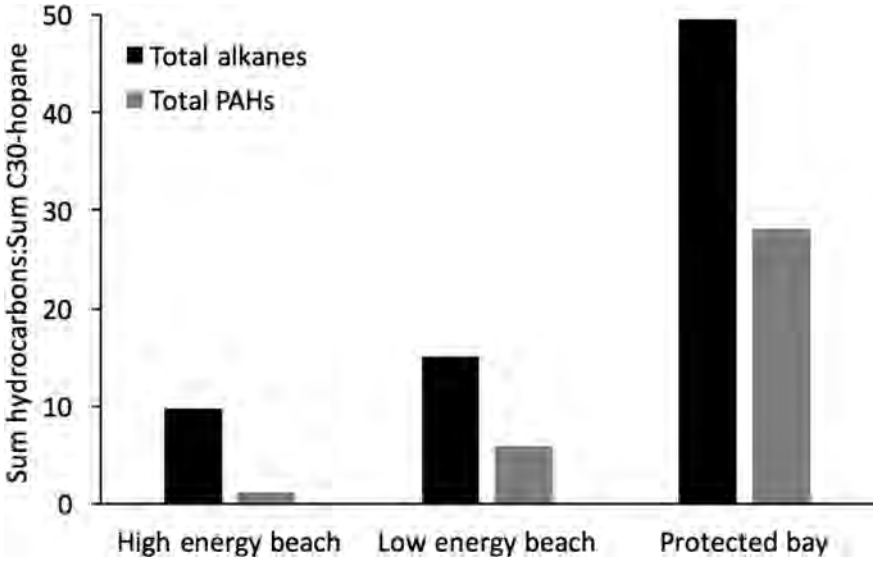

FIGURE 28.13 The sum of *n*-alkanes $C_{10\text{-}37}$ and the 16 priority EPA PAHs, normalized to internal recalcitrant biomarker C30-hopane, are presented for three samples collected between 678 and 694 days following the *Deepwater Horizon* oil spill. For both hydrocarbon categories, content is highest in a protected bay sediment sample and lowest in a high energy beach sediment sample, illustrating the effect of shoreline energy on hydrocarbon weathering.

We expanded this research by analyzing the compound-specific weathering patterns of the samples collected by Pendergraft and Rosenheim (2014) (Evans et al., 2017). After source confirmation using biomarker ratios, we quantified the *n*-alkane, PAH and alkylated PAH contents of these samples. This is an important expansion from the work of Pendergraft and Rosenheim (2014) as toxicity and bioavailability is determined on a compound-specific basis, whereas Pendergraft and Rosenheim's technique is useful to confirm the presence of labile versus recalcitrant hydrocarbons in general. The results of compound-specific analysis agree with the findings of Pendergraft and Rosenheim (2014). Across the three locations analyzed, samples collected at the same time showed the highest specific hydrocarbon content in an enclosed marsh, followed by a protected beach and finally, a high energy, oceanfront beach. Fig. 28.13 provides an example of this pattern observed between samples collected at different locations between 678 and 694 days following the spill for sum of *n*-alkanes C_{10-37} and the 16 priority pollutant EPA PAHs. Weathering patterns across time also confirmed that early samples were least weathered and older samples were most weathered, as evidenced by highest hydrocarbon concentrations in oil sheens and early oiled sediment. Importantly, however, at any one time, the most weathering took place in high energy environments. These two independent studies reach the same conclusion: following the *Deepwater Horizon* oil spill, weathering of petroleum in the coastal environments was highly dependent upon shoreline energy.

Shoreline energy is key in coastal zone weathering for two main reasons: (1) physical advection of oiled water/sediments advances weathering processes and (2) low energy sediment composition affects the sorption, biodegradation and retention of hydrocarbons. The most obvious driver behind this pattern is that physical advection breaks apart oil droplets, which creates greater surface area for dissolution of hydrocarbons into the surrounding water, evaporation of volatile hydrocarbons into the air and increases surface area and dissolved oxygen content for bacteria to break down petroleum hydrocarbons (Owens et al., 2008; Rashid, 1974). Less obviously, there are secondary effects of shoreline energy on the sediment characteristics and oxygenation profiles that may play a role in hydrocarbon degradation. For example, in the studies by Evans et al. (2017) and Pendergraft and Rosenheim (2014), high energy locations had medium grain size, characteristic of a high to mid energy beach, whereas the marsh sediment had very fine, clay/silt particles with lower dissolved oxygen content, characteristic of a low energy environment. Persistence of petroleum hydrocarbons in marsh sediments is partially a function of this low energy sediment type, which has higher sportive capacity and lower dissolved oxygen for biodegradation (Turner et al., 2014). In addition, organic pollutants are all relatively non-polar in nature; thus, presence of non-polar pollutants is likely to attract more non-polar pollutants, leading to aggregations of compounds such as PAHs in low energy sediments. This aggregation would be uncommon in high energy sediments as the grains are larger, thus decreasing surface area for sorption and increasing space for the penetration of oxygen that can be utilized by hydrocarbon-degrading bacteria. The weathering trends we observe, therefore, are not just a direct result of wave energy, but the combined effect wave energy has on the sediment composition, chemistry and thus, compound retention.

28.8 PRESSURE

Unlike many oil spills, the *Deepwater Horizon* oil spill intensely polluted deep sea waters and the sea floor. This is because not only the spill originated from a deep sea wellhead (16 MPa), but also the application of dispersants at depth prevented oil from rising. Seafloor pollution was magnified by the formation of marine snow formation at the surface, trapping petroleum hydrocarbons as it sunk, i.e., marine oil snow sedimentation and flocculent accumulation (MOSSFA). In total, up to 14% of petroleum oil from the *Deepwater Horizon* spill polluted the sea floor (Chanton et al., 2015; Scoma et al., 2016a). In addition, the majority of hydrocarbons spilled were concentrated in plume intrusions between 800 and 1200 m (Camilli et al., 2010; Valentine et al., 2014). Therefore, an integral challenge for scientists following the *Deepwater Horizon* oil spill was to investigate the effects of high pressure on petroleum weathering.

Petroleum weathering in the deep sea, however, does not have as many potential pathways as surface oil weathering, and primarily depends on biodegradation. Thus, a majority of research assessing high pressure weathering addresses hydrocarbon-degrading bacterial communities. Direct measurements of microbial activity in the *Deepwater Horizon* plume and contaminated sediments surrounding the wellhead indicate upregulation of genes related to hydrocarbon degradation in general (Lu et al., 2012; Scoma et al., 2016a). This suggests that bioremediation may be a viable option in the case of future deep sea spills. In the interest of developing such technology, laboratory studies have investigated the effects of hydrostatic pressure on hydrocarbon-degrading bacterium. In general, results indicate that growth of known hydrocarbon degraders, including *Alcanivorax dieselolei* KS_293, *Alcanivorax jadensis* KS_339, *Rhodococcus qingshengii* TUHH-12 and *Sphingobium yanoikuyae* B1, is negatively affected by increased hydrostatic pressure (Schedler et al., 2014; Scoma et al., 2016b). This indicates that although biodegradation may occur at depth, it is not optimal due to the gene function limitations created by high hydrostatic pressure. However, the bacteria used for these incubation experiments naturally inhabit the surface environment and atmospheric pressure.

Outside of these limited bacterial degradation studies, there has been minimal research investigating the direct relationship between pressure and hydrocarbon weathering. Future research is needed to elaborate on the mechanisms limiting bacterial degradation, such as specific pressures on protein polymerization. In addition, there is little research addressing the effects of pressure on the characteristics of oil droplet formation or dissolution. Thus, although high pressure was an integral factor in oil degradation following the *Deepwater Horizon* oil spill, more research is needed to characterize the direct effects.

28.9 CONCLUSIONS

The ultimate goal of oil spill science is to understand and mediate the organismal and ecosystem threats caused by petroleum pollution. Following the *Deepwater Horizon* oil spill, an unprecedented amount of research was funded in an effort to accomplish this goal. Here, we have focused on research that evaluated the weathering of petroleum hydrocarbons, particularly the biodegradation by bacterial communities. Weathering is the ultimate driver of petroleum hydrocarbon composition and as such, drives environmental toxicity threats. Weathering, however, is subject to combinations of environmental conditions including, but not limited to, bacterial community, temperature, solar radiation, nutrient content, pressure, oxygen, and shoreline energy. Some of the most notable recent advances in this field include characterizing bacterial community responses to petroleum hydrocarbons, describing photooxidation of surface oils and advancing chemical analysis techniques. The *Deepwater Horizon* oil spill was the ideal spill to advance this field as its pollution spread across many ecosystems including the deep sea, open ocean, coastal waters and surface ocean. As this field continues to expand, research should seek to characterize the synergistic effects of these many weathering drivers in order to predict and ultimately ameliorate the negative effects of future oceanic petroleum pollution.

References

Adhikari, P.L., Maiti, K., Overton, E.B., Rosenheim, B.E., Marx, B.D., 2016. Distributions and accumulation rates of polycyclic aromatic hydrocarbons in the northern Gulf of Mexico sediments. Environ. Pollut. 212, 413–423.

Aeppli, C., Carmichael, C.A., Nelson, R.K., Lemkau, K.L., Graham, W.M., Redmond, M.C., et al., 2012. Oil weathering after the Deepwater Horizon disaster led to the formation of oxygenated residues. Environ. Sci. Technol. 46, 8799–8807.

Bacosa, H.P., Erdner, D.L., Liu, Z., 2015a. Differentiating the roles of photooxidation and biodegradation in the weathering of Light Louisiana Sweet crude oil in surface water from the Deepwater Horizon site. Mar. Pollut. Bull. 95, 265–272.
Bacosa, H.P., Liu, Z., Erdner, D.L., 2015b. Natural sunlight shapes crude oil-degrading bacterial communities in northern Gulf of Mexico surface waters. Front. Microbiol. 6, 1325.
Bacosa, H., Suto, K., Inoue, C., 2010. Preferential degradation of aromatic hydrocarbons in kerosene by a microbial consortium. Int. Biodeter. Biodegr. 64 (8), 702–710.
Bacosa, H.P., Suto, K., Inoue, C., 2013. Degradation potential and microbial community structure of heavy oil-enriched microbial consortia from mangrove sediments in Okinawa, Japan. J. Environ. Sci. Health A 48, 1–12.
Bacosa, H.P., Thyng, K.M., Plunkett, S., Erdner, D.L., Liu, Z., 2016. The tarballs on Texas beaches following the 2014 Texas City "Y" Spill: modeling, chemical, and microbiological studies. Mar. Pollut. Bull. 109, 236–244.
Bælum, J., Borglin, S., Chakraborty, R., Fortney, J.L., Lamendella, R., Mason, O.U., et al., 2012. Deep-sea bacteria enriched by oil and dispersant from the Deepwater Horizon spill. Environ. Microbiol. 14, 2405–2416.
Beyer, J., Trannum, H.C., Bakke, T., Hodson, P.V., Collier, T.K., 2016. Environmental effects of the Deepwater Horizon oil spill: a review. Mar. Pollut. Bull. 110, 28–51.
Camilli, R., Reddy, C.M., Yoerger, D.R., Van Mooy, B.A.S., Jakuba, M.V., Kinsey, J.C., et al., 2010. Tracking hydrocarbon plume transport and biodegradation at Deepwater Horizon. Science 330, 201–204.
Campo, P., Venosa, A.D., Suidan, M.T., 2013. Biodegradability of Corexit 9500 and Dispersed South Louisiana Crude Oil at 5 and 25°C. Environ. Sci. Technol. 47, 1960–1967.
Chanton, J., Zhao, T., Rosenheim, B.E., Joye, S., Bosman, S., Brunner, C, Yeager, K.M., Diercks, A.R., Hollander, D., 2015. Using natural abundance radiocarbon to trace the flux of petrocarbon to the seafloor following the Deepwater Horizon oil spill. Environ. Sci. Technol. 49, 847–854.
Crone, T.J., Tolstoy, M., 2010. Magnitude of the 2010 Gulf of Mexico oil leak. Science 330, 634.
D'Auria, M., Emanuele, L., Racioppi, R., Velluzzi, V., 2009. Photochemical degradation of crude oil: comparison between direct irradiation, photocatalysis, and photocatalysis on zeolite. J. Hazard. Mater. 164, 32–38.
Dietrich, J., Trahan, C., Howard, M., Fleming, J., Weaver, R., Tanaka, S., et al., 2012. Surface trajectories of oil transport along the northern coastline of the Gulf of Mexico. Cont. Shelf Res. 41, 17–47.
Dutta, T.K., Harayama, S., 2000. Fate of crude oil by the combination of photooxidation and biodegradation. Environ. Sci. Technol. 34, 1500–1505.
DWH-NRDA. Deepwater Horizon Natural Resource Damage Assessment (NRDA)—DRAFT 2015—section 4. Injury to Natural Resources, 2015, p. 685.
Edwards, B.R., Reddy, C.M., Camilli, R., Carmichael, C.A., Longnecker, K., Van Mooy, B.A.S., 2011. Rapid microbial respiration of oil from the Deepwater Horizon spill in offshore surface waters of the Gulf of Mexico. Environ. Res. Lett. 6, 035301.
Evans, M., Liu, J., Bacosa, H., Rosenheim, B.E., Liu, Z., 2017. Petroleum hydrocarbon persistence following the Deepwater Horizon oil spill as a function of shoreline energy. Mar. Pollut. Bull. 115, 47–56.
Garrett, R.M., Pickering, I.J., Haith, C.E., Prince, R.C., 1998. Photooxidation of crude oils. Environ Sci. Technol. 32, 3719–3723.
Griffiths, M.T., Da Campo, R., O'Connor, P.B., Barrow, M.P., 2014. Throwing Light on petroleum: simulated exposure of crude oil to sunlight and characterization using atmospheric pressure photoionization Fourier transform ion cyclotron resonance mass spectrometry. Anal. Chem. 86, 527–534.
Hayes, M.O., 1996. An exposure index for oiled shorelines. Spill Sci. Technol. Bull. 3, 139–147.
Hayes, M.O., Gundlach, E.R., D'Ozouville, L., 1979. Role of dynamic coastal processes in the impact and dispersal of the Amoco Cadiz oil spill (March 1978) Brittany, France. In: International Oil Spill Conference Proceedings: March 1979, vol. 1, pp. 193–198.
Hazen, T.C., Dubinsky, E.A., DeSantis, T.Z., Andersen, G.L., Piceno, Y.M., Singh, N., et al., 2010. Deep-sea oil plume enriches indigenous oil degrading bacteria. Science 330, 204–208.
Hazen, T.C., Prince, R.C., Mahmoudi, N., 2016. Marine oil biodegradation. Environ. Sci. Technol. 50, 2121–2129.
Irvine, G.V., Mann, D.H., Short, J.W., 1999. Multi-year persistence of oil mousse on high energy beaches distant from the Exxon Valdez spill origin. Mar. Pollut. Bull. 38, 572–584.
John, G.F., Han, Y., Clement, T.P., 2016. Weathering patterns of polycyclic aromatic hydrocarbons contained in submerged Deepwater Horizon oil spill residues when re-exposed to sunlight. Sci. Total Environ. 573, 189–202.
Kallmeyer, J., Pockalny, R., Adhikaria, A.A., Smith, D.C., D'Hondt, S., 2012. Global distribution of microbial abundance and biomass in subseafloor sediment. Proc. Natl. Acad. Sci. U.S.A. 109, 16213–16216.
Kimes, N.E., Callaghan, A.V., Aktas, D.F., Smith, W.L., Sunner, J., et al., 2013. Metagenomic analysis and metabolite profiling of deep-sea sediments from the Gulf of Mexico following the Deepwater Horizon oil spill. Front. Microbiol. 4, 50.
King, S.M., Leaf, P.A., Tarr, M.A., 2011. Photochemistry of Deepwater Horizon oil. ACS Symp. Ser. 1086, 81–95.
King, S.M., Leaf, P.A., Olson, A.C., Ray, P.Z., Tarr, M.A., 2014. Photolytic and photocatalytic degradation of surface oil from the Deepwater Horizon spill. Chemosphere 95, 415–422.
Lewan, M.D., Warden, A., Dias, R.F., Lowry, Z.K., Hannah, T.L., Lillis, P.G., et al., 2014. Asphaltene content and composition as a measure of Deepwater Horizon oil spill losses within the first 80 days. Org. Geochem. 75, 54–60.
Liu, J., Bacosa, H.P., Liu, Z., 2017. Potential environmental factors affecting oil-degrading bacterial populations in deep and surface waters of the northern Gulf of Mexico. Front. Microbiol. 7, 2131.
Liu, Z., Liu, J., 2013. Evaluating bacterial community structures in oil collected from the sea surface and sediment in the northern Gulf of Mexico after the Deepwater Horizon oil spill. Microbiol. Open 2, 492–504.
Liu, Z., Liu, J., Zhu, Q., Wu, W., 2012. The weathering of oil after the Deepwater Horizon oil spill: insights from the chemical composition of the oil from the sea surface, salt marshes and sediments. Environ. Res. Lett. 7, 035302.
Liu, Z., Liu, J., Gradner, W.S., Shank, C., Ostrom, N.E., 2016. The impact of Deepwater Horizon oil spill on petroleum hydrocarbons in surface waters of the northern Gulf of Mexico. Deep-Sea Res. Part II 129, 292–300.

Lu, Z., Deng, Y., Van Nostrand, J.D., He, Z., Voordeckers, J., Zhou, A., et al., 2012. Microbial gene functions enriched in the Deepwater Horizon deep-sea oil plume. ISME J. 6, 451–460.
Mason, O.U., Hazen, T.C., Borglin, S., Chain, P.S.G., Dubinsky, E.A., Fortney, J.L., et al., 2012. Metagenome, metatran-scriptome and single-cell sequencing reveal microbial response to Deepwater Horizon oil spill. ISME J. 6, 1715–1727.
Mason, O., Han, J., Woyke, T., Jansson, J., 2014a. Single-cell genomics reveals features of a *Colwellia* species that was dominant during the Deepwater Horizon oil spill. Front. Microbiol. 5, 332.
Mason, O.U., Scott, N.M., Gonzalez, A., Robbins-Pianka, A., Bælum, J., Kimbrel, J., et al., 2014b. Metagenomics reveals sediment microbial community response to Deepwater Horizon oil spill. ISME J. 8, 1464–1475.
McGenity, T.J., Folwell, B.D., McKew, B.A., Sanni, G.O., 2012. Marine crude-oil biodegradation: a central role for interspecies interactions. Aquat. Biosyst. 8, 1–19.
McKenna, A.M., Nelson, R.K., Reddy, C.M., Savory, J.J., Kaiser, N.K., Fitzsimmons, J.E., et al., 2013. Expansion of the analytical window for oil spill characterization by ultrahigh resolution mass spectrometry: beyond gas chromatography. Environ. Sci. Technol. 47, 7530–7539.
McNutt, M.K., Camilli, R., Crone, T.J., Guthrie, G.D., Hsieh, P.A., Ryerson, T.,B., et al., 2012. Review of flow rate estimates of the Deepwater Horizon oil spill. Proc. Natl. Acad. Sci. U.S.A. 109 (50), 20260–20267.
Meng, L., Liu, H., Bao, M., Sun, P., 2016. Microbial community structure shifts are associated with temperature, dispersants and nutrients in crude oil-contaminated seawaters. Mar. Pollut. Bull. 111, 203–212.
Methé, B.A., Nelson, K.E., Deming, J.W., Momen, B., Melamud, E., Zhang, X., et al., 2005. The psychrophilic lifestyle as revealed by the genome sequence of *Colwellia psychtreryhraea* 34H through genomic and proteomic analysis. Proc. Natl. Acad. Sci. U.S.A. 102, 10913–10918.
Michel, J., Hayes, M.O., 1999. Weathering patterns of oil residues eight years after the Exxon Valdez oil spill. Mar. Pollut. Bull. 38, 855–863.
Michel, J., Owens, E.H., Zengel, S., Graham, A., Nixon, Z., Allard, T., et al., 2013. Extent and degree of shoreline oiling: Deepwater Horizon Oil Spill, Gulf of Mexico, USA. PLoS One 8, 65087.
Mills, H.J., Martinez, R.J., Story, S., Sobecky, P.A., 2004. Identification of members of the metabolically active microbial populations associated with *Beggiatoa* species mat communities from Gulf of Mexico cold-seep sediments. Appl. Environ. Microbial. 70, 5447–5458.
National Research Council Committee, 2003. Oil in the Sea III: Inputs, Fates, and Effects. The National Academies Press.
NOAA's Office of Response and Restoration- Environmental Response Management Application (ERMA). 2010. http://response.restoration.noaa.gov/about/media/mapping-fallout-deepwater-horizon-oil-spill-developing-one-tool-bring-unity-response.htm.
Orcutt, B.N., Joye, S.B., Kleindienst, S., Knittel, K., et al., 2010. Impact of natural oil and higher hydrocarbons on microbial diversity, distribution, and activity in Gulf of Mexico cold-seep sediments. Deep-Sea Res. II 57, 2008–2021.
OSAT-I, 2010. Summary Report for Sub-sea and Sub-surface Oil and Dispersant Detection: Sampling and Monitoring, Paul F. Zukunft, RADM, US Coast Guard Federal On-Scene Coordinator, DeepwaterHorizon MC252. Available online at: <http://www.restorethegulf.gov/release/2011/07/29/osat-summary-report-sub-sea-and-sub-surface-oil-and-dispersant-detection-ecotoxic>.
Owens, E.H., Taylor, E., Humphrey, B., 2008. The persistence and character of stranded oil on coarse-sediment beaches. Mar. Pollut. Bull. 56, 14–26.
Pendergraft, M.A., Rosenheim, B.E., 2014. Varying relative degradation rates of oil in different forms and environments revealed by ramped pyrolysis. Environ. Sci. Technol. 48, 10966–10974.
Peterson, C.H., Rice, S.D., Short, J.W., Esler, D., James, L., et al., 2003. Long-term ecosystem response to the Exxon Valdez oil spill. Science 302, 2082–2086.
Plata, D.L., Sharpless, C.M., Reddy, C., 2008. Photochemical degradation of polyaromatic hydrocarbons in oil films. Environ. Sci. Technol. 42, 2432–2438.
Radović, J.R., Aeppli, C., Nelson, R.K., Jimenez, N., Reddy, C.M., Bayona, J.M., et al., 2014. Assessment of photochemical processes in marine oil spill fingerprinting. Mar. Pollut. Bull. 79, 268–277.
Rashid, M.A., 1974. Degradation of Bunker C oil under different coastal environments of Chedabucto Bay, Nova Scotia. Estuar. Coast. Mar. Sci. 2, 137–144.
Ray, P.Z., Tarr, M.A., 2014a. Solar production of singlet oxygen from crude oil films on water. J. Photochem. Photobiol. 286, 22–28.
Ray, P.Z., Tarr, M.A., 2014b. Petroleum films exposed to sunlight produce hydroxyl radical. Chemosphere 103, 220–227.
Ray, P.Z., Tarr, M.A., 2015. Formation of organic triplets from solar irradiation of petroleum. Mar. Chem. 168, 135–139.
Ray, P.Z., Chen, H., Podgorski, D.C., McKenna, A.M., Tarr, M.A., 2014. Sunlight creates oxygenated species in water-soluble fractions of Deepwater horizon oil. J. Hazard. Mater. 280, 636–643.
Reddy, C.M., Arey, J.S., Seewald, J.S., Sylva, S.P., Lemkau, K.L., et al., 2012. Composition and fate of gas and oil released to the water column during the Deepwater Horizon oil spill. Proc. Natl. Acad. Sci. U.S.A. 109 (50), 20229–20234.
Redmond, M.C., Valentine, D.L., 2012. Natural gas and temperature structured a microbial community response to the Deepwater Horizon oil spill. Proc. Natl. Acad. Sci. U.S.A. 109, 20292–20297.
Romero, I.C., Schwing, P.T., Brooks, G.R., Larson, R.A., Hastings, D.W., Ellis, G., et al., 2015. Hydrocarbons in deep-sea sediments following the 2010 Deepwater Horizon blowout in the northeast Gulf of Mexico. PLoS One 10 (5), 1–23.
Ron, E.Z., Rosenberg, E., 2014. Enhanced bioremediation of oil spills in the sea. Curr. Opin. Biotechnol. 27, 191–194.
Ryerson, T.B., Aikin, K.C., Angevine, W.M., Atlas, E.L., et al., 2011. Atmospheric emissions from the Deepwater Horizon spill constrain air-water partitioning, hydrocarbon fate, and leak rate. Geophys. Res. Lett. 38, L07803.
Ryerson, T.B., Camilli, R., Kessler, J.D., Kujawinski, E.B., Reddy, C.M., et al., 2012. Chemical data quantify Deepwater Horizon hydrocarbon flow rate and environmental distribution. Proc. Natl. Acad. Sci. U.S.A. 109, 20246–20253.
Sammarco, P.W., Kolian, S.R., Warby, R.A.F., Bouldin, J.L., Subra, W.A., Porter, S.A., 2013. Distribution and concentrations of petroleum hydrocarbons associated with the BP/Deepwater Horizon oil spill, Gulf of Mexico. Mar. Pollut. Bull. 73, 129–143.
Sauer, T.C., Michel, J., Hayes, M.O., Aurand, D.V., 1998. Hydrocarbon characterization and weathering of oiled intertidal sediments along the Saudi Arabian coast two years after the Gulf War oil spill. Environ. Int. 24, 43–60.
Schedler, M., Hiessl, R., Valladares Juárez, A.G., Gust, G., Müller, R., 2014. Effect of high pressure on hydrocarbon-degrading bacteria. AMB Express 4, 77.

Schwarzenbach, R.P., Gschwend, P.M., Imboden, D.M., 2003. Environmental Organic Chemistry, second ed. John Wiley & Sons, Inc, Hoboken, NJ.
Scoma, A., Yakimov, M.M., Boon, N., 2016a. Challenging oil bioremediation at deep-sea hydrostatic pressure. Front. Microbiol. 7, 1203.
Scoma, A., Barbato, M., Hernandez-Sanabria, E., Mapelli, F., Daffonchio, D., Borin, S., et al., 2016b. Microbial oil-degradation under mild hydrostatic pressure (10 MPa): which pathways are impacted in piezosensitive hydrocarbonoclastic bacteria?. Sci. Rep. 6, 23526.
Shankar, R., Shim, W.J., An, J.G., Yim, U.H., 2015. A practical review on photooxidation of crude oil: Laboratory lamp setup and factors affecting it. Water Res. 68, 304–315.
Shiller, A.M., Joung, D., 2012. Nutrient depletion as a proxy for microbial growth in Deepwater Horizon subsurface oil/gas plumes. Environ. Res. Lett. 7, 4.
The Federal Interagency Solutions Group, 2010. Oil Budget Calculator Science and Engineering Team. Oil Budget Calculator Deepwater Horizon Technical Documentation. November 2010. <http://www.restorethegulf.gov/sites/default/files/documents/pdf/OilBudgetCalc_Full_HQ-Print_111110.pdf>.
Thibodeaux, L.J., Valsaraj, K.T., John, V.T., Papadopoulos, K.D., Pratt, L.R., Pesika, N.S., 2011. Marine oil fate: knowledge gaps, basic research, and development needs; a perspective based on the Deepwater Horizon spill. Environ. Eng. Sci. 28, 87–93.
Turner, R.E., Overton, E.B., Meyer, B.M., Miles, M.S., Hooper-Bui, L., 2014. Changes in the concentration and relative abundance of alkanes and PAHs from the Deepwater Horizon oiling of coastal marshes. Mar. Pollut. Bull. 86, 291–297.
Valentine, D.L., Fisher, G.B., Bagby, S.C., Nelson, R.K., Reddy, C.M., Sylva, S.P., et al., 2014. Fallout plume of submerged oil from Deepwater Horizon. Proc. Natl. Acad. Sci. U.S.A. 111, 15906–15911.
Wade, T.L., Sericano, J.L., Sweet, S.T., Knap, A.H., Guinasso, N.L., 2016. Spatial and temporal distribution of water column total polycyclic aromatic hydrocarbons (PAH) and total petroleum hydrocarbons (TPH) from the Deepwater Horizon (Macondo) incident. Mar. Pollut. Bull. 103, 286–293.
Yang, Z., Hollebone, B.P., Wang, Z., Yang, C., Brown, C., Zhang, G., et al., 2015. A preliminary study for the photolysis behavior of biodiesel and its blends with petroleum oil in simulated freshwater. Fuel 139, 248–256.
Zhuang, M., Abulikemu, G., Campo, P., Platten, W.E.I., Suidan, M.T., Venosa, A.D., et al., 2016. Effect of dispersants on the biodegradation of South Louisiana crude oil at 5 and 25°C. Chemosphere 144, 767–774.
Ziolli, R.L., Jardim, W.F., 2003. Photochemical transformations of water-soluble fraction (WSF) of crude oil in marine waters—a comparison between photolysis and accelerated degradation with TiO_2 using GC–MS and UVF. J. Photochem. Photobiol. 155, 243–252.

Further Reading

Yang, Z., Hollebone, B.P., Brown, C.E., Yang, C., Wang, Z., Zhang, G., et al., 2016. The photolytic behavior of diluted bitumen in simulated seawater by exposed to the natural sunlight. Fuel 186, 128–139.

CHAPTER

29

Using Stable and Radiocarbon Analyses as a Forensic Tool to Find Evidence of Oil in the Particulates of the Water Column and on the Seafloor Following the 2010 Gulf of Mexico Oil Spill

Samantha H. Bosman, Jeffrey P. Chanton and Kelsey L. Rogers

Florida State University, Tallahassee, FL, United States

BIOGRAPHIES

Samantha Bosman is a Research Assistant in the Department of Earth, Ocean & Atmospheric Science at Florida State University investigating the effects of the 2010 Gulf of Mexico oil spill in food webs and the environment through the use of isotopes. She has a Master of Science degree in fish ecology and a Bachelor of Science degree in marine biology, both from the University of New Brunswick. She had worked in the field of fish ecology for 6 years before joining the oil spill project in 2010. She has participated on 8 research cruises to the Gulf of Mexico to collect samples, prepared over 1000 samples for stable and radiocarbon analyses, and is a coauthor of 8 scientific journal publications.

Jeff Chanton is a Gulf Coast Native. His Acadian ancestors were married in Mobile in the late 1700s after being ejected from Nova Scotia for failing to support the British throne. He received his PhD from the University of North Carolina at Chapel Hill in 1985 and joined the faculty at Florida State University in the Department of Oceanography in 1989. He is an AGU fellow, an Aldo Leopold Fellow and was named the Florida Wildlife Federation's Conservation Communicator of the year. He has authored or coauthored over 260 papers in the peer reviewed literature and received over 60 grants and contracts to support his research. He has supervised 18 PhD dissertations, 35 Master's theses and 5 undergraduate honors theses. He currently supervises 4 graduate students and 2 postdoctoral fellows. He teaches classes at the graduate and undergraduate level and is the director of the University's Aquatic Environmental Science Graduate Program.

Kelsey Rogers is a PhD Candidate working with Jeff Chanton at Florida State University. She completed her Masters in Oceanography in 2014 from Florida State University and her Bachelor of Science in Geological Sciences from the University of North Carolina at Chapel Hill in 2012. Her work uses carbon isotopes in suspended particulates and sediment to study the incorporation of hydrocarbon into those two carbon pools. She has spent 12 weeks at sea in the Gulf of Mexico collecting water and sediment samples.

Oil Spill Environmental Forensics Case Studies.
DOI: http://dx.doi.org/10.1016/B978-0-12-804434-6.00029-X

29.1 INTRODUCTION

On April 20, 2010 a blowout occurred on the *Deepwater Horizon* (DwH) well, releasing over 600 million liters of oil (Ziervogel et al., 2014; Brooks et al., 2015; Vonk et al., 2015) and copious quantities of natural gas, mostly as methane (Valentine et al., 2010; Joye et al., 2011; Kessler et al., 2011), into the Gulf of Mexico before the well was capped on July 15, 2010. Accounting for the fate of these hydrocarbons that entered the environment after the blowout has been the subject of numerous studies as summarized in Joye et al. (2016). Lehr et al. (2010) estimated that 16%–17% of the oil was recovered at the wellhead, 12%–13% was dispersed into the water column, 20%–25% was evaporated or dissolved, 10%–20% was chemically dispersed into the water column, 5%–6% was burned, 2%–4% was skimmed, and 11%–30% was unaccounted for or listed as "other" (Lehr et al., 2010). Methane released into the Gulf appears to have been oxidized by methanotrophic bacteria and converted to CO_2, energy, and biomass (Kessler et al., 2011; Crespo-Medina et al., 2014).

A large portion of the "unaccounted" oil may have been deposited to the seafloor (Valentine et al., 2014; Brooks et al., 2015; Chanton et al., 2015; Stout et al., 2016). One possible mechanism for the transport of oil to the seafloor is by its interaction with marine snow. Marine snow occurs everywhere in the ocean and consists of materials such as phytoplankton, bacteria, or detritus that have collided and fused together (Passow et al., 2012; Daly et al., 2016), making it less buoyant and capable of sinking to the seafloor. Shortly after the oil spill, a large, mucus-rich, marine snow event was observed near oil contaminated surface water (Passow et al., 2012; Daly et al., 2016). Approximately 1 month after the observation, the marine snow had all disappeared from the surface and was presumed to have sunk (Passow et al., 2012). Through a series of experiments, Passow (2014) concluded that the presence of oil at the surface or subsurface of the water contributed to the large amount of microbial marine snow that sank to the seafloor. This marine snow event that aided in the transport of oil to the seafloor was later termed MOSSFA, Marine Oil Snow Sedimentation and Flocculent Accumulation (Kinner et al., 2014; Daly et al., 2016), and provides a crucial link of oil observed at the sea surface and oil found on the seafloor.

When oil and methane enter the environment, they are often significantly altered. For example, burning oil will leave a significantly altered residue. If oil or methane is taken up by bacteria and processed, it will be unrecognizable by traditional approaches for measuring oil as it could be converted into microbial biomass. Photooxidation of oil will lead to increasing oxygen content and increasing polarity of the molecules, likely increasing water solubility and decreasing the volatility of the resulting compounds (Ruddy et al., 2014). However, when these compounds are altered, their isotopic composition follows them into the new compounds and thus this isotopic composition is a unique and powerful tracer for following the carbon during these transformations from oil or methane to biomass, ash, or chemically altered compounds. It goes without saying of course, that the unaltered oil or methane will retain its unique isotopic signature. The resulting suite of compounds and organic materials from the release of oil and gas and their transformations are termed "petrocarbon" (Chanton et al., 2015). This term is unique from the term petrogenic carbon, which also infers ancient origin, but may also describe organic materials disseminated in rocks.

For example, microbes are particularly effective at converting hydrocarbon into petrocarbon or altered hydrocarbon. A hydrocarbon plume that was southwest of the DwH well, at 1000–1300 m depth (Camilli et al., 2010; Ryerson et al., 2012; Spier et al., 2013), contained a significant assembly of microbes dominated by *Oceanospirillales* and *Colwellia* (Hazen et al., 2010; Redmond and Valentine, 2012; Mason et al., 2012; Dubinsky et al., 2013). When exposed to oil from the wellhead, *Colwellia* has been shown to produce a floc containing oil, carbohydrates and cell biomass (Bælum et al., 2012). Furthermore, *Colwellia* was highly abundant in the sediments that were below the plume (Mason et al., 2014). *Colwellia* consumed hydrocarbons from the plume and converted them into biomass (Valentine et al., 2010, 2014; Redmond and Valentine, 2012, 2014). By our definition this microbial carbon would be petrocarbon. In addition, the film created by these bacteria (petrocarbon) further collected particles rich in petroleum which led to their accumulation on the seafloor.

Previous studies have found evidence of penetration of petrocarbon in the planktonic and possibly higher food web (e.g., Graham et al., 2010; Chanton et al., 2012; Wilson et al., 2016) and it was suggested that methane released from the blowout may have contributed to this through small particles derived at least in part from the methanotrophs that eventually entered the food web (Cherrier et al., 2014). Using a mass balance equation to determine the contribution of fossil carbon to isotopes $\delta^{13}C$ and $\Delta^{14}C$, Chanton et al. (2012) reached a conclusion that methane likely was more effective at entering the food web than oil.

29.1.1 Isotope Tracing

Stable isotope results, $\delta^{13}C$, are reported relative to VPDB, an international standard carbonate reference material as:

$$\delta^{13}C = \left(\frac{R_{sam}}{R_{std}} - 1\right) \times 1000,$$

where $R = {}^{13}C/{}^{12}C$, R_{sam} refers to the ratio in a sample and R_{std} refers to the ratio in the international standard.

Radiocarbon values are reported according to the Δ notation as described by Stuiver and Polach (1977). The Δ notation normalizes the radiocarbon content of any sample to a common $\delta^{13}C$ value (−25‰) and time point. What is particularly useful about the notation is that it is a linear scale starting at −1000‰ when a sample has 0% modern carbon (McNichol and Aluwihare, 2007). Modern carbon prior to atmospheric weapons testing had a value of 0‰ on this scale, but in the 1960s, additional radiocarbon was produced in the atmosphere. This additional radiocarbon is slowly mixing into the earth's pool of surface carbon so that contemporary CO_2 is about +30‰ to 40‰ (Graven et al., 2012).

Oil and methane have a unique isotopic signature that can be traced into the environment and food web using both stable and radiocarbon analyses (Fig. 29.1; Chanton et al., 2012; Wilson et al., 2016). Oil and methane formed millions of years ago and have been sequestered for this time period. Therefore, they are free of radiocarbon ($\Delta^{14}C$) and have an isotopic signature of −1000‰ on the $\Delta^{14}C$ scale (Fig. 29.1). The modern carbon endmember in the Gulf is +40‰ (Fig. 29.1; Chanton et al., 2012). The relative amount of fossil carbon in a simple mixture can thus be determined using a two endmember mixing model (Fig. 29.2), provided both endmembers are known. Such mixing models can be complicated by $\Delta^{14}C$ enriched material which has resulted from nuclear weapons testing in the 1960s (McNichol and Aluwihare, 2007; Graven et al., 2012).

Both oil and methane (the main constituent of natural gas) are also depleted in $\delta^{13}C$ compared to surface production in the open ocean (Graham et al., 2010; Crespo-Medina et al., 2014). Surface production in the open ocean is approximately −20‰ for $\delta^{13}C$, while oil from the DwH spill was analyzed to be −27‰ (Fig. 29.1). Methane released from the spill was found to be about −60‰ (Fig. 29.1), considerably depleted in $\delta^{13}C$, as is typical for methane (Valentine et al., 2010; Crespo-Medina et al., 2014).

Together, the isotopes provide excellent forensic tools for deducing the relative importance of fossil carbon to mixtures with surface carbon. However, the larger range in isotopic endmembers for $\Delta^{14}C$ relative to the $\delta^{13}C$ variation make it somewhat more useful for finding evidence of petrocarbon in the sediment or particulates in the water column following an oil spill. Due to the presence of modern carbon in sediment derived from photosynthetic fixed material at the surface, along with a mix of radiocarbon supplied from the atmosphere and rivers in the form of particulate organic carbon, we expect to find more depleted $\Delta^{14}C$ values in the sediment relative to modern carbon values, however, we also assume prespill sediment will have $\Delta^{14}C$ values more modern

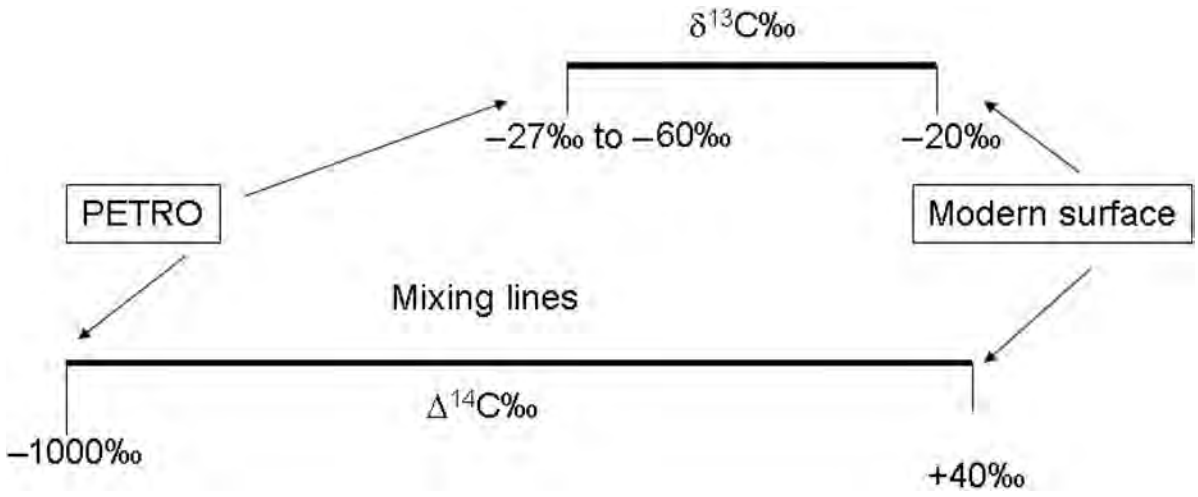

FIGURE 29.1 Schematic drawing of the stable and radiocarbon two endmember mixing lines. Positions located closer to the left indicate samples containing petrocarbon while positions located closer to the right indicate samples containing modern surface carbon in the northern Gulf of Mexico.

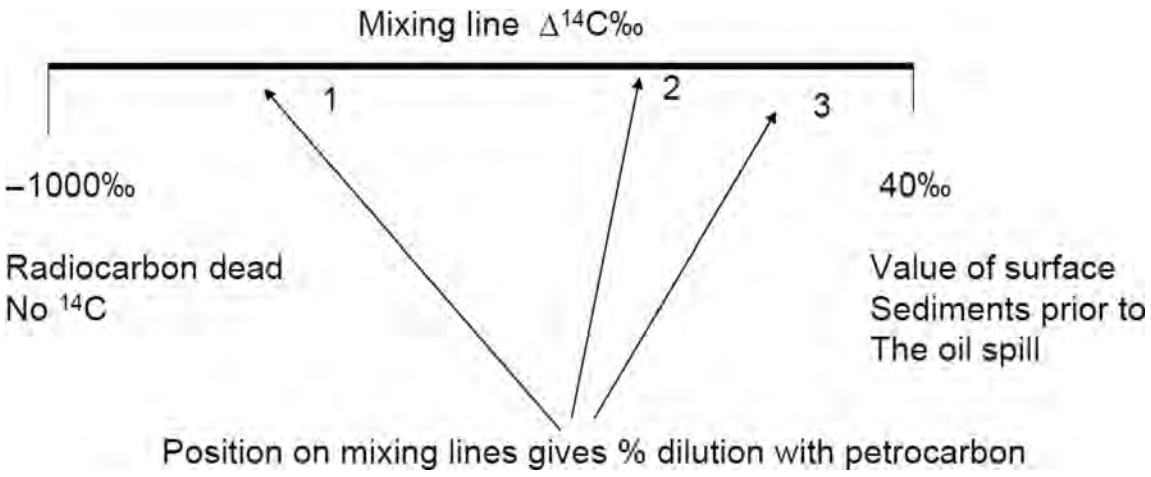

FIGURE 29.2 A schematic drawing of a two endmember mixing line for radiocarbon. Positions located closer to the left indicate samples containing petrocarbon while positions located closer to the right indicate samples containing modern surface carbon in the northern Gulf of Mexico. *Adapted with permission from Chanton, J., Zhao, T, Rosenheim, B., Joye, S., Bosman, S., Brunner, C., Yeager, K., Diercks, A., and Hollander. Using natural abundance radiocarbon to trace the flux of petrocarbon to the seafloor following the Deepwater Horizon oil spill.* Environ. Sci. Technol.*; 2015; 49(2), 847−854. Copyright 2015 American Chemical Society.*

(positive) than sediment deposited during the spill if oil is getting into the sedimentary carbon reservoir (Chanton et al., 2015). Based upon this assumption, the evidence for sedimentary oil contamination would consist of a $\Delta^{14}C$ depleted layer of sediment containing petrocarbon overlying a background (relatively $\Delta^{14}C$ enriched) sediment layer, consisting of a mixture of modern carbon and older carbon.

In this case study, we illustrate the use of stable and radiocarbon analyses as a forensic tool to find evidence of oil from the DwH well in the water column and accumulating on the seafloor. We provide a link between oil released into the environment and petrocarbon found in the water column and the seafloor.

29.2 METHODS

29.2.1 Suspended Particulate Organic Carbon (POC_{susp}) Samples

Water was collected at various depths throughout the water column using a niskin bottle rosette with CTD (Conductivity, Temperature, Depth) onboard the R.V. Weatherbird II in May of 2011 and 2012. The water column was sampled at four sites (DS1, 29.21 N, 87.06 W; DS2, 30.17 N, 86.66 W; DS3, 28.83 N, 88.27 W; DS4, 29.18 N, 87.75 W) in the DeSota Canyon (Fig. 29.3). At most sites, water was collected at the surface and near the seafloor, while some sites also included water collected in the middle of the water column. Water was drained from the niskin bottles into polycarbonate carboys and filtered through precombusted 0.7 μm, 47-mm glass fiber filters. Filters were stored in a freezer until ready for further preparation. Filters were thawed back at the lab and acid (HCl) fumed for 24 h. Once dried, one quarter of the filters were analyzed for $\delta^{13}C$ on a Carlo Erba elemental analyzer coupled to a Delta XP Thermo Finnigan isotope ratio mass spectrometer at the National High Magnetic Field laboratory. Filters analyzed for $\Delta^{14}C$ were combusted, converted to graphic targets, and analyzed by accelerator mass spectrometry at the Lawrence Livermore National Laboratory.

29.2.2 Sinking Particulate Organic Carbon (POC_{sink}) Samples From Sediment Traps

Sinking particulate organic carbon (POC_{sink}) samples were collected from a trap suspended 105 m above the seafloor and located approximately 7.4 km southwest of the DwH wellhead (28.71 N, 88.42 W) (Fig. 29.3). These samples are distinguished from suspended particulate organic carbon (POC_{susp}) samples collected on 0.7 μm glass filters by their larger size and by their mode of collection (Yan et al., 2016). POC_{sink} were collected in a series of cups between August 25, 2010 and October 19, 2011. A description and diagram of the funnel-shaped sediment trap setup is available in Yan et al. (2016). Samples collected in the cups were fixed in mercuric chloride at a salinity of 40 psu. Once samples were retrieved from the cups, they were stored in the dark at 4°C until ready for

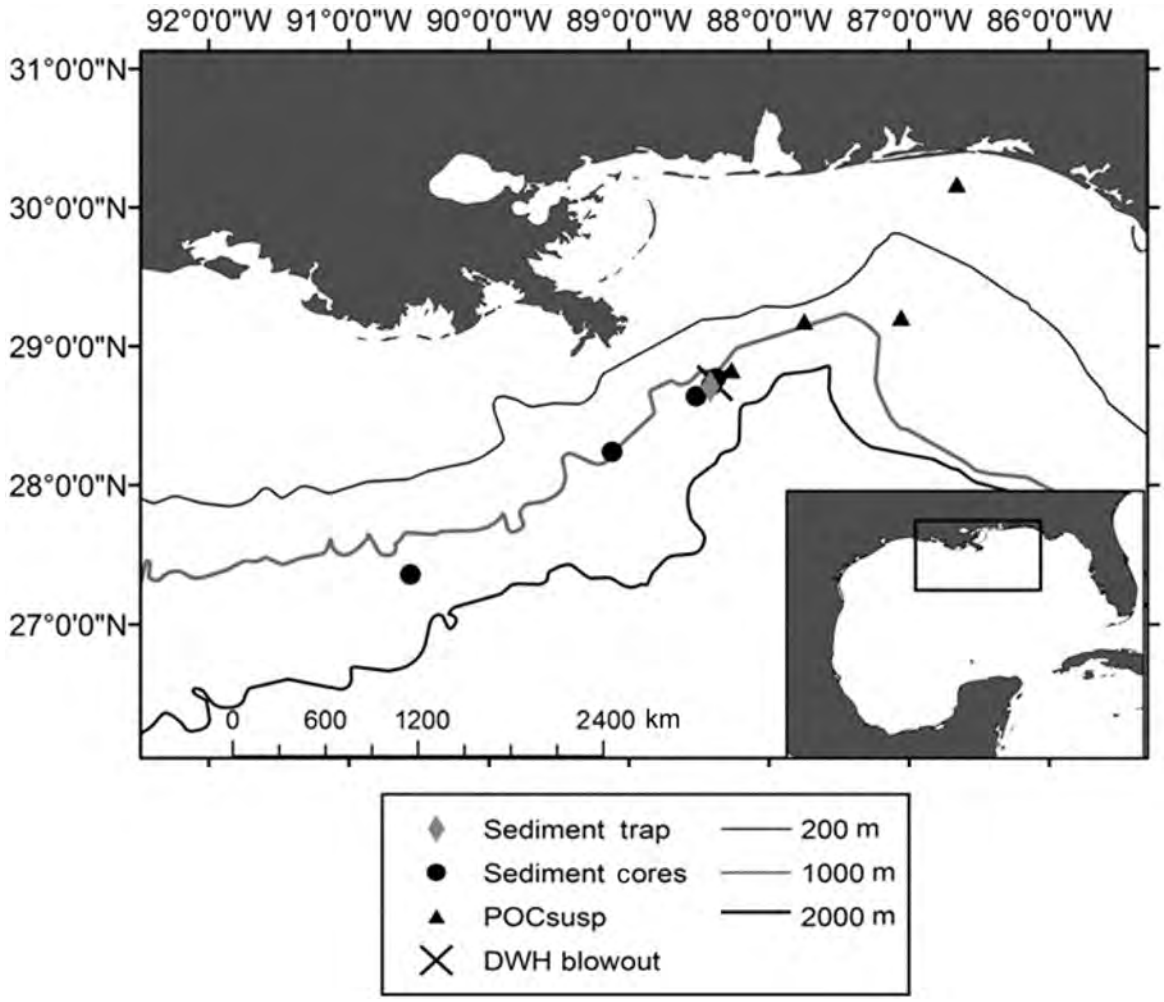

FIGURE 29.3 Map of the Gulf of Mexico with positions of sampling sites for suspended particulate organic carbon (POC_{susp}), shown as triangles, and sediment, shown as circles, and the location of the sediment trap, shown as the diamond. The location of the Deepwater Horizon (DWH) wellhead is shown as the cross.

further processing. Cups were gently mixed and then split repeatedly using a Folsom Plankton splitter (Yan et al., 2016). The 1/16 splits were used for isotope analyses. These samples were treated with 10% HCl to remove carbonates, rinsed with DI (deionized) water and then frozen prior to drying the samples in a freeze dryer. Dried samples were ground and then analyzed for $\delta^{13}C$ at the National High Magnetic Field laboratory. Samples for $\Delta^{14}C$ analyses were combusted in a muffle furnace and pure CO_2 from the samples were collected on a vacuum line using a series of cold traps to remove water vapor and noncondensable gases. Purified CO_2 samples were then prepared as graphic targets and analyzed at the University of Georgia Center of Applied Isotope Studies.

29.2.3 Sediment Samples From Cores

Sediment samples were collected using a multicore during research cruises to the Gulf of Mexico aboard several research vessels (R.V.s Cape Hatteras, Endeavor, Atlantis) in October 2010, September 2012 and April 2014. Four sites (GIP07, 28.24 N, 89.12 W; GIP16, 28.72 N, 88.41 W; GIP17, 28.64 N, 88.52 W; GIP24, 28.77 N, 88.38 W) were selected for analyses and were located as close as ~4 km from the DwH wellhead to as far as ~90 km from the wellhead (Fig. 29.3). One core site known to be a natural oil seep site (GC600, 27.36 N, 90.56 W) was also selected for analyses and was located over 180 km southwest of the wellhead (Fig. 29.3). Cores were stored in freezers until ready to be extruded back at the lab. Cores were thawed and sectioned at 1 cm intervals at the University of South Florida's College of Marine Science Paleo-Laboratory using an extrusion device. See Romero

et al. (2015) for a description of the extruder. Sectioned cores were immediately frozen and returned to Florida State University. Cores collected in the vicinity of the DwH wellhead were analyzed down to 5 cm of the core depth, while the core collected at site GC600 in 2012 was analyzed down to 3.5 cm and the core collected at the same site in 2014 was analyzed at a core depth of 10 cm. To prepare samples for stable and radiocarbon analyses, sediment samples were treated with 10% HCl to remove carbonates, rinsed with DI water and then frozen prior to drying the samples in a freeze dryer. Dried samples were ground using a mortar and pestle, and a high-energy ball mill. Stable carbon analyses were conducted at the National High Magnetic Field laboratory. Sediment samples for radiocarbon analyses were prepared at the National High Magnetic Field laboratory by combusting the samples in a muffle furnace and collecting the pure CO_2 from the samples on a vacuum line using a series of cold traps to remove water vapor and noncondensable gases. Purified CO_2 samples were then sent to the National Ocean Sciences Accelerator Mass Spectrometry Facility where the samples were prepared as graphic targets and analyzed by accelerator mass spectrometry (Vogel et al., 1984).

All data are publicly available through the Gulf of Mexico Research Initiative Information & Data Cooperative at https://data.gulfresearchinitiative.org; (doi: 10.7266/N7MK69V2, doi: 10.7266/n77942nj, doi: 10.7266/N7BR8Q6H); (doi: 10.7266/N7N58JB5, doi: 10.7266/N7FS77C7).

29.3 RESULTS

29.3.1 Suspended Particulate Organic Carbon (POC_{susp}) Samples

POC_{susp} samples collected throughout the water column in 2011 ranged in $\delta^{13}C$ values of −35.6‰ to −25.7‰, while those collected in 2012 ranged from −37.2‰ to −28.4‰. $\Delta^{14}C$ values ranged from −542‰ to −28‰ in 2011 and from −618‰ to −116‰ in 2012. In both years POC_{susp} samples appear to be considerably depleted both in $\delta^{13}C$ and $\Delta^{14}C$ relative to surface production, suggesting that these samples contain material contaminated with petrocarbon. POC_{susp} samples collected near the surface of the water column were more depleted in $\Delta^{14}C$ in 2012 compared to 2011 (Fig. 29.4). Furthermore, POC_{susp} collected near the seafloor were more depleted in $\Delta^{14}C$ than those collected near the surface (Fig. 29.4).

A positive relationship was observed between $\delta^{13}C$ and $\Delta^{14}C$, with more negative $\Delta^{14}C$ values associated with depleted $\delta^{13}C$ values (Fig. 29.5). The POC_{susp} samples collected from the Gulf of Mexico were generally more depleted than those sampled in the Mid-Atlantic Bight (MAB; Bauer et al., 2002) and in the North Central Pacific (NCP) and Sargasso Sea (SS; Druffel et al., 2003) (Fig. 29.5). POC_{susp} sampled in the MAB by Bauer et al. (2002)

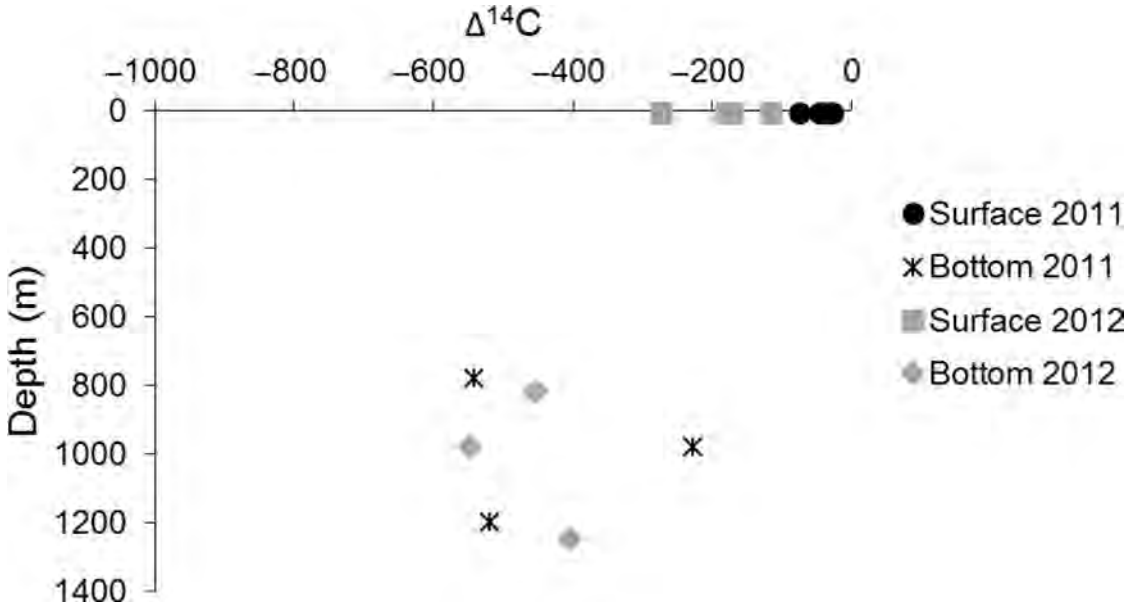

FIGURE 29.4 Radiocarbon values for suspended particulate organic carbon samples collected near the surface of the water column and near the seafloor in 2011 and 2012.

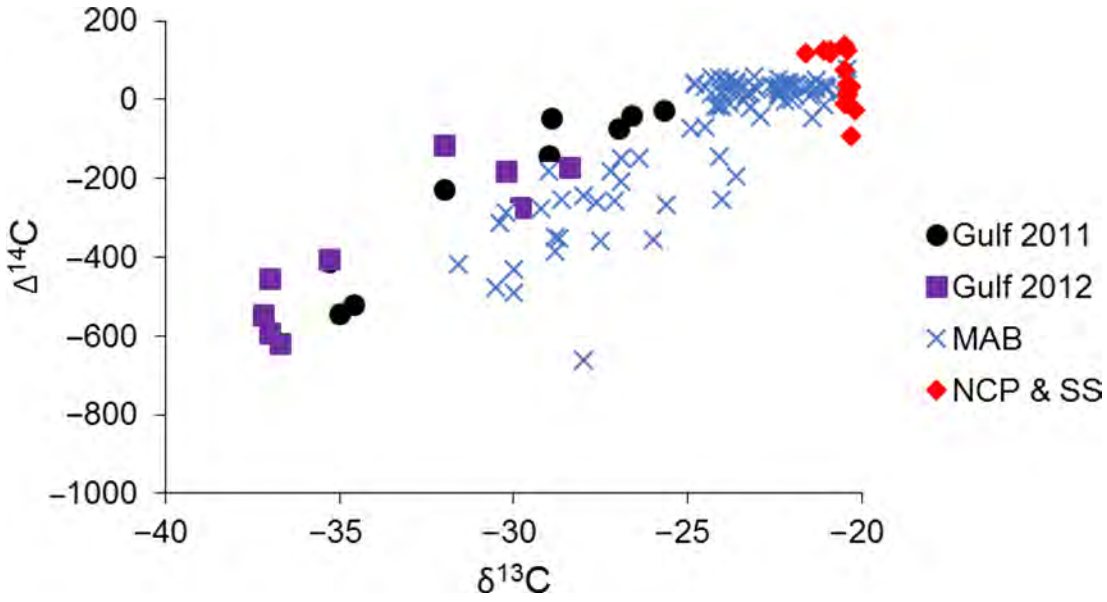

FIGURE 29.5 $\delta^{13}C$ values plotted against $\Delta^{14}C$ values of suspended particulate organic carbon samples. Circles are samples collected from the Gulf of Mexico in 2011 and squares are samples collected in the Gulf of Mexico in 2012. Crosses are data from Bauer et al. (2002) and were collected in the Middle Atlantic Bight (MAB), while diamonds are data from Druffel et al. (2003) and were collected from the North Central Pacific (NCP) and the Sargasso Sea (SS). *Adapted with permission from Cherrier, J., Sarkodee-Adoo, J., Guilderson, T.P., and Chanton, J.P. Fossil carbon in particulate organic matter in the Gulf of Mexico following the Deepwater Horizon event.* Environ. Sci. Technol. Lett.; *2014; 1, 108–112. Copyright 2014 American Chemical Society.*

ranged in $\delta^{13}C$ values from −31.6‰ to −19.6‰ and in $\Delta^{14}C$ values from −662‰ to +78‰, with more depleted values observed in deeper waters compared to shallower waters. POC_{susp} samples collected from the NCP and SS varied little in $\delta^{13}C$ (−21.6‰ to −20.2‰). However, $\Delta^{14}C$ values ranged from −92‰ to +138‰ (Druffel et al., 2003). Druffel et al. (2003) reported more depleted $\delta^{13}C$ values for samples collected at the surface compared to the seafloor; however, $\Delta^{14}C$ values were more depleted near the seafloor compared to the surface.

29.3.2 Sinking Particulate Organic Carbon (POC_{sink}) Samples From Sediment Traps

POC_{sink} captured in sediment traps from August 25, 2010 to September 7, 2011 ranged in $\Delta^{14}C$ values from −141‰ to +76.1‰. The positive $\Delta^{14}C$ value observed in September 2010 was reported to be the result of a large diatom bloom that contained modern $\Delta^{14}C$, canceling out the depleted $\Delta^{14}C$ found in oil contaminated material sinking to the seafloor (Fig. 29.6; Yan et al., 2016). After the diatom bloom, a rapid drop in $\Delta^{14}C$ was observed from September 15, 2010 to October 6, 2010 as oil contaminated material continued to sink from the sea surface to the seafloor (Fig. 29.6). $\Delta^{14}C$ continued to become more depleted up to the end of the year, before slowly becoming more modern throughout the 2011 sampling period. Based on these observations and supplementary findings reported in Yan et al. (2016), it is believed that material containing petrocarbon from the oil spill continued to sink to the seafloor for 5 months.

29.3.3 Sediment Samples From Cores

29.3.3.1 Deepwater Horizon Effected Sites

Surface sediment samples (0–1 cm) collected in the vicinity of the DwH wellhead ranged in $\delta^{13}C$ values of −23.1‰ to −22.0‰, while $\Delta^{14}C$ values ranged from −501.1‰ to −291.1‰ (Fig. 29.7). Below the surface (1–5 cm layers), $\delta^{13}C$ values ranged from −22.4‰ to −20.8‰ and $\Delta^{14}C$ values ranged from −252.7‰ to −163.7‰. The depletion in $\delta^{13}C$ and $\Delta^{14}C$ values in the surface sediment relative to $\delta^{13}C$ and $\Delta^{14}C$ values below the surface suggest the surface sediment contained petrocarbon deposited from the oil released from the DwH well blowout. The fairly constant $\delta^{13}C$ and $\Delta^{14}C$ values below the surface sediment layer give an indication of the background isotopic signature, or prespill condition, in the northern Gulf of Mexico.

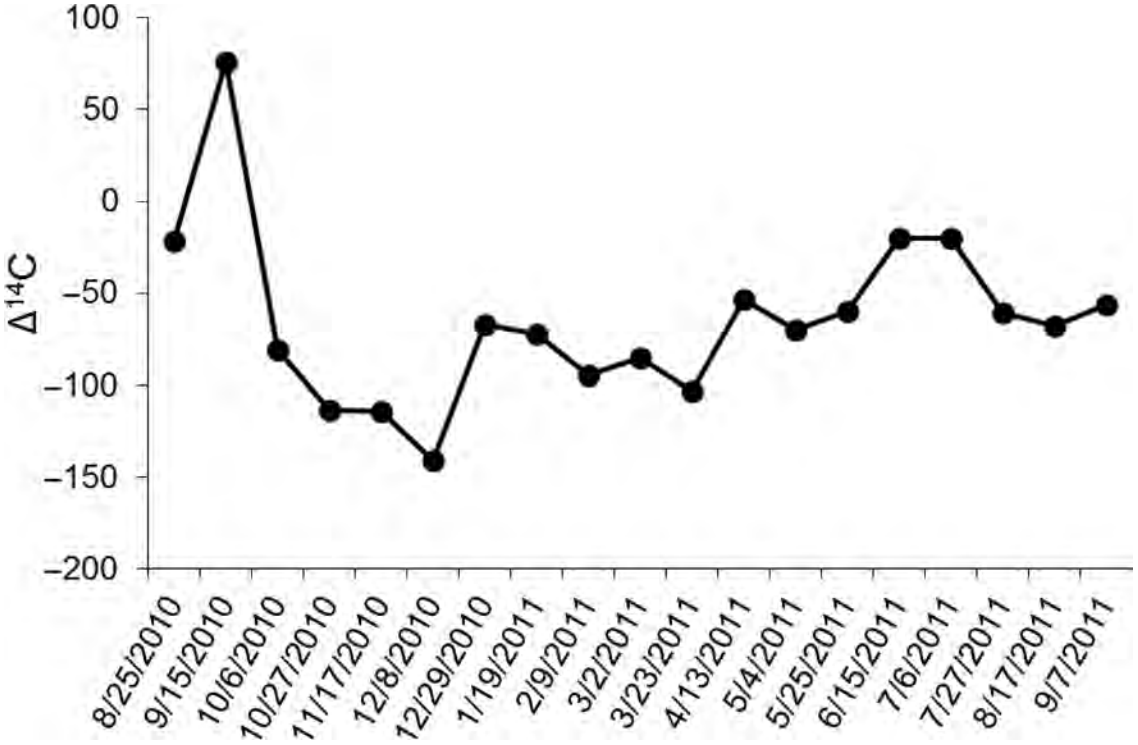

FIGURE 29.6 Time series of $\Delta^{14}C$ data measured from sinking particulate organic carbon samples collected from a sediment trap from August 25, 2010 to September 7, 2011. *Adapted with permission from Yan, B., Passow, U., Chanton, J.P., Nothig, E-M, Asper, V., Sweet, J., Pitiranggon, M., Diercks, A., and Pak, D. Sustained deposition of contaminants from the Deepwater Horizon spill.* Proc. Natl. Acad. Sci.*; 2016; 113: E3332–E3340.*

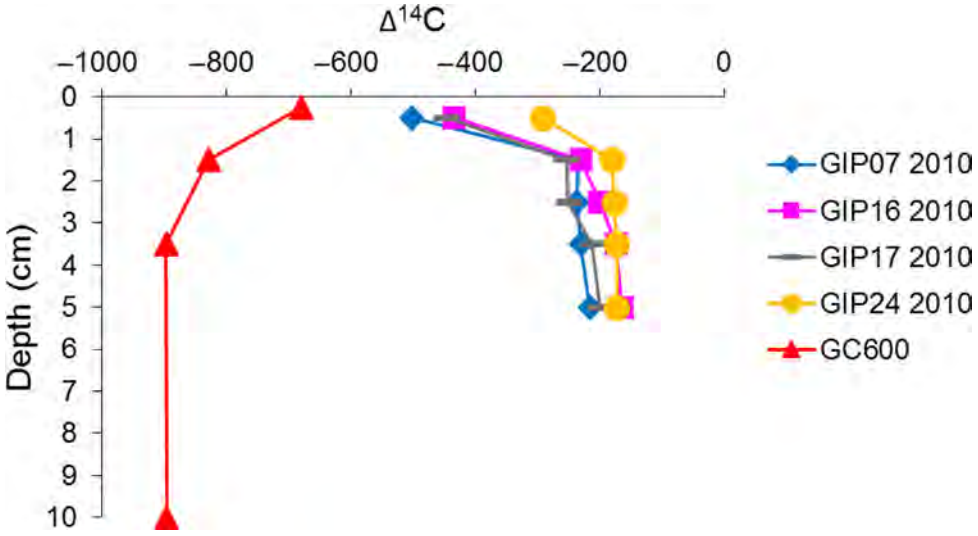

FIGURE 29.7 Radiocarbon depth profiles from sediment cores collected at sites in the vicinity of the Deepwater Horizon wellhead and a site of a known seep location (GC600). *Adapted with permission from Chanton, J., Zhao, T., Rosenheim, B., Joye, S., Bosman, S., Brunner, C., Yeager, K., Diercks, A., and Hollander. Using natural abundance radiocarbon to trace the flux of petrocarbon to the seafloor following the Deepwater Horizon oil spill.* Environ. Sci. Technol.*; 2015; 49(2), 847–854. Copyright 2015 American Chemical Society.*

29.3.3.2 GC600 Natural Seep Site

An opposite pattern is observed at the natural seep site, GC600, where $\delta^{13}C$ and $\Delta^{14}C$ become more depleted with increasing depth in the core (Fig. 29.7). Core depth 0–3.5 cm was analyzed from the same core collected in September 2012. The core depth taken at 10 cm came from a core collected at same site but in April 2014 and is included on the graph to show how $\Delta^{14}C$ continues to remain depleted down core,

which is expected at a natural oil seep site. In addition, both $\delta^{13}C$ and $\Delta^{14}C$ values are much more depleted at the seep site than those measured at the surface layer at sites in the vicinity of the DwH wellhead (Fig. 29.7).

29.4 DISCUSSION

The results from the $\delta^{13}C$ and $\Delta^{14}C$ isotopic analyses indicate that samples of particulate organic carbon and sedimentary organic carbon collected in the northern Gulf of Mexico contained petrocarbon from the DwH blowout.

29.4.1 Suspended Particulate Organic Carbon (POC_{susp}) Samples

POC_{susp} samples collected throughout the water column in 2011 and 2012 were depleted in $\delta^{13}C$ and $\Delta^{14}C$ relative to modern surface production. POC_{susp} have been known to remain in the water column for up to 7 years (Bacon and Anderson, 1982; Druffel et al., 2003), which can explain the observation of depleted isotope values 2 years after the spill. It was also noted that POC_{susp} collected near the seafloor were more depleted in $\Delta^{14}C$ than those collected near the sea surface. Druffel et al. (2003) reported similar findings for samples collected in the NCP. Druffel et al. (2003) suggested this was likely due to resuspended sediment along the continental shelf and slope or from sorption of dissolved organic carbon onto POC_{susp}. With one exception, similar findings were also reported by Bauer et al. (2002) for samples collected in the MAB. Younger POC_{susp} was observed on the shelf and shallow slope compared to deeper areas. Bauer et al. (2002) also suggested resuspended sediment due to tidal and wind mixing as the cause for this observation. It was also noted that terrestrial material was found in the sediment and could be incorporated into the POC_{susp} samples (Bauer et al., 2002). In the northern Gulf of Mexico, several major rivers, including the Mississippi River, drains into the Gulf, indicating that terrestrial input could influence the POC_{susp} which may help explain, in part, the pattern of older POC_{susp} near the seafloor and younger POC_{susp} near the surface for samples collected in the Gulf.

In the Gulf, $\delta^{13}C$ vs $\Delta^{14}C$ were found to be significantly correlated (Fig. 29.5; Cherrier et al., 2014). Cherrier et al. (2014) extrapolated the linear regression to the isotope data to determine the value of $\delta^{13}C$ at which $\Delta^{14}C$ was completely depleted. This value was about $-50‰$, indicating the importance of methane as the ultimate source of organic material. Cherrier et al. (2014) suggested that the methane was oxidized by two possible reactions, and partly retained in the particulate form by methanotrophic bacteria following the first reaction.

$$CH_4 + O_2 \rightarrow CH_2O + H_2O$$

$$CH_4 + 2O_2 \rightarrow CO_2 + 2H_2O$$

POC_{susp} material sampled in the Gulf was more depleted than those sampled in the central Atlantic and Pacific Oceans (Druffel et al., 1998, 2003). POC_{susp} material in Druffel et al. (1998, 2003) studies were likely derived from photosynthetic carbon fixed at the surface of the ocean. In Bauer et al. (2002)'s study in the MAB, the exceptional samples were those with $\Delta^{14}C$ values as low as $-660‰$ while $\delta^{13}C$ values were the lowest ever reported at the time the study took place with values of $-31.6‰$ to $-19.6‰$. Bauer et al. (2002) suggested these samples may be influenced by hydrocarbon seeps. The Bauer et al. (2002) data of the MAB, replotted on Fig. 29.5 with the Gulf of Mexico data, reveal a similar trend to the Gulf results and are also correlated. Cherrier et al. (2014) determined the $\delta^{13}C$ value at which $\Delta^{14}C$ is depleted for the MAB data, as done for the Gulf of Mexico data above, and found a value of $-46‰$. This value is similar to the Gulf value and also suggests methane input. Interestingly, after the publication of the Cherrier et al. (2014) paper, a large field of hydrocarbon seeps were discovered in the MAB supporting Bauer et al. (2002)'s suggestion of seep influence in their data (Skarke et al., 2014). Thus one could assume that collecting and analyzing particulate organic carbon is an excellent tool for geochemical prospecting.

Currently, we have no idea what the Gulf's isotopic baseline POC_{susp} prior to the spill was and to what extent the baseline values were determined by the relative importance of natural hydrocarbon seeps as opposed to photosynthetic carbon. As previously mentioned, POC_{susp} material can reside in the water column for up to 7 years (Bacon and Anderson, 1982; Druffel et al., 2003), and if the Gulf has a similar residence time, it could be years before oil from the DwH blowout no longer has an influence on the POC_{susp} material and we can determine how much natural hydrocarbon seeps have an influence on the POC_{susp}.

29.4.2 Sinking Particulate Organic Carbon (POC_{sink}) Samples From Sediment Traps

POC_{sink} that was captured in sediment traps consists of larger particles such as phytoplankton, zooplankton feces, and mucus that rapidly sink to the seafloor (Yan et al., 2016). Time series data plotted from August 25, 2010 to September 7, 2011 revealed evidence of oil contaminated POC that continued to descend from the sea surface or subsurface for 5 months (Fig. 29.6). Overall, the POC_{sink} radiocarbon data corroborated evidence from saturated and polycyclic aromatic hydrocarbon source indicators which indicated a contribution of crude oil derived carbon to the sinking particles in the 5 months following the capping of the well. These indicators lessened in the collections in the months following the spill (Fig. 29.6). Initially, the radiocarbon values of the sinking particulates reflected the input of a large diatom bloom in early September 2010 which was confirmed in the particles by microscopic examination and by measurements of biogenic silica (Yan et al., 2016). This bloom was largely dominated by *Skeletonema* sp. (Yan et al., 2016) and is known to be associated with oil spill events (Parsons et al., 2014).

Passow et al. (2012) determined that the large marine snow event observed shortly after the oil spill was the result of the oil present at or just below the surface. Through the use of experiments, Passow et al. (2012) came up with three mechanisms for the occurrence of a large marine snow event. First is the mucus formation by bacteria that allow other particles in the water to collide and stick together to create large masses of marine snow. The second was the colliding and sticking of particles in the presence of oil, forming flocs, and the third was the collision and sticking of cyanobacteria commonly found in the Gulf but in the presence of oil, contained oil droplets (Passow et al., 2014). Initially, the marine snow remains buoyant, but eventually with weathering of the oil and microbial activity, the marine snow sinks rapidly to the seafloor (Passow et al., 2012).

According to Yan et al. (2016), the diatom bloom was exceptionally large so that it diluted the influence of oil contaminated particles and hence a positive $\Delta^{14}C$ value was observed for samples collected during this time period. Following that bloom, the values became more negative, reflecting petrocarbon input, reaching a minimum in December 2010 (Fig. 29.6). The suggestion of resuspended sediment incorporated into the samples as mentioned by Bauer et al. (2002) and Druffel et al. (2003) for POC_{susp} samples is likely not the explanation for depleted $\Delta^{14}C$ observed in the POC_{sink} samples from the sediment trap. Planktonic foraminifera were present in the samples from the trap but no benthic species were found (Yan et al., 2016). Furthermore, the trap was suspended 105 m above the seafloor and it would be unlikely that sediment would resuspend to that height unless there was a large storm. Yan et al. (2016) also rejected the possibility of hydrocarbon influence from natural seeps due to the absence of any known seep sites within 2 km of the trap site.

Approximately 5 months after the oil spill, in late December 2010 and throughout 2011, POC_{sink} $\Delta^{14}C$ slowly began to recover, reaching values near 0‰ (Fig. 29.6), reflecting greater relative quantities of surface derived material. This observation further supports the notion that oil contaminated material can remain in the water column for a long period of time following the capping of the wellhead (Yan et al., 2016).

29.4.3 Sediment Samples From Cores

Sediment cores collected in October 2010 in the vicinity of the DwH well revealed evidence of oil in the surface layer (0–1 cm), indicated by a depletion in $\Delta^{14}C$ relative to surface production. In these cores, the data appear to be inverted, that is, older organic materials over younger more modern organic matter (Fig. 29.7). Our forensic analysis allows us to deduce that this is due to the presence of an oily sedimentation event overlying the surface sediments of the Gulf associated with the oil spill. Unlike the known seep site, GC600, where $\Delta^{14}C$ becomes more depleted down core, $\Delta^{14}C$ depletion seems to be confined to the upper 1cm sediment layer of the other four cores (Fig. 29.7). Confirmation that this deposition event was confined to the upper 1 cm layer of sediment may be found in Brookes et al. (2015) and Valentine et al. (2014). Furthermore, the lack of vertical mixing observed in the upper 1 cm layer of the core suggests this layer was deposited within a 4–5-month period (Brooks et al., 2015).

Chanton et al. (2015) mapped the distribution of $\Delta^{14}C$ values in the surface sediments and contoured them to estimate the spatial area within each contour on the seafloor within a polygon shaped area of 24,000 km^2 where 62 sediment cores were collected. They found evidence for oil contamination in 35% of this area, or 8400 km^2 of the area. This was in contrast to Valentine et al. (2014) who examined a 3200 km^2 area. By determining the amount of fossil organic matter above background in the sediments ($\Delta^{14}C = -200‰ \pm 29‰$), Chanton et al. (2015) were able to calculate a proportion of petrocarbon present in each contour in the 0–1-cm layer. From measurements of the sediment organic matter content, and the solid phase content of the sediments in this layer, they

extrapolated that this layer contained some 1.6 to 2.6×10^{10} g of petrocarbon, which represented 0.5% to 9.1% of the quantity released from the oil spill. The uncertainty of the estimate includes both the uncertainty of summing the oil on the seafloor, but also uncertainty about the quantity of oil actually released. The best estimate was 3.0%−4.9%. These authors acknowledged that the estimates might well be low as they focused only on a limited deep water area of the Gulf and not coastal areas, and that they used a fairly conservative value for the thickness of the layer. However, a similar approach using a biomarker (hopane) approach reported a range which varied from 1.8% to 14.4% (Valentine et al., 2014). Stout et al. (2016) also used hopane and estimated that 7%−8% of the spilled oil was on the seafloor, but they used a significantly smaller quantity for the spilled oil. Normalizing their result to that of Chanton et al. (2015) would give a more comparable result of 5%−6% of the spilled oil that went to the seafloor. The three studies converge extremely well.

29.5 CONCLUSION

The use of stable isotopes to trace contaminates released into the environment has become an important tool in environmental forensics (Philp, 2007). Due to the unique isotopic signature of contaminates, they can be used as tracers to determine their source (Miljević and Golobočanin, 2007). As mentioned previously, the petrocarbon from the oil spill has a $\Delta^{14}C$ value of −1000‰, radiocarbon dead, while surface modern carbon in the northern Gulf of Mexico is +40‰. Because of the wide range in the two endmembers, radiocarbon provides a much more sensitive tracer for petrocarbon released into the environment (Wilson et al., 2016). We used both stable and radiocarbon isotopes in this case study to reveal an important pathway of how oil released at the surface or subsurface from the DwH blowout reached the seafloor in the northern Gulf of Mexico.

Acknowledgments

This research was made possible by a grant from The Gulf of Mexico Research Initiative through its consortia: Ecosystem Impacts of Oil & Gas Inputs to the Gulf (ECOGIG) and Center for Integrated Modeling and Analysis of Gulf Ecosystems (C-IMAGE). Data are publicly available through the Gulf of Mexico Research Initiative Information & Data Cooperative (GRIIDC) at https://data.gulfresearchinitiative.org (doi:10.7266/N7MK69V2, 10.7266/n77942nj, 10.7266/N7BR8Q6H, 10.7266/N7N58JB5, 10.7266/N7FS77C7). This is ECOGIG Contribution #483.

References

Bacon, M.P., Anderson, R.F., 1982. Distribution of thorium isotopes between dissolved and particulate forms in the deep sea. J. Geophys. Res. 87, 2045−2056.

Bælum, J., Borglin, S., Chakraborty, R., Fortney, J.L., Lamendella, R., Mason, O.U., 2012. Deep-sea bacteria enriched by oil and dispersant from the Deepwater Horizon spill. Environ. Microbiol. 14, 2405−2416.

Bauer, J.E., Druffel, E.R.M., Wolgast, D.M., Griffin, S., 2002. Temporal and regional variability in sources and cycling of DOC and POC in the northwest Atlantic continental shelf and slop. Deep-Sea Res. II 49, 4387−4419.

Brooks, G.R., Larson, R.A., Schwing, P.T., Romero, I., Moore, C., Reichart, G.-J., et al., 2015. Sedimentation pulse in the NE Gulf of Mexico following the 2010 DWH blowout. PLoS One 10 (7), e0132341. Available from: http://dx.doi.org/10.1371/journal.pone.0132341.

Camilli, R., Reddy, C.M., Yoerger, D.R., Van Mooy, B.A.S., Jakuba, M.V., Kinsey, J.C., et al., 2010. Tracking hydrocarbon plume transport and biodegradation at Deepwater Horizon. Science 330, 201−204.

Chanton, J., Zhao, T., Rosenheim, B.E., Joye, S., Bosman, S., Brunner, C., et al., 2015. Using natural abundance radiocarbon to trace the flux of petrocarbon to the seafloor following the Deepwater Horizon oil spill. Environ. Sci. Technol. 49 (2), 847−854.

Chanton, J.P., Cherrier, J., Wilson, R.M., Sarkodee-Adoo, J., Bosman, S., Mickle, A., et al., 2012. Radiocarbon evidence that carbon from the Deepwater Horizon spill entered the planktonic food web of the Gulf of Mexico. Environ. Res. Lett. 7, 045303.

Cherrier, J., Sarkodee-Adoo, J., Guilderson, T.P., Chanton, J.P., 2014. Fossil carbon in particulate organic matter in the Gulf of Mexico following the Deepwater Horizon event. Environ. Sci. Technol. Lett. 1, 108−112.

Crespo-Medina, M., Meile, C.D., Hunter, K.S., Diercks, A.-R., Asper, V.L., Chanton, J.P., et al., 2014. The rise and fall of methanotrophy following a deepwater oil-well blowout. Nat. Geosci. 7, 423−427.

Daly, K.L., Passow, U., Chanton, J., Hollander, D., 2016. Assessing the impacts of oil-associated marine snow formation and sedimentation during and after the Deepwater Horizon oil spill. Anthropocene 13, 18−33.

Druffel, E.R., Bauer, J.E., Griffin, S., Hwang, J., 2003. Penetration of anthropogenic carbon into organic particles of the deep ocean. Geophys. Res. Lett. 30 (14), 1744. Available from: http://dx.doi.org/10.1029/2003GL017423.

Druffel, E.R.M., Griffin, S., Bauer, J.E., Wolgast, D.M., Wang, X.C., 1998. Distribution of particulate organic carbon and radiocarbon in the water column from the upper slope to the abyssal NE Pacific Ocean. Deep-Sea Res. 45, 667−687.

Dubinsky, E.A., Conrad, M.E., Chakraborty, R., Bill, M., Borglin, S.E., Hollibaugh, J.T., et al., 2013. Succession of hydrocarbon-degrading bacteria in the aftermath of the Deepwater Horizon oil spill in the gulf of Mexico. Environ. Sci. Technol. 47, 10860−10867.

Graham, W.M., Condon, R.H., Carmichael, R.H., D'Ambra, I., Patterson, H.K., Linn, L.J., et al., 2010. Oil carbon entered the coastal planktonic food web during the Deepwater Horizon oil spill. Environ. Res. Lett. 5, 045301.

Graven, H.D., Guilderson, T.P., Keeling, R.F., 2012. Observations of radiocarbon in CO_2 at LaJolla, California USA 1992-2007, Analysis of a long term trend. J. Geophys. Res. 117 (D2). Available from: http://dx.doi.org/10.1029/2011JD016533.
Hazen, T.C., Dubinsky, E.A., DeSantis, T.Z., Andersen, G.L., Piceno, Y.M., Singh, N., et al., 2010. Deep-sea oil plume enriches indigenous oil-degrading bacteria. Science 330, 204–208.
Joye, S.B., MacDonald, I.R., Leifer, I., Asper, V., 2011. Magnitude and oxidation potential of hydrocarbon gases released from the BP oil well blowout. Nat. Geosci. 4, 160–165.
Joye, S.B., Bracco, A., Özgökmen, T., Chanton, J.P., Grosell, M., MacDonald, I., et al., 2016. The Gulf of Mexico Ecosystem, six years after the Macondo Oil Well Blowout. Deep-Sea Res. II 129, 4–19.
Kessler, J.D., Vaentine, D.L., Redmond, M.C., Du, M., Chan, E.W., Mendes, S.D., et al., 2011. A persistent oxygen anomaly reveals the fate of spilled methane in the deep Gulf of Mexico. Science 331, 312–315.
Kinner, N.E., Belden, L., Kinner, P., 2014. Unexpected sink for Deepwater Horizon oil may influence future spill response. EOS 95 (21), 176.
Lehr, W., Bristol, S., Possolo, A., 2010. Federal Interagency Solutions Group, Oil budget calculator science and engineering team. Oil Budget Calculator. Technical document. <http://www.restorethegulf.gov/sites/default/files/documents/pdf/OilBudgetCalc_Full_HQ–Print_111110.pdf> (last accessed 24.07.14.).
Mason, O.U., Hazen, T.C., Borglin, S., Chain, P.S.G., Dubinsky, E.A., Fortney, J.L., et al., 2012. Metagenome, metatranscriptome and single-cell sequencing reveal microbial response to Deepwater Horizon oil spill. ISME J. 6, 1715–1727.
Mason, O.U., Scott, N.M., Gonzalez, A., Robbins-Pianka, A., Bælum, J., Kimbrel, J., et al., 2014. Metagenomics reveals sediment microbial community response to Deepwater Horizon oil spill. ISME J. 8, 1464–1475.
McNichol, A.P., Aluwihare, L.I., 2007. The power of radiocarbon in biogeochemical studies of the marine carbon cycle: insights from studies of dissolved and particulate organic carbon (DOC and POC). Chem. Rev. 443–466.
Miljević, N., Golobočanin, D., 2007. Potential uses of environmental isotopes in pollutant migration studies. Arh. Hig. Rada. Toksikol. 58, 251–262.
Parsons, M.L., Turner, R.E., Overton, E.B., 2014. Sediment-preserved diatom assemblages can distinguish a petroleum activity signal separately from the nutrient signal of the Mississippi River in coastal Louisiana. Mar. Pollut. Bull. 85 (1), 164–171.
Passow, U., 2014. Formation of rapidly-sinking, oil-associated marine snow. Deep-Sea Res. II 129, 232–240.
Passow, U., Ziervogel, K., Asper, V., Diercks, A., 2012. Marine snow formation in the aftermath of the Deepwater Horizon oil spill in the Gulf of Mexico. Environ. Res. Lett. 7, 035301.
Philp, R.P., 2007. The emergence of stable isotopes in environmental and forensic geochemistry studies: a review. Environ. Chem. Lett. 5, 57–66.
Redmond, M.C., Valentine, D.L., 2012. Natural gas and temperature structured a microbial community response to the Deepwater Horizon oil spill. Proc. Natl. Acad. Sci. 109, 20292–20297.
Romero, I.C., Schwing, P.T., Brooks, G.R., Larson, R.A., Hastings, D.W., Ellis, G., et al., 2015. Hydrocarbons in deep-sea sediments following the 2010 Deepwater Horizon blowout in the northeast Gulf of Mexico. PLoS One 10 (5), e0128371. Available from: http://dx.doi.org/10.1371/journal.pone.0128371.
Ruddy, B.M., Huettel, M., Kostka, J.E., Lobodin, V.V., Bythell, B.J., McKenna, A.M., et al., 2014. Targeted petroleomics: analytical investigation of Macondo well oil oxidation products from Pensacola Beach. Energy Fuels 28 (6), 4043–4050.
Ryerson, T.B., Camilli, R., Kessler, J.D., Kujawinski, E.B., Reddy, C.M., Valentine, D.L., et al., 2012. Chemical data quantify Deepwater Horizon hydrocarbon flow rate and environmental distribution. Proc. Natl. Acad. Sci. 109, 20246–20253.
Skarke, A., Ruppel, C., Kodis, M., Brothers, D., Lobecker, E., 2014. Widespread methane leakage from the sea floor on the northern US Atlantic margin. Nat. Geosci. 7 (9), 657–661.
Spier, C., Stringfellow, W.T., Hazen, T.C., Conrad, M., 2013. Distribution of hydrocarbons released during the 2010, MC252 oil spill in deep offshore waters. Environ. Pollut. 173, 224–230.
Stout, S.A., Rouhani, S., Liu, B., Oehrig, J., Ricker, R.W., Baker, G., et al., 2016. Assessing the footprint and volume of oil deposited in deep-sea sediments following the Deepwater Horizon oil spill. Mar. Pollut. Bull. Available from: http://dx.doi.org/10.1016/j.marpolbul.2016.09.046.
Stuiver, M., Polach, H.A., 1977. Reporting of 14C Data. Radiocarbon 19, 355–363.
Valentine, D.L., Kessler, J.D., Redmond, M.C., Mendes, S.D., Heintz, M.B., Farwell, C., et al., 2010. Propane respiration jump-starts microbial response to a deep oil spill. Science 330, 208–211.
Valentine, D.L., Fisher, G.B., Bagby, S.C., Nelson, R.K., Reddy, C.M., Sylva, S.P., et al., 2014. Fallout plume of submerged oil from Deepwater Horizon. Proc. Natl. Acad. Sci. doi 10.1073/pnas.1414873111.
Vogel, J.S., Southon, J.R., Nelson, D.E., Brown, T.A., 1984. Performance of catalytically condensed carbon for use in accelerator mass spectrometry. Nucl. Instrum. Methods Phys. Res. B5, 289–293.
Vonk, S.M., Hollander, D.J., Murk, A.J., 2015. Was the extreme and wide-spread marine oil-snow sedimentation and flocculent accumulation (MOSSFA) event during the Deepwater Horizon blow-out unique?. Mar. Pollut. Bull. 100 (1), 5–12. Available from: http://dx.doi.org/10.1016/j.marpolbul.2015.08.023.
Wilson, R.M., Cherrier, J., Sarkodee-Adoo, J., Bosman, S., Mickle, A., Chanton, J.P., 2016. Tracing the intrusion of fossil carbon into coastal Louisiana macrofauna using natural 14C and 13C abundances. Deep-Sea Res. II 129, 89–95.
Yan, B., Passow, U., Chanton, J.P., Nothig, E.-M., Asper, V., Sweet, J., et al., 2016. Sustained deposition of the contaminants from the Deepwater Horizon spill. Proc. Natl. Acad. Sci. 113, E3332–E3340.
Ziervogel, K., Joye, S.B., Arnosti, C., 2014. Microbial enzymatic activity and secondary production in sediments affected by the sedimentation pulse following the Deepwater Horizon oil spill. Deep-Sea Res. II 129, 241–248.

CHAPTER

30

Red Crabs as Sentinel Organisms in Exposure of Deep-Sea Benthos to Macondo Oil Following the *Deepwater Horizon* Oil Spill

Gregory S. Douglas, Bo Liu, Wendy Wong, Eric Litman and Jeffery Hardenstine

NewFields Environmental Forensics Practice, LLC, Rockland, MA, United States

BIOGRAPHIES

Gregory S. Douglas, Ph.D., received his doctorate in Oceanography from the University of Rhode Island and is a senior consultant and partner at NewFields Environmental Practice, LLC in Rockland, Massachusetts. Dr. Douglas received a B.S. in chemical oceanography from the Florida Institute of Technology and M.S. and Ph.D. degrees in chemical oceanography from graduate school of Oceanography at the University of Rhode Island. Dr. Douglas has over 30 years' environmental chemistry and forensic investigation experience and has developed innovative analytical tools for the monitoring and quantification of petroleum contamination and biodegradation in soil and sediments. His project experience includes many notable oil spill studies such as the *Exxon Valdez* (USA), *Haven* (Italy), *Trecate Blowout* (Italy), *OSSA II Pipeline* (Bolivia), *M/T Athos* (USA), *North Cape* (USA), *M/V New Carrissa* (USA), *T/V Selendang* (USA), 1991 *Gulf War Oil spills* (Saudi Arabia), and *2010 Gulf of Mexico Deepwater Horizon Oil Spill* (USA). He has written interpretive reports on more than 200 environmental site or incident investigations associated with retail gasoline stations, bulk fuel storage, facilities, refineries, petroleum pipelines, and exploration and production sites and has authored or coauthored over 50 papers published in scientific journals and scientific textbooks. His other areas of expertise include the measurement and environmental chemistry of industrial chemicals and solvents, modern and persistent pesticides, insecticides and fungicides, PCB congeners and Aroclors, dioxins and furans, metals, organometallic compounds, and petroleum-, natural gas-, coal-derived, and anthropogenic hydrocarbons in the environment.

Bo Liu is a senior consulting scientist at NewFields Environmental Forensics Practice, LLC in Rockland, Massachusetts. Ms. Liu has over 20 years of experience in the field of environmental chemistry. She received a B.S. in environmental chemistry from Nanjing University, China and a M.S. in environmental engineering from A. James Clark School of Engineering at University of Maryland. Her expertise includes the application of advanced analytical chemistry methods for the study of the fate and effects of organic contaminants such as PCBs, petroleum hydrocarbons in marine sediments, soil, waste, waste water, and biota. Ms. Liu has managed many major environmental investigations focused on aquatic and terrestrial environmental quality. Ms. Liu has worked on projects investigating major oil spill around the world, such as 1991 *Gulf War Oil spills* (Saudi Arabia), *2005 Murphy Oil refinery spill following Hurricane Katrina* (USA), 2007 *Cosco Busan Oil Spill* in San Francisco Bay (USA), 2011 *Bohai Oil Spill* (China), and *2010 Gulf of Mexico Deepwater Horizon Oil Spill* (USA). Her years of experience working in a laboratory provides her with the unique insight required to evaluate data quality through chemical reasonableness analysis. With the vetted data, Ms. Liu designs and constructs the

Oil Spill Environmental Forensics Case Studies.
DOI: http://dx.doi.org/10.1016/B978-0-12-804434-6.00030-6

appropriate database system for use within the Geographic Information Systems (GIS) to prepare relevant 2D and 3D spatial distributions and geostatistical analysis of the chemicals of concern. Ms. Liu has worked on more than 100 + projects with a broad spectrum of database and GIS requirements ranging from bulk fuel storage facilities to the Gulf of Mexico 2010 Deepwater Horizon (DWH) oil spill.

Jeffery Hardenstine is a senior consulting scientist at NewFields Environmental Forensics Practice, LLC in Rockland, Massachusetts. He holds a B.S. in Biology and has over 25 years of experience in environmental chemistry. His background is in the detailed chemical analysis and interpretation of organic contaminants such as petroleum products, PCBs, and manufactured gas plant residues and wastes, and their characterization using advanced instrumental methods and sophisticated chemometric data interpretation techniques (forensic chemical fingerprinting). He is particularly experienced in sample extraction and cleanup techniques related to sediment and tissues and data processing of gas chromatography/flame Ionization detection (GC/FID) and gas chromatography/mass spectrometry (GC/MS) analysis of hydrocarbons and other anthropogenic contaminants. He has designed and implemented bench scale treatability studies in the areas of biodegradation and weathering of petroleum constituents, PCB congeners, and Aroclors. He has managed the planning and technical work of over 50 projects involved with study of the fate and transport of organic contaminants in aquatic and terrestrial environments. Among those are the *Valdez Oil Spill* in Prince Williams Sound, Alaska, *North Cape* (USA), *M/V New Carrissa* (USA), *T/V Selendang* (USA), *Cosco Busan Oil Spill* in San Francisco Bay, and DWH in the Gulf of Mexico.

Wendy Wong is a consulting scientist at NewFields Environmental Forensic, LLC in Rockland, Massachusetts. Ms. Wong has 19 years of experience in the field of environmental chemistry and specializes in detailed chemical analysis, chemical fingerprinting, and applications of environmental forensic principles for advanced site investigation projects. Over the years, Ms. Wong has worked on numerous site assessment and investigative projects, including roles as analyst, consulting chemist, and technical project leader. She has managed laboratory operations during multiple large-scale oil spill investigations including the *Exxon Valdez*, Saudi/Gulf War, *Cosco Busan*, and DWH oil spills. As an experienced forensics chemist and a strong operations professional, she has optimized laboratory operations through staff training, process improvement, scaling of analytical capabilities, enhancement of real-time quality control measures, and augment client and laboratory communication to meet the demands of these high-profile, technical forensics programs.

30.1 INTRODUCTION

The DWH oil spill is unique because unlike most oil spills, a substantial fraction of the oil released from the Macondo well was deposited on the deep seafloor. As part of the Natural Resource Damage Assessment (NRDA) following the oil spill, tissue samples of benthic macrofauna that live in and on the deep seafloor were collected and chemically analyzed to determine the extent to which this sensitive ecosystem was exposed to the Macondo oil.

The presence of Macondo oil in the deep-sea sediment (spill zone) has been well documented through the chemical study of over 700 deep-sea sediment cores (Stout and Payne, 2016; Stout et al., 2016a, 2017). Transport of the oil from the wellhead to the underlying sediments occurred by multiple pathways (Stout and Payne, 2016; Fig. 30.1). Some oil was deposited on the seafloor within a direct fallout zone that extended approximately 3 km of the well, a process aided in part by the oil's cooccurrence with dense synthetic-based drilling mud (OSAT-1, 2010). Some of the Macondo oil that had ascended to the sea surface was transported back to the deep benthic sediments when bacteria-mediated mucus-rich marine snow formed in the near surface waters, and sunk, carrying some oil with it to the seafloor (Passow et al., 2012; Passow, 2014; Fu et al., 2014). Similarly, bacteria-mediated marine snow also formed within the deep-sea as indigenous bacteria proliferated while consuming dissolved gas and small oil droplets that had remained in the deep-sea within well-defined plumes (Camilli et al., 2010; Hazen et al., 2010; Socolofsky et al., 2011; Atlas and Hazen, 2011; Payne and Driskell, 2015a,b). This deep "marine oil snow" also sunk and carried oil to the seafloor (Baelum et al., 2012). The sinking of marine oil snow from both the sea surface and deep-sea plume to the seafloor led to the widespread accumulation of oil-bearing "floc" on the seafloor. The oil composition of this floc was found to consist of wax-rich, severely weathered Macondo oil, which tended to increase in the degree of weathering with increased distance from the well (Stout and Payne, 2016). Finally, some oil entrained within the deep-sea plume(s) directly impinged on sediments where bathymetry allowed resulting in elevated oil concentrations along the continental slope north of the well (i.e., "bathtub" ring; Stout et al., 2017; Fig. 30.1).

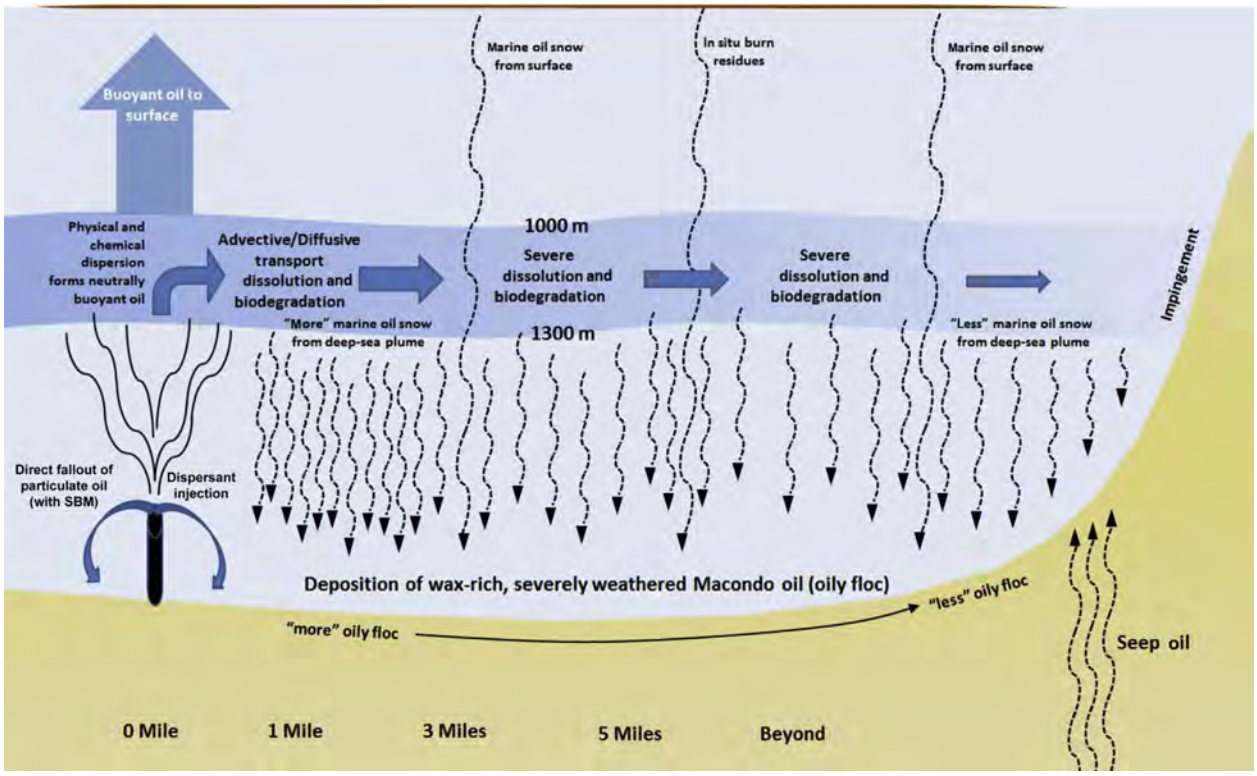

FIGURE 30.1 Conceptual model for Macondo oil deposition on the deep-sea floor. *Reprinted from Stout and Payne (2016) with permission from Elsevier.*

Deep benthic macrofauna living in and on these sediments were undoubtedly exposed to the oil and oily floc deposited on the seafloor through external contact with the oil (e.g., gills) or internal contact by ingestion of particulates and oil-impacted prey. A previous study had shown impacts of the DWH oil-derived floc occurred in deep-sea corals from northwest Biloxi Dome (MC294) where brown floc on coral was shown to contain Macondo oil (White et al., 2012; see also Stout et al., this volume). However, no large-scale study of the exposure of deep benthic macrofauna to Macondo oil or oil-derived floc has been conducted.

Assessing the amount and identity of oil present in biological tissue samples can be determined by oil fingerprinting. Oil fingerprinting typically relies on comparing the chemical fingerprint of the spilled oil vs that of the oil in environmental samples. If the oil component of the environmental sample is the same as the source oil, the fingerprints will "match." However, chemical fingerprinting of biological tissues must consider the effects that both the oil's weathering and any metabolism of the oil following uptake that may alter its composition, or fingerprint.

Benthic organisms can uptake oil-impacted, fine sediment particles present in the bottom mud and nepheloid layer by directly ingesting the material or through the exposure of external respiratory organs such as gills (Baumard et al., 1998; Lee et al., 1976). For example, the deep-sea red crabs (*Chaceon quinquedens*) studied herein eat a wide variety of infaunal and epifaunal benthic invertebrates that they find in silty sediments or pick off the seabed surface (NOAA, 2001). As such, ingestion of Macondo oil-impacted prey, sediment, or oil-derived floc by the red crabs is anticipated to have occurred as a result of the DWH spill.

Once incorporated within the benthic organism, metabolism and excretion of selected chemical compounds may occur [e.g., polycyclic aromatic hydrocarbons (PAHs)], further altering the chemical fingerprint of any oil remaining within the tissue. The accumulation of these compounds in benthic macrofauna is governed by the biotransformation capacities of the organism and by the PAH concentration of the prey they feed on (Baumard et al., 1998). The challenge for the forensic chemist is to (1) physically extract the weathered oil from the tissue and then (2) quantify the oil's diagnostic petroleum hydrocarbons, such as alkylated PAHs and petroleum biomarkers (e.g., triterpanes, such as hopane), in order to identify the presence and source of the oil in the tissue (Bartolome et al., 2007). At the most basic level, the presence of alkylated PAH homologs patterns that are

consistent with petrogenic sources is reliable proof that the organism has been exposed to petroleum (Douglas et al., 2007a; Stout and Wang, 2016). Additionally, the relative distribution of the PAH homologs in the tissue provides oil source and type information as well (Short and Babcock, 1996). However, as the PAH signature weathers in the environment and/or is metabolized/depurated in the tissue samples (Meador et al., 1995; Varanasi, 1989; Pruell et al., 1986), additional weathering resistant and source-specific petroleum biomarker compounds are extremely useful in establishing exposure and oil source identification (Stout, 2016; Wang and Stout, 2006; Wang et al., 2016). These triterpane and sterane compounds are highly resistant to weathering, including biodegradation (Prince et al., 1994; Douglas et al., 2012) and to tissue metabolism, thus providing a reliable measure of the source signature of petroleum in tissue samples (Ashton et al., 2000; Bartolome et al., 2007).

In addition to chemical fingerprinting of PAHs and biomarkers, other lines of evidence can be used to reach a forensic conclusion regarding the source of any oil detected in benthic tissues. These additional lines of evidence include temporal and spatial analysis of the data. With regards to temporal analysis, concentrations of hydrocarbons measured in benthic tissues are found to be highest following a spill and subsequently decrease over time. Therefore, the elevated concentrations measured soon after the spill can be reasonably concluded to have resulted from the spill. With regards to spatial analysis, if oil exposure is identified in animals living within the delineated oil spill zone then it can be reasonably concluded that the contamination is more likely than not related to the oil spill. In the case of the DWH oil spill, the spill zone of impacted deep seafloor has been quite well defined. Specifically, Stout et al. (2017) concluded that the total mass of Macondo-derived PAHs deposited on the seafloor was conservatively estimated between 2.00 and 2.26 mt and covered between 1030 and 1910 km^2 of the deep seafloor. Although numerous natural sources of oil (i.e., oil seeps) also were recognized to exist within this spill zone the impact of these were highly localized compared to the widespread impact of the Macondo oil and oil-derived floc on the seafloor [Stout et al., 2016a and thereby were excluded from the Stout et al. (2017) mass estimates]. In fact, at some seep area Macondo-derived oily floc was able to be recognized to have been deposited "atop" sediments impacted with naturally seeped oil (Stout et al., 2016a).

In this study, we report on the forensic evaluation—involving chemical fingerprinting and spatial/temporal analysis—of one particular type of benthic macrofauna present in the northern Gulf of Mexico, viz., deep-sea red crabs (*C. quinquedens*). Tissue samples collected from red crabs within the deep benthic DWH spill zone in 2010/2011 are studied and compared to those collected in 2014, 4 years after the spill. The objective of this work was to develop a reliable approach to identify Macondo-derived petroleum residuals in the deep benthic macrofauna tissue samples following the DWH oil spill, and thereby confirm their exposure to the spilled Macondo oil.

30.2 METHODS AND SAMPLES

30.2.1 Red Crab Sample Collection

The details regarding the collection of numerous red crab tissue types can be found in the NRDA Sampling Plans (NOAA, 2009, 2010a,b,c, 2011a,b, 2012, 2013a, 2013b, and 2014a). In summary, red crabs were collected in 2011 and 2014 as part of the NOAA R/V *Pisces* cruise from nearfield, historic, and seep locations. In total, collections were made from 69 unique locations, although not all locations sampled in 2011 were duplicated in 2014 due to poor sample capture success in those locations in 2011. For details on exact locations, refer to the NRDA Red Crab Sampling Plans referenced above.

Crab pots were baited and allowed to sit on the seafloor for approximately 18 hours at each sample station. Upon retrieval, crabs were removed from traps and immediately placed in a refrigerated seawater system set at 5°C. Crabs were maintained alive for a maximum of 24 hours until dissection onboard. Crabs were dissected using glass cutting boards, and ceramic or Teflon equipment. Dissected tissues provided for chemical analysis included hepatopancreas, gonads, gills, and muscle. Eggs were also collected from ovigerous females by removing the entire pleopod. All dissected tissues were stored frozen onboard at −20°C and maintained frozen during shipment to the laboratory (NOAA, 2011b, 2013b, 2014a). A limited number of whole body and external rinsate samples were also prepared and analyzed.

30.2.2 Red Crab Sample Analysis

Total of 1744 red crab tissue samples, which included 1321 samples collected in 2010−2011 and 423 samples collected in 2014, were evaluated in this study. In 2010−2011, these samples were composed of hepatopancreas (331),

gills (322), gonads (283), eggs, (52), muscles (328), whole body (1), and rinsates (4). In 2014, only hepatopancreas (423) were studied, owing to the fact that these tissues proved most useful in recognizing oil impacts among the 2010–2011 sample set. All of the tissue samples in this study were analyzed for detailed PAH and petroleum biomarker concentrations in accordance with the NOAA QAP prepared for the Mississippi Canyon 252 (DWH) NRDA (NOAA, 2014b).

30.2.3 Sample Preparation

Red crab samples were either delivered to the laboratory as predissected tissues (NOAA, 2013b, 2014a) or as the whole organism, which were then dissected into selected tissues (e.g., hepatopancreas, edible muscle tissue, gills, etc.) depending on size and gender. Samples requiring dissection were processed using stainless steel, or titanium and ceramic utensils (if metals analysis was to be performed). As an example, the carapace of the crabs was removed to gain access to the lipid-rich, hepatopancreas where environmental contaminants tend to accumulate making this the organ of choice (Meador et al., 1995; Varanasi, 1989). In some cases, the hepatopancreas was not always well defined possibly due to health of the animal or whether the animal was retrieved alive or was deceased for some time prior to retrieval. In these cases, all of the internal organs were removed for analysis and identified as such. Ancillary data (i.e., weight, length, or size) were collected from the whole body animals before they were dissected (Fig. 30.2).

Whole body and dissected parts were homogenized using a stainless steel or titanium (metals) Tissuemizer probe. Approximately, 10 g of homogenized tissue, or 5 g of fatty tissue (i.e., hepatopancreas), were dried with sodium sulfate to remove water, supplemented with surrogates, and serially extracted with dichloromethane (DCM) using a stainless steel tissuemizer probe (NOAA, 1993; Douglas et al., 2007a). The combined extract was concentrated using a Kuderna–Danish (KD) apparatus and an aliquot removed for lipid determination. Half of the extract was eluted through a combined silica/alumina gel column and concentrated using KD and nitrogen blowdown. Due to the high lipid content (readily extracted using DCM), tissues were further processed through a high-pressure liquid chromatography (HPLC) column to remove interfering lipids (EPA, 1994; Douglas et al., 2007a,b) which are not present in oil or sediments. Extracts were further concentrated and fortified with internal standards prior to instrumental analysis (Uhler et al., 2005; Douglas et al., 2007a).

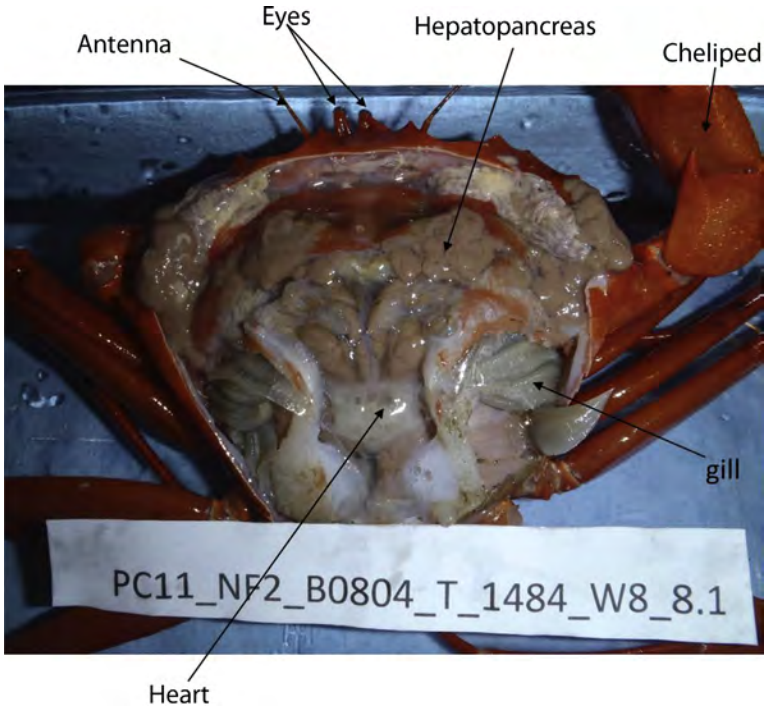

FIGURE 30.2 Red crab anatomy with carapace removed identifying hepatopancreas. Red crab photo is provided compliments of Barbara Viskup and Harriet Perry from South Regional Office of Mississippi Department of Environmental Quality at Biloxi, MS.

30.2.4 Instrument Analysis

Tissue samples were analyzed for PAHs using a gas chromatograph equipped with a mass spectrometer (GC/MS) operated in the selected ion monitoring (SIM) mode in accordance with a modified EPA Method 8270d (EPA, 2014; Douglas et al., 2007a,b; Douglas and Uhler, 1993; NOAA, 1993; Federal Register, 1994). This method determined the concentrations of 52 PAHs and alkylated PAHs including sulfur-containing aromatics (Table 30.1), total 49 PAH ($TPAH_{49}$) concentrations are calculated from the PAH analyte listed in Table 30.1. The concentrations of target compounds are presented herein as $\mu g/kg_{wet}$ for tissues. The concentration and distribution of PAHs provided greater detail and specificity about the type of contamination (petroleum, combustion byproducts, and background sources) in the field samples. For example, petroleum PAH patterns consist of a low parent PAH abundance relative to the alkylated PAHs, e.g., N0 < N1 < N2. By contrast, pyrogenic PAH patterns exhibit a high abundance of parent PAHs relative to the alkylated PAHs, e.g., N0 > N1 > N2, before weathering.

Selected tissue samples that contained a petroleum PAH pattern based on the initial PAH GC/MS analysis were further processed for biomarkers. Although the HPLC cleanup process discussed above is highly effective in removing lipid interferences for PAHs, it is less effective in removing lipid interferences among the biomarkers. This is due in part to the wide collection window on the HPLC required for biomarkers that also includes lipids (EPA, 1994; Douglas et al., 2007a). The narrow PAH collection window can be used to determine if some biomarkers are present (e.g., hopane), however, it does not capture the complete pattern. Therefore, in order to eliminate the lipid interferences and capture the full biomarker pattern, a portion of the pre-HPLC archive extract for the selected samples (i.e., those demonstrating petroleum PAH patterns) was solvent exchanged into hexane and processed through a silica gel column into an F_1 fraction (Fig. 30.3). Extracts were analyzed for biomarkers using a GC/MS operated in SIM mode in accordance with a modified EPA Method 8270d (EPA, 2014). This method determined the concentrations of petroleum biomarkers including tricyclic and pentacyclic triterpanes, regular and rearranged steranes (Table 30.1). The concentrations of target compounds are presented herein as $\mu g/kg_{wet}$ weight for tissues. The total concentration of all targeted biomarkers (Table 30.1) is described herein as TBIO.

High-resolution GC/FID fingerprints, total petroleum hydrocarbons (TPHs) and individual alkane concentrations were not generated for tissue samples due to the high lipid interferences that will obscure the chromatograms and produce false TPH and alkane detections (EPA, 1997; Clark and Brown, 1977). The preferred analytical methods for lipid-rich tissue samples are PAH and biomarker compounds analyses by GC/MS, as discussed above. All distributions of PAH or biomarkers presented in this study were evaluated at 3 times signal to noise and are calculated from surrogate uncorrected concentrations in order to eliminate the effect of surrogate correction on the chemical distributions. All analytical results for the samples studied were also reported through NOAA's Data Integration Visualization Exploration and Reporting (DIVER, 2015) system, which is a collection of tools and processes to standardize and make available a vast range of data associated with the NRDA surrounding the DWH spill. However, the concentrations reported therein were surrogate corrected.

30.2.5 Fingerprint Classification

The analytical results for each sample were examined and classified into one of the five categories: Fingerprint Classifications A through E (Table 30.2 and Fig. 30.4). In practice, a fingerprint classification of A through C indicated oil exposure was evident in the tissue but at decreasing levels of confidence. For example, samples assigned an "A" fingerprint classification exhibited reliable evidence of a Macondo oil source (Figs. 30.5 and 30.6), whereas samples identified with a "C" classification were considered less reliable. Samples classified with a "D" fingerprint classification were indeterminate and simply did not contain a sufficient chemical signature to reliably identify presence of Macondo oil in the sample (Table 30.2). Samples classified with a fingerprint classification of "E" had distinct chemical signatures that were different from the Macondo oil, indicating exposure to a different type of oil (e.g., natural seep oils). This sample classification system for red crab tissues paralleled that used in the assessment of deep-sea sediments (Stout et al., 2016a).

As discussed above, complicating factors affecting tissue chemical fingerprints were the weathering of the oil and any changes due to uptake or metabolism, all of which altered the chemical signature of the Macondo oil found in tissues. Close to the Macondo well (<1.6 km), oil exposures were clearly identified, however, with increasing distance from the well the chemical fingerprint signature declined and the degree of weathering increased (Stout and Payne, 2016). Dispersion of the oil, transportation in the water column, and floc formation and sedimentation (Fig. 30.1) all impacted the PAH distributions of the Macondo oil residues deposited on the

TABLE 30.1 Inventory of PAH and Petroleum Biomarker Analytes Analyzed in the Red Crab Tissues Studied

Abbrev.	Compound	$tPAH_{49}$
D0	*cis*/*trans*-Decalin	
D1	C1-Decalins	
D2	C2-Decalins	
D3	C3-Decalins	
D4	C4-Decalins	
BT0	Benzothiophene	
BT1	C1-Benzo(*b*)thiophenes	
BT2	C2-Benzo(*b*)thiophenes	
BT3	C3-Benzo(*b*)thiophenes	
BT4	C4-Benzo(*b*)thiophenes	
N0	Naphthalene	X
N1	C1-Naphthalenes	X
N2	C2-Naphthalenes	X
N3	C3-Naphthalenes	X
N4	C4-Naphthalenes	X
B	Biphenyl	X
DF	Dibenzofuran	X
AY	Acenaphthylene	X
AE	Acenaphthene	X
F0	Fluorene	X
F1	C1-Fluorenes	X
F2	C2-Fluorenes	X
F3	C3-Fluorenes	X
A0	Anthracene	X
P0	Phenanthrene	X
PA1	C1-Phenanthrenes/Anthracenes	X
PA2	C2-Phenanthrenes/Anthracenes	X
PA3	C3-Phenanthrenes/Anthracenes	X
PA4	C4-Phenanthrenes/Anthracenes	X
RET	Retene	
DBT0	Dibenzothiophene	X
DBT1	C1-Dibenzothiophenes	X
DBT2	C2-Dibenzothiophenes	X
DBT3	C3-Dibenzothiophenes	X
DBT4	C4-Dibenzothiophenes	X
BF	Benzo(*b*)fluorene	
FL0	Fluoranthene	X
PY0	Pyrene	X
FP1	C1-Fluoranthenes/Pyrenes	X
FP2	C2-Fluoranthenes/Pyrenes	X

(*Continued*)

TABLE 30.1 (*Continued*)

Abbrev.	Compound	$tPAH_{49}$
FP3	C3-Fluoranthenes/Pyrenes	X
FP4	C4-Fluoranthenes/Pyrenes	X
NBT0	Naphthobenzothiophenes	X
NBT1	C1-Naphthobenzothiophenes	X
NBT2	C2-Naphthobenzothiophenes	X
NBT3	C3-Naphthobenzothiophenes	X
NBT4	C4-Naphthobenzothiophenes	X
BA0	Benz[*a*]anthracene	X
C0	Chrysene/Triphenylene	X
BC1	C1-Chrysenes	X
BC2	C2-Chrysenes	X
BC3	C3-Chrysenes	X
BC4	C4-Chrysenes	X
BBF	Benzo[*b*]fluoranthene	X
BJKF	Benzo[*j*]fluoranthene/Benzo[*k*]fluoranthene	X
BAF	Benzo[*a*]fluoranthene	X
BEP	Benzo[*e*]pyrene	X
BAP	Benzo[*a*]pyrene	X
PER	Perylene	
IND	Indeno[1,2,3-cd]pyrene	X
DA	Dibenz[*ah*]anthracene/Dibenz[*ac*]anthracene	X
GHI	Benzo[*g*,*h*,*i*]perylene	X

Abbrev.	Compound
T4	C23 Tricyclic terpane
T5	C24 Tricyclic terpane
T6	C25 Tricyclic terpane
T6a	C24 Tetracyclic terpane
T6b	C26 Tricyclic terpane-22S
T6c	C26 Tricyclic terpane-22R
T7	C28 Tricyclic terpane-22S
T8	C28 Tricyclic terpane-22R
T9	C29 Tricyclic terpane-22S
T10	C29 Tricyclic terpane-22R
T11	18α-22,29,30-Trisnorneohopane-Ts
T11a	C30 Tricyclic terpane-22S
T11b	C30 Tricyclic terpane-22R
T12	17α(*H*)-22,29,30-trisnorhopane-Tm
T14a	17α/β,21β/α 28,30-Bisnorhopanes
T14b	17α(*H*),21β(*H*)-25-norhopane
T15	30-Norhopane

(*Continued*)

TABLE 30.1 (*Continued*)

Abbrev.	Compound
T16	18α(*H*)-30-norneohopane-C29Ts
X	17α(*H*)-diahopane
T17	30-Normoretane
T18	18α(*H*)&18β(*H*)-oleananes
T19	Hopane
T20	Moretane
T21	30-Homohopane-22S
T22	30-Homohopane-22S
T22A	T22a-gammacerane/C32-diahopane
T26	30,31-Bishomohopane-22S[a]
T27	30,31-Bishomohopane-22R
T30	30,31-Trishomohopane-22S
T31	30,31-Trishomohopane-22R
T32	Tetrakishomohopane-22S
T33	Tetrakishomohopane-22R
T34	Pentakishomohopane-22S
T35	Pentakishomohopane-22R
S4	13β(*H*),17α(*H*)-20S-Diacholestane
S5	13β(*H*),17α(*H*)-20R-Diacholestane
S8	13β(*H*),17α(*H*)-20S-Methyldiacholestane
S12	14α(*H*),17α(*H*)-20S-Cholestane/13b(H),17a(H)-20S-Ethyldiacholestane
S17	14α(*H*),17α(*H*)-20R-Cholestane/13b(H),17a(H)-20R-Ethyldiacholestane
S18	13β(*H*),17α(*H*)-20R-Ethyldiacholestane
S19	13α(*H*),17β(*H*)-20S-Ethyldiacholestane
S20	14α(*H*),17α(*H*)-20S-Methylcholestane
S24	14α(*H*),17α(*H*)-20R-Methylcholestane
S25	14α(*H*),17α(*H*)-20S-Ethylcholestane
S28	14α(*H*),17α(*H*)-20R-Ethylcholestane
S14	14β(*H*),17β(*H*)-20R-Cholestane
S15	14β(*H*),17β(*H*)-20S-Cholestane
S22	14β(*H*),17β(*H*)-20R-Methylcholestane
S23	14β(*H*),17β(*H*)-20S-Methylcholestane
S26	14β(*H*),17β(*H*)-20R-Ethylcholestane
S27	14β(*H*),17β(*H*)-20S-Ethylcholestane
RC26/SC27TA	C26,20R- + C27,20S-triaromatic steroids
SC28TA	C28,20S-triaromatic steroid
RC27TA	C27,20R-triaromatic steroid
RC28TA	C28,20R-triaromatic steroid

[a]*Not included in the total Biomarker summation due to interference.*
Abbreviations used in figures and list of 49 PAH analytes included in the total PAH ($tPAH_{49}$) concentrations discussed herein are indicated.

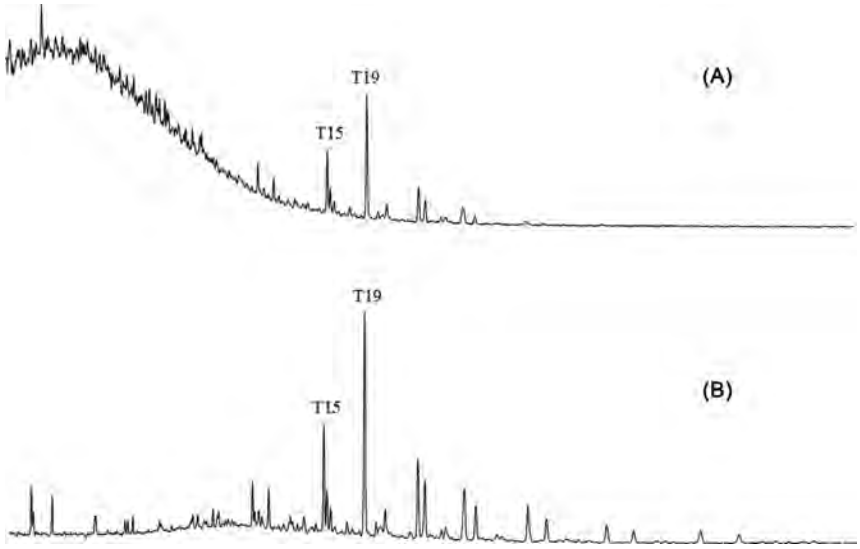

FIGURE 30.3 GC/MS of biomarker m/z 191 extracted ion plots for the extract from hepatopancreas from a single red crab prepared differently. (A) Post-HPLC extract showing obstructed biomarker pattern with only hopane (T19) and norhopane (T15) visible and (B) pre-HPLC extract processed through silica gel to obtain an F_1 aliphatic hydrocarbon fraction showing a full biomarker pattern. Sample identification in both: PC11_NF1_B0804_T_1478_W8_5.3H.

TABLE 30.2 Fingerprint Classifications Used in the Characterization of Hydrocarbons in Red Crab Tissue Samples

Fingerprint classification	Description	Practical conclusion to NRDA
A	Chemical fingerprints are consistent with weathered Macondo oil	Macondo crude oil is present
B	Chemical fingerprints are mostly consistent with weathered Macondo oil with any differences being reasonably attributable to low(er) concentrations, the effects of very severe weathering, and/or obvious interferences	
C	Chemical fingerprints are affected by mixing, interferences, or metabolic effects, although some Macondo oil may be present; concentrations often low	Equivocal; Macondo crude oil is possibly present
D	Chemical fingerprints are inconclusive, most often due to a very low hydrocarbon concentrations, or high proportion of background	No Macondo crude oil or indeterminate due to low target concentration
E	Chemical fingerprints are inconsistent with fresh or weathered Macondo oil and not attributable to weathering and/or mixing (i.e., a different type of oil is present)	Macondo oil is not present but a different petroleum is present

seafloor, which in turn, were then transferred to the exposed red crabs' tissue samples. Thus, comparisons of tissue fingerprints to the Macondo oil were performed using appropriate reference materials that were selected to account for both oil weathering and any uptake/metabolic or tissue matrix effects.

For example, in addition to comparisons to "fresh" Macondo oil, red crab tissue samples that were clearly impacted with substantial petroleum residues and located close to the Macondo well (<1.6 km) were adopted as "exposed tissue reference samples" because the hydrocarbons in these samples collectively incorporated weathering, uptake/metabolic, and tissue matrix effects on the Macondo oil residues found in these "exposed tissue reference samples." In addition, oily floc samples carefully collected from the seafloor and previously studied (Stout and Payne, 2016) were also used as Macondo oil reference samples for comparison to the tissue samples—rather than "fresh" Macondo oil. The characters of these different reference materials are described in Section 30.3.

Oil exposure was identified based on the distribution of alkylated PAH compounds and/or biomarker compounds in the samples. *Oil type* was determined by the range of those PAH compounds (e.g., alkylated naphthobenzothiophenes and chrysenes) and/or the presence of triterpane and sterane biomarker compounds (depending on available data and degree of PAH weathering). *Oil identification* was based on direct examination of the PAH (Fig. 30.5) and biomarker signatures (Figs. 30.6 and 30.7) and comparisons to appropriate reference

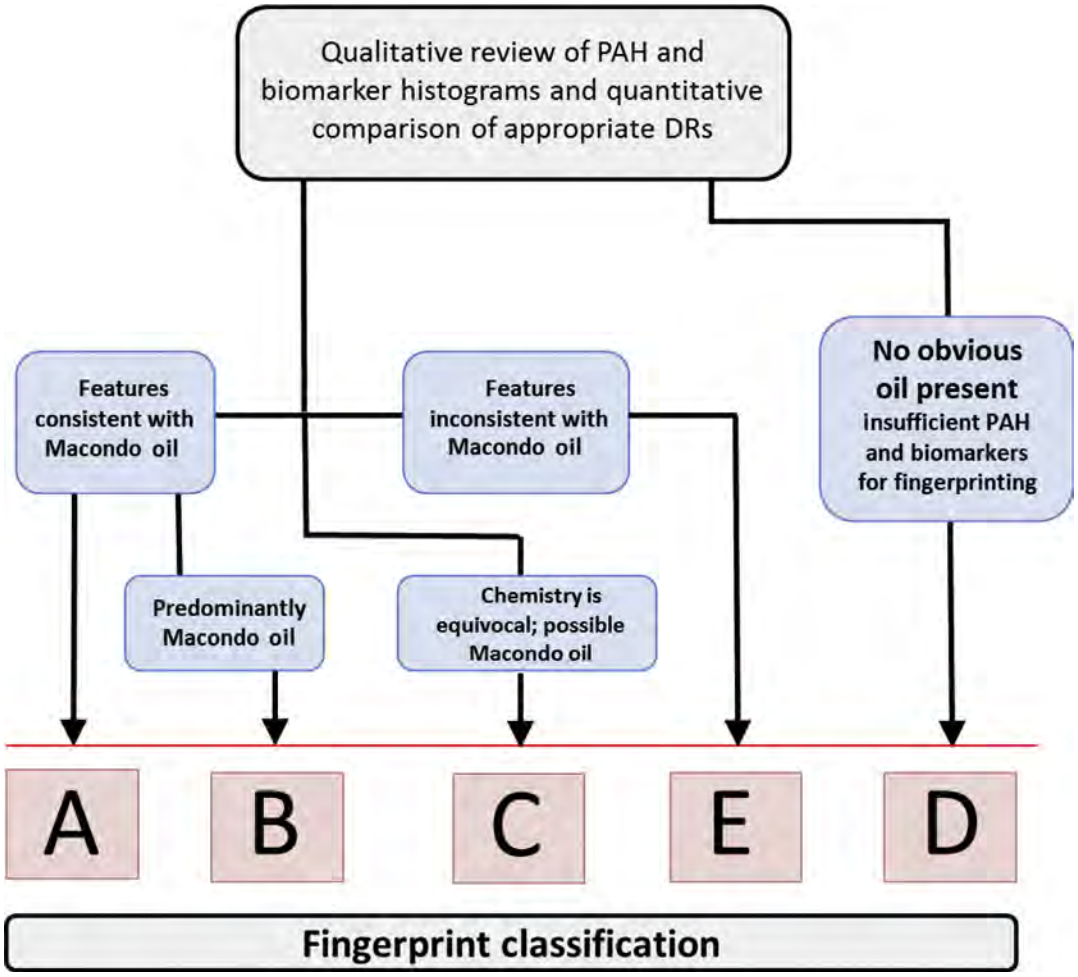

FIGURE 30.4 Flowchart depicting the tiered approach to fingerprinting red crab (and other deep benthic) tissue samples for the NRDA of the DWH oil spill.

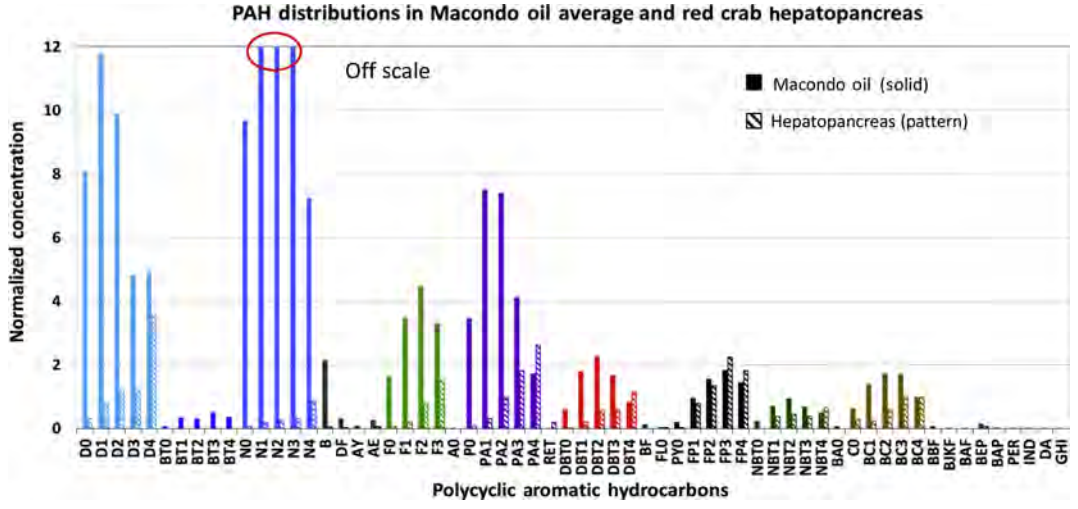

FIGURE 30.5 Histograms showing the concentrations of PAHs normalized to C4-Chrysene (BC4) comparing the fresh Macondo oil and a red crab hepatopancreas sample collected 1.2 km from the wellhead. This sample was assigned a fingerprint class "A." Sample ID: PC11_NF1_B0804_T_1478_W8_3.2H. Fresh Macondo average ($n = 6$) data from Stout et al. (2016b).

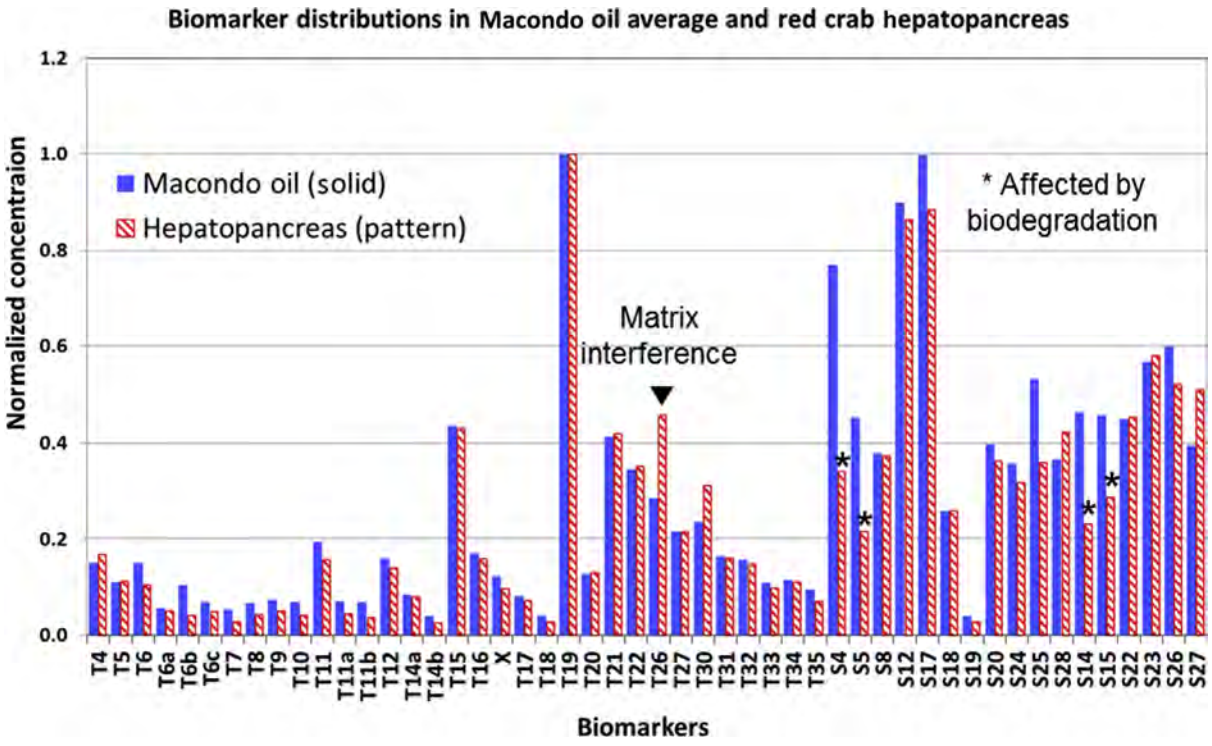

FIGURE 30.6 Histograms the hopane (T19) normalized concentrations of triterpanes (*blue* (filled bars)) and steranes (*red* (striped bars)) in fresh Macondo oil and a red crab hepatopancreas sample collected 1.2 km from the wellhead. This sample was assigned a fingerprint class "A." Sample ID: PC11_NF1_B0804_T_1478_W8_3.2H. Fresh Macondo average ($n = 6$) data from Stout et al. (2016b).

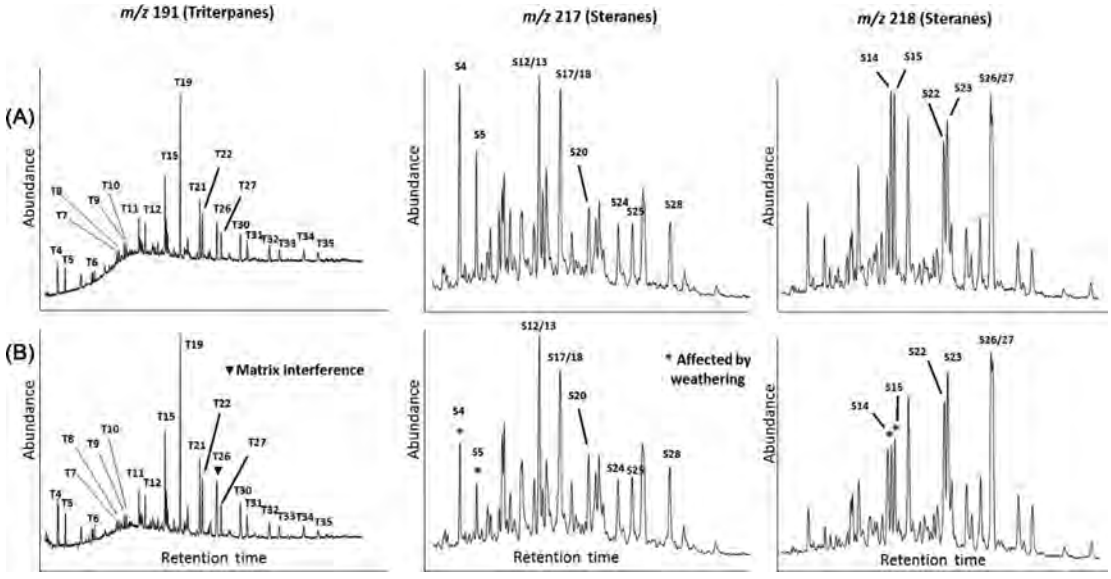

FIGURE 30.7 Partial m/z 191, 217 and 218 GC/MS ion profiles showing biomarker distributions in (A) fresh Macondo oil and (B) a red crab hepatopancreas sample collected 1.2 km from the wellhead. This sample was assigned a fingerprint class "A." Sample ID: PC11_NF1_B0804_T_1478_W8_3.2H. Note: T26 may be elevated due to matrix interference and S4, S5, S14, and S15 are depleted but recognized as susceptible to biodegradation in deep-sea sediments (Stout and Payne, 2016).

samples (i.e., Macondo oil, exposed tissue reference samples, and/or oily floc reference samples). To facilitate this comparison, 25 diagnostic ratios (DRs) calculated from the concentrations of highly specific, diagnostic PAH and biomarker compounds present in the tissue samples and the various Macondo reference samples were used to confirm the presence or absence of Macondo oil in the red crab tissue samples. The DRs used are typical of

those used in various oil spill source identification protocols (Stout et al., 2001; Daling et al., 2002; CEN, 2012). The selection of these DRs was based on a combination of published and long-established features recognized to depict differences among the specific geologic source and/or thermal history of a given crude oil (Peters and Moldowan, 1993). The level of confidence associated with each analysis is based on professional judgment of the degree to which the chemical fingerprints qualitative features and the calculated DRs matched an appropriate Macondo oil reference sample(s).

Additional consideration was given during the fingerprint classification process (Fig. 30.4) to the degree of "fit" between the chemical fingerprints of tissues and an appropriate Macondo reference sample(s), the location that the tissue sample was collected relative to the Macondo well, the tissue sample's proximity to surface sediments previously recognized to contain Macondo oil and oily floc (Stout and Payne, 2016) and its position within the recognized DWH spill zone "footprint" (Stout et al., 2017).

30.3 RESULTS AND DISCUSSION

A summary of the fingerprint classification for the red crab tissues from the 2010–2011 and 2014 sampling events are provided in Table 30.3. These results will be discussed in further detail later in this section.

Four basic forensic chemistry questions were addressed within the red crab study: (1) were red crabs exposed to Macondo oil, (2) could the benthic exposure be reliably measured by red crab tissues within the DWH spill zone, (3) what was the spatial extent of red crabs exposed to Macondo oil within the deep benthos, and (4) were the red crab tissues exposed to Macondo oil consistent with other independent studies of Macondo oil spill impacts (e.g., impact deep benthic sediments).

The answers to these questions are complicated by the fact that (1) forensic chemical analysis of crab tissues is an innovative approach, (2) tissue samples are generally small requiring sensitive and diagnostic analytical methods, (3) the Macondo oil hydrocarbon signature had been variably altered due to weathering, and (4) the Macondo oil was native to the geologic province in which it was spilled and, therefore, shared many chemical features with other northern Gulf of Mexico oils spilled or seeped within the same province.

The conceptual oil spill model prepared by Stout and Payne (2016) summarizes the various pathways that oil reached the seafloor during (April 20–July 15, 2010) and after the DWH spill (Fig. 30.1). The details and associated evidence are discussed in by Stout and Payne (2016) and were summarized in Section 30.1 herein. Various

TABLE 30.3 Summary of Results for the Forensic Fingerprinting Classes Assigned to Red Crab Tissue Samples Collected from Different Tissue Types in the 2010–2011 and 2014 Sampling Events

	2010–2011 Red crab								2014
Category	**Hepatopancreas**	**Gills**	**Gonads**	**Eggs**	**Muscles**	**Whole body**	**Rinsate**	**All 2010/11[a]**	**Hepatopancreas**
Total samples	331	322	283	52	328	1	4	1321	423
Mocondo oil matches A + B + C	137	3	18	11	2	0	1	172	343
Mocondo oil match A	62	0	0	0	0	0	0	62	4
Mocondo oil match B	41	1	5	1	1	0	1	50	72
Mocondo oil match C	34	2	13	10	1	0	0	60	267
Class D (indeterminate)	178	319	265	41	326	1	3	1133	59
Class E (nonmatch)	16	0	0	0	0	0	0	16	21
% Mocondo oil matches A + B + C	41%	1%	6%	21%	1%	0%	25%	13%	81%
Mocondo oil match A	19%	0%	0%	0%	0%	0%	0%	5%	1%
Mocondo oil match B	12%	0%	2%	2%	0%	0%	25%	4%	17%
Mocondo oil match C	10%	1%	5%	19%	0%	0%	0%	5%	63%
Class D (Indeterminate)	54%	99%	94%	79%	99%	100%	75%	86%	14%
Class E (nonmatch)	5%	0%	0%	0%	0%	0%	0%	1%	5%

[a]*17 Red crab samples (gonads, gills, muscles) not included. These are metals analyses only.*

mechanisms transferred Macondo oil to the seafloor and into the red crab habitat. Red crabs therefore were exposed to particulate-bound whole oil (often in association with synthetic-based drilling mud) near the well (<1.6 km), and to wax-rich, severely weathered Macondo-derived oily floc further from the well within the surface sediments.

30.3.1 Red Crabs as Sentinel Organisms in the Deep Benthos

Marine organisms are important biological indicators of chronic and transient pollutants in the environment (NOAA, 1991; Bence and Burns, 1995; Bender et al., 1988; Wade et al., 1989; Short and Babcock, 1996). Oil spill studies often collect tissue samples as a means to provide time-integrated measure of environmental exposure to oil or its components (e.g., PAHs, Porte et al., 2000; Bence and Burns, 1995; Glegg and Rowland, 1996). For oil spills with coastal intertidal impacts, bivalves (mussels and oysters) are the preferred organisms for monitoring environmental exposure. This is because their habitats are often proximal to the shoreline contamination, they are easy to sample, they are capable of bio-accumulating certain contaminants, their hydrocarbon metabolism (Lee et al., 1976; Bend et al., 1981; Little et al., 1985) and depuration rates (Pruell et al., 1986; Peven et al., 1996) are relatively slow, and there is a vast amount of scientific literature regarding their applications and limitations at oil spill sites.

Unfortunately, the preferred habitat for these previously studied sentinel organisms is not the deep benthos. Red crabs, however, are abundant in the deep benthic habitats proximal to the Macondo well and can be collected using baited crab pots. Their mobility (Ganz and Herrmann, 1975; Lockhart et al., 1990) is a positive factor in their use as sentinel organisms in that oil residues retained within their tissues would provide a spatially integrated signature relative to an immobile coral or bivalve, as the crabs actively moved through the seafloor's oily floc layer.

30.3.2 Red Crab Anatomy

Red crabs continuously filter fine sediment particles that are present in the bottom mud and nepheloid layer (NOAA, 2013b, 2014a). It is also suggested that red crabs are the major bioturbators of surface sediments through their feeding activities and are important biotic modifiers of the sea floor (Hastie, 1995). Crustaceans (e.g., crabs, lobsters, and shrimp) are often drawn to food based on the detection of dissolved material. Food is taken into the mouth, passes through the esophagus and into the stomach which consists of two chambers. The stomach is lined with hard chiton that serves to grind the material into a liquid paste on its way to the hepatopancreas (Ceccaldi, 1989).

The hepatopancreas (Fig. 30.2) is a lipid-rich dual organ in red crabs and other crustaceans, which performs the functions of both a liver and pancreas. The hepatopancreas is considered a major organ with many metabolic functions. This includes the synthesis and secretion of digestive enzymes, absorption of digested material from the stomach, distribution of stored reserves to muscle, gonads and other tissues, and storage of energy in the form of lipid and carbohydrate which can be later metabolized and the catabolism of organic compounds. In most decapods (e.g., crabs, lobsters, shrimp, etc.), it forms a pair of glans on either side of the stomach (Fig. 30.2) and can make up 2%–6% of the total body weight (Wang et al., 2014; Ceccaldi, 1989).

30.3.3 Uptake and Metabolic Effects

Fish and invertebrates can take up PAH contaminates from water and sediment through diffusion across their gills, integument and the ingestion of prey, detritus, and sediment. The major difference between PAHs is solubility in water, which is expressed as the log of the octanol:water partition coefficient (log K_{ow}) and is a measure of hydrophobicity (Mackay et al., 2006a,b; DiToro et al., 1991). As molecular weight increases, PAHs become more hydrophobic (higher log K_{ow}) and favor a less polar environment such as lipids (Meador et al., 1995). High concentrations of PAHs have been detected the hepatopancreas of lobsters and the blue crab compared to edible tissue and other organs indicating the hepatopancreas (rich in lipid) is the major organ for PAH uptake (McLeese, 1983; Lee et al., 1976).

PAH concentrations in tissues can decrease through metabolism and excretion. Metabolism is the process where PAHs that are introduced into an organism are biotransformed to polar metabolites (e.g., conversion of benzo[*a*]pyrene to hydroxybenzo[*a*]pyrene) and can be excreted out of the body via bile or urine. Fish have the ability to metabolize PAH rather quickly > Crustaceans (limited) > bivalves [poor (Meador et al., 1995; Neff et al., 1976)]. Lee et al. (1976) showed that 20 days after the transfer to clean water the hepatopancreas of the blue crab exposed to benzo[*a*]pyrene contained unmetabolized benzo[*a*]pyrene as well as metabolites indicating a slow metabolism by blue crabs. Bend et al. (1981) studied radio-labeled ^{14}C-benzo[*a*]pyrene in lobster where more than 80% of the ^{14}C-benzo[*a*]pyrene was still present in the hepatopancrease after 6.5 weeks.

The rate of PAH metabolism can also likely be affected by temperature. The excretion of radio-labeled ^{14}C-benzo[*a*]pyrene in the spiny lobster was slower at winter temperatures (13.5−16.5°C) compared to summer temperatures (26.5−29°C) (Little et al., 1985). It should be noted that metabolic rates can be species specific. Approximately 5% of the ^{14}C was left in the hepatopancreas of the spiny lobster at 3 days after dosing. The ambient temperature of the red crab deep benthic habitat studied herein is approximately 4°C (Steimle et al., 2001), which would reduce the metabolism of PAH compounds when compared to intertidal crabs from warmer environments. As will be discussed later, the hepatopancreas organ of red crabs provided the most reliable oil fingerprints for tissue classification and exposure assessment.

30.3.4 Macondo Oil Reference Samples for Comparison to Red Crab Tissues

Due to the alteration of the fresh Macondo oil during the oil spill, PAH and biomarker signatures from several reference samples were used to identify the presence of Macondo oil in the red crab tissue samples. These included (1) unweathered Macondo crude oil (Figs. 30.8A and 30.9A), (2) surface (0−1 cm) sediment collected

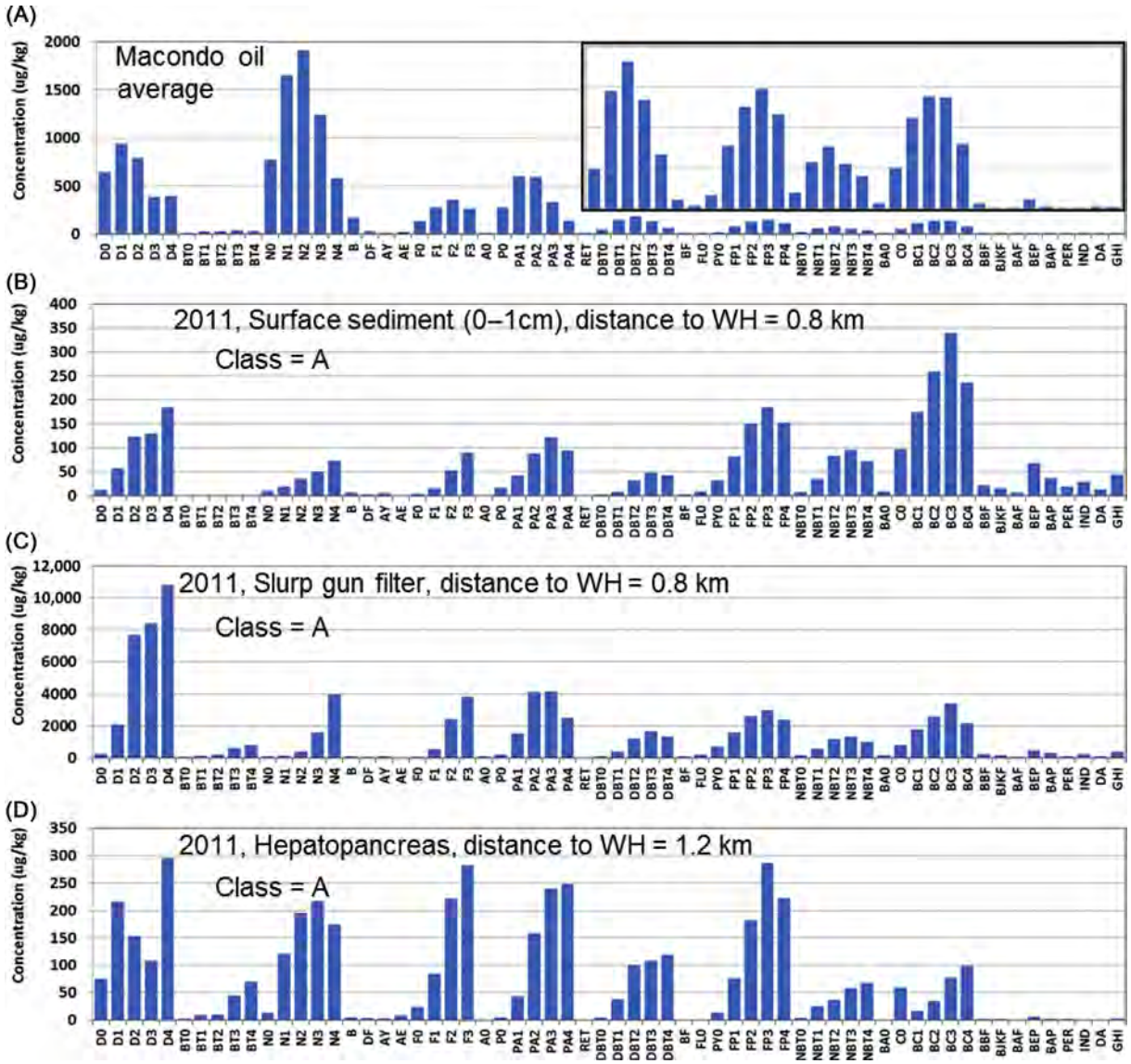

FIGURE 30.8 PAH distributions in four reference samples containing variably weathered/altered Macondo oil that were used in comparison to red crab tissues. (A) Fresh Macondo oil average, (B) surface sediment 0.8 km from the well (class = A), (C) slurp gun filter containing Macondo-derived oily floc, and (D) red crab hepatopancreas in reference crab collected 1.2 km from the wellhead. Sample IDs (A) fresh Macondo average ($n = 6$) from Stout et al. (2016b); (B) HSW2L2_FP0096_B0424_S_50_N2_885; (C) HSW2L2_FP0096_B0424_W_1495_50_P_Y_888; (D) PC11_NF1_B0804_T_1478_W8_1.2H.

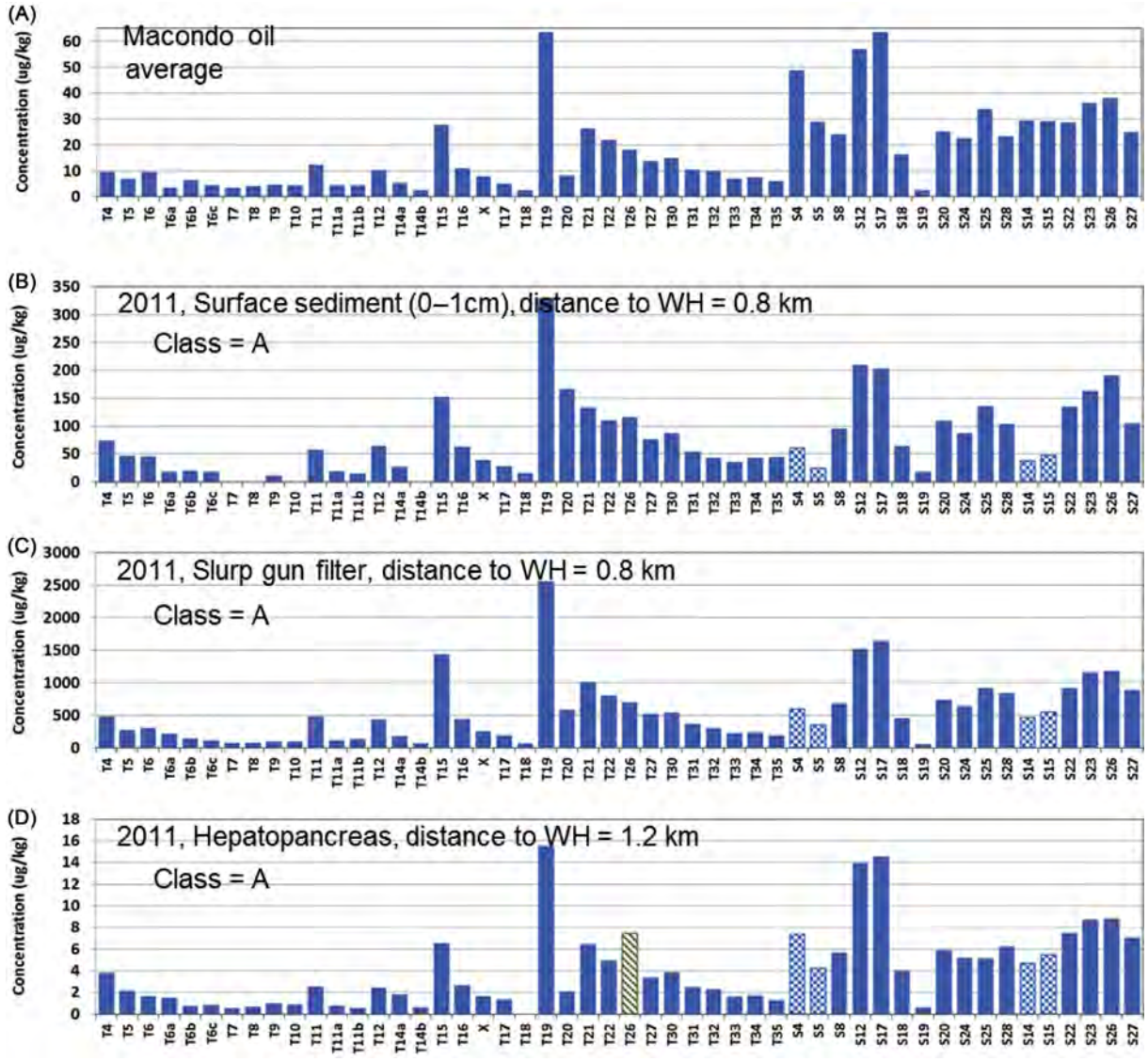

FIGURE 30.9 Biomarker distribution in our reference samples containing variably weathered/altered Macondo oil that were used in comparison to red crab tissues. (A) Fresh Macondo oil average, (B) surface sediment 0.8 km from the well (class = A), (C) slurp gun filter containing Macondo-derived oily floc, and (D) red crab hepatopancreas in reference crab collected 1.2 km from the wellhead. Sample IDs (A) fresh Macondo average ($n = 6$) from Stout et al. (2016b); (B) HSW2L2_FP0096_B0424_S_50_N2_885; (C) HSW2L2_FP0096_B0424_W_1495_50_P_Y_888; (D) PC11_NF1_B0804_T_1478_W8_1.2H.

0.8 km from the well and recognized to contain weathered Macondo oil (Figs. 30.8B and 30.9B), (3) a slurp gun filter sample used to collect Macondo-derived oily floc from the seafloor surface (Figs. 30.8C and 30.9C), and (4) a hepatopancreas collected from a reference crab collected less than 1.2 km from the Macondo well and obviously impacted by Macondo oil (Figs. 30.8D and 30.9D). The known biodegradation pathways of PAHs (Elmendorf et al., 1994) and selected biomarker compounds (triterpanes and steranes [Table 30.1, Douglas et al., 2007a,b]) were also included in the source identification of the oiled tissue.

30.3.5 Red Crab Reference Tissue Selection

For samples close to the Macondo well (less than 1.6 km), impacted red crab tissue results provided chemical fingerprints clearly indicative of Macondo oil exposure. Sediment and oil chemistry results show that the PAH distributions have been altered due weathering of the dispersed oil (Stout and Payne, 2016). The preferred tissue type to be used for forensic analysis (e.g., hepatopancreas vs gill) must provide maximum hydrocarbon

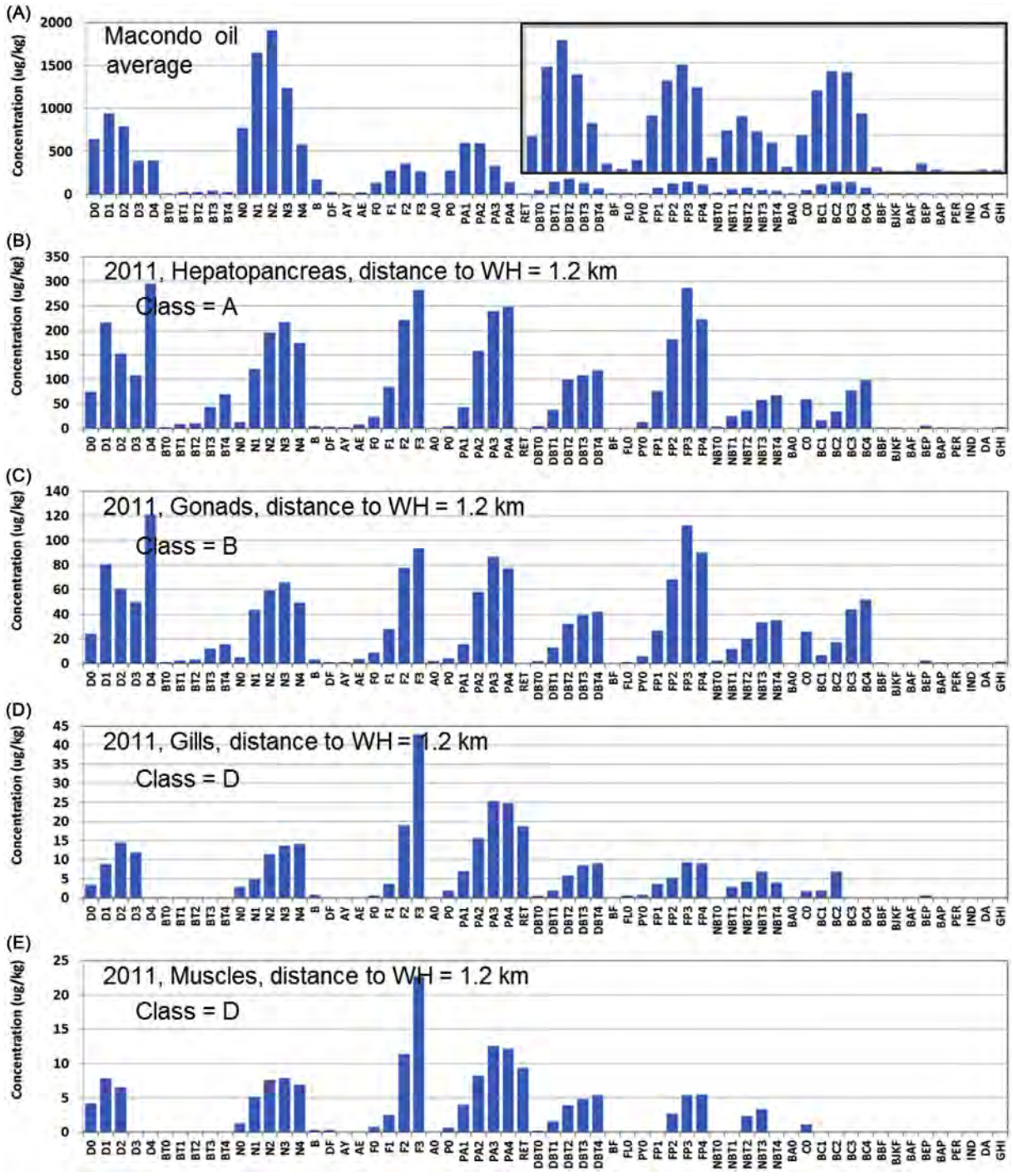

FIGURE 30.10 PAH concentrations and distributions in fresh Macondo oil and different tissue types collected from a single/individual red crab collected within 1.6 km from the wellhead. (A) Fresh Macondo oil average, (B) hepatopancreas (class = A), (C) gonads (class = B), (D) gills (class = D), and (E) muscle (class = D). Fresh Macondo average ($n = 6$) from Stout et al. (2016b).

sensitivity with minimum alteration of the weathered source oil signature. Fig. 30.10 shows the PAH distributions for Macondo oil and four different red crab tissues types—hepatopancreas, gonads, gills, and edible muscle—dissected from the same individual red crab collected from location NF1 (i.e., 1.2 km from the Macondo well) approximately 1 year after the oil spill (August 4, 2011).

Given that the various tissues/organs were derived from the same crab, the external sediment/water oil exposure was the same creating the opportunity to examine how oil signatures are altered by the crab biology

and exposure mechanism. Differences in hydrocarbon concentration and distribution among the different tissue types must be the result of the mechanism by which each tissue was exposed. For example, gills may be subject to more direct exposure to soluble and particulate-bound hydrocarbons, whereas hydrocarbons detected within the hepatopancreas are likely associated with the crab food selection and the digestion process. These varying methods of exposure may influence the hydrocarbon signatures observed in the respective tissue.

Inspection of the *y*-axis in Fig. 30.10 reveals the varying concentrations of PAHs in the different tissue types from the same individual crab. In order of detection sensitivity, the PAH concentrations were greatest within the hepatopancreas sample (Fig. 30.10B), and lowest in the muscle tissue (Fig. 30.10E). Gonads (Fig. 30.10C) ranked second and contained only about half the tPAH of the hepatopancreas (Fig. 30.10B); gills ranked third (Fig. 30.10D). Based on this comparative analysis of tissues within a single individual red crab, the hepatopancreas clearly provided the most sensitive measure of oil exposure compared to the other tissues.

$$\text{Hepatopancreas} > \text{Gonads} > \text{Gills} > \text{Muscles}$$

The PAH distribution or fingerprint relative to the spilled Macondo oil is the second component of tissue selection. For example, physical exposure of the gills to the water soluble fraction of the oil may result in a signature that is biased positive for the more soluble hydrocarbons and biased negative for the less soluble (e.g., benzanthracenes/chrysenes; Fig. 30.10D). The oil signature present in the hepatopancreas (Fig. 30.10B) and gonad samples (Fig. 30.10C) are almost identical and are most consistent with Macondo source oil, whereas the PAH distributions in the gill and muscle are qualitatively less robust, due largely to the small sample mass of these tissues and the resulting analytical sensitivity factors. Based on this comparison, the red crab hepatopancreas would clearly provide the highest PAH concentrations (Meador et al., 1995) and most comparably PAH distribution for the confirmation and identification of oil exposure within impacted red crabs. (it was for this reason that the 2014 red crab study was focused on hepatopancreas; Table 30.3).

The biomarker results for the same suite of crab tissues from an individual exposed red crab are shown in Fig. 30.11. The distribution of triterpane and sterane biomarkers in the hepatopancreas sample (Fig. 30.11B) is still consistent with the fresh Macondo oil more than one year after the spill. Because the biomarker concentrations are substantially lower in Macondo oil than PAHs, additional sensitivity issues were observed in the gonad (Fig. 30.11C) and gill tissues (Fig. 30.11D) with only limited detections of the targeted biomarkers. The muscle tissue was not analyzed for biomarker compounds. Thus, as was the case for PAHs, the biomarker results among different tissue types within a single exposed red crab also show that the hepatopancreas is the preferred tissue type for identifying petroleum exposure in red crabs.

30.3.6 Alteration of Source Oil Signatures by Red Crab Metabolism

The comparison of PAH concentration and signatures in the four red crab tissue types provides empirical evidence concerning PAH metabolism in red crabs. Currently, the scientific literature is limited with regards to crab metabolism of environmental contaminants (Lee et al., 1976; Baumard et al., 1998), although they have been proposed as sentinel organisms in some intertidal areas (Ikonomou et al., 2002). In addition, many of the studies where tissues were used to document oil exposure examine only the priority pollutant PAHs (Soriano et al., 2006; Wade et al., 1989) and few include the diagnostic alkylated PAHs (Bence and Burns, 1995; Glegg and Rowland, 1996; Short and Babcock, 1996) or biomarkers (Bartolome et al., 2007; Glegg and Rowland, 1996) that are the basis of forensic identification. Unlike fish and bivalves, little work has been done to examine deep benthic red crab metabolism of hydrocarbons during marine oil spills.

The current literature suggests that the efficiency of crabs' metabolism of PAHs lies somewhere between fish and bivalves (Meador et al., 1995). Most of this work was carried out on intertidal or subtidal sites where crabs are easily collected and are an important resource. To our knowledge, no work has been performed on deep benthic red crabs where factors such as low temperature may limit the ability of this species of crab to biotransform PAHs to more polar metabolites. Similarly, no research has been performed to examine the ability of deep benthic red crabs to metabolize alkylated PAH compounds or the more stable petroleum biomarker compounds.

The results of our study, summarized below, indicate that deep benthic red crabs do not rapidly metabolize oil spill-derived PAHs or biomarker compounds. These are important observations given the reliance on these chemical fingerprints when documenting oil exposure and identifying the source of that exposure. The following lines of evidence support the theory that red crabs do not rapidly metabolize oil spill-derived PAH or biomarker compounds.

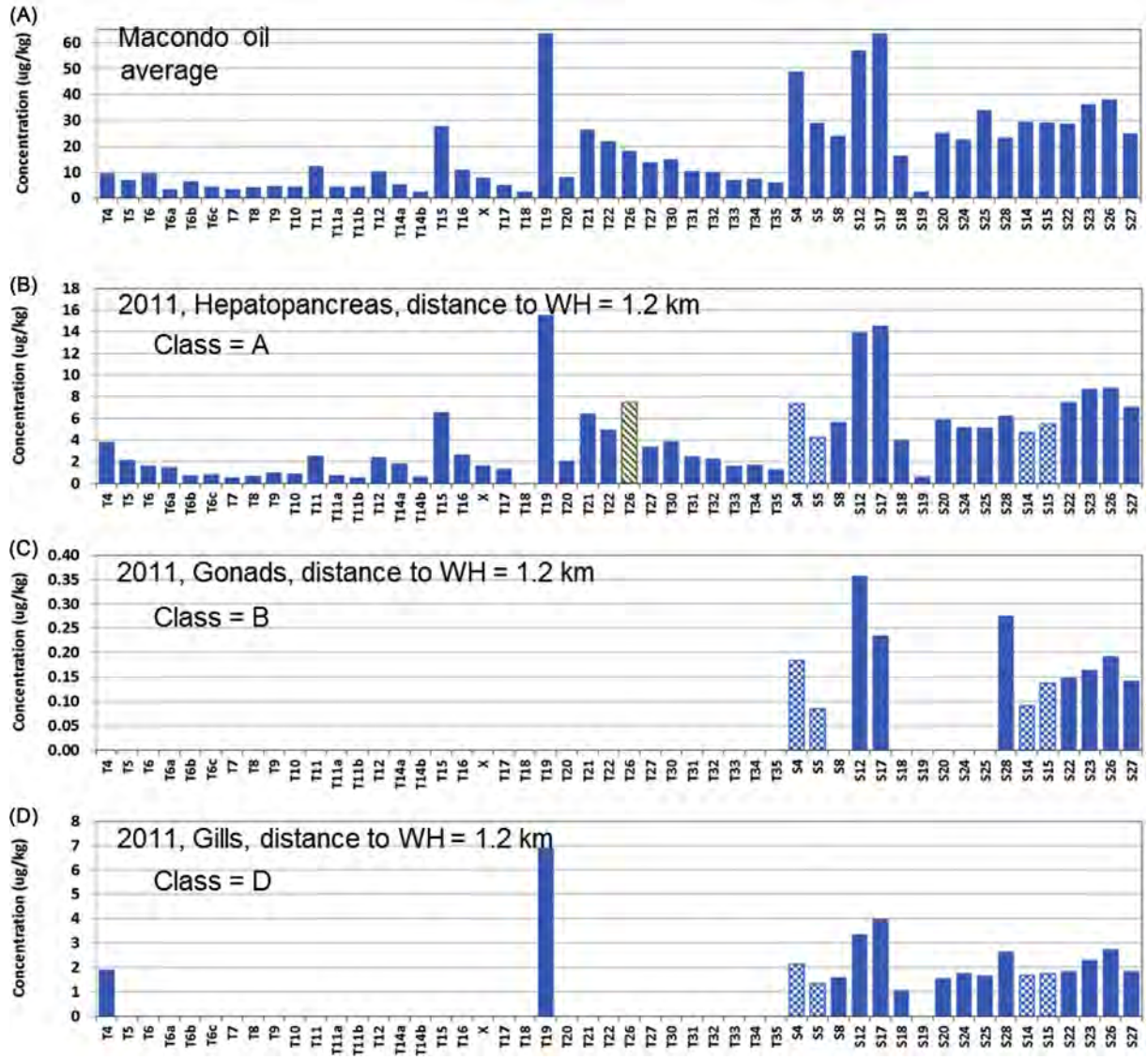

FIGURE 30.11 Biomarker concentrations and distributions in fresh Macondo oil and different tissue types collected from a single/individual red crab collected within 1.6 km from the wellhead. (A) Fresh Macondo oil average, (B) hepatopancreas (class = A), (C) gonads (class = B), and (D) gills (class = D). Fresh Macondo average ($n = 6$) from Stout et al. (2016b). Hatching reflects analytes affected by interferences (T26) or biodegradation (S4, S5, S14, and S15).

- More than 1 year after the DWH oil spill both the hepatopancreas (Fig. 30.10B) and gonad (Fig. 30.10C) in an exposed red crab still exhibit strong PAH signatures consistent with weathered Macondo oil.
- The PAH distribution in both the hepatopancreas and gonad samples is indicative of recognized oil weathering processes and not of compound-specific metabolite formation.
- Similar PAH distributions in crab tissues were observed in the surface sediments.
- If PAH metabolism were occurring, it would most likely occur within the hepatopancreas and not the gonads. Yet, the PAH signatures within these two different tissue types is almost identical suggesting that these different tissues were exposed to whole oil.
- The biomarker patterns present in the red crab hepatopancreas are still very similar (Fig. 30.11A vs Fig. 30.11B) to the Macondo oil and any small differences can be attributed to either (previously recognized) biodegradation in the source oil (e.g., depletion of selected sterane compounds S4, S5, S14, S15) in seafloor floc or interferences present in deep-sea sediment (T26; Stout and Payne, 2016).
- The water temperature in the deep subtidal is approximately 4°C which would reduce any enzyme-related PAH metabolism relative to crabs derived from warmer intertidal environments.

- If enzyme reactions were occurring in the red crab the residual PAH signature would not be expected to reflect the same weathered signature as is present in the impacted surface sediments.
- Given the chemical stability of the triterpane and sterane biomarkers, these compounds would be less likely to be impacted by enzymatic metabolism than the PAHs and would be more likely to accumulate in the marine organism (Ashton et al., 2000).

Based on these facts and observations, for this study, it is assumed that PAH and biomarker metabolism in red crabs is minimal and that the alteration of the Macondo oil signature recognized occurs primarily via external processes prior to uptake, such as weathering in the water column or surface sediments, which is known to have severely affected the Macondo oil residues deposited on the seafloor (Fig. 30.1; Stout and Payne, 2016).

30.3.7 Evidence for Macondo Oil Exposure in Red Crabs

Oil exposure in deep benthic tissue samples is indicated by the presence of petroleum-specific hydrocarbons in the sample such as alkylated PAHs. The presence of these PAH distributions (Fig. 30.10B–E) in red crab tissue samples from individual collected within the DWH spill zone is sufficient evidence to conclude that the oil present in these samples was *more likely than not* derived from the Macondo oil spill.

Fig. 30.12 shows the PAH signatures for Macondo oil, and four red crab hepatopancreas samples collected at increasing distances from the Macondo well in 2011. Figs. 30.12B and 30.12C represent PAH profiles in hepatopancreas samples collected 1.2 and 1.4 km from the Macondo well, where sediments were heavily impacted by the spilled oil (Stout and Payne, 2016). These exposed red crab hepatopancreas samples were clearly impacted and thereby could be used as reference tissue samples (for source identification further from the well). These reference samples provide a means to incorporate chemical fingerprint variations from weathering of the oil and any chemical changes that may be introduced during extraction and analysis of the tissue sample. This "reference tissue" approach was used on the *Cosco Busan* oil spill for tissue oil identification by both PRP and Trustee scientists (Driskell et al., 2010). In addition to these exposed reference tissue samples, as noted above, surface sediment and seafloor floc (slurp gun filter) PAH and biomarker distributions were also used as reference materials for the Macondo oil residues on the seafloor.

PAH distributions and concentrations in the red crab hepatopancreas samples decreased with distance from the DWH wellhead (Fig 30.12). This decrease is attributable to oil weathering/biodegradation and attenuation/dispersion of the oily floc (Fig. 30.1). As the PAH signature degraded, the more refractory biomarker signatures (Figure 30.13) retained sufficient resolution to identify the presence of Macondo oil in these tissues as far as 14 km from the wellhead (Fig 30.13E). Based on the combined PAH and biomarker patterns in these samples, their location within the known spill zone, and the documented presence of Macondo oil in sediments and floc proximal to the samples (Stout et al., 2016a), we concluded that Macondo oil was present in these tissue samples.

30.3.8 Red Crabs Tissues in 2014

Based on the results of the 2010–2011 red crab investigations, a second round of crab samples were collected in 2014 within the DWH spill zone to investigate temporal changes in the concentration and distribution of spill-related hydrocarbons in red crab tissues. Based on the results from 2010–2011, the 2014 study focused only on hepatopancreas tissues.

The PAH concentrations and distributions of representative hepatopancreas samples collected in 2014 at increasing distances from the Macondo well are shown in Fig. 30.14. In general, the PAHs were present at lower concentrations in the 2014 samples, and these tissues exhibited incomplete PAH patterns with the exception of the tissue sample collected 6.8 km from the wellhead (PC13-MC208B-E0829-T-W8-02-H2; Fig. 30.14D), which exhibited a sufficient PAH profile to indicate that the sample had been exposed to petroleum. Not surprisingly, the biomarker profiles for the same samples (Fig. 30.15) retained their forensic signature and provided the primary basis upon which to identify the presence of Macondo oil residues in all four of the samples—and many others from 2014 (per Table 30.3). These results suggest that the PAH concentrations in the 2014 hepatopancreas samples were generally lower and more weathered than those observed in the 2011 samples. However, the biomarker concentrations and distributions did not show the same degree of reduction/alteration as the PAHs likely due to the more refractory nature of the biomarker compounds (Fig. 30.15). As with the 2010–2011 samples, the locations of the oil-impacted hepatopancreas samples from 2014 were consistent with surface sediment samples collected in 2014 determined to have been impacted by Macondo oil (Stout et al., 2017).

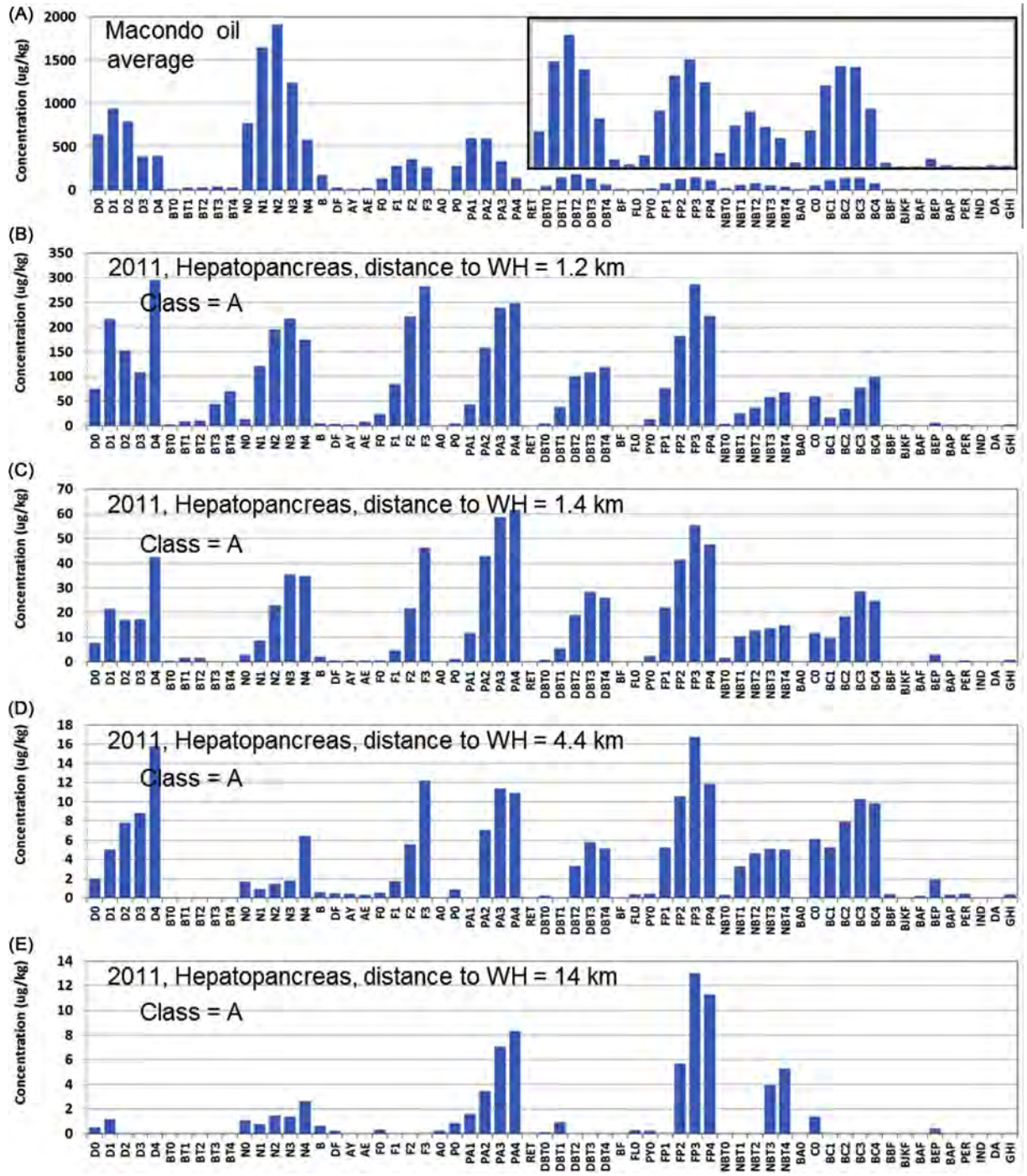

FIGURE 30.12 Examples of PAH distributions in four red crab hepatopancreas samples collected in 2011 at increasing distances from the wellhead. (A) Fresh Macondo oil average, (B) hepatopancreas 1.2 km from the wellhead, (C) hepatopancreas 1.4 km from the wellhead, (D) hepatopancreas 4.4 km from the wellhead, and (E) hepatopancreas 14 km from the wellhead. Sample IDs: (B) PC11_NF1_B0804_T_1478_W8_1.2H; (C) PC11_NF2_B0804_T_1484_W8_14.2H (class = A), (D) HSW6_FP10188A_B0827_T_1483_50_1WO_0078_INN, and (E) PC11_MC338_B0811_T_1396_W8_1.1H. Fresh Macondo average ($n = 6$) from Stout et al. (2016b).

Temporal data of tissue (and sediment) concentrations can provide supporting evidence regarding the source of petroleum contamination at a given site. For example, decreases in total TPH and TPAH concentrations over time following a spill is often used as supporting information to identify the source of the oil (Soriano et al., 2006; Glegg and Rowland, 1996). In the deep-sea DWH oiled sediments, one concern is the impact that natural seeps may have on the

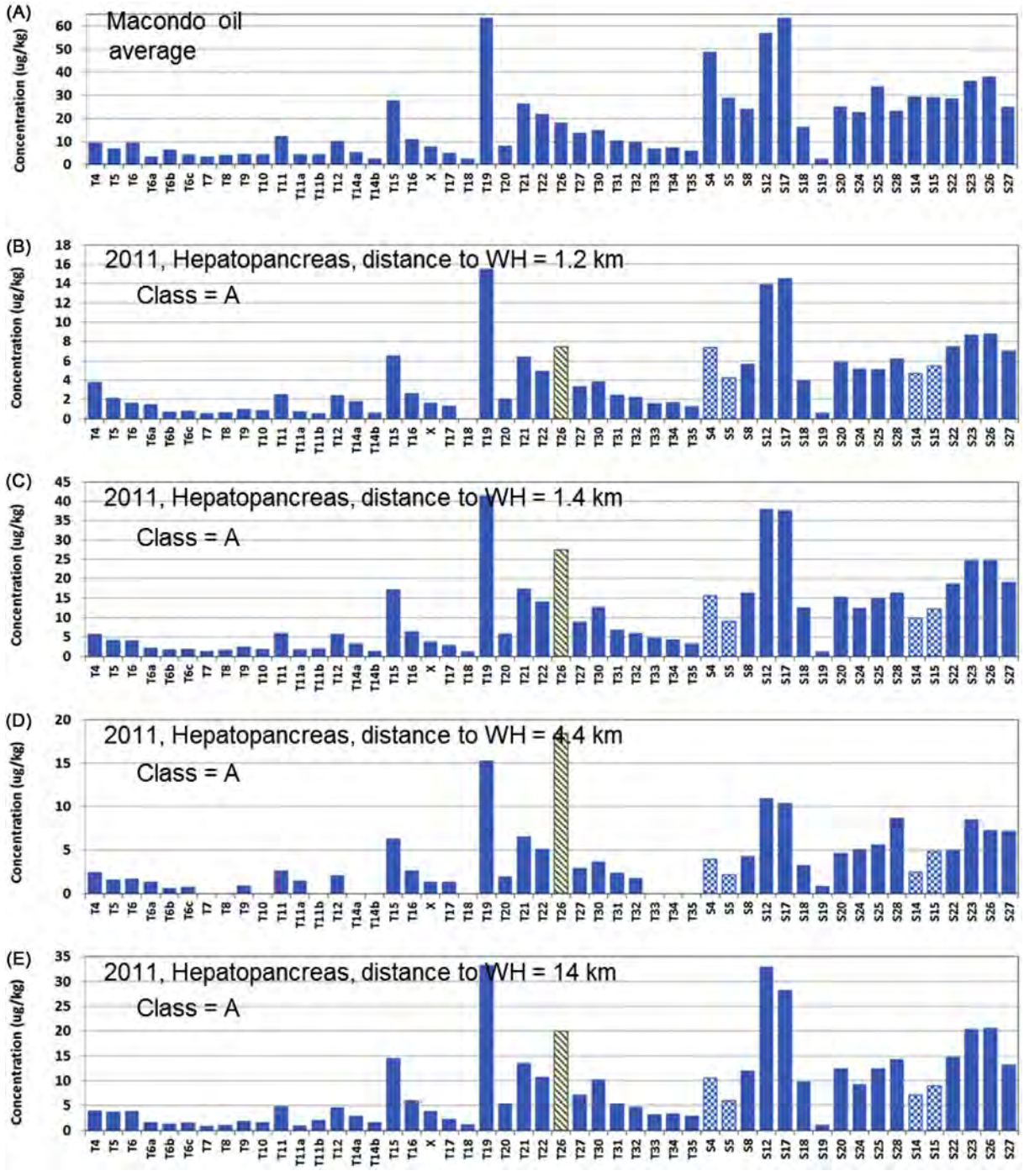

FIGURE 30.13 Examples of biomarker distributions in four red crab hepatopancreas samples collected in 2011 at increasing distances from the wellhead. (A) Fresh Macondo oil average, (B) hepatopancreas 1.2 km from the wellhead, (C) hepatopancreas 1.4 km from the wellhead, (D) hepatopancreas 4.4 km from the wellhead, and (E) hepatopancreas 14 km from the wellhead. Sample IDs: (B) PC11_NF1_B0804_T_1478_W8_1.2H; (C) PC11_NF2_B0804_T_1484_W8_14.2H (class = A), (D) HSW6_FP10188A_B0827_T_1483_50_1WO_0078_INN, and (E) PC11_MC338_B0811_T_1396_W8_1.1H. Fresh Macondo average ($n = 6$) from Stout et al. (2016b). Hatching reflects analytes affected by interferences (T26) or biodegradation (S4, S5, S14, and S15).

Macondo oil signature. Given that the Macondo oil and local seep oils are derived from similar geological provinces, and that the degree of weathering in the dispersed oil and oily floc present in the sediments was severe, chemical fingerprinting results alone may not always be sufficient to distinguish these impacts. Multiple lines of evidence are

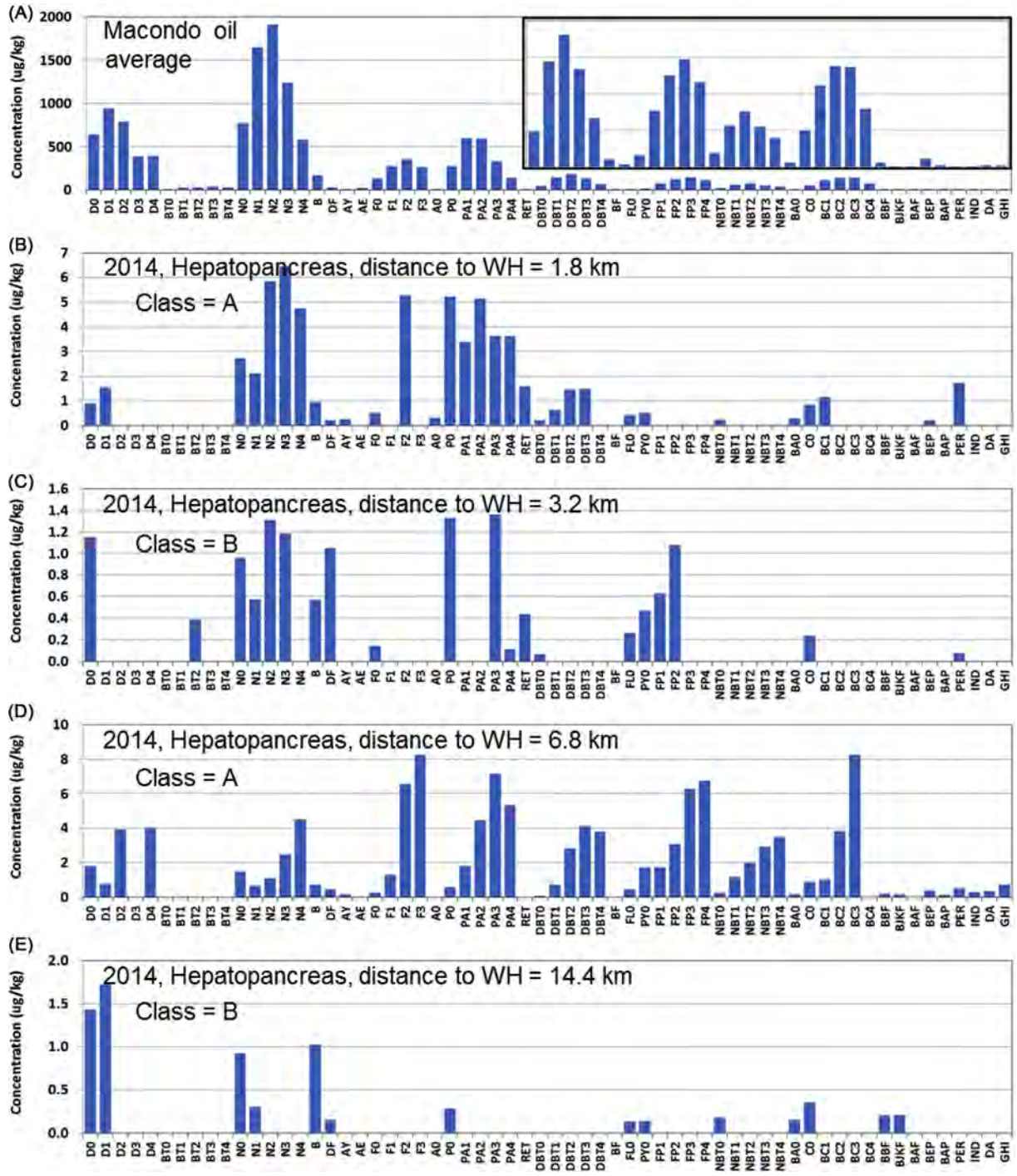

FIGURE 30.14 Examples of PAH distributions in four red crab hepatopancreas samples collected in 2014 at increasing distances from the wellhead. (A) Fresh Macondo oil average, (B) hepatopancreas 1.8 km from the wellhead, (C) hepatopancreas 3.2 km from the wellhead, (D) hepatopancreas 6.8 km from the wellhead, and (E) hepatopancreas 14.4 km from the wellhead. Sample IDs: (A) Fresh Macondo oil average ($n = 6$) from Stout et al. (2016b); (B) PC13-NF1-E0903-T-W8-04-H-2; (C) PC13-MC208A-E0904-T-W8-01-H-2; (D) PC13-MC208B-E0829-T-W8-02-H-2; and (E) PC13-NF3B-E0908-T-W8-05-H-2.

often required to determine if the oil present in tissue (or sediment) is more likely than not related to the Macondo oil spill.

For deep-sea sediments, the lateral and vertical delineation of Macondo impacts in the spill zone was one additional line of evidence that supported the conclusion that there are not widespread impacts of seep oil

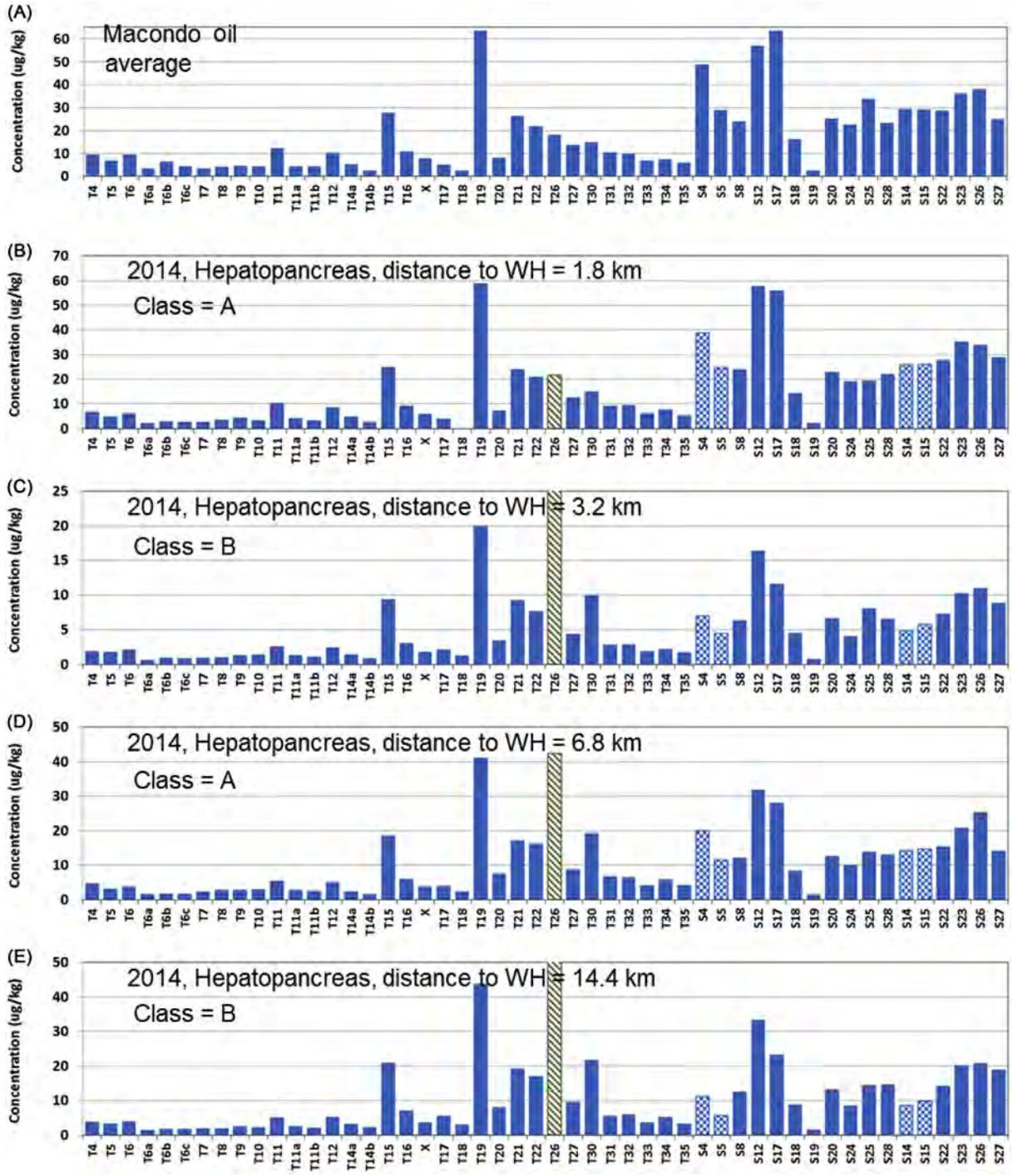

FIGURE 30.15 Examples of biomarker distributions in four red crab hepatopancreas samples collected in 2014 at increasing distances from the wellhead. (A) Fresh Macondo oil average, (B) hepatopancreas 1.8 km from the wellhead, (C) hepatopancreas 3.2 km from the wellhead, (D) hepatopancreas 6.8 km from the wellhead, and (E) hepatopancreas 14.4 km from the wellhead. Sample IDs: (A) Fresh Macondo oil average ($n = 6$) from Stout et al. (2016b); (B) PC13-NF1-E0903-T-W8-04-H-2; (C) PC13-MC208A-E0904-T-W8-01-H-2; (D) PC13-MC208B-E0829-T-W8-02-H-2; and (E) PC13-NF3B-E0908-T-W8-05-H-2. Hatching reflects analytes affected by interferences (T26) or biodegradation (S4, S5, S14, and S15).

throughout the DWH spill zone (Stout and Payne, 2016; Stout et al., 2016a, 2017). Unlike crab hepatopancreas samples where the exposure and identification are based on a single result, the identification of seep impacts in the deep-sea sediments were derived from many lines of chemical evidence and from multiple related samples. Stout et al. (2016a) delineated Macondo oil sediment impacts using spatial distribution of oil in hundreds of high-resolution sediment cores collected throughout the study area, including colocated cores, and vertical core

profiles of PAH, biomarker and GC/FID signatures and concentrations in order to assess the presence of Macondo oil in the sediments. Based upon a combination of chemical fingerprinting and spatial trends in and among cores, Stout et al. (2016b) concluded that seep oil impacts were highly localized.

Given that surface sediments are the primary exposure route for deep benthic red crabs, colocation of oil exposed crabs with Macondo oil-impacted surface sediments (Fig. 30.16) was one additional line of evidence that the oil identified in the tissue samples was derived from the spilled Macondo oil and not natural seeps. Of course, in known seep zones, the potential for commingled exposure to both Macondo oil and seep oil is possible.

A second line of evidence that seep inputs are not a widespread source of petroleum within the DWH spill zone is provided by the temporal changes in red crab hepatopancreas total PAH concentrations measured in 2010–2011 vs 2014. If after an oil spill event, such as the DWH oil spill, the petrogenic PAH signatures observed in the red crab tissue samples were derived from widespread natural seep oils, then given the chronic nature of those inputs over time, any significant temporal changes in petroleum contamination would be difficult to detect during the time scale of an oil spill investigation (e.g., 4 years) from a point-source release. The environmental weathering and degradation rates of the seep-related oils would be expected to be slower given that seep releases are not finely dispersed into the water column as was the case for the Macondo oil. Therefore, if the oil identified within the 2010–2011 crab hepatopancreas samples were indeed seep related, similar distributions and average concentrations of PAHs and biomarkers should exist in red crab tissues (hepatopancreas) throughout the deep-sea year-after-year indicating a relatively steady-state environment.

Fig. 30.17A shows a plot of the $TPAH_{49}$ concentration in 2010–2011 crab hepatopancreas samples vs their distance from the Macondo well. The $TPAH_{49}$ concentrations for the majority (75%) of samples with fingerprint

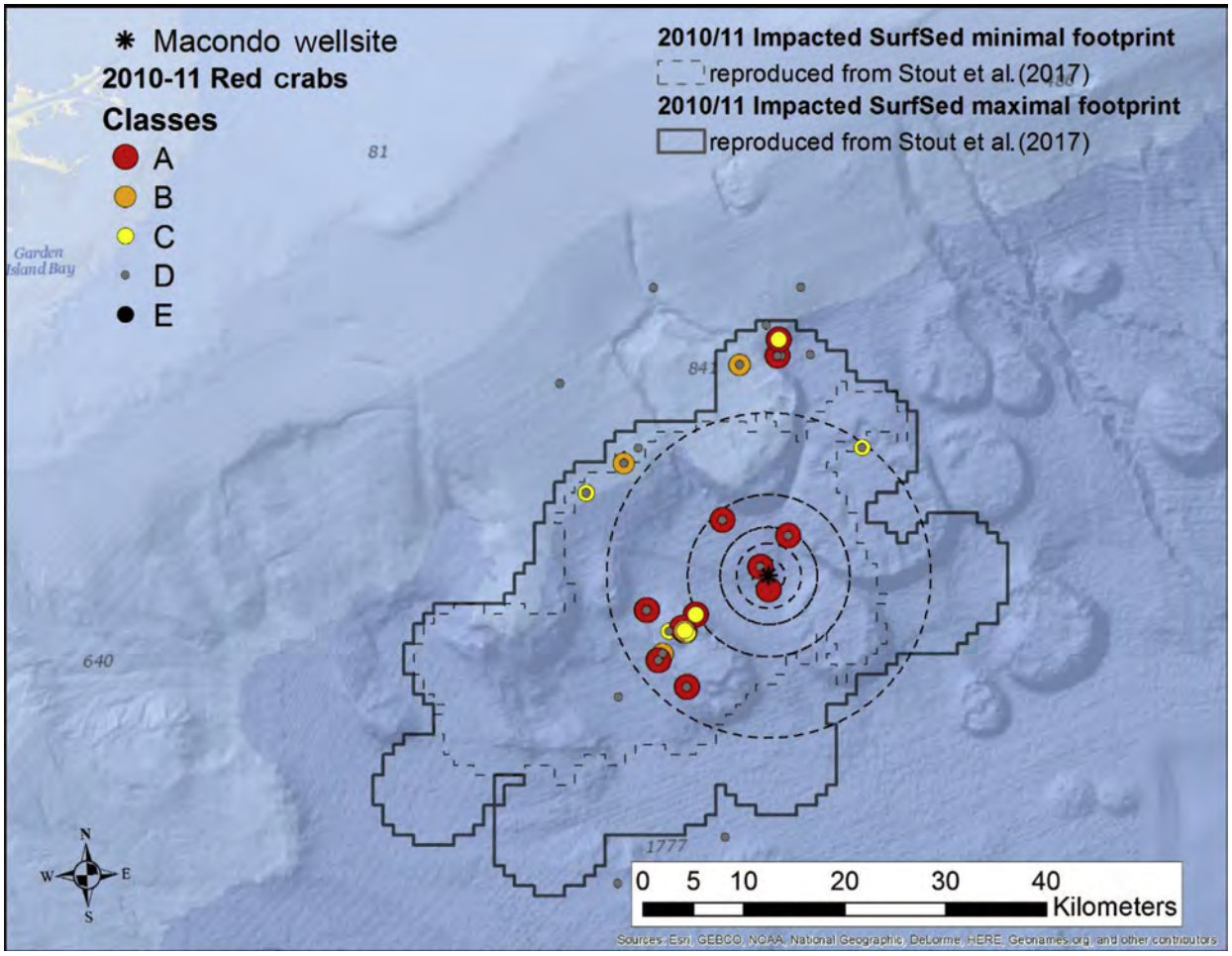

FIGURE 30.16 Map of red crab tissue samples by fingerprint classification collected in 2010–2011 superimposed upon surface sediment impact footprint from Stout et al. (2017). Over 900 individual red crab tissue samples are shown on this map, although at the resolution most appear superimposed at the 33 unique locations evident.

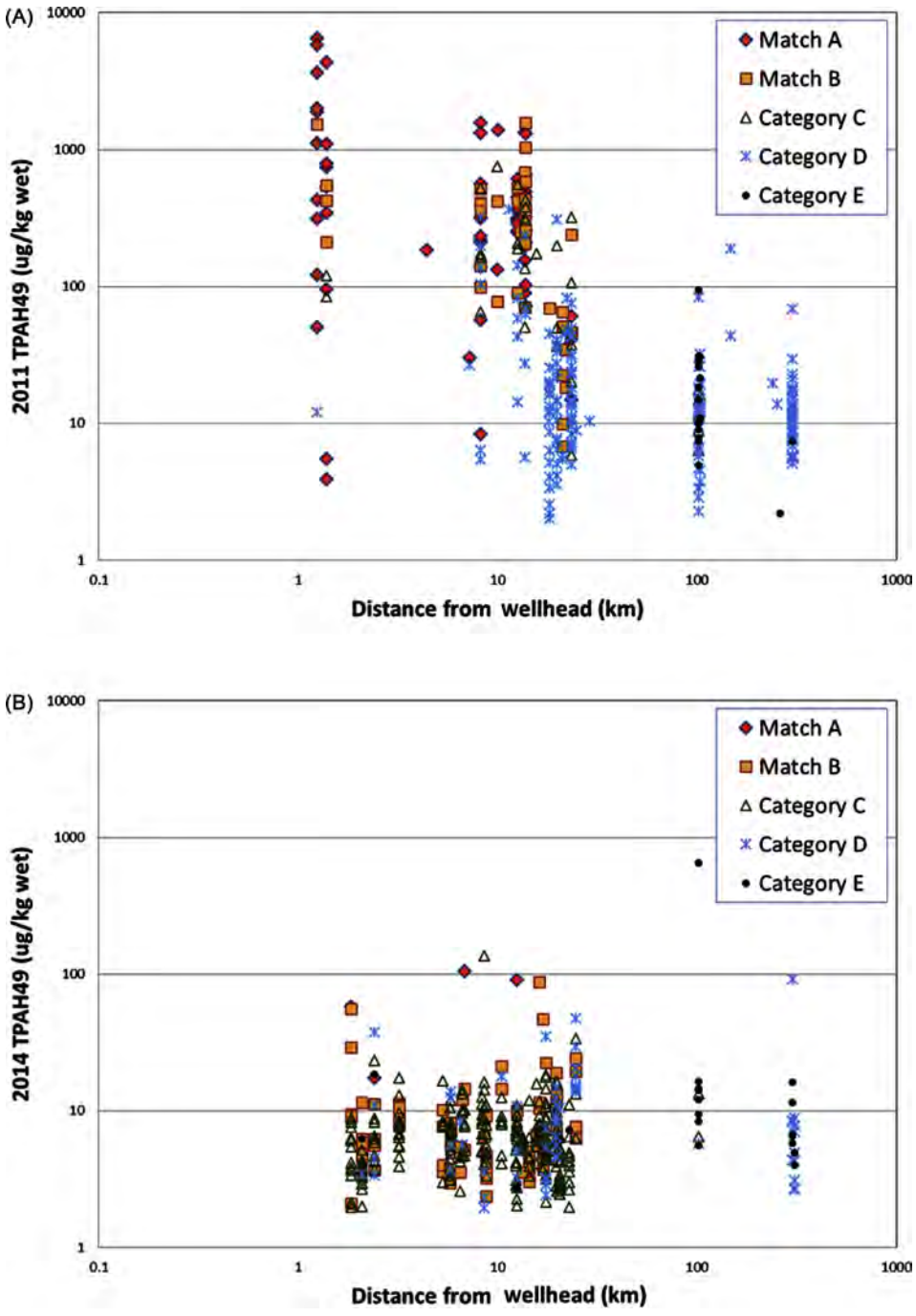

FIGURE 30.17 Graphs showing the concentrations of $TPAH_{49}$ in red crab hepatopancreas vs distance from the Macondo well by fingerprint class ("A" to "E;" per Table 30.3) in (A) 2010–2011 ($n = 331$) and (B) 2014 ($n = 423$).

classifications of A and B fall within a TPAH concentration range 100–9000 μg/kg and extend to a distance of approximately 14 km from the Macondo well. When these results are compared to the 2014 red crab hepatopancreas samples shown in Fig. 30.17B, the vast majority (99%) of $TPAH_{49}$ concentrations for samples with fingerprint classifications of A and B are below 100 μg/kg. This nearly two orders of magnitude decrease in TPAH concentration to a distance of approximated 14 km from the Macondo well cannot simply be due to differences in sample locations within the spill zone for the two sampling periods. These results show a clear temporal trend (decrease) in PAH concentrations in red crab hepatopancreas consistent with degradation of PAH residues within

the spill zone (which was also observed in the surface sediment data collected in 2014; Stout et al., 2017). Such temporal declines in tissue PAH concentrations are commonly observed after an acute oil spill incident (Glegg and Rowland, 1996). This decline in hepatopancreas PAH concentrations between 2010–2011 and 2014 (Fig. 30.17) is strong evidence of red crab exposure to an acute oil spill incident - and not due to chronic exposure of the crabs to seep oils within the spill zone.

A similar decline in PAH concentrations was observed by Stout et al. (2017) who reported that the 2014 surface sediment samples were on average lower in TPAH by more than an order of magnitude throughout the spill zone. Given that the oil and oily floc laden sediments are the exposure pathway for the red crab, the temporal decline in TPAH concentrations in both hepatopancreas and surface sediments is consistent with our current understanding of red crab behavior and the ongoing weathering of PAHs in the Macondo crude oil deposited on the seafloor in the 4 years since the DWH oil spill.

30.3.9 Evidence of Natural Seep Oil Exposure in Remote Red Crabs

As discussed above, the Macondo oil is native to the geologic province in which it was spilled, and therefore it shares many chemical features with other northern Gulf of Mexico oils spills/seeps within the province. Red crabs hepatopancreas can incorporate hydrocarbons associated with natural seeps. If the seep oil chemistry is sufficiently different from the Macondo oil it will be recognized as a different (non-Macondo) oil.

Fig. 30.18 shows a plot of the PAH distribution of Macondo oil vs a seep oil identified in a crab hepatopancreas located 102 km from the Macondo well—far beyond the recognized seafloor impact of Macondo oil. The TPAH concentration is consistent with the higher end of the TPAH concentrations identified in hepatopancreas samples exposed to Macondo oil within the spill zone. However, the distribution of PAHs indicates that the source oil in this remote hepatopancreas sample is from a different geological source than Macondo oil, and that it has not been severely weathered. Although the biomarker distributions are similar to Macondo oil several key source indicators are different, which allow us to recognize this oil is from a different geological source (e.g., the seep oil contains excess T15; Fig. 30.18b). Such differences were used during the fingerprint classification procedure to identify possible seep inputs in red crab hepatopancreas samples in both remote and more proximal locations. As with all of the tissue data, multiple lines of evidence were used to confirm the presence or absence of seep hydrocarbons in a given sample.

Exposure of red crabs to some seep oil within the spill zone *where seeps occur* is possible. However, multiple lines of evidence indicate that exposure of red crabs to seep oil was spatially limited to known seep areas and

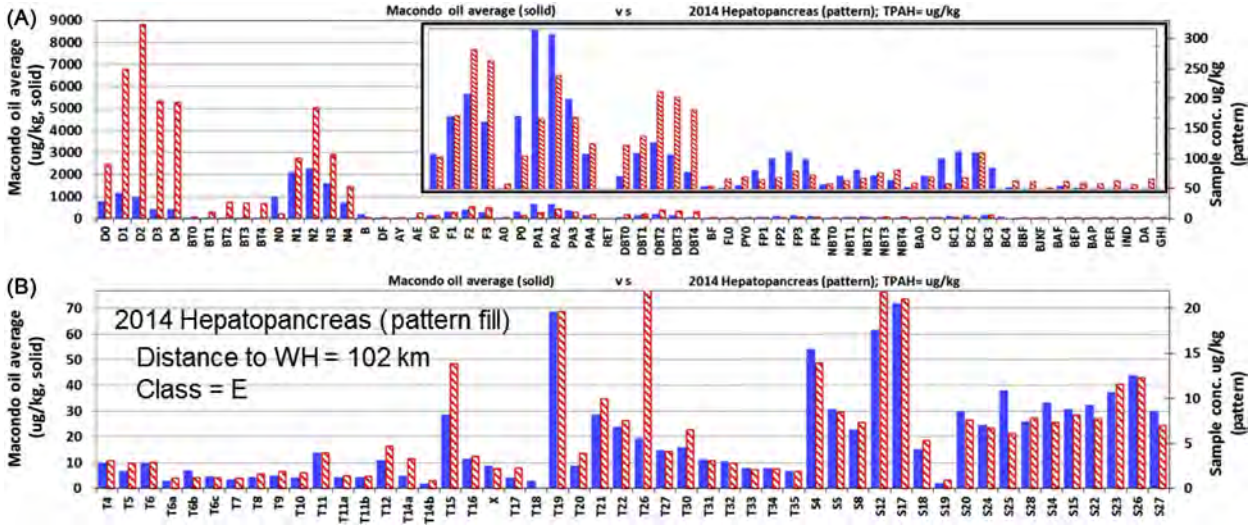

FIGURE 30.18 PAH and biomarker distribution in a red crab hepatopancreas tissue sample (*red* (striped bars)) collected 102 km from wellhead in 2014 vs fresh Macondo oil average (*blue* (filled bars)). (A) PAH distribution and (B) biomarker distribution. Differences between the hepatopancreas and Macondo oil indicate this red crab was exposed to seep oil—and not Macondo oil.

that the level of any exposure in these areas was be relatively consistent over time. Evidence against widespread and acute exposure of red crabs to seep oil include:

1. Surface sediment PAH concentrations have measurably declined in the spill zone within 4 years after the oil spill (Stout et al., 2017).
2. Red crab hepatopancreas PAH concentrations have measurably declined in the spill zone, including seep areas.
3. Despite lost PAH patterns due to degradation since 2010/2011, the biomarker patterns were retained in the crab hepatopancreas in both 2010/2011 and 2014 and was consistent with a Macondo oil source.
4. Macondo oil has positively been identified in surface sediments in the spill zone including areas proximal to red crab habitats.
5. The impact of naturally occurring oil seeps to surface sediment concentrations and distributions are highly localized and are not widespread within the spill zone (Stout et al., 2016a).

30.4 CONCLUSIONS

The impact of Macondo crude oil on the deep-sea sediment (within the spill zone) during and following the DWH blowout has been well documented (e.g., Stout and Payne, 2016; Stout et al., 2016a, 2017). Deep benthic macrofauna living in and on these sediments were subsequently exposed to the Macondo oil and oily floc through external contact with the oil (e.g., gills) or internal contact by ingestion of oily particulates and oil-impacted prey.

This study examined the exposure of benthic macrofauna through the study of indigenous deep-sea red crabs (*C. quinquedens*). Results demonstrated the red crabs were clearly exposed and that spatial extent of their exposure coincided with that recognized in (previously studied) surface sediments. We conclude that the red crabs acted as "sentinel" organisms for monitoring exposure to the spilled oil within the deep benthos ecosystem. The potential advantages of using the mobile red crab as a sentinel species include: (1) an integrated exposure to surface sediments where oil impacts are highest, (2) minimal metabolism of Macondo oil PAH and biomarker signatures, and (3) deployment of baited traps is less complex and costly than collection of sediment cores more than 1.6 km below the sea surface. The potential disadvantages include (1) incomplete coverage of red crabs across the spill zone and (2) more complex analytical procedures required for the preparation and analysis of tissue samples.

Based on the results from this study of multiple types of red crab tissues, the red crab's hepatopancreas provided the most robust chemical signatures of the Macondo crude oil compared to other tissue types (e.g., gills, eggs, muscle, gonads). The PAH and biomarker concentrations in hepatopancreas of crabs exposed to Macondo oil generally decreased with increasing distance from the failed Macondo well. The highest PAH exposures were found closest to the wellhead and though lower and were still identifiable as far as 14 km from the wellhead. The relative concentrations and distributions of PAHs and biomarkers in red crab hepatopancreas samples were consistent with those in (previously studied) impacted surface sediment (Stout et al., 2016a). Concentrations in Macondo-impacted hepatopancreas samples from 2010–2011 were, on average, two orders of magnitude higher than were found in impacted samples from 2014, which further argues the 2010–2011 impacts were attributable to the DWH oil spill and not persistent local seep oils. Finally, the PAH distributions observed in the red crab samples do not indicate that red crab rapidly metabolizes PAHs in this environment.

Acknowledgments

The authors wish to thank the efforts of Numerous Trustee and BP field teams that cooperatively planned and collected the red crab samples. In addition, we would like to thank the staff at Alpha Analytical laboratory that performed the sensitive chemical analyses required to fingerprint the tissue samples. The efforts of numerous NewFields staff who aided in the data review, management of the chemical analyses, database, and GIS are also acknowledged.

References

Ashton, B.M., East, R.S., Walsh, M.M., Miles, M.S., Overton, E.B., 2000. Studying and Verifying the Use of Chemical Biomarkers for Identifying and Quantitating Oil Residues in the Environment. Minerals Management Service: U.S. Department of the Interior.

Atlas, R.M., Hazen, T.C., 2011. Oil biodegradation and bioremediation: a tale of the two worst spills in US history. Environ. Sci. Technol. 45, 6709–6715.
Baelum, J., Borglin, S., Chakraborty, R., Fortney, J.L., Lamendella, R., Mason, O.U., et al., 2012. Deep-sea bacteria enrich by oil and dispersant from the *Deepwater Horizon* spill. Environ. Microbiol. 14 (9), 2405–2416.
Bartolome, L., Deusto, M., Etxebarria, N., Navarro, P., Usobiaga, A., Zuloaga, O., 2007. Chemical fingerprinting of petroleum biomarkers in biota samples using retention-time locking chromatography and multivariate analysis. J. Chromatogr. A. 1157, 369–375.
Baumard, P., Budzinski, H., Garrigues, P., Sorbe, J., Burgeot, T., Bellocq, J., 1998. Concentrations of PAHs (polycyclic aromatic hydrocarbons) in various marine organisms in relation to those in sediments and to trophic level. Mar. Pollut. Bull. 36 (12), 951–960.
Bence, A.E., Burns, W.A., 1995. Fingerprinting hydrocarbons in the biological resources of the Exxon Valdez Spill Area. Exxon Valdez Oil Spill: Fate and Effects in Alaskan Waters.
Bend, J.R., James, M.O, Little, P.J., Foureman, G.L., 1981. *In vitro* and *in vivo* metabolism of benzo(*a*)pyrene by selected marine crustacean species. In: Proceedings of the International Symposium of the Princess Takamatsu Cancer Research Fund, pp. 179–194.
Bender, M.E., Hargis, W.J., Huggett, R.J., Roberts, M.H., 1988. Effects of polynuclear aromatic hydrocarbons on fishes and shellfish: an overview of research in Virginia. Mar. Environ. Res. 24, 237–241.
Camilli, R., Reddy, C.M., Yoerger, D.R., Van Mooy, B.A.S., Jakuba, M.V., Kinsey, J.C., et al., 2010. Tracking hydrocarbon plume transport and biodegradation at deepwater horizon. Science 330, 201–204.
Ceccaldi, H.J., 1989. Anatomy and physiology of digestive tract of Crustaceans Decapods reared in aquaculture. Adv. Tropic. Aquacult. 9, 243–259.
CEN, 2012. Oil spill identification—waterborne petroleum and petroleum products—part 2: analytical methodology and interpretation of results based on GC-FID and GC-MS low resolution analyses. Technical Report CEN/TR; 15522-2.
Clark, R.C., Brown, D.W., 1977. Petroleum: properties and analyses in biotic and abiotic systems. effects of petroleum on arctic and subarctic marine environments and organisms. Nat. Fate Petrol. 1, 1–89.
Daling, P., Faksness, L.-G., Hansen, A.B., Stout, S.A., 2002. Improved and standardized methodology for oil spill fingerprinting. In: CEN/STAR Trends Analysis Workshop Discharges of Oil and Ballast Water Held in Copenhagen, Nordtest Technical Report 502.
Di Toro, D.M., Zarba, C.S., Hansen, D.J., Berry, W.J., Swartz, R.C., Cowan, C.E., et al., 1991. Technical basis for establishing sediment quality criteria for nonionic organic chemicals using equilibrium partitioning. Environ. Toxicol. Chem. 10, 1541–1583.
DIVER (Data Integration, Visualization, Exploration and Reporting), 2015. Web Application. Deepwater Horizon Natural Resource Assessment Data. National Oceanic and Atmospheric Administration. <https://dwhdiver.orr.noaa.gov/>.
Douglas, G.S., Uhler, A.D., 1993. Optimizing EPA methods for petroleum contaminated site assessments. Environ. Test. Anal. 2, 46–53.
Douglas, G.S., Emsbo-Mattingly, S.D., Stout, S.A., Uhler, A.D., McCarthy, K.J., 2007a. Hydrocarbon fingerprinting method. Introduction to Environmental Forensics. Elsevier, Amsterdam, pp. 201–309.
Douglas, G.S., Stout, S.A., Uhler, A.D., McCarthy, K.J., Emsbo-Mattingly, S.D., 2007b. Advantages of quantitative chemical fingerprinting in oil spill identification. Oil Spill Environmental Forensics. Elsevier, Amsterdam, pp. 257–292.
Douglas, G.S., Hardenstine, J., Liu, B., Uhler, A.D., 2012. Laboratory and field verification of a method to estimate the extent of petroleum biodegradation in soil. Environ. Sci. Technol. 46, 8279–8287.
Driskell, W.B., Payne, J.R., Douglas, G.C., 2010. Forensic fingerprinting of *Cosco Busan* samples containing mixed-oil sources. Presentation at the Society of Environmental Toxicology and Chemistry, Special Session on the *Cosco Busan* Spill. In: SEATAC 31st Annual Meeting, Portland, OR, November 7–10, 2010.
Elmendorf, D.L., Haith, C.E., Douglas, G.S., Prince, R.C., 1994. Relative rates of biodegradation of substituted polycyclic aromatic hydrocarbons. Bioremediation of Chlorinated and Polycyclic Aromatic Hydrocarbon Compounds. Lewis Publishers, Boca Raton, FL, pp. 188–202.
EPA, September 1994. Gel-Permeation Cleanup. Test Method. EPA/SW-846/3640A/Revision 1.
EPA, 1997. Test Methods for Evaluating Solid Waste. United States Environmental Protection Agency, Office of Solid Waste and Emergency Response, Chapter One – Quality Control. Washington, DC.
EPA, July 2014. Semivolatile Organic Compounds by Gas Chromatography/Mass Spectrometry. Test Method. EPA/SW-846/8270D/Revision 5.
Federal Register 1994. National Oil and Hazardous Substances Pollution Contingency Plan – Final Rule 40 CFR Parts 9 and 300.
Fu, J., Gong, Y., Zhao, X., O'Reilly, S.E., Zhao, D., 2014. Effects of oil and dispersant on formation of marine oil snow and transport of oil hydrocarbons. Environ. Sci. Technol. 48 (24), 14392–14399.
Ganz, A., Herrmann, J., 1975. Investigations into the Southern New England Red Crab Fishery. New England Fisheries Development Program (NOAA NMFS), Rhode Island Department of Natural Resources, Div. Fish. Wildl., Mar. Fish, 55 pp.
Glegg, G.A., Rowland, S.J., 1996. The Braer Oil Spill—hydrocarbon concentrations in intertidal. Mar. Pollut. Bull. 32 (6), 486–492.
Hastie, L., 1995. Deep-water geryonid crabs: a continental slop resource. Oceanogr. Mar. Biol. Ann. Rev. 33, 561–584.
Hazen, T.C., Dubinsky, E.A., DeSantis, T.Z., Andersen, G.L., Piceno, Y.M., Singh, N., et al., 2010. Deep-sea oil plume enriches indigenous oil-degrading bacteria. Science 330, 204–208.
Ikonomou, M.G., Fernandez, M.P., Knapp, W., Sather, P., 2002. PCBs in dungeness crab reflect distinct source fingerprints among harbor/industrial sites in British Columbia. Environ. Sci. Technol. 36 (12), 2545–2551.
Lee, R.F., Ryan, C., Neuhauser, M.L., 1976. Fate of petroleum hydrocarbons taken up from food and water by the blue crab *Callinectes sapidus*. Mar. Biol. 37, 363–370.
Little, P.J., James, M.O., Pritchard, J.B., Bend, J.R., 1985. Temperature dependent disposition of C-benzo(*a*)pyrene in the spiny lobster, *Panulirus argus*. Toxicol. Appl. Pharmacol. 77, 325–333.
Lockhart, F.D., Lindberg, W.J., Blake, N.J., Erdman, R.B., Perry, H.M., Waller, R.S., 1990. Distributional differences and population similarities for two deep-sea crabs (family Geryonidae) in the northeastern Gulf of Mexico. Can. J. Fish. Aquat. Sci. 47 (11), 2112–2122.
Mackay, D., Shiu, W.Y., Ma, K.-C., Lee, S.C., 2006a. Handbook of Physical–Chemical Properties and Environmental Fate for Organic Chemicals. Vol. I, Introduction and Hydrocarbons. CRC Press, Taylor & Francis Group, Boca Raton, FL.
Mackay, D., Shiu, W.Y., Ma, K.-C., Lee, S.C., 2006b. Handbook of Physical-Chemical Properties and Environmental Fate for Organic Chemicals. Vol. IV, Nitrogen and Sulfur Containing Compounds and Pesticides. CRC Press, Taylor & Francis Group, Boca Raton, FL.

McLeese, D.W., 1983. The Potential for Exposure of Lobsters to Creosote during Commercial Storage in the Maritime Provinces of Canada. Can. Tech. Rep., Fish Aquat. Sci.
Meador, J.P., Stein, J.E., Reichert, W.L., Varanasi, U., 1995. Bioaccumulation of polycyclic aromatic hydrocarbons by marine organisms. Rev. Environ. Contam. Toxicol. 143, 79–165.
Neff, J.M., Cox, B.A., Dixit, D., Anderson, J.W., 1976. Accumulation and release of petroleum-derived aromatic hydrocarbons by four species of marine animals. Mar. Biol. 38, 279–289.
NOAA, June 1991. Status and Trends in Concentrations of Selected Contaminants in Boston Harbor Sediments and Biota. NOAA, Seattle, WA.
NOAA, July 1993. Status and Trends. Sampling and Analytical Methods of the National Status and Trends Program National Benthic Surveillance and Mussel Watch Projects 1984–1992, Volume IV. Silver Spring, MD.
NOAA, 2001. Essential fish habitat source document: red deepsea crab, *Chaceon* (Geryon) *quinquedens*, life history and habitat characteristics. NOAA Technical Memorandum NMFS-NE-163, U.S. Department of Commerce.
NOAA, August 2009. Deepwater program: exploration and research of northern Gulf of Mexico deepwater natural and artificial hard bottom habitats with emphasis on coral communities. Reefs, Rigs, and Wrecks (Lophelia II).
NOAA, June 2010a. Work Plan for the Collection of Data to Determine the Impacts of the Deepwater Horizon Mississippi Canyon 252 Incident on Endangered and Protected Marine Mammals in the Northern Gulf.
NOAA, July 2010b. Mississippi Canyon 252 Incident NRDA Tier 1 for deepwater communities. Work Plan and SOPs.
NOAA, September 2010c. Water Column Injury Ephemeral Data Collections: Deepwater Horizon Oil Spill (DWHOS) Plan for Adaptive Water Column NOAA-NRDA Sampling (PAWNNS) Cruise Plan—HOS Davis 3.
NOAA, May 2011a. Assessment Plan for Sargassum Communities and Associated Fauna in the Northern Gulf of Mexico.
NOAA, July 2011b. MC252 *Deepwater Horizon* Oil Spill Deep Benthic Communities and Water Column Data Collection July–September 2011 HOS Sweetwater ROV Sediment and Bottom-Water Sampling Cruise Plan.
NOAA, August 2012. Mississippi Canyon 252 Deepwater Horizon Oil Spill, NRDA Sampling Plan, Mesophotic Reef Follow-Up Cruise Plan.
NOAA, January 2013a. Deepwater ROV Sampling to Assess Potential Impacts to Hardbottom Coral Communities and Associates from the *Deepwater Horizon* Oil Spill.
NOAA, March 2013b. Assessment of Impacts from the *Deepwater Horizon* Oil Spill on Red Crab.
NOAA, August 2014a. Addendum to the Assessment of Impacts from the *Deepwater Horizon* Oil Spill on Red Crab.
NOAA, May 2014b. Analytical Quality Assurance Plan, Mississippi Canyon 252 (*Deepwater Horizon*) Natural Resource Damage Assessment.
OSAT-1, 2010. Summary Report for Sub-Sea and Sub-Surface Oil and Dispersant Detection: Sampling and Monitoring, Operational Science Advisory Team.
Passow, U., 2014. Formation of rapidly-sinking, oil-associated marine snow. Deep-Sea Res. II: Topic. Stud. Oceanogr.
Passow, U., Ziervogel, K., Asper, V., Diercks, A., 2012. Marine snow formation in the aftermath of the deepwater horizon oil spill in the Gulf of Mexico. Environ. Res. Lett. Environ. Res. Lett. 7, 035301.
Payne, J.R., Driskell, W.B. August 2015a. 2010 DWH offshore water column samples—forensic assessments and oil exposures. PECI Report to the Trustees in Support of the DARP.
Payne, J.R., Driskell, W.B., August 2015b. Dispersant effects on waterborne oil profiles and behavior during the Deepwater horizon oil spill. PECI Report to the Trustees in support of the DARP.
Peters, K.E., Moldowan, J.M., 1993. The Biomarker Guide Interpreting Molecular Fossils in Petroleum and Ancient Sediments. Prentice Hall, Englewood Cliffs, NJ.
Peven, C.S., Uhler, A.D., Querzoli, F.J., 1996. Caged mussels and semipermeable membrane devices as indicators of organic contaminant uptake in Dorchester and Duxbury Bays, Massachusetts. Environ. Toxicol. Chem. 15 (2), 144–149.
Porte, C., Biosca, X., Pastor, D., Sole, M., Albaiges, J., 2000. The Agean Sea Oil spill. 2. Temporal study of the hydrocarbons accumulation in bivalves. Environ. Sci. Technol. 34, 5067–5075.
Prince, R.C., Elmendorf, D.L., Lute, J.R., Hsu, C.S., Haith, C.E., Senius, J.D., et al., 1994. 17α(*H*),21β(*H*)-hopane as a conserved internal marker for estimating the biodegradation of crude oil. Environ. Sci. Technol. 28 (1), 142–145.
Pruell, R.J., Lake, J.L., Davis, W.R., Quinn, J.G., 1986. Uptake and depuration of organic contaminants by blue mussels (*Mytilus edulis*) Exposed to Environmentally Contaminated Sediment. Mar. Biol. 91, 497–507.
Short, J.W., Babcock, M.M., 1996. Prespill and postspill concentrations of hydrocarbons in mussels and sediments in Prince William Sound. Am. Fish. Symp. 18, 149–166.
Socolofsky, S.A., Adams, E.E., Sherwood, C.R., 2011. Formation dynamics of subsurface hydrocarbon intrusions following the Deepwater Horizon blowout. Geophys. Res. Lett. 38, L09602. http://dx.doi.org/10.1029/2011GL047174, 6 p.
Soriano, J.A., Viñas, L., Franco, M.A., González, J.J., Ortiz, L., Bayona, J.M., et al., 2006. Spatial and temporal trends of petroleum hydrocarbons in wild mussels from the Galician Coast (NW Spain) affected by the prestige oil spill. Sci. Total Environ. 370, 80–90.
Steimle, F.W., Zetlin, C.A., Chang, S., 2001. Essential Fish Habitat Source Document: Red Deepsea Crab, *Chaceon* (Geryon) *quinquedens*, Life History and Habitat Characteristics. NOAA Tech Memo (NEFSC NMFS-NE-163).
Stout, S.A., 2016. Oil spill fingerprinting method for oily matrices used in the *Deepwater Horizon* NRDA. Environ. Forensics 17 (3), 218–243.
Stout, S.A., Payne, J.R., 2016. Macondo Oil in deep-sea sediments: part 1—sub-sea weathering of oil deposited on the seafloor. Mar. Pollut. Bull. 111, 265–380.
Stout, S.A., Wang, Z., 2016. Standard Handbook Oil Spill Environmental Forensics: Fingerprinting and Source Identification. Elsevier Publishing Co., Amsterdam.
Stout, S.A., Uhler, A.D., McCarthy, K.J., 2001. A strategy and methodology for defensibly correlating spilled oil to source candidates. Environ. Forensics 2, 87–98.
Stout, S.A., Payne, J.R., Ricker, R.W., Baker, G., Lewis, C., 2016a. Macondo Oil in deep-sea sediments: part 2—occurrence and distinction from background and natural oil seeps. Mar. Pollut. Bull. 111, 381–401.
Stout, S.A., Payne, J.R., Emsbo-Mattingly, S.D., Baker, G., 2016b. Weathering of field-collected floating and stranded Macondo oils during and shortly after the Deepwater Horizon oil spill. Mar. Pollut. Bull. 105 (1), 7–22.

Stout, S.A., Rouhani, S., Liu, B., Oehrig, J., Ricker, R.W., Baker, G., et al., 2017. Assessing the footprint and volume of oil deposited in deep-sea sediments following the Deepwater Horizon oil spill. Mar. Pollut. Bull. 114, 327–342.
Uhler, A.D., Emsbo-Mattingly, S.J., Liu, B., Hall, L.W., Burton, D.T., 2005. An integrated case study for evaluating the impacts of an oil refinery effluent on aquatic biota in the Delaware river: advanced chemical fingerprinting of PAHs. Human Ecol. Risk Assess. 11, 771–836.
Varanasi, U., 1989. Metabolism of Polycyclic Aromatic Hydrocarbons in the Aquatic Environment. CRC Press, Inc., Boca Raton, FL, pp. 69–91.
Wade, T.L., Kennicutt II, M.C., Brooks, J.M., 1989. Gulf of Mexico hydrocarbon seep communities: Part III. Aromatic hydrocarbon concentrations in organisms, sediments and water. Mar. Environ. Res. 27, 19–30.
Wang, W., Wu, X., Liu, Z., Zheng, H., Cheng, Y., 2014. Insights into hepatopancreatic functions for nutrition metabolism and ovarian development in the crab *Portunus trituberculatus*: gene discovery in the comparative transcriptome of different hepatopancreas stages. PLoS One. 9 (1), e84921.
Wang, Z., Stout, S.A., 2006. Spill Oil Environmental Forensics: Fingerprinting and Source Identification. Elsevier Publishing Co., Amsterdam.
Wang, Z., Yang, C., Yang, Z., Brown, C.E., Hollebone, B.P., Stout, S.A., 2016. Petroleum biomarker fingerprinting for oil spill characterization and source identification. Standard Handbook Oil Spill Environmental Forensics. Elsevier Publishing Co., Amsterdam, pp. 131–254.
White, H.K., Hsing, P., Cho, W., Shank, T.M., Cordes, E.E., Quattrini, A.M., et al., 2012. Impact of the *Deepwater Horizon* oil spill on a deep-water coral community in the Gulf of Mexico. PNAS. http://dx.doi.org/10.1073/pnas.1118029109.

Further Reading

Fisher, C.R., Demopoulos, A.W.J., Cordes, E.E., Baums, I.B., White, H.K., Bourgue, J.R., 2014. Coral communities as indicators of ecosystem-level impacts of the *Deepwater Horizon* oil spill. Bioscience 64 (9), 796–807.
Payne, J.R., Driskell, W.B., August 2015a. Offshore adaptive sampling strategies and field observations. PECI Report to the Trustees in Support of the DARP.
Wang, Z., Stout, S.A., 2007. Oil Spill Environmental Forensics: Fingerprinting and Source Identification. Elsevier Publishing Co., Amsterdam; Boston, MA.

CHAPTER

31

Modeling Distribution, Fate, and Concentrations of *Deepwater Horizon* Oil in Subsurface Waters of the Gulf of Mexico

Deborah P. French-McCay[1], *Matthew Horn*[1], *Zhengkai Li*[1], *Katherine Jayko*[1], *Malcolm L. Spaulding*[2], *Deborah Crowley*[1] *and Daniel Mendelsohn*[1]

[1]RPS-ASA, South Kingstown, RI, United States [2]University of Rhode Island, Narragansett, RI, United States

BIOGRAPHIES

Deborah French-McCay, Ph.D. is Director of Research and Model Development and a senior scientist at RPS ASA, South Kingstown, RI, USA. She received her bachelor's degree in Zoology from Rutgers in 1974 and her Ph.D. in Oceanography from the University of Rhode Island in 1984. Dr. French McCay specializes in quantitative assessments and modeling of oil and chemical releases for impact, risk, and natural resource damage assessments (NRDA); evaluating transport and fates, exposure, and effects of pollutants on individual organisms, populations, and aquatic ecosystems. Dr. French McCay leads development of RPS ASA's oil and chemical spill models SIMAP and CHEMMAP) and manages numerous projects utilizing these models to evaluate oil/chemical trajectory and fate, impacts, and ecological risks. In support of the government's NRDA for the *Deepwater Horizon* oil spill of April–July 2010 in the Gulf of Mexico, she modeled oil transport, fate, and exposure using SIMAP to evaluate injuries for water column organisms. She has been the principal investigator and primary author of more than 100 technical reports and papers and is an internationally recognized expert in oil spill fate and effects modeling.

Matthew Horn, Ph.D. is an executive director and senior scientist with RPS ASA, specializing in oil and chemical trajectory and fate modeling. He has experience working on Natural Resource Damage Assessments (NRDA), including the *Deepwater Horizon* oil spill and has provided evidence and expert testimony for regulatory hearings in Canada and the United States related to offshore development, pipeline projects, and rail. Dr. Horn received a B.S. in Science of Earth Systems, focusing on oceanography and climate dynamics from Cornell University in 2004, with distinction in research. He received a Ph.D. in oceanography from the University of Rhode Island, Graduate School of Oceanography in 2011. Dr. Horn has a range of modeling experience including determining the fate of spilled chemicals/hydrocarbons (HCs) within marine, estuarine, and freshwater environments (river and lake) both inland and offshore, overland trajectory and fate, hydrodynamic modeling, developing HC parameters used in modeling, biogeochemical cycling, chemistry, and other oceanographic processes.

Zhengkai Li, Ph.D., formerly with RPS-ASA, is currently a chief scientist of PureLine Treatment Systems in Chicago, IL. He conducts development and evaluation of advanced treatment and reclamation of industrial wastewater, particularly oil and gas water flood and produced water treatment. Previously, Dr. Li worked as a senior scientist with RPS ASA in Rhode Island, conducting research and development of oil spill fate and transport models, for *Deepwater Horizon* (DWH) oil spill Natural Resource Damage Assessment. Earlier, Dr. Li was a

Oil Spill Environmental Forensics Case Studies.
DOI: http://dx.doi.org/10.1016/B978-0-12-804434-6.00031-8

research scientist with Bedford Institute of Oceanography (BIO), working on oil spill response technology research and development. His work has been acknowledged by Canadian Government 2010 DFO ADM Award, and 2012 DFO BIO Crystal Award. Dr. Li has published more than 75 papers and technical reports in oil spill response and research area. He has Ph.D. in Environmental Engineering from Washington University in St. Louis. He is a registered professional environmental engineer.

Katherine Jayko, M.S. is a senior software engineer at RPS ASA. She received a B.S. in civil engineering from Ohio State University in 1977 and an M.S. in ocean engineering from the University of Rhode Island in 1982. Since joining RPS ASA in 1984, Ms. Jayko has developed pollutant transport models for many diverse and specialized applications. She has focused on developing the oil spill model codes for OILMAP-Deep and SIMAP, which are used worldwide for oil spill modeling-based assessments.

Malcolm L. Spaulding, Ph.D. is a Professor Emeritus, Ocean Engineering, University of Rhode Island (URI) and the Principal of Spaulding Environmental Associates (SEA), LLC. He served for 40 years on the faculty and over a decade as department chair. Dr. Spaulding has a long history in the development and application of oil spill models. He initiated and led the development of one of the most widely used oil spill transport and fate models in the world, OILMAP and established the foundation and fostered the development of ASA's spill transport and fate models. He led the development of OILMAP-Deep, which focuses on modeling of oil blowouts and the associated plume and oil droplet dynamics. Dr. Spaulding recently led the application and validation of OILMAP-Deep to the predict the blowout from the *Deepwater Horizon* spill, on behalf of NOAA's Natural Resource Damage Assessment (NRDA) office, making advances in developing and applying a fully integrated system, including pipeline release, plume, oil droplet size, dispersant treatment, and fountain and intrusion models. He has participated in major reviews of oil spill modeling over the past four decades and has recently (2017) published a review of the current state of the art.

Deborah Crowley is a senior consulting environmental scientist and project manager at RPS ASA. She has experience working on issues and projects related to various aspects of environmental science such as environmental data analysis, hydrodynamic and water quality modeling and analysis, oil and gas fate and transport assessment in the environment, operational discharge modeling and assessment, renewable energy project development assessment support, environmental impact assessment in coastal and marine environments, and permitting and regulatory compliance analysis and support. Areas of experience include numerical modeling, model development and application, field program design and support, data analysis and visualization in Matlab, and geospatial analysis in ArcGIS.

Daniel Mendelsohn is a senior scientist and project manager at RPS ASA. He has extensive experience in numerical model development and application with a focus on hydrodynamics, hydraulics, water quality, meteorology, thermal and pollutant, oil and chemical spill transport, and fates. Mr. Mendelsohn is internationally known for his applied research in the field of 3D oil spill fates modeling, for developments in the area of near neutrally buoyant emulsion products, the integration of Lagrangian and boundary conforming Eulerian modeling techniques for operational oil spill models, and most recently, for deepwater oil and gas blowout plume model development and application.

31.1 INTRODUCTION

The scope of the 2010 *Deepwater Horizon* (DWH) oil spill was extensive, with areas potentially affected including the entire northeastern Gulf of Mexico. Oil released from the broken riser both dispersed at depth and rose through nearly a mile of water before reaching the surface. Thus, there were logistical constraints in obtaining sufficient field sample data to completely characterize the contamination in space and time during and following the nearly 3-month duration of the oil and gas release. To evaluate the overall fate of the oil, a modeling effort was undertaken to analyze the deep water oil and gas blowout plume dynamics, rising oil droplets during their journey from the release through the water column to the surface, and fate of the oil in surface waters. The SIMAP (Spill Impact Model Application Package) oil fate model (French McCay, 2003, 2004) was used to evaluate concentrations of oil and fate of its components in the water column and on the surface resulting from the spill.

Fig. 31.1 illustrates the oil release features and models used to evaluate the buoyant plume and rising oil. The modeling analysis began with application of pipe-discharge, blowout plume, dispersant treatment, and droplet size models (i.e., OILMAP-Deep; Spaulding et al., 2015) to evaluate the release conditions and the height above the discharge where the oil and gas plume had entrained enough water and lost enough gas to dissolution to

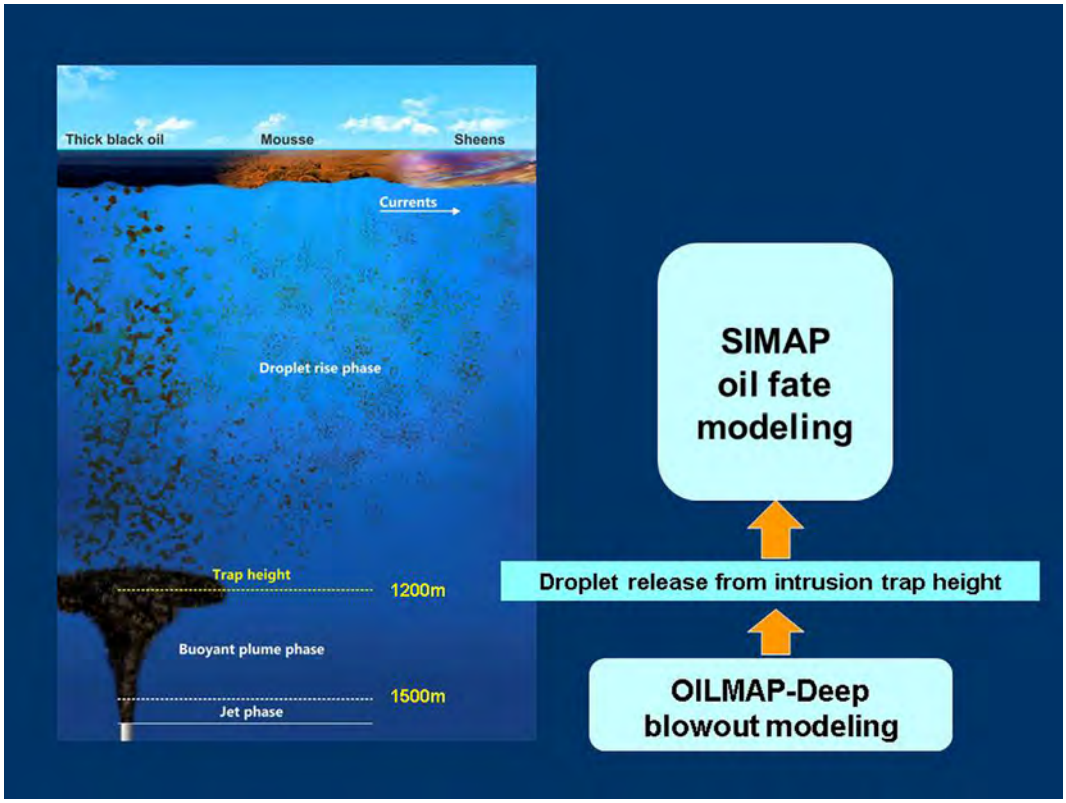

FIGURE 31.1 Conceptual model and approach for modeling the plume and rising oil.

become neutrally buoyant with the surrounding seawater. At this so-called trap height, oil droplets were released from an intrusion layer into the water and rose at varying rates toward the surface according to their individual droplet size (buoyancy). The analysis by Spaulding et al. (2015) provided the initial release conditions, i.e., oil mass and droplet sizes released at the trap height, that were used as input to the far field SIMAP oil fate model calculations.

The three-dimensional SIMAP oil fate model was used to estimate oil droplet and dissolved HC concentrations in the water column. Herein, the focus is on evaluation of the oil fate and concentrations from the trapping depth to just below the water surface, i.e., deeper than 40 m, the typical depth of the surface mixed layer. Model results for the surface layer above 40 m are to be reported elsewhere (RPS-ASA, in preparation). In the subsurface, the major weathering processes were dissolution and biodegradation. Oil droplets reaching 40 m rapidly surfaced to form floating oil slicks, which then further weathered via evaporation and emulsification. Surfaced oil was transported long distances (hundreds of kilometers) horizontally, as well as reentrained into the water column.

Below the surface water layer, the oil fate model estimates the distribution and mass of oil in the water column and settled to the seabed through time. Processes simulated by the physical fates modeling included oil droplet transport and dispersion, dissolution of soluble components into the water column, partitioning of oil components between water and suspended particulate matter (SPM), adsorption of oil droplets to SPM, sedimentation of oil droplets and SPM, and biologically mediated degradation (i.e., primary biodegradation). The model results include:

- rates of transformation of oil and its constituents,
- the concentrations of whole oil and individual HC components in the water, in both the droplet and dissolved phases,
- the overall mass balance of the spilled oil, and
- fluxes of HCs to the sediments over time.

As chemistry sampling during April–July 2010 was focused on the region within 10–20 km of the wellhead, model results were compared to field-collected data from within a 25-by-25-km box centered on the wellhead.

Measured currents over the depth of water affected were available at three stations within 10 km of the wellhead. Thus, model results using forcing from the application of eight (different) hydrodynamic models were compared to those using a current field derived from the current measurements.

The results demonstrate that use of current data from each of the eight hydrodynamic models as oil spill model input resulted in very different trajectory paths, and that the hydrodynamic models (to varying degrees) generally over-estimated the speed of the currents in the area of the wellhead. The concentrations of soluble and semisoluble HC components predicted by the model using the measured currents were compared with quality-controlled chemical measurements of samples collected by the Natural Resource Damage Assessment (NRDA) program to validate the model. Overall, the modeled concentrations below 40 m using the measured current data were distributed in accord with field observations and of the same order of magnitude as the measured concentrations.

31.2 METHODS

31.2.1 Oil Spill Models: OILMAP-Deep and SIMAP

Oil spill modeling of the DWH spill was performed sequentially using pipe-discharge, blowout plume, dispersant treatment, and droplet size models in OILMAP-Deep to predict the nearfield, and the oil transport and fate model SIMAP for the far field. The pipeline model utilized oil and gas flow rate, equations of state, pipe dimensions, aperture sizes, and conservation of mass and momentum equations to calculate the outflow from each aperture (e.g., riser and kink holes) over the 84 days of oil release (April 22–July 15, 2010). Before June 3, 2010, the oil and gas was discharged through the end of the broken riser and through holes in the kink in the pipe just above the blowout preventer (BOP), while after June 3, the oil and gas was discharged through the "Top Hat" on the cut pipe just above the BOP. The calculated oil and gas volume flow rates and exit velocities from each aperture over time were used as input to the OILMAP-Deep blowout model (for details, see Spaulding et al., 2015).

OILMAP-Deep was used to evaluate the nearfield dynamics of the blowout plume and the droplet sizes produced as a result of the turbulent mixing energy and application of dispersants (Spaulding et al., 2000; Crowley et al., 2014; Spaulding et al., 2015; Li et al., 2017). These results were used as the initial conditions for the SIMAP model, which was used to calculate transport and fate of the oil after release from the near-field buoyant plume. OILMAP-Deep includes two subordinate models, the plume model and a droplet size model. The plume model predicted the plume evolution through the water column (based on oil and gas flow rates, volumetric corrections for pressure and temperature at the release depth, and aperture size at the release point) and the droplet size model predicted the distribution of droplet sizes in response to the turbulence at the release and oil properties [density, viscosity, and interfacial tension (IFT)]. Subsurface dispersant application was implemented in the droplet model through incorporation of a reduced IFT associated with the dispersant treatment as a function of the dispersant-to-oil ratio (DOR) of the treated fraction of the release (Spaulding et al., 2015; Li et al., 2017). Reduction of IFT resulted in smaller oil droplets being released into the water column. The droplet size model was validated using experimental data reported by Brandvik et al. (2013), as described in Spaulding et al. (2015) and Li et al. (2017). The mass and droplet size distribution predicted by OILMAP-Deep was input to SIMAP, which then simulated the rise rate of the oil droplets (a function of droplet size and weathering state via its effect on oil density and hence buoyancy), dissolution (which is faster for smaller droplets), dilution, and degradation (which is faster for smaller droplet sizes because of increased surface area and dissolution and, therefore, bioavailability for biodegradation).

SIMAP (French McCay, 2003, 2004; French McCay et al., 2015a, 2017a) was used to quantify oil trajectory, concentrations of oil HC components (as part of droplets and dissolved) in the water column, areas swept by floating oil of varying mass concentrations and thicknesses, shorelines oiled to varying degrees, and the amount of oil settling to sediments. Processes simulated by SIMAP included spreading, evaporation of volatiles from surface oil, transport on the surface and in the water column, randomized dispersion from small-scale motions (mixing), emulsification, entrainment of oil as droplets into the water (natural and facilitated by dispersant application), dissolution of soluble and semisoluble components, volatilization of dissolved HCs from the surface water, adherence of oil droplets to SPM, adsorption of semisoluble aromatics to SPM, sedimentation, stranding on shorelines, and degradation (biodegradation and photooxidation). The model tracked soluble and semisoluble HC components of the oil (i.e., monoaromatic hydrocarbons (MAHs, such as benzene, toluene, ethylbenzene, and xylene [BTEX]), polynuclear aromatic hydrocarbons (PAHs), and soluble alkanes; i.e., S/SS HCs), as well as

insoluble volatile aliphatic HCs, separately from high-molecular weight nonvolatile and insoluble components of the oil. Whole oil (containing nonvolatiles and volatiles not yet volatilized or dissolved from the oil) were simulated as floating slicks, emulsions, and/or tarballs or as dispersed oil droplets of varying diameter (some of which may resurface). Sublots of the spilled oil were represented by Lagrangian elements ("spillets"), each characterized by mass of HC components and water content, location, thickness, diameter, density, and viscosity. A separate set of Lagrangian elements was used to track movements of the dissolved HCs.

Mechanical recovery and in situ burning were simulated using polygons defining time and spatial windows where oil was removed at specified rates (i.e., oil volume per unit time). These were based on recovery estimates made during the spill. Constraints due to weather (e.g., wind speed, wave height) and weathering state (i.e., viscosity) of the oil were defined in the model inputs. The model removed oil when weather conditions allowed to the extent that floating oil within an appropriate viscosity range was available at the time(s) and in the location(s) specified.

Surface dispersant applications were simulated in SIMAP by specifying as model inputs the applied dispersant volume, assumed effectiveness (percent of the oil treated), DOR (i.e., volume of oil treated per volume of dispersant encountering the oil), time and spatial window(s) when applied, and constraining weather and oil weathering characteristics (e.g., viscosity limit for dispersion via dispersant application). The SIMAP model's surface entrainment algorithm adjusted entrainment rate of a treated parcel of oil to reflect the DOR, level of turbulence (a function of wind speed), and oil characteristics (viscosity) at the time and location of dispersant application. This resulted in more floating oil dispersing into the water column and a change in entrained droplet size distribution to smaller droplet sizes (related to the DOR and level of turbulence), which in turn increased the surface area and dissolution rate of soluble components, and thus their biodegradation rates due to this increased bioavailability.

The model algorithms in SIMAP (French McCay, 2002, 2003, 2004; French McCay et al., 2015a, 2017a) were developed over the past three decades to simulate fate and effects of oil spills under a variety of environmental conditions. SIMAP was derived from the Natural Resource Damage Assessment Model for Coastal and Marine Environments (French et al., 1996), which was developed for the US Department of the Interior (USDOI) as the basis of Comprehensive Environmental Response, Compensation, and Liability Act of 1980 NRDA regulations (43 CFR PART 11 [1995], as amended at 61 Fed. Reg. 20609, May 7, 1996) for Type A. In addition to validating the model with data from the DWH spill, the model has been validated with data from more than 20 large spills, including the *Exxon Valdez* (French and Rines, 1997; French McCay, 2003, 2004; French McCay and Rowe, 2004), as well as test spills designed to verify the model (French et al., 1997).

Herein, we focus on the processes applicable to waters below 40 m. Thus, the model algorithms for subsurface processes (i.e., oil droplet transport and dispersion, dissolution of soluble components into the water column, partitioning of oil between water and SPM, sedimentation of oil, and biodegradation) are briefly described here. Further details on model algorithms are available in French McCay (2004) and French McCay et al. (2015a; 2017a).

31.2.1.1 Oil Components

Oil is a mixture of tens of thousands of HCs of varying physical and chemical characteristics and, thus, varying fates. In the SIMAP model, oil is represented by component categories, and the fate of each component is tracked separately. The "pseudocomponent" approach (Payne et al., 1984, 1987; French et al., 1996; Jones, 1997) is used, where chemicals in the oil mixture are grouped by physical–chemical properties, and the resulting component category behaves as if it were a single chemical with characteristics typical of the chemical group. The S/SS HCs were divided into chemical groups (components) based on volatility, solubility, and hydrophobicity (using the octanol–water partition coefficient, K_{ow}, of the chemicals). The water solubility of compounds having log (K_{ow}) values greater than about 6 is very limited (Di Toro et al., 2000, French McCay, 2002); thus, the oil was treated as being composed of aliphatic and aromatic components with $\log(K_{ow}) < 6$ as defined in Table 31.1. All but the residual oil component (representing nonvolatile and insoluble aromatics and aliphatics) dissolved at rates specific to the component. Solubility is strongly correlated with volatility, and the solubility of aromatics is higher than aliphatics of the same volatility. Of the aromatics, the MAHs are the most soluble, the 2-ring PAHs are less soluble, and the 3-ring PAHs slightly soluble (Mackay et al., 2006a,b). The solubility of the aliphatic HCs is much less than for the aromatics of similar molecular weight. Dissolved concentrations were calculated in the model for each of the soluble and semisoluble components (named AR1 to AR9). Note that nonaromatic (aliphatic) compounds that are soluble (i.e., C1–C10 *n*-alkanes, isoalkanes, and cycloalkanes) were included in the "AR9" component.

TABLE 31.1 The 19 Pseudocomponents Modeled in the SIMAP Oil Fate Model

AR or AL component number	All HCs	Soluble and semisoluble HCs (AR components)		Nonsoluble aliphatic HCs (AL components)	
	Volatility	Compounds	Range of log(K_{ow})	Compounds	BP range (°C)[a]
1	Volatiles	MAHs (BTEX[b], styrene)	1.9–2.8	Volatile aliphatics[a]	<150
2		C3-benzenes	2.8–3.6	Volatile aliphatics[a]	150–180
3	Intermediate volatility	C4-benzenes	3.1–3.8	Semivolatile aliphatics (C11)	180–200
4		Decalins	4.1–6.0	Semivolatile aliphatics (C12)	200–230
5		C0–C2 naphthalenes, C0–C2 benzothiophenes, biphenyl, acenaphthene, acenaphthylene	2.3–4.3	Semivolatile aliphatics (C13–C16)	230–280
6	Semivolatile	C3–C4 naphthalenes, C3–C4 benzothiophenes	4.2–5.20	Low-volatility aliphatics (C17–C18)	280–300
7		Fluorenes and C0–C1 3-ring PAHs	4.0–5.6	Low-volatility aliphatics (C19–C20)	300–350
8		4-ring PAHs and C2–C3 3-ring PAHs	4.9–6.0	Low-volatility aliphatics (C21–C23)	350–380
9	Highly volatile and soluble aliphatics	Low MW alkanes, isoalkanes, cycloalkanes	2.3–5.6	N.A. (used for dispersant indicators)	<180
Residual	Residual (nonvolatile)	High MW PAHs	>6.0	High molecular weight aliphatics (C24+)	>380

[a]*Composed of unmeasured nonsoluble compounds in the boiling point (BP) range.*
[b]*Benzene, toluene, ethylbenzene, and xylenes.*

The initial (at the point of release to the water column) mass concentrations of the eight soluble aromatic components (AR1–AR8) and the soluble aliphatic component (AR9) were computed using measured source oil sample hydrocarbon (HC) concentrations (see below). The mass concentrations of the eight nonsoluble aliphatic components (AL1–AL8) were based on measured weight fractions of a boiling curve for fresh source oil, using the boiling point ranges listed in Table 31.1. For components AL1 and AL2, all of the measured compounds are soluble, and so their mass concentrations were included in component AR9. Thus, AL1 and AL2 represent unmeasured compounds in their respective boiling ranges (where solubility is unknown and not considered in the model). This approach avoids "double counting" aliphatics that would otherwise be included in AL1 and AL2, as well as AR9. Component AL9 was reserved for tracking dispersant component(s) or other contaminants. Each of the components was tracked in both the whole oil (droplets and floating oil) and dissolved phases.

31.2.1.2 *Modeled Processes in SIMAP*

In the three-dimensional oil fate model SIMAP, sublots of the spilled oil are represented by Lagrangian elements ("spillets"), each characterized by mass of HC components, water content, location, thickness, diameter, density, and viscosity. A separate set of Lagrangian elements is used to track movements of the dissolved HCs. Each time step of the model, calculations of the transport and fate processes are made for each spillet, which below 40 m include transport (advection and turbulent dispersion), dissolution of soluble/semisoluble components into the water column, partitioning of soluble/semisoluble HCs between water and SPM, adhesion of oil droplets to SPM, sedimentation of oil droplets and SPM, and biodegradation.

Transport is the sum of advective velocities by currents input to the model, vertical movement according to particle (droplet or SPM) buoyancy (using Stoke's Law), and randomized turbulent diffusive velocities in three dimensions, with the horizontal values being much larger than those in the vertical. The modeling approach developed by Mackay and Leinonen (1977), which is based on Raoult's Law, is used in SIMAP for dissolution, applied to each of the S/SS HCs separately using component-specific properties. Once dissolved, S/SS HCs partition between dissolved and particulate (SPM) phases and the settling rate of the SPM is calculated based on

Stoke's Law using the density of the SPM. Adhesion of oil droplets to SPM is based on collision rate with SPM, a function of the concentrations of droplets and SPM. Modified Stoke's Law (White, 2005) is used to calculate the settling or rise rate of the combined particle, based on relative buoyancy and the particle diameter. Sedimentation of oil droplets and SPM occurs as these particulates reach the sea floor. These algorithms are described in French McCay (2004) and French McCay et al. (2015a).

HC degradation may occur as the result of photooxidation, which is a chemical process energized by ultraviolet light from the sun, and by biological (microbial) breakdown, termed biodegradation. Primary biodegradation is the first step in the breakdown by microbial action on HCs. Below 20 m, photooxidation is assumed negligible because the causal ultraviolet light does not penetrate this far into seawater. A first-order decay algorithm is used to estimate primary biodegradation (as described in French McCay, 2004; French McCay et al., 2015a), the rate being specified for each of the HC components modeled. Based on the NRC (2005) review of the different biodegradation pathways for the aromatic and alkane compounds, microbial degradation occurs primarily in the dissolved phase for soluble components, but in the particulate phase for the insoluble aliphatics. For the soluble and semisoluble components (AR1−AR9), biodegradation within subsurface droplets in the water column is assumed negligible, since biodegradation rates are much slower than their dissolution rates. Therefore, in the application of degradation rates in the oil fates model, biodegradation rates of the soluble and semisoluble components are calculated for the dissolved fraction, while the degradation rates of the insoluble alkanes are calculated for the dispersed particulate oil fraction. Biodegradation is assumed not to be inhibited by the presence of dispersant.

31.2.1.3 Estimation of Concentrations and Model Outputs

For subsurface oil, the model outputs after each time step include the location, dimensions, and physical−chemical characteristics of each spillet representing the oil; concentrations of each of the components in the particulate (oil droplet) and the dissolved phases in three dimensions; and total HCs and components deposited on the sediments.

The dissolved and droplet HC concentrations in the water column, by HC component, were calculated from the mass in the spillets, as follows. Concentration was contoured on a three-dimensional grid system. This grid was fixed in dimensions to provide concentration output of a consistent resolution throughout the model run. Distribution of mass around the spillet center was described as Gaussian in three dimensions, with one standard deviation equal to twice the local diffusive distance ($2D_x t$ in the horizontal, $2D_z t$ in the vertical, where D_x is the horizontal and D_z is the vertical spreading diffusion coefficient, and t is particle age). Concentrations depend highly on the resolution of the concentration grid used. Thus, a postprocessor was used to calculate concentrations in user-defined resolutions, as well as in specific spatial and temporal windows.

31.2.2 Oil Fate Model Inputs

31.2.2.1 Geographical and Model Grid

For geographical reference, SIMAP uses a rectilinear grid to designate the location of the shoreline, the water depth (bathymetry), and the habitat type. The bathymetric and shoreline grid resolution was 0.006 degrees of longitude and latitude, which is 650.4 m × 667.9 m at the spill site. Bathymetry for the Gulf of Mexico was obtained from the Gridded Global Relief Data (ETOPO2v2) supplied by the US Department of Commerce, National Oceanic and Atmospheric Administration (NOAA), National Geophysical Data Center (NOAA NGDC, 2012). The data were interpolated into the model grids for each area, by averaging all soundings falling within a cell. The shoreline was compiled from NOAA's ESI data: http://response.restoration.noaa.gov/esi. ESI shoreline data were reclassified to a simpler habitat classification, i.e., rocky, cobble, sand, mud, wetland, and artificial (man-made) shore types. Maps of the habitat types in this grid are available in French McCay et al. (2015a, 2017b).

31.2.2.2 Temperature and Salinity

Water temperature and salinity data used varied spatially, with depth, and by month. Climatic monthly mean water temperature and salinity data were obtained from the NODC Ocean Climate Laboratory's Monthly Climatology data set for the Gulf of Mexico (Boyer et al., 2005, 2009; Locarnini et al., 2010; Antonov et al., 2010). This NODC analysis uses all data for the region that had been collated in the World's Ocean Database to provide gridded monthly mean climatological data. The most recent version of the NODC database, which contains data through 2013 gridded on a 1/4-degree grid, was used.

31.2.2.3 Currents

Several current data sets were evaluated in model runs using SIMAP, including observational and hydrodynamic-model-generated data. A number of acoustic Doppler current profilers (ADCPs) moored in place along the continental slope of the northeastern Gulf of Mexico (Fig. 31.2), measured sufficient current data during 2010 before and during the spill period to evaluate the accuracy of the hydrodynamic models and to use as input for modeling subsurface transport of the released oil. During the spill period, ADCPs were deployed near the MC252 wellhead site, including a pair sampling the upper water column and waters deeper than 1000 m, set out by a cooperative NRDA plan (Mulcahy, 2010). The ADCP station closest to the DWH well is number "42916" (http://www.ndbc.noaa.gov/station_page.php?station = 42916), which was installed on the Development Driller 3 that operated one of relief wells within 1 km of the DWH wellhead. As an indication of the currents below 40 m, during the period from April–July 2010, the temporally averaged current velocity at 900 m at that station was 6.7 cm/s (0.13 knot), with standard deviation 4.7 cm/s (0.09 knot). Below 40 m, the mean current speeds, and their standard deviations, were <10 cm/s at all depths.

31.2.2.3.1 ADCP-Based Current Fields

ADCP data for 60 stations in the northern Gulf of Mexico were downloaded in March 2011 from the NDBC data archive at http://www.ndbc.noaa.gov/. Of these 60 stations, 19 ADCPs at 18 stations met the criteria for inclusion in the set used for modeling, i.e., the location was within the area potentially most affected by the spill (~26.5–30°N, ~87.5–93°W); the metadata were without obvious errors, change or inconsistencies in the locations or adjacent depth bins; and the data gaps did not exceed 50% of the period of interest, April 1–September 30, 2010. Details are provided in French McCay et al. (2017b).

ADCP data meeting the quality criteria were used in SIMAP model simulations for comparison with simulations run with hydrodynamic model results. The data for these 18 ADCPs at 17 stations were interpolated to

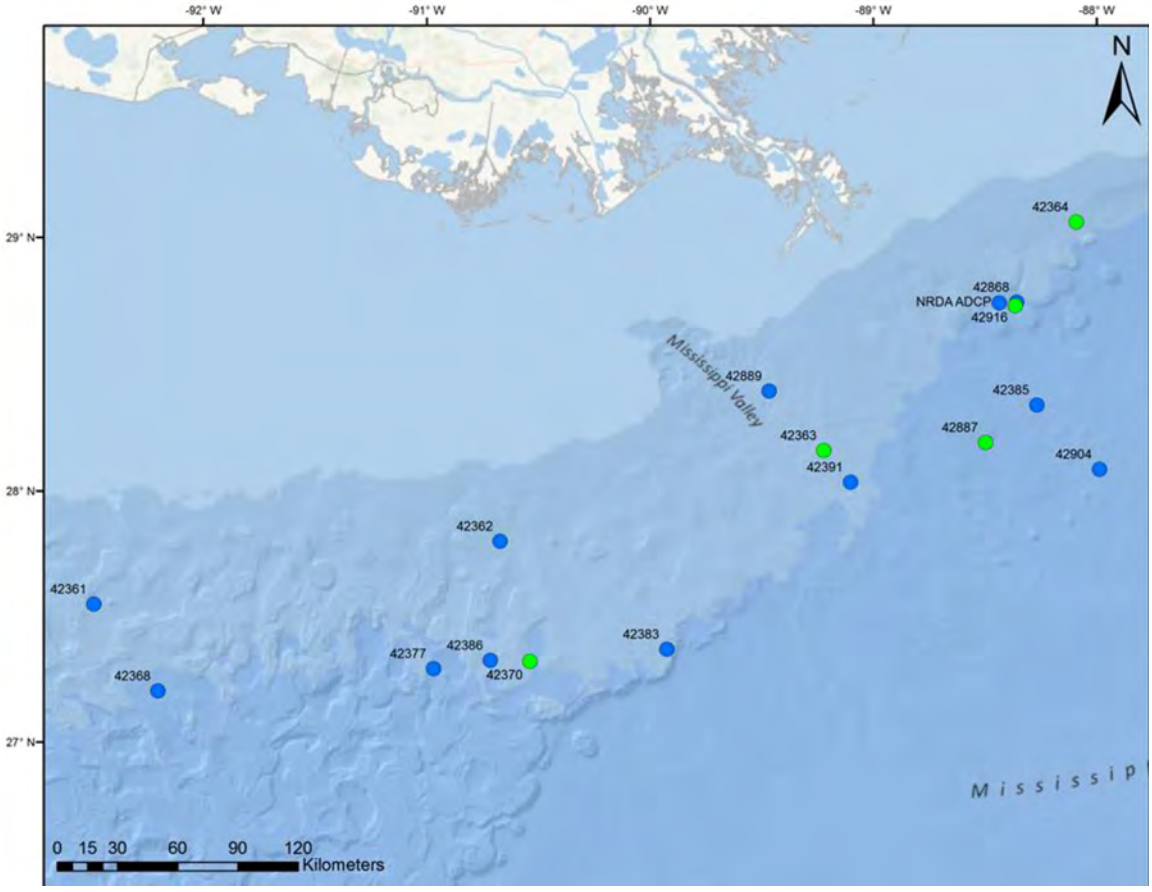

FIGURE 31.2 Locations of 18 ADCP moorings where sufficient data were available for 2010.

develop three-dimensional and time-varying current fields, using an inverse distance-weighted scheme employing all sensors, which could be used for transport calculations. The following steps were used in preparing and interpolating the ADCP data to develop the four-dimensional current field:

1. *Vertical registration*: The original ADCP data sets were first mapped to the same vertical locations (*bins*) extending from the top- to bottom-most data.
2. *Time registration*: All data sets were linearly interpolated in time so that all data were available at prescribed times and at fixed intervals of time (10 min).
3. *Spatial interpolation*: As is clear from Fig. 31.2, the ADCPs covered a limited portion of the spill-affected area horizontally. The vertical extent of the data was typically from depths between 50 and 1200 m. Little data were available near the surface (0–50 m) and from 1200 m to the bottom; the only such data being that from the NRDA ADCPs near the wellhead. This necessitated a process to extrapolate or interpolate the data to locations where it was needed. The methods used in both the vertical and horizontal are summarized below. This interpolation was implemented for each spillet at each time step in the spill model simulation.

   Horizontal interpolation/extrapolation: At the horizontal (latitude, longitude) location of the spillet, the currents are determined by inverse square distance weighting using the five closest horizontal neighbors.

   Vertical interpolation/extrapolation: If current observations were available both above and below the spillet location, then linear interpolation using the five nearest vertical neighbors was used to estimate the current vector. Above the shallowest bin where data were available, the closest vertical value was used. Based on coherence analysis, ADCP stations were grouped into five clusters (vicinity of the well and NE, S, SW, and distant SW of the well). A representative station in each cluster (lighter dots in Fig. 31.2) was selected to extrapolate values in the bottom-most bin to the seabed. The core assumptions are that currents are constant with depth above the shallowest and below the deepest observation (no or very weak vertical structure).

31.2.2.3.2 Hydrodynamic Models

Several hydrodynamic model simulations of currents in the northeastern Gulf of Mexico were available for the period and entire area of interest and therefore were used in model simulations. The hydrodynamic models are briefly described below.

HYCOM-FSU: The Florida State University (FSU) HYbrid Coordinate Ocean Model (HYCOM) uses a hybrid coordinate system, advantageous for resolving water bodies with large ranges of bathymetry (Chassignet et al., 2007, 2009). The hydrodynamic simulation used was provided to the USDOI, Bureau of Ocean Energy Management (BOEM) for the deep water blowout risk assessment study (Galagan et al., 2017). FSUs HYCOM has a 3–4-km horizontal resolution, 20 hybrid layers in the vertical, and provides current predictions every 3 hours. HYCOM-FSU was forced with NARR winds. Multiple observations were used for data assimilation to the hindcast including remotely sensed satellite Sea Surface Temperature and Sea Level Anomalies, in-situ temperature and salinity profiles obtained from ship surveys, moorings, profiling floats, and gliders. A statistical interpolation methodology called the Tendral–Statistical Interpolation System (T-SIS) was used (Halliwell et al., 2014) for data assimilation. Details of the model hindcast can be found in Chassignet and Srinivasan (2015).

NRL GLOBAL HYCOM: The US Naval Research Lab (NRL) provides its real-time operational GLOBAL HYCOM simulations on its government website, and many transport modelers download and utilize these data products. The model is forced with NOGAPS winds. Model resolution is 1/25° (~3.5 km) in the horizontal, with 20 vertical layers. Data for the Gulf of Mexico during 2010 were downloaded and formatted in netCDF files for use as input to SIMAP.

NRL HYCOM + NCODA GOM: The NRL's HYCOM + Navy Coupled Ocean Data Assimilation (NCODA) Gulf of Mexico 1/25° Reanalysis product GOMu0.04/expt_50.1 [http://tds.hycom.org/thredds/catalog/datasets/GOMu0.04/expt_50.1/data/netcdf/catalog.html and http://hycom.org/data/gomu0pt04/expt-50pt1] uses the NCODA system (Cummings, 2005, Cummings and Smedstad, 2013) for data assimilation. The Gulf of Mexico model has 1/25° equatorial resolution and latitudinal resolution of 1/25° cos(lat) or ~3.5 km for each variable at mid-latitudes. This version has 36 coordinate surfaces in the vertical. Wind data used to force the hydrodynamics, and for the oil spill modeling, were the NOAA NCEP Climate Forecast System Reanalysis (CFSR) Selected Hourly Time-Series Products, January 1979 to December 2010 (Saha et al., 2010) [http://rda.ucar.edu/datasets/ds093.1/].

SABGOM: SABGOM is a Regional Ocean Modeling System (ROMS) application that encompasses the entire Gulf of Mexico and South Atlantic Bight (Hyun and He, 2010; Xue et al., 2013). SABGOM ROMS employs a mesh with a horizontal resolution of ~5 km and 36 terrain-following vertical layers used to resolve the water column.

A one-way nesting approach was used, whereby the boundary conditions for SABGOM were provided by HYCOM/NCODA (1/12° equatorial resolution together with NRL Coupled Ocean Data Assimilation scheme, Chassignet et al., 2007). The implementation of SABGOM used was also provided to BOEM for a deep water blowout risk assessment study (Galagan et al., 2017). SABGOM was forced with NARR winds. Freshwater input from 49 coastal rivers was included in the model based on monthly mean climatological runoff data (except for the Mississippi river, for which daily USGS river gauge observations were used to define its discharge). During the simulation, a weak relaxation scheme was imposed to relax SABGOM interior temperature and salinity fields to their HYCOM/NCODA counterpart using a 20-day time scale. This procedure allowed SABGOM to evolve continuously according to its own high resolution dynamics, and at the same time be on par with HYCOM model prediction at low frequency. As HYCOM/NCODA assimilates satellite, XBT and Argo observations, this weak T/S relaxation scheme also provides a basic data assimilation capability for SABGOM. Current predictions were provided every 3 hours.

IAS ROMS: The Intra-Americas Sea (IAS) ROMS application consists of a single domain covering the entire Gulf of Mexico and much of the western Atlantic Ocean (between the equator and 40°N). SABGOM (Hyun and He, 2010) is the predecessor of IAS ROMS. The model has a grid resolution of ~6 km in the horizontal, with 30 levels in the vertical (Chao et al., 2014). The lateral boundary conditions for the model domain are provided by real-time global 1/12° HYCOM currents (Chassignet et al., 2009). Outputs were generated by the NRL at Stennis Space Center and distributed by Florida State University. Every 12 hours, IAS ROMS assimilated observational data (e.g., temperature, salinity, sea surface height, and the ADCP data described above) using its three-dimensional variational data assimilation algorithm (Li et al., 2008a,b). Twelve-hourly data were used as a direct input to SIMAP, as were hourly predictions between these 12-hour steps. The hourly results are a combination of the observational data and the model first-guess field, which is the 12-hour IAS ROMS forecast (without data assimilation) initialized from the previous nowcast. An IAS ROMS simulation (version "4C") for 2010, that included a 2-km nested grid within the larger IAS ROMS domain, was run as part of the trustees' NRDA program and provided by Chao et al. (2014) in April 2014. This simulation was forced with North American Mesoscale (NAM) winds.

NRL NCOM-Operational: The Global Navy Coastal Ocean Model (NCOM) was an ocean prediction system run (through 2013) by the Naval Oceanographic Office (NAVOCEANO) as the Navy's real-time operational global nowcast/forecast system. The NRL developed NCOM based on the Princeton Ocean Model (POM, developed by Dynalysis of Princeton) with time invariant hybrid (sigma over Z) vertical coordinates. For distribution [on http://ecowatch.ncddc.noaa.gov/global-ncom/], NAVOCEANO interpolates the output onto a regular latitude−longitude grid in the horizontal and a series of standard depths in the vertical and parses the global domain into 13 regions.

NRL NCOM Reanalysis: NRL also has publically provided a three-dimentional reanalysis product produced using the NRL NCOM (https://www.ncdc.noaa.gov/data-access/model-data/model-datasets/navoceano-ncom-glb), which uses CFSR winds [https://climatedataguide.ucar.edu/climate-data/climate-forecast-system-reanalysis-cfsr] for forcing. NCOM reanalysis product hydrodynamic data were downloaded in March 2015.

NGOM (NOAA/NOS/OCS): The NOS Gulf of Mexico Nowcast/Forecast Model (NGOM) is the NOAA/NOS Coast Survey Development Laboratory Gulf of Mexico implementation of the POM. NGOM was run as a nowcast in real time for 2010, forced with winds and river discharges. NOAA's surface winds (12 km resolution) and atmospheric forecasts from the NAM model were used. Synoptic river flow discharges are specified from 36 rivers at 29 discharge model locations along the US coastline, based on USGS and USACE gages. The resolution of NGOM is 2−3 km in the northwestern Gulf, 5−6 km in the northeastern and central basin, with 37 levels in the vertical. Predictions were provided every 3 hours.

31.2.2.4 Small Scale Dispersion (Diffusion)

In the simulations with currents, the horizontal dispersion (randomized mixing) coefficient was assumed to be 2 m^2/s in the upper 40 m and 0.1 m^2/s below 40 m in the water column. The vertical dispersion (randomized mixing) coefficient was assumed 10 cm^2/s in the upper 40 m and 0.1 cm^2/s below 40 m. These are reasonable values for oceanic waters based on empirical data (Okubo and Ozmidov, 1970; Okubo, 1971, Csanady, 1973, Socolofsky and Jirka, 2005), consistent with the various hydrodynamic models used and modeling experience.

31.2.2.5 Suspended Particulate Matter

Oil can adhere to SPM and be transported in the water column in accordance with the density, shape, and size of the combined oil-sediment particulates. Typically, for small spills of short duration, sedimentation of oil, via mineral-SPM interactions, becomes significant above suspended sediment concentrations of about 100 mg/L

(Payne et al., 1987; French McCay et al., 2004). After the DWH spill, components of the MC252 oil were identified on the sediments in the offshore area (Valentine et al., 2014; Stout, 2015d; Stout et al., 2015), indicating oil sedimentation. Because mineral SPM concentrations are typically very low in the offshore Gulf of Mexico (D'Sa et al., 2007, D'Sa and Ko, 2008; Salisbury et al., 2004), transport of oil dispersed in the water column to the seafloor likely resulted from oil droplets becoming less buoyant after weathering and biodegradation, facilitated by droplet adherence to organic matter and settling of marine snow (Passow et al., 2012; Passow, 2014), as well as the unsuccessful top-kill activities (i.e., injection of heavy drilling mud into the well) where considerable oil and SPM was ejected from the well into the water column. Given the large volume of oil and sediments released by the failed top kills, the density of the top-kill sediments (as opposed to near-neutral density of marine snow), and the majority of the oil in the footprint of contamination being focused very near the DWH wellsite (Valentine et al., 2014; Stout, 2015d; Stout et al., 2015), the top-kill material likely accounted for the majority of the oil flux to the sediments near the wellsite. Indeed, Stout et al. (2016b) and Stout and Payne (2017) have shown that a large fraction of the sedimented oil close to the wellhead was associated with synthetic drilling mud lost during the blowout or introduced into the oil within the drill pipe during the failed top-kill operations. The top-kill operation was not included in the modeling reported herein, and oil sedimentation was only mediated by baseline ambient SPM.

Based on a review of baseline SPM concentrations in the northern Gulf of Mexico, the mean SPM in offshore blue waters is 3 mg/L, while SPM concentrations in nearshore waters are ~5–10 mg/L and up to 50 mg/L near the Mississippi Delta (D'Sa et al., 2007; D'Sa and Ko, 2008; Salisbury et al., 2004). A synoptic map of SPM was developed by Galagan et al. (2017) for use in the oil spill model by combining results from field and modeling studies with satellite imagery depicting suspended sediment plumes (French McCay et al., 2016; based on Salisbury et al., 2004; D'sa et al., 2007; D'Sa and Ko, 2008; Lee et al., 2012).

31.2.2.6 Oil Properties

Table 31.2 provides a summary of the oil properties for the MC252 oil released into the far-field and used in the SIMAP modeling. The effects of the released gas were accounted for in the near-field blowout modeling, and gas was not tracked in the SIMAP model. Tables 31.3 and 31.4 summarize the fractional composition of MC252 oil by component group, based on measurements by Stout (2015a). The sum of the AR and AL components (i.e., the S/SS HCs) totals approximately 61% of the whole oil. The remaining 39% is treated as an insoluble and nonvolatile "residual" fraction.

31.2.2.7 Biodegradation Rates

Primary degradation, i.e., the loss of the initial HC compounds via biodegradation, was modeled using a first-order degradation equation and pseudocomponent specific rates. Biodegradation rates of HCs in seawater (Table 31.5) were based on reviews by French McCay et al. (2015a) and Li and French McCay (2017) to develop

TABLE 31.2 Oil Properties for MC252 Oil

Physical parameters	MC252 oil
Oil type	Light crude oil
Surface tension (mN m) at 20°C	3.43
Interfacial tension (mN m) at 20°C	19.63
Pour point (°C)	−28
Density at 30°C (g/cm^3)	0.8372
Density at 15°C (g/cm^3)	0.8483
Density at 5°C (g/cm^3)	0.8560
Dynamic viscosity (cP)@35°C	4.503
Dynamic viscosity (cP)@15°C	7.145
Resin content (wt%)	10.1
Asphaltene content (wt%)	0.27

Based on Stout, S.A., 2015b. Bulk chemical and physical properties of fresh and weathered Macondo crude oil. NewFields Technical Report to the Trustees in Support of the pDARP. <https://www.doi.gov/deepwaterhorizon/adminrecord>; Sample ID GU2988-A0521-09805.

TABLE 31.3 Fractional Composition of Whole MC252 Source Oil: Measured Soluble and Semisoluble Concentrations (Stout, 2015a) Were Summed by Component Group

Code	Hydrocarbon component	Fraction in oil (g/g oil)
AR1	BTEX and styrene	0.019124
AR2	C3-benzenes	0.007836
AR3	C4-benzenes	0.004674
AR4	Decalins	0.003786
AR5	C0–C2 naphthalenes	0.005634
AR6	C3–C4 naphthalenes	0.002434
AR7	Fluorenes and C0–C1 3-ring PAHs	0.002339
AR8	4-ring PAHs and C2–C3 3-ring PAHs	0.001667
AR9	Soluble alkanes	0.133190

TABLE 31.4 Fractional Composition of Whole MC252 Source Oil: Insoluble Component Concentrations in the Oil Were Based on Boiling Curve Cuts

Code	Hydrocarbon component	Fraction in oil (g/g oil)
AL1	Aliphatics: BP < 150	0.006923
AL2	Aliphatics: BP 150–180	0.060913
AL3	Aliphatics: BP 180–200 (C11)	0.034279
AL4	Aliphatics: BP 200–230 (C12)	0.053814
AL5	Aliphatics: BP 230–280 (C13–C16)	0.095099
AL6	Aliphatics: BP 280–300 (C17–C18)	0.036292
AL7	Aliphatics: BP 300–350 (C19–C20)	0.092923
AL8	Aliphatics: BP 350–380 (C21–C23)	0.049473
Σ AR#s + Σ AL#s	Total volatiles and semivolatiles	0.610400

Based on Stout, S.A., 2015a. Physical and chemical properties of the fresh MC252 Macondo-1 well crude oil. NewFields Technical Report to the Trustees in Support of the pDARP. <https://www.doi.gov/deepwaterhorizon/adminrecord>.

TABLE 31.5 Biodegradation Rates, Expressed as Half-Lives ($0.693/k_d$) for Components of Oil in the Water Column Used as Model Input

Insoluble component and boiling range (°C)	Half life (days)	Soluble component (log(K_{ow}) range)	Half life (days)
AL1 (<150°C)	2.9	AR1: MAHs/BTEX (1.9–2.8)	3.0
AL2 (150°C–180°C)	5.8	AR2: C3-benzenes (2.8–3.6)	2.4
AL3 (180°C–200°C)	11.6	AR3: C4-benzenes (3.1–3.8)	2.5
AL4 (200°C–230°C)	11.6	AR4: decalins (4.1–6.0)	11.6
AL5 (230°C–280°C)	11.6	AR5: C0–C2 naphthalenes (2.3–4.3)	2.5
AL6 (280°C–300°C)	13.9	AR6: C3–C4 naphthalenes (4.2–5.2)	3.9
AL7 (300°C–350°C)	17.3	AR7: fluorenes and C0–C1 3-ring PAHs (4.0–5.6)	4.6
AL8 (350°C–380°C)	17.3	AR8: 4-ring PAHs and C2–C3 3-ring PAHs (4.9–6.0)	6.9
Residual oil (>380°C)	34.7	AR9: low MW isoalkanes, cycloalkanes (2.3–5.6)	4.1

component-specific rates for the S/SS HCs (i.e., the AR pseudocomponents). The nonsoluble aliphatic (AL) components' biodegradation rates were obtained from the analyses of groups of similar molecular-weight aliphatics within separate boiling cut-based fractions by Brakstad et al. (2015) and Brakstad and Faksness (2000). Aromatic component rates were obtained by averaging measurements from studies designed to represent well-dispersed oil (i.e., Howard et al., 2005; Mackay et al., 2006a; Venosa and Holder, 2007; Prince and Walters, 2007; Prince et al., 2007, 2008, 2013; Campo et al., 2013; Brakstad and Faksness, 2000; Brakstad et al., 2004, 2015), as biodegradation of these compounds occurs mainly after their dissolution into seawater. The residual oil rates are applied to compounds that were not included in the AR or AL components. For floating and shoreline oil, the half-lives of AR and non-AR components are assumed 69 days and 690 days, respectively, based on reviews in French McCay (2004).

31.2.2.8 *Amounts and Timing of Oil Release*

The amount of oil released to the environment was assumed to be ~559 thousand metric tons (4.26 million bbl), based on information provided in the Flow Rate Technical Group (FRTG) report developed during the response phase of the spill (McNutt et al., 2011), as summarized in the Oil Budget Calculator (OBC) report, and including consideration of oil recovered at the release site and therefore not released to the environment (Lehr et al., 2010, referred to here after as OBC). Fig. 31.3 shows the timing of the release of oil, as well as the application volumes of dispersant (on surface oil and subsurface, injected into the blowout plume). The DWH Phase II Court finding of the total volume released (USDC, 2015), which was based on a mid-point of the FRTG and BP's estimates, was that 4.0 million bbls of oil were released from the reservoir and 3.19 million bbls of oil were discharged to the Gulf of Mexico, a total release to the environment that was 22% less than the OBC estimate used herein. In modeling performed for the NRDA, as described in French McCay et al. (2015a, 2016), the OBC estimates of the daily release volumes (April 22–July 15, 2010) made by the FRTG (McNutt et al., 2011) were proportionately reduced by 22% on each day of release, to match the Court's finding of the total discharge volume to the Gulf of Mexico.

The release of oil and gas to the water column varied in amount released per day, location, and the amount treated (subsurface) with dispersant throughout the spill event (Fig. 31.3). Early in the spill event, oil and gas

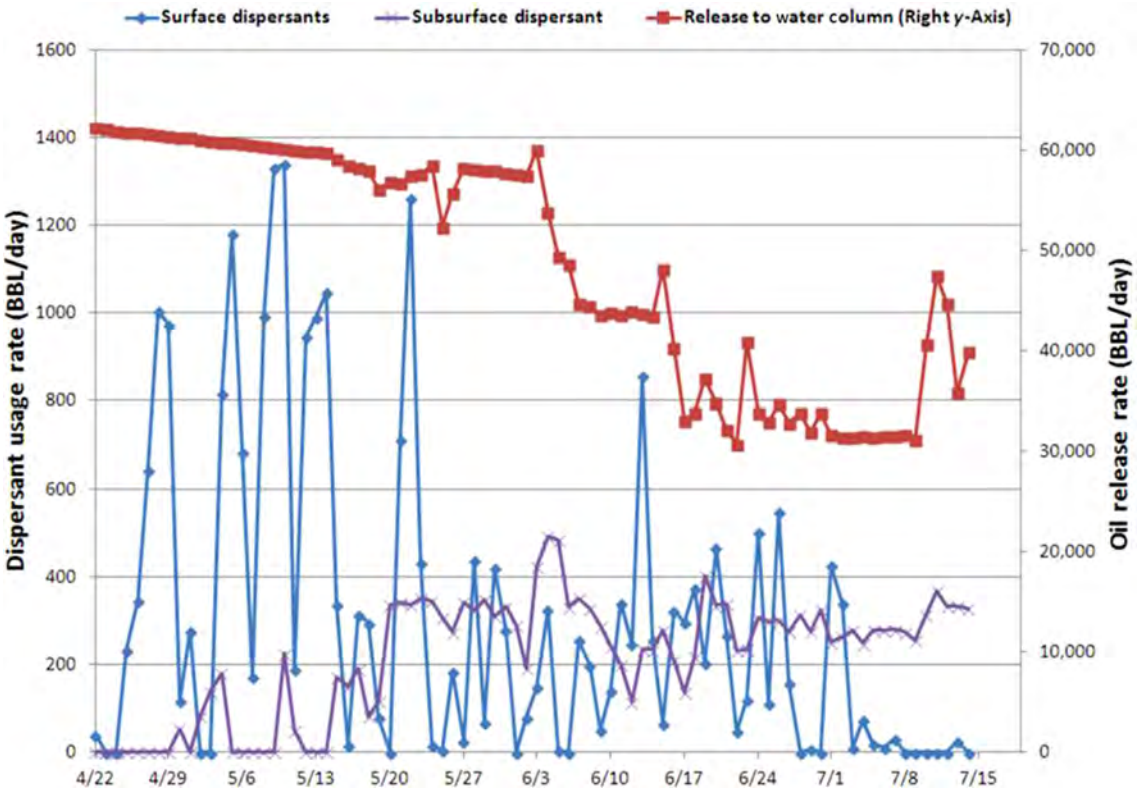

FIGURE 31.3 Oil release rate to the environment and application rates of dispersants on surface oil and subsurface in the blowout plume.

was only released from the end of the broken riser. After approximately 6 days, oil and gas were flowing from two different locations, the end of the broken riser and from holes in the riser, where a kink formed when the rig sunk and the riser collapsed. This division of flow between the riser and kink varied over time, with the kink release increasing with time due to the increase in the number of holes at the kink. With the increase in the number (2−6) and size (2.0−2.6 cm diameter) of the holes, the larger cross-sectional area of the exit openings allowed an increasing release from the holes at the kink. The kink flow occurred for 34 days, after which time the riser was cut just above the BOP (i.e., on June 3rd), and subsequently all the oil and gas was released from the cut end of the riser. Throughout the spill event, there were various levels of collection and dispersant treatment. While the amount of time precut versus postcut was the same (42 days each), the resulting mass of oil released to the water column during precut and postcut was 60% and 40%, respectively, based on the analysis by the FRTG (McNutt et al., 2011). Spaulding et al. (2015) provide a detailed discussion of the time line and sources of information used in the analysis. Oil collection at the release points, i.e., the Riser Insertion Tube (RITT) and the Top Hat, was assumed to not have entered the environment and therefore was not tracked in the oil fate modeling.

31.2.2.9 Trap Height of Buoyant Plume and Oil Droplet Sizes

The main objective of the blowout modeling (Spaulding et al., 2015) was to determine the blowout plume characteristics, namely the trap height of the oil above the release points. At this depth, the buoyancy of the plume became negligible due to the prior entrainment of seawater and the loss of gas to dissolution into the water column. A daily estimate of flow from each release type (kink, riser precut, and riser postcut) was made by Spaulding et al. (2015) based on total flow released from the reservoir, the amount collected, and the amount released from the kink holes, using the pipeline release model to determine the flow spilt between the kink holes (at 1503 m depth) and the riser outlet (at 1509 m depth precut and 1506 m postcut). The riser and kink releases were simulated in the blowout plume model to estimate the resulting trap height from these locations. The release from the kink trapped at a depth of about 1280−1310 m, whereas the (larger flow rate) release from the end of the riser trapped between 1150 and 1220 m (Spaulding et al., 2015). The trap heights were then used to initialize the depths of the oil droplets released in the (far field) oil fate model (SIMAP). Droplets were positioned randomly within a 130-m radius from the kink and 180-m radius from the riser, based on estimates of the dimensions of the near-field intrusion layer (see Spaulding et al., 2015).

The calculated droplet sizes reflected the effects of subsea dispersant applications (Spaulding et al., 2015). The analysis of the releases from the riser (pre or postcut on June 3) indicated that if all of the oil was effectively treated with dispersant, then the droplet size would range from 20 to 500 μm; if none the oil was treated, the range would be from 1000 to 10,000 μm. More than 99% of the dispersant-treated oil droplets would have diameters, d, ≤ 500 μm, whereas more than 99% of nontreated oil droplets would have $d \geq 1000$ μm. Because the droplets with $d \geq 1000$ μm would surface after a few hours from ~ 1500 m, the droplet size distribution remaining in the water column would be dominated by dispersant-treated oil (Spaulding et al., 2015). The analysis by Spaulding et al. (2015) indicates that during the preriser cut time period (prior to June 3), oil dispersion (formation of smaller droplets) was a result of mechanical processes (e.g., high exit velocities) at the kink holes and, to a more limited extent, dispersant application of low effectiveness at the end of the riser. During the postcut period, oil dispersion appeared to be primarily due to more effective dispersant treatment above the BOP. The daily droplet size predictions made by Spaulding et al. (2015), using the OBC release volume and their "best estimate" model, were used as input to the SIMAP model (Fig. 31.4). As a summary, the cumulative droplet size distribution over the 84 days of release is shown in Fig. 31.5.

31.2.2.10 Model Parameters

The start of the oil release was simulated as April 22, 2010 at 10:30 a.m. CDT (local time). The release duration was 2015 hours (84 days), i.e., until July 15, 2010 at 14:30 CDT.

The number of spillets, the time step, and the concentration gridding resolution were all model inputs. Below is a summary of model input parameters defining the model resolution:

- Number of spillets (Lagrangian elements):
  - Surface or subsurface oil: 100,000
  - Dissolved aromatics: 1,600,000
- Simulation time step: 0.5 hour
- Length of the simulation: 161 days (until September 30, 2010)

In order to obtain sufficient spatial resolution, model concentration mapping was performed using a 500-m resolution horizontal grid at 20-m depth intervals throughout the water column (40−1400 m).

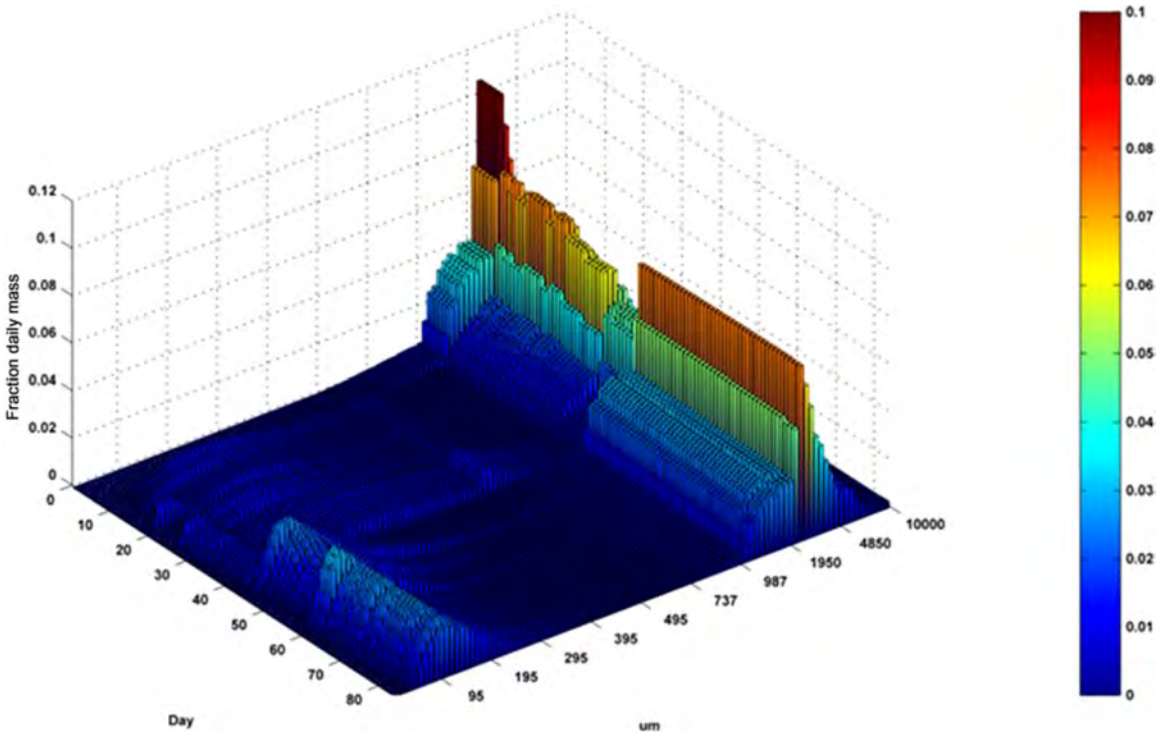

FIGURE 31.4 Daily fractional mass distribution by size bins (μm) throughout the release.

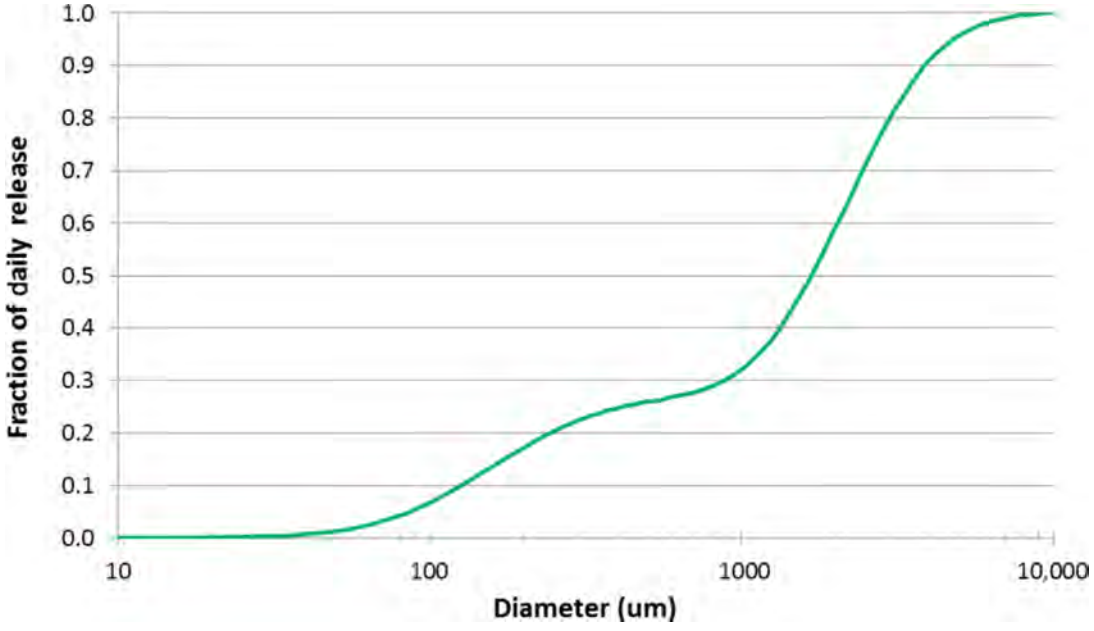

FIGURE 31.5 Cumulative droplet size distribution over the 84 days of release.

31.3 OBSERVATIONAL DATA

31.3.1 Literature Studies on DWH Oil Contamination in Deep Water

French McCay et al. (2015a) reviewed DWH observational data from offshore waters reported in published literature that were used for model validation, including water column chemistry and oil particle size information. When considered alongside the NRDA QA/QC'd data summarized below, and in more detail in the reports by

French McCay et al. (2015a), Horn et al. (2015a,b) and Payne and Driskell (2015a,b,c), a more complete understanding of the DWH spill becomes apparent, illustrating the transport, fate, and behavior of the oil and gas that was released into the environment.

HCs were repeatedly detected in the deep water at depths consistent with a trapped intrusion layer (Fig. 31.1). Camilli et al. (2010) detected a large plume at ~1000- to 1200-m depth and in some areas >2 km wide at ~ 4 km from the source during June 23–27, 2010. Their Sentry's methane m/z signal at 35 km from the source was only 53% less than that at 5.8 km, suggesting that plume extended considerably beyond the 35-km survey bound at that time. GC analysis focused on MAHs confirmed the presence of BTEX (50 μg/L) within the plume at 16 km downrange from the wellhead, suggesting a mechanism existed for direct HC transfer from the blowout source to the deep plume (i.e., rapid dissolution).

The larger droplets continued rising to the upper layer and the surface, in a volume described as a rising cone (e.g., Ryerson et al., 2012; Spier et al., 2013), due to the buoyancy of larger droplets relative to the ambient seawater. However, due to ADCP-documented current shear and varying rise rates for different diameter droplets, "plumes" of rising oil droplets would have followed different trajectories during their ascent toward the surface. In addition, while rising, the intermediate-sized droplets lost some of their relative buoyancy due to weathering (dissolution and biodegradation of the lighter HCs, fully weathered oil having a density of >920 kg/m^3, as compared to source oil with a density at 15°C of ~850 kg/m^3; Stout, 2015a), as well as potentially combining with SPM in the water column. Meanwhile, the ambient current higher in the upper water column is increasingly stronger than in deep water (Hyun and He, 2010), possibly causing separation of these intermediate sized droplets such that they left the cone and formed "multiple plumes" of slowly rising droplets in the upper layers mimicking the deep water plume.

Fluorescence anomalies (peaks) and water column HC chemistry data (Spier et al., 2013; Camilli et al., 2010; Valentine et al., 2010), as well as NRDA data, Horn et al. (2015a,b) and Payne and Driskell (2015a,b,c) show relatively high concentrations of HCs in finite "clouds" of particulate- and dissolved-phase oil at various depths above the intrusion at ~1100–1200 m (i.e., the deep plume is much more strongly evident in the data). This phenomenon is in agreement with the theoretical prediction of a multiphase flow plume model (Socolofsky et al., 2011), although the mechanism proposed by these authors differs from the model of rising independent droplets, and the possibility that some of the oil droplets alone or in combination with SPM, marine snow, or attached bacteria became nearly neutrally buoyant. If multiphase flow plumes occurred, one would expect similar fresh-oil chemistry signatures at the multiple depths, as opposed to more weathered oil signatures higher in the water column. Those shallower peaks appear to reflect oil droplets released at different times, which rose through currents that were highly variable in direction vertically and over time, such that "plumes" containing oil weathered to varying degrees were advected over the intrusion layer. We have not identified a vertical profile of samples containing similar fresh-oil chemistry signatures at the deep plume trap height and shallower depths. Instead, there is clear evidence of dissolution weathering as the oil rose through the water column. As a caveat, however, safety constraints precluded collecting sample profiles within 1–2 km of the release point. Samples taken from stations with vertical profiles having peaks at multiple depths further from the wellhead show complex and differing chemistry (Payne and Driskell, 2015a,b,c; Horn et al., 2015b), indicating oil of various droplet sizes and degrees of weathering being sheered and advected through the sampling locations at various times after release.

After the Top Hat became operational on June 3 (i.e., post riser cut), both the concentrations and the percentage of detectable chemistry results decreased in the deep water samples. In addition, there was a significant increase in the frequency of detections and sample concentrations with high dispersant indicator concentrations typically associated with less water-soluble compounds, including di- and polycyclic aromatics/alkylated aromatics and alkanes >C8, which is consistent with wider dispersion of reduced oil droplet sizes with application of dispersants (Chan et al., 2015; Payne and Driskell, 2015c).

Changes in chemical composition with depth also support the preceding description of the transport of dissolved compounds, dispersed oil, and larger droplets. Most water-soluble compounds such as benzene, alkylated MAHs, and soluble C5–C10 alkanes were enriched in the deep plume. Less water soluble compounds were present both in the deep water plumes and in the upper water column: C13–C22 PAHs and C11–C22 alkanes were found at 1175 and 865 m, as well as even deeper water and near the surface; C23–C40 alkanes were found at 1175 and 265 m, in surface waters, and also at lower concentrations in the 865-m plume (see Horn et al., 2015b, for details). These vertical changes in measured chemical composition indicate that dissolved HCs and (likely the smallest) droplets were trapped in the intrusion layer plume.

Valentine et al. (2010) focused on gas distribution and fate in the water column. They found that propane, ethane, and methane were most abundant at depths greater than 799 m and formed plume structures with dissolved

concentrations as high as 8, 16, and 180 μM for the three gases, respectively. Concentrations were orders of magnitude lower at shallower depths. The persistent plume at 1000- to 1200-m depth was located to the southwest of the spill site, consistent with other reports (Camilli et al., 2010; Hazen et al., 2010). Separate plumes were also identified by Valentine et al. (2010) at similar depths to the north and to the east. A distinctive shallower plume (or water layer containing HCs) was observed at 800- to 1000-m depth located to the east of the release site. Spier et al. (2013) calculated frequencies in each of eight cardinal directions of detectable HC concentrations in samples taken at various depths and within 45 km of the wellhead, not only finding the highest frequency of detectable results to the southwest, but also detections in the other directions. These findings, as well as other data sets compiled by the NRDA program, suggest that multiple plumes of HCs moved in varying and sometimes opposite directions, presumably originated at different times and indicative of complex current patterns in the area before sampling. This is consistent with the variability in the current speeds and directions from the ADCP data summarized above.

Davis and Loomis (2014) made measurements of the oil droplet size distribution using a holographic camera (*Holocam*) during the *M/V Jack Fitz* (JF) 3 cruise. The average volume median droplet diameter from the JF3 cruise (June 14–20, 2010) was 128 μm, with values ranging from 86 to 176 μm. Thus, the *Holocam* data provides evidence of small (volume mean diameter <300 um) chemically dispersed oil droplets in deep and intermediate waters. Further discussions of the *Holocam* and other particle size data are in Li et al. (2015).

Model simulations employing the well-known Stoke's Law (where rise rate increases with droplet diameter) provide additional evidence for the separation of small droplets (in the intrusion layer) from intermediate and large droplets (slowly or rapidly rising to the surface, respectively). For example, sensitivity analyses by North et al. (2011, 2015) showed that droplets with diameters of 10–50 μm would form distinct subsurface plumes that would be transported horizontally and remain in the subsurface for >1 month. Droplets with diameters ≥90 μm would rise to the surface, more rapidly at larger diameters.

31.3.2 Summary of NRDA Chemistry and Sensor Data

During the DWH blowout and resulting spill, a variety of environmental data were collected by samplers aboard numerous ships and analyzed using NRDA protocols, which included extensive quality control reviews and only reported concentrations above the method detection limit (MDL) for each investigated compound (Horn et al., 2015a,b). In addition to the collected chemical and forensic data, concurrent and continuous measurements of dissolved oxygen and fluorescence were recorded. A detailed description of the chemistry data used for validating the model may be found in Horn et al. (2015a,b). A detailed description of forensic findings may be found in reports by Payne and Driskell (2015a,b).

Considerable spatial heterogeneity was evident in the distribution of HCs at various depths and as a function of distance from the wellhead, resulting from variations in the oil release rate and subsea dispersant applications over time (changing droplet size distributions of the oil over time), spatially- and temporally varying currents throughout the water column, dissolution, dispersion, and biodegradation of HC constituents, as well as irregularly positioned sampling stations and different sampled depths. As discussed above, the multiple plumes observed moving in opposing directions presumably originated at different times and indicate the complex current patterns in the area before sampling.

Based on the analysis of the water column chemical and physical data, as well as the consideration of major events during response, four distinct periods of time are identifiable during the spill period in 2010. These are described as Observable Chemistry Regimes (OCR):

- OCR 1: pretop-kill (April 20–May 26)
- OCR 2: top-kill, riser-cutting, and initial top-hat (May 26–June 6)
- OCR 3: postcut and collection (June 6–July 15)
- OCR 4: postcap (after July 15) phase

Sampling of the active release of oil and gas during the three phases (OCR 1–3) was focused around the wellhead (<20 km), while more extensive and broad-scale sampling into the far-field (focused to the south and southwest of the spill site) did not commence until after the well shut-in was completed (OCR 4). [See French McCay et al. (2015a) and Horn et al. (2015a,b) for maps summarizing this data.] In-water concentrations remained elevated during the blowout and the released HCs began to dissipate just after the oil flow to the water column ceased on July 15, 2010.

In April and May, oil was released from the broken riser and the holes that developed at the kink in the riser pipe. The fluorescence and DO anomalies, chemical concentrations, and blowout models (Socolofsky et al., 2011; Spaulding et al., 2015) indicate that a considerable portion of the released oil rose from the depth of the release to several hundred meters above the release depth as part of the buoyant blowout plume. Several times during May 26–28, the spill responders attempted to fill the riser pipe with heavy drilling mud and bridging material, but the procedures did not stop the release and the mud and "junk" were forced out of the riser. Relatively high HC concentrations and fluorescence anomalies were observed during this period. During June 1–3, while the riser pipe was being cut, oil flowed freely from the riser, and this is evident in the data as elevated fluorescence peaks and HC concentrations between 1000 and 1300 m compared to periods prior to and after this event. In OCR 3, oil was released from the BOP from the opening of the Top Hat oil recovery installation or the gap between the Top Hat and the BOP. During OCR 4, after the release was stopped on July 15, in water HC concentrations decreased with increasing time and distance from the source.

The maximum HC and dispersant concentrations occurred at the surface (<40 m) and at depths between roughly 1100 and 1300 m deep (Horn et al., 2015a). With slow rise rates, the smallest droplets were trapped below 1100 m, where both whole oil and dissolved phase HCs were found concurrent with tracers from dispersants. Elevated dispersant concentrations were identified between 1000 and 1300 m near the wellhead and between 1100 and 1200 m to distances beyond 150 km. Forensically identified MC252 oil was commonly observed radially within roughly 50 km of the wellhead. See Payne and Driskell (2015a) and Driskell and Payne (this volume) for a full description of forensically identified MC252 oil in subsurface water samples, including as particulate- and dissolved-phase HCs.

Elevated HC concentrations at depth were observed in each of the groupings of investigated (i.e., measured) chemicals (i.e., components) ranging from BTEX (AR1) through to the soluble alkanes (AR9). The highest concentrations at depth were of the BTEX group and soluble alkanes. When considered together, the total soluble compounds, the total investigated compounds, and PAH groups, all had highest observed concentrations between 1000 and 1300 m. The highest measurements of total investigated compounds in the deep plume were >100–700 μg/L, with concentrations up to ~80 μg/L between 200 and 1000 m. When considered individually, soluble alkanes (AR9) typically had the highest concentrations between 1000 and 1300 m with values of >100–400 μg/L, while BTEX (AR1) were typically >100–200 μg/L, and PAHs were typically <120 μg/L (Horn et al., 2015a,b; French McCay et al., 2015a).

While most attention has been focused on HC concentrations in near surface waters and the region between 1000 and 1300 m, elevated concentrations in excess of the MDLs were identified throughout the water column beyond 150 km. Sampling in the depth range between 100 and 1000 m was much more sporadic. The highest concentrations at depth in this region were for the BTEX group and soluble alkanes. The spatial extent in these intermediate waters is slightly more proximal to the wellhead, with highest concentrations observed typically within 25 km of the wellhead (Horn et al., 2015a,b; Payne and Driskell, 2015a,b,c).

There were consistently observed fluorescence anomalies (relative high values or "peaks") and dissolved oxygen "sags" (i.e., relatively low values of dissolved oxygen in vertical profiles when compared to baseline profiles) at depths between approximately 1000–1300 m (JAG, 2010). Maximum anomalies occurred between roughly 1100 and 1200 m. The highest fluorescence values were observed near the wellhead; the fluorescence anomalies decreased as distance from the wellhead increased. Anomalies of high fluorescence values at depths of 1000–1300 m were typically associated with elevated HC concentrations in the water column, when water samples were collected concurrently with fluorescence measurements. These fluorescence peaks were observed mainly to the southwest of the wellhead. Although maximum fluorescence peaks were identified within a narrow range at depth, significantly elevated fluorescence values were noted throughout large portions of the profiles. Peak fluorescence values at depth typically tapered off to lower values in shallower waters. It was very common to observe significantly elevated fluorescence values as shallow as 600 m and occasionally shallower. As distance from the wellhead increased, dissolved oxygen anomalies first increased and then decreased. As sags decreased in magnitude, they frequently became slightly broader, covering larger depth ranges. These observations are indicative of microbial degradation (i.e., HC consumption) at depth followed by dispersion and mixing with surrounding waters above and below the plume (Horn et al., 2015b; French McCay et al., 2015a).

The consistent pattern of observed anomalies at depth supports the assessment of trapping of the buoyant oil and gas plume between 1100 and 1350 m. This subsurface region of HC contamination contained trapped oil, dissolved HCs (primarily BTEX, PAHs, and soluble alkanes), and dispersants, which were slowly dispersed and consumed at depth. Results from chemical and physical measurements suggest that, in general, before about July 1, HCs in this "deep plume" were advected in various directions and after July 1, the plume predominantly moved

to the southwest. The southwestward movement of the deep water contamination continued throughout the fall of 2010. Deep ocean currents in the region are dominated by cyclonic flows along the isobaths, which near the spill site are generally to the southwest (Schmitz et al., 2005); therefore, the chemistry and sensor indicators are consistent with understanding of the circulation in the area.

31.4 RESULTS OF OIL TRANSPORT AND FATE MODELING

31.4.1 Mass Balance

Fig. 31.6 summarizes the model-predicted mass balance of the oil, as percentage of the oil released to date, for the simulations using the ADCP currents and the HYCOM-FSU hydrodynamics, both with the winds used to force the HYCOM-FSU simulation (NARR). As described in the next section, below 40 m, the transport in the HYCOM-FSU simulation was most similar to that using ADCP currents. Mass balances using other hydrodynamic models varied somewhat by the hydrodynamics and wind data set used, which affected the percentage of oil on the water surface versus entrained or ashore. The main differences between runs with various

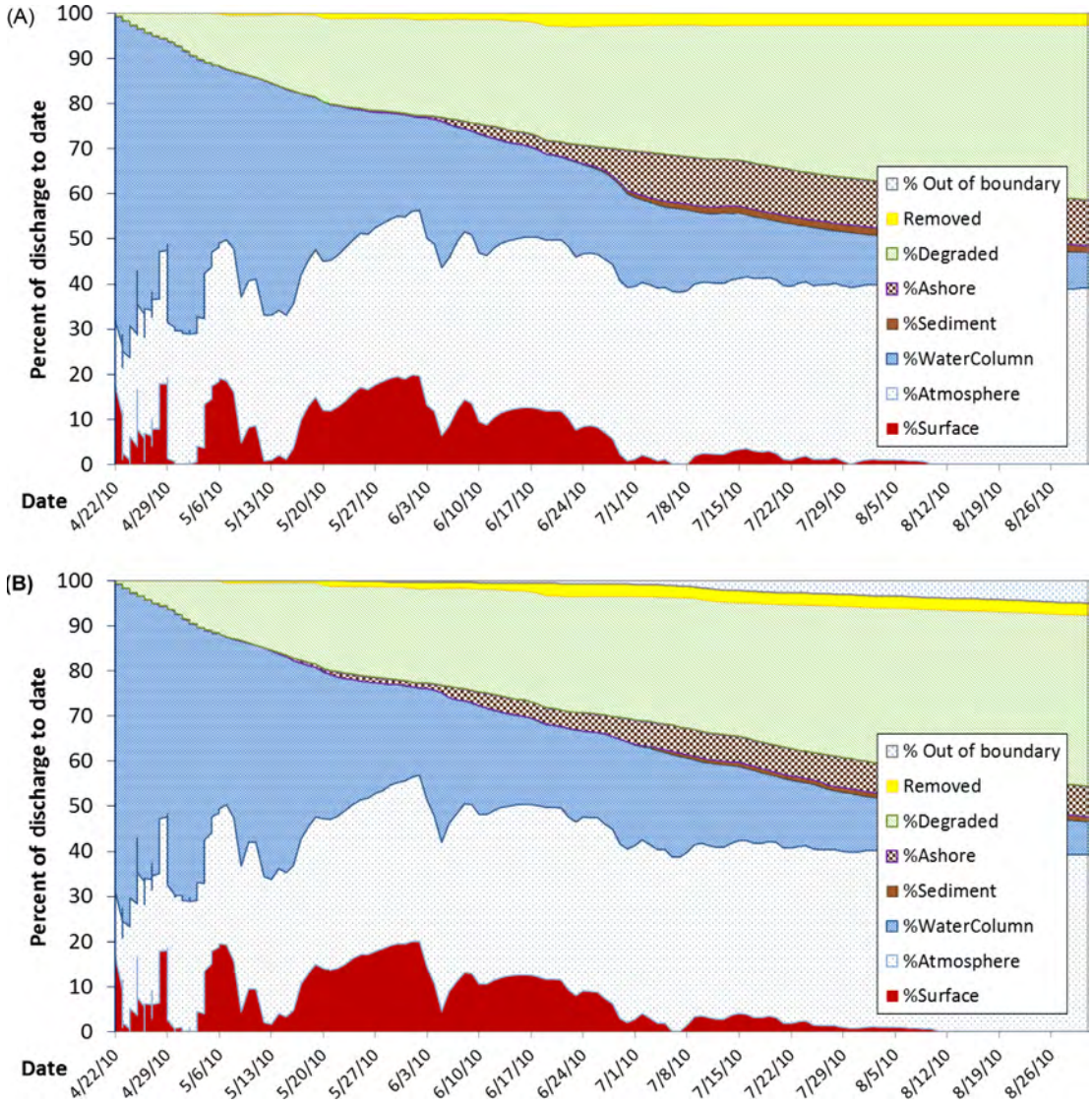

FIGURE 31.6 Mass balance, as percent of the mass released to date, for simulations using (A) ADCP and (B) HYCOM-FSU currents, both with NARR winds.

hydrodynamics were in the percentage (and locations) of oil coming ashore because of the differential transport (range 7%–15% by August 31, 2010). In the ADCP simulation, where currents over the shelf were assumed zero (due to lack of data), shoreline oiling is focused in Louisiana and higher than in the hydrodynamic model-forced simulations where transport east and west along the self is included.

In the model simulations, 85% of the oil passed through 40 m to the water surface. The remaining oil below 40 m was initially in the water column and ultimately biodegraded there or settled to the sediments. Of the surfaced oil, much of it evaporated or was entrained into the surface water via wind-driven waves and turbulence. The remainder was removed by mechanical means and burning, or came ashore.

The magnitude of the modeled amount of surface-floating oil agrees with estimates of surface oil volume made by MacDonald et al. (2015) based on analysis of Satellite Synthetic Aperture Radar (SAR) imagery (Fig. 31.7). In making their estimates, MacDonald et al. (2015) assumed an average thickness of 70 μm for SAR pixels identified as thick oil or emulsion by the Oil Emulsion Detection Algorithm (Garcia-Pineda et al., 2013a), assuming noncontinuous cover of emulsions in these areas. All other oil-covered regions identified in the SAR by Textural Classifier Neural Network Algorithm (Garcia-Pineda et al., 2013b) were classified as "sheen," set at ~1 μm following published standards (ASTM International, 2006). As in reality oil thickness varies considerably at small (and large) spatial scales, there is considerable uncertainty in the SAR-based estimates. However, the agreement in order of magnitude supports the overall mass balance of oil in the modeling, and the result that substantial amounts of oil surfaced before June 3, 2010 when subsea dispersant injection was brought into full operation and when subsea recovery via the RITT at the Top Hat began (Fig. 31.3).

Below 40 m, the overall mass balance was the same for all the current data sets, as the direction and speed of transport in the offshore environment did not greatly affect the fate process rates in the water column (i.e., dissolution, partitioning of soluble/semisoluble HCs between water and SPM, adhesion of oil droplets to SPM, sedimentation, and biodegradation). As shown in Fig. 31.8, oil released in the water column dissolved and biodegraded over time, with a small percentage in the sediments (~1–2% in the sediments in late July 2010). As noted above, the top-kill operation and resulting oil load to the sediments was not included in the modeling reported herein, and modeled oil sedimentation was only due to baseline ambient SPM without consideration of marine snow formation. Thus, the fraction of the oil sedimented in these simulations was low compared to the evidential amount in the sediments based on field data. By September 30, 2010, the model predicted that the subsurface oil (below 40 m) was highly weathered, with an average density of 930 kg/m^3 and average viscosity of 800 cP.

By September 30, 2010, 15% of the released oil remained in waters below 40 m in the model simulation, primarily as biodegradation products and microbial biomass. This falls within the estimated range of 4%–31% of the released oil that was sequestered in the deep-sea based on field data analysis by Valentine et al. (2014). Daling et al. (2014) estimated dissolution loss into the water during the ascent from 1500 m water depth to the

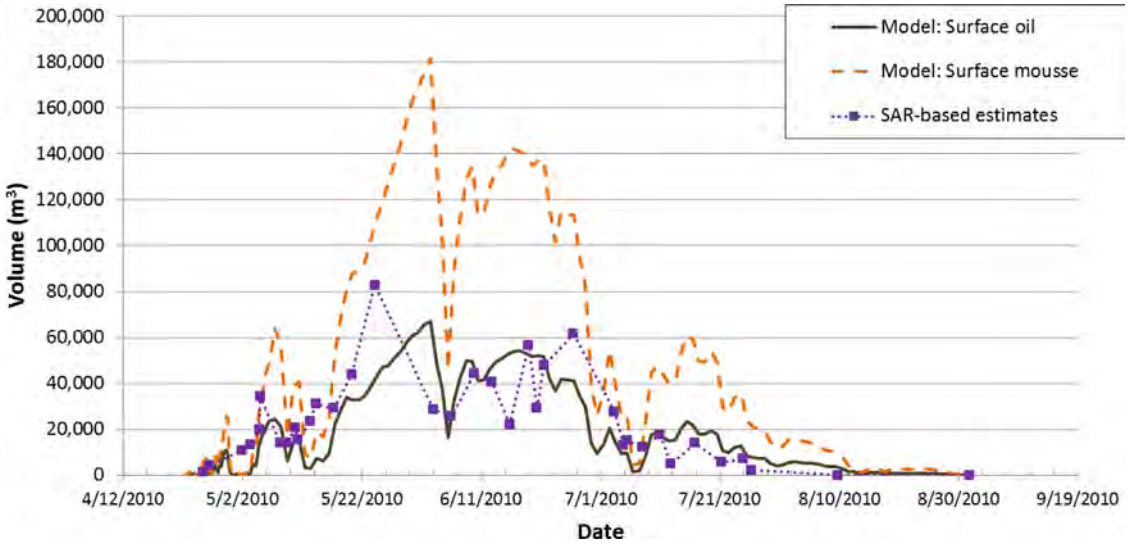

FIGURE 31.7 Modeled volume of surface-floating oil and water-in-oil emulsion (mousse), as compared to SAR-based estimates, for simulation using HYCOM-FSU currents and NARR winds.

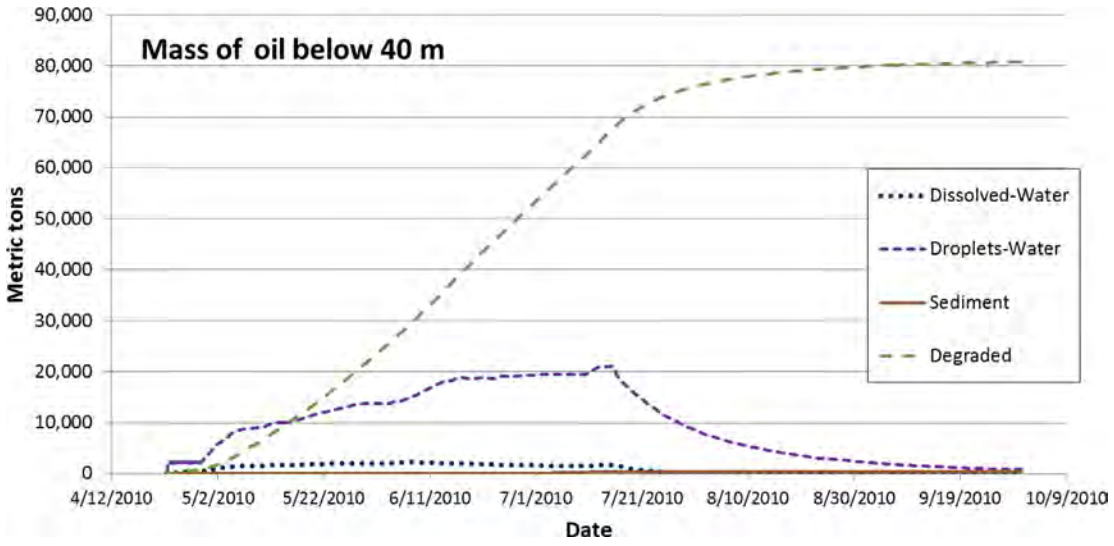

FIGURE 31.8 Mass of released oil, by compartment, below 40 m over time (simulation using ADCP currents).

surface was ~15% of the oil, composed of saturates <C7 (10 wt% of the stabilized source oil), BTEX (3 wt% of the source oil), and C-3-benzenes (1.5 wt% of the source oil). The 15% estimate accounts for all of the water soluble HCs in the released oil, so the implicit assumption made by Daling et al. was that dissolution of the soluble HCs was complete for all droplet sizes before the oil surfaced. Additionally, Daling et al. (2014) estimated about 18% of the total PAHs (TPAHs, PAHs representing 1.1 wt% of the total oil), corresponding to about 0.2 wt% of the source oil, was dissolved in the water before the oil surfaced. Based on analysis of freshly surfaced oil sampled in June 2010, Stout et al. (2016a) estimated that 20–25 wt% of the oil was lost to dissolution before the (larger droplets of) oil reached the surface.

In the SIMAP model results, 36% of the degraded mass below 40 m derived from dissolved soluble (AR1, AR2, AR3, AR5, and AR9; Table 31.1) and semisoluble (AR4, AR6, AR7, and AR8, i.e., PAHs; Table 31.1) HCs. On average over the entire spill, ~5% of the total oil HCs released into the environment dissolved before oil droplets reached 40 m on the way to the water surface. Since 18% of the released oil was soluble and semisoluble HCs, the remaining 72% of the soluble and semisoluble HCs rose through 40 m to the surface water, and either dissolved in the upper 40 m or volatilized. All soluble and semisoluble HCs in droplets remaining below 40 m dissolved and eventually biodegraded in the model simulation, whereas soluble components did not completely dissolve from the large droplets that rose to the surface in a few hours. One would expect this to be the case, as surfaced fresh oil did contain measurable BTEX and soluble alkanes (Stout, 2015c, Stout et al., 2016a), which volatilized rapidly. Ryerson et al. (2012) measured these volatiles in the atmosphere above the rising oil and fresh oil slicks.

Ryerson et al. (2012), using chemical analysis of HC data, estimated that, on June 10, 19%–20% of the total oil HC mass released to the environment was trapped in the deep plume, 8%–9% was in the surface slicks, 17.4%–18.4% was evaporated, leaving ~54% unaccounted for in their analysis. They presumed that the missing fraction of oil was biodegraded, suspended in the water column other than in the intrusion layer deep plume, and/or sunken to the seabed. The Ryerson et al. (2012) mass balance analysis has a number of sources of uncertainty, including that it depends on (1) an estimate of the total integrated DO anomaly from field samples by Kessler et al. (2011) and (2) the estimated ratios of Hazen et al. (2010) of alkanes to toluene in the plume phase versus in the leaking fluid phase (assumed to reflect the ratio of droplet to dissolved phase HCs—on the premise of the colocation of the dissolved versus droplet phases). To the extent that droplets rose (or sank) out of the deep plume preferentially leaving dissolved-phased HCs at depth (processes known to have occurred), the Ryerson et al. (2012) estimate of 19%–20% being in the deep plume is an overestimate. SIMAP model estimates for June 10 (Fig. 4.1) are about 24% in the water column (at all depths, with 15% below 40 m), 23% degraded (at all depths, with 9% below 40 m), 11% on the water surface, 38% in the atmosphere, and 3% ashore. As 61% of the fresh MC252 oil was volatile, at least 62% (38%/0.61) of the oil released to date surfaced by June 10, leaving less than 38% in deep water. Thus, the model estimates of 11% of the oil on the water surface and 15% of the oil remaining below 40 m are supported by their analysis.

31.4.2 Transport and Oil Trajectories

As the most uncertain model inputs for predicting oil transport and fate below the surface water layer were the three-dimensional and time-varying current data, simulations were performed for eight hydrodynamic input data sets, as well as ADCP-based measurements of currents. While the directions and speeds of the various hydrodynamic models varied in time and differed amongst the models, in all simulations, most of the oil mass (estimated as 68% on average over the 84 days of the release, Fig. 31.5), which was in droplet sizes greater than 1 mm diameter, passed through 40 m on the way to the surface within 10–20 km of the wellhead. Within ~11 km of the wellhead, there were four ADCPs at three stations with sufficient vertical coverage to reliably estimate the needed currents below 40 m. In the simulation using the ADCP data, most of the oil mass reached 40 m within 5 km of the wellhead.

Oil droplets 1 mm in diameter, weathered at depth by dissolution such that their density by the time they reached the surface approached 940 kg/m^3 (in agreement with measurements of "fresh" floating oil by Stout, 2015c, Stout et al., 2016a), rose to the surface in ~14 hours. ADCP-measured currents at the wellhead averaged <5 cm/s over the water column between 40 and 1400 m. Assuming a mean current of 5 cm/s, during their rise, 1 mm droplets would travel ~3 km horizontally. Payne and Driskell (2015d) reported observing fresh oil surfacing between 1.5 and 4 km from the wellhead on various dates in May and June 2010. Ryerson et al. (2012) observed fresh oil (as evidenced by measured volatiles in the air above it) surfacing at 1.0 ± 0.5 km from the wellhead during June 8–10, 2010, which based on ADCP measurements at that time implied a 10-hour surfacing time. Ryerson et al. (2012) noted that visual observations from response vessels suggested a ~3-hour lag time between deliberate intervention at the well and the onset of changes in the freshly surfaced oil. These observations imply the surfaced oil was composed of droplets millimeters in diameter. Droplets smaller than 1 mm rose over a longer period and so were carried progressively farther from the release point, e.g., 500 and 200 μm droplets with density 940 kg/m^3 would travel 7 and 39 km, respectively, in a 5-cm/s current. On average, estimates by Spaulding et al. (2015) indicate that 74% of the oil mass was released in >500 μm droplets, 83% was >200 μm, and 93% was >100 μm, leaving about 7% of the oil in <100 μm droplets (Fig. 31.5). Droplets less than about 100 μm did not rise appreciably (rise rate of a 100-μm weathered oil droplet in still water being 0.02 cm/s) and formed the deep water plume along with dissolved soluble HCs.

Transport to the southwest, particularly from July through the fall, was observed in fluorescence and dissolved oxygen indicators and chemistry samples collected in June through September 2010 (see reviews in Horn et al., 2015a,b; Payne and Driskell 2015a). Based on these and other observations (described in Section 31.3), the deep water plume was primarily transported to the southwest between the depths of 1100 and 1300 m. However, especially before July 2010, the deep plume was observed to extend in all directions from the wellhead at various times (Spier et al., 2013). Inspection of ADCP-measured currents at the wellhead (Station No. 42916) indicated that the currents in spring–fall 2010 were highly variable with depth (i.e., vertical variations in the horizontal currents) and over time. In the deep plume, the ADCP-measured speed averaged 3.9 cm/s (0.08 knot) to the southwest. Measured current speeds were <10 cm/s at all depths and for most of the period of the oil release.

In contrast, in the area of the DWH wellhead, many of the hydrodynamic models examined (three HYCOMs: HYCOM_FSU, NRL HYCOM + NCODA GOM, NRL GLOBAL HYCOM; two ROMS: SABGOM, IAS ROMS; and three POMs: NCOM-Operational, NCOM-Reanalysis, NGOM) calculated much higher speeds for the currents in the deep plume and water column below 40 m than is indicated by the ADCPs. This is evident in the differences between trajectories of oil droplets below 40 m. Concentrations of oil droplets were highly variable in space and over time, as the currents shifted. The concentration at any point in space or time changed rapidly, as the water and oil moved during the continuing release. Therefore, it is difficult to summarize the results in static figures. To portray the movement of the oil, the "age" of the spillets (time since each particle was released) was plotted. Example snapshots of the trajectory (for arbitrarily selected dates within each of the OCRs), integrating spillets over the water column, are shown in Figs. 31.9–31.14.

The simulations depict the extent to which currents transported and sheared the rising oil. There was substantial displacement as spillets moved in different directions. ADCP data in ~30–60 m vertical bins in the water column showed slow (<10 cm/s) currents in adjacent depths differing by as much as 120° in direction in the May–June 2010 timeframe. Transport in shallower layers sheared the oil plume in multiple directions. Some of the described shear is evident in Figs. 31.9–31.14, which depict the age of the spillets as they move throughout the simulation. Above 200–40 m, the spatial distribution of oil droplets was highly variable in time and between the various hydrodynamic inputs. All may be characterized as patchy and ephemeral.

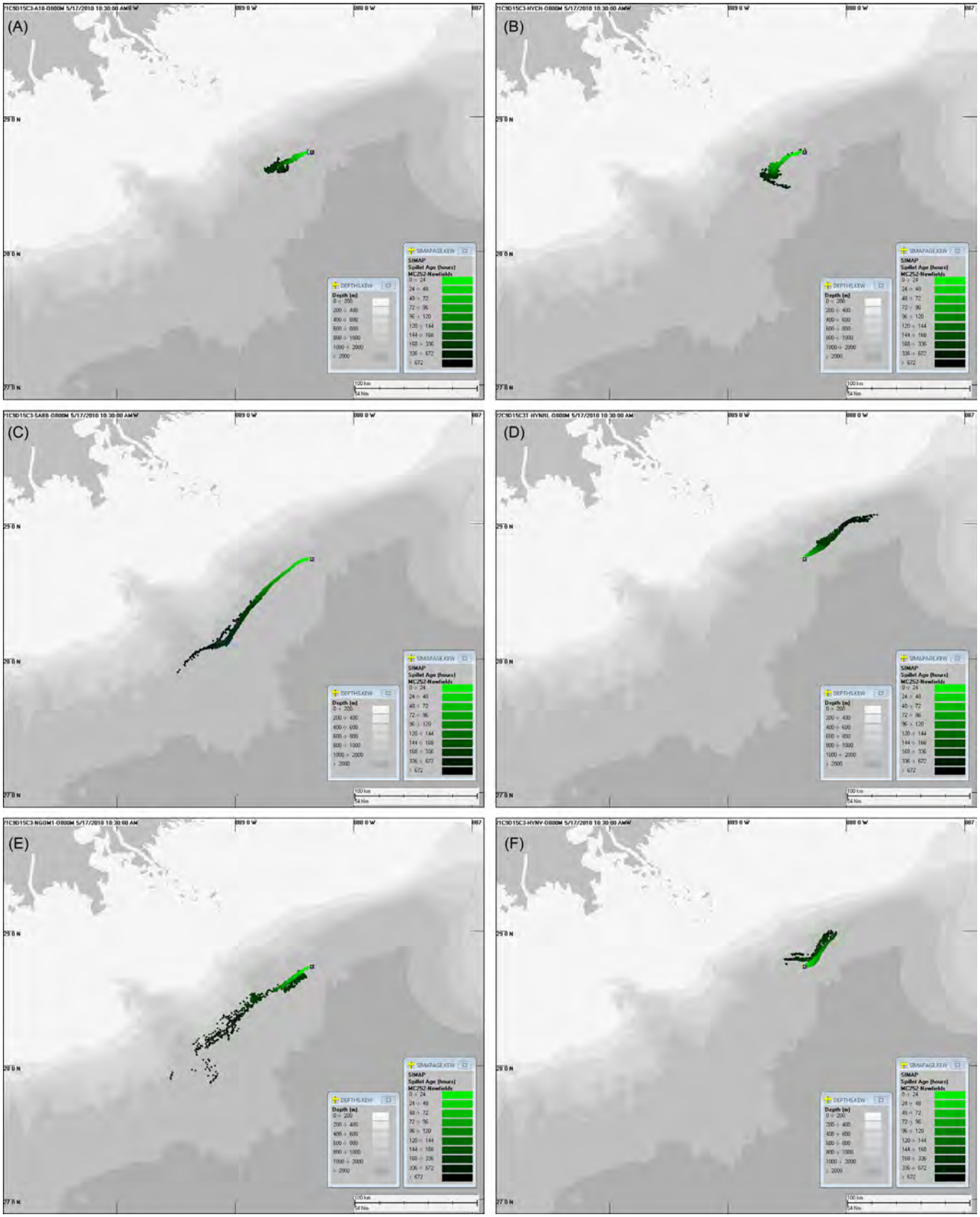

FIGURE 31.9 Cumulative trajectories to May 17, 2010 of subsurface oil droplets vertically integrated below 800 m (spillets shaded by age, i.e., hours since release): (A) ADCPs, (B) HYCOM-FSU, (C) SABGOM, (D) NRL HYCOM + NCODA GOM, (E) NGOM, (F) NRL GLOBAL HYCOM.

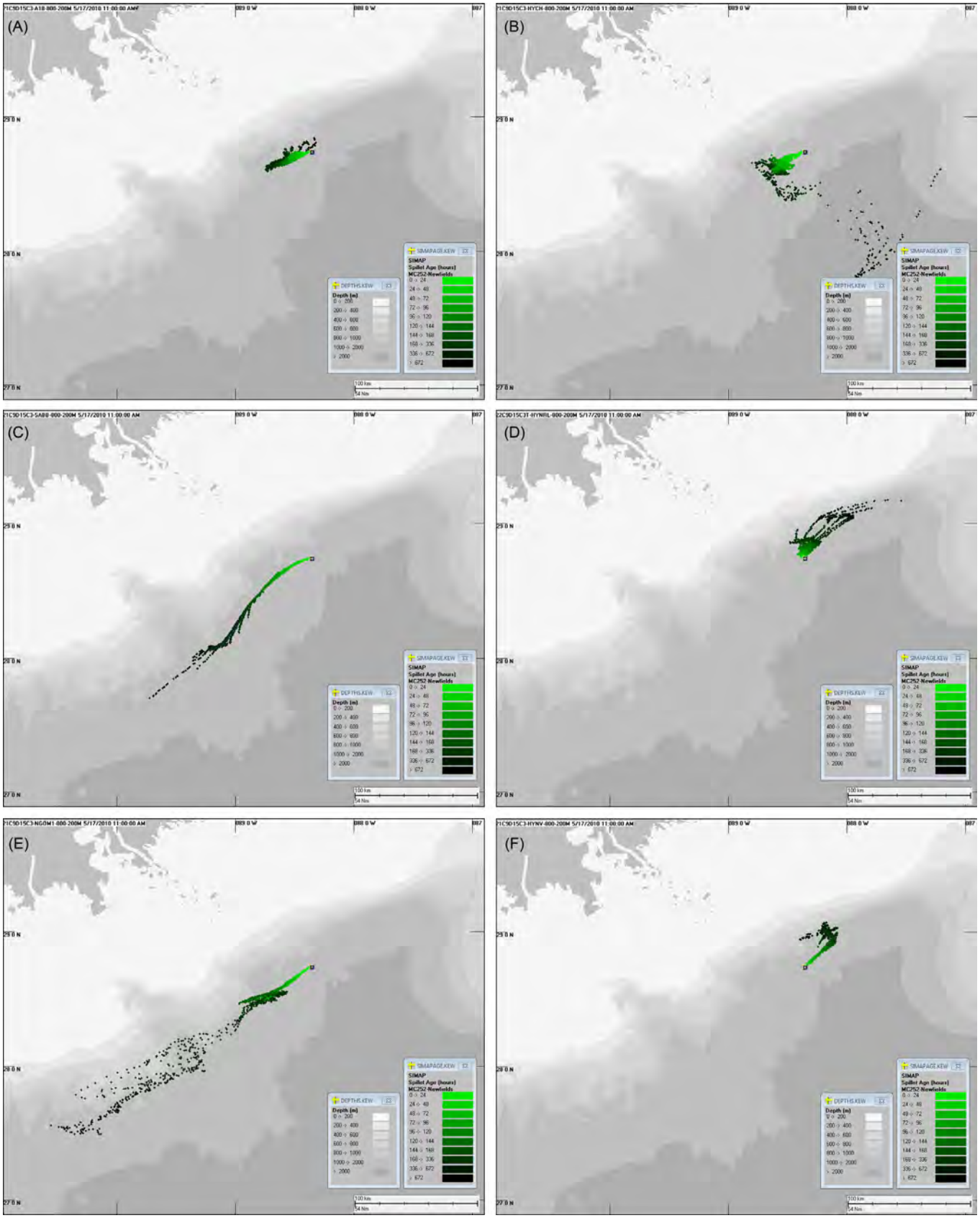

FIGURE 31.10 Cumulative trajectories to May 17, 2010 of subsurface oil droplets vertically integrated between 800 and 200 m (spillets shaded by age, i.e., hours since release): (A) ADCPs, (B) HYCOM-FSU, (C) SABGOM, (D) NRL HYCOM + NCODA GOM, (E) NGOM, (F) NRL GLOBAL HYCOM.

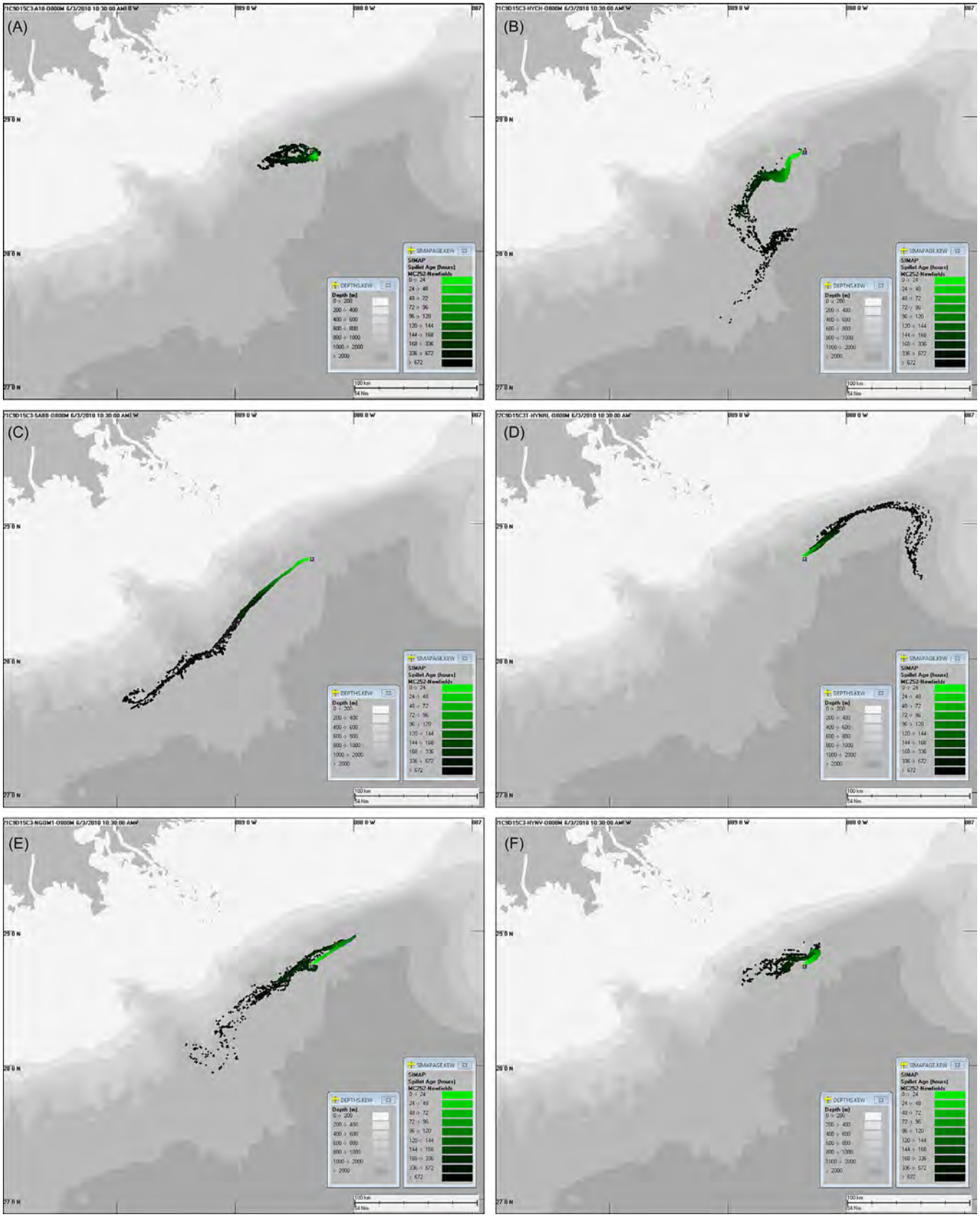

FIGURE 31.11 Cumulative trajectories to June 3, 2010 of subsurface oil droplets vertically integrated below 800 m (spillets shaded by age, i.e., hours since release): (A) ADCPs, (B) HYCOM-FSU, (C) SABGOM, (D) NRL HYCOM + NCODA GOM, (E) NGOM, (F) NRL GLOBAL HYCOM.

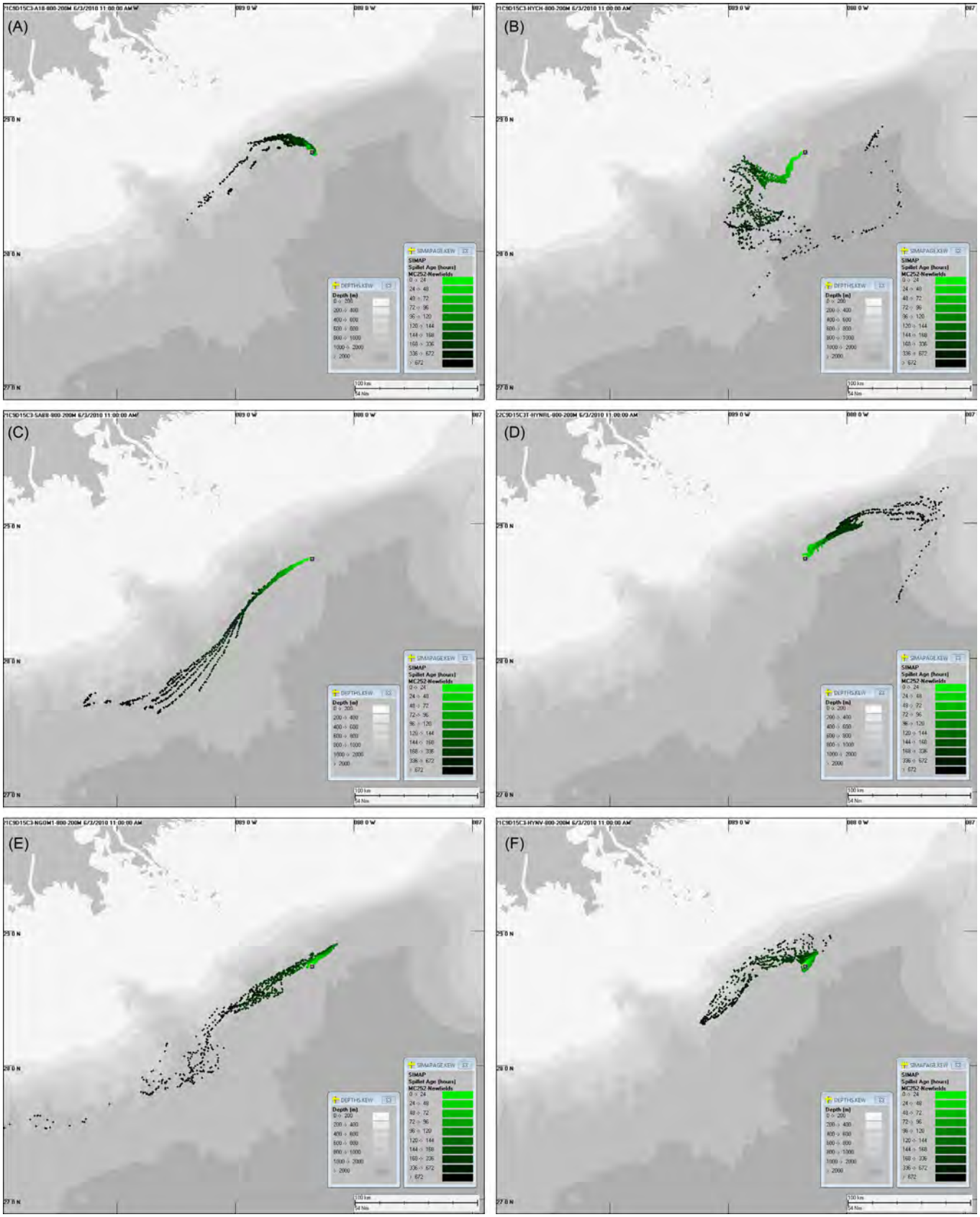

FIGURE 31.12 Cumulative trajectories to June 3, 2010 of subsurface oil droplets vertically integrated between 800 and 200 m (spillets shaded by age, i.e., hours since release): (A) ADCPs, (B)HYCOM-FSU, (C) SABGOM, (D) NRL HYCOM + NCODA GOM, (E) NGOM, (F) NRL GLOBAL HYCOM.

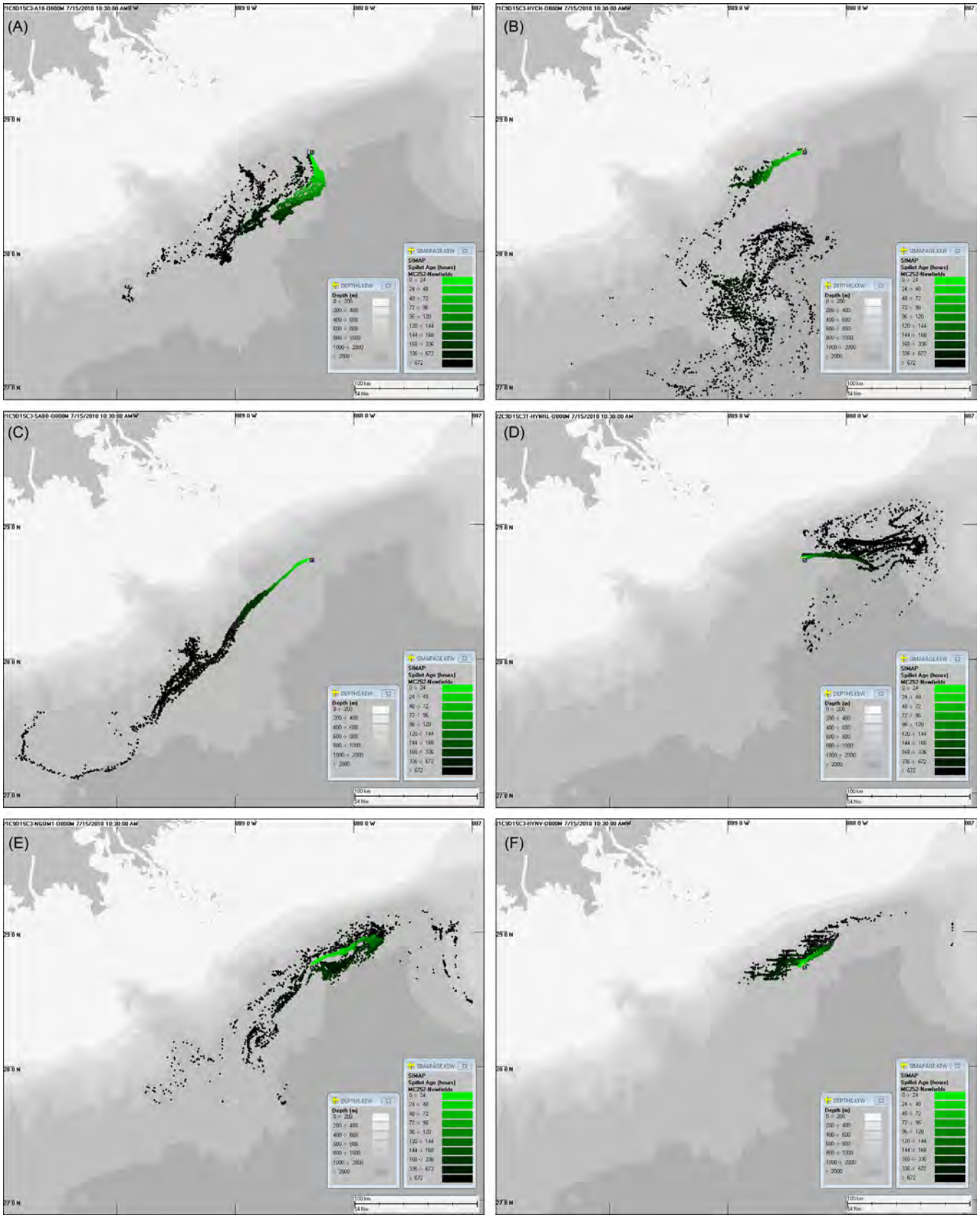

FIGURE 31.13 Cumulative trajectories to July 15, 2010 of subsurface oil droplets vertically integrated below 800 m (spillets shaded by age, i.e., hours since release): (A) ADCPs, (B) HYCOM-FSU, (C) SABGOM, (D) NRL HYCOM + NCODA GOM, (E) NGOM, (F) NRL GLOBAL HYCOM.

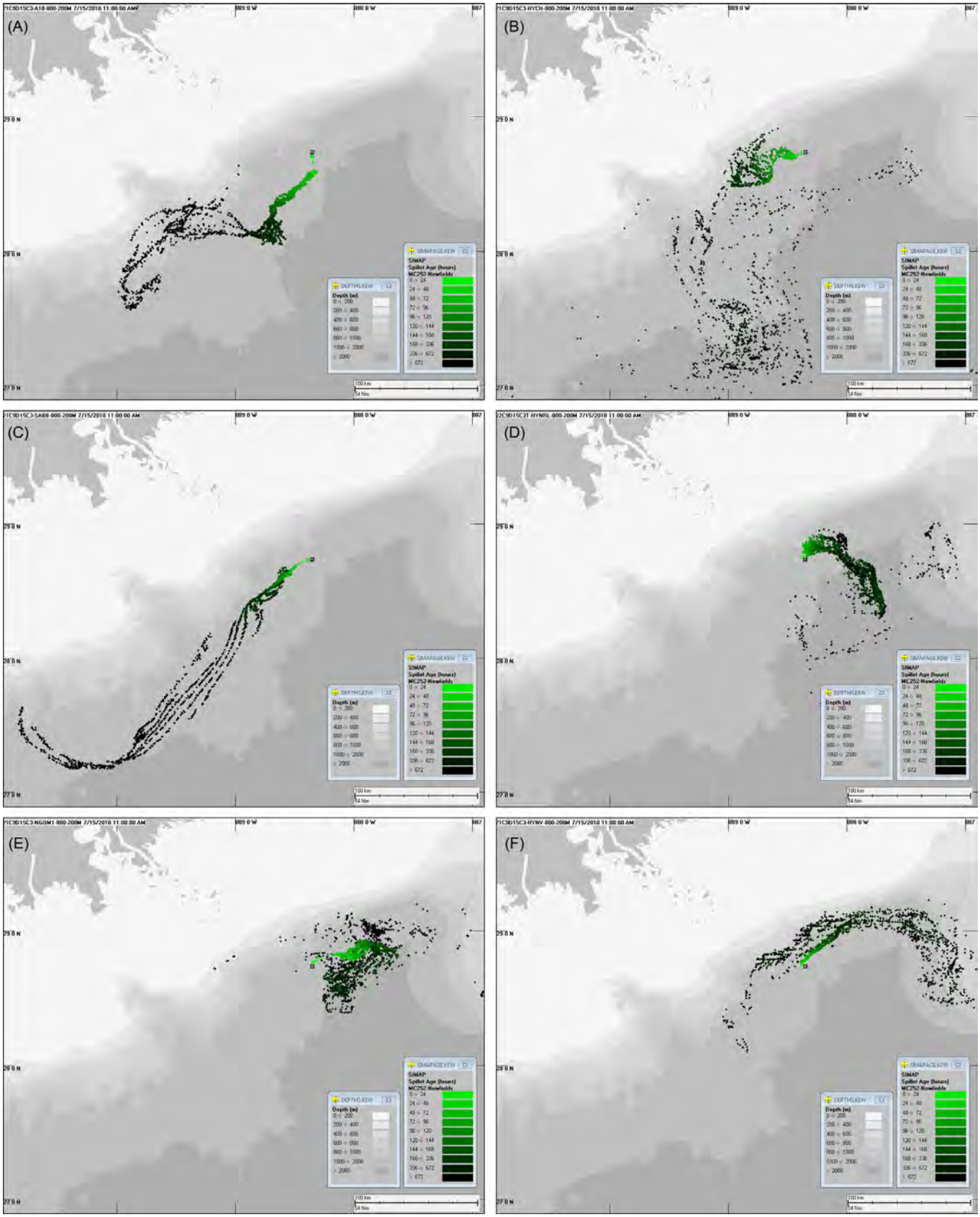

FIGURE 31.14 Cumulative trajectories to July 15, 2010 of subsurface oil droplets vertically integrated between 800 and 200 m (spillets shaded by age, i.e., hours since release): (A) ADCPs, (B) HYCOM-FSU, (C) SABGOM, (D) NRL HYCOM + NCODA GOM, (E) NGOM, (F) NRL GLOBAL HYCOM.

The hydrodynamic models produced current fields below 40 m that at times agreed with the ADCP data, and in other times diverged in direction and speed. The HYCOM-FSU model produced a trajectory of small droplets in deep water that was most similar to that using the ADCP data. The ROMs models tended to transport the small droplets along the bathymetry toward the southwest in narrow smooth flows much faster than indicated by the ADCP data. The IAS ROMS simulation was very similar to the SABGOM simulation shown in Figs. 31.9–31.14. The trajectory using IAS ROMS and modeled concentrations of oil components in the depth range of 1100–1400 m are available in French McCay et al. (2015a and 2016). The NRL GLOBAL HYCOM and NRL HYCOM + NCODA GOM both predicted the deep plume moved primarily northeastward from April through July of 2010, such that the deep plume did not reach southwestward in July as observed. The POM models (NGOM is shown in Figs. 31.9–31.14; NCOM results not shown) predicted movements at times to the northeast and other times to the southwest, but the timing of movements in these directions did not agree with the ADCP and observational data. The NRL NCOM model has been superseded by NRL's HYCOM, which produced more realistic (slower) currents at depth, and so these simulations are not considered further.

Thus, given the more narrow and accurate surfacing locations and reasonable data coverage within the 25-km × 25-km box around the wellhead, the simulation using ADCPs was considered the most realistic within that domain in all depth layers from 1400 m to 40 m. While the interpolation of the ADCP data is not a hydrodynamic model, which conserves mass and momentum, the ADCP current data field do indicate the actual flow field and which of the hydrodynamic models most closely simulates it (i.e., the HYCOM-FSU model).

31.4.3 Modeled Concentrations

As part of the NRDA analysis for the DWH Trustees (2016), for the purposes of estimating daily mean concentrations of PAHs in the exposure volume affected by rising oil and the deep plume, the oil fate model was run without currents. This simplification allowed daily averaging of concentrations in a stationary grid (25 km × 25 km, centered on the wellhead) and so generated a better representation of plankton exposures than possible with such spatial averaging if horizontal transport and displacements were included. The analysis assumed that the dissolved HCs and oil droplets remaining in the water column and the plankton all moved together; such that the gridded daily average concentrations based on the simulation without currents characterized the exposure experienced by plankton each day as they moved with the oil plume. Daily average exposure concentrations of total (dissolved plus particulate) PAHs (using 50 analytes, "TPAH50," Forth et al., 2015) were calculated for each horizontal grid cell and depth layer of the water column. See French McCay et al. (2015a and 2016) for the results and analysis of the simulation without currents, which provides a simplified picture of the concentration field.

Snapshots of the particulate (total HCs in droplets) and dissolved concentration distributions below 40 m produced by the simulation using ADCPs are shown in Figs. 31.15–31.22. The figures show top-down map views depicting the vertical maximum dissolved HC concentration in any 500 m × 500 m × 20 m cell within each 200-m layer of the water column, and a cross section along the line drawn on the map along the concentration plume. Concentrations of total dissolved HCs include all nine soluble and semisoluble components (AR1–AR9). Components AR5–AR8 are the PAHs, AR1 is BTEX, and AR9 includes the measurable soluble alkanes. Only concentrations greater than 1 μg/L (ppb) are plotted in the figures. Additional figures depicting the model results using ADCPs, HYCOM-FSU, and SABGOM are available in French McCay et al. (2017b).

In the simulations, the concentrations of droplets and dissolved constituents were highest close to the source (i.e., at and just above ~1200 or ~1300 m). Because the smaller oil droplets were spread out considerably by spatially and time-varying currents as they rose through the water column, the concentration profiles show much lower concentrations higher in the water column (Figs. 31.15–31.22). The soluble and semisoluble HC concentrations were in low concentrations in a narrow cylinder stretching toward the surface in April (not shown), when the release was not treated with dispersants at the release point and the oil was mostly in the form of large droplets >1 mm in diameter (Fig. 31.5). During May when the kink holes appeared and subsea dispersant began to be applied, such that small droplets were formed in addition to droplets >1 mm in diameter, the modeled subsurface concentrations were much higher and the contamination was dispersed over a wider area. After the riser was cut June 3, dispersant-treated and un-treated oil droplets were released at about 1200 m. The small droplets (<100 μm) remained in the deep plume layer of ~1100–1300 m, which was advected predominantly to the southwest, and progressively larger droplets rose to the surface at faster rates. The model results show more

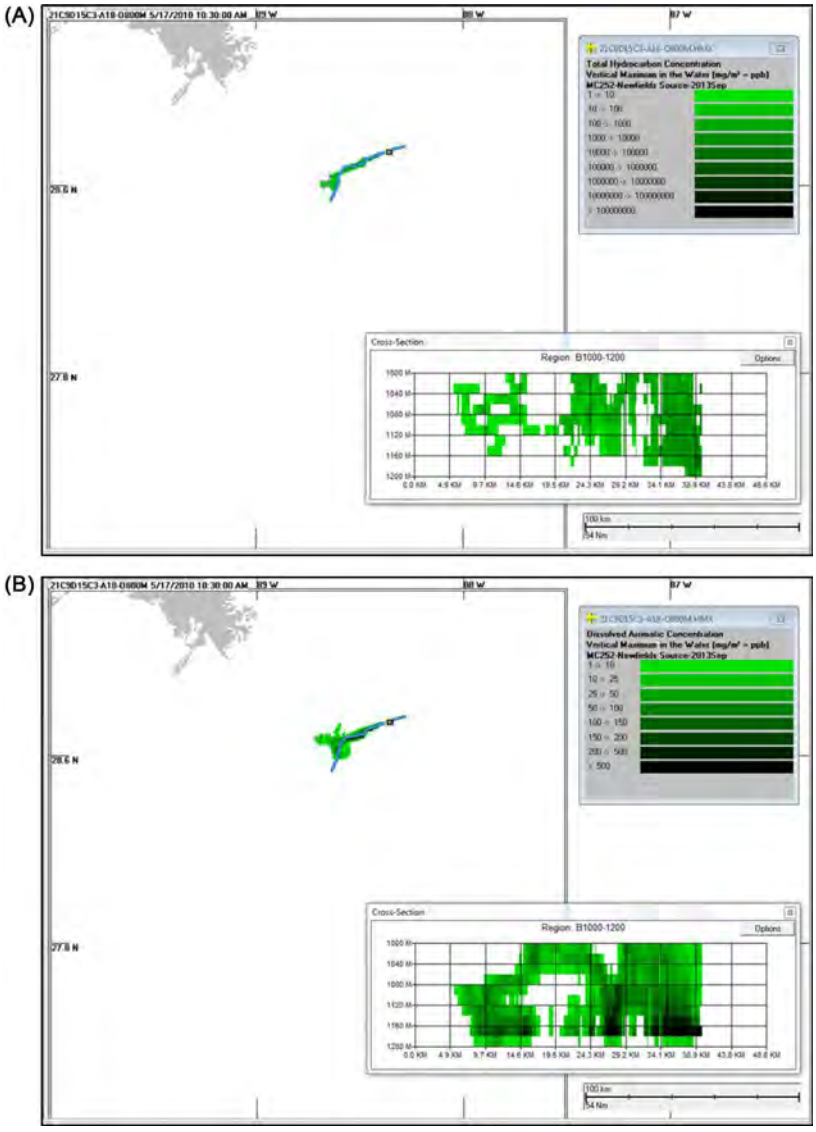

FIGURE 31.15 Snapshots of the particulate (total hydrocarbons in droplets, A) and dissolved (B) concentration distributions 1000–1200 m on May 17, 2010 produced by the simulation using ADCPs.

extensive plumes in deep water in June–July (OCR3) when more effective subsea dispersant applications were used than prior to June 3 (Spaulding et al., 2015).

Concentrations of dissolved components moved horizontally by current advection after dissolving from the droplets as they rose (Figs. 31.15, 31.16, 31.20 and 31.21). The dissolved components were diluted and biodegraded over time. On May 17, the deep plume between 1000 and 1200 m and contamination in waters at 800–1100 m consisted mainly of dissolved components, reflecting rapid dissolution of the most soluble components (MAHs [AR1, AR2, AR3], 2-ring PAHs, AR5, and soluble alkanes, AR9) from relatively large droplets that rose quickly to the surface (Figs. 31.15–31.16). Most of the 3-ring PAHs (AR6–AR8) remained in the particulate phase (i.e., oil droplets). After June 3, when subsea dispersant application was fully operational, the deep plume contamination included small droplets as well as dissolved components (Figs. 31.20–31.21) composed of all the S/SS HCs. The largest oil droplets rose directly to the surface and progressively smaller droplets were transported farther from the wellhead as they rose, yielding a cross-section that broadened higher in the water column (e.g., Fig. 31.16A). This displacement, along with current shear, made the concentrations higher in the water column patchy in space (Figs. 31.17–31.19, 31.21, and 31.22). Above 600 m, water with dissolved concentrations >1 μg/L were highly patchy and the volume

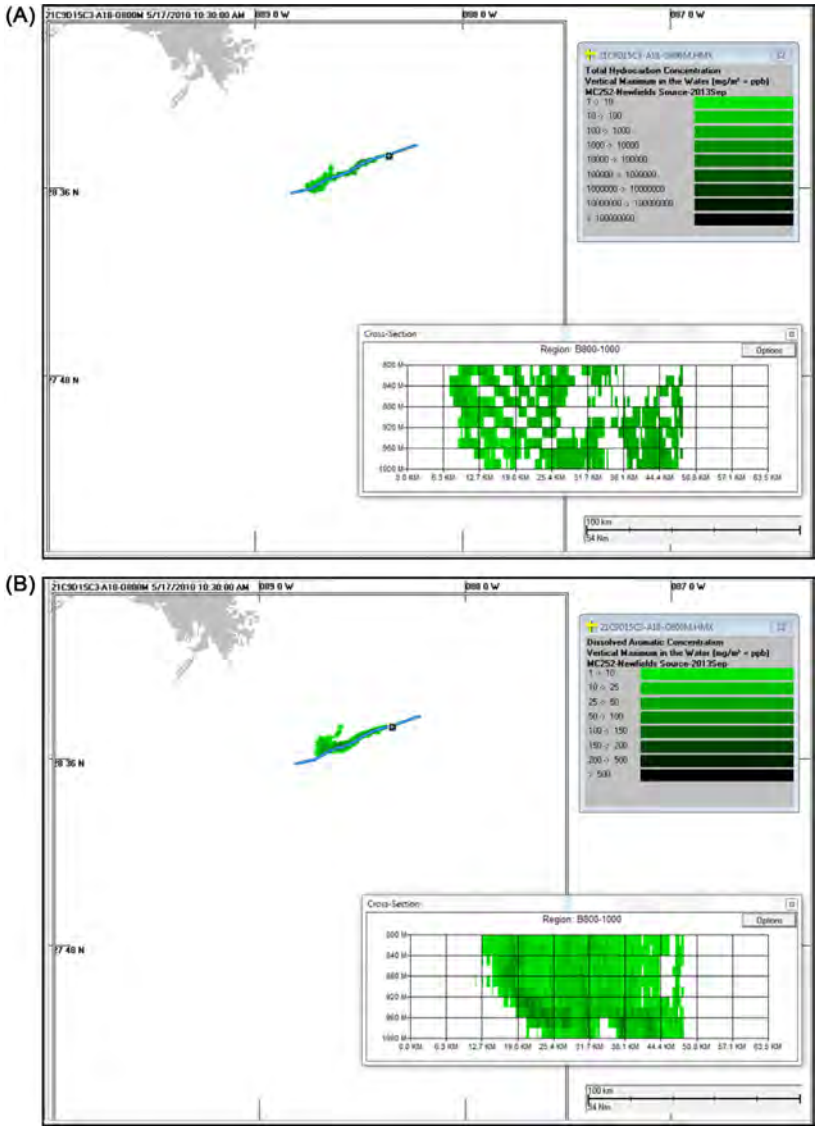

FIGURE 31.16 Snapshots of the particulate (total hydrocarbons in droplets, A) and dissolved (B) concentration distributions 800–1000 m on May 17, 2010 produced by the simulation using ADCPs.

contaminated was relatively low (Figs. 31.18 and 31.19, 31.22). [Note that successful sampling of such patches would be rare occurrences using a regularly spaced sampling design. For this reason, NRDA sampling was focused on locations in deep water where fluorescence and dissolved oxygen sensors indicated the potential presence of in-water HC concentrations (Payne and Driskell, 2015d). This targeted sampling approach was used on NRDA *Jack Fitz* 1–3 cruises of May and June 2010, but did not begin in earnest on the response vessels until late July and August of 2010.]

The modeled distributions of oil droplets and dissolved components agree with patterns discerned from field observations, as described in Section 31.3. Oil droplets >1 mm in diameter rose to the surface within ~4 km of the wellhead. The deep plume was enriched in dissolved soluble HCs and advected in various directions before July 2010, and to the southwest after 1 July, 2010. Less water-soluble compounds were present both in the deep water plumes and in the upper water column. Concentrations in the deep plume were consistently >1 μg/L, whereas higher in the water column, concentrations were very patchy and more widely dispersed.

In all simulations, in the layer from 1000 to 1200 m, concentrations peaked at over 500 μg/L near the release location and immediately downstream, but diluted rapidly such that concentrations over 100 μg/L were transported in a narrow plume to varying distances from the release point. In the ADCP simulation, concentrations in

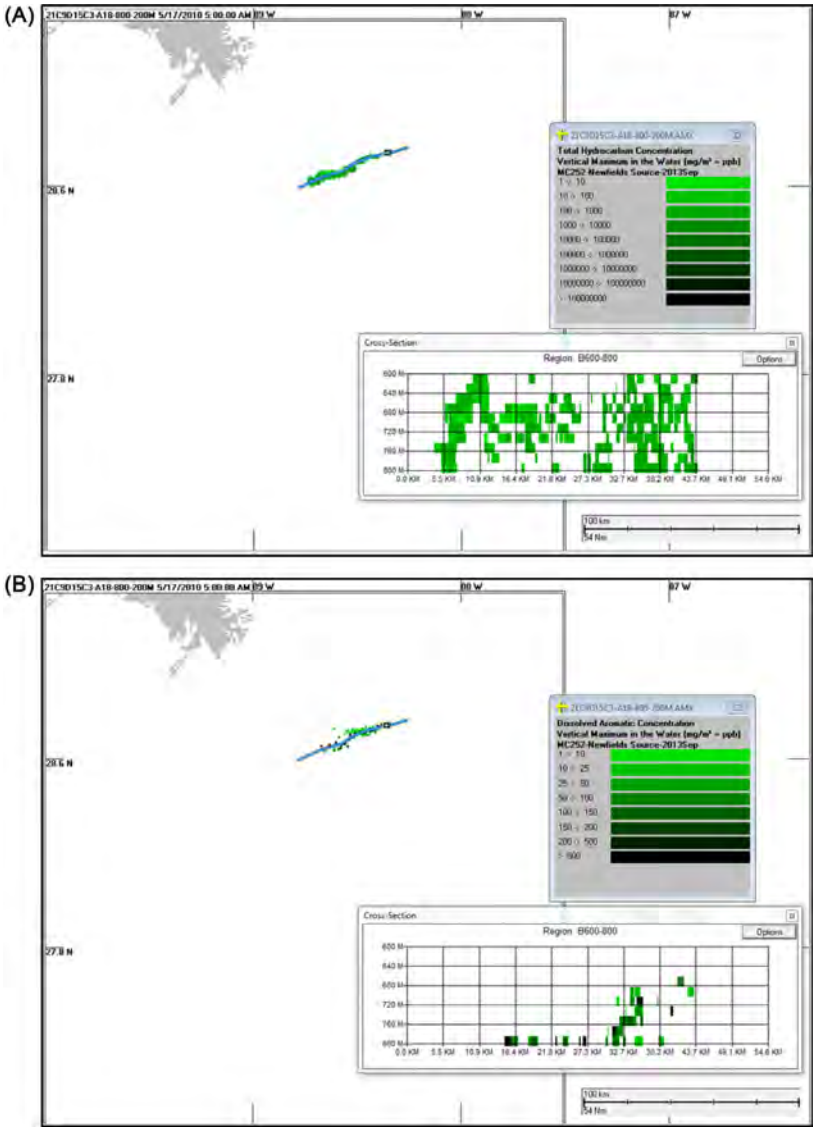

FIGURE 31.17 Snapshots of the particulate (total hydrocarbons in droplets, A) and dissolved (B) concentration distributions 600−800 m on May 17, 2010 produced by the simulation using ADCPs.

the deep plume >100 μg/L total dissolved HCs remain within ~25 km of the release point, and those >10 μg/L reached 30−40 km from the wellhead. In the HYCOM-FSU simulations, concentrations >100 μg/L were transported to ~40 km from the wellhead on most dates, to about ~50 km on some days; and concentrations >10 μg/L reached ~60 km from the wellhead on most dates, to about ~100 km in early July. In the SABGOM simulations, concentrations >100 μg/L were transported to ~60 km to as much as 100 km from the wellhead; and concentrations >10 μg/L reached ~110 km from the wellhead on many dates. (Maps showing concentrations for these three simulations are available in French McCay et al., 2017a,b.) The SABGOM results reflect much higher current speeds than in HYCOM-FSU, and HYCOM-FSU currents at the depth of the deep plume were generally higher than the ADCP data indicate. In the simulations with other hydrodynamics, the patterns are more complex, but transport and dilution is faster and in different directions than the ADCP and observational data indicate occurred in the field.

At depths of >1000 m, the majority of the field-measured concentrations greater than 10 μg/L were within approximately 30 km of the wellhead (Horn et al., 2015b, French McCay et al., 2015a). Furthermore, at higher depths in the water column but below 40 m, field-measured concentrations greater than 10 μg/L were within

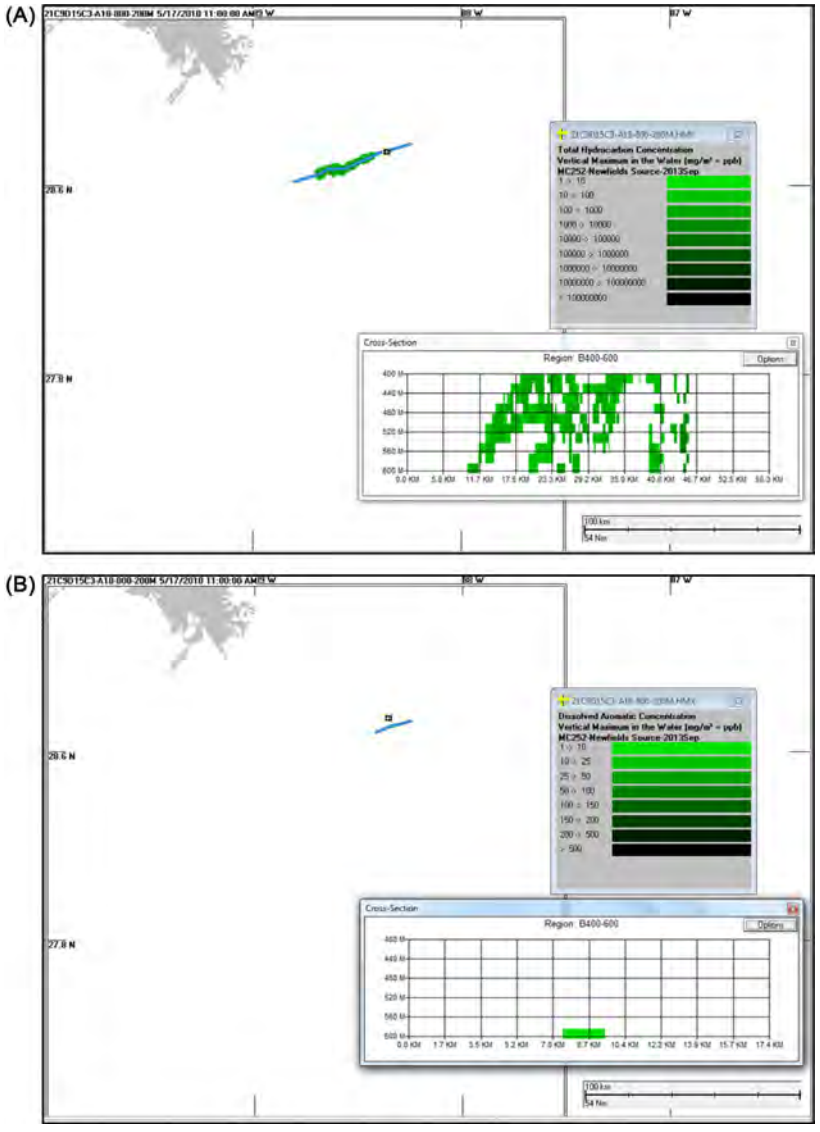

FIGURE 31.18 Snapshots of the particulate (total hydrocarbons in droplets, A) and dissolved (B) concentration distributions 400–600 m on May 17, 2010 produced by the simulation using ADCPs.

approximately 20 km of the wellhead. However, relatively few samples were taken between 40 and 1000 m at >25 km from the wellhead in April–July when the model depicts concentrations above 10 μg/L.

Thus, the simulation using ADCP current data produced concentrations in agreement with the distributions and concentrations measured in the field, whereas the simulations using the hydrodynamic model's currents resulted in total dissolved HC concentrations >10 μg/L that often extended too far from the wellhead and in the wrong directions. While it is possible that the field sampling missed the extended narrow plumes indicated by some of the hydrodynamic model-forced simulations, that distribution is unlikely given the comparison of the currents speeds predicted by the hydrodynamics models with measurement data showing the models over-estimated current speeds.

The highest measurements of total investigated HCs (including BTEX, other MAHs, PAHs, and soluble alkanes) in the deep plume were >100–700 μg/L, and concentrations up to ~80 μg/L were measured at other depths between 200 and 1000 m. The model-simulated dissolved concentrations (Figs. 31.15–31.22) depict similar peak concentrations in these depth ranges. Total HC concentrations were <100 μg/L in all locations below 40 m by August 20 and on September 15, they were <1 μg/L. In the simulations, dissolved soluble and semisoluble HC concentrations decrease to <1 μg/L in all locations below 40 m by August 20.

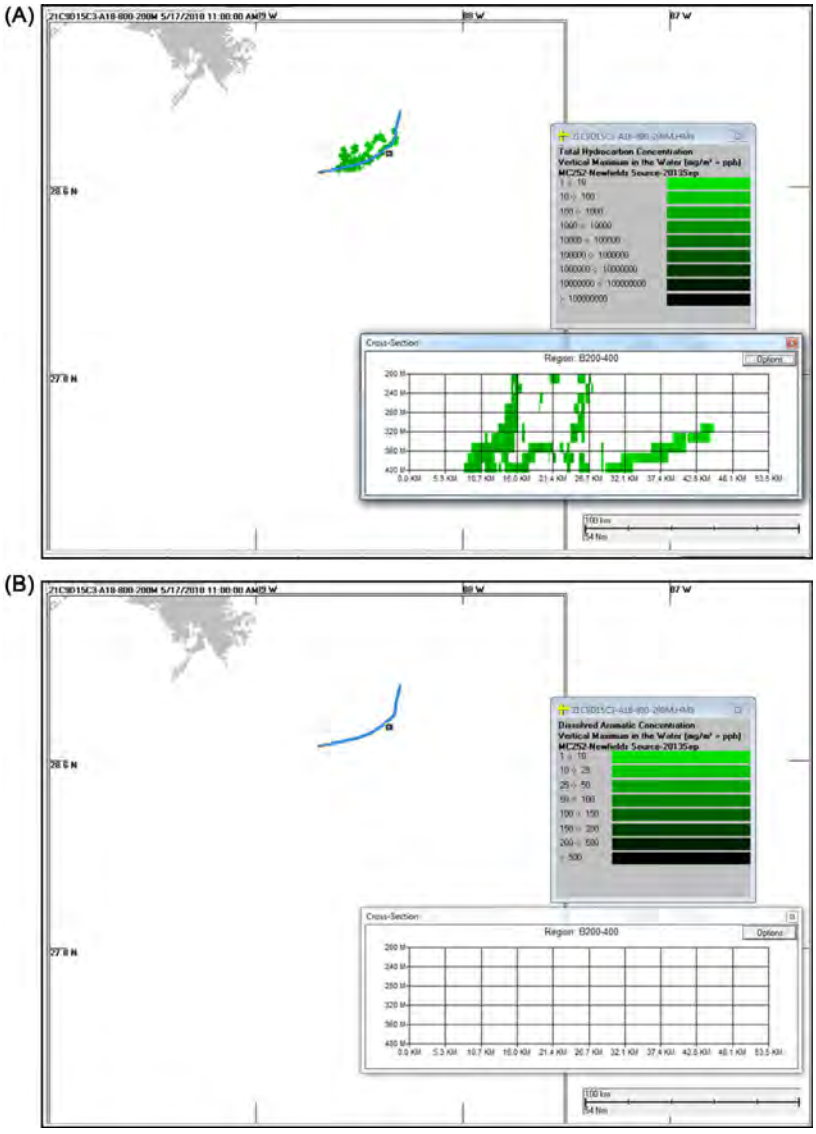

FIGURE 31.19 Snapshots of the particulate (total hydrocarbons in droplets, A) and dissolved (B) concentration distributions 400−200 m on May 17, 2010 produced by the simulation using ADCPs.

31.4.4 Comparison of the Modeled Concentrations to Field Measurements

As >75% of the oil rose to the surface within 11 km of the wellhead, and water sampling was also focused on this area (because the oil was observed surfacing within 4 km of the wellhead), modeled and observed HC concentrations below 40 m were compared in the 25-km × 25-km box centered on the wellhead. Since the ADCP-based current field was most realistic, the ADCP-forced scenario will be the focus of the presentation and discussion of the HC concentration results. For the hydrodynamic model-forced simulation using HYCOM-FSU, concentrations were similar to those simulated using the ADCP data (French McCay et al., 2017a,b); however, as noted above, the other hydrodynamic models that predicted much stronger currents than the ADCP measurements diluted the concentrations relative to the ADCP case.

The total HC concentrations in droplets that are predicted by the model are based on the total mass of the release (i.e., 553,889 MT), much of which cannot be chemically measured in water samples. Thus, the modeled total HC concentration is not comparable to a total petroleum HC measurement. For this reason, model-predicted concentrations of the soluble and semisoluble HCs, i.e., of the AR components, are compared to field sample measurements of those same chemical components. Note also that the aliphatic AL components are defined by

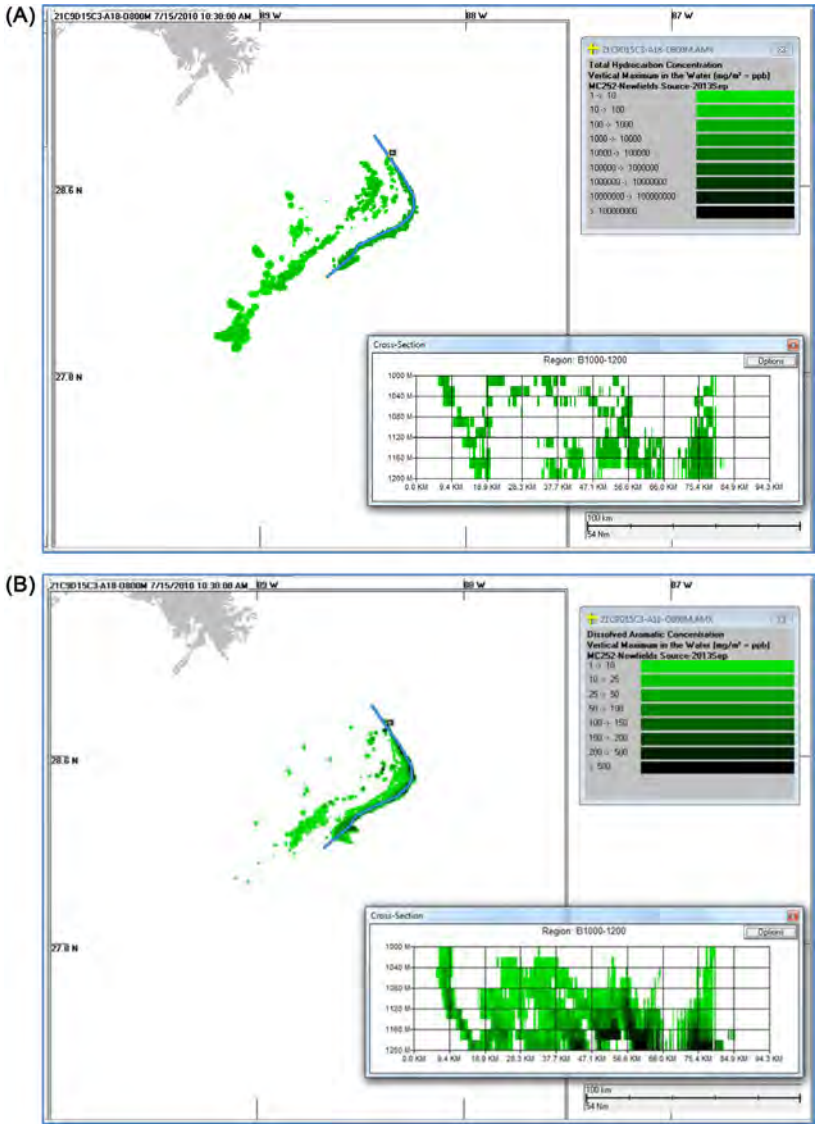

FIGURE 31.20 Snapshots of the particulate (total hydrocarbons in droplets, A) and dissolved (B) concentration distributions 1200−1000 m on July 15, 2010 produced by the simulation using ADCPs.

boiling point ranges, and so those components contain much more mass then is measurable within the boiling ranges using GC/MS or other existing techniques to measure individual aliphatic HCs in the water.

The modeled concentrations of AR components were compared to measurement data reported in the literature, as available, and from chemistry samples collected for the NRDA chemistry program (described in Horn et al., 2015a). Careful consideration was needed when comparing the model results to measurements from samples. Samples were not collected at the maxima directly above the wellhead, and therefore much lower concentrations would be anticipated further from the release locations. Furthermore, due to the differences between the modeled and actual field conditions and the patchiness of observed chemistry, there is the potential for displacement between modeled and observed concentrations in both space and time. Therefore, a direct overlay of the detectable chemistry measurements on the model would be insufficient for evaluating if the concentrations produced by the model are reasonable. To account for this displacement, results are plotted as probability distributions within a spatial and temporal window, containing a population of chemistry samples. The chemistry samples and modeled results were ordered by concentration so that the frequency distributions of concentrations may be compared.

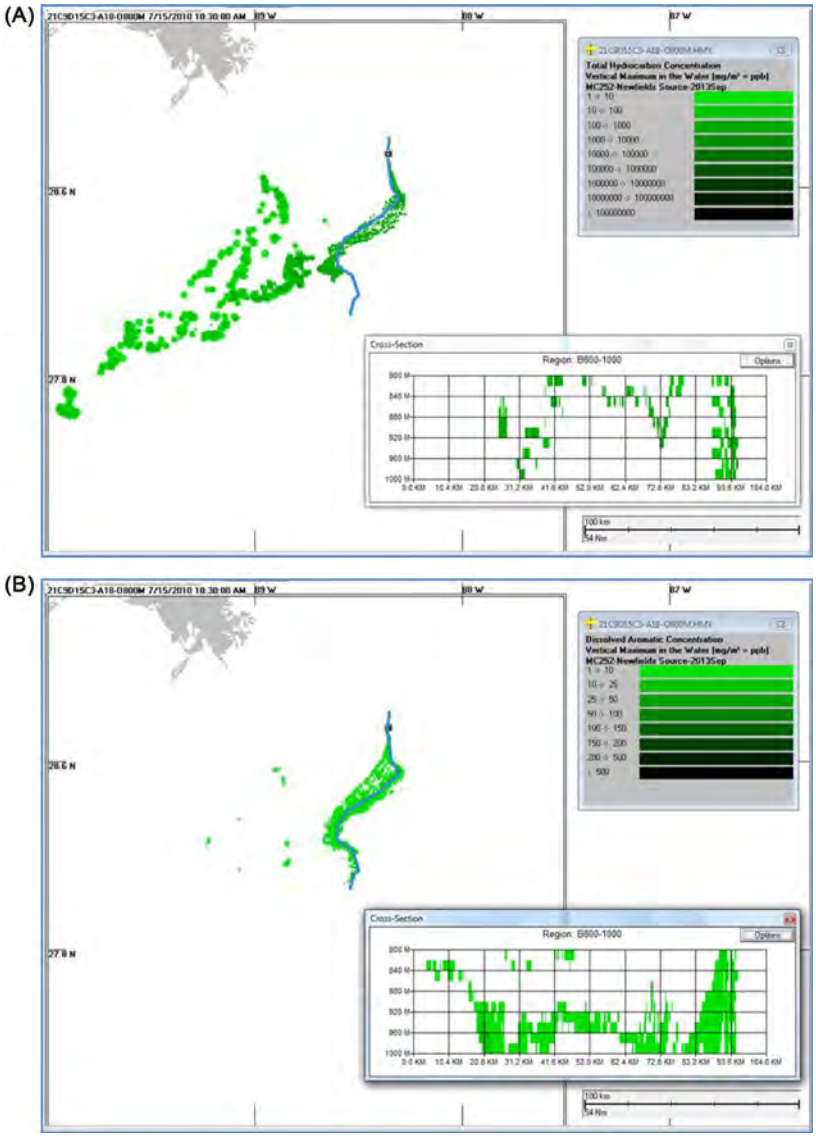

FIGURE 31.21 Snapshots of the particulate (total hydrocarbons in droplets, A) and dissolved (B) concentration distributions 800−1000 m on July 15, 2010 produced by the simulation using ADCPs.

Most of the chemistry samples were analyzed as whole water samples, which includes both the in-droplet and dissolved concentrations. The chemistry sampling was targeted at fluorescence peaks and dissolved oxygen sags in the deep plume, which indicated the presence of oil and preferentially targeted regions with higher chemical values (Payne and Driskell, 2015d). If a randomized sampling plan were used both horizontally and vertically, then many more samples would likely be present with nondetectable HCs. Therefore, only the modeled concentrations with HC concentrations greater than zero were compared to the chemistry results.

The comparisons were made for five vertical intervals (see below) within a 25-km-by-25-km box centered on the wellhead. Section 31.3.2 identifies the four time domains (OCRs) considered for the statistical analysis. However, only the OCR1, OCR2, and OCR3 time intervals had sufficient samples (>5 samples in each depth interval and the domain considered) for meaningful comparisons. The single latitude, longitude domain used is longitude: 88.5029°−88.2529°W; latitude: 28.6223°−28.8468°N. The depth range 40−1400 m was divided into five depth intervals: 40−200, 200−500, 500−800, 800−1100, and 1100−1400 m. Comparisons of the model-predicted concentrations with sample measurements were made for all nine AR components. Modeled concentrations were calculated in a grid with cell dimensions 500 m × 500 m × 20 m (width × length × depth).

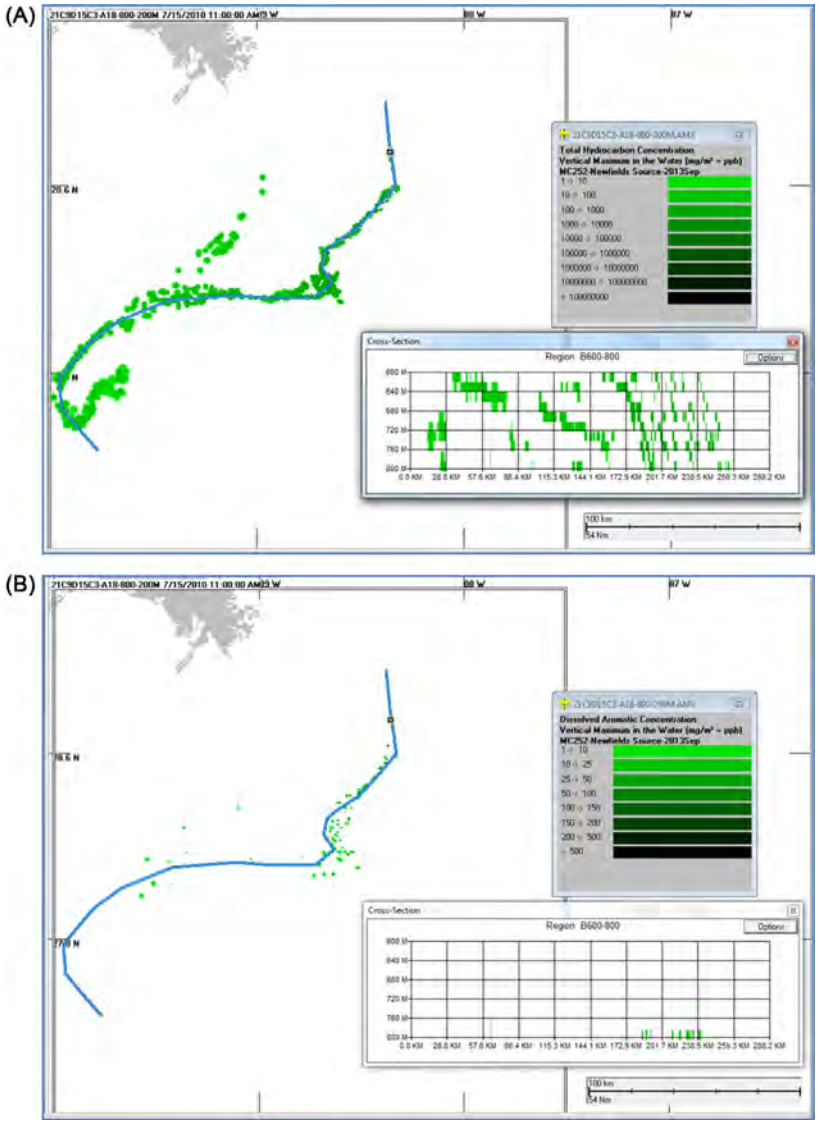

FIGURE 31.22 Snapshots of the particulate (total hydrocarbons in droplets, A) and dissolved (B) concentration distributions 600−800 m on July 15, 2010 produced by the simulation using ADCPs.

Histograms, in a cumulative percentile format, were used to compare the frequency distribution of the modeled concentrations within each grid cell to the frequency distribution of the measured samples. Figs. 31.23−31.31 show results for the depth intervals 800−1100 m and 1100−1400 m. For example, if the observed chemistry data (plotted as points) are above the cumulative frequency distribution for the SIMAP model prediction, then it indicates that there are more samples with low concentrations than the model predicts and the observed chemistry values as a whole are lower than the modeled values. If the model's cumulative frequency distribution is above that for the samples, the model has predicted lower concentrations than the samples indicate. If the observed and modeled frequency distributions cross each other, but the model distribution has a steeper slope, it indicates the modeled distribution had the higher concentrations in a broader area than the samples indicate.

In general, the modeled and measured concentrations were of the same order of magnitude. There was a statistically significant ($\alpha = 0.01$) decrease in both the sample concentrations and the percent detectable sample results taken in and just above the deep plume (800−1100 m) after the June 3 riser cut and Top Hat placement when oil recovery from depth began and the volume of oil released to the environment decreased substantially (Fig. 31.3). A decrease after June 6 is evident in the model results and the chemistry samples.

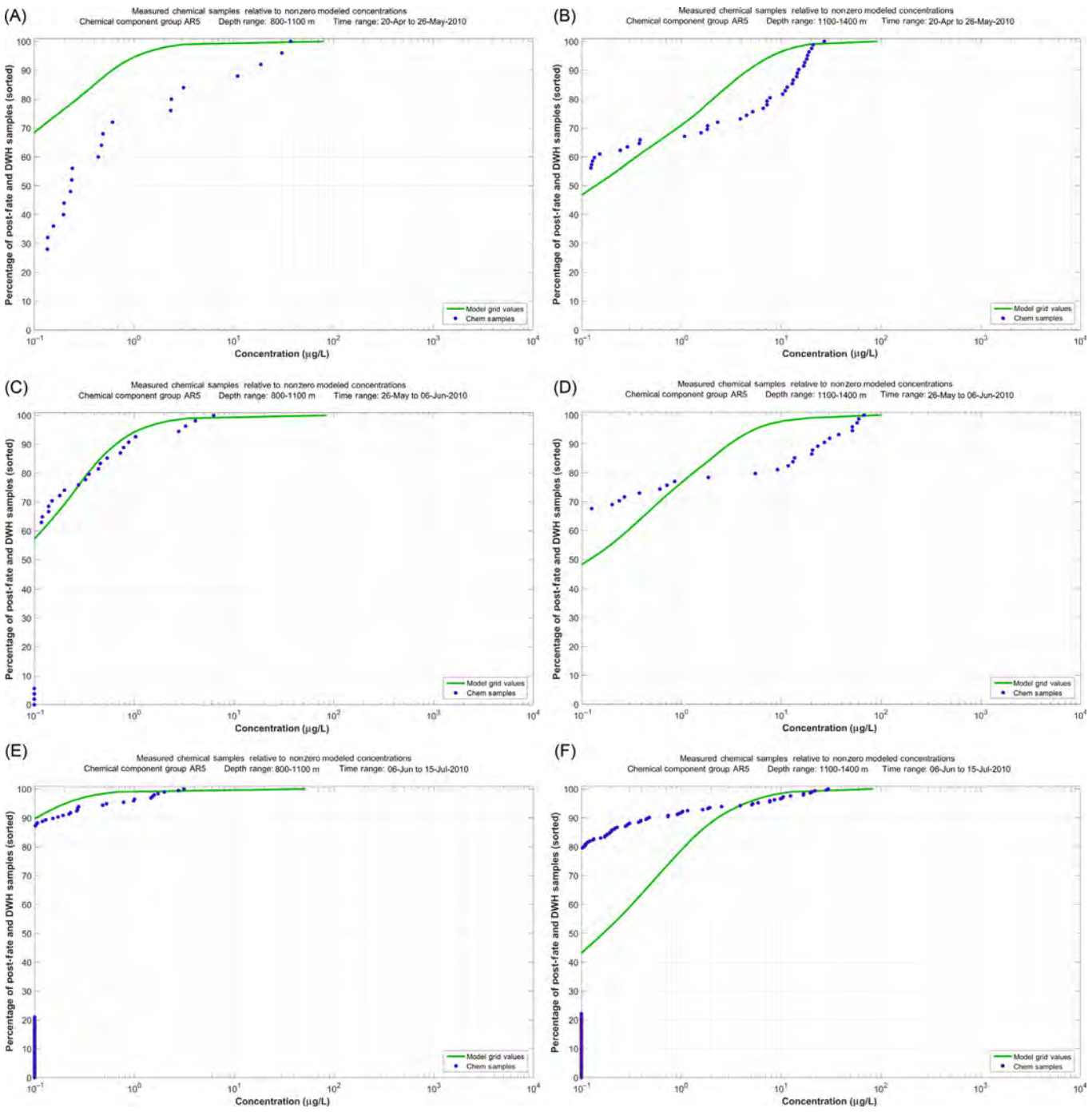

FIGURE 31.23 Comparison of total (in-droplet + dissolved) concentrations (μg/L) predicted by the model using ADCP data to measurements from chemistry samples of AR5 component (C0−C2 naphthalenes and C0−C2 benzothiophenes): (A) OCR1, 800−1100 m; (B) OCR1, 1100−1400 m; (C) OCR2, 800−1100 m; (D) OCR2, 1100−1400 m; (E) OCR3, 800−1100 m; (F) OCR3, 1100−1400 m.

The cumulative frequency distributions of the model and measured concentrations are more similar for PAH components than for some of the other components. Additionally, the modeled and measured concentrations compared more favorably in the deep plume (800−1100 m and 1100−1400 m depth intervals) than higher in the water column. There also were far fewer chemistry samples available from depths of 40−800 m, and those samples were typically taken on a vertical cast targeting the deep plume contamination. Thus, comparisons of modeled peak concentrations to samples in the lower layers where sampling targeted fluorescence peaks and

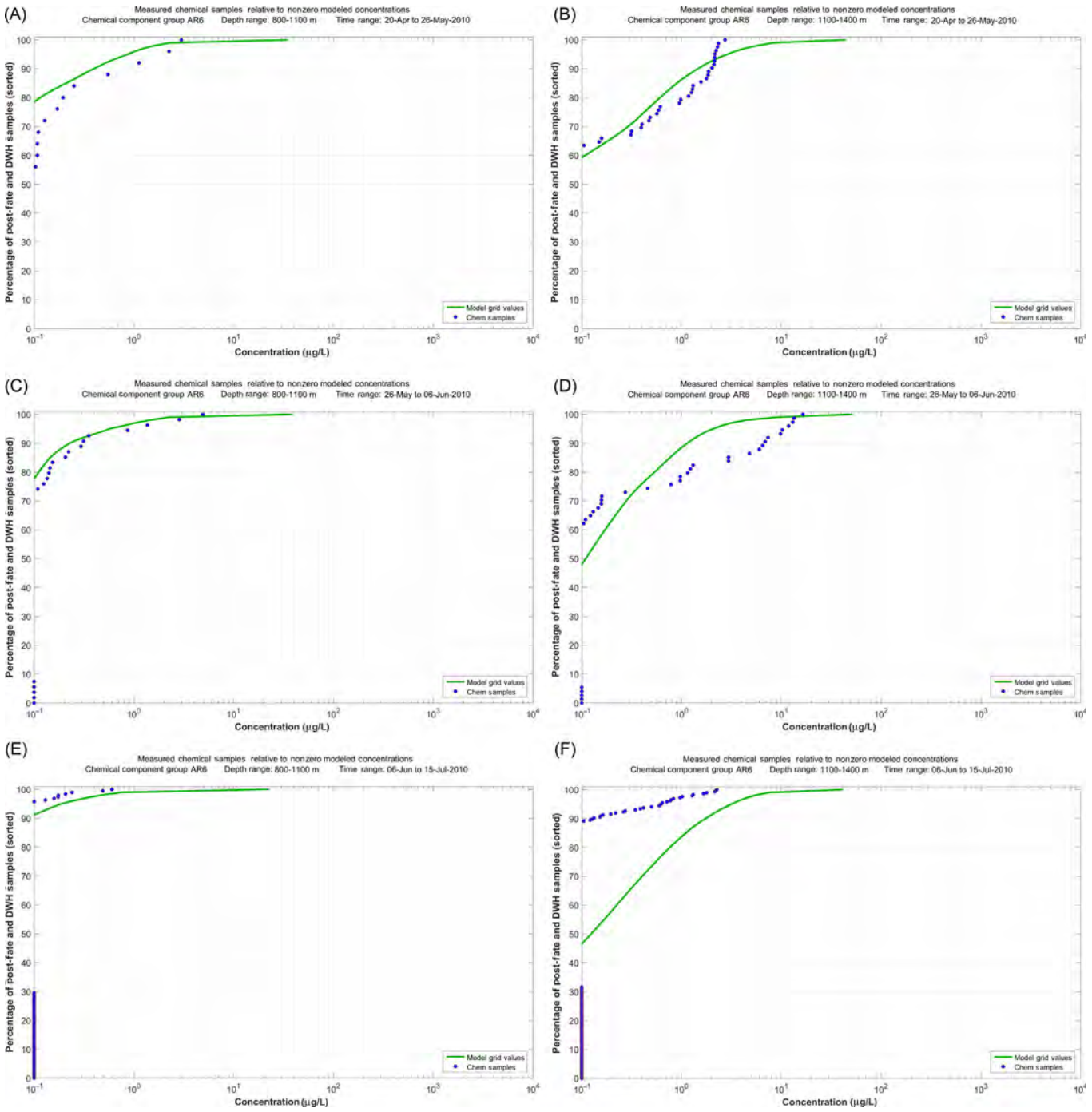

FIGURE 31.24 Comparison of total (in-droplet + dissolved) concentrations (μg/L) predicted by the model using ADCP data to measurements from chemistry samples of AR6 component (C3−C4 naphthalenes and C3−C4 benzothiophenes): (A) OCR1, 800−1100 m; (B) OCR1, 1100−1400 m; (C) OCR2, 800−1100 m; (D) OCR2, 1100−1400 m; (E) OCR3, 800−1100 m; (F) OCR3, 1100−1400 m.

dissolved oxygen sags are more meaningful than those in upper layers where sampling was infrequent, not targeted at peaks, and partially biased.

Components AR5 and AR6 include the C0−C4 naphthalenes and C0−C4 benzothiophenes. These comprise the semisoluble PAHs, whereas AR7 and AR8 include the slightly soluble 3-ring PAHs (Table 31.1). Figs. 31.22−31.25 show comparisons between the model concentrations and the sample measured concentrations for AR5 through AR8, respectively. The typical pattern for the comparison of modeled to measured AR5 and

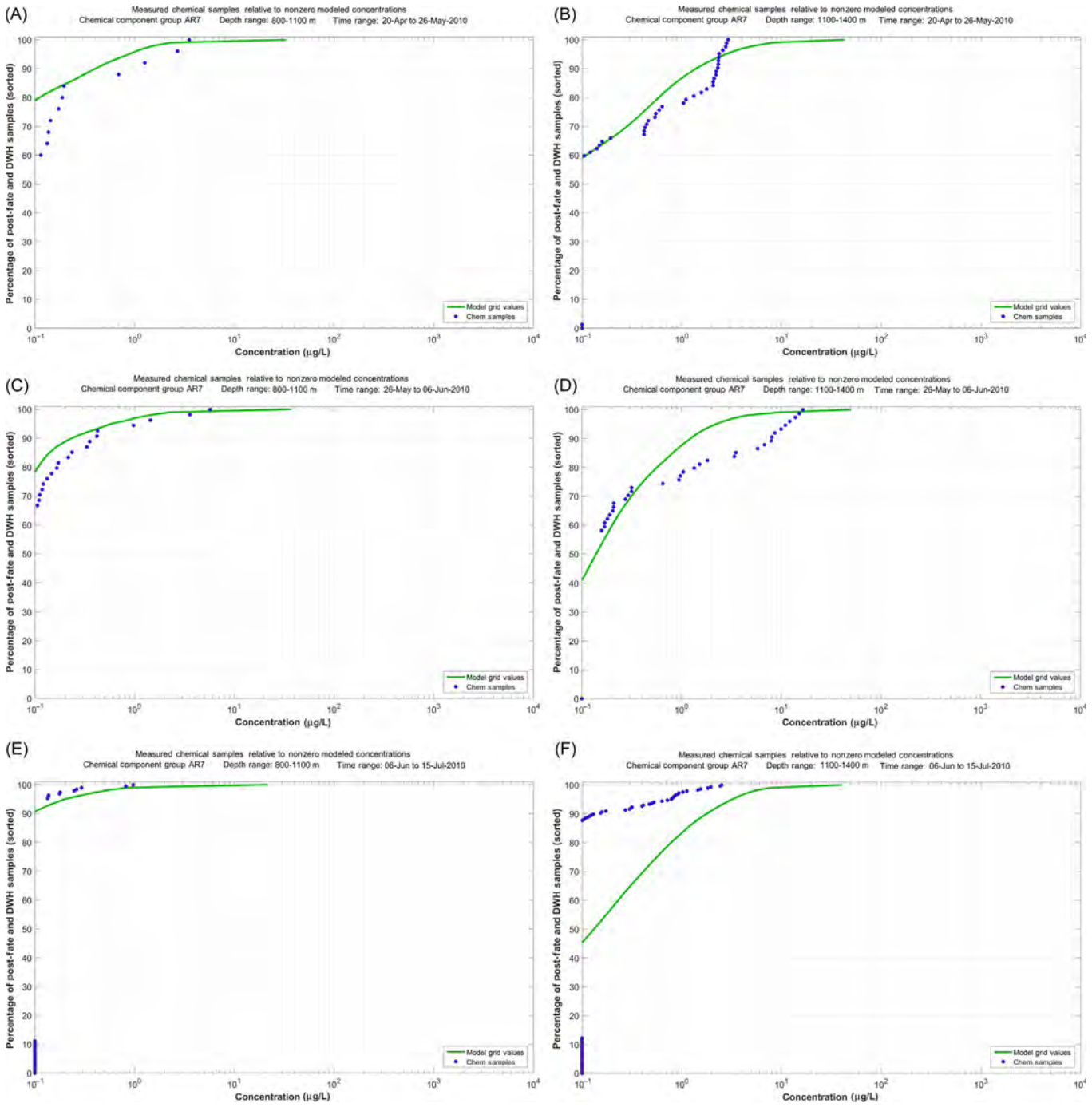

FIGURE 31.25 Comparison of total (in-droplet + dissolved) concentrations (μg/L) predicted by the model using ADCP data to measurements from chemistry samples of AR7 component (fluorenes and C0−C1 3-ring PAHs): (A) OCR1, 800−1100 m; (B) OCR1, 1100−1400 m; (C) OCR2, 800−1100 m; (D) OCR2, 1100−1400 m; (E) OCR3, 800−1100 m; (F) OCR3, 1100−1400 m.

AR6 concentrations is that the highest concentrations are of similar magnitude (~1−3 μg/L), but the frequency distributions among measured samples show somewhat higher concentrations than the model's frequency distribution of concentrations (i.e., there are more samples with concentrations >1 μg/L than there are grid cells with modeled concentrations of that magnitude). The comparisons for AR7 and AR8 at 1100−1400 m show a similar pattern as the naphthalenes (AR5 and AR6). Overall, considering all time windows and depth zones for all chemical components, the closest results to the observed are in the depth range 800−1000 m.

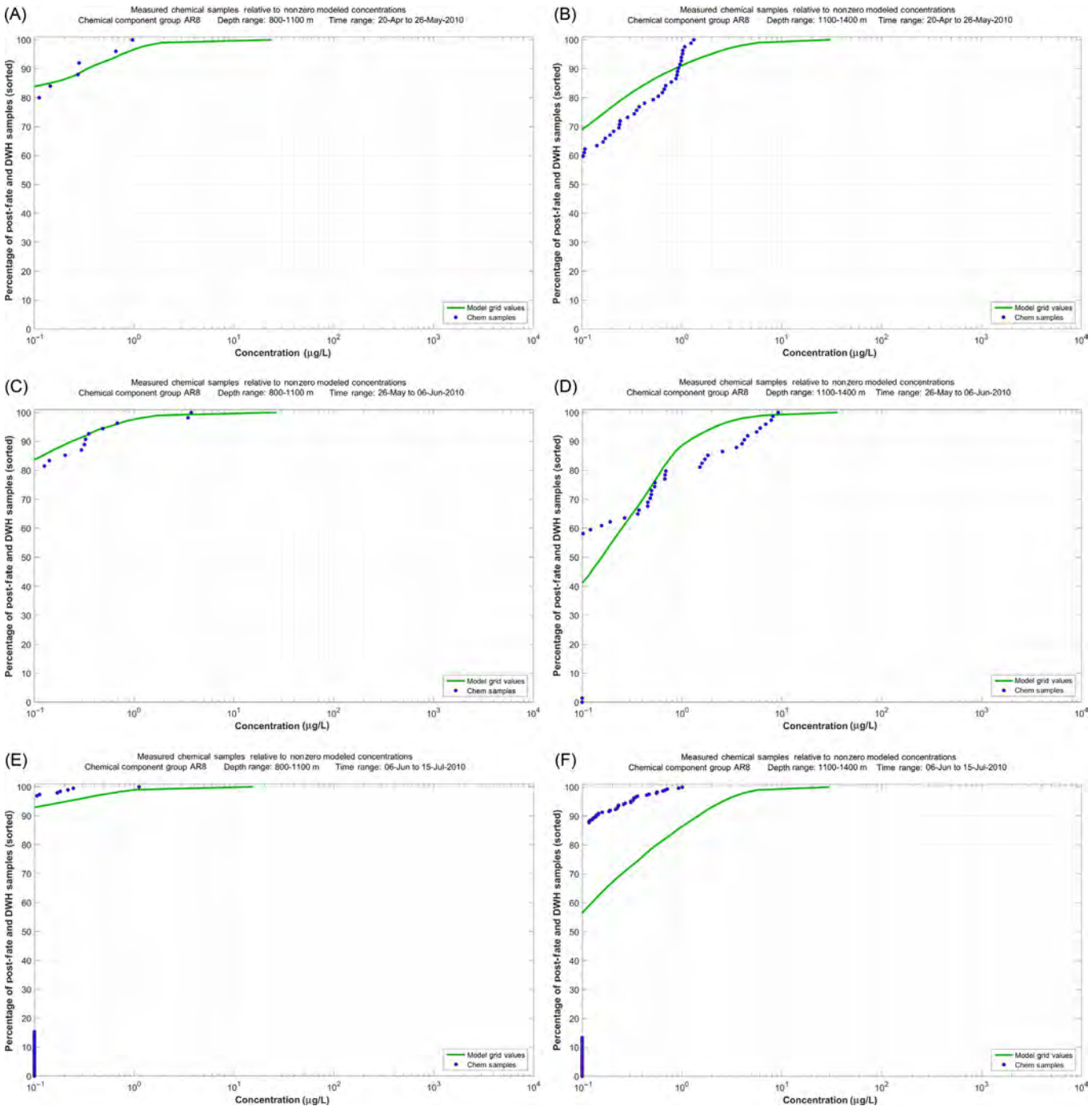

FIGURE 31.26 Comparison of total (in-droplet + dissolved) concentrations (μg/L) predicted by the model using ADCP data to measurements from chemistry samples of AR8 component (4-ring PAHs and C2–C3 3-ring PAHs): (A) OCR1, 800–1100 m; (B) OCR1, 1100–1400 m; (C) OCR2, 800–1100 m; (D) OCR2, 1100–1400 m; (E) OCR3, 800–1100 m; (F) OCR3, 1100–1400 m.

Concentrations at specific levels above 1 μg/L TPAH were assessed as acutely toxic (in waters below 20 m) by the DWH Trustees (Morris et al., 2015b; DWH Trustees, 2015). Thus, the focus of the model comparisons to observed data was on concentrations >1 μg/L TPAH. Only a few percent of the samples and model estimates within the 25-km-by-25-km box centered on the wellhead were above 1 μg/L PAH, and these modeled and observed concentrations compared well.

The maximum BTEX (AR1) concentrations predicted by the model were generally ~25–100 μg/L, with the exception of near the release location where concentrations >100 μg/L (Fig. 31.26). The typical pattern of the

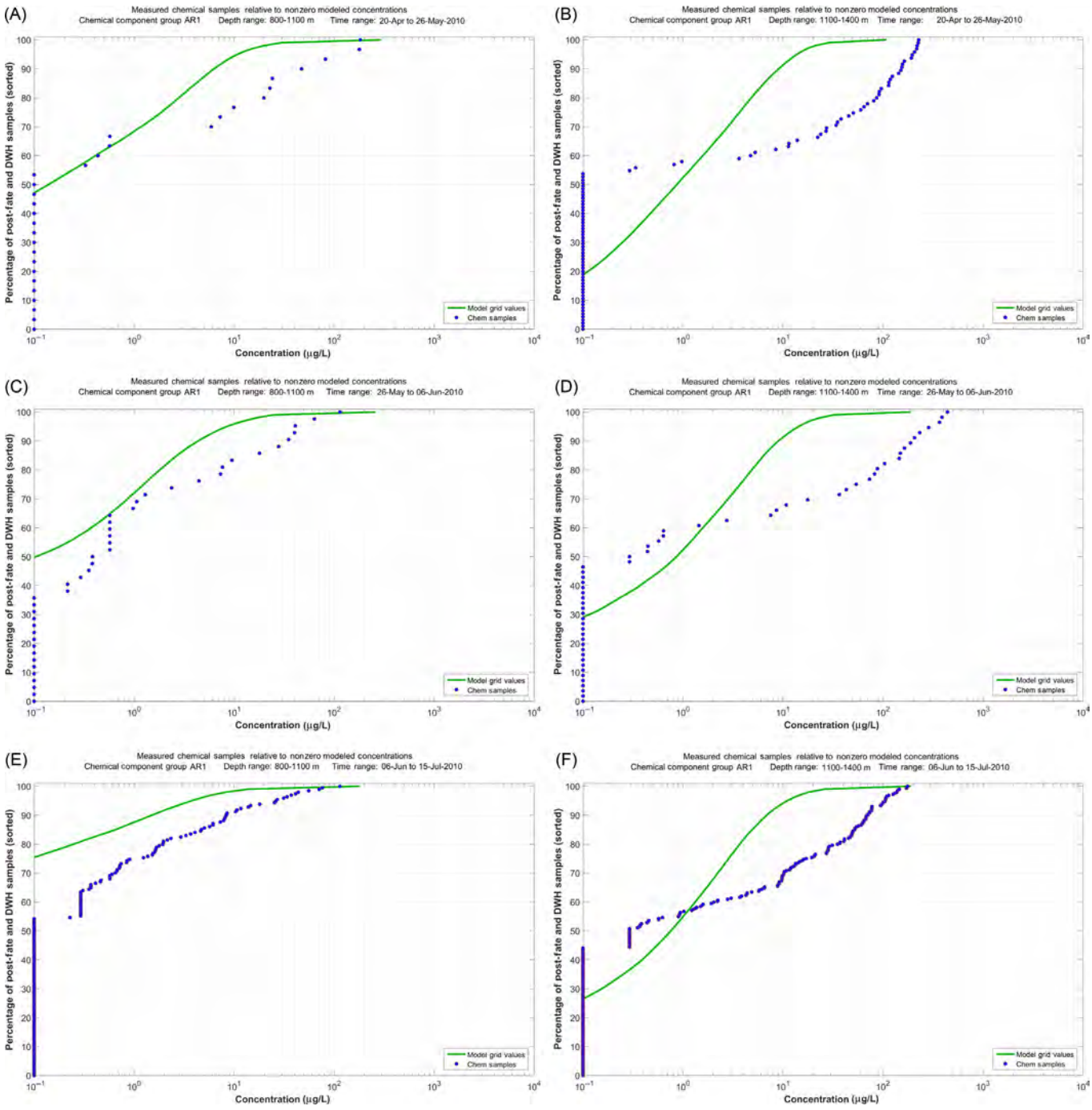

FIGURE 31.27 Comparison of total (in-droplet + dissolved) concentrations (μg/L) predicted by the model using ADCP data to measurements from chemistry samples of AR1 component (BTEX): (A) OCR1, 800−1100 m; (B) OCR1, 1100−1400 m; (C) OCR2, 800−1100 m; (D) OCR2, 1100−1400 m; (E) OCR3, 800−1100 m; (F) OCR3, 1100−1400 m.

comparisons was that there were occasional (a few percent of) sample concentrations measured above 100 μg/L and many observations less than the MDL, treated as zero for the observation, whereas the model results smoothly transition between these values. Thus, the nonzero concentration model results agree with the >MDL BTEX concentrations, but do not show as many (500 m × 500 m × 20 m) cells with concentrations >100 μg/L as there are samples with concentrations >100 μg/L (i.e., the chemical sample cumulative frequency distribution is often below the model distribution in Fig. 31.26). It should be noted that if a finer scale grid were used to calculate concentrations, the model concentrations would be higher in the core of the plume.

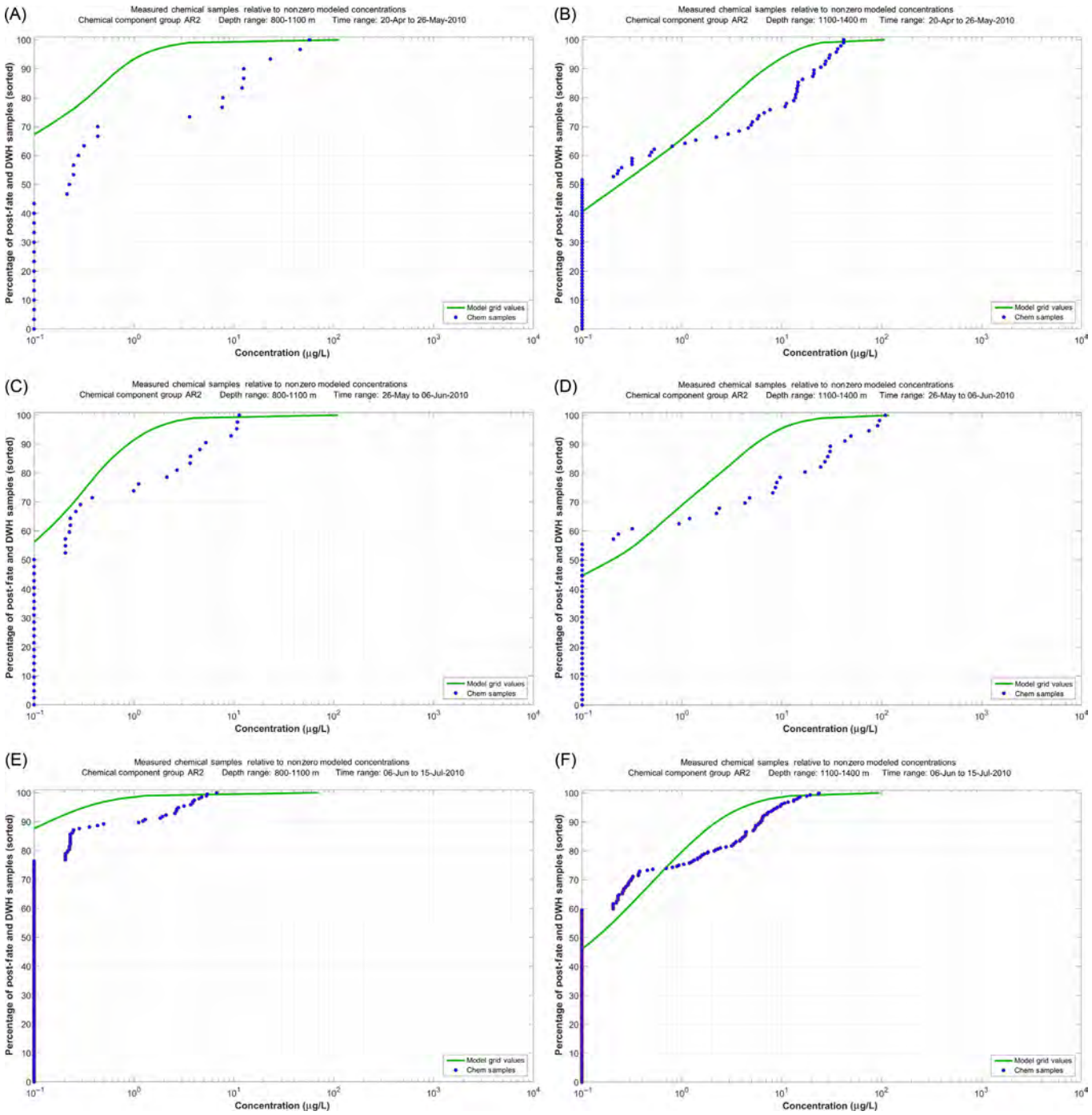

FIGURE 31.28 Comparison of total (in-droplet + dissolved) concentrations (μg/L) predicted by the model using ADCP data to measurements from chemistry samples of AR2 component (C3-benzenes): (A) OCR1, 800–1100 m; (B) OCR1, 1100–1400 m; (C) OCR2, 800–1100 m; (D) OCR2, 1100–1400 m; (E) OCR3, 800–1100 m; (F) OCR3, 1100–1400 m.

The modeled BTEX concentrations were also in agreement with published accounts of field observations, such as those by Reddy et al. (2012). Outside of a 1-km radius circle around the release location (where field samples could not be taken because of safety constraints), the maximum BTEX concentrations in the rising oil were predicted by the model to be 25–100 μg/L, in agreement with observations by Reddy et al. (2012) during June 19–28, 2010, which had a plume layer concentration as high as 78 μg/L. This is consistent with the NRDA cruise data (Horn et al., 2015a,b), in which, the precut (i.e., prior to June 3) plume layer median BTEX concentration value was 92 μg/L (range 4.5–228 μg/L) and the postcut plume layer median value 60 μg/L (range 4.9–176 μg/L).

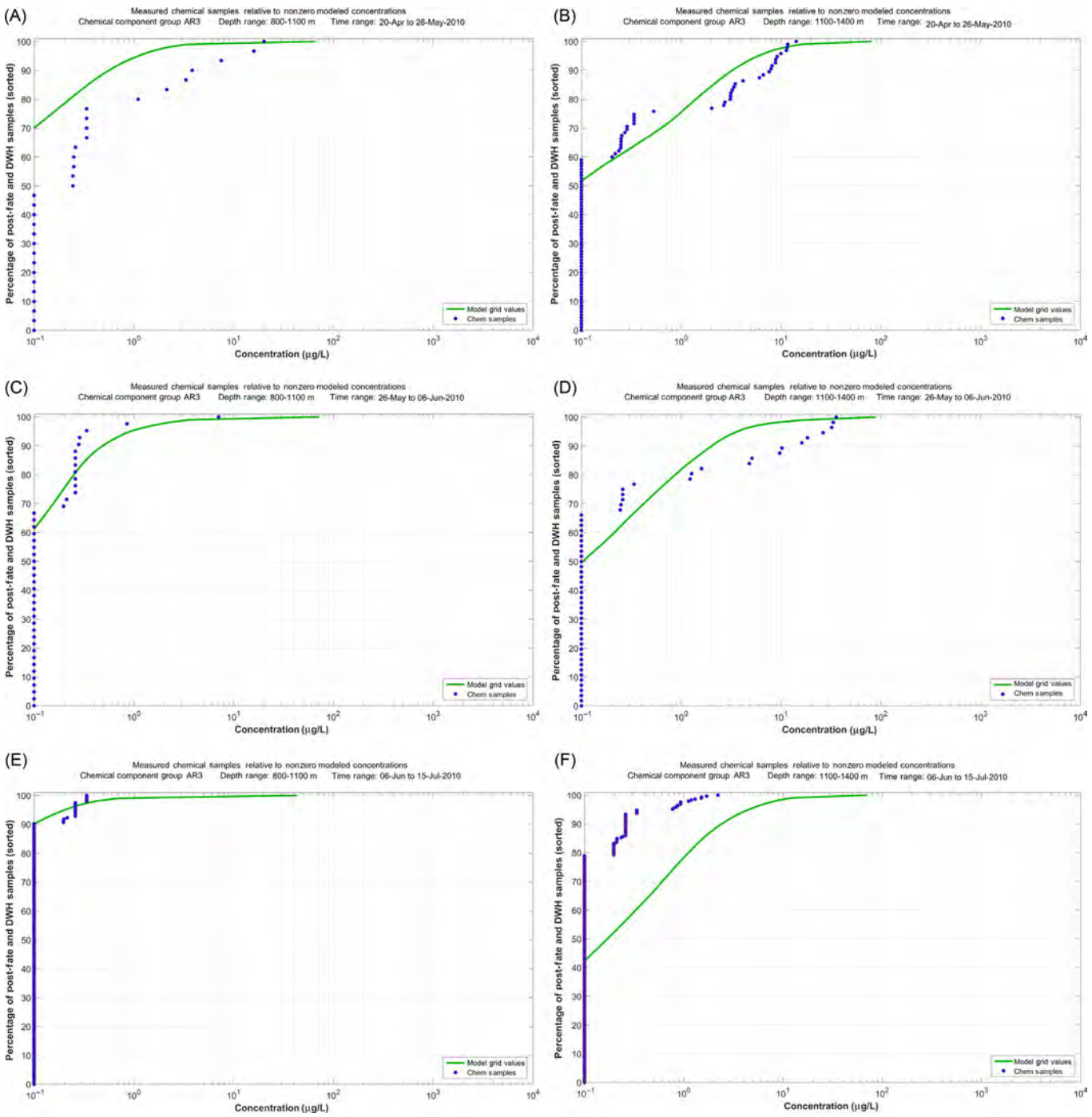

FIGURE 31.29 Comparison of total (in-droplet + dissolved) concentrations (µg/L) predicted by the model using ADCP data to measurements from chemistry samples of AR3 component (C4-benzenes): (A) OCR1, 800−1100 m; (B) OCR1, 1100−1400 m; (C) OCR2, 800−1100 m; (D) OCR2, 1100−1400 m; (E) OCR3, 800−1100 m; (F) OCR3, 1100−1400 m.

AR2 and AR3 are the pseudocomponents representing the substituted benzenes. The model and observed concentrations were similar in most time periods and depth zones (Figs. 31.27−31.29). During OCR1 (April 22−May 26), the model seemed to under-estimate the concentrations of substituted benzenes in the 800−1100-m depth zone, but after May 26, the model agreed well with the observed in this depth zone.

AR4 represents the decalins. Where sufficient numbers of measurements were available for meaningful comparisons, the model and observed concentrations were similar in most time periods and depth zones (Fig. 31.30).

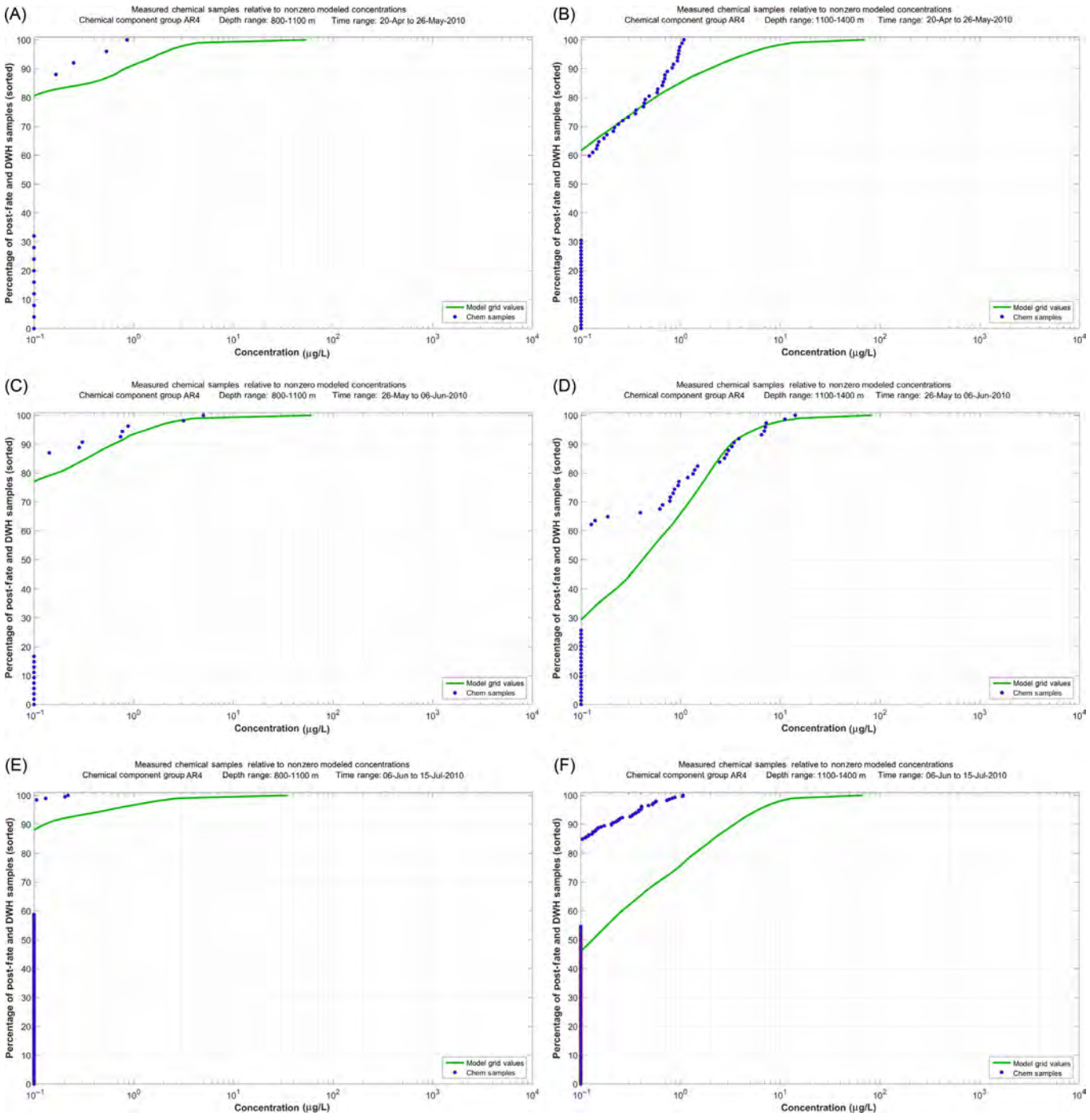

FIGURE 31.30 Comparison of total (in-droplet + dissolved) concentrations (μg/L) predicted by the model using ADCP data to measurements from chemistry samples of AR4 component (decalins): (A) OCR1, 800−1100 m; (B) OCR1, 1100−1400 m; (C) OCR2, 800−1100 m; (D) OCR2, 1100−1400 m; (E) OCR3, 800−1100 m; (F) OCR3, 1100−1400 m.

For the AR9 component (low molecular weight alkanes, isoalkanes, cycloalkanes), the modeled cumulative frequency distributions of concentrations are typically below the frequency distribution of the observations (Fig. 31.31). In and just above the deep plume, the maximum concentrations of the model are similar to the observed. This indicates that in the deep plume, the model predicted a broader volume contaminated at the highest concentrations than indicated by the measurements. The model may have overestimated the volume with these higher concentrations (perhaps due to underestimation of biodegradation rates for compounds included in

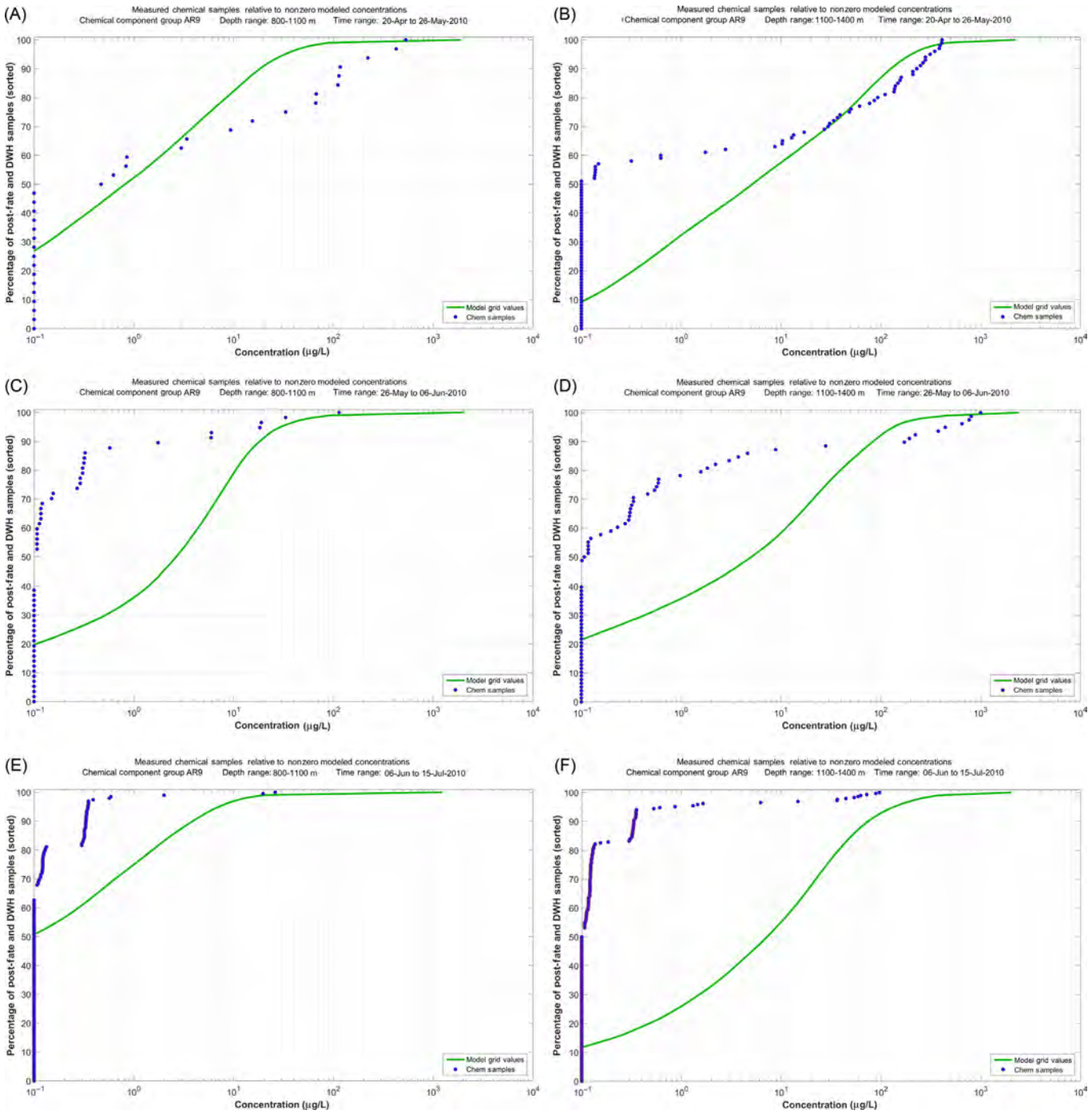

FIGURE 31.31 Comparison of total (in-droplet + dissolved) concentrations (μg/L) predicted by the model using ADCP data to measurements from chemistry samples of AR9 component (measured low molecular weight alkanes, isoalkanes, cycloalkanes): (A) OCR1, 800−1100 m; (B) OCR1, 1100−1400 m; (C) OCR2, 800−1100 m; (D) OCR2, 1100−1400 m; (E) OCR3, 800−1100 m; (F) OCR3, 1100−1400 m.

AR9) or the samples may not have been taken in areas were high concentrations occurred (which was the case for within 1 km of the wellhead and likely for sampling between 40 and 800 m). In addition, the measured percentage of the compounds included in AR9 was often well below 100% of the chemicals examined, which biases the chemistry results low as compared to the model results that include 100% of the chemical list. With the gaps in sampling and incomplete chemistry analyses, it is not possible to definitively determine which of these explanations are true.

It was clear that statistical analyses of the relationships between model predictions and measurements would be complex and dependent on the resolution of the model concentration grid cells; they are not attempted herein. However, in summary, the modeled concentrations of the various components are generally of the same order of magnitude as the measured concentrations. In order to be meaningful, comparisons need to be made on a component basis, as the components have different properties and behaviors (e.g., dissolution rates) that would cause their concentration distributions to vary. In many instances, the frequency distributions between the modeled concentrations and the measured samples compared well. However, in some cases, the model overestimated concentrations observed in the samples, whereas in others it underestimated the concentrations. The differences between observed and modeled concentrations were not large and there was no obvious bias, overall.

As the modeled TPAH concentrations were carried forward to the analysis of toxicity (Morris et al., 2015a,b) and injury (French McCay et al., 2015b), the comparisons of the PAH components AR5 through AR8 were of the most interest. The frequency distributions of the modeled and measured concentrations were more similar for PAH components than for some of the other components.

Uncertainties in these comparisons may result from the modeled transport or rate processes, field measurements of HC chemistry (e.g., GC/MS has constrained TPAH values only reflecting the target analytes amenable to analytical methods that can be measured, see Payne and Driskell, 2015b), or the input data used for modeling. In addition, the large gaps between sampling locations in both space and time contributed a considerable amount of uncertainty, which precludes any interpolation of the sample concentrations in this dynamic environment. Furthermore, the sampling efforts to depict HC distributions within the water column were complicated by the unavoidable heterogeneity in the water column and sampling logistics. Sampling was biased to sample within the concentration plumes below 800 m, but not all samples were taken with that objective (particularly, those taken above 800 m). For these reasons, sampling gaps in space and time can make conclusive interpretation of field observations quite difficult when attempting to assess the contaminant conditions on a larger scale. Furthermore, there is no evidence of either the presence or absence of oil in regions that were not sampled.

31.5 CONCLUSIONS

As the oil and gas was released from the DWH blowout near the seafloor, the jets and subsequently buoyant plumes of oil and gas mixture quickly rose through the water column, entraining ambient seawater and loosing buoyancy of the gas through dissolution until the plume reached neutral buoyancy due to the balance of densities from the increasing density of the plume and the decreasing density of ambient seawater (i.e., at the trap height; Spaulding et al., 2015). After being released from the trapped plume, oil was dispersed as oil droplets into the water column. The smaller droplets remained in the water column for an extended period of time due to their slow rise velocities (e.g., $<300\,\mu m$ weathered oil droplets would require >10 days to rise 1200 m), while larger droplets rose to the surface on the time scale of hours. The data and studies reviewed herein support the conceptual model that large droplets rose quickly in the immediate vicinity of the leaking wellhead, forming surface oil slicks in a relatively confined area near the wellhead (as described by Ryerson et al., 2012; Payne and Driskell, 2015d); intermediate sized droplets were transported further afield in the mid-water column as they were subject to dissolution weathering and continued to rise through the water column, surfacing tens of kilometers from the wellhead (consistent with observations by MacDonald et al., 2015); and small droplets ($<100\,\mu m$) remained suspended in the deep water column intrusion layer (as evidenced by the many observations of the deep plume).

Soluble and semisoluble HCs (primarily MAHs and PAHs, but also including low molecular weight alkanes) dissolved from oil droplets into the water column over time. The rates of dissolution of HCs from rising oil droplets are functions of the droplet sizes present (since it involves mass transfer across the surface area of the droplet); thus, the amount of HC mass dissolved increases with the oil mass, soluble HC content of the oil, and smaller droplet sizes (which are reduced by surfactant dispersants and mixing energy at the point of formation). Dissolution from small droplets is rapid and significantly enhanced by the application of dispersants (Payne and Driskell, 2015c). Thus, exposure of water column biota below 40 m to smaller droplets and dissolved components was much more wide spread than it was to the surfacing large droplets.

The modeled concentrations agreed well with field observations, based on comparisons with the NRDA chemistry results, data from multiple sensors that indicated the presence of oil, and reported information (e.g., water column HC concentrations and microbial activities) in the literature. Vertical distributions of dissolved and

TPAHs indicated the highest concentrations in the deep plume layer and up to about 800 m, with substantial concentrations throughout the water column. These model results compare favorably to fluorescence signals and DO sags indicating presence of oil HCs at these depths (JAG, 2010; Horn et al., 2015b; Payne and Driskell, 2015a,b) and literature reports of HC distributions in the water column (e.g., Diercks et al., 2010; Hazen et al., 2010; Camilli et al., 2010; Ryerson et al., 2012; Reddy et al., 2012; Spier et al., 2013). Model-predicted dissolved concentrations of BTEX and soluble alkanes were highest below 800 m, consistent with findings reported in the literature (e.g., Camilli et al., 2010; Reddy et al., 2012; Ryerson et al., 2012; Payne and Driskell, 2015a,b) in that the deep water plume layer was primarily composed of dissolved HCs, particularly BTEX and soluble alkanes.

The model successfully simulated the partitioning of PAHs between deep water and the surface. PAHs partially dissolved from droplets as they rose through the water column. Chemical measurements of floating oil and surface waters indicate that some of the PAHs remained in the larger oil droplets when they reached the surface; floating oil and surface water samples were observed to be enriched with 3- and 4-ring PAHs (Diercks et al., 2010; Spier et al., 2013; Stout, 2015c, Stout et al., 2016a; Payne and Driskell, 2015a,b). Diercks et al. (2010) noted that the PAHs in the deep plume were enriched in naphthalenes, as compared to surface samples where 3-ring PAHs were relatively enriched, a pattern consistent with water partitioning of more water soluble PAH compounds during transport to the surface. This pattern was consistent with model predictions.

Simulations using current data from eight hydrodynamic models as oil spill model input resulted in very different trajectories, and to varying degrees the hydrodynamic models generally over-estimated the speed of the currents in the area of the wellhead. Additional DWH oil trajectory simulations in the published literature (MacFadyen et al., 2011; Mariano et al., 2011; Weisberg et al., 2011; North et al., 2011, 2015; Paris et al., 2012; Dietrich et al., 2012; Boufadel et al., 2014; Testa et al., 2016; Lindo-Atichati et al., 2016) show highly variable paths and concentrations as well. However, the simulation using currents generated by the HYCOM-FSU hydrodynamics model resulted in a trajectory most similar to that predicted by the ADCP measurement-based current field below 40 m in the area of the wellhead.

As sampling during April–July 2010 was primarily performed within 20 km of the wellhead, and measured currents over the depth of water affected were available from three stations within 10 km of the wellhead, model predictions using measured currents were compared to field-collected data from within a 25-km-by-25-km box centered on the wellhead. Concentrations of soluble and semisoluble HC components predicted by the model agreed well with chemical measurements from samples both in magnitude and when compared as frequency distributions within depth zones of the water column, particularly in the deep-plume regions of 1200–1400 and 1000–1200 m. Agreements between observed and modeled in shallower waters were more variable, in part because modeled concentrations in the "plumes" were compared to untargeted samples at the shallower depth. The results showed that the soluble HCs primarily dissolved near the release depth in the intrusion layer, while semisoluble compounds were only partially dissolved at depth and as droplets rose, in agreement with observations. Based on model predictions, consistent with observations, most of the soluble and semisoluble compounds that dissolved at depth had biodegraded by fall of 2010.

By using a probability distribution approach for examining the HC carbon components in the water column, rather than point-to-point comparison of the predicted results with the measurements, a robust comparison of the model prediction and field observation data was made possible to account for the inevitable uncertainty in the transport by currents and the relatively sparse spatial and temporal sampling. The results verified that the processes included in the oil fate model and its predicted concentrations in the water column are reliable. The oil fate modeling described herein provides a holistic forensic analysis of the fate of the oil released during the DWH spill in the deep-sea environment.

Acknowledgments

Funding of this research was provided in part by the National Oceanic and Atmospheric Administration Damage Assessment, Remediation and Restoration Program (NOAA Contract No. AB133C-11-CQ-0050), and in part by the USDOI, BOEM, Environmental Studies Program, Washington, DC (BOEM Contract Number M11PC00028). Some of the information developed was used in the development of the Draft Programmatic Damage Assessment and Restoration Plan/Draft Programmatic Environmental Impact Statement (pDARP, DWH Trustees, 2015) for the DWH spill. The opinions expressed by the authors are their own and do not necessarily reflect the opinion or policy of the US Government. Any use of trade, firm, or product names is for descriptive purposes only and does not imply endorsement by the US Government. The authors are grateful to J. R. Payne of Payne Environmental Consulting Inc. (PECI) for his insightful and helpful comments on drafts of this work.

References

Antonov, J.I., Seidov, D., Boyer, T.P., Locarnini, R.A., Mishonov, A.V., Garcia, H.E., et al., 2010. World ocean atlas 2009, Volume 2: salinity. In: Levitus, S., (Ed.) NOAA Atlas NESDIS 69. US Government Printing Office, Washington, DC, 184p.

ASTM International, 2006. Standard guide for visually estimating oil spill thickness on water. In: ASTM International (Ed.), ASTM Committee F20 on Hazardous Substances and Oil Spill Response. ASTM International, West Conshohocken, PA, p. 4.

Boufadel, M., Abdollahi-Nasab, A., Geng, X., Galt, J., Torlapati, J., 2014. Simulation of the landfall of the *Deepwater Horizon* oil on the shorelines of the Gulf of Mexico. Environ. Sci. Technol. 48 (16), 9496–9505.

Boyer, T., Levitus, S., Garcia, H., Locarnini, R.A., Stephens, C., Antonov, J., 2005. Objective analyses of annual, seasonal, and monthly temperature and salinity for the world ocean on a 0.25 degree grid. Int. J. Climatol. 25, 931–945.

Boyer, T.P., Antonov, J.I., Baranova, O.K., Garcia, H.E., Johnson, D.R., Locarnini, R.A., et al., 2009. In: Levitus, S. (Ed.), World ocean database 2009. NOAA Atlas NESDIS 66. US Government Printing Office, Washington, DC, p. 216.

Brakstad, O.G., Faksness, L.G., 2000. Biodegradation of water-accomodated fractions and dispersed oil in the seawater column. Society of Petroleum Engineers (SPE) International Conference on Health, Safety and Environment in Oil and Gas Exploration and Production. International Society of Petroleum Engineers, Staganger, Norway.

Brakstad, O.G., Bonaunet, K., Nordtug, T., Johansen, O., 2004. Biotransformation and dissolution of petroleum hydrocarbons in natural flowing seawater at low temperature. Biodegradation 15, 337–346.

Brakstad, O.G., Nordtug, T., Throne-Holst, M., 2015. Biodegradation of dispersed Macondo oil in seawater at low temperature and different oil droplet sizes. Mar. Poll. Bull. 93, 144–152.

Brandvik, P.J., Johansen, Ø., Leirvik, F., Farooq, U., Daling, P.S., 2013. Droplet breakup in subsurface oil releases—Part 1: experimental study of droplet breakup and effectiveness of dispersant injection. Mar. Poll. Bull. 73, 319–326.

Camilli, R., Reddy, C.M., Yoerger, D.R., Van Mooy, B.A.S., Jakuba, M.V., Kinsey, J.C., et al., 2010. Tracking hydrocarbon plume transport and biodegradation at *Deepwater Horizon*. Science 330, 201–204.

Campo, P., Venosa, A.D., Suidan, M.T., 2013. Biodegradability of Corexit 9500 and dispersed South Louisiana crude oil at 5 and 25°C. Environ. Sci. Technol. 47 (4), 1960–1967.

Chan, G., Chow, A., Adams, E.E., 2015. Effects of droplet size on intrusion of sub-surface oil spills. Environ. Fluid Mech. 15 (5), 959–973.

Chao, Y., He, R., Farrara, J., Zhang, C., June 2014. ROMS hydrodynamic modeling. Report to NOAA OR&R NRDA Program, 64p.

Chassignet, E.P., Hurlburt, H.E., Metzger, E.J., Smedstad, O.M., Cummings, J.A., Halliwell, G.R., et al., 2009. US GODAE: global ocean prediction with the HYbrid Coordinate Ocean Model (HYCOM). Oceanography 22 (2), 64–75. Available from: http://dx.doi.org/10.5670/oceanog.2009.39.

Chassignet, E.P., Hurlbut, H.E., Smedstad, O.M., Halliwell, G.R., Hogan, P.J., Wallcraft, A.J., Baraille, R., Bleck, R., 2007. The HYCOM (HYbrid Coordinate Ocean Model) data assimilative system. J. Marine Syst. 65 (1–4), 60–83.

Chassignet, E.P., Srinivasan, A., 2015. Data assimilative hindcast for the Gulf of Mexico. US Dept. of the Interior, Bureau of Ocean Energy Management, OCS Study BOEM 2015-035, 40 pp.

Crowley, D., Mendelsohn, D., Whittier Mulanaphy, N., Li, Z., Spaulding, M.S., 2014. Modeling subsurface dispersant applications for response planning and preparation. Proceedings of the 2014 International Oil Spill Conference. American Petroleum Institute, Washington, DC, pp. 933–948.

Csanady, G.T., 1973. Turbulent Diffusion in the Environment. D. Reidel Publishing Company, Dordrecht, Holland.

Cummings, J.A., 2005. Operational multivariate ocean data assimilation. Q. J. R. Met. Soc., C 131 (613), 3583–3604.

Cummings, J.A., Smedstad, O.M., 2013. Variational data assimilation for the global ocean. In: Data Assimilation for Atmospheric, Oceanic and Hydrologic Applications, Vol II, Chapter 13, pp. 303–343.

Daling, P.S., Leirvik, F., Almås, I.K., Brandvik, P.J., Hansen, B.H., Lewis, A., et al., 2014. Surface weathering and dispersibility of MC252 crude oil. Mar. Poll. Bull. 87 (1–2), 300–310.

Davis, C.S., Loomis, N.C., 2014. Deepwater Horizon Oil Spill (DWHOS) Water Column Technical Working Group Image Data Processing Plan: Holocam, Description of Data Processing Methods Used to Determine Oil Droplet Size Distributions from In Situ Holographic Imaging during June 2010 on Cruise M/V Jack Fitz 3. Woods Hole Oceanographic Institution, MIT/WHOI Joint Program in Oceanography, 15 p. + Appendix. DWH-AR0047462.pdf. <https://www.doi.gov/deepwaterhorizon/adminrecord>.

Deepwater Horizon Natural Resource Damage Assessment Trustee Council (DWH Trustees), 2016. The Deepwater Horizon Oil Spill Final Programmatic Damage Assessment and Restoration Plan and Final Programmatic Environmental Impact Statement. National Oceanic and Atmospheric Administration, Office of Response and Restoration. <http://www.gulfspillrestoration.noaa.gov/restoration-planning/gulf-plan/>.

Diercks, A.R., Highsmith, R.C., Asper, V.L., Joung, D., Zhou, Z., Guo, L., et al., 2010. Characterization of subsurface polycyclic aromatic hydrocarbons at the *Deepwater Horizon* site. Geophys. Res. Lett. 37, L20602, 1–6.

Dietrich, J.C., Trahan, C.J., Howard, M.T., Fleming, J.G., Weaver, R.J., Tanaka, S., et al., 2012. Surface trajectories of oil transport along the Northern Coastline of the Gulf of Mexico. Cont. Shelf Res. 41, 17–47.

Di Toro, D.M., McGrath, J.A., Hansen, D.J., 2000. Technical basis for narcotic chemicals and polycyclic aromatic hydrocarbon criteria. I. Water and tissue. Environ. Sci. Technol. 19 (8), 1951–1970.

D'Sa, E.J., Ko, D.S., 2008. Short-term influences on suspended particulate matter distribution in the northern Gulf of Mexico: satellite and model observations. Sensors 8, 4249–4261.

D'Sa, E.J., Miller, R.L., McKee, B.A., 2007. Suspended particulate matter dynamics in coastal waters from ocean color: application to the northern Gulf of Mexico. Geophys. Res. Lett. 34, 6.

Forth, H.P., Morris, J.M., Cacela, D., August 2015. Explanation of analytes included in the total polycyclic aromatic hydrocarbon sums used by the Deepwater Horizon Natural Resource Damage Assessment Toxicity Group. DWH NRDA Toxicity Technical Working Group Report. Prepared for National Oceanic and Atmospheric Administration by Abt Associates, Boulder, CO.

French, D., Reed, M., Jayko, K., Feng, S., Rines, H., Pavignano, S., et al., April 1996. Final Report, The CERCLA Type A Natural Resource Damage Assessment Model for Coastal and Marine Environments (NRDAM/CME), Technical Documentation, Vol. I–V. Office of Environmental Policy and Compliance, US Department of the Interior, Washington, DC, Contract No. 14-0001-91-C-11.

French, D.P., Rines, H., 1997. Validation and use of spill impact modeling for impact assessment. Proceedings of the 1997 International Oil Spill Conference. American Petroleum Institute, Washington, DC, pp. 829–834, API Publ. 4651.

French, D.P., Rines, H., Masciangioli, P., 1997. Validation of an orimulsion spill fates model using observations from field test spills. Proceedings of the Twentieth Arctic and Marine Oil Spill Program (AMOP) Technical Seminar on Environmental Contamination and Response. Environment Canada, Ottawa, ON, pp. 933–961.

French McCay, D., Jayko, K., Li, Z., Horn, M., Kim, Y., Isaji, T., et al., September 2015a. Technical reports for Deepwater Horizon water column injury assessment—WC_TR.14: modeling oil fate and exposure concentrations in the deepwater plume and rising oil resulting from the Deepwater Horizon oil spill. DWH NRDA Water Column Technical Working Group Report. Prepared for National Oceanic and Atmospheric Administration (NOAA) by RPS ASA, South Kingstown, RI, USA. Administrative Record no. DWH-AR0285776. <https://www.doi.gov/deepwaterhorizon/adminrecord>.

French McCay, D., Rowe, J., Balouskus, R., Morandi, A., McManus, M.C., September 2015b. Technical reports for Deepwater Horizon water column injury assessment—WC_TR.28: injury quantification for planktonic fish and invertebrates in estuarine, shelf and offshore waters. DWH NRDA Water Column Technical Working Group Report. Prepared for National Oceanic and Atmospheric Administration (NOAA) by RPS ASA, South Kingstown, RI. Administrative Record no. DWH-AR0172019.pdf. <https://www.doi.gov/deepwaterhorizon/adminrecord>.

French McCay, D.P., Li, Z., Horn, M., Crowley, D., Spaulding, M., Mendelsohn, D., Turner, C., 2016. Modeling oil fate and subsurface exposure concentrations from the deepwater horizon oil spill, Proceedings of the 39th AMOP Technical Seminar on Environmental Contamination and Response, vol. 39. Environment Canada, pp. 115–150.

French McCay, D., Jayko, K., Li, Z., Horn, M., Isaji, T., Spaulding, M., 2017a. Simulation Modeling of Ocean Circulation and Oil Spills in the Gulf of Mexico—Appendix II. Oil Transport and Fates Model Technical Manual. Prepared for the US Department of the Interior, Bureau of Ocean Energy Management, Gulf of Mexico OCS Region by RPS ASA, New Orleans, LA. OCS Study BOEM 2017-xxx, xxx p (in press).

French McCay, D., Horn, M., Li, Z., Crowley, D., Spaulding, M., Mendelsohn, D., et al., Simulation Modeling of Ocean Circulation and Oil Spills in the Gulf of Mexico: Appendix VI. Data Collection, Analysis and Model Validation. Prepared for the US Department of the Interior, Bureau of Ocean Energy Management, Gulf of Mexico OCS Region by RPS ASA, New Orleans, LA. OCS Study BOEM 2017-xxx; 2017b; xxx p (in press).

French McCay, D.P., 2002. Development and application of an oil toxicity and exposure model, OilToxEx. Environ. Toxicol. Chem. 21, 2080–2094.

French McCay, D.P., 2003. Development and application of damage assessment modeling: example assessment for the *North Cape* oil spill. Mar. Poll. Bull. 47 (9–12), 341–359.

French McCay, D.P., 2004. Oil spill impact modeling: development and validation. Environ. Tox. Chem. 23 (10), 2441–2456.

French McCay, D.P., Rowe, J.J., 2004. Evaluation of bird impacts in historical oil spill cases using the SIMAP oil spill model. Proceedings of the 27th Arctic and Marine Oil Spill Program (AMOP) Technical Seminar. Emergencies Science Division, Environment Canada, Ottawa, ON, pp. 421–452.

French McCay, D., Whittier, N., Sankaranarayanan, S., Jennings, J., Etkin, D.S., 2004. Estimation of potential impacts and natural resource damages of oil. J. Hazard. Mater. 107 (1–2), 11–25.

Galagan, C.W., McStay, L., Rowe, J., Chaite, E., Crowley, D., French McCay, D., et al., 2017. Synthesis report—simulation modeling of ocean circulation and oil spills in the Gulf of Mexico. Prepared by RPS ASA for the US Department of the Interior, Bureau of Ocean Energy Management, Gulf of Mexico OCS Region, New Orleans, LA. OCS Study BOEM 2017-xxx, xxx p (in press).

Garcia-Pineda, O., MacDonald, I., Hu, C., Svejkovsky, J., Hess, M., Dukhovskoy, D., et al., 2013a. Detection of floating oil anomalies from the *Deepwater Horizon* oil spill with Synthetic Aperture Radar. Oceanography 26 (2), 124–137. Available from: http://dx.doi.org/10.5670/oceanog.2013.38.

Garcia-Pineda, O., MacDonald, I.R., Li, X., Jackson, C.R., Pichel, W.G., 2013b. Oil spill mapping and measurement in the Gulf of Mexico with Textural Classifier Neural Network Algorithm (TCNNA). IEEE J. Select. Top. Appl. Earth Observ. Remote Sens. 6 (6), 2517–2525.

Halliwell Jr., G.R., Srinivasan, A., Kourafalou, V., Yang, H., Willey, D., Le Henaff, M., Atlas, R., 2014. Rigorous evaluation of a fraternal twin ocean OSSE system in the open Gulf of Mexico. J. Atmos. Ocean. Technol. Available from: http://dx.doi.org/10.1175/JTECH-D-13-00011.

Hazen, T.C., Dubinsky, E.A., Desantis, T.Z., Andersen, G.L., Piceno, Y.M., Singh, N., et al., 2010. Deep-sea oil plume enriches indigenous oil-degrading bacteria. Science 330, 204–208.

Horn, M., Grennan, M., Decker, L., Zamorski, S., French McCay, D., Li, Z., August 2015a. Technical Reports for Deepwater Horizon Water Column Injury Assessment—Volume I. Water Column Chemistry Data from the Deepwater Horizon Blowout. RPS ASA, South Kingstown, RI. DWH-AR0023907.pdf. <https://www.doi.gov/deepwaterhorizon/adminrecord>.

Horn, M., French McCay, D., Payne, J., Driskell, W., Li, Z., Grennan, M., et al., August 2015b. Technical Reports for Deepwater Horizon Water Column Injury Assessment—Volume III. Water Column Chemical and Physical Data from the Deep Water Horizon Blowout. RPS ASA, South Kingstown, RI, USA. DWH-AR0024617.pdf. <https://www.doi.gov/deepwaterhorizon/adminrecord>.

Howard, P., Meylan, W., Aronson, D., Stiteler, W., Tunkel, J., Comber, M., et al., 2005. A new biodegradation prediction model specific to petroleum hydrocarbons. Environ. Tox. Chem 24 (8), 1847–1860.

Hyun, K.H., He, R., 2010. Coastal upwelling in the South Atlantic Bight: A revisit of the 2003 cold event using long term observations and model hindcast solutions. J. Mar. Syst. 83 (1–2), 1–13.

Joint Analysis Group (JAG), 2010. Review of R/V Brooks McCall Data to Examine Subsurface Oil. <http://www.ncddc.noaa.gov/activities/healthy-oceans/jag/reports/>.

Jones, R.K., 1997. A simplified pseudo-component of oil evaporation model. Proceedings of the 20th Arctic and Marine Oil Spill Program (AMOP) Technical Seminar. Environment Canada, pp. 43–61.

Kessler, J.D., Valentine, D.L., Redmond, M.C., Du, M., Chan, E.W., Mendes, S.D., et al., 2011. A persistent oxygen anomaly reveals the fate of spilled methane in the deep Gulf of Mexico. Science 331, 312–315.

Lee, Z., Huang, C., Lubac, B., Guo, L., Ko, D., Lohrenz, S., et al., 2012. Characterization of Suspended Particulates in the Northern Gulf of Mexico from Ocean Color Remote Sensing, Report Number NRL/PP/7320-10-0512. Naval Research Laboratory.

Lehr, B., Bristol, S., Possolo, A., 2010. (Oil Budget Calculator, OBC). Deepwater Horizon Oil Budget Calculator: A Report to the National Incident Command. The Federal Interagency Solutions Group, Oil Budget Calculator Science and Engineering Team. <http://www.restorethegulf.gov/sites/default/files/documents/pdf/OilBudgetCalc_Full_HQ-Print_111110.pdf> (accessed 1.04.12).

Li, Z., French McCay, D., 2017. Simulation Modeling of Ocean Circulation and Oil Spills in the Gulf of Mexico—Annex C to Appendix II. Oil Transport and Fates Model Technical Manual: Review of Biodegradation Rates of Crude Oil and Hydrocarbons in Seawater. Prepared by RPS ASA for the US Department of the Interior, Bureau of Ocean Energy Management, Gulf of Mexico OCS Region, New Orleans, LA, OCS Study BOEM 2017-xxx, xxx p (in press).

Li, Z., Chao, Y., McWilliams, J.C., Ide, K., 2008a. A three-dimensional variational data assimilation scheme for the Regional Ocean Modeling System. J. Atmos. Oceanic Technol. 25 (11), 2074–2090.

Li, Z., Chao, Y., McWilliams, J.C., Ide, K., 2008b. A three-dimensional variational data assimilation scheme for the Regional Ocean Modeling System: implementation and basic experiments. J. Geophys. Res., C: Oceans 113 (5), C05002. Available from: http://dx.doi.org/10.1029/2006JC004042.

Li, Z., Bird, A., Payne, J.R., Vinhateiro, N., Kim, Y., Davis, C., et al., August 2015. Technical Reports for Deepwater Horizon Water Column Injury Assessment—Volume IV. Oil Particle Data from the Deepwater Horizon Oil Spill. RPS ASA, South Kingstown, RI. DWH-AR0024715.pdf <https://www.doi.gov/deepwaterhorizon/adminrecord>.

Li, Z., Spaulding, M., French McCay, D., Crowley, D., Payne, J.R., 2017. Development of a unified oil droplet size distribution model with application to surface breaking waves and subsea blowout releases considering dispersant effects. Mar. Poll. Bull. 114 (1), 247–257.

Lindo-Atichati, D., Paris, C.B., Le Hénaff, M., Schedler, M., Valladares Juárez, A.G., Müller, R., 2016. Simulating the effects of droplet size, high-pressure biodegradation, and variable flow rate on the subsea evolution of deep plumes from the Macondo blowout. Deep-Sea Res. Part II, Top. Stud. Oceanogr. 129, 301–310.

Locarnini, R.A., Mishonov, A.V., Antonov, J.I., Boyer, T.P., Garcia, H.E., Baranova, O.K., et al., 2010. In: Levitus, S. (Ed.), World Ocean Atlas 2009, Volume 1: Temperature. NOAA Atlas NESDIS 68, US Government Printing Office, Washington, DC, 184 p.

MacDonald, I.R., Garcia-Pineda, O., Beet, A., Daneshgar Asl, S., Feng, L., Graettinger, G., et al., 2015. Natural and unnatural oil slicks in the Gulf of Mexico. J. Geophys. Res. Oceans 120. Available from: http://dx.doi.org/10.1002/2015JC011062.

MacFadyen, A., Watabayashi, G.Y., Barker, C.H., Beegle-Krause, C.J., 2011. Tactical modeling of surface oil transport during the deepwater horizon spill response. Monitoring and modeling the Deepwater Horizon oil spill: a record-breaking enterprise. Am. Geophys. Union, Geophys. Monogr. Ser. 195, 167–177. Available from: http://dx.doi.org/10.1029/2011GM001128.

Mackay, D., Shiu, W.Y., Ma, K.-C., Lee, S.C., 2006a. Handbook of Physical–Chemical Properties and Environmental Fate for Organic Chemicals. Vol. I, Introduction and Hydrocarbons. CRC Press, Taylor & Francis Group, Boca Raton, FL.

Mackay, D., Shiu, W.Y., Ma, K.-C., Lee, S.C., 2006b. Handbook of Physical–Chemical Properties and Environmental Fate for Organic Chemicals. Vol. IV, Nitrogen and Sulfur Containing Compounds and Pesticides. CRC Press, Taylor & Francis Group, Boca Raton, FL.

Mackay, D., Leinonen, P.J., 1977. Mathematical model of the behavior of oil spills on water with natural and chemical dispersion. Prepared for Fisheries and Environment Canada, Economic and Technical Review Report EPS-3-EC-77-19, 39 pp.

Mariano, A.J., Kourafalou, V.H., Srinivasan, A., Kang, H., Halliwell, G.R., Ryan, E.H., et al., 2011. On the modeling of the 2010 Gulf of Mexico oil spill. Dyn. Atmos. Oceans 52, 322–340.

McNutt, M., Camilli, R., Guthrie, G., et al., March, 2011. Assessment of Flow Rate Estimates for the Deepwater Horizon/Macondo Well Oil Spill. Flow Rate Technical Group Report to the National Incident Command, Interagency Solutions Group.

Morris, J.M., Krasnec, M.O., Carney, M., Forth, H.P., Lay, C.R., Lipton, I., et al., 2015a. Deepwater Horizon oil spill Natural Resource Damage Assessment comprehensive toxicity testing program: overview, methods, and results, DWH Toxicity NRDA Technical Working Group Report (TOX_TR.13). Prepared for National Oceanic and Atmospheric Administration by Abt Associates, Boulder, CO. <https://www.doi.gov/deepwaterhorizon/adminrecord>.

Morris, J.M., Lay, C.R., Forth, H.P., Cacela, D., Lipton, J., 2015b. Use of bioassay data in field exposure and toxicity modeling. DWH NRDA Toxicity Technical Working Group Report. Prepared for National Oceanic and Atmospheric Administration by Abt Associates, Boulder, CO. <https://www.doi.gov/deepwaterhorizon/adminrecord>.

Mulcahy, R., May, 2010. Water Column Injury Ephemeral Data Collection: ADCP Monitoring Plan (M/V Bunny Bordelon). Originated as a Requirement by D. French McCay, Y. Kim, and Laurie Sullivan, 2010. Deepwater Horizon NRDA <Administrative Record> Pre-assessment—Water Column. <http://www.doi.gov/deepwaterhorizon/adminrecord/Pre-assessment-Water-Column.cfm>.

North, E.W., Adams, E.E., Schlag, Z., Sherwood, C.R., He, R., Hyun, K.H., et al., 2011. Simulating oil droplet dispersal from the *Deepwater Horizon* spill with a Lagrangian approach. Monitoring and Modeling the Deepwater Horizon Oil Spill: A Record-Breaking Enterprise. American Geophysical Union, pp. 217–226, 195, Ch. 16, pp.

North, E.W., Adams, E.E., Thessen, A.E., Schlag, Z., He, R., Socolofsky, S.A., et al., 2015. The influence of droplet size and biodegradation on the transport of subsurface oil droplets during the *Deepwater Horizon* spill: a model sensitivity study. Environ. Res. Lett. 10 (2), 024016.

NRC, 2005. Understanding Oil Spill Dispersants: Efficacy and Effects. National Research Council, National Academies Press, Washington, DC, 400 p.

Okubo, A., 1971. Oceanic diffusion diagrams. J. Deep-Sea Res. 8, 789–802.

Okubo, A., Ozmidov, R.V., 1970. Empirical dependence of the coefficient of horizontal turbulent diffusion in the ocean on the scale of the phenomenon in question. Atmos. Ocean Phys. 6 (5), 534–536.

Paris, C.B., Hénaff, M.L., Aman, Z.M., Subramaniam, A., Helgers, J., Wang, D.-P., et al., 2012. Evolution of the Macondo well blowout: simulating the effects of the circulation and synthetic dispersants on the subsea oil transport. Environ. Sci. Technol. 46 (24), 13293–13302.

Passow, U., 2016. Formation of rapidly-sinking, oil-associated marine snow. Deep-Sea Research Part II: Top. Stud. Oceanogr. 129, 232–240.

Passow, U., Ziervogel, K., Asper, V., Diercks, A., 2012. Marine snow formation in the aftermath of the *Deepwater Horizon* oil spill in the Gulf of Mexico. Environ. Res. Lett. 7.

Payne, J.R., Driskell, W.B., 2015a., 2010 DWH offshore water column samples—forensic assessments and oil exposures. PECI Technical Report to the Trustees in Support of the pDARP. DWH-AR0039118.pdf. <https://www.doi.gov/deepwaterhorizon/adminrecord>.

Payne, J.R., Driskell, W.B., 2015b. Forensic fingerprinting methods and classification of DWH offshore water samples. PECI Technical Report to the Trustees in support of the pDARP, DWH-AR0039170.pdf. <https://www.doi.gov/deepwaterhorizon/adminrecord>.

Payne, J.R., Driskell, W.B., 2015c. Dispersant effects on waterborne oil profiles and behavior. PECI Technical Report to the Trustees in support of the pDARP. DWH-AR0039201.pdf, <https://www.doi.gov/deepwaterhorizon/adminrecord>.

Payne, J.R., Driskell, W.B., 2015d. Offshore adaptive sampling strategies. PECI Technical Report to the Trustees in support of the pDARP. DWH-AR0023786.pdf, <https://www.doi.gov/deepwaterhorizon/adminrecord>.

Payne, J.R., Kirstein, B.E., McNabb, Jr., G.D., Lambach, J.L., Redding, R. Jordan, R.E., et al., February, 1984. Multivariate analysis of petroleum weathering in the marine environment—sub Arctic. Environmental Assessment of the Alaskan Continental Shelf, OCEAP, Final Report of Principal Investigators, Vols. 21 and 22, 690p.

Payne, J.R., Kirstein, B.E., Clayton, Jr., J.R., Clary, C., Redding, R., McNabb, Jr., G.D., et al., 1987. Integration of suspended particulate matter and oil transportation study. Final Report. Minerals Management Service, Environmental Studies Branch, Anchorage, AK. Contract No. 14-12-0001-30146, 216p.

Prince, R.C., Walters, C.C., 2007. Biodegradation of oil hydrocarbons and its implications for source identification. In: Wang, Z., Stout, S.A. (Eds.), Oil Spill Environmental Forensics. Elsevier, Burlington, MA, pp. 349–379.

Prince, R.C., Parkerton, T.F., Lee, C., 2007. The primary aerobic biodegradation of gasoline hydrocarbons. Environ. Sci. Technol. 41 (9), 3316–3321.

Prince, R.C., Haitmanek, C., Lee, C.C., 2008. The primary aerobic biodegradation of biodiesel B20. Chemosphere 71 (8), 1446–1451.

Prince, R.C., McFarlin, K.M., Butler, J.D., Febbo, E.J., Wang, F.C., Nedwed, T.J., 2013. The primary biodegradation of dispersed crude oil in the sea. Chemosphere 90 (2), 521–526.

Reddy, C.M., Arey, J.S., Seewald, J.S., Sylva, S.P., Lemkau, K.L., Nelson, R.K., et al., 2012. Composition and fate of gas and oil released to the water column during the *Deepwater Horizon* oil spill. Proc. Nat. Acad. Sci. 109 (5), 20229–20234.

Ryerson, T.B., Camilli, R., Kessler, J.D., Kujawinski, E.B., Reddy, C.M., Valentine, D.L., et al., 2012. Chemical data quantify *Deepwater Horizon* hydrocarbon flow rate and environmental distribution. Proc. Nat. Acad. Sci. 109 (50), 20246–20253.

Saha, S., et al., 2010. NCEP Climate Forecast System Reanalysis (CFSR) 6-hourly Products, January 1979 to December 2010. Research Data Archive at the National Center for Atmospheric Research, Computational and Information Systems Laboratory. <http://dx.doi.org/10.5065/D69K487J>.

Salisbury, J.E., Campbell, J.W., Linder, E., Meeker, L.D., Muller-Karger, F.E., Vorosmarty, C.J., 2004. On the seasonal correlation of surface particle fields with wind stress and Mississippi discharge in the northern Gulf of Mexico. Deep-Sea Res. II 51, 1187–1203.

Schmitz Jr., W.J., Biggs, D.C., Lugo-Fernandez, A., Oey, L.-Y., Sturges, W., 2005. A synopsis of the circulation in the Gulf of Mexico and on its continental margins. In: Sturges, W., Lugo-Fernandez, A. (Eds.), Circulation in the Gulf of Mexico: Observations and Models. American Geophysical Union, Washington, DC, pp. 11–29.

Socolofsky, S.A., Jirka, G.H., 2005. Environmental Fluid Mechanics. Part I: Mass Transfer and Diffusion. Engineering—Lectures. Texas A&M University, College Station, TX, 184 p.

Socolofsky, S.A., Adams, E.E., Sherwood, C.R., 2011. Formation dynamics of subsurface hydrocarbon intrusions following the *Deepwater Horizon* blowout. Geophys. Res. Lett. 38 (9), L09602.

Spaulding, M.L., Bishnoi, P.R., Anderson, E., Isaji, T., 2000. An integrated model for prediction of oil transport from a deep water blowout. Proceedings of the 23rd Arctic and Marine Oil Spill Program (AMOP) Technical Seminar on Environmental Contamination and Response. Environment Canada, Ottawa, ON, pp. 611–636.

Spaulding, M.S., Mendelsohn, D., Crowley, D., Li, Z., Bird, A. 2015. Technical Reports for Deepwater Horizon Water Column Injury Assessment—WC_TR.13: Application of OILMAP DEEP to the Deepwater Horizon Blowout. RPS ASA, 55 Village Square Drive, South Kingstown, RI. Administrative Record no. DWH-AR0285366.pdf. <https://www.doi.gov/deepwaterhorizon/adminrecord>.

Spier, C., Stringfellow, W.T., Hazen, T.C., Conrad, M., 2013. Distribution of hydrocarbons released during the 2010 MC252 oil spill in deep offshore waters. Environ. Pollut. 173, 224–230.

Stout, S., Rouhani, S., Liu, B., Oehrig, J., 2015. Spatial extent ("footprint") and volume of Macondo oil found on the deep-sea floor following the Deepwater Horizion Oil Spill. Newfields Technical Report to the Trustees in Support of the pDARP. <https://www.doi.gov/deepwaterhorizon/adminrecord>.

Stout, S.A., 2015a. Physical and chemical properties of the fresh MC252 Macondo-1 well crude oil. NewFields Technical Report to the Trustees in Support of the pDARP. <https://www.doi.gov/deepwaterhorizon/adminrecord>.

Stout, S.A., 2015b. Bulk chemical and physical properties of fresh and weathered Macondo crude oil. NewFields Technical Report to the Trustees in Support of the pDARP. <https://www.doi.gov/deepwaterhorizon/adminrecord>.

Stout, S.A., 2015c. Range in composition and weathering among floating Macondo oils during the Deepwater Horizon oil spill. NewFields Technical Report to the Trustees in Support of the pDARP. <https://www.doi.gov/deepwaterhorizon/adminrecord>.

Stout, S.A., 2015d. Chemical evidence for the presence and distribution of Macondo oil in deep-sea sediments following the Deepwater Horizon oil spill. Newfields Technical Report to the Trustees in Support of the pDARP. <https://www.doi.gov/deepwaterhorizon/adminrecord>.

Stout, S.A., Payne, J.R., 2017. Footprint, weathering, and persistence of synthetic-base drilling mud olefins in deep-sea sediments following the Deepwater Horizon disaster. Mar. Poll. Bull. 118 (1–2), 328–340.

Stout, S.A., Payne, J.R., Emsbo-Mattingly, S.D., Baker, G., 2016a. Weathering of field-collected floating and stranded Macondo oils during and shortly after the *Deepwater Horizon* oil spill. Mar. Pollut. Bull. 105, 7–22.

Stout, S.A., Payne, J.R., Ricker, R.W., Baker, G., Lewis, C., 2016b. Macondo oil in deep-sea sediments: Part 2—Distribution and distinction from background and natural oil seeps. Mar. Pollut. Bull. 111, 381–401.

Testa, J.M., Adams, E.E., North, E.W., He, R., 2016. Modeling the influence of deep water application of dispersants on the surface expression of oil: a sensitivity study. J. Geophys. Res. Oceans 121 (8), 5995–6008.

USDC, The US District Court for Eastern District of Louisiana, 2015. Case 2:10-md-02179-CJB-SS Document 14021 Filed 01/15/15, Findings of Fact and Conclusions of Law Phase Two Trial, pp. 1–44. <http://www2.epa.gov/sites/production/files/2015-01/documents/phase2ruling.pdf>.

Valentine, D.L., Kessler, J.D., Redmond, M.C., Mendes, S.D., Heintz, M.B., Farwell, C., et al., 2010. Propane respiration jump-starts microbial response to a deep oil spill. Science 330, 208–211.

Valentine, D.L., Fisher, G.B., Bagby, S.C., Nelson, R.K., Reddy, C.M., Sylva, S.P., et al., 2014. Fallout plume of submerged oil from *Deepwater Horizon*. Proc. Nat. Acad. Sci. 111 (45), 15906–15911. Available from: http://dx.doi.org/10.1073/pnas.1414873111.

Venosa, A.D., Holder, E.L., 2007. Biodegradability of dispersed crude oil at two different temperatures. Mar. Poll. Bull. 54 (5), 545–553.

Weisberg, R.H., Zheng, L., Liu, Y., 2011. Tracking subsurface oil in the aftermath of the *Deepwater Horizon* well blowout, Monitoring and Modeling the Deepwater Horizon Oil Spill: A Record-Breaking Enterprise, 15. American Geophysical Union, Washington, DC, pp. 205–215., 195, Ch.

White, F.M., 2005. Viscous Fluid Flow, 3rd ed McGraw-Hill, New York, 656 p.

Xue, Z., He, R., Fennel, K., Cai, W.J., Lorentz, S., Hopskinson, C., 2013. Modeling ocean circulation and biogeochemical variability in the Gulf of Mexico. Biogeoscience 10 (11), 7219–7234.

Further Reading

Chao, Y., Li, Z., Farrara, J.D., McWilliams, J.C., Bellingham, J., Capet, X., et al., 2009. Development, implementation and evaluation of a data-assimilative ocean forecasting system off the central California coast. Deep-Sea Res. II 56, 100–126. doi:10.1016/j.dsr2.2008.08.011.

Fox, D.N., Teague, W.J., Barron, C.N., Carnes, M.R., Lee, C.M., 2002. The modular ocean data assimilation system (MODAS). J. Atmos. Ocean. Technol. 19, 240–252.

General Bathymetric Chart of the Oceans (GEBCO), 2009. Digital Atlas, Centenary Edition of the GEBCO Digital Atlas Published on Behalf of the Intergovernmental Oceanographic Commission (IOC) and the International Hydrographic Organization (IHO) as part of the General Bathymetric Chart of the Oceans. British Oceanographic Data Centre (BODC), Liverpool.

Stiver, W., Mackay, D., 1984. Evaporation rate of oil spills of hydrocarbons and petroleum mixtures. Environ. Sci. Technol. 18, 834–840.

Stout, S.A., Payne, J.R., 2016. Macondo oil in deep-sea sediments: Part 1—sub-sea weathering of oil deposited on the seafloor. Mar. Poll. Bull. 111, 365–380.

US Department of Commerce, National Oceanic and Atmospheric Administration, National Geophysical Data Center (NOAA NGDC), April 2012, 2-Minute Gridded Global Relief Data (ETOPO2v2). <http://www.ngdc.noaa.gov/mgg/fliers/06mgg01.html> (accessed 04.12).

CHAPTER

32

Louisiana Coastal Marsh Environments and MC252 Oil Biomarker Chemistry

Buffy M. Meyer, Puspa L. Adhikari, Gregory M. Olson, Edward B. Overton and Martin Scott Miles

Louisiana State University, Baton Rouge, LA, United States

BIOGRAPHIES

Puspa L. Adhikari is a postdoctoral research associate in the Department of Environmental Sciences at Louisiana State University, Baton Rouge, United States. He obtained his PhD in Chemical Oceanography from Louisiana State University in 2015. His research interest lies in utilizing various analytical/sampling tools and techniques to understand source, reactivity, bioavailability, transport, and fate of nutrients and particle-reactive organic compounds in various coastal marine environments. He is also interested in petroleum geochemistry, sediment-oil uptake kinetics, and oil spill forensics. He has utilized both direct observations and indirect geochemical proxy-based estimations to determine distribution, vertical and lateral transports, residence times, and sedimentary accumulation of hydrophobic organic compounds (HOCs), primarily polycyclic aromatic hydrocarbons, in the northern Gulf of Mexico.

Buffy M. Meyer is a senior research associate in the Department of Environmental Sciences at Louisiana State University, Baton Rouge, United States. She obtained her PhD in Environmental Sciences from Louisiana State University in 2016. For the past 17 years, she has been part of the Response and Chemical Assessment Team at LSU and has been dedicated to the instrumental analysis, primarily GC/MS, of oil residues during and after oil spills. As part of LSU-RCAT, she has been involved in the analysis of sediments and biota collected as part of NOAA-ERD's monitoring efforts after the *Exxon Valdez*, took part in the multiagency sampling and analysis of multiple oiling events caused by Hurricane Katrina, and provided laboratory support during the *Deepwater Horizon* oil spill. Dr. Meyer's research focuses on quantitative and statistical approaches to oil source fingerprinting, instrumental analysis techniques for oil spill research, and understanding the fate of oil biomarkers in coastal marsh environments.

Martin Scott Miles received his PhD in Environmental and Civil Engineering from Louisiana State University, Baton Rouge, United States. He received his MS in Environmental Sciences from LSU and holds undergraduate degrees in biology and environmental engineering from the Southeastern Louisiana University and LSU, respectively. He joined the Department of Environmental Sciences in 1990 and is currently the lead research associate for the Response and Chemical Assessment Team (RCAT). RCAT works closely with the National Oceanographic and Atmospheric Administration's (NOAA) Emergency Response Division (ERD) and has been involved in a wide range of environmental sampling and analysis efforts following Hurricanes Katrina, Ike, Gustav, and Isaac. In addition, LSU-RCAT has responded to most major oil/chemical spills in the United States, including the *Exxon Valdez*, the COSCO Busan, Texas City acid spill, and the *Deepwater Horizon*. His research interests focus on investigating the fate and transport of oil/chemicals in marine and riverine environments, water and sediment quality monitoring, bioaccumulation of toxic constituents in biota, and detection of contaminants in environmental matrices.

Oil Spill Environmental Forensics Case Studies.
DOI: http://dx.doi.org/10.1016/B978-0-12-804434-6.00032-X

Gregory M. Olson is a research associate in the Department of Environmental Sciences working with the Response and Chemical Assessment Team. He received his BS from McNeese State University, United States, and his MS from Louisiana State University, Baton Rouge, United States, before completing his doctorate in the Department of Environmental Sciences in 2015. His doctoral research focused on the concentrations of polycyclic aromatic hydrocarbons in Gulf menhaden tissue in the years following the Deepwater Horizon oil release. His current research involves crude oil analysis of various matrices as well as chemical fingerprinting of oil for the use in biomarker analysis. His research interests include crude oil fingerprinting and forensics, solvent chemistry, and GC/MS analytical techniques.

Edward B. Overton is Professor Emeritus in the Department of Environmental Sciences at Louisiana State University, Baton Rouge, United States. He received his BS (1965) and PhD (1970) from the University of Alabama, Tuscaloosa. His research interests include understanding the fates and distributions of hydrocarbons following an oil spill, the environmental chemistry of hazardous chemicals, and the detection of environmental pollutants in situ. He has been active in understanding the fate and effects of petroleum hydrocarbons in marine environments since the 1978 well blowout at the US DOE Strategic Petroleum Reserve West Hackberry Site, followed by the *Amoco Cadiz* tanker wreck and the IXTOC 1 blowout in 1979, the *Exxon Valdez* wreck in 1989, and currently the *Deepwater Horizon* fire and blowout in 2010. He has given hundreds of live interviews regarding the *Deepwater Horizon* oil spill to international print, radio, and TV media and news sources, and even appeared on the Late Show with David Letterman. He has also been an invited speaker at dozens of national and international scientific meetings and seminars on topics associated with oil spills. He held the Claiborne Chair in Environmental Toxicology and Air Quality prior to his retirement, was the 1996 Louisiana Technologist of the Year, honored as an LSU Distinguished Faculty in 2008, and was the 2010 Louisiana Communicator of the Year.

32.1 BACKGROUND

For more than 40 years, marine oil spills have been recognized as a prime source for major environmental impacts that cause significant and long-term ecological damages (NOAA-ERD, 2012; Stout and Wang, 2007; Wang and Fingas, 2003; Wang et al., 2006). The 1968 *Torrey Canyon* oil spill off the southwest coast of the United Kingdom accentuated the potential environmental threat posed by large volumes of oil spilled by accidents involving the then newly introduced "supertanker" transportation vessel. A production well blowout in 1969 off the California coastal city of Santa Barbara caused another major spill in the marine environment, further highlighting environmental concerns of oil pollution. There have been numerous spills around the world since the 1960s, including the infamous *Amoco Cadiz* (Brittany, France) and *Exxon Valdez* (Prince William Sound, Alaska) spills, which resulted in considerable media attention. Eventually, media attention and public outrage during the *Exxon Valdez* incident lead to the passage of the US Oil Pollution Act of 1990 (OPA 1990) that put liability on the responsible parties (i.e., spiller or spillers) to cleanup major oil spills. Presently, the most notable oil release to date is the *Deepwater Horizon* (DWH) disaster. The accidental release occurred in the Macondo prospect region located in the Mississippi Canyon lease block 252 (MC252) of the northern Gulf of Mexico (GoM), about 41 mi off the coast of Louisiana. Eleven people lost their lives, 17 people were injured, and an estimated 4.9 million barrels of crude oil and gas were released into the GoM between April 20 and July 15, 2010 (US DOI, 2010).

The principal questions asked when oil is released are the source of the oil, quantity in various compartments of the environment (i.e., air, water, sediment, biosphere, etc.), and the risk and consequences associated with various petrogenic (oil-derived) hydrocarbon concentrations within these compartments. The key to answering these questions is in the chemical composition of the spilled oil. Crude oil itself is a complex mixture of organic compounds derived from the partial decomposition of animal and plant materials that have long since been buried and acted upon by natural forces. On a geological time scale, the process of oil formation (e.g., diagenesis, catagenesis, and metagenesis) occurs very slowly and produces "simple" more reduced organic molecules (petroleum) from more complex organic structures (organic biomass) (Peters et al., 2005). These processes contribute to the formation of petroleum-type hydrocarbons which can exist as a gas (natural gas), a solid (tar, bitumen), and a liquid (crude oil). The physical and chemical properties of crude oil vary between regions of production, as well as reservoir zones within these regions because of differing geographic conditions and organic matter assemblages (Peters et al., 2005). These differences in composition are important from an environmental chemistry and oil forensics perspective because they are useful in determining the possible origins of the oil. These differences can also be used to predict how the oil will behave if spilled in the environment.

In general, all crude oils tend to be composed of the same hydrocarbon compounds, but the relative abundance of these compounds can vary significantly between oils of different origins. Oil constituents commonly targeted by analysis techniques like gas chromatography/mass spectrometry (GC/MS) can be classified into four general groups: (1) individual saturated hydrocarbons (the normal alkanes and isoprenoids); (2) polycyclic aromatic hydrocarbons (PAHs) including their dominant alkylated homologs; (3) sulfur heterocyclic aromatics and related alkylated homologs; and (4) oil biomarkers that are polycyclic aliphatics. Oil biomarkers are important compounds that typically suffer little interference from weathering and biodegradation effects because of their high molecular weights (Wang and Fingas, 1995; Peters et al., 2005; Wang et al., 2006; Hansen et al., 2007). Furthermore, oil biomarkers can be used to distinguish one oil from another, including oils with similar geographic origins. As a result, they are commonly used for oil source fingerprinting (Wang and Fingas, 1995; Stout et al., 2002; Wang and Fingas, 2003; Peters et al., 2005). The composition of crude oil in the environment is continually being altered by a variety of biological, chemical, and physical processes. The culmination of these processes over many months to years after an oil-spill event can and will affect all four of these general groupings.

32.1.1 Spilled Oil in the Environment

There are two major factors that affect spilled oil in the environment. The first major factor is the inherently heterogeneous distribution of spilled oil in the impacted environment. The phase separation of crude oil in water can mobilize pockets of crude oil beyond the initial shoreline impacts and into the near-shore and interior bodies of water, extending the potential environmental impacts of the spilled oil (Zengel et al., 2015; Turner et al., 2014; Ramsey et al., 2014). The second major factor is weathering which is the combined effect of different biological and physiochemical processes on the original oil's composition. Weathering includes evaporation, spreading, dispersion, dissolution, emulsification, oxidation, sedimentation, aggregation, and both microbial and photooxidation. These processes, both individually and in combination, continually alter oil composition and affect its distribution into different compartments of the environment (Overton et al., 2016; Tarr et al., 2016). In sum, weathering changes the physical and toxic properties of oil as well as the oil's appearance by changing its original composition after release.

As weathering proceeds, certain groups of oil constituents are lost in a predictable sequence. The first compounds to be depleted are the low molecular weight hydrocarbons that are lost to evaporation and dissolution. The normal (*n*) alkanes and isoprenoids usually degraded rapidly, followed by the lighter PAHs, then the remaining PAHs and their alkyl homologs (Prince and Walters, 2007; Stout and Wang, 2007; Wang and Fingas, 2003). Once oil is stranded on a beach or shoreline, further weathering is modified by the microenvironment in which the oil is entrapped; therefore, the degree of weathering is very site specific. An important component of this microenvironment is the microorganism assemblage and their ability to biodegrade oil in the presence or absence of oxygen. How biodegradation affects the composition of oil in the environment is highly dependent on the physical properties and amount of oil spilled, as well as factors like redox conditions, nutrient availability, temperature, and salinity. All of these factors greatly influence the microbial ecology and petroleum hydrocarbon degradation dynamics for any given microenvironment (Atlas et al., 2015).

32.1.2 Louisiana Coastal Salt Marsh Environments

The magnitude of the DWH oil spill has provided an opportunity to study the long-term effects of Louisiana coastal salt marsh environments on MC252 oil (i.e., the oil leaking from the DWH) residues deposited in these environments. According to Nixon et al. (2016), a total of 2104 out of 9545 km of surveyed GoM shorelines were determined to be oiled (on a scale of "trace" to "heavily oiled") by the Shoreline Cleanup and Assessment Technique (SCAT). Louisiana was disproportionally affected by the DWH oil spill and represented 65% of these oiled shorelines, and 95% of the total oiled marshes (Nixon et al., 2016; Michel et al., 2013). Even after initial shoreline impacts, oil residues (i.e., mousse, tarballs, stranded oil) continued to impact the Louisiana coastal shorelines and marsh environments after the wellhead was officially shut off on September 19, 2010 resulting in multiple oiling events (Turner et al., 2014).

Louisiana coastal salt marsh environments have unique and important interactive ecological roles. They provide a nursery habitat for estuarine organisms, a habitat for wildlife, provide water quality enhancements, and protection against shoreline erosion and storm surges (Lin and Mendelssohn, 1996; DeLaune et al., 1979; Rabalais and Turner, 2016). The trophic structure in these environments is heavily dependent upon primary producers including marsh grasses (e.g., *Spartina alterniflora*), phytoplankton, benthic plants, and epiphytic algae living on

the grasses (DeLaune et al., 1979). *S. alterniflora* is the most important primary producer in salt marsh environments as all estuarine animals either directly or indirectly depend on the detrital food it provides (DeLaune et al., 1979). Marsh health is often determined by the appearance of the marsh vegetation, specifically *S. alterniflora* when discussing Louisiana coastal salt marshes. The appearance of recovering or healthy vegetation after a catastrophic event, such as a major oil release, may obscure the possible arrested development of other vital ecosystem components (McClenachan et al., 2013; Rabalais and Turner, 2016; Zengel et al., 2015). Therefore, any adverse effects to *S. alterniflora* could result in adverse effects on salt marsh productivity that may have significant ramifications on the entire community structure (DeLaune et al., 1979; DeLaune and Wright, 2011; Rabalais and Turner, 2016; Zengel et al., 2015).

32.1.3 Oil in Coastal Salt Marsh Environments

The persistence of crude oil in some coastal salt marsh environments has been well documented (Teal et al., 1992; Reddy et al., 2002; Oudot and Chaillan, 2010; Lin and Mendelssohn, 2012; Natter et al., 2012). However, degradation of oil and oil biomarkers in other environments has also been documented (Wang et al., 2001; Aeppli et al., 2014; Radović et al., 2014). The difference between persistence and degradation of oil residues greatly depends on the environmental conditions where these residues are deposited.

The primary environmental factor influencing the fate of oil residues is the availability of oxygen (i.e., aerobic vs anaerobic conditions) (DeLaune et al., 1990; Atlas and Hazen, 2011). Under ideal aerobic conditions, most crude oil compounds are biodegradable (Prince and Walters, 2007; Atlas and Hazen, 2011). This is because there is a rich diversity of bacteria, archaea, and fungi that are widely distributed throughout the aerobic layer of soils and sediments. Further, petroleum is a reduced form of carbon and is readily oxidized. The most readily biodegradable compounds are normal and isoprenoid alkane hydrocarbons and one- and three-ringed aromatic hydrocarbons. For larger aromatic hydrocarbons, such as heavier PAHs and their associated alkyl homologs, the parent PAH is typically the first to enzymatically degrade, while the alkyl homologs are slower to degrade (i.e., increasing alkylation slows biodegradation) (Wang and Fingas, 2003).

Anaerobic degradation is accomplished by a consortium of bacteria along with methanogenic archaea and is driven by either methanogenesis, or sulfate, nitrate, and transitional metal reduction (Atlas et al., 2015). When compared to aerobic biodegradation, anaerobic biodegradation is a much slower process (Atlas, 1981). Thus, oil residues can remain relatively unaltered in anaerobic environments for longer periods of time. Additionally, these oil residues may even appear to be relatively "fresh" oil compared to the same oil residues exposed to aerobic conditions (Fig. 32.1). This is particularly true when oil residues become buried through the sedimentation process occurring within coastal salt marsh environments (refer to Section 32.2.3).

Coastal salt marshes tend to be low-energy and organic-rich environments with anaerobic (i.e., anoxic) conditions just below the surface, resulting in the preservation of some crude oil constituents, including the oil biomarkers. Sediments in these environments typically have a very thin (5–10 mm) oxidized soil layer at the sediment–water interface (DeLaune et al., 1979, 1990). Oil residues on the surface sediment are eventually buried and incorporated into the reduced soil layer that is under the oxidized soil layer (DeLaune et al., 1990). Organic matter content is one of the primary factors affecting the penetration, sorption, and degradation of oil residues in the soil and sediment; therefore, marshes with high organic matter content may be more susceptible to oil spill events (Lin and Mendelssohn, 1996).

It has been reported that only about 20% of the total oil released during the DWH oil spill was recovered with about 6% removed via in situ burning (US DOI, 2010; McNutt, et al., 2012; Camilli et al., 2012; Ryerson et al., 2012). Thus, the major fraction of the oil (approximately 75%) remained in the environment where it was subsequently acted upon by several weathering processes. While much of the weathered oil residues remained offshore or sank and were incorporated into seafloor sediments, a significant amount of weathered oil residues came ashore, impacting coastal marshes and beaches from as far west as Vermilion Bay, LA to near Apalachicola, FL in the east (Adhikari et al., 2015, 2016; Stout and Payne, 2016; Nixon et al., 2016; Michel et al., 2013). This weathered oil had a very heterogeneous distribution and was either stranded or buried along the impacted shorelines. Fig. 32.1 exemplifies the effects of an aerobic and anaerobic environment on oil residues. This figure showcases the range of chromatographic profiles of weathered to relatively fresh MC252 oil collected from the marsh surface and found buried in Bay Jimmy, LA.

Under the anoxic conditions of Louisiana coastal salt marshes, petroleum hydrocarbons are not readily utilized as an energy source for microbial metabolism, therefore buried oil residues tend to remain in the environment for longer period of times (DeLaune et al., 1979). The remobilization of buried oil and oiled sediments due to

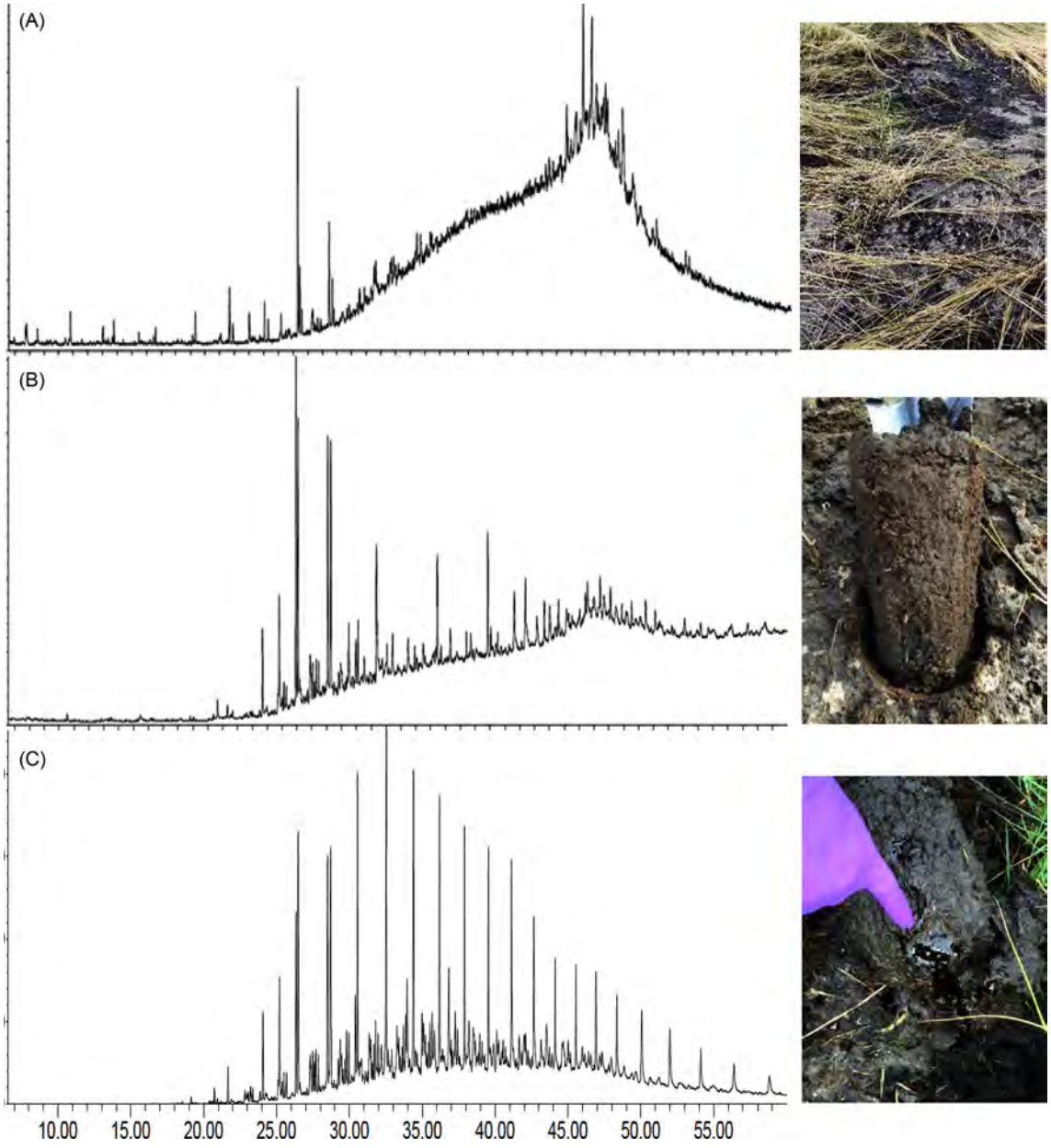

FIGURE 32.1 GC/MS chromatographic profiles of (A) clearly visible marsh surface oil residue, (B) near-surface oil residue without a clearly visible oil layer, and (C) oil residue buried ~17 cm below the surface with a clearly visible oil layer collected from Bay Jimmy, LA in 2016.

storm events and hurricanes is a significant concern for these salt marsh communities (Rabalais and Turner, 2016; Turner et al., 2014; Zengel et al., 2015). Storm events can force oil residues farther into the marshes, or can bury oil residues more deeply within associated soil pore space and animal burrows (Zengel et al., 2015). Thus, the remobilization of buried oil can cause chronic exposures that adversely distress the plant-dependent food web of these environments, as well as create exposure risk for nearby or adjacent habitats and wildlife (Turner et al., 2014; Zengel et al., 2015). Several tropical weather events, including Tropical Storm Lee in 2011 and Hurricane Isaac in 2012, crossed the coastal areas of Louisiana and resulted in a remobilization of the DWH oil residues from the initially oiled marshes (Zengel et al., 2015). This remobilization of oil is depicted in Fig. 32.2. The GC/MS *n*-alkane profiles (m/z 57) in Fig. 32.2 are from near-surface sediment samples collected from the same sampling location before and after Hurricane Isaac. Also, included in Fig. 32.2 is the *n*-alkane profile of MC252 source oil that was characteristic of the weathering stage of oil that impacted the Louisiana coastal salt marshes during the DWH event.

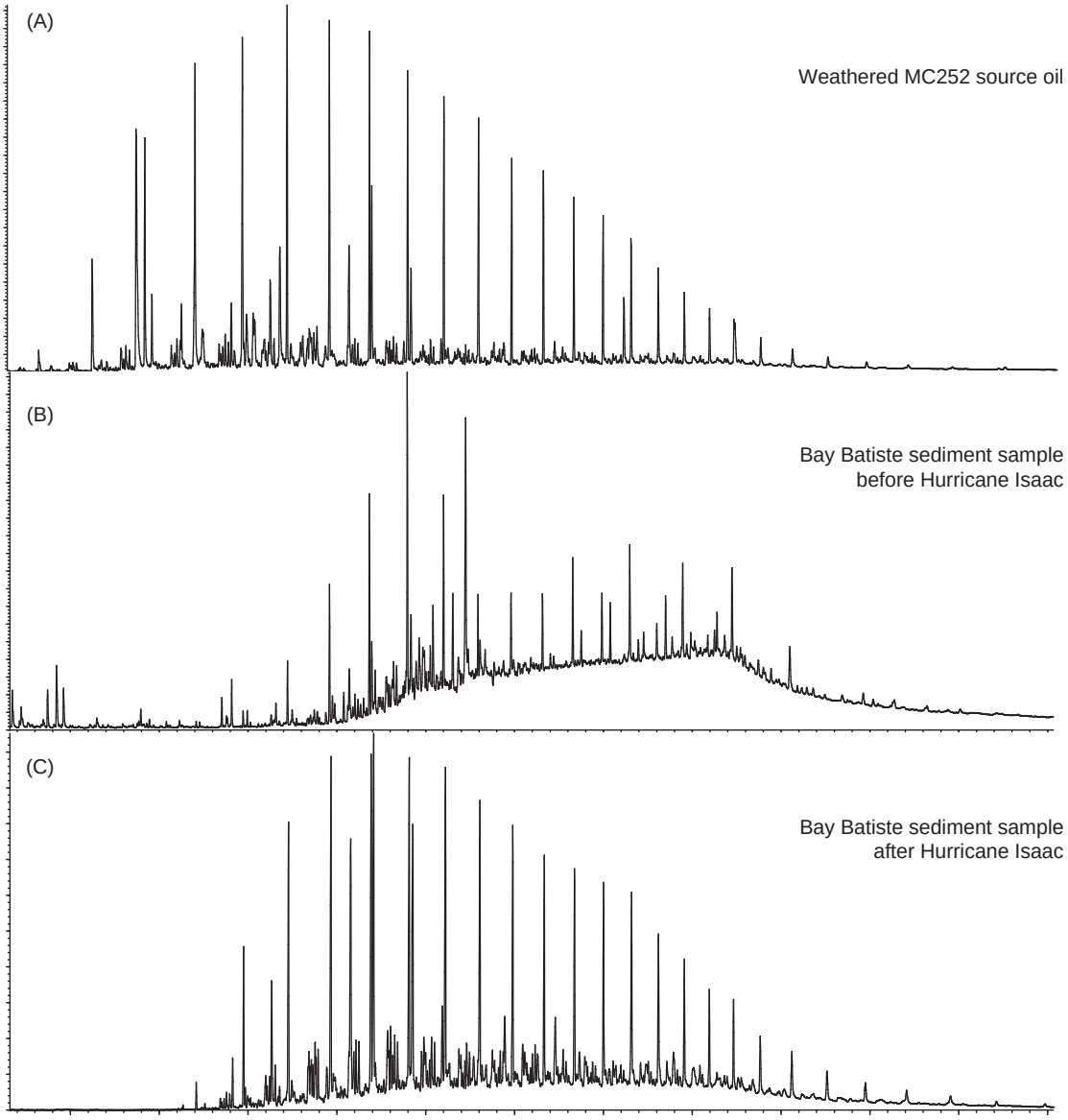

FIGURE 32.2 GC/MS normal alkane (m/z 57) chromatograms of weathered MC252 source oil (A), and a sediment sample collected from the same location in Bay Batiste, LA before (B) and after (C) Hurricane Isaac highlighting the potential for oil redistribution.

32.2 LOUISIANA COASTAL MARSHES AND MC252 OIL BIOMARKER CHEMISTRY

A total of 778 near-surface sediment samples (i.e., the top 5 cm of sediment) were collected throughout Louisiana coastal salt marshes from 2010 to 2015. Fig. 32.3 is a map showing the generalized areas of sample collection throughout the coastal region of Louisiana. More detailed sample site information is provided in Turner et al. (2014). The sampling locations in Fig. 32.3 were chosen because these areas sustained the most prominent oiling according to SCAT mapping and satellite imagery (Turner et al., 2014). Field sampling included these three general areas semiannually, but the same exact sites were not always resampled because of easement issues, erosion, or logistical issues (i.e., no longer boat accessible).

The chemical analyses of all sediment samples were accomplished using gas chromatography/mass spectrometry operated in selected ion monitoring mode (GC/MS-SIM). The GC/MS instrumentation was tuned every 12 hours using perfluorotributylamine to ensure optimum operational conditions. The inlet septa were changed prior to each instrument tune and inlet liners were replaced as necessary. Each analytical batch included a continuing calibration standard of oil analysis standard (Absolute Standards, Inc., Hamden, CT), an extract of unweathered MC252 source oil (from a riser pipe aboard the drillship *Discoverer Enterprise*, May 20, 2010), solvent blanks, and instrument blanks.

FIGURE 32.3 Generalized map of Louisiana coastal salt marsh sediment sample locations. The Google Earth image shown is indicated by the black box in the state image.

All of these samples were used to ensure quality control of the instrumental acquisition process. Sediment sample field identifications were excluded until after all data processing and oil fingerprinting was finalized to minimize bias.

After GC/MS-SIM analysis, all sediment samples were qualitatively examined and sorted as "background" or "oiled" based on the total ion chromatogram, the *n*-alkanes, and oil biomarker profiles. Only samples that were sorted as "oiled" underwent additional oil source fingerprinting. A total of 404 samples were deemed "oiled" out of 778 near-surface sediment samples. Also, at this stage of analysis, oiled samples were further sorted based on a postulated weathering pattern of MC252 regular steranes and diasteranes (m/z 217) described in Section 32.2.2.

32.2.1 MC252 Oil Biomarkers and Oil Source Fingerprinting

Three classes of oil biomarkers commonly used for oil source fingerprinting are (1) the triterpanes (including hopanes); (2) the steranes, including the diasteranes, regular steranes, and 14β(*H*)-steranes; and (3) the triaromatic steroids. Table 32.1 provides a list of oil biomarkers found in each of these three major classes. Oil biomarkers have cyclic structures of repeating subunits composed of mostly carbon, hydrogen, and sometimes other elements, indicating that their precursors were from living organisms. Steranes in petroleum originate from sterols in the cell membranes of eukaryotes. Prokaryotes use hopanoids rather than steroids in their cell structures which, in turn, accounts for the presence of hopanes (triterpanes) in petroleum (Peters et al., 2005).

Oil source fingerprinting is an environmental forensics technique that was adapted from the field of petroleum geochemistry. Source fingerprinting utilizes analytical chemistry to compare samples that contain recognizable oil profiles to a suspected source and was first used by Overton et al. (1981) to evaluate the environmental impacts resulting from an oil spill and fire at the US Strategic Petroleum Reserve Complex in West Hackberry, LA. Since that time, the use of specific oil biomarker compounds has become increasingly important to oil source fingerprinting because the relative distribution of these compounds are unique for different types and blends of petroleum products and source oils, and, as a result, represent an oil-specific fingerprint for oil source correlations (Daling et al., 2002; Wang et al., 2006; Hansen et al., 2007). Oil source fingerprinting gained new significance after the passage of OPA 1990. At this point, it was used to link released oil to a responsible party who would have to pay for mitigation and ecological damages. Fig. 32.4 displays MC252 source oil triterpanes, steranes, and triaromatic steroids.

TABLE 32.1 List of Common Oil Biomarker Compounds Used for Oil Source Fingerprinting

Abbreviation	Name	*m/z*	Abbreviation	Name	*m/z*
TC28R	C28-Tricyclic triterpene-22R	191	C27DBS	13β(*H*),17α(*H*)-Diacholestane-20S (diasterane)	217
TC28S	C28-Tricyclic triterpene-22S	191	C27DBR	13β(*H*),17α(*H*)-Diacholestane-20R (diasterane)	217
TC29R	C29-Tricyclic triterpene-22R	191	C27aaS	5α(*H*),14α(*H*),17α(*H*)-Cholestane-20S	217
TC29S	C29-Tricyclic triterpene-22S	191	C29DBaS	13β(*H*),17α(*H*)-Ethyldiacholestane-20S	217
C27Ts	C27-18α(*H*)-22,29,30-Trisnorhopane	191	C27aaR	5α(*H*),14α(*H*),17α(*H*)-Cholestane-20R	217
C27Tm	C27-17α(*H*)-22,29,30-Trisnorhopane	191	C29DBaR	13β(*H*),17α(*H*)-Ethyldiacholestane-20R	217
C28aB	C28-17α(*H*),21β(*H*)-28,30-Bisnorhopane	191	C28aaS	24-methyl-5α(*H*),14α(*H*),17α(*H*)-Cholestane-20S	217
C25nor	C29-17α(*H*),21β(*H*)-25-Norhopane	191	C28BBS	24-methyl-5β(*H*),14β(*H*),17β(*H*)-Cholestane-20S	217
C29aB	C29-17α(*H*),21β(*H*)-30-Norhopane	191	C28BBR	24-methyl-5α(*H*),14β(*H*),17β(*H*)-Cholestane-20R	217
C29Ts	C29-18α(*H*)-30-Norneohopane	191	C28aaR	24-Methyl-5α(*H*),14α(*H*),17α(*H*)-cholestane-20R	217
C30d	C30-15α-methyl-17α(*H*)-27-Norhopane (diahopane)	191	C29aaS	24-Ethyl-5α(*H*),14α(*H*),17α(*H*),24-cholestane-20S	217
C29Ba	C29-17β(*H*),21α(*H*)-Norhopane (normoretane)	191	C29BBR	24-Ethyl-5α(*H*),14β(*H*),17β(*H*)-cholestane-20R	217
C30 O	C30-18α(*H*)- and 18β(*H*)-Oleanane	191	C29BBS	24-Ethyl-5α(*H*),14β(*H*),17β(*H*)-cholestane-20S	217
C30aB	C30-17α(*H*),21β(*H*)-Hopane	191	C29aaR	24-Ethyl-5α(*H*),14α(*H*),17α(*H*)-cholestane-20R	217
C30Ba	C30-17β(*H*),21α(*H*)-Hopane (moretane)	191	C27BBR	5α(*H*),14β(*H*),17β(*H*)-Cholestane-20R	218
C31aBS	C31-17α(*H*),21β(*H*)-Homohopane-22S	191	C27BBS	5α(*H*),14β(*H*),17β(*H*)-Cholestane-20S	218
C31aBR	C31-17α(*H*),21β(*H*)-Homohopane-22R	191	C28BBR	24-Methyl-5α(*H*),14β(*H*),17β(*H*)-Cholestane-20R	218
C30G	C30-Gammacerane	191	C28BBS	24-Methyl-5α(*H*),14β(*H*),17β(*H*)-cholestane-20S	218
C32aBS	C32-17α(*H*),21β(*H*)-Bishomohopane-22S	191	C29BBR	24-Ethyl-5α(*H*),14β(*H*),17β(*H*)-cholestane-20R	218
C32aBR	C32-17α(*H*),21β(*H*)-Bishomohopane-22R	191	C29BBS	24-Ethyl-5α(*H*),14β(*H*),17β(*H*)-cholestane-20S	218
C33aBS	C33-17α(*H*),21β(*H*)-Trihomohopane-22S	191	C20TA	C20-Triaromatic steroid (pregnane)	231
C33aBR	C33-17α(*H*),21β(*H*)-Trihomohopane-22R	191	C21TA	C21-Triaromatic steroid (homopregnane)	231
C34aBS	C34-17α(*H*),21β(*H*)-Tetrahomohopane-22S	191	SC26TA	C26-20S-Triaromatic steroid (cholestane)	231
C34aBR	C34-17α(*H*),21β(*H*)-Tetrahomohopane-22R	191	RC26TA + SC27TA	C26-20R- + C27 20S-Triaromatic steroids	231
C35aBS	C35-17α(*H*),21β(*H*)-Pentahomohopane-22S	191	SC28TA	C28-Triaromatic steroid-20S (ethylcholestane)	231
C35aBR	C35-17α(*H*),21β(*H*)-Pentahomohopane-22R	191	RC27TA	C27-Triaromatic steroid-20R (methylcholestane)	231
			RC28TA	C28-Triaromatic steroid-20R (ethylcholestane)	231

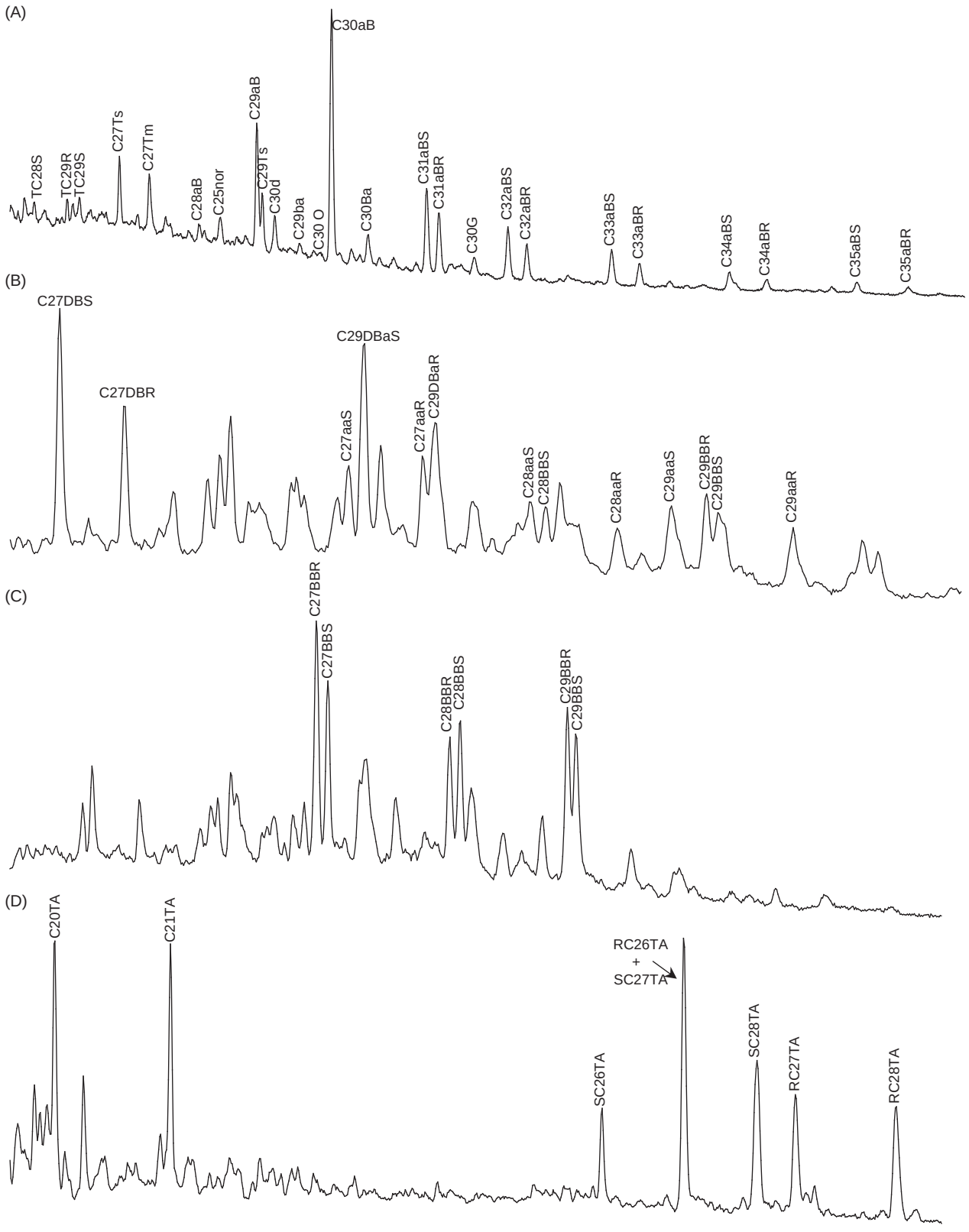

FIGURE 32.4 GC/MS extracted ion chromatograms of MC252 oil biomarkers. (A) Triterpanes, m/z 191; (B) diasteranes and regular steranes, m/z 217; (C) 14β(*H*)-steranes, m/z 218; (D) triaromatic steroids, m/z 231.

The profiles presented in Fig. 32.4 were qualitatively and quantitatively compared to oil residues detected in Louisiana coastal salt marsh sediments collected from 2010 to 2015. A visual, or qualitative, comparison was initially performed as outlined by ASTM 5739-00 (ASTM, 2000). Two different quantitative oil source fingerprinting techniques, diagnostic biomarker ratio analysis and chemometrics, were applied to the "oiled" samples if GC/MS abundances for targeted oil biomarker compounds were above three times the signal-to-noise ratio. The diagnostic biomarker ratio analysis was an adaptation of the Center for European Norms (CEN) methodology (Hansen et al., 2007; CEN, 2012). Chemometrics is used extensively to interpret quantitative data of all varieties but is particularly common in the field of petroleum geochemistry to determine oil−oil and oil−source rock correlations (Peters et al., 2007; 2008; 2013). The field of petroleum geochemistry forms the foundation of the oil source fingerprinting methods used currently during and after oil spills; therefore, the utilization of chemometrics as a quantitative oil source fingerprinting technique is also a logical extension of this field into the realm of oil spills.

Oil biomarkers were targeted in both quantitative techniques because they provide unique chemical fingerprinting information that can distinguish one oil from another, including oils with similar geographic origins (Wang and Fingas, 1995; Stout et al., 2002; Wang and Fingas, 2003; Peters et al., 2005). For that reason, the ability to differentiate MC252 source oil from seven other South Louisiana crude oils was included in both quantitative methodologies. The other South Louisiana crude oils included EPA South Louisiana Crude (SLC) standard, fresh and weathered oil from the Marlin platform in the Dorado field (VK915), Exxon OCS oil, and oil from three different pipelines (i.e., Cut Off, LA, Point Coupee Parish, LA, and SLC Blend). Alaskan North Slope crude oil was also included in the reference oil suite because it has a totally different geographic origin. All the source oils analyzed had been collected, preserved, and archived as part of other oil spill responses throughout the years, or from various oil spill related research.

32.2.1.1 Diagnostic Oil Biomarker Ratios

Diagnostic biomarker ratio analysis of Louisiana coastal marsh sediments was accomplished by identifying and integrating peak heights in GC/MS data of specific triterpanes, steranes, and triaromatic steroids that were then used to calculate diagnostic ratios specific to MC252 source oil. Hansen et al. (2007) recommends use of peak heights for diagnostic biomarker ratios because they tend to be more robust than area responses for peaks that may be poorly resolved and have noisy baselines. All ratio calculations were done using a corrected baseline value, and peak heights not exceeding three times the signal-to-noise value were not integrated. A total of 313 near-surface "oiled" sediment samples underwent diagnostic biomarker ratio analysis after applying the signal-to-noise criteria.

Establishing a set of diagnostic ratios unique to MC252 oil is a critical step in the oil source fingerprinting process. Therefore, a total of 44 separate GC/MS analyses of MC252 source oil were used to determine 15 MC252 diagnostic biomarker ratios (Table 32.2). All diagnostic ratios chosen had a percent relative standard deviation (% RSD) less than 5%, a quality criterion set forth in the CEN (2012) method. The same 15 MC252 ratios were calculated for oil residues detected in the near-surface coastal marsh sediment samples. The sample ratios were then statistically compared to the average ($n = 44$) MC252 source oil ratios using the critical difference (CD) method. The CD between a sample ratio and the MC252 ratio cannot be more than 14%, which represents the repeatability limit at a 95% confidence interval ($r_{95\%}$). Repeatability, in terms of diagnostic biomarker ratio analysis, is used to compare individual diagnostic biomarker ratios with the assumption that oil in the unknown sample is the same as the source oil in question. Once the CD was calculated for each ratio, each near-surface sediment sample was given a final oil source fingerprinting score. This score was calculated by dividing the number of "matching" ratios by 15 and multiplying by 100 to yield a percentage.

The diagnostic biomarker ratio analysis of oil residues detected in near-surface Louisiana coastal salt marsh sediments demonstrated that oil biomarker weathering had profoundly affected the calculation, and subsequent CD analysis of MC252 diagnostic biomarker ratios, rendering strict adherence to the CEN method's match criteria ineffective in these types of samples. All oil biomarker groups were affected by weathering, but the 14β(*H*)-steranes, the triaromatic steroids, and the homohopanes were the most affected. The CEN method is designed to be used as a short-term quantitative comparison technique (Stout, 2016). MC252 diagnostic biomarker ratios are the most robust during the early stages of a spill and its impacts (beginning of spill to up to ~1 year after), or in situations where oil residues have been buried and minimally altered by weathering. Stout (2016) has developed an alternative diagnostic biomarker ratio technique specific to oily matrices from the DWH oil spill that accounts for the effects of weathering throughout the long-term Natural Resource Damage Assessment, or NRDA, investigation of this oil spill.

TABLE 32.2 Suite of 15 Diagnostic Ratios for MC252 Source Oil Used to Oil Source Fingerprint Oil Residues in Near-surface Coastal Marsh Sediments

Ratio[a]	*m/z* Value
C27Ts/C27Tm	191
C29aB/C29Ts	191
C29aB/C30aB	191
C31aB(S + R)/C32aB(S + R) + C33aB(S + R)	191
C32aB(S + R)/C31aB(S + R) + C33aB(S + R)	191
C33aB(S + R)/C31aB(S + R) + C32aB(S + R)	191
C27DBS/C27DBR	217
C29DBaS/C29DBaR	217
C28aaR/C29aaR	217
C27BB(R + S)/C28BB(R + S) + C29BB(R + S)	218
C28BB(R + S)/C27BB(R + S) + C29BB(R + S)	218
C29BB(R + S)/C27BB(R + S) + C28BB(R + S)	218
C20TA/C21TA	231
SC26TA/SC28TA	231
RC27TA/RC28TA	231

[a]*Compound names for abbreviations are provided in Table 32.1 and peaks are labeled in Figure 32.4.*

An approach similar to Stout's may be feasible for oil residues in sediment samples. One analytical technique, gas chromatography/triple quadrupole mass spectrometry in multiple reaction monitoring (GC/MRM) mode, can improve oil source fingerprinting when trace levels of oil biomarker compounds are detected (Adhikari et al., 2017). Fig. 32.5 shows how the GC/MRM method effectively separates interferences from targeted oil biomarker compounds, significantly increases resolution, and improves baseline resolution when compared to using the conventional GC/MS–SIM method. These benefits, specifically improvement of the signal-to-noise ratio and baseline resolution, are especially useful for diagnostic oil biomarker ratio applications that will result in improved peak height integrations and integration reproducibility. Thus, GC/MRM can be a powerful analytical strategy for trace level analysis of oil biomarker compounds and warrants continued investigation.

32.2.1.2 Other Oil Source Fingerprinting Techniques

Since the CEN diagnostic ratio analysis loses effectiveness over time, a chemometric approach to oil source fingerprinting was tested. Chemometrics is an exploratory data analysis technique that recognizes patterns using multivariate pattern recognition algorithms and classifies samples into related groupings, or clusters (Peters et al., 2005; Peters et al., 2007; Peters et al., 2008; Lorenson et al., 2011; Peters et al., 2013). The two most common chemometric analyses are hierarchical cluster analysis (HCA) and principal component analysis (PCA). HCA groups samples based on cluster distance, which is a measure of similarity that accentuates the relationships among samples. A HCA also reveals samples that are contributing to a high variance. As a result, these samples can be excluded to improve the cluster results. A PCA simplifies a complex data matrix into a few components or factors to explain much of the variation in the data, while noise or irrelevant information comprises the remaining factors. A PCA also reveals samples that may be outliers. Visualization of data is a key component of chemometric analyses (Infometrix, 2014). Tribes and families determined by a HCA are simply displayed in a dendrogram based on cluster distance and natural groupings that reveals similarities among samples. A PCA employs 2D or 3D scatterplots to graphically display significant differences between sample clusters and to evaluate the HCA groupings. Chemometric analysis, therefore, reduces complex data into interpretable patterns without any assumptions regarding the distribution of the data (Infometrix, 2014).

Chemometric analysis has not been used previously as a quantitative oil source fingerprinting tool. The nature of the chemometric HCA and PCA allows for the separation of "genetically" related oils to a higher degree. This was important because the DWH oil spill impacted a region that has endured chronic oiling (i.e., natural seeps

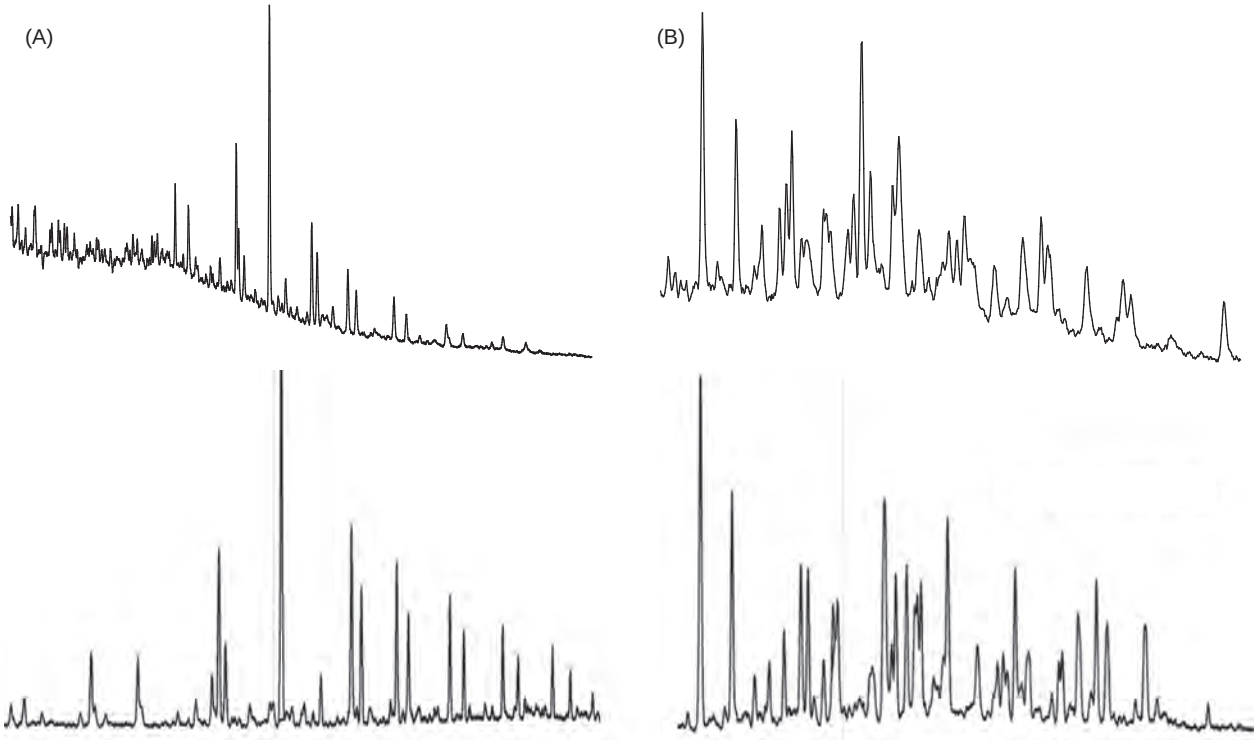

FIGURE 32.5 Comparison of extracted ion chromatograms of select MC252 oil biomarkers obtained using conventional GC/MS-SIM and GC/MRM. (A) Comparison of triterpanes, conventional GC/MS (top) and GC/MRM (bottom). (B) Comparison of diasteranes and regular steranes, conventional GC/MS (top), and GC/MRM (bottom).

and other oil spill events) of "genetically" related crude oils, which could cause a hindrance in the forensic assessment of oil residues in sediment samples. This potential application of chemometrics would prove especially important in fingerprinting oil residues in complex sample matrices, such as sediments, wherein CEN diagnostic ratio analysis loses its effectiveness. Therefore, it was important to verify whether or not chemometric analysis could effectively differentiate biomarkers in "genetically" related crude oils from the region before using utilizing the method for oil source fingerprinting of oil residues in coastal marsh sediments.

In order to test the effectiveness of chemometrics, one Alaskan North Slope crude oil, the seven different Southern Louisiana crude oils mentioned in Section 32.2.1, and MC252 oil were used to develop and validate the chemometric method. The extracted ion chromatograms (EICs) of the triterpanes (m/z 191), the diasteranes and regular steranes (m/z 217), the 14β(*H*)-steranes (m/z 218), and the triaromatic steroids (m/z 231) of each crude oil were first converted into peak intensity data points recorded approximately every second within a limited time window for each respective biomarker ion group. For example, the conversion of the GC/MS data of the diasteranes and regular steranes (m/z 217) from 42.5 to 52.0 minutes into peak intensity data resulted in 638 data points that were used as input variables in the chemometric analysis. The peak intensity data were then transferred into the chemometric software package Pirouette (*Infometrix*, Bothell, WA) for subsequent HCA and PCA analysis. The differentiation of the seven "genetically" related South Louisiana source oils was successful (Fig. 32.6). Not surprisingly, the Alaskan North Slope crude oil, which is from an entirely different oil province, was distinctly divergent from all the South Louisiana crude oils. Among all examined South Louisiana crude oils, the three pipeline oils from Point Coupee, Cut Off, and the SLC blend were dissimilar from the rest, with the Point Coupee pipeline oil being the most dissimilar South Louisiana crude. The EPA South Louisiana crude oil standard and the oils collected from production platforms (i.e., Exxon OCS, Marlin Platform, MC252) were more similar to one another as indicated by their positions in the PCA plot; however, HCA and PCA were capable of distinguishing MC252 from the other related South Louisiana crudes.

The results of the chemometric analysis of different sources of South Louisiana crude oils showed that chemometrics was effective in differentiating crude oil biomarkers from similar geographic origins and could be employed to determine which oil residues detected in Louisiana coastal salt marsh sediments were similar to MC252 oil. It was evident from the qualitative observations of the initial "background" vs "oiled" sorting phase,

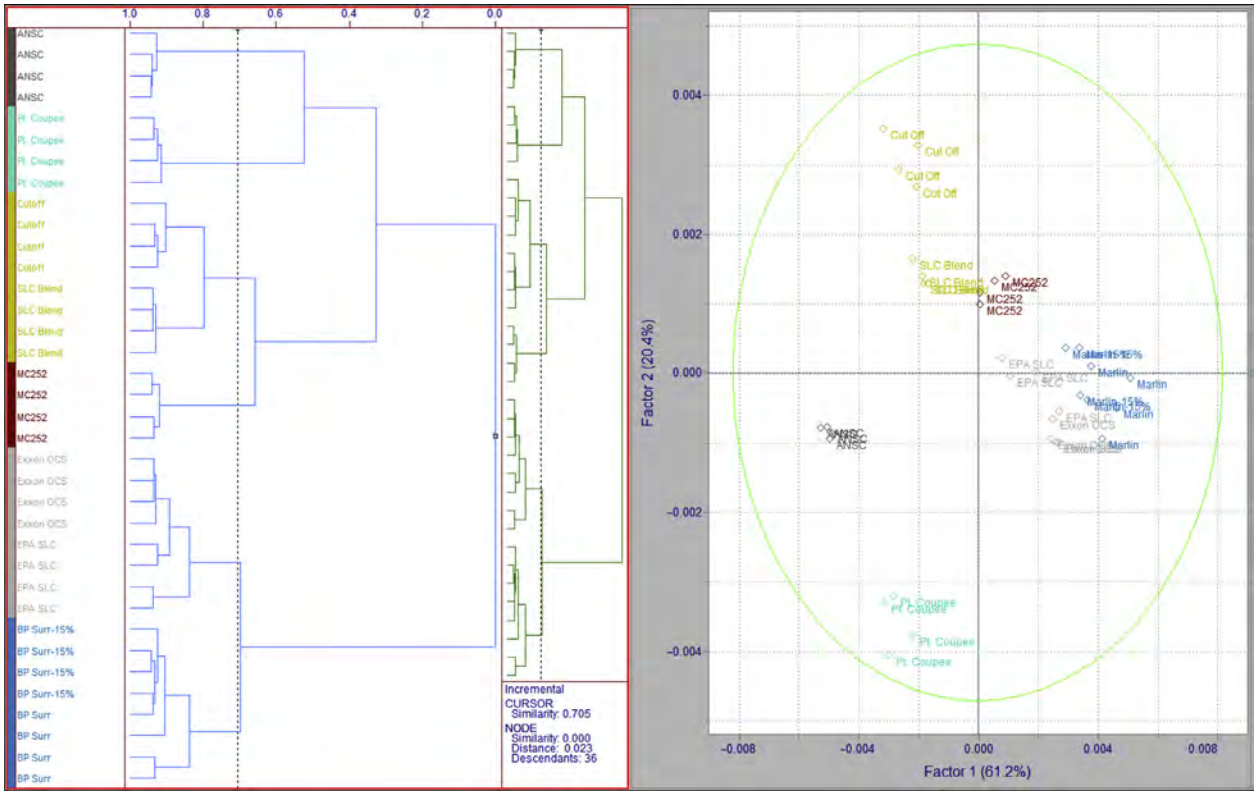

FIGURE 32.6 The chemometric differentiation of South Louisiana crude oils and Alaskan North Slope crude oil biomarker (diasteranes and regular sterane) peak intensity data ($n = 9$ oils w/4 reps, 638 variables).

and from the quantitative information gained from the diagnostic ratio analysis that the EIC for diasteranes and regular steranes (m/z 217) provided the most discriminating power of the four biomarker groups in the coastal marsh sediment samples impacted by MC252 oil. The EIC data for diasteranes and regular steranes for a total of 295 "oiled" coastal marsh sediments and the MC252 source oil sample included in each sample batch was converted into peak intensity data (638 input variables) in the same manner as the source oils described above. All peak intensity data were transferred into Pirouette for HCA and PCA analysis.

A total of 49 of the 295 "oiled" near-surface coastal marsh sediment samples were determined to be similar to MC252 oil based on the m/z 217 peak intensity data. Fig. 32.7 is a histogram that displays the percentage by year of coastal marsh samples clustering with MC252 source oil based on the diasteranes and regular steranes peak intensity data. The number of samples analyzed using chemometrics after 2012 did not decrease; however, the percentage of samples determined to be similar to MC252 oil decreased. Weathering, at this point, appears to have greatly affected the original diasteranes and regular steranes chromatographic pattern in the sediments and this is discussed further in Section 32.2.2.

Chemometric analysis is often used to answer questions, such as: Are the analytical data collected appropriate for classifying samples? Can different sample categories be determined based on chemical composition (Infometrix, 2014)? In this case, both questions were answered affirmatively. The benefit of chemometrics is that there are no assumptions about the distribution of data and large amounts of data can be quickly processed to understand natural groupings present in a dataset. However, weathering of biomarker compounds still affects the chemometric analysis. If an oiled sample has significant differences in peak intensities caused by weathering, the sample may not cluster with MC252 even if it would qualitatively match. The heterogeneous nature of oil residues in the environment is very similar to the heterogeneous gene expression found in humans. The same oil residue will be affected differently in the environment just like genetic expression varies from person to person and gene to gene. Genomic microarray analysis uses a technique called biclustering to overcome the inherent variation among large heterogeneous datasets (Shamir et al., 2005; Tanay et al., 2002). The goal of biclustering is to find subgroups that are significantly like each other, and as different as possible to the rest of the subgroups (Kaiser and Leisch, 2008). The main advantage of biclustering is that it provides probability levels and confidence

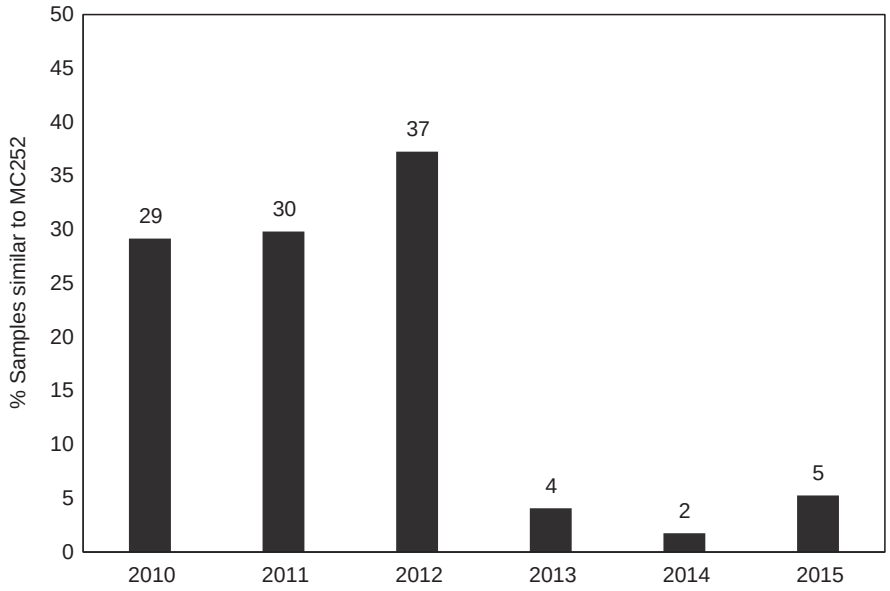

FIGURE 32.7 Percentage of coastal marsh sediment samples that are similar to MC252 source oil by year (2010–2015). The peak in 2012 is the result of the redistribution of buried oil by Hurricane Isaac.

limits that are absent in exploratory HCA and PCA analysis. Biclustering should be added to future work with the chemometric analysis of oil residues.

32.2.2 Weathering Pattern of MC252 Diasteranes and Regular Steranes

The qualitative analysis of the EICs for all the "oiled" surface sediment samples has led to a postulated weathering pattern of MC252 diasteranes and regular steranes, shown in Fig. 32.8. In Fig. 32.8, fresh and slightly weathered MC252 oil is represented by what we will identify as "pattern A;" moderately weathered MC252 oil is represented by what we will identify as "pattern AB;" severely weathered MC252 oil is represented by what we will identify as "pattern B;" and what we will identify as "pattern C" represents a pattern other than MC252 oil. Chemometric analysis was also used to validate the proposed MC252 diasteranes and regular steranes weathering pattern classification. All "oiled" surface sediment samples were qualitatively sorted as having pattern A, AB, B, or C in the initial stages of the oil source fingerprinting process. Then, after chemometric analysis, the samples within each cluster of the m/z 217 peak intensity HCA dendrograms were analyzed on an individual basis to determine if each cluster was dominated by pattern A, AB, B, or C.

A total of 49 of the 295 "oiled" coastal marsh sediment samples clustered with fresh MC252 oil based on the m/z 217 peak intensity data. Of these 49 samples, 78% were pattern A, 12% were pattern AB, and 10% were pattern B. The average concentration of total targeted aromatics was 24 parts per million (ppm) in the 49 samples that clustered with MC252 oil (minimum = 0.21ppm, maximum = 360 ppm). Further, the number of samples clustering with MC252 oil was much lower than the number of samples that were a qualitative match to MC252 oil, and samples that were qualitatively determined to be pattern A or AB didn't always cluster with MC252 oil. The reason for this could be due to settings used to determine clusters in the HCA dendrogram, the sum of squares approach used by HCA for determining clusters, or weathering within the oil biomarker EIC. For future spills, a weathered source oil sample should be included as another quality control sample in each analysis batch to improve the chemometric results, especially when an oil spill event will span several years.

Weathering from pattern A to AB to B significantly affects the m/z 217 chromatographic profile, which in turn will affect the chemometric pattern recognition algorithm. Therefore, if an oiled sample has significant differences in peak intensities due to weathering, it will be in a cluster other than MC252 even if it would be qualitatively matched to MC252. Also, there will be reoiling events that can distribute sequestered oil residues which have not undergone significant weathering caused by anaerobic conditions (i.e., buried oil), like Hurricane Isaac in 2012, and may result in a spike of patterns A and AB in near-surface sediments. The current inference is that MC252 oil residues with pattern A or AB are weathered to pattern B in near-surface marsh sediments, and to better

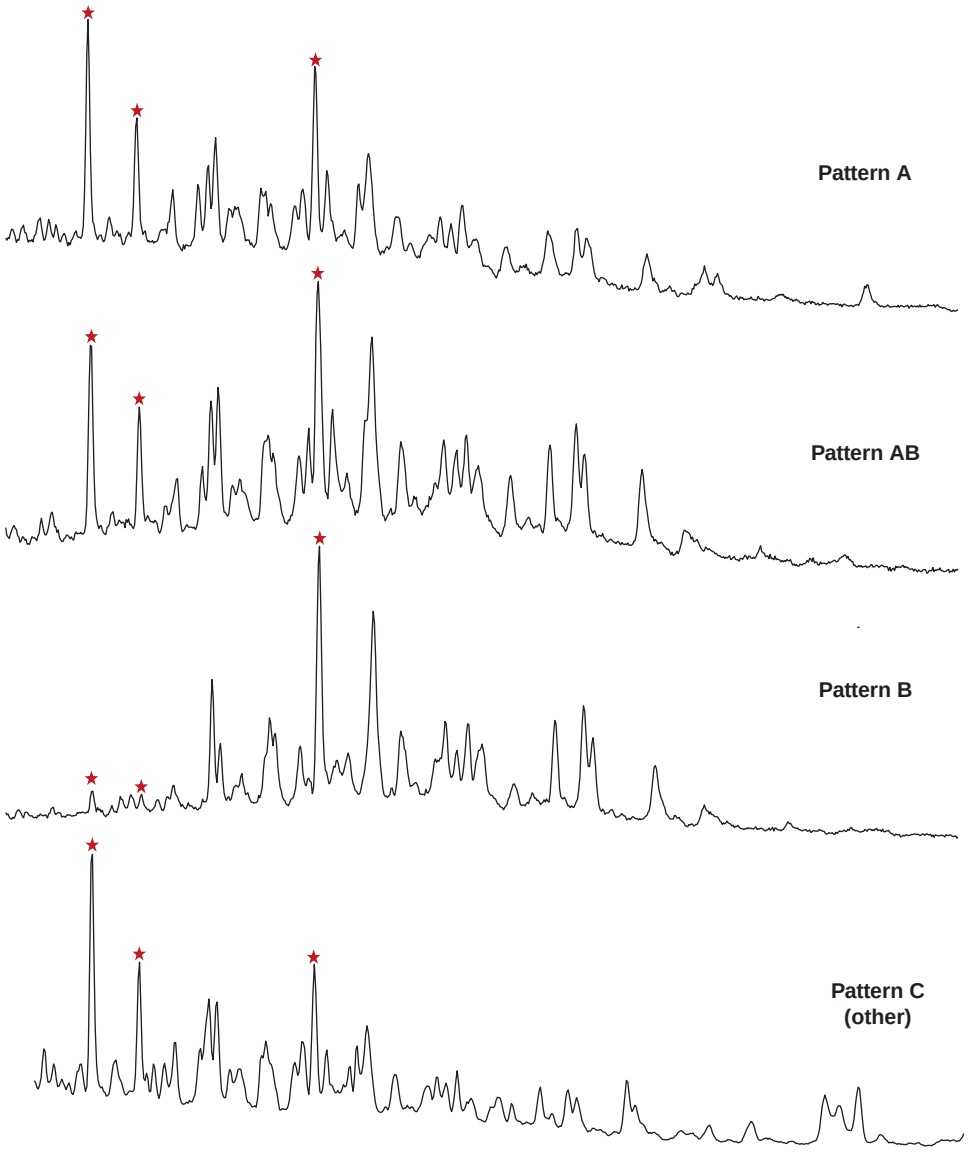

FIGURE 32.8 Weathering pattern of MC252 diasteranes and regular steranes (m/z 217). Pattern A: Fresh to slightly weathered MC252 oil. Pattern AB: Moderately weathered MC252 oil. Pattern B: Severely weathered MC252 oil. Pattern C: Other than MC252 oil. Stars highlight the most obvious peak differences between each pattern.

understand the complex interactions of oil residues in dynamic Louisiana coastal marsh environments, a series of mesocosm experiments are currently underway. The implementation of chemometric analysis to validate the proposed weathering of MC252 diasteranes and regular steranes was valuable overall; however, it was not absolute in clustering all oil residues with pattern A or AB with fresh MC252 source oil. This underscores the importance of using multiple oil source fingerprinting approaches and adapting these approaches to fit the unique circumstances of each oil spill.

32.2.3 Buried MC252 Oil Residues

The persistence of MC252 oil residues in Bay Jimmy, LA can be seen in Figs. 32.1 and 32.9. The chromatograms in Fig. 32.9 are from 2013 and 2016, 3 and 6 years after the DWH oil spill. These buried oil samples are a match to MC252 oil based on diagnostic biomarker ratio analysis and chemometric analysis. The diagnostic biomarker ratio analysis of buried oil in Bay Jimmy was accomplished by expanding the previous list of 15 MC252 diagnostic ratios (Table 32.2) to a suite of 24 ratios given in Table 32.3. The 24 MC252 ratios met the <5% RSD criteria

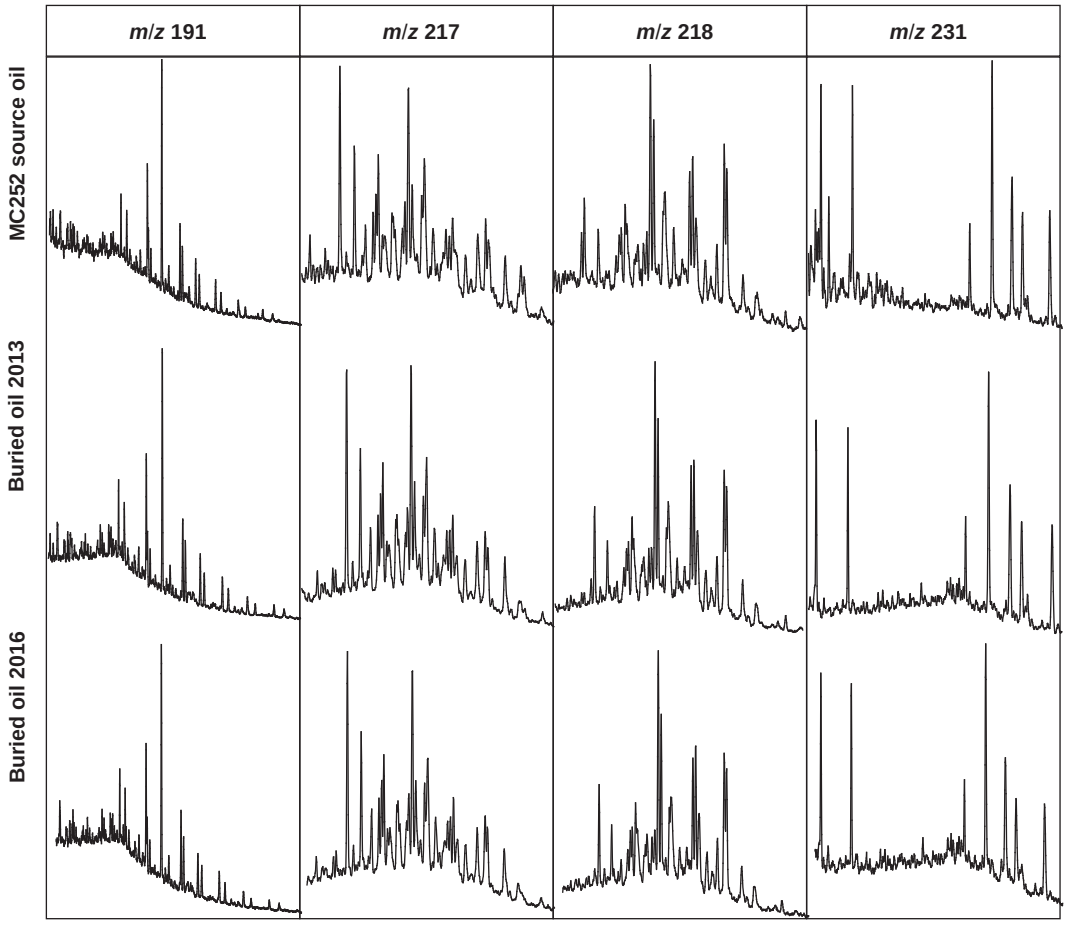

FIGURE 32.9 Biomarker EICs of buried oil collected in Bay Jimmy, LA from 2013 and 2016 compared to MC252 oil. These buried oil samples from Bay Jimmy were a match to MC252 source oil based on diagnostic ratio analysis and chemometrics.

described earlier in Section 32.2.1.1 and were based on 15 replicate analyses of the MC252 source oil. A final score (i.e., the percentage of the 24 ratios that matched MC252 oil based upon the CEN (2012) CD criteria) was calculated for each buried oil residue and based on the score, the sample was either a match (87–100%), probable match (79–86%), or inconclusive (<79%) to MC252 oil. These categories were established by analyzing both fresh and weathered MC252 crude oil, which provided information on how weathering affected the diagnostic biomarker ratio results for MC252 oil. Fresh MC252 source oil had scores that ranged from 87% to 100% with an average score of 93% ($\pm 3.0\%$, $n = 12$), while weathered MC252 oil had scores that ranged from 79% to 91% with an average score of 87% ($\pm 5.7\%$, $n = 12$). Therefore, the "match" and "probable match" categories were set based on the biomarker ranges identified in the fresh and weathered MC252 source oil and were used to oil source fingerprint buried oil in sediment cores from Bay Jimmy.

It is essential to detect and determine the vertical and lateral distribution of buried oil in Louisiana coastal salt marsh sediments to determine its long-term fate and potential redistribution during future tropical weather events; however, this is logistically very challenging. The most commonly used approach in detecting and determining oil distribution in marsh sediments is to take near-surface sediment samples that may not account for oil buried >15 cm below the marsh surface. Thus, sediment core sampling would be a more appropriate technique for detecting such buried oil; however, the vertical and lateral distribution of oil in the marsh is very patchy and would require the collection of many sediment cores followed by intensive and expensive lab analyses. More importantly, intensive sediment coring itself can adversely affect the fragile coastal marshes by promoting further erosion and land loss in these ecosystems.

In an effort to nonevasively screen for the vertical and lateral presence of subsurface DWH petroleum hydrocarbons in the coastal marshes, a real-time soil–gas probe monitoring system was deployed and tested both in the laboratory and in Barataria Bay, Louisiana. The small diameter, real-time soil–gas probe can be manually

TABLE 32.3 List of MC252 Diagnostic Ratios used for Oil Source Fingerprinting of Buried Oil in Bay Jimmy, LA

Class	Diagnostic ratio[a]
Tri- and pentacyclic triterpanes (hopanes) (*m*/*z* 191)	C27Ts/C27Tm
	C29aB/C29Ts
	C29aB/C30aB
	C31aB(S + R)/C32aB(S + R) + C33aB(S + R)
	C32aB(S + R)/C31aB(S + R) + C33aB(S + R)
	C33aB(S + R)/C31aB(S + R) + C32aB(S + R)
Diasteranes and regular 14α(*H*)-steranes (*m*/*z* 217)	C27DBS/C27DBR
	C29DBaS/C29DBaR
	C28aaR/C29aaR
	C29aaS/C29aaR
	C29BBR/C29BBS
	C29aaS/C29aa(R + S)
	C29BB(R + S)/C29aa(R + S)
14β(*H*)-Steranes (*m*/*z* 218)	C27BBR/C27BBS
	C28BBR/C28BBS
	C29BBR/C29BBS
	C27BB(R + S)/[C28BB(R + S) + C29BB(R + S)]
	C28BB(R + S)/[C27BB(R + S) + C29BB(R + S)]
	C29BB(R + S)/[C27BB(R + S) + C28BB(R + S)]
Triaromatic steroids (*m*/*z* 231)	C20TA/C21TA
	SC26TA/SC28TA
	RC27TA/RC28TA
Interion biomarker ratios (*m*/*z* 218/191)	C27BB(R + S)/C30aB
	C29BB(R + S)/C30aB

[a]*Compound names for abbreviations are provided in Table 32.1 and peaks are labeled in Figure 32.4.*

inserted into multiple sampling locations followed by measuring petroleum-related hydrocarbon vapors using a handheld photoionization detector (PID) monitoring device (Devine et al., 2014). The PID detects the vapors coming out of the buried oil and provides an indication of the presence of fairly unweathered oil, as well as a range of total petroleum hydrocarbons. PID monitoring allows for sediment sampling decisions to be made directly in the field and causes minimal disturbance in the coastal marsh environment. Sediment samples can be collected concurrently with the PID measurements and the presence of oil residues in the sediments can then be confirmed by analysis on laboratory analytical instrumentation with more specific detectors, like GC/MS or GC/MRM. Future research and development of nondestructive sampling techniques is imperative, especially for fragile ecosystems, as it greatly reduces the number of samples collected and subsequent laboratory analysis.

32.3 SUMMARY

The analysis of over 700 sediment samples collected throughout Louisiana coastal salt marsh environments has demonstrated that the fate of oil residues in these environments is greatly dependent on the dynamics of the ecosystem itself. The best case scenario for weathering and reduction of oil residues is for the residues to remain on or near the aerobic surface where they can be acted upon by the indigenous and adapted microorganism populations and by other weathering processes like photooxidation. Biomarker weathering is most prominent

in the near-surface (top 5 cm) sediment samples collected throughout Bay Batiste, Bay Jimmy, and Terrebonne Bay, wherein the weathering of the diasteranes and regular steranes is occurring in a predictable pattern (i.e., from pattern A to AB to B). The worst case scenario for the persistence of oil residues is to become buried and incorporated into the anaerobic soil layer where the residues have the potential to remain relatively unweathered for long periods of time. This phenomenon was observed in sediment cores sampled in Bay Jimmy, LA with buried oil residue at ~17 cm below the marsh surface. Buried oil in Louisiana coastal salt marsh environments represents a potential threat to these ecosystems. The redistribution of buried oil will occur during storm or hurricane events, as shown by the redistribution of MC252 oil in Bay Batiste, LA after Hurricane Isaac.

Oil residues deposited in Louisiana coastal salt marshes represent a unique challenge to oil source fingerprinting compared to oily matrices. Matrix interferences in organic-rich marsh sediments and severe weathering of conventionally stable oil biomarker compounds confounded the ability to maintain strict adherence to the quantitative oil source fingerprinting criteria set forth by the CEN (2012) methodology. Yet, qualitative oil source fingerprinting and two other quantitative techniques—HCA and PCA—were used to determine if oil residues detected in marsh sediment samples were MC252 oil from the DWH oil spill. The qualitative and quantitative methods were able to utilize GC/MS data generated from the standard analysis used for quantitating a targeted list of petroleum-related normal alkanes, isoprenoids, and PAHs, with oil biomarkers providing the greatest distinction between MC252 and other "genetically" related South Louisiana crude oils. Weathering of some biomarkers, particularly steranes and diasteranes was evident in the MC252 oil residues, which when recognized did not inhibit the ability to identify MC252 residues in marsh sediments. Hence, each GC/MS analysis can result in multidimensional data interpretation, and this saves instrument time and analysis costs. In the end, there are benefits to each oil source fingerprinting technique and the use of multiple techniques will result in higher confidence levels when it comes to making match/nonmatch determinations. And, as Stout (2016) states, an analyst with ample experience in oil fingerprinting is necessary to look at all the data to determine what makes sense.

Acknowledgments

Funding for this research was provided by the Gulf of Mexico Research Initiative, Coastal Waters Consortium. Reference to any specific commercial products, process, or service by trade name, trademark, manufacturer, or otherwise does not constitute or imply its endorsement, recommendation, or favoring by the authors. Data are publicly available through the Gulf of Mexico Research Initiative Information & Data Cooperative (GRIIDC) at https://data.gulfresearchinitiative.org.

References

Adhikari, P.L., Maiti, K., Overton, E.B., 2015. Vertical fluxes of polycyclic aromatic hydrocarbons in the northern Gulf of Mexico. Mar. Chem. 168, 60–68.

Adhikari, P.L., Maiti, K., Overton, E.B., Rosenheim, B.E., Marx, B.D., 2016. Distributions and accumulation rates of polycyclic aromatic hydrocarbons in the northern Gulf of Mexico sediments. Environ. Pollut. 212, 413–423.

Adhikari, P.L., Wong, R.L., Overton, E.B., 2017. Application of enhanced gas chromatography/triple quadrupole mass spectrometry for monitoring petroleum weathering and forensic source fingerprinting in samples impacted by the Deepwater Horizon oil spill. Chemosphere 184, 939–950.

Aeppli, C., Nelson, R.K., Radović, J.R., Carmichael, C.A., Valentine, D.L., Reddy, C.M., 2014. Recalcitrance and degradation of petroleum biomarkers upon abiotic and biotic natural weathering of Deepwater Horizon oil. Environ. Sci. Technol. 48, 6726–6734.

ASTM 5739-00, 2000. Oil Spill Source Identification by Gas Chromatography and Positive Ion Electron Impact Low Resolution Mass Spectrometry. ASTM International: West Conshohocken, PA.

Atlas, R.M., 1981. Microbial degradation of petroleum hydrocarbons: an environmental perspective. Microbiol. Rev. 45, 180–209.

Atlas, R.M., Hazen, T.C., 2011. Oil biodegradation and bioremediation: a tale of the two worst spills in US history. Environ. Sci. Technol. 45, 6709–6715.

Atlas, R.M., Stoeckel, D.M., Faith, S.A., Minard-Smith, A., Thorn, J.R., Benotti, M.J., 2015. Oil biodegradation and oil-degrading microbial populations in marsh sediments impacted by oil from the *Deepwater Horizon* well blowout. Environ. Sci. Technol. 49 (14), 8356–8366.

Camilli, R., Di Iorio, D., Bowen, A., Reddy, C.M., Techet, A.H., Yoerger, D.R., et al., 2012. Acoustic measurement of the Deepwater Horizon Macondo well flow rate. Proc. Nat. Acad. Sci. 109, 20235–20239.

Center for European Norms (CEN), October 2012. Oil spill identification—waterborne petroleum and petroleum products—part 2: analytical methodology and interpretation of results based upon GC–FID and GC–MS low resolution analysis. Technical Report 15522-2. Center for European Norms, Brussels, Belgium.

Daling, P.S., Faksness, L., Hansen, A.B., Stout, S.A., 2002. Improved and standardized methodology for oil spill fingerprinting. Environ. Forensics 3, 263–278.

DeLaune, R.D., Wright, A.L., 2011. Projected impact of *Deepwater Horizon* oil spill on US Gulf coast wetlands. Soil Sci. Soc. Am. 75 (5), 1602–1612.

DeLaune, R.D., Patrick Jr., W.H., Buresh, R.J., 1979. Effect of crude oil on a Louisiana *Spartina alterniflora* salt marsh. Environ. Pollut. 20, 21–31.

DeLaune, R.D., Gambrell, R.P., Pardue, J.H., Patrick Jr., W.H., 1990. Fate of petroleum hydrocarbons and toxic organics in Louisiana coastal environments. Estuaries 13 (1), 72–80.

Devine, C.E., Bennett, P., Synowiec, K., Nelson, S., Mohler, R., Einarson, M., 2014. Development and testing of a field screening method based on bubbling extraction and photoionization detection for measurement of benzene and total VOCs. Groundwater Monit. Remediat. 34 (3), 95–104.

Hansen, A.B., Daling, P.S., Faksness, L., Sorheim, K.R., Kienhuis, P., Duus, R., 2007. Emerging CEN methodology for oil spill identification. In: Wang, Z., Stout, S.A. (Eds.), Oil Spill Environmental Forensics: Fingerprinting and Source Identification. Academic Press, Burlington, MA, pp. 229–256.

Infometrix, Inc., 2014. Pirouette Multivariate Data Analysis Software, User's Guide, version 4.5. Infometrix, Inc., Bothell, WA. Available from <http://www.infometrix.com>.

Kaiser, S., Leisch, F., 2008. A toolbox for bicluster analysis in R. Department of Statistics, University of Munich. Technical Report Number 028. Available from <http://citeseerx.ist.psu.edu/viewdoc/download?doi=10.1.1.455.9770&rep=rep1&type=pdf>.

Lin, Q., Mendelssohn, I.A., 1996. A comparative investigation of the effects of South Louisiana crude oil on the vegetation of fresh, brackish, and salt marshes. Mar. Pollut. Bull. 32 (2), 202–209.

Lin, Q., Mendelssohn, I.A., 2012. Impacts and recovery of the *Deepwater Horizon* oil spill on vegetation structure and function of coastal salt marshes in the northern Gulf of Mexico. Environ. Sci. Technol. 46, 3737–3743.

Lorenson, T.D., Leifer, I., Wong, F.L., Rosenbauer, R.J., Campbell, P.L., Lam, A., et al., 2011. Biomarker chemistry and flux quantification methods for natural petroleum seeps and produced oils, offshore southern California. US Geological Survey Scientific Investigations Report 2011-5210, 45 p., OCS Study BOEM 2011-016.

McClenachan, G., Turner, R.E., Tweel, A.W., 2013. Effects of oil on the rate and trajectory of Louisiana marsh shoreline erosion. Environ. Res. Lett. 8 (2013), 044030.

McNutt, M.K., Camilli, R., Crone, T.J., Guthrie, G.D., Hsieh, P.A., Ryerson, T.B., et al., 2012. Review of flow rate estimates of the *Deepwater Horizon* oil spill. Proc. Nat. Acad. Sci. 109, 20260–20267.

Michel, J., Owens, E.H., Zengel, S., Graham, A., Nixon, Z., Allard, T., et al., 2013. Extent and degree of shoreline oiling: *Deepwater Horizon* oil spill, Gulf of Mexico, 2010. PLoS One 8 (6), e65087.

Natter, M., Keevan, J., Wang, Y., Keimowitz, A.R., Okeke, B.C., Ahjeong, S., et al., 2012. Level and degradation of *Deepwater Horizon* spilled oil in coastal marsh sediments and pore-water. Environ. Sci. Technol. 46, 5744–5755.

Nixon, Z., Zengel, S., Baker, M., Steinhoff, M., Fricano, G., Rouhani, S., et al., 2016. Shoreline oiling from the *Deepwater Horizon* oil spill. Mar. Pollut. Bull. 107, 170–178.

Oudot, J., Chaillan, F., 2010. Pyrolysis of asphaltenes and biomarkers for the fingerprinting of the Amoco-Cadiz spill after 23 years. Compt. Rend. Chim. 13, 548–552.

Overton, E.B., McFall, J.A., Mascarella, S.W., Steele, C.F., Antoine, S.A., Politezer, I.R., et al., 1981. Identification of petroleum residue sources after a fire and oil spill. Proc. Int. Oil Spill Conf. 1981 (1), 541–546.

Overton, E.B., Wade, T.L., Radović, J.R., Meyer, B.M., Miles, M.S., Larter, S.R., 2016. Chemical composition of Macondo and other crude oils and compositional alterations during oil spills. Oceanography 29 (3), 50–63.

Peters, K.E., Walters, C.C., Moldowan, J.M., 2005. The Biomarker Guide, second ed Cambridge University Press, Cambridge, UK.

Peters, K.E., Ramos, L.S., Zumberge, J.E., Valin, Z.C., Scotese, C.R., Gautier, D.L., 2007. Circum-Artic petroleum systems identified using decision-tree chemometrics. Am. Assoc. Petrol. Geol. Bull. 91 (6), 877–913.

Peters, K.E., Hostettler, F.D., Lorenson, T.D., Rosenbauer, R.J., 2008. Families of Miocene Monterey crude oil, seep, and tarball samples, coastal California. Am. Assoc. Petrol. Geol. Bull. 92 (9), 1131–1152.

Peters, K.E., Coutrot, D., Nouvelle, X., Ramos, L.S., Rohrback, B.G., Magoon, L.B., et al., 2013. Chemometric differentiation of crude oil families in the San Joaquin Basin, California. Am. Assoc. Petrol. Geol. Bull. 97 (1), 103–143.

Prince, R.C., Walters, C.C., 2007. Biodegradation of oil hydrocarbons and its implications for source identification. In: Wang, Z., Stout, S.A. (Eds.), Oil Spill Environmental Forensics: Fingerprinting and Source Identification. Academic Press, Burlington, MA, pp. 349–379.

Rabalais, N.N., Turner, R.E., 2016. Effects of the Deepwater Horizon oil spill on coastal marshes and associated organisms. Oceanography 29 (3), 150–159.

Radović, J.R., Aeppli, C., Nelson, R.K., Jimenez, N., Reddy, C.M., Bayona, J.M., et al., 2014. Assessment of photochemical processes in marine oil spill fingerprinting. Mar. Pollut. Bull. 79, 268–277.

Ramsey III, E., Meyer, B.M., Rangoonwala, A., Overton, E., Jones, C.E., Bannister, T., 2014. Oil source-fingerprinting in support of polarimetric radar mapping of Macondo-252 oil in Gulf Coast marshes. Mar. Pollut. Bull. 89, 85–95.

Reddy, C.M., Eglinton, T.I., Hounshell, A., White, H.K., Xu, L., Gaines, R.B., et al., 2002. The West Falmouth oil spill after thirty years: the persistence of petroleum hydrocarbons in marsh sediments. Environ. Sci. Technol. 36, 4754–4760.

Ryerson, T.B., Camilli, R., Kessler, J.D., Kujawinski, E.B., Reddy, C.M., Valentine, D.L., et al., 2012. Chemical data quantify *Deepwater Horizon* hydrocarbon flow rate and environmental distribution. Proc. Nat. Acad. Sci. 109 (50), 20246–20253.

Shamir, R., Maron-Katz, A., Tanay, A., Linhart, C., Steinfeld, I., Sharan, R., et al., 2005. EXPANDER—an integrative program suite for microarray data analysis. BMC Bioinform. 6, 232. Available from <http://bmcbioinformatics.biomedcentral.com/articles/10.1186/1471-2105-6-232>.

Stout, S.A., 2016. Oil spill fingerprinting method for oily matrices used in the *Deepwater Horizon* NRDA. Environ. Forensics 17 (3), 218–243.

Stout, S.A., Payne, J.R., 2016. Chemical composition of floating and sunken in-situ burn residues from the *Deepwater Horizon* oil spill. Mar. Pollut. Bull. 108, 186–202.

Stout, S.A., Wang, Z., 2007. Chemical fingerprinting of spilled or discharged petroleum –methods and factors affecting petroleum fingerprints in the environments. In: Wang, Z., Stout, S.A. (Eds.), Oil Spill Environmental Forensics: Fingerprinting and Source Identification. Academic Press, Burlington, MA, pp. 1–54.

Stout, S.A., Uhler, A.D., McCarthy, K.J., Emsbo-Mattingly, S., 2002. Chemical fingerprinting of hydrocarbons. In: Murphy, B.L., Morrison, R.D. (Eds.), Introduction to Environmental Forensics. Academic Press, London, UK, pp. 137–260.

Tanay, A., Sharan, R., Shamir, R., 2002. Discovering statistically significant biclusters in gene expression data. Bioinformatics 18 (S1), S136–S144. Available from <https://bi.snu.ac.kr/SEMINAR/ISMB2002/ISMB2002/S136PPT.pdf>.

Tarr, M.A., Zito, P., Overton, E.B., Olson, G.M., Adhikari, P.L., Reddy, C.M., 2016. Weathering of oil spilled in the marine environment. Oceanography 29 (3), 126–135.

Teal, J.M., Farrington, J.W., Burns, K.A., Stegeman, J.J., Tripp, B.W., Woodin, B., et al., 1992. The West Falmouth oil spill after 20 years: fate of fuel oil compounds and effects on animals. Mar. Pollut. Bull. 24 (12), 607–614.

Turner, R.E., Overton, E.B., Meyer, B.M., Miles, M.S., McClenachan, G., Hooper-Bui, L., et al., 2014. Distribution and recovery trajectory of Macondo (Mississippi Canyon 252) oil in Louisiana coastal wetlands. Mar. Pollut. Bull. 87, 57–67.

U.S. Department of Commerce, National Oceanic and Atmospheric Administration, Office of Response and Restoration, Emergency Response Division (NOAA-ERD), 2012. Responding to Environmental Catastrophes: An Evolving History of NOAA's Involvement in Oil Spill Response. Available from <http://celebrating200years.noaa.gov/transformations/spill_response/welcome.html#tech>.

U.S. Department of the Interior, 2010. Press Release, August 2010, US Scientific Teams Refine Estimates of Oil Flow from BP's Well Prior to Capping. Available from <http://app.restorethegulf.gov/release/2010/08/02/us-scientific-teams-refine-estimates-oilflow-bps-well-prior-capping>.

Wang, Z., Fingas, M., 1995. Differentiation of the source of spilled oil and monitoring of the oil weathering process using gas chromatography-mass spectrometry. J. Chromatogr. 712, 321–343.

Wang, Z., Fingas, M., 2003. Development of oil hydrocarbon fingerprinting and identification techniques. Mar. Pollut. Bull. 47 (9–12), 423–452.

Wang, Z., Fingas, M., Owens, E.H., Sigouin, L., Brown, C.E., 2001. Long-term fate and persistence of the spilled *Metula* oil in a marine salt marsh environment: degradation of petroleum biomarkers. J. Chromatogr. A 926, 275–290.

Wang, Z., Stout, S.A., Fingas, M., 2006. Forensic fingerprinting of biomarkers for oil spill characterization and source identification. Environ. Forensics 7, 105–146.

Zengel, S., Bernik, B.M., Rutherford, N., Nixon, Z., Michel, J., 2015. Heavily oiled salt marsh following the Deepwater Horizon oil spill, ecological comparisons of shoreline cleanup treatments and recovery. PLoS One 10 (7), e0132324.

CHAPTER

33

Novel Biological Exposures Following the *Deepwater Horizon* Oil Spill Revealed by Chemical Fingerprinting

Scott A. Stout[1], *Eric Litman*[1], *Gregory Baker*[2] *and James S. Franks*[3]

[1]NewFields Environmental Forensics Practice, LLC, Rockland, MA, United States
[2]NOAA, Menlo Park, CA, United States [3]The University of Southern Mississippi, Ocean Springs, MS, United States

BIOGRAPHIES

Dr. Scott A. Stout is an organic geochemist with 28 years of petroleum and coal industry experience. Since receiving his Ph.D. from The Pennsylvania State University in 1988, he has served on the faculty at Southern Illinois University and as a researcher at Unocal Corp. and Battelle Memorial Institute. Since 2004, he has been a Sr. Consultant at NewFields Environmental Forensics, LLC in Massachusetts, serving clients in both government and industry. Dr. Stout has extensive experience in the chemical compositions of natural/shale gas-, crude oil-, coal-, gasoline-, diesel-, and other fuel-derived sources of contamination in terrestrial and aquatic environments. He has authored or coauthored over 150 papers published in scientific journals and scientific textbooks and has provided expert testimony in state, federal, and foreign courts. Along with Dr. Zhendi Wang, he has coedited two editions of the *Oil Spill Environmental Forensics*, also published by Elsevier. He is member of the Society of Environmental Forensics, Oil Spill Identification Network (OSINET; Bonn Agreement), and European Association of Organic Geochemists.

Eric Litman is an environmental scientist with 15 years of laboratory and consulting experience specializing in applied chemistry and technical project management. Since 2010, he has been a consulting scientist at NewFields Environmental Forensics Practice, LLC in Rockland, Massachusetts working in support of governmental and industrial clients. During this time he has managed a variety of regulatory and industrial site investigations focused on the chemical characterization of environmental contaminants and conducted extensive research during the NRDA investigation following the *Deepwater Horizon* oil spill. His research interests include the optimization of analytical techniques and the development of emerging environmental technologies.

Gregory Baker is an environmental scientist with the National Oceanic and Atmospheric Administration (NOAA). He has a bachelor's degree in biology from the University of California, San Diego, and a master's in environmental science from the University of San Francisco. Throughout 17 years with the US Environmental Protection Agency he managed water, wastewater, and hazardous and solid waste regulatory programs. Two of these years were spent in Micronesia as the Executive Officer of the Trust Territory Environmental Protection Board. Mr. Baker has been a scientists with NOAA since 1998 conducting natural resource damage assessments of hazardous waste sites (Duwamish River in Seattle, Portland Harbor in Oregon, Montrose Chemical Corporation in Los Angeles) and oil spills (*Deepwater Horizon* in the Gulf of Mexico, *Cosco Busan* in San Francisco, *New Carissa* in Oregon). He is a frequent speaker on natural resource injury assessment methods and is engaged in research on the chemistry and toxicity of heterocyclic compounds derived from petroleum.

Oil Spill Environmental Forensics Case Studies.
DOI: http://dx.doi.org/10.1016/B978-0-12-804434-6.00033-1

James S. Franks is a marine fisheries biologist with 35 years of research experience in the Gulf of Mexico. He is a senior research scientist with the University of Southern Mississippi's (USM) Center for Fisheries Research and Development at the Gulf Coast Research Laboratory (GCRL) in Ocean Springs, MS. Since receiving his M.S. from the University of Mississippi in 1968, he has served in various research capacities with the GCRL and the Mississippi Department of Marine Resources. He is adjunct research faculty with the USM Department of Coastal Sciences and associate faculty with the USM Graduate School. He has authored or coauthored over 50 scientific papers on the biology and ecology of marine fishes, with special interest given large pelagic fishes and their critical habitats. He coauthored the contingency guide to the protection of Mississippi coastal environments from spilled oil. He has served as Field Chief on numerous offshore research cruises in the Gulf of Mexico. He is a member of fisheries resource management committees and boards, including the Western Central Atlantic Ocean Fishery Commission Scientific Advisory Committee. He is a recent past-Chair of the Gulf and Caribbean Fisheries Institute.

33.1 INTRODUCTION

During the *Deepwater Horizon* (DWH) oil spill about 3.2 million barrels of crude oil was released into the northern Gulf of Mexico (GoM) over 87 days (April 20 to July 15, 2010) from the failed Macondo well, which was located 66-km offshore and 1500-m below the sea surface. The unique circumstances of the DWH spill, aided by the action of physical and chemical dispersion, subsea and surface currents, wind and waves, spread the spilled Macondo oil throughout the deep benthos and water column and across the sea surface and shorelines in the northern GoM. As such, the ecological scope of the spill's impact was considered unprecedented (Trustees, 2016).

Graphic images of externally oiled animals and plants were widely distributed during the DWH oil spill. These images were in part used by the Trustees to establish the nature and extent of injuries from the DWH oil spill on the region's biota and other natural resources (water, sediment, etc.) and the services they provide (and also on human recreational uses, which are not dealt with herein). In keeping with Oil Pollution Act (OPA, 1990) regulations, the State and Federal Trustees performed the natural resource damage assessment (NRDA) wherein they sought to (1) determine the pathway(s) by which the spilled oil made its way to the area's natural resources, (2) provide direct or indirect evidence that those resources were exposed to the spilled oil, and (3) determine the nature and extent of natural resource injuries and the loss of services they provide (Trustees, 2016).

Chemical fingerprinting played a significant role in the DWH NRDA in both determining pathways and demonstrating exposure through the chemical analysis of over 30,000 field (oil, water, sediment, soil, and biological) samples. Samples' chemical fingerprints were compared to those of variably weathered Macondo oil collected over time from many areas in order to establish the presence and character of spilled oil in different habitats of the northern GoM, including the deep seafloor (e.g., Stout and Payne, 2016; Stout et al., 2016a, 2017), the deep-sea water column and "plume" (e.g., Payne and Driskell, 2015), the sea surface and shorelines (Stout et al., 2016b), and nearshore soils and sediments (Emsbo-Mattingly and Martin, 2015). Chemical fingerprinting of biological samples was used to demonstrate direct exposure to DWH oil on external wipe samples collected from sea turtles (Stout, 2015a) and dolphins (Stout, 2015b), external solvent rinsate samples from shoreline vegetation (Emsbo-Mattingly and Martin, 2015), and tissue samples from benthic invertebrates (Douglas and Liu, 2015), the latter including deep-sea red crabs (see Douglas et al., this volume; Chapter 30).

In this chapter, we present selected chemical fingerprinting for four different biological natural resources collected following the DWH oil spill that serve to demonstrate some novel biological exposures to Macondo oil that occurred due to the DWH oil spill. These four biological sample types are (1) floating *Sargassum*, (2) deep-sea coral, (3) osprey nests, and (4) dolphin lung tissue, as described sequentially in separate sections below.

33.2 SARGASSUM

Sargassum is a genus of brown macroalgae, which includes two buoyant (floating) pelagic species (*S. natans* and *S. fluitans*) that are found exclusively in the Atlantic Ocean, including the GoM. (Hereafter, we refer to these two pelagic species as *Sargassum*.) *Sargassum* can form floating mats that stretch tens of kilometers across the ocean. This floating habitat provides food, refuge, and breeding grounds for fishes, sea turtles (particularly

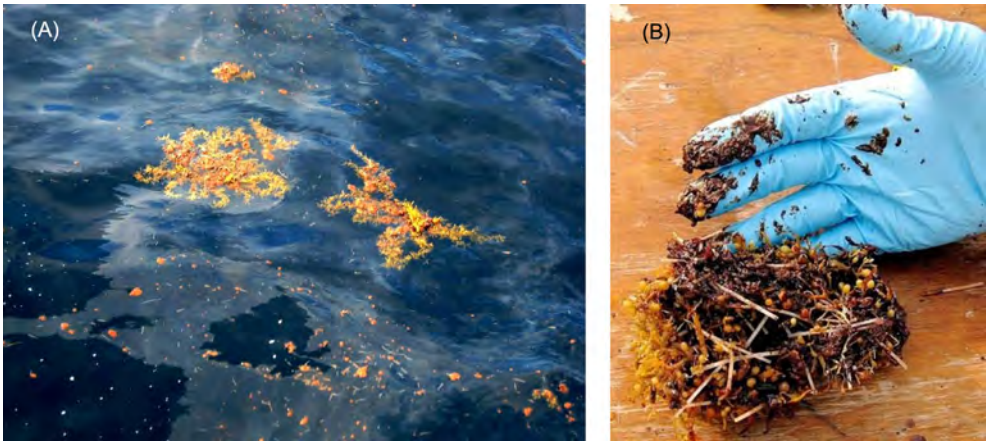

FIGURE 33.1 Photographs of (A) floating *Sargassum* in surface oil and (B) visibly oiled *Sargassum* collected May 23, 2010 (SARG3). Photos by J. Franks. *Reprinted with permission from Manolito G. Torralba, M.G., Franks, J.S., Gomez, A., Yooseph, S., Nelson, K.E., Nelson, et al. (2017) Effect of Macondo prospect 252 oil on microbiota associated with pelagic Sargassum in the Northern Gulf of Mexico. Microbial. Ecol. 73: 91–100.*

juveniles), marine birds, and invertebrates (crabs, shrimp, etc.). As such, *Sargassum* represents an important biological resource in the northern GoM (SAFMC, 2002).

Aerial surveys showed *Sargassum* was visibly exposed to floating Macondo oil during the DWH spill (Powers et al., 2013). Our own ground observations (JF) made during Sargassum collections confirmed large expanses of oil-infused Sargassum were floating among vast surface oil sheens (Fig. 33.1). High-resolution aerial photography and satellite imagery were used to estimate *Sargassum* coverage within the integrated floating oil footprint ranged from 736 and 1296 km^2 (Hu et al., 2016). The chemical fingerprinting results described below provide "on-the-water" validation that floating *Sargassum* was directly exposed to the spilled Macondo oil, and the chemical nature of that oil.

33.2.1 Sargassum—Samples & Methods

Table 33.1 summarizes the *Sargassum* samples analyzed, which consisted of 249 floating pelagic *Sargassum* samples collected from the sea surface as grab samples between May 19, 2010 and September 26, 2011. Only six samples were collected *during* the active 87-day spill between May 19 and 25, 2010 at three locations (2 samples from each location) referred to herein as Location A (~80 km northeast of the wellhead), Location B (~170 km southeast of the wellhead), and Reference (~480 km south of the wellhead; Fig. 33.2).

In addition, 3 to 4 months after the spill ended (on July 15, 2010), 17 additional floating *Sargassum* samples were collected between Oct. 27 and Nov. 13, 2010. Nine of these samples were collected at Location C (~100 to 150 km northeast of the wellhead) and the remaining eight samples were collected from a Reference location (~530 km east of the well head nearshore of Tampa Bay; Fig. 33.2).

Finally, 226 floating *Sargassum* samples were collected on various NRDA sampling cruises conducted between May and September 2011, i.e., 10 to 14 months after the spill ended (Table 33.1). These samples were collected 6 to 150 km, mostly north and to the west, of the Macondo wellhead (Fig. 33.2).

Only 1 of 249 *Sargassum* samples collected was visibly oiled (Fig. 33.1B). This sample was collected from Location B in May 2010 during the active DWH spill and was thereby prepared and analyzed as oily material. Oil was physically scraped from the exterior of this visibly oiled *Sargassum* sample, spiked with recovery surrogates, diluted with dichloromethane (DCM) and then passed through a filter containing glass wool and sodium sulfate. After filtration a 1-mL subaliquot was taken and spiked with internal standard for analysis. No silica gel fractionation of this sample was necessary.

All remaining 248 samples collected contained no obvious visible evidence of oil. These samples were prepared as vegetative tissues. These tissues were spiked with recovery surrogates and serially extracted (3 ×) using fresh DCM and agitation using a stainless steel tissue homogenization probe. The serial extracts were combined, dried with sodium sulfate, concentrated, and spiked with internal standards prior to analysis. Aliquots of each extract were put through a further silica gel fractionation to partition the aliphatic biomarker compounds from the aromatics, allowing greater resolution in quantifying aliphatic petroleum biomarkers.

TABLE 33.1 Inventory of Sargassum Samples collected from the Sea Surface During and Following the *Deepwater Horizon* Oil Spill that Were Analyzed via Chemical Fingerprinting to Determine Presence of Macondo Oil.

				Macondo oil present?	
NRDA study name	**Sample date range**	**Spill**	**Sample count**	**Yes**	**No**
Sargassum Samples-USM	May 2010	During	6	4	2[a]
MammalTurtle-Preassessment-Sargassum—2010	Oct–Nov 2010	After	17	0	17[b]
Wes Bordelon Cruise 08	May–June 2011	After	50	0	50
MammalTurtle-Preassessment-Sargassum—2011	May–Sept 2011	After	76	0	76
Tommy Munro Cruise 01	July–Aug 2011	After	44	0	44
Dry Tortugas Cruise 01 Leg 01	Aug. 2011	After	24	0	24
Dry Tortugas Cruise 01 Leg 02 2011	Aug–Sept 2011	After	12	0	12
Dry Tortugas Cruise 01 Leg 03	Sept. 2011	After	20	0	20
		Total	249	4	226

[a]*Reference locations.*
[b]*Includes eight reference locations.*
Additional sample details provided in Torralba et al. (2017).

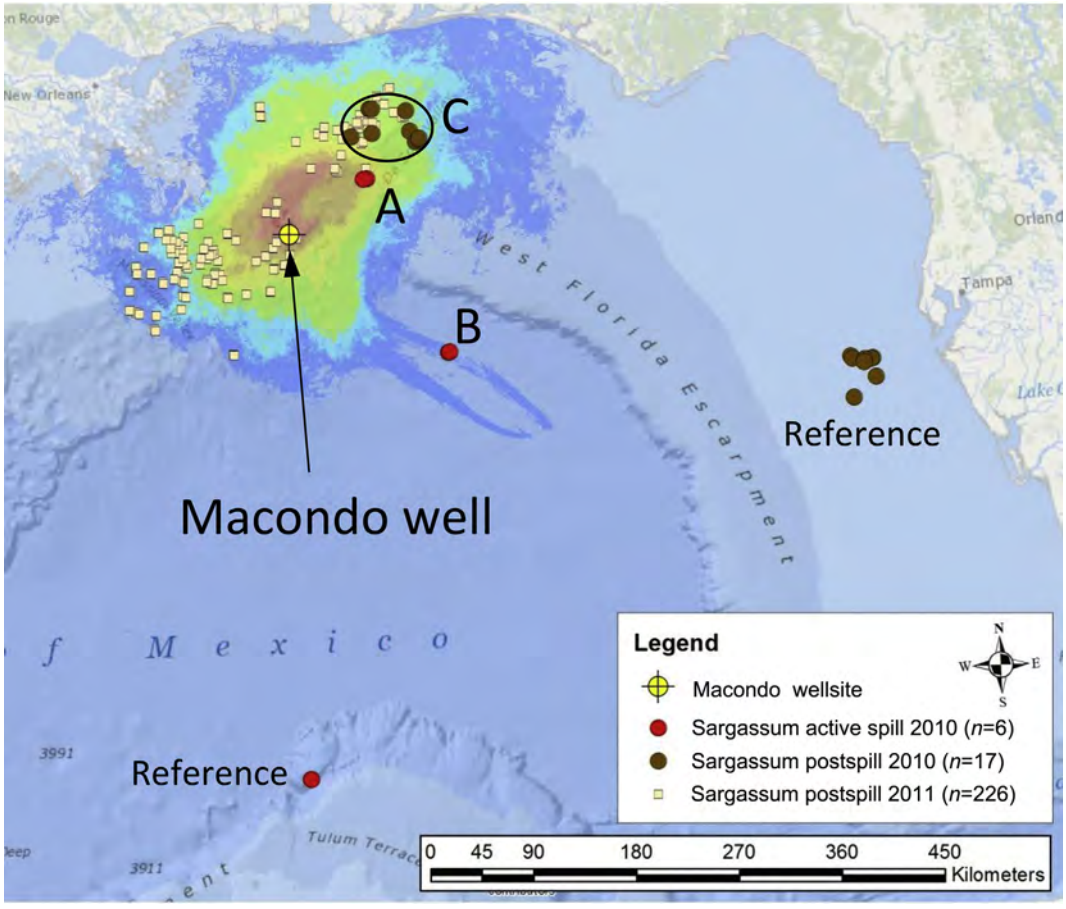

FIGURE 33.2 Maps showing the locations of *Sargassum* samples collected during the active spill, shortly after the spill in October–November 2010, and about 1 year after the spill in May–September 2011. Colored background shows cumulative surface oil "footprint" based on aerial and satellite imagery (after Graettinger et al., 2015). Red/dark area near center represents area where surface oiling existing more than 40 days during the active spill; blue/light area near margins represent area where surface oiling existed 1 to 5 days during the active spill.

All extracts were analyzed in accordance with NOAA (2014) as described in detail elsewhere (Douglas et al. 2015). Briefly, the single oily *Sargassum* sample was analyzed by gas chromatography–flame ionization detection (GC–FID) to obtain a detailed hydrocarbon fingerprint using a modified EPA Method 8015B. In addition, all 249 *Sargassum* sample extracts were analyzed by GC–mass spectrometry (MS) operated in the selected ion monitoring (SIM) acquisition mode to determine the concentration of (1) 61 semivolatiles (including decalins, polycyclic aromatic hydrocarbons (PAHs), alkylated PAH homologues, individual PAH isomers, and sulfur-containing aromatics) and (2) 54 tricyclic and pentacyclic triterpanes, regular and rearranged steranes, and triaromatic steroids (TASs; Table 33.2). TAS were not analyzed within the 248 silica-gel cleaned tissue extracts because these compounds are aromatic and do not elute in the aliphatic fraction containing the other biomarker compounds. The TAS were only analyzed in the oily sample. Concentrations of target compounds are reported in mg/kg of oil weight for the oily *Sargassum* sample and in μg/kg wet weight for the remaining 248 *Sargassum* tissue samples.

The chemical fingerprinting characteristics of each *Sargassum* sample were determined using oil spill fingerprinting methodology described in detail elsewhere (Stout, 2016). Briefly, this methodology involves the qualitative review of GC/FID chromatograms (for oily material only) and GC/MS extracted ion profiles, and the quantitative review of 29 diagnostic ratios (DRs) based upon measured concentrations of PAHs and petroleum biomarkers. For ease of fingerprinting comparison among matrices, all measured concentrations were normalized to the abundance of 17α(*H*),21β(*H*)-hopane (hopane) therein.

33.2.2 Sargassum—Results and Discussion

Table 33.1 provides a tabulated summary of the chemical fingerprinting results obtained for the samples studied. Looking first at the annual totals provided,

- All four samples collected from Locations A and B (Fig. 33.2) in May 2010 during the active DWH spill contained Macondo oil (while the two samples collected from the reference location contained no Macondo, or any other, oil); not surprisingly one of the oiled sample was the single sample that was visibly oiled (Fig. 33.1B).
- None of the nine samples collected from Location C (Fig. 33.2) in October and November 2010, 3 to 4 months after the spill ended, contained Macondo oil; the eight samples collected from the reference location contained no Macondo, or any other, oil.
- None of the 226 samples collected from May to September 2011, 10 to 14 months after the spill ended, contained Macondo, or any other, oil.

These general results indicate that the location and timing of *Sargassum* sample collection was critical in recognizing exposure of this resource to Macondo oil using hydrocarbon fingerprinting. The limited number and spatial extent of *Sargassum* samples collected during the active spill undoubtedly under-represented the extent to which floating *Sargassum* had been exposed to the oil during the active spill. Interpretation of aerial and satellite remote sensing data indicated there were between 736 and 1296 km^2 of *Sargassum* within the estimated 112,000 km^2 of sea surface found to have floating oil present for at least 1 day during the active spill (Graettinger et al., 2015; Hu et al., 2016). It is notable that all four *Sargassum* samples recognized herein to contain Macondo oil (Locations A and B) were collected from the sea surface in areas within the cumulative footprint of floating Macondo oil (Fig. 33.2).

Although floating oil was still observed in some locations for up to ~1 month after the spill ended in mid-July (Ramseur, 2010), none of the nine *Sargassum* samples collected from Location C in October or November 2010 contained any Macondo oil (Fig. 33.2). The apparent lack of oil in the nine *Sargassum* samples from Location C (collected 3 to 4 months after the spill) may be, at least in part, due to the widespread use of chemical dispersants in response to the spill. Specifically, over 1 million gallons of chemical dispersants (Corexit 9500/9527) were applied to surface waters of the GoM in response to the DWH spill, mostly within 80 km of the wellhead (BP, 2014). Mesocosm studies showed that the natural buoyancy of *Sargassum* was compromised when exposed to these dispersants or to chemically dispersed Macondo oil, and sunk within 24 to 48 hours of initial exposure (Powers et al., 2013). Perhaps for this reason, only *Sargassum* samples collected within days of exposure to the dispersants and/or chemically dispersed oil are likely to have remained afloat and been available for collection and chemical fingerprinting—during or only shortly after the spill ended. The more thorough sampling of 226 *Sargassum* samples in 2011 (Table 33.1; Fig. 33.2) showed no lingering Macondo oil had remained to impact *Sargassum* collected 10 to 14 months after the spill ended.

TABLE 33.2 Inventory of PAH and Biomarker Target Analytes and Abbreviations Used in Figures Herein

Abbrev	PAH and related analytes	Abbrev	Biomarker analytes
D0	*cis*/*trans*-Decalin	T4	C23 tricyclic terpane
D1	C1-decalins	T5	C24 tricyclic terpane
D2	C2-decalins	T6	C25 tricyclic terpane
D3	C3-decalins	T6a	C24 Tetracyclic Terpane
D4	C4-decalins	T6b	C26 tricyclic terpane-22S
BT0	Benzothiophene	T6c	C26 tricyclic terpane-22R
BT1	C1-benzo(*b*)thiophenes	T7	C28 tricyclic terpane-22S
BT2	C2-benzo(*b*)thiophenes	T8	C28 tricyclic terpane-22R
BT3	C3-benzo(*b*)thiophenes	T9	C29 tricyclic terpane-22S
BT4	C4-benzo(*b*)thiophenes	T10	C29 tricyclic terpane-22R
N0	Naphthalene	T11	18a(*H*)-22,29,30-Trisnorneohopane-Ts
N1	C1-naphthalenes	T11a	C30 tricyclic terpane-22S
N2	C2-naphthalenes	T11b	C30 tricyclic terpane-22R
N3	C3-naphthalenes	T12	17a(*H*)-22,29,30-Trisnorhopane-Tm
N4	C4-naphthalenes	T14a	17a/b(*H*),21b/a(*H*) 28,30-Bisnorhopane
B	Biphenyl	T14b	17a(*H*),21b(*H*)-25-Norhopane
DF	Dibenzofuran	T15	30-Norhopane
AY	Acenaphthylene	T16	18a(*H*)-30-Norneohopane-C29Ts
AE	Acenaphthene	X	17a(*H*)-Diahopane
F0	Fluorene	T17	30-Normoretane
F1	C1-fluorenes	T18	18a(*H*)&18b(*H*)-Oleananes
F2	C2-fluorenes	T19	Hopane
F3	C3-fluorenes	T20	Moretane
A0	Anthracene	T21	30-Homohopane-22S
P0	Phenanthrene	T22	30-Homohopane-22R
PA1	C1-phenanthrenes/anthracenes	T26	30,31-Bishomohopane-22S
PA2	C2-phenanthrenes/anthracenes	T27	30,31-Bishomohopane-22R
PA3	C3-phenanthrenes/anthracenes	T30	30,31-Trishomohopane-22S
PA4	C4-phenanthrenes/anthracenes	T31	30,31-Trishomohopane-22R
DBT0	Dibenzothiophene	T32	Tetrakishomohopane-22S
DBT1	C1-dibenzothiophenes	T33	Tetrakishomohopane-22R
DBT2	C2-Dibenzothiophenes	T34	Pentakishomohopane-22S
DBT3	C3-dibenzothiophenes	T35	Pentakishomohopane-22R
DBT4	C4-dibenzothiophenes	S4	13b(*H*),17a(*H*)-20S-Diacholestane
FL0	Fluoranthene	S5	13b(*H*),17a(*H*)-20R-Diacholestane
PY0	Pyrene	S8	13b(*H*),17a(*H*)-20S-Methyldiacholestane
FP1	C1-fluoranthenes/pyrenes	S12	14a(*H*),17a(*H*)-20S-Cholestane + 13b(*H*),17a(*H*)-20S-Ethyldiacholestane
FP2	C2-fluoranthenes/pyrenes	S17	14a(*H*),17a(*H*)-20R-Cholestane + 13b(*H*),17a(*H*)-20R-Ethyldiacholestane

(*Continued*)

TABLE 33.2 (*Continued*)

Abbrev	PAH and related analytes	Abbrev	Biomarker analytes
FP3	C3-fluoranthenes/pyrenes	S18x	Unknown sterane
FP4	C4-fluoranthenes/pyrenes	S19	13a(*H*),17b(*H*)-20S-Ethyldiacholestane
NBT0	Naphthobenzothiophenes	S20	14a(*H*),17a(*H*)-20S-Methylcholestane
NBT1	C1-Naphthobenzothiophenes	S24	14a(*H*),17a(*H*)-20R-Methylcholestane
NBT2	C2-naphthobenzothiophenes	S25	14a(*H*),17a(*H*)-20S-Ethylcholestane
NBT3	C3-Naphthobenzothiophenes	S28	14a(*H*),17a(*H*)-20R-Ethylcholestane
NBT4	C4-naphthobenzothiophenes	S14	14b(*H*),17b(*H*)-20R-Cholestane
BA0	Benz[*a*]anthracene	S15	14b(*H*),17b(*H*)-20S-Cholestane
C0	Chrysene/triphenylene	S22	14b(*H*),17b(*H*)-20R-Methylcholestane
BC1	C1-chrysenes	S23	14b(*H*),17b(*H*)-20S-Methylcholestane
BC2	C2-chrysenes	S26	14b(*H*),17b(*H*)-20R-Ethylcholestane
BC3	C3-chrysenes	S27	14b(*H*),17b(*H*)-20S-Ethylcholestane
BC4	C4-chrysenes	RC26/SC27	C26,20R- + C27,20S-triaromatic steroid
BBF	Benzo[*b*]fluoranthene	SC28	C28,20S-triaromatic steroid
BJKF	Benzo[*jk*]fluoranthene	RC27	C27,20R-triaromatic steroid
BAF	Benzo[*a*]fluoranthene	RC28	C28,20R-triaromatic steroid
BEP	Benzo[*e*]pyrene		
BAP	Benzo[*a*]pyrene		
PER	Perylene		
IND	Indeno[1,2,3-*cd*]pyrene		
DA	Dibenz[*a*,*h*]anthracene		
GHI	Benzo[*g*,*h*,*i*]perylene		

The chemical fingerprints for the four Macondo-oil-impacted *Sargassum* samples collected from Locations A and B in May 2010 were consistent with the presence of weathered Macondo oil. These four samples were identified as SARG4 and SARG1 (collected May 25, 2010; Location A) and SARG2 and SARG3 (collected May 23, 2010; Location B; Fig. 33.2). The last of these samples, SARG3, was the visibly oiled *Sargassum* shown in Fig. 33.1B. The GC/FID chromatogram for the visibly oiled *Sargassum* sample is shown, along with that of fresh Macondo oil, in Fig. 33.3. The oil present on the *Sargassum* consisted of a weathered Macondo oil quite typical of those found floating on the sea surface in the summer of 2010 (Stout et al., 2016b). The oil was dominated by a broad UCM and $C_{15}+$ *n*-alkanes that reached a maximum at *n*-C_{21}, indicating losses due predominantly to evaporation (Fig. 33.3B).

The distributions of PAHs and biomarkers in the four *Sargassum* samples studied that were impacted by Macondo oil were comparable to weathered Macondo oil collected from floating slicks and sheens during the active spill (Stout et al., 2016b). This comparability is demonstrated when the hopane-normalized distributions in the visibly oiled Sargassum sample are compared to those for average fresh and weathered (floating) Macondo oils (Fig. 33.4). The PAHs and biomarker in the other three floating *Sargassum* samples, which had not appeared visibly oiled, also exhibited comparable fingerprinting features, albeit these samples contained lower concentrations of oil (see below).

The weathered oil on *Sargassum* was dominated by 3-ring phenanthrenes (P0−PA4), having lost the more volatile and soluble 2-ring PAHs (N0−N4) and decalins (D0−D4) to the combined effects of evaporation and dissolution (Fig. 33.4A). Such PAH depletions were also typical of the floating oils collected during the active spill (Stout et al., 2016b). Some effect of photooxidation of the oil found on *Sargassum* is evidenced by the atypical pattern of PAHs among the naphthobenzothiophenes and benz(*a*)anthracenes/ chrysenes homologues. Specifically, these

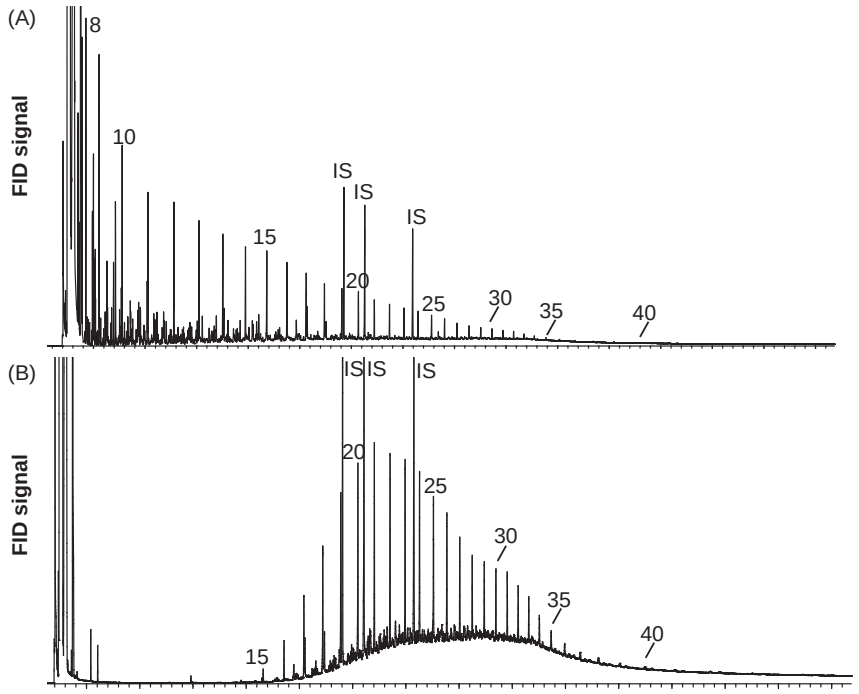

FIGURE 33.3 GC/FID chromatograms for (A) fresh Macondo oil and (B) weathered Macondo oil on floating *Sargassum* collected May 23, 2010 (SARG3) from location B (per Fig. 33.2). IS: internal standards; #—*n*-alkane carbon number.

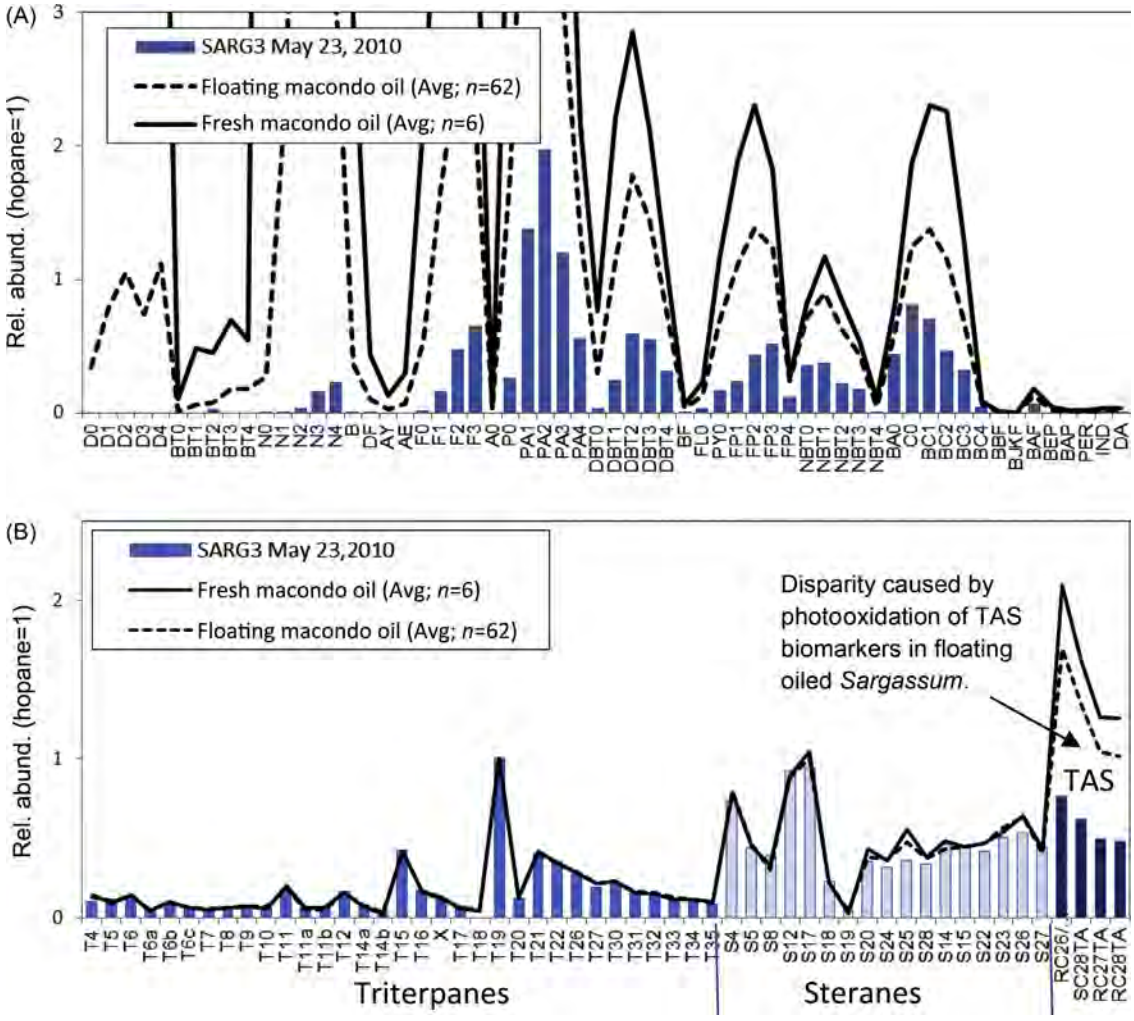

FIGURE 33.4 Comparison of hopane-normalized distributions of (A) PAH and sulfur-containing aromatics and (B) petroleum biomarkers in floating *Sargassum* collected May 23, 2010 (SARG3) from location B (per Fig. 33.2) compared to fresh and weathered (floating) Macondo oil. Fresh and weathered Macondo oil data from Stout et al. (2016b). See Table 33.2 for compound abbreviations.

homologues exhibited greater depletion of benz(*a*)anthracene over chrysene and relatively less depletion among the parent (nonalkylated) or C1-alkylated homologues, which is recognized as typical of photooxidation (e.g., Garrett et al., 1998; Plata et al., 2008; Radović et al., 2014). This feature was also observed among floating Macondo oils collected during the active DWH spill (Stout et al., 2016b).

The hopane-normalized distribution of biomarkers in the oiled *Sargassum* sample is highly comparable to those for the fresh and weathered (floating) oils collected during the spill (Fig. 33.4B). This is especially true among the triterpanes (T4 to T35) and steranes (S4 to S27), which exhibit the same profiles testifying to the persistence of these biomarker compounds during the weathering of floating oil. The oil from the *Sargassum*, however, exhibits a marked reduction in the relative abundance of TASs (TAS; four peaks to the far right; Fig. 33.4B). The reduction of these biomarker compounds is due to the effects of photooxidation on the floating oil, a phenomenon that has been observed in other Macondo oils collected from the sea surface and shorelines (Aeppli et al. 2012; Radović et al. 2014; Stout et al., 2016b).

Although less specific than chemical fingerprinting, the PAH concentrations measured on the floating *Sargassum* samples provided an additional line of evidence for exposure to Macondo oil. The concentration of TPAH50 in the biological tissue of the visibly oiled sample (Fig. 33.4A) was undoubtedly high, but because this sample was analyzed as an oil collected from the plant surface, the actual concentration of PAHs on the *Sargassum* tissue is unknown. However, the concentration of TPAH50 found on the other three *Sargassum* tissue samples collected from locations A and B during the active spill (in May 2010) that contained Macondo oil was calculated on a tissue wet weight basis.

Table 33.3 shows the total concentration of PAH analytes [TPAH50; sum of 50 analytes spanning from naphthalene to benzo(*ghi*)perylene] in the three (nonvisibly) oiled *Sargassum* samples from May 2010 contained 84, 4980, and 5162 μg/kg (tissue wet wt.) of TPAH50. In contrast, the two nonoiled *Sargassum* collected from the reference location in May 2010 (480 km south of the wellhead; Fig. 33.2) contained only 11 and 13 μg/kg; i.e., about 10- to 500-times lower than the oiled *Sargassum* (Table 33.3). Both of these reference location *Sargassum* tissues contained only trace concentrations of pyrogenic PAHs, viz., phenanthrene, fluoranthene, pyrene, and chrysene, most likely derived from atmospheric deposition of combustion particles. The markedly higher TPAH concentrations, and petrogenic character of these PAHs, supports the chemical fingerprinting results and confirms these three *Sargassum* samples were exposed to Macondo oil (even though it was not visibly evident).

The 17 *Sargassum* samples collected only 3 to 4 months after the spill ended were also not visibly impacted with oil, and chemical fingerprinting could not identify any samples that contained Macondo oil (Table 33.1). All 17 of these (apparently) nonoiled *Sargassum* samples from the Fall of 2010 contained only 11 ± 5 μg/kg (tissue wet wt.), which is comparable to the reference location *Sargassum* samples collected during the active spill (Table 33.3). These 17 *Sargassum* samples also contained only low concentrations of pyrogenic PAHs, indicating they too only contained "background" PAHs likely derived from atmospheric deposition of combustion particles. Thus, our limited data suggest that within 3 to 4 months of the spill the *Sargassum* sampled had no evidence of Macondo oil impact despite being collected from an area of the sea where floating oil had been present during the spill (Location C, Fig. 33.2). Perhaps not surprising given this result, none of the 226 Sargassum samples collected in 2011 contained any chemical fingerprinting evidence of exposure to Macondo oil (Table 33.1). These samples also contained only low concentrations of TPAH50 (9 ± 7 μg/kg tissue wet wt.; Table 33.3), consistent with "background" pyrogenic PAHs.

TABLE 33.3 Concentration of Total PAHs (TPAH50) Measured in Oiled and Nonoiled Floating *Sargassum* Samples Collected in 2010 and 2011.

	Oiled Sargassum			Nonoiled Sargassum			
	During the spill			During the spill		Postspill	
Sample ID	SARG2	SARG4	SARG1	SARG7	SARG5	Average Fall 2010 ($n = 17$)	Average 2011 ($n = 226$)
Date (2010)	23-May	23-May	25-May	19-May	19-May		
TPAH50	4980	84	5162	13	11	11 ± 5	9 ± 7

Concentrations are in μg/kg Tissue Wet Weight. One of the Four Oiled Samples Collected During the Active Spill (SARG3), is not Included Because It Was Analyzed as an Oily Material Rather Than as a Biological Tissue Sample. See Table 33.2 for Compound Abbreviations

33.2.3 Sargassum—Conclusion

Chemical fingerprinting demonstrated that pelagic *Sargassum* in the northern GoM was directly exposed to weathered Macondo oil released during the DWH oil spill. All four floating *Sargassum* samples collected from two locations within the known footprint of floating oil during the active spill (May–July 2010) contained weathered Macondo oil, although only one was visibly oiled upon inspection. The Macondo oil-exposed *Sargassum* samples were collected at two locations about 80 and 170 km from the wellhead, and in areas remote sensing had indicated floating oil had occurred. Sargassum from a reference location 480 km south from the wellhead contained only traces of pyrogenic PAHs attributed to atmospheric deposition of combustion particles (not oil).

Subsequent sampling of 17 floating *Sargassum* samples 3 to 4 months after the spill had ended showed no chemical (fingerprinting or PAH concentration) evidence for exposure to Macondo (or any other) oil. Similarly, none of the 226 floating *Sargassum* samples collected in 2011 showed chemical evidence for exposure to Macondo (or any other) oil.

The absence of Macondo oil in any floating *Sargassum* samples collected soon after the spill ended may be in part attributed to the reported "sinking" of oiled *Sargassum* where dispersants were applied (Powers et al., 2013).

33.3 DEEP-SEA CORAL

The failed Macondo well-injected oil (and gas) into the deep-sea at a depth of approximately 1500 m. One fraction of the oil remained at depth as physically- or chemically dispersed droplets, which were advected away from the well within a nonbuoyant plume centered at approximately 1000–1300 m depth (Camilli et al. 2010; Socolofsky et al. 2011). A second fraction of the oil rose to the ocean surface where it was dispersed by wind and currents over vast areas of the northern GoM over a period of nearly 3 months (Fig. 33.2; Graettinger et al., 2015). Some fraction of oil from both the deep-sea plume and sea surface was ultimately deposited on the seafloor as evidenced by the widespread accumulation of oil-laden "floc" in sediments (e.g., Valentine et al., 2014; Chanton et al., 2015; Stout et al., 2016a).

In places where carbonate hard bottoms occur, often in locations where natural oil seeps persist, colonies of hard, soft, and black corals often form the foundation of a diverse deep-sea habitat (Fisher et al. 2014). In November and December 2010, White et al. (2012a) observed a deep-sea coral community about 11 km southwest of the Macondo well, within block MC294 located on the southwest flank of Biloxi Dome (1370 m deep), where over half of the dozens of coral colonies examined were partially covered by brown floc (Fig. 33.5). Chemical analysis of triterpane biomarkers in floc collected from corals at MC294 indicated it to be consistent with Macondo oil (White et al., 2012a). This conclusion, however, was questioned owing to the occurrence of natural oil seeps in the MC294 area and the overall chemical comparability between Macondo oil and the region's natural oil seeps (Boehm and Carragher, 2012).

In our studies of the DWH oil spill's impact to deep-sea sediments (Stout and Payne, 2016; Stout et al., 2016a), we had the opportunity to analyze a large number of seep-impacted sediments in the MC294 area (Fig. 33.5), where both deep-sea coral communities and natural oil seeps exist. We also analyzed floc collected from a deep-sea coral colony within Block MC294 in December 2010 (Fig. 33.5), which allowed for the chemical fingerprinting comparisons described below.

33.3.1 Deep-Sea Coral—Samples & Methods

In December 2010, i.e., 6 months after the DWH spill had ended, a floc sample was collected from a coral colony (identified as specimen F6; Fig. 33.5B) in the MC294 area (Lat: 28.6722; Long: −88.4765) as part of the R/V *Atlantis* cruise. The floc sample was vacuumed from the coral surface by DVS *Alvin* into a 4-L canister, the contents of which was subsequently filtered (onboard) onto a precombusted 47-mm glass fiber filter (0.7 μm), which was wrapped in precleaned aluminum foil, frozen (−20°C), and shipped for study. The filter/floc sample's identification was GU2888-A1208-OE301B.

The filter and floc material was spiked with recovery surrogates and serially extracted (3×) on a shaker table using fresh DCM. The serial extracts were combined, dried with sodium sulfate, concentrated, and spiked with internal standards prior to analysis. No silica gel fractionation of the extract was performed.

The extract was analyzed in accordance with NOAA (2014) as described in detail elsewhere (Douglas et al. 2015). Briefly, the filter/floc sample was analyzed by (1) GC–FID to obtain a detailed hydrocarbon fingerprint using a modified EPA Method 8015B and (2) GC–MS operated in the SIM acquisition mode to determine the abundances of decalins, PAH, alkylated PAH homologues, individual PAH isomers, and sulfur-containing

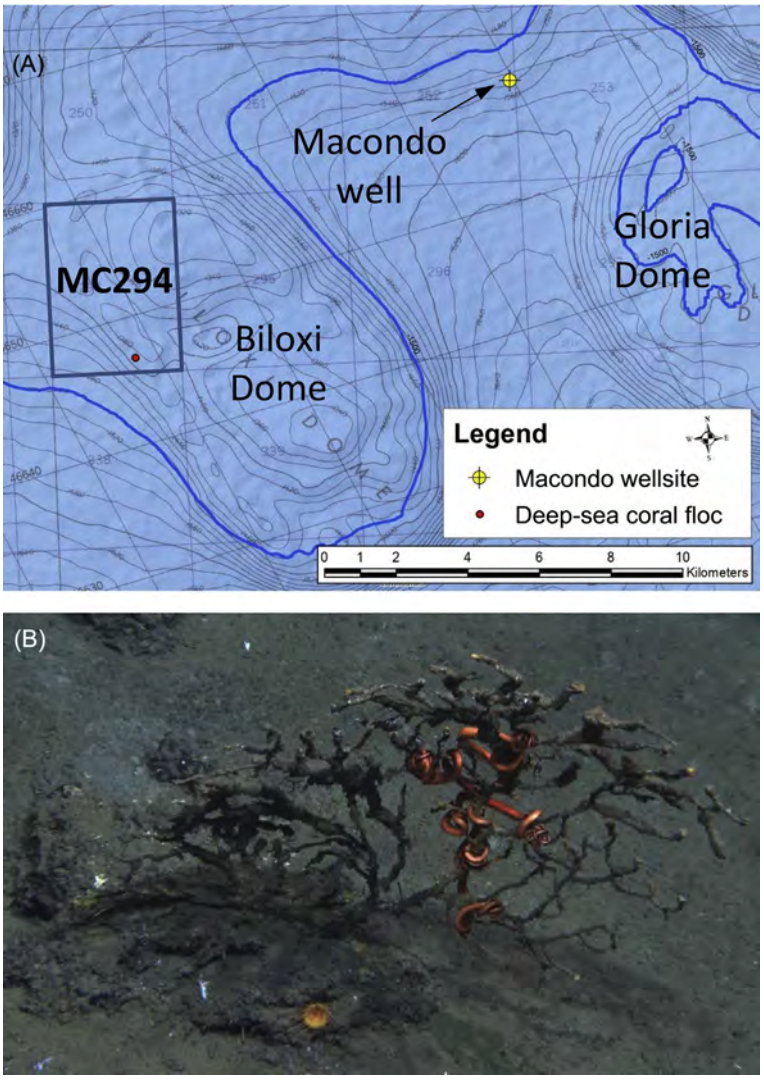

FIGURE 33.5 (A) Map showing the general locations of deep-sea coral communities identified within Mississippi Canyon Block 294 (MC294) west of Biloxi Dome and (B) photograph of impacted deep-sea coral colony (F6) from the MC294 site in November 2010. Photo in (B) courtesy of Woods Hole Oceanographic Institution and Charles Fisher (The Pennsylvania State University) taken using the ROV *Jason II*. *Reprinted with permission from White, H.K., P.-Y. Hsing, W. Cho, T.M. Shank, E.E. Cordes, A.M. Quattrini, et al., 2012b. Reply to Boehm and Carrangher: multiple lines of evidence link deep-water coral damage to Deepwater Horizon oil spill. Proc. Natl. Acad. Sci. 109(40), E2648*. MC294 block boundary, location of the F6 coral in MC294 studied herein (GU2888-A1208-OE301B), and 1500-m contour are indicated in (A).

aromatics, and (3) petroleum biomarkers (tricyclic and pentacyclic triterpanes, regular and rearranged steranes, and TASs) (Table 33.2). Amounts of target compounds are reported in ng/filter, and for fingerprinting comparison to sediments, were normalized to the abundance of 17α(*H*),21β(*H*)-hopane (hopane).

33.3.2 Deep-Sea Coral—Results and Discussion

The GC/FID chromatogram for the floc collected from deep-sea coral at MC294 is shown in Fig. 33.6A. Also shown for comparison are the chromatograms for a Macondo-oil-derived floc sample collected from the seafloor surface 6.9 km southwest of the Macondo well (Fig. 33.6B) and a nearby surface sediment containing local seep oil (Fig. 33.6C). All three samples exhibit the general features of severely weathered crude oils, although obvious differences are also evident.

Most of the mass within the deep-sea coral floc occurred within the unresolved complex mixture (UCM) within the $C_{25}+$ range, or residual range organics (RRO), with far less occurring in the diesel range organics ($C_{25}-$; DRO; Fig. 33.6A). Atop the UCM for the coral floc were numerous long-chain *n*-alkanes spanning from

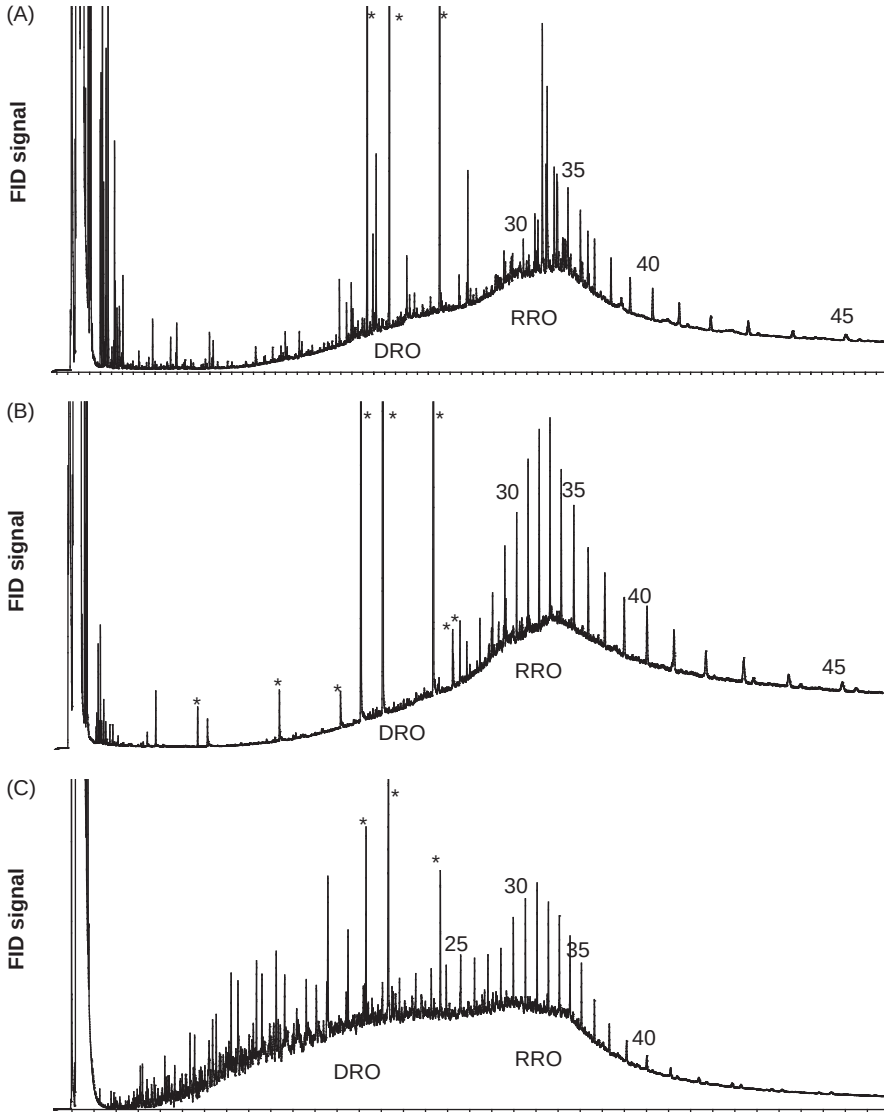

FIGURE 33.6 GC/FID chromatograms for: (A) Floc vacuumed from a deep-sea coral (F6) from MC294, (B) typical Macondo-derived floc as represented by a seafloor surface sediment 6.9 km west-southwest of the Macondo well (HSW6_FP8204A_B0830_S_1357_50M2_0313; Stout and Payne, 2016), and (C) local seep-impacted surface sediment near the deep-sea coral studied (HSW6L2_SLP3230_B1012_S_1385_50_P2_0158; Stout et al., 2016a). DRO-diesel range organics; RRO-residual range organics; #—*n*-alkane carbon number; *—internal standard.

n-C28 to *n*-C45 that reached a maximum at *n*-C33. (Scattered among the *n*-alkanes were numerous resolved peaks that remain unidentified but are attributed to naturally occurring organics vacuumed from the coral surface.)

The coral floc's general chromatographic features are highly consistent with those reported as typical of the oily floc derived from fallout from the deep-sea plume that was deposited on the seafloor beyond ~5 km from the well (Stout and Payne, 2016). Fig. 33.6B shows the GC/FID chromatograms of Macondo-derived floc collected from the seafloor 6.9 km southwest of the Macondo well (toward Biloxi Dome) that, as demonstrated through the chemical fingerprinting study of 2782 sediment samples from 729 deep-sea sediment cores (Stout and Payne, 2016; Stout et al., 2016a), represents the severely weathered (biodegraded and water-washed) residue of the dispersed Macondo oil droplets transported within the deep-sea plume.

The Macondo-derived floc found on the seafloor beyond ~5 km from the well was a wax-rich oil containing an abundance of longer-chain *n*-alkanes spanning from ~*n*-C_{25} to *n*-C_{44} with a maximum ~*n*-C_{33} (Fig. 33.6B). The preferential loss of *n*-alkanes below ~*n*-C_{30} was attributed to intense biodegradation within the deep-sea plume, which can preserve the longer chain *n*-alkanes as shorter chain *n*-alkanes are preferentially degraded (Prince et al., 2013). Accompanying the loss of *n*-alkanes in oil within the deep-sea plume was the progressive loss of isoprenoids (e.g., pristane and phytane) and the bulk of unresolved compounds within DRO (Stout and Payne, 2016). This loss in DRO caused a reduction in the size and concave shape of the UCM in the

DRO range—and corresponding retention/enrichment of the compounds within the RRO (Fig. 33.6B; Stout and Payne, 2016). The progressive loss in DRO compounds was also reasonably attributed to the combined effects of dissolution and biodegradation of the dispersed Macondo oil particles within the deep-sea plume.

The chromatographic character of the locally seeped oils, which have not experienced the same degree of weathering as the Macondo-derived floc, is distinct. Fig. 33.6C shows a surface sediment collected nearby that was determined to contain locally seeped oil (Stout et al., 2016a). Although the seeped oil also is enriched in more resistant long-chain *n*-alkanes, it contains an abundance of resolved compounds and unresolved mass within the DRO range (Fig. 33.6C)—in stark contrast to the Macondo-derived floc (Fig. 33.6B). The relative abundance of DRO in the seep oil owes to the fact that this oil has not experienced the same degree of weathering (dissolution and biodegradation) as the finely dispersed Macondo oil had within the deep-sea plume (Stout and Payne, 2016). Evidence for this was the increasing loss of DRO found with increasing distance from the Macondo well. Clearly, the floc recovered from the deep-sea coral at MC294 exhibits features consistent with those of Macondo-derived floc and inconsistent with the local seep oil.

Additional evidence for this conclusion is found in the distributions of PAHs and biomarkers in these samples. Fig. 33.7 shows the hopane-normalized distributions of PAHs (and related analytes) and petroleum biomarkers

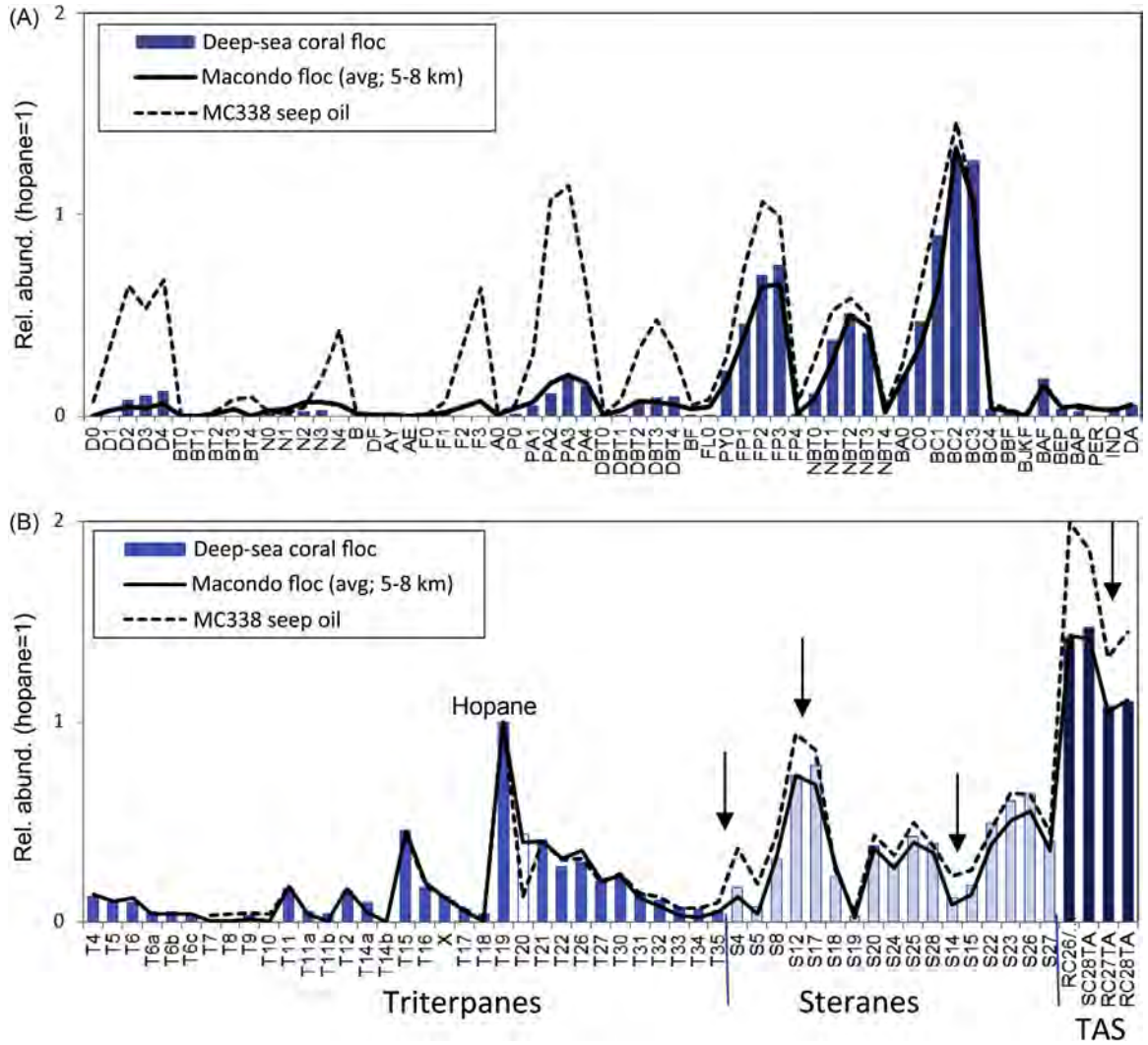

FIGURE 33.7 Hopane-normalized distributions of (A) PAH and related compounds and (B) petroleum biomarkers in the deep-sea coral floc from MC294. Distributions are compared to the average distribution for Macondo-derived floc in surface sediments (5–8 km; from Stout and Payne, 2016) and in local seep-impacted surface sediment collected near the deep-sea coral studied (HSW6L2_SLP3230_B1012_S_1385_50_P2_0158; Stout et al., 2016a). Arrows in B show steranes and TAS that identify the deep-sea coral floc as Macondo oil floc. Note T20 (moretane) in coral floc contains a prominent interfering terpane that is likely 17β(*H*),21β(*H*)-30-norhopane, a naturally occurring triterpane that can be prominent in recent marine sediments (Kennicutt and Comet, 1992). See Table 33.2 for compound abbreviations.

in the deep-sea coral floc compared to those of Macondo-derived floc and local seep oil from MC294. The PAHs in the deep-sea coral floc, Macondo-derived floc, and local seep oil all are dominated by C_3- and C_4-benz[*a*]anthracenes/ chrysenes (BC3 and BC4), testifying to their highly weathered states (Fig. 33.7). However, the deep-sea coral floc and Macondo-derived floc are also significantly depleted in fluoranthrenes/pyrenes (FP1-4), dibenzothiophenes (DBT0-4), phenanthrenes/anthracenes (PA0-4), and other lower molecular weight PAHs, including decalins (D0−D4), compared to the local seep oil. This difference is, as described above with respect to the decrease in DRO, attributable to the greater degree of weathering (dissolution and biodegradation) experienced by the finely dispersed Macondo oil within the deep-sea plume, than the seep oil experienced in its slow (geologic) rise to the seafloor (Stout and Payne, 2016).

The biomarkers further support the conclusion that the deep-sea coral floc from MC294 is derived from Macondo oil and not local seep oil. Fig. 33.7B (note arrows) shows that the Macondo-derived floc oil has experienced losses of selected dia- and regular steranes and TASs compared to the local seep oil. The most notable of these are marked reductions in the relative abundances of 13β(*H*),17α(*H*)-diacholestane epimers (S4 and S5) and 14β(*H*),17β(*H*)-cholestane epimers (S14 and S15; Fig. 33.7B). Some reduction was also evident in the coeluting epimers of 14α(*H*),17β(*H*)-cholestane and 13β(*H*),17α(*H*)-diaethylcholestane (S12 and S17; Fig. 33.7B). The preferential losses of 13β(*H*),17α(*H*)-diacholestanes and 14β(*H*),17β(*H*)-cholestanes have been observed previously in spilled oil and attributed to biodegradation, although over much longer time scales (Wang et al. 2001; Prince et al., 2002) and in vitro (Diez et al. 2005). As was the case for DRO and lower boiling PAHs (see above), the rapid biodegradation of these βα dia- and ββ regular C_{27} steranes in the Macondo-derived floc is attributable to accelerated biodegradation within the finely dispersed oil droplets in the deep-sea plume (Stout and Payne, 2016). Notably, comparable losses of 13β(*H*),17α(*H*)-diacholestanes and 14β(*H*),17β(*H*)-cholestanes were also reported by White et al. (2012a,b) in floc on deep-sea coral samples collected from MC294 (NW of our coral sample; Fig. 33.5). Finally, the Macondo-derived floc also contains a reduced abundance of TAS compared to the local seep oil (Fig. 33.7B), which also is attributed to dissolution and/or biodegradation of these aromatic biomarkers (Stout and Payne, 2016).

33.3.3 Deep-Sea Coral—Conclusion

The floc collected from the deep-sea coral (F6) at MC294 in December 2010, ∼5 months after the DHW oil spill ended, is comprised of oily-floc derived from severely weathered (biodegraded and water-washed) Macondo oil—and not from locally seeped oil. Despite the fact that Macondo oil and the local (MC294) seep oil are both Mississippi Canyon-type crude oils with similar geologic origins (and chemical features, e.g., biomarkers), the degree of weathering of the Macondo-derived floc exceeds that of the local seep oil(s), owing to the severity of biodegradation and water-washing experienced by the finely dispersed Macondo oil droplets within the deep-sea plume prior to deposition. The severity of weathering of the Macondo-derived floc allows it to be distinguished from the local seep oil—and matched to the deep-sea coral's floc.

33.4 OSPREY NEST MATERIAL

The DWH oil spill exposed dozens of species of birds to oil in a variety of northern GoM habitats. Exposure to oil occurred in several ways, including physical contact with oil in the environment, ingestion during preening or foraging, and consuming contaminated prey, water, or sediment (Trustees, 2016). Avian embryos within incubating eggs are particularly sensitive to crude oil (Finch et al., 2011) and can be exposed when adults build nests with oil-contaminated materials or when adults get oil on their feathers and carry it back to the nest. As the onset of the DWH oil spill coincided with the early stages of the nesting season for numerous bird species in the northern GoM, it has been estimated that between 4200 and 12,700 nests would have suffered a complete loss of fledglings in 2010 (Trustees, 2016).

In this section, we present chemical fingerprinting evidence that osprey nest materials collected 6 to 7 months after the DWH oil spill ended (i.e., January−February 2011) from multiple osprey nests located on Horn Island, a barrier island located in the Gulf Islands National Seashore (Alabama), contained weathered Macondo oil. Osprey living within these nest were exposed to the oil during the collection of these nesting materials and within the nests.

33.4.1 Osprey Nest Material—Samples & Methods

Nineteen osprey nest material samples from various areas of the Gulf Coast were provided for chemical fingerprinting (Fig. 33.8). Eleven of the samples were collected from nests southeast of Apalachicola Bay (Florida), three nests from the Pascagoula Naval Station (Mississippi), two nests from the mouth of the Mississippi River delta in (Louisiana), and three nests on Horn Island located in the Gulf Islands National Seashore. All of the samples were collected by researchers at the Center for Conservation Biology Research at William & Mary between

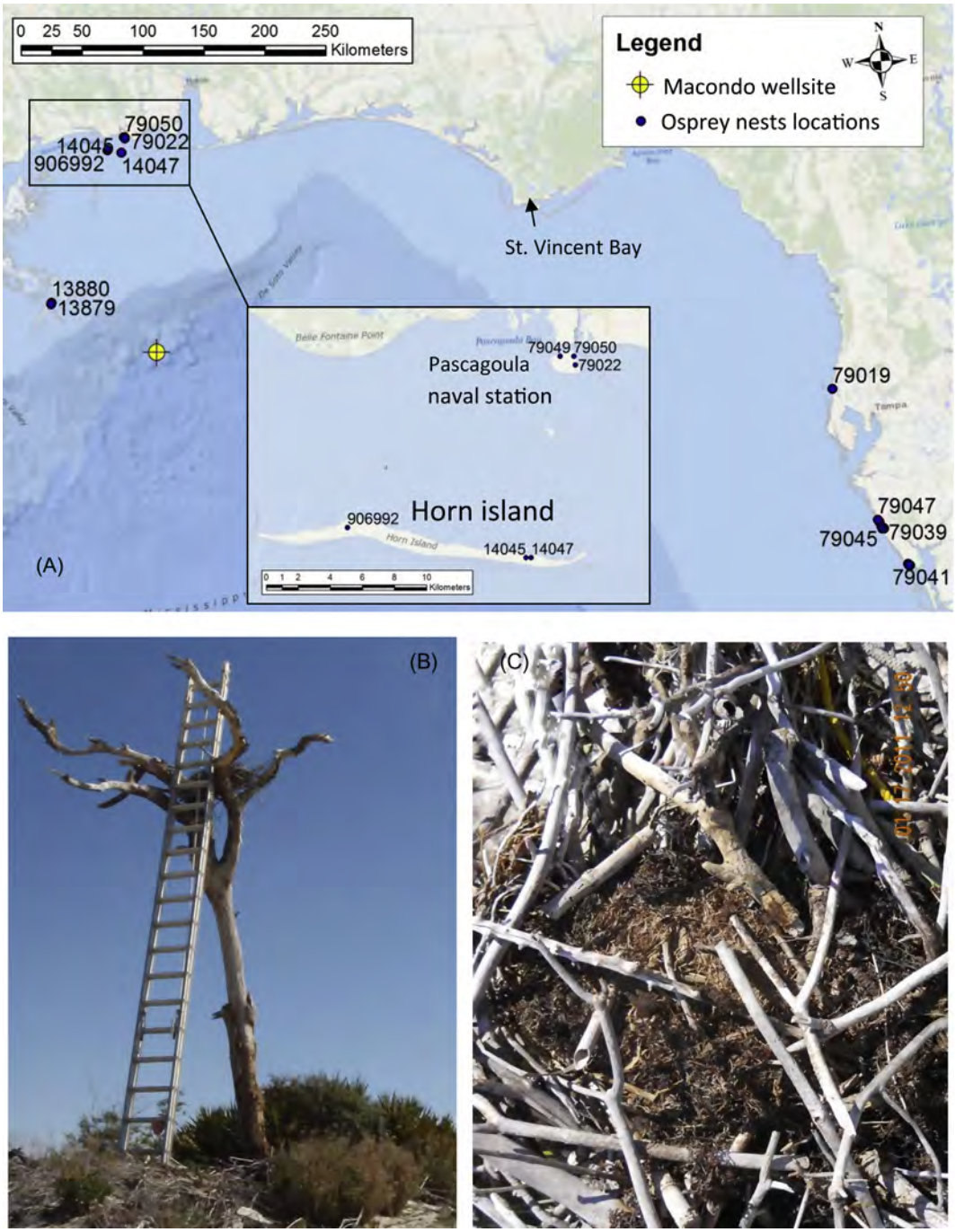

FIGURE 33.8 (A) Map showing the locations of the osprey nest materials analyzed and (B) and (C) photographs of nest sampled on Horn Island (sample ID: 14045; API-79). Inset shows locations of oiled nest materials collected from Horn Island and the Pascagoula Navel Complex. Labels refer to nest material sample identifications. Photos (B and C) courtesy of Libby Mojica. *Courtesy of The Center for Conservation Biology.*

January 17 and February 12, 2011; i.e., 6 to 7 months after the end of the DWH oil spill (Mojica et al., 2011). The samples consisted of various nesting materials including; twigs, seaweed, bark, grass, feathers, rope, paper, plastic, and pieces of clothing.

The osprey nest samples were analyzed as oily materials. Oil was removed from the exterior of the nest material when visible or the exterior was rinsed with DCM. The oil and rinsates were spiked with recovery surrogates and adjusted to a final volume in DCM, and passed through a filter containing glass wool and sodium sulfate. The extracts were then concentrated and cleaned using silica gel and elemental copper to remove the presence of sulfur. A 1-mL subaliquot was then taken and spiked with internal standard for chemical analysis.

The extracts were analyzed in accordance with NOAA (2014) as described in detail elsewhere (Douglas et al. 2015). Briefly, the filter/floc sample was analyzed by (1) GC−FID to obtain a detailed hydrocarbon fingerprint using a modified EPA Method 8015B and (2) GC−MS operated in the SIM acquisition mode to determine the abundances of decalins, PAH, alkylated PAH homologues, individual PAH isomers, and sulfur-containing aromatics) and (2) petroleum biomarkers (tricyclic and pentacyclic triterpanes, regular and rearranged steranes, and TASs) (Table 33.2). Concentrations were reported in mg/kg of oil weight (determined gravimetrically), although for fingerprinting comparisons the concentrations were normalized to the abundance of 17α(*H*),21β(*H*)-hopane (hopane).

33.4.2 Osprey Nest Material—Results and Discussion

Chemical fingerprinting (see below) determined that three of the 19 nest material samples analyzed contained weathered Macondo oil. All three of these were collected from the nests on Horn Island, located within Gulf Islands National Seashore in offshore Mississippi (Fig. 33.8). In contrast, three additional nest material samples collected from the Pascagoula Naval Station contained hydrocarbons that were inconsistent with Macondo oil, i.e., these nests' oils were derived from a source other than Macondo oil. No oil of any type was found in the remaining 13 osprey nest material samples collected from the Mississippi River delta terminus area ($n = 2$) or west coast of Florida ($n = 11$; Fig. 33.8). As this study was not an extensive survey involving a large number of osprey nests throughout the northern Gulf coast, (over)interpreting these results spatially (or statistically) is not appropriate. However, the absence of Macondo oil in all 11 nests collected from western Florida is not unexpected given they were located over 150 miles to the southeast of St. Vincent Bay, i.e., the easternmost extent of stranded Macondo oil (Fig. 33.8; Stout et al., 2016b). Similarly, the absence of Macondo oil in the two nest material samples collected in Mississippi River delta area may not be unexpected given that, based upon SCAT results, this *specific* area of the Birdfoot was not oiled during the spill (Michel et al., 2013). The analysis of the distances over which osprey may travel to gather nest materials, or over which these birds may range and encounter oil and then transfer oil to their nesting materials, is unknown and beyond the scope of our investigation.

The presence of Macondo oil in all three samples collected from nests on Horn Island in early 2011 (14047, 14045, and 906992) is not unexpected given this island was impacted by stranded oil on both the landward and seaward shorelines (Michel et al., 2013). In addition, chemical fingerprinting of stranded oils confirmed the presence of variably weathered Macondo oil around the entirety of Horn Island (Stout et al., 2016b).

Fig. 33.9 shows the GC/FID chromatograms obtained from two of the Macondo-impacted nests on Horn Island (Fig. 33.9A and B) and, for comparison, two nests from the Naval station that contained hydrocarbons from non-Macondo sources (Fig. 33.9C and D). The Horn Island osprey nests contained Macondo oil that was severely evaporated and variably biodegraded. The Macondo oil from the 14047 (and 14045, not shown) nest sample was markedly less biodegraded (Fig. 33.9A) than the oil in the 906922 sample, as evidenced by the latter's near absence of n-alkanes (Fig. 33.9B). This same variability in weathering was observed among stranded Macondo oils collected from shorelines on Horn Island in the 2010 (Stout et al., 2016b). Although weathering of the oil after reaching the nests cannot be ruled out, the observed variability suggests that adult osprey gathered variably weathered Macondo-oil-impacted nest materials, or had carried such oil to their nests (i.e., on their own bodies or their prey).

Nests from the Pascagoula Naval Station also contained oil, as evidenced by the prominence of UCM (Fig. 33.9C and D). The 79049 nest's UCM is lower boiling than those of the Macondo oil-impacted nests, and it exhibits a more Gaussian shape typical of refined oil (e.g., lubricating oil; Fig. 33.9C). The 79050 nest's UCM is broad boiling but is highly skewed toward high boiling compounds. This nest also contains an abundance of resolved peaks including prominent PAHs (fluoranthene, pyrene, chrysene, and benz(*a*)anthracene) (Fig. 33.9C). Although the prominent PAHs could implicate the presence of a tar-like product (e.g., weathered creosote),

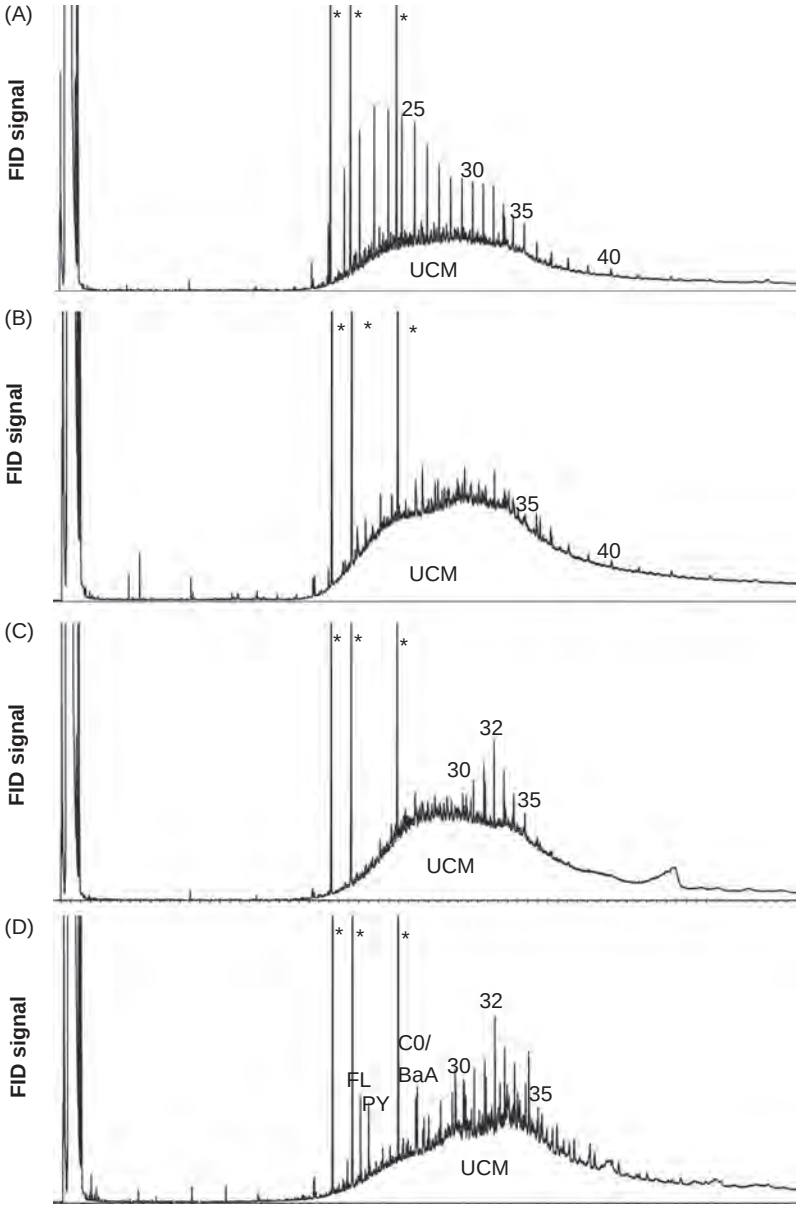

FIGURE 33.9 GC/FID chromatograms for oils in osprey nests: (A) Macondo oil in Horn Island nest (14047), (B) Macondo oil in Horn Island nest (906992), (C) non-Macondo oil in Naval Station nest (79049) and (D) non-Macondo oil in Naval Station nest (79050). IS: internal standards; #—*n*-alkane carbon number.

when considered together these features are more consistent with impacts by urban runoff (i.e., combination of petroleum and combustion particles; Stout et al., 2004).

Figs. 33.10 and 33.11 show the hopane-normalized PAH and petroleum biomarker histograms for the same four nests described in Fig. 33.9. In each of these, the distributions are compared to the average for 1174 stranded oil samples collected from shorelines across the northern GoM in 2010 (before Sept. 2, 2010: Stout et al., 2016b). As can be seen the oil present in the two Macondo-impacted nests from Horn Island are relatively depleted in PAHs compared to the average stranded Macondo oils (Fig. 33.10A and B). In addition, some effect of photooxidation of the Macondo oil is evidenced by the atypical pattern of PAHs among the benz(*a*)anthracenes/ chrysenes homologues, as was also observed in *Sargassum* (see above). The fact that the oil in the nests appear more photooxidized than the average stranded oils (Fig. 33.10A and B) suggests photooxidation of the oil likely continued within the nests (until their collection in early 2011). Thus, the Macondo oil present in these nests was likely to have continued to weather (e.g., water-wash and photooxidize) after being carried into the nests by adult osprey.

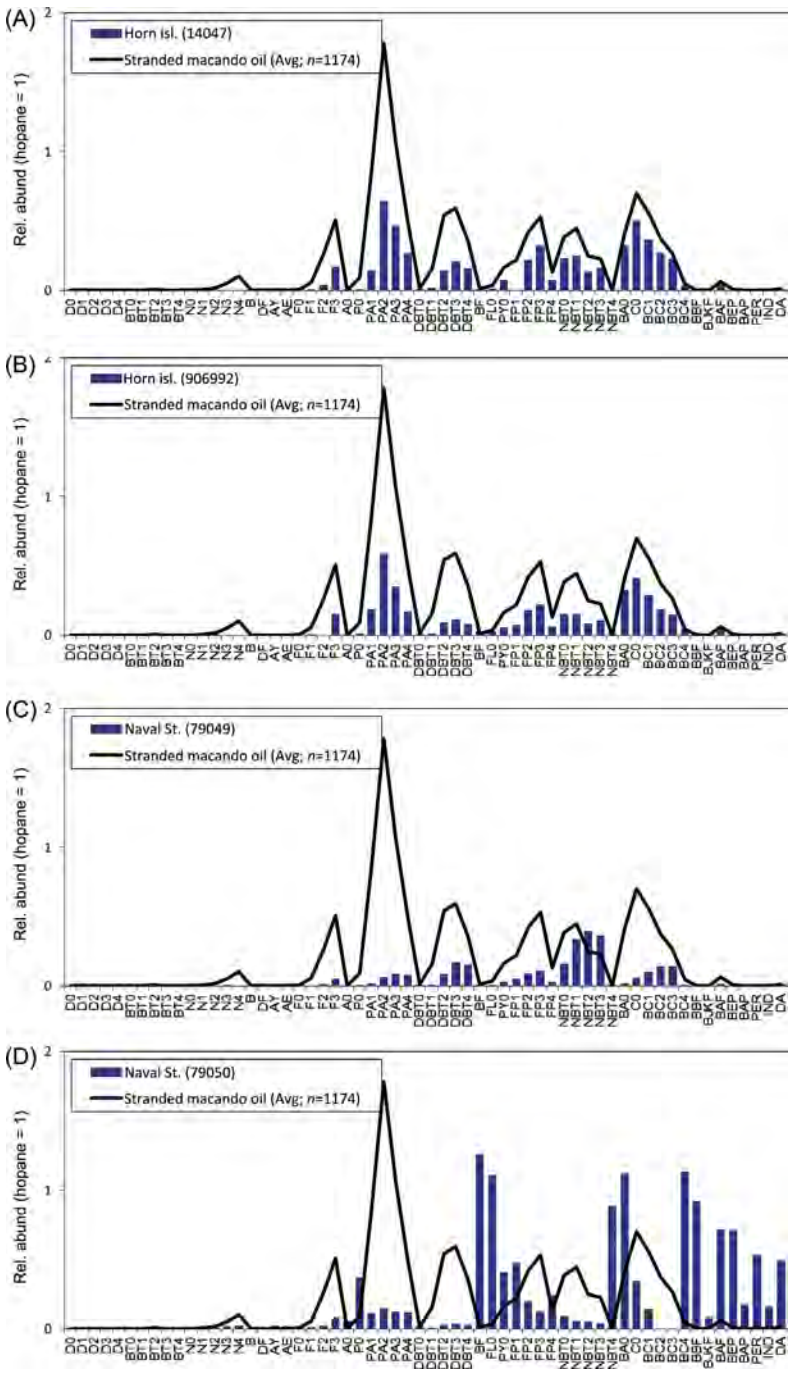

FIGURE 33.10 Hopane-normalized PAH distributions for oils in osprey nests: (A) Macondo oil in Horn Island nest (14047), (B) Macondo oil in Horn Island nest (906992), (C) non-Macondo oil in Naval Station nest (79049), and (D) non-Macondo oil in Naval Station nest (79050). The average stranded Macondo oil ($n = 1174$) is obtained from Stout et al. (2016b). See Table 33.2 for compound abbreviations.

The disparate distributions of the PAHs between the non-Macondo impacted nests from the Naval Station and stranded Macondo oil are obvious. The 79049 nest contained a weathered (high boiling) oil relatively enriched in naphthobenzothiophenes (Fig. 33.10C), whereas the 79050 nest contained prominent pyrogenic PAHs (as had been evident in the GC/FID chromatogram), which is consistent with a prominence of combustion-derived particles present in this nest.

Inspection of the hopane-normalized biomarker distributions confirms the presence of Macondo oil in the two nests from Horn Island (Fig. 33.11A and B). The 14047 nest (and 14045, not shown) exhibits a biomarker

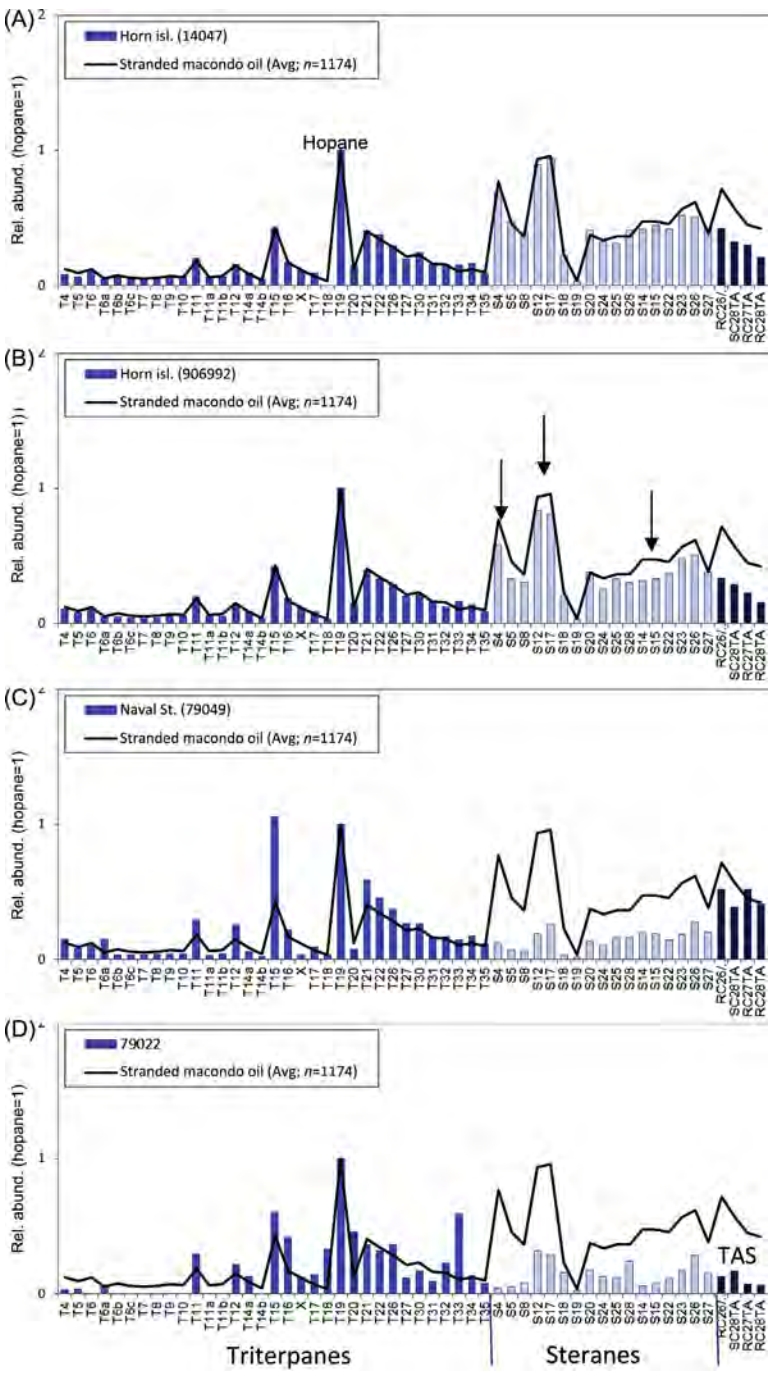

FIGURE 33.11 Hopane-normalized biomarker distributions for oils in osprey nests: (A) Macondo oil in Horn Island nest (14047), (B) Macondo oil in Horn Island nest (906992), (C) non-Macondo oil in Naval Station nest (79049), and (D) non-Macondo oil in Naval Station nest (79050). The average stranded Macondo oil ($n = 1174$) is obtained from Stout et al. (2016b). See Table 33.2 for compound abbreviations.

distribution highly consistent with the average stranded (weathered) Macondo oil collected from shorelines in 2010. The Macondo oil in both nests, however, are relatively depleted in TASs compared to average stranded oils. The depletion of the TAS is due to the effects of photooxidation, which had also been observed in other Macondo oils collected from the sea surface and shorelines in 2010 (Aeppli et al. 2012; Radović et al. 2014; Stout et al., 2016b)—and in the Macondo-impacted Sargassum described above (Fig. 33.4B). The greater loss of TAS in the osprey nests would seem consistent with continued photooxidation of the TAS after the oil had reached the nests (until their collection in early 2011).

It is notable that the more highly biodegraded Macondo oil present within the 906992 nest from Horn Island (that had lacked *n*-alkanes; Fig. 33.9B) also exhibits a slight depletion in the abundances of selected dia- and regular steranes compared to average stranded Macondo oils (see arrows in Fig. 33.11B). More advanced depletion in the relative abundances of 13β(*H*),17α(*H*)-diacholestane epimers (S4 and S5), coeluting epimers of 14α(*H*),17β(*H*)-cholestane and 13β(*H*),17α(*H*)-diaethylcholestane (S12 and S17) and 14β(*H*), and 17β(*H*)-cholestane epimers (S14 and S15) was also observed among deep-sea sediments (Stout and Payne, 2016), deep-sea coral floc (Fig. 33.7B; White et al., 2012a,b), and marsh sediment (Meyer et al., this volume), which in each case is attributed to biodegradation of these specific sterane biomarkers. Thus, the Macondo oil present in the 906992 appears to exhibit incipient biodegradation of these steranes.

The obviously disparate biomarker distributions of the oils collected from the Naval Station nests testifies these nests clearly contain different, non-Macondo sources of oil (Fig. 33.11C and D). These oils exhibit very different characteristics that are by no means attributable to weathering, and therefore provided the basis to conclude the nests from Pascagoula Naval Station contained different types petroleum from non-Macondo sources. This is reasonably attributable to their location in a more urbanize area (Fig. 33.8) where nesting materials collected by osprey were potentially impacted by multiple urban sources.

33.4.3 Osprey Nest Material—Conclusion

The exposure of osprey to Macondo oil following the DWH oil spill was assessed through a chemical fingerprinting study of materials collected from 19 osprey nests 6 to 7 months after the spill ended (Jan.–Feb., 2011). Chemical fingerprinting confirmed that osprey nest materials from the three nests on Horn Island (Gulf Islands National Seashore, offshore Mississippi) contained variably weathered Macondo oil. Thus, each nests' adult osprey may have (1) been directly exposed to the oil and carried it into their nests, (2) carried oil-contaminated prey to their nest, and/or (3) used oil-contaminated materials to construct their nests. In turn, any eggs and chicks in these nests had been potentially exposed to the oil.

In addition, the three nests from the Pascagoula Naval Complex contained hydrocarbons derived from sources other than Macondo oil while two nests from the Mississippi River delta terminus and 11 nests from western Florida did not contain Macondo oil (or any other hydrocarbon source).

33.5 DOLPHIN LUNG TISSUE

Marine mammals (whales, dolphins, and manatees) throughout the northern GoM and its shorelines were potentially exposed to the Macondo crude oil released during and after the DWH oil spill. Exposures could occur in several ways that included (1) direct external exposure to floating, submerged, or stranded oil, (2) inhalation or aspiration of volatile compounds or aerosol particles from floating oil, and (3) direct or incidental ingestion of oil from contaminated water, sediment, or prey (Trustees, 2016).

Direct external exposure to Macondo oil in the months following the spill was evident upon observations of dolphins swimming through floating oil with oil adhering to their skin (Schwacke et al., 2013; Dias, 2016). Inhalation exposure also was evident in Schwacke et al. (2013) wherein it was observed (using pulmonary ultrasound) a greater prevalence and severity of lung disease in dolphins captured (and released) from heavily oiled Barataria Bay, Louisiana—as compared to an unoiled reference site (Sarasota Bay, Florida) and to previously reported wild dolphin populations.

Chemical fingerprinting was used by both the US Coast Guard Marine Safety Laboratory (MSL, New London, CT) and by our group to show 13 out of the 36 common bottlenose dolphin (*Tursiops truncates*) carcasses stranded along the Port Fourchon and Grand Isle, and Isle Grand Terre beaches, Louisiana, between May 24, 2010 and February 23, 2012 (Fig. 33.12), and one Clymene dolphin (*Stenella clymene*) carcass recovered from Langdon Beach, Florida on June 23, 2010, had Macondo oil on their exteriors (Stout, 2015b). This exposure was demonstrated through chemical fingerprinting of swab samples collected from the dolphins' exteriors.

In some instances the timing of the exterior exposure was uncertain, and as Macondo oil was widely present along these shorelines, dead carcasses may have encountered the Macondo oil *postmortem*. Therefore, the lung tissue from a relatively fresh bottlenose dolphin carcass (Fig. 33.12) was also studied with the intent to determine if the animal had been exposed to Macondo oil prior to its death, through inhalation or aspiration of oil. Limited studies of internal tissue samples from marine mammals have been conducted, with varying success

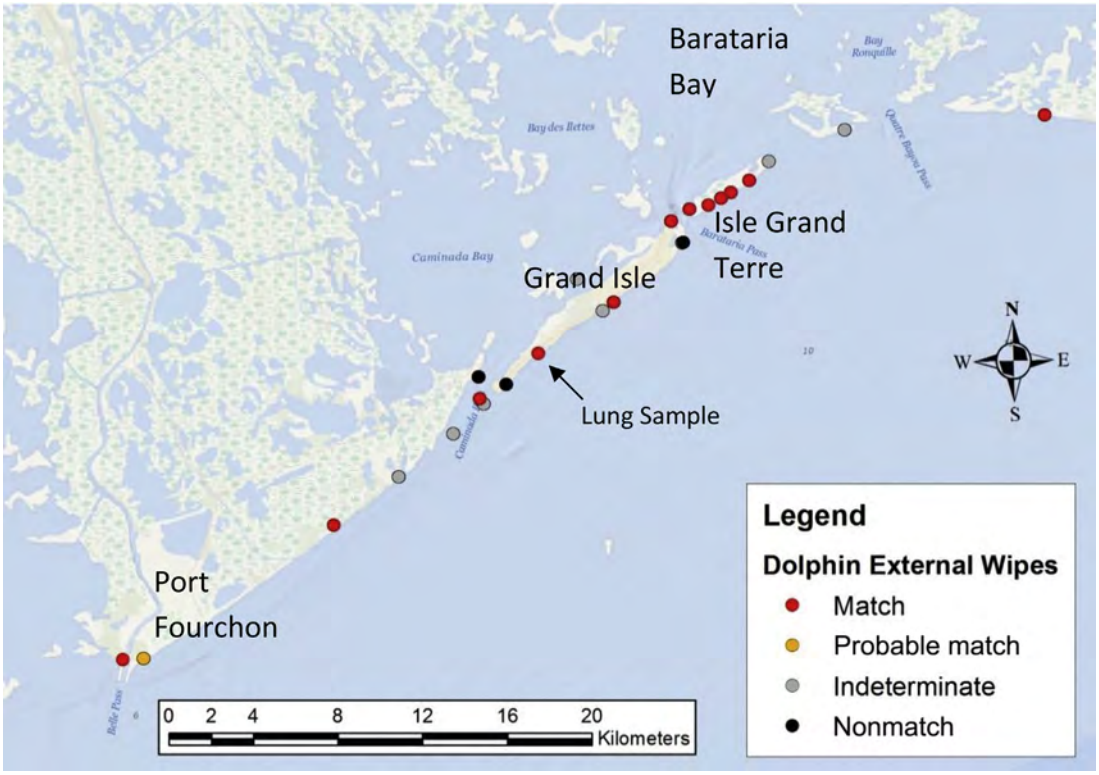

FIGURE 33.12 Map showing the locations of stranded dolphins from which external wipes of oil were chemically fingerprinted and compared to Macondo oil. Location of the lung sample studied herein is indicated. See Stout (2015b) for additional details.

(e.g., Bence and Burns, 1993; Bence et al., 1996). These workers had found that internal tissue fingerprints were significantly altered and thereby difficult to attribute to *Exxon Valdez* oil, unless additional evidence, such as external oiling of the individual, was available (as in our case).

Previous work had demonstrated the presence of volatile hydrocarbons in air samples collected less than 0.5 m above floating oil (Payne et al., 1980). Research during the DWH spill demonstrated the widespread occurrence of volatile *and* less volatile (intermediate and semivolatile) compounds in atmospheric plumes derived from the floating oil (DeGouw et al., 2011). As dolphins breathe just above the water-air interface it is anticipated that evaporated (volatile, intermediate, and semivolatile) constituents from the oil were inhaled by nearby marine mammals. It is also possible that liquid (or aerosolized) oil could enter the lungs of an animal swimming among floating oil.

While liquid (or aerosolized) oil within lung tissue could be directly compared to the Macondo source oil, the chemical fingerprint of the potentially inhaled vapors is of course, different from that of the floating liquid oil. However, as will be explained below, the composition/ chemical fingerprint of the vapor above the floating Macondo oil can be predicted using equilibrium partitioning theory. This approach has been previously applied to predict the chemical composition of soil gas and indoor air samples that may be present above an accumulation of liquid petroleum in the subsurface (Uhler et al., 2010).

33.5.1 Dolphin Lung Tissue—Sample and Methods

The lung tissue sample from a dead, female common bottlenose dolphin carcass collected from Port Fourchon Island on May 24, 2010, i.e., only 1 month after the DWH oil spill had commenced, was frozen and provided for our study (in August 2013) by scientists at NOAA's Northwest Fisheries Science Center. The sample had an identification of MCT20100524-LA001(LA28).

The lung tissue was thawed and homogenized using a stainless steel or titanium (metals) Tissuemizer probe. The homogenized tissue was dried with sodium sulfate to remove water, spiked with surrogates, and serially extracted with methylene chloride (DCM) using a stainless steel tissue homogenization probe. The combined

extract was concentrated and an aliquot removed for lipid determination. The extract was further processed using gel permeation chromatography and alumina–silica gel fractionation in order to obtain concentrated F1 (aliphatic) and F2 (aromatic) fractions, which were analyzed for petroleum biomarkers and PAHs, respectively (as described earlier in this chapter; see also Douglas et al., 2015). Concentrations of detected analytes were reported in μg/g on a lipid-free, wet tissue weight basis.

33.5.2 Predicting Breathing Zone Vapor Phase Fingerprint

The predicted distribution of hydrocarbons in breathing zone vapors above floating (weathered) Macondo oil was calculated using equilibrium partitioning theory, as described by Uhler et al. (2010). Briefly, the partial vapor pressure of each compound in equilibrium with a floating oil is first calculated from the compound's pure vapor pressure (VP) and its mole fraction in the oil using Raoult's Law:

$$\text{partial vapor pressure} = \text{pure vapor pressure} \times \text{mole fraction} \tag{33.1}$$

The mole fraction of each compound in the floating oil can be calculated from its measured mass in the floating oil, its molecular weight, and the average molecular weight for the floating oil. With the partial vapor pressure of each compound known, the estimated concentration of the compound in the vapor phase above the floating oil (mass per unit volume) can be calculated from the ideal gas law expressed as

$$\text{concentration in vapor} = (\text{partial vapor pressure})/(\text{universal gas constant} \times \text{temperature}) \tag{33.2}$$

Temperature and pressure above the floating oil were assumed to be 25°C (298°K) and 1 atm, respectively—and the average molecular weight of the floating oil was assumed to be 200 g/mole (assumed to be typical of light crude oil). While these assumptions influence the determination of absolute concentrations of individual chemicals predicted in the breathing zone vapor phase, they do not affect their relative proportions (and by extension, their fingerprint) which are of particular interest in this study. The only variable that affects this fingerprint is the composition of the floating oil (i.e., the moles of each compound in the floating oil).

A previous study of 62 floating Macondo oils collected in the spring and summer of 2010 demonstrated the range in weathering, mostly due to evaporation, among the floating oils present during and shortly after the active spill (Stout et al., 2016b). The compositions of a moderately evaporated floating Macondo oil from that study (sample: JF2-2km-surf-0net-20100527-N186) was used herein to calculate the predicted distributions (relative concentrations) of compounds in the breathing zone vapor phase above the floating oil (Table 33.4) using equilibrium partitioning theory. These distributions were qualitatively compared to those found in the dolphin lung sample (Table 33.4).

33.5.3 Dolphin Lung Tissue—Results

The concentrations of PAH analytes measured in the lung tissue are given in Table 33.4. The lung tissue had a TPAH50 concentration of 0.162 μg/g (wet). The most prominent PAHs were a suite of alkylated naphthalenes that were present in a "bell-shaped" distribution generally consistent with petrogenic PAH sources. In addition to naphthalenes, the lung tissue sample contained decalin and C1- and C2-alkylated decalins along with traces of benzothiophenes, biphenyl, and dibenzofuran (Table 33.4). Only trace amounts of higher boiling (3- to 5-ring) PAHs were present, with most of these also being present in the associated blank (Table 33.4).

No hopane or any other biomarkers were detected in the lung tissue. The fact that no higher molecular weight PAHs (Table 33.4) or biomarkers were detected in the lung tissue argues that no liquid or aerosol oil entered the lungs through aspiration, but (if anything) only as oil vapors. The distribution of hydrocarbons detected in the lung tissue sample (Table 33.4) was compared to the distribution of hydrocarbons predicted to occur in the breathing zone vapors above moderately evaporated floating Macondo oil—as described above and calculated in Table 33.4.

Fig. 33.13 shows the relative histograms of PAH analytes measured in a moderately evaporated floating Macondo oil (Fig. 33.13A), calculated to exist in that oil's vapor phase (Fig. 33.13B), and measured in the dolphin lung sample (Fig. 33.13C). There is a general comparability evident between the hydrocarbons predicted to occur within vapor phase above moderately evaporated Macondo oil and what was measured within dolphin lung. Most notably, the PAH fingerprint for the lung tissue contains almost exclusively the lighter aromatics that equilibrium partitioning theory predicts would be present in the breathing zone above a moderately weathered oil

TABLE 33.4 Molecular Weights and Pure Vapor Pressure for PAH Analytes, Measured Concentrations in and Predicted Vapor Phase Concentrations Above a Moderately Evaporated Floating Macondo Oil, and Concentrations Measured in the Dolphin Lung Sample

Abbrev	Analytes	Isomer used as proxy[a]	MW (g/mol)	Vapor pressure (atm; 25°C)[b]	Floating oil measured[c] (mg/kg oil)	Calculated conc in vapor above floating oil (g/L 25°C)	Dolphin lung measured (g/g wet)	
D0	cis/trans-Decalin	Decahydronaphthalene	138	5.89E − 04	11	5.38E − 02	0.006	J
D1	C1-decalins	1-Methyldecalin	152	2.82E − 04	32	7.38E − 02	0.014	
D2	C2-decalins	2,3-Dimethyldecahydronaphthalene	166	2.34E − 04	60	1.16E − 01	0.027	
D3	C3-decalins	1-Propyldecahydronaphthalene	180	2.95E − 05	59	1.43E − 02	nd	
D4	C4-decalins	1-Butyldecahydronaphthalene	194	8.91E − 06	180	1.32E − 02	nd	
BT0	Benzothiophene		134	1.15E − 04	1	4.93E − 04	0.001	J
BT1	C1-benzo(*b*)thiophenes	3-Methylbenzothiophene	148	6.61E − 05	5	2.76E − 03	nd	
BT2	C2-benzo(*b*)thiophenes	2,3-Dimethylbenzothiophene	162	2.40E − 05	11	2.09E − 03	0.003	J
BT3	C3-benzo(*b*)thiophenes	2,5,7-Trimethylbenzothiophene	176	1.6E − 06	37	3.81E − 04	0.008	J
BT4	C4-benzo(*b*)thiophenes	2,3,4,5-tetramethylbenzothiophene	190	1.32E − 06	42	4.55E − 04	nd	
N0	Naphthalene		128	2.00E − 04	19	3.04E − 02	0.026	
N1	C1-naphthalenes	2-methylnaphthalene	142	7.94E − 05	209	1.36E − 01	0.035	
N2	C2-naphthalenes	2,6-Dimethylnaphthalene	156	1.02E − 05	824	6.89E − 02	0.041	
N3	C3-naphthalenes	1,6,7-Trimethylnaphthalene	170	6.03E − 06	1179	5.81E − 02	0.023	
N4	C4-naphthalenes	2,3,6,7-tetramethylnaphthalene	184	1.62E − 06	744	9.86E − 03	0.011	
B	Biphenyl		154	4.07E − 05	53	1.76E − 02	0.008	J
DF	Dibenzofuran		168	3.98E − 06	17	5.53E − 04	0.005	J
AY	Acenaphthylene		152	1.45E − 05	4	5.10E − 04	nd	
AE	Acenaphthene		170	2.75E − 06	16	3.53E − 04	nd	
F0	Fluorene		166	2.45E − 06	112	2.24E − 03	0.002	J
F1	C1-fluorenes	1-Methylfluorene	180	8.32E − 07	375	2.55E − 03	nd	
F2	C2-fluorenes	9,9-Dimethyl-9H-Fluorene	194	3.55E − 06	546	1.58E − 02	nd	
F3	c3-fluorenes	9-Isopropyl-9H-fluorene	208	1.26E − 06	429	4.41E − 03	nd	
A0	Anthracene		178	9.77E − 08	12	9.85E − 06	nd	
P0	Phenanthrene		178	2.82E − 07	368	8.48E − 04	0.004	JB
PA1	C1-phenanthrenes/ anthracenes	2-Methylphenanthrene	192	1.15E − 07	924	8.68E − 04	0.003	JB
PA2	C2-phenanthrenes/ anthracenes	3,6-Dimethylphenanthrenes	206	1.41E − 08	977	1.13E − 04	nd	
PA3	C3-phenanthrenes/ anthracenes	1,4,5-Trimethylphenanthrene	220	1.15E − 08	500	4.69E − 05	nd	
PA4	C4-phenanthrenes/ anthracenes	1-Methyl-7-isopropylphenanthrene	234	5.50E − 09	224	1.01E − 05	nd	
DBT0	Dibenzothiophene		184	6.76E − 08	65	3.59E − 05	0.000	J
DBT1	C1-dibenzothiophenes	4-Methyldibenzothiophene	198	3.55E − 08	216	6.26E − 05	0.001	J
DBT2	C2-dibenzothiophenes	2,8-Dimethyldibenzothiophene	212	1.58E − 08	298	3.87E − 05	nd	
DBT3	C3-dibenzothiophenes	2,4,8-trimethyldibenzothiophene	226	1.48E − 09	240	2.91E − 06	nd	
DBT4	C4-dibenzothiophenes	1,2,3,4-tetramethyldibenzothiophene	240	1.35E − 10	124	1.37E − 07	nd	
BF	Benzo(*b*)fluorene		216	1.38E − 09	17	1.94E − 07	nd	

(*Continued*)

TABLE 33.4 (*Continued*)

Abbrev	Analytes	Isomer used as proxy[a]	MW (g/mol)	Vapor pressure (atm; 25°C)[b]	Floating oil measured[c] (mg/kg oil)	Calculated conc in vapor above floating oil (g/L 25°C)	Dolphin lung measured (g/g wet)	
FL0	Fluoranthene		202	3.72E − 08	3	1.03E − 06	0.001	JB
PY0	Pyrene		202	4.57E − 08	26	9.84E − 06	0.001	JB
FP1	C1-fluoranthenes/pyrenes	3-Methylfluoranthene	216	2.19E − 08	121	2.16E − 05	nd	
FP2	C2-fluoranthenes/pyrenes	8,9-Dimethylfluoranthene	230	7.76E − 10	210	1.34E − 06	nd	
FP3	C3-Fluoranthenes/Pyrenes		244	2.57E − 09	294	6.18E − 06	nd	
FP4	C4-fluoranthenes/pyrenes			na	266	0.00E + 00	nd	
NBT1	C1-naphthobenzothiophenes	7-Methylbenzo(*b*)naphtho(2,3-D)thiophene	248	4.57E − 11	95	3.55E − 08	nd	
NBT2	C2-naphthobenzothiophenes	Benzo(*b*)naphtho(2,3-D)thiophene, 7,8-dimethyl-	262	1.20E − 11	147	1.45E − 08	nd	
NBT3	C3-naphthobenzothiophenes			na	121	0.00E + 00	nd	
C0	Chrysene/triphenylene	chrysene	228	1.20E − 10	84	8.29E − 08	0.001	J
BC1	C1-chrysenes	1-Methylchrysene	242	3.31E − 11	213	5.77E − 08	nd	
BC2	C2-chrysenes	6-Ethylchrysene	256	1.02E − 10	275	2.30E − 07	nd	
BC3	C3-chrysenes	3,3,7-trimethyl-2,4-dihydro-1H-chrysene	274	8.71E − 11	264	1.88E − 07	nd	
BC4	C4-chrysenes	Tetramethylchrysene	284	4.47E − 12	196	7.17E − 09	nd	
BBF	Benzo[*b*]fluoranthene		252	3.63E − 11	9	2.73E − 09	nd	
BJKF	Benzo[*jk*]fluoranthene	benzo(*j*)fluoranthene	252	2.75E − 11	nd	0.00E + 00	nd	
BAF	Benzo[*a*]fluoranthene		252	1.20E − 10	nd	0.00E + 00	nd	
BEP	Benzo[*e*]pyrene		252	6.61E − 11	18	9.89E − 09	nd	
BAP	Benzo[*a*]pyrene		252	5.62E − 11	4	1.94E − 09	nd	
PER	Perylene		252	3.39E − 11	1	3.97E − 10	nd	
IND	Indeno[1,2,3-*cd*]pyrene		276	9.33E − 12	0.5	3.45E − 11	nd	
DA	Dibenz[*a,h*]anthracene		278	6.76E − 13	3	1.51E − 11	nd	
GHI	Benzo[*g,h,i*]perylene		276	8.32E − 12	3	2.13E − 10	nd	
						TPAH50	0.162	

[a]*Used to represent numerous isomers comprising each alkyl group.*
[b]*Obtained from EPA On-Line Tools for Site Assessment; http://www.epa.gov/athens/learn2model/part-two/onsite/sparcproperties.htm.*
[c]*JF2-2km-surf-0net-20100527-N186; collected May 27, 2010 ~ 2 km from wellhead (Stout et al., 2016c).*

slick. The lack of an "exact" match between the predicted vapor for this particular floating oil and the lung tissue sample is to be expected. Various factors can affect the predicted vapor phase fingerprints. For example, if a different isomer were to be used to represent some of the alkylated groups (Table 33.4), the predicted vapor phase distributions can be varied slightly. In addition, the actual chemical composition of the floating oil(s) in the vicinity of this particular dolphin at the time of potential vapor inhalation is not known and may have differed from the moderately evaporated sample used in the calculation of predicted partial vapor pressures. Finally, any influence of variably absorbing and incorporating these different chemicals into lung tissue on the lung sample's "fingerprint" is unknown. Despite these variables, the PAH pattern found in the lung tissue generally resembles the fingerprint expected in a petroleum vapor above a moderately weathered oil slick.

What is evident from this comparison (Fig. 33.13B and C), however, is that the decalins and naphthalenes found in the lung tissue of this particular dolphin—which remember, also was found to have Macondo oil on its exterior—could very reasonably have been derived from the inhalation of vapors from a moderately evaporated Macondo oil. Although the distribution of decalins and naphthalenes in the lung tissue is not by itself an unequivocal indicator of exposure to Macondo oil, the fact that this dolphin had Macondo oil on its exterior

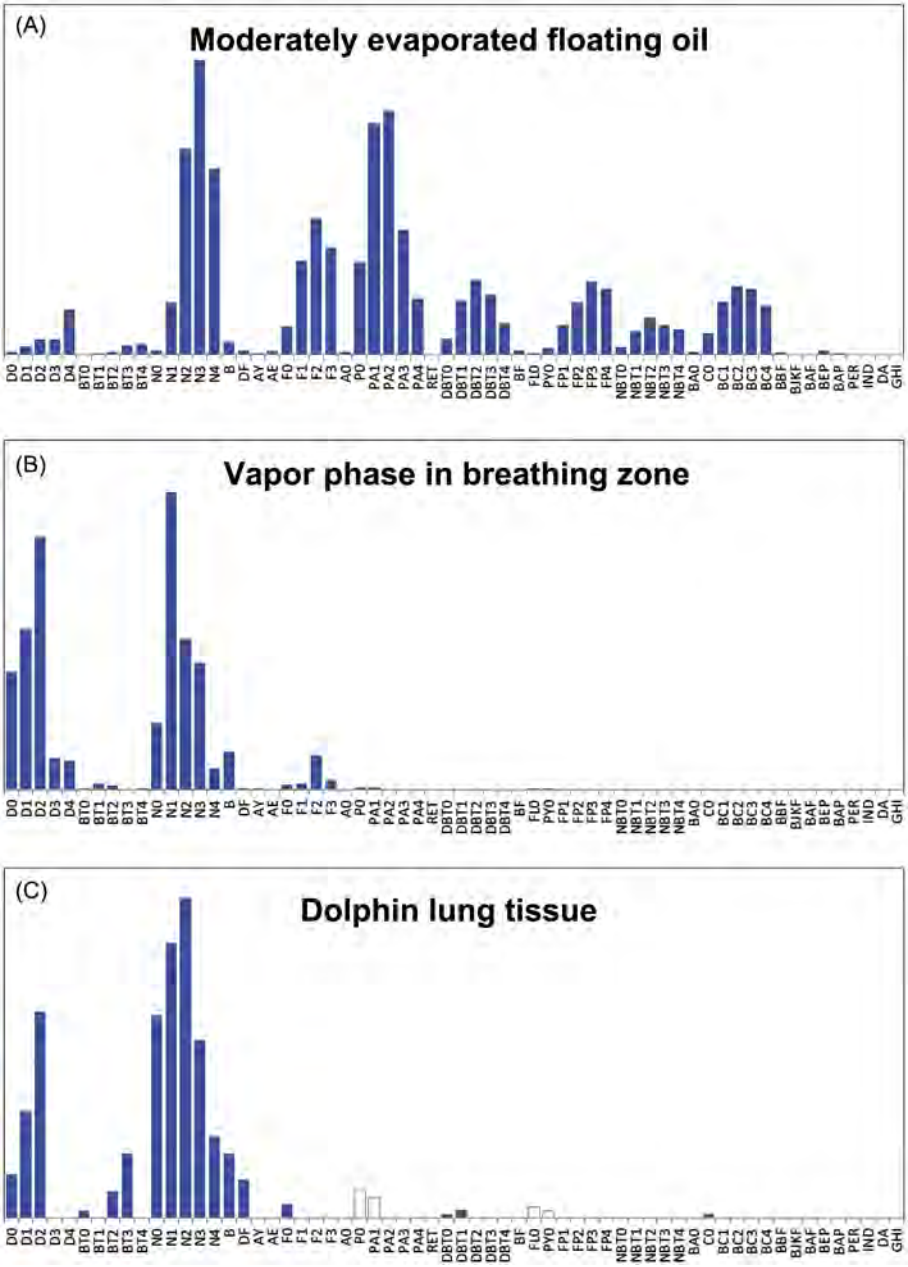

FIGURE 33.13 Histograms showing the distributions of PAH and related compounds in (A) moderately evaporated Macondo oil collected May 27, 2010 approximately 2 km from Macondo wellhead, (B) vapor predicted to exist in the breathing zone above a moderately evaporated floating Macondo oil and (C) a dolphin lung tissue sample. (A) sample id: JF2-2km-surf-0net-20100527-N186. All data from Table 33.4, but *y*-axes are unit-less and normalized to maximum analyte value for ease of comparison; White bars in (C) are compounds that were B-qualified, i.e., also detected in the method blank (Table 33.4).

bolsters the conclusion—in the same way that internal tissue exposures to *Exxon Valdez* oil were confirmed in individuals also exhibiting external exposure to the oil (Bence et al. 1996.) In addition, this particular bottlenose dolphin carcass was among the first to appear on shorelines (May 24, 2010) indicating it could reasonably have been exposed to the floating liquid oil and inhaled its vapors sometime within the 4 weeks since the spill began (April 20, 2010).

As previously mentioned, higher molecular weight (nonvolatile) PAHs and biomarkers were not found in the dolphin lung tissue sample indicating the exposure occurred via inhalation of vapors, not liquid oil or aerosols. A recently published study likewise found that higher molecular weight PAHs were absent from lung tissue

sampled from a visibly oiled Kemp's ridley turtle carcass collected in June 2010, although they were present in the turtle's other internal tissues (e.g., enteric contents and the liver; Ylitalo et al., 2017).

33.5.4 Dolphin Lung Tissue—Conclusion

The lung tissue from one of the common bottlenose dolphins confirmed to have had Macondo oil on its exterior, which was the first stranded dolphin sampled (May 24, 2010), contained 0.046 μg/g (wet) of decalins and 0.162 μg/g (wet) TPAH50, the latter comprised mostly of alkyl-naphthalenes.

The distribution of decalins and naphthalenes in the lung tissue was generally consistent with that predicted (using equilibrium partitioning theory) for the breathing zone vapor phase that would exist above moderately evaporated Macondo oil. Considering this carcass also had Macondo oil on its exterior, the hydrocarbons in the lung are reasonably attributed to indirect exposure through inhalation of Macondo oil vapors prior to death. The absence of nonvolatile PAHs and biomarkers in the lung tissue indicates liquid (or aerosolized) oil did not enter the lung before or after the animal's death.

33.6 CONCLUSION

Chemical fingerprinting, which is often thought of solely as a means to identify the source of a spilled oil, can play an important role in the assessment of natural resource exposed to oil following an oil spill from a known source. Impacts to the external surfaces of biological resources can be assessed through conventional oil spill fingerprinting methods. Internal tissue exposures, such as lung tissues studied herein, require consideration of the effects of chemical–physical processes and/or metabolic processes on the tissue fingerprints.

Acknowledgments

The authors wish to thank the efforts of numerous Trustee/BP and academic field teams that collected and provided the diversity of samples to the NRDA, some of which are described in this study. Specific thanks are extended to University of Southern Mississippi researchers (Bruce Comyns, Eric Hoffmayer, Richard Waller and Read Hendon) for participating in the collection of the *Sargassum*, US Fish & Wildlife biologist (Pete Tuttle) and contractor (Libby Mojica, EDM International, Inc.) for providing osprey nest materials, US Geological Survey and The Pennsylvania State University researchers (Amanda Demopolous and Chuck Fisher, respectively) for providing the deep-sea coral floc, and NOAA mammal biologists for providing the dolphin lung tissue sample.

The information in this chapter reflects the views of the authors and not necessarily the official positions or policies of NOAA or the Department of Commerce.

References

Aeppli, C., Carmichael, C.A., Nelson, R.K., Lemkau, K.L., Graham, W.M., Redmond, M.C., et al., 2012. Oil Weathering after the Deepwater Horizon Disaster Led to the Formation of Oxygenated Residues. Environ. Sci. Technol. 46 (16), 8799–8807.

Bence, A.E., Burns, W.A., 1993. Fingerprinting hydrocarbons in the biological resources of the *EXXON VALDEZ* spill area. In: Proceedings of Third ASTM Symposium on Environmental Toxicology and Risk Assessment: Aquatic, Plant, and Terrestrial, April 25–28, 1993, Atlanta, GA. pp. 46.

Bence, A.E., Kvenvolden, K.A., Kennicutt II, M.C., 1996. "Organic geochemistry applied to environmental assessments of Prince William Sound, Alaska, after *Exxon Valdez* oil spill—a review". Org. Geochem. 24 (1), 7–42.

Boehm, P.D., Carragher, P.D., 2012. Location of natural oil seep and chemical fingerprint suggest alternative explanation for deep sea coral observations. Proc. Natl. Acad. Sci. 109 (40), E2647.

British Petroleum, 2014. Gulf Science Data Reference Oil Characterization Data. Website: http://gulfsciencedata.bp.com/, directory: Other; subdirectory: Dispersant Application; filename: DispersantApplication_OTH-02v01-01.xlsx and DispersantApplication_OTH-02v01-02.xlsx (last accessed January 24, 2014).

Camilli, R., Reddy, C.M., Yoerger, D.R., Van Mooy, B.A.S., Jakuba, M.V., Kinsey, J.C., et al., 2010. Tracking hydrocarbon plume transport and biodegradation at *Deepwater Horizon*. Science 330, 201–204.

Chanton, J., Zhao, T., Rosenheim, B.E., Joye, S.B., Bosman, S., Brunner, C., et al., 2015. Using natural abundance of radiocarbon to trace the flux of petrocarbon to the seafloor following the *Deepwater Horizon* oil spill. Environ. Sci. Technol. 49, 847–854.

De Gouw, J.A., Middlebrook, A.M., Warneke, C., Ahmadov, R., Atlas, E.L., Bahreini, R., et al., 2011. "Organic aerosol formation downwind from the *Deepwater Horizon* oil spill.". Science 331, 1295–1299.

Dias, L.A., 2016. Evidence of marine mammals' direct exposure to petroleum products during the *Deepwater Horizon* oil spill in the Gulf of Mexico. In: DWH NRDA Marine Mammal Technical Working Group Report, Deepwater Horizion Admin. Record, https://www.fws.gov/doiddata/dwh-ar-documents/876/DWH-AR0305029.pdf.

Díez, S., Sabate, J., Vinas, M., Bayona, J.M., Solanas, A.M., Albaiges, J., 2005. The prestige oil spill. I. Biodegradation of a heavy fuel oil under simulated conditions. Environ. Toxicol. Chem. 24, 2203–2217.

Douglas, G.S. and Liu, B., 2015. Chemical Evidence for Exposure of Red Crabs and Other Deep Benthic Organisms to Macondo oil. U.S. Dept. of Interior, *Deepwater Horizon* Response & Restoration, Admin. Record, www.doi.gov/deepwaterhorizon/adminrecord, DWH-AR00260310, p. 47.

Douglas, G.S., Emsbo-Mattingly, S.D., Stout, S.A., Uhler, A.D., McCarthy, K.J., 2015. Hydrocarbon Fingerprinting Methods. In: Murphy, B.L., Morrison, R.D. (Eds.), Introduction to Environmental Forensics, third ed. Academic Press, Boston, pp. 201–309.

Emsbo-Mattingly, S.D. and Martin, C., 2015. Distribution and Weathering of Macondo Oil in Nearshore Soils, Sediments, and Tissues Collected between Spring 2010 to Spring 2012 based on Chemical Fingerprinting Methods. U.S. Dept. of Interior, *Deepwater Horizon* Response & Restoration, Admin. Record, www.doi.gov/deepwaterhorizon/adminrecord, DWH-AR00260533, p. 38.

Finch, B.B., Wooten, K.J., Smith, P.N., 2011. Embryotoxicity of weathered crude oil from the Gulf of Mexico in mallard ducks (*Anas platyrhynchos*). Environ. Toxicol. Chem. 30 (8), 1885–1891.

Fisher, C.R., Demopoulos, A.W.J., Cordes, E.E., Baums, I.B., White, H.K., Bourgue, J.R., 2014. Coral communities as indicators of ecosystem-level impacts of the *Deepwater Horizon* oil spill. BioScience 649, 796–807.

Garrett, R.M., Pickering, I.J., Haith, C.E., Prince, R.C., 1998. Photooxidation of crude oils. Environ. Sci. Technol. 32 (23), 3719–3723.

Graettinger, G., Holmes, J., Garcia-Pineda, O., Hess, M., Hu, C., Leifer, I., et al., 2015. Integrating Data from Multiple Satellite Sensors to Estimate Daily Oiling in the Northern Gulf of Mexico during the *Deepwater Horizon* Oil Spill. DWH Administrative Record, https://www.fws.gov/doiddata/dwh-ar-documents/790/DWH-AR0071445.pdf.

Hu, C., Hardy, R., Ruder, E., Geggel, A., Feng, L., Powers, S., et al., 2016. *Sargassum* coverage in the northern Gulf of Mexico during 2010 from Landsat and airborne observations: Implications for the *Deepwater Horizon* oil spill impact assessment. Mar. Pollut. Bull. 107 (1), 15–21.

Kennicutt, M.C., Comet, P.A., 1992. Resolution of sediment hydrocarbons sources: Multiparameter approach. In: Whelan, J.K., Farrington, J.W. (Eds.), Organic Matter: Productivity, Accumulation, and Preservation in Recent and Ancient Sediments. Columbia Univ. Press, New York, pp. 309–338.

Michel, J., Owens, E.H., Zengel, S., Graham, A., Nixon, Z., Allard, T., et al., 2013. Extent and degree of shoreline oiling: *Deepwater Horizon* oil spill, Gulf of Mexico, USA. PLoS ONE 8 (6), e65087.

Mojica, E.K., B.J. Paxton, F.M. Smith, and B.D. Watts, 2011. Natural Resource Damage Assessment Work Plan for Preassessment of Injury to Ospreys from the Deepwater Horizon (MC 252) Oil Spill (Bird Study #9): End of Study Draft Final Report. Center for Conservation Biology Technical Report Series, CCBTR-11-16. College of William and Mary and Virginia Commonwealth University, Williamsburg, VA. pp. 19.

NOAA, 2014. Analytical quality assurance plan, Mississippi Canyon 252 (*Deepwater Horizon*) natural resource damage assessment, Version 4.0. May 30, 2014.

OPA, 1990. Oil Pollution Act; 33 U.S.C. §2701 et seq.

Payne, J.R., Flynn, N.W., Mankiewicz, P.J., Smith, G.S., 1980. Surface evaporation/dissolution partitioning of low molecular weight aromatic hydrocarbons in a downplume transect from the IXTOC-I wellhead. In: Proc. Symp. Prelim. Results, Sept. 1979 Research/Pierce IXTOC-I Cruise, June 9-10, 1980, Key Biscayne, FL(NTIS Access. No. PB-246068): 239–263.

Payne, J.R. Driskell, W.B., 2015. 2010 DWH Offshore Water Column Samples—Forensic Assessments and Oil Exposures. U.S. Dept. of Interior, *Deepwater Horizon* Response & Restoration, Admin. Record, www.doi.gov/deepwaterhorizon/adminrecord, DWH-AR0039118, p. 37.

Plata, D.L., Sharpless, C.M., Reddy, C.M., 2008. Photochemical degradation of polycyclic aromatic hydrocarbons in oil films. Environ. Sci. Technol. 42, 2432–2438.

Powers, Sean P., Hernandez, Frank J., Condon, Robert H., Drymon, J. Marcus, Free, Christopher M., 2013. "Novel pathways for injury from offshore oil spills: direct, sublethal and indirect effects of the *Deepwater Horizon* Oil Spill on pelgaic *Sargassum* communities.". PLoS ONE 8 (9), e74802.

Prince, R.C., Owens, E.H., Sergy, G.A., 2002. Weathering of an Arctic oil spill over 20 years: the BIOS experiment revisited. Mar. Pollut. Bull. 44 (11), 1236–1242.

Prince, R.C., McFarlin, K.M., Butler, J.D., Febbo, E.J., Wang, F.C.Y., Nedwed, T.J., 2013. The primary biodegradation of dispersed crude oil in the sea. Chemosphere 90, 521–526.

Radović, J.R., Aeppli, C., Nelson, R.K., Jimenez, N., Reddy, C.M., Bayona, J.M., et al., 2014. Assessment of photochemical processes in marine oil spill fingerprinting. Mar. Poll. Bull. 79, 268–277.

Ramseur, J.L., 2010. *Deepwater Horizon* oil spill: The fate of the oil. In: *Congressional Research Service Report* 7-5700, Dec. 16.

Schwacke, Lori H., Cynthia, R. Smith, Townsend, Forrest I., Wells, Randall S., Hart, Leslie B., Balmer, Brian C., et al., 2013. "Health of common bottlenose dolphins (*Tursiops truncatus*) in Barataria Bay, Louisiana, following the *Deepwater Horizon* oil spill.". Environ. Sci. Technol. 48, 93–103.

Socolofsky, S.A., Adams, E.E., Sherwood, C.R., 2011. Formation dynamics of subsurface hydrocarbon intrusions following the *Deepwater Horizon* blowout. Geophys. Res. Lett. 38, L09602, http://dx.doi.org/10.1029/2011GL047174): p. 6.

South Atlantic Fishery Management Councel (SAFMC), 2002. Fishery Management Plan for Pelagic Sargassum Habitat of the South Atlantic Region. Charleston, SC., p. 153.

Stout, S.A., 2015a. Chemical Fingerprinting of Sea Turtle Wipe Samples from the Northern Gulf of Mexico during and after the *Deepwater Horizon* Oil Spill. U.S. Dept. of Interior, *Deepwater Horizon* Response & Restoration, Admin. Record, www.doi.gov/deepwaterhorizon/adminrecord, DWH-AR0038939, p. 15.

Stout, S.A. (2015b) Chemical Fingerprinting Assessment of Exposure of Dolphins to Macondo Oil during and after the *Deepwater Horizon* Oil Spill. U.S. Dept. of Interior, *Deepwater Horizon* Response & Restoration, Admin. Record, www.doi.gov/deepwaterhorizon/adminrecord, DWH-AR0038954, p. 30.

Stout, S.A., 2016. Oil spill fingerprinting method for oily matrices used in the *Deepwater Horizon* NRDA. Environ. Forensics 17 (3), 218–243.

Stout, S.A., Payne, J.R., 2016. Macondo oil in deep-sea sediments: Part 1—Sub-sea weathering of oil deposited on the seafloor. Mar. Pollut. Bull. 111 (1–2), 365–380.

Stout, S.A., Payne, J.R., Ricker, R.W., Baker, G., Lewis, C., 2016a. Macondo oil in deep-sea sediments: Part 2—Distribution and distinction from background and natural oil seeps. Mar. Pollut. Bull. 111 (1–2), 381–401.

Stout, S.A., Payne, J.R., Emsbo-Mattingly, S.D., Baker, G., 2016b. Weathering of field-collected floating and stranded Macondo oils during and shortly after the *Deepwater Horizon* oil spill. Mar. Pollut. Bull. 105, 7–22.

Stout, S.A., Rouhani, S., Liu, B., Oehrig, J., Ricker, R.W., Baker, G., 2017. Assessing the footprint and volume of oil deposited in deep-sea sediments following the Deepwater Horizon oil spill. Mar. Pollut. Bull. 114, 327–342.

Stout, S.A., Uhler, A.D., Emsbo-Mattingly, S.D., 2004. Comparative evaluation of background anthropogenic hydrocarbons in surficial sediments from nine urban waterways. Environ. Sci. Technol. 38 (11), 2987–2994.

Torralba, Manolito G., Franks, M.G., Gomez, J.S., Yooseph, A., Nelson, S., Nelson, K.E., et al., 2017. Effect of Macondo prospect 252 oil on microbiota associated with pelagic Sargassum in the Northern Gulf of Mexico. Microbial. Ecol. 73, 91–100.

Trustees, 2016. *Deepwater Horizon* Oil Spill: Final Programmatic Damage Assessment and Restoration Plan and Final Programmatic Environmental Impact Statement. Feb. 2016, available on-line: http://www.gulfspillrestoration.noaa.gov/restoration-planning/gulf-plan. Accessed: Dec. 1, 2016.

Uhler, A.D., McCarthy, K.J., Emsbo-Mattingly, D., Stout, S.A., Douglas, G.S., 2010. Predicting chemical fingerprints of vadose zone soil gas and indoor air from non-aqueous phase liquid composition. Environ. Forensics 11 (4), 342–354.

Valentine, D.L., Burch Fisher, G., Bagby, S.C., Nelson, R.K., Reddy, C.M., Sylva, S.P., et al., 2014. Fallout plume of submerged oil from *Deepwater Horizon*. Proc. Natl. Acad. Sci.10.1073/pnas.1414873111: p. 6.

Wang, Z., Fingas, M., Owens, E.H., Sigouin, L., Brown, C.E., 2001. Long-term fate and persistence of the spilled Metula oil in a marine salt marsh environment. Degradation of petroleum biomarkers. J. Chromatogr. A. 926, 275–290.

White, H.K., Hsing, P.-Y., Cho, W., Shank, T.M., Cordes, E.E., Quattrini, A.M., et al., 2012a. Impact of the *Deepwater Horizon* oil spill on a deep-water coral community in the Gulf of Mexico. Proc. Natl. Acad. Sci. 109 (50), 20303–20308.

White, H.K., Hsing, P.-Y., Cho, W., Shank, T.M., Cordes, E.E., Quattrini, A.M., et al., 2012b. Reply to Boehm and Carrangher: multiple lines of evidence link deep-water coral damage to Deepwater Horizon oil spill. Proc. Natl. Acad. Sci. 109 (40), E2648.

Ylitalo, G.M., Collier, T.K., Anulacion, B.F., Juaire, K., Boyer, R.H., da Silva, D.A.M., et al., 2017. Determining oil and dispersant exposure in sea turtles from the northern Gulf of Mexico resulting from the *Deepwater Horizon* oil spill. Endang. Species Res. 33, 9–24.

CHAPTER

34

Forensic Identification of Historical and Ongoing Tar Oil Releases in Nearshore Environments

Stephen Emsbo-Mattingly and Eric Litman

NewFields Environmental Forensics Practice, LLC, Rockland, MA, United States

BIOGRAPHIES

Eric Litman is an environmental scientist with 15 years of laboratory and consulting experience specializing in applied chemistry and technical project management. Since 2010, he has been a consulting scientist at NewFields Environmental Forensics Practice, LLC in Rockland, Massachusetts working in support of governmental and industrial clients. During this time he has managed a variety of regulatory and industrial site investigations focused on the chemical characterization of environmental contaminants and conducted extensive research during the NRDA investigation following the *Deepwater Horizon* oil spill. His research interests include the optimization of analytical techniques and the development of emerging environmental technologies.

Stephen Emsbo-Mattingly is a senior scientist at the NewFields Environmental Forensics Practice in Rockland Massachusetts. He has twenty-eight years of environmental chemistry and forensic investigation expertise. Mr. Emsbo-Mattingly specializes in the source identification of petroleum, tar, PAHs, PCBs, dioxins, and chlorinated solvent products in the environment. His chemical fingerprinting involve extensive research concerning the process chemistry associated with petroleum and tar refineries, coal operations, pavement producers, chemical manufacturers, metal fabricators, degreasing operations, dry cleaning, avionics, electrical utilities, wood treaters, pipelines, hydraulic fracturing, oil & natural gas development, railroading, automobile manufacturing and recycling, circuit board manufacturing, and wastewater treatment plants. He has authored or co-authored over 100 papers, book chapters, guidance documents, and presentations. Mr. Emsbo-Mattingly's research extends to natural ambient sources of contaminants, such as petroleum seeps, coal fires, sewage and storm-water runoff. He is member of the American Chemical Society, Society of Environmental Toxicology and Chemistry, Air and Waste Management Association, American Wood Protection Association, and Society for Industrial Archeology. His project portfolio reflects a wide range of public and private sector sponsors in support of site investigations, risk assessments, liability management, as well as civil and criminal litigation.

34.1 INTRODUCTION

Tar oils are nonaqueous phase liquid (NAPL) byproducts formed during the manufacture of gas and coke. A variety of tar oil types were generated at manufactured gas plants (MGPs) and coke oven plants: some were refined into saleable products (e.g., creosote, Tarvia, and pitch) and others were discharged into the environment. Historical waste management practices at some MGPs, coke manufacturers, and tar refiners represent significant historical sources of tar oil releases. Most of these plants closed when less expensive products, like natural gas,

Oil Spill Environmental Forensics Case Studies.
DOI: http://dx.doi.org/10.1016/B978-0-12-804434-6.00034-3

imported steel, and petrochemicals, became available. Closed plants ceased generating tar oil; however, some historical tar oil releases captured in subsurface soil or sediment bodies that did not evaporate or solidify, chronically leach or seep into shoreline environments, especially when disturbed. Contemporary tar and tar product producers generally comply with modern environmental regulations, which effectively reduce or eliminate ongoing tar oil releases. However, some tar products, like creosote treated marina pilings and bulkheads, represent ongoing sources of tar oil in nearshore environments. Both historical and contemporary tar oil discharges are commonly misidentified as petroleum spills and vice versa. Hydrocarbon fingerprinting is one of the most effective methods for accurately identifying fugitive tar oil impacts.

The hydrocarbon patterns of tar oil and petroleum exhibit significant chemical differences. Tar oil is dominated by parent polycyclic aromatic hydrocarbons (PAHs), while petroleum contains abundant saturated hydrocarbons. These dominant compositional features provide numerous metrics for distinguishing tar oil from petroleum and for allocating mixtures. However, tar oil also contains trace amounts of the parent coal or petroleum feedstock in use when the tar was generated. The feedstock is dominated by saturated hydrocarbons, which can be isolated and characterized by advance chemical fingerprinting techniques. The feedstock signature is particularly useful for distinguishing historical releases of coal tar and gas oil tars historically produced by MGPs from subsequent releases of unrelated crude and fuel oil. In this way, the tar oil signature is recognized in a wide variety of shoreline settings by (1) the dominant pattern of parent PAHs generated at high temperature and (2) the saturated hydrocarbon pattern of the original feedstock derived from geochemical and refining processes.

In this chapter, we describe the types of industrial processes capable of generating tar oil and the forensic strategies for differentiating tar oil from other hydrocarbon products commonly encountered in nearshore environments. Tar oils possess two important forensic source signatures. First, the dominant tar oil signature is primarily composed of benzenes and parent PAHs. Second, trace amounts of nearly unaltered feedstock reside in all crude and refined tar products. The feedstock is predominantly composed of saturated hydrocarbons and geochemical biomarkers. Laboratory methods for measuring each tar oil signature are presented. Forensic methods for confirming tar oil impacts are discussed in relation to four sediment case studies with alleged impacts from a variety of tar and petroleum products.

34.1.1 Tar Oil

The demand for inexpensive refined fuel dates back to the early industrial revolution. Heavy reliance on wood progressed to coal, petroleum, electricity, and eventually natural gas (Simmons, 2009). Each shift responded to the evolving needs of industry and consumers for heat, illumination, chemicals, and transportation. For example, coal was originally burned for heat before engineers developed methods for destructive distillation capable of generating gas for illumination, coke for metallurgy, and tar for chemicals. Gas and coke manufacturers carefully studied the effects of feedstock composition, plant equipment, and heating procedure to produce high quality gas, coke, or tar (Rhodes, 1945; Morgan, 1926). The production of one product required conditions that altered and typically diminished the quality of other products; for example, the high temperatures used to generate illuminating gas generated coke that was too brittle or otherwise poorly suited for steel making. The industrial site history helps forensic investigators identify components of the hydrocarbon signature that help track fugitive tar oil in a variety of nearshore environments.

Hatheway (2012) provides an integrated and detailed summary of historical tar oil generators and refiners with an emphasis on issues of concern to modern environmental professionals. Harkins et al. (1988) and Hatheway (2012) estimated the number of former MGPs in the United States between 1000 and 50,000, respectively, most frequently occurring in municipalities of 5000 or more residents. Hayes et al. (1996) estimated that former MGPs generated 3000 to 900,000 L of tar per site. The volume of tar oil generated by each process roughly corresponded to the volume of gas generated (Fig. 34.1). High temperature coal carbonization plants produced approximately 8% tar oil by weight of coal processed, which increased at lower carbonization temperatures. Carbureted water gas (CWG) plants produced 2% to 18% tar per volume of petroleum feedstock processed with lower yields from naphtha and higher yields from heavy petroleum distillates. The specialized nature of MGPs and coke plants largely explains why tar oils possess plant specific chemical signatures controlled by the composition of the feedstock, plant equipment, and plant operating conditions. Although coal gas dominated the industry in the 1800s, CWG gas was the dominant overall tar oil generating processes throughout the entire MGP period. A brief summary of the major tar oil producing industries links the manufacturing processes with the forensic hydrocarbon signatures.

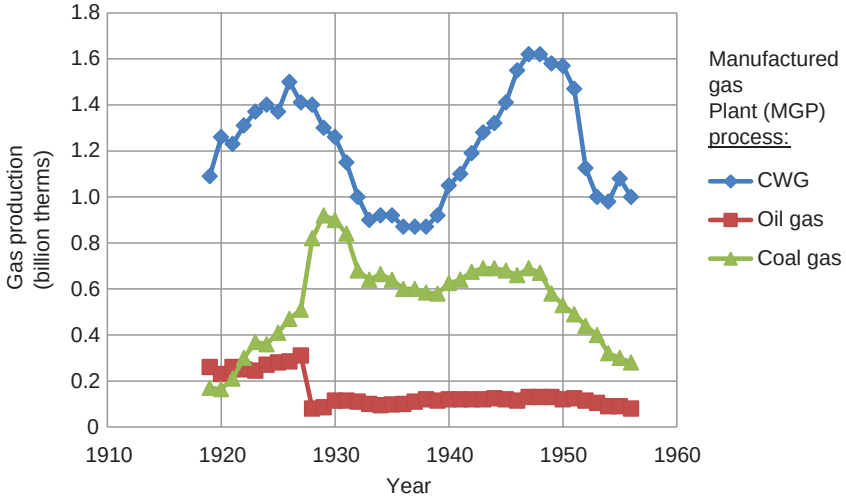

FIGURE 34.1 **Gas production by manufacturing process.** The three primary processes used to manufacture gas included coal carbonization (CC), carbureted water gas (CWG), and oil gas (OG) (Harkins et al., 1988). The volume of manufactured gas paralleled the generation of tar byproducts by the CWG, OG, and CC, respectively.

34.1.1.1 Coal Gas (1816–75)

Coal gas plants emerged in US cities that possessed easy access to coal bearing trains and barges plus close proximity to gas main networks. Coal gas generation began by filling retorts or ovens with bituminous coal, although other types of local coals were used when available. The ovens were sealed from ambient air and vents conveyed gases generated from the coal as it was heated indirectly to a temperature between 600°C and 800°C through the retort walls (Rhodes, 1945). The carbonized coal or coke that remained in the oven was effectively purified of moisture, heteroatomic carbon, volatile, and semivolatile hydrocarbons. Much of the coke was burned in the coal gas plant or sold locally as fuel. Metallurgists preferred coke because it burned hot, maintained its structure, and contained few impurities that could adversely affect the quality of the steel. As the retort gas cooled, larger hydrocarbons condensed into tar oil while the gases stabilized. The tar oil consisted of aromatic hydrocarbons (benzenes and PAHs) mixed with lower proportions of coal distillate and particulates (feedstock).

The gas primarily consisted of combustible hydrogen, methane, carbon monoxide, and ethane mixed with inert carbon dioxide, oxygen, and nitrogen with an energy content of approximately 615 Btu/ft^3. The gas was initially used to light streets, but production efficiencies eventually generated lower cost manufactured gas for residential commercial applications. Coal gas production declined when alternative illumination technologies arose in the form of kerosene and electricity. The coal gas generators were typically replaced or augmented with more efficient MGP technologies.

34.1.1.2 Byproduct Coke Ovens (1892–Present)

German industrialists developed the byproduct coke oven to minimize manufacturing waste and maximize recovery of valuable gas, coke, tar, phenols, ammonia, sulfur, cyanide and related chemicals (Bateman, 1922; Rhodes, 1945). Construction of byproduct coke ovens proliferated in areas with easy access to coal, steel manufacturing and transportation hubs. World Wars I and II stimulated the growth of these plants as critical producers of raw materials for munitions, pharmaceuticals, and metallurgy (Fig. 34.1). Although declining in number after World War II, byproduct ovens continue to produce coke (steel making), coal tar (wood preservative and chemicals), light oil (crude mixture of benzene, toluene, and xylene), naphthalene (plastic precursor), ammonia, and sulfur. The market value for these products fluctuated over time; however, the resale of one or more of the byproducts rendered them to be overall profitable over the long term. Coal gas plants and byproduct coke ovens shared the general principals of coal carbonization, but the byproduct coke ovens employed specialized equipment and procedures for isolating coke, gas, tar oil, light oil, ammonia, cyanide, sulfur, and others for reuse or resale.

34.1.1.3 Carbureted Water Gas (1875–1960s)

Thaddeus Lowe patented the CWG process in 1875 and the United Gas Improvement Company purchased the Lowe process in 1882 (Morgan, 1926; Harkins et al., 1988). The proliferation of CWG plants rejuvenated the MGP

industry in the face of mounting competition from cheap kerosene and Thomas Edison's incandescent light bulb (1881). The CWG process thrived because it required (1) less space, (2) less equipment, (3) less labor, and (4) less plant construction time (Morgan, 1926). By 1882, the CWG process generated more gas nationally than coal carbonization due in part to easily accessible sources of inexpensive petroleum. The initial use of naphtha quickly diminished after the invention of mass produced motorcars increased the demand and cost for naphtha-based gasoline in the 1920s. Gas oil composed of petroleum hydrocarbon distilled between kerosene and lubricating oil rapidly became the most widely used carburetion fluid when the proliferation of CWG plants first peaked (Fig. 34.1).

The CWG generator directed air and steam in alternating cycles through a bed of coke (preferred) or locally sourced anthracite or bituminous coal to produce water gas or blue gas primarily composed of hydrogen and carbon monoxide with an energy content of approximately 300 Btu/ft^3 (Morgan, 1926). The coke or coal was combusted in the generator, while producing ash and slag. The water gas traveled to a carburetor in which petroleum was sprayed onto hot refractory brick and cracked into light hydrocarbons raising the energy content to approximately 530 Btu/ft^3.

The composition of CWG gas resembled coal gas, but contained significantly more carbon monoxide and less methane and ethane. The CWG tar was enriched in aromatic hydrocarbons (benzenes and PAHs) mixed with lower proportions of unreacted feedstock (gas oil range saturated hydrocarbons). The lighter CWG tar differed from coal tar in that it contained little to no tar acids or tar bases, due to the fact that the gas oil feedstock contained relatively little oxygen and nitrogen compared to bituminous coal. The tar separation processes generated tar oil with high water content. The absence of tar acids and tar bases plus the high water content diminished the value of CWG tar for refiners. MGP operators struggled to find beneficial uses for CWG tar and incurred extra costs if they elected to dehydrate it. Consequently, CWG tar oil was often an unmarketable waste that was discharged to nearby waterbodies, and as such is commonly the dominant tar encountered during environmental investigations near former MGPs.

34.1.1.4 Pacific Oil Gas (1889–1929)

Leon Lowe patented the Pacific oil gas process in 1889, which proliferated in western US cities with easy access to petroleum and limited access to coal (Morgan, 1926; Harkins et al., 1988). The Pacific oil gas process resembled the CWG process with design features customized for cracking crude petroleum and residual fuel oil. The cracking temperature ranged from 690°C to 1100°C depending on the plant configuration, which yielded more tar at lower temperatures and more lampblack (graphitic carbon) at higher temperature (Morgan, 1926). The plants employed a superheater that forced the manufactured gas and pyrolyzed aerosols across additional hot brick surfaces to assure maximum gas generation from heavy carburetion fluids. Pacific oil gas plants did not survive well through the Great Depression (1929–39) and, with few exceptions, were replaced by more efficient sources of illumination and heating fuel.

34.1.1.5 High Btu Oil Gas (1945–60s)

In response to the arrival of natural gas pipelines, gas companies began purchasing a base load of natural gas from regional pipeline systems, but incurred surcharges and penalties for drawing excess natural gas during peak consumption periods (Harkins et al., 1988). In response, gas companies constructed high Btu oil gas plants during the transition from MGP to natural gas, which repurposed much of the existing CWG equipment to manufacture high Btu gas (1000 Btu/ft^3). Plant operators refitted the generator with high temperature refractory brick and carburetion fluid sprayers designed for mixtures of gas oil and MGP tar oil. The Hall oil gas design extended the array of refractory checkerbrick by converting secondary carburetors into superheaters. The renovated plants provided flexible systems for generating gas during peak consumption and consumed most to all of the tar byproducts.

34.1.1.6 Natural Gas (1925–Present)

North Americans living near natural gas fields enjoyed access to this fuel in the 19th and early 20th centuries (Castaneda, 2009). Numerous advances in pipeline technologies between 1925 and 1935 facilitated the widespread distribution of natural gas to urban and industrial centers over distances approaching 1000 miles. Natural gas gradually replaced manufactured gas as expanding pipeline networks delivered cheaper, cleaner, and more energetic (1000 Btu/ft^3) natural gas across the country. After World War II, the advancing network of natural gas replaced MGPs (Fig. 34.1). Former MGPs were redeveloped or converted into liquid natural gas supply and storage centers. The loss of MGPs limited the generation of tar oil in the United States to byproduct coke oven facilities.

34.2 HYDROCARBON SOURCE SIGNATURES

Source signatures are properties that differentiate one material from another. Manufacturers and refineries use a variety of terms and easily measured bulk properties (e.g., color, smell, density, viscosity, and miscibility) to differentiate hydrocarbon products. Context is important for interpreting these properties, especially in historical documents. For example, the term "oil" could refer to petroleum products at a fuel refinery or tar products at a byproduct coke oven plant. Similarly, the term "coal tar" is often used to collectively describe all types of MGP tar, regardless whether the tar was generated from coal (e.g., coal gas or coke oven plant) or petroleum (e.g., CWG or oil gas plant). Technically, coal tar only refers to tar generated during coal gasification or coke production, while petroleum tar refers to tar generated from the cracking of carburetion fluid during the CWG and oil gas processes.

Once released into the environment, further complications ensue. Evaporation, dissolution, oxidation, biodegradation, and other processes alter the bulk properties of fugitive hydrocarbon products and often yielding viscous black oils that sheen and stain. In other words, the appearance and physical properties of fugitive oil or impacted sediments/soils can be misleading in shoreline forensic investigations. The identity of hydrocarbon sheens and sediment staining near marinas and structural shorelines is particularly difficult, because pilings and bulkheads treated with creosote can leak into the proximal sediment and water.

Forensic investigators rely most heavily on chemical fingerprints to accurately identify the source of fugitive oil, especially in shoreline areas with multiple potential sources. The source signature of hydrocarbon products depends heavily on the type of product and the degree of environmental weathering. Volatile hydrocarbon patterns may be used when the products are fresh and semivolatile hydrocarbons work well when the products are moderately to severely weathered. As a general guideline, forensic investigations benefit greatly from the collection of site specific source samples in various stages of environmental weathering. The chemical fingerprints of these source samples can accurately delineate the nature and extent of fugitive oil among field samples collected from spatially diverse samples collected from the alleged area of impact.

By using multiple lines of chemical evidence, the ability to recognize and define independent source signatures increases and the distinctions among candidate source samples and ambient conditions becomes more resolved or specific. As modern chemical testing methods improve, the number of source signatures based upon diagnostic molecular features greatly expands. Source identification of liquid tar oil can be accomplished with volatile and semivolatile hydrocarbon fingerprinting if little to no weathering occurred. Semivolatile hydrocarbon signatures are particularly useful for weathered tar oil, because they represent some of the most abundant and environmentally stable hydrocarbons. The relative abundance of semivolatile hydrocarbons with the greatest stabilities generally works best for the widest range of samples collected as part of a forensic investigation involving tar oil. Source signatures based on ratios of PAH concentrations or standardized chromatographic peak areas of saturated hydrocarbon and geochemical biomarkers provide the relative abundances necessary to not only distinguish tar oils from spilled petroleum, but also for distinguishing among different types of tar oils.

34.2.1 Fossil Fuels

Petroleum formation is described well in numerous treatises (Peters et al., 2005; Tissot and Welte, 1984). To this larger discussion, it should be noted that coal is the terrestrial analog of crude petroleum. Most coal formed from the residues of terrestrial plants and trees that accumulated in marshes and swamps, while most petroleum formed from algae residues that accumulated in marine or lacustrine areas. The biomass mixed with varying amounts of inorganic materials (sediment) before burial over geological time. The weight of the overburden and heat from the earth over long periods of time transformed the terrestrial and marine biomass into fossil fuels. Although sometimes described differently by coal and petroleum scientists, the geochemical transformations that convert biomass into fossil fuels occurred in three general stages, often termed diagenesis, catagenesis, and metagenesis (Tissot and Welte, 1984).

Coal and petroleum theoretically exhibit formation-specific source signatures resulting from the accumulation of characteristics associated with the prehistoric biomass, depositional environment, and formation conditions. The collective processes of petrogenesis (Peters et al., 2005) and coalification (Taylor et al., 1998) imbue the fossil fuels with physical and chemical features that help forensic investigators differentiate fossil fuels and refined products from different geological formations. The chemical compositions—and thereby, source signatures—of fossil fuels varies considerably around the world. In their pure form, petroleum and coal exhibit distinct bulk properties as well as distinct molecular signatures evident in the patterns of saturated hydrocarbons, aromatic hydrocarbons, and geochemical biomarkers.

34.2.2 Modern Anthropogenic Effects

Polycyclic aromatic hydrocarbons are widespread environmental contaminants found in soil, sediments, and airborne particulates (Ohkouchi et al., 1999; Lima et al., 2005). While low levels of PAHs in the environment have natural origins (Wakeman et al., 1980), the majority of PAHs found in modern soils and sediments arise from myriad anthropogenic petrogenic and pyrogenic sources (Laflamme and Hites, 1978; Kennicutt and Comet, 1992; Stout et al., 2004). Tar oils and tar oil-refined products such as creosote produced from the industrial pyrolysis of coal or oil at former MGPs or in coking retorts are viscous, oily substances that contain significant concentrations of PAH (EPRI, 1993). The mole fraction of PAHs of environmental significance is lower in petroleum than in tar oil. When regulated PAH concentrations exceed the applicable regulatory standards, the nearest hydrocarbon point source is often expeditiously assumed to be the cause of the exceedance and potentially responsible parties are ordered to pay for the remedy. This assumption can be mistaken; however, hydrocarbon fingerprinting is well suited for correctly associating regulatory contaminants with specific historical operations or anthropogenic background (Costa et al., 2004; Uhler et al., 2005).

Anthropogenic hydrocarbons and natural organic matter (NOM) possess source-specific distributions of PAH compounds (Youngblood and Blumer, 1975; Boehm and Farrington, 1984; Colombo et al., 1989; Dickhut et al., 1995; Yunker and Macdonald, 1995; Sauer and Uhler, 1994; Lima et al., 2005). In particular, anthropogenic products exhibit characteristic PAH patterns (source signatures) that are a function of the geological formation and the chemical process (e.g., distillation, synthesis, cracking, etc.) used to reform the hydrocarbon pattern (Emsbo-Mattingly et al., 2003a; Costa et al., 2004). Although not true in all oil spill situations, investigations that occur over months and years emphasize diagnostic ratios constructed from the more environmentally recalcitrant 4-, 5-, and 6-ring PAHs, because the lighter PAHs are disproportionately affected by environmental weathering. The use of selected source ratios is based on the concept that hydrocarbons with similar properties (i.e., molecular weight, partial pressure, solubility, partition coefficients, and biotic/abiotic degradation) will weather at similar rates in the environment (Yunker and Macdonald, 1995; Costa and Sauer, 2005; Uhler and Emsbo-Mattingly, 2006).

34.2.3 Generation of Pyrogenic PAHs

There are two forms of heating that are significant in the generation of PAH, viz. carbonization and combustion (Scott, 1982). Carbonization is the complex process of concentrating and purifying carbon by denaturing organic matter with heat in the presence of little to no oxygen. Carbonizing petroleum or coal consists of four steps. First, heat distills the volatile and semivolatile hydrocarbons into a vapor phase. Second, surplus heat pyrolyzes larger hydrocarbons by breaking or "cracking" most of the carbon−hydrogen and carbon−carbon bonds to form smaller hydrogen and hydrocarbon gases. Pyrolysis also cleaves thermally unstable functional groups (e.g., saturated hydrocarbons and heteroatomic moieties). Third, surplus heat helps pyrosynthesize and condenses polymeric networks of aromatized carbon (i.e., soot). Fourth, the volatile and semivolatile hydrocarbons in the vapor phase condense into stable gases and PAH-rich liquid tar and particulate soot as the vapor phase cools. Collectively, carbonization of petroleum and coal produces coke, tar oil, soot, and hydrocarbon gases.

Combustion is the thermal decomposition of organic matter in the presence of oxygen. The processes of distillation, pyrolysis, pyrosynthesis, and condensation (described above) are largely the same during the combustion of petroleum and coal, except oxygen acts powerfully to transform most of the hydrocarbon vapors into nonhydrocarbon gases (e.g., carbon dioxide, nitrogen oxides, sulfur oxides, and water) (Swaine, 1990). Consequently, little or no liquid coal tar is produced from the combustion of coal. The combustion of oil predominantly generates nonhydrocarbon gases; however, this combustion is never complete and the partial combustion of the fuel generates soot consisting of very large carbon polymers mixed with low proportions of monocyclic and PAHs.

Carbonization and combustion preferentially pyrolyze alkylated functional groups producing three major changes in the hydrocarbon signature. First, saturated hydrocarbons and geochemical biomarkers experience dramatic reductions throughout the volatile and semivolatile range. Second, more thermally stable compounds, like PAHs, loose alkylated functional groups much more quickly than the aromatic ring structures (Fig. 34.2). In this way, the relative abundances of parent and alkylated PAHs act like internal thermometers for reconstructing the temperature at which the fossil fuels are carbonized or combusted. Higher temperatures and exposure to catalytic surfaces break aliphatic bonds transforming petrogenic PAH patterns into pyrogenic PAH patterns with high proportions of parent PAHs (e.g., naphthalene, phenanthrene, pyrene, chrysene, benzo[*a*]pyrene) and progressively creating more skewed profiles with increasing temperature (Fig. 34.2). Third, pyrosynthesis generates contorted PAHs with 5-member carbon rings (e.g., fluoranthene, benzo[*b*]fluoranthene, and dibenzo[*a*,*e*]fluoranthene) and linear configurations (e.g., benz[*a*]anthracene, pentaphene, and ananthrene). These PAH precursors grow very rapidly

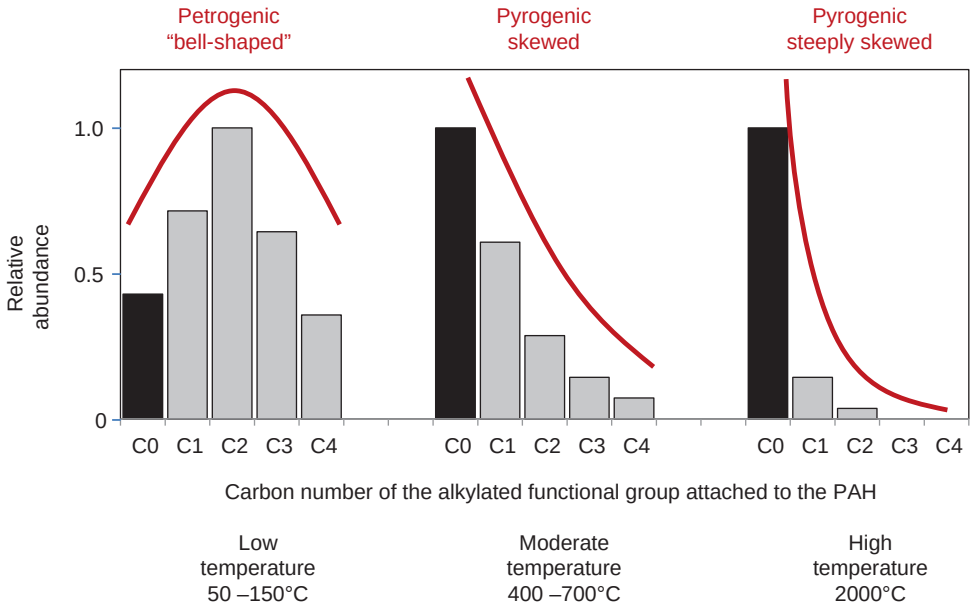

FIGURE 34.2 **Petrogenic and pyrogenic PAH patterns.** Petrogenic PAHs contain abundant alkylated functional groups, which preferentially break and release energy during pyrolysis shifts the PAH profile from a "bell" to a "sloped" shape (Blumer, 1976).

into larger soot molecules at high temperatures. The pyrosythetic PAH structures do not appear in appreciable concentrations when PAHs form geologically at lower temperatures through petrogenesis or coalification.

34.3 METHODS

Tar oils contain volatile and semivolatile hydrocarbons. The volatile hydrocarbons are organic compounds with boiling points between 35°C and 235°C, which correspond to hydrocarbons eluting from a gas chromatograph equipped with a nonpolar silicone capillary column between approximately *n*-pentane (*n*-C_5) and *n*-tridecane (*n*-C_{13}). The volatile fraction of tar oil primarily consists of benzene and alkylated benzenes. Semivolatile hydrocarbons are solvent-extractable organic compounds with boiling points between approximately 150°C and 545°C, which elute between approximately *n*-nonane (*n*-C_9) and *n*-tetratetracontane (*n*-C_{44}) on gas chromatography (GC) equipped with a nonpolar silicone capillary column. The semivolatile hydrocarbons in tar oil primarily consist of 2- to 7-ring parent PAHs. Lower relative abundances of coal and petroleum feedstock residues consist of normal alkanes, acyclic isoprenoids, alkylcyclohexanes, sesqui-, di-, and triterpanes, regular and rearranged steranes, mono- and triaromatic steranes among others. Tar oils are generally classified using patterns of parent and alkylated PAHs; however, more detailed analyses of saturates provide additional lines of evidence needed for more complex sites and commingled plumes.

The forensic methods used to characterize tar oils are typically employed as part of a tiered approach using a combination of screening and confirmatory testing methods (Douglas et al., 2015). High resolution hydrocarbon fingerprints help identify the major products and degree of weathering. The concentration and composition of PAHs, saturated hydrocarbons, and geochemical biomarkers help qualitatively and quantitatively identify specific sources and allocate mixtures. This chapter focuses on specific strategies for differentiating tar oils in NAPL and particulate samples (soil, sediment, and solids) with specific attention to differentiating tar oil spills from petroleum spills, and differentiating among tar oil spills derived from different feedstocks, within urban shoreline environments.

34.3.1 Sample Extraction

Tar oil dissolves readily in dichloromethane (DCM). Unweathered tar oil is a liquid that sinks in water although it can form sheens under certain circumstances. Weathered tar oil can range in appearance from a high viscosity liquid to a solid. Tar oil samples are initially homogenized before a small aliquot (2 g) is transferred to a dilution vessel (10 mL scintillation vial or equivalent) with Teflon lined cap. Approximately, 4 mL of DCM are added to the vial. The vessel is capped and shaken by hand, votexed, or sonicated for approximately 2 to

5 minutes. The sample is filtered through a power funnel containing anhydrous Na_2SO_4 that drains into a 10-mL volumetric. The extract is spiked with surrogate and brought up to 10 mL volume.

Solid particulate samples (soil and sediment) are extracted using a procedure developed for the extraction of semivolatile hydrocarbons from highly sequestered soil and sediment (NOAA, 1998). The sample is initially homogenized. Unless previously determined, approximately 5 g of solid particulate sample is weighed in an aluminum weigh boat on an electronic balance (+0.0001 g). After baking at 105°C for a minimum of 4 hours, the sample is reweighed and percent moisture determined by difference. A second aliquot of solid particulate sample (approximately 10 to 30 g) is placed in a solvent rinsed glass extraction vessel (8 oz jars with Teflon lined caps). An equal mass of anhydrous sodium sulfate (Na_2SO_4) is added to remove residual moisture.

The sample is spiked with a mixture of surrogate compounds that demonstrate the sample extraction efficiency. Thirty to sixty milliliters of DCM are added on top of the spiked and dried sample. The vessel is sealed and agitated on a shaker table for a minimum of 12 hours. The first extract is decanted through a powder funnel containing anhydrous Na_2SO_4 and collected in an Erlenmeyer flask. The extraction vessel is recharged with DCM (30 to 60 mL) and extracted a second time on the shaker table for at least one hour. After decanting, the extraction vessel is recharged with DCM (30 to 60 mL) and extracted a third time on the shaker table for at least one hour. The combined DCM extract is concentrated by Kuderna-Danish apparatus to known volume between 4 and 10 mL.

34.3.2 Extract Cleanup

Pure petroleum samples may not require cleanups due to the relative absence of hydrocarbon interferences. If the sample contains high concentrations of interferences, like polar (nitrogen-, sulfur-, and oxygen-containing) compounds or elemental sulfur, then one or more cleanups are recommended. The low proportion of saturated hydrocarbons from the feedstock residue within tar oil will not separate from the predominating PAHs and other aromatic hydrocarbons without aggressive fractionation in a laboratory setting.

34.3.2.1 Alumina Solid Phase Cleanup of Polar Organics

Alumina solid phase cleanup is used to remove polar organic compounds from the sample extract. This cleanup is recommended for sediment samples that commingle with high abundances of biogenic substances. The reference method is EPA Method 3611B (USEPA, 2009). A chromatography column is fitted with a Teflon stop cock. A glass wool plug is placed inside the column, on top of the stop cock. The column is packed with a 10-g bed of alumina (solvent rinsed and oven dried granular aluminum oxide) topped with 1 cm of anhydrous Na_2SO_4. The column is rinsed with 3 bore volumes of DCM. A suitable volume of extract containing 10 mg of extractable hydrocarbons is transferred to the top of the column and drawn into the solid phase packing by opening the stop cock. The column is then eluted with 30 mL DCM and collected into a concentrator tube. The extract is evaporated with a stream of high purity nitrogen gas to less than 1 mL. The extract is quantitatively transferred with rinses to a GC autosampler vial and brought up to 1 mL with DCM.

34.3.2.2 Copper Solid Phase Cleanup of Sulfur

Elemental sulfur and sulfide can interfere with the measurement of hydrocarbons. Marine sediments with high abundances of sulfur benefit from this cleanup step. The reference method is EPA Method 3660B (USEPA, 2009) or NOAA Status and Trends Program methods (NOAA, 1998). The granular copper (99% purity) is activated by suspension in 6N hydrochloric acid. While preventing exposure to air, the copper granules are rinsed with deionized water and stored in DCM. Approximately, 2 g of activated copper powder are placed in a 10-mL scintillation vial that contains the sample extract. The Teflon lined cap is closed and the sample is mixed by hand, vortex, or sonicator. If the copper turns black, the cleanup is repeated with a fresh aliquot of activated copper powder.

34.3.2.3 Silica Gel Fractionation of Aliphatic Hydrocarbons

Silica gel fractionation helps isolate aliphatic hydrocarbons from polar and aromatic hydrocarbon interferences. The aliphatic hydrocarbon interferences can include lipids, polymers, proteins, natural resins, cellular components, asphaltines, and others. The reference method is EPA Method 3630C (USEPA, 2009). The silica gel (100−200 mesh) is activated by baking at 120°C overnight. An aliquot of the sample extract is solvent exchanged to hexane. A gravimetric column with a glass wool plug is precleaned with DCM. Approximately, 5 g of silica gel are slurried with DCM, transferred to the gravimetric column and topped with 2 cm of Na_2SO_4. The gravimetric column is eluted with two bore volumes of pentane to remove the DCM. The sample extract is quantitatively transferred to the silica gel column and eluted with 20 mL of pentane. The elutriate is concentrated to known volume (1.0 mL) for the analysis of saturated hydrocarbons and geochemical biomarkers.

34.3.3 High Resolution Hydrocarbon Fingerprints

The high resolution hydrocarbon fingerprint (HRHF) resolves the dominant semivolatile hydrocarbons extracted from the field sample. The term, high resolution, refers to exceptional ability of the gas chromatograph equipped with a flame ionization detector (GC/FID) method to separate hydrocarbons as a function of the sample preparation procedure, GC operating conditions, capillary column design, detector sampling rate and detector sensitivity. It is expected that instrument manufacturers will improve the performance of these components over time; however, the HRHFs represented in this chapter are thought to reflect the maximum GC resolution available for resolution of the most forensically significant hydrocarbons. Often, this scan yields recognizable hydrocarbon patterns, but it frequently yields novel features that necessitate supplemental testing. Therefore, the high resolution scan is instrumental in determining the degree to which the sample resembles known hydrocarbon patterns, interesting variations of known patterns, or new patterns for geochemical inquiry.

The reference method for the high resolution hydrocarbon scan is EPA Method 8015C (USEPA, 2009). This analysis employs the semivolatile extract that is contains no more than 10 mg/mL of extractable material. Internal standards are added to the 1-mL extract to minimize the effects of evaporative loss during the sample analysis. The extract is injected into a GC instrument equipped with capillary column and a flame ionization detector (GC/FID). The extracts are injected into a GC/FID instrument equipped with a 95% dimethyl−5% diphenyl polysiloxane, fused silica capillary column with 0.25 mm inner diameter, 60 m length, and 0.25 μm film thickness. The instrument run program begins with the oven temperature set to 60°C for 2 minutes, then increases the temperature by 10°C/minute for 10 minutes, then increases the temperature by 25°C/minute for 2 minutes, then holds the oven temperature at 310°C for 3 minutes. The carrier gas is hydrogen with an isobaric flow rate of 3 mL/minute.

The instrument is initially calibrated with normal alkanes and selected isoprenoid hydrocarbon standards eluting between *n*-C_9 and *n*-C_{40} run at multiple concentrations between 1 and 200 μg/mL. The resolution of the instrument is assured by demonstrating that height of the valley between phytane and *n*-C_{18} is less than 40% of the height of phytane using a common baseline in a standard with equal concentrations of both compounds. In addition to developing relative response factors, the initial calibration standards are used to demonstrate the absence of mass discrimination by assuring the ratio of *n*-C_{36} relative to *n*-C_{20} is greater than 0.85. A crude oil reference sample is run with every initial calibration to verify comparable pattern resolution and quantitative precision over time. A continuing calibration standard is run every day to demonstrate quantitative precision over time. Once the instrument accuracy, precision, and sensitivity are assured, field sample extracts can be analyzed. The total hydrocarbon concentration is measured as all the hydrocarbons eluting between *n*-C_9 and *n*-C_{44} (TPH_{C9-C44}).

34.3.4 Polycyclic Aromatic Hydrocarbons

Virtually, all petroleum and tar oils contain PAH patterns with characteristics of hydrocarbon types or specific sources. The high-resolution hydrocarbon scan sometimes depicts the presence of PAHs; however, this method is incapable of comprehensively measuring the majority of PAHs due to the widely varying PAH concentrations and obscuring effects of coelution with non-PAH compounds. Mass spectrometry solves this problem because PAHs ionize with characteristic fragmentation patterns that are accurately measured and differentiated from coeluting compounds. The gas chromatograph equipped with a mass spectrometer (GC/MS) instrument provides the technological means for resolving the concentration of a full range of PAHs and revealing source specific patterns.

The reference method for the PAH analysis is EPA Method 8270D (USEPA, 2009). This analysis employs the semivolatile extract described previously. The sample extract should contain no more than 10 mg/mL of extractable material to maintain consistent instrument performance over time, as discussed previously. Internal standards are added to the 1-mL extract to minimize the effects of evaporative loss during the sample analysis. The extract is injected into a GC instrument equipped with capillary column and a mass spectrometer detector operated in the selected ion monitoring mode (GC/MS SIM). Based on personal experience, one of the better GC systems for the characterization of PAHs is the Agilent 6890 using a 95% dimethyl−5% diphenyl polysiloxane, fused silica capillary column with 0.25 mm inner diameter, 60 m length, and 0.25 μm film thickness. The instrument run program begins with the oven temperature set to 60°C for 2 minutes, then increase the temperature by 10°C/minute for 10 minutes, then increase the temperature by 25°C/minute for 2 minutes, then hold the oven temperature at 310°C for 3 minutes. The carrier gas is helium with an isobaric flow rate of 1 mL/minute.

The instrument is initially calibrated with forensic PAH isomers containing 2- to 6-rings at multiple concentration levels between 1 and 200 μg/mL (Table 34.1). The resolution of instrument is assured by demonstrating that height of the valley between benzo[*b*]fluoranthene and benzo[*k*]fluoranthene is less than 40% of the height of benzo[*b*]fluoranthene using a common baseline in a standard with equal concentrations of both compounds. In addition to

TABLE 34.1 Forensic PAH Analytes and Classifications (GC/MS)

Analytes	Abbrev	Rings	1° Ion	TPAH49	EPAPAH16	Parent (PAR22)	Alkylated (ALK27)	Diagenetic (DIA2)
Naphthalene	N0	2	128	X	X	X		
C1-Naphthalenes	N1	2	142	X			X	
C2-Naphthalenes	N2	2	156	X			X	
C3-Naphthalenes	N3	2	170	X			X	
C4-Naphthalenes	N4	2	184	X			X	
Biphenyl	B	2	154	X		X		
Dibenzofuran	DF	3	168	X		X		
Acenaphthylene	AY	3	152	X	X	X		
Acenaphthene	AE	3	153	X	X	X		
Fluorene	F0	3	166	X	X	X		
C1-Fluorenes	F1	3	180	X			X	
C2-Fluorenes	F2	3	194	X			X	
C3-Fluorenes	F3	3	208	X			X	
Anthracene	A0	3	178	X	X	X		
Phenanthrene	P0	3	178	X	X	X		
C1-Phenanthrenes/Anthracenes	PA1	3	192	X			X	
C2-Phenanthrenes/Anthracenes	PA2	3	206	X			X	
C3-Phenanthrenes/Anthracenes	PA3	3	220	X			X	
C4-Phenanthrenes/Anthracenes	PA4	3	234	X			X	
Retene	RET	3	234					X
Dibenzothiophene	DBT0	3	184	X		X		
C1-Dibenzothiophenes	DBT1	3	198	X			X	
C2-Dibenzothiophenes	DBT2	3	212	X			X	
C3-Dibenzothiophenes	DBT3	3	226	X			X	
C4-Dibenzothiophenes	DBT4	3	240	X			X	
Fluoranthene	FL0	4	202	X	X	X		
Pyrene	PY0	4	202	X	X	X		
C1-Fluoranthenes/Pyrenes	FP1	4	216	X			X	
C2-Fluoranthenes/Pyrenes	FP2	4	230	X			X	
C3-Fluoranthenes/Pyrenes	FP3	4	244	X			X	
C4-Fluoranthenes/Pyrenes	FP4	4	258	X			X	
Naphthobenzothiophenes	NBT0	4	234	X		X		
C1-Naphthobenzothiophenes	NBT1	4	248	X			X	
C2-Naphthobenzothiophenes	NBT2	4	262	X			X	
C3-Naphthobenzothiophenes	NBT3	4	276	X			X	
C4-Naphthobenzothiophenes	NBT4	4	290	X			X	
Benz[*a*]anthracene	BA0	4	228	X	X	X		
Chrysene/Triphenylene	C0	4	228	X	X	X		
C1-Chrysenes	BC1	4	242	X			X	

(*Continued*)

TABLE 34.1 (*Continued*)

Analytes	Abbrev	Rings	1° Ion	TPAH49	EPAPAH16	Parent (PAR22)	Alkylated (ALK27)	Diagenetic (DIA2)
C2-Chrysenes	BC2	4	256	X			X	
C3-Chrysenes	BC3	4	270	X			X	
C4-Chrysenes	BC4	4	284	X			X	
Benzo[*b*]fluoranthene	BBF	5	252	X	X	X		
Benzo[*k*]fluoranthene	BJKF	5	252	X	X	X		
Benzo[*a*]fluoranthene	BAF	5	252	X		X		
Benzo[*e*]pyrene	BEP	5	252	X		X		
Benzo[*a*]pyrene	BAP	5	252	X	X	X		
Perylene	PER	5	252					X
Dibenz[*a,h*]anthracene	DA	5	278	X	X	X		
Indeno[1,2,3-cd]pyrene	IND	6	276	X	X	X		
Benzo[*g,h,i*]perylene	GHI	6	276	X	X	X		
Total				49	16	22	27	2

developing relative response factors, the initial calibration standards are used to demonstrate the absence of mass discrimination by assuring the ratio of benzo[*g,h,i*]perylene relative to phenanthrene is greater than 0.85. A crude oil reference sample is run with every initial calibration to verify comparable pattern resolution and quantitative precision over time. A continuing calibration standard is run every day to demonstrate quantitative precision over time.

The 51 PAH analytes include 22 parent PAHs (enriched in combustion byproducts), 27 alkylated PAHs (enriched in petroleum), and 2 diagenetic PAHs (enriched in detrital vegetation). The sum of the 49 PAHs (TPAH49) commonly used in chemical fingerprinting includes parent and alkylated PAHs and sulfur-containing aromatics found in petroleum but excludes the two diagenetic PAHs (Table 34.1). The EPAPAH16 list includes a shorter list of parent PAHs used for regulatory compliance and risk assessment.

It is important to recognize that there are thousands of parents and alkylated PAH isomers and most hydrocarbon products contain tens to thousands of individual PAH isomers. The number of PAH isomers in the semivolatile range represented by the TPAH49 analytes is at least 19,303 of which the EPAPAH16 analytes represents 0.05% and the TPAH49 analytes represents 0.25% (Emsbo-Mattingly and Litman, 2016). One of the main reasons that these percentages are low reflects the fact few authentic PAH standards are not commercially available and many of the rare PAH standards are very expensive. The routine measurement of all 19,303 will never be technically or economically possible.

Forensic laboratories use commercially available PAHs as surrogate calibration standards for the measurement of many PAH isomers; for example, the naphthalene standard is used to generate a response factor for all of the alkylated naphthalenes. It is recognized that this practice is associated with a negative bias when measuring alkylated PAHs (Zeigler et al., 2008); for example, the negative bias for using naphthalene to measure methylnaphthalenes underestimates the sum of the 2- and 1-methylnaphthalene concentrations by approximately 20%. However, this bias does not significantly affect the forensic interpretation, because chemical fingerprinting is a comparative analysis. As long as the source and release samples are analyzed by methods with the same bias, the process of matching the source signature of the spilled product with samples collected from the alleged release area will produce scientifically valid results. The precision for the surrogate calibration method is demonstrated by the routine measurement of well-characterized reference samples and reflects a detailed review by the USEPA, NOAA, the National Environmental Laboratory Accreditation Program, and many independent laboratory auditors.

One of the primary challenges for applying new technologies to tar oil spills is the scaling factor. Tar oil spills can affect large areas and require the analysis of hundreds to thousands of samples. New technologies may be capable of identifying the oil and its degradation byproducts; however, the analysis and interpretation of the chemical signatures in hundreds to thousands of samples is prohibitive. The transformation of new technologies from the method development stage to the production or "workhorse" stage requires significant effort and compliance with established environmental quality assurance programs. This chapter presents the concentrations of thirty-seven additional parent and alkylated PAHs with demonstrated forensic value (Emsbo-Mattingly and

Litman, 2016) that are entering the "workhorse" phase (Table 34.2). The chemical signatures of these additional compounds are discussed later in the chapter. The procedure for identifying and quantifying these compounds reflects the use of authentic calibration standards and the use of surrogate calibration methods when authentic calibration standards were not available.

34.3.5 Saturated Hydrocarbons

The saturated hydrocarbon analysis confirms the molecular weight range of the spilled oil and its degree of environmental degradation. The primary analytes of interest include normal alkanes and isoparaffins (Table 34.3). These patterns are frequently obscured by interferences associated with tar oil aromatics plus NOM, sewage, degraded petroleum, and others. Many of the interferences are minimized or eliminated by using a mass spectrometer instrument.

The reference method for the saturated hydrocarbon analysis is EPA Method 8270D (USEPA, 2009). This analysis is typically conducted on the aliphatic fraction of the sample extract. A modified EPA Method 8270D is used to determine the relative abundance of saturated hydrocarbons from the *m*/*z* 85 extracted ion plot. There are other extracted ions that can be used, but the *m*/*z* 85 ion provides a suitable signature for evaluating a wider range of saturated hydrocarbons. The operation and run conditions of the instrument are identical to the PAH method. The saturated hydrocarbons resolved by GC/MS include *n*-C_9 to *n*-C_{40}, which is slightly narrower than the GC/FID technique (*n*-C_9 to *n*-C_{44}).

34.3.6 Geochemical Biomarkers

The geochemical biomarkers represent middle to heavy range hydrocarbons with molecular signatures primarily determined by the geological and industrial history of the hydrocarbon product. The saturated biomarkers are measured in the aliphatic fraction and include sesquiterpanes (Table 34.4), triterpanes (Table 34.5), and steranes (Table 34.5).

The monocyclic aromatic steroids (MAS) and triaromatic steroids (TAS) are measured in the whole sample extract analyzed for PAHs. These compounds are vulnerable to pyrolysis and their concentration declines rapidly to trace levels during coal carbonization and petroleum cracking. However, the manufactured gas processes were not perfectly efficient and the destruction of geochemical biomarkers was rarely, if ever complete.

The analysis of geochemical biomarkers in tar oils, other than MAS and TAS, is typically conducted on the aliphatic fraction of the sample extract. (As noted above, MAS and TAS are analyzed in the whole extract.) A modified EPA Method 8270D is used to determine the relative abundance of sesquiterpanes, triterpanes, steranes, MAS, and TAS using the *m*/*z* 123, 191, 217, 253, and 231 extracted ion plots, respectively. Secondary ions are used for confirmation purposes. Quantification can be completed using a combination of authentic and surrogate analyte methods depending on the available biomarker standards. The operation and run conditions of the instrument are identical to the PAH method.

34.3.7 Reference Samples

In this chapter, we present data from a series of reference samples as a means of demonstrating the variations among different types of tar and petroleum products. The reference samples included herein represent many of the hydrocarbon products potentially encountered during tar oil spill investigations. The actual hydrocarbon products encountered in any given investigation will differ from the reference standards described herein; however, many distinguishing chemical fingerprint features and weathering trends will likely manifest themselves to a comparable degree. The fossil fuel reference samples include a bituminous coal and two crude oils derived from distinct formations. The coal sample in this paper is from the coal storage area at a former byproduct coke oven site. One crude oil is from the Alaska North Slope (ANS), while the other is a crude oil from the EPA repository at the Oak Ridge National Laboratory and sold as Standard Reference Material (SRM) 1582 from the National Institute of Standards and Testing (NIST). The ANS crude is enriched in light molecular weight hydrocarbons with little to no biodegradation, while the NIST SRM 1582 is heavier and biodegraded. These crude oils demonstrate typical differences between fossil fuel samples from different formations and weathering states.

The reference samples also include a variety of refined products (Gary and Handwerk, 1984; Leffler, 2000). The naphtha sample is a light petroleum distillate used in the earliest CWG plants and subsequently in automotive gasoline. The diesel/fuel oil #2 is a middle petroleum distillate used in trucks, trains, and home heating systems. The molecular weight of the hydrocarbon reflects the typical distillation range of on-road and off-road

TABLE 34.2 Quantitative PAH Isomer Analytes

Analytes	Abbrev	Rings	1° Ion	Total (xPAH37)	Parent (xPAR14)	Alkylated (xALK23)	302
2-Methylnaphthalene	2MN	2	142			X	
1-Methylnaphthalene	1MN	2	142			X	
2,6-Dimethylnaphthalene	26DMN	2	156			X	
2,3,5-Trimethylnaphthalene	35DMN	2	170			X	
2-Methylfluorene	2MF	3	180			X	
1-Methylfluorene	1MF	3	180			X	
Methylfluorene	3/4MF	3	180			X	
3-Methylphenanthrene	3MP	3	192			X	
2-Methylphenanthrene	2MP	3	192			X	
2-Methylanthracene	2MA	3	192			X	
9/4-Methylphenanthrene	9MP	3	192			X	
1-Methylphenanthrene	1MP	3	192			X	
4-Methyldibenzothiophene	4MDT	3	198			X	
2/3-Methyldibenzothiophene	2MDT	3	198			X	
1-Methyldibenzothiophene	1MDT	3	198			X	
2-Methylpyrene	2MPy	4	216			X	
4-Methylpyrene	4MPy	4	216			X	
1-Methylpyrene	1MPy	4	216			X	
3-Methylchrysene	3MC	4	242			X	
2-Methylchrysene	2MC	4	242			X	
6-Methylchrysene	6MC	4	242			X	
5-Methylchrysene	5MC	4	242			X	
1-Methylchrysene	1MC	4	242			X	
Carbazole	CAR	2	167	X	X		
Benzo[*a*]fluorene	BaFl	3	216	X	X		
Benzo[*b*]fluorene	BbFl	3	216	X	X		
Benzo[*c*]fluorene	BcFl	3	216	X	X		
Cyclopenta[*cd*]pyrene	CcdPy	4	226	X	X		
Anthanthrene	ANT	6	276	X	X		
Coronene	COR	7	300	X	X		
Naphtho[2,3-a]pyrene	N23aP	6	302	X	X		X
Naphtho[2,3-e]pyrene	N23eP	6	302	X	X		X
Dibenzo[*a*,*l*]pyrene	DALP	6	302	X	X		X
Dibenzo[*a*,*e*]fluoranthene	DAEF	6	302	X	X		X
Dibenzo[*a*,*e*]pyrene	DAEP	6	302	X	X		X
Dibenzo[*a*,*i*]pyrene	DAIP	6	302	X	X		X
Dibenzo[*a*,*h*]pyrene	DAHP	6	302	X	X		X
Total			37	14	14	23	7

TABLE 34.3 Saturated Hydrocarbon Analytes

Analyte	Abbrev	1° Ion	SHC	Normal alkane	Isoprenoid hydrocarbon
n-Nonane	C9	85	X	X	
n-Decane	C10	85	X	X	
n-Undecane	C11	85	X	X	
n-Dodecane	C12	85	X	X	
n-Tridecane	C13	85	X	X	
n-Tetradecane	C14	85	X	X	
n-Pentadecane	C15	85	X	X	
n-Hexadecane	C16	85	X	X	
n-Heptadecane	C17	85	X	X	
n-Octadecane	C18	85	X	X	
n-Nonadecane	C19	85	X	X	
n-Eicosane	C20	85	X	X	
n-Heneicosane	C21	85	X	X	
n-Docosane	C22	85	X	X	
n-Tricosane	C23	85	X	X	
n-Tetracosane	C24	85	X	X	
n-Pentacosane	C25	85	X	X	
n-Hexacosane	C26	85	X	X	
n-Heptacosane	C27	85	X	X	
n-Octacosane	C28	85	X	X	
n-Nonacosane	C29	85	X	X	
n-Triacontane	C30	85	X	X	
n-Hentriacontane	C31	85	X	X	
n-Dotriacontane	C32	85	X	X	
n-Tritriacontane	C33	85	X	X	
n-Tetratriacontane	C34	85	X	X	
n-Pentatriacontane	C35	85	X	X	
n-Hexatriacontane	C36	85	X	X	
n-Heptatriacontane	C37	85	X	X	
n-Octatriacontane	C38	85	X	X	
n-Nonatriacontane	C39	85	X	X	
n-Tetracontane	C40	85	X	X	
n-Hentetracontane	C41	85	X	X	
n-Dotetracontane	C42	85	X	X	
n-Tritetracontane	C43	85	X	X	
n-Tetratetracontane	C44	85	X	X	
n-Pentatetracontane	C45	85	X	X	
2,6,10 Trimethyldodecane	1380	85	X		X

(*Continued*)

TABLE 34.3 (*Continued*)

Analyte	Abbrev	1° Ion	SHC	Normal alkane	Isoprenoid hydrocarbon
2,6,10 Trimethyltridecane	1470	85	X		X
Norpristane	1650	85	X		X
Pristane	Pr	85	X		X
Phytane	Ph	85	X		X
Total			42	37	5

TABLE 34.4 Sesquiterpane Analytes

Analyte	Abbrev	1° Ion	TSES	Drimane	Other
Rearranged C14	Q9	123	X		X
Rearranged C14	Q10	123	X		X
Rearranged C15	Q1	123	X		X
Rearranged C15	Q2	123	X		X
Rearranged C15	Q4	123	X		X
Rearranged C16	Q5	123	X		X
Rearranged C16	Q6	123	X		X
Rearranged C16	Q7	123	X		X
8β(*H*)-drimane	Q3	123	X	X	
8β(*H*)-homodrimane	Q8	123	X	X	
Total			10	2	8

diesels as well as number 2 fuel oils (Kaplan et al., 1997). The diesel sample is also a low-sulfur variety that was subjected to hydrodesulfurization (HDS). The light gas oil is a straight-run middle distillate that is consistent with the carburetion fluid formerly used in CWG MGPs. The heavy gas oil is a straight-run heavy distillate product consistent with carburetion fluids used in modernized CWG and high Btu oil gas MGPs.

Finally, the reference samples also include a range of tar oil reference samples with known operational histories. The crude tar oil reference samples include a coal carbonization tar (CT), CWG tar (CWG), and oil gas tar (OG). The creosote sample is a middle coal tar distillate used for wood treating. The Tarvia is a residual coal tar product formulated into roadway pavement prior to the 1960s which is solid at room temperature with slight plasticity. The pitch reference sample is a residual coal tar product processed to a brittle dry texture, which represents a highly devolatilized coal tar. Although a solid at room temperature, some pitch products were not devolatilized to this extent due to the need for some plasticity. Pitch was used to manufacture waterproofing, roofing, electrodes (aluminum smelting), coal briquettes (as a binder), sealing, and lubrication products. The refined coal tar products contain high proportions of PAHs with trace residues of the coal feedstock used to generate coke and crude coal tar.

34.3.8 Case-Study Samples

The case-study samples help illustrate compositional features that differentiate tar oils and other hydrocarbon products represented by the reference samples (above) as they appear in real world samples. Recognizing the heterogeneous nature of the sediment environment, the forensic interpretation begins with two sets of ambient background sediments representing the typical range of petroleum, combustion, and carbonization observed in remote and urban shoreline areas. The Remote Background Sediments are sandy sediments with no significant impacts based upon field observations. The Urban Background Sediments were collected in organic sediments proximal to a large US city with combined sewer overflows and storm sewer systems. These two sediment populations represent the range of residual petroleum and PAHs observed throughout the United States (Stout et al., 2004).

TABLE 34.5 Triterpane and Sterane Analytes

Analyte	Abbrev	1° Ion	Tricyclic triterpane	Tetracyclic triterpane	Pentacyclic triterpane	Sterane
C23 Tricyclic Terpane	T4	191	X			
C24 Tricyclic Terpane	T5	191	X			
C25 Tricyclic Terpane	T6	191	X			
C24 Tetracyclic Terpane	T6a	191		X		
C26 Tricyclic Terpane-22S	T6b	191	X			
C26 Tricyclic Terpane-22R	T6c	191	X			
C28 Tricyclic Terpane-22S	T7	191	X			
C28 Tricyclic Terpane-22R	T8	191	X			
C29 Tricyclic Terpane-22S	T9	191	X			
C29 Tricyclic Terpane-22R	T10	191	X			
C30 Tricyclic Terpane-22S	T11a	191	X			
C30 Tricyclic Terpane-22R	T11b	191	X			
18α-22,29,30-Trisnorneohopane	Ts	191			X	
17α(*H*)-22,29,30-Trisnorhopane	Tm	191			X	
17α/β,21β/α 28,30-Bisnorhopane	T14a	191			X	
17α(*H*),21β(*H*)-25-Norhopane	T14b	191			X	
30-Norhopane	NH	191			X	
18α(*H*)-30-Norneohopane-C29Ts	T16	191			X	
17α(*H*)-Diahopane	X	191			X	
30-Normoretane	T17	191			X	
18α(*H*)&18β(*H*)-Oleananes	T18	191			X	
Hopane	H	191			X	
Moretane	T20	191			X	
30-Homohopane-22S	T21	191			X	
30-Homohopane-22R	T22	191			X	
30,31-Bishomohopane-22S	T26	191			X	
30,31-Bishomohopane-22R	T27	191			X	
30,31-Trishomohopane-22S	T30	191			X	
30,31-Trishomohopane-22R	T31	191			X	
Tetrakishomohopane-22S	T32	191			X	
Tetrakishomohopane-22R	T33	191			X	
Pentakishomohopane-22S	T34	191			X	
Pentakishomohopane-22R	T35	191			X	
13β(*H*),17α(*H*)-20S-diacholestane	S4	217				X
13β(*H*),17α(*H*)-20R-diacholestane	S5	217				X
13β(*H*),17α(*H*)-20S-methyldiacholestane	S8	217				X
14α(*H*),17α(*H*)-20S-cholestane	S12	217				X
14α(*H*),17α(*H*)-20R-cholestane	S17	217				X

(*Continued*)

TABLE 34.5 (*Continued*)

Analyte	Abbrev	1° Ion	Tricyclic triterpane	Tetracyclic triterpane	Pentacyclic triterpane	Sterane
13β(*H*),17α(*H*)-20R-ethyldiacholestane	S18	217				X
13β(*H*),17α(*H*)-20S-ethyldiacholestane	S19	217				X
14α(*H*),17α(*H*)-20S-methylcholestane	S20	217				X
14α(*H*),17α(*H*)-20R-methylcholestane	S24	217				X
14α(*H*),17α(*H*)-20S-ethylcholestane	S25	217				X
14α(*H*),17α(*H*)-20R-ethylcholestane	S28	217				X
14β(*H*),17β(*H*)-20R-cholestane	S14	217				X
14β(*H*),17β(*H*)-20S-cholestane	S15	217				X
14β(*H*),17β(*H*)-20R-methylcholestane	S22	217				X
14β(*H*),17β(*H*)-20S-methylcholestane	S23	217				X
14β(*H*),17β(*H*)-20R-ethylcholestane	S26	217				X
14β(*H*),17β(*H*)-20S-ethylcholestane	S27	217				X
Total		50	11	1	21	17

The specific case studies represent urban sediments with a range of hydrocarbon impacts. While the names of the study area must remain anonymous, the compositional features are presented to illustrate the typical range of hydrocarbon signatures, environmental weathering, and mixing observed during forensic sediment investigations in urban depositional systems. In order to simplify the double ratio plots and reduce the high compositional variability found in urban background signatures, only the urban background sediments and the case-study samples with concentrations above the urban background threshold (EPAPAH16 >10 mg/kg) are presented.

The first case study's samples, denoted as "x" in the figures below, include sediments with alleged impacts from historical petroleum, MGP tar, and coke oven tar releases. The second case study's samples, denoted as "+,"include sediments with alleged impacts from petroleum tar oil; specifically, an MGP that employed the CWG and oil gas processes. The third case study's samples, denoted as "−," include sediments collected near a former coal tar refinery and creosote wood treater. The fourth case study's samples, denoted as "o," represent sediments collected near a petroleum refinery with suspected releases of mineral oil products and refinery wastes. Collectively, these four case studies represent realistic hydrocarbon patterns observed near facilities that handled crude and refined petroleum and tar products.

34.4 DOMINANT HYDROCARBON SIGNATURES

Tar and petroleum oils contain thousands of compounds in widely varying concentrations. The evaluation of these hydrocarbon mixtures benefits from the use of multiple analytical techniques. The GC/FID technique offers the greatest resolution of light, middle, and heavy range hydrocarbons over the widest concentration range. When optimized for forensic purposes, the GC/FID instrument generates a HRHF capable of identifying the dominant products by comparing known reference samples to samples collected in an alleged release area.

34.4.1 Petrogenic Products

Petrogenic products are hydrocarbon mixtures found in crude fossil fuels (e.g., petroleum and coal) and petroleum distillates generated without pyrolysis. Most petrogenic products contain thousands of individual hydrocarbons and heteroatomic compounds. The relative abundances of resolved and unresolved compounds provide the key features for determining the dominant hydrocarbon products in each sample. The HRHF of unweathered petrogenic materials typically exhibit hydrocarbon patterns that are dominated by saturated hydrocarbons. For example, bituminous coal contains a wide range of hydrocarbons eluting between *n*-octane (*n*-C_8) and *n*-tetratetracontane (*n*-C_{44}) (Fig. 34.3A). Branched and cyclic aliphatic

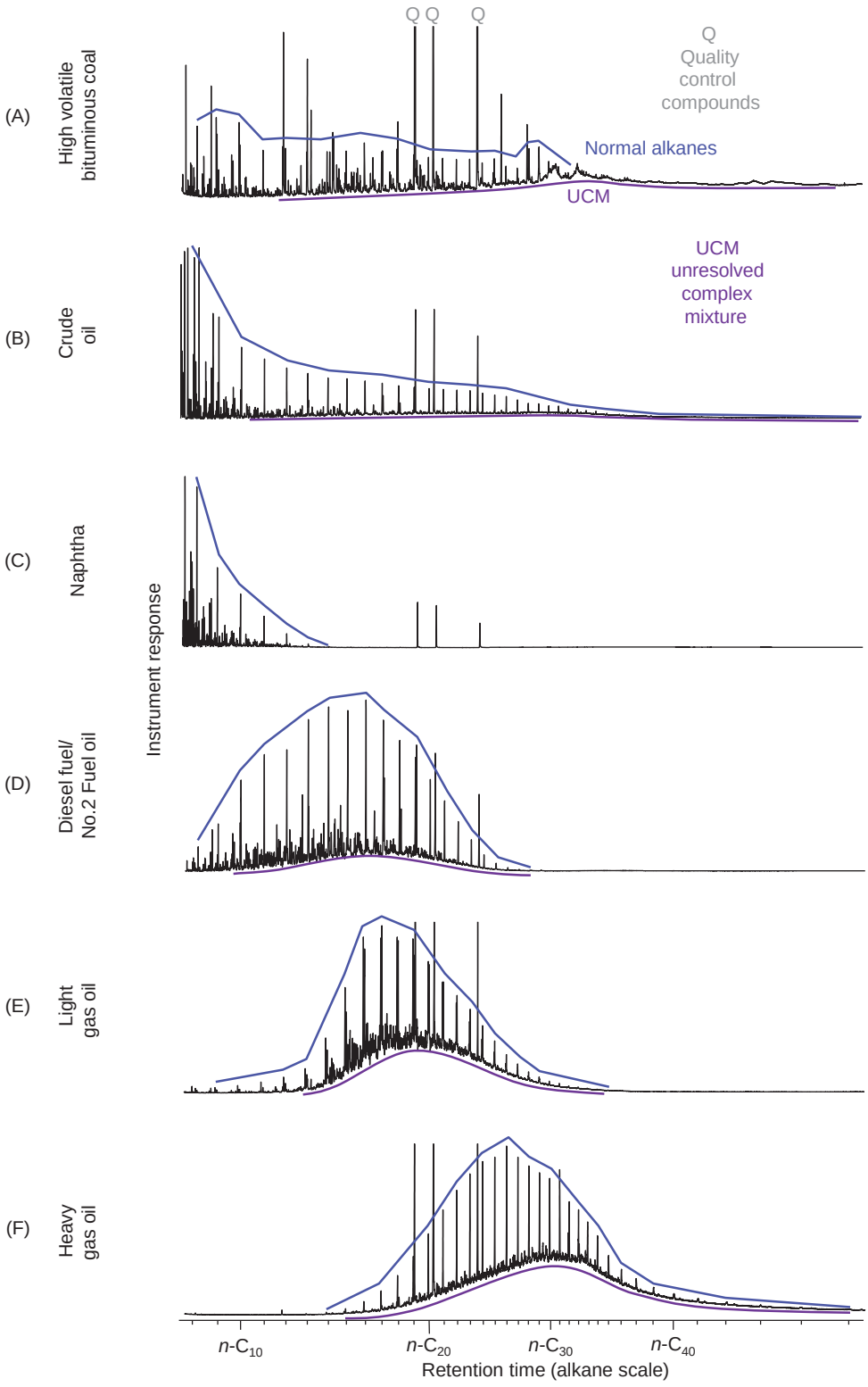

FIGURE 34.3 *FID fingerprints*: High resolution hydrocarbon fingerprints (GC/FID) of selected petroleum and tar products: (A) high volatile bituminous coal, (B) crude oil, (C) naphtha (light petroleum distillate), (D) diesel or fuel oil #2 (middle distillate), (E) light gas oil (middle distillate), and (F) heavy gas oil (heavy distillate). High resolution hydrocarbon fingerprints (GC/FID) of selected petroleum and tar products: (G) coal tar (coal carbonization byproduct), (H) CWG tar (cracked middle petroleum byproduct), (I) oil gas tar (cracked heavy petroleum byproduct), (J) creosote (middle coal tar distillate), (K) Tarvia road tar (residual coal tar), and (L) pitch (residual coal tar).

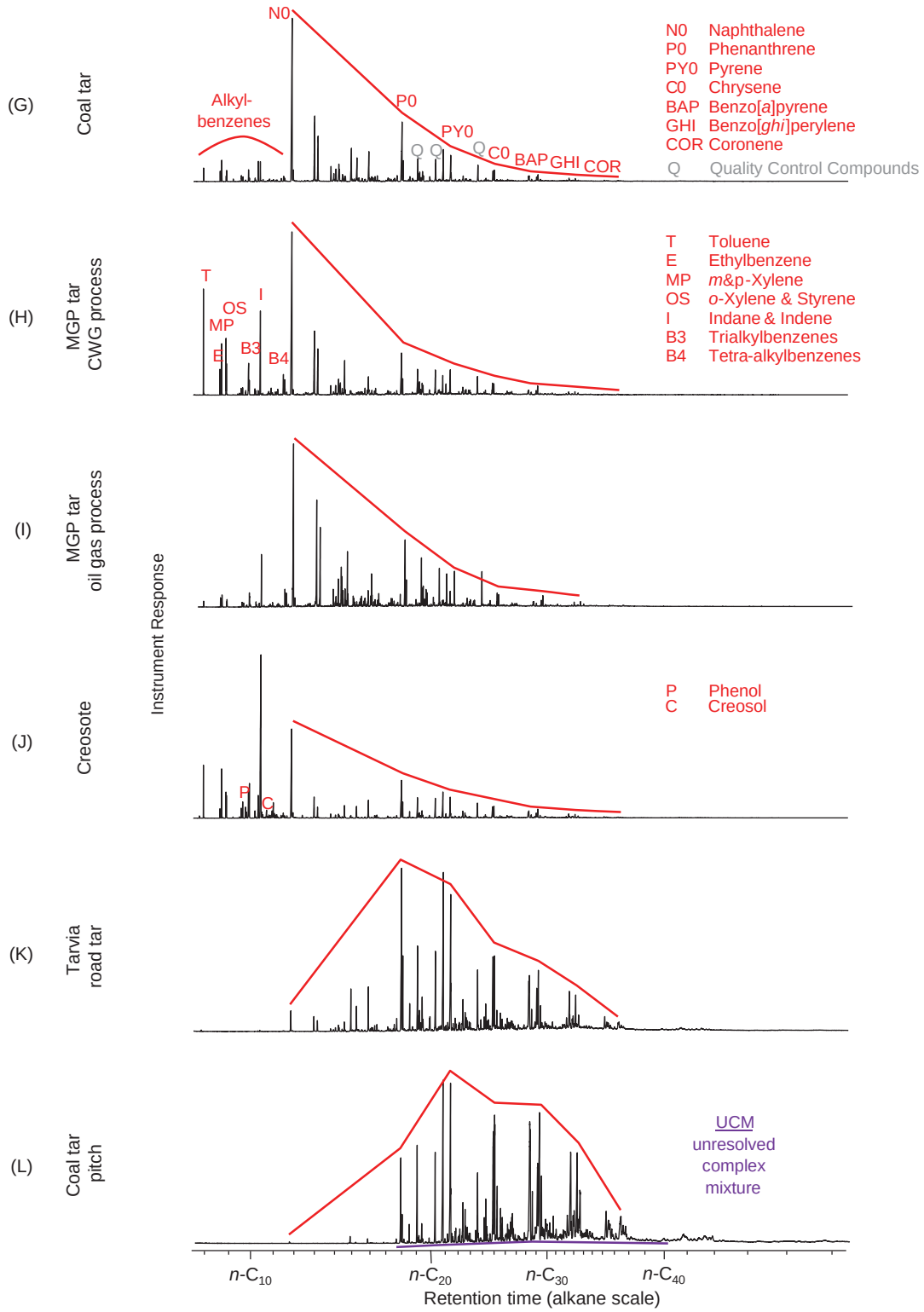

FIGURE 34.3 (Continued).

compounds too numerous to separate comprise the majority of hydrocarbons within the unresolved complex mixture (UCM), which also elutes between n-C_8 and n-C_{44}. Fossil fuels can contain volatile organic compounds that elute before n-C_8 and heavy hydrocarbons eluting after n-C_{44}; however, most forensic investigations focus on the hydrocarbons eluting between n-C_8 and n-C_{44} because many of these compounds

(1) occur above the method detection limits, (2) provide distinctive patterns for source identification, and (3) resist environmental weathering.

Many crude petroleum oils also contain a wide range of normal alkanes and a broad UCM (Fig. 34.3B). The pattern of normal alkanes and the shape of the UCM typically varies by fossil fuel type and formation. The molecular weight range of distillate product is necessarily narrower than the coal or crude oil from which it is refined. For example, naphtha primarily consists of hydrocarbons eluting between *n*-C_5 and *n*-C_{12} (Fig. 34.3C), diesel fuel primarily consists of hydrocarbons eluting between *n*-C_8 and *n*-C_{28} (Fig. 34.3D), light gas oil hydrocarbons elute between *n*-C_9 and *n*-C_{36} (Fig. 34.3E), and heavy gas oil elutes between *n*-C_{15} and *n*-C_{44} (Fig. 34.3F). These molecular weight distributions provide useful benchmarks for differentiating distillate products in the environment.

34.4.2 Pyrogenic Products

Pyrogenic hydrocarbon products are transformed by exposure to heat. Although coal is a solid fossil fuel, it generates both gas and liquid byproducts when destructively distilled. The resulting pyrogenic product is composed of hydrocarbons formed from a specific type of organic material heated to specific temperatures in the presence of metallic surfaces that catalyze the pyrolytic processes and then rapidly cooled and condensed. For example, coal gasification and coke oven plants carbonized coal and generated coal tar byproducts dominated by benzenes and parent (nonalkylated) PAHs (Fig. 34.3G). Naphthalene is the dominant component of unweathered crude coal tar. MGPs using the CWG (Fig. 34.3H) and oil gas (Fig. 34.3I) processes generate tar byproducts that resemble the benzene and parent PAH dominated HRHF of coal tar. Although significant differences are evident within the pyrogenic patterns, notice how the relative abundances of toluene, styrene, indane, and indene change within each tar. Other important differences within the saturate, PAH, and geochemical biomarker patterns are discussed later.

Tar refineries distill crude tar oils into saleable products. Light oils are distilled using roughly equivalent temperature ranges to naphtha, which generated variable mixtures of benzene, toluene, ethyl benzene, xylenes, and styrene with little to no saturated hydrocarbons. Creosote (Fig. 34.3J) is a middle tar oil distillate that effectively concentrates the trialkylbenzenes (B3), tetraalkylbenzenes (B4), naphthalene (NO), alkylated naphthalenes, phenol (PH), and creosols (CR). Creosote is an excellent wood preservative, because the enriched benzenes improved its penetration into wood, the phenols (PH) and cresols (CR) increased the toxicity to wood-consuming insects, and the heavy PAHs formed a hydrophobic skin on the exterior of the wood to reduce decay by microbes and water (Bateman, 1922; Emsbo-Mattingly et al., 2003b). Tar refineries used the residual fraction of crude tar oil to manufacture residual products, like Tarvia (Fig. 34.3K), as a hydrophobic and plastic binder of sand and gravel for the pavement of roadways, highways, and runways. Similar residual products included roofing shingles, tar paper for weatherproofing buildings, and roadway sealers. The tar refiners historically used elevated temperatures and vacuum pressure to remove the light oils and middle tar distillates to create solid pitch products (Fig. 34.3L) historically used for black ink, pencils, paint, and cosmetics.

The HRHF samples help illustrate the point that while petroleum (petrogenic) and tar (pyrogenic) products contain hydrocarbons in overlapping molecular weight ranges, the hydrocarbon composition of each product is distinct. Once released into the environment, however, the hydrocarbon patterns exhibited in the reference samples begins to systematically degrade and mix with other types of hydrocarbons. Multiple lines of evidence help monitor weathering and gauge mixing.

34.5 SATURATED HYDROCARBON SIGNATURES

Saturated hydrocarbon signatures help demonstrate several important features when accurately resolved. The mass spectrometer is well suited for resolving the saturated signature for petroleum products. The extracted ion chromatograms presented in this section are generated on a GC/MS instrument using the *m*/*z* 85 extracted ion plot, which helps isolate the saturated hydrocarbon patterns from aromatic and heteroatomic hydrocarbon interferences. However, the high proportion of aromatics ($>95\%$) obscures the aliphatics unless the aliphatics in pyrogenic products are carefully isolated during sample preparation using silica gel fractionation.

34.5.1 Biodegradation Patterns

Once isolated, the saturated hydrocarbon signatures confirm the molecular weight range of coal and petroleum products. Second, the homologous series of normal alkanes and cycloalkanes help estimate the degree of

evaporation based upon the principal that lighter hydrocarbons evaporate more rapidly than heavier hydrocarbons. Third, the degree of biodegradation is particularly clear in the relative abundances of normal alkanes, acyclic isoprenoids, and cycloalkanes. Microbes metabolize normal alkanes (e.g., *n*-heptadecane or *n*-C_{17}) more rapidly than comparable acyclic isoprenoid hydrocarbons (e.g., pristane or Pr) when oil contacts bacteria laden soils and sediment. Prior to contact with particulates, middle range petroleum with little to no biodegradation typically exhibits higher abundances of normal alkanes relative to isoprenoids (*n*-C_{17}/Pr > 1). The exact magnitude of the *n*-C_{17}/Pr > 1 ratio in an unweathered sample of the source oil helps oil spill investigators to estimate the degree of biodegradation. As microbes biodegrade the middle range petroleum hydrocarbons in coal and petroleum products, they preferentially metabolize the normal alkanes, while isoprenoid hydrocarbons degrade much more slowly. Light biodegradation is recognized as *n*-C_{17}/Pr approaches 1. Moderate biodegradation is recognized when *n*-C_{17}/Pr < 1. Heavy biodegradation is recognized when *n*-C_{17}/Pr approaches zero. Severe biodegradation is recognized when it is difficult to identify the isoprenoids among the variable peaks that comprise the baseline of the UCM.

34.5.2 Petroleum Patterns

Normal alkanes eluting between *n*-C_8 and *n*-C_{40} can dominate the bituminous coal (Fig. 34.4A) and crude oil reference samples (Fig. 34.4B). Light distillates, like naphtha (Fig. 34.4C), exhibit hydrocarbons eluting within the *n*-C_8 to *n*-C_{13} distillation range of the product. Petroleum distillates exhibit normal alkanes, acyclic isoprenoids, and cyclic alkanes within their respective distillation ranges. For example, diesel and fuel oil #2 elute between *n*-C_8 and *n*-C_{28} (Fig. 34.4D), light gas oil hydrocarbons elute between *n*-C_9 and *n*-C_{36} (Fig. 34.4E), and heavy gas oil hydrocarbons elutes between *n*-C_{15} and at least *n*-C_{40} (Fig. 34.4F).

34.5.3 Tar Oil Feedstock Residues and Product Patterns

The saturated hydrocarbon fingerprint of coal tar (Fig. 34.4G) represents the unreacted coal distillate devolatilized from the coal feedstock during the manufacture coal gas and coke. The feedstock residue contains hydrocarbons that elute between approximately *n*-C_8 and *n*-C_{40}. The saturated hydrocarbons in the CWG tar (Fig. 34.4H) elute between *n*-C_9 and *n*-C_{36}, indicating that a light gas oil feedstock was in use when this CWG tar was generated. Similarly, the saturated hydrocarbons in the oil gas tar elute between *n*-C_{10} and at least *n*-C_{40} (Fig. 34.4I), which is consistent with tar oil generated from a heavy gas oil feedstock. The saturated hydrocarbons in the creosote sample (Fig. 34.4J) elute between *n*-C_8 and *n*-C_{33} and reveal evidence of the distillation process used to manufacture this product. The abrupt change in slope between *n*-C_{12} and *n*-C_{13} indicates blending of light oil and middle coal tar distillate to achieve lower viscosity and higher penetration during wood treating. By contrast the heavier hydrocarbons in the Tarvia sample (Fig. 34.4K) elute between *n*-C_{11} and at least *n*-C_{40+}. More extreme thermal exposure is required to further isolate the *n*-C_{16} to *n*-C_{40+} saturated hydrocarbons in the pitch sample (Fig. 34.4L).

34.6 AROMATIC HYDROCARBON SIGNATURES

Aromatic hydrocarbons span a wide molecular weight range. Monocyclic aromatic hydrocarbons, such as benzene and alkylated benzenes, dissolve fairly readily in water. They provide evidence of contact and exposure to fugitive tar or petroleum oil in aquatic ecosystems. Polycyclic aromatic hydrocarbons possess two or more fused benzene rings and occur as homolog group with both parent and alkylated PAHs. Aromatic hydrocarbons exhibit predictable physical and chemical properties. Generally, they are slightly more soluble and less biodegradable than saturated hydrocarbons of equivalent molecular weight. Consequently, they provide complementary lines of evidence for delineating tar oil spills and monitoring changes in the character of the oil over time.

The pattern of aromatic hydrocarbons in petroleum and tar oils is controlled by many factors. The ancient biomass and geological conditions primarily control the concentration and composition of aromatic hydrocarbons in coal and petroleum. MGPs and coke plants transform saturated hydrocarbons into gas and tar oil, which effectively concentrates benzenes and parent PAHs from the fossil fuel and pyrosynthesizes new PAHs in the tar oil byproducts. Tar and petroleum refineries introduce tertiary effects by partitioning the hydrocarbons into distillate and residual fractions to achieve product performance specifications. Each of these natural and anthropogenic processes create and modify the patterns of aromatic hydrocarbons in forensically significant ways.

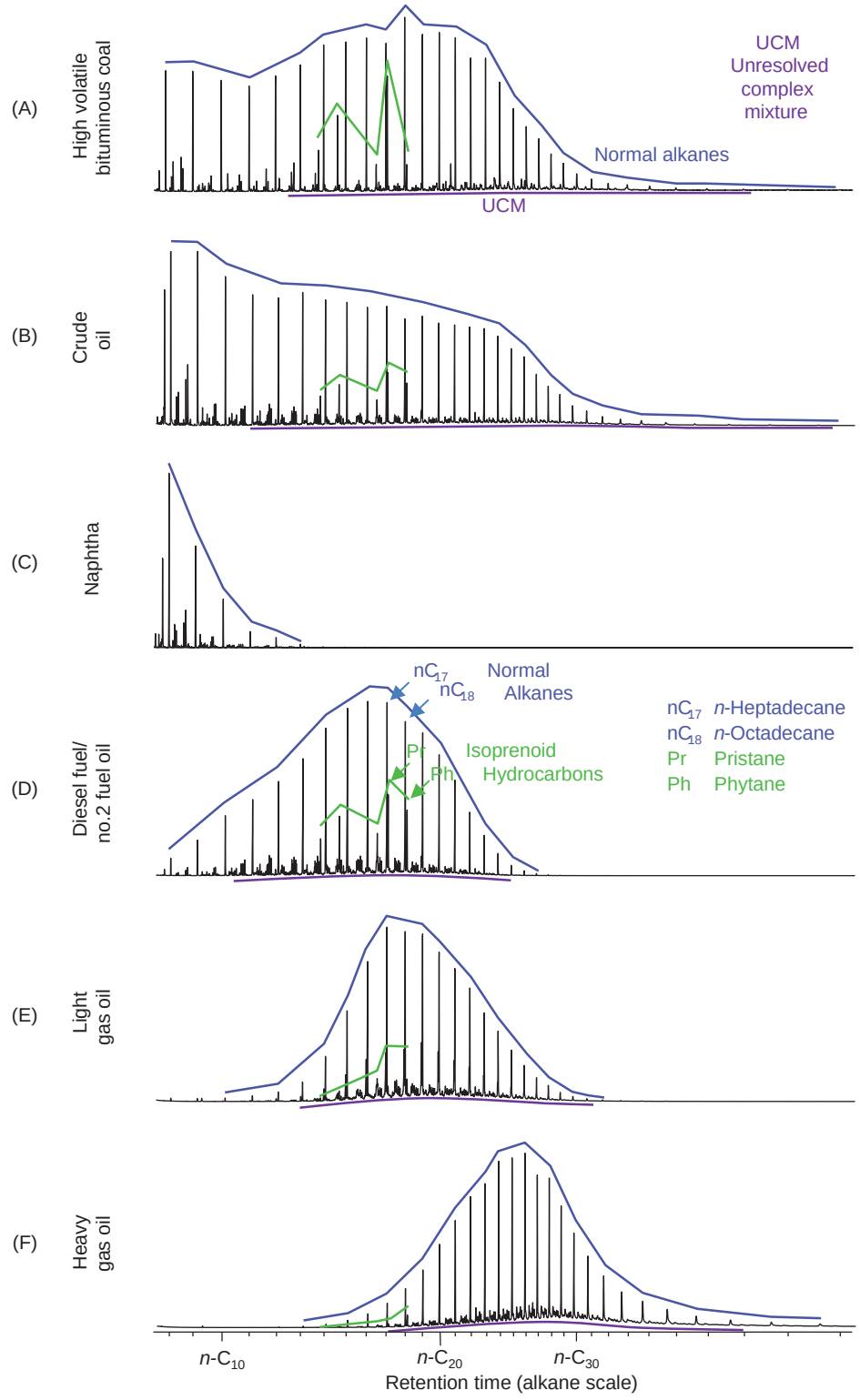

FIGURE 34.4 **Saturated fingerprints:** Saturated hydrocarbon fingerprints (GC/MS m/z 85) of selected petroleum and tar products: (A) high volatile bituminous coal, (B) crude oil, (C) naphtha (light petroleum distillate), (D) diesel or fuel oil #2 (middle distillate), (E) light gas oil (middle distillate), and (F) heavy gas oil (heavy distillate). Saturated hydrocarbon fingerprints (GC/MS m/z 85) of selected petroleum and tar products: (G) coal tar (coal carbonization byproduct), (H) CWG tar (cracked middle petroleum byproduct), (I) oil gas tar (cracked heavy petroleum byproduct), (J) creosote (middle coal tar distillate), (K) Tarvia road tar (residual coal tar), and (L) pitch (residual coal tar).

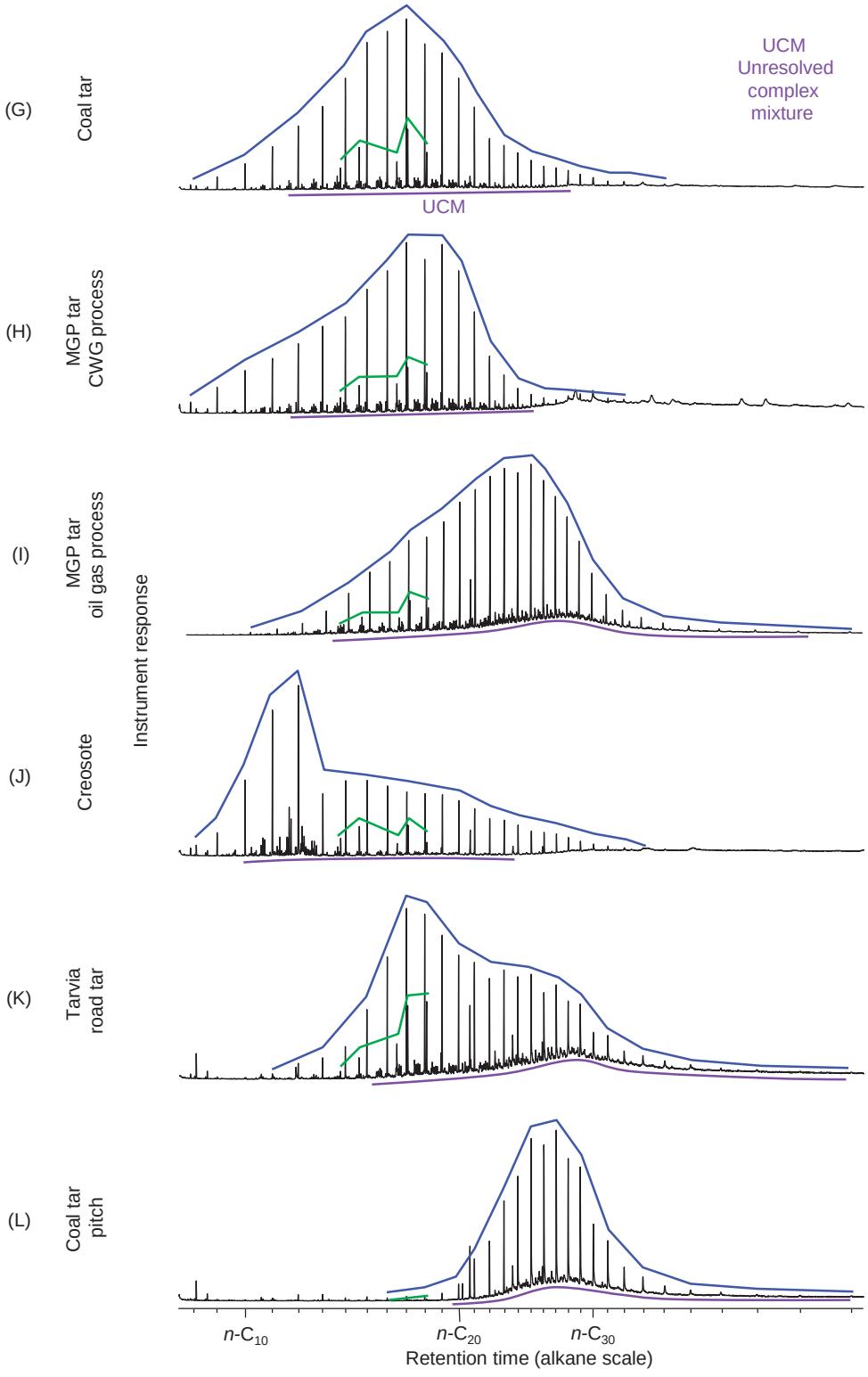

FIGURE 34.4 (Continued).

34.6.1 Petrogenic PAHs

The PAH patterns of the coal (Fig. 34.5A, left histogram) and crude oil (Fig. 34.5B, left histogram) reference samples demonstrate petrogenic patterns across a wide molecular weight range. The dominant feature of these fossil fuels are alkylated naphthalenes (N1 and N2) mixed with progressively lower proportions of alkylated

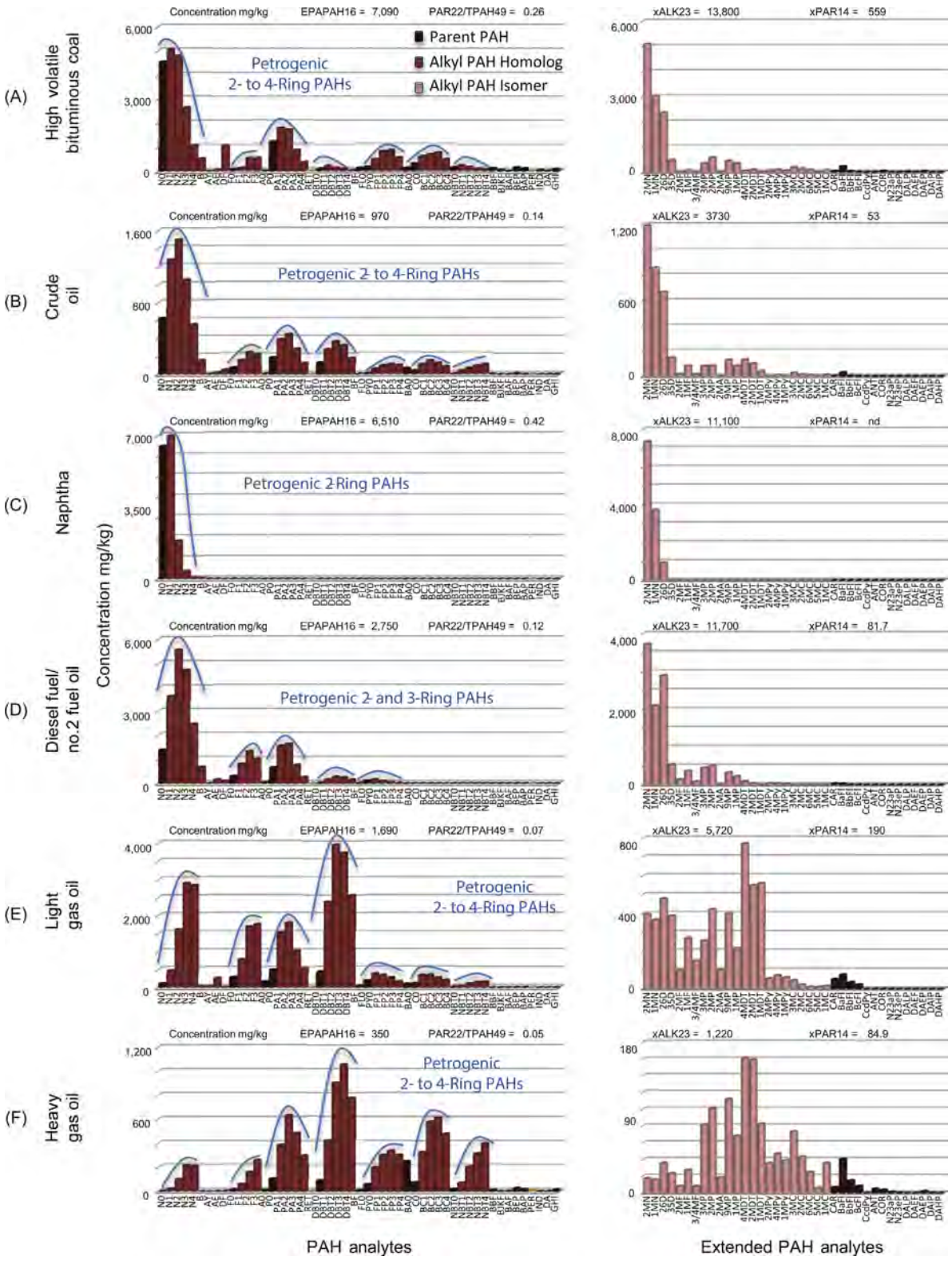

FIGURE 34.5 **PAH histograms:** Parent and alkylated PAH fingerprints (GC/MS) of selected petroleum and tar products: (A) high volatile bituminous coal, (B) crude oil, (C) naphtha (light petroleum distillate), (D) diesel or fuel oil #2 (middle distillate), (E) light gas oil (middle distillate), and (F) heavy gas oil (heavy distillate). Parent and alkylated PAH fingerprints (GC/MS) of selected petroleum and tar products: (G) coal tar (coal carbonization byproduct), (H) CWG tar (cracked middle petroleum byproduct), (I) oil gas tar (cracked heavy petroleum byproduct), (J) creosote (middle coal tar distillate), (K) Tarvia road tar (residual coal tar), and (L) pitch (residual coal tar).

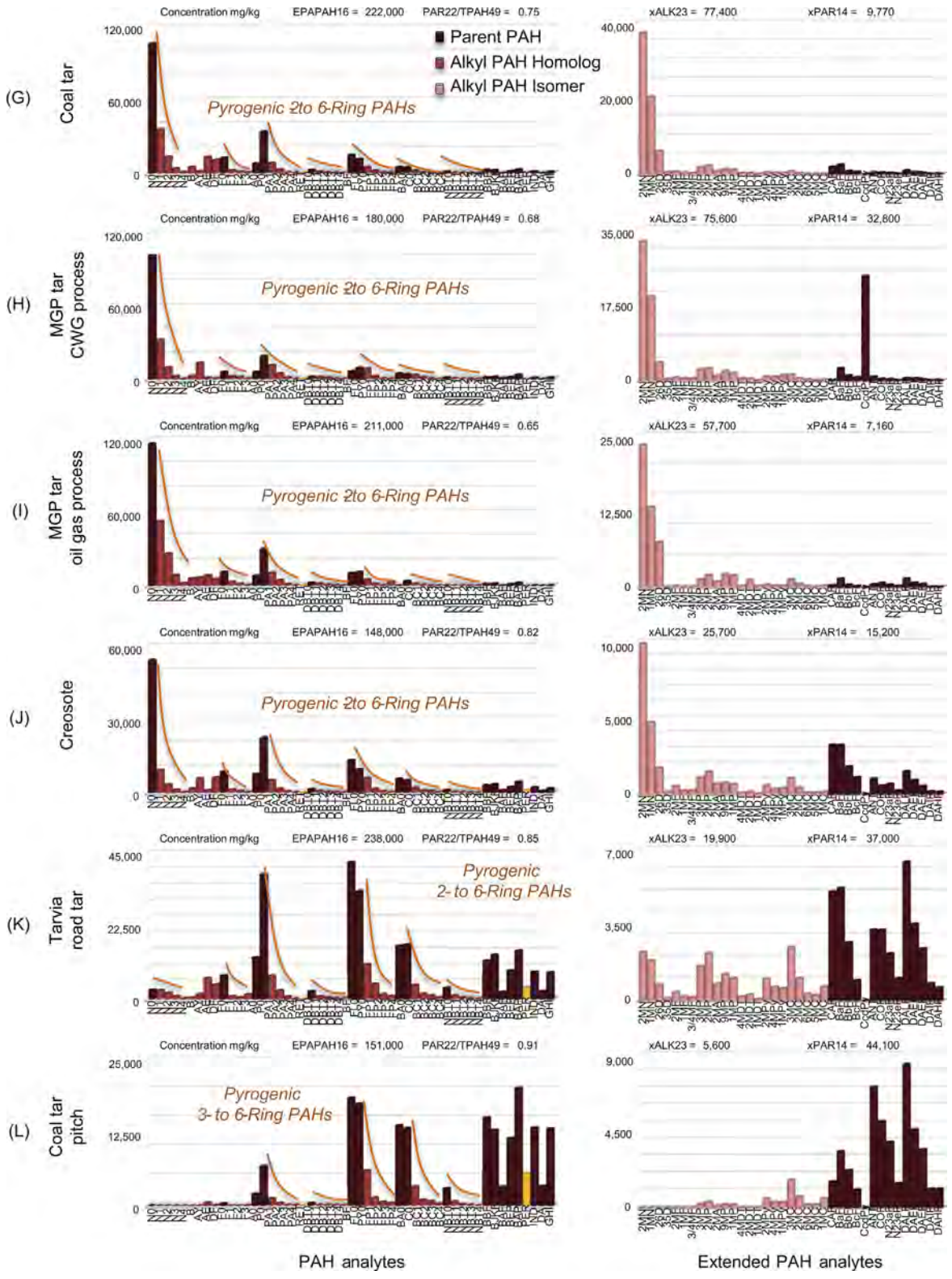

FIGURE 34.5 (Contiuned).

phenanthrenes and anthracenes (PA1 and PA2), fluoranthenes and pyrenes (FP2 and FP3), and benz[*a*]anthracenes and chrysenes (BC2 and BC3). The PAH isomer patterns within selected alkylated PAH homolog groups further exhibit petrogenic signatures in the form of low proportions of 2-methylanthracene (e.g., 2MA) relative to comparable methylphenanthrenes (e.g., 1MP, nonlinear structure). In addition, fossil fuels contain little to no 5- to 7-ring parent PAHs, because they are formed at low temperature. Source specific features, like the abundances of sulfur containing dibenzothiophenes, relative to comparable diatomic PAHs, like phenanthrenes and anthracenes, are discussed in the PAH ratio sections that follow.

Petroleum distillates retain the portion of the petrogenic PAH pattern that falls within the specific boiling point range of the refined product. For example, naphtha contains only parent and alkylated naphthalenes (Fig. 34.5C). Diesel and fuel oil #2 predominantly contain alkylated naphthalenes with lower proportions of alkylated fluorenes, phenanthrenes, anthracenes, and dibenzothiophenes (Fig. 34.5D). The reduced levels of dibenzothiophenes are consistent with low sulfur crude oil products or refined products exposed to extra refining procedures, such as hydrotreating or desulfurization. The low proportions of 4-ring PAHs indicate the limit of the distillation range. Light gas oil is heavier than diesel and fuel oil #2; consequently, alkylated 3-ring PAHs are more abundant than the alkylated naphthalenes and more 4-ring PAHs are evident (Fig. 34.5E). The high proportion of dibenzothiophenes in the gas oil sample suggests that this product is derived from a sour (high sulfur) crude oil and no attempt was made to reduce its sulfur content through advance refining technologies (e.g., hydrodesulfurization or HDS) as is now commonly necessary to comply with modern environmental regulations.

The heavy gas oil represents many features of heavy distillate products (Fig. 34.5F). The petrogenic PAH pattern is enriched in dibenzothiophenes mixed with lower proportions of phenanthrenes and 4-ring PAHs. The low proportions of alkylated naphthalenes suggest the sequential removal of lighter distillates before the manufacture of this heavy gas oil product. The high proportions of dibenzothiophenes relative to phenanthrenes and anthracenes plus the high proportion of naphthobenzothiophenes relative to benz[*a*]anthracenes and chrysenes are consistent with distillates manufactured from a sour crude oil, or distillates that have been blended to include high-sulfur intermediates, or distillates that have not been subjected to secondary refining steps, such as HDS.

34.6.2 Pyrogenic PAHs

The transformation of a petrogenic PAH pattern into a pyrogenic PAH pattern depends heavily on the fuel type, temperature, catalytic surfaces, and condensation process. Combustions scientists consider PAHs precursors to soot formation (Graham et al., 1975; Zevenhoven and Kilpinen, 2002). As a general rule of thumb, hotter conditions preferentially pyrolyze aliphatic hydrocarbons and alkylated PAHs in the feedstock and pyrosynthesize heavier 5- to 7-ring PAHs in the tar byproduct. For example, coal carbonization generates tar byproducts between 700°C and 1200°C (Rhodes, 1945) that coincides with steeply skewed PAH homolog patterns (Fig. 34.5G). The parent PAH concentrations decline progressively from naphthalene (N0) with increasing molecular weight. CWG tar (Fig. 34.5H) and oil gas tar (Fig. 34.5I) share these compositional features. CWG tar oils form in the carburetor at temperatures ranging from 800 to 1000°C (Morgan, 1926). The lower temperature of formation for CWG tar oils yields slightly lower abundances of the 22 parent PAHs relative to the total 49 parent and alkylated PAHs (PAR22/TPAH49 = 0.68) compared to the coal tar (PAR22/TPAH49 = 0.75). This ratio quantifies the slightly higher degree of skewedness in the coal tar compared to the CWG tar. These and other diagnostic PAH ratios exploit compositional features to distinguish among the multiple tar oil sources as discussed in the diagnostic ratio section later in the chapter.

Creosote is a tar distillate primarily composed of pyrogenic 2- to 6-ring PAHs (Fig. 34.5J). Distillation enriches the concentration of N0 relative to the other PAHs. By contrast, the residual tar products exhibit enriched concentrations of 4- to 7-ring parent PAHs. Tarvia contains high proportions of phenanthrenes and pyrenes (Fig. 34.5K). More extreme devolatilization conditions apply to the manufacture of pitch, which further reduce the phenanthrenes and concentrate the 4- to 7-ring PAHs (Fig. 34.5L). Thus, the molecular weight range of the PAHs in different tar products helps identify fugitive hydrocarbon products in the environment.

34.6.3 Geochemical Biomarkers

Geochemical biomarkers are cyclic aliphatic and aromatic compounds used by petroleum geochemists to identify crude oils based upon the biomass and the petrogenesis conditions within a particular formation or region. Coal and petroleum crude oil commonly contain terpanes, steranes, and aromatic steranes ultimately derived from lipids, pigments, and biomembranes from marine and terrigenous organisms (Tissot and Welt, 1978; Peters

et al., 2005). Refined products "inherit" these "genetic" signatures from the fossil fuel feedstock when the biomarkers fall within the specific boiling point range of a refined product. Bicyclic sesquiterpanes (Table 34.4) likely originate from higher plants, algae, or bacteria and elute between *n*-C_{13} and *n*-C_{16} providing source signatures for middle distillate products, such as kerosene, jet fuel, diesel, and fuel oil #2, and gas oils (Stout et al., 2005; Wang et al., 2007). Triterpanes (Table 34.5), including hopanes that originate from prokaryote (bacteria and cyanobacteria) membranes, elute from *n*-C_{23} to *n*-C_{38} with chemical patterns well suited for identifying heavy distillate and residual products, such as gas oils, heavy fuel oil, lube oils, pavement, asphalt, and pitch (Uhler et al., 2007; Wang et al., 2007). Steranes (Table 34.5) originate from eukaryote (algae, plants, and animals) sterols and elute from *n*-C_{26} to *n*-C_{34} with chemical patterns well suited for identifying heavier distillate and residual products, such as gas oils, heavy fuel oil, lube oils, pavement, asphalt, and pitch (Uhler et al., 2007; Wang et al., 2007). MAS and TAS (Table 34.6) progressively aromatize from steranes when archaeo-biomass matures into fossil fuel. The MAS pattern elutes from *n*-C_{25} to *n*-C_{31}, while the TAS pattern elutes from *n*-C_{24} to *n*-C_{33} and the chemical patterns are well suited for identifying heavier distillate and residual products (Wang et al., 2007).

The patterns of geochemical biomarkers clearly differ among the coal and petroleum reference samples. The coal sample exhibits high abundances of sesquiterpanes dominated by 8β(H)-homodrimane (Q08) with low proportions of pentacyclic triterpanes (hopanes), steranes and no detectable tricyclic terpanes, MAS or TAS (Fig. 34.6A). The petroleum crude oil is dominated by hopanes with lower proportions of TAS, steranes,

TABLE 34.6 Monoaromatic and Triaromatic Steroid Analytes

Analyte	Abbrev	1° Ion	Mono Aromatic Steroids (MAS)	Tri Aromatic Steroids (TAS)
C27 5β-cholestane (20S) + diacholestane (20S)	MAS01	253	X	
C27 5β-cholestane (20R) + diacholestane (20R)	MAS02	253	X	
C27 5α-cholestane (20S)	MAS03	253	X	
C28 5β-ergostane (20S) + diaergostane (20S)	MAS04	253	X	
C27 5α-chloestane (20R)	MAS05	253	X	
C28 5α-ergostane (20S)	MAS06	253	X	
C28 5β-ergostane (20R) + diaergostane (20R)	MAS07	253	X	
C29 5β-stigmastane (20S) + diastigmastane (20S)	MAS08	253	X	
C29 5α-stigmastane (20S)	MAS09	253	X	
C28 5α-ergostane (20R)	MAS10	253	X	
C29 5β-stigmastane (20R) + diastigmastane (20R)	MAS11	253	X	
C29 5α-stigmastane (20R)	MAS12	253	X	
C20 pregnane	TAS05	231		X
C21 20-methylpregnane	TAS06	231		X
C22 20-ethylpregnane (*a*)	TAS07	231		X
C22 20-ethylpregnane (*b*)	TAS08	231		X
C26 cholestane (20S)	TAS09	231		X
C26 cholestane (20R) + C27 ergostane (20S)	TAS01	231		X
C28 stigmastane (20S)	TAS02	231		X
C27 ergostane (20R)	TAS03	231		X
C28 stigmastane (20R)	TAS04	231		X
C29 24-*n*-propylcholestane (20S) (*a* + *b*)	TAS10	231		X
C29 24-*n*-propylcholestane (20R)	TAS11	231		X
C30 20-*n*-decylpregnane (20S)	TAS12	231		X
C30 20-*n*-decylpregnane (20R)	TAS13	231		X
Total		25	12	13

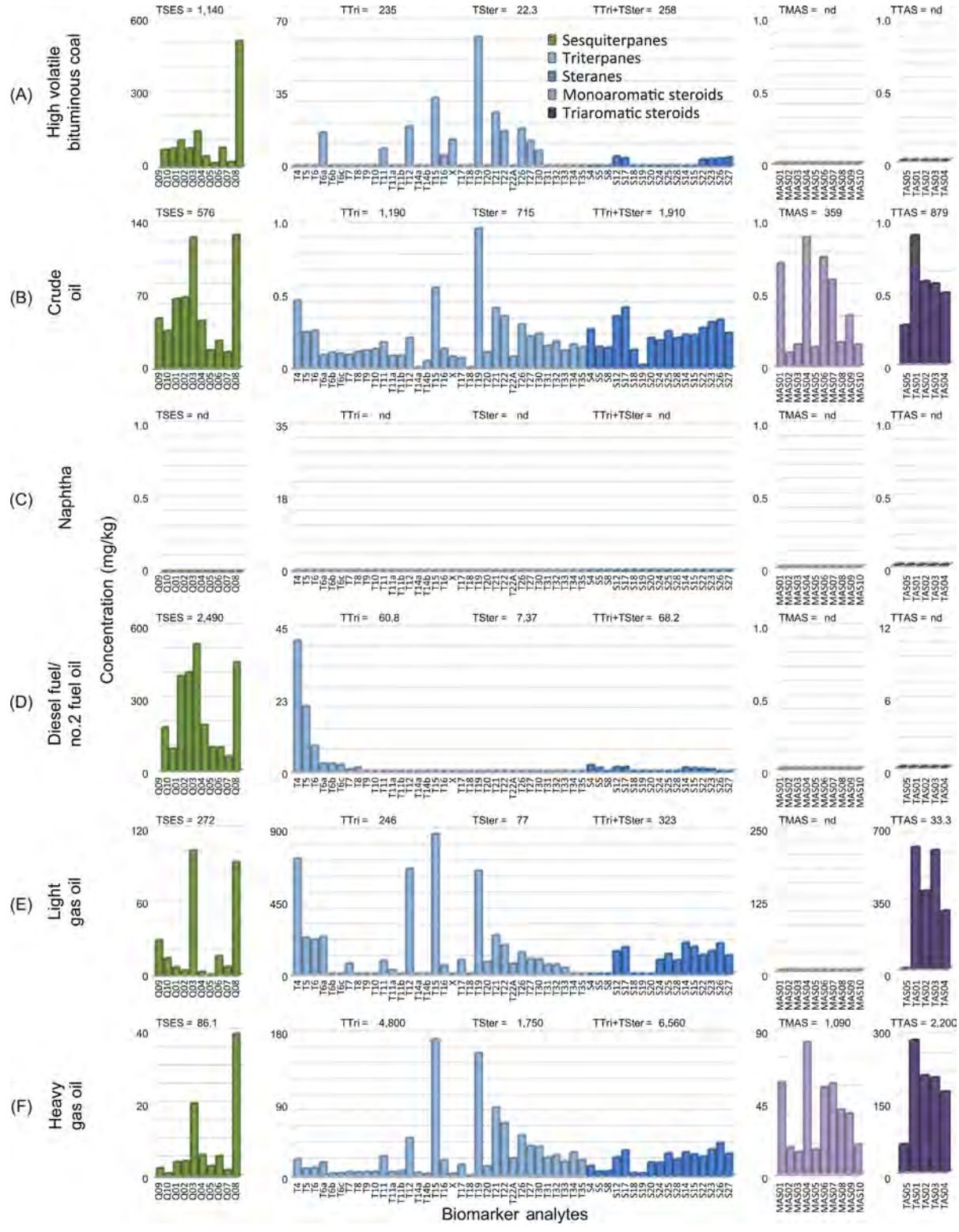

FIGURE 34.6 **Geochemical biomarker histograms:** Sesquiterpane, triterpane, sterane, and aromatic steroid fingerprints (GC/MS) of selected petroleum and tar products: (A) high volatile bituminous coal, (B) crude oil, (C) naphtha (light petroleum distillate), (D) diesel or fuel oil #2 (middle distillate), (E) light gas oil (middle distillate), and (F) heavy gas oil (heavy distillate). Sesquiterpane, triterpane, sterane, and aromatic steroid fingerprints (GC/MS) of selected petroleum and tar products: (G) coal tar (coal carbonization byproduct), (H) CWG tar (cracked middle petroleum byproduct), (I) oil gas tar (cracked heavy petroleum byproduct), (J) creosote (middle coal tar distillate), (K) Tarvia road tar (residual coal tar), and (L) pitch (residual coal tar). See text regarding nondetection of MAS and TAS in these samples.

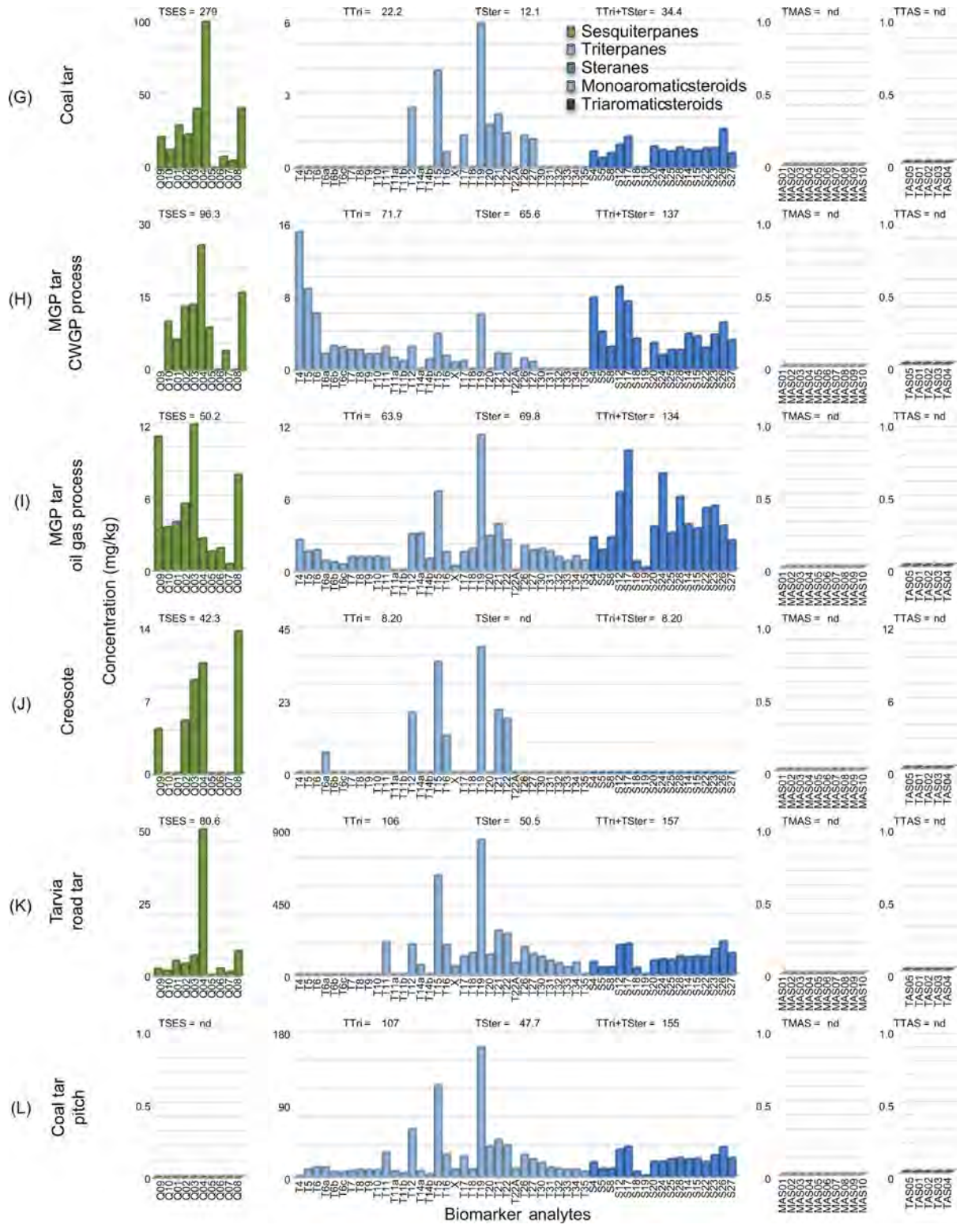

FIGURE 34.6 (Continued).

sesquiterpanes, and MAS (Fig. 34.6B). Naphtha is a light distillate (n-C_5 and n-C_{13}) no detectable biomarkers, because they are too heavy to fall in the naphtha distillation range (Fig. 34.6C). Diesel and fuel oil #2 are middle distillates (n-C_8 and n-C_{28}) with strong sesquiterpane signatures and some tricyclic terpanes, but little to no hopanes, steranes, MAS or TAS (Fig. 34.6D). The light gas oil is a higher boiling middle distillate (n-C_9 and n-C_{36}) than diesel or fuel oil #2 with abundant sesquiterpanes, hopanes, steranes, no MAS and trace TAS (Fig. 34.6E). The heavy gas oil is a heavy distillate (n-C_{15} and n-C_{44}) with trace sesquiterpanes and abundant hopanes, steranes, MAS and TAS (Fig. 34.6F). The biomarker source signature of each reference sample can be interpreted based on the relative abundances of all the compounds by class (e.g., total sesquiterpanes relative to total hopanes) or by analyte (e.g., Ts/[Ts + Tm]) as discussed in the diagnostic ratio section later in the chapter.

As a general rule, the pyrogenic substances contain low proportions of aliphatic hydrocarbons, like geochemical biomarkers, that are best resolved after removing the aromatic hydrocarbons that would otherwise interfere with their detection. Unfortunately, the MAS and TAS analytes are part of the aromatic fraction using the methods in this chapter; consequently, they are not detected in the aliphatic fraction (F1). Careful inspection of the pyrogenic sample extracts reveal that parent and alkylated PAH coelutions prevents the accurate measurement of MAS and TAS analytes in the unfractionated extract (UF) and aromatic fraction (F2); consequently, MAS and TAS analytes in the tar oil products are reported as not detected herein.

The coal tar reference sample is consistent with the coal sample discussed previously in that it is exhibits high abundances of sesquiterpanes with low proportions of hopanes, steranes and no detectable tricyclic terpanes (Fig. 34.6G). This pattern is fairly common among coals, because the tricyclic triterpanes are attributed to marine organisms and coal is predominantly formed from terrigenous eukaryotic biomass. The CWG (Fig. 34.6H) and oil gas (Fig. 34.6I) tar samples contain tricyclic triterpanes (dominant in the CWG tar sample), because they are formed from cracking petroleum, which contains marine-derived biomass. The creosote contains low proportions of sesquiterpanes, tetracyclic triterpane, and hopanes (Fig. 34.6J). The Tarvia sample contains low proportions of sesquiterpanes (Q04 dominated), tetracyclic triterpane, and hopanes, and steranes (Fig. 34.6J). The pitch sample is too heavy to contain sesquiterpanes but is does contain hopanes and steranes with low proportions of tricyclic triterpanes potentially indicating blending with petroleum pitch or petcoke.

34.6.4 Tar Oil Weathering

Tar oil weathering systematically alters the aromatic and aliphatic patterns with commensurate affects in tar acid and tar base constituents (Fig. 34.7). The specific gravity of tar oil is typically greater than 1.0, which indicates its propensity to sink in water and limit its exposure to sunlight and air. It is possible for tar oils to form sheens during ebullition (i.e., tar droplet mobilized by biogenic gas bubbles passing through tar impacted sediment); however, these special conditions are not widely observed. Most fugitive tar oil adheres to existing surfaces and forms mats with skins or rinds of heavily weathered tar on the outside and less weathered tar on the inside. As tar oil weathers, the viscosity increases, mobility decreases, solidification ensues, and bioavailability declines.

Tar oil weathers most quickly by evaporation and dissolution immediately after a tar oil spill. Evaporation accelerates when the tar oil spreads into a thin layer on surfaces exposed directly to air and warm temperatures. Dissolution is most pronounced when tar oil forms thin deposits in groundwater or mats on subtidal sediments. Biodegradation can also occur, but the rate of biodegradation is slower for aromatic-rich tar oils compared to petroleum. Biodegradation is most easily observed in the saturated hydrocarbon patterns of the uncombusted feedstock. Photodegradation can also occur in the surface microlayer of a tar deposit; however, its magnitude is not considered significant if the NAPL layer exhibits a measureable thickness, because light cannot penetrate far below the tar surface.

The cumulative effect of environmental weathering of tar oils occurs gradually in a predictable continuum of chemical changes. The rates of dissolution and evaporation reflect the water solubility and vapor pressure of each compound, which preferentially reduce the hydrocarbons in the following sequence: 1-ring > 2-ring > 3-ring > 4-ring and C0 > C1 > C2 > C3 > C4 PAHs. These abiotic weathering processes help explain why most PAH patterns observed in thick formations permanently below groundwater or surface water contain high proportions of 1- and 2-ring aromatics with phenols and cresols, while surface deposits predominantly contain 4- to 6-ring PAHs (Fig. 34.7). Naphthalene is the dominant compound in lightly weathered tar oil, phenanthrene is the dominant compound in moderately weathered tar, pyrene dominates heavily weathered tar, and chrysene or benzo[*a*]pyrene dominates severely weathered tar. Heavily and severely weathered tar oil exhibits corresponding losses

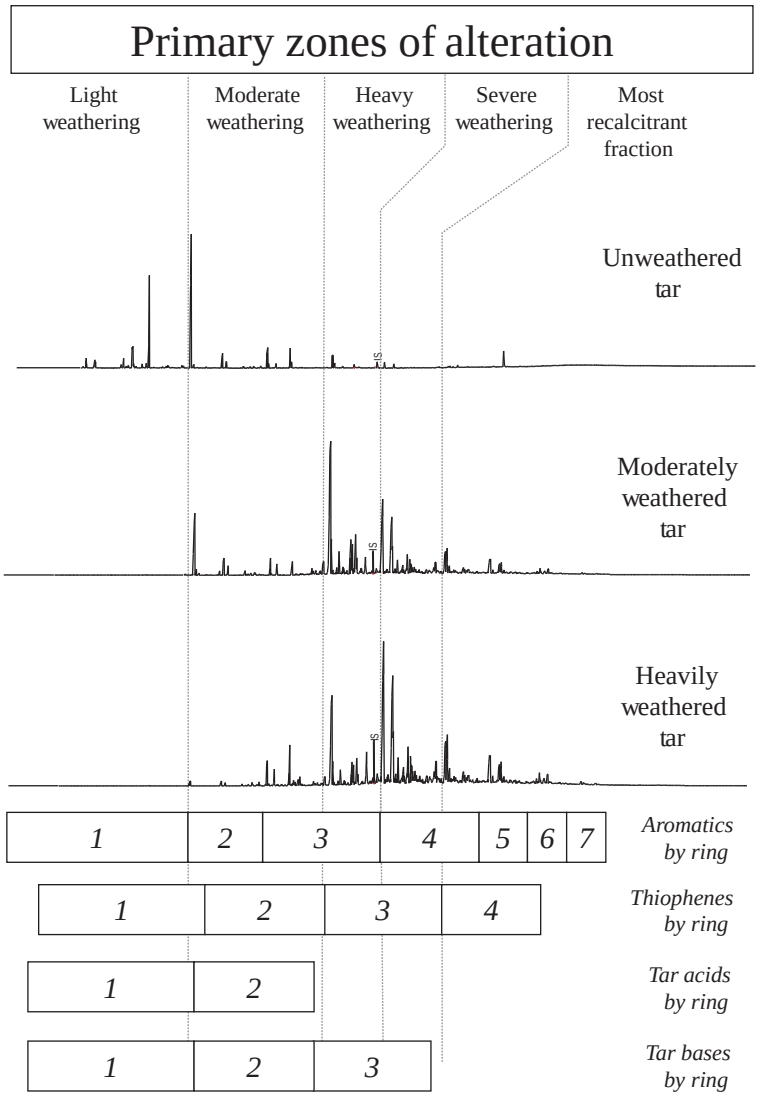

FIGURE 34.7 **Tar weathering:** Evaporation, biodegradation, dissolution and other weathering processes degrade lighter hydrocarbons (e.g., 1-ring PAHs) faster than heavier hydrocarbons (e.g., 2- to 3-ring PAHs) when exposed to the environment. The most recalcitrant hydrocarbons (e.g., 4- to 7-ring PAHs) can exhibit little to no chemical degradation over decades.

of aliphatics hydrocarbons, tar acids (e.g., phenols and cresols), tar bases (e.g., pyridines, anilines, quinolones, and carbazoles), and often the emergence of a late eluting UCM.

The PAH weathering rank (PWR) and PAH weathering index (PWI) provide semiquantitative and continuous indices for gauging tar oil weathering, respectively (Emsbo-Mattingly and Litman, 2016). The PWR is calculated using the concentrations of naphthalene (N0), phenanthrene (P0), pyrene (PY0), chrysene (C0), and benzo[*a*]pyrene (BAP); for example, the relative abundance of N0 is calculated as the concentration of N0/(N0 + P0 + PY0 + C0 + BAP), etc. The PAH with the highest relative abundance determines the rank as follows:

- PWR 1—Dominant naphthalene indicates light PAH weathering;
- PWR 2—Dominant phenanthrene indicates moderate PAH weathering;
- PWR 3—Dominant pyrene indicates heavy PAH weathering; and
- PWR 4—Dominant chrysene indicates severe weathering.

The PWR provides a robust framework for gauging environmental weathering in most hydrocarbon products that contain the most commonly measured PAH analytes.

The PWI is the ratio of the sum of 2- and 3-ring PAH concentrations (LPAH) divided by the TPAH49 concentration (Table 34.1). This PWI is simply an "a/(a + b)" version of the metrics proposed in Costa and Sauer (2005). This ratio provides a continuous variable for comparing relatively fresh hydrocarbon products and weathered hydrocarbon products.

34.6.5 Hydrocarbon Trends and Source Ratios

Hydrocarbon concentration trends and quantitative ratios help identify and track source signatures in urban environments. Careful inspection of the hydrocarbon chromatograms and patterns for each sample, as discussed previously, is a critical preliminary step for accurately interpreting the source ratios, because real world samples and laboratory data can possess interferences and anomalies that might otherwise bias or adversely affect the interpretation. That said, hydrocarbon trends and ratios are particularly effective at comparing hydrocarbon source signatures, weathering trends, and mixing gradients across large concentration ranges.

The selection of diagnostic ratios is flexible and requires knowledge about the properties associated with the compounds placed in the numerator and denominator. By placing one hydrocarbon analyte concentration in the numerator and a second hydrocarbon analyte concentration in the denominator, the ratio becomes dimensionless and concentration independent. In this way, hydrocarbon ratios from a high concentration source sample can be compared to a low concentration field sample potentially containing a small aliquot of the source material mixed with native sediment. The use of multiple hydrocarbon ratios can further increase the resolution of source and weathering signatures.

There are two general approaches to the construction of hydrocarbon ratios. First, the concentration of one hydrocarbon analyte can be divided by the concentration of another hydrocarbon analyte. This "a/b" structure is commonly used, but often requires further manipulation when the magnitude of the ratios vary widely. Second, the "a/(a + b)" structure is often preferred, because it scales the ratio to a decimal fraction between and including 0 to 1. The "a/(a + b)" structure helps standardize the range when comparing multiple hydrocarbon ratios to one another and serves as the primary structure used in the following quantitative analysis.

A comparison of candidate reference samples and field samples helps demonstrate the relationships between hydrocarbon concentrations and hydrocarbon ratios. This comparison focuses primarily on compositional differences among the candidate source reference samples introduced previously, because they represent the types of hydrocarbon signatures commonly encountered during tar oil investigations. The comparison also includes populations of sediments from four urban waterbodies with alleged impacts from tar and petroleum oils. The sediment samples represent varying concentrations and mixtures of hydrocarbons from multiple sources whose compositional trends and variability help illustrate real world conditions.

34.6.5.1 Aggregate Hydrocarbon Measurements

The TPH and EPAPAH16 concentrations in the reference samples are far greater than most of the sediment samples (Fig. 34.8A and B). The tar oil reference samples contain at least one order of magnitude greater PAH concentrations than the coal and petroleum reference samples. The remote sediment samples (TPH $<$ 200 mg/kg, EPAPAH16 $<$ 10 mg/kg) and urban background sediment samples (TPH $<$ 200 mg/kg and EPAPAH16 $<$ 300 mg/kg) are consistent with the hydrocarbons observed in other US sediments (Stout et al., 2004). Due to the high compositional variability among background samples, the subsequent plots retain only the urban background sediments and the case-study samples containing more than 10 mg/kg EPAPAH16, which signifies the approximate background concentrations for these field samples.

The general relationship between the source reference and case studies' field samples is explored by comparing the aggregate hydrocarbon concentrations and total PAH concentrations by ring number (Table 34.1). For example, the cross plot of the 2-ring/3-ring PAHs and 3-ring/4-ring PAHs depict the light PAH enrichment of fresh fossil fuels and refined products (upper right) compared to the devolatilized residual tar products, such as heavy gas oil, Tarvia, and pitch (lower left). The distillate and residual products mirror the range of weathering observed in the sediment samples (Fig. 34.8C). The case study sediment samples plotting between the urban sediment background samples and the light to medium distillate products suggest some degree of environmental weathering. The case-study samples on this plot reflect a combination of the product type and weathering trends. For example, the hydrocarbon fingerprints of the case-study samples collected near a petroleum refinery in the lower left exhibited heavy distillate fingerprints of mineral oil products most closely resembling lubricating oil, whereas the heavy petroleum in the samples plotting near the heavy gas oil sample exhibit a broad, late-eluting

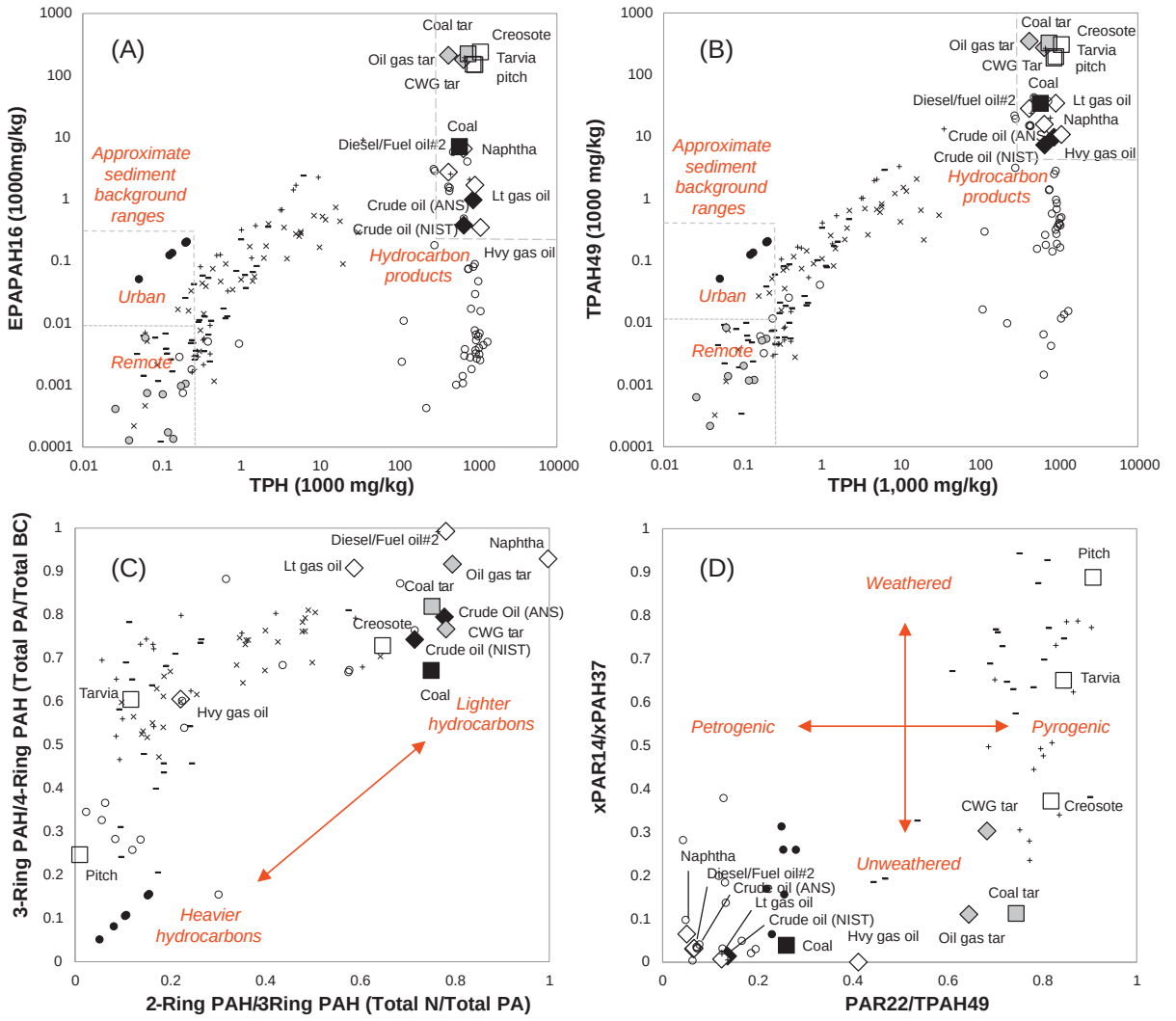

FIGURE 34.8 **Forensic hydrocarbon metrics:** The relative abundances of selected hydrocarbons help distinguish hydrocarbon sources and mixing gradients: (A) TPH and EPAPAH16 concentrations, (B) TPH and TPAH49 concentrations, (C) 2-, 3-, and 4-Ring PAH Ratios, and (D) Parent and Alkylated PAH ratios. See Tables 34.1 and 34.2 for metric definitions. The relative abundances of selected hydrocarbons help distinguish hydrocarbon sources and mixing gradients: (E) Alkylated Dibenzothiophene Ratios, (F) Alkylated Naphthobenzothiophene Ratios, (G) Petrogenic 4- and 5-Ring PAH Ratios, and (H) Diagenetic PAH Ratios. See Table 34.1 for compound identifications. The relative abundances of selected hydrocarbons help distinguish hydrocarbon sources and mixing gradients: (I) Fluoranthene and Benzofluoranthene Ratios, (J) Benz[*a*] anthracene and Indeno[1,2,3-*cd*]pyrene Ratios, (K) Methylnaphthalene and Methylfluorene Isomer Ratios, and (L) Methyldibenzothiophene Isomer Ratios. See Tables 34.1 and 34.2 for metric definitions. The relative abundances of selected hydrocarbons help distinguish hydrocarbon sources and mixing gradients: (M) Heaviest Petrogenic PAH Isomer Ratios, (N) Methylanthracene and Benzo[*b*]fluorene Isomer Ratios, (O) Methylchrysene and Ananthrene Isomer Ratios, and (P) Coronene and 302 PAH (Naphthopyrene, Dibenzopyrene, and Dibenzofluoranthene) Ratios. See Tables 34.1 and 34.2 for metric definitions. The relative abundances of selected hydrocarbons help distinguish hydrocarbon sources and mixing gradients: (Q) Sesquiterpane Ratios, (R) Triterpane Ratios, (S) Sterane Ratios, and (T) Hydrocarbon Ratio Allocation Model. See Tables 34.1 and 34.2 for metric definitions; "302" in (P) refers to sum of seven analytes per Table 34.2.

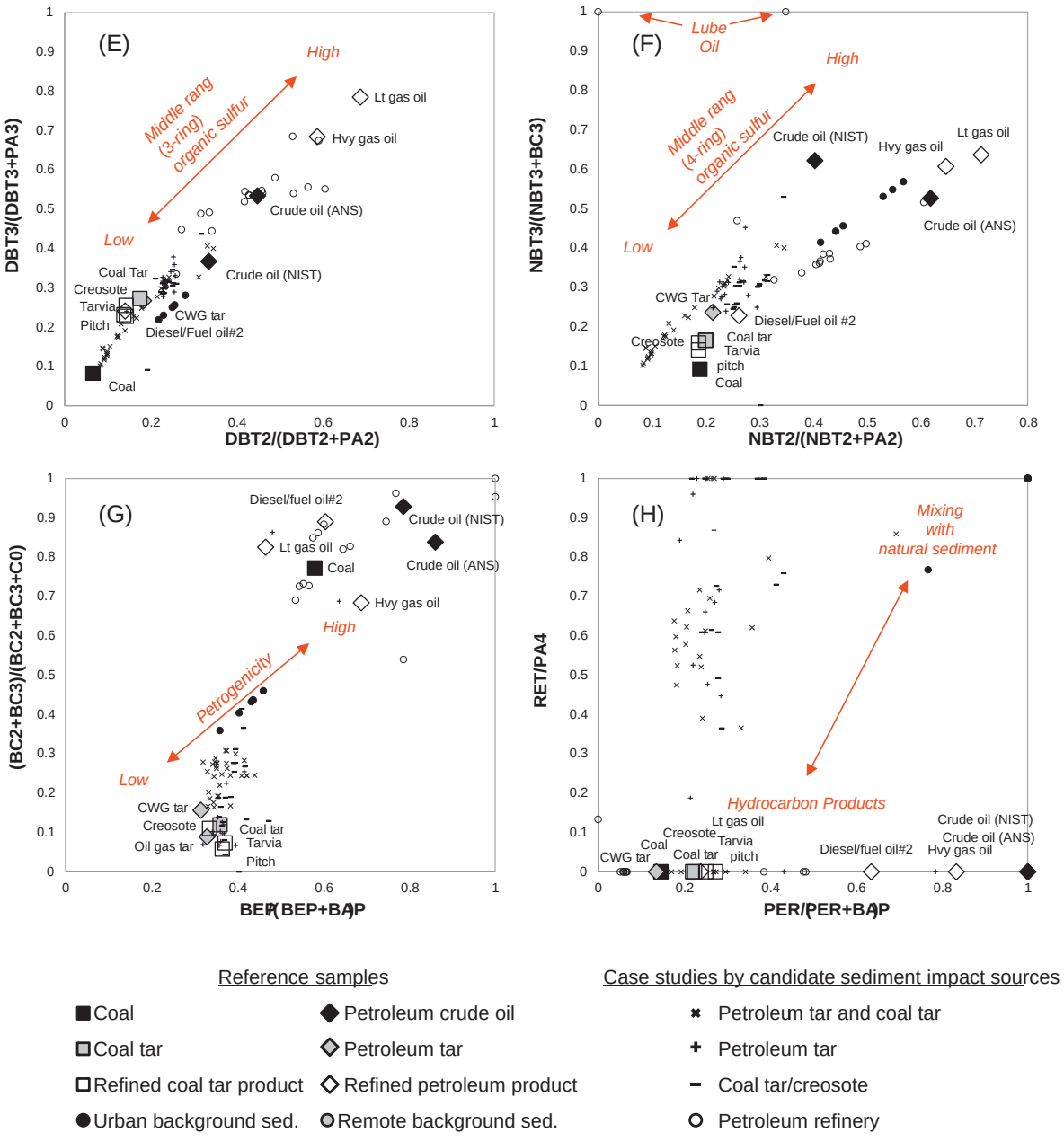

FIGURE 34.8 (Continued).

petroleum product attributed to abraded roadway pavement. Therefore, separating weathering and refining trends benefits from use of chromatographic data and additional hydrocarbon ratios.

The relative concentration of parent PAHs relative to total PAHs can be evaluated using a variety of analyte groupings. The plot of PAR22/TPAH49 from the forensic PAH analyte list (Table 34.1) and the xPAR14/xPAH37 from the extended PAH analyte list (Table 34.2) separates well samples with enriched petroleum product in the lower left, fresh tar oils in the lower right, and heavy hydrocarbon enrichment by weathering or refining toward the upper right (Fig. 34.8D). Consequently, the aggregate PAH analytes help explore source and weathering patterns across broad molecular weight ranges.

34.6.5.2 PAH Double Ratios

Environmental and geochemical scientists employ individual PAH analyte ratios for source identification purposes (Yunker and Macdonald, 1995; Dickhut et al., 1995; Emsbo-Mattingly et al., 2003a; Costa et al., 2004; Lima

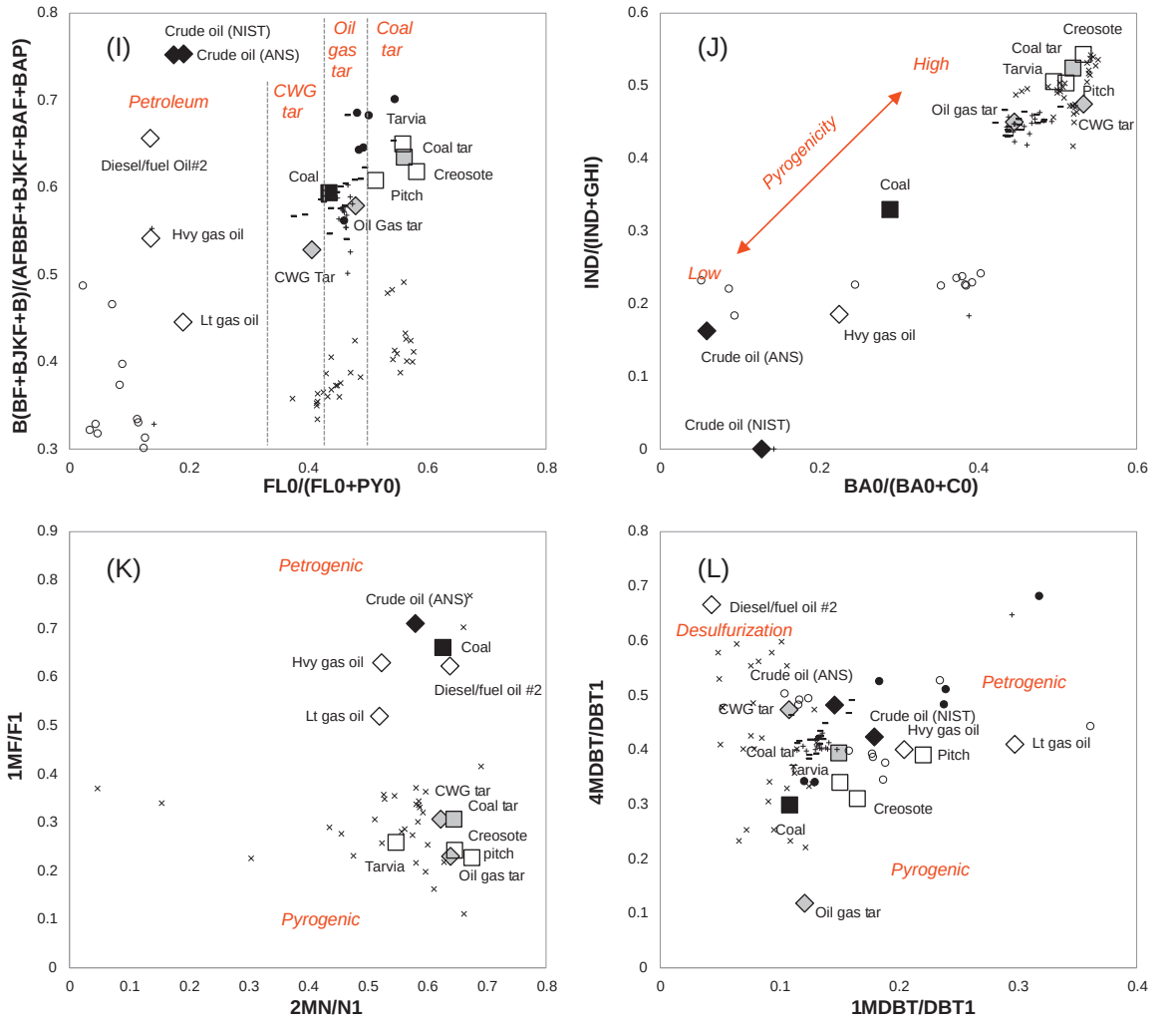

FIGURE 34.8 (Continued).

et al., 2005; Yunker et al., 2014; Stout et al., 2015). Studies of hydrocarbon product weathering under biotic and abiotic conditions demonstrate that some of the PAH source ratios are more affected by weathering than others (Uhler and Emsbo-Mattingly, 2006). PAH source ratios work best for tar oil spill investigations when the PAH analytes in the numerator and denominator exhibit similar propensities to degrade in the environment. As a rule of thumb, the PAH source ratio analytes should have similar molecular weights, vapor pressures, and aqueous solubilities. The following discussion focuses on the more recalcitrant PAH source ratios that demonstrate good source signature fidelity under light, moderate, and heavy environmental weathering conditions.

Dibenzothiophenes weather in the environment at similar rates as comparable phenanthrenes (Radke et al., 1991; Douglas et al., 1996). For this reason, the ratio of dialkyldibenzothiophenes relative to dialkylphenanthrenes and anthracenes (DBT2/PA2) and trialkyldibenzothiophenes relative to trialkylphenanthrenes and anthracenes (DBT3/PA3) are considered stable for most oil spill environments. The double ratio plot of DBT2/PA2 versus DBT3/PA3 provides a robust metric for distinguishing PAHs derived from independent sources based on differences in the

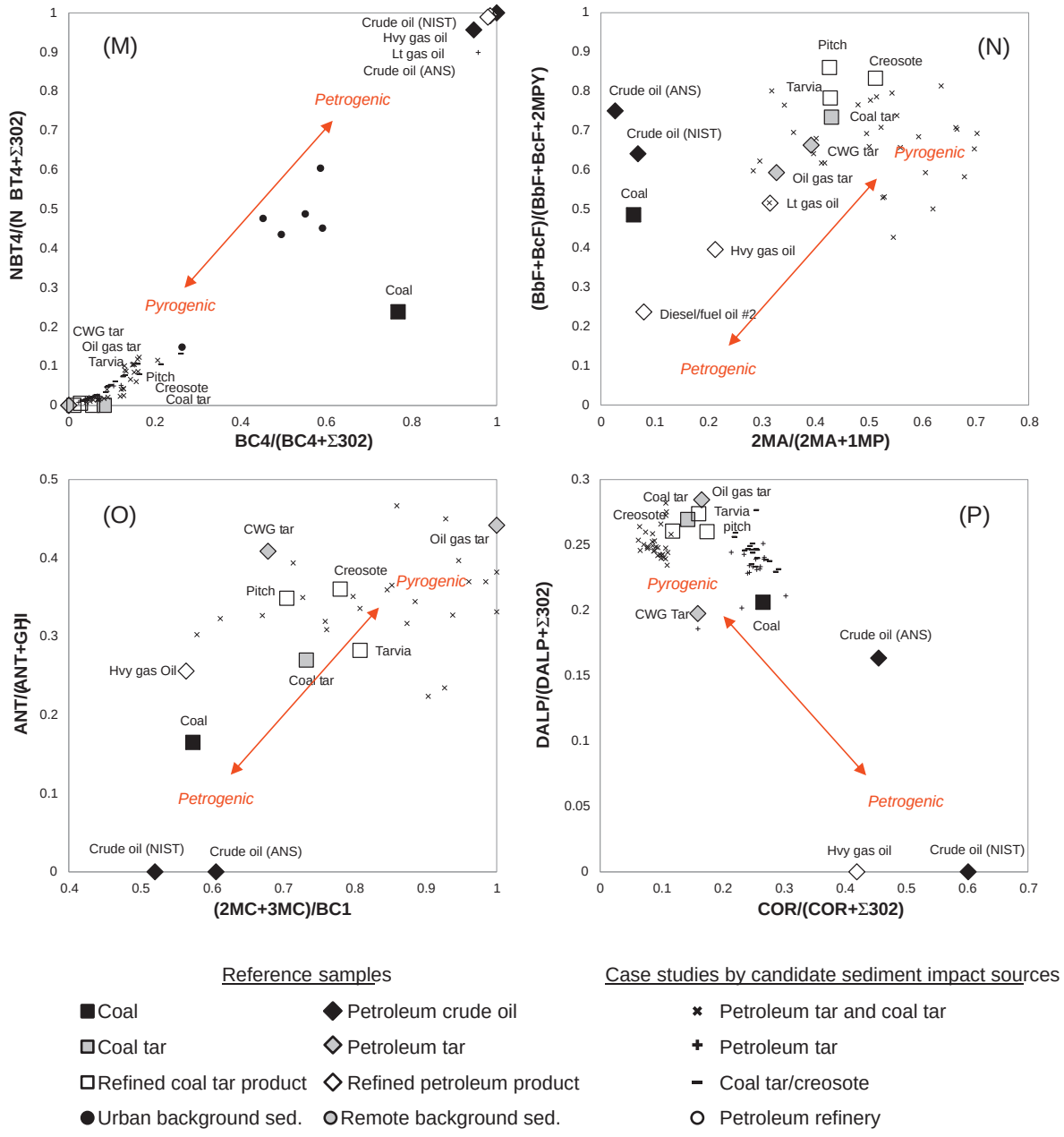

FIGURE 34.8 (Continued).

organic sulfur levels (Fig. 34.8E). The reference samples with the highest proportions of alkylated dibenzothiophenes include light gas oil and heavy gas oil likely due to the crude oil or the refining practices associated with each product. Inspection of the chromatograms indicates that most of the sediment samples with high organic sulfur contain mineral oil products resembling lubricating oils. The lowest proportions of alkylated dibenzothiophenes occur in the diesel sample and the tar oil products, which all experienced high temperature hydrocarbon catalysis associated with HDS and carbonization, respectively. This observation indicates that dibenzothiophenes are less thermally stable than comparable PAHs. Most of the sediment case-study samples contain low proportions of alkylated dibenzothiophenes, which suggests a combustion or carbonization origin.

Ratios of heavier PAHs with lower vapor pressures and solubilities are sometimes used when heavy petroleum products are involved or extreme weathering occurs; for example, ratios of dialkylnaphthobenzothiophenes relative to dialkylbenz[*a*]anthracenes and chrysenes (NBT2/BC2) and trialkylnaphthobenzothiophenes relative to trialkylbenz[*a*]anthracenes and chrysenes (NBT3/BC3) are considered stable for most oil spill investigations

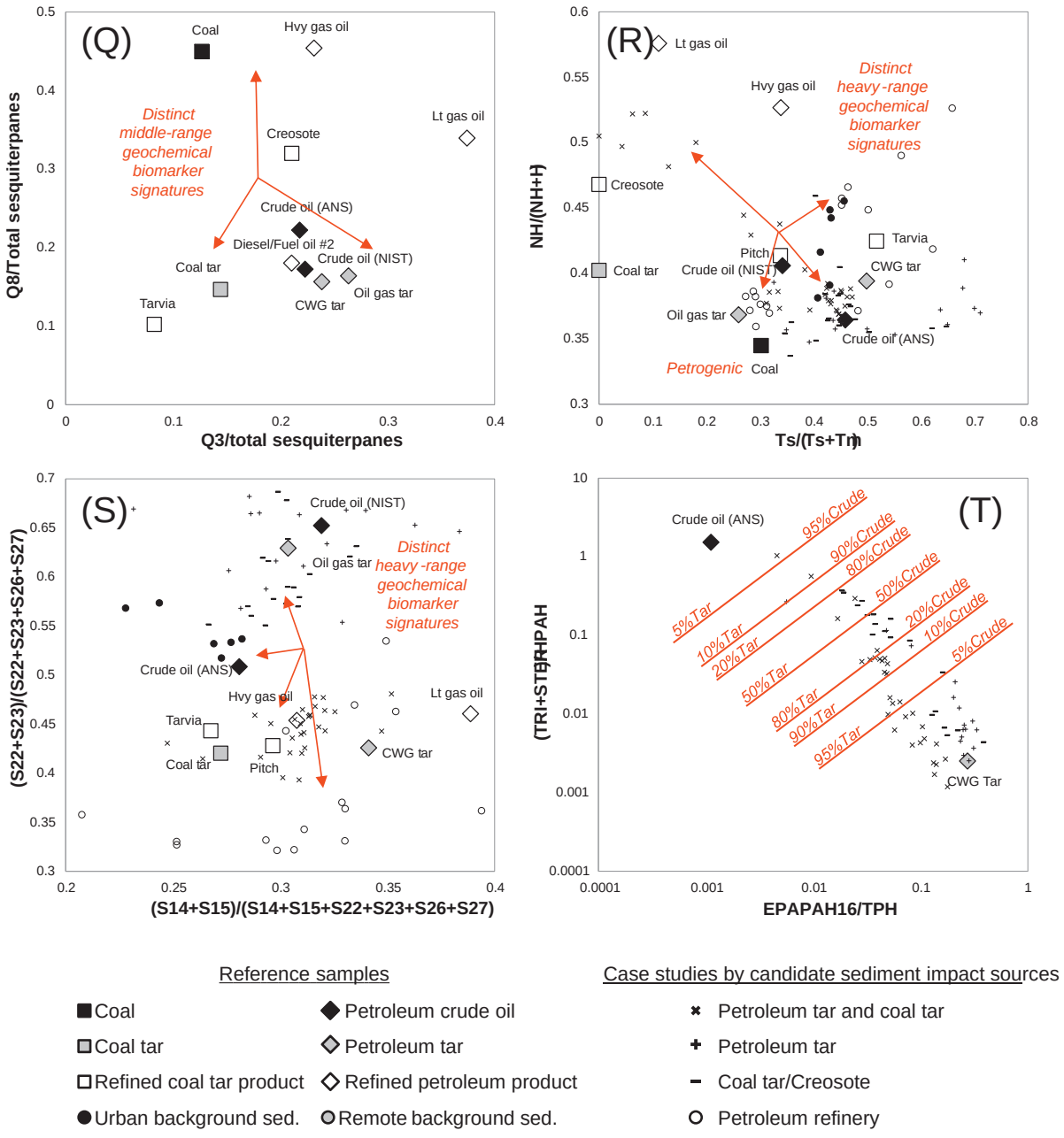

FIGURE 34.8 (Continued).

(Fig. 34.8F). The reference samples maintain similar positions relative to one another on the alkylated dibenzothiophene and naphthobenzothiophenes plots with differences largely explained by the molecular weight ranges of each hydrocarbon product. The case study sediment samples exhibit higher resolution in Fig. 34.8F compared to Fig. 34.8E. The chromatograms of the samples from the case study marked with "x" plotting closest to the origin exhibit weathered coal tar signatures with little UCM, while the remaining sediment from this case study plot closer to the CWG tar reference sample and exhibit a hydrocarbon fingerprint resembling tar oil with a heavy UCM. These observations suggest that the sulfur content of tar and petroleum oil residues possess useful hydrocarbon signatures within the 3- and 4-ring molecular weight ranges during tar oil spill investigations.

Petrogenic PAH source ratios emphasize differences among PAH analytes that are more abundant among fossil fuel products (Stout and Wang, 2008). For example, the BEP and alkylated benz[*a*]anthracene/chrysene concentrations tend to be higher than the BAP and parent benz[*a*]anthracene and chrysene concentrations in the

petroleum reference samples and sediment samples collected near a petroleum refinery (Fig. 34.8G). By contrast, reference samples and case study sediment samples enriched in pyrogenic PAHs plot in the lower left. This plot employs recalcitrant 4- and 5-ring PAHs to distinguish samples based on the degree of petrogenicity along a diagonal gradient from low petrogenicity in the lower left and high petrogenicity in the upper right. The chromatograms of the urban background samples confirm that they contain approximately equal proportions of petrogenic and pyrogenic PAHs. By extension, the case study sediment samples with alleged tar oil impacts appear to contain higher proportions of pyrogenic PAHs than explained by urban background sediment alone; consequently, tar oil impacts are possible.

Diagenetic PAH ratios help identify the presence of modern sediments in watersheds containing detrital vegetation from higher plants (Peters et al., 2005). The origin of perylene (PER) is debated; however, retene (RET) is attributed to the oxidation of conifer resin with an abietic acid origin. While these compounds can be measured in some coal and petroleum, the ratios of RET/PA4 and PER/BAP provide stable 4-and 5-ring metrics with source specific resolution (Fig. 34.8H). This cross plot demonstrates that the proportion of PER/BAP ranges widely among the reference samples, but none of the reference samples contain significant RET. This observation suggests that PER is more common or better conserved through petrogenesis, while RET is either more rare or less geochemically stable (Wakeman et al., 1980; Radke et al., 1991). In this way, RET serves an important function for the observation that many of the sediment samples that plot in the upper left contain naturally derived organic matter that is not associated with petroleum or tar reference samples.

Pyrogenic PAH source ratios emphasize differences among PAH isomers that are more abundant among combustion and carbonization products. The ratios of FL0/(FL0 + PY0) and (BBF + BJKF)/(BBF + BJKF + BAP) are particularly effective at differentiating PAHs for different pyrogenic sources. For example, uncombusted fossil fuels are thought to contain low proportions of fluoranthene, benzofluoranthene, and indeno[1,2,3-*c*,*d*]pyrene, because PAHs with 5-member rings are not geochemically favored relative to PAHs with 6-member rings, such as PY0, BAP, and GHI, respectively. The abundance of PAHs with 5-member rings increases with greater exposure to higher temperatures and catalytic cracking (Emsbo-Mattingly and Litman, 2016). Hydrocarbon residues generally exhibit the following trend:

Fossil Fuel: $0 \leq$ FL0/(FL0 + PY0) $<$ 0.33; Low BA0/(BA0 + C0); Low IND/(IND + GHI)
Low Temperature Process: 0.33 $<$ FL0/(FL0 + PY0) $\leq$ 0.5
High Temperature Process: 0.5 $<$ FL0/(FL0 + PY0); High BA0/(BA0 + C0); High IND/(IND + GHI)

Similarly, the configuration of PAHs with 3 or more linear rings, like anthracene (A0) and benz[*a*]anthracene (BA0), are less geochemically favored relative to bent PAHs, such as P0 and C0, respectively. Based on personal experience, the thresholds for FL0/(FL0 + PY0) are observed in many sites throughout the world; however, the threshold for pyrogenic PAH source ratios with BBF, BJKF, IND, A0, and IND are not as clearly defined and are often site-specific (Fig. 34.8I and J).

The use of quantitative PAH ratios is constantly expanding to include additional analytes with source specific properties. For example, petrogenic PAH isomer ratios can focused on the ratios of 2-methylnaphthalene relative to the total concentration of total methylnaphthalenes (2MN/N1) is typically greater than 0.5 except when the hydrocarbon product exhibits an atypical refinery signature or advanced weathering (Fig. 34.8K). The ratio of 1-methylflourene relative to total methylflourenes (1MF/F1) is generally high in fossil fuel products and low in pyrogenic products. These analytes were only measured for one of the case studies in this chapter. The case-study samples plotting in the lower right of the 2MN/N1 and 1MF/F1 cross plot contain tar oil residue. The sediments plotting in the lower left corner were among the most weathered, while the sediment plotting in the upper right most closely resembled petroleum asphalt with a large heavy UCM.

Some PAH ratios are particularly sensitive to pyrolysis, while others are thermodynamically stable. Among the methyldibenzothiophene isomers (DBT1), 1-methyldibenzothiophene (1MDT) is least stable and 4-methyledibenzothiophene (4MDT) is most stable (Farag et al., 2000; Schade et al., 2002). The cross plot of 1MDBT/DBT1 versus 4MDBT/DBT1 exploits differences in thermodynamic stability to differentiate hydrocarbon sources. This double ratio plot positions crude petroleum and straight distillates on the right, hydrodesulfurized distillates to the upper left, and pyrogenic hydrocarbons to the lower left (Fig. 34.8L).

Additional PAH isomer ratios help separate samples with heavier range petrogenic origins. The heaviest range alkylated PAHs BC4 and NBT4 are abundant in heavy fossil fuel residues. Some of the heaviest pyrogenic PAHs measured by advanced commercial laboratories are naphthopyrenes, dibenzopyrenes, and dibenzofluoranthenes with molecular weights of 302 amu (Table 34.2). The sum of the concentrations of these 6-ring PAHs is

collectively termed the "302" concentration. Double ratio plots of BC4/(BC4 + 302) and NBT4/(NBT4 + 302) separate heavy petrogenic from pyrogenic hydrocarbons dramatically (Fig. 34.8M).

Advanced forensic PAH testing methods are also capable of measuring a range of pyrogenic PAH isomers (Table 34.2). These additional isomer concentrations are used to construct pyrogenic PAH isomer ratios. For example, the ratios of 2MA/(2MA + 1MP) and (BbF + BcF)/(BbF + BcF + 2MPY) are high in pyrogenic products and low in petrogenic distillates (Fig. 34.8N). Similarly, the ratios of 2- and 3-methylchrysenes to the total sum of methylchrysenes ([2MC + 3MC]/BC1) and the concentration of ananthrene relative to the 302 PAHs (ANT/[ANT + 302]) are high in pyrogenic products and low in petrogenic products (Fig. 34.8O).

One of the more powerful new double ratio plots includes the ratios of coronene and dibenzo(a,l)pyrene relative to the sum of the 302 PAHs (COR/[COR + 302] versus DALP/[DALP + 302]). The reference samples that contain heavy petroleum are enriched in COR and plot in the lower right, soot laden samples in the upper half of the plot, and pyrogenic products plot in the upper left (Fig. 34.8P). Many of the sediment samples with petroleum tar impacts plot tightly near the creosote reference sample. Careful inspection of the PAH pattern of these sediment samples indicates an oil tar pattern based on the ratio of FL0/(FL0 + PY0). By comparison, the COR/(COR + 302) is significantly lower than the other case-study samples with alleged tar oil impacts. Therefore, this cross plot highlights ratios that are sensitive to differences in the type and condition of the feedstock pyrolysis and pyrosynthesis.

34.6.5.3 Geochemical Biomarker Double Ratios

Geochemical biomarker patterns focus on the genetic signature of the fossil fuel to differentiate hydrocarbon products. As discussed elsewhere in this book, there are many differences among the relative abundances of geochemical biomarkers that indicate different biomass types, geological periods, depositional environments, and maturity states. The novelty here is that the biomarker patterns of fossil fuels and refined petroleum products can be directly compared to those of the trace feedstock residues in tar oil products—when the latter are properly prepared (F1 fractions) and analyzed.

Sesquiterpanes exhibit distinct middle range hydrocarbon signatures. As previously discussed, the abundances of Q03 and Q08 relative to the total sesquiterpane (TSES) concentration provide the basis for constructing a cross plot of Q03/TSES versus Q08/TSES (Fig. 34.8Q). These metrics strongly separate the coal, light gas oil, heavy gas oil, coal tar, and Tarvia. Additional ratios could be drawn upon as needed to evaluate the biomarker patterns in the crude oil, diesel/fuel oil #2, and petroleum tars.

The cross plot of higher molecular weight triterpane biomarkers Ts/(Ts + Tm) versus NH/(NH + H) help distinguish the source signatures among most of the petroleum and tar oil reference samples (Fig. 34.8R). The source signatures of the "x" case-study samples cluster in several different groups signifying several potentially different sources (i.e., cluster 1 is proximal to the oil gas tar, cluster 2 is proximal to the ANS crude oil, cluster 3 is in the upper left, and cluster 4 is intermediate between the other cluster, likely indicating a "mixed" signature). The samples from the " + " case study primarily plot in the lower right quadrant indicating a distinct source relative to the "x" case study sediment samples.

Sterane biomarker patterns provide additional resolving power for the higher molecular weight range. The ratio of 14β(*H*),17β(*H*)-cholestanes (S14 + S15) and 14β(*H*),17β(*H*)-methylcholestane (C22 + C23) relative to total 14β(*H*),17β(*H*)-cholestanes + methylcholestanes + ethylchloestanes (S14 + S15 + S22 + S23 + S26 + S27) distinguishes the feedstocks in the " − " coal tar/creosote case study (upper quadrants), "x" petroleum and coal tar case study (middle), and "o" petroleum refinery case study (lower quadrants) sediment samples (Fig. 34.8S). Combining the triterpane and sterane biomarker ratios is especially useful when the case study compares source samples from multiple candidate source areas and proximal sediment samples.

34.6.5.4 Allocation

Double ratios help allocate the percentage of tar and petroleum oil in each sample. Allocations using double ratio plots are most easily completed by first using the chromatograms, signature plots, and double ratios to determine the samples that match the candidate source samples. Second, plot the source and impacted samples using aggregate measurements, if possible, because they are less sensitive to subtle shifts in the hydrocarbon source signature evident in specific analyte ratios (Fig. 34.8T). Third, mathematically mix specific ratios of each source sample and plot with the case-study samples. However, the mixing of ratios is not linear owing to the varying concentrations in source materials. Therefore any mixing models used for allocation must account for absolute concentrations of the ratios' analytes among the various source samples. The plot of EPAPAH16/TPH versus (TRI + STER)/HPAH illustrates how the mixtures of tar and petroleum oils are more widely mixed in the

"x" case study compared to the " + " case study. The mixing regression can be used to estimate the specific allocation of tar and petroleum oils in each impacted sample. Ultimately, these percentages can be used to allocate site investigation or remediation costs.

34.7 CONCLUSION

Hydrocarbons products contain a large number of individual compounds and patterns capable of identifying the source of tar oils, degree and type of weathering, and relative amounts of each product when mixing occurs. Tar oils form from fossil fuel products at high temperatures. Coal gas plants and coke byproduct ovens generate coal tar byproducts. CWG plants generate petroleum tars by cracking naphtha or gas oil in a carburetor. Pacific oil gas plants generated petroleum tar oils by cracking crude and residual oils, while high Btu oil gas plants used heavy gas oil carburetion fluids. The combination of fossil fuel feedstock (e.g., coal, naphtha, and gas oils), the temperatures of pyrolysis and pyrosynthesis, the presence of catalytic surfaces, and the process of tar condensation control the composition of the tar oil byproduct. Advance forensic analyses demonstrate the relationship between the manufacturing process and the hydrocarbon chemistry with a sufficient resolution for accurately identifying and differentiating pyrogenic and petrogenic products in the environment.

The wide range of hydrocarbons helps determine the type, origin, and source of the tar oils in the environment. Aromatic hydrocarbons are the dominant volatile and semivolatile hydrocarbons in tar oils. High resolution hydrocarbon fingerprints resolve the dominant 1- to 7-ring aromatics in tar oils and help match candidate source and field samples. Benzene, toluene, ethylbenzene, xylenes, styrene, indane, indene, phenols, cresols, and others help characterize fresh tar oils and differentiate them from crude oil and refined petroleum products. Detailed measurements of forensic PAHs include 22 parent, 27 alkylated, and 2 diagenetic PAH analytes are discussed for numerous tar and petroleum oil reference samples. These hydrocarbon patterns help distinguish fresh and weathered tar oil signatures in the environment. Extended measurements of 14 parent and 23 alkylated PAH isomers include a selection of heavier PAH isomers (i.e., "302") that offer high signature fidelity when needed. No single or small suite of metrics can universally distinguish tar oils from petroleum oils, or tar oils of different origins. However, when used in combination and in consideration of site-specific data the use of numerous metrics can provide a basis to distinguish these hydrocarbon sources and develop means for allocation among them.

Careful isolation of trace aliphatic hydrocarbons reveals the type of feedstock used to generate the tar. The aliphatic hydrocarbons, such as normal alkanes and acyclic isoprenoid hydrocarbons, are particularly well suited for determining the molecular weight range and the degree of biodegradation of tar oils. The geochemical biomarker patterns represent some of the more recalcitrant compounds in tar oils and serve well to differentiate tar and petroleum oil releases when mixtures occur in the environment. This chapter presents and discusses the signature diversity available by increasing the number of parent and alkylated PAH isomers for source identification and allocation purposes.

References

Bateman, E., 1922. Coal-Tar and Water-Gas Tar Creosotes: Their Properties and Methods of Testing. Professional Paper. United States Department of Agriculture Bulletin No. 1036. Government Printing Office, Washington, DC.

Blumer, M., 1976. Polycyclic aromatic hydrocarbons in nature. Sci. Am. 234 (3), 34–45.

Boehm, P.D., Farrington, J.W., 1984. Aspects of the polycyclic aromatic hydrocarbon geochemistry of recent sediments in the Georges Bank region. Environ. Sci. Technol. 18 (11), 840–845.

Castaneda, C.J., 2009. History of natural gas. In: Cleveland, C.J. (Ed.), Concise Encyclopedia of History of Energy. Elsevier, New York, pp. 163–174.

Colombo, J.C., Pelletier, E., Brochu, C., Khalil, M., 1989. Determination of hydrocarbon sources using *n*-alkane and polyaromatic hydrocarbon distribution indexes: Case Study—Rio de La Plata Estuary, Argentina. Environ. Sci. Technol. 23, 888–894.

Costa, H.J., Sauer, T.C., 2005. Forensic approaches and considerations in identifying PAH background. Environ. Forensics 6, 9–16.

Costa, H.J., White, K.A., Ruspantini, J.J., 2004. Distinguishing PAH background and MGP residues in sediments of a freshwater creek. Environ. Forensics 5, 171–182.

Dickhut, R.M., Canuel, E.A., Gustafson, K.E., Liu, K., Murray, K.Y., Walker, S.E., et al., 1995. Atmospheric inputs of selected polycyclic aromatic hydrocarbons and polychlorinated biphenyls to southern Chesapeake Bay. Mar. Poll. Bull. 30, 385–396.

Douglas, G.S., Bence, A.E., Prince, R.C., McMillen, S.J., Butler, E.L., 1996. Environmental stability of selected petroleum hydrocarbon source and weathering ratios. Environ. Sci. Technol. 30, 2332–2339.

Douglas, G.S., Emsbo-Mattingly, S.D., Stout, S.A., Uhler, A.D., McCarthy, K.J., 2015. Hydrocarbon fingerprinting methods. In: Murphy, B.L., Morrison, R.D. (Eds.), Introduction to Environmental Forensics, third ed. Academic Press, San Diego, CA, pp. 201–309.

Electric Power Research Institute, 1993. Chemical and Physical Characteristics of Tar Samples from Selected Manufactured Gas Plant (MGP) Sites. EPRI TR-102184.

Emsbo-Mattingly, S.D., Litman, E., 2016. Polycyclic aromatic hydrocarbon homolog and isomer fingerprinting. In: Stout, S.A., Wang, Z. (Eds.), Standard Handbook of Oil Spill Environmental Forensics: Fingerprinting and Source Identification, second ed. Elsevier Publishing Co., Boston, MA, ISBN 9780128038321.

Emsbo-Mattingly, S.D., Boehm P.D., Coleman, A., 2003a. Identifying PAHs from Manufactured Gas Plant Sites. EPRI Technical Report 1005289, Palo Alto, CA.

Emsbo-Mattingly, S.D., Stout, S.A., Uhler, A.D., and McCarthy, K.J., 2003b. Identifying Creosote Releases in the Environment. In: American Wood Preservers Association Proceedings, 99th Annual Mtg., Boston, MA.

Farag, H., Mochida, I., Sakanishi, K., 2000. H2S and aromatic effects on hydrodesulfurization of dibenzothiophenes over CoMo/C catalyst. In: Song, C., Hsu, C., Mochida, I. (Eds.), Chemistry of Diesel Fuels. Taylor & Francis, New York, pp. 123–138.

Gary, J.H., Handwerk, G.E., 1984. Petroleum Refining. Marcel Dekker, Inc., New York, NY.

Graham, S.C., Homer, J.B., Rosenfeld, J.L.J., 1975. The formation and coagulation of soot aerosols generated by the pyrolysis of aromatic hydrocarbons. Proc. R. Soc. London, Ser. A: Math. Phys. Sci. 344 (1637), 259–285.

Harkins, S.M., Truesdale, R.S., Hill, R., Hoffman, P., Winters, S., 1988. EPA /600/2-012, U.S. Production of Manufactured Gases: Assessment of Past Disposal Practices. EPA ORD Hazardous Waste Engineering Research Laboratory.

Hatheway, A.W., 2012. Remediation of Former Manufactured Gas Plants and Other Coal-Tar Sites. CRC Press, New York, p. 1354.

Hayes, T.D., Linz, D., Nakles, D., Leuschner, A., 1996. Management of Manufactured Gas Plant Sites, Vol. 1. American Scientific Publishers, Wastes and Chemicals of Interest pp. 599.

Kaplan, I.R., Galperin, Y., Lu, S.T., Lee, R.P., 1997. Forensic environmental geochemistry: differentiation of fuel-types, their sources and release time. Org. Geochem. 27 (5/6), 289–317.

Kennicutt, M.C., Comet, P.A., 1992. Resolution of sediment hydrocarbon sources: multiparameter approaches. In: Whelan, J.K., Farrington, J. W. (Eds.), Organic Matter: Productivity, Accumulation, and Preservation in Recent and Ancient Sediments. Columbia University Press, NY, pp. 308–338.

Laflamme, R.E., Hites, R.A., 1978. The global distribution of polycyclic aromatic hydrocarbons in recent sediments. Geochim. Cosmochim. Acta. 42, 289–303.

Leffler, W.L., 2000. Petroleum Refining, third ed. PennWell Corp., Tulsa, OK.

Lima, A.L., Farrington, J., Reddy, C., 2005. Combustion derived polycyclic aromatic hydrocarbons in the environment—a review. Environ. Forensics 6, 109–131.

Morgan, J.J., 1926. Manufactured Gas: A Textbook of American Practice, first ed. Jerome J. Morgan, New York, NY.

National Oceanic and Atmospheric Administration, 1998. Trace organic analytical procedures. Sampling and Analytical Methods of the National Status and Trends Program Mussel Watch Project: 1993–1996 Update. NOAA Technical Memorandum NOS/ORCA/CMBAD 130. National Oceanic and Atmospheric Administration, Silver Spring, MD.

Ohkouchi, N., Kawamura, K., Kawahata, H., 1999. Distributions of three-to seven ring polynuclear aromatic hydrocarbons on the deep seafloor of the Central Pacific. Environ. Sci. Technol. 33, 3086–3090.

Peters, K.E., Walters, C.C., Moldowan, J.M., 2005. The Biomarker Guide: Biomarkers and Isotopes in Petroleum Exploration and Earth History. Cambridge University Press, United Kingdom.

Radke, M., Welte, D.H., Willsch, H., 1991. Distribution of alkylated aromatic hydrocarbons and dibenzothiophenes in rocks of the upper Rhine Graben. Chem. Geol. 93, 325–341.

Rhodes, E.O., 1945. The Chemical Nature of Coal Tar. In: Lowry, H.H. (Ed.), National Research Council Committee Chemistry of Coal Utilization, Vol. II. John Wiley & Sons, Inc., United States, pp. 1287–1370. 1945; v.

Sauer, T.C., Uhler, A.D., 1994. Pollutant source identification and allocation: advances in hydrocarbon fingerprinting. Remediation, Winter Issue, pp. 25–50.

Schade, T., Roberz, B., Andersson, J.T., 2002. Polycyclic aromatic sulfur heterocycles in desulfurized Diesel fuels and their separation on a novel palladium(II) complex stationary phase. Polycyclic Arom. Comp. 22, 311–320.

Scott, L.T., 1982. Thermal rearrangements of aromatic compounds. Acc. Chem. Res. 15, 52–58.

Simmons, I.G., 2009. Environmental change and energy. In: Cleveland, C.C. (Ed.), Concise Encyclopedia of Energy. Elsevier, Boston, pp. 94–104.

Stout, S.A., Wang, Z., 2008. Diagnostic compounds for fingerprinting petroleum in the environment. Environ. Forensics. R. E. H. Hester, R.M. Lond. Spec. Publ. No. 26, 54–104.

Stout, S.A., Uhler, A.D., Emsbo-Mattingly, S.D., 2004. Comparative evaluation of background anthropogenic hydrocarbons in surficial sediments from nine urban waterways. Environ. Sci. Technol. 38, 2987–2994.

Stout, S.A., Uhler, A.D., McCarthy, K.J., 2005. Middle distillate fuel fingerprinting using drimane-based bicyclic sesquiterpanes. Environ. Forensics 6 (3), 241–252.

Stout, S.A., Emsbo-Mattingly, S.D., Douglas, G.S., Uhler, A.D., McCarthy, K.J., 2015. Beyond 16 priority pollutants: a review of PACs used in environmental forensics. Polycyclic Arom. Comp. 35, 285–315.

Swaine, D.J., 1990. Trace Elements in Coal. Butterworth & Company Publishers, London, p. 278.

Taylor, G., Teichmuller, M., Davis, A., Diesel, C., Littke, R., Robert, P., 1998. Organic Petrology. Gebruder Borntraeger, Berlin.

Tissot, B.P., Welte, D.H., 1978. Petroleum Formation and Occurrence: A New Approach to Oil and Gas Exploration. Springer-Verlag, Berlin Heidelberg, Germany, p. 460.

Tissot, B.P., Welte, D.H., 1984. Petroleum Formation and Occurrence. Second revised and enlarged edition. Springer-Verlag, New York, p. 699.

Uhler, A.D., Emsbo-Mattingly, S.D., 2006. Environmental stability of PAH source indices in pyrogenic tars. Bull. Env. Cont. Tox. 76, 689–696.

Uhler, A.D., Emsbo-Mattingly, S.D., Liu, B., Hall, L.W., Burton, D.T., 2005. An integrated case study for evaluating the impacts of an oil refinery effluent on aquatic biota in the Delaware river: advanced chemical fingerprinting of PAHs. Hum. Ecol. Risk Assess. 11, 771–836.

Uhler, A.D., Stout, S.A., Douglas, G.D., 2007. Chemical heterogeneity in Modern Marine Residual Fuel Oils. In: Wang, Z., Stout, S. (Eds.), Oil Spill Forensics. Associated Press, Boston, pp. 327–348.

United States Environmental Protection Agency, 2009. Test methods for evaluating solid waste (SW-846), Final Updates I, II, IIA, IIB, III, IIIA, IIIB and IV. USEPA Office of Solid Waste and Emergency Response, Washington, DC, <http://www.epa.gov/wastes/hazard/test-methods/sw846/online/index.htm>.

Wakeman, S., Schaffner, C., Giger, W., 1980. Polycyclic aromatic hydrocarbons in recent lake sediments—II. Compounds derived from biogenic precursors during early diagenesis. Geochim. Cosmochim. Acta. 44, 415–429.

Wang, Z., Yang, C., Fingas, M., Hollebone, B., Yim, U.H., Oh, J.R., 2007. Petroleum biomarker fingerprinting for oil spill characterization and source identification. In: Wang, Z., Stout, S. (Eds.), Oil Spill Forensics. Associated Press, Boston, pp. 73–146.

Youngblood, W.W., Blumer, M., 1975. Polycyclic aromatic hydrocarbons in the environment: homologous series in soils and recent marine sediments. Geochim. Cosmochim. Acta. 39, 1303–1314.

Yunker, M.B., Macdonald, R.W., 1995. Composition and origins of polycyclic aromatic hydrocarbons in the Mackenzie River and on the Beaufort Sea shelf. Arctic 48, 118–219.

Yunker, M.B., McLaughlin, F.A., Fowler, M.G., Fowler, B.R., 2014. Source apportionment of the hydrocarbon background in sediment cores from Hecate Strait, a pristine sea on the west coast of British Columbia, Canada. Org. Geochem. 76, 235–258.

Zeigler, C., Kevin MacNamarab, K., Wang, Z., Robbat, A., 2008. Total alkylated polycyclic aromatic hydrocarbon characterization and quantitative comparison of selected ion monitoring versus full scan gas chromatography/mass spectrometry based on spectral deconvolution. J. Chromatogr. A. 1205, 109–116.

Zevenhoven, R., Kilpinen, P., 2002. VOCs, PAHs, Soot, Tar, CO. In: Control of Pollutants in Flue Gases and Fuel Gases, Ch 6. ISBN 951-22-5527-8 p. 6-1 to 6-19.

Index

Note: Page numbers followed by "*f*" and "*t*" refer to figures and tables, respectively.

D

Q

R

S

T

OIL SPILL ENVIRONMENTAL FORENSICS CASE STUDIES

Edited by **Scott A. Stout** and **Zhendi Wang**

Review the recent developments in environmental forensics analysis methodologies frequently used in oil spill investigations.

- Each chapter presents one or more cases on the application of specific oil spill environmental forensic techniques
- Chapters written by international experts from both academia and practice as standalone contributions
- Relevant concepts and theories are elucidated in at least one chapter in each theme

Oil Spill Environmental Forensics Case Studies includes 34 chapters that serve to present various aspects of environmental forensics in relation to "real-world" oil spill case studies from around the globe. Authors representing academic, government, and private researcher groups from 14 countries bring a diverse and global perspective to this volume.

Oil Spill Environmental Forensics Case Studies addresses releases of natural gas/methane, automotive gasoline and other petroleum fuels, lubricants, vegetable oils, paraffin waxes, bitumen, manufactured gas plant residues, urban runoff, and, of course, crude oil, the latter ranging from light Bakken shale oil to heavy Canadian oil sands oil. New challenges surrounding forensic investigations of stray gas in the shallow subsurface, volatiles in air, dissolved chemicals in water (including passive samplers), and biological tissues associated with oil spills are included, as are the effects and long-term oil weathering, long-term monitoring in urbanized and non-urbanized environments, fate and transport, forensic historical research, new analytical and chemical data processing and interpretation methods.

RELATED TITLES

Fingas / *Oil Spill Science and Technology* / 9781856179430

Wang and Stout / *Oil Spill Environmental Forensics: Fingerprinting and Source Identification* / 9780123695239

Kletz / *What Went Wrong? Case Histories of Process Plant Disasters and How They Could Have Been Avoided* / 9781856175319

Engineering, Environmental Engineering, Management

ISBN 978-0-12-804434-6

9 780128 044346

ELSEVIER

Butterworth-Heinemann
An imprint of Elsevier
elsevier.com/books-and-journals